General Report of TC 212
Deep Foundations

Rapport général du TC 212
Fondations profondes

Katzenbach R.
Institute and Laboratory for Geotechnics, Department of Civil Engineering and Geodesy, Technical University Darmstadt, Darmstadt, Germany.

Choudhury D.
Department of Civil Engineering, Indian Institute of Technology Bombay, Mumbai, India.

Chang D.W.
Department of Civil Engineering, Tamkang University, New Taipei City, Taiwan.

ABSTRACT: This general report is prepared from the selected 62 papers of 18 ICSMGE which are related to the domain of studies for ISSMGE Technical Committee TC 212 – Deep Foundations. Paper IDs 1691~3105, which are presented during two sessions of TC 212 – Deep Foundations are from 26 member societies, which include Algeria (1), Argentina (1), Australia (6), Brazil (7), Bulgaria (1), Canada (3), China (2), Finland (2), Denmark (1), Egypt (3), France (4), Germany (1), Hungary (2), India (2), Iran (1), Italy (1), Japan (4), Korea (3), Mexico (1), Netherland (1), Poland (2), Russia (2), Thailand (1), UK (5), USA (4) and Vietnam (1). Value in parenthesis indicates number of papers from that particular member society. The subjects of these papers cover a variety of sub-themes like (i) foundation behaviour and performance (15), (ii) technologies for construction, rehabilitation and energy (6), (iii) analytical and numerical analyses on piles and pile-raft foundation (20), (iv) field measurements (5), (v) seismic hazard analysis (2), (vi) design methods and assessments (2), (vii) model testing, soil behaviours on soil-pile interactions (8), (viii) predictions from testing methods (4).

RÉSUMÉ : Ce rapport général est préparé à partir des 62 articles proposés au 18ème CIMSG concernant les Fondations profondes, le domaine du Comité Technique TC 212 de la SIMSG,. Les articles No. 1691 - 3105, qui sont présentés pendant les deux sessions du TC 212 - Fondation profondes, proviennent de 26 sociétés membres dont Algérie (1), Argentine (1), Australie (6), Brésil (7), Bulgarie (1), Canada (3), Chine (2), Finlande (2), Danemark (1), Egypte (3), France (4) Allemagne (1), Hongrie (2), Inde (2), Iran (1), Italie (1), Japon (4), Corée du Sud (3), Mexique (1), Pays-Bas (1), Pologne (2), Russie (2), Thaïlande (1), Royaume-Unis (5), Etats-Unis (4) et Vietnam (1). Les chiffres entre parenthèses montrent le nombre de papiers venant de chaque société membre. Les sujets des papiers couvrent plusieurs sous-thèmes comme (i) le comportement et les performances des fondations (15), (ii) les technologies de construction, réhabilitation et énergie (6), (iii) les analyses analytique et numérique des pieux et radiers sur pieux (20), (iv) les mesures in situ (5), (v) les risques sismiques (2), (vi) les méthodes de dimensionnement (2), (vii) la modélisation physique et le comportement des sols dans l'interaction sol-pieu (8), (viii) les prévisions à partir des essais (4).

KEYWORDS: pile, pile raft foundation, design, model test, in-situ measurements, construction, numerical and analytical methods.

1 INTRODUCTION

The 18th International Conference on Soil Mechanics and Geotechnical Engineering (18th ICSMGE) is being held at Paris, France during September 2 to 6, 2013 on the main theme 'Challenges and Innovations in Geotechnics'. Based on the main conference theme, two parallel technical sessions related to the sub-topic on 'Deep Foundations' are getting organized by the technical committee TC 212 – Deep Foundations of ISSMGE. Total sixty two (62) technical full length papers related to this sub-topic on deep foundations are grouped and distributed for the two parallel technical sessions.

The area of research and practice in the field of deep foundations is expanding day by day with new challenges and innovations in this area. All the technical papers for this sub-topic can be grouped into major three categories, viz. (i) field tests and monitoring of deep foundations, (ii) analytical and numerical methods for deep foundations and (iii) laboratory based tests including physical modelling of deep foundations. This conference is the best venue to share and exchange new innovations and difficulties in various countries for the subject matter on deep foundations. Papers received from twenty six (26) member societies of ISSMGE with wide range of research and practice data related to deep foundations will be extremely useful for the designers and practitioners worldwide.

2 REVIEW OF PAPERS

In this section, review of all 62 papers of the 18th ICSMGE, which are related to the topic of 'Deep Foundations' is carried out in the sequence of alphabetical order of authors' surname.

Allievi et al. discussed the process followed for designing the pile raft foundations of tall buildings by analyzing the governing limit states, assessing the geotechnical characterization of the soil deposits and using appropriate modelling techniques for studying the behaviour of the selected foundation system at different design phases. The piled raft was analysed using finite element software Oasys GSA 2010, where the superstructure, foundation and ground were modelled into a single soil – structure model. The effects of concrete in the raft and pile were considered since they influenced the long term behaviour of the foundation. It was observed that 50% of the total rat settlements occurred during construction.

Alnuiam et al. studied the performance of piled raft foundation systems under axial loads. 3D finite element model is established to analyze the piled raft foundation system installed in cohesionless soil with stiffness linearly increased with depth. The model was calibrated using geotechnical centrifuge test data. Conclusions are: The load carried by the piles is higher for a rigid raft (K_f > 10) due to the minimal interaction between the raft and subsoil compared to the perfectly flexible raft (K_f < 0.01). The spacing between piles can be used to evaluate the raft flexibility instead of its width (Eq. 2 in this paper). The load carried by piles increases as pile diameter increases. However, the rate of increase is higher for small size piles and diminishes as the pile diameter increases.

Ashlock and Fotouhi performed full-scale pile vibration test for steel HP piles installed to a depth of 6 m in a soft clay profile, with one pile being surrounded by a cement-deep-soil-mixed (CDSM) improved zone. Authors conducted multi-modal tests with vertical and coupled lateral-rocking vibrations using a shaker mounted on a rigid pile cap. It was observed that the improved soil zone significantly increased the stiffness of the measured vertical response, but had little effect on the lateral-rocking mode. Results of the forced vibration tests were analyzed using methods reported in the literature and it was found that the simplified model was able to capture the vertical response reasonably well in both the improved and native unimproved soil profiles along with the lateral response in unimproved soil.

Balakumar et al. developed a new design method for pile raft foundation in cohesionless soil for different densities. This design procedure constitutes two stages; First stage of design procedure regarding to determination of the optimum number of piles, pile length and diameter required to be placed in a strategic manner to produce the required settlement reduction along with the load shared by the pile group. Second stage of design procedure was developed a 3D model in ANSYS finite element analysis based software and performed an extensive parametric study. Authors were also performed 1g small scale model test on circular and square shaped pile raft foundation and concluded that that the equivalent pier theory could be used in combination with the pressuremeter test results to predict the load settlement and load sharing behavior of the piled raft foundation.

Basile described a practical analysis method for determining the response of piled rafts. Validity of the analysis was demonstrated through comparison with alternative numerical solutions and field measurements. The author suggests that the negligible computational costs make the analysis suitable not only for the design of piled rafts supporting high rise buildings (generally based on complex and expensive 3D FEM or FDM analyses) but also for that of bridges and ordinary buildings.

Basu et al. presented an approach using the variational principles of mechanics to analyze torsionally loaded piles in elastic soil. The total potential energy of the pile-soil system is minimized to obtain the differential equations governing the pile and soil displacements. The analysis explicitly takes into account the three-dimensional pile-soil interaction in multi-layered soil. The authors found that the soil layering does have an effect on the pile response, particularly for short, stubby piles with low slenderness ratio.

Berthelot et al. presented the necessary site investigations for continue flight auger piles in firm sites. The penetration in the grounds can be made only with a tool of specific attack extended by an experimental retractable point in the concreting. It also requires an important couple of rotation and the means of vertical pushes. These tests were implanted right adapted soils investigations highlight well the strong resistances and the very high modulus of this hard soil. They can validate the anchoring and help the specificities of each project to bring successful construction at the sites.

Bilfinger et al. adopted new approach to evaluate safety assessment of pile foundations which uses Bayesian inference to combine bearing capacity and field controls which may lead to economic design. Ultimate load prediction method was used for bearing capacity determination. Field controls methods were used to ensure pile settlement within limit. Bayesian inference which is statistical approach which consider local soil condition as variable and reported it in terms of equation. This approach provided sound justification to field operational rules that may lead to economical foundation solution while maintaining the same safety level as required by code.

Biswas and Manna conducted a comparative study on vertical vibration tests of full-scale single piles with three-dimensional FE analysis using Abaqus/CAE. The resonant frequency and amplitude obtained from 3D FE analysis were found compatible to field test results. The resonant frequencies are decreased with the increase of eccentric moments whereas the changes of resonant amplitudes are opposite. It increases gradually with the increase of eccentric moments, and stops below the ground water table.

Bouafia presented a practical method to construct the P-Y curves for analysis on lateral load-deflection behavior of single piles using data from pressuremeter test. Full-scale pile tests were conducted to validate the predictions. With the correlations between soil reaction modulus/resistance and pile/soil stiffness ratio via the parameters from PMT test, a step-by-step method was suggested to define the parameters of P-Y curves for single pile under in multi-layered soils. Formulations of the P-Y curves, methodology to construct the P-Y curve and the analytical features can be found in this paper.

Bretelle compared the French (Fascicule 62) and Australian (AS2159) approaches on pile design methodology and shows their difference with an example. French standard provides the relationship between measured characteristics and design parameters as well as a unique set of reduction factors on resistance. Australian standard leaves the choice to the engineers and defines different reduction factors on resistance depending on site geotechnical risk. The ways to account for pile testing is described is this paper with the example showing optimization opportunity when pile testing is undertaken on site.

Cannon described the high strain and low strain dynamic pile testing for assessing the foundation of Messa A Rail Bridge at Western Australia, which have caused a change in foundation type from bored pile foundation to a driven pile foundation. Cross – hole sonic logging (CSL) test was performed at the required site for testing the test pile statically in tension. However, during construction, serious problem with the constructability of the bored pile was detected by both high strain and low strain dynamic testing. Thus the bored pile was changed to a driven pile, after its integrity was tested using a Pile Integrity Tester. Hence, the dynamic pile testing confirmed the pile resistance, providing high level of confidence in the foundation.

Carvaldho and Albuquerque presented the test results of uplift behavior of bored piles in unsaturated sandy soil found in Southern central region of Brazil. Tests were conducted in on the campus of the University of São Paulo, located in the city of São Carlos on three bored piles having length of 10m and diameter of 0.35m, 0.4m and 0.5m respectively to ascertain load transfer mechanism to subsoil as well as ascertaining the applicability of the methods for calculating ultimate load that are available within the technical milieu. The ultimate loads (Q_{ult}) obtained on the three piles were 387kN, 440kN and 478kN respectively. The determination of the ultimate load using CPT demonstrates good results when the LCPC Method is adopted.

Christin et al. introduced the timber pile load test instrumentation with removable extensometer. As the timber piles become popularly used in France for retrofitting and reuse of all historical structures and sustainable development, the load test on such pile receives attentions. The authors present a research project “Pieux Bois” (2010-2013) to establish a database necessary for design methods on timber piles. The first pile loading test campaign was carried out in Rouen on piles instrumented with removable extensometers. Interesting results are discussed in this paper.

Dembicki et al. presented an analysis of raft foundation supporting the pylon of cable-stayed bridge in Rędzin. Important decision on the pile length was their shortening due to occurrence of confined aquifers which would cause soil liquefaction under the piles during installation. The decision could be undertaken after comprehensive numerical analyses as well as additional investigations of soil parameters. Load tests with measurement of the distribution of force along the piles with extensometers were found very useful, allowing the control of design assumptions. It was concluded that in-situ measurements with agreeable results from numerical analyses are the best proof of assumptions made in the design process.

EI – Sakhawy and Nassar investigated the behavior of soil – pile interaction during soil consolidation by performing several experimental tests for different conditions such as end bearing pile and floating tip pile for different soils at the tip of pile. From the test results authors concluded that;

1. The negative skin friction was developed along the pile shaft due to consolidation of the soil surrounding the pile under surcharge loads.
2. The neutral plane was moved closer to the tip of the pile with increase in the end bearing.
3. The depth of the neutral plane was increased with increase in the pile length.

Elsherbiny and El Naggar presented a 3D FE analysis using ABAQUS on helical piles for performance of the pile groups under axial compressive loads. Mohr-Coulomb plasticity model is used for soils, where numerical models are calibrated and verified using: full-scale load testing data of single piles; representative soil properties obtained from the borehole logs; and realistic modeling assumptions. It was found that the performance of a helical pile group in sand or clay is mainly affected by the pile-to-pile spacing. The practical range of inter-helix spacing (1D~3D) has negligible effect on the settlement ratio, R_s. The factor of safety could significantly affect R_s for piles in sand and has negligible effect for piles in clay. In general, R_s for helical piles with multiple helices spaced at a typical pile spacing of 3D is suggested to be 1.15 to 1.2 for both clay and sand.

Fakharian et al. adopted a numerical approach for studying the setup effects of a single pile embedded in layered soil strata by calculating the pile shaft resistance β – parameter. Authors adopted an axi-symmetric non – linear finite element scheme for simulating the cavity expansion which occurred due to pile driving followed by dissipation of pore water pressure and ageing. Finite element based numerical package ABAQUS was used for modelling the soil as elasto – perfectly plastic model. It was observed that an increase in the interface shear strength between pile – soil was considered to be the ageing component of the soil setup.

Goto et al. conducted model pile load tests on grouped piles in large tank of dry sand. 9 cylindrical model piles of 40mm diameter were tested under 50-200kPa load pressures. Test results were discussed at yielding point of the total load, tip stress distribution of the grouped piles, pressure distribution in the soil measured by the sensors and ground deformation after the loading tests. The authors suggested that the group pile of 2.5D spacing caused significant interactional effect between piles and it will behave as a block. In contrast, the piles in a pile group of 5.0D spacing was reported more independently.

Gusmão et al. presented main aspects of design, execution and control of shopping centre construction of 280,000 m2 area in Recife, Brazil. Geotechnical characterization revealed that soil consisted of silty clays. Static pile load tests were conducted on 400mm and 500mm diameter piles with allowable loads of 700 and 1,150 kN. The Van der Veen equation was used for extrapolating the results of the geotechnical rupture load for the load tests which may help in the design. It was found that as the number of sample increased standard deviation increases and probability density function around the mean decreases and the curve with flatter appearence can be observed. With increases in sample space, population dispersion is incorporated into sample and standard deviation was found to increase with increase in dispersion, reliability index decreases probability of failure was found to increase.

Gwizdala and Krasinski discussed the cases of bridge structures founded on driven displacement piles. It is pointed out that the general principles given by Eurocode 7 should aim at an unification of the methods for the calculation of bearing capacity of the pile. It would be important to create the international database with complete static and dynamic test results and the information regarding the soil resistances over the pile shaft and under the base referred to careful description of the subsoil and the in situ tests itself.

Haberfield described the design of piled raft for two buildings (Tall towers and Nakheel tower (1000m high)) in Dubai which is founded on weak carbonate rocks and a group of tall towers (up to 300 m high) founded in deep alluvial soil deposits based on serviceability condition to find out ground modulus based on various field testing adopted. To get accurate results pressuremeter, seismic crosshole test and Osterberg load cell test were used to evaluate the geotechnical properties of foundation material for two towers. Test result revealed that significant thickness of debris was found at the base of pile toe which made the elastic modulus estimation challenging and its estimation is made on unloading and reloading response of pile load test.

Hai and Dao performed two bidirectional loading tests on piles to determine pile capacities for the foundation of 12-story Sea Bank Building project in Da Nang City, Vietnam. Authors validated the capacities of pile with pile load test programme of the bidirectional O-cell test as it is the best suitable for the limited project. From the test results authors concluded that maximum upward movements were 3.3 and 7.4mm and maximum downward movements were 28mm and 49.3mm for the two tests, the maximum upward movement of pile head were 0.2 and 2.5 mm respectively and the shaft resistances above 30 m depth were not full mobilized.

Hamova et al. briefly described the effects of landslide of width in the top 55m, length 38m and depth 8 to 9m that occurred on main road and affected more than half of the roadway. From the analysis authors mentioned that ground water table raise, river erosion undermining the slope and the dynamic effects of transport were the main factors for slope instability. Authors designed and recommended cantilever retaining wall on driven pile foundation. Authors observed the proposed structure for period 2006 – 2012 and concluded that the landslide was successfully stabilized and new landslide deformations had not been established.

Herrmann et al. investigated the load-bearing behaviors of bored piles with different enlarged bases. According to DIN EN 1536, overboring of the bottom of drilled piles to increase the bearing resistance is permissible up to three times the pile diameter. To validate the supports of design specifications, model tests at a scale of 1:25 were performed. The tests showed that an enlargement contributes significantly. By the use of a reduction coefficient of 0.75 for the bearing resistance, covering the disturbance effects of the drilling the enlargement, the bearing resistance would be underestimated. The results were evaluated against the available results of large 1:1 drilled pile experiments.

Ishikura et al. discussed the technology of using surface stabilization and floating type deep mixing soil stabilization for acceptable settlement where the performance of piles on deep soft soil layers is maintained. Consolidation settlement properties and skin friction of model test of grouped piles were investigated. Two types of model tests and full scale FEM analysis were conducted. The full mobilization length of skin friction was found to be increased with elapsed time and it would converge to the constant value during the consolidation. Simple forms of the formulations are presented to calculate the skin friction of floating type column and equivalent conversion ratio defined as a ratio between the column length and the mobilized length for skin frictions.

Jeong and Cho studied the settlement behavior of piled raft foundations by 3D numerical analysis on case studies. Attention is given to the improved analytical method (YSPR) and interactive analysis considering raft flexibility and soil nonlinearity. It was found that the proposed method in present study is in good agreement with general trend of the field measurements. Conclusions are:. Proposed analytical method produces a considerably larger settlement than the results obtained by the conventional methods (GSRaft). The proposed method is shown to be capable of predicting the behavior of a large piled raft. Nonlinear load-transfer curve and flat-shell element can be used to improve the existing numerical methods.

Jung et al. introduced a new development of multiplexed Fiber-optic Bragg Grating (FBG) sensors to measure lateral pile displacements. With the pile displacement calculated under lateral load, the data were compared with the measured ones. Three optimization strategies—positioning sensors at regular intervals, positioning sensors at projected Gaussian points but not following the Gaussian rule, and positioning sensors exactly based on the Gaussian rule—were implemented. In both cases for the 1st and 2nd strategies, the measurement error decreases as the number of sensors increases. Moreover, positioning the sensors rigorously based on the Gaussian quadrature rule enhances the accuracy more than just using the Gaussian points.

Kaneda et al. presented the numerical simulation of field tests on bearing capacity of pile, raft, and piled raft foundations. The SYS Cam-clay model developed at Nagoya University was used. Material parameters were determined by laboratory tests considering the state of stress in the field. Agreeable results were found between predictions and field tests. Furthermore, it is found that the total bearing capacity of the raft and the piles is equal to that of the piled raft foundation. This was also confirmed via the simulations. The authors explained the reason of such phenomenon.

Kang et al. introduced the Fiber Reinforced Plastic (FRP) pile and applications. To improve axial and lateral load capacities, a Hybrid Concrete Filled FRP Pile (HCFFP) is suggested. The load-strain relation of CFFP was compared with finite element solutions. The confinement effect between FRP Pile and CFFP are shown. Load capacity of HCFFP member is increased if confining pressure and concrete strength are increased. In addition, the equations to predict the compressive and flexure strengths of the HCFFP member are proposed. It was confirmed that HCFFP is suitable to apply as the structural elements with the comparisons of CFFP member. It's suggested that the structural performance of connection between the segments of HCFFP, and constructability of HCFFP pile should be explored in the future for more practical applications.

Korff and Mair investigated the ground displacements related to deep excavations on a case study of North South Metro Line in Amsterdam. It was found that the response of buildings is governed by soil displacements resulting from the excavation. It is concluded that the surface displacement behind the wall is 0.3~1.0% of the excavation depth, if all construction works are included. The largest effect on the ground surface displacement (55~75%) can be attributed to the diaphragm wall construction, jet grout strut installation and construction of the roof and took in total about 4 years. The actual excavation stage caused only about 25-45% of the surface displacements. At larger excavation depths the influence zone is found significantly smaller than 2 times the excavation depth.

Lehtonen introduced the use of steel piles in retaining wall construction and energy transfer. Open section drilling for new micropile inventions is discussed. Drilled pile walls and energy transfer applications extend the use of drilled piles to sites where conventional piling is rarely seen as an option and where the drilled piles can be installed as hybrid structures, functioning as vertically loaded piles, or retaining structure, or a heating/cooling energy reservation system.

Levy and Richards confirmed that base suction may contribute significantly to footing performance. Field tests on full scale footings were carried. The suction developed is similar to physical model tests using centrifuge. The design uplift performance is not reached before the ultimate limit state displacement criterion set by UK design guidance. In the case where suctions did not develop, the uplift performance of the footings was extremely poor. Such a poor performance will require a re-evaluation of the use coarse granular material, when used in excavations bounded by London clay.

Look and Lacey implemented two land based test piles fitted with Osterberg cells for testing the shaft capacity of the sedimentary bedrock at the Gateway Bridge site. Based on the test data, the required magnitude of the input unconfined characteristic strength (UCS) of the rock were back calculated for various pile design methods. It was concluded by the authors that five of the examined methods produced results which matched the observed shaft capacities by adopting a design UCS value close to the UCS lower quartile "characteristic" value.

Lorenzo et al. described how to find out bearing capacity of piled raft foundation at ultimate stage which governs the design of PRs with a raft width between 6 to 14m using limit state approach. Author proposed the relation to find out ultimate bearing capacity of PR with the help of numerical model. To apply limit state method, floating piles behaviour is considered under ultimate or limiting capacity and design equation were presented. Global factor of safety considered in the design. Partial safety coefficient of resistant load was found out. Taylor series method was adopted to find bearing capacity of PR. This analysis is generalized method for the calculation for determining the bearing capacities of raft and pile groups separately.

Mayne and Woeller suggested a closed-form elastic continuum solution for upper and lower segment responses of bored piles subjected to bi-directional Osterberg load testing. Seismic piezocone tests (SCPTu) are used to provide data for assessing the capacity, while the shear wave velocity provides the fundamental stiffness for displacement analyses. A load test case study involving two levels of embedded O-cells for a large bridge in Charleston, South Carolina is presented to illustrate the approach. Results from the seismic piezocone testing provide the necessary input data to evaluate axial side and base resistances of the deep foundations, as well as the small-strain stiffness (G_{max}) needed for deformation analyses.

Mendoza et al. discussed the observations learned from Metro-Line 12 overpass in Mexico City soft clay. A pioneer foundation of footing or foundation slab with long skirts was used first time in the city. Geotechnical sensors and accelerometers were installed to monitor during the construction and long term operations as well as strong earthquakes A first earthquake of low intensity caused a sudden, reduced and transitory horizontal pressure decrease on the walls, but a rapid recovery of the sustained loads was observed. The Metro trains impose no significant changes in vertical pressure under the footing, nor on lateral pressures or pore water pressures on the sides of the perimeter walls.

Miller et al. discussed the applications of shaft grouting to improve pile foundation capacity in Georgia. Poor ground conditions and high loads were encountered and the deep bored piles were installed. Results from the strain gauges showed differences in the behaviour of the piles in different strata depending on the granular content of the material. It was found the shaft grouting improved the skin friction of the strata with a high sand and gravel content by a factor of 2.2~2.4. Some improvement was achieved in material with as little sand content (<10%). It was reported that the shaft grouting improved the load-displacement behaviour of the test pile with settlements reduced by approximately 50%.

Perälä presented a new technology called as polymer pillar. The product is patented and mainly made by injecting expanding high density geopolymer to a geotextile tube. It can be used as end bearing and/or friction piles with the dependence of soil conditions. While injected, the pillars volume expands fast, which will cause the surrounding soils displaced and compacted. Totally there have been over 500 projects so far. Some load tests and material tests are presented in this paper.

Poulos et al. performed pile load test for verifying the foundation design of a tower in South Korea. Four pile load test were performed on vertically loaded piles using the Osterberg cell method, while one was performed on a laterally loaded pile which were jacked against each other. Authors also carried out finite element analyses using the computer program PLAXIS for determining the effects of pile shape and quality of concrete which were used while conducting the pile load test. It was found that while pile load capacities were underestimated at over - break levels; they were overestimated during shaking, due to non – consideration of diameter of the pile during the analyses. It was concluded by the authors that non – uniformity of pile section and quality of concrete should be considered for accurate interpretation of pile load test data.

Powell and Skinner presented the data of tested piles on London clay which was located at Chattenden, northern Kent and was underlain by high plasticity London Clay to a depth of at least 44m. This paper presents testing of piles which is now in use onto the soil, pile tested at an age of up to 5 months, but mostly 2.5-3.5 months, by static incremental maintained load testing (ML). The Topic, RuFUS and RaPPER pile tests were undertaken using a combination of BRE load frames and a remotely operated hydraulic loading and control system. Through testing α (empirical factor for shaft resistance) was found out for different types of piles and reported and α will be incorporated in the design of pile capacity.

Puech and Benzaria presented an experimental study on the behaviour of piles under axial static load. Three mode of pile installation were considered: driving, boring, and screwing. Piles tested were instrumented with removable extensiometers and installed in the overconsolidated Franders clay. The results showed very high skin friction mobilized for driven pile (>150 kPa); that of bored pile and screwed pile are lower, 40 kPa and 60 kPa, respectively. The experimental results were finally compared to the prediction methods developed by Imperial College or recommended by French codes.

Ramadan et al. developed a model in PLAXIS 3D to study the importance of piled supporting system to the excavation adjacent to existing buildings in soft to medium clay. For the present study authors considered the excavation area as 10 x 10m and the foundation of adjacent building as three strip footings of length 10m and width 2m with 100kN/m^2 stress on the foundation level. From the analysis authors concluded that;

1. For stability number N_c = 4 the unsupported excavation was fail due to stress of the adjacent building.
2. Continuous pile wall support wall was decreased the lateral soil displacement between the foundation level of the adjacent building and the bottom of the excavation.

Ray and Wolf outlined the past history and present implementation of foundation design when subjected to seismic loading in Hungary as per Eurocode 8. Authors also used SAP 2000 finite element software for analyzing the influence of different support conditions on the bearing stresses of a superstructure on a typical reinforced concrete building. The building periods of the structure were computed using the Eurocode 8 formulae and modal analyses which considered fixed base and spring base supports, giving building periods of 0.85sec, 0.69sec and 0.79sec respectively. It was observed that foundations having spring base conditions reduced the bending moments near the base by 30%, with the reduction being less at the higher portion of the column. Moreover a decrease in fundamental period owing to different support conditions, resulted in an increase in magnitude of spectral ordinate and bending moment.

Rinaldi and Viguera performed pseudo-static load tests for evaluating the bearing capacity of large diameter piles. Authors showed that moderate loads, weighing between 10 to 20 tons, when dropped from a height of 10cm to 120cm, resulted in full mobilization of ultimate pile capacity. The loading generated a time controlled load which depended on the size and height of fall of the load, geometry and elastic properties of the elastomeric cushion which were included between the mass and top of the pile. It was concluded by the authors that pseudo-static methods allowed application of load increments in steps, repeatability of each loading step and simpler test setup, when compared to Statnamic tests.

Sakr and Nasr investigated the effects of inclined load on axial pile displacement and lateral pile response for single pile embedded in the level ground and near ground slope by conducting several experiments. Authors compared the results of single pile founded in the level ground with that in near ground slope and concluded that;

1. The ultimate axial and lateral load capacities of pile were decreased with increase in inclination of load with vertical.
2. The ultimate lateral load capacity of pile founded in dense sand subjected to inclined loads increased significantly with increase in slenderness ratio.
3. The lateral load capacity of pile was increased with increase in distance between pile head and slope crest for different densities of sand.

Salgado et al. proposed semi-analytical methods to calculate the response of laterally loaded piles with general-shape cross sections embedded in multilayered elastic soil. The method produces results with accuracy comparable with that of a 3D FE analysis but requires much less computational time. Analytical solutions for laterally loaded piles with rectangular and circular cross sections embedded in multilayered elastic media are obtained. The solutions for pile deflection, slope of the deflected curve, bending moment and shear force, are obtained iteratively and it depends on the rate at which the displacements in soil medium decreases with increasing distance from the pile.

Shulyatiev et al. described a new field test technique developed for the analysis of single pile and pile groups in Moscow International Business Center (MIBC) “Moskva-CITY” is a complex of 19 sky-scraper buildings. Authors were analyzed single pile and pile groups of length range 20 – 30m, diameter range 1.2 – 1.5m and spacing range 3 – 5m. Authors determined separately side resistance and tip resistance in the site by using that developed test technique and verified with analytical model developed in PAXIS 2D 8.2 software for single pile test data.

Silva et al. (a) proposed a method to mitigate risk in geotechnical constructions by using borings and pile load tests that enable the elaboration of bi and three-dimensional models, which gives assure that the correct analysis and evaluation of the associated risks to design and to the construction execution should be one of the targets of a Geotechnical Engineering. From the results authors concluded that the process of post-evaluation of the models developed in computer software requires geological/geotechnical experience of the region and knowledge of limitations and potential advantages of the computer software as the quantity of input attributes, working grid limit, interpolating devices and their limitations.

Silva et al. (b) proposed the use of SCCAP methodology to control the execution of CFA types foundation works which proposes formulations, routines and criteria for pile acceptance. To ensure quality and the design assumptions, the SCCAP routines introduces to the execution monitoring software for CFA piles the excavation quality control in real time and assure the execution piling process conditions for the piles to achieve the planned bearing capacity. Through SCCAP quality in the excavation can be assured whose results rely upon the bearing capacity and deformability through the decrease of the variability and the increase of reliability. SCCAP methodology also provides the stopping criteria for boring on the basis of statistical formulations.

Steenfelt and Schunk discussed the cavity remediation for piles underneath a cable stayed bridge. The cavity feature was pressure grouted and transfer of axial load across the cavity into Limestone was facilitated by insertion of grouted steel reinforcement assemblies. The success of the remedial measures was proven by carrying out an O-cell load test on the pile positioned over the maximum recorded depth of the cavity.

Szep and Ray predicted that soil – structure interaction could be better modelled using three dimensional geotechnical finite element packages where true soil – structure could be analyzed. The laterally loaded pile was analyzed using three numerical methods like (1) AXIS 10VM which is the fundamental structural design tool in Hungary, (2) GE04 and GE05 which are popular geotechnical codes and (3) PLAXIS and MIDAS GTS, which are 2D and 3D geotechnical finite element packages for ensuring realistic modelling of soil – structure interaction. Authors also used an optimization technique for translating the pile head displacements and rotations computed using finite element analyses to a small number of elasto – plastic subgrade springs, which could be used in various structural and geotechnical design software.

Teparaksa carried out damage assessment of the Bank of Thailand head office by means of finite element method for predicting its influence on the Tewavej Palace and Bangkhunphrom Palace with simulation of basement construction. The top down construction method was selected for basement construction and complete set of instrumentation was installed at the palaces, diaphragm wall and ground surface for monitoring the field performance during and after basement construction. The predicted wall movement obtained using finite element analysis agreed well with the field performance, and construction of basement was completed without affecting the stability of the palaces

Ter – Martirosyan et al. proposed a rheological equation based on modification of Maxwell rheological model to explain the shear deformations in partial saturated hardening – softening clay soil. Authors explained creep, relaxation and kinematic shear including decaying, stable and progressive creep, depending on shear stress intensity by using that proposed equation. Authors showed that in constant loading case that proposed equation described decaying, non-decaying and progressing soil creep as well as stress and shear strain relaxation processes in kinematic loading mode.

Tomisawa and Miura performed large-scale model experiments to suggest a design verification method for pile foundations combined with solidified improved columns with following suggestions. Specifications for solidified columns are related to ground conditions and the improvement depth depends on characteristic pile length 1/β. The design horizontal subgrade reaction P_{HU} should be smaller than the passive earth pressure of composite ground for inner stability and column soundness. The allowable horizontal pile displacement in normal conditions and during storms and Level-1 earthquakes should be reduced to 0.5% of the pile diameter instead of 1% (or 15 mm) for natural ground.

Tsuha et al. conducted experiments for determining the influence of soil characteristics and configuration of helical blades on the uplift capacity of multi – helix anchors. The experiments included centrifuge tests on dry Fontainebleau sand and tension load tests executed out in a tropical soil at Sao Carlos in Brazil. The authors inferred that the efficiency of the second helix of helical anchors embedded in sand decreased with an increase in relative density of the sand and diameter of the helix. Further it was also found that uplift capacity of triple helix anchor with tapered helices were superior compared to those with cylindrical helices.

Van Tol et al. presented the results of a study of concealed safety factors by performing centrifuge tests on single pile and group piles. For studying the time effect authors loaded single pile in centrifuge test at 1, 10, 100,1000 minutes after installation and for pile group also were followed the same pattern and the centrifuge test was continued to operate from the start of installation until the final load test. Authors showed that the quantification of the effect and the determination of the impact of load variations and recommended to continue with research into pile group effects of displacement piles.

Wang et al. presented the aspects of design and construction of super-long bored pile foundation together with a brief description of bearing behaviors of super-long bored piles. Deep buried firm soils are usually selected as the bearing stratum. The authors suggests that the application of the double steel sleeves, design of the pile top, construction and measurement requirements are essential to the design of the field load test. Calculation should consider the synergism of the superstructure, soils and pile foundation. Inspection and controlling standards of super-long bored piles are stricter than those of ordinary piles.

Wong presented the results of two case studies on rock socketed pile design and pile load testing in Sydney region of Australia, in one site underlain by medium to high strength shale, dynamic pile load testing was carried out, and on another site underlain by high strength sandstone, Osterberg Cell (O-Cell) testing was carried out to validate the designs. Author concluded that better understanding of load-deformation characteristics of pile foundations would lead to more cost-effective designs.

Yanjing et al. proposed new methods for calculating rebound and recompression deformations by analyzing the data from the consolidation-rebound-recompression test of in-situ soil, bearing test, model experiment and field measurement test, which were based on the stress history of ground soil, loading and unloading conditions. Authors established a mathematical relation between rebound and recompression deformation. Form the analysis authors concluded that;

1. The progress of rebound deformation exhibits three – phase's characteristics, and the critical unloading ratio was used to determine the calculating depth of rebound deformation.
2. The recompression deformation was larger than rebound one and the increase proportion vary with different kinds of soil.
3. The recompression deformation of foundation soil was computed as two-phase mode.

Zaghouani et al. described some difficulties related to the execution of large diameter deep piles in soft soils during the construction of the bridge "Rades-La-Goulette" in Tunisia. First, drilling piles of 2-m diameter up to 100-m depth in soft clay met various problems that increased seriously the time previously expected. That induced the horizontal displacement of the borehole's wall toward its centre. Displacement was first estimated using finite element modeling. Calculations show that this problem would modify only the stress related to the lateral friction but not that at the pile's toe. Second, difficulties related to the concreting phase were also described. Some faults have been detected along the piles by sonic inspections. The paper describes the techniques adopted to repair these faults.

Zhang et al. reported the results of axial static load tests of both full-scale instrumented pile groups and single piles. The single pile settlement was found smaller than the corresponding pile group settlement at the same average load per pile when the load was relatively large. Group effect was more pronounced for piles with smaller L/B ratios, and the impact of the pile spacing is greater than that of the pile length. The load at the top of the corner piles was observed to be the largest, followed by side piles and then center piles.

3 SUMMARY

Deep foundation is a broad area of foundation engineering ranging from conventional pile foundation to modern combined pile-raft foundation. As expected, for this important topic huge number of papers were submitted and finally 62 papers have been selected which is distributed over two technical sessions of this technical committee TC 212 – Deep Foundations. The subject matters of these papers cover various sub-topics of deep foundations viz., foundation behaviour and performance, technologies for construction, rehabilitation and energy, analytical and numerical analyses on piles and pile-raft foundation, field measurements, seismic analysis of deep foundations, design methods and assessments, model testing, soil-pile interactions and predictions from testing methods in deep foundations. This general report summarizes the various latest developments in research and practice in the area of deep foundations.

4 ACKNOWLEDGEMENT

Authors acknowledge the support provided by (i) A. M. Tang, Researcher, Laboratoire Navier/CERMES, Université Paris-Est, France, (ii) K. Chatterjee, Research Scholar, Department of Civil Engg., IIT Bombay, Mumbai, India and (iii) V. Dilli Rao, PG Student, Department of Civil Engg., IIT Bombay, Mumbai, India, for preparation of this general report.

5 REFERENCES

Allievi L., Ferrero S., Mussi A., Persio R. and Petrella F. 2013. Structural and geotechnical design of a piled raft for a tall building founded on granular soil. Proceedings of the 18th International Conference on Soil Mechanics and Geotechnical Engineering, Paper No. 2950.

Alnuiam A., El Naggar H. and El Naggar M.H.. 2013. Performance of piled-raft system under axial load. Proceedings of the 18th International Conference on Soil Mechanics and Geotechnical Engineering, Paper No. 2417.

Ashlock J.C. and Fotouhi M.K. 2013. Analysis of Full – Scale Random Vibration Pile Testsin Soft and Improved Clays. Proceedings of the 18th International Conference on Soil Mechanics and Geotechnical Engineering, Paper No. 2776.

Balakumar V., Oh E., Bolton M. and Balasubramaniam A.S. 2013. A design method for piled raft foundations. Proceedings of the 18th International Conference on Soil Mechanics and Geotechnical Engineering, Paper No. 2873.

Basile F. 2013. A practical method for the non-linear analysis of piled rafts. Proceedings of the 18th International Conference on Soil Mechanics and Geotechnical Engineering, Paper No. 2503.

Basu D., Misra A. and Chakraborty T. 2013. A variational approach for analysis of piles subjected to torsion. Proceedings of the 18th International Conference on Soil Mechanics and Geotechnical Engineering, Paper No. 2434.

Berthelot P., Cardona G., Glandy M. and Durand F. 2013. Anchoring of continue flight auger piles in hard soil : necessity of successful tools of drilling and adapted soils investigations. Proceedings of the 18th International Conference on Soil Mechanics and Geotechnical Engineering, Paper No. 1857 (in French).

Bilfinger W., Santos M. and Hachich W. 2013. Improved Safety Assessment of Pile Foundations Using Field Control Methods. Proceedings of the 18th International Conference on Soil Mechanics and Geotechnical Engineering, Paper No. 2601.

Biswas S. and Manna B. 2013. Three dimensional finite element nonlinear dynamic analysis of full-scale piles under vertical excitations. Proceedings of the 18th International Conference on Soil Mechanics and Geotechnical Engineering, Paper No. 1691.

Bouafia A. 2013. P-Y curves from the prebored pressuremeter test for laterally loaded single piles. Proceedings of the 18th International Conference on Soil Mechanics and Geotechnical Engineering, Paper No. 1714.

Bretelle S. 2013. French and Australian pile design comparison – load testing influence on design. Proceedings of the 18th International Conference on Soil Mechanics and Geotechnical Engineering, Paper No. 1813 (in French).

Cannon J.G. 2013. Dynamic Pile Testing at the Mesa A Rail Bridge. Proceedings of the 18th International Conference on Soil Mechanics and Geotechnical Engineering, Paper No. 2704.

Carvalho D. and Albuquerque P. 2013. Uplift behavior of bored piles in tropical unsaturated sandy soil. Proceedings of the 18th International Conference on Soil Mechanics and Geotechnical Engineering, Paper No. 2590.

Christin J., Le Kouby A., Reiffsteck P. and Rocher-Lacoste F. 2013. Timber pile load test instrumented with removable extensometers. Proceedings of the 18th International Conference on Soil Mechanics and Geotechnical Engineering, Paper No. 1716 (in French).

Dembicki E., Cudny M., Krasiński A. and Załęski K. 2013. Pylon foundation of a cable stayed bridge at the motorway ring road of Wrocław. Proceedings of the 18th International Conference on Soil Mechanics and Geotechnical Engineering, Paper No. 2475.

El – Sakhawy N. and Nassar A. 2013. Consolidating soil-pile interaction. Proceedings of the 18th International Conference on Soil Mechanics and Geotechnical Engineering, Paper No. 2809.

Elsherbiny Z. and El Naggar M.H.. 2013. The performance of helical pile groups under compressive loads: a numerical investigation. Proceedings of the 18th International Conference on Soil Mechanics and Geotechnical Engineering, Paper No. 2427.

Fakharian K., Attar I.H., Sarrafzadeh A. and Haddad H. 2013. Contributing factors on soil setup and the effects on pile design parameters. Proceedings of the 18th International Conference on Soil Mechanics and Geotechnical Engineering, Paper No. 3105.

Goto S., Aoyama S., Liu ., Towhata I., Takita A. and Renzo A.A. 2013. Model loading tests in large soil tank on group behavior of piles. Proceedings of the 18th International Conference on Soil Mechanics and Geotechnical Engineering, Paper No. 2014.

Gusmão A., Oliveira P., Ferreira S., Maia G.. and Amorim M. 2013. Probabilist analysis of the foundation of a shopping center in Brazil. Proceedings of the 18th International Conference on Soil Mechanics and Geotechnical Engineering, Paper No. 2585.

Gwizdala K. and Krasinski A. 2013. Bearing capacity of displacement piles in layered soils with highly diverse strength parameters. Proceedings of the 18th International Conference on Soil Mechanics and Geotechnical Engineering, Paper No. 2519.

Haberfield C. 2013. Practical experience with piled raft design for tall buildings. Proceedings of the 18th International Conference on Soil Mechanics and Geotechnical Engineering, Paper No. 2623.

Hai N.M. and Dao D.H. 2013. Non – conventional pile loading tests in Vietnam. Proceedings of the 18th International Conference on Soil Mechanics and Geotechnical Engineering, Paper No. 2897.

Hamova M., Frangov G. and Zayakova Hr. 2013. Slope stability structures for road landslide. Proceedings of the 18th International Conference on Soil Mechanics and Geotechnical Engineering, Paper No. 2770.

Herrmann R.A., Löwen M., Tinteler T. and Krumm S.. 2013. Research on the load-bearing behaviour of bored piles with different enlarged bases. Proceedings of the 18th International Conference on Soil Mechanics and Geotechnical Engineering, Paper No. 2394.

Ishikura R., Matsuda H. and Igawa N. 2013. Visualization of settlement behaviour for friction pile group during consolidation. Proceedings of the 18th International Conference on Soil Mechanics and Geotechnical Engineering, Paper No. 2346.

Jeong S. and Cho J. 2013. Interactive 3-D analysis method of piled raft foundation for high-rise buildings. Proceedings of the 18th International Conference on Soil Mechanics and Geotechnical Engineering, Paper No. 2167.

Jung Y.-H., Na S.-U. and Mok Y.-J. 2013. Optimal FBG sensor deployment via Gaussian Quadrature formula for measurement of displacement of laterally loaded piles. Proceedings of the 18th International Conference on Soil Mechanics and Geotechnical Engineering, Paper No. 2170.

Kaneda K., Honda Y., Shigeno Y. and Hamada J. 2013. Numerical simulation of the load tests on bearing capacity of piled raft foundations. Proceedings of the 18th International Conference on Soil Mechanics and Geotechnical Engineering, Paper No. 2298.

Kang I.-K., Kim H.-T., Baek S.-C. and Park S.-Y. 2013. The development and the structural behaviour of a new type hybrid concrete filled fiber-glass reinforced plastic pile. Proceedings of the 18th International Conference on Soil Mechanics and Geotechnical Engineering, Paper No. 2188.

Korff M. and Mair R.J. 2013. Ground displacements related to deep excavation in Amsterdam. Proceedings of the 18th International

Conference on Soil Mechanics and Geotechnical Engineering, Paper No. 2496.

Lehtonen J. 2013. Drilled pile technology in retaining wall construction and energy transfer. Proceedings of the 18th International Conference on Soil Mechanics and Geotechnical Engineering, Paper No. 2078.

Levy F.M. and Richards D.J. 2013. Full scale rapid uplift tests on transmission tower footings. Proceedings of the 18th International Conference on Soil Mechanics and Geotechnical Engineering, Paper No. 2480.

Look B. and Lacey D. 2013. Characteristic values in rock socket design. Proceedings of the 18th International Conference on Soil Mechanics and Geotechnical Engineering, Paper No. 2753.

Lorenzo R., Zubeldia H. and Chunha R. 2013. Safety theory in geotechnical design of piled raft. Proceedings of the 18th International Conference on Soil Mechanics and Geotechnical Engineering, Paper No. 2602.

Mayne P.W and Woeller D. 2013. Bored pile foundation response using seismic cone test data. Proceedings of the 18th International Conference on Soil Mechanics and Geotechnical Engineering, Paper No. 2158.

Mendoza M.J., Rufitar M., Ibarra E. and Mendoza S.A. 2013. Performance of a pioneer foundation of the skirt type for the Metro-Line 12 overpass on the Mexico City soft clay. Proceedings of the 18th International Conference on Soil Mechanics and Geotechnical Engineering, Paper No. 2304.

Miller M, Potts V., Skinner H. and Vaziri M. 2013. Improving the capacity of bored piles by shaft grouting. Proceedings of the 18th International Conference on Soil Mechanics and Geotechnical Engineering, Paper No. 2525.

Perälä A. 2013. Polymer pillar, a new innovation for underpinning. Proceedings of the 18th International Conference on Soil Mechanics and Geotechnical Engineering, Paper No. 2110.

Poulos H.G., Badelow F., Tosen R., Abdelrazaq and Kim S.H. (2013). Identification of Test Pile Defects in a Super-tall Building Foundation. Proceedings of the 18th International Conference on Soil Mechanics and Geotechnical Engineering, Paper No. 2617.

Powell J. and Skinner. J. 2013. A review of pile test results and design from a London clay site. Proceedings of the 18th International Conference on Soil Mechanics and Geotechnical Engineering, Paper No. 2531.

Puech A. and Benzaria O. 2013. Effect of installation mode on the static behaviour of piles in highly overconsolidated Flanders clay. Proceedings of the 18th International Conference on Soil Mechanics and Geotechnical Engineering, Paper No. 1704 (in French).

Ramadan E.H., Ramadan M., Khashila M.M. and Kenawi M.A. 2013. Analysis of piles supporting excavation adjacent to existing buildings. Proceedings of the 18th International Conference on Soil Mechanics and Geotechnical Engineering, Paper No. 2811.

Ray R.P. and Wolf A. 2013. Analysis and Design of Piles for Dynamic Loading. Proceedings of the 18th International Conference on Soil Mechanics and Geotechnical Engineering, Paper No. 2929.

Rinaldi V.A. and Viguera R. 2013. Pseudo-static Pile Load Test: Experience on Pre-bored and Large Diameter Piles. Proceedings of the 18th International Conference on Soil Mechanics and Geotechnical Engineering, Paper No. 2917.

Sakr M.A. and Nasr A.M. 2013. Behavior of vertical piles embedded in sand under inclined loads near ground slope. Proceedings of the 18th International Conference on Soil Mechanics and Geotechnical Engineering, Paper No. 2805.

Salgado R., Basu D., Prezzi M. and Tehrani F.S. 2013. Semi-analytical solutions for laterally loaded piles in multilayered soils. Proceedings of the 18th International Conference on Soil Mechanics and Geotechnical Engineering, Paper No. 2125.

Shulyatiev O.A., Ladyzhensky I.G and Yastrebov P.I. 2013. Skyscrapers of «Moskva-City» business center – tests of bored ples. Proceedings of the 18th International Conference on Soil Mechanics and Geotechnical Engineering, Paper No. 2678.

Silva C.P.L., Souza N.M. and Silva M.C. 2013a. Three-dimensional models of bearing capacity – case study. Proceedings of the 18th International Conference on Soil Mechanics and Geotechnical Engineering, Paper No. 2603.

Silva C., Carvalo J. and Cavelcante A. 2013b. Energy And Reliability Applied To Continuous Flight Augern Pilings – The Sccap Methodology. Proceedings of the 18th International Conference on Soil Mechanics and Geotechnical Engineering, Paper No. 2604.

Steenfelt J.S. and Schunk M. 2013. Cavity remediation for pylon foundation of the Transrhumel Viaduct in Constantine. Proceedings of the 18th International Conference on Soil Mechanics and Geotechnical Engineering, Paper No. 2408.

Szep J. and Ray R.P. 2013. Integrating Nonlinear Pile Behavior with Standard Structural Engineering Software. Proceedings of the 18th International Conference on Soil Mechanics and Geotechnical Engineering, Paper No. 2933.

Teparaksa W. 2013. Deep Basement Construction of Bank of Thailand Along Chao Phraya River closed to Tewavej Palace and Bangkhumphrom Palace. Proceedings of the 18th International Conference on Soil Mechanics and Geotechnical Engineering, Paper No. 3082.

Ter – Martirosyan Z.G., Ter – Martirosyan A.Z. and Sidorov V.V. 2013. Creep and long-term bearing capacity of a long pile in clay. Proceedings of the 18th International Conference on Soil Mechanics and Geotechnical Engineering, Paper No. 2675.

Tominsawa K. and Miura S. 2013. A design verification method for pile foundations used in combination with solidified improved columns. Proceedings of the 18th International Conference on Soil Mechanics and Geotechnical Engineering, Paper No. 2021.

Tsuha C.H.C., Santos T.C., Rault G., Thorel L. and Garnier J. 2013. Influence of multiple helix configuration on the uplift capacity of helical anchors. Proceedings of the 18th International Conference on Soil Mechanics and Geotechnical Engineering, Paper No. 2595.

Van Tol A.F., Stoevelaar R., Bezuijen A. and Hannink G. 2013. Compressive resistance of piles, an update. Proceedings of the 18th International Conference on Soil Mechanics and Geotechnical Engineering, Paper No. 2766.

Wang W., Wu J. and Li Y. 2013. Super-long bored pile foundation for super high-rise buildings in China. Proceedings of the 18th International Conference on Soil Mechanics and Geotechnical Engineering, Paper No. 2338.

Wong P.K. 2013. Case studies of cost-effective foundation design in rock. Proceedings of the 18th International Conference on Soil Mechanics and Geotechnical Engineering, Paper No. 2562.

Yanjing T, Jianmin LI and Shuguang W. 2013. Experimental study on the method of rebound and recompression deformation calculation in deep and large foundation design. Proceedings of the 18th International Conference on Soil Mechanics and Geotechnical Engineering, Paper No. 2684.

Zaghouani K., Chouikha A. and Haffoudhi S. 2013. Difficulty execution of large diameter deep piles in soft soils. Proceedings of the 18th International Conference on Soil Mechanics and Geotechnical Engineering, Paper No. 3058 (in French).

Zhang Y., Salgado S., Dai G. and Gong W. 2013. Load tests on full-scale bored pile groups. Proceedings of the 18th International Conference on Soil Mechanics and Geotechnical Engineering, Paper No. 2119.

Structural and geotechnical design of a piled raft for a tall building founded on granular soil

Conception géotechnique et structurelle du radier sur pieux d'un bâtiment de grande hauteur fondé sur des sols granulaires

Allievi L., Ferrero S., Mussi A., Persio R., Petrella F.
Arup

ABSTRACT: The process followed in designing the piled raft foundation of a tall building is discussed. This entails analysing the governing limit states, assessing the geotechnical characterisation of the soil deposit as well as deploying the appropriate modelling tool to study the behaviour of the chosen foundation system at each design phase. Non-uniform loading imposed by the superstructure, long-term creep effects for deeper soil layers and reinforced concrete elements, cyclic actions associated with wind loading and pile-raft connection detailing also influence the design process. As the design of this piled raft is mainly differential settlement governed, the interaction between the structural and geotechnical design is of the utmost importance.

RÉSUMÉ: On présente la démarche suivie dans la conception du radier sur pieux d'un bâtiment de grande hauteur. Cela implique l'analyse des états limite, la validation de la caractérisation géotechnique des sols ainsi que la mise en œuvre des outils de modélisation appropriés pour étudier le comportement du système de fondation choisi à chaque étape des études. Les charges variables induites par les superstructures, les effets de fluage long terme des couches sous-jacentes du sol et des éléments en béton armé, les actions cycliques associés aux charges de vent, ainsi que les spécificités de la connexion radier-pieux, sont autant d'éléments qui interviennent également dans le processus de conception. Comme la conception de ce radier sur pieux est principalement contrôlée par les tassements différentiels, l'interaction entre la conception géotechnique et celle de la structure est de la plus haute importance.

KEYWORDS: piled raft, settlement reducing piles, differential settlement, cohesionless soils

1 INTRODUCTION

Unlike conventional rafts or fully piled foundations, piled rafts are composite structures consisting of three bearing elements: piles, raft, and subsoil. The Isozaki Tower foundation falls under the category of "large piled rafts" and requires, according to Mandolini 2003, "differential settlement based design"; it is considered a "raft-enhanced pile group" as per the definitions given by Burland *et al.* 2012.

2 THE ISOZAKI TOWER

The Isozaki tower located in Milan comprises 52 storeys and has a total height of 202.2m from ground level (Figure 1).

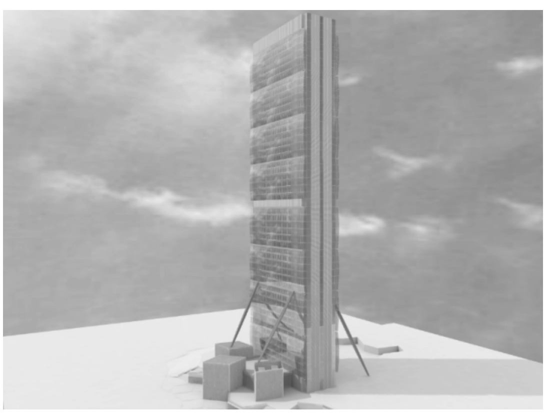

Figure 1 General view of the Isozaki Tower

Use is primarily offices with a few areas reserved for services. In plan the tower is approximately 54.8m long by 22.5m wide. The reinforced concrete raft is 2.5m to 3.5m thick and is supported by 10 no. 1.5m diameter piles and 52 no. 1.2m diameter piles. The piles are bored cast in-situ and 33.2m in length.
The unfactored total load applied at the base of the tower is 1350MN (Figure 2). Considering a raft footprint of 63.1m x 27.0m, the equivalent bearing pressure on the ground is 860kPa, including the raft self-weight.

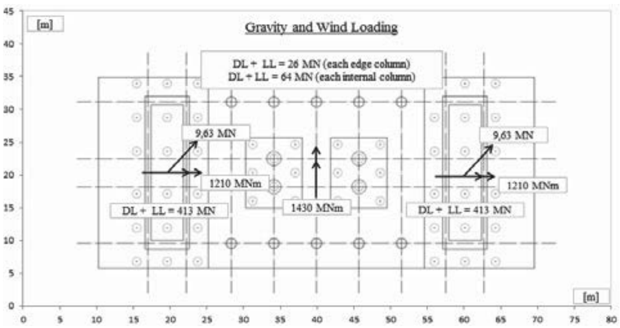

Figure 2 Piled-Raft foundation plan and loading.

3 GROUND CONDITIONS

The site is situated within the Padana Plain in northern Italy, underlain by a 100m thick deposit of Quaternary alluvial granular material. This consists of a normally consolidated coarse sand and gravel unit with the original ground level at +124m asl. The extensive site investigation (SI) included borehole drilling, down hole SPT and pressuremeter tests, permeability tests as well as a pumping test. The SI also comprised a set of geophysical investigations. Undisturbed samples collected from the cohesive layers were subject to oedometer tests and triaxial tests.

Within the granular deposit, three interbedded layers of clayey silts with a PI of 10-30% are found at +79m asl (layer D), +59m asl (layer F) and +45m asl (layer H) with a thickness of 3m, 4m and 2m respectively (Figure 3).

The cohesionless layers typically have a relative density of 45-65% and ϕ'_{cv}=36°. The soil stiffness profile at small strains was derived from V_S measured in situ; a good agreement with the empirical correlation to N_{SPT} values proposed by Stroud (1988) was found for the granular materials. For the cohesive layers, the secant stiffness was estimated from c_u and OCR according to Koutsoftas and Fisher 1980.

The two level basement requires a 16m deep excavation, so the raft formation level is at +108m asl. Extensive aquifer exploitation lowered the groundwater table from +120m asl to a minimum level of +100m asl in the mid 70's. With the relocation of industrial sites outside the urban area the groundwater table has risen to the current level of +106.5m asl, resulting in a lightly overconsolidated deposit, with OCR values ranging between 1.35 and 1.20 in the cohesive layers D to H.

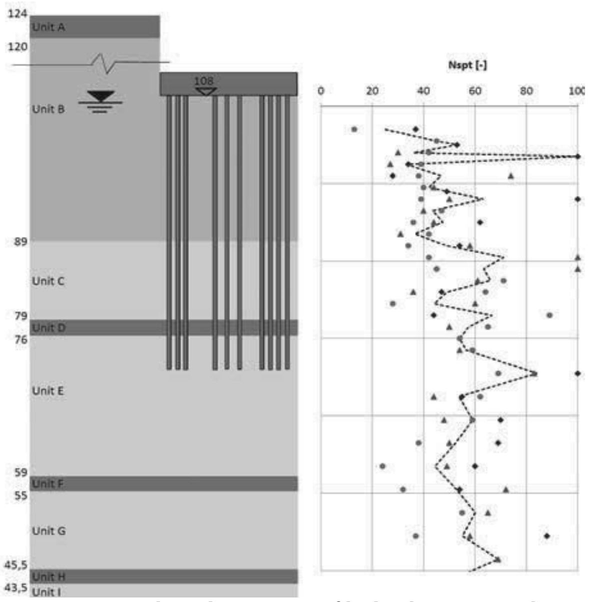

Figure 3 Stratigraphy and SPT tests profile (levels in metres asl)

4 FOUNDATION DESIGN

The Italian Construction Code (2008) covers mixed foundations and determines that where the raft alone is capable of satisfying the ULS, the piles can act as settlement reducers and their design should ensure the satisfaction of the SLS. This implies that the piles need to be checked for the structural limit states only.

The main design challenges consisted in accounting for the presence of deep cohesive layers and achieving a cost-effective solution. The absence of published data on the behaviour of existing high-rise buildings founded on mixed foundations in Milan is noted.

The structural and geotechnical design was developed in phases, with simplified methods being used for preliminary design (Poulos 2001; Mandolini *et al.* 2005).

From early design stages it was found that an unpiled raft could carry the load shed from the superstructure alone. The corresponding stresses, however, require a very thick and heavily reinforced raft which is not the most cost-effective or buildable foundation solution. Similarly, there was no feasible configuration for a fully piled solution, considering the pile length constraints explained below. The behaviour of an unpiled raft foundation solution was analysed to guide the selection of the settlement reducing pile locations and control the raft stresses and differential settlements (Figure 4).

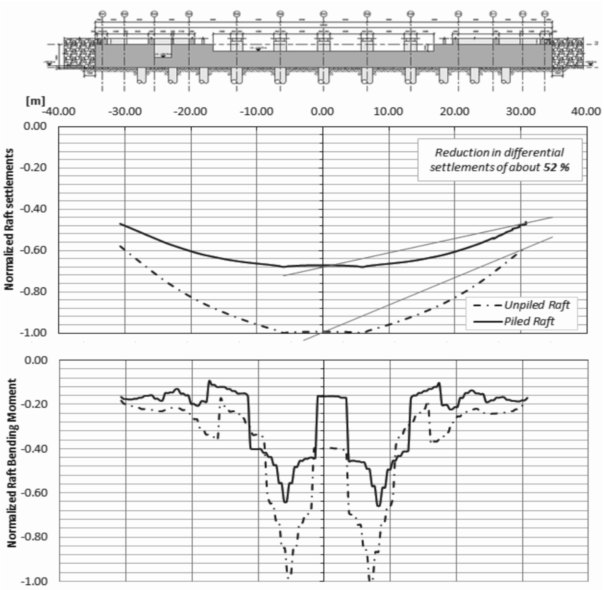

Figure 4. Unpiled Raft vs Piled Raft: Settlement and Bending Moment diagrams normalized to the unpiled raft maximum values.

Creep settlements of the cohesionless layers where estimated according to Burland & Burbidge 1985 for a design life of 100 years.

Due to permeability of cohesive layers ranging between 10^{-8}m/s (layers D and H) and 10^{-9}m/s (layer F) and their limited thickness it was evaluated that primary consolidation should take place during construction (assumed > 2 years). The secondary consolidation coefficient was estimated from *ad hoc* oedometer tests subject to a longer than standard duration (6 days ≈ one additional log-cycle) at the relevant design effective stress. The aim of limiting the impact of creep associated to the cohesive layers, led to positioning the pile base just below the cohesive layer D. This corresponds to a pile length to radius of equivalent circular foundation area ratio of 1.4 which, together with the pile group-raft area ratio, is identified as the most effective elements of the system geometry for the minimisation of the normalised differential settlements (Reul & Randolph 2004).

During the first phases of design the single pile axial resistance and load-settlement curve were estimated using the $K_s \cdot \tan\delta$ approach and the method proposed by Fleming 1992, respectively. The final design stage benefited from the availability of site-specific preliminary pile load tests which showed an average unit shaft resistance ranging between 90 and 120kPa and provided load-settlement curves for the calibration of the FE models. The piled-raft was analysed with the FEM software Oasys GSA 2010 which links the superstructure, foundation and ground into a single soil-structure model. The raft was modelled with 2D shell elements in contact with beam elements (piles) and a linear elastic soil mass within which displacements are calculated according to the Mindlin method. Each pile node has an associated pile-soil interaction coefficient curve which enables a non-linear response of the pile under vertical loading. The soil stiffness was developed considering the part of the load occurring in re-loading conditions and that in virgin compression as well as the estimated average soil shear

strain (γ=0.1%) derived from the stiffness degradation curves proposed by Seed & Idriss 1970 for cohesionless soils.
The GSA model was compared with a full 3D FE analysis developed with MIDAS GTS (Figure 5) which provided similar settlements, pile axial loads and raft stresses.

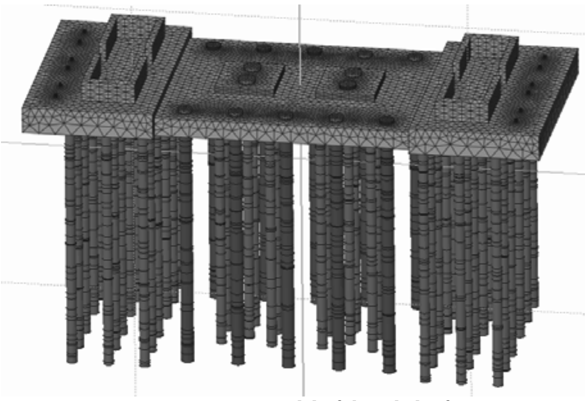

Figure 5. MIDAS GTS 3D FE model of the piled raft.

Creep effects of the concrete in the raft and piles were taken into account as these affect the long term behaviour of the foundation. A reduction factor of the young modulus of $1+\varphi_\infty$ was adopted with φ_∞=0.90 for the raft and 0.76 for the piles. In order to limit bending moments in the top of the piles due to raft deflection, no structural connection between the raft and the pile head was provided.
The piled raft behaviour under horizontal loads was analysed with PIGLET (Randolph 2006) and the Oasys software ALP and PDISP.
The effect of wind induced cyclic actions was estimated according to the methods described by O'Riordan 1991 (settlements) and Poulos & Davids 2005 (pile stiffness degradation).
Half of the maximum raft settlements were estimated to occur during construction, 33% were associated to creep, 13% to cyclic loading and 4% to planned nearby buildings. The potential for tilting due to variations in thickness of the cohesive layers was estimated to be negligible.
The load percentage split between the raft and the piles estimated from the FE analyses is 35/65: this matches well with that proposed by Mandolini *et al.* 2005 for $(s/d)/(A_g/A)$=4.75.
The 1.2m diameter piles have a factor of safety (FoS) ranging between 1.45 and 1.65, and the 1.5m diameter piles between 1.55 and 1.75.
Whilst stringent checks of pile construction (eg. cleaning of the base) are needed to ensure that the specified requirements are met, limiting the mobilisation of the piles shaft resistance minimises the sensitivity of the raft behaviour with respect to workmanship problems and local variations of soil conditions.
Accepting a FoS<2 for the piles required the use of a higher concrete class (C32/40) than in conventional piled foundations: this has cost implications and needs to be considered at optioneering stage. The overall cost of the piled raft was estimated to be 35-45% lower than that of a simple raft; the piled raft requires 50-60% less concrete and 35-45% less steel. The cost of the piles is 20% of the total foundation cost.
The piled raft has been constructed and is fully instrumented.

5 CONCLUSIONS

Mixed foundations are covered by the Italian Construction Code which allows the design of piles as settlement reducers if the raft alone can comply with the ULS requirements.
Simplified methods are used during the initial optioneering phase to develop a solution which can then be analysed with more rigorous tools.
GSA is a reliable and efficient tool for the final design stages which has shown to match the results of a parallel full 3D FE piled raft model.
Pile length to equivalent circular raft radius ratio and pile group-raft area ratio are important elements to consider during design.
A FoS<2 on piles results in higher working load in piles than would otherwise be the case; this requires additional consideration for their structural design.
Internal actions on the upper part of the piles are reduced by avoiding a structural connection between piles and raft without significantly affecting the raft behaviour. Limiting the mobilisation of the piles' shaft resistance minimises the sensitivity of the raft behaviour with respect to workmanship problems and local variations of soil conditions.
Assessment of the total settlements requires consideration of time-dependant phenomena.
Piled rafts can offer a cost-effective foundation solution for high-rise buildings.

6 ACKNOWLEDGEMENTS

The authors would like to thank Duncan Nicholson, Alessandro Baliva, and Matteo Minno for their contribution as well as Marco Beccati for his support from the client's side.

7 REFERENCES

Burland and Burbidge 1985. Settlement of foundations on sand and gravel. Proc. ICE, part 1.
Burland J., Chapman T., Skinner H. D. and Brown M. 2012. Manual of Geotechnical Engineering, Institution of Civil Engineers.
Decreto Ministeriale 14.1.2008 del Ministero delle Infrastrutture. "Nuove norme tecniche per le costruzioni". S.O. n. 30 alla G.U. del 4.2.2008, n. 29.
Fleming G.W.K. 1992. A new method for single pile settlement prediction and Analysis, Geotechnique 42, No. 3 pp 411-425
Koutsoftas, D., Fisher, J. 1980. Dynamic properties of two marine clays, ASCE J. Geotech Division 106 (GT6), pp. 145-157.
Mandolini A. 2003. Design of piled raft foundations: Practice and Development, Design of foundations on bored and auger piles, Van Impe ed., Rotterdam.
Mandolini A., Russo G. and Viggiani C. 2005. Pile Foundations: Experimental investigations, analysis and design. *ICSMGE*, Osaka.
MIDAS GTS Scientific Manual.
Oasys Ltd, Oasys Geo Suite v 19.1 ALP, GSA and PDISP Software Manual, London 2010.
O'Riordan N.J. 1991. Effects of cyclic loading on the long term settlements of structures, Cyclic loading of soils, Blackie.
Poulos H. G. 2001. Piled-raft foundation: design and applications. Geotechnique, 51(2), 95-113.
Poulos H. G. and Davids A. J. 2005. Foundation design for the Emirates Twin Towers Dubai, Canadian Geotechnical Journal, 42, 716-730.
Randolph M.F. 2006. PIGLET: Analysis and design of pile groups. Users' Manual, Version 5.2, Univ. Western Australia, Perth.
Reul O. and Randolph M.F. 2004. Design strategies for piled rafts subjected to nonuniform vertical loading, Journal of Geotechnical and Geoenvironmental Engineering, ASCE.
Seed H. and Idriss I. 1970. Soil moduli and damping factors for dynamic response analysis. EERC report n.70-10. Berkeley, CA.
Stroud, M.A. 1988. The standard penetration test – its application and interpretation.

Performance of Piled-Raft System under Axial Load

Performance du système radier pieux sous chargement axial

Alnuiam A.
University of Western Ontario, London, ON, Canada and affiliated with King Saud University, Riyadh, Saudi Arabia

El Naggar H.
University of New Brunswick, Fredericton, NB, Canada

El Naggar M.H.
University of Western Ontario, London, ON, Canada

ABSTRACT: Many high rise buildings are founded on piled raft foundation systems, which generated a significant interest in understanding the performance characteristics of this foundation system. The soil-structure interaction for piled raft foundations involves the interaction of different components including: the pile-soil interaction; pile-soil-pile interaction; raft-soil interaction; and piles-raft interaction. To account for this complicated interaction scheme, three-dimensional consideration of the problem is necessary. In this paper, a 3D finite element model is established to analyze the response piled raft foundation system installed in cohesionless soil with linearly increasing stiffness with depth. The model was calibrated/verified using geotechnical centrifuge test data. The calibrated model was then employed to investigate the effect of raft dimensions and piles diameter and spacing on the load sharing between piles and raft.

RÉSUMÉ : Durant ces dernières années, un grand nombre de projets ont été construit en utilisant le concept du système de fondation de radier sur pieux. C'est ainsi que de nombreuses études ont été menées afin d'examiner et de comprendre la performance de ce système soumis à des charges verticales. L'interaction sol-structure pour ce système implique différentes interactions comme l'interaction pieux-sol, pieux-radier, radier-sol et finalement l'interaction pieux-radier. Par conséquent, une analyse numérique tridimensionnelle est nécessaire dans un cas aussi complexe. Dans cet article, une modélisation 3-D par éléments finis a été effectués pour analyser la réponse d'un système radier pieux sur un sol sans cohésion et qui présente une rigidité qui augmente linéairement avec la profondeur. Ce modèle a été calibré à partir de résultats expérimentaux obtenus sur des essais en centrifugeuse. Les résultats numériques ont été utilisés pour étudier l'effet de plusieurs paramètres, comme l'épaisseur et la largeur du radier, l'espacement et le diamètre des pieux, sur le transfert des charges entre le radier et les pieux.

KEYWORDS: piled raft foundation, soil-structure interaction, 3D FEM, centrifuge, cohesionless soil, piled-raft load sharing.

1 INTRODUCTION

A piled raft foundation is a composite structure with three components: subsoil, raft and piles. These components interact through a complex soil-structure interaction scheme, including the pile-soil interaction, pile-soil-pile interaction, raft-soil interaction, and finally the piles-raft interaction.

The construction of a piled raft foundation system generally follows the same practices used to construct a pile group foundation in which a cap is normally cast directly on the ground. Although the construction of the cap in this manner should allow a significant percentage of the load to be transmitted directly from the cap to the ground, the pile group is usually designed conservatively by ignoring the bearing capacity of the raft (i.e. the pile cap). In many cases, the raft alone can provide adequate bearing resistance; however, it may experience excessive settlement. Therefore, the concept of employing piles as settlement reducers was proposed by Burland et al. (1977), where the piles are used to limit the average and differential settlements.

The vertical load applied to a piled raft foundation is assumed to be transmitted to the ground by both the raft and piles, which differentiates the design of a piled raft from a pile group. The percentage of load taken by each element depends on a number of factors, including: the number and spacing of piles, subsoil conditions, and the raft thickness.

A piled raft design offers some advantages over the pile group design in terms of serviceability and efficient utilization of materials. For a piled raft, the piles will provide sufficient stiffness to control the settlement and differential settlement at serviceability load while the raft will provide additional capacity at ultimate load. The raft in a piled raft design transmits 30% to 50% of the applied load to the soil (Clancy and Randolph, 1993). Typically, a piled raft design will require fewer piles in comparison to a pile group design to satisfy the same capacity and settlement requirements. Additionally, if any of the piles in a piled raft becomes defective, the raft allows re-distribution of the load from the damaged pile to other piles (Poulos et al. 2011). Furthermore, the pressure applied from the raft to the subsoil may increase the confining pressure for the underlying piles, which in turn increases the pile load carrying capacity (Katzenbach et al. 1998).

Analytical, numerical and physical modeling approaches were employed to evaluate the performance of piled raft foundations. The simplified Poulos-Davis-Randolph (PDR) method (Poulos 2001) combines the analytical methods proposed by Poulos and Davis (1980) and Randolph (1994) for the analysis of piled rafts. Clancy and Randolph (1993) proposed a plate-on-spring method in which the raft is represented by a plate and the piles are represented by springs. Additionally, there are methods that combine the finite element analysis for the raft and the boundary element analysis for the piles (e.g. Ta and Small, 1996), and methods that are based on three-dimensional finite elements modeling (e.g. Katzenbach et al.,1998). Piled raft behavior was also investigated employing physical modeling such as centrifuge testing (e.g. Horikoshi et al., 2002, 2003a and b; Matsumoto et al., 2004a and b).

This paper investigates the performance of piled raft foundations and their load sharing mechanism employing a 3D finite element model calibrated/verified using geotechnical centrifuge data.

2 DEVELOPMENT OF FINITE ELEMENT MODEL

The development of the FEM in this study consisted of three main steps. First, a 3D FEM was established to simulate the behavior of piled raft foundation considering an appropriate size mesh and number of elements. Second, the results of a centrifuge study of piled raft performed by others were used to calibrate the FEM created in this study. Lastly, the calibrated FEM was employed to perform a parametric study to evaluate the effect of different parameters on the overall performance of piled raft foundation.

2.1 *Description of FEM*

A finite element model (FEM) was developed using the Plaxis 3D software package (Plaxis bv. 2011). A quarter of the piled raft foundation system was modeled taking advantages of symmetry across the x and y-axes to reduce the computation effort and time. The boundaries of the model were set at a distance equal to 1.5B~2B (where B is raft width) measured from the edge of the raft, and the depth of the model was approximately two times the pile length as shown in Figure 1.

The model was built using about 275,000 3D 10-node tetrahedral elements. The average size of the element was approximately 110 mm. The large number of small size elements assured high accuracy of the results at locations where non-linear behavior is anticipated (e.g. raft base, pile base and pile circumference). The load was applied using uniform prescribed displacement applied at the top of the raft, and the corresponding load was evaluated.

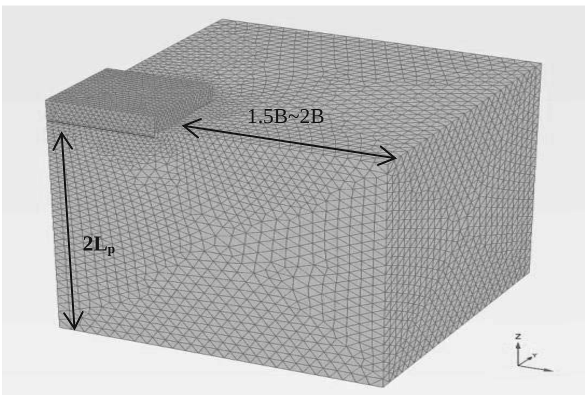

Figure 1. The FEM used in the current study.

2.2 *Centrifuge testing used to calibrate FEM*

Horikoshi et al. (2002, 2003a, b) employed geotechnical centrifuge testing in order to simulate the complicated soil-structure interaction problem for a piled raft under different types of loading. The results of the vertical loading case from their studies will be considered herein to calibrate the 3D finite element model. The tests were conducted under 50g centrifugal acceleration. The model consisted of four piles rigidly connected to the raft. The raft and piles models were made of aluminum. Toyoura sand was used as the model ground (Horikoshi et al. 2003a). Table 1 summarizes the dimensions of the model in both model and prototype scales.

Table 1. The dimensions of the model in both model and prototype scales.

	Model	Prototype (n=50)
Diameter (mm)	10	500
Wall thickness (mm)	1	Solid
Materials	Aluminum	Concrete
Pile length	170 mm	8.5 m
Modulus of Elasticity	71 GPa	41.7 GPa
Raft thickness	40 mm	2.0 m
Raft width (square)	80 mm	4 m
Pile Spacing	40 mm	2 m
Number of piles	4	4

Cone penetration tests (CPT) were performed in-flight to evaluate the sand strength using a miniature cone penetrometer. The cone tip resistance profile is shown in Figure 2. It is noted that the strength (and stiffness) increased with depth, which is expected for sand soil. This strength profile will be simulated in the FEM through the input parameters such as the initial modulus of elasticity and the incremental modulus of elasticity, which will account for the increase in stiffness with depth.

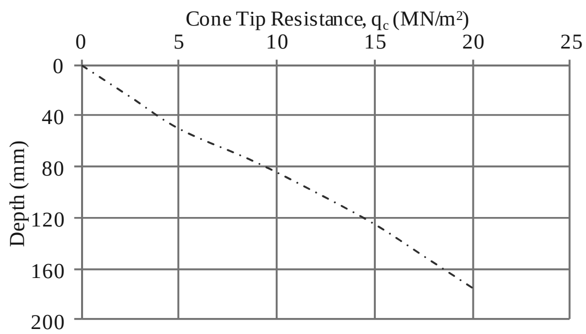

Figure 2. In-flight results for CPT (after Horikoshi et al. (2003a).

2.3 *Calibration of FEM*

The behavior of the Toyoura sand was simulated using a linear elastic-perfectly plastic Mohr-Coulomb constitutive model. Matsumoto et al. (2004b) reported that the peak friction angle, ϕ, for Toyoura sand is about 45° and the reduction factor, R_{int}, at the interaction surface between the pile and Toyoura sand is 0.43 (Horikoshi et al., 2003a). The modulus of elasticity was correlated to the cone tip resistance, q_c, using the relationship proposed by Tomlinson (1996), i.e.

$$E = 2\sim4\ q_c \qquad (1)$$

All input parameters used in the FEM are listed in Table 2.

The process of calibration was performed by refining the soil and interface properties in the FEM. This was done by adjusting the values of the interface reduction factor values at the pile-soil interface; and the estimated initial modulus of elasticity and incremental increase of modulus of elasticity with depth (i.e. within the range stipulated in Eq. 1). After a number of trials, the FEM a reasonable match with the centrifuge test results was achieved as demonstrated in Figure 3.

The slight nonlinear behavior observed at relatively low displacement is attributed to the movement of the pile caused by slippage at pile-soil interface and increased strains at the pile base, reaching plastic condition. This piles movement resulted in more intimate contact between the raft and soil, which resulted in a portion of the load to be transmitted through the contact at the raft-soil interface.

Table 2. The parameters used in the FEA.

	Soil	Concrete
Constitutive Modeling	Mohr-Coulomb	Linear Elastic
Unit Weight (kN/m^3)	14.6	23.6
Angle of internal friction	45°	-
Modulus of Elasticity	4500 kN/m^2	23.6 GN/m^2
Poisson's ratio	0.175	0.21
Stiffness increases with depth	Yes	No
Incremental Modulus of Elasticity (kN/m^2/m)	6500	-
Interface reduction factor	0.43	-

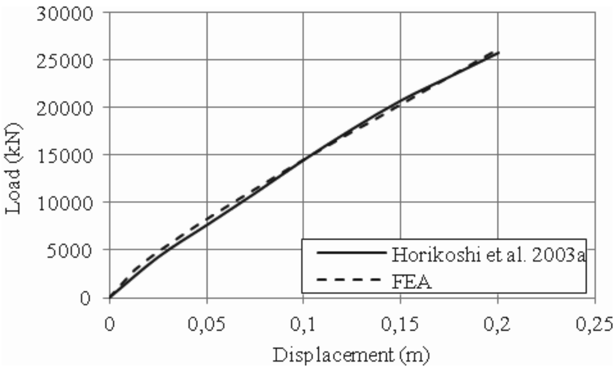

Figure 3. Comparison of the FEA and centrifuge test results.

3 EFFECT OF PILED RAFT PARAMETERS ON ITS LOAD SHARING SCHEME

In a piled raft, different factors affect the load sharing between the raft and piles but with varying influence on the load sharing. The raft flexibility, which is governed by its thickness and the spacing between the piles, affects the load sharing between the raft and piles, and will be investigated. For example, increasing the raft width is expected to increase the load transmitted by the raft. On the other hand, increasing the pile diameter is expected to increase the load transmitted through the piles. The effects of these two parameters are examined and the results obtained are discussed in this section. The load carried by the piles will be presented as a percentage of the total vertical load applied on the raft.

3.1 *Effect of raft thickness*

Brown (1969) evaluated the foundation flexibility using finite element analysis. He proposed a relationship between the thickness of the raft and its flexibility, given by:

$$K_f = \left[{}^{E_f}/{}_{E_s}\right]\left(\frac{2t}{s}\right)^3$$
(2)

Where E_f = Young's modulus for raft; E_s= average soil elastic modulus; t= raft thickness; and s= spacing between piles.

Thin or flexible rafts tend to deform more than rigid or thick rafts. This increased deformation of a flexible raft establishes intimate contact with the subsoil, resulting in increased load carried by the raft. Equation 2 may be used for the assessment of the flexibility of a piled raft, but considering the spacing between the piles instead of the raft width, B. Using the spacing between piles is appropriate in representing the flexibility of the piled raft as small pile spacing results in a s smaller deformation at the raft center in comparison with large spacing. Considering Eq. 2, the raft can be characterized according to the following conditions: (i) perfectly rigid if $K_f > 10$; (ii) perfectly flexible when $K_f < 0.01$; and (iii) intermediate flexibility at K_f varies between 0.01 to 10 (Mayne and Poulos 1999). The load sharing scheme for piled rafts with varying flexibility is investigated. Figures 4 and 5 show the load carried by the piles for two different pile spacing with various raft thicknesses as a function of the piled raft total displacement.

At initial small displacement, most of the load is carried by the piles; this is believed to be due to the lack intimate contact between the raft and subsoil. Similar behavior was reported by Horikoshi and Randolph (1996). As the displacement increases, the proportion of the load carried by the piles dropped significantly at about 7% of the total displacement and continued to decrease gradually after that. At about 80% of displacement, the load transmitted by the piles reached a plateau and became almost constant. The variation in load carried by the pile is noticeable at S/D=4; the load carried by the piles is about 35% and 45% for raft thickness, t= 0.3 m and t= 2 m, respectively. The raft flexibility, K_f = 0.2 and 8.73 for these two cases. On the other hand, K_f = 0.29 and 0.02 if the spacing is S/D=10 for the same raft thickness values. Due to the narrow range of K_f for the large spacing case, the variation in percentage of load carried by the piles is insignificant, and it is approximately 25%. This is attributed to the large pile spacing, which renders even the thick raft flexible, resulting in increased raft soil interaction, compared to the case of the raft with small pile spacing. Poulos (2001) reported a similar percentage of 25% of the load carried by the piles.

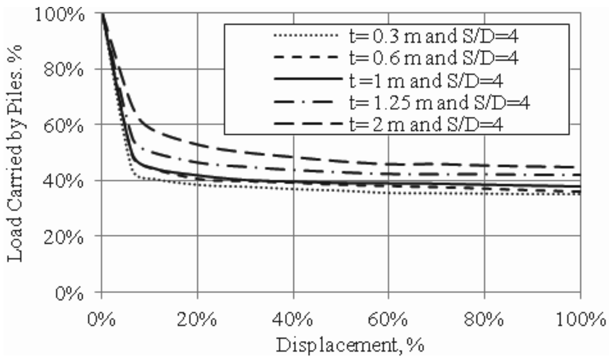

Figure 4. Load carried by piles with different raft thicknesses and S/D=4.

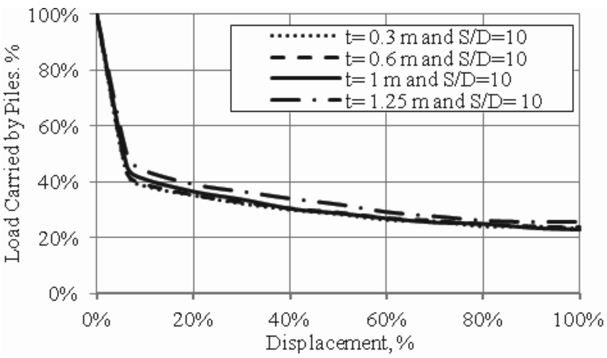

Figure 5. Load carried by piles piles with different raft thicknesses and S/D=10.

3.2 *Effect of raft size*

The raft width contributes to the bearing capacity of the raft. As the raft width increases, the contact area with the subsoil increases and hence the load carried by the raft increases. The load carried by the piles was evaluated for different raft widths varying from 4 m to 7 m with the same pile diameter (0.5m), spacing ratio (4D) and raft thickness (1.25 m) (i.e. relatively rigid raft) and the results are presented in Figure 6. As expected, Figure 6 shows that the load transmitted by the piles was reduced as the raft width increased. It is noted that the piles load decreased sharply until it reached a constant value at about 18% of the total displacement. As the raft width increased from 4 m to 7 m, the load transferred through the piles decreased by about 22%. As the load carried by the raft increases, however, it is important to carefully examine the total and differential settlements, which may rise due to the high level of stress beneath the raft.

3.3 *Effect of pile diameter.*

The pile diameter has a significant effect on its load carrying capacity and stiffness, which can affect the performance of the piled raft. To examine the effect of pile diameter on its load share in piled raft design, a raft with width, B = 7.2 m and piles spaced at S/D =4 is considered with pile diameter varying from 0.3 m to 0.9 m. Figure 7 demonstrates the percentage of load carried by the piles as the pile diameter changes. The load transferred by the piles increased from 18% to 33% of the total load as the pile diameter increased from 0.3 m to 0.9 m. The increase occurred because the piles started to interact with the soil across a larger surface area and thus more load carried by the piles. However, the effect of the pile diameter on the piles load share diminishes as the diameter reaches the higher end of the range considered. For example, the percentage of load taken by the piles increased by about 2% as the diameter increased from 0.7 to 0.9 m, while the difference for a smaller diameter was about 9% as the diameter increased from 0.3 to 0.5 m.

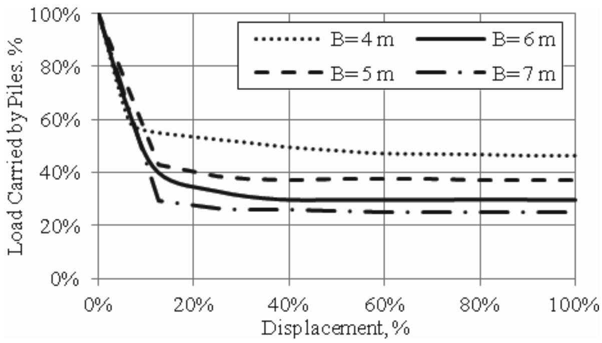

Figure 6. Load carried by the piles with different raft width.

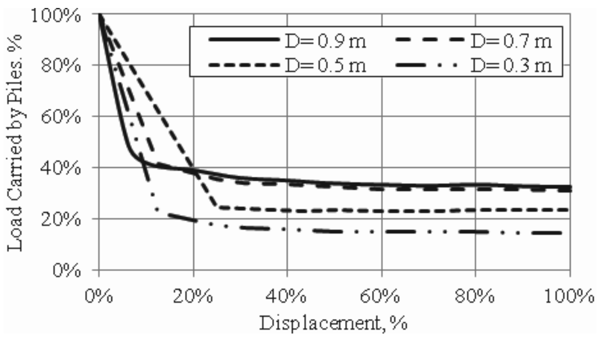

Figure 7. Load carried by the piles with different pile diameters.

4 CONCLUSIONS

Some of factors that affect the load sharing between the piles and raft in a piled raft foundation were examined using a 3D finite element model that has been calibrated/ verified by comparing its predictions with measurements made in a geotechnical centrifuge study. Based on the results of the 3D-FEA, a number of conclusions can be drawn as follows:

- The load share carried by piles is higher for a rigid raft (K_f > 10) due to the minimal interaction between the raft and subsoil compared to the perfectly flexible raft (K_f < 0.01).
- The spacing between piles can be used to evaluate the raft flexibility instead of its width using Eq. 2.
- The percentage of load transmitted by the piles decreases by about 22% as the raft width doubled within the range considered.
- The percentage of load carried by piles increases as the pile diameter increases. However, the rate of increase is higher for small size piles and diminishes as the pile diameter increases.

Additional studies are required to evaluate the performance of a flexible piled raft considering the number of piles, pile length and loading scheme.

5 REFERENCES

Brown, P. T. 1969. Numerical Analyses of Uniformly Loaded Circular Rafts on Deep Elastic Foundations. *Géotechnique* 19 (3), 399-404.

Burland, J. B., Broms, B. B., and De Mello, V. B. 1978. Behaviour of foundations and structures. *Proc. 9th ICSMFE.* Tokyo: V. 2, 496-546.

Clancy, P., and Randolph, M. F. 1993. An Approximate Analysis Procedure for Piled Raft foundations. *International Journal for Numerical and Analytical Methods in Geomechanics* 17(12),849-869.

Horikoshi, K., and Randolph, M. F. 1996. Centrifuge modelling of piled raft foundations on clay. *Géotechnique*, 46 (4), 741-752.

Horikoshi, K., Matsumoto, T., Hashizume, Y., and Watanabe, T. 2003b. Performance of Piled Raft Foundations Subjected to Dynamic Loading. *International Journal of Physical Modelling in Geotechnics*, 3 (2), 51-62.

Horikoshi, K., Matsumoto, T., Hashizume, Y., Watanabe, T., and Fukuyama, H. 2003a. Performance of Piled Raft Foundations Subjected to Static Horizontal Loads. *International Journal of Physical Modelling in Geotechnics* 3 (2), 37-50.

Horikoshi, K., Watanabe, T., Fukuyama, H., and Matsumoto, T. 2002. Behaviour of Piled Raft Foundations Subjected to Horizontal Loads. In R. Phillips, P. J. Guo, & R. Popescu (Ed.), *Procceding of the Internationa confrancePhysical Modelling in Geotechnics.* St John's, Newfoundland, Canada: Taylor & Francis.

Katzenbach, R., Arslan, U., Moorman, C., and Reul, O. 1998. Piled Raft Foundation: Interaction Between Piles and Raft. *Darmstadt Geotechnics, Darmstadt University of Technology* 4, 279-296.

Matsumoto, T., Fukumura, K., Horikoshi, K., and Oki, A. 2004b. Shaking Table Tests on Model Piled Rafts in Sand Considering Influnce of Superstructures. *International Journal of Physical Modelling in Geotechnics* 4 (3), 21-38.

Matsumoto, T., Fukumura, K., Pastsakorn, K., Horikoshi, K., and Oki, A. 2004a. Experimental and Analytical Study on Behaviour of Model Piled Raft in Sand Subjected to Horizontal and Moment Loading. *International Journal of Physical Modelling in Geotechnics*4(3),1-19.

Mayne, P. W., & Poulos, H. G. (1999). Approximate Displacement Influence Factors for Elastic Shallow Foundations. *125*(6), 453-460.

Plaxis bv. 2001. *Plaxis 3D Version 2001,Reference Manual.* Delft, The Netherlands.

Poulos, H. G. 2000. Practical Design Procedures for Piled Raft Foundations. In J. Hemsley, *Design Applications of Raft Foundations* 425-467. London: ICE Publishing.

Poulos, H. G. 2001. Piled Raft Foundations: Design and Applications. *Geotechnique* 51 (2), 95-113.

Poulos, H. G., and Davis, E. H. 1980. *Pile Foundation Analysis and Design.* New York: Wiley.

Poulos, H. G., Small, J. C., and Chow, H. 2011. Piled Raft Foundations for Tall Buildings. *Geotechnical Engineering Journal of the SEAGS and AGSSEA* 42 (2), 78-84.

Randolph, M. F. 1994. Design Methods for Piled Groups and Piled Rafts. *Proc. 13th ICSMFE*, 61-82. New Delhi, India.

Ta, L. D., and Small, J. C. 1996. Analysis of Piled Raft System in Layered Soils. *International Journal for Numerical and Analytical Methods in Geomechanics* 20 (1), 57-72.

Tomlinson, M. J. 1996. *Foundation Design and Construction.* London: Longman Publishing Group.

Analysis of Full-Scale Random Vibration Pile Tests in Soft and Improved Clays

Analyses à grande échelle de vibrations aléatoires sur pieux dans un sol argileux

Ashlock J.C., Fotouhi M.K.
Iowa State University, Ames, IA, USA

ABSTRACT: Full-scale pile vibration test results are analyzed for steel HP piles installed to a depth of 6 m in a soft clay profile, with one pile surrounded by a cement-deep-soil-mixed (CDSM) improved zone. Multi-modal tests with vertical and coupled lateral-rocking vibrations were conducted using a shaker mounted on a rigid pile cap. The improved soil zone significantly increased the stiffness of the measured vertical response, but had little effect on the lateral-rocking mode. Results of the forced vibration tests are analyzed using methods reported in the literature, including impedance functions and an approximate computational method which incorporates variation of soil properties with depth. The simplified model is able to capture the vertical response reasonably well in both the improved and native unimproved soil profiles, as well as the lateral response in unimproved soil. For the pile in improved soil, however, calibration of the model to the observed vertical mode results in a greatly stiffened lateral-rocking response which was not observed experimentally. To improve the simulation results, more sophisticated computational solutions are proposed for modeling the dynamic interaction of the pile and improved soil.

RÉSUMÉ : Les résultats d'essais de vibrations à grande échelle sur des pieux en acier (HP) et un pieu renforcé en tête par un mélange sol-ciment, installés sur 6 mètres de profondeur dans de l'argile, ont été analysés. Des tests multimodaux avec vibrations verticales et balancements latérales ont été réalisés à l'aide d'un actionneur monté en tête des pieux. Nous montrons que le renforcement du sol améliore la réponse verticale de manière significative mais n'a que peu d'effet sur la réponse latérale. Les résultats des essais ont été interprétés en utilisant des méthodes publiées dans la littérature, notamment une méthode qui prend en compte des fonctions d'impédance et une méthode numérique qui prend en compte les variations des propriétés du sol en fonction de la profondeur. Le modèle simplifié utilisé est capable de décrire correctement la réponse verticale pour les deux types du sol, avec ou sans renforcement, ainsi que la réponse latérale pour un sol non renforcé. Cependant, l'ajustement du model à partir de la réponse verticale rend compte d'une plus grande raideur latérale que celle observé expérimentalement. Ainsi, afin d'améliorer les résultats de nos simulations, nous proposons des modèles plus sophistiqués qui prennent en compte l'interaction dynamique des pieux avec le sol renforcé.

KEYWORDS: soil-pile interaction, soil dynamics, random vibration, pile, soil improvement, soft clay, impedance.

1 INTRODUCTION

Accurate characterization of the dynamic interaction between foundations and layered soils is an important issue for the design and analysis of foundations under seismic or vibratory loading. To date, several solutions ranging from simplified 2D approximations to 3D numerical models have been developed and employed to analyze soil-foundation interaction. However, validation and calibration of the various methods against full-scale field tests is essential for an understanding of their relative capabilities and limitations. While analytical and computational studies in the literature are numerous, the volume of full-scale field testing studies is comparatively limited. To help bridge the knowledge gap between theory and experimentation in soil-pile interaction problems, the current study investigates a series of full-scale dynamic field tests of two identical steel HP 250x63 (English HP 10x42) piles installed to a depth of 6 m in a soil profile featuring soft clay. The influence of local soil improvement on the dynamic pile response is also examined experimentally using a 1.2 m diameter, 4 m deep cement-deep-soil-mixed (CDSM) zone installed in the soft clay layer surrounding one of the piles. The piles were subsequently used for a reaction frame in a related study, which limited the pile spacing and diameter of the improved zone. The pile in the native unimproved soil profile is referred to as pile U, and the pile in the improved CDSM soil as pile I. The random vibration test procedures employed are described below, followed by analyses of the experiments via simplified 2D numerical models developed for dynamic interaction of piles with layered soils.

A newly developed servo-hydraulic shaker system was used to deliver three types and various levels of excitation. The excitation types used were chaotic impulse, random and swept-sine, denoted C, R and S, respectively. Theoretically, the broadband random (R) signal has a uniformly distributed energy over all frequencies while the swept-sine signals (S) concentrate the excitation's energy at a single frequency which is continually changing within a predefined interval. The chaotic impulse (C) excitation consists of a series of randomly timed impulses with randomly distributed amplitudes. In all tests, accelerations of the shaker and pile cap were measured in the horizontal (x) and vertical (z) directions in the plane of motion of the pile cap using six uniaxial accelerometers. Additionally, seven triaxial accelerometers were buried 6 inches below the soil surface at selected locations to record the near-surface vertical and horizontal motion. Figure 1 details the test setup including the soil profile, improved zone and sensor arrangement.

For data acquisition and real-time analysis in the time and frequency domains, a 20 channel dynamic signal analyzer was programmed in LabVIEW to record time histories and spectral quantities including FFTs, auto- and cross-spectral densities, transfer functions, and coherence functions. The stimulus for the transfer functions was taken as the force applied by the shaker's inertial mass in the direction of excitation, and all other accelerations of the pile cap and soil were treated as response quantities. Additionally, the full time histories of all sensors were simultaneously recorded on the nees@UCLA Kinemetrics Granite seismic recording systems to enable further interpretations such as time-domain analyses or different stimulus-response combinations.

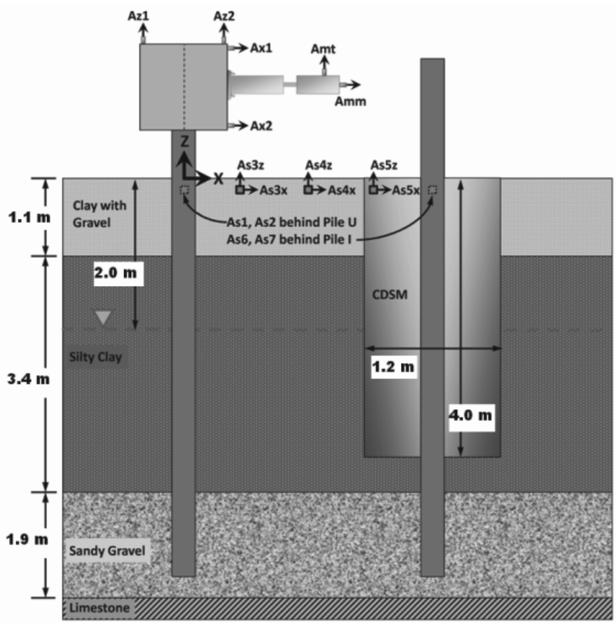

Figure 1. Soil profile, test set-up and sensor arrangement. Pile cap and shaker shown on pile U in native unimproved soil.

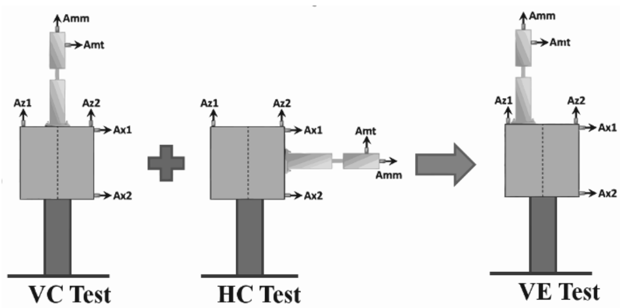

Figure 2. Inertial shaker configurations for the three test types.

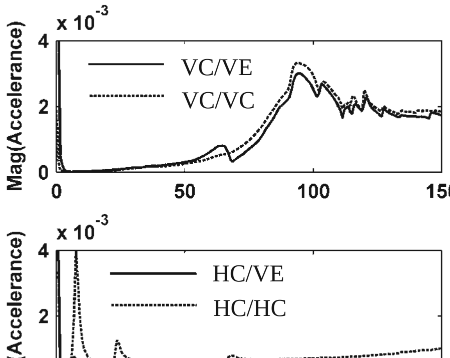

Figure 3. Comparison of VE test to combination of VC and HC tests for swept sine loading on pile I in improved soil. Top: VC response from VC and VE tests; Bottom: HC response from HC and VE tests.

For each combination of pile type (U or I), excitation type (C, R, or S) and intensity (1, 2, or 3), three separate tests were performed with the shaker mounted in the vertical-centric (VC), horizontal-central (HC), and vertically eccentric (VE) positions, shown schematically in Figure 2. The VC test primarily activates the vertical mode of vibration, while the HC test excites the coupled horizontal-rocking mode. These two tests have traditionally been performed independently, creating uncertainty as to the similarity of contact and soil conditions in the two separate tests. The VE tests were studied as a method to reduce such uncertainties and improve efficiency by activating the vertical and coupled horizontal-rocking modes simultaneously.

A total of 109 full-scale vibration tests were performed on the piles using the three excitation types and three shaker configurations described above, with a range of loading levels and excitation bandwidths. Typical experimental results are shown in Figure 3 for pile I. The results demonstrate that a single VE test can be used to characterize the vertical and horizontal-rocking modes normally obtained from separate VC and HC tests. Due to the difference in shaker orientation and location in the VE and HC tests, the HC response to HC excitation (HC/HC) differs from the HC response to VE loading (HC/VE). However, such differences are accounted for in the equations of motion of the shaker, pile cap, and un-embedded pile stem, and the HC and VE responses can be evaluated against their theoretical counterparts for both test types using a common set of soil-level impedance functions. A more detailed description of the test set up and experimental results can found in the Experimental Setup Report archived together with the data from all experiments described herein on the NEEShub at http://nees.org/warehouse/project/940.

To refer to the various tests, a naming convention of (Pile Type)-(Test Type)-(Excitation Type and Level) will be used. For example, U-HC-R3 refers to a test performed on pile U in unimproved soil with the shaker in the HC configuration, with random (R) excitation at the highest intensity level (3). In the naming convention, test types VC and HC can replace VE, and excitation types S (swept-sine) and C (chaotic impulse) can replace R. For any accelerometer, the accelerance is defined at each frequency as the ratio of the directional acceleration to the force applied by the moving mass of the shaker. Accelerance is used as the main frequency response function for comparing and analyzing experimental and analytical results. For example, VC/VE refers to the vertical-centric acceleration due to vertical-eccentric forcing. The pile-cap and stationary portion of the shaker are assumed to undergo rigid-body motion, and a set of vertical, horizontal and rotational accelerances at the centroid can therefore be easily calculated using acceleration measurements from three non-collinear points on the pile-cap.

2 THEORETICAL MODEL

The theoretical accelerance of the system is calculated using frequency-domain rigid-body equations of motion for the pile-cap and shaker, an Euler-Bernoulli beam-column formulation for the above-ground pile segment, and the aforementioned 2D approximate or 3D BEM formulations for impedance functions at the soil level to account for the dynamic pile-soil interaction (the BEM models are not discussed in this paper). The soil-pile impedance matrix relates the force and displacement of the pile cross-section at the soil surface elevation. Each component of the impedance matrix is frequency dependent and complex-valued, with the real part representing the dynamic stiffness of the pile-soil system and the imaginary part accounting for the material and geometric damping.

The 2D approximate pile-soil interaction model introduced by Novak and Aboul-Ella (1978) was used to calculate the soil impedances with account of the variation of soil parameters with depth. This model derives the soil reactions from a plane strain assumption and also incorporates the reaction of the soil at the pile tip. Upon constructing the stiffness matrices using the approach, the pile head impedances can be found by solving the global matrix equations for prescribed unit displacements and rotations of a pile section at the soil-surface. The model is limited to hysteretic damping behavior for the soil and a circular cross section for the pile. Circular sections with equivalent axial or bending stiffness as appropriate were therefore used to model the H-piles in this study. Additionally, the model requires that soil and pile properties are constant for each pile element.

The approach is fast compared to other numerical alternatives such as the finite element and boundary element methods, while offering good agreement with the more rigorous 3D computational methods for certain pile-soil configurations. However, the solution cannot easily model pile installation effects or soil-pile separation. Additionally, variation of the soil profile below the pile tip is not included in the formulation. The formulation was programmed in MATLAB for use in this study. More details on the theoretical approach can be found Novak and Aboul-Ella (1978).

3 PARAMETRIC STUDY AND RESULTS

The measured vibration data from full-scale tests were used in an inverse-analysis framework to calibrate the theoretical soil-pile model and identify the optimum values for each parameter in the solution. A sensitivity analysis was first conducted to determine the relative influence of the various parameters and estimate their possible range of variation for modeling the experimental observations. The properties of the pile-cap and shaker are known relatively accurately, and were therefore determined not to play a major role in the sensitivity analysis.

Attention was thus focused on the soil-pile interaction unknowns, including contact conditions and gapping near the surface, and profiles of soil shear modulus and damping. The parametric studies indicated that the un-embedded length of the pile can have a significant effect on the accelerance. Although the free un-embedded length of the pile can be measured accurately, slight gapping was observed in the field for pile U.

The sensitivity of accelerance to gapping effects was therefore examined by increasing the length of the free pile stem in the theoretical accelerance calculation, while decreasing the embedded pile length accordingly in the approximate 2D soil-pile impedance model. Figure 4 illustrates the effect of gapping on the theoretical accelerance, shown relative to the experimental HC/HC response for test U-HC-R4. As indicated in this figure, a 0.3 m soil-pile separation depth was found to produce an improved fit of the first experimental horizontal-rocking peak. Due to the non-destructive elastodynamic nature of the tests, the gapping depth was not observed to vary significantly between tests. Gapping was not observed for pile I in the field, likely due to its vibratory installation while the CDSM zone was still in a liquid state.

Figure 5 depicts the two shear modulus soil profiles that were used in the study of the unimproved soil-pile system. The profile labeled “CPT” was calculated from the CPT data using correlations to shear wave velocity presented in NCHRP Synthesis 368 (Mayne, 2007). Since correlations between CPT resistance and shear-wave velocity are not precise, the input values for the soil modulus are expected to incur some degree of error. Therefore, a second shear modulus profile based on Hardin and Drnevich (1972) was also examined, as shown in Figure 5. To model the soil damping profile, only three major layers corresponding to those shown in Figure 1 were distinguished along the length of the pile, compared to 38 finer layers used in shear modulus profiles.

Figure 6 demonstrates the effect of the two shear modulus profiles on the theoretical vertical and horizontal-rocking responses in VC and HC tests, respectively. The CPT profile generates a softer response in the vertical mode of vibration while yielding a slightly increased stiffness for the horizontal mode. This may be expected as the CPT-based modulus profile

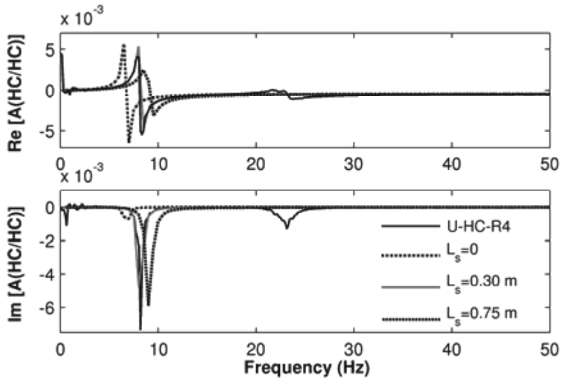

Figure 4. Effect of soil-pile separation depth on HC/HC response for pile U in native unimproved soil.

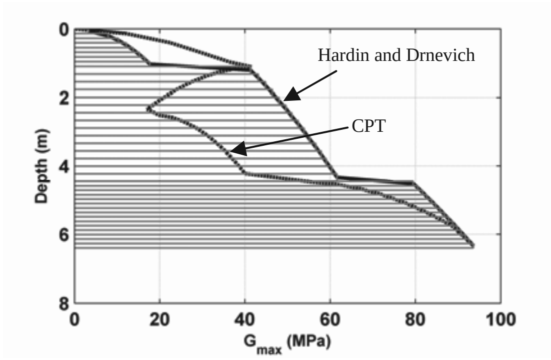

Figure 5. Two 38-layer shear modulus profiles used in the analyses based on interpretation of field CPT data and Hardin and Drnevich (1972).

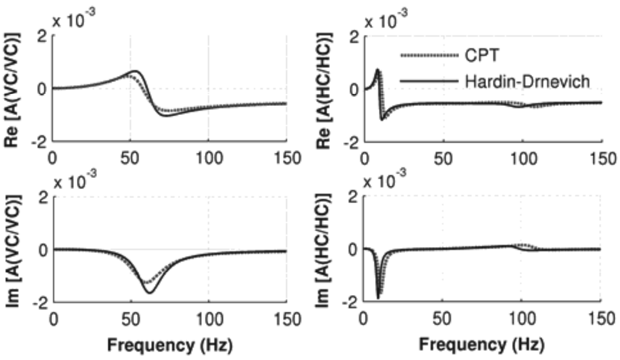

Figure 6. Effect of the two shear modulus profiles of Figure 5 on theoretical vertical response (left) and horizontal response (right).

is softer overall, but is stiffer near the surface region which has a greater influence on the bending behavior.

Both the vertical and horizontal rocking modes of the pile in the native unimproved soft clay can be nearly captured using the Hardin & Drnevich shear modulus profile together with the 0.30 m separation zone, but require application of scale factors to the modulus and damping within the three major layers shown in Figure 1. Figure 7 illustrates such a comparison using modulus reduction factors of 0.8, 0.8 and 0.5 for the top, middle and bottom layers, respectively, while increasing the damping in all layers by a factor of 10. The peak frequency of the vertical mode is fit reasonably well, but the experimental vertical response exhibits some deviation from the theoretical solution at higher frequencies. This is assumed to be a relic of a higher mode of the shaker’s stationary base frame which does not behave as a perfectly rigid body. The first peak for the horizontal response matches very well, although this is difficult to see in Figure 7 as the experimental and theoretical curves are nearly coincident at this frequency.

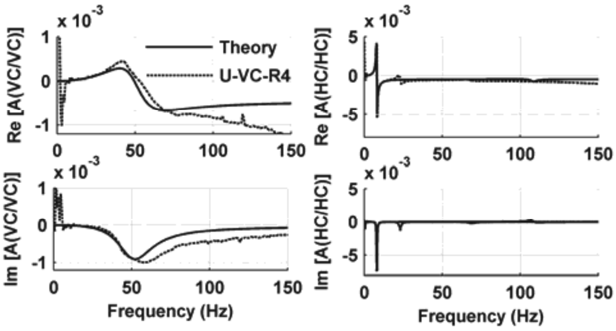

Figure 7. Comparison between experimental accelerance for pile in unimproved soil and theoretical model using the Hardin & Drnevich modulus profile with modification factors of (0.8 ,0.8, 0.5) for modulus and (10,10,10) for damping from top to bottom layers. Left: vertical response, Right: horizontal response.

Based on unconfined compression tests, the shear strength of the improved soil is more than 20 times greater than that of the unimproved soil. One approach for modeling pile I in the improved soil would therefore be to multiply the modulus values of Figure 5 by a factor of 20 for the first 4 m depth. On the other hand, the cement-like properties and mechanical mixing of the CDSM zone suggest the use of a more uniform modulus profile compared to the natural soil profile. These criteria may both be satisfied to some extent by using a modulus profile proportional to the fourth-root of depth (for curve fitting) and starting at 75 MPa at the soil surface. Such a profile will closely follow the natural soil profile below the improved zone. Although Figure 8 affirms that this modulus profile works very well for predicting the stiffened vertical mode for pile I in improved soil, Figure 9 illustrates that the corresponding experimental horizontal-rocking response was very similar for the native and improved soil profiles. Although a larger improved zone would likely be used in practice, the relatively unchanged dynamic lateral response in this study was unexpected considering the significant differences in native and improved soil properties. The similar lateral stiffness may be related to competing effects of a stiffer improved soil zone, but a relaxed state of stress in the surrounding soil due to installation of the CDSM zone, as well as separation between the CDSM region and surrounding soil from concrete shrinkage upon curing. The approximate 2D analytical model of Novak and Aboul-Ella (1978) is unable to incorporate such effects, and further study of more sophisticated 2-zone models may be necessary for modeling the observed behavior.

4 CONCLUSION

An experimental program was detailed for a series of full-scale pile vibration tests employing random vibration techniques. An approximate numerical elastodynamic model from the literature was employed to model the experimental results. Parametric studies revealed that an account of gapping between the pile and soil may be necessary to accurately model the observed behavior of the pile in unimproved native soft clay. However, the theoretical response was shown to be less sensitive to the modulus profile than to gapping, especially in the horizontal mode of vibration. The experimental response of the pile in soft clay was approximately fit by incorporating gapping over the first 0.3 m and scaling the modulus and damping in the three major soil layers. The vertical response of the pile in the improved cement deep soil mixed zone exhibited an increase in stiffness as expected. However, the horizontal response was relatively unchanged from that of the native soft clay profile. In practice, a larger lateral extent of soil improvement would be used, and a greater improvement in lateral stiffness expected. The numerical model can be fit to the stiffened vertical mode, but cannot simultaneously model the relatively unchanged horizontal stiffness encountered in this study. More sophisticated computational models will be examined to further model the latter behavior.

5 ACKNOWLEDGEMENTS

This material is based upon work supported by the National Science Foundation under Grant No. 0936627. This support is gratefully acknowledged. Any opinions, findings, and conclusions or recommendations expressed in this material are those of the authors and do not necessarily reflect the views of the National Science Foundation. This project was a payload to the NEESR-SG project 0830328. The assistance of the NEESR-SG project teams and the nees@UCLA team is appreciated.

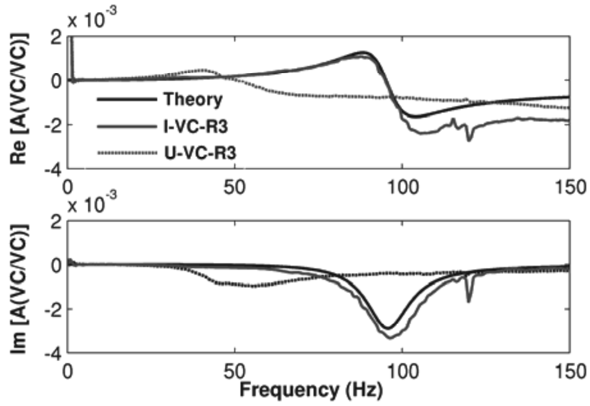

Figure 8. Experimental vertical response for pile in improved and unimproved soils with analytical model prediction for stiffened CDSM zone.

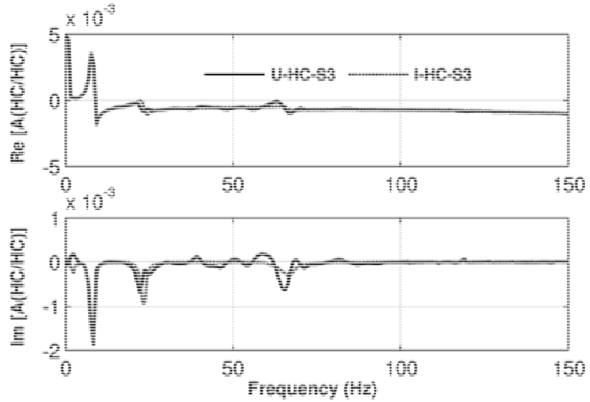

Figure 9. Representative experimental results for horizontal pile response in improved and unimproved soils exhibiting minimal difference.

6 REFERENCES

Ashlock, J.C. and Fotouhi, M.K. (2011). “Characterization of Dynamic Soil-Pile Interaction by Random Vibration Methods: Experimental Design and Preliminary Results”, Proceedings of 2011 NSF Engineering Research and Innovation Conference, Atlanta, Georgia (CMMI Grantee Conference), 11 pp. http://nees.org/warehouse/project/940

Fotouhi, M.K. and Ashlock, J.C. (2012). “Analysis of Experimental Dynamic Soil-Pile Interaction by Approximate Numerical Solutions ”, 15th WCEE, Lisbon , Portugal

Mayne, P. W. (2007). Cone Penetration Testing, NCHRP Synthesis 368. Transportation Research Board, Washington DC.

Novak, M. and Aboul-Ella, F. (1978). Impedance Functions of Piles in Layered Media. Journal of the Engineering Mechanics Division. 104:6, 643-661.

Hardin, B. O. & Drnevich, V. P. (1972). Shear modulus and damping in soils: design equation and curves. J. Soil Mech. Found. Engng. Div., ASCE 98, No. 7, 667–691

A Design Method For Piled Raft Foundations

Méthode de conception des fondations de type radier sur pieux

Balakumar V.
Simplex Infrastructures Limited, Chennai, Tamil Nadu, India.

Oh E., Bolton M., Balasubramaniam A.S.
Griffith University Gold Coast Campus, Brisbane, Australia.

ABSTRACT: The design of piled raft foundation involves two stages namely a preliminary stage and the final stage. The preliminary design stage involves the identification of the essential parameters namely the number of piles, their diameter and the length along with E_s value of the subsoil strata for an optimum design which can produce the required settlement reduction. The existing design methods, whose accuracy depends upon the accuracy of the evaluation of in-situ parameters like E_s although can produce satisfactory results, the computational efforts involved and the time does not justify the use of them for the preliminary analyses which will involve repetitions. This paper outlines a simple analytical procedure and the effectiveness of the pressuremeter tests in predicting the piled raft behaviour, so that the results can be used in the detailed design.

RÉSUMÉ : La conception des fondations de type radier sur pieux implique deux étapes, l'étape préliminaire et l'étape finale. L'étape préliminaire de conception implique la détermination de paramètres essentiels : nombre de pieux, leurs diamètres et leurs longueurs ainsi que la valeur de E_s de la couche de sol superficielle pour un design optimal qui pourra amener à la réduction requise du tassement. Les méthodes de conception existantes, dont la précision dépend de la précision sur la mesure des paramètres in situ conduisent à des résultats satisfaisants. Néanmoins les moyens numériques et le temps impliqués pour leurs réalisations ne sont pas justifiés pour l'analyse préliminaire qui nécessite des répétitions. Cet article synthétise une méthode analytique simple et efficace de tests de pression pour prédire le comportement des fondation de type radier sur pieux dont les résultats peuvent être utilisés pour des projet de conception.

KEYWORDS: piled raft, tri-linear pressuremeter.

1. INTRODUCTION.

The combined piled raft foundation system provides a skilful geotechnical concept wherein the applied load is transferred by means of a load sharing mechanism which is generated through a process of interaction between the pile soil and the raft. The piled raft foundation system differs from the traditionally designed pile supported raft in the fact that in the case of piled raft the presence of the raft and its contribution in sharing the load with the pile group is recognized. The piled raft foundation utilises the pile group for the control of settlement, with the piles providing most of the stiffness at the service loads while the raft elements provide the additional capacity at the ultimate load levels. The concept of piled raft system was born out of the fact that any structure has a certain magnitude of permissible settlement and the foundation system has to aim at reducing the settlement as close to the permissible value as possible rather than eliminating the settlement completely. In the last two decades researchers like Cooke (1986), Burland(1995), and Poulos(2001) have provided considerable insight into the behaviour of piled raft .

The development of sophisticated computational facilities and FEA codes like Defpig,Napra,and HyPr etc have enhanced the interaction process between the observational methods (Katzenbach etal., 2000 a; Balakumar and Ilamparuthy, 2007), small scale model studies (Horikoshi1995; Balakumar etal.,2005) and numerical and analytical simulations leading to the improvement of the design process. Consequent to this number of tall and heavily loaded structures have been supported on piled raft and the performance of some of these piled rafts have been monitored and the results may be used to refine the design in the future. (Poulos, 2008; Yamashita etal., 2010).

2. THE DESIGN PROCESS

In the design process of piled raft the initial stages of design involves the determination of the optimum number of piles, pile length and diameter required to be placed in a strategic manner to produce the required settlement reduction along with the load shared by the pile group. This process may require a large number of trials depending on the nature and requirement. Hence the analytical procedure has to be computationally simple so that the efforts and the time will be less. The existing methods although produce satisfactory results, involve more complicated computational efforts .Further in solving the complicated three dimensional problems such as piled raft, many simplified assumptions are to be made and the rigourousness of the method may have to be diluted to make the problem computationally viable. Therefore there is a need for a simple method that can solved by treating the problem as axisymmetric or plane strain problem in the case of preliminary design to establish parameters like pile length, numbers diameter and the layout to be used in the final design.

It is always recognized in geotechnical engineering that the most difficult part is the evaluation of the in-situ parameters particularly the elastic modulus. In most of the cases, such parameters are obtained either from laboratory tests or from standard correlations between tests like SPT and Es values, which can affect the accuracy of results. However over the past few years there is a considerable shift from the laboratory testing to in-situ testing and this has led to the use of the results from in situ tests such as CPT and pressuremeter tests extensively to determine the stress strain characteristics and essential parameters like the in-situ elastic modulus of the soil over the length of the pile. A well tried procedure for predicting such parameters along with the shaft friction development has been published by Roger Frank et al (1991) using pressuremeter tests. Therefore it was felt necessary to study whether such predictions can be used to evaluate the numerical details such as the number of piles, length, diameter, and layout required for the design of the piled raft.

3. SCOPE OF WORK

With the above in mind it was decided to study the various options available to idealise the piled raft model which would be amenable for a simple numerical procedure and will give the load settlement, settlement reduction and load sharing behaviour of the piled raft. Further in order to evaluate the elastic modulus and other parameters over the pile depth various in-situ test options were also studied. It was found that the equivalent pier approach would be the most suitable approach for modelling the piled raft. The paper presents the details of the study and the conclusions of the study.

4. THE STUDY

In the design of piled raft the requirement is the settlement reduction and the data for the design is the load shared by the raft and the pile group. It is only from the group capacity required, the number of piles required, diameter and the length can be evaluated. In order to study the load settlement response, a series of 1g small scale model tests were carried out on circular and square shaped piled raft placed on sand bed. Poorly graded sand was rained in pre-calibrated manner so that the required densities could be achieved; the tests were carried out on unpiled raft, free standing pile group and piled raft. Extensive parametric studies were also carried out but the presentation is restricted to the load settlement and load sharing response typically for circular piled raft under medium dense bed condition. The studies showed that the performance of the piled raft was identical in all the other cases. Details of the models test set up and other details are presented elsewhere (Balakumar etal., 2005)

5. LOAD SETTLEMENT AND LOAD SHARING RESPONSE.

Figure 1 presents the load settlement response of circular piled raft with varying pile lengths and and figure presents the charecterised form of the load settlement response.It is clearly seen that at any given settlement the load taken by the piled raft is more than the unpiled raft for the corresponding settlement.It is seen that the load taken by the piled raft with pile length of 200mm is far higher than the other lengths namely 75mm,100mm and 120mm. The typical characterisation curve of the piled raft shown with various pile lengths are given in Figure 2 for a pile diameter of 10 mm, which shows that irrespective of the pile length, the behaviour has three phases. Although the settlement up to which the linear elastic stage (portion OA of the curve) remains same as 1mm, the load corresponding to this varies. As can be seen at higher length the linear behaviour extends nearly upto 30% of the load taken by the piled raft corresponding to settlement equal to 10% of the pile length. The second stage of the curve AB is the stage where the behaviour tends to become elasto- plastic, which extends up to a settlement level 9 mm for 200 mm long pile, 7.5 mm for 120 mm long pile and 4.5 mm for 75 mm long pile.

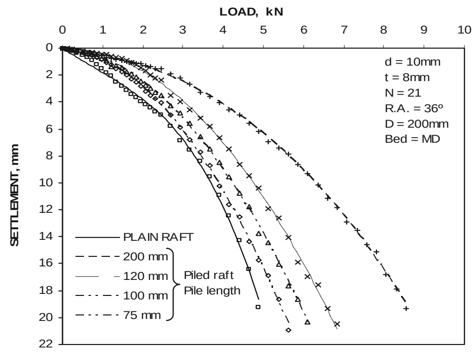

Figure 1. Load-Settlement Response of Circular Piled Raft with Various Pile Lengths

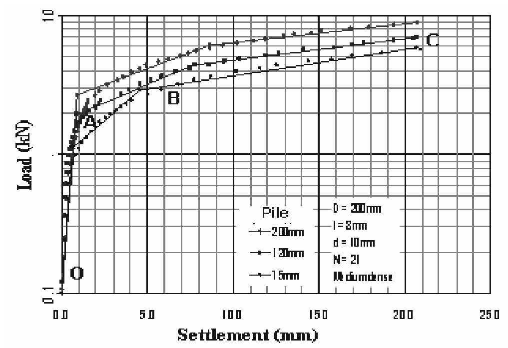

Figure 2. Characteristic Response of Piled Raft

To have better understanding on load sharing between the raft and pile group of piled raft, three dimensional nonlinear analysis was carried out using ANSYS code. Only quarter model of piled raft was analysed taking advantage of the symmetry (Figure 3).

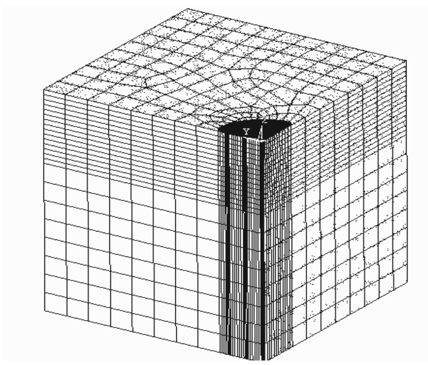

Figure 3. Finite Element Mesh of a Circular Piled

The bed density was kept as medium dense with φ = 37.5° and dry unit weight = 15.5 kN/m3. MISO material model was used for the soil. The continuum was modelled using solid 45 elements with three degrees of freedom at each node. In the analysis the bed dimensions were kept same as that of the model tested in the laboratory. The raft and piles were also modelled as solid 45 elements in order to maintain the elements compatibility. The load was applied as pressure in small increments till the load on the raft equal to the final test load. Figure 3 shows the quarter model including finite element meshing adopted in the analysis.

6. LOAD-SETTLEMENT BEHAVIOUR

Figure 4 presents the load settlement curves of circular piled raft obtained from 1g model test and the numerical model. Figure 5 presents comparison of characteristic load-settlement response of circular piled raft between experiment and numerical analysis. The results obtained from the 1g model test and numerical model agree very closely, till the settlement level of 4 mm.

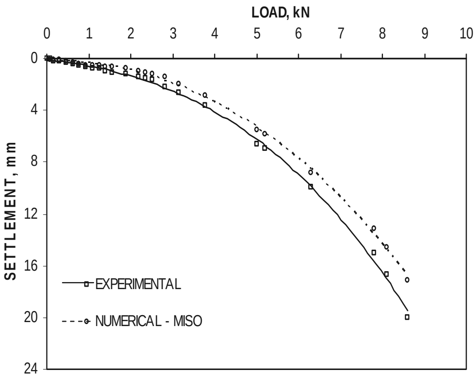

Figure 4. Comparison of Load-settlement

As the load increases, the difference in the settlement between the 1 g model and the numerical model results increased marginally. However the maximum variation in the load between the numerical model and the small scale model results was less than of 5%. This comparison indicates a close agreement between the numerical model and 1g model test. Similar observation is made in the analyses of piled raft in loose and dense sand. Thus the nonlinear analysis using MISO model idealization for the soil predicts the performance of piled raft reasonably well.

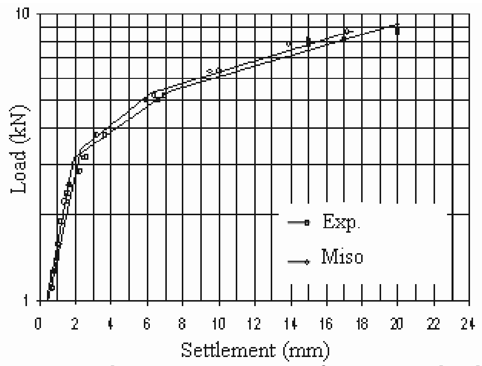

Figure 5. Characterisation Curves of Experimental and Numerical Analysis

Although it has been established that the characterised load settlement response predicted by analytical study and the 1g model tests have agreed very closely, the basic parameter namely the Es value of the soil was obtained from the direct shear tests and the standard correlations available from the literature The agreement in the results of 1g model and the numerical analyses can be attributed to the fact that the supporting medium was prepared under laboratory conditions. However in the case of field samples the accuracy of the parameters obtained largely depends upon the sampling efficiency and the care taken in the extrusion of the specimen and the preparation of test conditions. The probability of wide variation while correlating the field data with the laboratory test results cannot be ruled out. Therefore the evaluation of parameters from the in-situ tests gain considerable importance.A well tried procedure for predicting the shaft friction development has been published by Roger Frank et al., (1991) using pressuremeter is discussed below.

7. PREDICTION OF PILE BEHAVIOUR. PRESSSUREMETER AND ITS APPLICABILITY

The pressuremeter is an effective tool that has been extensively used to obtain the in-situ parameters and for the last three decades foundations have been designed based on the parameters obtained from the in-situ tests. The large volume of data collected over a period of time particularly the French Highway authorities has enhanced the confidence level of the designers in using them for the design of deep foundations. Frank etal., (1991) have studied the load settlement response of two piles forming a part of a bridge foundation. and had established that their behaviour can be predicted by conducting the pressuremeter test.Their prediction of pile behaviour is based on a tri-linear relationship for the skin friction mobilisation based on the pressuremeter tests The model they had used is given in Figure 6.

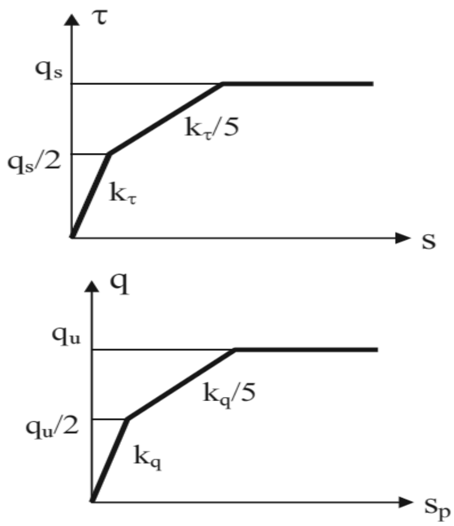

Figure 6. Tri-linear Model, Frank et al (1991)

The first segment has a constant slope .The slope of the second line as more flat and third segment represents the mobilisation of total skin friction. A typical tri-linear model of shaft friction mobilisation. The end of the second part is the limiting value of the friction .The evaluation of the friction is done in their case based on LCPC-SETRA (1985) RULES. The slopes of the lines depend upon the pressuremeter modulus and radius of the pile. The prediction experimental load distribution given by them has a similar trend as predicted by the numerical analyses of the 1g model tests.

8. APPLICABILITY TO PILED RAFT DESIGN

Figure 7 and Figure 8 present the shaft stress distribution over the length of the pile by pressuremeter test results and from the numerical analyses of the 1g model tests. it is seen that the trend of the shaft stress distribution obtained from both the cases agree closely,indicating that the tri-linear model assumed in the analyses of the pressuremeter results and the actual behaviour of piled raft obtained from the 1g model are identical.

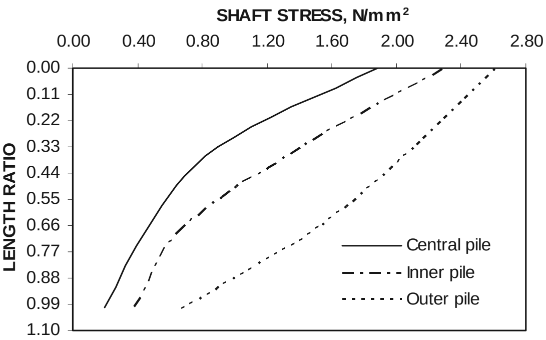

Figure 7. Variation of stress along the shaft of typical piles along the centre line of raft for 8.10kN

This establishes the fact that if the pile group of piled raft can be idealised as a single large pier,then the procedure adopted by Frank et al(1991) can be used to predict the behaviour of pile group of piled raft foundations. Poulos (2001) has shown that while studying the settlement behaviour of the pile group, that if the pile group with the soil prism can be considered as a single pier, then the procedure applied for a single pile behaviour can be used for the prediction of the load settlement response of the equivalent pier numerically using axisymmetric analyses.The equivalent pier modulus E_{eq} is given by the expression

$$EEQ = E_S + (E_P - E_S)\, A_T/A_G \qquad (1)$$

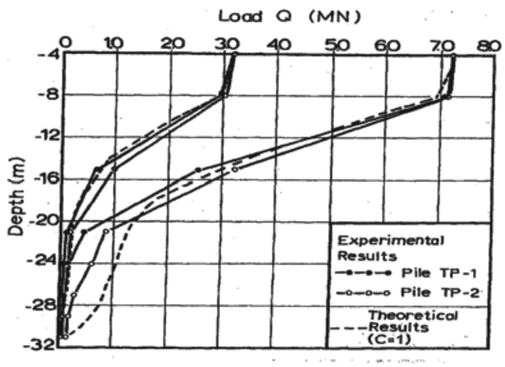

Figure 8. Comparison of Theoretical and Experimental Load Distributions for Test Piles (Roger Frank et al.,))1991)

The value of the Es can be the pressuremeter modulu,E_p is the pile material modulus, A_t is the total cross sectional area of the piles and A_g is the gross plan area of the group. The equivalent pier has the same plan area of the pile group and the length of the pile can be taken as the length of the pier.The load settlement response predicted by the pressuremeter with the shaft friction mobilisation can be compared with the equivalent pier analyses to validate the in-situ E_s value over the length of the pile (pile group) and the shaft friction over the length of the pile group. This will also establish the shaft stress distribution at any given settlement level and the in-situ E_s value which can be used in the detailed analyses.

9. CONCLUSIONS

The design economy in the piled raft design depends upon the optimum design of the pile group of piled raft. Therefore before the final design number of trials has to be made and also the evaluation of in situ parameters has a considerable influence. Keeping the above in mind the study carried out has shown that the tri-linear relationship for the shaft friction mobilisation adopted by Frank etal.,(1991)to study the performance of two single piles was in agreement with the trend of the characterised load settlement response of the piled raft. Also the trend of shaft friction mobilisation over the length of the pile agreed with the prediction made from the pressuremeter test results in the case of single pile. Based on the above it is concluded that the equivalent pier theory can be used in combination with the pressuremeter test results to predict the load settlement and load sharing behaviour of the piled raft adopting parameters determined from in-situ tests which are more reliable.

10. REFERENCES

Katzenbach R., Arslan V. and Moorman ch .2000a. Numerical Stimulations of Combined Piled Raft Foundations for the New High Rise Building, Max in Frankfurt am main, Proc. 2nd Int. Conf. on Soil Structure Interaction in Urban Civil Engineering.

Poulos H.G. 2001. Piled Raft Foundation: Design and Application, Geotechnique, 51(2),111-113

Horikoshi K. 1995. Optimum Design of Piled Raft Foundations, Dissertation submitted for the degree of Doctor of Philosophy, University of Western Australia.

Polous H.G. 2008. The Piled Raft Foundation for the Burj Dubai – Design & Performance. IGS – Ferroco Terzaghi, Oration – 2008.

Burland J.B. 1995. ‘Piles as Settlement Reducer’ 18th Italian Congress on Soil Mech., Pavia.

Balakumar V. and Ilamparuthi K. 2007. Performance Monitoring of a Piled Raft Foundation of Twelve Storied Building and Analytical Validation, Indian geotechnical Journal, 37(2), 94-115.

Yamashita.K , Hamada.J, Yamada.T. 2010. Field Measurements On Piled Rafts with Grid-Form Deep Mixing Walls on Soft Ground, Geaotechnical Engineering-SEAGS .42(2) .

Cooke R.W. 1986. Piled Raft Foundation on Stiff Clays – A Contribution to Design Philosophy, Geotechnique, 36(2),169 -203

Roger Franke, Nicholos Kateziotis , Michel Bustamante, Stavaros Christoulos .1991. Evaluation of Performance of Two piles Using Pressuremeter Methods - Journal of Geotechnical Engineering, 117(5), 695-713

Balakumar V., Kalaiarasi V. and Ilamparuthi K. 2005. Experimental and Analytical Study on The Behaviour of Circular Piled Raft on Sand, Proc. 16th Intl Conf. on Soil Mechanics and Geotechnical Engineering-2005, Osaka, Japan, 1943-1947.

A practical method for the non-linear analysis of piled rafts

Une méthode d'analyse pratique pour déterminer la réponse non linéaire des fondations mixtes de type radier sur pieux

Basile F.
Geomarc Ltd, London, United Kingdom

ABSTRACT: The paper describes a practical analysis method for determining the response of piled rafts. The key feature of the method lies in its capability to provide a non-linear complete boundary element solution of the soil continuum, while retaining a computationally efficient code. The validity of the proposed analysis is demonstrated through comparison with alternative numerical solutions and field measurements. Examples are given to demonstrate the importance of considering soil nonlinearity effects in piled rafts (given the relatively high load level at which the piles operate), thereby leading to more realistic predictions of the raft and pile response. The negligible computational costs make the analysis suitable not only for the design of piled rafts supporting high rise buildings (generally based on complex and expensive 3D FEM or FDM analyses) but also for that of bridges and ordinary buildings.

RÉSUMÉ: Cet article décrit une méthode d'analyse pratique pour déterminer la réponse des fondations mixtes de type radier sur pieux. La principale caractéristique de la méthode réside dans sa capacité à fournir une solution non linéaire de type « Boundary Element » du continuum sol, tout en conservant un code de calcul efficace. La validité de l'analyse proposée est démontrée par comparaison avec d'autres solutions numériques et des mesures *in situ*. Des exemples sont donnés pour démontrer l'importance de la prise en compte de la non-linéarité du sol dans l'analyse des radiers sur pieux, ce qui conduit à des prévisions plus réalistes de réponse du radier et pieu. Les coûts négligeables de calcul rendent l'analyse appropriée non seulement pour la conception des radiers sur pieux supportant des immeubles de grande hauteur (basé sur des analyses 3D en éléments ou différences finies, complexes et coûteuses), mais aussi pour celle des bâtiments ordinaires et des ponts.

KEYWORDS: CPRF, piled raft, pile group, non-linear, numerical analysis

1 INTRODUCTION

In conventional foundation design, it is assumed that the applied load is carried either by the raft or by the piles, considering the safety factors in each case. In recent years, an increasing number of structures have been founded on Combined Pile-Raft Foundations (CPRFs), an attractive foundation system which allows the load to be shared between the raft and the piles, thereby offering a more economical solution. In the design of piled rafts, a sufficient safety against geotechnical failure of the *overall* pile-raft system has to be achieved, while the piles may potentially be used up to their ultimate geotechnical capacity. Contrary to traditional pile foundation design, no proof for the ultimate capacity of each individual pile is necessary (Katzenbach 2012). Given the high load level at which the piles operate, consideration of soil nonlinearity effects is essential, and ignoring this aspect can lead to inaccurate predictions of the deformations and structural actions within the system.

Due to the 3D nature of the problem and the complexity of soil-structure interaction effects, calculation procedures for piled rafts are based on numerical analyses, ranging from simplified Winkler approaches (e.g. "plate on springs" methods) to rigorous 3D finite element (FEM) or finite difference (FDM) solutions using available packages. While Winkler models suffer from some restrictions mainly related to their semi-empirical nature and fundamental limitations (e.g. disregard of soil continuity), finite element and finite difference solutions retain the essential aspects of interaction through the soil continuum, thereby providing a more realistic representation of the problem. However, even though 3D FEM and FDM analyses are powerful numerical tools which allow complex geometries and soil behaviour to be modelled, such analyses are burdened by the high computational cost and specialist expertise needed for their execution, particularly if non-linear soil behaviour is to be considered. This aspect restricts their practical application in routine design, where multiple load cases need to be examined and where the pile number, properties and location may have to be altered several times in order to obtain an optimized solution.

In an attempt to provide a practical tool for the designer, the paper describes an efficient analysis method for determining the response of piled rafts. The main feature of the approach lies in its capability to provide a non-linear complete boundary element (BEM) solution of the soil continuum (i.e. the simultaneous influence of all the pile and raft elements is considered), while retaining a computationally efficient code. Validity of the proposed analysis is assessed through comparison with alternative numerical solutions and a published case history. Examples are given to highlight the significance of considering soil nonlinearity effects, thereby leading to more realistic predictions of the raft and pile response.

2 METHOD OF ANALYSIS

The safe and economic design of piled rafts requires non-linear methods of analysis which have the capacity of simulating all relevant interactions between the fondation elements and the subsoil, specifically (1) pile-soil-interaction (i.e. single pile response including shaft-base interaction), (2) pile-pile-interaction (i.e. group effects), (3) raft-soil-interaction, and (4) pile-raft interaction (Katzenbach 2012).

The proposed method is an extension of the BEM formulation employed in the pile-group program PGROUPN (Basile 2003) and widely used in pile design through the software Repute (Bond and Basile 2010). The originality of the approach lies in its ability to provide a complete BEM analysis of the soil continuum (in which all four of the above interactions are modelled), while incurring negligible computational costs. Indeed, compared to FEM or FDM analyses, BEM provides a complete problem solution in terms of boundary values only, specifically at the raft-pile-soil interface. This leads to a drastic reduction in unknowns to be solved for, thereby resulting in substantial savings in computing time and data preparation effort. This feature is particularly significant for three-dimensional problems such as piled rafts and makes the analysis suitable not only for the design of piled rafts supporting high rise buildings (generally based on complex and expensive 3D FEM or FDM analyses) but also for that of bridges and ordinary buildings.

A description of the BEM formulation adopted in PGROUPN for the case of pile groups has been presented by Basile (2003). In a similar fashion, the approach has been extended to include the raft analysis (including its reciprocal interaction with the piles) by discretizing the raft-soil interface into a number of rectangular elements (Fig. 1), whose behaviour is evaluated using the traditional Mindlin solution. Completely general loading conditions (axial, lateral and moments) on the piled raft can be examined, even though only the bearing contribution of the raft is considered (i.e. the raft-soil interface is assumed to be smooth). Similarly to the pile analysis, non-linear soil response is modelled, in an approximate manner, by adopting a hyperbolic stress-strain model within a stepwise incremental procedure which ensures that the specified limiting stresses at the raft-soil interface are not exceeded. Limiting values of raft-soil contact pressure (based on the traditional bearing capacity theory) are set for both compression and tension in order to allow for local bearing failure or lift-off of the raft from the soil.

The proposed PGROUPN analysis is currently restricted to the assumption of perfectly rigid raft. In practice, this assumption makes the analysis strictly applicable to "small" piled rafts (Viggiani et al. 2012), i.e. those rafts in which the bearing capacity of the unpiled raft is usually not sufficient to carry the applied load with a suitable safety margin, and hence the primary reason for adding piles is to increase the factor of safety. This generally involves rafts in which the width (B_r) amounts to a few meters (typically B_r<15m) and is small in comparison to the length (L) of the piles (B_r/L<1). Within this range (whose limits should however be regarded as tentative and indicative only), the raft response may be considered as truly rigid and hence the design should aim at limiting the maximum settlement (being the differential settlements negligible). In practical applications, a simple check on the validity of the assumption of rigid raft may be performed by calculating the raft-soil stiffness ratio (K_{rs}) as defined by Horikoshi and Randolph (1997):

$$K_{rs} = 5.57\frac{E_r}{E_s}\frac{1-\nu_s^2}{1-\nu_r^2}\left(\frac{B_r}{L_r}\right)^{0.5}\left(\frac{t_r}{L_r}\right)^3 \qquad (1)$$

where the subscripts r and s denote the raft and soil properties,

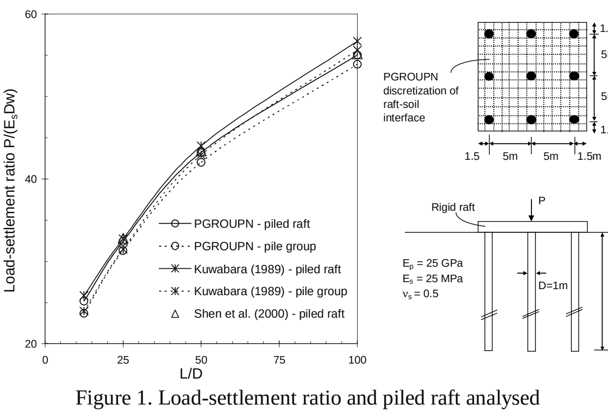

Figure 1. Load-settlement ratio and piled raft analysed

respectively, E is the Young's modulus, ν is the Poisson's ratio, B_r is the raft breadth, L_r is the raft length (with $B_r \leq L_r$), and t_r is the raft thickness. For values of K_{rs} > 5-10 the raft can be considered as rigid while a lower limit K_{rs} > 1.5 may be assumed for practical purposes (Randoph 2003). It is however observed that the above definition of K_{rs} does not include the additional stiffening contribution provided by the piles and by the superstructure which in effect increases the raft rigidity. Clearly, for "large" flexible rafts (in which B_r/L > 1 according to the definition by Viggiani), the assumption of rigid raft is no longer valid and the limitation of differential settlement becomes one of the design requirements. It is interesting to note that Poulos (2001) has shown that, except for thin rafts, the maximum settlement and the load sharing between the raft and the piles are little affected by the raft rigidity.

3 NUMERICAL RESULTS

3.1 *Comparison with Kuwabara (1989)*

The accuracy of PGROUPN is initially assessed in the linear elastic range for the piled raft (3x3 group) sketched in Fig. 1. The figure shows the dimensionless load-settlement ratio (P/E_sDw, where P is the total applied load and w is the settlement) of the piled raft for a wide range of pile length-diameter ratios (L/D). For comparison, results from the corresponding free-standing pile group are also reported and show the small influence of the raft contribution to the resulting settlement. However, the load distribution is considerably affected by consideration of the ground-contacting raft, as illustrated in Figure 2 which shows the percentage of the total load carried by the raft and by the corner pile as a function of the L/D ratio. For comparison, the load taken by the corner pile of the pile group is also reported, demonstrating a significant reduction of corner load in the piled raft as compared to the pile group. Both figures show a favourable agreement of PGROUPN with the boundary element solution of Kuwabara (1989) and the variational approach of Shen et al. (2000).

3.2 *Comparison with Poulos (2001)*

The effects of soil nonlinearity are examined in the piled raft (3x3 group) shown in Fig. 3, as reported by Poulos (2001). The non-linear load-settlement response predicted by PGROUPN agrees well with the corresponding settlement value obtained by Poulos using the program GARP (employing a FEM analysis for the raft and a BEM analysis for the piles), under the assumption of rigid raft (i.e. a raft thickness t_r = 1m giving K_{rs} = 6.1), and for a typical design load P = 12 MN (equivalent to an overall factor of safety of 2.15 against ultimate capacity). For consistency with the Poulos analysis, an elastic-perfectly plastic soil model has been adopted in PGROUPN with an assumed raft bearing capacity of 300 kPa and a pile load capacity of

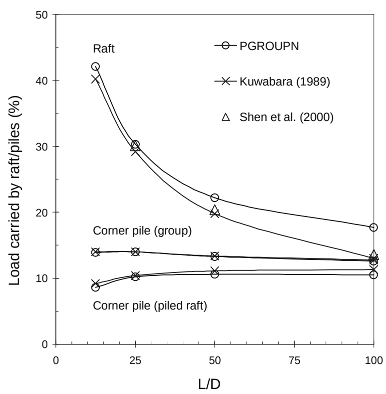

Figure 2. Load sharing between raft and piles

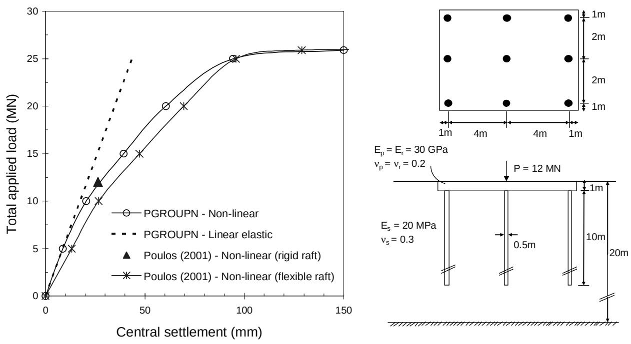

Figure 3. Load-settlement response and piled raft analysed

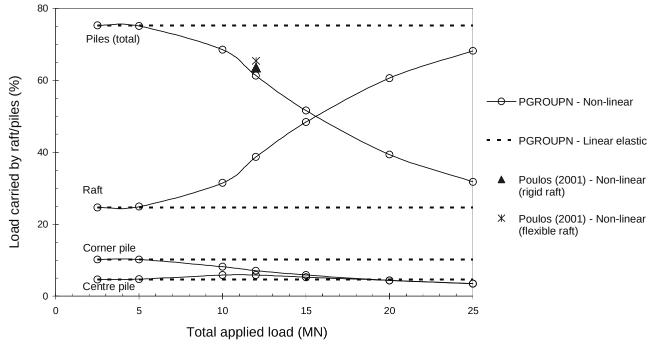

Figure 4. Load sharing between raft and piles

873 kN in compression and 786 kN in tension. The figure also shows a fair agreement with the load-settlement curve obtained by Poulos for a flexible raft (i.e. t_r = 0.5m giving K_{rs} = 0.8), as previously reported. It is noted that, as the load capacity of the piles becomes nearly fully utilized at a load of about P = 10-12 MN, the load-settlement behaviour reflects that of the raft, which is significantly less stiff than the overall pile-raft system, while the load carried by the raft starts to increase significantly (Fig. 4). As previously observed, the fact that some of the piles (usually the stiffer piles located around the perimeter of the group) are close to their ultimate capacity is not an issue for a piled raft and is actually inevitable for an efficient design.

The load sharing between the raft and the piles as a function of the total applied load reported in Fig. 4 shows a significant reduction of the total load carried by the piles with increasing load level. Under a total load P = 12 MN, the figure shows a good agreement with the load carried by the piles predicted by Poulos for the rigid raft and a slightly less agreement with that obtained for the flexible raft. Overall, the comparison shown in Figs. 3-4 demonstrates the importance of considering non-linear behaviour of the pile-raft system in order to obtain realistic predictions of the settlement and the load sharing between the raft and the piles. Assumption of linear elastic behaviour beyond a load of about 10 MN would lead to an under-estimation of the settlement and an over-estimation of the amount of load carried by the piles, with a consequent over-design of the requirements for structural strength of the piles. As emphasized by Poulos (2001), an analysis which accounts for soil non-linearity, even though in an approximate manner, is preferable to a complex analysis in which linear behaviour is assumed.

3.3 *Design example*

The hypothetical design example shown in Fig. 5 is described in order to demonstrate that, in suitable ground conditions, a significant reduction of the piling requirements can be achieved with the use of a piled raft as compared to a conventional pile foundation. Two foundation systems are evaluated:

(1) A 4x4 pile group (i.e. with no raft contribution) designed according to a traditional approach in which an overall (geotechnical) factor of safety FS = 2 is assumed to apply to the maximum axial force of the single pile;

(2) A piled raft (3x3 group) in which FS = 2 is assumed to apply to the total force acting on the whole pile-raft system.

A total force E_k = 25 MN is acting on the foundation and a maximum allowable settlement of 25mm has been prescribed. The analyses have been carried out using PGROUPN (non-linear soil model) with the parameters indicated in Fig. 5 (the raft may be considered as fully rigid being K_{rs} = 10.5). The initial solution of an unpiled raft (11m x 11m) has been discarded due to both bearing capacity and settlement requirements, given that the raft bearing capacity is equal to 54.5 MN (based on $q_u = 6C_u$) and the raft settlement results in 38mm. Thus, a pile-group solution is considered and is found that a group of 4x4 piles (30.5m long) at a spacing of 3D = 3m is required in order to achieve FS = 2 on the maximum axial force (V_{max}) of the corner pile, (i.e. Q_{all} = 2421 kN > V_{max} = 2390 kN). It is noted that the calculated pile-group settlement is equal to 14mm, i.e. below the allowable value of 25mm, thereby indicating that a design optimization may be achieved.

A piled raft solution (3x3 group with pile spacing of 4D = 4m and pile length of 20m) is then evaluated following the methodology outlined in the International CPRF Guideline (Katzenbach 2012). According to the guideline, a sufficient safety against failure of the overall pile-raft system is achieved by fulfilling the following inequation:

$$E_d \leq R_d \;\rightarrow\; E_k \cdot \gamma_F \leq \frac{R_{tot,k}}{\gamma_R} \;\rightarrow\; E_k \cdot \gamma_F \cdot \gamma_R \leq R_{tot,k} \qquad (2)$$

where E_k is the characteristic total force acting on the CPRF, γ_F and γ_R are the partial safety factors on actions and resistance, respectively, and the characteristic value of the total resistance $R_{tot,k}$ has to be derived from the load-settlement response of the CPRF and is equal to the load at which the increase of the settlement becomes increasingly superproportional, as determined from a "numerical" load test. In order to allow a direct comparison with the above pile-group solution, it is assumed that an overall FS = 2 applies to the force E_k (this assumption is equivalent to consider a value of $\gamma_F \cdot \gamma_R$ = 2). This implies that Equ. (2) is fulfilled by proving that $R_{tot,k} \geq 2E_k$ = 2·25 = 50 MN. Thus, using PGROUPN, a numerical load test has been performed to generate the typical relationship between the settlement and the total load (i.e. the CPRF overall resistance), as illustrated in Fig. 5. From this figure, it can be seen that, up to the loading of 50 MN, the increase of the settlement is not yet superproportional (i.e. $R_{tot,k}$ > 50 MN), implying that no significant failure of the CPRF has occurred. Thus, the ultimate bearing capacity (ULS) of the piled raft has been proved. It is noted that the maximum pile axial load is equal to V_{max} = 2210 kN, which would give FS = 1.5 (being the pile capacity Q_{ult} = 3358 kN); however, in contrast to conventional pile foundations, the proof of the bearing capacity

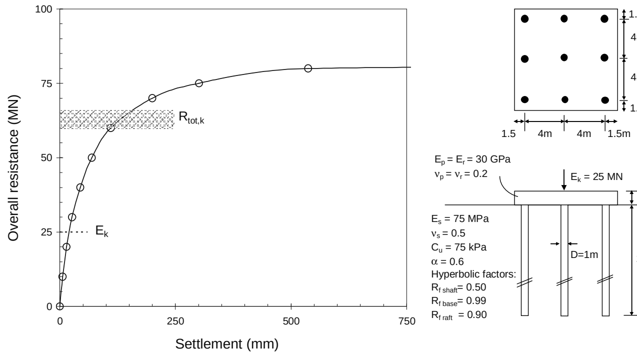

Figure 5. Load-settlement response and piled raft analysed

for single piles is unnecessary because this proof is inconsistent with the concept of piled rafts. Within the same numerical load test, proof of the serviceability limit state (SLS) for the piled raft can be performed and, under the total load of 25 MN, a settlement of 20mm is calculated, i.e. below the allowable value of 25mm. It may be observed that at this load level the raft carries 39% of the total load. Finally, it should be emphasized that the piled raft solution leads to a significant reduction in the required number and length (L) of the piles as compared to the conventional pile group, resulting in a saving of 63% in total pile length, i.e. from 488m for the 4x4 pile group (L = 30.5m) to 180m for the 3x3 piled raft (L = 20m).

4 CASE HISTORY

The case history for the Messe-Torhaus building in Frankfurt is presented (Sommer et al 1985). The building is supported by two separate piled rafts, each with 42 bored piles with a length of 20m and a diameter of 0.9m. The piles under each raft are arranged in a 6x7 rectangular configuration with a centre-to-centre spacing of 2.9m and 3.5m along the shorter and the larger side of the raft, respectively. Each raft is 17.5m x 24.5m in plan, 2.5m thick and is founded at 3m below ground surface.

The piled raft is embedded in the Frankfurt clay and, within PGROUPN, it is assumed that C_u increases linearly with depth from 100 kPa at the foundation level to 200 kPa at the pile base, with a correlation E_s/C_u = 600 and ν_s = 0.5. The same soil parameters were adopted in the variational approach by Chow et al (2001) so that a direct comparison between analyses may be made. For consistency with the non-linear Chow analysis, an elastic-perfectly plastic soil model has been adopted, while a total load of 181 MN is assumed to act on the piled raft (as only approximately 75% of the total structural load of 241 MN was applied at the time of the measurements reported herein). In addition, the following parameters have been assumed (as these were not reported by Chow): an adhesion factor (α) of 0.7 (in order to achieve an ultimate pile load of about 7 MN, given that the measurements showed that piles were carrying at least this amount of load), and a Young's modulus of 23.5 GPa for the piles and of 34 GPa for the raft. The latter value results in K_{rs} = 2.2 and hence the PGROUPN assumption of rigid raft is valid, as confirmed by the field measurements which showed that the raft actually behaved as fully rigid.

The settlement of the piled raft and the proportion of load carried by the raft are reported in Table 1 showing a good agreement between analyses and measurements. In this case, soil nonlinearity appears to have only a relatively small effect on the computed response (at least in terms of settlement and load carried by the raft). The rather low value of the measured load carried by the raft (20%) suggests that the effect normally intended by a piled raft was not realised, thereby indicating a quite conservative design. Indeed, the contact pressures between raft and soil are scarcely larger than those due to the dead weight of the raft (i.e. about 25 MN, resulting in a load proportion of 14%), so that almost the complete load of the superstructure is carried by the piles. It is also noted that, while the aim of reducing settlements of the foundation in comparison to a shallow foundation has been reached (resulting in a reduction of about 50%), a more efficient design could have been achieved using fewer piles of greater length. Indeed, PGROUPN shows that an identical value of settlement can be attained with a significantly smaller total pile length, specifically with 25.5m long piles in a 4x5 group configuration (at a spacing of 5.0m and 5.5m along the shorter and the larger side of the raft, respectively). In this case, a better ratio of the raft-pile load sharing could have been achieved (i.e. 23%) with a saving of 39% in total pile length, i.e. from 840m for the original 6x7 group (L = 20m) to 510m for the 4x5 group (L = 25.5m). Finally, it is noted that PGROUPN non-linear analyses for the 6x7 and 4x5 group configurations run in 3 and 1 min, respectively, on an ordinary computer (Intel Core i7 2.7 GHz), thereby resulting in negligible computing costs for design.

Table 1. Settlement and load proportion carried by raft

	Settlement (mm)	Load carried by raft (%)
Measured (Sommer et al 1985)	45	20
Chow et al (2001)	45	26
PGROUPN	44	21
PGROUPN (linear elastic)	43	21
PGROUPN (4x5 group, L= 25.5m)	44	23

5 CONCLUSIONS

The paper has described a practical analysis method, based on a complete BEM solution and implemented in the code PGROUPN, for determining the non-linear response of piled rafts. The method has been successfully validated against alternative numerical analyses and field measurements.

It has been shown that the concept of piled raft, generally adopted for "large" flexible piled rafts, can also be applied effectively to "small" rigid piled rafts (and to any larger piled raft in which the assumption of rigid raft is valid), making PGROUPN suitable to a wide range of foundations such as bridges, viaducts, wind turbines and ordinary buildings. In such cases, if the raft can be founded in reasonable competent ground (which can provide reliable long-term resistance), then the extra raft component of capacity can be used to significantly reduce the piling requirements which are necessary to achieve the design criteria (e.g. ultimate bearing capacity, settlement).

Given the relatively high load level at which the piles operate within a pile-raft system, the influence of soil nonlinearity can be significant, and ignoring this aspect can lead to inaccurate predictions of the deformations and the load sharing between the raft and the piles. Consideration of soil nonlinearity would also be required if PGROUPN is used to perform a numerical load test following the methodology outlined in the International CPRF Guideline. Due to the negligible costs (both in terms of data preparation and computer execution times), a large number of cases can be analysed efficiently, enabling parametric studies to be readily performed. This offers the prospect of more effective design techniques and worthwhile savings in construction costs.

6 REFERENCES

Basile F. 2003. Analysis and design of pile groups. In *Num. Analysis and Modelling in Geomech.* (ed. J.W. Bull), Spon Press, 278-315.

Bond A.J. and Basile F. 2010. Repute 2.0, Software for pile design and analysis. *Reference Manual,* Geocentrix Ltd, UK, 49p.

Chow Y.K., Yong K.Y. and Shen W.Y. 2001. Analysis of piled raft foundations using a variational approach. *Int. J. Geomech*. 1 (2), 129-147.

Horikoshi K. and Randolph M.F. 1997. On the definition of raft-soil stiffness ratio. *Géotechnique* 47 (5), 1055-1061.

Katzenbach R. 2012. *Combined Pile-Raft Foundations.* International CPRF Guideline.

Kuwabara F. 1989. An elastic analysis for piled raft foundations in homogeneous soil. *Soil and Foundations* 29 (1), 82-92.

Poulos H.G. 2001. Piled-raft foundation: design and applications. *Géotechnique* 51 (2), 95-113.

Randolph M.F. 2003. 43rd Rankine Lecture: Science and empiricism in pile foundation design. *Géotechnique* 53 (10), 847-875.

Shen W.Y., Chow Y.K. and Yong K.Y. 2000. A variational approach for the analysis of pile group-pile cap interaction. *Géotechnique* 50 (4), 349-357.

Sommer H., Wittmann P. and Ripper P. 1985. Piled raft foundation of a tall building in Frankfurt clay. *Proc. XI ICSMFE*, 2253-2257.

Viggiani C., Mandolini A. and Russo G. 2012. *Piles and pile foundations*. Spon Press, 278p.

A Variational Approach for Analysis of Piles Subjected to Torsion

Une approche variationnelle pour l'analyse des pieux soumis à torsion

Basu D., Misra A.
University of Waterloo

Chakraborty T.
Indian Institute of Technology Delhi

ABSTRACT: A framework is developed using the variational principles of mechanics for analyzing torsionally loaded piles in elastic soil. The total potential energy of the pile-soil system is minimized to obtain the differential equations governing the pile and soil displacements. Closed-form solutions are obtained for the angle of twist and torque in the pile as a function of depth. The analysis explicitly takes into account the three-dimensional pile-soil interaction in multi-layered soil. The results match well with the existing solutions and with those of equivalent finite element analyses.

RÉSUMÉ : Un cadre conceptuel est élaboré en utilisant les principles variationnels de la mécanique pour l'analyse de pieux chargés en torsion dans un sol élastique. L'énergie potentielle totale du système pieu-sol est minimisée pour obtenir les équations différentielles régissant le pieu et les déplacements du sol. Des solutions analytiques sont obtenues pour le couple et l'angle de torsion dans le pieu en fonction de la profondeur. L'analyse prend en compte explicitement les interactions pieu-sol tridimensionnelles dans un système multi-couches. Les résultats correspondent bien avec les solutions existantes ainsi qu' à celles obtenues par des analyses par éléments finis.

KEYWORDS: pile, torsion, multi-layered soil, elastic analysis, variational principles.

1 INTRODUCTION

Piles loaded laterally are often subjected to torsion due to eccentricities of applied lateral loads. The existing analysis methods are mostly based on numerical techniques such as the three-dimensional finite difference, finite element, discrete element or boundary element methods (Poulos 1975, Dutt and O'Neill 1983, Chow 1985, Basile 2010) although some analytical methods also exist mostly based on the subgrade-reaction approach (Randolph 1981, Hache and Valsangkar 1988, Rajapakse 1988, Budkowska and Szymcza 1993, Guo and Randolph 1996, Guo et al. 2007).

In this paper, a new analytical method is developed for torsionally loaded piles in multi-layered soil using the variational principles of mechanics. Based on a continuum approach, the analysis assumes a rational displacement field in the soil surrounding the pile, and explicitly captures the three-dimensional pile-soil interaction satisfying the compatibility and equilibrium between the pile and soil. Closed form solutions for the angle of twist and torque in the pile shaft are obtained. The analysis produces accurate results if the equivalent soil elastic modulus is correctly estimated.

2 ANALYSIS

A pile of radius r_p and length L_p embedded in a soil medium containing n layers is considered (Figure 1). The pile base rests in the n^{th} layer and the pile head is at the level of the ground surface. The pile has a shear modulus of G_p and is subjected to a torque T_a at the head. The soil layers extend to infinity in all horizontal directions and the bottom (n^{th}) layer extends to infinity in the downward vertical direction. The bottom of any layer i is at a depth of H_i from the ground surface; therefore, the thickness of the i^{th} layer is $H_i - H_{i-1}$ (note that H_0 = 0). The soil medium is assumed to be an elastic, isotropic continuum, homogeneous within each layer, characterized by Lame's constants λ_s and G_s. There is no slippage or separation between the pile and the surrounding soil or between the soil layers. For analysis, a polar (r-θ-z) coordinate system is assumed with its origin at the center of the pile head and z axis pointing downward.

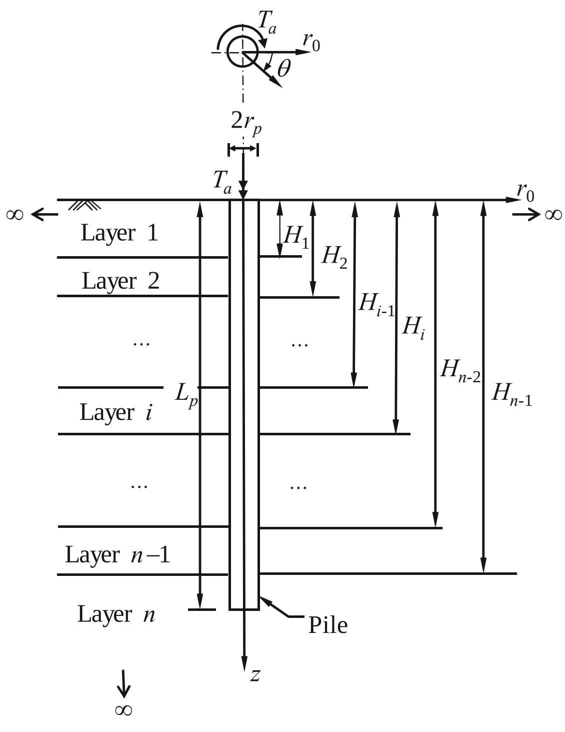

Figure 1. Torsionally loaded pile in multilayered soil.

Soil displacements u_r and u_z in the radial and vertical directions, generated by the applied torque T_a, can be assumed to be negligible (Figure 2). The tangential displacement u_θ in soil is nonzero and is assumed to be a product of separable variables as

$$u_\theta = w_p(z)\,\phi_s(r) = r_p\,\phi_p(z)\,\phi_s(r) \tag{1}$$

where w_p is the displacement in the tangential direction at the pile-soil interface (i.e., it is the tangential displacement at the outer surface of the pile shaft), ϕ_p is the angle of twist of the pile cross section ($w_p = r_p\phi_p$) which varies with depth z, and ϕ_s is a dimensionless function that describes how the soil displacement varies with radial distance r from the center of the pile. It is assumed that $\phi_s = 1$ at $r \le r_p$, which ensures no slip between pile and soil, and that $\phi_s = 0$ at $r = \infty$, which ensures that the soil displacement decreases with increasing radial distance from the pile.

Using the above soil displacement field, the strain-displacement and stress-strain relationships are used to obtain the total potential energy of the pile-soil system as

$$\begin{aligned}\Pi = {} & \frac{1}{2}G_p J_p \int_0^{L_p}\left(\frac{d\phi_p}{dz}\right)^2 dz + \frac{1}{2}\int_0^{\infty}\int_{r_p}^{\infty}\int_0^{2\pi}\left[G_s\left(r_p\frac{d\phi_p}{dr}\,\phi_s\right)^2 \right.\\ & \left. + G_s\left\{r_p\phi_p\left(\frac{d\phi_s}{dr}-\frac{\phi_s}{r}\right)\right\}^2\right] r\,d\theta\,dr\,dz \\ & + \frac{1}{2}\int_{L_p}^{\infty}\int_0^{r_p}\int_0^{2\pi}\left[G_s\left(r_p\frac{d\phi_p}{dr}\right)^2 + G_s\left(\frac{r_p\phi_p}{r}\right)^2\right] r\,d\theta\,dr\,dz - T_a\,\phi_p\big|_{z=0}\end{aligned} \tag{2}$$

where J_p $(=\pi r_p^4/2)$ is the polar moment of inertia of the pile cross section. Minimizing the potential energy (i.e., setting $\delta\Pi = 0$ where δ is the variational operator) produces the equilibrium equations for the pile-soil system. Using calculus of variations, the differential equations governing pile and soil displacements under equilibrium configuration are obtained.

The differential equation governing the angle of twist of pile cross section $\phi_p(z)$ within any layer i is obtained as

$$-\left(1+2\tilde{t}_i\right)\frac{d^2\phi_{pi}}{d\tilde{z}^2} + \tilde{k}_i\phi_{pi} = 0 \tag{3}$$

where

$$\tilde{t}_i = \begin{cases} \dfrac{\pi G_{si} r_p^2}{G_p J_p}\displaystyle\int_{r_p}^{\infty}\phi_s^2\,r\,dr & i = 1,\ 2,\ ...,\ n \\[2ex] \dfrac{\pi G_{sn} r_p^2}{G_p J_p}\left[\dfrac{r_p^2}{2} + \displaystyle\int_{r_p}^{\infty}\phi_s^2\,r\,dr\right] & i = n+1 \end{cases} \tag{4}$$

$$\tilde{k}_i = \begin{cases} \dfrac{2\pi G_{si} r_p^2 L_p^2}{G_p J_p}\displaystyle\int_{r_p}^{\infty}\left(\frac{d\phi_s}{dr}-\frac{\phi_s}{r}\right)^2 r\,dr & i = 1,\ 2,\ ...,\ n \\[2ex] \dfrac{2\pi G_{sn} r_p^2 L_p^2}{G_p J_p}\left[\ln r_p - \lim\limits_{\varepsilon\to 0}\left(\ln\varepsilon\right) + \displaystyle\int_{r_p}^{\infty}\left(\frac{d\phi_s}{dr}-\frac{\phi_s}{r}\right)^2 r\,dr\right] & i = n+1 \end{cases} \tag{5}$$

The boundary conditions of $\phi_p(z)$ are given by

$$-\left(1+2\tilde{t}_1\right)\frac{d\phi_{p1}}{d\tilde{z}} = \tilde{T}_a \tag{6}$$

at the pile head (i.e., at $z = \tilde{z} = 0$),

$$\phi_{pi} = \phi_{p(i+1)}$$

$$\left(1+2\tilde{t}_i\right)\frac{d\phi_{pi}}{d\tilde{z}} = \left(1+2\tilde{t}_{i+1}\right)\frac{d\phi_{p(i+1)}}{d\tilde{z}} \tag{7}$$

at the interface between any two layers (i.e., at $z = H_i$ or $\tilde{z} = \tilde{H}_i$), and

$$\left(1+2\tilde{t}_n\right)\frac{d\phi_{pn}}{d\tilde{z}} + \sqrt{2\tilde{k}_{n+1}\tilde{t}_{n+1}}\;\phi_{pn} = 0 \tag{8}$$

at the pile base (i.e., at $z = L_p$ or $\tilde{z} = 1$). The dimensionless terms in the above equations are defined as: $\tilde{T}_a = T_a L_p / G_p J_p$; $\tilde{z} = z/L_p$ and $\tilde{H}_i = H_i/L_p$. In the above equations, the n^{th} (bottom) layer is split into two parts, with the part below the pile denoted by the subscript $n + 1$; therefore, $H_n = L_p$ and $H_{n+1} = \infty$. In equation [5], $\tilde{k}_{n+1}$ is not defined at $r = 0$ as ln(0) is undefined; therefore, in obtaining the expression of $\tilde{k}_{n+1}$, the lower limit of integration was changed from $r = 0$ to $r = \varepsilon$ where ε is a small positive quantity (taken equal to 0.001 m in this study).

The general solution of equation (3) is given by

$$\phi_{pi}(\tilde{z}) = C_1^{(i)}\Phi_1 + C_2^{(i)}\Phi_2 \tag{9}$$

where $C_1^{(i)}$ and $C_2^{(i)}$ are integration constants of the i^{th} layer, and Φ_1 and Φ_2 are individual solutions of equation (3), given by

$$\Phi_1 = \sinh\beta_i\tilde{z} \tag{10a}$$

$$\Phi_2 = \cosh\beta_i\tilde{z} \tag{10b}$$

with

$$\beta_i = \sqrt{\frac{\tilde{k}_i}{1+2\tilde{t}_i}} \tag{11}$$

The constants $C_1^{(i)}$ and $C_2^{(i)}$ are determined for each layer using the boundary conditions given in equations (6)-(8).

The governing differential equation (3) resembles that of a column (or rod) supported by a torsional spring foundation undergoing a twist. The parameter $\tilde{t}_i$ accounts for the shear resistance of soil in the horizontal plane and $\tilde{k}_i$ represents the shear resistance of soil in the vertical plane. The torque $T(z)$ in the pile at any depth is given (in dimensionless form) by

$$\tilde{T}(\tilde{z}) = -\left(1+2\tilde{t}\right)\frac{d\phi_p}{d\tilde{z}} \tag{12}$$

where $\tilde{T}_a = T_a L_p / G_p J_p$. The torque $T(z)$ includes the shear resistance offered by the horizontal planes of both the pile and surrounding soil. The governing differential equation (3) describes how the rate of change of this torque T with depth is balanced by the shear resistance in the vertical planes of the soil. The boundary conditions at the interfaces of the adjacent layers ensure continuity of angle of twist and equilibrium of torque across these horizontal planes. The boundary condition at the pile head ensures that equilibrium between the torque $T(z = 0)$ and applied torque T_a is satisfied. The boundary condition at the pile base ensures equilibrium by equating the torque in the pile and soil at a horizontal plane infinitesimally above the base with the torque in soil at a horizontal plane infinitesimally below the base.

The differential equation of $\phi_s(r)$ is given by

$$\frac{d^2\phi_s}{dr^2} + \frac{1}{r}\frac{d\phi_s}{dr} - \left[\frac{1}{r^2} + \left(\frac{\gamma}{r_p}\right)^2\right]\phi_s = 0 \tag{13}$$

where

(17a)

$$\gamma = \frac{r_p}{L_p}\sqrt{\frac{\sum_{i=1}^{n} G_{si}\int_{\tilde{H}_{i-1}}^{\tilde{H}_i}\left(\frac{d\phi_{pi}}{d\tilde{z}}\right)^2 d\tilde{z} + G_{sn}\left[\phi_{pn}^2\big|_{\tilde{z}=1}\right]\sqrt{\frac{\tilde{k}_n}{8\tilde{t}_{n+1}}}}{\sum_{i=1}^{n} G_{si}\int_{\tilde{H}_{i-1}}^{\tilde{H}_i}\phi_{pi}^2 d\tilde{z} + G_{sn}\left[\phi_{pn}^2\big|_{\tilde{z}=1}\right]\sqrt{\frac{\tilde{t}_{n+1}}{2\tilde{k}_n}}}} \tag{14}$$

At the boundaries $r = r_p$ and $r = \infty$, ϕ_s is prescribed as $\phi_s = 1$ and $\phi_s = 0$, respectively, which form the boundary conditions of equation (13).

The solution of equation (13) subjected to the above boundary conditions is given by

$$\phi_s = \frac{K_1\left(\frac{\gamma}{r_p}r\right)}{K_1(\gamma)} \tag{15}$$

where $K_1(\cdot)$ is the first-order modified Bessel function of the second kind. The dimensionless parameter γ determines the rate at which the displacement in the soil medium decreases with increasing radial distance from the pile.

Equations (3) and (15) were solved simultaneously following an iterative algorithm because the parameters involved in these equations are interdependent. At the same time, adjustments were made to the shear modulus by replacing G_s by an equivalent shear modulus $G_s^* = 0.5G_s$. This was necessary because the assumed soil displacement field described in equation (1) introduced artificial stiffness in the system and replacing G_s by G_s^* reduced this stiffness.

3 RESULTS

The accuracy of the proposed analysis is checked by comparing the results of the present analysis with those of previously obtained analyses and of three-dimensional (3D) finite element analyses performed as a part of this study. In order to compare the results with those of the existing solutions, normalized angle of twist at the pile head I_ϕ (also known as the torsional influence factor) and relative pile-soil stiffness π_t (Guo and Randolph 1996) are defined for piles in homogeneous soil deposits (with a constant shear modulus G_s)

$$I_\phi = \frac{\phi_p\big|_{z=0}}{\tilde{T}_a} = \phi_p\big|_{z=0}\frac{G_pJ_p}{T_aL_p} \tag{16}$$

$$\pi_t = L_p\left(\frac{4\pi r_p^2 G_s}{G_pJ_p}\right)^{\frac{1}{2}} \tag{17}$$

Figure 2 shows the plots of I_ϕ as a function of π_t for piles embedded in homogeneous soil, as obtained by Guo and Randolph (1996), Hache and Valsangkar (1978) and Poulos (1975) and as obtained from the present analysis. It is evident that the pile responses obtained from the present analysis match those obtained by others quite well. Figure 3 also shows that, for a given soil profile (in which G_s and G_p are constants) and a given applied torque T_a, I_ϕ of a slender pile is less than that of a stubby pile. Further, for a given pile geometry, I_ϕ increases as G_p/G_s increases.

In order to further check the accuracy of the present analysis, one example problem is solved and compared with the results of equivalent three-dimensional (3D) finite element analysis (performed using Abaqus). A four-layer deposit is considered in which a 30 m long pile with 1.0 m diameter is embedded. The top three layers are located over 0-5 m, 5-10 m and 10-20 m below the ground surface. The fourth layer extends down from 20 m to great depth. The elastic constants for the four layers are $G_{s1} = 8.6 \times 10^3$ kPa, $G_{s2} = 18.52 \times 10^3$ kPa, $G_{s3} = 28.8 \times 10^3$ kPa and $G_{s4} = 40 \times 10^3$ kPa, respectively. This results in $G_{s1}^* = 4.3 \times 10^3$ kPa, $G_{s2}^* = 9.26 \times 10^3$ kPa, $G_{s3}^* = 14.4 \times 10^3$ kPa and $G_{s4}^* = 20.0 \times 10^3$ kPa. The shear modulus of the pile $G_p = 9.6 \times 10^3$ kPa and the applied torque at the head $T_a = 100$ kN-m. Figure 3 shows the angle of twist in the piles as a function of depth for the two examples described above. It is evident that the match between the results of the present analysis and those of the finite element analyses is quite good.

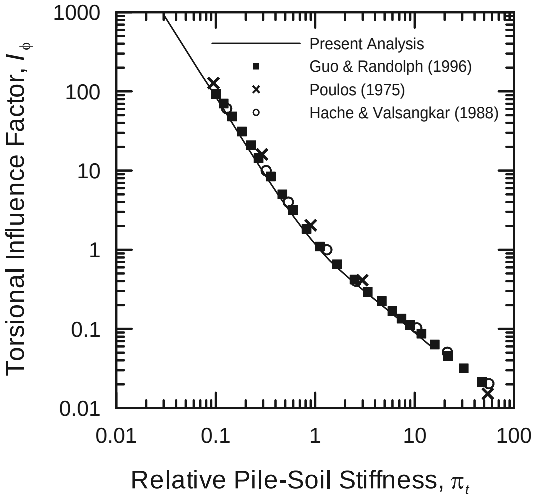

Figure 2. I_ϕ versus π_t for piles in homogeneous soil deposits.

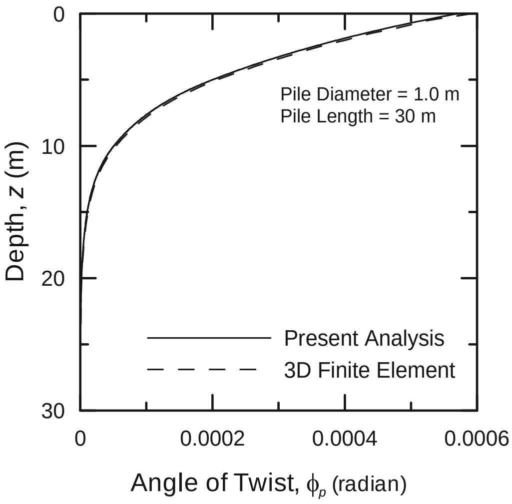

Figure 3. Angle of twist versus depth of a 10 m long pile in a 2-layer soil deposit.

The effect of soil layering is studied for piles in two-layer profiles with slenderness ratio $L_p/r_p = 20$ and 100 and for $G_p/G_{s1} = 1000$ (G_{s1} is the shear modulus of the top layer). I_ϕ is calculated using the above parameters for different values of H_1/L_p (H_1 is the thickness of the top layer) and G_{s2}/G_{s1} (G_{s2} is the shear modulus of the bottom layer). The values of I_ϕ thus obtained are normalized with respect to $I_{\phi,\mathrm{homogeneous}}$ calculated for piles in homogeneous soil profiles with $G_s = G_{s1}$. Figure 4 shows the normalized parameter $I_\phi/I_{\phi,\mathrm{homogeneous}}$ as a function of H_1/L_p. Note that $H_1/L_p = 0$ implies that the pile is embedded in a homogeneous soil with the shear modulus equal to G_{s2}. $H_1/L_p = 1$ implies that the entire pile shaft lies within the top layer and the pile base rests on top of the bottom layer. Also note that $I_{\phi,\mathrm{homogeneous}}$ corresponds to the case where $H_1/L_p = \infty$. It is evident from Figure 4 that, for long, slender piles with $L_p/r_p = 100$, the presence of the second layer affects pile head response only if the bottom layer starts within the top 25% of the pile shaft. For short, stubby piles with $L_p/r_p = 20$, the head response is affected even if the bottom layer starts close to the pile base.

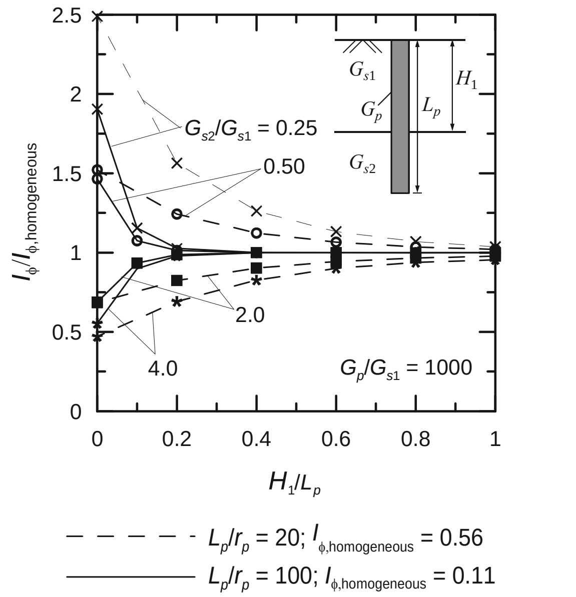

Figure 4. Angle of twist versus depth of a 10 m long pile in a 2-layer soil deposit.

The effect of soil layering is further studied with three-layer profiles for three different cases. For all the cases, the three layers divide the pile shaft into three equal parts of length $L_p/3$ and the pile base rests within the third layer, which extends down to great depth (Figure 5). Moreover, the shear moduli G_{s1}, G_{s2} and G_{s3} of the top, middle and bottom layers are so chosen that $(G_{s1} + G_{s2} + G_{s3})/3 = G_s$ for all the cases. Case I represents a soil profile in which the soil stiffness increases with depth — the top, middle and bottom (third) layer have a shear moduli equal to $0.23G_s$, $0.69G_s$ and $2.08G_s$, respectively. Note that, for this case, $G_{s3} = 3G_{s2}$ and $G_{s2} = 3G_{s1}$. For Case II, $G_{s1} = 0.69G_s$, $G_{s2} = 0.23G_s$ and $G_{s3} = 2.08G_s$. For case III, the soil stiffness decreases as depth increases with $G_{s1} = 2.08G_s$, $G_{s2} = 0.69G_s$ and $G_{s3} = 0.23G_s$. Figure 7 shows the I_ϕ versus π_t plots for these cases. The parameter π_t is calculated using the average shear modulus G_s. Also plotted in the figure is the I_ϕ versus π_t plots for homogeneous soil with shear modulus equal to G_s. As evident from Figure 5, the effect of layering is predominant for $\pi_t > 1.0$ for which $I_\phi < 1.0$. Similar plots can be obtained for cases with multiple layers.

4 CONCLUSIONS

The paper presents a method for analyzing piles in multi-layered elastic soil subject to a torque at the head. The analysis is based on a continuum approach in which a rational displacement field is defined and the variational principles of mechanics are used to develop the governing differential equations. The equations are solved analytically using which the pile response can be obtained using an iterative solution scheme.

The new method predicts the pile response quite accurately, as established by comparing the results of the present analysis with those obtained in previous studies by different researchers and with the results of equivalent three dimensional finite element analysis. A parametric study is performed for piles in layered soil profile. It is found that soil layering does have an effect on the pile response, particularly for short, stubby piles with low slenderness ratio.

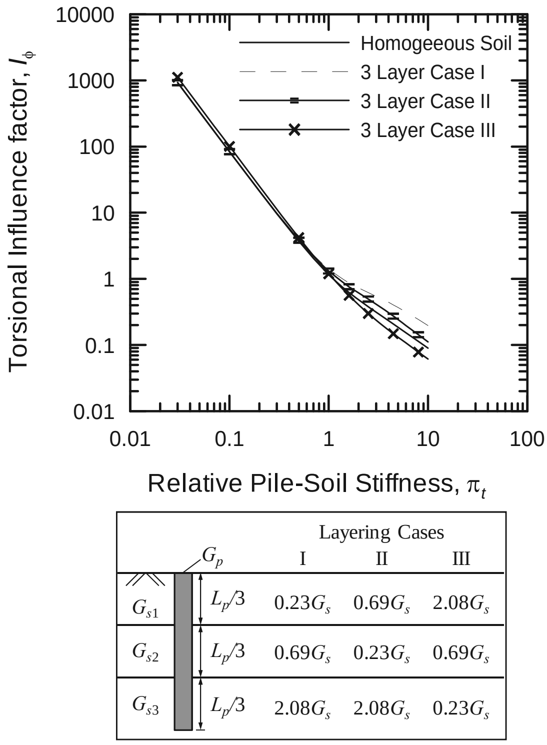

Figure 5. Response of piles in three-layer soil.

5 REFERENCES

Basile, F. (2010). Torsional response of pile groups. Proc. 11th DFI and EFFC Int. Conf. on Geotechnical Challenges in Urban Regeneration, June 26-28, London.

Budkowska, B. B. and Szymczak, C. (1993). Sensitivity analysis of piles undergoing torsion. Computers and Structures, 48(5), 827-834.

Chow, Y. K. (1985). Torsional response of piles in nonhomogeneous soil. Journal of Geotechnical Engineering, 111(7), 942–947.

Dutt, R. N. and O'Neill, M. W. (1983). Torsional behavior of model piles in sand. Geotechnical Practice in Offshore Engineering, ASCE, New York, 315–334.

Guo, W. D. and Randolph, M. F. (1996). Torsional piles in non-homogeneous media. Computers and Geotechnics, 19(4), 265-287.

Guo, W., Chow, Y. K. and Randolph, M. F. (2007). Torsional piles in two-layered nonhomogeneous soil. International Journal of Geomechanics, 7(6), 410–422.

Hache, R. A. G. and Valsangkar, A. J. (1988). Torsional resistance of single piles in layered soil. Journal of Geotechnical Engineering, 114(2), 216–220.

Poulos, H. G. (1975). Torsional response of piles. Journal of Geotechnical Engineering, 101(10), 1019–1035.

Rajapakse, R.K.N.D. (1988). A torsion load transfer problem for a class of non-homogeneous elastic solids. International Journal of Solids and Structures, 24(2), 139-151.

Randolph, M. F. (1981). Piles subjected to torsion. Journal of Geotechnical Engineering, 107(8), 1095–1111.

Ancrage des pieux tarière creuse type III dans des terrains indurés : nécessité d'outils de forage performants et de reconnaissances de sols adaptées

Anchoring of continue flight auger piles in hard soil: necessity of succesful tools of drilling and adapted soils investigations.

Berthelot P.
Bureau Veritas, Paris, France,
Cardona G., Glandy M.
Soletanche-Bachy-Pieux, Paris, France,
Durand F.
Fugro, Paris, France

RÉSUMÉ : Une des limites d'utilisation des pieux « tarière creuse » est la potentialité d'ancrage dans des terrains indurés (grès, poudingues, marno-calcaire compact, rocher, etc.). L'objet de l'article est de décrire les essais de faisabilité réalisés dans ces terrains préalablement aux travaux, essais mettant en exergue la sensibilité et la performance des outillages mis en œuvre provenant de tarière creuse de dernière génération. La pénétration dans ces terrains ne peut se faire qu'avec un outil d'attaque spécifique prolongé d'une pointe pilote télescopable au bétonnage. Elle nécessite aussi un important couple de rotation et des moyens de poussées verticales. Ces essais ont été implantés au droit de sondages de reconnaissance géotechnique adaptés (de type pressiomètres de haute pression, enregistrement de paramètres de foration, carottage,…) permettant de bien mettre en évidence les fortes résistances et les modules très élevés de ces terrains indurés. Ces essais de faisabilité prenant en compte ces adaptations de l'outillage et les résultats des reconnaissances géotechniques ont été mis en œuvre sur deux chantiers importants. Ils ont permis de valider les critères d'ancrage répondant aux spécificités de chacun des projets et de mener à bien ces deux chantiers.

ABSTRACT: One of the limits of continue flight auger piles is the potentiality of anchoring in hard soil (sandstone, compact malm-limestone, rock …) The object of the article is to describe feasibility tests realized in these grounds before the works, the tests highlighting the sensibility and the performance of the implemented equipments resulting of continue flight auger of last generation. The penetration in these grounds can be made only with a tool of specific attack extended by an experimental retractable point in the concreting. He also requires an important couple of rotation and the means of vertical pushes. These tests were implanted right adapted soils investigations (pressiometer high pressure, recording of parameters of foration, core drilling) allowing to highlight well the strong resistances and the very high modulus of this hard soil. These feasibility test taking into account these adaptations of the equipment and the soil investigation were operated on two important construction sites.They allowed to validate the criteria of anchoring answering the specificities of each projects and to bring a successful conclusion these two construction sites..

MOTS-CLÉS: tarière creuse, terrains indurés, outil de forage, essais pressiométriques, essais destructifs.
KEYWORDS: continue flight auger, hard soil, drilling tools, pressiometer test, destructive test

1 INTRODUCTION

Sur les sites de l'hôpital Robert Schumann à Metz, et des « Terrasses du Port » à Marseille, le contexte géologique, rocheux, voire induré, du substratum orientait le concepteur vers l'exécution de pieux forés tubés, avec mise en œuvre de moyen de pénétration adapté au terrain dur tel que le trépan ou le carottier
En variante, Soletanche-Bachy-Pieux a proposé la mise en œuvre du procédé Starsol (Cahier des Charges version 5, 2012) sous réserve d'un essai de faisabilité préalable aux travaux.
Ces essais de faisabilité avaient pour objet, d'une part de vérifier que les moyens mis en œuvre permettaient de réaliser les fondations, d'autre part de caler un critère d'ancrage en fonction des caractéristiques pressiométriques mesurés.
Sur le site de Marseille, ils ont été couplés à des essais pressiométriques supplémentaires haute pression
L'objet de cet article est d'exposer le contexte géotechnique de chaque site, de décrire les moyens mis en œuvre, de décrire les essais de faisabilité réalisés, et enfin de conclure sur les critères d'ancrage

2 CONTEXTE GÉOTECHNIQUE

Les deux sites ont fait l'objet d'une campagne de reconnaissance à partir principalement d'essais carottés et d'essais au pressiomètre avec p_{le} : valeur moyenne des pressions limites mesurées par couche et E_m : valeur moyenne des modules mesurés par couche.

2.1 Hôpital Robert Schumann à Metz

Le site a fait l'objet d'une campagne de reconnaissance par Fondasol, et a mis en exergue la géologie suivante au droit du sondage PR5 qui correspondait aux valeurs de module les plus élevées

- 0 à 6 m, argile de caractéristiques moyennes avec p_{le} = 0.7 MPa et E_m = 10 MPa ;
- 6 à 9 m, argile marneuse moyenne avec p_{le} = 1.5 MPa et E_m = 15 MPa
- 9 à 11 m, argile marneuse plus compacte avec ple = 2 MPa et E_m = 50 MPa
- Au-delà, marnes à passages calcaire de p_f (pression de fluage) > 5 MPa et E_m > 250 MPa, avec p_{le} retenue = 8 MPa

La classification des sols, notamment le distinguo entre marnes et argiles marneuses, repose sur la mesure des teneurs en carbonate C_aC_{O3}.

2.2 Terrasses du Port à Marseille

Le site a fait l'objet d'une première campagne de reconnaissance par Sobesol, puis par une campagne de reconnaissance pressiométriques avec essai haute pression et a mis en exergue la géologie suivante du substratum stampien qui présente la particularité d'être soit

- Marneux avec des p_{le} > 5 MPa et des E_m > 100 MPa
- Gréseux, avec des p_{le} > 10 MPa et des E_m > 200 MPa ;

La difficulté du site relevait de cette dichotomie entre la nature gréseuse ou marneuse du stampien, et des valeurs importantes des valeurs de E_m et de p_f mesuré

3 MOYEN MIS EN OEUVRE

Soletanche-Bachy a mis en œuvre les moyens matériels suivants :

- Foreuse IHC3500, couple de rotation 45 tm, et pulldown 40t
- Diamètre de la tarière 800 à 1350 mm
- Equipement Starsol
    - Tube plongeur 1.5 m
    - Tarières spécifiques au couple
    - Outils à dents carbure sur lame unique et pointe pilote adaptée
    - Enregistrement de paramètres affichés en temps réel,

Figure 1. Tube plongeur et dents en bout de l'outil d'attaque.

4 ESSAIS DE FAISABILITÉ

Les essais de faisabilité (NF EN 1536 -2010) réalisés en début de chantier permettent de vérifier la faisabilité et l'adéquation de la méthode d'exécution par rapport à la réalité du terrain réellement rencontré. Ils permettent également de vérifier la bonne application des critères fournis par le projet.

4.1 Hôpital Robert Schumann à Metz

Cet essai a été réalisé en présence du géotechnicien et du bureau de contrôle le 25 février 2010.
Il s'agit de 2 pieux de diamètre 820 mm, de longueurs 11.5 m et 19 m, ancrés de 1.5 m ou 9 m dans les marnes indurées.
Le deuxième pieu a fait l'objet d'un suivi par la géotechnicien.
Ce pieu a été équipé d'une cage d'armature et a aussi fait l'objet d'un essai dynamique de chargement.
A la demande de SBP, une analyse des teneurs en CaCO3 a été faite et a conclu au caractère argileux des 3 premiers mètres.
Le compte-rendu de cette campagne de faisabilité a été rédigé par Michel Bustamante, a été validé par la Maîtrise d'œuvre et par le géotechnicien, en validant une portance calée sur un critère d'ancrage
La note de calcul a alors été établie sur la base d'ancrage calé sur les vitesses d'avancement de cet essai, et sur une valeur de ple = 8 MPa. Le chantier s'est ensuite déroulé sans problème majeur, les enregistrements de paramètres en temps réel permettant de valider en toute transparence les ancrages réalisés.

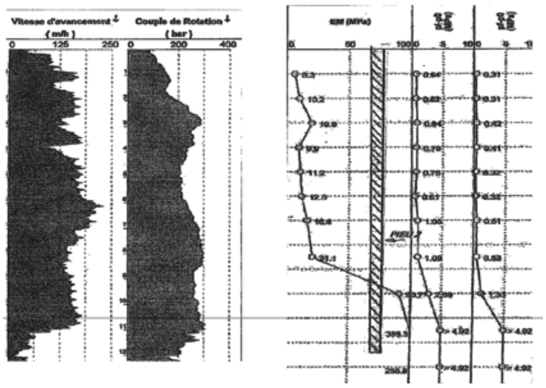

Figure 2. Metz : Comparaison avancement de l'outil Starsol et valeurs de l'essai au pressiomètre (E_m, p_f, p_l).

4.2 Terrasses du Port à Marseille

La campagne de faisabilité a eu lieu en présence du bureau de sol Fugro, de Vinci et du bureau de contrôle Veritas le 8 avril 2011. Trois pieux ont été réalisés : un au droit du stampien marneux, deux au droit du stampien gréseux.

4.2.1 Au droit du Stampien marneux

Le pieu a été réalisé au droit du sondage M2.1 correspondant à un ancrage de 9 m dans le stampien marneux à partir de 14 m de profondeur, et a mis en exergue une chute de vitesse d'avancement de l'ordre de 60 m/h

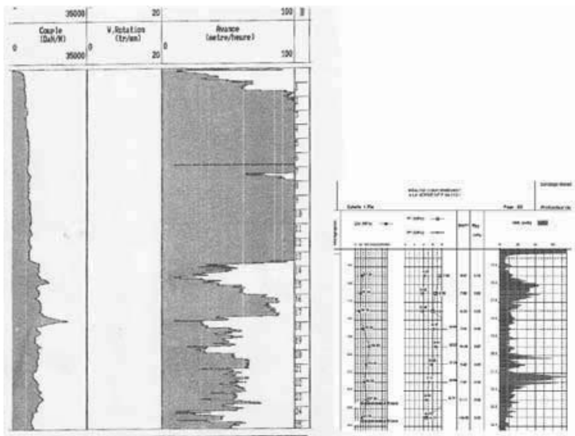

Figure 3. Marseille : Comparaison avancement de l'outil Starsol et valeurs de l'essai au pressiomètre (E_m, p_f, p_l; vitesse instantanée d'avancement.).

Le terrassement général de la fouille voisine sous le bâtiment M1 a permis de visualiser ce stampien marneux

Figure 4. Marseille : stampien marneux

4.2.2 Au droit du Stampien gréseux

Le pieu a été réalisé au droit du sondage M2.2 et du sondage carotté SC34 correspondant à un ancrage de 8m dans le stampien gréseux à partir de 18 m de profondeur

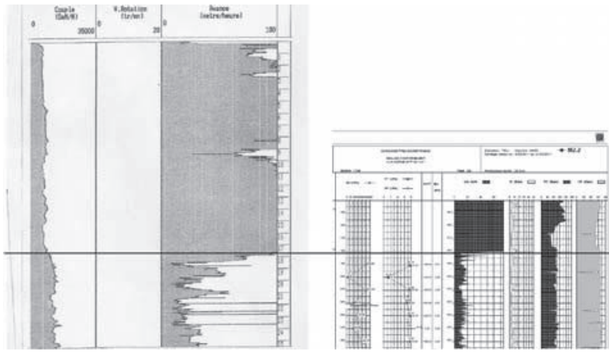

Figure 5. Marseille : Comparaison avancement de l'outil Starsol et valeurs de l'essai au pressiomètre (E_m, p_f, p_l; vitesse instantanée d'avancement.).

Le terrassement général de la fouille voisine sous le bâtiment M1 a permis de visualiser ce stampien gréseux

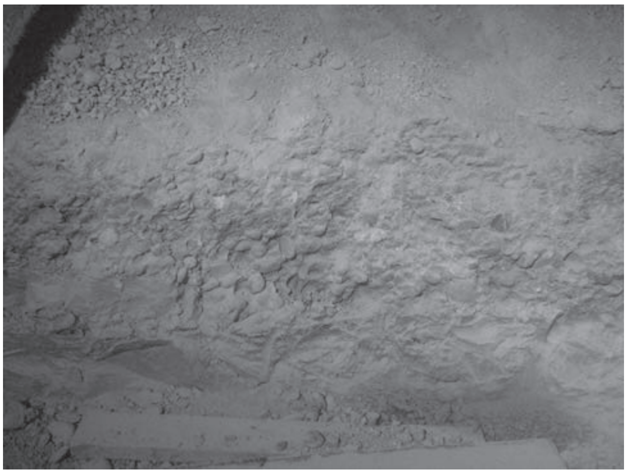

Figure 6. Marseille Stampien gréseux

4.2.3 Analyse

Au sens de l'essai destructif avec enregistrement de paramètres mené préalablement à la réalisation de l'essai pressiométrique, les vitesses instantanées d'avancement (v.i.a) montrent une très nette différence entre le Stampien marneux avec des v.i.a. de l'ordre de 20 à 40 m/h et le Stampien gréseux avec des v.i.a. inférieure à 20 m/h.
Les enregistrements en temps réel spécifiques réalisés par l'outillage Starsol et tracés directement sur papier grâce au système embarqué Enbesol permettent de retrouver cette dichotomie entre les deux types de Stampien. La pénétration dans le stampien marneux se caractérise par des vitesses d'avancement de l'ordre de 60 m/h, celle dans le stampien gréseux par des vitesses inférieures à 20 m/h.

5 CRITÈRE D'ANCRAGE ET PARAMÈTRES DE DIMENSIONNEMENT

5.1 Hôpital Robert Schumann à Metz

Nous n'avons retenu qu'un seul critère d'ancrage calé sur les vitesses d'avancement de l'outil Starsol, avec un minimum de 1 m, associé à une valeur caractéristique de pression limite égale à 8 MPa.

5.2 Terrasse du Port à Marseille

Les valeurs de pression limite des essais courants étant plafonnées à 5 MPa, que ce soit dans la marne ou que ce soit dans le grés et afin de bien caractériser les critères d'ancrage, les sondages pressiométriques complémentaire avec sonde haute pression ont été réalisés au droit de chaque type de substratum, avec possibilités de mesurer des pressions de fluage à plus de 9 MPa et ainsi de valider une pression limite de 10.5 MPa.
Nous avons alors différencié deux critères d'ancrage calées sur des vitesses d'avancement de l'outil de forage et vérifiés sur chaque pieu :

- Dans les matériaux à prédominance marneuses la vitesse retenue de l'outil Starsol est : V = 80m/h sur les 2 premiers m et 60 m/h au-delà. Dans ce type de matériaux le minimum d'ancrage permettant de justifier les critères de calcul de projet est de 3 m.
- Dans les matériaux à prédominance gréseux la vitesse retenue de l'outil Starsol est : V = 25 m/h. Dans ce type de matériaux l'ancrage minimum permettant de justifier les critères de calcul de projet est de 1.5 m.

Le chantier s'est ensuite déroulé sans problème majeur, supervisé par une mission G4 par Fugro, les enregistrements de paramètres en temps réel permettant de valider en toute transparence les ancrages réalisés.

6 CONCLUSION

Grâce à la puissance de la machine et surtout à la spécificité de l'outil d'attaque terminant le tube plongeur, la pénétration et donc l'ancrage du pieu tarière creuse de type III (Starsol) dans un sol très résistant (module pressiométrique > 200 MPa) et sur des longueurs ≥ 2 diamètres sont réalisables.
Seule l'utilisation d'outil spécifique particulièrement en base du tube plongeur permet l'ancrage, en évitant le patinage de la plaque classique que l'on trouve sur les tarières creuses sans tube plongeur
Les enregistrements de paramètres en temps réel permettent en toute transparence de réaliser le chantier conformément au dimensionnement
Des essais de faisabilité en début de chantier, bien positionnés par rapport aux essais géotechniques sont toujours nécessaires pour démontrer la parfaite adéquation entre les moyens mis en œuvre par l'entreprise de Fondations Spéciales et les critères fixés par le projet.
Il est utile de réaliser des essais pressiométriques haute pression pour valoriser le terme de pointe en fonction de la réelle valeur de mesure de p_l, voire d'une corrélation de cette valeur en fonction de la valeur mesurée de p_f

7 RÉFÉRENCES

Cahier des Charges Pieu Starsol 2012. Version 5. Soletanche-Bachy-Pieux.
NF EN 1536 (P 94-310) 2010.Exécution des travaux géotechniques : Pieux forés. AFNOR, Paris.

Improved Safety Assessment of Pile Foundations Using Field Control Methods

Évaluation améliorée de la sécurité des fondations sur pieux à l'aide de méthodes de contrôle in situ

Bilfinger W.
Vecttor Projetos, São Paulo, Brazil

Santos M.S.
Liberty Seguros, São Paulo, Brazil

Hachich W.
Polytechnic School – University of São Paulo, Brazil

ABSTRACT: The theme of foundation safety has historically deserved special attention in both theory and practice due to the need to find optimized solutions which balance cost and safety. Safety against bearing capacity failures (ultimate limit states) continues to be a key topic, particularly in pile foundations, as opposed to other foundation types in which serviceability limit states tend to dominate safety considerations. The paper presents a new approach, in which Bayesian inference is used to combine bearing capacity predictions and field controls, so as to improve reliability assessment and, possibly, lead to more economic design. For bearing capacity predictions semi-empirical procedures based on SPT blow-count are frequently used, and those are the ones addressed in the paper. Rebound and set obtained during pile driving are generally used for uniformity control only, but the paper explores the possibility of combining this duly interpreted information with the design predictions, so as to achieve more economical foundations, while maintaining the prescribed level of safety against failure. The extension of the approach to the case where pile load tests (both static and dynamic) are also available is straightforward and discussed in referenced papers.

RÉSUMÉ : Le thème de la sécurité des fondations a historiquement fait l'objet d'une attention particulière, dans la théorie et la pratique, en raison de la nécessité de trouver des solutions optimales entre coût et sécurité. La sécurité vis-à-vis des états limites ultimes est notamment importante dans le cadre des fondations sur pieux, par opposition aux autres types de fondations, dans lesquels les états limites de service dominent les considérations de sécurité. Cet article présente une nouvelle approche, dans laquelle l'inférence bayésienne est utilisée pour combiner les prédictions de capacité portante et les contrôles in situ, afin d'améliorer l'évaluation de la fiabilité et, éventuellement, conduire à un projet plus économique. Des procédures semi-empiriques fondées sur le SPT sont fréquemment utilisées pour la prévision de la capacité portante, et ce sont celles traitées ici. Le refus élastique et l'enfoncement obtenus au cours du battage des pieux sont généralement utilisés pour le seul contrôle de l'uniformité, mais cet article explore la possibilité de combiner ces informations, dûment interprétées, avec les prédictions de projet afin de parvenir à des fondations plus économiques, tout en maintenant le niveau prescrit de sécurité vis-à-vis de la rupture. L'extension de l'approche, au cas où des essais de chargement de pieux (statique et dynamique) sont également disponibles, est simple; elle est discutée dans les documents référencés.

KEYWORDS: pile, set, rebound, foundation, safety, bayesian, inference, ULS

1 INTRODUCTION

Foundation safety is a primary concern of civil engineers. Given the serviceability requirements of modern buildings, safety is frequently governed by serviceability limit states. Even if safety against such limit states must always be confirmed, pile foundations are most often designed on the basis of bearing capacity predictions, i.e., ultimate limit states. Semi-empirical procedures based upon field tests such as SPT or CPT are a common choice for such predictions.

The paper presents a new approach, in which Bayesian inference is used to combine bearing capacity predictions and field controls, so as to improve reliability assessment, and possibly lead to more economic design.

2 THE PROPOSED APPROACH

The idea behind the proposed approach is that foundation design based on semi-empirical bearing capacity prediction models can benefit from the incorporation of duly interpreted field controls during construction.

Even if field controls are almost always used exclusively to guarantee that uniform behavior is attained, it is believed that such controls carry quantifiable information that can be translated into more efficient foundation solutions.

The proposed incorporation mechanism is Bayesian updating. This paper relies heavily in the work of Baecher and Rackwitz (1982), which has been explored in detail by Santos (2007) and by Hachich and Santos (2006).

3 SEMI EMPIRICAL PREDICTION PROCEDURES

Bearing capacity prediction is one of the key analyses required by pile foundation design. Several semi-empirical procedures are available, based on different geotechnical investigation methods, such as SPT, CPT, pressuremeter, dilatometer, and others.

The use of the SPT to estimate bearing capacity of piles is still current practice in Brazil and other countries (Poulos et al. 2001). "Case 1" bearing capacity predictions, as categorized by Poulos (1989), are the commonly adopted procedure.

Several bearing capacity prediction methods using the SPT have been developed since Meyerhof (1956), including the relatively recent SPT 97, by the Florida DOT.

In Brazil the most widely used such method is D&Q, the Décourt and Quaresma method (Décourt and Quaresma 1978, Décourt 1982, Décourt 1991). For this reason, D&Q is retained in the paper as the ultimate load prediction method.

Table 1 presents the moments of the random variable $R=\log_{10}(K)$, where $K = P_{OBS}/P_{PRED}$. The first line is based on the values originally used to develop the method, where P_{OBS} was derived from static load tests on precast concrete piles and $P_{PRED}=P_{D\&Q}$. The second line is based on the statistical analysis of a database of 189 dynamic load tests in precast concrete piles

(Rosa 2000), revised to correlate static ultimate loads to CASE-dynamic ultimate loads (Bilfinger 2002).

Table 1. Moments of the distribution of R = log ($P_{OBS}/P_{D\&Q}$) from two different sources

Source	Mean	Variance
40 static load tests (original)	0.00610	0.01538
189 dynamic load tests reinterpreted	0.04157	0.04330

Figure 1 is a graphical representation of the distribution associated with the second line of Table 1.

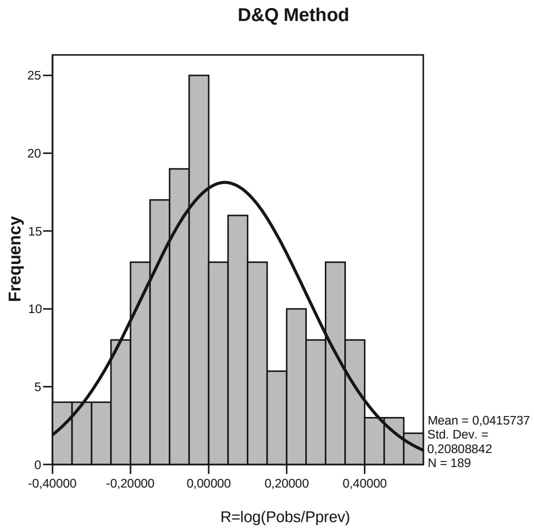

Figure 1. Distribution of R = log ($P_{OBS}/P_{D\&Q}$)

It is interesting to note that the variance of the original results used to develop the method is significantly lower than that associated with databases compiled from regular job sites. One can speculate that boreholes and tested piles were probably much closer to each other for the original formulation, so that intra-site variance was negligible. Moreover, the correlation between static and dynamic load tests adds to the uncertainty in the second database of Table 1. In any case, the higher coefficient of variation of $P_{OBS}/P_{D\&Q}$ in the second database (61.7%) is not incompatible with equivalent results found by other researchers: Briaud and Tucker (1988) published the results of 98 static pile load tests and showed that the coefficient of variation of P_{OBS}/P_{PRED}, for 12 different ultimate load prediction methods (using SPT, CPT, PMT and direct shear strength tests) varied between 42% and 74%.

For this reason, it seems reasonable to assume that ultimate load prediction methods based on industry-standard site investigation plans are prone to exhibiting high variability and could, therefore, benefit from information gathered during the pile driving operation itself.

4 FIELD CONTROL METHODS

Only a limited number of piles are usually subject to dynamic monitoring and testing. For the vast majority, field control methods are the only tools the engineer has at his disposal to check if the piles are being adequately driven.

Field control methods have been used since the early days of pile driving, and the best known is the set, the permanent settlement due to a hammer blow. There are a number of the so called pile driving formulas, which basically equate the energy delivered by the pile driving equipment to the work done by the soil forces that resist pile penetration.

Terzaghi (1943) thus expressed his realistic opinion about the relevance of those formulas: *In spite of their obvious deficiencies and their unreliability, pile driving formulas still enjoy great popularity among practicing engineers, because the use of these formulas reduces the design of a pile foundation to a very simple procedure.* The number of technical papers on such formulas is indeed significant; after all, it is also relatively easy to obtain field data. Even if some published results show good correlation between estimated and measured ultimate loads, the universal use of any particular formula must be questioned: pile length, pile diameter, hammer types, operational practices, soil types, to name a few, are factors which have significant impacts on the results. Figure 2 presents, for the database made available by Rosa (2000), the comparison of ultimate loads obtained by dynamic load tests and those predicted on the basis of some of the most popular (Poulos and Davis 1980) set-based pile driving formulas: Engineering News, Eytelwein (or Dutch), Weisbach, Hiley, Janbu, Danish and Gates. The scatter speaks for itself.

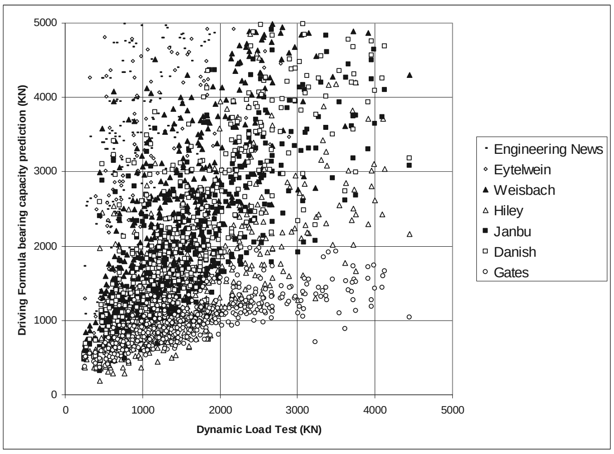

Figure 2. Comparison between measured and estimated bearing capacities using set-based dynamic formulas.

Janbu's formula led to the best correlation and the moments of the variable log(P_{OBS}/P_{CTL}), where CTL=Janbu, are presented in table 2.

Rebound, the elastic deformation caused by a hammer blow, is being increasingly used as a pile driving field control. The basic idea is to use the pile itself as a dynamometer that measures soil resistance to driving, but it is sometimes difficult to distinguish pile rebound from soil rebound. Moreover, measuring rebound requires continuous pile displacement recording during driving, which is more complicated than set measurement.

Figure 3 presents, for the database made available by Rosa (2000), the comparison of ultimate loads obtained by dynamic load tests and those predicted on the basis of two of the most popular (Aoki and Alonso 1989) rebound-based pile driving formulas: Chellis and Uto. In addition, it presents similar results for Rosa's modification of the Chellis formula (Rosa 2000). Comparison of the scatter in Figures 2 and 3 suggests that rebound-based formulas are more precise than set-based formulas. This is confirmed by the variances in Table 2. Also, the coefficient of variation of P_{OBS}/P_{JANBU} is 69.8%, while that of $P_{OBS}/P_{CHELLIS}$ is 45.0%.

Table 2. Moments of the distribution of log (P_{OBS}/P_{CTL}) for two different formulas

Pile driving formula	Mean	Variance
CTL=Janbu (set-based)	-0.01819	0.02657
CTL=Chellis (rebound-based)	0.01818	0.01113

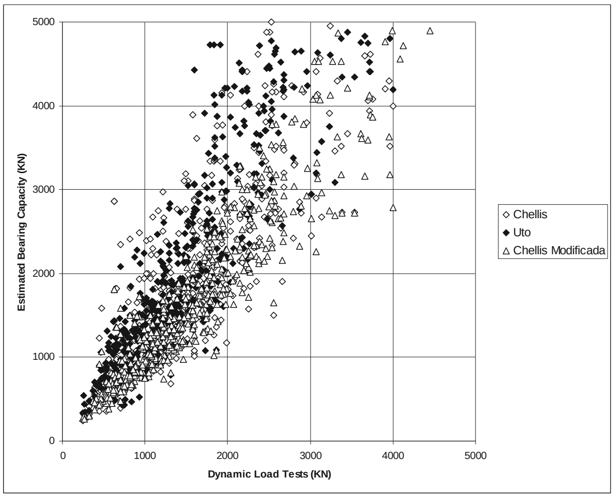

Figure 3. Comparison between measured and estimated bearing capacities using rebound-based dynamic formulas.

5 BAYESIAN UPDATING IN PILE FOUNDATION SAFETY

Baecher and Rackwitz (1982) define a random variable K = $P_{\mathbf{OBS}}/P_{\mathbf{PRED}}$ as the ratio of observed and predicted resisting forces, which is assumed to follow a lognormal distribution. Therefore, R=$\log_{10}$(K) is normally distributed (Gauss): R~N(ρ,h^{-1}), where ρ and h^{-1} are the usual parameters of a Gaussian distribution; ρ represents the central tendency and h^{-1} the dispersion. In more usual notation, h = $1/\sigma^2$, that is, parameter h, which is sometimes called precision, is the inverse of the variance. In the context of Bayesian inference, the parameters of $f_R(r)$, ρ and h, are themselves random variables, so that the (normal) distribution of R is conditional on the knowledge of those parameters: $f_R(r|\rho,h)$. Within this approach:

$$f_R(r) \propto \int_{\rho,h} f_R(r \mid \rho,h) \cdot f(\rho,h) d\rho dh \qquad (1)$$

The Bayesian updating procedure consists in deriving a posterior (or updated) distribution f "(ρ,h) from the prior distribution, f '(ρ,h), and statistics of a sample obtained in the field. Formally,

$$\mathrm{f}\,''(\rho,\mathrm{h}) = \frac{\mathrm{L}(\rho,\mathrm{h}) \cdot \mathrm{f}\,'(\rho,\mathrm{h})}{\int_{-\infty}^{\infty} \mathrm{L}(\rho,\mathrm{h}) \cdot \mathrm{f}\,'(\rho,\mathrm{h}) \mathrm{d}\rho \mathrm{dh}} \qquad (2)$$

f "(ρ,h) is the substituted into equation 1, so as to arrive at an updated version of $f_R(r)$.

Variability inherent to geological characteristics of the local subsoil, driving details and other local and circumstantial specificities make σ^2 vary from one site to the next; h is therefore named intra-site precision. Bilfinger and Hachich (2006) analyze some aspects of intra-site variability. Baecher and Rackwitz (1982) treat it as a random variable within the context of Bayesian inference (see equation 2). Many authors have treated variance as a known, generally estimated, deterministic parameter (Kay 1976, Kay 1977, Vrouwenvelder 1992, Zhang 2004). This is the approach adopted here.

Under such conditions of know variance, updating of a Normal process is significantly simpler and it can be demonstrated (Martz and Waller 1982) that the posterior distribution of ρ, the mean of $f_R(r)$, is also normal with two parameters obtained from equations 3 and 4.

$$h''_\rho m''_\rho = h'_\rho m'_\rho + n \cdot h \cdot \bar{r} \qquad (3)$$

$$h''_\rho = h'_\rho + n \cdot h \qquad (4)$$

The same authors (Martz and Waller 1982) show that, in the case of known variance, integration of the single nuisance parameter (ρ) leads to a predictive distribution of R (equivalent to equation 1) that is also Normal, with same posterior mean (equation 5) and a variance that satisfies equation 6.

$$m''_R = m''_\rho \qquad (5)$$

$$\frac{1}{h''_R} = \frac{1}{h''_\rho} + \frac{1}{h} \qquad (6)$$

The procedure described above can be readily applied to a situation in which the new information stems from a direct measurement of the resisting force (P_{OBS}), such as a static or dynamic load test (Hachich and Santos 2006, Hachich, Falconi and Santos, 2008).

In this paper, however, the idea is to incorporate whatever information is provided by field control procedures into the reevaluation of the safety of a pile foundation. The resisting force on a pile, $P_{\mathbf{PRED}}$, is predicted at the design stage by one of the semi-empirical procedures, which are based on SPT blow counts from a borehole that is seldom located at the exact point where the pile is being installed. The only information pertaining exactly to the location where the pile is installed is provided by the field control procedures, either set or elastic rebound, and it would be a waste not to take advantage of this location-specific information to revise the pile safety prediction.

For this, $P_{\mathbf{OBS}}/P_{\mathbf{PRED}}$ can be written as the product of $P_{\mathbf{OBS}}/P_{\mathbf{CLT}}$ and $P_{\mathbf{CTL}}/P_{\mathbf{PRED}}$, where $P_{\mathbf{CTL}}$ stands for the pile resistance inferred from the field control records, namely Janbu's expression based on set, or Chellis expression based on rebound. It is straightforward to derive the moments of $P_{\mathbf{OBS}}/P_{\mathbf{PRED}}$ from the moments of $P_{\mathbf{OBS}}/P_{\mathbf{CLT}}$ and $P_{\mathbf{CTL}}/P_{\mathbf{PRED}}$. It is understandable that the variance of $P_{\mathbf{OBS}}/P_{\mathbf{PRED}}$ thus obtained is significantly larger than the variance of the $P_{\mathbf{OBS}}/P_{\mathbf{PRED}}$ derived from pile resistances actually measured in pile load tests. This fact must be accounted for in the Bayesian updating procedure, since the actual observation is not a pile load test, but rather an estimate of ultimate load based on a field control measurement. It can be demonstrated that this is achieved in a statistically sound manner if the actual number of observations (n in equations 3 and 4) is replaced by an equivalent number that is adjusted downwards in proportion to the ratio of those two variances. In other words, one observation derived from a set measurement and application of Janbu's formula (or rebound and Chellis), is worth less than one observation in the Bayesian updating procedure.

The moments of $P_{\mathbf{OBS}}/P_{\mathbf{CTL}}$ are available from the proponents of the pile driving formulas and from correlation studies in the literature. Values relevant to the present application were presented item 4 above.

Moments of $P_{\mathbf{CTL}}/P_{\mathbf{PRED}}$ are the only missing piece of information for application of the Bayesian updating procedure just proposed.

Table 3 presents the moments of the random variable log ($P_{\mathbf{CTL}}/P_{\mathbf{D\&Q}}$), estimated from statistical analysis of the aforementioned database of 189 dynamic pile load tests (Rosa 2000), revised by Bilfinger (2002) to correlate static ultimate loads to CASE-dynamic ultimate loads. The database includes precast concrete piles with diameters of 17 to 70cm, lengths up to 39m, driven by free fall hammers of 13 to 80kN. The first line of Table 3 refers to the variable log($P_{\mathbf{JANBU}}/P_{\mathbf{D\&Q}}$), while the second refers to log($P_{\mathbf{CHELLIS}}/P_{\mathbf{D\&Q}}$).

Table 3. Moments of the distribution of R = log ($P_{CTL}/P_{D\&Q}$) for Janbu and Chellis formulas

Pile driving formula	Mean	Variance
CTL=Janbu (set-based)	0.05977	0.05339
CTL=Chellis (rebound-based	0.02339	0.04523

Once again correlations with the Chellis formula exhibit a smaller variance that those with Janbu's.

6 APPLICATION AND RESULTS

Application of the proposed procedure was guided by the final goal of developing plots that could provide sound statistical justification to field operational rules that will lead to more economical pile foundation solutions, such as shorter piles, with the very same probability of failure (or reliability index, β).

Figures 4 and 5, developed by means of equations 3 to 6 with data from Tables 1 to 3, show the updated global safety factor required to maintain the same reliability index (β) after the distribution of the predicted ultimate load of the pile is updated on the basis of field control measurements and the corresponding pile driving formulas. The x-axis values are possible observable results of the ratio P_{OBS}/P_{PRED}. In Figure 4, set is the field control and Janbu is the formula used for P_{OBS} prediction. In Figure 5 the performance of set and rebound are compared for an intra-site variance of 0.08, while results in Figure 4 explore four possible values of intra-site variance.

Figure 5 confirms previously discussed indications that rebound-based control is slightly superior to set-based control.

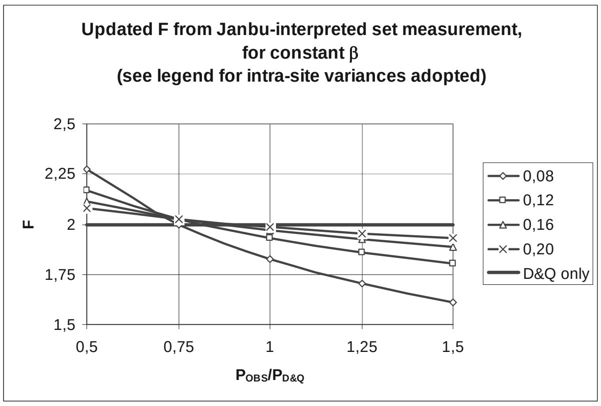

Figure 4 - Comparison of code-prescribed global safety factor (F=2) with set-updated F values, for the same reliability index (β)

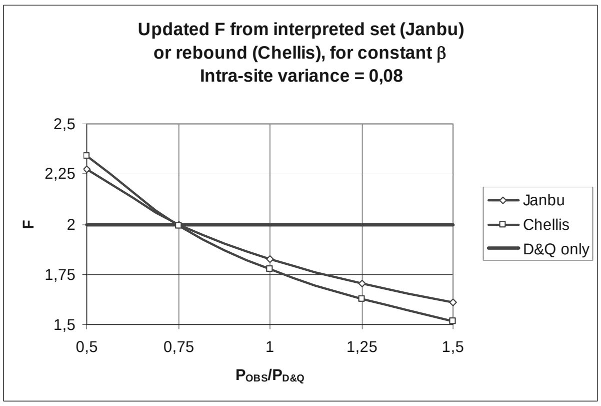

Figure 5 - Comparison of the performance of set and rebound field controls for updating the safety factor while preserving the same reliability index (β)

7 CONCLUSIONS

Duly interpreted field control measurements, recorded during pile driving, facilitate more economical pile foundation design, while maintaining the same safety level required by code-prescribed safety factors. Figure 5, for example, sets a sound foundation for operational rules that provide safe guidance for early interruption of pile driving.

8 REFERENCES

Aoki, N., Alonso, U. R. Correlation between different evaluation procedures of static and dynamic load tests and rebound. *XII ICSMFE – 12th International Conference On Soil Mechanics And Foundation Engineering*, Rio de Janeiro.

Baecher, G.B., Rackwitz, R. 1982. Factors of safety and pile load tests. International *Journal for Numerical and Analytical Methods in Geomechanics*, v. 6, 409-424.

Bilfinger, W. 2002. Safety criteria of foundations of driven piles using field control methods. *PhD Thesis. Polytechnic School, University of São Paulo* (in Portuguese).

Bilfinger, W., Hachich, W. 2006. Influence of pile length in the variability of axial resistance. *XIII COBRAMSEG – Congresso Brasileiro de Mecânica dos Solos e Engenharia Geotécnica*, ABMS, Curitiba (in Portuguese).

Briaud, J. L., Tucker, L. M. 1988. Measured and Predicted Axial Response of 98 Piles. *Journal of Geotechnical Engineering – ASCE*, 114 (9), 984-1001.

Décourt, L. 1982. Prediction of the Bearing Capacity of Piles based exclusively on N values of the SPT. *2nd European Symposium On Penetration Testing*, Amsterdam.

Décourt, L. 1991. Bearing Capacity of displacement piles in residual soils on basis of SPT. *SEFE II – 2O Seminário De Engenharia De Fundações Especiais, São Paulo*, São Paulo.

Décourt, L., Quaresma, A. R. 1978. Capacidade de Carga de Estacas a partir de Valores de SPT. *VI COBRAMSEF – 6o Congresso Brasileiro De Mecânica Dos Solos E Engenharia De Fundações*, Rio de Janeiro.

Kay, J.N. 1976. Safety factor evaluation for single piles in sand. *J. of the Geot. Engng. Div.*, ASCE, V. 102.

Kay, J.N. (1977) Factor of safety for piles in cohesive soils. *IX International Conference on Soil Mechanics and Foundation Engineering*, Tokyo.

Hachich, W., Falconi, F., Santos, M.S. 2008. Foundation safety: incorporating load test results. *11º Congresso Nacional de Geotecnia*, SPG, Coimbra, Portugal (in Portuguese).

Hachich, W., Santos, M.S. 2006. Safety updating for piles based on load tests. *XIII COBRAMSEG – Congresso Brasileiro de Mecânica dos Solos e Engenharia Geotécnica*, ABMS, Curitiba (in Portuguese).

Martz, H.F., Waller, R. A. 1982. *Bayesian reliability analysis*. John Wiley & Sons.

Meyerhof, G. G. 1956. Penetration Tests and bearing capacity of cohesionless soils. *J. Soil Mechanic and Foundation Division - ASCE*, 82 (SM1), 1-19.

Poulos, H. G., Davis, E. H. 1980. Pile Foundation Analysis and Design, New York.

Poulos, H. G. 1989. Pile behaviour – theory and application. *Géotechnique* 39(3), 365-415.

Poulos, H. G., CARTER, J. P., SMALL, J. C. 2001. Foundations and retaining structures – research and practice, *XII IXSMGE – 12th International Conference On Soil Mechanics And Geotechnical Engineering*, Istambul, 2001.

Rosa, R. L. 2000. Proposition for the modification of Chellis and Uto et. Al. Driving formulas using CASE method results. *MSc Thesis, Polytechnic School, University of São Paulo*.(in Portuguese).

Santos, M.S. 2007. Bayesian inference for the evaluation of foundation safety of displacement piles. *MSc Thesis, Polytechnic School, University of São Paulo* (in Portuguese), 183 p.

Terzaghi, K. 1943. Theoretical Soil Mechanics. *John Wiley and Sons*, New York.

Vrouwenvelder, A. 1992. Effects of inspection on the reliability of foundation piles. In: Barends, F.B.J. (ed), *Application of Stress Wave Theory to Piles*, Balkema, Rotterdam.

Zhang, L. 2004. Reliability Verification Using Proof Pile Load Tests. *Journal of Geotechnical and Geoenvironmental Engineering*, ASCE, V. 130, n.11.

Three Dimensional Finite Element Nonlinear Dynamic Analysis of Full-Scale Piles under Vertical Excitations

Analyse dynamique non linéaire en 3D par éléments finis des pieux à grande échelle soumis à des vibrations verticales

Biswas S., Manna B.
Research Scholar, Department of Civil Engineering, Indian Institute of Technology Delhi, New Delhi - 110016, India

ABSTRACT: The present investigation emphasised on a comparative study between vertical vibration tests of full-scale single piles (length of 22 m and diameter of 0.45 m) with the three-dimensional (3-D) finite element (FE) analysis using Abaqus/CAE. A 3-D finite element model was developed to predict the nonlinear dynamic response of pile foundations in layered soil medium based on field data. First, the FE analysis was carried out for static load for the validation of the finite element model and the results were compared with the test results. Then, the vertical vibration analyses were conducted on the finite element model to determine the frequency-amplitude response of the pile and the FE results were compared with the vertical vibration test results of full-scale pile. It was found that the resonant frequency and amplitude obtained from the 3-D FE analysis were very close to the field test results of the full-scale single pile. Based on the FE analysis the variation of the soil-pile separation length with the depth was presented in this paper for different eccentric moments. It was found that the 3-D finite element model was found to be very efficient for the prediction of the nonlinear frequency-amplitude response considering complex nonlinear phenomena of soil-pile system in layered soil medium.

RÉSUMÉ : La présente étude a mis l'accent sur une étude comparative entre les essais de vibrations verticales à grande échelle des pieux simples (longueur de 22 m et un diamètre de 0,45 m) à l’aide d’une analyse par élément finis (EF) à trois dimensions (3D) en utilisant Abaqus / CAE. Un modèle des éléments finis 3D a été développé pour prédire la réponse dynamique non linéaire des pieux dans les sols multicouches en utilisant les données in-situ. Tout d'abord, l'analyse par éléments finis a été réalisée pour la charge statique à fin de valider le modèle et les résultats ont été comparés avec les mesures in-situ. Ensuite, les analyses de vibrations verticales ont été modélisées par éléments finis pour déterminer la réponse en fréquence d'amplitude du pieu et les résultats EF ont été comparés avec les résultats d'essais aux vibrations verticales des pieux à pleine échelle. Il a été constaté que la fréquence de résonance et l'amplitude obtenues à partir de l'analyse ont été très proches des résultats des essais in-situ du pieu à pleine échelle. La variation de la longueur de la séparation sol-pieu avec la profondeur a été calculée dans ce papier pour différents moments excentriques. Il a été constaté que le modèle 3D est très efficace pour la prédiction de la réponse de fréquence non linéaire-amplitude, compte tenu des phénomènes complexes non linéaires du système sol-pieu dans un milieu multicouches.

KEYWORDS: Layered soils; Nonlinear response; Soil-pile separation; Vertical vibration; 3-D finite element analysis.

1 INTRODUCTION

Vibration of pile foundation from the operation of machine produces elastic waves within the soil mass. The determination of pile stiffness and damping parameters is an important step in the analysis of pile-supported structures subject to dynamic loading due to machinery and vibrating equipments etc. A key step to a successful design of the machine-pile foundation system is the careful engineering analysis of the pile foundation response to the dynamic loads from the anticipated operation of the machine. In recent years, a considerable amount of theoretical research has been accumulated in the area of dynamic behavior of piles, especially under linear elastic assumptions. On the other hand, the available literature on nonlinear soil-pile system subject to dynamic loading is limited.

The finite element method (FEM) was appropriate to study the response analysis of the pile by considering the nonlinearity of the soil medium and separation at the pile-soil interface. Kuhlemeyer (1979) introduced the finite element results of soil-pile system by a simple lumped mass model. Then Dobry et al. (1982) made a parametric study (stiffness and damping coefficients) of the dynamic response of single pile. Lewis and Gonzalez (1985) was investigated the nonlinear soil response of soil-pile system and soil-pile gapping using FE analysis. Bentley and El Naggar (2000) developed a 3-D finite element model that considers the soil nonlinearity, discontinuity conditions at the soil-pile interface, energy dissipation, wave propagation, and actual in-situ stress conditions, to evaluate the kinematic soil-pile interaction. Maheshwari et al. (2004, 2005) studied the significance of nonlinearity of soil-pile system by a three dimensional finite element programme. Ayothiraman and Boominathan (2006) was performed two-dimensional analysis using Mohr-Coulomb soil model to determine the soil-pile response by FE software package, PLAXIS. Manna and Baidya (2009) used a simple axisymmetric two-dimensional finite-element model for the prediction of the dynamic response of full-scale single pile. It was observed that the finite-element model predicted the natural frequency and peak displacement amplitude of pile reasonably well.

It can be concluded based on literature review that a very few studies are available to model of the full-scale pile-soil system using rigorous 3-D finite element model. Prediction of the boundary zone parameters and the soil-pile separation lengths are another key aspect of nonlinear response of pile foundation which has not been studied in details.Hence in the present study, the nonlinear response of the soil-pile system was investigated by a 3-D finite element package. Parametric study was performed based on the comparison between finite element analysis results and vertical vibration test results of full-scale single pile.

2 EXPERIMENTAL BACKGROUND

The vertical vibration tests on the full-scale single pile were conducted at I.I.T. Kharagpur Extension Centre, Block No. HC, Plot. 7, Sector - III, Salt Lake City, Kolkata, India (Manna and Baidya, 2009). In the field three bore holes were made and soil samples were collected. The depth of exploration below ground level was 30.45 m. Disturbed representative soil samples and undisturbed soil samples were collected from the field. During boring ground water was encountered in all the three boreholes and it was found that the position of standing water table was at 1.25 m below the ground level. Standard penetration tests (SPT) were carried out in the field and the SPT - *N* value was determined at different depths of the soil strata. Based on different laboratory observations and field test results the site soil was divided into six different layers. The RCC piles were constructed at site using cast in situ technique. The diameter and length of the pile were 0.45 m and 22 m respectively. Forced vibration tests were conducted on the piles in vertical direction. The mechanical oscillator (Lazan type) was used to induce unidirectional vibrations on pile foundation. The mechanical oscillator was connected by means of a flexible shaft with a motor and its speed was controlled by a speed control unit. The vibration measuring equipment consisted of a piezoelectric acceleration pickup and the associated vibration meter. The complete dynamic test set up is shown in Figure. 1. The amplitudes were measured at different frequencies for each eccentric setting. Tests were conducted for four different exciting moments (0.278, 0.366, 0.45, and 0.529 Nm) under different static loads (8 kN and 10 kN).

Figure. 1 Complete setup of vertical vibration test on full-scale pile

3 THREE DIMENSIONAL FINITE ELEMENT MODELLING

A 3-D FE model was developed to study the nonlinear soil-pile interaction using the finite element software, ABAQUS/CAE 6.11 (2010). A harmonic vibration load was applied i.e., rotating mass type machine at the top of a 0.45 m diameter single pile having 22 m length. Both the pile and soil mass were meshed using tetrahedral solid elements (10 nodded) where elements were more closely spaced near the pile compared to the outer region shown in Figure. 2(a). Boundary conditions were applied to those regions of the model where the displacements and/or rotations were known. Bottom soil boundary nodes were considered as fixed against displacements and rotations at all directions. At the side soil boundary, nodes displacement and rotation were allowed only in vertical Z direction.

The soil-pile interaction was modelled using surface-to-surface contact algorithm, where relative movement between soil and pile was allowed for considering friction. The tangential contact between the pile and the surrounding soil was defined using Coulomb's Law with a friction coefficient estimated by the tangent of the friction angle between the two materials. The normal behaviour was considered to be hard (no penetration to each other) allowing separation after contact.

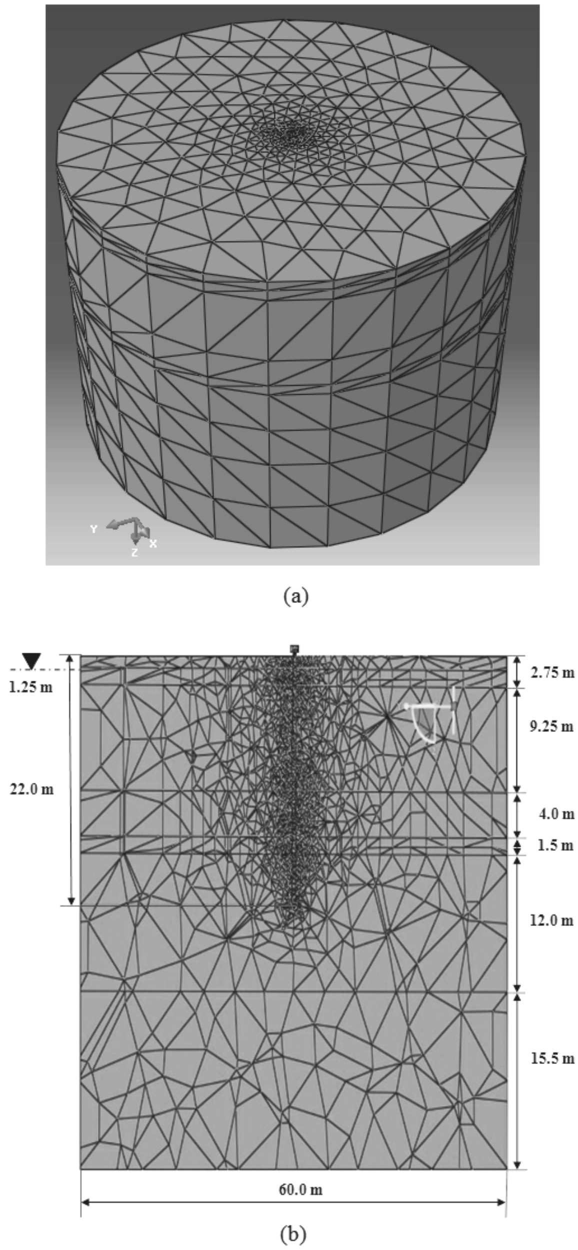

Figure 2. Three Dimensional Finite Element Model of Soil-Pile System: (a) 3-D view and (b) Sectional view.

The whole system was modelled in six layers of soil as found in site investigation (Manna and Baidya, 2009) and the sectional view of the model is shown in Figure. 2(b). The phreatic level was considered 1.25 m below the ground surface and the effective soil pressure was applied in the whole geometry according to this phreatic line. Soil behaviour was considered as elasto-plastic. The displacement of soil had both a recoverable and non-recoverable component under load. Therefore, there was a need to include a failure criterion in the elastic models to define the stress states that would cause the plastic deformation. Mohr-Coulomb model was adopted for soil to simulate the elasto-plastic behaviour. For analysis the FE model material damping was considered. The Rayleigh damping coefficients (α) and (β) was used to define in each layer and the coefficients were determined from the relationship given below:

$$\alpha + \omega_i^2 \beta = 2\omega_i D_i \tag{1}$$

where D_i = damping ratio corresponding to frequency of vibration ω_i

It was assumed that 60 rad/sec and 500 rad/sec were the limit of predominant frequencies in dynamic testing i.e., all damping values for different layers were less than the damping values (D_1, D_2) considered here in this frequency range. The damping values were taken from guidelines given by Bowles (1996). Finally the (α) and (β) coefficients were calculated by using Eq. (1).

The model was analysed in three calculation phases. First gravity analysis was performed only in soil mass in vertical *Z* direction. In the next step, the pile-soil interaction was introduced as well as static load was applied on the top of the pile. A steel plate was provided on the pile head to simulate the exact static load (8 kN and 10 kN) applied on pile. In the third phase the dynamic FE analysis was performed by applying sinusoidal vertical load on the pile using a dynamic multiplier function at wide range of frequencies (5 to 60 Hz). According to the values of eccentric moments (0.278 Nm, 0.366 Nm, 0.450 Nm and 0.529 Nm) and operating frequency of the motor, the dynamic load amplitudes were determined.

4 RESULTS AND DISCUSSION

4.1 Validation of finite-element model

To monitor the boundary effect, the model was analysed with different radius of boundaries. Based on the results, the boundaries of soil mass around the pile were considered with a radius of 30 m and height of 45 m to avoid the direct influence of the boundary conditions. Static load analysis was carried out and the results obtained from FE analysis were compared with the static load test results. The comparison of static load test results with the FE analysis is shown in Figure. 3. The predicted settlement obtained from FE analysis is approximately 1.45 mm and observed settlement is 1.45 mm and 2.3 mm for pile 1 and pile 2 respectively at calculated safe load (283 kN).

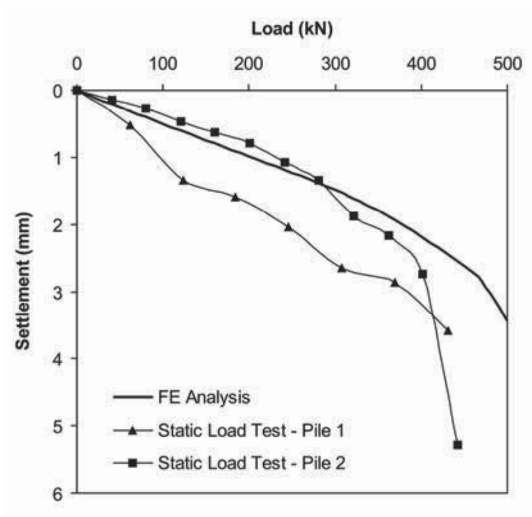

Figure 3. Comparison of load verses settlement curve obtained from FE analysis and static load test.

4.2 Comparison between finite-element analysis and dynamic test results

The time versus amplitude curves were obtained from FE analysis at different operating frequencies of machine for different static load and eccentric moments. A typical response curve is presented in Figure. 4 for static load of 10 kN. From the time versus amplitude curves, the frequency versus amplitude curves were obtained and compared with the field vibration test results.

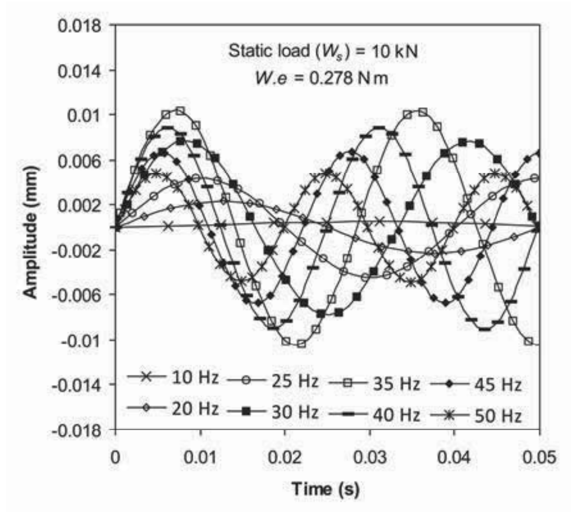

Figure 4. Time-amplitude response of pile at different frequencies (FE analysis).

The typical comparison of frequency-amplitude response obtained from FE analysis and test results are shown in Figure. 5 and Figure 6 for pile 1 and pile 2 respectively.

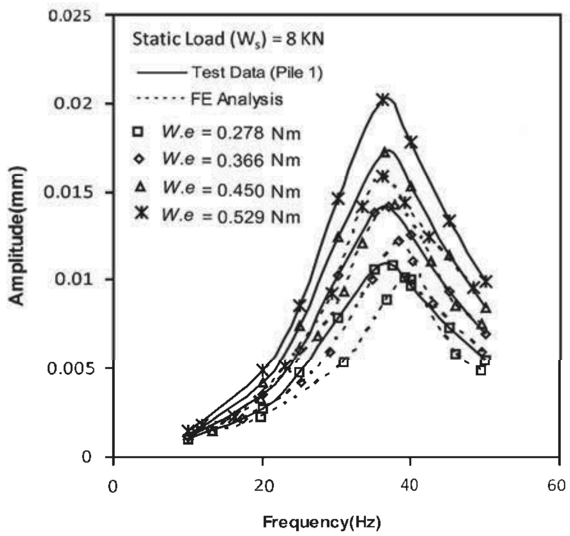

Figure 5. Comparison of frequency-amplitude curve obtained from FE analysis and dynamic test results (Pile 1).

It is found from these figures that the predicted resonant frequency and amplitude are very close to the vertical vibration test results. The resonant frequencies are decreased with the increase of eccentric moments under same static load. This phenomenon indicates the nonlinear behaviour of soil-pile system obtained from FE analysis which is similar to the field test results. This nonlinear response of the soil-pile system is due to the material nonlinearity which is nothing but reduction in shear modulus during vibration. The negligible difference in resonant frequencies with the test results are due to the average soil properties and stratifications considered in the FE analysis. Though there is a significance difference in amplitude values but it is understandable that it can be optimize by implementing precise represented field damping values of soil. In spite of nonlinearity, the FE model can also able to describe vibration theories by showing the pattern of reducing resonant frequency and amplitude values with the increase of static load on pile for same eccentric moment.

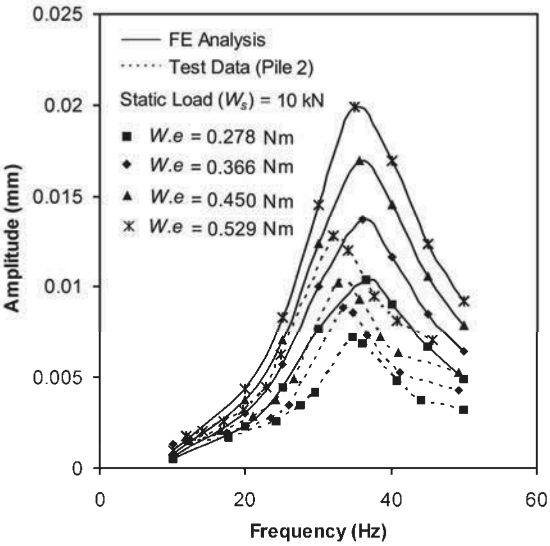

Figure 6. Comparison of frequency-amplitude curve obtained from FE analysis and dynamic test results (Pile 2).

4.3 Soil-pile separation from finite element analysis

The bonding between the soil and the pile is rarely perfect and the slippage or even soil-pile separation often occurs during vibration of pile. Furthermore, the soil region immediately adjacent to the pile can undergo a large degree of straining, which would cause the soil-pile system to be having in a nonlinear manner. Hence in the present study, the soil-pile separation length for different eccentric moment has been predicted from 3-D finite element analysis. The relative movement between pile and soil surface was measured at the resonant frequency. A small variation of the soil-pile separation length was found along the periphery of the pile. So the average of measurement at 45°, 135°, 225° and 300° along the pile cross section plane were taken. The amount of separation between the soil and pile for different eccentric moments along the depth is showed in Figure. 7. It can be observed that the amount of separation is reduced drastically with the increase of the depth. It is found that though the eccentric moment increases but separation length is not increase beyond the depth of water table which is very practical phenomena at the site. The accuracy of the predicted depth of separation from the FE analysis depends on the mesh size of the model.

5 CONCLUSIONS

In this study, the vertical vibration test results of two full-scale single pile were used to predict the nonlinear characteristics of the soil-pile system using 3-D finite element package. The complex soil-pile interaction as per actual field condition was simulated using 3-D finite element analysis. It is found from the FE analysis that the resonant frequencies are decreased with the increase of eccentric moments under same static load and resonant amplitudes are not proportional to the eccentric moments. This phenomenon indicates the nonlinear behaviour of soil-pile system obtained from FE analysis which is similar to the field test results. The frequency-amplitude responses obtained from FE analyses are found very satisfactory comparing with the dynamic test results.

A most critical parameter, soil-pile separation lengths for various eccentric moments were also determined from 3-D FE analysis. The soil-pile separation length is increased gradually with the increase of eccentric moments but there is no effect of soil-pile separation below the ground water table. The nonlinear 3-D finite element model is found to be very efficient for the prediction of dynamic response of full-scale pile in layered soil medium.

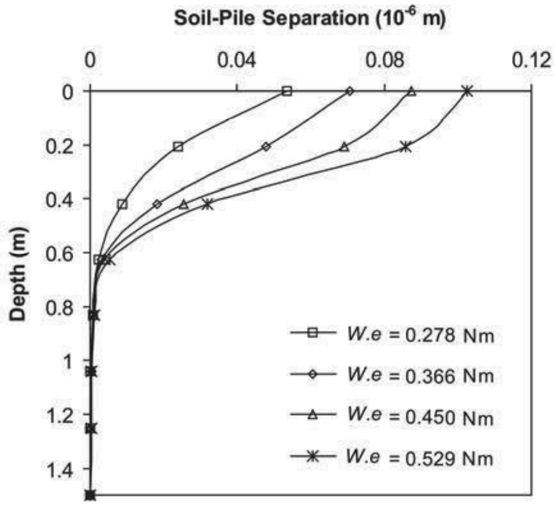

Figure 7. Amount of separation at soil-pile interface (FE Analysis).

6 REFERENCES

Abaqus Inc. 2010. Abaqus analysis user's manual. Version 6.11.

Ayothiraman R. Boominathan A. 2006. Observed and predicted dynamic lateral response of single pile in clay. *Proceedings of GeoShanghai. The Geo-Institute of ASCE Geotech Special Publication. Soil and rock behavior and modelling, Shanghai. Chaina* 367-374.

Bentley K.J. El Naggar M.H. 2000. Numerical analysis of kinematic response of single piles. *Canadian Geotechnical Journal* 37 (6), 1368-1382.

Bowles J.E. 1996. *Foundation analysis and design. 5th edition*. The McGraw-Hill Companies, Inc New York.

Dobry R. Vicente E. O'Rourke M. Roesset J. 1982. Horizontal stiffness and damping of single piles. *Journal of Geotechnical Engineering ASCE* 108 (3), 439-458.

Kuhlemeyer R.L. 1979. Vertical vibration of pile. *Journal of Geotechnical Engineering ASCE* 105 (2), 273-287.

Lewis K. Gonzalez L. 1985. Finite element analysis of laterally loaded drilled piers in clay. Proceedings *of 12th International Conference on Soil Mechanics and Foundation Engineering* 2, 1201-1204.

Maheshwari, B. K., Truman, K. Z., El Naggar, M. H., and Gould, P.L. 2004. Three- dimensional nonlinear analysis for seismic soil-pile-structure interaction. *Soil Dynamics and Earthquake Engineering* 24, 343-356.

Maheshwari B.K. Truman K.Z. El Naggar M.H. Gould P.L. 2005. Three- dimensional nonlinear seismic analysis of single piles using finite element model: effects of plasticity of soil. *International Journal of Geomechanics* 5 (1), 35-44.

Manna B. Baidya D.K. 2009. Vertical vibration of full-scale pile-analytical and experimental study. *Journal of Geotechnical and Geoenvironmental Engineering ASCE* 135 (10), 1452-1461.

P-Y curves from the prebored pressuremeter test for laterally loaded single piles

Courbes P-Y à partir de l'essai pressiométrique préforé pour les pieux isolés sous charge latérale

Bouafia A.
University of Blida Department of civil engineering P. O. Box 270 R. P Blida 09000 Algeria

ABSTRACT: The paper aims at presenting a practical method of constructing the P-Y curves for the analysis of the lateral load-deflection behaviour of single piles on the basis of the prebored pressuremeter test data. This method was derived from the interpretation of several full-scale lateral loading tests on fully instrumented piles in a variety of soils. After presenting the methodology of construction of the P-Y curve, the paper focuses on the validation of the proposed method, the comparison with the existing approaches and on the discussion of the concept of the critical deflection and the effect of the lateral pile/soil stiffness ratio on the P-Y curve parameters.

RÉSUMÉ : La communication a pour objectifs de présenter une méthode pratique de construction des courbes P-Y pour l'analyse du comportement en déflection des pieux isolés à la base des données de l'essai pressiométrique préforé. Cette méthode a été développée suite à l'interprétation de plusieurs essais de chargement latéral en vraie grandeur de pieux instrumentés dans une variété de sols. Après une présentation de la méthodologie de construction des courbes P-Y, la communication focalise sur la validation de la méthode proposée, la comparaison avec les méthodes existantes, ainsi que sur l'interprétation du concept du déplacement latéral critique et de l'effet de la rigidité latérale relative pieu/sol sur les paramètres de la courbe P-Y.

KEYWORDS: P-Y curve, Pile, Lateral load, Deflection, Pressuremeter test, Loading test, Full-scale.

1 INTRODUCTION.

During more than half a century the design methods of piles under lateral loads based on the P-Y curves concept demonstrated their capability to accurately predict the lateral pile response. The simple physical model of a spring at the pile/soil interface allows taking into consideration the non linearity of the pile/soil interaction as well as the non homogeneity of the soil properties along the pile.

As shown in figure 1, the P-Y curve is characterised by an initial slope denoted E_{ti} called the lateral reaction modulus, and a horizontal asymptote P_u corresponding to the lateral soil resistance.

The pressuremeter test PMT provides an experimental stress-strain curve describing the lateral expansion of the soil borehole under horizontal axisymmetric loads. Some methods of construction of P-Y curves assume some similarity in terms of stress and displacement fields between the lateral response of the pile and that of the PMT borehole (Baguelin et al, 1978), and relate the P-Y curve parameters E_{ti} and P_u to the ones of the PMT test, namely E_M and P_l which are respectively the Ménard deformation modulus and the PMT limit pressure, according to the following general equation at a given depth:

$$f(P_l^*, E_M, E_pI_p, D, B, P_u, E_{ti}) = 0 \quad (1)$$

P_l^*, E_pI_p, D and B are respectively the net PMT limit pressure, the pile flexural stiffness, the pile embedded length and the pile diameter (or the dimension perpendicular to the lateral load direction).

Dimensional analysis of this equation according to the Buckingham's theorem leads to the dimensionless equation:

$$g\left(\frac{E_{ti}}{E_M}, \frac{P_u}{P_l^* B}, \frac{D}{B}, \frac{E_p I_p}{E_M D^4}\right) = 0 \quad (2)$$

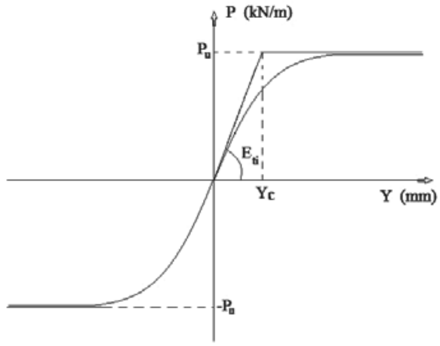

Figure 1. Schematic shape of the P-Y curve

The first ratio is noted K_E and called the modulus number such as:

$$E_{ti}=K_E.E_M \quad (3)$$

The second ratio is noted K_p and called the lateral resistance factor:

$$P_u=K_p.P_l^*.B \quad (4)$$

The third ratio is the pile slenderness ratio and the last one is noted K_R and called the lateral pile/soil stiffness ratio. Equation 2 shows that K_E and K_p are both functions of K_R and D/B.

Because of the three-dimensional aspect of the lateral pile/soil interaction and the multitude of the key parameters involved in such an interaction, a rigorous determination of K_E and K_p is rather complex. Alternatively, full-scale lateral loading tests on instrumented piles were carried out for more than half a century to investigate this topic. P-Y curves are usually derived from bending moment profiles measured by strain gauges along the pile. However, a few full-scale tests on instrumented piles were reported in the literature with successful derivation of the P-Y curves from double differentiation and integration of the bending moment profile. The main difficulty in deriving these curves is due to the high sensitivity of the lateral soil reaction P to the experimental conditions as well as to the method of fitting and differentiation of the bending moments (Bouafia and Garnier, 1991).

The method of construction of the P-Y curves presented in this paper in based on the interpretation of several full-scale lateral loading tests on fully instrumented piles carried out in a variety of quite homogeneous soils in France. A detailed description of the experimental sites, the test piles and the interpretation of the experimental P-Y curves was given by Bouafia (2005) and Bouafia and Lachenani (2005). The paper rather focuses on the formulation of K_E and K_p, the validation of the proposed P-Y curves by predicting the behaviour of test piles reported in the literature and the discussion of the concept of the critical pile deflection.

2 FORMULATION OF THE P-Y CURVE

The P-Y curve at a given depth is described by a usual hyperbolic formulation as follows (Reese, 1971; Garassino, 1976; Georgiadis et al, 1992):

$$P = \frac{y}{\frac{1}{E_{ti}} + \frac{|Y|}{P_u}} \tag{5}$$

The parameters E_{ti} and P_u may be computed according to equations (3) and (4) respectively.

The modulus number and the lateral resistance factor were found varying as a power with the pile/soil stiffness ratio K_R, such as (Bouafia, 2007):

$$K_E = aK_R^n \tag{6}$$

$$K_p = b + cK_R^m \tag{7}$$

Table 1 summarises the values of coefficients a, b, c, n and m. Due to the limited data regarding the behaviour of experimental piles in organic clays and in silty soils it was not possible to analyse K_E and K_p for such soils. Average values were nevertheless proposed in Table 1.

It should be emphasized that the influence of the lateral pile/soil stiffness on the P-Y curve was not accounted for by the current methods of construction of P-Y curves which simply correlate the parameters of the P-Y curve to those of the PMT test (Gambin, 1979).

The lateral pile/stiffness may be defined as follows:

$$K_R = \frac{E_p.I_p}{E_c.D_e^4} \tag{8}$$

E_c is the characteristic PMT modulus defined as the average value of the PMT moduli such as:

$$E_c = \frac{1}{D_e}\int_0^{D_e} E_M.dz \tag{9}$$

D is the embedded length of the pile and D_e is the effective embedded length of the pile, beyond which the pile segments do not deflect. It is computed as:

$$D_e = \min\{D, \pi L_0\} \tag{10}$$

The elastic length (or the transfer length) L_0 is given by:

$$L_0 = \sqrt[4]{\frac{E_p I_p}{E_{ti}^c}} \tag{11}$$

E_{ti}^c is the characteristic lateral reaction modulus of the equivalent homogeneous soil (or the average lateral reaction modulus) given by:

$$E_{ti}^c = \frac{1}{D_e}\int_0^{D_e} E_{ti}(z)dz \tag{12}$$

Table 1. Values of coefficients a, b, c, n and m

Soil	D/B	K_R	a	n	b	c	m
Sand	D/B ≥ 10	≥ 0.01	0.33	- 0.5	0.0	3.0	0.5
		< 0.01	3.40	0.0	0.0	0.31	0.0
Clay	D/B ≥ 5		1.85	- 0.2	0.3	1.0	1.0
Silt			5.50	0.0	2.30	0.0	0.0
Organic clay			3.70	0.0	0.14	0.0	0.0

3 METHODOLOGY OF CONSTRUCTION OF THE P-Y CURVE

The following step-by-step procedure helps using the method to define the P-Y curves parameters:

1. Subdivide the soil along the pile into N horizontal slices enough thin so that the PMT data (E_m, P_l) may be considered varying linearly within any slice. The value of any of these parameters at the mid-slice is then considered as representative within the slice.

2. If the soil is composed of n layers around the pile, compute the average PMT modulus E_M^i for each layer i supposed thick of h_i as follows:

$$E_M^i = \frac{1}{h_i}\int_0^{h_i} E_M.dz \tag{13}$$

3. Assume D_e=D that is to say the pile is assumed to be semi-rigid or rigid.

4. Compute the characteristic soil modulus E_c by equation 9. For practical purposes, replace the integration formula by that of the summation of trapezes:

$$E_c = \frac{1}{D_e}\int_0^{D_e} E_M(z)dz = \frac{\sum_{i=1}^{i=n} E_M^i h_i}{D_e} \tag{14}$$

5. Compute the lateral pile/soil stiffness ratio K_R according to the equation (8).

6. Compute the modulus number K_E^i of each layer i (i=1, n) on the basis of equation (6) and table 1.

7. Compute the average lateral reaction modulus E_{ti}^i of the layer i at the mid-segments of the pile:

$$E_{ti}^{i} = \frac{1}{h_i}\int E_{ti}(z)dz = \frac{K_E^i}{h_i}\int E_M(z)dz = K_E^i E_M^i \qquad (15)$$

8. Compute E_{ti}^{c} according to equation 12 as follows:

$$E_{ti}^{c} = \frac{1}{D_e}\int_0^{D_e} E_{ti}(z)dz = \frac{\sum_{i=1}^{i=n} K_E^i E_M^i h_i}{D_e} \qquad (16)$$

9. Compute the transfer length L_0 by equation 11.

10. Compute the effective embedded length D_e of the pile based on equation 10. If L_0 leads to $D>D_e$ (flexible pile), repeat steps 4 to 10 along an iterative process until the convergence of K_R.

11. Compute the values of E_{ti} and P_u for each segment according to equations (3) and (4) respectively.

12. Use a PC software to analyze the load-deflection response of the pile on the basis of the P-Y curves so built. SPULL (Single Pile Under Lateral Loads) developed at the University of Blida is a freeware available upon request sent by E-mail to the author.

4 VALIDATION OF THE METHOD

Lateral load-deflection response of some case studies reported in the literature was predicted. Piles are identified as mentioned in their references.

Five full-scale lateral loading tests in sandy soils were studied according to the proposed method.
The Lock & Dam 26 site is composed of alluvial deposits (poorly graded sand) 3 m thick and overlying glacial deposits (medium to coarse sand with gravel) 17 m thick. The bedrock is a hard limestone from the Mississipian age. Lateral load tests were performed on two identical HP-14x73 piles socketed in the limestone bedrock, jacked apart, and the lateral displacements of each pile were measured.

The Longjuemau site is located near Paris and composed of a tertiary silty fine sand, rather uniformly graded. Piles TG and TD are driven and loaded as in the above site.

The Roosevelt bridge site is composed of loose layer of sand thick of 4 m, overlying a thick layer of very dense partially cemented sand. The site was submerged by water up to 2 m above the ground level. Square prestressed concrete pile was driven and tested up to cracking under a load of 200 kN and concrete failure occurred under a load of 320 kN.

Figure 2 shows remarkable fluctuation of the 35 points of comparison around the ratio predicted to measured ground deflection of 1.11. Moreover, $Y_0^{pred.}/Y_0^{meas.}$ has a mean value of 1.22 and a coefficient of variation of 21%.

The experimental site located in Plancoët (Côtes-du-Nord, France) is a bi-layered soil composed of a clay (CL) thick of 4 m overlying a layer of sand (SM) thick of 4 m. The test pile is a driven rectangular pipe with 0.284 m of width and an embedded length of 6.5 m.

As shown in figure 3, very good agreement is noticed between the measured pile ground deflections and the ones predicted by the proposed method. The P-Y curves of Ménard and Gambin led to very pessimistic prediction (Hadjadji et al, 2002). The P-Y curves of the French code Fascicule-62 however overpredicted at small deflections and then underpredicted at larger deflections (Hadjadji et al, 2002).

Moreover, two other multi-layered experimental sites were studied.

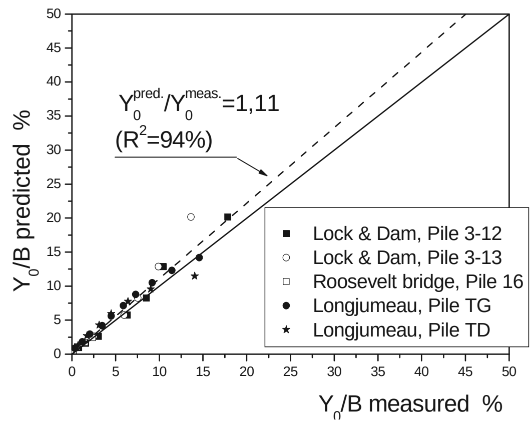

Figure 2. Comparison of predicted and measured deflections in sand

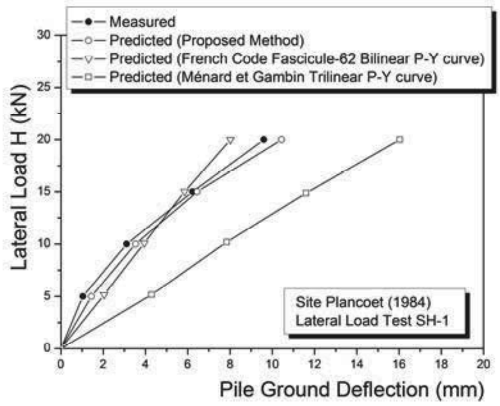

Figure 3. Comparison of predicted and measured deflections in bilayered soil

The first one is located in Vallée de Voulzie (Provins, France) and composed of 14 m de silt overlying 2.5 m of gravelly sand and then a layer of soft chalk becoming hard in depth. The test pile is a vibratory driven pipe having an outside diameter of 0.93 m and an embedded length of 23 m.

The second site is located in Livry-Gargan (France) and composed of clayey sand thick of 4 m, followed by a layer of marl thick of 10 m then a deep layer of chalk. The test pile is a bored pipe having an outside diameter of 0.7 m and an embedded length of 20 m (Moussard and kersale, 2011).

As illustrated by figure 4, the pile ground deflections were accurately predicted by the proposed method. The results of predictions are encouraging seeing the multitude of approximations made during the process of definition of the method.

5 ANALYSIS OF THE FEATURES OF THE METHOD

5.1. The modulus number

Equation 6 may be reformulated in case of a solid circular pile embedded in a homogeneous soil. For example, in sandy soils, combining equations 6 and 8 leads to:

$$K_E = \frac{3}{2}(D/B)^2 \frac{1}{\sqrt{K}} \qquad (17)$$

where $K = E_p/E_c$ is the pile/soil compressibility. This equation shows that the modulus number increases with the pile slenderness ratio and decreases with the pile/soil compressibility.

5.2. The lateral resistance factor

Equation 7 shows that the lateral soil resistance around a rigid pile is greater than the one around a flexible pile and it increases with the pile flexural stiffness and decreases with the embedded length of the pile. For example, in case of a homogeneous sandy soil, combining equations 7 and 8 gives:

$$K_p = \frac{2}{3}\frac{\sqrt{K}}{\left(\frac{D}{B}\right)^2} \tag{18}$$

In contrast with K_E, K_p decreases however with the pile slenderness ratio and increases with the pile/soil compressibility.

5.3. Concept of the critical deflection

As illustrated by figure 1, the critical deflection Y_c corresponds to the intercept of the initial linear portion with a slope equal to E_{ti}, and the horizontal asymptote corresponding to the lateral resistance P_u. Y_c is therefore defined as the threshold of large lateral deflections of the pile section and of full mobilisation of the lateral soil resistance according to the elastic plastic scheme of the P–Y curve. Based on Equations (6) and (7), the ratio Y_c/B may be expressed by the following function of K_R and the PMT parameters measured in sand:

$$\frac{Y_c}{B} = 9K_R \frac{p_L{*}}{E_M} \tag{19}$$

and in clay by:

$$\frac{Y_c}{B} = \frac{(0.3+K_R)}{1.84}\frac{p_L{*}}{E_M} \tag{20}$$

It is to be noted from equation 5 that the critical deflection Y_c corresponds to half the limit lateral reaction in the hyperpoblic formulation, say to a factor of safety of 2, and to all the limit lateral reaction in the elastic plastic formulation.

Equations (19) and (20) provide simple and useful tool to estimate the threshold of large lateral load-deflection behaviour.

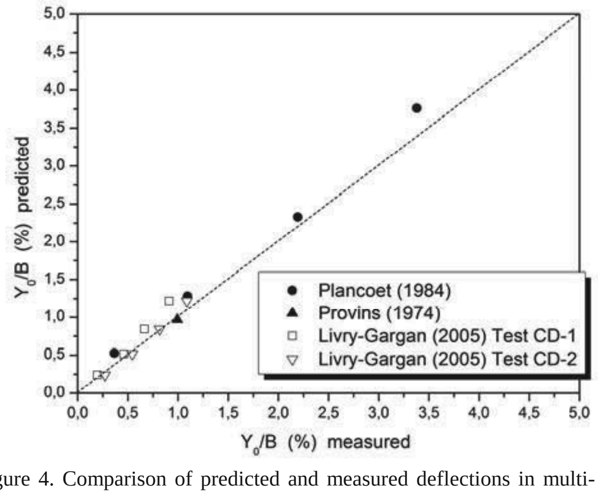

Figure 4. Comparison of predicted and measured deflections in multi-layered soil

CONCLUSION

The analysis of several full-scale lateral loading tests carried out on instrumented piles in a variety of soils led to the definition of hyperbolic P-Y curve whose parameters are correlated with the PMT data.

It was shown the lateral soil reaction modulus and the lateral soil resistance were correlated to the lateral pile/soil stiffness ratio and the parameters measured during the PMT test (PMT modulus and soil limit pressure).

A step-by-step methodology was presented to define the parameters of P-Y curves for single pile under lateral loading in multi-layered soils.

The proposed method of construction of P-Y curves was validated by predicting the load-deflection response of single piles laterally loaded in a variety of soils. The comparison of the predicted pile deflections with the measured ones showed very good predictive capability of the proposed pile/soil stiffness dependant P-Y curves method.

REFERENCES

Baguelin F., Jézéquel J-F., Shields D-H. *The pressuremeter and foundation engineering*, Series on rock and soil mechanics, Vol. 2 (1974/77), N° 4, 1st edition, 1978 Trans Tech Publications, Germany, 615 p.

Bouafia A and Garnier J, 1991. Experimental study of P-Y curves for piles in sand., Proceedings of the 1st international conference CENTRIFUGE'91, Boulder, Colorado, 13-14 Juin 1991, pp 261-268, A A Balkema.

Bouafia A. 2005. Evaluation of the Lateral Load-Deflection Behaviour of Single Piles from the Pressuremeter Test Data, Proceedings of the International Symposium on Pressuremeters ISP-05, Vol. 1, pp : 433-446, ISBN: 2-85978-417-9, Presses ENPC, August, 22-24, 2005, Paris.

Bouafia A and Lachenani A. 2005. Analysis of P-Y Curves for Single Piles from the Prebored Pressuremeter, Proceedings of the 16th International Conference on Soil Mechanics and Geotechnical Engineering, September 12-16, 2005, Osaka, Japan, pp : 1955-1958, ISBN: 978-90-5966-027-4.

Bouafia A. 2007. Single piles under horizontal loads-Determination of the P-Y Curves from the prebored pressuremeter, *International Journal of Geotechnical and Geological Engineering*, Springer-Verlag, ISSN: 0960-3182, Vol. 25, pp: 283-301.

Gambin, M. 1979. Calculation of foundations subjected to horizontal forces using pressuremeter data, *Sols-Soils* N° 30/31, pp 17-59.

Garassino A. 1976. Soil modulus for laterally loaded piles, Proceedings of the 4th European Conference on Soil Mechanics and Foundations Engineering, Vienna, 1976.

Georgiadis M. Anagnastopoulos C., Saflekou S. 1992. Centrifugal testing of laterally loaded piles, *Canadian Geotechnical Journal*, No. 259, pp 208-216.

Hadjadji T., Frank R. and Degny E. 2002. Analyse du comportement expérimental de pieux sous chargements horizontaux (in French), Rapport de recherche série Géotechnique et Risques Naturels no. GT-74, mai 2002, 303 p.

Moussard H. and Kersale J.-F. 2011. Etude expérimentale du comportement d'un pieu isolé sous l'effet de sollicitations horizontales de freinage et de démarrage de circulations ferroviaires (in French), *Revue Française de Géotechnique* No. 134-135, 1e-2e trimestres 2011, pp 87-98.

Reese L C. 1971. The analysis of piles under lateral loading, Proceedings of the Symposium Interaction structure-Foundation, University of Birmingham, 1971.

Comparaison des règlements australien et français pour le dimensionnement des pieux - Prise en compte des essais de chargement

French and Australian Pile Design Comparison – Load Testing Influence on Design

Bretelle S.
GHD, Perth, Australie

RÉSUMÉ : L'utilisation des pieux pour la réalisation de fondations d'ouvrages de toute taille est une méthode couramment utilisée dans le monde entier. L'approche réglementaire relative au dimensionnement de ces éléments de fondations reste différente, pour des raisons diverses comme la nature des sols dans chaque pays ou des raisons culturelles. Au-delà de la simple comparaison des approches réglementaires Française (Fascicule 62) et Australienne (AS2159) et à partir de l'étude comparative illustrée par un type de pieu et une stratigraphie de sol standard, cet article vise à montrer les principales caractéristiques des deux approches. L'une définit de manière précise les paramètres d'interaction à partir des résultats des essais en place (Approche Française), l'autre repose de manière plus importante sur l'interprétation de l'ingénieur pour le choix des paramètres, et insiste sur les essais de chargement en permettant leur prise en compte au travers de la définition d'un « facteur de risque » (Approche Australienne). Finalement, l'intérêt des essais de chargement est démontré au travers de l'estimation de la longueur optimale nécessaire à l'obtention des caractéristiques de portance requises.

ABSTRACT: Piling is commonly used as foundation system in all countries. Design standards remain quite different, for cultural reasons, but also due to the different types of soils encountered in each country. This paper compares French (Fascicule 62) and Australian (AS2159) approaches, describing the design methodology and comparing both approaches on a detailed example. French standard provides the relationship between measured characteristics and interaction design parameters, and a unique set of reduction factors on resistance. Australian standard lets the parameter choice to the geotechnical engineer and defines different reduction factors on resistance depending on site geotechnical risk. Finally, the way each standard accounts for pile testing is described, the example showing optimisation opportunity when pile testing is undertaken on site.

MOTS-CLÉS : Pieux, dimensionnement, pondération, essais chargement, comparaison

KEYWORDS: Pile, design, safety factors, risk, load testing, comparison.

1 INTRODUCTION

Les pieux constituent une solution de fondation couramment utilisée dans le monde entier pour des projets de toutes tailles. La pratique du dimensionnement géotechnique de ce type de fondation dans un contexte international met en exergue une variabilité importante des approches règlementaires.

La réalisation d'essais de chargement statiques ou dynamiques, pratique courante sur les grands projets, permet de valider les paramètres pris en compte dans le dimensionnement, mais aussi, de réduire les incertitudes qui entourent la définition des paramètres d'interaction sol pieu par une mesure directe. Elle se révèle donc une source d'information précieuse pour l'optimisation du dimensionnement.

Cet article présente dans un premier temps un rappel des méthodes et une revue des principales pondérations des actions et des résistances applicables au dimensionnement des pieux suivant les deux réglementations. Une synthèse sous forme de tableau et un exemple permettent d'apprécier les différences de longueur de pieu résultant des différentes approches règlementaires, en considérant des charges et un contexte géotechnique type.

Dans un deuxième temps, une comparaison des méthodes de prise en compte des résultats des essais de chargement dans le dimensionnement est détaillée. On se limite au cas où les essais de chargement confirment la capacité portante supposée, l'exemple est complété par la prise en compte des résultats des essais pour l'optimisation de la longueur des pieux.

2 RAPPEL DES MÉTHODES

2.1 *Pratique Française*

En France, la pratique usuelle est l'application du Fascicule 62 ou du DTU 13.2, pour le dimensionnement des pieux. Ces deux textes reposent essentiellement sur les essais pressiométriques, mais permettent aussi le choix des paramètres d'interaction à partir de pénétromètre statique (CPT).

Une première étape du dimensionnement consiste à choisir un profil de sol représentatif. Il relève de la pratique de l'ingénieur qui synthétise l'ensemble des données disponibles, puis définit un profil de calcul. Celui-ci ne correspond pas forcement exactement à chaque résultat de sondage. Toutefois, le Fascicule 62 propose une formulation qui permet d'effectuer des calculs directement à partir des valeurs mesurées. Dans ce cas, l'analyse de capacité portante peut se faire pour chaque sondage.

On reprend ci-après les grandes lignes du dimensionnement suivant le fascicule 62, pour les sables. Le lecteur se reportera au texte complet pour des compléments, en particulier pour les autres sols. Les habitués reconnaîtront aussi certains raccourcis pour le calcul des valeurs caractéristiques, qui ont bien sûr été simplifiés pour cet article.

Pour le dimensionnement des pieux, la capacité portante se décompose de la façon suivante :

- ✓ Le frottement extérieur $Q_{su} = \sum q_{si} \pi D l_i$ qui s'applique sur la surface périphérique (frottement à l'interface sol-pieu) ;

- ✓ La résistance en pointe Q_{pu} = S q_{pu} qui s'applique sur la section de pointe (la section complète dans le cas du pieu foré).

avec

- ✓ S = section totale de la pointe du pieu ;
- ✓ D = diamètre du pieu ;
- ✓ q_{pu} = contrainte ultime en pointe du pieu ;
- ✓ q_{si} = frottement latéral unitaire dans chaque couche i ;
- ✓ l_i = longueur du pieu dans chaque couche i.

La contrainte de rupture en pointe est donnée par l'expression :

$q_{pu} = k_c\, q_{ce}$

q_{ce}= ½ *∫ $q_c(z)$ dz (la résistance en pointe mesurée par le pénétromètre q_c est intégrée entre 0.5m au-dessus et 1,5m au-dessous de la pointe du pieu)

k_c est le facteur de portance. Il dépend du mode de mise en place des pieux et du type de sol (voir tableau 1).

Tableau 1. Facteur de portance k_c (Fascicule 62).

Nature des terrains	*Pieux mis en place sans refoulement de sol*	*Pieux mis en place avec refoulement de sol*
Argiles, limons	0.40	0.55
Sables, graves	0.15	0.50
Craies A - B	0.20 – 0.30	0.20 – 0.45

Les valeurs du frottement latéral sont déterminées en fonction du mode de mise en place et de la catégorie de sol, par l'intermédiaire du coefficient β : $q_s=q_c/\beta$ (Voir tableau 2)

Tableau 2. Choix du coefficient β (Fascicule 62).

Nature des terrains	β	*q_s max (kPa)*
Sables, graves Pieux forés	200	120
Sables, graves (q_c<15 MPa) Pieux forés tubés – tube récupéré	250	40
Sables, graves (q_c>20 MPa) Pieux forés tubés – tube récupéré	300	120

Les combinaisons d'actions prévalant au dimensionnement des pieux sollicités par des charges permanentes G sont les suivantes :

- ✓ ELU fondamental 1.35 G < (Q_{su} + Q_{pu}) / 1.4
- ✓ ELS quasi permanent G < (0.7 Q_{su} + 0.5 Q_{pu}) / 1.4

Les combinaisons de dimensionnement ne varient pas en fonction de la complexité du site, de la qualité de la reconnaissance de sol, ou de la spécificité du problème.

La parution de l'Eurocode 7, et la mise en place progressive des annexes nationales spécifiques aux pieux conduit à utiliser de nouvelles méthodes de dimensionnement. Elles ne sont toutefois pas encore usuellement mises en œuvre, l'annexe nationale Française portant sur le dimensionnement des fondations profondes étant parue en Juillet 2012.

2.2 *Pratique Australienne*

La réglementation Australienne diffère par son approche. Celle-ci accorde plus d'importance aux résultats des CPT et aux essais de laboratoire (donnant la cohésion et l'angle de frottement). Les méthodes de prise en compte de la variabilité des actions et des incertitudes sur les résistances diffèrent, non pas dans le principe, mais dans les coefficients utilisés.

L'AS 2159 ne propose pas de valeurs de frottement latéral ou de résistance en pointe. Il rappelle les principes nécessaires à la détermination de la capacité portante ultime :

- ✓ Analyser les paramètres géotechniques provenant de la reconnaissance de sol sur le site ;
- ✓ Analyser les résultats d'essais de chargement dynamique ou d'instrumentation de battage ;
- ✓ Analyser les résultats des essais statiques.

Dans le cas où des corrélations sont utilisées, elles doivent avoir été obtenues dans des conditions similaires (méthode d'installation, types de sol) et démonstration doit être faite de cette similarité.

La résistance ultime du pieu s'exprime alors comme dans le Fascicule 62, en respectant la logique de l'interaction :

$R_{d,ug} = f_{ms}\, A_s + f_b\, A_b$

Avec

- ✓ A_b = section totale de la pointe du pieu ;
- ✓ A_s = surface du fut du pieu (négligeant les 1.5 m supérieurs) ;
- ✓ f_b = contrainte ultime en pointe du pieu ;
- ✓ f_{ms} = frottement latéral unitaire (différencié dans chaque couche si nécessaire).

Les combinaisons d'actions prévalant au dimensionnement des pieux sollicités par des charges permanentes G sont les suivantes :

- ✓ ELU (ULS) 1.20 G < ϕ_g * $R_{d,ug}$
- ✓ ELS (SLS) vérification des tassements

Le coefficient de réduction de la résistance géotechnique (ϕ_g) est le paramètre qui constitue la plus grande différence entre les deux règlementations. Le facteur géotechnique (ϕ_g) est déterminé de la façon suivante :

- ✓ Les facteurs de risque sont évalués sur une échelle de 1 à 5 (risque très faible a risque très élevé) à l'aide du tableau 3 ; A chaque risque est attribué un poids (importance relative de ce risque dans l'ensemble du dimensionnement) ;
- ✓ Le risque global (ARR) est la moyenne pondérée de l'ensemble des risques identifiés ;
- ✓ La valeur de (ϕ_{gb}) est alors choisie en fonction du tableau 4 ;
- ✓ ϕ_g est calculé en fonction du nombre et du type d'essais, et est égal à ϕ_{gb} en l'absence d'essais.

Tableau 3. Choix des facteurs de risque (AS2159).

Risque Site	***Poids***
Complexité géologique	2
Importance de la reconnaissance de sol	2
Quantité et qualité des données géotechniques	2
Risque Dimensionnement	***Poids***
Expérience du même type de fondations dans le même contexte géotechnique	1
Méthode de détermination des paramètres de dimensionnement	2
Méthode de dimensionnement	1
Utilisation d'essais in situ et de mesures pendant l'installation	2
Risque Installation	**Poids**
Niveau de contrôle pendant la construction	2
Niveau de contrôle du la structure pendant et après la construction	0.5

Par exemple, pour évaluer le risque lié à la Complexité géologique, les exemples suivants sont proposés dans l'AS2159 :

- ✓ 1 (très faible risque) correspond à des couches subhorizontales, et à des caractéristiques de sols et de roches bien définies ;
- ✓ 3 (risque moyen) correspond à un site avec une variabilité notable, mais sans changements brusques de stratigraphies ;
- ✓ 5 (risque très élevé) est utilisé pour un site très variable, avec des karsts ou des failles impliquant le niveau de fondation.

Tableau 4. Choix du coefficient ϕ_{gb} (AS2159) pour un système de fondation redondant.

Moyenne pondérée du risque (ARR)	catégorie globale de risque	ϕ_{gb}
ARR < 1.5	Très faible	0.76
1.5<ARR<2.0	Très faible à faible	0.70
2.0<ARR<2.5	Faible	0.64
2.5<ARR<3.0	Faible à modéré	0.60
3.0<ARR<3.5	Modéré	0.56
3.5<ARR<4.0	Modéré à fort	0.53
4.0<ARR<4.5	Fort	0.50
ARR>4.5	Très fort	0.47

2.3 *Exemple de dimensionnement*

2.3.1 *Données géotechniques*

L'exemple retenu pour illustrer l'utilisation des deux règlements portera sur le dimensionnement de pieux forés (Pieux forés tubés – tube récupéré) de 60 cm de diamètre.

La capacité portante sera déterminée suivant le fascicule 62 et l'AS 2159, avec le pénétromètre statique dont le log est reporté sur la figure 1.

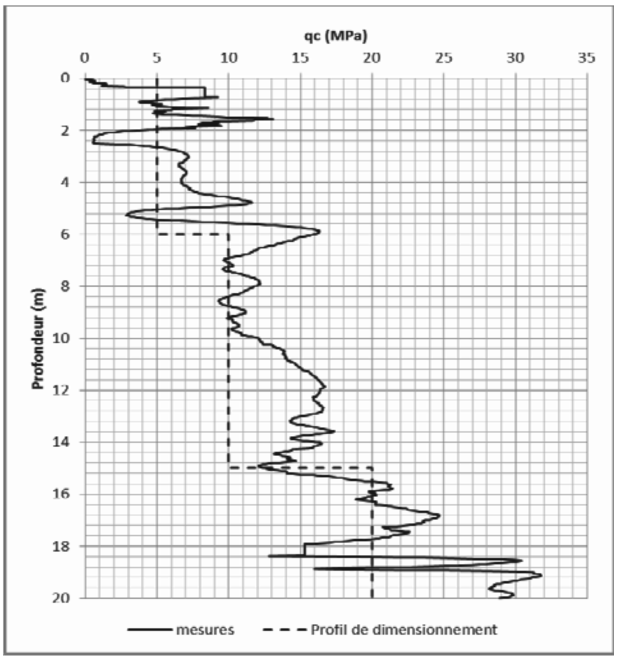

Figure 1. Caractéristiques de sol mesurées et profil de calcul

Les couches rencontrées sont constituées de :

- ✓ Un sable lâche avec q_c=5 MPa de 0 à 6m ;
- ✓ Un sable moyennement compact avec q_c=10 MPa de 6 à 15m ;
- ✓ Un sable dense avec q_c=20 MPa de 15 à 20 m.

Afin de simplifier la comparaison, un profil de dimensionnement unique est proposé sur le log. On se reportera aux commentaires spécifiques à chaque réglementation pour le choix du profil de dimensionnement.

La charge de dimensionnement non pondérée est de 1 100 kN, constituée essentiellement de charges permanentes.

2.3.2 *Dimensionnement suivant le Fascicule 62*

Les classes de sol applicables suivant les catégories du fascicule 62 sont :

- ✓ Un sable A (lâche de 0 à 6m),
- ✓ Un sable B (moyennement compact de 6m à 15m),
- ✓ Un sable C (dense de 15m à 20m).

Les caractéristiques de la pointe sont les suivantes :

K_c = 0,15 (sable pieu mis en place sans refoulement)
q_{ce} = 20 MPa
q_{pu} = 3 MPa
Résistance en pointe : $Q_{pu} = S\ q_{pu}$ = 850 kN

Pour ce qui concerne le frottement, les valeurs unitaires se décomposent comme suit :

- ✓ Sable de 0 à 6m : q_s = 20 kPa
- ✓ Sable de 6 à 15m : q_s = 40 kPa
- ✓ Sable de 15 à 20m : q_s = 65 kPa

La résistance en frottement est : $Q_{su} = \sum q_{si}\ \pi\ D\ l_i$

$Q_{su} = \pi * 0,6 * (20*6+40*9+65*5) = 1530$ kN

Les vérifications suivantes sont effectuées pour justifier qu'une longueur de pieu de 20m est juste suffisante :

Tableau 5. Vérifications de capacité portante (Fascicule 62).

Cas de charge	*Charge pondérée*	*Résistance pondérée du sol*
ELU fondamental	1.35 G = 1500	$(Q_{su} + Q_{pu})$ / 1.4= 1700
ELS quasi permanent	G = 1100	$(0.7\ Q_{su} + 0.5\ Q_{pu})$ / 1.4 = 1100

2.3.3 *Dimensionnement suivant l'AS2159*

Il n'y a pas de raisons pour choisir des paramètres d'interaction différents de ceux recommandés par le Fascicule 62, on peut d'ailleurs noter que les publications de M. Bustamante sont souvent citées en référence en Australie.

La résistance ultime du pieu de notre exemple est donc la même dans les deux approches. Seule la vérification pondérée de capacité portante va être différente.

Le risque est évalué pour un site relativement homogène, avec une reconnaissance de bonne qualité et un dimensionnement avec une méthode éprouvée dans les mêmes conditions. Par contre le contrôle pendant la construction est très limité ; les facteurs de risque choisis sont reportés dans le tableau 6.

La valeur de ARR déduite de l'évaluation détaillée dans le tableau 6 est de 2.4, ce qui va donner une valeur de ϕ_{gb} de 0.64, correspondant à un risque géotechnique faible.

Tableau 6. Evaluation des facteurs de risque (AS2159).

Risque	Poids * Risque
Site	
Complexité géologique	2 * 3
Importance de la reconnaissance de sol	2 * 1
Quantité et qualité des données géotechniques	2 * 1
Dimensionnement	
Expérience du même type de fondations dans le même contexte géotechnique	1 * 1
Méthode de détermination des paramètres de dimensionnement	2 * 1
Méthode de dimensionnement	1 * 1
Utilisation d'essais in situ et de mesures pendant l'installation	2 * 5
Installation	
Niveau de contrôle pendant la construction	2 * 5
Niveau de contrôle de la structure pendant et après la construction	0.5 * 5

Les vérifications de capacité portante suivantes sont effectuées :

Tableau 7. Vérifications de capacité portante (AS2159).

Cas de charge	*Charge pondérée*	*Résistance pondérée du sol*
ELU site à risque faible - pas de test	1.2 G = 1320	$(Q_{su} + Q_{pu})$ *0.64 = 1520
ELU cas le plus défavorable risque très élevé - ϕ_{gb} de 0.47	1.2 G = 1320	$(Q_{su} + Q_{pu})$ *0.47 = 1120

On note déjà que pour un site à risque faible, une réduction de longueur est possible (de 20 m à 18m), alors que dans le cas d'un site à risque très élevé, une longueur de 24 m sera nécessaire.

3 PRISE EN COMPTE DES ESSAIS

3.1 *Pratique Française*

Le fascicule 62 permet de prendre en compte les résultats des essais statiques pour déterminer (après une analyse critique des résultats des essais) les paramètres de frottement et de résistance en pointe. Un coefficient d'abattement de 1.2 sera appliqué sur les valeurs mesurées si le pieu n'est pas instrumenté le long du fût.

3.2 *Pratique Australienne*

La réalisation d'essais de pieux est fortement recommandée, voire obligatoire pour certains ouvrages. La prise en compte des essais de pieux est effectuée de la manière suivante :

$\phi_b = \phi_{gb} + (\phi_{tf} - \phi_{gb})$ K

Avec

- ✓ ϕ_{gb} déterminé ci-dessus ;
- ✓ ϕ_{tf} facteur pour prendre en compte le type de test (0.9 pour un test statique, 0,8 pour un essais dynamique avec « signal matching » de type CAPWAP, et ϕ_{gb} en l'absence de test) ;
- ✓ K dépend du nombre de tests p en pourcent du nombre total de pieux, $K=1.33\ p / (p + 3.3) \leq 1$.

3.3 *Exemple d'optimisation*

3.3.1 *Résultats des essais*

Lorsque le dimensionnement est effectué dans un contexte ou une zone où les paramètres d'interaction sont déjà bien connus, du fait de l'expérience de cas similaires, l'essai de pieu va surtout confirmer les paramètres déjà choisis pour le dimensionnement.

3.3.2 *Dimensionnement suivant le Fascicule 62*

Le fascicule 62 ne permet pas de modification du dimensionnement lorsque les essais de pieux ne modifient pas les paramètres d'interaction.

3.3.3 *Dimensionnement suivant l'AS2159*

La réalisation sur le site de 4% d'essais dynamiques permettra d'obtenir une valeur de ϕ_{gb} de 0.74.

Les vérifications de capacité portante sont alors modifiées comme suit :

Tableau 8. Vérifications de capacité portante avec essais (AS2159).

Cas de charge	*Charge pondérée*	*Résistance pondérée du sol*
ELU 4% test dynamiques ϕ_{gb} de 0.74	1.2 G = 1320	$(Q_{su} + Q_{pu})$ *0.74 = 1760
ELU 1% d'essais statiques - ϕ_{gb} de 0.72	1.2 G = 1320	$(Q_{su} + Q_{pu})$ *0.72 = 1710

La réalisation d'essais de pieux sur ce site permettrait une réduction de la longueur des pieux de 20m à 17m, soit une réduction de longueur de 15%.

La réalisation d'essais de pieux qui confirment les paramètres de dimensionnement permet systématiquement de réduire la longueur des pieux.

4 CONCLUSION

Cet article a permis de mettre en évidence les principales différences entre les règlementations Française et Australienne pour le dimensionnement des pieux. L'approche Française définit de manière précise les paramètres d'interaction à partir des résultats des essais en place, l'approche Australienne repose de manière plus importante sur l'interprétation de l'ingénieur pour le choix des paramètres, et insiste sur les essais de chargement en permettant leur prise en compte au travers de la définition d'un « facteur de risque ».

5 REMERCIEMENTS

Je tiens à remercier mon mari et mon fils pour leur patience pendant la période de rédaction de cet article, ainsi que pour leur relecture.

Bien entendu, cet article n'aurait pas vu le jour sans mon expérience en France, à Terrasol pour la maitrise des concepts géotechniques, chez Saipem, pour l'ouverture Internationale, chez Cathie Associates pour la compétence relative aux essais de pieux et enfin en Australie, où GHD me donne l'opportunité de travailler sur des projets avec des centaines de pieux.

6 REFERENCES

Fascicule 62 - Titre V du CCTG intitulé "Règles techniques de conception et de calcul des fondations des ouvrages de génie civil".

DTU 13.2 - Travaux de fondations profondes pour le bâtiment.

AS 5100.3-2004 Bridge design: Foundations and soil supporting structures.

AS 2159-2009 Piling: Design and installation.

Dynamic Pile Testing at the Mesa A Rail Bridge

Analyse dynamique d’essais de pieux au pont ferroviaire Mesa A

Cannon J.G.
Independent Geoscience Pty Ltd, Melbourne, Australia

ABSTRACT: The paper will describe high strain and low strain dynamic pile testing that was used to assess the foundations for this bridge and how the results led to an innovative decision during construction to change from a bored pile foundation to a driven pile foundation. The revised construction used minimal extra equipment and materials. The foundations originally comprised permanently cased bored piles socketed into rock. Dynamic pile testing identified significant problems with the concrete early in the project. A number of attempts were made to correct the problems but to no avail. In addition, the down-the-hole hammer system being used to install the casings was causing delays. The steel tube casings being used were substantial and a large hydraulic piling hammer was on site for dynamic testing. A decision was made to drive the casings into soft rock far enough to generate the required compression and tension resistance and to delete the concrete sockets. Dynamic pile testing was used to verify that the required resistances were achieved.

RÉSUMÉ : Cet article décrit l'analyse dynamique d’essais de pieux sous forte et sous faible déformation, effectuée pour évaluer les fondations du pont, et montre comment les résultats ont mené à une décision innovante pendant la construction, passant de fondations par pieux forés à des fondations par pieux foncés. Le changement de construction nécessita peu d'équipements et matériaux supplémentaires. Les fondations comprenaient à l'origine des pieux forés dans la roche maintenus de manière permanente par des conduites en béton. L'analyse dynamique des pieux mit en évidence un sérieux problème lié au béton dès le début du projet. Plusieurs tentatives pour le régler furent infructueuses. De plus, le système de marteau de fond de trou utilisé pour installer les pieux posait problème et créait des retards. Les conduites en acier utilisées étaie décision fut prise d'enfoncer les boitiers dans une roche meuble nécessaires et de supprimer les conduites en en béton. L'analyse dyna nécessaire était atteinte.

KEYWORDS: Dynamic pile testing, Bridge Foundations, PDA, CAP

1 INTRODUCTION.

The Mesa A bridge is located over the Robe River in the Pilbara Region of Western Australia. Iron ore is mined from various Mesa, or low flat-topped mountains, in the area. The iron ore is carried directly from near the mine face by rail to a processing and export facility about 200km away. The trains are some of the longest in the world and have some of the highest axle loads in the world. At the bridge site the Robe River is dry on the surface for much of the year but up to 15m deep and fast-flowing during the "wet" cyclone season. Significant scour of the foundations was expected. High lateral loading from river debris was also anticipated.

During the "dry" construction season conditions are arduous for construction work and, in particular, concreting with daytime temperatures typically 38-42° C and within the construction zone in the low-lying riverbed they were frequently higher.

The Specification for the work included a test pile separate from the bridge works, which was to be tested statically in tension, together with testing for integrity using cross-hole sonic logging (CSL). The contractor offered high strain dynamic testing with a Pile Driving Analyzer® (PDA) as an alternative to the static test. The client required PDA testing at 40kHz, which required the newest PAX model PDA.

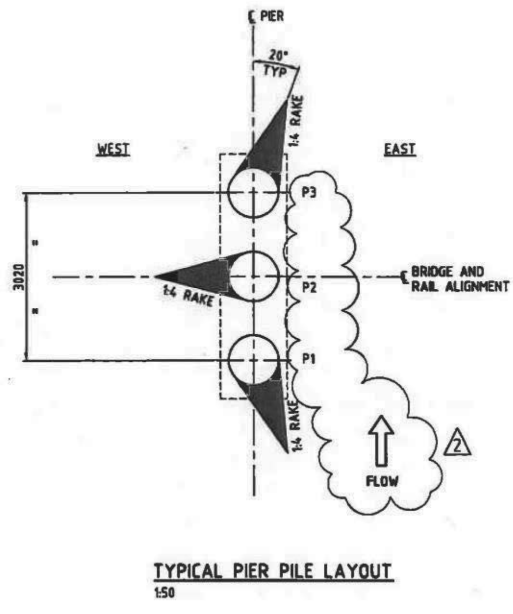

The Contractor submitted alternative pier foundations that comprised three raking piles in a tripod arrangement as shown below. (Figure 1). The tripod arrangement meant there were no redundancies and it was absolutely essential for every pile to perform as designed. Abutment foundations comprised four vertical piles. The size of the abutments meant there was the possibility of installing extra piles to augment any under-strength piles.

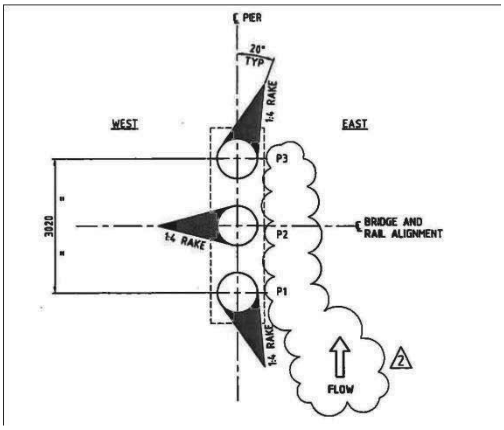

Figure 1 - Pier foundation Layout

The piles were 900mm OD with 20mm wall thickness steel tubes with a concrete socket in the rock. At this site the socket was 780mm diameter. The concrete was to be continued into the pile a sufficient distance to transfer the load by steel/concrete bond - about 8m. The concrete was to be heavily reinforced owing to high tension loading, with ten clusters of three 36mm diameter bars.

The contractor initially installed the casings with a large down-the-hole hammer. This used a 940mm hammer positioned at the bottom of the excavation and powered by compressed air. The hammer drags the casing behind it by engaging a collar at the bottom of the casing. Upon reaching rock the hammer can disengage the casing and bore a socket. At this site the hammer was removed after reaching the rock and a 780mm rock-roller drill was used to drill the socket. The method was well known to the contractor and is reputed to have excellent production rates in hard ground. However, at this site the gravels and cobbles were loose and saturated. There was frequently insufficient resistance to start the hammer and it stalled frequently. Progress was slow and delays were extensive.

Owing to the remote site concrete was produced by a mobile batch plant at the site but was otherwise unremarkable. The piles were concreted using a tremie pipe with the shaft full of water or drilling fluid.

4 SOCKETED TEST PILES

The first pile constructed at the site was a test pile that was not to be incorporated into the bridge. It was a vertical full sized pile. To provide for dynamic testing the socket concrete was extended to the top of the pile. The test gauges were initially attached to the concrete through "windows" in the steel tube and the pile was considered as a combined section. The top of the steel tube was cut back 25mm below the top of concrete to ensure the hammer acted on the concrete. A 19mm plywood cushion was used between the hammer and the pile.

Other than the permanent casing there was nothing unusual about the dynamic testing. Concreting had been completed about 14days prior to the test.

Very strange measurements were obtained initially, with almost no force measured in the concrete. (Figure 2). In addition it was observed after several blows that the concrete in the "window" had moved down relative to the steel.

The gauges were moved to the steel tube and again very strange measurements were obtained The only way the measurements made sense was to use the properties of the steel tube only and assume the concrete was not working as part of the pile. (Figure 3). The hammer was removed and it was noted the top was level with the steel. The hammer was indeed acting on the steel tube.

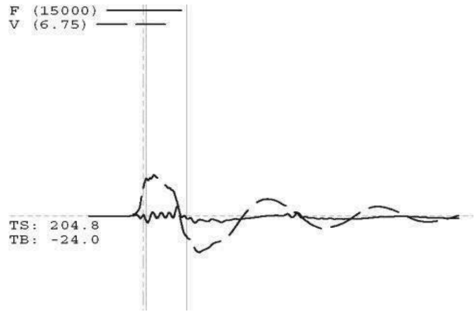

Figure 2 - PDA measurements on concrete

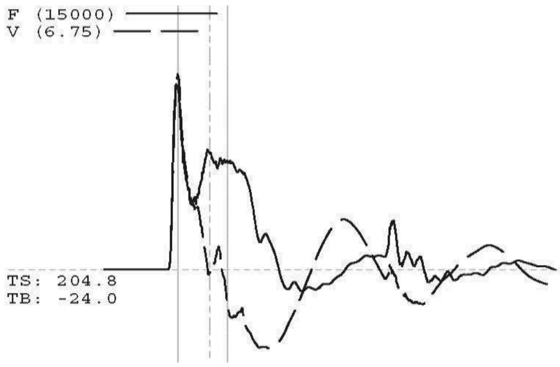

Figure 3 PDA measurements on steel

The concrete between the pile top and the gauges must have crushed by up to 44mm, being the 25mm upstand of concrete plus the thickness of the pile cushion. The hammer was replaced, with increased cushion, and more blows were applied with no improvement of the measurements and with further crushing of the concrete.

A second test pile was constructed and this time access tubes for CSL testing were cast in the pile. Concreting records showed potential problems near the toe and part way though the pour. Observations suggested the concrete had started to set early, possibly due to the extreme temperatures. CSL test results confirmed problems at the toe and between 15-20m below the pile top. (Figure 4).

Dynamic pile testing was also conducted and confirmed concrete problems. Gauges were attached to the concrete through windows in the steel casing. Results suggested there was a significant defect 15-20m down the shaft. The steel was also not contributing to the pile. Transfer of load by steel to concrete bond seemed unreliable. (Figure 5).

5 PRODUCTION SOCKETED PILES

As it was thought the cause of the concrete problems was known, and related to temperature and the behaviour of concrete additives, it was decided to proceed with production piles, but only at abutments, where repairs such as additional piles were possible.

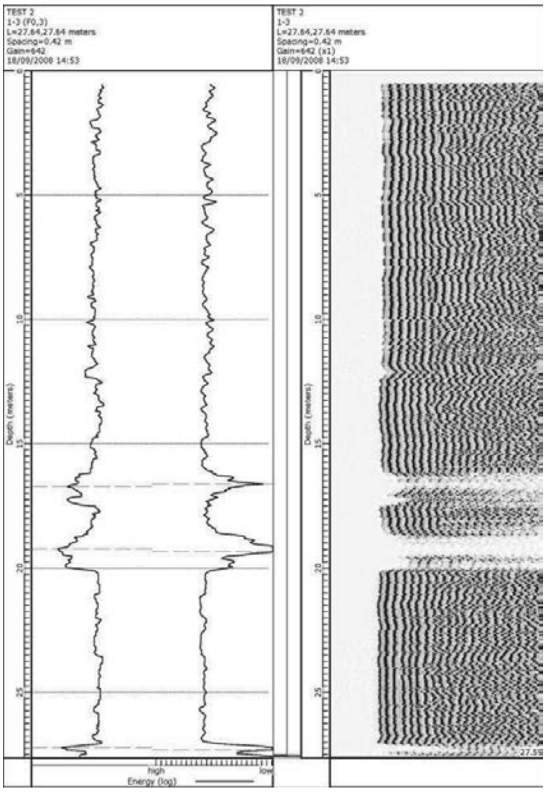

Figure 4 - CSL test results Test Pile 2

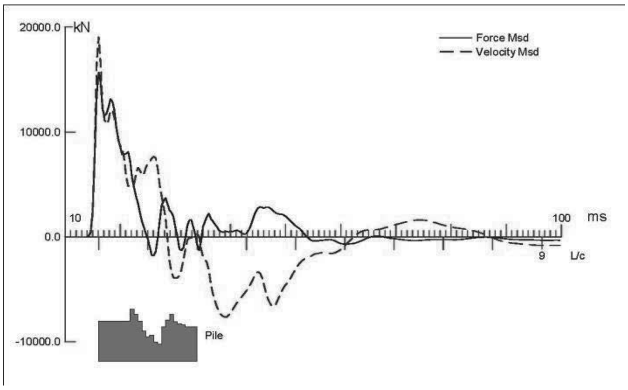

Figure 5 - PDA measurements Test Pile 2

At the same time the author was requested to conduct driveability predictions using wave equation analysis of piles (WEAP) to assess if the casings could be used as driven piles. One of the main criteria of interest was whether the piles could be driven far enough into the soft rock to achieve the required tension resistance, which was a controlling aspect of the tripod foundation design. This appeared to be the case, and with a smaller hammer than was being used for the dynamic testing.

Construction started on the East Abutment and, again, problems with the concrete quickly became obvious. CSL testing indicated a significant defect at 25m below the top. (Figure 6). Drill cores were conducted to investigate and repair the problem zone. Coring confirmed a zone of aggregate only with no cement - exactly as predicted by the CSL. (Figure 7).

Further attempts were made to improve the concrete but in every case problems were detected. If anything the concrete problems got worse, both in size and significance. (Figure 8).

Prior to the abandonment of socketed piles one further test was conducted on the last socketed abutment pile. No access tubes had been cast in this pile so low strain axial sonic pile integrity testing using a Pile Integrity Tester® (PIT) was conducted (Figure 9). No integrity problems were detected

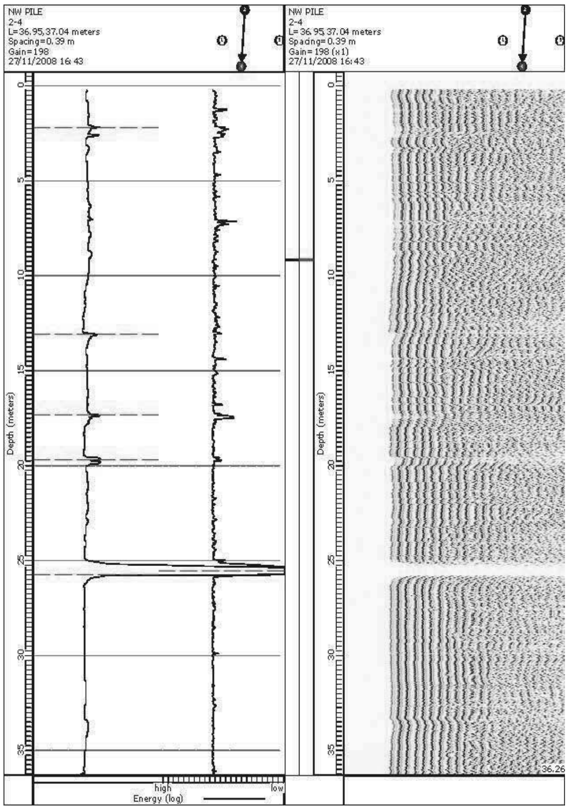

Figure 6 CSL test result East Abutment NW pile

Figure 7 - Core of East Abutment NW pile

using this method. A very slight increase in velocity was detected at the top of the socket but this was attributed to the change in diameter from 900mm to 780mm.

6 DRIVEN TEST PILE

Soon after the WEAP analyses were conducted a third test pile was installed. Again, this was positioned adjacent to the bridge location and was not to be incorporated into the contract works. The 900x20mm steel tube casing was modified by removing the bottom collar and installing a 900x50mm driving shoe of 0.8m length. This third test pile was driven with a Junttan HHK9A hammer, which has a 9t ram. The pile was driven through the gravels and cobbles and 12m into the soft rock at a final set of 2.9mm/bl. A restrike test was conducted the next day using the Junttan HHK16A hammer, which has a 16t ram. The pile had "set-up" to such an extent the set had reduced to 1.3mm/bl despite the hammer being significantly larger than the hammer used to drive the pile. The resistance demonstrated during the

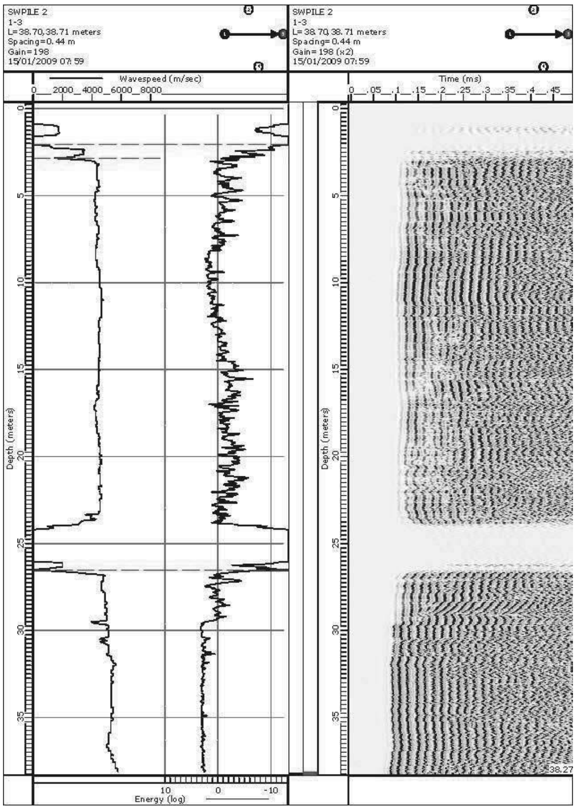

Figure 8 CSL result on production pile

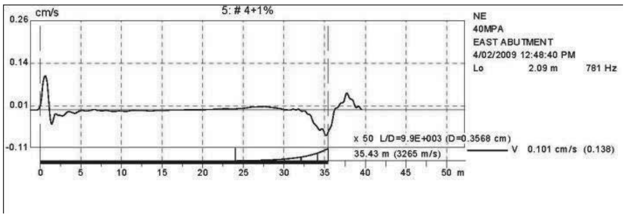

Figure 9 PIT results for East Abutment NW pile

restrike was adequate for all pile positions - upstream, downstream and longitudinal. (Figure 10).

The skin resistance distribution shown in the CAPWAP ® appears to reduce toward the toe because at such small sets not much of the energy of the input blow reached the lower part of the pile and the reduced energy did not strain the ground enough to generate the full resistance that was available. The available resistance probably does not reduce. If the pile could have been struck harder, then even more resistance would have been demonstrated.

7. DRIVEN PRODUCTION PILES

It was considered the driven pile created a more reliable foundation and repairs could be easily accomplished by re-driving if necessary. A decision was made to change the foundations for all piers from bored piles into driven piles. In addition repairs for the abutment piles were also to be driven piles.

The effect of this decision was to dramatically improve production rates on the pile foundations. Because the concrete was eliminated from the pile there were also considerable savings over the original design.

Owing to the numerous problems experienced during initial piling and the tripod design that provided no redundancy, the client required that all driven piles undergo PDA testing. Production testing was conducted remotely or by "stand-alone." (Likins, Hermansson, Kightley, Cannon and Klingberg 2009)

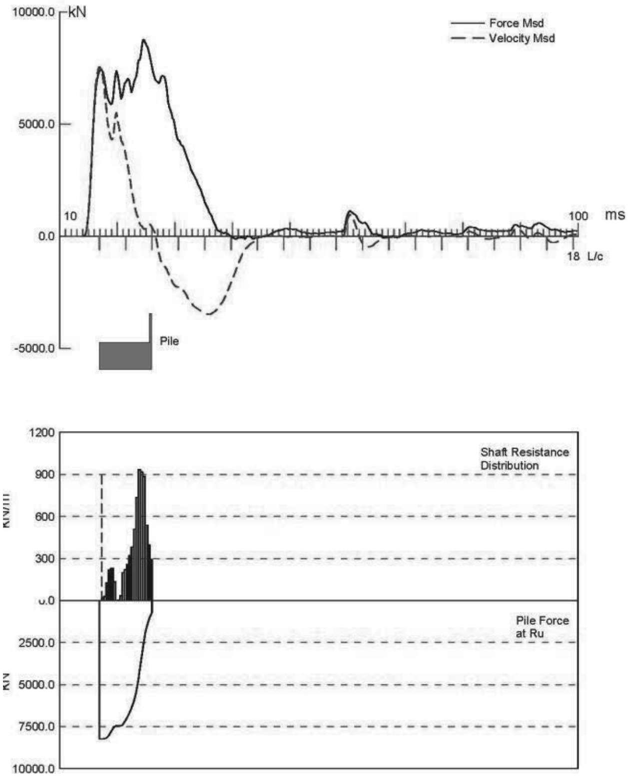

Figure 10 CAPWAP results for Test Pile 3

The shorter piles at the western end of the bridge could be tested with the smaller 9ton hammer, however from almost exactly the centre of the bridge it was necessary to use the larger 16t hammer to demonstrate the required resistance. In some cases it was necessary to wait for "set-up" and conduct restrikes at 1-7 days after driving.

Tension resistance, particularly on upstream piles, was of critical importance. In some cases the resistance demonstrated by CAPWAP appeared to be heavily concentrated near the toe and owing to concern about the ability of CAPWAP to accurately differentiate between skin friction near the toe and toe resistance the author was requested to provide an estimate of the "minimum likely" skin friction. The method adopted was purely arbitrary and comprised starting with "best match" and moving skin friction to toe resistance until the match quality increased by one percent, ie CAPWAP match quality increased from 3.1 to 4.1 percent error.

8. CONCLUSIONS

Low strain and high strain dynamic pile testing was incorporated into both the design revision and construction verification aspects of this successful project.

During construction both high strain and low strain dynamic testing demonstrated serious problems with the "constructability" of the original bored pile design.

An innovative decision was made to radically change the pile design, from a bored pile to a driven steel tube pile.

Dynamic pile testing was able to confirm pile resistance and provide a high level of confidence in the foundation. The bridge has been working as designed through 3 cyclone seasons carrying some of the heaviest train axle loadings in the world.

9. REFERENCES

Likins, Hermansson, Kightley, Cannon and Klingberg 2009 Advances in Dynamic Foundation Testing Technology IFCEE Orlando, Florida USA

Uplift behavior of bored piles in tropical unsaturated sandy soil

Comportement en traction de pieux forés en sol tropical sablonneux non saturé

Carvalho de D.
State University of Campinas, Brazil

Rocha de Albuquerque P.J.
State University of Campinas, Brazil

ABSTRACT: Large deposits of high-porosity, unsaturated, sandy soils are found in the southern central region of Brazil, to several meters of depth. This region regularly sees increases in uplift loads in structures such as wind energy and power transmission towers. For the current study uplift load tests were conducted on three bored piles,10m depth and with respective diameters of 0.35m, 0.4m and 0.5m. The piles were instrumented with strain gauges connected in full bridge at five depth levels. The load vs. displacement and the load transfer curves along the depth were obtained. The data obtained from the field tests (CPT, SPT) and laboratory tests (c, ϕ, γ_n) were used to predict the ultimate loads of the piles. The calculated ultimate load values were compared with those obtained in the piles load tests. The tests were carried out on the campus at the University of São Paulo, in the city of São Carlos. The average composition of the subsoil is sand (62%), clay (22%) and silt (16%), with an average porosity of 45%. The field tests produced average values of N_{SPT}=5, qc=1700kPa and fs=98kPa, respectively. The water table was encountered at a depth of 10m.

RÉSUMÉ : Dans la région centrale sud du Brésil on trouve de grands dépôts de sols sablonneux, non-saturés, jusqu'à plusieurs mètres de profondeur. L'augmentation des tensions verticales de soutien de charge est fréquente dans cette région pour des structures comme des tours d'éoliennes et des lignes de transmission d'énergie. Pour cette recherche ont été réalisés des essais d'arrachage sur trois pieux forés à 10m de profondeur et avec des diamètres de 0,35m, 0,40m et 0,50m. Les pieux ont été instrumentés avec des jauges de déformation connectées en ponts complets à cinq niveaux le long de l'encastrement. On a obtenu des courbes charge/déplacement et le transfert de charge le long de l'encastrement. Les données des essais in situ (CPT ,SPT) et des essais en laboratoires (c, ϕ, γ_n) ont été employées pour prévoir les charges ultimes des pieux. Les valeurs calculées ont été comparées avec les valeurs obtenues dans les essais de charge. Les essais ont été réalisés dans le Campus da Université de São Paulo, dans la ville de São Carlos. La composition moyenne du sous-sol est sable (62%), argile (22%) et limon (16%), avec porosité moyenne de 45%. Les essais in situ ont indiqué des valeurs moyennes de N_{SPT}=5, qc=1700kPa et fs=98kPa. Le niveau d'eau a été trouvé à 10m de profondeur.

KEYWORDS: uplift load test; unsaturated sandy soil; bored pile; instrumented pile.

1 INTRODUCTION

The southern central region of Brazil possesses vast areas of sandy soil where the water table is often deeper than 10 meters. This unsaturated soil condition, combined with the lateritic soil, enables the use of bored piles, with no need to line the boreholes in the vast majority of constructions. Where these foundations are subjected to uplift forces, there is some debate as to which method to use to calculate the ultimate load. Consequently, this study, by way of the performance of three uplift load tests on instrumented bored piles, analyzes the mechanism for transferring load to the subsoil as well as ascertaining the applicability of the methods for calculating ultimate load that are available within the technical milieu. This study was conducted on the campus of the University of São Paulo, located in the city of São Carlos, in the state of São Paulo, Brazil. Geographically, its location is defined by the coordinates 22º 01' 22" South and 47º 53' 38" West.

2 GEOTECHNICAL CHARACTERISTICS

The region sits on rocks of the São Bento Group, composed of sandstone of the Botucatu and Pirambóia formations and by ridges of basalt rocks of the Serra Geral formation. On top of these rocks appears sandstone of the Bauru Group, followed by Cenozoic sediment.

Close to the piles used in the study, five CPT tests and five SPT tests were carried out. Laboratory testing was carried out on both disturbed and undisturbed soil samples collected via an open hole down to the level of the water table, situated at a depth of 10 meters.

The tests characterized the subsoil down to a depth of 10 meters as being made up of two layers, primarily composed of fine lateritic sand separated by a line of boulders at a depth of 6.5 m. The soil in the first layer is characterized as Cenozoic sediment and in the second layer as sandstone of the Bauru Group. Table 1 shows the average values for the geotechnical parameters of the subsoil in the chosen location.

Table 1. Average geotechnical parameters

Depth	**1 m – 6 m**	**6 m – 12m**
Formation	**Sediment**	**Residual**
γ_n (kN/m^3)	16.3	18.9
w (%)	16	16
Gs	2.73	2.76
e	0.94	0.71
n (%)	48	42
Sr (%)	47	62
LL (%)	28	32
IP (%)	11	17
Sand (%)	62	61
Silt (%)	13	10
Clay (%)	25	19
c' (kPa)	6	20
ϕ' (º)	30	23
SPT - N_{72}	4	7
CPT – qc (MPa)	1.07	2.36
CPT – fs (kPa)	45	150

N.B. γ_n (bulk specific weight), w (water content), Gs (grain density), e (avoid ratio), n (porosity), Sr (degree of saturation), c’ (cohesion – CD triaxial); ϕ' (friction angle – CD triaxial)

4 PILES AND INSTRUMENTATION

Three 10m long auger bored piles were inserted with respective diameters of 0.35m, 0.4m and 0.5m. The boring was carried out without using water. The concreting was carried out immediately following the opening of the holes. The simple compression resistance of the concrete used was 26MPa at 28 days.

The reinforcement of the piles consisted of two 20mm and two 32mm corrugated steel bars, both 10m in length.

The instruments consisted of strain gauges at five levels along the depth (0.6m – reference section; 3.1m; 5.3m; 7.5m; 9.7m). The strain gauges were connected in full bridge to 20mm steel bars, 0.6m long, which were screwed to the reinforcement. At each level along the depth, two diametrically opposed, instrumented bars were installed (Figure 1).

Tell tales were also installed on the piles but these did not give precise readings for analysis due to the low displacement values measured.

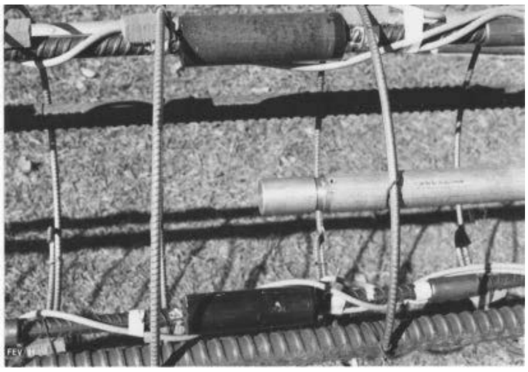

Figure 1. Instrumentation using strain gauges and tell tales.

3 LOAD TESTS

The load tests were of the slow maintained load type, with successive 40kN loads, observing the principles of Brazilian standard NBR 12131. The reaction system comprised root piles 16m long with a diameter of 0.25m, for a working load of 500kN, and four I-shaped steel beams with a load capacity of 2MN. Loads were measured using load cell with a capacity of 1MN and displacement was measured using four dial gauges to within an accuracy of 0.01mm. The ultimate loads (Q_{ult}) obtained were 387kN, 440kN and 478kN respectively. The load vs. displacement curves obtained are shown in Figure 2.

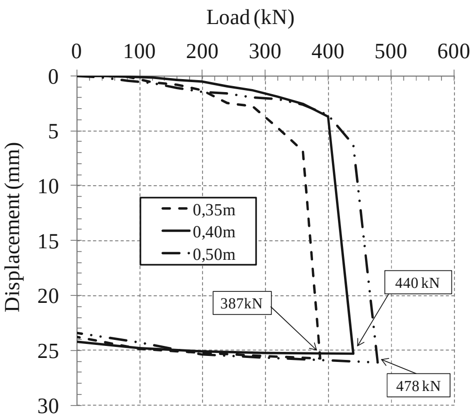

Figure 2. Load vs. displacement curves.

Figure 3 shows, for the ultimate loads and working loads, (Qult/2) the lateral friction for each pile segment, recognizing a rupture in the pile-soil interaction.

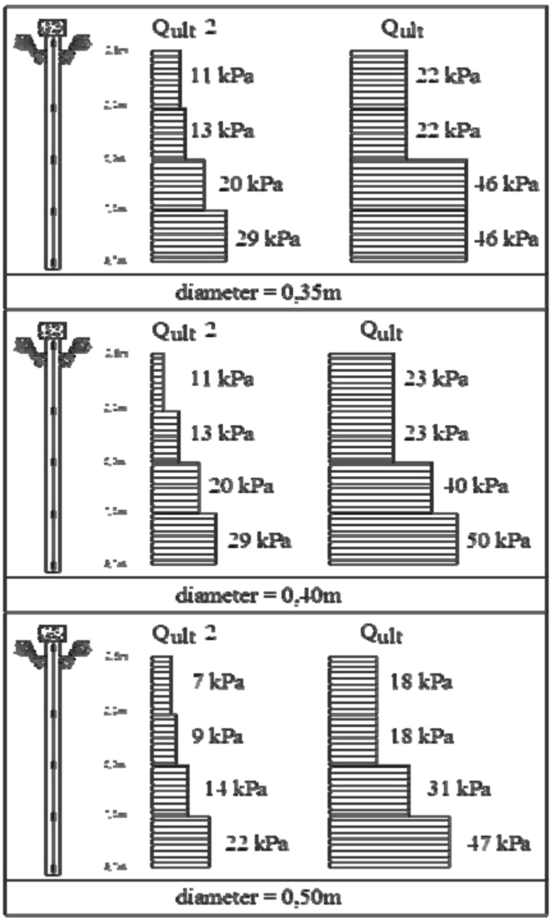

Figure 3. Lateral Friction Distribution Graph.

Figure 4 shows the average lateral friction curves resulting from shaft displacement. Tables 2, 3 and 4 show the load values at depth for all piles.

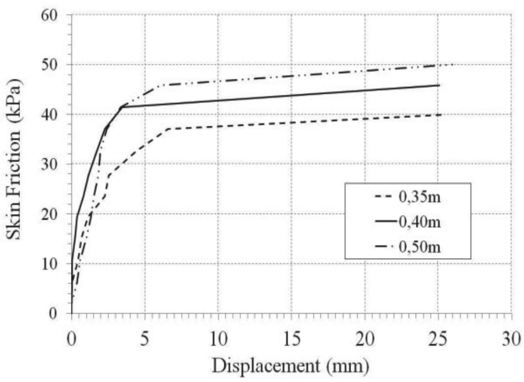

Figure 4. Average skin friction x shaft displacement curves.

Table 2. Load at depth for the 0.35m pile.

Load at top (kN)	Load at respective levels (kN)			
	3.1m	5.3m	7.5m	9.7m
40	35	29	27	21
80	76	47	41	23
120	107	90	70	23
160	146	119	80	21
200	171	140	91	23

240	210	167	103	25
280	253	196	115	27
320	280	222	126	23
360	315	253	154	23
387	-	272	161	23

Table 3. Load at depth for the 0.4m pile.

Load at top (kN)	**Load at respective levels (kN)**			
	3.1m	**5.3m**	**7.5m**	**9.7m**
40	37	35	32	1
80	64	56	46	3
120	118	104	75	11
160	150	126	83	11
200	187	158	110	11
240	217	185	123	11
280	249	211	136	11
320	284	233	144	11
360	318	265	163	11
400	340	278	166	8
440	-	302	190	8

Table 4. Load at depth for the 0.5m pile

Load at top (kN)	**Load at respective levels (kN)**			
	3.1m	**5.3m**	**7.5m**	**9.7m**
40	36	32	32	4
80	79	68	65	7
120	119	111	93	22
160	158	133	101	18
200	183	158	120	22
240	212	180	133	40
280	248	208	151	29
320	287	241	162	29
360	320	269	176	29
400	348	295	194	40
440	377	320	216	18
478	-	345	233	18

5 ANALYSIS

The load tests show, for the ultimate load, an average skin friction (sf) for the three piles of 21kPa (sf_1) for the Cenozoic sediment layer and 45kPa (sf_2) for the residual soil layer.

From Figure 4 it can be seen that the almost total mobilization of skin friction is for 5mm displacement.. Fellenius (2012) showed that, to mobilize the ultimate pile shaft resistance requires very small relative movement between the pile and the soil, usually only a few millimeters in inorganic soils and that the direction of the movement has no effect on the load-movement for the shaft resistance. That is, push or pull, positive or negative, the maximum shear stress is the same. Moreover, the movement necessary for full mobilization of the shaft resistance is independent of the diameter of the pile.

In analyses using semi-empirical formulae, the rupture in the pile-soil contact area was assumed. As the soil being studied was soft sand and the piles were relatively short, the tensile skin friction was assumed to be equal to the compression skin friction. Poulos (2011) states that for piles in medium dense to dense sands, this ratio typically ranges between 0.7 and 0.9, but tends towards unity for relatively short piles, and that a significant advance in the understanding of this problem was made by Nicola and Randolph (1993).

Table 5 shows the results obtained in the load tests ($P_{Ult.PC}$) compared to those obtained from the methods employed to predict the ultimate load of the piles ($P_{Ult.Cal.}$).

Table 5. Ratio of the ultimate load value obtained in the load test to the calculated value

Ratio $P_{Ult.PC}$ / $P_{Ult.Cal}$	**0.35m**	**0.4m**	**0.5m**
Meyerhof and Adams (1968)	2.03	1.79	1.26
Meyerhof (1973)	0.71	0.66	0.51
Das (1983)	1.21	1.00	0.85
Martin (1966) - Univ. Grenoble	0.82	0.81	0.68
LCPC (Fellenius, 2012)	1.21	1.19	1.00
Aoki and Velloso (1975) SPT	2.16	2.13	1.79
Aoki and Velloso (1975) CPT	2.30	2.29	1.99
Decourt (1996)	1.08	1.06	0.89
Philiponnat (1978)	1.44	1.14	0.96

For the two soil layers, the average skin friction ratios for the piles based on the results of the CPT tests are $sf_1=0.5.fs_1$, $sf_2=0.3.fs_2$, $sf_1=0.02.qc_1$, $sf_2=0.02.qc_2$, respectively. By expressing the ratios sf = k.fs and sf = C.qc, the values for k demonstrated by Slami and Fellenius (1977) range from 0.8 to 2 while those for C range from 0.008 to 0.018 for sandy soils. Bustamante and Gianeselli (1982) present the C coefficient ranging from 0.005 to 0.03, as governed by the magnitude of the cone resistance, type of soil and type of pile.

The LCPC Method (in Fellenius 2012), based on the experimental work of Bustamante and Gianeselli (1982), establishes that sf=C.qc, for bored piles in sand and with a qc of less than 5MPa, the value of C is equal to 1/60. Given these values, sf_1=19kPa and sf_2=39kPa can be computed, values which are close to those obtained in the load tests, namely 21kPa and 45kPa, respectively.

Using the method espoused by Décourt (1996), which uses SPT test data, tensile ultimate load values were calculated for the three piles. According to the current suggestion of the author, it is also necessary to use a correction coefficient (β_L) due to the soil being lateritic. In this case, β_L=1.2 was used, giving rise to the results presented in Table 3.

The method proposed by Martin (1966) and developed at the University of Grenoble, includes various important aspects such as cohesion, angle of friction, overload, specific soil mass and the weight of the foundations themselves. Moreover, it is recognized that the rupture surface forms an angle λ at the base of the pile. In the calculations performed, the hypothesis of angle λ equal to zero was the one which most closely approximated the load test results.

The method proposed by Meyerhof (1973) considers adhesion, pile-soil angle of friction, effective vertical stress and a pull-out coefficient that depends on the angle of friction of the soil and the type of pile. The method employed by Das (1983) was developed for sandy soils and includes the pile-soil angle of friction and a pull-out coefficient which depend on the relative density of the sand, the pile-soil angle of friction and the soil's angle of friction. The problem with these two methods lies in the correct definition of the abovementioned parameters.

In order to predict the ultimate loads from the load vs. displacement curves of the load tests, the method employed was that proposed by Décourt (1999) based on the stiffness concept (Fellenius 2012), which divides each load with its corresponding movement and plots the resulting value against the applied load, Figure 5. Ultimate load prediction simulations were performed, without using all of the load vs. displacement curve data and it was found that, starting from 70% of the maximum load in the test, the method presents good results in terms of determining the ultimate load.

The average tensile skin-friction values found are close to the values found in compression load tests with the same type of pile in the same soil.

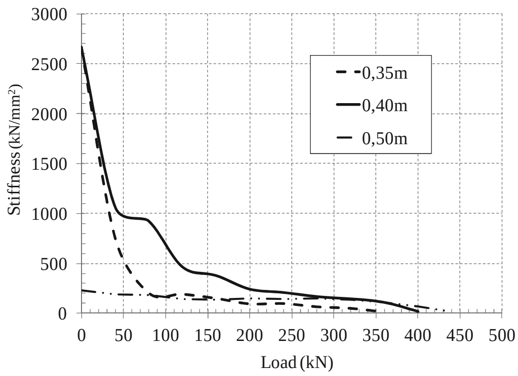

Figure 5. Stiffness curves

6 CONCLUSIONS

- The determination of the ultimate load using CPT demonstrates good results when the LCPC Method is used.
- The determination of the ultimate load using SPT demonstrates good results when using the Décourt (1996) method, assuming sandy soil and the adoption of an correction parameter (β_L = 1.2) due to the lateritic soil in the location;
- The Das (1983) method provides good results in determining ultimate load, however its use depends on the pile-soil angle of friction and a pull-out coefficient, parameters which are not always available for the particular soil being analyzed;
- The best prediction of ultimate load using the Martin (1966, 1973) method is obtained using a rupture surface inclination angle equal to zero, indicating rupture in the pile-soil interaction;
- The load transfer function presents good definition for unit skin-friction, finding that displacements in the order of 5mm were required for their almost total mobilization;
- The Décourt (1999) stiffness method demonstrated good results in the prediction of ultimate load based on the analysis of the load vs. displacement curve.

7 ACKNOWLEDGEMENTS

The authors wish to thank the São Paulo Research Foundation (Fapesp), the University of São Paulo (EESC-USP) and the university lecturers José Henrique Albiero and Judy N.R.Mantilla.

8 REFERENCES

Aoki N. and Velloso D. 1975. An approximate method to estimate the bearing capacity of piles. *Panamerican Conference on Soil Mechanics and Foundation Engineering*, V, Buenos Aires. V.1, 367-376

Bustamante M. and Gianeselli L.1982. Pile bearing capacity predictions by means of static penetrometer CPT. *Proceedings of the Second European Symposium on Penetration Testing*, ESOPT II, Amsterdam, May 24-27, A.A. Balkema, Vol. 2, pp. 493-500

Das B.J. 1983. A procedure for estimation of uplift capacity of rough piles. *Soils and Foundations* 23 (3), 72-77.

Décourt L. 1996. Analysis and design of deep foundations: piles. In: Hachich et al. (eds). Foundations: theory and practice. São Paulo. Pini. pp. 336 – 344. (in Portuguese)

Decourt L. 1999. Behavior of foundations under working load conditions. Pan-American conference on Soil Mechanics and Geotechnical Engineering, 11th. Brazil. V.4, 453-488.

Fellenius B.H. 2012. *Basics of foundation design*. Electronic Edition. www.fellenius.net, 384p.

Martin D. 1966. *Étude à la rupture de différents ancrages sollicitées verticalem*ent. Thése de Docteur-Ingénieur. Faculté des Sciences de Grenoble.

Martin D. 1973. Calcul des pieux et foundations à dale des pylons de transport d'energie électrique. Etude théorique et resultats d'essais en laboratorie et in-situ. *Annales de L' Institut Techinique du Batiment et Des Travaux Publies*, 307-308.

Meyerhof G.G. and Adams J.I. 1968. The ultimate uplift capacity of foundations. *Canadian Geotechnical Journal* 5 (4), 225-244.

Meyerhof G.G. 1973. Uplift resistance of inclined anchors and piles. *International Conference on Soil Mechanics and Foundations Engineering*, VIII, Moscow. V.2, 167-172

NBR 12131. 1986 – *Piles. Static load tests*. ABNT (in Portuguese)

De Nicola A. and Randolph M. F. 1993 Tensile and compressive shaft capacity of piles in sand. *ASCE Journal of Geotechnical Engineering*. 119 (12), 1952-1973

Philipponnat G. 1978. Méthode pratique de calcul des pieux à l'aide du pénétromètre statique. Paris. Soletanche Enterprise. *Informations Techiniques Bulletin* 16, 21p.

Poulos H.G. 2011. The de Mello foundation engineering legacy. *Soils and Rocks* 34 (1), 3-31.

Essais de chargement statique de pieux en bois instrumentés avec des extensomètres amovibles

Timber pile load test instrumented with removable extensometers

Christin J., El Kouby A.
Université Paris Est / IFSTTAR, Marne la vallée, France

Reiffsteck P.
Terrasol, Paris, France

Rocher-Lacoste F.
Sétra, Sourdun, France

ABSTRACT: Timber piles were used in France until the 19th Century. They cannot currently be proposed in projects as they are not implemented in the French pile design methods. Nevertheless, their domain of application has widened with retrofitting and reuse of all historical structures and sustainable development. The research project “Pieux Bois” (2010-2013) has the objective of beginning to establish a database necessary for design methods. The first pile loading test campaign carried out in Rouen on piles instrumented with removable extensometers, shows interesting results.

RÉSUMÉ : Les pieux en bois, utilisés en France jusqu’au 19ème siècle, ne peuvent pas à l’heure actuelle rentrer dans les méthodes de dimensionnement françaises basées sur le pressiomètre (développées dans les années 50). Néanmoins, leur domaine d’application trouve un écho favorable pour la réhabilitation de vieux ouvrages et dans la dynamique actuelle du développement durable. Le projet de recherche « Pieux Bois » (2010-2013) a pour objectif de commencer à établir la base de données nécessaire pour les règles de dimensionnement. La première campagne d’essais de pieux, instrumentés à l’aide de l’extensomètre amovible, réalisé sur le port de Rouen, donne accès à des résultats tout à fait intéressants.

KEYWORDS: Foundation, wood, timber pile, pile loading tests.

1 CONTEXTE ET ENJEUX

Le battage des premiers pieux en bois remonte à l’époque du néolithique, il y a plus de 6000 ans. A cette époque, ces pieux étaient enfoncés dans le sol à la force humaine. Les premières machines de battage dont on garde trace en Europe ont été développées au cours de l’époque romaine. Durant les époques qui suivirent l’ère romaine, de la Renaissance jusqu’à l’ère industrielle, les modes de fondations et les constructions sur pieux bois se sont développés et diversifiés, jusqu’à leur remplacement et abandon au 19ème siècle par du béton immergé.

La société actuelle française a hérité de ces périodes un patrimoine très riche d’ouvrages fondés sur pieux bois. Les ponts construits sur la Loire ou la Seine, le château de Chambord ou encore le Grand Palais en sont quelques exemples.

L’abandon des pieux en bois en France a été antérieur au développement du pressiomètre par L. Ménard dans les années 1950 ; dont les résultats des essais constituent aujourd’hui la base du dimensionnement des fondations profondes en France. Il n’existe donc à ce jour aucune règle professionnelle ni de contexte normatif français permettant d’asseoir le dimensionnement de fondations de cette nature sur le territoire. Les bases de données d’essais de pieux conduisant à l’élaboration des règles de calculs et abaques de la norme NFP94-262 (*AFNOR, 2012*) ont été construites à partir d’essais de chargement statiques de pieux en acier et béton instrumentés sur toute leur longueur avec des extensomètres amovibles.

Le projet Pieux Bois (2010-2013), initié et piloté par l’IFSTTAR, vise à promouvoir la technique de fondations de type pieux en bois dans la construction de bâtiments et petits ouvrages. La mise en place d’un contexte normatif passe par la proposition d’une courbe de frottement unitaire limite le long du fût des pieux. La construction de cette courbe doit être réalisée selon la même méthodologie que celle qui a prévalue pour l’élaboration des courbes de références de la norme.

Ce papier présente les premiers résultats de l’étude entreprise. Dans une première partie, les caractéristiques mécaniques des pieux en bois ainsi que la technique d’instrumentation sont résumées. La seconde partie de l’article est consacrée à la réalisation et l’interprétation des essais de chargement des pieux en bois réalisés sur un plot expérimental.

2 CARACTÉRISTIQUES DES PIEUX EN BOIS

1.1 *Essences de pieux*

Les pieux en bois instrumentés ont été fournis par la scierie GROUAZEL, partenaire du projet Pieux Bois. Quatre essences ont été retenues dans le cadre de cette expérimentation : le pin car il s’agit de l’essence la moins durable et ses ressources sont importantes, notamment dans le sud-ouest de la France ; le chêne car il est considéré comme l’essence la plus durable et constitue une ressource de proximité sur une partie importante du territoire français ; le hêtre qui présente des caractéristiques intermédiaire et l’acacia qui possède également une très grande durabilité, bien que la ressource soit à l’heure actuelle faible.

1.2 *Caractéristiques géométriques des pieux*

La conicité naturelle des troncs d’arbres a été conservée. Les pieux n’ont donc pas été équarris. Ils sont naturellement "cylindriques" et bruts. Le tableau 1 présente leur longueur, leur diamètre en tête et en pointe, ainsi que leur conicité.

Tableau 1. Caractéristiques géométriques des pieux en bois

Essence (numéro)	Longueur (m)	Diamètre tête (cm)	Diamètre pointe (cm)	Conicité (mm/m)
Hêtre (1)	5	27,2	24,4	2,8
Hêtre (2)	5	32,3	29,4	2,9
Pin (3)	5	26,7	24,2	2,5
Pin (4)	5	24,8	23,1	1,8
Chêne (5)	5	27,1	23,9	3,2
Chêne (10)	5	26,9	23,6	3,3
Acacia (8)	5	22,1	19,6	2,5
Acacia (9)	5	23,1	21,2	1,9

1.3 *Caractéristiques mécaniques des pieux*

La non-linéarité des pieux en bois rendant difficile le calcul de leur volume, la masse volumique des pieux a été déterminée en laboratoire à partir d'une tranche prélevée en tête de pieux.

La masse des pieux a été mesurée après usinage, c'est-à-dire après la taille de la pointe et la réalisation de la saignée accueillant les tubes logement du système de mesure.

Dans le but de disposer du module d'élasticité longitudinal moyen de chaque pieu, une analyse vibratoire couplée à un modèle aux éléments finis (MEF) a été mise en œuvre. Dans un premier temps, le profil en long de chaque pieu ainsi que leur masse totale ont été mesurés. En plaçant le pieu sur deux appuis, celui-ci a été mis en vibration libre. A l'aide de trois accéléromètres, la première fréquence propre a été obtenue par analyse fréquentielle. Après avoir réintroduit le profil en long du pieu et sa masse dans le MEF, le module moyen tenant compte d'un rapport E/G de 16 a été retrouvé pour chaque pieu.

Le tableau 2 présente les caractéristiques mécaniques des huit pieux.

Tableau 2. Caractéristiques mécaniques des pieux en bois

Essence (numéro)	Masse (kg)	Masse volumique (kg/m3)	Fréquence résonance (Hz)	Module d'Young (MPa)
Hêtre (1)	136	475	18,2	6400
Hêtre (2)	275	709	21,1	9100
Pin (3)	153	572	19,9	9370
Pin (4)	120	587	20,5	9900
Chêne (5)	201	723	16,4	8150
Chêne (10)	192	723	14,6	6980
Acacia (8)	150	806	15,2	10970
Acacia (9)	153	757	18,8	13320

1.4 *Instrumentation des pieux*

L'objectif de l'instrumentation des pieux en bois est de mesurer à différentes profondeurs le raccourcissement élastique du pieu en fonction de la charge appliquée en tête *(Bustamante et Jézéquel, 1975)*. La valeur du raccourcissement permet, via la section et le module d'élasticité de chaque tronçon, de déterminer la charge reprise par chaque tronçon du pieu et donc le frottement latéral entre le pieu et le sol à différentes profondeurs.

Dans la pratique courante, la chaine d'extensomètres amovibles est introduite dans un tube métallique solidaire du pieu, une fois le pieu foré ou battu dans le sol. La non-linéarité et la conicité naturelle du pieu, mêlées aux difficultés que représentent la fixation du tube en acier au bois rendent l'emploi de cette méthode difficile. Un dispositif d'instrumentation à l'aide d'extensomètres amovibles spécifique aux pieux en bois a donc été élaboré.

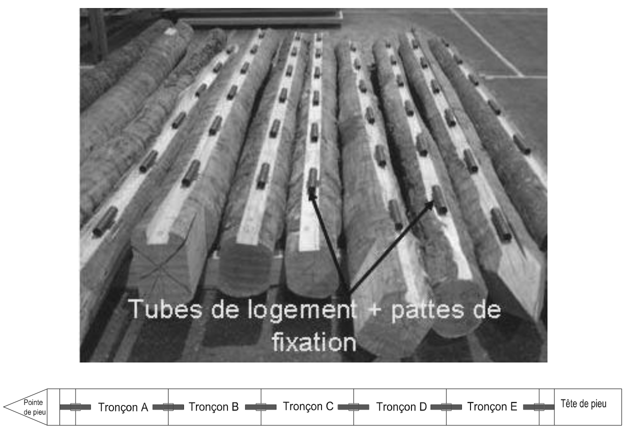

Figure 1. Usinage des pieux et fixation des tubes logement aux pattes

Dans un premier temps, une saignée de 80mm de largeur et de 60 mm de profondeur a été réalisée sur toute la longueur du pieu, au niveau de la section où le pieu était le plus rectiligne.

Des pattes de fixation, de 60mm de large et 80mm de long, ont été fixées dans la saignée au droit des futurs emplacements des bloqueurs. Les pattes étaient espacées les unes des autres de 75 cm (Figure 1).

Des fenêtres de 26cm de longueur et de 80mm de largeur ont été usinées sur un tube métallique à section rectangulaire de dimensions 80mm * 60mm. Ce tube métallique (qualifié de tube extérieur) est venu chapeauter et protéger l'ensemble « patte de fixation + tubes de logement » dans la saignée. Il a été fixé au bois avec des vis et des tirefonds (Figure 2).

La pointe des pieux a été usinée en forme pyramidale. L'extrémité du tube extérieur au niveau de la pointe a été biseautée de sorte que le biseau soit dans le prolongement d'une des faces de la pointe. La pointe a été renforcée avec 4 plats métalliques (un sur chaque face) dont l'un a été soudé au biseau du tube extérieur (Figure 2).

Deux plats diamétralement opposés et distants de 20 cm (distance constante sur tous les pieux) ont été usinés sur la tête du pieu. Ils avaient pour objectifs de faciliter la fixation du casque de battage au pieu lors de la phase chantier.

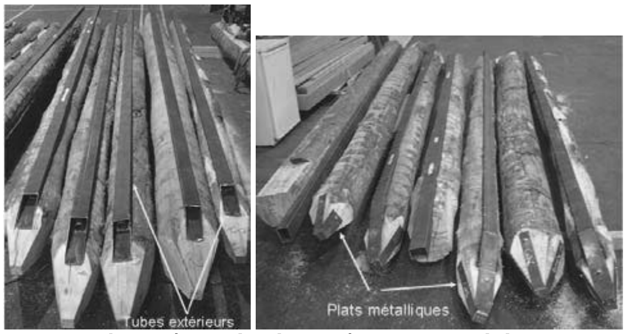

Figure 2. Tubes extérieurs dans la saignée et protection de la pointe

3 CONSTRUCTION D'UN PLOT EXPÉRIMENTAL

3.1 Caractérisation géotechnique du site

Le Grand Port Maritime de Rouen (GPMR) est un maître d'ouvrage public qui possède de nombreux quais fondés sur des pieux en bois de hêtre. Souhaitant s'impliquer dans le projet afin d'établir des solutions de confortement pour ses propres ouvrages, le GPMR a mis à disposition de l'IFSTTAR une parcelle en bordure de Seine sur laquelle le plot expérimental a été construit.

Trois sondages à la pelle mécanique ont permis d'identifier la géologie du site (Figure 3). Le niveau moyen d'eau de la nappe sujet à marnage a été mesuré à 3,80m de profondeur.

	0m
Remblai graveleux	**0,55m**
Limon-argileux (couleur gris foncé)	**2,50m**
Matériaux sablo-graveleux (couleur gris clair) *Grattage de la tarière à partir de 2,3m de profondeur, présence éventuelle de blocs de craies*	**4,20m**
Argile sableuse	**>7m**

Figure 3. Coupe géologique du site

Des essais d'expansion au pressiomètre Ménard, de pénétration dynamique avec un pénétromètre type PANDA, des essais de pénétration statique au piézocône (CPT) et des essais de pénétration au carottier (SPT) ont été réalisés sur le site expérimental, à proximité de la zone de battage des pieux (Figure 4).

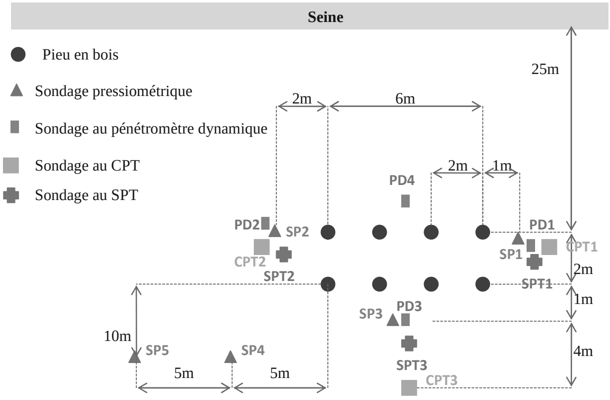

Figure 4. Plan d’implantation des sondages

Le tableau 3 présente les résultats des différents sondages réalisés, ainsi que le modèle géotechnique retenu pour le site.

Tableau 3. Caractéristiques géotechniques de sol et modèle de terrain

Couche /prof de fin de couche (m)	q_d (MPa)	p_l (MPa)	q_c (MPa)	N_{SPT}
Limon argileux / 2,50	$5,2<q_d<19,2$ $q_{d,moyen}=10,3$	$0,21<p_l<0,55$ $p_{l,moyen}=0,4$	$0,1<q_c<2,8$ $q_{c,moyen}=0,5$	$5<N_{SPT}<8$
Sable grave / 4,20	$7,5<q_d<41,1$ $q_{d,moyen}=14,3$	$0,80<p_l<1,40$ $p_{l,moyen}=1$	$1,1<q_c<10$ $q_{c,moyen}=4,5$	$18<N_{SPT}<33$
Argile sableuse / >6,70	X	$0,42<p_l<0,91$ $p_{l,moyen}=0,62$	$0,5<q_c<6,9$ $q_{c,moyen}=1,9$	$21<N_{SPT}<27$

3.2 *Battage des pieux*

Les pieux en bois ont été battus avec un trépideur pneumatique de 600kg. Ce marteau développait une énergie par coup comprise entre 2100 et 2360 joules, équivalent à la chute d’un mouton de 83kg d’une hauteur fictive de 2,63m.

Un casque de battage, constitué de 3 plats métalliques fixés à la tête de pieux et d’un HEB200 faisant office de raccord entre la tête des pieux et le marteau a été mis en place sur les têtes des pieux. L’objectif était de protéger la tête des pieux du marteau pneumatique et donc d’éviter toute fissuration ou fracturation du pieu (Figure 5).

Au niveau de la zone de battage, la couche de remblai a été remplacée par des regards en béton remblayés avec du limon argileux. Les pieux étaient distants les uns des autres longitudinalement et transversalement de 2m (Figure 5). Ils ont été mis en fiche à 4,6 m de profondeur en environs 3 minutes.

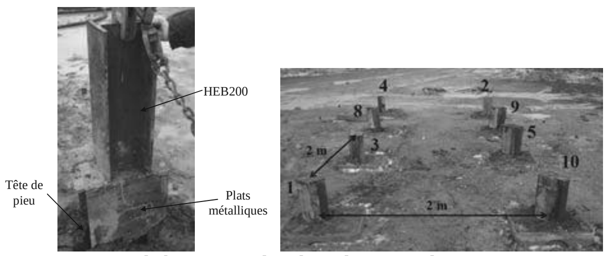

Figure 5. Casque de battage et plan d’implantation des pieux

4 ESSAIS DE CHARGEMENT

4.1 *Réalisation des essais de chargement*

Les 8 pieux en bois ont été chargés en compression. Le massif de réaction était composé d’une poutre de chargement consituée de 2 HEB900 accolés et soudés de 6,50m de long. Deux traverses étaient posées perpendiculairement aux extrémités de la poutre. Les micropieux du massif de réaction assurent alors la reprise des efforts.

L’effort en tête de pieu a été appliqué à l’aide d’un vérin hydraulique de 3MN et d’une pompe. Une rotule était installée au dessus du vérin afin d’éviter la transmission de moments de flexion. Les enfoncements verticaux de la tête du pieu ont été mesurés à l’aide de 4 comparateurs potentiométriques au 1/100^{e} mm, montés sur des bases de référence fixes. Malgré la protection de la tête des pieux par un casque métallique lors du battage, certaines têtes de pieux se sont fissurées sous les coups du marteau hydraulique. Afin d’éviter une fracturation de la tête des pieux lors des essais de chargement, un casque métallique a été installé (Figure 6).

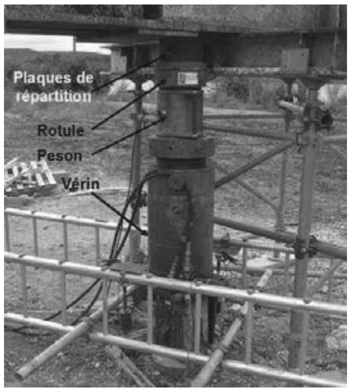

Figure 6. Dispositif de chargement

4.2 *Courbes de chargement et fluage des pieux*

La norme NFP94-262 (*AFNOR*, *2012)* stipule que la rupture du pieu sous charge axiale est atteinte lorsque l’enfoncement de la tête de pieu est supérieure à 10% de son diamètre. Ce critère de rupture a été retenu pour les essais de chargement.

La Figure 7 présente les courbes de chargement des 8 pieux testés. Aucun pieu n’a rompu au nivau de sa structure.

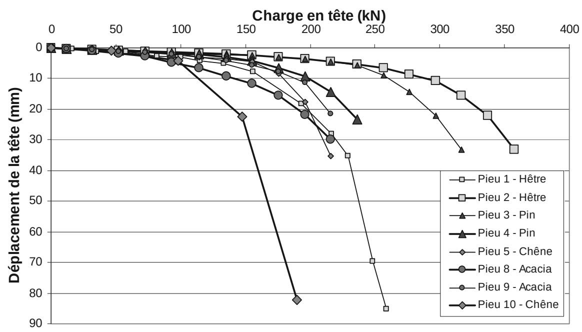

Figure 7. Courbes de chargement

4.3 *Mesures extensométriques*

L’instrumentation des pieux avec des extensomètres amovibles a permis de déterminer la distribution des efforts le long du fût et la résistance de pointe durant l’essai de chargement. L’hypothèse d’un comportement élastique linéaire isotrope de chaque tronçon de pieu a permis de déterminer l’effort repris par le tronçon i selon la loi de Hooke :

$$Q_i = \frac{E * S_i * \Delta l_i}{l_i} \qquad (1)$$

Avec E le module d’élasticité du matériau du pieu issu du tableau 2, S_i la section du tronçon i calculée à partir du tableau 1, l_i et Δl_i la longueur et le raccourcissement du tronçon i.

Le frottement latéral unitaire q_{si} repris par le tronçon i s’exprime de la façon suivante :

$$q_{si} = \frac{Q_i - Q_{i+1}}{S_{latérale}} \qquad (2)$$

La résistance de pointe a été calculée par extrapolation de l’effort repris par le tronçon du dessus : la différence des efforts repris par la pointe (Q_p) et le tronçon A (Q_A) était identique à celle des efforts repris par les tronçons A et B (Q_B), modulant les longueurs des tronçons.

$$Q_p = Q_A - (Q_B - Q_A) * \frac{H_p}{H_A} \qquad (3)$$

Les mesures des raccourcissements unitaires Δl ont été effectuées à l'aide d'un chapelet d'extensomètres amovibles délimitant 5 tronçons de mesure de 75 cm. Ils sont mesurés au micromètre.

La Figure 8 présente la déformation du bas de chaque tronçon du pieu n°1 en fonction de l'effort appliqué en tête, ainsi que la distribution des efforts le long du fût.

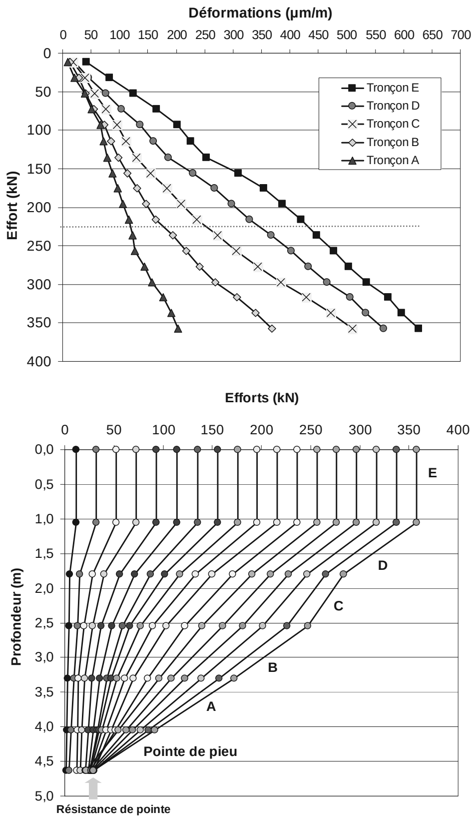

Figure 8. Déformation unitaires et distribution de charge du pieu n°1

A effort constant, les déformations les plus importantes sont mesurées sur le tronçon E, situé en dessous de la tête du pieu. La diminution progressive des déformations des tronçons E à A montre que les tronçons reprennent une partie de l'effort appliqué en tête de pieu par frottement avec le sol.

On observe une rupture de pente pour un effort de 220kN, plus marquée sur les tronçons A, B et C que sur les tronçons D et E. Cet effort marque la limite entre le domaine élastique et le domaine plastique du sol à l'interface sol-pieu.

Pour une charge inférieure à 220kN, les déformations des tronçons évoluent pseudo-linéairement avec l'effort appliqué en tête. On retrouve cette relation pseudo-linéaire entre la charge appliquée en tête et le tassement du pieu dans le sol. Jusqu'à 220kN, la mobilisation du frottement le long du pieu augmente avec la charge.

Pour une charge supérieure à 220kN, l'évolution des déformations des tronçons en fonction de l'effort appliqué en tête n'est plus linéaire. Le frottement à l'interface sol-pieu est intégralement mobilisé. Le sol à l'interface commence à fluer.

La distribution des efforts permet de remonter à la loi de mobilisation du frottement des tronçons du pieu en fonction de leur déplacement. Les courbes (Figure 9) sont caractérisées par une phase pseudo-linéaire, une rupture de pente puis un plateau (ou un pic) représentatif de l'atteinte du frottement latéral maximum.

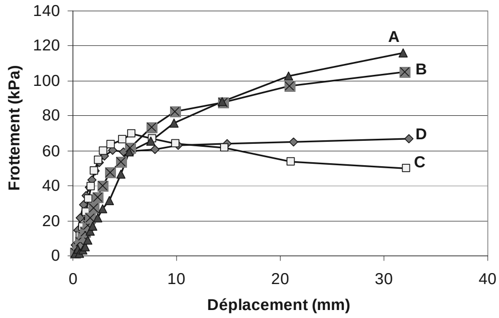

Figure 9. Mobilisation du frottement en fonction du déplacement - pieu n°1

4.4 *Synthèse des résultats*

Les valeurs du frottement latéral unitaire des pieux en fonction de la pression limite du terrain sont présentées sur la Figure 10.

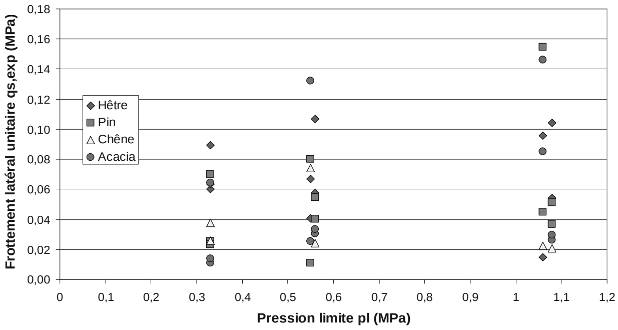

Figure 10. Frottement latéral unitaire en fonction de la pression limite

La dispersion des valeurs du frottement latéral unitaire en fonction de la pression limite montre que la nature de l'essence de bois n'a pas d'influence sur le comportement du pieu dans le sol.

Les mesures de résistance de pointe des pieux ont permis de déterminer un coefficient de portance $k_{p,exp}$. Il est défini comme le ratio entre la résistance de pointe unitaire $q_{p,exp}$ et la pression limite équivalente p_{le}^{*} sous la fondation qui a été prise égale à 0,75Mpa dans l'argile sableuse. La moyenne des coefficients de portance issus des résultats expérimentaux est de 2,15.

5 CONCLUSIONS

Les essais de chargement réalisés sur des pieux en bois de différentes essences ont permis de déterminer des premières valeurs du frottement latéral unitaire et de la résistance de pointe. Ces valeurs sont nécessaires à la proposition d'une courbe de frottement unitaire limite le long du fût des pieux en bois.

Ces essais ont mis en évidence que la nature de l'essence n'interviendrait pas dans les caractéristiques mécaniques de l'interface sol-bois.

6 REMERCIEMENTS

Les auteurs remercient le projet Pieux Bois, le GPMR le SETRA et l'entreprise GTS pour leur aide et leur contribution apportée durant le projet. Les auteurs remercient également le MEDDE pour le financement du projet dans le cadre du programme C2D2.

7 REFERENCES

Bustamante M. et Jézéquel J.-F. 1975. Mesure des élonguations dans les pieux et tirants à l'aide d'extensomètres amovibles, *Travaux* (489)

AFNOR, Norme NFP94-262. 2012. Justification des ouvrages géotechniques, normes d'application nationale de l'Eurocode 7.

Pylon foundation of a cable stayed bridge at the motorway ring road of Wrocław

Fondation d'un pylône du pont suspendu du périphérique de l'autoroute de Wrocław

Dembicki E., Cudny M., Krasiński A., Załęski K.
Gdańsk University of Technology, Faculty of Civil and Environmental Engineering,
Department of Geotechnics, Geology and Maritime Engineering

ABSTRACT: The largest bridge of the motorway ring road of Wroclaw is a cable stayed bridge over the Odra river near Rędzin. Due to hydrogeological conditions of the ground it was not convenient to use standard bored piles of high length. Instead shorter piles were applied with additional improvement by cement injections at the pile toes. This decision was possible by extending ground investigation program and application of numerical modeling of the soil-structure interaction with nonstandard material models of the overconsolidated clayey deposits. Sufficient stiffness and bearing capacity of piles was approved by field tests. Overall performance of the foundation was monitored during construction and after completion of the bridge. Comparison of settlements predicted during design and obtained in the monitoring is presented and discussed.

RÉSUMÉ : La plus grande construction sur le périphérique de l'autoroute de Wrocław est le pont suspendu sur le fleuve Odra à Rędzin. L'utilisation des pieux normalisés de grandes longueurs a été jugée inconvenable à cause des conditions hydro-géologiques. Les pieux de grands diamètres raccourcis avec un renforcement de la base par l'injection de ciment ont été donc utilisés. Une telle solution a été rendue possible grâce à un programme élargi de caractérisation du sous-sol ce qui a permit de réaliser les calculs du projet en utilisant des modèles de comportement non standards adaptés aux matériaux à grains fins surconsolidés. La rigidité et la résistance correspondante des fondations sur pieux ont été confirmées par les essais de chargement in situ. Le comportement de la fondation en entier a été contrôlé durant sa construction et durant la période d'exploitation après la fin des travaux. Les déplacements de la fondation évalués en cours de projet et après, par observation, ont été présentés et discutés.

KEYWORDS: piled-raft foundations, pile foundations, finite element analysis

1 INTRODUCTION

Main section of the bridge of 612m length will be suspended from a single pylon of 122m high. Large loading from the pylon structure causes the design of the foundation to be a challenging geotechnical problem due to high level of loads to be safely transmitted into the subsoil. In the case of the cable-stayed bridge over the Odra river the highest characteristic vertical load, considered among various combinations of loads analysed by the designer, transmitted onto the support was estimated to be 776.0 MN. Dimensions of the bridge makes it the highest object of that type in Poland.

2 SOIL AND WATER CONDITIONS

Designed foundation will be placed in the central part of Rędzin Island within the main Odra river bed. The island is connected with the river banks and mainland through two Rędzin locks, which are located ca. 70 m north and through historical weir, located ca. 110 m south-west. The area designated for foundation is 67.4 m x 28.0 m.

The terrain under foundation is basically flat with mean elevation of 112.8 m a.s.l. From the geomorphological point of view it is located in Wrocław-Magdeburg ice-marginal valley (Odra River valley), 10 km wide and filled with Pleistocene and Holocene river sediments with several terraces at various levels.

The surface layer of fills and normally consolidated river accumulation formations 2.0 m thick lies on dense coarse material of the thickness of 6-7 m with unconfined water table at the mean elevation of 107.6 m a.s.l. Below coarse sediments there are fine soils of tertiary origin represented by clays and locally silty sands. In this continuous, 15 m thick layer local water percolations are observed. Below it, thin layer (2.5 m) of silty sands and sandy silts with confined water table under high pressure was found.

Table. 1: Characteristic values of basic geotechnical parameters

Layer	**Soils**	**(γ/γ')** [kN/m^3]	**ϕ'** [°]	***c'*** [kPa]	$\boldsymbol{E_{oed}}$ [kPa]	**ν** [–]
IIa/IIb	Cl, siCl, Si	21,0/11,0	15,0	5,0	30 000	0,20
IIIa	MSa, CSa, FSa	19,0/10,0	33,0	1,0	85 000	0,20
IIIb	MSa, CSa, grCSa	20,0/10,0	35,0	1,0	150 000	0,15
IIIc	grCSa, Gr	20,0/10,0	35,0	1,0	220 000	0,15
Va	Cl, siCl,	21,5/11,5	23,0	18,0	40 000	0,20
Va*	Cl, siCl,	21,5/11,5	23,0	18,0	100 000	0,20
Vc	siSa	20,5/11,0	32,0	1,0	85 000	0,15

To the depth of 50 m below the subsoil surface there were no weak soils found. Tertiary clays are characterized by good strength and stiffness. The only problem related to the depth of the pylon foundation are local water percolations and high water pressures in confined aquifers. The most unfavorable foundation and execution conditions have been assumed for the further calculations and analyses, see Figure 1 and Table 1.

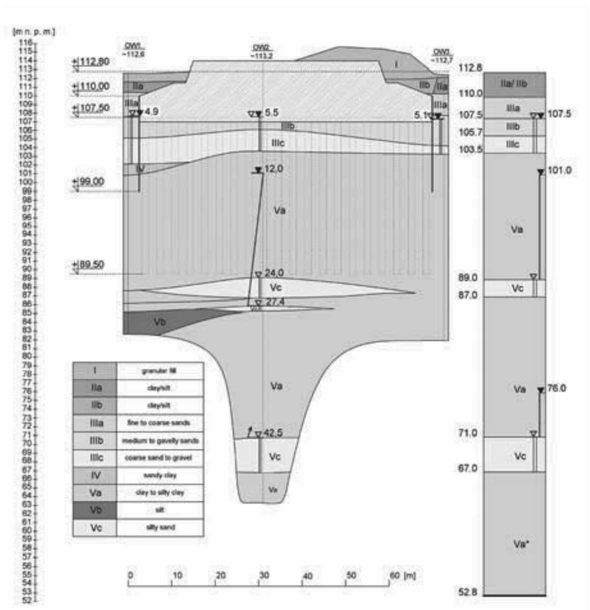

Figure 1: Characteristic geotechnical cross-section with the simplified system of layers.

3 TECHNOLOGICAL SOLUTION OF THE FOUNDATION

Four alternatives regarding the foundation of the pylon were being considered i.e.: shallow foundation in the layer of dense coarse soils, foundation on the diaphragm walls, foundation on the block made of jet-grouting columns and foundation on large diameter bored piles. Finally, the latest concept has been assumed for design. Additionally bored piles were strengthened by the injection under the pile base. Such solution was found to be optimal technologically in the soil conditions. The concept of shallow foundation was rejected due to small thickness of coarse material below the foundation level. In the case of diaphragm walls the problem might be low shaft bearing capacity. The foundation on the block made of injection columns has been rejected due to large volume and mass of the block.

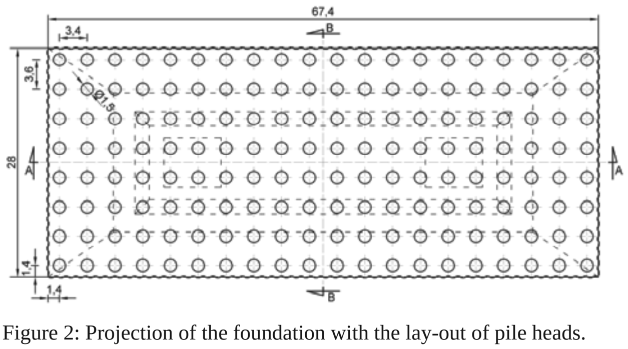

Figure 2: Projection of the foundation with the lay-out of pile heads.

The foundation foot has size of 67.4 m x 28.0 m and is founded on 160 large diameter bored piles. The piles have a rigid connection with the slab. The piles of diameter D=150 cm and length of 18 m are spaced in the rectangular grid 3.4 m x 3.6 m, (Fig. 2). The bottom of the foundation slab is localized at the elevation of 107.5 m a.s.l. and rests on the 0.5 m thick layer of blinding concrete. The perimeter of the foundation foot was protected by sheet pile wall of the length of 11.0 m (between elevations of 99 m to 110 m a.s.l.). The sheet pile wall is not a foundation element transmitting the loads into the subsoil but it is used as erosion protection.

The lack of high strength soil layer, did not allow to design base bearing piles, hence the raft foundation system was designed. In such system transmission of loads takes place both by piles as well as by foundation slab. The main layers deciding of bearing capacity and settlements of the foundation are layers of over-consolidated tertiary clays No. Va and Vc. The base level of the piles is designed in the upper part of geotechnical layer No. Va above the confined aquifer Vc. The confined aquifer is not considered as weak layer from the strength point of view, nevertheless it should be protected against any perforation due to high water pressure occurring in it. It was recommended to concrete the piles by dry method however this recommendation could not be fully achieved. The piles have been strengthen by injection under their bases. During the injection both grout pressure and pile heave were controlled.

4 CALCULATIONS

At the preliminary stage of the foundation design several schemes of pile foundation system were analyzed. In the simplest scheme no direct soil - foundation slab interaction as well as infinite stiffness of slab were assumed (rigid foundation method). Here, maximal compression force in pile was estimated at the level of 7200 kN for the envelope of maximum moments acting at the top of foundations, whereas minimum compression force was 5300 kN. In the next calculation stage the foundation was analysed as boundary-value problem solved by finite element method. The discretization was based on structural elements such as shells and beams resting on elastic supports. The characteristics of elastic supports have been calculated based on the stiffness of soil layers. The soil response under the slab was assumed as uniform passive ground pressure equal to 100 kPa. It allowed to assess the values of internal forces in the foundation slab and in the piles. These forces were necessary for design of the reinforcement. The maximum calculated axial force in the pile was 7367 kN and meets standard bearing capacity condition just on the edge of safety whereas maximum bending moment was 4742 kNm.

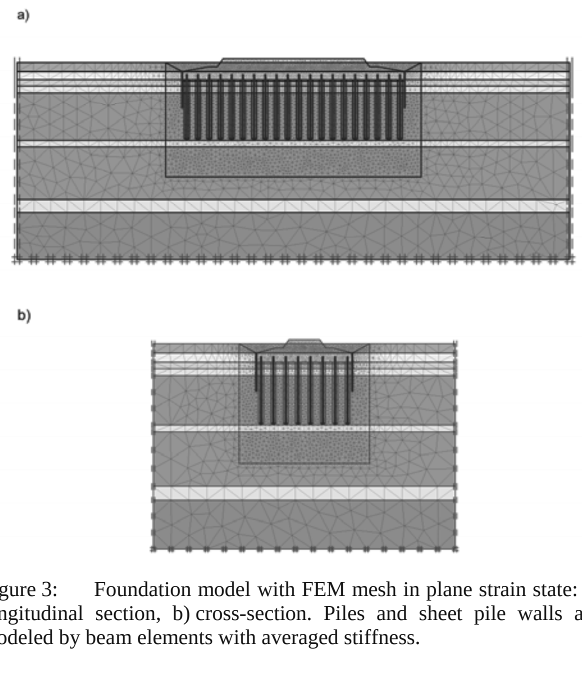

Figure 3: Foundation model with FEM mesh in plane strain state: a) longitudinal section, b) cross-section. Piles and sheet pile walls are modeled by beam elements with averaged stiffness.

Final calculation stage regarded numerical simulation of boundary-value problem by finite element method with discretization of the foundation body and geotechnical layers by continuum elements. The piles were discretised by beam elements directly interacting with soil elements. Calculations were carried out for simplified schemes in plane strain state with averaging stiffness of piles in rows and in the complex three dimensional model. In the later case alignment of beam elements is independent of the mesh representing soil (so called embedded piles). Bearing capacity of the pile base is modelled by equivalent force. Its value is calculated based on the stress state and bearing capacity of a soil at the level of pile base. Schemes of plane strain and three dimensional models are shown in Figs. 3 and 4.

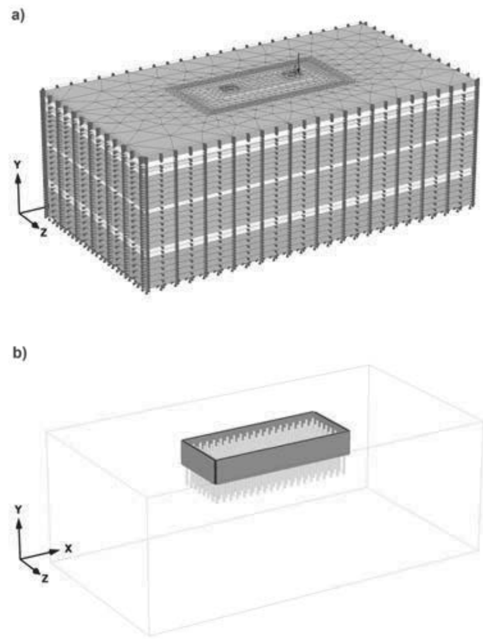

Figure. 4: 3D FEM mesh of foundation model: a) general view with boundary conditions, b) detail of pile elements (so called embedded piles) and sheet pile wall elements (plate elements). Foundation body modelled by continuum elements.

The main goal of the last calculation stage was a determination of the subsoil resistance and an assessment of the foundation settlements during the construction phase as well as during its operation. Besides strength of the soil layers which was modelled by either Coulomb-Mohr or Matsuoka-Nakai strength criteria, special attention was paid to possibly accurate description of the soil stiffness. For that purpose non-linear stiffness model including description of small strain behaviour of soil was adopted. Conventional implementation of constant stiffness with secant parameters (Table 1) leads to unrealistic overestimations of the settlements in majority of practical cases of raft foundations. It is well known from the laboratory and in situ investigations that the stiffness increase with the mean effective stress, however on the other hand it degrades due to accumulation of large shear strains (Atkinson, 2000), (Santos and Correia, 2000). The nonlinear small strain stiffness was included in the model for fine grained soils. Small strain stiffness moduli for the soil layers were determined in the triaxial tests equipped with bender elements, (report (2), 2008).

The value of current shear modulus G was calculated according to the following formulas:

$$G = G^{ref}\left(\frac{\sqrt{\frac{1}{3}\sum_{r=1}^{3}\sum_{s=1}^{3}\sigma_{rs}\sigma_{rs}}}{p_{ref}}\right)^{1-\beta} \quad (1)$$

$$G^{ref} = G_0\left(\frac{\gamma_{0.7}}{\gamma_{0.7}+\frac{3}{7}\gamma}\right), \quad (2)$$

where G and G^{ref} are current and reference tangent shear moduli respectively, $G^{ref} = E^{ref}/(2(1\text{-}\nu))$ at mean reference stress $p_{ref} = 200$ kPa; σ is the stress tensor; $\beta = 0.5$ is power parameter expressing the dependence of the stiffness on effective stress and $\gamma_{0.7}$ is shear strain at which shear modulus G^{ref} decreases about 30% with respect to G_0 – initial modulus at reference stress p_{ref} (see Fig. 5).

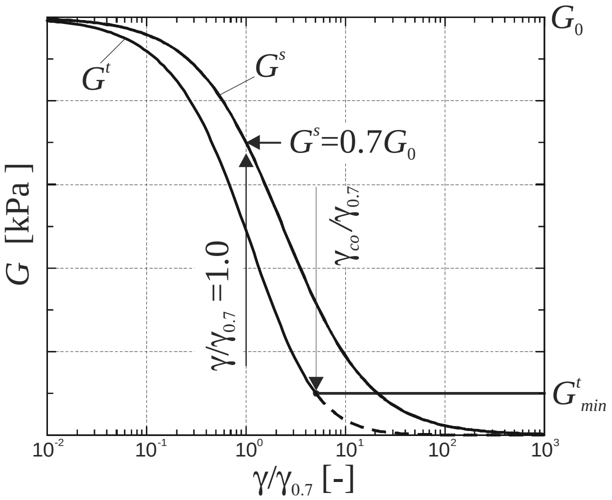

Figure 5: Dependence of shear modulus on shear strains. G_t=G_{ref} and G_s are tangent and secant shear moduli, respectively and G_{tmin} is a minimal shear modulus at the accumulation of shear strain γ_{co}.

The calculation results show that for estimated strength parameters of the soil layers stability of the foundation is preserved. In the numerical simulations the foundation was stable even for doubled loads. Minimum factor of safety for the foundation model received by ϕ-c reduction method was $F = 1.35$. The uniform settlement of the foundation was 0.08 m, whereas maximum settlement difference was 0.01 m. Exemplary distribution of vertical displacements for the calculation scheme assuming maximum horizontal loads has been shown in Fig. 6.

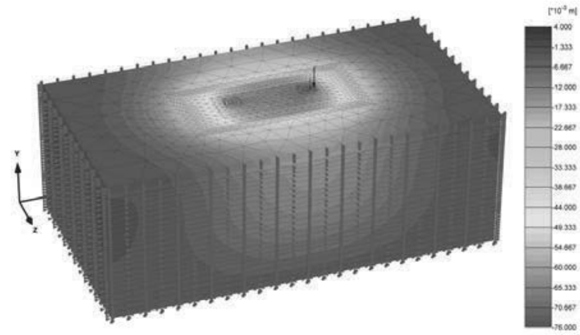

Figure. 6: Distribution of vertical displacement obtained for maximum lateral load calculation scheme.

5 LOAD TESTS OF INDIVIDUAL PILES.

In order to verify the design assumptions as well as to meet general recommendations regarding pile foundations, the bearing capacity of piles was investigated by static load tests. Due to importance of the construction as well as from the design assumptions, the load tests program was extended (after the agreement of the designer and investor). In order to examine the effectiveness of the pile base improvement by injection as well to control its quality, one of piles designated for testing was installed without the injection. Additionally, in three of the test piles, extensometer measuring system to control the distribution of force along the pile was installed. The goal of these measurements was to investigate the distribution of load transmitted by the pile shaft and base. It is also useful to assess the force generated at the pile base due to injection. Additionally, extensometer measurements were planned for the case of unfavorable bearing capacity test results. The measurement results would be useful for the analysis of the reasons of too low bearing capacity (shaft of pile or its base). The extensometers were installed at seven levels distributed along the pile length.

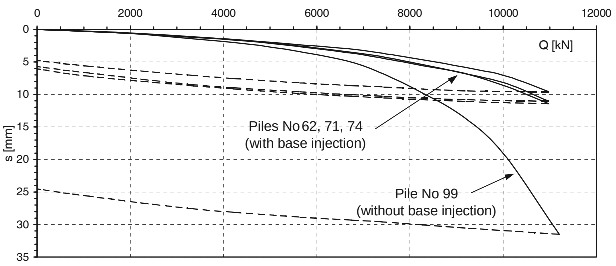

Figure 7: Pile load test results

Pile load tests were carried out according to the standard procedure i.e. to the maximum force Q_{max} = 11000 kN with intermediate unloading at the force Q_1 = Q_r = 7400 kN. The results of load tests confirmed the need of extended measuring program. The gained information proved the safety of the current and future foundation work. The important observation was proper work of the piles with injection and their advantage over the pile without base improvement. It is well visible in Fig. 7 where respective load-settlement curves are shown. The results of extensometric measurements in the form of distribution of force along the piles are shown in Fig. 8. They allowed for the examination of the work of the piles in the existing soil conditions. The essential portion of force was transmitted by the pile shaft what corresponded to the assumed concept of piles in the raft foundation system.

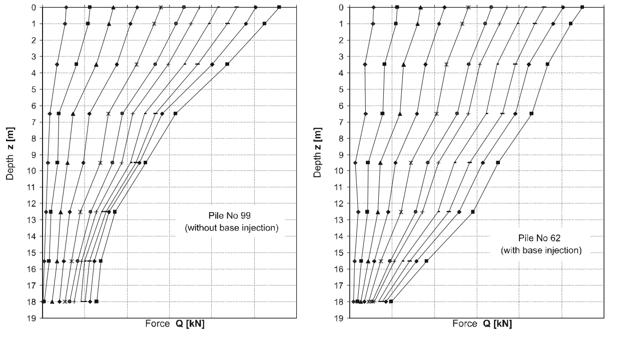

Figure 8: Distribution of forces along the pile form the extensometric measurements.

6 FIELD MEASUREMENTS

After piling and pylon slab construction, six benchmarks were placed on the slab surface in characteristic points (see figure X). Since 11.09.2009 till now the vertical displacements of foundation are geodetically monitored. After every stage of bridge loading vertical displacement were measured. Currently bridge is fully loaded, and settlements are in a stabilisation phase. Good agreement between measured displacements and numerical analysis results is observed (see Fig. 9).

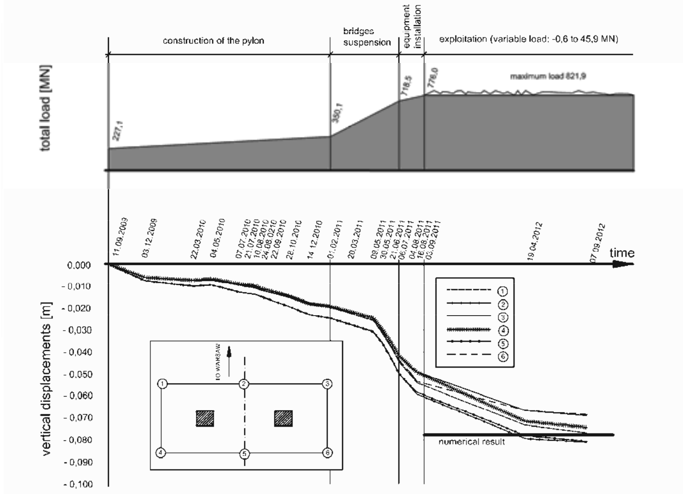

Figure 9: Settlements of foundation slab measured in 6 points in different phases of pylon loading.

7 SUMMARY

In the paper analysis of the raft foundation supporting the pylon of cable-stayed bridge in Rędzin being the part of Wrocław motorway A8 ring is briefly presented. Important decision related to the selection of the pile length was their shortening due to occurrence of confined aquifers which would cause the liquefaction of soils under the pile bases during installation. The decision could be undertaken after comprehensive numerical analyses as well as additional, non-standard investigations of soil parameters. Load tests with the measurement of the distribution of force along the piles with extensometers were very useful, allowing the control of design assumptions. The field measurements and their agreement with numerical analyses results are the best proof that assumptions made in the design process were correct.

8 REFERENCES

Atkinson, J.H. *Non-linear Soil Stiffness in Routine Design*, 40th Rankin Lecture, "Geotechnique", 2000, vol. 50 No. 5, 487-508.

Geological report (1), A-8 Motorway, AOW, GeoTech Ltd. Rzeszów 2006, (in Polish).

Kosecki M.: *Static of piling structures*, PZTB Szczecin branch, 2006, (in Polish).

Elaboration the way of foundation of the P14 support of cable-stayed bridge pylon in the motorway ring (A8) over the Odra river in Wrocław, Geosyntex Ltd., Gdynia 2008, (in Polish).

Santos, J.A, Correia A.G.: *Reference Threshold Shear Strain of Soils, Its Application to obtain a Unique Strain-Dependent Shear Modulus Curve for soil.* Proc. The 15th Int. Conf. On Soil Mech and Geot. Eng., Instanbul, 2000, vol. 1, 267-270.

Geological report (2) on the geotechnical and laboratory investigations under the pylon and permanent supports for construction of cable-stayed bridge over the Odra River in Wroclaw, Geoteko - Design and Geotechnical Consulting Ltd., Warszawa, 2008, (in Polish).

Consolidating Soil-Pile Interaction

Interaction pieux-sol en cours de consolidation

El-Sakhawy N., Nassar A.
Engineering College, Zagazig University, Zagazig, Egypt

ABSTRACT: Soft clay is consolidated upon any slight change in the effective vertical stress. Consolidation causes a downdrag movement to the shaft piles that penetrate this layer. The downdrag movement adds additional loads to the already loaded pile. This force is expressed as a negative skin friction. Negative skin friction extends to a depth depending on the consolidating soil-pile interaction. This depth is referred to as the neutral plan.

This paper presents a study on the behavior of soil-pile interaction during soil consolidation. Experimental work was developed to analyze the negative skin friction and the location of the neutral plane on a single pile embedded in soft clay layer. The pile is ended either in clay or sand soil, or is floated. The clay layer was allowed to consolidate. The study concluded that the neutral plane is located closer to the end of the pile as the end bearing increases. The depth of neutral plane increases by increasing the embedded length of the pile in the clay layer. Closed form equations of Shong, 2002, predict the experimental results in very well agreement.

RÉSUMÉ : Une argile molle se consolide sous l'effet d'une augmentation de la contrainte verticale effective. Cette consolidation provoque un déplacement vertical des pieux qui pénètrent la couche de sol. Ce mouvement ajoute des charges supplémentaires au pieu déjà chargé. Cette force peut être exprimée en frottement latéral négatif et s'étendre en profondeur en fonction de l'interaction sol-pieux en cours de consolidation. Cette profondeur est définie comme étant le plan neutre.

Cet article présente une étude sur le comportement de l'interaction sol-pieux lors de la consolidation des sols. Un travail expérimental a été développé pour analyser le frottement négatif et l'emplacement du plan neutre sur un seul pieu fondé dans une couche d'argile. La couche d'argile peut se consolider. L'étude montre que le plan neutre se situe près de l'extrémité du pieu ou la charge augmente. Ainsi, la profondeur du plan neutre augmente en même temps que la longueur du pieu. Ces résultats sont en accord avec ceux de Shong, 2002.

KEYWORDS: soft clay consolidation, pile foundation, negative skin friction, down drag movement neutral plane, floating piles

1 INTRODUCTION

Deep foundations are installed in different soil stratification. Usually the penetrated soil stratifications offer considerable resistance for the pile shaft deformation upon loading. This resistance is called shaft resistance or skin friction. This soil behavior can be reversed drastically if the penetrated soil encompasses soft clay.

Soft clay is consolidated upon any slight change in the effective vertical stress. Consolidation and settlement of soft clay surrounding a pile usually drag the pile downward (Walker and Dravall 1973, Sharif 1998, Leung, et al. 2004). The downdrag movement adds additional loads, downdrag force, to the already loaded foundation. Dragload heavily depends on the interface properties (friction coefficient, and adhesion), surface loading, and axial load (Sangseom Jeong, et al. 2004).

This force is the most common problem in the design and construction of pile foundations in soft soil (Maugeri et al. 1997, Van Der Veen 1986). (Briaud 2010) pointed out situations where downdrag force should be considered in the design.

The downdrag force can be expressed as a negative skin friction (N.S.F) as it acts in the opposite direction for the normally skin friction. The negative skin friction will be mobilized in the upper portion starting from the pile head to a neutral depth, ND, after which positive skin friction is mobilized in the lower portion. ND can also be defined as the depth at which the relative displacement between the pile and the soil is zero (Fellenius 1989, 2004, and 2006). (Bozozuk 1972) suggested that ND depends only on the embedded length of the pile in the clay layer. However, (Poorooshasb et al. 1996) stated that ND is not highly influenced by the surcharge. But that the presence of a strong soil layer at the tip of the pile would have a significant influence.

(Shong 2002) proposed closed form equations to locate the neutral plane depending on the elasticity of the soil and the pile. According to this approach, the depth of neutral plane, ND, to pile penetration length, L is:

$$\frac{ND}{L} = \sqrt{\frac{Q_u}{2Q_s}\left[(1 - \frac{Q_d}{Q_u})\right]} \tag{1}$$

Where

$$Q_u = \text{ultimate pile capacity} = Q_s + Q_t \tag{2}$$

Q_s, the pile shaft resistance over the whole shaft length, is:

$$Q_s = \int_0^L \beta\,(\pi D z)\,\sigma_z^{'}\,dz \tag{3}$$

L = length of the pile,
D = pile diameter,
Q_t, = the pile toe resistance:

$$Q_t = N_t . A_t . \sigma^{`}_{z=L} \tag{4}$$

A_t = the toe area of the pile,
Q_d = imposed load at pile top

Shong suggested a range of β varies between 0.25 - 0.35 for clay, and a value of 3 for N_t, toe bearing capacity coefficient.

Shong approach is adapted in the analysis of the results in this study.

This paper represents a study to investigate the behavior of soil-pile interaction during soil consolidation. Since full-scale testing of the influence of the large number of variables involved is economically unreasonable, a simulated laboratory experiment has been designated. A special rig was designed and constructed for this purpose. In order to carry out the investigations, experimental program was developed.

2 EXPERIMENTAL WORK

(Nasser 2010) arranged the experimental rig as shown in Figure 1. Three P.V.C circular model piles with different diameters of 1.5, 2 and 2.5 cm were chosen to model the pile in this study. Compression tests were carried out on a specimen of this P.V.C pipes to determine its modulus of elasticity. The modulus of elasticity of the pile material; P.V.C is 1500000 KN/m^2. The surface of the pile is smooth.

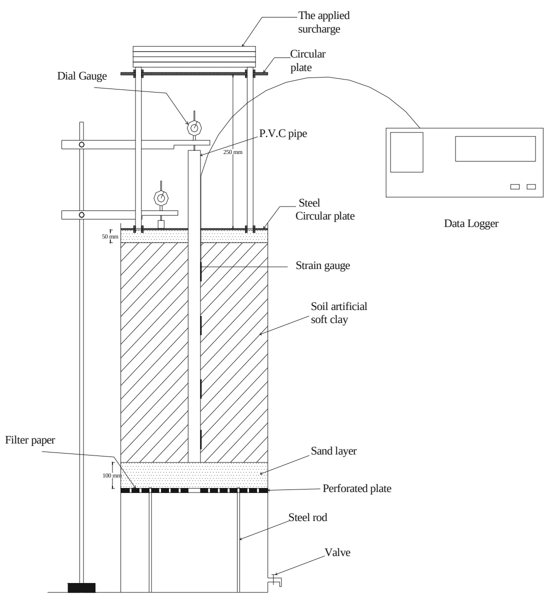

Fig. 1 The experimental rig

Two layers of sand with depth 5cm for each layer. One of these layers placed on the surface of soft soil and the second layer under the soil.

Bentonite soil has been adapted for the experimental investigation in this study. 85% water content provides a soft consistency of bentonite. For this condition initial void ratio is 2.38, bulk density is 16 KN/m^3.

A surcharge has to be applied to the soil layer for consolidation. Steel and lead plates of 1.2kN total weight were arranged for the surcharge. These loads simulate a surcharge of 1m fill of unit weight 17kN/m^3.

The vertical displacement of the model pile and the soil surface were measured using dial gauges. The displacement of the model pile is measured at its center. The soil settlement is measured at a point located at the mid distance between the pile shaft and the container wall.

Strain gauges are fixed at various depths of the length of the pile to measure the strains occurred on the pile during soil consolidation. Number and locations of the strain gauges are designed depending on the thickness of the clay layer.

Table (1) illustrates the experimental program. Three cases of boundary conditions were considered in this study. The first case is the pile ended in the clay layer. This represents clay end bearing case. The second case is the pile ended in the sand layer. And the last case represents floating pile. That is, the pile passes through the lower plate and not resting on any soil. This case is aimed to investigate the pure shaft resistance without the interference of the end condition.

Table (1) Different cases with code for each test

No.	Cases	Pile Diameter (cm)	L/d	Pile Length (cm)	Code	No. of Strain gages
1	CASE I (end bearing clay EC)	1.5	10	15	L15EC	3
2			15	22.5	L22.5EC	3
3			20	30	L30EC	4
4		2	10	20	L20EC	3
5			15	30	L30EC	4
6			20	40	L40EC	4
7		2.5	10	25	L25EC	4
8			15	37.5	L37.5EC	4
9	CASE II (end bearing sand ES)	1.5	10	15	L15ES	3
10			15	22.5	L22.5ES	3
11			20	30	L30ES	4
12		2	10	20	L20ES	3
13			15	30	L30ES	4
14			20	40	L40ES	4
15		2.5	10	25	L25ES	4
16			15	37.5	L37.5ES	4
17	Floating (F)	2.5	10	25	L25F	4
18			15	37.5	L37.5F	4
19			20	50	L50F	4

3 RESULTS AND ANALYSIS

3.1 Time–strain behavior of pile model

Figures 2 shows the axial strain with time of applying the surcharge, for pile model (L22.5Ec). From the Figure, it can be seen that the top strain is higher and occurs earlier than the middle and the bottom strains. However, it declines just after reaching the early peak. The other strains continue increasing until the end of the test.

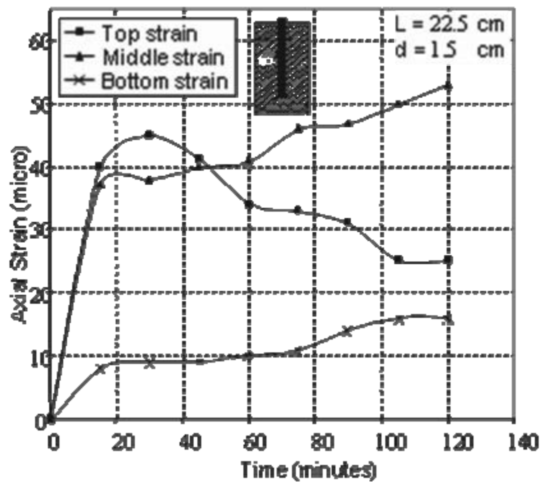

Fig. 2 Time-Axial strain curves of pile model (L22.5Ec)

It is clear that the top portion of the deposit go through consolidation due to the nearby surcharge faster than the remaining deposit. By the time being, the rate of water dissipation decreases, and, hence, the axial strain decreases. The middle axial strains continue increasing with lower rate than the initial one. The bottom strain is much less than the upper and middle ones. The stress increase, and hence the water dissipation and the soil consolidation, is moderate at the bottom strain compared with the other two locations.

Figure 3 illustrates the pile strains for pile model (L22.5Ec). It can be seen from the Figure that the bottom strains are generally larger when compared with the previous case of pile ended in clay. This can be attributed to the increased dissipation of pore water pressure through the bottom layer. Moreover, sand layers offer resistance to the pile movement; end bearing. This increases stresses in the bottom portion of the pile. Hence, there is increase in the monitored strain.

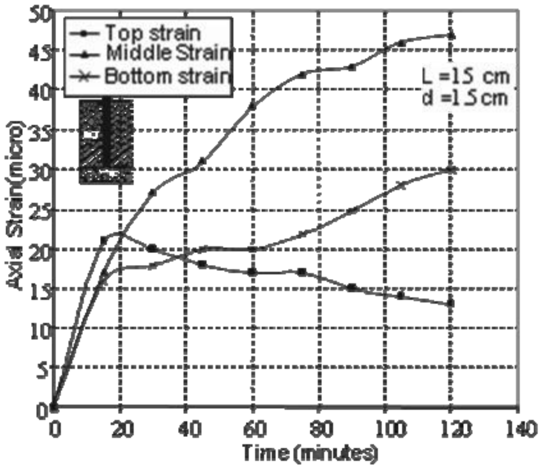

Fig. 3 Time- Axial strain curves of pile model (L15ES)

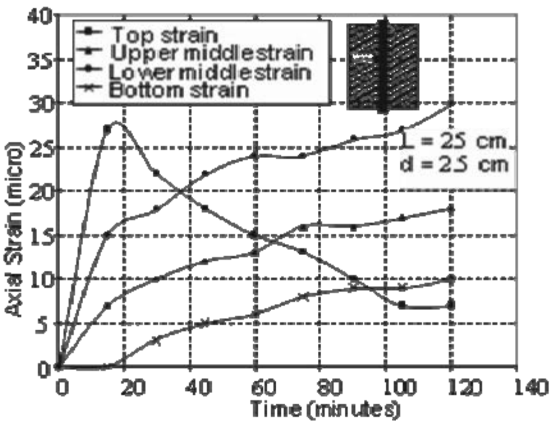

Fig.4 Time- Axial strain curves of pile model (L25F)

Figure 4 shows the pile strains for pile model (L25F). Here, the boundary condition at the pile tip does not allow for developing stresses at the bottom of the clay layer. Hence, the bottom strains are the least among all locations along the pile.

3.2 Distribution of normal strain and shear stress along the normalized depth of the pile

Figure 5 depicts the distribution of normal strain and shear stress along the normalized depth of the pile models (L15EC and L15ES). The shown strains are those monitored at the end of the test. As can be seen from the Figure, small values of strains are indicated in the upper part where the excess pore pressure had dissipated, and hence, consolidation process had decayed. The axial strain increases by the presence of a sand layer at the pile tip (case II). Strain increases until it reaches a peak value at an intermediate depth. Then, it decreases. Strain decrease reflects a decrease in the dragging force. That is the developing of positive shear resistance along the pile shaft. Hence, the zone of the peak strain is a transition zone from negative skin friction to positive skin friction. Obviously, the neutral plan is located at this peak point.

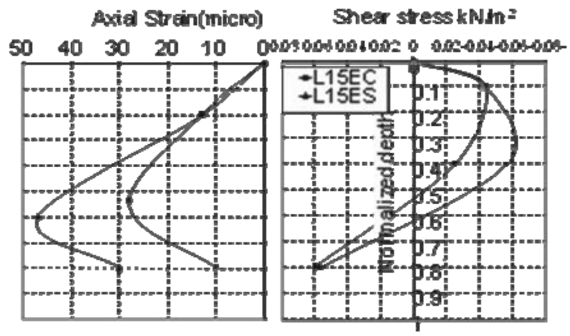

Fig. 5 Axial strain and shear stress distribution along pile length for cases (L15EC and L15ES)

The developed shear stress along the pile shaft is calculated from the monitored strain. Shear stress starts from zero value at the surface of the soil and increases until it reaches a peak negative value at an intermediate depth, then it decreases down to zero at the elevation of the neutral plane where the positive skin friction develops. Neutral plane is determined where shear stress changes from negative to positive. That is at the intersection of the curve with the vertical axis. As can be seen from the Figure the location of the neutral plane is matched from these two approaches.

As can be seen from Figure 5, the transition of pile ended in clay is located near to the middle of the pile. The transition zone of pile ended in sand is located near the pile toe. The neutral plane is located at the peak point of the transition zone. In addition, it can be seen that the normalized neutral depth is (0.53) and (0.61) for the cases of end bearing on clay and sand, respectively. That is the neutral plane is located closer to the end of the pile as the base layer gets stiffer.

This observation can be explained based on the simple equilibrium of vertical forces. (Accumulative negative skin friction = accumulative positive skin friction + bearing resistance). Since small-bearing resistance is available for case I, positive skin friction should be large enough to resist negative skin friction. Hence, negative skin friction will be reduced with the neutral plane being located further from the pile tip.

3.3 Effect of the pile length embedded in the clay layer on the location of neutral plane

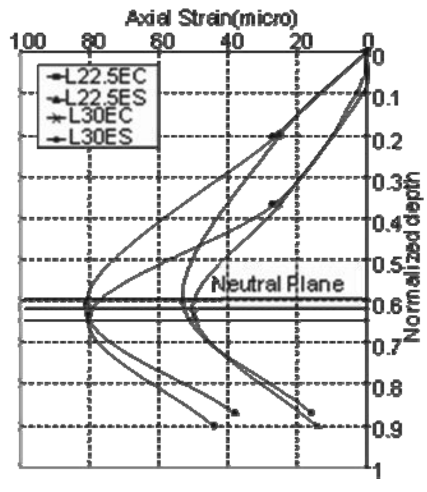

Fig. 6 Normalized neutral plane for piles ended in sand and clay (same L/d)

Figure 6 illustrates the normalized neutral depth as a function to the pile length embedded in the clay layer. The pile diameter is 1.5cm. Two cases; I, and II of tested piles are shown in the Figure. As can be seen from the Figure, the normalized neutral depth increases with the increase of the pile length embedded in the clay layer.

The explanation of the effect of the pile length on the neutral plane is due to the compressibility of the pile length. When negative skin friction is induced in a short pile, most of the downdrag is transmitted to the pile tip in the form of penetration to the bearing layer. Whereas, for long pile the downdrag is partly taken by the pile compressibility, and partly transmitted to the tip.

3.4 Determination of the Neutral Plane

Shong approach is adapted to locate the neutral plan. This approach is outlined in Section 1. The factor of safety of pile capacity against ultimate pile capacity, Fs is considered two, and β is taken 0.3.

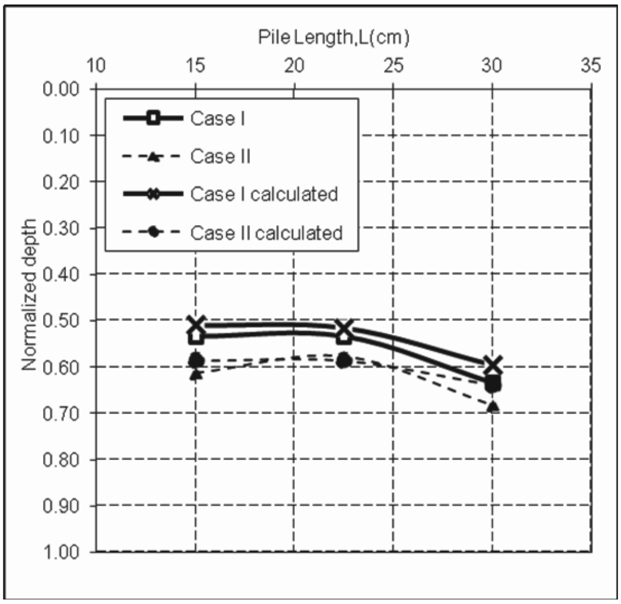

Fig. 7 Monitored and Calculated Location of the Neutral Plane

Figure 7 depicts the normalized neutral depth from both the monitored data and Shong approach. The pile diameter is 1.5cm. Two cases; I, and II, of tested pile are shown in the Figure. As can be seen from the Figure, the calculated normalized neutral depth is having the same trend as the monitored ones. The approach results into very good agreement with the normalized neutral depth.

4 CONCLUSION

This paper presents a study on the behavior of pile during soil consolidation. In order to carry out the investigations, experimental program was designated. A special rig was designed and constructed for this purpose. Based on test results the following conclusions are reached:

- Consolidation of the soil surrounding the pile due to surcharge loads induces negative skin friction on piles.
- The monitored strains along the pile length reflect the consolidation process with time. Strain increases from the pile top until it reaches a peak value at the location of the neutral plane.
- Sand layers, at the pile tip, offer resistance to the pile movement; end bearing. This increases stresses in the bottom portion of the pile. Hence, there is increase in the monitored strain, when compared with piles ended in clay, or floated.
- Shear stress is initiated from zero value at the surface of the soil and increases until it reaches a peak negative value at an intermediate depth. Then, it decreases down to zero at the elevation of the neutral plane where the positive skin friction develops.
- The neutral plane is located closer to the end of the pile as the base layer getting stiffer.
- The normalized neutral depth increases with the increase of the pile length.
- Shong approach for ND results into very good agreement with the monitored ones.

5 REFERENCES

Bozozuk M. 1972. Downdrag measurements on a 160-ft floating pipe test pile in marine clay. Canadian Geotechnique J. 9(2), 127-136.

Briaud J. L. 2010. Designing for downdrag on uncoated and coated piles. Piling and Deep Foundation. Middle East.

Fellenius B. H. 1989. Unified design of piles and pile groups. Transportation Research Record. 1169, 75-82.

Fellenius B. H. 2004, Unified design of piled foundations with emphasis on settlement analysis. ASCE. Geotechnical Special Publication. GSP 125, 253 - 275.

Fellenius B. H. 2006. Piled foundation design – clarification of a confusion. Geotechnical News Magazine. 24 (3), 53-55.

Leung C. F., B. K. Liao, and Chow Y.K. 2004. Behavior of pile subject to negative skin friction and axial load. Japanese Geotechnical society.44 (6), 17-26.

Maugeri M., Amenta G., Castelli F. and Motta E. 1997. Settlement of a piled foundation due to negative skin friction. Proc. 14th. int. Conf. on SMFE Hamburg. (2), 1111-1114.

Nassar A. E. 2010. Geotechnical Behavior of Pile during Soil Consolidation. Msc. Zagazig University. Zagazig. Egypt.

Poorooshasb H. B., Alamgi M. and Miura N.1996. Negative skin friction on rigid and deformable piles. Computers and Geotechnics, 18 (2), 109-126.

Sangseom J., Leea J. , Leeb C. J. 2004. Slip effect at the pile–soil interface on dragload. Computers and Geotechnics 31, 115.126.

Sharif, A. 1998. Negative skin friction on single piles in clay subjected to direct and indirect loading. M.Sc. thesis. Concordia university, Montreal. Quebec. Canda.

Shong Ir L. S. 2002. Pile design with negative skin friction, Geotechnical Engineering. 27 Puteri Pan Pacific Hotel.

Van Der Veen C. 1986. A general formula to determine the allowable pile bearing capacity in case of negative friction. International conference on deep foundations. Beijing. China, pp. 2.138-2.147.

Walker L.k., and Darvall,P. 1973. Downdrag on coated and uncoated pile. Proc. 8th int. conf. in soil mech. Eng. Moscow. 2(1), 257-262.

The Performance of Helical Pile Groups Under Compressive Loads: A Numerical Investigation

Performance d'un groupe de piles héliocoïdales sous chargement axial : une étude numérique

Elsherbiny Z.
Natural Resources, AMEC Americas Ltd., Calgary, Canada

El Naggar M.H.
Department of Civil and Environmental Engineering, University of Western Ontario, London, ON, Canada

ABSTRACT: An extensive finite element analysis (FEA) study on helical piles is conducted to evaluate the performance of helical pile groups subjected to axial compressive loads. Three-dimensional nonlinear analysis is conducted using the FE program ABAQUS. The Mohr-Coulomb plasticity model is used to represent the mechanical behaviour of soil. The numerical models are calibrated and verified using: full-scale load testing data of single piles; representative soil properties obtained from the borehole logs; and realistic modeling assumptions. A parametric study is then conducted on a wide range of varying parameters including: soil types (dry sand and saturated clay); and pile spatial parameters (inter-helix spacing and pile spacing). The numerical results are compared to available methods in the literature for conventional piles and design recommendations are provided.

RÉSUMÉ : Une étude numérique par éléments finis (MEF) sur des piles hélicoïdales est entreprise pour évaluer la performance d'un groupe de piles soumis à des charges de compression. Une analyse tridimensionnelle, non linéaire, est conduite en utilisant le code ABAQUS et le modèle de plasticité de Mohr-Coulomb est utilisé pour représenter le comportement mécanique du sol. Les modélisations numériques sont calibrées sur des essais complets sur simple pile avec les caractéristiques du sol obtenu sur des carottes en laboratoire et avec des hypothèses réalistes. Une étude paramétrique est alors entreprise sur un large éventail de paramètres comprenant: les types de sol (sable sec et argile saturé) et des paramètres géométriques (espacement inter-hélice et espacement des piles). Les résultats numériques obtenus sont comparés aux résultats issus de la littérature pour des piles conventionnelles et des recommandations de conception sont fournies.

KEYWORDS: helical pile, numerical modeling, group effect, interaction factor, settlement ratio, displacement ratio, efficiency factor

1 INTRODUCTION

Helical piles represent an efficient deep foundation system used in a wide range applications varying from anchors for transmission towers to foundations for bridges and large industrial installations. Helical piles are made of a steel shaft; either a solid square shaft or circular pipe, with one or multiple helices attached to it. They are installed by employing rotational force applied through a drive head. The piles could be installed to any depth and at any angle provided that the soil conditions are tolerable and the pile is designed to withstand the applied torque from a suitable drive head.

The current design methods of single helical piles are based on the same framework and theories of conventional piles, where the compressive capacity of the pile is provided by a combination of shaft resistance and bearing resistance on the helices (Mitsch and Clemence, 1985; Narasimha Rao, et. al, 1991; Zhang, 1999; and Livneh and El Naggar, 2008).

Pile foundations typically involve a group of piles connected by a common pile cap. A concrete cap is normally used to connect the pile heads in the group. Structural loads are applied to the cap, which in turn transfers them to the piles. The pile group behaviour is strongly affected by the soil type and the spacing between piles. However, currently there is no published research work on the compressive capacity and performance of helical pile groups which lead the designers to use methods available for conventional piles (i.e. bored piles and driven piles) to design helical pile groups.

The load transfer mechanism of helical piles is more complex than for conventional piles. The lack of particular guidance for helical piles motivated the present research work herein, with special emphasis on the group performance of helical piles and to provide design methods that are tailored for helical pile groups. This paper examines the effects of: inter-helix spacing; soil type; and pile spacing on the performance of helical pile groups.

1.1 *Review of Pile group Behaviour*

Piles in a group are expected to interact as the stress zones around the piles overlap. This interaction is strong for small pile spacing and diminishes as the pile spacing increases. The overlapped stress zones underneath the cap could affect the average capacity or average settlement of piles in the group compared to single piles subjected to average group load.

It is convenient to characterize the group effect on the performance of pile groups through the settlement ratio, R_s, as follows:

$$R_s = \frac{Settlement\ of\ the\ group\ (S_G)}{settlement\ of\ single\ pile\ (S_S)} \geq 1.0 \tag{1}$$

A practical approximation of the settlement ratio was derived by Randolph (Rowe, 2001):

$$R_s \cong n^w \tag{2}$$

where *n* is the number of piles in the group; and *w* is a factor depending on pile spacing, pile geometry, relative pile/soil stiffness, and the variation of soil modulus with depth. Typically, $w = 0.5$ for friction piles in clay and 0.33 for friction piles in sand spaced at 3 x pile diameters center to center.

Poulos and Davis (1980) proposed using the interaction factors, α_v, to represent the effect of a pile on a neighboring pile. In general, the interaction factor is a function of the relative pile/soil stiffness, pile length, pile diameter, center to center pile spacing, and the soil elastic modulus along the pile length and at its base (Poulos, 1988).

The settlement ratio can then be evaluated using the interaction approach as follows:

$$R_s = \alpha_{11} + \sum_{j=2}^{n} \alpha_{1j} \geq 1.0 \tag{3}$$

where *n* is the number of piles in the group; the interaction factor between reference pile and itself, $\alpha_{11=1}$; and α_{1j} is the interaction factor between reference pile 1 and pile j and j = 2,…, n.

2 FULL-SCALE TESTING

The field testing program consisted of performing five compression load tests on four non-instrumented piles of different sizes at two sites: site (A) is composed primarily of sand; and site (B) is mainly clayey soil. Two axial compressive load tests were conducted at Site (A) and three axial compression load tests were conducted at site (B). The piles installed at site (A) had single helix, while those installed at site (B) had double and triple helices. The load tests conformed to procedure A of ASTM D1143 for axial compression testing.

The subsurface soil condition at site (A) included a top 0.3m of an organic soil material followed by a thin brown clay layer that extends 0.5m and consists of silt and sand, and traces of gravel. Underlying the clay layer is a sand layer that extends to 9m below ground surface. The sand ranged from fine grained at the top to coarse grained with increasing depth. The Standard Penetration Test (SPT) blow count number indicated loose to medium dense sand conditions with depth. The natural moisture content was averaged at 20% along depth. The groundwater table was not observed at the time of drilling and the piles were installed and tested during the month of October.

The subsurface soil profile established from the boreholes at site (B) comprises a surficial fill layer of sand and gravel mixed with some organics and extends to 1.5m with an SPT number ranging between 5 and 6. Underlying the surficial layer is medium to stiff brown silt and sand that extends to depths between 2.3m to 4.6m below ground surface with an SPT number varying between 3 and 12. Further deep is a silty clay layer that extends to depths 6.1m and 7.6m below ground surface. The silty clay layer gets softer with increasing depth and the SPT number ranged from 6 to 0. The ground water table was encountered 1.0 m below the ground surface.

The tested piles geometrical properties were representative of typical helical piles geometry in projects that involve light to medium loading conditions and are summarized in Tables 1 and 2 for site (A) and site (B), respectively.

The test results were used exclusively to calibrate and verify the numerical models that were then used to perform the parametric study.

Table 1. Summary of tested piles configurations at site (A)

Test Pile	Depth (m)	Shaft Diameter (mm)	Helix Diameter (mm)
PA-1	5.5	273	610
PA-3	5.6	219	508

Table 2. Summary of tested piles configurations at site (B)

Test Pile	Depth (m)	Shaft Diameter (mm)	Helix Diameter (mm)
PB-1	7.2	178	610x610x610
PB-2	7.2	178	610x610x610
PB-4	3.2	114	406x406

3 NUMERICAL MODELING

A finite element model is developed using the program ABAQUS (SIMULIA, 2009) to simulate the experimental program. The soil continuum is modeled considering a 3D cylindrical configuration and the pile is placed along the axial z-direction of the cylinder. The helix is idealized as a planar cylindrical disk so that modeling of the pile and the surrounding soil can take advantage of the axisymmetric conditions as shown in Figure 1.

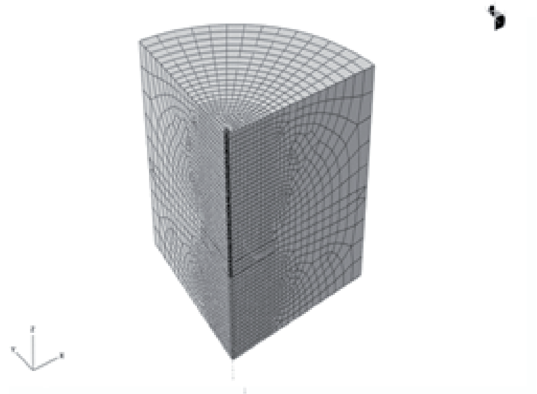

Figure 1. Numerical model geometry for a single pile subjected to axial load.

3.1 *Model description*

The 3-dimensional soil medium is discretized into 8-noded, first order, and reduced integration continuum solid elements (C3D8R). The element has three active translational degrees of freedom at each node and consists of one integration point located at the centroid. The pile is simulated using four-nodes, first order, reduced integration, general-purpose shell elements (S4R).

The boundaries are located such that there is minimal effect on the results. The radius of the soil column extends approximately 33 shaft diameters from the center of the pile shaft. The depth of soil deposits below the lower helix is a minimum of 6.5 helix diameters. The top soil surface is considered as stress-free boundary. The boundary conditions exploited symmetry to reduce the model size. The bottom of the soil cylinder is pinned. The back of the cylinder is constrained in the horizontal plane and is free to move vertically.

The soil is modeled as an isotropic elastic-perfectly plastic continuum with failure described by the Mohr-Coulomb yield criterion. The elastic behavior was defined by Poisson's ratio, v, and Young's modulus, E. The plastic behavior is defined by the residual angle of internal friction, φ_r, and the dilation angle, ψ, and material hardening is defined by the cohesion yield stress, c, and absolute plastic strain, ε_{pl}.

The pile-soil interface is modeled using the Tangential Behavior Penalty-type Coulomb's frictional model. The soil unit weight is accounted for in the numerical model as an initial stress through the geostatic equilibrium step.

3.2 *Calibration and verification*

Using some of the test results, the above model properties and configurations, and representative soil properties obtained from the boreholes and the literature, the numerical models are calibrated satisfactorily considering the soil conditions and load test results of piles PA-1 and, PB-1 and PB-2 as shown in Figures 2 and 3. The soil properties used in the analysis are assumed to be the disturbed properties due to pile installation.

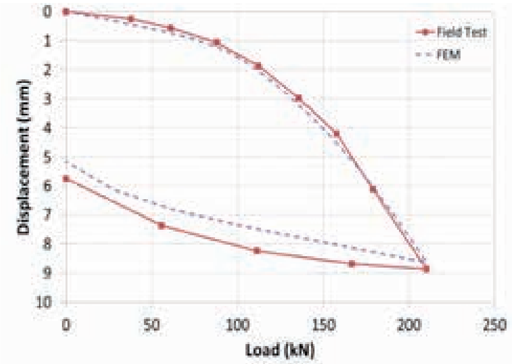

Figure 2. Calibrated numerical model compared to field test of PA-1

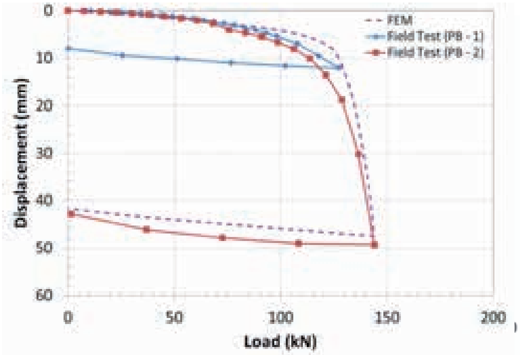

Figure 3. Calibrated numerical model of piles PB-1 and PB-2

In order to verify the ability of the calibrated models to accurately depict the behavior of helical piles under compressive and lateral loading, the calibrated models were utilized (considering the same soil properties and boundary and interface conditions) to analyze the remaining load test data and the results showed satisfactory agreement with actual test results of piles PA-3, and PB-4 as shown in Figures 4(a), and 4(b).

a)

b)

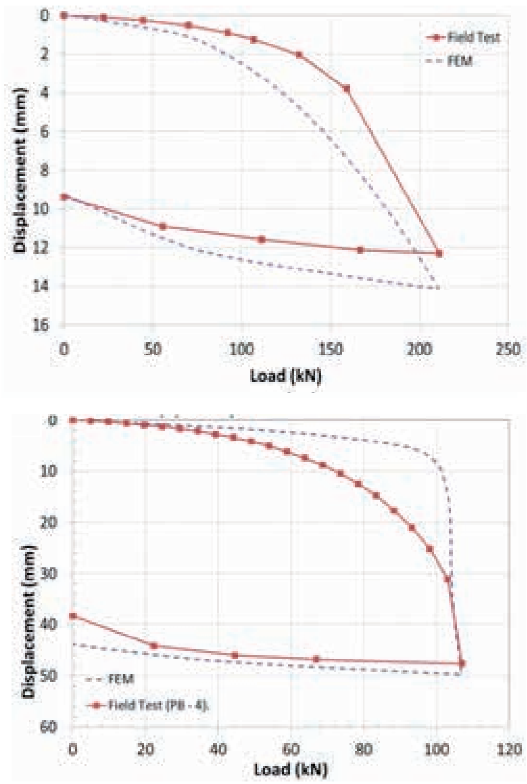

Figure 4. Verified numerical models: a) Pile PA-3; b) Pile PB-4.

Using the same soil properties that are established from the calibration of model considering pile PA-1 test data, the calculated response of neighbouring pile PA-3 is softer than the field test results as shown in Figure 4(a), but the calculated response of pile PB-4 is stiffer than the load test data. This is expected due to the natural spatial variability of soil properties.

3.3 *Parametric study*

Using the previously calibrated and validated models, a numerical parametric study is conducted considering different practical pile configurations and common soil types. The piles considered consist of a 273mm diameter steel pipe that has two 610mm helices attached to it. The inter-helix spacing ratio, S_r, ranges between 1 and 3 helix diameters (i.e. 1*D*, 2*D*, and 3*D*) with a pile embedment depth of 6 m. The piles are modeled as single, two, and four piles in a square arrangement with a center to center spacing, S_p, ranging between *2D* to *10D*.

The pile is modeled as elastic steel with E = 200GPa and ν = 0.3. For piles in sand, the sand is modeled as homogeneous with φ_r = 30° and ψ = 0° to represent loose to medium dense sand. The yield cohesion, c, is 0 kPa to represent purely frictional sand. The sand is assumed to have a bulk unit weight of 20 kN/m^3 and an initial coefficient of lateral earth pressure, K_o, equal 0.5. Moreover, the pile-soil interface friction angle, δ, is assumed to be 0.67φ_r which yields a friction factor of 0.38. Finally, the modulus of elasticity of the soil is assumed to be 100MPa and the soil Poisson's ratio, ν = 0.3.

For piles in clay, it is assumed that the helices are embedded into a very stiff clay layer with undrained shear strength, c_u = 100kPa and E = 50MPa, while the soil above top helix (i.e. along the shaft) is soft clay with c_u = 25kPa and E = 30MPa. The clay is modeled assuming the water level is at the ground surface, and the loading rate is assumed fast enough to invoke undrained conditions. Therefore, Poisson's ratio = 0.49 was considered in the analysis. The adhesion, c_a, between the pile and the soil is estimated from CFEM (2006): for c_u = 25 kPa, c_a = 25 kPa. A friction factor of 1.0 is used indicating that the frictional stresses along the shaft are equal to the contact pressure. However, to account for the adhesion strength, a shear stress limit along the interface is defined at which slippage occurs. This shear stress limit along the interface is c_a.

4 RESULTS AND DISCUSSION

For load-settlement curves with no visually distinctive failure point, as for the case of piles in sand, the failure loads are obtained at a practical settlement level equal to *5%D* (i.e. 30mm). The pile settlement is obtained at a service load equal to the failure load divided by a factor of safety, *FS*, equal to 3.

For a 4-pile group in sand, R_s could be as high as 1.3 at S_p = *2D* and as low as 1.1 at S_p = *5D*. R_s is the greatest at S_p = *2D* and decreases gradually with increasing S_p as shown in Figure 5. It is also found that S_r has a negligible effect on R_s. Moreover, R_s at service load considering *FS* = 2 is larger than R_s for service loads given by *FS* = 4, as shown in Figure 6. It is also found that R_s for a group of piles is not necessarily an algebraic summation of the interaction factors, α_{ij}, of the piles in the group. The existence of other piles in a group (other than the two under consideration) stiffens the soil. Therefore, the interaction factors would decrease relative to the case of a 2-pile group. Basile (1999) made similar observations and concluded that the interaction factors approach may lead to overestimation of pile response. Furthermore, Randolph (1994) stated that the interaction factors should only be applied to the elastic component of settlement since the plastic component of settlement is largely due to localized failure close to the pile and is not transferred to neighboring piles.

It is also found that the empirical equation suggested by Randolph (Equation 1) overpredicts the settlement ratio for four-pile groups by 22% for $S_p = 2D$ and by 45% for S_p greater than *3D*. In addition, using the equation proposed by Randolph and Poulos (1982) to obtain the interaction factor, α_v, for helical piles assuming straight shaft with diameter *D* for $S_p = 2D$ yields largely overestimated interaction effect. On the other hand, using a straight shaft pile diameter of *d* (i.e. helical pile shaft diameter) yields comparable values to the ones obtained by the parametric study.

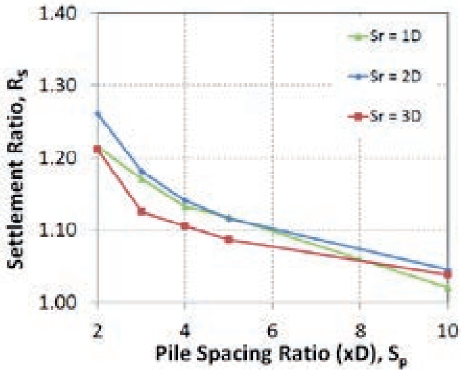

Figure 5. The settlement ratio for 4-piles group in sand with different S_r

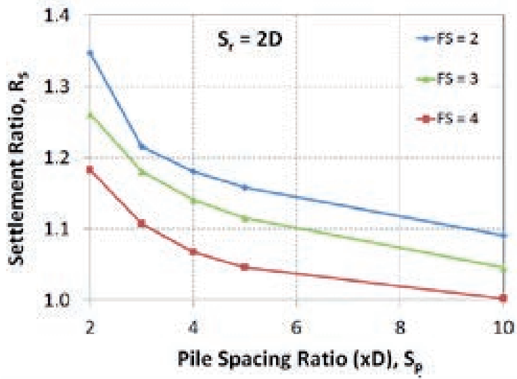

Figure 6. The effect of the factor of safety on the settlement ratio for 4-piles group in sand

For piles in clay, it is found that R_s could be as high as 1.33 for $S_p = 2D$ and as low as 1.1 for $S_p = 3D$, as shown in Figure 7. The settlement ratios are the highest at $S_p = 2D$ and decrease rapidly with increasing spacing. It is also found that S_r has a negligible effect on R_s.

Similar to piles in sand, it is also found that R_s for a group of piles is not a linear algebraic summation of the interaction factors, α_{ij}, of the piles in the group. It is found that the empirical equation suggested by Randolph (Equation 1) over-predicts R_s by 80% for piles spaced at *2D* and by 100% for S_p greater than *3D*. In addition, using Poulos (1979) charts and Randolph and Poulos (1982) equation, (Poulos, 1988), to obtain α_v assuming straight shaft piles diameter of *D* for $S_p = 2D$ is found to overestimate α_v. On the other hand, using the same charts and equation with a straight shaft pile diameter of *d* yields comparable values to the ones obtained by the parametric study.

Finally, in contrast to piles in sand, it is found that R_s at service load considering *FS* = 2 is lower than R_s for service loads given by *FS* = 4, however the effect is negligible.

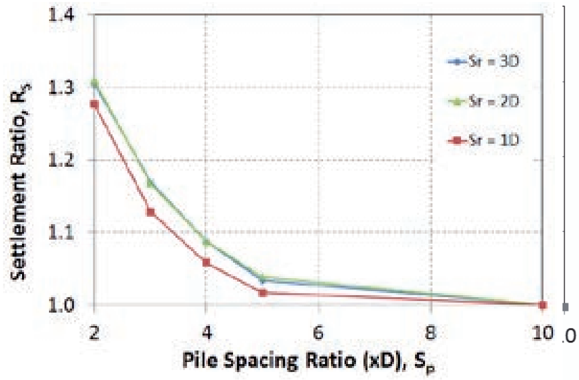

Figure 7. The settlement ratio for 4-piles group in clay with different S_r

5 CONCLUSIONS

The performance of a helical pile group in sand or clay is mainly affected by the piles center to center spacing. The practical range of inter-helix spacing (*1D* to *3D*) has negligible effect on R_s. The factor of safety, *FS*, could significantly affect R_s for piles in sand and has negligible effect for piles in clay. In addition, the settlement ratio, R_s, for a pile group is not simply an algebraic summation of the interaction factors, α_{ij}, of the piles in the group.

Finally, R_s can be conservatively estimated using the methods reported herein using a straight shaft pile with a diameter equal to the shaft diameter of the helical pile. In general, R_s for helical piles with multiple helices spaced at a typical pile spacing of *3D* is in the range of 1.15 to 1.2 for both clay and sand.

6 ACKNOWLEDGEMENT

The authors wish to extend their thanks to the National Science and Engineering Research Council of Canada (NSERC) for the generous financial support. The authors also extend their thanks and appreciation to Helical Pier Systems (HPS) and Almita Piling Inc. for their continuous support.

7 REFERENCES

ASTM. (2007). *Standard test methods for deep foundations under axial compressive load, D1143M-07.* West Conshohocken: ASTM International.
Basile, F. (1999). Non-linear analysis of pile groups. *Proceedings of the Institution of Civil Engineers (UK), Geotechnical Engineering,* 137(2), 105-115.
CFEM. (2006). *Canadian Foundation Engineering Manual* (4th ed.). Richmond, BC: BiTech Publishers Ltd.
Livneh, B., & El Naggar, M. H. (2008). Axial testing and numerical modeling of square shaft helical piles under compressive and tensile loading. *Canadian Geotechnical Journal*, 1142-1155.
Mitsch, M., & Clemence, S. (1985). The uplift capacity of helix anchors in sand. In S. Clemence (Ed.), *Proceedings of the Uplift Behaviour of Anchor Foundations in Soil* (pp. 26-47). Detroit: ASCE.
Narasimha Rao, S., Prasad, Y., & Shetty, M. (1991). The behaviour of model screw piles in cohesive soils. *Journal of Soils and Foundations, 31*, 35-50.
Poulos, H. (1988). *Marine Geotechnics.* London: Unwin Hyman Ltd.
Rowe, R. K. (2001). *Geotechnical and geoenvironmental engineering handbook.* Massachusetts: Kluwer Academic Publishers.
Randolph, M.F. (1994). Design methods for pile groups and piled rafts. *Proc. 13th Int. Conf. S.M. & Found. Eng.,* 5: 61-82
Int. Conf. S.M. & Found. Eng., 5: 61-82.
SIMULIA. (2009). *Getting Started with ABAQUS: Interactive Edition.* Providence: Dassault Systèmes Simulia Corp.
Zhang, D. J. (1999). *Predicting Capacity of Helical Screw Piles in Alberta Soils. Unpublished master's thesis.* Alberta, Canada: University of Alberta.

Contributing factors on soil setup and the effects on pile design parameters

Facteurs contribuant au durcissement du sol et leur effet sur les paramètres de conception des pieux

Fakharian K., Attar I.H., Sarrafzadeh A., Haddad H.
Department of Civil and Environmental Engineering, Amirkabir University of Technology, Tehran, IRAN,

ABSTRACT: Most of the pile setup studies in literature have focused on the variations of total capacityand/or tip and skin friction resistances. But it is of practical importance to propose realistic parameters for design applications such as pile shaft resistance β-parameter. Pile dynamic (PDA) and staticload test results are available for 5% of total of 6000 drivenpre stressed spun piles with OD of 450 mm at a petrochemical utility plant in southwest Iran.The range of β-parameter for each of the three layers along which the piles are embedded are determined for design applications in the regionwith back-calculationfromdynamic tests results at restrike. An axisymmetric finite element numerical model isused to simulate the cavity expansion developedduring pile driving and corresponding generation of excess pore water pressure (EPWP). The setup effects are evaluated allowing sufficient time for dissipation of EPWP and simultaneous increase in radial effective stresses along the pile shaft. The difference between shaft capacity obtained from the back-calculated β of the field data and that from the numerical model for EPWP dissipation analysisonly, is assumed to be attributed to aging effects. Increase in the interface shear strength between pile-soil with time isconsidered to account for the aging component of the soil setup. The results show that the dissipation of EPWP has been the dominant factor in soil setup corresponding to increase in the frictional resistance of the pile shaft of the study area in which 75% has been resulted from radial cosolidation (EPWP dissipation) and 25% from aging.

RÉSUMÉ : La plupart des études configuration de pieuxdans la littératureontmisl'accentsurles variations de la capacitétotale et / ou la pointe et les résistances de frottementlatéraldans le temps. Maisilestd'une importance pratique de proposer des paramètresréalistes pour les applications de conception telles le paramètre β décrivant la résistance de fût. Des essaisdynamiques (PDA) ainsique des résultatsd'essais de charge statiquesontdisponibles pour 5% des 6000 pieux de bétonpréfabriquésprécontraint d'un diamètreextérieur de 450 mm dansuneusinepétrochimique du sud-ouest de Iran. La plage des valeurs du paramètre β pour chacune des trois couches le long desquelles les pieuxsontenfoncésestdéterminée pour les applications de conception dans la région à partir de rétro-calculsd'après les résultatsd'essaisdynamiqueslors du rebattage. Un modèlenumérique par éléments finis axisymétrique estutilisé pour simulerl'expansion de la cavitédéveloppée au cours du battage de pieux et de la production correspondante de la pressiond'eauinterstitielle en excès (EPWP). Les effets de mise en place sontévaluées en permettant un temps suffisant pour la dissipation de l'augmentation de la pressiond'eau et l'accroissementsimultané des contraintes effectives radiales le long du fût du pieu. La différence entre la capacité de fûtobtenued'après les valeurs de β rétro-calculées à partir des données de terrain et cellesobtenues à partir du modèlenumériqued'analyse de dissipation de la pressiond'eauinterstitielle, estsupposéêtreattribués à des effets de vieillissement. L'augmentation de la résistance au cisaillementd'interface entre le pieu et le sol en fonction du temps supposétenircompte de la composante du vieillissement du durcissement du sol. Les résultatsmontrentque la dissipation de la pressioninterstitielle a été le facteur dominant dans le durcissement du sol correspondant à l'augmentation de la résistance de defûtdans la zone d'étudeoù 75% de l'augmentationestattribuable à la consolidation radiale (dissipation de la pressiond'eauinterstitielle) et 25% au vieillissement.

KEYWORDS: pile driving,numerical modelling,effective stress analysis, soil setup, aging, PDA test, cavity expansion

1 INTRODUCTION

Driven piles are frequently used in industrial projects in southern lowlands of Iran near Persian Gulf.One of the important issues in driven piles is variation of bearing capacity with time after the initial drive. This important issue is well-understood in literature and it is pointed out that depending on the soil type, either “soil setup” or “soil relaxation” may occur with time. Soil setup results in eventual increase in the pile capacity, whereas in the soil relaxation condition, the bearing capacity decreases with time.

Different reasons are stated for these phenomena and the types of soil in which either of the setup or relaxation may occur (Svinkin, 1996; Seidel and Kolinowski, 2000; Rausche et al., 2004; Bullock et al., 2005 and 2005b).In majority of reported cases however, the setup has occurred and relaxation has seldom been reported (Komurka et al., 2003; Axelsson, 2000). The bearing capacity variations are observed to be rapid with time initially, the rate of which substantially decreases with time elapse.

The stated reasons for setup can be summarized as: (1) generation of excessive pore water pressure during pile driving and subsequent dissipation with time, (2) aging. Most of the studies available in literature, however, have focused on pile capacity variation with time and it is stated that (for example by Svinkin, 2000) the most portion of setup is related to dissipation of effective pore water pressure. Little attention has been paid on distinguishing between the contribution of dissipation of EPWP and aging.

The main objective of this study is a numerical approach to study the setup effects on a single pile embedded in layered strata on the basis of back-calculated parameters from an industrial unit in southwest Iran. An axisymmetric nonlinear finite element scheme is adopted to simulate the cavity expansion as a result of pile driving and its subsequent dissipation of EPWP and aging effects. A case in fajr II utility have been carried out at End of Initial Drive (EOID) and, after 13 days, at Beggining of Resrtike (BOR) condition is selected to study the different components contributing to the setup effects.

2 CONSTRUCTION SITE AND TESTS

Fajr II is a 32-hectar utility plant in PetZone of Mahshahr, located in southwes Iran near Persian Gulf. The site accommodates a power plant, pre-treatment and treatment water units and air unit. Different types of precast and prestressed driven concrete piles at a total of nearly 7000 points have been constructed within the past three years. About 6000 points include 450 mm outside diameter prestressed spun piles with a wall thickness of 80 mm and closed-toe. The spun piles have been driven with Kobe-35 and Kobe-45 diesel hammers, or equivalents, down to embedment depths ranging between 14 through 22 m. The dominant soil layering across the construction site is a very soft to stiff silty clay, average of 15 m thick (layers I & II), overlain a medium dense to dense sand, 4 to 8 m thick (layer III). The pile tips are mostly embedded within the sandy layer. Table 1 shows the geotechnical parameters for construction site layers.

Nearly 5000 spun piles, 450 mm OD were driven to support 12 water tanks. Pile dynamic tests (PDA) and static load tests were carried out on 30 test piles & 221 construction piles, including, respectively, 54 & 251 PDA tests and 4 & 32 compressive static load tests. Static and PDA tests procedure comply with general guidelines and specification of ASTM D1143 and D4945, respectively. Some of the comparisons between static and dynamic load tests are presented in Fakharian et al. (2012). In fact about 5% of the construction piles were PDA tested and average of 2 piles were static load tested at each tank. With support of the test program, the factor of safety was lowered to about 2 to 2.2 and sometimes as low as 1.8, that resulted in considerable savings compared to previous projects in the region. The construction challenges and cost savings are presented in more details by Fakharian et al. (2012).

Further information about tank details, test piles and borehole location, pile arrangement and No. of construction pile tests can be found in Sarrafzadeh et al. (2012).

The dominant soil layering in the 32-hectar site is highly variable but classified in three layers, from top to bottom respectively, layer 1 with 8 m thickness as soft clay, layer 2, 7 m thick as medium stiff to stiff clay, and layer 3, sand down to 20 m. The incremental and cumulative shaft capacities from CAPWAP analysis are available, from which, β-factor versus depth is back-calculated. All the data points of five tanks were put together and the results are presented in Fig. 1.

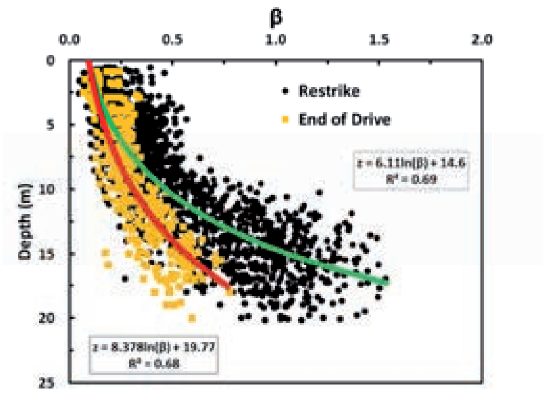

Figure 1.β variation with depth at EOD and Restrike for all tanks.

The lower and upper bounds of β-values and the average trend lines are plotted in Fig.2. The average trend line can be represented by empirical Eq. (1):

$$\beta = e^{\frac{z-14.6}{6.11}} \qquad (\beta < 1.5) \qquad (1)$$

in which, z (in m) is depth from ground surface.

Similarly, Eqs. (2) and (3) represent the upper bound,β_u, and lower bound, β_l, respectively. The β parameter variation with depth value is limited to 1.5 in all equations.

$$\beta_u = e^{\frac{z-11}{7.5}} \qquad (\beta < 1.5) \qquad (2)$$

$$\beta_l = e^{\frac{z-20}{5.5}} \qquad (\beta < 1.5) \qquad (3)$$

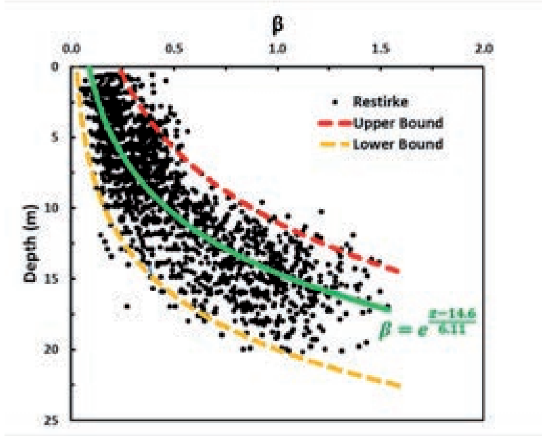

Figure 2. Mean β and lower and upper bounds at restrike.

3 NUMERICAL MODEL AND VALIDATION

Test pile No. 11 with 15.4 m embedment length is selected for modeling, PDA test was performed at End of Initial Drive (EOID) and, after 13 days, at Beggining of Resrtike (BOR) condition. an elastic isotropic cylindrical pile with radius of 225.5 mm and 15.4 m length has been generated using the FEM numerical package ABAQUS, in 2D axisymmetric condition. Elasto-perfectly plastic model has been considered for the soil material. Therefore, the required parameters for the elastic part include elastic modulus, E, and Poisson's ratio, ν, and Mohr-coloumb strength parameters for the shear failure. The soil surrounds the pile shaft with a radius of 5 m and length of 15.4 m. The brick soil elements have been generated 2.5x2.5cm adjacent to the pile skin with gradual increase in size to reach a maximum dimension of 2.5x12.5cm at the vertical boundary. The pile shaft is simulated by 2.5x2.5cm solid elements. Table 1shows the specified parameters for both pile and soil material.

Table 1. Soil and pile parameters in numerical model (for TP 11)

Layer #	Soil type	Depth (m)	γ' (kN/m³)	E (MPa)	K (m/s)	C (kPa)	φ'
I	Soft clay	0-7.4	10	20	1×10^{-9}	27	0
II	Medium to stiff clay	7.4-12.4	10	20-50	1×10^{-9}	27	0
III	Medium dense to dense sand	12.4-15.4	10	50	1×10^{-8}	1	30
Pile	Concrete	15.4	14	20,000	-	-	-

The solid element CAX4RP has been used for which simultaneous measurements of PWP and stress-strain are possible. It is assumed that drainage is possible from the ground surface only. Therefore, the top horizontal boundary was specified as a zero pressure surface. Interface elements were specified at the pile-soil contact surface. The interface parameters were specified as tangential interface.

The pile installation process has been simplified to an eventual expansion of the soil from a zero radius up to the 225.5 mm. In other words, cavity expansion has been simulated in axisymmetric condition, therefor effects of eventual pile shaft penetration are not considered in this study. The PWP at the end of cavity expansion (U_0) has the maximum magnitude, corresponding to t=0 in the presented results.

Validation of the numerical model was done by comparing the numerical model results with the results of instrumented case that is reported by Konrad and Roy (1987).It is noticed that the numerical model predictions compare reasonably well with measurements.For example, Figs. 3 representthe dissipation of EPWP resulted from driving at depth 6.1 m with time. The EPWP at any time t (U_t) is normalized with U_0 and expressed in percentage. Therefore U_t/U_0 at t=0 is 100% and supposed to approach 0 at sufficiently long periods of time, depending on the permeability of the soil material. More details of verification process may be found in Haddad et al. (2012).

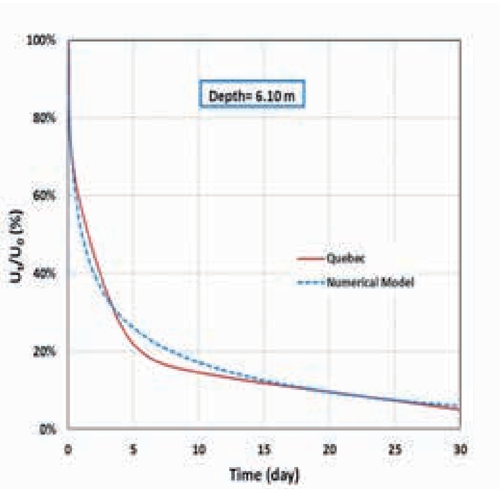

Figure 3.Dissipation of EPWP with time resulted from pile driving at depth 6.1 m.

4 ANALYSIS RESULTS

The main focus of this study is effect of setup on skin friction. The important factors contributing to variation of skin friction with time are radial effective stress and PWP adjacent to the pile shaft, as far as the effect of dissipation of EPWP is concerned. To account for aging effects, the interface shear strength parameters have been considered. The interface strength parameters have been specified applying the β′ reduction factor introduced by Fakharian and Iraji (2010) as:

$\tau_{int} = \beta'(c' + \sigma \tan\varphi')$

in which:

τ_{int}: shear strength at interface

c′: effective cohesion of adjacent soil

φ′: effective angle of internal friction of adjacent soil

Figure 4 shows the contour lines of effective radial stress along the pile shaft and up to the boundaries both at the end of initial drive (4a) and after 13 days (4b). It is observed that the radial stress has substantially increased as a result of dissipation of EPWP. Similarly, Fig. 5 presents the PWP at the end of initial drive (5a) and after 13 days (5b).Pore water pressure significantly increased due to the compressibility of the soft soil, except close to the ground surface that the dissipation has occurred rapidly due to short distance to the open boundary.

Comparing the results of Figs. 3 and 4 indicate that in zones that higher PWP has been generated at EOID, higher radial effective stress is developed after 13 days that about60% of EPWP has dissipated. Figure 6 presents the variation of effective radial stress with time between initial *in situ*condition up to end of EPWP dissipation along the pile shaft. It is of importance to note that the effective radial stress at EOID is considerably greater than initial *in situ* condition. This could be attributed to passive stress path outside the expanded cavity zone, indicating compaction of the soil. This requires further investigation with more advanced constitutional models and field measurements. The change in variations at depths of 7.4 and 12.4 m is because of soil layer differences.

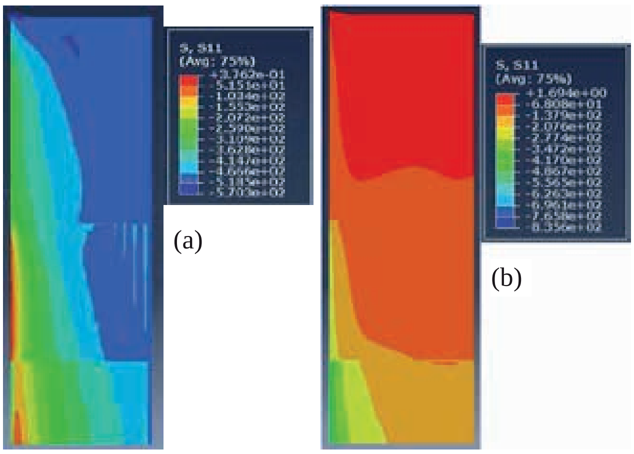

Figure 4.Radial effective stress distribution innumerical model: (a) EOID, (b) BOR after 13 days.

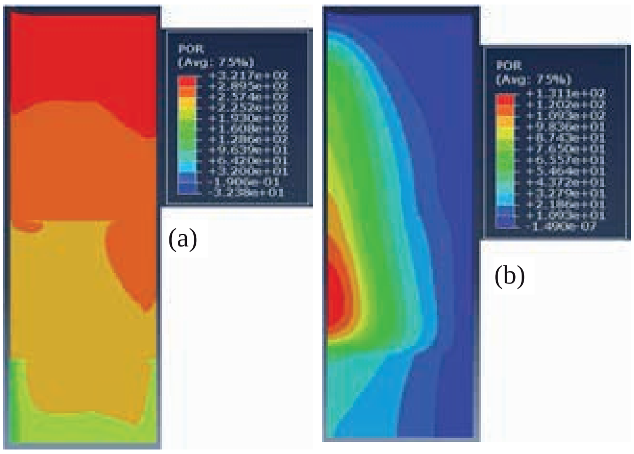

Figure 5.Excess pore water pressure distribution in numerical model: (a) EOID, (b) BOR after 13 days.

The main objective of this study has been attempting to distinguish between dissipation of EPWP and aging. As an example, variation of shaft capacity with respect to time are plotted in Fig. 7, resulted both from the back-calculation of field PDA tests and model predictions. The PDA test results are available for EOID and 13 days, depicted in Fig. 7 by for four solid square symbols.

In the numerical model, adopting a β′ of 0.235 has resulted in a good match between the EOID ofPDA test and model prediction. In other words, after the simulation of initial drive (cavity expansion), as an EOID condition, β′ was adjusted till the predicted and measured capacities have a good correlation. Then dissipation was allowed for 1, 4, 13 and 50 days (with the same β′) and the shaft capacity is calculated. The shaft capacity results from this procedure are plotted with green solid line (circled symbols) betweenEOID to 50 days. Considerably lower capacities are resulted compared to the measured capacities. This difference is thought to be attributed to the so-called aging effects.

To account for the aging setup effects, the interface frictional resistance coefficient, expressed by β′ factor in this study, has been increased until correlations are obtained between predicted and field measurements. This has been shown by the blue line in Fig. 7. The difference between the two green and blue lines in figure is assumed to be representing all the contributing factors to soil setup that are not effective-stress related. Such factors are referred to as “aging” in this study, and as explained, the β′ factor is assumed to account for it. Figure 7 shows that the contribution of dissipation of EPWP is 75% while the contribution of aging is 25%.

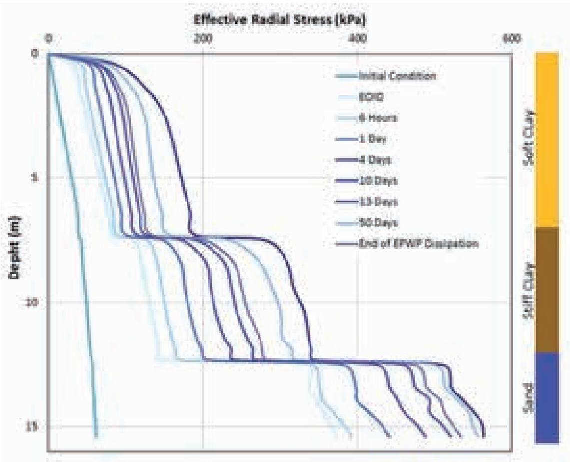

Figure 6.Radial effective stress changes with timealong the pile shaft.

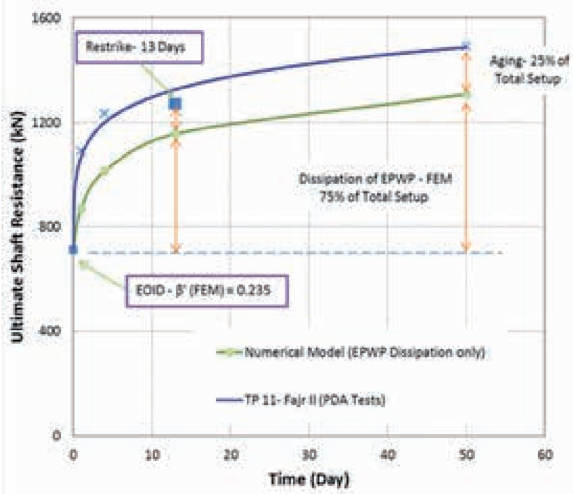

Figure 7.Increase in pile shaft capacity in numerical model.

5 CONCLUSION

The construction site ofFajr II utility plant,Mahshahr, Iranis selected to study the different components contributing to the setup effects using an elasto-perfectly plastic axisymmetric FEM model. Theadopted FEM model is capable of effective stress analysis and consideration of PWP effects and has been used to simulate the cavity expansion resulted from pile driving and subsequent dissipation of EPWP. The focus of study was to distinguish the effective stress-dependent and independent factors influencing the setup in layered strata. The findings of the study are listed below:

- -An empirical equation for calculation of shaft capacity after setup is presented for the study area.Two equations also are proposed as upper and lower bounds.
- - The numerical model predictions compare well with field measurements.
- -The generation of EPWP as a result of cavity expansion and subsequent dissipation with time has been predicted reasonably well.
- -The variation of interface shear strength reduction factor, β′is considered to represent the setup component attributed to aging.
- -In the layered media of the study site, the contribution of dissipation of EPWP and aging to soil setup has been estimated 75% and 25%, respectively, at about 50 days after initial drive.

6 ACKNOWLEDGEMENTS

The authors would like to thank Amirkabir University of Technology (AUT), Fajr Petrochemical Co., and Machine Sazi Pars Co., for financing the extensive dynamic and static load tests of this study.

7 REFERENCES

Axelsson, G. (2000). “Long-Term Set-up of Driven Piles in Sand” Ph.D Thesis, Royal Institute of Technology, Stockholm, Sweden

Bullock, P. J., Schmertmann. J., McVay. M, and Townsend, F. (2005). “Side Shear Set-up: Test Piles Driven in Florida.” Journal of Geotechnical & Geoenvironmental Engineering, ASCE, 131(3), 292-30

Bullock. P. J., Schmertmann. J., McVay. M. and Townsend. F. (2005b). “Side Shear Set-up. II: Results From Florida Test Piles” Journal of Geotechnical & Geoenvironmental Engineering, ASCE, 131(3), 301-310

Fakharian, K., Bahrami, T., Esmaili, F., and Hosseinzadeh Attar, I. (2012). “Dynamic and Static Tests for Optimization of Spun Piles of a Utility Plant near Persian Gulf - Case Study” The 9th International Conference on Testing and Design Methods for Deep Foundations, 18-20 September, 2012, Kanazawa, Japan.

Fakharian, K. and Iraji, A. (2010).“Numerical modeling of suction pile installation in Caspian Sea clay with effective and total stress analyses” International Journal of Offshore and Polar Engineers (IJOPE), Vol. 20, No. 4, pp. 313-320.

Haddad, H., Fakharian, K., and Hosseinzadeh Attar, I. (2012).“Numerical Modeling of Setup Effects on Pile Shaft Capacity and Comparison with an Instrumented Case” The 9th International Conference on Testing and Design Methods for Deep Foundations, 18-20 September, 2012, Kanazawa, Japan.

Komurka, E., Tuncer, B. E. and Wagner, A. (2003). “Estimating Soil/Pile Set-Up” Wisconsin highway Research Program #0092-00-14

Konrad, J. M. and Roy, M. (1987). “Bearing capacity of friction piles in marine clay” Geotechnique 37, No. 2, 163-175

Rausche, F. Robinson, B. and Likins, G. (2004). “On The Prediction Of Long Term Pile Capacity From End-Of-Driving Information” Current Practices and Future Trends in Deep Foundations (GSP 125) pp. 77-95.

Sarrafzadeh, A, Fakharian, K., and Hosseinzadeh Attar, I. (2012). “Investigation of bearing-capacity parameter variations with time using PDA test results: case study” The 9th International Conference on Testing and Design Methods for Deep Foundations, 18-20 September, 2012, Kanazawa, Japan.

Seidel, J. and Kolinowski, M. (2000). “Pile set-up in sands,” Procedures of the 6th Int. Conf. on the Application of Stress Wave Measurements to Piles, Sao Paulo, Brazil, Balkema, 267-274.

Svinkin, M. R. (1996). “Setup and Relaxation in Glacial Sand – Discussion,” Journal of Geotechnical Engineering, Volume 122, No. 4, ASCE, pp. 319-321.

Svinkin, M. R. and Skov, R. (2000). “Setup effects of cohesive soils in pile capacity” Proc. 6th International Conference on Application of Stress-Wave Theory to Piles, Sao Paulo, Brazil, Balkema, pp. 107-111.

Model loading tests in large soil tank on group behavior of piles

Essais de chargement modèle afin d'étudier le comportement de groupe de pieux dans un grand réservoir du sol

Goto S., Aoyama S., Liu B., Towhata I.
The University of Tokyo

Takita A.
Nippon Steel & Sumitomo Metal Corporation

Renzo A.A.
Anddes Asociados S.A.C., Lima-Perú

ABSTRACT: Model pile loading tests in dry sand were conducted with applying confining pressure of 50-200kPa at the surface of the model ground to investigate the behavior of a group pile. The group pile consisted of 9 cylindrical model piles of 40mm in diameter, while two kinds of the pile spacing between pile centers were used; 2.5 times of the diameter of the pile and 5.0 times of the diameter. For comparison, a single pile with a large diameter was also tested under the same condition. The test results were discussed based from the following 4 points of view; the settlement at the yielding point of the total load, tip stress distribution by the pile location in the group pile, pressure distribution in the soil measured by the tactile sensors and ground deformation after the loading tests. All discussion suggested that the group pile of 2.5D spacing caused significant interactional effect between piles and behaved in one block. In contrast, each pile in the group pile of 5.0D spacing behaved more individually.

RÉSUMÉ : Des essais de chargement de modèle de pieu dans un sable sec ont été effectués en appliquant une pression de confinement de 50-200 kPa à la surface du sol modèle pour d'étudier le comportement d'un groupe de pieux. Le groupe de pieux comprend neuf pieux modèles cylindriques de 40 mm de diamètre. Deux types d'espacement entre les pieux ont été utilisés dans le groupe de pieux modèles : 2,5 fois le diamètre du pieu et 5,0 fois le diamètre entre les centres des pieux. Afin de comparer, un seul pieu à grand diamètre a également été testé dans les mêmes conditions. Les résultats sont examinés selon les quatre points de vue suivants : le tassement à la limite élastique du chargement total, la distribution de contraintes en fonction de la position du pieu au sein du groupe, la distribution de la pression au fond du réservoir contenant le sol, mesurée par des capteurs tactiles, la déformation du sol après les essais de chargement. L'analyse suggère que le groupe de pieux de 2,5D d'espacement a provoqué une forte intéraction entre les pieux qui se sont comportés en tant qu'un seul bloc. En revanche, chaque pieu appartenant au groupe de pieux de 5D d'espacement s'est comporté de manière individuelle.

KEYWORDS: group pile, model test, interaction

1 INTRODUCTION

Group pile is the foundation that supports a footing with several piles. The behavior of a group pile is totally different from that of a single pile if the pile spacing becomes narrow enough because of the pile-soil-pile interaction. To investigate the effects of the interaction in the group pile, model tests were conducted by previous researchers [Whitaker (1957), Vesic (1967), and Itoh and Yamagata (1998)]. However, the bearing mechanism of the group pile is not so clear yet as that of a single pile. As a result, it is not yet understood clearly whether or not the bearing capacity of the group pile is greater or less than that of a single pile

To understand the bearing mechanism of a group pile, the interaction should be studied more scientifically. It is thus necessary to observe precisely the behavior of piles and the surrounding ground in detail during group pile loading. Additionally, a large-scale model is also required to make clear the effects of interaction in a group pile.

Therefore, loading tests on a group pile and a single pile were conducted in a large soil tank with several sensors; strain gauges in the piles, colored sand layers and tactile sensors. To investigate the effect of pile spacing on the interaction, two kinds of models with different spacing were tested. A single pile with a large diameter was also tested for comparison based on the comparison between the group piles and the single pile, the bearing mechanism of group pile was discussed.

2 TEST APPARATUS & TEST PROCEDURE

Group pile loading tests and single pile loading tests were conducted in a large rigid soil tank as shown in Fig. 1. Its internal dimension was 1600mm×1600mm (width)×1650mm (height). At the top of soil tank, a loading actuator was installed. Loading tests were able to be conducted everywhere in the soil tank by moving the actuator. The maximum capacity of the actuator was 500 kN and the loading was performed in a displacement control manner. Details of the device were described by Goto et al. (2012). Air bags were placed on the surface of the model ground to generate confining pressure. Thus, the present tests reproduced the in-situ situation around and above pile tips.

Tactile sensors were installed on the bottom and sidewall of the tank to measure how the earth pressure propagated in the ground. The advantage of this filmy sensor is the ability to measure the distribution of normal (effective) stress. The sensor covered 440mm * 480mm area, containing 2016 sensing cells spaced at 10mm interval in each direction as shown in Fig. 2. In the experiments, stress distribution was measured in a wider area by combining several tactile sensors.

Model ground measured 1200mm in height and was made of air-dried Silica sand No.5; D_{50} = 0.523mm, e_{max} = 1.09 and e_{min} = 0.66. It was constructed by spreading dry sand and manual compaction at every 150 mm lift. The total amount of sand was measured and the average relative density was calculated to be around 90%. The several layers of colored sand were installed

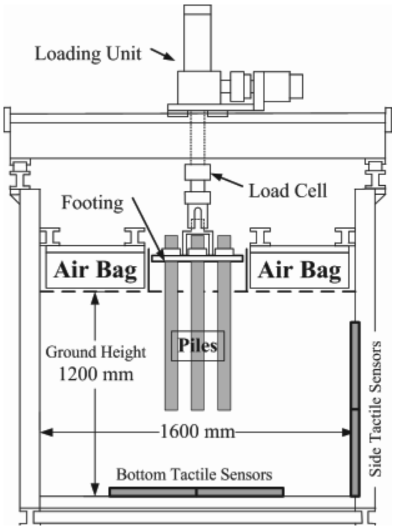

Figure 1. Cross section of the test equipment

Table 1. All conducted tests conditions

Case No.	Aim of the test	Number of piles	Pile Spacing	Pile length	Initial embeded depth
1	Loading test of the pile group	9	5.0 * D (200mm)	1000 mm	550mm
2			2.5 * D (100mm)		
3	Veritical pressure distribution under the pile group loading		5.0 * D	1300 mm	850mm
4			2.5 * D		
5	Loading test of the single pile	1		1000 mm	550mm

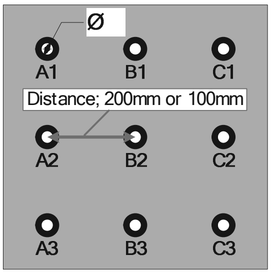

Figure 3. Pile layout in a pile group

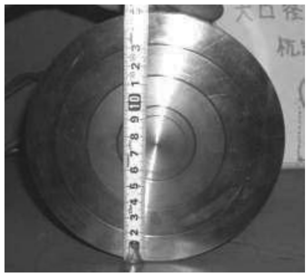

Figure 4. Annular load cells on the bottom

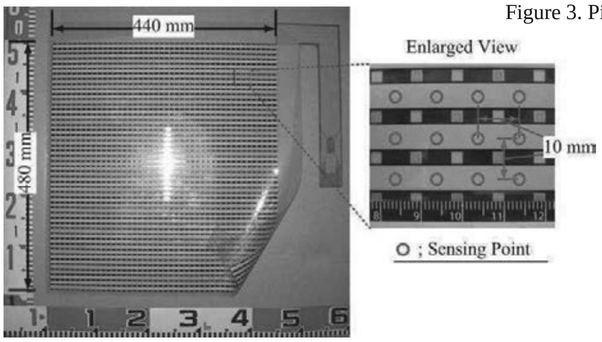

Figure 2. Tactile sensor sheet

in parallel below the initial height of the pile tips to observe the ground deformation after all loading tests were completed.

All conducted test conditions and main object of each test are shown in Table 1.

The models of Case 1 to Case 4 were composed of 9 cylindrical piles as shown in Fig. 3. Each pile was made of aluminum, 40mm in outer diameter, 4mm in thickness and 1000mm (Case 1 and Case 2) or 1300mm (Case 3 and Case 4) in length. The bottom of the piles was closed by a flat plate. Strain gauges were attached inside the piles at 5 levels along the piles and each level had 4 strain gauges to measure both the axial force and bending moments in two directions. Two kinds of the center-to-center spacing between piles were adopted; 5.0 times the pile diameter (200mm) and 2.5 times (100mm).

The diameter of a single large pile in Case 5 was 150mm in the outer diameter, while the thickness being 10mm and 1,000mm in length. Area of the pile tip is 1.5 times the total area of 9 piles in group piles. The strain gauges were attached inside at the same elevation as in the case of group piles. Moreover, the bottom of the large pile was closed by a load cell that was divided into annular 4 rings as shown in Fig. 4 and the contact pressures were measured individually by each ring.

After the ground was built up to le level of the pile tips, pile models were set on the ground. The initial embedded depth is shown in Table.1. Each head of pile in a group pile was fixed to a steel plate that is called “footing” in Fig. 1. After setting the models, the ground was built again up to 1200mm in height.

Group-pile loading tests were conducted in a displacement-control manner; 0.1mm/min. The footing, to which each pile was connected, was pushed down so that all piles would move together into the ground. The confining pressure was increased from 50kPa to 200kPa at an interval of 50 kPa. The loading were performed till 30mm settlement under each confining pressure, the loading was suspended at every 10mm settlement to measure the pressure distribution by tactile sensors..

Additional loading tests were also performed on individual piles before the group pile loading under each confining pressure. The each head of 9 piles was pushed down without any connection to the footing in the individual loading.

The single pile loading tests in Case 5 was also conducted in a displacement-control manner but the loading rate was different from that of the group pile; 0.2mm/min. Other conditions were same as that of the group loading tests.

3 TEST RESULTS & DISUCUSSION

3.1 *Load settlement curve and yielding point*

Figure 5 shows the relationships between total bearing load measured by at the top by the load cell and the settlement of the footing. The pile spacing was 5.0D in Case 1 and 2.5D in Case 2. Irrespective of the pile spacing, the greater confining pressure induced the greater bearing load. Although this was partially caused by the increased stress level under higher confining pressure, it is important as well that the ground below pile tips had been compressed during the previous pile loading.

The inflection points of each curve, so called yielding points, were marked by arrows in Fig. 5. The settlement at yielding points when the pile spacing was 2.5D is greater than that of 5.0D spacing under each confining pressure. The settlement at yielding point became slightly greater at the same pile spacing when the confining pressure was increased.

Figure 6 shows the load-settlement curve until 20mm settlement under the confining pressure of 100 kPa with both pile spacing. The curve of the single pile loading tests with the large diameter in Case 5 and the individual loading tests in Case 1 under the same confining pressure are also shown in the figure. The yielding point of each curve was marked by the arrow. The settlement at the yielding point became greater as the pile diameter increased in case of the single or individual loading. This implies that the settlement of a single pile would increase if the diameter of pile becomes larger.

In comparison with the case of the single pile, the settlement at the yielding point in the group pile of 5.0D spacing was similar with that in the single pile of the small diameter; the individual loading result in Case 1. On the other hand, the settlement in the group pile of 2.5D spacing was similar with that in the single pile of the larger diameter. These suggest that the group pile of 2.5D spacing behaved as a unified group, while each pile in the group pile of 5.0D spacing behaved independently.

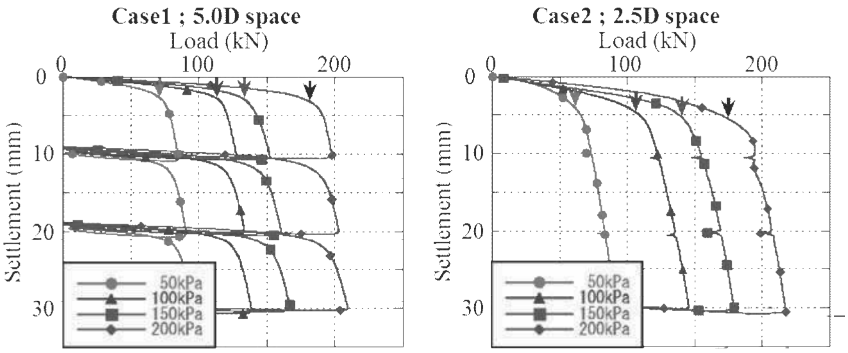

Figure 5. Total Load - settlement curve in the pile

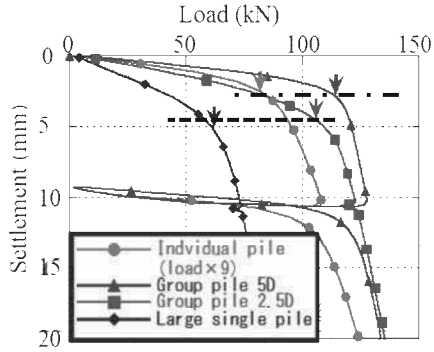

Figure 6. Total Load - settlement curve in both the single pile and the pile group

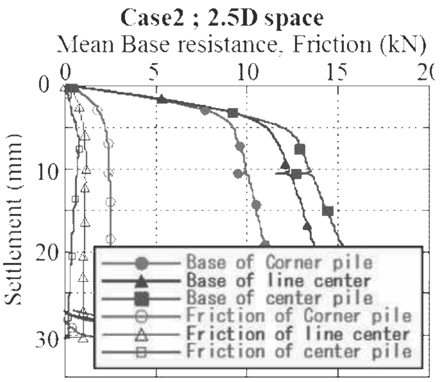

Figure 7. Mean base resistance and friction

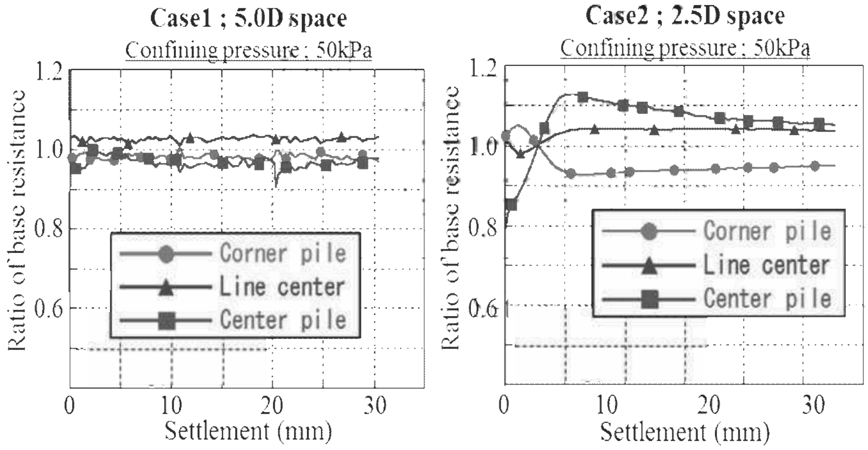

Figure 8. Ratio of base resistance

3.2 *Tip stress distribution by pile location in the group pile*

Figure 7 shows the mean pile tip resistance and skin friction changing with the location of piles – at the center (B2 pile in Fig.1), center of perimeter (A2, B1, B3 and C2), and corner (A1, A3, C1 and C3) in the group pile 2.5D spacing. The figure shows that the behavior of each pile in the group pile varies with the location if the spacing is small.

The skin friction of the corner pile was most significant and that of the center pile was the least for 2.5D spacing. The soil immediately below the tip of the central pile was affected by the other piles and moved down with piles as Fig.12 shows. That is why the skin friction of the center pile became smaller. In contrast, the corner piles were in contact with the outer ground that was less affected by pile displacement. Hence the skin friction on the corner pile was largest.

The tip resistance of the center pile was the largest and that of the corner pile was the smallest. This would be because the ground below the center pile was compacted by other piles.

To discuss the tip resistance more in detail, the resistance ratio was plotted in Fig. 8. This figure shows the tip resistance changing with the location of piles, normalized by the total tip resistance under the confining pressure of 50kPa. With 5.0D spacing, the ratio of each pile was almost equal to unity throughout the loading. It suggests that each pile behaved independently. In contrast, for 2.5D spacing, the ratio changed with the penetration of the group pile. The load concentration shifted from the corner piles to the center pile.

Figure 9 shows the tip resistance changing with the location within the bottom of the large pile that was measured by annular load cells as shown Fig.4. The stress concentration also shifted from the edge to the center of the pile. The tendency of the stress concentration changing in the bottom of one pile was similar to that of the 2.5D spacing group pile. This suggests that the significant interaction occurred in the 2.5D spacing group pile and all 9 piles behaved as a block.

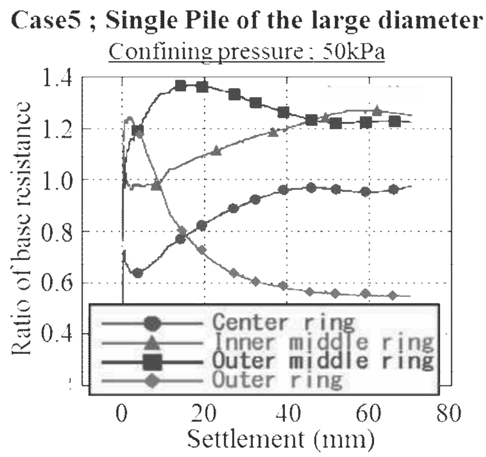

Figure 9. Distribution of contact pressure at base in a single pile with the large diameter

3.3 *Response of tactile sensor*

Figure 10 shows the normal pressure distribution at the bottom of the soil tank, measured by tactile sensors. The lighter color means higher pressure. The distance between the bottom of piles and the sensors was 290 mm. In both pile spacings, the highest pressure occurred below the center pile and the pressure decreased in an annular manner.

In contrast, the stress distribution near the tip of the piles varied with the spacing of piles. Fig. 11 shows the stress distribution when the distance between the pile tip and the sensor was 110 mm. For 5.0D spacing, the higher pressure occurred individually below the bottom of each pile. On the other hand, in case of 2.5D spacing, the pressure distribution looks like one block and the maximum pressure occurred in the zone between piles and formed a circular shape. This also suggests the strong interaction near the pile tip incase of 2.5D spacing.

3.4 *Observed ground deformation*

Figures 12 and 13 show the ground deformation after the completion of loading tests. The colored sand layers were installed in the horizontal direction with the equal interval prior to model construction. The dotted lines show the initial location of each colored sand layer. After the pile penetration of 240 mm, the distance of colored sand layers decreased to 5% of the original distance at the maximum below the pile bottom. This means that the ground just below the pile bottom was compressed severely. In the compressed core, heavy particle crushing was observed. These features occurred in both cases of pile spacing.

In contrast, the shape of ground deformation between or below piles was different according to the spacing. For 5.0D spacing, the ground below each pile moved down separately. On the other hand, in case of 2.5D space the ground under the group pile deformed in a continuous convex way. Furthermore, the ground between piles also moved down. This suggests that the ground not only below the pile but also between piles was compressed downward together in the case of 2.5D spacing.

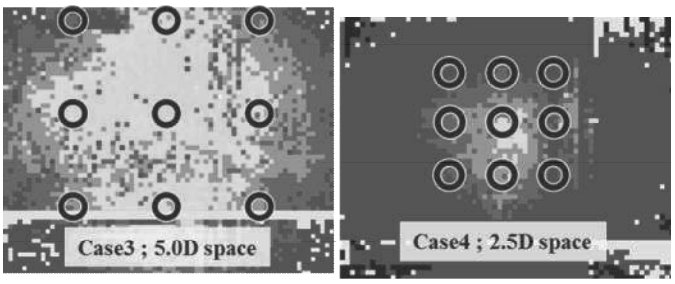

Figure 10. Pressure distribution at 290mm distance

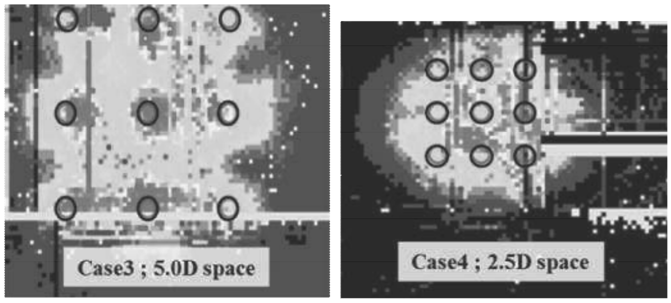

Figure 11. Pressure distribution at 110mm distance

4 CONCLUSIONS

The vertical loading tests of the group pile and the single pile were conducted. By comparing the bearing load, stress concentration by the pile location, pressure distribution and the ground deformation, the following conclusions may be drawn.

(1) For the narrower 2.5D pile spacing, the group pile yields at a larger settlement and the settlement was almost same as that in the loading of a pile of a large diameter. In contrast the settlement in the 5.0D pile spacing was similar to that in the loading of a single pile of the same diameter.
(2) For 2.5D pile spacing, tip resistance concentrated to the corner piles in the early state of loading. The concentrated load shifted to the center pile after the settlement increased. The same shift of the concentration occurred in the bottom of the single pile with the larger diameter as well.
(3) The higher ground pressure occurred below the bottom of each pile individually in 5.0D spacing group pile near the pile bottom. In contrast, the higher pressure was observed in a block manner and the highest pressure showed a ring distribution in 2.5D spacing group pile.
(4) The ground only below the bottom of each pile deformed downward individually in case of 5.0D spacing. Conversely, the ground under the group pile deformed in a contiguous convex curve for 2.5D spacing.

From these observations, it was concluded that individual piles in the group pile with 5.0D spacing behaved independently. In contrast, the group pile of 2.5D spacing behaved in a block, similar to one large single pile.

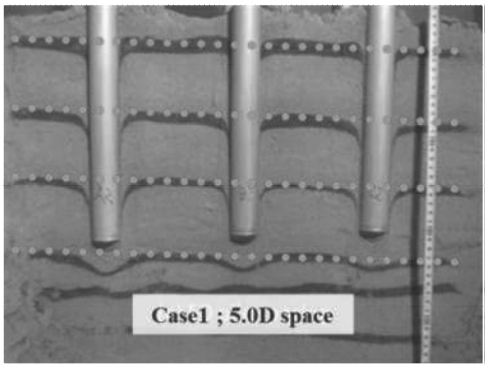

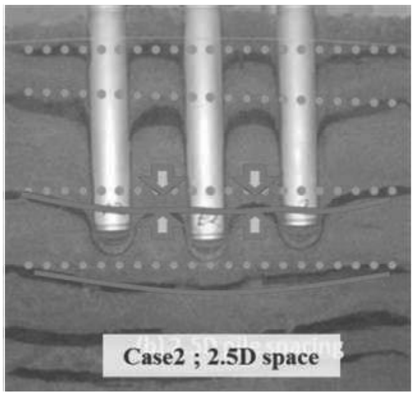

Figure 12. Ground deformation after all loading tests

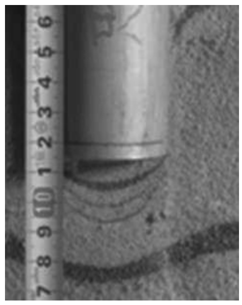

Figure 13. Ground deform. near the pile bottom

5 ACKOWREDGEMENT

Authors are thankful to Dr. Sadao Yabuuchi, President of Japan Pile Corporation for his invaluable support. Authors also appreciate the discussion made by members of the research committee on group pile that was sponsored by the Kanto Chapter of the Japanese Geotechnical Society.

6 REFERENCES

1) Whitaker, T. : Experiments with Model Piles in Groups, Geotechnique, Vol. 7, pp. 147-167, 1957
2) Vesic A.S. : A Study of Bearing Capacity of Deep Foundations, Final Rep., Project B-139, Georogia Inst. of Tech., 1967
3) Itoh, A. and Yamagata, K. : Vertical Loading Test of Model Group piles(Part 3: Influence of Pile Spacing), Proceedings of Annual conference AIJ, Structurel, pp. 661-662, 1988 (in Japanese)
4) Goto, S. Aoyama, S., Liu, B., AyalaAlarco, R., Takita, A. and Towhata, I. : Model pile and group pile bearing capacity in large scale soil tank test ,Proceedings of IS-Kanazawa 2012, 2012

Probabilist analysis of the foundation of a shopping center in Brazil

Analyse probabiliste des fondations d'un centre commercial au Brésil

Gusmão A.
University of Pernambuco and IFPE, Brazil

Oliveira P.
Gusmão Engineers, Brazil

Ferreira S.
Federal University of Pernambuco and Unicap, Brazil

Maia G., Amorim M.
Gusmão Engineers, Brazil

ABSTRACT: The Brazilian foundation code that was reviewed in 2010 defined the criteria for the use of probabilistic analysis in the design of foundation, and there is a perspective that such analyzes are increasingly used in practice. The greatest difficulty of the analysis is the small number of load tests available in the works, and particularly in the design phase. This article presents the main aspects of design, execution and control of the construction of a shopping center with 280,000 m^2 area in Recife, Brazil, where they were executed 4,000 continuous flight auger piles type (CFA piles). 40 static load tests were simultaneously performed with the execution of the piles (1% of the total number of piles as recommended by the Brazilian code). With the favorable outcome of the first 15 load tests, the design was reviewed and there was a significant reduction in the number of piles and the total cost of the foundation. It is presented a statistical analysis of results of static load tests, where it was verified the influence of the number of load tests considered on the shape of the curve of resistance, global factor of security, characteristic safety factor and probability of failure. The results showed that when it attained a number of load tests equivalent to 0.4% of the total number of piles, the probability of failure are not showed more substantial changes.

RÉSUMÉ : La norme brésilienne sur les fondations qui a été révisée en 2010 a défini les critères pour l'utilisation de l'analyse probabiliste dans la conception des fondations. Une telle analyse est susceptible d'être de plus en plus utilisée en pratique. La plus grande difficulté de l'analyse est le petit nombre d'essais de chargement disponibles et en particulier en phase de conception. Cet article présente les principaux aspects de la conception, l'exécution et le contrôle de la construction d'un centre commercial de 280 000 m^2 de surface à Recife, au Brésil, où ont été exécutés 4 000 pieux forés en continu (pieux CFA). 40 essais de chargement statique ont été réalisés simultanément à l'exécution des pieux (soit 1% du nombre total de pieux, tel que recommandé par la norme brésilienne). Avec les résultats satisfaisants des 15 premiers essais de chargement, la conception été révisée, entraînant une réduction significative du nombre de pieux et du coût total des fondations. Une analyse statistique des résultats des essais de chargement statique est présentée, permettant de vérifier l'influence du nombre d'essais de chargement considéré sur la forme de la courbe de résistance, le facteur global de la sécurité, le facteur de sécurité caractéristique et la probabilité de ruine. Les résultats ont montré que, quand on atteint un nombre d'essais de chargement équivalent à 0,4% du nombre total de pieux, la probabilité de ruine ne se trouve pas significativement modifiée.

KEYWORDS: Foundation, Statistical Analysis, Probability of Failure.

1 DESCRIPTION OF THE STRUCTURE AND SUBSOIL

The building analyzed is a precast reinforced concrete structure with openings, with approximately 280,000 m2 destined to shopping areas and garages. There are portions of the structure with up to six levels of concrete slabs. A total of 1,283 pillars support permanent vertical loads ranging from 200 to 9,000 kN. The arrangement of the loads also takes into account vertical, horizontal, and moments loads resulting from wind action. The project is designed with a ground floor level, deployed at an elevation of +3.00. From the standpoint of topography, the native terrain does not feature natural unevenness, with a median average of 2.00. From the geological standpoint, the site is located in the fluvial-marine plain, within an marine terrace (Gusmão et al., 1998).

The geotechnical characterization carried out with an arrangement of 61 percussion soundings permits, in a simplified form (Fig.1) characterization of the foundation ground, which is initially composed of a landfill layer of fine silty sand, light brown, soft to moderately compact, to a level of 1.00; followed by layers of sand with organic materials, or silty organic clays, dark gray, very soft, to a level of -3.00. Below this level are found subsequent layers of fine to medium sand, gray, lightly to moderately compacted, interspersed with layers of silty clays, medium, to levels of -21.00 -28.00. After this layer, a layer of silty clays, or silt with very fine sand, gray, compact, extends to the limit of the soundings that were performed (-35.00). The water level was found to vary in levels from 0.00 to +1.50.

2 FOUNDATION DESIGN AND VERIFICATION OF PERFORMANCE

CFA piles (400 and 500 mm diameter) were employed, with allowable loads of 700 and 1,150 kN, respectively. The client indicated that load tests be conducted over the course of the execution of the foundation, due to the time frame for completion and delivery of the project. At first, a total of 15 static load tests were performed, with satisfactory results. At this point, during this first step, 2,563 piles had been placed. Then, from the results of these pilot load tests, the project was revised, and loads for the 400 and 500 mm piles were altered to 800 kN and 1,300 kN (an increase of 14% and 13% respectively).

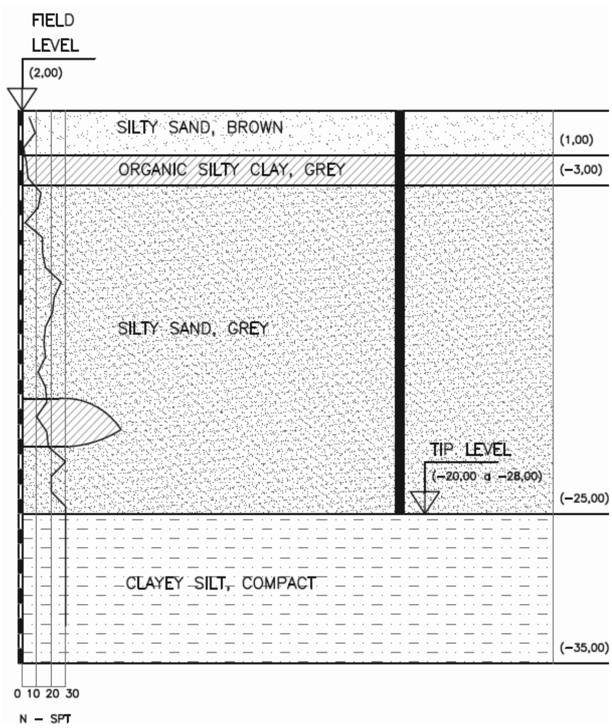

Figure 1. Subsoil profile

The final total of all piles placed, both before and after the revision, came to 3,838. A total of 38 static load tests were programmed throughout the project, 27 for 500 mm piles, 09 for the 600 piles, and 02 for 400 mm piles. However, two of the load tests, specifically the 33rd and 34th, indicated problems in the pile caps, and had to be redone. Figure 2a shows the diagram regarding load versus settlement for the piles analyzed in the study. The Van der Veen equation was used as a criterion for extrapolating the geotechnical rupture load for the load tests.

3 STATISTICAL ANALYSIS

A mean value (μR) can be imagined in a representative area where the resistances are distributed, and a standard deviation (σR) can measure the distance this data is from this mean average. Analogically, in designing the details of a project with deep foundations, normally the piles are not designed with expectations to have to withstand maximum admissible loads. Generally, verifiable loads are less than, but close to admissible, presenting an average (μS), and standard deviation (σS)..Since not all locations in the subsoil present the same resistance, it is possible that in a certain location, the resistance is found to be less than that which is required to withstand the load indicated. The likelihood that this phenomenon occurs is called the probability of failure.

Sample variation can be measured by the ratio between the standard deviation and the mean, this ratio is called the coefficient of variation. Reliability is a concept opposed to variability. The reliability index (β) is defined as the inverse of the coefficient of variation. The reliability index increases as the normal distribution is concentrated to a greater degree around the mean. The concept of a Safety Margin, which is defined as the difference between the requirements demanded, and the actual resistance, also is distributed normally, and through it can be obtained the parameters for analysis of potential for failure.

For the case of the project under study, we studied the probability of failure values before and after revision of the foundation design project for the piles with 500 mm diameters, since the number of samples was greater. This review only changes the curve for requirements, considering that the mean load (μR) per pile was reviewed. For the first step, which preceded the review, mean and standard deviation values were verified for operating loads of 985 and 91.5 kN, respectively. For the second step, values of 1,086 and 106.0 kN, respectively, were determined. Regarding load resistance, values of 536 and 3,167 kN were verified. A standard curve can only be set up using its mean value, and its standard deviation.

From the data obtained, standard curves were plotted for both steps, similarly for the requirements, and the resistances. They are presented in Figure 2b. For the first step, the Reliability Index (β) measured 3.99, and the Probability of Failure (pf) was 1/30,893. For the second stage, β measured 3.79, and the pf measured 1/13,373.

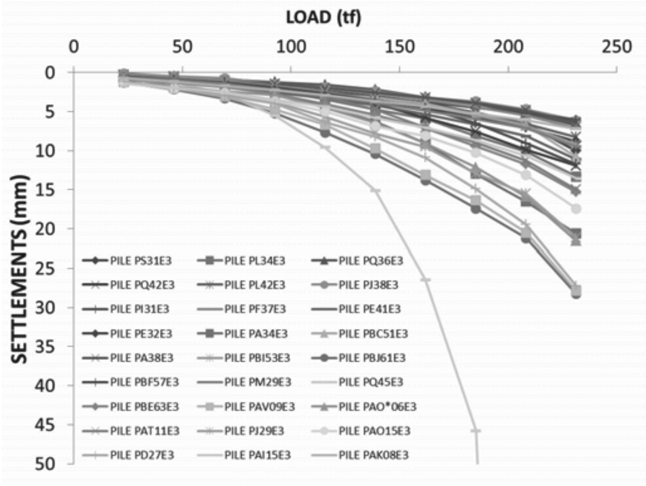

(a)

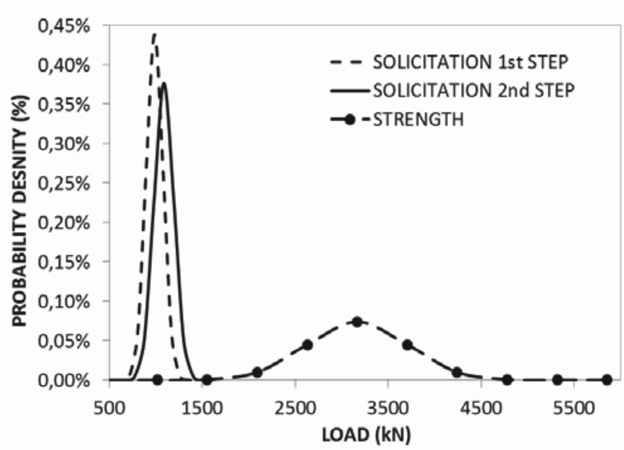

(b)

Figure 2. (a) Results of load tests for the 500mm piles; (b) Standard curves for the first and second phase compared to the normal curve of resistance.

The load tests carried out for the project were not conducted all at once, thus, during the course of testing, the standard resistance curves could be adjusted to include the last test performed. As each new test is considered, a different pair of mean and standard deviation values is obtained. In such a manner, it is possible to trace standard curves that consider different steps for implementing quality controls for the foundation, or for different quantities of static load test performed, varying the size of the sample until the completion of predictive control for the work.

As the sample increases, dispersion analysis is incorporated. This dispersion arises from the variability of the subsoil profile, the variability of the materials used, and from the uncertainties regarding measurements of the loads and settlement.

Thus, with sample growth, the standard deviation increases, and the probability density around the mean decreases, leaving the curve with a flatter appearance (recalling that the area considered between the standard curve and the abscissa is equal to the unity) . This can be seen in Figure 3, which depicts the variation of the shape of the standard curve, due to the growth of the sample until the final number of load tests performed (N = 27).

In a deterministic analysis, foundation safety is verified by means of the Global Safety Factor (FSg), which is the ratio between the mean resistance and mean requirement. However, for an analysis where the effects of sample dispersion are intended to be considered, as with Probability of Failure, the Safety Characteristic Factor (FSk) must be also considered. This factor is defined as the ratio between the Resistance Characteristic (Rk) and the Requirement Characteristic (Sk). The Resistance characteristic represents the mean resistance increased from Z.σR, as well as the characteristic that is obtained by minimizing the mean requirement in Z. σS (where Z represents the reliability interval, usually equal to 95%, equivalent to Z = 1.65). Figure 3b makes comparison between the Global Safety Factor, and the Safety Characteristic Factor as the sample increases.

As already seen, as sample space increases, population dispersion is incorporated into the sample, and the standard deviation tends to increase. In this manner, as dispersion increases, the reliability index represented by β decreases and eventually the Probability of Failure increases. Thus, on the basis of everything that has been presented, it was verified that with an increase in number of load tests, the probability of failure increased until practically constant between the values of 15 and 20 load tests performed, i.e. 0.35 to 0.48% of the project piles tested. Figure 5 shows the variation of failure probability in function of the increase of the number of load tests, compared with the limits set by the European code EN1990.

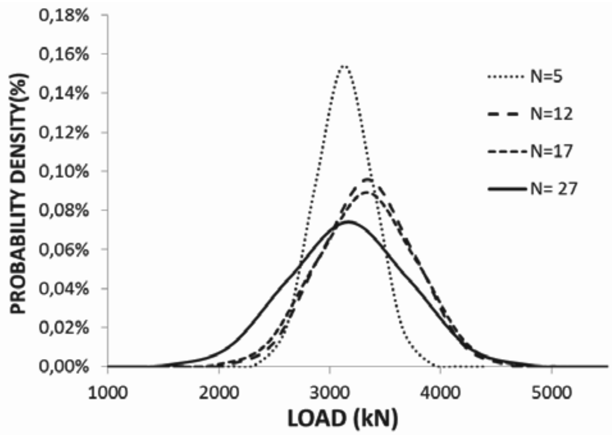

Figure 3. Standard curves varying according to the number of load tests analyzed.

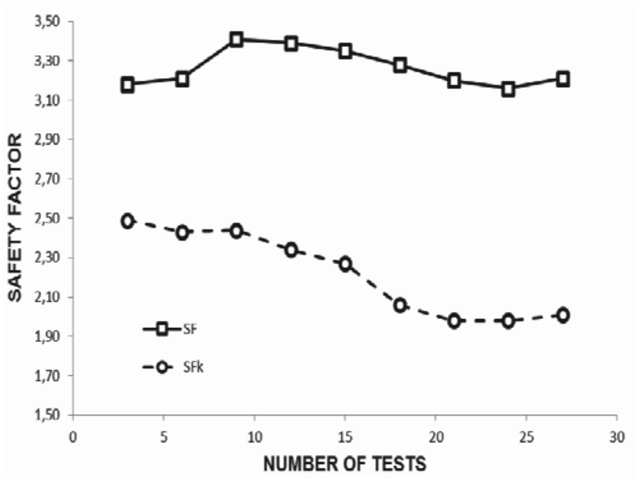

Figure 4. Variation of global and partial safety factors relative to the number of load tests.

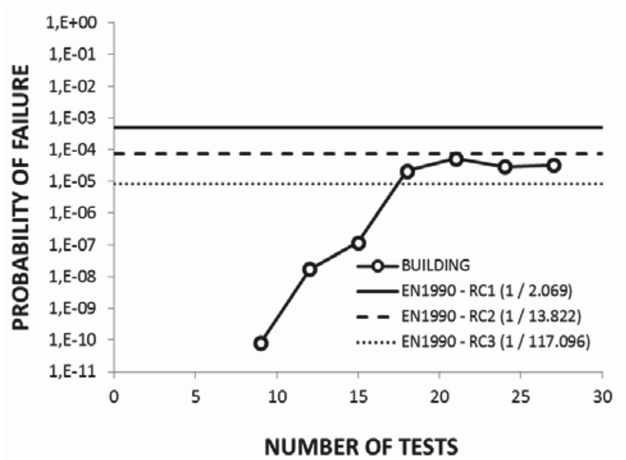

Figure 5. Variation of the probability of failure with an increase in the number of load tests.

3 CONCLUSIONS

With growth of the sample, the standard deviation increases, and probability density around the mean decreases, leaving the curve with a flatter appearance. As sample space increases, population dispersion is incorporated into the sample, and the standard deviation tends to increase. As the dispersion increases, the reliability index represented by β decreases, and probability of failure increases. It was possible to verify that with an increase in the number of load tests, the probability of failure increased until practically constant when reaching 15 and 20 load tests performed, and 0.35 to 0.48% of the project piles having been tested. The safety characteristic factor showed to be, as expected, always less than the global security factor, however, with values remaining above levels permitted by codes.

4 REFERENCES

Gusmão Filho, J.A; Gusmão, A.D. and Maia. G.B. 1998. Prática de fundações na cidade do Recife: Exemplos de Casos (in Portuguese). 12º Congresso Brasileiro de Mecânica dos Solos e Engenharia Geotécnica, Brasília, Vol.3, pp.1415-1422.

Bearing capacity of displacement piles in layered soils with highly diverse strength parameters

Capacité portante des pieux de deplacements battus dans les sols stratifiés avec des paramètres fortement differés de la resistance

Gwizdala K., Krasinski A.
Gdansk University of Technology, Gdansk, Poland

ABSTRACT: Reliable prediction of pile bearing capacity including the installation effects is still a serious research and engineering problem. Computational analyses should be related to the load-settlement characteristics comprising entire range of loads, up to the limit state. European standard Eurocode 7 includes only the general rules and some calculation concepts. In the analytical method of pile bearing capacity calculation a commonly applied static formula, based on pile base and shaft unit resistances, is proposed. It is also recommended that the calculating procedures and the values of unit soil resistances used in the calculations would be verified by field tests done on real piles. In the paper the cases of bridge structures founded on driven displacement Vibro and Franki piles are presented. The design assumptions and computational results were verified by static load tests of piles (SPLT). Soil profiles and geotechnical parameters of soil layers have been determined by CPTU tests. One of static load tests was carried out on instrumented pile equipped with extensometers.

RÉSUMÉ : Prediction rèliable de la capacité portante des pieux avec les effets d'installation constitue toujours un problème important de l'ingénièrie et de la recherche. Analyse devrait inclure les caractéristiques charge-tassement dans le cadre entière de la charge jusqu'au l'état limit. Le standard Eurocode inclue seulement des règles et une concéption générales de calculs. Une méthode analytic de la capacité portante est proposée par la formule statique considerant unitaires resistances de base et du frottement latérale. Il est récomandé que la procedure de calcul ansi que les valeurs unitaires de la résistance au sol soit verifier par un essais de chargèment d'un pieu réel. Quelques cas des fondations de ponts posés sur les pieux battus Vibro et Franki sont présentés. Les assumptions de dimmensionement et les résultats de calcul sont vérifiés par le chargement statique des pieux (SPLT). Le profil du sol et les paramètres de couches du sol sont détèrminés par les essais CPTU. Un essais de chargement statique est réalisé avec un pieu instrumenté avec éxtènsomètres.

KEYWORDS: pile bearing capacity, settlement of piles, displacement piles

1 INTRODUCTION

Reliable prediction of bearing capacity and settlements of piles is still quite a difficult task either from theoretical as well as from practical point of view. The analysis of the transmission of loads by the construction into the subsoil in terms of full relation between load and settlement (*Q*–*s*) is more adequate. Currently in Europe and also in Poland general Eurocode 7 rules are applied.

According to the Eurocode recommendations, a design of pile foundations should be made using one of the following approaches:

a) based on the static load test results, the consistency of which with other comparable experiences has been proved by calculations or in some other way;
b) based on empirical or analytical calculation methods, the reliability of which has been confirmed by static load tests in comparable conditions;
c) based on dynamic load test results, the reliability of which has been revealed by static load tests in similar soil conditions and for the same type of piles;
d) based on the observation of the behavior of comparable pile foundations, provided that the data were verified by field tests (site investigations and soil testing).

It should be pointed out that basic method for the evaluation of *Q-s* curve are static load tests. An example of the relation of shaft, base resistances, total load and pile shortening are presented in Fig. 1. According to Eurocode principles, the conventional ultimate load Q_u, corresponding to the settlement equal to 10% of pile diameter (s = 0,10D) has been indicated. In such approach, partial coefficients for loads and partial coefficients for shaft and base resistances should be correlated with assumed ultimate load level determined from *Q-s* curve.

Characteristic bearing capacity of the pile determined on the basis of geotechnical parameters from ground test results can be calculated from the following formulae:

$$R_{c;k} = R_{b;k} + R_{s;k} \tag{1}$$

$$R_{b;k} = A_b \cdot q_{b;k} \tag{2}$$

$$R_{s;k} = \sum A_{s;i} \cdot q_{s;i;k} \tag{3}$$

where:
$q_{b;k}$ – characteristic value of the unit resistance under the pile base,
$q_{s;i;k}$ – characteristic value of the unit resistance over the pile shaft in subsequent soil layers,
A_b – calculated area of the pile base,
$A_{s;i}$ – calculated area of the pile shaft in the subsequent soil layers.

All over the world there exists quite a lot of methods for the calculation of pile bearing capacity. Also in Poland proposals of $q_{b;k}$ i $q_{s;i;k}$ calculation in relation to various technologies of piles have been elaborated, see e.g. Gwizdala 1997, Gwizdala 2011, Gwizdala and Steczniewski 2007, Gwizdala et al 2010, Krasinski 2012. When the pile bearing capacity is concerned, the range of settlement curve for the given method should be precisely defined (Fig. 1). Possibly, some reserve ΔQ may be included in relation to critical load Q_c (see Gwizdala 1997).

Comparison of bearing capacities calculated by various methods reveals significant differences. Exemplary results of calculations for Vibro pile and for data presented in Fig. 2 are collated in Table 1.

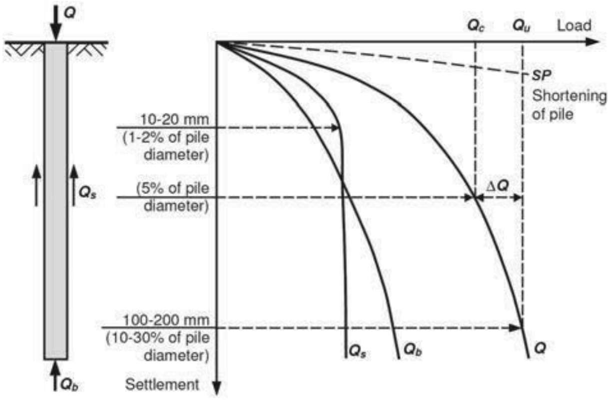

Figure 1. Generalized load-settlement curves of pile

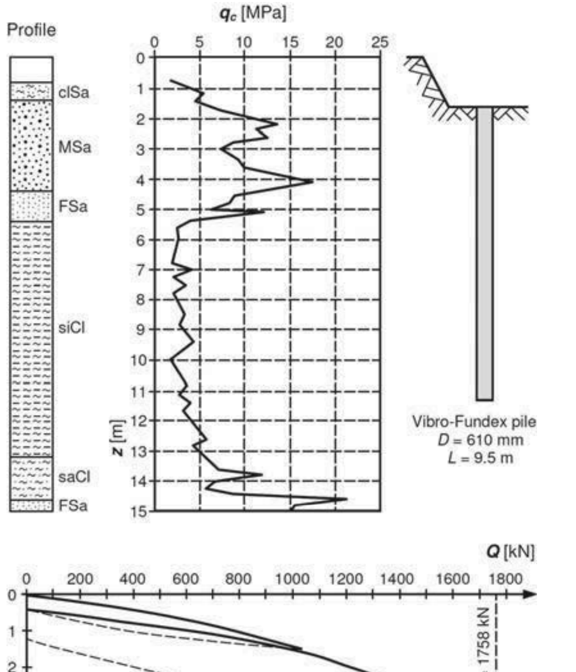

Figure 2. Data and static load test result of Vibro-Fundex pile, taken into calculation analysis

Currently big pressure is put on the development of calculation methods based on direct results of in situ tests, e.g. CPTU tests and making use of load-transfer t-z i q-z functions. Such method has been proposed by Gwizdala and Steczniewski 2007 (see example shown in Fig. 3) and for screw displacement piles by Krasinski 2012.

The problem becomes much complex for the piles installed in layered soils with highly diverse strength parameters. In such cases reliable results can be obtained from static load tests (SPLT).

Table 1. Static load test and calculation results for Vibro–Fundex pile

Method	Bearing capacity based on characte-ristic parameters [kN]	Corre-lation coeffi-cients	Chara-cteristic bearing capacity $R_{c;k}$ [kN]	Partial resis-tance factor γ_t	Calcula-ted bearing capacity $R_{c;d}$ [kN]
Design load Q_r	–	–	–	–	1034.0
PN-83/B-02482 based on SPLT	1758.0 ($R_c = Q_{max,SPLT}$)	–	–	$k = 0.8$	1406.0
EN 1997-1; 2004 based on SPLT	1758.0 ($R_c = Q_{max,SPLT}$)	$\xi_1 = 1.4$ $\xi_2 = 1.4$	1256.0	1.1	1142.0
EN 1992-2; 2007 (DIN 1054)	2378.0	$\xi_3 = 1.4$ $\xi_4 = 1.4$	1699.0	1.1	1545.0
LCPC Bustamante & Gianeselli (1982)	1980.0	$\xi_3 = 1.4$ $\xi_4 = 1.4$	1414.0	1.1	1285.0
α – method API (1984)	1538.0	$\xi_3 = 1.4$ $\xi_4 = 1.4$	1098.0	1.1	998.0
Gwizdala & Steczniewski (2007)	2308.0	$\xi_3 = 1.4$ $\xi_4 = 1.4$	1648.0	1.1	1498.0

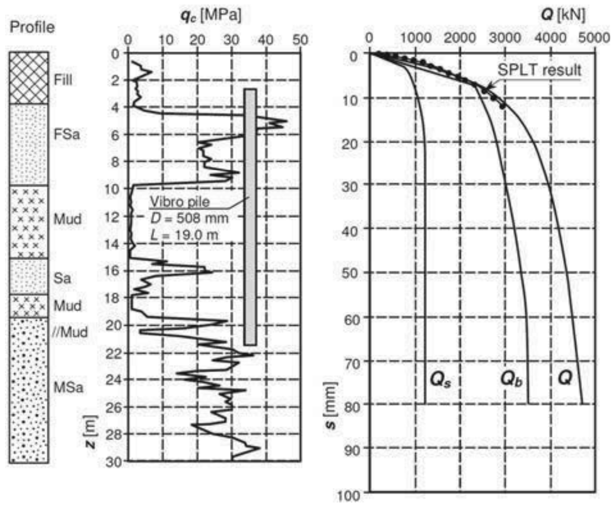

Figure 3. Example of Vibro pile calculation results obtained from load-transfer functions method (Gwizdala and Steczniewski 2007)

2. EXAMPLES OF IN SITU TESTS ON DRIVEN DISPLACEMENT PILES

Driven displacement piles are applied for constructions transmitting large loads and when small settlements are required, especially plastic settlements for designed load range. Very good characteristics of subsoil-pile interaction are obtained for driven cast-in-place displacement piles such as Virbo, Vibro-Fundex and Franki. (Fig. 3, 4 and 5).

2.1. *Tests on Vibro and Franki piles under bridge object of A1 highway*

In the frame of reconnaissance works for foundation of access flyover roads to large bridge over the Vistula river some tests on Vibro and Franki piles have been carried out. Vibro piles have the diameter of 508/560 mm and the length 25.4 m whereas Franki piles 560 mm and 23.5 m respectively. In Fig. 4 geotechnical conditions in the form of CPTU characteristics and settlement curves obtained from load tests are presented. Load –

settlement relations for both pile types are nearly linear. Due to conventional procedure of tests, the results did not provide any information regarding the distribution of loads transmitted by the shaft and by the base of piles into the subsoil.

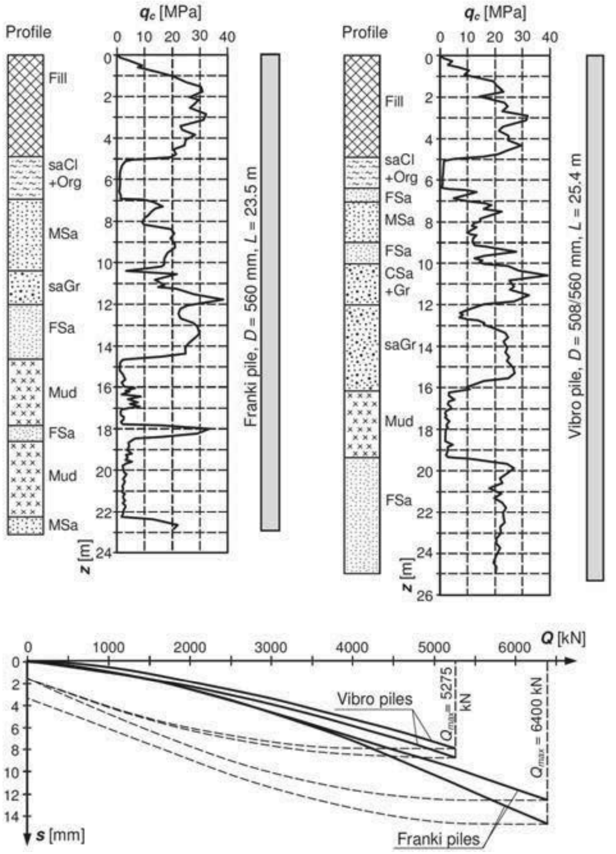

Figure. 4. Soil conditions and SPLT results of Vibro and Franki piles tested for bridge over the Vistula river project

2.2. *Tests on Vibro pile under road viaduct in Gdansk*

More advanced static load test has been carried out for ϕ508/560 mm Vibro pile installed under the foundation of road viaduct in Gdansk. In the test the distribution of load between shaft and base of the pile was measured. For this purpose a system of 7 extensometers have been installed inside the pile shaft in order to measure shaft strains. The principle of extensometric system work is commonly known, (Bustamante and Diox 1991, Hayes and Simmonds 2002, etc.). The assessment of axial load at various pile levels is based on the shortening measurement of individual pile sectors. Subsequently, the load transmitted into the particular soil layers over the pile shaft and under its base are determined.

Basic *Q-s* diagram representing settlement of the pile is presented in Fig. 5. In turn, the distribution of axial load in the pile for subsequent load levels obtained from the extensometric measurements is shown in Fig. 6. In Fig. 7 the results of further interpretation of the measurements in terms of unit friction resistances t_{si} over the pile shaft in particular soil layers and unit resistance under the pile base q_b are presented. The unit resistances have been expressed as a function of displacement of corresponding pile sectors.

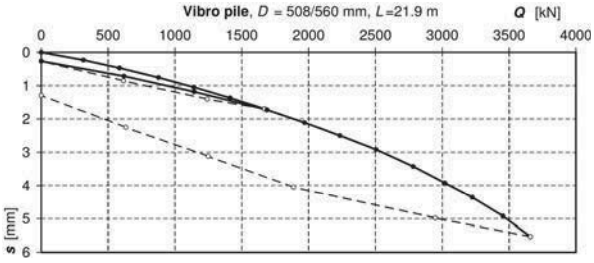

Figure. 5. Basic result from static load test of instrumented Vibro pile

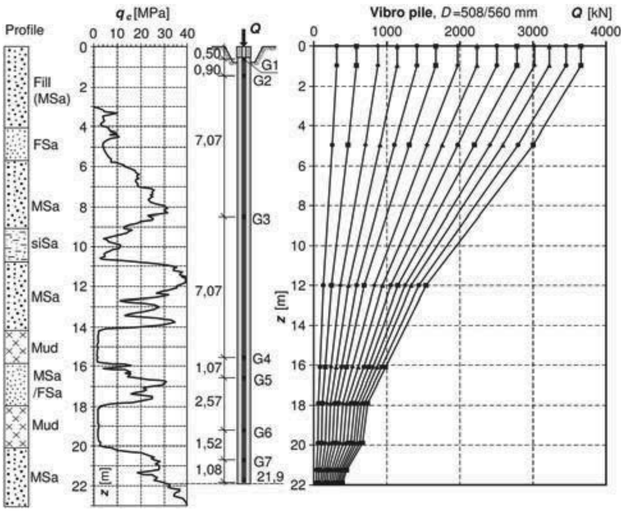

Figure. 6. Distribution of axial load in the instrumented Vibro pile

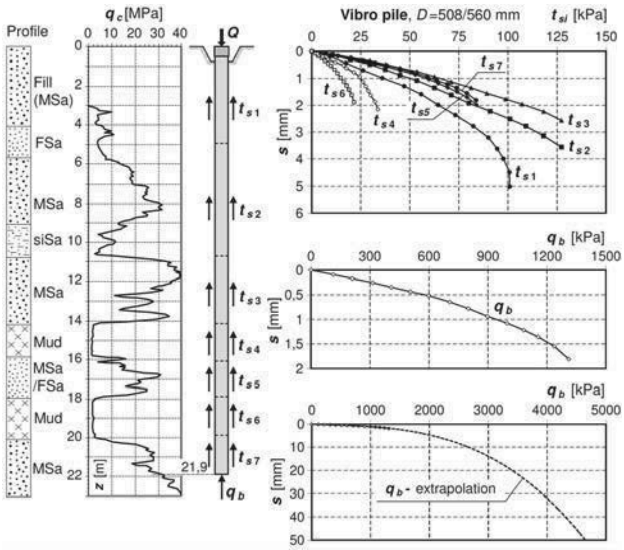

Figure. 7. Unit friction resistances t_{si} over the shaft in particular soil layers and unit resistance q_b under the base of instrumented Vibro pile

There are main observations and conclusions drawn from the analysis of the results of extensometric measurements:

- large part of external load applied to the pile head has been overtaken by the friction resistance of upper sandy soil layers which exist in the subsoil to the depth of 14 m, still over the mud layers;
- small portion of total load reached the level of pile base. The value of Q_b force transmitted by the pile base in the

final load phase was 400 kN approximately which is equivalent to 11% of total load Q_{max} = 3560 kN;

- essential portion of pile settlement (75% approximately) at the level of pile head (5.5 mm) is related to the shortening of the pile (4 mm approximately);
- settlement of the pile base in the final loading stage reached the value nearly 2 mm which explains small value of mobilized soil resistance under the base;
- values of mobilised unit friction resistances over the pile shaft t_s in sandy layers varied from 85 to 130 kPa whereas in mud layers from 25 to 35 kPa. Friction resistances in sandy layers directly under the soil surface (t_{s1}) reached full mobilization state corresponding to maximum value 100 kPa. In turn, the friction resistances of deeper sandy layers (t_{s2}, t_{s3}, t_{s5} i t_{s7}) did not reach maximum values due to small pile displacements against the soil occurring at the corresponding levels;
- mobilized unit resistance of the soil under the pile base q_b reached the value of 1300 kPa approximately and due to small displacements of the base is far from ultimate value. After extrapolation of the curve for the displacements corresponding to 10% of the pile diameter (50 mm), approximate value of limit unit resistance of soil under the base was about 4500 kPa.

Extensometric measurements performed during the load test revealed that upper subsoil layers took over large portion of the pile force which made difficult the reliable assessment of the bearing capacity of basic soil layers lying below. Thus the load applied in the load test should be much higher corresponding to Q_{max} of the order of 6000–7000 kN. However, due to capacity of loading stand it was not possible to apply such high loads. The described case may be a good example showing that the planning and interpretation of conventional loading tests requires always individual approach and analysis referred to the specifics of soil conditions, especially when we deal with layered subsoil. In such cases it is recommended to carry out the load tests accompanied by exetensometric measurements.

3 SUMMARY

Driven displacement piles of Vibro, Vibrex and Franki type have favorable load-settlement characteristics and reveal small settlements. General principles given by Eurocode 7 should aim at an unification of the methods for the calculation of bearing capacity of the pile. Current comparison of the calculation results obtained by various methods indicated significant differences in the assessment of the bearing capacity of the piles.

Experiences and comparative analyses with the results of load tests show that the most reliable results are obtained in terms of calculation methods which make use of in situ test results (CPT, CPTU, DLT, PMT). It would be of significant value to create the international database with complete static and dynamic test results of piles and the information regarding the measurements of soil resistances over the pile shaft and under the base referred to careful description of the subsoil and the in situ tests itself.

4 REFERENCES

Bustamante, M., Doix, B. 1991. A new model of LCPC removable extensometer. Fourth International Conference on Piling and Deep Foundations, Stresa, Italy.

Bustamante M., Gianeselli L. 1982. Pile Bearing Capacity Prediction by Means of Static Penetration CPT. *Proceedings of 2nd European Symposium on Penetration Testing, Amsterdam*, Vol. 2, 493-500.

De Cock F., Legrand C & Huybrechts N. 2003: Overview of design methods of axially loaded piles in Europe – Report of ERTC-Piles, ISSMGE Subcommittee. Praha. XIIIth, European Conference on Soil Mechanics and Geotechnical Engineering. Volume 3, 663-715.

Gwizdała K., 1997. Polish design methods for single axially loaded piles. *Design of Axially Loaded Piles - European Practice*. Brussels, 291-306.

Gwizdała K. 2011. Pile foundations . Vol. 1. Technologies and Calculations. (in Polish). PWN Publising House, 1-300.

Gwizdała K., Stęczniewski M. 2006. Determination of the bearing capacity of pile foundations based on CPT test results. *Proceedings of the 3rd International Seminar on Soil Design Parameters from In Situ and Laboratory Tests*. Poznań, September.

Gwizdała K., Brzozowski T., Więcławski P. 2010. Calculation aspects of pile foundation in Eurocode 7. Proc. of the XIV Danube-European Conf. on Geotechnical Engineering *From Research to Design in European Practice.* Bratislava, Slovak Republic, June 2-4, 141+Cd.

Hayes J., Simmonds, T. 2002. Interpreting strain measurements from load tests in bored piles. Proceedings of the 9th Int. Conference on Piling and Deep Foundations, Nice, 663-669.

Krasiński, A. 2012. Proposal for calculating the bearing capacity of screw displacement piles in non-cohesive soils based on CPT results. Studia Geotechnika et Mechanica, Vol. XXXIV, No 4, 41-51.

Tejchman A., Gwizdała, K., Kłos, J. 1985. Application of in situ tests for evaluation of pile bearing capacity. *Proc. 11th Int. Conf. Soil Mech. Found. Eng.* Vol. 3, San Francisco, 1479-1482.

EN 1997-1:2004, Eurocode 7. Geotechnical design – Part 1: General rules.

EN 1997-2:2007, Eurocode 7. Geotechnical design – Part 2: Ground investigations and testing.

EN 12699:2001, Execution of special geotechnical works. Displacement piles.

ISSMFE Subcommittee on Field and Laboratory Testing, Axial Pile Loading Test, Suggested Method. ASTM Journal, June 1985, 79-90.

ASTM Designation D 4945, Standard Test Method for High-Strain Dynamic Testing of Piles.

Polish Code PN-83/B-02482, 1983. Foundations. Bearing capacity of piles and pile foundations.

Practical experience with piled raft design for tall buildings

Expérience pratique de la conception de radiers sur pieux pour les immeubles de grandes hauteurs

Haberfield C.M.
Golder Associates Pty Ltd Melbourne, Australia

ABSTRACT: For many tall buildings, a practical and cost effective foundation solution is provided by a piled raft. Recent research and field observations have shown that in practically all cases, serviceability conditions control the behaviour of the footings. The design of a piled raft usually requires non-linear analysis in three dimensions, based on detailed knowledge of the ground conditions, the soil and rock properties (especially modulus and its variation with strain), structural loads and raft geometry. Information on ground properties can only reliably be obtained from a detailed ground investigation with a heavy reliance on quality insitu testing. Further information can be obtained from instrumented pile load testing. This paper describes the design of the pile rafts for two tall towers: the 1000 m Nakheel tower in Dubai, which is founded on weak carbonate rocks and a group of tall towers (up to 300 m high) founded in deep alluvial deposits.

RESUME: La construction de radiers sur pieux offre une solution pratique et économique pour les fondations de nombreux immeubles de grande hauteur. Les observations récentes faites sur le terrain et dans le domaine de la recherche ont montré que, dans pratiquement tous les cas, les conditions de service contrôlent le comportement de ces fondations. La conception d'un radier sur pieux nécessite généralement une analyse non linéaire tridimensionnelle, basée sur une connaissance approfondie de l'état du sol en profondeur, des propriétés du sol et de la roche (en particulier le module et sa variation avec la déformation), des charges appliquées par la structure et de la géométrie du radier. Les données sur les propriétés du sol et/ou de la roche ne peuvent être obtenues de manière fiable qu'à partir d'une campagne de reconnaissance géotechnique détaillée et avec des essais de bonne qualité. Des informations complémentaires peuvent être obtenues à partir d'essais de chargement de pieu. Cet article décrit la conception des radiers sur pieux de deux tours de grande hauteur: la tour Nakheel de 1000m de hauteur, à Dubaï, fondée sur des roches carbonatées de faibles caractéristiques et un groupe de tours (jusqu'à 300 m de hauteur), fondées en profondeur dans des dépôts alluvionnaires.

KEYWORDS: piled raft, insitu testing, settlement, pile load testing

1 FACTORS AFFECTING FOOTING PERFORMANCE

For a typical pile-supported footing, it is necessary to consider both individual pile, pile group and raft performance. These require consideration of the behaviour of the ground in critical locations:

- Immediately beneath the surface raft or footing, where the important factors are strength for bearing capacity and stiffness for settlement and interaction effects.
- Along the pile shaft where the factors of most interest are strength for bearing, excavatability and stability; stiffness for settlement and interaction effects; geology and permeability for pile stability and, most importantly, pile shaft resistance.
- At the pile toe where all the factors for the pile shaft are present and in addition the pile end bearing is of interest.
- Beneath the pile where stiffness for pile settlement is important for a depth of at least twice the building width.

Recent research and field observations have shown that in practically all cases, serviceability conditions control the behaviour of the footings. Therefore this paper concentrates on evaluation of ground modulus for the calculation of behaviour at serviceability limit state.

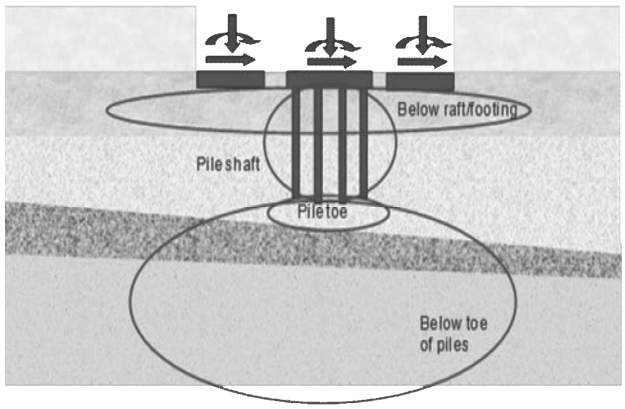

Figure 1 Areas of interest for footing design

2 METHODS OF GROUND INVESTIGATION

For many tall buildings, the ground investigation is required to extend to significant depths (e.g. up to 200 m for the Nakheel tower) due to the heavy loads and relatively large plan area of the building. Where footings do not found on relatively strong rock, a major component of settlement can result from compression of the soil or weak rock below the pile toe. The measurement of representative deformation and strength properties at this depth can be problematic.

2.1 Laboratory testing of core

Core samples subjected to laboratory testing are affected by disturbance and stress relief and can give erroneous results which usually represent a significant underestimate of the insitu stiffness of the material. This leads to over-design of footings, higher costs and in some cases the footings can be impractical to design or construct.

2.2 In situ testing by SPT or cone tests

Two of the insitu tests commonly used in ground investigations; standard penetration tests and cone penetration tests, are either not appropriate for testing at significant depths or cannot penetrate relatively competent founding materials. For example, the results of SPTs at reasonable depth (say 30 m) must be considered to be unreliable due to the rod weight and the resulting ineffectiveness of the impact from the hammer. It is also of very little value to report an 'SPT' value of 50 blows for some nominal (say 50 mm penetration). Such a result cannot be interpreted to give an estimate of ground stiffness.

Cone penetrometer tests are ineffective where they cannot penetrate moderately competent ground. Predrilling to overcome frictional resistance is not a solution since refusal often occurs at the tip.

2.3 Pressuremeter and cross-hole seismic tests

High quality pressuremeter testing and cross-hole seismic testing provide a practical method for obtaining estimates of the deformation parameters of the rock at different strain levels.

The crosshole seismic test provides estimates of small strain modulus which cannot be applied directly to analysis of footings where strains in the ground under dead, live and wind loading are significantly higher than those experienced during seismic testing. As deformation parameters depend on the strain level imposed in the test, this must be taken into account in the test interpretation.

The pressuremeter on the other hand provides deformation properties at strain levels which are commensurate with those of the ground when subjected to service loading from the building. On some sites however, for example in deep alluvial deposits, pressuremeter testing may result in significant disturbance to the ground and hence the results of such testing may not be of benefit. Self-boring pressuremeter tests can overcome this problem, however they may be impractical in relatively hard materials such as discussed in Section 4.

2.4 Instrumented pile load tests

Deformation properties of the ground under load can be obtained from an appropriately designed test on an instrumented pile. The results can be used to supplement those obtained from the tests described in Section 2.3 prior to final design of the footing system.

Load cells (typically Osterberg cells) are located in the pile at chosen depths, while displacement transducers can be located below the tip. By placing one Osterberg cell close to the base of the pile in conjunction with a displacement transducer, the load-displacement performance of the base of the pile can be measured. It is a relatively straight forward process to then back calculate a representative modulus for the material immediately below the pile toe.

By combining the results from pressuremeter and cross-hole seismic tests (adjusted to take into account strain levels), a reasonable level of confidence can generally be obtained to undertake the footing design.

The overall pile load-displacement performance can also be measured and provides a means of back-figuring pile and ground properties for use in a group settlement analysis package such as PLAXIS or FLAC.

2.5 Application of in situ testing to modulus estimates

The methods for estimating ground modulus described in Sections 2.3 and 2.4 are demonstrated for the design of footing systems for two towers. Section 3 describes the application to the design of the proposed 1000 m Nakheel tower in Dubai which is to be founded in a weak calcareous siltstone (UCS of about 2 MPa). Section 4 considers design for a group of tall towers (up to 300 m high) founded in deep alluvial deposits comprising very dense silty sand and hard sandy silt.

3 NAKHEEL TOWER, DUBAI

3.1 The tower and ground conditions

The Nahkeel Tower in Dubai was designed to extend to a height in excess of 1 km. With about 2,000,000 tonnes dead load, the structure would have been one of the heaviest ever built. The project was placed on hold in early 2009 at a stage when about half of the foundations had been constructed.

The high bearing pressures applied to the ground coupled with the soft calcareous rock ground conditions present at the site provided a significant challenge to the design of the footing system.

3.2 Foundation system

Based on prior but limited knowledge of the ground conditions in Dubai, the foundation system concept adopted for the tower was a piled raft. The raft design had a variable thickness, being up to 8 m under the most heavily loaded structural elements. Design founding depth was at about 20 m below ground level, and at the base of a 120 m diameter excavation supported by a circular, embedded diaphragm wall. Approximately 400 barrettes were proposed, for installation to depths of between approximately 60 m and 80 m below ground level. The design of the barrettes had to consider not only the control of ground response to the tower loading, but also various regulatory requirements and constructability issues.

3.3 Ground investigation

The ground investigation (Haberfield and Paul, 2011) comprised an extensive laboratory testing program on core samples together with pressuremeter and crosshole seismic testing. The self-boring pressuremeter tests extended to depths of up to 200 m below ground level. Cross-hole seismic testing was undertaken in arrays of 3 boreholes with 3 m centre-to-centre spacing between the boreholes.

Figure 2 shows the values of initial loading modulus (E_i) calculated from laboratory unconfined compression strength (UCS) tests, pressuremeter tests and cross-hole seismic tests.

The small-strain cross-hole seismic tests gave estimates of modulus which ranged between about 3 to 7 times those measured in the pressuremeter tests at the same depths. This difference is consistent with the effects of strain level on modulus. To obtain a modulus value for engineering design adopting the strain levels appropriate to field behaviour, the cross-hole values were reduced by a factor of five.

The modulus values measured in the UCS tests showed a wide scatter. An upper bound to the results over the depth of interest is around 600 MPa, which is about half the value estimated from the pressuremeter test results.

3.4 Instrumented pile load tests

The preliminary foundation design was based on the results of the in situ tests. However, prior to the detailed design stage, three test barrettes with cross-sectional dimensions of 1.2 m ×

2.8 m were installed to depths of 65 m and 95 m. Load testing of the barrettes comprised two levels of Osterberg cells in each test barrette with each level of cells designed to achieve a bi-directional load of up to 83 MN. The Osterberg cells were positioned to measure performance of the lower 20 m (approximately) of the barrettes .

The remaining instrumentation for each test barrette included strain gauges and tell-tales as well as a displacement transducer located in the rock below the toe in order to directly measure the displacement of the rock at this location. The displacement transducer at the toe of the barrettes was used to make a direct measurement of compression of the ground immediately below the toe.

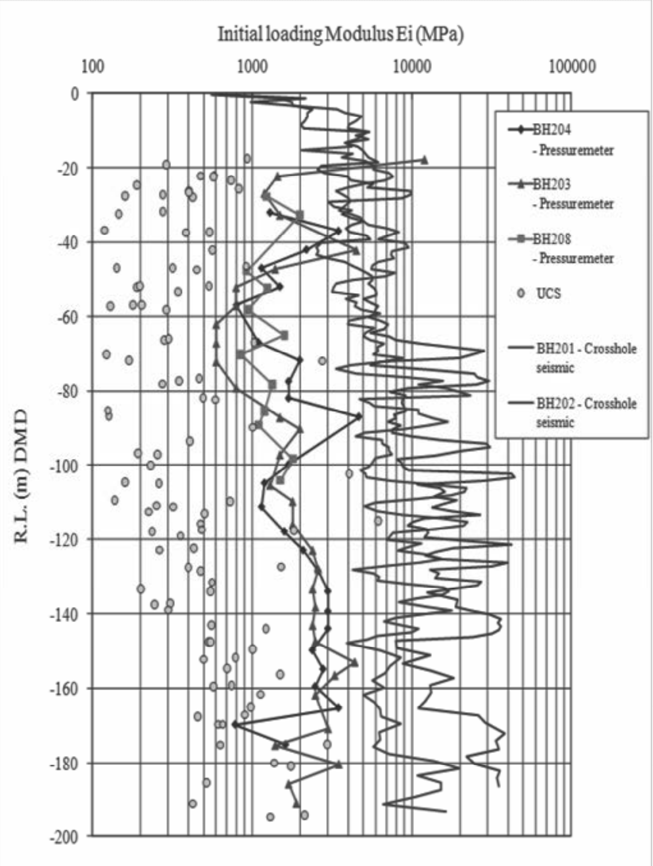

Figure 2 comparison of modulus values form UCS tests, pressuremeter and cross-hole seismic tests

3.5 *Comparison of modulus values*

The results of the three pressuremeter tests shown in Figure 2 show values of modulus of between about 1200 MPa and 2000 MPa at the depths corresponding to the bases of the barrettes. Reducing the modulus values from the cross-hole seismic tests by a factor of five gives results in the range of 1000 MPa to 4000 MPa (with the highest values being obtained in layers of gypsum).

Back analysis of the test data from the instrumented barrettes indicates a modulus (Ei) of the soft rock below the toe of between 1200 MPa and 1500 MPa.

The most optimistic assessment of the UCS results at the depths considered is about 600 MPa.

There is good agreement between modulus values from the test barrettes, the pressuremeter results and factored-down cross-hole seismic results. This gave confidence in the adoption of a value for final design. Adoption of the laboratory test results would have led to an overly conservative design (and, in fact, would have shown the design of a pile-supported raft to meet the settlement criteria to be impractical).

4 TALL TOWERS ON DEEP ALLUVIAL DEPOSIT

4.1 *Ground conditions and original investigation methods*

The author has recently been involved in the design of piled rafts for a series of towers from 50 levels to 80 levels. The site is located on a river flood plain and is underlain by very deep alluvial deposits comprising predominantly very dense silty sands and hard sandy silts.

The original ground investigation undertaken by others included SPT tests to about 100 m depth, with SPT refusal (more than 50 blows for less than 150 mm penetration) occurring for all tests below about 30 m depth. It was therefore not possible to make a reliable estimate of ground stiffness from the SPT results.

Menard pressuremeter testing was also performed. The Menard pressuremeter tests gave unrealistically low results, possibly the result of relatively poor drilling methods which caused significant disturbance of the borehole. Cone penetrometer testing was also attempted but the cone refused at relatively shallow depth. Continuation of cone testing beyond refusal depth using predrilling was not successful as cone refusal occurred within 0.5 m of the base of the predrill.

The information from the geotechnical investigation (undertaken by others) was not sufficient to be able to reliably design the foundations for the towers. In addition, preliminary calculations indicated that based on a reasonable interpretation of the ground investigation data, a pile only or pile raft solution of sufficient capacity and dimensions to support the towers could not be practically installed using available piling technology.

4.2 *Cross-hole seismic and pile load tests*

The author requested cross-hole seismic testing to be undertaken to supplement the original ground investigation data. Two cross-hole seismic tests were carried out to about RL 60 m (CHST1 and CHST2). The two deeper cross-hole seismic tests (CHST3a and CHST4a) were carried out to below RL 10 m. Figure 3 compares estimates of Young's modulus assessed from the various tests. The cross-hole seismic modulus results have been reduced by a factor of five to account for the increased strain levels appropriate to pile performance.

The resulting design line used for the analysis of the pile rafts is also shown in Figure 3.

The author also recommended that pile load testing be undertaken to provided additional information with respect to the properties of ground in the vicinity of the pile shaft and below the toe of the test pile. To maximize the amount of information from the pile testing, Osterberg cell testing using two levels of Osterberg cells was recommended. By using two levels of cells, the shaft resistance between the upper and lower cells could be directly measured without reliance on interpretation of strain gauges which can be problematic. By placing the lower Osterberg cell close to the base of the pile, the direct measurement of the base performance of the pile could also be measured directly. Interpretation of this load versus settlement performance would allow an estimate of the modulus of the ground below the toe of the test pile.

Load testing was carried out on a pile of 1.2 m diameter and about 47 m length, constructed from the basement excavation at about 20 m below surrounding ground level.

The results of the pile load test indicated an unknown but significant thickness of debris at the base of the pile, which made estimation of the modulus of the soil below the toe of the pile more difficult and less certain. An estimate of the modulus of the soil below the toe of the pile was therefore made on the basis of the unload-reload response of the pile load test. This estimate of 250 MPa is reasonably consistent with the results from the factored cross-hole seismic test results shown in Figure 3 at the pile toe elevation (about RL 33 m).

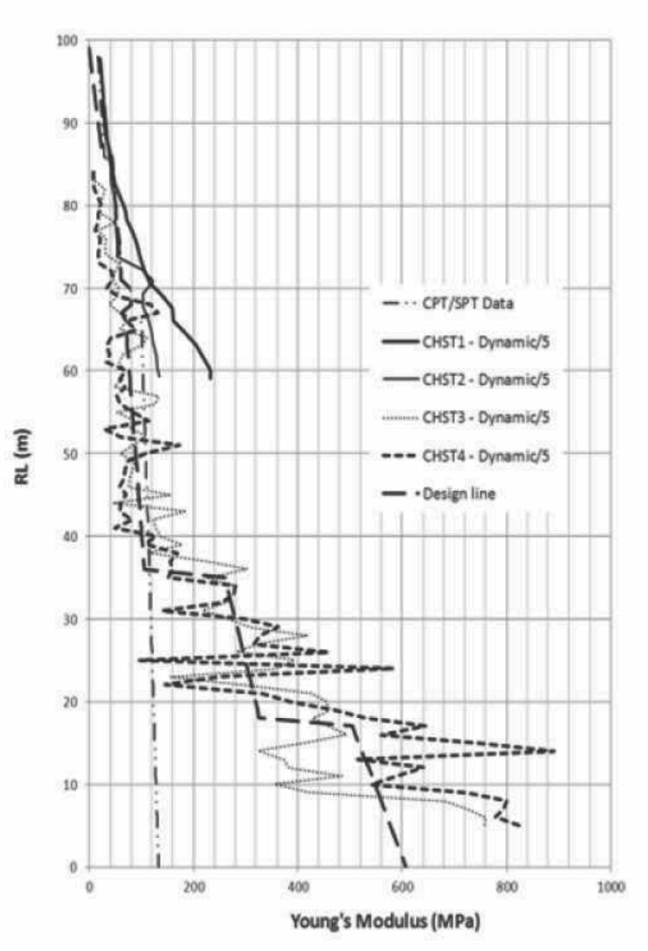

Figure 3 Estimates of modulus assessed from cone tests, SPTs and cross-hole seismic tests

5 CONCLUSION

Piled rafts often form practical solutions for the support of tall buildings on sites comprising weak rock or deep alluvial deposits. The analysis of piled rafts in these ground conditions requires a good understanding of the soil deformation modulus at the appropriate strain level.

Laboratory testing on core samples often underestimates the modulus because of stress relief and sample disturbance. In situ testing by cone penetrometer or by the use of standard penetration testing is often unsatisfactory or impossible in relatively stiff materials such as those encountered at the sites discussed in this paper.

Experience at the sites discussed shows that a careful evaluation of the results of pressuremeter tests, cross-hole seismic tests and instrumented pile load tests can provide a consistent picture of deformation modulus. This consistency provides confidence in the results of the analyses using these values.

6 ACKNOWLEDGEMENTS

The Author gratefully acknowledges the assistance of Nakheel, Soletanche Bachy, Intrafor Joint Venture and Fugro/ Load Test International. The author also acknowledges the assistance of Dr Jack Morgan in preparation of this paper.

7 REFERENCES

Haberfield, C.M. and Paul, D.R. 2011. Footing Design of the Nakheel Tower, Dubai, UAE in Workshop on soil-structure interaction and retaining walls. Proceedings of the Technical Meeting TC207 ISSMGE, Dubrovnik, pp 35 to 52

Non-Conventional Pile Loading Tests in Vietnam

Essais non conventionnels de chargement de pieux au Vietnam

Hai N.M.
Faculty of Civil Engineering, Thu Dau Mot University, Vietnam

Dao D.H.
Faculty of Bridge and Road Engineering, Da Nang University of Technology, Vietnam

ABSTRACT: Two bidirectional tests used single-level jacks were performed on strain-gauge instrumented bored piles in Da Nang City, Vietnam. The soil profile consists of medium dense silty sand followed by thick firm clay underlain by highly weathered sandstone. The piles, 800 mm and 1,000 mm in diameter, were installed to 34 m depth and constructed using bucket drill technique with bentonite slurry. The jack assemblies were attached to a reinforcing cage above the pile toe from 0.5 m through 0.8 m. The static loading tests were performed 21 days after constructed piles. The maximum bidirectional test loads ranged from 3.8 through 4.8 MN and the measured maximum upward and downward movements ranged from about 3 through 28 mm and 7 through 49 mm, respectively. The analysis of strain-gauge records showed that the Young's modulus values were about 25 and 22 GPa as calculated on the nominal cross section of the 800 and 1,000 mm diameter piles, respectively, the shaft resistances were strain-softening, and the pile toe stiffness was very soft and essentially linear. The measured load distribution corresponded to effective stress proportionality coefficients, ß, of about 0.2 through 0.3.

RÉSUMÉ : Deux essais bidirectionnels utilisés à un niveau sur les pieux instrumentés à jauges de contrainte ont été effectuées à Da Nang, Vietnam. Le profil géologique du site se compose d'une couche de sable limoneux moyennement dense au-dessus d'une couche d'argile ferme épaisse reposant sur les grès très altérés. Les pieux de 800 mm et 1000 mm de diamètre, ont été installés jusqu'à 34 m de profondeur en utilisant la technique de seau de forage avec les coulis de bentonite. Les ensembles de vérins étaient attachés à une cage d'armature de 0,5 m à 0,8 m au-dessus de la pointe des pieux. Les essais de chargement statique ont été effectués à 21ème jours après l'exécution des pieux. Les charges maximales des essais bidirectionnels varient de 3,8 à 4,8 MN et les déplacements maximaux mesurés vers le haut et vers le bas varient respectivement de 3 à 28 mm et de 7 mm à 49 mm. L'analyse des données enregistrées des jauges de contrainte a montré que le module de Young était d'environ 25 à 22 GPa, tel que calculé sur la section nominale des 800 à 1.000 mm pieux, respectivement, les résistances se ramollissaient et la rigidité de la pointe des pieux était très faible et essentiellement linéaire. Le coefficient de proportionnalité (β) entre la charge mesurée et la contrainte effective correspondante était de 0.2 à 0.3.

KEYWORDS: bidirectional test, bored piles, strain-gages, shaft and toe resistances, strain-softening, movements.

1 INTRODUCTION

The 12-story Sea Bank Building is built over a 7.35 m by 20.30 m area among existing high-rise Buildings in Da Nang City, Vietnam. The foundations were placed on 800 and 1,000 mm diameter bored piles constructed to 34 m depth designed for working loads of 3.8 and 4.8 MN, respectively..

To validate the capacity of the piles, a pile loading test programme was carried out by means of the bidirectional O-cell test (Osterberg 1989) as being the best suitable for the limited project area. Both test piles were equipped with vibrating wire strain gages.

The results of the tests are presented and correlated to the soil conditions of the site. The test data and back-analyses are considered to be of interest beyond the design of the piled foundations for the Sea Bank Building.

2 SOIL PROFILE

The soil profile consists of medium dense silty sand to 18.5 m depth followed by 14.5 m thick firm clay underlain by highly weathered sandstone. Figure 1 shows the distribution of water content, consistency limits, grain size distribution, and SPT N-indices. The natural water content ranges from about 20 % through about 30 %. The density of the silty sand above the firm clay is 1,940 kg/m^3 (from w_n = 25 %). Total saturated density is about 1,950 kg/m^3 throughout the firm clay.

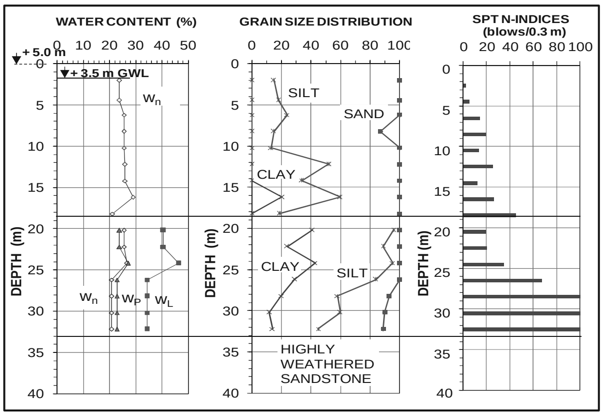

Figure 1. Water contents, grain size distrib., and SPT N-indices

Average of SPT N-indices is about 23 blows/0.3m to 27 m depth and more than 100 blows/0.3m below this depth. The underlain layer is highly weathered sandstones with rock quality designation of 0% through 10% and total core recovery of 12 through 21 % to 50 m depth below the original ground surface. Below this depth, the rock quality designation and total core recovery are 13 through 30% and 20 through 80%, respectively. The groundwater table is located at a depth of about 1.5 m below the ground surface.

3 PILE CONSTRUCTION AND TEST PROGRAMME

The two test piles, Piles TP01 and TP02 of 800 and 1,000 mm diameter, were constructed using bucket drill technique with bentonite slurry on 24 and 26 August 2012, to 34 m depth, respectively. The production piles were designed with the reinforcing cages of sixteen 20 and 22 mm bars to 11 m depth and eight 20 and 22 mm bars below this depth. The O-cells attached at 0.5 and 0.8 m above the pile toes, as shown in Figure 2. However, to avoid damage to the instrumentation during the lowering the reinforcing cages into piles the reinforcing cages of the test piles were supplied with sixteen bars.

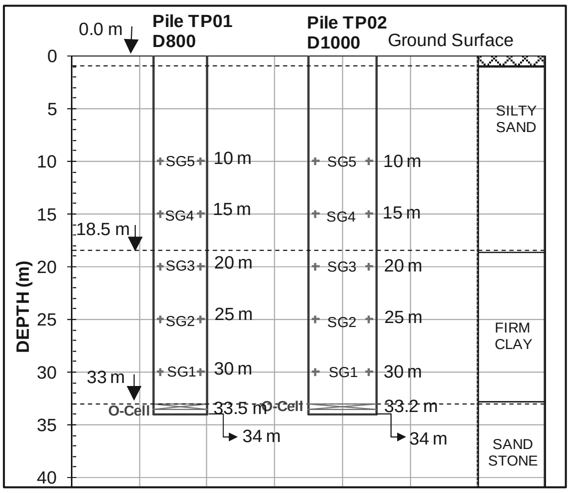

Figure 2. Details of instrumented test piles

The test piles were instrumented with a pair of diametrically opposed vibrating wire strain-gages at four levels and two pairs of diametrically opposed vibrating wire strain-gages at levels SG1 and SG4, respectively.

The test piles were constructed by first inserting 820 mm and 1,020 mm outer diameter temporary casings, respectively, to 7.6 m depth. Thereafter, the test piles were drilled to 34 m depth using a bucket drill with bentonite slurry. Before concreting each shaft, the shafts were cleaned and a reinforcing cage with the O-Cell assembly was lowered into the shafts. The O-cell assemblies consisted of three O-cells; 200 mm diameter in Pile TP01 and 220 mm in TP02.

On completion of the drilling, on August 24 and 26, 2012, a 219 mm diameter tremie pipe was inserted to the bottom of each shaft and tremie placing of the concrete was commenced, displacing the bentonite slurry.

The concrete cube strength was determined 28 days after casting to 40 MPa and 44 MPa for the concrete used in Piles TP01 and TP02, respectively.

The bottom 0.5 and 0.8 m length of Piles TP01 and TP02, respectively, was equipped with a 114 mm diameter coring tube attached to the reinforcing cage. The coring was performed after the concrete had cured and showed that an about 20 mm thick layer of debris and slurry existed below the toe of Pile TP01. Pile TP02 could not be cored because the coring tube was obstructed by steel reinforcement bars..

The static loading tests were performed on September 16 and 17, 2012, 23 and 22 days after concreting.

4 TEST RESULTS AND ANALYSIS

1.1 *Load – movement measurements*

The internal bond of the O-cells was broken at loads of at 190 and 480 KN load for Piles TP01 and TP02, respectively. Theoretically, the O-Cell does not impose an additional upward load until its expansion force exceeds the bond breaking load, the buoyant weight of the pile above the O-Cell and the residual load, if any, acting at the O-cell level. For both test piles TP01 and TP02, the initial upward movement records were taken at 570 and 960 KN; that is, these recorded loads included bond breaking load, the buoyant weight and residual load. The pile buoyant weights above the O-Cell for Piles TP01 and TP02 were 163 KN and 255 KN, respectively. Therefore, the residual loads determined at O-cell locations of Piles TP01 and TP02 are 217 and 225 KN, respectively.

Figure 3 shows the load-movement records of the two O-cell tests. After subtracting the buoyant weight of the piles TP01 and TP02 above the O-Cell, the maximum upward resistances were 3,636 and 4,544 KN, respectively. The maximum O-cell upward movements were 3.3 mm and 7.4 mm, the maximum O-cell downward movements were 28.0 and 49.3 mm, and the maximum pile head movements (upward) were 0.2 and 2.5 mm, respectively.

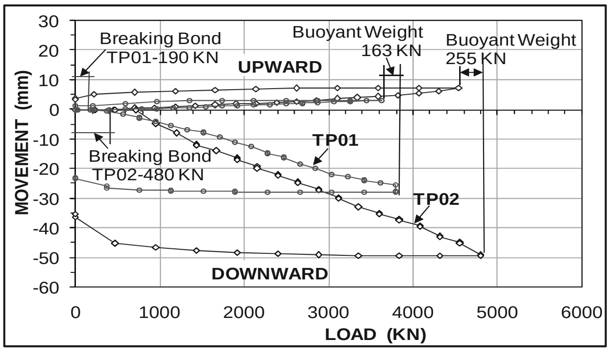

Figure 3. Load-movement curves of the piles

1.2 *Strain measurements and determining Axial Modulus*

To determine the secant modulus of the pile material, the best way is to use "tangent modulus" or "incremental stiffness" plot which is the applied increment of load over the induced increment of strain plotted versus the measured strain. The tangent modulus is then converted to the secant modulus (Fellenius 1989; 2011). The incremental stiffness plots for the two tests are shown in Figures 4 and 5. The incremental stiffness method assumes that for load increments applied after the shaft resistance at the studied gage level has been fully mobilized, the continued incremental stiffness values will plot along a slightly sloping line, representing the tangent modulus relation for the pile cross section. Because of the combined effect of the strain-softening and the scatter of values, the incremental stiffness method did not provide sufficiently precise values for the tangent and secant stiffnesses. Therefore, for this case, the authors have preferred to rely on the linear portions of load-strain relations and convert the measured strains using constant stiffnesses, AE, of 12.5 GN and 17.0 GN for Piles TP01 and TP02, respectively. Correlated to the nominal cross sectional areas, the values indicate that the E-modulus of Piles TP01 and TP02 is about 25 and 22 GPa, respectively.

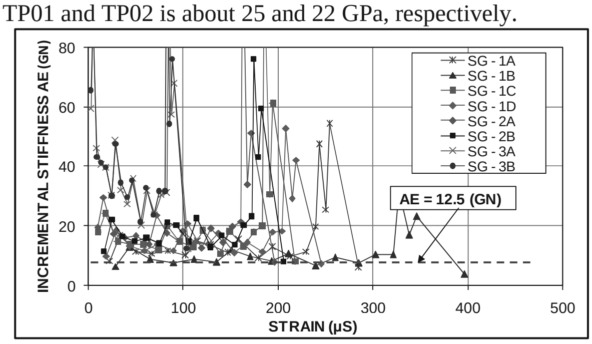

Figure 5. Increment stiffness plot of records from Levels 1 to 3, Pile TP01

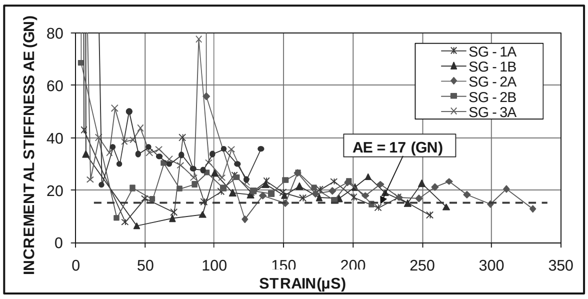

Figure 5. Increment stiffness plot of records from Levels 1 to 3, Pile TP02

1.3 *Load distribution along the pile shafts*

The evaluated stiffness (EA) values were used to convert the strain measurements to load. Figure 6 shows the so-evaluated load distributions. The shaft resistances shown along the upper about 30 m for both piles were not fully mobilized.

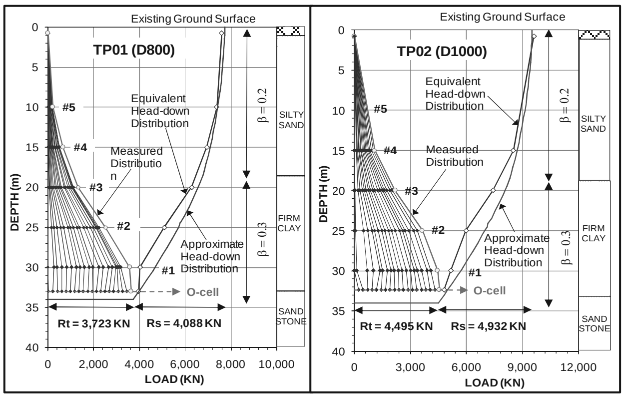

Figure 6. Load Distributions with Approximate Head-down Curve of Piles TP01 and TP02

As shown in Figure 1, the soil at the depth of SG1 to SG3 was a firm clay layer. It is a reasonable expectation that the load distributions would have shown a gentle shape with a decreasing slope toward depth, reflecting increasing shaft resistance as SPT N-indices increase with depth. That this is not the case is considered due to varying effect of the slurry filter cake and, possibly varying pile cross section.

Assuming that the shaft resistance would show a uniform proportionality to effective overburden stress, Figure 6 shows the actual and approximate equivalent head-down load-distribution curves. The latter are obtained by an effective stress calculation for ß-coefficient of 0.2 to 18.5 m depth and 0.3 below this depth to the pile toes. The effective stress analysis indicates the toe resistance and total shaft resistance of Pile TP01 are 3,723 and 4,088 KN, and of Pile TP02 are 4,495 KN and 4,932 KN, respectively.

1.4 *Unit stress versus movement for shaft resistances and pile toes*

The average unit shaft shear resistance between the gage levels can be determined as the difference in evaluated strain-gage load divided by the surface area between the gage levels. Figures 8 and 9 show those values plotted against movements for the particular gage levels. The maximum values of the unit shaft resistance evaluated between the O-cell and SG1 for both test piles showed the average unit shaft resistances of about 60 kPa. Because of strain-softening, the shear resistances were smaller than expected. Moreover, the resistances from SG1 through SG3 are smaller than between SG2 and SG3 for both piles.. It is probable that the construction process left a filter cake between the concrete and the soil and, therefore, the shear movement occurred in the filter cake. The curves also show that, for both piles, ultimate shaft resistance along the length above the O-cell level has not occurred excepting for the curves from O-cell to SG1. The uppermost gage level movements and loads were too small to produce meaningful curves in pile. The records of unit shear resistance between SG4 and SG5 in Pile TP02 were unreliable and are therefore omitted.

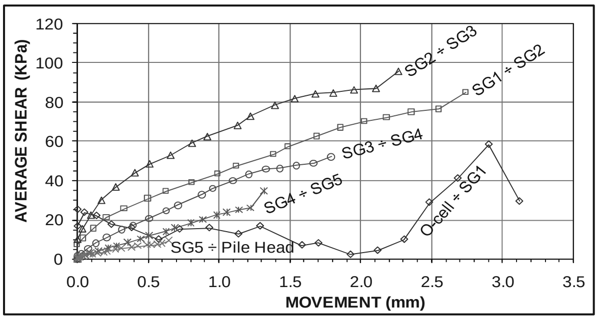

Figure 8. Average shear resistance between gage levels of Pile TP01

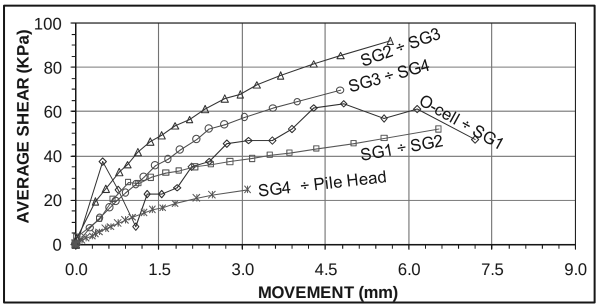

Figure 9. Average shear resistance between gage levels of Pile TP02

Figure 10 shows stresses applied to the pile toe versus the pile toe movements divided by the pile diameter in percent. The stresses are determined by dividing the measured load at O-cells with the nominal shaft areas below O-cell. The maximum toe movements were about 3 and 5 mm, respectively. The increasing stiffness measured for Pile TP01 is considered due to the debris at the pile toe having become compressed.

For both piles, the pile toe stress-movement response was essentially linear and showed no tendency toward an ultimate resistance. It is obvious that the pile toe response is not representative for pile toes placed in weathered sandstone or in sand. Similar observation for large diameter bored piles is reported by (Fellenius and Nguyen 2013).

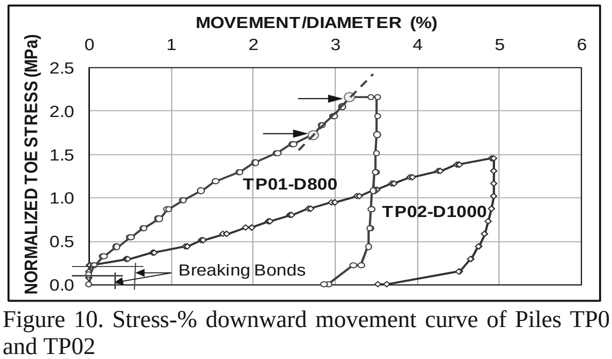

Figure 10. Stress-% downward movement curve of Piles TP01 and TP02

1.5 *Back-analysis to response long-term settlements of piles*

The back-analysis of two tested piles was performed by "The Unified Pile Design" method (Fellenius 1984; 1988; 2011).

The unified pile design approach is the combination of capacity, drag load, settlement, and downdrag. The main tenet of method includes the sustained working load, the shaft resistance distribution, and the soil settlement distribution; they interact with the neutral plane location, the downdrag, and the pile toe load-movement response.

The back-analysis of two tested piles is performed by the software UniPile (Goudreault and Fellenius 1999) and the results are presented in Figure 10. Figure 11 shows the long-term load distribution in the piles TP01 and TP02 starting from the 3.8 and 4.8 MN sustained load from the structure, respectively. Assuming that the drag loads accumulated from negative skin friction are fully mobilized, the maximum loads in the piles are about 5.8 and 7.2 MN at the neutral planes at 23 through 25 m depth below the ground surface. The maximum loads are well within the axial structural strength of both piles. The settlements at the neutral planes and the 'elastic' shortenings of the piles are about 11 through 13 mm and 9 through 11 mm, respectively.

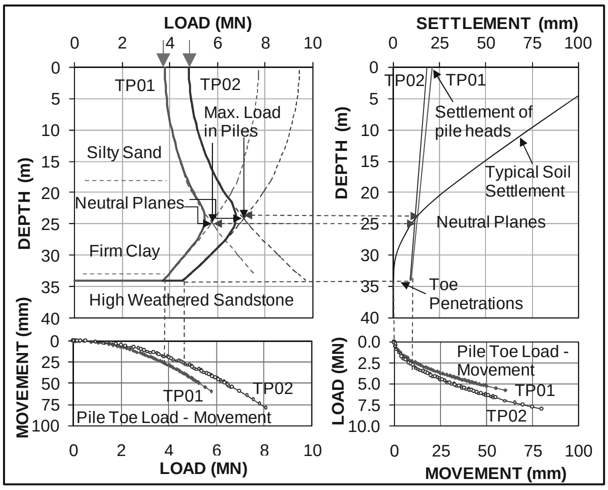

Figure 11. Long-term load distribution and settlement profile for working piles with same diameter and length as the two test piles.

As indicated in Figure 1, the soil at depths of the neutral planes is compressible; this can cause an increase of the pile penetration into the highly weathered sandstone, i.e., downdrag. However, this would partially be offset by the increase of the pile toe force with a subsequent lowering of the neutral plane.

For pile toe resistance, it is recognized that the pile toe does not exhibit an ultimate resistance but is a function of the pile toe stiffness response. Figure 11 also shows the pile toe load-movement curves established by the O-cell measurements. When drag loads in the piles TP01 and TP02 reach the maximum values, the pile toe resistances will increase to about 2.2 and 2.7 MN. The estimated final pile toe movements are about 10 and 9 mm, respectively.

The acceptable maximum long-term foundation settlement for the project is about 40 mm, which is larger than the estimated value. Thus, the testing and the design analysis indicate that there is no need for having the piles constructed deeper to bear on or in the bedrock.

5 SUMMARY AND CONCLUSION

The two bidirectional loading tests on Piles TP01 and TP02 established that the pile capacities satisfied the specified values.

The maximum load tests of 3.8 and 4.8 MN achieved maximum upward movements at the O-cell location of 3.3 mm and 7.4 mm and maximum downward movements of 28.0 and 49.3 mm, respectively. The maximum upward movements of the pile heads were 0.2 and 2.5 mm, respectively. The shaft resistances above 30 m depth were not full mobilized.

The evaluated pile Young's modulus, E, for the piles TP01 and TP02 correlated to 25 and 22 GPa for the nominal pile cross section of both piles. The shaft resistances were small and correlated to an effective stress analysis beta-coefficient of 0.2 and 0.3. The shaft resistances between O-cell and SG1 were strain-softening. It appears that the shaft resistances for both test piles were affected by presence of slurry filter cake between the concrete and the soil.

The measured pile toe stress-movements in percent of nominal diameters for the piles were essentially linear trend and have shown no tendency toward an ultimate resistance. The pile toe response was very soft and not representative for a pile in high weathered sandstone.

Back-analysis by the Unified Design method shows that the structure maximum long-term settlements of the piles will be about 20 mm, which is well below the acceptance value of 40 mm assigned to the project.

6 REFERENCES

Da Nang University of Technology, 2008. Reports on Bored Pile Testing for SeaBank Tower, Da Nang, Vietnam, 54p.

Fellenius, B.H., 1984. *Negative skin friction and settlement of piles.* Proceedings of the Second International Seminar, Pile Foundations, Nanyang Technological Institute, Singapore, 18 p.

Fellenius, B.H., 1988. Unified design of piles and pile groups. Transportation Research Board, Washington, TRB Record 1169, pp. 75-82.

Fellenius, B.H., 1989. Tangent modulus of piles determined from strain data. *ASCE, Geotechnical Engineering Division*, the 1989 Foundation Congress, F.H. Kulhawy, Editor, Vol. 1, pp. 500-510.

Fellenius, B.H., 2011. Basics of foundation design, a text book. Revised Electronic Edition, [www.Fellenius.net], 374 p.

Fellenius B.H. and Nguyen H.M., 2013. Large Diameter Long Bored Piles in the Mekong Delta. *International Journal of Geoengineering Case Histories*, 2(3), 196-207.

Goudreault, P.A. and Fellenius, B.H., 1999. UniPile Version 4.0 for Windows. Users Manual, UniSoft Ltd., Ottawa, [www.UnisoftLtd.com] 64 p.

Nguyen H.M., 2013. *Analysis of Bidirectional Test for Red River Bridge, Vietnam.* The 3th International Conference on Geotechnical Engineering, Hammamet, Tunisia, 9p.

Osterberg, J.O., 1989. *A new device for load testing driven piles and drilled shafts separates friction and end bearing.* Proc. of Deep Foundations Institute, Int. Conf. on Piling and Deep Foundations, London, May 15-18, pp. 421-427.

Slope stability structures for road landslide

Structures de stabilité de pentes pour glissement de terrain

Hamova M., Frangov G., Zayakova Hr.
Higher School of Civil Engineering "L. Karavelov" – Sofia, Bulgaria

ABSTRACT: Landslide had appeared on main road affecting more than half of the roadway and caused traffic difficulties. The landslide had a width in the top 55 m, length - 38 m and maximum depth of 8-9 m. Groundwater table rising, river erosion undermining the slope and the dynamic effects of transport were defined as key factors for slope instability. Cantilever retaining wall on driven pile's foundation, in addition with trailing plate and drainage facilities for landslide stabilization were designed and constructed. The monitoring of strengthened road section during the period 2006 - 2012, shows that the landslide was successfully stabilized and new landslide deformations have not been established.

RÉSUMÉ : Un glissement de terrain est apparu sur une route principale affectant plus de la moitié de la chaussée et perturbant terriblement le trafic. La surface de glissement avait les dimensions suivantes: largeur dans la partie supérieure - 55 m, longueur - 38 m sur une profondeur maximale de 8 à 9 m. On a considéré que l'instabilité de la pente était le résultat des facteurs suivants : nappe phréatique, érosion croissante provoquée par la rivière, effets dynamiques du trafic. Un mur de soutènement fondé sur des pieux, un sol renforcé par inclusion et des drainages ont été conçus et construits pour stabiliser l'ensemble. L'analyse du profil en travers de la route entre 2006 et 2012 montre que le glissement a été stabilisé et qu'aucun nouveau déplacement n'a été observé.

KEYWORDS: Landslide, slope instability, stabilization, cantilever retaining wall, driven piles, drainage facilities.

1 INTRODUCTION

Many landslides have appeared every year on the roads of Bulgaria triggering by various factors and causing serious traffic problems (Ivanov & Dobrev, 2006). Such landslide had occurred on the main road Ruse - Veliko Tarnovo in October, 2005. The landslide had affected more than half of the roadway and it had a width at the top 55 m. This part of the road for a few days had slide up to 70 cm. Wide open cracks had been clear observed on the roadway (fig. 1).

Tension cracks were hardly noticed without vertical escarp at the beginning of sliding. The impression was that only horizontal movement of the landslide had occurred toward the rest of the terrain. The appearance of the landslide was preceded by anomalously high precipitation. Overall it was a wet year, and the annual rainfall amounted to 163% compared to the norm. Rainfalls had formed significant surface runoff, increasing water levels in the river Yantra and the related increase in the levels of groundwater. The subsequent rapid drop in the river water levels had caused reverse filtration and occurrence of high groundwater gradient toward the river.

2 GEOLOGY AND CLIMATE

2.1. Geomorphology

The studied area represents a system of low hills with well-defined crests with west-east direction. More expressive heights are Tarnovo Hils with oversea levels - 300 to 400 m. Main artery Yantra River cuts through the Turnovo mountain forming pictorial Dervish Gorge. Belyakovo and Arbanasi Plateaus are located to the west and the east of the gorge. The northern slopes of Turnovo Hills are steep and there the Danube plain border is marked. The survey landslide is on the highway Ruse - Veliko Tarnovo on the left slope of the Yantra River. The slope is too steep to vertical at the top and low-grade - at the bottom.

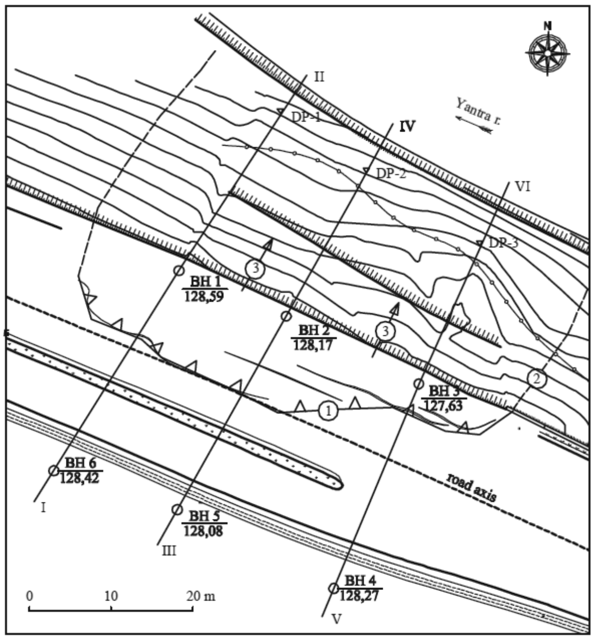

Figure 1. Location map of landslide: 1 - main scarp; 2 - lateral boundary; 3 - movement direction; BH 2 - borehole No 2; DP 1 - dynamic probing No 1; I - II - engineering geological cross-section

2.2. Geology

Territory in close vicinity of the site is made up of different by genesis and composition rock complexes (Chrischev, 1990):

Gornooryahovska Formation (gK1h-a). The Formation outcrops have wide area. The unit builds lower parts of the terrain and slopes of hills, crowned by a strong sandstone and limestone cliffs on its cover. It consists mainly of gray-blue to dove-gray clayey marl altered with some rare and thin layers of solid calcareous sandstones and softer unsorted clayey sandstones.

Balgarenska Terrigenous Formation (bnK1b-a). In the eligible area this formation consists of calcareous sandstones, silty clays and marls, which in places pass into lime-clay siltstones.

Emen Limestone Formation (eK1b). In Veliko Tarnovo region the lower parts of Emen Limestone Formation are presented. It is made of bio-detritus fine limestone, which are revealed in the ridge parts of the landscape. The thickness of the Formation is up to 200 m.

Quaternary diluvial and alluvial deposits are presented above rocky basement. Deluvial deposits are composed of sandy clays, coarse gravels and boulders. They are presented at the foot of the slopes. In some places deluvial clays have considerable thickness. Alluvial deposits build up fragments of first and second terrace above the Yantra River. Alluvial sediments include well graded gravels and sands and sandy clays.

The region belongs to the transitional zone between the Moesian platform and Fore Balkan. Southern boundary of the transition zone is traced unambiguously from Turnovo-Zlatarishky fault. On the surface, it is marked by longitudinal beam fractures, tearing sediments of Balvanska syncline. Northern border passes along the most significant gradient of facial changes and transitions sediment thickness formed during Middle Alpine stage. The transitional nature of the area is expressed in fold-block structure dominated by faults. The study area falls within the scope of the Tarnovo anticline.

2.3. Climate

Investigated area characterized by moderate continental climate. The average January temperature is -1 to -3,0° C and the average July temperature 23-24° C. The annual rainfall is 550-650 mm, with a minimum in February and a maximum in June. The west and northwest winds predominate. In 2005, significant rainfall exceeded the average monthly and annual rate (Table 1).

Table 1. Rainfall in the region before landslide (2005) (www.stringmeteo.com)

Month	Monthly Rainfall, mm	Compared Rate, %
05	113,3	138
06	148,7	179
07	212,2	322
08	90,0	141
09	236,6	538
10	47,8	126
Sum, 2005	1132,2	163

Precipitation in September was more than five times the average monthly rainfall. This reflected in the runoff, increase groundwater levels and the development of physical and geological processes and phenomena.

2.4. Geo-dynamical phenomena and processes

Landslides, weathering, erosion and karst are developed in the region. The presence of clayey sediments, very rugged terrain, tectonic structures and hydro geological characteristics determine the appropriate conditions for development of different type landslides. Their appearance and activation is caused by river erosion, increase groundwater levels, earthquakes, undercutting the slopes by excavations and overloaded the slopes with large embankments (Glavcheva & Dobrev, 2012).

The basic rocks are cracked and disintegrated at a depth of 5-7 m under the action of weathering agents. The weathered rocks are susceptible to sliding and erosion during high precipitation and runoff. Karst is highly developed in the limestone cliffs of Emen Formation and different caverns and caves are formed.

2.5. Methods of exploration works

The landslide was studied with 6 motor boreholes located in three longitudinal profiles (fig. 2). Drilling depths were 9.20 m to 12.00 m, depending on specific conditions. Dynamic probing in 3 points was carried out to determine the thickness of the Quaternary cover and landslide masses and for extending the profiles.

Core drilling was performed, without casing, on dry and short trips. This technology was applied in order to obtain the most reliable information about the boundaries of engineering geological layers and determining slip surface of the landslide. To characterize the physical and mechanical properties of soils 12 samples were taken.

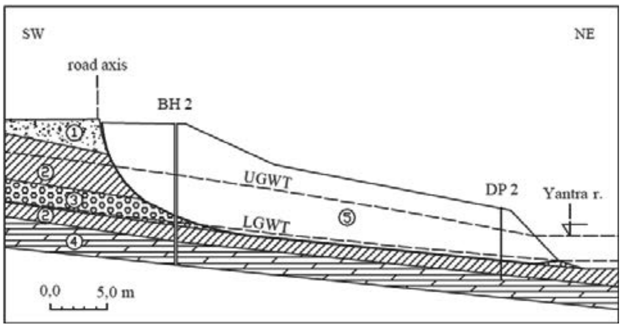

Figure 2. Engineering geological cross-section I - II

1 - road embankment; 2 - Quaternary diluvial clay; 3 - Quaternary gravels with sandy-clayey filler; 4 - Lower Cretaceous marls; 5 - Landslide masses; LGUT - lower ground water table; UGWT - upper ground water table

2.6. Engineering geological layers

According to Genesis, lithological characteristics and physico-mechanical properties of soils established in exploratory boreholes, five layers were separated (Table 2).

Layer 1 - Embankment. The layer builds the road bed. Its thickness is amended widely due to the slope of the natural terrain. The layer is composed of medium to coarse well graded gravel with a maximum thickness of 1.50 m on the coarse rounded gravel with a sandy-clayey filler.

Layer 2 - Quaternary diluvial clay. The layer is located below a layer 1, reveals the at the terrain surface or alternating with layer 3. It is represented by brown, tan to variegated stiff to firm clays with fine gravels. Large boulders up to 0.5 to 1.5 m diameter are found in some places. The thickness of the layer is between 4.70 m in borehole 5 (BH 5) to 9.20 m in BH 1.

Layer 3 - Quaternary gravels with sandy-clayey filler. The layer is set below the layer 1 in BH 1 or alternating layer 2 at different depths in the other boreholes. It is represented by medium to coarse angular to semi rounded gravels with soft sandy-clayey filler. Its thickness varies from 0.50 m in BH 1 to 2.30 m in BH 3.

Table 2. Physical and mechanical properties of the layers

Layer No	Unit wt. γ, κN/m³	Angle of internal friction, φ	Cohesion, c κN/m²
1	23,0	35°	0,00
2	20,5	14,9°	13,3
3	22,7	16,3°	15,8
4	21,6	12,1°	14,5
5	19,3	9,8°	10,2

Layer 4 - Lower Cretaceous marls. Layer 4 is established under the Quaternary cover at various depths below the surface of the terrain - from 3.90 m in dynamic probing 1 (DP 1) to 10.80 m in BH 2. The whole thickness of marls is not exceeded in exploratory drillings. According to visual macroscopic description marl is gray with a brownish tint. The texture is layered and it is built by calcite and clay minerals with some single quartz grains.

Layer 5 - Landslide masses. Landslide body is made of highly mixed clays with some gravels. The landslide movement caused violation of soil structure, changing natural water content and consistency. For the purposes of slope stability calculations three soil samples from slip surface were tested.

2.7. Hydro geological conditions

The region characterizes by middle ground water abundance. The presence of cracked karst limestone creates appropriate conditions for the formation of fissure-karst groundwater. They are drained underground in the Yantra river alluvium or by springs in contact zone between limestone and marl.

Groundwater is accumulated in the Lower Cretaceous karst and cracked limestone and Quaternary sand and gravel layers and lenses. Deep drainage of groundwater has been determined by highly dissected topography. The aquifer is confined with low to medium water pressure at the bottom of the slope depending on the position of ground water table. Groundwater flow is directed northeast to the Yantra.The feeding of ground water is performed by infiltration of precipitation in areas of outcropping of rocks. Groundwater levels are strongly influenced by the seasonal distribution of precipitation and levels of Yantra River. At high river water levels the groundwater upraise, where a sharp drop in river flow creates high-gradient groundwater and hence hydrostatic and hydrodynamic pressure in the slope.

3 SLOPE STABILIZATION

3.1. Overall stability of the slope

To compile a design model for determination of actual stability stage and its alternation due to different destabilizing factors have been reviewed geological and geomorphologic characteristics of the slope, physical and mechanical soil's parameters, sliding mechanism, etc. Main factors in landslide activation have been River Yantra's erosion, increasing of the water table levels and dynamic impact of the vehicles on the road. Additionally the slope stability is influenced from the restraining of gravitational movement of surface and ground waters due to the positioning of road embankment, the lack of effective drainage in the foot of the slope, weathering of the down part of the slope with high river levels, deterioration of shear strength of soils due to vibrations from heavy vehicles.

Position of the most unfavorable sliding surfaces is determined as following boundary conditions have been accepted: obtained main slope of the landslide, swelling on the landslide terrain and established sliding surfaces in drilling boreholes. The form of the sliding surfaces is circular. Janbu's "effective stresses" method is applied under consideration of following conditions: slope stability in natural and dry state and under a dynamic loading.

Table 3. Alternation of Factor of safety (Fs,min) for a different design states and for all of investigated geological profiles

Design state	Fs,min
After landslide activation, in natural state of the slope	0,94 - 1,04
Dynamic impact of the road traffic	0,91 – 0,99
Lower ground water level	1,05 – 1,20

Main conclusions from slope stability analyses can be generalized as follow:

- During the active stage at the time of in – situ investigations of landslide, the slope is in the state of limit equilibrium, near to the further movement.
- Under dynamic loading from the road traffic, the slope exhibits additional decrease of stability measured by the minimum coefficient of safety less than 1.
- Lowering of the ground water levels leads to the increase of its stability.

Analyses of slope stability show that the design of effective drainage system shall not be enough for ensuring the minimum values of factor of safety through all testing profiles, prescribed in national standard for construction in unstable slopes, including the value of Fs,min=1.1 set in National annex of EC7. To achieving the standard overall stability prescriptions the landslide should be strengthened by a retaining structure set in an upper part of slope near to the road (Kolev, 2006).

3.2. Landslide strengthening and drainage works

For recovering of the damaged road section, cantilever reinforced retaining wall on driving pile foundation and additional trailing plate has been designed (fig. 3). The retaining wall has a length of 60 m and it is divided into 12 sections long 5 m each with 2 cm gap between them. The height of retaining wall above the foundation is 4 m. Each section's foundation is composed by 8 driving piles 30/30/900 cm. Due to large horizontal loading from landslides materials at the foundation level the additional "trailing" plate has been designed (fig. 4). The transverse limit state design of pile group has to be done considering of the weight of the backfill above the plate and the activated friction beneath the plate and ground base. The width of trailing plate is 3.5 m and its height is 0.3 m. The piles are designed as end – bearing and embedded into a strong soil layer.

The drainage of landslide has been performed by deep horizontal interception drainage toward the slope. From the bottom of drainage have been constructed drainage shafts 2 m deep, in 10 m from each other. The shafts cross the impermeable soil layer and embedded into lower layer with high seepage capacity. The drainage of high ground water decreases the hydrostatic pressure on the landslide materials. Through the shafts water flows in drainage concrete pipes and then in concrete culvert beneath the road.

The soil beneath the foundation of retaining wall at a depth of 0.5 m is replaced with gravel connected with three deep trench drains with branches. Draining water flows gravitationally into the river.

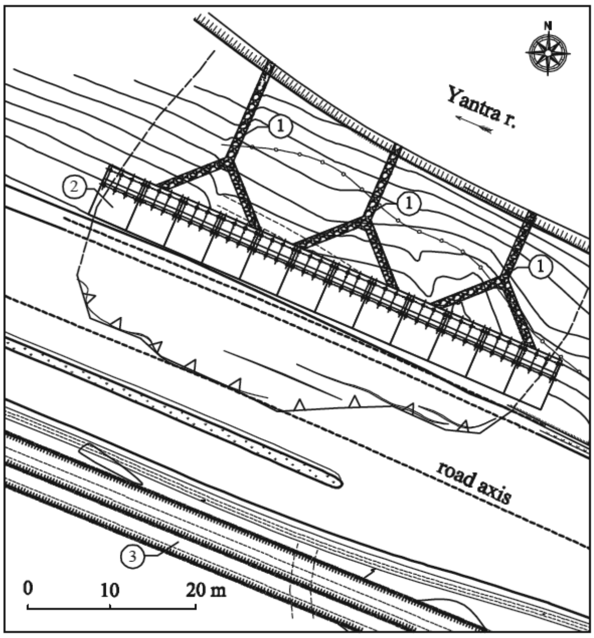

Figure 3. Layout of stabilizing structures

1 - deep trench drains with branches; 2 - retaining wall with trailing plate on driving pile foundation; 3 - deep horizontal interception drainage

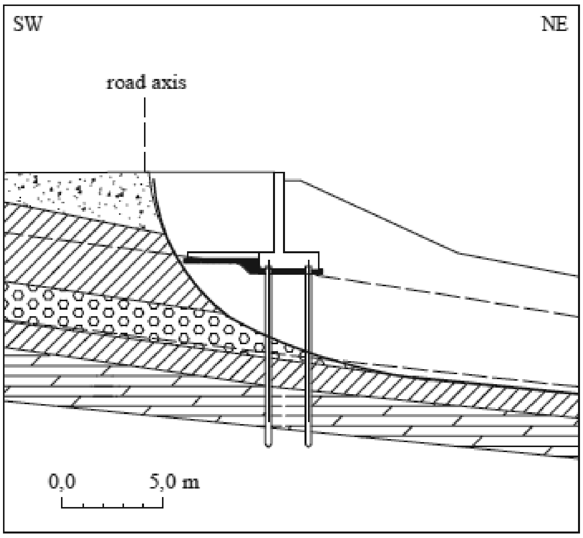

Figure 4. Cross-section through the retaining structure

4 CONCLUSIONS

Conducting investigation of activated landslide leads to following conclusions:

- The investigated slope consists of Quaternary deposits covering Lower Cretaceous marls. Activated landslide is caused by combining influence of river erosion due to high water tables of Yantra River, low strength parameters of quaternary clays, temporary rise of ground water levels from rain water infiltration, static loading from road embankment and dynamic impact of passing vehicles.
- For quality strengthening of road section passed trough activated landslide has been constructed reinforced retaining structure on pile foundation, combined with trailing plate. Piles are embedded in a strong soil layer beneath the sliding surface. The structure has been designed for the pressure from landslide materials and under earthquake condition.
- Drainage system includes interceptor trench drain aligned parallel to the road toward the slope and deep trench drains between the retaining wall and the river. The designed system allows the infiltrated surface water from rains and snow melting to be drawn aside through the culvert to the river without further moistening of landslides materials.
- The installed monitoring system for observation of displacement of stabilized road section shows that constructed retaining structure and drainage system are functioning successfully.

ACKNOWLEDGEMENTS

Present investigation has been funded by Road infrastructure agency part of Ministry of Regional Development and Public Works of Bulgaria.

REFERENCES

BS-EN 1997. Eurocode 7-1 "Geotechnical design. National annex"

Chrischev, Chr. (ed.). 1990. Geological map of Bulgaria. Sheet Veliko Tarnovo, scale 1:100 000. *Bulg. Geol. Survey*, 1.

EN 1997 Eurocode 7 " Geotechnical design "

Glavcheva R., and N. Dobrev. 2012. Inventory of past earthquakes in Bulgaria and searching for geodynamical effects at archaeological sites. *5th Int. Conf. 110 anniversary of the seismological survey in Azerbaijan, 2012, 487-499.*

Ivanov, P., N. Dobrev. 2006. Results from laboratory tests of samples from Fore-Balkan landslides. *Proc. National Sci. Tech. Conf. on Landslides and Erosional Processes in Bulgaria, Prof. M. Drinov*, 155-160.

Kolev, Ch. 2006. General criterion for optimization of complex retaining systems. *National Scientific conference" Conditions and controlling of landslides and erosion in R.Bulgaria" Academic Publisher "Prof. M.Drinov"*. pp.131-134.

www.stringmeteo.com/synop/prec_year.

Research on the Load-Bearing Behaviour of Bored Piles with Different Enlarged Bases

La recherche sur le comportement portante de pieux forés avec diverses bases élargies

Herrmann R.A., Löwen M., Tinteler T., Krumm S.
University Siegen, Siegen, Germany

ABSTRACT: According to DIN EN 1536 overboring of the bottom of drilled piles to increase the EC7-1: bearing resistance is permissible up to three times the pile diameter. The former German standard DIN 4014, however, permitted only an overboring of up to double the pile diameter. The bearing resistance was reduced to 75% in order to take into account the EDZ (excavation disturbed zone) caused by the overboring process. This special area of foundation engineering has been largely unexplored until the early tests by FRANKE/GARBRECHT, and reliable data is not yet available for the new possible pile-base enlargement according to DIN EN 1536. Therefore, model tests at a scale of 1:25 were performed. The experiments were also based on the geometry of the new-type overboring excavation method by BAUER. Thus, new knowledge was obtained on the bearing and settlement behavior of large overbored pile bases with enlargements of one-, two-, and three-times the pile diameter. The tests first showed that an enlargement contributes significantly to an increase in bearing resistance or in limiting pile settlement. More efficient pile foundations are technically possible. A further result is that by the use of a reduction coefficient of 0.75 for the bearing resistance, covering the effects of the drilling the enlargement, the bearing resistance is underestimated. The results were evaluated against the available results of large 1:1 drilled pile experiments. The results of the full-scale tests were assessed regarding their Serviceability Limit State. The available results are to be evaluated by further investigations.

RÉSUMÉ: Selon la norme DIN EN 1536 l'élargissement du fond des pieux forés pour augmenter la capacité de support de charge est permis jusqu'à trois fois le diamètre du pieu. L'ancienne norme allemande DIN 4014, cependant, est premise seulement pendant un alésage allant jusqu'à doubler le diamètre du pieu. Le palier de capacité a été réduite à 75% afin de tenir compte de l'EDZ (excavation zone perturbée) causée par le processus d'élargissement. Étant donné que cette région est en grande partie inexplorée à part les essais antérieurs de FRANKE/GARBRECHT et que les études pour l'élargissement de la nouvelle base de pile possible selon DIN EN 1536 ne sont pas encore disponibles, des essais selon un modèle à l'échelle 1:25 ont été effectués. Les essais se sont également basés sur la géométrie de la nouvelle méthode de type d'excavation de BAUER. Ainsi, de nouvelles connaissances relatives à la capacité de charge et au comportement de déformation, en cas d'élargissements du diamètre du pieu d'une, de deux et même trois fois ont ainsi été obtenues. Les essais ont montré, en premier lieu, qu'un élargissement selon cette nouvelle méthode contribue à une augmentation de la capacité portante ou à une limitation de tassement du pieu. Techniquement, des fondations plus efficaces des piles sont possibles. Une autre conséquence est que le coefficient de réduction de 0,75 pour la résistance de roulement, justifiée par l'influence de la technique de forage dans la production de l'expansion, conduit à une valeur calculée qui contient un facteur de sécurité élevé. Les résultats ont été évalués en fonction des résultats disponibles des essais de forage 1:1 des pieux. Les résultats des grands essais ont été évalués quant à leur fonctionnalité. Les résultats disponibles doivent être évalués par des enquêtes ultérieures plus approfondies.

KEYWORDS: Drilled Pile, Pile foot expansion, reducing coefficient, pile diameter, EDZ excavation disturbed zone

1 INTRODUCTION

Specialized foundation engineering literally lays the groundwork for almost any construction project. On poor, inadequate subsoils, the use of shallow foundations is not acceptable due to excessive settlements. Wooden piles were already being used more than 4000 years ago for foundation construction in weak soils. This made it possible to transmit loads into deeper soil layers with a higher load-bearing capacity. Today wooden piles are only used occasionally for small, temporary buildings.

Along with various other pile foundations, as for example driven piles, displacement piles and micropiles, bored piles are a current standard for deep foundations, especially when high loads must be supported. Special types of the bores piles are bored piles with bottom enlargement according to DIN EN 1536. With this system an increase of the load- bearing capacity is achieved through an enlargement of the supporting cross-sectional area. As a result of the larger area of the base in addition to the skin friction, larger bearing resistance can be attained where the area of the bottom, D², is larger or the enlargement will preserve the assigned Serviceability Limit State (SLS). Normally a pile with a base enlargement would first have the point bearing with the skin friction determined and then be designed predominantly based on a point-bearing pile (see also Herrmann, Lauber).

The aim of this test series was to test the load-bearing capacity the afore-mentioned pile system with different diameters. This need for the tests arose from the issuance of the European standard DIN EN 1536. This standard permits an expansion of up to twice the pile diameter, whereas DIN EN 1536, which replaces the old German standard DIN 4014, permits a cross-section enlargement of up to thrice the pile diameter (see DIN 4014 and Franke/garbrecht).

In order to obtain and afterwards compare the differences in the load-bearing behaviour due to the increased base areas, static axial tests (compression tests) were carried out on scale model piles (smooth probe rod (d= 36 mm) with turned pile foot (hard plastic)) at a scale of 1:25 (see Figure 1).

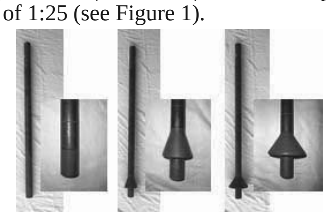

Figure 1. Pile models without (1xD), and with 2 - (2xD) and 3 -(3xD) times the pile diameter bottom enlargements

2 PILE SYSTEM

2.1 *General*

A drilled pile with base enlargement functions like a large drilled pile in accordance with DIN EN 1536 which is manufactured with or without suspension support depending upon the stability of the ground. Subsequently, the bottom of the borehole will be enlarged by the assistance of a special drilling tool, the Belling bucket (see Figure 2).

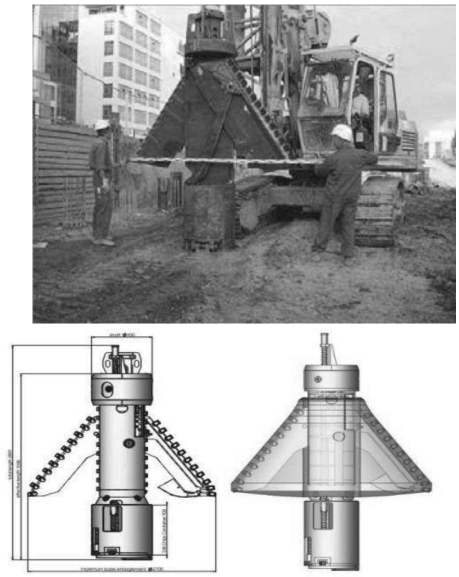

Figure 2. Belling bucket Bauer

This aforesaid drilling tool is denoted as a pile base extension cutter and generally consists of two cutting arms and a cutting body that functions as a borehole reamer to produce a pile (an under-pile) beneath the pile base enlargement.

2.2 *Advantages of the Pile Base Enlargement*

- Higher load-carrying capacity of the single pile or settlement reduction
- Fewer piles under concentrated loads
- Simple pile head construction (none or smaller pile head slabs)
- Reduced pile shaft diameter with shallower drilling depths
- Smaller drilling equipment (more favorable BE/BR, lower costs)
- Savings on pile concrete (more favorable relationship load/m^3 concrete)

2.3 *Pile geometry*

2.3.1 *Pile Shaft*

The drilled pile shaft exhibits a constant cross section, which is selected according to the static requirements for the internal bearing capacity from the top of the pile down to the beginning of the enlargement. Usually the pile is manufactured using a C30/35 concrete. Unreinforced or partially reinforced piles are permissible in principle, while at the same time the load distribution according to EC 2 must be considered. With wide base enlargements and high pile loadings, high-strength concrete can be used, permitted in accordance with DIN EN 1536, or steel fiber reinforcing would be useful.

2.3.2 *Pile base*

It must be noted foremost, that the widening of the foot of the pile is dependent on the basic geometry of the drilled pile, meaning the diameter of the shaft and the overboring equipment used. This is due to the different opening mechanisms of the cutting arms. Modern cutters, like those presented in the current paper, are able to produce flat bottoms within the area of the widening, which was not the case with older models. Also with these types of devices, depending on the manufacturer, an under-pile beneath the enlargement with the same diameter as the shaft is created. This has a positive influence on the friction of the base of the overboring to provide additional support and provides a stopper effect which mechanically increases the bottom of the pile. Investigations by BAUER showed that with these new type cutting devices, even the largest, all pile foot enlargements according to DIN EN 1536 can be manufactured in the soils envisioned for special foundation construction safer and with a higher quality.

According to DIN EN 1536 the area of the foot enlargement is reduced as follows depending of the soil in the base area:

- with cohesionless soils (See Figure 3):
  a) Foot height / Foot Overboring = h_{Base} / $Ü_F \geq 3$ (similar to DIN 4014)
  b) max. permissible pile foot diameter = 2 x pile shaft diameter, d_{Base}

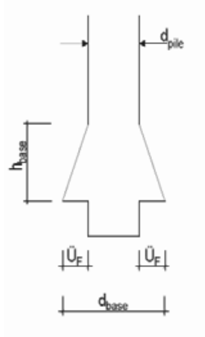

Figure 3. Pile foot base enlargement in cohesionless soils

- In cohesive soils (See Figure 4):
  a) Foot height / Foot Enlargement = h_{Base} / $Ü_F \geq 1.5$
  b) max. allowable pile foot diameter = 3 x pile shaft diameter, d_{Base} (1.5 fold value from DIN 4014)
  c) max. allowable pile foot area = 10 m² max. allowable pile foot diameter = 3.57 m

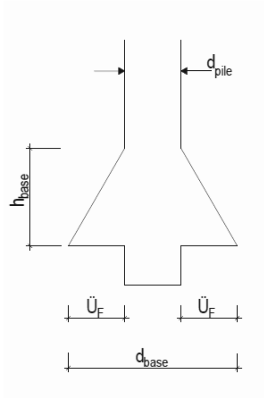

Figure 4. Pile foot base enlargement in cohesive soils

2.4 *Pile tests*

2.4.1 *Pile tests Description*

The investigation of the differences in the bearing capacities of the piles depending on the different pile foot base enlargements (see Tinteler, Herrmann) was carried out with load tests on scale models. (see figure 5).

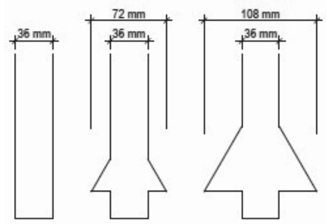

Figure 5. Cross section of the pile models (M = 1:25)

In each case two tests conditions were investigated: using a casing in order to eliminate skin friction and to measure point resistance R_b only, and without a casing to determine the entire pile resistance R_{b+s}. The experimental soil was a sand with a uniformity coefficient, U, of 2.5 – 2.8. It can further be said that this soil was prepared by an in-place compaction, I_D, of approximately 0.74, which corresponds to a dense condition.

For statistical reasons and to acquire meaningful strong results, for each case three identical loads (in each case three per cross section with and without casing – altogether 18 trials) were applied with the different models (See Figures 1 & 5).

3 TEST SEQUENCE

After complete installation of the appropriate test pile (see Installation- /Soil parameter Table 1):

1. Placement /Compaction 1. Layer
2. Placement /Compaction 2. Layer
3. Centering/Plumbing test pile in the container
4. Placement /Compaction 3.-6. Layer,

Table 1. Installation- /Soil parameter

Installation- /Soil parameter		
$d_{Container}$	[cm]	70
h_{layer} (1-6)	[cm]	14.5
M_{layer} (1-6)	[g]	15867
D	[g/cm³]	1.71
g_s	[g/cm³]	2.65
I_D	[-]	0.74

in the test soil (dense sand), the experimental container (steel cylinder) was centered under the cross beam and hydraulic press. After installation of the measuring bridge (See Figure 6) a seating load, F_i = 250 N, was applied to eliminate any slack in the loading system and to adjust the strain gauge.

The experimental models 1xD and 2xD were loaded in increments of 250N, and model 3xD in 500N steps. After each increment of loading the load was held for 10 minutes. Settlement readings were made after 0, 1, 2, 3, 5 and 10 minutes. The failure criterion for the test loadings was taken to be when the pile sank continuously into the soil under a constant load.

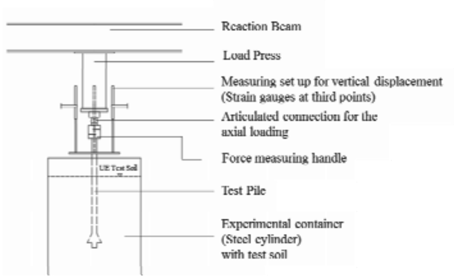

Figure 6. Test Set-Up

3.1 *Results of the Load Tests*

On the basis the measured values of the applied loads and associated vertical displacements, a graphic evaluation of the various test loads was made. The bearing resistance dependant on the pile settlement is illustrated in the following (see figure 7) by the average resistance-settlement curve (average values of the R_{b+s} and R_b test loadings).

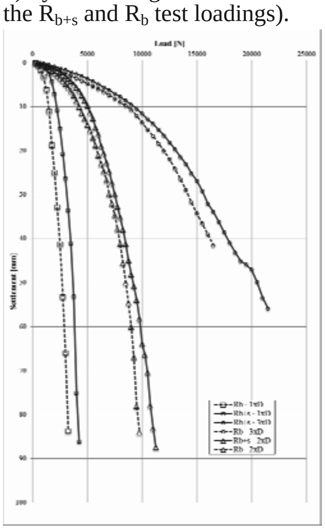

Figure 7. Load Test Resistance-Settlement Curves, R_{b+s} and R_b (average values in each case from 3 test load trials)

4 EVALUATION OF THE RESULTS

For the evaluation of the results and the comparative analysis, the three tests per pile were averaged. The calculated average values were used as the representative values for the respective pile models for all of the following comparisons and computations.

Table 1 shows that all three models had comparable mobilized skin frictions from 6131.1 to 762.0 N. The skin friction appears to be a constant value with it's proportion of the load decreasing greatly with increasing base enlargement so that a shift in the resistance occurs from a skin friction/point bearing to a predominantly point bearing pile. The existing technical assumption/theory that there is an "arching effect" regarding the stress distribution with a base enlargement by activating higher skin friction stresses cannot be substantiated by this test series.

Table 2. Results of Test Models 1xD, 2xD, 3xD, Comparison of results with and without skin friction

Test Pile	Point bearing (R_b) +Skin friction (R_S)	Point bearing	Skin friction (R_S)	
			Absolute	Relative
	R_{b+s} [N]	R_b [N]	[N]	[%]
Model 1xD	1645.4	1032.3	613.1	37.2
Model 2xD	4505.2	3743.2	762.0	17.1
Model 3xD	9684.5	9013.1	671.4	6.8

According to FRANKE the evaluation of the FRANKE/GARBRECHT investigations shows that for bearing structures with acceptable deformation ranges of 2 to 4 cm and different loadings, it is possible to equalize settlements by the use of pile foot base enlargement (see Table 4).

Table 3. Comparison of the results of model tests 1xD, 2xD, 3xD

Test Pile		1xD	2xD	3xD
Base diameter	[mm]	36	72	108
Contact area	[mm²]	1017.88	4071.5	9160.88
Settlement limit s_{gr}	[mm]	3.6	7.2	10.8
$R(s_{gr})_{b+s}$ from tests	[N]	1645.4	4442.5	9645.9
Proportional increase related to the 1xD-pile	[%]	-	270.0%	586.2%
$R(s_{gr})_b$ from tests	[N]	1032.3	3743.2	9013.1
Proportional increase related to the 1xD-pile	[%]	-	362.6%	873.1%

5 COMPARISON WITH IN SITU TESTS

For the evaluation of the results, there are at present only the investigations by FRANKE/GARBRECHT in the form of full-scale tests, which are drilled piles 6 to 14 m long with pile (b) and pile base diameters (b_f) from 1100 to 2100 mm hat were manufactured with and without base enlargements in medium dense sands and were load tested with deactivated skin friction (using a bentonite filled ring gap) (see Table 3).

The results of the investigations by Franke/Garbrecht indicate that the ratio of the breaking stress for the enlarged to the normal pile amounts to approximately 0.94 to 0.95 (see Table 4 $\sigma b(s_{gr})^{(1)}$ to $\sigma b_f(s_{gr})^{(1)}$). This with the reducing coefficient for characteristic pile resistances, $\alpha_{enlarged}$ = 0.75, verifies the manufacturer's partial safety factor, γ > 1.25 (see Eq. 1 resp. Eq. 2 / Table 4),

$$R_{bf}(s_{gr}) / (R_{bf}(s_{gr}) \cdot 0{,}75) > 1{,}25 \quad \text{(Eq. 1)}$$

$$\sigma b_f(s_{gr})^{(1)} / (\sigma b_f(s_{gr})^{(1)} \cdot 0{,}75) > 1{,}25 \quad \text{(Eq. 2)}$$

the acceptable safety representative of the researched pile foot base enlargement.

Table 4. Comparison of the results of Franke/Garbrecht with own Tests

FRANKE/GARBRECHT					
Pile	b resp. b_f	Ratio b_f resp. b	Pile foot base area	$\sigma b(s_{gr})^{(1)}$ resp. $\sigma b_f(s_{gr})^{(1)}$	$\sigma b(s_{gr})^{(1)}$ to $\sigma b_f(s_{gr})^{(1)}$
		[-]	[m²]	[N/mm2]	

	[m]				[%]
1** (b)	1.10	1.44	0.95	3.60	-5.90
2** (b_f)	1.58		1.96	3.40	
3++ (b)	1.50	1.36	1.77	4.20	-31.30
4++ (b_f)	2.04		3.27	3.20	
5## (b)	1.10	1.39	0.95	3.80	-5.60
6## (b_f)	1.53		1.84	3.60	
7*+ (b)	1.50	1.40	1.77	3.80	-5.00
8*+ (b_f)	2.10		3.46	4.00	
Own Tests					
Pile	b resp.b_f [m]	Ratio b_f resp. b [-]	Pile foot base area [m²]	$\sigma b(s_{gr})^{(1)}$ resp. $\sigma b_f(s_{gr})^{(1)}$ [N/mm2]	$\sigma b(s_{gr})^{(1)}$ to $\sigma b_f(s_{gr})^{(1)}$ [%]
1xD (b)	3.60		1017.90	1.01	-
2xD (b_f)	7.20	2.00	4071.50	0.92	-10.20
3xD (b_f)	10.80	3.00	9160.90	0.98	-3.00

(1) $\sigma b(s_{gr})$ resp. $\sigma b_f(s_{gr})$
$= R_b(s_{gr})$ resp. $R_{bf}(s_{gr})$ / ((b resp.bf) · π) / 4)
$s_{gr} = 0.1 \cdot$ b resp. b_f
**, ++, ##, *+ Comparable piles comparable lengths, Without base enlargement (b) /with base enlargement (b_f)

Note: Pile No. 4 is not comparable because of a shorter pile length, i.e. not included in the evaluation.

In summarizing, two informative results come from the test loadings on the scale model test piles. This is on the one hand the realization that the base enlargement of a drilled pile to three times it's shaft diameter would increase the load-bearing resistance expected due to the effect of D^2 was fair.

On the other hand it turned out that a pile base enlargement according to DIN 1054 (or EA-Pfähle) using the reducing coefficient $\alpha_{enlarged}$ = 0.75 for calculating the pile base resistance contains a high safety factor.

Fundamentally, it is to be noted, however, that in the context of this work the results obtained are based on tests at a small scale (model tests). Further, are factors (ground-water flows, inhomogeneous soils) that were left out of consideration, which could possibly have an influence on the bearing behavior of in situ piles. This is especially true if, due to pile settlement, a displacement of the soil in the area of the pile foot base can take place. Therefore no clear conclusions on the actual bearing behavior of large drilled pile with base enlargements can be drawn.

Table 5: Evaluation of In Situ Load Tests by Franke/garbrecht for various related Settlements, s/D

Pile	Pile base dia-meter [m]	Pile foot area [m²]	s/D(2) [-]	Settle-ment [cm]	$\sigma b(s)^{(3)}$ resp. $\sigma b_f(s)^{(3)}$ [N/mm2]	$R_b(s)$ resp. $R_{bf}(s)$ [MN]
1** (b)	1.10	0.95	0.02	2.2	1.7	1.6
			0.03	3.3	2.0	1.9
			0.10	11.0	3.6	3.4
2** (b_f)	1.58	1.96	0.02	3.2	1.8	3.5
			0.03	4.7	2.1	4.1
			0.10	16.0	3.4	6.7
3++ (b)	1.50	1.77	0.02	3.0	1.7	3.0
			0.03	4.5	2.3	4.1
			0.10	15.0	4.2	7.4
4++ (b_f)	2.04	3.27	0.02	4.1	1.4	4.6
			0.03	6.1	1.7	5.6
			0.10	20.4	3.2	10.5
5## (b)	1.10	0.95	0.02	2.2	1.5	1.4
			0.03	3.3	1.8	1.7
			0.10	11.0	3.8	3.6
6## (b_f)	1.53	1.84	0.02	3.1	1.3	2.4
			0.03	4.6	1.8	3.3
			0.10	15.3	3.6	6.6
7*+ (b)	1.50	1.77	0.02	3.0	1.5	2.7
			0.03	4.5	2.0	3.5
			0.10	15.0	3.8	6.7
8*+ (b_f)	2.10	3.46	0.02	4.2	1.9	6.6
			0.03	6.3	2.3	8.0
			0.10	21.0	4.0	13,9

(2) D = b_f resp.b
(3) $\sigma b(s)$ resp. $\sigma b_f(s)$ =
= $R_b(s)$ resp. $R_{bf}(s)$ / ((b resp.bf) · π) / 4)
s = s/D · b resp. b_f
**, ++, ##, *+ Comparable piles comparable lengths, Without base enlargement (b) /with base enlargement (b_f)

Note: Pile No. 4 is not comparable because of a shorter pile length, i.e. not included in the evaluation.

However, since there appears to be a discrepancy between theory and practice, a continuing analysis would be meaningful and necessary based on full-scale tests up to the 1:1 scale, since the reliable data collection on the influence of manufacturing variabilities can only be investigated in full-scale tests. This evaluation is valid in particular under the aspect that there are new techniques and geometries for pile base enlargement – as were considered in this presentation – to produce new types of pile foot base enlargements with positive influences on the bearing behavior or the piles.

Thus, these drilled piles represent a new system for deep foundation with a special capability regarding the loads and the deformation limitations. It is of special importance that all of the new pile cutting equipment for pile foot base enlargement according to DIN EN 1536 – including the largest – can assuredly manufacture piles in the soils envisaged for it by specialized foundation engineering.

If these investigations would lead to a confirmation of available findings, a safe and economic adjustment of the reducing coefficient would be possible. Therefore, the work on this topic should be continued.

6 REFERENCES

DIN EN 1536: Ausführung von Arbeiten im Spezialtiefbau – Bohrpfähle,Deutsche Fassung EN 1536:2010, Beuth-Verlag Berlin, 2010

DIN 4014: Bohrpfähle – Herstellung, Bemessung und Tragverhalten,Beuth-Verlag Berlin, 1990

Franke/Garbrecht: Lastsetzungslinien von Großbohrpfählen mit und ohne Fußverbreitung bei 2,5 m Einbindung in Sand und verschiedenen Pfahllängen (nach Franke/Garbrecht 1976). In: Smolczyk, U.: Grundbau-Taschenbuch, 4. Auflage, Teil 3, S. 210. Ernst & Sohn, Berlin, 1992

BAUER: Firma BAUER Spezialtiefbau Schrobenhausener Tage 2006 (unveröffentlicht) / Firmenunterlagen, 2006

Herrmann, Lauber: Vergleichende Untersuchungen zur Kompatibilität zwischen den nationalen und europäischen Grundbaunormen und sonstigen Regelwerken – Band 1: Bohrpfähle – Vergleich DIN 4014 mit DIN EN 1536, Beuth-Verlag Berlin, 2000

Herrmann, Lauber: Vergleich DIN 4014 mit DIN EN 1536, fahlsymposium 2001, TU Braunschweig, Heft Nr. 65, Braunschweig, 2001

Tinteler, Herrmann: Untersuchungen zum Tragverhalten von Großbohrpfählen mit unterschiedlichen Fußaufweitungen, Institut für Geotechnik der Universität Siegen, 2012

DIN 1054: Baugrund – Sicherheitsnachweise im Erd- und Grundbau,Beuth-Verlag Berlin, 2005 / 2010

EA-Pfähle: Empfehlungen des Arbeitskreises “Pfähle” der DGGT, 2007

Visualization of Settlement Behavior for Friction Pile Group during Consolidation

Visualisation du tassement pour un groupe de pieux frottant lors d'une consolidation

Ishikura R.
Kyushu University, Fukuoka, Japan

Matsuda H., Igawa N.
Yamaguchi University, Ube, Japan

ABSTRACT: Combined technology by using surface stabilization and floating type deep mixing soil stabilization has been developed as a method with acceptable settlement for maintaining the proper functioning of superstructures on deep soft soil layers. In this study, in order to apply for the practice of this ground improvement technique, settlement properties and skin friction were investigated by using two types of model tests and full scale FEM analysis in the consolidation process. For applying the image analysis to the model test, it was clarified that vertical strain of soft clay in the upper part of the improved portion was restrained by transferring the load to the deep soft soil layer. Further, from the analytic results, it was also found that full mobilization length of skin friction increased with elapsed time and converged to the constant value under the consolidation condition.

RÉSUMÉ : Une technologie combinée comprenant une stabilisation de surface et des fondations de type pieux sur sol renforcé a été développée pour limiter le tassement et assurer la stabilité des super structures dans les sols mous. Dans cette étude, afin d'analyser cette technique d'amélioration du sol, le tassement et le frottement ont été étudiés à l'aide de deux types de modèle numérique à grande échelle (MEF) pendant la phase de consolidation. Les essais sur modèles réduits ont montrés un transfert de la charge verticale de la partie supérieure du massif renforcé vers la partie profonde sur sol mou. En outre, à partir des résultats, il a également été constaté que la longueur de mobilisation du frottement augmente avec le temps et tend vers une valeur constante au cours de la consolidation.

KEYWORDS: ground improvement, skin friction, consolidation, floating soil pile

1 INTRODUCTION

Economy and environmental safety have recently become very important factors in the construction of soil structures. So it is essential to develop the rational construction technique to correspond with the diversity of performance. In this demand of society, it is beginning to recognize the importance of the technique that combines different individual methods.

Piled raft foundation has recently been considered as a rational foundation type in Japan. This technology can reduce raft settlement by combining piles with maintaining the safety of the foundation on deep soft soil layers.

In the ground improvement field, combined technology by using surface stabilization and floating type deep mixing soil stabilization has also been developed. This technology has the advantage to reduce the construction cost of soil structures on deep soft soil layers. The structural form of the floating deep mixing soil piles with shallow stabilization is similar to that of the piled-raft foundation. In order to apply for the practice, it is important to clarify the mechanical behavior of this improved ground in relation to the combined effect between pile and raft.

In previous studies, several model tests for simulating this type of improved ground were conducted to investigate the influence of the improvement parameters such as improvement ratio and improvement depth on the settlement (Bergado et al., 1994; Miki et al., 2004; Ishikura et al., 2006). A method for predicting the total settlement of this improved ground has been previously proposed (Ishikura et al., 2006). On the other hand, from the model tests of piled raft foundation conducted on soft ground, it has been clarified that the failure of piled raft foundations was caused by the block consisted of the pile and soft clay enclosed within the pile group by Whitaker (1957).

Figure1 shows the concept of the equivalent raft method. In this figure, H_1 is defined as the improvement depth. As shown in this figure, Tomlinson et al. (2008) suggested that the pile group transfers the load to the bearing layer at the elevation of the pile tips by an end-bearing-type mechanism. He also suggested that the pile group transfers the load to the soft soil layer at an elevation corresponding to 2/3 the pile length below the top of the piles. However, this method is still experimental and has not been sufficiently validated.

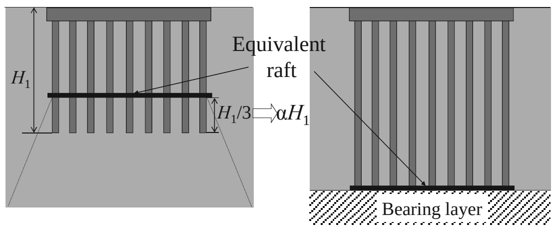

Figure 1. Equivalent raft method

In this study, in order to investigate the group effect of this improved ground in the consolidating ground, consolidation settlement behavior was observed by using two types of model tests. From the test results, the influence of improvement conditions on the consolidation settlement and skin friction was discussed. Secondly, ground behavior was observed through the rubber membrane of transparent plate. By using image analysis, several strain distributions of the model ground were clarified. Based on the model tests, group effects during consolidation were discussed. In particular, skin friction under different improvement conditions were formulated.

Finally, in order to consider the equivalent raft elevation in relation to the improvement conditions, full scale FEM analysis were performed in the consolidating ground using the different pile skin friction resistance. From the results, equivalent raft elevations were discussed in the consolidation process.

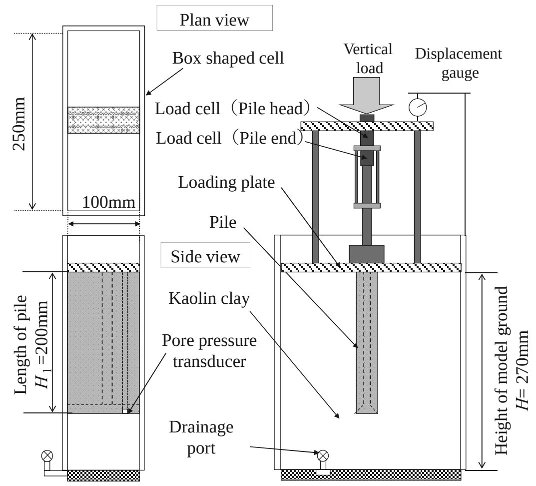

Figure 2. Loading model test under the plane strain condition

2 VISUALIZATION OF GROUND BEHAVIOR UNDER PLANE STRAIN CONDITION

2.1 *Outline of model test*

Figure 2 shows the apparatus used in the model test under the plane strain condition. The model tests were carried out with drainage at the upper and lower surfaces. Wall friction was reduced by a rubber membrane between the specimen and acrylic plate. The tests for the model ground were conducted under stress controlled conditions. The vertical load and consolidation settlement were also measured. This apparatus can also measure the pile head and end resistance individually at the center of model pile (Ishikura et al., 2012).

The model ground was prepared by using Kaolin clay and model pile. Kaolin clay was remolded in a slurry condition with a water content of about 80%. This slurry was then poured into the consolidation cell up to a depth of about 350mm. The specimen was consolidated under a pre-consolidation pressure of 20kPa using a bellofram cylinder until the end of primary consolidation. After pre-consolidation, a model ground with a height H of about 270mm was obtained.

The model piles are composed of aluminum and have 30mm in width D, 100mm in depth and 200mm in length H_1. Pore pressure transducer was placed at the bottom of model pile. After the model ground was prepared, consolidation pressure was applied and increased stepwise from σ =20kPa to 40kPa, 40kPa to 80kPa using bellofram cylinder. The loads are applied to unimproved ground and improved grounds with 1 or 3 piles.

2.2 *Test results and discussions*

Figure 3 shows the relationships between normalized settlement S/D, normalized incremental averaged skin friction $\Delta f/\Delta\sigma$ and elapsed time in the consolidation process with 1 pile. Incremental averaged skin friction Δf is the value that divides the load difference between the pile head and pile end by the surface area of the model pile. As shown in this figure, normalized settlement S/D increased with elapsed time and converged to the constant value. On the other hand, incremental averaged skin friction Δf initially increased just applying on the vertical pressure, however, after reaching the peak incremental skin friction Δf, these began to decrease with elapsed time and later converged to the constant values.

Figure 4 shows the corresponding relationships between the normalized settlement S/D and normalized averaged incremental skin friction $\Delta f/\Delta\sigma$ under several test conditions. It is considered that averaged incremental skin friction Δf is mobilized by acting relative displacement between the model pile and soft clay around the pile end surface during consolidation. As shown in this figure, normalized skin friction and normalized settlement curves with 1 pile are different from that with 3 piles under several consolidation pressures. However, normalized averaged incremental skin friction $\Delta f/\Delta\sigma$ increased initially with an increase of the normalized settlement and later converged to the constant value under all the test conditions.

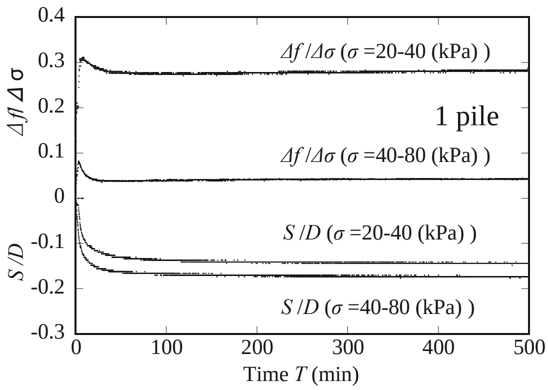

Figure 3. Relationships between skin friction and settlement

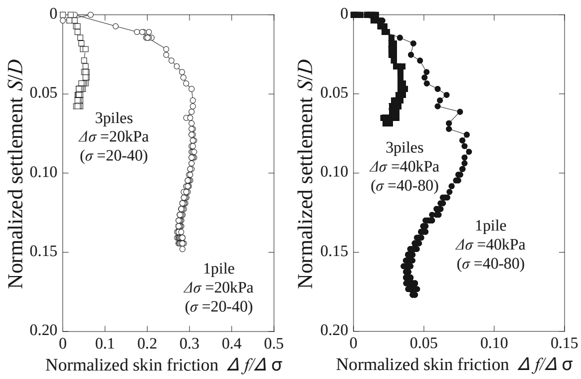

Figure4. Relationships between normalized settlement and skin friction

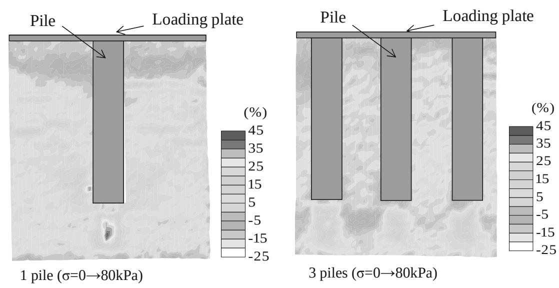

Figure5. Vertical strain distribution after consolidation

Figure 5 shows the vertical strain distributions with 1 pile and 3 piles. These strains can be obtained from the deformation vectors during loading model tests. Deformation vectors are obtained by observing the ground behaviors through the rubber membrane. As shown in this figures, vertical strain of soft clay just below the pile end increased significantly with 1 pile. It is considered that the applied load is transferred from the model pile to the soft clay. It is also observed that vertical strain of soft clay just below the pile end with 3 piles is smaller than that with 1 pile. On the other hand, soft clay just below the loading plate has little vertical strain in comparison with that of just below the pile end in both test conditions.

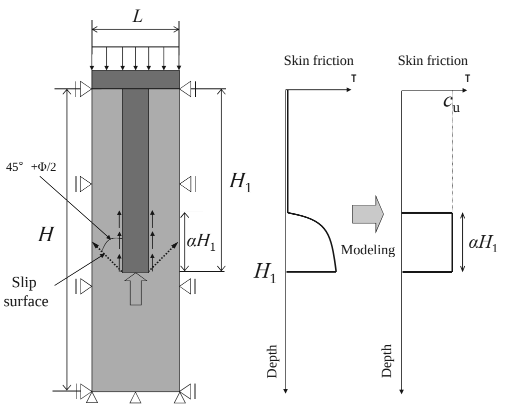

Figure6. Hypothesis of skin friction around the surface

2.3 *Prediction model for skin friction of floating-type column*

In this study, in order to evaluate the skin friction applied around the surface of floating-type columns, FEM analysis with the Cam-clay model as the constitutive equation was performed using axi-symmetric and plane strain models (Ishikura et al., 2006). H, H_1 and L denote the ground depth, the improvement depth and the distance between the improved columns or walls, respectively. The ground surface was deformed equally by the rigid plate on the assumption of shallow stabilized ground.
From the results of FEM analysis, the upward skin friction applied around the surface of the improved column is determined using the approximate formula given in Eq. (1).

$$\frac{\bar{\tau}}{p_0} = \frac{c_u}{p_0} \bullet \frac{1}{H_1/L} \quad (\bar{\tau} \leq c_u) \qquad (1)$$

p_0 denotes the pre-consolidation pressure of the soft clay. $\bar{\tau}$ denotes the averaged skin friction applied around the surface of the column. This value is obtained from the difference between the stress applied on and immediately below the improved column. Each value of $\bar{\tau}$ is normalized by the p_0. H_1 is normalized by the value of L. The normalized average friction $\bar{\tau}/p_0$ decreases with an increase in H_1/L. Furthermore, the maximum value of $\bar{\tau}/p_0$ is almost equal to the shear strength ratio c_u/p_0 . It is clarified that $\bar{\tau}$ changes under several conditions with different values of H, H_1, and L.

Here, c_u is the undrained shear strength. The approximate curve almost corresponds to the relationship between the upward averaged skin friction and the improvement parameters. It is considered that skin friction is mobilized around surface acting relative displacement between the column and soft clay. The combined foundation transfers the load to the pile group via the raft; hence soft clay between the friction piles in the upper part of the combined foundation is enclosed.
Figure 6 shows the hypothesis of skin friction around the surface of columns. As shown in this figure, if the slip surface that has inclination of 45 degrees from the pile end to the upper part has occurred, the intersection adjacent the column has been existed. When the length from this intersection to the column end is supposed the length that the skin friction is mobilized, the equivalent conversion ratio α which is defined as the ratio between the column length and the length that the skin friction is mobilized is introduced in Eq.(2).

$$\alpha = L/H_1 \qquad (2)$$

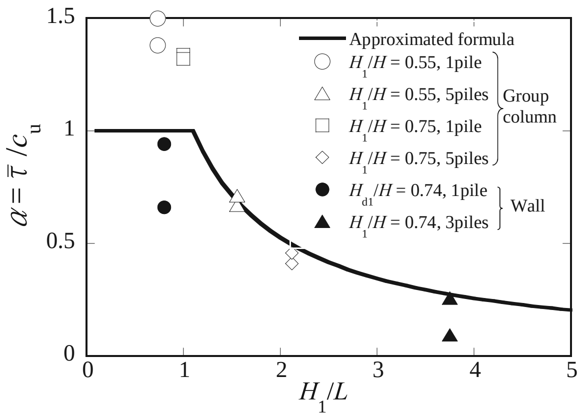

Figure7. Formulation of equivalent conversion ratio α

When c_u is defined as the undrained shear strength near the surface acting relative displacement between the column and soft clay, α is also given in Eq.(3) by using Eq.(1).

$$\alpha = \frac{\bar{\tau}}{c_u} = \frac{1}{H_1/L} \quad (H_1/L \geq 1) \qquad (3)$$

Figure7 shows the formulation of the equivalent conversion ratio α . Experimental values of two types of loading model tests were also plotted (group column type and wall type). As shown in this figure, equivalent conversion ratio α nearly corresponds with the calculated value from Eq.(2) or Eq. (3).

3 TENDENCY OF SKIN FRICTION MOBILIZATION IN THE CONSOLIDATION PROCESS

3.1 *Numerical modeling*

In this section, in order to evaluate skin friction mobilization of this type of improved ground during consolidation, time dependent behaviors of skin friction were investigated by using FEM analysis. Numerical analysis has already been performed to investigate the neutral plane of pile in the consolidating ground (Yan, W. M. et al., 2012). Figure 8 shows the Axi-symmetric model for evaluating skin friction in this study.

Elastic model was applied to the shallow stabilized ground (raft) and column (pile). Modified Cam-clay model was also used in the soft clay as the constitutive equation. In this figure, h means the thickness of shallow stabilized ground, H_1 and L means the column length and distance between columns. H and d also means the thickness of soft soil layer and column diameter. In this analysis, in reference to the field measurement (Ishikura et al., 2009), h, H_1, d, L was set to 1.0m, 6.5m, 1.0m, 2.0 m , respectively. Table1 shows the material parameters. The ground water level was located at the ground surface of model ground and drainage boundaries were set to the upper and lower part of model ground. After applying to the 1 kPa on the ground surface, 150 kPa of Δp was applied to the ground surface in the assumption of fill with 7.5m. In this study, full shear resistance of soil-pile interface was modeled by Eq.(4).

$$\tau_f = Rc' + R\sigma_n \tan\phi' \qquad (4)$$

Here, c' and ϕ' means the effective cohesion and friction angle of soil, σ_n means the normal effective stress applied to the interface and R means the interface friction coefficient. These R values were used in 0.90, 0.75, 0.50, 0.30, respectively.

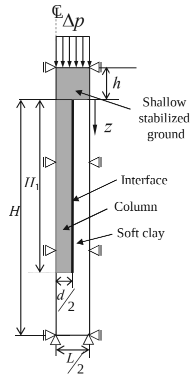

Figure8. Axi-symmetry analytic model

Table1. Material parameters for analysis

	Raft and Pile	Soil	Interface
γ_{sat}(kN/m^3)	16.8	16.8	
E(kPa)	1.0× 10^8		
ν	0.30	0.15	
λ		0.5 or 0.1	
κ		0.1 or 0.02	
c'(kN/m^2)		1.0	1.0
ϕ'(°)		30	30
OCR		1	
e_{ini} (at p'=1kPa)		1.8	
R			0.9,0.75,0.5,0.3

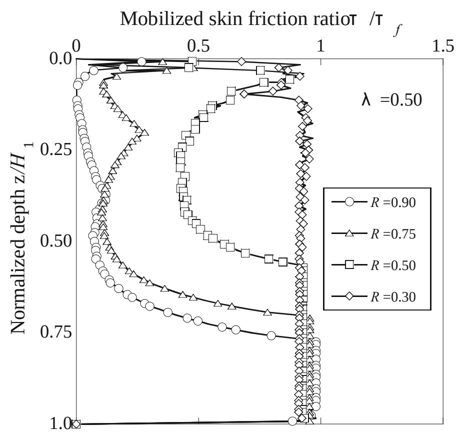

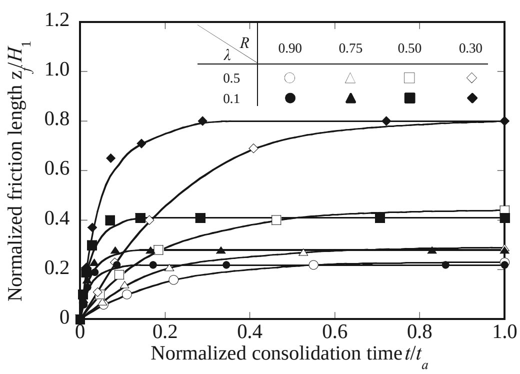

Figure9. Mobilized skin friction used in the different shear strength
Figure10. Time dependent tendency of friction mobilization

3.2 *Tendency of skin friction mobilization*

Figure 9 shows the relationships between degree of mobilized skin friction and normalized column depth after primary consolidation. Mobilized skin friction ratio was defined as the ratio of the current mobilized skin friction to the full skin friction resistance. Normalized depth was defined as the ratio between the column depth from just below the shallow stabilized ground and the column length. As shown in this figure, full mobilized skin friction length reduced with an increase of interface friction coefficient.

Figure10 shows the relationships between the normalized friction length and consolidation time by using different full shear resistance of soil-pile interface and soil properties. Normalized friction length means the ratio of full mobilized skin friction length to the column length. Normalized consolidation time was also defined as the ratio between the current time and the time that excess pore water pressure reached under 1 kPa in the soft clay. In all the conditions, full mobilized skin friction length increased with elapsed time and converged to the constant value. In this analysis, soil property λ has little influence on the full mobilized skin friction length. It is considered that skin friction is mobilized around the soil –pile interface acting relative displacement between pile and soft clay. So there is some possibility that the equivalent raft elevation can also be moved upward in the consolidation process.

4 CONCLUSION

In order to investigate the settlement behavior and skin friction of floating type improved ground with shallow stabilization during consolidation, loading model tests and full scale FEM analysis were performed. From the results, It was clarifed that vertical strain of soft clay in the upper part of the improved portion was restrained by the combined effect of pile and raft. Further, from the analytic results, it was also found that full mobilization length of skin friction increased with elapsed time and converged to the constant value in the consolidation process.

5 ACKNOWLEDGEMENTS

The authors wish to express their gratitude to many students, at graduate school of Yamaguchi University, for their supports. The first author is grateful to Prof. Y. Nakata of Yamaguchi University for his support of image analysis and is also grateful to Professor Noriyuki Yasufuku of Kyushu University and Professor Kiyoshi Omine of Nagasaki University for their advice and encouragement.

6 REFERENCES

Bergado, D.T., Chai, J.C., Alfaro, M.C. and Balasubramaniam, A.S. 1994. Improvement Techniques of Soft Ground in Subsiding and Lowland Environment, *Taylor and Francis*,pp.108 –121.

Ishikura, R., Matsuda, H., Yasufuku, N., Omine, K., Kashima, K., Igawa, N. 2012. Settlement behavior of piled raft foundation in soft ground, *Proceedings of the 9th International Conference of on Testing and Design Methods for Deep Foundation*, pp.485 -490.

Ishikura, R., Ochiai, H., Matsui, H. 2009. Estimation of settlement of in-situ improved ground using shallow stabilization and floating-type columns, *Proceedings of 17th International Conference on Soil Mechanics and Geotechnical Engineering*, pp.2394-2398.

Ishikura, R., Ochiai, H., Yasufuku, N., Omine, K., and Kobayashi,T. 2006. Estimation of the settlement of improved ground with floating-type cement-treated columns, *Proceedings of the 4th International Conference on Soft Soil Engineering*, pp. 628–635.

Miki, H.and Nozu, M. 2004. Design and numerical analysis of road embankment with low improvement ratio deep mixing method, *Geo-trans*, ASCE, 126(12), pp.1395-1402.

Tomlinson,M.J., Woodward, J. 2008. Pile design and construction practice, *5thEdition,Taylor and Francis*,pp.240-243.

Whitaker, T.1957. Experiments with model piles in groups. *Geotechnique*, l(4), pp.147-167.

Yan,W. M., Sun, T. K. and Tham, L. G. 2012.Coupled-consolidation modelling of a pile in consolidating ground, *Journal of Geotechnical and Geoenvironmental Engineering* ASCE, 138(7), 789-798.

Interactive 3-D Analysis Method of Piled Raft Foundation for High-rise Buildings

Méthode d'analyse 3-D interactive de fondations mixte radier pieux pour immeubles de grande hauteur

Jeong S.J., Cho J.
Department of Civil and Environmental Engineering, Yonsei University, Seoul, Korea

ABSTRACT: The settlement behavior of piled raft foundations were investigated by a numerical analysis and field case studies. Special attention is given to the improved analytical method (YSPR) and interactive analysis proposed by considering raft flexibility and soil nonlinearity. The proposed method has been verified by comparing the results with other numerical methods and field case studies on piled raft. In the interactive analysis of super- and sub-structure, the loading conditions of super-structure, stiffness of sub-structure and soil conditions were considered. Through comparative studies, it is found that the proposed method in present study is in good agreement with general trend observed by field measurements and, thus, represents a significant improvement in the prediction of settlement behavior.

RÉSUMÉ : La stabilité des fondations mixtes de type radier pieux, d'un cas d'étude, est analysée numériquement. Une attention particulière est portée à l'amélioration de la méthode analytique (YSPR) et à l'analyse interactive proposée en considérant la flexibilité du radier et la non linéarité du sol. La méthode proposée a été vérifiée en comparant les résultats obtenus à d'autres récupérés sur des cas d'étude. Avec l'analyse interactive de la super structure et de la sous structure, les conditions de chargement, la rigidité et les états du sol ont été considérés. En comparant les études, nous montrons que la méthode utilisée est en bon accord avec les observations de terrain. Elle représente donc une amélioration significative par rapport au risque de tassements prévisionnels.

KEYWORDS: High-rise buildings, Piled raft foundation, Interactive analysis, computer based analytical method

1 INTRODUCTION

In South Korea, a number of huge construction projects involving high-rise buildings are being undertaken and the application of piled rafts for high-rise building is becoming an important issue in foundation design. The behavior of a structure is affected by the 3D interaction between the soil, super- and sub-structure(piled raft foundation). Therefore, a proper analytical model is needed to evaluate these interactions.

Numerical methods, which are approximate, have been developed widely in the last two decades because numerical methods are less costly and may be used to consider many kinds of different soil and foundation geometries compared to field and model tests. There are three broad classes of numerical analysis methods: (1) simplified calculation methods (Poulos, 1994; Randolph, 1983) (2) approximate computer-based methods (Clancy and Randolph, 1993; Russo, 1998) and (3) more rigorous computer-based methods (Katzenbach et al., 1998; Lee et al., 2010). Poulos(2001) noted that the most feasible method of analysis was the three-dimensional linear/nonlinear FE method.

The overall objective of this study is focused on the application of interactive analysis method for predicting behavior of super- and sub-structures. An analytical method is proposed for the interaction between the superstructure and the piled raft. In this study, a numerical method is used to combine the pile stiffness with the stiffness of the raft, in which the flexible raft is modeled as flat shell element and the piles as beam-column element, and the soil is treated as linear and nonlinear springs. Based on the proposed analysis method, approximate analysis computer program of YSPR for raft and piled raft foundations are developed respectively. In order to examine the validity of YSPR, the analysis results are compared with the available solutions from previous researches. In the field case study, comparative analyses between YSPR and a three-dimensional finite element analysis are carried out for the settlement behavior.

2 APPROXIMATE ANALYTICAL METHOD FOR PILED RAFT FOUNDATIONS

2.1 Modeling of piled raft foundation

A raft was treated as a 4 node flat shell element including torsional degrees of freedom. An improved four-node flat shell element, which combines a Mindlin's plate element and a membrane element with torsional degrees of freedom as shown in figure 1, is adopted in this study. This element having six degrees of freedom per node permits an easy connection with other elements such as beams or folded elements.

A pile was modeled as a beam-column element in this proposed method. The behavior of individual piles in a group was controlled by using stiffness matrices of pile heads, and the soil-structure interaction between soil and pile was modeled by using nonlinear load-transfer curves (t-z, q-z and p-y curves).

As a final outcome, a numerical method was developed to analyze the response of a raft and a piled raft considering pile-soil-pile and raft-soil interactions. In the present method, the raft was simulated with four-node flat shell elements, the piles with beam-column elements, and the soil with nonlinear load transfer curves (figure 1(a)).

A nonlinear analysis algorithm was proposed using a mixed incremental and iterative technique in this study. The stiffness matrix of piles, soil and that of a flat shell element are combined and a coupled analysis method of a piled raft is developed including a nonlinear analysis algorithm. Figure 1(b) shows the flow chart of the present method (YSPR).

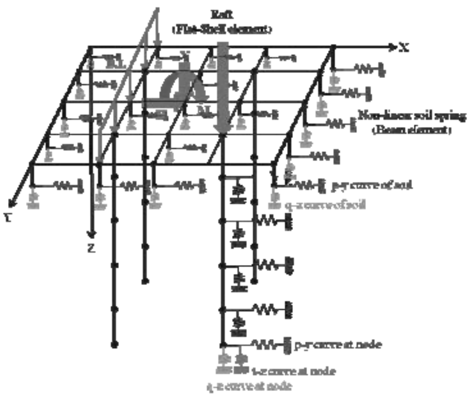

(a) Modeling of a piled raft

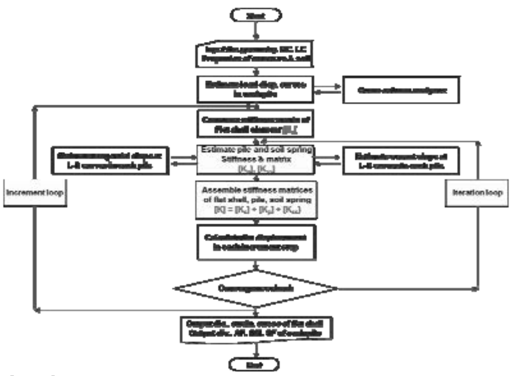

(b) Flowchart

Figure 1. YSPR(Yonsei Piled Raft)

2.2 Comparison with case history

The validity of the proposed method was tested by comparing the results from the present approach with some of the case history.

As shown in Fig. 2, preliminary design case of piled raft (OO super tower) conducted at high-rise building construction sites in Korea were representatively selected for the design application. The construction site is comprised mainly of normally banded gneiss, brecciated gneiss and fault core zones. Based on the results of pressure meter, Goodman Jack and plate load tests carried out in the field, a non-linear elastic modulus design line is established to represent the stiffness of the ground.

A schematic diagram of a raft foundation with piles is shown in Fig. 2. This structure consists of a raft, and 112 of ground strengthen piles. The piles have an embedded length of 30 m, a diameter of 1.0 m. A large raft size 71.7x71.7m with a thickness of 6.0 m is resting on a banded gneiss. The raft and ground strengthen piles, with a Young's modulus of 30GPa and 28GPa respectively, is subjected to a vertical load (P_{total}=6,701MN). Table 1 summarizes the material properties used in the case studies.

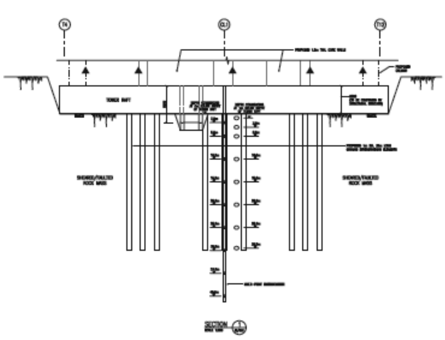

Figure 2. Preliminary design case

Table 1. Material propertiess

	Type	Depth(m)	E (MPa)	ν
Pile	Concrete	0~-30	28,000	0.2
Raft	Concrete	0~6.0	33,234	0.15
Soil	Gneiss	Soil spring stiffness (kPa/m)		
		0~204,250		

Fig. 3(a) and (b) shows the raft settlement at different section predicted by GSRaft and YSPR. Agreement between the GSRaft and YSPR of settlement is generally good; however there is a slight difference in prediction of settlement in the faulting zone which the sudden drop of the magnitudes were occurred. This can be attributed to the appropriate assumption of material properties due to no accurate ground investigation data on this section. As shown in this result, the prediction by the proposed method has a considerably larger settlement than the settlement calculated by the existing solution. This is because the existing method ignores lateral displacement due to membrane action of flexible raft and, thus, overestimates the lateral stiffness of raft and small displacement in raft lateral behavior. Although there are no measured profiles of raft settlement, the proposed analysis method showed reasonably good correspondence with well-known in-house program.

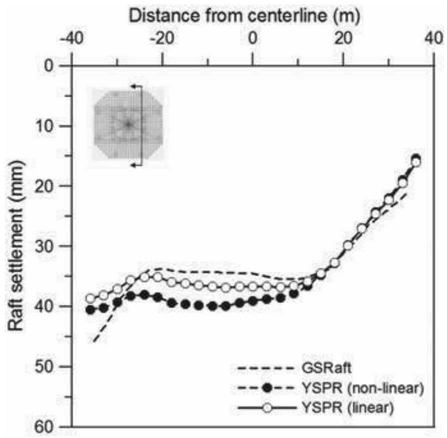

(a) Section1

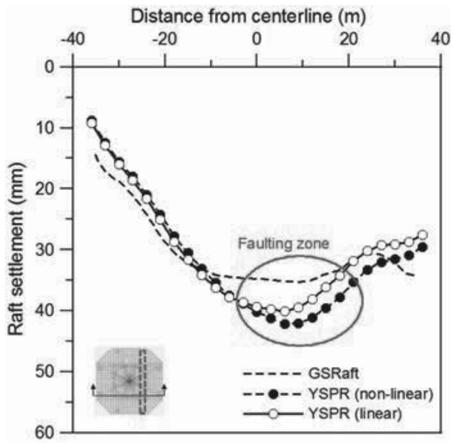

(b) Section2

Figure 3. Raft settlement distribution

3 INTERACTIVE ANALYSIS OF SUPER- AND SUB-STRUCTURE

3.1 General

The unified analysis of piled foundation in long span bridges and buildings has become an important issue in structure design. There has been much work done on pile-soil interaction. A relatively less work has been done on the unified analysis that includes both piled foundation and superstructures. Because the mechanism of load transfer between piled foundation and superstructures involves a complex interaction between structures, raft, piles, and surrounding soil. The analysis process is affected by many factors such as: column and wall geometry, design load, raft and pile group geometry, soil properties, and interaction between different structure elements. Accordingly, there are currently no methods available to predict behavior of the entire structures due to the difficulty and uncertainty in quantifying these factors.

Therefore, the overall objective of this study focuses on application of interactive analysis method for predicting behavior of entire structures. A series of numerical analyses was performed to verify the interactive analysis routine in comparison to the unified analysis method. For this purpose, the three-dimensional (3D) Finite-Element (FE) analysis has been carried out. For the unified analysis of super and sub-structures, the numerical analyses were performed via the FE code PLAXIS 3D foundation, with column, floor and piled raft foundation systems placed on a typical weathered soil in Korea.

3.2 Interactive analysis

In most of the design field, the analysis of super-structure was conducted without modeling the foundation system and the foundation was designed without considering the rigidity of super-structure. It may result in overestimation of forces, the bending moment, settlement of super- and sub-structure.

In this study, the interactive analysis procedure is proposed for predicting the behavior of entire structure by considering soil-foundation stiffness and rigidity of super-structure. The procedure of interactive analysis in this study include the following steps:

(a) Compute the reaction force of structure-foundation interface in fixed boundary condition.
(b) Construct the CSM(coupled stiffness matrix) of soil and foundation using reaction force.
(c) Re-compute the reaction force of interface in CSM boundary condition.
(d) Calculate the member force and displacement of foundation.
(e) Check the convergence of member force and displacement at interface node from step (c) and (d).

The procedure described above is iterated until the error between the super- and sub-structure displacements falls within a tolerance limit. Figure 4 shows a schematic diagram and flowchart of the interactive analysis.

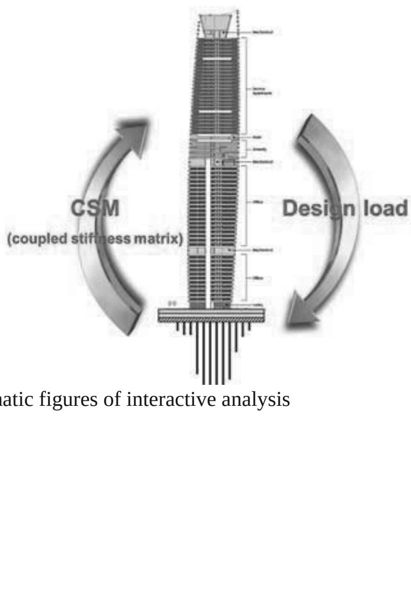

(a) Schematic figures of interactive analysis

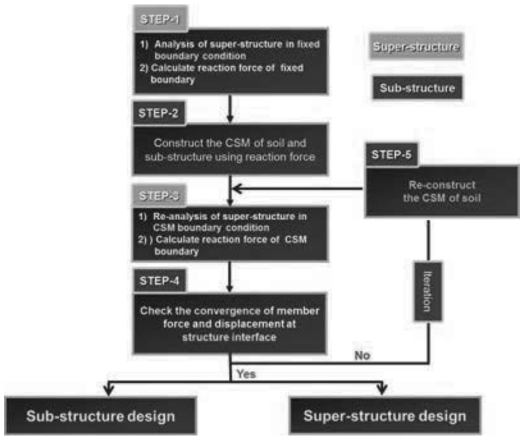

(b) Flowchart of interactive analysis

Figure 4. Interactive analysis between super- and sub-structure

3.3 Verification of proposed method with finite-element analysis

In this section, the validation of the proposed method with numerical analysis is discussed. The three-dimensional finite-element mesh used for the structure-foundation-soil system is shown in Figure 5. The structure consists of columns, 10 floors, a raft, and 25 identical vertical piles, which are spaced by 2.5m (= 2.5D, where D is a pile diameter).

The piles are 1m in diameter and 10m in embedded length. A square raft has a width of 15m with fixed pile head conditions. The columns are 3.5m in length and 0.6m in width. At the left- and right-hand vertical boundaries, lateral displacements were restrained, whereas fixed supports were applied to the bottom boundaries. The specified initial stress distributions should match with a calculation based on the self-weight of the material. After the initial step, the applied loading was simulated by a self-weight of super-structure.

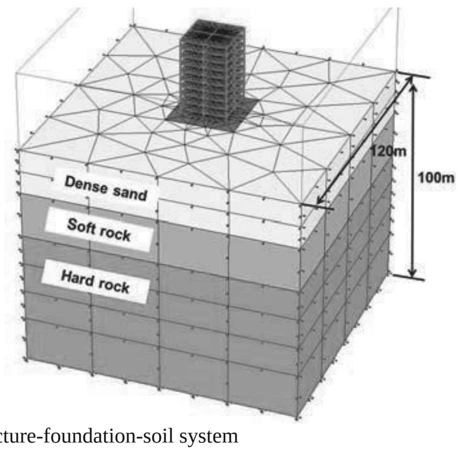

(a) Structure-foundation-soil system

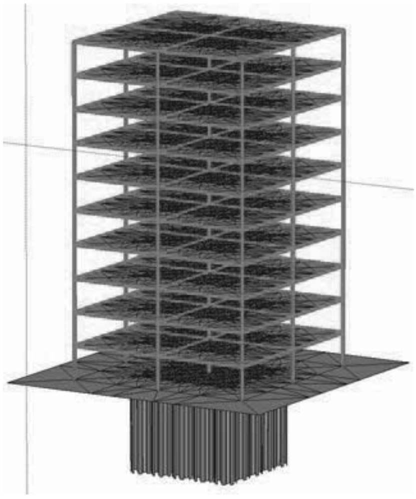

(b) Modeling of structure-piled raft foundation
Figure 5. Typical 3D model for FE analysis

The pile is considered as linear-elastic material at all times, while for the surrounding soil layer the Mohr-Coulomb non-associated flow rule is adopted. The interface element modeled by the bilinear Mohr-Coulomb model is employed to simulate the pile–soil interface. The interface element is treated as a zone of virtual thickness. It behaves as an element with the same material properties as the adjacent soil elements before slip occur. A decreased value of shear modulus is assigned to the interface element when a slip mode occurs in the interface element. The decrease of strength for the interface element is represented by a strength reduction factor R_{inter} in PLAXIS.

Fig. 6 shows the computed settlement of a raft with different analysis methods. It is observed that the unified method using PLAXIS 3D Foundation predicts smaller settlement compared with interactive analysis in fixed and CSM boundary condition. Although, a reasonably good agreement between the unified analysis method and the proposed interactive analysis was obtained for the same loading step, the fixed boundary analyses have a larger displacement than that of the proposed interactive analysis and unified analysis.

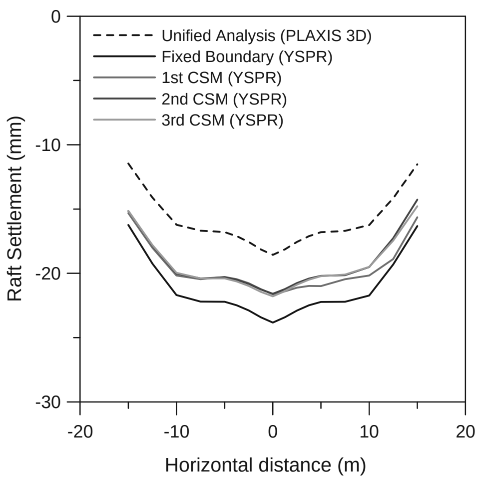

Figure 6. Raft settlement

Fig. 7 shows the computed bending moment of the raft. The figure also demonstrates a good agreement between the interactive analysis and the more rigorous finite element approach. These comparisons suggest that the proposed interactive analysis is fairly capable of predicting the deformation and load distribution of sub-structure.
Figure 7. Raft bending moment distribution

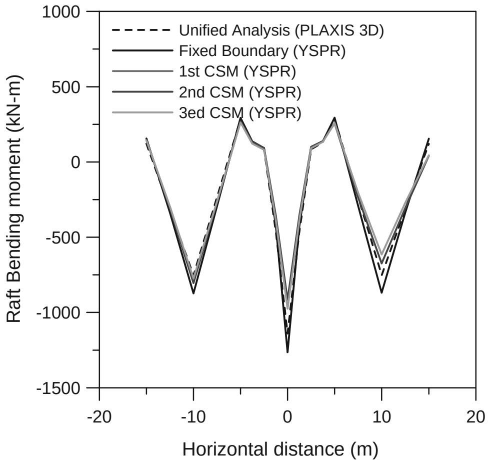

Figure 7. Raft bending moment distribution

4 CONCLUSIONS

The primary objective of this study was to propose improved analytical method and interactive analysis for super- and sub-structure. A series of analytical studies were conducted. Additionally, the analytical method is intermediate in theoretical accuracy between general three-dimensional FE analysis and the conventional numerical method. From the findings of this study, the following conclusions can be drawn:

Proposed analytical method produce a considerably larger settlement of piled raft than the results obtained by the conventional methods (GSRaft). When compared with the results of case histories, the proposed method is shown to be capable of predicting the behavior of a large piled raft. Nonlinear load-transfer curve and flat-shell element can overcome the limitations of existing numerical methods, to some extent, by considering the realistic nonlinear behavior of soil and membrane action of flexible raft. Therefore, the proposed method could be used in the design of large piled rafts for high-rise buildings.

Based on a numerical analysis for the structure-piled raft-soil system, it is found that the CSM boundary condition provide more realistic behavior of piled raft foundation than the result obtained by the fixed boundary condition.

5 REFERENCES

Clancy, P., and Randolph, M. F. (1993): An approximate analysis procedure for piled raft foundations, International Journal for Numerical and Analytical Methods in Geomechanics, 17(12), 849-869.

Katzenbach, R., Arslan, U., Moorman, C. and Reul, O. (1998): Piled raft foundation- Interaction between piles and raft, International Conference on Soil-Structure Interaction in Urban Civil Engineering, Darmstadt, 2(4), 279-296.

Lee, J. H., Kim, Y. H., and Jeong, S. S. (2010): Three-dimensional analysis of bearing behavior of piled raft on soft clay, Computers & Geotechnics, 37, 103-114.

Poulos, H. G. (1994): An approximate numerical analysis of pile-raft interaction, International Journal for Numerical and Analytical Methods in Geomechanics, 18 (2), 73–92.

Poulos, H, G. (2001): Piled raft foundations : design and applications, Geotechnique, 51(2), 95-113.

Randolph, M. F. (1983): Design of piled foundations, Research Report Soils TR143. Cambridge: Cambridge University Engineering Department.

Russo, G. (1998): Numerical analysis of piled rafts, International Journal for Numerical and Analytical Methods in Geomechanics, 22(6), 477-493.

Optimal FBG Sensor Deployment via Gaussian Quadrature Formula for Measurement of Displacement of Laterally Loaded Piles

Le déploiement optimal des capteurs à fibres optiques, par la formule de la quadrature de Gauss, pour la mesure du déplacement des pieux chargés latéralement

Jung Y.-H., Na S.-U., Mok Y.
Dept. of Civil Engineering, Kyung Hee University, Republic of Korea

ABSTRACT: A new approach to sensor deployment for measurement of lateral displacement of piles is introduced. To monitor a pile loaded by lateral loads, the multiplexed Fiber-optic Bragg Grating (FBG) sensors are used. For enhanced accuracy of measurement under budgetary limitation, optimal position of the FBG sensors inscribed along an intact optic fiber line is crucial. Herein, ideal test conditions under which test results could be verified through theoretical solutions were created. The integration points of the Gaussian quadrature formula were employed to determine the optimal positions to place sensors. By using differential equations on pile displacement subjected to lateral load, the measured and calculated displacements were compared. The comparative analysis shows that positioning sensors based on theoretical Gaussian quadrature formula reduces measurement errors. To minimize the errors in estimating lateral displacement under general in-situ conditions, a suggestion for the FBG sensor deployment has been given.

RESUME : Une nouvelle approche de déploiement des capteurs à fibres optiques pour la mesure du déplacement latéral des pieux est présentée. Pour surveiller un pieu chargé latéralement, les capteurs multiplexeurs à fibres optiques avec réseau de Bragg (Fiber-Optic Bragg Grating : FBG) sont utilisés. L'emplacement optimal des capteurs FBG inscrits le long d'une ligne intacte de fibre optique est crucial afin d’assurer une bonne précision de mesure, à un coût optimisé. Les conditions idéales d'essai dans lesquelles les résultats peuvent être vérifiés par des solutions théoriques ont été créées. Les points d’intégration de la formule de la quadrature de Gauss ont été utilisés pour déterminer les meilleurs emplacements des capteurs. En utilisant les équations différentielles des déplacements d’un pieu soumis à une charge latérale, les résultats des mesures et du calcul ont été comparés. L'analyse comparative montre que l'approche du déploiement des capteurs sur la base théorique de la formule de la quadrature de Gauss fonctionne très bien. Une suggestion du déploiement des capteurs FBG est donnée afin de minimiser les erreurs d’estimation du déplacement latéral sous les conditions générales *in situ.*

KEYWORDS: Gaussian quadrature, Sensor placement, Lateral-loaded Pile, Measurements

1 INTRODUCTION

FBG sensors have been widely applied to structural monitoring because optical sensors can overcome many limitations of existing electric sensors such as electronic interference and low durability. In addition, there is an advantage that it is possible for one strand of optical fiber to be inscribed with many sensors and used as a multi-point sensor. In regard to monitoring super-structures such as railroad bridges that are frequently exposed to electromagnetic waves, the FBG sensor is successfully used for the long-term maintenance system (Chung et al. 2005).

To measure the performance of geotechnical structures such as piles, FBG sensors are superior to other electric sensors because typically the measurement for geotechnical structures should be performed in adverse environments such as high confinement, strong chemical corrosion, and narrow space. Recently, there were several attempts to measure the performance of piles. Lee, et al. (2004) have attached FBG sensors to cast-in-place concrete piles and measured the vertical load transfer process, thus presenting the usability of FBG sensors in geotechnical structures. Habel and Krebber (2011) have used fiber-optic acoustic emission sensors to measure AE signals related to the shock waves of concrete pile heads, thus evaluating the soundness of concrete piles. However, few are cases that have systematically analyzed and verified the use of FBG sensors in geotechnical structures.

Compared to the conventional point-located sensors, FBG sensors multiplexed on a single strand of fiber has a great advantage in its small occupancy of space for attachment and installation. Despite such advantages, the use of FBG sensors has not prevailed because inscribing one FBG grating on an optic fiber is still more expensive than buying a conventional strain gage sensor. Therefore, minimizing the number of sensors and optimizing sensor positions are the most urgent issue for successful deployment of FBG sensors in the industry.

Sensors can generally be placed in an area of interest either deterministically or randomly. The choice of the deployment scheme depends highly on the type of sensors, application and the environment that the sensors will operate in. Without any preferance of interest, sensors would be placed uniformly along the pile, whereas those simple schemes do not consider any cost effectiveness or optimazation to reduce measurement errors.

In this study, a new deployment scheme for multiplexed FBG sensors on the single optical fiber strand is introduced. The Gaussian quadrature formula has been employed to minimize the error in measuring the displacement of a laterally loaded pile. A model cantilever beam is used to simulate the pile. The applicability of the Gaussian quadrature formula for optimizing sensor positions has been confirmed by comparing applied and computed displacements. Three different strategies for placing sensors along the aluminum bar which represents a laterally loaded pile are developed, and accordingly eight different schemes of the sensor placement are configured. One end of the bar specimen is clamped, and the other is displaced by using the calipers. The maximum displacement is calculated by integrating the slopes and moments at the FBG sensor positions, and compared with the actual magnitude of applied displacement to suggest its geotechnical applicability.

2 THEORETICAL BACKGROUND

1.1 *Fiber-optic Bragg Grating (FBG) sensors*

FBG sensors inscribe stripe-like grating on the photosensitive fiber optic core by exposing the latter to ultraviolet (UV) radiation by periodically distributing the strength of the light. Once formed, FBG sensors serve as reflectors that reflect light with a pattern-specific wavelength. This reflected wavelength is called the Bragg wavelength and is as in Equation (1). In other words, when broad-spectrum light beams are transmitted to the FBG, light with the Bragg wavelength is reflected and remaining light with other wavelengths passes through.

$$\lambda_b = 2n_e\Lambda \tag{1}$$

where λ_b is Bragg wavelength, n_e is the effective refractive index of the fiber-optic core, and Λ is the interval of the grating inscribed on the fiber-optic core.

Changes in strain and the temperature affect the effective refractive index, n_e, and the grating period, Λ, so that the Bragg wavelength comes to shift. In comparison with the initial Bragg wavelength, λ_0, the shifted amount of wavelength, $\Delta\lambda$, is given as

$$\Delta\lambda/\lambda_0 = (1-p_e)\varepsilon + (\alpha_f + \xi_f)\Delta T \tag{2}$$

where the first term of Eq. (2) is the amount shifted due to strain, p_e is the photoelatic constant, and ε is the strain underwent by the grating. The second term of Eq. (2) shows the shift of the wavelength caused by the change of temperature, α_f is the thermal expansion coefficient of the fiber optic, and ξ_f is the thermo-optic coefficient of the fiber optic. Because the experiments in the present study were conducted in a controlled laboratory environment, changes in the temperatures of the sensors themselves and their surroundings were negligible such that $\Delta T = 0$. Consequently, the second terms was eliminated so that it is possible easily to calculate strain from the wavelength shift as shown in Eq. (3).

$$\varepsilon = \frac{1}{1-p_e}\frac{\Delta\lambda}{\lambda_0} \tag{3}$$

where the photoelastic constant, p_e = 0.229, provided by the manufacturer.

1.2 *Integration by Gaussian quadrature*

In numerical analysis, a quadrature rule is an approximation of the definite integral of a function, usually stated as a weighted sum of function values at specified points within the domain of integration. An n-point Gaussian quadrature rule is a quadrature rule constructed to yield an exact result for polynomials of degree $2n-1$ or less by a suitable choice of the points x_i and weights w_i for i = 1, …, n. The domain of integration for such a rule is conventionally taken as [-1, 1], so the rule is stated as

$$\int_{-1}^{1} f(x)dx \approx \sum_{i=1}^{n} w_i f(x_i). \tag{4}$$

Gaussian quadrature as above will only produce accurate results if the function *f(x)* is well approximated by a polynomial function within the range between -1.0 and +1.0. If the integrated function can be written as $f(x) = W(x)g(x)$, where $g(x)$ is approximately polynomial, and $W(x)$ is known, then there are alternative weight w'_i such that

$$\int_{-1}^{1} f(x)dx = \int_{-1}^{1} W(x)g(x)dx \approx \sum_{i=1}^{n} w'_i g(x_i). \tag{5}$$

For the simplest integration problem, i.e. with $W(x) = 1$, the associated polynomials are Legendre polynomials, $P_n(x)$, and the method is usually known as Gauss-Legendre quadrature. With the nth polynomial normalized to give $P_n(1) = 1$, the i-th Gauss node, x_i, is the i-th root of P_n. Its weight is given by (Abramowitz and Stegun 1972)

$$w_i = \frac{2}{(1-x_i^2)[P'_n(x_i)]^2} \tag{6}$$

A few order rules for solving the integration problem are listed in Table 1.

Table 1. Position of Gauss points and corresponding weights.

Number of Gaussian points, n_{gp}	Location, ξ_i	Weight, w_i
1	0.0	2.0
2	±0.57732502692	1.0
3	±0.7745966692 0.0	0.555 555 5556 0.888 888 8889

An integral having arbitrary limits can be transformed so that its limits are from -1 to +1. With $f = f(x)$, and with the substitution $x = \frac{1}{2}(1-\xi)x_1 + \frac{1}{2}(1+\xi)x_2$,

$$\int_{x_1}^{x_2} f(x)dx = \int_{-1}^{1} \phi d\xi \approx \sum_{i=1}^{n} w'_i \phi(\xi_i). \tag{7}$$

Thus the integrand is changed from $f = f(x)$ to $\phi = \phi(\xi)$, where ϕ incorporates the Jacobian of the transformation, $J = dx/d\xi = (1/2)(x_2 - x_1)$. If the function $\phi = \phi(\xi)$ is not a polynomial, Gauss quadrature is inexact, but becomes more accurate as more points are used.

1.3 *The differential equations of the deflection for a cantilever beam subjected to a point load*

As shown in Figure 1, lateral displacement, y, which is produced when pile heads are subjected to a lateral load, P, and not to axial load, is expressed in terms of differential equation, as in Equation (8).

$$EI\frac{d^2y}{dx^2} = M = P(l-x) \tag{8}$$

where *E* is the Young's modulus of the pile material, *I* is the moment of inertia of the section area of the pile, *x* is the distance from the pile end, and *M* is the sectional moment. Integrating Eq. (8) yields the function of the slope, *S*, as

$$S = \frac{dy}{dx} = \int_0^x \frac{d^2y}{dx^2}dx = \frac{1}{EI}\left(Plx - \frac{Px^2}{2}\right) \tag{9}$$

For the cantilever beam, the slope, *S*= dy/dx , remains zero at the clamped end (i.e., *x* = 0). Integrating Equation (9) again yields an expression of the lateral displacement, *y*, as

$$y = \int_0^x \frac{dy}{dx}dx = \frac{1}{EI}\left(\frac{Plx^2}{2} - \frac{Px^3}{6}\right) = \frac{Px^2}{6EI}(3l - x) \tag{10}$$

As a result, the maximum deflection, y_{max}, occurs at the point of the lateral load, given as

$$y_{max} = \frac{Pl^3}{3EI} \tag{11}$$

Note that two sequential integrations are necessary to obtain the displacement function of Eq. (10) from the moment function of Eq. (8).

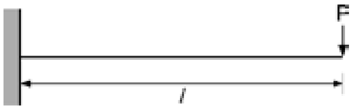

Figure 1. A cantilever beam with a concentrated load, simulating the pile subjected to a lateral load.

2 EXPERIMENTAL SETUP

2.1 *Experimental procedure*

A model cantilever beam is the aluminum bar specimen which has a physical properties listed in Table 1. Figure 1 shows the loading system including a clamp to fix one end of the bar and a calipers used to apply the displacement on the other end of the bar. In the middle points, two dial indicators were attached to measure the deflections of the bar during loading. Because the displacement is applied by using the calipers, the concentrated load, P, can be estimated as $P = (3EIy_{max})/l^3$. An optic fiber including FBG sensors inscribed at given positions was epoxied on the top surface of the bar specimen developing tensile strains during loading. Electric strain gages were glued together to validate the performance of the FBG sensors.

Figure 3. A model cantilever beam system.

Table 2. Properties of aluminum bar speciment

Length, *l* (mm)	255
Thickness, *h* (mm)	6
Width (mm)	25
Young's Modulus, *E* (Gpa)	70.56
Moment of inertial, *I* (mm^4)	450
Bending stiffness, *EI* ($N{\cdot}mm^2$)	31,752,000

As in Eq. (11), the lateral displacement, y, is obtained by integrating Eq. (10) which is a polynomial equation with degree 2 so that two Gaussian points, ξ_1 = -0.577 and ξ_2 = +0.577, are possibly chosen according to Table 1. As shown in Figure 4, sensors were located at two points projected from two Gaussian points. The FBG sensors measure the strains via Eq. (3). When the point load, P, is applied, the cantilever beam specimen is deflected. The curvature, 1/ρ, at a section can be calculated by the strains developed on upper and lower surfaces as

$$\frac{1}{\rho} = \frac{M}{EI} = \frac{\varepsilon_e - \varepsilon_c}{h} \tag{12}$$

where ε_e is the tensile strain on upper surface, ε_c is the compressive strain on lower surface of the bar, and h is the thickness of the section of the bar specimen. Assuming that both tensile and compressive strains have the same magnitude, the sensors were attached only on the upper surface of the bar specimen. Consequently, the moment at the sections where the sensors were placed can be measured as $M = 2\varepsilon_e EI/h$.

Figure 4. Optimal sensor positions for a cantilever beam

For a given displacement, theoretical values of the moment can also be computed via Eq. (9) and (11), thus $M = 3EIy_{max}(l - x)/l^3$ for a given y_{max} value. As shown in Table 3, errors in the measured moment to computed moment range between 0.15 and 1.54%, and average out to 0.82%.

Table 3. Measured and computed moments at two Gaussian points

Applied deflection, y_{max}	Moment, N-mm		
	Sensor position	x_1	x_2
1 mm	Measured	1153.6	295.3
	Computed	1155.3	309.6
	Error, %	0.15	0.46
2 mm	Measured	2290.4	612.8
	Computed	2310.7	619.2
	Error, %	0.88	1.03
3 mm	Measured	3435.6	914.458
	Computed	3465.9	928.8
	Error, %	0.88	1.54

2.2 *Optimizing sensor positions using Gaussian points*

Primary objective for deployment in this study is to minimize the error in measuring the maximum deflection at the point of loading, y_{max} . Herein, we developed three optimization strategies. The first strategy is positioning sensors at regular intervals, which is a simplest way to deploy. The second is positioning sensors at projected Gaussian points but not following the Gaussian quadrature rule. The third is positioning sensors exactly based on the Gaussian quadrature rule.

Figure 5 illustrates different deployment schemes according to first and second strategies. Four possible schemes at regular intervals are illustrated in figures on the left-hand-side column of Fig. 5, where n is the number of sensors used for each scheme. Figures on the right-hand-side column of Fig. 5 illustrate three deployment schemes using the projected Gaussian points for the number of Gaussian points, n_{gp} = 1, 2, and 3. For each case, the FBG sensors on a single strand were inscribed at positions marked as open symbols in Fig. 5. After applying y_{max} by the calipers, the strain at each sensor position was measured by FBG sensors. Subsequently two unknowns such as *P* and *l* in Eq. (8) were determined by using measured strains incorporated with the boundary condition at the clamped end, and then y_{max} was calculated via Eq. (11).

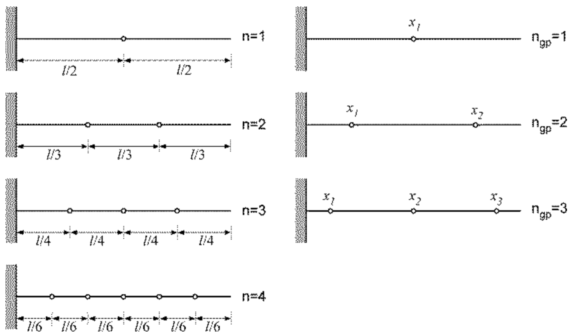

Figure 5. Different sensor deployments at regular and Gaussian points

The third strategy requires a double integral to calculate y_{max} using the moment values as described in section 2.3. Using the Gaussian quadrature rule, y_{max} can be obtained by integrating the slope function, S, which is the polynomials of degree 2, as

$$y_{max} = \int_0^l S(x)dx = \frac{l}{2}[w_1 S(x_1) + w_2 S(x_2)] \tag{13}$$

where w_1 and w_2 are weights for two Gaussian points given in Table 1, and x_1 and x_2 are the distances from the clamped end to projected Gaussian points as illustrated in Fig. 4. Because the moment function, $M(x)$, is a first order polynomial, Eq. (13) is solved by second integral with a single Gaussian point as

$$S(x_i) = \int_0^{x_i} \frac{M(x)}{EI} dx = \frac{x_i}{2} w' \frac{M(z_i)}{EI} \quad (13)$$

where $x_i = x_1$ or x_2 in Eq. (13), w' is the weight for the single Gaussian point (i.e., w' = 2.0, referring to Table 1), and z_i is the sensor position projected from the Gaussian point in the range between 0 to x_i. Note that z_i is in the middle of the target length according to Table 1. Figure 6 shows the exact locations of z_i in the testing configuration.

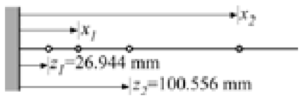

Figure 6. Optimal location of the sensors for cantilever beam

According to the different configurations for three different strategies illustrated in Figures 5 and 6, the FBG sensors were inscribed on the optic fiber attached to the bar specimen, and then the displacement was applied repeatedly by more than ten times. Table 4 compares applied and calculated values of y_{max} for the configurations with sensors positioned at the regular intervals. As the number of sensor increases, the error significantly decreases. Figure 7 shows the variation of errors against increasing applied deflection. When employing one or two sensors, the error increases as the applied deflection increases. When three or five sensors are used, the errors remain approximately constant irrespective of applied displacement.

Table 5 compares the applied and calculated values of y_{max} for the configurations with sensors positioned at the projected Gaussian points. Even in this case, the errors are also decreasing as the number of the sensors increases. For the same number of sensors, however, the error in the configuration according to the second strategy is smaller than that for the first strategy. This implies that positioning sensors deployed via the analytical formula exhibits better performance than uniformly distributed sensors.

As shown in Table 5, the error of sensors deployed with the third strategy yields much better performance than others. The average error for the third strategy is smaller by 0.2% than the error for the first strategy, and even smaller than the error for the second strategy by 0.03%. It is obvious that measuring displacement rigorously based on the Gaussian quadrature rule is superior to other cases because of its simple calculation, whereas the results indicates that increasing the number of sensors uniformly would give better measurement than employing the Gaussian quadrature rule.

Table 4. y_{max}, using sensors positioned at the regular intervals

Applied y_{max}, mm	y_{max} using 1st strategy			
	n=1	n=2	n=3	n=5
1	0.999	0.996	0.996	1.016
2	1.985	1.983	1.986	2.002
3	2.958	2.959	2.986	2.999
4	3.931	3.934	3.979	3.999
5	4.903	4.899	4.963	4.988
Average error, %	1.18	1.25	0.54	0.28

Table 5. y_{max}, using sensors positioned at projected Gaussian points

Applied y_{max}, mm	y_{max} using 2nd strategy			Using 3rd strategy
	n_{gp}=1	n_{gp}=2	n_{gp}=3	n_{gp}=2
1	0.999	0.996	0.991	1.000
2	1.985	1.982	1.995	1.982
3	2.958	2.972	2.976	2.967
4	3.931	6.949	3.943	3.941
5	4.903	4.917	4.958	4.921
Average error, %	1.18	1.04	0.84	1.01

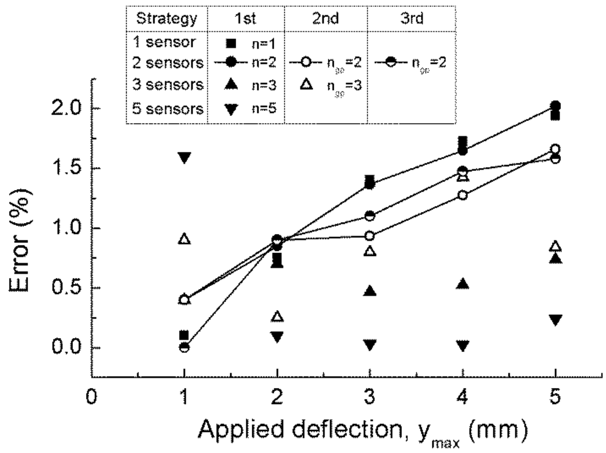

Figure 7. Errors in measurement using three different strategies

3 CONCLUSION

Using multiplexed FBG sensors require a careful deployment scheme to minimize errors in measuring lateral displacement of the pile through the least number of sensors. Herein, a new approach to deploy the FBG sensors for measurement of lateral displacement of piles was introduced. The Gaussian quadrature formula was adopted to minimize the error in measuring the deflection of a laterally loaded pile. The performance of Gaussian quadrature formula for optimizing sensor positions has been tested using the aluminum bar specimen representing a lab-scale cantilever beam with the clamped end. Primary objective for sensor deployment was set to minimize the error in measuring the maximum deflection at the point of loading. Three optimization strategies—positioning sensors at regular intervals, positioning sensors at projected Gaussian points but not following the Gaussian rule, and positioning sensors exactly based on the Gaussian rule—were implemented. In both cases for the first and second strategies, the measurement error decreases as the number of sensors increases. For the same number of sensors, however, the second strategy where the sensors were positioned at the projected Gaussian points reduces the errors by 0.2% than those for the first strategy. Positioning the sensors rigorously based on the Gaussian quadrature rule enhances the accuracy more than just using the Gaussian points. The experimental results suggested that the analytical deployment plan using the Gaussian quadrature rule can be helpful in crafting a placement in measuring the displacement of the laterally loaded pile accurately.

4 ACKNOWLEDGEMENTS

This work was supported by the National Research Foundation of Korea (NRF) grant funded by the Korean government (MEST) (No. 2009-0090774)

5 REFERENCE

Abramowitz, M. and Stegun, I.A. (1972), Handbook of Mathematical Functions, Dover, ISBN 978-0-486-61272-0

Chung, W., Kang, D.H., Choi, E.S., Kim, H.M. (2005), “Monitoring of a steel plate girder railroad bridge with fiber bragg grating sensors,” Journal of Korean Society of Steel Construction, Vol. 17, No. 6, pp. 681-688.

Habel, W.R. and Krebber, K. (2011), “Fiber-optic sensor applications in civil and geotechnical engineering,” Photonic sensors, Vol. 1, No. 3, pp. 268-280.

Lee, W., Lee, W.-J., Lee, S.-B., and Salgado (2004), “Measurement of pile load transfer using the Fiber Bragg Grating sensor system,” Canadian Geotechnical Journal, Vol. 41, No. 6, pp. 1222-1232.

Numerical Simulation of the Load Tests on Bearing Capacity of Piled Raft Foundations

Simulations numériques d'essais de chargement pour établir la capacité portante des fondations mixtes radier sur pieux

Kaneda K., Honda T., Shigeno Y., Hamada J.
Takenaka Corporation, Chiba, Japan

ABSTRACT: Field tests on the bearing capacity of pile, raft, and piled raft foundations are compared with simulations of the same tests. Those simulations used the SYS Cam-clay model developed by the Soil Mechanics Group of Nagoya University as the constitutive equations for material behavior. In this study, the material parameters and initial conditions were determined by laboratory testing performed on specimens collected in the area of the field tests. We found that the numerical simulations reproduced the experimental data well. Furthermore, in our experiments, the total bearing capacity of the raft and pile were found to be equal to that of the piled raft foundation. This was also confirmed via the simulations.

RÉSUMÉ : Cet article, qui traite de la capacité portante des pieux, des radiers et des fondations mixtes de type radier sur pieux, présente des résultats issus d'une comparaison entre des essais *in situ* et ceux obtenus par simulations numériques. Ces simulations utilisent le modèle de comportement SYS, développé par le groupe de mécanique des sols de l'Université de Nagoya. Les paramètres relatifs aux matériaux et aux conditions initiales ont été déterminés sur la base d'essais en laboratoire d'échantillons prélevés au même endroit où les essais *in situ* ont été exécutés. Ces simulations numériques ont convenablement reproduit les données expérimentales. Par ailleurs, lors des essais *in situ*, la capacité portante totale du radier et du pieu a été trouvée similaire à celle de la fondation mixte. Ce résultat a été aussi confirmé par les simulations.

KEYWORDS: piled raft foundations, numerical simulation, bearing capacity

1 INTRODUCTION

A significant number of studies have been carried out on the settlement and bearing capacity of pile, raft, and piled raft foundations. The designed bearing capacity for pile and piled raft foundations is considered to be the load at 10% settlement. In the present study, prototype vertical load simulations were carried out on such foundations to investigate the relationship between their settlement and bearing capacity at loads near their designed limits. This paper reports the results of these simulations and compares them to experimental data.

In this research, a combined soil and pile analysis was carried out. In the simulations, the SYS Cam clay model developed by the Soil Mechanics Group of Nagoya University was used as the constitutive mathematical model for the soil (Asaoka *et al.* (2000, 2002)). Since settlement exceeded 10% in the simulations, and since large soil deformations made the influence of geometrical non-linearity important, finite deformation analysis based on finite deformation theory was performed (Asaoka *et al.* (1994)). In addition, because the bearing capacity of saturated soils changes with loading rate, a soil-water coupled analysis was also carried out.

The remainder of the present paper is organized as follows. A brief outline of the experiments is first provided, followed by a discussion on the determination of material parameters and initial conditions for the vertical loading experiments based on laboratory tests. Next, the use of these parameters to perform soil-water coupled analyses based on simulated loading rates is described, and the results are compared to experimental data. Differences in the bearing capacities of pile, raft, and piled raft foundations are then discussed.

2 EXPERIMENTAL CONDITIONS

Details of the experiments and results are given in Honda *et al.* (2012). The experimental conditions and soil profile used in this paper are shown in Figure 1. From the top surface downwards, the soil layers consist of fill, loam, clay, two types of sand and silt. The N value around the pile is from 10 to 60 in the sand layer. Cases 1, 2, and 3 correspond to the raft, pile, and piled raft foundations, respectively. The raft has a square shape with 4 m sides, and the pile is 12 m long.

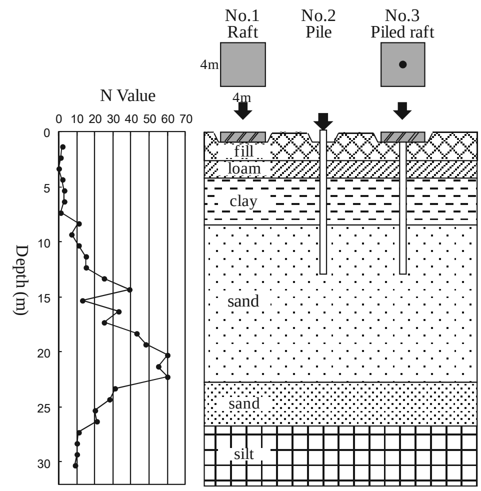

Figure 1: Experimental conditions

3 ANALYSIS MESH AND DETERMINATION OF MATERIAL PARAMETERS

Axisymmetric conditions are assumed for all simulations. Figure 2 shows the mesh used to analyze the piled raft foundation and the boundary conditions that were applied. The left edge corresponds to the central axis of a cylindrical section taken through the soil. Overall, the mesh contained 9,845 elements and 10,080 nodes, and it was made as fine as possible around the pile. It extended about four times the pile length in the vertical direction.

Although a full three dimensional (3D) analysis is preferable when studying problems involving piles, in the present study a two dimensional (2D) approach under axisymmetric conditions was used in order to reduce the computation time. This means that, even though the real raft shape was rectangular, a circular raft was simulated. The raft had a radius of 2.257 m, giving it the same area as the real raft. The pile had a radius of 600 mm and was straight, with no base enlargement. From the top surface, the simulated soil layers were clay 1 (4 m), sand 1 (4 m), sand 2 (13.5 m), clay 2 (6.5 m) and clay 3 (12 m), as shown in figure 2. The material parameters were determined by consolidation testing of clay 1 and drained triaxial compression testing of sand 2. Figures 3a (clay) and 3b (sand) compare the simulated and laboratory test results. For clay, the simulated and experimental results agree well, but for sand, the initial simulated modulus differs from the experimental data. This is because the parameters of the simulated sand were chosen to allow later simulation of a loading experiment. Table 1 shows the soil material parameters. Due to the lack of experimental data, some of the material parameters for clays 2 and 3 were set to be the same as those for clay 1, but with different initial void ratios. Similarly, some of the material parameters for sand 2 were set to be the same as those for sand 1. Table 2 shows the pile material properties, which correspond to the typical linear elastic parameters of pre-stressed high-strength concrete. Figure 4 shows the initial simulated soil profile. A load of 19.2 kPa was applied to the soil surface at the raft position to simulate the load of the raft. Displacement of raft elements in the x direction was restrained, but displacement in the y direction was allowed.
The stratified soil model was first prepared, after which elements with properties corresponding to the pile material were added. This was done while taking into account the force equilibrium between the soil and pile elements. After the excess pore pressure dissipated, a vertical displacement was applied to the pile elements for the three different cases: Case 1 models the raft alone, Case 2 models the pile alone, and Case 3 models the piled raft foundation. Figure 5 shows the step loading process followed during the actual physical experiment. The bearing capacity is dependent on the loading speed as well as the load magnitude. In the simulation, even though cyclic loading was not taken into consideration, the loading rate was set to a fixed value of 0.01 mm/sec in consideration of the final 10 cm settlement (Kaneda *et al.* (2012)).

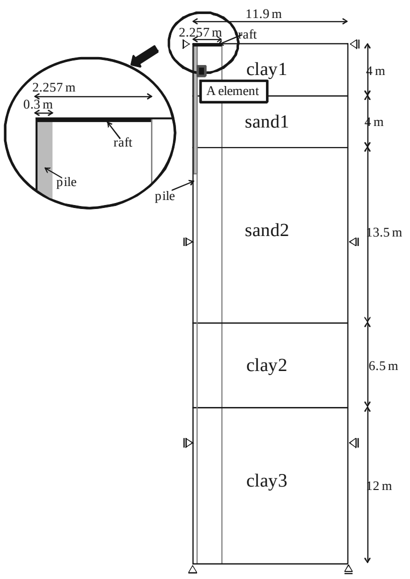

Figure 2: Boundary conditions

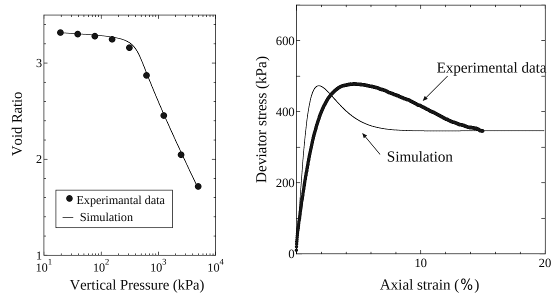

(a) Clay 1 (b) Sand 2

Figure 3: Experimental and simulation results

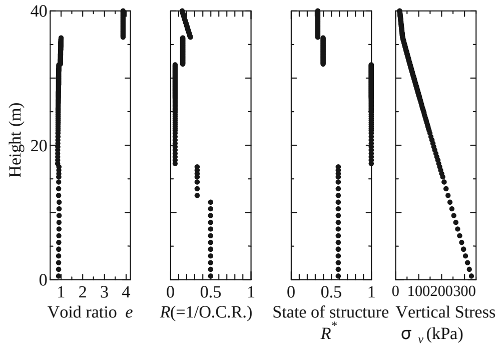

Figure 4: Initial soil conditions

Table 1: Material properties of soils

<Elasto-plastic parameter>	Clay 1	Sand 1	Sand 2	Clay 2	Clay 3
Compression index λ	0.50	0.050	0.050	0.10	0.10
Swelling index κ	0.02	0.012	0.012	0.015	0.015
Critical state constant M	1.45	1.36	1.36	1.26	1.26
NCL intercept N (at p' = 98 kPa)	4.3	1.98	1.98	2.00	2.00
Poisson's ratio ν	0.1	0.1	0.1	0.3	0.3
<Evolution parameters>					
Degradation parameter of structure a	0.8	2.2	2.2	0.8	0.8
Degradation parameter of structures b and c	1.0 2.0	1.0 1.0	1.0 1.0	1.0 1.0	1.0 1.0
Degradation parameter of overconsolidated state m	5.0	1.0	1.0	1.2	1.2
Evolution parameter b_r	0.001	1.00	1.00	0.150	0.150
Limit of rotation m_b	1.0	0.6	0.6	1.0	1.0
Permeability k (cm/sec)	1.0^{-7}	4.0^{-3}	4.0^{-3}	1.0^{-7}	1.0^{-7}
Density ρ_s (g/cm^3)	2.631	2.631	2.631	2.65	2.65
<Initial conditions>					
Void ratio e	3.87				
Overconsolidation ratio $1/R_0$		6.5	17.0	3.0	2.0
Degree of structure $1/R^*_0$	3.0	2.5	1.0	1.7	1.7
Degree of anisotropy ζ_0	0.545	0.545	0.75	0.545	0.545
Coefficient of lateral pressure K_0	0.6	0.6	0.5	0.6	0.6

Table 2: Pile material properties

	Pile
Elastic modulus E (kPa)	47360000
Poisson's ratio ν	0.2
Density ρ (g/cm^3)	2.3
Coefficient of lateral pressure K_0	0.0

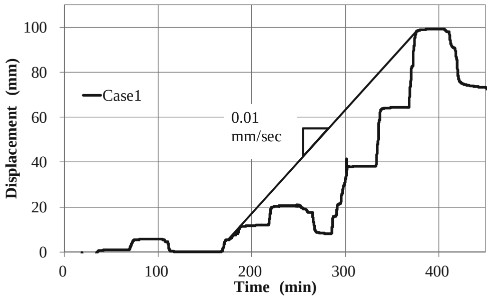

Figure 5: Experimental displacement versus loading time

4 COMPARISON OF EXPERIMENTS AND SIMULATIONS

Figure 6 shows both the experimental and simulated results for the relationship between settlement and load at the center of the load area. It can be seen that the simulation reproduced the experimental results in each case, including the initial modulus and the inflection point for Case 2. Figure 7 shows the shear strain contours at a settlement of 10 cm. For Case 1, the distribution of shear strain under the raft appears wedge shaped. For Case 2, the shear strain around the pile is high because of friction between the soil and the pile. Shear stain is also high at the toe of the pile. For Case 3, although the shear strain under the raft and around the pile is also high, the strain around the upper part of the pile is not. This is because the friction around the upper part of the pile is not sufficient to deform the soil under the raft into a wedge shape.

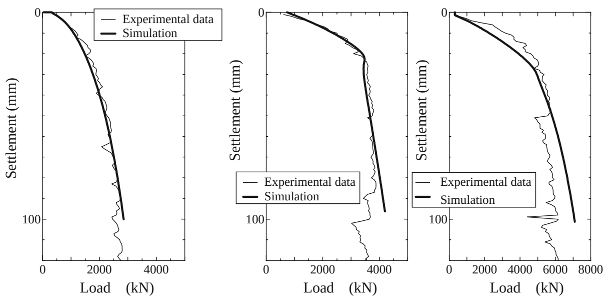

(a) Case 1 (b) Case 2 (c) Case 3

Figure 6: Relationship between settlement and load

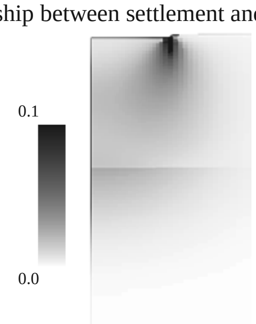

(a) Raft

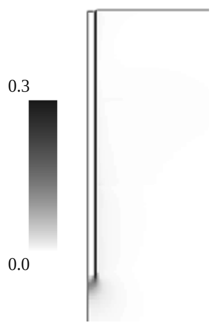

(b) Pile

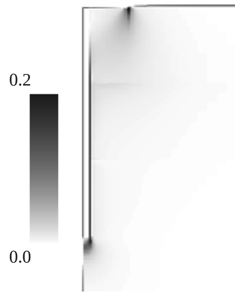

(c) Piled raft

Figure 7: Shear strain contours

Figure 8 shows the axial force distribution for loads of 1,000, 2,000, and 3,000 kN on the head of the pile. For Cases 1 and 2, the simulations reproduce the experimental results. For Case 3, no increase in axial force occurs from the soil surface to a depth of 2 m. As noted previously, this indicates that friction around the upper part of the pile is not effective in deforming the soil under the raft. Figure 9 shows the relationship between the vertical displacement at a soil depth of 1.0 m or 4.5 m and the raft settlement. The measurement point is shown in figure 1. It can be seen that there is good agreement between the experimental and simulation results. At a depth of 1.0 m, the displacement is almost the same as that at the surface, whereas at 4.5 m, it is consistently less. This is probably due to horizontal compression or deformation of the soil at a depth of 4.5 m.

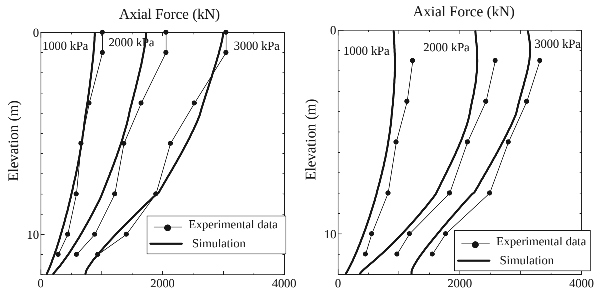

(a) Pile (b) Piled raft

Figure 8: Axial force distribution

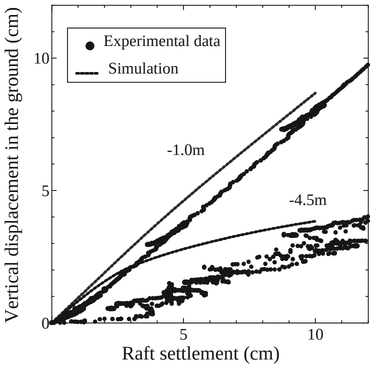

Figure 9: Relationship between vertical displacement at different depths and raft settlement

5 COMBINED BEARING CAPACITY OF PILE AND RAFT

Figure 10 shows the relationship between the settlement and load. Here, “Pile + raft (Exp.)” indicates the combined experimental load of the pile and the raft, “Piled raft (Exp.)” represents the experimental data for the piled raft foundation (Case 3) and “Pile + raft (Sim.)” shows the simulation results for the combined load of the pile and the raft. The simulation results for the piled raft foundation (Case 3) are omitted because they agree with the experimental results. In general, as discussed above, the amount of settlement for the piled raft foundation is less than the sum of that for the pile and the raft because the friction around the upper pile is not effective. In this case, in both the experiment and the simulation, the combined load of the pile and the raft is the same as that of the piled raft foundation.

Figure 11 shows the distribution of the mean effective stress for the raft, pile, and piled raft foundations. The stresses range from 0 to 300 kPa. The soil parameters around the pile are set to represent clay 1, sand 1, and sand 2. An increase in the mean effective stress can be seen in clay 1 for Case 1, sands 1 and 2 for Case 2, and sands 1 and 2 and clay 1 for Case 3. The stress increase in sand 1 is particularly large for Case 3. The reason why the combined load for the pile and the raft is the same as the load for the piled raft foundation is that the increased mean effective stress is transmitted deeper into the ground by the effects of both the raft and the pile. The mechanism by which the total load is carried can be better understood by considering the shear behavior of both clay and sand and the influence of the multi-layered structure.

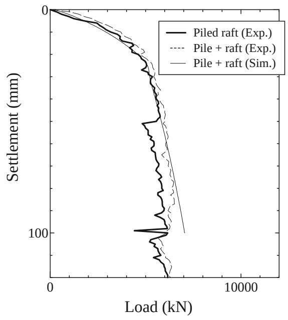

Figure 10: Relationship between settlement and load

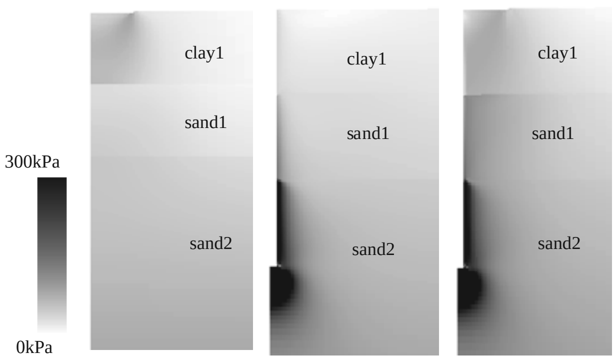

Figure 11: Distribution of mean effective stress

6 CASE STUDY OF COMBINED BEARING CAPACITY

In this phase of the research, additional case studies were performed on the combined bearing capacity between pile, raft and piled raft foundations. Clay 1, which is considered a relatively soft naturally sedimented soil, is assumed for all soils in Figure 12, which shows the simulation results. As can be seen in the figure, the bearing capacity of the piled raft foundation is slightly larger than that of the summation between the pile and raft. Figure 13 shows the element behavior at the A element of Figure 2, which is near the pile. The behavior near the pile can be seen in the softening observed in both the pile and piled raft foundations. As for the mean effective stress space, it was found that the stress of the piled raft foundation was slightly larger than that of the pile. This is because the confined effect of the raft is sufficient. It should be noted that this is a relatively simple example and that additional research into multi-layer soil systems, as well as the effects of soil materials, will be necessary in the future.

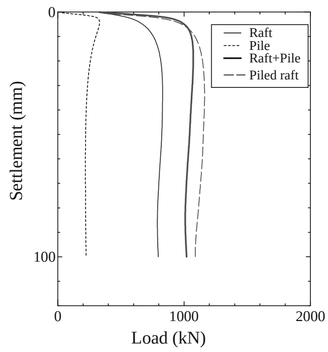

Figure 12. Relationship between settlement and load

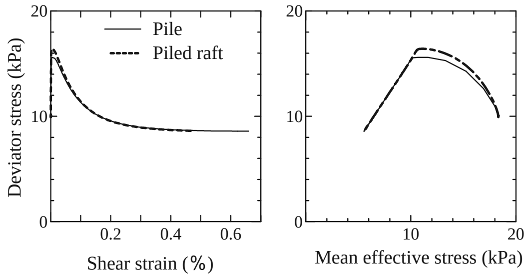

Figure 13. Element behaviors

7 CONCLUSIONS

Simulations of the bearing capacity of raft, pile, and piled raft foundations were performed and the results were compared with those obtained from experimental measurements. Material parameters and initial conditions were determined by laboratory testing of specimens collected in the field. The numerical simulations were found to reproduce the experiment data well.

These results indicated that the combined load for the pile and raft was the same as the load for the piled raft foundation, and this was confirmed by both experiments and simulations. We believe the reason for this is that the mean effective stress is transmitted to deeper parts of the ground by the combined presence of both the raft and the pile. However, more detailed numerical simulations will be required to fully clarify this issue.

8 CONCLUSIONS

The authors wish to express their sincere thanks to the Geotechnical Research Group, Nagoya University, Japan for their advice during the numerical analysis.

9 REFERENCES

Asaoka, A., Nakano, M. and Noda, T. (2000): Superloading yield surface concept for highly structured soil behavior, *Soils and Foundations*, 40(2), pp. 99-110.

Asaoka, A., Noda, T., Yamada, T., Kaneda, K., and Nakano, M. (2002): An elasto-plastic description of two distinct volume change mechanisms of soils, *Soils and Foundations*, 42(5), pp. 47-57.

Asaoka, A., Nakano, M. and Noda, T. (1994): Soil-water coupled behavior of saturated clay near/at critical state, *Soils and Foundations*, 34(1), pp. 91-105.

Honda, T., Hamada, J., Tanikawa, T., Yamada, T., Tsuchiya, T. and Yamashita, K. (2012): Large-scale load tests on bearing capacity of piled raft foundations, Testing and Design Methods for Deep Foundations, IS-Kanazawa, pp.497-502.

Kaneda, K., Shigeno, Y., Hamada, J. and Tanikawa, T. (2012): Numerical Simulation of Load Tests on the Bearing Capacity of Piled Raft Foundations, Testing and Design Methods for Deep Foundations, IS-Kanazawa, pp.491-496.

The Development and the Structural Behavior of a New Type Hybrid Concrete Filled Fiber-Glass Reinforced Plastic Pile

Développement et comportement structural d'un nouveau type de béton hybride rempli de fibre de verre renforcé par pile plastique

Kang I.-K.
Vniel Consultant Co., Ltd.

Kim H.-T.
Hongik University

Baek S.-C.
Andong National University

Park S.-Y.
Korea Engineering Research Co., Ltd.

ABSTRACT: Concrete and reinforced Concrete are the most frequently used material due to the superior strength, durability and affordability. But Concrete and reinforced Concrete are weak in a adverse external environment. Especially, corrosion and damage from sea water cause the serious durability deterioration on marine structures, such as piles. To avoid corrosion of steel and degradation of the durability of concrete, repair and reinforcement are needed. Fiber-glass Reinforced Plastic(FRP) material is widely used because of the excellent corrosion resistance, fatigue resistance, light weight. In the study, in order to enhance the durability and constructability of the pile foundation, a FRP pile is developed and its applicability considering construction is discussed. To improve the axial and transverse load carrying capacities longitudinal reinforcement is also needed additionally, and hence a new type hybrid Concrete Filled FRP Pile (HCFFP) is suggested. A new type HCFFP which is composed of pultruded FRP, filament winding FRP, and concrete filled inside of the FRP tube is proposed to improve compressive strength as well as flexural strength of the HCFFP. This paper studied compression structure behavior of Concrete Filled FRP Pile(CFFP) by using uniaxial compression test about CFFP. The load-strain relation of CFFP is compared with result from finite element analysis program, as well, gained the properties of FRP Pile and analyzed existing document relating to the study about CFFP. This paper proved the confinement effect comparing between FRP Pile and CFFP. Prediction model for the strength and load-strain relation of CFFP is suggested. Also, we present the results on experimental investigations pertaining to the structural behavior of HCFFP which is suggested in order to mitigate the problems associated with the concrete filled steel-concrete composite pile (CFSP) and the concrete filled fiber reinforced plastic pile (CFFP).

RÉSUMÉ : Les bétons concrets et renforcés sont les matériaux utilisés les plus fréquemment à cause de la force supérieure, la durabilité et l'abordabilité. Mais, les bétons concrets et renforés sont faibles dans un environnement externe défavorable. Particulièrement, la corrosion et le dommage de l'eau de mer causent la détérioration sérieuse de la durabilité sur des structures marines, par example, piles. Pour éviter la corrosion de l'acier et la dégradation de la durabilité du béton, la réparation et la renforcé sont nécessaires. Le matériel plastique renforcé en fibre-verre (en anglais, Fiber-glass Reinforced Plastic, FRP) est utilisé largement à cause de sa résistance excellente contre la corrosion et la fatigue, et son poids léger. Dan cette étude, afin d'améliorer la durabilité et la constructabilité de la fondation en piles, une pile en FRP est dévelopé et son applicabilité sur la construction en site est discutée. Pour améliorer la charge axiale et transverale qui transporte les capacités du renforcement logitudinal est composé du FRP est nécessaire plus, et donc un béton de nouveau type hybride remplie en pile FRP (HCFFP) est suggéré. Un nouveau type de HCFFP, qui est composé par le FRP pultrudé, le filament enroulant par FRP et le béton rempli à l'interieur d'un tube FRP, est proposé pour améliorer la force compressible et la force flextionnelle du HCFFP. Cet article présente le comportement compressible structural du béton rempli par FRP piles (en anglais, Concrete Filled FRP Pile, CFFP) en utilisant un essaie de compression uniaxiale sur CFFP. La relation entre la charge et la tension de CFFP est comparée avec des resultats obtenus de l'analyse de la méthode des éléments finis, les propriétés deu pile FRP, et l'analyse des documents existant relative à des études sur CFFP. Cet article prouve l'éffet de la détention comparant entrée le pile FRP et CFFP. Le modèle de prédiction pour la force et la relation entre la charge et la tension de CFFP est suggeré. En outre, nous présentons les résultats sur les investigations expérimentales concernant le comportment structural de HCFFP qui est proposé afin d'atténuer les problèmes associés au béton rempli par le pile composite de l'acier et le béton (en anglais, concrete filled steel-concrete composite pile, CFSP) et le béton rempli par pile plastique renforcé en fibre.

KEYWORDS: hybrid concrete filled FRP pile, FRP, fiber-glass reinforced plastic, pile, laboratory test

1 INTRODUCTION.

Due to the advantageous mechanical properties of the fiber reinforced polymeric plastics (FRP), their application in the construction industries is ever increasing trend, as a substitute of structural steel which is highly vulnerable under hazardous environmental condition (i.e., corrosion, humidity, etc.).

As a fundamental structural element, pile is constructed to transfer loads from superstructure to foundation. In general, since the pile foundation is constructed in the soil and/or under-water, it is difficult to maintain against the damages relating to corrosion. Moreover, it is even more difficult to estimate its durability. Accordingly, the requirement to be satisfied in the design of pile foundation is diversified. In recent years, as a new construction material in the pile foundation industries, fiber reinforced polymeric plastic (FRP) pile has been developed because it has a superior corrosion resistance, fatigue resistance, high specific strength/stiffness, etc. Therefore, such mechanical and physical properties can be used to mitigate the problems associated with the use of conventional construction materials.

When the reinforced concrete compression member (e.g., reinforced concrete pile) is wrapped with the fiber reinforced plastic, the axial load carrying capacity of the pile is increased due to the confinement provided by the fiber reinforced plastic. Such an effort to develop efficient concrete Column wrapped with FRP has been continued from the early of 20th century.

Hybrid FRP-concrete composite pile (HCFFP) is consisted of pultruded FRP unit module, filament winding FRP which is in the outside of mandrel composed of circular shaped assembly of pultruded FRP unit modules, and concrete which is casted inside of the circular tube shaped hybrid FRP circular tube as shown in Figure 1. Therefore, pultruded FRP can increase the flexural load carrying capacity, and the filament winding FRP tube and concrete filled inside of it can increase the axial load carrying capacity.

In this study, in order to use as the pile for foundation construction, we estimated the structural performance of HCFFP through the uniaxial compression tests. Mechanical properties of the FRP material are investigated. Based on the reviews of previous research results and the experimental studies conducted in this study, equation for predicting the ultimate axial compressive strength of the HCFFP is suggested.

1 HYBRID FRP-CONCRETE COMPOSITE COMPRESSION MEMBER

In this study, improved HCFFP system, an exterior filament winding FRP layer component and an interior pultruded FRP with concrete, is proposed as shown in Figure 1.

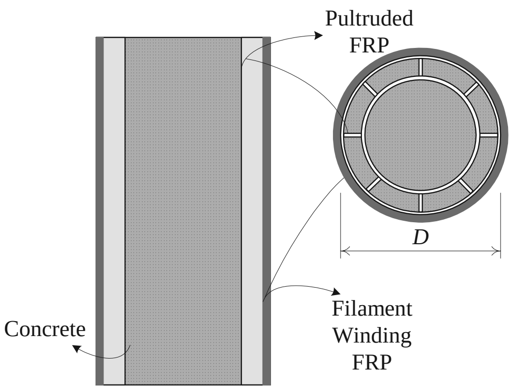

Figure 1 Hybrid FRP-concrete composite pile (HCFFP).

The exterior layer consists of a multilayer filament winding FRP. The interior reinforced concrete consists of pultruded FRP and concrete. Filament winding FRP may have various cross-sectional dimensions to satisfy the structural design requirements. A cylindrical concrete core is located in the filament winding FRP and pultruded FRP, where the interior pultruded FRP and the exterior filament winding FRP provide axial and circumferential reinforcement, respectively, for the concrete core.

The specimens of HCFFP members, which are the FRP circular tubes that had been manufactured by filament winding and pultrusion processes are shown in Figures 2 and 3, respectively. Filament winding process is surfaces of revolution, such as pipes, cylinders, and spheres. In filament winding, continuous reinforcements, such as roving, are wound onto a mandrel until the surface is covered and the required thickness is achieved. Pultrusion is a continuous manufacturing process used to manufacture constant cross section shapes with unlimited length. Pultrusion is a cost effective process because it achieves direct conversion of continuous fibers and resin into a finished part. The fibers are continuously impregnated and pulled through a heated die, where they are shaped and cured.

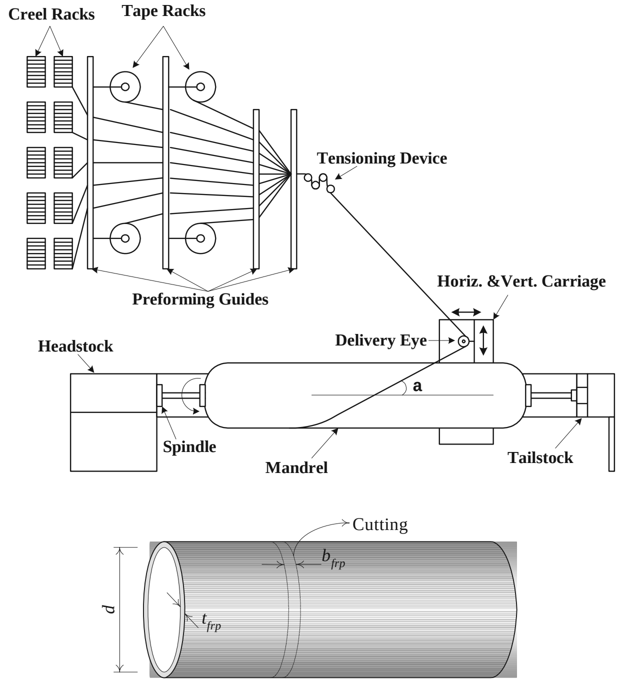

Figure 2 Manufacture of the filament winding FRP specimen.

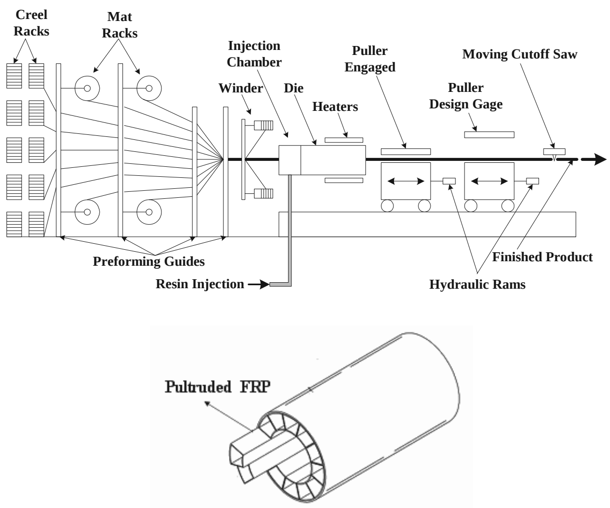

Figure 3 Manufacture of the pultruded FRP specimen.

2 LABORATORY TEST RESULTS

2.1 *Mechanical Properties of Materials*

Dimension of the filament winding FRP tube and pultruded FRP specimens are given in Table 1. A glass-fiber and a polyester resin were used to manufacture the FRP. Compressive strength of concrete was obtained from the uniaxial compression tests at the age of 28 days. Material properties tests of the filament winding FRP tube were split disk and compressive tests and pultruded FRP were tensile test. The split disk test of the FRP specimens was carried out at the Structures Laboratory in Hongik University, Korea. A total of 9 specimens were tested for the split disk test and the compressive test, respectively. A total of 9 specimens are tested, 3 for 3 tests, as given in Table 1.

The failure load, the ultimate strength, and the modulus of elasticity are determined and summarized as shown in Table 2, respectively. One of the failure modes of a tested specimen is also shown in Figure 4.

Table 1. Dimension of the FRP tube specimen

Classification		Number of specimen	Thickness (mm)	Width (mm)
Filament winding FRP	Split disk test	3	2.8	30
		3	4.2	
		3	5.6	
	Compressive test	3	2.8	L= 600 D= 300
		3	4.2	
		3	5.6	
Pultruded FRP	Tensile test of inner arc	3	3.9	25.3
	Tensile test of outer arc	3	3.7	28.5
	Tensile test of rib	3	3.1	24.7

Table 2. Test results

Classification		Thick ness (mm)	Failure load (kN)	Ultimate Strength (MPa)	Modulus of elasticity (MPa)
Filament winding FRP	Split disk test	2.8	62.3	294.6	22.2
		4.2	112.7	326.9	23.3
		5.6	157.7	318.8	22.6
	Compressive test	2.8	254.9	194.1	N/A
		4.2	507.4	258.2	N/A
		5.6	647.1	247.5	N/A
Pultruded FRP	Tensile test of inner arc	3.9	25.6	260.1	22.4
	Tensile test of outer arc	3.7	22.8	214.2	27.9
	Tensile test of rib	3.1	29.8	387.4	31.4

Figure 4 Failure mode.

The mechanical properties were determined from the experiments conducted by changing the thickness. In the test, three sets of tests with different thickness and each set consists of three specimens are prepared. Specimens were taken from the FRP tube and the properties were, then, calculated by averaging the results obtained from the split-disk test, compression test, and tensile test. From the tests result, it can be observed that the mechanical properties for the FRP tube specimens were almost similar. In the specimen preparation three different compressive strengths of concrete, i. e., 19.2MPa, 34.5MPa, and 44.0MPa, are used and the strength of concrete at the age of 28 days was measured by tests.

2.2 *Uniaxial Compression Tests of HCFFP*

For estimating the compressive strength of HCFFP, uniaxial compression tests on HCFFP members are conducted. It was observed that the HCFFP specimens are finally failed after the rupture of filament winding FRP. From the experiment, load versus displacement at the upper part of a loading plate and the load versus strain measured at the middle of the specimen are obtained. The axial stress versus axial strain of confined concrete specimen is shown in Figure 5.

It can be observed that the uniaxial compressive strength of HCFFP is increased if the concrete strength and the thickness of exterior filament winding FRP tube is increased. This tendency is also similar to that of existing CFFP member used currently in practice.

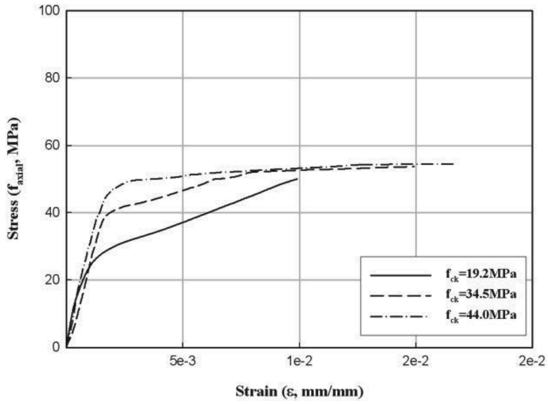

(a) 2.8mm FFRP

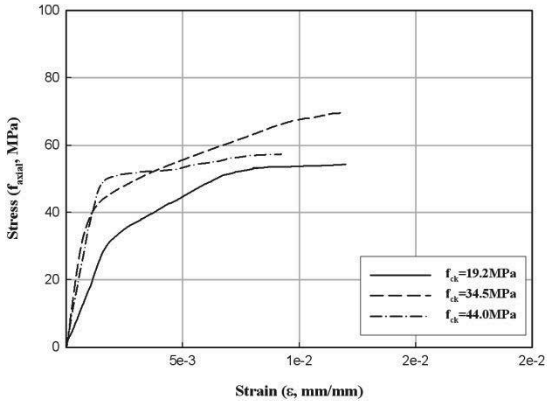

(b) 4.2mm FFRP

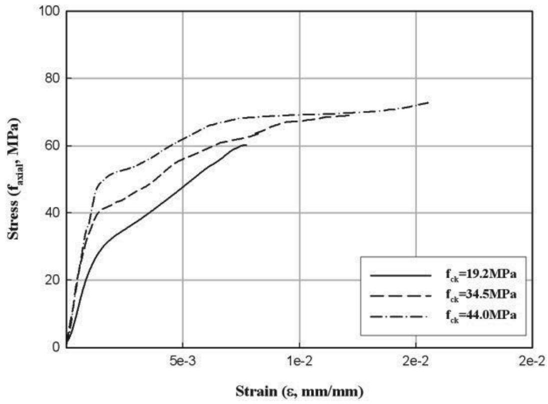

(c) 5.6mm FFRP

Figure 5 Axial stress-strain relationship of HCFFP specimen.

2.3 *Flexural Test of HCFFP*

For estimating the flexural strength of HCFFP, flexural tests on HCFFP members are conducted. A total of 9 specimens, 3 sets of test with 3 specimens for each set, were tested under four-point bending loads as shown in Figure 6. In the test, specimens with 3 different filament winding thicknesses, i.e., 2.8mm, 4.2mm, and 5.6mm, are used. It was observed that the HCFFP specimens are finally failed after the rupture of filament winding FRP. From the experiment, load versus displacement measured at the middle and quarter points of span length of the specimen is obtained.

It was observed that the moment estimated at failure of the HCFFP specimens is almost similar regardless of the differences in the thickness of exterior filament winding FRP tube. Moreover, the flexural moment versus vertical deflection at the time of cracking initiation of the specimen surface is shown in Figure 7.

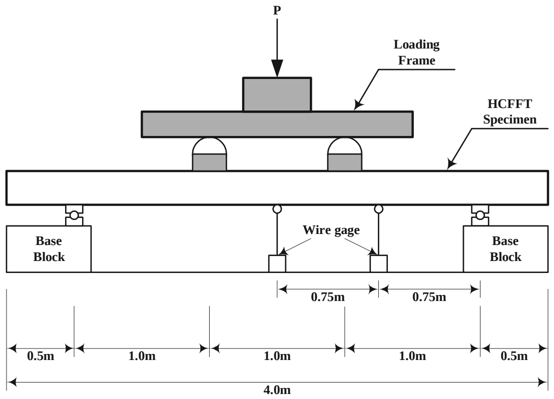

Figure 6 Loading and measurement location of HCFFP specimen.

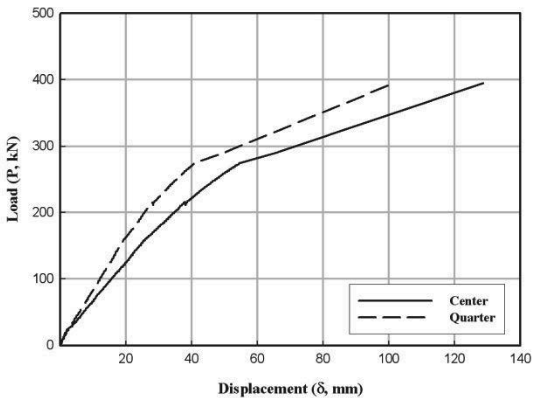

(a) 2.8mm FFRP

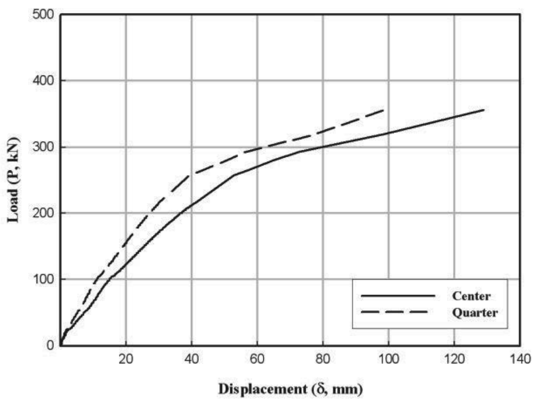

(b) 4.2mm FFRP

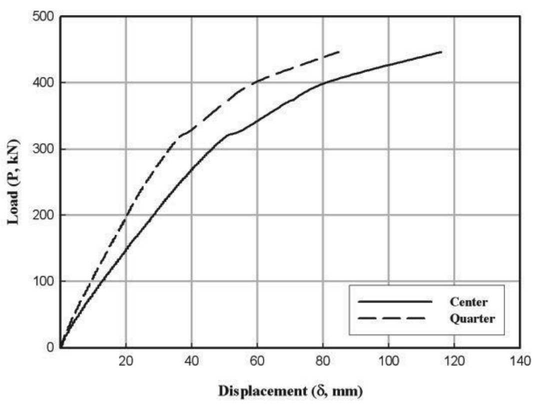

(c) 5.6mm FFRP

Figure 7 Moment-deflection relationship.

3 CONCLUSIONS

In this paper, we presented the structural behavior of HCFFP specimens under compression and flexure. The improvements of the load carrying capacity of HCFFP members compared with CFFP, based on the experimental investigations, are discussed. As expected, load carrying capacity of HCFFP member is increased if the confining pressure and core concrete strength are increased. In addition, the equations for predicting the compressive and flexure strengths of the HCFFP member are proposed. The results obtained by the analytical study are compared with the average experimental results. It was also provided that HCFFP member is suitable to apply as the structural member by performing the comparison with the strength of CFFP member.

For the future study, structural performance of the connection between the segments of HCFFP, and constructability of HCFFP pile should be explored and eventually its applicability in the construction field should be evaluated.

4 ACKNOWLEDGEMENTS

This research was supported by the Construction Technology Innovation Program (CTIP) (code: 11CCTI-C053526-03) of the Korea Institute of Construction & Technology Evaluation and Planning (KICTEP). The financial support provided by the KICTEP is acknowledged.

5 REFERENCES

An, D.J. 2011. *Structural Characteristics of Hybrid FRP-Concrete Composite Piles.* Ph.D. Thesis, Hongik University, Seoul, Korea.

Choi, J.W., Joo, H.J., Nam, J.H., and Yoon, S.J. 2010. Development of the Hybrid CFFT Pile. *Journal of the Korean Society for Advanced Composite Structures* 1 (2), 20-28.

Shin, K.Y. 2010. *Estimation of Load Carrying Capacity of Hybrid FRP-Concrete Composite Pile.* Ph.D. Thesis, Hongik University, Seoul, Korea.

Ground displacements related to deep excavation in Amsterdam

Déformations du sol liées à des excavations profondes à Amsterdam

Korff M.
Deltares and Cambridge University

Mair R.J.
Cambridge University

ABSTRACT: This paper explores the ground displacements related to deep excavations for a case study from the Netherlands, the construction of the North South Metro Line in Amsterdam. The overall goal of the analysis of the displacement is to study the interaction of deep excavations with piled buildings. The response of buildings is governed by the soil displacements resulting from the excavation. These displacements, at the surface level and at deeper levels, are described in this paper. The response of the piled buildings is described in a second, related paper in this conference.

RÉSUMÉ : Les auteurs ont analysé les déformations du sol liées aux excavations profondes de la ligne nord/sud du métro à Amsterdam. L'objectif principal de cette analyse des déformations est d'étudier l'interaction des excavations profondes avec les bâtiments sur pieux. La réponse des bâtiments est régie par les déformations du sol résultant de l'excavation. Ces déformations, de sub surface et de niveaux plus profonds, sont décrites ici. La réponse des bâtiments sur pieux quant à elle est décrite dans un article connexe de cette conférence.

KEYWORDS: deep excavation, ground displacement.

1 CONSTRUCTION OF THE NORTH-SOUTH LINE

1.1 *Deep excavation and soil conditions*

The North-South Line in Amsterdam passes under the historical centre of the city in twin tunnels. Five underground stations are currently under construction. Rokin, Vijzelgracht and Ceintuurbaan Station are three of the deep stations in the historic city centre. They are built using the top down method.

The soil consists mainly of Holocene and Pleistocene, soft clay, peat and sand deposits, underlain by a stiff, lightly over consolidated clay, with OCR=2. Fill and soft Holocene deposits are present to a level of about NAP –11.0m (ground level is around NAP +1.0m (NAP is Dutch Reference Level). These are underlain by the 1st sand layer. The 2nd sand layer is found at about NAP –16m, extending to NAP –25m. Below the 2nd sand layer the stiff clay layer of around 15m thickness (the Eem clay) is found, overlaying the 3rd sand layer. Phreatic ground water is found just under NAP and the piezometric levels in the aquifers are influenced by deep pumping for the polders surrounding the city to a level of about NAP-3m.

1.2 *Rokin Station and Vijzelgracht Station*

Rokin Station is the first of the Deep Stations for the North South metro Line in Amsterdam, following the line south from Central Station. The station is 24.5 m wide. The diaphragm wall is 1.2m wide and 38m deep. At 4 cross sections, surface measurements as well as inclinometer and extensometer measurements are taken, see Figure 1. Vijzelgracht Station is 250 m long, 22 m wide and the diaphragm walls extend to a depth of NAP - 44.5 m. Both stations had reached a depth between NAP-12 and NAP-15m at the time of the measurements presented here, while the final depth (results not presented in this paper) is about NAP-30m.

⊠ inclino/extensometer point
□ surface measurement point

Figure 1 Top view of cross section west of Rokin Station

1.3 *Ceintuurbaan Station*

Ceintuurbaan Station is 220 m long, only 11 m wide and a maximum of 31 m deep. It is also built by means of a top down construction, with 1.2m thick diaphragm walls extending to a depth of NAP-45 m. A cross section of the excavation, soil profile and monitoring instruments is shown in Figure 2. The monitoring instruments include extensometers behind the wall, inclinometers in the soil and in the wall, manual levelling of the surface and the buildings and automatic monitoring of the buildings. Details about the construction and monitoring of Ceintuurbaan Station are given in De Nijs & Buykx (2010).

Over a period of about 8 years, preparations for the construction and the subsequent excavation of the deep station took place, see Table 1. The preliminary activities include raising the ground level (≈0.7m), diaphragm wall construction, jet grout strut installation, excavation to NAP-2m, construction of the roof, backfilling above the roof and a pumping test for water tightness of the D-wall in the 1st and 2nd sand layers.

Table 1 Construction activities and dates for Ceintuurbaan

Construction activity	End date
Base monitoring start 2001	2003-11-01
Preliminary activities	2007-04-01
Excavation to NAP –6.2m	2007-09-13
Excavation to NAP –15.3 m	2007-12-10
Excavation to NAP –19.4 m	2008-03-01
Excavation to NAP –24 m	2008-08-01
Excavation to NAP –25.6 m, Floor construction, pumping test	2009-06-24

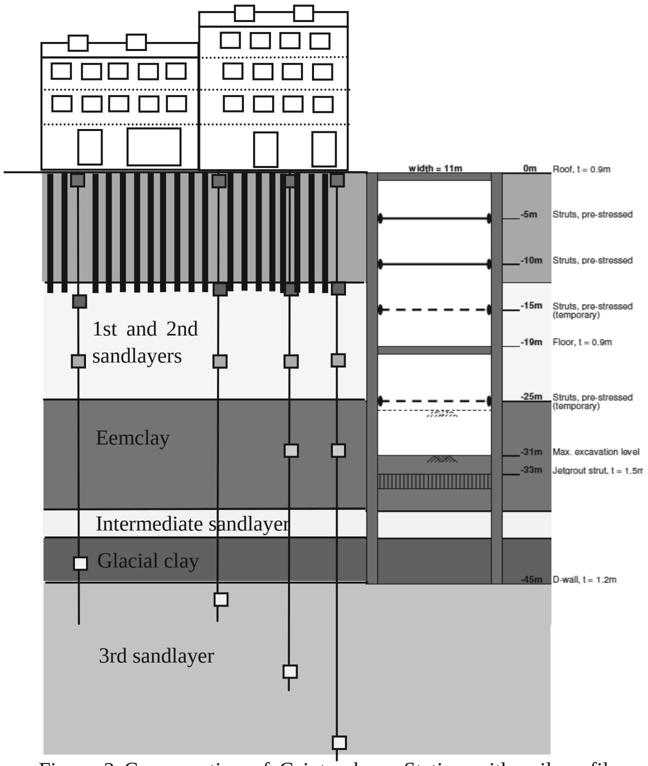

Figure 2 Cross section of Ceintuurbaan Station with soil profile and extensometer locations

2 SURFACE DISPLACEMENTS

In the Amsterdam deep excavations, the following construction effects contributed to the displacement of the ground surface:

- Installation of diaphragm wall including preliminary activities
- Excavation of the station box.

Figure 3 shows the measurements of the ground surface for all three stations, Rokin, Vijzelgracht and Ceintuurbaan, for various stages of the excavation. It should be noted that the excavations had not finished at the time these measurements were taken and so the long term consolidation settlement is not completely included. The total period of the displacement measurements was over 6 years (from 2003-2009). For each stage, the excavation depth H is mentioned in the figures. From Figure 3 it is concluded that the settlement profile found in Amsterdam falls within the limit of Zone 1, as described by Peck (1969), with the ground surface displacement falling within 1% of the excavated depth. The main displacements occur within 2 times the excavation depth as also suggested by Peck. More significant however is the effect of the excavation depth itself. In all three of the Amsterdam cases, the largest effect on the ground surface can be attributed to the preliminary activities, which took in total about 4 of the 6 years presented.

For each station, the average contribution of the preliminary activities to the surface displacements has been determined. The percentage of displacement caused by preliminary activities in 2003-2007 compared to the overall displacement between 2003-2009 or 2003-2010 for Ceintuurbaan Station is 70%. For Vijzelgracht Station this is 55% and for Rokin Station 74%. The percentage at Vijzelgracht is influenced by some leakage incidents (Korff et al. 2011), showing a larger effect during the excavation period after 2007. The percentages for all the stations are somewhat higher than the actual values would be if the displacements at the end of construction (after 2012) had been taken into account, although additional displacements between 2009-2012 have been very small. Such a high percentage of the settlements caused by preliminary activities was also reported by Fernie et al. (2001) for a case study in London (Harrods). The deflection of the retaining wall in a top-down construction there caused only a small fraction of the overall ground movements. The installation of a contiguous piled wall of bentonite-cement caused up to 40% of the total movement.

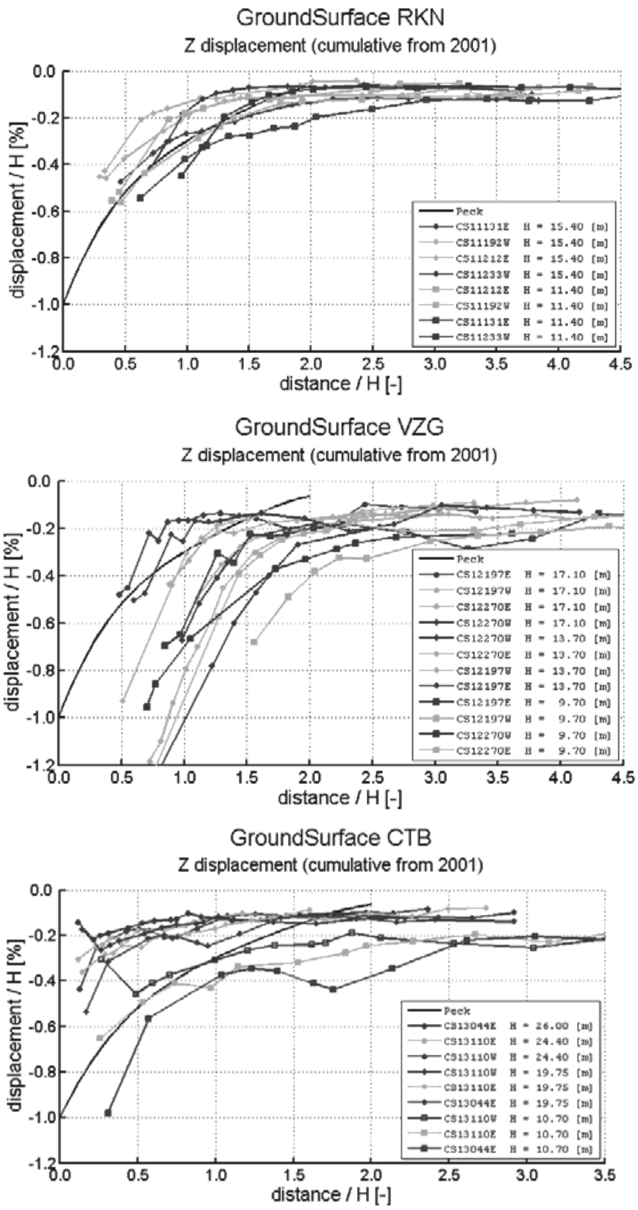

Figure 3 Settlements normalized with excavation depth H, compared with envelopes by Peck (1969)

Clough and O'Rourke (1990) evaluated the maximum displacement to be expected behind different types of retaining walls. In stiff clays, residual soils and sands the maximum ground displacement behind the wall is about 0.15% - 0.5% of the excavation depth, see Figure 4. The Amsterdam cases are plotted in a similar way in Figure 5.

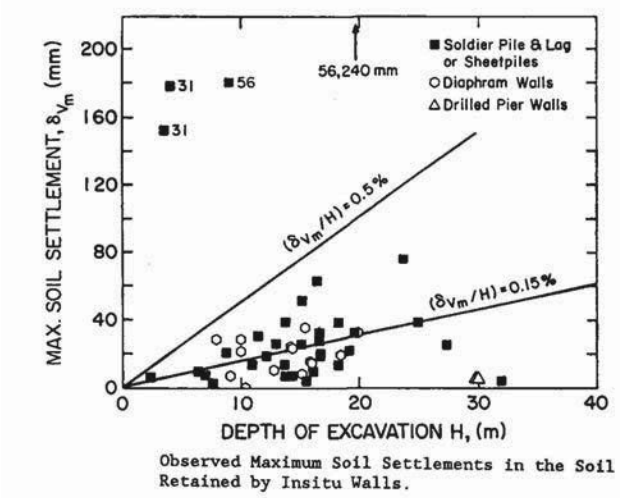

Figure 4 Observed maximum wall deflection and settlements for stiff clays, residual soils and sands (Clough and O'Rourke, 1990)

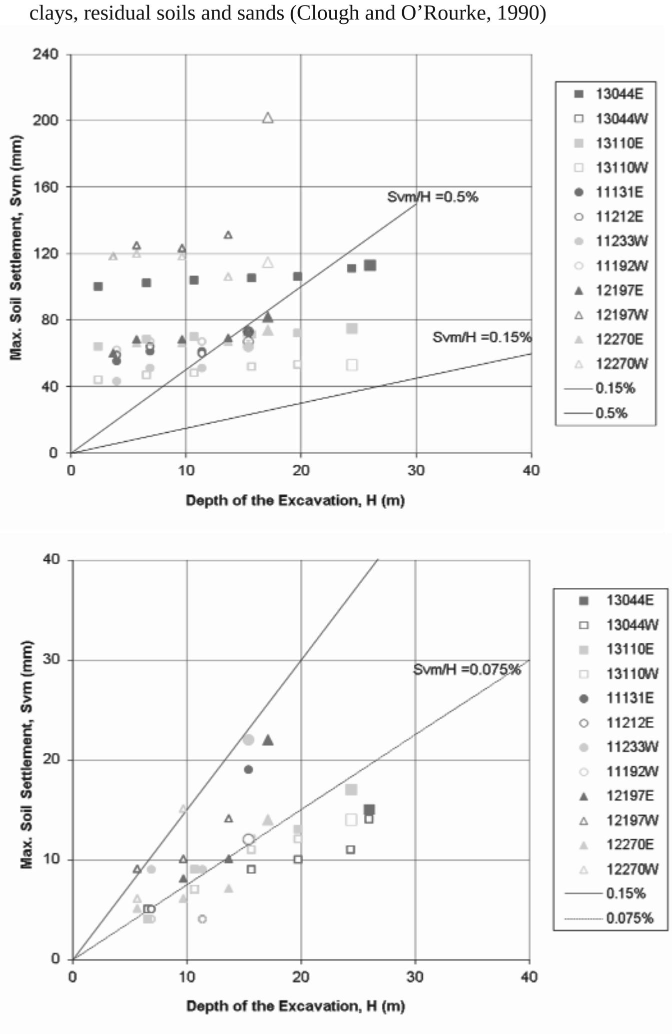

Figure 5 Observed Maximum surface settlements in Amsterdam for a) all construction effects (including preliminary activities) and b) for excavation only.

At the time of the end of the measurements presented here, Figure 5(a) shows the surface settlement to fall within the band of 0.15-0.5% times the excavation depth as determined by Clough and O'Rourke (1990), except for 2 incident locations (12197W and 12270W) as described in Korff et al. (2011). During the early stages of construction, the surface settlement is approximately 1% of the excavated depth. This can be attributed to the significant impact of the preliminary activities, mainly due to the presence of highly disturbed soil conditions. The final values (shown slightly bigger in Figure 5(a)) for the surface settlement average to 0.3 to 0.45% of the excavation depth, with 0.3% for Ceintuurbaan Station which had almost reached full depth and 0.45% for Rokin and Vijzelgracht Station, which were both excavated about halfway down. The additional displacement due to the deeper excavation steps is small compared to the preliminary activities.

If the preliminary stages are not taken into account, the values are given in Figure 5(b) look much more like the values found by Clough and O'Rourke. The surface settlement, due to excavation of the stations, is less than 0.15% of the excavated depth, with an average of 0.07%. This value was achieved through the use of the very stiff diaphragm wall in combination with a large number of struts, including the deep grout strut.

3 SHAPE OF THE SURFACE SETTLEMENT

The results of all three stations are combined in Figures 6 and 7. During the preliminary activities (Figure 6) a hogging displacement profile similar to that seen above tunnels fits the measurements reasonably well. Most of the displacement in this stage is caused by predrilling and raising of the ground level close to the edge of the excavation, both having the largest impact on the top layers, thus resulting in this curved profile.

During the excavation, shown in Figure 7, the shape of the surface displacement consists of both hogging and sagging parts. The sagging part could not always be captured, because some settlement markers close to the excavation were lost in the process of construction. The shape of the surface displacement profile suggested by Hshieh and Ou (1998) fits the curves reasonably well, although it sometimes extends further away from the wall.

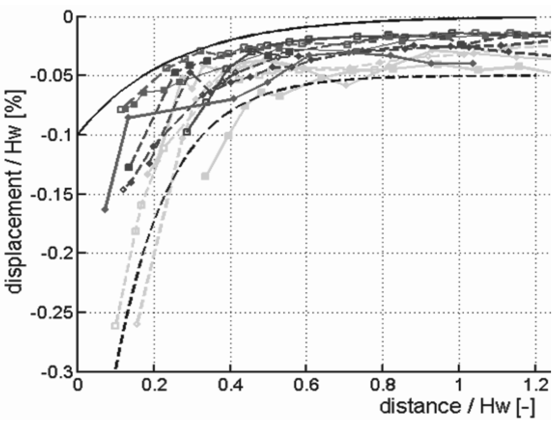

Figure 6 Measured surface displacements normalized with wall depth Hw for Amsterdam stations during preliminary activities, with upper bound (solid line) and lower bound (dashed line)

4 GROUND DISPLACEMENTS AT DEPTH

Especially for buildings with deep foundations, the displacements at deeper levels in the ground are important. Figure 8 shows the measurements of the vertical ground displacement at the surface compared to the extensometer data at two additional depths, NAP-12m and NAP-20m. At larger excavation depths the influence zone is significantly smaller than 2 times the excavation depth. The diagonal line from Aye et al. (2006) can be used as an estimate for the influence area; it is a conservative line. Also the curvature of the displacement profiles associated with it can be considered conservative. For a better fit, the maximum distance from the wall for significant surface displacements (D0) could be taken as 2 times the excavated depth, instead of 2.5 times as suggested by Aye et al. (2006).

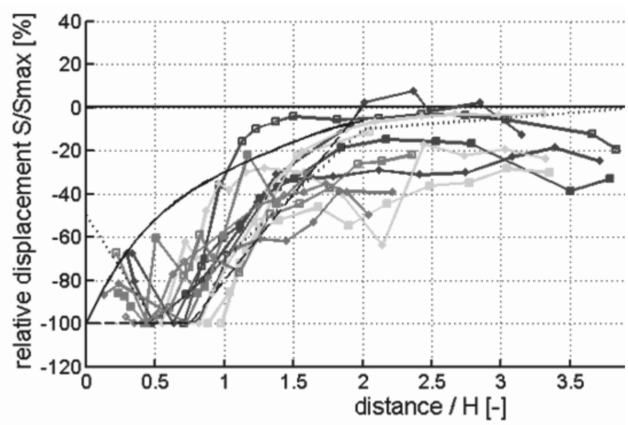

Figure 7 Measured surface displacements normalized with excavation depth H for three Amsterdam deep stations at the deepest excavation level available (2009-07-01), compared to settlement envelopes proposed by Peck (1969), Clough and O'Rourke (1990) and Hsieh and Ou (1998). With:

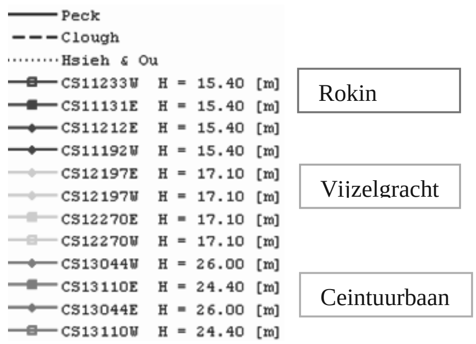

5 CONCLUSIONS

The settlement measurements for the Amsterdam deep excavations have been compared to several, mostly empirical, relationships to determine the green field surface displacements and displacements at depth.

It is concluded that the surface displacement behind the wall is 0.3 – 1.0% of the excavation depth, if all construction works are included. Surface displacements behind the wall can be much larger than the wall deflections and become negligible at 2-3 times the excavated depth away from the wall. The shape of the displacement fits the profile of Hshieh and Ou (1998) best.

In all three of the Amsterdam cases, the largest effect on the ground surface displacement can be attributed to the preliminary activities, which include amongst others the diaphragm wall construction, jet grout strut installation and construction of the roof and took in total about 4 years. The actual excavation stage caused only about 25-45% of the surface displacements, with 55-75% attributed to the preliminary activities. At larger excavation depths the influence zone is significantly smaller than 2 times the excavation depth.

5 ACKNOWLEDGEMENTS

This research was performed in cooperation with the Dutch Centre for Underground Construction (COB). The authors wish to thank the city of Amsterdam for permission to use the data.

6 REFERENCES

Aye, Z.Z., Karki, D. and Schulz, C. (2006) Ground Movement Prediction and Building Damage Risk-Assessment for the Deep Excavations and Tunneling Works in Bangkok Subsoil. *International Symposium on Underground Excavation and Tunnelling*, Bangkok, Thailand

Clough and O'Rourke (1990) Clough, G. W. and O. Rourke, T.D. (1990). Construction induced movements of insitu walls. *ASCE specialty Conference, ASCE Special Publication 25.*

Hsieh, P. G. and Ou, C. Y. (1998) Shape of ground surface settlement profiles caused by excavation, *Canadian Geotechnical Journal*, Vol. 35, pp. 1004-1017.

Fernie, R., Shaw, S. M, Dickson, R. A, St John, H. D, Kovacedic, N, Bourne-Webb, P. and Potts, D. M. (2001). Movement and deep basement provisions at Knightsbridge Crown Court, Harrods, *Int. Conf. Response of Buildings to Excavation Induced Ground Movements*. CIRIA, London..

Korff, M., Mair,R.J., Van Tol, A.F. and Kaalberg, F.J. (2011) Building damage and repair due to leakage in a deep excavation. *Forensic Engineering* Volume 164 (FE4), 165–177

de Nijs, R.E.P. & Buykx. S.M. (2010). Instrumentation and Monitoring at Deep Excavation in Historic City of Amsterdam. Design and Performance Analysis of Monitoring System at Ceintuurbaan Station. *ITA 2010*. Vancouver

Peck, R. B. (1969) Deep excavations and tunneling in soft ground, . 7th *Int.Conf. Soil Mech. Fdn. Engrg, Mexico City*, Sociedad Mexicana de Mecanica de Suelos, A.C.

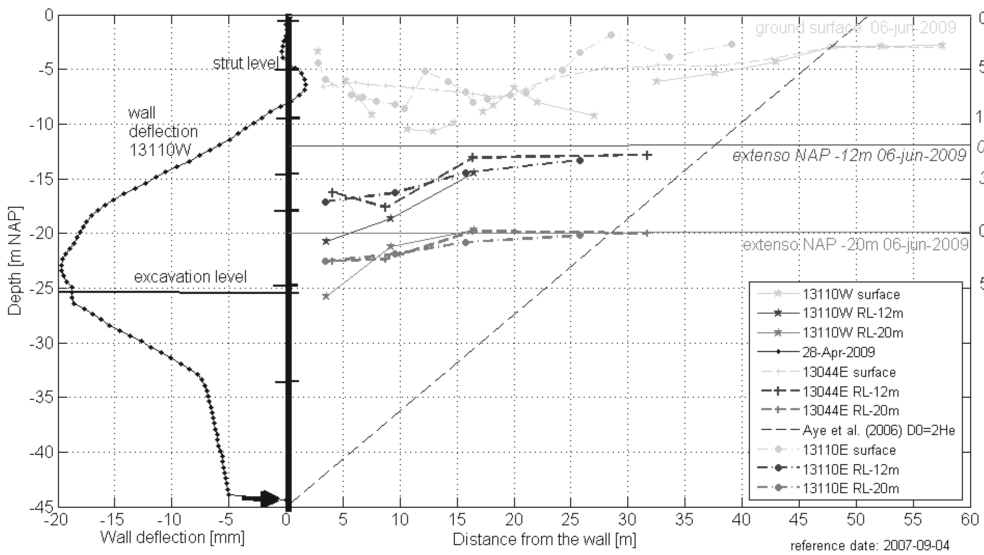

Figure 8 Measured ground displacements at Ceintuurbaan Station (13044E, 13110E and 13110W). Influence zone as described by Aye et al. (2006) but with D0=2He instead of 2.5He shown as diagonal line

Drilled pile technology in retaining wall construction and energy transfer

Application de la technologie des pieux forés à la construction des murs de soutènement et au tranfert d´énergie

Lehtonen J.
D.Sc.(Tech.), Turku University of Applied Sciences, Finland

ABSTRACT: The use of steel piles has grown substantially in the Nordic countries during the last few decades. The growth has been supported by active research and development contributing a versatile collection of pile types and applications. Open section drilling is an example of new micropile inventions. Drilled pile walls and energy transfer applications extend the use of drilled piles to sites where conventional piling has previously not been seen as an option and where the drilled piles can be seen as hybrid structures functioning partly as vertically loaded piles, partly as lateral capacity of the retaining wall, or a heating/cooling distribution system.

RÉSUMÉ : L'utilisation des pieux en acier a connu une forte croissance dans les pays nordiques au cours des dernières décennies. Cette croissance a été soutenue par beaucoup de recherche et de développement en contribuant une collection variée de types de pieux et d'applications. Le forage à section ouverte est un exemple de nouvelles inventions des micropieux. Les parois de pieux forés et les applications pour le transfert d'énergie étendent l'utilisation des pieux forés à des sites où les pieux conventionnel n'ont pas été considérés auparavant et où les pieux forés peuvent être vus comme des structures hybrides qui fonctionnent en partie comme des pieux chargés verticalement, et en partie comme la capacité latérale du mur de soutènement ou comme une installation pour la distribution de chaleur /refroidissement.

KEYWORDS: steel pile, micropile, open section drilling, energy pile, drilled pile wall.

1 INTRODUCTION

Development of drilled micropiles and versatile micropile applications have been subjects of extensive international cooperation since the 1990s. As a regular meeting, the International Workshop on Micropiles IWM has been held eleven times from 1997 until 2012. Since 2006, the IWM has been organised by the International Society for Micropiles (ISM 2013).

In Northern Europe, micropiles are commonly end bearing, in diameter 75…300 mm, drilled or impact driven, sometimes jacked, screwed or vibrated piles (Lehtonen 2011). Use of micropiles has grown significantly since 1980s; in Sweden, for instance, from 150.000 m/a (1991) to 687.000 m/a (2011) when the total market varied from 1.620.000 m (1991) to 2.200.000 (2001) (Swedish Commission on Pile Reseach 2012). Micropiles are in common use mainly for following purposes:

(i) Underpinning.

Hundreds of houses - detached or multi-storey houses - have been underpinned in Scandinavia by impact driven, steel micropiles. The main reason for underpinning is decay of existing wooden piles, which were an acceptable ground engineering method for houses up 1970s. Typical applications are driven or drilled piles of type RR115 (114,3x6,3) or RD140 (139,7x10) giving a service load about 300…1000 kN.

(ii) Light load on soft soil.

Typical load under a structural wall of detached or semi-detached houses is 20…30 kN/m giving a service load to a pile about 100…200 kN. A common application is a slender driven steel pile, as type RR90 (88,9x6,3) or RR115 (114,3x6,3).

(iii) Industrial construction.

There are a great number of manufacturing buildings in Scandinavia locating on very soft soils. Additional construction – between existing buildings and production machinery – is

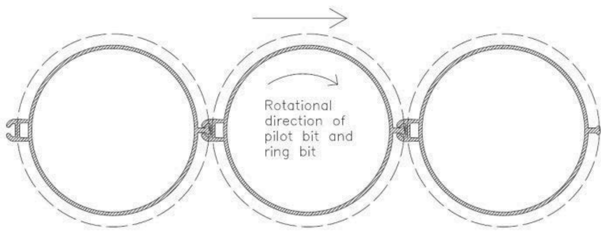

Figure 1. Drilled pile wall.

continued typically with driven micropiles of type RR140 or drilled RD170 (168,3x10), a service load respectively about 500…1400 kN.

The latest innovations in steel pile technology cover mainly drilling. There are several new methods for concentric and eccentric drilling developed in Finland since 1990s. Drilled piles have been used for new applications contributing hybrid techniques where the steel pile can be a part of a drilled retaining wall (Fig. 1) or energy transfer distribution system.

2 OPEN SECTION DRILLING

Traditionally, the drilled piles have been made of hollow steel sections and the drilling methods are often originally developed for oil or water well drilling. Drilled piles are embedded using either top hammer or down-the-hole (DTH) techniques. Drilled piles can be grouted or non-grouted; grouting can be done simultaneously during embedding or after drilling, using gravity of pressured grouting.

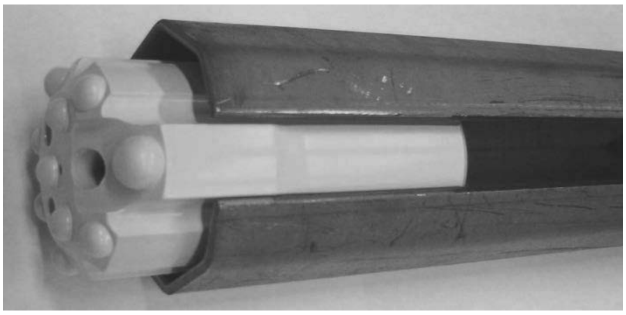

Figure 2. Drilling of an open C section can be done using an eccentric drilling bit.

A new invention has been introduced in Finland to drill an open section as a structural body of a drilled pile. Open section drilling can be done using an eccentric drilling bit (Fig. 2) and the eccentric part of the machinery can be removed from the pile body through the open side of the steel section. The drilling bit has been developed by Robit Rocktools Ltd and the C section has been developed by Emeca Oy. Drilling has been tested (Table 1) until now using the top hammer method but the DTH drilling could be applicable, too.

Table 1. Test sites for open section drilling in Finland.

Site	*Soil layers*	*Pile diameter*	*Lengthening coupler*
Masku 2010	gravel, bedrock	80 mm	no
Espoo 2011	gravel, clay	80 mm	no
Naantali 2012	clay, moraine	80 mm	yes

3 ENERGY PILES

The use of energy piles has grown since 1980s when concrete piles were started to utilize to transfer heating or cooling energy. When the end bearing steel pipe piles have become very common in the Nordic countries, development of energy type micropiles has been an interesting opportunity to face demand of greener energy and lower energy consumption. (Uotinen et al 2012)

3.1 *Steel pipe piles*

The pipe piles are easy applicable to use as energy piles due to hollow structure of the pile. Steel material has a good thermal conductivity reducing the thermal resistance of the energy pile. Steel pipe piles can be installed by driving, drilling, jacking or vibrating. The minimum outer pile diameter considering the heat collecting pipes is 88,9 mm but typically diameter for drilled energy piles is close to 200 mm or more.

3.2 *Heat collecting components*

Normally, the heat collecting pipes are made from high density polyethene, diameter between 20 to 40 mm. One or two U loops of collecting systems (Fig. 3) are installed inside of a steel pipe pile. Water-ethanol mixture is the most common liquid used in energy piles. (Uotinen et al 2012)

3.3 *Case study: an office building in Finland*

The first energy pile building in Finland was constructed to Jyväskylä. The 6-storey office building, base area ca. 1700 m^2,

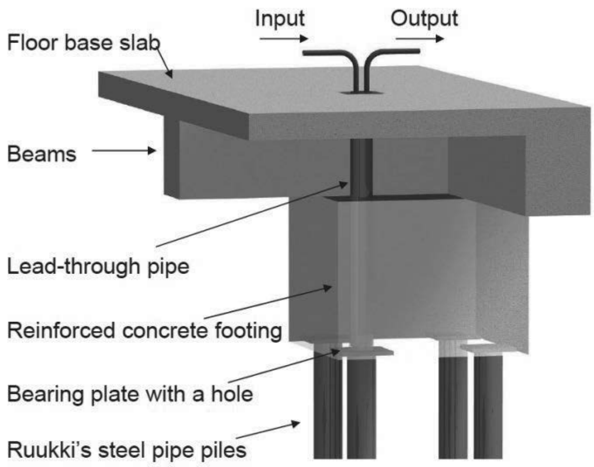

Figure 3. Loops of energy collecting components are installed inside of a steel pipe pile.

is equipped with 38 energy piles when totally 246 piles of 22 to 29 m length has been driven to fill, clay, silt and moraine layers.The piles are type RR170/10, RR220/10 and RR220/12,5, the pile load respectively 691 kN to 1350 kN. In addition, there are 65 precast concrete piles; all piles were driven with Junttan PM 20 LC piling rig and with 4 ton hydraulic hammer. The space between the energy piles varies from 5,5 m to 7,8 m. (Uotinen et al 2012)

4 DRILLED PILE WALLS

Drilled piles have been used for retaining walls have been constructed in Finland, Sweden and Norway since 2008. (Uotinen and Jokiniemi 2012) Drilled pile walls can be used in demanding soil conditions where installation of conventional sheet piles can face penetration problems or vibration risks. In Northern Scandinavia and Finland, hard and large boulders are common obstacles in the overburden limiting use of conventional sheet pile and retaining wall methods.

Two variations of drilled pile walls have been introduced based on either (i) Ruukki´s drilled steel pipe piles (RD piles) or (ii) an application of open section drilling utilizing C and CT profiles (Fig. 4). The RD pile wall cases are collected to Table 2 covering large variations of diameter and interlocking systems. Totally 2150 piles or 24500 m piles have been used for drilled RD walls until now.

The drilled pile walls can be used as a temporary or a permanent structure. Typically, the wall has capacity to take both high vertical and lateral loads when needed. (Uotinen & Jokiniemi 2012)

5 CONCLUSION

The market share of micropiles and other steel piles is remarkably high in the Nordic countries, partly due to active research and development during the past decades. There are versatile collection of applications available and many e.g. drilled pile techniques extend the use of piles to design solutions which are totally new for piles. The energy piles and the drilled pile walls have great potential for future ground engineering. Further research and development efforts will be needed to get all potential benefits linked to the inventions.

Table 2. The RD pile walls. (Uotinen & Vesamäki 2013)

Site	*Interlock*	*Oversize of the ring bit (mm)*	*Pile type*	*Pile length (m)*
Ylitornio, Finland 2009	Ruukki E21	47	test RD400	6
Ruoholahti, Finland 2009	Ruukki E21	47	test RD400	12
Motala, Sweden 2010	Ruukki E21	30	RD400	8-12
Trondheim, Norway 2010-2011	modified WOM-WOF	30	RD600	10-32
Tampere, Finland 2010	modified WOM-WOF	30	test RD170	3
Nummela, Finland 2010-2011	modified WOM-WOF	30	test RD400	12
Kiruna, Sweden 2010	Ruukki E21	47	RD500	10-15
Kalasatama, Helsinki 2011-2012	modified WOM-WOF	47/30	RD600	3-14
Metro sites, Helsinki 2011-2012	modified WOM-WOF	30	RD400 RD600	16-20
Messukeskus, Helsinki 2011	modified WOM-WOF	30	RD170	6
Tampere 2012	RM/RF	27	test RD400	6
Keskuskuilu, Espoo 2012	RM/RF	27	RD220	8-9
Fredriksdal, Stockholm 2012	RM/RF	27	RD400	10-15
Strömkajen, Stockholm 2012	RM/RD	27	RD220	5-9

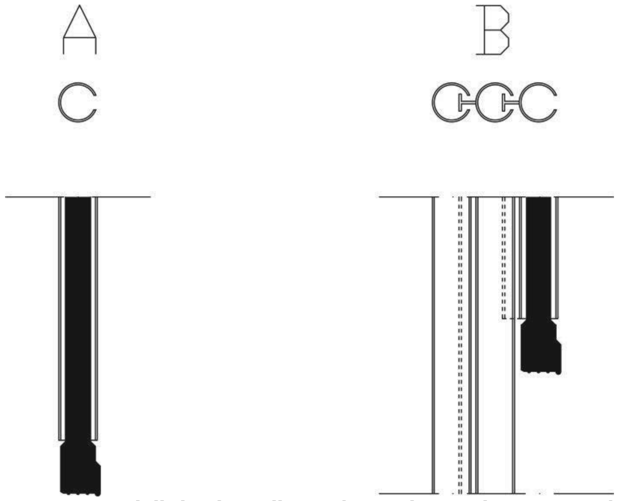

Figure 4. A drilled pile wall can be implemented starting with embedding of an open C section (phase A) and the wall can be extended using CT profiles.

6 ACKNOWLEDGEMENTS

Sari Loppela-Rauha has translated the abstract to French, Olli Rahkala has contributed the Figure 4 and Ville Hyyppä has fine-tuned the lay-out of the paper.

7 REFERENCES

Hyyppä V., Hattara J., Lautkankare R. and Helmisaari J. 2012. *FIN-C2M – New Micropile Innovations in Underpinning*. Proceedings of IWM2012, Milan.

ISM 2013. *International Society for Micropiles*. Retrieved 8 January 2013 from http://www.ismicropiles.org/ism-background

Lehtonen J. 2011. Underpinning project; owners´ views on technology, economy and project management. Aalto University publication series, doctoral dissertations 80/2011, Helsinki.

Swedish Commission on Pile Research 2012. *The pile delivery report*. Retrieved 1 December 2012 from http://www.palkommissionen.org/web/page.aspx?refid=16

Uotinen V.-M. and Jokiniemi H. 2012. *RD pile wall – a new way to build micropile retaining wall structures*. Proceedings of IWM2012, Milan.

Uotinen V.-M., Repo T. and Vesamäki H. 2012. *Energy piles – ground energy system integrated to the steel foundation piles*. Proceedings of NGM2012, Copenhagen.

Uotinen V.-M. and Vesamäki H. 2013. *Case histories on drilled pile walls in Finland, Sweden and Norway*. Proceedings of Teräspaalupäivä (steel pile day), Helsinki.

Three-Dimensional Models of Bearing Capacity – Case Study

Modèles tridimensionnels de capacité de portante – Étude de cas.

Leite da Silva C.P.
Federal Institute of Brazilia, Brazilia, Brazilr

Moreira de Souza N.
University of Brasília, Brazilia, Brazil

Medeiros Silva C.
Embre- Brazilian Engineering and Foundations, Brazilia, Brazil

ABSTRACT: To mitigate risk in geotechnical constructions by making borings and pile load tests that enable the elaboration of bi and three-dimensional models, which assure the correct analysis and evaluation of the associated risks to design and to the construction execution should be one of the targets of a Geotechnical Engineering. Generally, the analyses done in terms of design level are conducted under some uncertainties, especially concerning geological-geotechnical formation which has a great influence on the soil-foundation system, however, it has been looking for techniques that assure a good evaluation of such constructions, by the elaboration and usage of three-dimensional models, based on data from geotechnical and geological survey. The organization, treatment and specialization of soil data furnish models that help in the decision and mitigating process of risks involved in those constructions. The obtained results by the usage of the referred methodology show that data interpolation during the three-dimensional modeling process decrease uncertainties that come from the natural variability of the soil.

RÉSUMÉ : Pour atténuer les risques dans les constructions géotechniques en faisant des essais de chargement sur pieux et des tests de forages qui permettent l'élaboration de modèles bi et tridimensionnels, qui assurent la bonne analyse et la bonne évaluation des risques associés à la conception et à l'exécution de la construction devraient être l'un des objectifs de l'ingénierie géotechnique. En général, les analyses effectuées en terme de niveau de conception sont menés malgré certaines incertitudes, notamment en ce qui concerne la formation géologique-géotechnique qui a une grande influence sur le système sol-fondation, cependant, on a effectué des recherches de techniques qui assurent une bonne évaluation de ces constructions, par l'élaboration et l'utilisation des modèles en trois dimensions, à partir des données de l'enquête géotechnique et géologique. L'organisation, le traitement et la spécialisation des données du sol fournissent des modèles qui aident dans le processus de décision et d'atténuation des risques liés à ces constructions. Les résultats obtenus par l'utilisation de cette méthode montrent que l'interpolation des données pendant le processus de modélisation tridimensionnelles diminue les incertitudes qui proviennent de la variabilité naturelle du sol.

KEYWORDS: bearing capacity, three-dimensional model, geotechnical risk.

MOTS CLES : capacité de portant, model tridimentionnel, risque géotechnique.

1 INTRODUCTION

The estimation of the bearing capacity, the definition of the resistant surface, the tip elevation of the bases and the execution control of the foundations are in many times defined under uncertain conditions which are caused by nature and by the intrinsic characteristics of the soil and by the deficiencies and limitations of the preliminary studies which are the support for the elaboration of a design.

The ideal would be that the foundation could offer a minimum risk concerning the safety and the maximum economy about the costs. The satisfy such dual idea it is necessary to have wide range and consistent preliminary studies for the understanding of the geological-geotechnical behavior of the soil and its interaction with the foundation and the superstructure Silva (2011).

To handle such problem, the elaboration and the usage of three-dimensional models, based on data from geotechnical, geological and geo-physical surveys start to gain a space in civil engineering constructions, especially in foundation and excavation constructions. Based on such philosophy, firstly the design forces (loads) were defined; secondly, the sub-surface model (resistant surface) (soil layers) that would be used in the foundation solution was set.

It is known that to solve the referred problem there are many dimensioning methods which result in many possible foundation solutions. However not even the best method , that is, the one that best adapts itself to the local soil and to the construction's expectations can skip from the natural variability of the soil. Therefore, to understand such variability is the great task of the geotechnical engineering, which is the key point of this article, which proposes a way, for not saying a new one, but efficient to organize, treat and specify in a bi or tridimensional way the soil data, to furnish information that help in the decision making process and in the mitigation of the risks which take part in the foundation constructions.

To validate and measure the quality of the three-dimensional methods, results from load testes were used which decreased in a good way the uncertainties concerning the real execution condition and the foundations' behaviors, in terms of bearing capacity and deformability.

At the end, the obtained results from the three-dimensioning spacialization are shown throughout the proposed methodology. The results obtained from the application of the methodology show that on the contrary of the traditional methods, the data interpolation during the three-dimensional modeling process reduced the uncertainties of the natural variability of the soil.

2 MATERIALS AND METHODS

2.1 *Localization of the Study Area*

The refferred construction is located in an adjacent city called Guará II, Brasília, DF. The design consists of two residential towers with an underpark garage excavated in such a way that the three-dimensional spacialization of soil data was justified because of the great soil variability and because of that the difficulty in executing the foundations. In such construction, 33 SPT borings were made in a piece of land with 60 m by 150 m and lately load tests were also made which results were added to the three-dimensional models. The differential of that construction is that a three-dimensional model of bearing capacity was proposed for it, which was calibrated by the field load tests.

The UTM coordinates which limit the area are: Xmin = 180.941 m, Xmax=181.001 m, Ymin= 8.246.782 m, Ymax=8.246.932 m, Zone 23, datum Astro-Chuá with central meridian of 45º WGr. Figure 1 shows the study area location.

2.2 *Geological Context of the Study Area*

With the topographical ellevations around 1090-1108 m that area presents a plan topography. The river basin of Riacho Fundo is the fundamental factor of the local landscape evolution. The original rock, with a low degree of metamorphism shows an ordinary bright probably due to the sericita presence. The lithological characteristics and the geographycal situation of such occurance suggests its posisioning in the Fácies Ardósia (MNPpa), according to the statigraphical sequence proposed by Faria (1995).

2.3 *Three-dimensional Modeling of the Geotechnical Data*

The data modeling in a three-dimensional environment requires some methodological procedures (Silva & Souza, 2009). The more used parameters for three-dimensioning modeling are the lithological ones in the case of rock descriptions; statigraphical ones to describe soil layers or excavating material; Nspt values or any numerical measurement (geophysical data, geochemical data, strength parameters among others) which can be described in a local manner or between pre-defined intervals; water table; among other parameters that can be adapted to the RockWorks 15 software

I this case, the adopted calculating method for the foundations, continuous flight auger piles, was proposed by Decourt & Quaresma (1978). By the access to the geotechnical dimensioning and results of the load tests, load test models were generated for 50 and 60 centimeter diameter piles.

It is important to mention that the target of the load test was to calibrate the results obtained from the foundations' calculations, once the adjustment parameters for the shaft and tip calculation bearing capacity were initially assumed by the designer, and letting the model to spacialize the results to make possible a proper ajustment for the dimensioning adopted method. That is, it was not the objective of the work to review any foundation calculating method, but to show that it is possible to manage other types of three-dimensioning models and their applications on the field in the most direct way.

2.3.1 *Data Log*

The first step for the three-dimensional modeling is the data log in a data bank of the computer software which will be responsible for the modeling. The data log of the borings in the RockWorks 15 software is done in a sequence as follows:

1. Location of the borings. A simple procedure which requires the name of the boring, The East and North coordinates (x,y) and the elevation of the top of the boring (coordinate z), besides the total depth achieved by the drilling. If it is necessary, a symbol can be added represent the borings in the generated bi-dimensional charts.

2. After the location of the borings, the soil profile or the statigraphic log can be done. However, it is very important to evaluate all borings and to establish which will be the soil profile to be used by the model, which procedure can be a complex one because of the soil variability, and in some cases it will be impossible to elaborate the statigraphic model due to such variability.

3. Description of the punctual numerical values. That concerns to insert the numerical values described in the borings, normally the Nspt values.

3 RESULTS

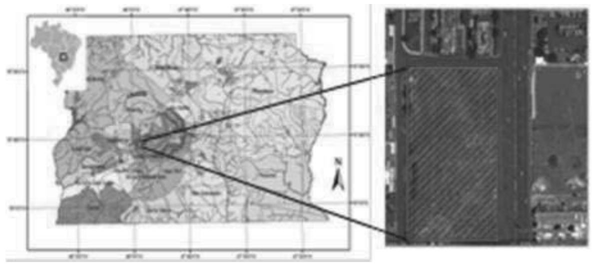

Figure 1. Location of the study area.

The first result obtained for the case study was the basic chart with the information concerning the borings' location, the "Verano" and "Blanc" constructions which gave the name of the case study, and the hipsometria values for the piece of land. In the case of this construction there was no compatibility of datum and the construction was not geologically referred, that is, the modeling was done based on the local reference, because the construction made its choice based on such reference.

It can be observed in Figure 2 the basic chart with the information geologically referred. It is important to mention that ground is general plan and later it was excavated 4 meters below because of the execution of the construction undergrounds.

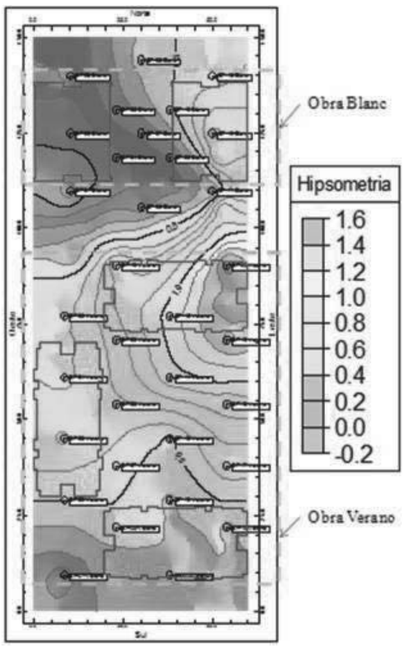

Figure 2. Hipsométrica chart with the SPT borings' location and the constructions' location.

Besides the wide red clay layer, observed in the SPT borings, the soil presented a great variability in the Nspt resistance values what justified the development of the modeling for such construction.

3.1 *Horizontal Slicing of Nspt Values*

To detect with more preciseness the places with soft soil many horizontal slicings were done where the values in grey color represent Nspt values below 30 blows (which do not represent trouble for the continuous flight auger equipments), the other values follow with the presented colors showed sequentially in Figures 3 to 5.

The slicing was done taking into account that the foundation would start 4 meters below the original ground level and that the foundation with continuous flight auger has a minimum execution depth, which in the case was considered 8 meters from the excavation, that is, 12 meters below the ground level (4 meters of excavation + 8 meters of minimum length for continuous flight auger piles).

It can be observed by such sequence of slicings that some places of the construction had soil areas with low Nspt resistance (values in grey color) which were in course and that the design should consider such fact. By taking the analysis of such problem that the idea of elaborating a bearing capacity model for the construction came up, which was done. By observing the great variability of the geological profile it was evident that the resistant surface was variable forcing the definition of different depths for each region of the construction by the detailed analysis of the three-dimensional model. However for the model to be convincing the over-position of the calculate piles in the design was done in the bearing capacity model

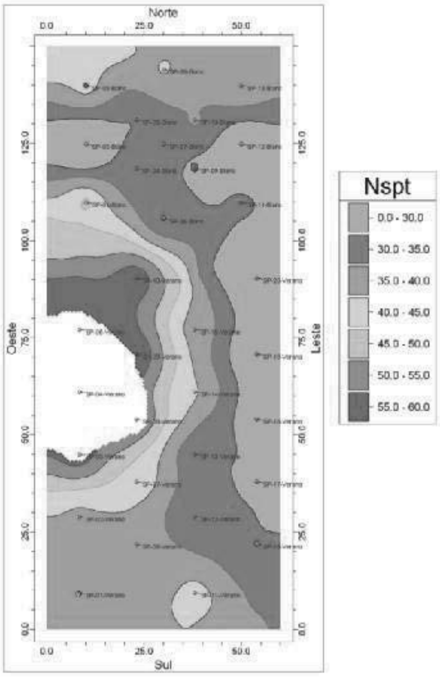

Figure 3. Horizontal Slicing Sequence of the Nspt Model – Decision Taking for the Execution of the continuous flight auger piles – 18 m depth.

3.2 *2D Sections of Bearing Capacity (tf)*

Because of the application of the new technique, in the beginning there was a resistance by the piling contractors concerning the usage of the obtained results from the bearing capacity models. Forcing the specialization of the majority of the piles to make it easier to understand the decision taking in terms of design level that were subsided by the bi and three-dimensional models.

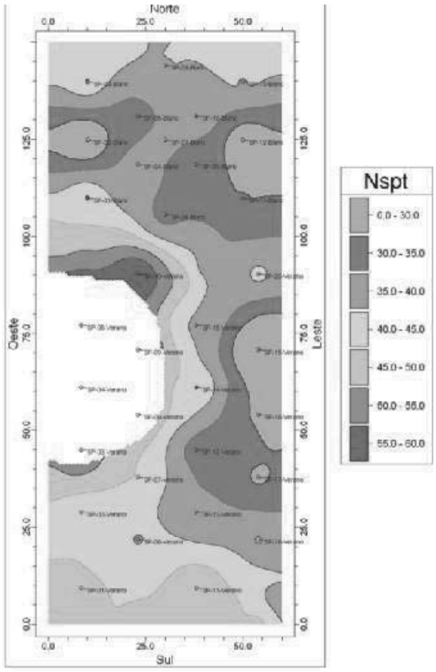

Figure 4. Horizontal Slicing Sequence for the Nspt Model – Decision Taking for the Execution of continuous flight auger piles – 19 m depth.

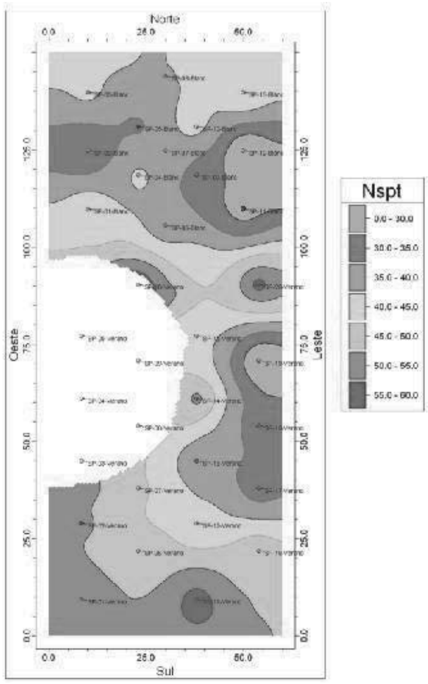

Figure 5. Horizontal Slicing Sequence for the Nspt Model – Decision Taking for the Execution of continuous flight auger piles – 20 m depth.

Most of the piles of interest which were to be executed in the construction had a depth of 20 m (length) with a prevailing diameter of 50 cm for 100 tf of bearing capacity, had their execution in terms of depth defined by the elaborated models.

The objective of the 2D sections of bearing capacity, which in the beginning was just to do the depth control reached by the execution, took new destinations when many piles start to present problems during the excavation. Figure 6 shows a section of interest for the construction in which some piles presented execution problems.

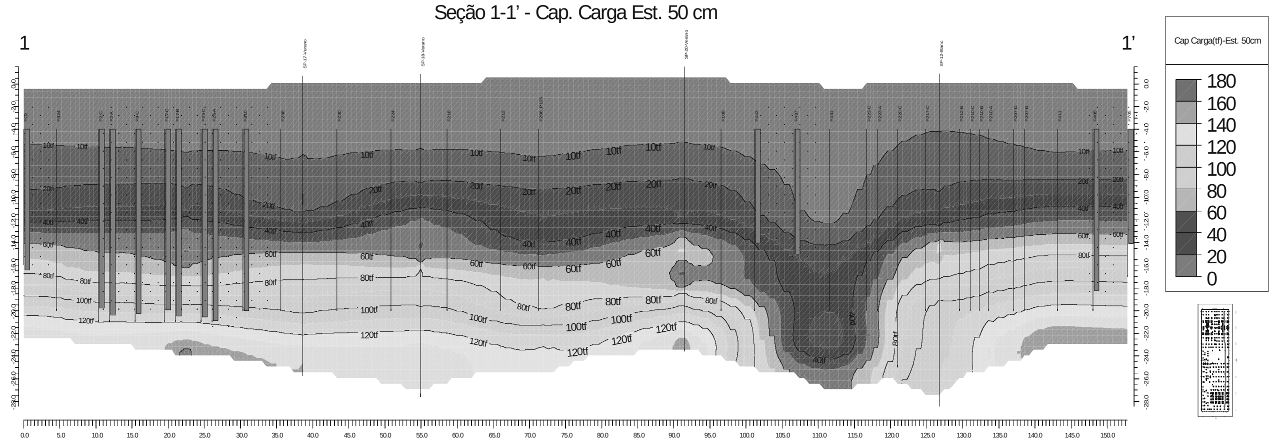

Figure 6. Section 1-1 of bearing capacity of the case study

3.3 *Horizontal Sections (2D) of Bearing Capacity*

The horizontal sections 2D of bearing capacity are very useful to see the results in a general way. Figure 7 shows the bearing capacity (tf), for 50 cm diameter and 16 meters depth and Figure 24 shows the bearing capacity surface for 20 meters depth, and those are in reality what can be called as 2,5D surfaces.

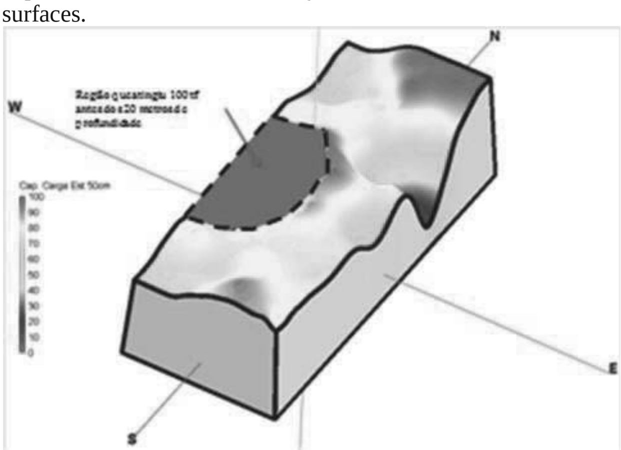

Figure 7. Horizontal Section of Bearing Capacity for 20meters depth of the case study.

The choice of the 20 meters depth was due to the fact to achieve most of piles in terms of bearing capacity and because many piles did not reach longer depths, once they were getting close to the maximum excavation limit of the equipment.

Finally it can be observed how often the resistant surface can vary in the construction and how can the models help in the problem analysis and in the search of more efficient solutions for the construction.

4 CONCLUSIONS

The three-dimensional mapping of the soil has the target to obtain the maximum knowledge of the geotechnical conditions of the construction location to make the engineers' analyses easier. On the contrary of traditional methods, the data interpolation during the 3D modeling process decrease the uncertainties of the natural variability of the soil.

The propose to produce a bearing capacity model was extremely satisfactory and with a practical value, however we must be careful in taking into account the traditional methods and the field tests, as the static load tests, with the objective to calibrate the bearing capacity model. Besides, the construction control with the spacialization of the design foundations and the executed ones, in the bearing capacity model, diminish a great deal the uncertainties in the construction and promote a greater economy for the foundation execution..

The process of post-evaluation of the models produced by the computer softwares must always be done with criterion. That is, the whole process of three-dimensional modeling of sub-surfaces or underground space requires geological/geotechnical experience of the region and knowledge of limitations and potential advantages of the computer softwares as the quantity of input attributes, working grid limit, interpolating devices and their limitations.

5 REFERENCES

DÉCOURT , L.; QUARESMA, A. R. Capacidade de Carga de estacas a Partir de Valores de SPT. 6º Congresso Brasileiro de Mecânica dos solos e Engenharia de Fundações, Rio de Janeiro, anais, v. 1, pp 45-53, 1978.

FARIA, A. (1995). Estratigrafia e Sistemas Deposicionais do Grupo Paranoá nas Áreas de Cristalina, Distrito Federal e São João D'aliança - Alto Paraíso De Goiás. Tese de Doutorado, 4, Instituto de Geociências, Universidade de Brasília, Brasília, DF, 199 p.

SILVA, C.M. (2011). Energia e Confiabilidade Aplicadas aos Estaqueamentos Tipo Hélice Contínua. Tese de Doutorado, Publicação G.TD - 070/11, Departamento de Engenharia Civil e Ambiental, Universidade de Brasília, Brasília, DF, 303p.

SILVA, C. P. L. & SOUZA, N. M. (2009). Desenvolvimento de Modelagem Tridimensional de Subsuperfícies. Livro Comemorativo dos Vinte Anos do Programa de Pós-Graduação em Geotecnia da Universidade de Brasília. Editora FT, ISBN 978-85-60313-15-0, Brasília, DF, 441-470 p.

SILVA, C. P. L. (2011). Cartografia Geotécnica Tridimensional do Setor Noroeste de Brasília. Tese de Doutorado, Publicação G.TD-072/2011, Departamento de Engenharia Civil e Ambiental, Universidade de Brasília, Brasília, DF, 274 p.

Full scale rapid uplift tests on transmission tower footings

Tests grandeur nature d'arrachement rapide sur les fondations d'une tour relais

Levy F.M., Richards D.J.
Geomechanics Research Group, Faculty of Engineering and the Environment, University of Southampton, UK

ABSTRACT: This paper describes results from a series of full scale tests on transmission tower footing at a London clay site in Kent. The testing series investigated the effects of rapid loading at field scale with footings founded directly onto clay or coarse granular material, with a clay or coarse granular material backfill. It was shown that footings founded on London clay mobilised significantly greater uplift capacities at smaller displacements than those with a breakaway condition. In a suite of centrifuge tests this enhanced capacity was shown to originate from suctions that formed on the base of model footings (Lehane et al. 2008). Back analysis of the field tests revealed that inferred normalised suctions were similar to those generated in the centrifuge tests. However the enhanced uplift capacity was not sufficient to cause the uplift resistance to reach design capacity by the displacement serviceability limit state of 10mm.

RÉSUMÉ : Cet article présente les résultats issus d'une série de tests grandeur nature sur les fondations d'une tour relais basées sur un terrain en argile de Londres (London clay), dans le Kent, Angleterre. Ces séries de tests ont été menées pour étudier les effets d'un chargement rapide en conditions réelles avec une tour remblayée et fondée dans un sol argileux ou un matériau granuleux. Il a déjà été prouvé que, pour de petits déplacements, des fondations basées sur de l'argile de Londres présentaient une résistance à l'arrachement plus importante que des fondations placées sur une base en gravier. Des essais en centrifugeuse ont montré que cette résistance à l'arrachement accrue provenait de succions sur la base de la maquette (Lehane et al. 2008). De nouvelles analyses sur le terrain ont révélé que les forces de succion calculées étaient similaires à celles générées durant les tests de centrifugeuses. Cependant cette meilleure résistance à l'arrachement n'a pas été suffisante pour satisfaire la limite de résistance imposée par le cahier des charges pour un déplacement fonctionnel de 10mm.

KEYWORDS: clays; footings; foundations.

1 INTRODUCTION

In the UK there are 22,000 high voltage transmission tower pylons supported by a pyramid (or pad) and chimney type footing under each tower leg. The majority of these towers have cable bundles (conductors) that are reaching the end of their design life (Clark et al. 2006) and due to demand increases and changing power generation patterns the majority of these cable bundles require uprating to transmit higher voltages. This will require larger cable bundles increasing the loads transmitted to the tower support foundations.

Recent studies undertaken by Southampton University for National Grid UK have shown that the design basis for transmission tower foundations may not be reliable. The uplift capacity derived from the conventional UK design practice is higher than that predicted by other models (e.g. American IEEE design methods (IEEE 2001)). The ultimate reliability of National Grid foundation systems in terms of their uplift capacity is therefore uncertain, particularly as the imposed loads transmitted to the foundations are likely to increase in both magnitude and frequency as climate change produces more extreme storm/loading events.

However, the failure of tower foundations/footing systems in service is extremely rare suggesting that although the design methodologies may be unsound as they are not based on actual failure mechanisms there are additional factors not considered in the simplified design methods used that are providing increased resistance to uplift, particularly under rapidly applied loading conditions. To examine these issues a series of full scale rapid uplift tests were carried out at the Building Research Establishment's London clay test site at Chattenden, Kent.

1.1 *UK design and construction practice*

The uplift capacity of transmission tower footings in the UK is calculated using the frustum method. This method assumes that there is no transfer of tensile resistance from the soil on the founding plane to the base of the footing and that a breakaway condition exits.

The design uplift resistance of a footing is derived from the footing mass (Wf) and the soil mass (Wf), contained within an inverted frustum extending to the surface from the base of the footing. The geometry of the frustum is governed by the in-situ soil properties. In accordance with TS 3.4.15 Issue 2 (National Grid 2004) in 'strong' soils (SPTN>20 or su>50 kN/m2) the angle of the failure plane to the vertical (frustum angle) is 25o. In all other cases the frustum angle is set to 15o.

The serviceability limit state (SLS) displacement criterion of shallow foundations is considered to be approximately 10% of footing width (B). However the serviceability displacement criterion of individual tower footings is very low to prevent buckling failure of the tower support structure members. Both the UK (National Grid 2004) and the United States (IEEE 2001) design codes set minimal SLS vertical footing displacements (w) regardless of footing size – 10mm and 13mm (0.5") respectively. These values are based on the assumption that the lattice tower has enough flexibility to redistribute load as a result of these maximal differential movements but will weaken considerably thereafter.

A truncated pyramid base with an inclined chimney is the most common footing type for lattice transmission towers in the UK. The chimney is constructed from steel reinforced concrete with the reinforcement extending into the base of the pyramid;

the pyramid is constructed of mass concrete. The footing is cast inside a large excavation which is typically backfilled using the excavated or imported material. In each case, the embedment (H) to width (B) ratio is typically between 1 and 1.5.

1.2 *Uplift resistance of footings*

It is conventional to express the uplift capacity (Q_u) of a footing as:

$$Q = W_f + q_0 B^2 \quad (1)$$

where

$$q_0 = N_{uc} s_u + \gamma H N_{us} \quad (2)$$

The contributions from any base tension and backfill are represented in Eq. 2 in the form of reverse bearing capacity factors N_{uc} and N_{us}, respectively. The value of N_{us} may be quantified by a number of back analysed failure surfaces (e.g. Murray and Geddes 1987) or through the use of design charts derived from parametric numerical analysis (e.g. Merifield and Sloan 2006).

Early physical testing at quasi static uplift rates investigated the variation N_{uc} with embedment ratio (H/B). There are therefore many solutions available (e.g. Rao and Datta 2001). However more recent centrifuge studies have shown that N_{uc} is also dependent on uplift rate (v_f) (Lehane et al. 2008). Under rapid loading (v_f = 30mm/s) it was found that a single footing founded on kaolin clay generated more than twice the capacity in comparison to a slow uplift rate (v_f = 0.3mm/s). The difference in uplift capacities between v_f = 0.1mm/s and v_f = 30mm/s was proportional to the reduction of pore water pressure below the footing base (Lehane et al. 2008). It was proposed that the slow uplift rate allowed suction relief to occur due to the gradual base/soil separation during uplift. This is sufficient to relieve suctions and at approximately w/B≥6% residual capacity was equivalent to a full breakaway condition.

At very fast uplift rates (v_f > 30mm/s) base separation does not occur due to the full development of suctions that eventually cause a reverse bearing failure to occur in the clay. This type of failure results in a clay wedge remaining adhered to the footing base post-pullout and capacity is determined by the undrained shear strength of the clay (fully bonded).

2 FIELD TESTS

The aim of the field tests was to reduce the uncertainty surrounding the in situ performance of transmission tower footings. Reduced scale physical model tests conducted in a geotechnical centrifuge demonstrated that during continuous pullout out at increasing velocities that uplift capacity may be significantly enhanced due to the development of suctions occurring across the footing base. It was shown that uplift capacity had a log linear relationship with the uplift velocity (Lehane et al. 2008). The source of this contribution was the formation of negative pore water pressures on the footing base. However it is only at field scale that these effects can examined and quantified in the context of realistic in situ soil conditions and construction variabilities associated with full scale footings..

To examine these issues a series of full scale tests were commissioned at the Building Research Establishment's London Clay test site at Chattenden, Kent (OS ref: TQ 75521 73987). The field tests aimed to bridge understanding of the load-displacement, load-rate and suction behaviour of soils from small scale and numerical modelling to field scale. By using different construction backfill materials to replicate as-built construction practices, uplift rate and base interfaces across five L4M tower type footings (Footings 1-5) that different uplift mechanisms at full scale could be revealed.

2.1 *Site layout*

Five L4M footings were constructed at the Chattenden site in August 2010. The footing geometry used is shown in Figure 1. The footings were designed and constructed to TS 3.4.15 Issue 2 (National Grid 2004). The design uplift resistance (Q_{des}) of the footings using TS 3.4.15 was 420kN based on a 25^o frustum angle as s_u>50 kN/m^3 on the founding plane (Butcher et al. 2009).

Each footing was installed with different base contact conditions and backfill material (see Figure 1.). These variables allowed the contribution of each resistance mechanism to be isolated. Footings 1 and 2 were backfilled with tumbled and compacted London clay – representing field/early construction practices. Footings 3-4 used DoT Type 2 backfill - a coarse granular material from recycled aggregate (Depart of Transport 2009). All footings were directly cast on the underlying clay apart from Footing 3, which had a Type 2 free drainage layer.

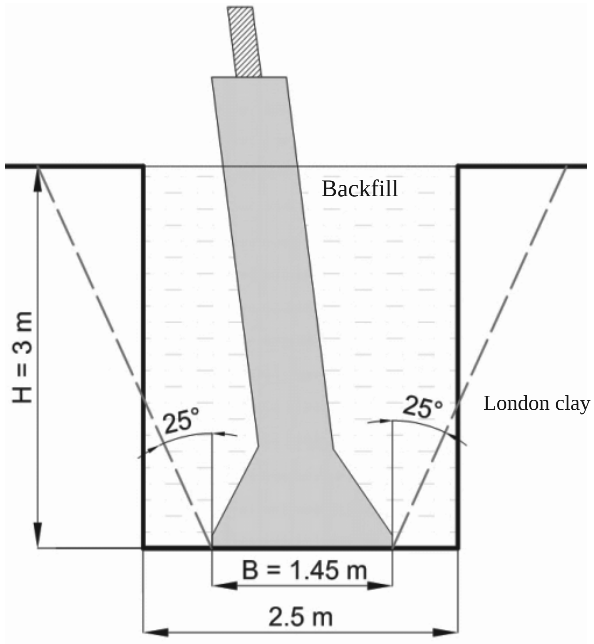

Figure 1. L4M footing with a 25^o frustum

Table 1. Footing specifications

Footing	*Backfill*	*Base*
1	Loose London clay	London clay
2	Dense London clay	London clay
3	Type 2	Type 2
4	Type 2	London clay
5	Type 2	London clay

2.2 *Ground conditions*

The Chattenden site has been used extensively for foundation testing due to the presence of the deep and uniform London clay strata (e.g. Butcher et al. 2009). The depth of the London clay strata is ~30m and it was evident that during the construction of the footings that the top 3m was heavily weathered and fissured. The foundation tests were conducted over a two week period in July 2012. The extremely wet summer of 2012, particularly in the weeks prior to the field tests resulted in the top layer of weathered clay became soft (~s_u=10kPa). It was also evident that the excavations backfilled with granular material were fully saturated leading to extreme softening (swelling) of the clay in the base of the excavations.

A total of five ~10m deep CPTs were used to characterise the site and backfill. Using a N_{kt} = 20 (Butcher et al. 2009) the variation of s_u and density (γ) of the London clay below 3m (the founding plane) corroborates with previous observations. A profile from Footing 5 is shown in Figure 2.

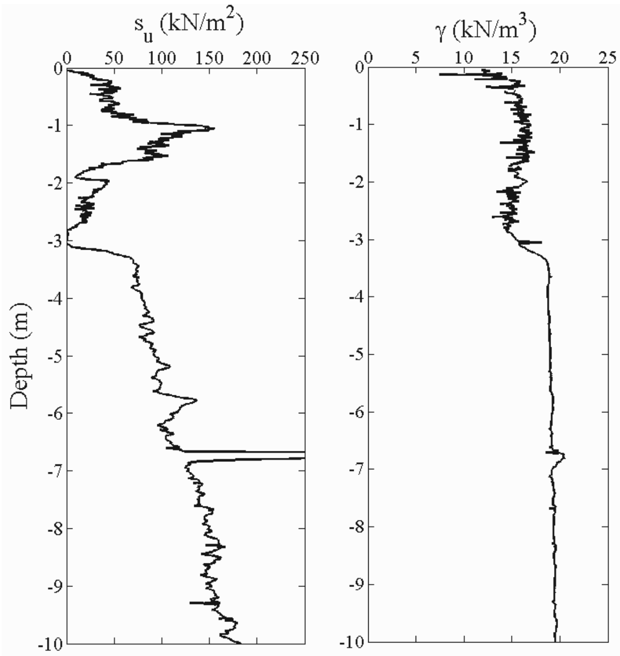

Figure 2. CPT profile of Footing 5

2.3 *Load schedule*

The footings tests were carried out over a period of six working days (18th - 25th July 2012). Table 3.2 shows the order with which the tests were carried out. The small displacement tests (denoted 'A') of Footings 2 and 3 examined the rate effect at small displacements in the fully bonded and breakaway conditions. The first load test on Footing 4 was a design test to BS EN61773:1997 (BSI 1997).

The load was applied to the footing stubs using a hydraulic jack system. The setup of the reaction beams and jack is shown in Figure 3. The reaction beams at the base were orientated parallel to the line of the excavations and outside the failure zone of a 30^o frustum. The cross beams with the hydraulic jack were inclined so that the footings could be pulled up in line with the footing chimney. Wedges were placed under the cross beam to achieve the required rake angles. The hydraulic ram had a total stroke length of 150mm (w/B=10%).

The resistance of the footing during uplift was measured using a load cell mounted above the hydraulic jack. The displacement of the footing was measured by mounting LVDTs on a reference beam. The LVDTs were vertically orientated and recorded the movement from the head of the chimney. The data from the instrumentation was acquired using a Campbell CR5000 data logger sampling at 10-100s/s.

3 FIELD TEST RESULTS

3.1 *Load-displacement behavior*

The load-displacement profiles of the tests conducted with a London clay base displayed an extremely stiff response (see Test 1-A and 5-A.

The loading rates during the first few millimetres of movement was in the range 276 kN/mm (Test 2-A) – 333 kN/mm (Test 1-A). The peak capacities of the footings were achieved between w/B = 2.1 - 4.7% versus the secondary test which were generally in excess of 7%. Although the Tests 1-A, 2-A and 5-A were conducted at different uplift velocities this did not affect uplift capacity. The measured uplift capacities were similar for both tests (<10% difference) during the first 10mm of uplift and at peak there is a difference of 50 kN versus Test 1-A and 5-A.

Test 3-A was used to examine the difference that base contact conditions at small displacements would have. Although the test did not reach its peak the stiffness response is comparable with Footing 2-A. This implies that the base condition contribution was similar to the footings tested on London clay and that the blinding did not fulfill its purpose of excluding suctions from uplift i.e. acted a free draining material.

Tests 3-B and 4-B indicated that the performance of Type 2 granular fill is extremely poor and could only mobilise ~50% of Q_{des} at w=10mm. Large displacements were required for the granular fill to mobilise sufficient strength to produce uplift capacities equivalent to Q_{des} (w = 60mm Test 3-B and w = 80mm Test 4-B). It should be noted on Test 5-A reached Q_{des} within a 10mm displacement.

Figure 3. Field test arrangement

Table 2. Load schedule

Footing	*Test*	*w (mm)*	*v_f (mm/s)*
1	1-A	150	35
2	2-A	15	5
2	2-B	150	15
3	3-A	15	15
3	3-B	150	10
4	4-A	BS EN61773:1997	
4	4-B	150	15
5	5-A	150	35

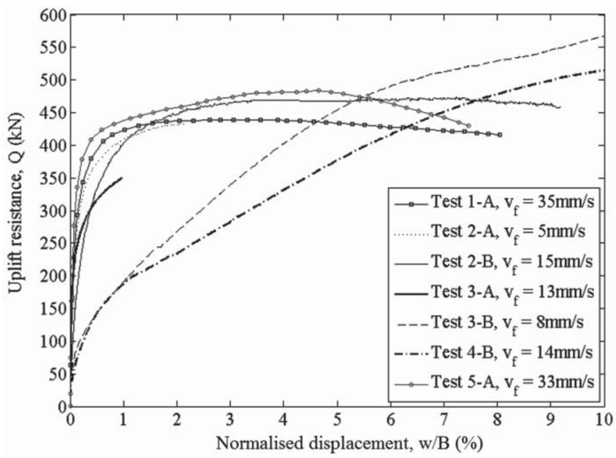

Figure 4. Load-displacement results for rapid uplift footings

3.2 *Suction*

In previous studies (e.g. Lehane et al. 2008) the degree of uplift capacity enhancement may be estimated as the difference between the suction and breakaway uplift resistances (Eq. 3). When the uplift capacities are evaluated using the slope method (BSI 1997) the average enhancement due to suction is 325 kN. This is equivalent to a pore water pressure drop of 155 kPa from hydrostatic. The magnitude of pore water pressure drop is similar to the values of pore water pressure measurements observed during undrained uplift of model footings (Lehane et al. 2008).

$$N_{uc} = (Q - Q_{br})/s_u B^2 \tag{3}$$

The effects of suction may be presented using a normalised velocity ($V = v_f B/c_v$) where c_v is the coefficient of consolidation of the underlying London clay (0.24, Skempton and Henkel 1957). The results from Lehane et al. (2008) are presented in this manner against the undrained bearing coefficient N_{uc}. Q_{br} was defined as the average uplift capacity values for second tests on Footing 3 and 4 using the slope method with Q the uplift resistance of the remainder.

Figure 5. shows the similarity between the results of the model tests at v_f = 30 mm/s and the field tests results on London clay. The range of N_{uc} of the tests on London clay is between 3.3 - 3.9 compared to 3.7 – 4.1 for v_f = 30 mm/s. The data point at N_{uc} = 1.9 corresponds to Test 3-A, which did not reach peak but evidently mobilised a degree of suction.

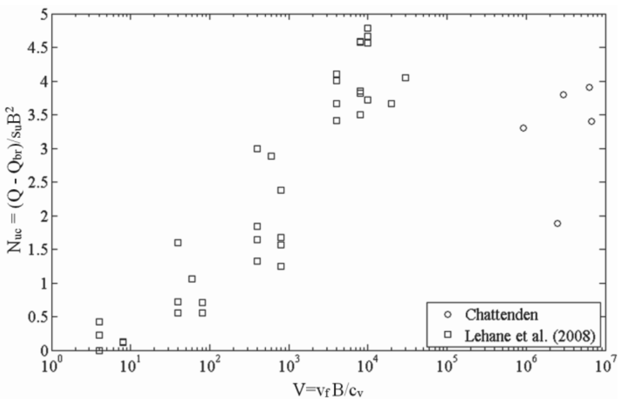

Figure 5. N_{uc} from tests on transmission tower footings

4 CONCLUSIONS

The series of field tests on a number of full scale L4M footings has confirmed that base suction may contribute significantly to footing performance. Preliminary analysis has shown that the magnitude of suction developed is similar to that observed in physical model tests conducted in a centrifuge.

The results have also shown that the design uplift performance is not reached (in general) before the ultimate limit state displacement criterion set by UK design guidance. This includes the performance of footings were suction developed. In the case where suctions did not develop, the uplift performance of the footings was extremely poor. Such a poor performance will require a re-evaluation of the use coarse granular material, specifically Type 2, when used in excavations bounded by London clay.

5 ACKNOWLEDGMENTS

The authors wish to thank National Grid UK for the financial support required to conduct the field tests. The authors gratefully acknowledge the work of Grid Line Foundations Ltd, Andrew Hewitt of Lankelma and PMC.

6 REFERENCES

BSI 1997. *Overhead lines - Testing of foundations for structures, BS EN 61773:1997*, London.

Butcher, A.P. et al. 2009. Comparison of behaviour of CFA piles in London clay as determined by static, dynamic and rapid testing methods. In *5th International Symposium on Deep Foundations on Bored and Auger Piles*. London, 205–212.

Depart of Transport, 2009. *MCHW Volume 1 SHW: Roads pavements - Unbound cement and other hydraulically bound mixtures*. London

IEEE, 2001 *Guide for transmission structures: Foundation design and testing, IEEE Std 691-2001*, New York.

Lehane, B.M., Gaudine C., Richards, D.J. and Rattley, M.J. 2008. Rate effects on the vertical uplift capacity of footings founded in clay. *Géotechnique* 58(1), 13–21.

Merifield, R.S. and Sloan, S.W. 2006. The ultimate pullout capacity of anchors in frictional soil. *Canadian Geotechnical Journal* 43(8), 852–868.

Murray, E.J. and Geddes, J.D. 1987. Uplift of anchor plates in sand. *Journal Of Geotechnical Engineering* 113(3), 202–215.

National Grid 2004. *Overhead line support foundations, TS 3.4.15 Issue 2*. Warwick, UK.

Rao, N.S. and Datta, M. 2001. A comparison of uplift and bearing behaviour of plate anchors in soft clay. In *Eleventh International Symposium Offshore and Polar Engineering Conference*. Stavanger. 560-565.

Skempton, A.W. and Henkel, D.J. 1957. Tests on London clay from deep borings at Paddington, Victoria and the South Bank. In *Proceedings of the 4th International Conference on Soil Mechanics and Foundation Engineering*. London, 100–106.

Characteristics Values in Rock Socket Design

Valeurs caractéristiques d'ancrage sur roche

Look B., Lacey D.
Sinclair Knight Merz Pty Ltd, Australia

ABSTRACT: The substructure of the Gateway Bridge comprises 1.5 metre diameter bored piers socketed into sedimentary rock. Characterisation of the rock strength properties, through goodness-of-fit tests, showed the use of non-normal distributions produced realistic characteristic strengths, while comparable predictions based on a Normal distribution showed unrealistically low values existed below the 20th percentile reliability. Since limit state codes imply characteristic design strengths should be derived from conservative (low) percentile values, erroneous characteristic strength values may be produced due to an assumption of a Normal distribution. Two land based test piles fitted with Osterberg cells tested the sedimentary bedrock for shaft capacity at the bridge site, and "Characteristic" rock strengths required by various rock socket design methods to replicate observed pile shaft capacity have been back-calculated. This paper assumes that all considered design methods are equally "correct", and compares the required design values (the selection of which are often subjective) to their relative location within the applied strength profile distributions.

RÉSUMÉ : L'infrastructure du pont "Gateway Bridge" a des piliers forés de 1,5 mètre de diamètre ancrés dans de la roche sédimentaire. La caractérisation des propriétés de résistance de la roche, faîte par le biais de test d'ajustement, a montré que l'utilisation de loi non-normale a produit des caractéristiques de résistance plausibles alors que des prédictions comparables basées sur une loi normale pouvaient devenir artificiellement basses pour un degré de probabilité au 20ième centile. Certaines normes d' états limites suggèrent que les caractéristiques de résistance devraient être dérivées à partir de valeurs (au bas mot) de bas centile, des valeurs de caractéristiques de résistance erronées pouvant être calculées en assumant une loi normale. Deux piliers tests installés sur terre-sèche avec des cellules d'Osterberg ont été utilisés pour tester la capacité de la roche sédimentaire par rapport au pilier mais les valeurs de résistance caractéristique de roche nécessitées par les diverses conceptions d'ancrage sur roche ont été rétro-calculées afin de reproduire la capacité observée des piliers. Cet article assume que toutes les méthodes de conception considérées sont tout aussi "correctes" et dérive les valeurs caractéristiques de conception requises (la sélection desquels est souvent subjective) afin de reproduire les capacités observées des piliers durant des tests à grande échelle.

KEYWORDS: Rock socket, bored piles, characteristic design value, statistical distribution, Osterberg pile tests, sedimentary rocks

1 INTRODUCTION

The Gateway Upgrade Project (GUP) was the largest road and bridge infrastructure project ever undertaken in Queensland, Australia. The six lane bridge structure spans 1.6 km between abutments with a main river span structure of 520 metres. This paper focuses on rock socket design procedures applied to two large-scale, land-based pile load tests conducted for this project.

The rock founding conditions varied across the bridge footprint as summarised in Table 1. Characterisation of rock strength properties included the derivation of site-specific correlation of Point Load Index ($I_{s(50)}$) data with Uniaxial Compressive Strength (UCS) test results, and a statistical analysis of resulting datasets.

The two test piles (TP1 and TP2) installed with Osterberg Cells were constructed to investigate the rock socket behaviour under high loads and identify any constructability issues prior to construction of the two river piers. This paper considers various accepted methods of pile rock socket design and compares their applicability to the load tests completed at this site.

Rock socket design methods typically have similar formulations for the estimation of side shear capacity, but produce varying results due to their method of derivation, and the available data or tested rock types used for formulation. While the rock type may be a governing factor, this paper assumes that all the methods produce "correct" pile designs, but require varying "characteristic" design input values to produce equivalent results. Reliability theory implies a moderately conservative or cautious estimate should be used as the characteristic design value, yet without a statistical basis the selection of appropriate characteristic values remains subjective.

Table 1. Background Data

Location / Pier	No. of Bored Piers	Key Geological Issue within Rock Founding Layers
Land 5 – Southern	10 (+ TP1)	Dipping Coal seam layer within zone of influence of pier.
River 6	24	Random Shear zones with varying length of piles
River 7	24	
Land 8 – Northern	10 (+ TP2)	Uncertain and inconsistent data with possible weak zones

1.1 *Background*

Whilst driven piles were used extensively across the GUP site, the river span of the Gateway Bridge is founded upon 1.5 metre diameter bored piers socketed into sedimentary rock. Piers 5 and 8 are located on the riverbank while Piers 6 and 7 are located within the river. River piers consisted of 24 piles that extended to a depth of over 50m below the river level, and each of the land based piers consisted of only 10 bored piers. Day et. al. (2009) provides further GUP foundation and project details.

For the bridge foundation the key geological features were:

- The basement rock consisted of Triassic aged material. This includes layers of sandstone, siltstone, mudstone and low grade coal formed about 220 to 180 million years ago. This material does not have any significant folding, but is known to have faulting as a consequence of crustal tension in the Tertiary period.
- Deposition of Quaternary Alluvium occurred in the recent past. This site is located close to the mouth of the

Brisbane River and generally has Holocene (young) overlying the Pleistocene (older) Alluvium.

2 STATISTICAL ANALYSIS OF DATA

Look and Wijeyakulasuriya (2009) carried out a statistical review of the intact rock strength data at Piers 6 and 7 for the sub-horizontally interbedded sedimentary layers at the GUP site, and defined Point Load Index ($I_{s(50)}$):UCS ratios of 40 and 25 for diametral and axial orientated $I_{s(50)}$ tests respectively. This highlighted the need to account for strength anisotropy in the rock socket design, due to the radial normal stresses on the socket wall. Via use of goodness-of-fit tests, Look et. al. (2004, 2009) has demonstrated that the use of non-normal distribution functions for describing rock strength datasets produces more realistic characteristic strength values than comparable values based on assumption of a Normal distribution. Use of a Normal distribution was reported to produce unrealistically low, or even negative, values at low percentile values of the rock strength.

Figure 1 compares the best fit distribution (Log-logistic) with the better known Log-normal and Normal distributions for all Pier 6 diametrally orientated $I_{s(50)}$ values completed in the interbedded sandstone layer (n = 330). The Log-normal distribution, while not the best fit, is observed to provide a much closer fit to the dataset than the Normal distribution does.

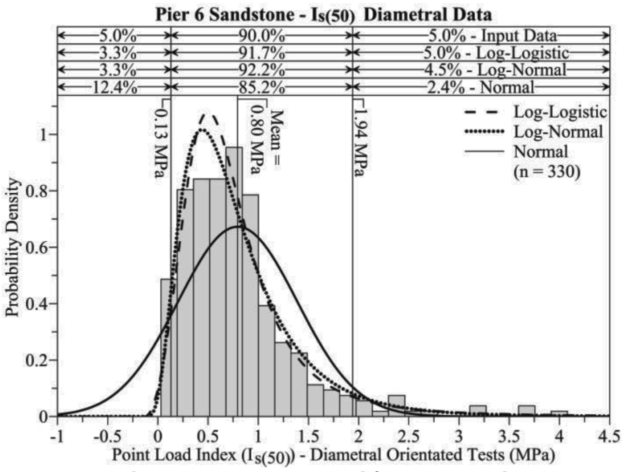

Figure 1. Distribution Functions compared for Pier 6 $I_{s(50)}$ data (n = 330)

2.1 *Characterisation of rock strength*

The test piles, TP1 and TP2, were completed upon the south and north riverbank respectively (~600m apart). TP1 was located approximately 160m from the location of Pier 6. Strength data was compiled by conversion of $I_{s(50)}$ values of tests completed along of the length of the instrumented pile to equivalent UCS values via use of the site calibrated conversion ratios of 25 and 40. Figure 2 compares statistical distribution functions fitted to the equivalent UCS strength results applicable TP2. Similar distribution fitting was also completed independently for TP1.

Tests related to TP2's rock socket indicated the presence of higher strength sandstone layers than encountered in TP1, which illustrated the localised material variation within the geological sequences that existed below the bridge footprint.

Both non-normal and Normal distribution functions were fitted to each test pile's strength dataset through application of the Anderson-Darling goodness-of-fit test. The resultant UCS values for selected fractiles of the fitted non-normal and Normal distributions are detailed in Table 2 for each test pile. At low percentile values (TP1 ≤ 15th percentile; TP2 ≤ 10th percentile), the use of a Normal distribution function would output a negative "characteristic" design value. This supports the assertion that a non-normal distribution is most appropriate for use in characterising rock strength data for this site.

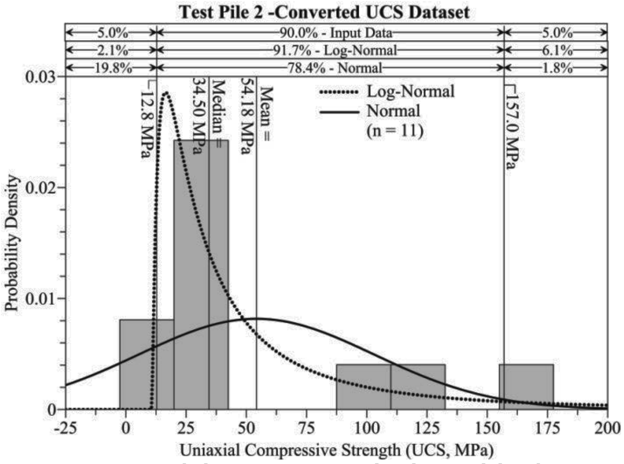

Figure 2. TP2 strength dataset – Log-normal and Normal distributions

Table 2 also shows the localized variation in rock strength for the interbedded sandstone layer. Numerical similarity is not apparent between TP1 and TP2, and the comparatively low number of strength tests available for each test pile should also be noted. Pier 6 can be considered geologically similar to TP1, in both strength data and as both were logged as having deep alluvium overlying rock. If a single characteristic rock strength value was selected to represent the entire GUP site, the location of the value upon the derived strength profiles would vary. If, arbitrarily, 10MPa was selected as the design characteristic rock strength, this could represent either the 40th or 30th percentile, depending on the distribution applied to the TP1 dataset, or either the 5th or 20th percentile for the TP2 rock strength data.

The data presented herein demonstrates that the choice of distribution function used to define such fractiles plays a critical role in the calculated design value, especially within the lower percentiles (below the 20th percentile). As the shear capacity of a rock socket is largely defined by the design rock strength, the selection of the distribution function applied to calculate the characteristic strength value can thus potentially have a large impact upon the resulting pile design and the required length of rock socket to withstand the design load.

Table 2. Test Piles UCS distribution

Distribution	Percentile	UCS (MPa)		
		TP1 $n = 8^+$	Pier 6 $n = 330^*$	TP2 $n = 11^+$
Normal	10%	-11.5	0.9	-8.4
	25%	9.2	9.9	21.2
	Median (50%)	32.1	19.9	54.2
	75%	55	29.9	87.1
Non-normal	10%	4.3	5.9	15.8
	25%	7.2	10.0	21.3
	Median (50%)	14.4	16.4	34.3
	75%	35.2	25.8	63.2

+Over length of Pile Shaft; *in equivalent interbedded sandstone layers

Approximate "equivalency" between the non-normal and Normal distributions occurs at the 25th percentile. Thus, if the inconsistencies associated with use of inappropriate distribution functions are to be minimised then the adopted design UCS value should be close to, or at, this fractile.

2.2 *Full Scale Load Tests*

Osterberg Cell (O-Cell™) data was recorded during cyclical loading / unloading of the two 1.2m diameter test piles. The rock socket of both test piles consisted of slightly weathered, medium to high strength, Triassic aged sedimentary rock (interbedded layers of mudstone, sandstone and siltstone).

In both TP1 and TP2 the shaft resistance of the section of rock socket existing between the level of the installed Osterberg Cell and pile tip was observed to have become fully mobilised during the application of a peak load (up to 56.6MN, approximately 3.1 times the expected SLS load).

The maximum shaft capacity of the 2.66m length of shaft that existed below the installed Osterberg Cell of TP1 was calculated to be 17.55MN, with a residual value of 16.4MN. The residual value represented a 7% decrease from the maximum observed value. Similarly, the peak shaft capacity of the 5.24m length of TP2 between the Osterberg Cell and pile tip was determined to be 29.2MN.

3 ROCK SOCKET DESIGN PROCEDURES

Early work for rock socket design occurred in Australia by Williams, Johnston and Donald (1980) who examined non-linear pile design in Melbourne Mudstones, and Rowe and Pells (1980) who calibrated elastic pile design with Sydney Sandstones and Shales. Horvath and Kenny (1979) undertook similar field and laboratory testing on mudstones in Canada while Meigh and Wolshi (1979) conducted comparable work in Europe. Side slip design was subsequently detailed by Rowe and Armitage (1987).

Kulhawy and Phoon (1993) showed the discontinuity in shaft friction between clays and various soft rocks (shales, mudstones and limestone). Seidel and Haberfield (1995) extended that work to demonstrate that rock socket performance is highly dependent on shaft roughness and socket diameter; whereby pile shaft friction reduces as the pile diameter increases.

Generally, rock socket design is governed by serviceability conditions rather than ultimate load conditions, and the load – deformation behaviour of the rock sockets are determined largely by the rockmass deformation properties. The rockmass modulus (E_m) value can be estimated from the modulus of intact rock (E_i) reduced for the frequency of rock defects. Relevant theory is discussed by Zhang (2004).

Various pile rock socket design procedures are now available which frequently calculate the design shaft capacity based on correlation with a “characteristic” compressive rock strength (q_{uc}) value. A good summary of the shaft shear capacity equations derived by design method researcher is provided in Kulhawy et al. (2005). Gannon et al. (1999) described four of these methods and showed, even when adopting consistent rock properties for design, the resulting design pile socket shear capacities ranged widely. The longest pile socket lengths for the example provided were predicted by the Carter and Kulhawy (1988) design method, while the Rowe and Armitage (1987) and Williams et al. (1980) procedures reduced the socket lengths by 40-60%.

This paper aimed to provide guidance on two key questions:

- Which rock socket design method should be used?
- What characteristic rock strength value should be selected (and does the selected method alter the required value)?

Ng et al. (2001) showed that the correlations presented by Rowe and Armitage (1987) and Hovarth et al. (1983) are applicable for sedimentary and volcanic rocks respectively.

Table 3. Unit side resistance formulas for considered rock socket pile design methodologies, normalised with atmospheric pressure (p_a)

Design Method	Normalised Unit Side Resistance Equation	
Hovarth and Kenny (1979)*	$\frac{f_{su}}{p_a} = 0.65\sqrt{\frac{q_{uc}}{p_a}}$	(1)
Meigh and Wolski (1979)	$\frac{f_{su}}{p_a} = 0.55(q_{uc})^{0.6}$	(2)
Williams, Johnson and Donald (1980)	$f_{su} = \alpha\beta(q_{uc})$	(3)
Rowe and Armitage (1987)	$\frac{f_{su}}{p_a} = 1.42\sqrt{\frac{q_{uc}}{p_a}}$	(4)
Carter and Kulhawy (1988)	Lower Bound: $\frac{f_{su}}{p_a} = 0.63\sqrt{\frac{q_{uc}}{p_a}}$	(5)
	Upper Bound: $\frac{f_{su}}{p_a} = 1.42\sqrt{\frac{q_{uc}}{p_a}}$	(6)
Kulhawy and Phoon (1993)	$\frac{f_{su}}{p_a} = C\sqrt{\frac{q_{uc}}{2p_a}}$	(7)
Prakoso (2002)	$\frac{f_{su}}{p_a} = \sqrt{\frac{q_{uc}}{p_a}}$	(8)

*Also confirmed by Zhang (1999) and Reese and O’Neill (1988)

3.1 *Back-analysis of rock socket design methodologies*

By using the measured ultimate shaft frictional capacity as the basis for back-analysis, “characteristic” q_{uc} input values could be determined for each considered rock socket design method.

Table 3 details the rock socket pile design methodologies considered and the published formulae used in each to calculate dimensionless unit side resistance values (f_{su}). These values are transformed to rock socket design capacities via multiplication of the calculated f_{su} value by the surface area of the segment of the rock socket that was loaded to capacity. In this study it has been assumed that the pile socket is effectively smooth and that concrete strength does not limit the shear capacity of the pile. No factors of safety have been applied as field data is being fitted back to design equations.

Notes relevant to the formulae presented in Table 3 include:

- Eq. (3) calculates shear capacity based on both the rock strength value and a mass factor (j) which is defined as the ratio of rock mass modulus to intact rock modulus. Based on the average logged RQD values (TP1 = 70%; TP2 = 55%), a mass factor (j) of 0.33 would be appropriate for TP1 (j = 0.20 for TP2). Also, in Eq. (3) α is directly related to the adopted q_{uc}, whilst β is estimated from the j value.
- Shaft capacity values for Eq. (4) are recommended to be multiplied by a partial factor of 0.7 to ensure the probability of exceeding design settlements is lower than 30%.
- The coefficient C in Eq. (7) is based on conservatism and rock socket roughness; C = 1 provides a lower bound estimate, C = 2 for mean pile behaviour and C = 3 for upper bound estimates or for rough rock sockets.
- The approach used to derive Eq. (8) was cited by Kulhawy et al. (2005) as providing the most consistent approach in evaluation of the constructed pile load dataset.

3.2 *Back-calculation Results*

Table 4 provides a summary of the various input UCS values required to achieve the ultimate shaft capacity values observed in each test pile. These values have been back-calulated via use of the equations detailed in Table 3. The 5th percentile closest to the required UCS value has been determined for both the normal and non-normal distribution functions fitted to each test pile’s strength data (refer Table 2).

Table 4. Typical Correlations between UCS and shaft friction

Design Method Equation	TP1 – $f_{su} =$ 1.64 MPa		TP2 – $f_{su} =$ 1.48 MPa	
	UCS (MPa)	Percentile (Pearson5 / Normal)	UCS (MPa)	Percentile (Log-Normal / Normal)
Hovarth and Kenny (1979)	62.6	80% / 85%	51.2	70% / 50%
Meigh and Wolski (1979)	28.3	70% / 45%	24.0	35% / 30%
Williams, Johnson and Donald (1980)	20.5 (α = 0.1) (β = 0.8)	60% / 35%	22.8 (α = 0.1) (β = 0.65)	30% / 25%
Rowe and Armitage (1987)	13.1	60% / 30%	10.8	< 5% / 20%
Carter and Kulhawy (1988)	66.6	85% / 85%	54.5	70% / 50%
	(Lower Bound Equation)			
	13.1	50% / 30%	10.7	< 5% / 20%
	(Upper Bound Equation)			
Kulhawy and Phoon (1993)	52.9 (C = 1)	85% / 75%	43.3 (C = 1)	60% / 40%
	13.2 (C = 2)	50% / 30%	10.8 (C = 2)	< 5% / 20%
Prakoso (2002)	26.5	70% / 45%	21.6	25% / 25%

The results indicate that various researchers appear to have assumed a Normal distribution in developing shear capacity formulae, with a lower quartile to mean / median value generally adopted (20th to 50th percentiles). Higher (≥50th) percentiles were required to replicate the observed ultimate capacity values for lower bound (conservative) pile capacity formulas. As the adopted design UCS value is commonly above the point of equivalency between the Normal and non-normal distribution ($q_{uc} \cong$ 25th percentile, refer Table 2), the comparable back-calculated design strength percentiles are generally higher for the non-normal distributions.

However, the more accurate distribution function has been shown to be non-normal. Using the best fitting distribution, the derived UCS values required to replicate the shaft capacity observed in TP1 were consistently at, or above, the median value. This suggests that all considered design methodologies would, if the non-normal 50th percentile value was adopted, provide overly conservative shear capacity values for this site.

To avoid the inconsistencies associated with use of incorrect distribution functions a characteristic q_{uc} value about the 20th to 30th percentile range was previously recommended. Using this percentile range of the Normal and non-normal TP1 rock strength (UCS) datasets, or the larger Pier 6 datasets (also assumed representative of TP1), the formula provided by Rowe and Armitage (1987), and upper bound equations from Carter and Kulhawy (1988) and Kulhawy and Phoon (1993) calculate pile shaft capacities closest to those observed. In the higher strength rock profile of TP2, the capacity equations provided by Meigh and Wolski (1979) and Prakoso (2002) displayed the closest match to the observed shaft capacity when the 20th, 25th or 30th percentiles of the UCS datasets were adopted.

4 CONCLUSIONS

Statistical analysis of the available GUP rock strength data shows that if a Normal distribution is assumed for characteristic value determination, then errors may result. To minimise inconsistencies associated with the use of ill-fitting distribution functions to describe strength data, then the selection of values near the lower quartile of the UCS dataset is recommended.

Two large-scale instrumented test piles were loaded beyond shaft capacity at the GUP site. Based on this test data, the required input UCS value has been back calculated for a number of pile design methods, and the indicative strength percentile reliability of the UCS value has been determined. Five of the examined methods have produced results that match the observed shaft capacities via the adoption of a design UCS value close to the UCS lower quartile "characteristic" value.

5 ACKNOWLEDGEMENTS

Some reliability concepts were formulated while the principal author was working on this project at Connell Wagner Pty Ltd together with Vasanatha Wijeyakulasuriya of Queensland Main Roads. Fugro-Loadtest undertook the field trials discussed.

6 REFERENCES

Carter, J.P., and Kulhawy, F.H., 1988. Analysis and design of drilled shaft foundations socketed into rock. *Report EL-5918*. Palo Alto: Electric Power Research Institute, 190p.

Day, R., Johnston, I. and Yang, D. 2007. Design of Foundations to Second Gateway Bridge – Brisbane. *7th Austroads Bridge Conference*, Auckland, N.Z., 12p.

Gannon, J.A., Masterton, G.G., Wallace, W.A. & Wood, D.M. 1999. *Piled Foundation in Weak Rock (CIRIA Report No.181). C*onstruction Industry Research & Information Assoc., UK, 80p.

Horvath, R.G. and Kenney, T.C. 1979. Shaft Resistance of Rock Socketed Drilled Piers. *Proc. Symp. on Deep Foundations*, ASCE, New York, N.Y., pp. 182–214

Horvath, R.G., Kenney, T.C. and Koziki, P. 1979. Methods of improving the performance of drilled piers in weak rock. *Canadian Geotech. Journal*, 20(4), pp.758-772

Kulhawy, F.H. and Phoon, K-K. 1993. Drilled Shaft Side Resistance in Clay Soil to Rock. *Geotechnical Special Publication No. 38: Design and Performance of Deep Foundations*, pp. 172–183

Kulhawy, F.H., Prakoso, W.A., & Akbas, S.O. 2005. Evaluation of Capacity of Rock Foundation Sockets. *Proc. 40th U.S. Symp. Rock Mechanics*, G.Chen et al. (Eds.), Anchorage, Alaska, paper 05-767

Look, B.G. and Griffiths, S. 2004. Characterization of rock strengths in South East Queensland. *Proc. of the 9th Australia New Zealand Conf. in Geomechanics*, Auckland, N.Z., Vol. 1, pp.187–194

Look, B.G. and Wijeyakulasuriya, V. 2009. The statistical modelling of rock strength for reliability assessment. *17th Int. Conf. on Soil Mechanics and Foundation Eng.*, Alexandria, Vol. 1, pp.60–63

Meigh, A.C. and Wolski. W. 1979. Design parameters for weak rock. *Proc., 7th European Conf. on Soil Mechanics and Foundation Eng.*, Brighton, UK, Vol. 5, pp.59-79

Ng., C.W.W., Yau, T.L. Li, J.H. and Tang, W.H. 2001. Side resistance of large diameter bored piles socketed into decomposed rocks. *Journal of Geotech. & Geoenvir. Eng.,* ASCE 127(8), pp.642-657

Prakoso, W.A. 2002. Reliability-Based Design of Foundations on Rock for Transmission Line & Similar Structures. *PhD Thesis.* Cornell University.

Reese, L.C. and O'Neill, M.W. 1988. Drilled shafts: construction procedures and design methods. *Report FHWA-HI-88-042*. McLean: Federal Highway Administration.

Rowe, R. K. and Armitage, H. H. 1987. A design method for drilled piers in soft rock. *Canadian Geotech. Journal*, 24(1), pp.126-142.

Rowe, R.K. and Pells, P.J.N. 1980. A Theoretical Study of Pile-Rock Socket Behaviour. *Proc., Int. Conf. on Structural Foundations on Rock*, Vol. 1, Sydney, Australia, pp.253-264

Seidel J.P. and Haberfield C.M. 1995. The axial capacity of pile sockets in rocks and hard soils. *Ground Eng.*, 28(2), pp.33 – 38

Williams, A.F., Johnston, I.W. and Donald, I.B. 1980. The Design of Sockets in Weak Rock. *Proc., Int. Conf. on Structural Foundations on Rock*, Vol. 1, Sydney, Australia, pp. 327–347

Zhang, L. 1999. Analysis and design of drilled shafts in rock. *PhD Thesis*, Massachusetts Institute of Technology, Cambridge, Mass.

Zhang, L. 2004. *Drilled Shaft in Rock: Analysis and Design.* A.A. Balkema Publishers

Safety theory in geotechnical design of piled raft

Théorie sur la sécurité pour la réalisation de radier sur pieux.

Lorenzo R., Zubeldia E.H., Cunha R.P.
University of Brasilia, GPFees Geotechnical Research Group (www.geotecnia.unb.br/gpfees)

ABSTRACT: A significant amount of literature describing and discussing the behavior of piled raft foundations have been produced in the last thirty years; nevertheless, a method to introduce the safety in the design of this kind of foundation has not been established yet. Hence, they have been omitted in most Standards and Codes around the world and have been used in just few cases. Until now, the performance of piled rafts has been analyzed using a global factor-of-safety approach. The application of the Limit State Method to geotechnical designs of this kind of foundation is presented with the purpose of establishing a methodology for the calculation of the bearing capacity of piled rafts. The partial coefficients necessary to describe the safety in this method are defined for the ultimate limit state. The application of the Safety Theory and probabilistic methods in the geotechnical design is presented, as well as the mathematic formulation for its implementation in piled raft foundation. A methodology for the adjustment of partial coefficients (to be used for the method of limit states) based on probabilistic methods is proposed. The expressions for the adjustment to be used in piled raft foundations using the selected design method are finally presented.

RÉSUMÉ : Une importante partie de la littérature décrivant et examinant le comportement de radier sur pieux a été réalisée au cours des trente dernières années. Néanmoins, une méthode pour introduire la sécurité dans la conception de ce type de fondation n'a pas encore été établie. En conséquence, on remarque son oubli dans la plupart des normes et des codes dans quasiment tous les pays et on relève son utilisation dans très peu de cas. Jusqu'à présent, la sécurité du radier sur pieux a été analysée en utilisant un facteur global permettant l'approche sécuritaire. L'application de la méthode des états limites pour la conception géotechnique de ce type de fondation est présentée dans le but d'établir une méthodologie de calcul de la capacité portante du radier sur pieux. Les coefficients partiels nécessaires pour incorporer la sécurité dans cette méthode sont définis pour les états limites ultimes. L'application de la théorie basée sur la sécurité et l'utilisation des méthodes probabilistes dans la conception géotechnique sont explicitées, ainsi que les formules mathématiques pour sa mise en œuvre en ce qui concerne les radiers sur pieux. Une méthodologie pour l'ajustement des coefficients partiels (à utiliser pour la méthode des états limites) basées sur des méthodes probabilistes est proposée. Enfin, les expressions pour l'ajustement à utiliser dans le cas des radiers sur pieux, en utilisant une méthode de conception spécifique, sont obtenues.

KEYWORDS: pile raft, safety theory, limit state, probabilistic method, partial coefficient.

1 INTRODUCTION

After the publication of the Technical Committee Report TC18 of the International Society of Soil Mechanics and Geotechnical Engineering (ISSMGE) in 2001, the use of piles as settlement reducers has increased, with the corresponding design savings. Nevertheless, this kind of foundation is seldom used, because of the complexity generated by the analysis of the load transfer mechanism between the piles and the raft, and also because of the difficulty in determining the *load-settlement* curves. All this mechanisms are influenced by the interaction between the elements (raft-piles-soil) of the system. (Sales, 2000).

It´s worth adding that, despite the TC18, the lack of Design Codes for piled raft foundation (PR) in many countries has had a great influence in the slow pace incorporation of this kind of foundation in engineering projects (Ahner, Soukhov, & König, 1997).

Based on the concepts of Limit States, most of the engineering schools (and Standards) use *partial coefficients* as safety approach. Notwithstanding, this is not applied in foundation design (Quevedo 2002, Eurocode 7 2005) and let alone in deep foundations in which the *global safety factor* approach is still used in most codes and standards. Some of the disadvantages of this approach are: a) it does not explicitly take into account the material´s variability y; b) it uses nominal loads, while the structural design uses design loads, i.e. characteristic loads affected by weighting coefficients (Caneiro 2003).

The definition of a global safety factor for a PR is very difficult, because it has to involve both the raft bearing capacity and the corresponding pile group capacity. A rigorous safety analysis has to take into account the interaction of these distinct elements (raft and piles) with the incorporation of the soil.

2 CALCULATION METHODS FOR THE ULTIMATE BEARING CAPACITY

The design of any foundation has two main stages: first, the bearing capacity analysis (ultimate state) and second, the design settlement estimation (service state). This article focuses in safety studies related to the ultimate (state) stage which, according to Mandolini (2003), is the stage that generally governs the design of PRs with a raft breath between 6 to 14m.

Methods for evaluating the bearing capacity of PR are based in empirical correlations or in numerical analyses calibrated by field tests. These are very simple methods, but they can only be used in similar conditions to those where the in situ tests or instrumentation were carried out.

One of the more recent methodologies for the PR design is the one developed by Sanctis & Mandolini (2006). The authors carried out a series of numerical analyses and proposed the following equation:

$$Q_{PR} = \alpha_{UR} \cdot Q_{UR,ult} + Q_{PG,ult} \tag{1}$$

Q_{PR}, Q_{UR} and Q_{PG} are the ultimate bearing capacities of the PR, the isolated raft and the isolated pile respectively; α_{UR} is a coefficient introduced to affect the raft bearing capacity when it is considered to be working in the pile-raft system.

Numerical models were generated inducing settlements of 10% of the raft width, which are considered to be capable of mobilizing all the strength capacity of the system. The results were used to make out a numerical correlation to obtain the relation between α_{UR} and the geometry of the PR, which led to the following expression:

$$\alpha_{UR} = 1 - 3\left(\frac{A_G}{A} \bigg/ \frac{s}{d}\right) \tag{2}$$

where A_G is the area enclosed by the piles; A is the raft area; s and d are the pile spacing and diameter respectively.

3 APPLICATION OF THE LIMITE STATE METHOD (LEM) TO THE PILED RAFT FOUNDATION DESIGN

The application of the Limit State Method (LEM) to the PR design to be described in this article is based on a design in which the piles behave as floating piles under ultimate or limiting capacity. It is one of the options that generate the greatest efficiency of the system, because it considers the piles working at their ultimate creep stages (Randolph 1994). This forces an analysis of the PR rather as a system than as independent elements, since the piles will be working at their ultimate stages and will consequently not satisfy any of the safety criteria established in pile design codes. Off course this obliges the contribution of the raft into design. Also, the safety coefficient of the mechanical characteristics of the soil can be applied to the mean values, as suggested by Quevedo (2002).
Figure 1 shows how LEM concepts are introduced in the PR design. The resisting loads function Y_2 is determined as the sum of the raft average bearing capacity plus the respective one of the pile group, as shown by the following equation:

$$Y_2 = Y_{2,PG} + Y_{2,R} \tag{3}$$

where $Y_{2,R}$ and $Y_{2,PG}$ are the raft and piles bearing capacity, respectively, calculated with average values of soil properties.
The design load function of each element of the system can be obtained from the following equations:

$$Y^*_{2,R} = \frac{Y_{2,R}}{\gamma_{g,R}}, \; Y^*_{2,PG} = \frac{Y_{2,PG}}{\gamma_{g,PG}} \tag{4}$$

where $Y^*_{2,R}$ and $Y^*_{2,PG}$ are raft and the pile´s resistant loads, respectively. They can be calculated from the design values of the soil mechanical properties.
By mean of the former definitions and Figure 1 it is possible to obtain the design equation for the ultimate limit state of a PR.

$$P^* \le \frac{Q^*_{PR}}{\gamma_S} \tag{5}$$

where P^* is the overall vertical design load; γ_S is a partial coefficient that considers the quality of the construction and the type of failure; Q^*_{PR} is the design load capacity of the PR obtained from equation 6.

$$Q^*_{PR} = \alpha_{UR} \cdot Q^*_{UR} + Q^*_{PG} \tag{6}$$

where Q^*_{UR} and Q^*_{PG} are the raft and the piles design bearing capacity respectively, calculated separately from the soil design values.
The overall vertical design load can be obtained as a sum of the individual characteristic load weighted by a particular coefficient, as shown in the following equation:

$$P^* = \sum\left(P_{ki} \cdot \gamma_{fi}\right) \tag{7}$$

where P_{ki} is the characteristic loads and γ_{fi} are the weighting coefficients for the loads.

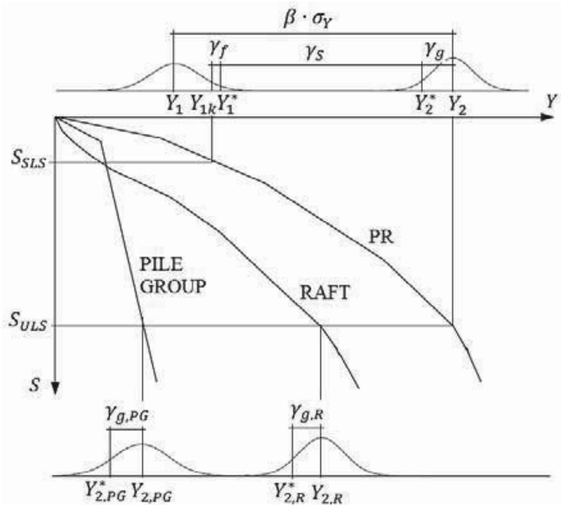

Figure 1. Introduction of safety by the LEM in PR (Lorenzo 2010)

In this article, the resistant load function and its design values are obtained in a manner that differs from the way they are normally obtained in structural analyses. As suggested by Quevedo (1987), Becker 1996), Gonzalez-Cueto (2000) and Lima (2006), the soil properties coefficients are applied directly to the mean values, while in structural design they are applied to the characteristics values.
The design soil properties are calculated from values obtained from the statistical processing of laboratory tests results, weighting them by partial coefficients, as shown in equations 8, 9 and 10.

$$\phi^* = \tan^{-1}\left(\frac{\tan\phi}{\gamma_{gtg\phi}}\right) \tag{8}$$

$$C^* = \frac{C}{\gamma_{gC}} \tag{9}$$

$$\gamma^* = \frac{\gamma}{\gamma_{g\gamma}} \tag{10}$$

where ϕ, C and γ are the mean values of the soil internal friction angle, cohesion and specific weigh, respectively; and $\gamma_{gtg\phi}$, γ_{gC}, $\gamma_{g\gamma}$ are the partial safety coefficients that affect each soil property.

4 APLICATION OF SAFETY THEORY TO THE GEOTECHNICAL DESIGN OF PRF

By means of probabilistic methods it is possible to calibrate the partial safety coefficients to be used in the LEM. This approach has not yet been introduced in the design codes. Consequently, the loads and resistance partial coefficients have not been establish as well. Nevertheless, the necessary expressions for the calibration of partial coefficients to use in the LEM can be developed by means of the general procedure described in Quevedo (1987). This author applied the procedure to the design of shallow foundations in cohesive soils and

subsequently, Gonzalez-Cueto (2000) applied it to the design of shallow foundations in frictional soils. Lima (2006) used the approach in the design of drilled caisson's foundation and anchorages.
The procedure to calibrate the weighting coefficients by this methodology requires the calculation of the global safety factor ($F_{s,d}$) and the optimal safety factor. The global safety factor is associated with the partial coefficients introduced in the design by the LEM. The optimal safety factor is determined with the application of the probabilistic methods.

1.1 *Global Design Safety Factor*

The weighting coefficient that are applied to adjust the soil specific weight and the mechanical properties of the soil can be respectively calculated from equations 12 and 13.

$$\gamma_{gi} = \frac{1}{1 - \frac{t_\alpha v_i}{\sqrt{n_i}}} \tag{12}$$

$$\gamma_{gi} = \frac{1}{1 - t_\alpha v_i} \tag{13}$$

Where t_α is the t-student function value for α = 0.95 at n-1 degrees of freedom; v_i is the coefficient of variation of the *i* soil property; n_i is the amount of repetitions of the test where the *i* soil property was obtained.
The partial safety coefficient of the resistant loads can be obtained from the following equation:

$$\gamma_g = \frac{Q_{PR,ult}}{Q_{PR}^*} \tag{14}$$

Where γ_g is the aforementioned coefficient.

In order to calculate $Q_{PR,ult}$ and Q^*_{PR} Equations 1 and 6 can be used, respectively.

The weighting coefficients of the loads can be calculated from equation 15.

$$\gamma_f = \frac{\sum P_{ki} \cdot \gamma_{fi}}{\sum P_{ki}\left(1 - t_\alpha \cdot v_i\right)} \tag{15}$$

Finally, the global design safety factor can be obtained as:

$$F_{s,d} = \gamma_f \cdot \gamma_g \cdot \gamma_s \tag{16}$$

1.2 *Optimal Safety Factor*

In order to obtain the optimal safety factor $\left(F_{s,o}\right)$ it is necessary to deal with equations that are more complex than those used to obtain the global safety factor. The load function (Y_1) and the resistant capacity function $\left(Y_2\right)$ can be defined by the following equations:

$$Y_1 = P \tag{17}$$

$$Y_2 = Q_{PR,ult} \tag{18}$$

Where *P* is the mean value of the loads.
In the design of a PR, the required safety level $\left(H_{req}\right)$ is related to the $F_{s,o}$ by means of the equation 19.

$$H_{req} = 0.5 + \phi_n\left[\frac{F_s - 1}{\sqrt{v_P^2 + F^2{}_S \cdot v_{QPR,ult}^2}}\right] \tag{19}$$

Where ϕ_n is the error function, v_P and $v_{Q_{PR,ult}}$ the coefficient of variation of the loads and the ultimate bearing capacity, respectively.

As v_P and $v_{Q_{PR,ult}}$ are unknown, they can be expressed as:

$$v_P = \frac{\sigma_P}{P} \tag{20}$$

$$v_{Q_{PR,ult}} = \frac{\sigma_{PR,ult}}{Q_{PR,ult}} \tag{21}$$

where σ_P and $\sigma_{Q_{PR,ult}}$ are the standard deviation of the total vertical load and the ultimate bearing capacity of the PR, respectively.
Taking into account that the total load is the result of the sum of independent loads, which are values that represent random variables, the standard deviation of the total vertical load can be obtained as the sum of the standard deviation of each load, as shown by the following equation:

$$\sigma_P^2 = \sum \sigma_{Pi}^2 \tag{22}$$

where σ_{Pi} is the standard deviation of the *i* vertical load.
The bearing capacity of the PR is a function that depends on several random variables. This increases the complexity of the calculation of the standard deviation. As shown in Lorenzo (2010), it is possible to apply the Taylor`s series method where the linearization of the function is combined with application of the general theorem of standard deviation. With this, the standard deviation can be expressed by:

$$\sigma^2_{Q_{PR,ult}} = \left(\frac{\partial Q_{PR,ult}}{\partial \tan\phi}\right)^2 \sigma^2_{\tan\phi} + \left(\frac{\partial Q_{PR,ult}}{\partial C}\right)^2 \sigma_\gamma - 2\left(\frac{\partial Q_{PR,ult}}{\partial \tan\phi}\right)\left(\frac{\partial Q_{PR,ult}}{\partial C}\right)\sigma_{\tan\phi}\sigma_C r_{C\cdot\tan\phi} \tag{23}$$

where $r_{C\cdot\tan\phi}$ is a correlation coefficient between the cohesion and the tangent of the friction angle.
The derivatives on Equation 23 can be obtained from the bearing capacity equations presented in (CTE 2006). This leads to equations 24 to 29. In order to simplify the expressions, the depth coefficients of the bearing capacity equations are considered to be 1. This does not introduce a significant error, because the contribution of the soil above the foundation is a small percent of the total load. Equations 24 to 26 can be used in a drained type analysis. These expressions become more simple for cohesive soils in an undrained analysis, leading to equations 27 to 29, as follows.

$$\frac{\partial Q_{PR,ult}}{\partial \tan\phi} = \alpha_{UR} A\left(C \cdot S_C \frac{dN_c}{d\tan_\phi} + \gamma_1 \cdot d \cdot S_q \cdot \frac{dN_q}{d\tan\phi} + \frac{1}{2} B \cdot \gamma_2 \cdot S_\gamma \cdot \frac{dN_\gamma}{d\tan\phi}\right) + n\eta\left[A_P \cdot \sigma'_{Vp} \cdot \frac{dN_q}{d\tan\phi} + A_F \cdot \sigma'_V \cdot k \cdot f\right] \tag{24}$$

$$\frac{\partial Q_{PR,ult}}{\partial c} = \alpha_{UR} \cdot A\left[S_C \cdot N_C\right] \tag{25}$$

$$\frac{\partial Q_{PR,ult}}{\partial \gamma} = \alpha_{UR} \cdot A\left[d \cdot N_q \cdot S_q + \frac{1}{2} \cdot B \cdot S_\gamma \cdot N_\gamma\right] + n\eta\left(A_p \cdot N_q \cdot L + A_F \cdot L \cdot k \cdot f\right) \tag{26}$$

$$\frac{\partial Q_{PR,ult}}{\partial \tan\phi} = 0 \tag{27}$$

$$\frac{\partial Q_{PR,ult}}{\partial c} = 5{,}14 \cdot \alpha_{UR} \cdot A + n\eta\left[A_p \cdot F_E + A_F \cdot \frac{100C_U\left(C_U + 200\right)}{\left(C_U + 100\right)^2}\right] \tag{28}$$

$$\frac{\partial Q_{PR,ult}}{\partial \gamma} = 0 \tag{29}$$

The standard deviation of the soils properties can be expressed by equations 30 to 32.

$$\sigma_{\tan\phi} = v_{\tan\phi}.\tan\phi \tag{30}$$

$$\sigma_c = v_c.C \tag{31}$$

$$\sigma_{\gamma} = \nu_{\gamma} . \gamma \qquad (32)$$

Some reference guiding values for the coefficient of variation of the geotechnical parameters are presented in Table 1.

Table 1. Reference values of geotechnical properties of de soil.

Parameter	Coefficient of variation
Specific weigh	0.05
Tangent of friction angle	0.07
Cohesion	0.1
Shear undrained resistance	0.15

In this way, it is possible to obtain the coefficient of variation of the load (ν_p) and the ultimate bearing capacity of the PR $(\nu_{Q_{PR,ult}})$. With this and a defined safety level, the $F_{s,o}$ can be calculated. Quevedo (2002) recommended to use a safety level $H = 0{,}98$, in the geotechnical designs by the ultimate limits states. It means a failure probability of 0.02.

In order to know if the partial safety coefficients used in a specific design are appropriated, a comparison between $F_{s,o}$ and $F_{s,d}$ has to be done. Generally, the coefficients used in regular designs are conservative and they have to be calibrated to find one or more combinations that make $F_{s,o}$ equal to $F_{s,d}$.

In practice, because the variability of the load is lesser known, or measured, than the geotechnical parameters, it is better to reduce the weighting coefficient of the parameters of the soil. Also, it is easier for engineers to use the same weighted load for structures and foundations projects alike. Figure 2 shows the algorithm that resumes the method of calibration.

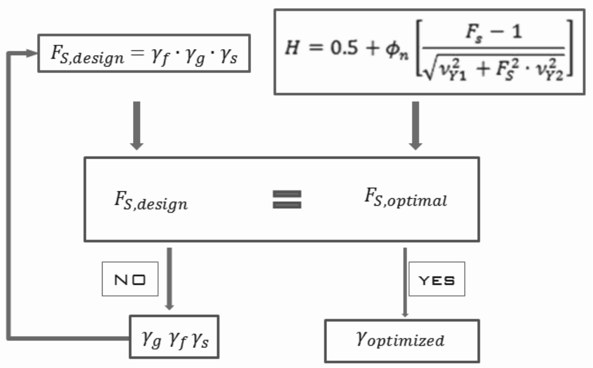

Figure 2. Algorithm for obtaining safety factors by LEM (Lorenzo 2010)

5 CONCLUSIONS

The cost of the (more) rational approach for the foundation design methods is the increase of the complexity level. Nevertheless, this cost is compensated by a proportional advantageous decrease of the execution costs. Besides, it will enhance the understanding of the design and yield a better assurance of its related variables. Thus, the use of the safety theory is the first step to obtain a more economical and rational design.

The PRF analysis approach for a foundation system leads to an effective and optimized use of its components (Cunha et al. 2001), as it allows the raft-soil contact contribution both in the overall stiffness and load capacity of the system. This analysis is a generalization of the calculation methods for determining the bearing capacities of raft and pile groups separately.

Based on the method proposed by Sanctis & Mandolini (2006), a methodology for the application of the LEM in the design of PR was established. The use of three sets of partial coefficients allow to separately consider the uncertainties introduced in the design of the materials, the loads and the working conditions.

By means of the methodology described by Quevedo (2002) it is possible to calibrate the partial safety coefficients which are necessary for the application of the LEM in the design of PRF systems. This makes it possible to better define and understand the safety level to be achieved in design.

6 ACKNOWLEDGEMENTS

The authors acknowledge the support of the National Brazilian Agency CNPq and the Geotechnical Graduation Prog. of the UnB for all related funds that allowed this particular research.

7 REFERENCES

Cunha, R.P., Poulos, H.G. and Small, J.C. (2001). “Investigation of design alternatives for a piled raft case history”. ASCE Journal of Geotechnical and Geoenvironmental Engineering, August, 127(8), pp. 635-641.

Poulos, H.G. & Davis, E.H. (1980). “Pile Foundation Analysis and Design”. John Wiley & SonsEd., New York.

Randolph, M. F. (1983). “Design of piled raft foundation”. Proc. Int. Symp. on Recent Developments in Laboratory and Field test and Analysis of Geotechnical Problems, Bangkok, pp. 525-537.

Sales, M.M. (2000). “Análise do comportamento de sapatas estaqueadas”. Tese de doutorado, Publicação GTD/0022. Universidade de Brasília-DF, pp. 229.

Carsten, A. & Dmitri, S. (1998). “Combined Piled-Raft Foundation (CBRF), Safety Concept”. Universitat Leizpig, pp. 13.

Quevedo, G. (2002). “Aplicación de los Estados Límites y la teoría de la Seguridad en el Diseño Geotécnico en Cuba”. Tesis de Doctorado en Ciencias, UCLV, Santa Clara, pp.163.

Eurocódigo 7. (2005). “Proyecto Geotécnico. Reglas generales”. European committee for standarization. Brussels, Bélgica, pp. 119.

Caneiro J. H. (2003). “Apuntes para libro Diseño de Hormigón Estructural”. Instituto Superior Politécnico José Antonio Echeverria. La Habana. Cuba.

Mandolini, A. (2003). “Design of piled raft foundations: practice and development”. Proc., Geotech. Int. Seminar Deep Foundation on Bored and Auger Piles, BAP IV, Van Impe and Haegeman, eds., pp. 59–80.

Sanctis de L. & Mandolini A., (2006). “Bearing Capacity of Piled Raft on Soft Clay Soils”. Journal of Geotech. and Geoenvironmental Eng. vol. 132, no. 12 , pp. 11.

Jiménez Salas, J.A.; Justo Alpañes, J. L.; Serrano, A. A. (1981) “Geotecnia y cimientos III : Mecánica del suelo y de las rocas.” 2da Edición. Madrid : Editorial Rueda, pp. 1188

Randolph, M.F. (1994). “Design Methods for Pile Groups and Piled Rafts”. Proc. of the 13th Inter.Conf. on Soil Mechanics and Found. Eng. New Delhi. 5, pp. 1-21.

Quevedo, G. (1987) “Aplicación del Método de los Estados Límites en el diseño de las cimentaciones superficiales”. Revista Ingeniería Estructural. 2(III), pp. 95 - 106.

González - Cueto, A. V. (2000). “Diseño Geotécnico de Cimentaciones Superficiales en Arenas.” Tesis de Doctorado, Universidad Central de Las Villas, Santa Clara, pp. 133.

Lima, R. (2006). “Diseño de cimentaciones sometidas a grandes esfuerzos de momentos y/o cortantes y axiales pequeños o de succión”. Tesis de Maestría. Univ. Central de Las Villas, pp. 99.

Becker D. E. (1996). “Eighteenth Canadian Geotechnical Colloquium: Limit States Design for Foundations”. Part I. An overview of the foundation design process.” Canadian Geotechnical Journal 33, pp. 956 – 983.

Lorenzo, R. (2010). “Diseño Geotécnico de Losas Pilotadas. Aplicación de la Teoría de Seguridad”. Tesis de Maestría. CEDEX, Madrid, pp.123.

CTE. (2006). “Código Técnico de la Edificación”. Ministerio de la Vivienda, España, 1061p.

Bored pile foundation response using seismic cone test data

Réponse des pieux à l'aide des données de piézocône sismique

Mayne P.W.
Georgia Institute of Technology, Atlanta GA USA

Woeller D.J.
ConeTec Investigations, Richmond, BC Canada

ABSTRACT: A closed-form elastic continuum solution is used to represent the upper and lower segment response of bored piles subjected to bi-directional Osterberg load testing. For geotechnical parameter input, seismic piezocone tests (SCPTu) are a most efficient and economical means because the penetrometer readings provide data for assessing the capacity of side and base components, while the shear wave velocity provides the fundamental stiffness for displacement analyses. A simple algorithm for modulus reduction is employed to allow nonlinear load-displacement-capacity behavior. A load test case study involving two levels of embedded O-cells for a large bridge in Charleston, South Carolina is presented to illustrate the approach.

RÉSUMÉ: Une solution analytique en élasticité est utilisée pour représenter la réponse des sections supérieures et inférieures de pieux forés soumis à des essais de chargement bidirectionnel Osterberg. Les essais sismiques utilisant des piézocônes (SCPTu) sont des moyens efficaces et économiques pour obtenir des paramètres géotechniques. Les mesures du pénétromètre sont généralement utilisées pour l'analyse du frottement latéral et de la capacité portante, tandis que les données de vitesse des ondes de cisaillement donnent le module de cisaillement initial lors de l'analyse des déplacements. Un algorithme simple pour la réduction du module est utilisé pour l'analyse non-linéaire du comportement charge - déplacement - capacité. Une étude de cas sur un essai de chargement Osterberg à deux niveaux effectué sur un grand pont situé à Charleston en Caroline du Nord est utilisée afin d'illustrer cette démarche.

KEYWORDS: bored piles, cone penetration, deep foundations, elastic solution, load tests, shear modulus, shear wave velocity

1 INTRODUCTION

The Osterberg load cell provides a novel alternative to conventional static load tests that either rely on large dead weight frames or anchored reaction beams. The O-cell occupies a minimal space in its setup, essentially the same space taken by the bored pile foundation itself (Osterberg 1998, 2000). In the original design, a single sacrificial hydraulic jack is situated at the pile base (O'Neill, et al. 1997). After concrete placement and curing, the jack is pressurized resulting in bi-directional loading to simultaneously mobilize end bearing downward while pushing the shaft segment upward (Fellenius, 2001). After loading, the O-cell is grouted to become part of the completed and working foundation. In fact, the O-cell can be positioned at mid-level elevations within the pile shaft to better match and optimize opposing segments. Moreover, multiple O-cells are now utilized to stage load separate pile segments and verify higher load capacities.

An elastic pile solution (Randolph and Wroth, 1978, 1979) is shown to accommodate the various O-cell configurations, as well as the more common top-down loading of bored piles. The results from seismic piezocone tests (SCPTu) are shown to be applicable for providing all the necessary input parameters to drive the computations and generate curves on the axial pile deformation response. A case study from South Carolina is used to illustrate the methodology.

2 ARTHUR RAVENEL BRIDGE

This newly-completed I-17 bridge over the Cooper River in Charleston, SC was supported by over 400 large bored pile foundations having diameters of 1.8 to 3 m and embedded lengths of between 45 to 72 m. The 4.0-km long cable-stayed concrete segmental bridge has a main span length of 471 m and connects the city of downtown Charleston with Drum Island and Mount Pleasant, replacing two old steel truss crossways known as the Pearman and Grace Memorial bridges.

In the region, all significant heavy building, port, and civil structures are founded on a deep overconsolidated formation termed the Cooper Marl that generally lies below elevations -15 to -20 m MSL (Camp, 2004). The uppermost soils consist of soft variable clays, loose sands, silts, and peats of Holocene age which are heterogeneous deposits from marine, deltaic, and alluvial origins

2.1 *Cooper Marl*

The Cooper marl is a marine deposit consisting of stiff green-gray sandy calcareous clay of Oligocene age that has been preconsolidated by erosional processes and natural cementation. The marl has a high calcite content on the order of 60 to 80 %.

Mean values of indices from laboratory tests include: w_n = 48%, w_L = 78%, and PI = 38% (Camp et al. 2002). Typical SPT-N values in the Cooper marl are between 12 and 16 blows/0.3 m. Triaxial tests consistently show high effective stress friction angles averaging $\phi' \approx 44^{\circ} \pm 3^{\circ}$. An equivalent prestress $\Delta\sigma_v' = (\sigma_p' - \sigma_{vo}')$ = 480 kPa captures the general trend of preconsolidation stress (σ_p') which increases with depth, as well as corresponding profile of overconsolidation ratio (OCR = σ_p'/σ_{vo}') that decreases with depth (Mayne 2007a).

For the bridge project, approximately 45 rotary drilled borings and 55 SCPTu soundings were completed to depths of 55 m. Two representative SCPTu soundings are presented in Figure 1. The SCPTu is a particularly efficient and economical means for site exploration as it provides five separate readings on soil response with depth, including: cone tip resistance (q_t), sleeve friction (f_s), porewater pressures (u_2), time rate of dissipation (t_{50}), and downhole-type shear wave velocity (V_s).

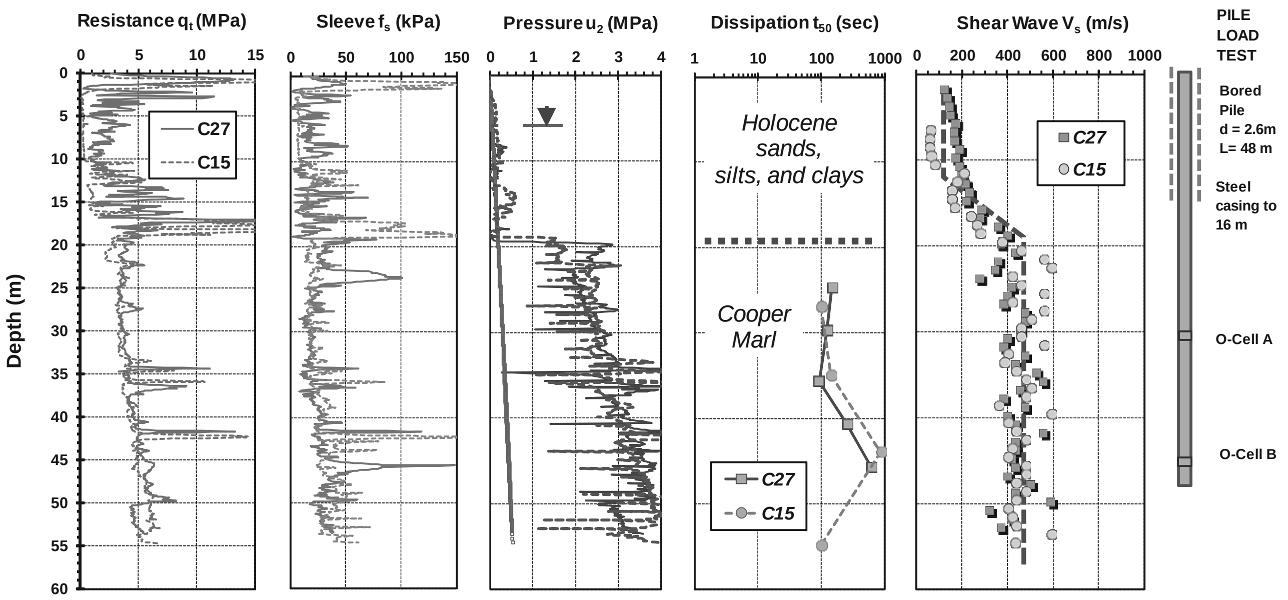

Figure 1. Soil profile with two representative seismic piezocone soundings (SCPTu) and O-cell setup for Arthur Ravenel Bridge, Charleston, SC

3 OSTERBERG LOAD TESTING

A fairly comprehensive load testing program of large diameter bored piles was performed at the site at the direction of the South Carolina Dept. of Transportation (Camp, 2004). This included 12 O-cell tests to measure static axial capacities and displacements. Three test sites were established to represent the conditions near Charleston, Drum Island, and Mount Pleasant.

The test setup for bored pile load test (MP-1) at the north end of the bridge at the Mt. Pleasant site had a constructed diameter d = 2.6 m and embedded length L = 48 m. The upper 16 m was cased with large diameter steel pipe to restrict load test results for pile side friction within the lower Cooper Marl. Two levels of Osterberg cells were installed at depths of 30 and 45 m to allow three-stages of loading.

The first stage involved pressurization of the lower O-cell resulting in a downward movement of the lower pile segment (d = 2.6 m; L = 2.53 m) while essentially no movement occurred in the upper shaft portions. Stage 1 involved base mobilization into the marl to evaluate end bearing resistance plus a small portion of side friction. The second stage involved pressurization of the upper O-cell with the lower cell ventilated (open). Stage 2 resulted in a downward motion of the mid-section shaft (d = 2.6 m; L = 14.0 m) with virtually no movements above the elevation -30 m mark. As such, stage 2 solely involved mobilization of the side friction in the Cooper Marl.

Finally, stage 3 was conducted by closing the lower O-cell and pressurizing the upper O-cell to push the top pile segment upward. Essentially no displacements were recorded in the lower pile portions (below -30 m). Stage 3 data provided information on the shear resistance in the Cooper marl in the non-cased zone from depth intervals from elev. -16 to -30 m.

4 EVALUATION OF AXIAL PILE RESPONSE

4.1 *Pile Capacity Assessment*

For pile capacity, CPT data can be utilized either directly or indirectly to assess the end bearing and side components (e.g., Eslami and Fellenius 1997; Mayne 2007b). Herein, a rational or indirect approach was followed using the CPT data to evaluate geotechnical parameters to determine the pile side friction (f_p) and base resistance (q_b).

For end bearing resistance of piles in clays, limit plasticity solutions detail that:

$$q_b = N_c \cdot s_u \tag{1}$$

where N_c = bearing factor (N_c = 9.33 for circular pile) and s_u = undrained shear strength. For a mode corresponding to direct simple shear (DSS), the strength can be obtained from:

$$s_u = \tfrac{1}{2} \sin\phi' \cdot OCR^{\Lambda} \cdot \sigma_{vo}' \tag{2}$$

where σ_{vo}' = effective overburden stress, exponent $\Lambda = 1 - C_s/C_c \approx 0.8$, C_s = swelling index, and C_c = compression index. In clays, an evaluation of the overconsolidation ratio from CPT data using the expression:

$$OCR = \tfrac{1}{3} Q \tag{3}$$

where $Q = (q_t-\sigma_{vo})/\sigma_{vo}'$ = normalized cone tip resistance. The CPT data indicate OCRs decreasing from 6 to 3 which are slightly higher than OCRs from the noted $\Delta\sigma_v'$ = 480 kPa.

The effective stress friction angle in clays can be evaluated from piezocone results using an effective stress limit plasticity solution developed by Senneset, et al. (1989). A simplified form can be expressed (Mayne, 2005):

$$\phi' = 29.5° \cdot B_q^{\,0.121} \, [0.256 + 0.336 \cdot B_q + \log Q] \tag{4}$$

where $B_q = (u_2-u_0)/(q_t-\sigma_{v0})$ = normalized excess porewater pressure. The equation is applicable for the following ranges: $20° \leq \phi' \leq 45°$ and $0.1 \leq B_q \leq 1.0$. For the Cooper Marl, the CPTu results indicate an effective $\phi' \approx 43°$, quite comparable to values measured from laboratory CIUC triaxial tests on undisturbed samples (Mayne 2005).

The corresponding calculated values of pile end bearing resistance using equations (1) through (4) are presented in Figure 2 as a function of σ_{vo}'. The q_b increase from 2 to 4 MPa and compare quite well with the measured values evaluated from the O-cell test results.

The pile side resistance (f_p) can be expressed in terms of the lateral stress coefficient (K_0) and interface friction between the pile surface and surrounding soil. As a first approximation, this "beta" method gives:

$$f_p \approx K_0 \cdot \sigma_{vo}' \cdot \tan\phi' \quad (5)$$

For soils with stress history of virgin loading-unloading, the geostatic lateral stress coefficient can be evaluated from:

$$K_0 = (1\text{-}\sin\phi') \cdot OCR^{\sin\phi'} \quad (6)$$

In consideration of pile material type and method of installation, the expression is modified to:

$$f_p \approx C_M \cdot C_K \cdot K_0 \cdot \sigma_{vo}' \cdot \tan\phi' \quad (7)$$

where C_M = interface roughness factor (= 1 for bored cast-in-place concrete, 0.9 prestressed concrete, 0.8 for timber, and 0.7 for rusty steel piles) and C_K = installation factor (= 1.1 for driven piles; 0.9 for bored piles).

Calculated values of pile side friction are shown in Figure 3 and vary between $150 < f_p < 250$ kPa. These are comparable in magnitude, and in some cases less than f_b determined from the O-cell load test series.

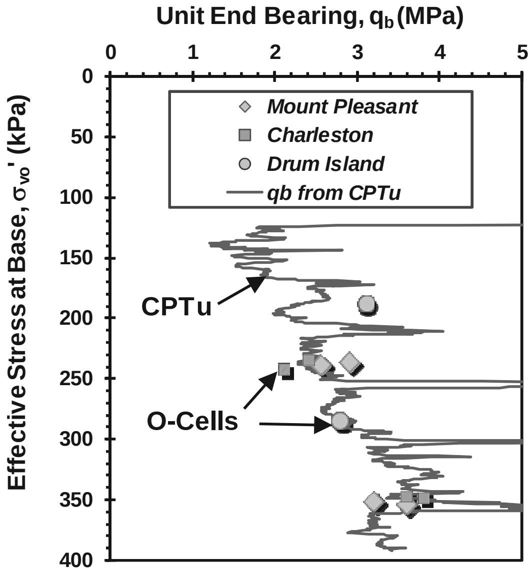

Figure 2. Measured and calculated unit end bearing resistances

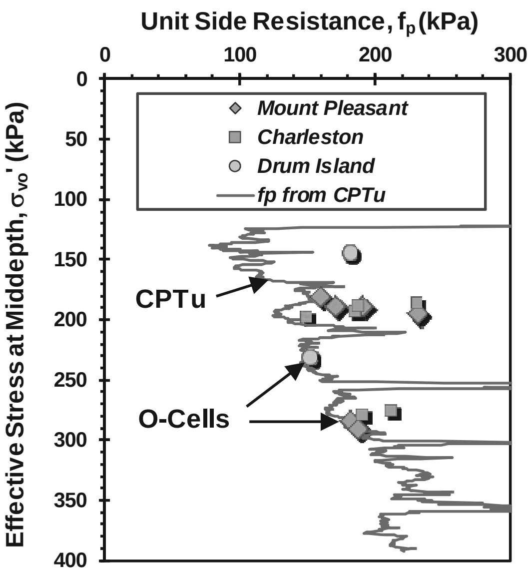

Figure 3. Measured and calculated unit side friction resistances

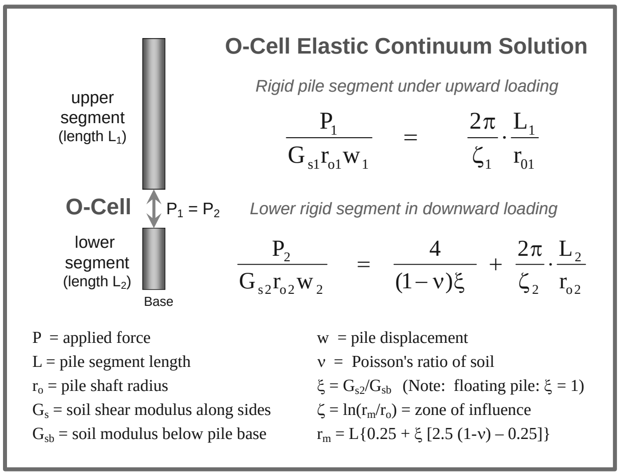

Figure 4. Elastic continuum solution for O-cell loading of piles

4.2. *Axial Pile Displacements*

The elastic continuum solutions for an axial pile foundation are detailed by Randolph and Wroth (1978, 1979) and Fleming et al. (1992) by coupling a pile shaft with a circular plate. This can be deconvoluted back into the separate components to represent the original O-cell arrangement or into stacked pile segments for a mid-shaft O-cell as well as for multi- staged O-cell setups. For the simple case of rigid pile segments, Figure 4 presents the elastic solution for a mid-section O-cell framework.

The stiffness of the surrounding soil is represented by a shear modulus (G). The initial fundamental small-strain shear modulus of the ground is obtained from the shear wave velocity measurements:

$$G_0 = \rho_T \cdot V_s^2 \quad (8)$$

where ρ_T = total mass density of the soil. This small-strain stiffness is within the true elastic region of soil corresponding to nondestructive loading. To approximately account for non-linearity of the stress-strain-strength behavior of soils, a modified hyperbola is adopted (Fahey, 1998):

$$G = G_0 \cdot [1 - (P/P_{ult})^g] \quad (9)$$

where P = applied force, P_{ult} = axial capacity of the pile segment, and the exponent "g" is a fitting parameter (Mayne, 2007a, 2007b). Thus when P = 0, initially G = G_0 and at all higher load levels the shear modulus reduces accordingly.

Data from monotonic loading in resonant column, torsional shear, and triaxial shear tests with local strain measurements on both clays and sands under drained and undrained conditions have been compiled to evaluate the nonlinear modulus trends. A summary of these data for a wide variety of soils has been compiled and presented in Figure 5 (Mayne 2007b). The y-axis (G/G_0) can be considered as a modulus reduction factor to apply to the measured small-strain stiffness attained from (8) using site-specific V_s field data. The x-axis (q/q_{max} = 1/FS) is a measure of the mobilized strength and can be considered as the reciprocal of the factor of safety (FS) corresponding to the load level relative to full capacity. In the case of pile capacity, the mobilized strength is obtained from the ratio of applied load to capacity (P/P_{ult} = 1/FS)

The modified hyperbola given by (9) is also presented in Figure 5 and can be seen to take on values of "g" exponent ranging from 0.2 (low) to 0.5 (high) when compared to the lab data. Usually, a representative exponent value g = 0.3 has been

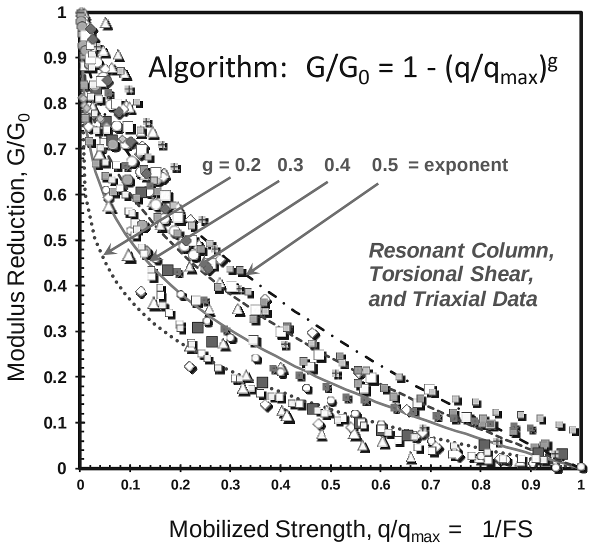

Figure 5. Modulus reduction algorithm for monotonic static loading

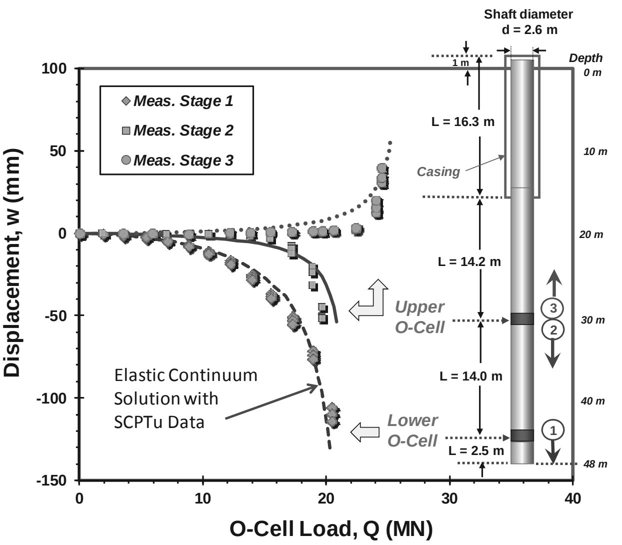

Figure 6. Measured and calculated O-cell response for test shaft MP-1 at Cooper River Bridge site

suggested for relatively insensitive clays, nonstructured soils, and uncemented quartzitic sands (Mayne 2007a). For the Cooper marl, the high calcium carbonate content would implicate a rather structured geomaterial, therefore an appropriate exponent "g" = 0.5 can be considered characteristic.

Using the aforementioned elastic continuum solution and axial pile capacity determined from CPT results, together with the initial shear moduli obtained from the V_s profile, the response of the three pile segments from the O-cell arrangements can be represented, as shown in Figure 6 for test shaft MP-1. A reasonable agreement is observed for all three loading stages of both O-cell jacks, including an approximate nonlinear load-displacement-capacity behavior.

If desired, a more realistic compressible pile solution is also available (Fleming et al. 1992), yet more complex as it involves a hyperbolic tangent function. In that case, the developed curves are quite similar to those shown herein.

5 CONCLUSIONS

The upward and downward pile segments of an O-cell load test can be conveniently represented by a versatile elastic continuum solution. Results from seismic piezocone testing (SCPTu) provide the necessary input data to evaluate axial side and base resistances of the deep foundations, as well as the small-strain stiffness (G_{max}) needed for deformation analyses. Modulus reduction is dependent upon mobilized capacity ($P/P_{ult} = 1/FS$) using a simple algorithm. A case study involving a two-level O-cell arrangement for a large bored pile situated in the calcareous Cooper marl formation of South Carolina was presented to illustrate the application.

ACKNOWLEDGMENTS

The writers thank Billy Camp of S&ME and the SCDOT for providing access to the load test results.

REFERENCES

Camp, W.M. 2004. Drilled and driven foundation behavior in a calcareous clay. *GeoSupport 2004* (GSP 124), ASCE, Reston, Virginia: 1-18.

Camp, W.M., Mayne, P.W., and Brown, D.A. 2002. Drilled shaft axial design values in a calcareous clay. *Deep Foundations 2002*, Vol. 2, GSP No. 116, ASCE, Reston/Virginia: 1518-1532.

Eslami, A. and Fellenius B. H. 1997. Pile capacity by direct CPT and CPTu methods applied to 102 case histories. *Canadian Geotechnical J.* 34 (6): 886-904.

Fahey, M. 1998. Deformation and in-situ stress measurement. *Geotechnical Site Characterization*, Vol. 1 (Proc. ISC-1, Atlanta), Balkema, Rotterdam: 49-68.

Fellenius, B.H. 2001. The O-cell: an innovative engineering tool. *Geotechnical News Magazine*, Vol. 19 (2): 32-33.

Fleming, W G K, Weltman A J, Randolph M F and Elson W K. 1992. *Piling Engineering, 2nd Edition*, Blackie /Halsted Press - Wiley & Sons, London: 122-128.

Mayne, P W. 2005. Integrated ground behavior. in-situ and lab tests. *Deformation Characteristics of Geomaterials*, Vol. 2 (IS-Lyon), Taylor & Francis Group, London: 155-177.

Mayne, P.W. 2007a. In-Situ Test Calibrations for Evaluating Soil Parameters, *Characterization & Engineering Properties of Natural Soils*, Vol. 3, Taylor & Francis Group, London: 1602-1652.

Mayne, P W. 2007b. *Synthesis 368 on Cone Penetration Testing*, National Cooperative Highway Research Program (NCHRP), National Academy Press, Washington, DC: 117 p. www.trb.org

Mayne, P.W. and Woeller, D.J. 2008. O-cell response using elastic pile and seismic piezocone tests. *Proc. Intl. Conf. on Foundations* (Dundee), British Geotechnical Association, IHS BRE Press, UK.

O'Neill, M W, Brown, D A, Townsend, F C, and Abar, N. 1997. Innovative load testing of deep foundations. *Transportation Research Record No. 1569*, Washington, D.C.: 17-25..

O'Neill, M W and Reese L C. 1999. *Drilled Shafts: Construction Procedures and Design Methods*, Vols. I and II, Publication FHWA-IF-99-025, Assoc. Drilled Shaft Contractors, Dallas: 758 p.

Osterberg J O. 1998. The Osterberg load test method for bored and driven piles. *Proc. 7th Intl. Conf. Piling and Deep Foundations* (Vienna), Deep Foundations Institute, NJ: 1.28.1-1.28.11.

Osterberg, J O. 2000. Side shear and end bearing in drilled shafts. *New Technological and Design Developments in Deep Foundations*, GSP No. 100 (Proc. GeoDenver), ASCE, Reston, Virginia: 72-79.

Randolph M F and Wroth C P. 1978. Analysis of deformation of vertically loaded piles. *Journal of Geotechnical Engineering Division (ASCE)*, Vol. 104 (GT12): 1465-1488.

Randolph M F and Wroth C P. 1979. A simple approach to pile design and the evaluation of pile tests. *Behavior of Deep Foundations*, STP 670, ASTM, West Conshohocken, Pennsylvania: 484-499.

Senneset, K., Sandven, R. and Janbu, N. 1989. Evaluation of soil parameters from piezocone tests. *Transportation Research Record 1235*, National Academy Press, Washington, DC: 24-37.

Energy and Reliability Applied to Continuous Flight Augern Pilings - The SCCAP Methodology

Énergie et fiabilité appliquées à l'excavation des pieux forés en continu - La méthodologie SCCAP

Medeiros Silva C.
Embre Empresa Brasileira de Engenharia e Fundações Ltda

Camapum de Carvalho J., Brasil Cavalcante A.L.
Dept. of Civil & Environmental Engineering, University of Brasilia

ABSTRACT: The SCCAP methodology was developed to control the execution of Continuous Flight Auger (CFA) type foundation works. The methodology SCCAP was based in the law of energy conservation, which is one of the basic fundaments from classical physics and quantifies the required energy, or developed work, to excavate each of the piles from any particular foundation site. It proposes formulations, routines and criteria for pile acceptance based on the statistical characteristics of the population or from an energy sample taken from this one. It has been incorporated into the monitoring and execution software from CFA piles machines, and it allows for local corrections on procedures and excavation depth at each executed pile from the site. Consequently it enhances the reliability and mitigates involved risks to the geotechnical job. The SCCAP methodology has been validated through the assessment that the necessary energy to excavate a particular pile is related to its bearing capacity, when the excavation process is monitored.

RÉSUMÉ : La méthodologie SCCAP a été développée pour contrôler l'exécution des pieux forés en continu (CFA). La méthode SCCAP est fondée sur la loi de conservation de l'énergie, qui est un des fondements de la physique classique et qui quantifie l'énergie requise - ou le travail à fournir - pour excaver chacun des pieux dans n'importe quel sol de fondation. Elle propose des formulations, des procédures et des critères pour définir la conformité des pieux, basés sur les caractéristiques statistiques de la population ou sur un échantillon d'énergie pris dans celle-ci. Cette méthode a été incorporée au logiciel de suivi et d'exécution des machines foreuses de pieux CFA et elle permet d'effectuer des corrections locales sur les procédures et la profondeur d'excavation de chaque pieu. Par conséquent, elle améliore la fiabilité et réduit les risques encourus lors du travail d'excavation. La méthode SCCAP a été validée par le fait que l'énergie nécessaire pour excaver un pieu particulier est en relation directe avec sa capacité portante, lorsque le processus d'excavation est contrôlé par monitoring.

KEYWORDS: Energy, Methodology SCCAP, Continuous Flight Auger (CFA) and Reliability.

1 INTRODUCTION

Safety analyses in Foundation Engineering when are done, are generally restricted to design and are deterministic, that is, in theory certainty of the parameters involved in dimensioning exists, accepting as precise the calculating methodology adopted. However, it is known that the greatest source of variability in Foundation Engineering is the geological-geotechnical formation., which affects the performance of the soil-foundation system that is strongly determined by the stratum variability through the soil profile as a whole.

In pilings the aim is to reach the design assumptions in terms of load capacity and deformability for them to be verified during execution. Consequentially, Foundation Engineering look for techniques that assure the good performance of the foundations concerning resistance and/or deformability. The ideal is to adopt procedures and routines during design phases especially during the quality control of the execution to identify the need of intervention during execution.

In this context, the SCCAP Methodology is presented for the control and uniformity of the bored pilings, especially for the continuous flight auger pile which is based on the interpretation of the necessary energy or the work done during the excavation of a pile. Such methodology was developed from the understanding of the force system of the boring equipment and the application of the universal energy conservation principle which when applied to the excavation process of a pile allows the enrgy quantification necessary for a pile. As a consequence of the confirmation that the bearing capacity is related to the necessary energy to excavate a pile, it was possible to incorporate the statistical concepts as SCCAP routines allowing to control the excavation process quality during the piling excavation.

For the confirmation of the SCCAP Methodology efficiency load tests and comparisons were used with predictions based on SPT tests. The developed methodology was presented in details in Silva (2011) and according to the author can be extended to any type of bored or other rotating excavations such as the ones for tunnels, only if it is possible to identify the force system to quantify the spent energy in the process.

The SCCAP proposed routines do not substitute the geotechnical engineer judgment but it can help him in the identification and mitigation of involved risks in any type of piling, especially for the ones that do don't have controls based on scientific concepts, as the excavated pilings.

1 ENERGY AS BASE FOR THE CONTROL OF PILINGS

Silva (2011) and Silva et al. (2012) presented the construction of the methodological structure that is the basis of a thesis which says that the control of mechanical excavations, especially for bored piles done by the determination of the required energy during the pile excavation consists of an element for technological control capable to offer a greater security and less risks to the constructions that use them. Coming from some hypothesis, Silva (2011) proposed an analytical formulation to quantify the total transferred energy by the system to the soil, which is obtained by the volumetric integration as a function of the soil temperature. Consequently the total energy of the system is obtained by:

$$E_{st} = \iiint_V \rho_s \, C_{ps} \, [T_s(r,z,t) - T_s(r,z,0)] dV \qquad (1)$$

Where: E_{st} = total energy of the system [J]; ρ_s = soil density [kg m^{-3}]; C_{ps} = specific soil heat [J m^{-3} ^{0}C^{-1}]; V = refering to volume [m^3].

The problem which was showed concerning heat transient transference in the soil is bi-dimensional (2D) and aximetric and it can be solved analytically, for example, through finite differences. However, Silva (2011) and Silva et al. (2012) considering Hamilton's principle it is possible to determine the variation of mechanical energy produced by the system, assuming that the presented energy of the system is conservative, that is, such energy cannot be created or destroyed, simply transformed. Considering such principle, Silva (2011) and Silva et al. (2012) applied the concept of work done to the excavating process of a pile, achieving the conclusion that the system of variable forces (*Fi)* produced by the continuous flight auger equipment, showed in Figure 1, applies to the boring device a movement from the initial elevation (*ci*) to a final elevation (*cf*) through a path (Δ*xi*). Accordingly, the work (*W*) done to excavate a pile is a pure number defined by Silva (2011) as the pure product of such two greatness, *Fi* e Δ*xi* given by:

$$W = \lim_{\Delta x_i \to 0} \sum_{i}^{n} F_i.\Delta x_i = \int_{ci}^{cf} F_i.dx \tag{2}$$

Where: W= Work [J]; F_i= Force applied to the body [N]; Δx_i= body path [m]; c_i= initial elevation of the body [m]; c_f= final elevation of the body [m].

Similarly, he defined the work done by the friction and adhesion present during the excavating process which represents parts done by the non-conservative forces through the same displacement, defined by:

$$W_c = -\lim_{\Delta x_i \to 0} \sum_{i} F_{ci}.\Delta x_i = -\int_{ci}^{cf} F_{ci}.dx \tag{3}$$

Where: W_c=work done by non-conservative forces [J]; F_{ci}=non conservative forces applied to the body [N].

Figure 1. Boring system and forces.

Moreover according to Silva (2011), another type of energy associated to the excavation of a pile is the potential energy which basically depends on the position and system configuration, in the case, the position of the helical device or of the auger, is given by:

$$W_g = F_g \Delta y = m.g.(y_2 - y_1) \tag{4}$$

where: Wg= work done by the gravity force [J]; Fg=*Gravity force or Weight Force* [N]; g = gravity acceleration [m/s^2]; m = system mass [kg]; $(y_2$-$y_1)$ = variation of the geo-reference position [m].

Silva (2011) also considered that the conservation energy principle summarized in Hamilton's principle is present in the excavation of a pile. Similarly to the structural system dynamics it can be simplified as mentioned by Clough and Penzien (1975):

$$\int_{t1}^{t2} \delta(T - V)dt + \int_{t1}^{t2} \delta(W_{nc})dt = 0 \tag{5}$$

Where: T = total kinetic energy [J]; V = potential energy including the deformation energy of any external conservative force [J]; W_{nc} = work done by non-conservative forces that act in the system, including cushion, friction and external forces [J].

Silva (2011) solved the problem considering Hamilton's principle represented by Equation 4, assuming that the total thermal and sound energy of the system (ΔE_{st} is equal to the mechanical energy applied to the system or the work done by external forces applied to the system (W_R), in the case, forces applied to the helical device during the excavation of a pile represented in Figure 1.

Then, knowing the torque applied to the helical device and the lever arm, he measured the tangent force applied to the helical device and knowing the angular and boring speed of the helical device, the track can be determined and consequently, the work of the tangent, which is the pure product of such force by the displacement through depth. Finally, the total work done by the external forces is the sum of the work done by the tangent force to the helical device, plus the work done by the gravity force and the work done by the downward force which is equal to the mechanical energy applied to the helical device. Thereby, the work is a pure greatness represented and defined by Silva (2011) and Silva et al. (2012) as:

$$W_R = \int_0^{z_b} m_{hc}.g.dz + \int_0^{z_b} Fd_i.dz + \int_0^{m2\pi} F_i.r.d\theta \tag{6}$$

Where: W_R = work done or required energy to excavate a pile [J]; Fi= force applied to the helical device [N]; m_{hc} = mass of the excating system [kg]; r = radius of the CFA pile [m]; g = acceleration of gravity [m/s^2]; z_b = pile length [m]; Fdi= downward force applied to the helical device [N]; m= number of turns of the helical device during excavation.

Silva (2011) and Silva et al. (2012) proved mathematically that Equation 6 is consistent in terms of the physical point of view and take to values close to the ones obtained by Van Impe (1998) proposal, that considers in its approach mean values to survey the required energy to excavate a pile type atlas.

3 SCCAP METHODOLOGY

In the traditional execution method, the pile depth is previously set by the designer and is generally not modified during the execution. However, in a profile with folded structural geology, the current practice can take to mistakes, mainly when the non-sampled soil, soil between boring tests appear in the depression zone of the synclines, achieving low resistance till the predicted design tip elevation.

To solve this problem, Silva (2011) proved that the work done in each pile of the foundation piling executed by a fixed process of the system machine/operator is proportional to the pile bearing capacity. When put together in a data file, these works make a population which fit in a normal probabilistic distribution that allow the authors to establish acceptance criteria related to the mean value and standard deviation of the population from an extracted soil sample of the piling. The methodology which is physically represented by Equation 6, was introduced in the monitoring system of CFA piles, allowing to quantify the work or required energy to excavate each pile of the piling and, consequently to control the piling based on on the required energy during the execution of the piling. Therefore, the SCCAP routines introduce to the execution monitoring software for CFA piles the excavation quality control in real time and assure to the execution piling process conditions for the piles to achieve individually the planed bearing capacity, assuring quality and the design assumptions. It is very clear that the final behavior of the pile will also depend, among other issues, for example, the concrete injection pressure which depending on the type of soil and its value will have a great influence on the pile behavior, such fact observed by Silva (2011).

Figure 2 presents the results obtained during the execution of seven load tests, construction on the Paranoá Lake shore in Brasília – Brazil and the total required energy to execute each pile. It can be seen in Figure 2 that the measured energy in each pile is proportional to its bearing capacity. In Table 1, the most important geometric and monitored data of the tested piles are shown. Moreover it’s also observed in Picture 2 that the ultimate load is rampant with the required energy increase during the excavation, independently of the failure criteria adopted, the one from Brazilian norm criterion (NBR 6122, ABNT) or the conventional one which corresponds to 10% of the pile diameter. In this case, all piles were excavated by a same set machine/operator.

Table 1. geometric features of the piles (modified from silva, 2011).

Pile	Length (m)	Medium pressure of concrete (kPa)	Diameter (cm)	Total Energy (MJ)
E110BA	17,12	100	42	9,64
EPC1BB	15,12	100	42	10,60
TC2BB	12,80	0-75	53	13,18
E55AA	14,24	25-100	37	7,06
EPC1C	10,80	50	42	4,73
GE 24C	20,92	0-50	52	13,36
EE6B	20,08	100	54	14,27

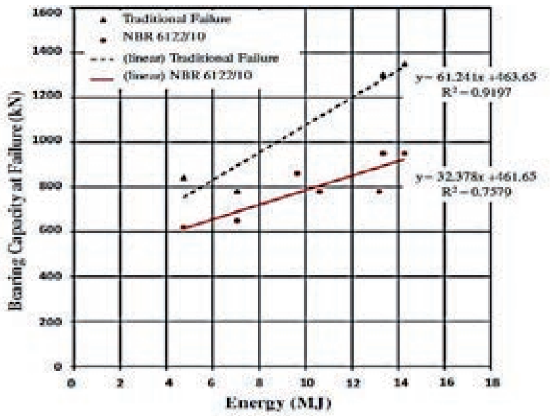

Figure 2. Ultimate bearing capacity versus work done (Silva, 2011).

By the confirmation that the bearing capacity of the pile is directly proportional to the work done and that the collected results in the piling (energy) when organized in frequency distribution conducted to a normal distribution, Silva (2011) proposed an acceptance for the piles based on Physics concepts (energy conservation) and on statistics characteristics of collected energy sample during the execution of the piling. Preferably they suggested that the population sample would be collected close to the load test once statistics properties of the sample could be associated to the real bearing capacity of a pile in the execution condition adopted in the construction. According to the authors, if the referred association is not possible, it is important that the sampling is done in a region with known geotechnical characteristics, for example, giving attention to regions where the field tests were executed and have little variability. Once the region to be sampled was chosen and its size, the results are put together by class fitting them to a normalized distribution. By that way, the mean (μ) and the standard deviation (σ), were calculated what made possible to establish reliability and acceptance criteria to applied in boring. From the beginning they proposed criteria tht should be chosen by geotechnical variability basis and the existing quality control in the construction, for example, it will be accepted the pile which when achieving the minimum design depth did during excavation a required and measured work (w) greater than the mean (μ) of the work measured from the sample (W≥μ).

Tabela 2. Caracterização Geotécnica – Ensaio SPT

Deep (m)	SPT by Layer				Type of Soil
	SPT 01	SPT 02	SPT 03	SPT 04	
1	7	6	6	6	Clay
2	4	4	5	5	
3	2	4	2	5	
4	2	4	4	7	
5	4	6	6	10	
6	4	6	8	15	
7	8	7	4	18	
8	7	7	13	13	
9	5	11	30	7	
10	14	24	30	5	
11	32	12	32	9	
12	58	31	56	14	Silt
13		52		18	
14				21	
15				19	
16				24	
17				27	
18				42	

In Table 3 the required energies to excavate each pile are presented. The tip elevations of the pile bases were defined based on the geotechnical characterization and its location in the construction site and three different depths were adopted, 10, 11 and 13 m. It is important to mention that the piles were executed from elevation -4,00m, which is related to the initial elevation of the borings because of the existence of an underground level.

Table 3. Energia demandada na escavação das estacas (Silva,2011)

Estaca	Prof. (m)	Energia (MJ)	Estaca	Prof. (m)	Energia (MJ)
E42A2C	13,12	6,0	E13A2D	13,12	4,7
E23A2F	13,12	6,4	E18A2A	13,12	4,8
E23A2B	13,12	3,9	E25A2C	13,12	4,9
E23A2D	13,36	6,3	E26A2C	13,12	4,3
E18A2E	13,12	5,8	E13A2C	13,12	6,1
E18A2D	13,12	3,6	E13A2B	13,12	8,2
E23A2E	13,12	4,0	E25A2A	13,12	7,5
E23A2C	13,12	4,9	E26A2A	13,12	6,6
E23A2A	13,12	5,8	E13A2A	13,12	5,1
E18A2F	13,60	5,1	E13GA	10,08	3,1
E18A2C	13,12	2,7	E20GB	10,08	3,6
E18A2B	13,12	3,5	E65DC	10,08	3,8
E25A2B	13,12	6,3	E19GB	10,08	5,1
E26A2B	13,12	6,8	E64DC	10,08	3,8
E10GB	10,08	5,1	E2B1E	11,12	8,5
E17GB	10,08	4,3	E11B1A	11,12	6,9
E23G	10,08	2,9	E17B1D	11,12	6,9
E63DB	10,08	2,8	E5B1A	11,12	7,8
E17GC	10,16	4,3	E2B1C	11,12	6,5
E10GC	10,16	4,9	E17B1B	11,12	6,1
E11B1E	13,04	5,6	E5B1B	11,12	5,4
E17B1E	12,96	8,8	E4B1B	11,12	6,7
E17B1A	13,04	6,6	E17B1C	11,12	6,5
E2B1A	11,12	7,6	E2B1D	11,12	6,6
E4B1A	11,12	7,1	E2B1B	11,12	7,2

For the 40 centimeter pile sample, the data of the works done, obtained during the excavation of 10,00 meter depth piles, once a load test was made on a pile with those characteristics, close to boring SPT 1 (Table 2), which results are marked with grey color in Table 2. Silva (2011) submited all the collected data to normality tests that evaluate if the frequency distribution of a data group adheres to the Normal Distribution and verified that the data adheres to the normal distribution. The central tendency measures, mean and median, the standard deviation and the variance are presented in Table 4.

Table 4– Características estatísticas da população e da amostra

Estacas	População	Amostra
Média (MJ)	5,56	3,97
Mediana (MJ)	5,70	3,80
Desvio Padrão (MJ)	1,56	0,84
Variância (%)	29	21

It is observed in this case that the mean and the variance of the sample was smaller than the population. Such fact was expected for the mean once it refers to a very folded profile, the load test was made on the pile with a small depth in favor of safety. The smaller value of variance is perfectly justified because in accordance with the methodology, a region with small variability must be chosen what was assured, in the case, by the sampling in a restricted area, on the contrary concerning the piling which was executed taking all the area and consequently all its variability. Then to assure that the bearing capacity could be achieved, the SCCAP methodology was applied during the piling execution, in the case, the first criteria by considering that the mean is a good representative of the population, the criterions are:

- It will be accepted the pile which when achieving the minimum design depth did during excavation a required and measured work (w) greater than the mean (μ) of the work measured from the sample (W≥μ);
- It will be accepted the pile which when achieving the minimum design depth did during excavation a required and measured work (w) greater than the mean (μ) plus the standard deviation (σ) of the work measured from the sample (W≥μ+σ);
- It will be accepted the pile which when achieving the minimum design depth did during excavation a required and measured work (w) greater than the mean (μ) plus two times the standard deviation (σ) of the work measured from the population sample where they belong (W≥μ+2.σ).

For the analyses, hypothetical applications were done from the first and second criterion. Comparing the work done (W) in each pile during its excavation (Table 3) with the mean (μ) of the required work to execute the piles of the sample, first criterion (W≥μ), it is observed that it would be necessary to correct or increase the depth of 4 piles with a diameter of 40 cm for them to present a cumulative work smaller than the mean obtained for the sample. By using the second criterion, which is more conservative, it is noticed that eliminating the piles which have been excluded from the previous analysis, even though 8 piles with a diameter of 40 cm would be refused.

Once the results presented in Table 3 were set in the chronological execution sequence of the piling and knowing that the piling was executed sequentially till the total area of the construction was covered, it can be verified, for example, in Table 3, that the piles refused by criterions 1 and 2 are arranged in group, that is, those piles are neighbors and probably are founded in regions with NSPT mean value smaller than what was expected or they were founded on synclinal folds.

It is clear that the adoption of the SCCAP methodology gives more reliability to the piling in terms of bearing capacity.

4 RELIABILITY

Trying to measure the reliability of CFA pilings, Silva (2011) from a data file made with energy or wok done records to execute each pile of the piling, he evaluated the reliability in bored pilings. He considered the concept that the bearing capacity of each pile and its deformability are directly related with the measured energy or the required work to bore it, he used the proposal of Ang & Tang (1984), which defined the continuous random variables, in the case, their probability distributions that define the demanding forces and piling resistance: X= resistance or resistant capacity of the system; Y= demanding load acting in the system.

The goal was to assure that the event (X > Y) happens during the whole life of the foundation. This condition or warranty can be verified in terms of the which represents the piling reliability. On the contrary, the probability of failure is the measurement which corresponds to the completing event.

Once fixed to the shape of the demanding action curves (loads on foundations) and of resistances (bearing capacity of piles); and knowing their coefficients of variety and the global safety factor of the piling, the reliability index can be determined and the probability of failure of the piling, interpreted by Cardoso e Fernandes (2001). From that proposal, Silva (2011) showed that the reliability index (β) of the piling increased a great deal, going from 2,69 to 3,14.

4 CONCLUSIONS

The routines of quality control proposed by the SCCAP methodology are showing their great importance in constructions controlled by such technique, assuring quality for the whole process of excavation. Mainly because it can assure that all design assumptions in terms of bearing capacity and deformability are guaranteed through the decrease of the variability and the increase of reliability. Another important issue which was observed is that the SCCAP methodology offers stopping criteria for the boring which has a complementary and corrective role, contributing to risk reduction in the construction once it reduces the probability of failure and increasing the reliability..

5 ACKNOWLEDGEMENTS

The authors would like to thank the foundation company Empresa Sul Americana de Fundações S/A and Embre Engenharia for the availability of the data files analyzed in this study.

6 REFERENCES

CARDOSO, A.S. & FERNANDES, M.M. (2001). Characteristic Values of Ground Parameters and Probability of Failure in Design according to Eurocode 7. Geotechnique 51, 6: 519-531.

CLOUGH, R.W. & PENZIEN, J. Dynamics of Structures, 1st Ed., New York-NW, McGraw-Hill, 634 p., 1975.

SILVA, C.M. Energy and Reliability in Continuous Flight Auger Type Foundation Works. PhD Thesis, Publication G.TD - 070/11, Civl and Environmental Department, University of Brasilia, Brasilia, DF, 303p, 2011. (in portuguese).

SILVA, C.M.; CAVALCANTE, A.L.B.; CAMAPUM DE CARVALHO, J. On Modelling Continuous Flight Auger Pilings by means of Energy. International Journal of Science and Engineering Investigations vol. 1, issue 9, October 2012, ISSN: 2251-8843.

Performance of a pioneer foundation of the skirt type for the Metro-Line 12 overpass on the Mexico City soft clay

Comportement d'un nouveau type de fondations de type radier à jupe, utilisé pour les tronçons en viaduc de la ligne 12 du Métro fondés sur les argiles molles de Mexico

Mendoza M.J., Rufiar M., Ibarra E., Mendoza S.A.
Instituto de Ingeniería, Universidad Nacional Autónoma de México, 04510 Mexico City

ABSTRACT: Given the extension and importance of Mexico City's Metro-Line 12, it was considered relevant to monitor the behavior of the foundation of one of the supports for the overpass solution, which is laid on very soft clayey soils. This pioneer foundation, a footing or foundation slab with long skirts, locally known as structural cell or "inverted glass" type, was used for the first time in the city. Geotechnical sensors and accelerometers were included in the foundation to follow its behavior, not only during its construction and long term operation, but to record significant variables during strong earthquakes. From measurements made to date (two years after the beginning of construction) it stands out the effective coefficient K of earth pressure, reaching values close to the unit, at the soil-concrete walls (cast in place) contact.

RÉSUMÉ : Au vu des dimensions et de l'importance de la Ligne 12 du Métro de la ville de Mexico, il a été jugé nécessaire de procéder à l'auscultation des fondations de l'un des appuis du tronçon de la ligne en viaduc, implantées dans des sols lacustres très mous. Les fondations, d'un type nouveau à Mexico, sont constituées par un radier avec une jupe de parois moulées et sont connues localement comme cellule structurée ou « verre renversé ». Des jauges géotechniques et accéléromètriques ont été insérées dans les fondations afin non seulement de suivre leur comportement durant la construction et à long terme mais aussi d'enregistrer certaines variables importantes durant les séismes intenses. Les mesures réalisées à ce jour mettent en évidence un coefficient de poussée des terres K effectif de l'ordre de l'unité au contact entre le sol et les parois de béton.

KEYWORDS: Foundations, Static and seismic performance, geotechnical instrumentation, soft clayey soils.

1 INTRODUCTION.

Construction of Mexico City's Metro-Line 12 has involved tunnel, semi-deep box, surface and overpass solutions along 25 km of development, connecting the southeast and southwest zones of the country's capital. Stratigraphic conditions along the layout have demanded novel solutions, mainly at the portion that runs into Lake zone subsoil consisting of very compressible and low strenght clayey lacustrine deposits. Such is the case of a pioneering type of foundation in Mexico City, known locally as structural cell or "inverted glass" which was used at the supports of an overpass almost 1.7 km long located near the Tláhuac terminal station. This reinforced concrete foundation consists of four perimeter walls, each 60 cm thick and 10.5 m long, cast in place, that constitute the skirting, Figure 1. The precast footing-column unit is integrated to the four perimeter walls by casting in place the rest of the footing's four sides, thus forming what is known locally as an "inverted glass".

The instrumented support is named ZP16, and is located between the Zapotitlán and Nopalera stations. The foundation's behavior is exposed based on vertical pressures measured under the footing, lateral pressures on the walls, and pore water pressures at the contact between clayey soil and walls, for which total pressure cells, push-in pressure cells, and piezometers were used, respectively. With the objective to improve our knowledge on the behavior since the construction process, in the long term and during an earthquake, the adopted instrumentation required long life trustworthy ad hoc equipment with sufficient precision and immediate dynamic response during seismic events. The latter required the adoption of an automatic recording system for these geotechnical data and the accelerations measured at the footing.

This paper describes the type of foundation, its construction process, the geotechnical and accelerographic instrumentation that was integrated into the foundation, and the monitoring carried out to learn about its geotechnical behavior, not only during construction and long term operation, but to record significant variables in the foundation precisely during a strong earthquake. The monitoring time period covers the constructive process and its evolution over almost two years. It also includes static measurements before and after two earthquakes of moderate intensity.

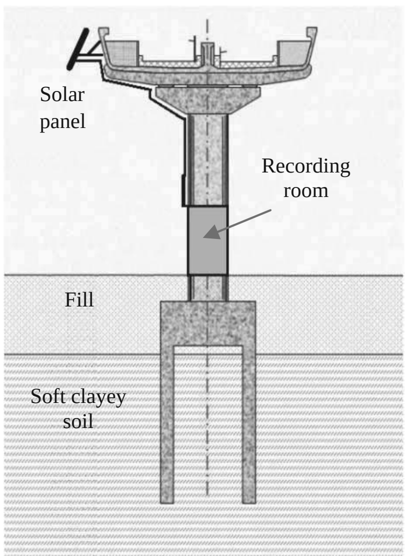

Figure 1. Overpass for Metro-Line 12. Support ZP-16.

2 SCOPE AND OBJECTIVES

The instrumentation's primary objective is to compare theoretical and semi empirical forecasts that have been assumed during the design stages, refering to load capacity and its movements, with the experimental results derived from instrument monitoring. Specific objectives contemplate 1) knowing the magnitude of total and effective lateral pressures in static and long term conditions; 2) the same, but during moderate and high intensity earthquakes; and 3) quantifying the footing base contribution to the bearing capacity of the foundation system against axial static loads. In this paper, field measurements and design forecasts will not be compared.

3 GENERAL DESCRIPTION OF THE STRUCTURAL CELL

For about 40 supports of the Metro-Line 12 overpass, an innovative foundation solution was used like the studied one, according to prevailing conditions at Tláhuac Avenue consisting of very thick soft clayey soils. The foundation's construction began with the excavation and casting of reinforced concrete walls with the diaphragm wall technique, forming a square plan section of 6.5 m exterior sides starting at 2.5 m depth. Once the central core soil was excavated to a depth of 3 m, a reinforced slab was built at the bottom, which temporarily received the precast footing-column unit, whose dimensions are smaller than the cell's inner dimensions, in order to allow its transport from the manufacturing plant. Once the monolithic footing-column unit was installed and leveled, its periphery was cast in place with high resistance concrete, ensuring a structural continuity along the footing's entire height (1.7 m) with its four perimeter walls, prior overlapping of their reinforcement bars.

4 STRATIGRAPHIC CONDITIONS OF THE SITE

There is a stratified formation of very soft clayey soils at the site, interbedded with sandy or volcanic ash soils strata of variable thicknesses (decimeters) at the more shallow portion. This lacustrine formation reaches a thickness of 79 m, with deep deposits below it consisting of sandy soils. A silty layer 3 m thick was detected at 56 m depth. Based on a nearby cone penetration test (CPT), the cone point's resistance q_c from surface to 3.1 m depth was defined at 1 MPa. A sandy stratum of 3.1 to 4 m reached a maximum q_c value of 6 MPa. But, below the 8 m depth, and down to the 25 m depth explored by CPT, there were very soft clay conditions, with very low q_c values. Undrained shear strength at these depths reached values of 28 to 50 kPa. In summary, it is a site of lacustrine deposit with very low shear resistance and high compressibility. Therefore, the foundation for a work of infrastructure like the one described here, with high applied loads per column, represents an engineering challenge.

5 GENERAL DESCRIPTION AND FOCUS OF THE GEOTECHNICAL AND SEISMIC INSTRUMENTATION

Following relevant guidelines of Terzaghi and Peck (1967), Peck (1960), and Dunnicliff (1988), among others, the foundation's design was outlined responding to specific questions of possible behavior and distinguishing the internal variables that determine and explain it. This also determined the type of sensors that would measure these variables and their location. Also, from an analysis of the expected level of stresses and deformations, transducer measurement intervals were defined.

It was not possible to place instruments in the body of the walls as was initially intended, because they had already been cast when it was decided to study this support. The initial plan was to measure pressures on the walls using jack-out pressure cells, in order to ensure their contact with the soil walls at the excavated ditch.

5.1 *Pressure cells at the soil-footing contact*

The instrumentation included the installation of seven pressure cells, Figure 2, under the thin bottom slab with which it is possible to measure total vertical stresses immediately below the slab on which the footing-column unit gravitates temporally. Six cells were of resistive type (SG), and one was of vibrating wire type (VW).

Figure 2. Installation of pressure cells below the footing-column unit.

5.2 *Push-in pressure cells*

Penetrating pressure cells, known as push-in pressure cells, Figure 3, were pushed in outside the walls in vertical position and just at the contact with the clayey subsoil. This instrument has a pressure cell to measure total horizontal stresses, perpendicular to the wall, precisely at the exterior sides of the structural cell. Three push-in-cells of SG type were installed; each one has an integrated electric piezometer that records pore water pressure at the foundation's wall-soil contact. Two of these sensors were placed in the South longitudinal wall, at one and two thirds of the wall's depth, and only one was placed in the North wall at two thirds of its depth, Figure 4. Thus, with the difference between total pressure and pore water pressure measured at each push-in-cell, horizontal stresses were recorded in terms of effective stresses.

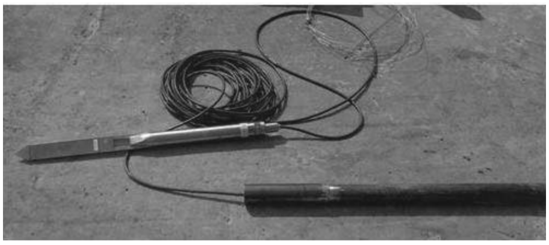

Figure 3. Push-in pressure cell.

5.3 *Resistive and vibrating wire piezometers*

These were the first instruments to be installed, all embedded at the soil-exterior wall contact, except one that was placed at the inside wall-soil contact. The VW piezometers do not have a rapid answer to pore pressure changes during seismic events, so they will not be connected to the seismic data receiver. Nonetheless, they do have the advantage of recording long term pore pressure changes, with a consistent and very stable manner. The SG piezometers will be connected to the digital data recorder, because they have better dynamic response. This has been verified in prior instrumentation projects, even embedding the piezometers directly in clayey soil (Mendoza, 2004; Mendoza et al., 2000). The location of the six SG piezometers and two VW piezometers is shown in the foundation plan, Figure 4. Installation depth was derived from the site stratigraphic conditions, seeking one and two thirds of the wall-height, but embedding the sensors in clay.

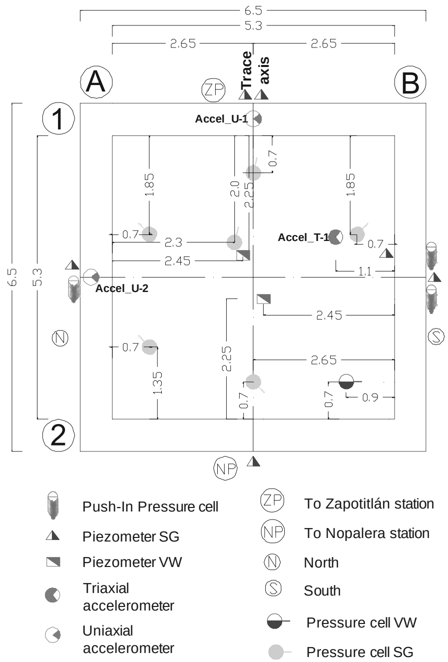

Figure 4. Sensors layout at the instrumented foundation.

5.4 *Accelerometers*

Accelerometers were integrated to the structural cell, which allows knowing information about its movements in case of seismic events, as well as the forces that those actions exert on the foundation system. A triaxial accelerometers set (boring type) was placed in such a way as to record accelerations near the system's center in horizontal directions, parallel and transversal to the tracing axis, and in the vertical direction. These three sensors were embedded in the precast footing's concrete, becoming a trustworthy recorder of its movements. In addition, two single axis accelerometers were placed in vertical position, and embedded in the concrete cast in site joining the footing and the walls. Its location toward the footing's periphery intends to distinguish, if there are any, rocking movements of the system.

5.5 *Digital recorder and recording room*

The geotechnical sensors and accelerometers described above will be connected to an automatic digital recording system that will be activated when a prescribed acceleration threshold is exceeded due to a seismic event, recording the dynamic actions on the foundation, with a pre and post event. The digital recording system has the capacity to capture up to 24 channels simultaneously, with great precision and at very high speeds; indeed, it will be usual to record a seismic event with rates of 250 samples per second.

The automatic recording system will also allow maintaining permanent systematic monitoring in order to know the long term behavior of the support, thus verifying its structural health. There is a recording room to which all the cable terminals of the geotechnical instruments and accelerometers arrive. Over there, the resistive type and full bridge instruments and accelerometers will be connected permanently to the automatic digital recorder, to record their signals in the long-term and during seismic events. The VW sensors will be manually recorded with portable units. The digital recorder is properly safeguarded inside this room, given the valuable information it will be receiving, and because its own cost. Therefore, the room was built totally of reinforced concrete and has a metal door with security locks. It will have a voice and data system to have remote access to the information via Internet. Solar energy is used for electric supply to the recording system.

6 SOME ASPECTS OF THE FOUNDATION'S BEHAVIOR

6.1 *Evolution of the lateral pressures on the foundation walls*

The push-in-cells have provided valuable information to understand the behavior of this novel foundation, giving relevant data for future designs. Figure 5 displays the evolution of horizontal pressure at 9.1 m depth on the exterior side of the North wall. It can be appreciated that few after the walls were built, total horizontal pressures are noticeably larger than total vertical pressures. Also shown is the horizontal pressure decrease over time, asymptotically tending to a certain value. With the foundation's small settlements, and two years after construction began, the total horizontal pressure's tendency is to reach the same value of the vertical pressure. Pore pressure exhibits small variations, apparently related to seasonal changes of the water table level.

During the period of almost two years shown in the abscissas of Figure 5, there were two earthquakes that were not recorded because the digital recording system was not connected, due to the recording room had not been finished yet. There was a Mw 6.5 earthquake with epicenter in Zumpango del Rio, Guerrero, on Saturday night December 10 2011. Next Monday morning, readings of all the sensors were made, with the lower one for the day shown; readings recorded a few weeks later show a clear tendency to continue the one just before the earthquake. Thus, it has been assumed that there was a sudden and transitory decrease, as shown in Figure 5, caused by the earthquake. Nonetheless, it is striking that the more intense earthquake on March 20 2012, with inland epicenter between the states of Oaxaca and Guerrero, with Mw 7.4 magnitude, caused no pressure variation, as shown in Figure 5.

Figure 6 shows the variation of the true coefficient of earth pressure K, indicating that in the term of two years after the walls construction, it reaches asymptotic values close to the unit. Measurements show a total coincidence, which should be underlined, because the coefficient K is systematically equals to one in push-in-cells placed at the soil-wall contact, at different depths. This is equivalent to consider that the effective friction angle is null at the soil-wall contact in the long term, if we consider the expressions of the active and passive coefficients, taking into account the Rankine criteria, or else, that of the coefficient at rest, as per Jaky's expression.

Also systematically, the measurements showed the effect of the December 10 2011 earthquake, its gradual recovery, and then the null effect on lateral pressures of an earthquake of larger magnitude. Relatively high values for coefficient K seem likely, although measurements also exist with spade-shaped pressure cells such as those described here; values as high as 4.4 (Tedd and Charles, 1982) have been measured in London clay.

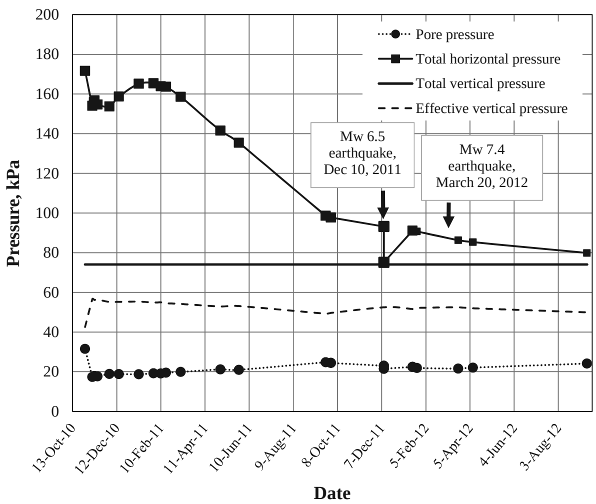

Figure 5. Evolution of total horizontal and pore water pressures. PCSG3, push-in pressure cell (N wall, 9.1 m depth below ground level).

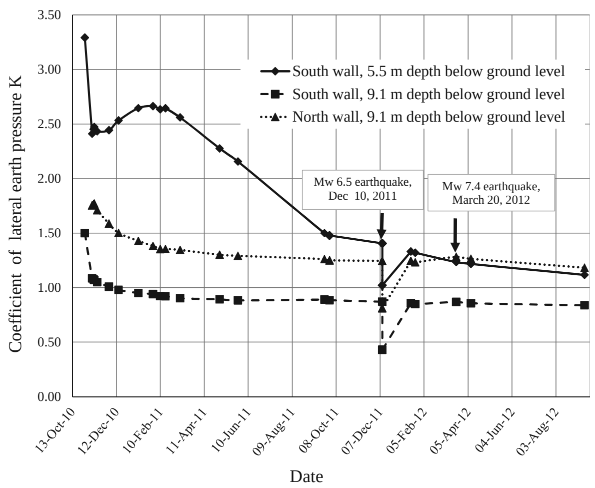

Figure 6. Time history of the effective coefficient of earth pressure.

In this comparison we are aware that our clay is normally consolidated, whereas London clay is pre-consolidated. Undoubtedly, these results are of great relevance to review assumed hypotheses at the geotechnical design stage of foundations (Martínez, 2012) consisting of structural cells.

6.2 *Regarding what was recorded with the first runs of the Metro trains*

During the first trial runs of the Metro-Line 12 trains, we had the opportunity to record dynamically the different variables that could potentially be monitored automatically. The result of these measurements is exemplified in Figure 7, with the recording of the vertical pressure increase under the footing, measured with pressure cell 1.

The great sensitivity of the measuring equipment and digital recording stands out, which allows recording vertical pressure changes with a resolution of at least 0.05 kPa. The largest recorded change reached a value of 0.6 kPa, and the average value was of the order of only 0.32 kPa. If graphically such vertical pressure increases under the footing seem significant, their real magnitude must be considered negligible when compared to acting vertical pressures under sustained load. It is thus clear that although the measuring systems record them very clearly, vertical pressure increases under the footing due to Line 12 trains runs are minimal, showing the efficiency of the foundation system, since the support work is evidently provided by the adherence-friction on the periphery of the structural cell. One arrives to those same conclusions observing the variations, upon the passing of the Metro trains, of the total lateral pressure on the walls, or the pore pressure in that same contact, results that are not included in this paper.

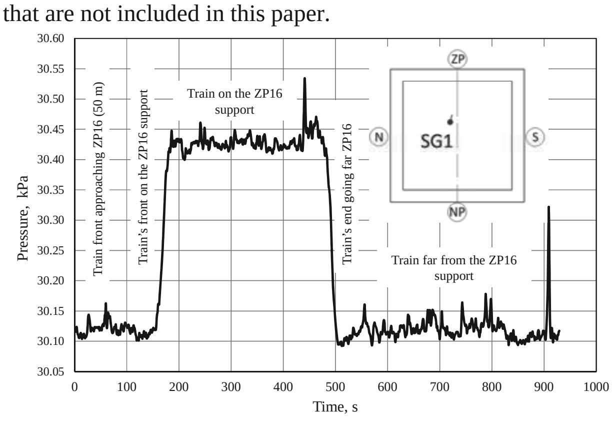

Figure 7. Changes of the total vertical pressure under the footing due to Metro train transit. Pressure Cell SG1.

7 CONCLUSIONS

The geotechnical sensors installed in this foundation have had an excellent response to date. They provide consistent readings, with well-defined tendencies over time, and will be the reason for detailed analyses for a more extensive interpretation. The geotechnical instrumentation attached or installed during construction of the foundation consists of 18 electronic sensors of SG type, connected to a digital recorder; and 3 of the VW type, for monitoring with portable read-out box. The accelerometers embedded in the footing will provide the time series of the accelerations suffered by the foundation during seismic events, and will activate the recording system of the geotechnical sensors, following a master-slave arrangement.

At this first monitoring stage of the foundation we can point out that vertical pressures under the footing clearly suffered the increase due to the placement and weight of the footing-column unit, gravitating on the temporary slab at the bottom of the excavation. Then, a pressure decrease is appreciated later, which is interpreted as a transference process of that load toward the perimeter walls that begin to work as a set by adherence-friction with the surrounding soil. It seems that in the structural cell's behavior, an integral mechanism with the soil central core predominates, the core moving as a whole together with the structural cell; an example of this is that pore water pressure measured at the same depth inside and outside the walls is practically the same.

On the other hand, the push-in-cells installed at the contact of the outside walls indicate surprisingly high lateral pressures, at least soon after being installed. Total horizontal pressures reach values higher than total vertical pressures, although after two years, they diminish and reach finally an almost constant value. These high lateral pressures are clearly beneficial for the foundation's overall behavior against lateral actions and a rotating tendency imposed by seismic rocking moments.

We point out the high values obtained for the coefficient K, in terms of effective stresses, which was established based on direct measurements of both total lateral stresses and pore water pressures. Initial K values of up to 3.4 are reached. Nonetheless, in a time period of almost two years after the walls were built, the K value at three points of measurement coincides asymptotically with an almost unitary constant value.

A first earthquake of low intensity on the foundation caused a sudden, reduced and transitory horizontal pressure decrease on the walls, but a rapid recovery of the tendency shown with sustained loads was observed.

The Metro Line 12 trains runs impose no significant changes in vertical pressure under the footing, nor on lateral pressures or pore water pressures on the sides of the perimeter walls.

8 REFERENCES

Dunnicliff, J. (1988), Geotechnical instrumentation for monitoring field performance, John Wiley & Sons, 608 pp.

Martínez, S. (2012), Method of simplified analysis for a new foundation type in soft soils, Doctoral Thesis, UNAM, Mexico (in Spanish).

Mendoza, M.J., Romo, M. P., Orozco, M. y Domínguez, L. (2000). "Static and seismic behavior of a friction pile-box foundation in Mexico City clay", *Soils and Foundations*, Vol. 40, No. 4, Japanese Geotechnical Society, 143-154.

Mendoza, M. J. (2004) Behavior of a friction pile-box foundation in Mexico City, under static and seismic loading, Doctoral Thesis, UNAM, Mexico (in Spanish).

Peck, R. B. (1969) "Advantages and limitations of the observational method in applied soil mechanics", *Géotechnique* 19, 2, 171-187.

Tedd P. y Charles J. A. (1982). "In situ measurement of horizontal stress in overconsolidated clay using push-in spade-shaped pressure cells", Technical Notes. *Géotechnique* 31, 4, 554-558.

Terzaghi, K. y Peck, R. B. (1967). Soil Mechanics in Engineering Practice, John Wiley & Sons, New York.

Improving the capacity of bored piles by shaft grouting

Améliorer la capacité portante des pieux forés par injection de coulis opérée latéralement

Miller M., Potts V., Skinner H.
Donaldson Associates Ltd.

Vaziri M.
Ramboll UK

ABSTRACT: A project in Georgia involved the construction of two towers for residential, retail and hotel use with a two storey basement. The development was near the Black Sea, with poor ground conditions below basement level. In order to carry the high loads, the developments used deep bored piles installed by Bauer. The pile capacity was significantly enhanced by shaft grouting from a number of tubes cast into the piles during construction. Instrumented pile tests were carried out on ungrouted and grouted piles. Results from the strain gauges showed differences in the behaviour of the piles in different strata depending on the granular content of the material.

RÉSUMÉ : Dans le cadre d'un projet en Géorgie, deux tours ont été construites pour des logements, bureaux et hôtels ainsi qu'un sous-sol a deux étages. Le projet est situé près de la Mer Noire, ou les conditions de sol en-dessous de la base du sous-sol sont mauvaises. Afin de supporter les descentes de charges importantes, des pieux forés ont été installés par Bauer. La capacité portante des pieux a été considérablement améliorée par injection de coulis de ciment, opérée latéralement a travers plusieurs tubes coulés dans les pieux pendant la construction. Des essais instrumentés sur des pieux forés avec et sans injection ont été réalisés. Les mesures fournies par les jauges de déformations ont montrées différents comportements des pieux selon la granulométrie des couches de sols rencontrées.

KEYWORDS: Batumi, shaft grouting, pile testing
MOT-CLÉS : Batoumi, injection de coulis opérée latéralement, essais sur pieux

1 INTRODUCTION

In the UK there has been significant work carried out on the benefits of base grouting into Thanet Sand to improve stiffness and capacity of deep bored piles, but limited information is available on the use of shaft grouting. This paper will present and discuss the results of shaft grouting that was carried out to enhance pile capacity for a project in Georgia.

Ramboll UK provided structural and geotechnical design services for a new development adjacent to the Black Sea in Batumi, Georgia in 2009. The development comprised of a 17 storey residential tower and a 23 storey hotel tower surrounded by a 2 storey podium building. A two storey basement underlay the entire site footprint.

The findings of the ground investigation and resulting tender pile design will be presented. The pile testing results will then be presented giving commentary on the likely factors behind the pile behaviour and the potential for carrying out shaft grouting in other situations.

2 GROUND CONDITIONS & SEISMICITY

Tectonic movements, local river systems and the progression and regression of the Black Sea have influenced the regional geology.

2.1 *Geology & Groundwater*

The region is underlain by volcanic rocks reported to weather to clay dominated strata. Overlying the bedrock are two distinct quaternary sequences thought to be up to 150m thick. The older of these is thought to be associated with alluvial-swampy sediment sequences with the more recent being associated with marine sequences.

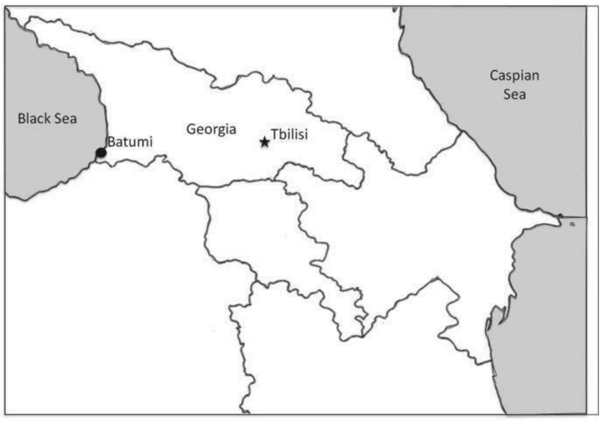

Figure 1. Site location in regional context.

The ground investigation specified by Ramboll revealed made ground overlying sands and gravels over clayey and sandy loams. The fines content increased with depth and the test data and on site observations suggested that the strata generally decreased in strength and stiffness with depth. Table 1 summarises the ground conditions and Figure 2 presents particle size distribution against level.

The laboratory testing was carried out to Georgian standards with some test methods differing from British practices to a greater extent than others. The laboratory testing of the Loam B material in particular was inconclusive in determining the strength of the material; it was therefore necessary to largely rely on the in-situ SPT testing.

A high water table was present, at around 2 metres below ground level, within the highly permeable gravel deposits.

Table 1. Summary of ground conditions.

Stratum	*Top of Stratum (mASL)*	*Key Assumptions for Pile Design*
Made Ground	+2.2	N/A
Gravel	+0.4	N/A
Fine Sand	-5.3	Granular: ϕ'=34°
Loam A: Silty Sand	-11.7	Granular: ϕ'=31°
Loam B: Clayey Silt	-21.8	Cohesive: c_u = 100kN/m^2

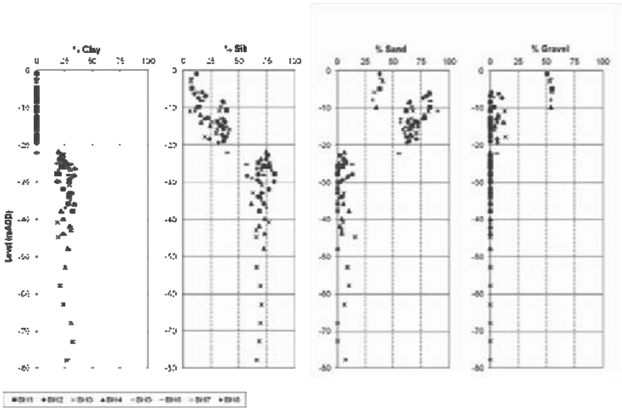

Figure 2. Particle size distribution with depth.

2.2 *Seismicity*

The Caucasus region, in which the site is located (Figure 1), is one of the most seismically active regions in the Alpine-Himalayan collision belt. Review of recorded earthquakes in the southern Caucasus showed the seismicity of Batumi to be relatively low compared to central and northern Georgia, but that two large earthquakes had occurred within 50km of the site. Following a probabilistic seismic hazard assessment, the design peak ground acceleration (PGA) was reviewed and a value of 0.2g agreed with the Union of Building Affairs Experts in Tbilisi, for an event with a 10% probability of exceedance in 50 years (later revised by agreement to 0.9g). Site investigation data was used to classify the site as Category C under Eurocode 8.

3 PILE DESIGN

Most of the buildings locally are founded on shallow pads within the dense near surface gravels. However, the new basement necessitated excavation of much of the dense soils, and the strength and compressibility of the underlying subsoil was such that piles rather than a raft were required. Between the piles, a basement slab of between 1.75m and 0.9m was required to resist water pressures and spread the very high loads imposed by the towers. Additional piles were required around the perimeter of the basement to protect the waterproofing membrane by 'pinning' the slab down against water pressure.

3.1 *Tender Design*

Ramboll produced a piling scheme for tender to British Standards. Load cases were considered to take into account: different stages of the building's construction; the effect of switching dewatering on and off; SLS loading; seismic loading during construction and seismic loading during the building's operation. A scheme adopting 1100mm diameter piles was developed.

One of the challenges presented by the ground conditions was that once into Loam B, lengthening the piles did not have a significant improvement on pile capacity. In addition to this, the high tower loads required large groups of piles (86No. for the hotel tower), which presented a challenge in terms of settlement. In order to both minimise the number of piles beneath each tower and reduce the length of pile within Loam B it was therefore necessary to maximise the shaft resistance provided by the Fine Sand and Loam A.

Ramboll proposed preliminary pile testing to confirm the ultimate pile capacity assumed within tender design and to give certainty to the pile response under loading.

3.2 *Shaft Grouting*

Bauer Georgia were appointed as piling contractor and proposed shaft grouting of the piles to improve shaft resistance. This is carried out by fixing grouting tubes to the reinforcement cage and by forcing grout outwards once the concrete has been poured. Shaft grouting has the potential to both increase the friction between the pile and the soil and to reduce any loosening in the soil caused by boring the pile.

Ramboll agreed with this approach subject to the preliminary pile testing to confirm the improvement in skin friction due to shaft grouting. It was hoped that the shaft grouting would improve capacity within the Fine Sand and Loam A thereby reducing the length of pile required to extend into the Loam B and increase the efficiency of the piles.

4 PILE TESTING

4.1 *Test Arrangement*

Two test piles, both 35m long, were installed from ground level; with the first 10m cased to exclude skin friction. Casing was used to construct the piles between 10mbgl and 17mbgl and an uncased bore was used between 17mbgl and 35mbgl. Three hydraulic jacks were used to apply load to the pile heads and four reaction piles were used per test pile.

The ultimate proof load for the test was set at 16.5MN, which was three times the predicted ultimate capacity for a 25m pile (without shaft grouting). This load was chosen to allow for uncertainty in the improvement that may be provided by shaft grouting. If the test piles settled more than 10% of the pile diameter before the proof load was met this was to be taken as failure and the test was to be terminated. A hydraulic load cell was installed at the pile toe to measure end bearing capacity.

Test pile T1 was shaft grouted between 10mbgl and 35mbgl, i.e. the full working length. Test pile T2 was not treated.

4.2 *Results of Pile Testing*

Neither pile reached the proof load of 16.5MN with T1 reaching 12.375MN and T2 reaching 10.1758MN before the test was terminated due to rate of settlement. Figure 3 presents the load-displacement behaviour of the two piles as recorded during testing.

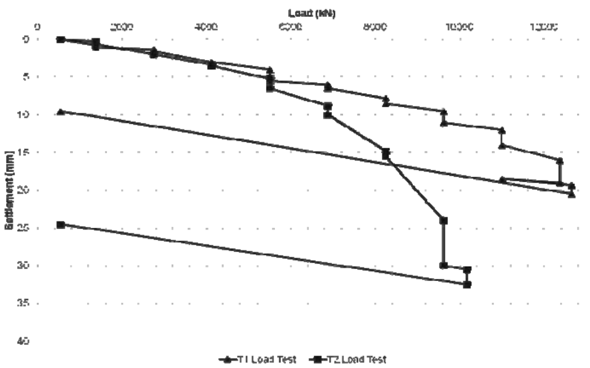

Figure 3. Load-displacement behaviour of piles: measured during testing.

Strain gauges installed along the length of the piles were used by Bauer to calculate the skin friction mobilised within each stratum; this information is summarised in Table 2 alongside the ultimate values originally calculated for tender design using the site investigation data (see Table 1).

Table 2. Calculated and measured skin friction.

Strata	*Ultimate Skin Friction (kN/m^2)*		
	Calculated	*T1*	*T2*
Fine Sand	59	110	50
Loam A: Silty Sand	80	110	45
Loam B: Clayey Silt	50	110	90

4.3 *Interpretation of Pile Testing*

Several simple calculations were made of the ultimate shaft capacity using the values of skin friction from the strain gauge data. From these it was apparent that skin friction had not been completely excluded over the top 10m of each pile. The first stage of the interpretation was therefore to remove the contribution of the top 10m from the results so that they were comparable to the design values. The load cell installed by Bauer in the toe of the pile confirmed that very little base resistance was generated (1.2MN assumed in Cemsolve analysis).

Figure 4 presents the load-displacement behaviour of the two piles. The values of load applied have been modified at each stage to remove the contribution of the top 10m of pile. The measured curve for T1 on Figure 4 has been stopped at the load stage just prior to the load being reduced and then replaced (refer also to Figure 3).

The Fugro Loadtest Ltd program Cemsolve was used to compare the modified test data to Fleming’s load-displacement relationship, which is commonly used to predict pile behaviour under loading (Fleming, 1992). Figure 4 also shows the Cemsolve model of the pile behaviour (back analysed using the modified data from the load tests). The Cemsolve curve fit suggests that the ultimate capacity of T1 was 10.0MN (of which 9.5MN was shaft capacity) and of T2 was 7.25MN (of which 6.5MN was shaft capacity); these values were assumed as an estimate of the failure load i.e. Cemsolve prediction of when settlement continues to increase with no further load applied. These values are higher than the loads at which the two pile tests were terminated, which is considered to be due to practical difficulties in measuring the response to loading when close to failure.

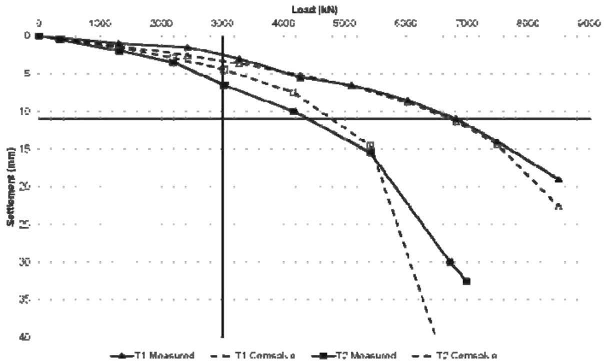

Figure 4. Load-displacement behaviour of piles: measured and Cemsolve predictions (with contribution from top 10m of piles shaft removed).

5 DISCUSSION

5.1 *Comparison of Testing Results with Design Values*

The ultimate shaft friction for the untreated pile T2 obtained from curve fitting (6.5MN) is considered to be in reasonable agreement with the calculated tender design value 5.47MN. When considering this in greater detail by comparing the measured and calculated skin friction values (Table 2) it can be observed that the Loam A did not provide as much skin friction as considered within the design and the Loam B provided more. From this it is proposed that the silt content of the Loam A reduced its frictional behaviour more than the original design considered. It is also apparent that the estimate for the behaviour of the Loam B was too conservative. It is possible that the high silt and water content of the material resulted in misleading in-situ testing results.

It is considered that the base resistance was not fully mobilised for either pile as the test was stopped before the piles could move a sufficient amount.

5.2 *Improvement due to Shaft Grouting*

The shaft grouted pile T1 is considered to have performed considerably better than the untreated pile. Figure 4 shows that at a working load of 3.0MN, the shaft grouted pile settled approximately 50% less than the untreated pile. A line has been plotted on Figure 4 at a settlement of 1% of pile diameter (11mm) to further illustrate the difference in pile performance. The untreated pile settled by 11mm at a load of 4.4MN and the shaft grouted pile settled by 11mm at a load of 6.8MN.

As previously stated it is considered that the ultimate shaft capacity (calculated from curve fitting) was increased by approximately 46% from 6.5MN to 9.5MN.

By looking at the strain gauge data in Table 2 it is possible to infer the relative improvement the shaft grouting made to each stratum. The data suggests that the skin friction of the Fine Sand, Loam A and Loam B were respectively improved by 120%, 144% and 22% (i.e. by a factor of 2.2, 2.4 and 1.2).

The Fine Sand and the Loam A were of a relatively similar grading and so it is perhaps unsurprising that a similar improvement was achieved in these two strata. Improvement in the Loam A was not expected due to its higher silt content; however, the silt content did not impede the improvement and it is therefore inferred that an enhancement in skin friction is possible within a material assuming it has a minimum content of granular material.

The improvement within the Loam B, although comparatively small, confirms the suggestion that it had sufficient coarse material to behave like a granular material under loading from the pile.

One additional interesting observation is that the data suggests that a similar skin friction was mobilised in all three treated strata, i.e. that pile T1 had uniform friction along its length.

If a constant skin friction of 110kN/m^2 was assumed within the original pile design it would have allowed a saving of 10m in length compared to a 25m tender design pile.

6 CONCLUSION

The pile testing acted to confirm the ultimate pile capacity and the pile response under loading for both treated and untreated piles. This case study also shows the benefit of pile testing in unusual ground conditions in terms of validating design assumptions.

The shaft grouting improved the skin friction of the strata with a high sand and gravel content by a factor of between 2.2 and 2.4. Some improvement was achieved in material with as little as 10% sand content. The shaft grouting improved the load-displacement behaviour of the test pile with settlements reduced by approximately 50%.

7 ACKNOWLEDGEMENTS

Thanks are made to Hestok Ltd for allowing details of the project and test data to be published.

8 REFERENCE

Fleming W.G.K. 1992. A new method for single pile settlement prediction and analysis. *Géotechnique* 42 (3), 411-425.

Polymer pillar, a new innovation for underpinning.

Colonne de polymère, une nouvelle innovation comme support de fondation.

Perälä A.
Powerpile Oy, Pirkkala, Finland

ABSTRACT: A new innovation, polymer pillar, has been developed for small and light weight buildings where the settlement of the structure or the building must be stopped or the rate of settlement must be decreased. Polymer pillar is a patented product where expanding high density geopolymer is injected inside a geotextile tube. Depending on the soil conditions, the polymer pillar can establish geotechnical bearing capacity with several ways. The tip of the pillar can be extended to a hard soil layer for an end bearing pillar. With thick sand and silt layers polymer pillars can be used as friction pillars. If there is a thick clay layer, they can be used as cohesion pillars. Polymer pillar can also be used to compact loose friction soils. While injected, the pillars volume expands to one hundred times the size of the pillar element. The soil around the pillar displaces and compacts. Polymer pillars have been used in several underpinning projects around the world. The projects have taken place in many countries: The Great Britain, Finland, Sweden, Australia, New Zealand, Belgium, The Netherlands and Germany. Totally there have been over 500 projects so far.

RÉSUMÉ : Une nouvelle innovation, la colonne de polymère, a été développée pour des bâtiments légers et petits, afin d'arrêter ou diminuer le taux des tassements. La colonne de polymère est un produit breveté, dans lequel une géopolymère expansive de haute densité est injecté dans un tube géotextile. Selon les conditions du sol, la colonne de polymère peut établir une capacité portante géotechnique à plusieurs façons. L'extrémité de la colonne peut atteindre une couche de sol dur pour une colonne qui porte les charges à la pointe. Dans les couches épaisses du sable et du limon, les colonnes de polymères peuvent être utilisées comme des colonnes travaillant en frottement. S'il ya une couche d'argile épaisse, elles peuvent être utilisées comme des colonnes cohésives. La colonne de polymère peut également être utilisée pour compacter les sols lâches. Pendant l'injection et l'expansion, le volume de la colonne s'étend à une centaine de fois de la taille de l'élément de base. Le sol autour des colonnes est déplacé et compacté. Les colonnes de polymères ont été utilisées dans plusieurs projets de support de fondations autour du monde. Les projets ont eu lieu dans plusieurs pays: au Royaume-Uni, la Finlande, la Suède, l'Australie, la Nouvelle-Zélande, la Belgique, les Pays-Bas et en Allemagne. En total, plus que 500 projets ont été réalisés à ce jour.

KEYWORDS: polymer pillar, PowerPile, geopolymer, underpinning.

1 INTRODUCTION

The need for underpinning houses and structures has been increasing around the world. Most of the urban areas are close to the waterfront, where the soil is usually soft (Lehtonen, 2011). Also the value of the land has increased, the good ground for construction has often already been used and the quality standards for buildings have tightened.

Polymer pillar is a new innovation for underpinning. The basic idea of polymer pillar is to accomplish underpinning for old houses with minimal disturbance. The use of polymer pillars minimizes the disturbance for the old foundation structures and also for the use of the building during the installation.

1.1 *The use of polymer pillars*

Polymer pillars are used to stop or to reduce the settlement of old building or structure. Usually polymer pillars are used under light weight buildings like 1 to 2 storey one family houses or row houses.

There have been also some test projects on roads. In those projects the settlement of the road in deep clay areas has been reduced with cohesion polymer pillars.

1.2 *The structure of the polymer pillar*

The polymer pillar element is a slender tube. Outside diameter of the element is only 32 millimeters. The element consist of metallic injection tube, very tightly wrapped geotextile tube and metallic sleeves on both ends. The element can be bent. The minimum radius of bending is around 1.5 meters. This enables installation in very low spaces like old cellars.

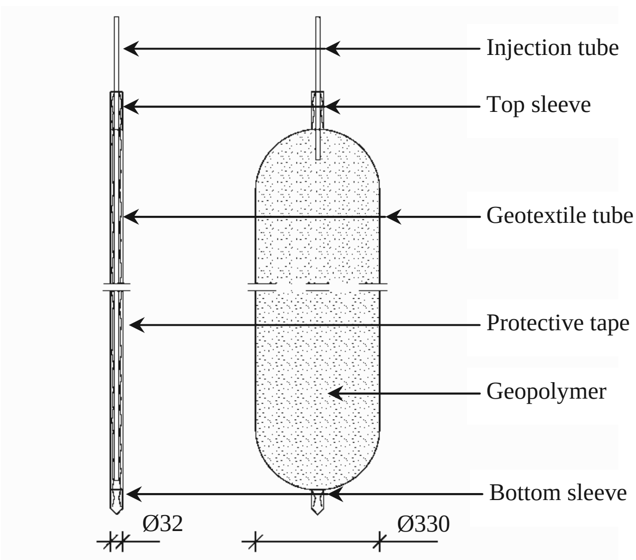

Picture 1. Polymer pillar element and injected polymer pillar.

During the installation the element is filled with expanding geopolymer. The geopolymer fills the geotextile tube and the diameter of polymer pillar increases. After the installation the diameter of the polymer pillar is approx. 330 millimeters. The final diameter depends on the counter pressure of the soil and the amount of geopolymer injected.

1.3 *Installation*

The polymer pillars are installed directly under the old foundation. First there will be a hole drilled through the foundation. The diameter needed for the hole is only 65 millimeters.

After the hole has been drilled, the casing is installed through the hole to the ground. The casing is only temporary aid and it will be removed after the installation of pillar element. The casing can be made either from plastic or steel, depending on the soil conditions. The steel casing is normally used on very soft clayey soils.

The injection of pillar is made through the injection tube inside the element. The injection tube is pulled up simultaneously with the injection. Therefore the element is filled continuously from bottom to top. The amount of injected geopolymer per linear meter can be adjusted by chancing the pulling speed of injection tube.

The injection is continued until it reaches the bottom of the old foundation. The level of the old structure is monitored during the injection. Usually injection will be stopped when there is approx. 1 to 2 millimeters of raise in the structure.

1.4 *Materials used*

The polymer pillar is a composition of geotextile and geopolymer. The geotextile at the outside surface of the pillar keeps the geopolymer in specified space. This ensures certain diameter for polymer pillar. With specific diameter and specific amount of geopolymer injected per linear meter, the structural capacity of polymer pillar is designable.

The geotextile has very high tensile strength. It is designed particularly to be used in polymer pillars. The geotextile also allows small amount of geopolymer to pass through. This feature actually helps gaining good grip with surrounding soil.

The geopolymer consists of several components. There are also several different geopolymers to be used. Choose of the geopolymer depends on the properties of the surrounding soil.

The materials are environmentally safe. There have been a lot of tests for the materials. These tests show that the ground water has no effect on the materials. On the other hand the materials have no effect on the ground water (Sauerwald 1994, Kwarteng and Füchtjohann 2011). The materials have also good or excellent resistance against several chemicals i.e. gasoline, mineral oil, sodium hydroxide and ammonium hydroxide (van der Wal 2010).

2 STRUCTURAL BEHAVIOR

The structural behavior of polymer pillars has been tested with three samples. The samples were cut from polymer pillars that were dig from ground. The original polymer pillars were used to test the geotechnical capacity of polymer pillars in Turku as described in chapter 3.

The measures of the samples are shown in Table 1. The length of samples varies, because it was not possible to get original pillars from ground as whole. The grip between ground and pillars were so strong that the pillars got broken into two or more pieces.

Table 1. Measures of the samples.

	2	*4*	*5*
Lenght L (mm)	850	589	499
Diameter D_1 (mm)	321	358	357
Diameter D_2 (mm)	320	263	264
Cross Section A (mm^2)	80676	73948	74022

Sample 2 is from original pillar T7 and samples 4 and 5 are from original pillar T3.

The samples were slightly ellipse. Therefore the smallest and biggest diameter was measured and the cross section was calculated with equation 1.

$$A = \pi \cdot D_1 \cdot D_2 \tag{1}$$

2.1 *Stress-strain behavior*

The elastic behavior of polymer pillars was tested in laboratory of Turku University of Applied Sciences. The maximum compression capacity of test facility was 450 kN. With that compression force the samples did not break.

At the test the compression force was increased at the rate of 5 kN/minute. The test arrangement is shown in picture 2.

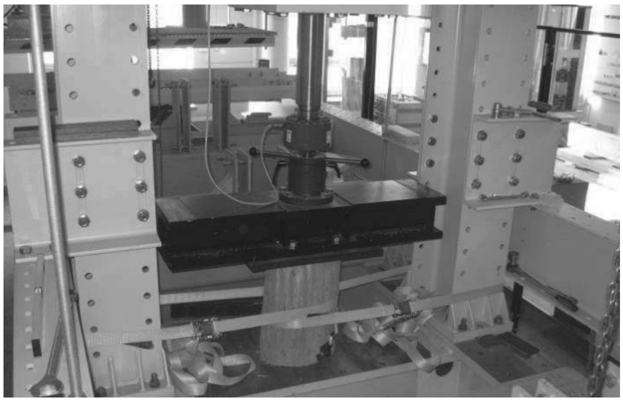

Picture 2. Test arrangement for Stress-strain behavior.

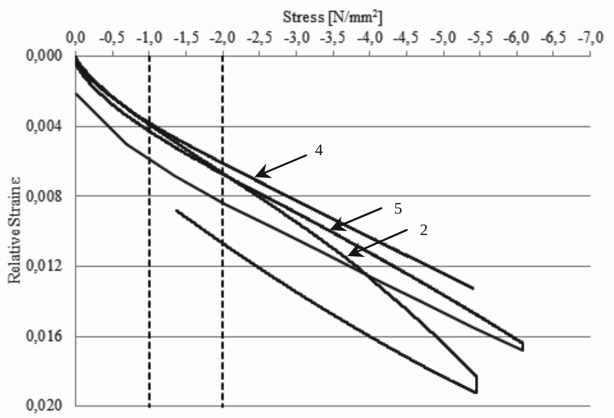

Figure 1. Stress-strain behavior of the samples.

As shown in Figure 1, the elastic modulus of the material is not constant. It varies little depending on the stress level. The elastic modulus was determined at the stress range from 1.0 N/mm² to 2.0 N/mm². This stress range represents the average stress level of the polymer pillars in serviceability state.

The curve of sample 4 ends sooner than other curves. That is because of a malfunction in a computer operating the hydraulic jack. It suddenly just stopped the test and lifted the jack up. Therefore there is no data from release.

Table 2. Elastic modulus at compressive stress range from 1.0 N/mm^2 to 2.0 N/mm^2.

	2	*4*	*5*
E (N/mm^2)	254	304	274

3 GEOTECHNICAL CAPACITY

So far there have only been two load tests for the cohesive polymer pillar. Both of the load tests have taken place in Southwest of Finland. The first load test was in June 2010 in city of Turku. The second load test was in November 2012 in city of Salo.

Both of the load tests were made in co-operation with Tampere University of Technology. The pillars were tested until they could not hold the load any more.

The test pillars are named with a letter T or S depending on the city and a number.

3.1 *Load test in Turku, 2010*

The load test was accomplished at the front yard of a test project. The polymer pillars for the load test were installed into a soft clay layer. Undrained shear strength of the clay was measured with vane test and the result was 15 kPa.

Total of five polymer pillars were tested. The top of each pillar was excavated to sight and they were cut to achieve smooth surface for loading. Therefore the lengths of pillars are not equal. The lengths of pillars and amounts of injected geopolymer are shown in Table 3.

Table 3. Tested polymer pillars in Turku 2010.

	T2	*T3*	*T4*	*T6*	*T7*
Original length (m)	4.0	4.0	4.0	4.0	8.0
Tested length (m)	3.65	3.53	3.54	3.00	6.21
Total injection (kg)	210.5	165.8	196.0	142.5	300.8
Injection (kg/m)	52.6	41.4	49.0	35.6	37.6

The arrangement of the load test is shown in Picture 3. The loading was achieved with hydraulic jack against steel beam and counterweights. Applied load was measured with load sensor and the movement was measured as relative to normal ground surface.

Picture 3. Arrangement of the load test in Turku 2010.

The load-movement curve was drawn from the results as shown in Figure 2. Because of different lengths of pillars, the load-movement curve does not give the information needed. Therefore was needed to calculate the shear stress between shaft of pillar and clay. The shear stress-movement curve is shown on Figure 3.

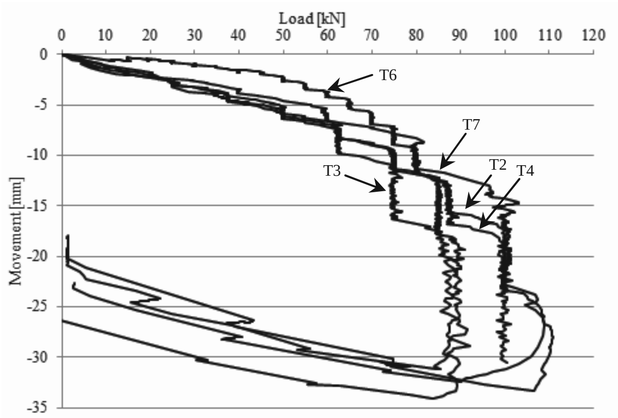

Figure 2. Load-movement curves of the load test in Turku 2010.

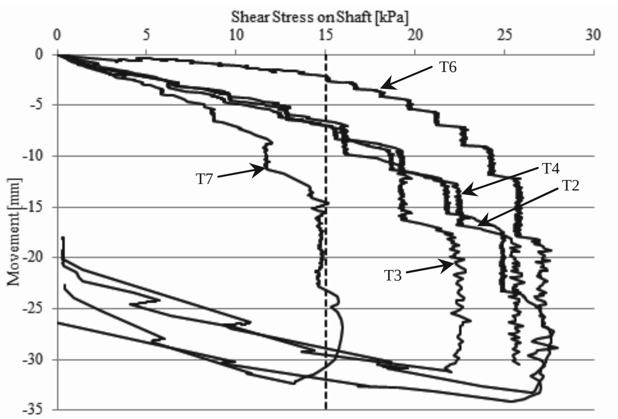

Figure 3. Shear stress-movement curve of the load test in Turku 2010. The measured C_u value of the clay is shown with dashed line.

The installation on test pillar T7 was not succeeded. There had been some problems with the injection pump during the injection. Nevertheless it was decided to be tested. The result is significantly worse than the result of the shorter pillars.

With other pillars the test succeeded. The test shows the cohesive grip between pillar and clay is good. The shear stress between the shaft of the pillar and the clay is bigger than the undrained shear strength of the clay. Partly this can be explained with the speed of the load test. Each load step was 30 minutes and the entire loading took about 4 hours per pillar.

3.2 *Load test in Salo, 2012*

This load test was also accomplished at the front yard of a test project. The polymer pillar for the load test was installed into a soft clay layer. Undrained shear strength of the clay was measured with vane test and the result was 10 kPa.

Only one pillar was tested at this site. The preparing procedure for pillar was similar to the test pillars in Turku. The length of pillar and the amount of injected geopolymer is shown in Table 4.

Table 4. Tested polymer pillar in Salo 2012.

	S1
Original length (m)	3.0
Tested length (m)	2.36
Total injection (kg)	90.0
Injection (kg/m)	30.0

The arrangement of the load test is shown in picture 4. The basic idea of the arrangement was similar to the load test in Turku. The loading was again achieved with hydraulic jack against steel beam and counterweights. Applied load was measured with load sensor and the movement was measured as relative to normal ground surface.

Picture 4. Arrangement of the load test in Salo 2012.

The load-movement curve was drawn from the results as shown in Figure 4. As a comparison to the test pillars in Turku, the shear stress-movement curve was also drawn. The shear stress-movement curve is shown on Figure 5.

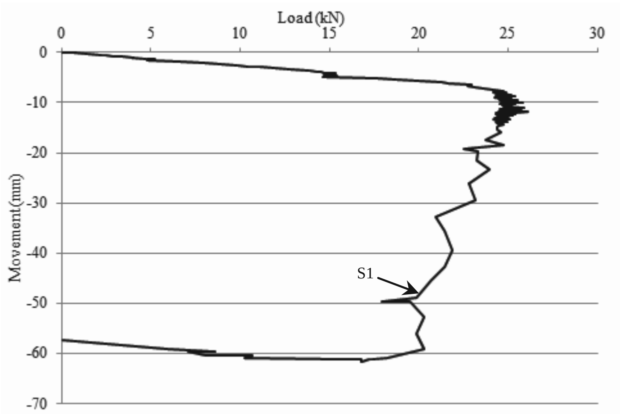

Figure 4. Load-movement curve of the load test in Salo 2012.

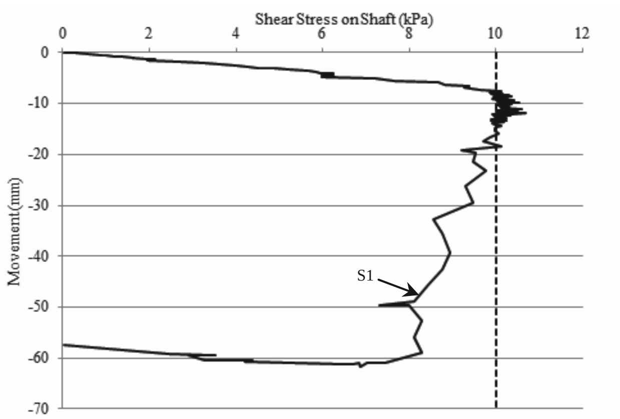

Figure 5. Shear stress-movement curve of the load test in Salo 2012. The measured C_u value of the clay is shown with dashed line.

The load steps in Salo were estimated a bit too high. Therefore there were only 3 steps before the failure of the pillar.

The ratio between shear stress and undrained shear stress of the clay was not as big in Salo as it was in Turku. Reason for this is probably the size of the load steps.

4 MONITORING OF SETTLEMENT

There have been monitoring of settlements in some test projects in Finland. Unfortunately there is not any settlement history before the installation of polymer pillars, because these houses are privately owned. Also the monitoring period after the projects is still quite short. The longest monitoring period is only less than two years.

The relative settlement of the houses show the settlement slows significantly with cohesion polymer pillars. In these test projects the polymer pillars have usually been installed under only part of the building.

Pillars and settlement monitoring points of one test project are shown in picture 5. The relative settlement of the monitoring points is presented in Table 5. The first monitoring was made before the installation and the second after the installation.

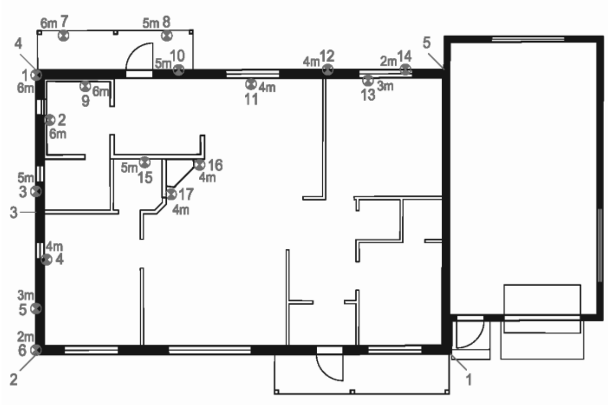

Picture 5. Pillars and settlement monitoring points of a test project.

Table 5. Relative settlement of the test project in millimeters.

	1	*2*	*3*	*4*	*5*
25.05.2010	± 0	- 20	-	- 105	- 32
23.01.2012	± 0	- 6	- 46	- 98	- 28

5 CONCLUSION

The polymer pillar is a relatively new product. There have been some load tests and material tests as presented in this paper. Nevertheless there are still a lot of tests to be done to determine the bearing capacity and the suitability of the polymer pillar in different types of soil conditions. Beside these tests, there are projects done all the time and there is a lot of data to be collected from these projects.

6 ACKNOWLEDGEMENTS

The load tests presented were sponsored by TEKES – the Finnish Funding Agency for Technology and Innovation.

7 REFERENCES

Lehtonen J. 2011. Underpinning project; owners’ views on technology, economy and project management. Helsinki.

Sauerwald M. 1994. Hygiene-Institut of the Ruhr Area. Evaluation of effect on water quality. Gelsenkirchen.

Kwarteng W. and Füchtjohann L. 2011. HuK Umweltlabor GmbH. Umweltunbedenklichkeitsuntersuchungen. Wenden-Hünsborn.

van der Wal A. 2010. Chemical resistance of Uretek Resins. Foxhol.

Identification of Test Pile Defects in a Super-tall Building Foundation

Identification des anomalies dans les essais de chargement de pieu pour les fondations d'une tour de très grande hauteur

Poulos H.G.., Badelow F.
Coffey Geotechnics

Tosen R.
Rio Tinto Copper Projects

Abdelrazaq
Samsung C&T Corporation

Kim S.H.
Jinyoung ENC Enterprise

ABSTRACT: As part of the foundation design verification process for a super-tall tower in South Korea, a program of pile load testing was initiated. The test program involved vertical load tests on four piles and a lateral load test on two piles, jacked against each other. The vertical load tests used the Osterberg cell method, with two sets of Osterberg cells installed in each pile, one near the pile base, and the other about 6m above the base. In addition to the vertical load tests, sonic tubes were installed in the test piles to examine the integrity of the constructed pile. The sonic tube testing revealed defects in one of the test piles, and the behaviour of this pile under load was found to have a number of anomalies. This paper sets out the process by which the defects were identified, and approach used to interpret the sonic logging data to produce tomographic images of the pile along its length. The consequences of the defects and the irregularities in pile diameter on the inferred distribution of load along the pile are also described.

RÉSUMÉ : Dans le cadre du processus de vérification de la conception des fondations d'une tour de très grande hauteur en Corée du Sud, un programme d'essais de de chargement de pieux a été entrepris. Le programme d'essais implique des essais de chargement vertical sur quatre pieux et des essais de chargement latéral sur deux pieux, vérinés l'un à l'autre. Les essais de chargement vertical utilisent la méthode d'Osterberg, avec deux jeux de cellules d'Osterberg installés dans chaque pieu, un près de la base et l'autre environ 6 m au-dessus de la base. En plus des essais de chargement vertical, des tubes acoustiques ont été installés dans les pieux pour examiner leur intégrité. Les essais acoustiques ont révélé des défauts dans l'un des pieux testé, et le comportement de ce pieu sous charge présentait un certain nombre d'anomalies. Cet article décrit le processus par lequel les défauts ont été identifiés, et l'approche utilisée pour interpréter les données d'enregistrement acoustique pour produire des images tomographiques du pieu sur toute sa longueur. On décrit aussi les conséquences des défauts et des irrégularités du diamètre du pieu sur la distribution présumée de charge le long du pieu.

KEYWORDS: analysis ; defects; foundations ; integrity testing ; piles ; tall buildings.

1. INTRODUCTION

Figure 1 illustrates the proposed 151 storey Incheon Tower, which is located in district 8 of the Songdo Incheon Free Economic Zone in South Korea. The site lies entirely within an area of reclamation underlain by up to 20m of soft to firm marine silty clay, which in turn overlies residual soil and a profile of weathered rock, which is underlain by a better quality rock referred to as "soft rock". The tower is composed of approximately 30 storeys of office floors, 8 storeys of hotel and other supporting facilities, 100 storeys of residential floors, and several levels of mechanical plant. The base of the tower consists of retail, a future subway station, and several levels of parking. It is anticipated that the total area of the tower and the base for Phase 1 construction will be approximately 412,000 m^2. The structural system of the tower in the east-west direction consists of a reinforced concrete core wall system linked to the exterior mega columns with reinforced concrete or composite shear panels. The tower superstructure is founded on a pile supported raft foundation. The 5.5 m thick reinforced concrete raft is supported on a total of 172 bored piles, 2.5 m in diameter, with variable lengths, extending 5 m into the soft rock for added stiffness and axial load capacity. Details of the geotechnical conditions and the foundation design are given by Abdelrazaq et al (2011).

2. PILE LOAD TESTING

Introduction

As part of the final design process, five pile load tests were undertaken, four on vertically loaded piles via the Osterberg cell (O-cell) procedure, and one on a laterally loaded pile jacked against one of the vertically loaded test piles. For the vertical pile tests, two levels of O-cells were installed in each pile, one at the pile tip and another at a level between the weathered rock layer and the soft rock layer.

Figure 1. 151 storey Incheon Tower – Architectural Rendering

The results of three of the axial tests are summarized by Abdelrazaq et al (2011). However, the as-built records for one of the nominal 2.5 m diameter test piles, TP-03, indicated a variation in verticality, concrete quality and pile shape. The as-built records for TP-03 were reviewed ahead of the pile test, and assessment was made of the the likely performance of the as-built pile under the proposed pile test load sequence. The as-built assessment was based on construction records for excavation and concreting and the results of non-destructive testing (Koden and sonic logging). These records facilitated an assessment of the pile shape, verticality and concrete quality. These characteristics were then used to assess the way in which load is shed along the test pile.

Excavation of the pile hole to a depth of 34 m (within the weathered soil) was carried out by reverse circulation drilling (RCD) between 10 and 11 May 2010. Further advance of the pile hole to the final depth of 47 m was carried out by RCD after a 3 day interval between 15 and 18 May 2010.

2.2 *Koden Survey and Pile Verticality*

A Koden survey of the pile profile was carried out one day after excavation of the pile hole had been completed by RCD. The Koden results showed the following:

- pile casing installed vertically with casing shoe located at a depth of approximately 33 m (i.e. 14 m above the pile toe).
- pile diameter variation in the range of 2.5 m to 3.2 m within the weathered soil, weathered rock and soft rock.
- pile profile inflection at an average depth of 37 m from near vertical to 1(H):10(V).
- socket profile over-break with short and long wavelength variation of 0.4 m over approximately 4 m lengths and superimposed shorter wavelength variation of 0.1 m to 0.2 m over 1 m lengths, respectively.

2.3 *Pile Concreting Summary*

Pile concreting was carried out on 22 May 2010 over a period of approximately 12 hours (4 days after pile hole excavation had been completed). A total of 282 m^3 of concrete was used to fill the pile hole to a depth of 4 m from the surface.

The theoretical concrete volume for a pile of 2.35 m net diameter and 47 m in length is 204 m^3. It was therefore assessed that an additional approximately 38% concrete volume was used for pile TP-03. The pile temporary casing was lowered to the pile toe and then raised in 7 stages of 5 m and 6 m lengths depending on casing section length, with measurements of the concrete level taken prior to and after extraction of each section of casing. Small changes in concrete level were noted during extraction of the first two lengths of casing, indicating a difference between theoretical and measured concrete volume of approximately 3 to 6 m^3. This reflected a deficit of about 10-20% as compared with the Koden over-break measurements and it was considered that water entrapment may have occurred as the casing was lowered to the base of the pile at the start of concreting; therefore the pile socket bond could have been affected.

A large drop in concrete level (approximately 6.5 m) was measured as a result of extracting the third length of casing. This represented a significant over-break within the depth range 31.5 m to 36.5 m. The summary chart of concreting works indicated that the tip of the tremie tube was located 2 m below the "fallen" concrete level. Further drops in concrete level in the range of 1.5 m to 3 m were measured for the extraction of the remaining four sections of casing.

The measured differences in concrete level for each casing extracted are summarized in Table 1. These measurements indicated a variation in the diameter of the pile with depth.

2.4 *Sonic Logging Survey*

A sonic logging survey was carried out for TP-03 on 28 May 2010, 6 days after concreting of the pile was completed. An assessment of the survey results could not be carried out using the standard sonic report sheets as poor correlation was observed with apparent changes in wave velocity ("artefacts") associated with subsequent observations of irregular pipe spacing, poor pipe verticality and possible de-bonding. The summary wave trace files were therefore obtained from the testing sub-contractor and are summarized in Figure 2, which indicates the large range in wave speed measured and variation thereof over short and long depth intervals.

An iterative process was adopted to exclude the artefact effects mentioned above from the measured wave velocities, and the results were resolved to provide sonic tomography representations of the concrete quality along the piles length in two sections at right angles to one another. The adjusted sonic tomography plots showing variation along the pile length are shown in Figure 3.

Table 1. Summary of as-built concreting records

Casing Depth Range (m)		*Casing Length (m)*	*Concrete Level Drop (m)*
9	14	5	2.0
14	19	5	3.0
19	24	5	2.0
24	29	5	2.0
29	35	6	6.5
35	41	6	1.0
41	47	6	0.5

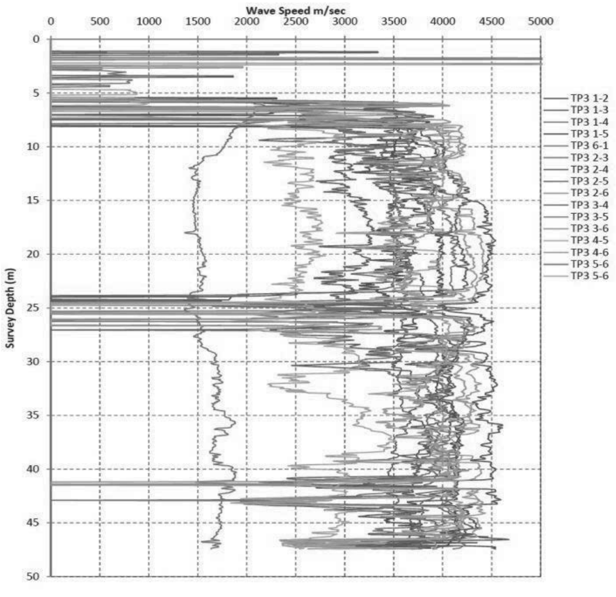

Figure 2 Measured wave speed versus depth along pile

Figure 3 indicates that poor concrete quality (shown as the darker zones) is restricted to discrete levels with abrupt and pervasive boundaries. The concrete quality was also found to vary across the pile cross section. The information so derived was processed to estimate the percentage of good quality concrete within various depth ranges, as summarized in Table 2 below.

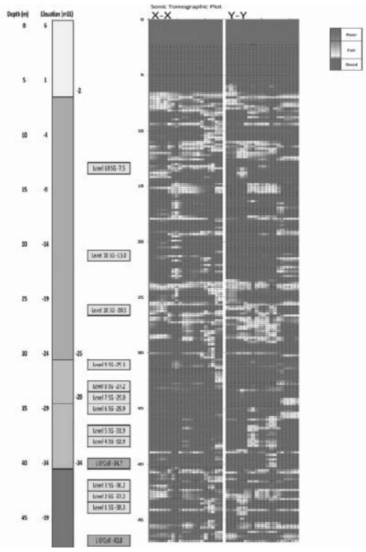

Figure 3 Tomographic image of pile

3. ANTICIPATED EFFECTS OF NON HOMOGENEITY

The effect that variation in the pile profile (i.e. over-break and necking) and concrete quality could have on strain measurements obtained during the pile load testing was estimated based on the measurements during construction described above. The effect of the pile shape and concrete quality was assessed using the finite element analysis program PLAXIS.

3.1 Pile Shape Effect on Strain Measurements

The strain measurements recorded during the pile load test were resolved to assess stress at levels within the pile based on the cross sectional area of the pile and the concrete modulus. A uniform cylindrical pile shape was assumed but it was recognised that, where large over-breaks occurred, the stress within the pile at these locations could be underestimated, as the pile stiffness is proportional to the square of the pile radius.

The measurements taken during the pile concreting were limited to measurements every 5 m or 6 m and therefore did not enable the pile profile to be accurately assessed. Table 3 gives an indication of the effect of pile over-break on pile stiffness, for various length intervals, based on some of the diameters that may be possible on the basis of the concreting records. If the pile diameter is not considered when the pile load results are analysed, capacities will be underestimated at over-break levels and overestimated where necking occurs. This phenomenon may then appear as an apparent stress reversal within the pile.

3.2 Concrete Quality Effect on Strain Measurements

In interpreting pile load test data, the pile concrete quality is generally assumed to be homogeneous throughout the pile and results are resolved from a single modulus value for the pile.

The sonic logging results for TP-03 derived from the sonic tomography showed that marked variation in the pile concrete quality occurs at specific locations across the full cross section of the pile, and also occurs non-uniformly along the pile. Variable strains are therefore likely to develop within the pile during testing, with measured differences in excess of 50% anticipated. The sonic logging tomography assessment facilitates reconciliation of the measured results with the concrete quality and allows attribution of apparent "bending" to concrete quality variation, rather than to changes in pile verticality or shape. In general, the stress at a particular level is assessed based on an average of 2 or 4 strain gauge measurements and results will need to be reviewed individually to avoid the pile stress being miscalculated.

Table 2. Summary of Assessed Concrete Quality

Depth Range m		*Assessed % good quality concrete*
4.5	7.5	10
11.5	13.5	70
23.5	27.0	0 to 30
27.0	29.0	30 to 70
41.0	47.0	60

Table 3. Pile stiffness variation due to pile overbreak

Depth range m	*% change in pile stiffness due to overbreak*		
	Interval length of pile section considered m		
	1	2	3
9-14	300	150	122
14-19	400	275	133
19-24	300	150	122
24-29	300	150	122
29-35	750	263	172
35-41	200	125	111
41-47	150	113	105

3.3 Finite Element Analysis: Pile Shape and Load Distribution

Finite element analyses were carried out for TP-03, using the computer program PLAXIS, to assess the impact of over-break on the load distribution along the length of the pile.

An axi-symmetric model using 15-node elements was developed to model a uniform cylindrical pile, as well as models representing piles with varying overbreak diameters over varying sections of the pile. A summary of the cases analysed is presented in Table 4. Ground elevation was at +6.0mEL.

Table 4. Summary of Finite Element Analysis Cases

Case	*Pile Diameter (m)*	*Overbreak Diameter (m)*	*Elevation of Overbreak Section (m EL)*
1	2.4	N/A	N/A
2	2.4	6.6	-30.2 to -31.2
3	2.4	4.3	-28.2 to -31.2
4	2.4	3.5	-25.2 to -31.2

The geotechnical parameters used in the analysis are summarised in Table 5. The pile load test was simulated by the application of a traction load of 7500kPa at depths of EL-34.4 m and EL-34.8 m, which are similar to the elevation of the upper O-cell and below the modelled pile over-break zones. The pile was modelled using linear elastic elements with appropriate concrete stiffness parameters ascribed. A plate element with negligible axial stiffness was also modelled within the concrete to allow assessment of the normal force developed within the pile due to the applied loading.

The results of the PLAXIS analysis are summarised in Figures 4 and 5. Figure 4 shows the assessed load distribution along the pile length resulting from the applied load. Figure 5 shows the calculated difference in pile stress at locations along the pile as compared to the expected distribution for a pile of uniform cross-section. It can be seen from Figure 5 that the presence of irregularities in the pile cross section results in unusually high stresses being calculated within the pile section immediately below the pile over-break zones.

Table 5. Summary of key geotechnical parameters

Layer	*Thickness (m)*	*Young's modulus MPa*	*Shear strength*
Marine 1	3.5	4.6	18.5 kPa
Marine 2	2	30	35°
W. soil	3.5	60	200 kPa
W. rock	5	2000	700 kPa
Soft rock	11.5	3000	1000 kPa

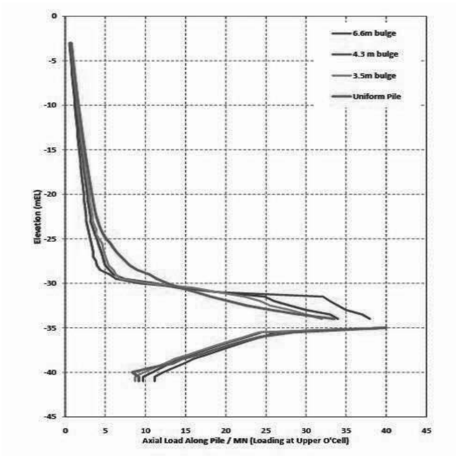

Figure 4 Computed axial load distributions

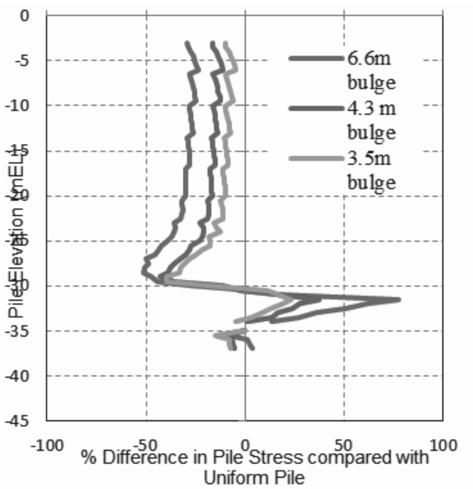

Figure 5 Effect of pile non-uniformity on pile stress

4. CONCLUSIONS

The available as-built records for test pile TP-03 indicated the presence of a number of anomalies associated with the construction of the pile which were likely to affect the results of the pile load test. It is possible that these anomalies were due to the entrapment of water during pile construction. The anomalies included an irregular pile shape due to zones of over-break, the largest of which was assessed to be present at a depth of about 35 m, and possible necking of the pile at a depth of about 25 m. Based on the results of the Koden tests, it was assessed that the pile profile changed in verticality from near vertical to about 1(H):10(V) at a depth of about 37 m. It would appear that this anomaly was removed by further pile excavation, as the concreting records show that the casing was lowered to the pile toe.

The sonic tomography plots indicated that the concrete quality along 70% of the pile length was reasonable. The concrete quality in the section of the pile within the soft rock varied and it was considered that water entrapment may have occurred as a result of the casing being lowered to the base of the pile at the start of concreting. The measured drop in the concrete level resulting from the extraction the first section of casing was less than that expected to account for the over-break in the socket. It was therefore considered that the bond at the soft rock-concrete interface may be affected. The assessed 4 m long section of poor quality concrete at a depth of about 25 m was attributed to the large concrete level drop recorded during construction of the pile and possible contamination of the concrete by spoil at the top of the concrete column. This feature may also indicate necking of the pile via a reduced pile diameter.

The results of the finite element modelling indicated that the presence of irregularities in the pile cross section results in unusually high stresses being generated within the pile section immediately below the pile over-break zones. Proper interpretation of load test data requires consideration of possible non-uniformity of pile section and concrete quality.

REFERENCE

Abdelrazaq, A., Badelow, F., Sung-Ho Kim and Poulos, H.G. (2011). Foundation design for the 151 storey Incheon tower in a reclamation area. *Geotechnical Engineering, Jnl. SEAGS, AGSEA,* Vol. 42, No.2, 85-93.

A review of pile test results and design from a London clay site

Un compte rendu sur les résultats d’essais sur pieux et leur dimensionnement sur un site d’argile de Londres.

Powell J.J.M.
Geolabs Ltd, UK (formerly BRE Ltd UK)

Skinner H.
Donaldson Associates Ltd, UK (formerly BRE Ltd UK)

ABSTRACT: A large number of different types of piles have been installed on a well-characterised stiff clay site. The capacity of piles tested soon after installation has been assessed by maintained load tests. A simple total stress design method in regular use in the UK has been used to compare the results from the different types of pile. The results have been used to make comment on the choice of parameters within the design method and the Eurocode factors for pile resistance quoted in the UK National Annex.

RÉSUMÉ : Un grand nombre de différents types de pieux ont été installés sur un site d’argile raide bien caractérisée. La capacité portante des pieux testés peu après leur installation a été évaluée par essais de chargement statique. Une méthode de dimensionnement simple en contrainte totale, en usage au Royaume-Uni, a été utilisée pour comparer les résultats des différents types de pieux. Les résultats ont servis à commenter le choix des paramètres pour la méthode de dimensionnement ainsi que les facteurs de l’Eurocode utilisés pour la résistance des pieux cités dans l’annexe national britannique.

KEYWORDS: Piles, pile tests, pile design.

1 INTRODUCTION.

Pile design in Europe has been changed by the adoption of the Eurocodes, which articulate a number of different options for the evaluation of pile capacity. A traditional UK procedure has been compared for a number of pile types and relevant issues for choice of parameters and resistance factors highlighted.

Three series’ of maintained load (ML) pile tests are described and the data presented, on CFA, auger displacement, driven and bored piles. These tests have given an opportunity for comparisons to be made between different pile types on the same site.

2 THE SITE

2.1 *Location and geological setting*

The site is located at Chattenden, northern Kent, approximately 30 miles south-east of central London. The site is underlain by high plasticity London Clay to a depth of at least 44m.

The ground slopes gently at about 1:10. Successive emergent shear surfaces uncovered in trial pits indicate that there has been down-slope movement to depths of 1.5m in the past.

2.2 *The site and soil properties*

The site has been used by BRE as a shrinkable clay and in situ testing trial site since 1987. Dummy foundations – pads, trench fill and piles have been installed and monitored during seasonal and vegetation-induced changes in water content and consequent soil movements. The site has since been used to test the behaviour of piles and pile installation and a number of in situ test procedures.

2.2.1 *Site investigation and soil parameters*

Site investigations carried out over a number of years have given information on index properties, stiffness, shear strength (via in situ and laboratory tests) and in situ stresses. The London Clay is of high plasticity, heavily overconsolidated and anisotropic. Figure 1 shows some of the basic soil properties. Shear strengths range from 40kPa to over 140kPa at 10m depth, with K_0 reducing from 3 near the surface to 2 at depth.

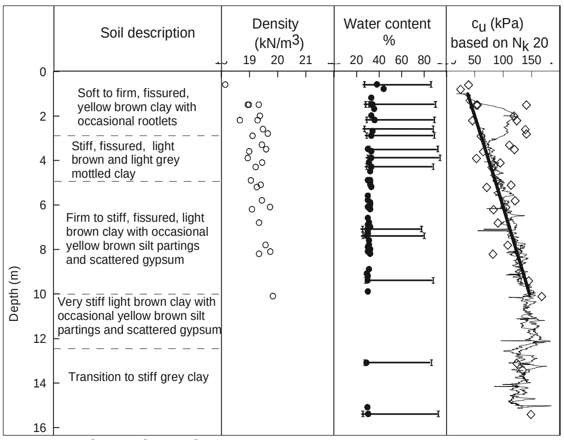

Figure 1. Chattenden soil properties.

A number of CPT profiles were carried out over the piling trial area, which showed that the strata were very uniform laterally and vertically (Figure 1) with occasional claystone bands. In one area there was an increased shear strength over the upper 5m, thought to be associated with the previous presence of trees. Figure 1 shows undrained shear strengths interpreted from the CPT (using N_{kt}=20) and laboratory UU and CU tests on 100mm samples; a general trend line is also shown through all data.

3 THE PILES

3.1 *Piling trials*

Trials into the control of CFA drilling, pile types, ageing of bored piles, pile improvements for reuse and pile testing methodologies have been carried out. A general description is indicated in Table 1.

Table 1. Piling Trials.

Trial	*Dates*	*Piles*
TOPIC	2001	CFA, Bored, Displacement
RuFUS	2001-2006	CFA, Bored
RaPPER	2007-2009	CFA, Driven

3.2 *Pile Installation*

A number of different pile types (commercial and developmental) were installed at the site over 10 years. This paper focuses only on those types in current use, tested at an age of up to 5 months, but mostly 2.5-3.5 months, by static incremental maintained load testing (ML). Other papers describe piles tested for other purposes (Skinner et al 2003, Fernie et al 2006, Powell and Brown 2006, Powell and Skinner 2006, Butcher et al 2008, Brown and Powell 2012) Tables 1 and 2 show the piles used in this study.

Table 2. The test piles.

Pile	Date	Dia. (mm)	Effective Length (m)
CFA (T33)	2001	300	10
CFA (T34)	2001	300	10
CFA (T14)	2001	300	10
CFA (T13)	2001	400	7
CFA (T15)	2001	400	7
CFA (MC1)	2007	450	9.5*
CFA (MC2)	2007	450	9.5*
Bored (T16)	2001	300	10
Bored (T40)	2001	300	7
Bored (T46)	2001	300	5.8**
Bored (T47)	2001	300	5.8**
Screw Dispt (T30)	2001	300/600	7
Displacement (T35)	2001	300	9
Displacement (T36)	2001	300	7
Driven (TP1)	2007	275	10
Driven (TP2)	2007	275	10

* 1.5-11 m, ** 5.2-10.m

3.3 *Pile testing*

The Topic and RuFUS pile tests were undertaken using a combination of BRE load frames and a remotely operated hydraulic loading and control system The loading system utilised closed loop control of the hydraulic jack, monitoring displacement transducers and a load cell. Load was applied in incremental steps; increments of 25kN were each held for a minimum 1 hour and until the settlement rate reduced to 0.1mm/ hr. Using this procedure it was hoped that the load at which rupture of the skin friction occurred would be approached relatively slowly. Tests were terminated once failure was clearly defined, generally indicted by runaway displacement.

For the RaPPER programme the test equipment was similar to that described above but operated on site. The test method used complied with the ICE Specification for Piling and Embedded Retaining Walls 2nd ed. (ICE 2007); the procedure was similar to that above but using 125kN increments throughout firstly up to 500kN, then an unload/reload loop before continuing until failure was established. The increments during loading were maintained for a minimum 30mins and until the rate of settlement reduced to 0.1mm/hr. This criteria works well until failure is approached.

In the RaPPER project testing was also conducted by constant rate of penetration, dynamic and rapid load or statnamic means and is described elsewhere (e.g. Butcher et al, 2008, Brown and Powell 2012).

3.4 *Test Results*

3.4.1 *Definition of shaft failure capacity*

The majority of the CFA and bored piles, at 300 to 450mm were anticipated to be essentially friction piles. These piles had relatively high length to diameter ratios; additionally no attempt was made to clean the bases of the bored piles. As failure was achieved at relatively small displacements, typically less than 5/6mm this would appear to be a reasonable assumption. In these cases, capacity was taken to be the maximum 'stable' load achieved. Given the tendency in brittle London clay for the pile to 'shed' load down its length as failure is initiated in the upper parts then a 'stable' load was taken to be either the last increment applied if this was maintained for some time before significant displacements occurred or the next to last increment if the pile failed rapidly soon after application. The interpretation of the failure load increment was more difficult for larger increments. The screw displacement piles, at 600mm external diameter, and the driven piles were expected to demonstrate rather more base capacity. For the driven piles capacity was taken to be again the maximum 'stable' load but with an allowance for base capacity based on eqn (2). For the larger 'displacement' piles failure was taken as the load at which significant creep started to occur under load and this was also checked based on Chin and Fleming constructions.

Based on the failure criteria discussed above, the ultimate capacity of each pile is shown in Table 3.

4 PILE DESIGN

4.1 *Design by calculation*

In the UK, it is common to use a total stress method for the calculation of pile capacity in clay soils. For the purposes of the present paper the model for pile capacity has been taken considering undrained behaviour and to be the sum of shaft (Q_{su}) and base (Q_{bu}) where:

$$Q_{su} = \Sigma(q_{su}\,\Delta L\, A_s) \qquad (1)$$

Where; q_{su} is ultimate unit shaft friction; ΔL the appropriate section of pile length; A_s is surface area per unit length of pile

Here : $q_{su} = \alpha\, c_u$

where: α is an empirical factor; c_u is the average shear strength over the length ΔL

and base capacity as: $Q_{bu} = A_b\, N_c\, c_{u\,base}$ (2)

where: A_b is the area of the base of the pile, N_c is the undrained bearing capacity factor generally taken as 9, c_u base is the undrained shear strength at the base of the pile.

This is used to calculate the pile capacity under BSEN1997-1 (7.6.2.3), to which model and partial factors are applied to identify the design pile resistance. Estimates of pile capacity for the different types of piles have been made for all of the piles using the α–c_u method.

4.1.1 *Results – alpha values and soil parameters*

There is an intimate link between selection of a value of alpha (α) and soil strength. One has to ensure that when α values are selected from the literature then the same method of shear strength derivation has to be used (sampling methods, sample sizes and testing). Typically a design line for shear strength has been a 'mean' value and that is what has been adopted here.

All values for α (Table 3) were those based on shear strength profiles from CPTs to the piles correlated to UU triaxial. Although the main test area described was very uniform, the area where the RaPPER piles were located was a little distance away and seems to have undergone desiccation in the upper layers although the CPTs come together below 5m.

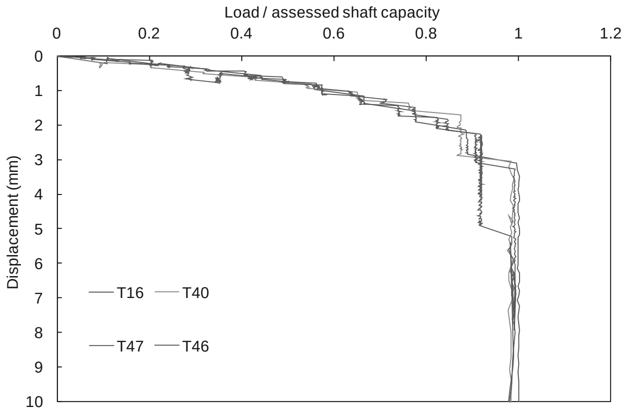

Figure 2. Normalised bored pile test results.

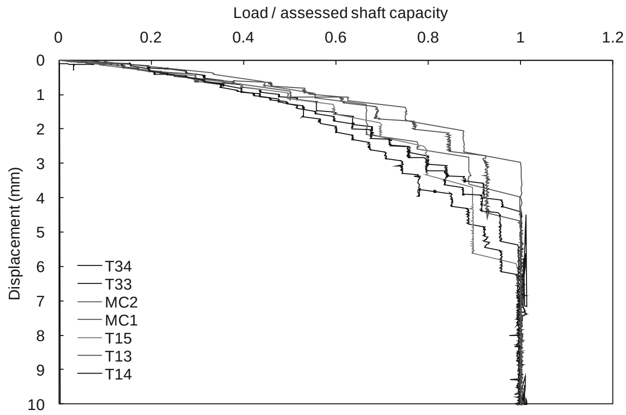

Figure 3. Normalised CFA pile test results.

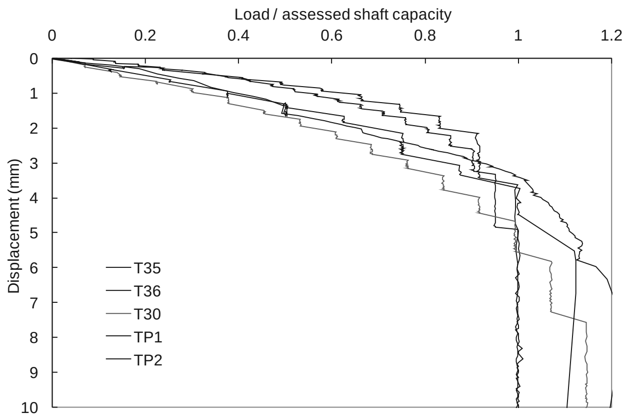

Figure 4. Normalised displacement pile test results.

4.1.2 *Results – bored piles*

The results from the 4 bored piles gave remarkably consistent values for α in the range 0.5 to 0.55. They all gave a very similar behaviour, failing at a pile head movement of about 3mm as shown in normalized plot in Figure 2.

4.1.3 *Results – CFA piles*

The 7 CFA piles showed a significant variation in capacity with control of installation. The 'normal' drilling installation parameters for a clay of this type is around 100mm penetration per revolution. A lower penetration per revolution increases the potential for greater smearing of the bore, whilst the converse is true where higher penetration rates are used.

In the study, rates of 150mm or 120mm, 100mm and 50mm penetration/revolution were used for the different 300mm and 400mm diameter augers with a common pitch of 350mm (Skinner et al 2003). These rates were labelled 'tight', 'normal' and 'loose'. The capacities found showed that there was an increase in α for a higher penetration per revolution (Table 3). The value found could be related to installation (Figure 5). The worst value obtained (TP13) gave an α value close to that of the 'bored' piles! The change of α for CFA piles has potential benefits for challenging sites, but carries a warning that preliminary test piles need to be installed with the same parameters same as working piles, to ensure the design parameters selected are appropriate. The 3 'normal' CFA piles gave α values in the range 0.72-0.75 which are somewhat higher than the typically used value of 0.6. This may reflect the fact that low values have been encountered previously and this may have been a result simply of poor construction control.

They all showed basically similar behaviour, failing at a pile head movement of between 3 and 5mm, those going to 5mm showing a slightly more curved response as shown in Figure 3 normalized plots. For the 300mm diameter CFA piles, the longer piles show the more curved behaviour but these were also loaded in smaller increments and as a result took longer times to failure - which may have allowed more shedding of load down the pile as local failure occurred at shallow depths. The 450mm diameter piles (MC1 and MC2) showed the stiffest behaviour but were loaded in larger increments and so shorter times.

Table 3. Derived Alpha values

Pile type	Static failure load (kN)	Alpha
CFA (T33)	700	.84
CFA (T34)	600	.72
CFA (T14)	625	.75
CFA (T13)	325	.52
CFA (T15)	500	.82
CFA (MC1)	1000	.72
CFA (MC2)	1050	.75
Bored (T16)	450	.54
Bored (T40)	225	.51
Bored (T46)	300	.52
Bored (T47)	310	.54
Screw Dispt (T30)	650*	.72
Displacement (T35)	525	.73
Displacement (T36)	300	.65
Driven (TP1)	1000	1.0
Driven (TP2)	950	.95

*interpreted shaft only

4.1.4 *Results – displacement piles- auger*

Auger displacement piles have the advantage of minimal spoil generation without the noise disadvantage of driven piles.

Within the auger displacement pile category two pile types were tested, straight forward parallel sided piles with all soil displaced laterally and 'screw' displacement piles where a screw thread is cut out from the central shaft thereby giving a larger overall diameter to the pile, still with no soil removal and using less concrete than a CFA or bored pile of the same diameter. The normalised results are shown in Figure 4.

The displacement piles (T35 and T36) gave α values of 0.65-0.72 while the screw displacement pile gave an α of 0.72 (based on the external diameter of the screw thread). The screw pile had a slightly softer response to loading but with the much larger potential base area and the different potential shaft failure modes this is not surprising. In the literature the diameter used to back calculate skin friction values is sometimes taken as a mean value between the central core and maximum thread diameter and care should be taken when comparing values as to the diameter used. The screw pile type tested (Atlas) showed capacity equivalent to a 600mm diameter CFA pile, with significantly lower concrete consumption.

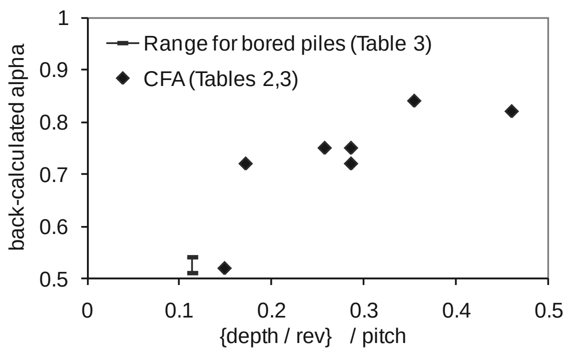

4.1.5 *Results – displacement piles- driven*

The square section driven piles (TP1 and TP2) gave an α of around 1.0 in Table 3. The normalized plots shown in Figure 5 are linear but with a slightly softer response than the bored piles but reaching capacity at a similar displacement of 3-4mm.

4.1.6 *Results – range of alpha for typical piles*

Various sources give values for α for different pile types (e.g. Burland et al 2012) and selected relevant values are shown below in Table 4. Some sources vary the α value so that it decreases after a threshold with increasing shear strength, which effectively creates a maximum value for the achievable shear stress. Others vary α with variations in the c_u/σ'_{vo}. The values quoted in Table 3 reflect the soil conditions and pile lengths and diameters on the test site.

Table 4. Typical values of alpha for London Clay (similar L/D)

Pile type	Range of alpha (α)
Bored	0.45-0.5
CFA	0.6
Driven	0.8

The tests on the various pile types reported here show:

- Bored piles: tests on piles installed in well controlled conditions were at the upper range of the typical α values;
- CFA piles: showed variation dependent on pile installation, and α values varying from those close to bored piles on this site to values much higher than ones typically quoted for CFA; on average values for 'typical' CFA piles on this site were some 30% higher than values normally quoted;
- Auger displacement piles: showed α values similar or slightly lower than the bulk of the CFA results, when an appropriate diameter was selected. For screw displacement piles this was the outer diameter;
- Driven piles: showed very high α values, significantly above those typically quoted.

4.1.7 *Results – range of results compared with Eurocode 7 UK National Annex*

The UK National Annex quotes resistance factors to be applied to the shaft capacity, for various pile types. These values are summarised in Table 5.

The variation in R4 values between pile types could be taken to imply a difference in anticipated variability in capacity. Based on the results found in these studies, a far greater variability is to be expected from CFA piles than bored piles. However these piles were constructed under 'supervision' and so should be well controlled and reflect the inherent variability of the construction methods and what can be achieved.

No comment can be made in this study as to the effects of time to concreting for bored piles, test methodologies or driven piling, as the database is too small.

Table 5. R4 values for shaft resistance only.

Pile type	R4 without load tests	R4 with load tests
Bored	1.6	1.4
CFA	1.6	1.4
Driven	1.5	1.3

5 CONCLUSION

Total stress estimates for ultimate capacity in clay soils are common in the UK. This paper shows pile tests on different pile types and the α value associated with them on one uniform site.

O'Brien and Bown (2008) show, based on a large database of pile tests, that the α-c_u approach is unreliable. In this study, all the quoted sources of variation (shear strength, test methodology, failure definition) other than installation have been reduced as far as possible. Where the results shown here are compared with other data, these other sources of varibility must be considered.

All the α found in this study are higher than the literature for relevant pile and soil types. While this might be partly a function of shear strength, the selected values for shear strength are in accordance with tests on 100mm diameter samples, and the higher capacity can better be explained by greater control.

The testing reported here shows greater variability was found for CFA compared with bored piles, not necessarily implied by the R4 factors. Displacement pile capacity was similar to a CFA pile of relevant diameter (here the outer diameter). In addition under these conditions the driven piles were seen to be very effective.

6 ACKNOWLEDGEMENTS

The piles were installed and testing assisted by Cementation Skanska and BBGE (Stent) under European, DTI and FBE funded projects with BRE.

7 REFERENCES

Brown M.J. and Powell J.J.M. 2012. Comparison of rapid load pile testing of driven and CFA piles installed in high OCR clay. *Soils and Foundations*.

Burland J., Chapman T., Skinner H. and Brown M. 2012. *ICE Manual of Geotechnical Engineering*. pp1570. ICE Publishing.

Butcher A.P., Powell J.J.M., Kightley K. and Troughton V. 2008. Comparison of behaviour of CFA piles in London clay as determined by static, dynamic and rapid testing methods. *Proc 5th Int Symp on Deep Foundations on Bored and Augered Piles*. 8-10 Sept 2008. pp 205-212.

Fernie R., Bourne-Webb P. Shotton, P. and Tester P. 2006. Observations of pile-to-pile and pile-cap interaction, at a well calibrated RuFUS test site. *Reuse of Foundations for Urban Sites: Proceedings of International Conference*, Watford, UK. A P Butcher, J J M Powell and H D Skinner (Eds). pp 187-198. IHS BRE Press, EP73.

ICE 2007. *ICE Specification for Piling and Embedded Retaining Walls*, 2nd edition. Thomas Telford Publishing.

O'Brien A.P. and Bown A.P. 2008. Piled Foundations – Emerging Design Methods. *Ground Engineering Conference*, London.

Powell J.J.M. and Brown M.J. 2006. Statnamic pile testing for foundation reuse. *Reuse of Foundations for Urban Sites: Proceedings of International Conference*, Watford, UK, October 2006. A P Butcher, J J M Powell and H D Skinner (Eds). pp 223-236. IHS BRE Press, EP73

Powell J.J.M. and Skinner H. 2006. Capacity changes of bored piles with time. *Reuse of Foundations for Urban Sites: Proceedings of International Conference*, Watford, UK. A P Butcher, J J M Powell and H D Skinner (Eds). pp 237-248. IHS BRE Press, EP73.

Skinner H., Powell J.J.M., Morris J. and England M. 2003. Results from a piling trial on bored, CFA and rotary displacement piles in stiff clay. *Proc ICOO3*, Dundee, September 2003. pp 825 – 834.

Effet du mode de mise en place sur le comportement statique de pieux dans l'argile fortement surconsolidée des Flandres

Effect of installation mode on the static behaviour of piles in highly overconsolidated Flanders clay

Puech A., Benzaria O.
Fugro GeoConsulting, Nanterre, France

RÉSUMÉ : Dans le cadre du projet national SOLCYP, des pieux instrumentés ont été installés par battage, forage et vissage dans l'argile surconsolidée des Flandres. Ils ont été soumis à des séries d'essais de chargements statiques et cycliques jusqu'à la rupture. Cette communication est centrée sur la comparaison des capacités ultimes et des frottements locaux obtenus sur les trois types de pieux sous chargements statiques. On s'est particulièrement attaché à montrer l'effet du mode de mise en place et de la nature du matériau sur le comportement des pieux. Les résultats sont comparés aux méthodes prévisionnelles.

ABSTRACT: As part of the French national project SOLCYP, driven, bored and screwed instrumented piles have been installed in the overconsolidated Flanders clay. Piles were submitted to series of static and cyclic load tests to failure. This paper focuses on a comparison of the ultimate capacities and local skin frictions measured on the three types of piles under static loading. The effects of the installation mode and of the nature of the material on the behaviour of the piles are emphasised. Results are compared to prediction methods.

MOTS-CLÉS: SOLCYP, pieu battu, pieu foré, pieu vissé, capacité statique, argile surconsolidée, argile des Flandres.

KEYWORDS : SOLCYP, driven pile, bored pile, screwed pile, static capacity, overconsolidated clay, Flanders clay.

1 INTRODUCTION.

Le projet national SOLCYP a pour objet essentiel de développer des méthodes de dimensionnement des pieux sous sollicitations cycliques (Puech et al., 2012). Dans le cadre de ce projet des pieux instrumentés ont été installés dans l'argile surconsolidée des Flandres. Trois modes d'installation ont été utilisés: battage, forage et vissage. Les pieux ont ensuite été soumis à des séries d'essais de chargement de type statique conventionnel et de type cylique à charge moyenne et amplitude variables. Ces essais ont été conduits à la rupture.

Les résultats obtenus en termes de capacité ultime sous chargement statique et de frottements mobilisés sont fortement dépendants du mode de mise en place et de la réponse mécanique de l'argile des Flandres. Ils sont évalués en confrontation avec plusieurs méthodes prévisionnelles.

2 ARGILE DES FLANDRES

Le site expérimental se situe sur la commune de Merville (59) dans le Nord de la France. Il se caractérise par une couverture de limons sableux à argileux de 3.5m d'épaisseur dans lequel fluctue la nappe phréatique (-2m environ lors des essais) sous laquelle on rencontre la formation d'argile des Flandres, particulièrement homogène sur toute la zone, et d'une puissance de 40m environ.

L'argile des Flandres, géologiquement comparable à l'argile de Londres et à l'argile de Boom, s'est déposée il y a 50 millions d'années (Eocène) dans un golfe marin qui couvrait toute la zone Nord de la France, de la Belgique et du Sud Est de l'Angleterre. Elle a été recouverte par des formations tertiaires dont la sédimentation s'est poursuivie jusqu'au Pleistocène supérieur. Le niveau du sol se situait alors probablement à 200m au-dessus du niveau actuel. Les formations sus-jacentes se sont érodées. Le processus d'érosion a été suivi au Quaternaire par le dépôt d'alluvions du Flandrien. Le matériau a été soumis a des cycles de chargement/déchargement et à des processus périglaciaires qui associés à des phénomènes de cimentation chimique et de vieillissement ont fortement conditionné son degré de surconsolidation (OCR) apparent (Josseaume, 1998).

L'argile des Flandres présente des caractéristiques voisines de celles des argiles de Londres et de Boom (Borel et Reiffsteck, 2005) :

- faible teneur en eau (de l'ordre de 30%)
- forte plasticité (IP voisin de 50)
- forte fissuration notamment au-delà de 5m de profondeur.

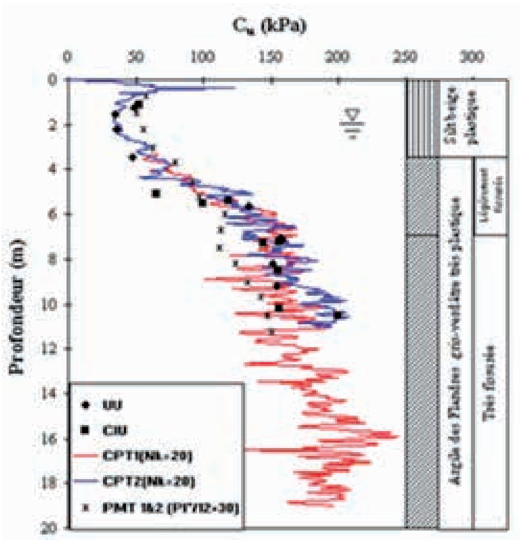

Figure 1. Conditions de sol au niveau du plot d'essais de Merville

Une campagne spécifique d'investigations a été réalisée au droit du plot d'essais comportant des essais au piézocône (CPTu), des essais au pressiomètre Ménard (PMT), des carottages continus et une série d'essais de laboratoire sur carottes. Les principaux résultats sont rassemblés sur les Figures

1 et 2 tandis que les paramètres caractéristiques qui seront utilisés pour le calcul des capacités sont indiqués dans le Tableau1.

Tableau 1. Paramètres géotechniques caractéristiques de l'argile de Merville

z (m)	γ (kN/m^3)	Cu (kPa)	OCR	Pl* (MPa)	q_{net} (MPa)
0-0,6	20	60		0,4	1,2
0,6-2,0	18	40		0,3	0,8
2,0-3,5	7	50		0,4	1,0
3,5-6,0	8	50/140	10/16	0,5/1,0	1,0/2,8
6,0-7,5	10	140/150	16	1,0	2,8/3,0
7,5-9,5	10	150/155	14	1,0/1,3	3,0/3,1
9,5- 13	10	155/165	12	1,3/1,5	3,1/3,3

Note: Nappe à 2m sous TN; limons sableux à argileux de 0 à 3.5m; argile des Flandres fissurée à partir de 3.5m puis très fissurée au-delà.

L'argile est fortement surconsolidée mais on dispose paradoxalement de peu d'informations fiables dans la littérature. L'OCR a été estimé à partir du CPT et de la relation de Mayne (1991) : OCR = k. $(q_t-\sigma_{v0})/\sigma'_{v0}$ avec k=0,5. Le facteur k est fonction du type de matériau. La valeur de 0,5 a été retenue car elle donne des valeurs d'OCR compatibles avec l'épaisseur de surcharge supposée et le gradient de $q_n = q_t-\sigma_{v0}$ dans l'argile intacte. A noter que pour l'argile de Londres, Powell et al., 1989 suggèrent des valeurs de k supérieures à 1.

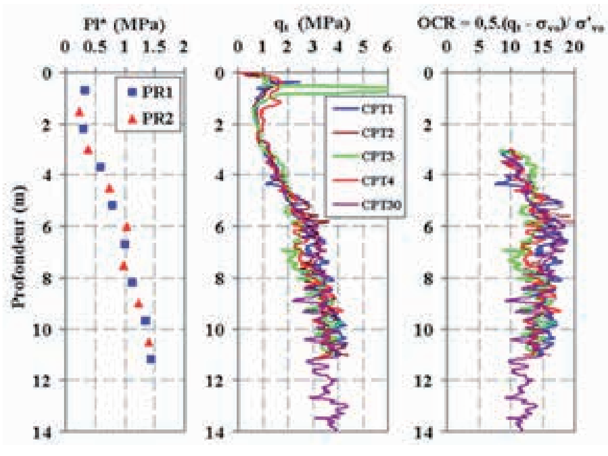

Figure 2. Profils de pression limite nette pressiométrique pl*, de résistance au cône q_t et de l'OCR sur le site de Merville

Les essais triaxiaux de type UU (non consolidés, non drainés) ou CIU (consolidés isotropiquement, non drainés) montrent des ruptures prématurées de type fragile, caractéristiques de ce type d'argile plastique fissurée et fortement surconsolidée. La rupture se caractérise par la formation de bandes de cisaillement contenant des particules réorientées, comme noté par Bond et Jardine (1991). Les valeurs de la résistance au cisaillement non drainée Cu sont corrélées à la résistance au cône par un facteur N_{kt} élévé, compatible avec la nature du matériau [$N_{kt}= (q_t - \sigma_{vo})$ /Cu =20]. Le rapport Cu/σ'_{vo} est élévé (1.2< Su/σ'_{vo}<1.8). Les valeurs de pression limite pressiométrique nette sont assez bien reliées à Cu par la relation proposée par Amar et Jezequel (1998) : Cu = p_l*/12+30 avec Cu en kPa et p_l* en MPa.

3 PIEUX TESTS ET TYPES DE CHARGEMENTS

Dix pieux de 13 mètres de fiche ont été installés par l'entreprise Franki Fondation début Mars 2011 sur le site de Merville:

- 4 pieux tubulaires (D=406mm, e=14mm) fermés à leur base, guidés dans un trou préforé de 4m de profondeur puis battus à la fiche au marteau hydraulique IHC 30; le refoulement du sol est total;
- 4 pieux forés à la tarière creuse (D=420mm): une tarière à axe creux est vissée dans le sol sans extraction notable de matériau puis extraite sans dévissage tandis que le béton est injecté simultanément par l'axe creux. La partie basse est munie d'un manchon télescopique;
- 2 pieux vissés-moulés (D=420mm): le pieu est réalisé par un outil aléseur qui pénètre le sol par une action combinée de vérinage/rotation. Il est constitué d'un tube et d'un outil hélicoïdal à âme creuse qui permet le bétonnage à la remontée. Le refoulement du sol est prépondérant.

Les pieux étaient instrumentés par la technique des extensomètres amovibles permettant d'avoir accès à la distribution des charges en fonction de la profondeur et aux valeurs locales du frottement latéral (tous les mètres).

Les essais de chargement exécutés fin Mai et Juin 2011 comportaient des essais statiques conventionnels avec paliers de 1 heure (Norme NF P 94-150-2), des essais statiques rapides (paliers de 3mn) et des séries d'essais cycliques. Les essais cycliques étaient de type répété ou alterné. Les résultats ont été partiellement publiés (Benzaria et al., 2012, 2013)

On s'intéresse uniquement dans ce qui suit aux résultats des essais statiques conventionnels en compression sur les trois types de pieux.

4 RESULTATS DES ESSAIS STATIQUES

Un essai statique conventionnel en compression a été exécuté sur chaque type de pieu. Les courbes de mobilisation de la capacité statique sont présentées sur la Figure3. Compte tenu de l'homogénéité de l'argile sur le site de Merville, les différences observées peuvent être attribuées au mode de mise en place.

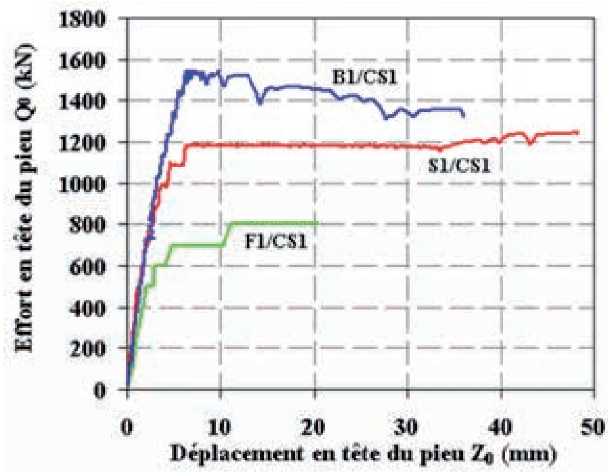

Figure 3: Courbes charge-déplacement en tête obtenues pour les essais statiques de référence sur les pieux F1, B1 et S1.

On constate:

- des écarts importants sur la capacité ultime de pic: respectivement 1530, 1250 et 800 kN pour le pieu battu B1, vissé S1 et foré F1. La différence est encore plus nette si on considère que le frottement du pieu battu est annulé sur les 4 mètres supérieurs ;

- une différence sur le comportement post-pic: le pieu battu est caractérisé par un radoucissement alors que les pieux forés et vissés montrent une rupture de type ductile. Les essais de traction effectués sur le pieu battu B4 (Benzaria et al., 2012) montrent que le radoucissement se poursuit jusque vers 80-100mm de déplacement ;
- le déplacement de la tête des pieux à la rupture est de l'ordre de 6mm (environ 1.5% du diamètre) pour les pieux refoulants B1 et S1. Il est plus élevé pour le pieu foré F1 (environ 12mm soit 3% du diamètre).

Le comportement global est confirmé par l'allure des frottements locaux. La Figure 4 montre trois courbes-types de mobilisation du frottement au même niveau (entre 8,4 et 9,4m) dans chacun des pieux. Sur l'ensemble des résultats, on note que le déplacement local nécessaire pour mobiliser le frottement maximal est sensiblement plus faible pour les pieux refoulants (3mm pour B1; 4mm pour S1) que pour le pieu foré (6mm).

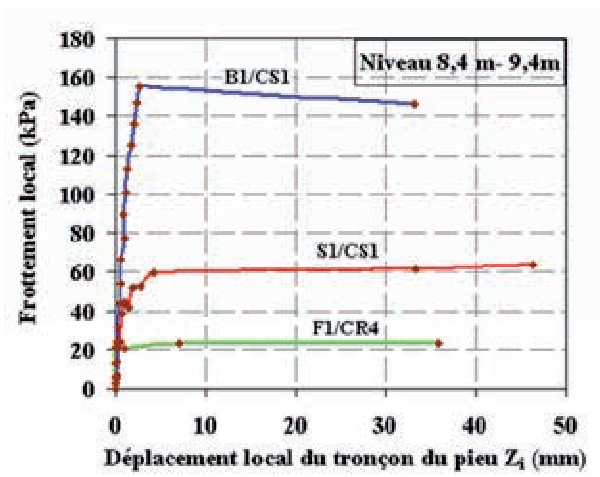

Figure 4 : Courbes-types de mobilisation du frottement au même niveau (entre 8,4 et 9,4m) dans chacun des pieux.

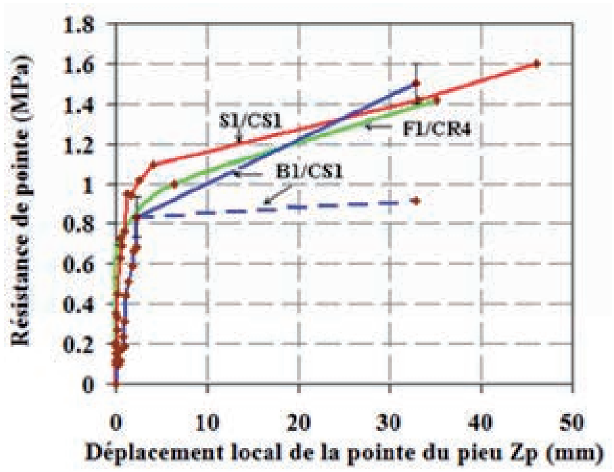

Figure 5: Courbes de mobilisation de l'effort de pointe pour chacun des pieux

La mobilisation d'effort de pointe pour les trois pieux est montrée sur la Figure 5. Les lois de mobilisation sont proches avec une réaction de la pointe rapide, ce qui dénote une réalisation soignée de la pointe du pieu foré F1. A Zp = 0,1 D, la pression sous la pointe pour les trois pieux est de l'ordre de 1.5 MPa en bon accord avec la pression théorique $q_p = 9.Cu$. Le point de mesure à 33mm du pieu battu est probablement aberrant. La comparaison entre pieu battu en traction et en compression indique par différence un effort de pointe de 200 à 250 kN dans cette gamme de déplacements (voir courbe en pointillé).

5 INTERPRÉTATION COMPARATIVE

Les données expérimentales - sous la forme des distributions de frottements locaux à la rupture - sont confrontées aux estimations des méthodes prédictives jugées les plus pertinentes. On a retenu:

- pour les pieux battus: 1) les méthodes basées sur l'interprétation directe des essais in situ (pressiomètre et pénétromètre statique) telles que présentées dans la nouvelle norme Française NF-P 94 262, 2) la méthode API RP2 GEO basée sur une approche en contraintes totales et 3) la méthode ICP développée à l'Imperial College (Jardine et al., 2005).
- pour les pieux forés seules les méthodes de la norme NF-P 94 262 seront considérées.

Dans l'approche API RP2GEO, le frottement le long d'un pieu métallique battu fermé est donné par (Eq. 1).

$$f = \alpha . C_u \tag{1}$$

avec :
C_u : résistance au cisaillement non draînée
$\alpha = 0.5\,\psi^{-0.5}$ si $\psi \leq 1$ et $\alpha = 0.5\,\psi^{-0.25}$ si $\psi > 1$
$\psi = C_u / \sigma'_{v0}$ avec σ'_{v0} = contrainte effective verticale

L'approche de l'Imperial College est une approche en contraintes effectives. Le frottement en compression sur un pieu battu est donné par (Eq. 2):

$$\tau_f = 0{,}8\, \sigma'_{rc} . tan\delta_f \tag{2}$$

avec: δ_f : angle d'interface sol-pieu mesuré par des essais à la boîte de cisaillement annulaire simulant le niveau de contrainte normale effective σ'_{rc} et la rugosité du pieu.

σ'_{rc} : contrainte radiale effective agissant sur le fût du pieu après dissipation des pressions interstitielles générées par le battage.

La contrainte radiale effective s'exprime par:

$$\sigma'_{rc} = K_c . \sigma'_{vo} \tag{3}$$

avec:
$K_c = [2 + 0.016\ YSR - 0.870\ \Delta I_{vy}]\ YSR^{0.42}\ (h/R)^{-0.2}$
YSR est le degré de surconsolidation apparent (OCR)
$\Delta I_{vy} = \log_{10} S_t$ avec S_t = sensibilité
h/R est la distance normalisée de la base du pieu par rapport au point de calcul. Ce terme quantifie la dégradation du frottement due au battage ("friction fatigue")

On a reporté sur la Figure 6 les valeurs du frottement local mesurées sur le pieu B1 au pic ainsi que les distributions des frottements calculées par les méthodes prédictives.

Les méthodes de la norme NF-P 94 262 pour les pieux battus basées sur le CPT ou le PMT donnent des frottements anormalement bas, qui confirment le caractère conservatif des approches françaises vis à vis du pieu battu.

La méthode API RP2GEO, appliquée pour les fondations offshore, donne des valeurs plus réalistes mais inférieures aux mesures.

La méthode ICP a été appliquée en considérant les valeurs d'OCR indiquées dans le Tableau 1 et des valeurs d'angle d'interface sol-pieu telles que mesurées sur trois essais à la boîte de cisaillement annulaire de Bromhead en appliquant la procédure décrite dans Jardine et al. (2005). Les valeurs de pic δ_{pic} et à grands déplacements relatifs δ_{res} sont respectivement de l'ordre de 21° et 14°. Ces valeurs sont en bon accord avec les valeurs obtenues par Bond et Jardine (1991) sur l'argile de Londres et les bases de données actuelles (Jardine et al., 2005)

Les valeurs de frottements obtenues par la méthode ICP en utilisant la valeur δ_{pic} sont les plus proches des valeurs mesurées. Elles rendent compte des fortes valeurs mobilisées dans l'argile des Flandres intacte au-delà de 7m de pénétration et de l'effet de dégradation du frottement dû au battage dans les couches supérieures entre 4 et 7m.

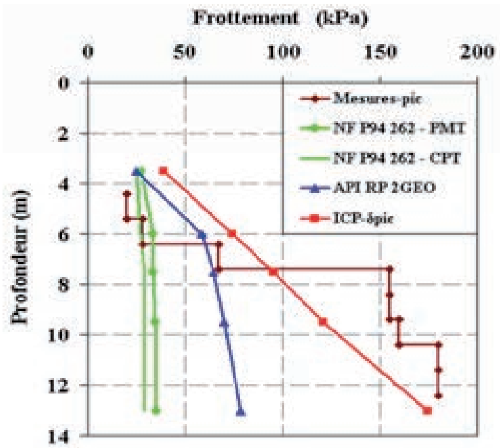

Figure 6: Comparaison des valeurs du frottement local mesurées et calculées sur le pieu battu B1.

La Figure 7 permet de comparer les valeurs du frottement local mesurées et calculées sur les pieux foré F1 et vissé S1.

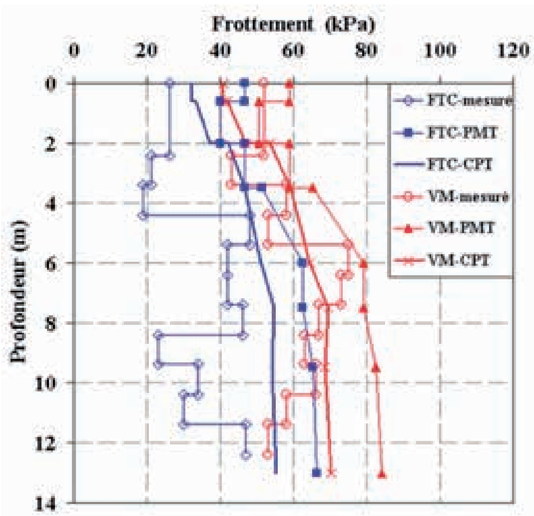

Figure 7: Comparaison des valeurs du frottement local mesurées et calculées sur les pieux foré F1 et vissé S1.

Les méthodes de la norme NF-P 94 262 pour les pieux vissés moulés donnent des frottements réalistes. Pour les pieux forés les frottements sont légèrement surestimés dans l'argile des Flandres.

6 CONCLUSION

Le mode de mise en place influe très fortement sur la capacité statique de pieux dans les argiles fissurées, fortement plastiques et surconsolidées telles que l'argile des Flandres.

Le pieu métallique battu fermé, fortement refoulant, mobilise des frottements très élevés (> 150kPa) égaux ou supérieurs à la valeur locale de la cohésion drainée du matériau.

Le pieu foré à la tarière creuse non refoulant mobilise des frottements nettement inférieurs (de l'ordre de 40kPa).

Le pieu vissé moulé partiellement refoulant mobilise des frottements sensiblement plus élevés (de l'ordre de 60kPa)

La méthode ICP en contraintes effectives est la seule méthode considérée qui permette, dans ce type de matériau, de rendre compte des très fortes valeurs de frottement enregistrées sur les pieux battus.

Les méthodes de la norme française NF-P 94 262 basées sur les essais in situ prédisent de manière assez réaliste le frottement des pieux vissés et surestiment légèrement celui des pieux à la tarière creuse. Elles sous-estiment fortement les frottements sur les pieux métalliques battus fermés.

7 REMERCIEMENTS

Les résultats présentés dans cette communication ont été acquis dans le cadre du Projet National Français SOLCYP. SOLCYP est un projet de recherche sur le comportement des pieux soumis à des sollicitations cycliques, regroupant 12 entreprises et bureaux d'études du génie civil et 6 organismes universitaires et de recherche. Il est piloté par l'IREX et financé par les partenaires, l'Agence Nationale de la Recherche, le Ministère de l'Ecologie, du Développement Durable et de l'Energie et la Fédération Nationale des Travaux Publics. Les auteurs remercient les partenaires du projet d'avoir autorisé la publication de ces données.

8 REFERENCES

AFNOR.1999. NF P 94-150-2. Norme Française. Sols: Reconnaissance et Essais – Essai statique de pieu sous effort axial – Partie 1: en compression et Partie 2: en traction.

AFNOR. 2012. NF P 94 262. Norme d'application de la Norme Française NF EN 1997-1. Fondations profondes

API RP2GEO (2011) API Recommended Practice, Geotechnical and Foundation Design Considerations, First Edition, April 2011.

Benzaria O., Le Kouby A. and Puech A. 2012. Cyclic axial load-tests on driven and bored piles in overconsolidated clay, *Offshore Site Investigation and Geotechnics*, SUT, London

Benzaria O., Puech A. and Le Kouby A. 2013. Essais cycliques axiaux sur des pieux forés dans une argile surconsolidée. *Proceedings 18th ICSMGE, Paris*

Bond A.J. and Jardine R.J. 1991. Effects of installing displacement piles in a high OCR clay. *Géotechnique*, 41(3) 341-363.

Bond A.J. and Jardine R.J. 1995. Shaft capacity of displacement piles in a high OCR clay. *Géotechnique*, 45: 3–23.

Borel S. and Reiffsteck P. 2006. Caractérisation de la déformabilité des sols au moyen d'essais en place. *Géotechnique et Risques Naturels*, LCPC, GT81.

Jardine R., Chow F., Overy R. and Standing J. 2005. ICP design methods for driven piles in sands and clays. *Thomas Thelford Publishing*, London

Josseaume H. 1998. Propriétés mécaniques de l'argile des Flandres à Dunkerque et Calais. Revue Française de Géotechnique, N°84.

Puech A., Canou J., Bernardini C., Pecker A., Jardine R., and Holeyman A. 2012. SOLCYP: a four year JIP on the behavior of piles under cyclic loading. *Offshore Site Investigation and Geotechnics*, SUT, London

Analysis of Piles Supporting Excavation Adjacent to Existing Buildings

Analyse de pieux de bâtiments existant en cours de fouilles sous-jacentes

Ramadan E.H., Ramadan M., Khashila M.M.
Civil Eng. Dept., Faculty of Engineering, Assiut University, Egypt

Kenawi M.A.
Civil Eng. Dept., Faculty of Engineering, Sohag University, Egypt

ABSTRACT: In urban environment, excavation adjacent to existing buildings is common. Supporting excavation is important to prevent damaging of the adjacent buildings. There are many factors affecting the selection of the supporting system. Some of them are soil behavior, type of foundation, foundation level of the adjacent buildings, and the budget of the project under construction. In order to reduce the surrounding soil movement due to deep excavation, a three dimensional Finite Element (3D FE) study was carried out in this paper, considering soil-structure interaction. A piled supporting system was selected because it is common and relatively economic to use in cohesive soil in Egypt. A parametric study was performed to study the effect of the stiffness of the supporting system on minimizing the ground deformation. From the results, some recommendations are given in terms of excavation depth, soil-pile stiffness, and pile embedded depth.

RÉSUMÉ : En milieu urbain, les excavations sous-jacentes aux bâtiments existants sont courantes. Soutenir les fouilles pour prévenir des endommagements sur les bâtiments est donc très important. Il y a plusieurs facteurs qui influencent les choix des systèmes de renforcement. Par exemple, le comportement du sol, le type de fondation, la profondeur des fondations et enfin le coût des travaux. Afin de limiter les désordres occasionnés par une excavation profonde, une étude numérique tridimensionnelle (méthode aux éléments fins) a été réalisée dans cet article en prenant en compte l'interaction sol-structure. Un ensemble de pieux supports a été considéré car il est relativement économique et très commun dans les sols Egyptiens. Une étude paramétrique a été réalisée pour étudier la rigidité du système qui minimise les déformations du sol. A partir des résultats, des recommandations sont données en termes de profondeur d'excavation, de rigidité sol-pieu, et de profondeur de fondation.

KEYWORDS: excavation, pile wall, clay, adjacent building.

1 INTRODUCTION

In urban environment in Egypt most buildings in the same block area are adjacent to each other. No distance between buildings exists due to high population intensity along the river Nile Valley. These conditions increased the tendency to build high rise buildings. Most of these new high rise buildings are built adjacent to old existing buildings. The adjacent old buildings condition is usually critical either due to the weakness of the structure system of the building or the foundation level is at shallow depth. High rise buildings with basements need deeper excavation than the foundation level of the adjacent building. With the presence of adjacent shallow foundation, the excavation will cause large soil movement and damage to the adjacent building, as shown in Fig. (1). Many failure cases were observed due to unsupported excavations. It is common, in Egypt, to use contiguous pile wall to support the excavation on the adjacent buildings sides. Such type of wall is economic and effective in cohesive soil. The excavation will cause lateral and vertical soil movement, the first component is considered to be more critical for adjacent piles. The design of these excavations should include an estimation of the ground movement as well as stability check of the adjacent buildings. The lateral loads resulting from the soil movements induce bending moments and deflections in the piles supporting excavation, which may lead to structural distress or failure of both the existing building and the excavation supporting system. Indeed, several instances of structural damage to piles have been reported in the literature, for example, Hagertry and Peck 1971 and Finno et al. 1991, as reported by Chen and Poulos 1997.

Many theoretical and empirical methods have been established for solving certain types of excavation problems, for example, Poulos and Chen 1995, Hashash and Whittle 1996, Ou et. al 1996, Poulos and Chen 1996, Chen and Poulos 1997, Poulos and Chen 1997 and Leung et. al 2000. They studied the failure of the excavation with no adjacent buildings or additional loads close to the excavation. In other cases, they studied the effect of soil movement during the excavation on the behavior of adjacent existing piles. However, the design of supporting system for excavation adjacent to existing building founded on shallow foundation is not studied enough. Many parameters could affect the design of pile supporting excavation. This includes excavation height, soil properties, the foundation type and the foundation level of the adjacent building.

The present study mainly aims to provide recommendations for the design of contiguous pile wall in cohesive soil. Three Dimensional Finite Element Modeling (3D FEM) was used to carry out the study. PLAXIS 3D Foundation software was used in the analysis. Different parameters were considered in the study. The ranges of the selected parameters were limited to the common cases in Egypt and as recommended by the Egyptian Code of Practice (ECP).

2 FINITE ELEMENT MODEL (FEM)

2.1 *Geometry and meshing*

FEM meshing and geometry is shown in Fig. (2). The figure shows a cut at the face of the excavation. Soil above the foundation level was removed only to show footing shape in the figure. However, it was included in the analysis. Model dimensions were selected so that the boundaries are far enough to cause any restriction or strain localization to the analysis. The excavation area is 10 x 10 m. For simplicity, the foundation of the adjacent building was assumed to be three strip footings of 10 m length and 2 m width each and in between distance of 2 m.

The foundation level was assumed to be at 1.5 m depth from the ground surface. The mesh was generated as fine mesh at piles where the stresses are expected to be high. Coarse mesh was used at the boundaries of the model where the stresses are low.

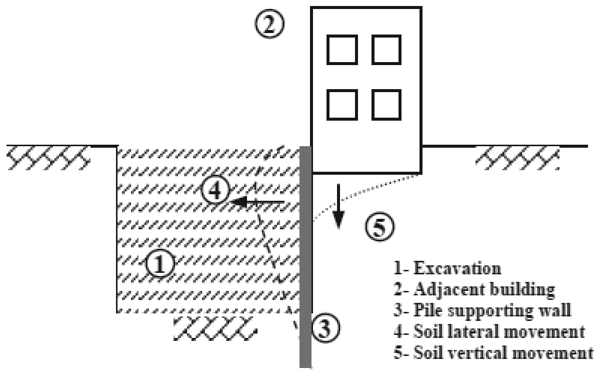

Figure 1. Problem under study

2.2 *Soil modeling*

Soil is assumed to be a deposit of clay. Fifteen node triangular element was used to model the soil. Soil material was assumed to behave as an elastic perfectly plastic material following Mohr-Coulomb model. The soil parameters are presented in Table 1.

2.3 *Pile and foundation modeling*

Piles were modeled as a massive circular concrete pile. Pile Young's modulus (E) was 2.1 x 10^7 kPa. Both pile diameters (d) of 0.3 m and 0.4 m was considered in the study. They have flexural stiffness (EI) of 8350 kN.m^2 and 26390 kN.m^2 respectively.

The adjacent building foundation is modeled as plate of thickness of 0.5 m. Foundation was idealized with six nodes triangular plate element in the analysis. Interface element was used to represent the contact between plate elements and soil.

Table 1. Clay input parameters in FEM

Parameter	Soft to Medium Clay	Medium Clay	Unit
Dry unit weight, γ_d	18	18	kN/m^3
Wet unit weight, γ_{wet}	20	20	kN/m^3
Young's modulus, E_s	4000	8000	kN/m^2
Poisson's ratio, υ	0.3	0.3	-
Undrained cohesion, c_u	25	50	kN/m^2
Friction angle, φ	12	14	degree
Dilatancy angle, ψ	0	0	degree
Interface reduction factor, R	1	1	-------

2.4 *Analysis procedure*

The variable parameters used in the analysis are the excavation height (H), pile embedded depth (D), and pile diameter (d) as shown in Fig. (2). Also, both soft to medium clay and medium clay soil were used in the analysis. Pile diameter was assumed to be 0.3 m and 0.4 m with spacing of pile diameter between pile edges.

The analysis was carried out in steps. The first step was applying the stress of the adjacent building at the foundation level without the pile wall and the excavation. The second step was activation of the pile wall in the soil. The third step was the excavation of the soil.

In the present paper, only bending moment of pile and pile lateral displacement outputs were used in the analysis. All the presented results are of the pile at the middle of the supporting wall. It was found from the results that this pile is the most critical in both lateral deflection and bending moment. The piles at the ends of the wall have the lowest lateral deflection and bending moment profiles. The stress on the foundation level was assumed to be 100 kN/m^2. This stress is corresponding to a bearing capacity factor of safety of 2 for the soft to medium clay case.

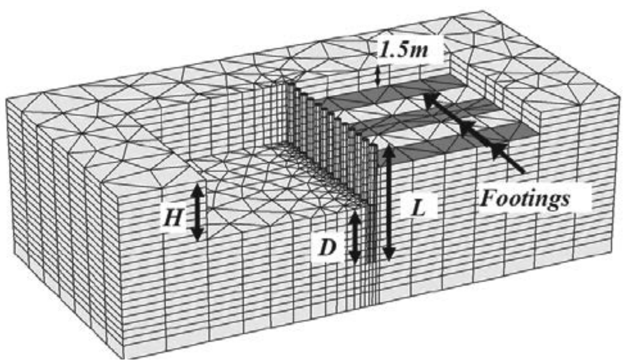

Figure 2. FEM geometry and meshing

3 FEM RESULTS AND DISCUSSIONS

3.1 *Effect of supporting excavation*

Excavation height (H) and cohesion of clay (c_u) are two main parameters in the design of the pile wall. It was found that results should better be related to a factor has both the effect of excavation height (H) and undrained soil shear strength (c_u). The stability factor (N_c) joins both H and c_u parameters in the following relationship as recommended by Polous and Chen (1996):

$$N_c = \frac{\gamma \cdot H}{c_u} \tag{1}$$

where γ is the unit weight of the soil.

Figure (3) shows lateral displacement profile (U_x) versus depth (Z). Both the profile of unsupported soil lateral displacement and pile lateral deflection are shown in Fig. (3). Large soil movement can be observed due to the stress of the adjacent building in the case of unsupported excavation. The lateral displacement increases rapidly as the excavation height increases. Maximum lateral displacement increased from about 0.06 m to 0.2 m when N_c increased from 1.9 to 3.2. However, the maximum lateral displacement increased to very large value of 1.2 m for N_c = 4.5. This means that the excavation is failed at N_c = 4.5. When the excavation is supported using contiguous pile wall, soil movement decreases in the zone above the excavation level. However, below the excavation level, there is no obvious decrease in soil movement. It should be noted that in all cases the pile wall is translated horizontally.

3.2 *Effect of excavation height*

Pile wall lateral deflection increases as excavation height (H) or the stability factor (N_c) increases. As N_c increases pile wall movement changes from translation (H =3 m) to both translation and rotation (H = 5 m and 7 m) as shown in Fig. (4). Maximum lateral deflection was observed at (0.6 to 0.8 H) with the lowest value for small N_c. Figure (5) shows normalized bending moment ($M.d/EI$) profiles for different N_c values. It is clear that bending moment increases by increasing N_c. The location of maximum bending moment is at (0.7 to 0.8 H) with the lowest value for small N_c.

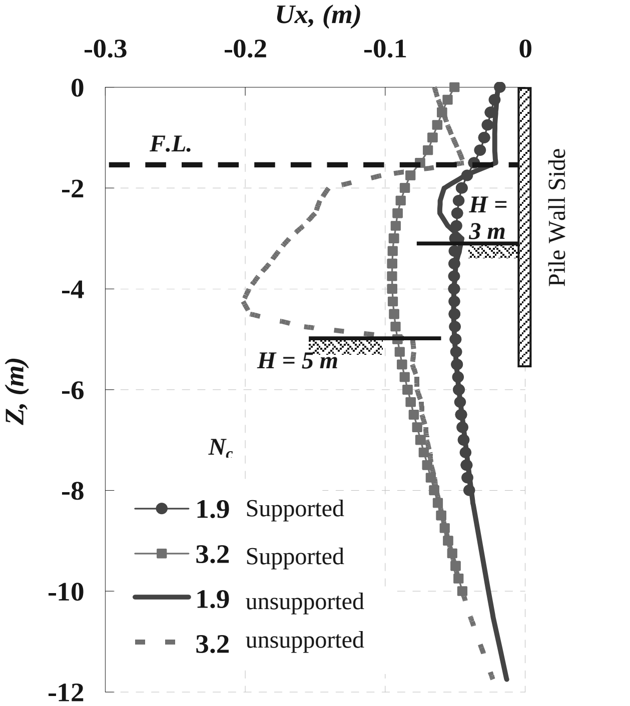

Figure 3. Lateral displacement profile of unsupported and supported excavation

3.3 *Effect of pile wall embedded depth*

Figures (4) and (5) show no change in the normalized lateral pile wall deflection (U_x / d) and ($M.d$ / EI), respectively, for N_c values of 1.9 and 3.2 and for D values of 3 m and 5 m. At N_c = 4.5, U_x / d decreases when D increases from 3 m to 5 m. The same trend can be seen in Fig. (5) for $M.d$ / EI. For N_c = 4.5 (H = 7m), the increase of D has a significant effect on both lateral deflection and bending moment of pile wall. By increasing D both U_x / d and $M.d$ / EI decreases. Figure (6) shows the relation between $U_{x\ max}$ / d versus D. The effect of D on the system stability is clear to be effective in case of N_c = 4.5. However, the increase of D more than 7 m (H/D = 1) has no contribution to the system stability.

3.4 *Effect of pile diameter and soil-pile stiffness*

The Egyptian Code of Practice recommends pile diameter ranges between 0.3 m and 0.5 m for contiguous pile wall. It is clear from Figs. (7) and (8) that increasing pile diameter (d) from 0.3 m to 0.4 m decreases both lateral deflection and bending moment. In Fig. (8), $M_{max}.d/EI$ increases with the increase of ($H^2/d.L_o$). L_o is soil-pile stiffness factor. The soil-pile

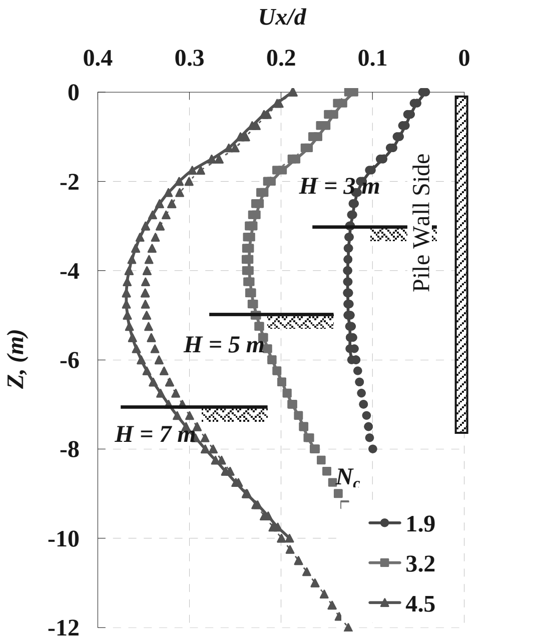

Figure 4. Lateral displacement profile of contiguous pile wall for different Nc values (solid line for D= 3 m, dashed line for D = 5 m)

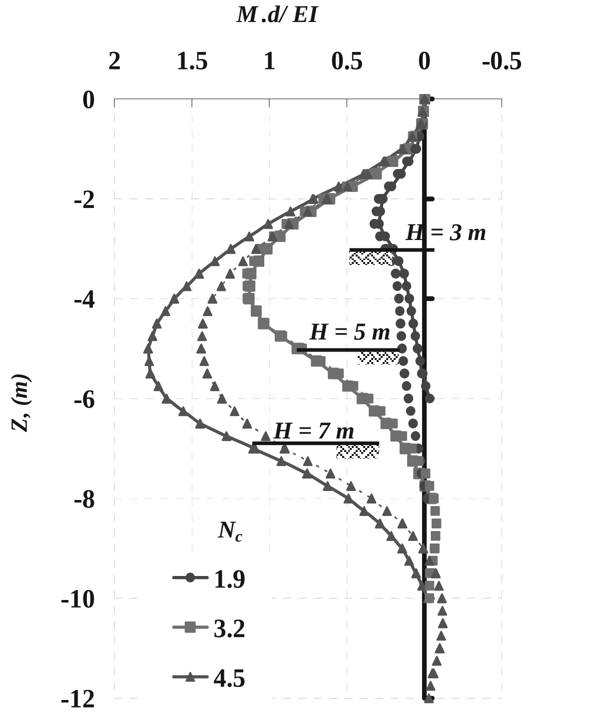

Figure 5. Normalized bending moment profile of contiguous pile wall for different N_c values (solid line for D= 3 m, dashed line for D = 5 m)

stiffness can be defined as follows:

$$L_o = \sqrt[4]{\frac{4EI}{E_s}} \tag{2}$$

It can be observed from Figs. (7) and (8) that at N_c = 4 both pile wall maximum lateral deflection and maximum bending moment are not increasing. This means that the pile wall starts to be more effective at N_c = 4 at which the unsupported excavation fails.

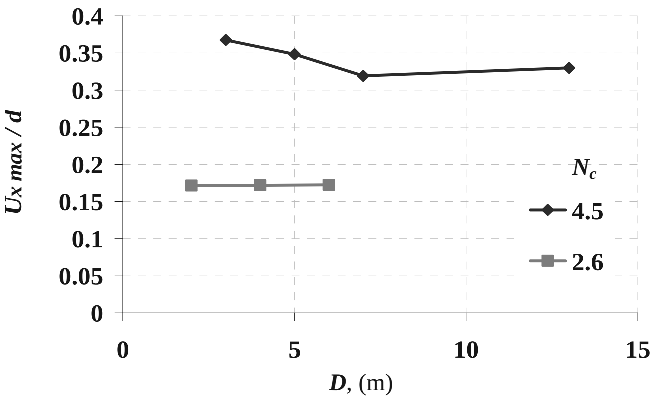

Figure 6. Normalized maximum lateral pile wall displacement versus pile wall embedded depth

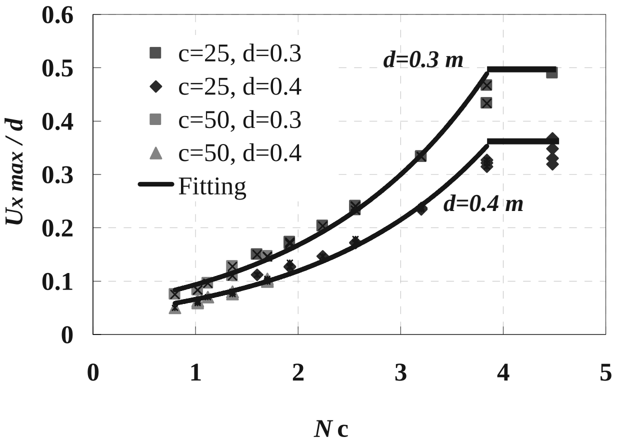

Figure 7. Normalized maximum lateral pile wall displacement versus the stability factor N_c

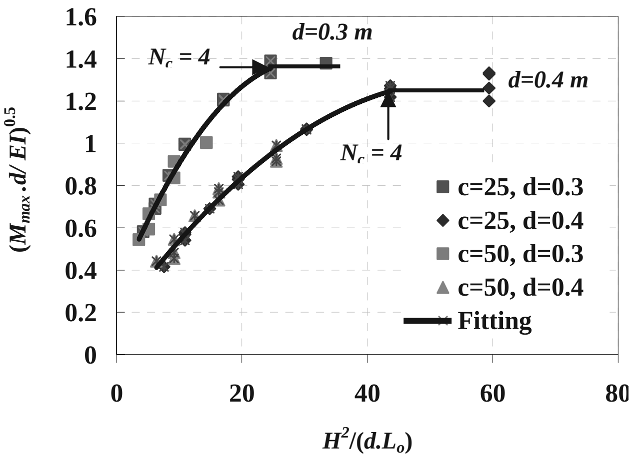

Figure 8. Normalized maximum bending moment of pile wall versus $H^2/(d*L_o)$

4 CONCLUSIONS

3D FEM study was carried out to provide recommendations for the design of contiguous pile wall in cohesive soil. Pile diameter was considered to be 0.3 m and 0.4 m as recommended by ECP. The vertical stress at the foundation level of the adjacent building assumed to satisfy a bearing capacity factor of 2 for soft to medium clay case. From the previous discussion the following design recommendations can be concluded:

1. At stability factor, $N_c = 4$, the unsupported excavation starts to fail due to the stress of the adjacent building.

2. Contiguous pile wall decreases the lateral soil displacement between the foundation level of the adjacent building and the bottom of the excavation. However, the pile wall does not decrease lateral soil displacement at the foundation level and below the bottom of the excavation.

3. Increasing pile diameter (d) from 0.3 m to 0.4 m decreases both lateral deflection and bending moment.

4. Pile wall embedded depth, (D) has no obvious effect on the stability of the supporting system for N_c value up to 4. It starts to be more effective for $N_c > 4$ up to $H/D = 1$. Using D values larger than $H/D = 1$ is ineffective and uneconomic.

5. Contiguous pile wall starts to be more effective when $N_c > 4$ as it prevents the unsupported excavation from failure.

6. It is recommended to check the use of connecting beam at piles head to improve the supporting system for excavation conditions of $N_c > 4$.

5 FUTURE RESEARCH

The present paper is the beginning of an ongoing research on designing deep excavation. The design of the contiguous pile wall will be extended to check the stability and safety of the adjacent building. Also, using braced excavation will be considered. A method will be derived to predict the earth pressure on the contiguous pile wall.

6 REFERENCES

Chen L.T. and Poulos H.G. 1997. Piles subjected to lateral soil movement. *Journal Geotechnical and Geoenvironmental Engineering*, 123(9), 802-811.

Hashash Y.M. and Whittle A.J. 1996. Ground movement prediction for deep excavations in soft clay. *Journal Geotechnical Engineering*, 122(6), 474-486.

Leung C.F., Chow Y.K. and Shen Y.K. 2000. Behaviour of pile subject to excavation-induced soil movement. *Journal Geotechnical and Geoenvironmental Engineering*, 126(11), 947-954.

M. M. Khashila 2013. *Analysis of piles supporting excavation adjacent to existing buildings.* M.Sc. thesis. to be submitted. Assiut University, Assiut, Egypt.

Ou C., Chiou D. and Wu T. 1996. Three dimensional finite element analysis of deep excavations. *Journal Geotechnical Engineering*, 122(11), 337-345.

Poulos H.G. and Chen L.T. 1995. Tests on single model piles subjected to lateral soil movement. *Soils and Foundations*, 35(4), 85-92.

Poulos H.G. and Chen L.T. 1996. Pile response due to unsupported excavation-induced lateral soil movement. *Canadian Geotechnical Journal*, 33, 670-677.

Poulos H.G. and Chen L.T. 1997. Pile response due to excavation-induced lateral soil movement. *Journal Geotechnical and Geoenvironmental Engineering*, 123(2), 94-99.

Analysis and Design of Piles for Dynamic Loading

Analyse et conception de fondations par pieux en chargement dynamique

Ray R.P., Wolf Á.
Széchenyi István University, Győr, Hungary

ABSTRACT: With the acceptance of Eurocode 8 in Hungary a new level of seismic design is now necessary. This paper outlines some of the past history and present implementation of foundation design for seismic loading as practiced in Hungary. It shortly describes the possibilities of modeling foundations (fix support, linear elastic support, non-linear elastic support) during the design of the superstructure, and introduces the Hungarian practice. The influence of the different support's methods for the bearing forces/stresses of a superstructure is analyzed on a typical reinforced concrete office building using SAP2000 finite element software. The results of the calculation are compared through the moment of a column, the deflection and the support reaction.

RÉSUMÉ : Il était nécessaire de modifier les principes de dimensionnement des fondations par pieux, vis à vis des charges sismiques, depuis l'entrée en vigueur en Hongrie de l'Eurocode 8. L'étude donne un apercue des méthodes précédentes et actuelles du dimensionnement dynamique des fondations. Elle montre aussi les possibilités de modelisations des fondations profondes pratiqués en Hongrie (rigide, élastique linéaire, élastique non-linéaire). La comparaison des differentes techniques de fondation est réalisé par elements finis sur une structure en béton armé et à l'aide du logiciel SAP2000. La comparaison des différents résultats est montré en terme de moment, de déplacement et de force de réaction d'appuis.

KEYWORDS: pile foundation, seismic design, Eurocode-8

1 INTRODUCTION

Acceptance of Eurocode 8 in Hungary has lead to a great many changes in how engineers think about designing for seismic loading. Since Hungary experiences only moderate seismic events over several hundred years, it is difficult to implement a practical yet thorough design procedure for seismic (and other dynamic) loadings. Much of the research and development in seismic design is driven by post-earthquake evaluation and large-scale testing. For regions with lower seismicity and modest research budgets, this approach becomes problematic. A more urgent problem is that of practical implementation: designers must do something. In order to develop a reasonable and rigorous approach to the problem, the Structures and Geotechnics Department at Széchenyi István University has pursued methods to link the latest approaches in earthquake engineering to standard structural and geotechnical design practice. To that end, part of the difficulty is pile design for seismic loading. This paper describes some of the ongoing efforts to use sophisticated analysis and testing in "code-based" design practice.

2 BRIEF REVIEW OF RESEARCH

Seismic behavior of piles and their contribution to structural response has been recognized for over 50 years. However, due to the difficulty in modeling this behaviour, only very simple models could be implemented. One early approach by Penzien (1970) illustrates that the complexity of the problem was acknowledged by even the best analysts. The early methods used a subgrade reaction approach where the soil is replaced by (usually linear) springs. Dashpots may be added as well to simulate both material damping of the soil as well as radiation of energy from the foundation. Additional refinements in the approach to modelling piles included visco-elastic media and analytical methods with relaxed boundary conditions (Novak and ElSharnouby 1984, Dai and Roesset 2004). Concurrent with the development of the relaxed continuum methods, finite element approaches became more practical and required less expensive computing resources. This rather complex evolution of hardware, programming and theory resulted in what are now the de-facto analysis methods for assessing seismic behavior.

In addition to these classes of analysis, four levels of progressively "complete" SSPSI analyses can be described (Wolf, 1985). The basic level consists of a single pile kinematic seismic response analysis, normally incorporating nonlinear response and performed as a pile integrity evaluation. A pseudo-static method for pile integrity evaluation consists of transforming the horizontal profile of soil displacement (derived from a free-field site response analysis) to a curvature profile, and comparing peak values to allowable pile curvatures. This method assumes piles follow the soil perfectly, and that no inertial interaction takes place. Alternatively, a displacement time history may be applied to nodal points along the pile in a dynamic pile integrity analysis. The kinematic approaches consider the difference in stiffness between piles and surrounding soil as seismic waves travel through both. The mismatch leads to stresses generated in the pile system that become more pronounced as the soil becomes softer (the mismatch becomes greater). This behavior is indeed difficult to measure, or even qualitatively assess in the field.

In a second level of analysis, pile head stiffness or impedance functions may be condensed from linear or nonlinear soil-pile analyses and assembled into a pile group stiffness matrix for use in a global response analysis. Secant stiffness values at design-level deformations are normally ascertained from nonlinear soil-pile response analyses. Third, both inertial and kinematic interaction may be evaluated from a substructuring type analysis to determine pile head impedance and foundation level input motions.

Finally, a fully-coupled SSPSI analysis may be carried out to define the complete system response.

Shake table and centrifuge models have offered a great deal of insight into the kinematic and inertial interaction between pile groups and soil, however, there remains a great deal of research yet to be done.

2.1 *SPSI*

Interaction of piles with structural components (inertial interaction) is perhaps better understood. However, simplifying assumptions to gain computational efficiencies and limit the complexity of the design process are often adopted. This is a common practice when performing structural design calculations when foundation alternatives have not been finalized. Most importantly, the design engineer wants to know what impact, if any, the foundation design will have on the seismic response of the structure.

EC-8.2 and 8.5 recommend values for applying seismic loading and estimating pile stiffness. The loadings and soil reactions are then applied to pile elements and included in the overall structural analysis/design process. These stiffness formulae are similar to those discussed by Gazetas and Dobry (1984) for low frequencies and typical ranges of pile-soil moduli.

2.2 *EC-8 Stiffness Formulae*

Eurocode 8 suggests formulae for estimating pile stiffness in seismic response analysis. One should note the effect of soil profile on behavior, especially for lateral loading. Load displacement curves based on EC-8 formulae are shown in Figure 1 for sand (E_s=20 Mpa) and clay (E_s=5 Mpa). As one moves down the legend the responses get stiffer. The lines marked with Cl or Sa are the clay and sand stiffness based on linear distribution, square root distribution, or constant with depth. E_s values were adjusted so that the average E values for a 12-m pile were equal for the respective distribution profile. Values for sand and clay are typical for Hungarian soils.

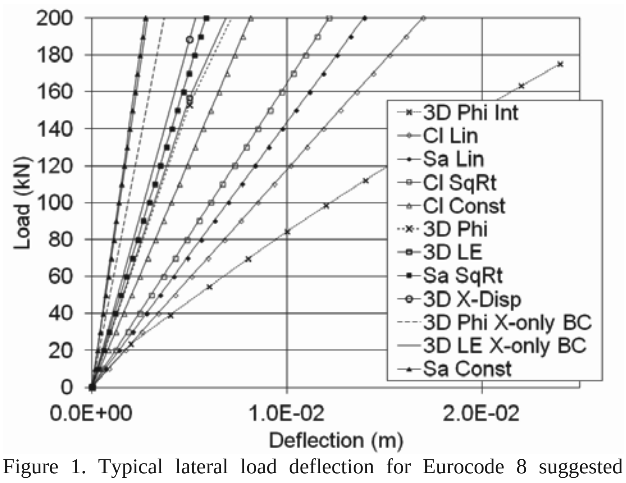

Figure 1. Typical lateral load deflection for Eurocode 8 suggested spring constants and corresponding FEA results for single piles.

These stiffness values are very high compared to what one would consider lateral load-deflection behavior for a single pile in a soil similar to the sand or clay shown. The lines marked 3D represent 3D FEA of the same pile with different conditions. The most flexible condition uses an elasto-plastic sand with a Mohr-Coulomb failure condition and E_s=20 Mpa, φ=30 deg and interface "slip" elements appropriate for the model. Progressively stiffer responses occur when the interface is removed, linear elastic (LE) behavior is used, or boundary restraints are applied. Finally, agreement is reached when the pile head is restricted to only horizontal displacement and linear elastic soil is used. Care should be taken when adapting one set of analysis or field test results for another design approach.

While dynamic conditions may influence the value of stiffness, other authors have pointed out that the first approximation to pile stiffness, especially in lower frequency ranges, is the static displacement profile (Gazetas and Dobry 1984; Blaney et al 1976; Novak and Nogami 1977). Damping will also reduce response, but to a lesser extent and it primarily shifts the pile response out of phase with the driving (earthquake) forces.

3 APPLICATION TO BUILDING DESIGN

The primary focus of research has been to establish more precisely the effects of SPSI on structural design considerations. To that end, an example design is used as a basis for study.

3.1 *Example Structure*

The structure is a 5-bay by 3-bay reinforced concrete frame with a ground floor, seven floors supported by columns, and a roof slab. Floor slabs are separated 3.2m c-c and columns are spaced uniformly 6.0 m c-c. Structural elements were dimensioned according to EC-2 using factors from the Hungarian National Annex. While this is a common design, one unique, and problematic feature of Hungarian designs is the integration of continuous floor slabs with floor beams. This makes it more difficult to model beam-column connections and properly account for stiffness distributions throughout each floor system. Columns are dimensioned 40x65 cm at the base and taper to 40x40 at the top while beams are uniformly 40x90cm and slab thicknesses are 20cm. Perspective and profile views are shown in Figure 2 a, b respectively.

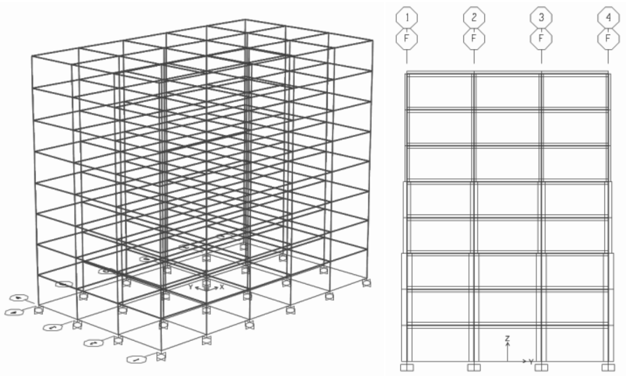

(a) (b)

Figure 2. Perspective and section view of RC frame. Note elastic supports added to base of columns.

3.2 *Seismic Loading*

Hungary is located in a region of moderate seismicity. Recurrence and intensities of earthquakes have been estimated by the National Seismological Observatory, Hungarian Academy of Science. A comprehensive discussion of seismicity as it applies to engineering design can be found in Tóth et al (2006). Based on the observatory's studies, maximum horizontal accelerations one would expect with 10 percent probability of exceedance over 50 years are shown in Figure 3. Design values for seismic loading in EC-8 Annex are presently being completed; however horizontal accelerations of 0.1-0.15g can be expected in some areas.

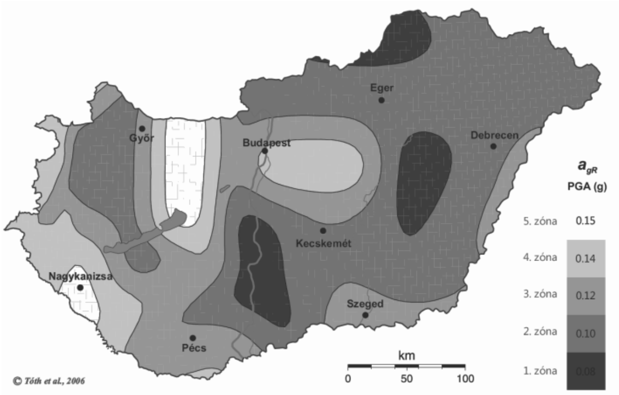

Figure 3. Five Seismic zones in Hungary showing contours of peak ground acceleration, PGA = 0.15,0.14,0.12,0.10,0.08 Tóth et al, (2006).

Acceptance of seismic code requirements by the structural design community in Hungary has been mixed; mainly due to perceptions that seismic requirements present an unnecessary financial burden on the builder. However, much of the design work, when properly executed, result in very little increase in materials and workmanship. Much of the difficulty lies in resorting to overly-conservative design assumptions and pseudo-static approaches that contribute to substantial increases in materials used in standard framing design. Of course, when viewed from this perspective, seismic design is certainly expensive. However, if new designs are carefully applied in a more sophisticated over-all approach, seismic requirements can be met with less difficulty. An added benefit is that the static design is more robust as well.

4 IMPACT OF ELASTIC PILE RESPONSE ON STRUCTURAL DESIGN

A more flexible foundation system will generally offer lower base shear at the cost of larger lateral deflections. What is more difficult to quantify is the re-distribution of member forces due to the greater component flexibility. That is, the relative stiffness of members changes when introducing a flexible foundation system.

4.1 *Response Spectra Method*

For this analysis, one of the methods used was elastic response spectrum. The spectrum approved for use in Hungary is the Type I spectrum (Figure 4). The two spectra are shown with respective soil profile values. Note that the Type II lines are the left-most of the plot lines.

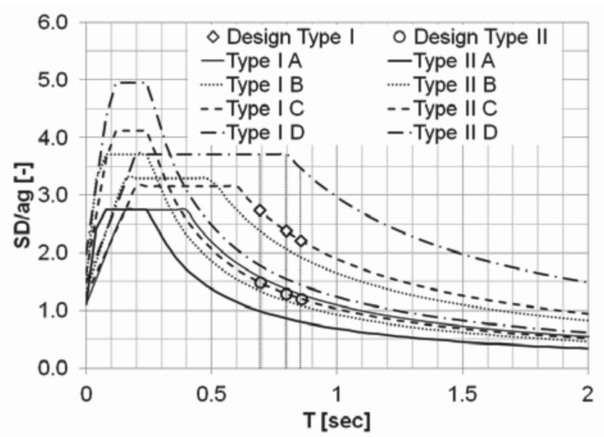

Figure 4. Elastic response spectra.

Building periods were computed from EC-8 formulae (T=0.85 sec) and modal analysis assuming fixed-base (T=0.69 sec) or spring-base (T=0.79 sec). In this range, the design spectral values for a Type I spectra (diamond symbols) are much higher than for Type II (circles). It is ironic that one of the reasons for adopting a Type I curve was the perception that it would yield lower factors and lower cost. However, for a large percentage of buildings in Hungary, the opposite is true, as just shown. Once the spectral factors are known, appropriate lateral loads may be computed for simulating seismic forces.

4.2 *Computing Structural Response*

Load combinations were applied to the structure through SAP2000 analysis program. Loads were based on floor and frame masses and distributed throughout the structure. As suggested in the software documentation (Wilson 2002) lateral load combinations consisted of 100% lateral load parallel to the direction of study and 30% perpendicular to it. This helps to determine the effects of slightly non-symmetrical geometry. Without the perpendicular loading, a feeling of false confidence in building resistance is possible. Three loading cases were examined based on the fundamental periods mentioned earlier: Eurocode-8 (EC-8), SAP fixed base (SapFB), and SAP spring base (SapSB). Since this study has a field component, most attention was focused on the site conditions with Type C soil.

In order to directly compare the difference between rigid and spring base conditions, the structure is first analyzed under a lateral load that was based on the distributed load from EC-8 section 4.3.3.2.3, equation 4.11. For this structure, load increases linearly with height from 8 to 54 kN/m. These values change with changing base shear forces computed from the spectral values discussed earlier. There are a total of six load/base fixity combinations presented here: 3 spectral values; 2 base fixities. While the overall maximum and minimum joint forces changed by moderate amounts, the re-distribution of forces was significant. Table 1 lists joint forces at the base of the structure for 100% force applied on the long side (parallel to the plane of Figure 2b, the y-direction in the model) direction and 30% applied perpendicular. Average percent changes in joint forces, related to the fixed-base condition are also shown.

Table 1. Joint reactions in rigid- and spring-base models

	Spring Base		Fixed Base		
Joint Rxn	Max (kN)	Min (kN)	Max (kN)	Min (kN)	Avg % Chg
Y-direction Reaction	430	278	443	255	20
Z-direction Reaction	3004	556	3165	-8	30

A comparison of forces and moments in selected members shows that the overall seismic effect is reduced, however for particular members, forces and moments may increase. Figure 5 presents interior column bending moments for the loading cases discussed previously. Spring-base conditions reduce bending moments near the base by about 30%. For higher portions of the column, the reduction is less. The same is true to a slightly lesser degree for the exterior columns. Since the EC8 spectral ordinate value is the smallest, lower moments are produced. As the fundamental period decreased for the other cases, spectral ordinate values, and moments, increased.

The other difference in behavior is increased lateral deflection due to the increased flexibility of the spring-base condition. Figure 6 shows lateral displacement of the same column and for the same loading conditions. Note that the foundation flexibility doubles the lateral displacement for almost all soil profiles. The slightly wavy nature of the deflection profiles is due to the abrupt cross-section changes in the column with increasing height.

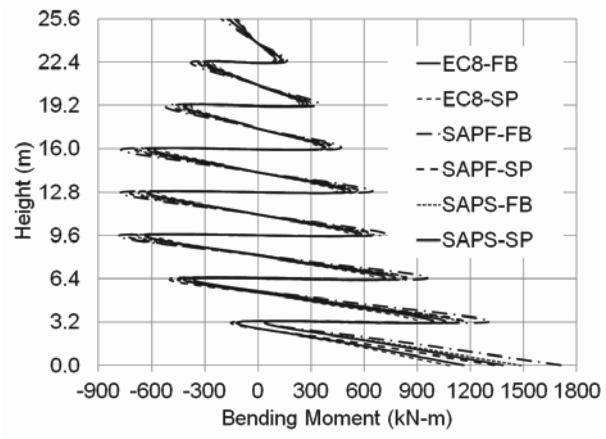

Figure 5. Column bending moments for rigid- and spring-base conditions.

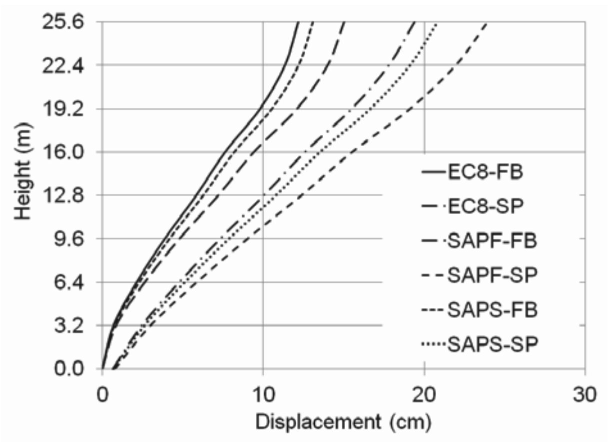

Figure 6. Lateral displacement vs. height for an interior column.

5 CONCLUSIONS AND FURTHER STUDY

The engineering community in Hungary has started to put the seismic provisions of Eurocode-8 into practice. Some parts of the provisions have been easy to deliver, while others require more experience and constructive feedback on their best application. The fact that Hungary has moderate seismicity makes delivery of the code a challenge: seismicity is strong enough to require substantial changes to design practice, but is not obvious to the public and professionals since no major earthquakes have been witnessed in recent history.

Implementing a useful but rigorous methodology for pile design for seismic loading is equally challenging. One of the major efforts in the author's department is to develop a continuously-improving system of analysis, design, testing and assessment of foundations and structures for seismic and other dynamic forces.

The authors are working on integrating sophisticated foundation modeling into the structural design work-flow. This includes methods to evaluate field data, laboratory testing, geotechnical modeling, and structural design. The final goal is a more seamless movement from site characterization to final design. Being able to bridge between geotechnical and structural analysis software is part of this process.

6 ACKNOWLEDGEMENTS

The authors acknowledge the financial support of the Széchenyi István University within the framework of TáMOP 4.2.2/B-10/1-2010-0010 application.

7 REFERENCES

Blaney G.W., Kausel E.and Roesset J. M., 1976. Dynamic Stiffness of Piles. *Second Intl Conf on Num Meth in Geomechanics*, Vol II, Virginia Tech, Blacksburg, Va. 1001-1012.

Dai W. and Roesset J.M. 2010. Horizontal dynamic stiffness of pile groups: Approximate expressions *Soil Dyn. & Eq. Engrg.* (30) 844-850.

Gazetas G. and Dobry R. 1984. Horizontal Response of Piles in Layered Soil, *Jour. Geotech. Engrg*. 110 (1), 20-40.

Novak M, ElSharnouby B. 1984. Evaluation of dynamic experiments on pile group. *Jour. Geotech. Engrg.* 110(6):738–56.

Novak M. and Nogami T. 1977. Soil–pile interaction in horizontal vibration. *International Journal of Earthquake Engineering and Structural Dynamics* (5) 263–281.

Penzien, J 1970. Soil Pile Foundation Interaction, Chapter 14 in *Earthquake Engineering*, R.L.Weigel ed., Prentice-Hall, 518 p.

Simonelli A.L. 2008. Fondazioni profonde in Metodi Innovativi per la Progettasione di Oere di Sosteno e la Valutasione della Stailita dei Pendii, *Rete dei Laboratori Universitari di Ingegneria Sismica* (Reluis), 1-71.

Tóth, L., Győri E., Mónus P., Zsíros T. 2006. Seismic Hazard in the Pannonian Region. *The Adira Microplate: GPS Geodesy, Tectonics, and Hazards*, Pinter N., Grenerczy G., Weber J., Stein S., Medak D. (eds), Springer Verlag, NATO ARW Series 61, 369-384.

Wilson E. 2002. Three-Dimensional Static and Dynamic Analysis of Structures. *Computers and Structures Inc*., Berkeley CA. 1-423.

Wolf J.P. 1985. *Dynamic Soil-Structure Interaction* Prentiss-Hall NJ

A new tool for the automated travel time analyses of bender element tests

Un nouvel outil pour les analyses automatisées du temps de déplacement des essais « bender element »

Rees S., Le Compte A., Snelling K.
GDS Instruments, UK

ABSTRACT: Whilst bender elements are increasingly used in both academic and commercial laboratory test systems, there still remains a lack of agreement when interpreting the shear wave travel time from these tests. Given such interpretation is often subjective, a software tool was developed to automate the interpretation process using a number of analysis methods recommend in the literature. The tool resulting from this development is accessed through two easy-to-use Microsoft Excel Add-Ins, allowing any digital bender element data to be interpreted. Initial assessment of the tool was provided by a series of tests conducted on a triaxial specimen of Leighton Buzzard sand at a mean effective stress of 100 kPa, with variation of the source element frequency. Travel times estimated from a time-domain cross-correlation showed relatively low scatter, equal to ± 7 µs, across a frequency range of 3.3 kHz to 14.3 kHz, whilst times estimated from a frequency-domain cross-spectrum calculation produced much larger scatter, equal to ± 138 µs. Finally comparisons with subjective observational analyses performed by a geotechnical academic showed good agreement, suggesting the tool can provide accurate, automated interpretation of bender element shear wave travel times.

RÉSUMÉ : Tandis que la technique des *Bender Elements* est de plus en plus utilisée dans les laboratoires commerciaux et de recherche, il subsiste encore une carence dans l'interprétation du temps de parcours des ondes de cisaillement. Pour pallier ce manque, un outil logiciel a été développé pour automatiser le processus en utilisant un certain nombre de méthodes d'analyses recommandées dans la littérature. Cet outil est accessible par la simple utilisation de deux applications Microsoft Excel, permettant d'analyser n'importe quelle donnée issue d'un essai de type *Bender Elements*. Les premiers tests de cet outil ont été effectués sur un échantillon triaxial de sable « Leighton Buzzard » pour une contrainte effective moyenne de 100 kPa, avec une variation des fréquences de l'élément source. Les temps de trajet estimés à partir d'une corrélation temporelle ont montré une dispersion relativement faible égale à +/- 7 µs pour des fréquences de 3,3 kHz à 14,3 kHz, tandis que les temps calculés à partir d'une corrélation spectre-fréquence indiquent une forte dispersion des résultats égale à +/- 138 µs. Enfin, les comparaisons réalisées avec des analyses classiques effectuées par un laboratoire de géotechnique académique ont montré de bonnes similitudes, suggérant que cet outil peut véritablement fournir des résultats précis et automatiques des temps de parcours des ondes de cisaillement.

KEYWORDS: bender elements, shear wave travel time, automated analysis, cross-correlation, cross-spectrum.

1 INTRODUCTION

Bender elements have seen increasing use in laboratory test systems since their initial development in the 1970s (Shirley and Hampton 1978), as they enable the small-strain shear modulus, G_0, of a soil specimen to be estimated using a simple methodology. This is achieved via determination of the shear wave velocity, V_S, estimated from the time required for a shear wave to propagate from one bender element (BE) to another. V_S can then be related to G_0 as shown in Equation 1, wherein ρ = bulk density of the soil, L = shear wave propagation distance, and t = shear wave travel time.

$$G_0 = \rho V_S^{\,2} = \rho (L^2 / t^2) \tag{1}$$

Early studies demonstrated good agreement between G_0 values obtained using bender elements and other small-strain test systems such as the resonant column (Dyvik and Madshus 1986). A number of issues were however subsequently identified that arise when interpreting bender element test results, including the near field effect (Sánchez-Salinero et al. 1986) and subjectivity in determining arrival time of the propagated shear wave (Jovičić et al. 1996). Such issues have meant that despite bender element systems being well-established within academic and commercial testing, there still remains the lack of a satisfactory model or standard for test interpretation (Viana da Fonseca et al. 2009, Alvarado and Coop 2012). Therefore whilst it is understood that potential errors in values of ρ, L, and t may each affect the estimated value of G_0, this paper focuses on a principal issue in interpreting bender element test data – the subjectivity in determining the shear wave travel time, t.

1.1 *Current recommendations for determining the shear wave travel time*

Primarily three different approaches have been identified for determining the shear wave travel time, t: observation of the source and received bender element signals, cross correlation of the signals, and a cross-power spectrum calculation of the signals (Yamashita et al. 2009). The two former approaches are typically considered as techniques applied in the time-domain (TD), with the latter viewed as a frequency-domain (FD) method. Recommendations made by the Japanese Geotechnical Society Technical Committee TC-29 suggest use of the two TD methods is generally more appropriate, given the variability in FD travel time estimates obtained from an international parallel test. It is however important to note the suggested observational techniques, which are the 'start-to-start' and 'peak-to-peak' methods, can be performed through visual analysis of the bender element data by a test operator, and thus may produce subjective travel time estimates. It is therefore considered useful to automate the travel time estimation process to decrease the subjectivity in such analyses.

2 DEVELOPMENT OF A MULTI-METHOD AUTOMATED TOOL FOR TRAVEL TIME ANALYSES

A new software tool was developed by GDS Instruments to perform automated analyses of bender element test data. The primary aim of this tool was to allow travel time estimations to be conducted objectively via a simple user interface, providing both visual and numerical representations of the estimated travel times. Implementation of the tool was completed by creating Add-Ins for Microsoft Excel, a decision based on the ubiquitous use of the software.

Based on the recommendations presented in Section 1.1, it was considered important to include a number of analysis methods within the tool, providing flexibility to the user when interpreting the results. Variations of the three primary approaches listed in Section 1.1 were therefore chosen for implementation: observation of points of interest within the received wave signal via software algorithm (TD); cross-correlation of the source and received signals (TD); group travel time calculation obtained from the absolute cross-power spectrum phase diagram (FD). Implementation of these methods is briefly discussed in Section 2.2 and 2.3, whilst the analysis tool is introduced in Section 2.1.

2.1 *GDS Bender Element Analysis Tool user interface*

The GDS Bender Element Analysis Tool (BEAT) is accessed via two Add-Ins for Microsoft Excel (version 2007 or later): the Interactive Analysis tool and the Batch Analysis tool. The Interactive Analysis tool is designed to analyse one BE test at a time, whilst allowing the user some interaction when performing the FD estimation. To use the tool, BE test data is firstly imported into Excel, with relevant test parameters then selected via the window interface displayed in Figure 1. Note this allows data obtained from any BE system to be analysed, assuming the data file can be loaded within Excel. The tool then performs the majority of the analysis before pausing to allow user alteration of the frequency window chosen for the FD estimation.

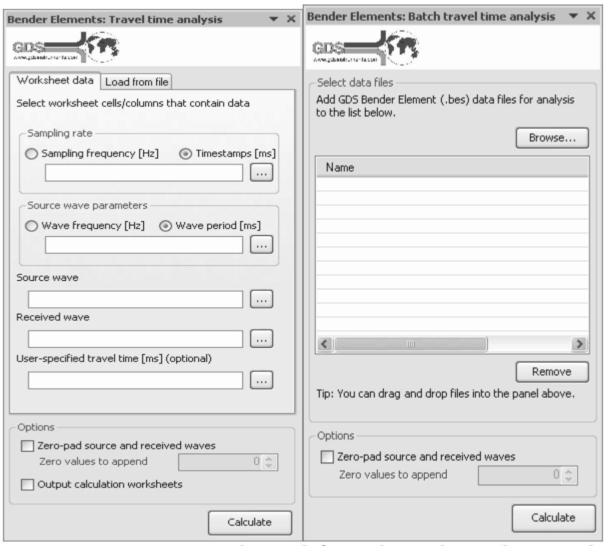

Figure 1. Interactive Analysis (left) and Batch Analysis (right) parameter / data file input windows within Microsoft Excel.

Conversely the Batch Analysis tool is designed to analyse multiple BE tests at a time, assuming the data is organised using the GDS Bender Element System (BES) output format (.bes). The tool is used by simple loading .bes files into the window interface shown in Figure 1 and clicking "Calculate".

2.2 *Observation of received wave signal via algorithm*

Figure 2 displays an idealised received shear wave signal containing the near field effect, with four points of interest noted: first deflection (A); first bump maximum (B); zero after first bump (C); major first peak (D) (Lee and Santamarina 2005). To observe the time at which each point occurs, relative to initial triggering of the source signal (time zero), an algorithm was included within BEAT to implement the following procedure:

- The major first peak (D) is located by scanning the signal and determining the maximum (i.e. most positive) output. The time signature corresponding to this maximum thus defines point D.
- Point B is determined next by scanning the signal from time zero up to point D and locating the minimum (i.e. most negative) output. The corresponding time signature defines point B.
- Point C is then found by scanning the signal between point B and point D to locate the output closest to zero. The corresponding time signature defines point C.
- Point A is located via an iterative process: beginning at time zero, the mean and standard deviation of 10 consecutive outputs (e.g. $n_1 - n_{10}$) are calculated, with the subsequent five outputs ($n_{11} - n_{15}$) then assessed to determine whether all are at least three standard deviations more negative than the calculated mean. If 'true', the time signature of the first of the five subsequent outputs (i.e. n_{11}) is used to define point A; if 'false', the iteration proceeds by determining the mean and standard deviation of the next set of 10 consecutive outputs (i.e. $n_2 - n_{11}$) until a 'true' condition is reached.

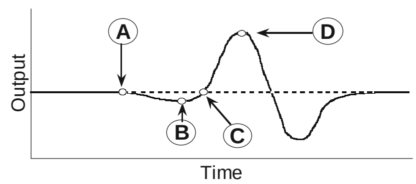

Figure 2. Idealised received shear wave signal containing the near field effect (reproduced from Lee and Santamarina 2005).

2.3 *Cross-power spectrum and cross-correlation of source and received wave signals*

Use of the cross-power spectrum and cross-correlation functions to provide travel time estimations has been extensively covered in the literature (Viggiani and Atkinson 1995, Leong et al. 2005), and as such only the two primary equations relating to each method used within BEAT are presented here. Equation 2 firstly displays the group travel time, t_g, where $d\varphi/df$ corresponds to the slope of the absolute cross-power spectrum phase diagram across a user-defined frequency range. Equation 3 provides the discrete cross-correlation function, CC_{xy}, with respect to source signal time shift, t_s, where T corresponds to the signal time record and $Y(T)$ and $X(T)$ correspond to the source and received signal outputs respectively.

$$t_g = \frac{1}{2\pi}\frac{d\varphi}{df} \tag{2}$$

$$CC_{xy}(t_s) = \frac{1}{T}\sum_{T=0}^{T-1} X(T)Y(T+t_s) \tag{3}$$

The time shift corresponding to the maximum value of CC_{xy} is used for the travel time estimate obtained from the TD analysis (i.e. $t = t_s$ when CC_{xy} = maximum), whilst a frequency window running from 0.8 to 1.2 times the source signal frequency is used to determine the group travel time t_g = t

(unless the user alters this frequency window when using the Interactive Analysis tool).

2.4 *GDS Bender Element Analysis Tool output*

Following the analysis process, BEAT produces two output tabs within Excel: these are Travel Time Report and Graphs. The Travel Time Report lists all relevant data numerically, including the data filenames, travel time estimates obtained from the TD and FD analysis methods, and various analysis metrics. The Graphs tab displays a number of plots for each data file, including the source and received wave signals with travel time estimates shown, frequency spectrums for each signal, the unwrapped phase angle, and values of the cross-correlation function. These outputs allow the user to further assess the validity of the analysis, and to use the travel time estimates in V_S and G_0 calculations.

3 BENDER ELEMENT TESTS ON LEIGHTON BUZZARD SAND TRIAXIAL SPECIMEN

To initially assess the performance of BEAT, a series of bender element tests were performed on a triaxial specimen of Leighton Buzzard sand Fraction D. The triaxial apparatus used was a GDS Dynamic Triaxial Testing System (DYNTTS), with bender element tests conducted via a GDS BES. The specimen, nominally 70 mm diameter by 144 mm in height, was prepared using a moist-tamping method similar to that previously employed by the authors (Rees 2010). Following saturation (B value ≥ 0.95), the specimen was isotropically consolidated to four mean effective stresses, p', with bender element tests being conducted at each stress level. The data presented herein focuses exclusively on the tests performed at p' = 100 kPa using a single sine-wave source.

Properties of the specimen are presented in Table 1, including void ratio, e, and relative density, D_r. Note values of the maximum and minimum void ratios used to estimate D_r were 1.01 and 0.72 respectively (Klotz 2000), with L equal to the element tip-to-tip distance.

Table 1. Properties of the Leighton Buzzard sand triaxial test specimen.

p' (kPa)	e	D_r (%)	ρ (t/m^3)	L (mm)
100	0.88 ± 0.03	43 ± 10	1.88 ± 0.02	139.1

The bender element tests were conducted by systematically varying the source wave frequency, as recommended by TC-29, from the chosen values of 14.3 kHz to 1.0 kHz. For each test frequency five separate source element triggers were applied to the specimen, with the received signal output then stacked in the time domain to remove random signal noise. Three examples of source and received signals obtained during these tests are presented in Figure 3.

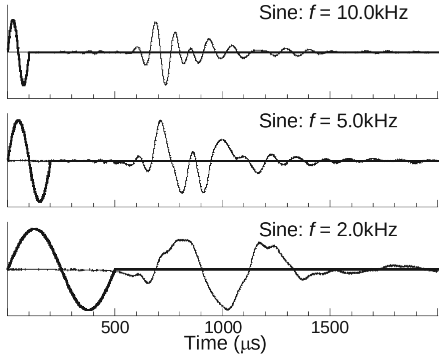

Figure 3. Source and received bender element signals obtained from the test specimen at p' = 100 kPa.

After completion of the bender element tests, the Batch Analysis Add-In tool was used to automate the data analysis and report the estimated travel times. Note the analysis was completed after approximately 45 seconds using a desktop PC running Windows XP SP3 with a 2.93 GHz Intel Core 2 Duo CPU and 2.00 GB RAM. Travel time estimates obtained from this process are presented in Table 2.

Table 2. Travel time estimates from the Batch Analysis tool.

Source f (kHz)	Shear wave travel time estimates, t (μs)					
	Observation of Received Signal (TD)				Cross-correlation (TD)	Cross-spectrum (FD)
	Point A	Point B	Point C	Point D		
14.3	221	635	651	675	662	620
12.5	224	637	655	681	663	703
11.1	224	641	658	685	663	663
10.0	225	643	662	689	662	641
8.3	227	646	667	698	662	697
6.7	226	652	671	706	661	678
5.9	278	650	671	712	662	613
5.0	497	650	672	713	662	495
3.3	227	653	676	719	674	771
2.5	229	654	682	784	669	735
2.0	488	655	690	828	657	767
1.7	450	657	696	846	645	642
1.4	404	658	700	855	640	633
1.3	398	659	707	858	632	515
1.1	442	658	716	862	632	325
1.0	443	659	744	868	640	235
Scatter for f ≥ 3.3kHz :	± 138	± 9	± 13	± 22	± 7	± 138

To compare the performance of BEAT with subjective analyses, a geotechnical academic at Warsaw University (WU) with previous bender element signal analysis experience was sent the test data (from 12.5 kHz – 1.0 kHz) and asked to provide travel time estimates using any observational, non-automated analysis methods they considered appropriate. This resulted in travel times being estimated with five separate methods, including the first arrival or start-to-start method (specified as point C in Figure 2) and the peak-to-peak technique. Travel time estimates produced by BEAT and the subjective analyses from WU were subsequently used to calculate V_S and G_0 values, which are presented in Figure 4. It should be noted a system delay of 42 μs was subtracted from all travel time estimates when calculating V_S, and that G_0 values are approximate (± 2 MPa) due to axis scaling when plotting both parameters in Figure 4.

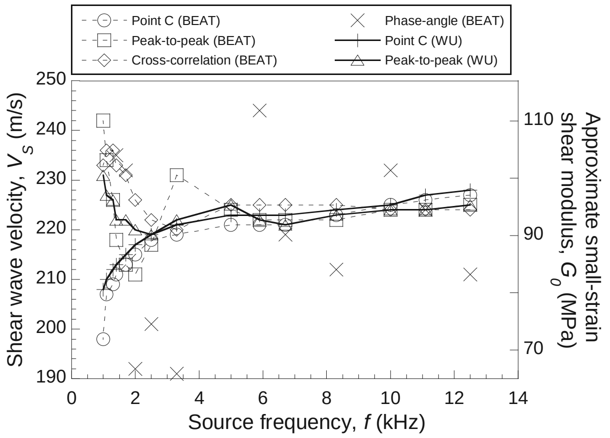

Figure 4. Shear wave velocity and approximate small-strain shear modulus values calculated from estimated travel times.

4 DISCUSSION

Table 2 lists the scatter in travel time estimates for source frequencies from 14.3 kHz to 3.3 kHz, as this provides an indication of the robustness of each analysis method. Note the lower limit of 3.3 kHz was chosen as this value corresponds to an approximate propagation distance-to-wavelength ratio equal to two, avoiding data which may include near field effects (Sánchez-Salinero et al. 1986). The values in Table 2 indicate significant variation in estimates obtained using the cross-spectrum calculation and first deflection observational algorithm (both ± 138 µs), suggesting estimates taken from either method may be unreliable if not validated by other data. In particular the scatter observed from cross-spectrum analyses has been previously been reported following other studies (Yamashita et al. 2009), with the sensitivity of estimates to the frequency window used within the analysis method also being highlighted (Viana da Fonseca et al. 2009). As such it is recommended the cross-spectrum method be used with caution, and it is recognized that a more advanced technique for determining the frequency window may be required for implementation within the Batch Analysis tool.

Conversely the scatter in estimates obtained from the cross-correlation function (± 7 µs) and first bump maximum observation (± 9 µs) were relatively minimal. These values suggest each method is relatively robust, an observation also made for the cross-correlation function after reviewing recent studies comparing analysis methods (Styler and Howie 2012).

Whilst the V_S and G_0 values presented in Figure 4 demonstrate the carry-on effect of scattered travel time estimates produced by the cross-spectrum calculation, they also display good comparison between values obtained via BEAT and the subjective WU observational analyses. It can specifically be seen that travel times based on a determination of point C (i.e. the start-to-start method) lead to V_S values generally within 2 m/s of each other, whilst the peak-to-peak estimates follow the same trend with variation in source frequency (e.g. increased V_S and G_0 values when f < 3.3 kHz). Such preliminary results suggest the use of BEAT may decrease subjectivity when interpreting travel times using standard observational techniques, whilst still allowing accurate estimates of the shear wave velocity and small-strain shear modulus to be calculated.

5 CONCLUSIONS

The subjectivity and lack of a satisfactory model for interpreting shear wave travel times from bender element test data has led GDS Instruments to develop BEAT, a tool designed to automate the interpretation process using a number of recommended analysis methods in both the time and frequency domains. The tool is accessed via two easy-to-use Microsoft Excel Add-Ins, allowing data derived from almost any bender element system to be analysed, either one test at a time, or in batches when organised using the GDS .bes file format. Outputs from the tool include numerical values of the travel time estimates and analysis metrics, as well as visual representations of the source and received bender element signals to assist with rapid data validation by the user.

An initial assessment of BEAT was made by conducting bender element tests on a saturated, isotropically consolidated triaxial specimen of Leighton Buzzard sand. During these tests the single sine-wave source frequency was systematically varied from 14.3 kHz to 1.0 kHz, allowing the robustness of each analysis method to be investigated. Results from BEAT when f ≥ 3.3 kHz showed significant scatter in travel time estimates obtained from a cross-spectrum calculation (± 138 µs), whilst the cross-correlation function produced relatively consistent estimates (± 7 µs) with variation in the source frequency. Observational analyses of the received bender element signals conducted by BEAT were also compared with subjective estimates provided by a geotechnical academic, demonstrating good agreement between calculated V_S and G_0 values. This has led to the preliminary conclusion that BEAT can provide accurate, objective interpretation of bender element test data via a simple user interface, however caution and engineering judgment are still recommended when making final decisions regarding the most suitable shear wave travel time estimate for further geotechnical calculations.

GDS BEAT is available for free download from www.gdsinstruments.com/gds-bender-elements-analysis-tool, which also includes further technical information and video demonstration of the software tool.

6 ACKNOWLEDGEMENTS

The authors wish to express their sincere thanks to Tomasz Szczepański of Warsaw University for providing observational analyses of the bender element test data presented in this paper, and Sophie Laliat for providing a French translation of the paper abstract.

7 REFERENCES

Alvarado G. and Coop M. R. 2012. On the performance of bender elements in triaxial tests. *Géotechnique* 62 (1), 1-17.

Dyvik R. and Madshus C. 1986. Lab measurements of Gmax using bender elements. *NGI Publication* 161, 1-7.

Jovičić V., Coop M. R. and Simić M. 1996. Objective criteria for determining Gmax from bender element tests. *Géotechnique* 46 (2), 357-362.

Klotz U. 2000. *The influence of state on the capacity of driven piles in sands*. PhD Thesis, City University, London.

Lee J-S. and Santamarina J. C. 2005. Bender Elements: Performance and Signal Interpretation. *Journal of Geotechnical and Geoenvironmental Engineering* 131 (9), 1063-1070.

Leong E. C., Yeo S. H. and Rahardjo H. 2005. Measuring Shear Wave Velocity Using Bender Elements. *Geotechnical Testing Journal* 28 (5), 1-11.

Rees S. D. 2010. *Effects of fines on the undrained behaviour of Christchurch sandy soils*. PhD thesis, University of Canterbury, Christchurch.

Sánchez-Salinero I., Roesset J. M. and Stokoe II K. H. 1986. *Analytical studies of body wave propagation and attenuation*. Geotechnical Engineering Report GR86-15, University of Texas, Austin.

Shirley D. J. and Hampton L. D. 1978. Shear-wave measurements in laboratory sediments. *Journal of the Acoustical Society of America* 63 (2), 607-613.

Styler M. A. and Howie J. A. 2012. *Comparing frequency and time domain interpretations of bender element shear wave velocities*. Proceedings of GeoCongress 2012, Oakland.

Viana da Fonseca A., Ferreira C. and Fahey M. 2009. A Framework Interpreting Bender Element Tests, Combining Time-Domain & Frequency-Domain Methods. *Geotechnical Testing Journal* 32 (2), 1-17.

Viggiani G. and Atkinson J. H. 1995. Interpretation of bender element tests. *Géotechnique* 45 (1), 149-154.

Yamashita S., Kawaguchi T., Nakata Y., Mikami T., Fujiwara T. and Shibuya S. 2009. Interpretation of international parallel test on the measurement of Gmax using bender elements. *Soils and Foundations* 49 (4), 631-650.

Pseudo-static Pile Load Test: Experience on Pre-bored and Large Diameter Piles

Tests de chargement pseudo-statique sur pieux: experiences sur pieux forés de grands diametres

Rinaldi V.A.
National University of Cordoba, Argentina.

Viguera R.
Principal Engineer, CIM SRL consultants, Cordoba, Argentina

ABSTRACT: Pseudostatic load test is usually employed as an alternative to the conventional static load test for piles. Recent developments showed that the well developed Statnamic tests can be substantially simplified by using a hanging weight falling over a cushion system that allows increasing the time length of the generated stress pulse. This work describes the design of the test method and a recently experience related to the application of the pseudostatic load test used to evaluate the bearing capacity of large diameter piles. The performed test showed that using moderate loads from 10 to 20 tons falling from 10 cm to 120 cm and cushions prepared at varied stiffness allowed to reach more than 800 tons of loading and the fully mobilization of the pile ultimate capacity. The main advantages of the proposed pseudostatic tests respect to the conventional Statnamic tests is the possibility to apply load increments by steps, the repeatability of each loading step and the simpler test setup required by the former.

RÉSUMÉ : Des essais de chargement pseudo-statique ont été récemment proposés comme alternative à l'essai de chargement statique classique sur pieux. Les développements expérimentaux récents ont montrés que ces tests peuvent être simplifiés par l'utilisation d'une masse suspendue qui tombe sur un système amortissant. Ainsi cette technique permet d'augmenter le temps de l'application de la charge impulsionnelle. Ce travail décrit la conception de l'expérience et les essais qui ont récemment été effectués pour évaluer la capacité portante de pieux de grand diamètre. Les tests effectués ont montrés que l'utilisation de charges modérées de 10 à 20 tonnes tombant d'une hauteur de 10 à 120 cm sur des amortisseurs à rigidités contrôlés, permettent de simuler plus de 800 tonnes de chargement et d'atteindre la charge ultime du pieu. Les principaux avantages des essais pseudo-statiques sont la possibilité d'appliquer des incréments de charge, une répétabilité de chaque chargement et un essai plus simple à réaliser.

KEYWORDS: Pile load test- Statnamic- pseudostatic test- bearing capacity-shaft resistance, tip resistance.

1 INTRODUCTION.

The in-situ determination of bearing capacity of the pre-bored piles has historically been performed by means of the conventional static load tests as described in the ASTM C1143-69. The implementation of this type of test on piles of very large ultimate capacity becomes cumbersome resulting fundamentally from the extremely heavy and complex system for the load reaction. The interpretation of the tests is straight forward however it may be affected by the proximity of the piles of reaction. To overcome these difficulties ather alternatives such as dynamic load test was proposed. In this test the load is applied by the impact of a falling mass dropped from various heights depending on the desired loading requirements. The maximum height depends on the capacity of the pile. The interpretation of this test is performed by using the wave equation (Smith, 1960) applied to a discrete soil-pile model, from which are determined the static shaft and tip soil resistance and the load-settlement curve of the pile. Conceptually the method is very robust; nevertheless its main limitation is that the applied test loads produce tensile stresses that may cause breakage of the pile shaft.

Pseudoestátic methods become an interesting alternative that significantly overcomes the limitations of the other types of tests. In this group can be mentioned the Statnamic method (see for example Bermingham and Janes, 1989), and the non-conventional tests based on free-falling and accelerated falling mass impinging on an special cushion (eg. Schellingerhout and Revoort, 1996; Matsuzawa et al., 2008; Miyasaka et al 2008).

The fundamental difference with respect to the dynamic tests is the of time of application of the load as shown in Figure 1. In pseudoestáticos methods, the time of application of the load should be:

$$t_{50} >> \frac{2l}{V_p} \tag{1}$$

Where l is the pile length and V_p is the wave propagation velocity of the pile shaft which for concrete is usually adopted a value of 4100 m/s.

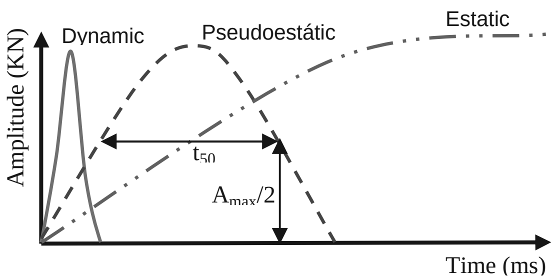

Figure 1. Loading functions of the different loading test for piles.

Usually it is recommended for a pseudo-static condition:

$$\lambda = V_p\, t_{50} > 7\, a 10\;\; l \tag{2}$$

If assumed the loading condition imposed by equation (1) and (2), the interpretation of the soil-pile interaction can be that of the simple physical model described in Figure 2.

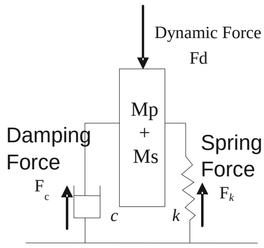

Figure 2: Model for the soil pile interaction in the peudoestatic model.

To increase the application time of loading, a high strength resilient material is required to be placed on the head of the pile in the area of impact. Assuming that the load is obtained by a falling mass of approximately 10% of the ultimate capacity of the pile (Fu) and also considering the charging triangular diagram of Figure 3, then:

$$t_{50} = \frac{m\sqrt{2gh}}{F_u} = \frac{\frac{0.1F_u}{g}\sqrt{2gh}}{F_u} = 0.1\sqrt{\frac{2h}{g}} \tag{3}$$

Where h is the falling height of the mass m. This cinematic equilibrium equation is an approximation since restitution forces has been overridden.

The maximum forces that can be exerted on the pile tip (F_{max}) due to the falling mass on a cushion material of elastic constant k_e can be calculated as:

$$m\ g\ h = \frac{1}{2} F_{\max}\ z_{\max} \tag{4}$$

Where z_{max} is the maximum deformation of the cushion material $z_{max} = F_{max}/k_e$. Then, replacing in equation (4),

$$F_{\max} = \sqrt{2\ m\ g\ h\ k_e} \tag{5}$$

Being the natural frequency of the mass-cushion system:

$$T = 2\pi\sqrt{\frac{m}{k_e}} \tag{6}$$

Since t_{50} is half of the natural frequency and assuming a triangular shape of the wave (see Figure 3):

$$\pi\sqrt{\frac{m}{k_e}} > t_{50} > \frac{2}{3}\pi\sqrt{\frac{m}{k_e}} \tag{7}$$

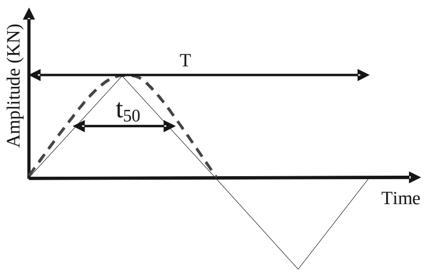

Figure 3: Simplified model of the stress pulse.

Equations (5) to (7) allows to evaluate the magnitude of the mass and the falling height to obtain a maximum force F_{max} according to the elastic constant k_e of the cushion material.

From Figure 2, the equilibrium equation can be derived as:

$$F_d - F_c - F_k = (M_s + M_p)\,a \tag{8}$$

Where M_s and M_p are the mass of the pile and the soil respectively and a is the acceleration of the movement. Equation (8) can be rewritten in terms the resistant forces as a function of the dynamic parameter $F_c = c\ v$, and $F_k = k\ u$, being u and v the displacement and velocity of displacement respectively:

$$F_d - c\ v - k\ u = (M_s + M_p)\,a \tag{9}$$

Equation (9) allows determine dynamic influence on the measured force at the point of where the velocity becomes zero and thereafter correcting the measured force by the dynamic effect.

2 TESTING PROCEDURE.

Figure 4 and 5 sketch the testing setup and electronic devices used for the pseudoestatic load test. This loading design generates a time-controlled load which will depend on the magnitude and height of the falling mass, and geometry and elastic properties of the elastomeric cushion included between the mass and head of the pile. The force pulse is captured by a load cell placed below the cushion. The displacement of the pile is obtained from the double integration of the signals captured by two accelerometer placed on the shaft and below one diameter from top of the pile. The weight of the mass to be used ranges between 5% and 10% of the servicebility capacity of the pile. The test requires the continuous increment of the height of drop of the mass. The output of the conditioners is then digitized by the dynamic analyzer and conveniently stored for subsequent laboratory analysis. In addition to the equipment shown, a proximeter is placed to capture displacements and permanent settlement of the pile. The maximum testing load is obtained when a permanent displacement is generated or until the 50% of the service load is reached.

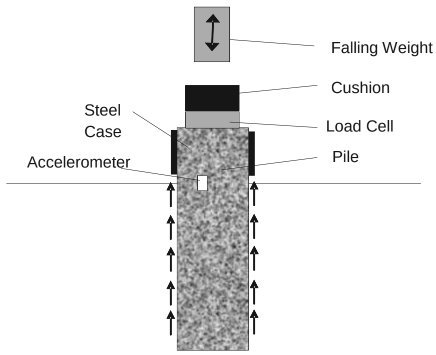

Figure 4. Testing setup for the pseudoestatic load test.

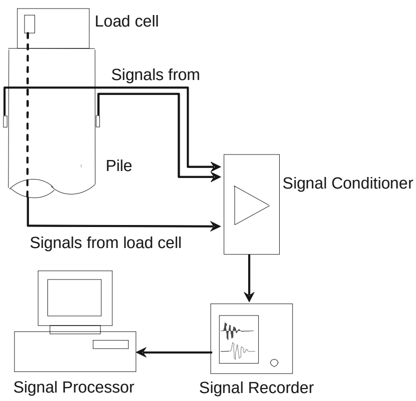

Figure 5. Testing electronic devices used for the pseudoestatic load test.

The impact mass can be made at the site usually employing a concrete slab or a steel casing filled with concrete depending on its size. For the purpose of centering the load, steel bars are used as guides for obvious safety reasons and ensuring the impact of the mass be centered avoiding the generation of moments. For the purpose of preventing the damage of the pile by the application of impact on the mass, the shaft is increased (1.5 to 2 times the diameter) by means of a steel case of the same diameter of the shaft. In all cases, the accelerometers must be positioned below this extension or in a window made on it. The load cell is cylindrical and of stainless steel of the same diameter as the damper.

3 CASE HISTORY.

This work describes the results of two pseudostatic load tests performed on large diameter piles buit for a bridge over the River Calchaquí on the state highway No 37, in the province of Santa Fe, Argentina. For this bridge were projected sixteen piles of 1.20 m in diameter and approximately 24 m long with preload cell. The soil profile of the site is characterized by the presence of reddish-colored silty clays with interbedded more greenish layers. The compactness of the soil has significant horizontally and vertically variations. At the foundation depth of 24 m the penetration resistance is higher than 50 blows of the normalized Standard Penetration Test. Ultrasonic cross hole tests (ASTM D6760) were performed in all the piles on the six prospecting pipes before and after the load test. The service load of each pile was designed for 4800 kN and the falling mass was 25 tn. The mass was hanged and dropped using a free fall crane (see Figure 6).

Figure 6. Picuture of one of the piles tested at the site.

Figures 8 to 10 show the typical curves of the recorded force, velocity and displacement for a single drop of the mass. Note that loading times exceed the 50 milliseconds which for the present case can be considered pseudostatic.

Figures 9 and 10 show the curves of load-settlement obtained for the two piles tested in this work. Notice that in these figures the results from all mass drops have been included. The envelope correspond to the total envelop and the corrected envelop to account for dynamic effect using equation (9) at the point where the velocity is zero or where the maximum displacement is attained.

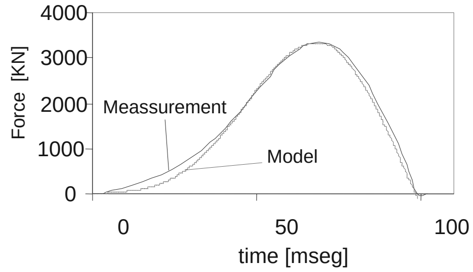

Figure 7. Force function for a falling weight of 25 tn from a drop height of h=2.2 m

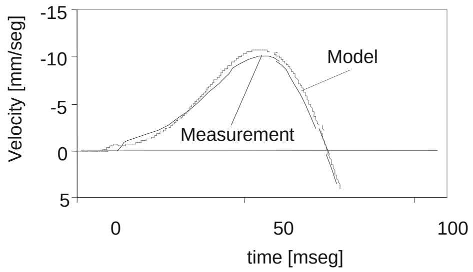

Figure 8. Velocity function for a falling weight of 25 tn from a drop height of h=2.2 m

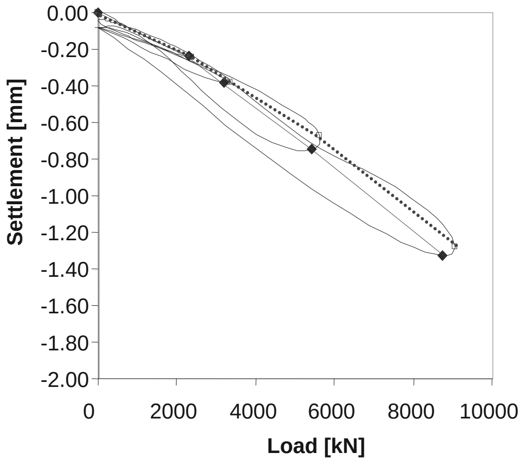

Figure 9. Load- settlement envelopes for the pile P2-S tested in this work. Dotted line corresponds to the total envelop and filled line to the corrected envelop by removing the dynamic effect.

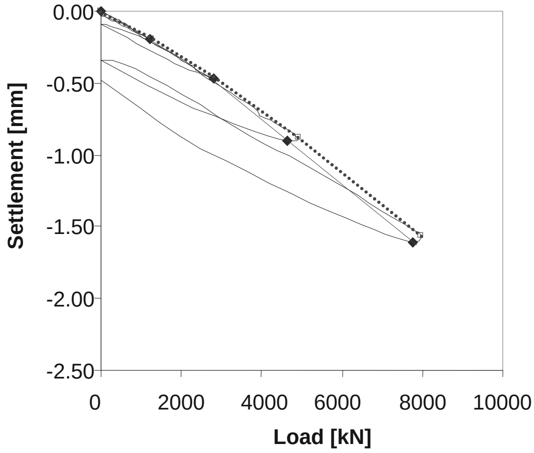

Figure 10. Load- settlement envelopes for the pile P3-S tested in this work. Dotted line corresponds to the total envelop and filled line to the corrected envelop by removing the dynamic effect.

.

Notice that the maximum loads were around 8000 kN and settlements were in between 1.4 mm and 1.50 mm for the maximum load imposed. At the service load is expected a settlement lower than 0.6 mm.

The piles were also modeled by using the wave equation model formulated by Smith (1960). The pile shaft was divided in sections of one meter ant the soil was modeled as spring and dashpots. The dynamic constants were varied until the best approximate of the model to the measurements were obtained. Figures 7 and 8 show the agreement of the modeled pile to the measurements. The distribution of reaction forces along the pile shaft is shown in Figure 11. It seems that most of the load is taken by the shaft an only 900 kN are taken by the tip at the maximum load of the test performed. The behavior of pile-soil systems corresponds to a quasi elastic phase with little plastic deformations.

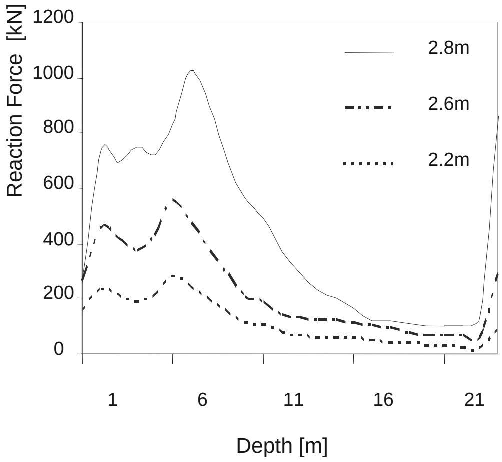

Figure11. Distribution of reaction forces along the pile shaft obtained from the solution of the wave equation for different drop height of the mass.

4 CONCLUSIONS

The conclusions of the work presented here can be summarized as follow:

a) The pseudostatic test can be performed for most piles using a proper design of the cushion system and falling weight.
b) The falling weight method is advantageous respect to most other pile loading test since it can be performed much easier, at lower costs and at higher productivity per day.
c) The pseudostatic test procedure has also the advantage that can be interpreted as the conventional static test and also using the Smith´s wave equation.
d) There is a need to compare the results from pseudostatic tests and static tests, however, since the pseudostatic test is physically identical to the Statnamic method, the well established comparison between Statnamic and static can be extended to the pseudostatic falling weight test.

5 REFERENCES

Bermingham P. and Janes M., 1989. Innovative Approach to Load Testing of High Capacity Piles, Proc. Int. Conference on Piling and Deep Foundations, London, pp. 409-413.

Goble G. and Likins G., 1996. On the Application of PDA Dynamic Pile Testing, Proc. 5th Intern. Conf. on the Application of Stress Wave Theory to Piles, Orlando, FL.

Matsuzawa K., Nakashima Y. and Matrsumoto T., 2008. Spring Hammer Rapid Load Tests Method and Its Validation, Proc. of the 2nd BGA International Conference on Foundations, Brennan A. And Knappedt J. Ed., pp.224-234.

Miyasaka T., Kuwabara F., Likins G. and . Rauche F., 2008. Rapid Load Test on High Bearing Capacity Piles", Science Technology and Practice, Dos Santos J. Ed., pp. 5001-5006.

Schellingerhout A.J.G. and Revoort E., 1996. Pseudostatic Static Pile Load Tester, Proc. Of 5th international Conference of Stress Wave Theory to Piles, Orlando, pp.1031-1037.

Smith, E. A. L. 1960. Pile Driving Analysis by the Wave Equation, Journal of the Soil Mechanics and Foundations Division , ASCE, Vol. 86, No. SM4, Proc. Paper 2574, pp. 35-61, Agosto, 1960

Behavior of Vertical Piles Embedded in Sand under Inclined Loads near Ground Slope

Comportement de pieux verticaux ancrés dans une couche de sable à proximité d'une pente

Sakr M.A., Nasr A.M.
Faculty of Engineering, Tanta University, Egypt

ABSTRACT: Pile foundations are used to support structures exposed to different types of loads. Among these loads are inclined loads which give axial and lateral loads. The main objective of the present paper is to investigate experimentally the effects of inclined load on axial pile displacement and lateral pile response for piles embedded in the level ground and near ground slope. The factors considered for this purpose are slenderness ratio for pile (L/D), relative density of sand (D_r), distance of the pile head from the slope crest (B/D), and the inclination of the applied load with the vertical. The behavior of the piles in the level ground was compared with the behavior of piles located near ground slope. Different results were obtained for combined axial and horizontal loading. From test results, the inclination of the applied load has a significant effect on the ultimate axial and lateral loads for pile, lateral pile deflection, and the bending moment along the pile shaft especially near ground slope. The coefficient of horizontal modulus of sub-grade reaction decreased when the inclination of the applied load increased.

ABSTRACT: Les fondations sur pieux sont envisages pour des structures soumises à différents types de chargement parmi lesquels on distingue ceux à composante latéral. Ce papier présente une étude expérimentale qui analyse l'influence de l'inclinaison d'un chargement sur le déplacement vertical et la réponse latérale d'un pieu ancré dans un sol à proximité d'une pente. Les paramètres d'influence sont l'élancement du pieu (L/D), la densité relative (D_r), la distance horizontale séparant le pieu de la pente (B/D) et l'inclinaison de la charge par rapport à la verticale. Le comportement des pieux dans un massif horizontal est comparé à celui de pieux à proximité de la pente à partir de résultats obtenus pour des chargements à composante verticale et horizontale. Il a été conclu que l'inclinaison du chargement à une influence considérable sur la capacité portante ultime sous charges verticale et latérale, le déplacement horizontal et le moment de flexion le long du fût du pieu, en particulier à proximité de la pente. Il a été également vérifié que l'augmentation de l'inclinaison du chargement conduit à une diminution du module de réaction horizontale.

KEYWORDS: Vertical piles, inclined load, sand slope, axial and lateral displacement.
MOTS CLÉS: Pieu vertical, charge incline, pente en sol sableux, déplacemenst vertical et horizontal

1 INTRODUCTION

Pile foundation for several types of structures is often subjected to simultaneous axial and lateral loading. According to current practice, piles are independently analyzed first for the axial load to determine their bearing capacity and settlement and then for the lateral load to determine the stresses and deflections. Several results of investigations on the behavior of piles subjected to inclined loading have been reported in the literature, e.g. by Chari and Meyerhof (1983), Sastry and Meyerhof (1990) and Abdel-Rahman and Achmus (2006).

Poulos and Davis (1980) suggested that the failure of a vertical pile exposed to an inclined load can be treated as the ultimate load capacity is a function of both the lateral resistance and the vertical load capacity of the pile. When the applied load deviates slightly from the axial direction, the failure will essentially occur due to the axial slip while lateral failure will occur when the inclination is large; that is the load becomes nearly perpendicular to the pile axis.

Six model tests were performed on aluminum closed-ended piles by Christos and Michael (1993) to investigate experimentally any possible effects of lateral loading on axial pile displacements and stresses as well as the influence of axial loads on the lateral pile response. The main findings were the following: the effect of axial loading on the lateral pile response was rather limited. The interaction between axial and lateral pile responses can be studied with a nonlinear finite-element analysis, while the conventional elastic half space and subgrade reaction methods of pile analysis cannot consider this interaction.

According to Vankamanidi and Geoffrey (1999), the lateral soil pressure, bending moments, pile displacements at the ground surface have been investigated. The results of these load tests are compared with theoretical estimates based on the concept of the effective embedment depth of equivalent rigid piles for ultimate and elastic case. Reasonable agreement has been found between the observed and the predicted behavior of flexible piles.

From the above literature, lack in the knowledge about the behavior of pile under inclined loads near ground slope was noted. Therefore, the main objective of this paper is use experimental model to study the behavior of pile adjacent to a slope crest under inclined loads.

2 MODEL DESCRIPTION

Vertical and lateral loads were conducted on the model pile in a rectangular steel test tank with the size of 1000 mm (length) x 500 mm (width) x 700 mm (height). The vertical edges of the tank were stiffened by using steel angle sections. The inner faces of the tank were graduated at 50 mm intervals to facilitate an accurate preparation of the sand bed in layers. The front long side was made of a 20 mm thick glass panel. The glass side allows the sand to be seen during the preparation and to minimize friction between the tank wall and sand particles.

Vertical loads were applied to the model pile by using a hydraulic jack. The magnitudes of applied loads were recorded with the help of a pre-calibrated sensitive proving ring. The lateral load was affected through a 2 mm diameter high-tension steel wire connected to the pile cap using an eye bolt. The other side of the wire ran over smooth adjustable pulley with a 70 mm diameter and supported a load plat form. In order to record the correct vertical settlement and lateral deflection of the pile for each load increment applied, four sensitive dial gauges of the least measurement of 0.01 mm were used, two for vertical and two for lateral and their average was taken.

A smooth steel model pile, with diameter of 10mm, and total length 110, 210, 310, and 410 mm were used in this study. The upper 10 mm of the pile is screwed part and the other length embedded in sand. The slenderness ratio (L/D) was chosen to be used in this research equal to 10, 20, 30, and 40. Five strain gages were stuck to the surface of the model pile with L/D = 40. The measurement of flexural strains can lead directly to bending moment curve.

The cap was designed as flexible as possible and the pile was not deeply seated through it, so that no restraint of the pile head rotation is available. One edge of the cap is bent up to allow horizontal dial gauges to be mounted. At the other side of the cap, a 1.5-cm hook was welded exactly at the center of this side.

3 SOIL PROPERTIES

The soil used in this study for all of the tests is clean sand, classified as poorly graded sand according to the Unified Soil Classification System. The moisture content (W_c) was about 2%. The following are the results of the sieve analysis test; effective grain size D_{10} = 0.14 mm and uniformity coefficient C_u = 4.357. The sand was placed to achieve three relative densities. The physical characteristics of these soils are shown in Table (1).

Table 1. Physical Properties of the Tested Soils.

Soil Condition	A	B	C
Relative density D_r (%)	25	45	68
Unit weight (kN/ m^3)	17.5	17.8	18.3
Voids ratio (e)	0.56	0.52	0.48
Porosity (n)	0.36	0.34	0.33
Angle of shearing resistance (Ø)	31^o	34^o	38^o

4 PREPARATION OF EXPERIMENTAL SETUP

Before sand slope preparation, the model pile was then placed at a specific position. Then, model sand slope 150- mm high with slope angle, θ, of 26.56^o (2H: 1V) was prepared in layers of 50 mm thick. The proposed testing geometry of the slope was first marked on the walls of the tank for reference. To obtain uniform density of the soil in the tank, controlled pouring and tamping techniques using a flat bottom hammer were applied. The pile was placed and fixed in its correct position before the formation of sand slope to simulate non displacement piles.

5 RESULTS AND DISCUSSION

An experimental testing program was designed to study the effect of inclined load on the behavior of vertical pile in sand on level ground and adjacent to ground slope. The geometry of the problem is illustrated in Fig. 1. As shown in this figure, the height of ground slope (H_{slope}) equal to 15 cm and its horizontal projection (X_{slope}) equal to 30 cm to achieve slope gradient (2H:1V). The location of the pile relative to the slope crest is the distance (B).

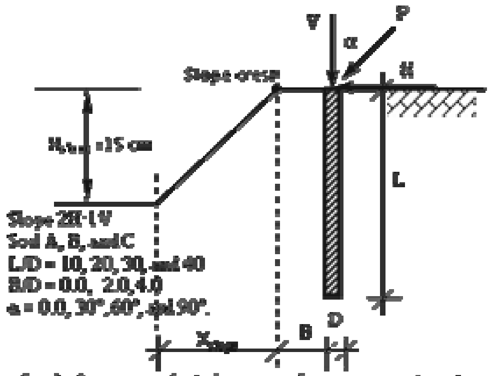

Fig. 1. Positions of pile in cases of experimental work.

The load-deflection curves were obtained by plotting the relationship between the vertical and lateral loads and its axial settlement and lateral deflections, respectively. According to Terzaghi (1942) and Tomilson (1980), the ultimate axial (V_u) and lateral (H_u) loads are defined as the loads, which cause a vertical or horizontal deflection of one tenth of the pile diameter (i.e. 10% of the pile diameter) to simulate the geotechnical failure in the soil.

5.1 *Ultimate capacity of pile in the level ground*

The ultimate axial load and lateral load of the pile increased during testing program when the slenderness ratio (L/D) was increased. As shown in Fig. 2, for dense sand (soil C), a significant increase for ultimate axial load (V_u) with increasing slenderness ratio. But for loose sand (soil A), the effect of slenderness ratio on the ultimate axial load found to be small. The ultimate axial load (V_u) decreased as the inclination of the applied load with the vertical (α) was increased.

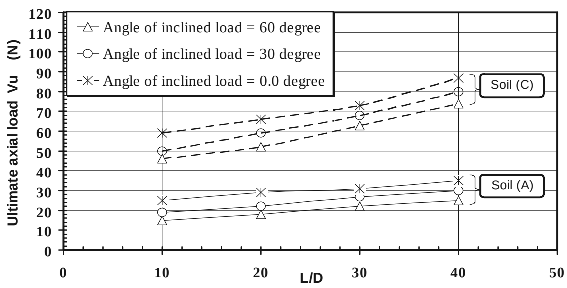

Fig. 2. Relationship between (L/D) and (V_u) for soil A and C.

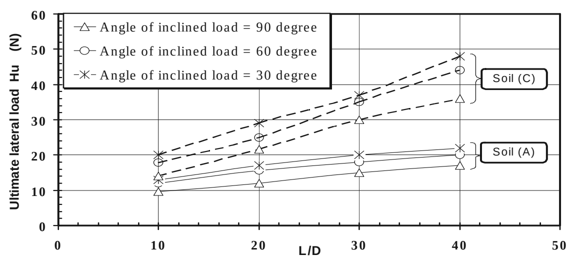

Fig. 3. Relationship between (L/D) and (H_u) for soil A and C.

From Fig. 3, it is clear that, the ultimate lateral load (H_u) dependent on the slenderness ratio (L/D). A significant increase on ultimate lateral load with increasing (L/D). This can be explained by the embedded length, for small (L/D) is not sufficient to create the full fixation of the pile. Increasing the inclination of the applied load (α) will increase the lateral load acting on the pile head. Therefore, the lateral piles displacement will increase and decrease the ultimate lateral load.

5.3 *Bending moment along the pile length*

Figures 4 and 5 presents the experimental bending moments along the pile length with L/D = 40 in sandy soil. The strain readings obtained experimentally are converted to bending moment. In general, the shape of the diagrams is compatible with the shapes investigated by Broms, 1964. It is obvious that, the increasing of (α) increased the maximum values of the bending moment along the pile length. The maximum bending moment in case of ($\alpha = 90^o$) for pile in soil (A) is about 29 % and 9 % larger than that in case of $\alpha = 30^o$ and 60^o respectively. These percentages are about 13 %, 8 % respectively for pile in soil (C). From the above mentioned figures, the bending moment may vanish before the end of the pile. The depth of the point of the maximum bending moment increases by increasing the inclination of the applied load with vertical (α).

It is obvious from the previous figures that, the maximum bending moments are usually higher for loose sand than the case of dense sand. Increasing the relative density of soil decreased the maximum bending moment along the pile length at the same (α).

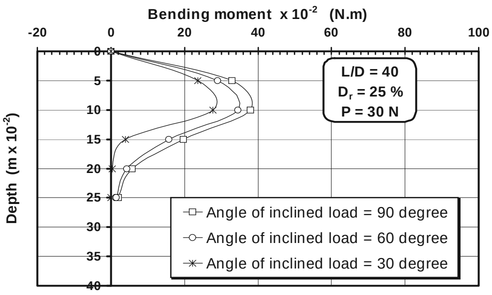

Fig. 4. Experimental bending moment along the pile length for soil A.

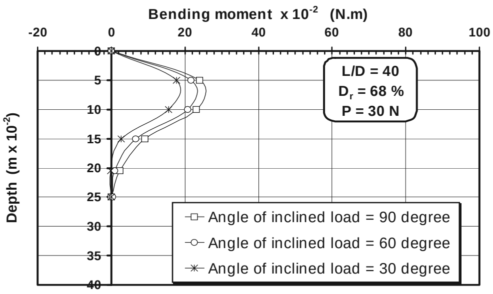

Fig. 5. Experimental bending moment along the pile length for soil C.

5.4 *n_h – deflection relationship*

According to Reese and Matlock (1956), the coefficient of horizontal modulus of sub-grade reaction (n_h) is related to the relative stiffness factor, (T) through the relation, $T = (E_p\ I_p / n_h)^{1/5}$ which is used in the analytical analysis. The value of (T) can be obtained from the following equation:

$$y_{gs} = y_{zg} \times H_{gs} \times T^3 / E_p\ I_p \qquad \text{(Valid for vertical pile only) (2)}$$

where: y_{gs} is the lateral deflection of the pile at ground surface, y_{zg} is a non-dimensional coefficient that depends on the ratio, embedded length / T (for embedded length / T > 4, $y_{zg} = 2.435$), H_{gs} is the lateral load at ground surface, $E_p\ I_p$ is the Flexural stiffness of the pile, and (T) is the relative stiffness.

From load – deflection curves and by using the above equation, the values of (n_h) were calculated at each deflection. The results show that the coefficient of horizontal modulus of sub-grade reaction is significantly dependent on the deflections at the low load levels and is relatively insensitive to deflections at high load levels. Figure 6 shows the coefficient of horizontal modulus of sub-grade reaction versus deflection in the free head case for pile with (L/D=40) and inclined load with ($\alpha = 30^o$). From this figure it is clear that the coefficient of horizontal modulus decreases with the deflection increase. This conclusion agrees with that drawn by Alizadeh and Davisson, 1970. It is obvious from that; relative density of sand has a significant effect on (n_h) values.

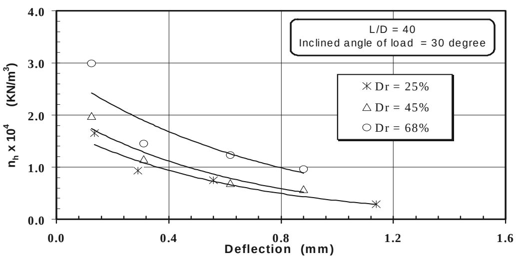

Fig. 6: n_h – deflection relationship for pile under inclined load = 30^o.

5.5 *Pile near ground slope*

There are many practical situations where piles are constructed near ground slope. Both axial and lateral loads were applied to the pile head at ground surface for pile near ground slope (2H: 1V). The test results from experimental model are presented. An important parameter defining the location of the pile head relative to the crest of the slope (B/D) is considered.

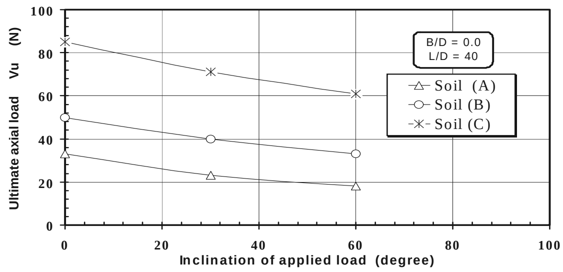

Fig. 7. Relationship between load inclination and (V_u) for pile at crest of slope 2H:1V.

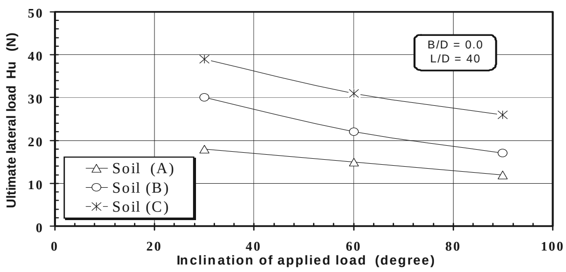

Fig. 8. Relationship between load inclination and (H_u) for pile at crest of slope 2H:1V.

The results in case of a ground slope are compared with the corresponding results obtained by considering the case of a horizontal ground surface. For pile with L/D = 40 and B/D = 0.0, the effects of the inclination of the applied load on the ultimate axial load (V_u) and the ultimate lateral load (H_u) are shown in Figs. 7 and 8. In these figures, the results are normalized with respect to the corresponding values in case of horizontal ground surface. The ultimate axial and lateral loads decreased as the inclination of the applied load with the vertical (α) was increased. Increasing the relative density of the soil will increase the ultimate load (axial and lateral) at the same load inclination (α). For soil (C) and (α = 60^o), the ultimate axial load in case of pile at crest of ground slope having an inclination 2H: 1V is about 18% smaller than that in case of horizontal ground surface. This percentage increases to 31% for ultimate lateral load.

The ratio (B/D) represents the closeness of the crest of the ground slope to the pile head. According to Sakr and Nasr (2010), the ratio (B/D) is very important on the lateral behavior for piles near ground slope. Therefore, the ultimate lateral load is plotted against the pile distance from the slope crest (B/D) in figure 9 for pile with (L/D = 40) and (α = 30^o). From the above mentioned figure, increasing of (B/D) will increase the ultimate lateral load for different soil densities. For soil (A), the effect of (B/D) on the ultimate lateral load can be neglected. For soil (C) and (B/D = 0.0), the percentage decrease in ultimate lateral load is about 21% than that in case of a horizontal ground surface. This percentage is 18% for soil (A).

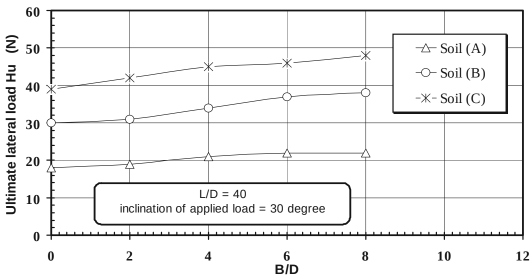

Fig. 9. Relationship between (B/D) and (Hu) for pile near ground slope 2H: 1V.

Figure 10 presents the experimental bending moments along the pile length for pile with (L/D = 40) embedded in loose sand (soil A) and (α) equal to 30^o, and 60^o respectively. From the above figure, increasing of (α) will increase the maximum bending moment. For example from experimental results and at (α = 60^o), the maximum bending moment is about 31% larger than that in case of (α = 30^o). It is clear that the depth of the point of the maximum bending moment is about 25% from the pile length measured from the ground surface.

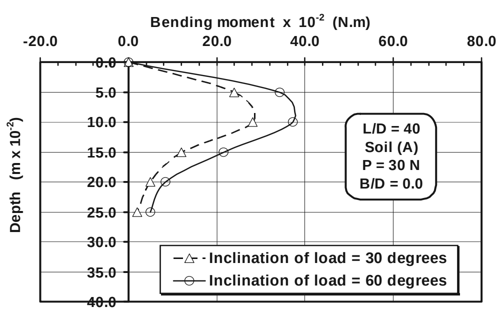

Fig. 10. Experimental bending moment along the pile length at different load inclination.

6 CONCLUSIONS

The results of an experimental model were presented in this research to study the general behavior of a single pile in sandy soil under inclined load. The following conclusions are drawn based on the results of tests for pile in the level ground and near ground slope 2H: 1V:

1- The ultimate axial and lateral loads decreased as the inclination of the applied load with the vertical (α) increased.
2- For pile embedded in dense sand and under inclined loads, a significant increase on the ultimate lateral load with increasing slenderness ratio (L/D).
3- Increasing the inclination of the applied load with vertical (α) will increase the lateral deflection along the pile length. For pile embedded in loose sand and at (α = 90^o), the maximum lateral deflection at ground surface is about 53% larger than that in case of (α = 30^o). This percentage is about 40% for pile in dense sand (soil C).
4- For the same soil and deflection, the values of (n_h) decreases by increasing the inclination of the applied load (α).
5- Increasing the distance of the pile head from the slope crest will increase the ultimate lateral load for piles embedded in different sand densities.

7 REFERENCES

Alizadeh, M. and Davisson M.T. 1970. Lateral Load Tests on Piles-Arkansas River Project.' Journal of the Soil Mechanics and Foundations Division, ASCE, Vol. 96, No. SMS, 1583 - 1604.

Abdel-Rahman K. and Achmus M. 2006. Numerical modeling of combined axial and lateral loading of vertical piles. 6th European Conference on Numerical Methods in Geotechnical Engineering, Graz, Austria.

Broms, B.B. 1964. Lateral Resistance of Piles in Cohesionless Soils. Journal of the Soil Mechanics and Foundations Division, ASCE, Vol. 90, No. SM3, 123 - 156.

Chari. T.R. and Meyerhof G. 1983. Ultimate capacity of single rigid piles under inclined loads in sand. Canadian Geotechnical Journal, Vol. 20, 849-854.

Christos A. and Michael G. 1993. Interaction of Axial and Lateral Pile Responses. Journal of Geotechnical Engineering Division, ASCE, Vol. 119, No. 4, April.

Poulos, H.G. and Davis E.H. 1980. Pile Foundation Analysis and Design. John Wiley and Sons.

Reese, L.C. and Matlock H. 1956. Non-Dimensional Solutions for Laterally loaded Piles with soil Modulus Assumed Proportional to Depth. Proceedings, Eighth Texas Conference on Soil Mechanics and Foundation Engineering, Austin, Texas.

Sakr, M.A. and Nasr A.M. 2010. Behavior of pile groups arrangement adjacent to a sand slope under lateral load. DFI 35th Annual Conference on Deep Foundations, Hollywood, California, 12 – 15 October, 315 – 323.

Sastry, V. and Meyerhof G. 1990. Behavior of flexible piles under inclined loads. Canadian Geotechnical Journal, Vol. 27, No. 1, 849-854.

Terzaghi K. 1942. Discussion of the Progress Report of the Committee on the Bearing Value of Pile Foundation. Proc. ASCE, Vol. 68.

Tomilson M.J. 1980. Pile Design and Construction Practice. A View Point Publication, London.

Vankamamidi V.R.N. and Geoffrey G.M. 1999. Flexible Pile In Soil Layered Under Eccentric and Inclined Loads. Soil and Foundations, Vol. 39, No. 1, Feb., 11 – 20.

Semi-Analytical Solutions for Laterally Loaded Piles in Multilayered Soils

Solutions Semi-analytiques pour des pieux soumis à des charges latérales dans les sols multicouches

Salgado R.[1], Basu D.[2], Prezzi M.[1], Tehran F.S.[1]

[1]*Purdue University, West Lafayette, Indiana, USA*
[2]*University of Waterloo, Waterloo, Ontario, Canada*

ABSTRACT: Piles subjected to lateral forces and moments at the head are often analyzed in practice with the p-y method. However, the p-y method is not capable of capturing the complex three-dimensional interaction between the pile and the soil. The continuum approach is conceptually more appealing but it requires the use of numerical techniques, such as the three-dimensional (3D) finite element (FE) method. In order to save computational time, researchers have explored the development of closed-form solutions based on linear elasticity that can be used to obtain lateral pile deflection with depth. In this paper, we present semi-analytical methods developed to calculate the response of laterally loaded piles with general-shape cross sections embedded in multilayered elastic soil. The displacement field of the pile-soil system is taken to be the product of independent functions that vary in the vertical and horizontal directions. The differential equations governing the displacements of the pile-soil system are obtained using the principle of minimum total potential energy and calculus of variations. The input parameters needed for the analysis are the pile geometry, the soil profile, and the elastic constants of the soil and pile. The method produces results with accuracy comparable with that of a 3D FE analysis but requires much less computational time.

RÉSUMÉ : Les pieux soumis à des charges latérales et des moments à la tête sont souvent analysés dans la pratique par la méthode p-y. Toutefois, cette méthode n'est pas capable de prendre en compte les interactions complexes trois dimensionnelles entre le pieu et le sol. L'approche continue est conceptuellement plus attrayante, mais elle nécessite l'utilisation de techniques numériques, tels que les des éléments finis (EF) en trois dimensions (3D). Afin de gagner du temps de calcul, les chercheurs ont étudié le développement des solutions analytiques basées sur l'élasticité linéaire qui peuvent être utilisé pour évaluer les déplacements latérales du pieu avec la profondeur. Dans cet article, nous présentons des méthodes semi-analytiques développés pour calculer la réponse des pieux chargés latéralement avec des sections transversales en forme générale incorporés dans le sol élastique multicouche. Le champ de déplacement du système pieu-sol est considéré comme le produit de fonctions indépendantes qui varient dans les directions verticale et horizontale. Les équations différentielles qui régissent les déplacements du système pieu-sol sont obtenues en utilisant les principes variationnels et le principe de l'énergie potentielle totale minimum. Les paramètres d'entrée nécessaires pour l'analyse sont la géométrie du pieu, le profil du sol, et les constantes élastiques du sol et du pieu. Cette méthode donne des résultats d'une précision comparable à celle d'une analyse par éléments finis 3D mais nécessite beaucoup moins de temps de calcul.

KEYWORDS: laterally loaded single piles, elastic soil, continuum method, energy principles.

1 INTRODUCTION

Piles subjected to lateral forces and moments at the head are analyzed in practice with the p–y method (e.g., Reese and Cox, 1969). According to the p–y method, the pile is assumed to behave as an Euler–Bernoulli beam with the soil modeled as a series of discretely spaced springs, each connected to one of the pile segments into which the pile is discretized. The springs model the soil response to loading through p–y curves (p is the unit resistance per unit pile length offered by the springs, and y is the pile deflection), which are developed empirically by adjusting the curves until they match actual load–displacement results (e.g. Cox et al., 1974; Ashour & Norris, 2000). However, the p–y method often fails to predict pile response (Anderson et al., 2003; Kim et al., 2004), for it is not capable of capturing the complex three-dimensional interaction between the pile and the soil.

The continuum approach is conceptually more appealing; however, in order to model the soil as a continuum, the use of numerical techniques such as the three-dimensional (3D) finite element (FE) method, finite elements with Fourier analysis, the boundary element (BE) method or the finite difference (FD) method is often required (Poulos, 1971a, 1971b; Banerjee & Davis, 1978; Randolph, 1981). The 3D FE or FD methods can capture the most important features of the complex pile–soil interaction, but three-dimensional analyses are computationally expensive for routine practice.

In this paper, an analysis is developed, based on variational principles, by which the deflection, slope of the deflected curve, bending moment and shear force of laterally loaded piles with rectangular and circular cross section can be obtained. A multi-layered, elastic soil deposit is considered. The analysis captures the 3D pile–soil interaction and produces pile response using closed–form solutions. As a consequence of the analysis, the lateral response of piles can be obtained with a degree of rigor and speed not previously possible. The method can be extended to capture the non-linear pile response due to soil non-linearity.

2 PROBLEM DEFINITION

A circular cross-section pile with radius r_p and a rectangular cross-section pile with cross sectional dimensions $2a \times 2b$ and both with length L_p embedded in a multilayered soil profile are considered (Figure 1). Each soil layer extends to infinity in all horizontal directions, and the bottom layer extends to infinity in the downward direction. The pile is subjected to a horizontal force F_a and a moment M_a at the pile head. The goal of the analysis is to obtain pile deflection as a function of depth caused by the action of F_a and/or M_a at the pile head.

The soil medium is assumed to be an elastic, isotropic continuum, homogeneous within each layer, with Lame's constants G_s and λ_s. There is no slippage or separation between the pile and the surrounding soil or between the soil layers. The pile behaves as an Euler–Bernoulli beam with a constant flexural rigidity E_pI_p.

3 ANALYSIS

3.1 *Soil Displacement Field*

A separable variable technique is used to define the horizontal displacement fields in the soil, and the soil displacement u_z in the vertical direction is assumed to be negligible. The horizontal displacements for rectangular and circular piles are given by

$$\begin{cases} u_x = w(z)\phi_x(x)\phi_y(y), u_y = 0 & \text{for rectangular piles} \\ u_r = w(z)\phi_r(r)\cos\theta, u_\theta = -w(z)\phi_\theta(r)\sin\theta & \text{for circular piles} \end{cases} \tag{1}$$

where $w(z)$ is a displacement function (with a dimension of length) varying with depth z that describes the pile deflection, $\phi_x(x)$ and $\phi_y(y)$ are dimensionless displacement functions varying along the x and y directions of the Cartesian coordinate system used for the rectangular-cross section pile, and $\phi_r(r)$ and $\phi_\theta(r)$ are dimensionless displacement functions varying along the r and θ directions of the cylindrical coordinate system used for the circular-cross section pile (Figure 1). The dimensionless displacement functions describe how the displacements in the soil mass (due to pile deflection) decrease with increase in horizontal distance from the pile. These functions are set to unity at the pile-soil interface, which ensures perfect pile-soil contact, and are set to zero at infinite horizontal distance from the pile center, which ensures that the displacements in the soil due to the laterally loaded piles decrease as the horizontal distance from the pile increases.

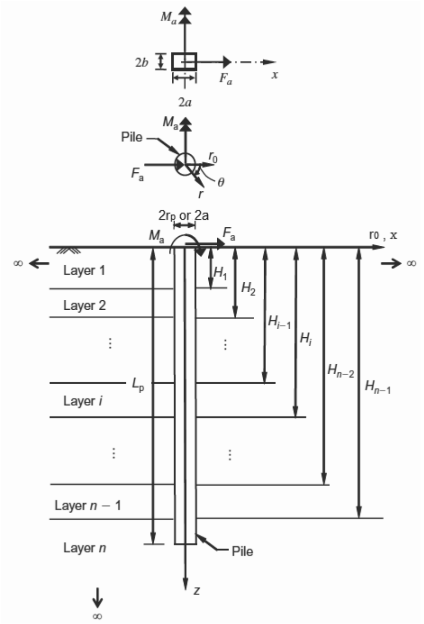

Figure 1. Laterally loaded pile in a layered elastic medium (Modified after Basu and Salgado 2008 and Basu et al. 2009)

3.2 *Potential Energy and its Minimization*

The total potential energy of the pile–soil system, including both the internal and external potential energies, is given by:

$$\Pi = \frac{1}{2}E_pI_p\int_0^{L_p}\left(\frac{d^2w}{dz^2}\right)^2 dz + \frac{1}{2}\int_{\Omega_s}\sigma_{mn}\varepsilon_{mn}d\Omega_s - F_a\, w\big|_{z=0} + M_a\frac{dw}{dz}\bigg|_{z=0} \tag{2}$$

where w is the lateral pile deflection; σ_{mn} and ε_{mn} are the stress and strain tensors in the soil, respectively (summation is implied by repetition of the indices m and n); and Ω_s represents the soil domain surrounding the pile that extends to infinity in the horizontal directions and from 0 to $+\infty$ in the z direction, but excludes the volume occupied by the pile. The first integral in Eq. (2) represents the internal potential energy of the pile, while the second integral represents the internal potential energy of the soil continuum. The remaining two terms represent the external potential energy.

The principle of minimum potential energy ($\delta\Pi = 0$) is used to obtain the differential equations governing the equilibrium condition of the pile-soil system:

$$\delta\Pi = E_pI_p\int_{z=0}^{z=L_p}\delta\left(\frac{d^2w(z)}{dz^2}\right)\left(\frac{d^2w(z)}{dz^2}\right)dz + \frac{1}{2}\int_{\Omega_s}\delta\left(\sigma_{mn}\varepsilon_{mn}\right)d\Omega_s - F_a\delta w(z)\big|_{z=0} + M_a\delta\left(\frac{dw(z)}{dz}\right)_{z=0} = 0 \tag{3}$$

The strain-displacement relationship for infinitesimal strains and the elastic stress-strain relationship, given by

$$\sigma_{mn} = 2G_s\varepsilon_{mn} + \lambda_s\varepsilon_{kk}\delta_{mn} \tag{4}$$

are used in Eq. (3) to express the first variation of the total pile-soil potential energy in terms of the soil elastic constants and the displacement functions described in Eq. (1). Thus Eq. (3) contains the first variations of the displacement functions w, ϕ_x and ϕ_y for rectangular pile and the first variations of the displacement functions w, $\phi_r(r)$ and $\phi_\theta(r)$ for circular pile. Since these variations are independent, the terms associated with each of these variations can be individually equated to zero, which produces the differential equations and boundary conditions of the displacement functions.

3.3 *Pile deflection*

The pile deflection equations corresponding to the i^{th} soil layer for both circular and rectangular piles is given by:

$$\begin{cases} E_pI_p\dfrac{d^4w_i}{dz^4} - t_i\dfrac{d^2w_i}{dz^2} + k_iw_i = 0 & 0 \le z \le L_p \\ -t_i\dfrac{d^2w_i}{dz^2} + k_iw_i = 0 & z \ge L_p \end{cases} \tag{5}$$

where, for rectangular piles:

$$t_i = \begin{cases} G_{s,i}\left(\displaystyle\int_{-\infty}^{+\infty}\int_{-\infty}^{+\infty}\phi_x^{\,2}\phi_y^{\,2}dxdy - 4ab\right) & 0 \le z \le L_p \\ G_{s,i}\displaystyle\int_{-\infty}^{+\infty}\int_{-\infty}^{+\infty}\phi_x^{\,2}\phi_y^{\,2}dxdy & z \ge L_p \end{cases} \tag{6}$$

$$k_i = \int_{-\infty}^{+\infty}\int_{-\infty}^{+\infty}\left[(\lambda_{s,i} + 2G_{s,i})\left(\frac{d\phi_x}{dx}\right)^2\phi_y^{\,2} + G_{s,i}\phi_x^{\,2}\left(\frac{d\phi_y}{dy}\right)^2\right]dxdy \tag{7}$$

and, for circular piles:

$$t_i = \begin{cases} \pi G_{s,i}\left[\int_{r_p}^{\infty}\left(\phi_r^{\,2}+\phi_\theta^{\,2}\right) r dr\right] & 0 \le z \le L_p \\ \pi G_{s,i}\left[\int_{r_p}^{\infty}\left(\phi_r^{\,2}+\phi_\theta^{\,2}\right) r dr + r_p^{\,2}\right] & z \ge L_p \end{cases} \quad (8)$$

$$\begin{aligned} k_i = \pi\Bigg[& (\lambda_{s,i}+2G_{s,i})\int_{r_p}^{\infty} r\left(\frac{d\phi_r}{dr}\right)^2 dr + G_{s,i}\int_{r_p}^{\infty} r\left(\frac{d\phi_\theta}{dr}\right)^2 dr \\ & + 2\lambda_{s,i}\int_{r_p}^{\infty}(\phi_r-\phi_\theta)\frac{d\phi_r}{dr}dr + 2G_{s,i}\int_{r_p}^{\infty}(\phi_r-\phi_\theta)\frac{d\phi_\theta}{dr}dr \\ & + (\lambda_{s,i}+3G_{s,i})\int_{r_p}^{\infty}\frac{1}{r}(\phi_r-\phi_\theta)^2 dr\Bigg] \end{aligned} \quad (9)$$

The boundary conditions for the differential equations are given below:

At $z = 0$:

$$\begin{cases} w_1 = w_0 \quad \text{or} \quad E_p I_p \dfrac{d^3 w_1}{dz^3} - t_1 \dfrac{dw_1}{dz} = F_a \\ \text{and} \\ \dfrac{dw_1}{dz} = \theta_0 \quad \text{or} \quad E_p I_p \dfrac{d^2 w_1}{dz^2} = M_a \end{cases} \quad (10)$$

At $z = H_i < L_p$:

$$\begin{cases} w_i = w_{i+1} \\ E_p I_p \dfrac{d^3 w_i}{dz^3} - t_i \dfrac{dw_i}{dz} = E_p I_p \dfrac{d^3 w_{i+1}}{dz^3} - t_{i+1}\dfrac{dw_{i+1}}{dz} \\ \dfrac{dw_i}{dz} = \dfrac{dw_{i+1}}{dz} \\ E_p I_p \dfrac{d^2 w_i}{dz^2} = E_p I_p \dfrac{d^2 w_{i+1}}{dz^2} \end{cases} \quad (11)$$

At $z = L_p$, for free-base pile base:

$$\begin{cases} w_i = w_{i+1} \\ E_p I_p \dfrac{d^3 w_i}{dz^3} - t_i \dfrac{dw_i}{dz} = -t_{i+1}\dfrac{dw_{i+1}}{dz} \\ E_p I_p \dfrac{d^2 w_i}{dz^2} = 0 \end{cases} \quad (12)$$

At $z = L_p$, for fixed-base pile base:

$$\begin{cases} w_i = w_{i+1} = 0 \\ \dfrac{dw_i}{dz} = 0 \end{cases} \quad (13)$$

As $z \to \infty$,

$$w_i = 0 \quad (14)$$

The above differential equations are solved analytically after applying the boundary conditions to obtain the response of piles. The details of the solution can be found in Basu and Salgado (2008) and Basu et al. (2009).

3.4 *Soil displacement functions*

The differential equations for the soil displacement functions in the case of rectangular piles are given by:

$$\begin{cases} -p_x \dfrac{d^2\phi_x}{dx^2} + q_x \phi_x = 0 \\ -p_y \dfrac{d^2\phi_y}{dy^2} + q_y \phi_y = 0 \end{cases} \quad (15)$$

where,

$$p_x = \left[\sum_{i=1}^{n+1}(\lambda_{s,i}+2G_{s,i})\int_{H_{i-1}}^{H_i} w_i^2 dz\right]\int_{-\infty}^{+\infty}\phi_y^{\,2} dy \quad (16)$$

$$\begin{aligned} q_x = & \left[\sum_{i=1}^{n+1} G_{s,i}\int_{H_{i-1}}^{H_i} w_i^2 dz\right]\int_{-\infty}^{+\infty}\left(\frac{d\phi_y}{dy}\right)^2 dy \\ & + \left[\sum_{i=1}^{n+1} G_{s,i}\int_{H_{i-1}}^{H_i}\left(\frac{dw_i}{dz}\right)^2 dz\right]\int_{-\infty}^{+\infty}\phi_y^{\,2} dy \end{aligned} \quad (17)$$

$$p_y = \left[\sum_{i=1}^{n+1}(\lambda_{s,i}+2G_{s,i})\int_{H_{i-1}}^{H_i} w_i^2 dz\right]\int_{-\infty}^{+\infty}\phi_x^{\,2} dx \quad (18)$$

$$\begin{aligned} q_y = & \left[\sum_{i=1}^{n+1} G_{s,i}\int_{H_{i-1}}^{H_i} w_i^2 dz\right]\int_{-\infty}^{+\infty}\left(\frac{d\phi_x}{dx}\right)^2 dx \\ & + \left[\sum_{i=1}^{n+1} G_{s,i}\int_{H_{i-1}}^{H_i}\left(\frac{dw_i}{dz}\right)^2 dz\right]\int_{-\infty}^{+\infty}\phi_x^{\,2} dx \end{aligned} \quad (19)$$

The differential equations for the soil displacement functions in the case of circular piles are given by:

$$\begin{cases} \dfrac{d^2\phi_r}{dr^2} + \dfrac{1}{r}\dfrac{d\phi_r}{dr} - \left[\left(\dfrac{\gamma_1}{r}\right)^2 + \left(\dfrac{\gamma_2}{r_p}\right)^2\right]\phi_r = \dfrac{\gamma_3^{\,2}}{r}\dfrac{d\phi_\theta}{dr} - \left(\dfrac{\gamma_1}{r}\right)^2\phi_\theta \\ \dfrac{d^2\phi_\theta}{dr^2} + \dfrac{1}{r}\dfrac{d\phi_\theta}{dr} - \left[\left(\dfrac{\gamma_4}{r}\right)^2 + \left(\dfrac{\gamma_5}{r_p}\right)^2\right]\phi_\theta = -\dfrac{\gamma_6^{\,2}}{r}\dfrac{d\phi_\theta}{dr} - \left(\dfrac{\gamma_4}{r}\right)^2\phi_r \end{cases} \quad (20)$$

where $\gamma_1^{\,2} = m_{s4}/m_{s1}, (\gamma_2/r_p)^2 = n_s/m_{s1}, \gamma_3^{\,2} = (m_{s2}+m_{s3})/m_{s1}$

and $\gamma_4^{\,2} = m_{s4}/m_{s2}, (\gamma_5/r_p)^2 = n_s/m_{s2}, \gamma_6^{\,2} = (m_{s2}+m_{s3})/m_{s2}$

with

$$m_{s1} = \sum_{i=1}^{n+1}(\lambda_{s,i}+2G_{s,i})\int_{H_{i-1}}^{H_i} w_i^2 dz \quad (21)$$

$$m_{s2} = \sum_{i=1}^{n+1} G_{s,i}\int_{H_{i-1}}^{H_i} w_i^2 dz \quad (22)$$

$$m_{s3} = \sum_{i=1}^{n+1} \lambda_{s,i}\int_{H_{i-1}}^{H_i} w_i^2 dz \quad (23)$$

$$m_{s4} = \sum_{i=1}^{n+1}(\lambda_{s,i}+3G_{s,i})\int_{H_{i-1}}^{H_i} w_i^2 dz \quad (24)$$

$$n_s = \sum_{i=1}^{n+1} G_{s,i}\int_{H_{i-1}}^{H_i}\left(\frac{dw_i}{dz}\right)^2 dz \quad (25)$$

As mentioned earlier, these displacement functions are equal to unity at the pile-soil interface and they are equal to zero at the boundaries of the domain at infinity.

The above differential equations of the soil displacement functions for rectangular piles can be solved analytically as shown in Basu and Salgado (2008), while the coupled differential equations that govern the soil displacement surrounding the circular piles can be solved numerically using the finite difference method as shown in Basu et al. (2009).

As evident from Eqs. 5, 15, and 20, the responses of the pile and soil to the lateral loading are interrelated. Therefore, these differential equations are solved simultaneously following an iterative algorithm until they converge to a unique solution for a given soil profile, pile geometry and applied loading.

4 RESULTS

To illustrate the use of the analysis, a 15-m long drilled shaft with a diameter of 0.6 m and pile modulus E_p = 24 GPa, embedded in a four-layer soil deposit with H_1 = 2.0 m, H_2 = 5.0 m, and H_3 = 8.3 m; E_{s1} = 20 MPa, Es_2 = 35 MPa, E_{s3} = 50 MPa and E_{s4} = 80 MPa; ν_{s1} = 0.35, ν_{s2} = 0.25, ν_{s3} = 0.2 and ν_{s4} = 0.15 is considered (E_{si} and ν_{si} are the soil Young's modulus and Poisson's ratio for the i^{th} layer). A horizontal force F_a = 300 kN acts on the pile. The pile head and base are free to deflect and rotate. Figure 2 shows the pile deflection profile obtained using the present analysis and an analysis performed using the 3D FE method.

Figure 2. Deflection of a circular cross-section pile of 15 m length

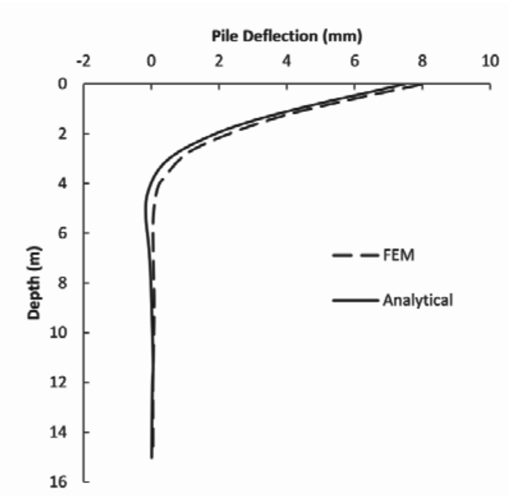

As shown in Figure 2, the results match those of the FE analysis closely. The difference in the head deflection obtained from the present analysis and FE analysis is 6.6%.

Analyses were also performed on a square pile of 0.53m × 0.53m (which has the same flexural rigidity as that of the circular pile described above) embedded in the same soil profile as of Figure 2. Figure 3 compares the response of the square cross-section pile and the circular cross-section pile.

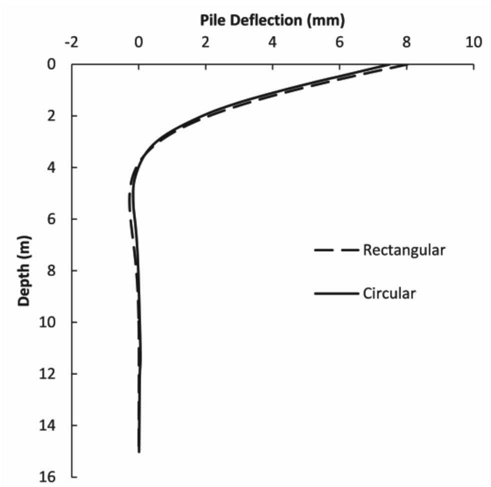

Figure 3. Deflection of a circular and rectangular cross-section piles of 15 m length and same flexural rigidity

Figure 3 shows that, if the second moment of inertia is the same for the piles, they will have (approximately) the same response under lateral loading even if the shapes of their cross sections are different. So, in summary, rectangular piles can be analyzed for lateral loads by replacing them with circular piles having the same second moment of inertia. However, this would work well for linear elastic soil in which knowledge of the appropriate soil constants is presumed, but would not be justified for an analysis that takes full account of soil non-linearity in which knowledge of the operative values of the soil 'constants' is not available a priori and must be obtained from the calculations themselves.

5 CONCLUSIONS

Analytical solutions for laterally loaded piles with rectangular and circular cross sections embedded in multilayered elastic media are obtained. The solutions produce the pile deflection, slope of the deflected curve, bending moment and shear force as functions of depth if the following are known: the pile cross-sectional dimensions and length, thicknesses of the soil layers, Young's modulus of the pile material, the Young's modulus and Poisson's ratio (or any pair of elastic constants) of the soils in the various layers, and the magnitudes of the applied force and moment. The governing differential equations for the pile deflections are obtained using the principle of minimum potential energy. The solution to all the governing differential equations is obtained iteratively and depends on the rate at which the displacements in the soil medium decreases with increasing distance from the pile. The shape of the pile cross section has a bearing on the pile response; however, it was shown that the piles with the same second moment of inertia produced the same response in elastic medium. The analysis presented in the paper can be used to make realistic predictions of the response of laterally loaded rectangular and circular piles.

6 REFERENCES

Anderson, J. B., Townsend, F. C. & Grajales, B. (2003). Case history evaluation of laterally loaded piles. *J. Geotech. Geoenviron. Engng*, ASCE, 129(3), 187–196.

Ashour M, Norris G. (2000). Modeling lateral soil–pile response based on soil–pile interaction. *J. Geotech. Geoenviron. Engng*, ASCE, 126(5):420–428.

Basu D, Salgado R., Prezzi, M. (2009). A continuum-based model for analysis of laterally loaded piles in layered soils, *Geotechnique* 59(2), 127–140.

Basu D, Salgado R. (2008). Analysis of laterally loaded piles with rectangular cross sections embedded in layered soil, *Int. J. Numer. Anal. Meth. Geomech.* 32:721–744.

Banerjee, P. K. & Davies, T. G. (1978). The behaviour of axially and laterally loaded single piles embedded in nonhomogeneous soils. *Geotechnique* 28(3), 309–326.

Cox WR, Reese LC, Grubbs BR. (1974). Field testing of laterally loaded piles in sand. *Proceedings of the 6th Offshore Technology Conference*, vol. 2, Houston, TX; 459–472.

Kim, B. T., Kim, N.-K., Lee, W. J. & Kim, Y. S. (2004). Experimental load-transfer curves of laterally loaded piles in Nak-Dong river sand. *J. Geotech. Geoenviron. Engng*, ASCE, 130(4), 416–425.

Poulos, H. G. (1971a). Behavior of laterally loaded piles: I – single piles. *J. Soil Mech. Found. Div*. ASCE 97, No. SM5, 711–731.

Poulos, H. G. (1971b). Behavior of laterally loaded piles: III – socketed piles. *J. Soil Mech. Found. Div*. ASCE 98, No. SM4, 341–360.

Randolph, M. F. (1981). The response of flexible piles to lateral loading. *Geotechnique,* 31(2), 247–259.

Reese LC, Cox WR. (1969). Soil behavior from analysis of tests of uninstrumented piles under lateral loading. *Performance of Deep Foundations*; 444:160–176.

Skyscrapers of «Moskva-City» Business Center - Tests of Bored Piles

Gratte-ciel du centre d'affaires « Moskva-City » – Essais de pieux forés

Shulyatiev O.A., Ladyzhensky I.G. Yastrebov P.I.
Gersevanov Research Institute of Bases and Underground Structures, Moscow, Russia

ABSTRACT: The Moscow International Business Center (MIBC) "Moskva-CITY" is a complex of 19 sky-scraper buildings. The buildings are supported by 20-30 m long 1.2-1.5 m dia piles, spaced at 3-5 m. Behavior of a pile within such a group differs from that of a standalone single pile. Therefore, analysis of such a footing requires prior determination of pile side and tip resistance. The paper describes a known test technique, based on application of a jacking system, and specially developed for «Moskva-CITY» system, with the test load applied downward with the help of a measuring system and jacks that act separately on the pile tip and on its side surface. The obtained test data was used for the project design analysis to verify the applied analytical model and the respective soil parameters.

RÉSUMÉ : Le Centre d'Affaires International de Moscou "Moskva-CITY est un complexe de 19 gratte-ciels. Les bâtiments sont fondés sur des pieux de 20 à 30m de long, de 1,2 à 1,5 m de diamètre, espacés de 3 à 5 m. Le comportement d'un pieu dans un groupe est différent du comportement du pieu seul. L'analyse de telles fondations demande d'abord la détermination du frottement latéral et de la résistance de pointe. La communication décrit un essai technique, basé sur l'application d'un système de vérins, élaboré spécialement pour le projet «Moskva-CITY», avec la charge appliquée vers le bas grâce à un système de mesure et des vérins qui agissent séparément sur la pointe du pieu et sur sa surface latérale. Les résultats obtenus ont été utilisés pour l'analyse de la conception du projet, afin de vérifier la modèle analytique et les paramètres du sol adoptés.

1 INTRODUCTION

MBIC is located on the Krasnopresnenskaya embankment and consists of a group of unique high-rise buildings (Figure 1) in one architectural complex. The terrain, divided into 20 sites, will include a central transport hub yet to be erected (with 2 conventional subway lines and a mini-subway line), a complex of intricate underground structures, transport intersections, etc.

Figure 1. MIBC photo (August 2012).

The downtown location of MIBC gives easy access to the complex. The 15 sky-scrapers are designed up to 150 to 400 m high with different numbers of stories. Most of them feature a frame-shaft design i.e., the staircase-elevator core is fixed together with ventilation shafts and other service premises, to which the building framework columns are fixed by floor discs.

CITY Geology of the terrain is characterized by Carbon deposits (C3, Figure 2). The soils top down from the surface are represented by an upper fill (1), underlain by limestone alluvium (2), alternating limestone, marl and hard clay layers (3-8). Such soil conditions dictated application of raft footings, pile footings and piled raft footings (Petrukhin et al, 2008). The pile footings under the high-rise buildings, bearing more than 0,4MPa mean pressure, consist of 1,0-1,5 m dia bored piles, spaced at 3 – 5 m. The piles are long so that they penetrate through softer clays, marls and fissured limestone to rest on medium-hard and hard Suvorovsky bed (Figure. 2, geotechnical element 7) and Podolsky-Myachikovsky bed (Figure 2, geotechnical element 8), having Rc=20 – 40MPa.The footing under the tower on the site is an exception in that the supporting piles rest on Ratmirovsky medium strength limestone (geotechnical element 5).

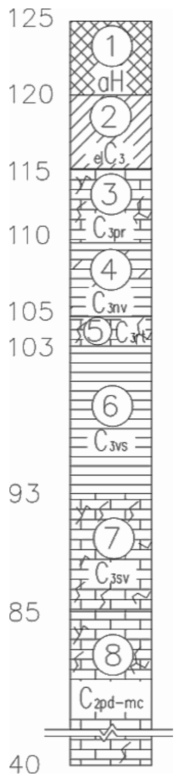

Figure 2. Geotechnical section

Pile footing analysis showed that the piles are loaded non-uniformly both in plan and along their length. The peripheral piles bear times 1,5-2,5 greater loads then the internal ones (Petrukhin et al, 2008; Kharichkin A. et al, 2009), and this was taken into account in the project design, therefore, some corner piles (site 4) have larger diameter (1,5 m) than that of internal ones (1,2 m). Distribution of forces along the pile length is different for different piles and is essentially different for a single pile. Therefore, such footing design requires 3D numeric analysis. In order to perform such analysis it is necessary to determine pile side and tip resistances on the basis of pile test data.

The paper presents data of pile tests, conducted by different methods, this data was compared and the application in design practice was analyzed.

2 RESULTS OF PILE TESTS

As has already been discussed above, it was necessary to erect cast piles of high bearing capacity (2000-3000 ton) within the bounds of the Moskva-CITY area. These pile tests, conducted by standard technique (load applied from the top), encountered technical difficulties and costs, as it was necessary to install anchor piles, to assemble a load transferring frame and a system of jacks. Worldwide such pile tests, Moskva-CITY skyscrapers inclusive, are done as per the Osterberg method, using submersible jacks. The jacks were installed in the pile body, the tested pile (its upper part) serving as their stop.

Within the Moskva-CITY area in order to determine side and tip resistances in particular soil layers there were installed gauges in the piles to measure relative deformations of the pile shaft and forces in reinforcement. Stresses were determined, using the elastic modulus values of concrete

Figure 3 shows the 1,2 m diam. 22,6 m long test pile TP1 longitudinal section on site 11 with jacks locations shown (elevation 84,93) and gauges at three elevations (1…3) bottom-up: 84,43 m (1.5 m below jacks); 89,0 and 92,0 m (4 and 7 m above jacks).

The test showed that for maximum load 20,1MN, the jack upper plate displacement was 1,7 mm, that of the lower one 2,3 mm, the forces at level 1 were 12,5 MN (elevation 84,43 m); at level 2 – 3,4 MN (elevation 89,0 m) and at level 3 – 0,8 MN (elevation 92,0 m).

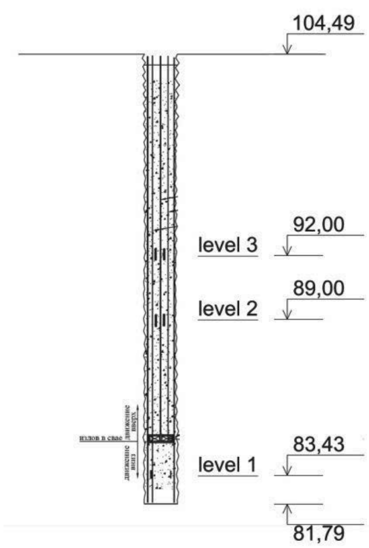

Figure 3. Cross section schematic of TP1 test pile (site 11)

Evidently, internal forces in the pile decrease fast to less than 5% at 7 m distance from the jacks (Figure 4). This shows high values of strength and deformation parameters of the soil.

The obtained distribution of forces in the pile body yielded the pile design side resistance F_i:

$$F_i = (N_0 - N_i)/A_i, \qquad (1),$$

with F_i as pile design side resistance over area A_i between two levels of sensors i and jacks 0;

N_0 and N_i as forces in jacks and in piles at the level of sensor i respectively.

The analysis, based on equation 1, yielded design side resistance for 1…3 to be F1= 1,34МПа; F2= 1,1МПа; F3=0,73МПа. The difference of the analytical values is due to difference of design resistances mobilization rates at different levels, depending on pile versus soil displacements, as well as to certain peculiarities of the surrounding soil properties.

Similarly equation 1 gave measured values of side resistance over other segments, that were obtained on other sites. The values were within 12-20 MN (Table 1), mainly 18 – 20MN. The causes of this scatter are similar to those mentioned above for test pile TP1.

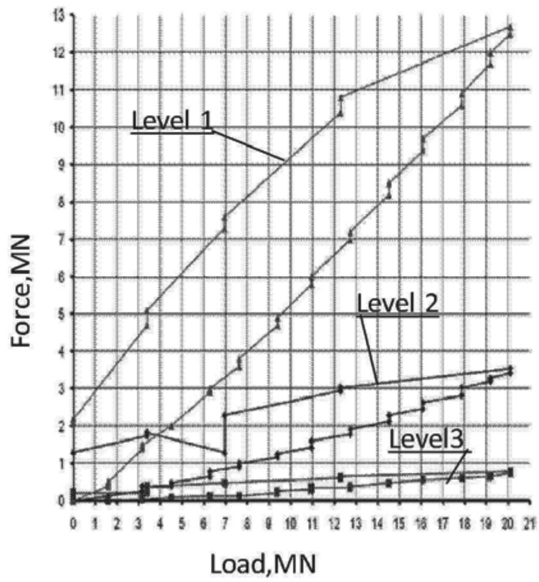

Figure 4. The distribution of forces in the body of the pile.

Force

At sites 12 and 13 there were staged special tests to establish pile side resistances. A 10,5 m long 1,2 m diam. pile fragment was tested at site 12 with the help of jacks, installed at 4 m distance from the pile fragment top (elevation 81,6 m).For maximum 33,30 MN load the fragment settlement was 3,2 mm. The calculated pile side resistance was F = 2,55 MN/m^2.

Similar tests of two 1.5 m diam. pile fragments 6 m long (item 2,3, Figure 5a) and3 m long (item 2,3, Figure 5b) were done at site 13 (Zaretsky Yu.K., Karabajev M.I. 2006; Duzceer R. et al, 2009).

The fragments were cast at 14,6 m and 23,3 m depths from the ground surface (Figure 4). The boreholes above the fragments were filled with rubble. The test side resistances of the pile fragments were F = 2,00 – 2,20 MN/m2. Therein, the 3 m long fragment 2 (Table 1, pile 13c, Figure 5b) displaced 17 mm (i.e. ultimate side resistance was mobilized) F = 2,20 MN/м2.The 6 m long fragment 2 (Table 1, pile 13a, Fig.5a) – 2,00 MN/m2. Other results are given in Table 1.

a) b)

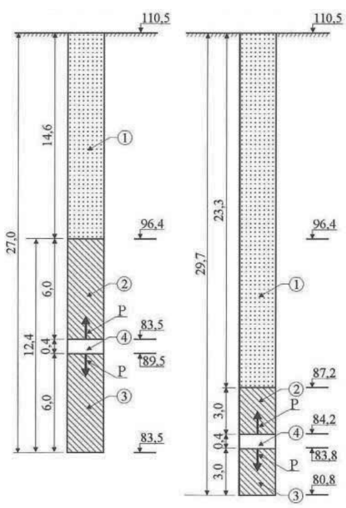

Figure 5. Pile cross section and test set-up on site 13

Pile test data yielded high ultimate side resistance F = 2,20 – 2,55 MN/m2.

To prove that the above design solutions are valid and safe there was developed a special set-up on site 16 (Figure 6) and a procedure for cast piles static tests by 36 MN vertical static load.

Table 1. Result of pile test.

Site (Pile)	Pile parameters				Max load, MN	Max displacement head/tip, mm	Side resistance determination method	Pile side resistance MN/m^2
	Ø, m	L, m	Head level, m	Jack level, m				
3(1)	1,2	28	113	86,1	20	3,1/1,5	D	1,20
3(2)	1,2	28	113	86,1	20	1,8/2,5	D	1,20
4(1)	1,2	28,6	110,4	87,4	26,5	4,1/1,7	D	-
4(2)	1,2	28,0	110,4	84,4	24,5	3,4/1,4	D	-
11(1)	1,2	22,6	104,5	85	20,00	1,8/2,1	D	1,30
11(2)	1,2	22,6	104,5	85	16,50	1,0/1,5	D	1,80
12	1,5	10,5	85,1	81,6	33,30	3,2/7,5	D,F(4)	2,55 (1,55)*
13А	1,2	27	109	89	33,3	6,1/3	F(6)	2,00
13Б	1,2	29,7	109	83,7	25,13	17/6	F(3)	2,20
14 (1)	1,5	19,2	103,2	88,4	33,33	8/65	D	2,00
14 (2)	1,5	19,2	103,2	92,6	33,33	16/4	D	1,90
15 (1)	1,5	20,4	103,8	93,4	1350	4/150	D	200
15 (2)	1,5	19,4	103,8	86,4	3333	10/10	D	200
16(1)	1,5	24,3	118,5	114	3000	8,3**	F(19)	33
16(2)	1,5	24,3	118,5	114	3200	7,2**	F(19)	36

*2,55(1,55) – values with no brackets were determined from tensometer data analysis , in brackets from fragment test data;** top-down fragments tests ; D, F – side resistance was determined as per equation 1 and from pile fragment test data ; F(4) – fragment length m.

In order to separate side and tip resistances the pile consisted of two parts: inside part 1 (630 mm external diam.) and outer part 2 (1500 and 820 mm ring diam.). The hollow space between the pile segments (3) was filled with elastic material to let the parts to freely slide against each other. The interior part (1) was connected with a stiff plate (4). In order to isolate the pile exterior top (2) from the soil mass an external casing tube was installed on the top (5). The loaded system included two steel box cross beams (Figure 7), connected with service piles, used as anchors.

The tests were started by load application to the interior part of the pile (1) and through it to the plate (4) (pile tip test).

Then the set-up was adjusted to step wise load application to the exterior part of the pile (2), and pile side resistance was determined.

The initial plate test and elastic spacers between pile parts prevent data distortion in the pile exterior side test.

The test results (Figure 8,9) show that the central part of the plate displacement largely exceeds that of the pile-shell.

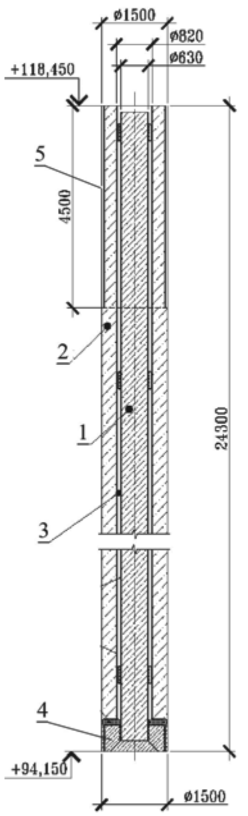

Figure 6. Loading set-up

The pile tip resistance for equal displacements was one order of magnitude less than that of the side resistance and several orders of magnitudes less than the analytical value. This fact shows presence of mud on the borehole bottom, which could not be removed during drilling operations.

Soil resistance below pile tip at other sites demonstrated its strong dependence on the quality of the bottom face and on the quality of special operations (soil grouting), e.g. on site 4 grouting was done to 5 m below the pile tip.

This shows the necessity for extra operations to clean and to compact the bottom, e.g. by grouting the soil under pile tip, by compacting the bottom, e.g. by ramming broken stone or stiff concrete into the bottom, etc. (Petrukhin et al, 2011).

Figure 7. Loading set-up

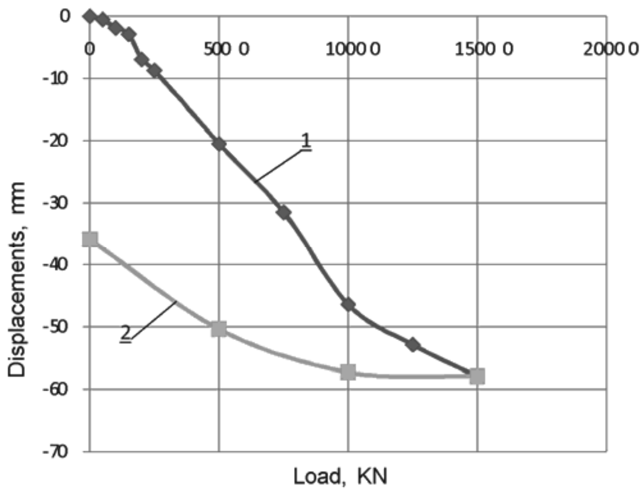

1 – loading, 2 - unloading

Figure. 8. Pile tip test diagram

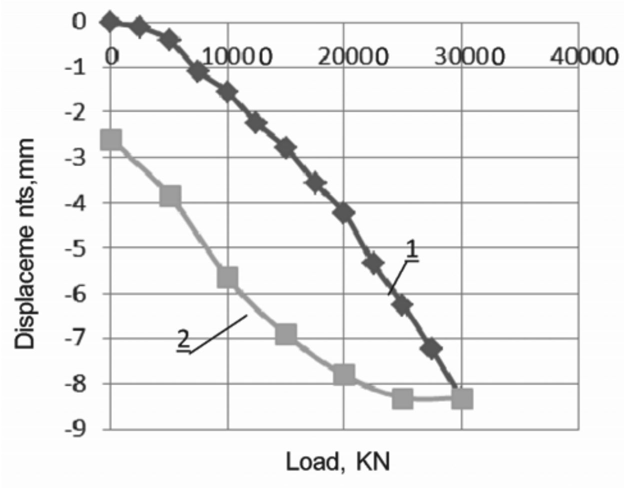

1 – loading, 2 - unloading

Figure. 9. Pile 5 side test diagram

3 PRACTICAL APPLICATION OF PILE TEST RESULTS

As was mentioned above, analysis of pile footings of MIBC Moskva-CITY sky-scrapes mainly consists in determination of pile side and tip resistances (maximum values and their dependence on displacements). Analysis of such piles can be done numerically with the help of 3D software.

The analytical soil model, developed for such analysis, shall be verified by solutions of test problems. The test problems in this case are single pile tests. In the process of test solutions design parameters are specified (side resistance as well as soil strength and deformation parameters).

Figure 10 gives analytical and test data of pile tests, obtained by submersible jacks at site 11.The numerical simulation was done with the help of PLAXIS 2D 8.2 software. The analytical model was the ideal elasto-plastic model with Mohr-Coulomb strength criterion.

The following assumptions and prerequisites were adopted for the analysis:

- the input values of physico-mechanical parameters of geotechnical elements were adopted as for the 2nd limit state analysis;
- static loads alone were adopted for the analysis. Shock, dynamic, vibration and other technological loads and actions due to construction operations were not taken into consideration;
- pile material was considered elastic.

In order to harmonize the results of tests and analyses there were used improved parameters of surrounding soil. 3 interlinked parameters: E, φ and c were selected. There were done several analyses, in which soil parameters were chosen as approximation of experimental data by analytical data, which were upper and lower jacks plates displacements and variation of forces and deformations in the pile at different levels along the pile length.

Final results are presented on Figure 10. Their comparison with experimental data showed their sufficient proximity: the scatter does not exceed 10%. The analyses showed that with practically identical soil strength parameters the soil stiffness modulus values, obtained from the analyses is times greater than the one, obtained from geotechnical investigations, that was further accounted for in soil analysis.

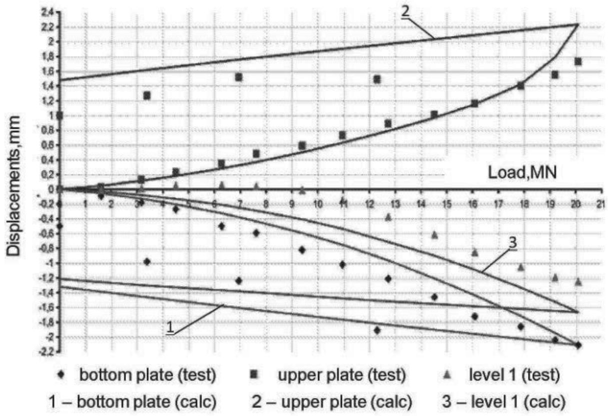

Figure 10. Data from pile tests by Osterberg method, compared with numerical simulation data.

4 CONCLUSIONS AND RECOMMENDATIONS

Pile side and tip resistance rather than a single pile bearing capacity are important for designing MIBC «Moskva-CITY» footings.

Side and tip resistance can be determined by tests of pile fragments, separate side and tip tests by means of a specially developed method, described in the paper, or by means of pile tests with gauges, installed in the pile body, to measure distribution of forces along pile length.

It is recommended to verify pile footing interaction with soil and to verify the analytical model, using single piles test data.

It is recommended to verify the values of design mechanical soil properties, obtained from geotechnical survey, by back analysis, using single pile tests.

It is admissible to adopt cast pile side surface resistance equal to 1,8MPa (180t/m2) for Suvorovsky and Podolsk-Myachikovsky medium-strength and strong limestones.

In order to activate cast pile tips it is necessary to apply special measures to clean and to compact borehole bottom face, e.g. to grout pile tip – soil interface, to compact the bottom face by filling rubble or by stiff concrete ramming, etc.

5 REFERENCES

Osterberg J. O. New Device for Load Testing Driven Piles and Drilled Shafts Separates Friction and End Bearing/ Proceeding: International Conf. on Pilling and Deep Foundation, London, A.A. Balkena, 1989

State Standard 5686-94 "*Methods of field pile tests*"

Petrukhin V.P., Shulyatjev O.A., Kolybin I.V., Mozgacheva O.A., Bezvolev S.G., Kisin B.F. Construction of MIBC «Moskva-CITY»/ Russian Architectural and Building Construction Encyclopedia, v.XII. Underground Construction, 2008.

Kharichkin A., Syuljatjev O., Besvolev Stepan. Soil-Pile Interaction in Pile Foundation and Pile Reactions Monitoring/ International Conference on Deep Foundations – CPRF and Energy Piles. Frankfurt am Main, 2009.

Analysis of a High-Rise Tower on Site №2-3 of MIBC Moskva-CITY. High-RiseBuildings. №1/11, 2011.

Zaretsky Yu.K., Karabajev M.I. Analysis of Test Piles-Ground Interaction and Comparison with Test Data. Messenger of Moscow State Construction University, №1, 2006.

Duzceer R, Gokalp A., Adatepe S. Load Testing and Bearing Capacity of Bored Piles in Limstone/ Proceeding of the 17 International Conference on Soil Mechanics and Geotechnical Engineering. Alexandria, Egypt, 2009.

Petrukhin V.P., Shulyatjev O.A, Bokov I.A. Review of Pile Tip Prestressing and Grouting Possibility and Applicability/Coll.Works №100 NIIOSP of Gersevanov, 2011.

Cavity remediation for pylon foundation of the Transrhumel Viaduct in Constantine

Résolution des problèmes de cavité sous les fondations du Viaduc Trans-Rhumel de Constantine

Steenfelt J.S., Schunk M.
COWI A/S, Denmark

ABSTRACT: The geology of Constantine, Algeria is highly influenced by previous seismic activities and the erosional feature by the river Rhumel. The Transrhumel Viaduct is a new river crossing featuring a 749 m long cable stayed bridge with a main span of 259 m and 80 m clearance. The soil/rock deposits are dominated by Marls of different strength underlain by Marlstone and very competent Limestone. However, exploratory boreholes for the foundation piles of Pylon P4 indicated the presence of possible cavities of up to 1 m high within the Limestone at the base of the upper weathered zone. To save 15 m of time consuming drilling of the 14 Ø2 m foundation piles into competent Limestone it was decided to end the foundation piles above the possible cavity feature in the Marlstone. The paper describes the innovative remedial measures carried out to safeguard the capacity of the individual foundation piles and ensure acceptable individual and overall displacements. The cavity feature was pressure grouted and transfer of axial load across the cavity into Limestone was facilitated by insertion of grouted steel reinforcement assemblies. The success of the remedial measures was proven by carrying out an O-cell load test on the pile positioned over the maximum recorded depth of the cavity.

RÉSUMÉ : Les conditions géologiques de la ville de Constantine en Algérie sont pour une grande part le résultat d'évènements sismiques passés et de l'érosion de l'oued Rhumel. Le viaduc Trans-Rhumel est un nouvel ouvrage qui traverse le court d'eau comprenant un pont à hauban de 749 m avec une travée principale de 259 m placée à une hauteur de 80 m. Les sols de fondation sont majoritairement composés de marne de compétence variable supportée par des roches marno-calcaire et roches calcaires très compétentes. Les sondages par forages effectués au droit du pylône P4 ont cependant révélé la présence de cavités d'une hauteur jusqu'à 1 m dans le calcaire à la base de la zone érodée supérieure. Afin d'économiser 15 m de forage onéreux pour les 14 pieux de 2 m de diamètre dans la roche calcaire, il a été décidé de stopper les pieux de fondation au-dessus de la zone de présence probable des cavités des roches marneuses. Cet article décrit les mesure innovantes mises en place pour assurer la capacité portante de chaque pieu de fondation et garantir des déplacements globaux et individuels acceptables. Un coulis de ciment a été injecté dans la cavité et le transfert des efforts axiaux au travers de la cavité fut assuré par l'insertion d'assemblages d'armatures placées dans le ciment. Le succès de cette méthode a été démontré en exécutant des essais de charges O-cell sur le pieu fiché à la hauteur maximale de la cavité.

KEYWORDS: natural hazards, cavity, bored piles, pile load test, pressure grouting, Marls, Limestone.

1 BRIEF PROJECT DESCRIPTION

The Constantine Viaduct (Figure 1) is a new bridge, crossing the River Rhumel in Constantine, Algeria. Constantine is situated on a plateau at 640 metres above sea level. The city is framed by a deep ravine and has a dramatic appearance with a number of bridges and a viaduct crossing the ravine.

Figure 1. Artist's impression of completed cable stayed bridge (Pylon P4 to the left).

The main bridge features a cable-stayed bridge as well as access and ramp bridges. The project includes very extensive road works of approximately 10 km, with 13 over and underpasses, 1 km of up to 45 m deep steep cuts stabilised with ground anchors and soil nails, 4 km retaining walls of which 1 km embedded retaining walls were stabilised with ground anchors (up to 32 m retained height).

The total length of the bridge between the main abutments is 749 m with an 80 m clearance over the river bed.

The Owner is Direction des Travaux Publics de la Wilaya de Constantine – DTP and the contractor is Andrade Gutierrez - AG from Brazil with COWI A/S Denmark as designer.

2 GEOLOGY WITH FOCUS ON PYLON P4

The geology of the site is highly influenced by previous seismic activities (medium severity) and the erosional feature by the River Rhumel.

The soil/rock deposits are dominated by Marls of different strength underlain by Marlstone and very competent Limestone. At the original position of Pylon P4 a very dramatic ancient fault was discovered where the Limestone surface dips near vertically and hence the Pylon was moved 14 m to the north, thus enabling the foundation to be completely based on bored piles with the toe well into the Limestone formation (Figure 2).

The borehole B4/03 at the location of Pile P4/3 indicates a soil profile as summarized in Table 1.

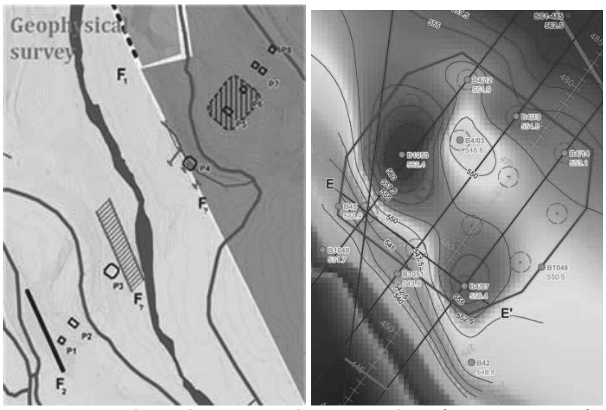

Figure 2. Geophysical survey and contour plot of Limestone surface based on boreholes (F_1 denotes the main fault at P4 location)

Table 1. Soil profile at borehole B4/03 (at pile 4/3) and assumed lower bound characteristic soil parameters ($\tau = 0.37\ c_u$ assumed for design in soils and formula (4.25) from Fleming et al. 2009 in rock).

Soil/rock layer	Top level [1] (m)	Undrained shear strength c_u (kPa)	Shaft friction τ (kPa)	Toe bearing capacity (MPa)
Fill from ground	+586.6	61	23	
Marl 1	+579.9	141	52	
Marl 2	+570.4	335	124	
Marlstone	+565.3	6750	1520	11
Pile toe	+559.5			
Weathered Limestone	+557.8	3500		
Limestone (intact)	+548.3	9000		

[1] Datum in Fuse 32

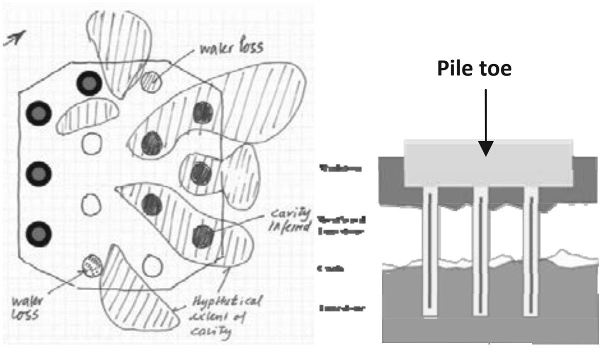

Figure 3. (a) Hypothetical extent of cavity feature (piles with bold outline were drilled into Limestone); (b) Schematic cross section at pile toe in Marlstone with pre-drilling holes below pile toe.

The unconfined compressive strength in the weathered Limestone (5 to 9 m layer between Marlstone and top of intact Limestone) had to be re-assessed from dried out samples and hence the average value of σ_c = 13.1 MPa (7 MPa as 95% lower fractile) was deemed conservative.

The strength of the Marlstone was σ_c = 13.5 whereas σ_c >> 18 MPa for the Limestone, i.e. above the strength of the concrete.

The toe bearing for the Marlstone was conservatively calculated as for a soil (11 MPa) as opposed to 45 MPa if rock parameters were used.

However, the drilling subcontractor TREVI experienced excessive time delays when drilling the 2 m diameter bored piles, 42 to 46 m long, into the Limestone, even after executing five Ø178 mm pre-drilling holes to the pile toe level within the foot print of each pile.

Moreover, the exploratory boreholes indicated the presence of cavities within the Limestone, at the base of the upper weathered zone and with heights up to 1 m.

The indicators were severe water loss and/or a sudden drop of the drill string.

Based on the observations the extent of the cavity feature was hypothesized as shown in Figure 3.

3 REMEDIATION AND MONITORING STRATEGY

The existence of the five Ø178 mm pre-drilling holes to the level of intended pile toe in Limestone turned out to be both a blessing and a curse. By re-opening the holes it would be possible to insert a "reinforcement" to transfer the load across the cavity feature but the holes at the same time prevented pressure grouting of the cavity as un-grouted holes would function as venting holes.

The solution adopted consisted in inserting a 12 m long steel reinforcing assembly composed of 6 Nos. of T40 mm reinforcement bars tack welded together around a central spacer ring into each pre-drilled hole. This solution was chosen in order not to cause delays by delivery to Africa of the preferred Ø90 mm GEWI piles and to utilize on site material. The reinforcement provided by the T-bars corresponds by and large to the reinforcement in the lower part of the Ø2 m bored pile.

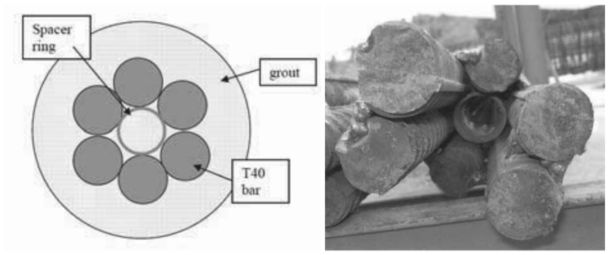

Figure 4. (a) Cross section through pre-drilling hole with assembly of T-bars; (b) Photo of T-bar assembly with spacer ring

The rationale of the solution is to transfer the axial load from the pile toe in Marlstone through the weathered Limestone and the cavity feature into the competent Limestone without risking excessive (differential) vertical displacement of the piles. Grout around the reinforcing assembly ensures stability of the reinforcement throughout the 12 m length. The reason for choosing this solution was that the pre-drilled holes were already available and it was not considered feasible to pressure grout the very localised weathered zones in the Limestone when grouting from just a few boreholes. The different degree of weathering across the foundation footprint could cause different settlement behaviour for individual piles, especially as the weathered zone would be directly below the pile toe where the loads are most concentrated.

The sequence of the reinforcement installation is: (i) re-open a pre-drilling hole, (ii) install 12 m long reinforcement assembly, with tremie pipe through the centre, so the top level is approximately 0.5 m below pile toe level, (iii) grout to the pile toe level allowing grout to permeate into potential cavities around the hole.

Grout of relatively high viscosity (Marsh viscosity 35- 50 sec.) was used. It consisted of Portland cement 42.5 with w/c ratio of 0.45 and thinner adjuvant type Rheobuilt with w/a ratio of 0.5 - 1.0%. Settling at 4 h < 5%. It would be expected that the grout could travel some 3-5 m away from the pre-drilling hole.

However, as the cavity (cavities) may have a considerable horizontal extent also outside the foundation footprint as visualized in Figure 3a it was considered a must to also perform pressure grouting (of cavities) to ensure the design capacity of the pile group and to safeguard against excessive or differential overall displacements.

The grouting scheme devised consisted of primary and secondary grouting holes in staggered sequence as shown schematically in Figure 5. To maximize the effect the sequence of grouting is staggered.

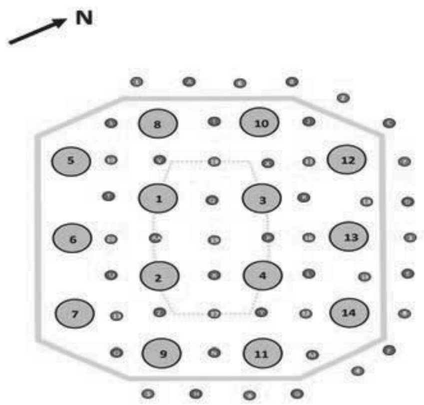

Figure 5. Schematic grouting scheme with primary grout holes in Arabic numbers and secondary grout holes in letters (pile numbers of the 14 Ø2 m piles shown for reference; piles 5, 6, 7 and 8 were drilled into the competent limestone prior to the remediation scheme).

The holes for pressure grouting (40 m deep) were drilled "destructively" from the ground surface using a Ø141 mm drill in the Marl (with casing) and a Ø105 to 115 mm drill to the full depth (without casing). The grout take was carefully measured using the same type of grout as before, but now with a settling <5% after 2 hours. The uncased part passing through the cavity feature was pressure grouted using packers with 12 bar pressure. The cased part was gravity grouted as the casing was withdrawn.

4 MONITORING OF REMEDIATION MEASURES

Based on the surface texture of the holes drilled for the piles (very uneven surface) the actual consumption would be expected to be higher than the theoretical consumption based on the bore and grout hole diameters. The consumption of concrete when casting the Ø2000 mm piles was:

- Piles P4/5 to P4/8 (46 to 50 m length): 113% ± 3.7%
- Remaining 10 piles (22 to 28 m length): 108% ± 1.8%

i.e. roughly 10% excess consumption.

As the Ø178 mm holes were re-drilled it seems likely that actual nominal consumption would be 115% of the theoretical consumption. Using this as baseline the excess grout take from the five reinforcement-holes below each of the ten Ø2000 mm piles are shown in Figure 6. In some cases re-grouting of the holes took place and hence a sequence number in excess of five occurs for some of the piles.

Although there is considerable scatter the excess grout take decreases by and large as a function of the sequence as would be expected as any cavity feature will be more readily filled during the initial grouting. Piles 3, 9, 11, 12 and 14 show grout take above average which is interpreted as a more persistent cavity feature at these locations.

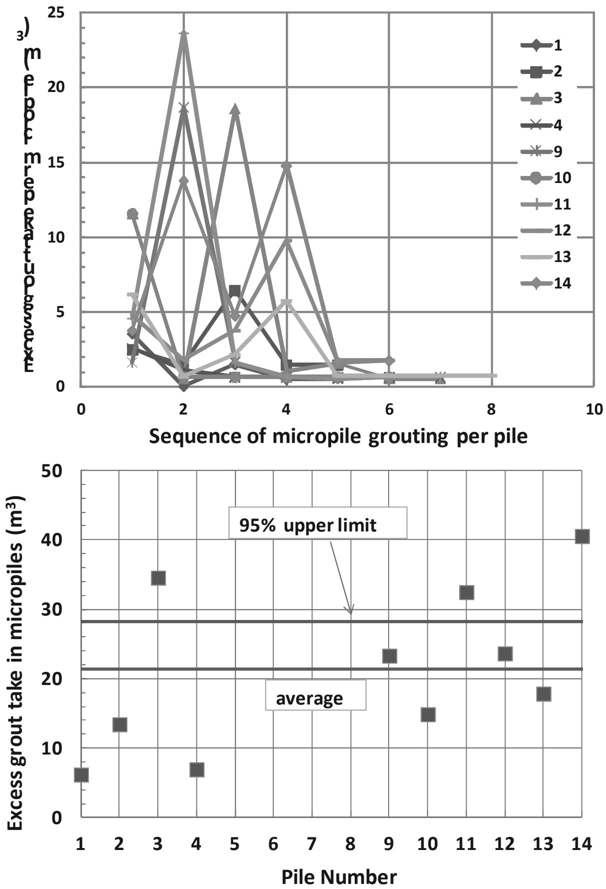

Figure 6. Excess grout take in "micropile" holes; (a) as function of sequence (2-6 weeks from grouting of fist to last pile); (b) accumulated values per pile location

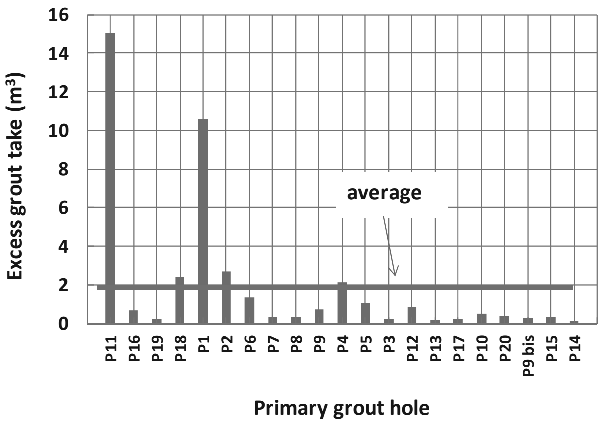

Figure 7. Excess grout take versus sequence for primary grout holes

The actual sequence of the subsequent pressure grouting in primary (Figure 7) and secondary (Figure 8) deviated slightly from the sequence in Figure 5 but followed the principal intent. The theoretical grout take was based on the nominal drilling diameters but with reference to the considerations for the piles and pre-drilling holes this may entail some 15% underestimation of take.

As seen in Figure 7 and Figure 8 the excess grout take was very limited in the majority of holes.

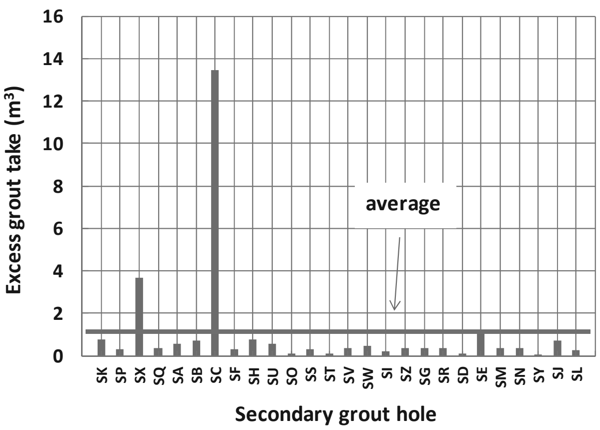

Figure 8. Excess grout take versus sequence for secondary grout holes

The excessive grout takes over the average value are by and large concentrated in areas where a cavity feature had already been indicated by the "micropile" grouting. Furthermore, it is clear that the grout take during primary grouting (1.9 m^3 ± 3.8 m^3) compared to the secondary grouting (1.1 m^3 ± 2.6 m^3) is an indirect confirmation of the success of the grouting scheme.

Excluding the seven values exceeding the average value the excess grout take is 0.6 m^3 ± 0.5 m^3 for primary and 0.4 m^3 ± 0.3 m^3 for secondary grout holes compared to the minimum theoretical grout take of 0.5 m^3.

The tentative evaluation in terms of cavity feature extent, based on the combined result in terms of excess grout take, is shown in Figure 9. The Figure lends credibility to the conclusion that the horizontal extent of the cavity feature was relatively modest and close to the hypothetical extent envisaged (Figure 3).

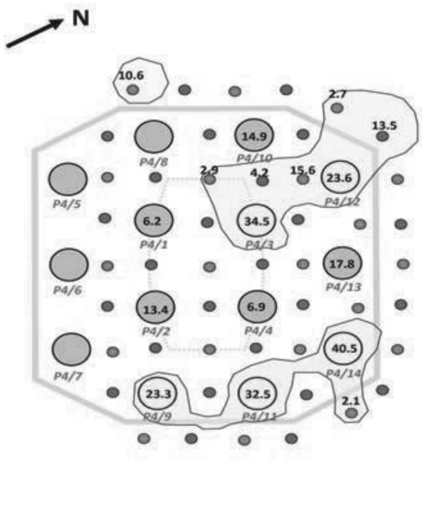

Figure 9. Tentative evaluation of the extent (shading) of the cavity feature below Pylon P4.

5 VERIFICATION BY PILE LOAD TESTING

To verify the capacity of the piles with pile toe in Marlstone the most onerous pile in relation to the cavity, P4/3, was tested by means of an O-cell load test carried out by Fugro LOADTEST.

The principle of the test is shown in Figure 10. In this case two Ø870 mm O-cells were placed 1 m above the intended toe level of the pile.

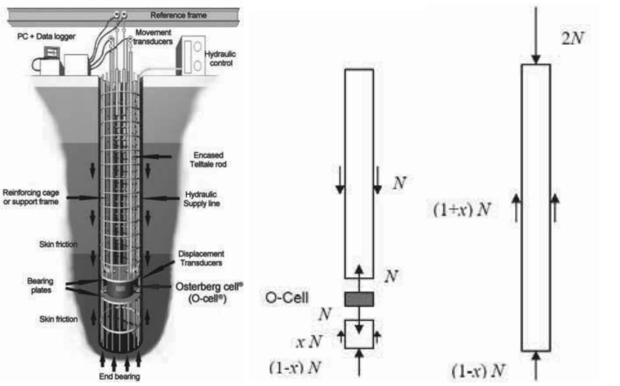

Figure 10. O-cell load test for a bored pile. (a) schematic set-up; (b) load distribution in O-cell test; (c) load distribution in top down loading

The 1 m pile length below the O-cells safeguards against tilting of the cells, due to uneven strength/stiffness distribution at the toe of the pile. The pile length above the O-cell is 26.1 m.

Note that when loading top down (the design load situation) it takes the double axial load to mobilise the same shaft and toe bearing as with the O-cell test and hence a greater elastic pile compression will occur.

For the test the pile was fitted with strain gauges, at six levels in the Marlstone, and tell-tales at four levels including the toe in order to be able to get a detailed understanding of the stress distribution along the shaft. Unfortunately, these measurements were inconsistent and deemed unreliable except for tell-tales 1 (level +560.5), 2 (level +565.3) and 3 (level +571.0). These measurements were combined with reliable values of the upwards and downwards displacement of the O-cell and the bi-directional O-cell load with a maximum load of 40.1 MN in each direction.

The capacity of the O-cell was higher, but in order to safeguard against any detrimental effect from the testing on the working pile the Owner decided to limit the load on the pile to 1.5 SLS.

The load test included three step-wise loading unloading cycles:

(i) to a level corresponding to the maximum SLS load in the pile group i.e. 26.5 MN
(ii) to 1.5 SLS ~ 40.1 MN (which exceeds the highest ultimate state load for earth quake of ULS-EQ = 32.4 MN for Pile P4/3) and
(iii) to SLS = 26.5 MN.

Creep was observed for up to 120 minutes for the designated loading steps and during shorter periods (typically 10 minutes) for the unloading steps.

The downward displacement of the bottom plate of the O-cells as a function of the gross downward O-cell load is shown in Figure 11.

A load of some 3 to 4 MN is required before displacements are initiated. This corresponds reasonably well to the tension capacity of the concrete section less the O-cell area (1.95 m^2) assuming $\sigma_t \sim 0.06\ \sigma_c = 0.06 \times 35.5 = 2.1$ MPa and thus a breaking load of $1.95 \times 2.1 = 4.1$ MN.

This is slightly higher than the load required for breaking the tack welds initially holding the O-cells closed (reported as 2.94 MN).

From Figure 11 it is apparent that the load-displacement curve is almost linear until the maximum load of 40.1 MN applied.

The creep rate increases with load level with a maximum of 2.0 mm/log cycle of time for the maximum load.

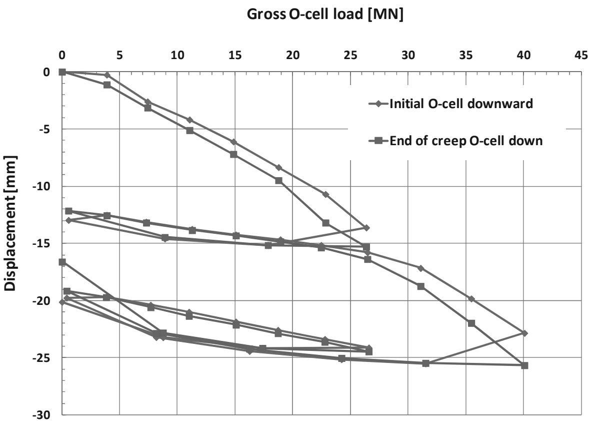

Figure 11. Displacement of lower O-cell plate versus applied downward gross O-cell load

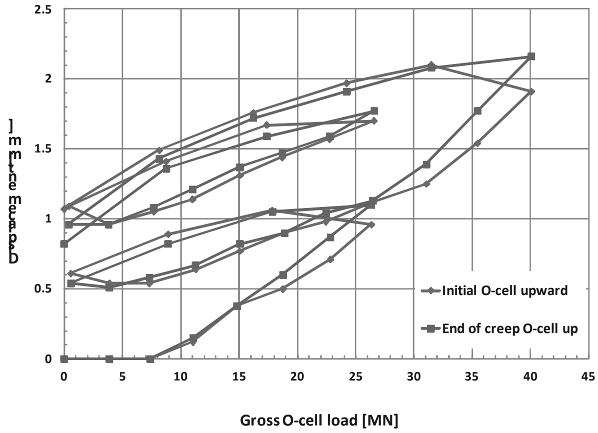

Figure 12. Displacement of upper O-cell plate versus applied upward gross O-cell load

Considering, that the major part of the load below the O-cells is taken by toe bearing the creep rate is acceptably low. The corresponding creep rates for the top plate of the O-cells are an order of magnitude smaller and hence insignificant.

The load-displacement curve for the upward O-cell displacement is shown in Figure 12. The upwards displacements are significantly less than the downward displacements (Figure 11) and they are only initiated at an O-cell load of 7 MN after which the load-displacement curve is essentially linear. It is apparent that shaft stresses are locked into the system at unloading resulting in a non-recoverable displacement of approximately 1 mm after unloading from the gross O-cell load of 40.1 MN (net load 38.8 MN after subtraction of pile weight).

From the readings of tell tales 2 and 3 it is apparent that the displacements decrease very significantly with the distance from the O-cells and that initiation of displacements requires significantly greater O-cell loads than needed to initiate downward displacement.

Tell tales 2 are at the transition from Marlstone to Marl 2 and hence the difference between tell tales 1 (top of O-cells) and 2 indicate the "rock socket" shortening in the Marlstone as shown in Figure 13.

This deformation corresponds to the accumulated displacement between pile and rock for developing the shaft resistance. As seen from the Figure the displacement is very small and almost mirrors the upward displacement of the O-cell upper plate (Figure 11). It means that the displacement between pile and rock at the top of the Marlstone is only 0.6 mm and thus the pile capacity is very significantly higher.

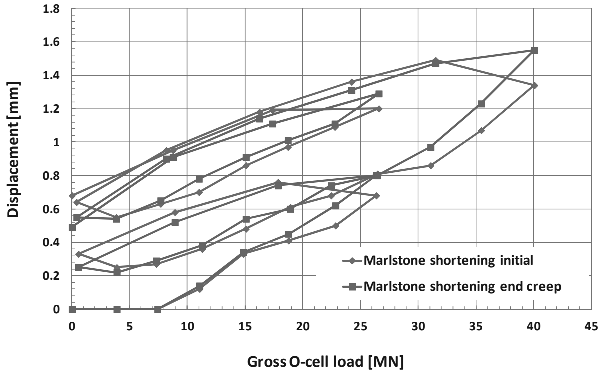

Figure 13. Shortening of the pile ("rock socket") in Marlstone between tell tales 1 and 2 versus applied O-cell gross load.

The recorded working curves for the upper pile shaft and the lower pile segment may be fitted by "linear fractional" (hyperbolic) functions, i.e. $y = (ax + b)/(cx + d)$. This facilitates extrapolation of the working curves and production of synthesized top load settlements curves.

The methodology by Fleming (1992) was used to produce the predicted top load settlement curve shown in Figure 14.

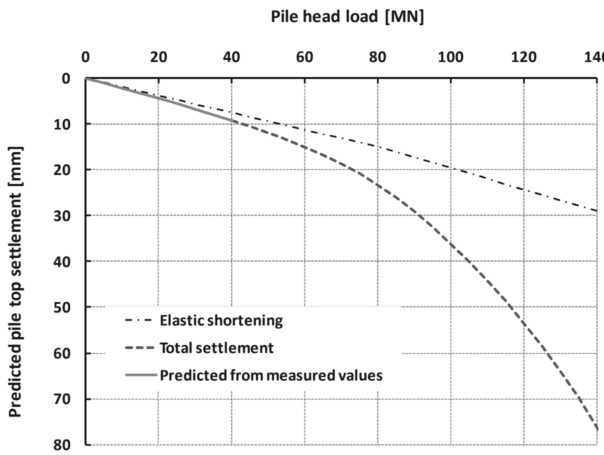

Figure 14. Predicted top load settlement curve for Pile P4/3

It is apparent from Figure 14 that a top loading of 26.5 MN (corresponding to the maximum SLS load in the P4 Pylon pile group) will cause a pile head settlement in the order of 6 mm. Twice the load, 53 MN (twice the SLS load and larger than the maximum ULS load of 45.5 MN in the pile group) will result in only 13 mm settlement.

Thus, even for the ultimate limit state (ULS-EQ) loading of the actual pile of 29.6 MN the predicted settlements are only slightly larger than the elastic part of the working curve.

6 EVALUATION OF ROCK SOCKET CAPACITY

The maximum toe and shaft design loads for pile P4/3 are 4.5 to 4.9 MN and 21.0 to 26.5 MN, respectively. The range reflects upper and lower bound soil stratification and soil spring assumptions. As seen from Figure 11 and Figure 12 the load test indicates much higher values even within near elastic load-displacement behaviour.

For the toe bearing of the rock socket the mobilisation of the resistance may be assumed to vary roughly proportional to the square root of the mobilised displacement, where $\delta_{ult,t}$ (toe bearing) ~ $0.1 \cdot D$ = 200 mm:

$$\frac{\sigma_{mob}}{\sigma_{ult,t}} = \sqrt{\frac{\delta_{mob}}{\delta_{ult,t}}} \tag{1}$$

For the development of shaft resistance the following expression may be tentatively used (Steenfelt & Abild, 2011):

$$\frac{\tau_{mob}}{\tau_{ult,s}} = \sqrt{\frac{4\,\delta_{mob}}{3\,\delta_{mob} + \delta_{ult,s}}} \tag{2}$$

where $\delta_{ult,s}$ (shaft resistance) is of the order 3-10 mm.

Based on the lower bound characteristic ultimate shaft friction resistances indicated in Table 1 and $\delta_{ult} = 5.5$ mm a total shaft resistance above the O-cell for the 26.1 m pile of 38.8 MN is found based on the mobilisation ratios inferred from Eq. (2). Average displacements in Marlstone, Marl 2, Marl 1 and fill, based on the tell tale measurements, have been used in this assessment. The corresponding ultimate shaft resistance at 100% mobilisation is 54.2 MN.

For the toe resistance and δ_{mob} =25.7 mm full development of 9.5 MN shaft resistance is assumed on the lower 1 m pile ($\delta_{mob} > \delta_{ult}$). This means that the mobilised toe resistance is 30.6 MN and by application of Eq. (1) an ultimate toe resistance of 85.5 MN may be deduced.

Thus, based on conservative estimates for the characteristic shear strength of the layers involved an ultimate capacity of the P4/3 pile of almost 140 MN is inferred. This would be close to the characteristic structural capacity of the pile as it corresponds to a maximum characteristic stress of 44.6 MPa at the pile toe.

Considering that conservative parameters have been applied it is concluded that the pile has more than sufficient capacity and that there is no reduction of capacity from the presence of the cavity feature or the weathered Limestone below the toe of the pile

7 SUMMARY & CONCLUSION

The recorded cavity feature below the foundation for Pylon P4 necessitated remedial measures. At the same time the Contractor preferred pile toes at a higher level, above the cavity feature, in order to reduce construction time. These issues were addressed by:

- the installation and grouting of five 12 m long reinforcing elements ("micro piles") from 0.14 to 0.78 m distance below the pile toe level and into the intact Limestone
- pressure grouting of 20 primary and 26 secondary grout holes over and slightly beyond the foot print of the P4 Pylon
- load testing of Pile P4/3 situated at the most onerous position over the recognised cavity feature

It was concluded that the cavity feature was not a consistent feature but was concentrated around piles 3, 9, 11, 12 and 14. Even if some additional cavity feature should exist to the west of pile 8 or to the north of pile 12 it is entirely unlikely that this would have any detrimental effect on the bearing capacity of the pile group.

The remediation measures were therefore deemed successful and required no further tertiary grouting to be carried out.

The main conclusions following the load test were as follows:

- There is no evidence of any detrimental effects from the cavity feature on the pile capacity.
- Both the shaft and the toe capacity are far from being exhausted at the maximum bi-directional load of 40.1 MN.
- A maximum characteristic toe bearing stress of 11 MPa was conservatively assumed in the design. This stress was almost reached in the test but at a toe displacement of only some 25 mm, corresponding to a low degree of mobilisation (of the order 24%). Thus, the cavity remediation works, including the reinforcement of the weathered Limestone, has been successful and allows for a high toe bearing capacity in ULS (cf. Figure 11).
- Extrapolation of shaft and toe resistances to 200 mm toe displacement and >5 mm shaft/soil displacement show capacity at or above the structural capacity of the concrete pile of approximately 110 MN (at the 7 days compressive concrete strength of 33.5 MPa).

Based on the thorough investigation of the cavity feature and the closely monitored remediation work it was possible to successfully conclude the foundation works for the Pylon P4 and start the casting of the Pylon as seen in Figure 15.

Figure 15. Status of P4 construction December 2012

8 ACKNOWLEDGEMENTS

The authors gratefully acknowledge fruitful discussions and interaction with the Contractor's site team in Constantine as well as the permission by the Contractor Andrade Gutierrez and the Designer COWI to publish the paper.

9 REFERENCES

Fleming, W.G.K. 1992. A new method for single pile settlement prediction and analysis. *Géotechnique 42*, No. 3, pp 411-425.

Fleming, W.G.K., Weltman, A,J. Randolph, M.F., Elson, W.K. 2009. *Piling Engineering, Third ed*., Taylor & Francis.

Steenfelt, J.S.. and Abild, J. 2011. Capacity of rock sockets in weak Mud/Siltstone. *Proceedings XVth European Conference on Soil Mechanics and Geotechnical Engineering*, 12-15 Sept. 2001

Integrating Nonlinear Pile Behavior with Standard Structural Engineering Software

Analyse non linéaire de fondations par pieux à l'aide d'un code industriel

Szép J., Ray R.P.
Széchenyi István University, Győr, Hungary

ABSTRACT: It is common in the practice of bridge design to analyze the superstructure, substructure, and foundation components separately. Applying this kind of modeling, soil-structure interaction effects can only be approximated with moderate accuracy. The foundation stiffness can greatly influence the internal forces, stresses, and displacements of superstructure. This is especially true for portal frame and integral bridges. Better modeling of soil-structure interaction can use three-dimensional geotechnical FEM programs, where the true soil-stucture environment can be analyzed. It is possible to use nonlinear constitutive models; capable of modeling soil behavior accurately, however it is difficult, time consuming, and costly in day-to-day practice.

RÉSUMÉ : Dans la pratique, le dimensionnement des structures et des fondations se fait dans des notes de calcul séparées. En conséquence les interactions sols-structures ne sont décrites qu'approximativement. Par exemple, la rigidité de la fondation peut affectée la répartition des charges et les déplacements de la structure. Cela est d'autant plus vraie dans le cas de fondations par pieux réparties sur une ou deux rangées. Le recourt à des codes de calcul tridimentionnel permet une approche plus réaliste des interactions sols-structures et la prise en compte de lois de comportement non linéaire pour le sol. La presente étude vise à comparer les rigidités des fondations par pieux réparties sur une ou deux rangées à l'aide d'un code de calcul industriel.

KEYWORDS: piles, nonlinear, structural, software

1 INTRODUCTION-DESIGN TRANSITIONS

Geotechnical and structural engineering software has evolved to where most common design tasks are performed on the computer. However, the levels of sophistication of these software packages are somewhat divergent. Geotechnical engineers prefer to consider soils as nonlinear materials with properties that vary throughout a site. These properties may also vary over time and loading conditions, yielding a highly complex set of behaviors. While this is an encouraging trend, structural engineers are often required to take a step back from such a sophisticated and time-consuming approach. The need for a timely and straightforward design that meets all aspects of building code requirements as well as budget and time constraints often forces structural designers to simplify geotechnical solutions. This is often reflected in structural design software that use beam elements and elasto-plastic spring elements to represent soil support behavior. This paper examines the methods to achieve these simplifications without creating an overly conservative or incorrect design.

Representing the full spectrum of three-dimensional soils-foundation-structure interaction is a laudable goal, but rarely achievable within the present design environment, hardware, and software. As a reasonable approximation, one may model the foundation system via sophisticated geotechnical software (Plaxis, Midas, Flac) and produce a family of foundation response curves which can then be approximated in the structural design model with simpler elements and material behaviors (Strom and Ebeling 2001).

2 SPECIFIC FOUNDATIONS CONSIDERED

This paper examines several simple examples of single piles and pile groups that support a bridge abutment. The structural concept of the foundation is rather simple: vertical loading due to structural loads, traffic, and other factors is generally small. Lateral loading due to wind, braking forces, temperature, and seismic contributions may control design. However, the geotechnical loading requirements can be quite demanding: approach embankments add lateral stresses to the piles; soft layers may exist in widely different thicknesses; and effects of consolidation may need to be considered (Szép et al 2009).

Additionally, the determining design quantity may be limiting lateral displacements. At the foundation, this will mean both lateral translation and rotation are important. Such deformations play an important role in the determination of global stiffness, hence deformations and moment/stress distribution throughout the structure. This is especially true for types of bridges (portal bridges, integrated bridges) where the connection between the foundation and the superstructure is moment-resistant (Hetényi 1964). In this paper we limit our investigation to determining how the stiffness of single row and double row pile foundations compare. In other words, what is the meaning of the common design approach, expressed in numbers, that the double row pile foundation is much more rigid than the single row one.

To accomplish this task we used several methods; all commonly used by structural and geotechnical designers. However we try to specifically address the problem of moving across the "structural-geotechnical divide" in the analysis/design process. We combine the results of structural analysis and geotechnical modeling software of varying levels of sophistication, especially when it comes to the treatment of piles and pile groups.

2.1 *Pile and Pile Cap Arrangements*

Figure 1 shows the basic pile configurations studied here. A series of progressively more complex pile foundations were examined: one, two, three, and five piles in a single row, then two, four, six and ten piles in a double row. Pile lengths and center-to-center spacing were identical.

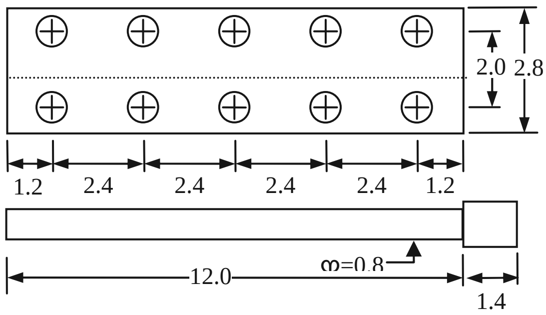

Figure 1. Model dimensions for pile study.

Single-line piles have become a favorite design alternative for bridge foundations in Hungary. Based on construction methods and materials, it is usually the most economic alternative. Pile type is the Continuous Flight Auger (CFA). There is some debate about how to model the pile structurally since its diameter is variable and difficult to estimate. The choice of diameter=0.8m seems to work best when compared to past pile load test data and examination of excavated prototypes.

With the new, advanced geotechnical packages more realistic modeling of soil-structure interaction becomes possible. For some critical problems, calculations show more favorable mechanical behavior than it was assumed based on routine bridge design calculations. Calculations show that the piles in the abutment have significantly lower loads on them than suggested by the Winkler-style models (Reese and Wang 1997) while the piles of the intermediate supports suffer more significant horizontal displacements and are subject to greater loads than previously assumed (Szép 2011).

2.2 *Analysis Methods*

As a first step, a single laterally loaded pile (*Fig. 1*) was analyzed using three different numerical methods. Results of bending moment distribution and displacements were then compared. The three numerical methods are:

- AXIS 10VM, the fundamental structural design tool in Hungary;
- GEO4 (and GEO5), an increasingly popular geotechnical design code;
- PLAXIS and MIDAS GTS, 2D and 3D geotechnical FEM packages that provide more realistic modeling for soil-structure interaction.

The AXIS and GEO software use similar subgrade reaction approaches to determine lateral pile behavior. The GEO software allows the user to calculate subgrade reactions as they are distributed down the pile and can allow for different backfill levels on either side as well as adjusting for passive and active conditions. AXIS uses a more direct approach in placing the subgrade reaction springs along the pile at discreet points. Both software packages will model the soil response as elastic or elasto-plastic with a specified strength limit.

3 2-D ANALYSIS AND RESULTS

The first level of analysis was a 2-D simplification of the actual geometry. This is a common design and analysis simplification that allows the engineer to evaluate the effects of 1-row or 2-row pile group as well as estimating the deflections, rotations, and bending moments generated within the model. Due to the relative ease of analysis, many design alternatives can be considered on a trial basis, and decisions made to further refine the design alternative or discard it. The two candidates for analysis are shown above (Figure 2) with element meshes generated by Plaxis. Material properties used in the analyses are presented in Table 1. Pile dimensions are identical to those

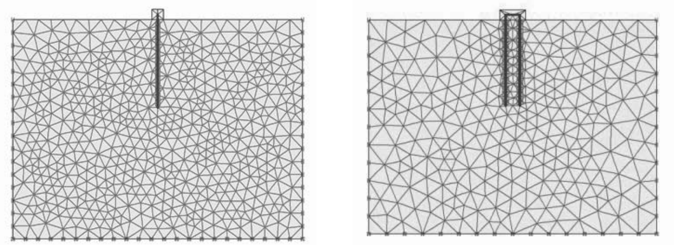

Figure 2. Two dimensional model for 1-row and 2-row pile groups.

Table 1. Material properties for analysis

			Sand	Clay	Concrete
Young's Modulus	E	kN/m^2	20 000	5 000	20 000 000
Poisson's-Ratio	ν	–	0.3	0.3	0.15
Dry unit weight	γ_d	kN/m^3	20.0	20.0	24.0
Wet unit weight	γ_t	kN/m^3	20.0	20.0	–
Cohesion	c	kN/m^2	0	20	–
Angle of Friction	φ	°	30	20	–

presented in Figure 1. Interface elements were also used to better represent soil/pile interaction. Results from the analysis are summarized in Figure 3. Lines most closely paired in the figure are one- and two-pile geometries indicating that doubling the number of piles has less effect than doubling, or halving the applied load. While the group-effect for this configuration has been studied before (Bak et al, 2010), the structural design implications can be more difficult to assess. The altered flexibility of the substructure now comes into play when dimensioning structural elements for the superstructure.

From Figure 3 one may also see that the rotation of the pile head for single-row groups is far greater, leading to greater deflections above the foundation. Most noticeable is the degree of rotation for sand where the soil is relatively much weaker near the surface than at depth, causing a very pronounced curvature in the pile. Comparing the Plaxis results with AXIS and GEO4 is a challenge. One may choose a wide variety of subgrade reaction values for AXIS and GEO4 and produce a corresponding wide variety of answers. In this study, a great deal of effort was spent trying to follow recommendations of the software providers and base subgrade reaction values on formulae and soil properties consistent with the other analyses.

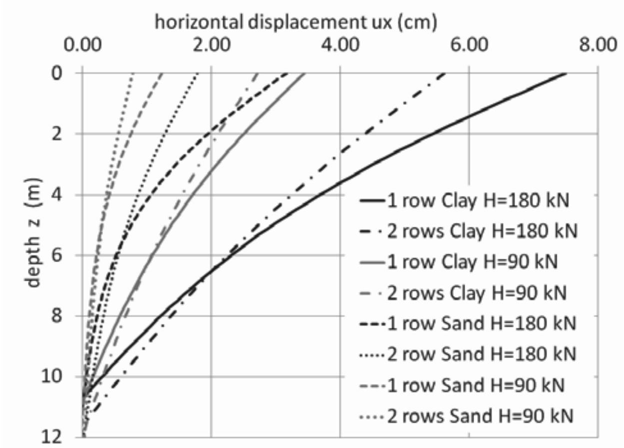

Figure 1. Lateral deflections for 1- and 2-row pile groups.

Table 2 lists the calculated lateral deflections consistent with the loads and soils shown in Figure 3. While the elastic/plastic behavior allowed for nonlinear load-displacement curves, deflections from these two programs were consistently lower than Plaxis-2D. There is also reason to believe that the two subgrade reaction programs may better represent single piles (as in 3D, discussed later) than as a 2D "pile wall" as represented in Figure 1.

Table 2. Summary of reaction coefficients and displacements

Spring Mode	Axis		Geo 4	
	k (MN/m/m)	ux (cm)	Ch (MN/m^3)	ux (cm)
Elastic	15-45	0.66	19-56	0.88
Elas/Plas	15-45	1.35	19-56	1.70
Elas/Plas	30-90	1.09	19-56	0.65

4 COMPARING 3-D ANALYSES

3-D methods highlight the same behavior but to different degrees. Using similar soil properties, one may compare the benefit of a two-pile system. The 3D model also made use of interface elements and a thin pile element placed within the solid element pile in order to determine shear and bending moments (MIDAS 2009). This time, the benefit is more pronounced, due to the more efficient process of spreading reaction loads throughout the soil in three dimensions.

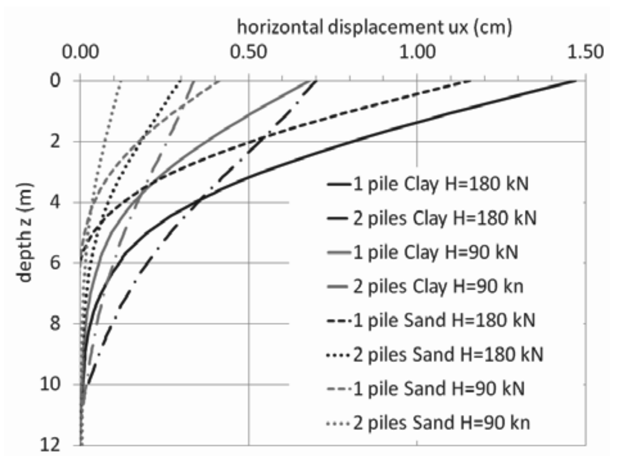

Figure 2. Displacement profiles for 1, 2 piles; Sand, Clay; 90,180 kN.

Displacement magnitude is much less for all combinations of load and soil. Surface displacements are smaller than those in Figure 3 by a factor of about 5-8x. This time the number of piles resisting movement is more influential in reducing displacement than the soil modulus. This is evidenced by the fact that the displacement profiles are grouped by number of piles and load magnitude (1 pile Sand H=180 is most near to 1 pile Clay H=180, etc.) The single piles also show a very pronounced slope at the surface which will again translate to rigid body rotation of the bridge pylons.

5 COMBINING ANALYSES

Presently the research group is adapting an optimization method to translate pile head displacement and rotations computed from 2D and 3D finite element analyses to a small number of elasto-plastic subgrade springs for use in structural or geotechnical design software (such as GEO and AXIS). The method assumes the pile has identical structural properties as the original (more sophisticated) analysis software. Four to six lateral springs are placed on the pile at various depths. One spring is always placed at the surface, another at the pile tip. The remaining springs will be placed in optimal positions to produce similar responses at the top of the pile.

The procedure seeks to optimize three quantities for each spring: elastic constant, k; plastic limit, c; and depth were the spring is attached to the pile, z. The pile structural element is modeled as a series of beam elements with nodes located at the pile tip, point of application of the middle springs, and the pile top. For a four spring model, the pile will consist of four nodes and three elements (Figure 5).

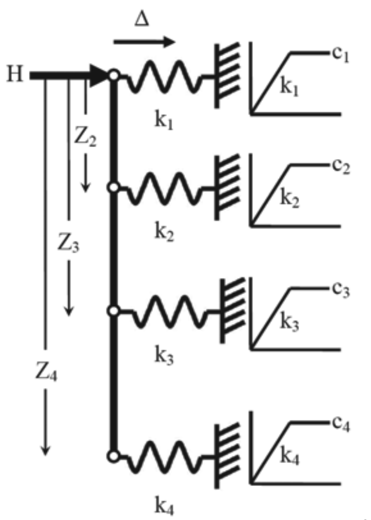

Figure 3. Four element pile with elasto-plastic springs.

The optimization process varies the eight spring parameters and two depths (the other two are the fixed length of the pile and zero) to minimize the least squares error between the deflection, Δ, computed above and the displacement generated from the finite element model for the same load, H. When the sum of least-squares error is minimized, the problem is solved. This is the same process one uses for fitting trend lines to data. The program is written in Visual Basic for Applications (VBA) and runs within an Excel spreadsheet. Computing deflections for the various loads is done with a small, nonlinear matrix structural analysis program that is called as an Excel function and returns the computed deflection value to the spreadsheet. The optimization makes use of the Solver add-in found in Excel. The parameters that are varied in the solver are those discussed above, the target value to minimize is the sum of the squared errors. Sample output for the optimization process is shown in Figure 6.

The optimization process can also be applied to pile load test data or any other method that generates the necessary values. The example here fits only horizontal deflections at the pile top. A better, slightly more complex approach is to fit both deflection and pile head rotation data. Since this involves more statistical degrees of freedom (double the number just demonstrated) more springs would be necessary. Data that is being compared can be assigned weighting (importance) values if some data is more reliable or vital than others.

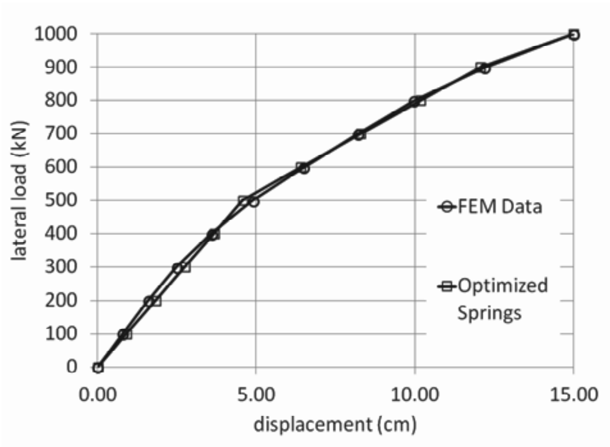

Figure 4. Finite element data with optimized spring response fit.

6 CONCLUSION AND FURTHER STUDY

Harmonizing structural and geotechnical design methods is a worthwhile challenge. Implementing the recently adopted design methods of Eurocode opens the possibility to teach new professionals a more integrated approach to design. However, in order to accomplish this, design methods and software must be better integrated and understood from both the structural and geotechnical perspectives. In this paper several methods were presented that Hungarian designers use for geotechnical and structural projects. Due to the more rigorous demands of modern designs, the substructure and superstructure components must work together seamlessly.

As part of ongoing research at Széchenyi University, the authors have presented several methods for analyzing and designing piles for lateral loads. Ideally the methods would be totally integrated; however this is not always possible due to the nature of design contracts, project timing, and available design software. Ideas and methods to overcome these limitations have been given and it is hoped they will engender further discussion by the engineering community.

Further research will focus on more complex structural and geotechnical systems where the entire construction process is modeled. By understanding the nuances of excavation, earthwork, falsework, concrete placement and finish schedules, further design efficiencies and enhancements can be found.

7 ACKNOWLEDGMENTS

The authors acknowledge the financial support of the Széchenyi István University within the framework of TáMOP 4.2.2/B-10/1-2010-0010 application.

8 REFERENCES

AxisVm, 2010. *Finite Element Analysis & Design Program*, users manual, InterCad Ltd, Budapest.

Bak E., Koch E., Ray R., Sharle P., Szepesházi R. 2010. Parametric study of combined pile-raft foundation. *Proc. of the XIVth Danube-European Conference on Geotechnical Engineering*, Bratislava, Slovakia, p. 13.

Hetényi M. 1964. Beams on elastic foundation, *Theory with applications in the fields of civil and mechanical engineering*, University of Michigan Press, Ann Arbor, Michigan.

MIDAS 2009. *MIDAS GTS users manual*, Information Technology Co., Ltd. Delft, Netherlands.

Reese L.C., Wang S.T 1997. *LPILE Plus 3.0 Technical manual of documentation of computer program*, Ensoft, Inc., Austin, Texas,.

Szép J., Murinkó G., Szepesházi R. 2009. Modelling bridge substructures, (in Hungarian) *Geotechnika conference*, Ráckeve, Hungary, p. 22.

Szép J. 2011. FEM - modeling of abutment, *10th Slovak Geotechnical Conference - Geotechnical Problems of Engineering Constructions*, Bratislava, Slovakia, 30-31 May, 207-218.

Strom R. W., Ebeling R. M. 2001. State of the practice in the design of tall, stiff, and flexible tieback retaining walls, *Technical Report ERDC/ITL TR-01-1*, US Army Corps of Engineers 1-225.

Experimental Study on the Method of Rebound and Recompression Deformation Calculation in Deep and Large Foundation Design

Etude expérimentale sur la méthode de calcul des déformations de résilience et de recompression pour les fondations larges et profondes

Teng Y., Li J., Wang S.
Institute of Foundation Engineering China Academy of Building Research

ABSTRACT: By analyzing the data from the consolidation-rebound-recompression test of in-situ soil, bearing test, model experiment and field measurement test, the calculating methods of rebound and recompression deformation are proposed, which based on stress history of ground soil, the loading and unloading conditions. Some conclusions can be drawn: i) the progress of rebound deformation exhibits three-phases characteristics, and the critical unloading ratio could be used to determine the calculating depth of rebound deformation; ii) the recompression deformation of foundation soil can be computed as two-phase mode, in fact, the controlled deformation emerges when the reloading ratio exceed the critical reloading ratio; iii) the recompression deformation is larger than rebound one, and the increase proportion varies with different kinds of soil; iv) in actual constructions, the parameters of rebound and recompression deformation can be gotten by compression-rebound-recompression test on in-situ soil of corresponding depth in the site, or bearing test in site that include the process of load-unload-reload. Then the recompression deformation can be calculated by using the parameters responding to the real stress history. According to model experiment and in-situ tests, the calculated rebound and recompression deformation has a well agreement with measured datum, and the accuracy of predicted deformation is improved.

RÉSUMÉ : Par une analyse de données d'essai de compression sur sol intact, de test de portance, d'expérimentation à grande échelle, et de mesure faites in situ, il est possible de proposer une méthode de calcul des déformations de résilience et de recompression pour fondation profonde et large sur la base de l'histoire des contraintes (conditions de chargement et déchargement lors de l'exécution des travaux). Les résultats importants de cette étude se synthétisent comme suit: 1. l'évolution de la résilience et de la recompression du sol de fondation se caractérisent par trois phases et la profondeur de résilience calculée peut être utilisée pour déterminer celle de profondeur critique; 2. La déformation de recompression du sol de fondation est calculée en deux phases; en fait au cours de la réalisation des travaux les grandes déformations se produisent durant la phase où la charge excède la recharge critique; 3. La valeur de la déformation globale de recompression est supérieure à celle de déformation de résilience; 4. Dans un cas réel de réalisation des travaux, le calcu de déformation de recompression de sol de fondation se fait suivant les paramètres recueillis de l'épreuve dite compression-rebond-recompression avec un échantillon du sol original prélevé in situ par sondage à une profondeur convenable, ou de l'essai s'applique in situ soit chargement-déchargement-rechargement sur le bloc de charge du sol de fondation, avec ces paramètres de résilience et de recompression, on peut procéder au calcul de déformation dans l'état réel des chargements de travaux. L'affirmation des résultats de l'essai de modèle et de l'épreuve in situ, les paramètres obtenus par calcul de déformation de résilience et de recompression correspondent bien à ceux recueillis par les essais in situ; dans ce cas-là, on peut dire que la précision de prédiction de déformation est acceptable.

KEYWORDS: deformation control design, rebound-recompression deformation, critical depth, critical reloading ratio.

1 INTRODUCTION

In the past decades, with the developing of engineering technique, building foundation engineering in china shows some new features such as bulky, deeply buried, large load differences, multiple-storey buildings or high-rise buildings built on the basis of the same large area raft foundation. For this kind of buildings, the deformation-controled foundation design is very important, and some deformation index should be pay more attention to prevent structure from cracking or damaging, such as overall deflection of main buildings, differential settlement between the main and podium buildings, etc. In the process of construction and normal service of this kind of buildings, the foundation soil deformation unually includes rebound deformation of foundation soil caused by the excavation of deep foundation pit, recompression deformation and consolidation deformation caused by addtional stress. The deeper the foundation buried, the proportion of recompression deformation to total settlement is larger. So the calculation of foundation deformation is more complicated. There are some mature methods to calculate consolidation deformation caused by addtional stress, but the reasearch and calculating mathod to rebound-recompression deformation are seldom reported. In this paper, the calculating methods of rebound and recompression deformation are proposed by analyzing the data from the consolidation-rebound-recompression test of in-situ soil, bearing test, model experiment and field measurement test. According to model experiment and in-situ tests, the calculated rebound and recompression deformation has a well agreement with measured datum, and the accuracy of predicted deformation is improved.

2 THE LAW OF REBOUND AND RECOMPRESSION DEFORMATION

2.1 The Law of Rebound Deformation

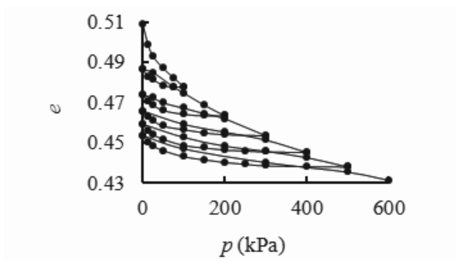

Figure 1. The typical *e-p* curves of soil.

The typical *e-p* curves of soil by the consolidation-rebound-recompression test are shown as figure 1. The basic law of rebound deformation under unloading condition and recompression deformation under reloading condition, usually can be described by some parameters such as unloading ratio R, modulus of resilience E_c, rebound ratio, critical unloading ratio R_{cr}, limit unloading ratio R_u, and some new parameters[1, 2] such as rebound proportion, reloading ratio R', recompression ratio r' are proposed, and some relation curves can be used to analyze rebound deformation and recompression deformation, such as the relation curves of unloading ratio-rebound proportion, the relation curves of unloading ratio- modulus of resilience, the relation curves of reloading ratio-recompression ratio etc.

(1) The relation curves of unloading ratio-rebound proportion

In the process of unloading, figure 2 shows that: i) as the unloading ratio is less than 0.4, the rebound deformation is less than 10% of the total rebound deformation; ii) as the unloading ratio increases to 0.8, the rebound deformation is about 40% of the total one; iii) as the unloading ratio increases from 0.8 to 1.0, the rebound deformation is about of 60% of the total one. So unloading ratio is the key influencing factor of rebound deformation.

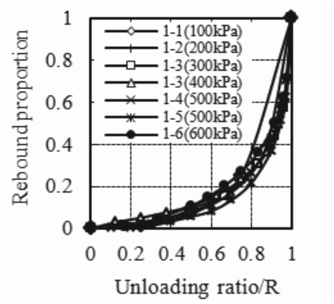

Figure 2. The relation curves of unloading ratio-rebound proportion of clay soil sample

(2) The relation curves of unloading ratio-modulus of resilience

The modulus of resilience is not a constant, see Figure 3. It varies with the unloading ratio and exhibits three-phase character*istics. For the soil of the same depth, the modulus of resilience is varied according to the excavation depth. The relation curves of R-E_c can be divided into two lin*e segments, see figure 3(a), and the unloading ratio of intersection of the two line segments can be defined as critical unloading ratio R_{cr}. When $R<R_{cr}$, E_c increases sharply and rebound deformation could be negligible. The relation curves of R- lgE_c also can be divided into two line segments approximately, see figure 3(b), and the intersection point of the two line segments can be defined as limit unloading ratio R_u. When $R>R_u$, E_c decreases sharply and the most rebound deformation occurs.

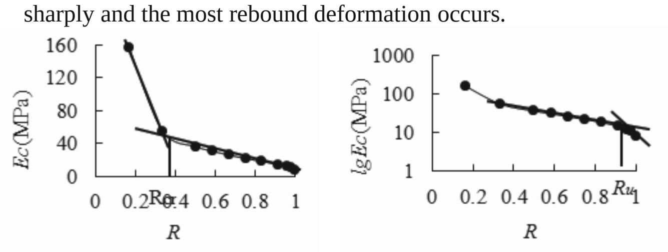

(a) (b)

Figure 3. The relation curves of R-E_c and R-lgE_c of clay soil sample

The relation curves of unloading ratio-modulus of resilience can be used to determine the calculation depth of rebound deformation. In calculation, the depth of R_{cr} can be calculated. The rebound deformation beneath the depth is negligible, and rebound deformation of this depth can be calculated. The rebound deformation result meets the requirments of engineering.

2.2 The Law of Recompression Deformation

(1) The relation curves of reloading ratio-recompression ratio[3]

In the process of recompression, the curves of reloading ratio-recompression ratio of clay soil, see figure 4, shows that: i) as the reloading ratio R' is 0.2, the recompression deformation is about 40% ~60% of rebound deformation; ii) as the reloading ratio increases to 0.4, the recompression deformation is about 70% of rebound deformation; iii) as the reloading ratio increases to 0.6, the recompression deformation is about 90% of rebound deformation; iv) as the reloading ratio reaches 0.8, the recompression is roughly euqal to the rebound deformation; v) for this kind of soil, as the reloading pressure is equal to the unloading pressure, the recompression deformation is 1.2 times to the rebound deformation. A large amount of testing data show that, the recompression deformation is not equal to the rebound deformation in value as the reloading ratio is equal to 1.0. Generally the recompression deformation is larger, and the increase proportion of deformation varies with different kind of soil[4].

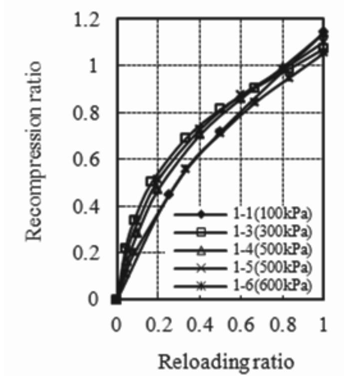

Figure 4. The curves of reloading ratio-recompression ratio of clay soil

2.3 Verification by Model experiment

In order to verify the law of rebound and recompression, the model experiment was carried out in the laboratory of Institute of Foundation Engineering, China Academy of Building Research. In the model experiment, soil deformation was monitored during excavating and backfilling. The dimension of the test pit is 13.0m×5.3m, the excavation depth is 3.5m, and the backfilling depth is about 3.5m. Rigid measure points were installed into the soil in different depth to measure the deformation during the model experiment[1, 5, 6].

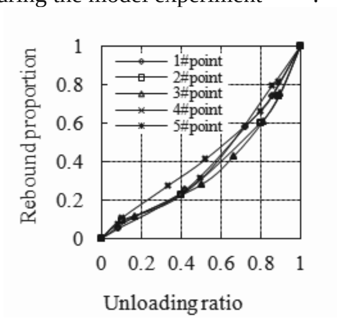

Figure 5. The curves of unloading ratio-rebound proportion of soil at the bottom of excavation

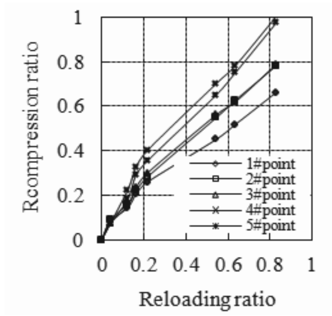

Figure 6. The curves of reloading ratio-recompression ratio of soil at the bottom of excavation

The curves of unloading ratio-rebound proportion of soil at the bottom of excavation, see figure 5, reflect the similar law of rebound deformation with curves of soil tests, but the curves are relatively flat, compared with the curves of soil tests.

In the process of backfilling, the curves of reloading ratio-recompression ratio of soil show as figure 6. The recompression deformation of soil can be divided into two line segments, and the reloading ratio of the intersection point of the two line segments is about 0.2, similar as the law of soil tests. As the reloading ratio is still low, the recompression deformation is obvious. As the reloading ratio of soil at the bottom of excavation increases to 0.8, the recompression deformation is roughly equal to the rebound deformation.

3 THE CALCULATION METHOD OF REBOUND AND RECOMPRESSION DEFORMATION

3.1The Calculation Method of Rebound Deformation

The systematic analyzing method of rebound deformation is as follow[1]:
i) get no less than 6 samples for each solum by investigation, and then obtain the basic data of soil by consolidation-rebound-recompression test;
ii) analyz the data by graphing curves of unloading ratio-rebound proportion and curves of unloading ratio- modulus of resilience, determine the value of R_{cr};
iii) determine the calculation depth of rebound deformation according to R_{cr}, divide the calculation depth to several layers, and calculate both unloading ratio R and modulus of resilience E_c of every layer;
iv) calculate rebound deformation of every layer and add them together to get the total rebound deformation.
The rebound deformation can be calculated as formula 1:

$$s_c = \sum_{i=1}^{n} \frac{p_c}{E_{ci}} (z_i \bar{\alpha}_i - z_i \bar{\alpha}_{i-1}) \tag{1}$$

Where：

s_c - rebound deformation of foundation soil, *mm*;

p_c - gravity of soil upon foundation base, *kPa*, buoyancy should be deducted underneath ground water;

E_{ci} - modulus of resilience, it can be determined from soil test directly or calculated from the relation curves of R-E_c and R-lgE_c;

n – number of layers which the calculation depth is divided;

z_i, z_{i-1} – distance between foundation base and the bottom of No. i , No. $i-1$ layer；

$\bar{\alpha}_i$, $\bar{\alpha}_{i-1}$ – additional stress coefficient of No. i , No. $i-1$ layer.

In this method, both E_c and R_{cr} must be determined by corresponding stress state of soil and stress history. This method is not only simplifying the process of calculation but also improving accuracy.

3.2 The Calculation Method of Recompression Deformation

According to the law of recompression deformation, the recompression deformation can be calculated as formula 2[7]:

$$s_c' = \begin{cases} r_0' s_c \dfrac{p}{p_c R_0'} & p < R_0' p_c \\ s_c [r_0' + \dfrac{r'_{R'=1.0} - r_0'}{1 - R_0'} (\dfrac{p}{p_c} - R_0')] & R_0' p_c \le p \le p_c \end{cases} \tag{2}$$

Where:

s_c' - recompression deformation of foundation soil, *mm*;

s_c - rebound deformation of foundation soil, *mm*;

r_0' - the critical recompression ratio. The curves of reloading ratio-recompression ratio of soil can be divided into two line segments. The recompression ratio of intersection of the two line segments is critical recompression ratio, and its value can be determined in the curves of reloading ratio-recompression ratio from soil test;

R' - the critical reloading ratio. Similar to r_0' , the reloading ratio of intersection of the two line segments is critical reloading ratio, and its value also can be determined in the curves;

$r'_{R'=1.0}$ - The value of recompression ratio, when $R' = 1.0$. it is equal with the increase proportion of recompression deformation.

4 ENGINEERING APPLICATION

In Beijing there is a 20-storeyed building with 4-storeyed basement. The foundation area is about 6000 m^2, and the excavation depth is 19.1m. In the process of the building's construction, research on rebound and recompression deformation was carried out by Institute of Foundation Engineering China Academy of Building Research. Rebound deformation was monitored during the excavation, and settlement was also observed in the process of construction.

4.1 Calculation of Rebound Deformation

According to the data of soil tests, the expression of R-E_c and R-lgE_c, and the value of R_{cr}, R_u of soil can be determined. For example, for sample 1-3: $R_{cr}=0.33$, R_u=0.92, and the expression of R-E_c is listed in table.1.

Table 1 The expression of R-E_c of sample 1-3

Condition of R	*expression*
$0 < R \le 0.33$	$E_c = 257533.3 - 386300R$
$0.33 < R \le 0.92$	$E_c = 181009.2 - 165111.8R$
$0.92 < R \le 1.0$	$E_c = 219419.9 - 203110.2R$

The rebound deformation can be calculated as formula 1. The calculated deformation contour of the foundation pit shows as figure 7. The rebound deformation of the foundation pit is not the same, the maximum of rebound deformation is 35 mm in the center of foundation base, and it reduces gradually to 6 mm at the edge of foundation base. The measured rebound deformation is about 32 mm.

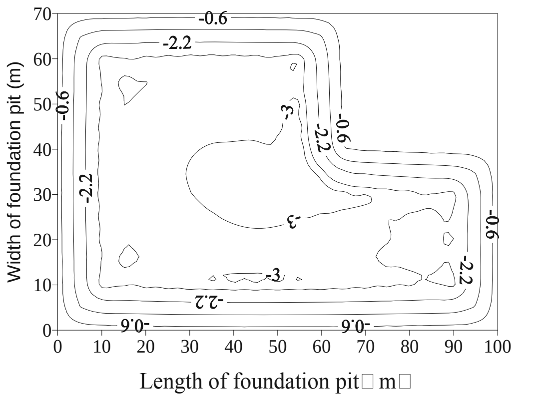

Figure. 7 the deformation contour in foundation pit of calculating

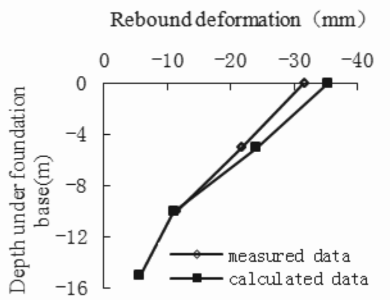

Figure. 8 the rebound deformation distribution along depth

The rebound deformation distribution along depth is shown as figure 8. The curve of calculating deformation by this method is approximate to the curve of measured deformation. The rebound deformation beneath 12.0m depth under foundation base is less than 30% of the total deformation.

4.2 Calculation of Recompression Deformation

For this foundation pit, the estimating unloading stress is about 353.35kPa. For the main buildings, since the pressure under the foundation is larger than unloading pressure, the settlement of foundation soil includes both recompression deformation and consolidation settlement. Recompression deformation can be calculated as formula 2. Firstly the curves of reloading ratio-recompression ratio of soil can be obtained by soil tests. By analyzing the curves, the expression of reloading ratio-recompression ratio can be determined and listed in table 2.

Table 2 The expression of reloading ratio and recompression ratio

NO.	*Consolidation Pressure（kPa）*	*Condition of R'*	*expression*
1-3	*300*	$0 < R' \le 0.125$	$r' = a_1 + b_1 R'$ $a_1 = 0.0541 \quad b_1 = 2.8726$
		$0.125 < R' \le 1.0$	$r' = a_2 + b_2 R'$ $a_1 = 0.5173 \quad b_1 = 0.5643$
1-4	*400*	$0 < R' \le 0.125$	$r' = a_1 + b_1 R'$ $a_1 = 0.0264 \quad b_1 = 3.551$
		$0.125 < R' \le 1.0$	$r' = a_2 + b_2 R'$ $a_1 = 0.4206 \quad b_1 = 0.6625$

Estimate the reloading stress of each construction stage according the construction progress to get the recompression ratio of each stage. Then recompression deformation of each stage can be calculated as table.3. When the reloading pressure is equal to the unloading pressure, the compression deformation is about 36.7mm.

Table 3 The calculating table of recompression deformation under main building in each conditions

NO.	*Reloading kPa*	*Unloading kPa*	R'	r'	S_c *mm*	S'_c *mm*
(1)	*80.3*	*353.35*	*0.2272*	*0.5711*	*35.0*	*19.99*
(2)	*103.4*		*0.2926*	*0.6144*		*21.50*
(3)	*134.9*		*0.3818*	*0.6735*		*23.57*
(4)	*145.4*		*0.4115*	*0.6932*		*24.26*
(5)	*176.9*		*0.5006*	*0.7522*		*26.33*
(6)	*218.9*		*0.6195*	*0.8310*		*29.08*
(7)	*250.4*		*0.7086*	*0.8900*		*31.15*
(8)	*302.9*		*0.8572*	*0.9885*		*34.60*
(9)	*318.9*		*0.9025*	*1.0185*		*35.65*
(10)	*334.9*		*0.9478*	*1.0485*		*36.70*

The consolidation settlement caused by additional stress is calculated by the layer-wise summation method recommended by Code for Design of Building Foundation [7]. By calculating, the consolidation settlement is 10.24mm. So the final settlement of the main building is 46.94 mm.

Usually the settlement of foundation is observed after raft foundation construction, and observation points are set on the raft foundation, so the recompression caused by gravity of raft foundation can't be monitored. According to the basic law of recompression deformation, the recompression deformation cannot be ignored, when reloading stress is low. The recompression deformation caused by gravity of raft foundation can be calculated as No. (1) in table 3. In this stage of construction, since the concrete strength of foundation had not formed completely and the superstructure had not constructed generally, there is no additional stress caused by the recompression deformation.

The settlement curves of calculation and observation of the main building are shown as Figure 9, and the line of dashes shows the calculated final settlement. Both the calculated settlement and monitored settlement have the same development tendency, but the calculated settlement is little higher than the corresponding one monitored.

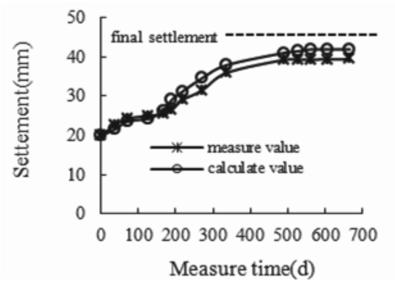

Figure. 9 the developing curves of settlement from calculating and measuring of main building

5 CONCLUSIONS

Through the soil test, model experiment and engineering application, the conclusion of rebound and recompression deformation can be summarized by the following clauses:

(1) The dimensionless parameters such as rebound proportion, reloading ratio, recompression ratio are proposed and used in research, and the basic law of rebound deformation and recompression deformation can be got, and then the calculation methods of rebound deformation and recompression deformation are put forward. Mathematical relation between rebound and recompression deformation is established;

(2) R_{cr} can be determined by the curves of R-E_c, and the calculation depth of rebound deformation can be calculated according to R_{cr}. E_c must be determined by corresponding stress state of soil and stress history. This method is not only simplifying the process of calculation but also improving accuracy.

(3)The calculation method of recompression deformation proposed by this paper can compute deformation of each construction stage.

(4) In initial stage of construction, the reloading stress is low, but the deformation is obvious. Meanwhile, the concrete strength of foundation had not formed completely and the superstructure had not constructed generally, so there is no additional stress caused by the recompression deformation. It is beneficial for the deformation control.

REFERENCES

1 LI Jianmin.2010. *Research on the calculation method of resilient deformation in ultra-deep foundation pit*[D]. Beijing: china academy of building research.

2 TENG Yanjing, LI Jianmin. 2011.*Research on the analyzing and calculation method of resilient deformation in ultra-deep foundation pit*[R]. Beijing: china academy of building research.

3 LI Jianmin, TENG yanjing. 2010.Model test on rebound deformation in foundation pit excavation. *Chinese Journal of Geotechnical Engineering*, 32(S2): 81-84.

4 LI Jianmin, TENG Yanjing. 2011.Reaching for the character of rebound deformation of foundation pit excavation by compression and resilience test of different sorts of soil[J]. *Building Science*, 27(1): 72-77.

5 LI Jianmin, TENG Yanjing.2010. Experimental study on the characteristics of the rebound and the recompression deformation of soil under unloading. *Geotechnical Investigation & Surveying*, 38(12): 9-14.

6 LI Jianmin, TENG Yanjing.2011. Test study of law of recompression deformation of soil[J]*Rock and Soil Mechanics*, 32(S2): 463-468.

7 National Standard of the People's Republic of China.2011. GB50007—2011 Code for design of building foundation. Beijing: China Architecture and Building Press, (in Chinese).

Deep Basement Construction of Bank of Thailand Along Chao Phraya River closed to Tewavej Palace and Bangkhumphrom Palace

Construction du sous-sol profond de la Banque de Thaïlande le long de la Chao Phraya près des palais de Bangkhumphrom et Tewavej

Teparaksa W.
Associate Professor, Department of Civil Engineering, Chulalongkorn University, Bangkok, 10330, Thailand

ABSTRACT: The Bank of Thailand (BOT) head office is a large building constructed in the inner Ratanakosin Island of Bangkok along Chao Phraya River, a main river of Bangkok, where high-rise building construction with more than three stories is not permitted. The BOT building consists of five basements with excavation depth of 15.8 meters and only three stories of super structure. The basement construction was constructed only five meters away from Tewavej Palace and ten meters away from Bangkhunphrom Palace. The damage assessment by means of Finite Element Method (FEM) with simulation of basement construction method was carried out to predict the influence on both palaces. Finally, the top-down construction method was selected for basement construction with one meter thick and 20 meters long of diaphragm wall which was designed together with the 50 meters long bored pile to support the whole building. The full set of instrumentation was installed at the palaces, diaphragm wall and ground surface for monitoring the field performances during and after basement construction. The field measurement and FEM prediction will be compared and the time dependent of lateral wall movement will be discussed. The construction was completed without any damage or effect to both palaces.

RÉSUMÉ : Le siège social de la Banque de Thaïlande (BDT) est un grand édifice construit sur l île intérieure de Rattanakosin dans Bangkok le long de la Chao Phraya, un fleuve principal de Bangkok, ou la construction de bâtiments haut de plus de trois étages est interdite. La BDT est constituée de cinq niveaux de sous sols avec excavation jusqu'à 15.8 mètres de profondeur et seulement trois étages de superstructure. La construction du sous-sol a été effectuée seulement à cinq mètres du Palais de Tewavej and à dix mètres du Palais de Bangkhunphrom. L'évaluation des dégâts par simulation de la construction du sous-sol par méthode des éléments finis (MEF) a été effectuée afin de prédire l'impact sur les deux palais. Enfin, la méthode de construction 'du haut vers le bas' a été sélectionnée pour la construction du sous-sol ainsi qu'une paroi moulée d'un mètre d'épaisseur et 20 mètres de long qui a été dimensionnée avec des pieux forés de 50 mètres de long pour supporter l'intégrité du bâtiment. Les mesures sur le terrain ainsi que les prédictions par MEF sont comparées et la dépendance en temps du mouvement latéral du mur est discutée. La construction a été effectuée sans qu'il n y ait de dégâts ou d'impacts sur les deux palais.

KEYWORDS: Deep Basement, FEM Analysis, Deep Excavation, Historical Building, Palace.

1 INTRODUCTION

The demand for deep underground basement construction is increasing in Bangkok city especially in the inner zone due to the optimized land use for underground car park and retail of the department store. The design and construction of deep basement in the large city have to take the impact of the nearby structure as well as public utilities into account. The designs of the deep basement in Bangkok subsoil done by the author are the Bai Yok II tower with 12 m. deep (Teparaksa, 1992), Library of Thammasat University with 14 m. deep (Teparaksa, 1999a), Central World with 9 - 14 m. deep and Millennium Sukhumvit hotel next to Bangkok Mass Rapid Transit (MRT) Tunnel with 14 m. deep (Teparaksa, 2007).

The head office, Bank of Thailand (BOT) is located in the inner Ratanakosin Island where high-rise building construction more than three stories is not allowed. The location of the new head office of BOT is planned along Chao Phraya riverbank and closed to two historical palaces; Tewavej Palace and Bangkhunphrom Palace as shown in Fig. 1.

The design and construction of the deep basement for head office of the BOT consists of five basements for underground car park with 15.8 m deep excavation and three floors of head office above ground surface.

The analysis and the diaphragm wall design as well as the impacted assessment of two palaces were carried out by Finite Element Method (FEM) analysis by simulating the full method of excavation and construction in the model. The instrumentation was installed in both diaphragm wall and at the palaces to monitor the safety and stability of the palaces. The behavior of diaphragm wall movement will also be discussed and compared with FEM prediction.

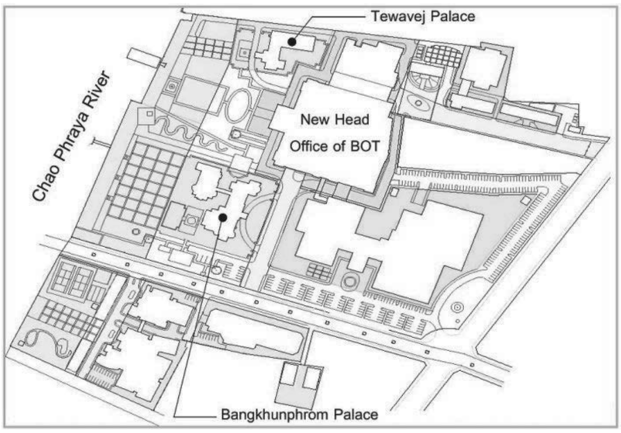

Figure 1. The location of new head office, Bank of Thailand (BOT) and the surrounding palaces.

2 SOIL CONDITIONS

The soil conditions at BOT site based on nine boreholes soil investigation consists of 12.5 m. thick soft dark grey clay and followed by medium stiff clay and stiff to hard clay until reached the first dense sand layer at about 28.5 m. deep. The second very dense sand where the pile tip of the building is seated is found at about 46 m. deep below ground surface. Table 1 presents the soil condition and the engineering properties.

Table 1. Soil conditions and engineering properties.

Depth (m.)	Soil Description	γt	Su	N	Eu	E'
0 - 12.5	Soft Clay	16.0	15	-	8750	-
12.5 - 15.0	Medium Stiff Clay	16.5	40	-	18000	-
15.0 - 20.0	Stiff to Very Stiff Silty Clay	19.0	-	12	85000	-
20.0 - 28.5	Hard Clay	20.0	-	35	300000	-
28.5 – 39.0	Dense Silty Sand	20.0	-	40		80000
39.0 – 46.0	Hard Silty Clay	20.0	-	45	-	-
46.0 – 65.0	Very Dense Silty Sand	20.0	-	>50	-	-

Note: γt = Total Unit Weight (kN/m^3)
Su = Undrained Shear Strength (kN/m^2)
N = SPT N-Value (Blows/ft)
Eu, E' = Undrained and Drained Young's Modulus (kN/m^2)

3 PROJECT DESCRIPTION

The basement design and construction of the new head office of bank of Thailand aims to solve the problem of car park from both staff as well as visitors. The surface area of excavation is approximately 10790 m^2 with 5 m. and 10 m. away from Tewavej Palace and Bangkhumphrom Palace accordingly as shown in Fig 2. The Tewavej Palace and Bangkhunphrom Palace are the historical palace constructed by brick and bearing wall seated on shallow foundation. In order to minimize the influence on these two palaces, the basement of BOT was designed to be constructed by top-down construction method which has been used only in Bangkok city restricted area such as the subway station of MRT project.

The diaphragm wall (D-Wall) of 1.0 m. thick and 20 m. deep was designed as the temporary wall for 15.8 m. deep excavation and used as permanent wall at the final stage. Five basement floors consist of F_1 ,P_1 ,P_2 ,P_3 and P_4 floor at -1.20 m., -4.70 m., -7.70 m., -10.70 m., and -13.70 m. deep respectively as illustrated in Fig 3.

The top-down construction method was started by casting the first basement F_1 at -1.20 m. then moving to third basement floor (P_2) at -7.70 m. and constructing the fifth basement floor and mat foundation at -13.70 m. deep as shown in Fig 3. Loading of the permanent basement floor during construction was transferred through the stanchion at the centerline of the column which was installed into the bored pile during construction of the bored pile.

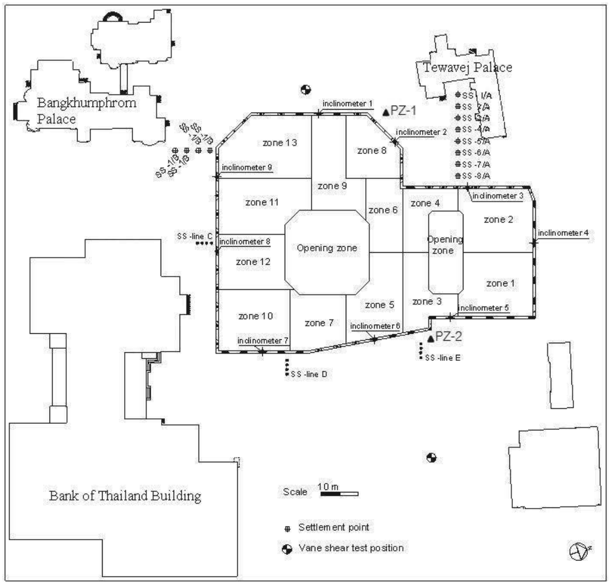

Figure 2. The BOT project plan view.

4 INSTRUMENTATION

The head office of BOT was constructed in the large area of more than 10790 m^2; therefore, the excavation area for top-down construction was divided into 13 zones as presented in Fig 2. Two large opening zones were provided for excavation work. The excavation at the deeper basement required to excavate step by step from far corner to the opening zone where the excavated soil was moved out of the project area. For safety reason and to monitor basement wall behavior, the full scheme of instrumentation was installed at the palaces on the ground surface and in the diaphragm wall as shown in Fig 2 and Table 2.

5 ANALYSIS AND DESIGN OF DIAPHRAGM WALL

The analysis and design of the diaphragm wall was carried out by means of the FEM. The construction sequence was simulated in the FEM analysis. The sequence of basement construction consists of 8 steps as follows:

1.Excavating to -1.75 m. deep and casting lean concrete.
2.Casting the first permanent basement floor at -1.20 m. (thickness 0.45 m.)
3.Excavating to the third basement floor at -8.10 m. deep and casting lean concrete.
4.Casting the third permanent basement floor at -7.70 m. (thickness 0.30 m.)
5.Excavating to the fifth basement floor (base slab) at -15.60 m. deep and casting lean concrete.
6.Casting the fifth basement floor (base slab) at -13.70 m. (thickness 1.30 m.)
7.Casting the permanent fourth basement floor at -10.70 m. (thickness 0.30 m.)
8.Casting the permanent second basement floor at -4.70 m. (thickness 0.30 m.)

The detail of construction sequence is presented in Fig. 4.

The analysis and design of the diaphragm wall for 15.6 m. deep excavation were carried out by FEM. As the basement constructed in soft clay layer, the undrained concept based on bi-linear Mohr-Coulomb failure theory was used for FEM analysis. The Young's modulus (Eu) was used in terms of an undrained shear strength (Su) of Eu/Su = 500 and 1000 for soft clay and stiff clay respectively (Teparaksa, 1999b). The value of Young's modulus is also presented in Table 1.

The Young's modulus or shear modulus (G) of clay depends on the shear strain of the system as proposed by Mair (1993) as shown in Fig. 5. The relationship of the Eu/Su and strain level presented in Fig. 6 is the modulus of soft and stiff Bangkok clay based on the results of self-boring pressuremeter test during construction of MRT Subway Blue Line in Bangkok city. Fig. 7 presents deformed mesh of the FEM analysis at the final stage of excavation at 15.6 m deep.

The result of FEM analysis presents the envelope of lateral movement of D-wall at final stage of excavation in the order of 28.2 mm. and maximum ground surface settlement of 23.7 mm. This maximum ground surface settlement behind the D-wall and lateral movement of the D-wall was set as the trigger level to control the method of excavation as well as the stability of Tewavej Palace.

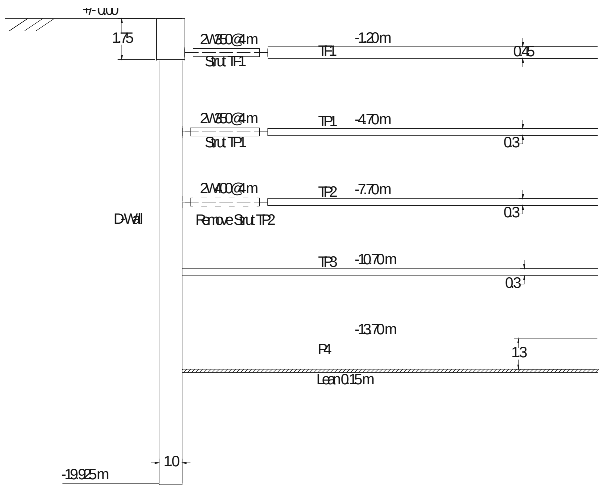

Figure 3. Typical section of underground basement.

6 INSTRUMENTATION AND PERFORMANCE OF DIAPHRAGM WALL

The full set of the instrumentation was proposed to monitor the behavior of the diaphragm wall and surrounding palaces as presented in Table 2 and Fig. 2. The results of the piezometer monitoring by pneumatic type in soft clay was constant with hydrostatic pore water pressure of ground surface water at 1.00 m. below ground surface.

Table 2. Instrumentation at the Palaces and Diaphragm Wall.

Instrumentation	Location	Purpose
Vibration Sensor	At Tewavej Palace and Bangkhunphrom Palace.	Vibration at the palace
Tiltmeter	At Tewavej Palace and Bangkhunphrom Palace.	Tilt of the palaces
Ground Surface Settlement point	Ground Surface	Ground Surface Settlement
Inclinometer	In the Diaphragm Wall	Lateral D-Wall movement
Piezometer	Outside the D-Wall	Ground water level

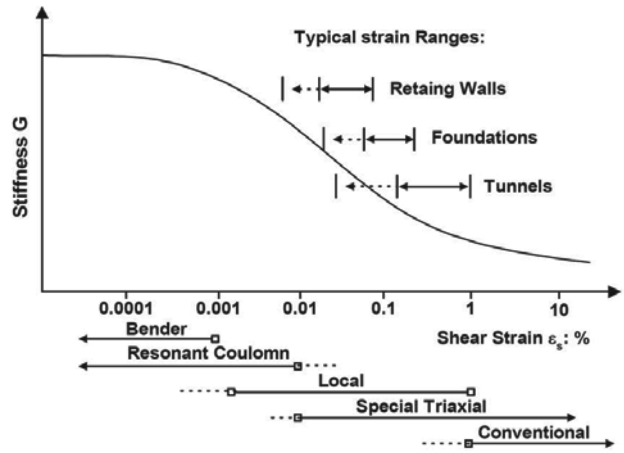

Figure 5. The relationship between modulus and shear strain level (Mair, 1993).

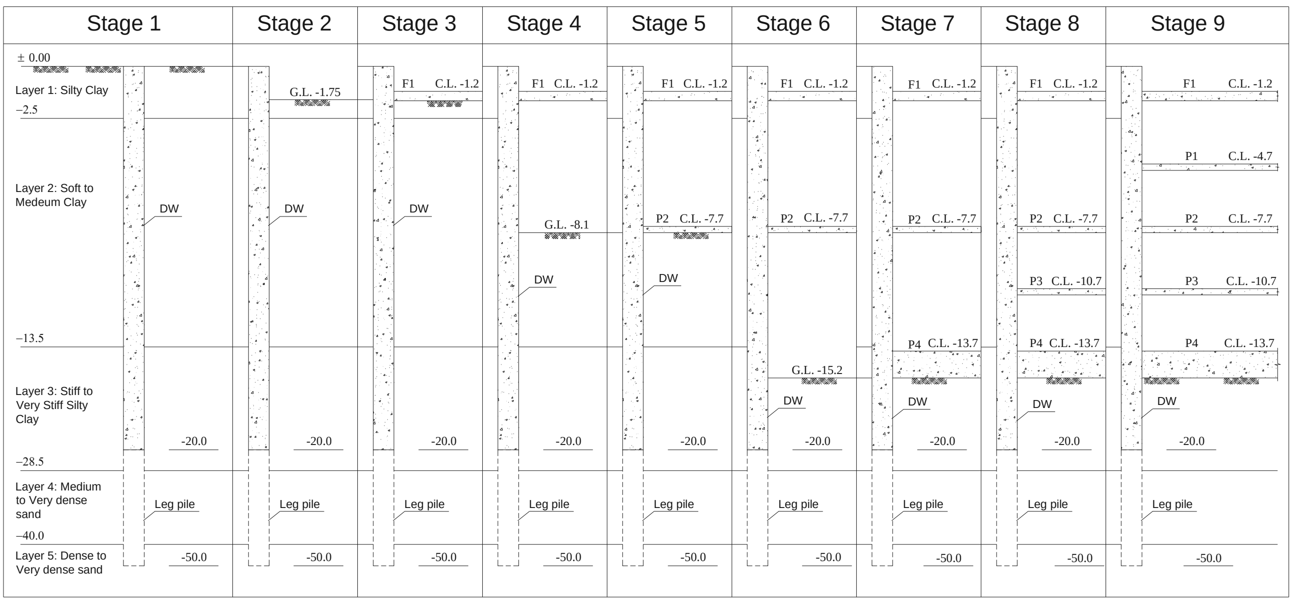

Figure 4. Detail of construction sequences.

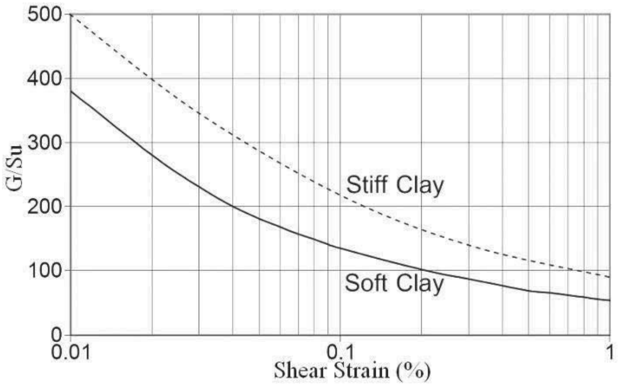

Figure 6. The relationship between modulus and shear strain level of soft and stiff Bangkok clay (Teparaksa, 1999b).

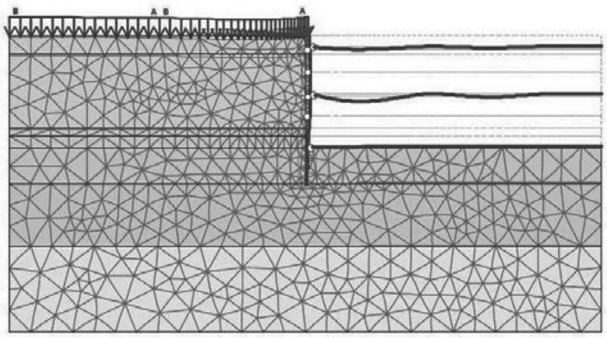

Figure 7. Deformed mesh of FEM analysis at the final stage excavation at -15.6m.

The measurement of the lateral diaphragm wall movement at all steps of excavation and basement floor casting at inclinometer no. I-3 next to Tewavej Palace is shown in Fig. 8 together with the predicted maximum envelope of diaphragm wall movement estimated by FEM.

It can be seen that the predicted wall movement by FEM agrees well with field performance. The tiltmeter measured at the Tewavej Palace is also less than the trigger level. The basement construction of the new head office of Bank of Thailand was completed without any disturbance to both Bangkhunphrom Palace and Tewavej Palace.

7 CONCLUSIONS

The basement of 15.6 m. deep excavation was constructed at the new head office of Bank of Thailand. The deep basement consists of 5 basement floors at -1.20 m., -4.70 m., -7.70 m., -10.70 m. and -13.70 m. depth. The basement constructed area is closed to two palaces; Bangkhunphrom Palace and Tewavej Palace, which are the historical buildings and also located close to the Chao Phraya river bank. The top down construction method was used for basement construction. The prediction of diaphragm wall movement and its effect to the palaces were carried out by FEM analysis. The instrumentation was installed in D-wall, ground surface and the palaces in order to measure the wall behavior and their effect. The lateral movement of D-wall by means of inclinometer at all stages of construction is compared with FEM prediction. The FEM prediction agrees well with measured values. The deep basement was completed without any disturbance to both palaces.

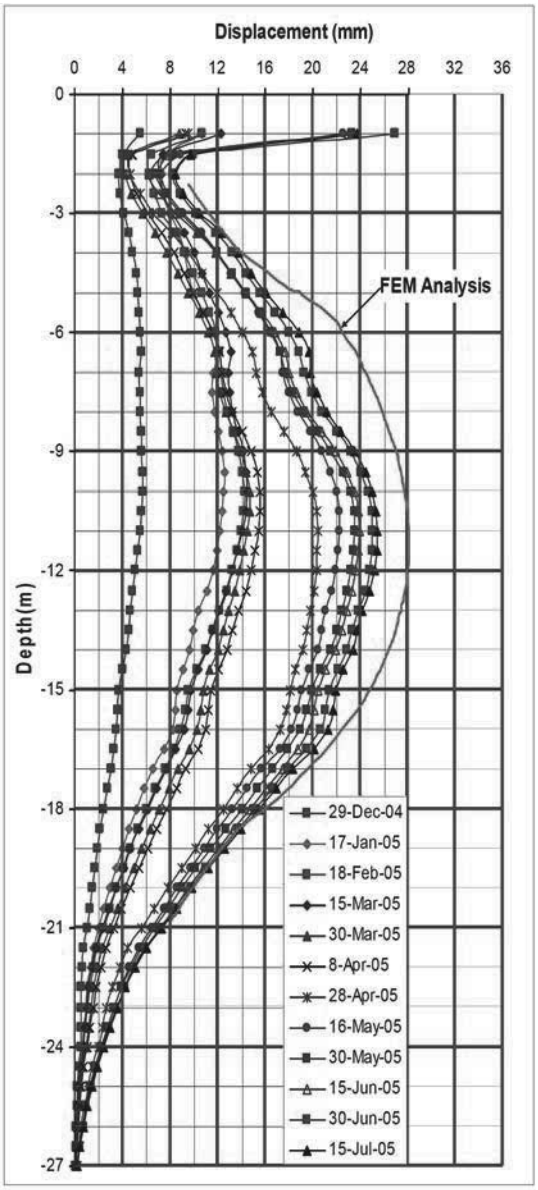

Figure 8. The inclinometer I-3 monitoring results with the predicted maximum movement by FEM analysis.

8 REFERENCES

Mair R.J. 1993. Unwin Memorial Lecture 1992 Developments in geotechnical engineering research: application totunnels and deep excavations. *Proceeding of the Institution of Civil Engineers. Civil Engineering.* Vol. 97, No. 1, 27-41.

Teparaksa W. 1992. Deep basement construction in Bangkok soft clay by sheet pile braced cut system. Journal of Engineering of Thailand. 97-106. (in Thai)

Teparaksa W., Thassananipan N. And Tanseng P. 1999a. Analysis of lateral movement for deep braced excavation in Bangkok subsoil. *Civil and Environmental Engineering Conference-New Frontier & Challengers, AIT, Bangkok.*

Teparaksa W. 1999b. Principal and application of instrument for the first MRTA Subway Project in Bangkok. *The 5th Int. Symposium on Field Measurement in Geomechanics.* Singapore. 411-416.

Teparaksa W. 2007. Deformation of subway tunnel induced by deep basement excavation in MRT Protection Zone, Bangkok. *Theme Speaker. 13th Asian Regional Conference in Soil Mechanics and Geotechnical Engineering*, Decrmber, Kalkate, India.

Creep and long-term bearing capacity of a long pile in clay

Fluage et capacité portante à long terme d'un long pieu dans de l'argile

Ter-Martirosyan Z.G., Ter-Martirosyan A.Z., Sidorov V.V.
Moscow State University of Civil Engineering, Moscow,Russia

ABSTRACT: A rheological equation is proposed to describe shear deformations in party saturated hardening-softening clay soil, based on modification of Maxwell rheological model. It is shown that the proposed equation describes creep, relaxation and kinematic shear with identical parameters, including decaying, stable and progressive creep, depending on shear stress intensity.

RÉSUMÉ : Une équation rhéologique est proposée pour décrire les distorsions au sein d'une argile partiellement saturée, avec durcissement et radoucissement, basée sur une modification du modèle rhéologique de Maxwell. Il est montré que l'équation proposée décrit le fluage, la relaxation et le cisaillement cinématique avec des paramètres identiques, y compris la diminution stable et progressive du fluage, en fonction de l'intensité de la contrainte de cisaillement.

KEYWORDS:long-time bearing capacity, hardening, softening, kinematic shear,stress relaxation, progressive creep.

1 INTRODUCTION

1.1 *Investigation of clay soils in shear [1…16] shows that rheological curves can be summarized for static loading ($\tau = const$) as creep curves (Fig.1, a); for kinematic loading ($\dot{\gamma} = const$, $\dot{\varepsilon}_1 = const$) as curves $\tau(t) = f(\dot{\gamma},\sigma)$ (Fig. 1, b); for given fixed strain value ($\gamma(0) = const$, $\tau(t) \neq const$) as relaxation curves $\tau(t) = f(\gamma_0,\sigma)$ (Fig. 1, c), with τ and σ as shear and compression stresses, γ and $\dot{\gamma}$ as shear strain and its rate, ν – as shear strain rate, t - time.*

In each case the curves are quantified as empirical dependencies, based on rheological models [1…16].

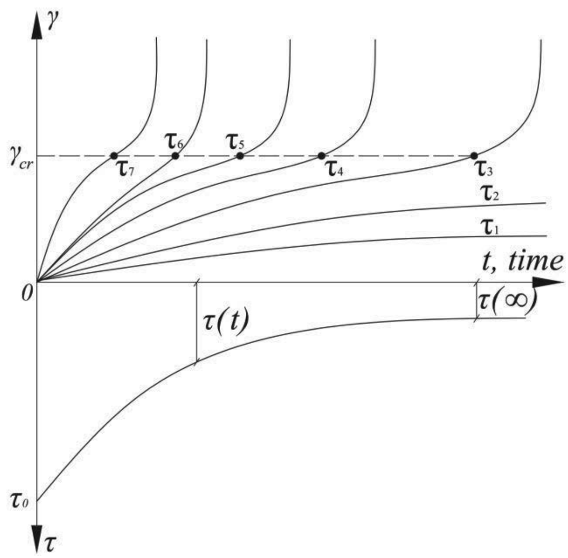

(a)

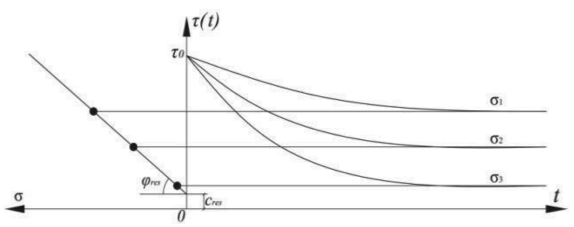

(b)

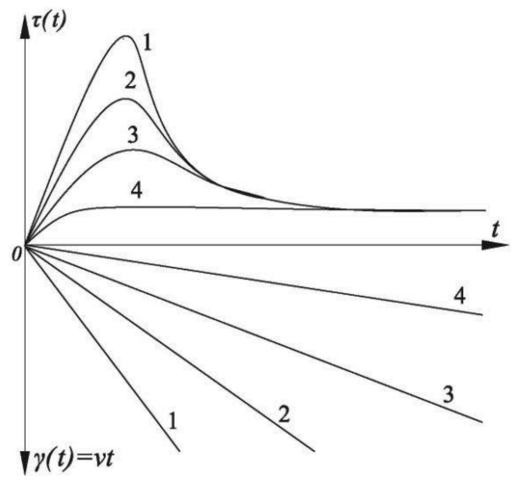

(c)

Fig.1. Rheological curves:

a) creep and long-term strength, ($\tau_1 < \tau_2 \ldots < \tau_7$ – critical values of τ in case of γ_{cr} = const);

b) shear stresses τ(t) for different shear rates $\dot{\gamma} = const$, and $\dot{\gamma}_1 > \dot{\gamma}_2 > \dot{\gamma}_3 > \dot{\gamma}_4$;

c) stress relaxation for different values of σ (right) and limit straight line of residual (long-term) shear strength (left)

The paper presents a rheological equation to describe shear deformations of clay soil with strong rheological properties and Maxwell rheological creep threshold τ^* for strengthening and softening, depending on accumulated shear strain (Fig. 2).

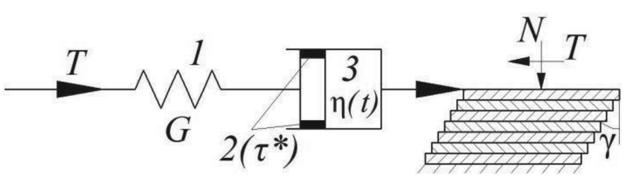

Fig. 2. Maxwell rheological model, having strengthening, softening and shear structural strength properties:
1 – elastic element, 2 – structural strength, 3 – viscous element.

The concept of simultaneous strengthening and softening of deforming clay soil was repeatedly stressed by S.S.Vyalov, M.N.Goldstein, G.I.Ter-Stepanayan, and it was also proved by experiments [1…5].

While summarizing these investigations S.S. Vyalov [1] emphasized that soil creep is accompanied by mutually opposite events of soil hardening and softening. If hardening dominates, then it leads to decreasing of deformations, if softening then it leads to failure. And he developed a kinematic theory of soil strength and creep, based on Ya.I.Frekel molecular theory of soil flow.

The equation below relates to the flow theory, in which strain rate isthe sum of elastic $\dot{\gamma}^{e}$ and visco-plastic $\dot{\gamma}^{vp}$ strain rates i.e., $\dot{\gamma}=\dot{\gamma}^{e}+\dot{\gamma}^{vp}$ where viscosity and cohesion variation rates versus time are taken into account:

$$\dot{\gamma}=\frac{\tau-\tau^{*}}{\eta(t)}\cdot\left(\frac{e^{\alpha\gamma}}{a}+\frac{e^{\beta\gamma}}{b}\right)+\frac{\dot{\tau}}{G} \qquad (1)$$

1.2 *witha ,b , α , β as strengthening and softening parameters, G as shear modulus; τ^{*} as creep threshold:*

$$\tau^{*}=\sigma\grave{}tg\varphi+c(t) \qquad (2)$$

with σ` as effective stress, c(t) as time dependent cohesion.

For triaxial compression eq. (1) looks similar if index i is added to all parameters that means transfer to strain ratesγ_i due to shear stresses τ_i , τ_i^{*} andσ`. Consider rheological processes on the basis of eq. (1) below.

2 CREEP AND LONG-TERM STRENGTH

Analysis of eq. (1) with constant cohesion ratio ($c(t)=const$) and volume deformation showed that at flexure points of creep curves (see Fig.1 a, top portion) the critical values of γ_{cr} , based on condition $\ddot{\gamma}=0$, are constant and are described by equations as

$$\gamma cr=\frac{1}{\alpha+\beta}\ln\frac{a\beta}{\alpha b}=const \qquad (3)$$

with respective stresses $\tau_{cr}(\gamma_{cr})$ depend on applied τ и γ_{cr}, i.e., $\tau_{cr}=f(\tau,\gamma_{cr})$, $t_{cr}=f(\tau,\gamma_{cr})$.

The creep curve flexure time point t_n can be determined from the curve (see Fig. 1) i.e., from the crossing points of lines $\gamma(t)$ and γ_{cr}=const. Hence, each τ corresponds to τ_{cr} and t_{cr}.Thus, (1) and (3), based on parameters of creep curves, yield long-term strength curve $\tau_n(t_n)$, using parameters τ_0 and τ_∞ (see Fig. 1a, bottom part).

Eq. (1) can be used for analyzing laboratory test data. In order to describe creep in soil mass asin (1) the following equation can be applied:

$$\dot{\gamma}=\frac{\tau-\tau^{*}}{\eta}\left(\frac{e^{\alpha_1 t}}{a_1}+\frac{e^{-\beta_1 t}}{b_1}\right)+\frac{\dot{\tau}}{G} \qquad (4)$$

If $\tau=const$:

$$\dot{\gamma}=\frac{\tau-\tau^{*}}{\eta}\left(\frac{e^{\alpha_1 t}}{a_1}+\frac{e^{-\beta_1 t}}{b_1}\right) \qquad (5)$$

Solution (5) can be expressed as follows:

$$\gamma(t)=\frac{\tau-\tau^{*}}{\eta}\left(\frac{e^{\alpha_1 t}}{\alpha_1 a_1}-\frac{e^{-\beta_1 t}}{\beta_1 b_1}\right) \qquad (6)$$

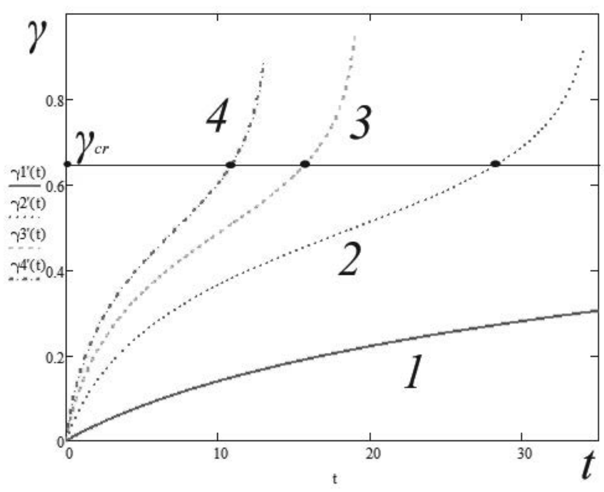

Fig. 3. Curves γ (in decimals) and$t$ (in hours) for clay soil with different values of tangential stresses in simple shear conditions, according to eq. (1) with known parameters α,β, a, b и η and $\tau>\tau^{*}$, $\tau_1<\tau_2<\tau_3<\tau_4$

Calculation as per (5) demonstrates that dependence $\gamma(t)$ features double curvature same as in case (1) i.e., depending on the level of stress τ , and parameters a_1 ,b_1 , α_1 , β_1 that depict decaying, non-decaying and progressive creep (Fig. 3). Such result is due to the difference of exponential functions in brackets in eq. (4), the first of which describes strengthening while the second relates to softening.

Eqs. (1) and(5) are identical, as they give the same results.In order to apply eq. (5) for solving boundary problems it is necessary to determine parameters a_1 ,b_1, α_1, β_1 from experiments that can differ from parameters in Eq.(1).

3 KINEMATIC SHEAR

Soil sample deviator loading is a broadly applied triaxial test, following hydrostatic compression with constant axial deformation rate $\dot{\varepsilon}_1=const$. In simple shear (distortion) under kinematic loading ($\dot{\gamma}=const$) eq. (1) with $\dot{\gamma}=const$ looks, as follows:

$$\dot{\gamma}=\frac{\tau-\tau^{*}}{\eta}\left(\frac{e^{\alpha v t}}{a}+\frac{e^{-\beta v t}}{b}\right)+\frac{\dot{\tau}}{G} \qquad (7)$$

with$v$ as angular strain rate $\dot{\gamma}=v=const$

We obtain from eq. (7)

$$\dot{\tau}+\frac{\tau G}{\eta}\left(\frac{e^{\alpha v t}}{a}+\frac{e^{-\beta v t}}{b}\right)=v\eta G+\frac{\tau^{*}G}{\eta}\left(\frac{e^{\alpha v t}}{a}+\frac{e^{-\beta v t}}{b}\right) \qquad (8)$$

Solution of this differential equation, obtained numerically with the help of MathCad software for various shear strain values $\dot{\gamma}_1,\dot{\gamma}_2...\dot{\gamma}_n$, enablesplotting a family of curves $\tau(t)$ - γ (Fig. 4). The calculations showed that they haveextreme points at characteristic time t^{cr} =const and acommon asymptote. It is obvious thatfrom those curves wecan plotcurves $\tau_{max}(\sigma)$ и $\tau_{min}(\sigma)$ in case of $\dot{\gamma}=const$.

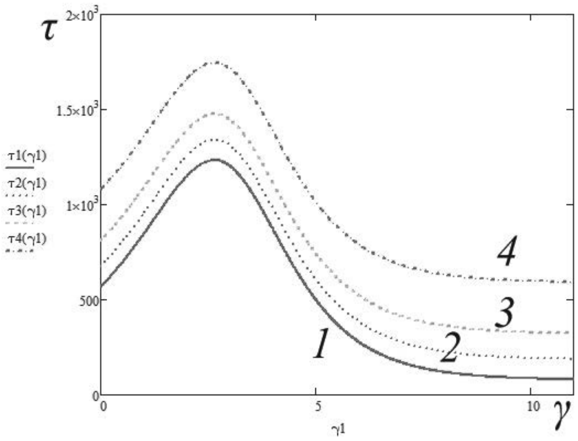

Fig. 4. Curves of τ (kPa), depending on γ *(%)*, in kinematic loading $\dot{\gamma} = const$ at various values of compacting loading σ (7) and $\sigma_1 > \sigma_2 > \sigma_3 > \sigma_4$

4 STRESS RELAXATION

Equation (1) demonstrates a stress relaxation process for $\dot{\gamma} = 0$ i.e., with $\gamma(t) = \gamma(0) = const$ and with initial $\tau(0) = \tau_0 > \tau^*$ and $\tau(t) \neq const$. Solution (1) in this case looks, as follows:

$$\tau(t) = \tau_{\text{res}}\left(1 - e^{-At}\right) + \tau_0 e^{-At} \tag{9}$$

with $$A = \frac{G}{\eta}\left(\frac{e^{\alpha\gamma_0}}{a} + \frac{e^{-\beta\gamma_0}}{b}\right),\ \tau_{res} = f(\sigma) \tag{10}$$

τ_{res}as residual strength

Let us determine the limit curve of residual strength from relaxation curves for different values of compressive stresses σ (see Fig.1, c, on the left side).

5 SOME PROBLEMS OF APPLIED SOIL MECHANICS

The problem of a pile interaction with rheological soil can be reduced to determining regularities of constant force N distribution between side resistance and bottom resistance (fig.5) and $N = R(t) + T(t)$

with $N = \pi a_0^2 p_i$, $T = 2\pi a_0^2 l$, $R = \pi a_0^2 p_2$, a_0, $b_0$as pileradius and pile influence area; l as pile length, p_1, p_2 as stresses at pile head and under its tip respectively.

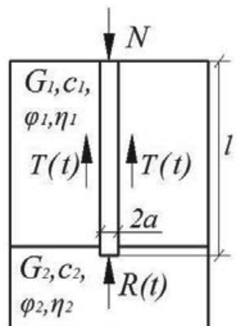

Fig.5 Principal schematic of interaction between pile and 2-layer soil massive, where G, φ, c и η are parameters of deformation, strength and viscosity respectively

In order to solve this problem the pile settlements, caused by forces $T(t)$ and $R(t)$, shall be calculated and then related to the pile deformation modulus E_p that is much greater than the surrounding soil modulus E_s i.e., $E_p >> E_s$. Consider various cases of bi-layer soil with upper layer, having viscoelastic properties as in eq. (4) while the lower one being elastic, viscoelastic, elastic-plastic and viscous.

5.1*Linear deforming soil under pile tip*

Let us determine pile settlement rate due to friction $T(t)$ from solution, based on the assumption for the shear mechanism of soil displacement around pile with volume deformations being neglected [11]. For $\tau^* = 0$

$$\dot{S}_T = \frac{a\tau_a}{\eta_1(t)}\ln(b_0/a_0) + \frac{a_0\dot{\tau}_a}{G_1(t)}\ln(b_0/a_0) \tag{12}$$

with $\tau_a = T/2\pi al$ and $\dot{S}_T$ as pile settlement rate. $\dot{\tau}_a$ - rate of changing τ_a

$$\eta_1(t) = \eta_1 \Big/ \left(\frac{e^{\alpha_1 t}}{a_1} + \frac{e^{\beta_1 t}}{b_1}\right) \tag{13}$$

The rate of settlement, generated by force $R(t)$ is also determined from solution for a circular stiff plate, pressed in elastic medium

$$\dot{S}_T = \dot{p}_2 \frac{\pi a_0(1-\nu_2)K_1}{4G_2} \tag{14}$$

With $K(l) \leq 1$ as coefficient, accounting for the depth of load application to the plate; p_2 и $\dot{p}_2$ - applied stress and rate of its changing.

By comparing eq. (12) and eq. (14) with the account of eq. (11) we obtain:

$$\frac{a_0^2(p_1 - p_2)}{2l\eta_1(t)}\ln(b_0/a_0) - \dot{p}_2\frac{a_0^2\ln(b_0/a_0)}{2lG_1} = \dot{p}_2\frac{\pi a\left(1-\nu^2\right)K_1}{4G_2} \tag{15}$$

After some transformations we get the following differential equation:

$$\dot{p}_2 + p_2 P(t) = p_1 Q(t) \tag{16}$$

with

$$P(t) = \frac{B(t)}{A},\ Q(t) = \frac{D(t)}{A};\ A = \frac{\pi\left(1-\nu^2\right)K_1}{4G_2} + \frac{a_0}{2l}\frac{\ln(b_0/a_0)}{G_1};$$

$$B(t) = \frac{a_0}{2l}\frac{\ln(b_0/a_0)}{\eta_1(t)};\ D(t) = \frac{a_0}{2l}\frac{p_1\ln(b_0/a_0)}{\eta_1(t)} \tag{17}$$

Solution (16) for initial condition $p_2(0) = 0$, obtained with the help of MathCad software, yielded that p_2 varies versus time with different rates and tends to constant values (Fig. 6). The pile settlement is also determined from eq, (14), by introducing $p_2(t)$ instead of $\dot{p}_2(t)$.

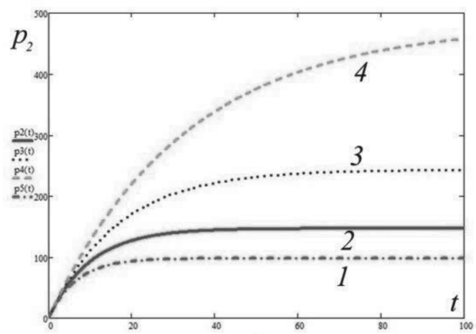

(a)

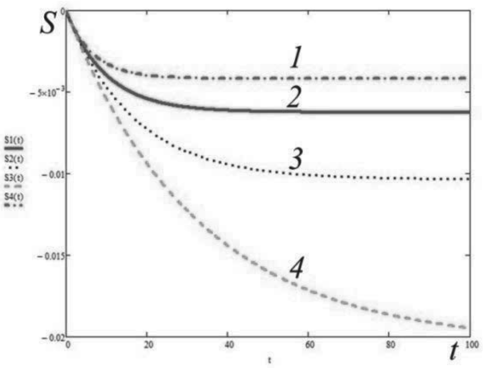

(b)

Fig. 6. Here $p_2(t)$ (kPa) - t (hours)(a) and *s(*in meters*)* (b) curves from (16) and (14) respectively with input parameters from (15)

5.2*Elasto-plastic bed under pile tip*

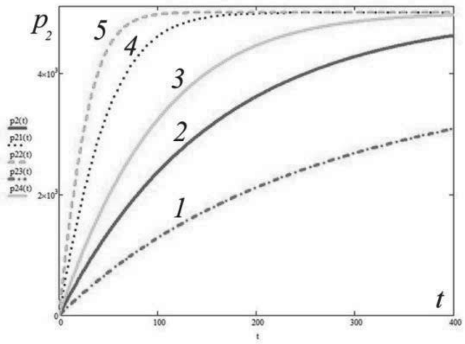

(a)

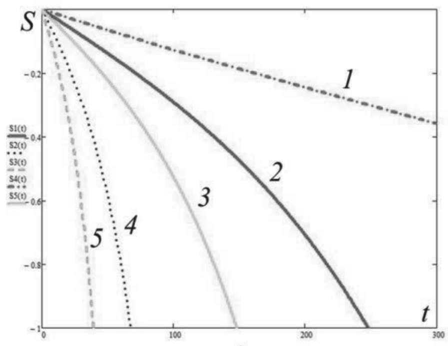

(b)

Fig. 7.p_2(kPa) - t (hours) (a) according (19) and *s(meters) - t(hours)* (b) according (18) plots for different viscosity and elasticity parameters of soil around pile and different elasto-plastic parameters of soil under pile tip.

The settlement rate of soils under pile tip is roughly approximated as:

$$\dot{S}_r = \dot{p}_2 \frac{\pi a(1-\nu_2)}{4G_2} \frac{p_2^*}{p_2^* - p_2} \quad (18)$$

With p_2^* as limit load on soil bed, determined from known solutions [11].

Eq. (1) yields that $p_2 \rightarrow p_2^*$ if $\dot{S} \rightarrow \infty$

Comparison ofeqs. (4) and (18) according (11) yields a differential equation versus p_2:

$$\frac{a_0^2(p_1 - p_2)}{2l\eta_1(t)} \ln(b_0/a_0) - \dot{p}_2 \frac{a_0^2 \ln(b_0/a_0)}{2lG_1} = \dot{p}_2 \frac{\pi a(1-\nu^2)}{4G_2} \frac{p_2^*}{p_2^* - p_2} \quad (19)$$

Analysis of solution (19) showed that p_2 decays versus time at different rates and tends to constant values (Fig. 7) while the settlement can decay or not decay, depending on the intensity of applied load $p_1 = N/\pi a^2$ (Fig. 7b).

6 CONCLUSIONS

1. A rheological equation is proposed to describe soil shear, based on the modified Maxwell model, having clay strengthening and softening parameters.
2. Analysis of the equations has shown that for the case of constant loading it describes decaying, non-decaying and progressing soil creep as well as stress and shear strain relaxation processes in kinematic loading mode.
3. In the pile-soil interaction problem solution the distribution of applied force between the side surface and the lower tip is time-related, and it can result either in decaying or in non-decaying pile settlements, depending on the parameters of soil around the pile and under its tip.

7 REFERENCES

Vyalov S.S. 1978. Rheological bases of soil mechanics.[in Russian], Vysshajashkola, Moscow.

ZaretskiyYu.K. 1988. Visco-elastic behavior of soil and calculations of structurers. [in Russian], Stroiizdat, Moscow.

Osipov V.I. 1979. Nature of strength of clay soil.[in Russian] Moscow State University, Moscow.

Ter-Martirosyan Z.G. 2010.Soil Mechanics. [in Russian], ASV, Moscow.

Ter-Martirosyan A.Z. 2010. Interaction between foundations and rheological soil under cyclic and vibration loads.[in Russian] *Author's abstract of dissertation for Ph.D. degree*, Moscow.

Skempton A.W. 1964. Long-term stability of clay slopes. "Geotechnique".Vol. 14.- №2. - P.p. 77-101.

Murajama S. and Sibata T.1961.Reological properties of clay. // Proc. 5-th ICSMFE. Paris, Vol. I. - P.p. 269-173.

Compressive resistance of piles, an update

Résistance à la compression des pieux, une mise à jour

Tol van A.F.[1,2], Stoevelaar R.[1], Bezuijen A.[1,3]
[1]Deltares; [2]Delft University of Technology, Netherlands; [3]Ghent University, Ghent, Belgium.

Jansen H.L.
Fugro Geoservices,Netherlands

Hannink G.
Engineering Consultancy Division, City of Rotterdam, Netherlands

ABSTRACT: The research consortium Delft Cluster/CUR recently published the results of a study of axial pile capacities. It emerged that the capacity of displacement piles calculated using the Dutch method considerably overestimates the actual capacity measured in static pile load tests. The identification and quantification of any concealed safety factor is a possible way of preventing the reduction of the pile capacity factors that could follow from the test results at least in part. This paper presents the results of a study of concealed safety factors. The conclusion of the study is that it is useful to examine time effects in greater detail, primarily focusing on the quantification of the effect and the determination of the impact of load variations. It is recommended to continue with research into the impact of compaction on pile-base capacity in combination with the sequencing of installation of displacement piles.

RÉSUMÉ: Le consortium de recherche Delft Cluster/CUR a récemment publié les résultats d'une étude sur la capacité axiale des pieux. Il est apparu que la capacité des pieux de déplacement calculée à l'aide de la méthode néerlandaise surestime considérablement la capacité réelle mesurée lors des essais de chargement statique. L'identification et la quantification des facteurs de sécurité cachés est un moyen de prévenir la réduction des facteurs de capacité dans la méthode NEN, du moins en partie. Cet article examine les résultats d'une étude des facteurs de sécurité cachés. La conclusion de l'étude est qu'il est utile d'examiner les effets du temps plus en détail, en se concentrant principalement sur la quantification de l'effet et la détermination de l'impact des variations de charge. En outre, nous recommandons la poursuite des recherches sur l'impact de la compaction sur la capacité de la base du pieu en combinaison avec le séquençage de l'installation de pieux de déplacement.

KEYWORDS: pile capacity, displacement pile, set-up, group effect.

1 INTRODUCTION

Research looking at the axial capacity of foundation piles (van Tol et al., 2010) has shown that calculating the capacity using the method set out in the Dutch standard (NEN 9997-1, 2012) results in a considerable overestimation of the capacity as compared to measurements in load tests. The study referred to properly equipped load tests conducted in France, Belgium and the Netherlands in which it was possible to distinguish between pile-base capacity and shaft capacity. It emerged that adequate tests for the reliable validation of the design rules (French, Belgian and Dutch) were available only for driven, soil-displacement, prefabricated piles (concrete and close-ended tubular piles). Calculations of the shaft capacity in accordance with the NEN standards proved to be a good match for the values generated by load tests, although the coefficient of variation is large at approximately 30%. The measured pile-base capacities, however, proved on average to be only 70% of the predicted values. The overestimation of capacity increased with the depth driven in the sand, see Figure 1. Piles located at a depth of more than 8 D in the sand layer were found to have a pile base capacity of 60% of the predicted value.

Since the capacity calculation is too optimistic, and since no failures have been observed in practice, it is thought that there must be concealed safety factors in the system. The identification and quantification of those factors may prevent a future reduction of the installation factors in the Dutch standard in whole or in part.

This paper will focus primarily on the results of the literature study looking at concealed safety factors. It will discuss the following areas: *i* the improvement in capacity over time *ii* residual stresses in the pile *iii* limit values *iv* group effects and *v* wind load in relation to negative skin friction.

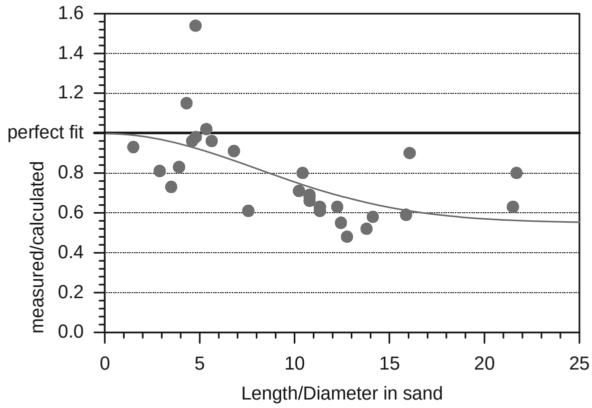

Figure 1. Comparison of measured and calculated pile-base capacities as a function of penetration in the sand (Stoevelaar et al. 2011).

2 IMPROVEMENT OF CAPACITY IN TIME

Extensive research has been conducted into the increase of pile capacity over time. In the past, it was mainly thought that this phenomenon was a factor related to piles in clay, but it has also emerged that the capacity of piles in sand increases with time. Most research involved steel tubular piles and the load tests were usually conducted under tension loading. Axelsson (2000) conducted a study of time effects in prefabricated concrete piles loaded in compression. This study will be discussed further here.

In predominantly silty sand, an instrumented prefabricated concrete pile with a cross-section of 235 x 235 mm was driven to a depth of 13 m below ground level. The pile was equipped with a pressure sensor at the pile base, and pressure sensors at the shaft. Static load tests were conducted 1, 5, 8, 141 and 667 days after the installation of the pile. Figure 2 shows the load-displacement curves for the load tests. This shows that the total capacity of the pile increases substantially over time. The increase in the pile-base capacity is at maximum approximately 10%. The increase in capacity is therefore mainly caused by an increase in the shaft capacity.

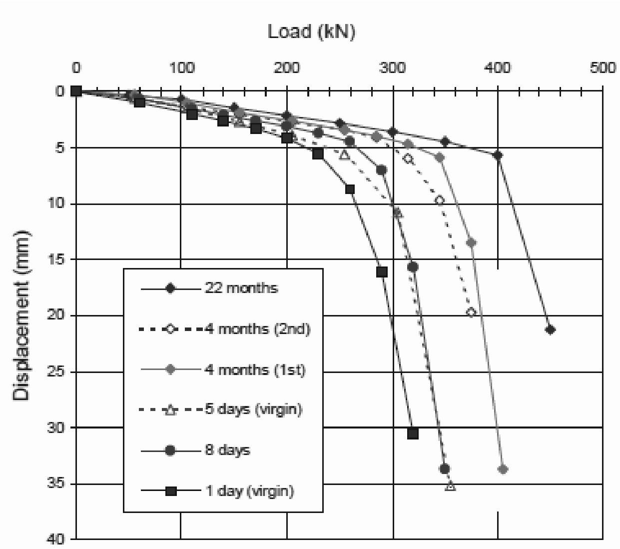

Figure 2. Head displacement, static tests, Axelsson (2000)

This is confirmed by the horizontal effective stress on the pile shaft. A distinction is made between the horizontal stress on the pile in loaded and unloaded conditions. The difference between the contact pressure in loaded and unloaded conditions is caused by dilatant behaviour. The increase over time of the horizontal stress during loading is primarily a result of increasing dilatant behaviour, which indicates a change in particle structure where the pile and the soil meet (Axelsson, 2000).

The increase in capacity over time is expressed by a range of authors as an increase with the logarithm of time in line with the equation below (Skov and Denver, 1988):

$$Q_t = Q_0\left(1 + A.\log_{10}\frac{t}{t_0}\right) \quad (1)$$

Where:
Q_t is the pile capacity at time t
Q_0 is the pile capacity at t_0
A is a factor – dependent of the type of soil
t_0 is the time for Q_0

The values for A used in the literature for clay and sand respectively are 0.6 and 0.2. This means that capacity increases by 60% per decade in clay and by 20% in sand. The lower limit generally used for piles in sand is 15%. However, Axelsson's study stated a much higher value of A=37.5% for a driven concrete pile in silty sand, see Figure 3.

The literature relating to set-up, the usual term for the phenomenon of increasing capacity over time, shows that the following factors are important in determining the set-up level (Axelsson, 2000; Sobolewsky; 1995, Chow & Jardine, 1997; Joshi et al., 1995; Baxter & Mitchell, 2004):

- Relative density and stiffness of the soil: set-up increases with density
- Particle-size distribution: set-up in silty sand is higher than in coarser sand
- Particle strength: set-up is higher in strong sands
- Particle structure and form: angular particles result in higher set-up
- Soil humidity: very high set-up is observed in unsaturated sand
- Stress level: at high stress levels, dilatant behaviour is a more significant factor
- Installation process determines the stress conditions after installation and therefore set-up
- Diameter of pile: higher set-up with smaller diameter

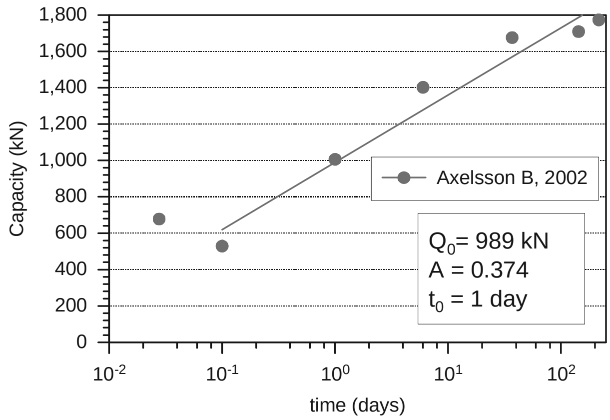

Figure 3. Measurements from Axelsson, 2000, fitted with equation (1)

Before the positive effect of time can be included in the regulations, the most important of these factors will have to be investigated. Another important question is the extent to which the increase in capacity persists after varying loads have been imposed. A study by Jardine et al. (2006) demonstrated that the repeated testing of piles in sand resulted in lower capacity measurements than tests on piles that have not been subjected to loads in the past. Tensile capacity in repeat testing approximates the trend line of Chow at al. (1997) which corresponds, according to their findings, with A is approximately 27.5%.

Subsequent research will, then, have to take this into account, as well as the effects of varying loads.

3 RESIDUAL STRESSES

In loading tests with driven piles, the strain gauges used to measure the forces in the pile are normally reset to 0 after the installation of the pile or installed as a string of gauges cemented into a tube in the pile, also after installation. That means that any residual stresses present in the pile base (after pile-driving) are not included in the measurement of the base capacity in pile load tests. This could explain why the pile-base capacity in the load tests was low (and lower than the value resulting from the design rule). However, any increase in the base capacity resulting from this consideration will be at the expense of the shaft capacity.

Xu et al. (2008) showed that the residual stress at the pile base is negligible in the case of piles when penetration is less than 20D; substantial residual stresses occur only when the driven depth exceeds 30D in the load-bearing layer. This phenomenon does not therefore explain the low pile-base resistance as shown in Figure 1, where the penetration depth of all the piles is less than 25D.

4 LIMITING – LIMIT VALUES

Another explanation for the lack of problems with the capacity of driven piles in practice could therefore be that the limit values prescribed in the Dutch standard (15 MPa for pile-base resistance and 150 kPa for shaft resistance) are too conservative. On the basis of a comparison between foreign standards and research looking at measured pile-base stresses in sand layers with very high cone resistances, it can be concluded that:

- The literature that was examined confirms the current limit value for base resistance (API, 2007; Foray et al., 1998).
- The limit value for shaft friction seems to be on the low side. Higher shaft resistances have been measured and also approved in other, foreign, standards (Foray et al., 1998; Bustamente et al., 2009).

5 GROUP EFFECTS

Group effects include both the effect of the installation and the consequences of the higher load in the ground as a result of the loading of the piles. Both effects are taken into account when calculating the capacity of tensile piles according to the Dutch standard. The installation effect of soil-displacement piles with factor f1 and the effect of the load (in the case of tensile piles, this is a negative effect) with factor f2.

Factor f1 (NEN 9997-1, 2012) is determined by converting the volume of the piles into compaction combined with an empirical relationship that, at a constant vertical stress, links density to cone resistance qc.

Factor f1 is the ratio of increased to initial qc, and it is included in the Dutch standard calculation method of the shaft capacity of a tensile pile. In principle, this factor should also be included when calculating the compressive shaft capacity of jacked or driven piles. It is under discussion whether compaction also occurs to this extent below the level of the pile base and to what depth, and therefore whether this factor can be included in the calculation of the pile-base capacity. For this purpose, the depth to which compaction extends must be determined, as must the effect of the pile-driving sequencing. Upward pile movement has been noted during the driving of piles close to piles that have already been installed; the piles in place move upward. This could have a negative effect on the pile-base capacity.

The compaction factor f1 determined as described above may result in a considerable increase in cone resistance and consequently of shaft capacity.

Figure 4 shows, for a symmetric pile field, factor f1 as a function of the centre-to-centre distance between the piles. For a symmetrical pile field with a centre-to-centre distance s of, for example, 4Deq, f1 is approximately 1.5, with a small variation due to differences in initial density. The compaction percentage expressed as pile surface to total surface is 5% here, which is not an extreme value.

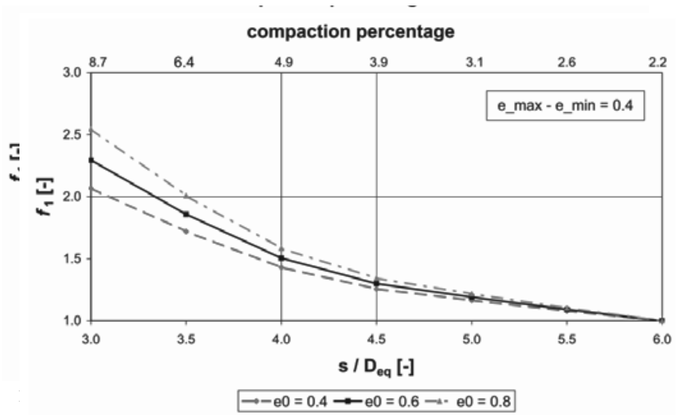

Figure 4. Compaction factor f_1 for a pile in a symmetrical pile field

The densification was checked in several projects by conducting CPTs before and after the installation of the displacement piles, (van Tol & Everts, 2003). It emerged that the value f1, as determined in NEN 9997-1 (2012) is a safe estimate of the installation effect; the compaction found in practice is usually higher than the predicted value. This is advisable in a design guideline, particularly because any over-estimate of the effect will only be noticed during the execution of the work, with all the associated consequences.

It should be pointed out that the actual installation effect with soil-displacement (driven) piles is much more complex than in an approach complying with NEN 9997-1 (2012).

- In addition to compaction, there is also an increase of stresses. If the initial density is already high, the increase of stresses will actually be dominant with respect to compaction.
- Not the full volume of the pile is involved in compaction; soil is also moved upwards.
- In the immediate vicinity of the pile shaft, in stead of compaction there is also dilatant behaviour. However, in the immediate vicinity of the shaft, there may also be relaxation, which is known as “friction fatigue” as a result of the up-and-down movement of the shaft during the pile-driving.
- Particularly in dense sands, crushing occurs, and the increase of stresses is therefore limited.

The conclusion with respect to the group effect is that, in principle, the compaction factor f1 can also be used for driven piles loaded in compression.

The following, more specific, topics must therefore be studied in more detail related to the factor f1:

- Does f1 also apply to the pile-base capacity and, if so, down to what depth below the pile base does compaction occur and what role is played by pile-driving sequencing?
- Does f1 also apply to small, highly compact, groups of piles?
- Is the value of f1 affected by the properties of the sand such as particle-size distribution, form, strength and the silt concentration?

6 WIND LOAD AND NEGATIVE SKIN FRICTION

In the current design approach, wind load is transferred to the load-bearing sand layer. In the western part of the Netherlands, where the Pleistocene sand is covered by a thick layer of Holocene clay and peat layers, piles are subjected to negative skin friction. The loads generated by negative skin friction can be very considerable, rising to more than 30% of the total pile load. Wind load is another major, temporary, component of the total load, particularly in the case of high-rise buildings. In the case of piles in which negative skin friction is fully developed, wind load will initially result in the pile being pushed downwards, decreasing the amount of negative skin friction. A number of calculations have been conducted for this phenomenon using an interaction model. Figure 5 shows a calculated result for the fluctuation of forces in a pile shaft, first when the pile is subjected only to a permanent load of 1000 kN and 550 kN negative skin friction. Then there is an additional temporary wind load of 600 kN. Negative skin friction drops from 550 to 300kN. In other words, (550-300) / 600 = approximately 40% of the wind load is transferred to the upper Holocene layers.

This factor can therefore certainly not be neglected and, in this case, represents a concealed safety factor in current design practice.

However, it should be kept in mind that wind load makes a significant contribution only when the height of the building exceeds 40 m. The contribution in the total load in that case is approximately 10% (so much smaller than in the example of figure 5). This means that the wind load transferred to the upper layers is therefore only a concealed safety factor in specific conditions of high buildings.

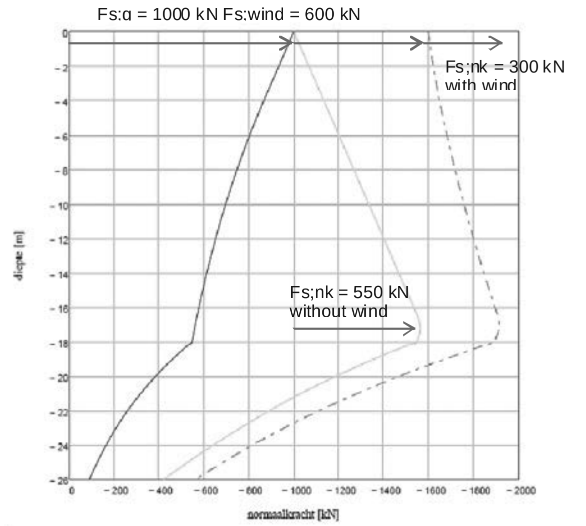

Figure 5. Normal forces as function of depth and a wind load of 600 kN

7 CONCLUSIONS AND FOLLOW-UP

The conclusion of the study of concealed safety factors is that the time effects and the pile group effects are the two effects most likely to contribute to concealed safety. It will therefore be useful to look at time effects more closely. The primary focus should be on quantifying and understanding the effect, determining the impact of load variations and identifying the applicable limitations. Furthermore, it is recommended to continue with research into pile group effects of displacement piles: the impact of compaction, focusing in particular on the impact on pile-base capacity in combination with the sequencing of installation.

7.1 Pilot tests in geotechnical centrifuge

The follow-up research will include pilot testing in a geotechnical centrifuge looking at concealed safety factors. This test will look at the time and the group effect. The design of this pilot test will focus primarily on determining whether the phenomena in question can be studied in the centrifuge. It is generally thought that creep (the process underlying set-up) cannot be modeled in a centrifuge because time cannot be scaled during testing. However, longer centrifuge testing can lead to the determination of the size of factor A in equation 1. If this is the case, research can be conducted in the centrifuge, precluding the need for more expensive field studies and allowing controlled conditions.

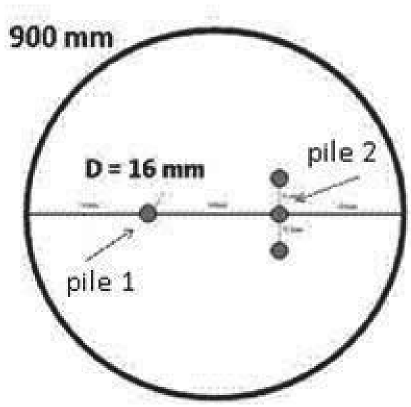

Figure 6. Centrifuge test design, test piles with a diameter of 16 mm in a 900 mm diameter container.

The test set-up is shown in Figure 6. Two instrumented test piles will be installed in a single sample preparation in the container, one single pile and a pile in a group of 3 piles. The two test piles and the other piles in the group will be installed in flight. To study the time effect, pile1 will be test loaded at 1, 10, 100 and 1000 minutes after installation. Then pile 2 will be loaded in the group using the same time schedule. The centrifuge will continue to operate from the start of the installation until the final load test.

8 REFERENCES

Axelsson, G. 2000. *Long-Term Set-up of Driven Piles in Sand.* Div. of Soil an Rock Mechanics. Dep. of Civil and Environmental Engineering. Stockholm, Royal Institute of Technology.

API 2007. Recommendations RP-2A-WSD

Baxter C.D.P. & Mitchell, J.K. 2004. Experimental study on the ageing of sand. *J. of Geotechnical and Environmental Engineering* 130 (10); 1051-1062.

Bustamente, M., Gambin, M. & Gianeselli, L. 2009. Pile design at failure using Menard pressuremeter; an update. *ASCE Geotechnical special publication* (GSP 186), 127-134.

Chow, F., Jardine, R.J., Nauroy, J.F., Brucy, F. 1997. Time related increases in the shaft capacities of driven piles in sand. *Geotechnique* 47 No2.: 353-361.

CUR 2010. CUR 229: *Axiaal draagvermogen van palen*. Gouda.

Foray, P.L., Balachowski & Colliat, J.L. 1998. Bearing capacity of model piles driven into dense overconsolidated sands. *Can. Geotechn. J.* 35 374-385.

Jardine, R.J., Chow, F. C., & Standing J.R. 2006. Some observations of the effects of time on the capacity of Piles driven in Sand. *Geotechnique* 56 no 4: 227-224.

Joshi, R.C., Gopal Achari, Shenbaga Kaniraj, R. Wijeweera, H. 1995. Effect of ageing on penetration resistance of sands, *Can. Geotechn. J.* 325: 767-782.

NEN-9997-1, 2012, *Geotechnical design of structures,- Part 1: General rules*, NEN, Delft

Skov, R. and Denver, H. 1988. Time-dependence of bearing capacity of piles. *Proc. 3rd. Int. Conf.on Application of Stress-wave Theory to Piles*, Ottawa, Canada.

Sobolewsky, D.Y. 1995. *Strength of dilating soil and load-holding capacity of deep foundations*. Rotterdam, A.A. Balkema, ISBN 90 5410 164 4.

Stoevelaar, R, Bezuijen, A., Lottum, H. van & Tol, A.F. van. 2011. Effects of crushing on point bearing capacity in sand tested in a geotechnical centrifuge. *15th European Conf. ISSMGE Athens*.

Van Tol, A.F., Stoevelaar, R. and Rietdijk, J. 2010. Draagvermogen van geheide palen in internationale context. *Geotechniek* december.

Van Tol, A.F. and Everts, H.J. (2003). New foundation technology - The limits of driving prefabricated concrete piles. In I. Vanicek & R. Barvinek (Eds.), *Geotechnical Problems with man-made and man influenced grounds* (pp. 503-510). Praag: The Czech Geotechnical Society CICE.

Xu, X., Schneider, J.A.& Lehane, B.M. 2008. Cone penetration test CPT methods for end-bearing assesment of open- and closed-ended driven piles in siliceous sand. *Can. Geotech. J.* 45: 1130.

A design verification method for pile foundations used in combination with solidified improved columns

Une méthode de vérification de la conception des pieux en combinant avec des colonnes de sol améliorés

Tomisawa K.
International member, Civil Engineering Research Institute for Cold Region

Miura S.
International member, Hokkaido University Graduate School of Engineering

ABSTRACT: In this study, research and development were conducted on a method of forming composite ground around piles mainly with solidified improved columns and reflecting the increased shear strength in pile design to support progress with a new foundation type for application in soft ground. The use of this approach, which is referred to as the composite ground pile foundation method, in line with site conditions is expected to reduce construction costs and improve the earthquake resistance of foundations. To systematize the technique, the study examined a design verification method based on the results of a large-scale model experiment.

RÉSUMÉ : Dans cette étude, une méthode de l'amélioration du sol autour des pieux à l'aide des colonnes solidifiées améliorées a été développée. L'effet de l'augmentation de la résistance au cisaillement dans la conception des pieux a été étudié pour un nouveau système de fondation dans les sols mous. L'utilisation de cette approche, appelé la méthode fondation composite, avec les conditions du site devrait permettre de réduire les coûts de construction et d'améliorer la résistance au séisme des fondations. Afin de systématiser la technique, l'étude a porté sur une méthode de vérification de la conception basée sur les résultats d'une modèle expérimentale à grande échelle.

1 INTRODUCTION

To support progress with a new foundation type for soft ground, research and development were conducted concerning a rational design method (Tomisawa *et al.* 2005, Tomisawa *et al.* 2007) in which composite ground consisting mainly of solidified improved columns is formed around piles and shear strength enhanced by such ground improvement is reflected in the form of horizontal resistance and bearing capacity. Although the use of this approach (tentatively referred to as the composite ground pile foundation method) in line with site conditions is expected to reduce construction costs, partial improvement to the support mechanism of piles alone is not enough; it is also necessary to ensure the seismic performance of foundations (Japan Road Association 2002) and to fully systematize the design and construction involved in the method.

Accordingly, this study closely investigated past research results (Tomisawa *et al.* 2005, Tomisawa *et al.* 2010) on the static and dynamic mechanical behavior of pile foundations used in combination with solidified improved columns, and examined the concept of a design verification method for composite ground pile foundations in line with existing design approaches (Japan Road Association 2002, Architectural Association of Japan 2001) based on the results of a large-scale model experiment.

2 DESIGN CONCEPTS

The concept of the composite ground pile foundation is based on reducing the foundation size to cut construction costs and improve seismic performance. Figure 1 shows a comparison of pile foundation specifications with the conventional method and composite ground foundation. For very soft ground, the number of piles is increased to ensure safety against the permissible horizontal displacement, and especially against the reaction force of the superstructure (Japan Road Association 2002). More than ten rows of cast-in-place piles measuring 1,000 mm in diameter are needed for preliminary design at an actual site, as shown in the figure.

Conversely, if a composite ground pile foundation is used for the same site, construction costs (including expenses incurred for ground improvement) can be cut by approximately 30% because only two rows of piles are required and the substructure and building frame sizes are reduced considerably.

The key points in the design of composite ground pile foundation are listed at the bottom of Fig. 1. In the new basic design method, the horizontal subgrade reaction/bearing capacity of piles is converted into the modulus of ground deformation E based on the increased shear strength, and the necessary range of ground improvement (i.e., the range of horizontal resistance of the piles) is set as a three-dimensional quadrangle that includes an inverted cone raised to the gradient of the passive slip surface θ= (45° + ϕ/2) (ϕ: angle of soil shear resistance) from the depth of the characteristic length of piles $1/\beta$. In other words, the elastic subgrade reaction design method for piles is applied with the improvement strength of solidified improved columns set relatively low (equivalent to q_u = 200 kN/m^2). The validity of this method of handling solidified improved columns around piles as a reaction mass has been confirmed statically in horizontal/vertical loading and centrifuge model tests involving actual piles at several sites (Tomisawa *et al.* 2009). Centrifugal excitation testing and dynamic nonlinear finite element analysis have also verified seismic performance improvement effects, such as the reduction of pile foundation deformation by almost half compared to the conventional design method for unimproved ground, against Level 1 (acceleration: approx. 150 gal) and Level 2 (acceleration: approx. 750 gal) earthquake motion (Tomisawa *et al.* 2008).

However, for pile foundations used in combination with solidified improved columns to satisfy the performance requirements of the current design method (Japan Road Association 2002, Architectural Association of Japan 2001), it is considered necessary to develop a design verification technique to ensure the soundness of solidified improved columns, especially in relation to the dynamic behavior of piles.

Against this background, a large-scale model experiment was conducted for the purpose of establishing a new design verification method for composite ground pile foundations. The experiment focused on the manifestation of horizontal subgrade reaction (i.e., the feasibility of the elastic subgrade reaction design method for piles) in particular when the strength and depth of solidified improved columns were changed.

3 LARGE-SCALE MODEL EXPERIMENT

3.1 *Experiment overview*

The large-scale model experiment involved static horizontal cyclic loading tests on piles in composite ground with solidified improved columns using a laminar shear box (1,200 mm in width (loading direction) × 800 mm in depth × 1,000 mm in height) and a 15-tiered shear frame) (Japanese Geotechnical Society 2010). Photo 1 shows the experimental setup.

The test ground had an upper layer with solidified improved columns and a lower layer of natural soil to simulate a composite ground pile foundation. The natural soil was the sandy type with an *N* value of 10, and was formed with a compaction water content of w = 5%. The required strength of the composite ground with solidified improved columns was achieved using bentonite as the base material and adding early-strength cement (Public Works Research Center 2004). The test piles were the point-bearing steel pipe type simulating the actual scale (pile diameter D = 101.6 mm, thickness t = 4.2 mm, length L = 1,110 mm).

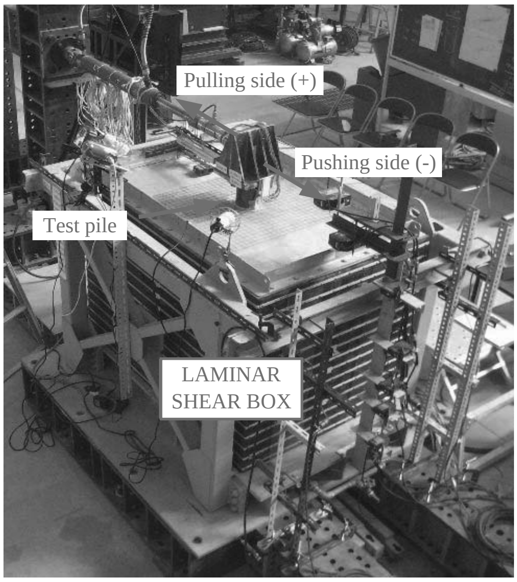

Photo 1. Setup of the large-scale model experiment

In the static horizontal loading experiment, peak-to-peak alternate loads were applied repeatedly with displacement controlled. Each loading step was performed three times with the maximum horizontal displacement of piles at the road

[Conventional design method]

Pile design method for soft ground: Horizontal resistance is insufficient and the foundation is large; the design method is not feasible.

(Site example) Cast-in-place pile foundation

Pile diameter 1,000 mm / 10 or more rows

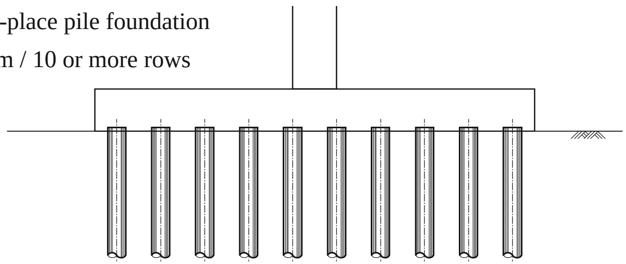

Design-related problems: (1) group pile design method, (2) bearing capacity of piles depending on arrangement, (3) bending rigidity of footing

Problems with other methods: (1) lightweight embankment method: seismic performance; (2) inclined pile foundation: axial force, bending stress

[Composite ground pile foundation]

Concept: reduction of foundation size and improvement of seismic performance based on the use of piles in combination with ground improvement

(Site example) Cast-in-place pile foundation

Pile diameter 1,200 mm / 2 or more rows

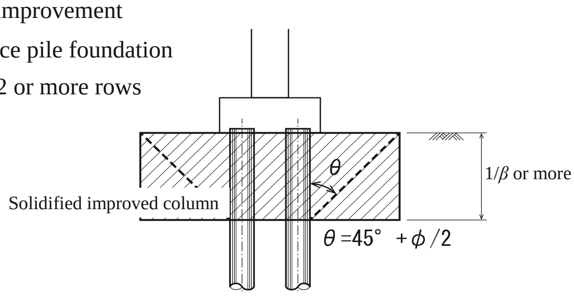

Key points of design: (1) composite ground design method, (2) range of $1/\beta$ or more, θ= 45° + ϕ/2), (3) strength: q_u = 200 to 500 kN/m^2

Key points of the actual design method:
(1) Normal conditions: elastic subgrade reaction method (sliding/horizontal subgrade reaction verification)
(2) During Level-1 earthquake motion: seismic coefficient method (permissible horizontal displacement/cross-sectional force of piles at the boundary)
(3) During Level-2 earthquake motion: verification of horizontal load bearing capacity during earthquakes (permissible response ductility), dynamic nonlinear analysis

Figure 1. Comparison of the conventional design method for pile foundations in soft ground and composite ground pile foundations

Table 1. Experiment cases

Experiment case	Ground condition	Unconfined compressive strength q_u (kN/m^2)	Remarks
CASE-1	Entire layer: natural ground 1.00 m	-	No improved ground (natural ground)
CASE-2	Upper layer: solidified improved columns 0.50 m (= 1/β); lower layer: natural ground 0.50 m	200 (actual strength: 223)	Standard strength
CASE-3	Upper layer: solidified improved columns 0.50 m (= 1/β); lower layer: natural ground 0.50 m	1000 (actual strength: 1,440)	Varied improvement strength
CASE-4	Upper layer: solidified improved columns 0.25 m (= 1/2β); lower layer: natural ground 0.75 m	200 (actual strength: 205)	Varied improvement depth

surface y (1) 0.5 mm, (2) 1.0 mm, (3) 2.5 mm and (4) 5.0 mm, which was set at the time of design to simulate normal and earthquake conditions.

The large-scale part of the model experiment was conducted for the four cases listed in Table 1. Case 1 involved natural ground with no improvement and an N value of 10 for the entire layer. Case 2 involved two-layered ground where the unconfined compressive strength of the solidified improved columns in the upper layer qu was close to the standard value of q_u = 200 kN/m^2 (223 kN/m^2 in actual strength) and the improvement depth was $1/\beta$ = 50 cm in accordance with the basic design method for composite ground pile foundations. Case 3 involved two-layered ground where the improvement depth of solidified improved columns in the upper layer was $1/\beta$ = 50 cm and the unconfined compressive strength q_u was around 1,000 kN/m^2 (1,440 kN/m^2 in actual strength), which was about five times as large as that of Case 2 (ratio in actual strength: 1,440 kN/m^2 / 223 kN/m^2 ≈ 6.5 times). Case 4 involved two-layered ground where the unconfined compressive strength of solidified improved columns in the upper layer was similar to that of Case 2 (205 kN/m^2 in actual strength) and the improvement depth was half ($1/2\beta$ = 25 cm).

3.2 *Results of horizontal subgrade reaction experiment*

Tables 2 to 4 summarize the experimental results regarding the horizontal subgrade reaction in Cases 2 to 4 as obtained from the large-scale model experiment. The actual modulus of subgrade reaction k in the horizontal direction in the table was found via back-calculation from the basic equation of the elastic subgrade reaction method for finite piles (Eq. (1)) based on the H-y relationship at each displacement as found from the static horizontal cyclic loading experiment (Japan Road Association 2002).

$$y = (C_1 + C_2) / (2EI\beta^3) \quad (1)$$

Here, C_1 and C_2 are the integral constants of the pile head fixation condition, β is the characteristic value of piles (m^{-1}) $\beta = \sqrt[4]{(kD)/4EI}$, D is the pile diameter (m) and EI is the pile bending rigidity (kN/m^2). The measured horizontal subgrade reaction P_H was set as the product of the modulus of subgrade reaction in the horizontal direction k and the displacement of piles at the ground surface (maximum displacement).

The design modulus of subgrade reaction in the horizontal direction k' was calculated as the modulus of deformation E for the solidified improved columns. The design horizontal subgrade reaction P_{HU} was assumed to be the upper-limit value of the horizontal subgrade reaction, which is the passive earth pressure strength of composite ground with solidified improved columns as calculated using Eq. (2) (Japan Road Association 2002).

Table 2. Modulus of subgrade reaction in the horizontal direction k and horizontal subgrade reaction P_H in Case 2

Experiment case	Pile displacement at the ground surface (ratio to pile diameter)	Experiment value		Design value	
		Modulus of subgrade reaction in the horizontal direction k (kN/m^3)	Horizontal subgrade reaction P_H (kN/m^2)	Modulus of subgrade reaction in the horizontal direction k' (kN/m^3)	Horizontal subgrade reaction P_{HU} (kN/m^2)
CASE-2	0.5 [0.5%]	383,466	191.7	Composite ground with solidified improved columns 395,642	Upper-limit value for solidified improved columns 334.5
	1.0 [1.0%]	233,577	233.6		
	2.5 [2.5%]	121,290	303.2	Natural ground with an N value of around 10 110,165	
	5.0 [5.0%]	73,880	369.4		

Table 3. Modulus of subgrade reaction in the horizontal direction k and horizontal subgrade reaction P_H in Case 3

Experiment case	Pile displacement at the ground surface (ratio to pile diameter)	Experiment value		Design value	
		Modulus of subgrade reaction in the horizontal direction k (kN/m^3)	Horizontal subgrade reaction P_H (kN/m^2)	Modulus of subgrade reaction in the horizontal direction k' (kN/m^3)	Horizontal subgrade reaction P_{HU} (kN/m^2)
CASE-3	0.5 [0.5%]	2,150,363	1,075.2	Composite ground with solidified improved columns 3,098,529	Upper-limit value for solidified improved columns 2,160.0
	1.0 [1.0%]	1,056,491	1,056.5		
	2.5 [2.5%]	412,912	1,032.3	Natural ground with an N value of around 10 110,165	
	5.0 [5.0%]	202,867	1,014.3		

Table 4. Modulus of subgrade reaction in the horizontal direction k and horizontal subgrade reaction P_H in Case 4

Experiment case	Pile displacement at the ground surface (ratio to pile diameter)	Experiment value		Design value	
		Modulus of subgrade reaction in the horizontal direction k (kN/m^3)	Horizontal subgrade reaction P_H (kN/m^2)	Modulus of subgrade reaction in the horizontal direction k' (kN/m^3)	Horizontal subgrade reaction P_{HU} (kN/m^2)
CASE-3	0.5 [0.5%]	295,440	147.7	Composite ground with solidified improved columns 240,555	Upper-limit value for solidified improved columns 307.5
	1.0 [1.0%]	188,945	188.9		
	2.5 [2.5%]	104,641	261.6	Natural ground with an N value of around 10 110,165	
	5.0 [5.0%]	66,922	334.6		

$$P_{HU} = a_S \cdot q_u \cdot a_p \quad (2)$$

Here, α_S is the correction factor for composite ground in which solidified improved columns are used, and was set as 1.5 as in the calculation for cohesive soil ground in consideration of related physical properties.

The experiment results were examined as described here. First, the modulus of the subgrade reaction in the horizontal direction measured in the large-scale model experiment k was compared with the design value for the upper layer of composite ground with solidified improved columns k'. In Case 1 with natural ground whose N value was 10 for the entire layer, the measured value k roughly corresponded to the design value k' when the permissible horizontal displacement was 1.0% of the pile diameter, which is the standard value set in existing design methods (Japan Road Association 2002, Architectural Association of Japan 2001). In Case 2 where the improvement depth was $1/\beta$ and the unconfined compressive strength q_u was used as the standard strength, the k and k' values were similar for pile displacement at the ground surface when the displacement was 0.5% of the pile diameter (y = 0.5 mm). However, when displacement at the ground surface was 1% or more of the pile diameter, the measured value k did not satisfy the design value k'. While the measured value satisfied the design value at the same displacement in Case 4 where the improvement depth was $1/2\beta$, pile strain increased in the bottom layer of the solidified improved columns because no binding effect could be expected from them in the deep section, and the measured bending moment of piles tended to be underestimated. In Case 3 where the unconfined compressive strength of solidified improved columns q_u was extremely high, the measured value did not satisfy the design value at all displacement levels. In other words, although a certain degree of reaction effect can be expected, the elastic subgrade reaction design method for piles is not feasible if solidified improved columns are very strong.

Accordingly, to enable application of the basic design method for composite ground pile foundations, the improvement depth should always be $1/\beta$, and q_u = 200 kN/m^2 should be set as the standard value for the unconfined compressive strength of solidified improved columns. At the same time, the permissible horizontal displacement of piles used for composite ground pile foundations should be reduced to 0.5% of the pile diameter instead of 1% (or 15 mm) for natural ground.

Next, the measured horizontal subgrade reaction P_H in Cases 2, 3 and 4 was compared with the design value P_{HU}. It can be seen from the table that the measured P_H in Cases 2 and 4 satisfied the design value P_{HU} when pile displacement at the ground surface was up to around 2.5% of the pile diameter (y = 2.5 mm). However, the measured P_H in Case 3 was less than half of the design value P_{HU} at all displacement levels, indicating that the elastic subgrade reaction design method for piles is not feasible when the strength of solidified improved columns is extremely high as seen in the examination of the modulus of subgrade reaction in the horizontal direction.

4 CONCLUSION

Based on the results of a large-scale model experiment, the following findings were obtained in regard to a design verification method for pile foundations used in combination with solidified improved columns (i.e., composite ground pile foundations):

(1) In the basic design method for composite ground pile foundations, specifications for solidified improved columns should be based on engineering grounds, the improvement depth should be based on the characteristic pile length $1/\beta$, and q_u = 200 kN/m^2, with which constitutive laws of soils (Public Works Research Center 2004) can be followed, should be applied as the standard value for the unconfined compressive strength of solidified improved columns.

(2) While the limit state of damage to solidified improved columns in composite ground pile foundations is assumed to be reached within the range of pile deformation to around 2.5% of the pile diameter, it should be verified that the design horizontal subgrade reaction P_{HU} calculated as a product of the design pile displacement y and the design value k' is smaller than the passive earth pressure strength of composite ground given by solidified improved columns to provide inner stability and ensure column soundness. The use of this index is expected to help prevent cracking in improved columns and other types of damage caused by pile behavior in normal conditions and during Level-1 earthquakes.

(3) To sustain the reaction effect and ensure the external stability of solidified improved columns in composite ground pile foundations, the permissible horizontal displacement of piles in normal conditions and during storms and Level-1 earthquakes should be reduced to 0.5% of the pile diameter instead of 1% (or 15 mm) for natural ground. The elastic subgrade reaction design method for piles can be considered feasible when the above design verification method is applied.

In this paper, a new design verification method for composite ground pile foundations with consideration for the limit state of solidified improved columns was presented based on past results from research on pile foundations used in combination with solidified improved columns. Using these results and the outcomes of discussions by a technical exploratory committee consisting of foundation engineering experts from the government, universities and industries, guidelines on design and construction methods for composite ground pile foundations have been established (Civil Engineering Research Institute for Cold Region 2010).

5 REFERENCES

Architectural Institute of Japan 2001: *Recommendation for the Design of Building Foundations*, pp. 173 –326.

Civil Engineering Research Institute for Cold Region 2010: *Guidelines on design and construction methods for composite ground pile foundations in Hokkaido*, pp. 1 – 189.

Japan Road Association 2002: *Specifications for Highway Bridges V – aseismic design*, pp. 4 – 118.

Japan Road Association 2002: *Specifications for Highway Bridges IV – substructure*, pp. 348 – 433.

Japanese Geotechnical Society 2010: *Method of horizontal loading test of piles and instruction manual*, pp. 22 – 28.

Public Works Research Center 2004: *Design and construction manual for the deep mixing method in work on land*, pp. 76 – 127.

Tomisawa, K. and Nishikawa, J. 2005: A design method concerning horizontal resistance of piles constructed in improved ground, *16th International Conference on Soil Mechanics and Geotechnical Engineering*, pp. 2187 – 2192.

Tomisawa, K. and Nishikawa, J. 2005: Pile design method in composite ground formed by deep mixing method, *Journal of the Japan Society of Civil Engineers* No. 799/III-72, pp. 183 – 193.

Tomisawa, K., Nishimoto, S. and Miura, S. 2009: Evaluation of mechanical behavior and examination of seismic performance of pile foundation in composite ground, *Journal of Structural Engineering* Vol. 55A, pp. 1182 – 1195.

Tomisawa, K. and Miura, S. 2007: Mechanical behavior of pile foundation constructed in composite ground and its evaluation, *Soils and Foundations*, Vol. 47, No. 5, pp. 961 – 972, 2007.

Tomisawa, K. and Miura, S. 2010: Method of evaluating the seismic performance of piles in composite ground, *Society of Materials Science, Japan, Material* Vol. 59, No. 1, pp. 26 – 31.

Tomisawa, K., Miura, S. and Watanabe, T. 2008: Influence of the improved strength and the range of improvement of composite ground on the seismic behavior of piles, *Journal of the Japan Society of Civil Engineers*, C, Vol. 164, No. 1, pp. 127 – 143.

Influence of multiple helix configuration on the uplift capacity of helical anchors

Influence de la configuration des hélices sur la résistance à l'arrachement de pieux hélicoïdaux

Tsuha C.H.C., Santos T.C.
University of São Paulo at São Carlos, Dept. of Geotechnical Engineering

Rault G., Thorel L., Garnier J.
Université Nantes Angers Le Mans, IFSTTAR, Centre de Nantes, Département GER, Physical Modelling in Geotechnics Group

ABSTRACT: The uplift capacity of multi-helix anchors usually depends on the helical blades configuration (including the number and the diameter) and the soil characteristics. An evaluation of those parameters is based on the results obtained from two different experimental programs. The first experiments were performed in centrifuge on dry Fontainebleau sand. For the second testing program, tension load tests were carried out in field at São Carlos in Brazil in a tropical soil. The geometrical effect (cylindrical or tapered helices) is also presented.

RÉSUMÉ : La capacité portante en traction des pieux hélicoïdaux dépend de la configuration des hélices (dont le nombre et le diamètre) et des propriétés du sol. Deux programmes expérimentaux permettent d'éclaircir l'influence relative de ces paramètres. L'un est réalisé sur modèles réduits centrifugés dans du sable sec de Fontainebleau, l'autre est mis en œuvre *in situ* sur un site test à Sao Carlos au Brésil, constitué de sols tropicaux. L'effet de la géométrie (hélices inscrites dans un cylindre ou dans un cône) est présenté.

KEYWORDS: helical anchor, tension capacity, centrifuge modeling, field load tests.

1 INTRODUCTION

Helical anchors have been employed in the construction of structures to sustain tension loads. Uses for helical anchors include transmission tower foundations, utility guy anchors, pipelines, braced excavations, retaining wall systems, etc. They are composed of helical bearing plates welded to a steel shaft, and installed into the ground by application of torsion to the upper end of the shaft (Figure 1).

The most common methods to estimate the uplift capacity of helical anchors are two: individual bearing and cylindrical shear methods. The individual bearing method assumes that the total capacity of a multi-helix anchor is equal to the sum of the individual capacities of each plate, estimated using the Terzaghi's (1943) general bearing capacity equation.

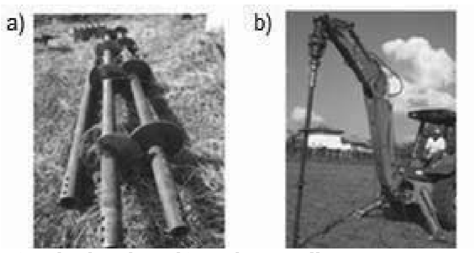

Figure 1. a) Helical anchors; b) Anchor installation.

The cylindrical shear method, described in Mitsch and Clemence (1985) and Mooney et al. (1985), supposes that the failure mechanism consisting of the bearing capacity failure above the top helix and of a cylindrical failure zone developed along the perimeter section between the helices.

The failure mechanism of helical anchors depends principally on the helix spacing ratio (ratio of helix spacing to helix diameter). Kulhawy (1985) stated that if the helices are widely spaced, the multi-helix anchor behaves as a sum of various single-helix anchors. According to the results of a field investigation on the behaviour of multi-helix anchors in clay, presented in Lutenegger (2009), there is no distinct transition from cylindrical shear to individual bearing behaviour. For helical anchors in sand, Lutenegger (2011) found that this transition occurs at a helix spacing ratio of about three.

For the application of these two prediction methods, used in helical anchor design, reductions in the values of some soil parameters have been suggested in the literature to consider the effect of the soil disturbance above the helices caused by the anchor installation.

As reported by Kulhawy (1985), significant disturbance does occur within the cylindrical installation zone of the helical anchor. Mitsch and Clemence (1985) cited that the installation of helical anchors induces significant stress changes in soil due to the disturbance produced by screwing the anchor into the sand and that these changes influence the anchor uplift behaviour.

Tsuha et al. (2012) mentioned that when a helical anchor is installed into the ground, the soil traversed by the helices is sheared and displaced laterally and vertically. According to these authors, the disturbance caused by the anchor installation is normally more pronounced in the soil above the upper plates than above the lower plates, because the upper soil layers are penetrated more times.

Some experimental investigations on helical anchors (Clemence et al. 1994, Sakr 2009, and Lutenneger 2011), with relative helix spacing of three times the plate diameter, have demonstrated that, the amount of increase in the uplift capacity of helical anchors with the increase in the number of helices is not as expected. The gain in the uplift capacity of helical anchors due to the addition of one more plate is variable, and depends of the anchor configuration and soil characteristics.

For this reason, considering that a thorough understanding of the influence of helices configuration on the uplift behaviour of helical anchors is fundamental to give accurate estimates of the helical anchors capacity, the purpose of this paper is to evaluate the geometry effect on the soil disturbance due to anchor installation and its influence on the anchor capacity. Two different experimental programs were performed to this aim. Initially, centrifuge model experiments were carried out on scaled models of helical anchors with different dimensions in sand, at the "French Institute of Science and Technology for Transport, Development and Networks" (IFSTTAR) in Nantes, France, to investigate the variability of the rate of capacity gain due to the addition of one more helix to a helical anchor.

Considering that the use of helical anchors as tower foundation has being increased in Brazil, and tropical soils covers a significant part of the Brazilian territory, the second experimental program of the present investigation was carried out at a site of tropical soil, to evaluate the influence of the helical anchor configuration on the installation torque and on its uplift capacity.

2 EXPERIMENTS

2.1 Centrifuge testing modeling

A centrifuge model program was performed at the IFSTTAR, in France, to verify the influence of the diameter and number of helices on the multi-helix anchor uplift capacity in sand. The purpose of centrifuge modeling is to reproduce a full-scale response, with the possibility of comparisons between helical anchors with different dimensions, as the model anchors were installed in a uniform sand mass.

Nine small-scale anchor models (Figure 2; Table 1) were tested in two different samples of dry NE34 Fontainebleau silica sand (Table 2), with relative densities of 56% (container 1) and 85% (comtainer 2), respectively. The samples were prepared by the air-pluviation technique in two containers with dimensions of 1200 mm × 800 mm in plan area and a height of 340 mm.

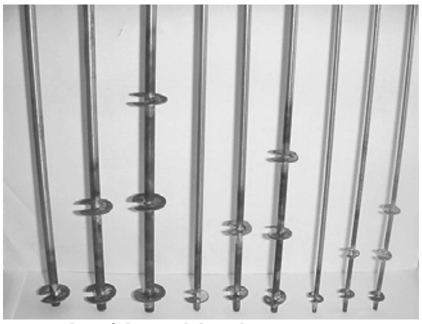

Figure 2. Photography of the model anchors.

For this investigation, tension load tests were performed on reduced-scale model piles, without helical plates (P10 to P12), to separate the shaft resistance, Q_s, from the total helical anchor uplift capacity, Q_u (see Figure 3 and 4). The cylindrical model anchors (multi-helix with same plate diameter), shown in Figure 2, were fabricated with the spacing between any two helices of three times the helix diameter.

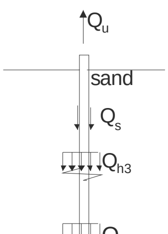

Figure 3. Resisting forces to upward movement of a multi-helix anchor in sand according to the " individual bearing" failure mechanism.

Table 1. Dimensions of model anchors (M) and prototype anchors (P).

Pile	Nº of helix	Shaft diameter d_M (d_P) mm)	Helix diameter D_M (D_P) (mm)	Prototype tip depth (m)
P1	1	3.0(64.3)	10(214)	3.1
P2	2	3.0(64.3)	10(214)	3.1
P3	3	3.0(64.3)	10(214)	3.1
P4	1	4.5(97.7)	15(326)	4.6
P5	2	4.5(97.7)	15(326)	4.6
P6	3	4.5(97.7)	15(326)	4.6
P7	1	6.0(132)	20(440)	6.2
P8	2	6.0(132)	20(440)	6.2
P9	3	6.0(132)	20(440)	6.2
P10	-	3.0(64.3)	10(214)	3.1
P11	-	4.5(97.7)	15(326)	4.6
P12	-	6.0(132)	20(440)	6.2

Table 2. Sand properties.

Property	Value
Unit weight of soil particles (kN/m^3)	25.90
Maximum dry density (kN/m^3)	16.68
Minimum dry density (kN/m^3)	14.13
Maximum void radio	0.834
Minimum void radio	0.550
Maximum porosity	0.455
Minimum porosity	0.355
Container 1	
Unit weight (kN/m^3)	15.46
Density index (%)	56
Friction angle (º)	31
Container 2	
Unit weight (kN/m^3)	16.30
Density index (%)	85
Friction angle (º)	41

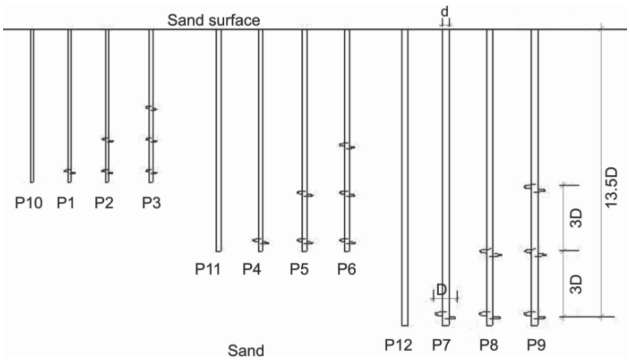

Figure 4. Model piles installed in the sand sample.

A total of 18 tensile loading tests were carried out on the model anchors, nine in the sand container 1, and nine in the container 2. The model anchors were installed at three different depths as illustrated in Figure 4. Further details of this experimental investigation are described in Tsuha et al. (2007).

2.1.1 Results of centrifuge tests

Figure 3 shows examples of load–displacement curves of tensile tests performed on the model anchors of 214mm helix (prototype) diameter, installed in the container 2 (denser sand). The curves of the other loading tests carried out for this investigation are presented in Tsuha et al. (2012).

From the results of this investigation, the fractions of the total helix bearing capacity (Q_h), related to each helical plate of the double-helix anchors ($F_{Qhi} = Q_{hi}/Q_h$, where Q_{hi} is the uplift helix bearing capacity of helix i), were calculated. The portion of helix bearing capacity related to the second helix (Qh_2) of the double-helix anchors was determined by the difference between the Q_h results of double-helix and single-helix anchors with same helix diameter and tip depth. A similar procedure was used to calculate the Q_h fractions of middle and upper helical plates of triple-helix anchors, and these results are included in Tsuha et al. (2012). Figure 4 shows the fractions of helix bearing capacity related to the second helix (F_{Qh2}) of the double and triple-helix anchors tested in this investigation.

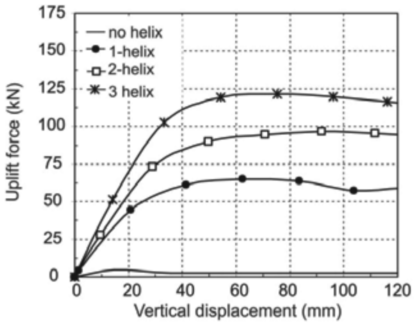

Figure 3. Load–displacement curves of tensile tests performed on model anchors of 214mm helix (prototype) diameter in container 2.

The results of tests performed on the model anchors with helix diameter of 214 mm in the looser sand are influenced by some local heterogeneity. For this reason, the contribution of the second helix of the anchors P2 installed in the container 1, was not shown in Figure 4.

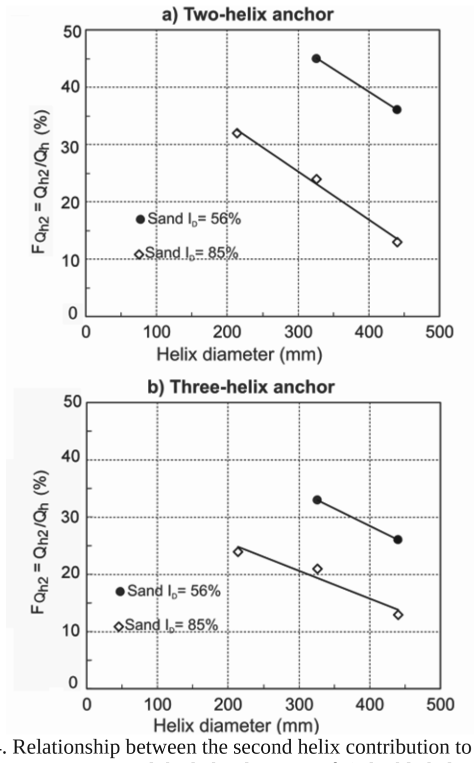

Figure 4. Relationship between the second helix contribution to total helix bearing capacity and the helix diameter of a) double helix and b) triple-helix anchors (Tsuha et al. 2012).

2.1.2 Efficiency of the second helix

Figures 4 shows that the efficiency of the second helix, of double and triple-helix anchors, depends linearly of the helix diameter, and also of the initial sand relative density (I_D).

2.1.3 Effect of sand compactness

The results of Figure 4 illustrate the influence of the relative density on the efficiency of the second plate of multi-helix anchors installed in sand. According to Tsuha et al. (2012), for dense sand, the difference in compactness between the sand penetrated by a helix one time and the sand penetrated two or three times is significant. Differently, for the looser tested sand, after anchor installation, the final relative densities of the sand above the three helices are similar. This hypothesis is detailed in Figure 5.

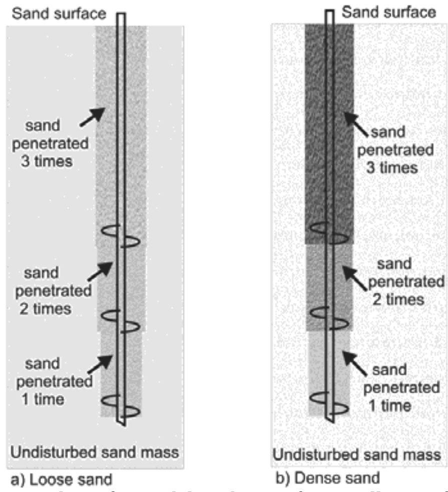

Figure 5. Hypothesis for sand disturbance after installation of a three-helix anchor: (a) loose sand; (b) dense sand (Tsuha et al. 2012).

2.1.4 Effect of helix diameter

The efficiencies of the second plates of the tested anchors decrease with the increase in helix diameter, as observed in Figure 4. This fact indicates that the effect of the helical anchor installation on the sand mass is more significant for helical anchors with larger plates. As the region of disturbed sand around the cylinder circumscribed by the anchors helices after installation is larger for larger helix diameter (increases with the helix diameter), the failure surface mobilized during the anchor loading is more distant from the undisturbed sand. Consequently, the efficiency of the second helix of cylindrical helical anchors decreases with the increase in diameter.

2.2 Field testing program

Eight helical anchors (Figure 6), with different configurations (multi-helix anchors with the same plate diameter and with increasingly larger diameter helices up the central shaft) were installed and tested at the CRHEA site of the São Carlos School of Engineering, São Carlos city, Brazil.

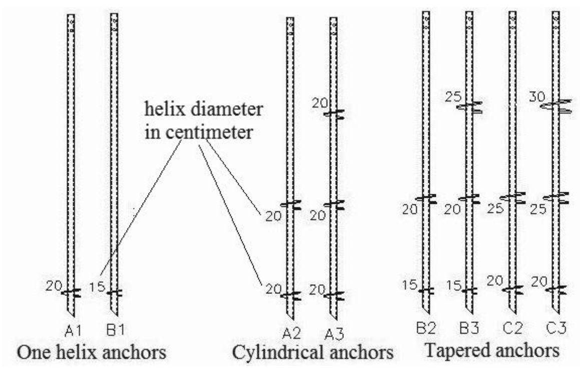

Figure 6. Prototype helical anchors tested at the CRHEA site.

The soil of the CRHEA site is material formed from igneous rock (basalt) from Serra Geral Formation (Figure 7). The top layer is a porous colluvial sandy clay with about 8 meters depth. Below this layer there is a residual soil (from igneous rock) limited by a thin layer of pebbles. The nature of this tropical soil is porous and has unstable structure due to the connections between particles by bonds attributed to soil water suction and cementing substances.

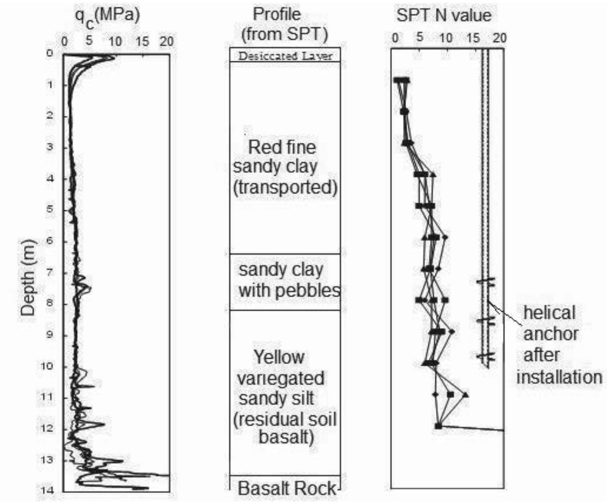

Figure 7. Soil profile at the CRHEA site.

2.2.1 Results of field tests

All anchors of this field investigation were installed with the anchor tip at a depth of 10 meters as illustrated in Figure 7. After installation, tension load tests were carried out on the anchors shown in Figure 6. More complete details of this investigation are available in Santos (2012).

The ultimate capacity (Q_u) of all tests was taken as the load producing a relative displacement of 10% of the helix average diameter. Table 3 presents the results of ultimate capacity (Q_u) of the tested anchors, and also the fractions of uplift capacity related the upper plates. Considering the homogeneity of this site, the fractions of uplift bearing capacity of the second plate of the multi-helix anchors (F_{Qh2}) were calculated by the difference between the ultimate capacity of anchors with two helices and of one helix (same bottom helix diameter). The fractions of uplift capacity due to the third plate (F_{Qh3}) of three-helix anchors were calculated by using the same procedure.

The comparison between the double-helix anchor A2 (cylindrical) and B2 (tapered) shows that the contribution of the second helix to the total capacity is better for tapered configuration. The second helix of the anchor B2 is larger than the bottom helix, and installed in a less disturbed soil layer compared to the second helix of the cylindrical anchor A2.

Table 3. Contribution of the upper plates to the total anchor uplift capacity.

Anchor	Helices diameters (mm)	Q_u (kN)	F_{Qh1} + Q_s fraction (%)	F_{Qh2} (%)	F_{Qh3} (%)
A1	200	14,5	100.0		
A2	200/200	25	58.0	42.0	
A3	200/200/200	36	40.3	29.2	30.6
B1	150	13,5	100.0		
B2	150/200	31	43.5	56.5	
B3	150/200/250	39	34.6	44.9	20.5
C2	200/250	48	30.2	69.8	
C3	200/250/300	57	25.4	58.8	15.8

However, from the comparison between the third helix contribution to the total capacity (F_{Qh3}) of three-helix anchors A3, B3, and C3, it could be observed that the efficiency of the third helix decreases with the third plate diameter, even for the tapered anchors. A similar trend was observed in the centrifuge tests presented in this paper. However, further investigation is needed to confirm this behaviour.

2.2.2 Cylindrical and tapered helices

The results of the final installation torque and the uplift capacity of helical anchors with same average plate diameter (A3 and B3) were compared. From this comparison it was found that the gain in uplift capacity for the tapered anchor is about 8%. However, to install the tapered model, it was necessary to apply a torque 20% larger than the needed to install the cylindrical model.

This difference is explained by the fact that during the tapered anchor installation, the upper helices pass through intact soil, differently of the upper helices of cylindrical anchor. However, during the loading of the both anchors, the both surfaces of soil mobilized above the plates are disturbed by the installation of the helices.

3 CONCLUSIONS

Two different types of experimental programs were carried on helical anchors to verify the effect of the helices configuration on the anchor uplift capacity. Based on the results of these tests, the most important conclusions are:

- The efficiency of the second helix of helical anchors in sand decrease with the increase of the relative density and the helix diameter.
- The uplift capacity of a triple-helix anchor with tapered helices is slightly superior then the one of cylindrical helices, with same average plate diameter in a tropical soil.

4 ACKNOWLEDGEMENTS

The authors wish to thank FAPESP (Fundação de Amparo à Pesquisa do Estado de São Paulo) project n°2010/19039-6, and the international Cooperation USP/Cofecub project n°2012.1.678.1.9.

5 REFERENCES

Clemence, S.P., Crouch, L.K., and Stephenson, R.W. 1994. Prediction of uplift capacity for helical anchors in sand. In Proceedings of the 2nd Geotechnical Engineering Conference, Egypt. Vol. I: 332–343.

Kulhawy, F.H. 1985. Uplift behaviour of shallow soil anchors — an overview. In Uplift Behaviour of Anchor Foundations in Soil. ASCE: 1–25.

Lutenegger, A.J. 2009. Cylindrical Shear or Plate Bearing? – Uplift Behavior of Multi-Helix Screw Anchors in Clay. Contemporary Issues in Deep Foundations, ASCE: 456-463.

Lutenneger, A.J. 2011. Behavior of multi-helix screw anchors in sand. *In Proceedings of the 14th Pan-American Conference on Soil Mechanics and Geotechnical Engineering*, Toronto, Ont. [CD ROM].

Mitsch, M.P., and Clemence, S.P. 1985. Uplift capacity of helix anchors in sand. In Uplift Behaviour of Anchor Foundations in Soil, ASCE: 26-47.

Mooney, J.S., Adamczak, S.J, and Clemence, S.P. 1985. Uplift Capacity of Helix Anchors in Clay and Silt. Uplift Behaviour of Anchor Foundations in Soil, ASCE: 48-72.

Sakr, M. 2009. Performance of helical piles in oil sand. *Canadian Geotechnical Journal* 46: 1046–1061.

Santos, T.C. 2012. The effect of helices configuration on the uplift capacity of helical piles in a tropical soil. Dissertation (master's degree) – Escola de Engenharia de São Carlos, Universidade de São Paulo, São Carlos.

Terzaghi, K. 1943. *Theoretical soil mechanics*. John Wiley & Sons, New York.

Tsuha, C.H.C., Aoki, N., Rault, G., Thorel, L., and Garnier, J. 2007. Physical modeling of helical pile anchors. *International Journal of Physical Modelling in Geotechnics* 7(4): 1–12.

Tsuha, C.H.C., Aoki, N., Rault, G., Thorel, L., and Garnier, J. 2012. Evaluation of the efficiencies of helical anchor plates in sand by centrifuge model tests. *Canadian Geotechnical Journal* 49: 1102–1114.

Super-long bored pile foundation for super high-rise buildings in China

Fondation profonde sur pieux de très grandes longueurs pour les immeubles de grandes hauteurs en Chine

Wang W., Wu J.
Department of Underground Structure & Geotechnical Engineering, East China Architectural Design & Research Institute Co., Ltd. Shanghai, China

Li Y.
Department of Geotechnical Engineering, Tongji University, Shanghai, China

ABSTRACT: In China, super-long bored piles are commonly used as deep foundations to support very heavily loaded super high-rise buildings. This paper presents some aspects of design and construction of super-long bored pile foundation together with a brief description of bearing behaviors of super-long bored piles. The issues of selection of pile type and pile tip bearing stratum, load test pile design, single pile design, pile foundation design, key construction technique and pile quality inspection are discussed with some engineering practices of super-long pile foundation. These will provide reference and help for futural engineering practice of super-long pile foundation for super high-rise building.

RÉSUMÉ : Les pieux de très grandes longueurs sont généralement utilisés en Chine pour les fondations profondes afin de supporter les immeubles de grandes hauteurs. Cet article présente certains aspects du désign et de la construction de ce type de pieux au travers notamment de leurs caractéristiques de chargement. La méthode de sélection de ces pieux, les tests de chargement, le désign du pieu lui-même, les aspects clé de la technique et enfin la méthode d'inspection sont discutés sur la base de certains cas pratiques. Cette discussion pourra apporter une référence et une aide pour les prochaines utilisations des pieux de très grandes longueurs.

KEYWORDS: super-long bored pile ; super high-rise building ; field load test ; double steel sleevs ; post grouting technique

1 INTRODUCTION

With the rapid economic growth in the past two decades, numerous super high-rise buildings have been built in Chinese riverside and coastal cities and there are more and more super high-rise buildings under construction or planned to be constructed. According to statistics, the number of tall buildings with height of more than 152m will be larger than 1000 in China during the next 10 years. Moreover, many of them will be more than 600m in height. Super high-rise buildings, especially those constructed in soft soil areas, have brought new challenges to geotechnical engineers. In order to obtain sufficient bearing capacities, super-long pile foundations are often adopted for super high-rise buildings. As shown in Table 1, super-long pile foundations were designed for some high-rise buildings in China by East China Architectural Design and Research Institute Co., Ltd. (ECADI) (Wang et al, 2011).

Table 1 A survey of pile foundations of some high-rise buildings in China

Building name	Height (m)	Floors	Pile type	Pile diameter (mm)	Pile length (m)	Pile tip bearing stratum
New CCTV Tower	234.0	51	Bored pile	1200	51.7	Sand and gravel
Tianjin Tower	336.9	75	Bored pile	1000	85.0	Silty sand
Tianjin 117 Tower	597.0	117	Bored pile	1000	98.0	Silty sand
Shanghai White Magnolia Plaza	320.0	66	Bored pile	1000	85.0	Medium sand with gravel
Wuhan Tower	438.0	88	Bored pile	1000	65.0	Moderately weathered mud rock and sand rock
Suzhou International Financial Center	450.0	92	Bored pile	1000	90.0	Fine sand
Wuhan Green Land Tower	636.0	125	Bored pile	1200	60.0	Slightly weathered mud rock

Until now the experience of design and construction of super-long pile foundation is very limited. Many of the traditional methods cannot be applied with any confidence since they require extrapolation well beyond the realms of prior experience. Therefore, geotechnical engineers are being forced to summary engineering experience and utilize more sophisticated methods for design and construction of super-long pile foundations (Poulos, 2009).

Base on some engineering practices of super-long pile foundations of super high-rise buildings in China, this paper presents some aspects of design and construction of super-long bored pile foundation. Some bearing behaviors of super-long piles will be reviewed firstly. Then selection of pile type and pile tip bearing stratum, design of field load test pile and pile foundation will be discussed. Moreover, some key construction techniques and pile quality control inspection standards are also presented. The methods and technical measures of super-long pile foundation, which are summarized and analyzed in this paper, can provide some valuable experience, reference and help for future super high-rise building foundation projects.

2 BEARING BEHAVIORS OF SUPER-LONG BORED PILE

Super-long bored piles mainly refer to piles with length larger than 50m and slenderness ratio larger than 50. Both theoretical research and engineering practice show that the bearing behaviors of super-long bored piles are different from those of short and middle long piles. The vertical loads supported by super-long bored piles are substantial. There are many soil layers around the pile shaft. The soils characteristics are usually complex. Construction of super long bored piles is complicated. It is difficult to control the construction quality. Furthermore, because of the large length and slenderness ratio of the super-long bored pile, the stiffness of pile-soil system is relative small. This directly influences the bearing characteristics of the super-long bored pile. According to the analysis of filed load tests results (Zhang and Liu, 2009), the basic bearing behaviors of super-long bored piles can be summarized as follows:

1. The pile load versus settlement curve (Q~s curve) has no significant change in slope if sediment under the pile tip is cleaned up or the pile tip is post grouted.
2. Under the ultimate bearing load, the pile top settlement is mainly caused by pile shaft compression, especially the compression of the upper half pile shaft. Moreover, the pile shaft presents large plastic compression deformation under very high load.
3. The mobilization of the pile shaft friction is asynchronous. In other words, the pile shaft friction in the shallow soil layers is mobilized before that in the deep layers. In the shallow soil layers, due to the large relative displacement between the pile shaft and the around soils, the pile shaft friction usually reaches ultimate value, and is prone to softening. The mobilization of the pile shaft friction in the deep soil layers and the pile tip resistance is hysteretic due to the small relative displacement between the pile shaft and the around soils. The pile tip resistance is difficult to be mobilized adequately due to the small pile tip deformation. The pile shaft friction resistance occupied a fairly large proportion of the pile ultimate bearing capacity. Therefore, super-long bored pile can usually be identified as friction pile.
4. The mobilization of the pile shaft friction is correlated with support condition at the pile tip. Not only the pile tip bearing capacity is low but also the pile shaft friction resistance can be cut down severely, when the bearing stratum is soft or the sediment is thick under the pile tip. However, both the pile tip resistance and pile shaft friction can be increased significantly after the support condition is improved by post grouting at pile tip.

3 SELECTION OF PILE TYPE AND PILE TIP BEARING STRATUM

Considering post grouting or not, super-long bored pile can be divided into normal pile, tip post grouted pile and tip and shaft post grouted pile. It is difficult to guarantee the bearing performance of the normal bored pile usually due to the problems of pile shaft mud cake and pile tip sediment. The sediment problem can be effectively solved by pile tip grouting technique, which can help to improve the bearing behaviors of the pile tip and pile shaft, and accordingly, the bearing capacity of the pile can be greatly increased. Therefore, the pile tip grouting technique is recommended for super-long bored pile. When the pile tip is embedded very deeply, or soils around the pile shaft are soft or settlement control of the pile is very strict, pile shaft grouting can be implemented, which can further improve bearing behaviors of the pile shaft and increase the pile shaft friction. Post grouting technique was adopted for all the projects listed in Table 1.

Although super-long bored pile is usually identified as friction pile, the pile tip bearing condition has a great influence on the mobilization of the pile shaft friction and the bearing capacity and deformation characteristics of the pile. Therefore, the deep and solid soil layers, such as rock, gravel layer and sand layer, are often selected as bearing stratums for super-long bored pile tip bearing stratums. As bearing behaviors of the soil at the pile tip and the pile bearing capacity are improved by post grouting, the shallower solid soil layer can be possibly selected as bearing stratum. The depth of pile tip extended into the bearing layer can also be decreased for this reason. Thus post grouting technique has expanded the range of selection of pile tip bearing stratum. This technique is benefit to shorten the length of the pile, save engineering quantity, and achieve optimization design of pile foundations.

4 FIELD LOAD TEST PILE DESIGN

Static filed load test is a basic and reliable method to obtain the bearing behaviors of the super-long bored pile. It is also a necessary link of inspection and optimization design of the pile foundation. As a design principle of the test pile, test data and technical parameters should be got as many as possible for design and construction of pile foundation. Besides the general contents, double steel sleeves, pile head, construction and measurement requirements should be especially concerned during the test pile design process.

4.1 DOUBLE STEEL SLEEVES DESIGN

The base rafts of the super high-rise buildings are often deeply buried. Therefore, it is necessary to concern how to reasonably deduct the pile shaft friction in the excavation segment when the load test is carried out at the ground surface. The pile test with double steel sleeves isolating pile-soil contact in the pit excavation segment can reasonably reflect the bearing behaviors of pile (Wang et al, 2011). Double steel sleeves have been applied in the pile load tests of several super high-rise building projects, such as the Shanghai Center Tower, The Tianjin 117 Tower, The Wuhan Green land Tower, et al. The design diagrams of double steel sleeves for the test piles of the Shanghai Center Tower project are shown in Figure 1.

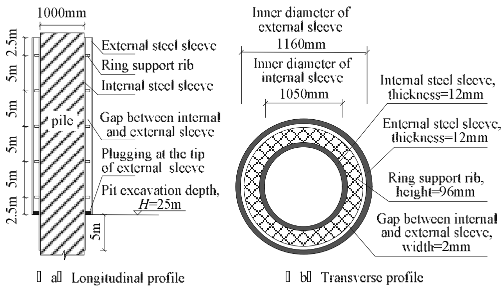

Figure 1 Design diagrams of double steel sleeves for the test piles of the Shanghai Center Tower project

4.2 PILE HEAD DESIGN

Super-long bored test piles often bear very large loads. For example, the load applied to the field test pile of Wuhan Green Land Tower reached 45000kN. Therefore, the test pile head need to be special designed. According to loading condition and test requirements, the pile head should be formed to provide a plane surface which is normal to the axis of the test pile and large enough to accommodate the loading and measuring equipments. The pile head should be adequately reinforced or protected to prevent damage caused by the concentrated loads applied from the loading equipment. The pile head should be concentric with the pile. The strength of the joint between the pile head and the pile should be equivalent to that of the pile. If the double steel sleeves are adopted for the test pile, measures should be made to ensure that the head and the external sleeve would not connect together during the construction process. Figure 2 shows the design schematic diagrams of the test pile head for the Shanghai Center Tower project. The anchor pile-cross beam reaction devices were used in this field test. The maximum load was 30000kN, which was applied using 8 hydraulic jacks. The capacity of each jack was 5000kN.

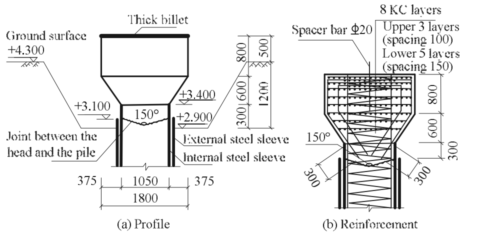

Figure 2 Design schematic diagrams of the test pile head for the Shanghai Center Tower project

4.3 CONSTRUCTION AND MEASUREMENT REQUIREMENTS

Practical construction conditions should be simulated in the construction process of the test piles. Artificial drilling fluid and desanding device should be used when the borehole is drilled through the deep sand layers. Vertical deviation of the borehole should be not more than 1/250. Thickness of the sediment at the borehole tip should be less than 50mm after the secondary tip cleaning. If post grouting technique is adopted for the test pile, the grouting construction parameters should be determined. The construction machineries, techniques and parameters are also need to be determined to form a guideline for pile construction.

Measurement items of super-long bored pile load test are illustrated as follows: (1) Drilling fluid density, viscosity, sand content and other technical indexes in different depth of the borehole. These parameters should be continuously monitored for not less than 36 hours in the construction process. (2) Concrete quality of the test pile, including pile shaft integrity and concrete strength. (3) Sediment and grouting effect under the test pile tip. (4) Ultimate bearing capacity of the test pile. (5) Pile shaft axial force and pile shaft friction. (6) Pile shaft deformations, including deformations of pile top, pile tip, section at the rock surface, and other pile shaft sections under each load level.

5 SINGLE PILE DESIGN

5.1 PILE ULTIMATE BEARING CAPACITY

The ultimate bearing capacity of super-long bored pile is determined by filed load test. If the load versus settlement curve of the test pile shows a slowly change in slope, the load corresponding to the pile head settlement of 40mm~60mm or 5% of the pile diameter can be used as the ultimate bearing capacity of the pile. For pile foundation under a condition of deep excavation, some factors, such as the soils gravity and pile shaft friction in pit excavation segment and unloading rebound of the soil at the bottom of the pit, should be concerned to determine the ultimate bearing capacity of engineering pile (Wang et al, 2012).

Due to the problems of pile shaft mud and pile tip sediment, measured values of the ultimate bearing capacities of the normal super-long bored piles are often lower than the values estimated by empirical methods. Test results of 10 field test piles from 5 different sites in Shanghai district were collected by the authors. It illustrates that the ratios of the measured values of the ultimate bearing capacities of the piles to the values estimated by empirical method range from 0.5 to 0.97. The average ratio is 0.69. The pile bearing capacity can be greatly improved by post grouting technique. Measured data of 28 post grouted piles from 9 Shanghai project sites indicate that the average ratio of the measured values of the piles ultimate bearing capacities to the values estimated by empirical method is 1.32. Therefore, the post grouting technique should be adopted for super-long bored piles in deep soft soils.

5.2 PILE SHAFT STRENGTH AND COMPRESSION

Due to the application of the post grouting technique, the bearing capacities of the foundation soils around the super-long pile are improved greatly. Therefore, the strength of pile shaft should match well with the bearing capacities of the foundation soils in the design of a single pile. The application of high-strength concrete is helpful to achieve this object. As shown in Table 2, in order to make the piles shaft strength meet the piles bearing capacities requirements, Grade C45 and even Grade C50 concrete were adopted for the foundation piles of several super high-rise buildings in China. Meanwhile, concrete strength can be enhanced by the effect of stirrup constraint. Thus, the spacing of spiral stirrups at the pile top within a scope of about 3*D*~5*D* (*D* is the pile diameter) should be appropriate reduced to increase the bearing capacity of pile shaft.

Table 2 Pile shaft strength of several projects in China

Project name	Concrete strength grade	*UCS* (MPa)
Shanghai Center Tower	C50	40.0
Shanghai magnolia square	C45	44.3
Tianjin 117 Tower	C50	59.3
Wuhan Center Tower	C50	54.6

Note: *UCS* is the average unconfined compressive strength of the concrete drilled from the shaft.

Pile shaft compression is a part of the pile top settlement deformation. It is often estimated by the following empirical formula:

$$S = \frac{1}{AE_{\mathrm{p}}}\int_0^L \left[Q_0 - \pi d \int_0^z q_{\mathrm{s}}\left(z\right) dz \right] dz = \xi_{\mathrm{e}} \frac{Q_0 L}{AE_{\mathrm{p}}} \qquad (1)$$

Where Q_0 is the load applied at pile top; L is the pile length; A is the pile section area; E_{p} is the elastic modulus of the pile shaft; ξ_{e} is the pile shaft compression coefficient. For friction pile, ξ_{e} =1/2~2/3.

According to measured data of nearly 40 super-long bored test piles from 15 sites, diagram of the relationship between the measured values of the pile shaft compression and the calculated value of Q_0L/AE_{p} was drawn, as shown in Figure 3. As can be seen from the graph, under the working loads, the pile shaft compression coefficients are less than 1/2. Therefore, the value of ξ_{e} for calculating super-long bored pile shaft compression by formula (1) should be not larger than 1/2.

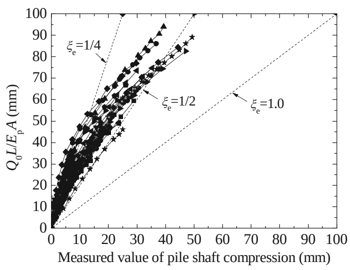

Figure 3 Diagram of the relationship between the measured values of the pile shaft compression and calculated values of Q_0L/AE_{p}

6 PILE FOUNDATION DESIGN

The synergism of the superstructure, foundation soils and pile foundations should be considered in the design calculation of pile foundations for super high-rise buildings. According to this, a practical method for analysis and calculation of the pile foundation is given in this paper. The theoretical framework and procedures of this method are illustrated in Figure 4. The general calculation process is shown in Figure 5.

Design calculation of the pile foundation consists of four parts, including foundation settlement calculation, bearing capacity calculation of the grouped piles, bending stress calculation of the raft, punching and shearing capacities calculation of the raft. The wind and earthquake actions need to be considered in the process of design calculation of the pile foundation for high rise building. The following load cases should be considered in the design. (1) Gravity load (dead load and live load); (2) Combination of gravity load and wind load; (3) Combination of gravity load and frequently earthquake load; (4) Combination of gravity load, wind load and frequently earthquake load; (5) Combination of gravity load and fortification intensity earthquake load.

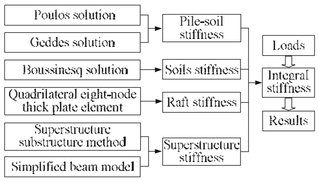

Figure 4 Theoretical framework and procedures of a practical method for analysis and calculation of pile foundation

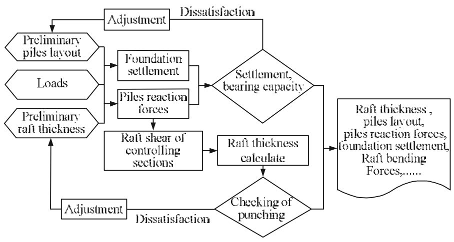

Figure 5 A general design calculation process of pile foundation

The lateral forces imposed by wind load and earthquake action may be very high for super high-rise buildings. When the eccentric vertical forces caused by wind load and earthquake action were accounted for in the design calculation process of the pile foundation, the characteristic value of the vertical bearing capacities of the piles can be increased about 20% and 50%, respectively. Moreover, if tension and compression zones generate in the foundation caused by the action of earthquake, for example as shown in Figure 6, the tension and compression bearing capacities of the piles in those zones should be checked.

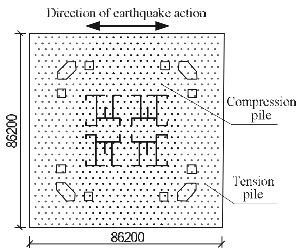

Figure 6 Distribution of tension and compression zones in the pile foundation of the Tianjin 117 Tower under the earthquake action

7 KEY CONSTRUCTION TECHNIQUES AND PILE QUALITY INSPECTION

Suitable drilling machine, techniques and some other auxiliary measures are key factors for successful construction of super long bored piles. Slewing drilling machine can be used in soft soils. But in the hard soils or soft rock layers, the construction efficiency of rotary drilling rig is higher than that of Slewing drilling machine. For example, in the Wuhan Tower project, which site soil stratigraphy consists of some dense slit, sand and moderately to slightly weathered mud rock within the drilling depth, about 79 hours were saved to construct a single pile when the rotary drilling rig was used instead of slewing drilling machine. Different types of rotary drilling rig bit can be selected for different soils in the borehole depth range. Different drilling machines can be combined to drill the boreholes in the complicated project site. For example, in the Wuhan Green Land Tower project, the rotary drilling rig was adopted for clay, sand and intense weathered mud rock layers, while the slightly weathered mud rock and sand rock were drilled by percussion drilling machine. In the process of the borehole drilling, sand content in the drilling fluid should be strictly controlled. Moreover, the density of the drilling fluid should be increased appropriately to ensure the stability of the super deep borehole wall. For example, in the Shanghai Center Tower project, the boreholes need to be drilled through about 60m thick sand layers. The indexes of the drilling fluid used in this project are shown in Table 3. If the borehole is very deep or located in coarse grained soil layers, the technique of pump suction or air-lift reverse circulation need to be utilized in the drilling construction process.

Table 3 Drilling fluid indexes of the Shanghai Center Tower project

index	Value
Density (g/cm^3)	1.1~1.2
Viscosity (s)	16~20
Sand content (%)	<4

Inspection and controlling standards of super-long bored piles are stricter than those of ordinary piles. Quality of the piles should be controlled in the process of construction. The borehole quality, including depth, diameter, verticality and sediment, need to be comprehensively inspected. The number of boreholes to be inspected should be not less than 30% of the total number of boreholes. The pile shaft quality should be evaluated mainly by sonic logging and core drilling methods. The number of piles to be inspected should be larger than 10% of the total number of engineering piles.

8 CONCLUSIONS

According to a great number of engineering practices of super-long bored pile foundations for super high-rise buildings in China, the paper systematically describes some key technical measures of design and construction of the super-long bored pile foundation together with a briefly summary of the bearing behaviors of the super-long bored pile. Post grouting technique is recommended for the super-long bored pile. Deep buried solid soils are usually selected for the pile tip bearing stratum. Application of the double steel sleeves, design of the pile top, construction and measurement requirements are essential issues that should be considered in the design of the field load test pile. Design calculation of the pile foundation should consider the synergism of the superstructure, soils and pile foundation. Inspection and controlling standards of super-long bored piles are stricter than those of ordinary piles. Quality of the piles should be controlled in the process of construction.

9 REFERENCES

Wang, W.D. Zhu, H.H and Li, Y.L. 2011. Urban geotechnical engineering and new technology. Chinese Journal of Undergrouond Space and Engineering, 7(s1): 1274-1291 (in Chinese).

Poulos, H.G. 2009. Tall building and deep foundations-Middle East challenges. Proceeding of the 17th International Conference on Soil Mechanics and Geotechnical Engineering, Alexandrie, Egypte, Volume 4: 3173-3205.

Zhang, Y. and Liu, J.B. 2009. Pile Foundation Handbook, China Building Industry Press, Beijing (in Chinese).

Wang, W.D., Li, Y.H. and Wu, J.B. 2011. Field loading tests on large-diameter and super-long bored piles of Shanghai Center Tower. Chinese Journal of Geotechnical Engineering, 33(12): 1817-1826 (in Chinese).

Wang, W.D., Li, Y.H. and Wu, J.B. 2012. Reply to disscussion on “Field loading tests on large-diameter and super-long bored piles of Shanghai Center Tower”. Chinese Journal of Geotechnical Engineering, 34(6): 1167-1168 (in Chinese).

Case Studies of Cost-effective Foundation Design in Rock

Études de cas sur la conception de la Fondation rentable dans Rock

Wong P.K.
Coffey Geotechnics Pty Ltd, Australia

ABSTRACT: In the Sydney region of Australia, the design of rock socketed piles in medium to strong rock is generally governed by settlement criteria, and designs are typically carried out using presumptive "serviceability" values quoted in the literature. The benefits of using a load-settlement performance rock socketed pile design method, rather than using "presumptive" values, are presented via two case studies in the Sydney region. On one site underlain by medium to high strength shale, dynamic pile load testing was carried out, and on another site underlain by high strength sandstone, Osterberg Cell (O-Cell) testing was carried out to validate the designs. The case studies presented clearly demonstrated that better understanding of load-deformation characteristics of pile foundations will lead to more cost-effective designs. Project owners have a tendency to resist spending money on testing, but the savings that can be achieved by adopting shorter rock socket lengths on medium to large projects far exceed the cost of pile load testing. The adoption of shorter rock socket lengths is generally the objective of project owners and contractors, but at the same time, has the benefit of preserving natural resources and reduction in CO2 emissions.

RÉSUMÉ : Dans la région de Sydney, de l'Australie, la conception des haldes encastrés dans un milieu à forte rock est généralement régie par critères de règlement, et conceptions sont généralement réalisées en utilisant les valeurs présumées « fonctionnalité » cités dans la littérature. Les avantages de l'utilisation d'un rocher de rendement de charge-tassement encastrés conception de pieux méthode, plutôt que d'utiliser les valeurs « présumées », est présentée par l'intermédiaire de deux études de cas dans la région de Sydney. Sur un même site sur des moyennes et schiste de haute résistance, essai de chargement de pieux dynamique a été réalisée, et sur un autre site sur des grès de haute résistance, Osterberg cellules (O-) essais a été réalisée pour valider les modèles. Les études de cas présentées a clairement démontré que meilleure compréhension des caractéristiques de contrainte-déformation des fondations sur pieux aboutira à des conceptions plus rentables. Maîtrise d'ouvrage ont tendance à résister à dépenser de l'argent sur les essais, mais les économies qui peuvent être obtenus en adoptant plus rock socket courtes sur moyens et grands projets bien dépassent le coût des tests de charge de pile. L'adoption de plus courtes longueurs de douille de roche est généralement l'objectif de la maîtrise d'ouvrage et les entrepreneurs, mais en même temps, a l'avantage de préserver les ressources naturelles et la réduction des émissions de CO2.

KEYWORDS: Rock sockets, bored piles, dynamic load test, Osterberg cell test, Sandstone, Shale, Serviceability

1 INTRODUCTION

The design of pile foundations in Sydney Sandstone and Shale in Australia has been carried out largely on the basis of "recipe book" approach, using the well-known references of Pells et al (1978) in Working Stress format, and Pells et al (1998) in Limit State format. Virtually in all cases, piles founded in rock are governed by serviceability limit (i.e. settlement criteria) rather than strength limit. Yet, there is little information on the deformation characteristics of piles founded in Sydney Sandstone and Shale. The use of presumptive design values quoted in references often leads to conservative designs.

Table 1. Design Values for Shale based on Pells et al (1998)

Shale Class(1)	Typical UCS (MPa)	Serv. Base, f_{ba} (MPa)	Ult. Base, f_{bu} (MPa)(2)	Ult. Shaft, f_{sa} (MPa)	Typical Field Modulus, E (GPa)
I	> 16	8	> 120	1	> 2
II	> 7	6	30 - 120	0.6 - 1	0.7 - 2
III	> 2	3.5	6 - 30	0.35 - 0.6	0.2 - 1.2
IV	> 1	1	> 3	0.15	0.1 - 0.5
V	> 1	0.7	> 3	0.05 - 0.1	0.05- 0.3

Table 2. Design Values for Sandstone based on Pells et al (1998)

Sandstone Class(1)	Typical UCS (MPa)	Serv. Base, f_{ba} (MPa)	Ult. Base, f_{bu} (MPa)(2)	Ult. Shaft, f_{sa} (MPa)	Typical Field Modulus, E (GPa)
I	> 24	12	> 120	3	> 2
II	> 12	12	60 - 120	1.5 - 3	0.9 - 2
III	> 7	6	20 - 40	0.8 - 1.5	0.35 - 1.2
IV	> 2	3.5	4 - 15	0.25 - 0.8	0.1 - 0.7
V	> 1	1	> 3	0.15	0.05 - 0.1(3)

(1) Rock Classification also depends on defect spacing and amount of seams
(2) Not more than 0.5 x UCS for Classes I, II and III Rock
(3) Not sure why this is less than modulus values for shale

Based on Pells et al (1998), the typical values adopted for design of rock socketed piles in Sydney Shale and Sandstone are tabulated in Tables 1 and 2 respectively. Pells et al (1998) suggested that the "serviceability" end bearing values given are for settlement < 1% of the minimum footing dimension, and that "ultimate" values occur at settlement > 5% of the minimum footing dimension. No "serviceability" values are given for shaft friction, because under serviceability loads, the pile shaft may take a majority of the load and the mobilized shaft resistance, particularly towards the top of the pile shaft, may reach close to the "ultimate" values.

It can be seen from Tables 1 and 2 that in conventional working stress terms, the ratio of ultimate end bearing value to the serviceability value would give rise to equivalent factors of safety of about 3 for the poorer quality rock, to 10 or more for Class I Shale and Sandstone. While it may be "safe" to adopt the presumptive "serviceability" values based on the notion that settlement will be less than 1% of the minimum footing size, there is no assessment on "how much less than 1%". Also, 1% of a relatively small diameter pile (say 0.6m dia.) would be very different to 1% of a 2m square footing (i.e. < 6mm compared to < 20mm settlement).

The difference between conducting a design based simply on presumptive "serviceability" values and a more detailed assessment of load-deformation response of a 1.8m diameter pile socketed 6m into rock (1m in Class V Sandstone, 2m in Class IV Sandstone, and 3m in Class III Sandstone) is illustrated in Figure 1 below. In both cases, the ultimate load capacity of the pile was assessed using the same values (f_{su} of 0.1MPa, 0.5MPa and 0.8MPa in Class V, IV and III Sandstone respectively, and f_{bu} of 20MPa for the Class III Sandstone). Using these parameters, the ultimate load for this pile was assessed to be 70MN. However, the load-deformation curves were in one case assessed using the method described by Poulos (1979), while in the other case as an extrapolation of a linear line between zero and the assessed ultimate load, with the line intersecting an assumed settlement of 1% at the pile load computed using the presumptive "serviceability" design values given by Pells et al (1998).

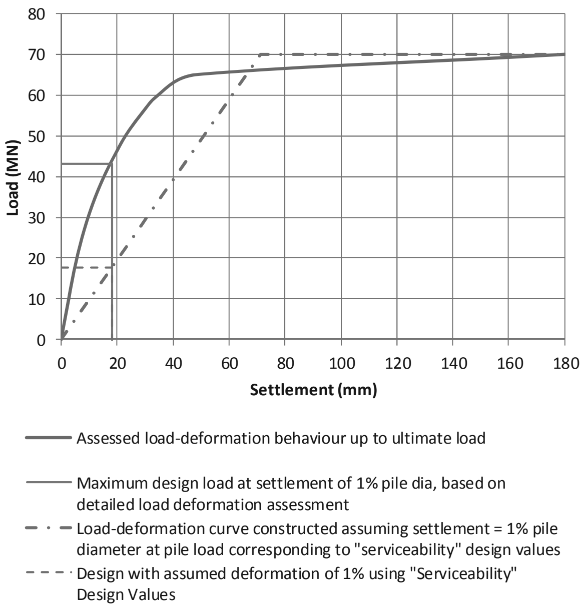

Figure 1. Load-deformation curves for Illustrative Example

Figure 1 shows that for the case corresponding to a presumptive settlement of 1%, the computed "serviceability" capacity would be limited to 18MN which corresponds to a relatively high factor of safety of 3.9. However, based on the more detailed load-deformation assessment, the maximum load to cause the same settlement of 18mm could be as high as 43MN. It should be pointed out that Pells et al (1998) acknowledges that the "elastic" design method is conservative, and supports that design be based on non-linear sidewall slip methods. It is therefore not surprising that the use of more sophisticated, non-linear load-deformation assessment methods would result in more economic foundation designs than adopting presumptive "serviceability" design values.

However, the accurate prediction of pile settlement relies heavily on knowledge of the foundation material stiffness in addition to adopting appropriate evaluation methods. Therefore, the author is of the opinion that using a performance based design, with pile load testing to validate the load-deformation response assessed, is more likely to achieve cost-effective designs, and increase confidence of meeting design objectives. This performance based design approach is illustrated in two case studies described below.

2 CASE STUDY 1

The first case study involves the testing of a 600mm diameter continuous flight augered pile socketed into weathered Ashfield Shale in Campbelltown, an outer south-western suburb of Sydney. The testing was carried out using dynamic technique with wave matching using the CAPWAP method.

The subsurface stratigraphy at this site comprised 7.3m of stiff to very stiff compacted clay fill and residual soil, underlain by a thin veneer (0.3m) of very low to low strength, highly to moderately weathered shale (Class IV Shale), followed by medium to high strength shale with Point Load Strength Index typically between 0.5MPa and 1.5MPa. Based on a typical correlation factor of 20 for Sydney Shale and Sandstone (although the range may be between 10 and 30), the approximate unconfined compressive strength of the medium to high strength shale is 10MPa to 30MPa, and the rock was classified as Class II Shale based on Pells et al (1998). The test pile was socketed 0.3m through the very low to low strength shale and penetrated only 0.1m into the medium to high strength shale so that its end bearing pressure can be readily assessed.

The dynamic load testing was carried out using an 11 tonne drop hammer and a purpose built testing frame as shown in Figure 2.

Figure 2. Dynamic pile load test set up in Case Study 1

The CAPWAP analysis results provided an estimated mobilized total capacity of 12.39MN, with a mobilized shaft resistance of 1.25MN and a mobilized pile toe resistance of 11.14MN. The mobilized end bearing resistance therefore corresponded to 39.4MPa. The mobilized pile toe settlement during the test blow was less than 6mm and the inferred static load-displacement response was relatively stiff with no suggestion that the ultimate end bearing resistance was reached.

Based on the test results, a "serviceability" design capacity of 3.4MN (i.e. 12 MPa end bearing pressure) was adopted. If the piles had been designed using a presumptive "serviceability" end bearing pressure of 6MPa, the design serviceability load would have been limited to 1.7MN (i.e. 50% less). The benefit of the dynamic load test in providing design confidence and economic design was clearly demonstrated in this example.

3 CASE STUDY 2

This is a recent case study associated with the Barangaroo South Stage 1A Development located on the western fringe of the Sydney CBD, on the eastern shoreline of Darling Harbour.

The site is situated over reclaimed land in an eroded and infilled paleovalley, with rock ranging in depth from 0m to 30m as shown in Figure 3. As such, most of the weathered rock has been removed during the erosional process, and replaced with overlying Holocene alluvial sand, silt, clay, and manmade fill.

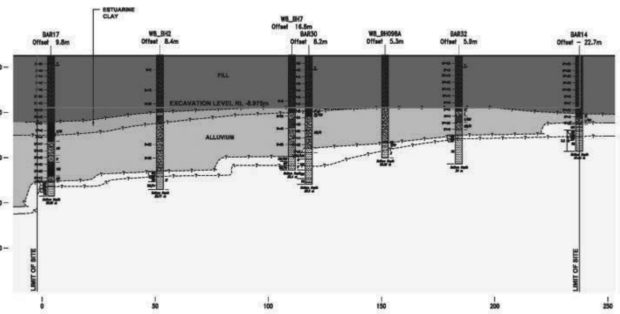

Figure 3. Stratigraphic profile at the site of Case Study 2

The rocks at the site comprise Hawkesbury Sandstone, with average Point Load Strength Index ranging from 0.05MPa to 1.5MPa between 1m to 3m below rock surface, thereafter having an average Point Load Strength of about 1.5MPa as shown in Figure 4. These Point Load Strength index tests suggested the unconfined compressive strength of the rock to be on average about 30MPa below 3m depth, but layers having strengths as high as 60MPa to 80MPa are likely to exist.

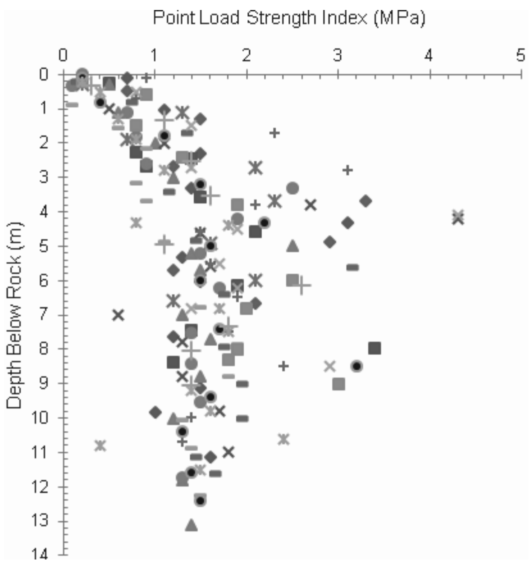

Figure 4. Point Load Strength Test Results (Case Study 2)

The sandstone rock at the site was classified in accordance with Pells et al (1998), and preliminary design parameters for pile design were assigned as summarized in Table 3. The project required nearly 1000 piles with diameters ranging from 1m to 2.4m to support 3 towers of up to 34 storeys in height and a number of low rise buildings over a 4ha site. The design serviceability pile loads ranged from 7MN to 14MN for 1m diameter piles, to 72MN to 81MN for the 2.4m diameter piles.

The structural engineer for the project was particularly concerned about long-term differential settlement effects on the tower structure, and therefore specified tight pile settlement criteria. A pile toe settlement limit of 0.3% of the pile diameter was stipulated at the pile toe. This was an unusual specification but it was adopted by the structural engineer so that equivalent structural "springs" could be adopted for the piles in his structural model of the superstructure, to include modeling of the piles due to the varying pile lengths on the project.

Table 3. Design Values Adopted for Design (Case Study 2)

Sandstone Rock Class	**Elastic Modulus* (GPa)**	**Poisson's Ratio**	**Ultimate End Bearing Pressure (MPa)**	**Ultimate Shaft Friction (MPa)**
IV	0.5	0.3	10	0.5
III	1.0	0.3	20	0.8
II or better	2.0	0.2	80	2

***** These represented the initial tangent modulus values.

A non-linear analysis using the following equation was adopted to describe the secant modulus:

$E_{sec} = E_t\,[1 - R_f(p/p_f)]$

where:

E_t = initial tangent elastic modulus (values given in the table)

R_f = hyperbolic curve-fitting constant (R_{fs} = 0.25 adopted for shaft and R_{fb} = 0.7 adopted for base)

p = mobilized pile-soil stress

p_f = limiting value of pile-soil stress (values of fb and fs given in table)

Because of concerns that dynamic testing would not be able to provide sufficient test load and would not capture the potential creep effect of the rock at high loads, pile load testing was conducted on two 750mm diameter prototype piles fitted with Osterberg Cells (O-Cell). Load-settlement prediction, pile load testing, and back-analyses of the pile load testing results for the project has been described in Wong and Oliveira (2012). In brief, the two test piles had rock socket lengths of 7.85m (SC-01) and 6.38m (SC-02); both founded with the pile toe socketed more than 3.5m in Class II Sandstone. The O-Cell was located at the toe of the test piles and the maximum O-Cell load reached was 22.6MN for SC-01 and 26MN for SC-02.

The test results for SC-02, together with results of back-analyses using the embedded pile element method in the commercial finite element analysis program FLAC (3D), are presented in Figure 5.

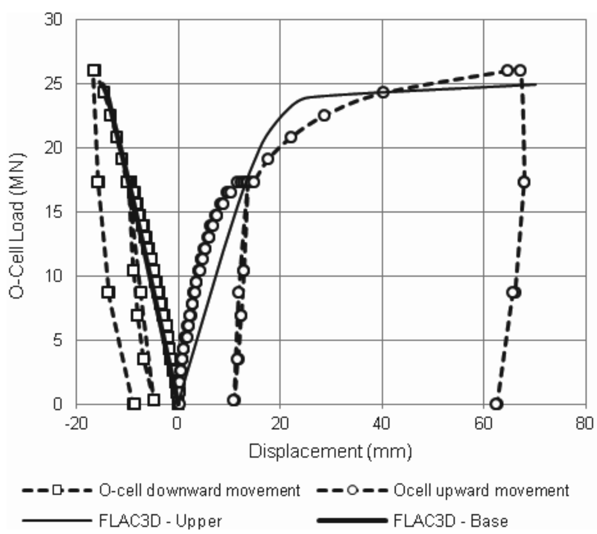

Figure 5. O-Cell Test and Back-analysis Results (Test Pile SC-02)

The key findings of the O-Cell testing are summarized below:

End Bearing Resistance

- Maximum mobilised resistance = 59MPa (ultimate end bearing pressure not reached)
- Little or no creep at an end bearing pressure of 38MPa (this pressure was held for 30 minutes)

Shaft Resistance

- Creep started at an average shaft resistance (over 5.5m length) of 1.06MPa and was significant at 1.3MPa
- The shaft response became "plastic" at a movement of about 30mm, with a corresponding average shaft resistance of 1.74MPa

The O-Cell test results confirmed the ultimate design values adopted for design, and as in Case Study 1, demonstrated that significantly higher serviceability end bearing pressure could be considered in the design of rock socketed piles in Sydney rock. If the presumptive end bearing pressure given in Table 2 for Class I and II Sandstone was adopted, the serviceability end bearing resistance would have been limited to 12MPa. The O-Cell test clearly demonstrated that significantly higher serviceability end bearing could be adopted, provided the base of the rock socket is adequately cleaned. The pile construction aspect of this case study to ensure adequate rock socket roughness and base cleanliness is described in Sethi et al (2012). However, it should also be stressed that under serviceability loading, a large proportion of the applied load may be carried by the pile shaft depending on the length to diameter ratio of the rock socket. Therefore, the use of excessively high serviceability end bearing pressure may not be warranted. A detailed assessment of the rock-socket load-deformation response is necessary for each specific case.

In the above case study, the non-linear load-deformation behavior observed from the O-Cell test is of particular interest. Using the back-analyzed test results, and by close inspection of the load-deformation behavior of both the shaft and base, it was possible to deduce the operating secant modulus of the rock socket material at various mobilized base and shaft resistance as shown in Figures 6 and 7.

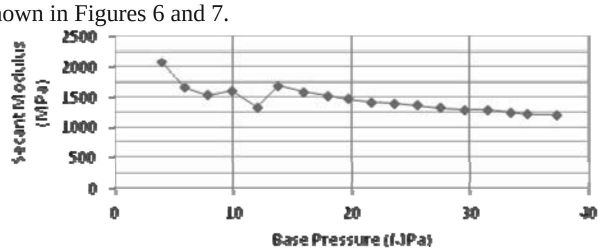

Figure 6. Deduced Secant Modulus of Rock below Pile Base

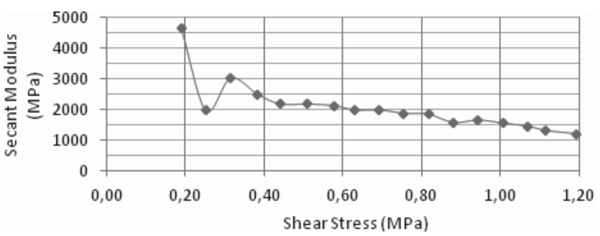

Figure 7. Deduced Secant Modulus of Rock around Pile Shaft

It can be seen from Figure 6 that there was a rapid drop in the inferred secant modulus of the rock below the pile base when a base pressure of 5MPa was reached, and remained at approximately 1.6GPa to 1.7GPa until a base pressure of 14MPa was reached. Above this pressure, the inferred secant modulus continued to drop steadily and reached a value of 1.3GPa at a base pressure of 30MPa. The initial drop in secant modulus at a base pressure of 5MPa to 14MPa could be attributed to compression of disturbed material or residual debris at the base of the socket, and the gradual drop of secant modulus beyond a base pressure of 14MPa is considered to be representative of the actual rock mass behavior.

From Figure 7, it can be seen that the inferred secant modulus of the rock socket material was initially very high (over 5GPa), then dropped rapidly to 2.5GPa at an average shaft resistance of 0.4MPa, then continued to drop steadily to 1.2GPa at a mobilized shaft resistance of 1.2MPa. Comparing these results with the non-linear function to describe the secant modulus adopted for design as shown in Table 3, it may be concluded that different initial rock modulus should be applied to describe the base and shaft response. However, for simplicity of design, and considering the operating stresses at the serviceability loads for the piles on this project, it was concluded that an initial tangent modulus value of 2GPa would still be appropriate for the Class II Sandstone if the hyperbolic pile base and shaft factors, R_{fb} and R_{fs} (see Table 3), were modified to 0.55 and 0.8 respectively. These values correspond to secant modulus values of approximately:

- Pile Base Response – 1.7GPa and 1.2GPa for the rock below the pile base, for end bearing pressures of 14MPa and 30MPa respectively, and
- Pile Shaft Response – 1.8GPa and 1.2GPa for the rock around the pile shaft for shaft resistance of 0.4MPa and 1.2MPa respectively.

However, these changes would only make very small changes ($\leq$ 3mm) to settlement prediction values at serviceability loading. Therefore, the original design parameters were adopted without changes for subsequent designs.

Supported by the O-Cell pile load testing, significant reduction in pile lengths and cost savings were achieved for this project as a result of the load-deformation analyses and performance based design carried out.

4 CONCLUSIONS

Other than very weak to weak rock, socketed pile design is generally governed by serviceability requirements rather than ultimate capacity. In such circumstances, economy pile designs can be achieved if accurate predictions of load-deformation behavior of the piles are made, rather than adopting recipe style presumptive values. Pile load testing should be carried out for such performance based design method.

Two case studies of rock socketed pile design and pile load testing have been presented in this paper, both of which clearly illustrated the advantages of this performance based design approach, with significant cost savings in foundation works. The use of the O-Cell testing method in Case Study 2 demonstrated the non-linear nature of high strength rock commonly encountered in the Sydney area of Australia.

5 REFERENCES

Pells P.J.N., Douglas D.J., Rodway, B., Thorne, C.P. and McMahon, B.R. (1978) Design Loading for Foundations on Shale and Sandstone in the Sydney Region, *Australian Geomechnics.* Jnl. Vol. 8, 31-39.

Pells P.J.N., Mostyn G., and Walker, B.F. (1998) Foundations on Sandstone and Shale in the Sydney Region, *Australian Geomechnics*. Jnl. No. 33 Part 3, 17-29.

Poulos, H.G. (1979) Settlement of Single Piles in Non-homogenous Soil, Jnl. Geot. Eng. Div., ASCE, Vol. 105, No. GT5, 627-641.

Wong, P.K. and Oliveira, D. (2012) Class A Prediction versus Performance of O-Cell Pile Load Tests in Sydney Sandstone, *Australian Geomechanics* Jnl,. Vol 47, No. 3, 89-96.

Sethi, P.L., Geng, I. and Wong, P.K. (2012) Construction of Rock Socketed Piles in Sydney Sandstone to Meet Performance Requirements, *Australian Geomechan.* Jnl., Vol 47, No. 3, 97-102.

Difficulté d'exécution des pieux profonds de grand diamètre dans des sols mous

Difficulty execution of large diameter deep piles in soft soils

Zaghouani K., Chouikha A.
Terrasol Tunisie

Haffoudhi S.
Hydrosol Fondations

RÉSUMÉ: La réalisation des pieux forés de 2m de diamètre et de 100 m de profondeur dans la vase de Tunis (cas des fondations principales du pont à haubans 'Rades-la-Goulette' à Tunis) ont posés de sérieux problèmes aux différents stades de leur exécution : notamment lors du forage, mais également lors du curage du fond du pieu, lors de la descente de cage d'armature et puis lors du bétonnage. L'article décrit les causes des difficultés rencontrées ainsi que les dispositions constructives adoptées en vue de valider les pieux contestables moyennant les calculs justificatifs nécessaires.

ABSTRACT : The achievement of 2m diameter, 100 m deep bored piles in the specific compressible soft clay soil of Tunis (the main foundations case of the cable-stayed Rades-la-Goulette bridge of Tunis) has posed serious problems at different execution steps: particularly during drilling, when cleaning the bottom of the pile, during the reinforcing cage drop, and then during concreting. The paper describes the causes of encountered difficulties and the adopted constructive arrangements to validate the debatable piles through the necessary supporting calculations.

KEYWORDS: deep piles, drilling, concreting, reinforced piles, loading test, bearing capacity

MOTS CLÉS : pieux profonds, forage, bétonnage, pieux renforcés, essai de chargement, capacité portante

1 INTRODUCTION

Le pont 'Rades-La-Goulette' reliant la Goulette à Radès et la banlieue Nord à la Banlieue Sud de Tunis, est l'un des plus grands ouvrages d'art en Tunisie. Cet ouvrage permet de desservir également trois départements: Tunis, l'Ariana et BenArous.

Ce pont haubané, le premier du genre en Tunisie, et en Afrique est d'une hauteur de 20 mètres au-dessus du niveau de la mer (Figure 1). Il est fixé par deux tours d'une longueur de 45 mètres chacune, reposant sur les deux piles principales P12 et P13 distantes de 120m. Ces piles, dans le projet initial d'appel d'offre, étaient prévues fondées chacune sur un groupe de 8 pieux de 2m de diamètre et ancrés à 100 m de profondeur. Les deux autres piles de rive P11 et P14 sont prévues fondées sur un groupe de 6 pieux de 1.5m de diamètre et de profondeur 60m de profondeur. Le dimensionnement des pieux a été basé sur les méthodes pressiométriques (Baguelin et al. 1986 ; Bustamante et al. 2009 ; Frank et Zhao 1982 ; Frank 1994 ; Melt 1991). Seuls les pieux profonds de la pile P12, exécutés en premiers, (pieux C et G) ont fait l'objet de difficultés d'exécution. Nous présentons dans cet article le cas du pieu G, les différentes difficultés rencontrées ainsi que la démarche de calcul justificatif en vue de simuler l'effet mécanique sur la portance et les dispositions constructives de renforcement adoptées.

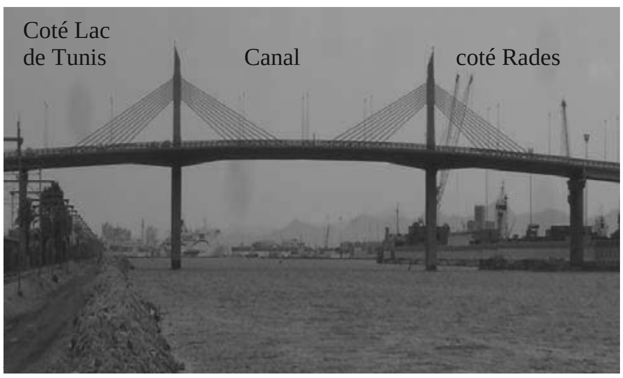

Figure 1. Photographie de l'ouvrage en service

d'épaisseur ne dépassant guère le mètre. On rencontre en moyenne de haut en bas :

- sous le TN (cote +1 NGT environ), un horizon superficiel I de vases très molles épaisse de 8 m ;
- une première couche II de sables et sables argileux moyennement denses, épaisse de 8 à 9 m ;
- une couche III d'argiles moyennement compactes, épaisse de 7 à 8 m ;
- une deuxième couche IV de sables fins plus ou moins argileux très denses, épaisse de 10 à 12 m ;
- une couche profonde V d'argiles plastiques moyennement raides à raides, de compacité croissante avec la profondeur, depuis 35 m de profondeur jusqu' à la base des sondages (115 m).

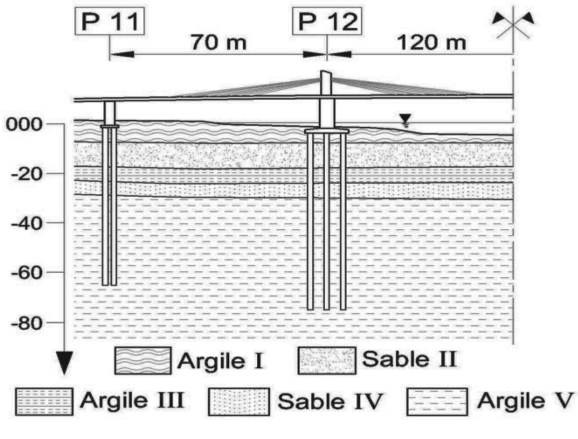

Figure 2. Demi-profil longitudinal de l'ouvrage et coupe géologique

3 DIFFUCULTÉS RENCONTRÉES LORS DU FORAGE DES PIEUX

La méthode de forage des pieux préconisée, prévoit deux techniques différentes successives:

- Forage classique 0 à 50 m de profondeur avec utilisation d'une foreuse à « bucket » type Soilmec, spécialement adaptée pour cette profondeur, sous confinement d'une boue bentonite.

- Jusqu'à 100 m, il était prévu l'utilisation du système RCD (Revese Circulation Drilling). Cette méthode consiste à descendre un outil à lames multi-formes à trois faces triangulaires et à attaque ponctuelle du sol. Le train de tige est constitué d'une tubulure creuse et une masse poids afin de maintenir la verticalité du forage. Le train de tige est actionné par une table de rotation hydraulique posée sur la tête du pieu. Le « cuttings » est envoyé par la voie de tubulure centrale moyennant une pression d'air comprimé envoyée depuis la surface. Cette méthode s'apparente à la technique d'air-lift utilisée souvent pour le pompage ou bien parfois pour le nettoyage de fond de forage.

Lors du forage du premier pieu (pieu G de la pile P12), après avoir atteint 33m le premier jour au bout de 8h avec la technique du « bucket », une certaine déviation de la verticalité a été constatée, ce qui a nécessité le recourt à une correction moyennant le RCD. Le changement de technique de forage et la mise en œuvre de la circulation inverse se sont traduits par de nombreuses difficultés et modifications sur l'outil. La profondeur de 50 m n'a pu être atteinte qu'au bout de 8 jours, mais par la suite la profondeur de 76m a pu être atteinte en quelques heures. Cependant à partir de cette profondeur, l'argile compacte et collante s'est mise à obstruer l'orifice d'aspiration, de telle sorte que, après plusieurs tentatives et modifications, le forage a été arrêté à 79,5 m . A ce stade, en attente de prise de décision, le forage a été comblé par de la grave concassée (5/8mm) jusqu'à 13 m de la surface. Ce temps d'attente a permis de reprendre les calculs afin d'étudier l'opportunité de limiter la profondeur des pieux.

Ainsi, on conclut que la méthode de forage classique au-delà de 33m a montré des problèmes de maintien de la verticalité du forage. Cette difficulté est due à la longueur du « kelly », et du jeu qui pourrait avoir lieu entre les éléments télescopiques notamment sous l'effet du poids important du « buket » de 2m de diamètre. Cet aléa est accentué par le manque de stabilité de la plateforme de travail, mise en place sur le terrain support constitué de vase molle. Puis, la méthode de circulation inverse a permis de corriger la dérive du forage par rapport à la verticale. C'est pour cette raison qu'il a été décidé de la conserver en dépit des difficultés apparues.

3.1 *Déplacements des parois du forage durant et après l'excavation d'un pieu*

Le profil et diamètre du forage ont été contrôlés à chaque étape, par des mesures au « KODEN », qui donnent les déformations en plusieurs points de la circonférence du forage, mesurées en continue le long du forage. Il a été constaté un resserrement de l'ordre de 25cm maxi sous boue bentonitique.

Nous avons procédé à des simulations de cette déformation moyennant un calcul EF avec le logiciel Plaxis afin de déterminer un ordre de grandeur des déplacements de la paroi du forage terminé et rempli de bentonite, puis par de la grave concassée, dans les deux cas :

- à court terme juste après l'excavation ;
- à long terme une fois que toutes les surpressions interstitielles dans les argiles autour de la paroi se sont dissipées.

La déformation de la paroi est simulée dans le modèle numérique de calcul à partir du module d'élasticité E :

- à court terme E a été déduit du module pressiométrique EM (Combarieu 2006) ;
- à long terme E a été déduit de l'indice de gonflement au déchargement C_s mesuré par les essais oedométriques (module consolidation de Plaxis).

$$\lambda^* = \frac{Cc}{2.3\,(1+e_0)} \quad ; \kappa^* = \frac{2\,Cs}{2.3\,(1+e_0)} \qquad (1)$$

avec C_c/C_s =10

Les calculs EF d'un modèle axisymétrique (Figure 3), donnent des valeurs faibles du déplacement de la paroi à court terme (de l'ordre du cm à quelques cm au plus). En revanche, à long terme les valeurs de ce déplacement dans les argiles sont beaucoup plus fortes : 18 cm au maximum dans la partie supérieure de la couche V et en moyenne 10 cm dans la partie moyenne de la même couche V.

Le calcul pour les différentes phases, indique que le pieu aurait subi une déformation maximale de 4 cm environ après un jour d'attente sous confinement par de la boue bentonitique. Elle concerne la partie supérieure de la couche V pour laquelle le déplacement maximal à très long terme est de 18cm, sous confinement par de la grave concassée.

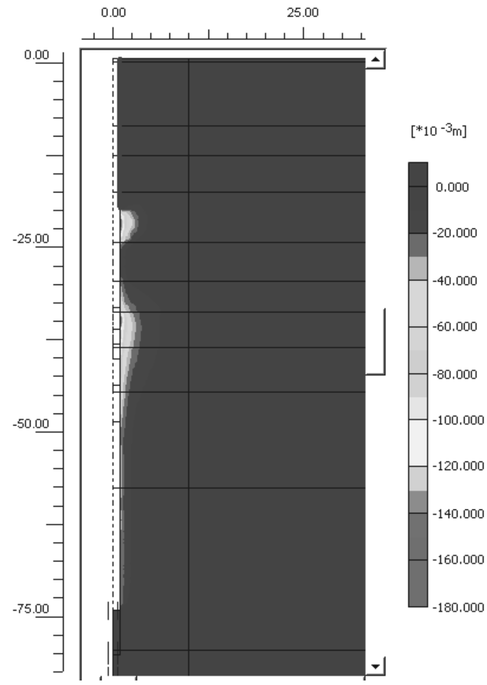

Figure 3. Déformation horizontale de la paroi du forage (max 174 mm)

Tous ces calculs, dont les résultats sont obligatoirement très approximatifs, montrent que le forage de grand diamètre dans l'argile, peut subir, durant la période de confinement sous boue, des déplacements non négligeables suite au mécanisme de relaxation du sol encaissant. Aussi, dans ces conditions, on comprend que, si la période de forage du pieu sous boue est trop longue, les couches compactes subjacentes (sable IV) peuvent présenter un risque d'éboulement.

3.2 *Effet de la relaxation du sol encaissant sur la portance du pieu isolé*

Afin de vérifier si la portance du pieu dont le sol encaissant aurait subi une altération, nous avons supposé que ceci a un effet direct sur le terme de frottement latéral q_s qui est fonction de la pression limite de terrain P_l. Le terme de pointe a été considéré peu affecté. Par mesure de sécurité, il a été recommandé de procéder à des travaux d'injection de la pointe.

Ainsi, le pieu G de la pile P12, a fait l'objet d'une reconnaissance complémentaire basée sur un sondage pressiométrique réalisé à proximité immédiate du pieu et un deuxième sondage un peu plus loin dans une zone supposée non affectée. Une étude paramétrique reliant un facteur de surdimensionnement (Q_{adm}/Q+W) à un coefficient réducteur sur les pressions limites noté r(%) a été effectuée :

$$r(\%) = 1 - (Pl_{réduite} / Pl_{initiale}) \quad (2)$$

avec Q_{adm} : la mobilisation du sol, Q : charge de service et W : poids du pieu déjaugé du sol encaissant (pour les pieux de grandes dimensions, le poids propre a une influence non négligeable qu'il faudrait intégrer à la descente des charges). On distingue pour la suite r_i et r_g, respectivement les coefficients réducteurs pour le pieu isolé et pour le groupe.

Dans le cas du pieu isolé, cette étude conduit au graphique suivant (Figure 4), qui montre que la réduction sur les valeurs des pressions limites du terrain encaissant ne doit pas dépasser 23% pour que le pieu soit justifié vis-à-vis de la portance, avec :

$$q_{s(réduit)} = (1 - r).q_s \; ; (0 \leq r \leq 1) \quad (3)$$

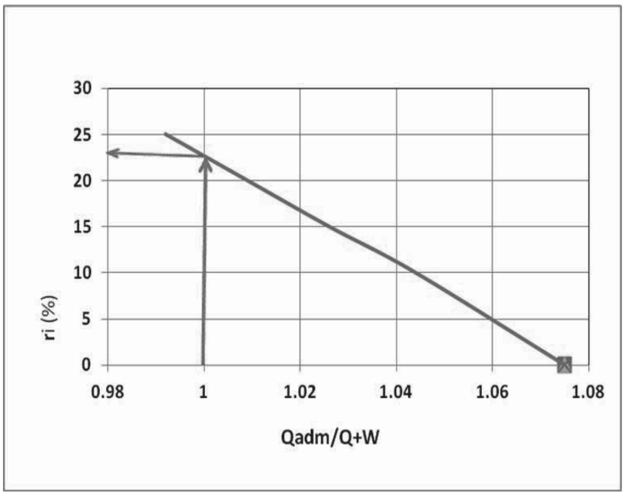

Figure 4. Coefficient réducteur de la portance en fonction du facteur de surdimensionnement : cas du pieu isolé

3.3 *Effet sur la portance du groupe de pieux*

La pile P12, a nécessité un groupe de 9 pieux arrêtés tous à 79.5m au lieu de 8 pieux initialement prévus descendre à 100m (Guilloux et al. 2009).

La même démarche précédente est conduite afin de déterminer une borne inferieure du coefficient réducteur r_g sur les caractéristiques du sol, afin de justifier la portance du groupe. Le groupe de pieux est modélisé par un pieu équivalent permettant ayant la même surface que l'enveloppe extérieure circonscrite aux 9 pieux, comme l'indique le schéma (Figure 5) suivant :

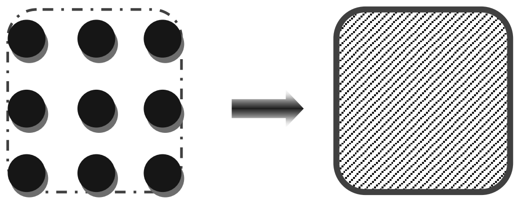

Figure 5. Principe du pieu équivalent au groupe de pieux

Le graphique suivant (Figure 6) montre que le groupe de pieux reste justifié vis-à-vis de la charge de service même en considérant un coefficient réducteur de 100% sur les valeurs de P_l, donc sur q_s. En effet, la capacité admissible du groupe a une répartition entre les efforts de pointe et de frottement latéral tout à fait différente de celle du pieu isolé. Alors que dans le pieu isolé la charge admissible en tête est essentiellement reprise par le frottement latéral, il n'en est plus de même dans le groupe où la pointe est beaucoup plus sollicitée. Ce calcul de pieu équivalent est justifié dans la mesure où le rapport de l'entraxe des pieux à leur diamètre est inférieur à 3, ce qui conduit à ce que les pieux et le sol qu'ils enserrent aient un comportement à peu près monolithique (Schlosser et al. 2009).

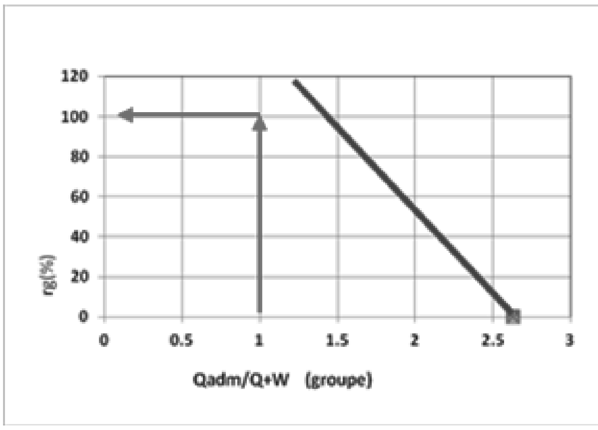

Figure 6. Coefficient réducteur de la portance en fonction du facteur de surdimensionnement : cas du groupe de 9 pieux.

3.4 *Effet de la relaxation du sol encaissant sur la raideur du groupe*

Une étude paramétrique de calcul de tassement du groupe de pieux a été également effectuée en considérant plusieurs cas de taux de dégradation qui affectent les 8 pieux extérieurs du groupe. En conditions normales de forage, sans dégradation de la paroi, le tassement du pieu équivalent est de 26mm. Le graphique suivant (Figure 7) montre que cette valeur sera doublée si l'on atteint un taux de dégradation de 50%. Ainsi, la raideur du groupe de pieux sera sensiblement affectée.

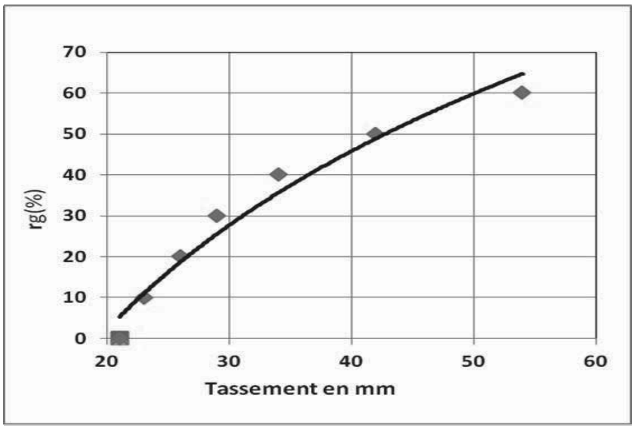

Figure 7. Coefficient reducteur affectant le groupe de 9 pieux en fonction du tassement admissible choisi

4 DIFFICULTÉS LORS DU BÉTONNAGE DES PIEUX

L'opération de bétonnage du pieu G a également posé des difficultés après reprise du forage. Un éboulement de la couche de sable a eu lieu. Des essais d'auscultation soniques ont révélés une anomalie au sens de la norme, très marquée et dont l'épaisseur est importante qui a affecté l'intégrité du pieu G vers 40 m de profondeur. Cette coupure de béton a été confirmée par des sondages carottés (présence de sable et gravier). Ce pieu a nécessité un traitement particulier de renforcement.

4.1 *Traitement des anomalies*

Deux carottages dans le pieu ont été réalisés et ont été descendus sous la pointe du pieu. Par ailleurs, les six tubes métalliques prévus pour l'auscultation soniques ont été percés par un procédé spécialement conçu à cet effet : perçage par oxycoupage au plasma (Figure 7).

Figure 8. Procédé de perforation par oxycoupage au plasma

Figure 9. Essai préalable de perforation sur un tube extérieur

Ainsi, au travers les perforations multiples (Figure 9) le long des tubes métalliques d'auscultation, et des sondages carottés, on a procédé au nettoyage des cavités avec la circulation d'eau sous pression.

Une auscultation endoscopique par une caméra, au travers les carottés dans le pieu, a permis de s'assurer de la qualité du nettoyage des zones d'anomalies.

4.2 *Renforcement mécanique du pieu*

Le long des anomalies, ainsi qu'au niveau de reprise du bétonnage, des micropieux ont été réalisés pour assurer une liaison mécanique et restituer l'intégrité du pieu. 23 barres HA 50 ont été réparties sur la section du pieu G et ont été scellées au coulis de ciment, en même temps que le comblement des cavités.

4.3 *Amélioration de la portance en pointe*

Le sol sous la pointe du pieu a été injecté en vue d'améliorer la portance pour se placer du côté de la sécurité. En effet, ce traitement a permis d'éviter un mauvais curage du fond de forage du pieu qui était jugé inefficace avec la méthode RCD

5 CONCLUSION

Les déplacements de la paroi du forage peuvent être importants dans les argiles lorsque le temps de forage sous bentonite est très long comme fut le cas pour le pieu G de la pile P12 du Pont Rades-La-Goulette. La dégradation de la résistance du sol par suite de ces déplacements de paroi a affecté l'effort de frottement latéral, mais pas l'effort de pointe. Si cet effet peut être important sur le pieu isolé, il est pratiquement sans effet sur la portance du groupe de pieux dans lequel l'effort de frottement latéral n'est plus du tout la part essentielle vis-à-vis de l'effort de pointe, comme c'est le cas pour la charge admissible du pieu isolé. Seule, la raideur peut en être sensiblement affectée.

6 RÉFÉRENCES

Baguelin, F., Bustamante, M., Frank, R. 1986. The pressuremeter for foundations: French experience. *Proc. Conference on the Use of In-Situ Tests in Geotechnical Engineering, Blacksburg, VA, ASCE, Geot. Special Pub*(6),31-46.

BUSTAMANTE, M., Gambin, M., Gianeselli, L. 2009. Pile Design at Failure Using the Ménard Pressuremeter: an Up-Date, *Proc. IFCEE '09, ASCE.*

Combarieu, O. 2006. L'usage des modules de déformations en géotechnique. *Revue Française de géotechnique*,(114), p. 332.

Frank, R., Zhao S.R. 1982. Estimation par les paramètres pressiométriques de l'enfoncement sous charge axiale des pieux forés dans les sols fins. *Bull. Liaison Labo P. et Ch.*, n° (119), 17-24.

Frank, R. 1994. The new Eurocode and the new French code for the design of the deep foundations. *Proc. Int. Conf. Design and Construction of Deep Foundations. Orlando. Florida. FHWA*(1), 279-304.

Guilloux, A., Berthelot, P., Zaghouani, K., Schlosser, F., 2009. Les fondations du pont de Radès La goulette (Tunisie) ; reconnaissances, conception et essais de pieux. *17th International Conference on Soil Mechanics and Geotechnical Engineering (17th ICSMGE) October 2009, Alexandria, Egypt.*

M.E.L.T.1991. Design Rules for Foundations, Tender Documents for Public Works. CCTG, Fasc. n° 62, TitreV (in French). Imprimerie Nationale Paris.

Schlosser, F., Gouilloux, A., Zaghouani, K. Berthelot, P. 2010. Rades Bridge Drilled Shafts Designed and Tested Using Menard Pressuremeter. *International Foundation Congress and Equipment Exhibition, Expo IFCEE 09, Orlando, Mars 2009*

Load Tests on Full-Scale Bored Pile Groups

Essais de chargement sur des groupes de pieux forés

Zhang Y., Salgado R.
Purdue University, USA

Dai G., Gong W.
Southeast University, China

ABSTRACT: Pile groups are commonly used in foundation engineering. Due to the difficulties and cost of full-scale load tests, most pile group tests are scaled down regardless of whether performed in the field or laboratory. Very limited experimental data are available on the loading of full-scale bored pile groups in the field. This paper reports the results of axial static load tests of both full-scale instrumented pile groups and single piles. Experiments vary in the number of piles in the group, the pile spacing, the type of pile groups and pile length. All piles have a diameter of 400 mm. Two-pile groups, four-pile groups and nine-pile groups with pile lengths of 20 m and 24 m are tested. Since the isolated piles and some piles in the pile groups are instrumented, the load transfer curve and the load-settlement curve of both of piles in isolation and individual instrumented piles in the groups are obtained. The interaction coefficient for each pile in the group is back-calculated from the measured data by optimization. The interaction coefficients are shown to depend on pile proximity, as usually assumed in elastic analyses, but also on settlement and on the size of the group.

RÉSUMÉ : Les groupes de pieux sont couramment utilisés dans les travaux de fondation. En raison des difficultés et du coût des essais de chargement à grande échelle, la plupart des essais de groupe de pieux sont réalisés à petite échelle indépendamment de la réalisation des essais en laboratoire ou in-situ. Très peu de données expérimentales sont disponibles sur le chargement en pleine échelle groupes des pieux forés in-situ. Cet article présente les résultats d'essais de chargement statique axial à grande échelle des groupes de pieux et des pieux simples instrumentés. Les expériences varient en nombre de pieux dans le groupe, l'espacement des pieux, le type de groupes et de longueur des pieux. Tous les pieux ont un diamètre de 400 mm. Des groupes composés de deux, quatre ou neuf pieux, avec des longueurs de 20 m et 24 m sont testés. Comme les pieux isolés et quelques uns des pieux dans les groupes sont instrumentées, la courbe de transfert de charge et la courbe de charge-tassement des pieux isolés et en groupe sont obtenus. Le coefficient d'interaction pour chaque pieu dans le groupe est évalué par calcul inverse à partir des données mesurées par l'optimisation. Il a été montré que les coefficients d'interaction dépendent de la proximité des pieux, comme habituellement supposé dans des analyses élastiques, mais également du tassement et de la taille du groupe.

KEYWORDS: pile groups, load transfer, interaction coefficient

1 INTRODUCTION

Settlement analyses of pile groups (e.g., Poulos 1968; Randolph and Wroth 1978, 1979; Poulos and Randolph 1983; Poulos 1989; Randolph 2003; Leung et al. 2010) are based on a variety of approaches, which include boundary-element methods, the hybrid load transfer approach, and the finite element method. Despite some theoretical advances in the analyses and prediction of pile group behavior in the last few decades, analyses are still largely based on simplifications of the problem and of the constitutive behavior of the soil. Due to the difficulties and cost of full-scale load tests, most pile group tests were scaled down regardless of whether performed in the field or laboratory. There are few *in situ*, full-scale bored pile group load tests reported in the literature.

The present paper aims to start filling this knowledge gap by reporting the results of *in situ*, full-scale bored pile group tests. The aim of the tests was to investigate the following crucial issues in particular: (*i*) what the rates of pile head and pile base load mobilization with settlement are; (*ii*) how the shaft resistance, which is responsible for the difference between these two rates, varies between single piles and piles in a group in various arrangements; (*iii*) the proportion in which load applied on a pile cap is shared between the piles in the group; (*iv*) how pile group efficiency varies with settlement.

2 EXPERIMENTAL PROGRAM

The field load tests on bored piles were performed on: (*i*) an isolated single pile with length L = 20 m; (*ii*) an isolated single pile with L = 24 m; (*iii*) a two-pile group with spacing s_p = 2.5B (B, the pile diameter) and L = 20 m; (*iv*) a two-pile group with s_p = 3.0B and L = 24 m; (*v*) a four-pile group with s_p = 2.5B and L = 20 m; (*vi*) a four-pile group with s_p = 3.0B and L = 24 m; (*vii*) a nine-pile group with s_p = 2.5B and L = 20 m; and (*viii*) a nine-pile group with s_p = 3.0B and L = 24 m. All piles in the experiments had a diameter B of 400 mm. The concrete strength (f'_{cd}) was 25 MPa for both the piles and the caps. The concrete reinforcement cover was 70 mm in the caps and 35 mm in the piles. In this paper, tests on isolated single piles are denoted by DZ. Pile group tests are denoted by QZ. The suffix L is used to indicate that the pile length L is 24 m. A dash after the pile group reference followed by a number indicates a specific pile within that group.

One auger boring was drilled at the test site to a depth of 29.50 m. This boring showed a uniform, thick soft clay layer starting at 17m and extending all the way to the bottom of that boring. This auger boring depth was 11B deeper than the test pile base for piles with 24 m length. Static cone penetration tests (CPTs) were performed in the vicinity of the boring to give a continuous record of the soil resistance with depth. The subsoil profile includes multiple layers of silt and clay. The ground water level was found at a depth of 2.60 m. The detailed soil properties for each layer at this test site are given by Dai et al (2012).

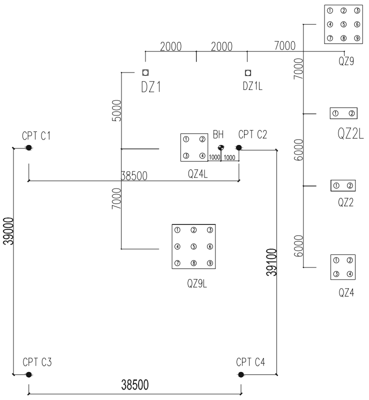

Figure 1. Layout plan of test piles and pile groups (all dimensions in millimeters).

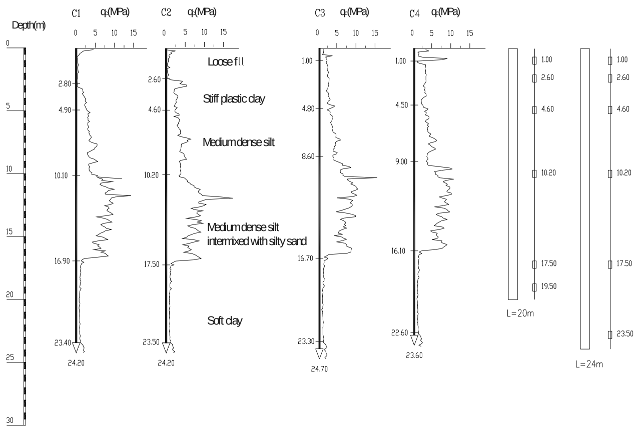

Figure 2. The CPT site logs and the layout of strain gauges in the test piles (all dimensions in meters).

The piles were installed using the slurry method. A 0.4-m-, 0.8-m- or 1.2-m-thick reinforced concrete cap was subsequently poured on the pile groups and single piles. Figure 1 shows a layout plan of the test piles and pile groups. The pile caps rested on the ground and may be considered rigid for practical purposes. The pile spacing was 2.5B in groups QZ2, QZ4 and QZ9 and 3.0B in groups QZ2L, QZ4L and QZ9L.

The axial loads transferred along the instrumented piles were measured by strain gauges, which were installed evenly at each cross section for all test piles. There were 6 instrumented sections in each instrumented pile (Figure 2). A vibrating-wire load cell measured the pile top load of each pile in the pile groups during the loading process. The load tests were performed by the kentledge load method. The load tests were slowly maintained load tests. There were no unload-reload loops. Load was applied by hydraulic jacks. Settlements were measured at four locations on the upper surface of the cap by four displacement transducers.

3 ANALYSIS OF LOAD TEST RESULTS

The load-settlement curves for the two single piles (Figure 3) show that these two curves are almost identical for $Q \leq 900$ kN, corresponding roughly to $0.6Q_{ult}$, with ultimate bearing capacity , Q_{ult}, defined based on the traditional 10% relative settlement criterion (Salgado 2008). For $Q > 900$ kN, the settlement at the pile top is greater for DZ1 than for DZ1L at the same load. The ultimate bearing capacity Q_{ult} is 1430 kN for DZ1 and 1540 kN for DZ1L according to the 10% criterion.

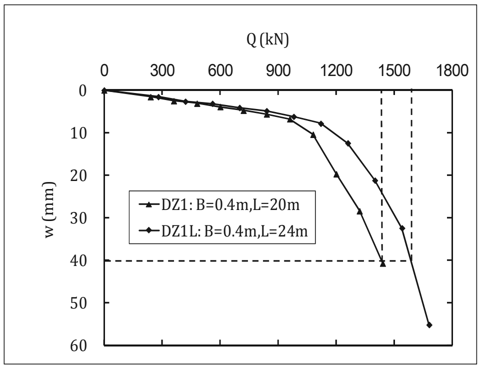

Figure 3. Load settlement curves for single pile tests.

Figure 4 and Figure 5 show the axial load transfer curves for DZ1 and DZ1L throughout the loading process. There is significant transfer of load from the pile to the soil between 2.6 m and 17.5 m for both DZ1 and DZ1L, which makes the resistance at the pile base for both DZ1 and DZ1L comparatively small. At the end of the test, the pile head load for DZ1 is 1440 kN while the pile base load is 31 kN. For DZ1L, the corresponding numbers are 1540 kN and 62 kN. These results suggest minimal and potentially zero base mobilization, which means that essentially all of the loads applied at the pile head are carried by shaft resistance. So both pile DZ1 (L/B = 50) and pile DZ1L (L/B = 60) derive their resistance from shaft resistance at values of relative settlement conventionally associated with the ultimate load. Complete shaft resistance mobilization in friction piles crossing soft soil layers may require large pile head settlement because of large axial pile compressibility.

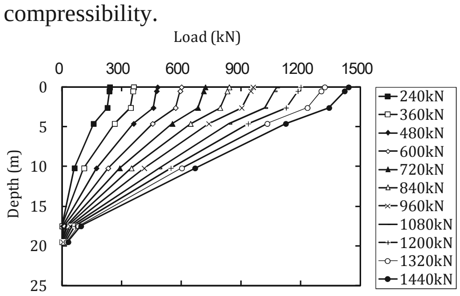

Figure 4. Axial force distribution for 20m-long single pile.

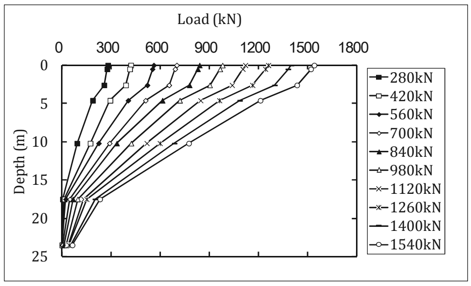

Figure 5. Axial force distribution for 24m-long single pile.

Figure 6(a) shows the load-settlement curves for the single pile and the average load-settlement curves for the pile groups with L = 20 m. The average load per pile in a group is less than the load on a single pile at the same settlement except for pile group QZ2. This exception is likely caused by variability in the soil properties around that group or some variability in construction. The equivalent figure for L = 24 m is Figure 6 (b), which shows a much more clear separation between the responses of the single pile and the average response of each pile group.

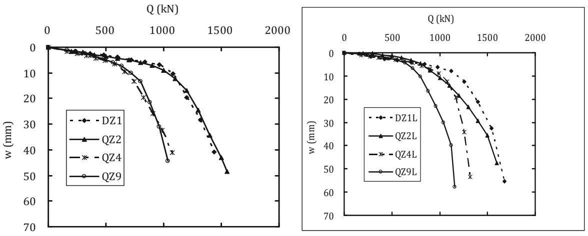

(a) (b)

Figure 6. Load-settlement curves for the single pile and the average load-settlement curves for the pile groups: (a) L = 20 m; (b) L = 24 m.

Figure 7 (a) and (b) show group settlement ratio R_s, the ratio of the settlement of a pile group to that of single pile at the same average load per pile (Poulos and Davis 1980).The values of R_s of both four-pile group and nine-pile group tend to increase with settlement. The single pile settlement is generally smaller than the corresponding pile group settlement at the same average load per pile when the load is relatively large. The R_s values for the two-pile groups are however close to unity. The initial values of R_s (at small loads) are also close to unity, indicating little interaction between the piles.

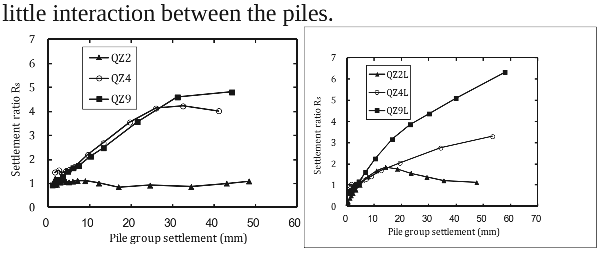

(a) (b)

Figure 7. Settlement ratio Rs versus pile group settlement for all pile groups: (a) with L = 20 m; (b) with L = 24 m.

Figure 8 shows the distributions of unit shaft resistance both for the single pile DZ1L and for some instrumented piles in groups QZ2L, QZ4L and QZ9L at intermediate load steps during the load tests.

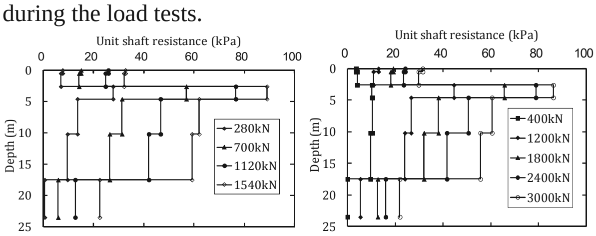

(a) (b)

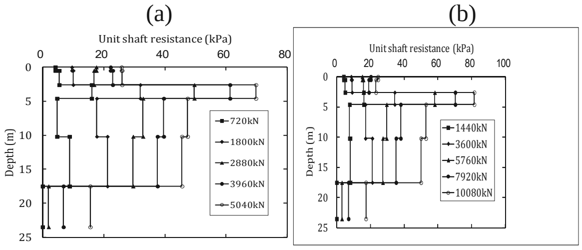

(c) (d)

Figure 8 Distribution of unit shaft resistance for the single piles and for the instrumented piles in the pile groups: (a) DZ1L; (b) QZ2L-1; (c) QZ4L-1; (d) QZ9L-1.

The limit shaft resistances were calculated by using the pile design methods proposed by Salgado et al. (2011), which capture the dependence of the unit shaft resistance on the clay undrained shear strength, the normal effective stress on the pile shaft and the difference between the critical-state friction angle and the minimum residual friction angle. Figure 8 shows that the unit shaft resistance is close to a limit value at shallower locations, but that is not the case for deeper locations along the pile. In practical terms, this means that the end of the load tests on the single piles corresponds to state at which the shaft resistance mobilized along the entire pile is less than the limit shaft resistance.

The pile head and base loads versus pile group load are shown in Figure 9 for piles of the 9-pile groups under different load levels. The corner piles have the largest pile load, followed by side and then central piles. This confirms intuition based on elasticity solutions that if the pile cap is flexible and the loads on every pile are as a result the same, the center pile with lowest stiffness would be expected to settle the most, showing that it has the lowest stiffness. When imposing the same settlement on all piles, we would therefore expect the center pile to carry the smallest load, as indeed observed. The experimental results seem to capture an aspect of pile group response that is not often commented on. The base of the pile located towards the center of the group is more constrained because of the surrounding piles, which may lead to a greater base resistance.

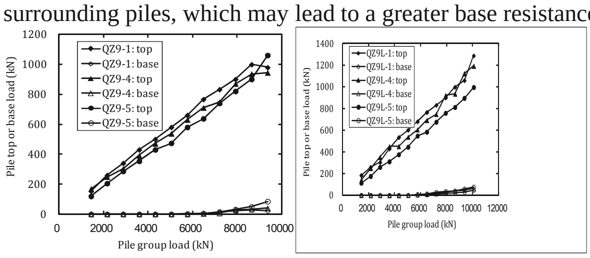

(a) (b)

Figure 9 Pile head and base loads versus pile group load for the nine pile groups: (a) L = 20 m; (b) L = 24 m

Because of symmetry, the head and base loads for piles in two-pile and square four-pile groups are expected to be the same. However, that is not the case for the piles in the nine-pile groups. The ratio Q_i/Q_{av} of the individual pile load to the average individual load in the group is shown in Figure 10. The load on the outer piles of each group is observed to be greater than the average load Q_{av}.

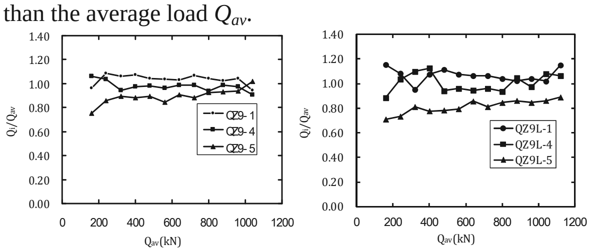

(a) (b)

Figure 10 The ratio Q_i/Q_{av} of the individual pile load to the average individual load in nine pile groups: (a) L = 20 m; (b) L = 24 m.

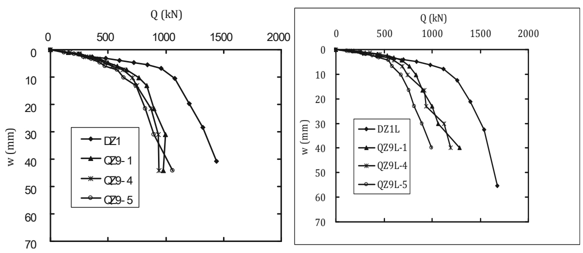

(a) (b)

Figure 11 Individual pile load versus group settlement relationship for the two nine pile groups: (a) L = 20 m; (b) L = 24 m.

Figure 11 shows individual pile load versus group settlement curves for QZ9 and QZ9L. For comparison, the load-settlement curves of DZ1 and DZ1L are also shown in Figure 11. For small group loads, for which linear elastic solutions would be most applicable, a random load distribution is obtained, with no definite pattern. When $Q_{10\%}$ is approached, there is a redistribution of the load, and position of the pile within the group begins to influence the load it carries. Generally, at the same settlement, the load on an individual pile within the group is always less than the load for the corresponding single pile.

4 IMPLIED INTERACTION COEFFICIENTS

This interaction between piles is expressed through the concept of the coefficient of interaction α_{ij}, which is equal to the ratio of the settlement of pile *i* to the settlement of pile *j* when pile *j* is loaded. Using this concept, the settlement of any pile *i* in a group with a rigid cap is expressed through (Salgado 2008)

$$w_i = \sum_{j=1}^{n} \alpha_{ij} \frac{Q_j}{K_{tj}} \tag{1}$$

where w_i is the settlement of pile *i*, α_{ij} is the influence factor between *i* and *j*. Q_j is the load acting on pile *j*, and K_{tj} is the stiffness of pile *j* (in the sense of how much load is required to have unit pile head stiffness). Details on how to obtain the interaction coefficients using these equations by linear optimization can be found in Dai et al. (2012).

The influence coefficients versus pile group settlements are shown in Figure 12. In general, with the increase of group settlement, the interaction coefficient increases, with an inflection point for small settlements (marking the transition from little interaction for small settlements to a higher level of interaction) and later a tendency of stabilization at large settlements, which is consistent with more intense localization of shear strain around the piles at large settlements, which leads to a reduction in the interaction for incremental settlement.

The results for the 2-pile groups QZ2 are inconsistent with the other results, with the interaction coefficient being practically zero. This may be because of spatial variability of the soil or other variability in the pile installation or pile cap. For the four-pile groups, the pile spacing has a larger effect on interaction than pile length, which is to be expected. The interaction coefficient in group QZ4 with s_p = 2.5*B* and *L* = 20 m is on average larger than that of group QZ4L with s_p = 3.0B and *L* = 24m. For the nine-pile group, the interaction coefficients are distributed proportionally to pile center-to-center spacing. The interaction coefficients for the piles in the four-pile group are larger than comparable coefficients (at the same spacing) for the nine-pile group. The presence of additional piles around interacting piles likely interferes with load or settlement transmission between the interacting piles.

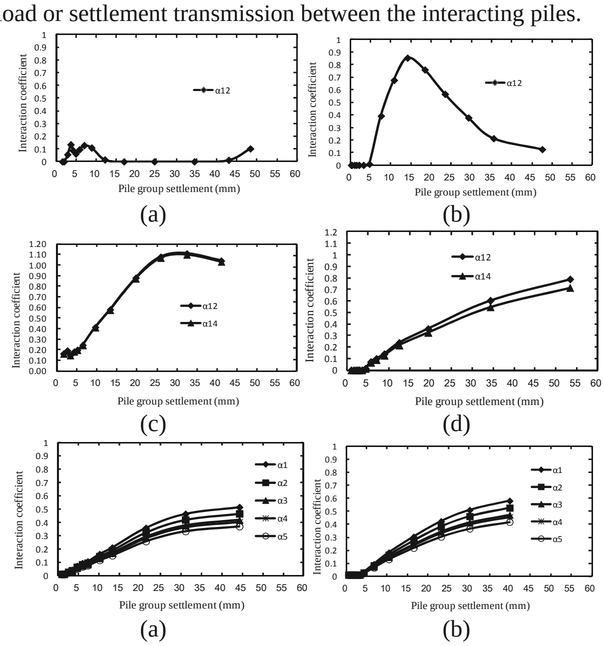

Figure 12.Interaction coefficients versus settlement in each pile group: (a) QZ2; (b) QZ2L; (c) QZ4; (d) QZ4L; (e) QZ9; (f) QZ9L.

5 CONCLUSION

A field pile load testing program was carried out on isolated bored piles and bored pile groups (with two, four, and nine piles with different pile lengths and pile spacing) installed in a soil profile with mixed layers of clay and silt. Based on the analysis of the field test results, the following conclusions can be reached:

(1) Based on the traditional 0.1*B* relative settlement criterion, the two single piles DZ1 (*L/B* = 50) and DZ1L (*L/B* = 60) mobilized essentially only shaft resistance, with loads measured at the strain gauge level closest to the pile base accounting for only 2.2% of the total load for the 20-m-long pile and 4% of the total load for the 24-m-long pile.
(2) The general response of an individual pile in the 2-pile groups was observed to be very close to that of the corresponding single pile, suggesting minimal interaction between piles in the two-pile groups.
(3) The values of settlement ratio of both the four-pile and nine-pile groups tended to increase with settlement. The single pile settlement was observed to be generally smaller than the corresponding pile group settlement at the same average load per pile when the load was relatively large.
(4) Group effect was more pronounced for QZ4 than for QZ4L and for QZ9 than for QZ9L, showing that the impact of the pile spacing is greater than that of the pile length on group load response.
(5) The load at the top of the corner piles was observed to be the largest, followed by side piles and then center piles. However, the load differences were not large, particularly for side versus corner piles.
(6) The interaction coefficient was seen to be a function of settlement and the size of the group. With the increase of group settlement, the interaction coefficient was observed to increase.

6 ACKNOWLEDGEMENTS

The research was supported by the National Natural Science Foundation of China (Grant No.50908048) and a project funded by the Priority Academic Program Development of Jiangsu Higher Education Institutions (PAPD).

7 REFERENCES

Dai, G., Salgado, R., Gong, W., and Zhang, Y. 2012. Loads tests on full-scale bored pile groups. Canadian Geotechnical Journal, accepted.

Leung, Y. F., Soga, K., Lehane, B.M. et al. 2010. Role of linear elasticity in pile group analysis and load test interpretation. J. Geotech. Geoenviron. Eng., 136 (12), 1686 - 1694.

Poulos, H. G. 1968. Analysis of the settlement of pile groups. Geotechnique, 18 (4), 449 - 471.

Poulos, H. G., Randolph M. F. 1983. Pile group analysis: a study of two methods. J. Geotech. Eng., 109 (3), 355 – 371.

Poulos, H. G., and Davis, E. H. 1980. Pile foundation analysis and design, Wiley, New York.

Poulos, H. G. 1989. Pile behave – theory and application. Geotechnique, 39 (3), 365 - 415.

Randolph, M. F. 2003. Science and empiricism in pile foundation design. Geotechnique, 53 (10), 847 - 875.

Randolph, M. F. and Wroth, C.P. 1978. Analysis of vertical deformation of vertically loaded piles. J. Geotech. Eng., 104 (12), 1465 – 1488.

Randolph, M. F. and Wroth, C.P. 1979. An analysis of the vertical deformation of pile groups. Geotechnique, 29 (4), 423 - 439.

Salgado, R., Prezzi, M., Tehrani F. S. 2011. "Soil Property-Based Methods for Design of Nondisplacement Piles." 2011 Pan-Am CGS Geotechnical Conference.

Salgado, R. 2008. The Engineering of Foundations. McGraw-Hill.

General Report of TC 214
Soft soils

Rapport général du TC 214
Sol mous

Ovando-Shelley E.
Universidad Nacional Autónoma de México

Rangel-Núñez J.L.
Universidad Autónoma Metropolitana

ABSTRACT: The papers in the Soft Soils session cover almost comprehensively the main topics related to soft soil engineering. The 15 papers that were submitted came from countries located in at least four continents, thus demonstrating that soft soils are widely spread and that research into their properties and characteristics is still of paramount importance for an increasing large number of geotechnical engineers worldwide. Theses papers will provide readers an opportunity to learn many aspects of soil engineering from the experiences shared by other colleagues around the world. In almost all of the papers the importance of characterizing soft soils properly is highlighted. It is also evident that thorough soil exploration as well as field and laboratory testing are necessary to achieve this purpose. The papers also show the extensive and extended use of exploration techniques that were rare only a few decades ago. It is also notable that most contributions refer to case histories in which basic soil mechanics concepts have been successfully applied and in which instrumentation was used judiciously to monitor and interpret soil behavior. Also, improved field instrumentation systems have had a positive influence on the development of many projects.

RÉSUMÉ : Les articles de cette session sur les sols mous couvrent presque complètement les principaux sujets liés à la géotechnique des sols mous. Les 15 communications qui ont été présentées proviennent de pays situés dans au moins quatre continents, démontrant ainsi que les sols mous sont largement répandus et que la recherche sur leurs propriétés et caractéristiques est toujours d'une importance capitale pour un grand nombre croissant d'ingénieurs géotechniques dans le monde entier. Ces documents donneront aux lecteurs l'occasion de découvrir de nombreux aspects de l'ingénierie des sols à partir des expériences partagées par d'autres collègues à travers le monde. Dans la plupart des articles est mise en lumière l'importance de la caractérisation des sols mous, et il est donc nécessaire d'avoir une reconnaissance et des essais sur le terrain et en laboratoire d'excellente qualité. Les documents montrent également l'utilisation intensive et prolongée de techniques d'exploration qui étaient rares il y a seulement quelques décennies. Il faut aussi noter que la plupart des contributions se réfèrent à des études de cas dans lesquels les concepts de base de mécanique des sols ont été appliqués avec succès et dans lequel l'instrumentation a été utilisée à bon escient pour contrôler et interpréter le comportement du sol. En outre, l'amélioration des systèmes d'instrumentation sur le terrain ont eu une influence positive sur le développement de nombreux projets.

KEYWORDS: Soft soils, soil improvement, historical cases, characterization of soft soils, analysis, numerical modeling & fracturing.

1 INTRODUCTION.

Urban expansion in many cities around the world as well as the construction of large industrial facilities and associated infrastructure have often made it necessary to build large projects in very soft soils where complex foundation solutions may be are required. Proper characterization of these soils is a crucial first step in applying specific analysis and design methods.

Geotechnical problems related to the presence of soft soils can appear in every other country around the world and in some regions geotechnical engineers face them on a day to day basis. Specialists now make reference to soft, very soft and even ultra-soft soils, depending on their specific properties. This is why characterization of these materials may also require the use of innovative means and even terminology to describe and identify them. Constitutive models for these soils have continued to appear over the last years as well as new conceptual solutions for foundation systems. New constitutive methods and new methods for improving the characteristics of these soils are also available.

The fifteen papers submitted to the Session deal with these topics and cover almost totally the subjects related to soft soil engineering. Three of the papers deal with analytical studies, one of them describes construction procedures, studies related to the determination of mechanical properties are discussed and described in two papers and one paper focused on discussing soil fracturing and fissuring within the context of regional subsidence. The eight remaining papers describe case histories in which characterization, analysis, design and construction related topics are dealt with.

2 METHODS OF ANALYSIS

Espinoza and Li (2013) present a hybrid drained-undrained model to design prefabricated vertical drains to improve the drainage characteristics of soft soil when surcharge loads are applied (Espinoza et al 2011). The model is based on the concept of virtual sand piles, where the soils located closer to prefabricated vertical drains dissipate excess pore pressures generated during construction faster than the soils located farther away. The authors show the influence of the construction rate on the maximum generated excess pore pressure. Their model considers the radial variation of excess pore pressure between drains. In their analyses the authors selected the magnitude of excess pore pressure that would have a negligible effect on the berm stability and then back-calculated the separation between drains necessary to yield this value. Soil columns around each prefabricated vertical drain mobilize their drained shear strength during loading, whereas the soil outside the virtual sand piles develops an undrained shear strength response during loading. This methodology was applied during construction of a high mechanically stabilized earth berm over very soft, low permeability and extremely compressible soil in the Cherry Island Landfill, located in the USA, in Wilmington, Delaware.

Müller and Larsson (2013) investigate and discuss the differences between six of the available analytical models to evaluate the average degree of consolidation U describing the characteristics of the disturbed zone around prefabricated vertical drains (eq 1), and evaluate the influence on the results of the variables incorporated in these models.

$$U = 1 - e^{\frac{-8xT_h}{F}} \tag{1}$$

where $T_h = c_h \times t/d^2$ is the time factor for horizontal consolidation, $c_h = k_h \times M_v/\gamma_w$ is the undisturbed horizontal coefficient of consolidation in the clay, t is the consolidation time, d is the diameter of the assumed unit cell dewatered by a single drain and the expression F is dependent on the model.

The influence of each variable x_i (i.e. F, T_h and κ) on can be assessed through the parameter α:

$$\alpha_i = \frac{\partial U/\partial x_i}{\sqrt{\sum_{i=1}^{n}(\partial U/\partial x_i)^2}} \tag{2}$$

The authors concluded that "although more realistically models may capture the nature of the smear zone, the impacts on the assessment of U of the more complex models are insignificant under the assumptions made in this paper. Hansbo´s simplified model "is still useful for practical engineering purposes due to its simplicity". They also state that "it is more important to put an effort into reducing the uncertainty in c_h the trying to investigate s and m in ordinary engineering projects".

Juárez-Badillo (2013) applies his general time-settlement equation (eq 3), provided by his principle of natural proportionality on the evaluation of settlements in soft soils for the Kansai International Airport.

$$S = \frac{S_T}{1 + \left(\frac{t}{t^*}\right)^{-\delta}} \tag{3}$$

where $t^*=t$ at $S=1/2S_T$, and S_T and d are parameters which may be obtained from experimental data. Using experimental data from Kansai International Airport and calibrating his equation, his estimates of total settlements in the long term tend to be similar to the observed data.

3 CONSTRUCTIVE PROCESS

Lui *et al.* (2013) study the application of X-section cast-in-situ concrete piles as a method for improving soft soils. They describe a construction method with a special pile-driving machine. The quality of piles driven with this machine was verified excavating the surrounding soil. They also used static and low-strain integrity testing methods making reference in all the process to the amount of concrete poured during concreting. A large scale model test program was carried out on X concrete piles and circular ones, to obtain the load transfer behavior of both pile types under three different loading modes: compression, uplift, and lateral loads. The authors also report the results of a field test.

Lui and his co-workers reached concluded that X piles have a larger contact area at the pile-soil interface and a larger inertia factor or lateral stiffness (*EI*) than circular piles for the same volume of concrete used.

4 DETERMINATION OF MECHANICAL PROPERTIES OF SOFT SOILS

Two papers were presented regarding about this issue:

Equihua-Anguiano and Orozco-Calderón (2013) estimated the undrained shear strength of marine soft soils based on the vertical penetration of a horizontal cylinder of 3.35 to 9m long and 1 to 2m in diameter, using steel and PVC tubes. An experimental program was carried out to validate the results of this device using a large rigid tank where a reconstituted marine soft soil was placed. The undrained shear strength was estimated from the analysis of the penetration of the cylinder and from miniature vane shear tests. The results show that the two methods yield similar values of the undrained shear strength.

Bobei and Locks (2013) present the results and interpretations of data collected during the procurement phase of a motorway upgrade in New Zealand. The strength and consolidation characteristics are investigated for a soil identified as a sensitive soft soil, Late Pleistocene–Holocene marine sediment. The estimate of undrained shear strength based on empirical methods is found to have limitations to predict the undrained shear strength of the sensitive soil. The authors propose that one-dimensional compression response of the virgin sensitive may be estimated using a relationship between the liquidity index and the vertical effective stress. The predictive capability of this relationship is demonstrated by numerical simulations of settlement monitored during the construction and post-construction phase of the original SH16 motorway embankment. The soil sensitivity represents an indicator of soil micro-structural bonding or development of inter-particle forces between particles or their aggregates. The disturbance to the soil structural bonding during loading could have some serious consequences such as: (a) strength reduction; and (b) changes in the overall soil behaviour due to an increase in soil compressibility properties.

The measure of soil sensitivity (S_t) adopted in this study is based on the ratio between peak undisturbed strength (s_u) and the remould strength (s_r) when the soil reaches its residual state. The results of shear vane tests were interpreted to determine the strength sensitivity manifested by virgin AH soil as shown in Figure 1b.

(3)

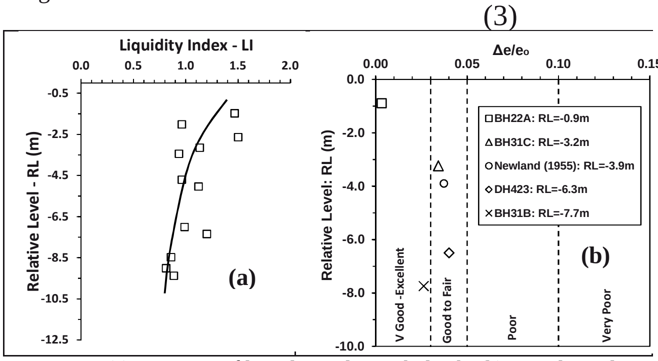

Figure 1. (a) Variation of liquidity index with depth; (b) Sample quality assessment based on (Lunne *et al.* 1997) classification system.

The main findings of the paper are summarized below:

- The undrained shear strength of virgin sensitive soils increase linearly with depth.
- The compressibility of virgin AH soil in one-dimensional testing displays non-linear characteristics when stresses exceed the pre-consolidation pressure.
- The assessment of undrained shear strength of virgin AH soil is not readily predicted by methods such as SHANSEP.
- The one-dimensional response of virgin AH soil is found to uniquely relate *LI* and σ'_v. The predictive capability of a proposed relationship is

demonstrated by numerical simulations of settlement monitored during the construction and post-construction phase of SH16 motorway embankment.

5 CASE HISTORIES

Eight papers on case histories were presented: Tashiro *et al.* (2013), Kim *et al.* (2013), Tan *et al.* (2013), Popovic and Stanic (2013), Massad *et al.* (2013), Ooi *et al.* (2013), Asiri and Masakasu (2013) and De Silva and Fong (2013). All of them dealing with aspects of embankments or earth structures over soft soils where soil improvement was applied.

Tashiro *et al.* (2013) study the case of a large field test performed on a trial embankment (150 by 27m) resting over a peaty soft soil deposit 50m thick. Upon the application large surcharges, the embankment settled 11m on average, after four years. Nearby structures were affected on account of lateral displacements and relative emersions of 2 and 1m, respectively. The authors analyzed several strategies for reducing settlement in the trial embankment and its surroundings by means of either sand drains or card board drains (wick drains). Field observations and comprehensive soil testing was carried out to characterize the soft soil.

The effects of countermeasures to prevent excessive deformations and settlements such as ground improvement with sand drains, replacement of the existing embankment with lightweight materials, and reduction of the loading rate, were also investigated using numerical analysis. These analyses were performed using the soil-water coupled finite deformation analysis program GEOASIA, in which the SYS Cam-clay model was mounted as the constitutive equation for the soil skeleton. The results showed that improvement of the mass permeability and the slow or lightweight banking are effective means of improving the stability during loading and reducing the residual settlement after entry into service. The results analyzed in this paper were applied to the actual construction design of a culvert and the lightweight embankment surrounding it.

Kim *et al*. (1013) present a case history about the expansion of the second branch of the Namhae Expressway in Korea which overlies a 53m thick soft soil deposit. The original design plans were reviewed, problems were discussed and solutions for the problems were proposed. With the improved plan, it was not necessary to dispose of soil and asphalt concrete removed from the existing road. The constructability of the project would be improved because the sequence of activities would be simplified and issues related to the difficulty of installing PBD (Plastic Board Drains) by drilling on the slope of the existing road could be avoided. The improved plan reduces the construction cost. Installation of PBD beneath the existing road would involve additional costs for drilling or removing gravel and crushed stone underneath the existing road. In addition, there would be a cost for disposal of the waste asphalt concrete. If PBD is used to improve the soil under the existing road, it is expected that coupled settlement will occur near adjacent structures due to the soil settlement. The improved plan does not involve improvement of the soft soil and consequently protects the stability of structures located near the existing road.

Tan *et al*. (2013) studied another trial embankment constructed over a 15m thick deposit of very soft clay whose relevant mechanical properties are shown in Figure 2. Pre-fabricated vertical drains (PVD) were installed in the soft soil deposit following a triangular pattern (1.2 m separation). The trial embankment was 50m long and 14.2m wide, a 50cm thick sand layer was placed at the bottom of the embankment as well as a geotextile sheet.

The embankment was instrumented with inclinometers, displacements markers, extensometers, vibrating wire piezocones, settlement gauges, stand pipes. Experimental observations were used to back analyze the embankment using the Plaxis computer software, using the "soft soil model" for the clays and the "hardening soil model" for sandy strata. Their analyses included indirectly the presence of PVDs. To achieve this, the authors used an equivalent vertical permeability for the soft clay stratum. The back analysis yielded a value of this equivalent permeability which turned out to be almost six times larger than the original permeability of the soft soils.

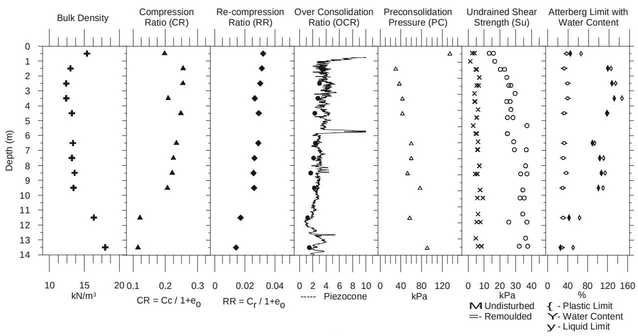

Figure 2. Mechanical properties of the trial embankment (Tan *et al*. 2013).

Popovic and Stanic (2013) analyze soil-structure interaction and effectiveness of soil improvement through back-analyses based on measurements conducted during the early stages of the construction of a new container terminal in the port of Ploce in Croatia. The soil profile is formed by a surface layer of silty sand and low plasticity silt of 8m of thickness followed by a low to high plasticity clay that reaches 33m of depth. After that, a low plasticity poorly graded silty sand is founded. Subsoil treatment consisted in dense and sparse stone columns (triangular grid 2x2m and square grid 2.8x2.8m, respectively).

Back analyses were performed based data on soil settlement and pile displacement measured with instruments installed to monitor the progress of construction. The objective of back analyses was to establish "actual" soil parameters and the condition of internal forces and displacements in the structure. The authors were able to verify the efficiency of planned works aided by the geotechnical measurements described in the paper.

Finally, the results of numerical models were used as a means for controlling the construction processes. The authors point out that it is necessary to perform back analyses during and after the construction of complex projects in difficult geotechnical environments on the basis of measurements and through the collaboration of structural and geotechnical engineers.

The paper by Massad *et al.* (2013) is based on data from a work in Santos Harbor, in São Paulo State, Brazil, in which three experimental fills were built and monitored, one of them partially with geodrains. The monitoring of earth fills built on soft clays has been done frequently through the Brazilian coastline. As the most common measurement is the settlement along time, the interpretation of the results is usually done by Asaoka's Method, generally involving extrapolations that have given rise to doubts (for instance, about the secondary consolidation effect) and to a double interpretation, and even to controversies, especially when it comes to evaluating the effectiveness of vertical geodrains to accelerate settlements.

The uppermost soil stratum is the SFL clay, a sedimentary material (fluvial-lagoon-bay) of the Pleistocene that has become lightly overconsolidated due to erosion, sea level oscillations and dune action. The authors describe and comment on the results of extensive soil exploration as well as field and laboratory testing with which a detailed and thorough characterization of the SFL clay was possible, for the sites at the three trial embankments.

In the first experimental site an earth fill was placed in area reclaimed from the sea. Application of loads was carried out in three stages and that made it possible to apply Asaoka's Method, as shown graphically in the paper. A second experimental fill (Pilot Embankment 2) was built with a maximum height of 5.2m. The values of the end of primary settlement (ρ_f) and c_v/H^2_d were determined from instrumental data for the two loading stages. The authors interpreted measurement to find equivalent c_v values, after roughly 5 months when at least 95% of the primary settlement was reached. In the third experimental fill, with a maximum hight of 6.7, they also inferred c_v values from instrumental observations. A third experimental fill (Pilot Embankment 3), built also in Area 3, with a maximum height of 6.7m, behaved in a similar way, with c_v/H^2_d averaging $1.8.10^{-2}$/day; the *EOP* settlement was ~80 cm and 95% of this value was reached after ~6 month.

Due to the relatively high *OCR* values of the SFL Clays, the c_v were also high, of the order or $10^{-2}cm^2/s$. As a consequence, there was no need to use geodrains in the Embraport site.

This conclusion was supported by instrumental observations in three experimental earth fills without geodrains and, more important, by the monitoring of settlements in the area where temporary surcharges were used. These results show that controversies that after arise about the use of geodrains can be overcome with proper characterization of soils present in the field and from thorough and careful interpretation of instrumental observations from properly instrumented trial fills.

The paper by Ooi *et al.* (2013) discusses the development of geogrid applications in soft ground in Malaysia starting in 1984 when a road pavement field trial was first carried out. Other experiences followed in the following years and in this paper they report another project in which geogrids with geocells were used. They compare the performance of three cases in which geogrids were used, a fabrication yard, a heavy duty working platform and a container yard working platform. They compare and assess the pavements used in them and the magnitude of settlement they underwent under construction and later operations. All the three platforms were built over soft clays 4.5 to 10m thick and applied stresses due to heavy equipment was as high as 500kPa and axial loads of heavy vehicles reached 105tonnes. Granular fill of varying thicknesses were used in all three working platforms. The authors state that mechanically stabilized soils using biaxial and triaxial geogrids with granular fill with or without geocell mattress performed satisfactorily in terms of platform settlement performances to support the heavily loaded platforms.

The case history presented by Asiri and Masakasu (2013) deals with the design and performance of a highway embankment constructed in Sri Lanka over very soft soils and alluvial clays. The project required that settlements be limited to less that 15cm after three years and those residual differential settlements be less than 0.3%. Soils were improved by means of wick drains, heavy tamping, pre loading with surcharges and vacuum consolidation. The soil improvement method was adjusted depending local geotechnical conditions. The major steps in ground improvement method and illustrated in Fig 3 are: a) placing surcharge loads with or without drains for soft clays of shallow thickness; b) removal of peaty soil, replacing it rock fragments; c) applying heavy tamping or, alternatively, vacuum consolidation for deeper strata. Heavy tamping was only effective down to 3.5 to 4.0m

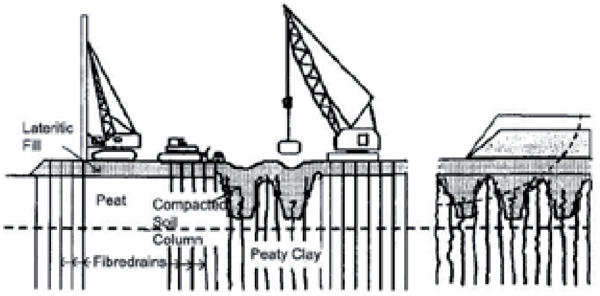

Figure 3. Major steps in heavy tamping ground improvement method (Asiri and Masakasu , 2013)

Vacuum consolidation was applied using band drains with a spacing of 1m. Primary consolidation settlements were compensated and secondary consolidation deformation minimized by applying a vacuum pressure of 70kPa. There were places where it was not possible to apply vacuum and in those cases, soil improvement was carried out by applying surcharge.

The continuous assessment of the improvement of soft ground was carried with field instruments: settlement plates, pyrometers, a vacuum pressure monitoring unit and a water discharge meter. The decision to remove the surcharge was made on the basis of the monitoring data obtained during the surcharge period. The aim was to eliminate 100% of the primary consolidations settlement and enough secondary settlement.

De Silva and Fong (2013) describe and discuss the case of the Cotai Landfill, the main receiving facility in Macau for building construction waste. As the dumping site is underlain with a thick layer of very soft to soft marine clay deposits, the uncontrolled end-tipped material has generated mud waves and they were encroaching the piles supporting the Macau International Airport taxiway nearby. In order to prevent future potential damage to the taxiway, the Macau Government commissioned the design of a containment bund adjacent to the taxiway to retain the waste and to prevent further generation of mud waves that would affect the taxiway.

This paper presents the design approach of the containment bund including the results of a limit equilibrium stability analysis and the numerical analyses carried out that demonstrated that the solution is appropriate as the bund will contain the landfill with minimal impact on the taxiway bridge piles. The analyses also demonstrated that the impacts during construction are also negligible. The sustainable design comprised the installation of vibrocompacted stone columns installed in over 20m thick, very soft to firm, moderately sensitive marine clay and alluvial clay, as the foundation to the waste retention bund, thereby avoiding the dredging and off-site disposal of a significant volume of dredged sediments. This paper presents the design approach and construction of the stone columns and the behaviour of the completed seawall.

The authors show instrumental observations to monitor during the taxiway and seawall during construction. Survey results indicated that the installation of the stone columns and construction of the bund had minimal impact on the taxiways foundation piles. The seawall was been completed in November 2011.

6 SOIL FRACTURING

Auvinet and Mendez (2013) present updated information concerning land subsidence and associated soil fracturing in Mexico City. Subsidence was estimated from the evolution of the elevations of 2064 benchmarks and other references located in former Texcoco Lake. Geodesic and topographic surveys carried out in the middle of the XIXth century proved to constitute an excellent initial reference for subsequent measurements of land subsidence. Extensive use was made of new geocomputing tools to process these data. Results of surveys of soil fracturing associated to subsidence are also presented and discussed

The demographic development in Mexico City has created an accelerated demand of services, mostly of potable water. One of the cheapest ways to meet this demand has been the exploitation of the local aquifer by pumping water from deep wells. This has produced a water pressure drawdown in the subsoil that in turn is causing general subsidence of the former lacustrine area and soil fracturing. This problem has been around for almost a century but is now reaching new worrying dimensions. Although regional land subsidence is an old phenomenon, it has not been possible to control it. In fact, it is expected to continue in the future for many more years since, due to the high cost of other alternatives, water pumping from the local aquifer cannot be suspended. Studies and analyses are thus necessary to rethink criteria and strategies to mitigate future effects

The authors describe the efforts of their research group to monitor the subsidence phenomenon of the lacustrine zone of Mexico City, as well as of others aspects of the problem, like soil fracturing. A Geographic Information System was developed to this end, using as a support a similar system developed previously by the authors. Up to now, 868 fracturing sites have been documented. About 45 sites where cracks had been reported were discarded when, during the field visits, it became evident that no fracturing could be detected and that defects in the soil surface could be attributed to other factors (mainly scour).

Figure 4. A dramatic example of soil fracturing in a site near Mexico City

Engineers and practitioners as well as local and federal authorities will surely profit for the crack and fissure maps produced by the authors, not only for assessing the feasibility of specific projects but also in the planning of urban development schemes or land usage regulations.

7 CONCLUSIONS

The papers in the session cover almost comprehensively the main topics related to soft soil engineering. The 15 papers that were submitted came from countries located in at least four continents, thus demonstrating that soft soils are widely spread and that research into their properties and characteristics is still of paramount importance for an increasing large number of geotechnical engineers worldwide. Sharing experiences with problems associated to soft soils is also very important. The papers submitted to the session will provide readers an opportunity to learn many aspects of soil engineering from the experiences shared by other colleagues around the world.

In almost all of the papers the importance of characterizing soft soils properly is highlighted. It is also evident that thorough soil exploration as well as field and laboratory testing are necessary to achieve this purpose. The papers also show the extensive and extended use of exploration techniques that were rare only a few decades ago.

It is also notable that most contributions refer to case histories in which basic soil mechanics concepts have been successfully applied and in which instrumentation was used judiciously to monitor and interpret soil behavior. Also, improved field instrumentation systems have had a positive influence on the development of many projects. In this respect, the submitted papers, especially those presented in the case histories, show different manners in which the observational method can be applied successfully, under a wide range of geotechnical conditions and within the context of a variety of problems.

8 REFERENCES

Karunawardena A. and Toki M. 2013. Design and Performance of Highway Embankments Constructed Over Sri Lankan Peaty Soils. *Proceedings of the 18th International Conference on Soils Mechanics and Geotechnical Engineering*, International Society for Soil Mechanics and Geotechnical Engineering, Paris.

Auvinet G., Méndez E. and Juárez M. 2013.Soil fracturing induced by land subsidence in Mexico City. *Proceedings of the 18th International Conference on Soils Mechanics and Geotechnical Engineering*, International Society for Soil Mechanics and Geotechnical Engineering, Paris.

Bobei D.C. and Locks J. 2013. Characterization of Sensitive Soft Soils for the Waterview Connection Project, New Zealand. *Proceedings of the 18th International Conference on Soils Mechanics and Geotechnical Engineering*, International Society for Soil Mechanics and Geotechnical Engineering, Paris.

De Silva S. and Fong L. T. T. 2013. Design and Construction of a Landfill Containment Bund cum Seawall Supported on Stone Columns Installed in Very Soft Marine Mud in Cotai, Macau. *Proceedings of the 18th International Conference on Soils Mechanics and Geotechnical Engineering*, International Society for Soil Mechanics and Geotechnical Engineering, Paris.

Equihua-Anguiano L. N. and Orozco-Calderón M. 2013. Estimation of undrained shear strength of soft soil obtained by cylinder vertical penetration. *Proceedings of the 18th International Conference on Soils Mechanics and Geotechnical Engineering*, International Society for Soil Mechanics and Geotechnical Engineering, Paris.

Espinoza, D., and Chunling Li 2013. The Application of a Novel Design Approach for Construction over Soft Soils: The Hybrid Undrained-Drained model. *Proceedings of the 18th International Conference on Soils Mechanics and Geotechnical Engineering*, International Society for Soil Mechanics and Geotechnical Engineering, Paris.

Espinoza R.D., Houlihan M.F., and Ramsey, T.B. 2011. Design of high soil berm over soft soil. *Geo-Strata*, March-April, pp 52-54.

Juárez-Badillo, E. 2013. Kansai International Airport. Theoretical settlement history. *Proceedings of the 18th International Conference on Soils Mechanics and Geotechnical Engineering*, International Society for Soil Mechanics and Geotechnical Engineering, Paris.

Juárez-Badillo, E. 1985b. General volumetric constitutive equation for geomaterials. Special volume on Constitutive Laws of Soils. *XI International Conference on Soil Mechanics and Foundation Engineering*. San Francisco. Japanese Society for Soil Mechanics and Foundation Engineering, Tokyo, pp 131 135.

Kim, K.H., Jung, T.M., Jung, J.H., Kim, T.H., Kim, S.R. and You, S.H. 2013. Design improvements for expansion of a roadway on a thick layer of soft soil. *Proceedings of the 18th International Conference on Soils Mechanics and Geotechnical Engineering*, International Society for Soil Mechanics and Geotechnical Engineering, Paris

Lui, H.L., Kong G.Q., Ding X.M., Yu, T. and Yang G. 2013. Case study on X-section cast-in-place pile-supported embarnkment over soft clay. *Proceedings of the 18th International Conference on Soils Mechanics and Geotechnical Engineering*, International Society for Soil Mechanics and Geotechnical Engineering, Paris.

Massad F., Henriques Teixeira A., Carvalho C. T. and Grangé Luiz F.A. 2013. Settlements of earth fills on thick layers of overconsolidated soft clays without geodrains. *Proceedings of the 18th International Conference on Soils Mechanics and Geotechnical Engineering*, International Society for Soil Mechanics and Geotechnical Engineering, Paris.

Müller, R., and Larsson, S. 2013. Aspects of the modelling of smear zonaes around vertical drains. *Proceedings of the 18th International Conference on Soils Mechanics and Geotechnical Engineering*, International Society for Soil Mechanics and Geotechnical Engineering, Paris.

Ooi, T.A., Tee, C.H., Chan, C.B. and Ong, R. 2013. A review of geogrid working platform in soft ground in Malaysia. *Proceedings of the 18th International Conference on Soils Mechanics and Geotechnical Engineering*, International Society for Soil Mechanics and Geotechnical Engineering, Paris.

Popovic, N., and Stanic, B. 2013. Container terminal on soft soil. *Proceedings of the 18th International Conference on Soils Mechanics and Geotechnical Engineering*, International Society for Soil Mechanics and Geotechnical Engineering, Paris.

Tan, Y.Ch., Lee P. T. and Koo, K.S. 2013. Instrumented trial embankment on soft ground at Tokai, State of Kedah, Malaysia. *Proceedings of the 18th International Conference on Soils Mechanics and Geotechnical Engineering*, International Society for Soil Mechanics and Geotechnical Engineering, Paris.

Tashiro, M., Inagaki M. and Asaoka A. 2013 Prediction of and countermeasures for embankment-related settlement in ultra-soft ground containing peat. *Proceedings of the 18th International Conference on Soils Mechanics and Geotechnical Engineering*, International Society for Soil Mechanics and Geotechnical Engineering, Paris.

Soil Fracturing Induced by Land Subsidence in Mexico City

Fracturation des sols induite par la subsidence de la ville de Mexico

Auvinet G., Méndez E., Juárez M.
Instituto de Ingeniería, UNAM, Mexico

ABSTRACT: Updated information concerning land subsidence and associated soil fracturing in Mexico City is presented. Subsidence was estimated from the evolution of the elevations of 2064 benchmarks and other references located in former Texcoco Lake. Geodesic and topographic surveys carried out in the middle of the XIXth century proved to constitute an excellent initial reference for subsequent measurements of land subsidence. Extensive use was made of new geocomputing tools to process these data. Results of surveys of soil fracturing associated to subsidence are also presented and discussed.

RÉSUMÉ: On présente des données récentes sur la subsidence et la fracturation des sols à Mexico. La subsidence a pu être évaluée grâce à des levés topographiques portant sur 2064 points de nivellement et d'autres repères situés dans l'ancien lac de Texcoco. Les relevés géodésiques et topographiques du milieu du XIXème siècle constituent une excellente référence initiale pour les mesures suivantes. On a utilisé de nouveaux outils informatiques pour traiter ces données. Des résultats de relevés concernant la fracturation des sols sont également présentés et commentés.

KEYWORDS: Subsidence, soil fracturing, soft clays, surveys, geocomputing.

1 INTRODUCTION.

The demographic development in Mexico City has created an accelerated demand of services, mostly of potable water. One of the cheapest ways to meet this demand has been the exploitation of the local aquifer by pumping water from deep wells. This has produced a water pressure drawdown in the subsoil that in turn is causing general subsidence of the former lacustrine area and soil fracturing. This problem has been around for almost a century but is now reaching new worrying dimensions.

Today, the subsidence phenomenon, at eighty years from Roberto Gayol's discovery (1925), and at more than sixty years from its scientific explanation by Nabor Carrillo (1947), persists with cumulative effects through time which cause differential settlements in colonial and modern structures of Mexico City. Installations as important as the subway system, the Gran Canal, and the water system network are also severely affected.

During the last decades, an increasing number of soil fractures have been detected in Mexico City valley. Such cracks are a matter of growing concern for the population and authorities since they have caused a series of accidents and serious damage to constructions and public services. It is now acknowledged that the soil fracturing problem is an important risk factor and that the best scientific tools and techniques should be mobilized to define prevention and mitigating measures.

Soil fracturing can occur as a consequence of any condition leading to large tensile stresses or extension strains in the soil. Accordingly, cracks in the soil have different origin, including contraction of compressible clays by drying, stresses induced by the weight of constructions, hydraulic fracturing of soft soils (Auvinet & Arias, 1991, Figure 1), seismic movements, etc. However, the largest and more destructive fractures are generally a direct consequence of land subsidence associated to pumping of water in the local aquifer.

Figure 1. Crack in Chalco

1 LAND SUBSIDENCE

1.1 Assessing regional subsidence

Although regional land subsidence is an old phenomenon, it has not been possible to control it. In fact, it is expected to continue in the future for many more years since, due to the high cost of other alternatives, water pumping from the local aquifer cannot be suspended. Studies and analyses are thus necessary to rethink criteria and strategies to mitigate future effects.

1.2 Local values of subsidence

Thanks to the historic information which was gathered with the support of different institutions among which stands out the Water System of Mexico City (SACM) of the Federal District Government (Pineda & Pelaez, 2009), the subsidence history in three sites of the Historic Center of Mexico City could be reconstituted (Figure 2).

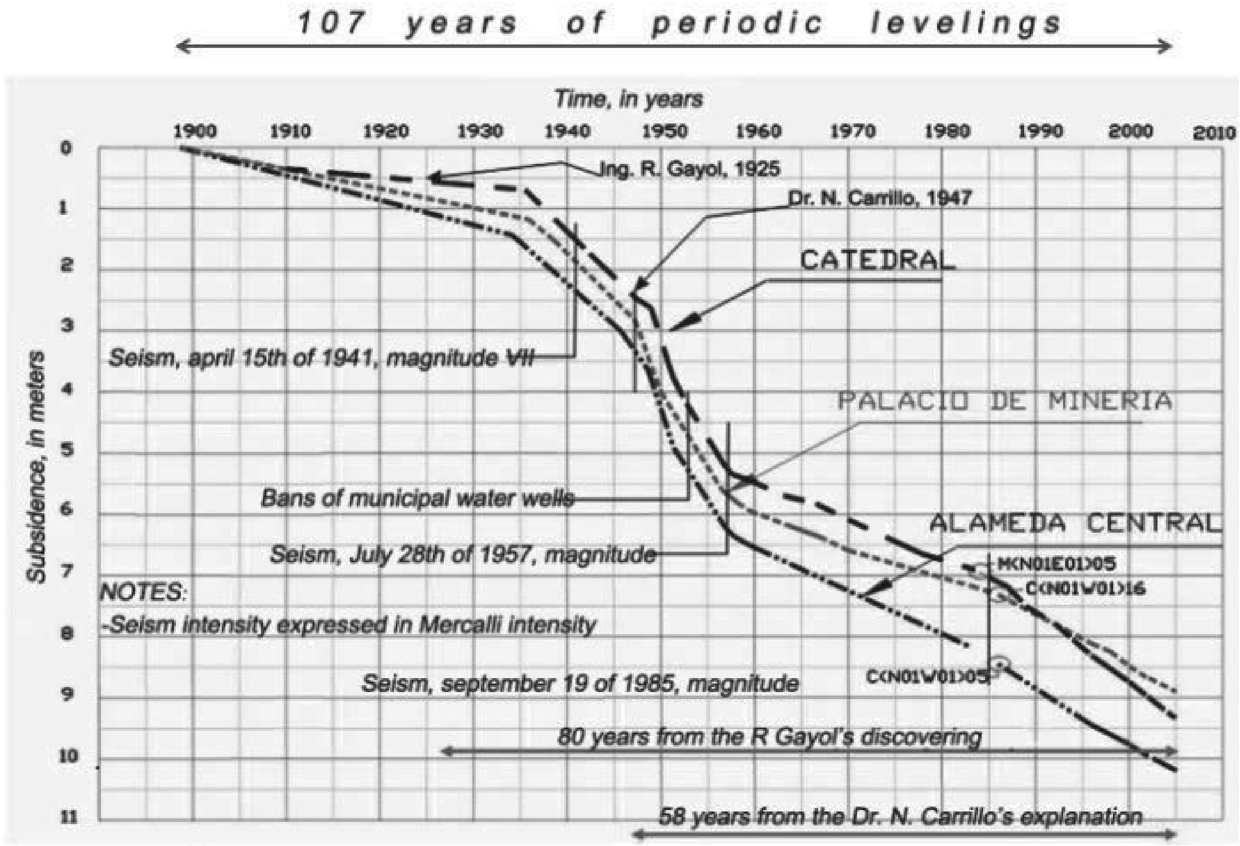

Figure 2. Local evolution of subsidence for the 1898-2005 period.

In the figure 2, it is observed that the subsidence rate reached a 29cm/year peak during the 1947-1957 period, and is still of the order 10cm/year for these three sites.

The accumulated settlement since the end of the XIXth century is of the order of 10m for these sites but, in other points of the valley, accumulated subsidence values as high as 13.5m have been observed (Pérez, 2009).

Some physical evidences of the general subsidence such as former well casings protruding from the subsiding surrounding soil can be observed in the city (Figure 3). The authorities have been asked to protect such evidences.

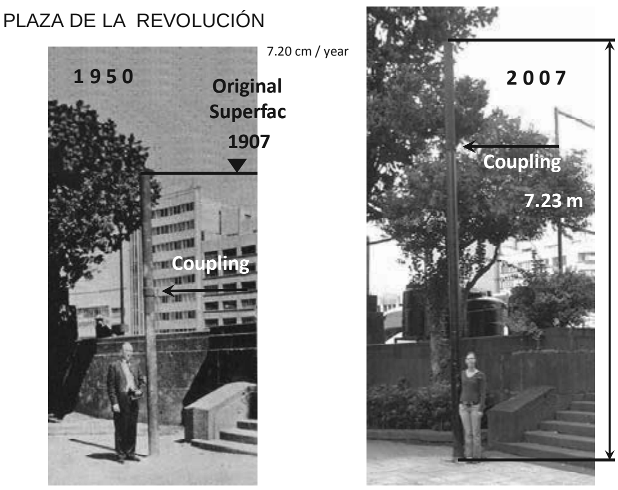

Figure 3. Old well casing protruding from the subsiding soil.

1.3 Spatial distribution of the subsidence phenomenon

In order to assess the spatial distribution of the subsidence in the former lacustrine area, it was necessary to build a Geographic Information System (SIG-BN) to process the data obtained from surveys of the existing benchmarks. Geodesic and topographic surveys carried out in the middle of the XIXth century were reviewed and proved to constitute an excellent initial reference for subsequent measurements. From the contour map obtained by geostatistical methods it was possible to develop a model of the present configuration of the surface relief of the bottom of the former lakes of Mexico valley (Figure 4).

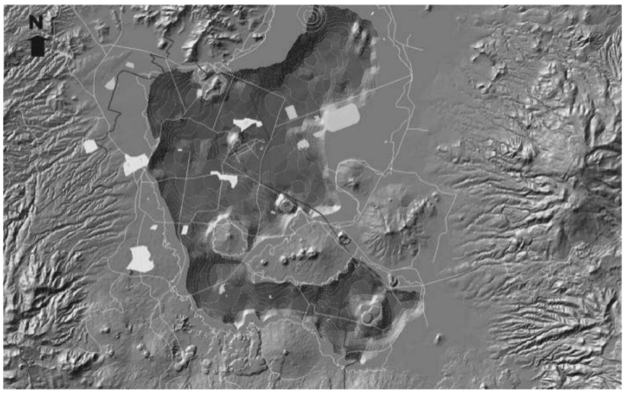

Figure 4. Relief of the former lakes of Mexico Valley.

1.4 Spatial distribution of the subsidence rate

Figure 5 shows the spatial distribution of the subsidence rate for the 1998-2002 period. The sites with the highest rate (40 cm/year) are located east of Tlahuac, in the Chalco Lake, and in Nezahualcoyotl City, in front of the Marquez hill.

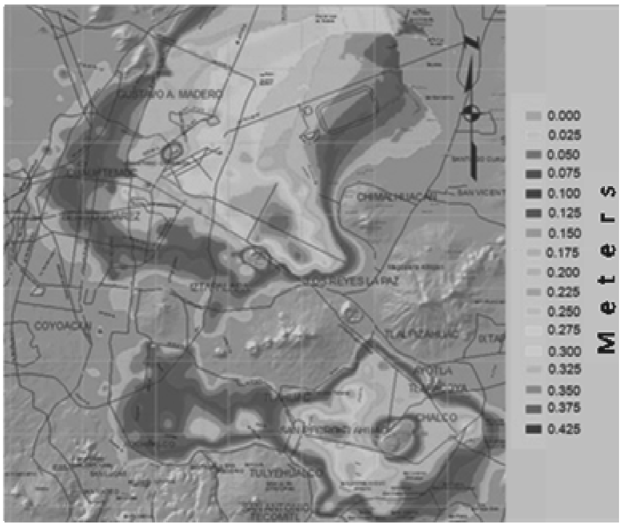

Figure 5. Subsidence rate in m/year during the 1998-2002 period.

2 SOIL FRACTURING

The Geocomputing Laboratory group of the Engineering Institute, UNAM, has undertaken a systematic study of the fracturing phenomenon, including both descriptive aspects and theoretical interpretation. For that purpose, a Geographic Information System was developed, using as a support a similar system developed by the authors to describe geotechnical characteristics of Mexico Basin subsoil (Auvinet *et al*., 1995).

Field work consisting of direct surveys of fractures in situ was carried out. Use was made of Geodesic control techniques recurring to differential Global Positioning Systems (GPS) equipped with double frequency antennas. At this moment, 868 fracturing sites have been documented. About 45 sites where cracks had been reported were discarded when, during the field visits, it became evident that no fracturing could be detected and that defects in the soil surface could be attributed to other factors (mainly scour).

The amount of information stored in the data base regarding the exact location as well as the description of the geometric characteristics and special features of each fracture has increased steadily. This database has been called: SIG-G. Figure 6 shows the spatial distribution of the 868 sites included until now in SIG-G.

The most important and destructive cracking mechanism is a direct result of subsidence. It is observed in abrupt transition zones between firm and soft soils. Cracks of this type are characterized by a step toward the compressible zone where larger settlements are observed (Figure 7). The Iztapalapa precinct, with 30 kilometers of abrupt transition, is the most affected by this phenomenon.

Using an extensive photographic file of cracks, a digital album is being elaborated in order to facilitate the analysis of evolution of each fracture through the years. This album is integrated by a set of files; each file contains from two to six photos of the same crack taken during one of the 1996, 1999, 2001, 2002, 2005, 2006, and 2007 campaigns. A complementary file includes photos of the damage caused by the fracture in adjacent buildings or negative effects in the vital lines of the city.

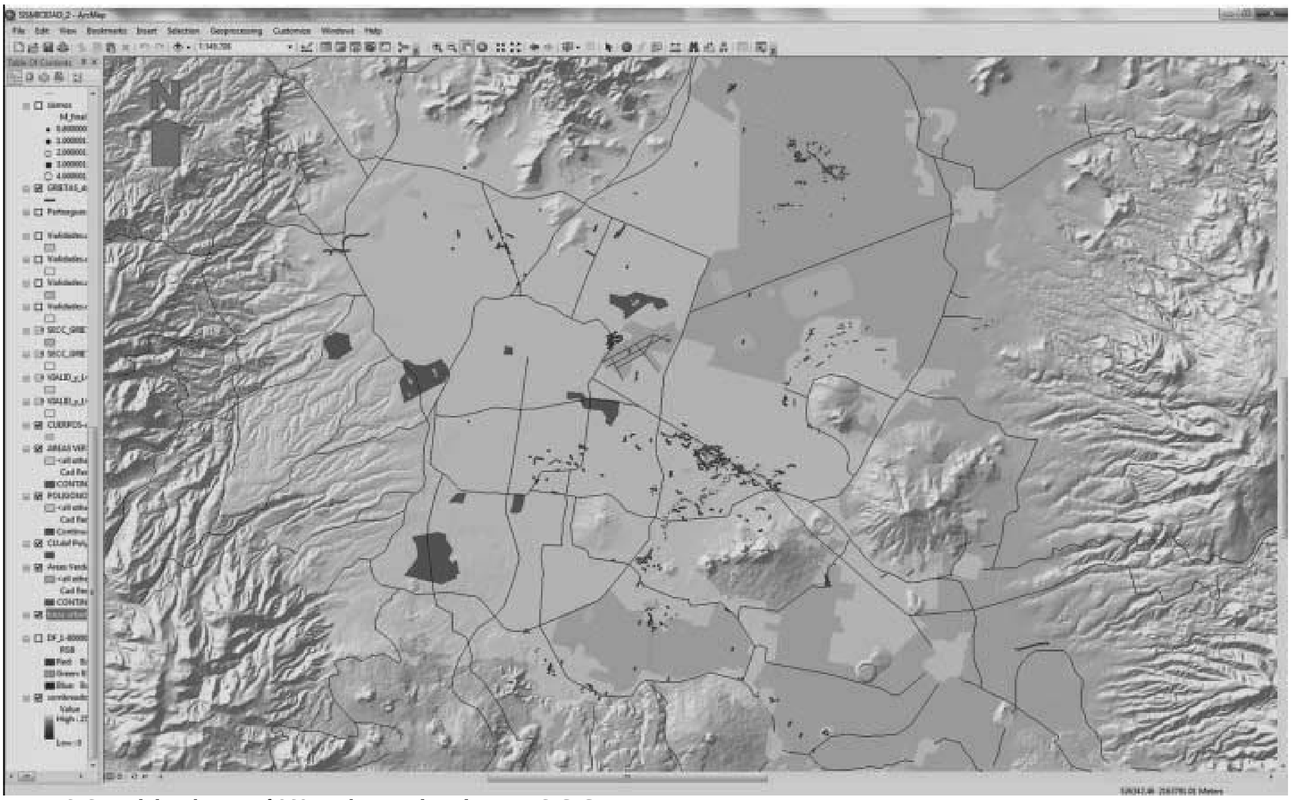

Figure 6. Spatial distribution of 868 cracks stored until now in SIG-G.

Figure 7. Crack in an abrupt transition area.

Initially, fracturing was only observed in the sediments of former Texcoco lake but, in the last years, the phenomenon has been widely reported in five areas of Mexico Valley: a) South zone: Xochimilco, Tláhuac and Chalco; b) East zone: Iztacalco, Iztapalapa, Nezahualcoyotl, Chimalhuacan and Los Reyes; c) Center area: Peñon de los Baños and Venustiano Carranza; d) North-West zone: Naucalpan, Azacapotzalco and G. A. Madero and e) North-East zone: former Texcoco lake.

3 CONCLUSIONS

Land subsidence is an ongoing process that affects the former lacustrine zone of Mexico City. Soil fracturing associated to land subsidence causes serious problems to the citizenship and the infrastructure of the metropolitan area of Mexico valley. Until now, actions in this regard have been isolated, and only short term solutions have been implemented without really trying to understand the problem in greater depth and to evaluate the true efficiency of these solutions.

Efforts by different groups, in particular by the Geocomputing Laboratory of II UNAM to achieve a better monitoring of the subsidence phenomenon of the lacustrine zone of Mexico City, as well as of others aspects of the geotechnical problematic, like soil fracturing, have allowed to obtain useful results but they just constitute the first stage of a huge monitoring work which should be followed on in a systematic way in the future. Institutional will to give continuity to these studies and availability of the required resources for its realization are essential to obtain satisfactory and up to date results.

4 REFERENCES

Auvinet, G. & Arias, A. (1991) Propagación de grietas. Memoria, Simposio sobre "Agrietamiento del suelo", Sociedad Mexicana de Mecánica de Suelos, pp. 21-31, august, México, D. F.

Auvinet, G. et al. (1995) Sistema de Información Geográfica para Sondeos Geotécnicos, Proceedings, Xth Pan-American Conference on Soil Mechanics and Foundation Engineering, Vol. 1, pp. 312-324, Guadalajara, Mexico.

Carrillo, N. (1947) Influence of Artesian Wells on the Sinking of Mexico City. 2nd Internation Conference on Soil Mechanics and Foundation Engineeering, Nederland.

Gayol, R. (1925) Estudio de las perturbaciones que en el fondo del valle de México ha producido el drenaje de las aguas del subsuelo por las obras del Desagüe, y rectificación de los errores a que ha dado lugar una incorrecta interpretación de los hechos observados. Revista Mexicana de Ingenieros y Arquitectos. Vol. III, Number 2, Mexico, D.F.

Marsal, R. & Mazari, M. (1959) The subsoil of Mexico City. Contribution to Ier Pan-American Soil Mechanics and Foundation Enginering Conference, Facultad de Ingeniería, UNAM, México. Reedited (spanish-english) in 1969.

Pérez, D. (2009) Modelado del hundimiento de la zona lacustre del valle de México. Aspectos estratigráficos y piezométricos. Master degree thesis, Escuela Superior de Ingeniería y Arquitectura, IPN, México D.F.

Pineda R. & Pelaez T. (2009) Procedimiento de medición del hundimiento de la ciudad de México, Geotechnical Engineering in urban areas affected by land subsidence, Proceedings, workshop organized by ISSMGE TC36, Instituto de Ingeniería and Sociedad Mexicana de Ingeniería Geotécnica, Mexico, D.F.

Characterization of Sensitive Soft Soils for the Waterview Connection Project, New Zealand

Caractérisation de sols mous sensibles pour le projet de raccordement Waterview en Nouvelle-Zélande

Bobei D.C.[1], Locks J.[2]
Aurecon Group Pty Ltd
[1] Level 2, 116 Military Road, Neutral Bay, Sydney, Australia
[2]Level 4, 139 Carlton Gore Road, Newmarket, Auckland, New Zealand

ABSTRACT: The paper presents the results and interpretations of data collected during the procurement phase of SH16 motorway upgrade. The strength and consolidation characteristics are investigated for a soil unit, labeled AH, which is identified to manifest a response typical for a sensitive soft soil. The estimateof undrained shear strength based on empirical methods is found to have limitations to predict the undrained shear strength of the sensitive AH soil. The one-dimensional compression response of the virgin AH soil is proposed to estimate using a relationship between the liquidity index and the vertical effective stress. The predictive capability of this relationship is demonstrated by numerical simulations of settlement monitored during the construction and post-construction phase of the original SH16 motorway embankment.

RÉSUMÉ : Cet article présente les résultats et les interprétations des données recueillies lors de la phase de projet de mise à niveau de l'autoroute SH16. La résistance et les caractéristiques de consolidation sont étudiées pour un type de sol, noté AH, qui est représentatif d'un sol mou sensible. L'estimation de la résistance au cisaillement basée sur des méthodes empiriques est peu adaptée pour prédire la résistance au cisaillement non drainée du sol sensible AH. La réponse en compression unidimensionnelle du sol vierge AH est modélisée par une relation entre l'indice de liquidité et la contrainte effective verticale. La capacité prédictive de cette relation est démontrée par des simulations numériques des tassements mesurés pendant la phase de construction et post-construction du remblai original SH16 de l'autoroute.

KEYWORDS: clay, sensitive soil, critical state soil mechanics, SHANSEP, settlement.

1 INTRODUCTION

The Western Ring Route (WRR) is an ambitious project initiated by New Zealand Transport Agency (NZTA) toprovide a 48km alternative route for improvement of traffic flow around the Auckland city center. One significant work component of the WRR project is the upgrade of the State Highway 16 (SH16), where part of the route is passing through an estuarine environment. This section of the motorway, referred to as the Causeway, has experienced significant settlements over a period of 60 years of service life. Today the traffic lanes are prone to flooding during storm and king tide events.

2 PAPER OBJECTIVES

NZTA has commissioned Aurecon to undertake an in-depth investigation into the soil conditions present along the Causeway Section. The geotechnical investigation includes over one hundred exploratory holes, in addition to numerous older holes drilled during the planning phase for the original Causeway in the late 1950s.

The field investigations were complemented by laboratory testing for the purpose to provide details on strength and compressibility of the Causeway estuarine soil materials.The compressibility and behaviour of AH soils is investigated in the critical state framework. The ability of SHANSEP formulation to predict the undrained shear strength is investigated based on the piezometer (CPTu) data.

Based on the non-linear one-dimensional compression manifested by the sensitive AH soil, a framework of analysis is proposed to predict the non-linear one-dimensional compression of AH soil. An example of soil settlement analysis is carried out to predict the magnitude and rate of settlement development of the original SH16 motorway embankment during the construction and post-construction stages.

3 GEOLOGICAL CONDITIONS

A detailed geological model was developed from the information collected during five (5) stages of site investigations. The ground profile consists of geological conditions which adopt a layering code system as summarized in Table 1.

Table 1.Geological layer codes adopted for SH16 Causewayalignment.

Geologic Age	Unit	Layer Code	Description
Late Pleistocene – Holocene	Marine Sediments	AH	Marine clays and silts – estuarine muds
Pliocene - Pleistocene	Tauranga Group	ATcl	Clays and Silts
		ATs	Sands and Silty Sands
		ATo/ATp	Organic Clay/Peat
		ATv	Rhyolitic Silt and Sand (volcaniclastic)
Miocene	East Coast Bay Formation (ECBF)	ER	Residual ECBF Soil
		EW	Weathered ECBF Sandstone – Soil and Rock Fractions (20 < N < 50)
		EU	Unweathered ECBF Rock – Sandstone and Siltstone (N > 50)

The marine sediments (AH soil unit) belong to the Late Pleistocene-Holocene age with a deposition environment starting between 8,000 to 14,000 years ago, which still carries on today.

The AH deposit generally consists of uniform normally consolidated Silty Clays. The very soft strength characteristic of the AH soils is in direct contrast to the typically overconsolidated soils present in the underlying Tauranga Group alluvium.

In the Causeway Section, the depth of the Holocene layer is typically 12.0m to 13.0m, with a reduced depth of 1.5m where the ECBF rock head is present at a shallow depth.

4 UNDRAINED SHEAR STRENGTH

The undrained shear strength was assessed by in-situ testing methods such as: (a) field shear vanes; and (b) piezocones (CPTu).

The field shear vanes are commonly used to determine the undrained shear strength (s_u) of soft to medium stiff clays. In this project, a typical field vane was used with a diameter of 50 to 65mm and a height to diameter ratio of 2.

The piezocone testing was conducted using a standard cone: cone angle of 60 degrees, a cross-sectional area of 10 cm^2, and a porous element located immediately behind the cone. The cone was advanced during field probing at a standard rate of 20mm/sec. The data was measured electronically to include the tip resistance (q_c), sleeve friction (f_s) and the penetration pore water pressure (u). The cone correction factor (N_k) for estimatesof s_u values, was assessed based on correlations against the field shear vane test results.

The shear vane profile for the virgin AH soil is presented in Figure 1a. All shear vane readings were corrected adopting the empirical correction factor (μ) recommended by (Bjerrum 1973). The undrained shear strength is showing an increasing trend with depth in accordance with a linear relationship that can be expressed as follows:

$$s_u = 6 + 1.9 \times depth \quad (1)$$

5 SOIL SENSITIVITY

The soil sensitivity represents an indicator of soil micro-structural bonding or development of inter-particle forces between particles or their aggregates. In this study these effects are referred to as structural bonding. The disturbance to the soil structural bonding during loading could have some serious consequences such as: (a) strength reduction; and (b) changes in the overall soil behaviour due to an increase in soil compressibility properties.

The measure of soil sensitivity (S_t) adopted in this study is based on the ratio between peak undisturbed strength (s_u) and the remould strength (s_r) when the soil reaches its residual state. The results of shear vane tests were interpreted to determine the strength sensitivity manifested by virgin AH soil as shown in Figure 1b.

Several classifications of soil sensitivity have been proposed in the technical literature. According to (Rosenqvist 1953) the AH soil falls in the range of a Very Sensitive soil (i.e. $4 < S_t < 8$).

6 ATTERBERG LIMITS

The consistency limits, liquid limit (LL) and plasticity limits (PL), besides serving the basic means of soil classification, they have also been shown to provide estimates of strength and deformation parameters via empirical correlations (Wroth and Wood 1978, among many others).

For this project, the method to assess the LL has adopted the "fall cone" method for the AH soils. The PL was determined by the method of thread rolling according to BS 1377-2:1990.

Figure2a shows the liquidity index (LI) for a soil profile at Chainage 1,860m. The values of LI are generally greater than 1 which is indicative of a soil micro-fabric that is able to accommodate additional resistance over the remoulded state due to development of structural bonds.

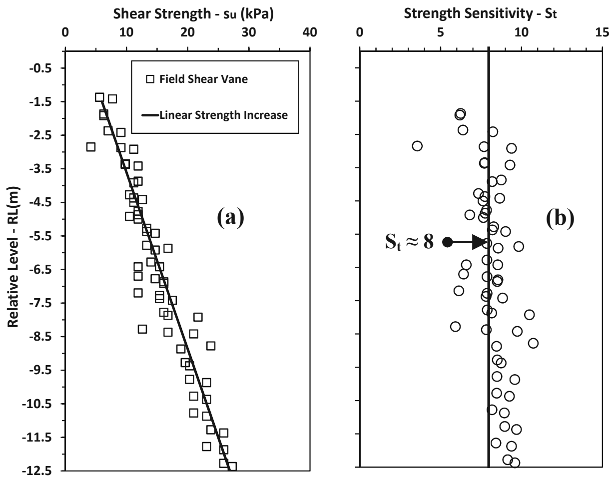

Figure 1. (a) Undrained shear strength profile; and (b) Soil sensitivity profile.

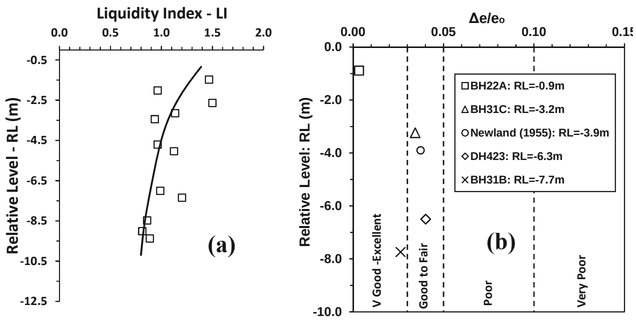

Figure 2. (a) Variation of liquidity index with depth; (b) Sample quality assessment based on (Lunne et al. 1997) classification system.

7 SAMPLE DISTURBANCE

An evaluation of the soil sample quality is essential, as disturbance may lead to a laboratory measured soil behaviour that is different from its in-situ response. Efforts were made to minimize the sample disturbance, but it inevitably occurs due to stress changes associated with soil sampling.

(Lunne et al. 1997) proposed to estimate the quality of soil samples based on the ratio $\Delta e/e_0$, where the change in void ratio Δe is measured during soil re-consolidation phase to in-situ vertical stress σ'_{v0} with consideration of void ratio $e_0$at the beginning of this phase.

Figure 2b presents an assessment of soil sample quality of "reliable" oedometer tests (i.e. sample designation falling in the range of good to excellent). Given the very soft consistency of the virgin AH soil, a significant number of samples were found to have an undesirable quality.

For brevity and clarity of the paper presentation these values have not been included in Figure 2b, and the associated oedometer and triaxial test results have been discarded from further consideration.

8 OEDOMETER TESTS

The tests were carried out using a fixed-ring oedometer with drainage allowed at top and bottom of the test soil sample. The soil samples were 31mm in diameter and 16mm in height. The settlement of the soil sample was monitored by a Linear Vertical Displacement Transducer (LVDT). Each load increment was applied over a time period of 24 hours, with the end of primary consolidation determined using the square-root-of-time method (Taylor 1942).

An AH sample was vigorously remoulded on a glass plate using a spatula to form a soil slurry at a water content equal to the liquid limit (Burland 1990).

The results of AH oedometer tests are presented in Figure 3 in a semi-logarithmic plot of void ratio, e, against the logarithm of the vertical effective stress, log(σ'_v). The virgin AH soil manifests initially a negligible amount of compression before reaching the pre-consolidation stress, σ'_p. When the stress values exceed σ'_p, the consolidation curve displays a non-linear response with a gradient significantly higher compared to the remoulded sample. At high pressures, the compression curve of virgin soil is seen to approach the remould consolidation line in an asymptotic trend.

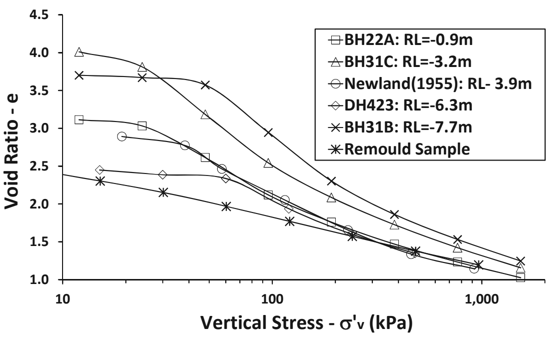

Figure 3. One-dimensional consolidation test results.

9 TRIAXIAL TESTS

The triaxial tests were carried out on virgin soil samples of diameters varying between 50 and 70mm. For all the tests the sample saturation was achieved by raising the back pressure to a maximum of 300kPa. Over the duration of saturation, the stress state was maintained at an effective stress of 20kPa. Full saturation was achieved when Skempton's pore pressure parameter B has achieved a value equal or greater than 95%.

On completion of soil saturation, the samples were isotropically consolidated before the start of undrained shearing. The undrained shearing was conducted in a deformation controlled mode to large axial strains between 15 to 20%.

Figure 4 presents the results of undrained shearing as plots of effective stress paths: deviatoric stress $q = \sigma'_1 - \sigma'_3$ vs. mean effective stress $p' = (\sigma'_1 + 2\sigma'_3)/3$.

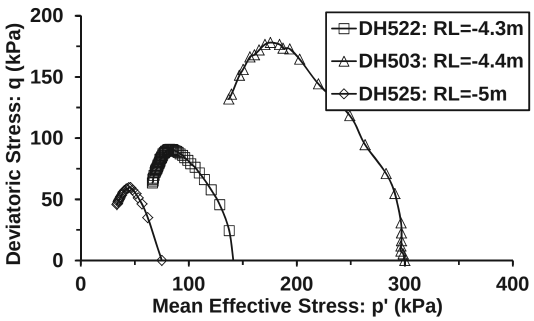

Figure 4. Effective stress paths of AH soil samples in undrained shearing for a range of confining pressures p'_0 = 75 to 300 kPa.

The behaviour manifested by the virgin AH soil is of a contractive type. The stress paths climb to a maximum deviatoric stress, q_{max}, before plummeting towards the origin of the stress path. The strain softening past q_{max} is a distinctive feature of this suite of tests.

10 CRITICAL STATE

The critical state is a fundamental concept in soil mechanics as it represents a reference state to assess the state and behaviour of soil under loading. It was firstly introduced by (Roscoe et al. 1958) to describe the behaviour of remoulded clays, and nowadays the concept was extended to represent a more general framework of soil behaviour for: (a) Sands (Been et al 1991); and(b) Combinations of sand with various percentages of plastic and non-plastic fines (Bobei et al. 2009).

The results of undrained triaxial tests conducted on AH soil are interpreted in the framework of critical state as illustrated in Figure 5. The soil samples were considered to reach the critical state when the following conditions are satisfied: dq=0, dp'=0, du =0 while $d\varepsilon_q \neq 0$.

The CS is found to plot along a linear relationship. On consideration of initial soil state being located above the CS line, and the contractive behaviour manifested during undrained loading (refer to Figure 4), the virginAH soil appears to fully conform to the framework laid out by CS.

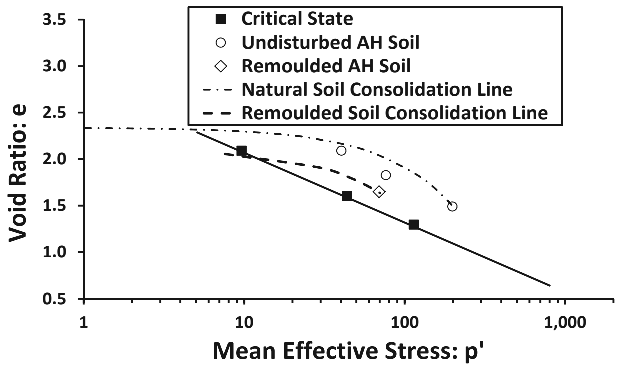

Figure 5. Critical state and soil state of AH soil before undrained loading.

11 SHANSEP PROCEDURE

SHANSEP (Stress History and Normalized Soil Engineering Properties) was proposed by (Ladd and Foot 1974) as an empirical method to adopt in engineering practice to estimate the undrained shear strength on consideration of stress history effects arising from geological unloading. The over-consolidation ratio (OCR = σ'_p/σ'_v) is chosen as a parameter to encapsulate the stress history effects, with the OCR values determined by high quality oedometer data. In mathematical terms, SHANSEP correlates the undrained shear strength with the soil OCR as follows:

$$\frac{s_u}{\sigma'_v} = S \times OCR^m = \left(\frac{s_u}{\sigma'_v}\right)_{OCR=1} \times OCR^m \qquad (2)$$

where: S = intercept with vertical axis at OCR = 1; and m = gradient of linear relationship.

A plot of undrained shear strength ratio (s_u/σ'_v) with OCR based on CPTu data is shown inFigure 6. The CPTu data was found to manifest a linear response, with slope gradients within the bounds of linear relationships shown with dashed lines. In the normally consolidation range, all linear relationships intersect the vertical axis at a constant $(s_u/\sigma'_v)_{OCR=1} = 0.35$.

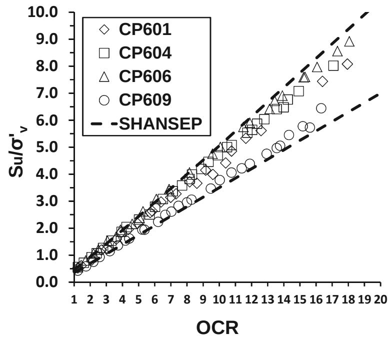

Figure 6. Interpretation of CPTu data based on SHANSEP normalization procedure.

12 FRAMEWORK OF SETTLEMENT ANALYSIS

Previous examinations of the one-dimensional response of a large number of clay soils (Skempton and Northey 1952), suggest the possibility to develop a correlation between the soil sensitivity and liquidity index. The oedometric results of virgin AH soils are interpreted in Figure 7 using LI as a normalizing parameter.

The one-dimensional compression curves are observed to "bundle together" in the stress range greater than pre-consolidation stress, σ'_p. Such normalization procedure may be modeled by a non-linear relationship expressed as follows:

$$\sigma_v^{'} = \frac{90}{(LI + 0.21)^2} \tag{3}$$

The predictive capability of equation (3) is illustrated in Figure7 by the dotted line.

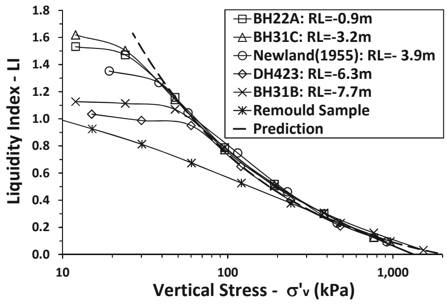

Figure 7. Prediction of non-linear oedometer compression curves.

13 SETTLEMENT PREDICTION

The embankment construction progressed gradually on the surface of soft marine muds to form a series of containment cells, to be later in-filled with granular (sand and shell) and cohesive clay material.

An in-house spreadsheet was developed to incorporate the non-linear relationship (3) to describe the compression response of the virginAH soil.The main features embedded into the spreadsheet include: (a) multi-layered soil configuration; (b) vertical stress increase with depth calculated based on 2D embankment geometry; (c) reduction in σ'_v due to submergence of fill embankment below the ground water table; (d) calculation of primary consolidation using Terzaghi's 1-D consolidation theory; and (e) calculation of creep settlement.

The prediction is found to simulate considerably well the magnitude and rate of settlement development with time as shown in Figure 8.

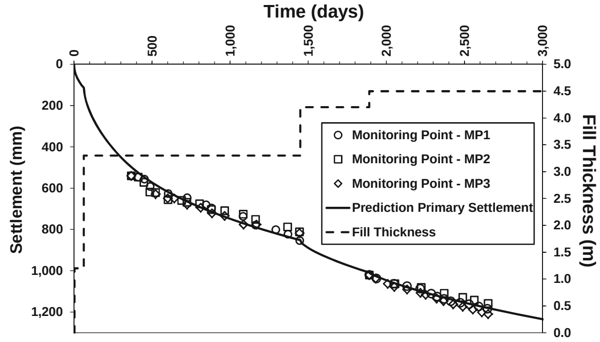

Figure 8. Settlement prediction at the centerline of motorway embankment.

14 CONCLUSIONS

The paper presents some of the results collected as part of an extensive geotechnical investigation carried out into the sub-surface conditions of the Causeway Section of SH16. The main findings of the paper are summarized below:

1. The undrained shear strength ofvirginAH soils manifests a linear increase with depth.
2. The compressibility of virginAH soil in one-dimensional testing displays non-linear characteristics when stresses exceed the pre-consolidation pressure.
3. The assessment of undrained shear strength of virginAH soil is not readily predicted by methods such as SHANSEP.
4. The one-dimensional response of virginAH soil is found to uniquely relate LIandσ'_v. The predictive capability of a proposed relationship is demonstrated by numerical simulations of settlement monitored during the construction and post-construction phase of SH16 motorway embankment.

15 REFERENCES

Been K. and Jefferies M.G. 1985. A state parameter for sands, *Géotechnique*, 35 (2), 99-112.

Bjerrum L. 1973. Problems of soil mechanics and construction on soft clays, *Proceedings of 8th International Conference on Soil Mechanics and Foundation Engineering*, Moscow, 3, 111-159.

Bobei D.C. Lo S. R. Wanatowski D. Gnanendran C. T. and Rahman, M. M. 2009. A modified state parameter for characterizing static liquefaction of sand with fines, *Canadian Geotechnical Journal*, 46 (3), 281-295.

Burland J.B. 1990. On the compressibility and shear strength of virgin clays, *Géotechnique*, 40(3), 329-378.

Ladd C.C. and Foot R. 1974. New design procedure for stability of soft clays, *Journal of Geotechnical Engineering Division*, ASCE, 100(7), 767-787.

Lunne T. Berre T. and Strandvik S. 1997. Sample disturbance on soft low plastic Norwegian clay, *Proceeding of the International Symposium on Recent Developments in Soil and Pavement Mechanics*, Rio de Janeiro, Brazil, 25-27.

Roscoe K.H Schofield A.N. and Wroth C.P. 1958. On yielding of soils, *Géotechnique*, 8, 22 - 53.

Rosenqvist I. Th. (1953) - Considerations of the sensitivity of Norwegian quick clays, *Géotechnique*, 3(5), 195-200.

Skempton A.W. and Northey R.D. 1952. The sensitivity of clays, *Géotechnique*, 3, 30-53.

Taylor D.W. 1942. Fundamentals of Soil Mechanics, New York, Wiley Publishers, 229-239.

Wroth, C.P. and Wood, D. M. 1978. The correlation of index properties with some basic engineering properties of soils, *Canadian Geotechnical Journal*, 15(2), 137-145.

Design and Construction of a Landfill Containment Bund cum Seawall Supported on Stone Columns Installed in Very Soft Marine Mud in Cotai, Macau

Conception et construction d'un remblai de depôts avec une enceinte sur des colonnes ballastées installées dans un sol marin très mou à Cotai, Macao

De Silva S., Fong L.T.T.
AECOM Asia Co. Ltd. Hong Kong.

ABSTRACT: The Cotai Landfill is the main receiving facility in Macau for building construction waste. As the dumping site is underlain with a thick layer of very soft to soft marine clay deposits, the uncontrolled end-tipped material has generated mud waves and they were encroaching the piles supporting the Macau International Airport taxiway nearby. In order to prevent future potential damage to the taxiway, the Macau Government engaged AECOM Asia Co. Ltd.(AACL), to design a containment bund adjacent to the taxiway to retain the waste and to prevent further generation of mudwaves that would affect the taxiway. The sustainable design prepared by AACL comprised the installation of vibrocompacted stone columns installed in over 20 m thick, very soft to firm, moderately sensitive marine clay and alluvial clay,as the foundation to the waste retention bund, thereby avoiding the dredging and off-site disposal of a significant volume of dredged sediments. This paper presents the design approach and construction of the stone columns and the behaviour of the completed seawall.

RÉSUMÉ : La décharge de Cotai est la principale installation de réception de déchets de chantiers de construction à Macao. Comme le site d'immersion repose sur une épaisse couche de dépôts d'argile marine très molle à molle, les matériaux en vrac ont généré des écoulements de boue et ils interpénétraient les pieux soutenant les voies de circulation de l'aéroport international de Macao. Afin d'éviter des dommages potentiels futurs à la voie de circulation, le gouvernement de Macao a engagé AECOM Asie Co. Ltd.(AACL), pour concevoir une enceinte de confinement adjacente à la voie de circulation pour retenir les déchets et prévenir une nouvelle génération de coulée de boue qui aurait une incidence sur la voie de circulation. La conception durable établie par AACL comprend l'installation de colonnes ballastées installées dans des couches de plus de 20 m d'épaisseur, constituées d'argiles marines de consistance très molles à ferme, moyennement sensibles et d'argile alluviale, comme la fondation de l'enceinte de rétention des déchets. Ceci permet d'éviter le dragage et l'élimination hors du site d'un volume significatif de sédiments dragués. Cet article présente l'approche de conception et la construction des colonnes ballastées ainsi que le comportement de l'enceinte terminée.

KEYWORDS : Soft Clay, Ground Treatment, Stone Column, Mudwaves, Seawall.

1 INTRODUCTION

In 2000s, Macau experiencing a major construction boom, the site formation and building works for major casinos, roads and infrastructure on reclaimed land as well as demolition of existing structures generated a large volume of construction waste. It comprised predominantly of spoil materials from basements excavations and piling works.

Cotai Landfill is the main receiving facility in Macau for building construction waste materials. Due to the rapid development activities in late 2000s, the landfill material is being generated at a much faster rate than initially anticipated. In 2008, it was observed that dumping of the construction waste have spread out as well as caused the underlying soft marine mud to displace in the form of mudwaves towards the Macau International Airport (MIA) Southern Taxiway Bridge (STB) and the cooling water intake at the Coloane power plant located in the vicinity of the Landfill (Figure 1).

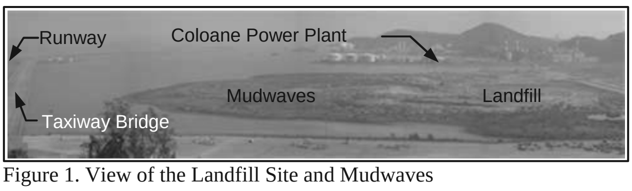

Figure 1. View of the Landfill Site and Mudwaves

This paper present the work for the initial phase of the protection measures against the mudwaves along the STB of MIA. The purpose of the proposed works is to achieve the following objectives:

a) prevent the propagating of mudwaves toward the MIA to protect the STB;
b) maintain the operation of the landfill site as well as maximise the capacity of the landfill site, and;
c) to facilitate the future development of the MIA extension project.

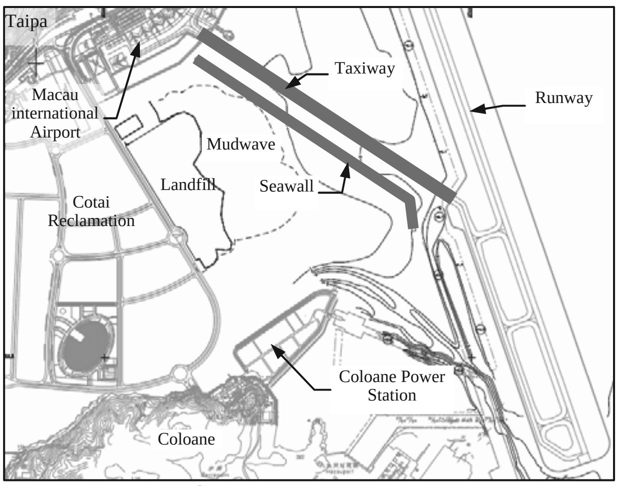

Figure 2. Site Layout Plan

2 SITE GEOLOGY

The superficial deposits within the study area comprise marine deposit (MD) of the Holocene age overlying a layer of alluvium of the Pleistocene age. Underlying the alluvium is the saprolitic soil consisting of completely decomposed granite (CDG). The solid geology comprises coarse-grained granite of Jurassic-Cretaceous age. Fill material has been subsequently placed over the marine soft clay deposit by the landfilling activities. Figure 3 shows the typical geological section of the site. Table 1 shows the typical thickness and constituentcy of the strata.

Table 1. Summary of Geological Strata

Strata	Thickness (m)	Constituent
Fill	4 to 7	C&D waste comprised disturbed mud, silty clayey, sand, concrete, bricks, wood, steel
Marine Mud	13 to 28	Very soft to soft, dark grey, clay to silty clay with occasional shell fragments.
Alluvium	0 to 58 average 30	Soft to stiff, mottled yellowish brown light grey to brown, silty CLAY, CLAY/SILT Medium dense to very dense, yellowish brown to yellowish grey, silty fine to coarse SAND.
CDG	0 to 10	Sandy silty to silty fine to coarse SAND
Bedrock	-	Moderately strong to strong, moderately to slightly decomposed granite.

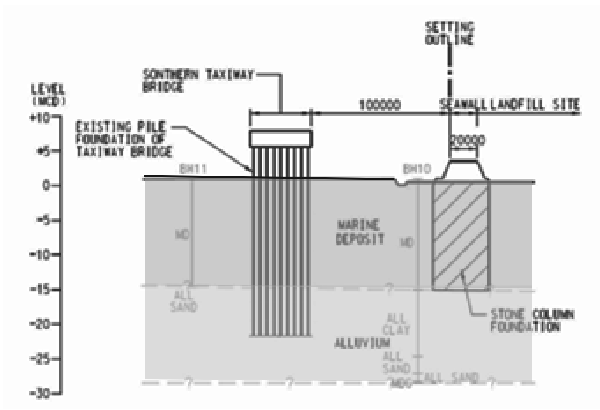

Figure 3. Typical Geological Section

3 DESIGN OF THE SEAWALL

The purpose of the seawall is to contain the dumped surfical clayey and other materials from spreading towards the STB, to prevent the further generation of the mudwaves that would impact the STB and to provide a stable and secure edge to the landfill. Since the founding material of the seawall is very soft to soft marine clay, ground treatment, by means of stone columns, are required to strength the foundation of the seawall in order to ensure the stability. It also improved the shear strength and stiffness of the soil mass to minimise the influence of the lateral load induced by the landfill soil mass that could possibly cause disturbance to the STB.

3.1 *Principle of Ground Improvement by Stone Column*

Stone column construction involves the partial replacement of the very soft subsurface soils with compacted, vertical columns of stone that completely penetrates the weak strata. The stronger and stiffer material will attract more stresses (i.e. the stone columns) and therefore the composite ground comprising stone columns and soft clay (Barksdale, R.D. & Bachus R.C. 1983) will be stronger and stiffer and capable of carrying a larger load originating from the landfill behind,preventing the formation of mudwaves. The stone columns will also act as vertical drains within the soft clay facilitating the rapid dissipation of the excess pore pressures allowing it to quickly consolidate and gain in strength, thus further increasing the stiffness of the composite soil mass over time.

The strength of the composite ground depends on the percentage of soil replaced by the stone columns, i.e. the replacement ratio,a_s, as defined by (1) and illustrated in Figure 4.

$$a_s = C_1\left(\frac{D}{s}\right)^2 \tag{1}$$

D - Diameter of the compacted stone column
s - Centre to centre spacing of stone columns
C_1 - Constant depending on stone column configuration pattern

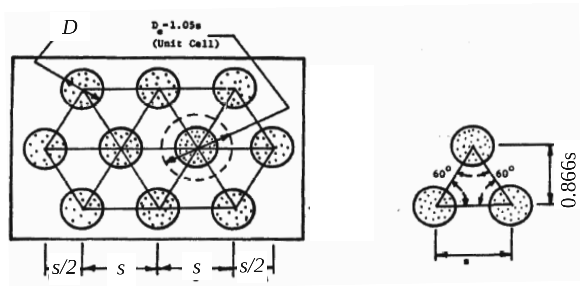

Figure 4. Replacement Ratio of Stone Columns

For this project, a 1.2 m diameter stone column at 2.5 m c/c spacing in a triangular pattern was adopted. The replacement ratio $a_s$is about 21%. Since the stone aggregate columns are much stiffer than the soft clay, the stresses will concentrate at the stone columns. The distribution of the stresses can be expressed by the stress concentrated factor *n*, defined as:

$$n = \frac{\sigma_s}{\sigma_c} \tag{2}$$

σ_s= stress in the stone column
σ_c= stress in the surrounding cohesive soil

The stresses over the soft soil and the stone column in term of $a_s$from (1) and the average overall stress on the ground surface, σ, is illustrated in a unit cell concept in Figure 5.

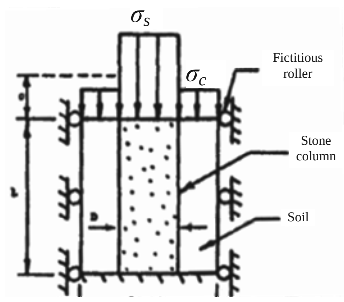

σ_s - Stress in stone
σ_c -Stress in clay

Figure 5. Ideal Unit Cell of Stone Column

$$\sigma_s = n\,\sigma / [1+(n-1)\,a_s] = \mu_s\,\sigma \tag{3}$$

$$\sigma_c = \sigma / [1+(n-1)\,a_s] = \mu_c\,\sigma \tag{4}$$

μ_s =Ratio of stress in stone in relation to σ
μ_c= Ratio of stress in cohesive soil in relationto σ

Using the expression of $\mu_s$in (3), the stone column foundation can be modeled as a composite material with the average shear resistance expressed as:

$$c_{avg} = (1 - a_s)\, c \quad (5)$$

$$\phi_{avg} = tan^{-1}\,(\mu_s a_s \tan\phi_s) \quad (6)$$

3.2 Stability Analysis

The stabilityanalyses of the stone column seawall were carried out using the computer software "Slope/W" with automatic circular failure mode and sliding block failure modes. The stone column foundation was modelled as a composite material with the embankment of landfill in place behind the seawall(Figure 6). With a_s of about 21%, the average cohesion of the composite material immediately after placing the stone columns will range from 2.8 kPa to 12.7 kPa; and the average friction angle of the composite material is 20.4°.

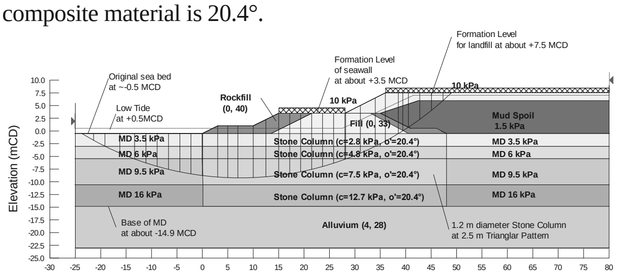

Figure 6. Geological Model for Slope Stability Analyses

To maintain the seawall stability, a 50m wide stone column treatment zonewas required. The seawall revetment and the landfill embankment slope profileswere proposed at a gradient of 1V:2H. A toe bund is provided as counterweight to stabilise the rockfill revetment. A typical section is shown in Figure 7.

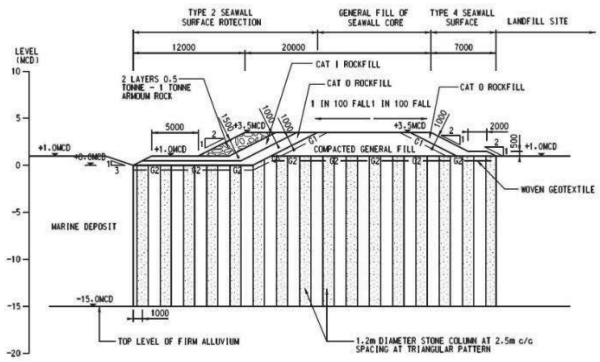

Figure 7. Typical Cross Section ofthe Seawall

The stone columns will also act as vertical drains to provide drainage path for the excess pore water pressures arising from the vertical load of the embankment. With a typical 15 m thick marine deposit and an equivalent rectangle embankment width of about 30 m, the average increase in the effective stress of Marine Mud is only 25 kPa. Based on the radial consolidation theory and settlement reduction by the stone columns, 0.6 m settlement will occur within a year. Due to uncertainty in the drainage performance of the stone columns, the increase in the strength of the marine clay as a result of consolidation was not taken into account in stability analyses.

3.3 Assessment of Impact on Taxiway Pile Foundation

Since the STB is a critical facility to the MIA any damage to the STB will significantly affect the operation of the MIA. In order to control the additional load imposed from landfill site to the STB, numerical modelling was carried out to assess the impact to the STB during installation of the stone columns, construction of the seawall and when filling behind the seawall as part of the landfilling operation.

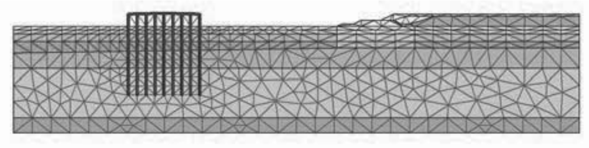
Figure 8. Finite Element Model

A Finite element model was developed (see Figure 9) using PLAXIS. The model adopted a geological profile with the deepest seabed level and thickest alluvium of the entire length of the seawall. The analyses were carried out with the marine clay behaving as an undrained material, which is considered to be an appropriate approach to model the actual behaviour of the soft clay. The structural elements included the beams and the PHC piles of the STBwere modelled as a continuous beam/wall element in the PLAXIS modelwith an influence zone of 3 times the diameter being adopted (LECM 2008b). The model simulates the full history of the site including the original ground conditions, formation of the STB, installation of the stone columns, formation of the seawall and landfilling operation behind it.

The results from numerical modeling show that the maximum additional bending moment due to stone column installation, seawall construction and landfilling activities is only 6 kNm near the top of the STB piles and the total load of the pile is still within the acceptable limit of the original design. The additional shear force is considered to be not significant. The maximum predicted movement of the nearest piles to the seawall is about 8 mm (Figure 9). This predicted lateral movement is likely to span across a few spans of the taxiway and the actual magnitude of relative movement between each span of taxiway structure is unlikely to be a concern asmovement joints have been provided between the taxiway spans and it should be capable of withstanding this relative movement.

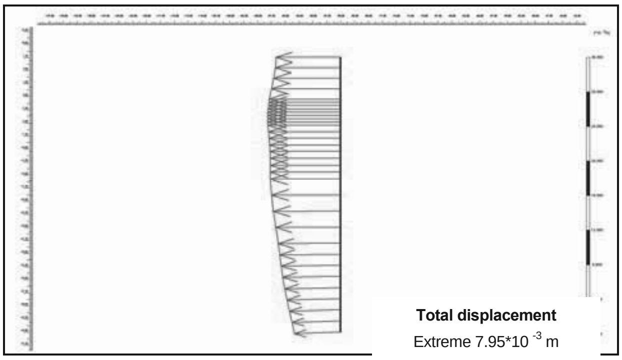

Figure 9. Predicted lateral Displacement of the Taxiway Foundation

3.4 Construction

Since the site is situated close to the MIA, there are certain physical constrains imposed by the Civil Aviation Authority of Macau on construction activities. The entire site is within the navigation restriction zone of the MIA (Figure 10). Marine access to the site is restricted and no mooring of vessels was allowed within the navigation restriction zone around the Airport. To avoid any disturbances on the movement of aircraft along the STB, all works were required to be carried out outside a zone of 57.5m from the centreline of the STB. Based on the information from the Civil Aviation Authority of Macau (AACM), the height restriction in the vicinity of the MIA along the runway is stringent and the use of high cranes was restricted. As a result, dredged seawall was adopted near the eastern end of the seawall.

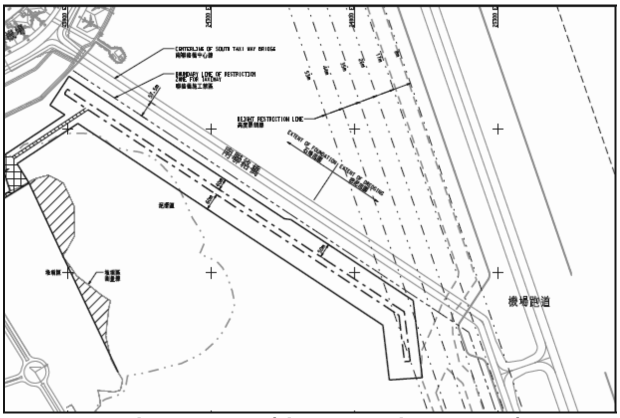

Figure 10. Height Restriction of the Site near the Runway of MIA

There was no readily available land access to the site as it is restricted by the landfill site and the MIA. Marine access was also limited due to the shallow draft and the contractor had to carry out additional dredging for navigation. The original design proposed a temporary platform for landbased stone column construction. During the construction stage, the contractor changed to marine based method for installation of the stone columns.

To ensure the mud will not be mixed with the stone aggregates due to collapse of hole or necking, wet bottom feed method was adopted (Figure 11). Acceptance of the stone column was based on the depth vsSC diameter plot, and degree of compaction (volume of aggregate, energy consumed)from the installation records. Site trial was carried out to determine the optimum arrangement on apparatus, setup, minimum required compaction time, amount of aggregate consumption per metre length, andmaximum energy consumption (Figure 12).

Figure 11. Stone Column Plant for Wet Bottom Feed installation

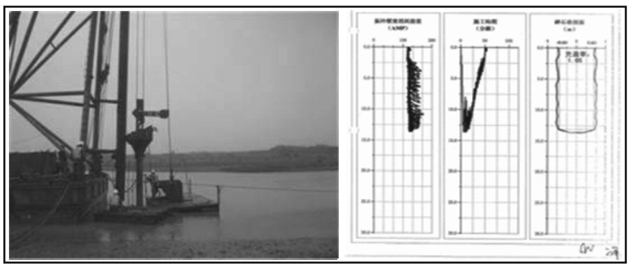

Figure 12. Site Trial Establishingthe Acceptance Criteria

3.5 *Monitoring of Taxiway and Taxiway Piles*

The movement of the taxiway pile foundation and the MIA seawall were closely monitored during the seawall construction phase. No significant movement of the taxiway, the piles and the seawall was measured. Monitoring will continue during the future landfilling operation stage when the loading is maximized in the landfill.

4 SUMMARY AND CONCLUSIONS

Construction waste was dumped over very soft marine mud at the Cotai Landfill of Macau. This uncontrolled dumping pushed the very soft mud and generating mudwaves that were then encroaching onto the piles supporting the taxiway bridges of the Macau International Airport.

Due to the seriousness of the problem, government of Macau commissioned AECOM Asia Co. Ltd., to develop a robust solution to contain the construction waste being dumped in the area and to protect the taxiway bridge of the Macau Airport. The design solution developed was to construct a containment bund/seawall that is founded on a stiffened and strengthened soil block by improving the soft clay with stone columns. This paper presented the design approach of the containment bund including the limited equilibrium stability analysis and the numerical analyses carried out that demonstrated that the solution is appropriate as the bund will contain the landfill with minimal impact on the taxiway bridge piles. The analyses also demonstrated that the impacts during construction are also negligible.

During construction, the taxiway and seawall was monitored by independent parties and survey results indicate the installation of the stone columns and construction of the bund had minimal impact on the taxiways foundation piles. The seawall has been completed in November 2011 (Figure 13).

Figure 13. The Completed Stone Column Seawall

5 ACKNOWLEDGEMENTS

This paper is published with the permission of the Head of Gabinete para o Desenvolvimento de Infra-estruturas of the Macau SAR Government.

6 REFERENCES

Barksdale, R.D. & Bachus R.C. 1983. *Design and Construction of Stone Columns – Volume 1*. US department of Transport.

Laboratório de Engenharia Civil de Macau 2008a. *Inspection Report of Southern Taxiway Bridge Piles*. LECM, Macau

Laboratório de Engenharia Civil de Macau 2008b. *Numerical analysis report on the landfill mudwaves impact to Southern Taxiway Bridge*.LECM, Macau

Estimation of undrained shear strength of soft soil obtained by cylinder vertical penetration

Estimation de la résistance au cisaillement d'un sol mou en conditions non-drainées obtenue par la pénétration verticale d'un cylindre

Equihua-Anguiano L.N.
UPAEP University, Puebla, Mexico

Orozco-Calderon M.
Geotechnical consultant, Ciudad del Carmen, Campeche, Mexico

Foray P.
Laboratoire 3SR,Grenoble, France

ABSTRACT: Determination of undrained shear strength (s_u) in cohesive soils is essential for the design of the offshore pipelines/flowlines, especially when burial depth is small (in the order of twice of the pipeline diameter). This paper presents experimental results of the undrained shear estimation, obtained by the vertical penetration of a cylinder in a soft normally clay with deep water characteristics. Results obtained were compared with analytical solution for a cylinder embedded in a cohesive soil, as well as with experimental s_u values obtained using laboratory vane test. The results between the two techniques are very close

RÉSUMÉ : La détermination de la résistance au cisaillement en conditions non-drainées des sols est nécessaire dans le design des conduits/*flowlines offshore,* particulièrement dans le cas où profondeur d´enfoncement est de l´ordre de deux fois le diamètre du conduit. Cet article présent les résultats d´une étude expérimentale conduisant à la détermination de la résistance au cisaillement non drainée d´un sol argileux très mous, en utilisant l´enfoncement d´un cylindre. Enfin, concernant l´aspect modélisation, une solution analytique correspondant à l´enfoncement d´un conduit dans un sol cohérent a été utilisée. Les résultats ont été comparés avec ceux obtenues avec un scissomètre du laboratoire et montrent une bonne approximation.

KEYWORDS: undrained shear strength, deep water, offshore geotechnics, pipeline, vane test..

1 INTRODUCTION.

Deep water soils present special characteristics with respect to the other soils. Examples of the particular parameters correspond to undrained of strength and plasticity. In field, high plasticity values (liquidity index close to 1) and low undrained shear strength (s_u) have been found, this last parameter varies approximately from 1 to 3 kPa on the seabed surface.

Undrained shear strength parameters is main in the marine pipeline conception as well as, its variation with depth, especially in the first tens centimeters. In practice, CPT, T-bar and recovery of intact samples with the Box corer and mini-Tbar are used *in situ* (ISSMGE-TC1 2005, Puech et al. 2010) to obtain geotechnical design parameters. In the same way, laboratory test are done for s_u determination to little depth in the soil, using experimental techniques well known as: vane shear laboratory (AFNOR, 1995), fall cone (Hansbo 1957, Orozco Calderon & Mendoza 2002), T-bar penetrometer (Stewart & Randolph 1991), among others. These techniques allow obtaining s_u to the surface level, at a point or continuously with depth. In this context, the article presents an option to measure s_u from testing cylinders in laboratory as is described below.

1.1 *Objective*

An alternative to estimate experimental undrained shear strength variation with depth was developed. Procedure and laboratory tests were done penetrating a cylinder in a soft soil with deep water characteristics. First, the cylinder was placed horizontally in the soil surface and then, it was penetrated vertically into the soil. The vertical displacement (z) was applied with an electromechanical actuator and the vertical force (F_v) was recorded and were compared with a theoretical solution, in order to determine the undrained shear strength. Finally, the results were compared with s_u values obtained with a laboratory vane. Figure 1 shows the schematic cylinder and nomenclature used.

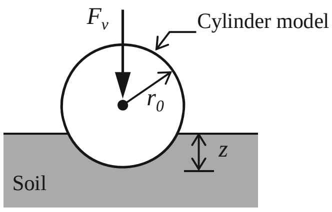

Figure 1. Schematic cylinder penetration.

2 PARTIAL PENETRATION OF A CYLINDER

2.1 *Theoritical solutions*

A theoretical solution to the failure load or collapse for a pipe on the soil was given by Murff et al. (1989) analyzing a pipe partially embedded on the soil and the undrained shear strength (c) uniform with the depth. The solution takes into account the type of surface roughness of the pipe through the concept of adherence a_d=αc, and consider a value of α=0 as smooth surface and α=1 as rough surface.

Vertical force on the cylinder (or a pipe) to a certain depth z on a soil with horizontal surface, is given by equation (1):

$$\frac{F_v}{2r_0c} = \left[\begin{array}{l} \cos(\Delta+\omega)+2\mathrm{sen}\left(\frac{\Delta}{2}\right)+(1+\Delta+2\omega)\cos\omega+ \\ +2\cos\left(\frac{\Delta}{2}\right)-2\mathrm{sen}\,\omega \end{array}\right] \quad (1)$$

where: a_d = adhesion at the interface soil-cylinder; c=undrained shear strength; Δ=sen^{-1} α; ω=sen^{-1} (1-z/r_0); r_0=cylinder radius; z=penetration depth of the cylinder.

The equation (1) can be represented by an expression of type power, in function of depth penetration z, the radius r_0, coefficient a and exponent b, as follows:

$$\frac{F_v}{2r_0 c} = a\left(\frac{z}{2r_0}\right)^b \qquad (2)$$

From the above equations, it follows that it is possible to obtain the resistance undrained shear if the vertical force F_v required to penetrate the pipe is known. Considering equation (1) as the theoretical solution, experimental values and resistance undrained shear as the unknown value, namely:

$$\left[\frac{F_v}{2r_0 c}\right]_{\text{theoretical}} = \left[\frac{F_v}{2r_0 s_u}\right]_{\text{experimental}} \qquad (3)$$

The s_u value for each depth of the cylinder penetration is represented by the equation (4). The undrained shear strength average for the entire depth z is represented by equation (5), where N=total values of cylinder penetration during the laboratory test.

$$(s_u)_i = \frac{\left[\dfrac{F_v}{2r_0}\right]_{\text{experimental}}}{\left[\dfrac{F_v}{2r_0 c}\right]_{\text{theoretical}}} \qquad (4)$$

$$\overline{s_u} = \frac{\sum_{1}^{N} (s_u)_i}{N} \qquad (5)$$

Another alternative to obtain s_u for the entire depth (z) of the cylinder penetration is solving the equation (3), applying numerical methods, for instance the least squares method.

In this case, the adjustment evaluation is minimizing the sum of squared residuals (E), which corresponds to the squared distance of the experimental values and the theoretical curve based on their, as shown in equation (6).

$$E = \sum_{i=1}^{N} \left\{ \left[\frac{F_v}{2r_0 s_u}\right]_i - \left[\frac{F_v}{2r_0 c}\right]_i \right\}^2 \qquad (6)$$

where: $\left[F_v / 2r_0 s_u\right]$ corresponds to the values obtained experimentally and s_u is an unknown; $\left[F_v / 2r_0 c\right]$ is the vertical collapse load normalized by the pipe diameter and the soil shear strength for different values of α (Murff et al. 1989).

Substituting equation (2) into (6) it is possible to obtain E (equation 7) with three unknowns values: the undrained shear strength s_u, coefficient a, and the exponent b.

$$E = \sum_{i=1}^{N} \left\{ \left[\frac{F_v}{2r_0}\right]_i - \left[s_u a \left(\frac{F_v}{2r_0}\right)^b\right]_i \right\}^2 \qquad (7)$$

Solution of equation (7) represents the value of s_u for the entire depth (z), where the values a and b allow to fit the experimental data to approximate the theoretical solution (equation 1).

Using the expressions (4), (6) and (7) it is possible to obtain s_u. Calculated values of s_u by these equations were compared with experimental values as shown in next sections.

3 CYLINDER MODELS AND SETUP

3.1 *Cylinder models and setup*

Two cylinder models with different geometrical and material characteristics were used: a steel pipe model with a diameter of 100 mm and a length of 335 mm, the second pipe model in PVC with 200 mm diameter and 900 mm length.

Tests were performed in the tank *VisuCuve* of Laboratoire 3S-R in Grenoble. Its internal dimensions are 2m-length, 1m-width and 1m-depth. For the experimental tests it was filled only 0.4 m-depth with the soft soil.

The vertical force F_v was applied on the cylinders using an electromechanical actuator. The vertical force and displacements were recorded during the penetration test via a control and data acquisition system (Fig. 2).

The large rigid tank *VisuCuve* was used in others laboratory studies to visualize in order to visualize the failure mechanism around a mini penetrometer T-bar (Puech et al. 2010) and study models anchor plates (Equihua-Anguiano et al. 2012).

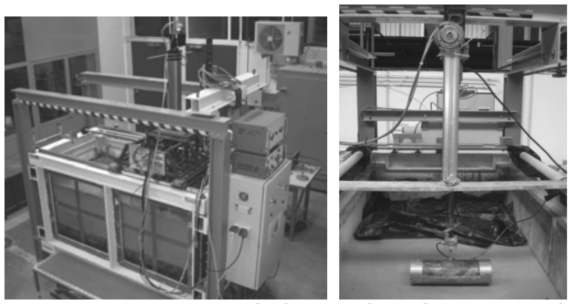

Figure 2. VisuCuve setup and electromechanical actuator used to penetrate a pipeline model vertically into a soft soil.

3.2 *Tested soil*

The reconstituted soil used in this study was composed of a mixture of bentonite and kaolin in equal proportions (50B/50K) with w=110% and 200%, w_L=163% and PI=132%. Its characteristics are very similar of deep water (Gulf of Guinea w=150-200%, w_L=170% and PI=125%). In the same way, this reconstituted soil has been used in other researches, for example a study of T-bar penetrometer and soil-pipeline interaction (Orozco-Calderon 2009).

3.3 *Experimental program*

Table 1 shows nine experimental tests program. For the pipe model of 100 mm diameter two soils were tested (s_u=6 kPa and 3 kPa). In the case of pipe 200 mm diameter only two penetration tests were performed in a soil with s_u=3 kPa.

Table 1. Dimensions of the pipe models used in the experiments.

Test No.	Pipe model	Pipe diameter (mm)	Material pipe model	Soil No.	w (%)	s_u (kPa)
1	10-110-1	100	Steel	1	110	6
2	10-110-2	100	Steel	1	110	6
3	10-110-3	100	Steel	1	110	6
4	10-110-4	100	Steel	1	110	6
5	10-150-5	100	Steel	2	150	3
6	10-150-6	100	Steel	2	150	3
7	10-150-7	100	Steel	2	150	3
8	20-150-8	200	PVC	2	150	3
9	20-150-9	200	PVC	2	150	3

4 RESULTS

Results for numerical and experimental testing are presented in the next sections.

4.1 *Force vertical and depth penetration of pipe model tests*

Figure 3 shows some typical experimental results and a comparison with those calculated from equations (4), (6) and (7).

Results presented in Figure 3(a) correspond to the curves of type s_u-z/r_0 (solution of equation 4) which represent undrained shear strength for each depth of the penetration. The results of Figure 3a the equation (5) could be used to obtain an average value of the s_u throughout the depth analyzed.

The second type of curves, Figures 3(b) and 3(c), corresponds to the vertical force F_v normalized respect to the diameter of the pipe and the undrained shear strength ($F_v/2r_0s_u$) versus the penetration normalized respect to the radius or diameter. The use of these curves represents the solution of the equations (6) and (7).

In the case of Figures 3(a) and 3(b) the calculated values correspond to depths of $z/2r_0 \leq 0.5$, since the theoretical solution is used for normalized force (Murff et al. 1989, equation 1), valid for a penetration less than or equal to the radius of the pipe. Values of the undrained strength calculated considering two types of surface, while the surface of the laboratory model was the same during the tests, and that can be interpreted as the minimum and maximum values.

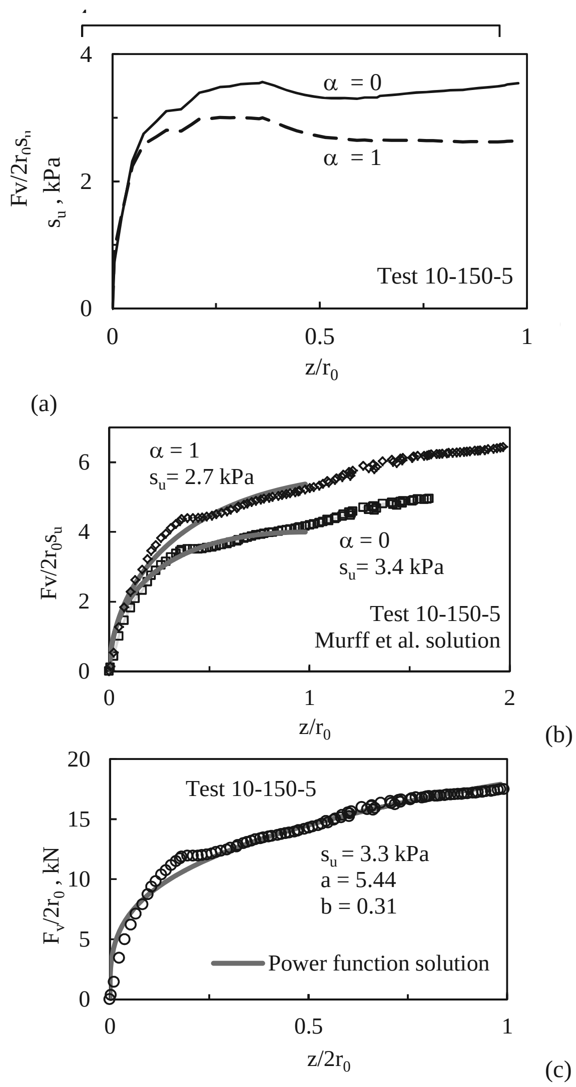

Figure 3. Estimating of undrained shear strength using a vertical penetration of a cylinder (Test No. 5). Solution using the equation (4) in (a). Calculated values of s_u considering the solution Murff et al. for α=0 and α=1 (equation 4) in (b). Value of s_u by fitting set of experimental data with a power function solution (equation 7) in (c).

For the results in Figure 3(c) the adjustment takes into account the values of $z/2r_0 \geq 0.5$, which represents an advantage over the equations (4) and (6), and the solution corresponds to a unique value of s_u, also at the same time, *a* and *b* values were calculated.

4.2 *Calculated undrained shear strength*

Results of undrained shear strength of all tests are summarized in Figure 4. Figure 4(a) represents the mean value of the s_u calculated with equation (5) for the typical results included in Figure 3(a). Interpretation of the results takes into account the variation of pipe surface. It can be noticed immediately the difference in the results for soils with different undrained shear strength.

Results are concentrated around the soil resistance obtained with miniature vane shear test. In case of analysis with α=0 the estimated values s_u are higher than corresponding to a rough surface (α=1). Horizontal lines included in the Figure 4(a) represent the average value of considering all the values of each soil and roughness. The experimental pipe models used had a surface intermediate, therefore it is expected that the corresponding s_u value is between two limits.

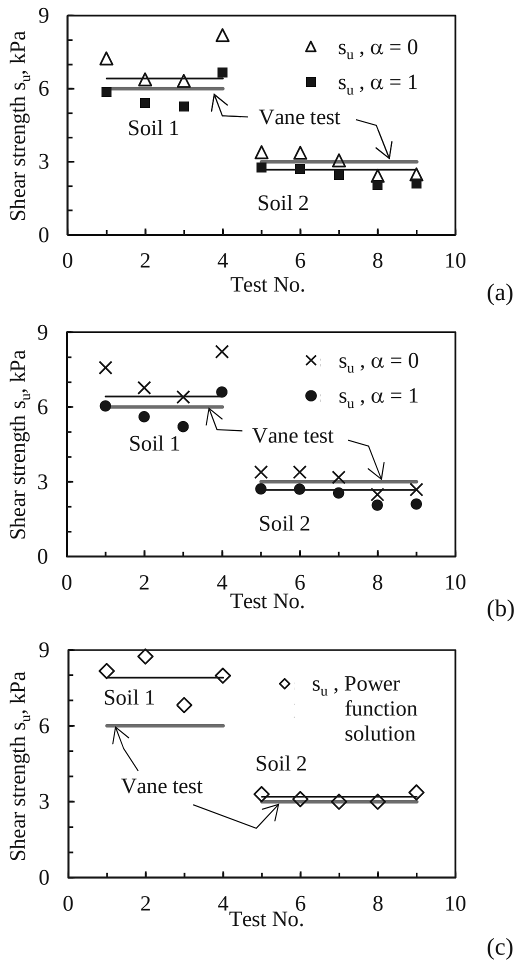

Figure 4. Undrained shear strength obtained from the equation (5) for a penetration depth of $z/2r_0 \leq 0.5$ (a). Values of s_u calculated from the equation (6) and the solution Murff et al. (equation 1) for α=0, α=1 and $z/2r_0 \leq 0.5$ (b). Values of s_u calculated from the equation (7) whereas the total depth of penetration of the pipe model (c).

Figure 4(b) shows the results for the case of the estimated value from the equation (6). Their values are grouped for each soil and the tendency of behavior is similar to the results of Figure 4(a), the difference is clearly distinct between the two undrained shear strength. Similarly, the horizontal line represents the mean value s_u estimated of each soil.

The calculated results from Equation (7) are included in Figure 4(c). Values are generally higher than those of the preceding Figures 4(a) and 4(b), this can be understood as such calculation does not take into account the theoretical solution (Equation 1), and the roughness of the pipeline is implied by the value of the coefficient *a* and the exponent *b* of the numerical curve fitting. In this case, the average value of the coefficient is a=5.12 with a standard deviation of σ=±0.48, to the exponent average value of b=0.32 and σ=±0.09. Figure 5 shows the variation of *a* and *b* values.

The estimated values of the undrained strength and standard deviation for each soil are included in Table 2. There are similarity of the values calculated from equations (4) and (6) and roughness respectively. For the type of power adjustment, which represents a simple solution compared to the strict theoretical equation, the values are generally higher. It is important to note that the value of the standard deviation is high, which encourages to study this alternative to estimate experimental undrained shear strength with a large number of experimental test for different soils with different undrained shear strength.

The technique using cylinders penetration in order to obtain the soil shear strength provides good results, one limitation is consider the undrained strength constant with depth.

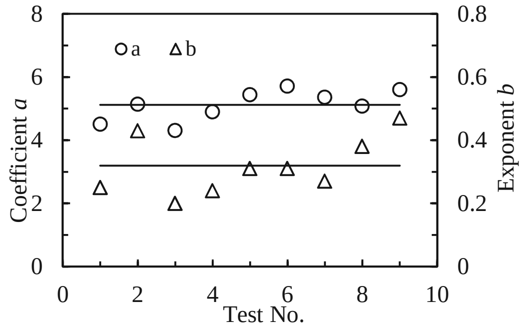

Figure 5. Variation coefficient *a* and exponent *b* for all experimental tests, obtained from fitting of experimental values with equation (2).

Table 2. Values of the average undrained shear strength calculated from vertical penetration tests cylinder models.

Soil No.	Values*	Equations (4)		(6)		(4) & (6)	(7)
		α=0	α=1	α=0	α=1	α=0 and 1	...
1	$\overline{s_u}$ (kPa)	7.0	5.8	7.3	5.9	6.5	7.9
	±σ (kPa)	0.9	0.6	0.8	0.6	1.0	0.8
2	$\overline{s_u}$ (kPa)	2.9	2.4	3.0	2.4	2.7	3.2
	±σ (kPa)	0.5	0.3	0.4	0.3	0.3	0.2

* $\overline{s_u}$: average undrained shear strength, σ: standard deviation.

5 CONCLUSIONS

This article presents experimental tests, as an option to obtain the undrained shear strength of soft soils using vertical penetration of a cylinder into the soil.

Experimental results takes into account theoretical solution for a pipe penetrated in a homogeneous medium, characterized by a constant undrained strength with depth.

Experimental tests were performed on two soils with different undrained shear strength, the results are close to the value of s_u obtained with a laboratory miniature vane.

The standard deviation of the experimental results of this paper is relatively high, which encourages study with a larger number of soils.

One limitation of the test is the depth shallow for soil characterization, however it is considered appropriate for the case of marine pipeline design.

6 ACKNOWLEDGEMENTS

The authors acknowledge the *GéO* team of the *Laboratoire 3S-R* at Grenoble, France, for the facilities and support to perform the experiments.

7 REFERENCES

AFNOR. 1990. *Essai scissométrique en laboratoire, sols: reconnaissance et essais*, Norme NF P 94-072, Association Française de Normalisation, Paris, La Défense, 325-337.

Aubeny C.P., Shi H. and Murff J.D. 2005. Collapse load for cylinder embedded in trench in cohesive soil, *International Journal of Geomechanics*, Vol. 5(4), 320-325.

Equihua-Anguiano L.N., Orozco-Calderon M. and Foray P. 2012. Numerical finite element method and experimental study of uplift capacity anchors, *Seventh International Conference on Offshore Site Investigation and Geotechnics, OSIG 2012*, London, U.K.

Hansbo S. 1957. A new approach to the determination of the shear strength of clay by the fall-cone test, Stockholm: Royal Swedish Geotechnical Institute, Proceedings 14.

ISSMGE-TC1 2005. Geotechnical and geophysical investigations for offshore and near shore developments, TC1, ISSMGE.

Murff J.D., Wagner D.A. & Randolph M.F. 1989. Pipe penetration in cohesive soil, *Géotechnique* Vol. 39(2), 213-229.

Orozco-Calderon M. 2009. *Etude de l'interaction cyclique sol-pipe dans les grands fonds marins*. Thèse, Institut Polytechnique de Grenoble, Laboratoire Sols, Solides, Structures – Risques, France.

Orozco-Calderon M. and Mendoza M.J. 2002. Quick and reliable determinations of water content, liquid limit and undrained shear strength for fine-grained soils (in Spanish), *XX National Meeting of Soil Mechanics*, SMMS, Oaxaca, Mexico, Vol. 2, 53-62.

Puech A., Orozco-Calderon M. and Foray P. 2010. Mini Tbar testing at shallow penetration, *Proceedings Frontiers in Offshore Geotechnics II*, Perth, W.A., Australia, 305-310.

Stewart D.P. and Randolph M.F. 1991. A new site investigation tool for the centrifuge, *Proceedings of CENTRIFUGE 91*, 531-538.

The Application of a Novel Design Approach for Construction over soft soils: The Hybrid Undrained-Drained model

L'application d'une nouvelle méthode de conception pour des constructions sur sols mous: le modèle hybride non drainé - drainés

Espinoza D., Li C.
Geosyntec Consultants, Columbia, Maryland, USA

ABSTRACT: The number of case histories of construction of high mechanically stabilized earth (MSE) berms over soft foundations, such as dredge disposal sites, is limited for obvious reasons: it is difficult to build without risking foundation instability. The purpose of this paper is to describe the challenges of designing and building embankments over extremely soft foundations using innovative design and construction techniques. The case history site for this paper is located in Wilmington, Delaware, where a 2400-m long, 21-m high MSE berm was completed in July 2010. The completion of this 1.5-million-cubic-meter berm represents a significant engineering achievement considering the size of the embankment and the 30-m deep layer of very soft soils (undrained shear strength as low as 10 kPa) over which the berm was constructed. The project was recently selected by the American Society of Civil Engineering among the five finalists for the 2012 Outstanding Civil Engineering Achievement Award.

RÉSUMÉ : Le nombre d'études de cas de construction de digues en terre compactée (MSE) sur des couches de fondations molles, comme le sont les sites de dépôts de dragage, est limité pour des raisons évidentes : il est difficile de construire sans risquer l'instabilité de la fondation. Le but de cet article est de décrire les défis de la conception et de la construction sur des fondations extrêmement molles en utilisant une conception innovante et des techniques de construction appropriées. Le site de cette étude de cas se trouve à Wilmington, dans le Delaware, où sur 2400 m de long une digue de 21 m de haut a été achevée en Juillet 2010. La réalisation de cette digue d'1,5 millions de mètres cubes représente une réalisation technique importante compte tenu de la taille du remblai et la couche de 30 m d'épaisseur des sols très mous (résistance au cisaillement non drainée voisine de 10 kPa) sur laquelle l'ouvrage a été construit. Le projet a été récemment choisi par la Société américaine de génie civil parmi les cinq finalistes pour le prix d'excellence 2012 des réalisations de génie civil.).

1 INTRODUCTION

This paper presents a case history of a reinforced earth structure constructed over extremely soft soils. The design and construction techniques developed for this project are applicable to many of the dredge management, levees, and other waterfront earthen structures.

Figure 1. Site Location Plan

The site where this case study was developed is the Cherry Island Landfill (CIL), located in Wilmington, Delaware, which was constructed over an area that was partly reclaimed from the Delaware River in the early 1900s (see Figure 1) and that had been used for many years as a dredged material disposal site for the U.S Army Corps of Engineers (USACE). Under the dredge layer lies an alluvium deposit with similar geotechnical characteristics as the overlying dredge. As a result, the subsurface at the site consist of unconsolidated, very soft, low permeability and extremely compressible materials with undrained shear strengths as low as 10 kPa and thickness ranging from 18 to 30m. Under the alluvial deposit lies the Columbia Formation (a 12m to 15m thick deposit of medium-to-coarse, medium-dense-to-dense sand).Because of the dredge layer's thicknessand permeability, it was initially estimated that it would take over 30 years for any excess pore pressures to dissipate.

To meet the growing demands for waste disposal in the Wilmington area, an additional 17 million cubic meters (mcm) of waste disposal capacity (i.e., 20 plus years capacity at the disposal rates at the time of design) was estimated. Because of the subsurface conditions, the additional airspace required to satisfy the needs of the state could not be obtained by increasing either the landfill sideslopes (8Horizontal:1Vertical in the original landfill layout) or the landfill height without compromising the overall foundation stability.Because the site is located at the confluence of the Delaware and Christina Rivers (See Figure 1), the potential for a horizontal expansion was limited;hence, the main alternative to obtain additional capacity at this facility was to expand it vertically.In order to obtain the required capacity, the only option available that would provide the additional disposal capacity was to build a 2400-m long and 21-m high mechanically stabilized earth (MSE) berm around the facility and place waste behind this structure. The preliminary feasibility study indicated that, in order to build the 21-m high MSE berm, the foundation shear strength needed to be improved from 10 kPa to 160 kPa as a minimum. The preliminary conceptual solution for achieving this strength gain was to use deep soil mixing (DSM), a technique that consists of mixing soil with cement. Because of the depth, length, and width of the soft soils that needed to be improved, the volume of soil that needed to be treated was approximately 2.5 mcy. At the time the construction of the soil improvement took place (2006), cement prices were significantly higher because of global demand, and the estimated cost for the DSM option was estimated to be \$150 million (2011 US dollars).

2 PREFABRICATED VERTICAL DRAINS FEASIBILITY STUDY

Installation of prefabricated vertical drains (PVDs) is a cost-effective foundation improvement technique at sites where a surcharge load will be applied (e.g., an MSE berm). In general, PVDs are installed in soft soils to improve the drainage characteristics hence accelerating the dissipation of excess pore pressures generated during stage construction of embankments. The time it takes for pore pressures to dissipate depends upon the permeability of the dredge and the spacing between PVDs and it can be estimated using well known radial flow equations (e.g., Barron, 1948).

Initially, the use of PVDs to improve the foundation strength appeared unfeasible due to the massive weight of the proposed 21-m high MSE berm which was required to gain the needed airspace. Typically, the maximum height of an MSE berm on soft soils is dictated by the undrained shear strength of the underlying soft material. At the CIL site, the maximum height that could have been built using standard design techniques would have been on the order of 7.5-m (i.e., about 13.5 m shorter than required to achieve the target airspace of 17 million cubic meters).

Standard design techniques assume that when PVDs are installed in soft soils: (i) the excess pore pressures generated between PVDs during loading is uniform; and (ii) only undrained shear strength is mobilized during loading. The maximum excess pore pressures (U_{max}) generated after placement of a soil lift (i.e., 3 m for the CIL project) is estimated assuming that the soil lift is placed at once and it generates excess pore pressures (i.e., the pressure of the water stored within the dredge) approximately equal to the weight of the soil lift. Although it is recognized that excess pore pressures at the PVD location is nil and increases with radial distance from the PVD (Figure 2), it is typically assumed that excess pore pressures between PVDs are uniform and equal to U_{max}.

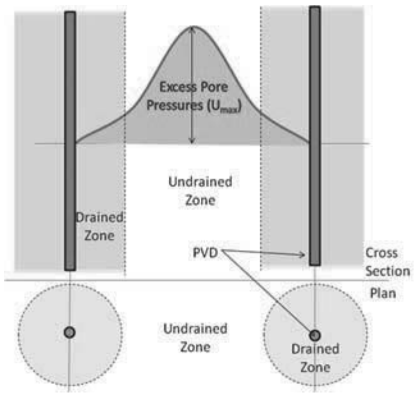

Figure 2. Pore Pressure Model

Because piezometers are located to monitor the maximum pore pressure, the radial variation is usually neglected. However, this conservative assumption made for computation and monitoring expedience not only neglects the fact that the excess pore pressures is not uniform but also does not take into consideration how PVDs change the dredge response to loading. In theory, drained parameters could be used to represent the shear strength of soft soils with PVDs if the applied loads (i.e., construction of the MSE berm) are imposed slowly enough to allow all excess pore pressures to dissipate as loading takes place. In practice, this could not be implemented because the rate of loading would need to be too slow to be feasible.

3 VIRTUAL SAND PILES: HYBRID DRAINED-UNDRAINED MODEL

The centerpiece of innovation for the design and construction of this massive MSE berm was the improvement of the weak dredge/alluvium foundation material using the concept of 'virtual sand piles', also described as the Hybrid Drained-Undrained (HDU) model (Espinoza et al., 2011).

The virtual sand pile concept is illustrated Figure 2. As shown in this figure, the closer the dredge is to the PVD the smaller the generated excess pore pressure and the faster that are dissipated. Hence, depending upon the speed of construction, it can be assumed that there are two distinct zones with different shear strength characteristics during loading: a drained zone, near the PVDs, and an undrained zone further from the PVDs. This concept constitutes a significant departure from standard design of soft cohesive soils with PVDs and it is the central element of the design. The development of the novel HDU design methodology for PVD design, to analyze the strength characteristics of the soft foundation soils during construction made the use of PVDs feasible for the CIL Project.

Subsequently, a more realistic model was developed to consider that: (i) the soils located closer to PVDs dissipate excess pore pressures generated during construction to more quickly than the soils located farther away from PVDs (Figure 2); and (ii) the rate of construction influences the maximum excess pore pressure that could be generated (i.e., pore pressures dissipate as the soil lift is placed). To simplify the model development, the rate of berm placement construction was assumed constant and equal to R_c. For each lift of soil, it was assumed that excess pore pressures starts to dissipate soon after it was placed (see Figure 3). Assuming an exponential decay function, the resulting excess pore pressure equation as a function of time is:

$$u(t) = \frac{R_c}{\alpha}\left[1 - e^{-\alpha t}\right] \quad \text{for} \quad t \le t_p \tag{1}$$

where: t_p is the time that takes to place the fill and α is a parameter that is related to Barron's Equations (1948) developed for sand drains:

$$\alpha = \frac{2}{F_n}\left(\frac{c_v}{r_i^2}\right) \tag{2}$$

$$F_n = \frac{n^2}{n^2 - 1}\ln(n) - \frac{3n^2 - 1}{4n^2} \tag{3}$$

$$n = \frac{r_i}{r_e} \tag{4}$$

and$c_v$is the coefficient of consolidation; r_i is the radius of influence of the PVDs; and r_e is the equivalent radius of the PVD. The maximum pore pressure takes place at $t = t_p$. It follows that after fill placement, it is assumed that excess pore pressure dissipates according to the same decay function, then:

$$u(t) = \frac{R_c}{\alpha}\left[1 - e^{-\alpha t_p}\right]e^{-\alpha (t - t_p)} \quad \text{for} \quad t > t_p \tag{5}$$

4 SELECTING THE DIAMETER OF THE VIRTUAL SAND PILE

Equations (1) through (5) were used to select the appropriate PVD spacing along with the corresponding rate of construction such that the soils near the PVDs would generate significantly smaller pore pressures that would allow to model the dredge around the PVD as a virtual sand pile. This meant that these soils could be considered to have a drained response during loading. The modified procedure consists of selecting the magnitude of excess pore pressure that would have negligible effect on MSE berm stability and then back-calculate the distance from the PVD that corresponds to this value. As a result, the dredge/alluvium materials enhanced with PVDs could be viewed (and analyzed) as a soft soil layer enhanced with virtual sand piles. In other words, the soil columns around the PVDs (hereafter, virtual sand piles) develop a drained shear strength during loading, whereas the soil outside the virtual sand piles develops an undrained shear strength response during loading.

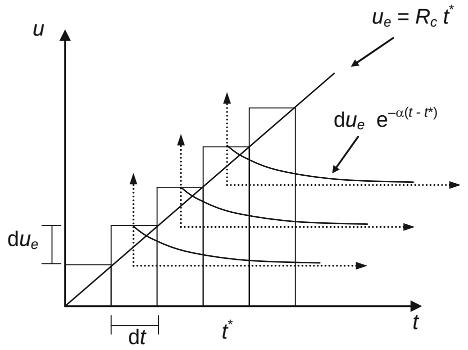

Figure 3. Pore Pressure Model

For the rate of construction (approximately 1 m of fill placed per week) and site-specific soils at this site (c_v = 0.0022 cm^2/s), approximately 1.8 million meters of prefabricated vertical drains (PVDs) were installed at a 1.5-m spacing to allow 90% dissipation of the excess pore-water pressures that were generated during construction of the overlying MSE berm within approximately 90 days. The berm was specified to be constructed 3-m high at a time at a rate of 1 m per week every 3 months (90 days). For a fill unit weight of 19.7 kN, the initial maximum pore pressure was 60 kPa (i.e., 6.1 m of water). For these conditions, it was estimated that if the average pore pressure generated within a certain distance from the PVD was about 15% of the maximum estimated excess pore pressure, the material could be considered drained. Based on this, it was estimated that the dredge/alluvium located within a 46-cm radius of the PVDs would be drained during each stage of MSE berm construction.

5 STABILITY ANALYSIS

The main purpose of the proposed methodology was to allow design engineers to use typical tools for analysis and design (i.e., limit equilibrium based methods). The HDU methodology expedited the stability analysis during the design stage as it was readily implemented using conventional limit equilibrium methods taking into consideration the soil strengths in the drained and undrained zones. In that way, hundred of different cross-sections were evaluated to optimize the design (i.e., minimize the MSE berm volume while still providing the same airspace for the same factor of safety). Accordingly, for slope stability analysis using limit equilibrium methods, the dredge/alluvium near the PVDs was considered to be drained with effective stress parameters given by ϕ' = 34º (obtained from triaxial tests), whereas the area further away from the PVDs was considered undrained with undrained parameters normalized with effective overburden given by S_u/σ' = 0.29 (parameters obtained from an extensive cone penetration tests and field vane shear tests). Figure 4 shows the soil stratigraphy during construction used inlimit equilibrium analysis. As shown in this figure, the soft dredge under the MSE berm is modeled as vertical strips of interchanging parameters (drained and undrained) to represent the HDU model. As shown in the model, the width of the soil columns does not need to represent the actual width of the virtual sand column (i.e., 0.92 m in diameter); only the ratio between drained to undrained areas needs to be taken into account. This can be simply estimated as:

$$A_r = \left(\frac{2r_s}{D_{pvd}}\right)^2 \times 100 \tag{6}$$

where: D_{pvd} is the distance between PVDs and r_s is the radius of the virtual sand (1.5 m and 0.46 m for this project, respectively). Hence, the percentage of drained area respect to the total area for this project is:

$$A_r = \left(\frac{0.92}{1.5}\right)^2 \times 100 = 38\%$$

Hence, when modeling using limit equilibrium methods, as long as the vertical strips represent approximately 38% of total area with PVDs, the actual width of the vertical strips is immaterial. However, the number of vertical strips should be selected in a wayit does not have an influence on the failure mechanism. For instance, two vertical strips would not be appropriate. Another powerful application of the HDU model is that PVDs outside the loaded area also have a positive effect on stability as 38% dredge can be modeled using drained parameters, hence increasing the overall shear strength along the potential failure surface. As shown in Figure 4, the zone with PVDs extended beyond the toe of the MSE berm to increase the factor of safety against sliding during construction. Typical design procedures would only account for the shear strength increase due to the overburden pressure located above the PVDs, hence PVDs outside the MSE berm footprint would not be installed as it would not be considered in the analysis.

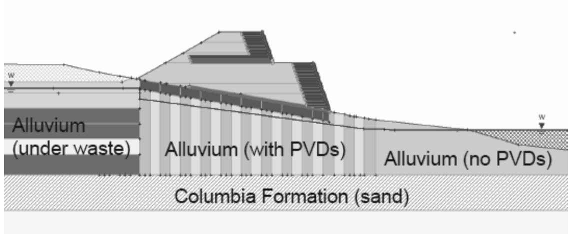

Figure 4. Limit Equilibrium Model of Enhanced Dredge with PVDs

In addition, to improve the stability of the MSE berm during construction, over 200.000 m^2 of high strength geotextile was installed at the base of the berm. The strength specified (1.170 kN/m) was one of the strongest materials ever manufactured by Tencate at the time of construction. The proposed solution for foundation improvement was significantly cheaper than DSM. The total cost of installing the PVDs including the high-strength geotextile was approximately $11 million, thus resulting in significant savings from the initial design. Although more engineering was required for design and construction, the total cost was significantly less than the DSM alternative.

6 CONSTRUCTION MONITORING AND MODELING

In order to prevent unacceptably high pore pressures from developing, construction was conducted in stages and each stage of berm construction was limited to a 3-m thick lift followed by a 3-month pore pressure dissipation period, estimated initially. To monitor the performance of the foundation during the stages of construction, data was collected from a total of 85 geotechnical monitoring instruments along 17 lines spaced approximately 150 meters apart along the length of the MSE berm including 51 piezometers to measure pore pressures generated within the dredge/alluvium during loading at three different depths, 17 settlement sensors to measure the compressibility (i.e., vertical displacement) of the dredge/alluvium during berm construction, and 17 slope inclinometers at the toe of the berm to obtain a profile of horizontal displacement with depth during loading.

Although the use of limit equilibrium analysis expedites the analysis during design when dozens of cross sections are analyzed during the design stage, during construction, the recorded displacements (horizontal and vertical) could not be used in conjunction with limit equilibrium methods. Moreover, the monitoring data do not indicate the stability condition of the MSE berm directly.

Several finite element models (FEM) were developed for evaluating the stability of the MSE berm during construction using PLAXIS® software. The soil consolidation parameters obtained from laboratory and pilot tests were used as an initial model calibration. These parameters were adjusted during the initial 3-m lift placement and then used to predict pore pressures, lateral and vertical displacements during construction for subsequent lifts. The calibrated FEM models were used to closely monitor the construction of the MSE berm. After construction of each stage, the predicted horizontal and vertical displacements and excess pore water pressure were compared to the measured values at selected cross sections to verify whetherthe MSE berm was performing as expected. In addition, using ashear strength reduction method, factors of safety (FS) at each stage of construction was estimated by the FEM model. The procedure consisted of reducing the soil shear strength parameters by a factor in an iterative procedure until large displacements of the FEM model were observed. The ultimate factor achieved represented the factor of safety against instability using PLAXIS.Figure 5 shows an example of the comparison between the measured and predicted pore pressures.

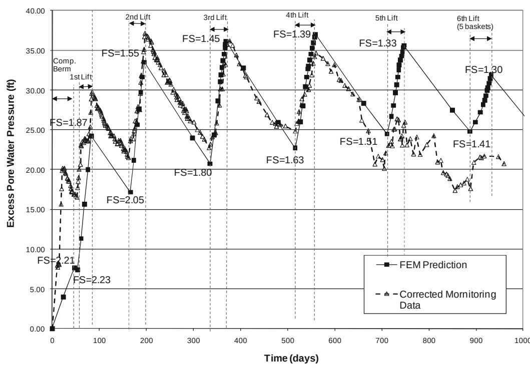

Figure 5. Example of monitoring results vs. predicted ones

The calculated FS at each stage of the construction are also shown in Figure 5.Although the construction schedule was initially established based upon estimated rates of pore pressure dissipation using the simplified drainage model described above, the schedule was constantly adjusted during construction based on the interpretation of the stability condition.

The MSE berm has undergone significant deformation.A settlement of approximately 4m was initially estimated.The recorded maximum vertical and horizontal displacements were approximately 4.2 m and 1.7 m, respectively.

7 BERM CONSTRUCTION

Construction of embankments designed using the HDU model requires close interaction between the designer, the contractor, and the owner, to allow timely geotechnical review and interpretation of monitoring data and communication of findings. During the initial stage of the project, it was found that the rate of pore pressure dissipation varied by sections of the MSE berm due to the localized subsurface geotechnical conditions. Because of the difference in consolidation rates, the contractor was required to alter its original construction sequence for the berm, moving back and forth between the different sections.By providing clarity to all parties on when subsequent berm lifts were likely to be feasible in any particular location, flexibility in construction task management and minimized disruption to the overall construction schedule could be achieved. With daily review of geotechnical data and frequent review of finite-element modeling output prepared for numerous berm cross sections, the designer was able to identify areas of construction on a “just-in-time” basis for the contractor to continue uninterrupted work. Eventually, the original plan of building a 3m-thick lifts over 600m to 900m length of the berm every 90 days evolved into construction of lifts in thicknesses as thin as 1m and/or berm lengths as short as 300m, which were patched together as review of geotechnical data would allow. The contractor’s ability to reorganize its efforts to construct the various sections of the berm based on week-to-week feedback from the designer became a critical piece of the success of the project. In this way, by August 2010, 36 months after starting, MSE berm construction was completed. A detailed description of the berm construction is presented by Espinoza et al (2008) and (2011).

8 CONCLUSIONS

The completion of this 1.8 million cubic meters MSE berm (see picture below) represents a significant engineering achievement considering the size of the embankment, the deep layer of very soft soils over which the berm was constructed, and the amount of settlements during construction. The successful design and construction of a 2,400m long, 21m high MSE berm over extremely soft dredge using innovative design and construction techniques opens opportunities not only for extending the capacity of existing disposal facilities over dredge disposal sites but also for very cost effectively raising levees and dykes at critical locations prone to flooding.

Figure 6. View of Completed MSE berm

The use of PVDs at this site, which was shown to be feasible using the HDU methodology, resulted in savings of over $150 million when compared to conventional ground improvement techniques such as DSM.

9 REFERENCES

Espinoza R.D., Lazarte, C.A., Germain, A.M., and Houlihan M.F. 2008. Design Considerations for Expansion of an Existing Landfill Over Extremely Compressible Soils. *Geo-Strata*, March-April 2008, pp. 38-43.

Espinoza R.D., Houlihan M.F. and Ramsey, T.B.Design of High Soil Berms over Soft Soils.*Geo-Strata*, March-April 2011, pp. 52-54.

Barron, R.A. (1948). Consolidation of Fined-Grained Soils by Drain Wells. ASCE Trans, paper 2346, V. 113, 718-724.

Land reclamation on soft clays at Port of Brisbane

Construction d'un terre-plein sur des sols argileux dans le port de Brisbane

Ganesalingam D., Sivakugan N.
School of Engineering and Physical Sciences, James Cook University, Australia.

Ameratunga J.
Coffey Geotechnics, Brisbane, Australia.

Schweitzer G.
Port of Brisbane Pty Ltd, Brisbane, Australia.

ABSTRACT: Land reclamation work is being carried out for the Port of Brisbane (PoB) Future Port Expansion Project, in the State of Queensland, Australia, which would develop a new reclaimed area of 235 ha. The mud excavated during maintenance dredging operations is pumped into the containment paddocks within the reclamation area. The dredged mud is soft and fine grained in nature, placed in a remoulded dilute slurry form at water content of at least 200%. The reclamation site is underlain by weak Holocene clays of depths up to 30 m. With such a large compressible thickness of both dredged fill and the underlying in situ Holocene clays, the total settlement under development loads during the primary consolidation will be significant. The secondary compression will be another considerable component of settlement to deal with. This paper briefly addresses the maintenance dredging works and the background of the PoB land reclamation project. It mainly focuses on the site conditions, the design of surcharge loading and installation of vertical drains to accelerate the consolidation settlement and minimize the post construction secondary compression. Furthermore, the in-situ and laboratory tests undertaken and the soil parameters obtained from these tests are discussed along with empirical correlations used to estimate appropriate soil parameters.

RÉSUMÉ : Des travaux d'aménagement s'inscrivant dans le cadre du « Future Port Expansion Project » (Projet d'extension du futur port) sont menés dans le Port de Brisbane, dans l'Etat du Queensland en Australie. Ce projet prévoit la création d'une étendue de terre de 235 ha gagnées sur l'eau. Les boues issues des opérations de dragage de maintenance sont pompées vers des bassins au sein même de la zone aménagée. Ces boues naturellement molles et fines forment une suspension diluée contenant au minimum 200% d'eau. Le site repose sur des terres argileuses datant de l'Holocène sur une profondeur allant jusqu'à 30 m. Avec une telle épaisseur d'argile compressible d'origine in-situ ou provenant du dragage, le tassement total dû aux charges de développement lors de la consolidation primaire sera significative. La compression secondaire constituera une composante supplémentaire à prendre en compte pour le tassement. L'article présente brièvement les travaux de dragage de maintenance et le contexte du projet de terre-plein dans le Port de Brisbane. Il se concentre principalement sur les caractéristiques du site, la conception des suppléments de charge et l'installation de drains verticaux pour accélérer la consolidation de l'installation et minimiser la compression secondaire liée à la construction. Les tests menés en laboratoire et sur le site ainsi que les paramètres du sol obtenus à partir de ces tests, et les corrélations empiriques utilisées pour estimer ces paramètres sont également abordés.

KEYWORDS: land reclamation, dredged mud, sedimentation, consolidation, vertical drains

1 INTRODUCTION

Dredging and land reclamation is a billion dollar industry asscociated with the ports throughout the coastal region of Australia. Maintenance dredging is carried out regularly in many major Australian ports and in some cases the dredged mud is reused as filling materials in the land reclamation works undertaken near the coast. The land reclamation works carried out in the Port of Brisbane (PoB) expansion project, Australia is one of the examples.

The Port of Brisbane is located at the mouth of the Brisbane River at Fisherman Islands, and it is the major port in the state of Queensland, Australia. In order to expand the port to accommodate additional facilities to meet the development expected in the next 25 years, the Port of Brisbane has embarked on a land reclamation process adjacent to the existing land mass, which will ultimately see 235 ha of new reclaimed land area, at the completion of the project. The 4.6 km long rock and sand seawall constructed around the perimeter of the site in Moreton Bay bounds the area which is being reclaimed (Ameratunga et al. 2010a). The seawall extends up to 1.8 km into Moreton Bay (Fig.1).

Annually around 300,000 m^3 of mud is extracted from the adjacent Brisbane River during the maintenance dredging works carried out in the navigation channel and berths. Land reclamation is undertaken by reusing these dredged materials in an environmentally friendly manner, as a way of disposing the dredged mud. The reclamation area is partitioned into a number of containment paddocks. Dredged mud is pumped into the containment paddocks in a slurry form of water content of at least 200 % and allowed to undergo self weight consolidation. The height of the dredged mud placement varies from 7 m to 9 m.

Dredged mud is a weak, fine grained soil with predominantly 40% silt and 50% clay constituents. The dredged mud fill is underlain by highly compressible in-situ Holocene clays, with thickness varying from 9 m to as much as 30 m. Since both in-situ clays and dredged mud are highly compressible and have low permeability characteristics, they are treated with preloading together with vertical drains to accelerate the consolidation process. Selecting appropriate soil properties is essential for reliable prediction of the degree of consolidation and future settlements. Hence, both horizontal and vertical consolidation parameters are required when vertical drains are used.

The paper outlines the land reclamation works with the design of preloading and vertical drains. Detailed review of the design strength, consolidation and compressibility parameters used for the recent dredged mud fill is given. In addition, laboratory tests results are discussed which were conducted on reconstituted dredged mud specimens prepared simulating the sedimentation and consolidation process at the reclamation site.

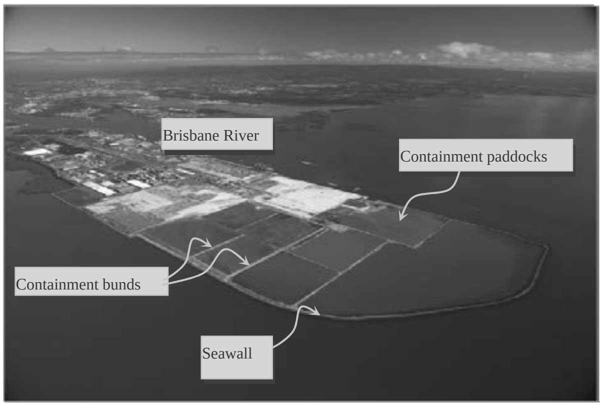

Figure 1: Aerial view of land reclamation site at Port of Brisbane, Queensland, Australia

2 SITE CONDTIONS

The Holocene clay layers include upper and lower Holocene clay layers. The upper Holocene layer consists of sand layers with interspersed soft clays and silts, thus the pore water pressure dissipation and the settlement rate is relatively fast. The lower Holocene clay layer, where the sand and silt layers are relatively few, controls the rate of settlement at the site because of its large compressible thickness. As both the in-situ Holocene clays and dredged mud fill are highly compressible, settlement due to filling alone could be as high as 2 m even before any service loads are imposed. It is predicted that it would take as much as 50 years for the area to be consolidated considering preloading as the only soil treatment option. Therefore vertical drains are incorporated to speed up the consolidation process. Ground improvement by combined preloading and vertical drains is designed to accelerate the majority of expected primary settlement and limit the long term postconstruction settlement. According to the design requirement of the Port of Brisbane, the long term residual settlement should not exceed 150 mm over a period of 20 years for applied pressures up to 50 - 60 kPa in areas where the Holocene clay thickness is less but the settement limit is greater for the deeper Holocene clay areas (Ameratunga et al. 2010a).

Maximum vertical stress exerted under the development loads (i.e buildings, traffic) can vary over the site between 15 kPa and 60 kPa depending on the different purposes the land would be used. In addition, the total thickness of compressible clays is variable over the site. The above two factors decide the amount of preloading to be applied at the ground level. Preloading is applied by both sand capping and vacuum preloading. Thickness of sand capping layer varies from 6 m to 9 m across the site. Initially, a number of vacuum trials was conducted at several test sites within the reclamation area itself in order to assess the effectiveness of wick drains to be used as a ground improvement measure (Ameratunga et al. 2010b)

The subsoil layers at the reclamation site is subjected to a preloading higher than the expected post construction design load, so that the underlying soil will generally be in an over consolidated state under design loads. In the over consolidated stage (recompression range), the settlements in both the primary consolidation and secondary compression range are significantly less than in the normally consolidated stage, which will be discussed later.

2.1 *Design Parameters of dredged mud fill*

The design strength and consolidation parameters of dredged mud fill used at the site are estimated from both in-situ and laboratory tests. In the absence of the above, correlations with physical properties of the clays are used for the preliminary assessment of properties. Atterberg limit values of dredged mud are in the range of 80-85% (Liquid limit- LL), 34-37% (Plastic limit- PL), 18-19% (Linear shrinkage- LS) and 44-46% (Plasticity Index- PI). The major constituents in the PoB dredged mud are 50% clay and 40% silt. From the Atterberg limits and particle size distribution, the PoB dredged mud can be classified as high plasticity clayey soil.

The undrained shear strength of recent dredged fill is evaluated from in situ vane shear and piezocone (CPTu) dissipation tests. In some instances, the shear strength parameters are estimated from the following empirical correlations incorporating PI values.

$$c_u / \sigma_v' = 0.11 + 0.0037 * PI \tag{1}$$

$$\sin \phi' = 0.8 - 0.094 * \ln(PI) \tag{2}$$

where c_u and ϕ' are the undrained shear strength and drained friction angle respectively.

Piezocone dissipation test results are also used to estimate the consolidation properties such as coefficient of consolidation c_v or c_h and approximate permeability. The c_v values calculated from the in situ tests are verified from the back calculations using Asaoka's method from field monitoring. A c_v value of 1 m^2/yr is used for the dredged mud fill and the coefficient of consolidation in the vertical and horizontal directions (c_v and c_h) are assumed to be equal.

At the PoB reclamation site, there are insufficient records yet for long time period settlements, thus the secondary compression parameters are estimated only from the laboratory tests and correlations. The subsoil is subjected to preloading higher than the expected post construction design load. As a result, the underlying soil will generally be in an over consolidated stage under design loads. The coefficient of secondary compression $C_{\alpha e}$ depends on the over consolidation ratio (*OCR*), and it drops quickly with a small increment in the *OCR* ratio (Ameratunga et al. 2010b; Alonso et al. 2000; Wong, 2007). For the reduction of $C_{\alpha e}$ with the *OCR* the following exponential law has been adopted (Eq.3).

$$C_{\alpha e}(OC) / C_{\alpha e}(NC) = [(1-m)/e^{(OCR-1)n}] + m \tag{3}$$

m is taken as 0.1, which is equivalent to ratio of C_r/C_c (Mesri,1991) and n is equal to 6. At the PoB reclamation site the underlying soil is generally over consolidated to an *OCR* ratio of 1.1-1.2. An average value of 0.008 was adopted for design $C_{\alpha e}$.

The design compression ratio *CR*, given by $C_c/(1+e_o)$ (e_o - Initial void ratio), is taken as 0.2 to 0.3 based on laboratory tests. Recompression ratio *RR* (= $C_r/1+e_o$) is generally taken as 0.1 times the compression ratio.

3 LABORATORY TESTS

The sedimentation and consolidation of dredged mud were simulated in the laboratory using the dredged mud samples obtained from the PoB reclamation site. The objective of the laboratory tests is to evaluate some of the consolidation parameters (c_v and c_h) and compressibility properties (*CR* and *RR*) of reconstituted dredged mud sediment and make comparison with the design values. In addition, potential anisotropy that can exist between the horizontal and vertical coefficients of consolidation and permeability was investigated. Series of oedometer tests were conducted in the present laboratory studies.

The mud was initially sieved through a 2.36 mm sieve to eliminate all the broken shells and debris and then mixed with sea water at a water content of 270 % in a slurry form. Sea water obtained from Townsville (in Queensland) was used to mix the slurry (Salt concentration 370 N/m^3). The dredged mud slurry was placed in a cylindrical tube of 100 mm diameter and 800 mm height and allowed to undergo sedimentation. When the dredged mud column accomplished most of its self weight consolidation settlement, it was sequentially loaded with small weights in the range of 500 to 3000 g. The soil column was allowed to consolidate under each vertical stress increment for two days before the next weight was added. Pore water dissipation was allowed through the porous caps placed at the top and bottom of the dredged mud column. The soil column was loaded up to a maximum vertical stress of 21 kPa over a duration of 8 weeks. The final thickness of the column at the completion of consolidation was around 300 mm.

From the final sediment, specimens were extruded for the oedometer tests. Six oedometer specimens of 76 mm diameter, 20 mm height, were extruded at three different depth levels as shown in Fig. 2. Three specimens were subjected to standard vertical consolidation tests (denoted by 'V') and three were tested to radial consolidation tests (denoted by 'R'). The procedure for the radial consolidation tests is explained below briefly.

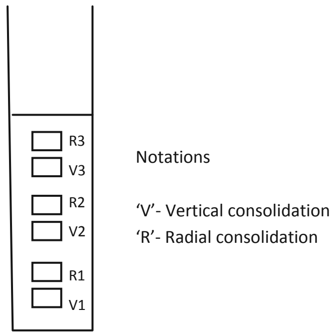

Figure 2: Specimen locations for oedometer tests

Specimens R1, R2 and R3 were tested for radial consolidation with an outer peripheral drain. The material used for outer peripheral drain was 1.58 mm in thickness. The strip drain was aligned along the inner periphery of the oedometer ring. A special cutting ring of diameter of 72.84 mm was used to cut specimens. The cutting ring had a circular flange at its bottom. A groove was carved along the inner periphery of the flange, which had a thickness equal to the thickness of the bottom edge of oedometer ring plus peripheral drain. The oedometer ring was placed tightly in the groove, to make it align properly with the cutting ring (Fig. 3). The specimen in the cutting ring was then carefully transferred to the oedometer ring using a top cap, without causing any disturbance. The porous bottom and top caps used for standard vertical consolidation tests were replaced with two impermeable caps, for radial consolidation tests.

All the specimens were loaded in the oedometer apparatus approximately between a vertical stress range of 9 kPa to 440 kPa (9 kPa, 17 kPa, 30 kPa, 59 kPa, 118 kPa and 220 kPa and 440 kPa). A load increment ratio of around 1.0 was adopted throughout the loading stage. From the settlement – time data of the specimens under each load increment, the vertical and radial coefficients of consolidation c_v and c_h were estimated. Taylor's square root of time method was used for estimating c_v. c_h was obtained from the curve fitting procedure given in McKinlay (1961) for radial consolidation with a peripheral drain.

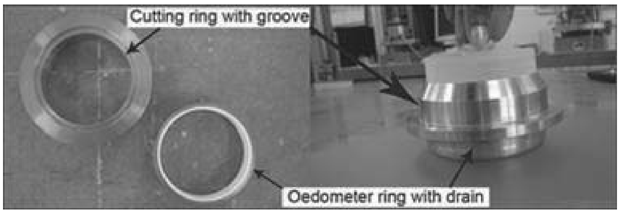

Figure 3: Specimen preparation for radial consolidation test

3.1 Results and discussion

Figs. 4(a), (b) and (c) show the comparison of c_v and c_h for pairs V1-R1, V2-R2 and V3-R3 respectively at different effective vertical stresses σ'_v. The degree of anisotropy, given by (c_h/c_v) is plotted against σ'_v in Fig. 4(d) for the three pairs of specimens.

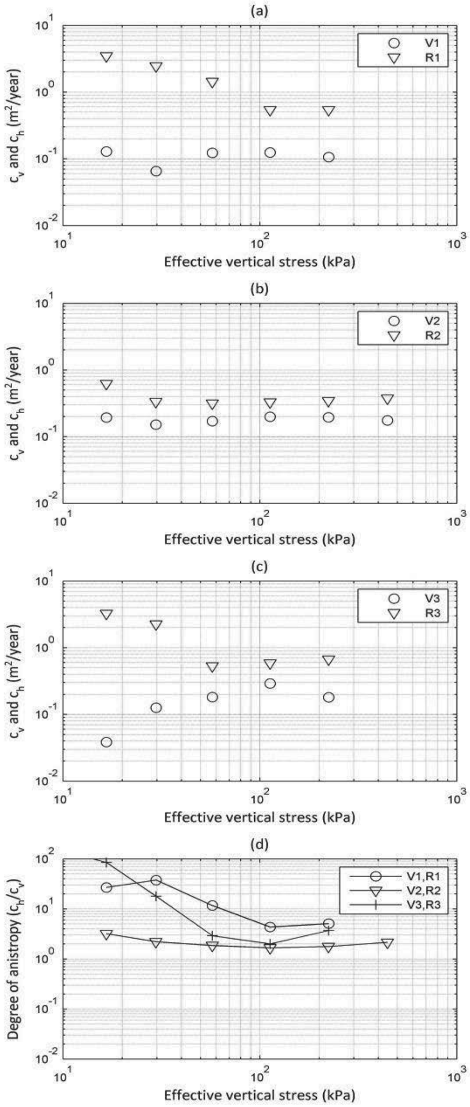

Figure 4: Comparison of c_v and c_h for specimens (a) V1, R1 (b) V2, R2 (c) V3, R3 (d) Degree of anisotropy

As clearly observed, the horizontal coefficient of consolidation is higher than that in the vertical direction at all three depths. The ratio c_h/c_v generally decreases with the increase in σ'_v. At low σ'_v (σ'_v < 20 kPa), the ratio c_h/c_v varies from 2 to as much as 100. The average degree of anisotropy in permeability (k_h/k_v) for the various stress levels is given in Table 1. The ratio k_h/k_v lies between 1 to 4. The horizontal permeability and coefficient of consolidation are higher than those in the vertical direction.

In remolded young clay sediment, the permeability and coefficient of consolidation are expected to be isotropic at low stress levels, since the particles are arranged in a random way, and there will be less fabric anisotropy (Clennell et al. 1999; Lai and Olson 1998). However, similar observations of higher c_h and k_h values than c_v and k_v have been reported elsewhere for remolded normally consolidated clays at low stress levels (Sridharan et al. 1996; Robinson 2009). In Fig. 4(d), at the moderate stress levels (50 – 60 kPa), the degree of anisotropy lies in the range of 2 to 10. Based on the above observation, the assumption of equal design c_v and c_h values for the recent dredged mud fill may have to be reviewed.

Table 1: Anisotropy in permeability (k_h /k_v)

σ'_v (kPa)	k_h/k_v
50-100	2.0
100-200	3.5
200-300	1.1

For a vertical stress levels between 50 – 60 kPa, c_v values of specimens V1, V2 and V3 varies between 0.1 – 0.2 m^2/year (Fig. 4). When compared to the design c_v obtained from in situ tests, this is about 5 to 10 times smaller. It has been reported that the laboratory tests generally result in lower c_v values than in situ test values for southeast Queensland clays (Ameratunga et al. 2010a).

The compression ratio (*CR*) and recompression ratio (*RR*) are given in Table 2 for all the six specimens. The *CR* values of specimens varies between 0.15- 0.36 and the *RR* values lie in the range of 0.02-0.035. These values agree well with the design *CR* and *RR* values discussed in the previous section.

Table 2: Compression and recompression ratio of specimens (*CR* & *RR*)

Specimen	*CR*	*RR*
V1	0.228	0.031
R1	0.378	0.035
V2	0.153	0.019
R2	0.219	0.062
V3	0.204	0.029
R3	0.159	0.020

4 CONCLUSIONS

In the paper, a review of the Port of Brisbane land reclamation works is given including the site conditions, design of vertical drains and soil parameters. The sedimentation and consolidation process of the dredged mud at the reclamation site was simulated in the laboratory. Standard vertical and radial consolidation tests were conducted on the reconstituted dredged mud specimens.

The results show that a large degree of anisotropy can exist between the horizontal and vertical coefficients of consolidation and permeability in young clay sediment. The c_v values obtained from the laboratory tests were found to be 5 to 10 times smaller than the field values. The compression ratio *CR* and recompression ratio *RR* are in good agreement with the design values.

5 ACKNOWLEDGEMENTS

The writers would like to acknowledge Warren O'Donnell (Senior Engineering Technician, Geomechanics Laboratory, School of Engineering & Physical Sciences James Cook University, Townsville, Australia) for his assistance in conducting the laboratory experiments. The cash and in-kind support provided by the Australian Research Council, Port of Brisbane Pty Ltd and Coffey Geotechnics are gratefully acknowledged.

6 REFERENCES

Alonso, E.E., Gens, A. and Lloret, A. 2000. Precompression design for secondary settlement reduction. Goetechnique, 50(6), 645-656.

Ameratunga, J., De Bok, C., Boyle, P. and Berthier, D. 2010a. Ground Improvement in Port of Brisbane (PoB) Clay- Case History, ISSMGE Bulletin, 4(2), 28-54.

Ameratunga, J., Boyle, P., De Bok, C. and Bamunawita, C. 2010b. Port of Brisbane (PoB) clay characteristics and use of wick drains to improve deep soft clay deposits, The 17th Southeast Asian Conference, Taipei, Taiwan, 2P-257, 1-4.

Clennell, M. B., Dewhurst, D. N., Brown, K. M., and Westbrook, G. K. 1999. Permeability anisotropy of consolidated clays. Special Publications - Geological Society, London, 158(1), 79-96.

Lai, J. R., and Olson, R. E. 1998. Discussion on Consolidation behavior of clayey soils under radial drainage by A. Sridharan, K. Prakash, and S. R. Asha. Geotechnical Testing Journal, 21(1), 66-67.

McKinlay, D. G. 1961. A Laboratory study of rates of consolidation in clays with particular reference to conditions of radial porewater drainage. Proc.5th Int.Conference on Soil Mechanics and Foundation Eng, Vol 1,Dunod,Paris.

Mesri, G. 1991. Prediction and performance of earth structures on soft clay. Proc.1st Int. Conference on Coastal development,Yokohama, Japan, Vol 2, G2.1-G2.16.

Robinson, R.G. 2009. Analysis of radial consolidation test data using a log-log method. Geotechnical Testing Journal, 32(2), 119-125

Sridharan, A., Prakash, K., and Asha, S. R. 1996. Consolidation behavior of clayey soils under radial drainage. Geotechnical Testing Journal, 19(4), 421-431.

Wong, P.K. 2007. Preload design to reduce post construction creep settlement. Soft soils and ground improvement workshop. Proc. 10th Australia New Zealand Conference on Geomechanics, Brisbane, Australia, 23-31.

7 NOTATIONS

C_c - Compression index
c_h - Horizontal/ Radial coefficient of consolidation
CR - Compression ratio
C_r - Recompression index
c_u - Undrained shear strength
c_v - Vertical coefficient of consolidation
$C_{\alpha e}$ - Coefficient of secondary compression
e_0 - Initial void ratio
k_h - Horizontal permeability
k_v - Vertical permeability
LL - Liquid limit
LS - Linear shrinkage
NC - Normally consolidated
OC - Over consolidated
OCR Over consolidation ratio
PI - Plasticity index
PL - Plastic limit
RR - Recompression index
σ'_v - Effective vertical stress
Ø´ - Drained friction angle

Kansai International Airport. Theoretical settlement history

Aéroport international de Kansai. Historique théorique du tassement

Juárez-Badillo E.
Graduate School of Engineering National University of Mexico

ABSTRACT: The settlements measured in the last eight years 2004-2011 in the Kansai International Airport are compared with the theoretical curve provided by the Principle of Natural Proportionality and published by the author in the 16th International Conference on Soil Mechanics and Geotechnical Engineering, Osaka 2005, in the paper"Kansai International Airport, future settlements".

RÉSUMÉ : Les tassements mesurés au cours des huit dernières années 2004-2011 sur le site de l'aéroport international de Kansai sont comparés avec la courbe théorique fournie par le principe de proportionnalité naturelle et publiée par l'auteur dans la 16e Conférence internationale de Mécanique des Sols et de la Géotechnique, Osaka 2005 : le papier "Aéroport International du Kansai, les tassements futurs".

KEYWORDS: Principle of Natural Proportionality, Kansai International Airport, settlement.

1 INTRODUCTION

"Kansai International Airport, future settlements" is the title of a paper presented by the author in the 16th International Conference on Soil Mechanics and Geotechnical Engineering, Osaka 2005, where the Principle of Natural Proportionality (Juárez-Badillo 1985b) was applied to the settlement data already published of the airport, to obtain the theoretical equation of its settlement.

In Juárez-Badillo (2005) is mentioned that the general equations provided by the principle of natural proportionality (Juárez-Badillo 1985 b), have been proven to describe the mechanical behavior of geomaterials: solids, liquids and gases. They have been applied to describe the stress strain time temperature relations of rocks, granular and fine soils and concrete (Juárez-Badillo 1985 a, 1988, 1997 a, 1999 a, 1999 b, 1999 c, 2000, 2001). A general equation for the evolution of settlement of engineering works has already been applied to the settlement data of embankmens, they are the settlements for the accommodation building (A) at Gloucester (Juárez-Badillo 1991) and to the settlements in the Fraser River delta (Juárez-Badillo 1997 b). This time this general equation is applied to the experimental data of the Kansai International Airport built in an artificial island 5 km from Osaka in Japan.

2 GENERAL TIME SETTLEMENT EQUATION

Consider an engineering work like an embankment that applies a load at the soil at time t=∞. The settlement S will increase from S=0 at t=0 to a total value $S=S_T$ at t=∞. These concepts S and t are the simplest concepts to describe the phenomenon, that is, they are proper variables. The relationships between them, according to the principle of natural proportionality, should be through their proper functions, that is, the simplest functions of them with complete domains, that is, functions that vary from 0 to ∞. The simplest function of S and t with complete domainare $z=1/S-1/S_T$ and t. When t varies from 0 to ∞, z varies from ∞ to 0. The principle of natural proportionality states that the relationships between them should be (Juárez Badillo, 2010):

$$\frac{dz}{z} = -\delta \frac{dt}{t} \qquad (1)$$

where: δ is the coefficient of proportionality called the "fluidity coefficient"

integration of (1) gives

$$z^{\delta} = \text{constant} \qquad (2)$$

which may be written

$$\left(\frac{S_T}{S} - 1\right) t^{\delta} = \text{constant} = \left(t^*\right)^{\delta} \qquad (3)$$

where $t^*=t$ at $S=1/2S_T$ and we may write

$$S = \frac{S_T}{1 + \left(\frac{t}{t^*}\right)^{-\delta}} \qquad (4)$$

Figs. 1 and 2 show the graphs of (4) for different values of δ in natural and semi-log plots respectively. From Fig. 1 we may observe that it appear that we should have $\delta \leq 1$.

Juárez Badillo (2005) specify that the parameter values to be obtained are S_T, δ and t*. They may be obtained from good experimental points. The author prefers, however, to obtain them from semi-log plot, Fig. 2. It can be shown (Juárez Badillo 1985 a) that the middle third of the settlements S_T is practically very close to a straight line. So, if one is able to determine from the settlement data the beginning of this straight line, one is able to determine the three parameters since this straight line extends l cycles in the graph, where

$$\frac{0.6}{\delta} = l \text{ cycles} \qquad (5)$$

From (4) it may be obtained the slope at t=t* as

$$\left(\frac{dS}{d\log t}\right)_{t=t^*} = \frac{2.3}{4}\delta S_T \tag{6}$$

and the settlement rate, from (4) is given by

$$\left(\frac{dS}{dt}\right) = S_T\frac{\delta}{t}\frac{\left(\frac{t}{t^*}\right)^{-\delta}}{\left[1+\left(\frac{t}{t^*}\right)^{-\delta}\right]^2} \tag{7}$$

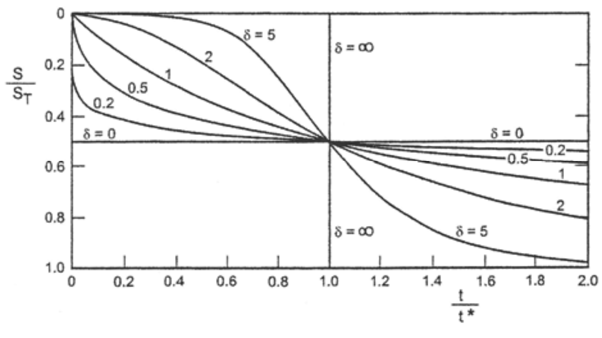

Figure 1. Graphs of $\frac{S_T}{S} = \left[1+\left(\frac{t}{t^*}\right)^{-\delta}\right]^{-1}$

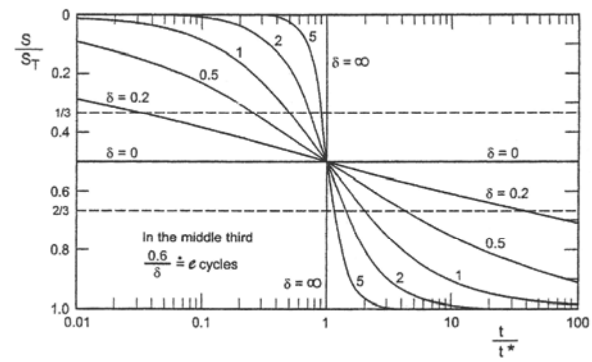

Figure 2. Graphs of $\frac{S}{S_T} = \left[1+\left(\frac{t}{t^*}\right)^{-\delta}\right]^{-1}$

3 KANSAI INTERNATIONAL AIRPORT

The Kansai International Airport was built in an artificial island 5 km from Osaka, Japan (Juárez Badillo, 2005). Fig. 3 shows the experimental compressibility curve (Tsuchida 2000) of undisturbed Pleistocene clay to which is attributed any further settlements. Its compressibility coefficient γ in the general equation (Juárez Badillo 1969).

$$\frac{V}{V_1} = \frac{1+e}{1+e_1} = \left(\frac{\sigma}{\sigma_1}\right)^{-\gamma} \tag{8}$$

where γ=0.19 and (σ_1,e_1) is a known point. Fig. (3) shows the theoretical points from (8). The laboratory quasi OCR=1.0-1.5 and the predicted settlement was 11.6 m calculated following the traditional way of calculation (Tsuchida 2000). The traditional coefficients m_v and C_c at any point are given by

$$m_v = \frac{\gamma}{\sigma_v} \tag{9}$$

$$C_c = 2.3\gamma(1+e) \tag{10}$$

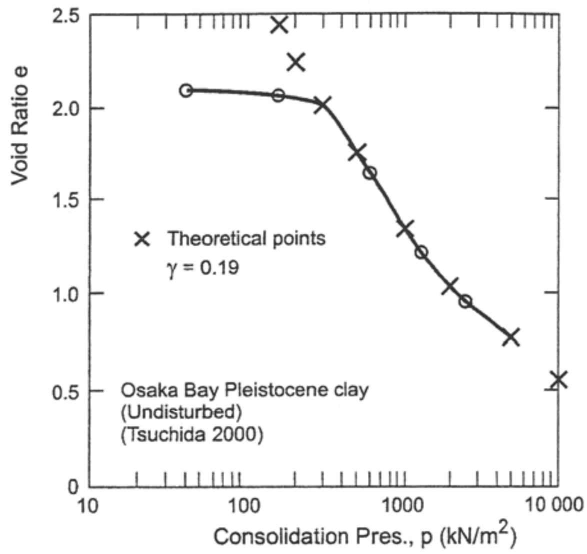

Figure 3.e-log p curve of undisturbed Pleistocene clay

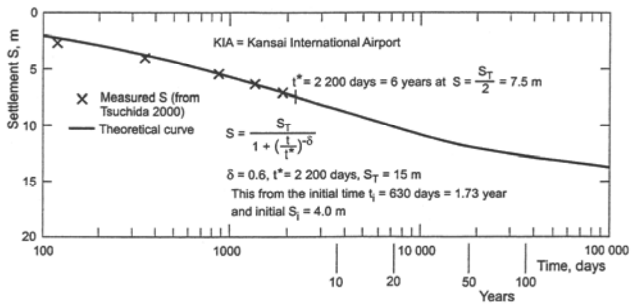

Figure 4.Settlements in KIA island

The construction of KIA started by Sept. 1987 and the opening of the Airport was seven years later, by Sept. 1994 when the first phase of construction was complete. During the period of construction from about the day 530 to about the day 630 the overburden stress by reclamation increased from about 200 to 450 kPa. By the day 1,300 the applied total load increased to about 500 kPa (Tsuchida 2000). The author took as origin of the final stage of construction the initial time t_i=630 days, (when the 90% of the total load was already in place), with an initial settlement S_i=4.0 m. Figs. 4 and 5 show application of (4) and (7) to this important case. As mentioned above the origin of time for these figures is around year 1989 and application of (4) and (7) for the present year 2004 (t=15 years) gives a total settlement of 9.50+4=13.50 m and a settlement rate of 14 cm/year. The total settlement at t=∞ will be S_T=15+4=19 m. In Fig. 5 the times from the considered initial time, year 1989, appear in parenthesis (Juárez Badillo 2005).

Fig. 5 presents also in this paper the eight settlement rates corresponding to the last eight years 2004 to 2011. As may be observed they are tending towards the theoretical curve.

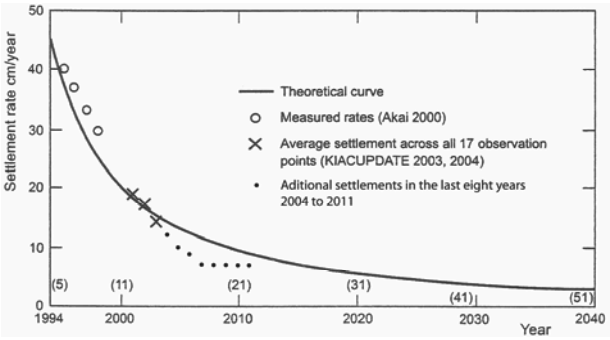

Figure 5.Settlements in KIA Island

4 CONCLUSIONS

Juárez Badillo (2005) maintain that the magnitude and evolution of the settlement of embankments in practice are described by the general equation (4). The total settlement S_T may be obtained from the EOS (end of secondary) compressibility curve (Juárez Badillo 1988) of the subsoil using the compressibility coefficient γ in equation (8) for its determination. The fluidity coefficient δ and the characteristic time t* require, at present, experimental test fills to study the factors that influence their values in a certain place. A very important point is to have a clear distinction between the two compressibility curves: the EOP (end of primary) and the EOS (end of secondary). Quasi OCR of 1 to 1.8 in practice correspond to a true OCR=1 in many cases. The difference has been illustrated in this paper by the application of Eq. (4) to the important case of the Kansai International Airport.

The important conclusion for this paper is precisely the fact that the settlement rate in the last eight years tend towards the theoretical curve obtained by the Principle of Natural Proportionality.

5 REFERENCES

Juárez-Badillo, E. 1969. Pore pressure and compressibility theory for saturated clays. Specialty session No. 12 on advances in consolidation theories for clays. Seven International Conference on Soil Mechanics and Foundation Engineering, Mexico. University of Waterloo, Canada, pp. 49 116.

Juárez-Badillo, E. 1985a. General time volume change equation for soils. XI International Conference on Soil Mechanics and Foundation Engineering. San Francisco, Vol. 1:519 530.

Juárez-Badillo, E. 1985 b. General volumetric constitutive equation for geomaterials. Special volume on Constitutive Laws of Soils. XI International Conference on Soil Mechanics and Foundation Engineering. San Francisco. Japanese Society for Soil Mechanics and Foundation Engineering, Tokyo, pp 131 135.

Juárez-Badillo, E. 1988. Postsurcharge secondary compression equation for clays. *Canadian Geotechnical Journal*, 25:594 599

Juárez-Badillo, E. 1991. Thirty years of secondary consolidation in sensitive marine clay: Discussion. Canadian Geotechnical Journal 28:466 467.

Juárez-Badillo, E. 1997 a. General equations to describe the mechanical behavior of granular soils. XIV International Conference on Soil Mechanics and Foundation Engineering, Hamburg, Vol. 1:133 138.

Juárez-Badillo, E. 1997 b. Case histories illustrate the importance of secondary type consolidation settlements on the Frase River delta: Discussion. Canadian Geotechnical Journal 34:1007 1008.

Juárez-Badillo, E. 1999 a. Secondary compression of peat with or without surcharging: Discussion. Journal of Geotechnical and Geoenvironmental Engineering, ASCE 125 (2):162 164.

Juárez-Badillo, E. 1999 b. General equations to describe the mechanical behaviour of concrete. Fourth International Conference on Constitutive Laws for Engineering Materials, Rensselaer Polytechnic Institute, Troy, New York, pp, 403 408.

Juárez-Badillo, E. 1999 c. Static liquefaction of very loose sands: Discussion. *Canadian Geotechnical Journal* 36:967 973.

Juárez-Badillo, E. 2000. General equations to describe the mechanical behavior of rocks. Year 2000 Geotechnics, Asian Institute of Technology, Bangkok, Thailand, pp. 39 52.

Juárez-Badillo, E. 2001. General relaxation equations for soils. XI International Conference on Soil Mechanics and Geotechnical Engineering, Istanbul, Vol. 1:141 144.

Juárez-Badillo, E. 2005. Kansai International Airport, future settlements. 16th International Conference on Soil Mechanics and Geotechnical Engineering, Osaka, Vol. 2:1053 1056.

Juárez-Badillo, E. 2010. Theoretical Geoscience. Ed. by Sociedad Mexicana de Ingeniería Geotécnica AC, México DF, 130 pages.

Tsuchida, T. 2000. Mechanical properties of Pleistocene clay and evaluation of structure due to ageing. Special Lecture, International Symposium on Coastal Geotechnical Engineering, IS Yokohama 2000:39 79.

Design and Performance of Highway Embankments Constructed Over Sri Lankan Peaty Soils

Conception et performance de remblais d'autoroute construits sur sols tourbeux au Sri Lanka

Karunawardena A.
National Building Research Organization, Sri Lanka

Toki M.
Oriental Consultants Co., Ltd., Japan

ABSTRACT: The construction of the Southern Expressway in Sri Lanka involved extensive ground improvement work as many parts of the Expressway traverses through flood plains and marshy ground consisting of very soft peat, organic soils, and clays. Depending on the ground conditions, various ground improvement methods including remove and replacement, preloading, preloading with vertical drains, dynamic compaction and vacuum consolidation were applied to improve the soft soil to build the embankments with heights varying from 2m to 12m. The performance of the ground improvement was evaluated in terms of the degree of consolidation, improvement of the physical and engineering properties, increase in preconsolidation pressure and gain in shear strength of the peaty soil. The results indicate that the properties of the peaty soil have been improved significantly, providing the required control over future settlements while ensuring embankment stability. The results of the post construction surface settlement monitoring of the expressway carried out up to date reconfirm that the ground improvement work was very successful and the expected residual settlements are well below the allowable limit of the contract.

RÉSUMÉ : La construction de la Southern Expressway au Sri Lanka a nécessité un important travail d'amélioration des sols. En effet plusieurs sections de la voie rapide traversent des zones inondables et du sol marécageux constitué de tourbes très meubles, de sols organiques et d'argiles. Selon les conditions du sol, différentes méthodes d'amélioration (excavation et remplacement, préchargement, préchargement avec drains verticaux, compactage dynamique et consolidation sous vide) ont été utilisées pour renforcer le sol mou et construire des remblais de tailles allant de 2 à 12m. La performance de l'amélioration des sols a été évaluée par rapport au degré de consolidation, à l'amélioration des propriétés techniques et physiques, à l'augmentation de la pression de préconsolidation et au gain de résistance au cisaillement de la tourbe. Les résultats indiquent que les propriétés de la tourbe ont été améliorées significativement, permettant le contrôle nécessaire des tassements à venir tout en assurant la stabilité des remblais. Les résultats du suivi après construction des tassements en surface sur la voie rapide confirment que l'amélioration des sols a été une réussite et les tassements résiduels prévus sont très inférieurs aux limites imposées contractuellement.

KEYWORDS: peat, embankment, monitoring, secondary consolidation, over consolidation ratio

1 INTRODUCTION

The Southern Highway is Sri Lanka's first E Class highway that links the Sri Lankan capital Colombo with Matara, a major city in the south of the island. The 96 km long section from Colombo to Galle was completed and opened to traffic in November 2011. Many parts of the highway traverses through flood plains and marshy ground consisting of very soft peat, organic soils, and clays. Especially, in the major flood plains of Welipenna river, Bentota river and Gingaga river areas, thick peat and organic clay deposits were found. The construction of road embankments over peat deposits is quite problematic, and thus, it is often done after first improving the properties of the peaty soil through the utilization of appropriate ground-improvement techniques.

This paper presents the ground improvement methods applied in the Southern Expressway between Ch.0.000 km to Ch.66.500 km to improve the peaty soil, with some background information on the design methodology. In the first 34.5 km of the highway, about 50% of the area is covered in soft ground and from 34.5 km to 66.5 km, the area covered by soft ground is around 12 km. In this project, embankments of about 4 km in length were constructed by improving the peaty soil mainly through the application of the heavy tamping method. The length of the embankments that were built by improving the peaty soil by vacuum assisted surcharging was around 2.5 km. The problems encountered during ground improvement and embankment construction work and the solutions given for the same are highlighted and discussed. The details of the laboratory and field investigations carried out before and after ground improvement, field instrumentation program and field monitoring program that was carried out during and after the construction of highway embankment to assess the soft ground improvement are presented.

2 TYPICAL SUBSOIL CONDITION OF SOFT GROUND

Many geotechnical investigations have been carried out since the inception of the project in order to assess the condition of the soft ground. At the preliminary stage, to provide information to bidders and to facilitate initial designs, boreholes were carried out at 500 m intervals. After commencement, boreholes were carried out at about every 50 m intervals in order to provide the necessary information for the detailed design.

Site investigation consisted of bore holes with Standard Penetration Test (SPT), hand augering, Cone Penetration Test with pore pressure measurement (CPTu) as in-situ testing and a series of laboratory tests such as index property tests, unconsolidated undrained triaxial compression tests and conventional consolidation tests.

The investigation identified that the soft ground area of the highway mainly consisted of peat, organic clay, alluvial clay and lose sand deposits. The distribution of soft soil deposits along the highway trace from Kottawa to Kurundugahahetekma is shown in Figure 1. Silty clay and silty sand were found as a top soil in most of the lowland areas up to a depth of 1.5 m to 3.0 m. This was followed by the sand to lateritic soil and the thickness of the layers varied from 1 m to 5 m.

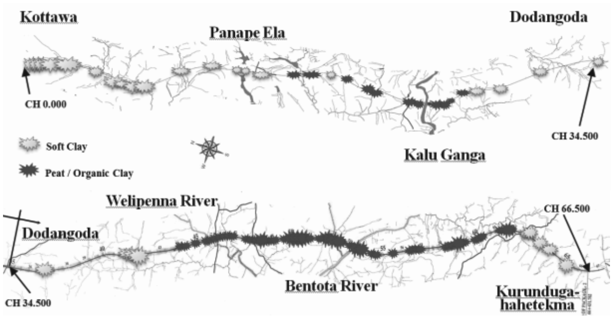

Figure 1. Distribution of soft ground areas

In the flood plains of Panape, Kalu Ganga, Welipenna and Bentota river areas sub soil consisting of mainly peat, organic clay, very soft inorganic clay and silt layers was found. The total average thickness of the compressible layer was in the range of 4 m to 11 m. In some areas loose silty sand layers were present under the above compressible layers. In the valley areas between hillocks, instead of cohesive inorganic clays, very loose to loose silt and sand were found ranging from 0.5 m to 4m thickness. The details of the Geotechnical properties of the subsoil have been given in Karunawardena and Nithiwana (2009) and Karunawardena and Toki (2011).

3 SOFT GROUND IMPROVEMENT DESIGN

Soft ground improvement design had to be carried out in order to control the settlements and to ensure the stability of the highway embankment as required in the technical specification. According to the technical specification, the embankment had to be designed and constructed by improving the soft ground in order to control the continued settlement to 15cm at the road center after a period of 3 years following the acceptance of the paving. In addition, the maximum residual differential settlement had to be not more than 0.3% change in grade over longitudinally within 3 years after construction. In order to achieve the above criteria, most or all of the primary settlement and some of the secondary settlement that would have occurred under the final embankment height alone were forced to take place by improving the soft ground.

The soft ground was improved mainly by using the following methods based on the subsoil conditions. Soft clay of shallow thickness was improved by placing a surcharge load. Shallow peat and organic clay deposits were removed and replaced with rock in order to support the embankments. The subsoil with relatively thick soft clay layers were improved by installing vertical drains and placing a surcharge load. The embankments on the relatively thick peat and organic deposits were constructed by improving the ground by heavy tamping method and the vacuum consolidation method from 0.0 km to 34.5 km and from 34.5 km to 66.5 km respectively.

In rock replacement method, all compressible layers of the sub soil were removed and replaced with rock, completely eliminating the settlements. In the ground improvement method of application of surcharge load with or without vertical drains, future settlement of the highway embankment was controlled as required in the contract by designing an appropriate surcharge load. Most or all of the primary settlement and some of the secondary settlement that would have occurred under the final embankment height alone were forced to take place under the surcharge load. In addition, it was expected that the soil beneath the embankment would become over consolidated or stiffer due to the surcharging of ground. The aim of applying the surcharge was to eliminate 100% of primary consolidation settlement and enough secondary settlement such that the residual settlement is within acceptable performance limits. The residual settlement for a given length of time after construction was estimated as the remaining secondary settlement that occurs during the required time after the eliminated equivalent time of secondary compression has elapsed. In the design of surcharge, it was expected to have 1.1 over consolidation ration (OCR) for inorganic clays and 1.2 to 1.3 OCR for peat and organic clays in order to reduce the secondary settlements during the operation period.

4 EMBANKMENT CONSTRUCTION ON PEATY SOILS

Embankments over peaty deposits in the Southern Expressway between Ch. 0.000 km to Ch 34.500 km were constructed by improving the peaty soil using the heavy tamping method whereas vacuum consolidation technique was applied to improve the peaty soil in the Section between Ch.34.500 km to 66.500 km. This Chapter presents the details of the heavy tamping method and the vacuum consolidation techniques applied in the project.

4.1 Heavy Tamping Method

Heavy tamping method was designed to enforce the settlements that would be caused by the construction of earth embankment on soft ground by applying impact energy. Different energy levels had to be imparted by considering the anticipated settlement of the compressible layer under the respective designed embankment heights. In the estimation of settlements, all primary consolidation settlements and secondary settlements at the end of 3 years after construction were considered. First, the soft soil which was to be consolidated, was overlain by a working platform of lateritic soil to facilitate the movement of machinery. Then, a strong type fibre drain (band drain) was installed by a machine in the soft subsoil in a square pattern with a spacing of 1 m in order to prevent high excess pore water pressure development in the underneath soil due to the applied energy. The required energy was applied to the soil by dropping a large weight on the ground surface repeatedly in phases on a grid pattern over the entire full base width of the embankment using multiple passes.

During tamping, once the depth of the crater formed by pounder exceeded the height of the pounder, the crater was back filled and leveled with soil. The dimension of the crater was recorded in order to calculate the volume of soil introduced. The above process was continued in all phases of the tamping operation. Using the crater fill volumes, the enforced settlement was calculated and if the enforced settlement was less than what was required then another phase of tamping was introduced until the required settlement was achieved.

After application of heavy tamping, borehole investigation was carried out in order to assess the ground improvement. Investigations revealed that the layer thickness of peat has been reduced to 20% to 50% of its original thickness after the heavy tamping. The SPT values of peat layer at a 3m to 4m depth increased from 0 to a range of 4 to 8. Consolidation test results showed that the value of the compression index (c_c) and coefficient of secondary consolidation (c_α) has decreased significantly. It was also noted that the pre-consolidation pressure, P_c , of peaty soil has increased from 32, to as high as 85. This increase of pre-consolidation pressure means the peaty soil is in an over-consolidated state during the service life of the highway. All these observations confirmed that the expected primary and secondary consolidation settlements due to the embankment load would be very small in the areas improved by heavy tamping.

However, it was observed that the peat layers at the deeper depths had not achieved the above improvement. This was investigated and it was found that the practically possible improvement depth that could be achieved in the present operation was about 3.5 m to 4 m. These underneath deeper soft layers were improved after the heavy tamping operation by keeping a surcharge load for a sufficient period of time as reported by Karunawardena and Toki (2011). Figure 2 illustrates the major steps in the heavy tamping ground improvement method adopted in the project.

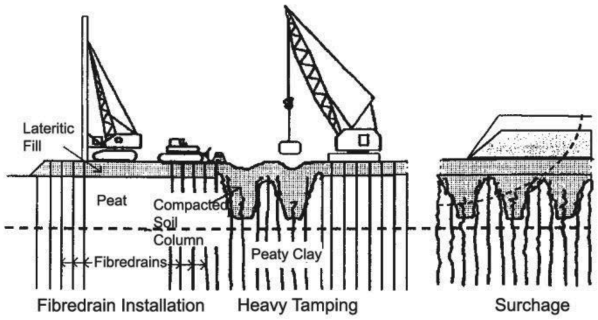

Figure 2. Major steps in heavy tamping ground improvement

4.2 Vacuum consolidation method

In the application of vacuum consolidation method, about a 1.0 m to 1.5 m thick fill was constructed on the original ground surface to form a working platform for the band drain installation machine. Band drains were installed by a machine up to a designed depth from the original ground surface in a square pattern with a spacing of 1 m. Thereafter, flexible horizontal drains (300 mm wide and 4 mm thick) were laid on top of the fill with a horizontal spacing of 1 m and then connected to the vertical band drains in order to ensure adequate horizontal drainage capacity. Subsequently, the tank system was installed and connected to the designed pipe systems. Small ditches were excavated perpendicular to the horizontal drains at 20 m intervals and filled with aggregates after placing perforated pipes. Instrumentation such as settlement plates, displacement stakes, electrical piezometers and differential settlement gauges were also installed at the designed depths. After installation of vertical drains, horizontal drains, perforated pipes and separator tanks, the surface of the treatment area was covered by a protection sheet. Thereafter, an air tight sheet was laid on top and the periphery trench system was constructed to provide air tightness and the necessary anchorage at the boundary of the treatment area. Vacuum pressure was then applied using a vacuum pumping system patented by Maruyama Industry Co. Ltd, Japan by connecting the suction and water hoses to the vacuum pump. After confirming that there were no leaks through the air tight sheet, filling was commenced.

It was expected to apply the surcharge by means of a vacuum pressure of 70kPa to compensate the primary consolidation settlements and to minimize the secondary settlements that can take place in the proposed highway embankment. However, in many areas the applied vacuum pressure was less than the designed value and therefore the above designed surcharge was applied by means of both vacuum pressure and embankment fills. The designed load was kept until the expected settlement completed.

5 ASSESSMENT OF THE SOFT GROUND IMPROVEMENT

The continuous assessment of the improvement of soft ground was carried out by conducting the field monitoring program. In addition, the soft ground improvement was assessed by conducting appropriate field and laboratory testing.

5.1 Field monitoring program

The improvement of the soft ground was monitored through the measurement of settlement and the excess pore water pressure during the construction period. Settlement plates were installed at the top of the soft layer or on top of the pioneer layer and piezometers were installed at the middle of the soft layer. The settlement stakes were installed near the toe of the embankments to check the stability during the construction. In addition to the above, in the areas improved by vacuum consolidation, a vacuum pressure monitoring unit was used to measure the vacuum pressure at the pump and under the air tight sheet. Also, a water discharge meter was used to measure the rate and the total discharged water flow due to the vacuum operation. An automatic data acquisition unit was connected with the piezometer, vacuum pressure monitoring unit and water discharge meter to keep continuous records.

The decision to remove the surcharge was made on the basis of the monitoring data obtained during the surcharge period. The aim was to eliminate 100% of primary consolidation settlement and enough secondary settlement such that the residual settlement was within acceptable performance limits. The primary consolidation settlement was assessed by estimating the degree of consolidation and in this project it was estimated by the method outlined by Asaoka (1978). The degree of consolidation was also calculated based on the pore water pressure (PWP) measurements, and laboratory consolidation testing of peaty samples after the treatment program. The comparison of the degree of consolidation for each method for some areas improved by the vacuum consolidation method is shown in Table 1.

Table 1. Estimation of the degree of consolidation

Location	Degree of Consolidation		
	Asaoka Method	Laboratory Data	PWP
Ch. 45.380 – Ch. 45.430	97.83%	83.10% 73.87%	79.46%
Ch. 47.850 – Ch. 47.920	97.10%	100.00% 100.00%	100.00%
Ch. 52.950 – Ch. 53.000	97.57%	80.21% 90.91%	100.00%
Ch. 53.660 – Ch. 53.730	96.65%	96.70% 83.62%	68.71%

If the degree of consolidation from the PWP measurement is assumed to be accurate, Asaoka Method accurately estimates the degree of consolidation in treatment areas Ch.47.850 to Ch.47.920 and Ch.52.950 to Ch.53.000 whereas Asaoka method over predicts the degree of consolidation in treatment areas Ch. 45.380 to Ch. 45.430 and Ch.53.660 to Ch. 53.730. However, in treatment area Ch.53.660 to Ch.53.730 the degree of consolidation from the laboratory test results agreed very well with the same estimated from the Asaoka method. Therefore, based on this investigation it can be concluded that the degree of consolidation estimated from the Asaoka method is reasonably accurate.

In order to assess the secondary settlements, for each monitoring point, the long-term settlement was predicted by extrapolating the secondary settlement rate over a period of 3 years. Predictions were made by preparing a plot of displacement against log (time) for each settlement plate, with the best-fit line through the data extended to define the likely settlement after 3 years. The surcharge was removed only after confirming the residual settlement by considering both the primary and secondary consolidation settlements as described above.

5.2 Investigation to confirm the ground improvement

Site investigation was carried out to assess the actual ground improvement in the areas improved by the vacuum consolidation method just before the removal of surcharge. Investigation was carried out in the improved as well the adjacent unimproved area in order to assess the ground improvement. Investigation revealed that initial thickness of the peat layer has been reduced by 50%-60% after ground improvement. The above reduction agreed reasonably with the percentage change of water content and void ratio values obtained from peaty soil collected from the improved and unimproved areas. Consolidation tests revealed that the compression index of the peat layer has reduced from a range of 2.65 to 2.13, to as low as 0.90 as a result of the ground improvement. The average reduced value is about 1.65. The results of long term consolidation tests carried out in the improved and unimproved peaty samples show that that the coefficient of secondary consolidation has reduced from a range of 0.10 to 0.13 to a range of 0.03 to 0.06. Subsequently the ratio of C_α / C_c has decreased from 0.050 to 0.029 due to ground improvement (Karunawardena and Nithiwana, 2009).

Consolidation test results also indicated that the pre-consolidation pressure of the peaty soil found under the embankment has increased as shown in Table 2. Table 2 also shows the expected load induced on the peaty layer due to the proposed embankment and the subsoil over consolidation ratio. According to the data in Table 2, the sub soil will behave under the over consolidated state with an OCR of 0.98 to 1.33. It should be noted here that even though the applied vacuum pressure and the fill surcharge load is adequate to yield an OCR value in the range of 1.2 to 1.3, sometimes the calculated OCR is less than that the anticipated value. This might be due to the inaccurate Preconsolidation Pressure (P_c) value obtained from the consolidation test as a result of sample disturbance.

Table 2. Increment of preconsolidation pressure and undrained cohesion

Location	Expected Load (kPa)	P_c (kPa)	OCR	C_u (kPa)	C_u / σ'$_v$
Ch.45.380-Ch.45.430	160.0	180	1.13	79.0	0.49
		160	1.00	57.0	0.36
Ch.47.850-Ch.47.920	145.0	200	1.37	55.0	0.36
		180	1.25	70.0	0.45
Ch.52.950-Ch.53.000	152.5	150	0.98	41.5	0.27
		170	1.11	38.2	0.25
Ch.53.660-Ch.53.730	150.0	170	1.13	54.0	0.36
		147	0.98	50.5	0.34

The strength gained due to ground improvement was investigated by calculating the ratio between the undrained shear strength of peaty soil and the effective stress (C_u / σ'$_v$). The ratio between the undrained shear strength of peaty soil and the effective stress (C_u / σ'$_v$) after the treatment program was obtained to be 0.25 to 0.49.

5.3 *Observed settlement after pavement construction*

The surface settlement of the highway embankment constructed over the improved soft ground was monitored by installing the settlement markers at 50 m intervals after construction of the road pavement. Initially, for about a 6 month period, before the road was opened to traffic, surface settlement was monitored at both the center and the edge of the embankment. The observed settlements were in the range of 0 mm to 5 mm in most of the ground improved sections except at very few locations where high embankments were constructed over thick peat deposits improved by the vacuum consolidation method. The observed surface settlement in those areas was around 10 mm to 20 mm at the end of six months after the construction of pavement. After the highway was opened to traffic in November 2011, settlement monitoring was carried out only along the edge of the highway embankment due to safety reasons. The observed total surface settlement up to September 2012, ten months after the highway was opened to traffic, is shown in Figure 3. The observed settlement was less than 5 mm in most of the sections and in only two locations the settlement exceeded 20 mm. The maximum observed settlement was 35 mm and the settlement prediction using the monitoring data indicates that the estimated residual settlement is less than 15 mm at the end of 3 years after the handing over of the project.

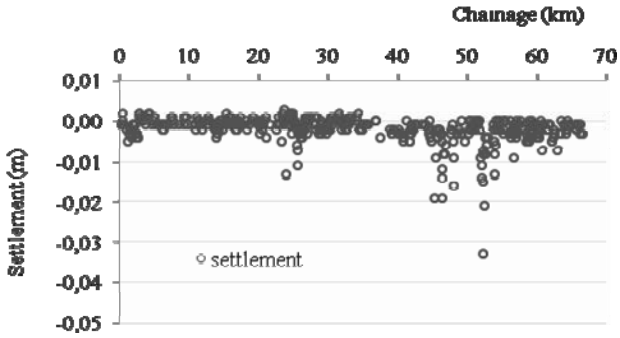

Figure 3. Results of the surface settlement monitoring

6 CONCLUSION

This paper presents successful application of ground improvement work carried out in the construction of Southern Highway project in Sri Lanka. Ground improvement methods such as heavy tamping method and vacuum consolidation techniques were applied to construct the high embankments over thick peaty deposits. In both methods, a surcharge load had been applied to over consolidate the peaty soil. Field monitoring data obtained during the construction period indicates that the primary consolidation settlement due to final load of the highway embankment has already been completed and the secondary settlement had been reduced to control the residual settlement within acceptable performance limits. Investigations carried out at the site show that both physical and mechanical properties of the peat have improved significantly and the peaty soil will behave in an over consolidated state with a ratio of 1.2 to 1.3 during the service life of the highway. The results of the post construction surface settlement monitoring of the expressway carried out up to date reconfirm that the ground improvement work was successful and the expected residual settlements are well below the allowable limit in the contract.

7 ACKNOWLEDGEMENTS

The authors are grateful to the Road Development Authority of Sri Lanka, for the necessary approval and support extended towards writing this paper.

8 REFERENCES

Asaoka A. 1978. Observational Procedure of Settlement Prediction. *Soil and Foundation*, 18(4): 87-101

Karunawardena A. and Nithiwana W. 2009. Construction of a trial embankment on peaty ground using vacuum consolidation method for a highway construction project in Sri Lanka. Proc. of 17th International Conference on Soil Mechanics and Geotechnical Engineering. Alexandria,Vol. 3. 2200-2203.

Karunawardena A. and Toki M. 2011. Application of the Heavy Tamping Method on Sri Lankan Peaty Clay for the Construction of a Highway Embankment. Proc. of 14th Asian Regional Conference on Soil Mechanics and Geotechnical Engineering. Hong Kong, China.

Design improvements for expansion of a roadway on a thick layer of soft soil

Un projet d'amélioration pour l'élargissement d'une autoroute sur une argile molle

Kim K.-H., Jung T.-M., Jung J.-H.
Korea Expressway Corporation, Korea

Kim T.-H.
Korea Maritime University, Busan, Korea

Kim S.-R.
Dong-A University, Busan, Korea

You S.-H.
Samyoung Technology Corporation, Busan, Korea

ABSTRACT: Expansion of a roadway on a soft soil can cause settlement of the existing road during embankment construction due to the consolidation characteristics of the soft soil. Many problems related to construction and maintenance, such as deterioration of the surface, decreased safety, and decreased structural stability, could affect the existing road. This scenario is especially true if the roadway foundation is a thick layer of soft soil. Therefore, the characteristics of the soil layer should be considered in the design and construction of the roadway expansion. In this study, the expansion of the second branch of the Namhae Expressway was selected as the target site because the expressway is constructed on a soft soil layer approximately 53 m thick. The original design plans were reviewed, problems were discussed and solutions to the problems were proposed.

RÉSUMÉ : L'élargissement d'une autoroute sur un sol d'argile sensible risque d'entraîner des tassements pour les voies actuelles pendant le remblayage sous l'effet de la compression des sous-sols argileux. D'importants problèmes liés à la construction et à la maintenance sont posés : dégradation de la surface, instabilité structurelle, insécurité des usagers. Le scénario présenté s'avère particulièrement important lorsque le sous-sol de l'autoroute en question est constitué d'une couche épaisse de sol argileux. Il faut donc tenir compte des caractéristiques du sol pour le projet d'élargissement de l'autoroute. Dans cette étude, nous prendrons comme exemple le cas de l'autoroute Namhae dont la seconde voie repose sur une couche argileuse atteignant 53m d'épaisseur. En examinant son plan de construction original, on étudiera les problèmes posés et on suggérera diverses solutions.

KEYWORDS: deep thick soft soil, roadway expansion, settlement, construction, design.

1 INTRODUCTION

Stress can exist at a point in a soil not only because of loading above the point by a superstructure but also by loading on adjacent points. For saturated clay, this stress can result in consolidation due to dissipation of excess pore water pressure. Localized nonuniform settlement can cause unevenness and cracking in the road and cracks in a superstructure. To minimize the likelihood of this problem occurring, it is best to apply a uniform embankment preload to the entire roadway area. In a road-widening project, however, it is difficult to accomplish this because of the need to divert traffic and comply with the construction schedule.

Recently, the traffic on the second branch of the Namhae Expressway has been approaching the traffic capacity of the roadway because of the increase in national income and increased desire for leisure. Severe traffic jams have diminished the comfort of drivers and the operating speeds of vehicles on the expressway. Expansion of the roadway from 4 lanes to 8 lanes is in progress because of the expansion of SOC (social overhead capital) and the economic growth of the country (Korea Expressway Corporation, 2008a; 2008b; 2008c).

As part of the original design for this project, embankment construction was planned after removal of the existing road and installation of vertical drains. Differential settlement might not be a problem if sufficient time were available for consolidation of the soil after construction of the embankment. However, differential settlement could occur because the overconsolidation ratio of the soil and the load history of the expanded and existing portions of the roadway are different. In addition, PBD (plastic board drain) are to be installed after removing the soil of the existing road. This installation may be difficult because of the resistance of granite material, such as crushed stone and gravel, used in the exiting roadway construction. The strength of the soil could also be reduced by disturbance during the installation of the PBD.

The original design plans call for expanding the roadway from 4 to 8 lanes by banking soil on the existing road and raising the longitudinal grade of the roadway. However, settlement of more than 2 m, and in some locations up to 5.4 m, was expected because the construction section of the second branch is located on soft soil up to 53 m thick. As an alternative, embankment construction after removal of the existing road and improvement of the underlying soil was planned. However, this strategy was also expected to be complicated and time-consuming. Moreover, this construction was expected to cause settlement in the surrounding area due to disturbance to the soil under the existing roadway that had been stable for more than 30 years. Consequently, complaints about damage to nearby farmlands, factories and houses were anticipated.

Expansion of a roadway typically involves diversion of traffic. Expansion of a roadway on a soft soil could cause settlement of the existing road during embankment construction due to the consolidation characteristics of the soft soil. Many problems related to construction and maintenance, such as deterioration of the surface, decreased safety, and decreased structural stability, could affect the existing road. This scenario is especially true if the roadway foundation is a thick layer of soft soil.

Accordingly, design and construction methods need to be identified to minimize the problems that can occur during construction of the expansion and minimize the expenditures associated with such problems, including future maintenance costs. This paper outlines the problem of designing and constructing the expansion of the second branch of the Namhae Expressway and suggests solutions to the problems involved.

2 STRIBUTION OF SOFT SOIL ON THE PROJECT SITE

Construction of the expansion of the second branch of the Namhae Expressway is in progress. The project has been divided into four construction zones (A, B, C and D). The distribution of soft soil in each zone is as follows (Korea Expressway Corporation, 2008d; 2008e; 2008f).

In zone A, which has a total length 6.40 km, soft soil is present at thicknesses in the range of 0.0~15.4 m in a segment 890 m in length, from station 5+110 to station6+000. According to the results of the boring investigation, the soft soil consists of clayey silt and silty clay. Zone B has a total length of 5.50 km and is located across the Joman River (5+140 to 5+500). The soft soil is present at thicknesses in the range of 2.0~50.8m throughout zone B, except between stations 0K+000 and 1K+000. Zone C is located across the W. Nakdong River (6K+160) and Pyeonggang Creek (8K+080 to 8K+230) and has a total length of 3.56 km. This section also has soft soil present at thicknesses in the range of 2.0~53 m. In the area of the W. Nakdong River, sandy soil is present to a depth of 10~12 m due to sedimentation from the river, and soft clay soil is present below the sandy soil. In zone D, soft sandy soil is present at thicknesses of 2.9~11.4 m, and soft clay soil is present at thicknesses of 8.0~25.2 m. The soft clay soil consists of clayey silt or silty clay.

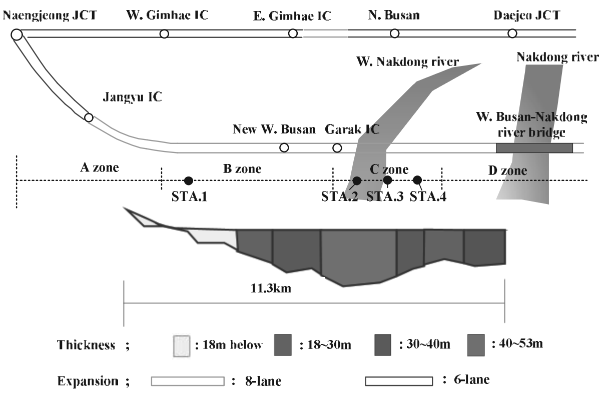

Figure 1. Route map of expansion construction for the second branch of the Namhae expressway and distribution of soft soil along the route.

3 THE ORGINAL DESIGN

Most of the new construction zones were planned to be expanded bordering the existing road in the direction of Naengjeong, except for a portion of the zones in which the horizontal alignment was to be adjusted. An accelerated consolidation method was applied to satisfy the requirement of 10 cm of allowable residual settlement. PBDs were selected as the vertical drain type to be used in the consolidation acceleration. For horizontal drainage, fiber drains were to be used in parts of zones C and D where sandy soil is present in the upper layer. In the remainder of the zones, a crushed stone mat was to be used for drainage.

For the existing road, prefabricated vertical drains (PVD) were installed along 1.2 km of the roadway, equivalent to 6% of the total length 19.6 km when it was constructed in May of 1978 (Korea Expressway Corporation, 1982). Long-term and continuous consolidated settlement occurred in the remainder of the zones because an embankment was built during the operation of the road after constructing MAT using sand and gravel and crushed stone. Thus, the construction method below was designed for and applied to the existing road because it was thought to be an economical method of ensuring the long-term stability of the roadway, allowing residual settlement by removing the existing soil, installing vertical drains for consolidation acceleration and preloading with counterweight fill.

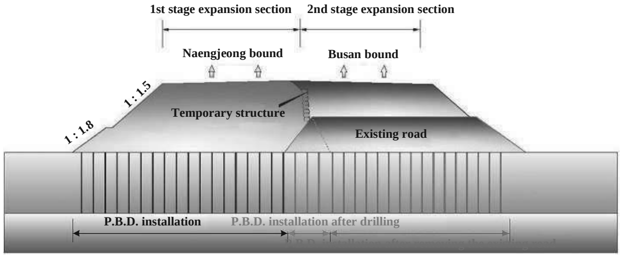

Figure 2. Overview of original design of road expansion.

4 EXAMINATION OF PROBLEMS WITH THE ORIGINAL DESIGN

4.1 *Low constructability and increased costs*

According to the original design, an improvement method should be applied to the soft soil after removing the soil under the sting road. When constructing the existing road, only a part of the sections improved with paper drains, and the remainder of the sections banked using sand, gravel, and crushed stone on the lower part without vertical drains being installed. The sand, gravel and crushed stone rested on the lower part of the natural soil during construction and use of the road. Thus, these objects pose obstacles to the installation of vertical drains under this expansion construction.

Therefore, it is expected that the constructability would be very poor because of the difficulty of removing the settled crushed stone and transport the soils removed from the existing roadbed. It is also expected that the costs would be increased by the need to transport and dispose of the waste asphalt concrete resulting from removal of the existing road. Examination of the cores reveals that the thickness of the asphalt concrete at an abutment is 1~1.5 m, due to repeated overlays of the pavement necessitated by settling of the soil over a long period of time.

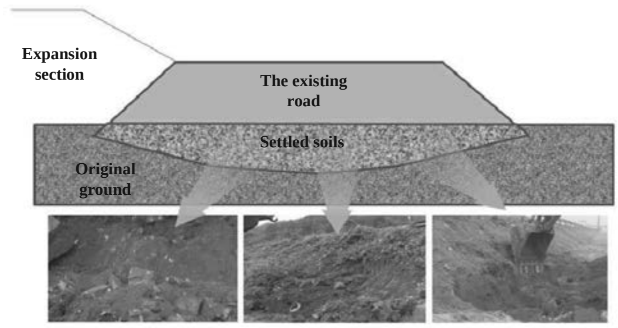

Figure 3. Results of field survey of the existing road.

4.2 *Problems of PBD construction on the existing Road*

Typical PBD construction is not expected to be possible because of resistance from the crushed stone and other coarse materials in the existing roadbed. Thus, special drilling and excavation are necessary, but these activities will delay construction and increase costs. If the existing roadbed soil is

completely removed, the stability of the soil may be disrupted by PBD construction. If a drilling PBD method is applied on the slope of the existing road, it is expected that construction will be delayed due to the additional time required for construction processes such as drilling and filling the drilled hall.

4.3 *Shortage of time for construction*

In the initial stage of construction, it was impossible to start the improvement of the soft soil on time because of civil complaints and delays in obtaining agreements for purchasing land. Multi-phase construction work such as "PBD construction after removing the existing road" may reduce the time available to improve the soft soil. For example, in the case of the Namhae line, on which construction was completed in 1996, it was expected that it would take 24 months to improve the soft soil in two sections of expansion and existing roads. However, it took more than 24 months just to improve the soft soil in the expansion section. Thus, at that time, the construction plan was modified to reduce the time spent improving the soft soil of the existing road (Korea Expressway Corporation, 2006).

4.4 *Allowable residual settlement*

For the construction of the expansion of the second branch, 10 cm of allowable residual settlement was applied equally, in spite of the great differences in the depths of the soft soil in the different zones. However, the problems and phenomena vary depending on the conditions of the soft soil. If the 10 cm standard is applied equally to all zones, it may produce an inefficient effort. For example, it is necessary that more than 98% of the consolidation occur during the construction period to satisfy the 10 cm residual settlement requirement, based on the assumption that the thickness of the soft soil is 50 m and the total settlement is 450 cm, applying Terzaghi's consolidation theory. In this situation, the cost and time required to improve the soft soil are excessive.

The road design manual clearly states that "For a road, it can be applied 10 cm as the residual settlement after pavement, but it should be appropriately applied by considering the factors such as the purpose of use, importance, ground characteristics, construction period, constructability and economic feasibility, etc." Accordingly, the standard needs to be adjusted.

5 IMPROVEMENTS IN DESIGN

5.1 *Establishment of improvement direction*

The original design was made to satisfy a grade of 0.5% and for traffic to be diverted during construction of the expansion, so that in both directions (to Busan and to Naengjeong), where the soft soil is present, the longitudinal grade could be raised and the road could be widened. To satisfy the 10 cm residual settlement requirement within 1,500 days (the construction time allowed), the soil of the existing road was to be removed, the soft soil improved and counterweight fill applied after banking. This design approach poses many problems. For example, long-term settlement can be induced by raising the longitudinal grade, dividing the median strip bilaterally and counterweight filling (banking), as well as not treating the existing road. Thus, improvements to the plan are needed to solve these problems.

Table 1. Improvements in design.

Original design	Improved design
Removing the embankment of the existing road + PBD + preloading ⇒ Satisfy the residual settlement requirement during the construction period	Non-improvement of the existing road + Preloading ⇒ Inducing long-term settlement
Upward adjustment of the longitudinal grade and connecting the two alignments	Controlling the upward adjustment of the longitudinal grade and dividing the median strip bilaterally

5.2 *Improvement factors*

5.2.1 Lowering the longitudinal grade

To minimize the settlement due to overburden load on none improved existing road, the embankment height was adjusted by changing the standard for the minimum slope (from 0.5% or more to 0.3% or more) given in the Manual and Guideline for Standards of Road Structures stipulated by the Ministry of Construction and Transportation (2003). Additionally, the embankment height was changed to be similar to the longitudinal grade of the existing road by changing a bridge type (from passing below to passing above) that crosses the main line and adjusting the height of the bridge to provide sufficient overhead clearance.

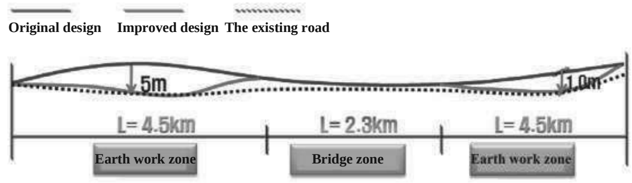

How to adjust	Descriptions	Applicable length	Remark
Change the way to cross a bridge	Underground rigid frame bridge ⇒ Pedestrian bridge	1.0km	- 5m
Adjustment of minimum Longitudinal slope	0.5% ⇒ 0.3%	4.5km	- 1m
Adjustment of passing extra height of bridge	Secure the minimum overhead clearance	3.5km	- 0.8m

Figure 4. A plan to adjust the longitudinal grade.

5.2.2 Change in the standard for allowable residual settlement

Disregarding the initial soil conditions (the depth of the soft soil), the design standard for uniformly applied allowable residual settlement is 10 cm. However, this standard was changed based on the depth of the soft soil, as shown in Table 2.

Table 2. Design criteria for allowable residual settlement.

Thickness of soft soil	Allowable residual settlement	Degree of consolidation
10 m below	10 cm	90% above
30 m below	20 cm	
30 m above	30 cm	

5.2.3 Line separation

To minimize damage due to differential settlement induced by the different loading histories of the soil in each direction, installation of a green belt 3~6 m wide on the median strip and line separation for each direction were suggested. For the existing road, an overlay was applied to match the finished grade with a slight adjustment of the longitudinal grade. The soil underneath the existing road was not improved.

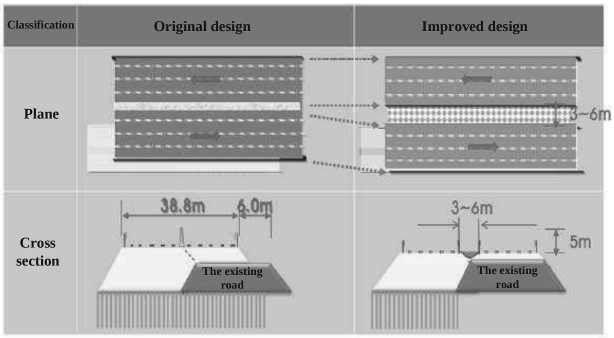

Figure 5. A plan for the road separation.

5.3 *Feasibility of improvement factors*

5.3.1 Constructability aspect

Reducing the number of construction steps from six to one makes it possible to reduce the time required for construction by more than 10 months. This reduction in construction time offsets the delays due to land purchases, civil complaints, etc. at the initial stage of this project.

The improved plan does not require disposal of soils and pavement materials removed from the existing road. The constructability would be improved because the sequence of work activities is not limited and issues such as the difficulty of PBD installation by drilling on the slope of existing road can be avoided.

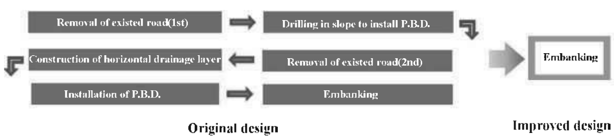

Figure 6. Simplification of construction phases.

5.3.2 Economic aspects

If PBD is installed in the soil of the existing road, additional expense is involved in drilling or removing the gravel and crushed stone underneath the existing road. In addition, a cost for disposal of the asphalt concrete is also incurred. However, the improved plan would result in a decreased net volume of the embankment and length of drainage material and consequently a decrease in the construction cost.

5.3.3 Stability aspects

If PBD is installed to improve the soil under the existing road, it is expected that a coupled settlement will occur near adjacent roads, railways, farmland, facilities, and other structures due to the soil settlement. The improved plan does not involve improvement of the soft soil of the existing road and consequently protects the stability of structures located near the existing road.

6 CONCLUSIONS

This study was conducted to develop improved design and construction methods for expansion of a roadway on a deep layer of soft soil. The project that was the focus of this study was the expansion of the second branch of the Namhae Expressway. The original design plans were reviewed, problems were discussed and solutions for the problems were proposed.

With the improved plan, it does not necessary to dispose of soil and asphalt concrete removed from the existing road. The constructability of the project would be improved because the sequence of work activities is simplified and issues related to the difficulty of installing PBD by drilling on the slope of the existing road can be avoided.

The improved plan reduces the construction cost. Installation of PBD beneath the existing road would involve additional costs for drilling or removing gravel and crushed stone underneath the existing road. In addition, there would be a cost for disposal of the waste asphalt concrete.

If PBD is used to improve the soil under the existing road, it is expected that coupled settlement will occur near adjacent structures due to the soil settlement. The improved plan does not involve improvement of the soft soil of the existing road and consequently protects the stability of structures located near the existing road.

7 ACKNOWLEDGEMENTS

This study was performed with the support and cooperation of the Naengjeong–Busan Construction Agency of the Korea Expressway Corporation.

8 REFERENCES

Cheong H.-I., Lee Y.-S., Cheong G.-S., Jin H.-S., Cheong M.-G., Woo J.-Y., Cho S.-D., Kim Y.-J., Ahn T.-B., Kim I.-D., Koh G.-S. and Park Y.-M. 1999. *A study of the consolidation characteristics of soft ground*

Cheong J.-H., Cho S.-M., Kim H.-J., Cheong G.-J., Park J.-G. and Kim D.-S. 2005. A study of the settlement evaluation and maintenance of long-term settlement for the highway on the soft grounds. Expressway & Transportation Research Institute

Choi Y.-C., Cheon S.-S., Park Y.-S. and Yang H.-S. 2003, A Study of Compaction Density of Surcharge on Soft Ground. Expressway & Transportation Research Institute, pp.200

Kim H.-J., Cho S.-M., Cheong J.-H., Cheong G.-J., Soe J.-W. and Lee J.-Y. 2004. Countermeasures for maintenance of highway on soft ground (II). Expressway & Transportation Research Institute, pp.46

Kim S.-H. and Noh H.-S. 1995. A study on the settlement estimation of soft ground. Expressway & Transportation Research Institute, pp.300

Korea Expressway Corporation. 1982. Documents for Busan~Masan Expressway Construction

Korea Expressway Corporation. 2002. Road design manual

Korea Expressway Corporation. 2008a. General report for the expansion project between Naengjeong and Busan of Highway No. 104 in the Namhae Expressway: Section No.3-1

Korea Expressway Corporation. 2008b. General Report for the Expansion Project between Naengjeong and Busan of Highway No. 104 in Namhae Expressway: Section No.3-2

Korea Expressway Corporation. 2008c. The Expansion Project between Naengjeong and Busan of Highway No. 104 in Namhae Expressway: Section No.4

Korea Expressway Corporation. 2008d. Ground Survey Report for the Expansion Project between Naengjeong and Busan of Highway No. 104 in Namhae Expressway: Section No.3-1

Korea Expressway Corporation. 2008e. Ground Survey Report for the Expansion Project between Naengjeong and Busan of Highway No. 104 in Namhae Expressway: Section No.3-2

Korea Expressway Corporation. 2008f. Ground Survey Report for the Expansion Project between Naengjeong and Busan of Highway No. 104 in Namhae Expressway: Section No.4

Korea Expressway Corporation. 2008g. Completion Documents for Pavement Rehabilitation Construction in Gyeongnam Branch(1996 ~ 2008.

Korea Land Corporation. 1992. Study on Settlement Measurement in Soft Ground Improvement (I)

Korean Geotechnical Society. 2005. Soft Ground

Ministry of Construction and Transportation. 2003. Manual and Guideline for Standards of Road's Structure and Facilities

Ministry of Land, Transport and Maritime Affairs. 1991. Handbook for Road Pavement Maintenance

Case Study on X-section Cast-in-place Pile-Supported Embankment over Soft Clay

Étude de cas pour un remblai renforcé par des pieux de section en X coulés en place dans de l'argile molle

Liu H.L., Kong G.Q., Ding X.M, Yu T., Yang G.

Key Laboratory for Ministry of Education for Geomechanics and Embankment Engineering, College of Civil and Transportation Engineering, Hohai University, Nanjing, Jiangsu, P. R. China

ABSTRACT: Pile-supported embankments are widely used for highway, railway, seawall, etc. over soft soils because of their effectiveness in minimizing deformation and accelerating construction. A new method of using X-section cast-in-situ concrete piles (referred to as XCC pile) which can improve bearing capacity, reduce settlement and costs effectively for foundations over soft clay is developed by Hohai University of China. In this paper, construction method, quality assurance (QA), and quality check (QC) involved in this method are described. A large-scale model test program on a XCC pile and a circular pile, both constructed with the same amount of concrete volume, was carried out to obtain the load transfer behavior of both piles under three different loading modes: compression, uplift, and lateral loads. One XCC pile-supported embankment application was presented. The large -scale load test indicated that load carrying capacity of XCC pile is slightly higher than that of circular pile, when the same amount of concrete volume was used. It is worth pointing out that this XCC pile type can be constructed rapidly, quality assurance (QA) and quality checked (QC) easily, and cost-effectively. The results of this study can provide reference for practical XCC pile-supported embankment design and construction.

RÉSUMÉ : Les remblais renforcés par pieux sont largement utilisés pour les autoroutes, les voies de chemin de fer, les digues, etc …construites sur des sols mous en raison de leur efficacité à minimiser les déformations et à accélérer la construction. Une nouvelle méthode développée par l'Université de Hohai en Chine consiste à utiliser des pieux en béton de section en X coulés in situ (appelés pieux XCC) qui peuvent améliorer la capacité portante, réduire efficacement le tassement et les coûts pour des fondations dans de l'argile molle. Dans cet article, méthode de construction, assurance qualité (AQ) et contrôle de qualité (QC) impliqués dans cette méthode sont présentés. Un programme d'essai sur des modèles à grande échelle avec un pieu XCC et un pieu circulaire, construits avec la même quantité de béton, a été réalisé pour obtenir le comportement de transfert de charge pour les deux pieux sous trois modes différents de chargement : compression, soulèvement et latéral. Une application pour un remblai renforcé par des pieux XCC est présentée. Le test de chargement à échelle réelle indique que la capacité portante du pieu XCC est légèrement supérieure à celle du pieu circulaire, pour la même quantité de volume de béton. Il est intéressant de souligner que ce type de pieu XCC peut être construit rapidement avec des assurances qualité (AQ) et contrôles de qualité (QC) faciles et à moindre coût. Les résultats de cette étude peuvent servir de référence dans la pratique pour la conception et la construction des remblais renforcés par les pieux XCC.

KEYWORDS: XCC pile, pile supported embankment, soft clay, case study.

1 INTRODUCTION.

Pile-supported composite foundation is one of useful soft soils treatment methods. It is widely used to construct highways, railways, and seawall on soft soils due to their rapid construction, small total and differential deformations, and low costs compared to other traditional soft soils improvement methods (such as, deep cement mixing (DCM) piles (Arulrajah *et al*. 2009), stone columns (Gniel *et al*. 2009), and precast prestressed piles (Han & Gab 2002; Dzhantimirovk *et al*. 2009; and Bakholdin *et al*. 2009)). Many cases using pile-supported embankments, such as, the railway widening projects (Jones et al. 1990; and Eekelen & Bezuijen 2008), the retaining wall projects (Alzamora et al. 2000), the vertical wall breakwaters (Suh *et al*. 2006), and the freeway embankment in USA and China (American Association of State Highway Officials/Federal Highway Administration 2002; Liu *et al*. 2009; and Chen *et al*. 2010*a*).

There are some ways to optimization pile-supported composite foundation designs by coordinating load share ratio of pile-soil. Special shape piles can improve the contact areas of pile-soil interface and lateral stiffness in specific direction effectively, which means the friction of pile shaft, and lateral load capacity can be improved in the same concrete consumption. It can coordinating load share ratio of pile-soil more suitable. Barrette pile (Lei *et al*. 2001), H-pile (So *et al.* 2009), and steel pipe pile (Arulmoli *et al*. 2010) etc, are widely used for pile foundation. While these special concrete piles have low costs and are more suitable for soft soils treatment. Y-section cast-in-situ concrete pile use for pile-supported embankment is reported (Chen *et al*. 2010*b*), while the lateral stiffness of these piles is not easy to control.

Hence, this paper presents one new method of soft soils treatment: XCC pile-supported composite foundation method. The construction method, quality assurance, and quality check involved in this method are described. A large-scale model test program on a XCC pile and a circular pile, both constructed with the same amount of concrete volume, was carried out to obtain the load transfer behavior of both piles under three different loading modes: compression, uplift, and lateral loads. A case study that illustrates the application of this method in a pile-supported composite foundation over soft clay is presented. The pile shaft of XCC pile are measured and analyzed.

2 CONSTRUCTION METHOD

Cast-in-situ rather than precast concrete X-section piles are used. This is because it is difficult to transport and install X-section piles without affecting the integrity of the pile, particularly when the piles are not reinforced in the corner part of piles. For this purpose, a special pile driving machine and methods have been designed to install the XCC pile (Liu *et al*. 2007). Pictures of the piling machine in action and the flap pile shoe are shown in Fig. 1.

The construction procedures for XCC piles are as follows: First, the vibratory pile driver is connected to the X-section steel casing by flange. Next, the X-section steel casing is connected with the flap pile shoe. Then, the vibratory driver drives the X-cross section steel casing into the desired elevation. After reaching the required penetration depth, concrete is then fed through the X-section steel casing inlet mouth. Finally, use the vibrating driver to extract the casing to the ground. Thus, XCC pile is formed. Pile cap can be constructed after casing is removed.

Figure 1. Physical diagrams of pile-driving machine: (a) XCC pile-driving equipment and pile mould; and (b) Pile driver locating and flappable pile shoes.

3 QUALITY ASSURANCE AND QUALITY CHECK

In order to improve the quality of pile, the withdrawing rate should be controlled within 1.0 to 1.5 m/min under normal circumstances. The casing should vibrate for 10 s before withdrawal. Subsequently for every 1 m withdrawal, the pulling should be stopped temporarily to vibrate the casing for 5 to 10 s until the casing is completely withdrawn. The vibratory effect applied to the casing during withdrawing also helps the concrete to be compacted. The maximum depth of the XCC pile is controlled by the height of the XCC piling machine and is normally within 25 m, and too long pile casing will reduce the install speed. The maximum advantages of XCC pile is the contact areas of pile-soil interface improvement with special cross-section. The most difficult part of XCC pile construction is the shape of pile head, overflow concrete may change the shape as the lateral soil pressures near ground are low.

To check the quality of the pile after formation, the following four methods can be used: (1) excavate the surrounding soil of pile to check the shape of piles, (2) static pile load testing, (3) low-strain integrity testing, and (4) amount of concrete poured in during concreting. To excavate the surrounding soil of pile for visual inspection and for taking concrete samples from the XCC pile is a good way to check the quality of XCC pile. Obviously, static pile load testing, and low-strain integrity testing can be also used for XCC pile.

4 LARGE-SCALE MODEL TEST

4.1 *Summary of Model Test Conditions*

A large -scale test facility is composed of a fairly rigid model container, a loading system, and a data measuring system. The model container is measured as 5 m × 4 m × 7 m (length × width × height). The loading system consists of hydraulic jacks, beams, reaction walls, and hanging baskets and bolts, etc. The data measuring system consists of load cells, reinforcement bars, earth pressure cells, frequency instrument device, and LVDTs.

The soils used to fill the model container consist of both sand and clay, taken from Hexi District of Nanjing, China. The sand is uniformly graded with uniformity coefficient (C_u) and curvature coefficient (C_c) equal to 1.58 and 0.99, respectively. The soil layers are filled in the container by controlling the density of the in-place dry soils. The dry density for sand and clay is 1.54 ~ 1.57 g/cm^3 and 1.47 ~ 1.51 g/cm^3, respectively. The mechanical properties of the soils with the specified density are shown in Table 1. The soil layers in the model test container are as follows: sand of 2.4 m deep at the top, clay of 3.9 m deep in the middle, and crushed rock of 0.3 m at the bottom.

Two pile types (XCC pile and circular pile) were subjected to three different modes of loading (axial compression, uplift, and lateral load) at the top of the pile for deriving load transfer behavior. The experimental set up is summarized in Table 2.

Table 1. The mechanical indices of test soil with the specified density

Materials	Cohesion, c (kPa)	Internal friction angle, φ (°)	Compression modulus, E_s (MPa)	Moisture content, ω (%)	Control density, ρ (g.cm^{-3})
Sand	17.60	25.90	17.00	5.10	1.55
Clay	27.60	21.20	4.60	16.70	1.50

Table 2. Summary of model test conditions

Types	XCC pile		Circular pile	
Section size	Diameter, a (m)	0.530	Diameter, R (m)	0.426
	Distance of arc, b (m)	0.110		
	Open arc, θ (°)	90		
Pile length, L (m)	5.0		5.0	
Cross-section area, A (m^2)	0.1425		0.1425	
Pile perimeter, C (m)	1.759		1.338	
Pile modulus, E (GPa)	28.5		28.5	
Moment of inertia, I (cm^4)	186430.6		161580.0	
Loading types	Compressive		Compressive	
	Uplift		Uplift	
	Lateral		Lateral	

The dimension of XCC pile constructed in the test facility is as follows: 5.0 m in length (L), 0.53 m in the diameter of outsourcing (a), 0.11 m in the spacing of two open arcs (b), and 90° in angle of open arc (θ**).** The reinforcement cage of the XCC pile is made of four reinforcing bars, with 12 mm in diameter and 0.35 m in the distance between the opposite reinforcing bars. The 28-day compressive strength of model pile concrete is equal to 28.5 GPa (JGJ94). Reinforcement sister bars were attached to the reinforcing bars, earth pressure cells were laid on pile tip and the surrounding soils, respectively. During the load tests, the total load applied to the pile head was measured by a load cell placed on the pile head, while the axial force along pile depth was calculated from the attached sister bars. The soil pressures were measured by the earth pressure cells, while the settlement of the pile head was recorded by two LVDTs installed symmetrically at the pile head. Data from the load cells and LVDTs during the load test were captured by a data acquisition system.

In order to perform a comparative analysis between the XCC pile and the circular section pile, a typical circular pile was also constructed and tested in the test facility. The dimension of the circular section pile is as follows: 5.0 m in length (L) and 0.426 m in diameter (R). The cross section area of the circular pile is equal to 0.1425 m^2 which is the same as that of XCC pile.

However, the perimeter of the circular pile is 1.338 m, which is smaller than that of the XCC pile of 1.759 m. Thus, with the same cross section area, the pile-soil interface contact area of the XCC pile is 31.5 % more than that of the circular pile.

4.2 Analysis of Test Results and Discussions

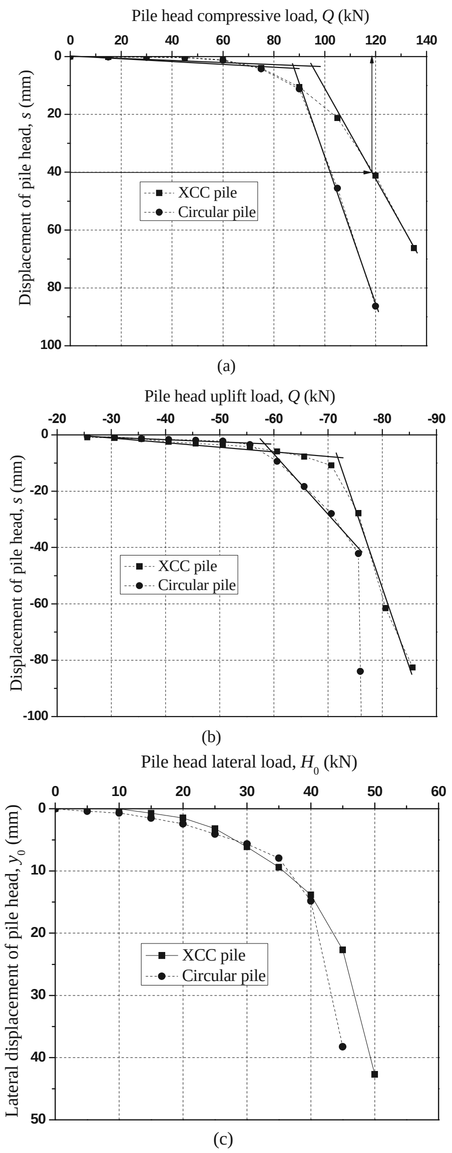

Figure 2. The curves of load versus displacement: (a) compressive load-displacement; (b) uplift load-displacement; (c) lateral load-displacement.

Fig. 2(a) shows load-displacement curves of the XCC pile and the circular section pile at the pile head. The ultimate compressive load-carrying capacity of the circular pile and XCC pile is equal to 90 kN, and 111 kN, respectively. The ultimate compressive capacity was improved nearly 24.0 % by changing the pile cross section from common circular section to X-section when the same amount of concrete volume was used. Fig. 2(b) shows the load-displacement curves under uplift load for the two different pile sections. The uplift capacity of XCC pile and circular pile was found to be -70.6 kN and -56.1 kN, respectively. The ultimate uplift capacity was improved nearly 25.8 % by changing the pile cross section from a circular section to an X-section for the same amount of concrete volume used. The test result of the lateral load versus lateral deflection at pile head is plotted in Fig. 2(c) for two different pile sections. The lateral H_0-y_0 curve of XCC pile is similar with that of circular pile. For the same lateral capacity, the amount of concrete volume used in a XCC pile is about 6.9 % less than in a circular pile.

5 FIELD TEST CASE STUDY

5.1 Summary of Field Test Conditions

The test site locates at north bridge of Nanjing city, where the landform is Yangtze River floodplain. By geological exploration, and laboratory soil test, the physical and mechanical parameters and distribution of soil layers are shown in Table 3.

Table 3. The soil layers and soil parameters in field test site

Soil symbol	Name	Depth h (m)	Water content w (%)	Unit weight γ (kN/m^3)	Modulus E_s (MPa)	Void ratio e
□	Filled back soil	0.20				
□$_2$	Mucky silty clay	1.30	38.60	17.60	3.50	1.11
□$_{2A}$	Silty sand	1.00	25.30	19.20	10.77	0.70
□$_2$	Mucky silty clay	1.50	38.60	17.60	3.50	1.11
□$_{2B}$	Silty sand	1.80	26.10	19.30	8.00	0.71
□$_2$	Mucky silty clay	2.30	38.60	17.60	3.50	1.11
□$_3$	Fine sand	9.40	26.30	18.90	11.83	0.76

The pile layout in Fig. 3 shows that the piles distribute as equilateral triangles, and the distances between two adjacent piles for single pile test and 2×2 pile groups test equal 1.85 m, and 1.80 m, respectively. In static loading tests of 2×2 pile group composite foundation, the loading plates are rhombic with side length of 3.6 m, which covers four piles. A layer of gravel cushion with the thickness of 30 cm is paved between pile top and loading plate. During the load tests, the total load applied to the loading plate was measured by a load cell placed on the loading plate, the axial force of pile shaft along pile depth was measured by reinforcement stress meters, the soil pressures and pile head pressures were measured by earth pressure cells, and settlement of the pile head was recorded by two LVDTs installed symmetrically at the loading plate. Data from the load cells and LVDTs during the load test were captured by a data acquisition system.

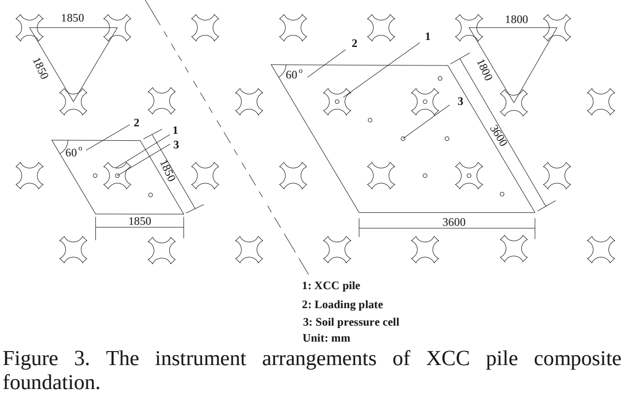

Figure 3. The instrument arrangements of XCC pile composite foundation.

5.2 Analysis of Test Results and Discussions

Fig. 4 shows the changes of axial forces result in the variations of side friction. When the load is relatively large, the side friction from the depth of -1 m to -2 m is negative, which is the typical characteristic of composite foundation. The load applied on loading plate causes the non-uniform settlement between the soil and piles. When the load is not very large, the differential settlement is in apparent, so the negative friction is extremely small. As the increase of the load step, the load shared by the piles also increases, and then the pile top tends to penetrate into the cushion, at the same time the soil subsidence occurs under the load shared by the soil, so the differential settlement is increscent. Because the compressibility of the soil is far greater than the pile, the settlement of the soil is far larger than the pile, as a result, the displacement of the soil is downward with respect to the pile and the downdrag is generated, that is the negative friction. The larger the load pressure, the greater the negative friction. The results in Fig. 4 also show that the location of neutral points is about -2 m, which is almost unchanged as the increase of the load.

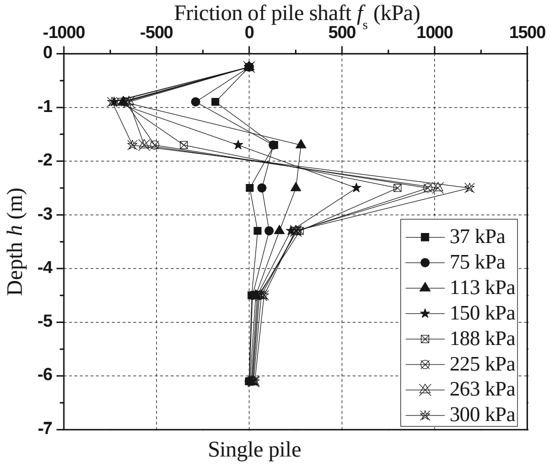

Figure 4. The distributions of friction of pile shaft along pile depth under different vertical load.

6 SUMMARY AND CONCLUSIONS

Based on large-scale load tests and field test of a XCC pile carried out in this paper, the following conclusions may be drawn.

(1) Regarding the contact area of pile-soil interface and EI of piles, XCC piles can increase these values in comparison to circular piles for the same amount of concrete volume used. The large-scale test in a load testing facility indicated that load carrying capacity of XCC pile exhibit a slightly higher capacity than circular pile when the same amount of concrete volume was used. Under the same working load level, XCC pile can be constructed with less concrete volume and exhibits smaller settlement when compared to the circular piles.

(2) The X cross section type offers a more reasonable section form as compared with other traditional pile sections from on the standpoint of offering contact areas of pile-soil interface and lateral stiffness. The contact areas of pile-soil interface can be improved obviously without the increasing of concrete consumption. XCC pile is also an economic environment new pile type. With less concrete usage can get the same treatment effect. In this case study, the maximum values of axial force of pile shaft is located on the -2 m deep, the location of neutral points is about -2 m of pile depth.

7 ACKNOWLEDGEMENTS

The authors acknowledge the financial support from the National Science Joint High Speed Railway Foundation of China (No. U1134207), and the National Science Foundation of China (No. 51008116, 51278170).

8 REFERENCES

Alzamora, D. E. , Wayne, M. H. , and Han, J. (2000). “Performance of SRW supported by geogrids and jet grout columns.” *Proc., Sessions of ASCE Specialty Conf. of Performance Confirmation of Constructed Geotechnical Facilities* , A. J. Lutenegeer and D. J. DeGroot, eds., ASCE Geotechnical Special Publication, Reston, Va., Vol. 94 , 456–466.

American Association of State Highway Officials/Federal Highway Administration (2002). Innovative technology for accelerated construction bridge and embankment foundations, Preliminary Summary Rep. Prepared for Federal Highway Administration, U.S. Dept. of Transportation, Washington, D.C.

Arulrajah, A., Abdullah, A., Bo, M. W., and Bouazza, A. (2009). “Ground improvement techniques for railway embankments.” *Ground Improvement*, 162(1), 3-14.

Arulmoli, A. K., Varatharaj, R. S., Posadas, J., Afewerki, R., Jaradat, O., and Lim, A. (2010). “Geotechnical challenges associated with the design of a new marine oil terminal at the port of Los Angeles.” In: *Ports 2010: Building on the Past, Respecting the Future Proceedings of the Ports 2010 Conference*, ASCE, Florida, 252-261.

Bakholdin, B. V., Yastrebov, P. I., and Chashchikhina, L. P. (2009). “Resistance characteristics of soils in the beds of precast piles.” *Soil Mech. Found. Eng.*, 46(2), 39-44.

Chen, R. P., Xu, Z. Z., Chen, Y. M., Ling, D. S., and Zhu, B. (2010*a*). “Field tests on pile-supported embankments over soft ground.” *J. Geotech. Geoenviron. Eng.*, 136 (6), 777-785.

Chen, Y. H., Wang, X. Q., Liu, H. L., Jiang, L., and Zhang, T. (2010*b*). “In-situ study on stress distribution of foundation improved by Y-section pile.” In: *Ground Improvement Technologies and Case Histories*, Leung et al. ed., Geotechnical Society of Singapore, Singapore, 319-330.

Dzhantimirovk, H. A., and Yalaev, R. R. (2009). “Form-free procedure for fabrication of prestressed piles with no transverse reinforcement.” *Soil Mech. Found. Eng.*, 46(2), 69-76.

Eekelen, S. J. M. van, and A. Bezuijen (2008). “Design of piled embankments, considering the basic starting points of the British Design Guideline.” *Proc. of EuroGeo 4,* Sep. 2008, Edinburgh UK.

Gniel, J., and Bouazza, A. (2009). “Improvement of soft soils using geogrid encased stone columns.” *Geotext. Geomembr.*, 27(3), 167-175.

Han, J., and Gab, M. A. (2002). “Numerical analysis of geosynthetic-reinforced and pile-supported earth platforms over soft soil.” *J. Geotech. Geoenviron. Eng.*, 128(1), 44-53.

JGJ94. (2008). “Technical code for building pile foundations.” Beijing, China Architecture and Building Press. (in Chinese)

Jones, C. J. F. P. , Lawson, C. R. , and Ayres, D. J. (1990). “Geotextile reinforced piled embankments.” *Proc., 4th Int. Conf. on Geotextiles, Geomembranes and Related Products*, International Geosynthetics Society, 155–160.

Lei, G. H. (2001). “Behavior of excavated rectangular piles (barrettes) in granitic saproletes.” Ph.D. thesis, The Hong Kong University of Science and Technology, Hong Kong.

Liu, H. L. (2007). “In-situ X-section reinforced concrete pile construction method.” China patent ZL200710020306.3.

Liu, H. L., Chu, J., and Deng, A. (2009). “Use of large-diameter, cast-in situ concrete pipe piles for embankment over soft clay.” *Can. Geotech. J.*, 46(7), 915-927.

So, A. K. O., and Ng, C. W. W. (2009). “Performance of long-driven H-piles in granitic saprolite.” *J. Geotech. Geoenviron. Eng.*, 135(2), 246-258.

Suh, K., Shin, S., and Cox, D. (2006). “Hydrodynamic Characteristics of Pile-Supported Vertical Wall Breakwaters.” *J. Waterway, Port, Coastal, Ocean Eng.*, 132(2), 83–96.

Settlements of Earth Fills on Thick Layers of Overconsolidated Soft Clays without Geodrains

Tassements des remblais sur d'épaisses couches d'argile molle, surconsolidée, sans géodrains

Massad F.
EPUSP – São Paulo, Brasil

Teixeira A.H.
A.H. TEIXEIRA CONSULTORIA E PROJETOS– São Paulo, Brasil

Carvalho C.T., Grangé L.F.A.
ODEBRECHT INFRAESTRUTURA – Brasil

ABSTRACT: The monitoring of earth fills built on soft clays has been done frequently through the Brazilian coastline. As the most common measurement is the settlement along time, the interpretation of the results is usually done by Asaoka's Method, generally involving extrapolations that have given rise to doubts (for instance, about the secondary consolidation effect) and to a double interpretation, and even to controversies, especially when it comes to evaluating the effectiveness of vertical geodrains to accelerate settlements. Doubts about the soil disturbances around the geodrains that have been of concern among us and abroad. The paper is based on data from a work in Santos Harbor, in São Paulo State, Brazil, in which 3 experimental fills were built and monitored, one of them partially with geodrains. Many laboratory and field tests were available besides local experience that proved decisive in the evaluation of the measurements and in making decision. It is shown that the controversies can be overcome with information of the soil and of similar works in the region and details of geodrain installation, confirmed by the behavior of the landfills of the work.

RÉSUMÉ: La surveillance des remblais construits sur argiles molles a souvent été effectuée le long de la côte brésilienne. Comme la mesure la plus courante est le tassement au cours du temps, l'interprétation des résultats est généralement faite par la méthode d´Asaoka, impliquant généralement des extrapolations qui ont donné lieu à des doutes (par exemple, à propos de l'effet de la consolidation secondaire), à une double interprétation, et même à des controverses, surtout quand il s'agit d'évaluer l'efficacité des géodrains verticaux pour accélérer les tassements. Ces doutes sur les remaniements du sol autour des géodrains ont été une préoccupation pour nous et à l'étranger. L´article est basé sur les données de travaux au Port de Santos, dans l'État de São Paulo, au Brésil, au cours duquel trois remblais expérimentaux ont été construits et surveillés, l'un d'entre eux avec des géodrains. De nombreux essais en laboratoire et in situ étaient disponibles en plus de l'expérience locale qui s'est avérée décisive dans l'évaluation des mesures et en prise de décisions. Il est démontré que les controverses peuvent être surmontées avec la connaissance des sols,des travaux similaires dans la région, et le mode d´installation des géodrains. Ceci est confirmé par le comportement des remblais en service.

1 INTRODUCTION

A port terminal (Embraport) is under construction in the left side of the Santos Harbor Channel, close to the Barnabe Island, as shown in Figure 1. The total area that is being filled, roughly 800,000m², is delimited by Sandi and Diana Rivers. The Area 3 of Figure 1, alongside the Santos Channel, will be used for containers storage and part of it was reclaimed underwater. The final level of the earth fills in the area will be 3.5m.

2 GEOLOGICAL AND GEOTECHNICAL ASPECTS

Many geological evidences show that the sedimentary clays of the Santos Coastal Plain ("Baixada Santista") were formed during two Quaternary depositional cycles, with an intermediate erosive process. This gave origin to two different types of clays: the Pleistocene (Transitional) Clays and the Holocene Clays. The former ones, also called Transitional Clays (AT), deposited 100,000 to 120,000 years BP (Before Present), are medium to hard clays, pre-consolidated due to a sea-level lowering of 130 m at the peak of the last glaciation (15,000 years BP); as a consequence, these sediments were also deeply eroded. The latter ones, also called SFL clays (from Sediments-Fluvial-Lagoon-Bay), originated since 10,000 years BP by sedimentation where the Pleistocene sediments had been eroded, are very soft to soft clays, lightly over consolidated due to such occurrences as short negative sea-level oscillations (i.e., bellow present sea level) or dune action. Included in this last category are the mangrove sediments, which are still forming.

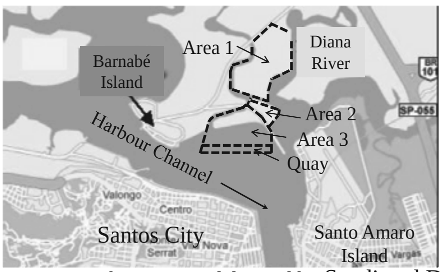

Figure 1.Embraport site delimited by Sandi and Diana Rivers.

In the site of the terminal occur fluvial sediments, originating alternate and discontinuous layers of sand and clay. But it is close to Santo Amaro Island, where a lagoon-bay type of sedimentation took place, with deep layers of SFL (SPT ~1 to 4). This way, both characteristics were found.

In fact, an extensive field investigation, including SPT percussion borings, Vane Tests and CPTUs, revealed: a) a fluvial sedimentation that led to a sandy or clayey mangrove deposition, 0 to 2m width (SPT=0); b) an intermediate sedimentation of a fluvial-bay type, 25 to 35m width, in a mix environment (turbulent and calm), that gave origin to layers of clay with sand lenses, with SPTs varying from 1 to 4; c) the presence of layers of Transitional Clay (AT) at greater depths, with SPTs>5; and d) at last, the occurrence of sands with gravel and residual soils from gneiss. Figure 2 illustrates the local subsoil, without the Transitional Clay and the residual soils.

Eolic deposits were always present in the area, including Santo Amaro Island and Santos City Plain. Their weights were responsible for the higher values of SPT, ranging from 2 to 4 as well as the overconsolidation of the deposits.

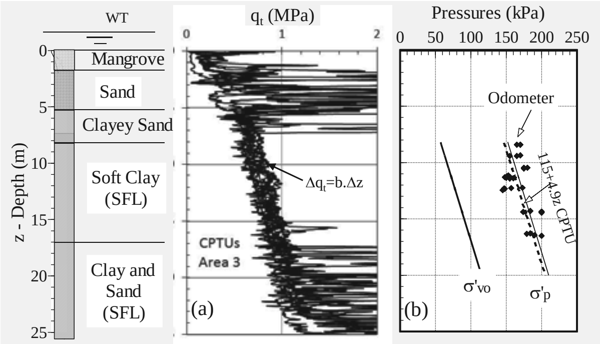

Figure 2. Odometer tests vs. 7 CPTUs at Area 3 of Figure 1.

The main properties of the marine clays are presented in Table 1, separated in two parts: the upper one emphasizes the differences and the lower one stresses the similarities. As it can be seen, their index properties are almost the same and they differ in their "state properties", like undrained shear strength, void ratio and SPT. It is interesting to mention that negative B_q values were observed for the Pleistocene Clays, whose preconsolidation, with high OCR, was confirmed by consolidation tests on undisturbed samples (Massad 2009-a).

Table 1.Properties of the Marine Holocene and Pleistocene Clays

Group	Item	Man-grove	SFL	AT
Differences	Depth(m)	≤5	≤50	20-45
	SPT	0	0-4	5-25
	B_q	-	0.4-0.9	-0.1-0.2
	q_t(MPa)	-	0.5-1.5	1.5-2.0
	e	>4	2-4	<2
	σ'p(kPa)	<30	30-200	200-700
	OCR	1	1.1-2.5	>2.5
	s_u(kPa)	3	10-60	>100
Similarities	γ_n(kN/m^3)	13.0	13.5-16.3	15.0-16.3
	%<5μ	-	20-90	20-70
	w_L	40-150	40-150	40-150
	I_P	30-90	20-90	40-90
	$C_c/(1+e_o)$	0.36	0.43	0.39
	Cr/Cc(%)	12	8-12	9
	R_f(%)	-	1.5-4.0	1.5-2.0

Legend: SI Symbols used

Data from 3 borings in Area 3 are presented in Figure 3.

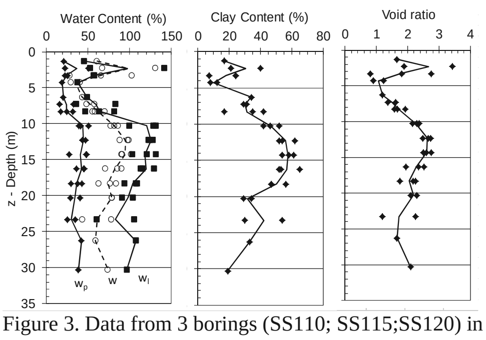

Figure 3. Data from 3 borings (SS110; SS115;SS120) in Area 3.

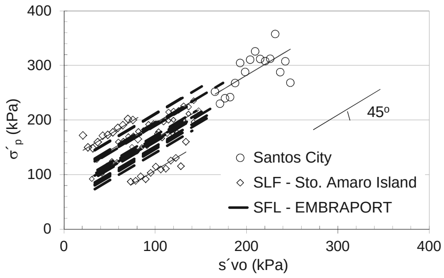

Figure 4. σ'p from CPTUs as a function of the σ'vo.

About 20 stress history profiles, from odometer tests and CPTUs, carried out in sites of the Santos Plain, like Figure 2, showed that equation (1) holds; C_1 and C_2 are constants.

$$\sigma'_p - \sigma'_{vo} = C_1 \quad \text{or} \quad \sigma'_p = C_2 + \gamma'.z \qquad (1)$$

Figure 4 illustrates its validity and Table 2 shows values of C_1 for the 4 Classes of SFL Clays (Massad 2009-a). These findings have a practical consequence: more than 12 experimental earth fills settled in a wide range of values (ε_{EOP}=1 to 12%) and of velocities ($c_v \cong c_h$~3.10^{-3} to 5.10^{-2} cm^2/s), depending on *OCR*. Note that for the SFL clays $c_v \cong c_h$ (Massad 2009-a).

Table 2.Classes of Holocene Clays (SFL). Santos Coastal Plain

Class	Clay Profile	Site	Consolidation Mechanism	OCR	σ'p- σ'vo (c_o)kPa
1	Out-cropping	Baixada Santista	Neg. Sea level Osc.	1.3-2.0	20-30 (5-20)
2		St.Amaro I Embraport.	Dune Action	>2.0	50-120 (25-45)
3	Beneath 8-12m of sand layer	Santos City	Neg. Sea level Osc	1.0-1.3	15-30 (10-30)
4		Santos City	Dune Action	>1.4	40-80 (>35)

Legend: SI Symbols used; stresses and c_o(of Eq. 3) in kPa;

For the SFL clays of Santos Coastal Plain there is a linear increase of q_t with depth, with a rate b. Massad (2009-b) used this fact and equation (1) to estimate the empirical factor $N_{\sigma t}$ of Kulhaway and Mayne (1990), as shown in Equation 2.

$$\sigma'_p = \frac{q_t - \sigma_{vo}}{N_{\sigma t}} \quad \text{with} \quad N_{\sigma t} = \frac{b - \gamma_n}{\gamma'} \qquad (2)$$

The use of equation 2 with *b*=34MPa/m for the SFL clay layer of Embraport site (see Figure 2-a) resulted in $N_{\sigma t}$ =3.9 and the constant C_2 of equation 1 varying from 80 to 115kPa, revealing the great heterogeneity of the soil (see also Teixeira 1960 on this feature). The high values of σ'p for the Embraport site are associated with *OCR*>2 at mid height of the layer, as shown in Table 2. Furthermore, Figure 2-b shows also data of odometer tests (dashed line is the average) carried out by Andrade (2009) that agree with the σ'_p of the nearest CPTU.

The shear strength of the SFL clays follows the equation $s_u=c_o+c_1.z$, with $c_1=0.4\gamma'$.For Embraport site the c_o values are higher (Table 2), as those found in Santos City (Teixeira 1994).

Figure 5 shows that: a) the c_h for the overconsolidated range (o.c.) varies from 4.7x10^{-3} to 1.5x10^{-1} cm^2/s (mean value of 2.1x10^{-2} cm^2/s) for the soft clay (SFL) layer (8 to 17m depth); and b) the upper sand and the lower clay/sand layers are highly permeable. In cases like this there is no need to use drains, as shown by Pilot (1991) besides local practice (Massad, 2009-a).

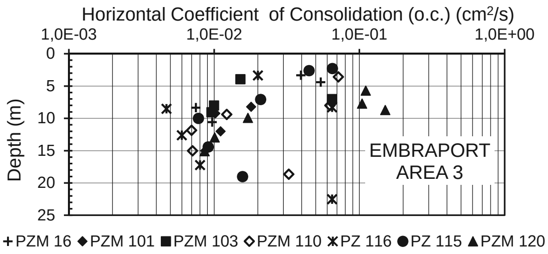

Figure 5: Data from dissipation tests of 7 CPTUs at Area 3.

3 PILOT EMBANKMENT 1

An experimental earth fill – the Pilot Embankment 1 - was built in the Area 3 before it was reclaimed underwater. It was divided in three parts (see Figure 6), Segments 1 and 2 with square meshes of geodrains 25m length, spaced 1,2m and 2.4m, respectively, and Segment 3, without vertical drains.

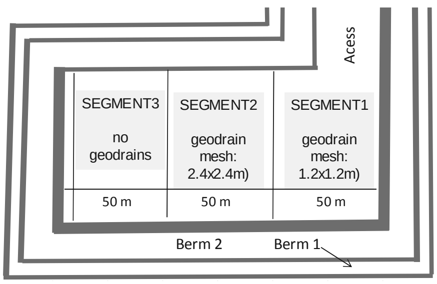

Figure 6: Relative positions of the Segments. Pilot Embankment 1

Detailed information about the construction and the instrumentation is found in Rémy et al (2010). It is worth mentioning that the rate of loading was distinct among the segments. And it was also distinct in Segment 3, comprising two sides, North and South, with different heights. Figure 2 shows the subsoil in the site.

Many difficulties arose in the interpretation of the data of the Embankment Pilot 1. They refer to the following drawbacks:

a) the Segments 1, 2 and 3 were too close and the earth fill loads were applied at different rates; for Segments 1 and 2, the 4 loading stages were applied during 354 and 452 days, respectively; for Segment 1, the 2 stages required 142 days;
b) the installation of the geodrains involved the use of a temporary casing 2 inches inside diameter and flushing water to pass through the upper sand layers (see Figure 2) besides the fact that the soil resistance was high; and
c) there occurred two problems with the measuring probe of the magnet extensometers. The first one in Nov., 13th, 2008 (day 400 in Figure 7) when the measuring probe was changed; ant the second one between Feb.,19th, 2009 (day 485) and Sept., 16th, 2009 (day 694), that is, 209 days with no measurements, due to damage in the probe device.

Figure 7 shows the measured settlements of the Soft Clay (SFL) layer, between 8 and 17m (see Figure 2) of Segment 3. The plot reveals: a) the interference between the Segments 2 and 3, due to their proximity and the differences in the rate of loading, as mentioned above; and b) the 3 stages of loading that occurred, making it possible to apply Asaoka's Method, as shown in Figure 8. Table 3 presents the results of this analysis.

Table 3: Results of the Application of Asaoka's Method

Stage	c_v (cm^2/s)	ρ_f EOP(cm)	ρ_f /H (%)	$\sigma'_{vf}/\sigma'_{vo}$ (*)
1	3.10^{-2}	3.5	0.37	1.29
2	2.10^{-2}	13.5	1.42	1.88
3	2.10^{-2}	15.3	-	-

Note: (*) in the center of the SFL Clay layer

With the preconsolidation pressures indicated in Figure 2-b it follows an average *OCR*=2.2 for the center of the Soft Clay (SFL) layer. The conclusion is that the SFL Soft Clay of Embraport site behaved as an overconsolidated clay, of Class 2 of Table 2. Moreover, note that the c_h~c_v given by Figure 5 agrees with the values of Table 3 and with local experience.

Due to the second difficulty and to the highly permeable layers, the geodrains of Segments 1 and 2 were disregarded, a position that differs from that of Rémy et al (2010) being a different view. Table 4 endorses this position: the indicated plates were installedat the base of the earth fills and the values of c_v are equivalent in the sense that they refer to all layers. It can be seen that the drain installation greatly affected the *EOP* settlements but lesser the time of its occurrence. These conclusions are in consonance with the research by Saye (2001) with the Florence Lake Clay, in Omaha, Nebraska (USA).

Table 4: Influence of soil disturbance due to drain installation

Segment	Geodrains	Plate	Max. Level	c_v/H_d^2	ρ_f EOP(cm)
1	2.4x2.4m	PR 02	7.27m	4.2*10^{-3}/day	194
2	1.2x1.2m	PR 08	6.95m	3.5*10^{-3}/day	~137
3	without	PR 11	7.70m	7.0*10^{-3}/day	89

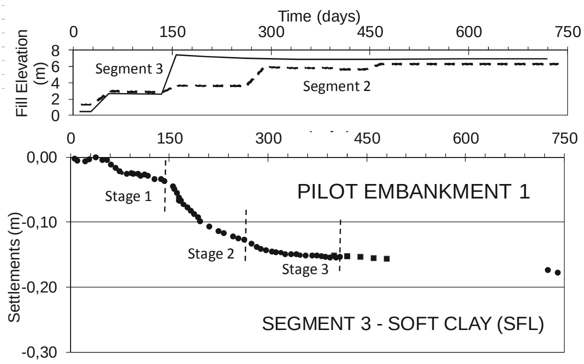

Figure 7: Compression of the Soft Clay (SFL) layer. Segment 3

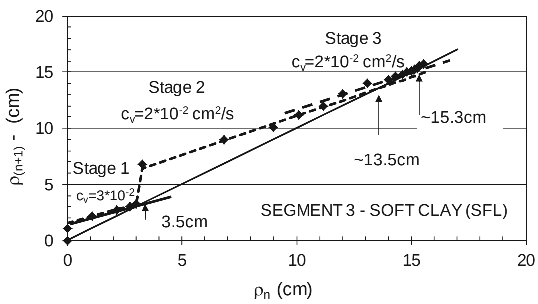

Figure 8: Asaoka's Method - Pilot Embankment 1

4 PILOT EMBANKMENTS 2 AND 3

A second experimental fill (Pilot Embankment 2) was built in Area 3, with a maximum height of 5.2m. Figure 9 displays de subsoil profile and gives information about the initial and final stresses, the preconsolidation pressures and the *OCR*.

The values of the end of primary settlement (ρ_f) and c_v/H^2_d were determined as illustrated in Figure 10 for one of the 4 plates installed at the earth fill base for the two stages shown in Figure 11-a. Note again that c_v is equivalent in the sense that it refers to all layers and that, after roughly 5 month, at least 95% of the primary settlement was reached.

The Figures 11-a and 11-b show also the very good fittings of the theoretical and measured values of settlements and the product *v.t* (velocity*time) along the primary consolidation time. For the secondary range, *v.t* reached a constant value, allowing the estimation of $C_{\alpha\varepsilon}$=0,85%, consistent with the values obtained for the Santos' Buildings (for more details,

Massad 2005 2010).
A third experimental fill (Pilot Embankment 3), built also in Area 3, with a maximum height of 6.7m, behaved in a similar way, with c_v/H^2_d averaging $1.8.10^{-2}$/day; the *EOP* settlement was ~80 cm and 95% of this value was reached after ~6 month.

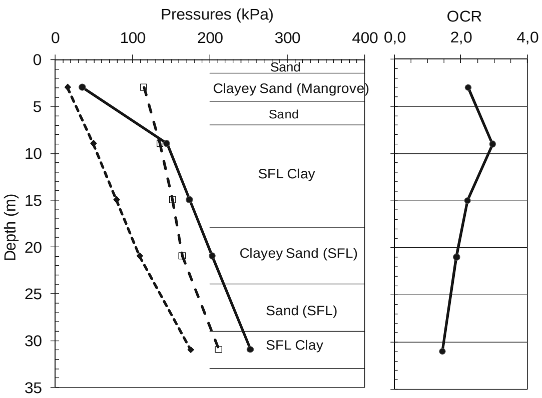

Figure 9: Subsoil profile, pressures and OCR – Pilot Embankment 2

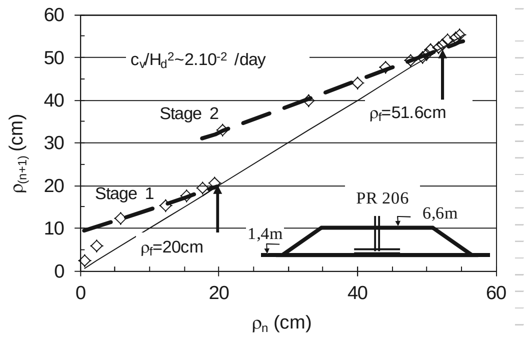

Figure 10: Asaoka's Method - Pilot Embankment 2

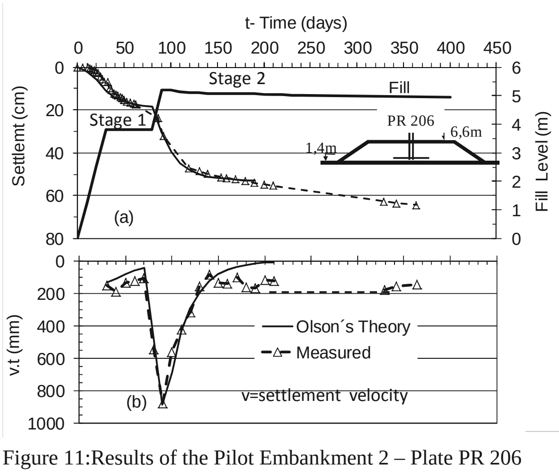

Figure 11:Results of the Pilot Embankment 2 – Plate PR 206

5 BEHAVIOR OF THE EARTH FILLS OF THE WORK

The earth fills in Area 3 of Figure 1 were built with a temporary surcharge, in general of 80kPa. Tens of plates were installed to monitor the settlements. The time of surcharge removal, set to reach 95% of consolidation, was fixed between 6 and 8 months, or even more, depending on the time of construction.
The settlements of two of these plates are shown in Figures 12-a and 12-b, together with the fittings with Olson´s Theory of Consolidation; the c_v/H^2_d values were determined using the Method of Baguelin (1999), alternative to Asaoka´s Method. In these cases, 6 months was enough for surcharge removal.

6 CONCLUSIONS

Due to the high *OCR* values of the SFL Clays, the c_v were also high, of the order or 10^{-2}cm^2/s. As a consequence, there was no need to use geodrains in the Embraport site.
This conclusion was supported by 3 experimental earth fills without geodrains and, more important, by the monitoring of settlements in Area 3, where temporary surcharges were used.

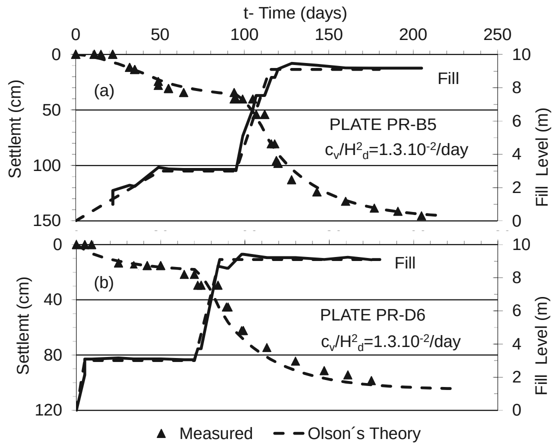

Figure 12:Analysis of settlements of earth fills of Area 3

7 ACKNOWLEDGEMENTS

The authors are grateful to the disposal of data by ODEBRECHT INFRAESTRUTURA and EMBRAPORT S.A.

8 REFERENCES

Andrade M. E. S. 2009. Contribution to the Study of the Soft Clays of Baixada Santista. MSc Thesis, COPPE, 397p. (in Portuguese).

Baguelin F. 1999. La détermination des Tassements Finaux de Consolidation: une Alternative à la Méthode d´Asaoka. Revue Française de Géotechnique no 86: 9-17.

KulhawayF.H. and Mayne P. N. 1990.Manual on Estimating Soil Properties for Foundation Design. Report EL-6800, Electric Power Research Institute, Palo Alto.

MassadF. 2005. Marine Soft Clays of Santos, Brazil: BuildingSettlements And Geological History. Proc. 16th ICSMGE. Osaka, Japan. v. 2: 405-408.

MassadF. 2009-a. Marine Clays of BaixadaSantista – Characteristics and Geotechnical Properties.S.Paulo: Ofic.Textos (in Portuguese).

MassadF.2009-b.Stress history and preconsolidation pressure evaluation from SCPTU.Proc.17th ICSMGE. Alexandria, Egypt, v.2. p.961 - 964.

MassadF.2010. Tall buildings in Santos City: unexpected behavior of the old shallow foundations and the newly long piles.New Techniques on Soft Soils.S.Paulo: Ofic.deTextos, v.1, p. 269-288.

Olson,R. E. 1977. Consolidation Under Time Dependent Loading. Journal of the Geotechinical Division, ASCE, 103 (GT1): 55-60.

PilotG. 1981. Methods of Improving the Engineering Properties of Soft Clays.In: Soft Clay Engineering. Edited by Brand, E. W. e Brenner, R. P.. Elsiver. p. 637-691

Rémy J. P. P.;Martins I.S.M.; Santa Maria P.E.L and Aguiar V.N. 2010. The Embraport Pilot Embankment – primary and secondary consolidations of Santos soft clay with and without wick drains. New Techn. Soft Soils.S.Paulo : Ofic. de Textos, v.1, p. 289-329.

SayeS. R. 2001. Assessment of soil disturbance by the instalation of displacement sand drains and prefabricated vertical drains. GSP no. 119, ASCE (American Society of Civil Engineers), USA.

Teixeira A.H. 1960. Typical Subsoil Conditions and Settlement Problems in Santos, Brazil. Congresso Panamericano de Mecánica de Suelos e Cimentaciones, México, I: 149-177 (in Portuguese).

Teixeira A.H. 1994. Shallow Foudations in Baixada Santista. In: Solos do Litoral Paulista, ABMS - NRSP: 137-154 (in Portuguese)

Aspects on the modelling of smear zones around vertical drains

Aspects de la modélisation de la zone remaniée autour des drains verticaux

Müller R.
Tyréns AB, Borlänge, Sweden / KTH Royal Institute of Technology, Stockholm, Sweden

Larsson S.
KTH Royal Institute of Technology, Stockholm, Sweden

ABSTRACT: The analytical design of vertical drains in soft clay requires knowledge of the coefficient of consolidation and also of the disturbance effects induced during the installation of the drains. Several analytical models describing the disturbance effects in different ways are proposed in the literature. The earliest and simplest models describe the disturbance effect in terms of concentric cylinders around a drain where a reduced and constant permeability is assumed, while more recent models attempt to describe the disturbance more realistically via more complex mathematical formulations. Although these new models describe the real in situ behaviour more realistically than the early ones, they may not always be suitable for practical use as many of the required variables are difficult to assess by standard investigation methods. This study investigates and discusses the difference between some of the available models and evaluates the influences on the results of the variables incorporated in the models.

RÉSUMÉ: L'étude analytique des drains verticaux dans les argiles molles nécessite la connaissance du coefficient de consolidation et des effets du remaniement produit par l'installation des drains. Ces effets peuvent être modélisés de plusieurs façons. Les modèles les plus anciens et les plus simples décrivent le remaniement à l'aide de cylindres concentriques autour d'un drain en supposant que la perméabilité est réduite et constante, tandis que des modèles plus récents s'efforcent à décrire le remaniement de façon plus réaliste à l'aide de formulations mathématiques avancées. Bien que ces modèles décrivent le comportement in situ de manière plus réaliste que leurs prédécesseurs, leur utilisation pratique est souvent limitée car plusieurs des paramètres requis sont souvent difficiles à évaluer à l'aide de sondages, forages et essais classiques. Cette étude s'intéresse aux différences entre certains des modèles existants et évalue l'influence des divers paramètres sur les résultats.

KEYWORDS: Vertical Drains, Design, Modelling

1 INTRODUCTION

During the installation of prefabricated vertical drains (PVDs) in soft clay, the original soil fabric is disturbed. The disturbance occurs when the installation device, the mandrel, is pushed through the clay displacing the soil material. According to e.g. Hird and Moseley (2000) this results in a disruption of the initial soil fabric, e.g. the destruction of any permeability anisotropy (the ratio of horizontal to vertical permeability k_h/k_v), and causes excess pore pressures that trigger a subsequent reconsolidation of the clay and an associated decrease in void ratio that in turn decreases the permeability (e.g. Tavenas et al. 1983). The nature of the disturbance is highly complex and depends on many factors such as the characteristics of the soil material, the shape, surface roughness and size of the mandrel, the installation rate and the soil movement after the mandrel has been removed (e.g. Onoue et al. 1991, Hird and Moseley 2000). Laboratory studies investigating the spatial characteristics of the disturbed zone show that the degree of disturbance (i.e. the reduction in k_h) is most pronounced in the vicinity of the drain where k_h approaches k_v and decreases with increasing radial distance from the drain (Onoue et al. 1991, Bergado et al. 1991, Madhav et al. 1993, Indraratna and Redana 1998, Hird and Moseley 2000, Sharma and Xiao 2000, Sathananthan and Indraratna 2006).

For the design of PVDs and the assessment of the average degree of consolidation (U), several theoretical models describing the characteristics of the disturbed zone have been proposed over the years. The early rather simple models (Barron 1948, Hansbo 1979) assumed a unit cell soil cylinder dewatered by one centric drain and a disturbed (smear) zone with a constant and reduced horizontal permeability (Figure 1). According to Basu et al. (2006), previous studies based on this model suggest that the extent (diameter) of the smear zone (d_s) is 2 to 4 times larger than the equivalent diameter of the PVD (d_w) and that the reduced horizontal permeability (k_{hs}) is 2 to 10 times lower than the undisturbed permeability (k_{h0}), i.e. $s = d_s/d_w \approx$2-4 and $\kappa = k_{h0}/k_{hs} \approx$2-10. However, the cited laboratory studies have indicated that the extent of the disturbed zone can be as large as d_s/d_m =9 (where d_m is the equivalent diameter of the mandrel).

More recent models attempt to capture the nature of the smear zone more realistically, describing the variation of k_h within the disturbed zone (e.g. Walker and Indraratna 2006, Basu et al. 2006, Chung et al. 2009). In addition, temporal effects, such as the reconsolidation of the clay after drain installation, affecting the characteristics of the disturbed zone have been incorporated in the models presented by Indraratna et al. (2005) and Walker et al. (2012).

To a practising engineer creating a design involving PVDs, the choice of model and the widely varying suggestions regarding the values of s and κ may be confusing. This paper investigates the differences between six of the analytical models available in the literature and the influences of the involved variables on the assessment of U. All the models investigated can be written on the form:

$$U = 1 - e^{\frac{-8\times T_h}{F}} \tag{1}$$

where $T_h = c_h \times t/d^2$ is the time factor for horizontal consolidation, $c_h = k_h \times M_v/\gamma_w$ is the undisturbed horizontal coefficient of consolidation in the clay (where M_v is the vertical

Table 1. Characteristics and formulations of F in the investigated models (valid for $n > 10$ [A] and neglecting well resistance)

no.	*Characteristics*	*Formulation* [A]	*Reference and comments*
I	No smear zone, c_v is used instead of c_h [B]	$F_{\mathrm{I}} = \ln(n) - 0.75$	Kjellman (1949), smear effects accounted for by adopting c_v instead of c_h
II	$k_h = k_{hs}$ and constant in the smear zone	$F_{\mathrm{II}} = \ln(n/s) - 0.75 + \kappa \ln(s)$	Hansbo (1979), equal to model no. I for s =1
III	Equal to no. II, k_h dependent on the void ratio	$F_{\mathrm{III}} = \dfrac{2F_{II}}{1 + (1 + \Delta p/\sigma_i)^{1-C_c/C_k}}$	Indraratna et al. (2005), valid for normally consolidated clays, equal to model no. II for $C_c/C_k = 1$
IV	Parabolic variation of k_h in the smear zone	$F_{\mathrm{IV}} = \ln(n/s) - 0.75 + \dfrac{\kappa(s-1)^2}{(s^2 - 2\kappa s + \kappa)} \ln\left(\dfrac{s}{\sqrt{\kappa}}\right) - \dfrac{s(s-1)\sqrt{\kappa(\kappa-1)}}{2(s^2 - 2\kappa s + \kappa)} \ln\left(\dfrac{\sqrt{\kappa} + \sqrt{\kappa - 1}}{\sqrt{\kappa} - \sqrt{\kappa - 1}}\right)$	Walker and Indraratna (2006)
V	$k_h = k_{hs}$ in the inner smear zone thereafter linear variation	$F_{\mathrm{V}} = \ln(n/s) - 0.75 + \kappa \ln(m) + \dfrac{s - m}{s/\kappa - m} \ln\left(\dfrac{s}{\kappa m}\right)$	Basu et al. (2006), case b, equal to model no. VI for m =1
VI	Linear variation	$F_{\mathrm{VI}} = \ln(n/s) - 0.75 + \dfrac{s - 1}{s/\kappa - 1} \ln\left(\dfrac{s}{\kappa}\right)$	Basu et al. (2006), case d

[A] *$n = d/d_w$; σ_i & Δp=initial stress & stress from the applied load; C_c & C_k=compression & permeability indices; $m = d_i/d_w$*

[B] $c_v = c_h/1.5$ was used based on suggestions in Tavenas et al. (1983) for the anisotropy in permeability in homogeneous clays.

compression modulus and γ_w is the unit weight of water), t is the consolidation time, d is the diameter of the assumed unit cell dewatered by a single drain (cf. Figure 1) and the expression F is dependent on the model.

1 METHODS

The characteristics and formulations of the expression F in the six investigated models are presented in Table 1 and Figure 1b.

Denoting the variables in Eq. 1 and in the formulations of F (i.e. $T_h, n, s, \kappa, \Delta p/\sigma_i, C_c/C_k, m$) as $x_1, x_2, \ldots, x_n$, the partial derivative of U with respect to the variable x_i, i.e. $\partial U/\partial x_i$, can be obtained and the influence of each variable on U can be assessed:

$$\alpha_i = \frac{\partial U/\partial x_i}{\sqrt{\sum_{i=1}^{n} (\partial U/\partial x_i)^2}} \qquad (2)$$

This was done for all of the aforementioned models, assigning $d = (1.1, 1.6, 2.1)$ metres and for values of t resulting in assessments of U ranging from 0 to 1. In addition, the uncertainties in the assessments of U (expressed as the variance, Var_U) were evaluated. In these analyses, the variables c_h, s, κ and C_c/C_k were treated stochastically, while the other variables were assumed to be deterministic, and the variances in the four variables were propagated through Eq. 1 via second order Taylor series approximations (e.g. Fenton and Griffiths, 2008 pp. 30-31). The contribution to Var_U from each variable was then assessed as (e.g. Christian et al. 1994):

$$dVar_{U,i} = \frac{(\partial U/\partial x_i)^2 Var_i}{\sum_{i=1}^{n} [(\partial U/\partial x_i)^2 Var_i]} \qquad (3)$$

Values assigned to the variables adopted in the analyses are presented in Table 2.

2 RESULTS

2.1 *Assessments of U from the six models*

In Figure 2, the degrees of consolidation U assessed from the six models are presented as a function of t for the three values

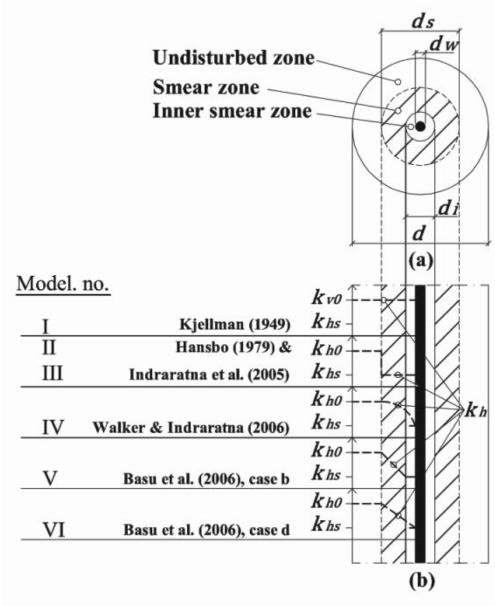

Figure 1. a) Plan view of the unit cell; b) Vertical section of the unit cell and illustration of the analytical models investigated.

of d. In the figure, a span representing two standard deviations (SD), i.e. $2 \times \sqrt{Var_U}$, is presented for d =1.1 m. The appearance is similar for the other two values of d. The curves plot at a close distance and well within the span of 2xSD for the respective values of d, i.e the uncertainties in the variables had a greater impact on the assessed value of U than the choice of model.

Table 2. Values assigned to the variables in the analyses, μ is the average value and COV is the coefficient of variation

Variable	μ_i	COV_i	*Comment*
c_h	5x10^{-8} m^2/s ^{A}	0.35	μ considered representative for soft clays and COV chosen based on Lumb (1974)
d_w	0.066 m ^{B}	Det.	Rectangular PVD 0.003 m x 0.1 m
d_m/d_w	1.7 ^{B}	Det.	Rectangular mandrel 0.06 m x 0.12 m
d_s/d_m	4.7	0.34	^{C}
s	8	0.34	$s = d_m/d_w \times d_s/d_m$
κ	1.6	0.34	^{C}
$\Delta p/\sigma_i$	2	Det.	Arbitrary chosen
C_c/C_k	0.75	0.34^{D}	μ arbitrary chosen
m	2	Det.	^{C}

^{A} *5x10^{-8}/1.5=3.3x10^{-8} m^2/s for model I*

^{B} *Equivalent diameter evaluated as proposed by Hansbo (1979)*

^{C} *μ and COV evaluated from the cited laboratory tests*

^{D} *$COV_{Cc/Ck} = \sqrt{COV_{Cc}^2 + COV_{Ck}^2}$ where COV_{Cc} =0.3 (Lumb 1974) and COV_{Ck} =0.15 (from compilation in Müller and Larsson 2012)*

2.2 *The influences of the variables on the assessments of U*

The influences of the variables T_h and κ (Eq. 2) are shown vs. assessed values of U in Figure 3 for d =1.6 metres. The appearance is similar for the other two values of d. In models I, II, IV, V and VI, the influences of the other variables were <0.045 for all values on U. However, formodel III, the influences of $\Delta p/\sigma_i$ and C_c/C_k were equal to that of κ, so that the curves for $\alpha_{\Delta p/\sigma i}$ and $\alpha_{Cc/Ck}$ coincide with the curve for α_κ (the short-dashed curve). Model I was excluded from this figure, as α_{Th} was equal to 1 for all values of U. In the figure, it can be seen that α_{Th} >0.8 for U <0.8, whereafter α_{Th} decreases rapidly and α_κ (and in case III also $\alpha_{\Delta p/\sigma i}$ and $\alpha_{Cc/Ck}$) become progressively more influential.

2.3 *The variables' contribution to Var_U*

In Figure 4, the relative influences of the four variables treated stochastically on Var_U are shown for d =1.6 metres. The appearance is similar for the other two values of d. It can be seen that $Var_{U,Th}$ contributes more than 50% to Var_U in all the analyses, that $Var_{U,\kappa}$ accounts for most of the remainder and that the contributions from s and C_c/C_k are smaller.

3 DISCUSSION

3.1 *Values on the variables*

The values assigned to the variables in the analyses were chosen by the present authors based on suggestions in the literature and are considered to be representative for soft clays. In the framework of this study (results not presented), μ for the variables were varied within reasonable ranges one at a time rendering a similar appearance in the results to that presented. Other combinations of the variables might render results that deviate from the results presented here, but it is the authors' belief that the appearance of the results is typical for most cases.

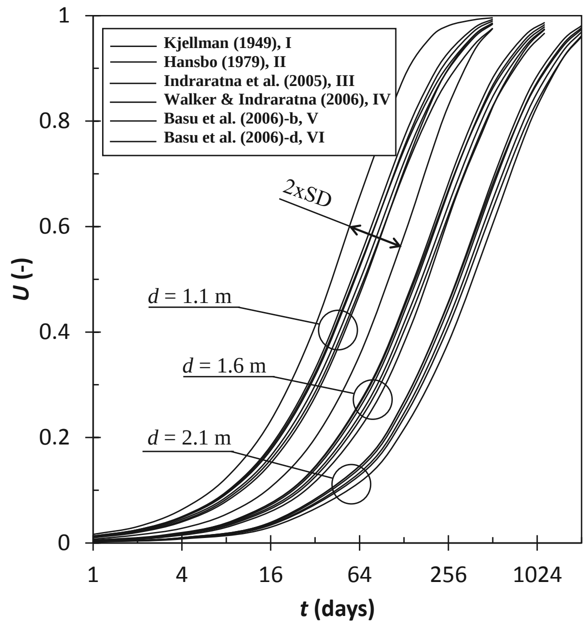

Figure 2. U assessed via the six models for different values of d.

3.2 *The assessed U and the influences of the variables*

As seen in Figure 2, model I followed by model II were the most conservative, predicting the slowest consolidation rate. Comparing the formulations for F in model II with those in models IV-VI (Figure 1b and Table 1), this is obvious since model II assigns a constant value of k_h over d_s whereas k_h is successively increased in the other three models. In this context, it should be noted that model III gives lower values of U than model II at corresponding t for C_c/C_k >1 (0.75 in this study). The finding that model I was the most conservative emphasises the relative importance of c_h compared to the modelling of the smear zone. Model I does not take the smear zone into account but adopts c_v instead of c_h (c_v was assumed to be 1.5 times less than c_h in this study). The relative importance of c_h is also shown in Figure 3 where α_{Th} predominates in the assessment of U for all but the last parts of the consolidation sequences.

The significance of (re)consolidation effects and the associated decrease in k_h (incorporated in model III) is confirmed by the results of laboratory oedometer tests presented by Indraratna and Redana (1998), Sharma and Xiao (2000) and Sathananthan and Indraratna (2006). The results presented in their studies suggest that the resulting decrease in void ratio when the consolidation stresses are increased by 25-50 kPa lead to a more pronounced decrease in k_h than the disturbance induced by the installation process. Hence, in most cases it is more important to consider the change in k_h that occurs due to the decrease in void ratio during consolidation than the disturbance effects.

3.3 *The uncertainty in U*

To reduce the uncertainty in the assessment of U via any of the investigated models, it is obvious that attention should be directed primarily towards c_h, since the uncertainty in T_h is dependent on Var_{ch} via $Var_{Th} = Var_{ch} \times t^2/d^4$, and secondarily towards κ (Figure 4). Hence, site investigations intended for the design of PVDs should focus on reducing the level of uncertainty in c_h and possibly the degree of disturbance in the smear zone (i.e. κ).

In ordinary engineering projects involving clay, investigations of c_v (e.g. via oedometer tests) are far more frequent than investigations of c_h and it might therefore be worth considering model I. However, if model I is used for design purposes, care must be taken as c_v is used instead of c_h

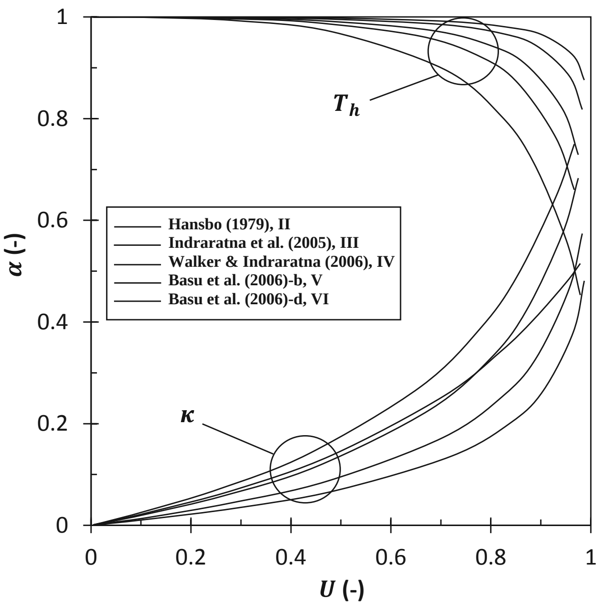

Figure 3. The influence on U of T_h and κ for d =1.6 metres.

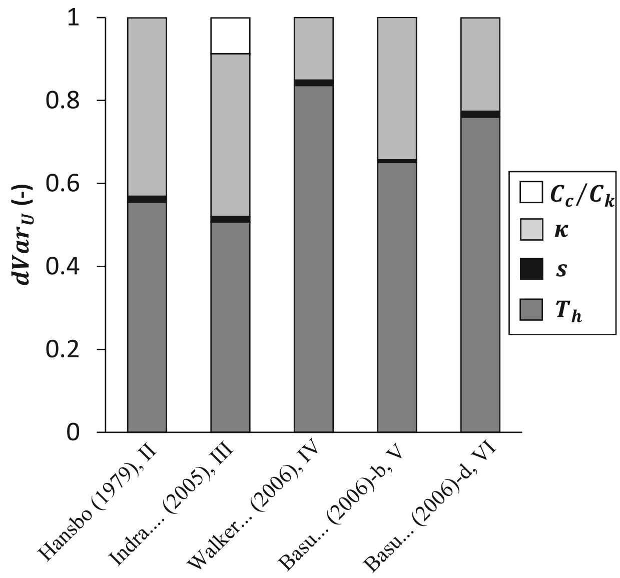

Figure 4. The contribution to Var_U of the variances in T_h, s, κ and C_c/C_k.

and the results are therefore highly dependent on the permeability anisotropy in the clay of interest. For instance, if $k_h \approx k_v$, the consolidation rate might be overestimated.

4 CONCLUSION

Although they may capture the nature of the smear zone more realistically, the impacts on the assessment of U of the more complex models (III-VI) rather than model II are insignificant under the assumptions made in this study and, as argued by Onoue et al. (1991) and Hird and Moseley (2000), model II (Hansbo 1979) is still useful for practical engineering purposes due to its simplicity. This study shows that the even more simple model suggested by Kjellman (1949), neglecting the smear zone but adopting c_v instead of c_h, might give satisfactory results. Care should however be taken, as assessments using this model are dependent on the permeability anisotropy in the clay of interest.

It is the authors' opinion that it is more important to put an effort into reducing the uncertainty in c_h (or c_v for use in model I) than trying to investigate s and m in ordinary engineering projects. It is also important to consider the change in c_h that occurs as a result of the decrease in void ratio as consolidation of the clay proceeds (e.g. via model III).

5 ACKNOWLEDGEMENTS

The Tyréns Foundation is acknowledged for funding this study.

6 REFERENCES

Barron R.A. 1948. Consolidation of fine grained soils by drain wells. *Transactions of ASCE* 113, 718-742. Reprinted in: A history of progress, ASCE, Reston, 1, 2003, 324-348.

Basu D., Basu P. and Prezzi M. 2006. Analytical solutions for consolidation aided by vertical drains. *Geomechanics and Geoengineering: An International Journal* 1 (1), 63-71.

Bergado D.T., Asakami H., Alfaro M.C. and Balasubramaniam A.S. 1991. Smear effects of vertical drains on soft Bangkok clay. *Journal of Geotechnical Engineering* 117 (10), 1509-1530.

Christian J.T., Ladd C.C. and Beacher G.B. 1994. Reliability applied to slope stability analysis. *Journal of Geotechnical Engineering* 120 (12), 2180-2207.

Chung S.G., Lee N.K. and Kim S.R. 2009. Hyperbolic method for prediction of prefabricated vertical drains performance. *Journal of Geotechnical and Geoenvironmental Engineering* 135 (10), 1519-1528.

Fenton G.A. and Griffiths D.V. 2008. *Risk Assessment in Geotechnical Engineering*. Wiley, Hoboken, NJ, USA.

Hansbo S. 1979. Consolidation of clay by band-shaped prefabricated drains. *Ground Engineering* 12 (5), 16-25.

Hird C.C. and Moseley V.J. 2000. Model study of seepage in smear zones around vertical drains in layered soils. *Géotechnique* 50 (1), 89-97.

Indraratna B. and Redana I.W. 1998. Laboratory determination o smear zone due to vertical drain installation. *Journal of Geotechnical and Geoenvironmental Engineering* 124 (2), 180-184.

Indraratna B., Rujikiatkamjorn C. and Sathananthan I. 2005. Radial consolidation of clay using compressibility indices and varying horizontal permeability. *Canadian Geotechnical Journal* 42 (5), 1330-1341.

Kjellman W. 1949. *Record of the activities at the Swedish Geotechnical Insitute 1944-1948*. Swedish Geotechnical Institute, Stockholm.

Lumb P. 1974. *Application of statistics in soil mechanics*. A memorial collection of selected papers and memoir of Professor Peter Lumb. Ed: Yeung A, p. 507. University of Hong Kong, Hong Kong.

Madhav M.R., Park Y-M. and Miura N. 1993. Modelling and study of smear zones around band shaped drains. *Soils and Foundations* 33 (4), 135-147.

Müller R. and Larsson S. 2012. Hydraulic conductivity and coefficient of consolidation of two sulphide clays in Sweden. *Geotechnical and Geological Engineering* 30 (1), 173-186.

Onoue A., Ting N., Germaine J.T., and Whitman R.V. 1991. Permeability of disturbed zone around vertical drains. *ASCE Geotechnical Special Publication* 27, 879-890.

Sathananthan I. and Indraratna B. 2006. Laboratory evaluation of smear zone and correlation between permeability and moisture content. *Journal of Geotechnical and Geoenvironmental Engineering* 132 (7), 942-945.

Sharma J.S. and Xiao D. 2000. Characterization of a smear zone around vertical drains by large-scale laboratory tests. *Canadian Geotechnical Journal* 37 (6), 1265-1271.

Tavenas F., Leblond P., Jean P. and Leroueil S. 1983. The permeability of natural soft clays. Part II: Permeability characteristics. *Canadian Geotechnical Journal* 20 (4), 645-660.

Walker R. and Indraratna B. 2006. Vertical drain consolidation with parabolic distribution of permeability in smear zone. *Journal of Geotechnical and Geoenvironmental Engineering* 132 (2), 937-941.

Walker R., Indraratna B. and Rujikiatkamjorn C. 2012. Vertical drain consolidation with non-Darcian flow and void-ratio-dependent compressibility and permeability. *Géotechnique* 50 (1), 89-97.

A Review of Geogrid Working Platform in Soft Ground in Malaysia

Analyse du comportement de plateformes renforcées par géogilles en Malaisie

Ooi T.A.
TAO Consult Sdn Bhd, Kuala Lumpur, Malaysia

Tee C.H., Chan C.B.
Mega Geoproducts And Services Sdn Bhd, Kuala Lumpur, Malaysia

Ong R.
Tensar International Ltd, Malaysia Regional Office, Petaling Jaya, Malaysia

ABSTRACT: This paper discusses the development of geogrid applications in soft ground in Malaysia. The Sungei Way trial during 1984 was conducted to assess the performance of geogrid in road pavement field trial conditions and a forerunner to the use of geogrid in working platform on soft grounds in Malaysia. Two layer biaxial geogrids system was first used in 1987 to rehabilitate an offshore fabrication yard in Pasir Gudang in Johor in Malaysia. Recently. geocell mattress and mechanically stabilised layer (MSL) formed with TriAx geogrids were used in offshore fabrication yard in Vung Tau in Vietnam. Similar concept was then adopted for a container yard in Gebeng, Kuantan in Malaysia constructed in 2011. The settlement performances of all heavy duty working platform reinforced with biaxial and TriAx geogrids with geocells were all satisfactory.

RÉSUMÉ: Cet article présente le développement d'applications des géogrilles en terrain meuble en Malaisie. Des essais à Sungei Way ont été effectués au cours de l'année 1984 pour évaluer la performance d'une géogrille lors de la construction d'un revêtement routier dans des conditions in-situ. C'est le test précurseur pour l'utilisation de géogrilles en plateforme de travail sur sols mous en Malaisie. Un système de géogrilles biaxiales à deux couches a été utilisé pour la première fois en 1987 pour réhabiliter le chantier de fabrication offshore de Pasir Gudang à Johor en Malaisie. Récemment, un matelas geocellulaire et une couche stabilisée mécaniquement (MSL) formée par des géogrilles TriAx ont été employés dans le chantier de fabrication offshore de Vung Tau au Vietnam. Un concept similaire a ensuite été adopté dans un chantier de conteneurs construit à Gebeng (Kuantan, Malaisie) en 2011. Les performances de comportement des plateformes d'ouvrages lourds renforcées par des géogrilles biaxiales et TriAx avec géocellules ont toutes été satisfaisantes.

KEYWORDS: geogrids, working platform, soft grounds, reinforcement, road pavement, ground stabilisation.

1. INTRODUCTION

This paper discusses the development of geogrid in soft ground in Malaysia. The Sungei Way trial during 1984 was conducted to assess the performance of geogrid in road pavement field trial conditions (Ooi et al., 2004). The results of the Sungei Way trial were verified by the more rigorous Transport Research Laboratory (TRL) full scale laboratory trials (Chaddock, 1988). Based on the results of the full scale trials, it was concluded that punched and stretched biaxial geogrids (i.e., stiff biaxial geogrids) in granular base or subbase is effective in achieving the following results: -

a) Interaction by interlocking between the geogrid and the granular material is mobilised with minimal deformation of the geogrid;
b) Tensile strains and deformations in subgrade are minimised;
c) Interlock provided by the geogrids confines the granular materials and minimises their lateral displacement; and
d) Reduction in rut depth for similar pavement life.

The trials have shown the physical form of geogrid (e.g., rib thickness, stiffness and shape, aperture size, rigidity and stability, junction strength and secant modulus at low strain as subsequently reported by Webster (1992)) and its ability to interlock effectively have major effect on performance of the mechanically stabilised layer (i.e., soils stabilised with geogrids). The important findings arose out of the full scale trial on the benefits of using stiff biaxial geogrid in the road pavement led to the construction of loading platform using geogrid to overcome the deformation and rutting of platform surfaces during service. In particular, the deterioration of platform surfaces caused by ground softening as a result of ponding of water on the platform of offshore fabrication yard during rainfall season. In ground stabilisation, especially for working platforms, the loading applied to the geogrid is multi-directional. A geogrid that can offer the properties of stiff biaxial geogrids and possess near-uniform tensile stiffness in all radial directions would be best suited for such application. Watts and Jenner (2008) conducted as series of large-scale laboratory load tests to assess the effectiveness of geogrids to stabilise granular working platforms and concluded the use of geogrids will significantly increase the bearing capacity of working platforms. The research also shows that triaxial geogrid with near-uniform tensile stiffness in the radial sense (i.e., TriAx) outperformed the biaxial geogrid and almost doubled the bearing capacity offered by the un-stabilised granular blanket of similar thickness.

Apart from using multiple layer of geogrids to stabilise granular material in working platform application, geocell mattresses are also used in some cases. Geocell mattress is a series of interlocking cells formed using stiff polymer geogrid reinforcement to contain and confine granular material providing stiff and rough foundation to an embankment that maximises the bearing capacity of the soft soil beneath it. Jenner et al. (1988) used the slip line fields to assess the improvement in bearing capacity of soft ground under geocell mattress installed at the base of an embankment. This provided a useful analytical method of assessing the horizontal stresses in the geogrid elements.

In Malaysia, the first loading platform using mechanically stabilised layer (MSL) for the fabrication yard to use geogrid was in Pasir Gudang, Johor in 1987 (Figure 1). Two layers of stiff biaxial geogrids were used to stabilise a metre thick of compacted quarry waste layer that form the top portion of the loading platform. During lifting operation the crawler crane track can exert contact pressure of up to 500 kPa (Yong et al., 1990, Chan, 2000, Ooi et al., 2004). Many similar loading platforms were built later. Recently, MSL has been combined with geocell mattress for the construction of a heavy duty working platform over soft soil in Vung Tau in Vietnam using one metre thick of geocell mattress to support a two metre thick MSL as a loading platform for the heavy crawler crane exerting a contact pressure of 500 kPa (Ong et al., 2011). The two loading platform performances are compared and it is found that both loading platforms performed satisfactorily with settlement of less than 50 mm. In 2011, geocell mattress and MSL were used in another project on soft ground for a container yard in Gebeng, Kuantan in Malaysia. In this case one metre thick of geocell mattress were used to support the container pavement of 760 mm thick aggregate base course stabilised with two layers of TriAx geogrid (MSL) and interlocking paving block finishes.

Figure 1. General condition of working platform without gegorids. (after Yong, Chan et al., 1990)

2 PASIR GUDANG FABRICATION YARD

The rehabilitation of the muddy platform started by removing the top 700 mm of residual soil fill (Figure 2). One layer of the biaxial geogrid was then placed on top of the compacted clay fill at excavated level. Backfilling using compacted quarry waste, a granular material, carried out after suitable subsoil drains were laid (Figure 3). Another layer of biaxial geogrid was placed before filling with compacted quarry waste for a further 300 mm.

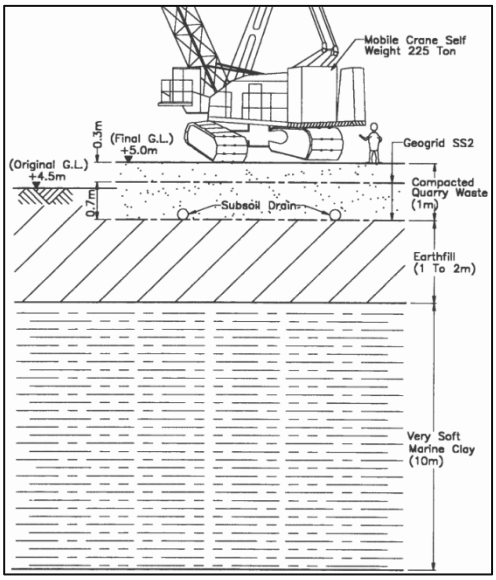

Figure 2. Schematic section of rehabilitated working platform. (after Chan, 2000)

The completed platform formation was tested and at 30 passes of the 2.3 MN crawler crane carrying 700 kN load and the resulting deformation measured was 37 mm (Chan, 2000), with decreasing rate of deformation after each pass, which was acceptable by the fabricator. Settlements on the subgrade and outside the crane track were measured (Figures 4 & 5). The rehabilitated fabrication yard was in use after handing over to the fabricator (Figure 6).

Figure 3. Platform rehabilitation work in progress. (after Yong, Chan et al., 1990)

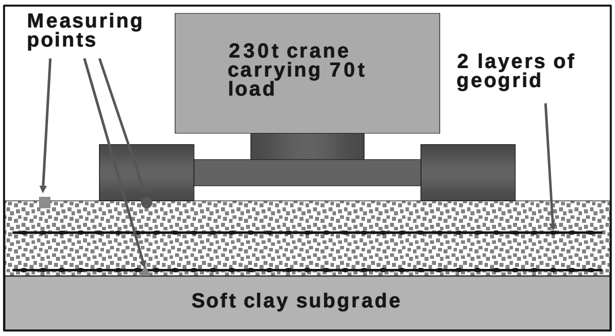

Figure 4. Settlement measuring points.

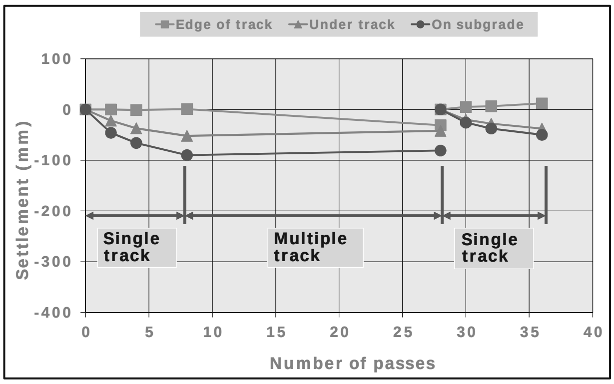

Figure 5. Plot of settlement versus number of passes.

3 WORKING PLATFORM IN VUNG TAU

In Vietnam, the geocell mattress with MSL was adopted for the construction of the working platform for an offshore facilities fabrication yard in Vung Tau, Vietnam (Ong et al., 2011). The working platform was required to take loading from heavy crawler crane tracks up to 50 t/m². The exhibited design uses conventional reinforced concrete pile-raft foundation system to support the working platform. However, in order to accelerate the construction works, alternative solutions using geocell mattress with MSL was selected not only will it reduce the construction time but also being more economic and sustainable. This geocell mattress with MSL was designed to form a working platform to support the movement of crawler cranes with 2 m wide and 13.7 m long crane tracks separated by a clear distance of 7.6 m. The maximum load to be supported on each track area is up to 50 t/m². The foundation soil is 10 m thick soft bluish clay with an average undrained shear strength of 23 kPa from vane shear test results.

Figure 6. Rehabilitated fabrication yard in use.

In the calculations, the angle of load spread for the fill material reinforced with TriAx geogrid within the MSL is taken to be 1 vertical to 1 horizontal (i.e., 1V:1H) whereby the load distribution through the geocell mattress was taken as 1 vertical to 2 horizontal (i.e., 1V:2H) to model the very stiff nature of the construction (Figure 7).

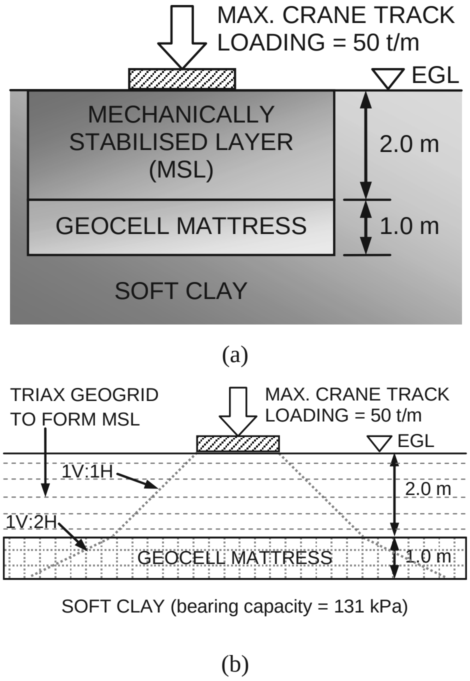

Figure 7. Geocell mattress and MSL platform (after Ong et al., 2011)

Five layers of TriAx geogrids were used to form the 2 m thick MSL. Stiff uniaxial geogrids were used to form the interlocking cells of the 1 m thick geocell mattress and a layer of TriAx geogrid was placed at the base. The aggregate to be used as backfill material for the MSL and geocell mattress was specified as well graded granular material with particle size less than 75 mm. Full scale plate bearing test (PBT) was conducted to ascertain the performance of the geocell mattress in meeting the acceptance criterion (i.e., total settlement less than 100 mm under loading of 50 t/m²). The loading on the steel plate was increase in six steps: 10 t/m², 20 t/m², 30 t/m², 40 t/m², 50 t/m² and 60 t/m². Settlement versus applied load and settlement versus time were plotted. It was found that the specified settlement requirement was satisfied with total settlement of 41 mm under 60 t/m² load.

4 CONTAINER YARD IN GEBENG, KUANTAN

In this project, a working platform in the form of container yard was built on soft subgrade with California bearing ratio (CBR) of 1% to 2%. The container yard was designed to support the following loadings:

- 6 m by 2.4 m container with maximum weight of 30 tonnes. Maximum staking of containers was 2 containers.
- Container handler machine with maximum axle load of 105 tonnes. Therefore maximum wheel load of 525 kN including dynamic factors.
- Total number passes of the container handler machine was designed as 250,000 during service life.

The terms of reference are:

- To reduce thickness of unbound granular layer platform.
- To mitigate differential settlement.
- To provide stable storage area and to increase load spread using geocell mattress and mechanically stabilised layer (MSL) with TriAx geogrids.

The analysis conducted indicated that the loadings from the trafficking movement due to container staker would be more critical than the static loadings due to the staking of 2 containers. Thus, the requirement for total platform thickness was assessed based on heavy duty pavement design (Knapton, 2008). By using geocell mattress and MSL, the thickness of granular fill required to construct the container yard has been reduced up to 810 mm. This resulted in substantial savings in terms of construction time and cost.

For the heavy duty pavement construction of the container yard, 1 m high geocell mattress was placed on one layer of TriAx geogrid at subgrade level. The geocell mattress is to provide a firm and relatively rigid platform with a perfectly rough interface between the mattress and the soft foundation. This stiff platform is created by the high tensile strength of polymer grid material used in the cellular construction to confine the granular fill which enables an even distribution of load onto the foundation. On top of the geocell mattress is MSL of 500 mm to 750 mm compacted well graded granular fill with 3 layers of TriAx geogrids. Granular layers reinforced with TriAx geogrids perform as composite due to the interlock phenomenon. The configuration of the geogrid ribs and the integral junctions provide lateral restraint to the aggregate particles as they partially penetrate the apertures by a process of interlock. This interlock effectively stiffens the aggregate and enables any imposed load to be distributed over a wider area. The container platform was finished with interlocking paving blocks. The construction of the container yard is expeditious starting from placement of TriAx geogrids, forming of geocells, filling with granular materials according to prescribed grading envelope, construction of MSL geogrid reinforced layers and installation of the paving blocks (Figures 8 to 12).

5 DISCUSSION AND CONCLUSION

Comparison is made in the pavement details and settlement performance of the working platform (Table 1). From Table 1 it can be seen that all the 3 platforms consist of soft clay layer of thickness varying from 4.5 m to 10 m. The crane track pressure exerted on the working platform was up to 500 kPa and axle load exerted by the reach stacker on the working platform is 105 tonnes. Granular fill of varying thicknesses were used in all three working platforms. It appears that MSL constructed using biaxial and TriAx geogrids with granular fill with or without geocell mattress performed satisfactorily in terms of platform settlement performances to support the heavily loaded crawler crane or stacker machine for the fabrication or container yard.

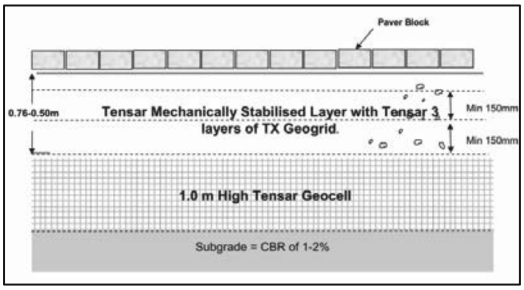

Figure 8. Typical section of proposed pavement

Figure 9. Laying of TriAx geogrids

Figure 10. Install diaphragm with Tensar uniaxial gegorid and filling of geocells with granular materials.

Figure 11. Construction of MSL with granular materials.

Figure 12. Placement of interlocking paving blocks.

Table 1. Comparison of the working platforms

	Pasir Gudang, Johor	**Vung Tau, Vietnam**	**Gebeng, Kuantan**
Subsoils	10 m soft clay	10 m soft clay	4.5 m soft clay
Working Platform	Fabrication Yard	Fabrication Yard	Container Yard
Handling Equipment	Crawler Crane (250T)	Crawler Crane (track pressure $50t/m^2$)	Reach Stacker (105T axle load)
Pavement Details	1m thick quarry waste	1 m high geocell; 2 m thick MSL with TriAx	1 m high geocell; 500-750 mm thick MSL with TriAx
Geogrids	2 layers SS2	5 layers TriAx	3 layers TriAx
Granular Materials	Quarry Waste	75mm down aggregates	75mm down aggregates
CBR	2%	1%	1%-2%
Settlement	< 40 mm	< 100 mm	Recipe design

REFERENCES

Chaddock, B. C. J. 1988. Deformation of road foundations with geogrid reinforcement, *TRL Research Report 140*.

Chan, S.F. 2000. Reinforced soil structures using geogrids. *Proceedings 2nd Asian Geosynthetics Conference*, Kuala Lumpur. 1, 95-110.

Jenner, C.G., Bassett, R.H. & Bush, D.I. 1988. The use of slip line fields to assess improvement in bearing capacity of soft ground by a cellular foundation mattress installed at the base of an embankment. *Proc. Int. Geotech. Symp. on Theory and Practice of Earth Reinforcement*, October, Fukuoka, Japan, 209–214.

Knapton, J. 2008. The structural design of heavy duty pavements for ports and other industries, Edition 4, *Interpave*, Precast Concrete Paving and Kerb Association.

Ong, R., Song, W.K., Tran, N.M., Pham, X.T. 2011. Geocell mattress for heavy duty working platform over soft soil. *Proc. Geotec Hanoi 2011 Conference*, Hanoi, Vietnam.

Ooi, T. A., Tee C. H. & Dobie, M. 2004. Some Malaysian experiences in the application of geosynthetics in soft ground. *Proc. 15th Southeast Asian Geotechnical Society Conference*, Bangkok. 486-492.

Watts, K. and Jenner, C. G. 2008, Large-scale laboratory assessment of geogrids to reinforce granular working platforms, *Proc. EuroGeo4*, Scotland, Paper #222.

Webster, S.L. 1992. Geogrid reinforced base course for flexible pavements for light aircraft: test section construction, behavior under traffic, laboratory tests and design criteria, *Report Number DOT/FAA/RD-92/25*, US Army Corps of Engineers.

Yong, K. Y., Chan, S. F. & Lee, K. K. 1990. Reinforced soil working platform for offshore jacket fabrication yard. *Proc. 4th International Conference on Geotextiles, Geomembranes and Related Products*, The Hague. 223-226.

Container Terminal on Soft Soil

Terminal de conteneurs sur un sol mou

Popovic N., Stanic B.
OpusGEOd.o.o., Zagreb, Croatia

ABSTRACT: This paper analyzes soil - structure interaction and effectiveness of soil improvement through the back- analyses based on measurements conducted on the example of a new container terminal in the port of Ploce. The terminal was built on part of the Neretva River delta, which is dominated by Quaternary sediments represented by delta deposits over 100 m thick, accumulated over carbonates. Coastal construction is based on bored vertical reinforced concrete piles and hammered steel battered piles. Storage areas (fibre-reinforced concrete slabs) are located behind the coastal structure, and they are founded on soil improved by vibrated stone columns. Construction of container terminal was divided into four main phases. Each phase of the project is analyzed through interactive collaboration of construction designers and geotechnical designers. The applied measurement system consisted of geodetic and geotechnical measurements - geodetic points, vertical inclinometers-deformeters in the vertical piles, horizontal inclinometers, vertical deformeters, tiltmeters and load testing of piles. Works were success fully completed and verified by test loads.

RÉSUMÉ : Cet article analyse l'interaction sol – structure et l'efficacité de l'amélioration des sols en utilisant une analyse en retour, basée sur des mesures effectuées sur le cas du nouveau terminal à conteneurs du port de Ploče. Ce terminal a été construit sur une partie du delta du fleuve Neretva dont le sous-sol est constitué par des sédiments quaternaires formés des dépôts deltaïques de 100 mètres d'épaisseur, surmontant une base calcaire. La construction repose sur des pieux forés en béton armé et des pieux en acier inclinés. La zone de stockage des conteneurs du terminal (dallage de béton renforcé de fibres), située en retrait des constructions côtières, est construite sur les colonnes ballastées. La construction du terminal à conteneurs a été divisée en quatre grandes phases. Chaque phase du projet est analysée grâce à la collaboration entre les ingénieurs de génie civil et les ingénieurs en géotechnique. Le système de mesures utilisé comportait des mesures géodésiques et géotechniques : points de contrôle géodésiques, tassomètres et inclinomètres dans les pieux verticaux, inclinomètres horizontaux, tassomètres verticaux, capteurs de rotation et tests de charge des pieux. Ces travaux ont été réalisés avec succès et puis contrôlés lors de la mise en oeuvre des tests de charge.

KEYWORDS: Container terminal, soft soil, bored vertical piles, vibrated stone columns, field mesaurements, back analyses.

1 INTRODUCTION

The container terminal is located in the Port of Ploče, which is situated in a part of the large Neretva River Delta. Quaternary deposits represented by delta sediments, accumulated over limestone paleorelief dominate in this area. The thickness of Quaternary deposits exceeds 100 m. Deposits have different grain size distribution. One contrasting environment in the vertical geological profile is represented by gravels, and partly sands.

The coast for containers is a surface structure at the level +3.0 m a.s.l., of width 27.4 m and berth length of 280.0 m. The coastal structure is divided in three segments by length. The total length of coastal structure is 88.6 + 102.8 + 109.5 = 300.9 m. The coast is 15.1 m in depth, for vessels of bearing capacity up to 60,000 DWT and draught of 13.5 m. The coastal structure is founded on drilled reinforced-concrete vertical piles (Benoto) of nominal diameter 1,500 mm, and on hammered steel battered piles of diameter 812.8 mm. Vertical piles end in a layer of gravel at the depth of -44 m a.s.l. They are made in single sided formwork from -20 to -44 m or double sided steel formwork down to the depth –20.0 m. Axial distance of piles in longitudinal direction is 7.1 m and in the transversal 8.0 m (four pile rows along coast width).

Storage and traffic surfaces are located behind the coastal structure. Pavement structure consists of fibre-reinforced concrete slabs which are founded on soil improved by stone columns. Stone columns are of 110 cm diameter on a grid 2x2 m to 2.8x2.8 m, of depth down to -15 m a.s.l., i.e. -20 m a.s.l.

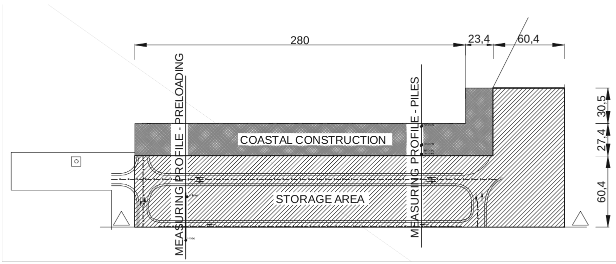

Figure 1 Plan view of the container terminal.

As a part of site investigations, a total of 27 CPT probes were made and 7 boreholes on an area of 15 ha. The lengths of CPT probes range from 22 m to 43 m, while the lengths of boreholes were from 42 m to 58 m. Out of in-situ testing in boreholes, vane tests and standard penetration tests were performed. Laboratory tests included the following: testing of grain size distribution, direct shear test, consolidated undrainedtriaxial test, etc.

2 GEOTECHNICAL SOIL PROFILE

Through implementation of geotechnical investigations and laboratory tests, the following geotechnical soil profile in the area of the container terminal was established:

- Surface layer is represented by siltysand and low plasticity silt, of thickness 8 m.
- Under the surface layer, clays of low to high plasticity dominate. This layer is 25 m thick.
- Low plasticity silt to sand, poorly graded.
- Well-compacted gravel of layer thickness 10m.
- Gray to gray-green clay of stiff consistency.

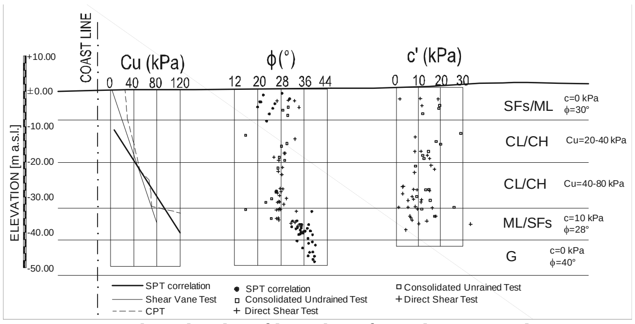

Figure 2 Geotechnical soil profile with performed in-situ exploratory works and laboratory tests.

3 MEASURMENTS AND CONSTRUCTION PHASES

Terminal construction was divided into four main phases: execution of vibrated stone columns and preloading in the storage area, execution of piles from the coast on previously prepared terrain, excavation and underwater embankments, and construction of the coastal structure.

There are two zones of execution in stone columns: dense (triangular grid 2x2m) and sparse improvement (square grid 2.8x2.8m). Dense soil improvement was carried out down to -8m a.s.l. Sparse improvement was performed down to -15m a.s.l. i.e. -20m a.s.l. in such a way that every other column of dense improvement is extended down to the required depth. The role of stone columns is to provide global stability, and settlement reduction and acceleration.

Because of terminal construction dynamics, pre-loading of storage areas was, due to limitations of material for preloading, performed independent of phases, on the condition that they are executed before the execution of coastal structure. Preloading was executed in three segments (fields).

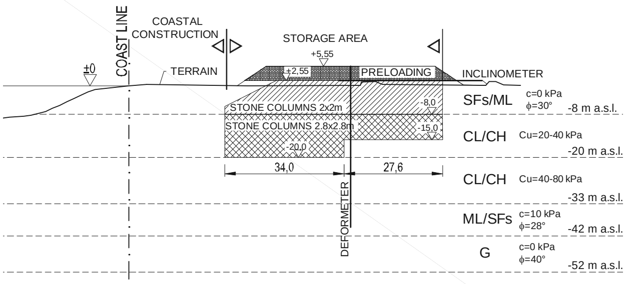

Figure 3 Construction phase I: improvement of foundation soil with stone columns and pre-loading in the area of storage and traffic surfaces.

Each construction phase was monitored through geotechnical and geodetic measurements. Geotechnical measurements in the area of storage and traffic surfaces consisted of measuring vertical displacements by horizontal inclinometers, and settlement measurements by layers using vertical deformeter (see Figure 3). A net of geodetic points was placed on the top of pre-load.

Pre-loading was performed in three fields, in such a way that the material was transferred from one field to another. Settlement of the first field was measured by horizontal inclinometer and vertical deformeter, and with a net of geodetic points 12x12 m. Measurements showed the settlement of 70 cm in the period of 105 days, and they are shown on Figure 4. The difference in settlement between the inclinometer and deformeter is caused by the fact that the deformeter's reference point is at 44 m and underneath it there are compressible layers which could not be followed by the deformeter.

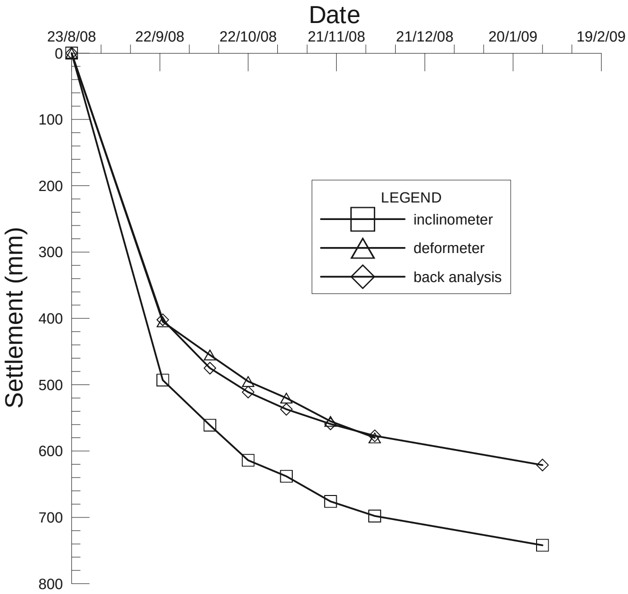

Figure 4.Inclinometer and deformeter settlement measurements together with the settlement curve obtained by back analyses in the first field of preloading.

The requirement for duration of preloading of 90 days was obtained by analysing the consolidation curve. For the other two fields, the same preloading duration requirement was set.

Settlement measurements in the second and third field were performed on geodetic points. Measurements in the second field have shown settlement of 30 cm, and in the third of 50 cm. The reason for smaller measured settlement is longer time of placing pre-loading, and the fact that the reference measurements were performed only after preloading was completed.

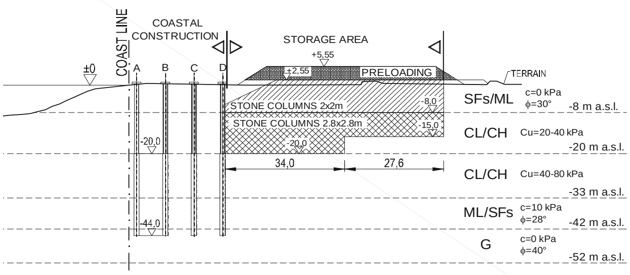

Figure 5 Construction phase II: execution of piles from the coast on previously prepared terrain.

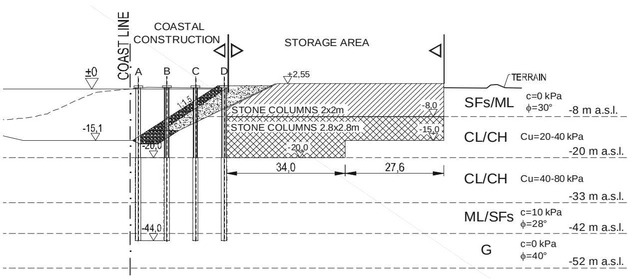

Figure 6 Construction phase III: undersea excavation and execution of undersea embankment.

Geotechnical measurements on the coastal structure consisted of measurements in vertical inclinometers-deformeters inside the pile. Measuring equipment was installed in one profile, so that one vertical inclinometer-deformeter was placed in tensile zones of each of piles A and C. In pile D, two vertical inclinometers-deformeters were placed –one in the compressive zone and the other in the tensile zone. The tops of inclinometers-deformeters were at the same time geodetic points, whose displacements were geodetically followed. Inclinometer measurements showed displacements up to 40 cm at the top of the pile before superstructure was placed. Measurements in the phase of test load have shown minimum displacements, which are within the limits of elastic deformation of concrete.

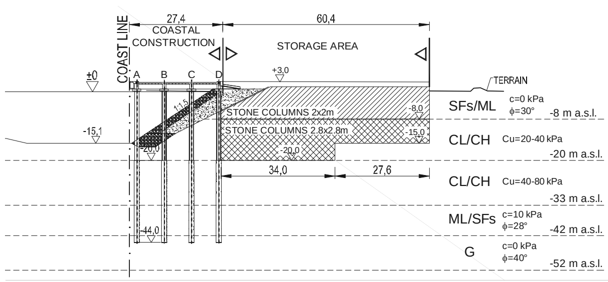

Figure 7 Construction phase IV: construction of coastal structure over piles.

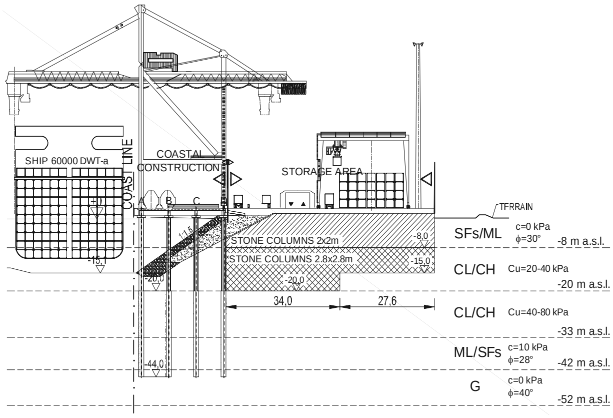

Figure 8 Use of container terminal.

4 BACK ANALYSES

Design and monitoring during construction by means of back analyses based on data obtained by measurements were carried out by the same design team. The design team was made up of designers of the coastal structure and geotechnical engineers. Soil-structure interaction was taken into account through cooperation of design teams in the design process and construction.

Based on measured data on soil settlement and pile displacement back analyses were performed. The objective of back analyses was to establish “actual” soil parameters and internal forces in the structure.

Two models were made for the implementation of back analyses. Inclinometer and deformeter measurements on storage areas through back analyses were processed in Model 1. Material parameters used in Model 2 were obtained on Model 1 based on actual displacements. In Model 2, analysis of pile displacements during terminal construction (up to phase III) was performed, as well as the comparison with measured displacements. Internal forces in piles were calculated on the model calibrated in this manner.

Since the measurements after execution of superstructure on piles and during test loading showed minimum displacements within the limits of elastic deformation of concrete, these construction phases will not be discussed in this paper.

Model 1 was made in Settle 3D software. The soil was set as a linear material through the coefficient of compressibility and vertical consolidation coefficient, and the parameters obtained by back analyses are shown in Table 1. A soil profile was made by means of deformeter measurements, which approximately describes the actual condition in the soil. Figure 9 shows the settlement curve from the vertical deformeter and the curve obtained through back analyses. The curves show soil settlement by layers after 90-day preloading period.

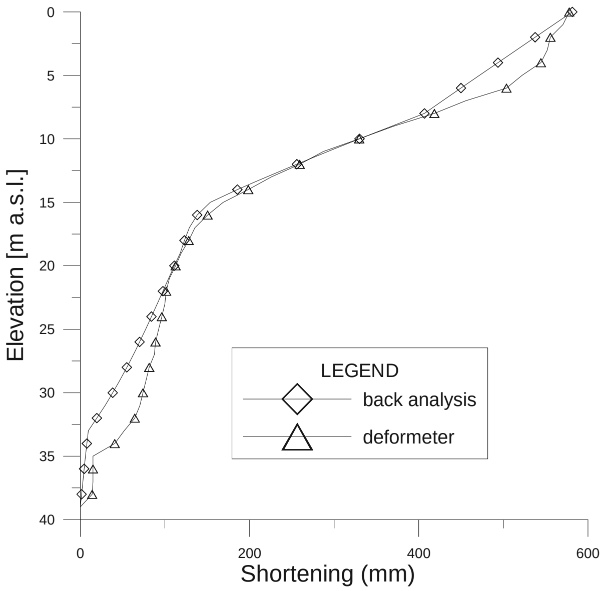

Figure 9 Soil settlement by layers in vertical deformeter, and according to back analyses after 90 days of preloading.

Table 1.Modules of compressibility and vertical consolidation coefficients for back analysis in Model 1.

Parameter / Soil	*Elev. [m]*	*Ms [MPa]*	*Cv [m²/s]*	*Ch / Cv*
SFs / ML	0 -8	4.5	$1.15 \cdot 10^{-5}$	4
CL / CH	8 -15	2.5	$3.5 \cdot 10^{-7}$	2
CL / CH	20 – 33	5	$8.1 \cdot 10^{-6}$	-
ML / SFs	33 - 39	30	$1.5 \cdot 10^{-5}$	-

Figure 10 shows the ratios of modules of compressibility assumed in the design and those obtained by back analysis. For design values, the improvement of compressibility parameters due to soil improvement by stone columns was not taken into consideration. The scope of ratios ranges from 0.625 to 1.5.

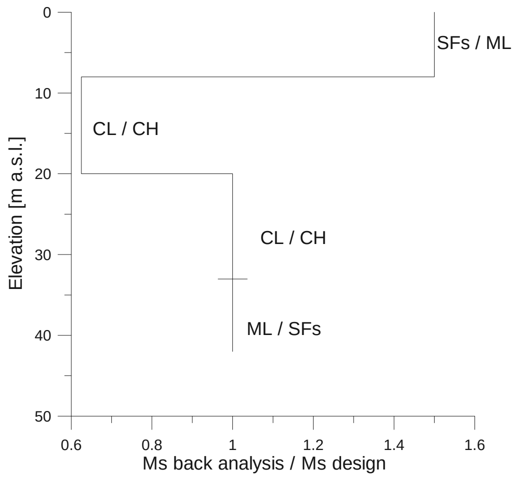

Figure 10 Ratios of modules of compressibility according to back analyses and design values.

Thus in parts where vibrated stone columns are placed in a triangular grid 2x2m, the value of soil improvement factors of 1.5 was obtained, which falls within the design assumptions. It is interesting to consider the ratio that was lower than 1, which was in the layer where stone columns were placed in a square grid 2.8x2.8m. Therefore, instead of obtaining an increase in module of compressibility due to soil improvement by stone columns, we got a decrease with respect to the design values. From there it follows that the compressibility of the CL/CH layer was overestimated in the design. Other layers according to the obtained measurement results were correctly determined in the design in terms of the modules of compressibility.

Based on the calculated parameters of compressibility from Model 1, a numerical model of finite elements was made in Plaxis 2D-Model 2. The soil was described as an isotropic elastoplastic material with linear elasticity properties until failure and by Mohr-Coulomb strength law for stresses at failure. A comparison of horizontal pile displacements before superstructure execution was carried out through the model obtained by back analysis. Also, the comparison of bending moment diagrams obtained by back analyses and on the basis of measured displacements was also carried out.

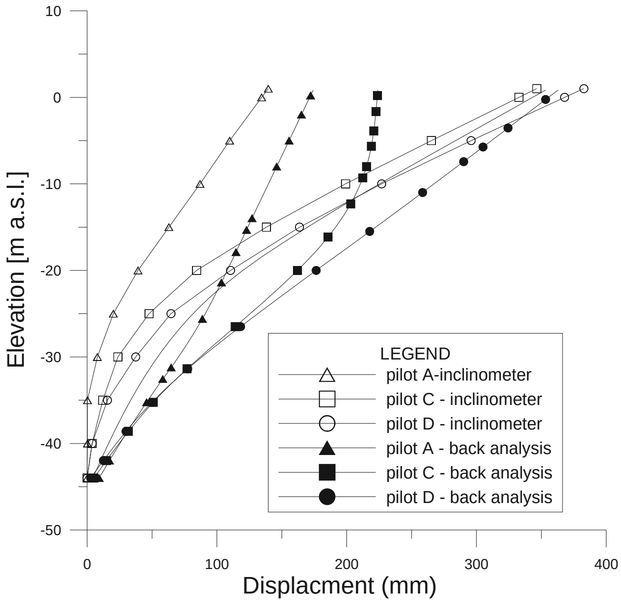

Figure 11 Horizontal displacements of piles A, B and C obtained by measurements in horizontal inclinometer and by back analysis through Model 2.

Figure 11 shows horizontal pile displacements during construction, before construction of coastal structure. Differences in horizontal displacements at the top of the piles obtained by measurements and through model 2 are within tolerance limits. The shapes of displacement curves do not coincide, and therefore the distribution of internal forces is also different. From Figure 11 it follows that the layers from -20 m to -44 m are less compressible than in data obtained based on back analyses through models 1 and 2.

Figure 12 shows bending moments obtained on the basis of measurements and back analyses through models 1 and 2 for pile D (last pile landwards).Diagrams show the temporary phase of bending moment before the construction of coastal structure. Maximum bending moments appear in the case obtained on the basis of measurements of horizontal displacements in inclinometer.

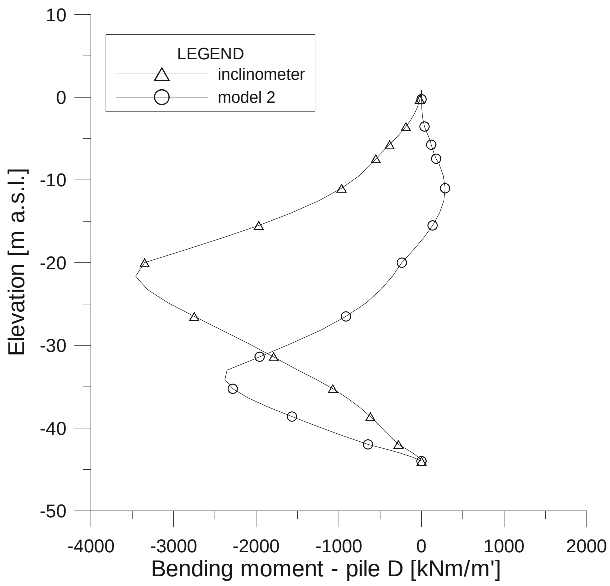

Figure 12 Bending moments in pile D, on the basis of displacements in vertical inclinometer and for back analyses model 2.

5 CONCLUSION

The paper aims to describe the design process and control of execution of a demanding structure –coastal structure, which takes into account soil-structure interaction.

The procedure was carried out iteratively through collaboration of design teams of structural engineers and geotechnical engineers.

The geotechnical model was made based on delivered loads and design assumptions of soil parameters. Through the geotechnical model and finite element method, the coefficients of soil reaction were determined through soil pressure and displacements. Ground reaction coefficients were delivered to the designers of the structure. By means of such procedure in several steps, through collaboration of design teams, soil-structure interaction assumed in the design was obtained.

Verification of efficiency of planned works was performed through geotechnical measurements described in the paper.

Based on geotechnical measurements, back analysis of soil parameters (Model 1) and the condition of internal forces and displacements of the structure (Model 2) was performed.

In this paper, we wanted to point out that it is necessary to perform back analyses during and after execution of demanding structures on the basis of performed measurements and through collaboration of structural and geotechnical engineers.

6 ACKNOWLEDGEMENTS

The authors would like to give special thanks for collaboration and support shown by Mr. Rene Lustig and Mr.DarkoPavokovic, the designers of the coastal structure from Rijekaprojekt.

7 REFERENCES (TNR 8)

Rocscience, 2009.*Settle 3D Version 1.0.*,Rocscience Inc. 31 Balsam Ave., Toronto, Ontario, M4E 1B2, Canada

Brinkgreve R.B.J., Engin, E. and Swolfs W.M., 2012. *Plaxis 2D 2012* Plaxisbv P.O. Box 572, 2600 An Delft, Netherlands

Priebe HJ1995, The design of vibroreplacement, *Grounding Engineering, December*, p. 31-37

Instrumented Trial Embankment on Soft Ground at Tokai, State of Kedah, Malaysia

Embankment essai instrumenté sur un sol mou à Tokai, État de Kedah, en Malaisie

Tan Y.-C., Lee P.-T., Koo K.-S.
G&P Geotechnics Sdn Bhd, Malaysia.

ABSTRACT: The geometrical tolerance of railway tracks at high operating speed is generally very stringent. Hence, when long stretches of the railway embankment traversing through soft alluvium deposits, cost effective designs meeting the design performance and construction schedule are required. A cost effective treatment such as prefabricated vertical drain (PVD) with temporary surcharging was designed to meet the stringent performance requirements. In addition, basal reinforcement was adopted to allow higher embankments to be built without compromising on the embankment stability during construction and to meet the tight construction schedule. Therefore, a fully instrumented trial embankment was carried out at Tokai, State of Kedah, Malaysia to verify the design philosophy of the ground treatment method adopted. This paper presents the consolidation settlement behavior and excess pore water pressure responses of the trial embankment during construction and surcharge waiting period. Back analyses using Finite Element Modeling (FEM) was performed to evaluate the performance of the ground treatment and to verify the subsoil parameters used in the design.

RÉSUMÉ : La tolérance géométrique des voies ferrées à grande vitesse de fonctionnement élevée est généralement très strictes. Ainsi, lorsque de longues étendues de la voie ferrée traversant remblai par des dépôts d'alluvions souples, efficaces coûtent conceptions répondant à la performance de la conception et du calendrier de construction sont nécessaires. Un traitement rentable telles que vidange verticaux préfabriqués (PVD) avec surcharge temporaire a été conçu pour répondre aux exigences de performance rigoureuses. En outre, le renforcement de base a été adopté pour permettre aux plus digues pour se construire sans compromettre la stabilité de remblai lors de la construction afin de respecter le calendrier de construction serré. Par conséquent, un remblai d'essai entièrement instrumenté a été effectuée à Tokai, État de Kedah, en Malaisie afin de vérifier la philosophie de conception de la méthode de traitement des sols adopté. Cet article présente le comportement tassement de consolidation et de l'excès de pression d'eau interstitielle des réponses du remblai d'essai pendant la construction et la période d'attente. Retour à l'aide des analyses de modélisation par éléments finis (FEM) a été réalisée afin d'évaluer la performance du traitement des sols et de vérifier les paramètres du sous-sol utilisés dans la conception

KEYWORDS: Instrumented trial embankment, soft ground, consolidation settlement .

1 INTRODUCTION

The construction of the electrified double track project in northern part of Peninsular Malaysia commenced in year 2007. As most of the embankments are founded on soft alluvium deposit, cost effective ground treatment such as PVD with temporary surcharging was widely adopted to meet the stringent settlement requirements and tight construction schedule. In view of this, a fully instrumented trial embankment was constructed at Tokai, State of Kedah as shown in Figure 1 to verify the design philosophy of the ground treatment method adopted. This is to study the consolidation settlement behavior, excess pore water pressure response and lateral displacement at the toe of embankment as indicator of consolidation process and embankment stability during construction filling and rest period.

This paper presents the settlement behaviour and excess pore water pressure response of the trial embankment. Back analyses using Finite Element Modelling (FEM) was also performed to evaluate the performance of the ground treatment and to verify the subsoil parameters adopted in the design.

2 SUBSOIL CONDITION

The subsoil is relatively homogenous consisting of very soft to soft CLAY (15m thick) overlying dense silty sand to sand from depth of 15m to 24m. Hard layer with SPT'N' value of more than 50 was found below 24m. The general subsoil properties including bulk density, compression ratio (CR), re-compression ratio (RR), over consolidation ratio (OCR), pre-consolidation pressure (Pc), undrained shear strength (s_u) and Atterberg limit are plotted in Figure 2. The interpreted subsoil parameters based on the field and laboratory tests are summarized in Table 1.

3 GROUND TREATMENT AND INSTRUMENTATION

The general ground treatment details for trial embankment are summarised in Table 2. The instrumentation scheme includes settlement gauges, extensometers, inclinometers, ground displacement markers, vibrating wire piezometers, standpipe and surface settlement markers as shown in Figure 3. Settlement at centre of embankment was measured by settlement gauges SG2, SG5 and SG8. Whilst, settlements at edge of embankment were measured by settlement gauges SG1, SG3, SG4, SG6, SG7 and SG9. Settlements at various depths were measured by extensometers EXT1, EXT2 and EXT3. The multistage construction with higher height of up to 7.6m was carried out due to site condition and problems such as delay in view of wet monsoon season, no borrow source, etc. The original intent is to construct the trial embankment in single stage loading of up to 5.9m

4 BACK ANALYSIS BY FEM MODELLING

Back analyses were carried out by using finite element modelling (FEM) software (Plaxis). Soft Soil Model (SSM) was adopted to simulate the behaviour of the soft clay under loading condition and coupled consolidation process for each stage of construction. Stress dependent stiffness (logarithmic compression behaviour) between volumetric strain and mean effective stress is assumed in SSM. Distinction between primary loading and unloading-reloading stiffness based on the modified index λ* (CR/2.3) and κ* (2RR/2.3) were obtained from 1D Oedometers tests. In addition, SSM is able to memorise the pre-consolidation stress with OCR input in the initial stage. Whilst, Hardening Soil Model (HSM) was utilised to model the underlying silty sand layer and the fill materials.

From a macro point of view, PVD increases the subsoil mass permeability in vertical direction (Lin et al, 2006). Therefore, an equivalent vertical permeability, k_{ve}, approximately represents the effect of both the vertical permeability of natural subsoil and radial consolidation by PVD was established to simulate the PVD behaviour in the back analyses. Based on the back analyses results, k_{ve} is about 5.8 times more permeable than the vertical permeability of the original subsoil (soft clay). The geometry of FEM is shown in Figure 4.

5 MEASUREMENT VERSUS CALCULATION

5.1 *Settlement*

The calculated results of the FEM analyses are compared with the measured settlement. Figure 5 shows the settlement profile of the embankment at the centre and the edge versus embankment filling time. The measured settlements at the end of surcharging period are averagely 1963mm and 1545mm at the centre and edge of the embankment respectively. This correspondences to 26% and 20% of the total constructed embankment height. The calculated settlement at the centre of embankment is 1932mm which is 31mm or 1.6% lower than the measured value. In general, the back-calculated settlement profile is fairly close to the measured settlement profile especially during first stage of filling (within 200 days) up to a fill thickness of 3.9m.

Figure 1. Location and overview of trial embankment.

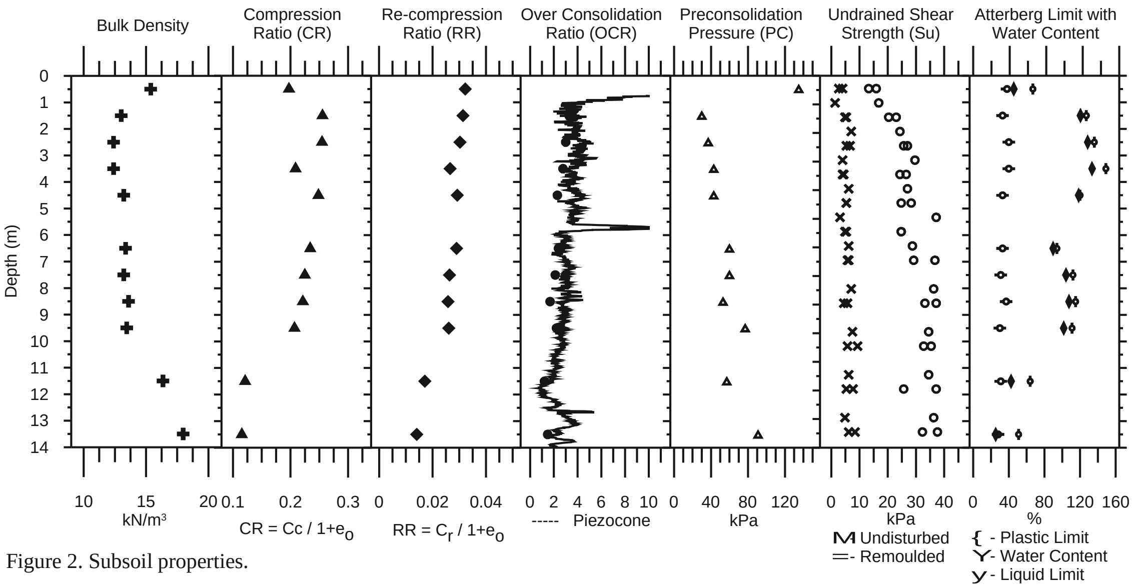

Figure 2. Subsoil properties.

Table 1. Interpreted subsoil parameters.

Depth	Soil type	SPT'N	γbulk (kN/m3)	c' (kPa)	ϕ' (°)	CR	RR	OCR	su (kPa)
0m to 5m	CLAY	0 - 1	13	5	21	0.25	0.03	3.0 - 4.4	15 - 25
5m to 10m	CLAY	0 - 1	13	5	21	0.22	0.027	1.7 - 2.7	25 - 35
10m t o15m	CLAY	1 - 4	16.5	5	21	0.12	0.017	1.2	30 - 35
15m to 24m	silty SAND	12 - 21	18	5	30				
24m to 30m	silty SAND	> 50	18						

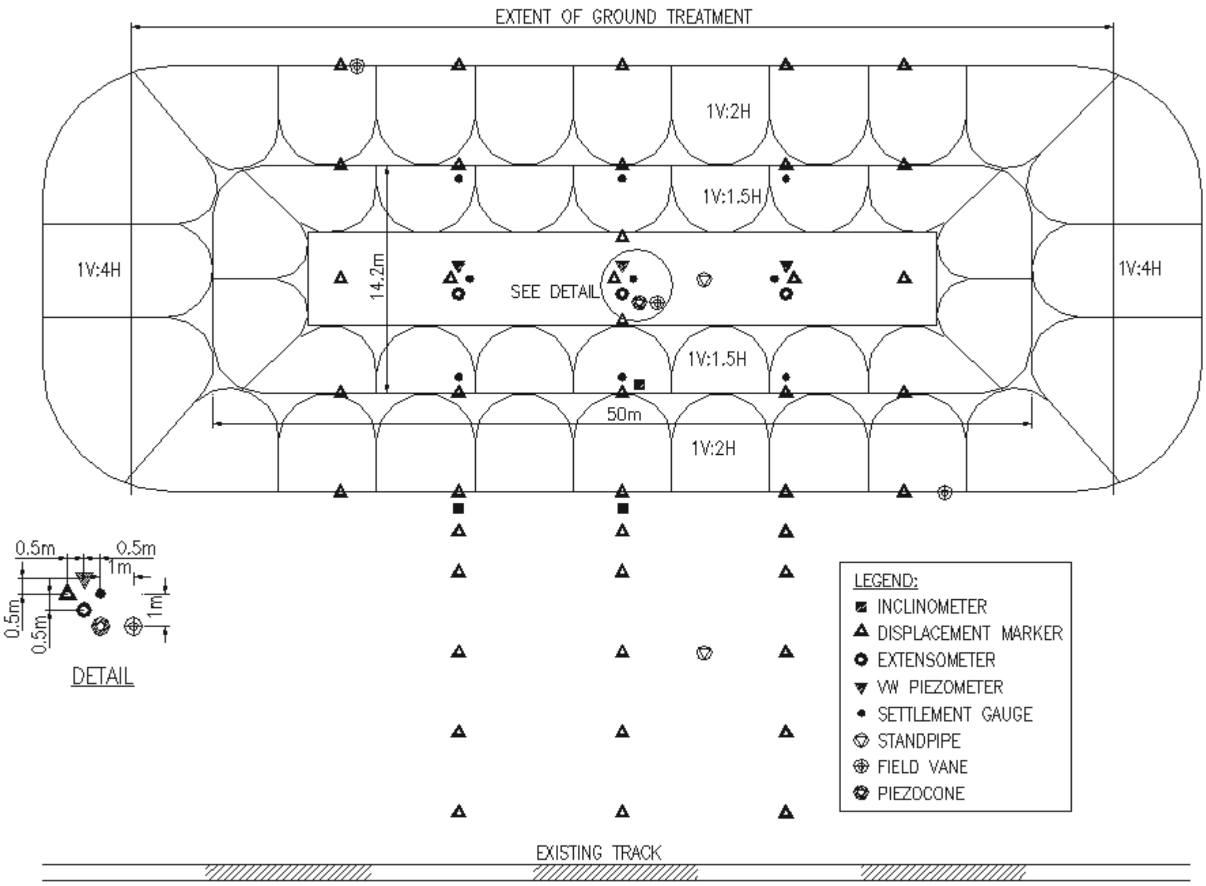

Figure 3. Instrumented layout plan.

Table 2 Design Criteria and ground treatment details

Design criteria:	Maximum settlement of 25mm and maximum differential settlement of 10mm for a chord of 10m (1:1000) over 6 months.
Soil replacement:	1m deep
PVD details:	15m long with 1.2m spacing in triangle pattern.
Sand blanket:	500mm thickness
Basal reinforcement:	Geotextile with ultimate tensile strength of 200kN/m
Surcharge:	1.5m thickness
Stages loading:	1. 3.9m thick fill and rest for 4 months. 2. 5.8m thick fill and rest for 3 months. 3. 7.6m thick fill and rest for 3 months.

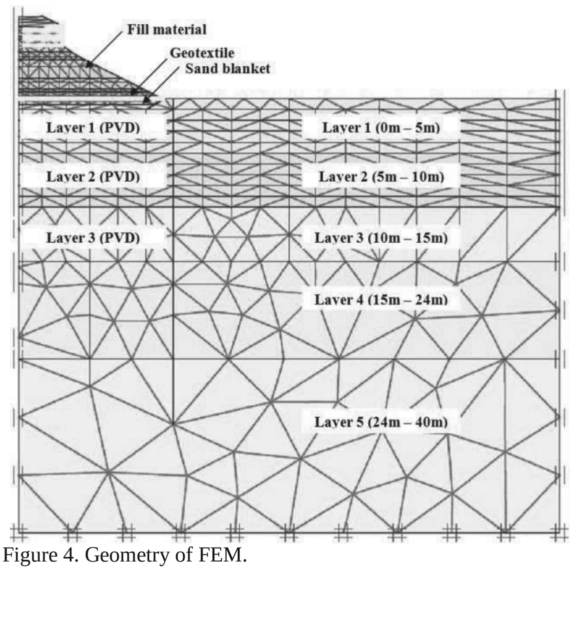

Figure 4. Geometry of FEM.

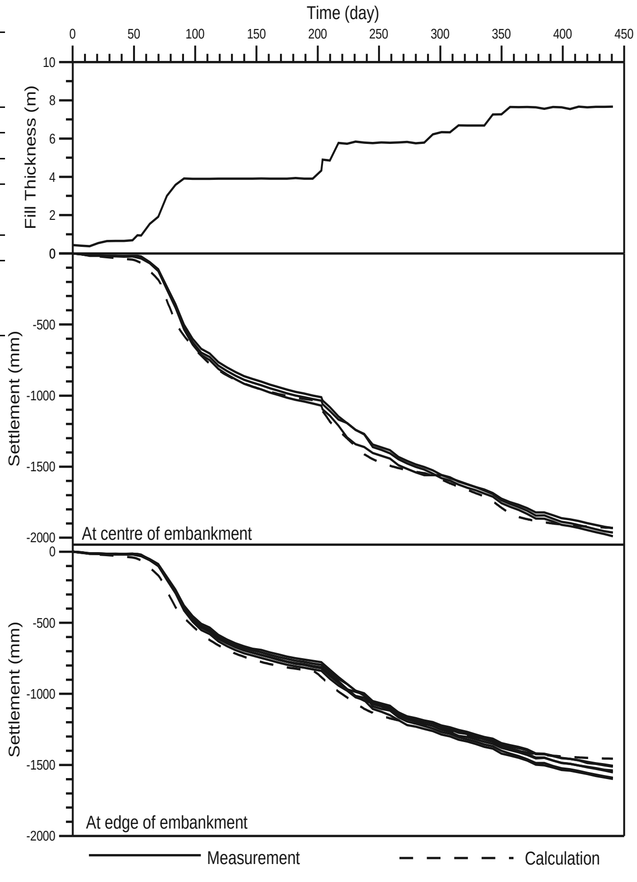

Figure 5. Settlement of embankment.

5.2 *Excess Pore Water Pressure*

The calculated results are compared with the measured excess pore water pressure at varies depths. Excess pore pressures were monitored using vibrating wire (VW) piezometers installed at centre of trial embankment. Figure 6 shows the excess pore water pressure profiles at depths of 2m, 3m, 4m, 8m and 10m versus embankment filling time. Generally, the measured pore water pressure increased during filling and dissipated during surcharge period. At 1st stage of filling (up to 3.9m), the VW piezometers indicated that the excess pore pressure at depth of 2m, 3m, 4m, 8m and 10m were 21kPa, 27kPa, 32kPa, 35kPa and 31kPa respectively. The measured excess pore pressure at depth of 2m is about 6kPa less than calculated result. However, the measured excess pore pressures at 3m depth and below are less than the calculated result with various pressure of 7kPa to 22kPa. The calculated result over predicted the excess pore pressure by more than 50% for depth at 4m and below. At 2nd stage of filling (up to 5.8m), the difference between measured and calculated results were less than 5kPa for depth of 4m and below. However, the calculated result over predicted the excess pore water pressure by more than 50% for depth of 3m and above.

VW piezometer results were corrected based on the measured settlement from extensometer at various depths. This is because the VW piezometers embedded into subsoil will settle together with subsoil during consolidation process. Some of the extensometers were damaged at 3rd stage of filling works. Therefore, the VW piezometer results at depth of 8m and 10m were not presented for 3rd stage filling.

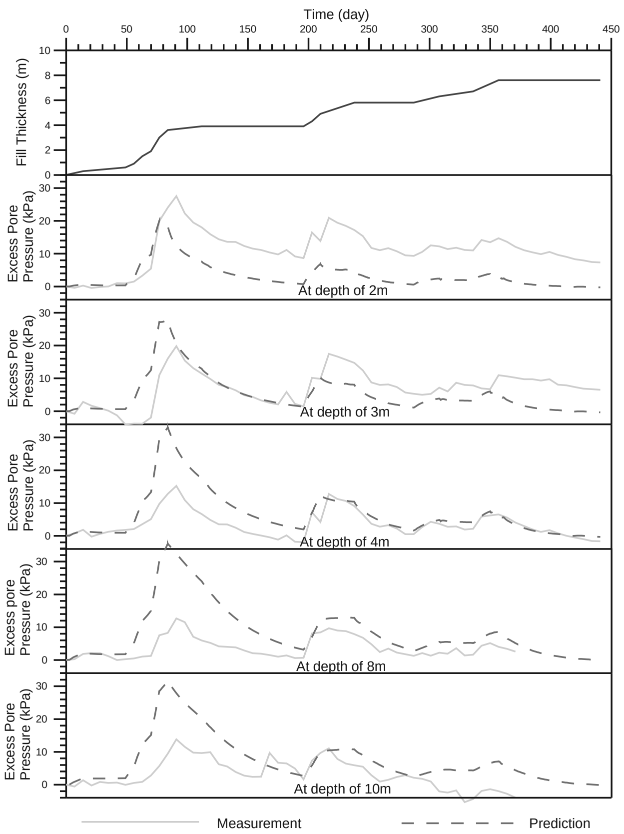

Figure 6. Measured excess pore pressure of embankment at depth of 2m, 3m, 4m, 8m and 10m.

5.3 *Lateral Displacement*

The measured lateral displacements of the embankment and subsoil compared with the predicted values at the end of surcharging period are presented in Figure 7. As refer to Figure 3, the lateral displacement of trial embankment were monitored by three inclinometers with two inclinometers located at the toe of embankment and one inclinometer located at the slope of embankment. The maximum measured lateral displacement at the toe of embankment is 172mm at depth of 2.5m below ground. The calculated values were over predicted by 79% (134mm). For the lateral displacement measured at the slope, the maximum measured lateral displacement is 258mm at depth of 3.2m below ground. The calculated displacement was over predicted by 62% (162mm).

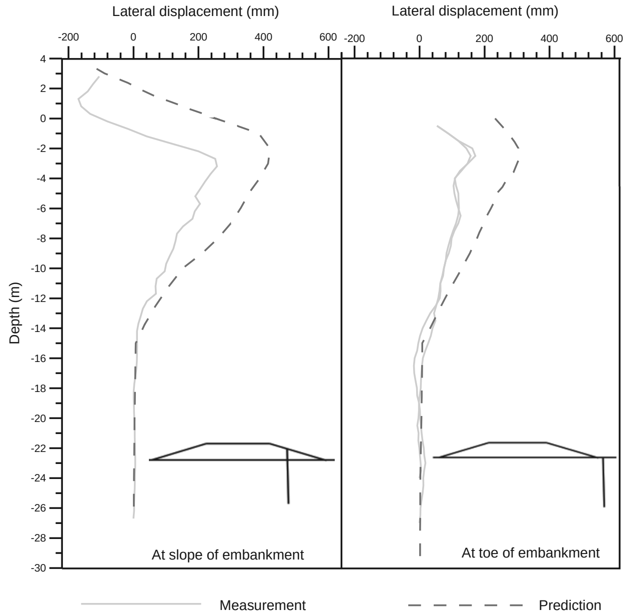

Figure 7. Measured lateral displacement of embankment.

6 CONCLUSIONS

Based on observations of the trial embankment performance and the analyses results, the following conclusions are made:

a) The total settlement at the end of surcharge period is about 26% of the constructed embankment height.
b) The measured settlements at original ground level were about 1.6% to 5.7% (31mm to 88mm) more than the calculated settlement.
c) In finite element modelling, an equivalent vertical permeability, k_{ve}, approximately represents the effect of both the vertical permeability of natural subsoil and radial consolidation by PVD can be adopted to simulate the PVD behaviour.
d) Back analyses using equivalent vertical permeability method for PVD treatment is about 5.8 times more permeable than the original subsoil permeability.
e) The settlement measured for the first stage filling up to 3.9m has good agreement with the settlement computed using FEM. The settlements measured and computed at the end of surcharging period only differ by about 6%.

7 REFERENCES

D.G.Lin, W.T.Liu and P.C.Lin. 2006. Numerical analysis of PVD improved ground at reference section of second bangkok international airport. *Journal of the Southeast Asian Geotechnical Society*, 157 – 170.

Prediction of and countermeasures for embankment-related settlement in ultra-soft ground containing peat

Prédiction et contre-mesure sur les tassements de remblais dans les sols ultra-meubles contenant de la tourbe

Tashiro M.
Nagoya University, Japan

Inagaki M.
Central Nippon Expressway Company Limited, Japan

Asaoka A.
Association for the Development of Earthquake Prediction, Japan

ABSTRACT: In the Mukasa area of the Maizuru-Wakasa expressway in Japan, delayed settlement as large as 11 m has occurred by test embankment loading on a ground that includes approximately 50 m of ultra-soft sediment layers containing peat and clay. In this paper, based on deductions of the initial in-situ soil conditions, simulations were carried out on the settlement and pore water pressure observed until now at the site, and predictions were made of the settlement that could occur in the future. In addition, the effects of countermeasures such as ground improvement by sand drain, replacement of the existing embankment with lightweight materials, and reduction of the loading rate, were also investigated using numerical analysis. These analyses were performed using the soil-water coupled finite deformation analysis program *GEOASIA*, in which the SYS Cam-clay model was mounted as the constitutive equation for the soil skeleton. The results showed that improvement of the mass permeability and the slow or lightweight banking are effective means of improving the stability during loading and reducing the residual settlement after entry into service. The results analyzed in this paper were applied to the actual construction design of a culvert and the lightweight embankment surrounded it.

RÉSUMÉ : Sur l'autoroute Maizuru-Wakasa au Japon, un tassement différé de près de 11m s'est produit suite à des essais de chargement de remblai sur un terrain incluant près de 50 m de couches de sédiments ultra-meubles contenant de la tourbe et de l'argile. Dans cet article, des simulations de tassement et de pression de l'eau interstitielle observées jusqu'à maintenant sur le site ainsi que des prédictions de tassement pouvant survenir dans le futur ont été réalisées en déduisant les conditions initiales de sols in situ. En outre, les effets des contre-mesures, comme l'amélioration du sol par drain de sable, le remplacement des remblais existants avec des matériaux légers, et la réduction de la vitesse de chargement, ont également été étudiés par analyse numérique. Ces analyses ont été employées en utilisant le programme d'analyse de déformations finies sol-eau couplées *GEOASIA*. Les résultats ont montré que l'amélioration de la perméabilité de masse, un tassement lent et léger sont des méthodes efficaces pour atteindre la stabilité pendant le chargement et la diminution du tassement résiduel après l'entrée en service. Les résultats analysés dans ce document ont été appliqués à la conception de la construction réelle d'un ponceau et du léger remblai qui l'entourait.

KEYWORDS: peat, prediction of settlement, soil-water coupled analysis

1 INTRODUCTION

In the Mukasa area of the Maizuru-Wakasa expressway, the ground consists of ultra-soft sediment layers comprising peat and clay with N-values on the order of 0 to 1 and a maximum depth of 50 m. Delayed settlement in excess of 11 m has occurred due to test embankment loading for approximately four years. While the construction of the embankment did not induce catastrophic sliding failure, it did dramatically impact the surrounding ground, causing substantial lateral displacement of up to 2 m and ground upheaval of up to 1 m (Inagaki et al 2010b).

In this paper, we simulated the large-scale ground settlement behavior observed in the region based on soil-water coupled finite deformation analysis, and in addition to predicting future settlement, we demonstrated that ground improvement by drain, and reduction in loading rate and weight are effective means of improving stability during embankment loading and reducing residual settlement of ultra-soft sediments containing peat. Numerical analyses were conducted using the SYS CAM-clay model (Asaoka et al. 2002) as an elasto-plastic constitutive equation mounted on the *GEOASIA* analysis program (All Soils All States All Round Geo-Analysis Integration: Asaoka and Noda 2007, Noda et al. 2008). The simulation results were applied to the actual construction design of a culvert and the lightweight embankment surrounding it.

2 SUMMARY OF THE TEST EMBANKMENT

Figure 1 presents a longitudinal cross-section of the soil strata underlying the test embankment that is the subject of this study. Three types of test embankments were established utilizing the

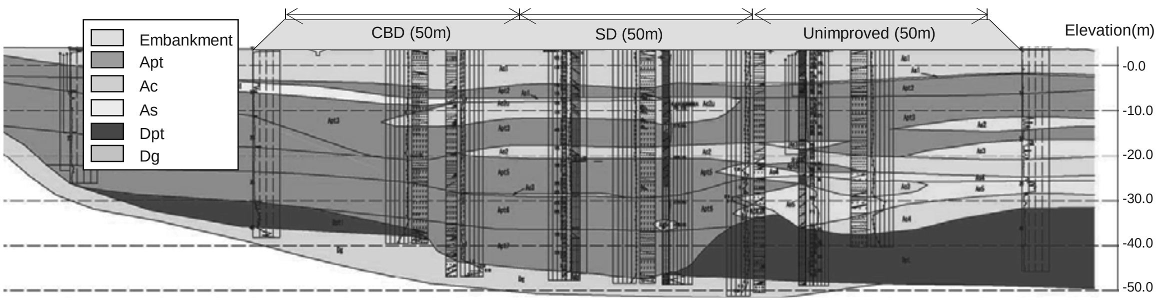

Figure 1. Schematic of test embankment and underlying soil strata (longitudinal cross section).

card-board drain (CBD) method, the sand drain (SD) method, or no improvement, with the aim to select a countermeasure for soft ground. Among these, the soft ground layer was thickest directly under the test embankment established using the SD method. When taking into consideration the settlement of all layers up to the deep peat layers, the total settlement, estimated prior to embankment construction, was 8.6 m. In practical terms, however, as presented in Figure 5, this meant that in order to achieve the planned embankment height of 7 m, the embankment had to be 15 m (embankment height + settlement) thick.

The large-scale settlement has been accompanied by substantial changes in an extensive area surrounding the embankment. Ground upheaval of up to 1 m and lateral displacement of up to 2 m have been observed in the vicinity of the toe of the slope. The surrounding ground has also experienced an inclination of waterways and cracking of the soil surface. At this point, 4 years after the establishment of the test embankment, settlement has reached 11 m, representing a settlement rate of 3.0 cm/month with little sign of convergence.

1 PREVIOUS RESEARCH

The long-term settlement that accompanies embankment loading is referred to as “delayed compression” or “secondary consolidation” and is a problem frequently encountered in sensitive naturally-deposited clay. For example, according to the construction records of the former Japan Highways Public Corporation, approximately 20% of embankments on soft ground in Japan have experienced 1 m or more of residual settlement after entry into service, which has necessitated substantial sums of money and labor for maintenance and repair including the expansion of road shoulders and rectification of level differences. However, we know from experience that settlement predictions based on Terzaghi’s Theory of Consolidations (Terzaghi 1943) and observational methods such as the Asaoka method (Asaoka 1978) tend to underestimate the magnitude and time span of settlement in such sites. Meanwhile, because settlement estimates based on visco-plastic theory (e.g. Šuklje 1957) assume perpetual delayed compression, it is difficult to explain why and under what conditions delayed compression occurs and the efficacy of particular countermeasures.

Mounting the SYS Cam-clay model as an elasto-plastic constitutive equation for the soil skeleton structure into the soil-water coupled finite deformation analysis program *GEOASIA*, we have explained the mechanism of delayed compression as a consolidation phenomenon accompanied by plastic compression due to progressive failure of the soil skeleton structure (Noda et al. 2005). While, we have also proposed a simple method for assessing the risk of delayed compression based on a laboratory mechanical test and a novel method for predicting long-term settlement accompanied by delayed compression (Inagaki et al. 2010a). In addition, we have applied these methods to the analysis of embankment loading sites built on soft clay ground that has actually experienced long-term settlement (Tashiro et al. 2011).

The elasto-plastic constitutive SYS Cam-clay model that serves as the basis for the above simulations enables the wide range of soil components, from sand to clay, to be treated within the same theoretical framework. Furthermore, the *GEOASIA* analysis program into which the model is integrated, enables all manner of mechanical conditions, including ground consolidation, deformation, stability and failure to be analyzed in series. In this paper, we apply the various insights gained from soft clay ground to peat ground and attempt to describe, predict, and evaluate countermeasures related to large-scale settlement behavior.

2 DEDUCTION OF INITIAL GROUND CONDITIONS

Prior to conducting the simulation, in order to estimate the initial ground conditions, we examined historical data related to ground formation as well as various survey data, including pore water pressure. The area is located between faults, and it is believed that the soil was deposited through the repeated upheaval, settlement, and deep sediment of organic components in a valley that experienced continuous artesian conditions. In this paper, the initial distribution of pore water pressure and effective overburden pressure of the ground prior to embankment loading is estimated in Figure 2. For reference, the distribution when artesian pressure is not taken into consideration is included as a dotted line. This represents an unusual case in which the initial effective overburden pressure p_0 becomes greater than the consolidation yield stress p_c ($p_0 > p_c$). In this region, it is expected that the increase in artesian pressure accompanying the increase in soft ground thickness resulted in a continuous low effective pressure in the deep ground.

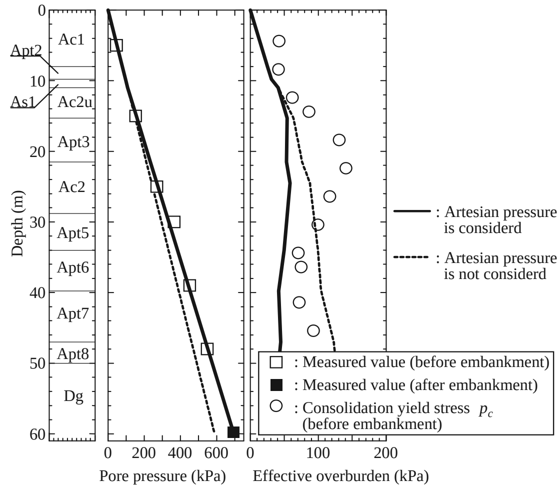

Figure 2. Estimated distribution of initial pore water pressure and effective overburden pressure

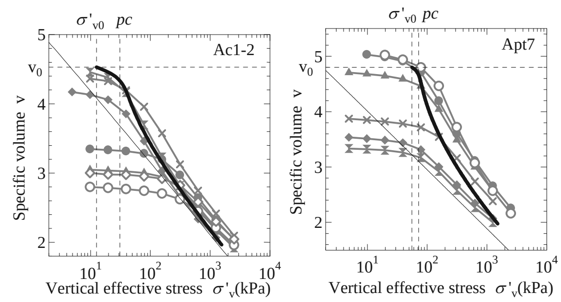

Figure 3. Examples of compression curves for undisturbed samples (gray lines) and estimated compression curves for in-situ soil (thick black lines).

Next, through laboratory tests, we attempted to determine the material constants and initial conditions. As presented in Figure 3, based on previous research on naturally deposited clay (Inagaki et al. 2010), we estimated compression curves for in-situ soil from the compression curves for undisturbed samples, taking into consideration the various “disturbances” that might occur during sampling, removal from the sampling tube, specimen preparation and setting-up on the testing machine. However, we observed considerable heterogeneity among samples from the deep peat layers with regard to factors such as mixing of plant fibers. In addition, it was expected that these samples were substantially impacted by “disturbances,” given their poor strength resulting from their high water content. For this reason, we conducted simulations based on a range of assumed initial conditions and determined the initial conditions that best reproduced the measured settlement. With regard to the permeability coefficient *k*, given the high compressibility of the peat layers, we assumed that the void ratio e was related to *k* by the expression $e=C\ln k/k_0+e_0$ and, for the other layers, we assumed a constant permeability coefficient. In addition, in order to represent the improvement by SD, we assigned a 100-fold greater permeability to finite elements corresponding to the SD area.

3 PREDICTION OF FUTURE SETTLEMENT BEHAVIOR

The finite element mesh and boundary conditions are presented in Figure 4. For simplicity, in this analysis, the SD section of Figure 1 was modeled assuming ground stratification.

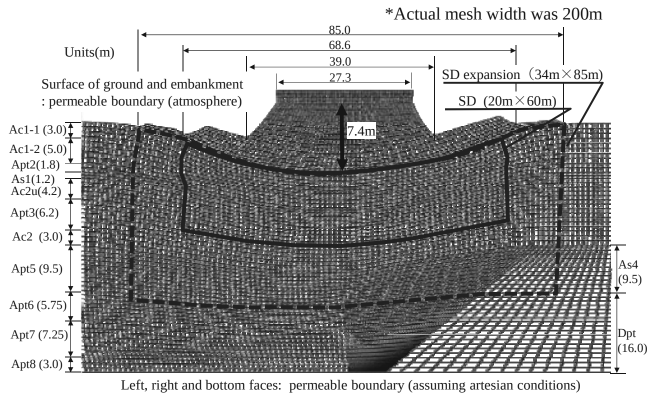

Figure 4. Finite element mesh (after embankment construction).

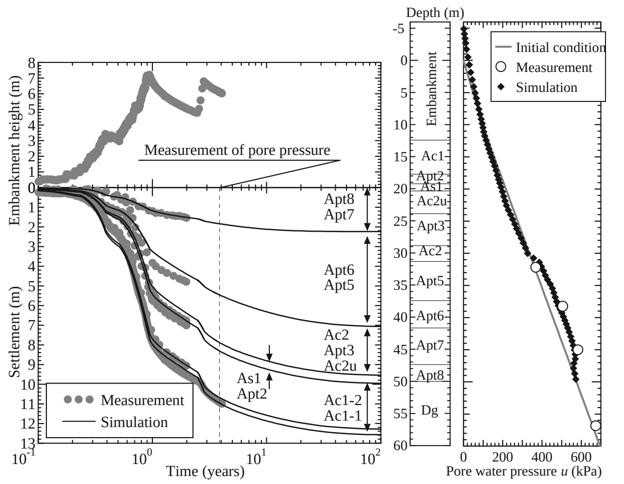

(a)Prediction of future settlement (b)Distribution of pore pressure

Figure 5. Simulation results (directly below the embankment center).

Figure 5(a) shows the predicted settlements at ground surface and for all layers directly below the center of the embankment. After adjusting the initial conditions and permeability coefficients to reproduce the observed settlement values, the simulation was allowed to continue to predict future settlement behavior. According to this analysis, additional residual settlement on the order of 1.5 m is expected to occur over the next 70 years. Figure 5(b) shows a comparison of the measured and simulated pore water pressure approximately 1,400 days after the entry of embankment loading (dotted line in Figure 5(a)). It can be seen that the simulation closely reproduces the distribution of excess pore pressure. Although the initial high void ratio for the deep peat layers experiences an rapid compression as a result of embankment loading, after a certain degree of volume compression has occurred, the layers then exhibit extremely poor permeability and have trouble dissipating excess pore pressure. Consequently, large settlement continues over a long term in these layers.

4 COUNTERMEASURES FOR SOFT PEAT GROUND

4.1 *Effect of ground improvement using SD method*

We evaluated the effect of SD on the test embankment ground by simulating the following three cases:

Case 1: Simulating the actual SD-improved area of the test embankment (20 × 60m (L ×W))
Case 2: No SD-improvement
Case 3: Expanding the SD-improved area in accordance with specific site conditions. (34 × 85 m (L × W), i.e., the entire area directly under the embankment down to the Apt5 layer)

In each case, based on actual records at the construction site, the simplest construction history was used (constant increasing the embankment thickness at a rate of 2.35 cm/day).

Although the magnitude of the settlement during initial embankment construction is lowest in Case 2, it was shown that because the poor permeability induces shear deformation under undrained condition, large-scale circular slip extends to the deep ground layers below the embankment center (Figure 6). From this result, it appears that ground improvement using SD in this area was effective in preventing catastrophic slip failure.

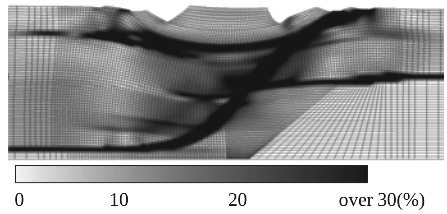

Figure 6 Circular slip during loading (Case 2: No SD-improvement)

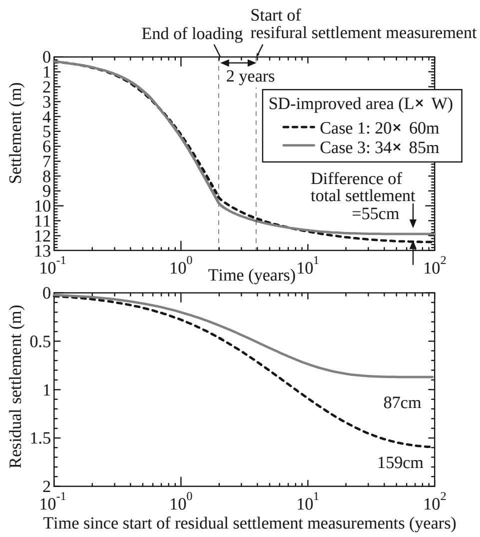

Figure 7 Comparison of SD-improvement area.

Case 3 resulted in stability, particularly of the deep peat layers, and early settlement convergence. Figure 7 shows the settlement for Cases 1 and 3. The residual settlement starting at a point 2 years (assuming the entry into service) after embankment construction is also illustrated in the lower panel. Expansion of the SD-improved area, particularly in the deep peat layers, reduces lateral displacement due to undrained shear deformation and settlement associated therewith. The total settlement is reduced by 55 cm across the entire area of ground under the embankment. Furthermore, residual settlement was reduced by approximately half due to the fact that the settlement approached convergence earlier. However, because consolidation of the deep peat layers also occurred earlier, deformation was concentrated in the upper peat layers, and upheaval of areas near the toe of the slope increased (Figure omitted). Potential countermeasures for this problem associated with expansion of SD-improved area, include expanding the area and load of the counterweight embankment and reducing the rate of embankment loading, particularly in the initial stages.

4.2 *Effect of slow banking method*

Table 1 shows the results of simulations performed under the same conditions as Case 3 above, but with lower (1.5 cm/day) or higher (3.0 cm /day) rates of embankment loading. Reducing the rate of loading allowed for greater drainage during loading, which resulted not only in earlier convergence of settlement and reduction in residual settlement but also a slight but significant reduction in total settlement. Although the data is not presented here due to space constraints, the lower loading rate was effective in reducing lateral displacement of the shallow ground layers and upheaval of the soil surface, and resulted in an earlier shift from outward deformation to inward deformation in the embankment loading process.

Table 1. Effect of rate of embankment loading.

Loading rate (increase in embankment thickness/day)	Total settlement (m)	Residual settlement (cm)
1.5cm/day	11.7	74
2.35cm/day	11.9	87
3.0cm/day	12.0	94

Although construction of the test embankment shown in Figure 5 (a) was managed so that the embankment “height” generally increased at a rate of 3.0 cm/day, because obvious settlement occurred during embankment construction, the actual rate of loading per unit time (increase in embankment “thickness”) was higher than that specified in any of the above simulations. Although no catastrophic slip failure occurred, this rapid construction resulted in increased lateral displacement and upheaval. Slow embankment loading is effective not only for increasing stability during construction but also for reducing residual settlement and impacts on the adjacent ground. When it is not possible to secure adequate time for embankment construction, combinations with other countermeasures such as vacuum consolidation should be considered.

4.3 *Effect of lightweight banking method*

Figure 8 shows the effect of weight reduction of the existing embankment with lightweight materials. For simplicity, in the simulation, the reduced loading was represented by removal of the embankment. Greater reduction in loading was accompanied by less residual settlement and earlier occurrence of settlement convergence. Furthermore, although not shown here, it was demonstrated that greater reduction in loading resulted in reduced inward deformation of the ground surrounding the embankment.

Based on these simulations, the culvert in actual construction site has been designed with a 1.2-m freeboard, and in order to reduce differential settlement, the material of the embankment in the vicinity of the culvert is planned to be replaced with lightweight material.

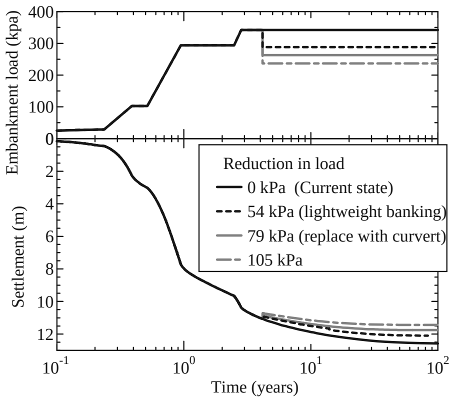

Figure 8 Effect of weight reduction of the existing embankment.

5 CONCLUSION

In this paper, we attempted to simulate the large-scale settlement in excess of 11 m and predict future settlement of ultra-soft ground containing peat due to loading by a test embankment. When the stress state of peat exceeds the consolidation yield stress under heavy loading, the undrained shear deformation resulting from poor permeability causes large lateral displacement to occur, which can lead in severe cases to slip failure. Furthermore, because rapid compression occurs even under drained conditions in peat layes, permeability improvement using SD, reduction of the loading rate, and the more drastic countermeasure of reducing the load itself are effective in increasing stability during loading, reducing the deformation of the ground surrounding the embankment, and reducing residual settlement after the enter into service.

6 REFERENCES

Asaoka, A. 1978. Observational procedure of settlement prediction, *Soils and Foundations*, 18(4), pp.87-101.

Asaoka, A., Noda, T., Yamada, E., Kaneda, K. and Nakano, M. 2002. An elasto-plastic description of two distinct volume change mechanisms of soils, *Soils and Foundations*, 42(5), pp.47-57.

Asaoka, A. and Noda, T. 2007. All soils all states all round geo-analysis integration, *International Workshop on Constitutive Modeling - Development, Implementation, Evaluation, and Application*, Hong Kong, China, 11-27.

Inagaki, M., Nakano, M., Noda, T., Tashiro, M. and Asaoka, A. 2010a. Proposal of a Simple Method for Judging Naturally Deposited Clay Grounds Exhibiting Large Long-term Settlement due to Embankment Loading, *Soils and Foundations*, 50(1), 109-122.

Inagaki, M., Sakakibara, K., Yamada, K., Tashiro, M., Noda, T. Nakano, A. and Asaoka, A. 2010b. Estimation of the initial conditions of a very soft peat ground which causes large delayed settlement due to test embankment loading, 45th Japan National Conference on Geotechnical Engineering, 751-752 (in Japanese).

Noda, T., Asaoka, A., Nakano, M., Eiji, Y. and Mutsumi, T. 2005. Progressive consolidation settlement of naturally deposited clayey soil under embankment loading, *Soils and Foundations*, 45(5), 39-51.

Noda, T., Asaoka, A. and Nakano, M. 2008. Soil-water coupled finite deformation analysis based on a rate-type equation of motion incorporating the SYS Cam-clay model, *Soils and Foundations*, 48(6), 771-790.

Šuklje L. 1957. The analysis of the consolidation process by the isotaches method, *Proc of 4th Int. Conf. on Soil Mech. Found. Engng.*, London, 1(1), 200-206.

Tashiro, M., Noda, T., Inagaki, M., Nakano, M. and Asaoka, A. 2011. Prediction of Settlement in Natural Deposited Clay Ground with Risk of Large Residual Settlement due to Embankment Loading, *Soils and Foundations*, 51(1), 133-149.

Terzaghi K. 1943. Theoretical soil mechanics, *John Wiley and Sons*.

Numerical simulation of energy consumption of artificial ground freezing applications subject to water seepage

Simulation numérique de la consummation d'énergie des applications pour la congélation artificielle du sol soumise au flux de l'eau souterraine

Ziegler M., Schüller R.
Geotechnical Engineering, RWTH Aachen University, Germany

Mottaghy D.
Geophysica Beratungsgesellschaft mbH, Aachen, Germany

ABSTRACT: The energy consumption of artificial ground freezing applications results from the necessary (consumed) refrigeration capacity. The determination of the refrigeration capacity requires the numerical modeling of heat transfer processes within the freeze pipe. Therefore a new module has been implemented in the Finite Difference Program SHEMAT. An approach for calculating the heat transfer processes and finally the refrigeration capacity is presented in this paper. Thus numerical simulations are carried out to determine the influence of groundwater flow on the refrigeration capacity and the related energy consumption for artifical ground freezing applications.

RÉSUMÉ : La consommation d'énergie des applications pour la congélation artificielle du sol résulte de la capacité nécessaire de réfrigération. La détermination de cette capacité de réfrigération exige un modèle numérique des processus de transfert de la chaleur dans le tuyau de congélation. C'est pourquoi un nouveau module a été implémenté dans le programme SHEMAT. Une approche pour calculer le transfert de la chaleur et finalement la capacité de réfrigération est présentée dans cet exposé. Ainsi, des simulations numérique ont été réalisées pour déterminer l'influence du flux des eaux souterraines sur la capacité de réfrigération et la consommation d'énergie qui en résulte des applications pour la congélation artificielle du sol.

KEYWORDS: artificial ground freezing, refrigeration capacity, heat transfer, Nusselt number

1 INTRODUCTION

The ground freezing method aims to provide artificially frozen soil which increases the strength of the ground and makes it impervious to water seepage. In recent years the artificial ground freezing method is more often used not only in tunneling but also in the construction of common basement stories. However, the regular application often fails as the energy consumption and its related costs are expected to be excessively high.

In the last few years several numerical simulations using the program SHEMAT (Simulator for Heat and Mass Transport) were carried out at the chair of Geotechnical Engineering of RWTH Aachen University. The Finite-Difference Program SHEMAT had been developed by a group of Prof. Clauser at the chair of Applied Geophysics of RWTH Aachen University for the simulation of geothermal processes in porous rocks (Clauser 2003). Mottaghy and Rath (2006) implemented a phase change model including latent heat effects due to freezing and thawing of subsurface fluids, as well as temperature dependent thermal properties. As part of the dissertation of Baier (2009), this work has been extended in terms of varying freezing curves and additional thermal and hydraulic ground properties and their temperature dependence. The numerical simulations carried out showed that significant reductions of the freezing time can be achieved by flow-adapted freeze pipe arrangements (Ziegler et al. 2009).

To increase the regular application of the artificial ground freezing method not only the freezing time but also the energy consumption has to be reduced. Therefore it is necessary to take into consideration the operating phase which essentially affects the total energy consumption of artificial ground freezing applications. The energy consumption can be estimated by determining the refrigeration capacity of artificial ground freezing applications first.

The aim of this paper is to highlight the determination of the refrigeration capacity by numerically modelling the heat transfer processes in the freeze-pipe itself and at the transition to the soil.

2 DETERMINATION OF REFRIGERATION CAPACITY

To ensure a realistic determination of the refrigeration capacity the freeze pipe has to be examined in detail. That implies the consideration of the so far neglected heat transfer within the freeze pipe itself.

2.1 *Basic heat transfer within freeze pipes*

The heat transport mechanisms, occuring during the ground freezing process, can be split into mechanisms in the soil, in the freeze pipes and in the transition of both. In the soil the heat transport consists of conduction and forced convection (advection) due to water seepage. These processes are not part of the current research and therefore not illustrated in detail. For a detailled explanation see e.g. Baier (2009).

In the following, the heat transfer processes in the freeze pipes are described in detail.

In general freeze pipes are coaxial pipes that consist of an inner pipe of polyethylene where the refrigerant moves downwards and an outer pipe of steel where the refrigerant moves upwards. In most cases a calcium chloride brine is used as refrigerant. The heat extraction of the surrounding soil warms the refrigerant in the outer pipe moving upwards. Therefore the refrigeration capacity can be determined from the temperature difference of inlet and outlet refrigerant temperature, the pump rate Q and the volumetric heat capacity of the refrigerant c_v (see Eq. 1).

$$P = c_V \cdot Q \cdot (T_{inlet} - T_{outlet}) \quad (1)$$

For a realistic determination of the outlet temperature the ongoing heat transfer processes ($\dot{Q}_s / \dot{Q}_e$) within the freeze pipe have to be considered (see Figure 1).

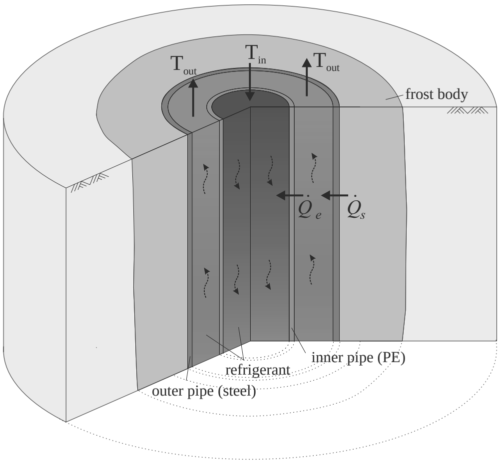

Figure 1. Freeze pipe in detail with occurring heat flow.

The heat flow $\dot{Q}_s$ between the soil and the outer freeze pipe comprises conductive heat flow through the outer freeze pipe and convective heat flow due to the flowing refrigerant. The heat flow $\dot{Q}_e$ between the down- and upstream via the inner freeze pipe can be divided into two mechanisms. On the one hand, conductive heat flow through the inner freeze pipe and on the other hand convective heat flow both inside and outside the inner freeze pipe. In case of a flowing refrigerant the vertical heat transfer is dominated by advection which is already considered in the horizontal heat flow. Therefore the vertical conductive heat flow within the refrigerant is neglected.

The heat transfer due to conduction can be determined by using Fourier's law. The conductive heat flow for a coaxial freeze pipe for n conductive layers with the thermal conductivity of the pipe material λ_i [W/(mK)] results in:

$$\dot{Q}_{conduction} = \sum_{i=1}^{n} 2 \cdot \pi \cdot \lambda_i \cdot \frac{\Delta T_i}{ln(r_{out,i}/r_{in,i})} \quad (2)$$

The convective heat flow depends on the heat transfer coefficient α_i [W/(m²K)]:

$$\dot{Q}_{convection} = \sum_{i=1}^{n} 2 \cdot \pi \cdot r_i \cdot \alpha_i \cdot \Delta T \quad (3)$$

The heat transfer coefficient depends on the freeze pipe geometry and the flow and material properties of the refrigerant. As a function of the Nusselt number Nu the heat transfer coefficient is defined as (Baehr and Stephan 2006):

$$\alpha = \frac{Nu \cdot \lambda_F}{d_{hydraulic}} \quad (4)$$

with the thermal conductivity of the refrigerant λ_F and the hydraulic freeze pipe diameter $d_{hydraulic}$. The hydraulic diameter of the inner freeze pipe corresponds to its inner diameter (see Figure 2).

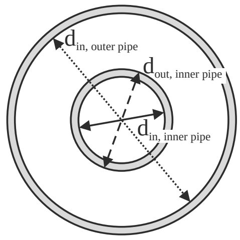

Figure 2. Freeze pipe diameters to calculate hydraulic diameter.

The hydraulic diameter for the annular space is:

$$d_{hydraulic} = d_{in,outerpipe} - d_{out,innerpipe} \quad (5)$$

The Nusselt number Nu depends on the flow type – laminar or turbulent. To differ between the two flow types the Reynolds number Re can be used, which depends on the refrigerant flow velocity v_F, the kinematic viscosity ν and the hydraulic diameter (VDI Heat Atlas 2010).

$$Re = \frac{v \cdot d_{hydraulic}}{\nu_F} \quad (6)$$

In the literature (Gnielinski 1995, VDI Heat Atlas 2010) it is generally mentioned that a full developed turbulent fluid flow in a pipe exists for $Re > 10^4$. For $Re < 2300$ a laminar fluid flow occurs. In the range of $2300 < Re < 10^4$ the transition from laminar to turbulent flow takes place. Furthermore, for all flow types a distinction has to be made between a modified fluid flow in the inlet area and a thermic and hydrodynamic fully developed fluid flow behind this area (VDI Heat Atlas 2010). Due to the spatial separation of the mechanical refrigeration plant and the inlet area of the freeze pipes, it can be assumed that the fluid flow reaching the inlet area is already fully developed.

Moreover, the VDI Heat Atlas (2010) indicates the differentiation between flow inside a pipe and in a concentric annular gap. In this paper only the Nusselt numbers for the inner freeze pipe are outlined. The equations for the calculation in the annular gap can be found in VDI Heat Atlas (2010).

In general the Nusselt number depends on the Reynolds number Re, the Prandtl number Pr, the inner pipe diameter d_i and the length of the pipe l.Thus the Nusselt number in case of a laminar flow and a constant heat flux density along the freeze pipe can be calculated with:

$$Nu_{m,q} = \left[4{,}364^3 + 0{,}6^3 + \left(1{,}953 \left(Re\,Pr \frac{d_i}{l} \right)^{1/3} - 0{,}6 \right)^3 \right]^{1/3} \quad (7)$$

In case of a turbulent flow, there is no need for a differentiation between the boundary conditions "constant wall temperature" and "constant heat flux density" since the Nusselt numbers are nearly equal. Thus the Nusselt number for turbulent flow is defined as:

$$Nu_m = \frac{(\xi/8)\,Re\,Pr}{1 + 12{,}7\sqrt{\xi/8}\left(Pr^{2/3} - 1\right)} \left[1 + \left(\frac{d_i}{l} \right)^{2/3} \right] \quad (8)$$

with:

$$\xi = \left(1{,}8 \log_{10} Re - 1{,}5 \right)^{-2} \quad (9)$$

According to Gnielinski (1995) the following interpolation function for the transition region between laminar and fully turbulent flow should be used:

$$Nu_m = (1 - \gamma) \cdot Nu_{m,L,2300} + \gamma \cdot Nu_{m,T,10^4} \quad (10)$$

with:

$$\gamma = \frac{Re - 2300}{10^4 - 2300} \; and \; 0 \le \gamma \le 1$$

Besides the Reynolds number the Prandtl number Pr is needed for the calculation of the Nusselt number. The Prandtl number characterizes the material properties of the refrigerant (kinematic viscosity ν, thermal conductivity λ_F and volumetric heat capacity c_F) (Baehr and Stephan 2006):

$$Pr = \frac{\nu \cdot c_F}{\lambda_F} \quad (11)$$

2.2 *Numerical modeling*

For a realistic calculation of all heat transfer mechanisms described afore the use of numerical methods becomes necessary. To avoid a very fine discretization which causes long simulation times a seperate module "freezrefcap" for the calculation of the heat transfer processes within the freeze pipe has been developed in cooperation with Geophysica

Beratungsgesellschaft mbH. This module is based on a Finite Difference formulation for simulating borehole heat exchanger developed by Mottaghy and Dijkshoorn (2012) and has been modified for the simulation of artificial ground freezing applications.

Adapted from the Kelvin line source theory the freeze pipes are modeled as line sources and the horizontal heat transfer is determined, using the concept of thermal resistances (Hellström 1991). To realize the coupling of the module “freezrefcap” with SHEMAT the soil temperature calculated in SHEMAT T_{Soil} is passed to the new module. In turn, a cooling generation $\dot{Q}_s$ returns to SHEMAT (see Figure 3).

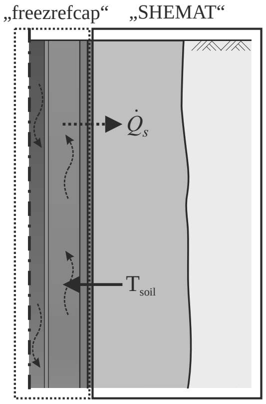

Figure 3. Coupling of “freezrefcap” module and SHEMAT.

The numerical model includes the afore-mentioned heat transfer conditions for the calculation of the thermal resistances. For the numerical model the inner freeze pipe and the annular space are divided into grid cells that are connected via thermal resistances (see Figure 4). Assuming a steady state solution the temperature of all grid cells is calculated considering the heat balance equation in every time step. Due to the high flow rate inside the freeze pipes and the comparatively short freeze pipe length this simplified steady state solution is a good approximation.

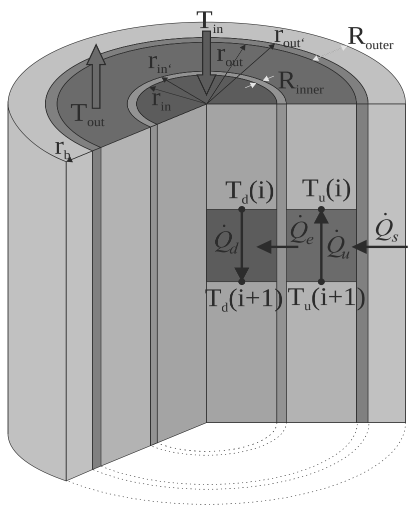

Figure 4. Calculation basis of module “freezrefcap” according to Mottaghy and Dijkshoorn (2012).

The module “freezrefcap” offers the opportunity to activate and deactivate freeze pipes, which provides the basis for the simulation of different modes during the operating phase. The distinction between “flow” and “no flow” case requires different calculations of thermal resistances and the temperature distribution inside the freeze pipe. In this paper only the “flow” case is described.

For the determination of the heat flow $\dot{Q}_s$ between the soil and the outer pipe and $\dot{Q}_e$ between the inner and the outer pipe the temperatures calculated in the previous time step (t-1) are used (see Eq. 12 and Eq. 13). The thermal resistances R_{inner} and R_{outer} are also calculated considering the results of the previous time step. Because of the flowing refrigerant the different grid layers i need to be taken into account.

$$\dot{Q}_s = \frac{T_{soil}(i) - T_u^{t-1}(i)}{R_{outer}} \tag{12}$$

For the determination of the heat flow between the outer and the inner pipe adjacent temperatures in the downstream and in the upstream are used (see Eq. 13).

$$\dot{Q}_e = \frac{T_u^{t-1}(i+1) - T_d^{t-1}(i)}{R_{inner}} \tag{13}$$

The temperature in the downstream $T_d^t(i+1)$ of the actual time step t is determined based on the downstream temperature $T_d^{(t-1)}(i)$ of the overlying grid cell i for the previous time step (t-1) because of the flowing refrigerant.

$$T_d^t(i+1) = T_d^{t-1}(i) + \frac{\dot{Q}_e}{q_F \cdot c_F} \tag{14}$$

$$T_u^t(i) = T_u^{t-1}(i+1) + \frac{-\dot{Q}_e + \dot{Q}_s}{q_F \cdot c_F} \tag{15}$$

c_F indicates the volumetric heat capacity of the refrigerant and q_F the flow rate.

Besides the flow rate the inlet temperature or the refrigeration capacity can be choosen as input parameters. Furthermore the simulation of different refrigerants requires just a simple implementation of the temperature dependent fluid parameters.

3 NUMERICAL SIMULATION

Former numerical simulations at the Chair of Geotechnical engineering showed that groundwater flow has an important influence on the freezing process. The results outlined that the freezing time increases disproportionately and the frost body development decreases with an increasing flow velocity.

To further investigate the influence of groundwater flow on the refrigeration capacity a numerical simulation of a simplified model with only one freeze pipe has been carried out using the module “freezrefcap”. Because of a missing module validation against measured data from laboratory model tests only the qualitative influence of groundwater flow is outlined. For this example a freeze pipe with an outer diameter of 10 cm, an inner diameter of 5 cm and a length of 9.5 m has been chosen. The inner pipe was assumed to consist of polyethylene and the outer pipe of steel. As refrigerant a 29 % $CaCl_2$ brine has been chosen. The results of the numerical simulation are displayed in Figure 5.

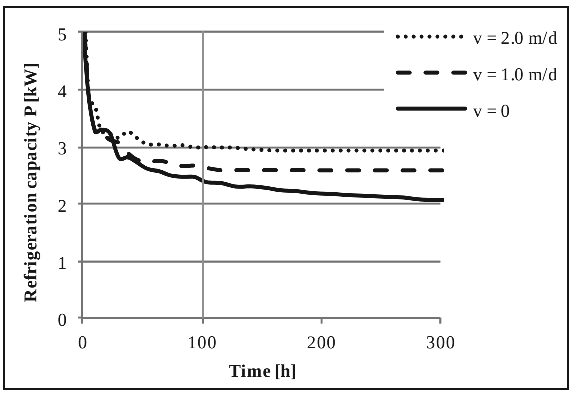

Figure 5. Influence of groundwater flow on refrigeration capacity of one freeze pipe.

It is obvious that an increase in flow velocity causes not only a reduced frost body development but also an increased refrigeration capacity. The reason for this increase is the additional convective heat flow caused by the groundwater flow. The flow velocity influences the artificial ground freezing application twice, because the increased refrigeration capacity has to be hold up for a longer time period to freeze the required frost body contour and during the operating phase.

Figure 5 displays that the refrigeration capacity with groundwater flow decreases with time due to an increasing frost body. However, the refrigeration capacity for a flow velocity of 1.0 m/d and 2.0 m/d proceeds constant. This implies an stagnating frost body growth, a steady state. Such a steady state indicates a thermal equlibrium of the heat supplied by the groundwater flow and extracted by the freeze pipes.

Monitoring points in the soil around the freeze pipe also indicating a stagnation in temperature course confirm this assumption (see Figure 6).

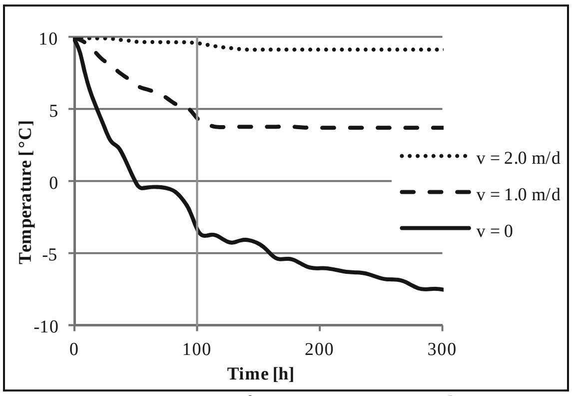

Figure 6. Temperature course of a monitoring point in the upstream.

Comparing the refrigeration capacity after 100 hours, when frost body still grows for all flow velocities, it becomes clear that the refrigeration capacity increases about 10 % for a flow velocity of 1.0 m/d and even about 25 % for a flow velocity of 2.0 m/d

4 CONCLUSION

An approach for the realistic determination of the refrigeration capacity by calculating the heat transfer processes within a freeze pipe was presented. By separating the “freezrefcap” module from SHEMAT and defining only two necessary interfaces for the coupling a very fine discretization and long computing times as a consequence can be avoided. The module offers the opportunity to calculate the outlet temperature and as a result the refrigeration capacity by entering the inlet temperature and the flow rate of the refrigerant. Thus the influence of different refrigerants on the refrigeration capacity can be estimated by numerical simulations.

The aim of further research is to validate the “freezrefcap” module by simulating a laboratory model test influenced by groundwater flow. Thus quantitative statements on the outlet temperature and the refrigeration capacity can be given for various artificial ground freezing applications subject to water seepage.

At this point qualitative statements already indicate that the refrigeration capacity increases disproportionally with an increasing flow velocity. In the further research process the influence of the operating phase on the total refrigeration capacity and the related energy consumption is determined. The aim of the research project is the simulation and optimization of artificial ground freezing applications regarding both time and energy aspects already in the design phase.

5 ACKNOWLEDGEMENTS

The displayed results have been gained from an ongoing research project “Energetic saving potential for the construction of complicated basements using the artificial ground freezing method” funded by the Federal Office for Building and Regional Planning (BBR). Sincere thanks are given to the BBR. Furthermore the Wayss & Freytag Ingenieurbau AG, the Züblin Spezialtiefbau GmbH and the Deilmann-Haniel Shaft Sinking GmbH deserve our thanks for the financial support. Our thanks also go to the Geophysica Beratungsgesellschaft mbH for their active support in the further development of SHEMAT.

6 REFERENCES

Baehr S. and Stephan K. 2006. *Wärme- und Stoffübertragung*. Springer, Berlin.

Baier Ch. 2009. *Thermisch-hydraulische Simulationen zur Optimierung von Vereisungsmaßnahmen im Tunnelbau unter Einfluss einer Grundwasserströmung*. Dissertation, Lehrstuhl für Geotechnik im Bauwesen der RWTH Aachen.

Clauser C. 2003. *Numerical Simulation Of Reactive Flow in Hot Aquifers – SHEMAT and PROCESSING SHEMAT*. Springer, New York.

Gnielinski V. 1995. *Ein neues Berechnungsverfahren für die Wärmeübertragung im Übergangsbereich zwischen laminarer und turbulenter Rohrströmung*. Forschung im Ingenieurwesen, Vol.61, No. 9, pp. 240-248.

Hellström G. 1991. *Ground heat Storage – Thermal Analyses of Duct Storage Systems*. Ph.D. thesis, Theory. Dep. Of Mathematical Physics, University of Lund.

Mottaghy D. and Dijkshoorn L. 2012. *Implementing an effective finite difference formulation for borehole heat exchangers into a heat and mass transport code*. Renewable Energy 45, pp.59-71.

Mottaghy D. and Rath V. 2006. *Latent heat effects in subsurface heat transport modelling and their impact on palaeotemperature reconstructions*. Geophysical Journal International 164, p. 234-245.

Verein Deutscher Ingenieure 2010. *VDI Heat Atlas*, 2nd ed. Springer, New York.

Ziegler M. and Baier Ch. and Aulbach B. 2009. *Optimization of artificial ground freezing applications for tunneling subject to water seepage*. Safe tunneling for the city and for the environment: proceddings ITA-AITES World Tunnel Congress, Budapest.

General Report of TC 215
Environmental Geotechnics

Rapport général du TC 215
Géotechnique de l'environnement

Bouazza A.
Monash University, Melbourne, Australia

ABSTRACT: Twenty two (22) papers have been allocated to this session. They originated from twelve (12) countries and five (5) continental regions (Asia, Europe, North America, South America and Oceania). They described and presented laboratory and field studies and numerical modelling addressing numerous topics which included novel materials, chemical compatibility of barrier materials, unsaturated behaviour of geosynthetic liners, soil-geosynthetic liner interface behaviour, waste geotechnical properties, phytoremediation, permeable reactive barriers, soil and groundwater remediation, image analysis, natural leaching of heavy metals and biogeotechnology. This general report offers a review of all the papers submitted to this session and highlights the major findings reported by the authors of these papers.

RÉSUMÉ : Vingt-deux (22) communications ont été allouées à cette session. Elles proviennent de douze (12) pays et de cinq (5) régions continentales (Asie, Europe, Amérique du Nord, Amérique du Sud et Océanie). Ces communications décrivent et présentent des études de laboratoire et sur site ainsi que des études de modélisation numérique. Elles traitent de nombreux sujets comprenant les nouveaux matériaux, la compatibilité chimique des matériaux d'étanchéisation, le comportement insaturé des géosynthétiques, le comportement de l'interface sol-géosynthétique, les propriétés géotechniques des déchets, la phytoremédiation, les barrières réactives perméables, l'assainissement des sols et des eaux souterraines, l'analyse d'images, le lessivage naturel des métaux lourds et la biogéotechnologie. Ce rapport général présente une revue de tous les documents soumis à cette session et met en évidence les principaux résultats rapportés par les auteurs de ces documents.

KEYWORDS: biogeotechnology, containment barriers, geotechnical properties, groundwater, soil, remediation, waste,

1 INTRODUCTION

Environmental Geotechnics has evolved dramatically from the 1980s/1990s practice where the focus was on addressing problems related to contaminated sites as well as waste management. Nowadays, the discipline has expanded dramatically to tackle new challenges brought about by a continuous evolving world. Energy (geothermal energy, CO2 sequestration, coal seam and shale gas, methane hydrates, etc.), oil and gas resources, mining, reservoir engineering, effect of climate change on built structures and biogeotechnical engineering, are examples of areas Environmental Geotechnics has expand to. Consequently, this had the effect of bringing other different disciplines (chemistry, biology, soil science, etc.) even closer than before.

Significant and rapid progress in research and development has enabled the development of Environmental Geotechnics as a discipline to the level where it is now. This is reflected by the contributions made to this session which includes novel materials to deal with very aggressive solutes to biological approaches to restore land devastated by natural events.

Twenty two (22) papers have been allocated to this session. They originated from twelve (12) countries and five (5) continental regions (Asia, Europe, North America, South America and Oceania). Most papers have presented laboratory studies. Papers including field studies and numerical modelling were also presented. The papers have been grouped into the following themes:

- Containment barriers
- Municipal solid waste and other types of waste geotechnical properties
- Soil and groundwater remediation
- Biogeotechnology

This general report offers a review of all the papers submitted to this session. It highlights the major findings reported by the authors of these papers.

2 CONTAINMENT BARRIERS

Bohnhoff et al. describe a study on bentonites that have been chemically modified to achieve greater chemical compatibility when used as containment barriers such that the desirable engineering properties of the bentonites are not compromised. They have considered three bentonites. These bentonites include **(1)** a natural Na-bentonite polymerized with acrylic acid to form polyacrylate polymerized bentonite, referred to as a bentonite polymer nanocomposite or BPN, **(2)** a propylene carbonate (PC) modified Na-bentonite, referred to as "multiswellable bentonite" or MSB, and **(3)** Na-bentonite amended with sodium carboxymethyl cellulose (Na-CMC), referred to as "HYPER clay" or HC. Two potential applications were considered: 1) soil bentonite (SB) vertical cut off walls and 2) geosynthetic clay liners. In both cases hydraulic conductivity to water and $CaCl_2$ solutions were compared with those of three natural Na-bentonites commonly used in geoenvironmental containment applications. Permeation with deionised water, DIW, (plotted at 0.1 mM $CaCl_2$ in Fig. 1) resulted in low k_w (i.e., 4.2 x 10^{-12} to 3.4 x 10^{-11} m/s) regardless of the bentonite type. However, the BPN, HC2, and MSB exhibited superior hydraulic behaviour (i.e., lower k_c) relative to the GCL bentonites. The influence of $CaCl_2$ on the k of backfill specimens containing 5.7 % NB1 or 5.6 % MSB and specimens containing 7.1 % NB2, 2.4 % BPN, and 5.5 % BPN is shown in Fig. 2b. All of the specimens were susceptible to an increase in k, i.e., k_c/k_w > 1, where k_c = hydraulic conductivity to the $CaCl_2$ solution, when permeated with ≥ 10 mM $CaCl_2$ solutions. The increases varied from approximately two-fold to 15-fold depending, in part, on the bentonite content. The authors indicated that the differences in behaviour among these novel bentonites illustrated in this paper highlight the need for further research into the specific mechanisms affecting the performance of such new materials. At the same time, the paper shows the potential that such bentonites can have in addressing aggressive solutes.

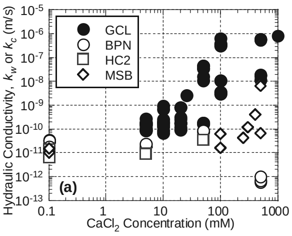

Figure 1 Hydraulic conductivity of bentonite specimens as a function of (a) $CaCl_2$ concentration in the permeant liquid (Bohnhoff et all., 2013)

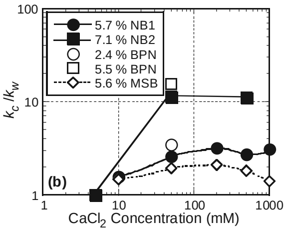

Figure 2. Permeation results for sand-bentonite backfills: ratio of hydraulic conductivity to $CaCl_2$ solution, k_c, relative to hydraulic conductivity to water k_w as a function of $CaCl_2$ concentration (Bohnhoff et al., 2013)

Brianzoni et al. report the results of a research study aimed at evaluating and predicting the long term hydraulic performance of cement bentonite (CB) mixtures used in cut off walls when in contact with saline solutions (K_2SO_4) or acidic solutions (H_2SO_4) at different concentrations. Hydraulic conductivity tests were conducted for this purpose and lasted in some cases for 2 year to assess the CB mixtures chemical compatibility. This paper shows that the saline and acidic solutions can adversely affect the hydraulic performance of CB mixtures depending on SO_4^{2-}concentration and pH. At concentration of the order of 25 g/l or more, both solutions produced an initial decrease in the k value, followed by an increase and finally an almost constant trend of hydraulic conductivity with curing time. Swelling and a dense net of fixtures were detected on both samples after permeation due to ettringite formation. Sample thickness was found to affect the response of the CB mixtures when permeated with saline solutions. The authors indicated that the chemical conditions adopted in the tests are not expected to occur continuously in the field if a pumping system is provided so that there is an advective flow of groundwater and not of pollutant across the barrier.

Indrawan et al. present the findings of the work they have conducted on the effects on the hydraulic conductivity of compacted clays, commonly used for lining coal seam gas (CSG) water storage ponds, of moisture conditioning and permeation with CSG water. Four kaolinite-dominant clays were mixed with CSG and deionised waters and compacted to varying compaction degrees at different gravimetric moisture contents before permeation. Tests were conducted in a rigid wall permeameter (100 kPa hydraulic loading) and in an oedometer (100 kPa axial stress). The hydraulic conductivity of clays moisture-conditioned, compacted and permeated with saline CSG water (k= $1x10^{-11}$ m/s) was found to be similar to that of the same clays moisture-conditioned, compacted and permeated with deionised water. In both CSG and deionised waters, the compacted clay particles dispersed and the hydraulic conductivity decreased to a very low value of about $1x10^{-11}$ m/s. The hydraulic conductivities measured using a compaction mould permeameter were found to be comparable to, and a little higher than, those calculated from oedometer test data for the same compacted clays. The authors concluded that the clays investigated would be suitable as a liner for a CSG water storage pond.

Hanson et al. present the results of a laboratory investigation aimed at determining the moisture-suction relationships of geosynthetic clay liners (GCLs) under as-received conditions (moisture contents in the range of 14-27%) and subsequent to wet-dry cycles (20 cycles at 50% moisture content). Tests were conducted on three types of needle punched GCLs which contained granular bentonite. Two of the GCLs were of the conventional types whereas the third GCL was of a multi-component type (i.e. the carrier geotextile was composed of a non woven geotextile and a geofilm). Differences were observed between the conventional and multi-component GCLs and between the as-received and wet-dry cycled GCLs. The air entry suction value for the multi-component GCL was found to be lower than that for the conventional GCLs for the drying branches of the moisture suction curves and higher for the wetting branches of the curves. The residual suction value for the multi-component GCL was found to be higher than the residual suction values for the other two GCLs. The extent of hysteresis decreased and the differences between drying and wetting curves reduced for the wet-dry cycled specimens compared to the as-received specimens. Macro- and micro-structural variations determined through grain size distribution and SEM analyses (Fig. 3) indicated increasing void sizes and non-uniformity in fabric due to wet-dry cycling, supporting the observations made for variations in moisture-suction response.

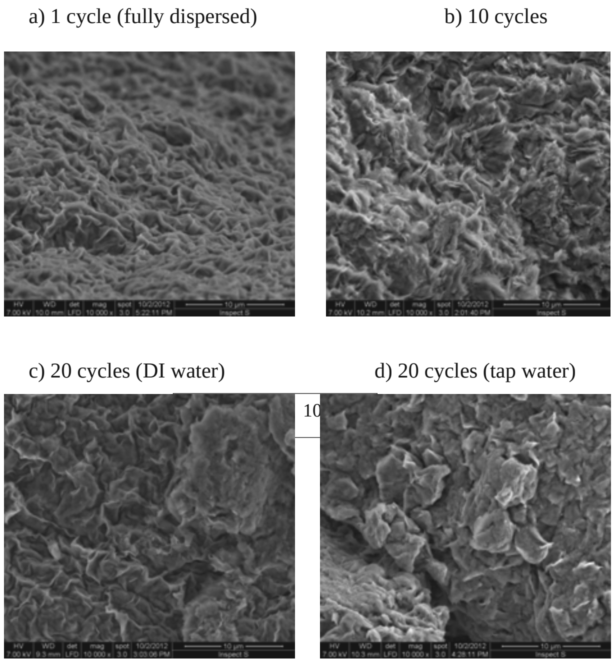

Figure 3. SEM images of bentonite from GCL specimens (Hanson et al. 2013)

Rayhani and Sarabadani describe a laboratory simulation study undertaken to quantify the hydration progress of Geosynthetic Clay Liners (GCLs) from underlying subsoils under simulated landfill conditions, before and after having been covered by municipal solid waste. GCL hydration was shown to be highly dependent on GCL manufacturing techniques, grain size distribution and initial moisture content of the subsoil. In particular, the difference in suctions between the GCLs and the type of subsoils was found to be an important factor governing the hydration process. The thermally treated, scrim-reinforced GCL demonstrated higher rate and degree of hydration compared to the other GCL products tested under similar conditions mainly due to the better anchorage of the connection layer against swelling of bentonite upon hydration.

Thermal cycles were found to severely suppress the moisture uptake of the GCL to as low as 15% of the moisture content observed under isothermal conditions. Seasonal cooling was shown to not guarantee sustainable hydration of the GCL provided that the GCL is subsequently exposed to daily thermal cycles. The authors suggest that the construction of a leachate collection system could provide the sufficient normal stress (2-5 kPa) for an adequately high rate of hydration as well as degree of hydration.

Monteiro et al., present the results of ramp and direct shear tests conducted on different geomembrane products (PVC and smooth and textured HDPE) in contact with a sandy soil prepared at various degrees of saturation. The results presented show that the interface friction angle between soil and geomembranes was insensitive to the variation of the soil degree of saturation. A progressive interface failure mechanism was observed in the tests with PVC geomembrane due to the more extensible nature of this type of geomembrane. The largest values of interface friction angles were obtained as expected with the textured HDPE geomembrane, whereas similar lower values were obtained with the smooth PVC and HDPE geomembranes.

3 MUNICIPAL SOLID WASTE AND OTHER TYPES OF WASTE GEOTECHNICAL PROPERTIES

Chen et al. propose a Bio-Hydro-Mechanical (BHM) coupled model to investigate solid-liquid-gas interaction behaviour in landfills containing municipal soils waste (MSW) with high organic content. The model also takes into account the release of moisture caused by the MSW biodegradation process. The development of the model is based on laboratory and in-situ investigations conducted on MSW to assess their hydraulic conductivity, gas permeability, and compressive and shear strength characteristics. The model was applied to hypothetical waste samples 5 m thick with properties similar to MSW from Qizishan landfill, China and Orchard Hills landfill, USA, to predict leachate production, gas pressure and settlement. Key problems relevant to waste management are also discussed in particular slope stability issues which can be caused by the presence of high organic content and consequently high water content and entrapment of gas pressures. Figure 4 shows that a mixture of leachate and landfill gas being ejected to a height of up to 5 m when drilling vertical extraction wells in Xiaping landfill, China. It indicates that the presence of very high pore and gas pressures may exist in the waste body if not managed properly and can be detrimental to the slope stability of a landfill.

Figure 4 . Ejection of leachate/gas (Chen et al., 2013)

Singh reports on the shear strength properties of municipal solid waste (MSW) and indicates that a factor which has not been paid much attention to is the highly compressible nature of MSW. It is suggested that due to the large compressibility of MSW at high normal stresses, a single Mohr Coulomb shear envelope for a landfill may not be applicable. A new approach based upon the use of 'Strength versus Depth' plot has been proposed. It is argued that the use of strength versus depth plot is more appropriate for characterizing shear strength of MSW, especially for high landfills.

Cañizal et al. discuss the importance of determining the mechanical properties of MSW and their implication on landfill design. The paper highlights the difficulties in measuring these properties due to the nature of the material tested. The lack of samples representativeness for laboratory work and difficulties in interpreting field tests based on the experience gathered with conventional geotechnical materials have been cited as being major hurdles in obtaining reliable assessment of MSW mechanical properties. Back-analysis of failures was suggested as another possible approach to gather further information. However uncertainties still exist with this approach since failure cases are not frequent; and in the few cases which have occurred, it was difficult to detect the failure surface. A compilation of strength parameters obtained from laboratory and in situ tests and from failures (Figure 5) was presented.

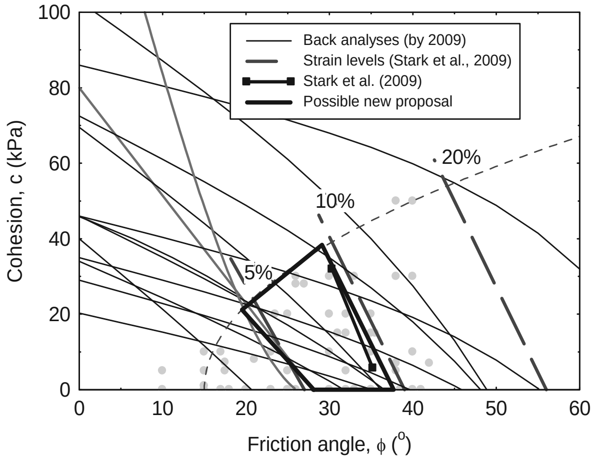

Figure 5. MSW strength parameters (Cañizal et al., 2013)

Lavoie and Sinclair discuss the properties of a waste sludge which comprises primarily clay and iron-sands/grit originating from iron sands mining and in relation to its disposal in cells . This wet sludge waste is landfilled in cells to heights up to 25m. This paper shows that the characteristics of the sludge in situ are governed both by the nature of the material and the operation procedures. Key to the process is the limited height of each lift, together with the period of desiccation between lifts. To investigate the properties of the sludge for design input, boreholes and CPT's were put down through completed landfill cells of different ages. Field tests (boreholes and CPT's) on completed landfill cells of different ages showed that the in situ sludge experiences significant strength increase with time and depth, with pore pressures well below hydrostatic conditions. The sludge was assessed to be non-liquefiable based CPT data and Atterberg Limits gathered for this project.

4 SOIL AND GROUNDWATER REMEDIATION

Fronczyk and Garbulewski present a study on the influence of MSW landfill leachate on the hydraulic conductivity of zeolite-sand mixtures (with 50% and 20% content of zeolite). Results of the study indicate that the hydraulic conductivity of the reactive material has changed almost by two orders of magnitude (from 9.25×10^{-5} to 1.25×10^{-5} m/s). This change is believed to have been caused by the reduction of the effective porosity due to pore clogging. Analysis of calcium carbonate content showed no significant increase of carbonates in the samples, while scanning electron microscope study showed increased calcium content and formation of crystals of calcium carbonate in the samples indicating that a precipitation process took place. Moreover, biological growth was observed indicating the presence of microbial activity.

Courcelles presents a study conducted on reactive filters for use in Permeable Reactive Barriers (PRB) to treat contaminants. One of the main geometric filter configurations consists in constructing an upward vertical filtration in a reactive filter. Crossing several meters of filter can generate excessive head losses, modify the regional flow and lead to a bypass of the system. A new radial-flow filter with a reduced filtration length has been developed to minimize these head losses. Physical tests have confirmed its hydraulic benefits since a reactive material with a hydraulic conductivity of 2.10^{-4} m/s after clogging was found to reduce the head loss by a factor of 4.5 when subjected to a radial filtration instead of a conventional vertical upward filtration. However, this result is strictly dependent on the ratio between the hydraulic conductivities of the coarse material and the reactive material. A minimum ratio of 50 was necessary to ensure a pseudo-vertical flow. This observation will improve the design of radial filters for tests at the pilot scale. It was concluded that in general, the use of radial hydraulic filter allows selection of the finest reactive materials, which is advantageous in chemical terms and makes it easier to meet the requirement for minimum ratio between the hydraulic conductivities of the coarse material and the reactive material.

Umezaki and Kawamura describe a zero-emission system to preserve the ecosystem in a closed water body such as a lake. The system is based on three processes: a) dredging of the lake bed soil; b) dehydration and purification to absorb nutrient salts; c) consolidation to reduce the volume of the dredged material after its return to the lake. Consolidation tests and column tests for bed mud and lake water sampled in Lake Suwa, Japan were conducted to simulate these processes. Natural zeolite powder was used as the absorbent for purification. Consolidation tests were carried out on the lake bed soil with natural zeolite powder as absorbent, and column tests were conducted to monitor the release inhibition of nutrient salts on the treated soil and lake water. It was reported that by applying about 30 kPa of low consolidation pressure, water contents approached the liquid limit and the volume decreased to about two-thirds. In the column test for bed mud with no treatment, total nitrogen (T-N), total phosphorus (T-P), and chemical oxygen demand (COD) surpass water quality standards for lakes in Japan. The release of nutrient salts from bed mud was clearly recognizable and algae developed in the water. To inhibit eutrophication, dehydration under 30 kPa and purification using natural zeolite powder was conducted; the contents of T-N and T-P were found to meet water quality standards for lakes. T-N decreased because of absorption of nitrogen by natural zeolite. Algae did not grow. The release inhibition effect for nutrient salts of natural zeolite was proved. However additional countermeasures against COD are still required.

Lugli and Mahler describe an in-situ remediation technique involving the uptake of contaminants by plant roots and their subsequent accumulation in plant tissues. The technique is referred to as Phyto-extraction. A numerical evaluation, using Hydrus 1-D, was conducted to evaluate the effectiveness of phytoremediation of Pb^{2+} and Zn^{2+}. The simulations considered soil and climatological data representative of the coastal lowlands of the municipality of Rio de Janeiro in Brazil and were organized in three steps: pre-contamination (analysis of the hydrological conditions), contamination (analysis of the contamination plume before planting) and remediation. It was indicated that, by modifying root depth and introducing irrigation, the phyto-extraction process could be optimized for contaminants characterized by low (e.g. Zn^{2+}) (Figures 6 and 7), and high (e.g. Pb^{2+}) retardation factors.

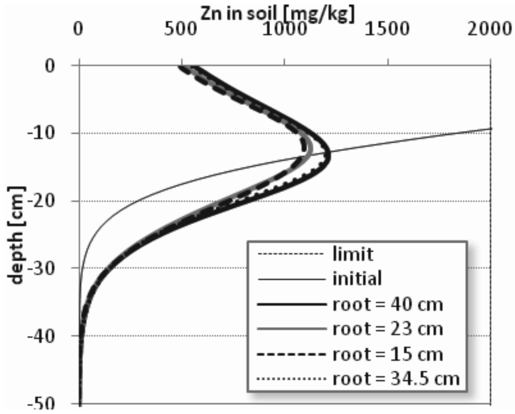

Figure 6: Zn^{2+} plumes: initial and after 10 years of remediation with different root depth (Lugli and Mahler, 2013)

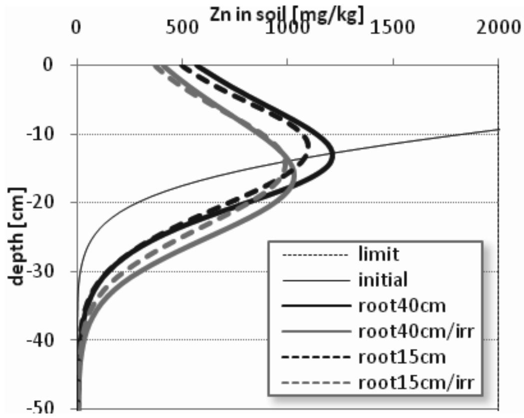

Figure 7: Zn^{2+} plumes: initial and after 10 years of remediation with different root depth and presence of irrigation (Lugli and Mahler, 2013)

Saadaoui et al. describe a new soil remediation technique using thermal in-situ desorption treatment (without excavation) referred to as NSRCityTM. The technique is based on heating the soil by conduction and extraction of the vapours of hydrocarbons released due to the heating process. The technique has already been used successfully on many urban and industrial sites in Europe and the United States. This technique was recently used in Belgium. The site contained a floating 0.5 m thick layer of hydrocarbons located at a depth of 3 m. A spacing of 1.5 m between heating tubes, allowed the site to be treated within 70 days.

Jones describes the integration of geotechnical, environmental and groundwater investigations for the Terminal 4 Project in Newcastle, Australia, aimed at identifying appropriate remediation measures to protect human health and environmental values. It discusses the various remediation methods proposed for the safe development of the site. Methods considered (see Fig. 8) include soil-bentonite cut off walls to deal with tar waste, permeable reactive walls to tackle asbestos/lead contaminants, multi-phase extraction (MPE) to extract free-phase LNAPL contamination, followed by monitored natural attenuation (MNA) for residual dissolved phase hydrocarbon contamination and installation of a low-permeability geosynthetic clay liner (GCL) over the site for protection purposes. The Terminal 4 Project (Fig. 8) is expected to improve the long-term environmental condition of a site previously contaminated by industrial waste, while protecting the surrounding sensitive environment.

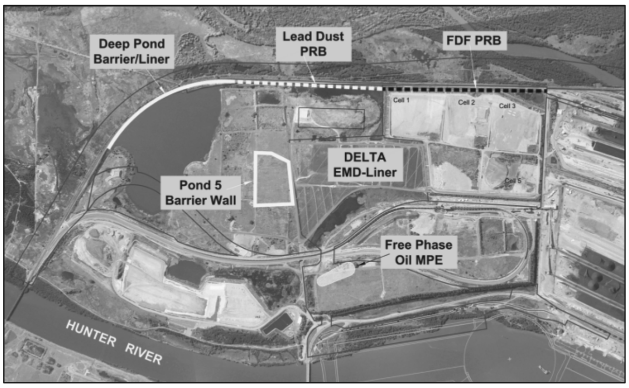

Figure 8. Remediation Plan (Jones, 2013)

Flores et al. present a simplified image analysis method to assess the saturation distribution of water and Non-Aqueous Phase Liquids (NAPLs) of different densities and viscosities ($0.73 \leq \rho \leq 1.20$ g/cm^3; $1.4 \leq \nu \leq 1000$ mPa·s) in granular soils subject to fluctuating groundwater conditions. This study has confirmed that the relationship between Optical Density (D_i) and water and LNAPL saturation values (S_w and S_o) is approximate linear, as predicted by the Beer-Lambert Law of Transmittance, for ten different NAPLs. Based on these findings, it was concluded that the Simplified Image Analysis Method can be safely used to assess water and NAPL saturation distributions in porous media subject to dynamic conditions, for a broad range of NAPLs. Furthermore, the authors applied this method to study the behaviour of five different NAPLs in experimental columns subject to drainage and imbibition processes, and confirmed that light NAPLs can effectively get trapped below the water table, despite their lower densities than water.

Inoue et al. describe a new methodology based on using spatial moment analysis linked with image processing of a dye tracer behaviour in porous media to estimate dispersivities in longitudinal and in transverse directions. Laboratory and field tracer experiments using a relatively mobile dye tracer referred to as Brilliant Blue FCF were conducted under saturated and unsaturated flow conditions. Dispersivities were found to exhibit an increasing and decreasing tendency associated with water content and showed a dependency on infiltration rates. Experimental results showed the effectiveness of the new methodology for simultaneous assessment of transverse and longitudinal dispersion in unsaturated soils in field as well as in laboratory.

Inui et al. address the issue of excavating stratums that naturally contain heavy metals due to their geologic histories. This paper addresses the long term leaching characteristics of arsenic and lead in several rock materials, which were weathered in outdoor for more than two years. Several laboratory tests were conducted to estimate the long term leaching characteristics of As and Pb in several rock materials, and then comparing to the results obtained from outdoor exposure tests.It was concluded that total contents of trace metals can be regarded possibly as screening values to judge whether detailed evaluation of leaching characteristics is necessary. The leaching amount of As obtained in the conventional batch leaching test was found to be a good index of field leaching amount, and the accelerated oxidation tests were shown that they could simulate the outdoor leaching amount on the safe side.

5 BIOGEOTECHNOLOGY

Omine et al. describe a geo-environmental approach used to restore farmed land which was damaged by salinity, due to tsunami water triggered by the mega earthquake that hit the pacific coast of the Tohoku region in Japan in March 2011. As a consequence of this event, the pH and EC of the agricultural soil increased and exceeded the safer limits for cultivated crops. Compost containing Halo bacteria/salt tolerance bacteria was used to restore the farmland. Chemical analysis and potting cultivation were performed on the saline soils. It was shown that the compost containing salt tolerance bacteria can reduce the excessive salts and consequently reduce the salinity problem. It was also confirmed that the compost was effective for growth of rice plants. The compost also provided necessary nutrients to the soil and plant. However, it was not easy to distinguish clearly in the field application the effect of the compost with salt tolerance bacteria due to decrease of salt concentrations caused by rainfall and vegetation.

Sassa et al. describe a new Ecological Geotechnics approach. They investigated the linkage between the waterfront environment and the burrowing activity of six species of invertebrates in intertidal flats through a series of controlled laboratory experiments on the benthos-soil systems. The experimental results show that there exist both suitable and critical environmental conditions for the burrowing activities of the diverse species irrespective of burrowing types, growth stages and weights. On the basis of these results, an ecohabitat chart was developed revealing complex interrelationships among species between suitable and critical environmental conditions. Validation of the chart was conducted through an integrated field observations, surveys and analyses of the waterfront environment and the species distributions at five natural and artificial intertidal flats. The results demonstrate that the way and where the diverse species lived are well consistent with the ecohabitat chart developed in this study. It was concluded that the results obtained succeed not only in answering the fundamental question of why intertidal flats foster a complex ecosystem by the diverse species, from a view point of Ecological Geotechnics, but also established a new rational basis which can facilitate the conservation and restoration of habitats with rich natural ecosystems in intertidal zones.

Stewart et al. review techniques from molecular biology for characterising microbial populations that are accessible to Geotechnical or Geo-Environmental Engineers. With reference to data from contaminated land studies, the paper discusses which techniques might be appropriate to use in an engineering context, how the data generated can be visualised and interpreted, and the dangers of over interpretation. Polymerase chain reaction (PCR), a technique for replicating a selected section of a DNA fragment, based methodologies have been proposed to manage populations of microorganisms available in soils. PCR permit the detection of the microbes present and how they change with changing conditions. It is relatively easy to use in an engineering setting and the availability of reagents in kit form along (with detailed protocols) means that the barriers to adoption are reasonably low. The paper stress the fact that this is a rapidly moving field and the advent of high throughput deep sequencing technologies have led to the development of ‘metagenomics’ and ‘metatranscriptomics’ which investigates the composite genetic potential of an ecological niche. The authors indicate that instrumentation and cost of sample analysis are still relatively high but likely to fall as capacity and technology increase. In addition, the sheer volume of data generated poses a significant challenge in terms of bioinformatics and fully exploiting these technologies will require multidisciplinary collaborations between engineers, molecular biologists and informaticians.

6 CONCLUSIONS

Twenty two (22) papers have been allocated to this session. They described and presented laboratory and field studies and numerical modelling addressing numerous topics which included novel materials, chemical compatibility of barrier materials, unsaturated behaviour of geosynthetic liners, geosynthetic liner interface behaviour, waste geotechnical properties, phytoremediation, permeable reactive barriers, soil remediation, image analysis, natural leaching of heavy metals and biogeotechnology This general report offers a review of all the papers submitted to this session and highlights the major findings reported by the authors of these papers.

List of papers submitted to this session

Bohnhoff, G., Shackelford, C., Malusis, M. Scalia,J., Benson, C., Edil, T., Di Emidio, G., Katsumi, T. and Mazzieri, F. (2013). Novel bentonites for containment barrier applications. Proceedings of the 18th International Conference on Soil Mechanics and Geotechnical Engineering, Paris 2013

Brianzoni, V., Fratalocchi, E. and Pasqualini, E. (2013). Long term performance of cement-bentonite cut-offs in saline and acidic solutions. Proceedings of the 18th International Conference on Soil Mechanics and Geotechnical Engineering, Paris

Cañizal, J., Lapeña, P. Castro,J. A. da Costa, A., Sagaseta, C.(2013). Determination of shear strength of MSW. Field tests vs. laboratory tests. Proceedings of the 18th International Conference on Soil Mechanics and Geotechnical Engineering, Paris

Chen, Y.M., Zhan, L.T., Xu, X.B. and Liu, H.L. (2013). Geo-environmental problems in landfills of MSW with high organic content. Proceedings of the 18th International Conference on Soil Mechanics and Geotechnical Engineering, Paris

Courcelles, B. (2013). Experimental study of radial filtration in Permeable Reactive Barriers (PRB). Proceedings of the 18th International Conference on Soil Mechanics and Geotechnical Engineering, Paris

Flores, G., Katsumi, T., Inui, T. and Takai, A. (2013). Measurement of NAPL saturation distribution in whole domains by the Simplified Image Analysis Method. Proceedings of the 18th International Conference on Soil Mechanics and Geotechnical Engineering, Paris

Fronczyk, J. and K. Garbulewski, K. (2013). Hydraulic conductivity of zeolite-sand mixtures permeated with landfill leachate. Proceedings of the 18th International Conference on Soil Mechanics and Geotechnical Engineering, Paris

Hanson, J.L., Risken, J.L. and Yeşiller, N. (2013). Moisture-ruction relationships for geosynthetic clay liners. Proceedings of the 18th International Conference on Soil Mechanics and Geotechnical Engineering, Paris

Indrawan, I.G.B, Williams, D.J. and Scheuermann, A. (2013). Hydraulic conductivity of compacted clay liners moisture-conditioned and permeated with saline coal seam gas water. Proceedings of the 18th International Conference on Soil Mechanics and Geotechnical Engineering, Paris

Inoue, K., Shimada, H. and Tanaka, T. (2013). Simultaneous estimation of transverse and longitudinal dispersion in unsaturated soils using spatial moments and image processing. Proceedings of the 18th International Conference on Soil Mechanics and Geotechnical Engineering, Paris

Inui, T., Katsumi, T., Takai, A. and Kamon, M. (2013). Evaluating the long-term leaching characteristics of heavy metals in excavated rocks. Proceedings of the 18th International Conference on Soil Mechanics and Geotechnical Engineering, Paris

Jones, S. (2013). Geo-environmental challenges of a major coal terminal development in Australia. Proceedings of the 18th International Conference on Soil Mechanics and Geotechnical Engineering, Paris

Lavoie, J.L.N. and Sinclair, T.J.E. (2013). Characterisation of landfill steel mill sludge waste in terms of shear strength, pore water pressure dissipation and liquefaction potential. Proceedings of the 18th International Conference on Soil Mechanics and Geotechnical Engineering, Paris

Lugli, F. and Mahler, C.F. (2013). A numerical analysis of phytoextraction. Proceedings of the 18th International Conference on Soil Mechanics and Geotechnical Engineering, Paris

Monteiro, C.B., Araújo, G.L.S., Palmeira, E.M. and Cordão Neto, M.P. (2013) Soil-geosynthetic interface strength on smooth and texturized geomembranes under different test conditions. Proceedings of the 18th International Conference on Soil Mechanics and Geotechnical Engineering, Paris

Omine, K., Moqsud, MD. A and Hazarika, H. (2013). Geoenvironmental approach to restoration of agricultural land damaged by tsunami. Proceedings of the 18th International Conference on Soil Mechanics and Geotechnical Engineering, Paris

Rayhani, M.T., and Sarabadani, H. (2013). Factors affecting hydration of Geosynthetic Clay Liners in landfill applications. Proceedings of the 18th International Conference on Soil Mechanics and Geotechnical Engineering, Paris

Saadaoui, H., Haemers, J. and Denecheau, P. (2013). Utilisation de la désorption thermique pour l'élimination in situ des couches flottantes d'hydrocarbures. Proceedings of the 18th International Conference on Soil Mechanics and Geotechnical Engineering, Paris

Sassa, S., Watabe, Y. and Yang, S. (2013). Development and verification of ecohabitat chart based on ecological geotechnics. Proceedings of the 18th International Conference on Soil Mechanics and Geotechnical Engineering, Paris

Singh, S. (2013). A new approach for characterizing shear strength of municipal solid waste for landfill design. Proceedings of the 18th International Conference on Soil Mechanics and Geotechnical Engineering, Paris

Stewart, D.I, Fuller, S.J., Burke, I.T., Whittleston, R.A., Lockwood, C.L. and Baker, A. (2013). The role of molecular biology in geotechnical engineering. Proceedings of the 18th International Conference on Soil Mechanics and Geotechnical Engineering, Paris

Umezaki, T. and Kawamura, T. (2013). A system of dehydration, purification, and reduction for dredged soil – Release inhibition of nutrient salts from bed mud using natural zeolite. Proceedings of the 18th International Conference on Soil Mechanics and Geotechnical Engineering, Paris

Novel bentonites for containment barrier applications

Bentonites novatrices pour des applications comme barriers de confinement

Bohnhoff G., Shackelford C.
Colorado State University, Fort Collins, Colorado, USA

Malusis M.
Bucknell University, Lewisburg, Pennsylvania, USA

Scalia J., Benson C., Edil T.
University of Wisconsin, Madison, Wisconsin, USA

Di Emidio G.
Ghent University, Zwijnaarde, Belgium

Katsumi T.
Kyoto University, Kyoto, Japan

Mazzieri F.
Universita` Politecnica delle Marche, Ancona, Italy

ABSTRACT: Sodium bentonite (Na-bentonite) commonly is used in geoenvironmental containment barriers to control liquid flow and contaminant migration, but is known to be thermodynamically unstable in environments where multivalent cations are present. As a result, a host of novel, chemically-modified bentonites designed for improved resilience have been developed. The objective of this paper is to illustrate selected properties of some of these bentonites being considered for containment barrier applications. The bentonites considered in this paper include Na-bentonite polymerized with acrylic acid (bentonite-polymer nanocomposite, or BPN), Na-bentonite amended with sodium carboxymethyl cellulose (HYPER clay), and a propylene carbonate modified Na-bentonite (multiswellable bentonite, or MSB). Engineering properties of the novel bentonites relevant to two specific types of barriers (i.e., cutoff walls and geosynthetic clay liners) are compared and contrasted with those of natural Na-bentonites. The results illustrate the potential for improved hydraulic performance of barriers containing the novel bentonites. However, further research is needed elucidate the mechanisms responsible for differences in behavior and performance among these bentonites.

RÉSUMÉ : La bentonite à base de sodium (bentonite-Na) est utilisée couramment comme barrière de confinement géo-environmentale pour contrôler les flux de liquides et la migration de contaminants ; elle est cependant connue pour être instable thermodynamiquement dans des environnements qui contiennent des cations multivalents. Pour palier cet inconvénient, diverses bentonites novatrices modifiées chimiquement et conçues pour présenter une résistance améliorée aux écoulements ont été développées. L'objectif de cet article est d'illustrer certaines propriétés techniques de quelques unes de ces bentonites étudiées leur utilisation dans les barrières de confinement. Cet article présente les propriétés de la bentonite-Na polymérisée avec de l'acide acrylique (« bentonite-polymer nanocomposite », ou BPN), de la bentonite-Na modifiée avec de la carboxymethylcellulose sodique (ou « HYPER Clay ») et d'une bentonite-Na modifiée avec du carbonate de propylène (« multiswellable bentonite », ou MSB). On a procédé à une analyse comparative des propriétés des bentonites novatrices correspondant à deux types spécifiques de barrières (c.a.d., parois de séparation et revêtement par des géomembranes synthétiques) et celles des bentonites-Na naturelles. Les résultats illustrent le potentiel d'amélioration de la performance hydraulique que présentent des barrières contenant les nouvelles bentonites. Des recherches supplémentaires sont cependant nécessaires pour comprendre les mécanismes susceptibles d'expliquer les différences de comportement et de performance entre ces bentonites.

KEYWORDS: Bentonite; Bentonite slurry; Cutoff wall; Geosynthetic clay liner; Hydraulic conductivity; Polymerized bentonite

1 INTRODUCTION

Bentonite is a natural clay composed primarily of the mineral montmorillonite, a member of the smectite group of clay minerals. Montmorillonite is characterized by large surface area (100-800 m^2/g), a net negative charge typically on the order of 80 to 150 $cmol_c/kg$, and exchangeable surface cations (Grim 1968). These characteristics, in turn, impart a strong affinity by bentonite for water, resulting in swelling, sealing, and adhesive characteristics (Eisenhour and Brown 2009).

Bentonite commonly is used to control flow (seepage) and contaminant transport in a variety of hydraulic containment applications, such as soil-bentonite (SB) groundwater cutoff walls, barriers for waste containment (e.g., landfills, wastewater ponds, manure lagoons, nuclear storage, etc.), secondary containment in petroleum tank farms, and seals in monitoring and water supply wells. In all of these applications, sodium bentonite (Na-bentonite) typically is used, meaning that sodium (Na^+) is the predominant cation on the exchange sites of the individual bentonite particles. The preference for Na-bentonite stems from desirable engineering properties, such as low hydraulic conductivity to water, k_w (typically < 10^{-10} m/s), and the existence of semipermeable membrane behavior, the latter giving rise to hyperfiltration, chemico-osmotic flow, and reduced diffusion (Malusis et al. 2003). Unfortunately, Na-bentonite is thermodynamically unstable in environments where multivalent cations (e.g., Ca^{2+}, Mg^{2+}) are present, including most naturally occurring pore waters as well as waste streams containing heavy metals (e.g., landfill leachates, acid mine drainage) or radionuclides. Under such conditions, multivalent cations replace exchangeable monovalent cations, thereby reducing or eliminating osmotic swelling of the bentonite and the ability of bentonite to function effectively (e.g., Gates et al. 2009).

In response to the susceptibility of natural Na-bentonites to chemical attack and poor hydraulic performance, recent research has been undertaken to investigate novel bentonites that have been chemically modified to achieve greater compatibility with the surrounding environment, such that the desirable engineering properties of the bentonites are not compromised. For example, anionic polymers have been added to Na-bentonite to attain rheological properties needed for drilling fluids, and organobentonites (i.e., bentonites with organic cations on the exchange sites) have been created for applications where an organophilic material is needed for containment of organic compounds (e.g., Lee et al. 2012). Also, Na-bentonites complexed with various organic chemicals (e.g., polymers) have attracted considerable interest as potential substitutes for natural Na-bentonites in containment barriers, such as SB cutoff walls and geosynthetic clay liners (GCLs) (e.g., Katsumi et al. 2008, Mazzieri et al. 2010). The objective of this paper is to illustrate the potential improvement in engineering properties that can be attained with some of these novel bentonites when used in containment barriers. This objective is achieved by comparing engineering properties of the novel bentonites, including hydraulic conductivity to water and chemical solutions, with those of natural Na-bentonites.

2 NOVEL BENTONITES

Three novel bentonites are considered herein. These bentonites include (1) a natural Na-bentonite polymerized with acrylic acid to form polyacrylate polymerized bentonite, referred to as a bentonite polymer nanocomposite or BPN, (2) a propylene carbonate (PC) modified Na-bentonite, referred to as "multiswellable bentonite" or MSB, and (3) Na-bentonite amended with sodium carboxymethyl cellulose (Na-CMC), referred to as "HYPER clay" or HC.

The BPN was supplied by Colloid Environmental Technologies Co. (CETCO, USA), and was produced with polyacrylic acid (PAA) using methods similar to those used for the production of polymer nanocomposites (Bohnhoff 2012, Scalia 2012). A monomer solution was prepared by dissolving acrylic acid in water, and then the solution was neutralized with sodium hydroxide. Next, a natural (unmodified) Na-bentonite was added to the monomer solution in concentrations ranging from 30 to 50 % by weight to form bentonite-monomer slurry, followed by the addition of sodium persulfate, which served as an initiator. Polymerization then was induced by raising the temperature of the slurry above the decomposition temperature of the initiator molecule. Following polymerization, the PAA polymerized bentonite was oven dried, milled, and screened.

The MSB, supplied by Hojun Corp. (Japan), was created by compounding Na-bentonite with PC that expands the clay lattice and forms a hydration shell around the interlayer cations. The resulting Na-bentonite-PC complex can undergo osmotic swell in both fresh water and electrolyte solutions (hence the term "multiswellable"), including sea water (~500 mM NaCl) and solutions containing multivalent cations (e.g., Onikata et al. 1999). The MSB contained 25 % PC by dry weight.

The HC was created by combining Na-bentonite with Na-CMC, the sodium salt form of the anionic polymer CMC that has been used in industrial applications as a thickener (Di Emidio 2010). The base Na-bentonite was combined with a Na-CMC solution to form slurry. The slurry was dried at 105 °C, and the resulting solids were ground with a mortar grinder. The Na-CMC penetrates the interlayer regions between the clay platelets, resulting in expansion of the clay lattice and enhanced osmotic swell. Test results for HYPER clay containing either 2 % Na-CMC or 8 % Na-CMC are presented herein, where the former is designated as HC2 and the latter is designated as HC8. In both cases, the base Na-bentonite was the same base Na-bentonite used to create the MSB (designated herein as NB3).

The index properties of the novel bentonites (BPN, HC2, HC8, and MSB) are summarized in Table 1 and compared with those of two natural Na-bentonites designated as NB1 (NaturalGel®, Wyo-Ben, Inc., USA) and NB2 (Volclay®, American Colloid Company, USA) and the base Na-bentonite, NB3, used to create HC and MSB. Both NB1 and NB2 are commonly used for SB cutoff walls. The unusual behavior that can be exhibited by polymer modified bentonites is illustrated in the case of the BPN, wherein the BPN exhibits the highest free swell and cation exchange capacity (*CEC*), despite the lowest liquid limit (*LL*) and an overall nonplastic behavior. This unusually high swell and *CEC* have been attributed to the high swelling potential of the hydrophilic polymer used in the BPN (also used in baby diapers) and the tendency of the polymer to bind cations (Bohnhoff 2012, Scalia 2012). In contrast, the *CECs* for HC2, HC8, and MSB are only marginally higher than that of NB3. However, HC2, HC8, and MSB exhibited markedly higher *LLs* relative to NB3, presumably due to the addition of Na-CMC and PC, respectively.

Table 1. Index properties of bentonites examined herein (NB1 = NaturalGel®; NB2 = Volclay®; NB3 = Hojun Na-Bentonite; BPN = Bentonite Polymer Nanocomposite; HC2 and HC8 = HYPER Clay with 2 % and 8 % Na-CMC, respectively; MSB = Multiswellable Bentonite).

Property	Standard	Value						
		NB1	NB2	NB3	BPN	HC2	HC8	MSB
Soil classification	ASTM D 2487	CH	CH	CH	CH	CH	CH	CH
Liquid limit (%)	ASTM D 4318	583	420	466	255	650	742	547
Plasticity index (%)		530	381	421	NP	594	681	502
Distilled water swell index (mL/2 g)	ASTM D 5890	35	32	26	73	37[c]	48[c]	29
Montmorillonite content (%)	a	69	91	77	76	78	78	74
Cation exchange capacity, *CEC* ($cmol_c$/kg)	b	83.4	78.0	44.5	143	47.3	46.7	49.8
Exchangeable metals ($cmol_c$/kg):	b							
Ca^{2+}		4.9	28.1	5.6	9	11.4	12.7	7.7
Mg^{2+}		8.8	13.3	7.9	3	6.2	5.5	6.1
Na^{+}		73.4	34.3	26.3	128	34.2	44.5	33.3
K^{+}		1.1	1.6	0.2	3	0.3	0.2	0.5
Sum		88.2	77.3	40.0	143	52.1	62.9	47.6

[a] Based on energy dispersive X-ray diffraction analysis;
[b] Procedures for NB1, NB2, and MSB given by Shackelford and Redmond (1995); procedures for BPN given by Scalia (2012); procedures for HC2 and HC8 given by Di Emidio (2010);
[c] Values likely underestimated (see Di Emidio 2010).

3 RESULTS

3.1 *Soil-Bentonite Vertical Cutoff Walls*

Soil-bentonite (SB) cutoff walls are commonly constructed in the US using the slurry trench method in which a trench is excavated and filled with bentonite-water slurry (typically 4-6 % bentonite) to maintain trench stability, the trench spoils are mixed with dry bentonite (as needed) and slurry to create a homogeneous, high-slump SB backfill, and the backfill is placed into the trench to create the wall. The slurry viscosity must be sufficiently high to maintain trench stability, yet sufficiently low to be easily displaced by the backfill. The slurry also should form an adequate filter cake along the trench sidewalls to minimize slurry loss during construction. Recommended slurry properties include a Marsh viscosity of 32-40 s and a filtrate loss of < 25 mL (Evans 1993). Also, the backfill must exhibit a low hydraulic conductivity, typically ≤ 10^{-9} m/s for geoenvironmental containment applications.

The influence of bentonite content on the Marsh viscosity and filtrate loss (API 13A-B) of slurry containing untreated bentonite (NB1, NB2) or treated bentonite (HC8, BPN, MSB) is illustrated in Fig. 1. Slurries containing 3-5 % NB1, NB2, or MSB exhibit viscosities within the range of 32-40 s (Fig. 1a). For these clays, a bentonite content of 5 % likely would be selected to obtain a greater slurry density and reduce filtrate loss (Fig. 1b). In contrast, the viscosities of slurries containing ≥ 3 % HC8 or BPN were > 40 s and increased drastically with increasing bentonite content due to thickening caused by the polymer. Thus, slurry containing 2 % HC8 or BPN would be appropriate for slurry trench construction based on viscosity. Finally, the filtrate losses for 2 % HC8 and BPN are equal to or lower than the filtrate losses for 5 % MSB or NB1.

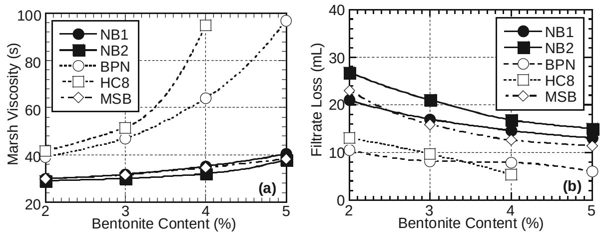

Figure 1. Properties of bentonite-water slurries as a function of bentonite content: (a) Marsh viscosity; (b) filtrate loss (NB1 and MSB data from Malusis et al. 2010; NB2 and BPN data from Bohnhoff 2012).

Hydraulic conductivity and chemical compatibility of model SB backfills comprised of sand and NB1, NB2, MSB, or BPN were investigated in recent studies by Malusis and McKeehan (2012) and Bohnhoff (2012). Although the sands used in both studies were clean and poorly graded, the sand used by Malusis and McKeehan (2012) in the NB1 and MSB backfills was a fine sand (D_{50} = 0.20 mm) whereas the sand used by Bohnhoff (2012) in the NB2 and BPN backfills was a medium sand (D_{50} = 0.45 mm). In both studies, the specimens were tested in flexible-wall cells at low confining stresses (≤ 34.5 kPa). The specimens were permeated with tap water until a steady k_w was achieved, and then were permeated with $CaCl_2$ solutions (5-1,000 mM) until termination criteria for chemical equilibrium between the influent and effluent were achieved (see cited references for further details).

The measured k_w values from these studies are presented in Fig. 2a along with k_w values measured recently at Bucknell University for sand-bentonite backfill specimens containing HC8 and the same fine sand used by Malusis and McKeehan (2012). The backfills containing the polymer-modified bentonites (BPN or HC8) generally exhibited lower k_w relative to the backfills containing similar percentages of MSB or Na-bentonite (NB1 or NB2), indicating that less BPN or HC8 is needed to create backfill with an acceptable k_w (i.e., ≤ 10^{-9} m/s).

The influence of $CaCl_2$ on the k of backfill specimens containing 5.7 % NB1 or 5.6 % MSB (Malusis and McKeehan 2012) and specimens containing 7.1 % NB2, 2.4 % BPN, and 5.5 % BPN (Bohnhoff 2012) is shown in Fig. 2b. All of the specimens were susceptible to an increase in k, i.e., $k_c/k_w > 1$, where k_c = hydraulic conductivity to the $CaCl_2$ solution, when permeated with ≥ 10 mM $CaCl_2$ solutions. The increases varied from approximately two-fold to 15-fold depending, in part, on the bentonite content. For example, the specimen containing the most bentonite (7.1 % NB2) exhibited the highest k_c/k_w (~15) of all the specimens. Also, the 2.4 % BPN specimen exhibited a lower k_c/k_w relative to the 5.5 % BPN specimen permeated with the same $CaCl_2$ solution (50 mM). However, k_w for the 5.5 % BPN backfill (2 x 10^{-12} m/s) was well below the typical regulatory limit (10^{-9} m/s), whereas k_w for the 2.4 % BPN backfill was unacceptably high (10^{-7} m/s; see Fig. 2a). Thus, the lower BPN content (2.4 %) was advantageous in terms of chemical compatibility, but was insufficient for achieving regulatory compliance in terms of k.

For the specimens with similar bentonite contents (i.e., 5.7 % NB1, 5.6 % MSB, and 5.5 % BPN), the 5.6 % MSB specimens exhibited the greatest resilience. The higher values of k_c/k_w for the 5.5 % BPN specimens relative to 5.6 % MSB and 5.7 % NB1 specimens permeated with the same $CaCl_2$ solution were attributed to two primary factors, viz., the greater reactivity of the 5.5 % BPN specimens, as reflected by the lower k_w for this backfill relative to those containing 5.6 % MSB or 5.7 % NB1 (see Fig. 2a), and the use of a coarser (i.e., more permeable) sand in the BPN backfills relative to the MSB and NB1 backfills. However, the lower k_w for the 5.5 % BPN backfill also allowed for a greater increase in k to occur without exceeding the typical regulatory limit of 10^{-9} m/s.

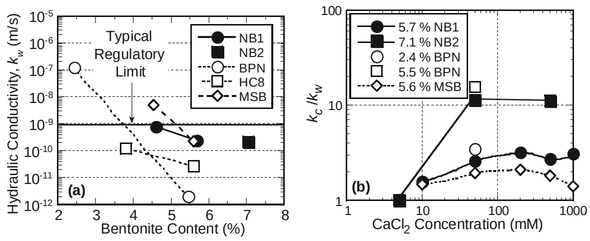

Figure 2. Permeation results for sand-bentonite backfills: (a) hydraulic conductivity to water, k_w, as a function of bentonite content; (b) ratio of hydraulic conductivity to $CaCl_2$ solution, k_c, relative to k_w as a function of $CaCl_2$ concentration (NB1 and MSB data from Malusis and McKeehan 2012; NB2 and BPN data from Bohnhoff 2012).

3.2 *Geosynthetic Clay Liners (GCLs)*

Values of k_c for BPN, HC2, and MSB specimens representing a typical GCL are shown in Fig. 3a. Data for specimens of Na-bentonite taken from actual GCLs (Bentomat® DN, CETCO, USA) are included in Fig. 3a for comparison. All specimens were permeated in flexible-wall cells under low effective stresses (14 to 30 kPa) until the hydraulic termination criteria of ASTM D 5084 were satisfied. Also, most of the specimens were permeated until chemical equilibrium (defined as the ratio of outflow and inflow electrical conductivity within 1.0 ± 0.1) was achieved, with the exceptions being the specimens permeated with deionized water (DIW) and the HC2 specimens. The results reflect a "worst-case" testing condition in that the specimens were not prehydrated prior to permeation (Shackelford et al. 2000). Permeation with DIW (plotted at 0.1 mM $CaCl_2$ in Fig. 3a) resulted in low k_w (i.e., 4.2 x 10^{-12} to 3.4 x 10^{-11} m/s) regardless of the bentonite type. However, the BPN, HC2, and MSB exhibited superior hydraulic behavior (i.e., lower k_c) relative to the GCL bentonites. These results illustrate the potential advantage of novel bentonites in solutions typically incompatible with conventional GCLs. Although higher $CaCl_2$ concentrations resulted in $k_c > k_w$ for HC2 and MSB, the increases were lower than those for the GCL bentonites. The BPN specimens exhibited similar increases in k_c relative to k_w for 5-50 mM $CaCl_2$, but exhibited $k_c < k_w$ for 500 mM $CaCl_2$.

The relationship between *k* and swell index, *SI* (ASTM D 5890), in the same solution (DIW or $CaCl_2$) for the bentonites in Fig. 3a is illustrated in Fig. 3b. The treated bentonites generally exhibited lower *k* for a given *SI* than the GCL bentonites, including MSB and HC2, which exhibit superior hydraulic behavior because of the activation of osmotic swelling (Di Emidio et al. 2011). However, the BPN exhibited both a low k_c and a low *SI* (8 mL/2 g) in 500 mM $CaCl_2$, illustrating that the hydraulic behavior of BPN was decoupled from swell. The BPN exhibited higher swelling in DIW relative to the other bentonites (see Table 1) due to the presence of the super-swelling polymer (Scalia 2012). However, polymer swelling does not account for the low k_c of BPN permeated with 500 mM $CaCl_2$, given the *SI* of only 8 mL/2 g. This atypical behavior of BPN illustrates that *SI* is not necessarily an accurate indicator of hydraulic conductivity for chemically modified bentonites.

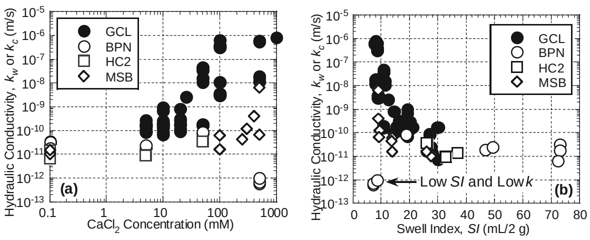

Figure 3. Hydraulic conductivity of bentonite specimens as a function of (a) $CaCl_2$ concentration in the permeant liquid, and (b) swell index in the same solution (GCL data from Jo et al. 2001, Jo et al. 2005, Lee and Shackelford 2005, Lee et al. 2005; MSB data from Lin and Benson 2000, Katsumi et al. 2008; HC2 data from Di Emidio et al. 2011; BPN data from Scalia 2012).

4 CONCLUSIONS

The hydraulic conductivity to water (k_w) and $CaCl_2$ solutions (k_c) of three novel (chemically modified) bentonites (BPN, HC, MSB) were compared with those of three natural Na-bentonites commonly used in geoenvironmental containment applications. The overall hydraulic performance is a function of not only the magnitude of chemical resistance (k_c/k_w) but also the baseline value of k_w. In terms of SB backfills, the use of BPN or HC8 generally exhibited lower k_w compared to MSB or Na-bentonites, implying that less BPN or HC8 is required to create backfills with an acceptable k_w. However, the backfill containing 5.5 % BPN exhibited the highest k_c/k_w, whereas the backfill containing 5.6 % MSB indicated low k_w and a k_c/k_w that was lower than that for the 5.5 % BPN backfill. Overall, the product of k_w and k_c/k_w for the backfills containing 5.5 % BPN and 5.6 % MSB resulted in superior hydraulic performance in terms of the providing the lowest values of k_c. In terms of GCLs, all three novel bentonites (BPN, HC, MSB) showed not only low k_w but also far superior resistance to chemical attack than the natural bentonites. Thus, the potential use of chemically modified bentonites in applications involving SB backfills and GCLs is promising. However, the differences in behaviors among the novel bentonites illustrated in this paper highlight the need for further research into the specific mechanisms affecting the performance of such novel bentonites.

5 ACKNOWLEDGEMENTS

Financial support for portions of the work presented herein was provided by the U.S. National Science Foundation (NSF), Arlington, VA, under grants CMMI-0757815 and CMMI-0758334. The opinions expressed in this paper are solely those of the authors and are not necessarily consistent with the policies or opinions of the NSF. The authors also appreciate the assistance of Mike Donovan and Jerry Darlington of CETCO, USA. Finally, the authors are grateful to Wyo-Ben, Inc., Hojun Corp., and American Colloid Company for providing materials.

6 REFERENCES

Bohnhoff, G. 2012. *Membrane behavior, diffusion, and compatibility of a polymerized bentonite for containment barrier applications.* PhD Dissertation, Colorado State Univ., USA.

Di Emidio, G. 2010. *Hydraulic conductivity and chemico-osmotic performance of polymer treated clays*. PhD Dissertation. Univ. of Gent, Belgium.

Di Emidio, G., Van Impe, W., and Flores, V. 2011. Advances in geosynthetic clay liners: polymer enhanced clays. *GeoFrontiers 2011*, ASCE, Reston, VA, USA, 1931-1940.

Eisenhour, D. and Brown, R. 2009. Bentonite and its impact on modern life. *Elements* 5 (2), 83-88.

Evans, J. 1993. Vertical cutoff walls, Ch. 17, *Geotechnical Practice for Waste Disposal*, D. Daniel, ed., Chapman & Hall, London, 430-454.

Gates, W. Bouazza, A., and Churchman, G. 2009. Bentonite clay keeps pollutants at bay. *Elements* 5 (2), 105-110.

Grim, R. 1968. *Clay mineralogy*, McGraw-Hill, New York.

Jo, H., Benson, C., Shackelford, C., Lee, J., and Edil, T. 2005. Long-term hydraulic conductivity of non-prehydrated geosynthetic clay liner permeated with inorganic salt solutions. *Journal of Geotechnical and Geoenvironmental Engineering* 131 (4), 405-417.

Jo, H., Katsumi, T., Benson, C., and Edil, T. 2001. Hydraulic conductivity and swelling of non-prehydrated GCLs permeated with single-species salt solutions. *Journal of Geotechnical and Geoenvironmental Engineering* 127 (7), 555-567.

Katsumi, T., Ishimori, H., Onikata, M., and Fukagawa, R. 2008. Long-term barrier performance of modified bentonite materials against sodium and calcium permeant solutions. *Geotextiles and Geomembranes* 26 (1), 14-30.

Lee, S., Oren, A. Benson, C. and Dovantzis, K. 2012. Organoclays as variably permeable reactive barrier media to manage NAPLs in ground water. *Journal of Geotechnical and Geoenvironmental Engineering* 138 (2), 115-127.

Lee, J. and Shackelford, C. 2005. Impact of bentonite quality on hydraulic conductivity of geosynthetic clay liners. *Journal of Geotechnical and Geoenvironmental* Engineering 131 (1), 64-77.

Lee, J., Shackelford, C., Benson, C., Jo, H., and Edil, T. 2005. Correlating index properties and hydraulic conductivity of geosynthetic clay liners. *Journal of Geotechnical and Geoenvironmental Engineering* 131 (11), 1319-1329.

Lin, L. and Benson, C. 2000. Effect of wet-dry cycling on swelling and hydraulic conductivity of geosynthetic clay liners. *Journal of Geotechnical and Geoenvironmental Engineering* 126 (1), 40-49.

Malusis, M. and McKeehan, M. 2012. Chemical compatibility of model soil-bentonite backfills containing multiswellable bentonite *Journal of Geotechnical and Geoenvironmental Engineering*, in press.

Malusis, M., McKeehan, M., and LaFredo, R. 2010. Multiswellable bentonite for soil-bentonite vertical barriers. *Proc., 6th Int. Conf. Environ. Geotech.* McGraw-Hill, New York, 764-769.

Malusis, M., Shackelford, C., and Olsen, H 2003. Flow and transport through clay membrane barriers. *Engineering Geology* 70 (2-3), 235-248.

Mazzieri, F., Di Emidio, G., and Van Impe, P. 2010. Diffusion of calcium chloride in a modified bentonite: impact of osmostic efficiency and hydraulic conductivity. *Clays and Clay Minerals* 58 (3), 351-363.

Onikata, M., Kondo, M., Hayashi, N., and Yamanaka, S. 1999. Complex formation of cation-exchanged montmorillonites with propylene carbonate: osmotic swelling in aqueous electrolyte solutions. *Clays and Clay Minerals* 47 (5), 672-677.

Scalia, J. 2012. *Bentonite-polymer composites for containment applications*. PhD Dissertation, Univ. of Wisconsin-Madison, USA.

Shackelford, C., Benson, C., Katsumi, T., Edil, T., and Lin, L. 2000. Evaluating the hydraulic conductivity of GCLs permeated with non-standard liquids. *Geotextiles and* Geomembranes 18 (2-4), 133-161.

Shackelford, C. and Redmond, P. 1995. Solute breakthrough curves for processed kaolin at low flow rates. *Journal of Geotechnical Engineering* 121 (1), 17-32.

Long term performance of cement-bentonite cut-offs in saline and acidic solutions

Perméabilité à long terme des parois ciment-bentonite en solutions acides et salines

Brianzoni V., Fratalocchi E., Pasqualini E.
Università Politecnica delle Marche, Ancona, Italy

ABSTRACT: The paper presents the results of a research aimed at evaluating and predicting the long term performance of CB mixtures in terms of hydraulic conductivity, k. A low k value is the necessary (even if not sufficient) requirement for a cut-off wall to isolate polluted sites. Aqueous sulphate solutions of different nature (acidic, saline) and concentrations were used as permeants in column tests performed for long time (one year or more) in order that full effects of physical and chemical reactions may occur. Results of these tests are here analysed mainly with the aim to find a criterion to predict how long a cement-bentonite cut-off wall can keep a proper hydraulic performance.

RÉSUMÉ: L'article présente les résultats d'une recherche ayant pour objectifs l'évaluation et la prévision de la perméabilité (k) à long terme des mélanges ciment-bentonite (CB). Une perméabilité faible est une condition nécessaire (bien que non suffisante) pour jouer le rôle d'écran de confinement sur les sites pollués. On a utilisé des solutions aqueuses de sulfates de différents natures (acide, saline) et concentrations dans des essais d'infiltration de longue durée (une année voire plus), pour s'assurer du développement complet des interactions chimiques and physiques. Les résultats de ces essais sont analysés avec l'objectif principal de trouver un critère pour prévoir les performances hydrauliques à long terme des parois en ciment-bentonite.

KEYWORDS: cut-off, acid, sulphate, cement-bentonite

1 INTRODUCTION

Few data are available in literature on the long term performance and durability of cement-bentonite (CB) cut-off walls (e.g. Jefferis 1992, 1993; Jefferis and Fernandez 2000; Fratalocchi et al. 2006, 2010) although this kind of vertical barriers (single or composite with geomembrane sheets) is frequently used to isolate polluted soils and groundwater (e.g. Manassero et al. 1995).

The authors are being performing a research aimed at evaluating and predicting the long term performance of CB mixtures in terms of hydraulic conductivity, k. A low k value is indeed the necessary (even if not sufficient) requirement for a cut-off wall to isolate polluted sites. Aqueous sulphate solutions of different nature (acidic, saline) and concentrations were used as permeants in column tests performed for long time (one year or more) in order that full effects of physical and chemical reactions may occur. Results of these tests are here analysed mainly with the aim to find a criterion to predict how long a cement-bentonite cut-off wall can keep a proper hydraulic conductivity.

2 MATERIALS AND TESTING METHODS

The CB mixture was selected in order to get a good hydraulic performance when permeated with water. To this purpose blast furnace slag cement was chosen (70% slag) as well as Na-bentonite (activated) and a special additive. The mix design is: cement/water = 0.22, bentonite/water = 0.0456, additive = 2 l/m^3 of mixture. Details on the mixing and sampling procedures are given in Fratalocchi et al. (2010). Typical values of density (11.4 kN/m^3), Marsh viscosity (50 s) and bleeding (1.0%) were obtained on the mixture at the fluid state, according to the practice requirements.

After a curing time of 10-14 days, each sample was permeated with a different saline or acidic solution of K_2SO_4 or H_2SO_4. Details of the permeant solutions are given in Table 1. The thickness of all the samples was in the range of 3.0-5.7 cm except two samples permeated with the same less concentrated acidic solution (sample A was 9.0 thick, sample B was 2.2 thick).

Flexible wall permeameters with bladder accumulators were used in order to control the effective confining pressure (40 kPa), the sample volumetric strains and to collect the effluent liquid. Constant head test were performed at hydraulic gradient, i, ranging from 25 to 100. Samples of the effluent liquid were periodically taken for concentration measurements to get the breakthrough curve (Fratalocchi et al. 2010; Brianzoni 2012) and to know the starting time at which the pore liquid fully consists of the inlet liquid. Permeation was kept for long time (months up to almost 2 years) in order to verify the long term performance.

Table 1. Main data of the permeant solutions

Solution	SO_4^{2-} (mg/l)	pH
K_2SO_4 (5.0)	2756	6.8
K_2SO_4 (27.5)	15159	7.0
K_2SO_4 (50)	27562	7.3
K_2SO_4 (95)	52368	8.0
H_2SO_4 (1.0)	9789	1.0
H_2SO_4 (1.5)	1176	1.5
H_2SO_4 (2.0)	310	2.0

3 RESULTS

Figure 1 shows the hydraulic conductivity trend over time of the mixture permeated with the salt solutions of K_2SO_4 at different concentrations together with the k trend of the same mixture permeated with water. With reference to the performance in water, the mixture shows the decrease of k with time typical of the well selected CB mixtures: k values of the order of 10^{-8} cm/s can be reached just after two months of curing. The reduction of k is significant during the first year of curing.

As far as the hydraulic conductivity with the salt solutions is concerned, each sample shows an initial decrease in the k value (no effluent SO_4^{2-} concentration were detected in this period), followed by an increasing hydraulic conductivity. Finally an almost constant trend of hydraulic conductivity with curing time occurs with the effluent SO_4^{2-} concentration that was measured to be equal to the inlet one. From Figure 2 it is also evident that the rate of reduction or increase of k with time depends on the permeant concentration: the higher the concentration, the faster the reduction and the successive increase in the k value with time, as well as the shorter the curing time at which the inversion of the k trend occurs. The reduction in the hydraulic conductivity exibited by the mixture during the first month of curing is equal or even higher than that of the mixture permeated with water. Significant (increasing) concentrations of SO_4^{2-} were measured at the effluent only when the k values increase with time; this transient phase lasted when the k values starts to be constant with time (Fratalocchi et al. 2010; Brianzoni, 2012).

In order to explain the results of Figure 1 it is necessary to consider the reactions occurring between sulphates and cementitious materials. Sulphate attack initially develops from the reation between SO_4^{2-} and both calcium hydroxite, $Ca(OH)_2$, and (partially) calcium hydro-silicate, C-S-H, with the consequent precipitation of gypsum ($CaSO_4 \cdot 2H_2O$) and release of OH^-. The subsequent (damaging) reactions take place between the sulphate and the hydrated calcium alluminate or calcium alluminate monosulphate hydrate (Bensted 1995; Gollop and Taylor, 1992, 1995) to produce ettringite with a consequent expansion.

All the aforesaid interaction mechanisms are progressive through the sample with curing time: the initial gypsum precipitation into the pores (reaction confirmed by the high pH values measued at the effluent, pH = 12-12.4) causes clogging of pores and contributes to the reduction of the hydraulic conductivity with time. This contribution tends to reduce and become negligible as the ettringite starts to form along the reaction front; such an expansive reaction is able to progressively invert the hydraulic conductivity trend with time up to a rapid increase. The expansive reaction of ettringite was confirmed by the increase in volume on the samples equal to 7-10% (Fratalocchi and Pasqualini 2007) and by a net of diffuse fissures observed on the samples at the end of the tests. The fissures give rise to preferential pathways that are responsible of the overall constant value of k (2-3 x 10^{-6} cm/s) at the end of the interaction mechanisms.

Samples of the same mixtures were permeated also with three aqueous solutions of sulphuric acid at different pH (Table 1). Two samples of different thickness (sample A and B) were permeated with the same H_2SO_4 solution (pH = 2.0) in order to evaluate the interaction effect taking into consideration different curing time. Figure 2 shows the hydraulic conductivity trends over time of all the samples. It is evident that the hydraulic conductivity trends versus time are similar to those measured on the samples permeated with the salt solutions. The main chemical reactions are indeed the same, with the addition of the dissolution of the cement hydration products (mainly calcium hydroxide and C-S-H) by the acidic solutions. SO_4^{2-} being equal, the increase in hydraulic conductivity tends to be faster when the mixture is permeated with the acidic solution. This is evident if we compare the k trend of the samples permeated with the salt solution at concentration of SO_4^{2-} of 2756 mg/l and the acidic solution of 1176 mg/l: both samples show a fast decrease followed by an increase of hydraulic conductivity but with the acidic solution the increase in k starts after about 250 days of curing whereas the increase of k occurs much more later (about 520 days) when the CB mixture is permeated with the saline solution, notwithstanding the lower concentration of SO_4^{2-}.

Considering the chemical reactions occurring between the different solutions and the mixture, it is necessary to point out that the overall hydraulic conductivity trend measured on the samples in Figures 1 and 2 depend on the sample thickness and on the flow rate through them. Therefore, in order to define how long the mixture is able to keep a good performance, the curing time cannot be considered as a reference parameter. To this purpose, the pore volume of flow, PV, is an appropriate parameter. Different criteria can be adopted to establish a satisfactory hydraulic performance for the CB mixture: for example, hydraulic conductivity lower than a maximum allowable value, or k lower than the k value measured with water, etc.; among them, the number of pore volumes of flow until k is decreasing, PV*, can be appropriate for the following reasons:

- at brief curing, both for K_2SO_4 and H_2SO_4, whatever concentration, the reduction of k with time is equal or lower than that with water;
- in the long term, if there is no inversion of the k trend with time, low k values can be reached;
- it is not necessary to establish a target k value (that would be related to a particular curing time);
- an increasing k trend with time does not imply a bad performance at least immediately; therefore, the criterion is on the safe side.

Therefore, the number of pore volumes of flow at which the k value stops decreasing (named “critical pore volumes”, PV*) was assumed as the reference value for the mixture good performance. This value (calculated assuming a porosity of the mixture equal to 0.6) was related to the concentration of SO_4^{2-} for the different salt and acidic solutions, as shown in Figure 3. Referring to the samples permeated with the acidic solution at pH = 2.0, only the thin one (sample B) showed a stop in decreasing of k after about 49 PV (500 days of curing) whereas the other one (sample A) still shows a decreasing k with time after 850 days of curing (at this time only 4 PV permeated the sample). Therefore, data of sample A could not be considered in Figure 3.

Figure 3 shows that PV* decreases as the sulphate ion concentration increases; the relation is well represented by a bi-logarithmic correlation. In particular, for concentrations of the order of g/l or more, that is, in aggressive conditions, the critical number of pore volumes assumes the same trend for both the solutions (saline and acidic). For concentrations of SO_4^{2-} lower than 1 mg/l, data are currently available only for the H_2SO_4 solution; the critical PV* should be lower for the H_2SO_4 solution than that of the salt solution considering its combined deleterious effect due to ettringite formation and dissolution of cement hydration products. Data are necessary to confirm this hypothesis.

Even assuming the criterion of good performance as the PV value until the k trend over time be not increasing (instead of decreasing), the data in Figure 3 would be practically the same except for the data with the lowest concentration of SO_4^{2-} which would have a PV* slightly higher (equal to about 57). It is important to point out that a little increase in PV* means a significant longer lasting for the mixture when the k value is low.

The results in Figure 3 can be useful from the practical point of view to estimate the durability of a cement-bentonite cut-off wall on the basis of the flow rate through it (i.e. on the basis of the hydraulic boundary conditions and assuming, safely, the minimum hydraulic conductivity value measured at brief curing). Since a high value of PV* results in case of low concentration of SO_4, this means that a good long term performance can be always expected because the hydraulic conductivity values after few months of curing are sufficiently low so that very few pore volumes of flow can pass through a cut-off wall in case of typical hydraulic heads of the order of units.

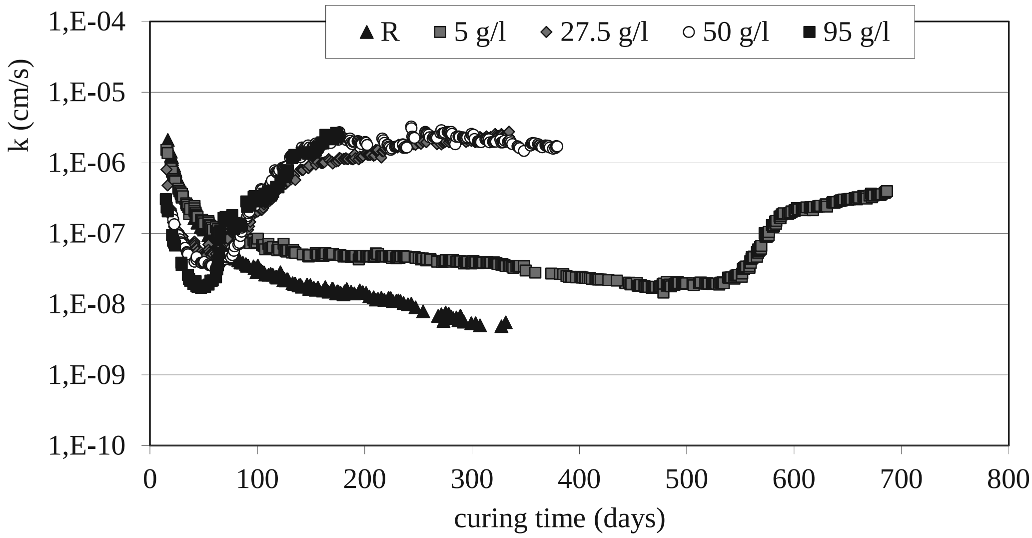

Figure 1. Hydraulic conductivity trend with curing time of the sample of the CB mixture permeated with water (R) and with solutions of K_2SO_4 at different concentrations (in the legend)

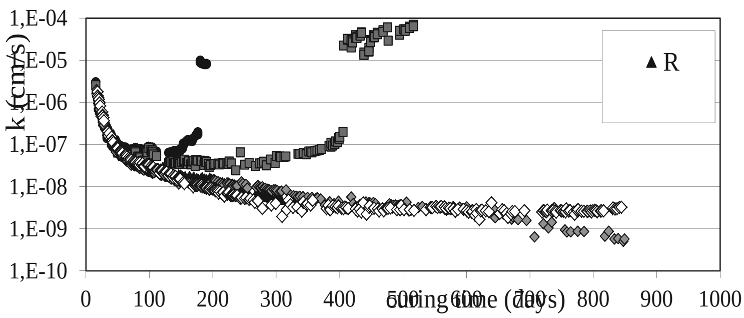

Figure 2. Hydraulic conductivity trend with curing time of the sample of the CB mixture permeated with water (R) and with solutions of H_2SO_4 at different pH (in the legend)

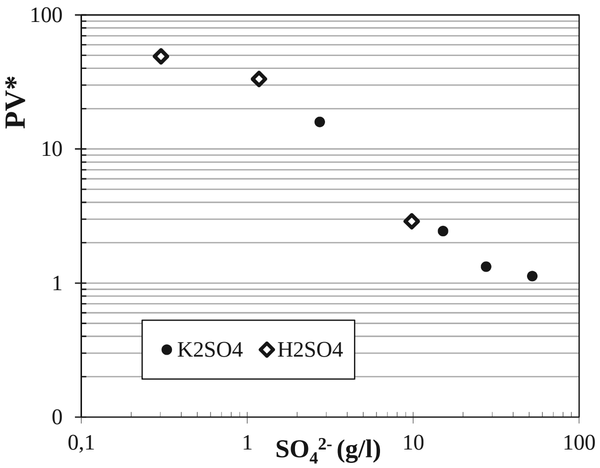

Figure 3. Critical number of pore volumes, PV*, as a function of the SO_4^{2-} concentration in sulphuric acid and potassium sulphate solutions.

4 CONCLUSIONS

On the basis of the available results it is possible to state that aqueous solutions of H_2SO_4 and K_2SO_4 may adversely affect the hydraulic performance of CB mixture depending on SO_4^{2-} concentration and pH. At concentration of the order of g/l or more, both solutions produce an initial decrease in the k value, followed by an increase and finally an almost constant trend of hydraulic conductivity with curing time. Swelling and a dense net of fixtures were detected on the samples after permeation mainly due to ettringite formation, both in samples permeated with the acidic and saline solutions.

The number of pore volumes of flow at which the change in the k trend occurs is greater the higher the SO_4^{2-} concentration. The PV at which this change of trend occurs (PV*) does not seem to be affected by the pH when SO_4^{2-} concentration exceeds 1 g/l.

A correlation between PV* and SO_4^{2-} concentration was found that can be useful from the practical point of view to estimate a cut-off wall durability on the basis of the expected flow rate through it. This criterion is on the safe side because it is based on the PV related to the requirement of decreasing k with time: a constant or increasing k with time does not necessarily imply a bad performance, at least immediately. Moreover, the chemical conditions adopted in the tests are not expected to occur continuously in the field if a pumping system is provided so that there is an advective flow of groundwater and not of pollutant across the barrier.

5 REFERENCES

Bensted J. 1995. The standardisation of sulphate-resisting cements. Part I + Part II. World Cement, Vol. 7 and 8.

Brianzoni V. 2012. Factors affecting the hydraulic performance of plastic cut-off walls for confinement of polluted sites. Ph.D. Thesis, Università Politecnica delle Marche (in Italian).

Fratalocchi E., Giorgini S. and Pasqualini E. 2010. Migration of sulphate solutions through cement-bentonite diaphragms. Proc.VI Int. Congress on Envir. Geotech., NewDelhi, India.

Fratalocchi E., Pasqualini E., Balboni P. and Mozzi R. 2005. Durability assessment of the confinement cut-off wall for a phosphogypsum landfill. Proc. 16th ICSMGE, Osaka, Japan.

Gollop R.S. and Taylor H.F.W. 1992 Microstructural and microanalytical studies of sulphate attack. I. Ordinary Portland cement paste. Cement & Concrete Research, 22 (6), 1027-1038.

Gollop R.S. and Taylor H.F.W. 1995. Microstructural and microanalytical studies of sulphate attack. III. Sulphate-resisting Portland cement: reactions with sodium and magnesium sulphate solutions. Cement & Concrete Research, 25 (7), 1581-1590.

Jefferis S.A. 1992. Contaminant-grout interaction. Proceedings of the Specialty Conference on Grouting, Soil Improvement and Geosynthetics, New Orleans, 1393-1402.

Jefferis S.A. 2003. Long term performance of grouts and the effects of grout by-products. Proc. 3rd International Conference on Grouting & Ground Treatments, New Orleans, ASCE Geotechnical Special Publication, No. 120.

Jefferis S.A. and Fernandez A. 2000. Spanish dyke failure leads to developments in cut-off wall design. Proc. Int. Conference on Geotechnical and Geological Engineering, Melbourne, Australia.

Manassero M., Fratalocchi E., Pasqualini E., Spanna C., Verga F. 1995. Containment with Vertical Cutoff Walls, ASCE Geotechnical Special Publication No. 46, 1142-1172.

Determination of shear strength of MSW. Field tests vs. laboratory tests.

Détermination de la résistance au cisaillement des déchets urbains (MSW). Essais in situ *vs* essais de laboratoire.

Cañizal J., Lapeña P., Castro J., Costa da A., Sagaseta C.
University of Cantabria. Santander, Spain

ABSTRACT: The knowledge of the mechanical properties of MSW has many implications on landfill design. The shear strength of the wastes determines the inclination to be given to the landfill slopes, which in turn governs the landfill capacity.
The measurement of these properties is not an easy task. Different approaches are possible. Conventional geotechnical laboratory tests face two main problems: the lack of representativeness of the samples, and the environmental difficulties associated to testing these materials in laboratories usually placed in general use buildings (odour problems). Due to these limitations, the number of published results is relatively short. The use of in situ tests has become an attractive alternative, because it eliminates the above two problems. However, the interpretation of these tests is based on the experience with conventional geotechnical materials (soils, rocks, compacted fills), but MSW have a different behaviour, with a seemingly unlimited strain, and no definite "failure" in most cases. A third approach is the back-analysis of the monitored behaviour of actual landfills. Some of these cases have been published, and even some compilations are available.

RÉSUMÉ : La connaissance des propriétés mécaniques des déchets urbains (MSW) a de nombreuses implications quant à la conception d'une décharge. La résistance au cisaillement des déchets détermine l'inclination des talus, qui se répercute sur la capacité de la décharge.
La détermination de ces propriétés n'est pas facile, différentes approches sont possibles. Les essais conventionnels de laboratoire présentent deux problèmes : le manque de représentativité des échantillons et les difficultés associées aux aspects environnementaux du fait que les laboratoires sont généralement situés dans des bâtiments à usage général (problèmes olfactifs). À cause de ces limitations, le nombre de résultats publiés dans la littérature est relativement faible. La pratique d'essais in situ est devenue une alternative intéressante, car elle élimine les deux problèmes ci-dessus. Cependant, l'interprétation de ces essais est basée sur l'expérience tirée des matériaux géotechniques conventionnels (sols, roches, remblais compactés), mais les déchets ont un comportement bien différent, avec une déformation apparemment illimitée et sans indice précis de "rupture". Une troisième possibilité repose sur l'analyse inverse du suivi de cas réels instrumentés. Quelques cas ont été publiés, et certaines compilations sont disponibles.

KEYWORDS: MSW, municipal solid wastes, landfill, site exploration, mechanical properties, shear strength.

1 INTRODUCTION

The stability of a landfill relies on the shear strength of its elements. It depends on the characteristics of the waste materials disposed in it, as well as in the characteristics of the materials that form the protection, isolation and sealing layers. As far as the waste material is concerned there are several factors influencing the strength characteristics such as composition, age, confining pressure, details of landfill operation, existence of soil layers as waste cell coverage, etc. In any case the shear strength of the wastes determines the inclination to be given to the landfill slopes, which in turn governs the landfill capacity. The necessity of establishing berms at mid-height of the slopes has also an important role in the capacity.

Municipal Solid Wastes (MSW) have some special characteristics making a clear distinction with soils in terms of behaviour. However, in landfill stability analyses the behaviour of MSW is usually based on models derived from soils, mainly the Mohr-Coulomb failure criterion, defined by two parameters: cohesion (c) and friction angle (ϕ).

Strength parameters of MSW can be obtained testing samples in the laboratory or conducting in-situ tests. In addition to these methods there is also a third way to obtain parameters using back-analysis of real scenarios, most of the times from landfill failure cases.

Both laboratory and in-situ tests, in their different variations, have several advantages and disadvantages, due to that, a pros-and-cons analysis of the different methods using the existing bibliography was conducted, considering their methodology, operative issues, reliability and repeatability of the results to determine the test procedure that fits best to our purposes.

2 OVERALL STRENGTH CHARACTERISTICS OF MSW

MSW show some overall strength characteristics that are reflected in almost all the existing bibliography. They can be summarized as follows (Bray et al., 2009; Stark et al., 2009):

- As a general trend, MSW shear strength increases with the average confining pressure in a nonlinear way, and the slope of the shear strength envelope decreases with the level of normal stress. For very low confining pressure, there is some strength provided by the fibrous material contained in the waste, giving rise to an equivalent cohesion.
- Fitting this non-linear strength envelope with a linear Mohr-Coulomb criterion line must be done for the range of interest of normal stress, and the values of frictional angle and cohesion have to be defined accordingly.
- Test results are influenced by test conditions and sample preparation.
- Within the usual ranges, variations in density do not produce large changes in MSW strength.
- Degradation and aging seem to have an important effect on the shear strength, decreasing the cohesive term and increasing the friction.

- The shear stress-strain curve of the MSW shows a noticeable hardening (Grisola et al., 1996; Jessberger et al., 1993; Eid, 2000; Zhan et al., 2008), and a horizontal asymptotic level is not reached even with large deformations. So it is necessary to define a certain level of deformation in which it is assumed that the failure situation is being reached.

3 METHODS FOR OBTAINING MSW STRENGTH

The methods for obtaining cohesion and frictional angle parameters can be grouped in three kinds: laboratory test, in-situ test and back-analysis of actual failures.

3.1 Laboratory tests

3.1.1 Sample conditions

Although laboratory tests are the most direct method for obtaining the strength parameters of a material, they show several problems that make difficult both their usage and the subsequent interpretation when working with MSW.

The first problem is to find representative samples. Samples obtained in the same landfill show a large dispersion in composition due to the heterogeneity of the waste mass. Some research has been done on "synthetic" samples, reconstituted with the average composition of the MSW mass in the landfill region or country (Sivakumar Babu et al., 2010).

On the other hand, among the MSW there are elements with a medium to large size. So it is necessary to take large samples, this is quite easy for MSW that have just arrived to the landfill, or for recently disposed and superficial waste, but makes it necessary to bore large diameter bore-holes (over 760 mm in diameter) (Bray et al., 2009) for deep waste.

It is very hard to take undisturbed samples from MSW, particularly at great depth. Densification is produced during the sampling process due to the large deformability of MSW. Because of the low cohesion, the loose nature of the material and the differences in size and stiffness among the different constitutive elements, alterations and collapses are produced during the sampling and trimming operations.

For these reasons, tests are made using samples prepared and compacted to in-situ density and moisture content, and with the prevailing composition. The uncertainties associated to these conditions make that this procedure can be only considered as an approximation of actual landfill conditions. Besides, the elements with a size over 1/5-1/10 of the minimum size of the specimen to test, usually fibrous materials such as paper, plastic, wood or metallic pieces, have to be removed or cut to fit this size in order to not interfering with the movement of the test equipment invalidating the results obtained. Furthermore, the tensile strength of fibrous elements introduces an anisotropic behaviour, making the strength obtained in the test depend on the preferred direction of the fibres (Bray et al., 2009).

3.1.2 Test types

The tests used to obtain strength parameters are direct shear, triaxial and simple shear tests.

From 23 research works revised by Stark et al. (2009), dated from 1990 to 2005, 48% used laboratory direct shear tests, 22% triaxial tests, and just one simple shear tests. The rest of them are in-situ direct shear tests. Recently, Bray et al. (2009) have presented the results of simple shear tests on 400x300 mm rectangular samples.

In general test specimens have a relative large size. It is frequent for the direct shear test probes to have a length of 300 millimetres or more and using triaxial specimens with over 200mm in diameter. Besides, the test equipment has to be prepared to provide large deformations. This circumstance is stated on plenty of the revised researches, and makes it necessary to modify the original design of the equipment.

3.1.3 Other aspects

In tests on MSW samples, the applied shear stress increases monotonically with deformation, and in most cases a maximum or asymptotical value is not reached even with the application of large displacements. The plots shown in Figures 1 and 2 belong to a compilation of results from several authors made by Stark et al. (2009). It is shown that shear stress does not grow only with the applied normal stress, but it also increases with the deformation or the displacement reached. Those authors attribute this behaviour to the reinforcement action of the wastes' fibrous elements when deformation increases.

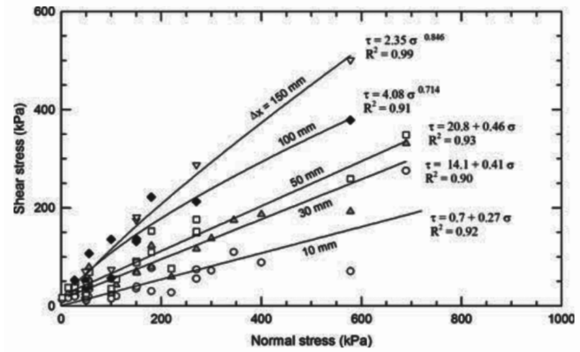

Figure 1. Summary of direct shear lab tests (Stark et al., 2009)

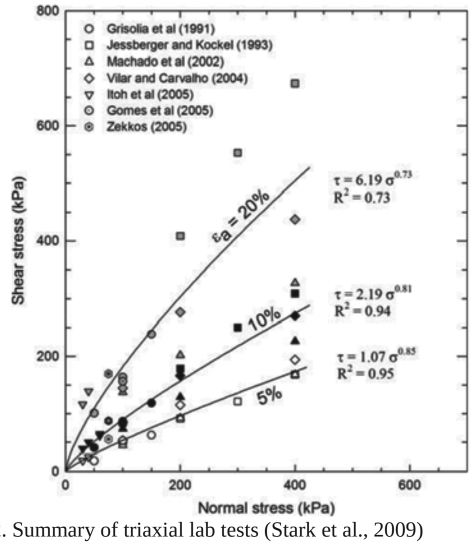

Figure 2. Summary of triaxial lab tests (Stark et al., 2009)

It has to be taken into consideration that in regular landfill operation the possible deformation is much smaller than during a test. Movement compatibility between MSW and the more rigid sealing layers, and also with the deformation limit of draining elements, gas evacuation elements, etc., limits waste deformation to acceptable levels, forcing the definition of strength parameters to an imposed deformation value (Machado et al., 2002).

The environmental conditions where the laboratory tests are conducted are problematic because of the odour and the hazardous sample management, making necessary to fit out a specific area, isolated from the rest of the laboratory. In some research it is necessary to carry out most of the tests in facilities belonging to the landfill grounds.

The difficulty in obtaining truly representative samples and test environmental conditions affects negatively to the possibility to undertake systematic shear strength laboratory test campaigns. The revised bibliography shows that there are a scarce number of tests executed for the amount of means mobilized (Bray et al., 2009, Sivakumar Babu et al., 2010).

3.2 In situ tests

3.2.1 Comparison with laboratory tests

In-situ tests are an alternative to the execution of laboratory tests on landfill samples. With in-situ tests there is no need to take and manipulate samples, with the subsequent alteration, very high when dealing with MSW. In-situ tests are made over the material in real conditions, not in a simulated laboratory scenario.

Besides, scale is larger in field tests, affecting more material. This bigger scale reduces the influence of MSW heterogeneity, making possible to take into consideration medium to large fibrous elements. However, these advantages over laboratory tests bring some additional problems:

- Although the alteration produced by taking the sample is removed, effects produced by the installation of the testing elements appear.
- Field tests control (stress state, displacements, drainage) is lesser than in laboratory tests.
- Even though the area affected by field tests is larger than the regular specimen size, scale problems are still present.
- Results obtained from some in-situ tests cannot be analysed using theoretical models to obtain strength parameters, the only way to obtain them are using empirical correlations.
- Interpretation complexity is higher for in-situ tests in comparison with those conducted in a laboratory. If the theoretical model depends on two or more parameters, like Mohr-Coulomb failure criterion, it is only possible to obtain the relationship between them. This implies that only a curve for different possible values for cohesion and frictional angle can be obtained.

In any case, most of the in-situ test procedures are quite fast and economical, making possible to execute multiple tests in a reasonable period of time and covering a large volume of material, which is a clear advantage over laboratory tests.

3.2.2 Test types

The in-situ tests commonly used in MSW are: penetration test, plate loading tests, pressuremeter tests and in-situ shear tests.

Penetration tests, both dynamic (DPSH, DPH, SPT) and static (CPT, CPTU) provide an index value for MSW strength, and from these indexes it is possible to empirically obtain strength parameters and other characteristics. Their main advantages are their easy usage and their low time and means consumption, as well as the possibility to check different penetrations in time and space to establish tendencies for the variation of the resistance to penetration.

Use of penetration test for landfill characterization is frequent, being one of the pioneers Sowers (1968) who used dynamic tests. The University of Cantabria (UC) Geotechnical Group has researched about the strength characteristics of landfills using dynamic and static penetration tests (Palma, 1995; Sánchez et al., 1993). In a recent research, Zhan et al. (2008) used, among others, static penetrometers.

Furthermore, the interpretation of plate loading tests is not as straightforward as in soils, due to the heterogeneity of the landfill. It is advisable to use large diameter plates (>600 mm), which is feasible because there is no need to apply large loads in order to produce the needed deformations or even to reach failure due to the soft nature of the MSW.

Several researchers have used this method for deformability and strength characterization of MSW. The UC Geotechnical Group (Palma, 1995; Sánchez et al, 1993) used load plates, interpreting the results using a multi-layer model for MSW and covering layers. In some occasions the rigid plate has been replaced by a container full of material, achieving larger size but lower pressure.

Pressuremeter tests, both with previous borehole execution and using self-boring systems have been recently used in landfills (Dixon et al., 2006).

There are several experiences with in-situ shear tests using parallelepipedic and cylindrical samples with sizes of 500 mm and even 1m in landfills (Withiam et al., 1995; Caicedo et al., 2002).

3.3 Back-analysis of real failures

Failure back-analysis is a widely used method in geotechnical activity and can be easily extrapolated to the study of MSW shear strength (Huvaj-Sarihan and Stark, 2008).

However, this method faces also some uncertainties. First, generalized failure cases are not frequent, and in the few cases occurred it is difficult to detect the failure surface. Besides, failure generally affects to the bottom sealing layers and the foundation ground as well as to the waste mass itself. In other cases the situation analysed is far from failure so a safety factor greater than the unit has to be assumed with no precise justification. Furthermore, the values for material density and phreatic level position are not known exactly and must be estimated. In any case, if the Mohr-Coulomb failure criterion is used, the result of the analysis is only a relationship between cohesion and frictional angle as in some in-situ tests. Only in very few cases, the precise knowledge of the sliding surface position can provide some guidance about the relative ranges for the two parameters. Otherwise, the result is a line plotted in a c-ϕ diagram. This diagram must be used with care, because it does not mean that all the points on the line are valid, but instead, only one point is the correct result, but it is not possible to identify it within the whole line (Figures 3 and 4).

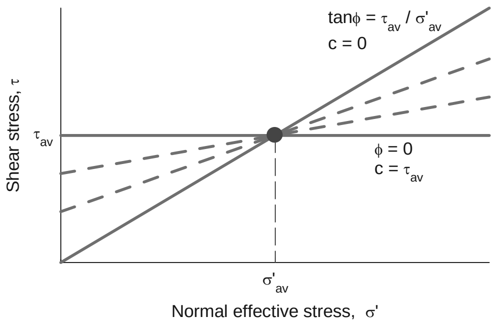

Figure 3. Mohr's plane of the results of a back-analysis

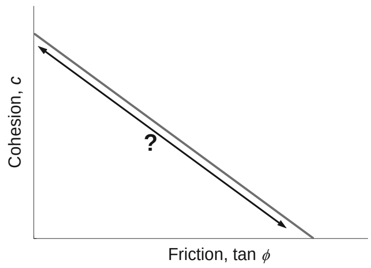

Figure 4. c-ϕ diagram of the results of a back-analysis

4 MOHR-COULOMB STRENGTH PARAMETERS PROPOSAL

Although the research in strength parameters dates back more than two decades, the special characteristics of MSW limit the obtained results. In several publications a compilation of parameter values is shown, but they do not only refer to test results, it also does to representative values deduced by the authors of other previous compilations and to values successfully used in particular cases of landfill design. Besides, the available results belong to different test type and methodology, carried out on MSW of different composition, age, density, etc. Furthermore, due to strain hardening behaviour, different values can be established for the same test according to the deformation level considered as critical.

Regarding the back-analysis of failures, the uncertainties commented above limit their use.

One of the first proposals was due to Singh and Murphy (1990), but with no attempt to reduce the wide ranges of cohesion and friction resulting from real failures.

Based on the limited data available at the time, Sánchez et al. (1993) proposed a joint consideration of the results of laboratory and in situ tests and back-analysis of failures. The first ones gave a set of pairs of values of cohesion and friction, increasing with the strain. The real failure cases help to identify the relevant strain level, and reciprocally, the lab tests help to identify the real c/ϕ ratio. In situ tests can also give information on that respect. The result is shown in Figure 5.

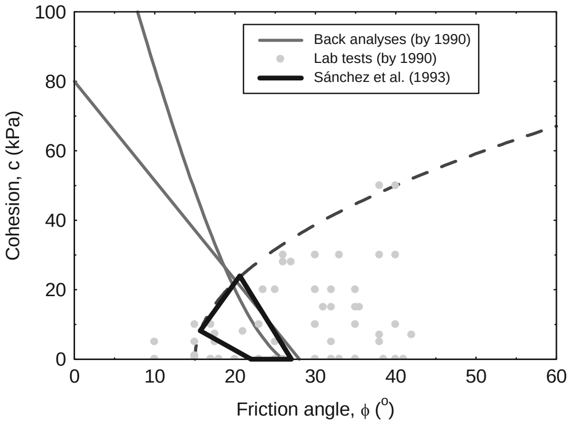

Figure 5. Strength parameters. Early design recommendations (Sánchez el al., 1993)

In the last two decades, some additional results have been published, from laboratory and in situ tests and from real failures (see, for instance, the compilation by Stark et al. (2009), among others). Considering these data, the recommended values in Figure 5 can be increased. Figure 6 includes the results of failures compiled by Stark et al. (2009), and their recommended values, based on the proposal by Eid et al. (2000).

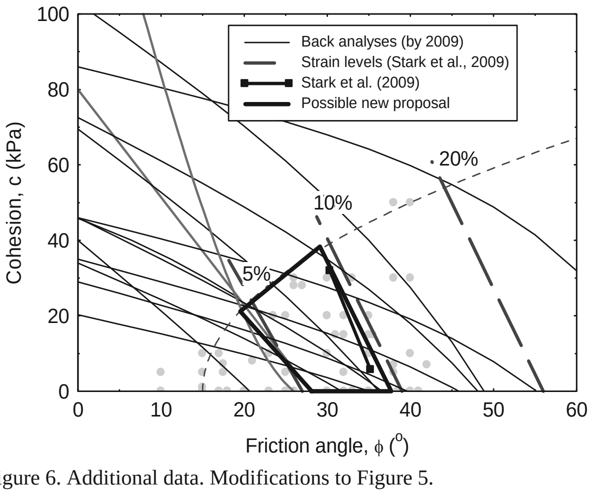

Figure 6. Additional data. Modifications to Figure 5.

5 CONCLUSIONS

Prior work has shown that it is no easy to obtain the mechanical properties of the waste mass.

After merging the data from the revision of existing bibliography and the experience of the U.C. Geotechnical Group, new research is being undertaken in order to establish a method to perform that task during the next three years. The study will be based on the use of field tests, complemented with medium to large scale laboratory direct shear tests. It will cover several landfills, with conventional MSW, together with wastes subjected to mechanical and biological pre-treatment (MBT), introduced in Spain in the last years (projects GEORES-03.2843.64001 and PROMERSU-BIA2012-34956).

The study will be performed in several landfills. In parallel with the test campaign, numerical modelling of the landfills under study will be undertaken to obtain feedback and refine the data acquisition process.

After all the data are gathered and the process is considered optimum, a method to obtain the mechanical properties of a landfill using field tests and a new proposal for the design strength parameters will be obtained as a result of the research.

6 REFERENCES

Bray, J.D., Zekkos, D., Kavazanjian, E., Athanasopoulos, G.A. and Riemer, M. F. 2009. Shear strength of municipal solid waste. *Journal of Geot. and Geoenv. Eng.*. ASCE 135(6),709-722.

Caicedo, B., Yamin, L., Giraldo, E. and Coronado, O. 2002. Geomechanical properties of municipal solid waste in Doña Juana sanitary landfill. *Proc. 4th Env. Geotechnics – 4th ICEG*, Rio de Janeiro 1,177-182.

Dixon, N. and Jones, R. 2005. Engineering properties of municipal solid waste. *Geotextiles and Geomembranes* 23,205–233.

Dixon, N., Whittle, R.W., Jones, D.R. V. and Ng'ambi, S. 2006. Pressuremeter tests in municipal solid waste: measurement of shear stiffness. *Géotechnique* 56(3),211–222.

Eid H, Stark T.D., Evans W.D. and Sherry P. 2000. Municipal solid waste slope failure I: Waste and foundation properties. *Journal of Geot. and Geoenv. Eng.*. ASCE 126(5),397-407.

Grisolia, M. and Napoleoni, X. 1996. Geotechnical characterization of municipal solid waste: choice of design parameters. *Proc. 2nd Int. Cong. on Env. Geotechnics*, Osaka, Japan 2,641–646.

Huvaj-Sarihan, N. and Stark, T.D. 2008. Back analyses of landfill slope failures. *VIth Int. Conf. on Case Histories in Geot. Eng. and Symp. in Honor of Prof. James K. Mitchell*. Paper 2.34.

Jessberger, H.L. and Kockel, R. 1993. Determination and assessment of the mechanical properties of waste materials. *Proc. Sardinia 93, 4th Int. landfill Symp.*, Cagliari, Italy,1383–1392.

Kavazanjian, E. 2003. Evaluation of MSW properties using field measurements". *Proc.17th GSI/GRI Conf.* Las Vegas, USA.74-113.

Machado, S. L., Carvalho, M.F. and Vilar, O.M. 2002. Constitutive Model for Municipal Solid Waste. *Journal of Geot. and Geoenv. Eng*. ASCE. 128(11),940-951.

Palma, J. 1995. *Comportamiento geotécnico de vertederos controlados de residuos sólidos urbanos*. PhD Thesis. Univ. of Cantabria.

Sánchez, J.M., Palma, J., Sagaseta, C. and Cañizal, J. 1993. Mechanical properties of wastes in a sanitary landfill. *Waste Disposal by Landfill. (R.W. Sarsby, ed.)*. Bolton, U.K. 357-364.

Singh, S., and Murphy, B. 1990. Evaluation of the stability of sanitary landfills. *Geotechnics of Waste Fills — Theory and Practice*, ASTM STP1070,240–258.

Sivakumar Babu, G.L., Reddy, K.R. and Chouksey, S.K. 2010. Constitutive model for municipal solid waste incorporating mechanical creep and biodegradation-induced compression". *Waste Management* 30,11–22.

Sowers, G.F. 1968. Foundation problems in sanitary landfills. *Journal of the Sanitary Div.*, ASCE 94(SA1),103-116.

Stark, T., Huvaj-Sarihan, N. and Li, G. 2009. Shear strength of municipal solid waste for stability analyses. *Environ Geol.* 57,1911–1923.

Withiam, J.L., Tarvin, P.A., Bushell, T.D., Snow, R.E. and Germann, H.W. 1995. Prediction and performance of municipal landfill slope. *Proc. Int. Conf. Geoenv. 2000*, GSP46, ASCE, New Orleans, Lousiana, 2,1005-1019.

Zekkos, D., Athanasopoulos, G. A., Bray, J. D., Grizi, A. and Theodoratos, A. 2010. Large-scale direct shear testing of municipal solid waste. *Waste Management* 30(8-9),1544-1555.

Zhan, L.T., Chen, Y.M., Ling, W.A. 2008. Shear strength characterization of municipal solid waste at the Suzhou landfill, China. *Eng. Geol.* 97,97-111.

Geo-environmental problems in landfills of MSW with high organic content

Problèmes géo-environnementaux dans les sites d'enfouissement de déchets urbains à hautes teneurs organiques

Chen Y.M., Zhan L.T., Xu X.B., Liu H.L.
MOE key Laboratory of Soft Soils and Geo-environmental Engineering, Zhejiang University, Hangzhou 310058, China

ABSTRACT: The municipal solid wastes (MSWs) in China are high in organic and moisture content, as compared with the MSWs in developed countries. Large amounts of leachate and landfill gas are generated and significant settlement takes place during the decomposition process of the MSWs. A build-up of leachate mound and gas pressure might take place in the landfills of MSWs. Waste stability is highly concerned for such landfills having excessive pore-water and pore-gas pressure. A bio-hydro-mechanical coupled model is presented in this paper, based on laboratory and in-situ investigations, to predict leachate production, gas pressure and settlement. Based on the prediction obtained by the proposed model, discussions are made on the geo-environmental problems in landfills of MSW with high organic content. The work is valuable for the development of bioreactor landfilling technologies in the Asian developing countries such as China.

RÉSUMÉ : Les déchets urbains en Chine ont des teneurs élevées en matières organiques et en humidité, par rapport aux déchets produits dans les pays développés. De grandes quantités de lixiviats et de gaz sont dégagées et un tassement significatif apparait lors du processus de décomposition des déchets. Il peut se produire dans les décharges une augmentation de l'accumulation des lixiviats et de la montée en pression des gaz. La stabilité de l'entreposage de ces déchets est fortement impactée par l'augmentation de pression du fluide et du gaz dans les vides. Un modèle couplé bio-hydro-mécanique est proposé dans cet article, basé sur des études expérimentales de laboratoire et in situ, pour prévoir la production de lixiviat, la pression de gaz et le tassement. Sur la base des résultats obtenus par le modèle proposé, les discussions portent sur les problèmes géo-environnementaux dans les sites d'enfouissement de déchets à hautes teneurs organiques. Le travail est très utile pour le développement des technologies de bioréacteurs dans les pays asiatiques en voie de développement telle que la Chine.

KEYWORDS: MSW, organic content, gas, leachate, settlement, stability

1 INTRODUCTION.

Municipal Solid Wastes (MSWs) contain biodegradable component, which results in the difference in engineering property between MSWs and traditional soil. Landfilling will remain the dominant disposal method for MSWs in China for the foreseeable future. An understanding of engineering characteristics of MSWs and landfill behavior is important for the planning, design, and operation of landfills.

The MSWs in China contain much more putrescible organic waste and higher initial moisture content than the MSWs generated in developed countries (Chen et al. 2010a). In this paper, engineering properties of MSWs with high organic content are discussed, and a Bio-Hydro-Mechanical (BHM) coupled model is proposed to estimate a series of coupled phenomena in such landfills. Based on the simulation results, geo-environmental problems associated with this kind of landfills of MSWs were discussed. The work is valuable for the development of bioreactor landfilling technologies in the Asian developing country such as China.

2 ENGINEERING PROPERTIES OF MSW WITH HIGH ORGANIC CONTENT

2.1 *MSW composition*

MSW typically consists of food and vegetable wastes, paper products, plastics, textiles, wood, cinder, and soils. Table 1 shows a comparison of waste composition among China, India, Korea, Singapore, UK, and USA as of 2000. The MSWs in China and India contain much more putrescible organic wastes (i.e., kitchen food and vegetable wastes which account for 40-50%) than the MSWs generated in UK, and USA. The content of mineral materials (i.e., cinder, dust, concrete, etc.) in China and India is also higher than that in UK and USA. These differences are likely attributable to the differences in cooking styles and the living standard among the countries.

Table 1. Comparison of MSW composition among China, India, Korea, Singapore, UK, and USA generated in 2000 (%) (Chen and Zhan 2007)

Country	Food Vegetable	Dust Cinder	Paper	Plasitc Textile Wood Rubber	Metal Glass	Others
China	43.6	23.1	6.7	16.7	3.4	6.5
India	41.8	40.3	5.7	8.2	4.0	0
Korea	24.6	NA	25.8	NA	13.5	NA
Singapore	23.5	17.1	21.6	11.1	24.0	2.7
UK	20.0	12.0	34.0	21.0	15.0	0
USA	15.3	10.9	29.8	29.4	12.7	1.9

2.2 *Initial moisture content and moisture retention characteristic of the MSWs*

For Chinese MSWs, more than 40% of the waste in wet weight is occupied by moisture for most of the data reported, as illustrated in Figure 1. At the rainy seasons, the initial moisture content (wet/wet) of the waste may reach 70% in the humid regions of southern China (Chen et al. 2010a). Compared with Chinese wastes, the MSWs of developed countries commonly have a lower initial moisture content (< 30%, Qian et al. 2002). High content of organic component (see Table 1) is the main factor that contributes to the high initial moisture content of Chinese MSW.

According to the literatures, the field capacity of wastes is generally assumed to be equivalent with the water content corresponding to a matric suction of 10 kPa, and its value for the Chinese wastes ranges from 33% to 45% (Chen et.al. 2010a), greater than that of the UK waste (22%) and the US waste (22.4%)(Sharma and Lewis 1994). For decomposed wastes filled in landfills for a long time, the average value of field capacity of MSWs in different countries is 37% (Chen et.al. 2010a).

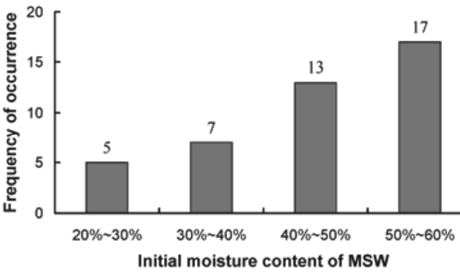

Figure 1. Initial moisture content of MSWs in China

2.3 *Hydraulic conductivity and gas permeability of the MSWs*

Results of laboratory tests on borehole samples and in situ pumping tests of Qizishan landfill, Suzhou, China show that hydraulic conductivity (k_s) of MSW decreases with an increase in burial depth or overburden pressure due to compaction and degradation of waste (Chen et al. 2010a). Results of laboratory tests on the borehole samples also indicate that (see Figure 2) the gas permeability decreases with an increase in the degree of saturation (or a decrease in volumetric gas content, θ_g), and the decrease is much more significant at the high range of degree of saturation (S_r) (Wei 2007).

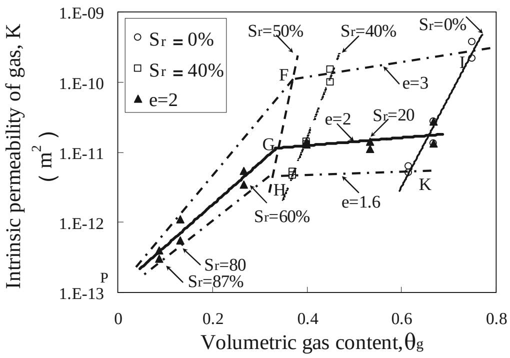

Figure 2. Gas permeability for MSW sampled from the Qizishan landfill, China (Wei 2007)

2.4 *Compression characteristics of the MSWs*

The compression characteristics of MSWs are of greater complexity than soils, whose solids can be normally regarded as inert materials. Based on laboratory tests on borehole samples and artificial wastes, it was found that creep is usually insignificant compared with the sum of primary and biodegradation compression for MSWs under favorable decomposition conditions, and the modified primary compression index tends to decrease with an increase of waste depth and age (Chen et al. 2009, 2010b). Laboratory study showed that MSW with a higher organic content tends to have larger C_C'(see Eq. 1) and secondary compression potential (Liao et al. 2007, Xu 2012). A one-dimensional compression model which considers the coupled effect of stress and age is proposed to express mechanical compression of MSWs (Chen et al. 2010b):

$$\varepsilon = C_C^{'} \lg \frac{\sigma'}{\sigma_0'} + \varepsilon_{tS}(1 - e^{-ct}) \quad (1)$$

where ε is the total strain corresponding to σ' and t, C_C' is the modified primary compression index for fresh wastes, σ' (Pa) is effective stress, σ_0' (Pa) is the initial stress for fresh MSWs, ε_{tS} is ultimate secondary strain which can be calculated as the ultimate strain under long-term compression minus the primary compression strain of fresh wastes, and c (s^{-1}) is the secondary compression rate constant related to biodegradation process.

2.5 *Shear strength characteristics of MSW*

Groups of consolidated drained triaxial compression tests were carried out to investigate the shear strength characteristics of borehole samples obtained from Qizishan landfill (Zhan et al. 2008). The results showed that the MSW samples exhibited a strain-hardening and contractive behavior (see Figure 3). As the fill age of the waste increased from 1.7 years to 11 years, the cohesion mobilized at a strain level of 10% was found to decrease from 23.3 kPa to 0 kPa, and the mobilized friction angle at the same strain level increasing from 9.9° to 26°. For a confinement stress level greater than 50 kPa, the shear strength of the recently-placed MSW seemed to be lower than that of the older MSW. The observed changes of shear strength with the fill age can be explained by considering the change in the MSW composition with age (Zhan et al. 2008).

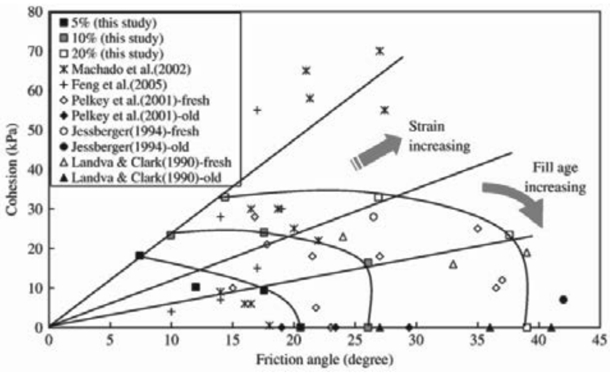

Figure 3. Summary of mobilized shear strength parameters reported in the research literatures (Zhan et al. 2008)

3 BHM COUPLED MODEL AND CASE STUDY

A Bio-Hydro-Mechanical (BHM) coupled model was proposed to investigate solid-liquid-gas interaction behaviors in landfilled MSWs with high organic content (Xu 2011, Chen et al. 2012). Apart from solid mass loss and gas generation, another key issue during biodegradation process is the release of celluar moisture within biodegradable matter, especially for MSWs high in organic content. Based on first-order kinetics, the source terms of liquid $f_{L,t}$ ($kgm^{-3}s^{-1}$) and gas $f_{G,t}$ ($kgm^{-3}s^{-1}$) due to biodegradation are expressed as:

$$f_{L,t} = \frac{\eta dm_{Sd}}{(V_S + V_V)dt} = \frac{\eta \sum (m_{dSi} c_i' f_{water} e^{-c_i' f_{water} t})}{(1-\varepsilon)(V_{S0} + V_{V0})} \quad (2)$$

$$f_{G,t} = \frac{(1-\eta) dm_{Sd}}{(V_S + V_V)dt} = \frac{(1-\eta) \sum (m_{dSi} c_i' f_{water} e^{-c_i' f_{water} t})}{(1-\varepsilon)(V_{S0} + V_{V0})} \quad (3)$$

where η is the reaction coefficient, m_{Sd} (kg) represents solid mass loss at the time t(s),V_S and V_V(m^3) are the volumes of solid matter and void space respectively, m_{dSi} (kg) is the initial mass of biodegradable component i, c_i' (s^{-1}) is the decomposition rate constant of biodegradable component i, V_{S0} and V_{V0} (m^3) are the initial volumes of solid matter and void space respectively, ε is the compression strain, and f_{water} is the water impact factor.

Mass conservation equations and Darcy's law for liquid and gas are used to model fluid flow in landfills (see Eqs. 4 and 5). Hydraulic conductivity, gas permeability and water retention characteristics of MSW are estimated based on laboratory studies as discussed in section 2.2 and 2.3.

$$\frac{\partial(\rho_L n S_L)}{\partial t} = f_{L,t} - \frac{\partial(\rho_L v_L)}{\partial z} \quad (4)$$

$$\frac{\partial(\rho_G n S_G)}{\partial t} = f_{G,t} - \frac{\partial(\rho_G v_G)}{\partial z} \quad (5)$$

where ρ_G and ρ_L are liquid density and gas density respectively, n is the porosity which is determined by m_{sd} and ε, S_L and S_G are liquid saturation and gas saturation respectively, v_L and v_G (m/s) are liquid velocity and gas velocity respectively.

Mechanical compression of MSW is expressed by the one-dimensional compression model expressed as Eq.1. The effective stress σ' is expressed as Bishop's equation for unsaturated soils (Bishop 1959).

Main governing equations of the BHM coupled model are shown as Eqs.1-5.The BHM coupled model is numerically solved by the finite difference method and Gauss-Newton method.

Based on Chen et al. 2009 and Reddy et al. 2008, two hypothetical waste samples with a height of 5m are studied for MSWs in Qizishan landfill, China and Orchard Hills landfill, USA, respectively. As shown in Figure 4, top boundary is impervious for liquid but free for gas flow, and the bottom boundary is impervious for gas but free for liquid flow. The total stress is set to be zero at the top boundary, and compression strain is set to be zero at the bottom boundary. Each element is 0.5m high, and the time step is 10^{-5}day^{-1}. Parameters applied are shown in Table 2. Gas pressure, leachate/gas production and settlement are analysed through the BHM coupled model.

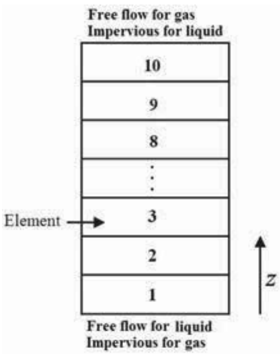

Figure 4. Schematic diagram of a hypothetical waste sample

Table 2. Parameters applied in the BHM coupled model

m_{ds1}/m_{s0}	m_{ds2}/m_{s0}	m_{ds3}/m_{s0}	w_0(wet)
0.35*	0.20*	0.10*	0.60*
0.05#	0.25#	0.20#	0.44#
f_{water}	d_S	γ_0(kN/m^3)	e_0
1.0*	1.87*	7.5*	3.0*
1.0#	0.85#	5.0#	1.4#
C_C'	$C_{C\infty}$'	σ_0' (kPa)	$\varepsilon_{tS}(\sigma_0')$
0.25*	0.17*	10*	0.38*
0.28#	0.17#	10#	0.20#
m_{vG}	n_{vG}	α_{vG}(m^{-1})	γ_{vG}
0.26*#	1.35*#	25.6*#	3.0*#
μ_L(kgm^{-1}s^{-1})	μ_G (kgm^{-1}s^{-1})	Mol_G (kgmol^{-1})	R (m^{3}PaK^{-1}mol^{-1})
1.0×10^{-3}*#	1.4×10^{-5}*#	0.03*#	8.314472*#
c_1'(day^{-1})	c_2'(day^{-1})	c_3'(day^{-1})	c (day^{-1})
0.00023*#	0.00013*#	0.00003*#	0.0016*#
k_0(m^2)	θ_S	θ_r	η
10^{-11}*#	0.75*#	0.035*#	-0.11*#
T (K)	g (ms^{-2})	ρ_L(kgm^{-3})	P_a(Pa)
303*#	9.8*#	994.13*#	101320*#

Note: * is for MSWs in Qizishan landfill, China
is for MSWs in Orchard Hills landfill, USA

As shown in Table 2, waste sample from Qizishan landfill has higher organic content (i.e. m_{ds1} which represents highly degradable component) and initial moisture content (i.e.w_0), compared to that from Orchard Hills landfill. Two samples are both assumed to have an optimum biodegradation condition (i.e. f_{water}=1.0). Simulation results are shown in Figure 5-8. It indicates that gas pressure of waste sample from Qizishan landfill have larger gas pressure during the early stage. Gas generation rate, gas production, leachate production and surface settlement of waste sample from Qizishan landfill are all much greater than that from Orchard Hills landfill.

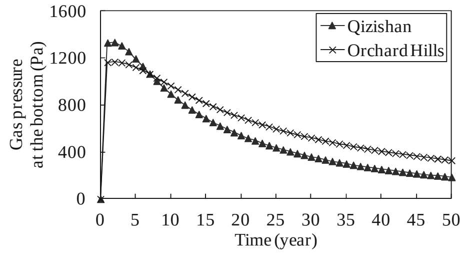

Figure 5. Gas pressure at the bottom of waste samples

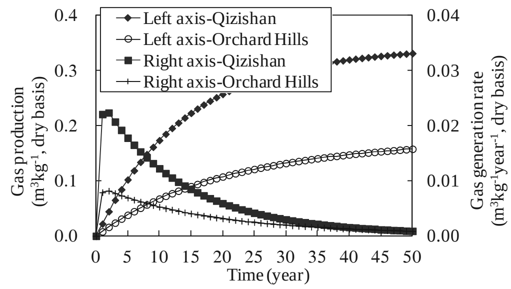

Figure 6. Gas generation rate and gas production of waste samples

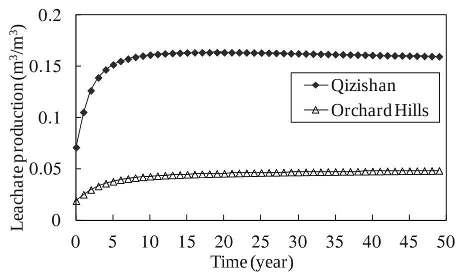

Figure 7. Leachate production per volume of waste samples

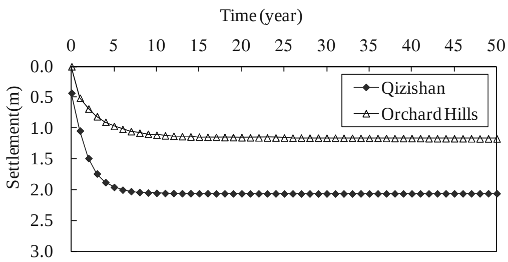

Figure 8. Settlement of waste samples

4 GEO-ENVIRONMENTAL PROBLEMS IN LANDFILLS WITH HIGH ORGANIC CONTENT

4.1 *Leachate generation*

As mentioned in section 2.2, the difference between the initial moisture content and the field capacity of the Chinese MSW is greater than that of western countries, which is the main factor causing high leachate production. Simulation result (see Figure 7) also shows that MSW with higher organic content and moisture content has larger leachate production. Therefore, calculation of leachate production in landfills with high organic content MSW cannot neglect the effect of initial moisture content and moisture release via decomposition of organic. Under certain circumstances (e.g. clogging of leachate collection system, etc.), high leachate mound might be resulted due to the high leachate production in Chinese landfills.

4.2 *Settlement in landfills*

The biodegradation-induced settlement rate is highly dependent on the decomposition condition of landfill. Under optimum biodegradation condition, Figure 8 shows that both samples will accomplish their settlement within about 5 years. Therefore, if the condition is adjusted via leachate recirculation or air injection, most settlement would occur during landfilling stage, which can significantly decrease post-closure settlement of landfill. Figure 8 also shows that instant settlements (i.e., t = 0) of the two samples are close to each other. It is mainly due to the relatively higher C_C' for Orchard Hills sample which is pre-shredded before tests. However, MSW from Qizishan landfill has much more long-term compression, which indicates the necessity of accelerating the biodegradation-induced settlement of landfills with high organic content.

4.3 *Landfill stability*

Based on the method of slices and the effective stress equation proposed by Bishop 1959, the factor of safety for the *i*th slice can be written as the following equation by neglecting lateral forces (see Figure 9):

$$F_S = \frac{R_i}{T_i} = \frac{\left[c_i' l_i + \left[W_i \cos\alpha_i - \left((1-\chi)u_{ai} - \chi u_{wi}\right) l_i\right] tg\varphi_i'\right]}{W_i \sin\alpha_i} \tag{6}$$

where R_i and T_i are resisting shear force and shear force acting along the slip surface respectively, c_i' and φ_i' are cohesion and the the effective stress friction angle respectively, α_i' is the slope angle, W_i is the self weight, l_i is the bottom length which equals $b_i/cos\alpha_i$', b_i is the width of each slice, and u_{ai} and u_{wi} are the pore gas pressure and pore liquid pressure.

Landfill stability need to be assessed during the whole bio-hydro-mechanical coupled processes as:

(i) Higher organic content and moisture content may promote gas generation. However, more gas may be trapped in high moisture content MSW due to the lowered gas permeability (see Figure 2). Figure 10 shows that a mixture of leachate and landfill gas was ejected to a height of up to 5 m when drilling vertical extraction wells in Xiaping landfill, China. It indicates that very high pore pressure (u_{ai} and u_{wi}) may exist in waste body, which will decrease F_S and cause a decrease in slope stability.

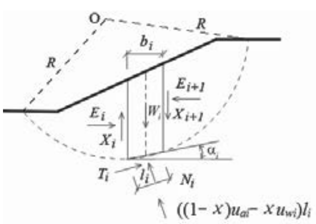

Figure 9. Method of slices

Figure 10. Ejection of leachate/gas

(ii) Higher moisture content will increase the self weight of waste body especially under leachate recirculation. As indicated by Eq.6, F_S will decrease with an increase of W_i.

(iii) During the bio-hydro-mechanical coupled process, the cohesion and friction angle mobilized at a certain strain level tend to change with an increase of waste age (see Figure 3). This makes the determination of F_S even more complex.

5 CONCLUSION

Engineering properties of landfilled MSWs with high organic content in Asian developing countries are distinguished from those in developed countries. Numerical study through the BHM coupled model showed that landfilled MSWs with higher organic content tend to have larger leachate production, long-term settlement and possibility of slope failure. The model developed can be used to study the application of bioreactor landfilling technologies in landfills with high organic content.

6 ACKNOWLEDGEMENTS

The work was supported by the National Natural Science Foundation of China (Grant Nos. 10972195, 51010008), and the National Basic Research Program of China (“973” Project) (Grant No. 2012CB719800)

7 REFERENCES

Bishop A.W. 1959. The principle of effective stress. *Tecnisk Ukeblad*, 106(39):859–863.

Chen Y.M. and Zhan L.T. 2007. Geo-environmental issues associated with landfills of municipal solid wastes. *13rd Asian Regional Conference on Soil Mechanics and Geotechnical Engineering*. Kolkata, India.

Chen Y.M., Zhan L.T., Wei H.Y. 2009. Aging and compressibility of municipal solid wastes. *Waste Management*, 29(1): 86-95.

Chen Y.M., Zhan T.L.T., Li Y.C. 2010a. Development of leachate mounds and control of leachate-related failures at MSW landfills in humid regions, invited lecture, *6th International Congress on Environmental Geotechnics*, New Delhi, India:76-98.

Chen Y.M., Ke H., Fredlund D.G., Zhan L.T., Xie Y. 2010b. Secondary compression of municipal solid wastes and a compression model for predicting settlement of municipal solid waste landfills. *Journal of Geotechnical and Geoenvironmental Engineering*, ASCE, 136(5), 706-717.

Chen Y.M., Xu X.B., Zhan L.T. 2012. Analysis of solid-liquid-gas interactions in landfilled municipal solid waste by a bio-hydro-mechanical coupled model. *SCIENCE CHINA-Technological Sciences*., 55(1):81-89.

Liao Z.Q., Shi J.Y., Mao J. 2007. Experimental study and mechanism analysis of primary compression index of MSW. *Journal of Hohai University (Natural Sciences)*, 35(3), 326-329.

Qian X.D., Koerner R.M., Gray D. H. 2002. *Geotechnical aspects of landfill design and construction*, New Jersey, Prentice-Hall, Inc.

Reddy K.R., Hettiarachchi H., Parakalla N.S., Gangathulasi J., Bogner J.E. 2008. Geotechnical properties of fresh municipal solid waste at Orchard Hills landfill, USA. *Waste Management*, 29(2): 952-959.

Sharma H.D. and Lewis S.P. 1994. *Waste Contaminant Systems, Waste, Stabilization, and Landfills Design and Evaluation*, New York, Wiley

Wei H.Y. 2007. Experimental and Numerical Study on Gas Migration in Landfill of Municipal Solid Waste Department of Civil Engineering. Dissertation of Doctoral Degree. Hangzhou, Zhejiang University.

Xu X.B. 2011. Bio-hydro-mechanical coupled analysis of solid-liquid-gas interactions in landfilled municipal solid wastes and its application. Dissertation of Doctoral Degree. Hangzhou, Zhejiang University.

Zhan T.L.T., Chen Y.M., Ling W.A. Shear strength characterization of municipal solid waste at the Suzhou landfill, China. *Engineering Geology*, 2008, 97(3-4): 97-111.

Étude expérimentale d'une technique de filtration radiale pour une application au sein de Barrières Perméables Réactives (BPR)

Experimental study of radial filtration in Permeable Reactive Barriers (PRB)

Courcelles B.
École Polytechnique de Montréal

RÉSUMÉ: Les Barrières Perméables Réactives (BPR) constituent une technique de réhabilitation environnementale utilisant le gradient naturel de l'eau souterraine pour la diriger vers un filtre réactif capable de traiter les contaminants. Une des principales configurations géométriques consiste à canaliser l'eau vers un filtre réactif dans lequel l'écoulement est vertical ascendant. La traversée de plusieurs mètres de filtre peut toutefois générer des pertes de charges importantes, qui perturbent l'écoulement régional et conduisent au contournement du système. Afin de limiter ces pertes de charges, un nouveau filtre à écoulement radial visant à réduire la longueur de cheminement dans le matériau réactif a été conçu à l'École Polytechnique de Montréal. La présente étude vise à vérifier expérimentalement les hypothèses du concept de filtre radial et à caractériser ses performances hydrauliques comparativement aux filtres traditionnels. Les résultats démontrent que les filtres radiaux permettent effectivement de limiter les pertes de charges, améliorant ainsi substantiellement l'hydraulique des filtres et augmentant le champ d'application des BPR, en particulier aux aquifères n'autorisant que peu de pertes de charges sous peine de contournement du système de traitement.

ABSTRACT: Permeable Reactive Barriers (PRB) constitute an environmental remediation technique in which natural gradients are exploited to channel the groundwater towards a reactive filter. One of the main geometric configurations consists in realizing an upward vertical filtration in a reactive filter able to treat the contaminants. Crossing several meters of filter can however generate excessive head losses, modify the regional flow and lead to a bypass of the system. To minimize these head losses, a new radial-flow filter consisting in reducing the filtration length has been developed at Polytechnique Montreal. The present study aims to experimentally verify the assumptions of the radial filtration and characterize its hydraulic performances compared to traditional filters. The results show that radial filters can effectively reduce head losses, improve substantially the hydraulic of filters and increase the scope of PBRs, in particular to aquifers allowing few head losses to prevent any bypass.

MOTS-CLÉS: barrières perméables réactives, filtration, milieux granulaires, réseau d'écoulement, décontamination.

1 INTRODUCTION

Pour faire face aux problèmes d'augmentation des sites contaminés, les Barrières Perméables Réactives (BPR) constituent une technique de réhabilitation in situ efficace pour le traitement des eaux souterraines (Blowes et al. 1995). Leur originalité réside dans l'exploitation des gradients naturels pour diriger l'eau souterraine vers un matériau réactif capable de la décontaminer par dégradation, adsorption ou précipitation. Cette technique ne nécessite ainsi aucun apport d'énergie externe, ce qui réduit considérablement les frais d'exploitation lors de la réhabilitation d'un site contaminé (RECORD, 2010).

Les BPR sont habituellement mises en œuvre selon trois grandes configurations géométriques: (1) un mur continu constitué de tranchées remplies de matériau réactif ou de puits d'injection de réactifs (Blowes et al 1995), (2) une configuration avec porte filtrante (usuellement dénommée « funnel-and-gate ») composée de deux parois imperméables canalisant le panache contaminé vers une zone réactive (Starr et Cherry 1994), et (3) une configuration en caisson qui est une variante de la précédente dans laquelle la filtration s'effectue de manière verticale ascendante (Porter 1998, Warner et al. 1998).

Les murs continus représentent la configuration la plus commune pour les BPR (Blowes et al. 1995). Ils sont habituellement composés de matériaux réactifs installés en aval d'un panache de contamination, perpendiculaire à l'écoulement des eaux souterraines. Comme ils constituent la configuration historique de BPR, ces murs continus ont été largement mis en œuvre et leur efficacité a été documentée dans la littérature (O'Hannesin et Gillham 1998). Une méthode de conception est également dédiée à cette configuration et s'appuie sur le temps de séjour des polluants dans le milieu réactif (Gavaskar et al. 1998, Powell et al. 1998).

Dans la configuration « funnel-and-gate », deux parois imperméables sont préalablement réalisées dans le sol. Il peut s'agir de parois minces, de parois composites, de palplanches ou encore de murs en coulis bentonite-ciment. Un matériau réactif est ensuite mis en place à l'exutoire de ces parois imperméables après excavation, sol-mixing ou tranchage. Dans cette configuration, le support réactif est placé verticalement et perpendiculairement à l'écoulement des eaux souterraines et la filtration est réalisée horizontalement.

Comme variante de la géométrie précédente, une configuration avec écoulement vertical ascendant dans un caisson réactif a été mise au point. Ces caissons sont la plupart du temps de forme cylindrique ou parallélépipédique et deux configurations différentes ont été développées et brevetées par Soletanche-Bachy (filtres cylindriques) et l'Université de Waterloo (filtres parallélépipédiques). Cet écoulement vertical ascendant dans des filtres réactifs manufacturés est ainsi plus uniforme (Elder 2000) et facilite la maintenance (Courcelles 2007).

La conception de BPR repose principalement sur trois aspects techniques: (1) le milieu réactif doit être adapté aux contaminants et sa sélection doit tenir compte de facteurs tels la géochimie, les conditions biologiques et hydrogéologiques du site, (2) la taille des filtres doit être sélectionnée pour assurer un temps de séjour suffisant et garantir des réactions complètes (Shoemaker et al. 1995, O'Hannesin et Gillham 1998, Warren et al. 1995), et finalement (3) le matériau réactif doit avoir une conductivité hydraulique supérieure à celle de l'aquifère environnant pour empêcher tout contournement du système (Starr et Cherry 1994). Afin de répondre aux contraintes hydrauliques et limiter les pertes de charges dans les filtres, un nouveau concept de filtre radial pouvant être mis en œuvre dans les caissons a été développé à l'École Polytechnique de Montréal. Sur le plan théorique, ce filtre permet, à volume de réactifs égaux, de diminuer les pertes de charges par rapport à un filtre classique et d'en améliorer les performances chimiques (Courcelles 2012). Toutefois, des expérimentations étaient nécessaires pour vérifier la principale hypothèse du filtre radial, à savoir la parfaite verticalité des équipotentielles dans le filtre. Les résultats d'essais de laboratoire visant à vérifier cette hypothèse sont présentés dans la suite du document.

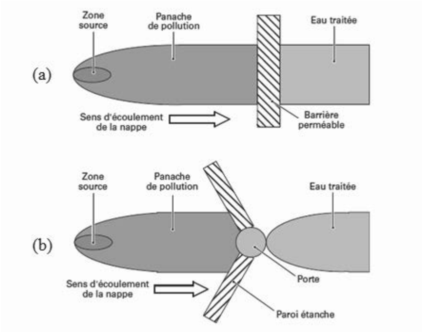

Figure 1. Principe des Barrières Perméables Réactives : (a) configuration en mur continu, et (b) configuration « funnel-and-gate » ou en caisson, d'après Roudier (2005).

.

2 PRINCIPE DU FILTRE RADIAL

La conception du nouveau filtre repose sur l'application directe de la loi de Darcy, qui énonce que le débit traversant une section d'un milieu granulaire est proportionnel au gradient hydraulique et à sa surface. Ainsi, à débit et volume de filtre constants, les pertes de charges sont moindres lorsque la section du filtre est augmentée et sa longueur proportionnellement réduite. Le filtre radial est ainsi un cylindre réactif ou l'écoulement peut se faire de son axe central vers la périphérie ou inversement. De fait, la longueur de filtration se limite au rayon du cylindre, ce qui est très intéressant compte-tenu des dimensions classiques des filtres, qui peuvent être particulièrement élancés avec des diamètres compris entre 0,5 et 1 m et des longueurs pouvant atteindre plusieurs mètres.

Comme illustré sur la Fig. 2, le filtre cylindrique est composé de trois matériaux coaxiaux : un matériau grossier inerte au centre, entouré un matériau réactif et d'un autre matériau inerte à l'extérieur. Les matériaux grossiers au centre et à la périphérie du filtre constituent les zones d'entrée ou de sortie d'eau dans le filtre, selon les pertes de charges appliquées. Les avantages d'un tel filtre sont multiples comparativement à la configuration classique et touchent l'hydraulique, mais également les performances chimiques des filtres.

Considérant que le filtre radial et le filtre classique de la Fig. 2 ont des longueurs identiques et un même volume de matériau réactif (R_{ext}^2-R_{int}^2=R'^2), les pertes de charges sont, à débits égaux, plus faibles dans le filtre radial car la longueur de filtration est réduite (R_{ext}-R_{int} comparativement à L dans une filtration classique). Un filtre radial permettrait ainsi d'augmenter la durée de vie hydraulique des BPR, puisqu'il permet de limiter les contraintes sur la conductivité hydraulique minimale du matériau réactif.

Sur le plan chimique, les temps de contact des deux filtres de la Fig. 2 sont identiques puisque les volumes des vides sont les mêmes. Par ailleurs, même si l'écoulement dans un filtre radial peut être centripète ou centrifuge, l'étude théorique a permis de démontrer qu'un écoulement centripète améliore les performances chimiques des filtres des BPR. En effet, la vitesse relative de l'eau contaminée par rapport aux grains réactifs est plus faible à la périphérie, c'est-à-dire là où les concentrations en contaminants sont les plus fortes dans le cas d'un écoulement centripète (Courcelles 2012). Dans le cas d'une rétention par adsorption des contaminants, la percée du filtre peut ainsi être retardée.

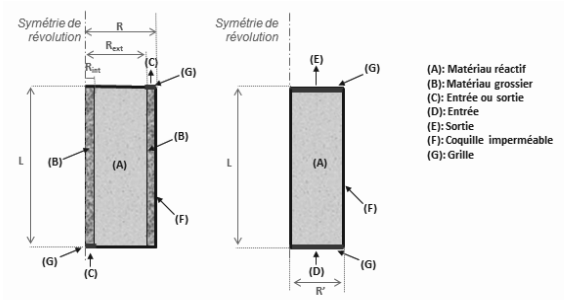

Figure 2. Concept de filtre radial

3 MATÉRIEL ET MÉTHODE

Afin de vérifier les conditions d'écoulement dans les filtres radiaux, des essais de laboratoire ont été réalisés sur un filtre miniature. Les conditions d'essais sont précisées dans la présente section.

3.1 Géométrie de filtration

Le filtre possédait une hauteur de 30 cm et un rayon de 15 cm. Tel que représenté en axisymétrie sur la Fig. 3, il comprenait un cylindre de matériau grossier de 15 mm de rayon au centre et un autre matériau grossier sur 15 mm d'épaisseur à la périphérie.

La filtration a été réalisée de manière centripète, soit du matériau grossier extérieur vers le matériau grossier intérieur. L'exutoire du filtre radial se situait au sommet de ce matériau grossier central.

Les charges hydrauliques ont été mesurées à l'aide de piézomètres implantés dans le matériau réactif sur une section verticale. Ces piézomètres constituent un maillage réparti selon trois rayons, de 15, 75 et 135 mm, et trois hauteurs de mesure, à 6, 15 et 24 cm. Chaque piézomètre est identifié par son rayon (1 à 3), suivi de son niveau (a à c).

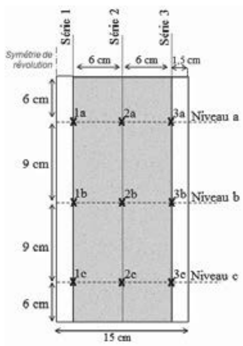

Figure 3. Localisation des mesures de pression sur une section verticale de filtre radial

3.2 Matériaux réactifs et solution filtrée

Le matériau réactif sélectionné pour les essais est de l'oxyde de magnésium, FlowMag® PWT de la compagnie Magnesia Specialties. Habituellement utilisé pour le traitement de l'eau potable, ce matériau permet de relever le pH de la solution filtrée et de retenir les contaminants métalliques par précipitation d'hydroxydes. Durant les essais, le pH est resté constant à une valeur de 9.8, particulièrement propice à la précipitation d'hydroxydes à partir d'ions métalliques divalents (Zn, Mn, Cu, Pb, Ni, Co ou Cd). La granulométrie du matériau réactif était comprise entre 1,2 et 3,35 mm, ce qui permettait d'assurer une bonne surface spécifique sans pénaliser la conductivité hydraulique. Le matériau grossier était quant à lui constitué de graviers inertes, de diamètres compris entre 3 et 10 mm.

L'objectif des essais étant de caractériser le comportement hydraulique des filtres radiaux, ces derniers ont été réalisés sur une eau non contaminée. Toutefois, la dureté de cette eau a été ajustée par adjonction de $NaHCO_3$ à une concentration de 500 mg/L. En effet, les eaux particulièrement chargées en ions carbonates sont particulièrement préjudiciables au fonctionnement des filtres d'oxyde de magnésium, puisque l'augmentation du pH conduit à la formation de calcite ($CaCO_3$), pénalisant ainsi la conductivité hydraulique des filtres (Courcelles 2007). Des conditions pénalisantes ont ainsi été sélectionnées pour ces essais hydrauliques afin d'observer l'évolution de la conductivité hydraulique du matériau réactif et son influence sur le réseau d'écoulement dans le filtre radial. En effet, l'étude théorique des filtres radiaux avait démontré qu'il existait un rapport de conductivité hydraulique minimal $k_{grossier}/k_{réactif}$ permettant de garantir un écoulement parfaitement radial (Courcelles 2012). La mise en œuvre d'un matériau à conductivité hydraulique évolutive en fonction de la quantité de précipités formés permet ainsi de déterminer expérimentalement le rapport minimal permettant de garantir l'hypothèse d'écoulement radial. Les essais ont été réalisés grâce à une alimentation par une pompe péristaltique à un débit constant de 150 mL/min.

4 RÉSULTATS EXPÉRIMENTAUX

Les mesures des charges hydrauliques totales en fonction du temps sont présentées dans la présente section et interprétées grâce à une interpolation spatiale par krigeage et une modélisation numérique de l'écoulement dans le filtre de laboratoire.

4.1 Évolution de la charge hydraulique totale

L'évolution de la charge hydraulique totale en fonction du renouvellement des vides est présentée sur la Fig. 4 pour les différents piézomètres. À l'entrée du filtre radial, c'est-à-dire au droit du rayon 3, on remarque que la charge hydraulique est identique pour les trois niveaux de mesure. Le matériau grossier assure donc son rôle de conducteur hydraulique permettant de limiter les pertes de charges à l'extérieur du matériau réactif. On notera toutefois l'augmentation simultanée de la charge hydraulique pour les piézomètres 3a à 3c en fonction du renouvellement des vides, ce qui traduit un colmatage progressif du filtre réactif.

Au droit des rayons 1 et 2, l'évolution de charge hydraulique totale est toutefois différente pour chacun des trois niveaux de mesure. Les charges diminuent en effet avec l'élévation dans le filtre, ce qui démontre que l'écoulement n'est pas parfaitement horizontal, mais possède également une composante verticale.

Tout comme pour le rayon 3, la charge au droit des rayons 1 et 2 présente une augmentation progressive avec le renouvellement des vides suite au colmatage par la formation de $CaCO_3$. Des régressions polynomiales d'ordre 2 ont été réalisés pour chacun des piézomètres afin d'illustrer l'augmentation de la charge hydraulique en fonction du renouvellement des vides.

4.2 Interprétation par krigeage et modélisation

Afin de représenter l'évolution spatiale des charges hydrauliques totales, les équipotentielles ont été interprétées par krigeage et sont fournies sur la Fig. 5 pour le début et la fin de l'essai de filtration.

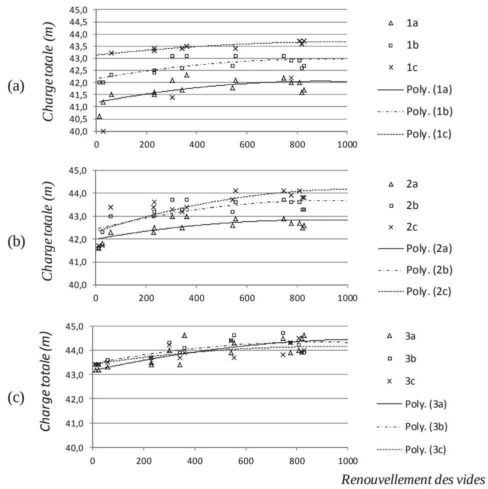

Figure 4. Évolution de la charge hydraulique totale en fonction du renouvellement des vides du matériau réactif pour : (a) la série 1, (b) la série 2 et (c) la série 3.

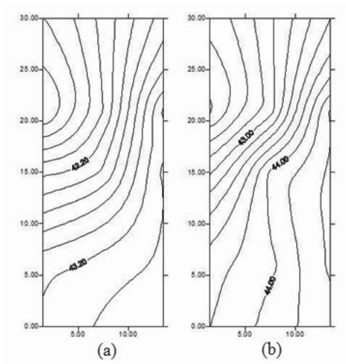

Figure 5. Interpolation des équipotentielles par krigeage : (a) début de la filtration et (b) après 900 renouvellement des vides. Échelle des axes et charge hydraulique totale en cm.

La localisation des équipotentielles sur la Fig. 5 démontre ainsi que l'écoulement n'est pas parfaitement radial, mais plutôt orienté vers le sommet du matériau grossier au centre du filtre. En ce sens, cette orientation n'est pas conforme aux hypothèses du modèle théorique, puisque la longueur de cheminement n'est pas, en moyenne, réduite par rapport à un écoulement vertical classique. Toutefois, après un renouvellement des vides de 900 fois et la diminution de la conductivité hydraulique, les équipotentielles deviennent plus verticales et l'écoulement s'approche d'un écoulement radial. Le rapport entre des conductivités hydrauliques des matériaux grossier et réactif ($k_{grossier}/k_{réactif}$) joue donc un rôle prépondérant dans l'orientation des lignes d'écoulement. Afin d'illustrer ce comportement, une modélisation numérique a été réalisée à l'aide du logiciel Comsol Multiphysics pour les dimensions du filtre expérimental et différents rapports de conductivités hydrauliques.

La Fig. 6 présente les résultats de la modélisation numérique pour des rapports $k_{grossier}/k_{réactif}$ de 5, 50 et 500. Le rapport de 5 correspond au début de la filtration, puisque des essais de perméabilité ont permis de déterminer des conductivités hydrauliques respectives de 10^{-1} et 2.10^{-2} m/s pour le matériau grossier et le matériau réactif. Au début de la filtration, la théorie corrobore ainsi les résultats expérimentaux puisque l'écoulement est essentiellement orienté vers le sommet de l'axe central. Après réduction de la conductivité hydraulique du matériau réactif ($k_{grossier}/k_{réactif}$=50), l'écoulement est moins oblique et son allure générale est semblable aux observations faites après un renouvellement des vides de 900 fois. Finalement, l'écoulement ne devient parfaitement radial que lorsque le rapport de conductivités hydrauliques atteint 500 (Fig. 3c).

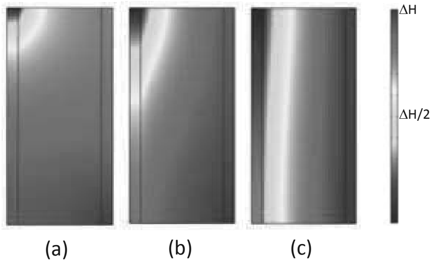

Figure 6. Résultats des simulations numériques pour différents ratios $k_{grossier}/k_{réactif}$: (a) 5, (b) 50 et (c) 500. (Bleu foncé: pression atmosphérique, rouge foncé: charge imposée à l'entrée du filtre).

Ces résultats expérimentaux assortis de la modélisation numérique démontrent ainsi que le rapport minimal $k_{grossier}/k_{réactif}$ permettant de garantir l'hypothèse d'écoulement radial est supérieur à 50. Au-dessus de ce rapport, le filtre radial commence à remplir sa fonction de limitation des pertes de charges.

4.3 Estimation de la conductivité hydraulique après colmatage

Dans le cas d'équipotentielles parfaitement verticales dans un filtre radial et en négligeant les pertes de charges dans le matériau grossier, le débit en fonction de la perte de charge dans le filtre peut être calculé selon l'équation 1 par analogie avec un puits dans un aquifère captif.

$$Q = k_{reactif} \cdot 2 \cdot \pi \cdot L \cdot \frac{H_{ext} - H_{\text{int}}}{\ln\left(\frac{R_{ext}}{R_{\text{int}}}\right)} \tag{1}$$

où Q représente le débit dans le filtre et H_{ext}-H_{int} la différence de charge appliquée entre l'entrée et la sortie du filtre.

Cette expression peut toutefois se réécrire selon l'équation 2, qui où k' représente la conductivité hydraulique apparente du filtre, c'est-à-dire celle qu'un observateur calculerait s'il ignorait que l'écoulement était radial dans le filtre.

$$Q = k' \cdot \pi \cdot \left(R_{ext}^2 - R_{\text{int}}^2\right) \frac{H_{ext} - H_{\text{int}}}{L} \tag{2}$$

$$k' = \frac{2 \cdot k_{reactif} \cdot L^2}{\left(R_{ext}^2 - R_{\text{int}}^2\right) \cdot \ln\left(\frac{R_{ext}}{R_{\text{int}}}\right)} \tag{3}$$

Afin d'évaluer l'état de colmatage du filtre radial à la fin de la filtration et l'ordre de grandeur de la conductivité hydraulique, des équipotentielles quasi-verticales ont été considérées et la conductivité hydraulique $k_{réactif}$ calculée à partir de l'équation 1 et des mesures au niveau b. En moyenne, les pertes de charges étant plus importantes au niveau a et plus faibles au niveau c, le calcul ne donne qu'une approximation de la conductivité hydraulique moyenne du filtre. Considérant la perte de charge de 1,48 cm au niveau b, nous obtenons ainsi une conductivité hydraulique de 2.10^{-4} m/s pour le matériau réactif. Cette valeur corrobore les résultats expérimentaux obtenus en filtration axiale avec un matériau réactif et des concentrations en $NaHCO_3$ identiques, à savoir un rapport de 2.10^{-2} entre les conductivités hydrauliques initiale et finale du matériau réactif (Courcelles 2011).

Le filtre radial "apparaît" cependant 4,5 fois plus perméable qu'un filtre classique puisque, d'après l'équation 2, les pertes de charges mesurées correspondent à une conductivité hydraulique $k' = 9.10^{-4}$ m/s pour une même hauteur de filtre et des sections identiques de matériau réactif.

5 CONCLUSION

Les essais physiques réalisés sur un filtre à écoulement radial ont permis de confirmer les avantages hydrauliques de ce dernier, puisqu'un matériau réactif possédant une conductivité hydraulique après colmatage de 2.10^{-4} m/s permet de réduire les pertes de charges d'un facteur de 4,5 lorsqu'il est soumis à une filtration radiale au lieu d'une filtration verticale ascendante classique. Toutefois, ce résultat est strictement dépendant du rapport entre les conductivités hydrauliques $k_{grossier}/k_{réactif}$. Dans les essais, un rapport minimal de 50 était nécessaire pour assurer un écoulement pseudo-vertical. Cette observation permettra de parfaire le dimensionnement des filtres radiaux pour des essais à l'échelle pilote, pour lesquels le rapport $k_{grossier}/k_{réactif}$ sera évalué numériquement en fonction de la géométrie retenue. D'une manière générale, les avantages hydrauliques du filtre radial permettent de sélectionner des matériaux réactifs plus fins, ce qui est avantageux sur le plan chimique et qui permet de respecter plus facilement le critère de rapport minimal $k_{grossier}/k_{réactif}$.

6 REFERENCES

Blowes D., Ptacek C., Cherry J., Gillham R., et Robertson W. 1995. Passive Remediation of Groundwater Using In Situ Treatment Curtains. *Geoenvironment 2000: Characterization, Containment, Remediation, and Performance in Environmental Geotechnics*, Daniel, D. and Acar, Y. (Eds.), ASCE, GSP 46, 1588-1607.

Courcelles B. 2007. *Étude du comportement physico-chimique des filtres de barrières perméables réactives : Modélisation et expérimentation à l'échelle pilote*. Thèse de doctorat, École Centrale Paris.

Courcelles B, Modaressi A., Gouvenot D., Esnault-Filet A. 2011, Influence of precipitates on hydraulic performance of permeable reactive barrier filters, *International Journal of Geomechanics*, April 2011, Vol. 11, Iss. 2, p.142-151.

Courcelles B. 2012. Filters of Permeable Reactive Barriers: A new design approach. *2nd International Conference on Environmental Pollution and Remediation, Montreal, Quebec, Canada*, 28-30 August.

Elder C. R. 2000. *Evaluation and Design of Permeable Reactive Barriers amidst Heterogeneity*. PhD Thesis, University of Wisconsin-Madisson.

Gavaskar A., Gupta N., Sass B., Janosy R., O'Sullivan D. 1998. *Permeable Barriers for Groundwater Remediation: Design Construction, and Monitoring*. Battelle Press, Columbus, OH.

O'Hannesin S. and Gillham R. 1998. Long-Term Performance of an In Situ "Iron Wall" for Remediation of VOCs. *Ground Water*, 36(1), 164-170.

Porter J. 1998. Greener Process. *Ground Engineering*, July, 32-33.

Powell R., Blowes D., Gillham R., Schultz D., Sivavec T., Puls R., Vogan J., Powell P., and Landis R. 1998. *Permeable Reactive Barrier Technologies for Contaminant Remediation*. EPA/600/R-98/125, Washington DC.

RECORD 2010, *Barrières Perméables réactives (BPR) : Retours d'expériences, perspectives d'application et enjeux de recherche pour le traitement des pollutions métalliques. Actualisation de l'état de l'art RECORD 2004*, 2010, 272 p, n°08-0331/1A.

Roudier 2005, Techniques de réhabilitation des sites et sols pollués : Fiches de synthèse, *Techniques de l'ingénieur,* TIB551DUO.

Shoemaker S., Greiner J., and Gillham R. 1995. "Permeable Reactive Barriers". Assessment of Barrier Containment Technologies: A Comprehensive Treatment for Environmental Remediation Application, Rumer, R. and Mitchell, J. Eds., *International Containment Technology Workshop, Baltimore, Maryland*, August 29-31, 301-353.

Starr R. and Cherry J. 1994. In Situ Remediation of Contaminated Ground Water: The Funnel-and-Gate System. *Ground Water*, 32(3) 465-476.

Warner, S., Yamane, C., Gallinatti, J. and Hankins, D. 1998. Considerations for Monitoring Permeable Ground-Water Treatment Walls. *Journal of Environmental Engineering*, 124(6), 524-529.

Warren K., Arnold R., Bishop T., Lindholm L, and Betterton E 1995. Kinetics and Mechanisms of Reductive Dehalogenation of Carbon Tetrachloride Using Zero Valent Metals. *Journal of Hazardous Materials*, 41, 217-227.

Measurement of NAPL saturation distribution in whole domains by the Simplified Image Analysis Method

Mesure de la distribution de la saturation de liquide en phase non-aqueuse couvrant tout le spectre de l'étude par la méthode simplifiée d'analyse d'image

Flores G.
Graduate School of Engineering, Kyoto University

˙Katsumi T., Inui T., Takai A.
Graduate School of Global Environmental Studies, Kyoto University

ABSTRACT: A *Simplified Image Analysis Method* devised to assess the saturation distribution of water and *Non-Aqueous Phase Liquids* (NAPLs) in granular soils subject to fluctuating groundwater conditions was developed and tested for ten different NAPLs of different density and viscosity values ($0.73 \leq \rho \leq 1.20$ g/cm^3; $1.4 \leq \nu \leq 1000$ mPa·s). The *Simplified Image Analysis Method*, which is based on an extension of the *Beer-Lambert Law of Transmittance* that predicts the existence of a linear relationship between the saturation of water (S_w), NAPL (S_o), and their corresponding average optical densities (D_i), was tested by photographing samples of Toyoura sand mixed with different amounts of water and NAPLs, using two digital cameras with different wavelength band-pass filters (λ = 450 nm and 640 nm), and obtaining the linear equations relating S_w, S_o and D_i for the each NAPL. Once the linear relationships were confirmed, this method was used to assess the behavior of two different NAPLs subject to fluctuating groundwater tables, demonstrating that this *non-intrusive* and *non-destructive* method can be used as a reliable tool to provide water and NAPL saturation distributions in full domains, when studying the effects of porous soil contamination by NAPLs under dynamic conditions.

RÉSUMÉ: Une *méthode simplifiée d'analyse d'image* visant à mesurer la distribution de la saturation d'eau et des *liquides en phase non-aqueuse* (NAPLs) des sols granuleux soumis aux fluctuations des eaux souterraines, a été développée et testée dans dix différents NAPLs ($0.73 \leq \rho \leq 1.20$ g/cm^3; $1.4 \leq \nu \leq 1000$ mPa·s). La méthode simplifiée d'analyse d'image, une extension de la *lois de Beer-Lambert* qui établit une relation linéaire entre la saturation d'eau (S_w), de NAPL (S_o) et leurs densités optiques respectives (D_i), a été testée en photographiant à l'aide de deux cameras digitales ayant des filtre passe-bande de longueur d'onde différente (λ = 450 nm et 640 nm) des échantillons de sable de Toyoura, mélangés avec des quantités différentes d'eau et des NAPLs, et en obtenant les équations linéaires qui lient S_w, S_o et D_i à chacun de NAPL. Après confirmation de la relation linéaire, cette méthode a été utilisée pour évaluer le comportement de deux différents NAPLs soumis aux fluctuations des nappes phréatiques; et pour démontrer que cette méthode non intrusive et non destructive, peut être utilisée de manière fiable pour obtenir les distributions de saturation d'eau et de NAPL dans tout le spectre lors des explorations des effets de contamination des sols poreux par des NAPLs sous les conditions dynamiques.

KEYWORDS: NAPL, simplified image analysis, saturation, optical density, column test

1 INTRODUCTION

When released in the vadose zone, *Non-Aqueous Phase Liquids* (NAPLs) pose significant contamination risks to the groundwater (Mercer and Cohen 1990; Capiro, Stafford et al. 2007). Remediation of these releases in an efficient and cost-effective way should be guided by field data interpreted by numerical models using the appropriate assumptions (Kechavarzi, Soga et al. 2000). To verify the accuracy of these models, laboratory tests should be run and precise saturation information should be obtained, especially under the dynamic conditions usually present in nature (Lenhard and Parker 1987; Fagerlund, Illangasekare et al. 2007; Flores, Katsumi et al. 2011). In this study, we aim to validate the *Beer-Law of Transmittance*, the basis of the *Simplified Image Analysis Method* for ten different NAPLs with different density and viscosity values, and then use this method to assess the behavior of five different NAPLs subject to fluctuating groundwater conditions, which may have a significant effect on the behavior of NAPLs, particularly with regards to their residual saturation. For this, residual saturation values at the end of drainage and imbibition stages will be compared for our different NAPLs.

2 SIMPLIFIED IMAGE ANALYSIS METHOD

The *Beer-Lambert Law of Transmittance* states that when a beam of monochromatic radiation I_0 strikes a block of absorbing matter perpendicular to a surface, after passing through a length b of the material, its power is decreased to I_t as a result of absorption:

$$D_i = \varepsilon bc = \log_{10} \frac{I_0}{I_t} \tag{1}$$

where D_i is the optical density, ε a numerical constant, b the length of the path, c the number of moles per liter of absorbing solution, I_0 is the initial radiant power, and I_t the transmitted power (Skoog et al. 2007). For digital images, the average optical density D_i is defined for the reflected light intensity as:

$$D_i = \frac{1}{N}\sum_{j=1}^{N} d_{ji} = \frac{1}{N}\sum_{j=1}^{N}\left(-\,log_{10}\left(\frac{I_{ji}^r}{I_{ji}^0}\right)\right) \tag{2}$$

where N is the number of pixels contained in the area of interest and, for a given spectral band i, d_{ji} is the optical density of the individual pixels, I_{ji}^r is the intensity of the reflected light given by the individual pixel values, and I_{ji}^0 is the intensity of the light that would be reflected by an ideal white surface (Kechavarzi et al. 2000).

It has been shown (Flores et al. 2011) that the *Beer-Lambert Law of Transmittance* establishes a linear relationship between optical density and the concentration of a dye:

$$D_t = c\ \cdot D_0 \tag{3}$$

where D_0 is the optical density of a solution of unit concentration, and D_t the optical density of a solution of concentration c. Therefore, when two cameras with band-pass filters (wavelengths $\lambda = i$ and j) are used, and when water and NAPL are mixed with dyes whose predominant color wavelengths are also i and j, we can obtain two different sets of linear equations that can be solved for S_w and S_o:

$$\begin{bmatrix} D_i \\ D_j \end{bmatrix}_{mn} = \begin{bmatrix} \left(D_i^{10} - D_i^{00}\right) \cdot S_w + \left(D_i^{01} - D_i^{00}\right) \cdot S_o + D_i^{00} \\ \left(D_j^{10} - D_j^{00}\right) \cdot S_w + \left(D_j^{01} - D_j^{00}\right) \cdot S_o + D_j^{00} \end{bmatrix}_{mn} \quad (4)$$

where m and n are the dimensions of the matrix, $[D_i]_{mn}$ and $[D_j]_{mn}$ are the values of average optical density of each mesh element for wavelengths i and j; $[D_i^{00}]_{mn}$ and $[D_j^{00}]_{mn}$ are the average optical density of each mesh element for dry sand; $[D_i^{10}]_{mn}$ and $[D_i^{10}]_{mn}$ for water saturated sand; and $[D_i^{01}]_{mn}$ and $[D_i^{01}]_{mn}$ for NAPL saturated sand. This is the base of the *Simplified Image Analysis Method*.

3 MATERIALS

For this study, 10 NAPLs (Table 1) were used as non-wetting fluids after being dyed red with Sudan III (1:10000). Their names were obtained from different national pollutant registry lists (Australia DSEWPC 1999; Environment Canada 2010; UK Environment Agency 2011; US EPA 2011) for their frequency as contaminants, as well as for their immiscibility (or negligible solubility) in water. Water, dyed blue with Brilliant Blue FCF (1:10000), was used as wetting fluid. Toyoura sand (Soil particle specific gravity, G_s = 2.64; uniformity coefficient, C_u = 1.36) was the porous media.

Table 1. Physical characteristics of NAPLs

NAPL	Solubility in Water	Density ρ (g/cm^3)	Viscosity ν (mPa·s)
Diesel 2	Immiscible	0.850	4
Ethylbenzene	0.0169 g/l	0.860	1.5
Low Viscosity Paraffin	Immiscible	0.880	7
Motor Oil	Immiscible	0.858	129
N-decane	0.009 ppm	0.730	1.4
N-dodecane	Immiscible	0.750	1.9
NEOVAC	Negligible	0.930	108
Nitrobenzene	0.019 g/l	1.199	3.1
Paraffin Liquid	Immiscible	0.870	170
Silicone Oil	Negligible	0.963	1000

4 TRANSMITTANCE TEST

For equation (3) to truly represent a linear relationship, the colorimetric characteristics of the solution of concentration c (i.e., each NAPL) must not greatly change throughout the test. To verify that our selected NAPLs satisfy this condition, samples of each one were analyzed before and after being freely let evaporate at laboratory conditions.

For every NAPL (Table 1), 50 ml were dyed with Sudan III (1:10000), their transmittance curves were obtained with the Shimadzu UV-VIS Spectrometer, and were let evaporate inside 50 ml glass centrifuge tubes ($ø$ = 29 mm, h = 117 mm) for 168 h at a constant room temperature of 20° C and humidity of 70%, after which their transmittance curves were once again calculated.

Graphics were prepared comparing transmittance before and after the 168 h period, for both samples that were dyed and extra samples that were kept undyed. Results show very little variation on the transmittance behavior of all NAPLs. As an example of the obtained results, Figure 1 shows the plots corresponding to two of our analyzed NAPLs: N-decane and Ethylbenzene. Similar results were obtained for all other NAPLs.

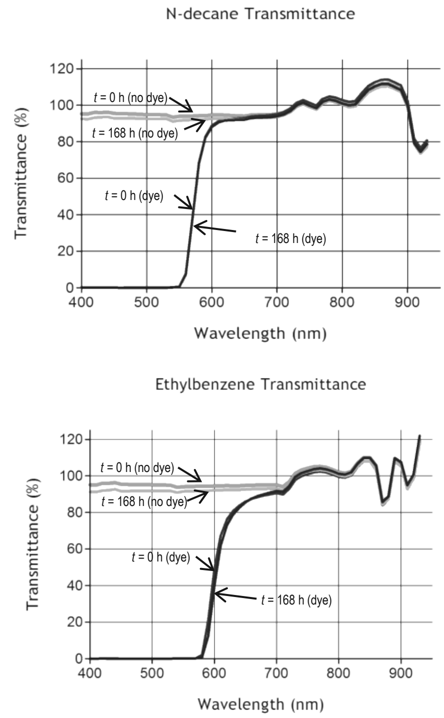

Figure 1. Test of Transmittance for N-decane and Ethylbenzene

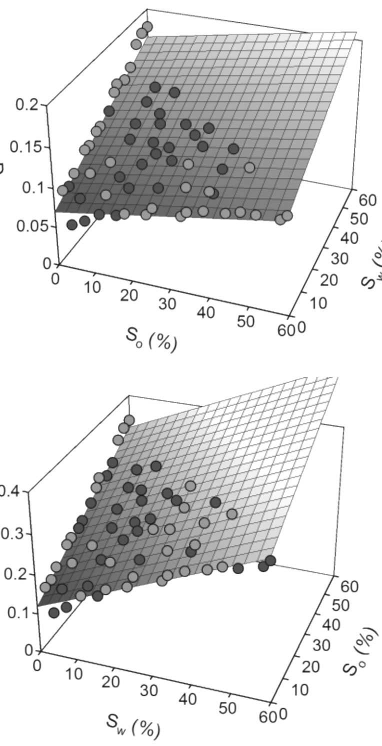

Figure 2. Water and NAPL Saturation vs. Optical Density Relationship for N-decane

5 SATURATION VERSUS OPTICAL DENSITY TEST

Sixty soil samples were prepared with each NAPL by mixing known amounts of water, NAPL and porous media in 25 cm^3 cylindrical sample containers ($ø$ = 40 mm, h = 20 mm). The prepared samples were positioned approximately 1.5 m in front of two cameras, two 500 W lights were turned on, and one picture was taken with each camera (one with a λ = 450 nm band-pass filter, and the other one with a λ = 640 nm one). To account for differences in lighting, a Kodak gray scale and a Gretamacbeth white balance card were placed next to each soil sample, and were part of each picture as well. Both cameras were set to manual mode so that aperture, shutter speed and white balance were kept constant. Room temperature was kept at 20 °C and humidity at 70%. Pictures were recorded in NEF format and then were exported to TIFF format using ViewNX 1.5.0. The TIFF images were then analyzed by an ad-hoc program written in MATLAB Release 2007a. Graphics were prepared for each NAPL, comparing water and NAPL saturation versus optical density values, for each wavelength. Figure 2 shows the plots corresponding to one of our analyzed NAPLs, N-decane, for both 450 and 640 nm. The linear fit for the first graphic (450 nm) has a coefficient of determination R^2 = 0.89, and for the second one (640 nm), R^2 = 0.96, showing that, as predicted by equation (3), the relationship between water and NAPL saturation, and optical density is linear. The regression equations and corresponding values for the coefficients of determination (R^2) for the ten studied NAPLs are as shown in Table 2.

6 COLUMN TESTS

Once linear relationships between water and NAPL saturation values, and optical density, were confirmed for a broad spectrum of NAPLs, we can apply the *Simplified Image Analysis Method* to study the behavior of different NAPLs in whole domains. Five NAPLs (Diesel 2, Ethylbenzene, Low Viscosity Paraffin, N-decane, and Paraffin Liquid) were selected for the column tests based on their diverse viscosity values (1.4 < ν < 170 mPa·s), and densities (0.730 < ρ < 0.880 g/cm^3). Similar amount of each NAPL (28 g) was injected from the top of their corresponding column and subjected to two cycles of Drainage-Imbibition in separate 3.5 × 3.5 × 40 cm columns (Figure 3) filled with fully saturated Toyoura Sand. Both drainage stages lasted 72 hours (h = -5 cm), and both imbibition stages lasted 24 hours (h = 40 cm). Total duration of each test was 192 hours. Two simultaneous pictures were taken of each column every 30 minutes, and were analyzed following the *Simplified Image Analysis Method* described in Flores *et al* (2011). Saturation distributions of NAPL and water for the whole domains were plotted for all cases at t = 0, 72, 96, 168, and 192 hours, representing initial conditions, end of the first drainage, end of the first imbibition, end of the second drainage, and end of the second imbibition. Saturation distribution graphics of N-decane are shown in Figure 4, but similar graphics were prepared for all NAPLs.

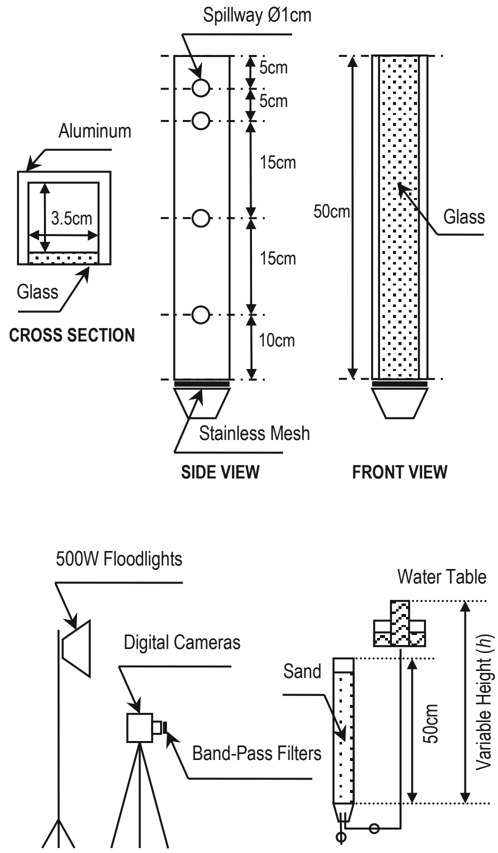

Figure 3. Column design (top) and Experimental setup (bottom)

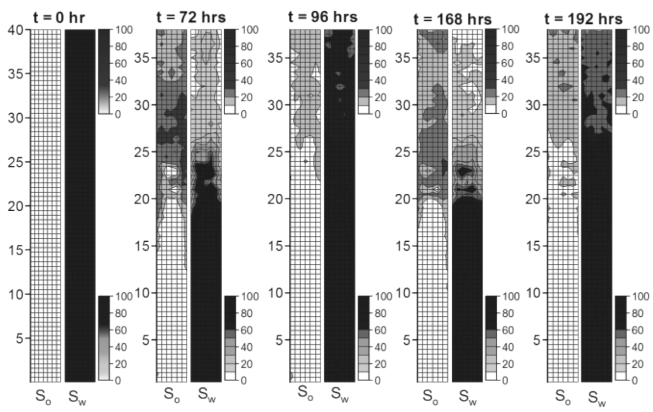

Figure 4. NAPL (S_o) and Water (S_w) saturation distribution matrices at different times, for N-decane

Table 2. Regression equations for different NAPLs, for wavelengths λ = 450 nm and 640 nm

NAPL	D_{450}	R^2	D_{640}	R^2
Diesel 2	0.0180 S_o + 0.0035 S_w + 0.2457	0.83	0.0030 S_o + 0.0025 S_w + 0.1283	0.95
Ethylbenzene	0.0175 S_o + 0.0007 S_w + 0.0680	0.81	0.0033 S_o + 0.0037 S_w + 0.1220	0.90
Low Viscosity Paraffin	0.0160 S_o + 0.0008 S_w + 0.0710	0.89	0.0029 S_o + 0.0036 S_w + 0.1300	0.93
Motor Oil	0.0150 S_o + 0.0006 S_w + 0.0750	0.91	0.0028 S_o + 0.0033 S_w + 0.1300	0.92
N-decane	0.0150 S_o + 0.0008 S_w + 0.0700	0.89	0.0033 S_o + 0.0040 S_w + 0.1200	0.96
N-dodecane	0.0160 S_o + 0.0007 S_w + 0.0700	0.88	0.0030 S_o + 0.0035 S_w + 0.1300	0.95
NEOVAC	0.0140 S_o + 0.0008 S_w + 0.0700	0.85	0.0025 S_o + 0.0036 S_w + 0.1300	0.95
Nitrobenzene	0.0130 S_o + 0.0007 S_w + 0.0730	0.85	0.0026 S_o + 0.0036 S_w + 0.1300	0.94
Paraffin Liquid	0.0140 S_o + 0.0007 S_w + 0.0087	0.88	0.0026 S_o + 0.0040 S_w + 0.1360	0.96
Silicone Oil	0.0120 S_o + 0.0009 S_w + 0.0690	0.93	0.0023 S_o + 0.0040 S_w + 0.1200	0.97

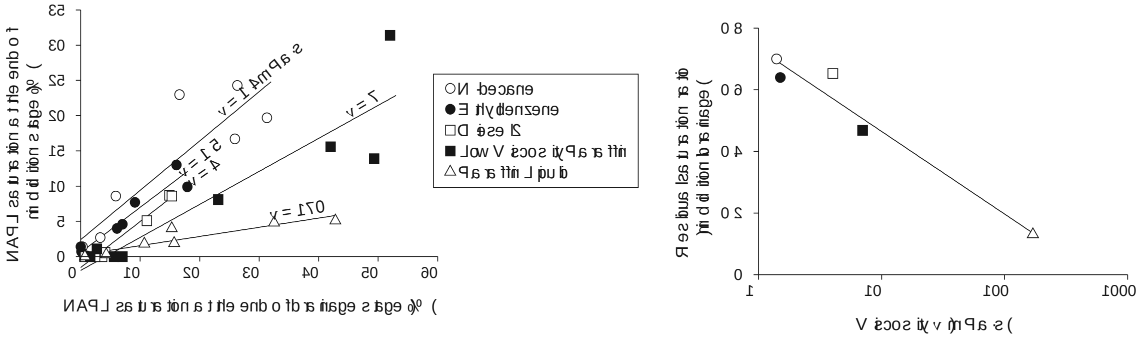

Figure 5. Comparison of residual saturation at the end of drainage and imbibition stages for 5 different NAPLs (left) and relationship between their viscosity and residual saturation ratio (right)

From Figure 4 we can observe the whole domain distribution of N-decane at the end of each stage, and it is clear how a light NAPL can actually get trapped below the water table after subsequent drainage and imbibition processes. We can also observe and quantify how less N-decane penetrated the column after the second drainage process, when compared to the first drainage process, mostly due to loss of NAPL trough the top spillway during imbibition. When comparing the depth and infiltration initial speed of the five studied NAPLs, no relationship was found with either density or viscosity values. More studies are necessary to compare these migration parameters with other physical properties of NAPLs. Finally, we can also observe how regions within the column that had higher NAPL saturation values at the end of the drainage processes, had also high saturation values by the end of the imbibition. This behavior was found on all five NAPLs, as shown in Figure 5 (left).

Figure 5 (left) shows, for each one of the five different studied NAPLs, the relationship between their residual saturation values at the end of the drainage stage, when compared to their residual saturation values at the end of the imbibition stage. As can be seen, the relationship between both values is linear for each NAPL, and the general ratio of imbibition over drainage is less than 1.0 for all NAPLs, which confirms that some contaminant is removed by water during the imbibition stages. It can also be noticed how the residual saturation ratio (imbibition/drainage) is different for each NAPL, and follows the progression (from larger to smaller) N-decane > Ethylbenzene > Diesel 2 > Low Viscosity Paraffin > Paraffin Liquid, which is their exact inverse order when comparing their viscosity values. In fact, if we plot viscosity versus residual saturation ratio, we will find a logarithmic relationship between them (Figure 5, right), which could help us predict the residual saturation of any NAPL after imbibition processes, if the residual saturation after the drainage process is known. Additional NAPLs need to be tested to improve the accuracy of this relationship.

7 CONCLUSIONS

We have confirmed that the relationship between Optical Density (D_i) and water and LNAPL saturation values (S_w and S_o) is approximate linear, as predicted by the *Beer-Lambert Law of Transmittance*, for ten different NAPLs with very different density and viscosity values ($0.73 \leq \rho \leq 1.20$ g/cm^3; $1.4 \leq \nu \leq 1000$ mPa·s). Due to this finding, the *Simplified Image Analysis Method* can be safely used to assess water and NAPL saturation distributions in porous media subject to dynamic conditions, for a broad range of NAPLs. In our research, we applied this method to study the behavior of five different NAPLs in experimental columns subject to drainage and imbibition processes, and confirmed that light NAPLs can effectively get trapped below the water table, despite their lower than water density values. We also found a logarithmic relation between viscosity and residual saturation ratios of different NAPLs that will help us predict their residual saturation values after imbibition processes, when their respective value after drainage processes are known. In the next step of this study, additional NAPLs will be tested to improve the accuracy of this relationship.

8 REFERENCES

Australia DSEWPC. 1999. Substance list and thresholds: National pollutant inventory. Retrieved 01/02/2012, from http://www.npi.gov.au/substances/list-of-subst.html.

Capiro, N. L., Stafford, B. P., Rixey, W. G., Bedient, P. B. and Alvarez, P. J. J. 2007. Fuel-grade ethanol transport and impacts to groundwater in a pilot-scale aquifer tank. *Water Research* 41(3): 656-664.

Environment Canada. 2010. National pollutant release inventory. *Canada Gazette*. 144.50: 3112-3142.

Fagerlund, F., Illangasekare, T. H. and Niemi, A. 2007. Nonaqueous-phase liquid infiltration and immobilization in heterogeneous media: 1. Experimental methods and two-layered reference case. *Vadose Zone J* 6(3): 471-482.

Flores, G., Katsumi, T., Inui, T. and Kamon, M. 2011. A simplified image analysis method to study LNAPL migration in porous media. *Soils and Foundations* 51(5): 835-847.

Kechavarzi, C., Soga, K. and Wiart, P. 2000. Multispectral image analysis method to determine dynamic fluid saturation distribution in two-dimensional three-fluid phase flow laboratory experiments. *Journal of Contaminant Hydrology* 46(3-4): 265-293.

Lenhard, R. J. and Parker, J. C. 1987. Measurement and prediction of saturation-pressure relationships in three-phase porous media systems. *Jnl. of Contaminant Hydrology* 1(4): 407-424.

Mercer, J. W. and Cohen, R. M. 1990. A review of immiscible fluids in the subsurface: Properties, models, characterization and remediation. *Journal of Contaminant Hydrology* 6(2): 107-163.

Skoog, D. A., Holler, F. J. and Crouch, S. R. 2007. *Principles of instrumental analysis*. Belmont, CA, Thomsom Brooks/Cole.

UK Environment Agency. 2011. Pollution inventory substances: Pollution inventory. Retrieved 01/02/2012, from http://www.environment-agency.gov.uk/pi.

US EPA. 2011. Toxics release inventory (TRI): Toxic chemical list. Retrieved 01/02/2012, from http://www.epa.gov/tri/trichemicals/index.htm.

Hydraulic conductivity of zeolite-sand mixtures permeated with landfill leachate

Conductivité hydaulique de mélanges zéolithe-sable infiltrés par des écoulements de décharge de déchets

Fronczyk J., Garbulewski K.

Department of Geotechnical Engineering, Warsaw University of Life Science, Warsaw, Poland

ABSTRACT: The study presented in this paper has been undertaken to evaluate the influence of leachate from landfill collected the municipal solid wastes at Warsaw district onto the hydraulic conductivity of zeolite-sand mixtures (with 50% and 20% content of zeolite). The long-term hydraulic conductivity tests with distilled water and landfill leachate collected from the landfill drainge were carried out using Trautwein equipment. Results of study indicated that hydraulic conductivity of reactive material tested have changed almost by two orders of magnitude (from 9.23E-5 to 1.24E-6 m/s). The decrease of hydraulic conductivity can be caused by reduction of the effective porosity due to pore clogging. The analysis of the calcium carbonate content using Scheibler method showed no significant increase of carbonates in the samples, while research in scanning electron microscope showed increased calcium content and crystals of calcium carbonate in the samples. Moreover, the presence of microbial activity had been observed. The conclusions drawn based on tests results should be considered in designing of PRB.

RÉSUMÉ : L'étude présentée dans cet article a été entreprise afin d'évaluer l'influence des écoulements des sites d'enfouissement des déchets du district de Varsovie sur la conductivité hydraulique de mélanges de zéolithe et de sable (avec 50% et 20% de teneur en zéolithe). La conductivité hydraulique à long terme a été mesurée avec de l'eau distillée et un liquide provenant du drainage d'une décharge, à l'aide d'un appareil de Trautwein. Les résultats de l'étude ont montré que la conductivité hydraulique du matériel réactif testé a changé de deux ordres de grandeur (de 9,23E-5 à 1,24E-6 m/s). La diminution de la conductivité hydraulique peut être due à la réduction de la porosité effective due à l'obstruction des pores. L'analyse de la teneur en carbonate de calcium en utilisant la méthode de Scheibler n'a montré aucune augmentation significative de carbonates dans les échantillons, alors que l'analyse par microscopie électronique à balayage a montré une augmentation de la teneur en calcium et des cristaux de carbonate de calcium dans les échantillons. En outre, la présence d'une activité microbienne a été observée. Les conclusions basées sur le résultat de ces essais doivent être prises en compte dans la conception des barrières réactives de protection.

KEYWORDS: permeable reactive barrier, landfill leachate, reactive materials, hydraulic conductivity.

1 INTRODUCTION

Throughout the world the pollution of groundwater by hazardous substances (e.g. landfill leachate) is one of the most crucial environmental problems. To protect the natural groundwater environment many technologies were developed in the last decade. One of the most effective and simultaneously low-cost technology is a method based on permeable reactive barriers - PRBs - that improves natural attenuation processes (Fig. 1). PRBs can be an effective remedy in many environmental settings with varying hydrogeologic and geochemical conditions.

According to ITRC publication (2011), ideal case for PRB application is ground containing cohesive silts and sands with hydraulic conductivity values lower than 3.5E-6 m/s. However, ITRC proposes to extend this criteria and also check the ground with hydraulic conductivity and groundwater velocity in range of 3.5E-6 to 3.5E-5 m/s as the most suitable conditions for application of PRBs.

The proper functioning of PRBs depends on the hydraulic properties of reactive materials that fullfield reaction zone of the barriers. The hydraulic criterion in the evaluation of reactive materials such as zeolites and zeolite-sand mixtures is expressed as the ratio of hydraulic conductivity of the reactive material (k_s) to the hydraulic conductivity of the aquifer (k_g), which, according to common recommendation, should be higher than one. This parameter governs the rate of occurring processes (sorption, biological and chemical reduction etc.) and in some circumstances can lead to changing groundwater flow direction ever to wrap the PRBs by contaminated groundwater. In this regard, it is necessary to identify changes of hydraulic conductivity as a result of contact with liquid pollutants.

The hydraulic conductivity of reactive materials and their changes during exploitation should be taken into account for design of PRB, particularly their thickness (b), which can be estimated from the equation (Czurda and Haus 2002):

$$b = \frac{t_{PRB} \cdot k \cdot i}{R} \tag{1}$$

where:
t_{PRB} - "working time" (s), time required for contaminant reduction to acceptable level,
k - hydraulic conductivity (m/s),
i - hydraulic gradient,
R - retardation factor, that depend on sorption processes intensity.

The changes of permeability of zeolite-sand mixtures, proposed as low-cost reactive materials, caused by landfill leachate are presented in this paper. The leachate samples were taken from municipal solid waste site in Warsaw (Radiowo site).

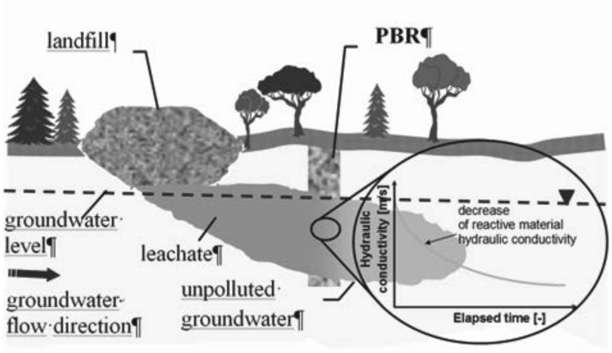

Figure 1. A concept of permeable reactive barriers.

1 MATERIALS AND TEST METHODS

Tests, result of which are presented in this paper, were carried out on zeolite-sand mixtures with 50% - ZS50, 20% - ZS20 content of Na-form of Slovak zeolite having 0.5-1.0 mm particle sizes. The mineral composition of the Slovak zeolite is as follows:

$$(Ca;K_2;Na_2;Mg)_4Al_8Si_{40}O_{96}\cdot 24H_2O \qquad (2)$$

The zeolite-sand mixtures considered as a reactive materials have specific surface areas from 3,65 m^2/g for ZS20 to 29,04 m^2/g for ZS50. The crystal structure of zeolite is presented by 3-dimentional aluminosilicate framework with the developed system of micropores and channels occupied by water molecules and exchangeable cations. Crystal habits of zeolite include blocky and thin-tabular crystals with good monoclinic crystal forms (Sprynsky et al. 2004). According to the results of scanning electron micrographs study unit cell parameters of crystals are close to each other (Fig. 2).

To determine the effect of synthetic leachates (containing 360 mgNH_4^+/L, 100 mgCa/L, 200 mgMg/L and 100 mgCu/L) and landfill leachate on the hydraulic conductivity of ZS50 and ZS20, constant-head permeability tests were performed using flexible wall permeameter (Fig. 3). In the tests the natural leachate from municipal landfill in Warsaw was used. Chemical composition of leachate is listed in table 1. Due to the character of these studies, it was necessary to use equipment made from materials not reacting with contaminated water. The hydraulic gradient of 2 was obtained by establishing an elevation difference between the liquid surface of inflow and outflow ends. Before leachate tests, specimens were pre-saturated with distilled water until establishing the constant flow through the samples. Samples were placed between two porous plates, that's hydraulic conductivity was more than 1.0E-3 m/s. The samples were making with mixed materials having 10% of water content. The specimens tested were 0,07 m in diameter and 0,12 m in height. In this study specimens were compacted to relative density equal 0.6. The confining pressure was 50 kPa.

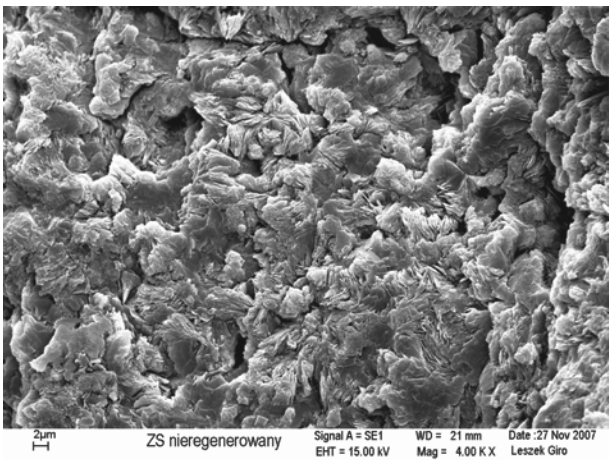

Figure 2 Scanning electron micrograph of zeolite (Katzenbach et al. 2008)

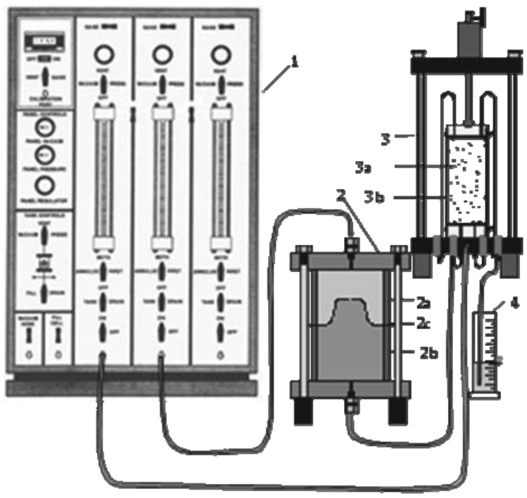

Figure 3. Scheme of a flexible-wall permeameter: 1-control panel, 2-bladder accumulator, 2a-water, 2b-liquid other than water, 2c-elastic membrane, 3-chamber, 3a-sample, 3b-latex membrane, 4- measuring cylinder (acc. to Trautwein Soil Testing Equipment Co.).

Table 1. Chemical composition of leachate from municipal landfill in Warsaw.

Parameter	*Value*
BOD (mg/l)	127.0
COD (mg/l)	960.0
Ammonia – N (mg/l)	52.0
Total P (mg/l)	3.94
Chloride (mg/l)	1400.5
Sulfate (mg/l)	419.0
Sodium (mg/l)	917.0
Potassium (mg/l)	396.0
Calcium (mg/l)	81.2
Magnesium (mg/l)	88.8
Iron (mg/l)	1.28
Chromium (mg/l)	0.13
Zink (mg/l)	1.83
Copper (mg/l)	0.2
Conductivity (µS/cm)	6480
pH	8.21

The hydraulic conductivity was calculated using equation (ASTM D 5084 - 00):

$$k = \frac{V}{i \cdot A \cdot \Delta t} \tag{3}$$

where:
k – hydraulic conductivity (m/s),
V – volume of effluent (m^3),
i – hydraulic gradient,
A – area of the specimen (m^2),
t – permeation time period (s).

2 RESULTS AND DISCUSSION

The hydraulic conductivity tests were performed with distilled and tap water, synthetic and landfill leachate. The results obtained are presented in Fig. 4. The hydraulic conductivity of samples is presented in relation to pore volume of flow, which may be calculated using equation:

$$PVF = \frac{k \cdot i \cdot t}{n_e \cdot L} \tag{4}$$

where:
PVF – pore volume of flow,
k – hydraulic conductivity (m/s),
i – hydraulic gradient,
t – elapsed time (s),
n_e – effective porosity,
L – length of the sample (m).

The hydraulic conductivity of materials tested using tap water was 9.8 E-5 m/s and 8.7E-5 of ZS50 and ZS20, respectively. The hydraulic conductivity slightly decrees with time at the beginning of the permeation with synthetic leachates but stabilized after 100 pore volume of flow. After 800 pore volume of flow hydraulic conductivity of ZS50 was 3.4E-5m/s and of ZS20 6.8E-5 m/s. This represented about a 2.90- and 1.30-fold decrees as compared with the results of hydraulic conductivity to tap water. The test results indicated that the permeation synthetic leachate influence negligible the hydraulic conductivity of zeolite-sand mixtures. Franciska and Glatstein (2010) observed the similar relation for compacted soil liners permeated with landfill leachate. Results of study with landfill leachate indicated that hydraulic conductivity of ZS50 have changed almost by two orders of magnitude (from 9.23E-5 to 1.24E-6 m/s). Observed permeability changes can be caused through inorganic compounds precipitation, mainly $CaCO_3$, and bioactivity (VanGulck and Rowe 2004, Asadi et al. 2011). The analysis of the calcium carbonate content using Scheibler method showed no significant increase of carbonates in the samples, while research in scanning electron microscope showed increased calcium content and crystals of calcium carbonate in the sample. Achieved results allow to conclude, that permeability changes of zeolie-sand mixtures may influence the operation conditions of PRB.

3 DESIGN CONSIDERATION

Considering the test results obtained the hydraulic criterion in the evaluation of reactive materials such as zeolites and zeolite-sand mixtures should be expressed as follows:

the ratio of hydraulic conductivity of the reactive material (k_s) to the hydraulic conductivity of the aquifer (k_g)

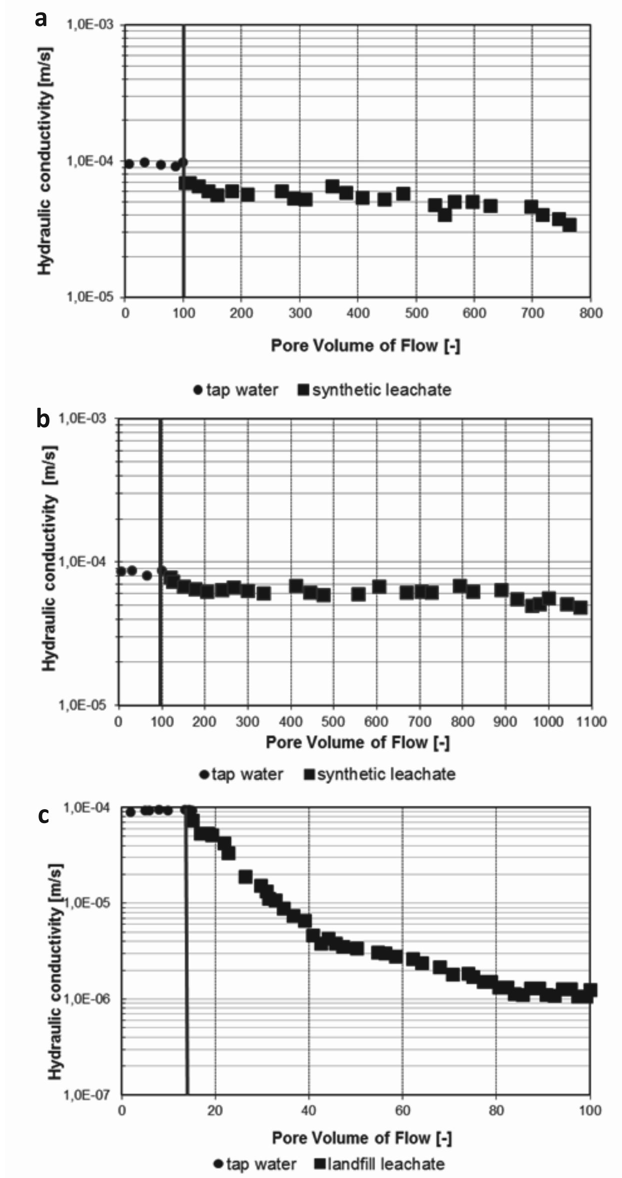

Figure 4. Hydraulic conductivity of ZS50 (a) and ZS20 (b) to tap water and synthetic leachate and ZS50 to landfill leachate (c).

$$\frac{k_s}{k_g} \geq 10 \tag{5}$$

Criterion (5) results from the necessity of taking into account changes of the hydraulic properties of materials during PRB exploitation. Laboratory studies showed a decrease of hydraulic conductivity values of zeolite and zeolite-sand mixtures under the influence of landfill leachate. In the case of zeolite-sand mixtures with a zeolite content Z (dimensionless value), estimation of hydraulic conductivity k_s in m/s at relative density I_D requires the application of the following equation (Fronczyk 2008):

$$k_s = A \cdot Z \cdot I_D^{-0.328} \tag{6}$$

For mixtures made of zeolite with particle size of 1.0–2.5 mm, A = 3.0 · 10-4, whereas at particle size of 0.5–1.0 mm, A = 2.6 · 10-5.

4 CONCLUSION

The choice of the reactive material for PRBs requires determining the hydraulic conductivity of reactive materials with regard to the relative density and strain conditions (effective stress) in the barrier. It is necessary to carry out “compatibility tests”, i.e. test of contaminated groundwater influence on hydraulic properties of the selected material.

Achieved results for synthetic leachate showed less than 3-fold decrease of zeolite-sand mixtures permeability. Landfill leachate caused decrease of hydraulic conductivity almost by two orders of magnitude due to inorganic precipitation and biological growth.

5 ACKNOWLEDGEMENTS

This research was partly supported by Grant no. NN523 561638 from Ministry of Science and Higher Education. Warsaw. Poland.

6 REFERENCES

Asadi A., Huat B.B.K., Moayedi H., Shariatmadari N., Parsaie A. 2011. Changes of hydraulic conductivity of silty clayey sand soil under the effect of municipal solid waste leachate. *International Journal of the Physical Sciences* 6 (12), 2869-2874.

ASTM D 5084 – 00. Standard test methods for measurement of hydraulic conductivity of saturated porous materials using flexible wall permeameter.

Czurda K.A. and Haus R. 2002. Reactive barriers with fly ash zeolites for in situ ground water remediation. *Applied Clay Science* 21, 13-20.

ITRC Interstate Technology & Regulatory Council 2011. *Permeable Reactive Barrier: Technology Update*. Washington DC.

Francisca F.M. and Glatstein D.A. 2010. Long term hydraulic conductivity of compacted soils permeated with landfill lechate. *Applied Clay Science* 49, 187-193

Fronczyk J. 2008. Fronczyk J., 2008: Zeolite-sand mixtures in permeable reactive barriers in the landfill surroundings. PhD thesis, Faculty of Engineering and Environmental Science WULS.

Katzenbach R., Fronczyk J., Garbulewski K. 2008. Evaluation of zeolite-sand mixtures as a reactive material towards landfill leachate. 11th *Baltic Sea Geotechnical Conference*, PG Publisher, 875-882.

Sprynsky, M., Lebedynets, M., Namiernik, J., Buszewski, B. 2004. Porous structure of clinoptilolite and problems connected with its characterization. XI Zeolite Forum, Poland.

VanGulck J.F. and Rowe R.K. 2004. Influence of landfill leachate suspended solids on clog (biorock) formation. *Waste Management* 24, 723 – 738.

Moisture-Suction Relationships for Geosynthetic Clay Liners

Courbes de rétention des membranes géotextiles chargées en argile

Hanson J.L., Risken J.L.
California Polytechnic State University, San Luis Obispo, U.S.A.

Yeşiller N.
Global Waste Research Institute, San Luis Obispo, U.S.A

ABSTRACT: A laboratory investigation was conducted to determine the moisture-suction relationships for Geosynthetic Clay Liners (GCLs) under as-received conditions (moisture contents in the range of 14-27%) and subsequent to wet-dry cycles (20 cycles at 50% moisture content). The moisture-suction relationships were developed using combined pressure plate, filter paper, and relative humidity methods over a wide range of suction. Tests were conducted on three types of common GCLs (two conventional and one multi-component) that contained granular bentonite and bonded with needlepunching. The responses of conventional and multi-component GCLs and as-received and wet-dry cycled GCLs were different. For the multi-component GCL, the air entry suction was lower for drying and higher for wetting than for the conventional GCLs. Residual suction for the multi-component GCL was higher than that for the other GCLs. The extent of hysteresis decreased and the differences between drying and wetting curves reduced for the wet-dry cycled specimens. Macro- and microstructural variations determined in grain size distribution and SEM analyses indicated increasing void sizes and nonuniformity in fabric due to wet-dry cycling supporting the observations of moisture-suction variations.

RÉSUMÉ : Une étude en laboratoire a été menée pour déterminer les courbes de rétention des membranes géotextiles chargées en argile dans les conditions de teneur en eau du commerce (de l'ordre de 14-27%) et suite à des cycles de mouillage-séchage (20 cycles à 50% d'humidité). Les courbes de rétention ont été mesurées en utilisant une plaque de pression et du papier filtre, et des méthodes de contrôle en humidité relative sur une large gamme de succion. Les tests ont été effectués sur trois types de membranes (deux conventionnelles et une multi-composants) qui contenaient de la bentonite granulaire et assemblés par aiguilletage. Les réponses des géomembranes conventionnelles et multi-composants étaient différentes selon les conditions d'essai. Pour la membrane multi-composants, la succion d'entrée d'air était inférieure après séchage et supérieure après mouillage à celle des membranes conventionnelles. La succion résiduelle pour la membrane multi-composants était également supérieure à celle des membranes conventionnelles. L'amplitude de l'hystérésis a diminué, de même que les différences entre les courbes de mouillage et séchage se sont réduites pour les échantillons ayant subi des cycles de mouillage-séchage. Les variations de la macro- et microstructure, en termes de distribution de la taille des grains et des analyses au MEB, ont montré une augmentation de la taille des vides et une non-uniformité de la structure induites par les cycles de mouillage-séchage. Ces résultats confirment les observations des courbes de rétention.

KEYWORDS: Geosynthetic Clay Liner, GCL, suction, moisture-suction curve, fabric, shrinkage, unsaturated.

1 INTRODUCTION

Geosynthetic clay liners (GCLs) are increasingly used to replace compacted clay liners in containment systems due to various perceived advantages of the GCLs including low thickness, low hydraulic conductivity, ease of installation, self-healing capability, and resistance to environmental conditions (e.g., cyclic freeze-thaw or wetting-drying). Even though GCL use has become commonplace in containment systems, concerns remain regarding the long-term field performance (NRC 2007).

Significant variations in the field moisture content of GCLs (e.g., Meer and Benson 2007, Scalia and Benson 2011) have been reported. Moisture transfer between GCLs and soils also has been reported (e.g., Olsen 2011). In general, GCLs remain unsaturated in service based on reported moisture contents. Limited information is available on moisture-suction relationships and water retention characteristics of GCLs, which control mechanical, hydraulic, and thermal properties of the GCLs as well as directly influence moisture transfer between GCLs and soils. Data for conventional GCLs indicated that the structure of GCLs affected moisture retention characteristics (Beddoe et al. 2011). Data are not available for multi-component GCLs or GCLs that have undergone wet-dry cycling.

This investigation was conducted to determine the influence of GCL type and wet-dry cycling on moisture-suction relationships. The investigation was supplemented by microscopy analysis of the bentonite component of the GCLs.

2 EXPERIMENTAL TEST PROGRAM

The test program included investigation of three types of GCLs (Table 1) representative of typical materials used in practice in the U.S. All of the GCLs were bonded by needlepunching and contained granular bentonite:

- WN2: conventional medium weight GCL with a lightweight slit-film woven geotextile and heavyweight nonwoven geotextile
- NN1: conventional heavyweight GCL with two heavyweight nonwoven geotextiles
- WNT: multi-component medium weight GCL with a lightweight slit-film woven geotextile and heavyweight nonwoven geotextile/textured geofilm (0.5 mm HDPE)

The GCL specimens were tested at as-received conditions and subsequent to 20 wet-dry cycles. The cycles consisted of wetting the specimens to 50% moisture content for 8 hours and then oven drying the specimens at 60°C for 12 hours for a total cycle duration of 24 hours. A common moisture content range of 45-62% was reported for GCLs exhumed from composite barriers in landfill covers (Scalia and Benson 2011). The 50% moisture content was selected as this moisture content is common in the field and also represents the threshold hydration water content to maintain low hydraulic conductivity (Scalia and Benson 2011).

Table 1. Properties of the GCLs used in the test program

Property	WN2	NN1	WNT
Cover geotextile	Nonwoven	Nonwoven	Woven
Cover mass (g/m^2)	200	200	105
Carrier geotextile	Woven	Nonwoven	Nonwoven/ Geofilm
Carrier mass (g/m^2)	105	200	200/605
Avg. bent. mass (g/m^2)	4000	3900	4000
As-received water content (%)	15-19	19-27	14-15

The moisture-suction characteristics of the GCLs were determined using combined pressure plate, filter paper, and relative humidity methods for the low (30-300 kPa), medium (10-100000 kPa), and high (5000-400000 kPa) suction ranges, respectively. Use of the three methods was required to investigate the wide range of moisture contents and associated suctions for the GCLs. The pressure plate tests were conducted in accordance with ASTM D6836 (Method C), the contact filter paper tests were conducted in accordance with ASTM D5298, and the relative humidity tests were conducted using procedures similar to the tests presented in Beddoe et al. (2011). Specimen diameters were 50, 100, and 100 mm for pressure plate, filter paper, and relative humidity methods, respectively. For drying branches, specimens were submerged to reach saturation whereas for wetting branches, specimens were hydrated with an atomizing sprayer to target moisture contents. Tests were conducted using deionized (DI) water to investigate solely the moisture-suction response of the GCLs without potential effects of chemical interactions from ionic species present in tap water. Microstructure of the specimens was investigated using scanning electron microscopy (SEM). Relatively undisturbed specimens were obtained by sampling clay from the GCL and then fracturing and pulling (instead of cutting and shearing) a subspecimen for image analysis.

3 RESULTS AND DISCUSSION

The results of the moisture-suction tests for the GCLs are presented in Figures 1-3 and Figure 4 for as-received and wet-dry cycled specimens, respectively. Gravimetric moisture contents were used due to the complexities and uncertainties associated with using volumetric moisture content for GCLs. The experimental data were modeled using the Fredlund and Xing (1994) and Pham and Fredlund (2008) methods. The Fredlund and Xing (1994) model commonly has been used for soils and also applied to GCLs (e.g., Beddoe et al. 2011). The Pham and Fredlund (2008) model had been developed to provide gravimetric moisture-suction relationships over the entire range of soil suction for soils that undergo volume change with suction and was adopted for this test program. The results of the Fredlund and Xing (1994) model are presented in Figures 1-4 and the model parameters for the two methods are provided in Tables 2 and 3. Data for air entry and residual suctions also are provided in the tables.

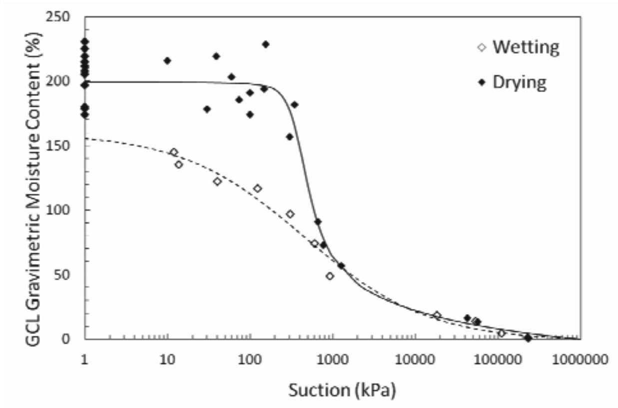

Figure 1. Moisture-suction relationships for WN2.

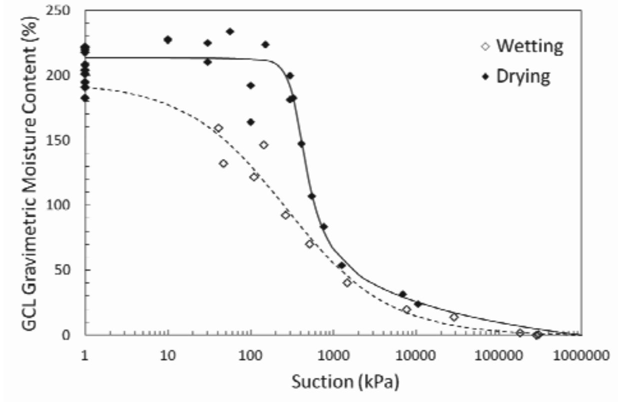

Figure 2. Moisture-suction relationships for NN1.

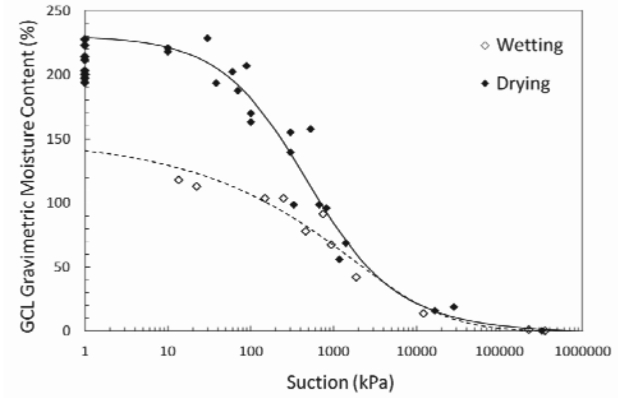

Figure 3. Moisture-suction relationships for WNT.

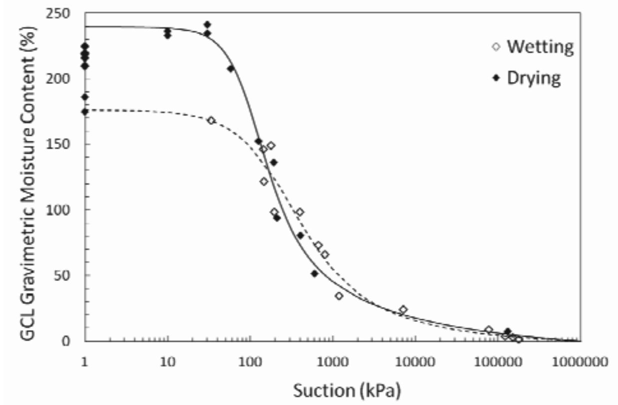

Figure 4. Moisture-suction relationships for NN1 at 20 cycles.

Table 2. Model parameters for drying branches

Parameter	WN2	NN1	NN1-20	WNT
a_f[1]	358	339	91.3	355
m_f[1]	0.678	0.626	0.93	2.01
n_f[1]	4.72	5.78	2.23	0.819
S_1[2]	15.5	0.974	6.86	15.4
S_2[2]	134	114	152	88.1
S_3[2]	11.5	13.5	8.74	8.76
ψ_{ae}[3] (kPa)	176	137	46.5	63
ψ_r[3] (kPa)	1620	1600	650	5220

[1]Fredlund and Xing (1994)
[2]Pham and Fredlund (2008)
[3]Based on Fredlund and Xing (1994)

Table 3. Model parameters for wetting branches

Parameter	WN2	NN1	NN1-20	WNT
a_f[1]	218	210	203	100000
m_f[1]	1.03	2.19	1.28	11.9
n_f[1]	1.28	0.695	1.29	0.368
S_1[2]	25.1	21.7	29.6	43.2
S_2[2]	74.8	72.2	101	115
S_3[2]	8.72	8.12	10.3	6.47
ψ_{ae}[3] (kPa)	78	30.3	66.9	125
ψ_r[3] (kPa)	8960	4250	2260	25000

[1]Fredlund and Xing (1994)
[2]Pham and Fredlund (2008)
[3]Based on Fredlund and Xing (1994)

The general shape and trends for the GCL moisture-suction relationships for the tested GCLs were similar to soils with discernable air entry and residual moisture characteristics and hysteresis observed between drying and wetting curves. The moisture-suction characteristics of as-received WN2 and NN1 were relatively similar, whereas the air entry suction value for the WNT specimens were lower than WN2 and NN1 for drying (Table 2) and higher for wetting (Table 3). Residual suction values for WNT were higher than those for WN2 and NN1 (Tables 2 and 3).

The extent of hysteresis observed for WNT was higher than that for WN2 and NN1. The similar moisture-suction relationships of WN2 and NN1 were attributed to the relatively similar structures of the GCLs. The presence of the geofilm impacted the response of WNT in line with the observations of Beddoe et al. (2011) indicating effects of GCL structure on material behavior.

Hysteresis observed in the tests was quantified for selected moisture levels for GCLs representing as-received/as-placed, common field exhumed, and limiting air entry and residual conditions for NN1 using as-received and wet-dry cycled conditions (Table 4). Wetting and drying cycles affected moisture-suction behavior of NN1 (Figures 2 and 4 and Tables 2-4). For drying, air entry and residual suctions decreased with cycling and for wetting, the opposite trend was observed (increasing air entry and residual suctions with cycling). The extent of hysteresis decreased (i.e., less difference between drying and wetting curves) in response to cycling (Table 4). The limited level of hysteresis observed for cycled specimens was consistent with findings reported by Fredlund et al. (2012) indicating that laboratory water retention tests provide extreme trends (i.e., bounds of limiting envelope) for wetting and drying branches of soil water characteristic curves (SWCCs), whereas in-situ soils are expected to demonstrate less extreme trends bound within the envelope. The GCL data were observed to be similar, in that data for the cycled GCLs representing in-service conditions were generally inside the limiting envelope.

Table 4. Extent of hysteresis between wetting and drying branches

Conditioning	Suction	Wetting Curve ψ (kPa)	Drying Curve ψ (kPa)	Hysteresis (kPa)
No cycles	ψ_r	4245	1602	266
	$\psi_{w=50\%}$	1215	1711	496
	$\psi_{w=75\%}$	521	829	308
	$\psi_{w=100\%}$	249	591	342
	$\psi_{w=125\%}$	118	480	362
	ψ_{ae}	30.3	137	107
20 cycles	ψ_r	2260	650	769
	$\psi_{w=50\%}$	1170	815	356
	$\psi_{w=75\%}$	577	386	191
	$\psi_{w=100\%}$	330	247	83
	$\psi_{w=125\%}$	190	178	12
	ψ_{ae}	66.9	46.5	55

Both macroscopic and microscopic changes occurred in the bentonite due to wet-dry cycling. On a macroscale, the agglomerated particles (i.e., granules) became larger in response to cycling. Grain size distributions of the granules were determined for as-received and cycled conditions. The percent retained on a No. 10 (2.0 mm) sieve for the cycled specimens was 10% greater than the percent retained for the as-received specimens. A photograph of the exposed bentonite component for as-received and cycled conditions is presented in Figure 5.

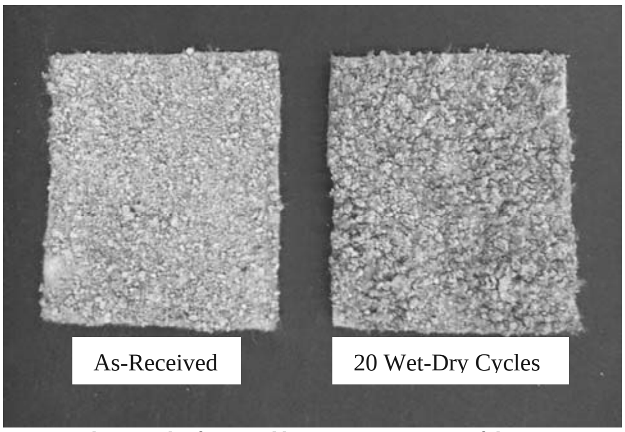

Figure 5 Photograph of exposed bentonite component of the GCLs.

Selected SEM images of bentonite from GCLs at varying stages of wet-dry cycles are presented in Figure 6. All images are presented using the same scale. Variation in the microstructure of the bentonite was observed in the images. The baseline (i.e., dispersed fabric) image for bentonite saturated with DI water (Figure 6a) is consistent with microscopic analysis of pulverized montmorillonite presented by Egloffstein (2001). The bentonite became progressively less oriented and more random with increasing wet-dry cycles. Spaces between particle agglomerations became visible, in particular for the specimens that underwent cycles with tap water. Ultimate shrinkage of the GCLs had occurred by the end of the 20 wet-dry cycles as presented in Olsen et al. (2012).

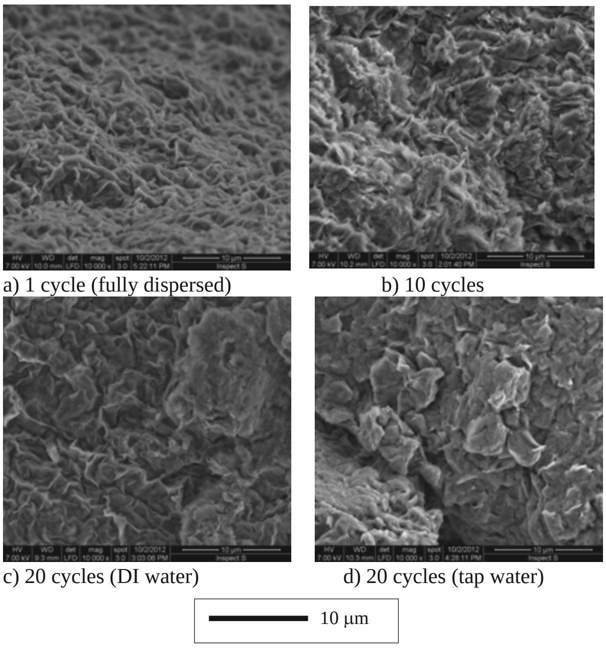

a) 1 cycle (fully dispersed) b) 10 cycles

c) 20 cycles (DI water) d) 20 cycles (tap water)

Figure 6. SEM images of bentonite from GCL specimens

Both macroscale and microscale effects observed due to wetting and drying may have promoted presence of larger voids and therefore lower values of suction for a given moisture content. The lower suction may have forced the drying curve closer to the wetting curve reducing the extent of hysteresis as observed in the test program for the cycled specimens.

4 CONCLUSION

A laboratory investigation was conducted to determine the moisture-suction relationships for GCLs under as-received conditions (moisture contents in the range of 14-27%) and subsequent to wet-dry cycles (20 cycles at 50% moisture content). The moisture-suction relationships were developed using combined pressure plate, filter paper, and relative humidity methods over a wide range of suction. Tests were conducted on three types of common GCLs (two conventional GCLs and one multi-component GCL) that contained granular bentonite and were bonded with needlepunching. Differences were observed between the conventional and multi-component GCLs and between the as-received and wet-dry cycled GCLs. The air entry suction value for the multi-component GCL was lower than that for the conventional GCLs for the drying branches of the moisture suction curves and higher for the wetting branches of the curves. The residual suction value for the multi-component GCL was higher than the residual suction values for the other two GCLs. The extent of hysteresis decreased and the differences between drying and wetting curves reduced for the wet-dry cycled specimens compared to the as-received specimens. Macro- and microstructural variations determined through grain size distribution and SEM analyses indicated increasing void sizes and nonuniformity in fabric due to wet-dry cycling, supporting the observations for variations in moisture-suction response. The moisture-suction data and model parameters obtained in the test program can be adapted for use for similar GCLs.

5 ACKNOWLEDGEMENTS

This study was partially supported by the Global Waste Research Institute and the South Central Solid Waste Authority. CETCO provided testing materials. Mr. Chris Athanassopoulos provided technical information.

REFERENCES

Beddoe R.A., Take W.A., and Rowe, R.K. 2011. Water retention behavior of geosynthetic clay liners, Journal of Geotechnical and Geoenvironmental Engineering, 137(11), 1028-1038.

Egloffstein T.A. 2001. Natural bentonites—influence of the ion exchange and partial desiccation on permeability and self-healing capacity of bentonites used in GCLs. Geotextiles and Geomembranes, 19, 427-444.

Fredlund D.G. and Xing A. 1994. Equations for the soil-water characteristic curve. Canadian Geotechnical Journal, 31(4), 533-546.

Fredlund D.G., Rahardjo H., and Fredlund M.D. 2012. Unsaturated soil mechanics in engineering practice. Wiley, Hoboken, New Jersey.

Meer S.R. and Benson C.H. 2007. Hydraulic conductivity of geosynthetic clay liners exhumed from landfill final covers. Journal of Geotechnical and Geoenvironmental Engineering, 133(5), 550-563.

National Research Council – NRC. 2007. Assessment of the performance of engineered waste containment barriers. The National Academies Press, Washington DC.

Olsen G.R. 2011. Dimensional stability of geosynthetic clay liners in landfill applications, M.S. Thesis, Cal Poly, San Luis Obispo, California, http://digitalcommons.calpoly.edu/theses/651/.

Olsen G.R., Yesiller, N., and Hanson, J.L. 2012. Dimensional stability of geosynthetic clay liners under varying hydration conditions. Proceedings, GeoAmericas 2012, 2nd Pan-American Congress on Geosynthetics, Lima, Peru, May 1-4, 2012.

Pham H.Q. and Fredlund D.G. 2008. Equations for the entire soil-water characteristic curve of a volume change soil. Canadian Geotechnical Journal, 45(4), 443-453.

Scalia J. and Benson C.H. 2011. Hydraulic conductivity of geosynthetic clay liners exhumed from landfill final covers with composite barriers. Journal of Geotechnical and Geoenvironmental Engineering 137(1), 1-13.

Hydraulic conductivity of compacted clay liners moisture-conditioned and permeated with saline coal seam gas water

La conductivité hydraulique de l'humidité argile compactée doublures conditionné et imprégné avec de l'eau salée gaz de houille couture

Indrawan I.G.B., Williams D.J., Scheuermann A.
The University of Queensland, Brisbane, Australia

ABSTRACT: The effects on the hydraulic conductivity of compacted clays, commonly used for lining coal seam gas (CSG) water storage ponds, of moisture conditioning and permeating with CSG water are investigated. Four kaolinite-dominant clays were mixed with CSG and deionised waters, compacted to varying degrees at different gravimetric moisture contents. The compacted specimens were subjected to 100 kPa hydraulic loading with CSG or deionised waters in compaction mould permeameters, and 100 kPa applied stress in oedometers, with the specimens placed in a bath of CSG or deionised water to match the water used to prepare the specimens. The 100 kPa loading represented the expected maximum pond water depth. The test results show that the hydraulic conductivity of clay specimens moisture-conditioned and permeated with both CSG and deionised waters decreased with time due to rearrangement of the clay particles. At the end of the tests with CSG and deionised waters, the clay specimens were found to have very low hydraulic conductivities of the order of 1E-11 m/s. The hydraulic conductivity values measured using the compaction mould permeameters were found to be reasonably comparable to those calculated from oedometer test data.

RÉSUMÉ: Les effets du contrôle en humidité et de l'imprégnation en eau venant de la production du gaz de houille, sur la conductivité hydraulique des argiles compactées (couramment utilisés pour le revêtement des bassins de stockage de cette eau) sont étudiés. Quatre argiles majoritairement kaolinites ont été mélangées avec le gaz de houille et de l’eau dé-ionisée, compactés à des degrés divers et à différentes teneurs en eau gravimétrique. Les échantillons compactés ont été soumis à un chargement hydraulique de 100 kPa avec le gaz ou l’eau dé-ionisée dans des perméamètres à moules de compactage, à une contrainte appliquée de 100 kPa dans des œdomètres, les échantillons étant placés dans un bain de gaz ou d'eau dé-ionisée pour correspondre à l'eau utilisée pour préparer les échantillons. Le chargement de 100 kPa correspondait à la profondeur maximale prévue pour le bassin d'eau. Les résultats des essais montrent que la conductivité hydraulique des échantillons d'argile à l'humidité contrôlée imprégnés à la fois de gaz de houille et d’eau dé-ionisée a diminué avec le temps en raison du réarrangement des particules d'argile. A la fin des essais avec le gaz et l’eau dé-ionisée, les échantillons d'argile ont présentés une très faible conductivité hydraulique de l'ordre de 1E-11 m/s. Les valeurs de conductivité hydraulique mesurée en utilisant les perméamètres à moules de compactage ont été jugées raisonnablement comparables à ceux calculés à partir des données de test œdométriques.

KEYWORDS: compacted clay liner, dispersion, hydraulic conductivity, kaolinite, oedometer, compaction mould permeameter.

1 INTRODUCTION

Rigid-wall hydraulic conductivity testing can be carried out using a compaction mould permeameter or an oedometer. A compaction mould permeameter allows the direct measurement of hydraulic conductivity, while hydraulic conductivity is calculated from the rate of consolidation in an oedometer test and the values obtained have been found to be too low (e.g., Taylor 1942; Mitchell & Madsen 1987).

Natural and compacted clays have been used in Queensland, Australia, as a liner for the storage of saline water produced during coal seam gas (CSG) production to limit seepage to the underlying soil and groundwater. Under the prevailing semi-arid climatic conditions, the available clays are typically dry and require moisture conditioning to achieve the moisture content specified for compaction. The most readily available water for moisture conditioning is the saline CSG water. This paper investigates the effects of moisture conditioning and permeating with CSG water on the hydraulic conductivity of these clays, with testing using deionised water used as a reference.

2 MATERIALS TESTED

Kaolinite-dominated clay samples, labelled herein as SB1, SB2, SB3 and DT, were obtained from a CSG production site in Queensland, Australia. The sand, silt and clay fractions are shown in Table 1. The liquid limits of SB1, SB2, SB3 and DT were 64.4%, 44.0%, 61.9% and 65.9%, and the plasticity indices were 43.6%, 25.2%, 45.2% and 51.1%, respectively. According to the Unified Soil Classification System (USCS), SB1 and DT were classified as clays of high plasticity (CH), SB2 was classified as a sandy clay of low plasticity (CL), and SB3 was classified as a sandy clay of high plasticity (CH).

Table 1. Particle size distributions of clay samples.

Sample	Particle size		
	Sand (%)	Silt (%)	Clay (%)
SB1	4.1	26.1	69.8
SB2	26.2	24.7	49.1
SB3	20.6	18.6	60.8
DT	13.3	19.9	66.8

The electrical conductivity (EC) of the saturated paste extracts, corresponding to about the liquid limits, were 13.4 dS/m, 8.7 dS/m, 14.6 dS/m and 14.6 dS/m, for SB1, SB2, SB3 and DT, respectively. The exchangeable sodium percentages were 41.3%, 33.2%, 39.0% and 45.1%, respectively. Based on these two parameters, the clay samples were classified as saline-alkali soils (Richards 1954).

Sample preparation for the hydraulic conductivity testing involved moisture conditioning with saline CSG water (CW) and deionised water (DW), and compaction to 90%, 95%, 98% and 100% of the maximum dry densities (MDD) at the optimum moisture contents (OMC) and at a nominal 3% wet of the optimum moisture contents (wet of OMC), based on the compaction curves shown in Figure 1. The concentrations of the major ions, EC, and pH of the CW are presented in Table 2.

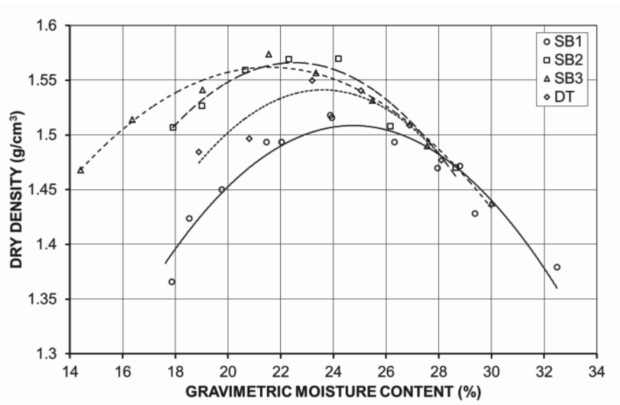

Figure 1. Compaction curves for clay samples.

Table 2. Chemistry of saline CSG water.

Cl^- (mg/l)	Na^+ (mg/l)	Mg^{2+} (mg/l)	Ca^{2+} (mg/l)	K^+ (mg/l)	EC (dS/m)	pH
789	1484	11	8	8	5.8	9.6

3 HYDRAULIC CONDUCTIVITY TESTING

3.1 *Compaction mould testing*

Specimens were compacted to the specified dry density at the specified moisture content in a 144 mm diameter by 130 mm high modified compaction mould permeameter. The initial height of each compacted specimen was limited to 50 mm, to allow space for the specimen to swell to its maximum capacity, as would occur in the field. Prior to a test, no attempt was made to saturate the specimen, simulating the field condition in which a clay liner will not be fully saturated prior to the ponding of CSG water. A 100 kPa constant water pressure was gradually applied to top of the specimen to simulate a 10 m deep pond of CSG water.

To minimise bypass flow along the wall of the permeameter under the high applied hydraulic gradient of 200, a well-graded sand was glued to the wall to roughen its surface. The effectiveness of the sand coating in preventing bypass flow was verified by conducting hydraulic conductivity tests under a 100 kPa constant water pressure using CW applied to SB1 mixed with CW and compacted to 90% of the MDD at OMC, and 95% of MDD wet of OMC. A 101.9 mm diameter by 5 mm thick sharp-edged divider ring was installed centrally on top of the base plate, on which a 3 mm thick medium sand layer was placed to act as a drainage layer. The divider ring had an area of about 50% of the open permeameter area and penetrated about 2 mm into the base of the compacted clay specimen. In addition to an outlet located at the centre of the base plate, two outer outlets between the permeameter wall and the edge of divider ring were provided. The flow rates from each of the outlets were calculated assuming vertical only flow. The measured flow rates from each of the outlets for the 90% MDD at OMC specimen are shown in Figure 2, in which there are no appreciable differences between the central and outer flow rates, indicating that the roughened permeameter wall was effective in minimising bypass flow. A similar result was obtained for the 95% MDD wet of OMC specimen.

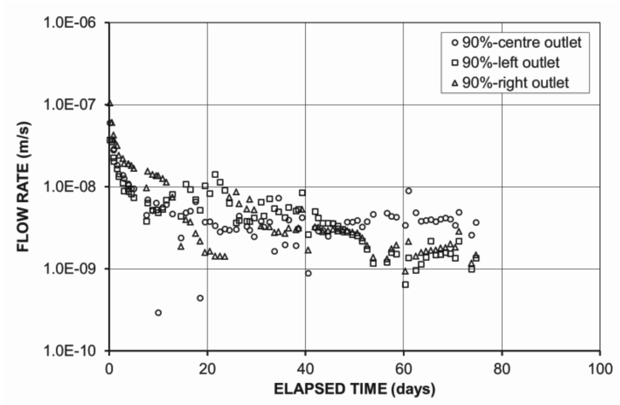

Figure 2. Flow rates from centre and outer outlets during testing of 90% MDD at OMC specimen with roughened permeameter wall.

A set of hydraulic conductivity tests was conducted on SB3 compacted to 90% of the MDD at the OMC, 95% of MDD at OMC and wet of OMC, 98% of MDD at OMC and wet of OMC, and 100% of MDD at OMC, to study the effects of dry density and moulding moisture content on hydraulic conductivity. Another set of hydraulic conductivity tests was conducted on all samples compacted to 95% of MDD wet of OMC, and mixed and permeated with DW and CW, to investigate the effects of moulding and permeating water type on hydraulic conductivity. These dry densities and moisture contents were selected because the clays in the field are usually compacted to 95% of MDD wet of OMC.

It was expected that moisture conditioning wet of the OMC would show significant differences in the compacted hydraulic conductivity compared to that following moisture conditioning to the OMC, since additional water would be available to fill the initially air-dried voids. The permeameter tests were terminated once a relatively constant flow rate and salt concentration of the outflow had been achieved. The EC and pH values of the outflows were measured using a portable EC-pH meter, while concentrations of major anions (Cl^-) and cations (Na^+, Mg^{2+}, Ca^{2+} and K^+) were measured using inductively-coupled plasma and inductively-coupled plasma-optical emission spectrometry methods, respectively.

3.2 *Oedometer testing*

Oedometer tests were conducted on standard 76 mm diameter by 20 mm thick compacted specimens mixed with and in a water bath of CW or DW. Each specimen was subjected to incremental applied stresses of 10 kPa, 50 kPa, 100 kPa and 150 kPa, from which data the coefficients of consolidation and coefficients of volume decrease, and hence hydraulic conductivities, were calculated. During the tests, the oedometer cells were covered with Glad wrap to prevent any change in the salt concentration or pH of the water bath due to evaporation.

4 TEST RESULTS AND DISCUSSION

4.1 *Compaction mould hydraulic conductivity*

The measured hydraulic conductivities of all compacted SB3 specimens are shown in Figure 3. Figure 3 shows that specimens compacted to 90% of MDD at OMC tend to have the highest hydraulic conductivities, while specimens compacted to 100% of MDD at OMC and 98% of MDD wet of OMC tend to have the lowest hydraulic conductivities. Comparing the data for specimens compacted at 98% and 95% of MDD, it appears that those compacted wet of OMC tend to have lower hydraulic conductivities than those compacted at OMC.

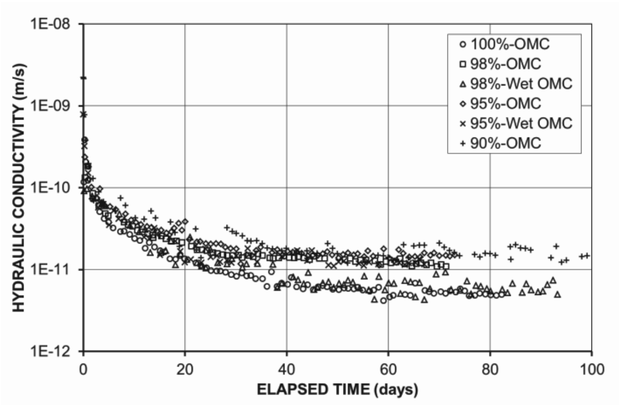

Figure 3. Hydraulic conductivity of SB3 specimens compacted to various dry densities at various moisture contents.

The change in the EC of the outflow from the SB3 specimens during the hydraulic conductivity tests is shown in Figure 4. The samples were originally saline, with an EC at their natural moisture content much higher than that of the CW. As the ponded CW infiltrated the compacted specimens, ionic exchange occurred between the infiltrating CW and the original pore water. This caused the EC of the outflow to decrease with time and eventually approach that of the CW, as salts in the compacted specimens were washed out, as shown in Figure 5.

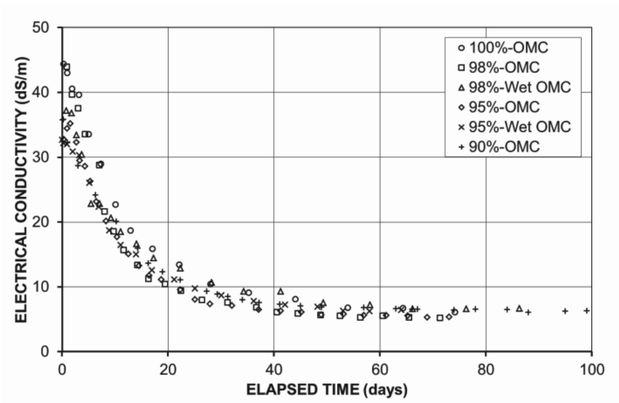

Figure 4. Electrical conductivity of SB3 specimens compacted to various dry densities at various moisture contents.

The pH of the pore water squeezed from SB3 mixed with CW to a gravimetric moisture content of 29% was 5.7, and at the OMC (21.8%) the pH was expected to be lower. Figure 6 shows that the pH of the outflow from SB3 specimens compacted to various dry densities at different moisture contents increased with time, exceeding the pH at the point of zero charge (PZC) at the edges (E) of the kaolinite particles, in the pH range 5 to 7 (Kretzschmar et al. 1998, Wang and Siu 2006). Below the PZC, the edges of kaolinite particles carry positive charges, while above the PZC, the edges carry negative charges. The faces (F) of kaolinite particles are always negatively-charged, resulting in a lower pH than at the edges (Wang and Siu 2006). Below the PZC, kaolinite particles tend to develop an E-F flocculated structure. When the pH is greater than that at the PZC, E-F interaction is prevented, since both E and F are negatively-charged, and kaolinite particles tend to have a dispersed structure.

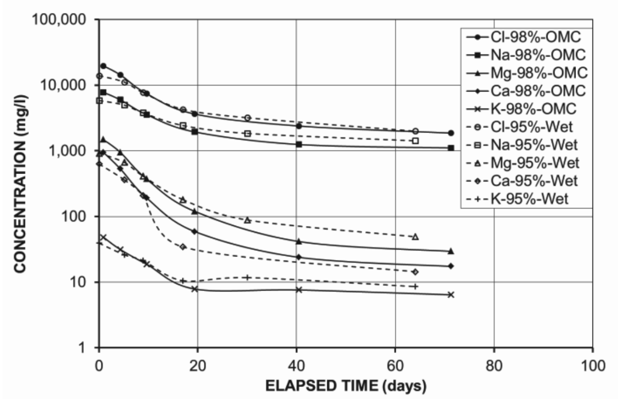

Figure 5. Concentrations of major ions in outflow from SB3 specimens compacted to 98% and 95% of MDD.

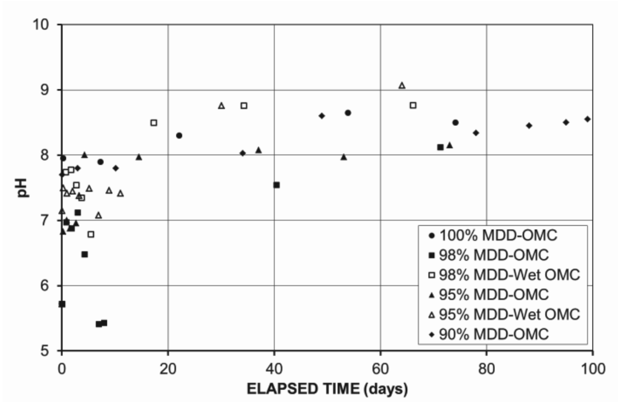

Figure 6. pH of SB3 specimens compacted to various dry densities at various moisture contents.

The hydraulic conductivity was initially high due to a flocculated clay structure, and decreased with time as the kaolinite particles became aligned and developed a dispersed structure. In addition, high clay dispersion was observed in the upper 3 to 5 mm layer of the compacted specimens. Clay dispersion is likely to clog the compacted pores and hence contribute to the observed decrease in hydraulic conductivity.

Similar to the compacted specimens permeated with CW, the hydraulic conductivity of all compacted specimens permeated with DW also decreased with time, as shown in Figure 7. Again, the kaolinite particles tend to develop a dispersed structure when the PZC of the edges is exceeded. As the pH of DW is 7, slightly above the PZC of the edges of kaolinite particles, the infiltration of DW eventually raises the pH of the outflow to 7, resulting in a dispersed structure and the decrease in the hydraulic conductivity with time observed in Figure 7.

Table 3 shows that there is no a clear trend of hydraulic conductivity of specimens moisture-conditioned and permeated with DW and CW in the compaction mould permeameter tests. The differences are considered to be within the accuracy of outflow measurements at these low hydraulic conductivities, due to susceptibility to environmental conditions such as evaporation. Moisture-conditioning with CW and DW is likely to affect the kaolinite structures only after mixing, or at the beginning of the hydraulic conductivity tests. Rearrangement of the kaolinite particles as the tests proceeded resulted in their eventual exposure to permeating CW.

4.2 *Oedometer hydraulic conductivity*

Despite the reduced reliability of the oedometer test for determining the hydraulic conductivity of a compacted clay, the values obtained from the oedometer test data under an applied stress of 100 kPa were reasonably comparable to, or a little higher than, those measured using the compaction mould permeameter under a 100 kPa applied water pressure, as seen in Table 3. However, it is important to note that the underlying flow mechanisms in the compaction mould permeameter and oedometer tests are quite different.

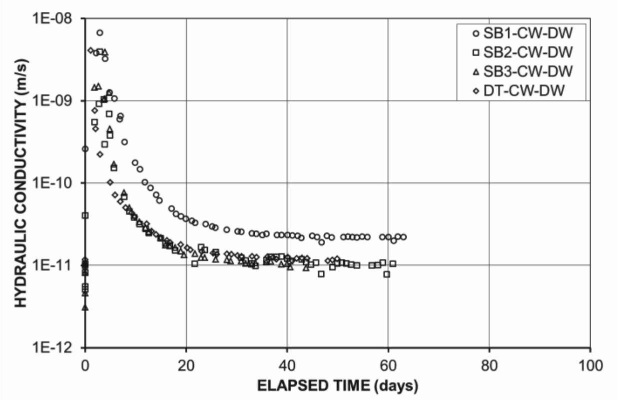

Figure 7. Hydraulic conductivity of all specimens moisture-conditioned with CW, compacted, and permeated with DW.

Table 3. Compaction mould permeameter and oedometer hydraulic conductivities of specimens compacted to 95% of MDD wet of OMC.

Sample	Hydraulic conductivity under 100 kPa	
	Compaction mould	Oedometer
SB1-DW-CW	1.2E-11	3.0E-11
SB1-CW-CW	6.5E-12	7.0E-12
SB1-CW-DW	2.2E-11	1.1E-11
SB2-DW-CW	1.2E-11	1.3E-11
SB2-CW-CW	1.8E-11	1.2E-11
SB2-CW-DW	1.1E-11	7.2E-11
SB3-DW-CW	1.0E-11	1.5E-11
SB3-CW-CW	1.2E-11	1.2E-11
SB3-CW-DW	1.0E-11	1.9E-11
DT-CW-CW	1.1E-11	5.9E-11
DT-CW-DW	1.2E-11	-
Averages	1.2E-11	2.5E-11

In the compaction mould permeameter, ponded water is forced under a pressure of 100 kPa to flow into the compacted specimens, causing their moisture content to increase significantly and the specimens to swell by about 70% of their initial height, with the upper 3 to 5 mm layer reaching a final gravimetric moisture content of about 70%. Swelling allowed the rearrangement of the clay particles from flocculated to dispersed.

In the oedometer specimens, matric suctions of 40 to 50 kPa were measured using tensiometers, and swelling pressures were likely to be greater than 10 kPa. As a result, under an applied stress of 10 kPa bath water was adsorbed and the compacted specimens swelled, allowing the rearrangement of the clay particles. At applied stresses of 50 kPa and greater, water is forced to flow out of the specimens, as indicated by the reduction in vertical strain with increasing applied stress shown in Figure 8. Since the amount of pore water is reducing, physico-chemical interaction between the pore water and the clay particles is likely to be limited. The main mechanism is therefore consolidation, a reduction in the void ratio, and a consequent reduction in the hydraulic conductivity.

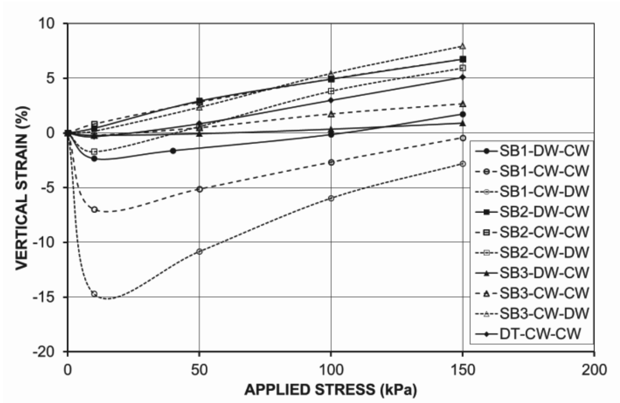

Figure 8. Vertical strains measured during oedometer tests.

5 CONCLUSION

The hydraulic conductivity of clays moisture-conditioned, compacted and permeated with saline CSG water was found to be similar to that of the same clays moisture-conditioned, compacted and permeated with deionised water. The hydraulic conductivity of the clay specimens decreased with increasing compaction from 90% to 100% of MDD, achieving a low value at 100% of MDD. The clays *in situ* would have a high dry density of at least 100% of their MDD, and hence would be suitable as a liner for a CSG water storage pond.

In both CSG and deionised waters, the compacted clay particles dispersed and the hydraulic conductivity decreased to a very low value of about 1E-11 m/s. The hydraulic conductivities measured using a compaction mould permeameter were found to be comparable to, and a little higher than, those calculated from oedometer test data for the same compacted clays.

6 ACKNOWLEDGEMENTS

The research on which this paper is based was carried out under an Australian Research Council Linkage Project in collaboration with QGC Pty Ltd and Golder Associates Pty Ltd. The assistance of David Truce and Sam Bass of Golder Associates Brisbane Office in collecting the clay samples, and undergraduate student Yunpeng Zhang and graduate student Gwenvael Cochet in assisting with the testing, is gratefully acknowledged.

7 REFERENCES

Kretzschmar, R., Holthoff, H., and Sticher, H. 1998. Influence of pH and humic acid on coagulation kinetics of kaolinite: a dynamic light scattering study. *Journal of Colloid and Interface Science*, 202, 95-103.

Mitchell, J.K. and Madsen, F.T. 1987. Chemical effects on the clay hydraulic conductivity. In: *Geotechnical practice for waste disposal*. ASCE, New York, 87-116.

Richards, L.A. 1954. *Diagnosis and improvement of saline and alkali soils*. Agriculture Handbook No. 60.

Taylor, D.W. 1942. *Research on consolidation of clays*. 82. Massachusetts Institute of Technology, Department of Civil Engineering, Cambridge.

Wang, Y.-H. and Siu, W.-K. 2006. Structure characteristics and mechanical properties of kaolinite soils. I. Surface charges and structural characterizations. *Canadian Geotechnical Journal*, 43, 587-600.

Simultaneous estimation of transverse and longitudinal dispersion in unsaturated soils using spatial moments and image processing

Estimation simultanée de la dispersion transversale et longitudinale dans des sols insaturés au moyen de la méthode des moments pour l'analyse des données spatiales et du traitement d'images

Inoue K., Shimada H., Tanaka T.
Graduate School of Agricultural Science, Kobe University, Japan

ABSTRACT: A new methodology using spatial moment analysis linked with image processing of a dye tracer behavior in porous media was developed to estimate dispersivities not only in longitudinal but in transverse directions. Laboratory and field tracer experiments using a relatively mobile dye tracer Brilliant Blue FCF were conducted under saturated and unsaturated flow conditions. Dye tracer in field moved through the soils in a preferential path pattern, which induced higher dispersivities in more irregular pore patterns as compared with those in laboratory. Experimental results demonstrated the effectiveness of the developed methodology for simultaneous assessment of transverse and longitudinal dispersion in unsaturated soils.

RÉSUMÉ : Nous avons développé une nouvelle méthodologie utilisant l'analyse par la méthode des moments associée au traitement d'images pour suivre le comportement d'un traceur colorant en milieu poreux afin d'estimer les dispersivités, aussi bien dans la direction longitudinale que transversale. Nous avons mené des expériences de traçage en laboratoire et sur le terrain au moyen d'un traceur colorant bleu brillant FCF relativement mobile dans des conditions de flux saturé et insaturé. Sur le terrain, le traceur colorant s'est déplacé dans les sols suivant un modèle de trajet préférentiel et, comparé à celles constatées en laboratoire, a présenté des dispersivités induites plus élevées dans les profils d'interstices plus irréguliers. Les résultats de ces expériences ont démontré l'efficacité de la méthodologie que nous avons mise au point pour évaluer simultanément la dispersion transversale et longitudinale dans des sols insaturés.

KEYWORDS: longitudinal and transverse dispersion, dye tracer, image processing, spatial moment, unsaturated soils.

1 INTRODUCTION

The movement of groundwater in porous media is subject to convection and dispersion, independently of any material being transported (Vanderborght and Vereecken, 2007). Dispersion results from the irregular movement of water in porous formations where tortuosity of flow paths is induced. The importance of local transverse dispersion is now identified as a key factor in the smoothing of concentration fluctuations and controlling the rate of dilution of conservative and non-conservative solutes. Despite the importance of transverse dispersion, transverse dispersivity is rarely determined due to the lack of data in the experimental and quantitative difficulties associated with such determinations. Recently, a few of the dye tracer experiments combined with image analysis techniques have been conducted to quantify the behavior of dye tracers (McNeil et al., 2006).

The popularity of dyes is attributable to their low detection limits, visualization potential and ease of quantification by chemical analysis (Flury and Flühler, 1995). Application of image analysis has shown that a time series of digitized images reflecting the movement of dye tracer could be successfully used to monitor solute transport in porous media as well as to estimate transport parameters such as dispersion coefficient, dispersivity (Forrer et al., 1999) and retardation factor (Flury and Flühler, 1995). However, there are many aspects of solute dispersion in unsaturated porous media that still be poorly understood. In the present study, a new methodology using spatial moment analysis linked with image processing of a dye tracer behavior was developed to estimate dispersivities not only in longitudinal but in transverse directions. This technique was applied to dye tracer experiments both in laboratory and field.

2 DYE TRACER EXPERIMENTS

2.1 *Materials and method*

Dye tracing has been widely used to characterize water flow and solute transport behavior in porous media. Previous work demonstrated that colored dye tracers could be successfully used to visualize and monitor solute transport in a porous medium confined in a transparent container (Flury and Flühler, 1995). In this study, one of the soluble dyes, Brilliant Blue FCF, was employed as a dye tracer with the initial concentration of 1.0 mg/cm^3. Although the initial concentration of dye tracer was determined to be low enough to avoid density-induced flow effects, there was no denying the effect of gravity on solute transport during the course of movement.

Tracer experiments were carried out in a two-dimensional and vertically placed water tank with the dimensions of 100 cm width, 100 cm height and 3 cm thickness. The water flow tank allowed to contain soils in order to form transparent quasi two-dimensional solute transport phenomena and consisted of two glass plates with 2 cm thickness. Schematic diagram of experimental apparatus is shown in Figure 1.

In dye tracer experiments, silica sand with a low uniformity coefficient was selected in order to simulate a sandy aquifer. In addition, Andisols, which are volcanic ash soils and have unique properties such as a low bulk density, were taken from a maize field, dried at 110ºC and passed through a 2-mm sieve. Grain sizes less than 0.2 mm were excluded to avoid the adsorption of dye onto the surface of silt or clay. Physical properties for both soils (silica sand and Andisol) are listed in Table 1. In Figure 2, the relationship between suction and volumetric water content for the drying process is plotted with fitting curves based on van Genuchten's formula (van Genuchten, 1980).

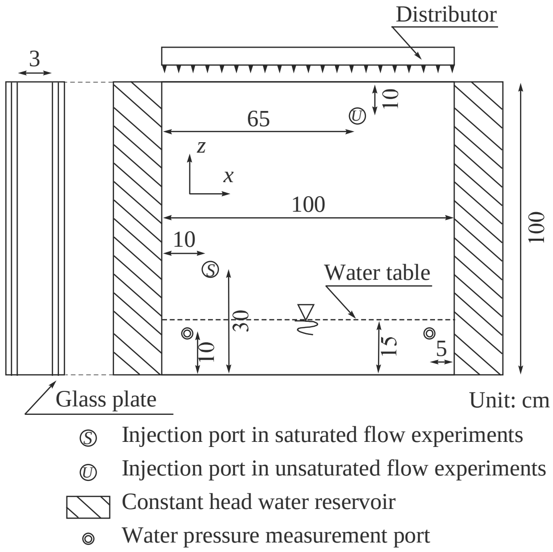

Figure 1. Schematic drawing of an experimental apparatus.

Table 1. Properties of soils.

	Silica sand	Andisol
Particle density (g/cm^3)	2.68	2.40
Mean diameter of particle (cm)	0.085	0.076
Uniformity coefficient (-)	1.80	2.74
Hydraulic conductivity (cm/s)	0.751	0.0341
Porosity (-)	0.42	0.64

2.2 Experimental procedure

Soils were completely washed and saturated before packing to remove organic chemicals attached to the particle surface, to avoid entering air and to conduct experiments under the saturated condition. In the process of creation of flow field, water flow tank was filled with water and soil material of interest from bottom to top in 5 cm layers to achieve uniform packing. In this process, soil was funneled using an extended funnel. Each layer of interest was compacted prior to filling the next layer, resulting in 0.42 and 0.64 of the porosity for silica sand and Andisol, respectively. The porosity of each flow field was able to be estimated indirectly from measurements of the particle density and the dry soil bulk density.

After packing, water was applied to the flow tank under a specific hydraulic gradient controlled by constant head water reservoirs at the upstream and downstream sides, while maintaining saturated condition of porous media. A steady saturated flow field was established when fluctuations in the observed drainage rate, which was effluent from the constant head water reservoir, and piezometer readings could become negligible. After reaching steady state flow conditions, dye tracer with the volume of 25 cm^3, which made flow paths visible, was uniformly injected along the whole thickness of the flow tank. During the experiment, the profiles of tracer migration were periodically recorded using a digital camera.

Dye tracer experiments under unsaturated conditions were conducted in a similar manner. Internal drainage using constant head reservoirs allowed for one day to create an unsaturated flow field after the flow tank was filled with water and sand of concern. After steady state condition was established, water was applied using a distributor placed 10 cm above the soil surface. Three rainfall rates of 0.09, 0.21 and 0.63 mm/min, were set with no rainfall case. Experimental cases are listed in Table 2.

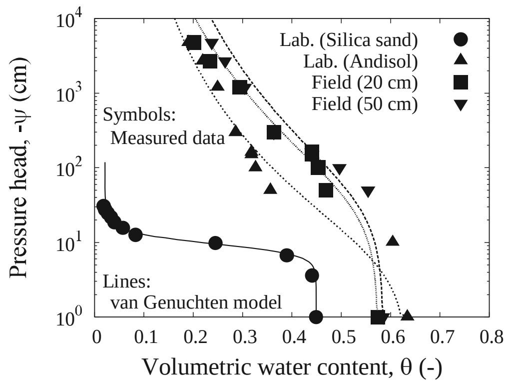

Figure 2. Water characteristic curves for both soils.

Table 2. Experimental cases.

		Rainfall intensity (mm/min)			
Soil type	Saturated	0	0.09	0.21	0.63
Silica sand	S-S	S-1	S-2	S-3	-
Andisol	A-S	A-1	A-2	A-3	A-4

2.3 Image processing and spatial moment approach

Each of the pixels representing an image has a pixel intensity which describes how bright that pixel is. In order to establish the relationship between the pixel intensity of a pixel and dye tracer concentration, a calibration was conducted. Under identical experimental conditions, a known concentration of dye tracer was injected into a corresponding porous formation without a hydraulic gradient. The spread of dye was captured by the digital camera. The same procedure was repeated using different concentrations of dye tracer. Consequently, the concentration of the dye tracer as a function of the pixel intensity varied over the range of 0 mg/cm^3 to 1.0 mg/cm^3.

A commonly used measure of dilution is the spatial moments of aqueous concentrations, which are calculated from snapshots of tracer plume at given times as follows (Tompson and Gelhar, 1990).

$$M_{ij}(t) = \int_{-\infty}^{\infty}\int_{-\infty}^{\infty} c(x,z,t)x^i z^j dxdz, \quad i,j = 1,2 \tag{1}$$

where x and z are the Cartesian coordinates, c is the solute concentration, t is the time, M_{ij} is the spatial moments associated with the distribution of tracer plume at a certain time, and i and j are the spatial order in the x and z coordinates, respectively.

The pixel intensity distribution can be converted to a concentration distribution by the calibration, providing an analogy between Eq.(1) and Eq.(2).

$$M_{ij}(t) = \int_{-\infty}^{\infty}\int_{-\infty}^{\infty} H(x,z)B(x,z,t)x^i z^j dxdz, \quad i,j = 1,2 \tag{2}$$

where $H(x,z)$ is the area per unit pixel and $B(x,z,t)$ is the intensity at a corresponding pixel. The centroid of plume concentration distribution is calculated as the normalized first order spatial moment by the following equation.

$$x_c = \frac{M_{10}}{M_{00}}, \quad z_c = \frac{M_{01}}{M_{00}} \tag{3}$$

where x_c and z_c are the centroid locations of plume concentration distribution in the x and z coordinates, respectively. The second order spatial moments are also computed as follows.

$$\sigma_{ij} = \begin{pmatrix} \sigma_{xx} & \sigma_{xz} \\ \sigma_{zx} & \sigma_{zz} \end{pmatrix} = \begin{pmatrix} \dfrac{M_{20}}{M_{00}} - x_c^2 & \dfrac{M_{11}}{M_{00}} - x_c z_c \\ \dfrac{M_{11}}{M_{00}} - z_c x_c & \dfrac{M_{02}}{M_{00}} - z_c^2 \end{pmatrix} \tag{4}$$

where σ_{ij} is the second order spatial moments.

Longitudinal and transverse dispersivities from spatial moments of the distributed tracer plume are calculated as the following equations (5) and (6) under saturated and unsaturated conditions, respectively.

$$\alpha_L = \frac{1}{2}\frac{\sigma_{xx}}{\xi_c}, \quad \alpha_T = \frac{1}{2}\frac{\sigma_{zz}}{\xi_c} \tag{5}$$

$$\alpha_L = \frac{1}{2}\frac{\sigma_{zz}}{\xi_c}, \quad \alpha_T = \frac{1}{2}\frac{\sigma_{xx}}{\xi_c} \tag{6}$$

where α_L is the longitudinal dispersivity, α_T is the transverse dispersivity and ξ_c is the travel distance of the center of tracer plume in the mean flow direction at a given time t.

3 DISPERSIVITY IN LABORATORY

3.1 *Longitudinal dispersivity*

The results of longitudinal and transverse dispersivities as a function of travel distance for silica sand and Andisol are shown in Figures 3 and 4, respectively. Longitudinal dispersivity estimates under unsaturated conditions are larger than those under saturated conditions. The increase of dispersivity may be induced from diversity of solute movement due to the effect of air. Several studies have pointed out the same tendency in unsaturated soils (Vanderborght and Vereecken, 2007).

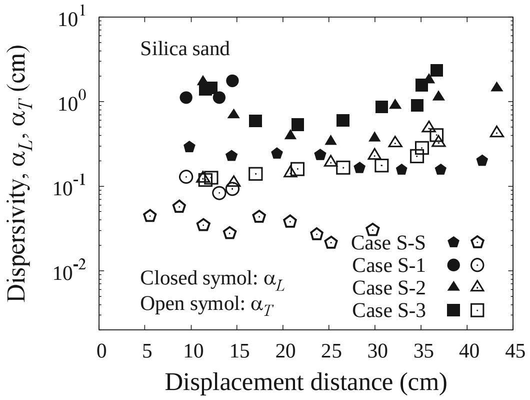

Figure 3. Longitudinal and transverse dispersivity estimates with displacement distance in silica sand.

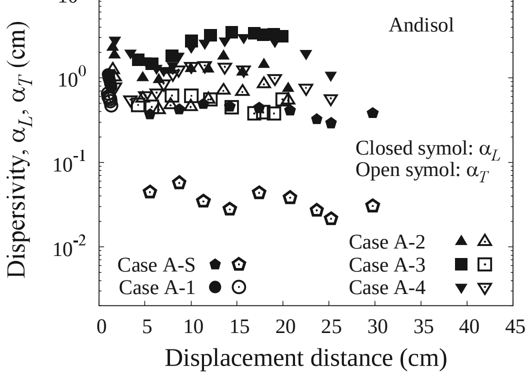

Figure 4. Longitudinal and transverse dispersivity estimates with displacement distance in Andisol.

Table 3. Soil properties in maize field.

	Depth from the ground surface 20 cm	50 cm
Dry density (g/cm^3)	0.95	1.13
Mean diameter of particle (cm)	0.021	0.10
Uniformity coefficient (-)	23.7	85.7
Hydraulic conductivity (cm/s)	0.00884	0.0239
Porosity (-)	0.59	0.57

Longitudinal dispersivity estimates also exhibit an increasing and decreasing tendency and show a dependency on infiltration rates. Water applied to the ground surface infiltrates and reaches an upper part of dye tracer. Because flow velocity is larger than solute velocity in unsaturated zone and affects the change of tracer migration, shape of dye tracer distribution is shrunk longitudinally. This duration may correspond to the decreasing process of the longitudinal dispersivity. After water reaches a front of dye tracer, dye tracer migrates with interstitial water. However, part of dye tracer has relatively low velocities due to the effect of air. Therefore, shape of dye tracer extends longitudinally, leading to the increase of longitudinal dispersivity estimates. Similar tendency can be seen in Andisol in Figure 4. A difference of the longitudinal dispersivity estimates between silica sand and Andisol is attributed to the difference of the uniformity coefficient.

3.2 *Transverse dispersivity*

As for Figures 3 and 4, transverse dispersivity slightly increases under unsaturated conditions or remains constant under saturated conditions with displacement distance. It is inferred that transverse solute displacement depends largely on mixing of water and air whose distribution varies with the depth. The degree of increase of water content induced from rainfall application decreases as rainfall intensity is lower. Since diversity of solute movement pathway in porous media increases at lower saturation this process would make mobile region of water complicated and result in larger values for longitudinal dispersivity. Hence, transverse dispersion phenomenon under unsaturated conditions is clearly different from longitudinal dispersion phenomenon.

4 DISPERSIVITY IN A FIELD

4.1 *Experimental setup*

Developed methodology for quantifying transverse and longitudinal dispersivities was applied to a maize field soil with approximately 100 cm depth from the ground surface under water-unsaturated conditions. Soil cores were taken at the depth of 20 cm and 40 cm. Physical properties are shown in Table 3 and water characteristic curves are also shown in Figure 2.

Brilliant Blue FCF tracer of 1000 cm^3 with the initial concentration of 2.0 mg/cm^3 was leached into the ground surface from two line sources (referred to as Plot 1 and 2) with 65 cm length and 3cm depth and subsequent tracer distributions were photographically recorded at vertical soil profiles excavated perpendicular to the line source. Artificial rainfall intensity was set to 0.12 mm/min for the application duration of 15 minutes. At a site near Plot 1 and 2, the two relations between the dye concentration and the pixel intensity at the upper and lower zones, which are 3 cm to 40 cm and are 40 cm to 80 cm below the ground surface, respectively, were obtained over the range of 0 mg/cm^3 to 2mg/cm^3. In a similar manner to laboratory tracer experiments, transverse and longitudinal dispersivities were quantified using spatial moments and image processing techniques.

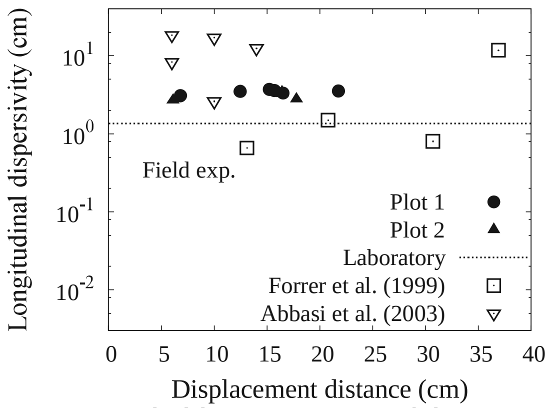

Figure 5. Longitudinal dispersivity estimates with distance.

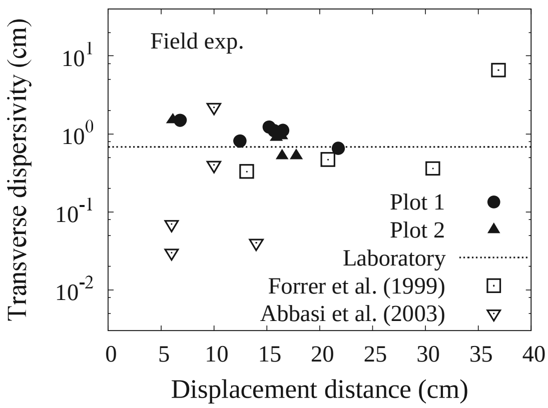

Figure 6. Transverse dispersivity estimates with distance.

4.2 *Longitudinal and transverse dispersivities*

Figures 5 and 6 illustrate the estimates of longitudinal and transverse dispersivities in comparison with the mean value of laboratory experiments and reported values (Forrer et al., 1999; Abbasi et al., 1995). Longitudinal and transverse dispersivity estimates ranged from 1.00 cm to 3.72 cm and from 0.52 cm to 2.35 cm respectively, which are good agreement with reported values, indicating the effectiveness of the developed methodology. Also, the ratio of longitudinal to transverse dispersivities was in the range of 1 to 5.4, which is in the lower range of dispersivity ratios reported in porous media (Persson and Berndtsson, 2002).

As a whole, both dispersivity values are slight larger than those identified in the laboratory. This is attributed to the difference between undisturbed soil in the field and disturbed soil in the laboratory. In addition, dye tracer moved through the soils in a preferential flow pattern, which induced higher dispersivities in more irregular flow patterns as compared with estimates obtained in laboratory tracer experiments. At the experimental site, some macropores were confirmed and influenced seepage and solute pathways in porous media.

Figure 7 shows the relation between the applied rainfall intensity and the dispersivity estimates in the field as well as in the laboratory. Mean values in each experiment are plotted in this figure. Despite of the rainfall intensity, both dispersivities remain constant. This is attributed to a relatively low degree of heterogeneity in the field of concern, while homogeneous packing of soil in the laboratory was reflected as a less variation of dispersivity estimates.

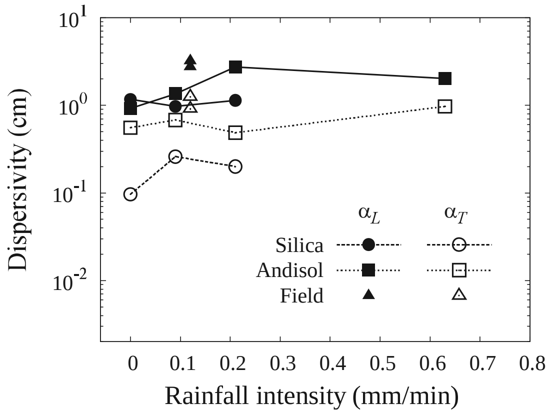

Figure 7. Relation between rainfall intensity and dispersivity estimates.

5 CONCLUSIONS

In the present study, a new methodology using spatial moment analysis linked with image processing of a dye tracer behavior was developed to estimate dispersivities not only in longitudinal but in transverse directions. Laboratory and field tracer experiments under unsaturated flow conditions were conducted with dye, Brilliant Blue FCF. Dispersivities exhibited an increasing and decreasing tendency associated with water content and showed a dependency on infiltration rates. Laboratory and field studies were extended by a literature search to compare the new results with earlier work, demonstrating a good agreement between the experimental and published results. Experimental results indicated the effectiveness of the developed methodology for simultaneous assessment of transverse and longitudinal dispersion in unsaturated soils in a field as well as in a laboratory.

6 ACKNOWLEDGEMENTS

The authors thank Mr. K. Suzuki for valuable discussion and Mr. H. Watanabe for giving us the permission to conduct the tracer experiments in his maize fields. The work reported here was supported by JSPS Grant-in-Aid for Young Scientists (B).

7 REFERENCES

Vanderborght J. and Vereecken H. 2007. Review of dispersivities for transport modeling in soils, *Vadose Zone J.*, 6, 29-52.

McNeil J.D., Oldenborger G.A. and Shincariol R.A. 2006. Quantitative imaging of contaminant distributions in heterogeneous porous media laboratory experiments, *J. Contam. Hydrol.*, 84, 36-54.

Flury M. and Flühler H. 1995. Tracer characteristics of Brilliant Blue FCF, *Soil Sci. Soc. Am. J.*, 59(1), 22-27.

Forrer I. Kasteel R., Flury M. and Flühler H. 1999. Longitudinal and lateral dispersion in an unsaturated field soil, *Water Resour. Res.*, 35(10), 3049-3060.

van Genuchten M.Th.1980. A closed-form equation for predicting the hydraulic conductivity of unsaturated soils, *Soil Sci. Soc. Am. J.*, 44, 892-898.

Tompson A.F.B. and Gelher L.W. 1990. Numerical simulation of solute transport in three-dimensional, randomly heterogeneous porous media, *Water Resour. Res.*, 26(10), 2541-2562.

Abbasi F., Simunek J., Feyen J., van Genuchten M.Th. and Shouse P.J. 1995. Simultaneous inverse estimation of soil hydraulic and solute transport parameters from transient field experiments: homogeneous soil, *Trans. ASAE*, 46(4), 1085-1095.

Persson M. and Berndtsson R. 2002. Transect scale solute transport measured by time domain reflectometry, *Nord. Hydrol.*, 33, 145-164.

Evaluating the long-term leaching characteristics of heavy metals in excavated rocks

Évaluation des caractéristiques de lixiviation à long terme de métaux lourds dans les roches excavées.

Inui T., Katsumi T., Takai A.
Kyoto University, Kyoto, Japan

Kamon M.
Kagawa National College of Technology, Takamatsu, Japan,

ABSTRACT: When excavation works are executed at stratums that naturally contain heavy metals due to their geologic histories, time-saving and reliable assessment of contamination potential by these metals is a current geotechnical challenge. This paper addresses the long term leaching characteristics of arsenic and lead in several rock materials, which were weathered in outdoor for more than two years. In addition, applicability of several time-saving laboratory test methods were verified as a tool to estimate the actual leaching behaviour of heavy metals.

RÉSUMÉ : Lorsque des travaux d'excavation sont effectués dans des strates contenant naturellement des métaux lourds en raison de leurs antécédents géologiques, une évaluation fiable et économe en temps du potentiel de contamination par ces métaux pose à l'heure actuelle un problème géotechnique. Ce document traite des caractéristiques de lixiviation à long terme de l'arsenic et du plomb dans plusieurs matériaux rocheux, ces derniers ayant été exposés à l'extérieur aux intempéries pendant plus de deux ans. En outre, l'applicabilité de plusieurs méthodes de test en laboratoire économes en temps a été vérifiée comme outil d'évaluation du comportement de lixiviation réel des métaux lourds.

KEYWORDS: natural contamination, rock, arsenic, leaching test, outdoor exposure test

1. INTRODUCTION

When excavation works are executed at stratums that naturally contain heavy metals due to their geologic histories, time-saving and reliable evaluation to judge the contamination potential by these metals and metalloids is required for proper management of geomaterials with unacceptable contamination potentials. Heavy metals existing naturally in stratums are fundamentally stable and immobile under the anaerobic depositional environment. However, in some cases, leaching of these constituents is triggered when exposed to water and oxygen after excavation works. Acid drainage, which comes mainly from the interactions between water, oxygen, and sulfide minerals in soils and rocks, often produces sulfide acid and increases the leaching concentrations of metals Thus, development of testing methodologies to assess their long-term leaching potential and behavior has been a great geoenvironmental issue in Japan (e.g. Hattori et al. 2003, Okumura et al. 2007). Generally, conventional batch and/or column leaching tests have been widely employed for evaluating the leaching potential of contaminated soils and waste-based geomaterials. However, when they are employed for rock materials, sample preparation including sampling and crushing is more likely to influence the leaching amount of trace elements (Inui et al. 2010). In addition, effects of oxidation after excavation on the leaching behavior should be considered since the acid rock drainage due to dissolution of sulfide minerals in rock is one of the main mechanisms which promote the leaching of heavy metals.

This study firstly presents the results of more than 27-month outdoor exposure tests conducted for five rock samples to assess their in situ leaching characteristics. They contain certain concentrations of natural-derived lead and arsenic, which are expected to be released if they are exposed to water and oxygen. The main focus is placed on the comparison of leaching characteristics of trace metals in outdoor exposure tests with those in various conventional laboratory tests, which include the total trace metal content test, conventional batch leaching test, accelerated oxidation tests and column leaching test. Laboratory leaching tests were validated as an index of the long term leaching characteristics of trace metals by comparatively assessing the results with the outdoor leaching behaviors

2 MATERIALS AND METHODS

2.1 *Materials*

Five different rocks materials were used. They were generated in construction works such as excavation and tunneling, which were executed in mountainous areas far from industrial and urban areas in Japan. Thus, it can be considered that heavy metals contained are derived from natural resources. Five rock samples consist of black shale, andesite, and three mudstones (MS-1, 2 and 3). They were all stored with their natural water content under the temperature of approximately 20 ºC in sealed condition to prevent the exposure to oxygen and water. Table 1 shows their appearances and the total contents of As and Pb as well as chemical compositions which were determined by the X-ray fluorescence analysis. According to the Japanese guideline, excavated materials containing more than 9 mg-As/kg or 23 mg-Pb/kg should be assessed in terms of their contamination potential (Ministry of Land, Infrastructure, Transport and Tourism, Japan 2010). All the samples used in this study contains more than 9 mg-As/kg. Pb higher than this standard was detected only in black shale.

Figure 1 shows pH values of rock samples for distilled water and H_2O_2 solutions with 3% and 30% concentrations. pH measurement using H_2O_2 solutions were employed to evaluate the possible pH change of geomaterials when they are oxidized under weathering conditions. Geomaterials with pH < 3.5 for 30% H_2O_2 solution are considered to have acidification potentials (Japanese Geotechnical Society 2009). In this study, 3% H_2O_2 solution was also used to evaluate the acidification potential against weaker oxidization effects. Black shale and andesite are fundamentally acidic even for distilled water. Three mudstone are considered to be alkaline rocks without oxidization effects. However, pH value of MS-2 for 30% H_2O_2 solutions were drastically reduced to 2-3, and pH values of MS-3 for 3% and 30% H_2O_2 solutions were lower than 3. These results supported that MS-3 is most easily acidifying among three mudstones.

Table 1. Chemical properties of rock samples used in this study

Sample ID	Black shale	Andesite
Appearance	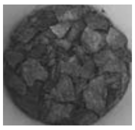	
As content (mg/kg)	28	26
Pb content (mg/kg)	23	5
Chemical composition (% in mass)	SiO_2: 43.6, Fe_2O_3: 21.4, Al_2O_3: 4.6, CaO: 0.2, K_2O: 16.5, SO_3: 8.8, TiO_3: 3.0, Others: 1.9	SiO_2: 59.0, Fe_2O_3: 11.6. Al_2O_3: 13.5, CaO: N.D., K_2O: 8.9, SO_3: 5.4, TiO_3: 1.0, Others: 0.6
MS-1	MS-2	MS-3
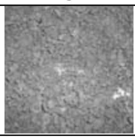	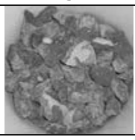	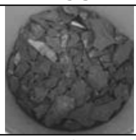
23	15	23
13	6	1
SiO_2: 54.2,Fe_2O_3: 15.3, Al_2O_3: 10.4, CaO: 7.9, K_2O: 5.2, SO_3: 4.0, TiO_3: 1.4, Others: 1.5	SiO_2: 54.2, Fe_2O_3: 18.7, Al_2O_3: 12.3, CaO: 2.7, K_2O: 7.2, SO_3: 2.5, TiO_3: 1.9, Others: 0.5	SiO_2: 64.6, Fe_2O_3: 11.6, Al_2O_3: 9.9, CaO: 1.1, K_2O: 5.2, SO_3: 3.9, TiO_3: 1.5, Others: 0.5

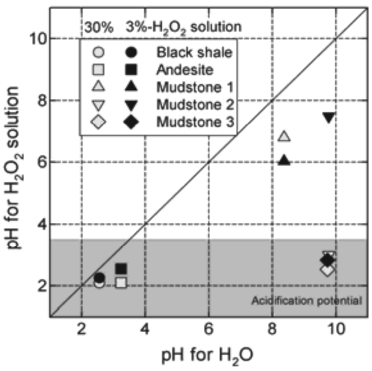

Figure 1. pH of each rock sample for distilled water and H_2O_2 solutions.

Photo 1. View of outdoor exposure test

2.2 *Outdoor exposure test*

Outdoor exposure tests have been conducted for five rock samples since October 2009. This paper presents the experimental results obtained until February 2012 (about 27 months). Each sample was crushed into 9.5 to 37.5 mm in grain size (2.0 to 9.5 mm in diameter for mudstone 1 due to its crushability). 4000g of rock sample with natural moisture content was stored in a cylindrical plastic container with a cross section of 0.05 m^2 with the dry density of 2.0 Mg/m^3 for black shale, 1.1 Mg/m^3 for andesite, 1.2 Mg/m^3 for mudstone 1 and 1.6 Mg/m^3 for mudstone 2 & 3, and exposed to the rainfall and air throughout the test (Photo 1). Rainfall intensity and percolation volume were continuously monitored. The leachate was periodically collected and subjected to chemical analyses.

2.3 *Laboratory leaching tests*

Leaching concentrations of As and Pb were analyzed according to the batch leaching test method for the soil quality regulated by the Notification No.46 of Japanese Ministry of the Environment in 1991. In the batch test, air-dried rock samples were crushed until its parcentage passing at 2 mm became 100%. In addition, for black shale, the sample subjected to accelerated oxidation was also prepared. Accelerated oxidation was promoted by storing the crushed sample in an incubator under 80% O_2 and 100% humidity condition in 200 days.

As and Pb leaching concentations during the aforementioned pH measurement using H_2O_2 solutions were analysed to evaluate the effects of accelerated acidification on the leaching behavior.

Tank leaching tests were conducted for monolithic rock samples with approximately 400 g in dry mass by submerging into distilled water for 28 days. The liquid to solid ratio (mL/g) of 10 was employed. Column leaching tests were performed for about 750 g rock samples, which were crushed until its percentage passing at 4.75 mm became 100%. A cylindrical specimen was prepared by vibratory compaction in an acrylic column (55 mm in inner diamete) and then permeated with the permeant by maintaining the constant water head (24 mL/hour in flow rate). The permeant was distilled water after its pH was adjusted to 4.7 using the nitric acid.

An atomic absorption spectrophotometer (Shimadzu, AA-6800) with a hydride generator and an electrothermal atomization system was used to determine the concentration of As and Pb in the solution. Chemical parameters of the solution (pH, Eh, Electrical conductivity (EC)) were also monitored.

3 RESULTS OF OUTDOOR EXPOSURE TESTS

Figure 2 show profiles of percolation volume, pH, EC, Eh, temperature and concentrations of As and Pb of the leachate sample with time. This paper describes the results for black shale and andesite rock samples only. Cumulative flow volumes ranged from 16 to 19 in the liquid to solid ratio (mL/g) after 27 months since due to the difference in permeability.

The leachate from the black shale was acidic, and pH values ranged between 2.1 and 2.5 (Figure 2(a)). As concentrations were higher than 0.1 mg/L in the first three months, then decreased with time and reached 0.02 mg/L. Temperature rising during summer (July-September) were followed by slight decrease in pH and increase in EC and leaching concentrations. This is because the rock samples were subjected to wet and higher temperaure conditions in summer and dissolution of the minerals was promoted due to the oxidization produces.Leaching of Pb was also detected but with much lower concentrations than As.

Testing results for the andesite (Figure 2(b)) had similarities with those for the black shale. pH values were ranging from 2.4 to 4.0. At the initial stage, EC values and As leaching concentrations were relatively high and then gradually decreasing and stabilized. However, 10 months after, with gradual lowering of pH values, the values of both parameters were getting larger particularly in summer as same as black shale. These profiles of pH, As leaching concentrations and EC were well explained well by the results of the accelerated oxidation test using H_2O_2 solutions (see Figure 1). Obvious pH drops were observed against the oxidization by H_2O_2 solutions. The andesite sample was gradually oxidized during the outdoor exposure test, and leaching of As and other minerals were promoted accordingly. Pb leaching higher than 0.01 mg/L were rarely observed throughout the test.

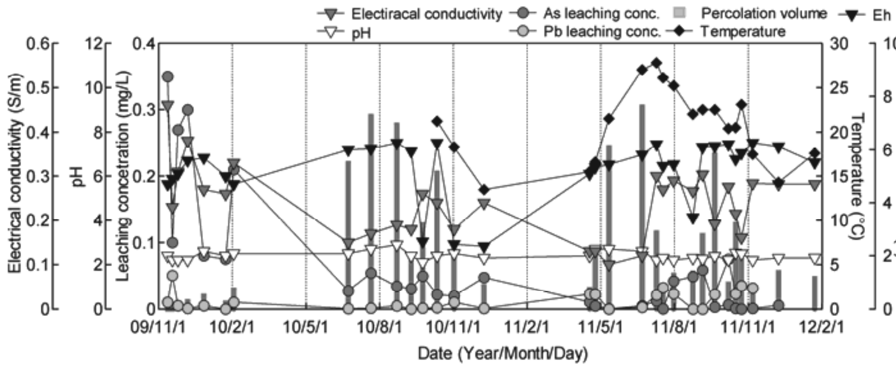

(a) Black shale

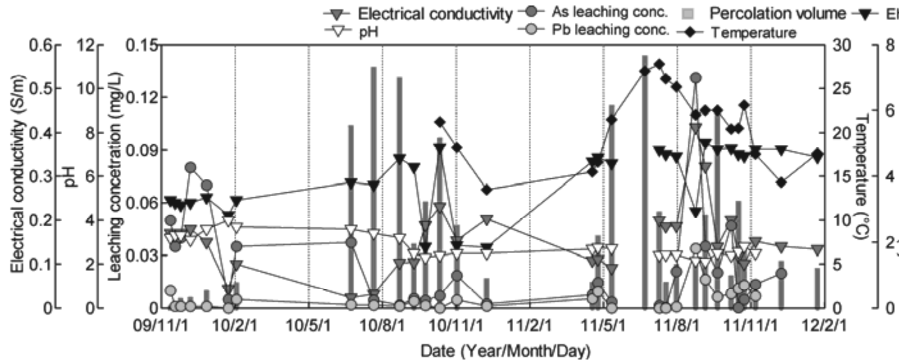

(b) Andesite

Figures 2. Profiles of pH, Eh, heavy metal concentrations, rainfall intensity and infiltration in outdoor exposure tests

4 DISCUSSION

In Figure 3, pH and Eh values of the leachate samples collected in both outdoor exposure tests and laboratory leaching tests for black shale are plotted on the pH-Eh/pe(electron activity) diagram of dominant forms of As and Fe in As-Fe-S-H_2O system (Zhu & Merkel 2001).

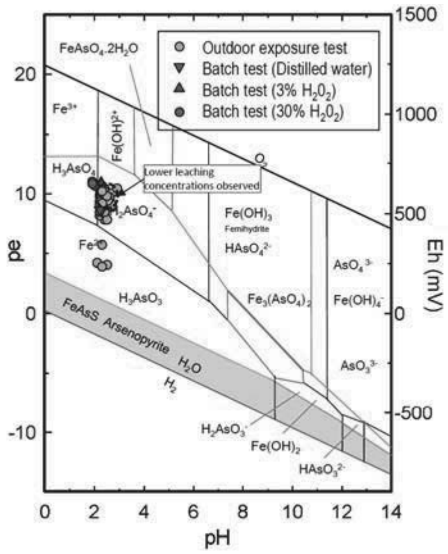

Figure 3. pH and Eh values observed in outdoor exposure tests and laboratory leaching tests combined with pH-Eh diagram of dominant forms of As and Fe in As-Fe- S-H_2O system (Zhu & Merkel 2001).

In the outdoor exposure test, higher leaching concentrations of As were observed even when Eh values were relatively low, where dominant forms of iron and arsenic are Fe^{2+} and H_3AsO_3 (arsenous acid), respectively. When lower leaching concentrations were observed (see the circle in Figure 3), the dominant form of As is expected $HAsO_4^-$, which is more easily absorbed to iron compounds and less mobile than H_3AsO_3. Comparing pH and Eh values monitored in laboratory leaching tests with those in outdoor exposure test, pH values in the batch test using 30% H_2O_2 solution was lowest, and pH for 3% H_2O_2 solution was almost similar to those in the outdoor exposure test. This indicates that 30%H_2O_2 solution is more influential than outdoor exposure in more than two years in terms of acidification, and accelerated acidification by 3% H_2O_2 solution is almost comparable to a few years outdoor exposure. This trend was consistent in all the rock samples used in this study and it can be concluded that pH changes against 3% and 30% H_2O_2 solutions could classify acidification potentials under the weathered condition, but the acceleration by 30 % H_2O_2 solution possibley overestimate the acidification progress in outdoor even for two years.

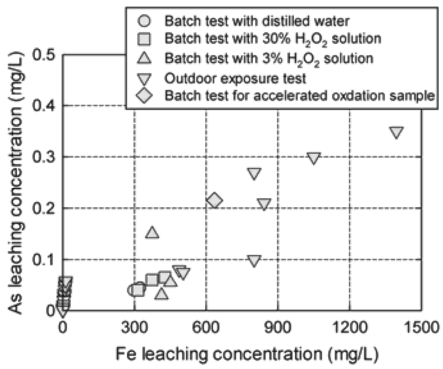

Figure 4. Relationship between Fe and As leaching concentrations in various leaching tests

Figure 4 shows a relationship between Fe and As leaching concentrations in both outdoor exposure tests and laboratory leaching tests. A clear correlation between them indicates that dissolution of iron pyrite due to oxidization is a main driver for As leaching. In addition, Fe and As concentrations are correlated in laboatory leaching tests as well. From these observations, dissolution of pyrite due to oxdization was well simulated by the accelerated acidification/oxidization methods, such as adding H_2O_2 solutions and long term exposure to 80%

O_2 and water, which were employed in this study.

Figures 5 shows As leaching amounts of all the samples in outdoor exposure test and several laboratory leaching tests described in section 2.3. The leaching amounts of As from unit weight of each rock sample are plotted with the cumulative volume of solvent or percolated water contacting with the rock sample during laboratory leaching tests and outdoor exposure tests, which is represented by the liquid to solid ratio (L/S).

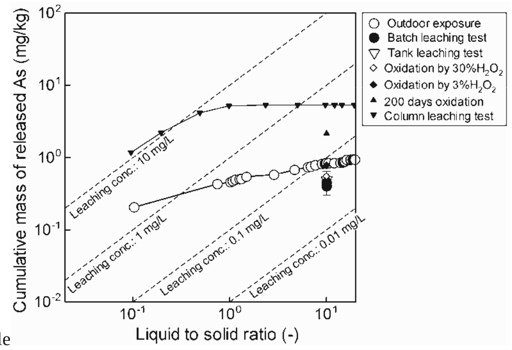

(a) Black shale

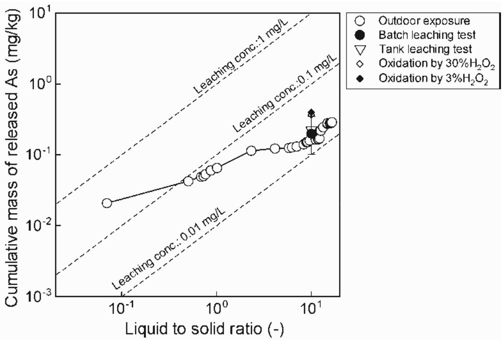

(b) Andesite

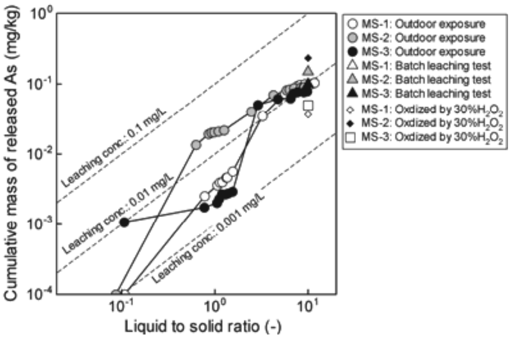

(c) Mudstones

Figures 5. Comparison of As leaching amounts obtained in 27 months outdoor exposure test and laboratory leaching tests.

For the black shale (Figure 5(a)), the leaching amount at L/S = approximately 10 reached 0.84 mg/kg, which is slightly larger than those in the conventional batch leaching test as well as the accelerated acidification test, which were conducted with L/S = 10. Considering that chemical activity of the black shale is relatively since EC values of the leachate collected were largest among all the rock samples, the chemical equilibrium achieved in the closed batch leaching systems was likely to limit the dissolution of As. Column leaching test gave 10 times larger leaching amount than the outdoor exposure test, probably because a crushed sample (< 4.75 mm in diameter) was used, and the permeant was continuoulsy renewed in the column leaching test. Thus, sample preparation in the laboratory leaching test is also a key issue for the rock sample.

For the andesite (Figure 5(b)), the overall trends were almot similar to those of the black shale. However, a slope for the outdoor exposure test became steeper as the percolation volume increased (L/S > 10), since aforementioned As leaching associated with the oxidation was observed. For MS-2 and 3 (Figure 5(c)), the leaching amounts at L/S = approximately 10 were almost equal to those in the conventional batch leaching test as well as the accelerated oxidation batch leaching test. However, similar to the black shale, MS-1 had a high chemical activity, and its leaching concentration in the batch leaching tests was limited to a negligible level although 0.1 mg/kg of As was released in the outdoor exposure test at L/S = 10.

From these testing results, the leaching amount of As obtained in the conventional batch leaching test can be a good index of the insitu leaching amount until L/S = 10 in the cases of rock samples with relatively low chemical activities. The accelerated oxidation tests using H_2O_2 solutions can simulate the in situ leaching amount for the safe side. However, the chemical equilibrium may limit the leaching of trace metals in the batch leaching test as observed in black shale and MS-1.

Pb leaching concentrations were negligible for all rock samples. According to the aforementioned criterion for total Pb content suggested by MLIT, all the rock samples are considered safe in terms of Pb leaching. These testing results support the validity of the criterion for total content of Pb.

5 CONCLUDING REMARKS

This manuscript verified several laboratory tests for estimating the long term leaching characteristics of As and Pb in several rock materials, by comparing the results of outdoor exposure tests. Total contents of trace metals can be regarded possibly as screening values to judge whether detailed evaluation of leaching characteristics are necessary. The leaching amount of As obtained in the conventional batch leaching test can be a good index of field leaching amount, and the accelerated oxidation tests can simulate the outdoor leaching amount for the safe side. These observations confirm the validity of a series of laboratory leaching tests as a tool to estimate the in situ leaching behavior of heavy metals in excavated rocks.

ACKNOWLEDGEMENTS

This research was financially supported by the Grant-in-Aid for Scientific Research (B) (No. 20360211), Japan Society for the Promotion of Science. The authors acknowledge Ms. A. Dejima and Ms. M. Katayama, former graduate students of Kyoto University, for their great efforts in laboratory experiment works.

REFERENCES

Hattori, S., Ohta, T. and Kiya, H. 2003. Engineering geological study on exudation of acid water from rock mucks -Evaluation methods of rocks at the Hakkouda Tunnel near mine area, *Jour. Japan Soc. Eng. Geol.*, 43 (6), 359-371.

Inui, T., Katsumi, T., Katayama, M. and Kamon, M. 2010. Effects of friability and grain size on the leaching of heavy metals in excavated rock materials, *Environmental Geotechnics for Sustainable Development*, M. Datta et al. (eds.), Tata McGraw Hill, New Delhi, 730-733.

Japanese Geotechnical Society. 2009. *Japanese Standards and Explanations of Laboratory Tests of Geomaterials*, 314-315.

Ministry of Land, Infrastructure, Transport and Tourism, Japan. 2010. *Technical Manual on the Countermeasures against Soils and Rocks Containing Natural-Derived Heavy Metals in Construction Works (Draft)*, 10.

Okumura, K., Sakurai, K., Nakamura, N. and Morimoto, Y. 2007. Environmental impacts of naturally occurring heavy metals and countermeasures, *Journal of Geology*, 116 (6), 892-905.

Zhu, Y. and Merkel, B.J.. 2001. The dissolution and solubility of Scorodite, $FeAsO_4{\cdot}2H_2O$: Evaluation and simulation with PHREEQC2, *Wiss. Mitt. Inst. fur Geologie*, TU Bergakedemie Freiberg, Germany, 18, 1-12.

Geo-environmental challenges of a major coal terminal development in Australia

Défis géo-environnementaux du développement d'un terminal majeur de charbon en Australie

Jones S.R.
Douglas Partners Pty Ltd

ABSTRACT: This paper describes the integration of geotechnical, environmental and groundwater investigations for the Terminal 4 Project in Newcastle, Australia, aimed at identifying appropriate remediation measures to protect human health and environmental values. The site presented a series of complex challenges due to its geological setting, previous uses for waste disposal and adjacent environmentally sensitive areas. Past industrial wastes have caused contamination of soil and groundwater. The site and adjoining wetlands form habitats for protected flora and fauna species. Without mitigation measures, the proposed coal terminal development would have the potential to increase the mobilisation and flow of contaminants off site into the wetlands and other environmental receptors. Geotechnical and groundwater modelling was undertaken, resulting in a series of remediation and mitigation measures for specific identified risks. The implementation of the proposed remediation and mitigation measures for the project will protect environmental values, and is expected to improve the long-term environmental condition of the project area and immediate surrounds.

RÉSUMÉ : Ce document décrit l'intégration des études géotechniques, environnementales et de sondages des eaux souterraines du Projet Terminal 4, afin que des mesures d'assainissement appropriées puissent être mises en œuvre pour protéger la santé humaine et l'environnement. Le site présente plusieurs défis complexes en raison de son contexte géologique, de son utilisation historique pour déposer des déchets et de sa proximité avec des zones à caractère environnemental sensible. Les déchets industriels ont entraîné la contamination des sols et des nappes souterraines. Le site forme avec les marécages adjacents des habitats pour des espèces protégées de la flore et de la faune. Le développement proposé du terminal de charbon a le potentiel d'accroître la mobilisation et la circulation des contaminants hors du site, et par là-même de contaminer les marécages adjacents ainsi que d'autres récepteurs de l'environnement. Les résultats des modélisations géotechniques et d'écoulement des eaux souterraines ont entraînés une série de mesures d'atténuation des risques identifiés. La mise en œuvre du projet d'assainissement et des mesures d'atténuation pour le projet protégera les valeurs environnementales, et devrait permettre d'améliorer sur le long terme l'état de l'environnement.

KEYWORDS: coal export, landfill, soil and water contamination, barrier wall, permeable reactive barrier, multi-phase extraction.

1 INTRODUCTION

Kooragang Coal Terminal on Kooragang island near Newcastle, Australia is the world's largest coal export facility with an export capacity of 120 Mtpa. It is planned to substantially increase the size of the facility by construction of a new adjoining terminal, known as Terminal 4. The location of the site is shown in Figure 1.

The site has a total area of 246 ha and comprises reclaimed land over soft alluvial soils. For 40 years the site was used for dumping of various industrial wastes, leading to significant soil and groundwater contamination.

Industrial landfill cells were constructed in the 1970s and 80s by pushing out slag bund walls and filling in between; no base or side liners were installed. It is proposed to fill and level the site by dredging approximately 5 million m^3 of sand from the nearby Hunter River. The development will impose significant loads to the ground and the sand will also be used as surcharge material for ground improvement purposes.

The groundwater system comprises dual aquifers connected to the adjacent Hunter Estuary Wetlands that support endangered flora and fauna. These sensitive wetlands are a national park and listed by the Ramsar Convention as having international importance. The wetlands and two arms of the nearby Hunter River represent the environmental receptors requiring protection.

The complex conditions presented many geotechnical and environmental challenges to the project. The project is unique to Australia, and relatively unusual worldwide, whereby multiple remediation technologies will be implemented on a large scale. Some of the proposed remediation measures have had only limited previous application in Australia.

The work included extensive field investigations, laboratory testing, water level monitoring, groundwater flow modelling and contaminant transport modelling.

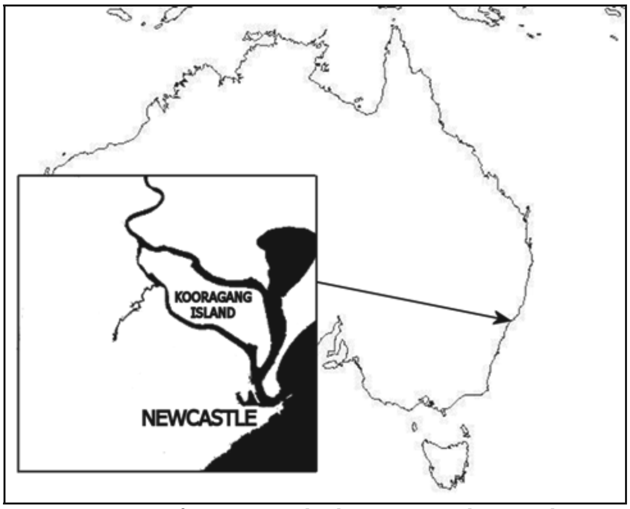

Figure 1. Location of Kooragang Island, near Newcastle, Australia.

2 GEOLOGY AND HYDROGEOLOGY*Geology*

Kooragang Island is located on the lower reaches of the Hunter River and is about 10 km long by 3 km wide. The island was formed by the reclamation of a number of former islands, channels and mudflats using dredged sandy materials from the river. The geology at the site comprises Permian aged Tomago Coal Measures overlain by Quaternary alluvium. The Tomago Coal Measures consist of shale, siltstone, sandstone, conglomerate and coal. The depth to rock ranges from 30 m to more than 70 m.

The overlying alluvium comprises fine to medium grained estuarine sediments with some gravel zones, overlain by fluvial sands with further fine grained estuarine deposits at the top of the natural profile including soft silty clays up to 14 m thick.

The natural profile is overlain by significant fill materials resulting from the former disposal of waste from steel making and dredging activities. The fill is up to 12 m in thickness and comprises a wide range of materials, including coal washery reject, slag, coal fines, oil/tarry sludge, clayey silt filter cake, kiln wastes, cell scale (gypsum and manganese dioxide), asbestos, steel-making flue dust, lime sludge, timber dunnage and various sporadic inclusions. The consistency of the fill ranges from very soft to very dense/cemented.

2.2 Hydrogeology

Groundwater beneath the site is known to be present in two principal aquifers: an upper unconfined aquifer within the fill strata (Fill Aquifer), and a deeper confined aquifer within the estuarine sediments (Estuarine Aquifer). The upper soft natural clays form a slightly ‘leaky’ aquitard that separates these aquifers. Figure 2 shows a conceptual groundwater model.

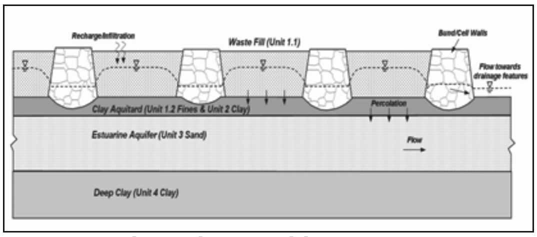

Figure 2. Conceptual groundwater model.

As the degree of contamination in the Fill Aquifer is considerably worse than the Estuarine Aquifer, the continuity and integrity of the clay aquitard is of important to the hydraulic and environmental performance of the site.

3 INTEGRATED INVESTIGATION

The investigation of the project site featured integration of geotechnical, environmental and groundwater aspects to achieve savings in terms of time and cost. Prior to commencing the field work program a desktop review was undertaken to collate pre-existing data on sub-surface conditions and contamination. This identified data gaps and was used to plan the investigation.

The integration of the disciplines during the investigation program was achieved by:

- Geotechnical boreholes were used to collect samples for both geotechnical testing and contamination testing.
- The use of staff trained in geotechnical logging, environmental logging and the appropriate collection of contamination samples.
- Extensive use of cone penetration tests, especially piezocone tests, to better delineate soil stratigraphy, layer permeability and potential flow paths.
- The boreholes were also used for the installation of environmental grade monitoring wells, so that water samples could be collected for contamination testing.
- Groundwater wells were also used to conduct in-situ permeability tests in both aquifers
- New and existing wells (over 150 in total) were gauged on the same day to provide a reliable snapshot of groundwater levels in both aquifers, which could then be used to prepare groundwater contours that for the first time accurately represented the groundwater regime of the site.

It was undesirable for the investigations to create hydraulic connections between the two aquifers, so all boreholes and CPTs were grouted upon completion to seal the aquitard.

Groundwater modelling was undertaken using MODFLOW (with Vistas), MODFLOW-SURFACT and PEST for preliminary parameter estimation. The modelling consisted of calibration of the model to existing conditions followed by modelling the effects of site filling, dredging, salinity and capping the site. Contaminant transport modelling was then undertaken using CONSIM to assess the potential off-site impacts of the proposed development.

4 CONTAMINATION

The investigations identified widespread general contamination and areas of more specific contamination, each with particular characteristics and potential to impact the environment. The main contamination issues are described below.

4.1 Tar Waste Ponds

An area known as Ponds 5 and 7 was found to contain large volumes of non-aqueous phase liquid (NAPL) tar waste to depths of approximately 8 m. The tar waste is generally in the form of a viscous sludge containing high concentrations of polycyclic aromatic hydrocarbons (PAH) and total petroleum hydrocarbons (TPH). Groundwater impact was also recorded in wells immediately surrounding Ponds 5 and 7. The groundwater impact was primarily within the Fill Aquifer, with some elevated concentrations also recorded in the underlying Estuarine Aquifer. Key findings included:

- Groundwater modelling indicated that the ‘squeezing’ effect of T4 Project loading would lead to temporarily increased flow of contaminants towards off-site receptors;
- Contaminant transport modelling indicated that contaminant flow rates would increase during dredging and preloading of the site, up to twice for naphthalene, compared to the no development case;
- There would be potential for long term off-site migration of contaminants with or without the T4 Project, however the risks are higher during dredging and preloading stages; and
- Following development over the area of Ponds 5 and 7 (by the proposed coal stockyard), it would not be practical to implement mitigation measures, should off-site impacts become evident.

4.2 Asbestos / Lead Area

The site history review found that an area containing asbestos burial pits also contained lead dust (from steelworks) co-disposed with the asbestos in polyethylene bags.

It was assessed that elevated concentrations of lead could potentially reach the wetlands to the north of the disposal area, for the following reasons:

- The asbestos/lead area is close to the northern boundary of the T4 Project area and the groundwater flow direction in this part of the site is to the north;

- At least 50 % of the asbestos and lead dust burial pits would be expected to come into permanent or frequent contact with groundwater following settlement induced by preloading and subsequent T4 Project loads;

- The long-term integrity of bags containing lead dust could not be guaranteed (i.e. potential for existing bags to be damaged, or become damaged due to loading and settlement, or degradation over time); and

- The lead dust is expected to be highly leachable when in contact with groundwater.

4.3 Free Phase Hydrocarbon Area

Free-phase hydrocarbon impact, comprising Light Non-aqueous Phase Liquid (LNAPL), was encountered in the Fill Aquifer at two monitoring well locations in the southern part of the site. The apparent thickness of floating product was found to be up to 2 m. Fingerprint analysis of the free product found that the sample was degraded mineral lubricating oil with trace amounts of diesel. The analysis concluded that the oil was not a recent release and may have been used in diesel engines.

The degree of impact generally diminished with distance from the wells suggesting that the extent of free product was relatively localised. Groundwater samples collected from the Estuarine Aquifer wells recorded minor hydrocarbon impact in the vicinity of free-phase impact.

4.4 Fines Disposal Facility

A 45 ha portion of the site known as the Fines Disposal Facility (FDF) was used to receive dredged fine sediments during various stages of construction of the existing coal terminal. The dredged fines contain PAHs and heavy metals. A leachate collection system generally maintains the groundwater level below the contaminated sediments. Preload and site development, however, will induce significant settlements which are likely to impact on the leachate collection system. This combined with the capping of the site is expected to result in a rise water table level with the result that the lower 1.5 to 2.0 m of dredge spoil will end up below the water table in the long term.

4.5 Manganese Dioxide Waste Area

This 25 ha former waste site contains electrolytic manganese dioxide waste and localised hydrocarbon contamination (TRH and PAH). The groundwater study identified that the main risk associated with the manganese waste site would be vertical infiltration of saline water during dredging due to the presence of a thinner and more permeable clay aquitard below fill materials compared to elsewhere on the T4 site. This presents a risk of migration of contamination into the Estuarine Aquifer, and increased groundwater effects on nearby surface water bodies, in particular increased salinity levels in nearby surface water ponds during dredging.

5 REMEDIATION

5.1 Review and Ranking of Available Options

A review of available remediation and management technologies was undertaken prior to assessing the preferred options for each of the contamination issues identified. Of the many remediation technologies available, only well-established, proven technologies were considered for the T4 Project. Relevant regulatory guidelines and policies were also considered when determining preferred options for remediation and management.

Alternative and emerging remediation technologies were also reviewed but discounted due to lack of experience and uncertain effectiveness; these included electrochemical remediation technologies (ECRT), supercritical fluid technology (SCF) and nanotechnology, in particular the use of nano-scale zero-valent iron (nZVI). Due to the site conditions preference was given to in-situ technologies that do not require excavation or removal of the contaminated soil and/or water to remediate the area. Ex-situ technologies require the contaminated soil or water to be removed from the ground for treatment, which can either occur on- or off-site.

The remediation options for each contamination issue were evaluated against the following attributes and weightings:

- Technical Effectiveness (20%): the suitability of the method to treat or manage the contaminant(s) of concern, also considering geotechnical impacts (beneficial or adverse);

- Track Record in Australia (5%): whether or not the method has been successfully used in Australia;

- Availability (5%): the number of contractors who have the expertise and equipment to implement the method; can include international contractors who could bring the technology into Australia;

- Ease of Implementation (10%): consideration of site constraints, regulatory hurdles and logistics;

- Verification (5%): effectiveness of construction quality control and ability to verify that specifications have been achieved;

- Sustainability (10%): the principles of environmentally sustainable development and the use of resources, energy inputs, waste generation, on-going management and maintenance;

- Stakeholder Acceptance (5%): the likely degree of satisfaction of regulators, owner, neighbours and the community with the remediation option;

- Risk of off-site Migration (10%): effectiveness of the method to inhibit contaminant transport;

- Cost (20%): including trials, design, construction and operation; and

- Time to Implement (10%): trials, design and construction.

The attributes were each scored from 0 to 5 based on a combination of quantitative and qualitative inputs, with zero being ineffective, unavailable or very costly and 5 being the best credible outcome. The total score was calculated as:

$$\Sigma S_i.W_i \tag{1}$$

where S_i is the score for attribute i, and W_i is the weighting for attribute i. The result was an overall score out of 5.

Based on the ranking system described, the preferred remediation options for each of the identified contamination issues were selected, as summarised in Table 1. In each case the three options with the highest score were identified so that alternatives were not ruled out for the detailed design stage.

Table 1. Summary of Selected Remediation Options

Contamination Issue	Preferred Remediation Option	Second Ranked Option	Third Ranked Option
Pond 5/7 tar waste	Barrier Wall	Permeable Reactive Barrier	Cap and Monitor
Lead Dust / Asbestos	Permeable Reactive Barrier	Barrier Wall	Interception Drain and Monitor
Free Phase LNAPL	Multi Phase Extraction	Pump and Treat	Barrier Wall
Fines Disposal Facility	Permeable Reactive Barrier	Cap and Monitor	Interception Drain and Monitor
Manganese Dioxide area (EMD) - Dredging Phase	Liner (GCL) prior to dredging	Barrier Wall	Interception Drain and Monitor

5.2 Tar Waste Ponds

The soil-bentonite barrier wall enclosing the Pond 5/7 tar waste would be approximately 1 km long and 10 m deep, keyed into the clay aquitard. The design of the wall will take into account the hydraulic conditions of the contained volume under initial loading (especially preload), which would be a one-off event during construction. Key design issues for the barrier wall were:

- Pre-trenching through the existing slag cell walls and other cemented layers in the fill for slurry trench construction;
- Mix Design of the bentonite slurry, including compatibility with site groundwater and soil conditions;
- Mix design of the soil-bentonite backfill, including compatibility with site groundwater and soil conditions;
- Global and local stability of the slurry trench;
- Density and viscosity of the slurry and backfill materials, such that trench stability is maintained, while permitting the backfill to displace the slurry; and
- Provision of vertical drainage (e.g. wick drains or sand drains) internal to the enclosed barrier wall to control pore pressures generated during preloading.

5.3 Asbestos / Lead Area and Fines Disposal Facility

The ‘precautionary principle’ was applied to the potential risk resulting from the asbestos/lead dust area. The permeable reactive barrier (PRB) would be designed to maintain northerly groundwater flows while ‘treating’ lead leachate in the event that lead dust comes into contact with the groundwater.

The PRB at the fines disposal facility would also be designed to maintain northerly groundwater flows while ‘treating’ leachate potentially generated by dredged sediments coming into contact with the groundwater. The target contaminants are metals (mainly aluminium) and PAH.

The two PRBs will be a ‘funnel and gate’ type comprising ‘gates’ of reactive medium with intervening panels of impermeable barrier wall. This system allows for more convenient maintenance and, if needed, replenishment of the reactive media. The Operational Environmental Management Plan for the terminal will incorporate regular monitoring and maintenance of the reactive media.

The PRBs will be installed along the northern boundary of the site and keyed into the clay aquitard at a depth of about 4 m to 5 m.

Key design considerations and aspects of the design and life cycle of the PRBs included the panel and gate widths, reactive media and treatment process, hydrogeology, contaminant distribution, geochemistry; reaction kinetics and residence time; and installation methods. The ratio of panel width to gate width was selected as 6:1 following groundwater modelling of flows and residence times through the gates.

It is also proposed to extend the wall as a continuous low-permeability barrier to the west, adjacent to a surface water body now as Deep Pond to protect the wetlands to the west and north from the saline water during dredging.

5.4 Free Phase Hydrocarbon Area

The preferred remediation option for the free-phase LNAPL contamination is multi-phase extraction (MPE). MPE is an in-situ remediation technology for simultaneous extraction of vapour phase, dissolved phase and separate phase (e.g. LNAPL) contaminants from the vadose zone, capillary fringe, and saturated zone soils and groundwater. It will likely be followed by monitored natural attenuation (MNA) for residual dissolved phase hydrocarbon contamination.

5.5 Manganese Dioxide Waste Area

The preferred remediation option to manage risks associated with dredging activities within the manganese dioxide waste site is to install a low-permeability geo-synthetic clay liner (GCL) over the site prior to dredging.

An overall plan showing the location and extent of the preferred remediation options is presented in Figure 3.

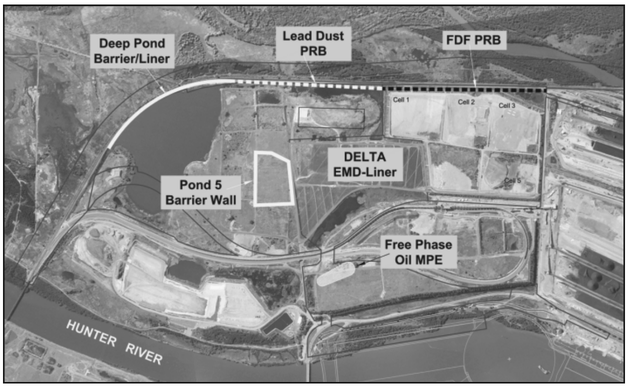

Figure 3. Remediation Plan.

6 CONCLUSIONS

The Terminal 4 Project is planned to be constructed at a site that presents complex geotechnical and environmental conditions. The investigation required close integration of geotechnical, contamination and groundwater assessments. The project will beneficially re-use a highly degraded site by implementing several remediation measures on a large scale, making the project unique to Australia and unusual worldwide. The method of selecting the preferred remediation options is described, and the key design considerations discussed. The Terminal 4 Project is expected to improve the long-term environmental condition of a site previously contaminated by industrial waste, while protecting the surrounding sensitive environment.

7 ACKNOWLEDGEMENTS

The author thanks Port Waratah Coal Services Limited for providing permission to publish this paper. The staff at Douglas Partners’ Newcastle office is acknowledged for their hard work and commitment to this important and complex project.

Characterisation of landfill steel mill sludge waste in terms of shear strength, pore water pressure dissipation and liquefaction potential

Caractérisation de la résistance au cisaillement, de l'évolution des pressions d'eau interstitielle et du potentiel de liquéfaction des boues d'aciérie dans un centre de stockage.

Lavoie J.L.N., Sinclair T.J.E.
Tonkin &Taylor Ltd, 105 Carlton Gore Road, Newmarket, Auckland, 1026; PH (+64) 9-355 0703; FAX (+64) 9-307 0265

ABSTRACT: The unique method of iron sands mining undertaken at the New Zealand (NZ) Steel Mill, produces an inert waste sludge comprised primarily of clay and iron-sands/grit. This wet sludge waste is landfilled in cells to heights up to 25m. The purpose of this paper is to characterise the sludge waste and to investigate its potential for liquefaction. This paper presents an investigation of the sludge in the existing landfill based on in situ and laboratory testing. Design parameters such as shear strength, and pore water pressure are developed and confirmed for the sludge material. Liquefaction potential of the sludge due to earthquake shaking is investigated using a CPT-based assessment and Atterberg limits test results. The paper concludes with a discussion of liquefaction potential and recommended total stress and effective stress parameters for detailed design of a new landfill development.

RÉSUMÉ : La méthode unique pour l'extraction de minerai de fer utilisée par New Zealand (NZ) Steel Mill produit une boue inerte résiduelle composée principalement d'argile et de sable ferreux. Cette boue liquide est stockée dans des casiers sur une hauteur pouvant atteindre 25m. L'objectif de cet article est de caractériser la boue résiduelle et d'évaluer son potentiel de liquéfaction. Cet article présente les résultats des essais in-situ et en laboratoire, réalisés sur la boue présente dans le centre de stockage existant. Les caractéristiques telles que la résistance au cisaillement et l'évolution des pressions d'eau interstitielle sont développées et confirmées pour cette boue. Le potentiel de liquéfaction de la boue lors d'un tremblement de terre est évalué par des essais réalisés au moyen de pénétromètres coniques ainsi que par la détermination des limites d'Atterberg. L'article conclut par une discussion sur le potentiel de liquéfaction et sur les valeurs de contrainte totale et contrainte efficace recommandées pour la conception et le développement d'un nouveau centre de stockage.

KEYWORDS: sludge, landfill, liquefaction, shear strength, pore water pressure

1 INTRODUCTION

The objectives of this paper are to characterise landfilled sludge waste in situ and to investigate the potential for liquefaction of the sludge. Various in situ test results are presented and parameters for detailed design of a proposed landfill are recommended. The potential for liquefaction of the sludge due to earthquake shaking is investigated.

2.1 *New Zealand Steel Mill*

The NZ Steel Mill is located approximately 60 km Southeast of Auckland and is the only mill in the world to manufacture iron and steel from titanomagnetite iron sands. The iron sands are found along the western coast of New Zealand's North Island and are the remains of rocks which once formed the flanking volcanoes of Mount Taranaki (located about 250 km south of the mill). They are the largest reserves of metal ore in New Zealand.

2.2 *Waste streams*

As a result of the unique nature of the NZ Steel sand mining and iron/steel making processes, a number of waste streams are produced and landfilled onsite. These wastes include: wet sludge, slag, reduced primary concentrate and char (RPCC), ironbearing dusts and general works debris.

The sludge waste is a mixture of clay slimes that result from the slurry pumping operation and the byproducts of pollution control operations. It is generated at a rate of approximately 80,000m^3/year and forms approximately half of the waste deposited in the landfill. The sludge waste is a mud-like fine grained material with a solids content of 15 to 20% by weight when it is carted to the landfill. It is comprised of clay, coal ash, ironbearing dusts and carbon.

2.3 *Landfill history*

For over 20 years, the sludge (and other wastes) have been deposited into the existing West Landfill facility in a series of cells. A new East Landfill facility has recently been designed to replace the existing West Landfill which is nearing its capacity. The East Landfill has an expected life of 30 years and a final fill volume of 4.7 million m^3. It will accept approximately 160,000m^3/year of waste.

The materials to be stored in the East Landfill are the same materials that have been landfilled in the West Landfill. As this existing facility has been in operation since 1992, it offers an ideal means for testing and characterising the sludge materials in situ for the design of the new East Landfill.

3 SLUDGE CHARACTERISTICS

3.1 *Prior to landfilling*

Prior to landfilling, the clay slimes and black waste are deposited into separate settling ponds to reduce the moisture content to approximately 80% to 85%. The clay slimes and black waste are then landfilled into the cells, forming a sludge waste. The sludge typically exhibits no free water, but some decant water is produced during excavation from the settling ponds. When tipped into the landfill, the sludge exhibits a degree of run-out (approximately 30 to 80m), but drains and desiccates relatively quickly.

3.2 *Operation of Landfill Cells*

The landfills are formed in a series of cells. Each cell is constructed by first constructing a containment bund of the high strength granular RPCC waste and then placing the sludge material behind it. After a sludge depth of 2.4m is achieved within the cell, the sludge is allowed to dry and desiccate for periods of 8 to 12 weeks. The next "lift" of the cell is then carried out by constructing another 2.4m high bund of RPCC on top of the previous one, and continuing the filling process with sludge in the same way as before. Because each new bund is half on the old bund and half on the sludge, the overall crest of the cell tends to move generally up the valley and is commonly termed "upstream" construction.

3.3 *In situ sludge characteristics*

3.3.1 *General*

Once the sludge has been deposited into the landfill, it gains strength relatively quickly. The surfaces of the sludge cells rarely pond rainwater and testing has shown the sludge mass does drain and consolidate over time.

To investigate the nature of the sludge within the landfill, boreholes and cone penetration tests (CPTs) were drilled through three different completed cells. Locations were chosen to represent the characteristics of both older and younger sludge materials. A variety of tests were completed in situ and on tube samples. The sludge was found to have the following typical properties:

- Bulk density: 1.4t/m^3
- Undrained shear strength (after initial settling, desiccation and consolidation): 30kPa and increasing to greater than 100kPa at depth
- Liquid limit (LL): 60% to 100%
- Plasticity index (PI): 10 to 53
- Effective angle of internal friction: 36° – 39°

3.3.2 *Shear strength*

The in situ undrained shear strength (s_u) was assessed using Geonor vane, hand-held vane, CPT and triaxial CUP tests and short term stability back analyses. The resultant shear strength data from all approaches is summarized in a single plot in Figure 1. Discussion about each method follows.

Geonor Vane: This is the most direct in situ test method and is given the highest weighting. Results show a clear indication of strength increase with depth.

Hand-held Vane: Measurements were taken with a small blade vane at the end of the open borehole barrel. Results show significantly lower values than the Geonor vane and triaxial CUP data and a generally slightly decreasing trend with depth. Such trends indicate a strong influence of sample disturbance and this data should therefore be disregarded.

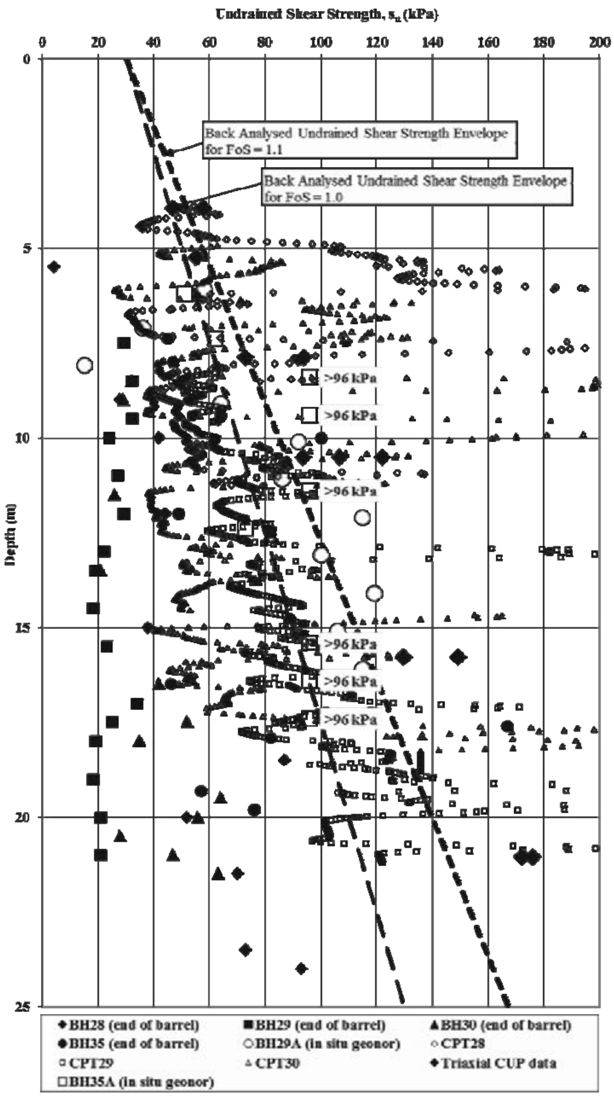

Figure 1. Undrained shear strength of sludge material with depth

CPT: A method of deriving the undrained shear strength from CPT data is given by Lunne, Robertson & Powell (1997). The data show a clear trend of increasing strength with depth and also, by comparing the different test locations, a clear indication of strength increase with the length of time the sludge has been in place.

Triaxial Tests: The consolidated undrained triaxial tests with pore pressure measurement (CUP tests) give a measure of undrained strength (s_u) with consolidation pressure (p´) and also a s_u/p´ relationship. This relationship gives an indication of the expected increase in strength with depth after full consolidation. The CUP data depth plotted on Figure 1 is based on the effective consolidation stress applied to the sample for each test, to represent a comparable overburden stress.

Back analysis: Based on historical annual survey data, the maximum free-standing slope face height for an operating cell was 24.5m with a slope of 1.2H: 1V. A back-analysis of this maximum free standing slope has been carried out using equilibrium software (Slope/W). An undrained shear strength profile for the sludge material of 30kPa at the surface, increasing at 4kPa per meter with depth is required for a safety factor of unity. Similarly, an undrained shear strength profile for the sludge material of 30kPa at the surface, increasing at 5.5kPa per meter with depth is required for a safety factor of 1.1.

Bund failure has never occurred at the site. Therefore, it can be inferred that the undrained shear strength of the sludge material is higher than the back-analysed undrained shear strength envelope (assuming a safety factor of unity). The back-analysed shear strength envelopes (refer Figure 1) show that the Geonor vane and triaxial undrained shear strength data closely fit the back analysed shear strength envelope for a safety factor of 1.1 and is therefore more representative of the sludge undrained shear strength characteristics.

3.3.3 *Pore pressure monitoring*

Six pore water pressure transducers were installed in two boreholes at various depths below the ground surface. Pore water pressures were measured over a period of one month.

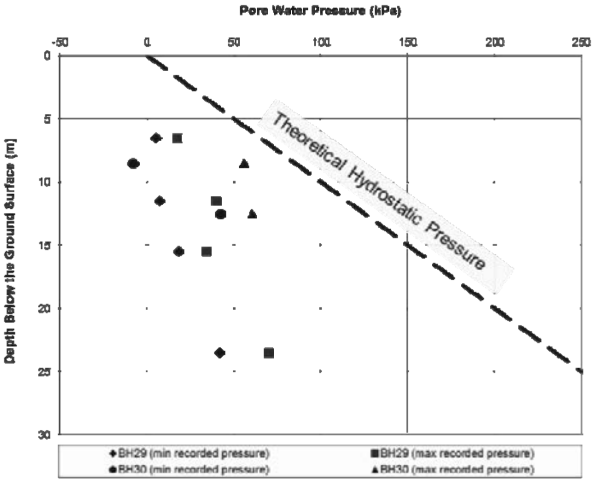

Figure 2. Pore water pressure distribution in sludge with depth

The sludge pore water pressure monitoring results are presented in Figure 2. The maximum and minimum ground water pressures measured by the transducers are presented as a function of depth below the ground surface. The results indicate that the pore water pressures in the sludge material range from 10kPa to 60kPa and are significantly lower than the theoretical pore water pressures for hydrostatic conditions with the water table at the ground surface. These results demonstrate the sludge mass is able to dry out and desiccate prior to subsequent placement of the above sludge layers and that the sludge mass is able to drain within the landfill cells.

4 LIQUEFACTION

The assessment of liquefaction potential of the sludge waste has been approached using CPT data and Atterberg Limits.

4.1 *CPT-based liquefaction assessment*

Liquefaction analyses using the CPT data have been undertaken using the assessment methods developed from the 1998 NCEER/NSF Workshop, supplemented and updated with the more recent recommendations for liquefaction assessment including the works of Zhang et al. (2002), Cetin et al. (2004), Moss et al (2006a), and Moss et al. (2006b).

The CPT data show that the sludge materials are very cohesive (i.e. they have Ic values greater than 2.6) and therefore, in theory, are not susceptible to liquefaction. The calculated liquefaction factor of safety (derived from $CRR_{7.5}$) for the majority of the CPT data was above 1.0 for a peak ground acceleration of 0.17g (10% probability of exceedance for a 30 year period).

4.2 *Liquefaction Susceptibility using Atterberg limits*

Over the past few decades it has been assumed that fine-grained soils (silts and clays) do not liquefy. Recent research has shown that, under some circumstances, fine grained soils (such as sludge) may be susceptible to liquefaction and there have been various suggested criteria for defining the limits.

Seed et al. (2003) recommended an area on the Casagrande Plasticity Chart within which soils should be classified as "potentially liquefiable". Out of nine, eight results are all well outside the potentially liquefiable region. Therefore the waste mass as a whole is not susceptible to liquefaction according to these criteria. Some small pockets or zones may be more susceptible than others, but will not govern the behaviour of the overall material mass.

Bray & Sancio (2006) suggested criteria based on PI and the ratio of natural water content to the liquid limit (w/LL). Again, only one result out of nine plots within the "Susceptible" region.

Boulanger & Idriss (2006) suggested that materials can be expected to exhibit clay-like behaviour (i.e. non liquefiable) if they have PI value of greater than 7 and that fine-grained soils with PI values less than 7 should be considered as potentially exhibiting "sand-like" behaviour (i.e. liquefiable). The PI data for the sludge range from 10 to 53 and fall into the "clay-like" category, indicating the material is not susceptible to liquefaction.

4.3 *Liquefaction conclusion*

It is concluded that the landfill materials are not susceptible to liquefaction under any credible level of shaking. In addition to this, however, it should be noted that the level of shaking under operating conditions (10% probability of exceedance in 5 years) is only 0.06g, and this is unlikely to exceed the strain threshold for liquefaction to occur for any type of material, except very loose sands.

In the long term the final landfill geometry will have a maximum slope of 5H: 1V and will be made up of consolidated sludge in many separated cells with numerous effective RPCC "chimney drains" extending up full-height through the fill. Even if liquefaction could occur, it would be localised and confined within the cells, with little risk of significant displacement.

5 DESIGN

Based on in situ and laboratory testing at the West Landfill, the sludge design parameters that have been selected for the cell design of the East Landfill are summarised in Table 1.

A seismic reduction factor was adopted for the sludge shear strength envelope to account for potential cyclic strain softening that may occur within the sludge during seismic loading. For a 7.5 magnitude earthquake, Boulanger and Idriss (2007) recommend a ratio of cyclic undrained to static strength for natural clays/silts is 0.8. Therefore the static strength was reduced by 20%.

Table 1. Sludge design parameters used for design of East Landfill

Test Method	Undrained	Drained	
	s_u (kPa)	c' (kPa)	ϕ' (deg)
Back Analysis (FOS=1.1)	30+5.5z[1]	0	35
Triaxial (CUP)	N/A	0	36-39
Geonor vane	15 to 120 with depth	N/A	N/A
CPT	25 to > 200 with depth	N/A	N/A
Design (static)	0 (for z < 2.5m depth) 30 + 4z (for z > 2.5m depth)	0	0 (for z<2.5m depth) 32 (for z>2.5m depth)
Design (seismic)	0 (z<2.5m depth) 24+3.2z (z>2.5mdepth)	0	27

[1] Most likely lower bound, assuming a factor of safety of 1.1

6 CONCLUSIONS

The design of a new landfill has been based on the properties and performance of an existing landfill that has been operating for 20 years. The landfills are operated in cells, with facing bunds retaining sludge, constructed in lifts using “upstream” construction. The characteristics of the sludge in situ are governed both by the nature of the material and the operation procedures. Key to the process is the limited height of each lift, together with the period of desiccation between lifts.

To investigate the properties of the sludge for design input, boreholes and CPT’s were put down through completed landfill cells of different ages. The tests showed the in situ sludge to have significant strength increase with time and depth, with pore pressures well below hydrostatic conditions. The need to check liquefaction potential is self-evident. The sludge was assessed to be non-liquefiable by a number of methods.

7 ACKNOWLEDGEMENTS

The authors thank New Zealand Steel Ltd. for their permission to publish this paper.

8 REFERENCES

Boulanger, R.W. & Idriss, I.M. 2006. Liquefaction susceptibility criteria for silts and clays. *ASCE Journ. Of Geotech. and Geoenv. Eng*., Vol. 132, No. 11, November.

Boulanger, R., and Idriss, I. M. 2007. Evaluation of Cyclic Softening in Silts and Clays. *Journal of Geotechnical and Geoenvironmental Engineering*, 133:6, 641-652.

Bray, J.D. and Sancio, R.B. 2006. Assessment of the liquefaction susceptibility of fine-grained soils. *Journal of Geotechnical and Geoenvironmental Engineering*, ASCE, July 2008, Vol. 134, No. 7, pp. 1031-1034.

Cetin, K. O., Seed, R. B., Der Kiureghian, A., Tokimatsu, K., Harder, L. F., Kayen, R. E., and, Moss, R. E. S. 2004. Standard Penetration Test-Based Probabilistic and Deterministic Assessment of Seismic Soil Liquefaction Potential. *Journal of Geotechnical and Geoenvironmental Engineering,* 130, 1314-1340.

Lunne, T., Robertson, P.K. and Powell, J.J.M. 1997. *Cone Penetration Testing*. Spon Press, London.

Moss, R. E. S., Seed, R.B., and, Olsen, R. S. 2006a. Normalizing the CPT for Overburden Stress. *Journal of Geotechnical and Geoenvironmental Engineering*, 132, 378-387.

Moss, R. E. S., Seed, R.B., Kayen, R. E., Stewart, J. P., Der Kiureghian, A., and, Cetin, K.O. 2006b. CPT-Based Probabilistic and Deterministic Assessment of In-Situ Seismic Soil Liquefaction Potential. *Journal of Geotechnical and Geoenvironmental Engineering*, 132, 1032-1051.

Seed, R.B., Cetin, K.O., Moss, R.E.S., Kramer, A., Wu, J., Pestana, J., Riemer, M., Sancio, R.B., Bray, J.D., Kayen, R.E. and Faris, A. 2003. Recent advances in soil liquefaction engineering: A unified and consistent framework. Keynote presentation, *26th Annual ASCE Los Angeles Geotechnical Spring Seminar*, Long Beach, California.

Zhang, G., Robertson, P.K., and Brachman, R. W. I. 2002. Estimating Liquefaction-Induced Ground Settlements from CPT for Level Ground. *Canadian Geotechnical Journal. 39*, 1168-1180.

A numerical analysis of phytoextraction processes

Une analyse numérique des processus de phyto-extraction

Lugli F., Mahler C.F.
COPPE/UFRJ, Rio de Janeiro, RJ, Brasil

ABSTRACT: Phytoextraction is an in situ remediation technique involving the uptake of contaminants by plant roots and their subsequent accumulation in plant tissues. Despite its many advantages, phytoextraction is not widely used because of difficulties in estimating its efficiency and the required remediation time. The objective of our research was to numerically evaluate the effectiveness of phytoremediation of Pb^{2+} and Zn^{2+} using a previously calibrated Hydrus-1D software package. The simulations considered soil and climatological data representative of the coastal lowlands of the municipality of Rio de Janeiro in Brazil and were organized in three steps: pre-contamination (analysis of the hydrological conditions), contamination (analysis of the contamination plume before planting) and remediation. Several conditions were tested, including different root depth and irrigation schemes. Although the results are specific for the assumed scenarios, it was possible to identify several trends in the simulations. While more elaborate calibrations may be needed using long-term field data, the numerical analysis provided useful insight into the phytoextraction process important for the design of future experiments.

RÉSUMÉ : La phyto-extraction est une technique de dépollution in situ basée sur l'absorption de contaminants par les racines des plantes puis de leur accumulation dans les tissus végétaux. Malgré ses nombreux avantages, la phyto-extraction est peu utilisée en raison de la difficulté à estimer son efficacité et la durée de traitement qu'elle implique. L'objectif de notre étude était d'évaluer numériquement l'efficacité de la phyto-extraction du Pb^{2+} et du Zn^{2+} à l'aide d'un logiciel préalablement étalonné Hydrus-1D. Les simulations ont pris en compte pour le sol et la climatologie des données représentatives de la plaine côtière de la municipalité de Rio de Janeiro au Brésil et ont été organisées en trois étapes : la pré-contamination (analyse des conditions hydrologiques), la contamination (analyse du panache de contamination avant le semis) et la dépollution. Plusieurs conditions ont été testées, en particulier diverses profondeurs des racines et différents systèmes d'irrigation. Bien que les résultats soient spécifiques aux scénarios pris en compte, il a été possible d'identifier plusieurs tendances dans les prédictions. Si des étalonnages plus élaborés peuvent être nécessaires en utilisant des données de terrain à long terme, l'analyse numérique fourni des indications utiles sur le processus de phyto-extraction qui sont importantes à prendre en compte pour la conception des expériences futures.

KEYWORDS: contaminant transport, plant solute uptake, irrigation, root density.

1 INTRODUCTION

Phyto-extraction is a remediation technique based on contaminant uptake by plant roots. Pollutants are generally accumulated in plant tissues. Plant based remediation processes are currently used for many classes of contaminants, including hydrocarbons, pesticides, explosives, metals, radionuclides, chlorinated solvents, and waste landfill leachate. These techniques can be complementary or alternative to chemical and mechanical treatments. Their applicability depends basically on the resistance of the plant to contaminants. In addition, the efficiency of the process depends strongly on the site characteristics such as soil, climate, hydrology and soil-contaminant interactions. Due to this variability, it is difficult to estimate the cost and the time necessary for a phytoremediation project. Some studies (ITRC, 2009; Truong et al., 2010) show that the costs due to installation, instruments and labor can be significantly lower compared to other techniques.

The present research was focused on numerical modeling of soil-plant-atmosphere continuum, proposing a method for the calculation of:

1. time required for remediation (according to Brazilian Law),
2. efficiency, defined as the ratio between contaminant mass withdrawn from the soil and contaminant mass previously leached into the soil.

The software Hydrus-1D (Šimůnek et al., 2009) was applied to scenarios of contamination by Pb^{2+} and Zn^{2+} chosen for their different reactivity with the soil solid phase. The remediation was carried by Vetiver grass (*Chrysopogon zizanioides*). Soil and climate data were relative to an industrial area of the municipality of Rio de Janeiro. The model parameters, relative to the crop, were determined and calibrated in a previous study, based on greenhouse experiment (Lugli et al., 2011).

2 MATERIALS AND METHODS

2.1 *Numerical Model*

The *Hydrus-1D* code uses linear finite element method of *Galerkin* type for spatial discretization and finite difference method for time discretization of the Richards equation (variably saturated flows). For solute transport, *Hydrus-1D* is based on the resolution of the advection-dispersion equation by finite elements (Šimůnek et al., 2009).

The main hypotheses of this study were:

1. one-dimensional approach,
2. absence of preferential flow paths,
3. invariance of the potential root contaminant uptake,
4. remediation process based only on direct extraction of the contaminant,
5. absence of growth, senescence, intoxication phenomena,
6. contaminants are considered separately.

2.1.1 *Water uptake model*

Water uptake was calculated by *Hydrus-1D*, through a macroscopic approach determining the sink term in *Richards equation* (Feddes et al., 1978; Vogel, 1988). In this study water stress was considered according to Feddes' formulation (Feddes et al., 1978).

The root water uptake was calculated directly by *Hydrus* code, through a macroscopic approach determining the sink term in the Richards equation. This term, s [T^{-1}], was calculated from the equation

$$s(h,h_\phi,x,t) = \alpha(h,h_\phi,x,t)\, b(x,t)\, T_p(t) \qquad (1)$$

where $T_p(t)$ [LT^{-1}] was the normalized root distribution [L^{-1}], a function of space and time (in the case of root growth). The function α [-] represented the response to plant stress ($0 \le \alpha \le 1$), by varying the hydraulic and osmotic head.

2.1.2 *Contaminant uptake model*

Roots contaminant uptake, when present, was calculated with models defined as passive and active. The first assume that the solute uptake is locally proportional to root water uptake and the concentration of the solute dissolved in water:

$$p(x,t) = s(x,t)\, c(x,t) \qquad (2)$$

The active root solute uptake $a(x,t)$ [$ML^{-3}T^{-1}$] was calculated using *Michaelis-Ment*en kinetics (Jungk, 2002). The theoretical maximum uptake value was called as potential active solute uptake $A_p(t)$ [$ML^{-2}T^{-1}$], characteristic of the pair plant-solute and function of time (Šimůnek and Hopmans, 2009).

$$a(x,t) = \frac{c(x,t)}{K_m + c(x,t)}\, b(x,t) A_p(t) \qquad (3)$$

K_m was defined as *Michaelis-Menten constant* [ML^{-3}]. Applied values were K_m = 1,32 μg/cm^3 and A_p = 0,4757 μg·cm^{-2}/day for Pb^{2+}.

2.1.3 *Soil*

The soil analyzed is a *Halpic Gleysol*. In the simulations only the unsaturated zone was modeled. The water table was assumed to have a fixed depth (90 cm). Two horizons were considered: *A*, clay and *C*, sandy clay loam. The parameters of *van Genuchten - Mualem hydraulic model* (van Genuchten, 1980) were estimated for each horizon using pedotransfert functions proposed by Tomasella et al. (2003).

Table 1. Hydraulic parameters of the *van Genuchten - Mualem model* (van Genuchten, 1980) relative to Halpic Gleysol

horizon	θ_r [cm^3/cm^3]	θ_s [cm^3/cm^3]	α [cm^{-1}]	n [-]	K_s [cm/day]
A	0.1555	0.5688	0.0654	1.1910	61.66
C	0.0900	0.4265	0.0450	1.3154	68.02

2.1.4 *Boundary conditions*

The top boundary conditions were imposed using daily values of precipitation, potential evaporation and transpiration. The reference evapotranspiration was determined using the equation of *Penman-Monteith* (Allen et al., 1989; Allen et al., 1998).

Pressure head h was considered constant and equal to zero at the bottom of the profile.

2.1.5 *Soil-contaminant interaction*

Ion sorption in soil solid phase was considered using a linear model for both horizons. The distribution coefficients (K_d) were inferred from a study (Soares, 2004) about tropical soils with similar characteristics, using 1500 cm^3/g and 70 cm^3/g, respectively, for Pb^{2+} and Zn^{2+}. Standard values for the diffusion coefficients in free water were applied (Shackelford and Daniel, 1991).

2.1.6 *Simulation phases*

The numerical simulations were organized in three phases: pre-contamination, contamination and remediation. The first phase (one year) was necessary to fix average pressure head profile. The presence of shrubby vegetation was included in the top *BC*.

During the contamination phase, the presence of containers, leaching metal ions in presence of rain, was simulated. It was also estimated that the vegetation suffered degradation due to toxicity of the contaminants. Therefore, transpiration values were considered equivalent to 20% of the reference. In this phase, no contaminant uptake was considered. The simulated period was of five years.

For remediating the soil, original vegetation was substituted by *Chrysopogon zizanioides*. According to the experimental study by Tavares (2009), this variety doesn't suffer any toxicity effect at considered concentrations. The *Feddes´* parameters where estimated by analogy with similar plants from *Poaceae* family (Wesseling, 1991). The solute uptake model selection and the determination of the relative parameters were performed in Lugli (2011). An active model was used for Pb^{2+} and a passive model for Zn^{2+}. The process was considered complete when the soil concentration of each contaminants would be punctually lower than the Brazilian standard values for industrial areas (CONAMA, 2009) respectively 900 mg/kg and 2000 mg/kg for Pb^{2+} and Zn^{2+} .

2.2 *Previous studies*

Lugli and Mahler (2012) showed that, by increasing the fraction of contaminant sorbed on the solid phase, the phyto-extraction process became less effective. No relevant consequences were observed in the remediation of Pb^{2+}. For contaminants characterized by low retardation factors (e.g. Zn^{2+}), the remediation process resulted more efficient.

Moreover, water stress partially inhibited contaminant uptake, but prevented plume migration towards water table. The results also showed that phyto-extraction process becomes more efficient by increasing the amount of transpiration at the expense of the portion of evaporation (e.g. increased crop density).

In the present study, some results form Lugli and Mahler (2012) were revisited analyzing the influence of root depth. The focus was to study if an engineered choice of plant species in terms of root distribution could promote (or not) an improvement in remediation process. For both Pb^{2+} and Zn^{2+} three different root models were analyzed and compared with the reference (root depth = 40 cm). All of them where static and linear interpolated with the lowest value corresponding to zero; the depth was determined multiplying the plume depth for each contaminant by 2/3, 1 and 1.5.

3 RESULTS AND DISCUSSION

3.1 *Influence of root distribution*

3.1.1 *Lead Ion*

In the case of lead ion (high retardation factor) it is known that the remediation process is not efficient (Lugli and Mahler, 2012).

Modified roots caused the remediation time to exceed 120 months (test 2, 3 and 4 in Table 2). This happens because the plume is substantially blocked due to the hydraulic conditions (Figure 1). According to the Brazilian Law, this result is not favorable. Despite of this, root modification implied an increase in the amount of contaminant extracted in comparison with the reference (test 1 in Table 2), This, together with the smaller mobilization of the plume, can be evaluated as an improvement from the environmental point of view. It could be identified that the most favorable configuration corresponded to a root depth of 3.5 cm: this value is less than the initial plume depth (5 cm).

Table 2. Transport and Pb^{2+} uptake with different root distributions

test	Ion	Root max depth	remediation time [months]	contaminant extracted/initial	plume depth [cm]
1	Pb^{2+}	40	90	1.68%	12.23
2	Pb^{2+}	7	>120	1.74%	6.34
3	Pb^{2+}	5	>120	6.43%	7.04
4	Pb^{2+}	3.5	>120	6.95%	7.16

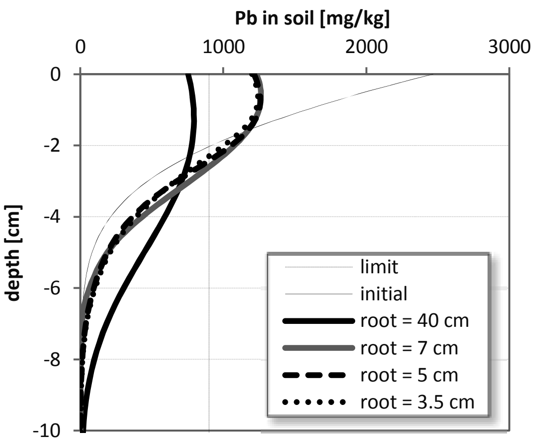

Figure 1: Pb^{2+} plumes: initial and after 10 years of remediation with different root depth

3.1.2 *Zinc Ion*

The same improvement observed in the previous paragraph for lead ion was present also for a more mobile ion such as zinc (Table 3). In this case all the indicators of remediation process register a favorable trend: remediation time, amount of contaminant extracted and plume depth. Differently from the previous case, the reduction of the concentration values took place in all the rizosphere (Figure 2). The most favorable configuration, also for Zn^{2+}, corresponded to a root depth lower than the initial plume depth (23 cm).

Table 3. Transport and Zn^{2+} uptake with different root distributions

test	Ion	Root max depth	remediation time [months]	contaminant extracted/initial	plume depth [cm]
5	Zn^{2+}	40	48	41.6%	35.87
6	Zn^{2+}	34,5	48	42.7%	36.09
7	Zn^{2+}	23	46	42.7%	35.76
8	Zn^{2+}	15	42	46.6%	35.65

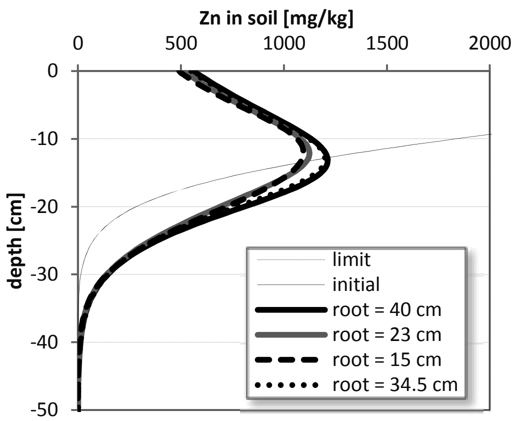

Figure 2: Zn^{2+} plumes: initial and after 10 years of remediation with different root depth

3.2 *Influence of water balance*

The object of this paragraph was to verify if the effects due to the addition of irrigation (Lugli and Mahler, 2012), persisted in the case of the optimized root depth. These effects were mainly:

- enhanced contaminant extraction,
- displacement of the contaminant plume downwards.

In Table 4 and Figure 3 it could be notice that both effects are present also in the case of the reduction of root depth.

Table 4. Transport and Zn^{2+} uptake with different root distributions and presence of irrigation

test	Ion	irrigation	Root max depth	remediation time [months]	contaminant extracted/initial	plume depth [cm]
5	Zn^{2+}	0	40	48	41.6%	35.87
8	Zn^{2+}	0	15	42	46.6%	35.65
9	Zn^{2+}	330 mm/year	40	42	42.8%	36.60
10	Zn^{2+}	330 mm/year	15	36	48.2%	38.29

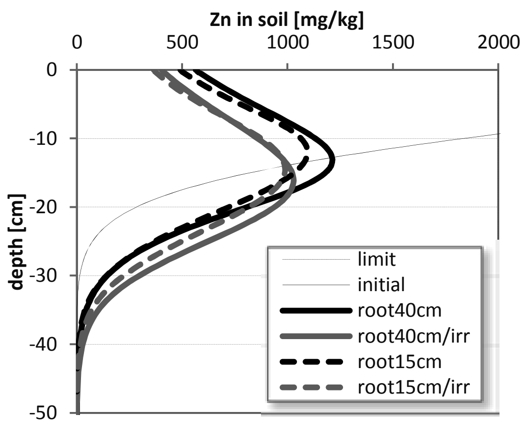

Figure 3: Zn^{2+} plumes: initial and after 10 years of remediation with different root depth and presence of irrigation

4 CONCLUSION

The present study examined an example of optimization of a phyto-extraction process in the presence of metal ions, based on numerical modeling. According to the assumptions related to the model and the analyzed scenarios, it was highlighted that, by modifying root depth and introducing irrigation, the phyto-extraction process could be optimized for contaminants characterized by low (e.g. Zn^{2+}), and high (e.g. Pb^{2+}) retardation factors. Moreover, both cases studied evinced better performances for root distribution shallower than plume contamination.

As a general consideration, the proposed methodology provided important data for the design and evaluation of a phyto-extraction process.

5 ACKNOWLEDGEMENTS

The authors would like to thank the Institutions of the Brazilian Government CAPES and CNPq for the scholarships, and FAPERJ, for the constant support on research.

6 REFERENCES

Allen R.G., Jensen M.E., Wright J.L., Burman R.D. 1989. Operational estimates of reference evapotranspiration. American Society of Agronomy. Madison, WI, USA.

Allen R.G., Pereira L.S., Raes D., Smith M. 1998. Crop evapotranspiration: guidelines for computing crop water requirements. FAO Irrigation and Drainage Papers. Food and Agriculture Organization of the United Nations. Rome, Italy.

CONAMA 2009. Resolução no 420. Publicação DOU nº 249, do 30/12/2009.

Feddes R.A., Zaradny H.K., Kowalik P.J. 1978. Simulation of Field Water Use and Crop Yield. John Wiley & Sons Inc. New York, NY, USA.

ITRC 2009. Phytotechnology Technical and Regulatory Guidance and Decision Trees, Revised, PHYTO-3. Interstate Technology & Regulatory Council, Phytotechnologies Team, Tech Reg Update. Washington, D.C.

Jungk A.O. 2002. Dynamics of nutrient movement at the soil-root interface. in Plant roots: The Hidden Half. Marcel Dekker, Inc. New York. 587-616.

Lugli F. 2011. Numerical Modeling of Phytoremediation Processes of Soils. M.Sc. Thesis. Civil Engineering Department. COPPE / Federal University of Rio de Janeiro. Rio de Janeiro.

Lugli F. and Mahler C.F. 2012. Modeling vadose zone contaminant transport and root solute uptake in a phyto-extraction processes. 10th World Congress On Computational Mechanics. São Paulo.

Lugli F., van Genuchten M.T., Mahler C.F. 2011. Phytoremediation: Simultaneous calibration of contaminant soil sorption and plant uptake. SETAC Europe 21st Annual Meeting. Milan.

Shackelford C.D. and Daniel D.E. 1991. Diffusion in Saturated Soil .1. Background. J Geotech Eng-Asce. Vol. 117, 467-484.

Šimůnek J. and Hopmans J.W. 2009. Modeling compensated root water and nutrient uptake. Ecological Modelling. Vol. 220, 505-521.

Šimůnek J., Šejna M., Saito H., Sakai M., van Genuchten M.T. 2009. The HYDRUS-1D Package for Simulating the Movement of Water, Heat, and Multiple Solutes in Variably Saturated Media, Version 4.08. Department of Environmental Sciences, University of California. Riverside, California, USA.

Soares M.R. 2004. Distribution Coefficient (Kd) Of Heavy Metals In Soils Of The State Of São Paulo. PhD Thesis. Agronomy Department. Agriculture School "Luiz de Queiroz" / USP. Piracicaba, São Paulo.

Tavares S.R.d.L. 2009. Phytoremediation of Soil and Water in Areas Contaminated by Heavy Metals from the Provision of Hazardous Waste. PhD Thesis. Civil Engineering Department. COPPE / Federal University of Rio de Janeiro. Rio de Janeiro.

Tomasella J., Pachepsky Y., Crestana S., Rawls W.J. 2003. Comparison of two techniques to develop pedotransfer functions for water retention. Soil Sci Soc Am J. Vol. 67, 1085-1092.

Truong P.N.V., Foong Y., Guthrie M., Hung Y.-T. 2010. Phytoremediation of Heavy Metal Contaminated Soils and Water Using Vetiver Grass. in Environmental Bioengineering. Humana Press. 233-275.

van Genuchten M.T. 1980. A Closed-Form Equation for Predicting the Hydraulic Conductivity of Unsaturated Soils. Soil Sci Soc Am J. Vol. 44, 892-898.

Vogel T. 1988. SWMII-Numerical model of two-dimensional flow in a variably saturated porous medium. Research report nr. 87. Vakgroep Hydraulica en Afvoerhydrologie. LUW (1988) 120 pp.

Wesseling J.G. 1991. Meerjarige simulatie van grondwaterstroming voor verschillende bodemprofielen, grondwatertrappen en gewassen met het model SWATRE. DLO-Staring Centrum. Wageningen.

Soil-geosynthetic interface strength on smooth and texturized geomembranes under different test conditions

Résistance au cisaillement des interfaces entre sols et membranes géo-synthétiques lisses ou rugueuses sous différentes conditions

Monteiro C.B., Araújo G.L.S., Palmeira E.M., Cordão Neto M.P.
Department of Civil and Environmental Engineering, FT, University of Brasilia,70910-900, Brasilia, DF, Brazil

ABSTRACT: Potential ground contamination from landfills justifies the use of sub-systems such as soil and geosynthetic layers as barriers at the landfill bottom and slopes. In configurations of barrier systems, geomembranes have often been used. For this type of application, the mechanisms of interaction between soil and geomembrane must be properly understood and failures along soil-geomembrane interfaces in slopes have been observed. This paper presents experimental results of shear strength mobilization along soil-geomembrane interfaces for different types of geomembranes and degrees of saturation of the underlying soils. Direct shear and ramp tests were used in this study. The results showed a little or no increase on values of interface friction angles with increasing degree of saturation of the soil. The highest values for interface shear strength were obtained for the texturized HDPE geomembrane.

RÉSUMÉ: Le potentiel de contamination des décharges sanitaires justifie l´utilisation de techniques d'imperméabilisation sur les fonds et les talus latéraux, tels que des couches de sols et des membranes géo-synthétiques. Pour ces systèmes d'imperméabilisation, on a souvent eut recours à des géo-membranes comme matériau imperméabilisant de protection. Pour ce type d'application, les mécanismes d´interaction entre le sol et la géo-membrane sont encore peu connus, la rupture le long de ces interfaces a été observée sur des talus par des phénomènes de glissement du sol sous la géo-membrane. Cet article présente des résultats expérimentaux de mobilisation de la résistance au cisaillement pour des interfaces sol/géo-membrane, pour différents types de géo-membranes et différents degrés de saturation des sols. Ces résultats montrent une augmentation légère voire nulle des valeurs d'angle de frottement des interfaces avec l´augmentation du degré de saturation des sols. Les valeurs de résistance au cisaillement les plus élevées ont été obtenues pour des géo-membranes en polyéthylène haute densité (PEHD) présentant une texture.

KEYWORDS: Interface strengh, geosynthetics, landfill, geomembranes.

1 INTRODUCTION

Geomembranes are often used as landfills barriers aiming at avoiding contamination of underneath soils or ground water. Some projects using these systems have a soil layer above the synthetic materials. Sometimes this soil layer is executed with sand for leachate drainage. Interaction between soil-geomembrane in landfills slopes still need a better understanding. Improper evaluation of soil-geosynthetic interation parameters for this kind of construction has yielded to slope failures along that interface (Dwyer *et al.* 2002, Gross *et al.* 2002, Palmeira 2009, for instance).

Shear strength interfaces studies of different kinds of materials can be found in the literature (Fleming *et al.* 2006 and Khoury *et al.* 2011, for instance). An increasing number of studies on soil-geosynthetic interface strength has been observed due to the risk of failures along these interfaces.

Failures due to soil sliding on a geomembrane in slopes under low stress levels can be more accurately modelled using ramp tests (inclined plane tests). Conventional direct shear tests sometimes is a adopted for this type of study, but some studies have demonstrated that for low values of normal stresses (typical in barrier systems of landfills), this kind of test may overestimate interface shear strength interface parameters (Girard et al. 1990, Giroud et al. 1990 and Gourc et al. 1996, for instance).

Some aspects related to soil-geosynthetic interface strength still need to be properly understood. With this regard, it might could be expected that soil moisture content may influence the interface strength parameters. Soil moisture content can increase due to saturation by leachate or due to infiltration of rain water.

This paper presents and discusses results from ramp and conventional direct shear tests on differents kinds of soil-geomembrane interfaces with varying soil degree of saturation.

1.1 *Parameters and interface shear strength*

Nowadays there are some studies about interface shear strength parameters using ramp tests, with several of them having addressed the use of GCL´s as lining materials. Briançon *et al.* (2002) verified that for six types of interfaces between geosynthetics and geocomposites, the effect of increasing GLC bentonite moisture content can reduce friction angles between 20 and 40%. Viana (2007) evaluated interface shear strength between soil and GCLs and found reductions of up to 43.5% on the interface friction angle.

Mello (2001) highlights the importance of studies on the influence of unsaturated soil conditions on displacements stabilization and mobilized loads in the geosynthetic layer with time. According to the author even after 120 hours using the same inclination, it was not observed reduction of the adhesion component or system failure. Besides, during this time the displacements of the sample and the transferred loads to the geosynthetic remained the same value.

Interface parameters between soils and geosynthetics are usually evaluated using Mohr-Coulomb failure criteria (Lima Júnior 2000, Mello 2001, Aguiar 2003 and Viana 2007 - see Eq. 1):

$$\tau = \alpha + \sigma.\tan\delta \tag{1}$$

Where:
α = Adesion;
σ = Normal stress;
δ = Interface friction angle.

2 MATERIALS AND METHODOLOGY

Works in the literature have shown that conventional direct shear tests under low normal stresses levels can overestimate the values of interface friction angle (Girard *et al.* 1994, Izgin and Wasti 1998, Koutsourais *et al.* 1998, Lopes 2001, Rebelo 2003). Because of this limitation ramp tests have been increasingly used. ISO 12957-2 (2005) normalizes the execution of this type of test.

In this work ramp and conventional direct shear tests for interface shear strength evaluation were carried out varying the soil degree of saturation between 5.5 and 66%.

The soil used in the tests had 12% of fines. Table 1 shows soil proprieties.

Table 1. Soil proprieties.

Propieties	Value
γ_s (kN/m^3)	2,63
γ_d (kN/m^3)	14,14
e_{max}	1,05
e_{min}	0,67
Relative Density (%)	50

The soil retention curve was estimated using Arya and Paris' model (1981), and is presented in Figure 1. PVC and HDPE (smooth and texturized) geomembranes were tested (See Table 2).

Table 2. Proprieties of geomembranes.

Propriety	PVC	Smooth HDPE	Textured HDPE
Thickness (mm)	1.0	1.0	1.0
Mass per unit area (g/m^2)	1.2-1.35	0.947	0.946
Maximum force at Failure (kN/m)	14	35.5	33

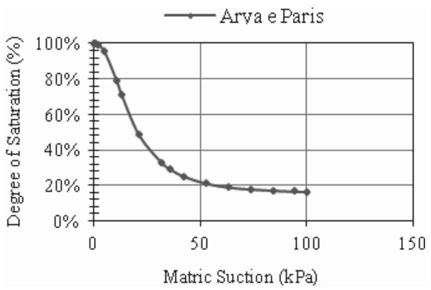

Figure 1. Estimated retention curve obtained from Arya and Paris (1981).

Seventy five ramp tests were performed where the following parameters were evaluated: interface friction angle (ϕ_{sg}); maximum relative soil displacements immediately before failure ($\delta_{máx}$) and mobilized tensile load in the geomembrane (F). In addition, 50 conventional direct shear tests were also carried out with the same soil and PVC and HDPE geomembranes.

The dimensions of the specimens and normal stresses in the ramp tests were equal to 51 cm x 51 cm and 1.2 kPa, 3.2 kPa and 7.2 kPa, respectively. These values were based on others studies and they aimed at simulating low confining pressures when only a thin cover soil (or drainage layer) is on the geomembrane in a slope of a waste disposal area.

(a) (b)

Figure 2. (a) Ramp test and (b) Conventional direct shear test.

Double layers of lubricated plastic films were used underneath the geomembrane specimen to reduce friction between the geomembrane and the ramp smooth metallic surface. This procedure was adopted to maximize the mobilization of tensile force in the geomembrane. The top extremity of the geomembrane specimen was fixed to the ramp structure by a clamping system connected to a load cell. This allowed the measurement of mobilized tensile forces in the geomembrane during the test. Figure 2 (a) presents a general view of one of the ramp tests performed.

For the conventional direct shear tests, the specimens had a plan area of 100 cm^2 (10 cm x 10 cm, Fig. 2b) and higher confining pressures were used, with values equal to 25 kPa, 55 kPa and 150 kPa.

3 RESULTS OBTAINED

3.1 *Interface friction angle*

Table 1 and Figure 3 present values of interface friction angles obtained from ramp and conventional direct shear tests for the range of degree of saturation tested. Mean and standard deviation values are also presented in Table 1.

The interface friction angles obtained were rather insensitive to changes in the soil saturation degree (S_r) for the interfaces tested. The variations of results can be considered to be within the expected scatter of results in this type of test. The standard deviation varied between 1.5^o and 3^o with large variations having occurred for the direct shear tests. The highest interface friction angle in the test with the texturized HDPE geomembrane was obtained for the highest value of degree of saturation. However, it was noticed that for higher values of S_r a certain amount of soil intruded between the soil box and the ramp, influencing the results to some extent. The same can be noticed for the test with the smooth PVC geomembrane.

A progressive failure mechanism was observed in the tests with the PVC geomembrane because of the extensible nature of this geomembrane. Figure 4 shows a view of the anchored extremity of the geomembrane specimen in one of the tests with the PVC geomembrane, where it can be seen that a greater amount of soil adhered to the geomembrane for the lower value of degree of saturation, probably due to the greater soil-geomembrane adhesion under low moisture content. The results of interface friction angle obtained in the on the smooth HDPE geomembrane were smaller than those obtained for the texturized geomembrane, as expected, and also insensitive to the variation of soil degree of saturation.

Table 1. Interface Friction angles obtained in ramp and direct shear tests.

S_r (%)	$\phi_{S\text{-}PVC\ S}$ (°)		$\phi_{S\text{-}HDPE\ S}$ (°)		$\phi_{S\text{-}HDPE\ T}$ (°)
	RT	DS	RT	DS	RT
5.5	29	30	26	27	32
10.8	30	30	28	29	33
15.7	30	31	27	27	34
20.3	30	32	29	32	30
26.3	31	33	29	31	36
45.1	31	33	30	31	37
58.4	30	33	27	29	36
66	34	39	27	31	39
Average (°)	30.6	32.6	27.9	29.6	34.6
Median (°)	30.5	33.0	29.0	33.0	33.0
Variance (°)	2.3	8.3	1.8	3.7	8.6
Standard Deviation (°)	1.5	2.9	1.4	1.9	2.9
Coefficient of variation (%)	4.9	8.8	4.9	6.5	8.4

DS: Direct shear tests
RT: Ramp tests
PVC S – Smooth PVC geomembrane
HDPE S – Smooth HDPE geomembrane
HDPE T – Texturised HDPE geomembrane
S_r – soil degree of saturation

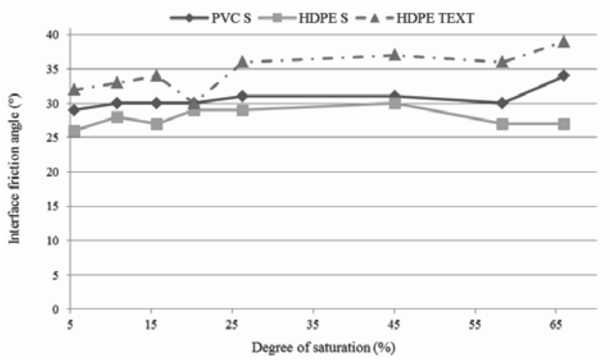

Figure 3. Interface friction angle (ϕ_{sg}) *versus* degree of saturation.

The higher values of interface friction angle were obtained in the tests on the texturized HDPE geomembrane. Figure 5 shows images of tests on the texturized HDPE geomembrane for different values of soil degree of saturation. Greater amount of soil adhered to the geomembrane for the lower value of degree of saturation as also observe in the test with the smooth PVC geomembrane.

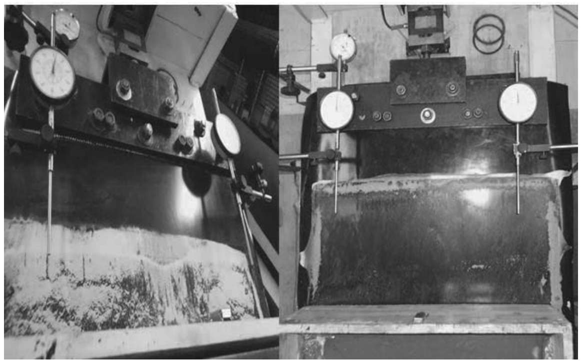

(a) (b)

Figure 4. Tests on smooth PVC geomembrane: (a) degree of saturation of 5.5% and (b) degree of saturation of 66%.

(a) (b)

Figure 5. Tests on texturized HDPE geomembrane: (a) degree of saturation of 5.5% and (b) degree of saturation of 66%.

3.2 *Additional parameters to interface shear strength*

Table 2 sumarizes results of maximum box displacements (δ_{max}) immediately before interface failure as well as mobilized tensile forces (F) in the geomembrane. Some increase on δ_{max} with soil degree of saturation can be noted for the tests with the PVC geomembrane.

Table 2. Maximum box displacements and mobilised force in the geomembranes obtained in ramp tests.

S_r (%)	PVC L		PEAD L		PEAD T	
	δh_{max} (mm)	F (kN/m)	δh_{max} (mm)	F (kN/m)	δh_{max} (mm)	F (kN/m)
5.5	39.2	0.61	70	1	70.3	1
10.8	43.7	0.6	68.6	0.9	67.5	1
15.7	51.7	0.6	71.5	0.8	72	1.3
20.3	51.2	0.7	82.4	1.1	74.4	1
26.3	54.58	0.52	67.66	0.8	73	1.2
45.1	49.7	0.5	73.7	0.8	69.6	1.3
58.4	45	2	71.54	1.2	47.5	1.5
66	43.9	0.9	73.36	0.8	69.2	1.1
Average	47.4	0.8	72.3	0.9	67.9	1.2
Median	52.89	0.61	75.0	1.0	73.7	1.1
Variance	27.0	0.2	21.0	0.0	73.1	0.0
Standard Deviation	5.2	0.5	4.6	0.2	8.6	0.2
Coefficient of variation (%)	11.0	62.1	6.3	17.1	12.6	15.6

For the HDPE geomembranes δ_{max} was rather insensitive to the variation of degree of saturation. The mobilized tensile force in the geomembrane was also insensitive to the variation of soil degree of saturation, with some higher values for some tests, but without allowing a conclusion on the influence of moisture content on the value obtained (probably a result of test scatter).

The highest values of F were obtained in the tests with the texturized HDPE geomembrane, whereas the lowest ones were obtained in the tests with the smooth PVC geomembrane. The smallest values of δ_{max} were also obtained in the tests with the smooth PVC geomembrane.

4 CONCLUSIONS

This paper presented results of ramp and direct shear tests on different geomembrane products in contact with a sandy soil. The degree of saturation of the soil was varied during the test to assess possible influence of this parameter on the adherence between soil and geomembrane. The results obtained showed that the interface friction angle between soil and geomembranes was insensitive to the variation of soil degree of saturation for the conditions employed in the test programme. A progressive interface failure mechanism was observed in the tests with PVC geomembranes due to the more extensible nature of this type of geomembrane.

The largest values of interface friction angles were obtained in the tests with the texturized HDPE geomembrane, whereas similar lower values were obtained in the tests with the smooth PVC and HDPE geomembranes. As a consequence of higher adherence with soil, the largest mobilized tensile forces were obtained in the tests with the texturized HDPE geomembrane.

5 ACKNOWLEDGEMENTS

Authors would like to thanks Maccaferri, Sansuy e Nortene Geosynthetics Ltd. for having supplied the geomembrane products tested. The authors are also indebted to the University of Brasilia, CAPES-Brazilian Ministry of Education and CNPq-National Council for Scientific and Technological Development for the financial support.

6 REFERENCES

Arya, L. M., Paris, J. F. 1981. A physico-empirical model to predict the soil moisture characteristic from particle-size distribution and bulk density data. Soil Science Society of America Journal, 45: 1023-1030.

Aguiar, V. R. de. (2003). Ramp tests for soil-geosynthetic shear strength interface studies. MSc Dissertation, Graduate Program on Civil Engineering, Federal University of Rio Grande of Sul, Porto Alegre, RS, Brazil, 121p (in Portuguese).

Briançon, L.; Girard, H.; Poulain, D. (2002). Slope stability of lining systems-experimental modeling of frictional at geosynthetic interfaces. Geotextiles and Geomembranes, 13 (5): 147-172.

Dwyer, S.F.; Bonaparte, R.; Daniel, D.E.; Koerner, R.M.; Gross, B. (2002). Technical guidance for RCRA/CERCLA final covers. US Environmental Protection Agency, Office of Solid Waste and Emergency Response, Washington, DC, USA.

Fleming, I. R.; Sharma, J. S.; Jogi, M. B. (2006). Shear strength of geomembrane-soil interface under unsaturated conditions (in English). Geotextiles and Geomembranes, (24): 274 - 284.

GEO-SLOPE International Ltda. (2004). GeoStudio Tutorials (includes student edition lessons). Calgary, Alberta, Canada.

Girard, H.; Fisher, S.; Alonso, E. (1990). Problems of friction posed by the use of geomembranes on dam slopes-examples and measurements. Geotextiles and Geomembranes 9 (2), 129-143.

Giroud, J.P.; Swan, R.H.; Richer, P.J.; Spooner, P.R. (1990). Geosynthetic landfill cap: laboratory and field tests, design and construction. 4th International Conference on Geotextiles, Geomembranes and Related Products, The Hague, The Netherlands, Vol. 2, 493-498.

Girard, H.; berroir, gourc, J. P.; matheus, G. (1994). Friction behavior of geosynthetics and slopes stability of lining systems (in English). Fifth International Conference on Geotextiles, Geomembranes and Related Products, Singapore, (1): 339 - 342.

Gourc, J.P.; Lalarakotoson, S.; Müller-Rochholtz; H., Bronstein, Z., (1996). Friction measurements by direct shearing or tilting process – development of a European standard. 1st European Conference on Geosynthetics - EUROGEO 1, Maastricht, The Netherlands, Vol. 1, 1039-1046.

Gross, B.A.; Bonaparte, R.; Giroud, J.P. (2002). Waste containment systems: problems and lessons learned. Appendix F, Assessment and Recommendations for Optimal Performance of Waste Containment Systems, EPA, USA, 214 p.

International Organization for Standardization. (2005). ISO 12957-2: Geosynthetics - Determination of friction characteristics - Part 2: Inclined plane test. 10p.

Khoury, C. N.; Miller, G. A.; Hatami, K. (2011).Unsaturated soil – geotextile soil interface behavior. Geotextiles and Geomembranes, (29): 17 - 28.

Izgin, M. & Wasti, Y. (1998). Geomembrane – sand interface frictional proprieties as determined by inclined board and shear box tests (in English). Geotextiles and Geomembranes, 16 (4): 207 – 219.

Koutsourais, M.; Sandri, D.; Swan, R. (1998). Soil Interaction characteristics of geotextiles and geogrids (in English). Sixth International Conference on Geosynthetics, pp. 739 – 743.

Lima Júnior, N. R. (2000). Soil-geosynthetic interaction study for environmental protection constructions using ramp test equipment. MSc Dissertation, Publication G.DM – 071A/2000, Department of Civil and Environmental Engineering, University of Brasília, Brasília,DF, Brazil, 48 p (In portuguese).

Lopes, C. P. F.C. (2001). Study of soil and geosynthetic interaction by shear tests and inclined board tests. MSc Dissertation, Civil Engineering University, Porto City, Portugal, 186p (in Portuguese).

Mello, L. G. R. de (2001). Soil-geosynthetic interaction study for waste landfills slopes. MSc Dissertation, Publication G.DM – 085A/01, Department of Civil and Environmental Engineering, University of Brasilia, Brasília, DF, Brazil, 137 p (In portuguese).

Palmeira, E.M. (2009). Soil-geosynthetic interaction: Modelling and analysis. Geotextiles and Geomembranes 27: 368-390.

Rebelo, K. M. W. (2003). Soil-geomembrane interface strength by Righ Shear tests. MSc Dissertation, Graduate Program on Civil Engineering, Federal University of São Paulo, São Carlos, SP, Brazil, 216p (in Portuguese).

Viana, H. N. L. (2007). Study of stability and permeability of conventional and alternative covering systems for waste landfills. DSc Thesis, Publication G.TD – 048/07, Department of Civil and Enrironmental Engineering, University of Brasília, Brasília, DF, Brazil, 259p (In portuguese).

Geoenvironmental Approach to Restoration of Agricultural Land Damaged by Tsunami

Approche géo-environnementale de la restauration de terres agricoles endommagées par Tsunami

Omine K.
Nagasaki University

Moqsud M.A.
Yamaguchi University

Hazarika H.
Kyushu University

ABSTRACT: In this study a geo-environmental approach was used for the restoration of the farmed land which was damaged by salinity, due to tsunami water water in the pacific coast of Tohoku region in Japan. The mega earth quake that hit on 11th March, 2011 has triggered a Tsunami in the coastal areas of Tohoku region. The huge water severely affected various environmental and geo-environmental parameters in that area. Soil salinity in the agricultural land has become a great concern for the after disaster geo-environmental restoration. Various approaches are being tried to get rid of the salinity problem of the agricultural land. In this study, major chemical properties (pH, electrical conductivity) of soil in Rikuzentakata city (one of the most affected areas due to tsunami) were measured in the field test during May and June, 2011. An innovative approach by using compost containing Halo bacteria/salt tolerance bacteria in this area was tested to restore the saline soil. This method can be useful for reducing the excessive salts from the soil. The compost can also provide necessary nutrients to the soil and plant.

RÉSUMÉ : Dans cette étude une approche géo-environnementale a été appliquée à la restauration de terres cultivées qui ont été endommagées par l'eau saline amenée par un tsunami dans la région côtière de Tohoku au Japon. Le méga tremblement de terre qui a frappé le 11 mars 2011 a déclenché un tsunami dans cette région. Cette énorme quantité d'eau de mer a affecté fortement les caractéristiques environnementales et géo-environnementales de la zone. La salinité de la terre agricole notamment est devenue une préoccupation majeure. Plusieurs approches sont expérimentées afin de se débarrasser du problème de la salinité de la terre agricole. Dans cette étude, les propriétés chimiques majeures du sol (pH, conductivité electrique) dans la ville de Rikuzentakata (une des régions les plus affectées par le tsunami) ont été mesurées in situ durant les mois de mai et juin 2011. Une approche novatrice a été mise en œuvre pour restaurer le sol salin ; elle utilise un compost qui contient des bactéries de type archées halophiles. Les bactéries de ce type peuvent utiliser les sels excédants du sol et par conséquent réduire le taux de salinité. Ce compost peut fournir aussi des éléments nutritifs nécessaires au sol et aux plantes.

KEYWORDS: salt damage, agricultural land, restoration, microorganism

1 INTRODUCTION

A disaster is the tragedy of a natural or man-made hazard (a hazard is a situation, which poses a level of threat to life, health, property, or environment) that negatively affects society or environment. A natural disaster is a consequence when a natural hazard (e.g., volcanic eruption or earthquake) affects humans. Tsunamis and earthquakes are two of the most dangerous, and yet the most common, hazards to affect population centres and economic infrastructures worldwide. Generally, tsunami flooding results from a train of long-period waves that can rapidly travel long distances from where they were generated by deep-ocean earthquakes, submarine landslides, volcanic eruptions, or asteroid impacts (Morton et al. 2007). Due to tsunami, the sea water carries sediments and salt. There have been many studies on recent (Nishimura and Miyaji 1995) and ancient tsunami deposits (Minoura et al. 1996, Bourgeois et al. 1988). These include descriptions of tsunami deposits in coastal lake, estuary, lagoon, bay floor and shelf environments, and even the farmland (Shiki and Yamazaki 1996). The mega earthquake and consequent tsunami caused a great damage to, not only human life and infrastructure, but also the agricultural land and crops in Tohoku region, Japan. The after math of the tsunami has created many problems to environment and geo-environment of the affected areas. Soil pollution with high salinity, which made the farmland unusable for cultivation, is one of the major geo-environmental problems. The objective of this study is to know the extent of change of soil chemical properties due to tsunami and to apply an innovative approach to control the salinity of the agricultural land (Omine 2012).

2 TOHOKU REGION PACIFIC COAST EARTHQUAKE

The great east Japan Earthquake (Higashi Nihon Daishinsai in Japanese) of magnitude 9.0 was an undersea mega thrust earthquake off the coast of Japan that occurred at 14:46:23 JST on Friday, 11 March 2011. The location of the epicentre (38.3220 N, 142.3690 E) of this earthquake was 70 kilometres east of the Oshika Peninsula of Tohoku and the hypocenter at an underwater depth of approximately 32 km. It was the most powerful known earthquake to have hit Japan, and one of the five most powerful earthquakes in the world since modern record-keeping began in 1900. The earthquake triggered extremely destructive tsunami waves of around 40 m in height in Miyako, Iwate and Tohoku, in some cases traveling up to 10 km inland. In addition to loss of life and destruction of infrastructure, the tsunami caused a number of nuclear accidents in the power plant in Fukushima that caused evacuation zones affecting hundreds of thousands of residents. The sea water inundated large areas of agricultural land and turned soil saline.

3 SOIL INVESTIGATION

Field test was conducted in Rikuzentakata city of Iwate prefecture to determine chemical properties of soil. Figure 1 shows the damaged area in Rikuzentakata city. This city was

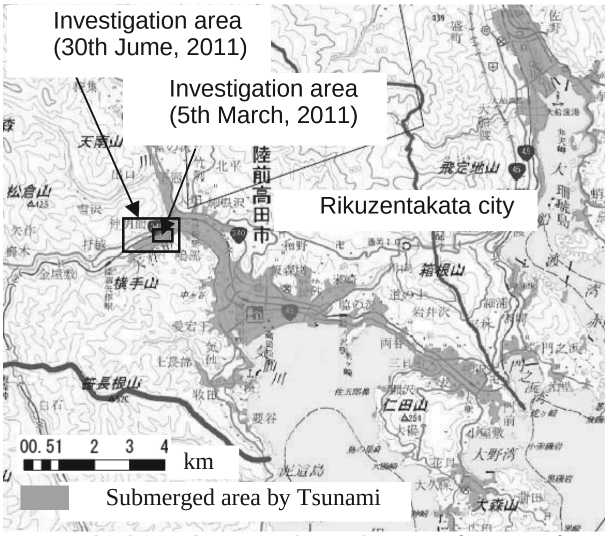

Figure 1. The damaged area in Rikuzentakata city of Iwate Prefecture (The Geospatial Information Authority of Japan, http://www.gsi.go.jp/common/000059844.pdf)

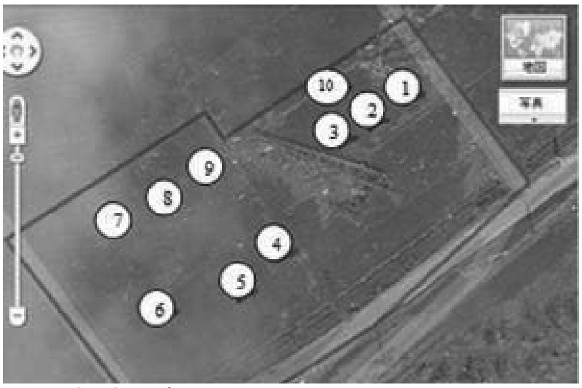

Figure 2. The place of investigation on 5 May 2011

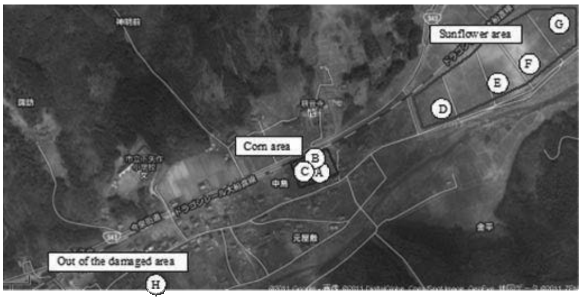

Figure 3. The place of investigation on 30 June 2011

one of the major affected areas by the tsunami on 11 March 2011. Figure 2 shows the place of soil investigation on 5 May 2011 and Fig. 3 shows the place of investigation on 30 June 2011. The sampling area shown in Fig. 1 corresponds to No. F in Fig. 2.

The pH and electric conductivity (EC) of the damaged agricultural land were measured by a digital pH meter (Horiba, D-54SE). The EC of the soil was also measured by using digital an EC meter (Oakton, PCSTEST35). The salinity of the soil was calculated from EC. It is said that normal plants are affected by salt if soil EC exceeds 0.3-0.7 mS/cm. Some parts of the land showed very high EC on 5 May 2011. Table 1 shows the test result of EC and pH. There is the following empirical relationship between Cl (Chlorine) and EC;

Cl content (mg/100g) = EC(mS/cm)×166

The investigation on 30 June 2011 was done in a wide area including the place investigated on 5 March 2011. Table 2 shows the test result of EC and pH. In Fig. 3, No. A~C is corn area, No. D~G is sunflower area and No. H is out of damaged area. The ECs of several soils were low, possibly due to the start of rainy season. Some soils however still showed high EC.

Table 1. Electrical conductivity (EC) and pH of the soils measured on 5 May 2011

(a) EC (mS/cm)

Depth	1	2	3	4	5	6	7	8	9	10
5cm	1.51	0.36	0.39	1.49	1.26	0.47	1.20	1.77	1.01	0.25
10cm	3.04	2.00	1.94	2.93	3.16	1.32	2.77	3.43	1.83	1.15
15cm	2.23	2.43	2.81	4.03	2.21	1.84	0.97	3.46	2.4	2.25

(b) pH

Depth	1	2	3	4	5	6	7	8	9	10
5cm	7.21	8.47	8.06	7.55	7.22	8.39	7.71	7.62	7.19	8.27
10cm	5.75	5.68	6.5	5.78	5.71	6.57	5.98	5.6	6.74	6.52
15cm	6.22	5.48	5.69	5.2	6.13	5.84	7.12	5.64	5.77	5.82

Table 2. Chemical properties of the soils (30th June, 2011)

(a) EC (mS/cm)

Depth	A	B	C	D	E	F	G	H
Surface	0.56	0.11	0.13	0.083	0.09	0.064	0.13	-
5 cm	-	-	-	-	-	-	-	0.032
10 cm	0.97	1.19	0.62	-	0.093	0.15	-	-
15 cm	-	-	-	-	-	-	0.21	-
20 cm	1.83	1.58	1.64	0.21	0.096	0.46		0.026
25 cm	2.15	-	-	-	-	-	-	-
30 cm	-	-	1.65	-	-	-	-	-

(b) pH

Depth	A	B	C	D	E	F	G	H
Surface	7.2	8.1	7.4	8.3	9.0	8.4	8.0	-
5 cm	-	-	-	-	-	-	-	6.9
10 cm	6.6	5.9	6.7	-	9.1	8.4	-	-
15 cm	-	-	-	-	-	-	6.7	-
20 cm	6.1	5.6	5.9	7.0	8.0	7.1	-	6.9
25 cm	6.4	-	-	-	-	-	-	-
30 cm	-	-	5.7	-	-	-	-	-

4 ATTEMPT OF RESTOATION OF AGRIGULTURAL LAND

4.1 *Methods of Restoration*

The aim of soil salinity control is to prevent soil degradation by salinization and to reclaim already degraded soils. Various attempts are now being tested to control salinity of the agricultural land.

The primary method of controlling soil salinity is to permit 10-20% of irrigation water to leach through the soil; the leached water is then drained and discharged through an appropriate drainage system. The salt concentration of the drainage water normally becomes 5 to 10 times higher than that of the

Figure 4. Growing sunflower at the agricultural land

Figure 5. Growing corn at the agricultural land

Figure 6. Building up the compost by mixing rice bran, oil cakes, grinds of fish bones and water

Figure 7. Processing of compost after 3 days

irrigation water. In this process, if export of the salt matches with the import of the salt, then there will be accumulation of salt in the field soil. However, it will take a long time and efforts for such a design of the salinity removal method.

Another method is to establish salt tolerant plants for reducing the salinity of soil biologically. Volunteers for Rikuzentakata (Cheering group of Ganbappeshi Fukuoka) discussed with the authors and proposed to plant sunflower and corn at the saline lands.

They sent a large number of seeds to the local residents and planted sunflower on 9.3 ha and corn on 0.6 ha on 5 June 2011 (Figs. 4 and 5). This method for salinity reduction may not be sufficient for the vast areas.

In this study, an innovative idea was tested for reducing the salt concentration from the agricultural soils. Mr. Usugami who is a researcher of Fukushima produced special compost containing salt tolerant bacteria or halo bacteria for many years (Rural Culture Association Japan , http://www.ruralnet.or.jp/oyaku_image/usu_01.pdf). The volume of the compost can be increased by mixing rice bran, oil cakes, grinds of fish bones and water in a specific ratio. The authors received 2 kg compost from him and increased up to 300 kg. After mixing each material, temperature of the compost was increased to 48˚C for 2 days and turned over for aeration (Figs. 6 and 7). The compost containing the halo bacteria was made ready for application in the tsunami affected large areas of Rikuzentakata for the purpose of reducing salinity of the agricultural land.

For improving the agricultural land damaged by Tsunami, the compost of 10 kg per 1000 m2 and the rice bran of 100 kg per 1000 m2 are needed. The rice bran is nutrition for increasing the halo bacteria/salt tolerance bacteria on site. The rice bran of 30 kg, oil cake of 10 kg, fish lees of 2 kg and water of 35 kg are mixed with the original compost of 2.5 kg using mixer. It was difficult to mix and turn over a large amount of the compost several times, so that the compost was cured in a soil bag with aeration effect as a simple method. Finally, 1 ton of the compost was made and it was brought to Rikuzentakata city together with 4 tons of the rice bran. These materials (compost and rice bran) were disseminated at the agricultural land of 6 ha together with oil-seed rape or rye as green manure crop.

Soil investigation at the site was performed on March 2012. Due to the rail fall and vegetation of sunflower, the salt concentration decreased gradually and the highest EC at the site was 0.25 mS/cm on September 2011. The value of EC decreased furthermore on March 2012. Therefore, it was difficult to distinguish the effect of the compost with halo bacteria/salt tolerance bacteria clearly. It is considered that the compost contains necessary nutrition and the soil is improved.

4.2 *Isolation of Salt Tolerant Bacteria/Halo bacteria*

The sample was collected separately in sterile plastic sheets, and brought to the laboratory for microbiological analysis. For isolation and enumeration of microorganisms, soil sample was serially diluted in sterile distilled water and plated on Luria–Bertani agar (LB g/L:Peptone-10; yeast extract-5; Nacl-10; Agar-15; pH-7.0-7.4) supplemented with 1% sodium chloride (NaCl) level. The plates were incubated at 30oC for 72 hours. Colonies differing in morphological characteristics was isolated in pure form and used for further studies. The screened Halo bacteria was confirmed their growth in specific medium, Mannitol salt agar (g/L: Enzymatic digest of Casein-5; Enzymatic digest of animal tissue-5; Beef extract- 1; D-Mannitol- 10; Sodium chloride- 75; Phenol red- 0.025 g; Agar-15; pH- 7.4) is a selective and differential medium salt tolerance. It contains 7.5% high salt concentration. The salt tolerant bacteria grow in mannitol salt agar and ferment the mannitol, an acidic by product is formed that will cause the phenol red turn to yellow colour.

The salt tolerance was determined in LB agar supplemented with NaCl. The growth was monitored after 72 hours incubation at 30^{o}C. Finally, six types of Halo bacteria were isolated from the compost. At present, Halo bacteria exhibiting 15% salt tolerance was determined in LB agar. Figure 8 shows microscopic view of salt tolerance bacteria isolated from the compost. Figure 9 shows the result of salt tolerance test on the compost. The salt tolerant bacteria exhibited salt tolerance ranged from 16-18 % in LB agar. Optimum growth test of bacterial was not conducted, so that the salt tolerance bacteria are not identified as Halo bacteria herein.

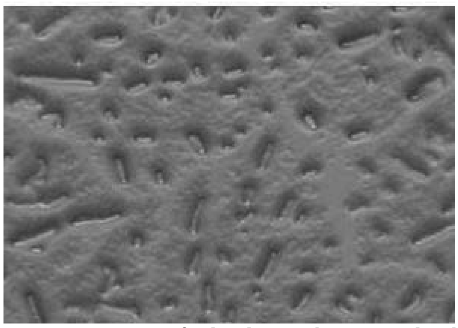

Figure 8. Microscopic view of salt tolerance bacteria isolated from the compost

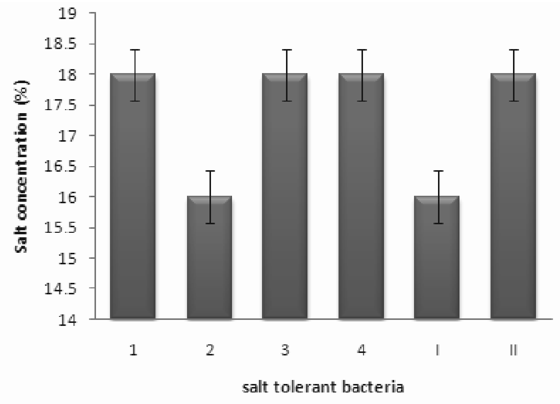

Figure 9. Result of salt tolerance test on the compost

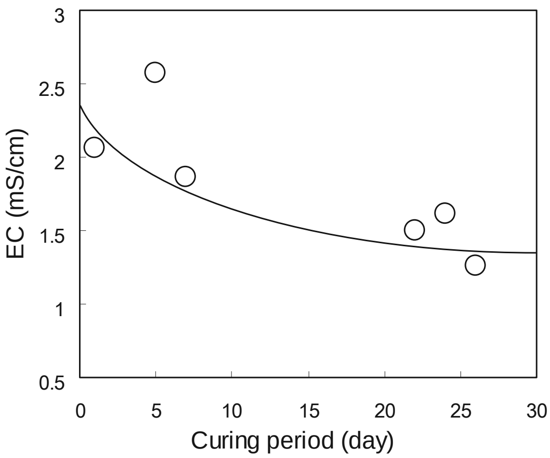

Figure 10. Relationship between electric conductivity and curing period on soil with salt

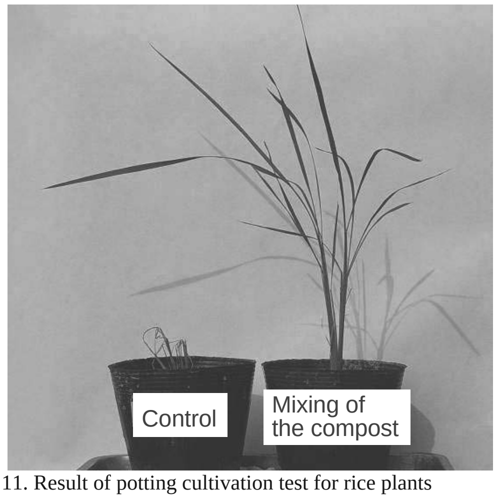

Figure 11. Result of potting cultivation test for rice plants

4.3 *Laboratory tests of Saline Soil*

In order to confirm the effect of the compost with salt tolerance bacteria, laboratory tests of the saline soil were performed.

For making clear the effect, natural salt of 400mg/100g-dry soil was added to a soil sampled from agricultural field at Rikuzentakata city. The compost of 1g and rice bran of 10 g ware mixed with the soil of 330 g. Electric conductivity of the sample were measured continuously as shown in Fig.10. The value of EC decreases with increase in curing period and becomes almost a half after one month.

The farmers in Rikuzentakata city are not able to start a cultivation of rice, because the agricultural land has contained a large size of disaster wastes in the soil still now and tractor cannot work correctly.

It was therefore that the potting cultivation test for rice plants was conducted. Figure 11 shows the test result after one month. In the case of control without the compost, rice plants were died during one week. On the other hand, the plants using the compost have grown steadily.

Thus, the compost with salt tolerance bacteria can reduce the soil salinity and it is also confirmed that the compost is effective for growth of rice plants and restoration of agricultural land.

5 CONCLUSIONS

The mega earthquake and consequent huge tsunami has done a great damage to the entire areas of the pacific regions in Tohoku, Japan. The sea water that overflowed the agricultural lands in the area has created a critical situation for the farmers. The farmers lost not only the crops they were cultivating but also the soil of the agricultural field was seriously damaged by salinity and other pollutants. The pH and EC of the soil have increased and exceeded the safer limit for cultivated crops.

The compost containing salt tolerance bacteria was used at the agricultural land damaged by Tsunami for restoration of the saline soil. However, it was not easy to distinguish the effect of the compost with salt tolerance bacteria clearly due to decrease of salt concentration by rail fall and vegetation. The laboratory tests of chemical properties and potting cultivation were also performed on the saline soil. From the test results, the compost containing salt tolerance bacteria can reduce the excessive salts from the soil and consequently reduced the salinity problem. It was also confirmed that the compost is effective for growth of rice plants. The compost also provided necessary nutrients to the soil and plant.

6 ACKNOWLEDGEMENTS

The authors wish to acknowledge the financial support by Grant-in-Aid for Scientific Research (21360227, 23656299) from Japan Society for the Promotion of Science and JST revitalization promotion program (A-step) (241FT0057). The authors also wish to thank Mr. T. Hashimoto for his valuable help in the experiments and Cheering group of Ganbappeshi Fukuoka.

7 REFERENCES

Bourgeois J, Hansen TA, Wiberg PL and Kauffman EG. 1988. A tsunami deposit at the Cretaceous-Tertiary boundary in Texas. Science, Vol. 241, 567-570.

Morton R.A., Gelfenbaum G. and Jaffe B.E. 2007. Physical criteria for distinguishing sandy tsunami and storm deposits using modern examples. Sedimentary Geology, 200, 184-207.

Minoura K., Gusiakov V.G., Kurbatov A., Takeuti S., Svendsen J.I., Bondevik S., Od, T. 1996. Tsunami sedimentation associated with the 1923 kamchatka earthquake. Sedimentary Geology, 106, 145-154.

Nishimura Y. and Miyaji N. 1995. Tsunami deposits from the 1993 Southwest Hokkaido earthquake and the 1640 Hokkaido Komagatake eruption, northern Japan, Pure and Applied Geophysics. 144 (3-4), 719-733.

Omine K., Fujikawa T., Sugimoto S. and Maeda H. 2012. Investigation of Rikuzentakata city of Iwate prefecture and geo-environmental Approach - Ground settlement, waste materials and restoration of saline agricultural land -, Japanese Geotechnical Journal, 7 (1), 231-241 (in Japanese).

Shiki T. and Yamazaki T. 1996. Tsunami-induced conglomerates in Miocene upper bathyal deposits, Chiba Peninsula, Central Japan. Sedimentary Geology, 104, 175-188.

Factors affecting hydration of Geosynthetic Clay Liners in landfill applications

Facteurs influençant l'hydratation des géosynthétiques bentonitiques dans les applications d'enfouissement

Rayhani M.T., Sarabadani H.
Department of Civil and Environmental Engineering, Carleton University, Ottawa, Canada

ABSTRACT: The progression of hydration of Geosynthetic Clay liner (GCL) from underlying subsoil was studied for three GCL products under simulated landfill conditions, before and after being covered by municipal solid waste. GCL hydration is shown to be highly dependent on the GCL manufacturing techniques, the grain size distribution and initial moisture content of the subsoil. The hydration behaviour of the GCL was also affected by the exposure conditions in the landfill. Prior to waste placement, the composite liner may be exposed to daily and seasonal thermal cycles for a period of time (weeks to months). These cycles significantly suppressed the hydration of the GCLs and kept the equilibrium moisture content of the GCLs far less than what expected under isothermal conditions at room temperature (22°C). After waste placement, the GCL may experience elevated temperatures that occur during waste decomposition in municipal solid waste landfills. Results indicated that as the temperature increased (from 22 to 55°C), the final equilibrium moisture content decreased, from about 96% at room temperature to about 14% at 55°C. Moreover, the normal stress of 2 to 5 kPa was shown to induce an adequately high rate of hydration and the maximum equilibrium moisture content.

RÉSUMÉ: La progression de l'hydratation de Géosynthétique Bentonique (GSB) du sol a été étudiée pour trois GSB produits dans des conditions simulées d'enfouissement, avant et après avoir été recouverts par des déchets solides municipaux. Hydratation est dépendante des techniques de fabrication GSB, la distribution de granulométrie et la teneur en humidité initiale du sol. Hydratation de GSB a également été affectée par les conditions d'exposition d'enfouissement. Avant déposer des déchets, le revêtement composite peut être exposé à des cycles journaliers et saisonniers thermiques pendant une période de temps (quelques semaines ou mois). Ces cycles ont supprimé l'hydratation des GSBs de manière sévère et ont gardé la teneur en humidité d'équilibre des GSB beaucoup moins ce que prévue dans des conditions isothermes à température ambiante (22°C). Après déposer des déchets, le GSB peut subir des températures élevées qui se produisent lors de la décomposition des déchets dans les sites d'enfouissement des déchets solides municipaux. Les résultats ont montré que lorsque la température a été augmentée (de 22 à 55 °C) le contenu d'humidité d'équilibre final a été diminué de manière sévère, de 96% à la température ambiante à environ 14% à 55 °C. En outre, la pression normale de 2 à 5 kPa a été montrée de causer un taux suffisamment élevé d'hydratation et de la teneur maximale en humidité d'équilibre.

KEYWORDS: Geosynthetic Clay Liners (GCL), hydration, thermal gradient, normal stress

1 INTRODUCTION

Geosynthetic Clay Liners (GCLs) are utilized as part of a barrier system while covered by a geomembrane liner to prevent the escape of contaminants form solid waste landfills (Rowe 2005, Benson et al. 2010, Gates and Bouazza 2010). The GCLs typically consist of a core of bentonite encapsulated by nonwoven or woven geotextiles. The hydraulic performance of the GCL depends on the degree of hydration from the pore water of the underlying soil prior to contact with leachate (Rowe 2005). Previous studies have shown that the hydraulic performance of the GCL is influenced by the GCL manufacturing techniques as well as the grain size distribution, and initial moisture content of the subsoil (e.g., Chevrier et al. 2012, Beddoe et al. 2010 and 2011, Rayhani et al. 2011). Beddoe et al. (2011) showed that the GCL manufacturing techniques affect the Water Retention Curve (WRC) of the GCL, indicating that the hydration of the GCL depends on the WRCs of both GCL and subsoil. Also, a reduction of approximately 12.5 % in the final moisture content of a needle-punched GCL with sand subsoil was observed as the initial normal stress of 7 KPa was increased to 28.2 KPa (Chevrier et al. 2012).

Composite liners in landfill applications might be left exposed to daily thermal cycles induced by solar radiation for a period of time prior to waste placement. Rowe et al. (2011) reported that the daily thermal cycles significantly suppressed the rate of hydration of GCLs placed on silty sand subsoil. Also, constant thermal gradients applied to the GCLs placed over subsoil have shown to induce loss of moisture and, hence, desiccation and cracking of the GCLs. The temperature at the base of bioreactor landfills and also the Municipal Solid Waste (MSW) landfills where the Leachate Collection System (LCS) has failed could increase up to 40-60ºC after placing the waste (Azad et al. 2011). Furthermore, the temperature within the aquifer is significantly lower which in turn causes temperature gradients. This induces downward flux of vapor (diffusion) from the GCL to the subsoil which causes the moisture loss of GCLs and the desiccation cracking of the GCLs (Barclay and Rayhani 2012, Azad et al. 2011, Southen and Rowe 2005). This paper summarizes the results of an extensive testing program which was initiated to evaluate the effect of field conditions such as the elevated temperatures and normal stresses on the GCL hydration from different underlying subsoils. Also, the effect of the GCL manufacturing techniques and the initial water content of the subsoil are investigated.

2 EXPERIMENTAL PROGRAM

This research analyzes the hydration behavior of the GCL from underlying soil under different field exposure conditions, including daily thermal cycles before waste placement, and constant temperatures induced by the waste decomposition after waste placement. Also, the effect of normal stresses provided by the overlying layers (e.g., Leachate Collection System (LCS), cover soil) is investigated. The hydration progression of three GCL products (GCL1, GCL2, and GCL3) which have significantly different manufacturing techniques has been evaluated in this study. Ontario Leda clay (CL in USCS classification system, ASTM D2487), clayey sand (SC), silty sand (SM), and ordinary construction sand (SP) were used to investigate the effect of the subsoil grain size distribution on GCL hydration. The hydration process was monitored by measuring the gravimetric moisture content (i.e. mass of water/mass of dry material) of the GCL up to 40 weeks.

2.1 *GCL properties*

GCL 1 and GCL2 contained fine granular sodium bentonite with D_{50} of 0.35 mm while GCL3 was coarse granular with D_{50} of 1 mm. All GCLs had NW cover geotextiles. The main difference of the GCLs was the connection layer and also the type of the carrier geotextile (Table 1). GCL1 and GCL2 had similar swell and plasticity indices of 24 ml/ 2g min. and 216% (ASTM D 4318), respectively. GCL3 had a swell index of 23 ml/ 2g min. and plasticity index of 262%. The water retention curves for these GCLs have been presented by Beddoe et al. (2011). The submerged moisture content, i.e., the maximum gravimetric moisture content which the GCL could attain while immersed in water is also given in Table 1.

Table 1. GCL properties

GCL	Total dry mass/area (g/m^2)	Carrier/ Cover Geotextile	Connection Layer	Submerged Moisture Content
1	4555-4988	W/ NW	NPTT	150±10
2	3312-4006	SRNW/ NW	NPTT	118±5
3	4499-5295	W/ NW	NP	190±10

W = Woven, NW = Nonwoven, SRNW = Scrim reinforced nonwoven, NP = Needle punched, NPTT = Needle punched and thermally treated.

2.2 *Soil properties*

The basic geotechnical properties of the four subsoils were determined through laboratory testing (Figure 1). The sand (SP), silty sand (SM), and clayey sand (SC) contained 5%, 35%, and 21% fines passing through the 0.075 mm sieve, respectively. The plasticity indices of the clay and the fine portion of clayey sand were measured at 21.6%, and 4%, respectively (ASTM D 4318). The maximum dry densities of the sand, silty sand, clayey sand, and clay were measured at 1.68, 1.83, 1.96, and 1.43 Mg/m^3 with the corresponding optimum moisture contents of 10%, 11.4%, 11.3%, and 28.3%, respectively (ASTM D 698).

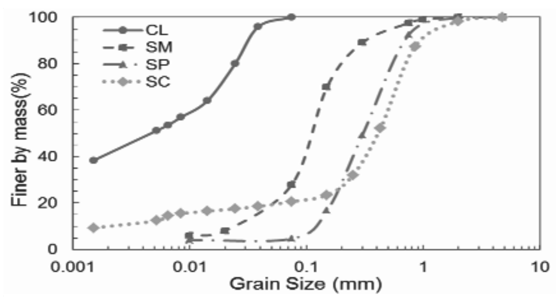

(a)

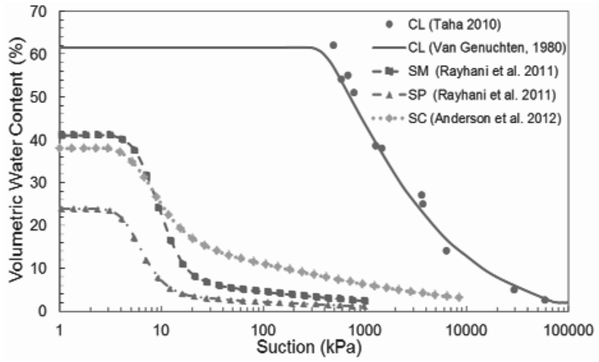

Figure 1. (a) Grain size distribution and (b) matric suction curves for the subsoils examined.

2.3 *Sample preparation*

Figure 2 demonstrates the diagram of instrumented test cells used for simulating GCL hydration from subsoil. To simulate the profile of a composite liner, the soil under examination was placed in cells having a diameter of 150 mm and a height of up to 500 mm. Tap water with an average calcium concentration of 40 mg/L was mixed with bulk samples of dried soils to the wet of optimum moisture content (w_{opt} + 2%). Some soil samples were watered to other gravimetric moisture content to evaluate the effect of the initial moisture content (10%). The soil samples were wrapped in airtight plastic bags to cure overnight. Afterwards, the soil was compacted into the PVC cylinders in five layers with a final height of 250 mm, and a dry density corresponding to approximately 90% of the maximum dry density. The GCL sample was placed over the subsoil and overlain by geomembrane. A steel seating block with a known weight corresponding to a specific level of normal stress (0-8 kPa) was placed on the liner. The test cells were closed and sealed to prevent any loss of moisture, and were opened weekly to determine the mass before returning them to the cells.

2.4 *Experimental procedure*

In order to investigate the effect of constant temperature on GCL hydration after waste deposition, heating blankets set to the temperatures of 35, 45, and 55°C were placed on top of a series of test cells. Some cells were left in room temperature (22°±2C) for isothermal and control experiments. Also, heat was applied for 8 hours to the top of some cells before they were subsequently left in room temperature (22°C) for 16 hours to simulate daily thermal (heating and cooling) cycles induced by solar radiation. The sides of all cells were surrounded by fibreglass insulation while their bottom was maintained at room temperature to simulate vertical thermal gradients developed in the field. Also, after 6 weeks of daily thermal cycles, the heating cycles were brought to a halt for a period of 6 weeks to simulate seasonal cooling periods before they were resumed.

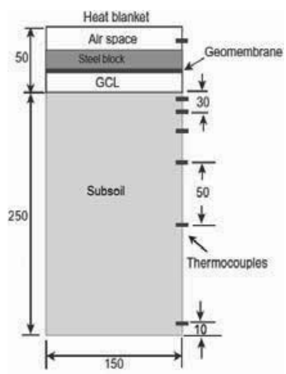

Figure 2. Diagram of instrumented test cells used for simulating GCL hydration from subsoil (numbers in mm)

Moreover, the normal stresses of 0, 0.5, 1, 2, 5, and 8 kPa were applied to some GCL specimens to evaluate the effect of the normal stress on the GCL hydration.

3 RESULTS AND DISCUSSION

The evolution of GCL hydration was monitored up to 40 weeks. In this paper, the effect of daily and seasonal thermal cycles, elevated constant temperatures, and external loading as well as the GCL manufacturing techniques and grain size distribution of subsoil on GCL hydration is discussed.

3.1 *Subsoil grain size distribution*

GCLs are placed over different subsoils depending on the availability of the type of the soil where a solid waste landfill is constructed. As mentioned earlier, the GCL hydration depends on the water retention curves of both subsoil and the GCL (Beddoe et al. 2011). In order to investigate this phenomenon, the isothermal hydration progressions of GCL2 from four different subsoils (SP, SM, SC, and CL) at 10% initial gravimetric moisture content were juxtaposed for comparison (Figure 3). GCL2 in close contact with clay subsoil stabilized with the equilibrium gravimetric moisture content of 48% while this value ranged between 79 to 88% for the other subsoils.

The rate of moisture uptake from the clay subsoil was also found to be lower compared to the other subsoils (SP, SC, and SM). As shown in Figure 3, the gravimetric moisture content after the first week for the GCL sample in close contact with clay (13%) subsoil was less than the other sandy subsoils which varied from 31% to 44%. This could be attributed to the fact that the difference between the suction of the GCL and the subsoil decreased as the portion of fine particles within the subsoil increased which in turn induced lower rate of hydration and equilibrium moisture content for the GCL.

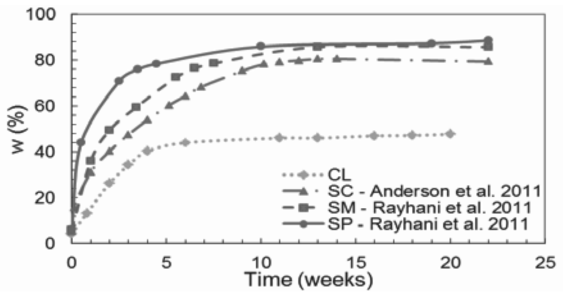

Figure 3. Hydration response of GCL2 from different subsoils at w_{fdn}=10% initial moisture content (CL: Clay, SC: clayey sand, SM: silty sand, SP: poorly graded sand)

3.2 *Daily and Seasonal Thermal Cycles*

Figure 4 compares the hydration progression of GCL2 from the clay subsoil at 30% initial gravimetric moisture content under the simulated daily thermal cycles with that of the isothermal condition (22°C). The GCL sample stabilized at the equilibrium gravimetric moisture content of 14% (week 6) while subjected to daily thermal cycles. Comparatively, the same GCL experienced the equilibrium moisture content of 61% under isothermal condition. Similarly, the results for GCL3 indicated that the equilibrium moisture content under thermal cycles was approximately 15% of the moisture content expected under isothermal conditions. As shown in Figure 4, a meager increase of 5% in moisture content was observed after cooling in each thermal cycle; however, the equilibrium moisture content under the daily thermal cycle was significantly suppressed and was much less than that attained under isothermal condition.

The daily thermal cycles were also stopped for a period of 6 weeks to simulate and evaluate the effect of seasonal cooling cycle on the GCL hydration. This led to an increase of the moisture content from 18% at the end of the daily thermal cycle period (week 6) to 44% at the termination of the cooling period (week 12). However, the moisture content of the GCL sample dropped to its initial level as the thermal cycles resumed. This shows that cooling periods followed by daily thermal cycles, which could normally occur during winter, may not guarantee the sustainable hydration of the GCL.

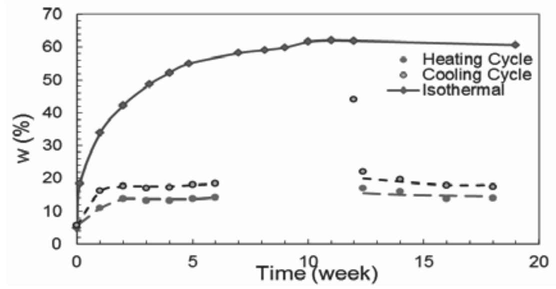

Figure 4. Effect of daily and seasonal thermal cycles on hydration of GCL2 (subsoil=CL, w_{fdn}=30%) (Sarabiam and Rayhani, 2012)

3.3 *GCL manufacturing techniques*

GCL manufacturing process was shown to affect the swelling of the bentonite upon hydration, and in turn the hydraulic conductivity of the GCL by controlling the level of constraint between the carrier and cover geotextiles (e.g. Lake and Rowe 2000, Beddoe et al. 2011). Particularly, Beddoe et al. 2011 reported that the type of the connection layer significantly influenced the WRC of GCLs in low ranges of suctions (i.e. high values of moisture content).

In order to compare the effect of GCL manufacturing techniques on the degree of hydration of GCL, the normalized equilibrium moisture content defined as the ratio of equilibrium moisture content of the GCL to its submerged moisture content (w/w_{ref}) was utilized. GCL3 demonstrated the least effective anchorage of geotextiles inducing the least normalized hydration values for all subsoil moisture contets. The normalized equilibrium moisture content of GCL1 which was thermally treated was 5-10% less than GCL2. GCL2 reached the highest normalized moisture content and in turn degree of hydration (Figure 5). The improved anchorage of the thermally treated scrim-reinforced GCL provided less swelling and final bulk void ratio which is expected to improve the hydraulic performance. Moreover, there was a positive correlation between the equilibrium moisture content of the GCL and the subsoil initial moisture content due to higher levels of suction at the GCL-subsoil interface in higher subsoil moisture contents (Figure 5).

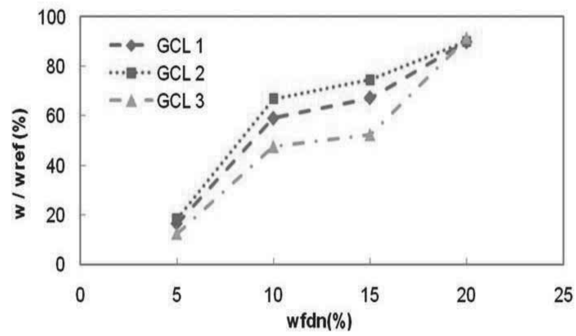

Figure 5. Normalized moisture uptake (w/wref) for all GCLs from clayey sand (SC) subsoil with different initial moisture contents (Barclay and Rayhani 2012) (w: equilibrium moisture content)

3.4 *Constant temperature*

In order to investigate the effect of the high constant temperatures induced by waste biodegradation, the hydration of GCL samples while subjected to the constant temperatures of

22, 25, 45, and 55°C were compared. The results demonstrated that the rate of hydration of both GCLs was significantly suppressed after 1 day of hydration while exposed to elevated temperatures, as opposed to continuous moisture uptake for months under the isothermal condition (22°C). Figure 6 demonstrates the hydration of GCL 2 and GCL3 from either sand or clay subsoil for all the aforementioned temperatures. The addition of 35°C heat source significantly decreased the average equilibrium moisture content (of all experiments) by 3/4, from an average value of 96 to 24%. Also, the GCL average equilibrium moisture content reduced from 24 to 14% as the applied constant temperature increased from 35 to 55°C. These results are notably similar to certain previous findings on GCL hydration under daily thermal cycles discussed above. The thermal gradients initiated by biodegradation of waste after depositing the waste or solar radiation before waste placement could induce severe loss of moisture in GCL and, hence, higher hydraulic conductivity.

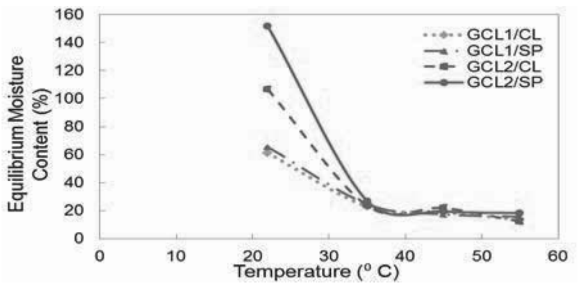

Figure 6. GCL moisture uptake vs. temperature (Barclay & Rayhani, 2012)

3.5 *External loading*

The level of normal stress provided by the leachate collection system or the cover soil could affect the swelling characteristics and hence the degree of hydration of the GCL. Figure 7 demonstrates the variation of equilibrium moisture content versus the normal stress for 4 different conditions. In general, the normal stress of 2-5 (for a typical leachate collection system) induced the highest equilibrium moisture uptake. The rate of moisture uptake also increased significantly as the level of the normal stress increased. GCL2 with sand subsoil (12% moisture content) achieved 62% gravimetric moisture content under 8 kPa normal stress after one week of hydration which was significantly more than that of the unconfined condition (36%). The normal stress enhanced the contact between the GCL and the subsoil leading to significantly higher rate of hydration as well as more equilibrium moisture content.

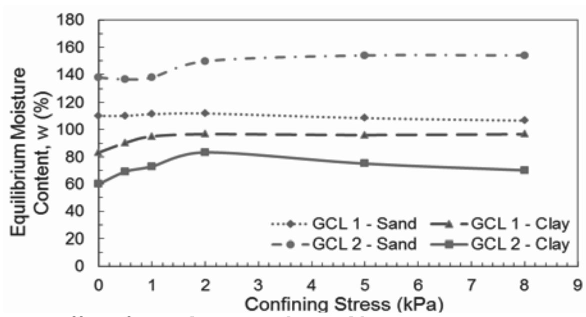

Figure 7. Effect of normal stress on the equilibrium moisture content

4 CONCLUSIONS

The hydration of three GCL different products from the subsoil pore water under simulated landfill conditions was studied. The following conclusion points could be extracted:

- The hydration potential of the GCL was found to be dependent on the difference between the suction of the GCL and the subsoil. The small grain size and high levels of matric suction associated with clay compared to other sandy soils was seen a limiting factor for the GCL hydration.
- The thermally treated, scrim-reinforced GCL (GCL2) demonstrated higher rate and degree of hydration compared to the other GCL product under similar conditions mainly due to the better anchorage of the connection layer against swelling of bentonite upon hydration.
- Thermal cycles severely suppressed the moisture uptake of the GCL to as low as 15% of the moisture content observed under isothermal conditions. Seasonal cooling was shown to not guarantee sustainable hydration of the GCL provided that the GCL is subsequently exposed to daily thermal cycles.
- Elevated constant temperatures at the bottom of landfills could significantly decrease the rate of hydration, the equilibrium moisture content of the GCL, and consequently the hydraulic performance of the GCLs.
- Employing the cover soil or the construction of leachate collection system could provide the sufficient normal stress (2-5 kPa) for an adequately high rate of hydration as well as degree of hydration.

5 ACKNOWLEDGEMENTS

This research was financially supported by the Natural Science and Engineering Research Council of Canada (NSERC). The writers are grateful to their industrial partner Terrafix Geosynthetics Inc., however the views expressed herein are those of the authors and not necessarily those of our partner.

6 REFERENCES

ASTM D 2487. 2005. Standard Practice for Classification of Soils for Engineering Purposes, ASTM, West Conshohocken, PA, USA: 249-260.

ASTM D 4318. 2005. Standard Test Method for Liquid Limit, Plastic Limit, and Plasticity Index of Soils, ASTM Standard 04.08, ASTM, West Conshohocken, PA, USA: 1-13.

Anderson, R., Rayhani, M.T., and Rowe, K., 2012. Laboratory investigation of GCL hydration from clayey sand, *Geotext. & Geomemb.*, Vol. 31, pp 31-38.

Azad, F. M., Rowe, R. K., El-Zein, A., Airey, D. W., 2011. Laboratory investigation of thermally induced desiccation of GCLs in double composite liner systems. Geotext. & Geomemb., 29 (6), 534-543.

Barclay, A., and Rayhani, M.T., 2012. Effect of temperature on hydration of Geosynthetic Clay Liners in landfills, *Journal of Waste Management Research*, (DOI: 10.1177/0734242X12471153).

Beddoe, R.A., Take, W.A. and Rowe, R.K., 2011. Water retention behaviour of Geosynthetic clay liners. *ASCE J. Geotech. Geoenviron. Eng.*, 137 (11), 1028–1038.

Benson, C.H., Kucukkirca, I.E., Scalia, J., 2010b. Properties of geosynthetics exhumed from a final cover at a solid waste landfill. *Geotext. & Geomemb.*, 28 (6), 536-546.

Chevrier, B., Cazaux, D., Didier, G., Gamet, M., Guyonnet, D., 2012. Influence of subgrade, temperature and confining pressure on GCL hydration. *Geotext. &Geomemb.*, 33, 1-6.

Gates, W.P., Bouazza, A., 2010. Bentonite transformations in strongly alkaline solutions. *Geotext. & Geomemb.*, 28 (2), 219-225.

Lake, C.B. Rowe, R.K., 2000. Swelling characteristics of thermally treated GCLs. *Geotext. & Geomemb.*, 18 (2), 77-102.

Rayhani, M.T., Rowe, R.K., Brachman, R.W.I., Take, W.A., and Siemens, G. (2011) Factors affecting GCL hydration under isothermal conditions. *Geotext. & Geomemb.*, 29, 525-533.

Rowe, R. K., 2005. Long-term performance of contaminant barrier systems. *Geotechnique*, 55 (9), 631–678.

Sarabian, T., and Rayhani, M.T., 2012. Rate of hydration of GCLs from clay soil. *J. of Waste Management*, 33(2013): 67-73.

Southen, J. M., and Rowe, R. K., 2007. Evaluation of water retention curve for GCLs. *Geotext. & Geomemb.*, 25 (1), 2–9.

Taha, M., A. Interface shear behavior of sensitive marine clays-leda clay. *M.Sc. thesis, University of Ottawa*, Ottawa, ON, Canada.

Utilisation de la désorption thermique pour l'élimination in situ des couches flottantes d'hydrocarbures

Use of thermal desorption for removing in-situ floating oil layers

Saadaoui H., Haemers J., Denecheau P.
TPS Tech, Bruxelles, Belgique

Cédou C.
G.T.S (groupe NGE), Saint Priest, France

RÉSUMÉ : NSRCity^{TM}, (breveté par TPSTECH) est une nouvelle technologie de traitement des sols par désorption thermique in situ (sans excavation). La technique utilise le chauffage du sol par conduction (circulation des gaz chauds dans un circuit placé dans le sol) et l'aspiration des vapeurs de contaminants produites dans le sol. Le système comporte des éléments chauffants (deux tubes concentriques) équipés chacun d'un brûleur à gaz, des tubes perforés pour la récupération des vapeurs et un ventilateur pour la circulation des gaz chauds. La technique est déjà utilisée avec succès sur plusieurs sites urbains et industriels en Europe et aux États-Unis. NSRCity^{TM} a été récemment testé sur deux sites : en Belgique et en France. Le site Belge renferme une couche flottante d'hydrocarbures de 0,50 m d'épaisseur (en moyenne) située à 3 m de profondeur. Le site Français renferme une couche flottante d'huiles de moteurs de 2 m d'épaisseur située à 2,50 m de profondeur contaminée par des solvants chlorés. Les résultats obtenus sont très encourageants.

ABSTRACT: NSRCityTM (patented by TPSTECH) is a new technology of soil by thermal in-situ desorption treatment (without excavation). The technique uses the soil heating by conduction (movement of hot gases in a circuit placed in the ground) and the fumes of contaminants produced in the soil. The system consists of heating elements (two concentric tubes) each burner gas tubes perforated for vapour recovery and a fan for the movement of hot gases. The technique is already used successfully on many urban and industrial sites in Europe and the United States. NSRCityTM was recently tested at two sites: one in Belgium and one in France. The Belgian site contains a floating layer of hydrocarbons from 0.50 m of thickness in 3 m deep. The French site has a floating layer of oils for engines of 2 m thick located at a depth of 2.50 m, contaminated by chlorinated solvents. The results are very encouraging.

MOTS-CLÉS : NAPL, couche flottante, traitement thermique in situ, conduction

KEYWORDS: NAPL, floating layer, thermal in-situ desorption, conduction

1 INTRODUCTION

Les NAPL (Non-Aqueous Phase Liquids), tels que les produits pétroliers et les solvants organiques volatils, sont les principaux polluants de l'air, du sol et des eaux souterraines. La pollution du sol par ces produits est généralement accidentelle et provient de plusieurs sources : fuites de réservoir et de tuyauterie de stockage extérieure ou souterraine, flaques d'huile, dépôts des déchets chimiques. Une fois présents dans le sol, ces produits tendent à se déplacer en profondeur par gravité en laissant dans leurs sillages des quantités résiduelles dans la matrice du sol (Power & Abriola, 1992 ; Mayer & Miller, 1992). Une couche flottante apparaît lorsqu'une certaine quantité d'hydrocarbures (plus légère que l'eau) atteint les eaux souterraines. Le liquide s'accumule alors dans la zone capillaire, juste au-dessus du niveau supérieur de la nappe. La couche flottante (ou surnageante) se forme lorsque cette accumulation atteint une valeur critique. Due à la fluctuation de la nappe (sur une saison), le L-NAPL est piégé sous forme de poches séparées et immobiles dans la zone saturée.

Le traitement d'une couche flottante ou/et de la zone saturée présente plusieurs difficultés.

- Accès difficile : généralement, la zone polluée se trouve à des profondeurs considérables ce qui nécessite des moyens d'intervention beaucoup plus sophistiqués et donc très onéreux.
- Présence d'eau : la présence des eaux souterraines limite l'efficacité de l'intervention (temps de traitement plus long, persistance de la pollution dans la zone saturée,...).

Les méthodes de traitement les plus connues actuellement sont l'excavation, le pompage classique «pump and treat» et l'écrémage. Ces méthodes sont trop coûteuses, peu efficaces et ne sont pas toujours physiquement possibles (Oswer, 2002). Le traitement thermique in situ peut être une alternative possible à ces méthodes. En effet, le chauffage du sol mène à des changements brutaux des conditions thermodynamiques du sol et rend le contaminant beaucoup plus mobile (Lingineni & Dhir, 1992). Les principaux effets sont décrits ci-dessous.

- La pression de vapeur du contaminant augmente nettement avec la température. Le chauffage du sol de 20°C à une température moyenne de 100°C augmente la pression de vapeur du contaminant d'au moins un facteur 10. Ceci améliore le transfert massique de la phase liquide vers la phase gazeuse.

- Dans les endroits où le contaminant et l'eau sont présents, l'ébullition du mélange peut se produire à des températures en dessous de 100°C.

- Les coefficients d'adsorption sont réduits pendant le chauffage, menant au dégagement du contaminant à partir de la matrice de sol ou de roche.

- La viscosité, la densité liquide du contaminant et les tensions capillaires entre le contaminant et l'eau sont réduites par le chauffage, favorisant le déplacement du contaminant.

La technologie NSRCity^{TM} développée récemment par TPS Tech est une nouvelle méthode de traitement thermique in-situ des sols. Un descriptif de la méthode sera exposé ici, ainsi qu'un exemple d'application sur un site en Belgique.

2 DESCRIPTION DE LA TECHNIQUE NSRCITY^{TM}

2.1 Principe

La technologie NSRCity^{TM} développée par TPS Tech traite par désorption thermique les zones saturée et non saturée du sol. Elle consiste à chauffer le sol par conduction (utilisation d'éléments chauffants ; figures 1 et 2). Les vapeurs produites dans le sol sont extraites par aspiration. Une partie des vapeurs est détruites in situ par plusieurs mécanismes (cf. §3.1). La technologie s'applique à tout contaminant dont le point d'ébullition à pression atmosphérique n'excède pas les 500°C. Elle est très flexible et peut être mise en œuvre facilement in situ (sans excavation de la terre polluée) ou sur site après excavation par le placement d'un circuit de chauffage constitué d'éléments chauffants. Chaque élément chauffant est constitué de deux tubes concentriques et d'un brûleur à gaz (Figure 1). Les gaz chauds (800°C) produits par le brûleur parcourent le tube interne puis remontent le long du tube externe avant de quitter le circuit. Les vapeurs de contaminant sont récupérées par un tube perforé en acier. Ce tube est placé à côté de l'élément chauffant.

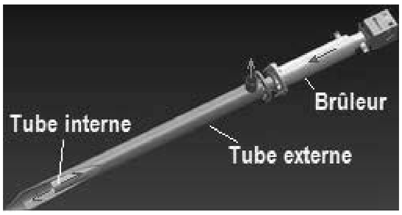

Figure 1. Élément chauffant complet - NSRCity$^{TM.}$

L'installation comporte plusieurs éléments chauffants déposés généralement en triangles isocèles (Figure 2).

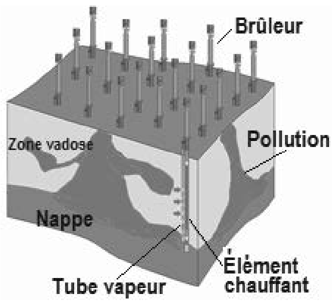

Figure 2. Installation NSRCity^{TM} : Traitement du sol et des eaux souterraines polluées par des produits pétroliers (L-NAPL).

2.2 Evolution de la température du sol

Dans la zone non saturée, l'évolution de la température du sol passe par trois phases (Figure 3).

- Chauffage jusqu'à 100°C (T°C d'ébullition de l'eau),
- Evacuation de l'humidité du sol à 100°C,
- Chauffage du sol jusqu'à la température finale de traitement.

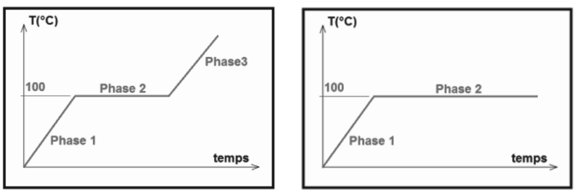

Figure 3. Evolution théorique de la température dans la zone du sol non saturée (à droite) et zone saturée en eau (à gauche).

En présence d'une quantité importante d'eau (présence de la nappe phréatique) et à cause de la vapeur d'eau, la température du sol se stabilise à 100°C (cf. Figure 3).

3 LES MECANISMES DE TRAITEMENT

3.1 Les différents mécanismes

Quand le sol est chauffé, les contaminants organiques sont évaporés ou détruits par plusieurs mécanismes qui sont fonction de la température du sol. Ces mécanismes comprennent :

<u>Pour T≤ 100°C</u>

- Evaporation
- Traitement à la vapeur d'eau
- Ebullition (pour certains contaminants avec $T_{éb}$ <100°C)

<u>Pour T> 100°C</u>

- Ebullition
- Pyrolyse
- Hydrolyse
- Oxydation

Pendant le traitement, le contaminant sous forme liquide se vaporise par ébullition, par évaporation dans l'air, ou par entraînement à la vapeur d'eau. Dans la zone à haute température (près des tubes; épaisseur quelques cm), des réactions de destruction sont mises en œuvre (Hydrolyse/Pyrolyse/Oxydation). Le chauffage du sol conduit aussi au rabattement de la nappe tout près des tubes (Figure 4), favorisant ainsi l'acheminement de la couche flottante vers la zone de destruction (Figure 4).

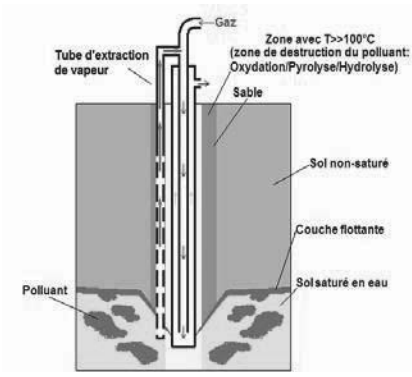

Figure 4. Régime stable de fonctionnement de la technique NSRCity^{TM} en présence d'une couche flottante.

A haute température (T>>100°C), la destruction du polluant se fait par pyrolyse, hydrolyse et en présence d'oxygène. Les réactions suivantes résument les processus de destruction :

- Pyrolyse

$$C_xH_y \rightarrow xC_{(s)} + y/2H_2 \quad (1)$$

- Hydrolyse

$$C_xH_y + 2xH_2O \rightarrow xCO_2 + (2x+y/2)H_2 \quad (2)$$

$$C_{(s)} + 2H_2O \rightarrow CO_2 + 2H_2 \quad (3)$$

- Oxydation

$$C_xH_y + (x+y/4)O_2 \rightarrow xCO_2 + y/2H_2O \quad (4)$$

$$C_{(s)} + O_2 \rightarrow CO_2 \quad (5)$$

$$H_2 + 1/2O_2 \rightarrow H_2O \quad (6)$$

En présence de la nappe et en dehors de la zone de haute température (zone autour de l'élément chauffant), la température du sol se stabilise à 100°C à cause de la présence de la vapeur d'eau en permanence. Dans cette zone, le mécanisme de dépollution est principalement l'évaporation et/ou l'entraînement à la vapeur d'eau. Cette technique est largement répandue dans les raffineries de pétrole et dans les procédés pétrochimiques, où elle est désignée généralement sous le nom de "Stripping vapour».

3.2 Traitement à la vapeur d'eau

La présence d'eau en abondance permet le traitement par entrainement à la vapeur d'eau. Le mécanisme fonctionne de la façon suivante : Lorsqu'un mélange de deux liquides pratiquement non miscibles est chauffé tout en étant agité pour exposer les surfaces des deux liquides à la phase vapeur, chaque constituant exerce indépendamment ses propres pressions de vapeur en fonction de la température, comme si l'autre constituant n'était pas présent. En conséquence, la pression de vapeur du système entier augmente. L'ébullition commence quand la somme des pressions partielles des deux liquides non miscibles excède la pression atmosphérique (approximativement 101,3 kPa au niveau de la mer). De cette façon, beaucoup de composés organiques insolubles dans l'eau peuvent être bien épurés à une température au-dessous du point auquel la décomposition se produit.

La quantité du contaminant présente dans la vapeur d'eau peut être évaluée de la manière suivante. Pour les liquides non miscibles, la fraction molaire d'un composant en phase gazeuse est donnée par la loi de Dalton :

$$Y_i = \frac{n_i}{n_t} = \frac{P_i^0}{P_t} = \frac{P_i^0}{\sum_i P_i^0} \quad avec \quad 1 = \sum_i Y_i \quad et \quad P_t = \sum_i P_i^0 \qquad (7)$$

d'où, pour un mélange gazeux de N composants, on a :

$$y_{i,m} = \frac{1}{1 + \frac{M_1 P_1^0}{M_i P_i^0} + \ldots + \frac{M_{i-1} P_{i-1}^0}{M_i P_i^0} + \frac{M_{i+1} P_{i+1}^0}{M_i P_i^0} + \ldots + \frac{M_N P_N^0}{M_i P_i^0}} \qquad (8)$$

La pression partielle (ou de saturation), P_i^0, d'un composant peut être obtenue à partir de la loi de Clapeyron :

$$\ln P_i^0 = A + \frac{B}{C + T} \qquad (9)$$

avec A, B et C : des constantes propres à chaque composant.

Pour un mélange binaire (par exemple C_xH_y/Eau), on a:

$$y_{C_xH_y,m} = \frac{1}{1 + \frac{M_{eau} P_{eau}^0}{M_{C_xH_y} P_{C_xH_y}^0}} \qquad (10)$$

Le Tableau 1 donne les fractions massiques d'un mélange eau/composé organique à 100°C et à pression atmosphérique.

Tableau 1. Fractions massiques en phase vapeur à 100°C d'un mélange Eau/Benzo-cyclopentane et Eau/N-Hexadécane.

Composé	$T_{éb}$(°C) à 1 atm	M_{CxHy} (g/mole)	T (°C)	y_{CxHy} (%)
Benzo-cyclopentane (C_9H_{10})	177	118	100	40,60
n-Hexadecane ($C_{16}H_{34}$)	287	226	100	1,10

Dans le cas des liquides miscibles, les mêmes équations seront utilisées en rajoutant la loi de Raoult qui corrige la pression partielle d'un composant par sa fraction molaire en phase liquide :

$$P_t = \sum_i P_i = \sum_i x_i P_i^0 \qquad (11)$$

4 CAS D'ÉTUDE SUR UN SITE BRUXELLOIS

4.1 Présentation du site et du pilote

Le site se localise sur le terrain d'une entreprise belge qui a des activités de distribution de voiture en Belgique et dans le monde. Suite à des activités de l'entreprise (nettoyage de voitures, traitement de carrosseries, etc.) et à l'utilisation de produits chimiques, des quantités importantes d'hydrocarbures ont étés versées sur le sol. Après des années d'exploitation, une couche flottante s'est formée à la surface de la nappe phréatique présente à 3 m de profondeur. Cette couche flottante, de hauteur variable selon l'endroit (0,20 à 0,80 m), s'étend sur une superficie de 2000 m^2. En plus de la couche flottante, les analyses effectuées sur des échantillons du sol et des eaux souterraines ont révélé la présence d'huiles minérales, des BTEX et des HAP (Tableau 2).

Un test pilote par désorption thermique in situ est réalisé sur site courant de l'année 2010. L'objectif principal de ce test était de vérifier l'efficacité de la technologie pour ce type de pollution, d'évaluer la consommation énergétique et le temps de traitement.

4.2 Les polluants du site

Comme mentionné ci-dessus, le polluant est composé d'un mélange d'huiles minérales, des BTEX et des HAP. Le Tableau 2 regroupe les résultats d'analyses effectuées sur des échantillons du sol et des eaux souterraines, prélevés avant traitement.

Tableau 2. Analyse des polluants présents sur le site (sol + eau).

Echan.	**BTEXS** (mg/kg-ms)	**C10-C40** (mg/kg-ms)	**HAP (16)** (mg/kg-ms)
Sol (1m)	< 0,25	997,40	0,06<x<0,81
Sol (2m)	< 0,25	-	<0,80
Sol (4m)	< 0,25	848	1,46<x<1,91
Echan.	**BTEXS** (µg/L)	**C10-C40** (g/L)	**HAP (16)** (µg/L)
Liq. (eau)	414	1,3	740

4.3 Installation du pilote

L'installation pilote, utilisée pour ce test, comporte 3 tubes de chauffages verticaux (4 m de long chacun). Ces tubes sont placés en triangle équilatéral à 1,5 m de distance. La surface totale de la zone traitée est de 5,3 m^2. Les tubes externes sont placés à 4 m de profondeur (niveau du sol). Les tubes internes sont placés à 3 ,5 m de profondeur (niveau du sol). L'ensemble est connecté à un réseau de tubes horizontaux (pour la circulation des gaz), et au ventilateur de circulation (Figure 5).

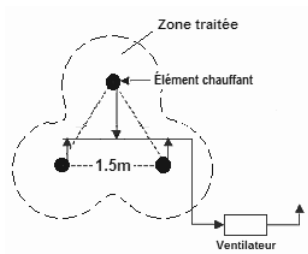

Figure 5. Installation du pilote test sur le site (Bruxelles / Belgique).

Pour réduire les pertes thermiques, l'ensemble de l'installation-sol a été isolé. Une couche de 0,15 m de béton a été mise en place sur le sol en surface, afin d'empêcher des fuites de gaz vers l'extérieur.

4.4 *Mesures et suivi du pilote test*

Huit thermocouples sont placés sur le circuit de gaz et sept thermocouples dans le sol à différentes profondeurs (1, 2 et 4 m). Les thermocouples sont de type K. Les températures sont enregistrées avec une fréquence de 12 mesures par heure. L'acquisition des données est effectuée via la carte Microlink 751. Les gaz sont analysés trois fois par jour à différents endroits du circuit. Les gaz analysés sont: les oxydes d'azote (NO et NO_2), le monoxyde de carbone (CO), le dioxyde de carbone (CO_2), l'oxygène (O_2), le dioxyde de soufre (SO_2) et les hydrocarbures (HCT). L'appareil utilisé est l'MRU Variousplus.

Pour suivre l'évolution de la couche flottante, trois puits de 5 m de profondeur sont creusés. Le premier est situé au centre du triangle formé par les tubes, les deux autres sont à l'extérieur de la zone de traitement (à 1 et 5 m de l'installation). La température des gaz et la concentration en oxygène à la sortie de la chambre de combustion constituent les paramètres les plus importants de fonctionnement du procédé. Les valeurs choisies devraient permettre d'avoir un bon rendement de combustion et une température élevée des gaz à l'entrée des tubes de chauffage. Le réglage du brûleur (débits d'air et de carburant) permet de mieux contrôler ces paramètres. Vu la longue durée de traitement (plusieurs semaines), l'installation est équipée en permanence d'un système de surveillance. En cas d'arrêt, un message SMS d'alerte est envoyé automatiquement.

5 RÉSULTATS ET DISCUSSION

Le test pilote a duré au total et sans interruptions 70 jours.

5.1 *Evolution de la température*

La Figure 6 donne la température du sol traité.

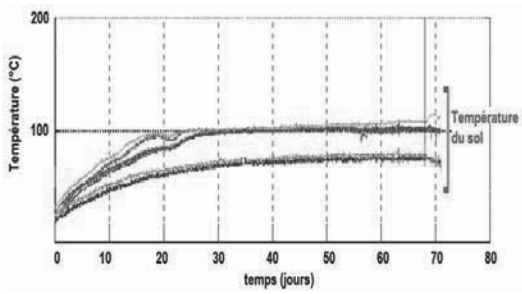

Figure 6. Evolution de la température du sol traité.

On distingue clairement deux phases de chauffage.

- Une première phase de 20 jours pendant laquelle la température du sol augmente jusqu'à 100°C (température d'ébullition de l'eau).

- Une deuxième phase de 50 jours où la température se stabilise à 100°C (sauf pour la zone autour des tubes). Pendant cette phase, l'énergie transmise au sol est utilisée pour l'évaporation de l'eau et du contaminant. Cette phase constitue la phase de traitement (entraînement par la vapeur d'eau).

5.2 *Evolution de la couche flottante*

Pendant le traitement, et pour suivre l'évolution de la couche flottante, des mesures sont effectuées dans les trois puits de contrôles. Seul le puits central présentait une diminution de la couche flottante. Après 70 jours de traitement, la couche flottante est totalement éliminée (Figure 7).

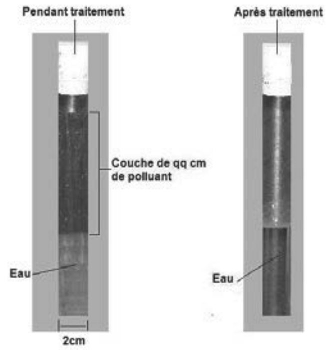

Figure 7. Echantillons liquides du puits central, pendant et après traitement.

5.3 *Analyse des sols*

Le Tableau 3 regroupe les résultats d'analyses effectuées sur des échantillons du sol et des eaux souterraines, prélevés avant et après traitement.

Table 3. Comparaison des résultats des polluants (sol + eau) avant et après traitement.

Echan.	**BTEXS** (mg/kg-ms)	**C10-C40** (mg/kg-ms)	**HAP (16)** (mg/kg-ms)
Sol (1m) Avant	<0,25	997,40	0,06<x<0,81
Sol (1m) Après	-	<50	0,10
Sol (2m) Avant	<0,25	-	<0,80
Sol (2m) Après	-	240	<0,05
Sol (4m) Avant	<0,25	848	1,46<x<1,91
Sol (1m) Après	-	180	<0,80
Echan.	**BTEXS** (µg/L)	**C10-C40** (µg/L)	**HAP (16)** (µg/L)
Liq(eau) Avant	414	1 300	740
Liq(eau) Après	-	6,40	-

6 CONCLUSION

Ces travaux ont démontré l'efficacité de la technologie NSRCity^{TM} de désorption thermique in situ pour le traitement des sols pollués en présence d'une couche flottante.

Dans le site étudié, avec une distance entre tubes de 1,50 m, 70 jours étaient suffisants pour l'élimination totale d'une couche de polluants d'épaisseur 50 cm. L'entraînement par la vapeur d'eau provenant de la nappe et la création d'une zone de haute température près des tubes ont permis ce traitement.

7 REFERENCES

Lingineni, S. & Dhir, V. 1992. Modelling of soil venting processes to remediate unsaturated soils. *J. Environmental* Engineering, 118(1): 135-152.

Mayer A. S., Miller C. T. 1992. The influences of porous medium characteristics and measurement scale on pore-scale distributions of residual nonaquous phase liquids. *J. Contam. Hydrol.*, 11, 189-213.

Oswer, P. 2002. Elements for Effective Management of Operating Pump and Treat Systems. November 2002. OSWER 9355.4-27FS-A.

Power S. E., Abriola L. M., Weber W. J. 1992. An experimental investigation of NAPL dissolution in saturated subsurface systems: study state mass transfer rates. Water Resours. Res., 28, 2691-2705.

Development and Verification of Ecohabitat Chart based on Ecological Geotechnics

Développement et Vérification de Ecohabitat Diagramme ont basé sur Écologique Géotechnique

Sassa S., Watabe Y.
Port and Airport Research Institute, Japan
Yang S.
Jeju National University, Korea

ABSTRACT: By utilizing our new approach in Ecological Geotechnics, we performed series of controlled laboratory experiments on benthos-soil systems with six species of invertebrates that belonged to Arthropoda, Mollusca, and Annelida. The experimental results demonstrated that for each of the burrowing activities, there exist optimal, transitional and critical geoenvironmental conditions, which were found to differ considerably between species, body sizes and weights. On the basis of these results, we have constructed an ecohabitat chart which enables an interspecific comparison of the burrowing performances and capabilities of the diverse benthic fauna in light of the associated geoenvironments in the field. The results of integrated field observations and surveys at various natural and artificial intertidal flats further demonstrate the validity and effectiveness of the ecohabitat chart in not only evaluating but also predicting the linkage between the species distributions and the ensuing geoenvironments. Hence, the present findings, together with the developed chart will effectively contribute to a new horizon of the performance-based geoenvironmental assessment, design and management for the conservation and restoration of habitats with rich ecosystems in intertidal zones.

RÉSUMÉ : En utilisant notre nouvelle approche dans Écologique Géotechnique, nous avons exécuté série d'expériences de laboratoire sur les systèmes du benthos-sol avec six espèces d'invertébrés qui ont appartenu à Arthropoda, Mollusca et Annelida. Pour chacun des activités fouisseuses, là a existé des optimales, transitionnelles et critiques geoenvironmental conditions qui ont différé considérablement entre espèces, dimension du corps, et poids qui ont permis le développement d'un diagramme de l'ecohabitat. Ce diagramme a été validé à travers champ études de l'intertidal naturels et artificiels. Les conclusions contribueront à un nouvel horizon de du geoenvironmental performance-basée estimation et gestion pour la conservation et restauration d'habitats avec les écosystèmes riches dans les intertidal zones.

KEYWORDS: ecological geotechnics, geoenvironment, intertidal flat, ecosystem.

1 INTRODUCTION

Biodiversity in oceans has received increasing attentions in recent years, particularly following the COP10 initiative to conserve and restore the valuable ecological systems. Intertidal zones are the vital elements in the sustainability of estuarine and coastal environments since they foster rich natural ecosystems. Previous research in the fields of ecology and water science has been directed to understanding the diversity of ecosystems, their water purification functions and associated hydroenvironments. However, geoenvironments as habitats and their linkage with biological activity remain poorly understood, although their complete understanding is crucial to the conservation and restoration of habitats.

Recently, we developed an integrated continuous observation system that enables close inspection of the geoenvironmental dynamics that take place in the zones relevant to benthos diversity and applied it to intertidal flats (Sassa and Watabe, 2007). Through the combined use of field, experimental and theoretical investigations, we have found that the dynamics of suction associated with tide-induced groundwater level fluctuations play a substantial role in controlling the geophysical environments of habitats (Sassa and Watabe, 2007), and there is a close linkage between the waterfront geophysical environment and the ecology of intertidal flats (Sassa and Watabe, 2008; Kuwae et al., 2010; Sassa et al., 2011).

The paper reports our recent findings from such new cross-disciplinary research field which we call “Ecological Geotechnics” (Sassa and Watabe, 2009). Specifically, the present study aims to investigate systematically the burrowing performances and capabilities of diverse species that belong to Arthropoda, Mollusca, and Annelida, and to develop an ecohabitat chart by which to evaluate the interrelationships between suitable and critical geoenvironment among species. The validity of the ecohabitat chart is assessed in light of the results of integrated field observations and surveys of the waterfront geoenvironment and species distributions at various natural and artificial intertidal flats.

2 DEVELOPMENT OF ECOHABITAT CHART

For the purpose of the present study, we targeted diverse species such as bivalves, worms, crabs, shrimp and decapod crustacean and realized an integrated comparison of the burrowing performances though a range of controlled laboratory experiments of benthos-soil systems. For the materials, we used tidal flat soils as well as agar based on the study of Sassa & Watabe (2009). In the series of the experiments, we simulated and varied the vane shear strength according to the procedures described in Sassa & Watabe (2009), and investigated the burrowing responses of each of the six species used, for one hour period. In cases where burrowing was possible, an individual burrowed under the soil surface. In contrast, in cases where burrowing was impossible, the whole body remained on the soil surface. For the bivalves and shrimp, partial burrowing manifested, and thus in order to elucidate their burrowing capabilities, we examined their responses for six hour period. All of the individual species were collected from natural intertidal flats such as Banzu, Ena, Nojima and Furenko intertidal flats, and acclimated in a water tank for the period of one month under constant air and water temperatures. We used

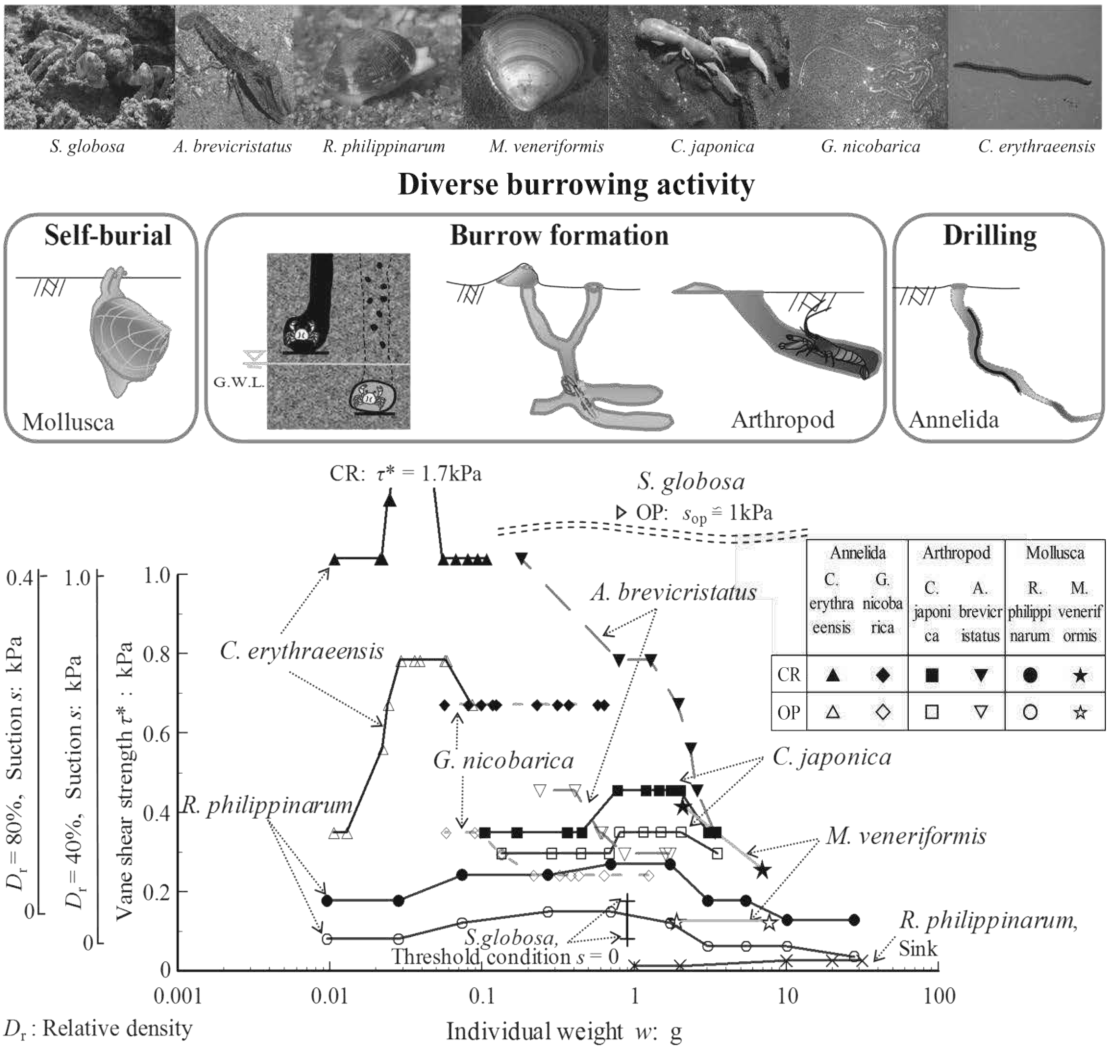

Figure 1. Ecohabitat chart and the interrelationships between optimal and critical geoenvironment among species in intertidal flats

a total of 835 individuals whose body sizes ranged from 2mm to 88mm and whose body weights ranged from 0.004g to 31.6g.

The experimental results are summarized in Fig. 1. This figure shows three burrowing regions, namely, an optimal region (below OP) where all individuals burrowed, a transitional region (between OP and CR) where burrowing success and failure mixed, and a critical region (above CR) where all individuals failed to burrow, in light of the vane shear strength. The associated suction ranges for the two different relative densities, 40% and 80%, were obtained on the basis of the calibration experiments of the tidal flat soils. The data are plotted for each species and growth stage as characterized by the individual weights. Note here that the threshold condition represents the situation where the sand bubbler crab cannot form burrows without suction. Figure 1 shows that for all the species and growth stages, there existed both suitable and critical conditions for burrowing, which differed considerably between species in a complex manner. This burrowing performance chart is named here the ecohabitat chart, which will be clarified in detail below.

3 VERIFICATION OF ECOHABITAT CHART

We performed field surveys at five natural and artificial intertidal flats located in Japan from 2009 to 2011. Specifically, we conducted integrated surveys of the geophysical environment and the species distributions during spring low tides at the Nojima intertidal flat in March 2009 and September 2010, at the Shirakawa intertidal flat in September 2009, at the Isumigawa intertidal flat in August 2009, at the Naha intertidal flat in June and December 2009 and February and September 2011, and at the Tokuyama artificial intertidal flat in September 2010 and June 2011. At each intertidal flat, we measured the spatial distributions of suction, groundwater level and vane shear strength, and collected undisturbed samples of surficial sediments of 50mm thickness, and subjected them to a series of laboratory soil tests to determine their grain size distributions, water content ratio w, specific gravity G_s, void ratio e, relative density D_r and the degree of saturation $S_r = G_s \cdot w/e$. At each location of the geophysical measurements described above, we took four core samples of 200mm diameter and 100mm thickness to obtain the density distributions (mean ± SE) of the two different bivalves of various growth stages, *R. philippinarum* (Manila clam) and *M. veneriformis* at the Shirakawa intertidal flat, and the burrow density distributions of the sand bubbler crab *S. globosa* and the decapod crustacean *C. japonica at* the Naha and Isumigawa intertidal flats, and measured and identified the species, individual densities and weights for each category of Arthropoda, Mollusca, and Annelida at the Tokuyama artificial intertidal flat. We compared the species distributions with the corresponding geophysical measurements obtained through these field surveys and laboratory tests, and analyzed them in light of the ecohabitat chart developed in this study.

At all the five natural and artificial intertidal flats, there

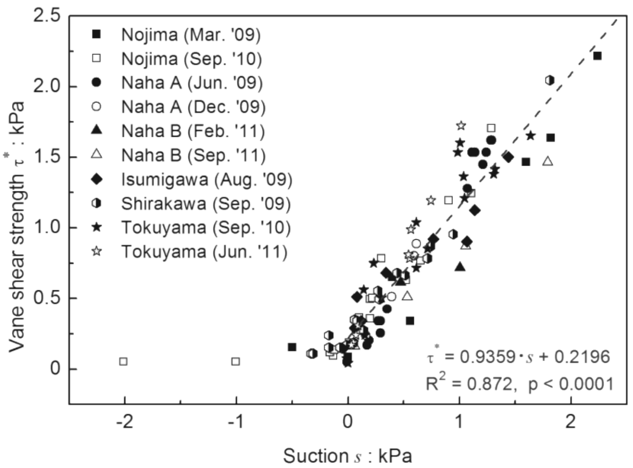

Figure 2. Relationship between suction and vane shear strength at five natural and artificial intertidal flats

was a strong correlation and unique interrelationship between suction and hardness of the surficial intertidal flat soils (Fig. 2). Indeed, the vane shear strength varied by a factor of 20–50 due to suction, that stemmed from the combined effects of suction development and suction-dynamics-induced cyclic elastoplastic soil compaction in the essentially saturated states (Sassa and Watabe, 2007). Such suction is found to be closely linked with the distributions of the various species as described below.

For the purpose of later discussion, the relationship between the shell lengths and wet weights of the two different bivalves, *R. philippinarum* (Manila clam) and *M. veneriformis* at the Shirakawa intertidal flat are shown in Fig. 3. We categorized adult and juvenile bivalves according to the shell length distributions in Fig. 4a. The individual densities of the juvenile and adult bivalves (mean ±SE) are plotted in Fig. 4b and c. The figure shows that for both Manila clam and *M. veneriformis,* the juveniles inhabited the area even where suction developed, but, the adults, particularly the adult Manila clams inhabited only the waterfront area where suction did not develop. Also, the peak density of the adult *M. veneriformis* manifested where the developed suctions were higher than those for the adult Manila clam. These field results are well consistent with the ecohabitat chart indicating the following. Namely, the burrowing capability of the Manila clam decreased considerably toward adult stages when the shell lengths exceeded 20mm corresponding to the wet weigths 1.5 to 2g in Fig. 3. This means that the adult Manila clam could not effectively burrow in denser soils as a consequence of the suction dynamics. Furthermore, the suitable geoenvironment for the adult *M. veneriformis* was above that for the adult Manila clam in the chart. This fact also conforms to the observed results.

Figure 5 shows the relationship between suction and burrow densities of the sand bubbler crab *S. globosa* and the decapod crustacean *C. japonica* at the Naha and Isumigawa intertidal flats. Both species inhabited the geoenvironment particular to each species, irrespective of the survey locations and periods. In fact, the individual densities increased markedly at suction equal to 1kPa for the *S. globosa*, and about 0.2kPa for the *C. japonica*. This observation conforms quantitatively to the ecohabitat chart showing that the suitable geoenvironment for *S. globosa* was well above that for *C. japonica*.

Figure 6 shows the relationship between suction and individual densities of Arthropoda, Mollusca, and Annelida at the Tokuyama artificial intertidal flat. The survey was conducted soon, one and half year, after the reclamation. It is seen that in the unsaturated region where suction exceeded the air-entry suction of the soils, the densities of all species declined, indicating the importance of water retention in soils for the survival of species. In the saturated region, the density of *C. erythraeensis* outnumbered the other species. This fact is also

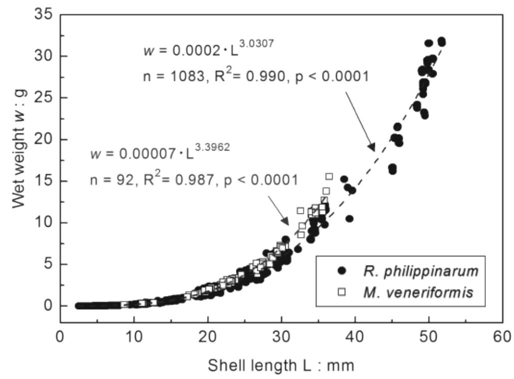

Figure 3. Relationships between shell length and wet weight of *R. philippinarum* and *M. veneriformis*

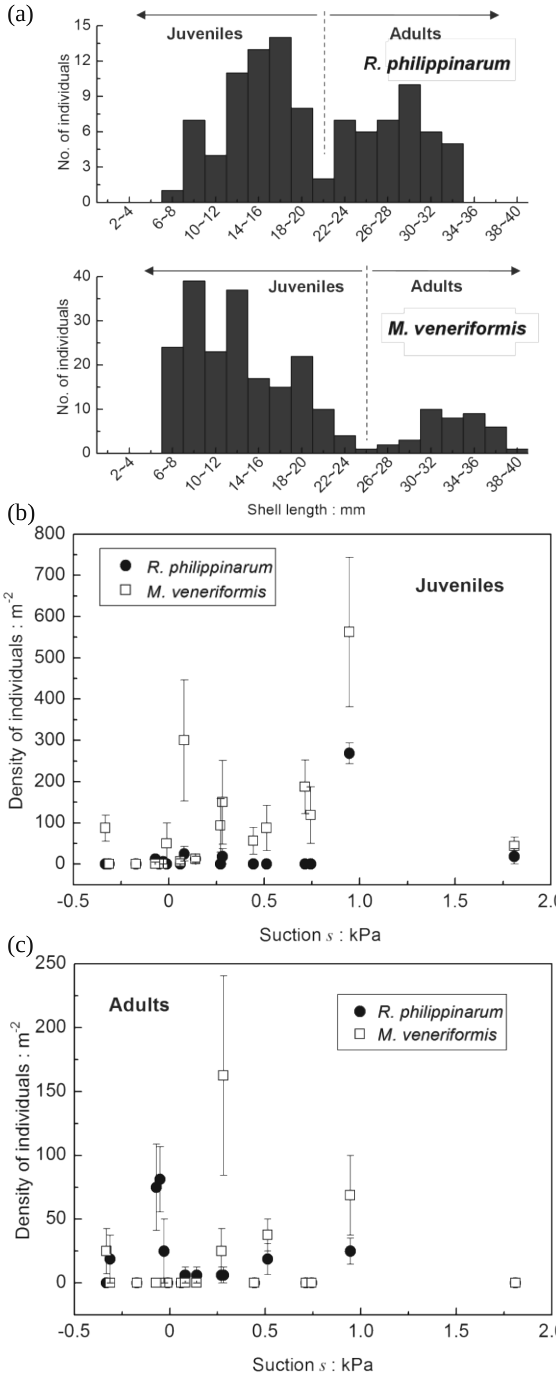

Figure 4. Relationships between suction and individual densities of the two different bivalves at the Shirakawa intertidal flat

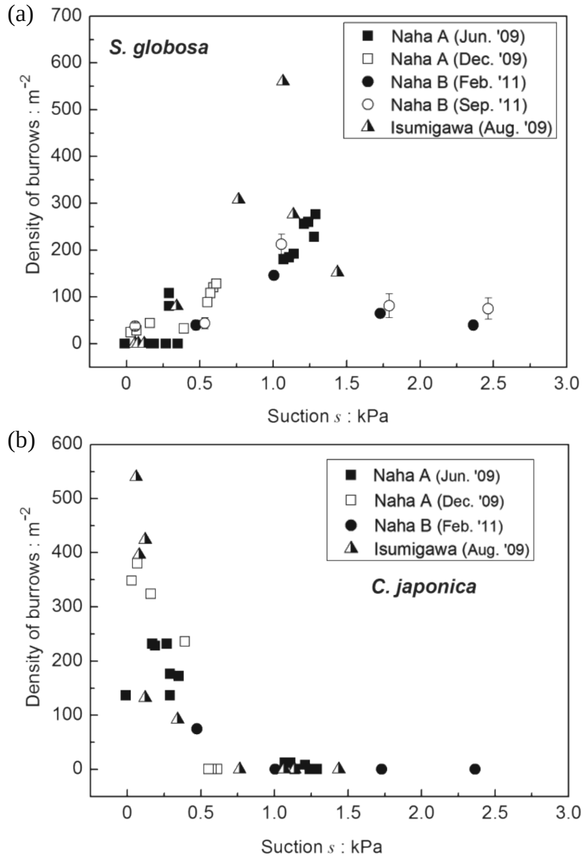

Figure 5. Relationships between suction and individual densities of the sand bubble crab and the decapod crustacean at three intertidal flats

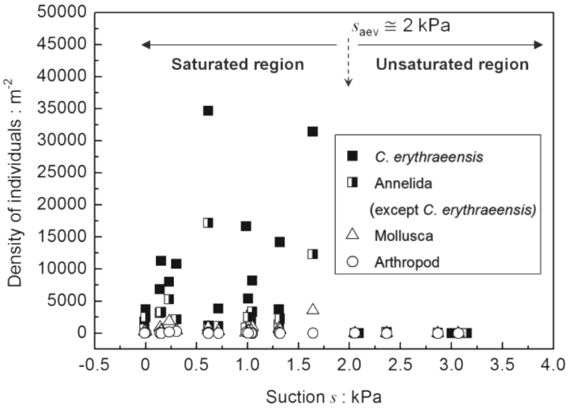

Figure 6. Relationships between suction and densities of Arthropoda, Mollusca, and Annelida at the Tokuyama artificial intertidal flat

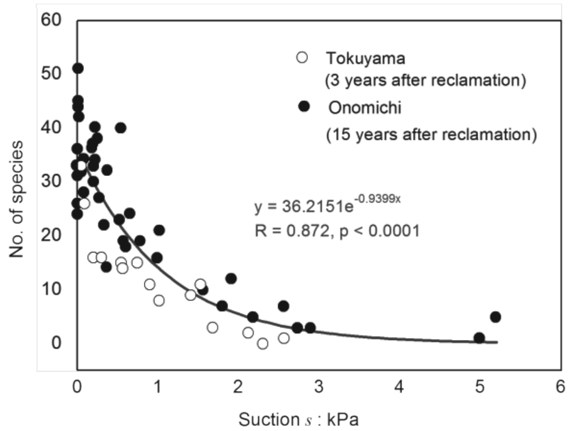

Figure 7. Relationships between suction and diversity of species at two different artificial intertidal flats

consistent with the ecohabitat chart showing that the burrowing capability of *C. erythraeensis* was markedly higher than other species and thereby exhibited the characteristics as the initial species inhabiting the reclaimed soils.

Figure 7 shows the relationship between suction and the number of species that was obtained three years after the reclamation at the Tokuyama artificial intertidal flat. For the purpose of comparison, the results of the field surveys conducted fifteen years after the reclamation at another artificial intertidal flat, the Onomichi flat, are also plotted in this figure. One can observe that there is a close correlation between the diversity of species and suction. This fact is in agreement with the ecohabitat chart demonstrating that the suction-induced geoenvironment governs the manifestation of suitable and critical conditions for the diverse species, and the number of species, which can adapt to a severer geoenvironment, decreases with increasing suction and shear strength. As such, these results indicate that the difference in the suitable and critical geoenvironment among species contributes significantly to the distributions of the diverse species inhabiting there.

4 CONCLUSION

In the present study, we investigated systematically the linkage between the waterfront geoenvironment and the burrowing activity of six species of invertebrates in intertidal flats through a series of controlled laboratory experiments on the benthos-soil systems. The experimental results elucidate for the first time that there exist both suitable and critical geoenvironmental conditions for the burrowing activities of the diverse species irrespective of burrowing types, growth stages and weights. On the basis of these results, we have developed an ecohabitat chart which reveals complex interrelationships between such suitable and critical geoenvironment among species.

In order to clarify the validity of the chart, we performed integrated field observations, surveys and analyses concerning the waterfront geoenvironment and the species distributions at five natural and artificial intertidal flats. The results demonstrate that the way and where the diverse species lived are well consistent with the ecohabitat chart developed in this study.

Overall, these results succeed not only in answering the fundamental question of why intertidal flats foster a complex ecosystem by the diverse species, from a view point of Ecological Geotechnics, but also establishing a new rational basis which can facilitate the conservation and restoration of habitats with rich natural ecosystems in intertidal zones.

5 REFERENCES

COP10. 2010. Strategic Plan for Biodiversity 2011-2020, tenth meeting of the Conference of the Parties (COP10).

Kuwae T., Miyoshi E., Sassa S. and Watabe Y. 2010. Foraging mode shift in varying environmental conditions by dunlin *Calidris alpine*. *Marine Ecology Progress Series* 406, 281-289.

Sassa S. and Watabe Y. 2007. Role of suction dynamics in evolution of intertidal sandy flats: Field evidence, experiments, and theoretical model. *Journal of Geophysical Research* 112, F01003, doi:10.1029/2006JF000575.

Sassa S. and Watabe Y. 2008. Threshold, optimum and critical geoenvironmental conditions for burrowing activity of sand bubbler crab, *Scopimera globosa*. *Marine Ecology Progress Series* 354, 191-199.

Sassa S. and Watabe Y. 2009. Ecological Geotechnics: Performance of benthos activities controlled by suction, voids and shear strength in tidal flat soils. *Proc. 17th Int. Conf. on Soil Mechanics and Geotechnical Engineering*, ISSMGE, Egypt, 316-319.

Sassa S., Watabe Y., Yang S. and Kuwae T. 2011. Burrowing Criteria and Burrowing Mode Adjustment in Bivalves to Varying Geoenvironmental Conditions in Intertidal Flats and Beaches. *PLoS ONE* 6, No.9: e25041, doi:10.1371/journal.pone.0025041.

A New Approach for Characterizing Shear Strength of Municipal Solid Waste for Land Fill Design

Une nouvelle approche pour la caractérisation de la résistance au cisaillement des déchets urbains pour la conception des décharges

Singh S.
Santa Clara University

ABSTRACT: Many researchers have characterized shear strength properties of municipal solid waste (MSW) by proposing Mohr-Coulomb strength envelopes derived from their experimental data. Still others reported results in terms of the same parameters after obtaining the data from back-calculations of failed landfills. A factor which has not been paid much attention to is the highly compressible nature of MSW. Variability in the unit weights, due to high compressibility of MSW, observed in the samples tested at increasing confining pressures invalidate the use of a common Mohr-Coulomb envelope for these samples. This paper critically examines the impact of the high compressibility of MSW on the development of Mohr-Coulomb strength parameters. It is argued that a single Mohr-Coulomb envelope does not account for the high compressibility of MSW. A new approach based upon the use of 'Strength versus Depth' plot has been proposed.

RÉSUMÉ : De nombreux chercheurs ont caractérisé les propriétés de résistance au cisaillement des déchets urbains (MSW) en proposant des enveloppes de résistance de type Mohr-Coulomb issues de leurs données expérimentales. D'autres encore ont présenté des valeurs obtenues par analyse inverse de ces mêmes paramètres, à partir de cas de glissements observés dans des décharges. Un facteur auquel n'a pas été accordé beaucoup d'attention est la nature hautement compressible des déchets. La variabilité massique, du fait de la forte compressibilité des déchets, qui est observée dans les échantillons soumis à une pression de confinement croissante invalide l'utilisation d'une enveloppe de Mohr-Coulomb pour ces échantillons. Cet article examine de manière critique l'impact de la forte compressibilité des déchets sur le développement des paramètres de résistance de Mohr-Coulomb. Une enveloppe unique de Mohr-Coulomb ne permet pas de tenir compte de la forte compressibilité des déchets. Une nouvelle approche basée sur la dépendance de la résistance avec la profondeur est proposée.

KEYWORDS: Municipal Solid Waste, Shear Strength, Mohr-Coulomb concept.

1 INTRODUCTION

Every day, the United States alone generates millions of tons of municipal waste solid waste (MSW) that must be processed. Landfilling is the least expensive method of waste disposal and landfills are being built to unprecedented heights. Landfill failures can expose the public to a variety of health hazards and can also create ecological and environmental disasters. These and other reasons make the determination of design parameters for landfills a growing field of interest. Geotechnical parameters are important for the design of each of the subsystems such as waste mass slope and height and the containment systems.. The parameter of shear strength is important for both seismic and static slope stability. Over the past decade, there have been several publishing's on shear strength of MSW as it pertains to seismic and static slope stability. The data presented in these publishings, however, reflects the variability of MSW in regards to constituents and location. . Many question the applicability of Mohr Coulomb concept with MSW and the effect of age and compressibility on the evaluation of its strength parameters still remains unanswered. Nearly vertical slopes in the MSW landfills observed all over the world cannot be explained by the frictional strength envelopes derived using Mohr-Coulomb Approach. Accordingly, no clear cut way for characterizing the shear strength of MSW has emerged. This paper attempts to progress in this direction.

2 ALTERNATIVES FOR CHARACTERIZING STRENGTH OF MUNICPAL SOLID WASTE

In the slope stability analysis of Municipal Solid Waste (MSW) landfills, shear strength properties of the MSW are of high importance. There have been different approaches to characterize the shear strength properties of MSW. Fassett, et al. (1994) presented a summary and analyses of MSW strength properties and brought into focus the limitation of existing approaches used to characterize shear strength properties of MSW. Characterization has essentially been attempted in two ways. Singh and Murphy (1990) summarized existing data from laboratory test back-calculations and from in-situ testing and recommended a range of strength parameters for MSW; cohesion (*c*) and internal friction angle (Φ). Howland and Landva (1992) used an alternate method and expressed MSW strength in terms of mobilized shear strength (τ_m) and normal stress (σ_n). Howland and Landva considered the strength of MSW to be primarily frictional in nature. In terms of Mohr-Coulomb parameters, the relationship between shear strength and normal stress developed by Howland and Landva gave a *c* equal to 10 kPa and Φ equal to 23 degrees as a lower bound to their data. Howard and Landva summarized MSW strength data reported in the literature on four cases (New Jersey Landfill Failure, California Landfill Load Test, Laboratory Direct-Shear Tests and Field Direct Shear Tests). The data (figure 3 of their paper) was plotted as mobilized shear strength and average normal stress. Only the lower bound values were reported. No upper bound values were estimated or reported. Kavazanjian, et al. (1995) used an approach similar to that of Howland and Landva, however, Kavazanjian relied more on back calculationed data from case histories and in-situ testing than they did on laboratory data. Kavazanjian adopted a bilinear representation of the MSW shear strength using Mohr-Coulomb parameters. Their data suggested that up to the normal stress of 30 kPa no increase in the shear strength was noted. Accordingly, they suggested that at normal stress below 30 kPa, the Mohr-Coulomb parameters were $\Phi = 0$ and $c = 24$ kPa, and above normal stress of 30 kPa, the parameters were $c = 0$ and $\Phi = 33°$. More recently, Kavanzanjian, 1999, Zekkos, 2005, and Bray et al., (2009), have characterized shear strength properties by proposing Mohr-Coulomb strength envelopes derived from their experimental data (Fig. 1).

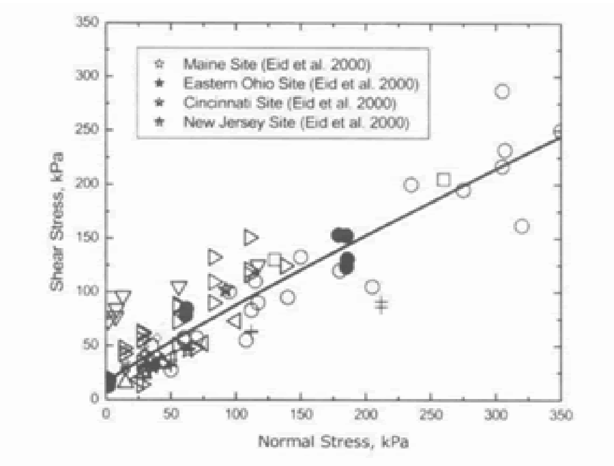

Figure 1 Recommended static shear strength of MSW based primarily on direct shear tests and field observation of slope stability. Bray et al. (2009)

Still others reported results in terms of the same parameters after obtaining data from back calculations of failed landfills (Kavazanjian, 2001, Eid, et al. 2000). Figure 2 presents data from various sources.

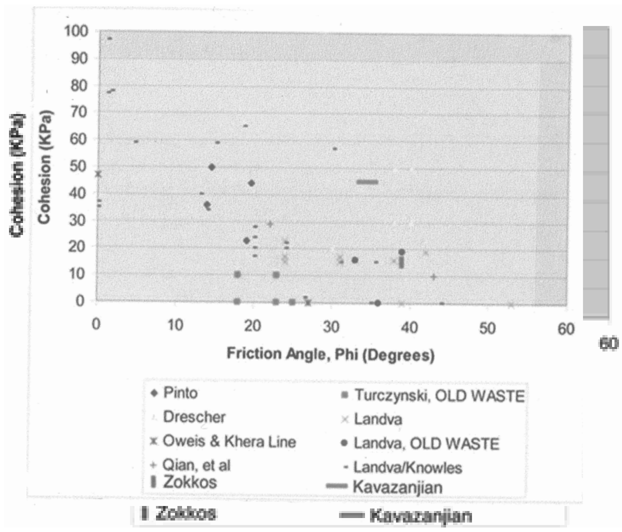

Figure 2 Lab Test or Institute Testing on MSW

Other researchers believed the variability they observed in their samples was too great for Mohr-Coulomb parameters to be usefully developed for each sample tested (Siegel, et al., 1990). For example, Siegel, et. al, (1990) tested samples from the OII landfill, perhaps the most studied landfill, in Monterey Los Angeles area and made the observation that given the refuse variability, deriving Mohr-Coulomb angles of internal friction and cohesion intercepts for individual samples was inappropriate. Singh and Murphy (1990) suggested that Mohr-Coulomb's theory might not be applicable to characterizing the shear strength of MSW.

The cause of this controversy is that while shearing, the strength mobilization rates for MSW and soils are quite different. The MSW behaves as a strain hardening material, i.e., even at large shear strains, it will continue to mobilize additional shear stress without exhibiting a leveling off or drop in shear stress or developing a failure plane typical of soils. In limit equilibrium analyses, such as what is used in slope stability analysis, the basic assumption is that the peak strength mobilization occurs at the same time along the entire failure surface. Because of the incompatibility of strains at which peak strength is mobilized in MSW, in soils, and along liner interfaces, the limit equilibrium analyses need to use reduced shear strength of MSW or the residual strength of soil and the interfaces (Mitchell et al. 1995).

3 COHESIVE PROPERTIES OF MUNICIPAL SOLID WASTE

The shear strength of the MSW is similar to a soil in many ways. It can be thought of for conceptual purposes (and many argue for other purposes as well) as a fibrous soil (Zekkos, 2008). Direct shear tests by Landva and others have shown that the shear strength of MSW depends on the nature of the test (Qian et al., 2002).

MSW can exhibit a kind of behavior while shearing, which is typically cohesion, but is seen by others as only apparent cohesion. Some call this apparent cohesion-'adhesion' (Qian et. al., 2002). This behavior comes about mainly because MSW is a hodgepodge of different materials with different shapes. The interlock of these odd-sized 'grains' causes the MSW to exhibit behavior similar to what is called cohesion in clay soils. In clay, cohesion is the result of water and associated electrical charges, although the critical state concept considers cohesion even in clays resulting from interlocking (Schofield, 2005). The cohesion in the MSW is the result of mechanical interlock. As MSW degrades with age the effect of the interlock would decrease and the cohesion should drop. Accordingly, cohesion in MSW cannot be treated as a constant parameter. Though, the root cause of the behavior differs from that in soils, the observed behavior is quite similar. Cohesion is observed in MSW although it can be correctly termed apparent cohesion. Cohesion has been observed in data on actual waste than in model wastes. The cohesive behavior of MSW is also reinforced in practice by the abundance of incidents in which vertical or nearly vertical cuts remain stable for years without any signs of failure (Qian et. al., 2002).

4 DATA FROM MODEL WASTE EXPERIMENTS

Testing of artificial waste and model waste provided data points with no cohesion (Thusyanthan et al, 2004).

5 DATA FROM CASE HISTORIES

As was mentioned earlier, another method of collecting shear strength data is back-calculations based on case histories. In almost all of the cases, the shear strength data was obtained after a landfill failure. The most common method was to assume a factor of safety equal to unity and back-calculate the shear strength of the MSW involved using standard geotechnical analysis. In this study, only case studies using a factor of safety equal to one for failure analysis were reported. Other case studies estimate the factor of safety and then back-calculate shear strength parameters. However, the shear strength values are very sensitive to changes in the factor of safety, and the factor of safety can't be known with certainty unless failure occurs. The most common details presented by the researchers, and the techniques used to calculate the shear parameters are given in Qian, et al., 2002 and Zekkos (2005) among others.

It is of interest that every case history for which shear strength was found, yielded data with cohesion. It should also be noted that the lowest cohesion is reported by Seed and Boulanger (1992), and it is the lower bound for five case studies reported by Howland and Landva (1992). All the case history data led to the determination that MSW does indeed have cohesive properties. However, no clear trendline emerged from the data, although a general decrease in cohesion as the friction angle increases was observed.

6 COMPRESSIBLITY OF MSW

An additional factor which has not been paid much attention is the highly compressible nature of MSW. Most of the test data on the shear strength of MSW has been presented without accounting for the significant volume changes that take place associated with high confining pressures. Tests at high confining pressures by Chen et al. (2008) (fig 3) showed that owing to the high compressibility of MSW, volume changes at high confining pressures are significant. Accordingly, these high volume changes should result in changes in the unit weight and hence in the shear strength. Bray et al. (2009) noted that the effect of unit weight on the shear strength is significant. Accordingly, the large compressibility of MSW would invalidate the attempt to use a single Mohr Coulomb envelope to tests on samples at widely varying unit weights at high normal stresses.

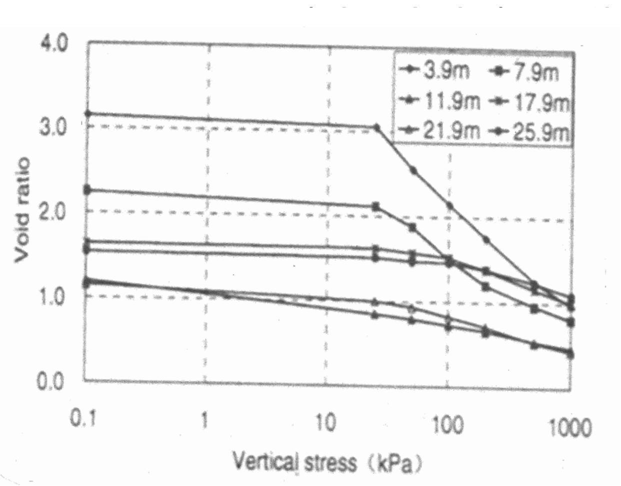

Figure 3 Compression curves for the samples taken from BH5 (chen et al, 2008).

It is therefore suggested that for high landfills, a plot of shear strength verses depth can better represent the effect of compressibility, unit weight, and high confining pressures than a single Mohr Coulomb envelope. Also, field measurements of density and shear strength supplemented with back calculation of well documented case histories appear to be the most logical mean of obtaining MSW strength information. These are some of the important issues which should be considered when applying geotechnical considerations in characterization of shear strength of MSW.

6 CONCLUSIONS

1. It is suggested that due to the large compressibility of MSW at high normal stresses, a single Mohr Coulomb shear envelope for a landfill may not be applicable.

2. The use of strength versus depth plot is more appropriate for characterizing shear strength of MSW, especially for high landfills.

7 ACKNOWLEDGEMENTS

Melanie Massie and Paige Rogalski's assistance in the preparation of this paper is gratefully acknowledged.

8 REFERENCES

Bray, Jonathan D., Zekkos, D., Kavazanjian, E., Athanasopoulos, G. A., Riemer, M. F. (2010) "Shear Strength of Municipal Solid Waste." ASCE Journal of Geotechnical & Environmental Engineering. June 2009.

Chen, Y., Zhan, T.L.T., and Ling, Wei-an, (2008), Mechanical Properties of Municipal Solid Waste from Suzhou Landfill in China, "Proceedings of Geo-Congress 2008, ASCE New Orleans March 9-12, 2008.

Fassett, J. B., Leonards, G.A., and Repetto, P. C. (1994) "Geotechnical Properties of Municipal Solid Wastes and Their Use in Landfill Design," Proc. WasteTech '94, Charleston, SC, National Solid Waste Management Association, Washington, D.C.

Howland, J. D. and Landva, A. O. (1992), "Stability Analysis of a Municipal Solid Waste Landfill." Proceedings, Stability and Performance of Slopes and Embankments – II, Vol, 2, Geotechnical Special Publication No. 31, ASCE, New York, NY.

Kavazanjian, E., Jr., Matasović, N., Bonaparte, R., and Schmertmann, G. R. (1995) "Evaluation of MSW Properties for Seismic Analysis" Accepted for publication, Proc. GeoEnvironment 2000, Special Geotechnical Publication, ASCE.

Kavazanjian, E, Jr., Mataxovic, N. and Bachus, R.C. (1999). "Large-diameter static and cyclic laboratory testing of Municipal Solid Waste." Proceedings, Sardinia 1999, 7th International Waste Management and Landfill Symposium, 4-8 October.

Mitchell, R.A., and Mitchel, J.K., (1992) "Stability Evaluation of Waste Landfills," Proceedings of ASCE Specialty Conference on Stability and Performance of Slopes and Embankments – II, Berkeley, California, June 28 – July 1.

Singh, S. and Murphy, B.J., (1990), "Evaluation of the Stability of Sanitary Landfills," In: *Geotechnics of Waste Fills – Theory and Practice*, ASTM STP 1070, pp. 240-258.

Zekkos (Zeccos), D. P. (2005), Evaluation of static and dynamic properties of Municipal Solid-Waste," Dissertation submitted in partial fulfillment of the requirements for the degree of Doctor of Philosophy, Department of Civil and Environmental Engineering, University of California, Berkeley, Fall. Also available at http://waste.geoengineer.org

The role of molecular biology in geotechnical engineering

Le rôle de la biologie moléculaire en géotechnique

Stewart D.I. , Fuller S.J.
School of Civil Engineering, University of Leeds, Leeds, UK

Burke I.T., Whittleston R.A., Lockwood C.L.
School of Earth and Environment, University of Leeds, Leeds, UK

Baker A.
School of Biology, University of Leeds, Leeds, UK.

ABSTRACT: This paper reviews techniques from molecular biology for characterising microbial populations that are accessible to Geotechnical or Geo-Environmental Engineers. With reference to data from contaminated land studies, it discusses which techniques it might be appropriate to use in an engineering context, how the data generated can be visualised and interpreted, and the dangers of over interpretation. Finally it reports on the capabilities of the latest high throughput next-generation sequencing platforms, and speculates on what engineering developments may result from this technological advance.

RÉSUMÉ: Ce document passe en revue les techniques de la biologie moléculaire pour la caractérisation des populations microbiennes qui sont accessibles aux ingénieurs géotechniques ou géo-environnementaux. En faisant référence aux données provenant d'études de terres contaminées, il aborde les techniques qu'il pourrait être approprié d'utiliser dans un contexte d'ingénierie, la manière dont les données générées peuvent être visualisées et interprétées, et les dangers d'une sur-interprétation. Enfin, il rend compte de la capacité des plateformes les plus récentes de séquençage à haut débit de prochaine génération, et s'interroge les développements techniques qu'il pourrait résulter de cette avancée technologique.

KEYWORDS: Geo-environment, Molecular Biology, DNA, rRNA, 16S gene sequencing

1 INTRODUCTION

In recent years Geotechnical and Geo-Environmental Engineers have started to exploit soil microorganisms, nature's catalysts, to deliver sustainable engineering solutions to big problems facing society. Such microorganisms obtain energy from catalysing thermodynamically favourable chemical reactions between natural soil constituents, but in the process can also catalyse chemical reactions that are of engineering interest. To date approaches such as monitored natural attenuation and active bioremediation have become well-established for the treatment of soils contaminated with petroleum hydrocarbons and organic solvents. However this field is about to expand rapidly, with techniques such as the reductive precipitation of contaminant metals and radionuclides, microbial induced calcite precipitation to improve soil strength, bacterially mediated phosphate recovery from waste streams and bacterially enhanced carbon capture likely to emerge from a research setting and into engineering practice in the near future.

What all these applications have in common is that they involve managing populations of microorganisms to bring about chemical transformations within an engineering context. Thus, if engineers are to manage these populations effectively, they need to characterise microbial populations to identify whether the necessary organisms are present, or better still to determine the genetic potential of the population to perform particular chemical transformations. In the near future engineers seeking better process control might wish to identify which metabolic pathways are active under particular conditions in order to predict which chemical transformations are about to occur.

To be able to quantify the contributions of microorganisms to a process, and ultimately to control that contribution, it is necessary to first know what organisms are present, secondly how this population changes with the conditions, and thirdly which organisms and conditions are the most important for achieving the desired outcome. Traditional microbiology methods involve culturing, identifying and enumerating the microorganisms present. However these suffer from a number of disadvantages; not all microorganisms can be cultured, the culture conditions selected can favour some species over others, and identification requires a high level of expertise in microbial taxonomy. In contrast methods based on nucleic acids, DNA and RNA the genetic material of all organisms, have become quick, simple and relatively cheap. A modest investment of a few thousand pounds can equip a laboratory for such analyses.

With the exception of some viruses the genome of all organisms is made up of DNA, Watson and Crick's famous double helix, in which two strands that run anti-parallel to one another are held together by H-bonds between complementary bases; A (adenine) always bonds with T (thymine), and G (guanine) with C (cytosine). This complementary base pairing allows each strand to provide the information for synthesis of its complementary strand during DNA replication. In the cell this process is carried out by enzymes called polymerases using building blocks called deoxynucleotide triphosphates (dNTPs) and is essential for cells to replicate. The DNA contains all the genes necessary to specify all structures and functions of the cell. As some processes (such as synthesising proteins) are fundamental to all cells, some genes are very similar in all organisms. Others play much more specialised roles and their presence can be used to infer the presence of specific organisms (see section 4). Fundamental to all the methods to be discussed is the ability to amplify and determine the sequence of specific sections of DNA from environmental samples. This allows inferences to be drawn about the presence or absence of organisms or to gain insights into the populations present and their dynamics.

2 THE POLYMERASE CHAIN REACTION (PCR)

The polymerase chain reaction (PCR) is a technique for replicating a selected section of a DNA fragment. It starts with one or two copies of the target section, and increases that by several orders of magnitude. PCR involves repeatedly heating and cooling the DNA using a piece of equipment known as a thermocycler. There are usually three discrete temperature steps. The first step is denaturation, which involves the highest temperature in the cycle (typically 94-95°C; Promega, 2012; Roche, 2011a). This separates the strands of double stranded DNA to act a template for DNA synthesis. The second step is annealing, which involves the lowest temperature in the cycle. In this step PCR primers become attached to the template DNA. PCR primers are short fragments of DNA which are designed and synthesised to match to the ends of a target section of DNA, and serve as a starting point for DNA replication. The annealing temperature depends on the properties of the primers being used, but is usually 42–65°C (Brown, 2001). The third step is extension where double stranded DNA is reconstructed base-pair by base-pair from dNTPs in the reaction mixture by the polymerase enzyme acting at the 3' end of the annealed primer (typical temperature 68-72°C). This three step cycle is repeated many times, with the amount of the target DNA fragment doubling (in theory) in each cycle. In practice there is initially exponential amplification, but it levels off with increasing numbers of cycles as the polymerase enzyme loses activity and the reagents (dNTPs and primers) are consumed until, eventually, no further product is produced. If the primers have been appropriately designed and the reaction conditions optimised only the target DNA fragment should be amplified.

The very high amplifications achieved by repeated cycling make PCR a very powerful technique, but users need to be aware of potential artefacts that can arise. The three main ones are contamination, polymerase errors and bias. The highly sensitive nature of PCR means that even low levels of contaminating DNA (from other samples or the laboratory environment) can lead to amplification of products that don't originate from the sample. Thus scrupulous cleanliness and the use of negative controls (where no DNA sample is added to the reaction) are mandatory. Small errors and slight biases in a single amplification cycle can over the course of many cycles lead to gross distortions in the representation of different fragments in the final PCR product. Thus, as a rule, data from an analysis involving a PCR reaction should be treated as qualitative rather than quantitative (the exception being where the more advanced tool of qPCR is used). PCR errors can arise due DNA polymerase errors (the Taq polymerase error rate is $\sim 3 \times 10^{-5}$ per nucleotide per duplication; Acinas et al. 2004), the formation of chimeric molecules, and the formation of heteroduplex molecules. The best way to avoid this type of problem is to avoid unnecessary over-amplification because such errors are cumulative (i.e. use the smallest possible number of PCR amplification cycles compatible with the intended application; Qiu et al. 2001; Acinas et al. 2005). For some purposes it may also be necessary to use a "proof-reading" polymerase enzyme with a far lower intrinsic error rate than Taq. PCR bias arises because of intrinsic differences in the amplification efficiency of different templates (e.g. due to differences in the GC-content). In late stages of amplification self-annealing of the most abundant templates can hinder their further amplification. PCR bias is reduced by using high template concentrations, performing fewer PCR cycles (Polz & Cavanaugh 1998) and by using a thermocycler that ramps quickly between the cycling temperatures (Acinas et al. 2005).

In Geo-Environmental Engineering PCR is most frequently used to characterise microorganisms or microbial populations. PCR is often used to amplify the same section of the same gene of different species of microorganisms in an environmental sample. The 16S rRNA gene is frequently used to identify microbes, and to study diversity, because it is present in all prokaryotic organisms (those without a nucleus, like bacteria). In this case the primers are targeted at two conserved regions of the gene where the base sequence is almost identical between widely different organisms because that part of the molecule encodes a function necessary for life so that the intervening region, which is more divergent, is amplified. The difference in sequence between the divergent regions can be used to infer evolutionary distance. PCR is also used to amplify sections of DNA between genes since these are often very variable in length and/or base sequence even for quite closely related species. An example of this approach is rRNA Intergenic Spacer analysis (RISA), which is often used for community fingerprinting with the aim of identifying when there has been a significant change in the microbial population.

3 CHARACTERISING MICROBIAL POPULATIONS

Simple PCR based techniques can identify that a particular gene is present within a microbial population, and to "fingerprint" bacterial populations to identify significant changes in population over time or under different conditions (section 4), but actually identifying the bacterial species present in a sample requires some method of separating out the individual DNA fragments in an environmental sample, and sequencing them.

The traditional approach to this problem is "cloning and sequencing" (see e.g. Islam et al. 2004). This approach starts with a PCR reaction on environmental DNA using broad specificity primers that target a suitable gene (usually the 16S rRNA gene). The resulting PCR product contains multiple copies of the target gene from all the species in the sample. These double stranded DNA fragments are then ligated to (joined-into) a standard cloning vector (e.g. pGEM-T, TOPO, etc.) to form circular double-stranded DNA molecules called plasmids. This is achieved with standard molecular biology kits available from suppliers such as Promega or Life Technologies. Each plasmid will contain a different DNA fragment from the PCR reaction. The plasmid is then "transformed" (inserted) into specially weakened laboratory strains of E-coli that lack resistance to antibiotics. The standard cloning vectors are designed to confer antibiotic resistance to any cell into which they are inserted, allowing selection of those cells that take up a plasmid. An important feature of the transformation is that it is very inefficient (which is why selection is necessary), and thus it is unlikely that more than one plasmid is inserted into a cell. The cells are then plated out on agar plates containing the antibiotic, so that only cells containing the plasmid grow. If this is done with care then bacterial colonies will grow on the plates so that each colony has grown from a single cell, and will thus contain copies of a single DNA fragment from the environmental sample. These cells can be harvested, and the plasmid they contain sent for gene sequencing. Figure 1 shows the bacterial population of soil from near a lime kiln waste tip determined by this technique (Burke et al. 2012). This showed that the bacterial population of the sample of buried soil was dominated by a single, unidentified species within the Comamonadaceae family of β-proteobacteria. Determination of the geochemical conditions allowed this study to postulate a link between anaerobic respiration of this specie and the

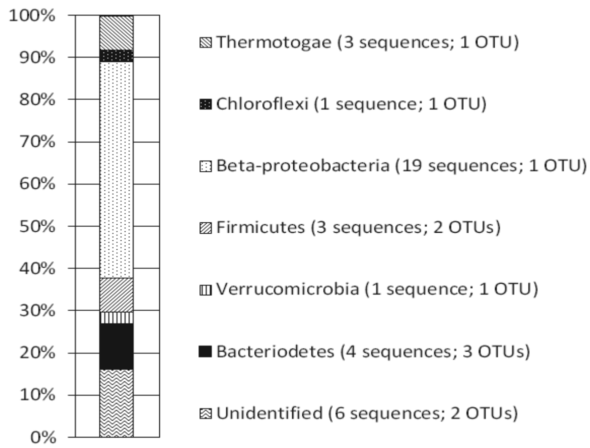

Figure 1. Phylogenetic diversity of 16S rRNA gene sequences extracted from sample. Key shows the number of OTUs within each phylum

reduction of nitrate in the groundwater.

DNA sequencing is relatively expensive, and therefore cheaper techniques for monitoring microbial populations are useful in order to decide whether more detailed analysis is required. There are several ways of "fingerprinting" a microbial population, the most useful of which, due to its simplicity of use and low cost, is probably RISA (Borneman, 1997). RISA exploits differences in the length of bacterial DNA between two genes: the 16S and 23S rRNA genes. This varies between 150 and 1500bp. The analysis uses a PCR that amplifies the intergenic spacer region using primers that target conserved sections of DNA (within the 16S and 23S genes) that flank the region (Cardinale, 2004). The PCR product is then size separated using agarose gel electrophoresis; the patterns in the bands that are visible on the gel image are a fingerprint for the bacterial population. Figure 2 shows a RISA gel image from a study of a soil/groundwater system investigating the effect of different amendments (bicarbonate and acetate) on the microbial population. The gel image shows that microbial populations were significantly different 175 days after amendment.

High-throughput sequencing (or next-generation sequencing) technologies read many thousands of sequences in parallel. There are a variety of "platforms" for high-throughput sequencing (see Metzker 2010 for a review), but for brevity this paper will focus on 454 pyrosequencing as, possibly, the most straight-forward approach to creating a 16S rRNA gene library. It employs an initial PCR reaction on a DNA sample to isolate the gene fragment of interest and attach "adapter" sequences to both ends of that fragment. Unique identifier codes can also be incorporated between the adaptor and the gene fragment at this stage so that several samples can be sequenced at same time and separated during subsequent analysis (potentially offering a cost saving). During pyrosequencing fragments of the template DNA are isolated by attaching them to microscopic DNA capture beads using the adaptor. These beads are suspended inside water droplets in an oil solution in separate picoliter-volume wells on a multi-well plate. A PCR reaction using a luciferase then generates a light signal from each well as individual nucleotides are added to a DNA strand, which can be read in parallel.

The Roche GS FLX Titanium system can sequence fragments of up to 600bp, including the adaptor sequences (Roche, 2011b), which is why it is suited to 16S rRNA library construction. However, because it requires an initial PCR to

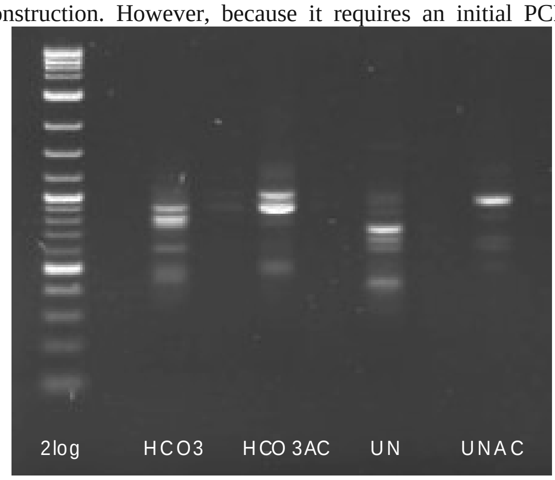

Figure 2. RISA signatures for soil-groundwater incubations with different amendments on day 175. HCO3 $\rightarrow HCO_3^-$ amended; HCO3AC $\rightarrow HCO_3^-$ & acetate amended; UN $\rightarrow$ unamended; UNAC $\rightarrow$ acetate amended, 2log $\rightarrow$ NEB 2-log DNA ladder

attach the adaptors, it does not escape from problems associated with PCR errors and bias, although a proof-reading polymerase and a low number of PCR cycles will minimise these effects. Other high-throughput sequencing approaches can directly sequence environmental samples without a PCR reaction to attach an adaptor sequence. These currently yield shorter read lengths than the approach described above, and the post sequencing analysis to identify the gene of interest is more complex, but it should be noted that this is a particularly fast moving area of scientific development, and direct sequencing of environmental samples may become the norm in the near future.

4 PCR TECHNIQUES FOR IDENTIFYING THE PRESENCE OF A MICROORGANISM

PCR is also used to identify the presence of a particular gene within a bacterial population. An example of this approach is to use a PCR reaction using primers that target the invA gene to identify the presence of Salmonella in a sample as this gene has very high specificity to Salmonella strains (Sunar et al. 2009). Figure 3 shows a gel image of a product from a PCR targeting invA gene of Salmonella (product at 285 bp). In this experiment DNA from an environmental sample was mixed with increasing concentrations of a competitor fragment (length 183bp), so that the number of gene copies could be estimated (so called competitive PCR).

5 IDENTIFYING THAT A SPECIFIC GENE IS BEING EXPRESSED UNDER THE PREVAILING CONDITIONS

DNA contains the genes of an organism but for these genes to perform their actions in the cell they must first be copied into RNA which is then usually converted into proteins. Proteins may be structural, or carry out chemical reactions. This process of copying genes into RNA is called transcription and when a gene is transcribed it is said to be expressed. Some genes are expressed under all or almost all conditions others are only expressed in specific situations, for example in the presence of a particular electron donor or acceptor. To monitor gene expression RT-PCR is commonly used. RT stands for reverse transcription and describes the process of copying RNA into DNA. In most cells information flows one way from DNA to RNA to protein (the central dogma) but enzymes called reverse transcriptases, isolated from some viruses, can copy RNA into DNA. PCR only works on DNA so to amplify sequences derived from RNA isolated from a sample an RT step has to be carried out first. Then PCR is carried out using primers for the gene whose expression is to be tested. This information will generally be qualitative unless conditions are carefully optimised to obtain quantitative data. Quantitative or qPCR generally monitors amplification in real time to ensure that the level of product in different reactions are compared within the exponential phase of the cycle, and by comparison to known standards either a relative or absolute number of gene copies can be calculated. qPCR allows monitoring of 10s of genes but

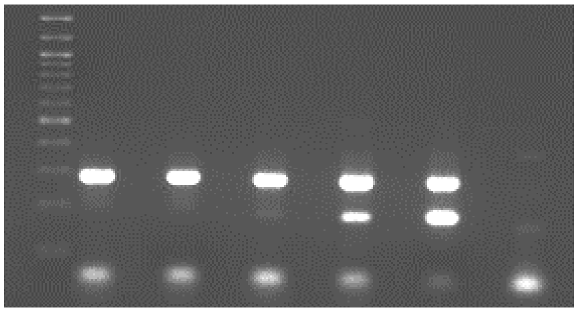

Figure 3: Agarose-TBE gel image showing the presence of the Salmonella invA gene (product at 285 bp). Samples contained an increasing concentration of a competitor fragment (product at 183bp)

high throughput technologies (RNA-seq: Wang et al. 2009) now allow analysis of all the genes being expressed by an organism at a given time (the transcriptome). However the use of this for environmental samples 'metatranscriptomics' is in its infancy (e.g. Marchetti et al. 2012).

6 GENE SEQUENCE DATA ANALYSIS

Sequence data is usually provided in a text file in FASTA format, where there a description line and then the sequence of nucleotides reported as single-letter codes (A,G,C,T). In a Geoenvironmental context, the purpose of sequencing a gene is usually to identify the species from which the sequence came. This is done by comparison with open-access databases such as GenBank (http://www.ncbi.nlm.nih.gov/genbank/), the EMBL nucleotide sequence database (http://www.ebi.ac.uk/embl/), or the DNA Data Bank of Japan (http://www.ddbj.nig.ac.jp/). These databases are maintained by public bodies in the USA, Europe and Japan collaborating as the International Nucleotide Sequence Database Collaboration (http://www.insdc.org/). Sequences obtained from samples can be compared with sequences in the database using a variety of free, public domain software. BLAST (Basic Local Alignment Search Tool) makes pair-wise comparisons with sequences in the chosen database and reports the statistically most significant matches. SEQMATCH available from the Ribosomal Database Project (http://rdp.cme.msu.edu/index.jsp) performs a similar function, and readily allows the user to restrict the quality of sequences to which matches are reported (e.g. type species, isolates, long read lengths, “good” quality).

CLASSIFIER, which is also available from the Ribosomal Database Project, is a naïve Bayesian Classifier that can place bacterial 16S rRNA sequences within Bergey’s Taxonomic Outline of the Prokaryotes (Wang et al. 2007). It is easy to use, and can be used for classifying single rRNA gene sequences or for the analysis of libraries of thousands of sequences.

For some types of analysis it may be necessary to align sequences from the same gene of different species prior to detailed analysis. An alignment is a way of arranging gene sequences to identify regions of similarity that indicate functional, structural, or evolutionary relationships between the sequences (Mount, 2004). There is a variety of open-access software available for aligning gene sequences, two of the more popular of which are ClustalW (Cluster Analysis) and MUSCLE (MUltiple Sequence Comparison by Log-Expectation) both of which are available from the European Bioinformatics Institute website (amongst other sources). Phylogentic relationships between the aligned sequences can be displayed as phylogenetic trees using software such as TreeView (http://taxonomy.zoology.gla.ac.uk/rod/treeview.html Page, 1996), or organised into “operational taxonomic units” (OTUs) using software such as MOTHUR (http://www.mothur.org/; Schloss et al., 2009). In this context an OTU is a grouping defined by sequence similarity, which can be set by the user to correspond roughly with phylum, class, order, family, genus, species, as appropriate. Rarefaction analysis (which can also be undertaken by MOTHUR) can characterize the diversity of a clone library using either rarefaction curves or a numerical indicator such as the Shannon Index (Krebs, 1999).

Next generation sequencing can produce 2-3 orders of magnitude more data than traditional approaches based on cloning and sequencing. Thus, while the basic stages in analysis are similar to the traditional approach, the task of applying it to many thousands of sequences in parallel usually requires the use of different software. The RDP project (described above) has a pyrosequencing pipeline that “processes and converts the data to formats suitable for common ecological and statistical packages”. Similarly, QIIME (Quantitative Insights Into Microbial Ecology) is an open source software package for analysing high-throughput amplicon sequencing data, such as 16S rRNA gene sequences (http://qiime.org/).

7 DISCUSSION AND CONCLUSIONS

Microbes can be expected to impact most if not all processes occurring in the geo-environment, and geotechnical engineers should be aware of the potential for harnessing microbial metabolism to bring about desired aims. PCR based methodologies permit the detection of the microbes present and how they change with changing conditions. PCR is relatively easy to use in an engineering setting and the availability of reagents in kit form along (with detailed protocols) means that the barriers to adoption are reasonably low. However this is a rapidly moving field and the advent of high throughput deep sequencing technologies have led to the development of ‘metagenomics’ and ‘metatranscriptomics’ which investigates the composite genetic potential of an ecological niche. Instrumentation and cost of sample analysis are still relatively high but likely to fall as capacity and technology increase. The sheer volume of data generated poses a significant challenge in terms of bioinformatics and fully exploiting these technologies will require multidisciplinary collaborations between engineers, molecular biologists and informaticians.

8 REFERENCES

Acinas S.G. et al. 2004. Fine-scale phylogenetic architecture of a complex bacterial community. Nature 430(6999), 551-554

Acinas, S. G. et al. 2005. "PCR-Induced Sequence Artifacts and Bias: Insights from Comparison of Two 16S rRNA Clone Libraries Constructed from the Same Sample." Appl. Environ. Microbiol. 71(12): 8966-8969.

Borneman, J. & Triplett, E.W. 1997. Molecular microbial diversity in soils from eastern Amazonia: evidence for unusual microorganisms and microbial population shifts associated with deforestation. Appl. Environ. Microbiol. 63:2647-2653

Burke, I.T. et al 2012. Biogeochemical reduction processes in a hyper-alkaline affected leachate soil profile. Geomicrobiology Journal 29 (9), 769–779.

Cardinale, M. et al. 2004 Comparison of different primer sets for use in automated ribosomal intergenic spacer analysis of complex bacterial communities. Appl. Environ. Microbiol. 70, 6147-6156.

Krebs, C.J. 1999. Ecological Methodology. Addison-Welsey Educational Publishers Inc, Menlo Park, CA.

Islam, F.S.. et al. 2004. Role of metal-reducing bacteria in arsenic release from Bengal delta sediments. Nature, 430, 6995, 68-71.

Marchetti, A., et al. 2012 Comparative metatranscriptomics identifies molecular bases for the physiological responses of phytoplankton to varying iron availability. PNAS www.pnas.org/cgi/doi/10.1073 /pnas.1118408109

Metzker, M.L. 2010 Sequencing technologies the next generation. Nature Reviews Genetics 11, 31-46.

Mount, D.W. 2004. Bioinformatics: Sequence and Genome Analysis. Cold Spring Harbor Laboratory Press: Cold Spring Harbor, NY.

Polz, M. F. and C. M. Cavanaugh 1998. "Bias in Template-to-Product Ratios in Multitemplate PCR." Appl. Environ. Microbiol. 64(10): 3724-3730.

Promega 2012. GoTaq® DNA Polymerase Protocol. http://www.promega.com/. Last accessed 4th December 2012

Qiu, X., Wu, L. et al. (2001). "Evaluation of PCR-Generated Chimeras, Mutations, and Heteroduplexes with 16S rRNA Gene-Based Cloning." Appl. Environ. Microbiol. 67(2): 880-887.

Roche 2011a. FastStart Taq DNA Polymerase dNTPpack: Version 7. https://cssportal.roche.com/. Last accessed 4th December 2012.

Roche 2011b. 454 Sequencing System Guidelines for Amplicon Experimental Design. http://my454.com/. Last accessed 10-12-12.

Sunar, N.M. et al. 2009. Enumeration of salmonella in compost material by a non-culture based method. Sardinia 2009: 12th Int. Waste Management and Landfill Symp., 1005-1006.

Page, R.D.M. 1996. TREEVIEW: An application to display phylogenetic trees on personal computers. Computer Applications in the Biosciences 12: 357-358.

Wang, Q. et al. 2007. Naive Bayesian classifier for rapid assignment of rRNA sequences into the new bacterial taxonomy, Appl. Environ. Microbiol. 73 5261–5267.

Wang, Z. et al. 2009. RNA-seq a revolutionary tool for transcriptomics. Nature Review Genetics 10 57-63

A System of dehydration, purification, and reduction for dredged soil – Release inhibition of nutrient salts from bed mud using natural zeolite

Un système de déshydratation, d'épuration et de réduction de sols dragués - Prévention du relâchement de sels nutritifs des lits de boue à l'aide d'une zéolithe naturelle

Umezaki T., Kawamura T.
Department of Civil Engineering, Shinshu University, Japan

ABSTRACT: In a closed water body such as a lake, many nutrient salts such as nitrogen and phosphorus are contained in bed mud deposited on the bottom. Their release is one of the causes of eutrophication. We propose a zero-emission system to preserve the ecosystem in a closed water body. Applying the system obviates landfill sites for dredged soil and reduces countermeasure costs. In the system, the bed mud is dredged and then reduced to the bottom after dehydration and purification treatments that reduce their volume and absorb nutrient salts. To realize a suitable bottom environment, reclaimed soil requires moderate flexibility. Consolidation tests were conducted on the bed mud with natural zeolite powder as absorbent, and column tests were also conducted for release inhibition of nutrient salts on the treated soil and lake water. Based on test results, the effectiveness of dehydration and purification was investigated. Main conclusions are as follows: Applying about 30 kPa of low consolidation pressure, water contents approach the liquid limit and the volume decreases to about two-thirds. For simulating the proposed system, the release of nutrient salts is inhibited and development of algae is prevented.

RÉSUMÉ : Dans un plan d'eau fermé tel qu'un lac, le lit de boue déposé au fond contient des sels nutritifs tels que l'azote et le phosphore. Leur libération est l'une des causes de l'eutrophisation. Nous proposons un dispositif sans émission pour préserver ce type d'écosystème. Le système permet d'éviter la mise en décharge de ces sols dragués et réduit les coûts économiques. Dans ce principe, le lit de boue est dragué puis redéposé au fond après déshydratation et purification pour en réduire son volume et absorber les sels nutritifs. Pour réaliser un environnement convenable au fond du plan d'eau, le sol récupéré exige une souplesse modérée. Des tests de consolidation sur de la boue avec de la poudre de zéolithe naturelle comme absorbant ont été effectués, ainsi que des essais en colonne pour inhiber le relâchement de sels nutritifs dans le sol traité et l'eau du lac. L'efficacité de la déshydratation et de la purification ont été étudiées sur la base de ces résultats. Les principales conclusions sont que l'application d'une pression de consolidation faible d'environ 30 kPa permet d'approcher la limite de liquidité des sols dont le volume diminue d'environ deux tiers. L'avantage du système proposé est de prévenir le relâchement de sels nutritifs et le développement d'algues.

KEYWORDS: closed water body, eutrophication, nutrient salts, bed mud, natural zeolite, consolidation, protection of ecosystem

1 INTRODUCTION

In a closed water body such as a lake, eutrophication is accelerated by nutrient salts such as nitrogen and phosphorus that inflow from rivers and which are released from bed mud deposited on the bottom. Many algae develop in the water, causing problems such as water pollution and offensive odors. Dredging of bed mud has been used as a countermeasure. However, dredging work is rarely conducted because of high transportation costs of dredged soil with high water content. Moreover, landfill sites are scarce.

As described herein, we propose a zero-emission system for ecosystem preservation in a closed water body. The system, as shown in Figure 1, dredges, dehydrates, purifies, and reduces bed mud. First, the system outline is discussed. Next, consolidation tests and column tests of bed mud simulating this system were conducted to verify the system effectiveness. Based on test results, dehydration, volume reduction, and release inhibition of nutrient salts from the treated soil were discussed.

2 A ZERO-EMISSION SYSTEM FOR ECOSYSTEM PROTECTION

Figure 1 shows an outline of the proposed system, which has three processes: (a) dredging, (b) dehydration and purification, and (c) reduction. The system concept is the following.

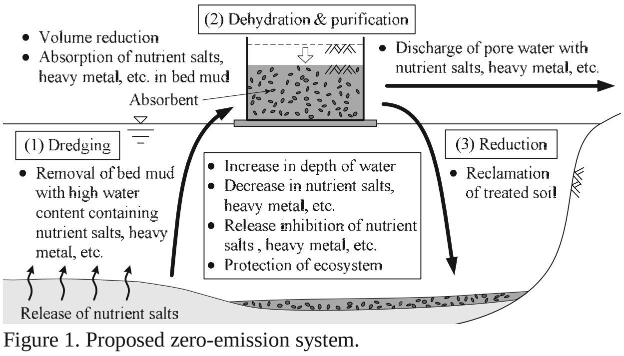

Figure 1. Proposed zero-emission system.

(1) To remove nutrient salts, heavy metals, etc. from the bed mud, the bed mud is dredged.
(2) By adding an environment-friendly adsorbent such as natural material to the bed mud, nutrient salts and heavy metals are adsorbed and immobilized.
(3) The volume of bed mud is reduced by dehydration, and nutrient salts and heavy metals are removed with drained water. After water quality analysis and suitable treatment, the drainage water is discharged.
(4) The treated soil is reclaimed to the bottom of the water and a zero-emission system is realized. The soil should be deformed flexibly with self-weight to avoid increasing the volume of reclaimed soil and release of nutrient salts from

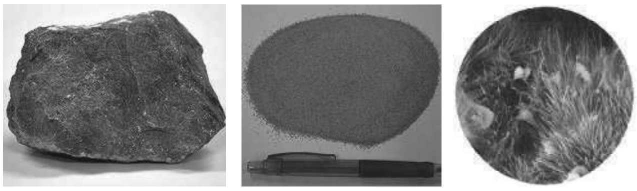

(a) Natural zeolite consists primarily of mordenite (b) Natural zeolite powder (under 0.5 mm) (c) Electron micrograph (MINDECO, 2012)

Photo 1. Natural zeolite (Shimane Prefecture, Japan).

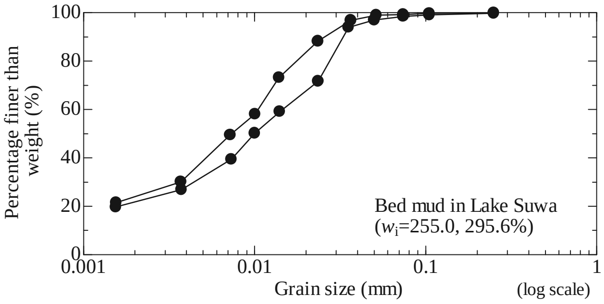

Figure 2. Grading curve of bed mud sampled in Lake Suwa.

Table 1. Physical properties of bed mud sampled in Lake Suwa.

w_i	255.0–295.6%	L_i	15.4–16.2%
ρ_s	2.520–2.582 g/cm^3	Clay fraction (%)	30–40%
w_L	155.0–165.0%	Silt fraction (%)	58–69%
w_P	102.0–104.2%	Sand fraction (%)	1–2%
I_P	53.0–61.3		

Table 2. Nutrient salt contents of dry bed mud.

Total nitrogen, T-N	3990–4200 mg/kg
Total phosphorus, T-P	1800–2000 mg/kg
Ammonia nitrogen, NH_4-N	248–258 mg/kg

Table 3. Nutrient salt contents of lake water.

Total nitrogen, T-N	0.48–0.52 mg/L
Total phosphorus, T-P	0.014–0.022 mg/L
Ammonia nitrogen, NH_4-N	0.03–0.09 mg/L
Chemical Oxygen Demand, COD	2.8–3.8 mg/L

no dredged bed mud. Simultaneously, a suitable environment for living things on the bottom of water, such as plants, insect nymphs, and shellfish, is formed.

(5) Increased water depth, release control of the nutrient salts, and immobilization of heavy metals are realized, and an ecosystem is preserved.

3 SAMPLES AND TEST PROCEDURES

3.1 *Natural zeolite*

Natural zeolite powder with particles smaller than 0.5 mm produced in Shimane Prefecture, Japan was used as an environment-friendly adsorbent (see Photo 1). The main mineral composition is mordenite (see Photo 1(a)), a light green, natural, inexpensive, and safe mineral produced from a mine. Zeolite, which contains large cavities and channels of angstrom scale (JSPS, 2006), exhibits characteristics of ion exchange and gas adsorption within its structural space. For the natural zeolite used for this study, the cavity size was 6.7–7.0Å (Photo 1(c), (MINDECO, 2012)) and the cation exchange capacity is CEC = 120–180 meq/100 g. The main application is soil improvement, water quality purification, etc., and it is useful to absorb ammonia, hydrogen sulfide, and nitrous acid from water, which cause bad odors (MINDECO, 2012). Moreover zeolite is effective as a bacteria carrier to resolve nutrient salts in the water (e.g. Popovici et al., 2011).

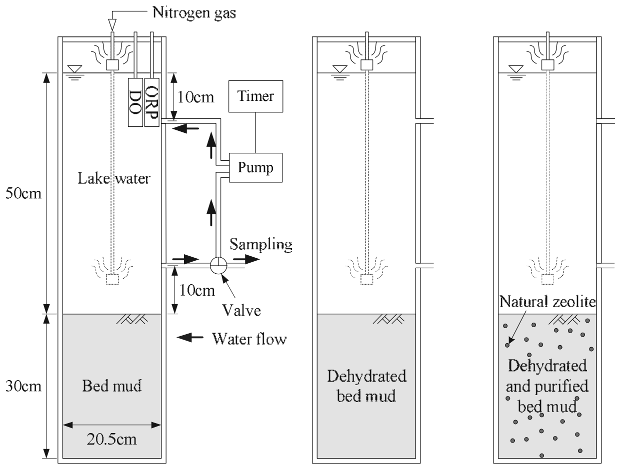

(a) Case A: Bed mud without treatment (b) Case B: Dehydrated bed mud (c) Case C: Dehydrated and Purified bed mud

Figure 3. Column test apparatus and test conditions.

Table 4. Conditions of column tests.

Case	Test conditions
Case A	Bed mud without treatment (water content, w_i=255.0%)
Case B	Bed mud (w_0=160.3%) dehydrated by consolidation
Case C	Bed mud (w_0=152.0%), to which was added 10% of natural zeolite powder for dry mass and dehydrated by consolidation

3.2 *Bed mud and lake water*

Bed mud was dredged using a grab type sampler at Lake Suwa in Nagano Prefecture, Japan. Lake water was sampled at the lakefront of Lake Suwa. The particle size distribution and physical properties of bed mud and content of the nutrient salts in bed mud and lake water are presented, respectively, in Figure 2 and Tables 1–3. In that figure and tables, w_i stands for the initial water content at dredging, ρ_s signifies the density of soil particle, w_L denotes the liquid limit, w_P represents the plasticity limit, I_P is the plasticity index, and L_i is the ignition loss. Tables 2 and 3 show contents of nutrient salts in bed mud as 3000–150,000 times greater than those in lake water. To improve eutrophication, countermeasures against bed mud are required.

3.3 *Consolidation test*

Two cases of the consolidation test of bed mud were conducted with and without natural zeolite powder. In one case, consolidation was conducted without natural zeolite (Case B in column test). In another case, 10% of natural zeolite powder (see Photo 1(b)), of which particle size is less than 0.5 mm, for the dry mass of bed mud was added and consolidation was conducted (Case C in column test). Consolidation pressure was increased step by step and the loading was continued until the water content calculated using drainage mass became w_L. Water quality analysis of the drainage water was conducted after consolidation. Analytical items are the total nitrogen (T-N), total phosphorus (T-P), ammonia nitrogen (NH_4-N), and chemical oxygen demand (COD). The analytical method followed Japanese Industrial Standards (JIS).

3.4 *Column test for release of nutrient salts*

Three column tests were conducted in reference to a manual of the Japan Sediments Management Association (2003). The outline and conditions of the test are presented in Figure 3 and Table 4. The bed mud was filled to 30 cm height into the acrylic cylinder with 20.5 cm inner diameter and 100 cm height. Moreover, lake water was poured carefully to 50 cm on the bed mud. A dissolved oxygen amount (DO) meter and oxidation reduction potential (ORP) meter were installed, and the top of the column was covered with a lid. Then, by the aeration of nitrogen gas near the bottom, lake water became an anaerobic condition (DO<1 mg/L), in which nutrient salts were released easily from bed mud. During the test, discharge of a slight amount of nitrogen gas was continued near the water surface to maintain an anaerobic condition. Circulation of lake water was performed. Tests were continued through 80 days. To verify the release inhibition effect, water quality analysis was conducted during a fixed period. All tests were conducted in a thermostatic chamber with room air temperature of 23±1°C in which the fluorescent light was illuminated continuously.

4 TEST RESULTS AND DISCUSSIONS

4.1 *Volume reduction and removal of nutrient salts through dehydration*

The relation of the water content w and the consolidation pressure p obtained from the consolidation tests is shown in Figure 4. A normal consolidation line was also obtained from the consolidation test using incremental loading. Initial water contents of the bed mud, w_i, were about 300% (Cases A and B). Furthermore, it is a slime-like condition as shown in Photo 2(a). The water content after adding natural zeolite powder, w_i^*, decreases slightly (Case C). However in Cases B and C, by application of 30 kPa of low consolidation pressure, the relation between w and p is almost identical. The volume decreased to about two-thirds and the water content becomes about w_L. The bed mud condition changes to a moderate consistency with flexibility by self-weight (see Photo 2(b)). The bed mud with w_L has workability for reclamation. Furthermore, it is expected that a suitable environment for living things on the bottom and realize inhibition of nutrient salts (see 2(3) and 2(4)). If 200 kPa of consolidation pressure is applied, then the water content becomes about w_P. The condition with w_P is hard and flexibility passes away. The consolidation pressure of the filter press, which is generally used to dehydration work, is too high. Using a simple dehydration machine, the countermeasure cost can be curtailed.

Figures 5(a)–5(d) show contents of T-N, T-P, NH_4-N, and COD in the drainage water and lake water. In Case B without natural zeolite, these contents are 28, 62, 4.2, and 2.4 times of lake water respectively, the nutrient salts in bed mud can be removed with drainage water. For Case C with natural zeolite powder, they are, respectively, 7.9, 11, 6.8, and 3.9 times. The contents of T-N and NH_4-N decrease to about one-fourth and one-sixth of Case B because of the adsorption effect of natural zeolite. The values of T-N, T-P, and COD are larger than those of water quality standards for lakes in Japan. However, the contents of all cases are much smaller than in original bed mud (Table 2). The values of contents in bed mud for Cases B and C differ only slightly from the initial value.

4.2 *Release inhibition of nutrient salts from bed mud*

The conditions of lake water at the initial stage and after 40 days are presented in Photos 3(a)–3(d). The lake water at the beginning of test is almost clear (Photo 3(a)). In Cases A and B without natural zeolite powder, the lake water gradually becomes turbid (Photos 3(b) and 3(c)). In Case A with no treatment, algae begin to increase in the lake water after about 20 days; the color becomes green. After 40 days, the luxuriance of algae reaches a peak, with adhesion of algae on the inner surface of container (Photo 3(b)). The algae in the column are cyanobacteria, which generate oxygen by photosynthesis because of increase in DO from 30 days, which is not shown. After about 60 days, the green water gradually pales. In Case B,

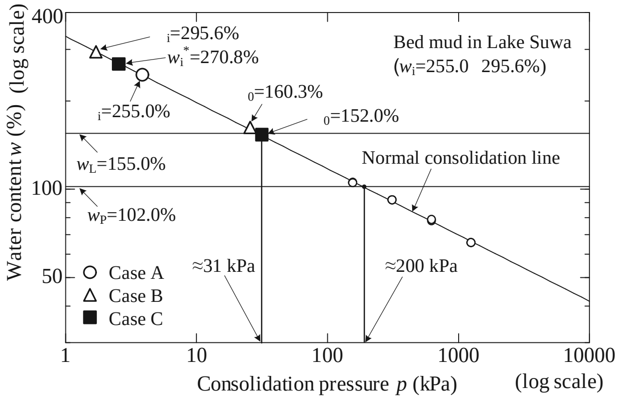

Figure 4. Relation between water content and consolidation pressure.

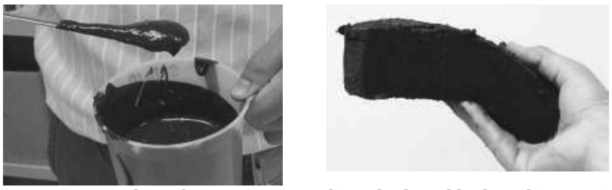

(a) Initial condition (b) Dehydrated bed mud (Case C)

Photo 2. Dehydration of bed mud by consolidation.

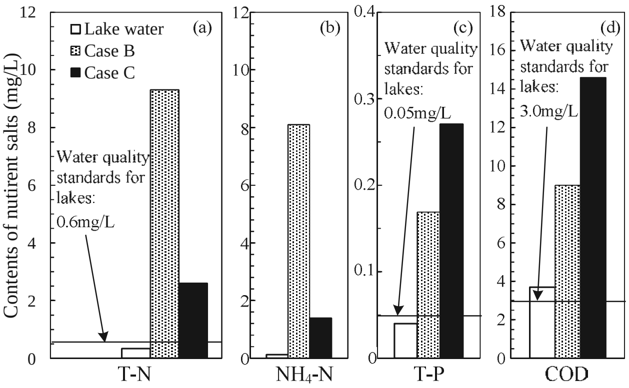

Figure 5. Nutrient salt contents in drainage water.

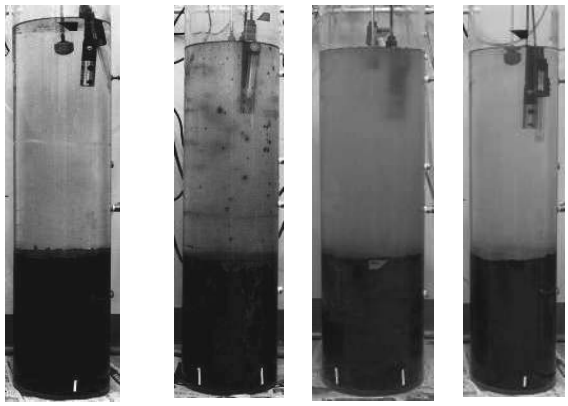

(a) Initial condition (b) Case A (c) Case B (d) Case C

Photo 3. Test results obtained after 40 days.

which was dehydrated by consolidation, algae regarded as cyanobacteria increase and the lake water color changes as well as Case A (Photo 3(c)). However algae are not observed on the container inner surface. In Case C, to which was added natural zeolite powder and dehydrated by consolidation, algae cannot be found in the lake water, and the lake water color changes only slightly (Photo 3(d)).

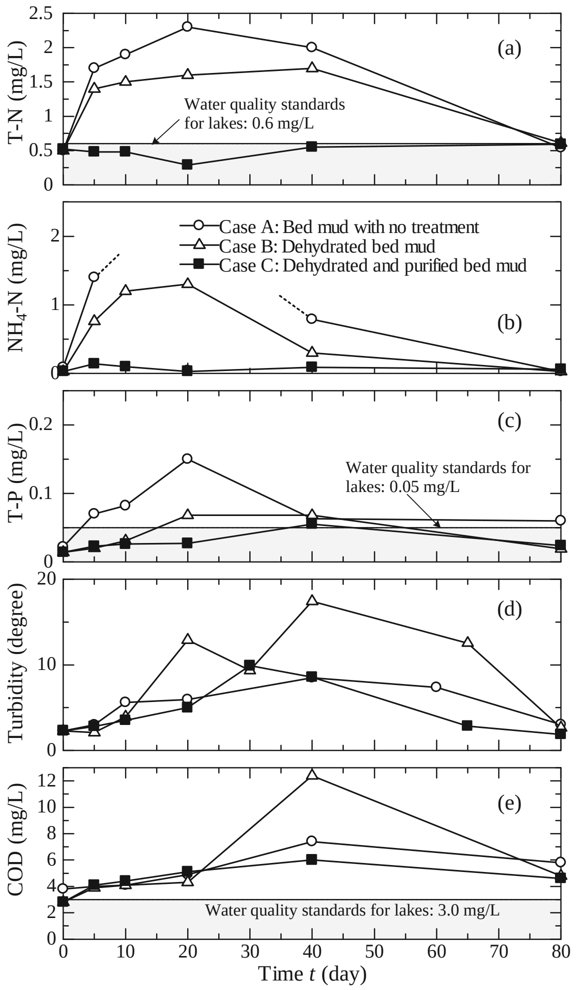

Figure 6. Analysis results of water quality.

Figures 6(a)–6(e) present some analysis results of lake water. The initial T-N and T-P values are about 0.5 and 0.02 mg/L, which are below the water quality standards for a lake in Japan. The initial values of COD are 3–4 mg/L, that of Case A is slightly larger than the standard value.

In Cases A and B without natural zeolite powder, the values of T-N, NH_4-N, and T-P increase greatly with elapsed time until after about 20 days (Figures 6(a)–6(c)). Compared to the water quality standards for a lake in Japan, the values of T-N after 20 days are 3.8 and 2.7 times, and those of T-P after 20 days are 3 and 1.4 times, respectively. The release of nutrient salts from bed mud is great and no release inhibition effect by dehydration is observed. Subsequently, these values decrease gradually. The values of T-N and NH_4-N after 80 days decrease nearly to initial values and that of T-P decreases to the standard value after 40 days. The decrease in nutrient salts is thought to result from digestion of cyanobacteria. The turbidity and COD increase gradually and reach a peak after about 40 days; they decrease gradually thereafter (Figures 6(d) and 6(e)). These tendencies are likely related to cyanobacteria development.

However, in Case C with natural zeolite powder, the values of T-N and T-P are maintained as lower than the values of water quality standards, and that of NH_4-N is almost maintained initial value. The value of T-N after 20 days decreases to half the standard value (Figures 6(a)–6(c)). Algae do not grow in the lake water (Photo 3(d)). The release inhibition effect of natural zeolite is recognized. The absorption effect for nitrogen in the lake water is also recognized. However, the values of turbidity and COD increase gradually as well as Cases A and B (Figures 6(d) and 6(e)). The value of COD exceeds the standard value. It is probably the increase in dissolved organic matter in lake water. Therefore, additional countermeasures against COD are required.

5 CONCLUSIONS

A zero-emission system was proposed for preservation of the ecosystem in a closed water body. The system has three processes: (a) dredging, (b) dehydration and purification, and (c) reduction. Consolidation tests and column tests for bed mud and lake water sampled in Lake Suwa, Japan were conducted simulating this system. Natural zeolite powder was used as the absorbent for purification. Based on the test results, the effectiveness of the system was examined. Main conclusions are as follows.

(1) Applying about 30 kPa of low consolidation pressure, the volume of bed mud with high water content can be decreased to about two-thirds. The water content reaches the liquid limit, w_L. The bed mud condition changes to a moderate consistency and workability for reclamation is obtained. For reclaimed soil with w_L, a suitable environment for habitation of living things is formed at the bottom of the water. Moreover, reclaimed soil volume is reduced, because it can be deformed flexibly with self-weight.

(2) In the column test for bed mud with no treatment, total nitrogen (T-N), total phosphorus (T-P), and chemical oxygen demand (COD) surpass water quality standards for lakes in Japan. The release of nutrient salts from bed mud is clearly recognizable and many algae developed in the water. To inhibit eutrophication, it is necessary to control the release of the nutrient salts from bed mud.

(3) For bed mud dehydrated by 30 kPa, T-N, T-P, and COD in the lake increase as in the case with no treatment. Dehydration of bed mud alone is insufficient for release inhibition of nutrient salts.

(4) For bed mud dehydrated by 30 kPa and purified using natural zeolite powder, the contents of T-N and T-P meet water quality standards for lakes. Especially, total nitrogen decreases because of absorption of nitrogen in the water by natural zeolite. Algae do not grow. The release inhibition effect for nutrient salts of natural zeolite is recognized. However additional countermeasures against COD are required.

6 ACKNOWLEDGEMENTS

This research was conducted as part of study of countermeasures against water pollution in Lake Suwa entrusted by the Suwa Branch at Construction Office of Nagano Prefecture. Natural zeolite powder was offered by Mitsui Mineral Development Engineering Co. Ltd. (MINDECO). Mr. Moussa Garba-Say Zoulkanel, a graduate of Shinshu University, performed the column tests for graduation research. The authors are deeply grateful to them.

7 REFERENCES

Japan Sediments Management Association. 2003. Release test for nutrient salts (nitrogen and phosphorus). *Manual for investigation and test for bed mud*, 31-40. (in Japanese)

Mitsui Mineral Development Engineering Co., Ltd. (MINDECO) 2012. *Mindeco Iwami Profile Iwamilite*, (in Japanese)

Popovici S., Ichim M., Raceanu G.H., Velea S., Pasarin D.G., Albulescu V., Faraon V., and Avram M. 2011. On-site treatment of wastewaters using integrative systemic biofilter technologies. *Romanian Biotechnological Letters* 16 (6), 6776-6780.

Zeolite sub-comittee, No. 111 Comittee, JSPS. 2006. *Natural Zeolite, qualification guides and data for application.* Japan Society for the Promotion of Science.

General Report du TC 301
Monuments, historic sites and case histories

Rapport général du TC 301
Monuments, sites historiques et études de cas

Flora A.
DICEA, University of Napoli Federico II, Italy

ABSTRACT : This general report presents and discusses papers dealing with the preservation of monuments and historic sites, as well as with some case studies related to problematic soils and to the design challenges they pose. The papers deal with a variety of issues and sometimes report different design approaches. They show that the themes discussed in this session are among the most challenging the geotechnical engineers and researchers have to face. In some cases, solutions have to be found taking into account the essential contributions of experts from different cultural fields.

RÉSUMÉ : Ce rapport général passe en revue une série d'articles portant sur la conservation des monuments et des sites historiques, ainsi que sur quelques études de cas concernant les sols difficiles et les défis qu'ils posent à l'ingénieur géotechnicien. La grande variété de problématiques traitées dans ces articles montre bien que les thèmes abordés dans cette session figurent parmi les plus complexes que les chercheurs en géomécanique et les ingénieurs géotechniciens soient appelés à résoudre. Souvent des solutions ne peuvent être trouvées qu'à travers les efforts combinés d'experts issus de différentes cultures disciplinaires.

KEYWORDS: Monuments, historic sites, preservation, problematic soils, case studies, seismic protection.

1 INTRODUCTION

This session combines two themes: *Preservation of Monuments and Historic Sites* and *Case Studies*. While the five papers that belong to the previous theme are homogenous, the nine papers belonging to the Case Studies theme can be conveniently subdivided in two categories: soil characterization (3 papers), and geotechnical design (6 papers).

Table 1 reports the list of the 14 papers belonging to the session. In the report, the papers will be presented and discussed following these categories, in the order adopted in Table 1. Citations of papers belonging to this session will be mentioned in Italics in the text.

2 PRESERVATION OF MONUMENTS AND HISTORIC SITES

2.1 *General considerations*

This topic has always been of interest to geotechnical engineers and, after the X ICSSMFE in Stockholm (1981) in which for the first time a full session was devoted to it, a technical committee was appointed (at that time TC19, now TC301) to work specifically on the preservation of monuments and historic sites. Since then, it has become an increasingly important topic in our community, along with the increasing awareness of the importance of heritage in our life.

Two specific conferences have been dedicated to the theme by the technical committee (Napoli, 1997 and 2013), and a theme lecture dedicated to Jean Kerisel has been established starting from this International Conference.

Furthermore, TC301 has produced a volume (Geotechnics and Heritage 2013) collecting a number of relevant case histories on the role of Geotechnical Engineering in the preservation of monuments and historic sites. The volume can be considered as the outcome of many years of activity of TC 301 (previously TC19): in fact, because of the complexity of the topic, it is difficult to imagine mandatory guidelines or recommendations summarizing what should be done and prescribing activities to carry on, intervention techniques, design methods. Therefore, the technical committee concluded that it is probably more effective to offer, as the volume does, a collection of well described examples of preservation activities which may inspire the geotechnical engineer dealing with monuments and historic sites, suggesting an approach rather than a solution.

Dealing with valuable sites and buildings poses a number of peculiar problems, and it has been recognised for a long time that their preservation is an interdisciplinary activity. The general principles of restoration and maintenance, and the constraints to interventions, have been stated in time from the Athens Charter (1933) first and Venice Charter (1964) subsequently. The principles contained in these fundamental reference documents apply not only to the superstructure but to the whole Ground-Monument System (Jappelli 1991), and their relevance for geotechnical engineering has been recalled many times (*e.g.* Jappelli 1997, Viggiani 1997, Aversa 2005).

The Nara Document (1994) and, more recently, the Krakow Charter (2000) have added complementary information and principles to these documents, recognising that the concept of preservation and even the definition of authenticity and heritage are somewhat elusive, and must be referred to considering the different cultural contexts existing around the world and not only in Europe, where the culture of preservation originally started.

Some of the papers belonging to this session deal directly or indirectly with authenticity, and different interpretations of its meaning are shown. An enlightening example of the elusiveness of the concept can be taken with reference to the conservation of some structures in Japan: up to the mid of the 19th century, several wooden Shinto shrines periodically underwent complete reconstruction ever since the inception of this custom in the 7th century. Such a practice had the character of an important religious ritual, but was probably answering to the need of

Table 1. List of papers belonging to the session on the Case Studies, Monuments and Historic Sites.

Category	Authors	Country	Title
Preservation of Monuments and Historic Sites	Akazawa Y. *et al.*	Japan	Reconstitution of foundation platform of Prasat Suor Prat by compaction of original soil with slaked lime, Angkor Ruins, Cambodia
	Iwasaki Y. *et al.*	Japan, Kazakhstan	Authenticity of Foundations for Heritage Structures
	Mimura M. and Yoshimura M.	Japan	Geotechnical Assessment for the Restoration of Garandoya tumulus with the Naked Stone Chamber
	Sesov V. *et al.*	Macedonia	Geotechnical aspects in sustainable protection of cultural and historical monuments
	Valore C. and Ziccarelli M.	Italy	The preservation of Agrigento Cathedral
Case Studies: soil characterization	Hawkins A.B. and St John T.W.	England	Importance of understanding the development and significance of sulphates in the London Clay
	Puppala A.J. *et al.*	USA	Heaving Mechanisms in High Sulfate Soils
	Vasquez A. *et al.*	Chile	Geotechnical characteristics of glacial soil deposits at Punta Arenas in Chilean Patagonia
Case Studies: geotechnical design	Hofman R. *et al.*	Austria, Germany	Rockfall-protection embankments – design concept and construction details
	Fedorovsky V. *et al.*	Russia	Geotechnical aspects of design and construction of the mountain cluster Olympic facilities in Sochi
	Petrukhin V.P. *et al.*	Russia	Geotechnical features of Sochi Olympic facilities project designs
	Slyusarenko Y. *et al.*	Ukraine	Modern methods of geotechnical defence of buildings in the difficult geological conditions of Ukraine
	Usmanov R.A. *et al.*	Tajikistan	Geotechnical problems at development of territories in the conditions of the Republic of Tajikistan
	Zhussupbekov A.Z. *et al.*	USA, Kazakhstan, India	Geotechnical issues of megaprojects on problematic soil ground of Kazakhstan

Figure 1. Ise shrine, which undergoes ritual reconstruction every 20 years ever since the 7th century.

Figure 2. The façade of the library of Celsus in Ephesus (Turkey), a magnificent example of *anastylosis*.

substituting spoiled or damaged parts. Later on, all the Shinto shrines but one (Ise shrine, Figure 1) stopped the periodic reconstruction because of political and economic changes.

Nowadays, while the Ise shrine still keeps its ritual reconstruction every 20 years, all the other shrines are protected by law as architectural heritage, assuming as an indicator of their relevance the material value. In fact, the interruption of the rebuilding process was an accident and not the norm, the Iso shrine being the only one to follow its originally conceived life cycle. So, the question is: what is authentic in this case? The frozen material situation of the 19th century or the immaterial heritage preserved by the ritual reconstruction of the Ise shrine?

Out of such a peculiar case, the preservation of authenticity usually asks to avoid reconstruction of monuments, which as explicitly stated by the Venice Charter "should be ruled out a priori". Only *anastylosis* (meaning in Ancient Greek "to erect a structure again"), that is to say, the reassembling of existing but dismembered parts can be permitted (Venice Charter, article 15). However, it can be done only when possible without misinterpreting the original structural scheme (Figure 2).

If static problems univocally indicate that interventions are necessary, clearly recognizable additions of new materials or elements should be preferred, which may eventually contribute to a long lasting life of the monument.

Nice examples can be found in the past, as shown by the Royal Palace of Napoli (Figure 3), whose façade may appear homogeneous but underwent a number of modifications in a period of about three centuries, some of which were caused by static problems, or in the present, as shown for instance by the

Figure 3. The Royal Palace of Napoli, built in the 17th century, whose façade was modified blinding some of the arches in the 18th century by architect Luigi Vanvitelli. Statues were added in the blinded arches in 1888.

Figure 4. Neues Museum, Berlin, in which the restoration project be architect David Chipperfield has been carried out with new materials.

nice restoration of the Neues Musem in Berlin (Figure 4) with completely new and recognizable materials.

As proposed by Jappelli (1991) and explicitly stated by the Krakow Charter, the basic requirements to be fulfilled when using new techniques in monument restoration are:

- chemical and mechanical *compatibility* between new and existing materials;
- *durability* of the new materials;
- *reversibility* of the intervention, in order to have the possibility of removing it without causing damages to the structure.

Indeed, most times the latter requirement seems impossible to fulfil for geotechnical engineers, who are often involved in restoration when possible critical mechanisms may involve the Ground-Monument System. In such cases, most times the geotechnical contribution is required to solve the static problem, and as a consequence additions (for instance, underpinning) may be tolerated, even though the ideal geotechnical solution would obviously be to mitigate the risk of failure without modifying the foundation scheme. The worldwide famous Pisa tower is an enlightening example, as the preservation was successfully obtained by careful underexcavation (Burland *et al.* 2013), therefore just removing some soil. However, it may also be seen as a misleading example, in the sense that it was obtained after almost one century of careful and detailed studies, investigations and monitoring, with no major economic constraints, with the support of politics and public opinion, involving world leading experts in different disciplines. Such an exceptional circumstance is rarely reproducible and cannot be considered as a routine situation, even in the case of extremely valuable monuments or historic sites. If foundation reinforcement may solve the problem, therefore, it should not be excluded *a priori*, and the solution should be considered case by case, obviously taking into account all the possible alternatives and privileging the least invasive ones.

Furthermore, often monuments as we see now are the result of continuous transformations that have taken place in time. Therefore, modifications based on sound cultural and mechanical bases should not scare the designers, being possible to consider them as part of the life of a monument, which should not be necessarily frozen to the present, intrinsically assumed as a reference time out of an historical pattern. The lack of a general theory and therefore of a clear indication of the best solution to preserve monuments impose the need to be extremely more cautious than with new constructions, and technical convenience or cost effectiveness must not be the guiding lights in this case. Engineers have to cope with values usually out of their skill, and have to agree on the solutions with archaeologists, architects, art historians and officials in charge of monuments preservation. Indeed, “a satisfactory equilibrium between safety and conservation, between engineers and restorers, may be found only in the development of a shared culture” (Viggiani 2013).

The role of research is fundamental to this aim, as new monitoring and investigation capabilities or new technical solutions may come to help in finding solutions as soft as possible, thus making the compromise simpler to reach. A good example is the seismic protection of monuments, which is a key issue often approached with extremely invasive solutions: recent experimental and numerical research activities seem to prove that by introducing a grouted layer with a low dynamic impedance at a certain distance from the building to protect (Figure 5), a relevant mitigation of seismic risk can be obtained (Kirtas and Pitilakis 2009; Lombardi *et al.* 2013). Ground improvement (actually, worsening in this case!) of the soil with appropriate grouts (Lombardi *et al.* 2013) then becomes a fully satisfactory solution, as it is carried out far from the structure to protect, therefore preserving its authenticity.

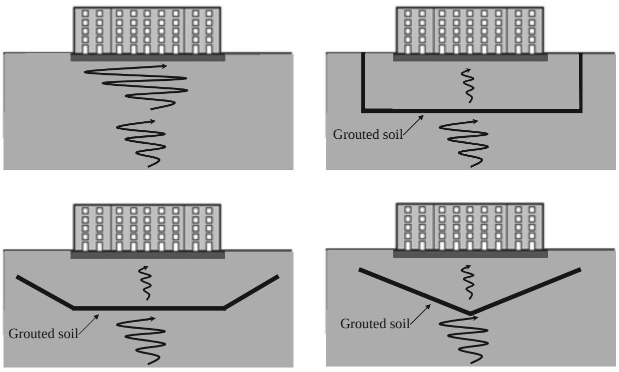

Figure 5. Different geometrical examples of grouted curtains realized to mitigate seismic risk on an existing building, which fully preserve the integrity of the structure (Lombardi *et al.* 2013).

2.2 *Papers presented to this session*

The subsession on the preservation of monuments and historic sites gathers five papers, all dealing with case studies.

The first, interesting case is presented by *Akazawa et al. (2013)*, concerning the restoration of a tower (named N1, Figure 5) belonging to the Angkor ruins (Cambodia). The tower is a three story masonry structure made of laterite blocks, about 10x10 m^2 at the base and 20 m in height. The tower is founded on a 5 m thick mound of compacted sand, overlaying a natural formation made of silty sands with clayey layers. It has experienced in time large settlements, with the largest value of

Figure 5. N1 tower in the Angkor ruins (Cambodia) before reconstruction (*Akazawa et al. 2013*).

about 40 cm measured on the side facing a nearby pond. The large structural damages, with wide cracks and a clear tilting of the structure towards the pond, were ascribed to a local bearing capacity failure of the wall facing the pond (Figure 6). As a consequence, it was decided to strengthen the compacted sandy foundation layer, mixing it with slaked lime and inserting layers of geotextiles, which was done completely dismantling the tower and reconstructing it after ground improvement completion. Even though this may seem an extremely invasive intervention and may pose problems in terms of the overall integrity and authenticity of the structure, it solved the static problems posed by the differential settlements experienced by the structure, which was on the verge of collapse.

The theme of overall integrity and authenticity is also dealt with in this session by *Iwasaki et al (2013).*

Mimura and Yoshimura (2013) present the very interesting case of the preservation works to be carried out on a monumental structure in Hita (Japan), one of the so called Garandoya Tumuli. These earth mounds were erected over stone chambers, in some cases with coloured mural paintings. Nowadays, the mounds have been destroyed and the stone chambers are exposed at the atmosphere. In order to protect from weathering one of them adorned with colourful paintings, it has been recently decided to rebuild its earth mound, introducing a large curved shelter between it and the stone chamber (Figure 7).

The strategy seems convincing, as the mound will somehow resemble the outside original earth structure, hiding and preserving the chamber, but the large shelter (18 m in diameter) will keep the chamber clearly separated from the new structure, ensuring a clear distinction between the new and the original structure, thus preserving its authenticity. The paper shows the careful investigations carried out to study the isolation effectiveness of the proposed restoration works against water and temperature changes.

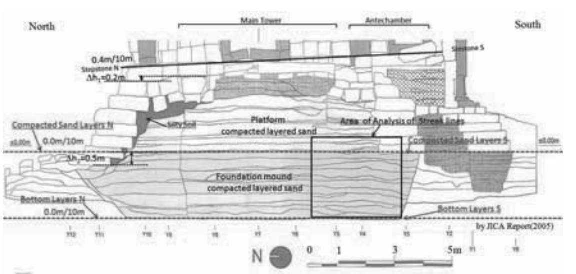

Figure 6. Local failure mechanism observed at the base of the N1 tower in the Angkor ruins (Cambodia) (*Iwasaki et al. 2013*).

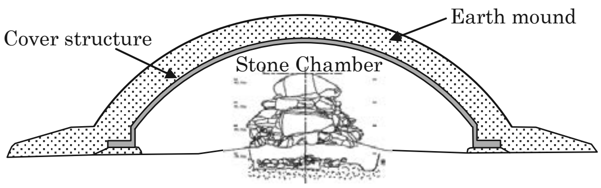

Figure 7. Schematic view of the restoration plan for the Garandoya Tumulus (*Mimura and Yoshimura 2013*).

As previously mentioned, seismic risk assessment of historic buildings is becoming a relevant issue, and procedures to get to reliable quantifications have been proposed in literature (e.g. D’Ayala and Ansal 2013). *Sesov et al (2013)* deal with this up to date topic in their paper, reporting on the efforts made in Macedonia to set up a rational procedure to assess seismic risk of some valuable historic buildings. The relevance of seismic site amplification analyses is addressed in the paper, and showed reporting some examples (Figure 8) of relevant structures having different natural frequencies and resting on different soils. Even though the approach is certainly appropriate, the paper does not give details on the considered case histories, and some of the conclusions appear obscure.

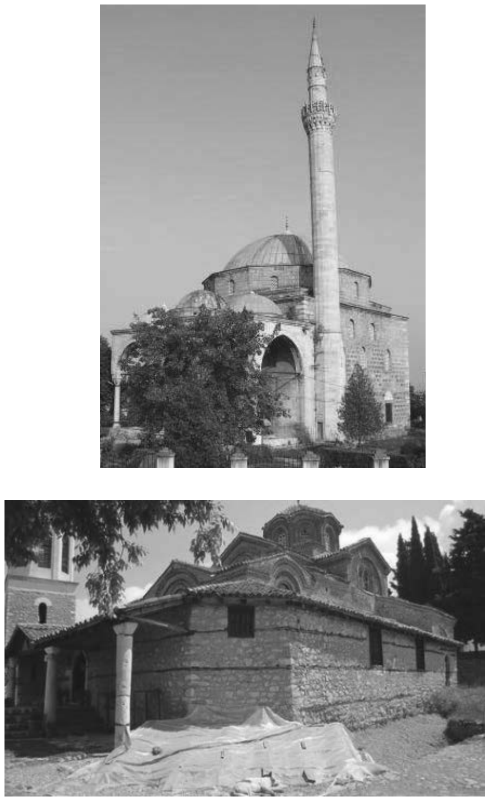

a)

b)

Figure 8. a) Mustafa pasha Mosque (15th century), b) St. Mary Peribleptos church (13th century) (*Sesov et al. 2013*).

However, the paper remarks the need to carry out seismic performance analyses expressing the seismic demand via comprehensive functions as the spectral acceleration Sa(T). The damages suffered during the different earthquakes experienced by the analysed structures could be somehow explained by the analyses briefly reported in the paper.

The last paper belonging to this subsession is the one by *Valore and Ziccarelli (2013)* on the preservation of the Agrigento Cathedral, in Italy. The cathedral was built in the 11th century on the top edge of a steep slope (Figure 9). It soon

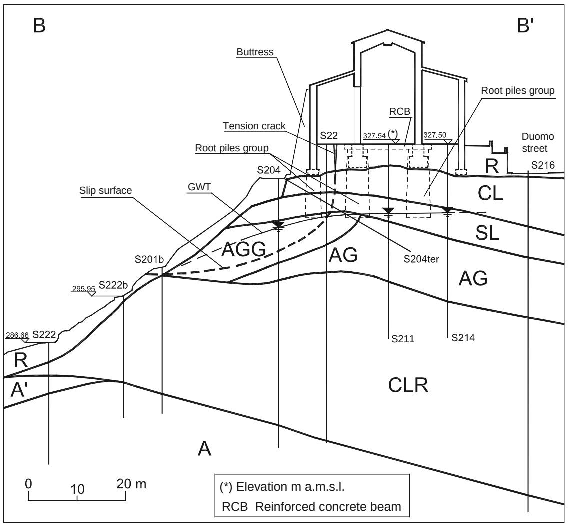

Figure 9. The Agrigento Cathedral, with an indication of subsoil stratigraphy and the supposed slope sliding mechanism (dotted line) *(Valore and Ziccarelli 2013).*

started to suffer differential settlements and structural problems which led to a number of modifications from the 14th to the 17th century. In a completely unsuccessful attempt to solve the problems, in the period 1976-1980 a large underpinning intervention with root piles was carried out.

The paper is a nice example of the correct geotechnical approach to the preservation of monuments, and is paradigmatic in the sense that shows how useless – or even detrimental – an intervention without a clear understanding of the mechanisms do be faced can be. Underpinning had no positive effects because it was conceived assuming that the settlements were due to the high deformability of the upper soils.

By simply monitoring with inclinometers the slope, *Valore and Ziccarelli (2013)* demonstrate that an active and extremely slowly evolving shear surface exists, mostly developing in a clayey soil stratum (AGG in Figure 9). This slope movement is consistent with the observed pattern of fissures, and can be considered responsible of the observed displacements. Back calculations of the slope safety factor indicate that the safety margins are actually low and reduce as the displacements increase and the shear strength tends to its residual value, for which global equilibrium would not be granted.

Monitoring, careful characterization of the subsoil and of the superstructure and a sound mechanical interpretation of the observed mechanisms are indeed the only tools geotechnical engineers have in their hands to tackle problems as the one of the Agrigento Cathedral.

It is also worth pointing out that in this case a timely correct interpretation of the observed settlements would have led to interventions aimed to stabilize the slope more than to underpin the structure, eventually contributing to preserve the overall integrity of the structure.

3 CASE STUDIES

3.1 *Characterization of problematic soils*

Soil characterization is an essential part of the activity of geotechnical engineers, and the success in design or in the interpretation of mechanisms often depends more on it than on the calculation methods adopted. Therefore, the topic never ends to be of great interest. This subsession includes three papers dealing with soil characterization, with reference to some peculiar cases.

In their paper, *Hawkins and John (2013)* report on the behaviour of the very well known London Clay, looking at it from an unusual point of view as they investigate the chemical properties of the unsaturated/seasonally aerated zone of the formation. The London Clay Formation is a silty clay deposit which, in its upper part, is weathered and mostly aerated, thus getting a typical brown colour. The deeper part of the deposit, saturated, is grey. In the transition (mottled) zone among the brown and the grey London Clay, peculiar chemical conditions exist, often with the presence of enriched acid soluble sulphate with a corresponding low pH. As well known, this is a rather aggressive environment for buried structures and foundations, and may lead to their deterioration, as demonstrated for instance by the case history of the St. Helier Hospital in Surrey. *Hawkins and John (2013)* have monitored the sulphate content in the soil during the construction of an underground car park at different depths, confirming that the upper brown London Clay has a certain amount of sulphate, whose largest values correspond to the brown-grey mottled transition zone. The authors argue that the heat generated by concrete hydration may enhance the formation and mobilization of sulphates, and appropriate countermeasures should be taken to protect concrete from its attack in underground construction activities.

In their paper, *Puppala et al. (2013)* focus on the heave mechanisms occurring in high sulphate soils after the addition with calcium based stabilisers (lime and/or cement), as a consequence of the formation of two expansive compounds (namely ettringite and thaumasite). The authors show several experimental results on two high sulphate soils treated by hydrated lime, highlighting the advantages of the mellowing technique - firstly proposed by Harris *et al.* (2004) - in reducing the swelling behaviour due to the expansive compounds formation. The role played by factors such as soil mineralogy and treatment parameters are clearly discussed in the paper.

A large scale geotechnical and geological soil characterization project for the city of Punta Arenas, in the Chilean Patagonia, is described by *Vasquez et al (2013)*. The urban expansion of Punta Arena has posed a number of geotechnical problems, as soft and complex soils are spread out in the area. *Vasquez et al (2013)* propose a classification of the city area in different zones having homogeneous properties and characteristics. Even though specific investigations are always necessary and large scale classifications cannot give design parameters at the scale of the single structure, an overall picture of the subsoil characteristics and the problems they pose may be of great help in planning urban development.

3.2 *Geotechnical design in problematic soils*

The papers belonging to this subsection report design considerations or experimental results mostly with reference to new geotechnical structures. Some of the papers refer to peculiar regional problems, some to specific projects, and some to specific structures. In most of them, reference is made to codes, either existing or missing, as they represent some of the design constraints.

A paper analysing a specific geotechnical structure is the one by *Hoffmann et al. (2013)*, in which the authors deal with the very interesting case of embankments conceived as rock-fall protection elements. Such structures may be more convenient than rock-fall protection nets, because they may absorb larger impact energies and usually present advantages in terms of longevity and construction cost. The paper briefly describes the results of a large number of 1g small scale experimental tests (Figure 10) carried out on model embankments having different characteristics (unreinforced, reinforced with geotextiles, or unreinforced with a rip-rap up-hill facing).

The tests allowed to find interesting correlations between the geometry of the embankment, its characteristic and the energy and position of the impact. Based on the experimental observations, the authors give geometric indications to avoid the hitting rock block (or sphere, in the small scale experiments) to roll on or jump over the embankment crest, and also propose a simple design chart to estimate the penetration δ into the embankment as a function of a non dimensional energetic parameter E* (Figure 11).

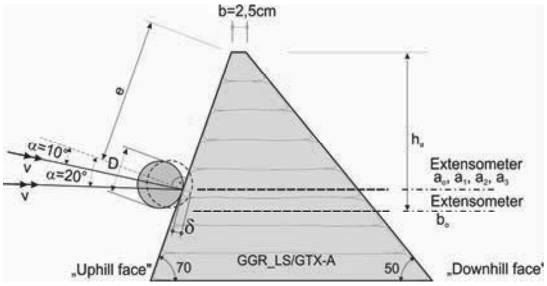

Figure 10. Small scale model rock-fall protection embankment used in the tests (*Hoffmann et al. 2013*).

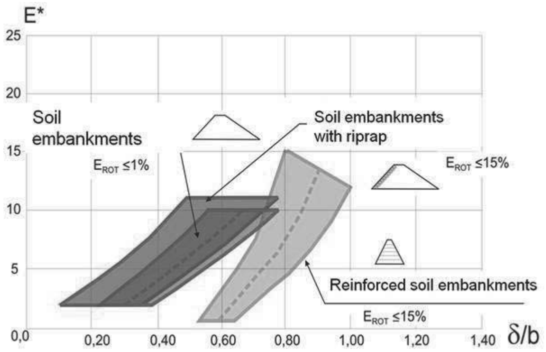

Figure 11. Summary of the results of the rock-fall experimental tests on small scale embankments (*Hoffmann et al. 2013*). E* is a dimensionless energetic parameter defined by the authors as relative impact energy, δ is the depth of penetration of the hitting sphere and b is the crest width (see Figure 10).

The other five papers belonging to this subsession share the characteristic of referring to geotechnical problems encountered in the problematic soils and in the extremely seismic areas of Eastern Europe and Western Asia, in states which were recently born after the collapse of Soviet Union.

Two of these papers deal with the large works under course in Sochi (Russia), where the XXIIth Winter Olympic Games and the XIth ParaOlympic Games will be held in 2014. The papers describe the geological and geotechnical features of the sites in which the Olympic Village and the sport facilities will be located. Two clusters are under construction: one in the coastal area and one on the mountains, giving rise to what claims to be the most compact venue ever for such an event. The whole area is highly seismic.

Fedorovsky et al. (2013) describe the complex geological conditions of the mountainous cluster, with chaotic, widely graded superficial soils over a base argillite formation. Since in some cases the facilities had to be realized operating slope cuts, slope stability analyses were carried out using different methods. Eventually, stabilizing interventions were conceived to meet safety requirements: soil nails were adopted to avoid local instability around the slope cuts, while rows of piles (in some cases anchored at the top) were used to stabilize the slope. No details are given in their paper on the design of the stabilizing interventions, and more than one doubt exist on the effectiveness of the adopted numerical approach for the design of rows of slope stabilizing piles. As a matter of fact, it is well known that piles give a contribution only if the slide is active, as the stabilizing shear forces they generate are the result of soil-structure interaction. What they usually do is slowing down more than stopping the slide (Lirer and Flora 2008, Lirer 2012), unless extremely heavy structures are realized. A realistic numerical calculation should allow soil flow among the piles, otherwise completely unrealistic interaction pressures may be calculated. Even though this seems to indicate than only complex 3D analyses are necessary, some codes allow such a flow even in 2D analyses.

The second paper on the new constructions in Sochi is the one by *Petrukin et al. (2013)*, who describe some of the geotechnical problems posed by the design of three large buildings in the coastal area, gives some information on the foundation solutions proposed, and briefly discuss the issue of pipelines design. The first building is the Big Ice Arena, seating 12000 people, resting on a complex deposit composed of layers ranging from coarse gravels to sandy clayey. Shallow foundations were chosen for this large building, made of a number of rafts having thicknesses from 0.6 m to 1.4 m, separated by joints. The displacements induced by the construction were monitored, and compared with the predicted ones (Figure 12). The reported comparison refers to the end of construction, and shows a general underestimate of the values of the absolute displacements. The authors do not say anything on the progress of consolidation settlements, and therefore it is not said if further displacements are expected in time because of pore pressure increments dissipation. However, the calculations were able to give the order of magnitude of the absolute and relative settlements. The second case described in this paper is the one of a tall building hosting the Organizing Committee of the Olympic Games. The building is founded on a thick layer of clay which,

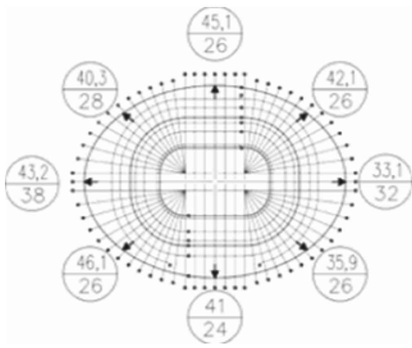

Figure 12. Mean values (mm) of measured (numerator) and calculated (denominator) settlements of the Big Ice Arena raft footing in Sochi (Russia) (*Petrukin et al. 2013*).

below a depth of few meters, has extremely poor mechanical properties. Consequently, the building has been founded on piles, whose seismic design was the geotechnical challenge. A refined solution was chosen in this case (Figure 13): a layer (40 cm) of dense sand reinforced with geogrids was interposed between the piles and the foundation raft. With such an elegant solutions, the piles solve the static problem in terms of bearing capacity and settlements, but do no interact (neither kinematically nor inertially) with the superstructure during earthquakes, thus avoiding the risk of large seismically induced bending moments at the piles caps.

A similar solution was adopted for part of the foundations of a hotel, which is the third building analysed in this paper, while the remain part of the foundations were shallow, because directly resting on a thick deposit of sand and gravel. *Petrukin et al. (2013)* claim that the interposition of an intermediary sand

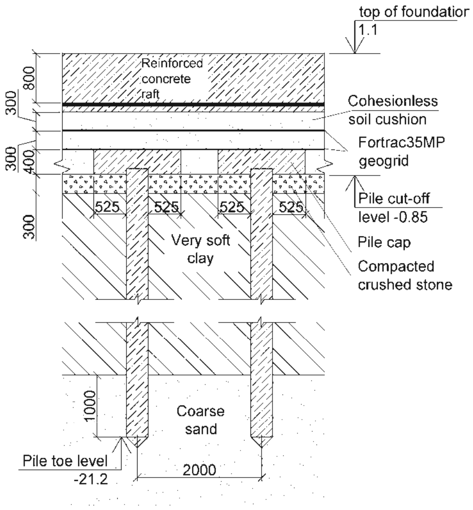

Figure 13. Foundation of the Organizing committee Building in Sochi (Russia). Detail of the pile foundation disconnected from the raft (*Petrukin et al. 2013*).

layer between piles and raft has started in seismic areas of the USSR in the 1960s, and this is very interesting as only few, and more recent, experiences (e.g. Thornburn *et al.* 1983, Jamiolkowski *et al.* 2009) are described in literature.

The critical geological conditions of the territory of Ukraine are described by *Slyusarenko et al. (2013)*, which are of concern as about 60% of the territory is interested by formations of collapsible soils or unstable slopes. Considering the geotechnical problems posed by such soils, the authors describe two case histories: one pertaining to an underground parking lot realized with a top-down procedure, the other referring to the reparation works carried out to preserve a valuable 18th century baroque church. As far as the latter is concerned, a number of static problems affected the structure in time, with leaning parts and diffused crack patterns. The church is positioned on top of a hill, which was found to be not far from limit equilibrium conditions. *Slyusarenko et al. (2013)* shortly report the list of investigations and of the numerical analyses carried out. They also describe in some detail the adopted solutions, even though no details on soil properties, slope geometry and stability analyses are given in the paper. Along with extensive restoration of the superstructure, it was finally decided to underpin the church with jet grouting (Figure 14). As previously discussed (see §2.1), this is a rather invasive intervention which irreversibly compromises *authenticity* of the monument. Even though underpinning cannot be excluded a priori, it should be carried out only if no alternatives are available which would induce similar beneficial static effects. Since slides were observed along the slope, and slope stability safety margins were extremely reduced, it would have been interesting to know if slope superficial and deep displacements were monitored, for instance with inclinometers. In fact, such displacements may have caused at least part of the static problems experienced by the church, as shown in this session by *Valore and Ziccarelli (2013)* with reference to the similar case of a church placed on top of a hill with a slope close to failure.

In any case, *Slyusarenko et al (2013)* have used jet grouting to underpin the church instead of more traditional techniques, as for instance micropiles. This choice may be convenient, because large columns can be formed drilling small holes into the soil by correctly tuning the treatment energy (Flora *et al.* 2013). However, extreme caution should be adopted when using jet grouting close to very sensitive buildings (Croce *et al.* 2013). Furthermore, it is well known that the highly energetic grout jet may cause undesired settlements when used in unsaturated collapsible soils as the upper ones seem to be under the church. In any case, the authors report that the underpinning works were successful, as the displacements have stopped.

Referring to similarly problematic soils, *Usmanov et al. (2013)* summarise the typical foundation systems in the very critical geotechnical conditions encountered in most of the territory of the Republic of Tajikistan. Even though the described systems are traditional, the site conditions in which they are applied are sometimes extreme, being the area highly seismic, with largely spread thick layers of unsaturated collapsible loess and weak saturated soils. The authors report that even in such critical conditions, the foundation solution reported in the paper have proven to be successful for medium rise buildings (up to 12 storeys).

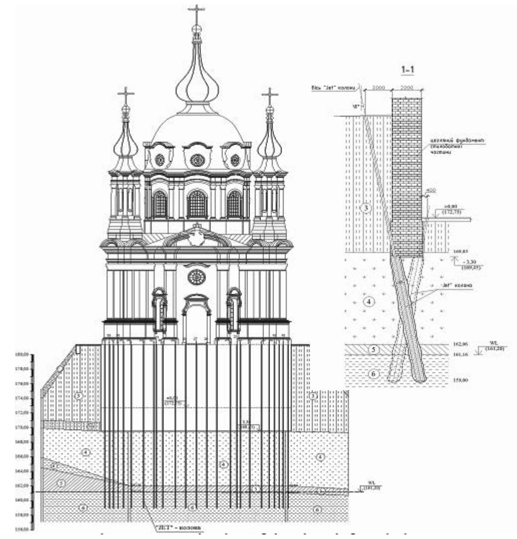

Figure 14. Underpinning with jet grouting columns of St. Andrew Church in Kyiv (Ukraine) (*Slyusarenko et al. 2013*).

Recently, a number of large projects has started in the new born state of Kazakhstan, and in its capital Astana in particular. The town is located in the Kazakh steppe, and the subsoil is constituted of erratic layers of soft and hard soils; in the most superficial part, soil freezes during the extremely severe winter. Because of these complex geotechnical conditions, deep foundations are usually adopted, and new technologies in pile construction and testing considered too. *Zhussupbekov et al. (2013)*, for instance, in their paper summarize some experiences relative to continuous flight auger piles (CFA piles, usually classified as replacement piles, even though the soil is partially displaced during installation) and displacement screw piles (in the paper named DDS piles). They show an interesting comparison between static and dynamic loading tests: in the cases reported in the paper, the dynamic tests largely underestimate the ultimate axial load of the piles, being also very sensitive to the kind of hammer adopted in testing. The authors also discuss the use of alternative testing procedures which may be more convenient, as the Osterberg Cell tests (Russo, 2013). Even though the paper contains interesting experimental data, it is very difficult to get an insight on them as information are given neither on the properties of the soils in which the test piles were realized, nor on the piles themselves.

4 CONCLUSIONS

The session deals with a number of complexities, related to the structures to preserve (monuments and historic sites), to the soils to characterize or to the design constraints posed for new structures by difficult regional conditions in highly seismic areas. Indeed, some of the most challenging issues for geotechnical engineers and researchers.

Generally speaking, and with some exceptions, the papers do not deal with new design methods or new technologies. They present case studies in which traditional tools were used to try and face complexity, the interest of the papers essentially being in the engineering solutions proposed. As obvious, the ones adopted for monuments and historic sites are usually less invasive than the ones conceived for new constructions, confirming that the design strategies have to be different in the two cases. This key issue certainly needs to be discussed.

In some cases, the differences in the approaches and in the solutions depend on different cultural backgrounds and environments. The discussion should deal with such differences. With specific reference to monuments and historic sites, it should be also debated to what extent interventions may alter integrity and authenticity, posing a question on its final goal: to preserve heritage or to the aim of touristic fruition?

5 REFERENCES

5.1 *Papers belonging to this sessions*

Akazawa Y., Fukuda M., Iwasaki Y., Nakazawa J. 2013. Reconstitution of foundation platform of Prasat Suor Prat by compaction of original soil with slaked lime, Angkor Ruins, Cambodia. *Proc. Of the 18th ICSMGE, Paris.*

Fedorovsky V., Kurillo S., Kryuchkov S., Bobyr G., Djantimirov K., Iliyn S., Iovlev I., Kharlamov P., Rytov S., Skorokhodov A., Kabantsev O. 2013. Geotechnical aspects of design and construction of the mountain cluster Olympic facilities in Sochi. *Proc. Of the 18th ICSMGE, Paris.*

Hawkins A.B. and St John T.W. 2013. Importance of understanding the development and significance of sulphates in the London Clay. *Proc. Of the 18th ICSMGE, Paris.*

Hofman R., Vollmert L., Molk M. 2013. Rockfall-protection embankments – design concept and construction details. *Proc. Of the 18th ICSMGE, Paris.*

Iwasaki Y., Zhussupbekov A. and Issina A. 2013. Authenticity of Foundations for Heritage Structures. *Proc. Of the 18th ICSMGE, Paris.*

Mimura M. and Yoshimura M. 2013. Geotechnical Assessment for the Restoration of Garandoya tumulus with the Naked Stone Chamber. *Proc. Of the 18th ICSMGE, Paris.*

Petrukhin V.P. Kolybin I.V., Budanov V.G., Isaev O.N., Kisin B.F., Bokov I.A. 2013. Geotechnical features of Sochi Olympic facilities project designs. *Proc. Of the 18th ICSMGE, Paris.*

Puppala A.J., Talluri N., Gaily A., Chittoori B.C.S. 2013. Heaving Mechanisms in High Sulfate Soils

Sesov V., Cvetanovska J., Edip K. 2013. Geotechnical aspects in sustainable protection of cultural and historical monuments. *Proc. Of the 18th ICSMGE, Paris.*

Slyusarenko Y. Chervinsky Y., Karpenko Y., Dvornik S., Malikov S., Rozenvasser G., Lavshuk I. 2013. Modern methods of geotechnical defence of buildings in the difficult geological conditions of Ukraine. *Proc. Of the 18th ICSMGE, Paris.*

Usmanov R.A. Saidov R.S., Mangushev R.A. 2013. Geotechnical problems at development of territories in the conditions of the Republic of Tajikistan. *Proc. Of the 18th ICSMGE, Paris.*

Valore C. and Ziccarelli M. 2013. The preservation of Agrigento Cathedral. *Proc. Of the 18th ICSMGE, Paris.*

Vasquez A., Le Roux J.P., Foncea C. 2013. Geotechnical characteristics of glacial soil deposits at Punta Arenas in Chilean Patagonia. *Proc. Of the 18th ICSMGE, Paris.*

Zhussupbekov A., Ling H.I., Baitassov T.M., Lukpanov R.E., Tulebekova A.S., Yenkebayev S.B., Popov V.N., Krasnikov S.V., Boominathan A. 2013. Geotechnical issues of megaprojects on problematic soil ground of Kazakhstan. *Proc. Of the 18th ICSMGE, Paris.*

5.2 *Other papers*

Aversa S. 2005. Preserving cities and monuments. *General Report in session 4.3 on Preserving Cities and Monuments in Urban Areas, Proceedings of the XIV ECSMGE,* Madrid.

Burland J.B., Jamiolkowski M., Squeglia N., Viggiani C. 2013. *The leaning tower of Pisa.* In Geotechnics and Heritage, Bilotta E., Flora A., Lirer S., Viggiani C. Eds., Taylor & Francis, London & New York.

Croce P., Flora A., Modoni G. 2013. *Jet Grouting*. Taylor & Francis, London & New York.

D'Ayala D., Ansal A. 2013. Local site conditions and seismic risk assessment of historic buildings. *Proc. Of the 2nd Int. Conf. on Geotechnical Engineering for the Preservation of Monuments and Historic Sites*, Bilotta B. Flora A., Lirer S., Viggiani C. Eds., Taylor and Francis.

Flora A., Modoni G., Lirer S., Croce P. 2013. The diameter of single, double and triple fluid jet grouting columns: prediction method and field trial results. *Geotechnique*, in press.

Harris J.P., Sebesta S., Scullion T. 2004. Hydrated lime stabilization of sulphate-bearing vertisols in Texas. *Transportation Res. Record 1868*, TRB, National Research Council, Washington D.C., 31-39.

Iwasaki Y., Akazawa Y., Fukuda M., Nakazawa J., Nakagawa K., Shimoda I., Nakagawa T. 2013 Dismantling for Reconstitution of N1 Tower of Prasat Suor Prat, Angkor Thom, Cambodia. *Proc. Of the 2nd Int. Conf. on Geotechnical Engineering for the Preservation of Monuments and Historic Sites*, Bilotta B. Flora A., Lirer S., Viggiani C. Eds., Taylor and Francis.

Jamiolkowski M.B., Ricceri G., Simonini P. 2009. Safeguarding Venice from high tides: site characterization and geotechnical problems. *Proc. 17th ICSMGE*, M. Hamza, M. Shahien and Y. El Mossallamy Eds., Millpress, Amsterdarm, 4, 3209-3230.

Jappelli R. 1991. *Contribution to a systematic approach.* in The Contribution of Geotechnical Engineering to the preservation of Italian historic sites. AGI Associazione Geotecnica Italiana.

Jappelli R. 1997. An integrated approach to the safeguard of monuments: the contribution of Arrigo Croce. *Proc. of the Arrigo Croce Memorial Symposium – Geotechnical Engineering for the Preservation of Monuments and Historic Sites*, Napoli, A.A. Balkema, Rotterdam.

Kirtas, E. & Pitilakis, K. 2009. Subsoil interventions effect on structural seismic response. Part II: parametric investigation. *Soil Dynamics and Earthquake Engineering*, 13 (3), 328-344.

Lirer S. and A. Flora 2008. Numerical analysis of the effectiveness of rows of piles in slope stabilisation. *Proc. Of the Int. Conference on Development of Urban Areas and Geotechnical Engineering*, Ulitsky V.M. Ed., NPO, Saint Petersburg, Russia, 16-19 June, 2, 279-286.

Lirer S. 2012. Landslide stabilizing piles: experimental evidences and numerical analyses. *Engineering Geology*, 149-150, 70-77.

Lombardi D., Flora A., Lirer S., Silvestri F. 2013. An innovative approach for reducing the seismic risk of existing buildings and historic sites. *Proc. Of the 2nd Int. Conf. on Geotechnical Engineering for the Preservation of Monuments and Historic Sites*, Bilotta B. Flora A., Lirer S., Viggiani C. Eds., Taylor and Francis.

Lombardi D., Flora A., Lirer S., Silvestri F. 2013. Soil grouting for the seismic protection of existing buildings. *Ground Improvement*, in press.

Russo G. 2013. Experimental investigations and analysis on different pile load testing procedures. *Acta Geotechnica*, 8, 17–31.

Thorburn S., Laird C, Randolph M.F. 1983. Storage tanks founded on soft soils reinforced with driven piles. *Proc. of the Conf. on Recent Advances in Piling and Ground Treatment*. ICE, London, 157-164.

Viggiani C. 1997. Opening address. *Proc. of the Arrigo Croce Memorial Symposium – Geotechnical Engineering for the Preservation of Monuments and Historic Sites*, Napoli, 1996., A.A. Balkema, Rotterdam.

Viggiani C. 2013. *Cultural Heritage and Geotechnical Engineering: an introduction.* In Geotechnics and Heritage, Bilotta E., Flora A., Lirer S., Viggiani C. Eds., Taylor & Francis.

Reconstitution of foundation platform of Prasat Suor Prat by compaction of original soil with slaked lime, Angkor Ruins, Cambodia

Reconstitution de la plate-forme de la fondation de Prasat Suor Prat par compactage du sol d'origine additionné de chaux éteinte, sur les ruines d'Angkor, au Cambodge

Akazawa Y.
Japan Cultural Heritage Consultancy Co. Ltd.

Fukuda M.
Taisei Geo-Tech Co. Ltd.

Iwasaki Y.
Geo-Research Institute

Nakazawa J.
Tokyo Engineering Consultants Co. Ltd.

ABSTRACT: Angkor ruins are situated at Siem Reap in Cambodia and are composed of many masonry structures of temples, moats and large earth embankment for a reservoir. They were constructed from the 9th to the 15th centuries. These cultural heritages in ancient Angkor have been in dangerous states that have resulted in collapse from various severe natural forces. The individual masonry towers of Prasat Suor Prat at Angkor Thom were studied and investigated. The N1 Tower was deemed as the most dangerous tower among them for restoration work. It has inclined 6.6 degrees towards a nearby pond with a northwest direction. The compacted sandy formation was found from -1.5m from the original ground surface and to +3.5m above the ground. The safety factor for the ground bearing capacity in rainy season was calculated with S.F=1.1. When its bearing strata were reconstituted, it was designed to have a sufficient safety factor value of S.F>1.5. To achieve this purpose, the original sandy soils were mixed with slaked lime and compacted by tamping with Geo-textile. The material soil used for the platform was a mixture of different soils of original sandy soil, clayey soil and lateritic soil at weight ratios of 70%, 15% and 15%. Slaked lime was added to the mixed soil 1 at a rate of 0.1.

RÉSUMÉ: Les ruines d'Angkor sont situées à Siem Reap au Cambodge et sont composées de nombreux temples à structure en maçonnerie, de fossés et d'une grande digue autour d'un réservoir. Ils ont été construits entre les 9e et 15e siècles. Ces héritages culturels de l'ancien Angkor sont dans un état dangereux résultant d'écroulements résultant de forces naturelles sévères. La maçonnerie particulière des tours de Prasat Suor Prat à Angkor Thom a été l'objet d'études et d'investigations. La Tour N1 a été jugée la plus dangereuse parmi celles-ci, justifiant un travail de restauration. Elle est inclinée de 6.6 degrés en direction d'un étang proche, vers le nord-ouest. Une formation sablonneuse compactée a été identifiée de -1.5m de la surface originelle jusqu'à 3.5m au-dessus. Le facteur de sécurité en terme de capacité portante en saison des pluies a été évalué à S.F =1.1. Quand les couches portantes ont été reconstituées, le facteur de sécurité a été amélioré jusqu'à la valeur S.F >1.5 considérée comme suffisante. Pour parvenir à ce but, les sols sablonneux originaux ont été mélangés avec de la chaux éteinte, compactés et renforcés avec du géo-textile. Le sol utilisé pour la plate-forme était un mélange de différents sols, constitué du sol sablonneux original, de sol argileux et lateritique selon des ratios en poids de 70%, 15% et 15%. La chaux éteinte a été ajoutée au mélange à raison de 0.1 pour 1.

KEYWORDS: Angkor ruins, cultural heritage, reconstitution, foundation, soil improvement, slaked lime,

1 INTRODUCTION

Angkor ruins are situated at Siem Reap in Cambodia and are composed of many masonry structures of temples, moats and large embankment for reservoir, that were constructed from the 9th to the 15th centuries. These ruins were registered as Cultural Heritages Sites by UNESCO in 1992. At the same time these were listed as Endanger World Heritages Site. Afterwards, in 2004 these were removed the list by many conservation activities around groups from the world. However they are still under dangerous states resulting in collapse by human activities and natural forces that sometimes may cause collapses, etc.

In 1993, Japanese Government team for Safeguarding Angkor was organized and has been working at on investigating and conserving them (Nakagawa 1996-2005).

This paper reports on a conservation project was carried out (Nakagawa 2005, Akazawa et al. 2009).

2OUTLINE OF OBJECTIVE STRUCTURE

Prasat Suor Prat in Angkor Thom is composed of 12 towers and terraces. The towers are masonry structures. They are constructed materials out of laterite blocks. They are designed to look like three stories. Each tower constructed differently and has different structure problems, for example, openings of wall joints and leaning of towers etc...

Photo. 1. N1 tower (Before reconstitution)

N1 tower was selected as the most dangerous tower among them for restoration work (Photo. 1). This tower had inclined 6.6 degrees towards a nearby pond in a northwest direction. The dimensions of the tower are 21m in height and 9.2m×10.5m in width and length at base level.

3RESULTS OF INVESTIGATION

To advance the design of N1 tower's restoration, case histories were collected of restoration of similar building. The existing states of N1 tower structure and investigations of ground under it were carried out (Iwasaki et al. 2013).

Based on these results, principals, guidelines and methods for the N1 tower's restoration project were decided.

3.1 Case history

N3 tower (one of Prasat Suor Prat) was restored by École française d'Extrême-Orient in 1950, and its superstructure was dismantled and rebuilt.

50 years after its restoration, it inclined once again and structure materials for its openings were broken. It has been recognized that N3 tower is at risk of collapse. This leaning of N3 tower is supposed to have occurred during restoration work or just after it. It was thought to be caused by fact that superstructure was treated, and its platform and its base ground were not treated.

3.2 Survey of existing state

The change in N1 tower's inclination with progressing time has been monitored by plumbing, however there was no significant change. During the rainy season in October in 1997, when there was wind velocity of over 10m/s blew for a few days, 0.5mm/m of the lateral displacement was measured. Figure 1 shows this monitoring data with inclinations, wind velocity, rainfall and temperature for N1 tower. This fact shows that the tower's displacement was increased by the external force acting against the tower (in this case, gust wind during rainy season), and this displacements will be accumulated.

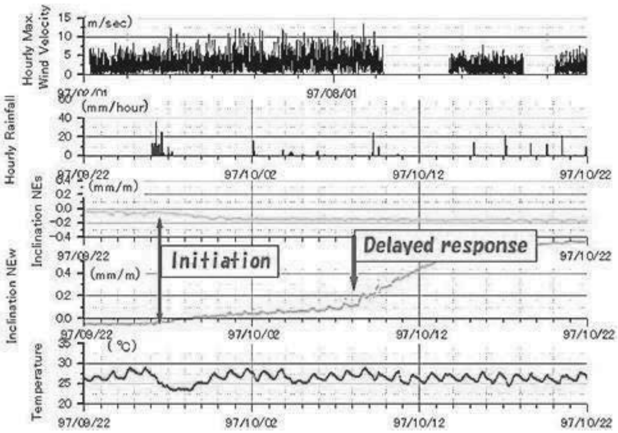

Figure 1. The measuring results of the amount of inclinations, the wind velocity, precipitation, and temperature of N1 tower.

Based on these facts, it is recognized that the foundation platform and the ground under it should be investigated in detail. First, a soil survey by hand auger was carried out, but results of it were insufficient to clarify the soil strata under the platform. It was concluded that the investigation of the tower state should be done by dismantling them, including excavating the base ground. Moreover, it is decided that these results will be used for designing of other ruins' restoration projects in future.

Photo. 2 and Figure 2 show soil strata under the platform of N1 tower. The compacted sandy formation was found from -1.5m from the original ground surface and to +3.5m above the ground, which the average thickness of one stratum was measured about 20cm. Figure 3 shows the grain size distribution curve of them. Figure 4 shows N-value distribution (by using standard penetration test) with depth. In figure white dots show the values in the dry season and the polygonal line shows them in the rainy season.

Photo. 2. Soil strata under the platform of N1 tower

Figure 2. North-South Section of N1 tower (Before restoration)

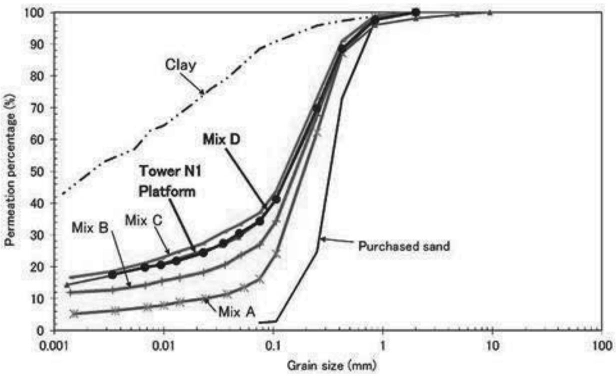

Figure 3. Grain size distribution curve of each soil

The average in-situ dry density of the compacted strata was measured at 1.69g/cm^3 at center of it and 1.73g/cm^3 directly under laterite blocks. Because the maximum dry density by Proctor's compaction test was measured at 1.88g/cm^3, these compacting layers were assumed to have been tamped with about 90% on degree of compaction.

Plate bearing in-situ test of plate loading on original compacted sandy ground showed the yield load of 290 - 340 kN/m^2 under wet condition. Since the contact pressure in the ground beneath the foundation of the tower was estimated at 270kN/m^2, the safety factor against the ground bearing capacity in rainy season was calculated at SF=1.1, which was considered as small and not safe. When the external force acts on the tower in the rainy season, the inclination, the subsidence and the differential settlement of them will increase.

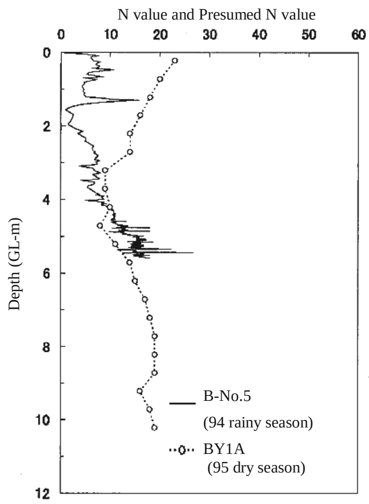

Figure 4. N-value distribution

4CONSTRUCTION METHOD

The principle for this reconstitution is to adopt the original tamping method for excavated original soils. However, if the bearing layers are reconstituted by the original tamping method with original soils, their bearing capacities will be same as original states and capacity reduction in rainy season will not be avoided. When constructed with the original excavated soil, it is concluded that it should be improved with some stabilizing materials for soils.

In the case of surface soil stabilization in place, Portland cement or hydrated lime is used as a hardening agent. Hydrated lime should be accepted for this case, because it is easy to buy it near the jobsite and to handle it for working. Moreover it is used for long time.

5MIXING TEST OF SLAKED LIME-SOIL AND RESULTS

Table 1 shows the proportions of material soils to be prepared and slaked lime to be mixed for them. In Table 1, item “sand” means excavated sandy soil which was used at the tower’s erection. Each mixed soil is mixed this “sand”, clayey soil and lateritic soil with weight ratio in Table 1. Slaked lime, which is a stabilizing material, is added to the mixed soil 1 at rates of Table 1. The mixing purpose of clayey soil is expected the stabilized effect with chemical reaction of clay minerals and slaked lime. Also, on lateritic soil mixing, it is intended that the ferromagnetic ion and aluminum ion in it will promote chemical hardening reactions. Grain size accumulation curves of mixed soils are shown in Fig.3. Results of the test were evaluated by comparison of unconfined compression strengths on treated specimens.

Table 1. Proportion of mixed soil

items	sand (excavated sandy soil)	clayey soil	lateritic soil	slaked lime mixture rate (%)
mixture A	100	0	0	5, 10, 15
mixture B	85	15	0	5, 10, 15
mixture C	70	30	0	5, 10, 15
mixture D	70	15	15	5, 10, 15

1) Unconfined compression strengths of treated specimens were increased as the mixing rates of slaked lime were increased.

2) The unconfined compression strengths and the deformation moduli of tested specimens increased with their curing times, and proportional relation between them was recognized. Relation between the curing time and the unconfined compression strength on mixed soil D is shown in Figure 5.

3) The changes of their dry densities by curing time were not recognized.

Figure 5. Relation of unconfined compression strength and curing time

Based on above-mentioned results, the material soil used for the foundation platform and its base ground was a mixture of three different soils of the original sandy soil, clayey soil and lateritic soil at weight ratios of 70%, 15% and 15%(mixing soil D proportion). Slaked lime, which was a stabilized material, was added to the mixed soil 1 at a rate of 0.1.

6CONSTRUCTION PROCEDURE AND UTILIZATION OF GEO-TEXTILE

It is decided that mixed soil D proportion should be used for material soil and slaked lime should be used for a stabilized material at adding to the mixed soil 1 at a rate of 0.1. The construction method will be applied by tamping method.

The construction procedure on jobsite is as follows.

1) The material soil treated by slaked lime should be spread at 15 cm of its thickness, after then it should be compacted to a thickness of about 7.5cm. By the repeat of this work, the base ground should be developed to the designated level.

2) Compacting work is decided by the field trial work to be composed of 3 steps. Primary compaction should be conducted using a wooden rod (dia.3cm) with man power’s tamping, and followed by secondary compaction using a flat steel plate (15cm×15cm×1cm) as the same manner. Finally, surface compaction should be conducted by using of a tamping rammer.

3) The designated base ground for the tower will be made of laminated structure with 7cm thickness tamping layers. Since there is a smooth surface among each layer, its existence may make a week point on the mechanical standpoint. In order to secure the bond of each layer, roughening work for each compacted surface should be done before tamping of the next layer. The surface roughening work should be performed by using of steel rakes with manpower.

When allowable bearing capacity is 1.2MN/m^2, it is assumed that the compressive strength in-place should be about 60 percent of the strength obtained in the laboratory test. This means that the target value should be 2 MN/ m^2. In the case of mixed soil D, it would be take a curing time of more than 90 days to achieve a value of 2MN/m^2. However, since the reconstitution work for the superstructure will be needed to be executed without waiting 90days, some measure to reinforce the improved soil should be needed until the onset of its strength. As above-mentioned consideration, it is decided that Geo-textile should be applied for temporally reinforcement of improved soils until the onset of its strength.

The designing study was preceded on a section of base ground in Figure 6 which spread and inserted 3 layers of Geotextile. Table 2 shows the specification of Geotextile which was utilized. One of the effects of Geo-textile is to work as reinforced materials of shear resistance for soil mass. When using this effect for the designing base ground, it is expected that it increases safety factor to the sliding failure by about 20 percent.

Figure 6. Section of spreading Geo-textile

Table 2. The specification of Geotextile

items	contents
type	KJV-6000
base texture	high-strength vinylon
width	2,000mm
weight	320g/m^2
tensile strength	59.0kN/m
reduction coefficient	0.6

On the other hand, when the curing time of treated soil is short, it is considered that the strength of base ground is insufficient for the bearing capacity. The base ground, which is composed of tamping layers and Geo-textile, may not have uniformly mechanical behaviors. It is supposed that only Geo-textile resists the overturning moment, which generates from the tower's load. As a result, it is simulated that Geo-textile will be able to share 26 percent of the total overturning moment. When converting this value to the settlement, it is estimated 40cm.

Based on above-mentioned result, Figure 7 shows a decided section for reconstitution of the foundation platform.

7CONCLUSION

This project has been achieved in May, 2005. After that, monitoring for these structures is being done. Until present after the reconstitution, there is no trouble on them.

A consensus, which cultural heritages should be conserved and saved from various collapsing factors, is changing in recent. If modern materials and modern methods will be applied for restoration works of heritages, the historic value on it may be spoiled. Therefore it is demanded that materials and methods for restoration works will not spoil the historic values of heritages. From these viewpoints, a concept about "authenticity and heritage" is discussing now, especially on consideration of designing and working for heritage geo-technology. The authors desire for this paper to become a reference for the same purpose.

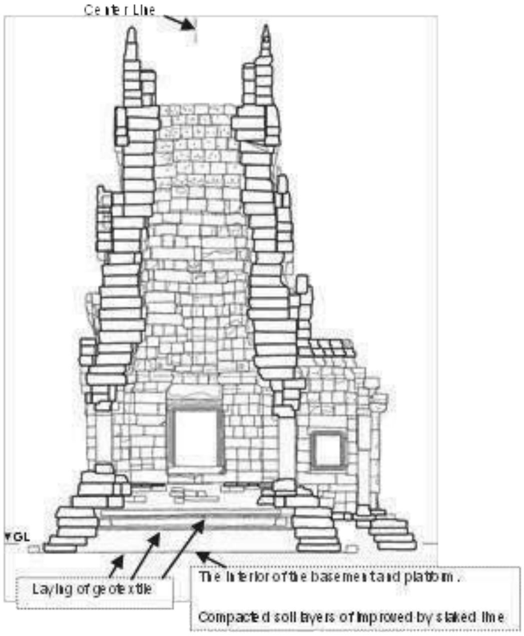

Figure 7. Decided section for reconstitution of the foundation platform

8ACKNOWLEDGEMENTS

The authors would like to express their sincere thanks to Professor Takeshi Nakagawa of Waseda University. The project, on which this paper is based, was supervised and promoted by him responsible the entire.

9REFERENCES

Nakagawa T. (Supervisor) 1996-2005. Annual Report on the Technical Survey of Angkor Monument 1995-2004, Japanese Government Team for Safeguarding Angkor (JSA), Japan International Cooperation Center

Nakagawa T. (Supervisor). 2005. Report on the Conservation and Restoration Work of the Prasat Suor Prat Tower, Royal Plaza of Angkor Thom, Kingdom of Cambodia, Japanese Government Team for Safeguarding Angkor (JSA), Japan International Cooperation Center.

Akazawa Y, Nakagawa T, Mizoguchi A, Nakazawa J, Iwasaki Y, Fukuda M. 2009. Development and reserch of the restoration methods for basement and platform of Prasat Suor Prat Tower N1, AIJ Journal of Technology and Design vol. 30, 567-572.

Iwasaki Y, Akazawa Y, Fukuda M, Nakazawa J, Nakagawa K, Shimoda I, and Nakagawa T. 2013. Dismantling for Reconstitution of N1 Tower of Prasat Suor Prat, Angkor Thom, Cambodia (TC 301- IS NAPOLI 2013, Currently, submitted).

Geotechnical Aspects of Design and Construction of the Mountain Cluster Olympic Facilities in Sochi

Les aspects géotechniques des projets et de la construction des sites olympiques situés dans les pays montagneux autour de la ville Sotchi

Fedorovsky V., Kurillo S., Kryuchkov S., Bobyr G., Djantimirov Kh., Iliyn S., Iovlev I., Kharlamov P., Rytov S., Skorokhodov A.
Gersevanov Research Institute of Foundations and Underground Structures, Moscow, Russia, e-mail: vfedor43@mail.ru

Kabantsev O.
Moscow State Building Construction University, Moscow, Russia

ABSTRACT: Construction of Olympic Facilities in Krasnaya Polyana, mountainous area near Sochi, was a real challenge to Russian geotechnical engineers for the lack of construction expertise in the area as compared to the Alpine mountain resorts with extensive record of such activities. The geotechnical challenges of construction in this mountainous cluster include, as follows:
- assessment of deformation and strength parameters of eluvial and half-rock soils, including rubbly and gravely ones;
- selection of reliable techniques to analyze stability of natural, transformed and strengthened slopes;
- design of footings and counter-slide structures in order to ensure adequate safety accounting seismic actions and soil condition variations.

The paper describes three case histories of Olympic construction projects within the mountainous cluster to illustrate how the above problems were solved.

RÉSUMÉ : Les travaux de construction des bâtiments olympiques dans le massif montagneux de Krasnaya Polyana aux environs de Sotchi ont causé nombre de difficultés aux géotechniciens russes. Cela s'explique par le manque de l'expérience nécessaire en ce domaine dans cette région, contrairement au cas des stations de ski des Alpes, qui ont une plus ancienne et plus riche histoire de développement. Les problèmes géotechniques essentiels liés à la construction dans la dite région consistent en les points suivants:
- évaluation des paramètres de déformabilité et de résistance des sols éluviaux et en partie rocheux, incluant des remblais rapportes ;
- choix de méthodes pertinentes de calcul de stabilité des pentes naturelles, aménagées et renforcées;
- conception de fondations et de structures installations para-glissements garantissant un niveau adéquat de stabilité, y compris pendant les séismes ou un changement d'état des sols.

Dans cet article, on décrit trois études de cas relatifs à la construction des installations olympiques dans la région montagnarde pour illustrer comment ces problèmes ont été résolus.

KEYWORDS: slope stability analyses, counter-slide structures.

1 INTRODUCTION

Erection of Olympic facilities within the Sochi mountainous cluster (Krasnaya Polyana area) forced construction engineers, particularly geotechnical engineers, to face quite a few complicated problems due to tight deadlines, absence of expertise of such large-scale projects in the area, complicated geological conditions and seismicity. The situation dictated that the leading research organizations such as Gersevanov Research Institute of Foundations and Underground Structures would take part in the design of some facilities and structures along with expert evaluation of the project designs. The paper describes the main challenges of the above work on three Olympic projects and their respective solutions.

2. GEOLOGICAL ENVIROMENT

The project (highway from Krasnaya Polyana to “Roza-Khutor” ski resort”, bobsleigh/luge track and a complex of ski-jumps) are allocated on the left-bank slope of Mzymta river and plateau expansion of Aigba ridge offspur at 950…1100 m altitudes with the valley bottom at 485…490 m. The terrain varies from gentle 5…15° slopes to steep 35…40° slopes. The area is cut with streams – tributes to Mzymta.

Geologically there are features from quaternary to underlying Jurassic deposits. The latter are mainly represented by argillites, interlayered with sandstones and limestones. Stratified partly outcropping argillites occur below 10…20 m depths (Fig. 1).

In terms of geotechnical engineering the main rocks are quaternary, mostly formed from of argillite bedrocks. Closer to the surface gravelly clay-filled soils contain more clay and less rock debris and gravel (Fig. 2).

Fig. 1. Outcropping argillite

Such grain size composition complicates any tests to determine soil deformation and, especially, strength parameters. Therefore, pillar shear test was the main method along with large-size sample (∅40 cm) direct shear test that required application of large-size test equipment. Additionally, pillar tests show the natural anisotropy of argillite properties due to its stratified structure.

Fig. 2. Gravely clay soil

At the initial stage gravely soil strength parameters were determined indirectly from results of crushing dry soil in a pebble mill (DalNIIS technique, 1989). Then the obtained parameters were corrected, because the natural slope stability analyses yielded faulty results (slope stability factor $k_{st} < 1$). Later the obtained experience made it possible to correlate the values of soil strength parameters with soil composition and state and thus to identify essential errors.

Essential reduction of soil shear resistance after moistening was a specific feature of the terrain. The relief usually prevented long-term moistening by torrents and/or melting snow. However, soil strength parameters variation had to be taken into account in stability analysis as an action.

Seismicity is yet another special action. Design seismicity of the terrain is reportedly from 8 to 9 points. In the analyses the seismic acceleration was generally assumed to be horizontal, but in some cases a more unfavorable direction had to be taken into account i.e., at 30° versus the horizon.

3. KRASNAYA POLYANA – ROZA-KHUTOR ROAD

Research and technological support of the motor road project was the authors' first effort. Therefore, the basic analytical and design concepts were tested on this very project.

The first soil data was obtained by DalNIIS method (1989) and initially looked dubious. It was especially so for gravel and pebble soils with clay fill, for which internal friction angle was 23.8° and 26.6°, cohesion 13.6 kPa and 11.3 kPa respectively. For coarse-grain soils the values of φ were evidently underestimated. This fact was proved by natural slope stability analysis. For some road cross sections the value of k_{st} with characteristic values of c and φ dropped down below 1.0 and even below 0.8.

This was demonstrated after two stability analyses: by the method of variable level of shear-strength mobilization (MVLM), proposed by the authors (Fedorovsky, Kurillo, 1998, 2001), and by finite elements analysis (Brinkgreve, Vermeer, 1998). Both methods MVLM and FEM (PLAXIS) yielded close k_{st} values that were much lower than those obtained with the well-known Bishop, Morgenstern-Price and Janbu methods, applied by the surveyors. This fact demonstrates that the new methods are certainly better for the analysis of essentially heterogeneous soils. The new methods are also more accurate, as is shown by comparing solutions of problems, having exact solutions (such as bearing capacity problems).

After φ and c of the two above-mentioned soils were corrected to 36°, 32.6° and 16.4 kPa, 19.7 kPa respectively, all the analyzed sections yielded stability factor slightly over 1. This was due to the fact that in the least stable sections the critical slip-lines passed through these very two engineering geological elements..

The road is constructed by cutting into the rock massif and sometimes by filling soil and by enlargement toward the lower slope. The objective was to select such strengthening solution for the upper and the lower slopes that would ensure the minimum value of k_{st}, at least 1.15,for the main load (including 10 kPa load on the road proper) and 1.05 for the special (seismic) load. Where necessary, the upper slope was to be retained by anchors, inserted into the primary rock (argillite). In order to minimize the impact on the natural environment the upper slope retaining wall was made rather steep (60° versus the horizon) and 8…16 m high. In order to ensure adequate stiffness and strength of the slope plane 6..8 m long soil nails were proposed (Fig. 3).

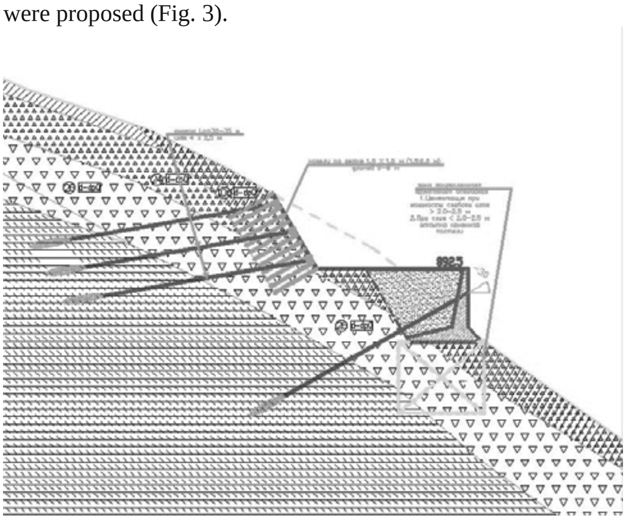

Fig. 3 Counter-landslide structures for the motor road.

Where the lower slope fill is insignificant, no extra measures were required. However, at some locations an angle-shaped retaining wall, strengthened by a row of anchors, was to be erected. However, it was insufficient for one of the cross-sections, as the wall was supported by soft soil. It was proposed to replace the soil by broken stone fill or to strengthen it by grouting (рис. 3).

Notably, application of anchors "neutralizes" both local landslides of the upper and lower slopes along with the global ones, initiated above the road and ending below it.

The anchors were directly simulated in PLAXIS (with the account of transfer from 3D to 2D). In MVLM method the plane, to which the anchors are fixed, is loaded to simulate stressed anchor action on the slope. Both methods demonstrated that the pulling force, applied to 2.5 m spaced anchors (along the road), per 4 m along the slope is 40…45 tons.

Just a few words on seismic numeric simulation. Russian standards recommend to apply proportional inertia forces to soil weight with AK_1 factor. Here A depends on the terrain seismic intensity(A = 0.2 for magnitude 8), and K_1 depends on allowable soil deformations. If a soil slope is viewed as a structure with limited (landslide) deformations then $K_1 = 1$. If then the road subgrade is considered separately from the counter-slide structures and the plastic non-destructive deformations of the structure are allowed then $K_1 = 0.25$. Finally, it is only logical to assume (geometrical) mean value of $K_1 = \sqrt{1 \cdot 0.25} = 0.5$, even more so that the result coincides with recommendations of Eurocode 8.

4. BOB-SLEIGH/LUGETRACK

This project was more difficult than theprevious one due to considerable relief altitude drops and to diverse hydrogeological conditions.

Bobsleigh/luge track (BLT) is located in the lower part of the Aibga ridge northern slope near Krasnaya Polyana.

Orographically the BLT terrain is located in a mid-mountain relief zone with 650-800 maltitude drop. Within the area next to the survey terrain Esto-Sadok and East-Achikhinsky fault zones occur. The South-Esto-Sadok fault passes at the south of the surveyed zone close to the "Bean Storage Area". One of the feathering faults, occurring from north-west to south-east, passes across the northern end of the designed trough. The massif is water-logged via aquifer zones all the way down to the investigated depth, the water heads correlate with the cut depths through the surface valley due surface flows of the Shumikhinsky stream.

Geological slope cuts are mainly represented by high density gravely clay loam or by gravely soils with clay loam fill. The clay loams and clay loam fills feature liquid-plastic to hard consistency.

At 16-40 m depths the quaternary deposits are underlain by low-strength argillites. Depending on the water table the argillites and their fills feature liquid plastic to hard consistency.

The seismicity of the construction project location is 8.5 points as per micro-seismic zoning.

The survey identified three slope terrains, on which development of landslide processes is possible under design seismic action. In order to confirm slope instability the authors performed verification analysis of the above-mentioned slope terrains with the help of PLAXIS as they were and in the case of BLT structures erection. According to the analytical results the stability factor was below the admissible level of 1.1 for 8.5 points seismic action(Figs. 4, 5).

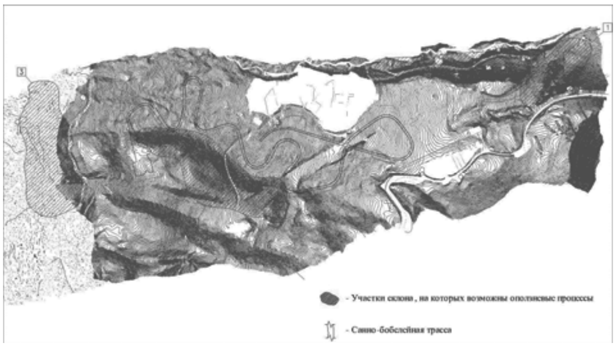

Fig. 4. Topographic map of BLT terrain. Black domains - landslide prone zones; the curved line - bobsleigh/luge track

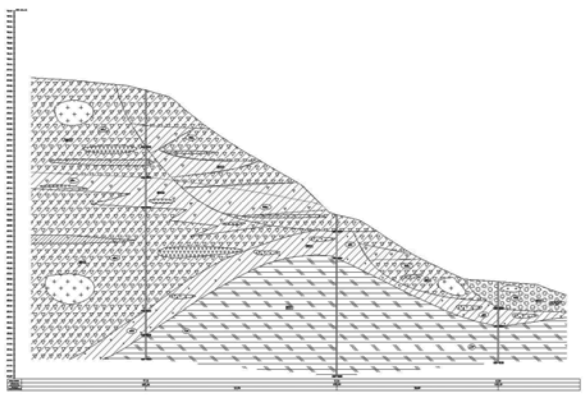

Fig. 5. Land-slide prone slope cross section at terrain 1

Then the authors proposed measures to provide for the required values of stability factor i.e., to erect retaining walls of various configurations, depending on the internal forces in them (one or two rows of bored piles, groups of bored tangent piles with the stiff pile capping beam).

Herein, application of piles as counter-slide structures shall be discussed. Spaced piles, located as a row across a slope would not let soil move between them at whatever landslide pressure (the effect of "non-pushing through", Fedorovsky, 2006) with the critical clearing between piles being larger the greater is the internal friction angle. However, the drawback of such pile strengthening consists in that the bending forces in the piles are so high that often surpass their bending strength. Therefore, in difficult cases the bending moments are reduced by respective measures (pile heads anchoring), or the piles stiffness or strength are increased (larger diameter up to 1.5 m) or installation of buttresses or several piles instead of single piles. In this case there were proposed bored tangent piles with a strong pilework on top. Bored secant piles with dedicated reinforcement are more effective.

Pile walls along the slope feature one more advantage. If their spacing across the slope is less than the wall length then the active (landslide) soil pressure is, as a rule, less than that of the ultimate thrust (Nazarova et al., 1995). The above structures were widely applied for the next facility, discussed below.

5. SKI-JUMP COMPLEX

The complex of K-125 and K-95 ski-jumps geological environment is similar to that of BLT, however, the altitude drops are greater, but hydro-geological situation is better.As different from BLT the counter-slide structures are partly combined with footings of the proper ski-jumps, of the landing slope, of the start and the referee towers.

Fig. 6. Ski-jump site at the beginning of construction operations

Fig. 7. The same terrain during footing erection

This is due to some factors. Firstly, the initial slope (Fig. 6) has k_{st} = 1.04 for soil design parameters while k_{st}< 1.0 for seismic conditions. The ski-jump track is located in a cut 8…10 m deep that undercuts the side slopes and deteriorates the landslide situation (Fig. 7).

In order to overcome these difficulties buttress rows of 3…5 of 0.88 m dia bored secant piles were selected, with some of these piles being anchored at their heads (Fig. 8). The pile fabrication process is shown on Fig.7.

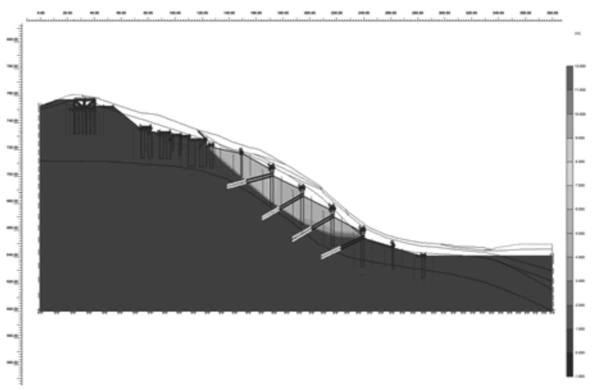

Fig. 8. Analytical scheme of a group of ski-jump footings in PLAXIS

The analysis of the row of buttresses was made in two steps. At the first step it is proved that the limit resistance of the structures to soil flow around is greater than the active (landslide) pressure. To this end a FEM analysis was made of the push-through pressure with the layer depth, represented by the value of pressure on rear side of the row. At the second stage FEM analysis was made either, this time reduced soil strength parameters technique was assumed to assess the slope stability factor with piles and anchors present.

Beside the ski-jumps proper, engineering protection of the terrain was to be taken care of. In order to reinforce the side slopes, retaining walls on piles were proposed. For lower slopes soil nails were assumed in the central portion rather than along the whole height. Such reinforcement divides the slope in two short segments: the upper and the lower one, with the stability factor for each one being greater than that of a single deep landslide of the whole slope.

6. CONCLUSIONS

Application of up-to-date slope stability analysis methods enabled improvement of Olympic facilities project designs in the Sochi mountain cluster in terms of engineering protection of the terrain and of the facilities.

For landslide control structures, sometimes combined with footings, various options were proposed, adjusted to local conditions: soil nails, anchors, retaining walls on subsoil or on piles, rows of piles and buttresses. These structures were applied as combinations rather than separately.

The above analytical techniques, FEM particularly, proved to be effective in the analysis of interaction of landslide-control structures and footings with soil.

Combinations of all these factors ensured construction of Olympic projects to meet the tight deadlines and to provide their adequate safety.

7. REFERENCES

Brinkgreve R.B.J., Vermeer P.A. (eds) 1998. *PLAXIS.Finite Element Code for Soil and Rock Analyses*. Balkema

DalNIIS. 1989. *The method of strength and compressibility assessment for macrofragmental soils with silty and clayey fill and silty and clayey soils with macrofragmental inclusions*.(in Russian). Stroyizdat, Moscow

Fedorovskii V.G. and Kurillo S.V.. 1998. Method of a variable level of shear-strength mobilization for calculation of the strength of soil masses. *Soil Mechanics and Foundation Engineering* , 35 (4-5), 121-126

Fedorovsky V.G. and Kurillo S.V. 2001. Method of a variable level of shear strength mobilization for calculation of the strength of soil masses. *Proc. XVth ICSMGE*, v.1, Stambul, 687-690

Fedorovskii V.G. 2006. Limiting pressure on rows of strip plates and the “no-force-through” effect. *Soil Mechanics and Foundation Engineering* 43 (3), 85-91

Nazarova N.V., Stavnitser L.R., Shvets V.B. 1995. Characteristics of longitudinal retaining walls used as slide-restricting structures *Soil Mechanics and Foundation Engineering* 32 (5), 167-173

Importance of understanding the development and significance of sulphates in the London Clay

L'importance de comprendre le développement et la signification des sulfates dans l'Argile de Londres.

Hawkins A.B., St John T.W.
University of Bristol

ABSTRACT: Although the differences in the engineering properties of the brown and grey London Clay are generally appreciated, less is known about the chemical changes in the unsaturated/seasonally aerated (mottled) zone. With pyrite and calcite present, calcium sulphates accumulate at this horizon.
The paper describes the formation of pyrite, its various forms and the significance of its oxidation in the mottled zone. It comments on the acid soluble sulphate results measured at 0.2 m vertical intervals which show a pronounced SO_4 peak at the brown/grey junction. However, two chemical profiles only 35 m apart illustrate a pronounced variability in chemistry. The mobilization of sulphates associated with the heat of hydration is discussed and the engineering implications of this, the sulphate-rich zones and the associated low pH are considered with particular reference to the significance for any concrete/steel emplaced at this depth.

RÉSUMÉ : Bien que les différences dans les propriétés techniques de l'argile marron et gris de Londres soient généralement appréciées, moins est connu au sujet des changements chimiques dans la zone non saturée/aérée saisonnièrement (tachetée). Quand la pyrite et la calcite sont présentes, les sulfates de calcium s'accumulent à cet horizon.
Le papier décrit la formation de pyrite, ses diverses formes et l'importance de son oxydation dans la zone tachetée. Il commente les résultats de sulfates solubles acides mesurés à intervalles verticaux de 0,2 m qui montrent une crête prononcée de SO_4 à la jonction du marron/gris. Cependant, deux profils chimiques séparés de seulement 35m montrent une variabilité chimique importante. La mobilisation des sulfates associées à la chaleur d'hydratation est discutée et on considère ses implications techniques, ainsi que ceux des zones riches en sulfate et le niveau faible de pH y associé. Une référence particulière est faite à la signification pour tout béton ou acier mis en place à cette profondeur.

KEYWORDS: sulphate, pyrite, London Clay, gypsum, sulphate attack.

1 INTRODUCTION

The London Clay Formation (LCF) is a Tertiary marine deposit up to 150 m in thickness. The sequence is predominately composed of silty clays with thin silt bands and is typically sand-rich towards the base. Selenite, the euhedral form of gypsum (calcium sulphate) is particularly common in the upper weathered zones, whilst pyrite, present as nodules, replacement of organic matter and framboids, is abundant in the unweathered Clay. During deposition, the climate was warm and rivers draining the adjacent land mass would have carried a high proportion of organic matter. The organic content would vary laterally and may have changed with time during deposition. As a result of variations in sea bed terrain and sea level, the deposits often accumulated in anoxic conditions.

2 SULPHIDES IN THE LONDON CLAY

Many dark grey/black sediments have high organic contents, the organic matter decaying the burial process. Oxygen is consumed by bacteria such that the sulphates are reduced to sulphides. When ferric iron is present in these oxygen-depleted environments, it too is reduced and reacts with the H_2S produced by the sulphate-reducing bacteria, ultimately to form pyrite (iron sulphide) (Figure 1).

Pyrite is typically found in well-bedded fine grained sediments which are dark in colour due to the high organic (carbonaceous) content. Whilst a pyrite content of some 2-4% is present throughout the grey LCF, it is often abundant in the silt/sand-rich horizons near the base and where similar horizons occur elsewhere.

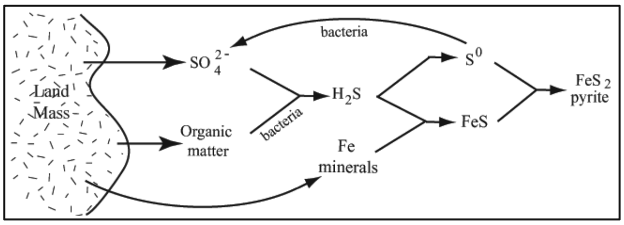

Figure 1. Sedimentary pyrite formation (after Berner, 1984).

Four major forms of pyrite are present in the LCF:
a) Large crystals with varying habits (cubic, octahedral etc)
b) Groups of microcrystals which have clustered together to form framboids up to 10-15 µm in diameter (eg Figure 2)
c) Irregular, often greenish-coloured pyrite nodules
d) Replacement of organic matter

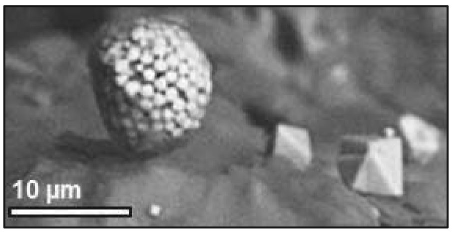

Figure 2. Pyrite framboid and octahedra in the LCF.

3 SULPHATES IN THE LONDON CLAY

As the LCF is a randomly fissured, jointed material, its secondary permeability is such that during past climates or de-watering phases, the weathering extended to considerably greater depths than would be anticipated in the present climate. Commonly the brown LCF extends to some 6-8 m depth and in rare cases, as recorded by Chandler (2000), to 15 m. Between the saturated (grey) and aerated/oxidized (brown) material there is a mottled grey/brown zone. In the upper brown LCF much of the pyrite has decomposed. In the mottled zone the pyrite experienced a wetting/drying environment such that the iron sulphides were oxidized to produce sulphuric acid and ferrous sulphate (Eq. 1).

$$FeS_2 + H_2O \rightarrow 2FeSO_4 + 2H_2SO_4 \qquad (1)$$

Although in stronger, more calcareous materials the ferrous sulphate may produce a significant initial expansion, in the weaker LCF this is less apparent. However, the formation of sulphuric not only changes the pH of the soil but reacts with calcium carbonate to produce calcium sulphate (Eq. 2). Detailed chemical reactions are given in Hawkins and Pinches (1987) and Hawkins (2013).

$$H_2SO_4 + CaCO_3 + H_2O \rightarrow CaSO_4.2H_20 + CO_2 \qquad (2)$$

Gypsum can grow within the Clay in various forms including:

a) Euhedral, monoclinic prisms, often known as selenite
b) Stellate (star shaped) or “rosette”-like, crystals (Figure 3)
c) Void infill, with irregular shapes
d) Apparently amorphous “sucrose” crystals

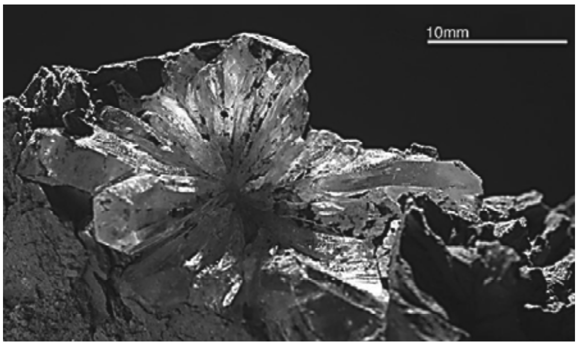

Figure 3. Stellate gypsum from the LCF at Camberwell (6-7 m depth).

The stellate form is typical of crystals which have developed over relatively long periods of time. As such crystals are common between 6 and 7 m depth, it is clear the pressure of crystallisation must have exceeded 100 kPa.

Gypsum is often associated with sandy horizons in the LCF (Bessey and Lea, 1953). The porous and relatively permeable nature of these bands will encourage water movement in wet periods and facilitate the ingress of oxygen during dry periods. As a consequence, oxidation takes place in the adjacent Clay and gypsum may be precipitated from the sulphate-rich solutes.

The development of gypsum on exposed clays can occur in a matter of weeks. Grey LCF borehole arisings from a site investigation in Camberwell left open to weathering showed fine (< 2 mm) white crystals after only four weeks while in an oven at 105 °C they formed within 1-2 days. Microscopic examination confirmed that the crystals were gypsum.

4 CHEMICAL TESTING

Although from a geotechnical point of view the sub-division between the grey Clay and the brown Clay is useful, rarely is there an explanation highlighting the importance of the chemistry of the mottled zone, which frequently contains enriched acid soluble sulphate with a corresponding lower pH.

Hawkins (2013) reports results obtained from the Camberwell site investigation in February 2012. Two boreholes only 35 m apart were tested for total sulphur (TS), acid soluble sulphate (AS) and water soluble sulphate (WS). Table 1 also shows the calculated total potential sulphate (TPS), oxidisable sulphides as sulphate (OS) and equivalent pyrite according to the Canadian Standard CTQ-M200 (Comité Technique, 2001).

Table 1. Sulphur chemistry for Camberwell boreholes, February 2012.

Depth (m)	AS (% SO_4)	WS (mg/l SO_4)	TS (% S)	TPS (% SO_4)	OS (% SO_4)	Eqv. Pyr. (%)
Borehole 1						
2.6	0.02	118	0.01	0.03	0.01	0.01
3.6	0.02	10	0.01	0.03	0.01	0.02
4.4	0.33	116	0.11	0.33	0.00	0.20
5.5	0.91	10	0.38	1.14	0.23	0.71
6.4	0.21	906	0.21	0.63	0.42	0.34
7.6	0.25	10	0.54	1.62	1.37	1.01
8.5	0.28	685	0.48	1.44	1.16	0.85
10.6	0.24	501	0.50	1.50	1.26	0.90
12.5	0.26	505	0.56	1.68	1.42	1.02
14.6	0.24	621	1.53	4.59	4.35	2.82
16.6	0.23	405	0.67	2.01	1.78	1.23
17.4	0.17	366	0.57	1.71	1.54	1.04
Borehole 2						
Depth (m)	AS (% SO_4)	WS (mg/l SO_4)	TS (% S)	TPS (% SO_4)	OS (% SO_4)	Eqv. Pyr. (%)
3.1	0.05	110	0.05	0.15	0.10	0.09
4.1	4.94	10	2.40	7.20	2.26	4.49
5.1	1.12	1850	0.38	1.14	0.02	0.60
6.0	0.62	1410	0.15	0.45	-0.17	0.19
7.1	0.73	1550	0.70	2.10	1.37	1.21
8.0	0.28	715	0.61	1.83	1.55	1.10
9.1	0.31	1050	0.63	1.89	1.58	1.11
10.1	0.31	898	0.63	1.89	1.58	1.12
12.0	0.28	970	0.44	1.32	1.04	0.76
14.0	0.34	10	1.88	5.64	5.30	3.51
16.0	0.23	10	1.19	3.57	3.34	2.22
18.0	0.20	10	0.52	1.56	1.36	0.97
18.9	0.14	10	0.45	1.35	1.21	0.84

At the Camberwell site, the brown-grey junction is at approximately 6-7 m depth while the groundwater level is at 1-2 m depth. To a depth of around 3 m the LCF is depleted of sulphates due to leaching, while a number of elevated values were recorded from between 4 and 8 m. Below 8 m the AS content is relatively uniform at 0.25-0.3 % SO_4. The TS in both boreholes attains a high value of between 1.5 to 2 % S at around 14 m depth, approaching the base of the LCF. The sulphur at these depths is likely to be related to pyrite nodules. With the exception of 4 m depth in BH 2, the equivalent pyrite is highest towards the base of the boreholes. Several pyrite nodules from this depth were noted in nearby borehole cores. Despite being only 35 m apart, there are stark differences between the two boreholes. For example, at 4 m depth, the AS is 0.3 % and the TS almost 0.1 % in BH 1 compared with an AS of almost 5 % and a TS of 2.4 % in BH 2.

The high SO_4 values at 4 m depth in BH 2 are probably due to the presence of coarse gypsum in the sample. As the sample mass used in these tests is less than 5 g, it is quite possible for a crushed gypsum crystal to occupy a large proportion of the sample and hence contribute to anomalously high sulphur and sulphate test results. This may in part be related to the presence of two mature trees within < 3 m of BH 2 (Hawkins 2013).

As a consequence of this significant variation, in September 2012 a new set of samples was taken at 0.2 m intervals close to the original BH 2. The sulphate and pH of these samples was determined (Figure 4).

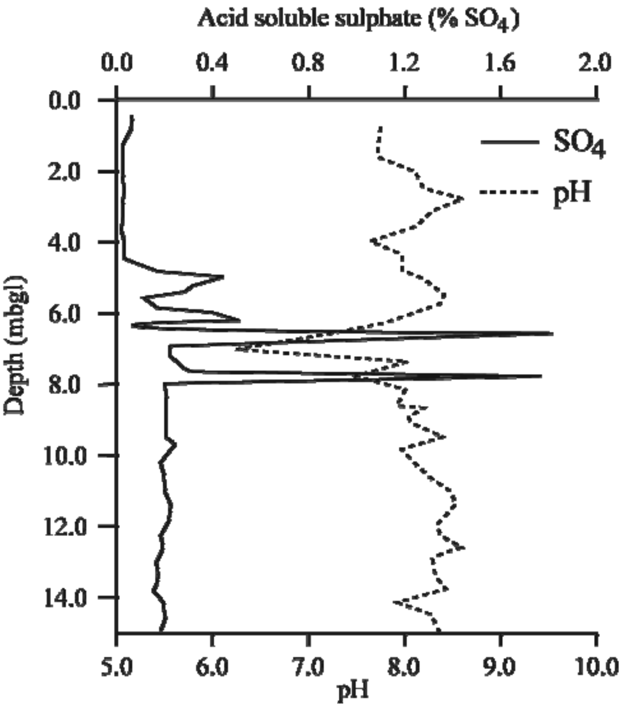

Figure 4. Sulphate and pH profile for the additional borehole at Camberwell.

The results shown in Figure 4 can be summarised as follows:

a) To 4.5 m depth the clay is almost devoid of any sulphate, below which there is a 2 m zone of minor sulphate peaks
b) A zone of sulphate enrichment is present at c. 6.5-8 m with a maximum of 1.8 % SO_4. This is over 2.5 times higher than the peak in the original BH 2. This highlights the need for an appreciation of the potential variation in sulphate profiles, in this case from boreholes only 5 m apart
c) Below 8 m the AS is relatively constant at c. 0.2 % SO_4

5 ENGINEERING IMPLICATIONS

The significance of sulphates in the LCF has been appreciated for many years such that in the 1930s the Institution of Civil Engineers set up a research sub-committee to examine this, although it was interrupted by the war years (Bessey and Lea, 1953). During their investigations, Bessey and Lea undertook total sulphur and water soluble sulphate analyses, which until the early 2000s was the common procedure. The determination of acid soluble sulphate is now favoured, taking into consideration the potential for acidic ground conditions to develop. In addition, sulphate values were originally presented as % SO_3 whereas % SO_4 is now used.

A well-known case study of concrete attack due to sulphate-bearing ground is that of the St Helier Hospital in Surrey. The 750-bed hospital at Carshalton was constructed in 1938 and by 1959 it was found that some of the concrete foundations placed in the brown LCF had seriously deteriorated. The remedial work in the early 1960s involved supporting the hospital on piles (Legget and Karrow, 1983).

5.1 *Seasonal variation in sulphate concentration*

Bessey and Lea noted the marked difference in sulphate values taken in dry and wet conditions. For instance, following a very dry summer/autumn, when measured in December the sulphate values in two boreholes at Benfleet were as high as 0.30 % SO_4. However, following the wet winter, by March they had dropped to 0.042-0.070 % SO_4. Whilst the seasonal influence on the shrink-swell of the LCF is well known, the effect on ground sulphates is not appreciated by many geotechnical engineers. Bessey and Lea also report sulphate contents taken from six boreholes between three different depths where the average acid soluble sulphate varied between 0.024-3.38 % SO_4 (Table 2).

Table 2. Difference in AS values given by Bessey & Lea (1953) with averages of all six samples and of the highest two, which BRE (2005) recommend should be taken as the characteristic value.

Depth (m)	Range, SO_4 (%)	Avg. six samples, SO_4 (%)	BRE avg. top two, SO_4 (%)
0.3-0.9	0.024-0.372	0.1	0.22
0.9-1.83	0.036-0.516	0.23	0.44
1.83-2.74	0.444-3.38	0.78	1.99

Table 2 highlights the significance of appropriate sampling. Although this has been in the literature for nearly 60 years, too frequently samples are taken without due consideration of the variation in sulphur/sulphate concentration with depth. Field sampling should always take into account the depth at which it is proposed to place concrete or steel in dark weathered clays.

Although Bessey & Lea draw attention to the fact that gypsum is often present in the sandier horizons, this is also true with calcareous/limestone bands which may become aerated in dry periods, resulting in oxidation of the adjacent pyritic mudrocks/clay.

5.2 *Harrow on the Hill*

Raison (1992) indicated the boundary of the LCF/Woolwich and Reading Beds Formation (Lambeth Group) was at 35.5 m AOD at Harrow. The relatively low liquid limit (c. 50 %) and a moisture content below the plastic limit at the base of the LCF are consistent with the presence of a silty-sandy horizon – the Basement Beds. Although Raison shows the groundwater level obtained during the investigation period to be at 50 m AOD (15 m deep) attention is not drawn to the difficulty of obtaining a realistically quick piezometric response in clay-rich soils. Detailed logging of continuous U_{100} samples from a supplementary borehole at Harrow on the Hill indicated the brown LCF to some 7 m has selenite crystals up to 10 mm long below which is a 1 m mottled horizon in which selenite crystals of around 6 mm length are present. Chemical analyses of the borehole samples gave the results in Figure 5.

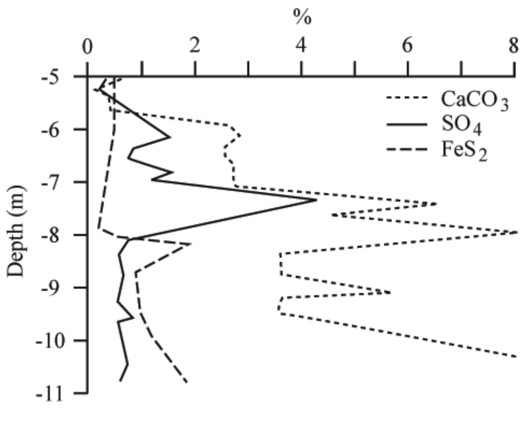

Figure 5. Borehole chemistry at Harrow on the Hill.

The results can be summarised as follows:

a) To a depth of 7.5 m the pyrite content is relatively low (0.2 - 0.5 %). Below 8 m the pyrite content is > 0.75 % with a peak of 1.8 % at 8.5 m depth
b) The calcite content is low to a depth of 6 m – frequently < 0.5 %. Although it rises to 2.5 % between 6 and 7 m, the main rise to 5-8 % is below 7 m

c) The acid soluble sulphate content is relatively low (< 0.5 %) to a depth of 5 m, rises between 5.25 and 7 m and has a significant peak of 4.2 % SO_4 at 7.25 m, below which it is in the order of 0.6 % SO_4

During the construction of an underground car park the opportunity was taken to collect samples at 10 mm intervals between two 600 mm CFA piles, 320 mm apart (Figure 6).

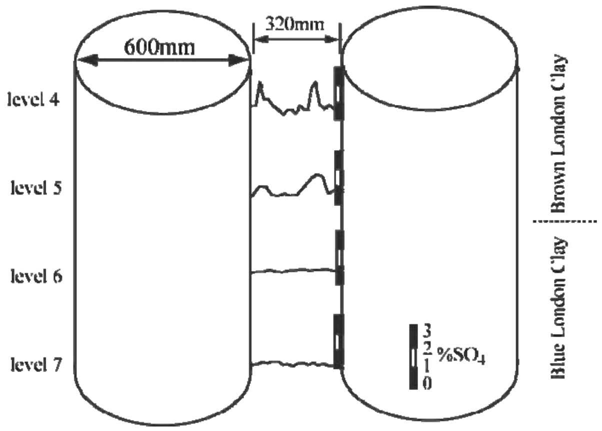

Figure 6. SO_4 content with distance from concrete piles in the LCF. Note variation in the brown Clay.

As noted by Hawkins and Higgins (1997), the sulphate level in the brown LCF was generally in the order of 0.5 % SO_4 but between the 4th and 5th floors rose to 2 %, approximately 30 mm from each of the piles. In the underlying saturated grey LCF (6th and 7th floors) where the pyrite and calcite had not chemically reacted, raised SO_4 values were not present. It is considered that when the sulphates are mobilized as a consequence of the heat of hydration, the sulphate-rich solutions move into the zone of shear which commonly occurs in the *in situ* ground adjacent to material affected by the auger torque.

A laboratory experiment was undertaken by Hawkins and Higgins to determine the influence of temperature when the LCF was heated in a moist environment at 30 °C for four, six and eight weeks, the acid soluble sulphate rose from 0.22 to 1.32 %. This six-fold rise emphasises the effect of the heat of hydration on the ground chemistry close to CFA piles, and hence the care required when assessing the concrete aggressivity class if concrete piles are to be installed in ground containing or likely to develop sulphates.

To assess the outward migration of heat from the hydrating concrete, Hawkins and Higgins undertook an experiment by placing a copper pipe in an augered hole in the LCF. Three thermometers were installed at 7.5, 15 and 30 mm from the pipe. When water at 65 °C was placed in the copper pipe the temperature of the Clay rose by a maximum of 8 °C in six minutes at 7.5 mm; by 5 °C in six minutes at 15 mm and by 4 °C in 35 minutes at 30 mm (Figure 7).

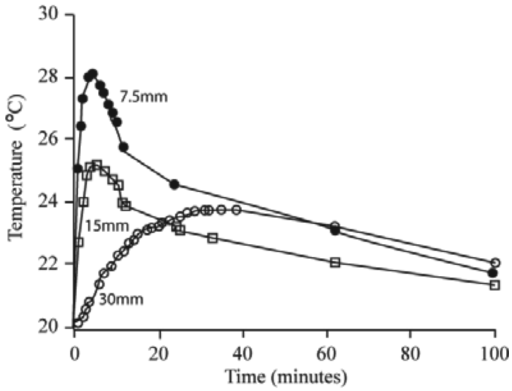

Figure 7. Variation in ground temperature with time at given distances from a heated pipe in the LCF.

6 CONCLUSIONS

a) Sulphur is present in the LCF predominantly as pyrite and gypsum. The distribution and abundance of these forms can be highly variable
b) Planning of site investigation works should appreciate the spatial variation (lateral and vertical) in ground sulphur, as well as the type and location of sub-surface structures
c) Appropriate laboratory testing would include a full suite of chemical testing including AS, WSS and TS
d) The determination of detailed sulphate and pH profiles is advocated
e) The heat of hydration of concrete may result in a concentration of sulphates and appropriate measures should be taken to protect concrete from sulphate attack

7 ACKNOWLEDGEMENTS

The authors would like to thank marcus hawkins for assistance in the preparation of figures.

8 REFERENCES

Berner R.A. 1984. Sedimentary pyrite formation: An update. *Geochimica et Cosmochimica Acta* 48, 605-615.

Bessey G.E. and Lea F.M. 1953. The distribution of sulphates in clay soils and groundwaters. *Proc. Inst. Civ. Eng.* 2, 159–181.

BRE. 2005. *Concrete in aggressive ground. Special Digest 1.* Building Research Establishment, Bracknell, UK.

Chandler R.J. 2000. Clay sediments in depositional basins: the geotechnical cycle. *Quart. Jnl. Eng. Geol. Hydro.* 33, 7-39.

Comité Technique Québécois D'étude Des Problèmes De Gonflement Associés à La Pyrite. 2001. *Appraisal procedure for existing residential buildings*. Procedure CTQ-M200, Version 2.0, June 4.

Hawkins A.B. 2013. Engineering Implications of the Oxidation of Pyrite: an overview, with particular reference to Ireland. In Hawkins, A.B. (ed) *Implications of pyrite oxidation for engineering works*. Springer. In press.

Hawkins A.B. and Higgins M.D. 1997. The generation of sulphates in the proximity of cast in situ piles. In: Ground Chemistry: Implications for Construction. A.B. Hawkins (ed). Balkema, Rotterdam.

Hawkins A.B. and Pinches G.M. 1987. Cause and significance of heave at Llandough Hospital, Cardiff - a case history of ground floor heave due to gypsum growth. *Quart. Jnl. Eng. Geol*. 20, 41-57.

Legget R.F. and Karrow P.F. 1983. *Handbook of geology in civil engineering*. McGraw-Hill.

Raison C.A. 1992. Deep basement construction at College Road, Harrow. P*roceedings of the Conference on Piling, European Practice and Worldwide Trends*, Institution of Civil Engineers.

Rockfall-protection embankments – design concept and construction details

Merlons de protection contre les chutes de pierres - modèle de conception et d'exécution

Hofmann R.
Ziviltechnikerbüro Dr. Hofmann, Perchtoldsdorf, Austria

Vollmert L.
BBG Bauberatung Geokunststoffe GmbH & Co. KG, Espelkamp, Germany

Mölk M.
Geologische Stelle des Forsttechnischen Dienstes für Wildbach- und Lawinenverbauung, Innsbruck, Austria

ABSTRACT: In the past, protection embankments were often erected in situations in which high design energies were anticipated; it was assumed that these embankments, if constructed appropriately, would provide adequate protection for such load cases. Rockfall-protection embankments are favoured in cases where the slope geometry and the space available allow their construction. In comparison with rockfall-protection nets, whose capacity to absorb energy is currently limited to 8000 kJ, embankments have advantages in terms of longevity, construction costs, and – depending on the construction – energy-absorbing capacity. To describe the failure mechanism associated with a dynamic impact on such an embankment, and to develop a design approach, model testing was carried out on conventional soil embankments, on reinforced embankments, and on embankments with stone facings. The objective of these model tests was to investigate the effects of rock impact on built-up embankments of various types, and to develop a concept for their design.

RÉSUMÉ : Dans le passé, les merlons de protection étaient souvent construits à haute énergie en supposant que ces merlons aient une capacité suffisante pour ces cas de chargement. Les merlons de protection contre les chutes de blocs sont construits, de préférence, dans les cas où la géométrie du talus et l'espace disponible permettent un tel ouvrage. En comparaison avec des filets protection contre les chutes de blocs, dont la capacité d'absorption d'énergie est actuellement limitée à 8000 kJ, les merlons ont des avantages, notamment en termes de durabilité, de coût de construction et - selon l'ouvrage - de capacité d'absorption d'énergie. Afin de décrire les surfaces de rupture des merlons causées par un impact dynamique et pour la mise en place d'une approche de conception, des modèles expérimentaux ont été réalisés avec des merlons en sol pur, des merlons renforcés et merlons en sol avec un parement en pierres. L'objectif du projet pilote était d'étudier les effets des éclats de blocs sur les différents types de merlons et de développer un dimensionnement.

KEYWORDS: rockfall protection, embankments, impact, energy absorption, design, model test, prototype, geosynthetics

1 INTRODUCTION

In the virtual absence of design rules for dynamic actions on pure soil structures, in the past 15 years designers have often resorted to the use of concepts used in the design of rockfall-protection galleries. The required parameters were derived from model testing (and, in a few cases, from full-scale tests) carried out since the late 1990s mainly in Switzerland, Austria, Italy and France (Blovsky (2002), Labiouse & Heidenreich (2009), Lambert et. Al (2011), Peila (2007) and Pichler et al. (2005)) In some cases, numerical calculations (Peila (2007) and Plassiard & Donze (2010)) were performed. In contrast to a rockfall-protection embankment, a rockfall-protection gallery is a stiff, reinforced-concrete construction overlain by a cushioning layer of various materials with differing thicknesses.

The construction of protection embankments has increased markedly in areas with a high risk of rockfall. No suitable design models for soil embankments currently exist which enable a geotechnical assessment of the stability of such structures. 1g model tests were therefore performed to obtain a picture of the failure mechanism under impact forces, and to use this to devise a design model.

A total of 150 tests with different structures (soil embankments, reinforced embankments, embankments with rip rap facing, embankments with cushioning elements), cross-sectional profiles, impact angles, freeboards, and impact energies were performed. The length of the embankment, and its height, were kept constant in all the tests. Several significant parameters have been varied, see 2.2. The test series were complemented with model embankments with rip rap facing and cushioning elements, and with geosynthetics. The model-scale geosynthetics were manufactured and delivered by NAUE.

2 SCALED MODEL TESTS

2.1 *Model tests*

The tests serve as experimental model tests, and the questions to be answered are limited to the shape of the failure body created in an embankment by a dynamic impact. A model scale of 1:33 was chosen to correspond to the energy involved in practice. The objective of these qualitative model tests was to depict with model embankments in the laboratory the failure mechanism generated in embankments by rock impact, see Hofmann & Mölk (2012).

The sphere was impacted against the embankment at three velocities (v1 = 4,5 m/s, v2 = 3,5 m/s, v3 = 6,0 m/s). Using the model scale of 1:33, these correspond to velocities of: v1 = 25,8 m/s, v2 = 20,1 m/s, v3 = 34,4 m/s in real life. The plastic displacements in the embankment and the penetration depth of the sphere were measured after each impact at two levels using several model extensometers (Figure 1).

2.2 *Structure types investigated*

Different slope angles β_{UPHILL} (4:5, 50°, 60° and 70°) and $\beta_{DOWNHILL}$ (2:3, 50°, 60° und 70°) and crest widths (b_1 = 2,5 cm, b_2 = 5,0 cm, b_3 = 10 cm and b_4 = 20 cm) were investigated and the impact height of the sphere (measured along the slope from the lowest point of the sphere up to the crest h_1 = 8 cm, h_2 = 16 cm, h_3 = 12 cm and h_4 = 20 cm) was varied.

Property	Unit	$F_{M,k}$ GGR_LS	λ	$F_{P,k}$
		Geogrid		Geogrid
Tensile strength md	kN/m	0.25	1089	272.3
Extension ε, md	%	5	-	5
Tensile strength cmd	kN/m	0.14	1089	152.5
Extension ε, cmd	%	5	-	5

Table 1: Tensile properties of the model geosynthetics

Property	Unit	GGR_LS	GTX_A
		Geogrid	Nonwoven
Mass per unit area	g/m²	28	39
Thickness	mm	0.24	0.25
Tensile strength md	kN/m	0.25	0.36
Extension ε, md	%	5	16
Tensile strength cmd	kN/m	0.14	0.09
Extension ε, cmd	%	5	55

Table 2: Conversion of characteristic strength properties model/prototype (Index k: characteristic)

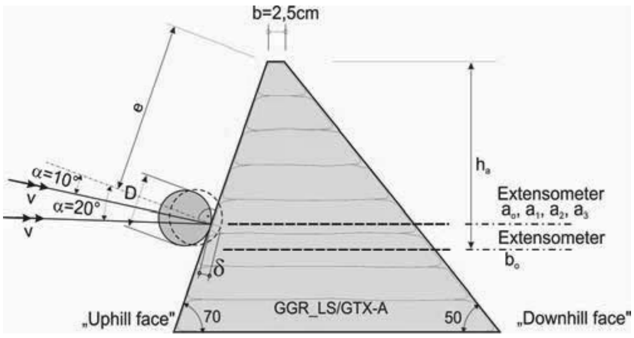

Figure 1. Cross section with extensometers

2.3 *Model embankments with geosynthetics*

The model embankment was reinforced with geosynthetics GGR_LS and GTX_A supplied by NAUE (Table 1).
If the model laws are observed, then a line load in this model has a transfer factor $\lambda^2 = 33^2 = 1089$ [-]. The characteristic values given in Table 2 are derived using this and equate to the full-scale values characteristic for the prototype.at a scale of 1:1.

The effective tensile strengths in the model are obtained using a factor of A2 = 1.2 for installation damage resulting from sub-base placement and compaction, as are the strengths $FP_{,d}$ relevant for the prototype after application of all reduction factors e.g. installation damage (Table 3).

2.4 *Model embankments with stacked-rock facing*

In some tests, a rip rap facing was used on the uphill face of the embankment (Figure 2).

Property	Unit	$F_{P,d}$	$J_{P,d@5\%}$
		Geogrid	
Tensile strength md	kN/m	226.9	4538
@ Extension ε, md	%	5	-
Tensile strength cmd	kN/m	127.1	2542
@ Extension ε, cmd	%	5	-

Table 3: Required values for reinforcement of the prototype
(Index d: design)

3 BASIS FOR DESIGN MODEL

3.1 *Evaluation using relative impact energy and penetration depth*

In the model tests, the size and shape of the failure body created by the sphere were recorded. With the help of a non-dimensional evaluation of the test results, diagrams were drawn up to enable the results to be transferred to the full-scale situation, Hofmann & Mölk 0.

For the evaluation, an activated soil body was defined near the embankment crest (Figure 3). A non-dimensional depiction of the results is shown in Figure 4. The relative impact energy E* was introduced and plotted against the non-dimensional value δ/b, where δ is the depth of penetration of the sphere into the embankment and b is the crest width. The upper extensometers (a_0, a_1, a_2, a_3) were positioned at the mid-point of the sphere in the axis of the embankment; one extensometer was positioned at the level of the bottom of the sphere. The following variables are introduced:

$$E^* = E / (\gamma * A_a * D * h_a) \; (-) \qquad (1)$$
$$E = m v^2/2 \; (\text{Joule}) \qquad (2)$$
$$\gamma = \rho * g \; (\text{N/m}^3) \qquad (3)$$
$$A_a = (b+c)/2 * h_a \; (\text{activated area}) \; (\text{m}^2) \qquad (4)$$

where E* is the relative impact energy, m is the mass of the sphere in kg, v its velocity in m/s (v_1;v_2;v_3), ρ the soil density in kg/m³, g the gravitational acceleration in m/s², D the diameter of the sphere in m, h_a the activated height in m and b the crest width in m.

3.2 *Lessons learned from the tests*

3.2.1 *Lessons from the model tests for all construction types*

- In the vicinity of the impact, the body of the embankment undergoes significant compaction, and the crest is displaced upwards.
- The slimmer the construction, the larger the failure body on the downhill face of the embankment.
- A comparison of the different model tests clearly shows the more pronounced elasto-plastic behaviour of the embankment reinforced with geogrids compared with the unreinforced case (Figure 4).

3.2.2 *Lessons from trials without rip rap facing and without geosynthetics*

- A comparison shows how the deformations increase significantly from the lowest point of the sphere upwards. Observation of the model tests shows that a freeboard of at least twice the diameter D of the sphere is required to prevent the sphere rebounding over the embankment crest on the first impact.

- The maximum width of the activated embankment body is 5 to 6 times the sphere diameter.
- In the tests it was found that the failure planes from the second impact onwards tended increasingly to form in an upward direction.
- The pictures taken with the high-speed camera clearly show quite significant elastic deformations during the period of impact.

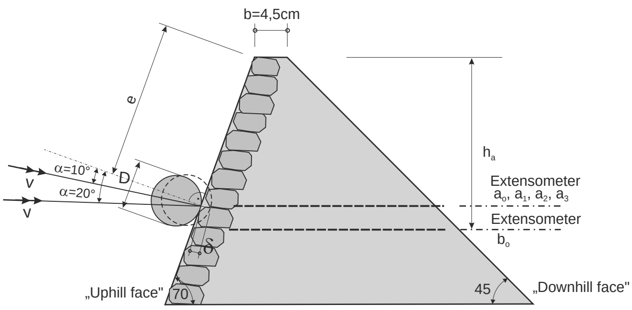

Figure 2. Model embankment with rip-rap facing

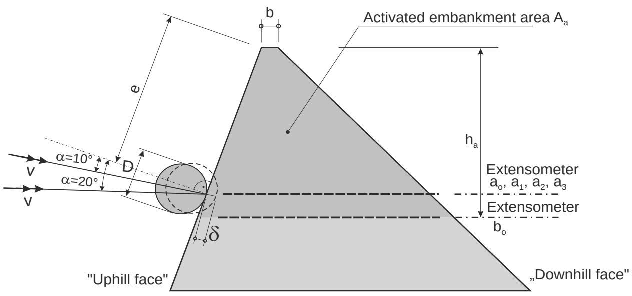

Figure 3. Model embankment system

3.2.3 Lessons from trials with rip rap facing and without geosynthetics

The following additional observations were made on embankments with rip rap facing:

- Slope angles ≥ 50° require a freeboard of at least 1 x the diameter of the sphere.
- After the impact, the sphere scarcely changes its height, whereas in the case of pure soil embankments, and reinforced structures, it tends to jump or roll in the direction of the crest.

3.2.4 Lessons learned from the tests with geosynthetics

- The model tests with the geosynthetics all showed a significantly larger lateral distribution (influence width) of the displacements. An influence width of at least 8 - 9 times the diameter of the sphere can be estimated from the measurements and the pictures taken with the high-speed camera.
- Very slim constructions with uphill and downhill slope angles of 70° and 60° were also investigated. These exhibited a noticeably more elastic behaviour than pure soil embankments.
- However, they require a markedly greater freeboard than embankments with rip rap facing. For geogrid-reinforced structures, a freeboard of 1.5 times the sphere diameter can be considered as being on the safe side.

4 DESIGN MODEL FOR ROCKFALL-PROTECTION EMBANKMENTS

4.1 *Principles*

A characteristic failure body for different structures was derived from the 1g model tests. An important and consistent parameter was the activated width of the embankment in the direction normal to the impact. The basic concept of the proposed design method is to derive a non-dimensional relationship between the penetration depth and the crest width (δ/b) using the relative impact energy E*, Hofmann & Mölk (2012).

4.2 *Activated failure body*

Normal to the impact direction, the size of the activated failure body is a function of the embankment structure. Whereas the width of the failure body in unreinforced embankments (both with and without rip rap facing) is at least 5 to 6 times the diameter of the block (the sphere in the model), this value increases to 8 to 9 times the diameter of the block for reinforced structures.

4.3 *Required freeboard*

Freeboard is defined here as the distance between the upper surface of the block and the upper surface of the embankment, measured along the slope (Section 3.2)

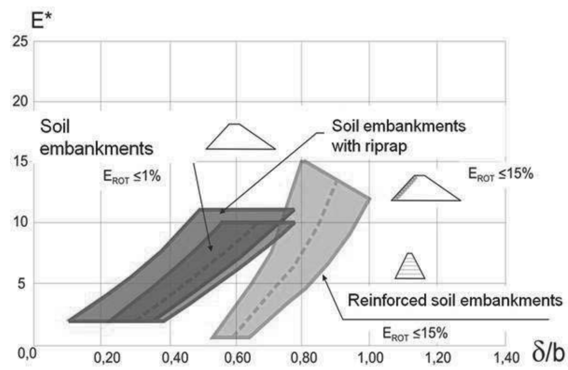

Figure 4. Comparison of the different structures

4.4 *Estimate of the equivalent static force*

An estimate of the equivalent static force is made using equation (5), on the assumption that the force initially increases, and then decreases, in a linear manner, and that the velocity decreases in a linear manner according to Blovsky (2002) (Figure 5). The equivalent static force is then distributed over the activated embankment width involved.

$$F = v^2 \, m / \delta \quad (5)$$

$$F = 2 \, v \, m / \Delta t \quad (6)$$

$$\Delta t = 2 \, \delta / v \quad (7)$$

$$\delta = (0{,}8 \text{ bis } 0{,}85) \, m \, v^2 / F \quad (8)$$

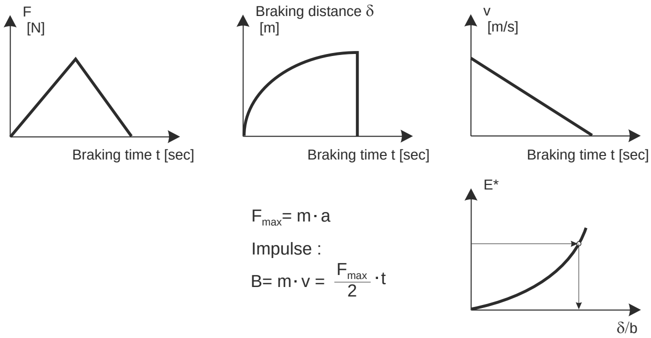

Figure 5. Assumptions for the evaluation (a = deceleration)

4.5 *Structure configuration*

The constructive aspects of rockfall-protection embankments are just as important as their numerical design. Rockfall incidents inevitably result in damage and wear on the facing. If at all possible, the facing should therefore effectively protect the outer surface of the reinforced earth body; it should also require little maintenance and ideally allow inspection, in case partial damage requires repair (ONR 24810 (2013) und ÖNORM B 1997-1-1 (2007)).

If rockfall-protection embankments are constructed as reinforced-soil bodies with steep side slopes, the reinforced body must have a wrap-round front surface to guarantee adequate anchorage for individual reinforcing layers at the edge of the structure. A facing is required to protect the structure against UV and impact. Figure 6 shows an example of a slim gabion solution which allows inspection and can be built independently of the supporting embankment body. The thickness, the area weight of the protective layer, and the quality of the steel elements must reflect the anticipated stressing/loading.

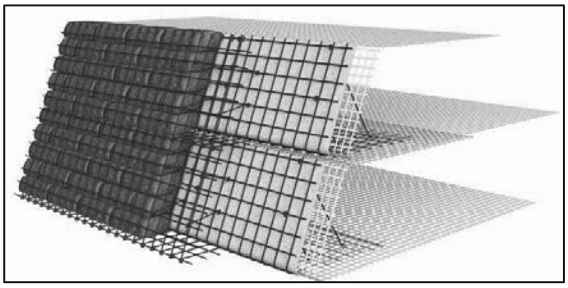

Figure 6. Inspectable outer facing-system (double-wall-system) to protect the load-bearing structure built using the wrap-around method (System NAUE DW)

5 COMPARISON OF DESIGN MODEL WITH FULL-SCALE TESTS

The results of model testing form the basis for the application of the results to full-size construction. To investigate the applicability of the design proposal, it will be necessary to evaluate existing protection embankments and the damage observed to have resulted from rockfall. This means that, after an incident, at the very least the block size and the penetration depth will have to be documented. Additionally, the velocity will have to be back-calculated using a rockfall-impact simulation program. The diagram in Figure 4 was confirmed at least by the full-scale tests of Peila et al. (2007), Lambert et al.(2011), and the observations of protection embankments in Tirol and Voralberg. The comparisons of observations on actual structures with the results obtained using the design proposals are summarised in Table 4. It can be seen that there is very good agreement.

		Observations from full-scale tests				Determined with diagram 15		
	Construction type	Energy	Crest width	Penetration depth		E*	Derived parameter	Penetration depth
Source		(kJ)	b (m)	**δ (m)**		()	δ/b	**δ (m)**
PEILA et al. [8]	Earth embankment + gabions	2500	0,9	**0,6**		9,85	0,75-0,88	**0,68-0,80**
PEILA et al. [8]	Earth embankment + gabions	4500	0,9	**0,95-1,10**		20,8	1,00-1,20	**0,90-1,08**
Observation Embankment	Earth embankment + stones	2700	1	**0,50-0,60**		7,5	0,40-0,70	**0,40-0,70**
LAMBERT et al. [7]	Gabions	2000	3	**0,70-0,80**		3,6	0,20-0,40	**0,60-1,20**

Table 4: Comparison of full-size tests with design proposal

9 REFERENCES

Blovsky S. (2002). Reinforcing possibilities with geosynthetics Dissertation. Technische Universität Wien. Institut für Grundbau- und Bodenmechanik.

Labiouse V. and Heidenreich B. (2009). Half-scale experimental study of rockfall impacts on sandy slopes. - Nat. Hazards Earth Syst. Sci. 9, pp. 1981–1993.

Lambert S., Heymann A. and Gotteland P.(2011). Real-scale experimental assessment of cellular rockfall protection structures. Proceedings interdisciplinary workshop on rockfall protection – ROCEXS, Innsbruck 2011.

Peila, D., Oggeri, C. and Castiglia, C. (2007). Ground reinforced embankments for rockfall protection: design and evaluation of full scale tests. Landslides 4, pp. 255-265.

Pichler B., Hellmich C., and Mang H. (2005). Impact of rocks onto gravel – design and evaluation experiments. – International Journal of Impact Engineering 31, pp. 559-578.

Plassiard J.P. and Donze F.V. (2010). Optimizing the design of rockfall embankments with a Discrete Element Method. Engineering Structures, 32, pp. 3817-3826.

Hofmann R. und Mölk M. (2012). Bemessungsvorschlag für Steinschlagschutzdämme. Geotechnik 35, Heft 1, Verlag Ernst & Sohn.

ONR 24810 (2013). Technischer Steinschlagschutz – Begriffe, Einwirkungen, Bemessung und konstruktive Durchbildung, Überwachung und Instandhaltung(Technical protection against rockfall –Terms and definitions, effects of actions, design, monitoring and maintenance) Entwurf, Ausgabedatum: 2013-01-01.

ÖNORM B 1997-1-1 Eurocode 7 - Entwurf, Berechnung und Bemessung in der Geotechnik - Teil 1 (2007). Allgemeine Regeln - Nationale Festlegungen zu ÖNORM EN 1997-1 und nationale Ergänzungen.

Authenticity of Foundations for Heritage Structures

Authenticité des fondations pour les structures du patrimoine

Iwasaki Y.
Geo Research Institute, Osaka, Japan

Zhussupbekov A., Issina A.
Eurasian National University, Astana, Kazakhstan

ABSTRACT: Foundation system is a basic part to support structure of cultural heritage but has been considered only as a function to keep authenticity of the heritage upper structure. Recent trend has changed the situation. Foundation becomes to be considered as an important part of structure and sometimes to be evaluated as an element of authenticity of heritage based upon unique characteristic in region as well as of the period that the heritage belongs. This paper describes a short history of authenticity of cultural heritage and discuss several examples of the authenticity of foundation systems including leaning Pisa Tower, stone masonry in Angkor, Cambodia, and wooden pile foundation of Great Gate at Itsukushima shrine, Hiroshima, Japan.

RÉSUMÉ : Le système de fondation est un élément fondamental pour soutenir la structure du patrimoine culturel mais il ne lui a été longtemps considéré comme une fonction que de garder l'authenticité de la structure patrimoniale supérieure. La tendance récente a changé la situation. La fondation devient un élément important de la structure elle-même et est parfois tenue comme un élément de l'authenticité du patrimoine basé sur une caractéristique régionale unique ainsi que sur la période à laquelle appartient le patrimoine. Cet document décrit un bref historique de l'authenticité du patrimoine culturel et discute de l'authenticité de plusieurs exemples de systèmes de fondation, tels que la Tour Penchée de Pise, la maçonnerie en pierres à Angkor au Cambodge, et les fondations sur pieux en bois de le Grande Porte à Itsukushima, Hiroshima, au Japon.

KEYWORDS: cultural heritage, authenticity, foundation, Pisa Tower, Angkor, Itsukushima shrine

1 INTRODUCTION

Geotechnical engineering plays one of the important role to safeguarding cultural heritages and has made such key contribution as in restoration work for the inclined Pisa Tower. However, foundations are generally considered as simply nothing but to support the heritage sturctures and not considered as a part of the heritage.

However recent trend of conservation of heritage indicates foundation system has become to be considered as one of the basic components of the heritage structure. Recent renewal of an international standard of ISO 13822 on assesment of structural safety added an Annex “Heritage Structures” and stressed the importance of the foundation.

In this paper, the new concept of “authenticity of foundation” is discuused as well as the characteristic elements of authenticity that should be evaluated and restored.

2 AUTHENTICITY

Authenticity was defined in the Venice Charter of 1964 as heritage composed from original material, original position, original design as well as original procedure. The comcept of the Venice Chapter is called “anastylosis(Greek),” which means “take column back to original position.” Anastylosis implies that original stone columns spread over in a historical ruin shall be rebuilt at the original positions. Anastylosis does not give any values of heritage to such repaired materials as often seen in wooden structures in Japan. The principle of the anastylosis was developed along the base of conservation of stone structure in Europe and resulted in the Venice Chapter.

Later in 1994, the concept of the authenticity was expanded by the Nara Document on Authenticity to cover various methods characterized by region to which the heritage belongs. Region specific method that developed in some area is also accepted as the characteristic of authenticity.

Character-defining elements are defined as historic materials, forms, locations, spatial configurations, morphology, concept and details, structural design, uses, and cultural associations that contribute to the heritage value of a structure that shall be retained in order to preserve its heritage value

3 AUTHENTICITY OF FOUNDATION

In 2005, ISO 13822(Bases for design of structures – Assessment of existing structures) was reviewed for renewal. ISCARSAH(International Scientific Committee on the Analysis and Restoration of Structures of Architectural Heritage under ICOMOS) had proposed to include heritage structures in the standard and worked together for five years. The ISO 13822 has been updated in 2010, and added an Annex-I (informative) Heritage Structure, which has expanded the heritage structure to include foundation as a part of the structures.

The Annex I clearly states as in a paragraph of I.5.3 Authenticity of foundation that “ From the point of view of conservation, foundations are not different from the rest of the structure and should be assessed and rehabilitated taking into consideration their heritage value. This involves the requirement to identify their authenticity and character-defining elements.”

3.1 Leaning Tower of Pisa

The inclined Pisa Tower was registered in 1987 as World Heritage by UNESCO.

The construction of the tower started in 1173 and completed in 1372 on a thick soft clayey ground in northern Italy as shown in Figure 1. In 1970’, Italian government called for internaional competetion of proposal to remedy and to restore the monument but did not carry out due to finacial shortage. In 1990’, international committee was organized to discuss the restoration how to conserve the inclined state of the upper structure of of the tower as it was. After heated discussions, a method to extract upper soft clay of the northen side by boring was adapted in 1998 as a trial test. The soil extraction was succefully applied and completed in 2001 (Burland,2009).

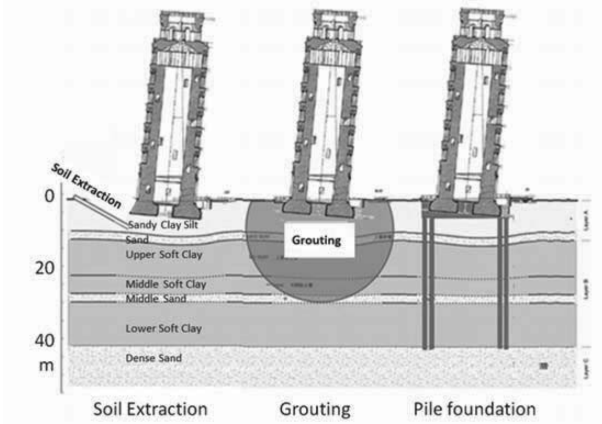

Figure 1. Possible contermeasures for restoration

Figure 1 shows three possible methods to restore the Pisa Tower. During the selection of possible various methods, discusions had been focussed upon the keeping the specific character of the Tower and the structural safety of the upper strcture. There was a choice to restore the tower at upright condition without any inclination. However, the state of being inclined is the specific value of the Pisa Tower, the characteristic element of the authenticity, the restoring method is only valid to keep the inclined state within some safety margine.

We could compare other methods of grouing or pile foundation to the soil extraction on the base of the authenticity as follows.

The inclination of the Tower is one of the characteristic element of the authenticity as an essential factor of the heritage. There are also important geotechnical factors to have caused the inclination of the characteristic of the heritage. These are thick soft clay ground and direct shalllow foundation that also constitute the characteristic elements of the authenticity.

3.2 Stone masonry in Angkor

Angkor monuments are distributed in a wide region of ancient Khmer Empire whose basic activities was in a Angkor plain from Kulen Mountains Ton le Sap Lake in Cambodia as shown in Figure 2.

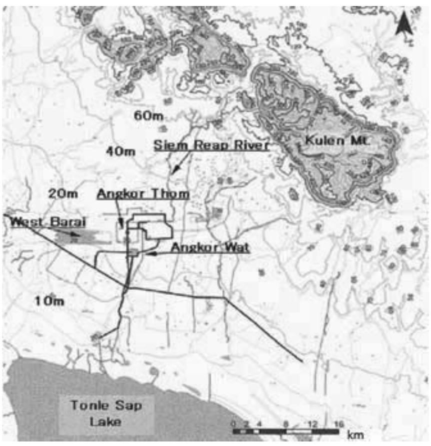

Figure 2. Angkor Plain

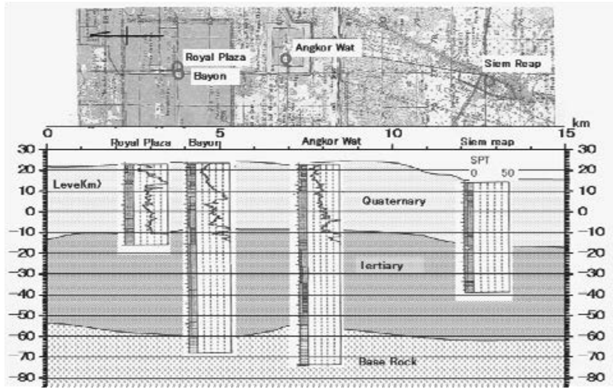

Figure 3. Geological section in Angkor plain N-S direction

Figure 3 shows geological section of the central part of the Angkor plain. Angkor plain consists of surface soil layers of Quaternary with 30-40meters in thickness followed by tertiary deposit and base rock.

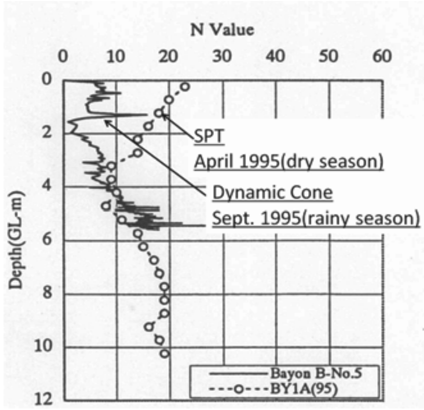

Figure 4. Seasonal change of N value in Angkor

Angkor belongs to monsoon region and shows distinctive climate of rainy season from May to October and dry season from November to April in a year.

Figure 4 shows changes of strength of SPT N-values at the same site in Bayon for dry and rainy season. The soil is silty fine sand and shows the STP value of about N=20 at the surface in dry season but drops to about N=5 during rainy season.

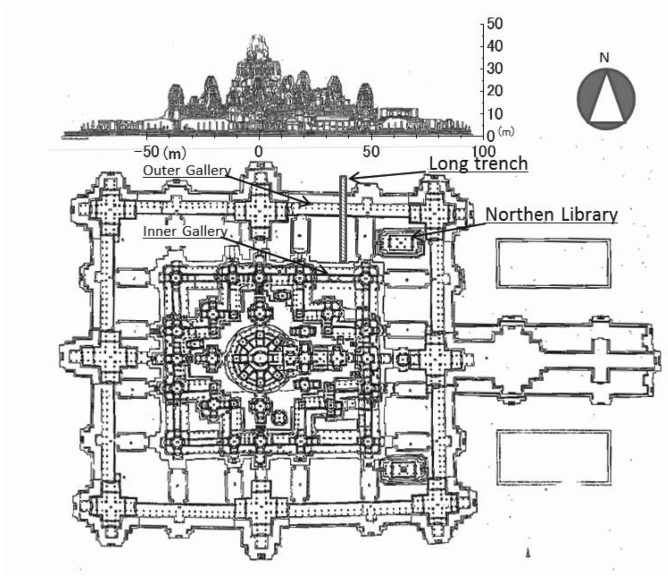

Figure 5. Bayon temple plan and section

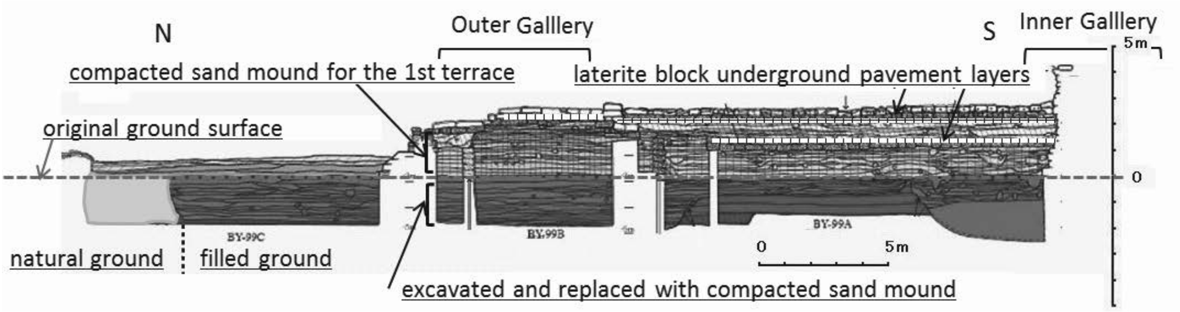

Figure 6. Long trench at north side of Bayon in N-S direction (Narita,2000)

The reason is change of water level and suction pressure. In dry season, the underground water drops around WT=GL-5m and rises to the ground surface during rainy season. The top of ground surface of a few meters in thickness has effects of seasonal change of the underground water.

To study foundation system, JSA (Japanese Government Team for Safeguarding Angkor) carried out a long trench at the north western corner as shown in Figure 5, which shows plan and section of Bayon, the central temple in the Angkor Thom.

The trench starts from the north edge of inner gallery extending to north including the lowest terrace and outer gallery until the natural original ground. The original ground was found about 10m from the north edge of the Outer Gallery as shown in Figure 6. The lowest terrace between Inner and Outer Gallery was excavated until the natural soil layer was found. Based upon the results of archaeological excavation, ancient Khmer engineers excavated 2-3m from the ground surface in the construction area including additional outer area of 10m in width before the construction.

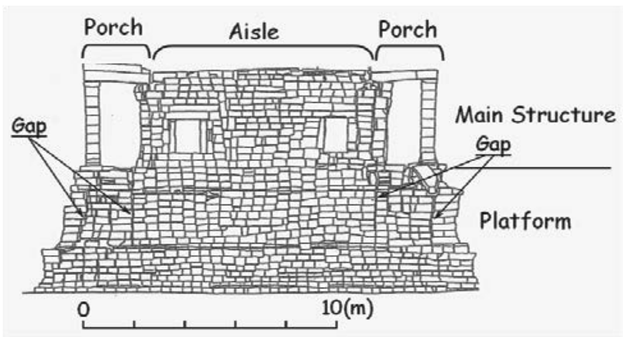

Figure 7. Vertical side view of Northern Library, Bayon

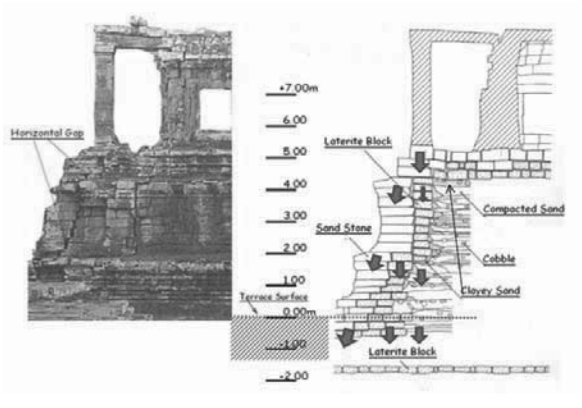

Figure 8. Trenched section at west end of Northern Library

The excavated area was filled to the original ground surface by sandy soils with dense compaction. Additional mound of about 2.5m was further compacted in the area of the lowest terrace. Within the lowest terrace, two layers of laterite block pavements were identified beneath the surface sand stone of the mound and at the depth of 1.5m below the surface.

JSA dismantled the Porch part of Northern library, Bayon before reconstitution of the Library as shown in Figure 7. Some vertical gaps are noted in the side sand stones beneath the porch section. These gaps look like to be caused by sliding of the edge part caused by the load of the upper structure of Porch.

Excavated section is shown in Figure 8. The plat form of the library consists of main body of compacted sand mound with 5m in height surrounded by retaining wall of laterite blocks in side with sand stones outside surface of the wall.

The clayey sand was found at a boundary between main body of sandy soil mound and laterite blocks as well as at top of the mound beneath the pavement of laterite block and sandstone. The clayey sand is estimated as to prevent water infiltration into the main mound (JSA, 2000).

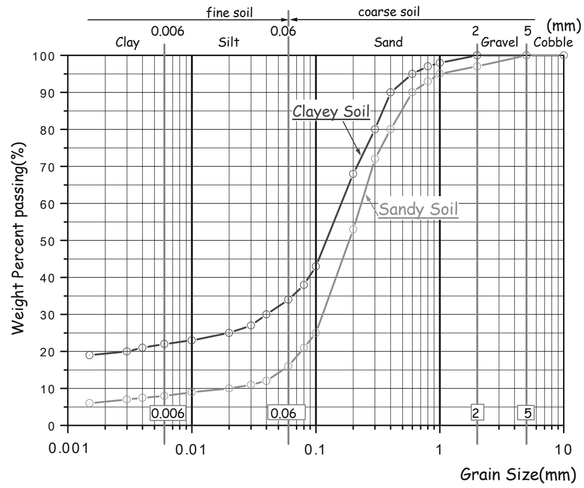

Figure 9. Grain size distribution for sand and clayey soils for mound

Figure 9 shows grain size distribution curve for these sand and clayey soils used for filled mound in Angkor.

There is no evidence of sliding along the gaps on side stones. The setting of the stone, laterite block, and compacted sand layer is shown in Figure 8 with estimated flow of the load of the upper structure to the foundation system. The load of the upper structure is supported by laterite blocks and sand stones at +4m in height, sand stones, laterite blocks, and compacted sand at +2m and +0m in height. The direction of these forces is always towards vertical or outwards. Khmer engineer seems to have treated these different materials as to show the same characters. The gaps are considered to be caused by the tendency of horizontal outwards of forces as well as horizontal expansion of compacted soils.

The elements of foundation system of ancient Khmer structure in Bayon may be characterized as follows,
1) Deep trench and backfilled foundation
2) Materials for foundation system; sandy and clayey soils, laterite block, and sand stones
3) High and steep retaining system for dense compacted mound that composes from sand stone, laterite block, and clayey soil

3.3 Great Gate of Itsukushima Shrine, Hiroshima

Photo-1 shows Great Gate for Itsukushima Shrine.

Photo-1 Great Gate for Itsukushima Shrine, Hiroshima

In 1950, during restoration work, foundation of the gate was excavated for study the foundation system, which is in Photo-2.

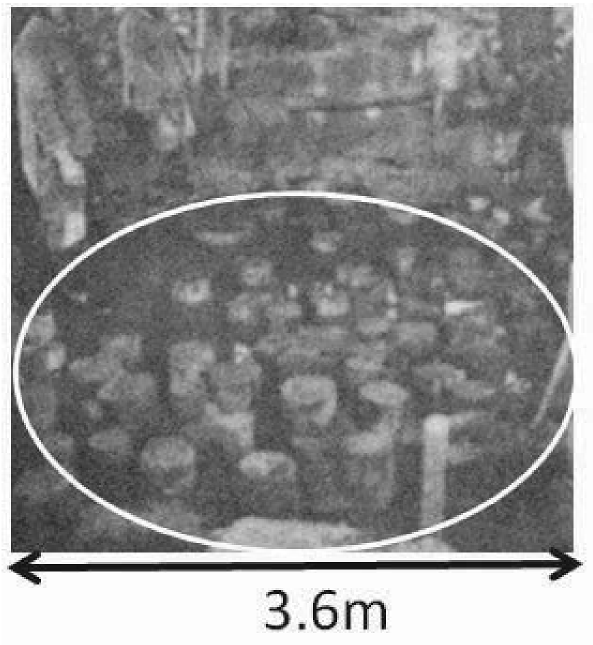

Photo.2 Thousand pile foundation for Itsukushima Shrine

Wooden pine piles with about 30cm in diameter were found as driven in dense condition. The surface soil is weathered granite with15m in thickness followed by granitic base rock.

The diameters of the piles are around 30cm and some piles of the existing foundation were pulled out and were measured as about 2m. The ground around the site consists from loose and medium dense soils of weathered granite with about 15m in depth followed by granitic rock. (Itsukushima Shrine Restoration Committee,1958).
The wooden pine piles were not rotten under sea water and reused for conservation work.
The characteristic element of foundation system for the Great Gate is thousand piles foundation, which composes of many densely driven piles with short length compared to depth to base rock.

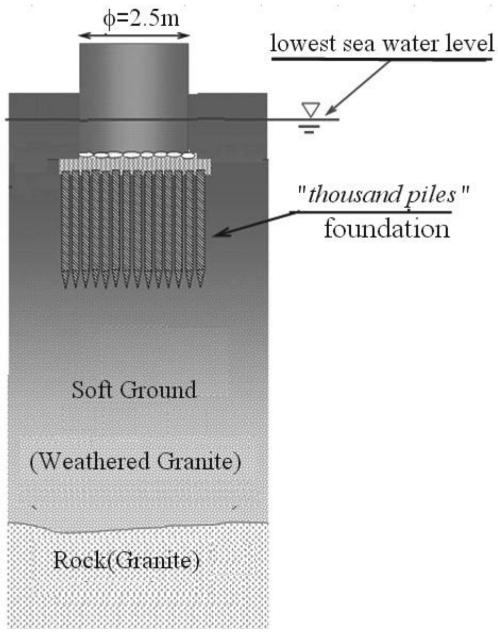

Figure 10 Schematic section of thousand piles for the Great Gate

4 CONCLUSIONS

So far, we discussed with characteristic element of foundation system for three World Heritage sites.
Shallow direct foundation and soft soil condition for Pisa Tower, Deep foundation trench and unique conbination of geo-materials for Angkor, and thousand piles system of Great Gate for Itsukushima Shrine are discussed as the characteristic element of the foundation. Since the foundation sysytem is usually hiddened underground and never exposed to public. We, geotechnical professon, need to explain these specialities to public.

5 REFERENCES

Burland J.B., Jamiolkowski M.B., Viggiani C.2009. Leaning Tower of Pisa: Behaviour after Stabilization Operations. International Journal of Geoengineering Case histories, http://casehistories. geoengineer. org, Vol.1, Issue 3, p.156-169

Narita.G.,Nishimoto.S.,Shimizu.N.,Akazawa.Y.2000.Trench at Outer Gallery of Bayon Temple, JSA Annual Report.2000.3-18, Color Fig.1, 317

JSA.2000, Chapter 5 Restoration Work, JSA Report on the Conservation and Restoration Work of the Northern Library of Bayon, Angkor Thom, Kongdom of Cambodia, JSA, 211-320

Itsukushima Shrine Restoration Committee.1958, Report on National Treasure of Itsukushima Shrine from1948 to1957

Geotechnical Assessment for the Restoration of Garandoya tumulus with the Naked Stone Chamber

Évaluation géotechnique de la restauration du tumulus de Garandoya et grottes en pierres nues

Mimura M.
Graduate School of Engineering, Kyoto University, Kyoto, Japan

Yoshimura M.
Soil and Rock Engineering Co. Ltd., Osaka, Japan

ABSTRACT: Garandoya Tumulus was constructed on the terrace of Mikuma River and famous for mural paintings. The soil mound that originally covered the stone chamber has been destroyed. Due to instability of the naked stone chamber, it has been decided to restore the tumulus with the construction of round soil mound with a diameter of 25 to 30m. The necessary strength together with the compacted density of the restored mound soils are investigated through various laboratory tests. A series of laboratory test results confirm that the stability of the restored mound is achieved with the possible in-situ density. Water resistant and adiabatic structure is required to protect the mural paintings inside the stone chamber. Based on the chamber model test results, the double-layered earth mound has been introduced for the restored tumulus mound, namely, the well compacted soil with the enough strength to stabilize the restored tumulus mound underlain by the well permeable gravel layer to support the drainage for rainfall water. The heat conduction chamber tests on the mound soils are carried out to investigate the capacity to protect the heat transfer into the chamber. A series of the stability and environmental assessments has successfully assisted to develop the design of the restored tumulus mound.

RÉSUMÉ : Le tumulus de Garandoya, très connu pour ses peintures murales dans ses grottes, est construit sur le banc de la rivière Mikura. Le monticule de terre qui recouvrait les grottes est désormais dénudé, ce qui mène à l'instabilité des pierres nues des grottes, ainsi que la vulnérabilité des peintures murales à l'eau. On propose des travaux de restauration du tumulus en construisant un monticule de forme circulaire de diamètre de 25 à 30m pour le recouvrir. On étudie la résistance du sol compacté et la restitution de la densité in situ en faisant des tests au laboratoire. La texture du sol compacté doit être étanche pour protéger les peintures murales contre l'infiltration des eaux dans la grotte. Les résultats de tests sur un modèle réduit de la grotte préconisent une bi-couche pour restaurer le tumulus, càd une couche de sol compacté recouvrant une sous-couche de gravier pour permettre le drainage. On a aussi fait des tests de conductivité thermique sur le sol compacté pour évaluer l'isolation de la grotte. Des études de la stabilité environnementale du monticule ont aussi fait partie du design de la restauration du tumulus.

KEYWORDS: heritage, tumulus, mound, water retention characteristic, capillary barrier, heat conduction

1 INTRODUCTION

The Garandoya Tumuli, the national heritage are located at Hita city in Oita prefecture (Figure 1) with the mural paintings in the stone chamber. Although three tumuli were discovered, all of them have lost their earth mound and the stone chambers are exposed. The tumuli have been determined to be restored to conserve the stone chamber as well as the colored mural paintings drawn on the surface of the chamber stones. In order to protect the mural paintings from deterioration, the water resistant and adiabatic structure is strongly required because the main factor for the damage of the mural paintings is luxuriant growth of mold due to dew condensation induced by the intruded water by rainfall and the rise in heat by solar radiation.

In the present paper, the geotechnical assessment for the conservation of the tumuli including the mural paintings through the in situ and laboratory tests is reported. The behavior of underground water at the site is investigated through the in situ tests with emphasis on the possibility of suction-induced water intrusion. The necessary drainage function against the rain water is also discussed. The layered structure such as the compacted earth underlain by the permeable coarse gravel for the restored earth mound is proposed considering the assisting effect of capillary barrier at the border of these layers. Discussion is extended to the adiabatic structure of the earth mound, which is expected with the heat conduction characteristics of soils. For the purposes, a series of chamber model tests are conducted.

Figure 1. Location of Garandoya tumulus

2 GENERAL VIEW OF THE RESTORATION PROJECT

2.1 Restoration plan

In order to keep the preferable environment for the mural paintings on the chamber stones as well as to enable general public presentation of the stone chamber, the Hita Municipal Board of Education has determined to construct the shelter building which covers the stone chamber covered by the restored earth mound as shown in Figure 2. The shelter building

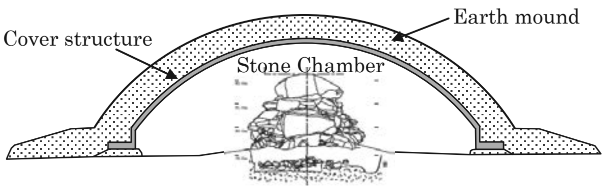

Figure 2. Schematic view of the restoration plan for the Garandoya Tumulus

whose diameter and height is 18 m and 6 m respectively. The restored earth mound will be constructed with a diameter of about 25 m based on the archaeological knowledge.

2.2 Examination subjects

Degradation of the colored paintings drawn on the surface of the chamber stone is most greatly subject to the influence of moisture. Development of the water resistant structure is required to prevent dew condensation and intrusion of water into the stone chamber. The possible phenomena to be considered are 1) the underground water exudation from the foundation, 2) the leakage of water from the joint of the reinforced concrete panel of the shelter building, 3) the inflow from surrounding ground. Technical procedures to overcome the above-mentioned problems have to be discussed together with the control of the temperature inside the stone chamber caused by the solar radiation.

3 INVESTIGATIONS OF MOISTURE IN THE GROUND

In order to consider the seepage of groundwater from the ground, the condition of groundwater was investigated in the observation well that is made from a vinyl chloride pipe with outer diameter 60 mm and inner diameter 52mm (Figure 3) currently installed in the nearest to the tumulus. The inserted type RI densimeter and moistmeter of the shape of a pillar stick of 42.7 mm in diameter and about 1000 mm in length is applied to detect the moisture content as well as the density of the ground. The RI densimeter and moistmeter is inserted to the bottom of the well at the depth of 9 m from the ground surface followed by conducting the scanning logging by pulling up at the rate of 1 m/min. Investigation was conducted in a rainy season when the groundwater level heightens due to sufficient rainfall as well as in a dry season when the groundwater level

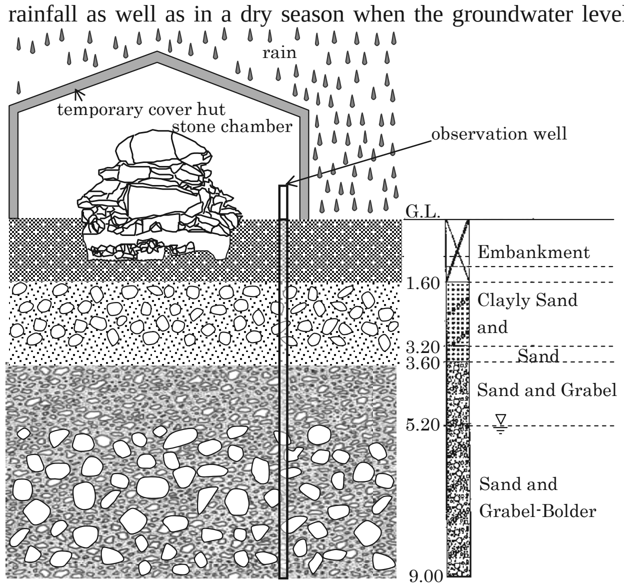

Figure.3 Cross section of the foundation of the Garandoya Tumulus

lowers. As far as the condition at the investigation is concerned, the temporary shelter structure was equipped to cover the stone chamber to avoid rainfall. The stone chamber was however not completely free from the infiltration of water through the surrounding ground.

According to the boring log, the subsurface condition of the Grandoya Tumuli is as follows: The artificial fill consisting of fine grained soil with gravel appears from the ground surface to GL-1.6 m underlain by the clayey sand with gravel and boulder from GL.-1.6 m to -3.2 m. The sand layer is found from GL-3.2 m to -3.6 m underlain by the sand and gravel from GL.-3.6 m to -5.2 m. Then the gravel and boulder deposit appears from GL-5.2 m to -9.0 m. Because the clayey sand above GL-3.2 m is expected to have a low permeability enough to hinder infiltration into the ground, the water by rainfall is expected to exude inside the stone chamber.

The measured results of the density and moisture logging are shown in Fig. 4. The groundwater level is found to change at G.L. -5.04 m in the rainy season and G.L.-8.45 m in the dry season. It is natural that the degree of saturation is kept almost

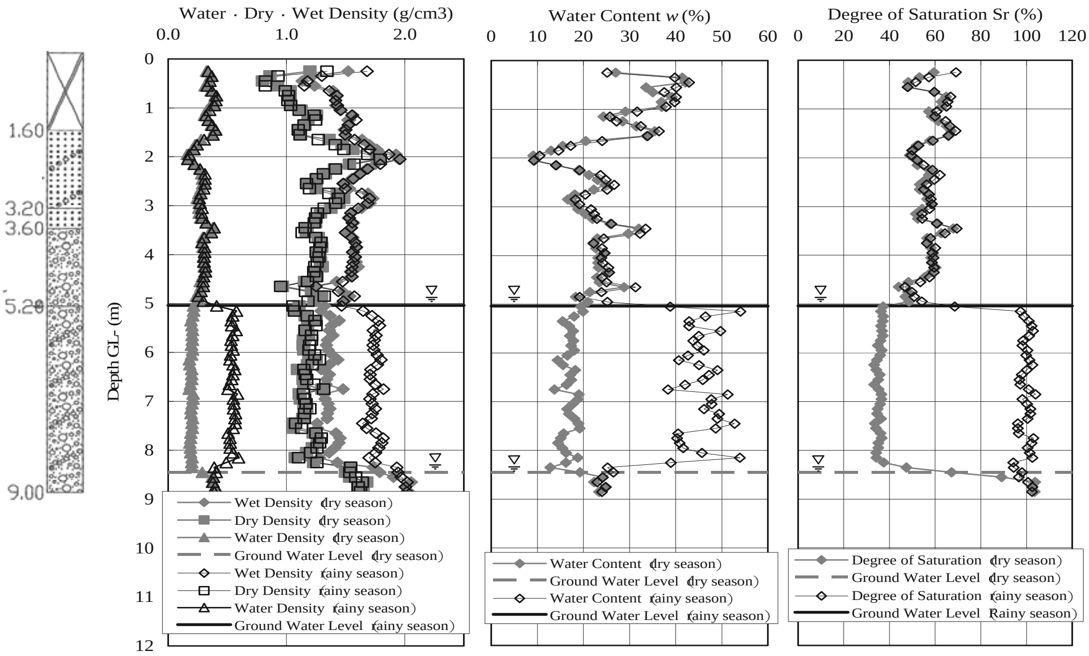

Figure 4 Measured results of the density and moisture content of the foundation ground at the Garandoya Tumulus

100 % and when the underground water level lowers in the dry season, the degree of saturation from G.L. -5.04 m to – 9.0 m significantly drops to about 35%. On the contrary, the degree of saturation above G.L. -5.04 m is about 60% in the rainy season, and it is noteworthy that the degree of saturation in the layers above the groundwater level of does not change at all irrespective of the underground water level. From these results, the seepage of the water to the layers above the groundwater level due to suction can be ruled out. It is hence not necessary to consider the problem of exudation of the underground water into the stone chamber from its base.

4 ASSESSMENT OF WATER RESISTANT STRUCTURE

The shelter building is planned to be constructed for the conservation of the naked stone chamber of the Garandoya Tumulus. It is true the intruded rain water is intercepted by the shelter building but it is preferable that the intruded water does not reach the surface of the shelter building to avoid possible leakage due to loss of function of the waterproof processing equipped among the concrete panels of the shelter building. The earth mound has been selected to cover the shelter building to reproduce the original shape of the tumulus together with the consideration of the adiabatic effect. The layered structure, namely the well compacted soil underlain by the well permeable coarse gravel has been adopted for the restored earth mound in order to provide a good drainage function. The adopted layered earth mound structure consequently give a possible function of a capillary barrier at the border of the compacted soil and gravel layers due to the different capacity of suction in those layers.

A series of the chamber tests on the layered foundation is carried out to confirm the occurrence of capillary barrier at the border of the upper compacted soil layer and the underlying coarse gravel layer. The model chamber is shown in Figure 5. The selected parameters for this chamber test are the inclination angle of the foundations and the intensity if precipitation. The size of the model chamber is 1100 mm in length, 600 mm in height, and 120 mm in width. The equipment for precipitation has eight hypodermic needles per 100 cm^2 at the bottom of the tank, and can give the raindrop from the needle tip to the surface of the model foundation. Intensity of precipitation is adjusted by the hydrostatic pressure in terms of the level of water in the tank that can be controlled by the Marriott siphon.

The soil with which the present experiment is conducted is the candidate material of the tumulus restoration that is the graded grain material extracted from the quarry in the proximity of the tumulus. The coarse gravel is also extracted from the same quarry. The particle size distribution of the materials is shown in Figure 6. The candidate material is a well-graded sandy soil. The initial water content of soil was adjusted as natural water content equivalent to the one for the actual restoration. A series of compaction tests is conducted with the different compaction energy on the material under the natural water content. Based on the experimental results, the density of the soil for the chamber test is determined by supposing the compaction energy at the construction of restored earth mound. The relation of the moisture content by volume and the suction is separately investigated from the unsaturated seepage test. The adopted testing apparatus for the unsaturated seepage test with the radioisotope system is shown in Figure 7.

Figure 8 shows the experimental results between the tangent of the inclination angle of the foundation and the limit length *L* that denotes the resistant distance for the capillary barrier under the prescribed intensity of precipitation of 3.6 mm/hr. In the present study, the thickness of the compacted earth mound is 300mm. A set of electric sensors to detect water is put at the top of the underlying coarse gravel layer. When infiltrated water leaks to the gravel layer, we can detect the location of the breaking point of capillary barrier by the occurrence of short-circuit. As shown in the figure, there is a definite linear relationship between the limit length *L* and the inclination angle of the foundation in terms of tanα. It is found that the water resistant structure with capillary barrier at the border of the layered earth mound is expected to function under the condition of the inclined foundation such as tumulus mound.

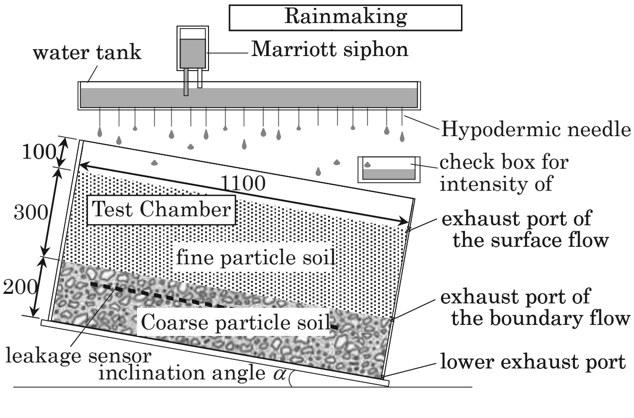

Figure.5 Schematic view of the model chamber of the test for capillary barrier

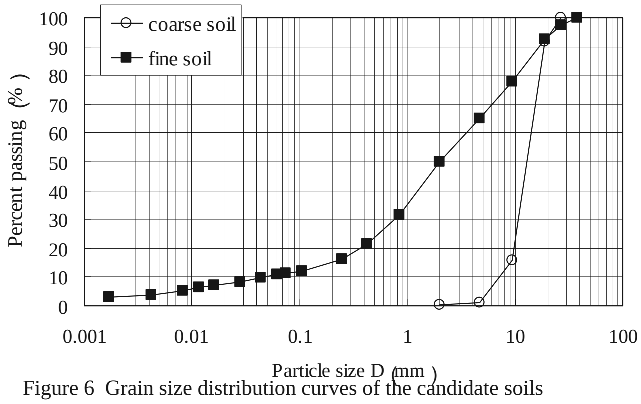

Figure 6 Grain size distribution curves of the candidate soils

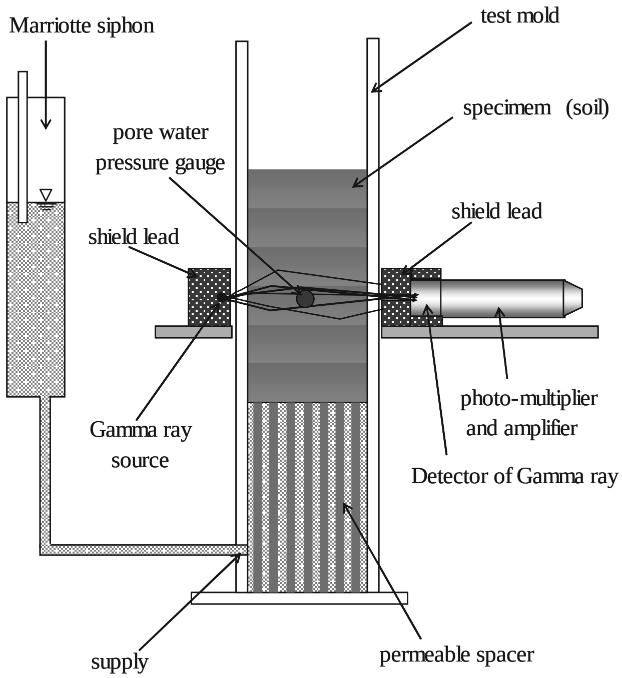

Figure 7 Schematic view of the unsaturated seepage test device

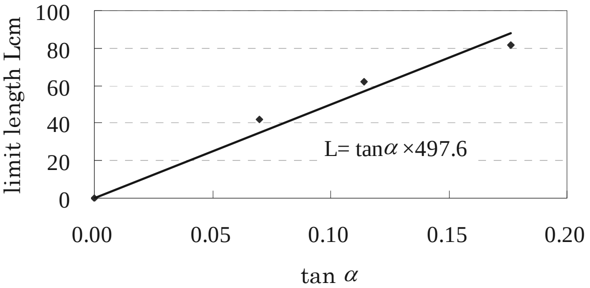

Figure 8 Relation of the inclination angle of the foundation α and the limit length L for capillary barrier

5 ASSESSMENT FOR HEAT CONDUCTIVITY OF SOILS

Subterranean preservation of food using the adiabatic effect of the ground is widely performed from ancient times. The shelter building for the Garandoya Tumulus has hence been covered with soils to ease the temperature change in the tumulus because the variation in temperature has a harmful influence on the conservation of the mural paintings in the stone chamber. The chamber model test is carried out in order to derive the characteristics of the heat conductivity of the soil that is used for the restoration of the tumulus. The schematic view of the experimental device is shown in Figure 9. The soil is prepared by compacting to 50mm per layer and the specimen of ten-layer structure is developed. Then, the specimen is prepared with 200 mm in diameter and 500 mm in height in the cylindrical container of acrylics covered by the thermal insulated styrene foam with a thickness of 100 mm. As is shown in the figure, the temperature sensors have been arranged at the prescribed depth in the specimen. The heat source of aluminum board is set at the top of the container.

The sequence of heat supply is set to provide 40°C of heat for 8 hours from the top of the specimen followed by removal of heat for 16 hours (1-day cycle model). During the time without heat supply, the temperature of the specimen surface is falling to the one of the room (about 15°C). Figure 10 shows the experimental results of the heat conductivity on the soil used for the restoration of the tumulus. The setup condition is equivalent to the prescribed one for the restoration of the tumulus. As shown in Figure 10, 4 cycles of heat supply and removal are conducted. The increasing rate of temperature tends to be higher in inverse proportion to the distance from the heat source. The absolute value of temperature is so high that it is close to the heat source, and there is the tendency for time to reach the

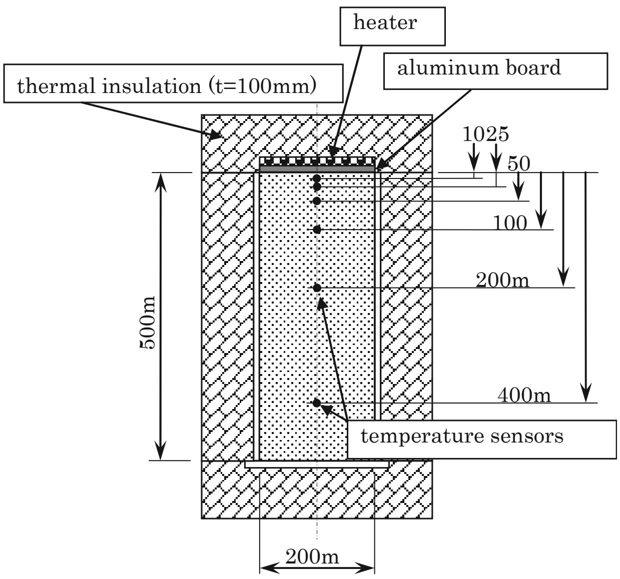

Figuare.9 Outline of the experimental device about heat conduction

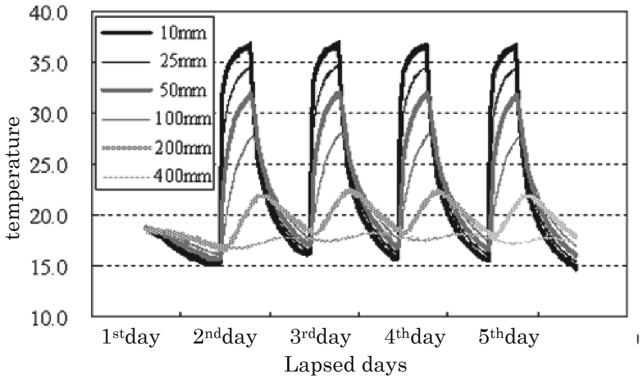

Fiigure.10 Experimental results on variation of temperature in the soil

maximum to be overdue in proportion to the distance from the heat source. It is shown that the heat conduction inside the specimen is accompanied by a time lag and attenuation. The one-dimensional equation of heat conduction is solved by the finite difference method. By fitting these data, the coefficient of heat conduction κ=8.04x10^{-5} (J/ms°C) is obtained. On the basis of the heat conductivity chamber test results, the candidate soil for the restored mound is found to have a sufficient capacity as an adiabatic material.

6 CONCLUSIONS

Geotechnical assessment was conducted to conserve the Garandoya Tumulus with the naked stone chamber in which the colored mural paintings are drawn. The preferable environment in the stone chamber is found to be achieved by equipping the shelter building covered by the earth mound. The seasonal change of the underground level that is interlocked with the river level has been monitored. The rise of the water content in the capillary zone above the groundwater level was not detected irrespective of the season. Underground water hence does not infiltrate into the stone chamber from the ground. The layered structure of the restored mound, namely the drained gravel layer overlain by the compacted earth is expected to provide the capillary barrier at the border of the layers. The chamber model test results showed the linear relationship between the limit length, L and the tangent of the inclination angle of the soil layers. Capillary barrier effect is found to possibly assist for the water resistant structure of the tumulus mound. The adiabatic effect by the restored earth mound is experimentally confirmed through the one-dimensional heat conductivity chamber test. On the basis of the experimental results, the necessary thickness of the restored earth mound has been proposed to maintain the desirable thermal environment in the stone chamber.

7 REFERENCES

Hita Municipal Board of Education, 2010: The investigation report of accompanying preservation maintenance of the historical site of Garandoya ancient tomb

Hita-City, 2008: A historical site of Garandoya ancient tomb drilling survey commissioned business report.

T. Morii, A. Horie, M. Kikuchi, Y. Takeshita, and M. Inoue, 2005: Prediction of the capirally barrier effect of gravel ground, Proceedings of the 40th geotechnical engineering research exhibition, pp.1325-1326.

Geotechnical Features of Sochi Olympic Facilities Project Designs

Les aspects géotechniques de la conception des installations olympiques de Sochi

Petrukhin V.P., Kolybin I.V., Budanov V.G., Isaev O.N., Kisin B.F., Bokov I.A.

Gersevanov Research Institute of Foundations and Underground Structures (NIIOSP), Moscow, Russia

ABSTRACT: The key facilities of the XXII-th Olympic Games 2014 in Sochi have been erected on the Imeretin lowland, characterized by complicated geological environment and high seismicity. Leading Russian organizations have been invited to tackle the related geotechnical issues. The paper describes specific aspects of geotechnical design of the Olympic facilities. There have been reviewed project design solutions for the footings of buildings, structures and underground service lines, developed either by NIIOSP or with its participation.

RÉSUMÉ : Les importantes installations des XXII^{èmes} Jeux Olympiques de Sochi en 2014 ont été réalisées dans la plaine d'Imeretin, caractérisée par un environnement géologique complexe et une sismicité élevée. Les autorités Russes ont été invitées à résoudre les problèmes géotechniques posés par ce projet. Cet article présente les particularités de la conception géotechnique des ouvrages Olympiques: les solutions adoptées pour les projets de fondations, de bâtiments et de lignes des services, développés par le NIIOSP ou avec sa participation.

KEYWORDS: OLYMPIC FACILITIES, IMERETIN LOWLAND, DESINGING, FOOTINGS, SOFT SOILS, SEISMICITY.

1 INTRODUCTION

In 2014 Russia will host the XXII-th Winter Olympic Games and the XI-th ParaOlympic Games to be held in Sochi which has humid subtropical climate.

The Olympic sports and infrastructure facilities are divided into two clusters: coastal and mountainous. The paper is dedicated to the geotechnical issues of Olympic facilities erection in the coastal cluster, which includes 6 main sport palaces, IOC quaters, hotels and tourist attractions. The coastal Olympic cluster is located on 1240 Ha up to 2 km wide Imeretin lowland terrain that extends 7 km along the coast (Fig.1).

The terrain is protected against cold winds by the Greater Caucausus Mountain Ridge so the winters here are not cold. The area features subtropical climate of Mediterranian type. Mean annual air temperature is + 13,7º C. The coldest month is January with mean air temperature + 5,3º C.

The mountainous cluster, where ski and biathlon competitions will be held and a ski jump and a bobsleigh center, are located at 48 km from the main Olympic facilities.

The seaside cluster terrain is a flatland, transferring into a gently sloping hillside piedmont. The geological survey of deposits down to 50 m (Fig. 2) depth revealed occurrence of several lithological features, represented by soft soils (peat, silt, including peat-containing clay soils of liquid-plastic consistence), sand loams, sands (from fine to coarse-grained composition), by gravel and pebble containing soils. Young modulus of soft soil which is present in most of the seaside area rarely exceeds 5 MPa value. Ground water table is just 1...3 m below ground surface.

The area seismicity magnitude is 9 i.e. extreme seismic risk. The soils on the site belong to seismic class II (sand loams, gravel pebble soils) and class III (water-saturated sands and soft clays).

More than 100 various buildings and structures are being built within the area.

The main Olympic sports facilities are erected on 240 Ha. area of "Olympic Park". This is the 40000 seats central Olympic stadium, a 12000 seats Big ice hockey arena, 12000 seats Ice sports palace with 60 x 20 m arena, a training rink for figure skating and for short track skating with 60 x 30 m arena, 8000 seats Indoor skating center, 7000 seats Ice hockey area, Ice arena for curling (see Fig.1). Auxiliary facilities are being built on the western side of the "Olympic Park" – IOC hotel, hotels for the Olympic family and ParaOlympic committee, technical and international zones, a service center. Media Center, 3*, 4*, 5* hotels and various auxiliary buildings are located to the east of the Olympic Park.

The lowland ground is slightly above the sea level, 1,5…4,0 m on the average. Large areas are subjected to flooding and waterlogging. Prior to construction works it was planned to protect the area from waterlogging and preserve existing ground water table. Thus the area was filled up to 2,5 ÷ 3,5 m average level with drainage at the bottom of the fill. The drainage ensures an excess of the fresh ground water table above the sea level that prevents sea water intrusion into the deposit rock. In order to avoid salination of ground water the depth of drainage is limited by at least 0.6 m level above the sea. This condition is maintained by limiting fresh water consumption especially in summer and autumn periods, which may be compensated from water supply system or other sources in the event of overconsumption.

Upfilling the terrain level prior to construction activities in the areas of soft clay soils, peat and peat-containing soils results in long-term settlements due to soft clayey soil consolidation.

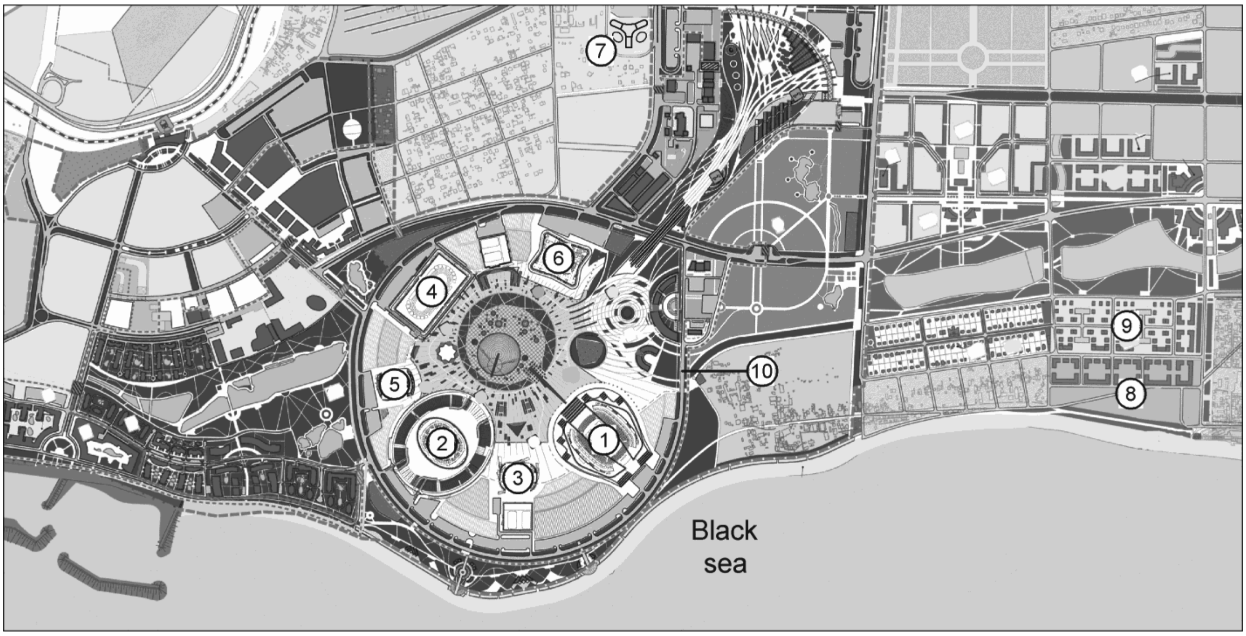

Figure. 1. Overview of Imeretin lowland with indicated construction sites. 1 – Olympic Stadium “Fisht”; 2 – Big Ice Arena; 3 – Minor Ice Arena “Ice Puck”; 4 – Skating Stadium “Adler Arena”; 5 - Curling Center “Ice Cube”; 6 – Winter Sports Palace “Iceberg”; 7 –Organizing Committee Building; 8 – Plot D1; 9 – Plot 17; 10 – Olympic park.

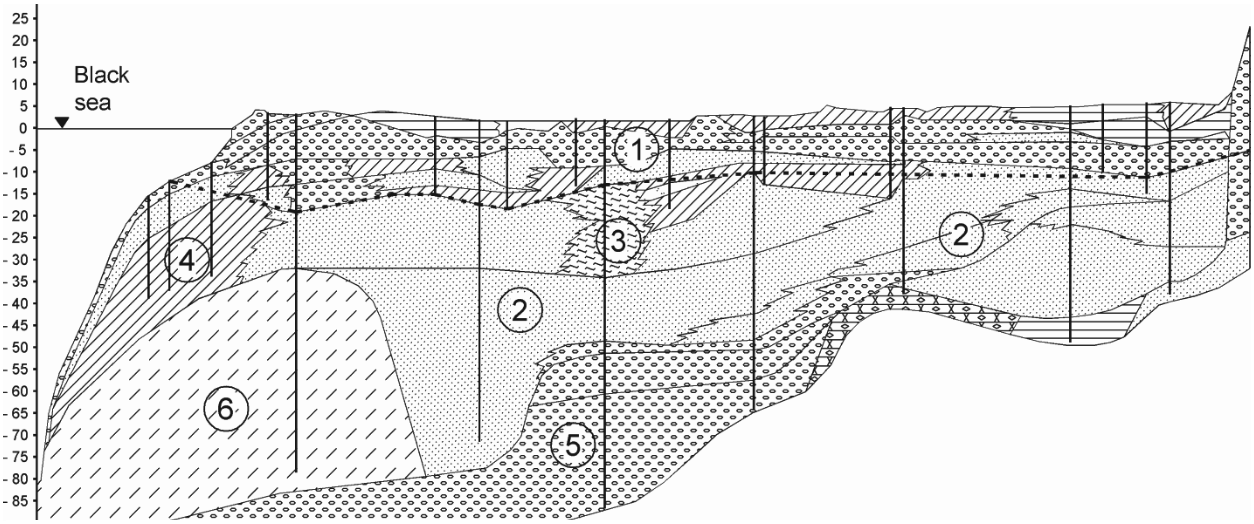

Figure. 2. Typical soil profile for Imeretin lowland.
1 – Interbedding of man-made ground and soft water saturated soils; 2 – Sands with inclusions of peat; 3 – Sands and clays with high peat content; 4 – Loam ; 5- Neogene gravel and pebbles, mudstone; 6 – Sandy loam.

2 THE BIG ICE ARENA

The Big Ice Arena (BIA), having 12000 seating capacity, will be used for competitions and workouts of ice-hockey teams. The arena comprises a complex of facilities, subdivided in to two independent volumes: the Big Arena structure and its stylobate. The stylobate is separated from the main arena by compensation joints. The stylobate periphery is backfilled with soil with access stairs on the soil slopes and drive-in ramparts for access to the building (Fig. 3).

Typical geological conditions of the area are shown on the profile (Fig. 4). Soil on BIA site is essentially better as to their strength and deformation properties than soft soils on other terrains of the Imeretin lowland.

The upper part of the geological profile down to 7,5 m consists of gravelly coarse and medium sands, gravel and pebble soils, having Young modulus of 20…32 MPa, that can ensure footing stability and its admissible deformations, therefore, a raft was preferred as a footing for BIA structure. According to triaxial dynamic compression test results the saturated sands below the building are not sensitive to vibro-liquefaction.

The cast concrete raft of BIA is divided by compensation joints into separate rafts for each structure (Fig. 5).

The raft under the main arena is 1 m thick while it is 1.4 m thick along the 11 m wide ring at locations of staircases and columns, transferring loads from roof cover trusses to the raft. The stylobate raft thickness is 0,6 m, and it is 1 m thick at column supports locations.

The absolute elevation of all footing rafts bottom is 2,3 m. The top soils and soft sand loam soils at the rafts bottom elevations are replaced by compacted crushed stone and gravel fill. The footing is protected from seasonal ground water table rise by local ring drainage system that is included into the system of engineering protection of the area.

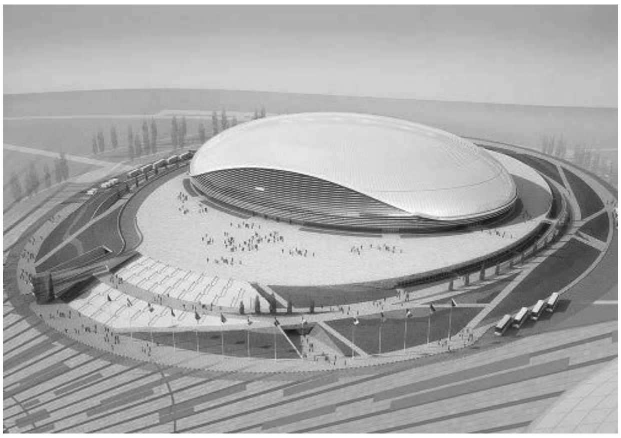

Fig. 3. Overview of Big Ice Arena.

Raft analysis was performed with the account of joint footing-superstructure analysis for the service and ultimate limit states. ULS analysis included the main and characteristic combinations of design loads with seismic action in both directions along the structure main axes. For characteristic combination the analysis included the raft shear along its bottom while for stylobate structures the exess of the vertical component of the design eccentric load over vertical force of limit state force in the case of one-sided soil upthrust, caused by seismic action. Shear verification was done for horizontal force, defined as a geometrical sum of horizontal loads in characteristic combination along the principle axes.

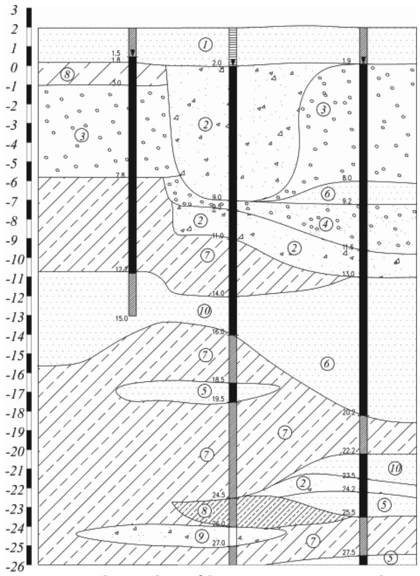

Fig. 4. Arena geological profile: 1. Coarse grained sand; 2. Gravelly soil; 3. Pebble soil with sand fill; 4. Gravely sand 5. Fine to medium sand, with thin seams of sandy clay; 6. Sand; 7. Plastic sandy loam; 8. Sandy loam with pebbles; 9. Gravel and pebble mixture; 10. Fine sand.

The values of loads, applied to the footing rafts, were determined with the account of safety factor К = 1,2 for important structures. Soil stiffness parameters were reduced as per К = 0,9. Soil base values were calculated as per the geological columns data within the structure footprint the soil base was simulated by linearly deforming layer. The 3D rafts analysis was done with the help of finite elements technique. The results enabled determination of cross section configuration of the rafts, internal forces in them and the required reiforcement.

During BIA construction period settlements of the main arena raft were measured. The measured settlements by the end of construction period were close to those predicted (Fig.6).

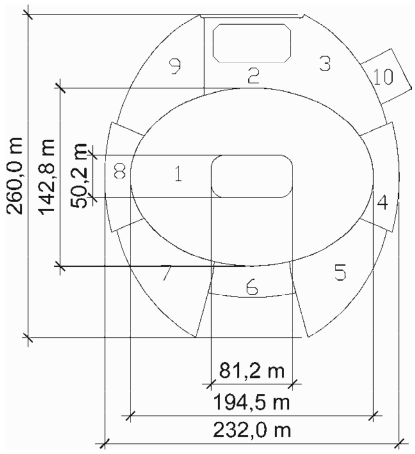

Fig. 5. Layout of Rafts of Big Ice Arena. 1. Raft of Main Arena; 2. Raft of workout arena; 3... 9 Rafts of service premises and bypass road; 10. Raft of refrigeration center.

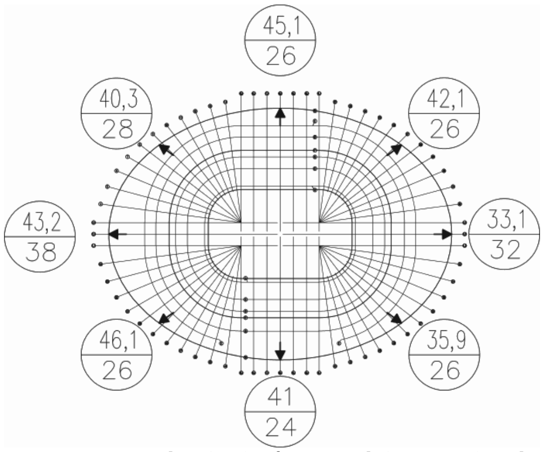

Figure 6. Mean value (mm) of measured (numerator) and analytical (denominator) settlements of arena raft footing.

3 OFFICE BUILDING OF ORGANIZING COMMITTEE

Office building of Organizing Committee of Olympic Games is located at 1200 m distance from the main facilities. The building consists of 9-storey main part and 3-storey parts, surrounding it (Fig. 7). A one-level parking lot is designed under the whole building is similar to a trifolium (one leave width is 18,7 m). The high-rise part of the building is divided into counter-seismic blocks, sitting on the solid raft. The structural design of the building consists of a framework with stiffness diaphragms in each antiseismic block. The main bearing structural elements of the building are made of cast concrete. The construction site dimensions are 120x90 m.

High-rise and low-rise sectors are divided by compensation joints. Mean design distributed load on the soil base from the 9-story component is 200 kPa, that from the 3-story is100 kPa.

The office building of the Organizing Committee of Olympic Games is located on the site that is certainly the most unfavorable as to its geotechnical conditions. Top ≈4,5 m layer composed of relatively strong clays. Underneath the top layer soft and liquid plastic clays of very low strength are lying up to 21 m depth. Some boreholes showed peat pockets at 9 to 17 m depth. At 21…23 m depth there occur coarse sands, below 23 m depth gravel-pebble muxture. Clay soils on the site feature organic content up to 10…15%.

Fig. 7. Organizing Committee Building under construction.

Table 1. Soil conditions of the Organizing Committee Building site.

Soil element	Depth, m	E, MPa	φ, deg	c, kPa
Clay	0…4,5	6	13	22
Very soft clays	4,5…21	0,7	10,6	10,3
Coarse sand	21…23	27	29	0
Mixture of gravel and pebbles	>23	53	35	0

Table 1 shows that application of spread footings is not possible, as it would result in excessive settlement. Soil improvement such as strengthening, reinforcement, replacement, etc. are not applicable because of thick layers of soft clays. Installation of drains for soil consolidation together with preloading of soil mass could not be applied due to tight project deadlines. Therefore, pile footing was the only alternative. At the stage of pile type selection there were considered prefabricated piles, bored cast piles, jet-piles, gravel piles in geosynthetic shell, etc.

The condition that complicates pile foundation design is that in order to ensure a footing seismic stability the piles shall bear the total lateral seismic load. The soil stratum capable to adequately resist to the lateral load usually occurs at over 21 m depth. In conditions of the site in question pile design bearing capacity to vertical load is times 40…60 greater that to the lateral load. In order to bear the vertical load of the 9-storey sector of the building 511 piles with 0.35x0.35 cm2 cross section are required while it requires 2030 piles to resist to lateral seismic load, i.e. times 4 as much.

Mass application of pile foundations with intermediary sand layer has started in 1960s in seismic areas of the USSR. The results of full-scale experiments demonstrated that in such foundations the lateral seismic load does not practically apply to the piles. Such foundation is recommended for practical application on sites having magnitude 7…9 seismicity. Application of pile foundation with intermediate cohesionless soil layer is not recommended by construction codes for sites with soils containing more than 10% of organic matter, collapsible soils, on karstic terrains, etc. This ban comes from possibility of collapse of loose soil and its disrupture that may result in extra deformations of the building. In order to enable application of such foundation a specific approach was required for foundation analysis and design.

Expanded pile caps together with cushion of cohesoinless soil reinforced by two layers of geosynthetics were used. Existing calculation method proposed by construction codes was developed with regard to aforementioned additions. The improved method took into account elasto-plastic properties of soils of the base; pile group effect, geometric and stiffness properties of deep footing (pile caps, reinforcement nets, etc.); stiffness parameters of foundation rafts (pile rafts); seismic conditions of construction site, etc.

The foundation design approved for implementation is shown on Fig. 8. Pile foundation below 9-th storey sector consists of 0.35x0.35 m prefabricated piles spaced over 2x2 m and for the 3-storey sector with 4x4 m square grid. The pile cap dimensions are 1,4x1,4x0,4 m. The intermediate cushion is 600 mm thick, reinforced by two layers of Fortrac 35MP geogrid. The raft thickness under 9-storey and 3-store sectors 800 and 600 мм respectively.

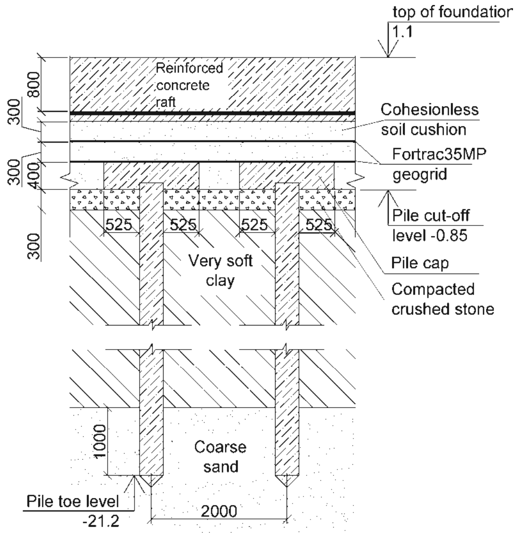

Fig. 8. Foundation cross-section for Organizing Committee Building.

The most essential factors predominant for the effectiveness of a such footing are: thickness of the intermediate layer above pile heads; pile caps overview dimensions; pile-to-pile spacing; pile cross sections; number of layers and stiffness of geogrid.

The building settlements monitoring data demonstrated that the settlement is close to analytical value and is compatible with actual standard pile footing settlements. Typical time-settlement diagrams based on measured values are shown on Fig.9.

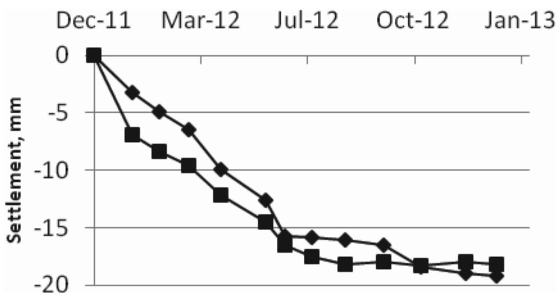

Figure 9. Time-settlement diagrams for Organizing Committee Building.

4 PLOT D1 AND PLOT 17.

Hotel complexes 3* and 4* are being constructed on plots 17 and D1.Plot D1 is located a slightly little closer to the shore.

Construction of 12 multistorey hotels (up to 8 floors) and buildings of public entertainment area is planned on plot 17. Each of the hotel building consists of two sections with dimensions of 36 x 14.9 m. Dimensions of the plot 17 is 265 x 220 m. Overview of the complex is shown in Fig. 12. Soil conditions of the site vary significantly due to its large area. The typical cross section of the site top down consists of 4 m thick fill, less frequent are peats, sludge and water-saturated silty sands, underlain at different depths (3…11 m) by gravely sands and gravel and pebble soils.

Driven concrete 30x30 cm 4-12 m long piles are applied. The length of piles depends on the depth of the bearing gravel and pebble layer, in which the pile tips are at least 0.5 m deep.

Due to variations of geological conditions within the construction site two types of footings were used in the project design (fig. 10)

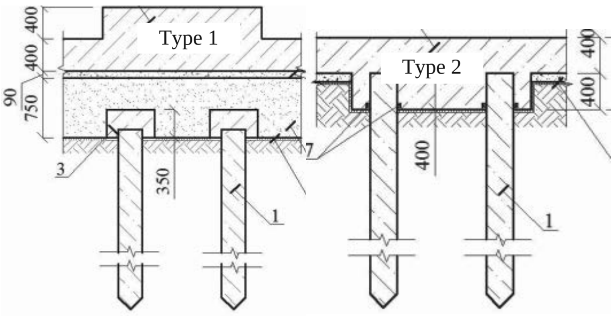

Figure 10. Foundation types for plot 17.

Type 1 (Fig. 10, left) is a concrete raft 400 mm thick with greater, up to 800 mm thickness, under bearing structures with flat bottom on pile foundation with intermediate sand and gravel layer. Presence of this layer practically excludes lateral seismic load transfer. The intermediate 0.75 m thick layer, consisting of local sand and sand-gravel soils, compacted layer by layer, is a damper, it is filled over pile heads having concrete caps. A layer of geotextile is placed between piles and under their caps separated from piles by shockproof polystyrol layer.

Type 2 (Fig. 10, right) is applied for the buildings, sitting on soil base, containing peats and peaty soils, having Young modulus of 5…6 MPa. Here a solid raft is designed of variable thickness, leveled on top, with pile heads fixed in the raft. The piles, bearing lateral seismic loads, have strong reinforcement in accordance with construction codes.

The pile field is designed to withstand the main and the special (seismic) combination of loads.. The design load, applied to the piles, is 750 kN for the main combination and 1000 kN for the special one. The piles bearing capacity of 1000 kN was proved by static load tests. The design lateral load on the piles does not exceed 35 kN for pile-raft rigid fixation.

Hotel, apartments and support services at plot D1 are located in the single building, separated by settlement and anti-seismic joints into sections (Fig. 11). Overall dimensions of the building are 150x264m.

Soil conditions of the plot D1 vary significantly within the building footprint, which determined the choice of different types of foundations within the same building.

On the part of the site (blocks 1-7, 10, 11 on figure 11), located close to the shore, surface part of the geologic section consists of large thick deposits of sand and gravel, underlain by gravel-pebble soils. For these conditions, the foundation is designed as a cast reinforced concrete raft with thickness of 400 mm. Under heavily loaded walls and columns 800 mm thick upward ribs are provided to increase stiffness of raft.

A further from the shore (Blocks 1A, 4A, 7A, 8, 8A and 9 in Figure 11) upper part of geological section consist of weak man-made soil, covered by fill produced during engineering preparation of the construction site. Due to low strength of these soils, they can not be used as the foundation base. Therefore, to minimize the differential settlements of adjoining blocks, pile

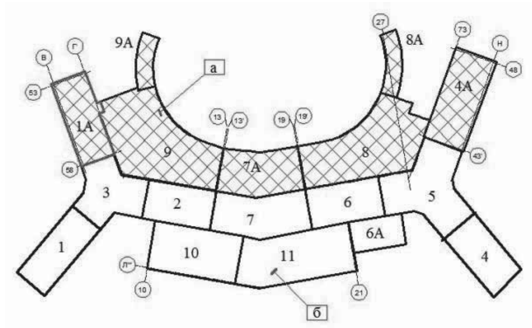

foundation with intermediate cohesionless soil cushion were designed similar to the one designed at plot 17 (Fig. 10 left).

Figure 11. Foundation layout for building on site D1. Hatched areas represent pile foundation, blank areas – raft foundation.

5 GEOTECHNICAL FEATURES OF UNDERGROUND PIPELINES DESIGN.

In order to ensure operation of the main Olympic facilities on Imeretin lowland terrain it was necessary to build a multi-kilometer long and dense network of various underground service lines for various purposes (heat and water lines, sewage and rainwater systems), of various liquid transportation principles (non-pressurized and pressurized), made of various pipeline materials (steel, polyethelyne, polypropelene), of various pipe diameters (250…1580 mm), with and without protection.

The main issue in foundation design for service lines is the account of potential considerable differential settlements of soft consolidating soils and, as a consequence, those of pipelines, caused by fill loading of the terrain. According calculation results the settlements of 5…20 m thick soft soils could be up to 0.7 m and could develop for several months or years even if special geotechnical techniques are applied to accelerate soil consolidation (sand and geosynthetic drains, temporary loading fill, jet stabilization, etc.). Application of other techniques of soil stabilization (stone columns, soil reinforcement, jet stabilization, etc.) was neither possible for financial and tight schedule reasons.

In view of the project of such scale the NIIOSP specialists had to develop special recommendations for service lines that outlined admissible deformations, missing in Russian construction codes (see Table 2). The assumed approach was based on limit state design analyses. This enabled selection of effective foundations types for the whole spectrum of numerous waterlines. Thereafter (Fig. 13) some service lines were designed to sit on driven concrete piles, other ones on cast concrete strip footing on natural or on improved ground, made by complete or partial replacement of soft laguna deposits by

Table 2. Ultimate admissable deformations of service lines.

Verification analysis type	Service lines			
	Pressure lines		Gravity lines	
	Water supply line (polyethylene)	Hot water line (steel)	Domestic sewage line (polypropylene)	Runoff water line (polypropylene)
Pipe line strength check	$r \geq r_{\min} = 50$ м	$r \geq r_{\min} = 400$ м	-	-
Pipeline gravity flow check	-	-	$i \geq i_{\min} = 2{,}5 \cdot 10^{-3}$	$i \geq i_{\min} = 0{,}8 \cdot 10^{-3}$
Pipeline plumbing check	-	-	$\varphi_{max} \leq 1^0$	$\varphi_{max} \leq 1^0$
Concrete duct crack resistance check	-	$r \geq r_{\min} = 16{,}7$ км	-	-

Note. r and $r_{\min}$ are design and minimally admissible radius of pipeline curvature; i and $i_{\min}$ are design and minimally admissible pipeline slopes; φ and $\varphi_{\max}$ are design and maximally allowable angle of rotation in pipeline joints.

gravel and pebble fill.

Figure. 12. Overview of plot 17.

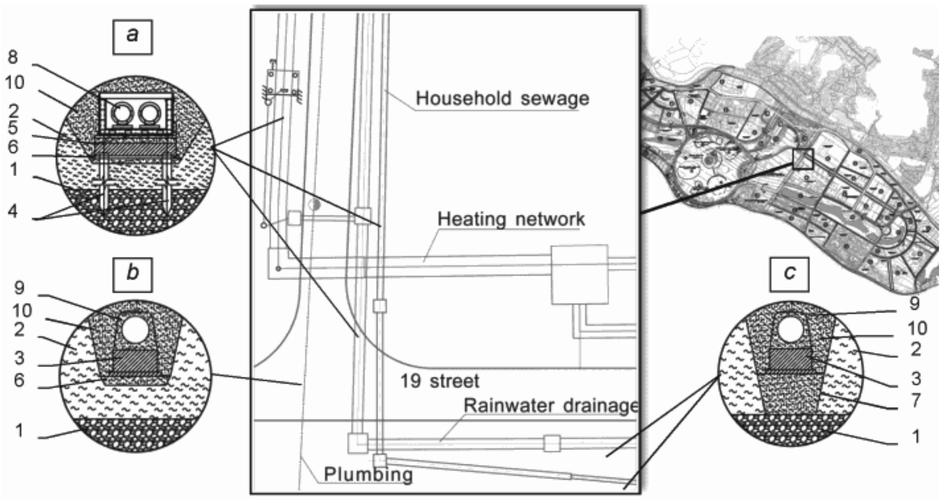

FIGURE. 13. Design solutions for foundations of underground water lines within Imeretin lowland terrain: a – driven pile footing; b – concrete strip footing on natural soil; c – concrete strip footing on replaced soil (replacement of soft soils by sand and gravel mixture). (1 – sand and gravel soils; 2 – soft clay soils; 3 – concrete strip footing; 4 – concrete driven pile; 5 – concrete raft; 6 – sand and gravel fill; 7 – replacement of soils with sand and gravel fill; 8 – pipeline in protective duct; 9 – pipeline wrapped around with geotexticle in sand fill; 10 – sand backfill).

6 CONCLUSIONS

Imeretin lowland, where main Olympic facilities are erected, features complicated geotechnical conditions, presence of thick soft clay deposits, high underground water level, and high seismicity of the area.

The above factors as well as the necessity of construction within tight deadlines of many sports facilities, including unique buildings and structures, made the designing engineers to face complicated challenges, which they finally coped with thanks to the accumulated experience of the national geotechnical community as well as to application of new approaches and effective design solutions.

Heaving Mechanisms in High Sulfate Soils

Mécanismes de soulèvement dans les sols à contenu élevé en sulfates

Puppala A.J.
Professor, Department of Civil Engg. University of Texas at Arlington

Talluri N., Gaily A., Bhaskar, Chittoori C.S.
Doctoral Student, Doctoral Student and Faculty Research Associate, Department of Civil Engg., University of Texas at Arlington

ABSTRACT: Pavement distress caused by chemically treated sulfate soils are considered as major maintenance problems to highway agencies. In view of this, researchers across the world have conducted studies on heave mechanisms in chemically treated sulfate soils. Many of these studies are focused on soils with soluble sulfate contents below 10,000 parts per million (ppm). Heave mechanisms in soils with sulfate contents above 10,000 ppm still need to be understood as sulfate measurements indicate that the soil sulfate levels of certain regions are well above 10,000 ppm and may exceed 50,000 ppm in some cases. In order to understand the behavior of treated soils containing sulfates above 10,000 ppm, a research study was initiated. Two soils with different soil classification are studied. Lime is used as a chemical stabilizer for these soils. Chemical and mineralogical tests as well as engineering swell tests were conducted to compare the changes in swelling, mineralogical and chemical compositions of the soils from the lime-sulfate reactions. Results will explain the need to look for replace the classical treatments by alternate ones for these high sulfate soils for civil infrastructure projects.

RÉSUMÉ : La dégradation des chaussées causée par les sols à contenu de sulfates traités chimiquement sont considérés comme des problèmes d'entretien majeurs par les agences routières. Compte tenu de cela, les chercheurs du monde entier ont mené des études sur les mécanismes de soulèvement dans les sols à contenu de sulfates traités chimiquement. La plupart de ces études portent sur des sols à teneurs en sulfates solubles en inférieures à 10.000 parties par million (ppm). Les mécanismes de soulèvement dans les sols à teneurs en sulfates supérieures à 10.000 ppm doivent encore être étudiés car des mesures de taux de sulfates indiquent que les niveaux de sulfates du sol de certaines régions sont bien au-dessus 10.000 ppm et peuvent même dépasser 50.000 ppm dans certains cas. Afin de comprendre le comportement des sols traités à contenu de sulfates supérieurs à 10.000 ppm, une étude a été lancée. Deux sols réputés différents selon la classification des sols ont été étudiés. De la chaux a été utilisée comme stabilisant chimique de ces sols. Des tests chimiques et minéralogiques ainsi que des tests d'ingénierie du gonflement ont été menés pour comparer les gonflements, et la composition minéralogique et chimique des sols à la suite des réactions chaux-sulfate. Les résultats exposés expliqueront la nécessité de chercher des traitements alternatifs aux traitements classiques pour ces sols à contenu élevé en sulfates dans les projets d'infrastructures civiles.

KEYWORDS: Sulfate, Swell, Mellowing, Ettringite, Expansive Soil

1 INTRODUCTION

Chemical stabilization of expansive soils using lime and cement has been a favourite option for practitioners over the years (Hausmann, 1990). In last few decades, premature failure of roads, highways and infrastructure facilities around several parts of the globe lead to question the validity of calcium based stabilization. It was reported that when soils contain sulfate minerals such as gypsum ($CaSO_4.2H_2O$) and sodium sulfate (Na_2SO_4) in their natural formation and are treated with calcium based stabilizers, adverse reactions occur causing heave and pavement distress. (Mitchell 1986, Hunter 1988, Puppala et al. 1999, 2003, 2012). These adverse reactions are attributed to the formation of expansive minerals such as Ettringite ($Ca_6.[Al(OH)_6]_2.(SO_4)_3.26H_2O$) and Thaumasite ($Ca_6.[Si(OH)_6]_2.(SO_4).(CO_3)_2.24H_2O$). This phenomenon is termed as “Sulfate Induced Heave” in literature. Repair and re-construction of the the failed infrastructure is costing millions of dollars to the tax payers. Under favourable moisture, humidity and temperature conditons these minerals grow causing further swell. Lime/cement treatement of sulfate soils can be regarded as the man made expasive soil problem.

In view of the past sulfate induced failures researchers have developed “Threshold Sulfate Levels” beyond which calcium based stabilization is to be cautioned. Berger et al., 2001 stated that sulfate levels below 0.3 percent can be safely treated with calcium stabilizers. Sulfate levels between 0.3 percent to 0.8 are to be handled with caution and sulfate levels greater than 0.8 percent should be avoided. Puppala et al., 2003 indicated that sulfate levels below 1000 ppm are of no concern and soils with sulfate levels between 1000-2500 ppm can be treated with additional amount of lime. Sulfate levels above 2,500 ppm are to be completely avoided. Harris et al., 2004 confirmed that in soils with sulfate levels greater than 7,000 ppm lime stabilization is not a viable option. There is no conclusive agreement between the threshold sulfates since in most cases of sulfate induced failures sulfate contents varied from as low as 320 ppm to as high as 43,500 ppm.

Based on previous recommendations researchers have studied heave mechanisms and developed alternative stabilization techniques for treating sulfate soils. Many of these studies were focused on soils with sulfate contents below 10,000 ppm. However, a further understanding about the soils with sulfate contents above 10,000 ppm and higher is needed. Researchers named these soils as “High Sulfate Soils”. In view of this aspect the current study focuses on heaving mechanisms and remedial options for high sulfate soils. Two soils from the state of Texas with sulfate contents above 20,000 ppm are considered in the current study. These soils were lime stabilized using mellowing technique and various engineering and mineralogical tests were conducted to understand the swell shrinkage characteristics of chemically stabilized high sulfate soils. Based on test results and analysis recommendations about the validity of mellowing technique, an attempt to look for alternative treatments was made.

2 MATERIALS AND EXPERIMENTAL PROGRAM

2.1 Test Soils and Basic Tests

Criteria for selection of the test soils is as follows: soils have to belong to different geological formation and classification. Based on these criteria Sherman and Childress, Texas soils were sampled for the testing program. As per USCS classification, Sherman soil is classified as 'CH' whereas Childress is classified as 'MH' soil. Gypsum is the sulfate source for both the soils. Soluble sulfate contents were determined using the TxDOT method (Tex-145-E, Colorimetric method). A 1:20 initial soil/water dilution ratio is used in this method. Turbidity caused by the presence of sulfate is determined using "Colorimeter" and converted in to ppm. Soluble sulfate content of Childress and Sherman soils are 24,000 ppm and 44,000 ppm respectively. Based on the classifications mentioned above these two soils are termed as "high sulfate soils".

Hydrated lime is used as the stabilizer for the soils understudy. Lime dosage is determined as per "Eades and Grim" test. Test soils were treated with various percentages of lime and pH test was conducted. The dosage at which soil pH reaches a value of 12.4 is considered as the optimum lime dosage. The optimum dosage of lime for both soils is 6% by dry weight. Optimum moisture content and dry density of natural and treated soils were obtained by conducting standard proctor tests as per ASTM standard procedures (ASTM D-698). It was observed that maximum dry density decreased and optimum moisture content increased up on lime treatment. Classification and standard Proctor test results are summarized in Table 1.

Table 1. Classification and Proctor Test Results

Soil	Atterberg Limits			Untreated Soil		6% Lime Treated Soil	
	LL	PL	PI	OMC (%)	MDD, psf	OMC (%)	MDD, psf
Sherman	72	30	42	27	89	28	87
Childress	71	35	36	21	103	22	96

Note: LL – Liquid Limit; PL – Plastic Limit; PI – Plasticity Index; OMC – Optimum Moisture Content; MDD- Maximum Dry Density

A series of chemical tests were conducted on test soils to determine the cation-exchange capacity (CEC), specific surface area (SSA) and total potassium (TP). Based on the mineralogical test results, clay mineralogy of the test soils was assessed as per the procedure outlined by Chittoori and Puppala (2011). Clay mineralogy indicated the dominance of Montmorillonite mineral in Sherman soil and Kaolinite mineral in Childress soil. Both soils exhibited swell potential upon hydration.

2.2 Engineering Tests and Mineralogical Tests

Engineering tests were performed on untreated test soils to assess the swell, shrinkage and strength characteristics. These tests include three dimensional (3-D) volumetric swell, shrinkage and unconfined compressive strength (UCS) tests. As alumina and silica constitute the chemical composition of Ettringite and Thaumasite, measurement of alumina and silica is essential. Alumina and silica that participate in the sulfate reactions are called "reactive alumina and silica". Reactive alumina and silica measurements were conducted as part of the mineralogical tests. All the engineering tests were conducted at optimum moisture content (OMC) and wet of optimum moisture content (WOMC) corresponding to 95% of maximum dry density. Wet of optimum moisture content is 2% and 3% higher than the optimum moisture content for Childress and Sherman soils.

Mellowing technique has been successful in stabilizing soils with sulfate concentration up to 7,000 ppm (Harris et al., 2004). Applicability of mellowing for high sulfate soils has not been studied so far. To assess the validity of mellowing technique in high sulfate soils both the soils are treated with 6% lime and corresponding moisture from the proctor curve. Lime treated soils were mellowed for periods of 0 and 3 days in a moisture controlled environment. Since lime treatment makes the soil dry, to compensate for the moisture loss during the mellowing process, additional 3% moisture is provided for 3 day mellowed soils. Another reason for provision of additional moisture is to increase the solubility of gypsum and early depletion as the sulfate reactions occur during the mellowing period. After the elapsed mellowing periods, soil samples were recompacted and engineering tests were conducted. Data from the engineering tests is compared with untreated soils to witness the sulfate reactions occurring in high sulfate soils. Reactive alumina and silica measurements were performed on the samples subjected to swelling and loss of aluminates and silicates were calculated. A brief description of the tests conducted is given below:

2.2.1 Three Dimensional Volumetric Swell (3-D Swell) Test

3-D swell tests were conducted on natural and treated soils to determine the maximum possible volumetric swell which is a combination of vertical and radial swell. These tests are conducted on 4 in. (101.6 mm) diameter and 4.6 in. (116.8 mm) height samples. The samples are prepared using a gyratory compactor machine. Porous stones are placed at the top and bottom of the sample and a rubber membrane is placed around the sample. The samples are double inundated and a dial gauge is placed on the top of the sample to record the vertical swell with time. Vertical swell readings are collected with time until there is no further swell for 24 hours. Radial swell of the sample is measured after the completion of the test using a pi-tape. Double inundation provides the worst possible scenario in field where the soil is 100% saturated and maximum swell is expected in this case. Researchers across United States and UK have successfully used double inundation technique for measuring the volumetric swell.

2.2.2 Three Dimensional Volumetric Shrinkage Test

3-D shrinkage tests were conducted as per the procedure developed by Puppala et al., 2004 to measure the decrease in the total volume of soil specimens due to the loss of moisture content in field samples during a dry spell. In order to replicate the worst possible conditions, drying from a compacted state to completely dry state is considered in this test. Soil samples were compacted to 2.26 in. (57 mm) diameter and 5 in. (127 mm) height using a static compaction machine. Initial sample height and diameter are measured at three locations and averaged. Samples are prepared at optimum and wet of optimum moisture contents and dried on bench top for 12 hours followed by oven drying for 24 hours. Steps used in sample preparation and extraction are similar to the UCS sample except the sample sizes are different. After 24 hours, samples are removed from the oven and sample dimensions are taken. Volumetric shrinkage is calculated as the difference of initial and final volume divided by the initial volume expressed in percentage.

2.2.3 Unconfined Compressive Strength (UCS) Test

Unconfined Compressive Strength (UCS) tests were conducted as per ASTM D 2166 method. The main intention of these tests is to determine the strength changes during the mellowing process. Soil samples are treated with lime and allowed to mellow for 0 and 3 days. After the mellowing period soil samples were compacted to 2.8 in diameter (70 mm) and 5.6 in. (140 mm) height and moist cured in a 100% relative humidity environment for 7 days. After the curing period soil samples are loaded to failure at a constant strain rate of 1.27 in/minute in a triaxial compression machine.

2.2.4 Reactive Alumina and Silica Measurements

Reactive alumina and silica are the aluminum and silica present in amorphous or poorly crystalline Al/Si phases including amorphous alumino silicate, organically complexed alumina and hydroxyl-Al polymers present in Montmorillonite interlayers. Reactive alumina and silica measurements were conducted by a procedure modified after Foster (1953). To determine the reactive alumina and silica, 15g of soil was mixed with 150 ml of 0.5 N NaOH and heated. Once the solution starts boiling, heating is discontinued and the solution is allowed to cool, followed by centrifuging at 8000 rpm. After centrifuging the extract is filtered using a 0.1 µm membrane type filter paper. The extract obtained was stored in a plastic bottle and the ICP analysis was performed on a clear extract. If the extract obtained in the last step is not clear it is treated for organics and iron oxides which inhibit the alumina and silica measurements in ICP analysis.

3 RESULTS AND DISCUSSON

3.1 Results of the Testing Program

3.1.1 Three Dimensional (3-D) Swell Test

3-D swell tests were conducted on natural and treated soils as per the procedure described above. Natural swell of Sherman and Childress soils at optimum moisture content is 16.2% and 7.5% respectively. The observed swell is less at wet of optimum moisture content. Additional swell tests were conducted on both the soils at 7-day mellowing. Results of the swell testing are presented in Figure 1 and Figure 2. It can be observed from the figures that for both the soils at 0 days mellowing, the treated swell is higher than the natural swell indicating the dominance of sulfate reactions over stabilization reactions which is common in lime treated high sulfate soils. In case of Sherman soil, the observed swell is below the natural swell for 3-day mellowing which further decreased with 7-day mellowing indicating the effectiveness of mellowing in Sherman soil. In Childress soil, with 3-day mellowing the reduction in swell is observed though it is not significant since the treated swell is higher than the natural swell. With 7-day mellowing, the treated swell further increased indicating mellowing is not effective for Childress soil. Reasons for this behavior are explained in the subsequent sections.

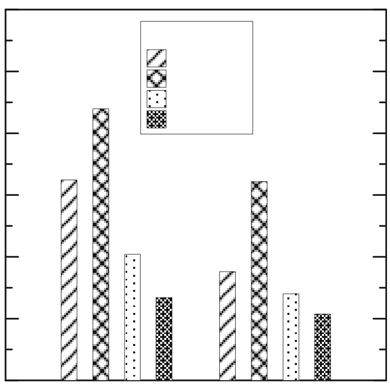

Figure 1. 3-D Volumetric Swell (SHERMAN Soil)

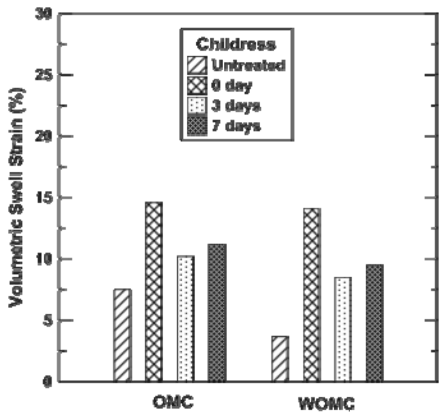

Figure 2. 3-D Volumetric Swell (Childress Soil)

3.1.2 3-D Shrinkage Test

3-D volumetric shrinkage tests were conducted on natural and treated soils at optimum and wet of optimum moisture contents. 3-D shrinkage test results are shown in Table 2.

Table 2. 3-D Shrinkage Test Results

Soil	**Natural**		**6%L, 0 day mellowing**		**6%L, 3 day mellowing**	
	OMC*	**WOMC***	**OMC***	**WOMC***	**OMC***	**WOMC***
Sherman	-15.8	-20.0	-7.6	-8.9	-6.3	-9.4
Childress	-14.3	-15.4	-2.4	-2.6	-3.1	-4.0

Note*: Negative sign indicates shrinkage

From Table 2, it can be observed that volumetric shrinkage reduced with lime treatment irrespective of the sulfate content. Volumetric shrinkage is higher at WOMC condition owing to the high moisture at wet of optimum than optimum. Volumetric shrinkage of the 3 day mellowed soils is slightly higher than the 0 mellowed soils due to additional moisture provided during the mellowing process. It can be concluded that sulfate heave reactions do not have significant influence on the shrinkage behavior of lime treated soils.

3.1.3 UCS Test Results

Unconfined compressive strength (UCS) tests were conducted on natural and treated soils (0 day and 3 day mellowing). The results of UCS tests are presented in Table 3. From Table 3. it can be observed that UCS strengh of treated soils is 2-5 times higher than the natural soil. There was a slight decrease in strength in case of 3 day mellowed samples which could be attributed to the addition of extra moisture during mellowing.

Table 3. UCS Test Results (psi)

Soil	**Natural**		**6%L, 0 day mellowing**		**6%L, 3 day mellowing**	
	OMC	**WOMC**	**OMC**	**WOMC**	**OMC**	**WOMC**
Sherman	33	19	81	60	70	46
Childress	23	16	108	78	103	56

3.1.4 Discussion

Reactive alumina and silica measurements on natural (untreated soils) and treated soils (after the samples have been subjected for swell testing) at different mellowing periods were performed as per the procedure outlined above. Table 4 shows the results of these tests and the loss of alumina and silica in treated soils at different mellowing time periods. It can be seen from the Table 4 that the initial reactive alumina and silica contents are very low in Childress soil when compared to that of Sherman soil. The main intent of mellowing is to allow the Ettringite formation reactions in initial stages. During remixing and compacting the initial Ettringite is broken and further Ettringite formation is hence not possible due to the lack of reactive sulfates.

It is reported in the literature that Ettringite formation depends on the amount of reactive alumina present in the system. For example, low alumina contents in soils favor the trisulfate hydrate (Ettringite) formation. High alumina contents, on the other hand, lead to simultaneous formations of pozzalonic and ettringite reactions. As a result, attractive forces formed from pozzalonic formation will resist the disruptive forces caused by Ettringite hydration reactions. This explains low heaving in high alumina soil (Sherman soil) of the present research.

Low initial reactive alumina contents coupled with high sulfate contents in Childress soils are attributed to large heaving and here the mellowing is deemed ineffective primarily due to low alumina content in the soil. Also, the loss of alumina and silica at both 0 day and 3 day mellowing periods were higher in case of Childress soil compared to Sherman soil. Though the loss of alumina and silica is less in 3-day mellowed soils, this soil still exhibited high swelling due to high sulfate content (44,000 ppm) present.

Table 4. Reactive Alumina and Silica (ppm) in present soils

Soil	Untreated (Natural)		6%L, 0-day mellowing		6%L, 3-day mellowing	
			% loss		% loss	
	Al(ppm)	Si(ppm)	Al	Si	Al	Si
Sherman@OMC	279	137	58	66	53	64
Sherman@WOMC	279	137	57	64	52	63
Childress@OMC	76	13	63	54	61	46
Childress@WOMC	76	13	62	62	58	54

Also, authors have made attempts to link the formation and growth of Ettringite to the compaction density/void ratio of the soil specimens. Based on specific gravity and maximum dry density (@OMC condition), the compaction void ratio is calculated. Compaction void ratios of Childress and Sherman soils are 0.52 and 0.86, respectively. In soils with high void ratio (Sherman), the initial Ettringite formation, growth and heaving on hydration can be accommodated in the soil matrix provided there is no further nucleation of new compounds. If there had been further Ettringite growth, heave would have been higher in Sherman soil. In soil with low void ratio such as the present Childress soil, the dense soil matrix could not accommodate both initial Etringite formation and their growth on hydration and as a result, this soil exhibited higher heaving.

Overall, both alumina amounts and compaction void ratio conditions contribute to soil sulfate heaving and this information is used in the development of alternate chemical treatments for high sulfate soils.

4 CONCLUSIONS

1. In Sherman soil containing sulfates of 30,000 ppm or less, the mellowing effectively reduced the swell potential. Childress soil, containing larger amounts of sulfates of more than 30,000 ppm, exhibited sulfate induced heaving even at longer mellowing periods.
2. Volumetric shrinkage behavior is unaffected by the presence of sulfates and mellowing periods indicating that the shrinkage behavior was succesfully reduced with lime treament.
3. Low alumina contents facilitated Ettringite formation and heaving (Childress soil) whereas at high alumina contents both Ettringite and pozzolonic reactions occur simultaneously but due to dominance of pozzolonic reactions less heave is observed in this case (Sherman soil).
4. Compaction void ratio is an important parameter that need to be emphasized in lime treament of sulfate soils because Ettringite induced heaving is more critical in dense soil matrix compared to loose matrix.

5 ACKNOWLEDGEMENTS

Authors would like to thank Texas Department of Transportation (TxDOT) for the funding the project. Authors would like to thank Mike Arellano and Richard Williammee of TxDOT as well as Pat Harris of Sam Houston State University for their assistance with the research.

6 REFERENCES

Berger, E., Little, D. N. and Graves, R. (2001). Technical Memorandum: Guidelines for Stabilization of Soils Containing Sulfate. http://www.lime.org/publications.html Accessed October, 2012.

Chittoori, B., and Puppala, A. J., (2011). Quantitative estimation of clay mineralogy in fine-grained soils. Journal of Geotechnical and Geoenvironmental Engineering, v 137, n 11, p 997-1008, 16 December 2011.

Foster, M. (1953) Geochemical Studies of Clay Minerals III. The determination of free silica and free alumina in Montmorillonites, *Geochemica Cosmochimica Acta*, Vol. 3, pp. 143-154.

Harris, J. P., Sebesta, S., and Scullion, T. (2004). Hydrated Lime Stabilization of Sulfate-bearing Vertisols in Texas. Transportation Research Record 1868, TRB, National Research Council, Washington, D.C., 2004, pp. 31-39.

Hausmann, M. R. (1990). Engineering principles of ground modification, McGraw–Hill, New York.

Hunter, D. (1988). Lime-Induced Heave in Sulfate-Bearing Clay Soils,. Journal of Geotechnical Engineering, ASCE, Vol. 114, pp. 150-167.

Mitchell, J. K. (1986). Practical Problems from Surprising Soil Behavior. Journal of Geotechnical Engineering Division, ASCE, Vol. 112, No. 3, pp. 259-289.

Puppala, A. J., Hanchanloet, S., Jadeja, M., Burkart, B. (1999). Sulfate InducedHeave Distress: A Case Study. Proceedings, Transportation Research Board Annual Meeting, Washington D.C, USA.

Puppala, A. J., Wattanasanticharoen, E. and Punthutaecha, K. (2003). Experimental Evaluations of Stabilization Methods for Sulphate-rich Expansive Soils. *Ground Improvement* Vol. 7, No. 1, 2003. pp. 25-35.

Puppala, A.J., Katha, B., Hoyos, L.R. (2004) Volumetric Shrinkage Strain Measurements in Expansive Soils Using Digital Imaging Technology. ASTM Geotechnical Testing Journal, Vol. 27, No. 6, November, 2004, pp.547-556.

Puppala, A.J., Naga S. Talluri., Bhaskar S. Chittoori and Ahmed Gaily . (2012). Lessons Learned from Sulfate Induced Heaving Studies in Chemically Treated Soils. Proceedings of the International Conference on Ground Improvement and Ground Control. Research Publishing, Vol. 1, November, 2012, pp.85-98.

Geotechnical aspects in sustainable protection of cultural and historical monuments

Les aspects géotechniques de la protection durable des monuments culturels et historiques

Sesov V., Cvetanovska J., Edip K.
University "Ss Cyril and Methodius" - Skopje
Institute of Earthquake Engineering and Engineering Seismology

ABSTRACT: This paper describes the geotechnical aspects of comprehensive methodology that has been developed at Institute for Earthquake Engineering and Engineering Seismology for protection of cultural and historical heritage. The methodology has been applied on numerous domestic and international projects. Primarily focus is given on geotechnical conditions related to seismic actions because the history showed that many of the historical monuments have been heavily damaged due to earthquakes. Multidisciplinary approach was used to have clear insight of key parameters that driven the seismic potential of the sites. Seismic hazard and risk analysis defined the level of the seismic potential of the sites. Practical implementation of the methodology is described through three case studies for protection of cultural and historical monuments in Macedonia: the St. Mary Peribleptos Church, from the 13th century, located in old town of Ohrid; the mosque Mustafa Pasha in Skopje, from the 15th century and the 19th century Clock Tower located in the city of Prilep. The obtained results point out the significance of involving local site conditions into the seismic assessment and retrofit of historical structures in general.

RÉSUMÉ : Dans cet exposé sont présentés les aspects géotechniques d'une méthodologie complète qui a été développée à l'Institut de génie sismique et d'ingénierie parasismique pour la protection des monuments historiques et culturels. La méthodologie est appliquée à plusieurs projets domestiques et internationaux. L'attention est particulièrement portée sur les conditions géotechniques liées au chargement sismique, puisque l'histoire a démontré que beaucoup de monuments historiques avaient très endommagés pendant le séisme. Pour obtenir une idée claire des paramètres clés du potentiel sismique des localités, on a utilisé une approche multidisciplinaire. A partir de l'analyse du danger et du risque sismique, on a défini le niveau du séisme potentiel sur les localités. L'implémentation pratique de la méthodologie est décrite sur trois exemples d'étude pour la protection des monuments historiques et culturels en Macédoine: l'église Sainte Marie Peribleptos du 13 siècle, dans le vieille ville d'Ohride, la mosquée Mustafa Pasha de Skopje datant du 15 siècle et la tour de horloge de Prilep construite au 19 siècle. Les résultats obtenus montrent l'importance de la prise en compte des conditions locales dans l'estimation des paramètres sismiques et plus généralement, des informations en retour sur les constructions historiques à partir de leur état initial.

KEYWORDS: geotechnical aspects, sustainable protection, historical monuments

1 INTRODUCTION

Located in the south east part of Europe, having central position in Balkan region, Republic of Macedonia is characterized with significant cultural and historical heritage, which originated from early ancient until recent modern periods. For such long life times these monuments have experienced many unexpected loading actions which produced different consequences, from minor cracks to heavily damages and collapses. Common thing for these 'destructive' situations is when the monument is heavily damaged or collapsed the new monument is built on the foundation of previous-older monument so the location of the monuments remains the same. This is very common situation in Macedonia where several civilization and empires passed through this territory and everyone leaves monuments from their own period. This emphasis the importance of the information and data for the site conditions where these monuments are located toward sustainable preservation and protection of cultural and historical heritage. Comprehensive approach for sustainable protection involving geotechnical aspects is presented through three chosen case studies of very unique and specific type of historical monuments: the Mustafa Pasha mosque in Skopje, from the 15th century, the church of The Holy Mother of God Peribleptos, from the 13th century, located in the old town of Ohrid and the Clock Tower, from the 19th century, located in the city of Prilep.

2 METHODOLOGY

The ground conditions in the seismic design process are usually taken into account through determination of the base seismic shear force, where the coefficient, which represents the ground conditions, is multiplied by other coefficients to calculate the seismic force. Then quasi-static analysis can be performed in order to design the structural elements and check the seismic performance of the structure. In cases where the design engineer has the task to design buildings of higher importance such as historic monuments, there should be no doubt that the engineer has to perform a time history analysis of the structure subjected to seismic loading (Sesov et al., 2012). This analysis has to be based on the seismic parameters which are defined by the results from the in-situ and laboratory investigations performed for the site.

This paper is primarily focused on application of this methodology on historical structures, which are by themselves and in most of the cases, unique structures of significant cultural importance and as such deserve a multidisciplinary approach to their strengthening and preservation. No matter how sophisticated the structural analysis may be (starting from linear-elastic, pushover and nonlinear time history analysis), yet the variation and the uncertainty associated with the local soil conditions, the design seismic input parameters, determine considerably the response of the structure.

The applied methodology for definition of the seismic input parameters in the case studies presented in this paper follows the following steps:

- The first step, Figure1 includes characterization of the design seismic motion based on existing earthquake catalog and seismotectonic data and the seismic hazard through attenuation of ground motion intensity.
- The second step is definition of the subsurface profile of the studied area based on geological geotechnical, geophysical and topographic data. Site characterization is mainly done by geotechnical boreholes, Standard Penetration Test (SPT), Cone Penetration Test (CPT), PS-Logging, Refraction Microtremor (ReMi), seismic reflection and refraction measurements and laboratory index test results to provide engineering bedrock (Vs > 750m/s) depths.
- The next step is selection of earthquake input motions which are applied on the bedrock level and PGA acceleration to which the earthquake motions are scaled based on the results from the seismic hazard analysis
- The third step is to evaluate, for each location within the studied area, all the aspects of the seismic ground response, namely, the elastic response spectra. The local site effects are assessed by carrying out one-dimensional (1-D) ground response analysis) using borehole data and shear wave velocity profiles within the investigated area (Ordonez, 2011).
- Seismic risk analysis;
- Definition of seismic design parameters at different levels (PGA, site design spectra, time histories of accelerations) to be used in the evaluation of the existing seismic stability of the structures.

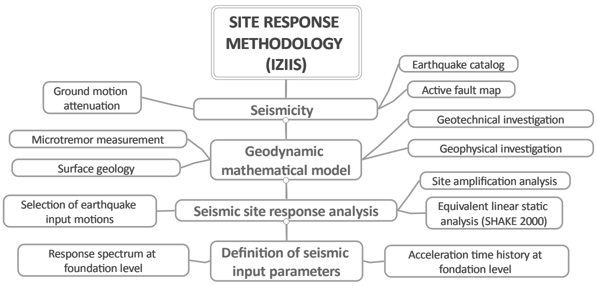

Figure 1. Flow chart of the applied methodology

1 CASE STUDY 1 - MUSTAFA PASHA MOSQUE

As the first case study, presented are the investigations related to the local site conditions in the seismic assessment of a historical structure in Macedonia: the Mustafa Pasha mosque in Skopje, dating back to the 15th century, as shown in Figure 2.

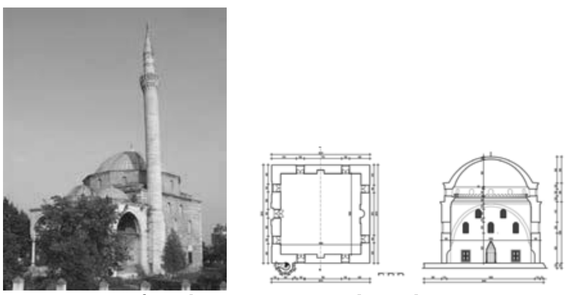

Figure 2. Mustafa pasha Mosque, view, plan and section

The Mustafa Pasha mosque in Skopje is located in the Skopje valley, which was created as a result of neotectonic movements of the surrounding structures. The geological characteristics of the location play an important role as to the amplitude and frequency content of the seismic action. Soils in the region of Skopje in Macedonia are relatively uniform according to stiffness so that the variations along soil depth lead to different levels of damage to structures.

The representative soil models have been defined based on comprehensive geotechnical and geophysical investigations arried out at the location of the mosque. The soil profile mainly consists of sand, clay as well as marl below depth of 12m. For the needs of this project, the effect of the local geotechnical media has been defined by analyses of the dynamic response of representative mathematical models of the foundation soil.

The input motions at bedrock have been selected as a result of the hazard investigations and taking into consideration the regional seismogeological characteristics. The maximum accelerations have been selected as amax=0.20(g) and amax =0.30(g) which are the expected maximum accelerations at the selected location. The acceleration spectra are given in the following figure 3.

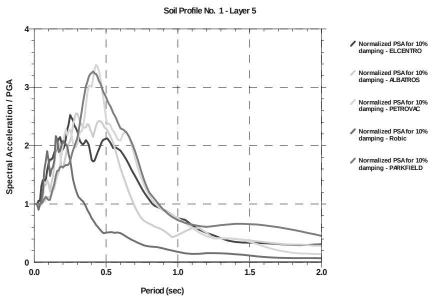

Figure 3. Normalized response spectrum for 10% damping

From the obtained spectra, it is seen that, for the presented MODEL1, the amplitudes occur in the period range of 0.15 - 0.25 s, and in the period of 0.4 s (more dominant) for the analysed input excitations. The obtained results on the response spectra of the soil models have carefully been analysed and taken into account in modelling and analysing the seismic resistance of the mosque.

The main parameters of seismic design, the maximum accelerations have been defined based on the results from the seismic hazard and risk analysis under the following assumptions:

- The serviceability period of the structure is 100 plus years;
- For the design earthquake, the acceptable level of seismic risk is 30-40%
- For the maximum earthquake, the acceptable level of seismic risk is 10-20%

The obtained spectral amplification factors can be used in probabilistic seismic hazard assessments, because, unlike the code site factors, the proposed site amplification factors include quantification of the underlying uncertainty in the site-dependent ground motion estimate. For the analysed structure, an average amplification factor DAF of 1.35 has been adopted.

For dynamic analysis, it is also necessary to know the time histories of accelerations that reflect the characteristics of earthquakes and the time duration of intensive excitation. Having no records on strong motion accelerations in the region of the investigated site, the time histories have been defined by selection of the characteristic previously mentioned records, whose frequency content covers the frequency range of interest for dynamic analysis (Sesov et al., 2007).

2 CASE STUDY 2 - ST. MARY PERIBLEPTOS CHURCH

As the second case study, presented are the investigations related to the local site conditions in the seismic assessment of a historical structure in Macedonia: the St. Mary Peribleptos church in Ohrid (figure 6) , dating back to the 13tn century.

The parameters for analysis of the structure of St. Mary Peribleptos church in Ohrid for the effect of seismic excitations expected at the site, have been defined on the basis of the results obtained from the performed investigations that are described in details in the previous case study.

Based on the realized investigations and the obtained results on the seismic potential of the site of the St. Mary Peribleptos church in Ohrid, the following conclusions are drawn:

The data on the seismic activity of the wider area of the site point to moderate exposure to earthquake effects with expected maximum magnitudes of M=6.9.

Figure 4. St. Mary Peribleptos church, Ohrid

The maximum expected accelerations at bedrock have been obtained by seismic hazard analysis. The results for the representative return periods (Table 2) range between 0.20 and 0.25 g, in accordance with the recommendations given in Eurocode 8: Design of Structures for Earthquake Resistance - Part 1: General Rules, Seismic Actions and Rules for Buildings for Damage Limitation Requirements – TDLR=95 years and Non-Collapse Requirements TNCR =475 years

The geotechnical boreholes and geophysical measurements confirmed the existence of a dominant geological formation at the site: below surface - plate-like limestone with presence of superficial alluvial zone with humus cover. The measured velocities of seismic waves show the existence of ground type "B" in accordance with the Eurocode 8 classification.

The performed analyses of seismic response of the site point to several important issues, namely that the predominant periods of the site are in the range of T=0.13-0.15 s . According to the data received from the design engineers, the predominant periods of the structures range between Tchurch =0.2 s, Tbellfry= 0.29 s and Tlodging=0.17s. If a comparison is made with the predominant periods of the site, it can be concluded that there is no danger as to occurrence of resonance effects.

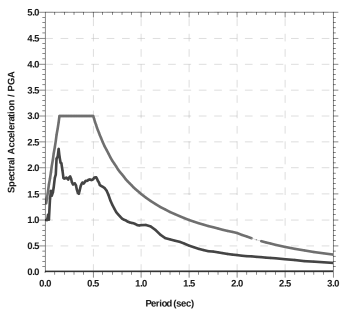

Figure 5. Mean normalized response spectrum and normalized spectrum in accordance with EC8 – ground type B, for 5% damping

The results from the analysis of the seismic response of the site show that the effects of amplification of the local soil are not much expressed (Sesov et al., 2011). The dynamic amplification factor ranges within 1.15 – 1.20.

Based on the analyses of the seismic risk, the maximum acceleration as one of the main seismic parameters for seismic analysis is given in function of the return period and the design engineer also has the possibility to adopt a maximum acceleration level based on the adopted level of acceptable risk and serviceability period of the structure which will indirectly provide the return period**.** In the case of the St. Mary Peribleptos church in which the soil conditions are mainly represented by stiff soils and rock, the amplification does not play a significant role regarding the response of the structure.

3 CASE STUDY 3 - CLOCK TOWER

The Clock Tower in Prilep (Figure 5) was built in 1858, on the location of an older wooden Clock Tower, which was burnt to the ground. It is an particularly important structure in Republic of Macedonia and beyond, in the Balkan region. It is a unique structure of this kind that has been preserved until present in its authentic architectonic and structural form.

A problem which is to be solved as soon as possible is the evident inclination of the tower, i.e., the displacement of the vertical axis in respect to the vertical line in west and southwest direction by which the existing stability of the tower is disturbed in static, and particularly dynamic conditions. Since 1998, there have been different kinds of research works for the purpose of precise measurement of the extent and the direction of the inclination and defining the reasons for this problem.

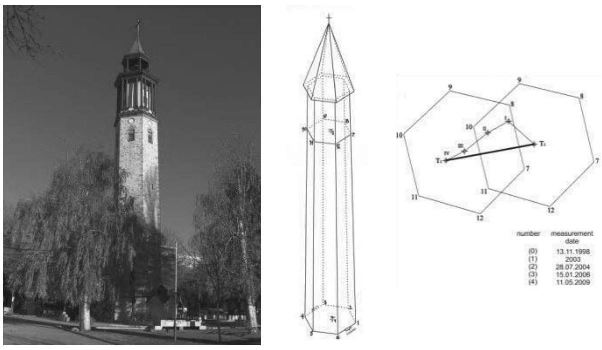

Figure 5. The Clock Tower in Prilep, Macedonia

For the purpose to analyze the existing structure together with the soil condition, a superstructure principle more detailed explained by Wolf, 1985 is applied. The application of the superposition principle, in case of linear i.e. equivalent linear methods, enables the dynamic soil-structure interaction problem to be analyzed in phases so that each phase is solved independently. As first step the structural components of the tower are analyzed where the soil is simulated by springs stiffness, and as second step the stress strain conditions in the soil are analyzed together with the foundation structure where the tower is added as continuous load.

The main model has been analyzed for the effects of dead weight of the tower and seismic forces according to the national regulations. The effects of the seismic forces increase the inclination in the direction as well as reduce the global safety coefficient. The inclination angle of the tower in this case of effects has increased for 40% in respect to the situation with the effects only due to the dead weight. This situation clearly points out that the capacity of the existing state is limited and that the deformation capacity of the tower along with the foundation soil is exhausted regarding maintenance of a satisfying level of safety. Therefore decision for strengthening the Tower has been made.

The main concept of this technical solution for strengthening is to reduce and prevent further uncontrolled inclination of the tower by means of additional structural elements (RC jackets, pile slab and piles) that are connected and make an integral structure (figure 7). This structural unit enables that additional effects contributing to further inclination be sustained and transferred to the soil layers with good strength-deformability characteristics and provides, at the same time, the required stability and safety of the Tower under seismic loads that, in the case of the present inclined position, may cause catastrophic consequences.

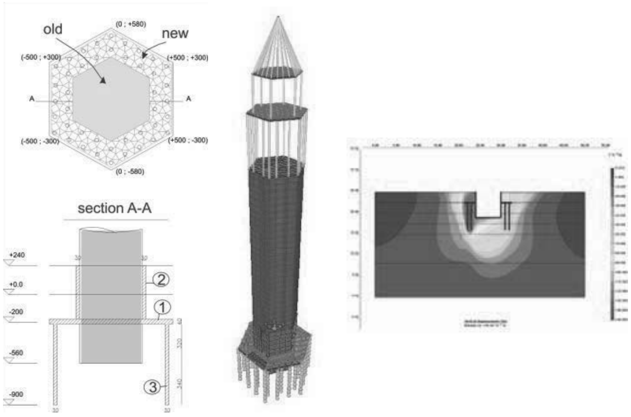

Figure 7. Tehnical solution for strengthening, numerical model of the structure and soil

Based on the obtained results (presented in figure 8) it can be noted that the deformations and the stresses in the soil significantly decrease compared to the existing conditions.

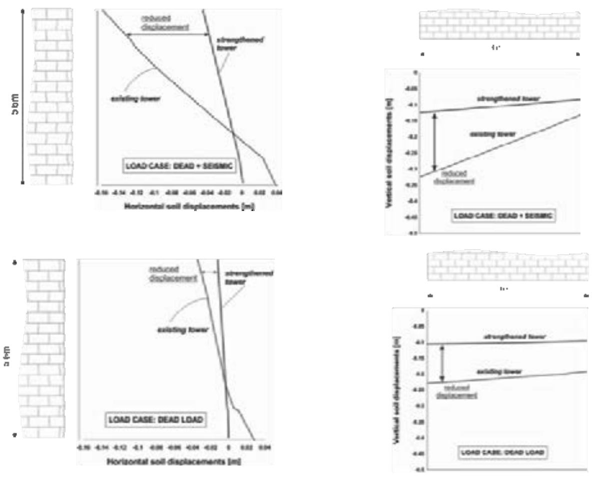

Figure 8. Horizontal and vertical displacements in soil due to dead load and dead + seismic forces

A particularly indicative element is the global coefficient of safety obtained through the incremental “phi-c” analysis which shows the ultimate state of the soil. The results are presented in table 1 for cases of effects due to dead weight and dead weight along with the effect of seismic forces. The increase of the global coefficient points to the fact that the newly designed solution enables a more uniform distribution of the effects of additional loads and their transfer to deeper soil layers with better strength-deformability characteristics.

Table 1. Coefficient of global safety through incremental “phi-c” analysis

Conditions	Load case	Safety coefficient
Existing conditions	Dead weight	2.44
	Dead weight + seismic load	1.91
Conditions of a strengthened structure	Dead weight	4.90
	Dead weight + seismic load	4.02

4 CONCLUSIONS AND RECOMENDATIONS

Large scale restoration and retrofitting projects were under concern at two of the important historical monuments in Macedonia, Mustafa Pasha Mosque and the St. Mary Peribleptos church, which have suffered considerable damages during their life time. Within the scope of these projects, detailed soil investigations and site response analyses have been carried out in order to understand the causes of structural damage during the past earthquakes and determine the dynamic parameters needed for structural analysis and retrofitting design for a probable future earthquake. In this paper, the findings from the investigation of the effects of the local soil conditions on the soil amplification in the mentioned case studies are presented. The objective of the described procedure is to take into consideration the regional and microlocation geological and seismological parameters as correctly as possible in order to define the input seismic parameters for dynamic analysis of important structures. The obtained results point out the significance of involving the local site conditions into seismic assessment of historical structures.

The site specific earthquake parameters are used in dynamic analysis of structures and to develop retrofitting techniques to increase the level of safety against future earthquake damages. As a result of this investigation, it is concluded that the local soil conditions which led to amplification of the ground motions in the case of the Mustafa Pasha Mosque during the past earthquakes had played a major role as to the structural damage experienced by the mosque. For the future safety of this valuable monument, the structural system and the elements are strengthened to withstand the inertial forces compatible with the dynamic behavior of the foundation layers during a probable earthquake. In the case of the St. Mary Peribleptos church in which the soil conditions are mainly represented by stiff soils and rock, the amplification does not play a significant role regarding the response of the structure. The presented methodology has been proved to be successful in preservation of the safety level in historical monuments which require strengthening and rehabilitation. This approach is recommended to be used in future rehabilitation and strengthening of old monuments of significant cultural importance located in seismically prone regions.

Based on the analyses of the existing conditions of the Clock Tower and considering the state in which this important cultural historic structure is, a technical solution for consolidation elaborated to a level of a main project has been proposed.

The main concept of the proposed technical solution involves design of new additional structural elements to prevent further inclination of the Clock Tower and raise, at the same time, the safety of this structure to a satisfying level of functioning in the next period. It should be pointed out that most of these new structural elements are anticipated to be constructed below the terrain level, meaning that the anticipated solution will have a minimal impact upon the external façade of the structure.

5 REFERENCES

Berilgen M. M. (2007) Evaluation of Local Site Effects on Earthquake Damages of Fatih Mosque. Engineering Geology 91. 240–253

Marchi M et al. [2011]. "Stability and strength analysis of leaning towers". Geotechnique, 61(12), 1069-1079

SAP 2000. Computers and structures inc.

Sesov, V. et al. (2007) Definition of Seismic Input Parameters for Evaluation of the Seismic Stability of Mustafa Pasha Mosque (in Macedonian). IZIIS Report 2007047

Plaxis V9.0 [2011]. Tutorial Manual, Balkema / Rotterdam / Brookfield publications

Wolf [1985] “Dynamic soil structure interaction” Prentice Hall Inc

Modern methods of geotechnical defense of buildings in the difficult geological conditions of Ukraine

Méthodes modernes pour la défense géotechnique de bâtiments dans les conditions géologiques difficiles de l'Ukraine

Slyusarenko Y., Chervinskyy Y.
Research institute of building constructions, Kiev, Ukraine

Karpenko Y., Dvornik S.
Ukraine-France enterprise «Osnova-Solsif», Kiev, Ukraine

Malikov S., Rozenvasser G., Lavshuk I.
DE Donetsk Promstroyniiproekt, «Pushkin» Complex Ltd, Donetsk, Ukraine

ABSTRACT: Ukraine is characterized by the considerable variety of geological conditions which complicate the construction and maintenance of buildings and structures. Among them – structurally unsteady collapsible soils (more than 60% territory of country), underworked areas and karsts, landslide slopes, seismic districts. The most widespread types of difficult geological conditions are collapsible soils and underworked areas because of mining. For construction the new methods, directed on defense and normal maintenance of buildings, are constantly developed. In this paper the examples of geotechnical defense methods for new and historical buildings in difficult geotechnical conditions are presented.

RÉSUMÉ : L'Ukraine est caractérisée par la variété considérable de conditions géologiques qui compliquent la construction et l'entretien de bâtiments et de structures. Parmi eux – les sols pliants structurellement instables (le territoire de plus de 60 % de pays), regions travaillées peu et karsts, des pentes d'éboulement, des régions sismiques. Les types les plus répandus de conditions géologiques difficiles sont de sols pliants et des régions travaillées peu à cause de l'exploitation minière. Les nouvelles méthodes pour la construction, orientees sur la défense et l'entretien normal de bâtiments, sont constamment développées. Dans ce journal les exemples de méthodes de défense géotechnique pour les bâtiments nouveaux et historiques dans les conditions géotechnique difficiles sont présentés.

KEYWORDS: underworked areas, landslide slopes, collapsible soils, measures of defense

1. CONSTRUCTION OF NEW BUILDING ON THE UNDERWORKED TERRITORY.

1.1. Description of object.

The hotel complex «Pushkin» in Donetsk is built on territory, underworked by mining. The innovative decisions of geotechnical and structural defense of complex (the 5-storey underground parking under 24-storey building) are realized at planning, building and scientific accompaniment (Fig. 1, 2, 3).

Fig. 1. General view of the «Pushkin» complex building.

The draft design of complex is developed by *Schwitzke* (Germany), the general designer is *Donetsk Promstroyniiproekt*, main contractor – *the Ukraine-France enterprise Osnova-Solsif*.

Fig. 2. Type of parking at 1 level.

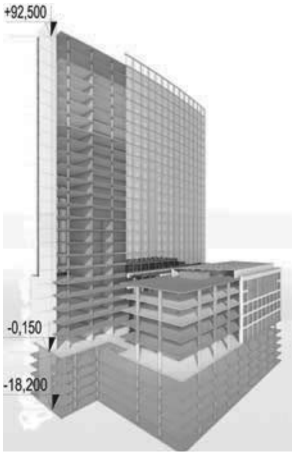

Fig. 3. The 5-storey underground parking.

The design decisions of building are accepted on a rigid structural concept both in parking and in above-ground part.

The kerns of rigidity are set equally on all height of building. They are located in middle part of lay-out and on butt ends as two parallel walls.

Underground parking has horizontal sizes 76x15 m under height part and 54x20 m under 5-storey part.

Framework of parking is executed with the diaphragms of rigidity, columns and disks of ceiling of 300 mm thickness; on a ground level the thickness of ceiling is 1500 mm.

Foundation under building is designed as cast-in-place concrete slab of 2000 mm thickness. The columns of parking have the sections 600x600 and 600x1200 mm. Thickness of bearings walls is 600 mm.

Because in underground construction the technology determines the structural decisions and methods of calculation of structures, the design decisions of underground parking are orientated on technology «wall in soil» (wall thickness 800 mm) and method of erection «UP-DOWN» to a depth of 21-24 m (Fig. 4).

Fig. 4. Construction of parking by the method «UP-DOWN»

At the same time the wall in soil have the functions of exception of the influence between existing and new buildings.

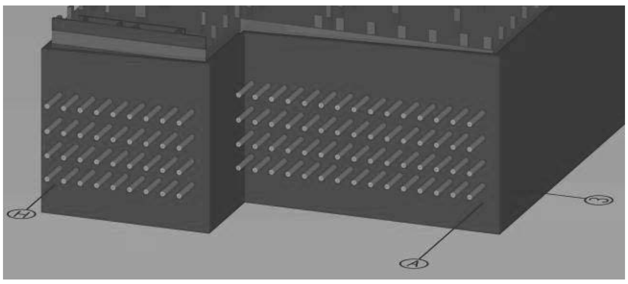

Fig. 5. The multi-tier off-loading system

1.2. The principle design decisions on defense of underground parking.

Design deformations of underworked base are: inclinations $i_p = \pm 3{,}1$ mm/m; relative horizontal deformations $\varepsilon_p = \pm 1{,}9$ mm/m; radius of curvature $R_p = \pm 19{,}8$ km.

Protection from the influence of compression deformations is carried out by the erection of the many-tier off-loading system (Fig. 5). This system consists of horizontal hard members as soil-cement piles, arranged within parking after excavation on the areas of subsequent erection of disks of ceiling or diaphragms of rigidity. Thus soil-cement piles unite with the walls by the members of resolving durability. The length of the off-loading system members is 5.0 m, diameter is 400 mm, the step of setting is 2.0-3.0 m.

Apparently on Fig. 6, the off-loading system reduces frontal pressure on protections to active one.

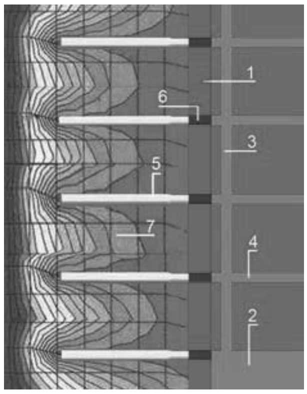

Fig. 6. Mode of distributing of frontal pressure of soil on the wall of parking: 1 - wall is in soil; 2 - foundation; 3 - column; 4 - ceiling; 5 - members of the off-loading system; 6 - support of resolving durability; 7 – picture of pressures (moving) of soil.

Protection from influence of horizontal tension deformations is foreseen by the reinforced concrete preparation and sliding joint (Fig. 7, 8). Preparation of 150 mm thickness has a single-row reinforcement. The chopping-off of «wall in soil» by contraction joints on compartments of 15-18 m length is foreseen.

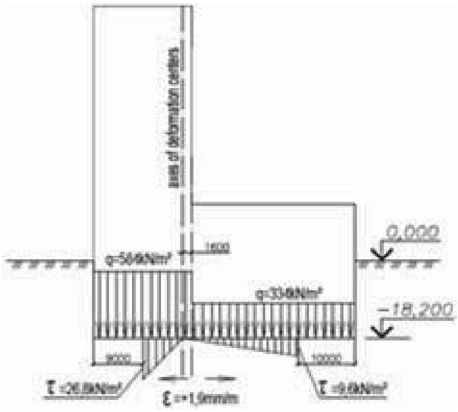

Fig. 7. To the calculation of the reinforced concrete preparation

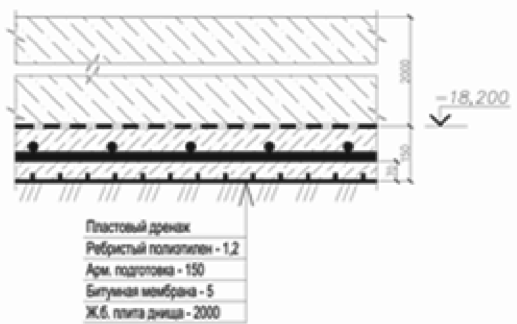

Fig. 8. Design of the reinforced concrete preparation

Other deformation influences as curvature and inclinations are perceived due to strengthening of bearings structures.

The design decisions of underground parking provided the structural and geotechnical safety of building in the terms of straitened construction and influences of uneven deformations of underworked ground massif.

2. DEFENSE OF HISTORICAL BUILDING LOCATED ON TERRITORY WITH DIFFICULT GROUND CONDITIONS.

2.1. Description of building.

The St. Andrew's church is unique sight of history and architecture of 18th century, built in Kyiv on the design of the famous Italian architect F. Rastrelli. The church is built in baroque style, which formality, dynamic of architectural forms, riches of decor, game of light and shade, is characteristic for. A church is erected on tailings of earthen fortress of 17th century. Building is crowned with the central dome and four angular decorative towers. Sizes of church are: length 32 m, width 20 m, height from a terrace to the top of cross of central dome 50 m.

Fig. 9. The St. Andrew's church.

The territory of the St. Andrew's church is located in overhead part of central historical part of Kyiv. The marks of hill surface change from 181.7 m (the planned ground round a church) to 118.5 m (the hill bottom). Slopes are dismembered by spring-beam network, an active slide and erosive processes developed and develop on them.

Within the building area, the unfavorable physical and geological processes take place:

- landslide and landslide-prone slopes;
- considerable layer of collapsible soils;
- substantial heterogeneity of soils on the building area;
- mechanical suffusion of silt particles of sandy loam and sand to the existent neglected gallery;
- surface erosion of the hill massif.

Visible part of the church building leans against greater in lay-out underground two-story fundamental part. An entrance to the church is arranged by cast-iron stairs which connect a street with parvis. A stylobate – two-story building, coverage of which is a part of parvis, joins to underground fundamental part of church.

Foundation is executed of masonry posts of 3 to 5 m width. The foundation base of the church beds on different marks: in western part – from 166,6 to 165,8 m; in east part which hangs over a hill – from 165,7 to 167,8 m.

Basis of foundations of the south, west and north facades are eolian-deluvium loess sandy loams which are collapsible at saturation. The moraine loams serve as basis of foundations of east part.

The hydrogeology terms are characterized by the presence of underwater of two levels.

It was discovered at the complex inspections of building, that it had substantial damages, main of them were through cracks, local destructions of clout layer and build solution of masonry. The uneven settling of basis, conditioned the presence of collapsible soils and slope slides appeared the principal reason of found out damages.

The technical state of church building was appraised as unapt for normal maintenance that caused the necessity of urgent implementation of reconstruction works.

2.2. General conception of reconstruction works

The reconstruction works of the St. Andrew's church were executed after the followings directions:

- geotechnical measures;
- repair and strengthening of the damaged structural members of building;
- restoration of facades and interiors;
- improvement of the technical state of surrounding territory.

The geotechnical measures were:

- research and analysis of geological conditions of the territory of the St. Andrew's church;
- research, analysis and prognosis of changes in geological conditions and mode of hydrogeology of adjoining territory with development of hydrogeology model;
- research and analysis of slope stability on the area of the St. Andrew's church and adjoining territory;
- research of modern erosive processes of slopes on this area;
- research and analysis of stress-strain state of the ground basis of building.

On the results of geotechnical researches the design decisions were developed.

2.3. Realization of geotechnical researches.

- Improvement of the hydrogeology mode.

For adjusting of underwater level, in addition to existent drainage system, a new drainage pipeline, located in the space after retaining wall on a slope, is erected.

The basic setting of the drainage system is an intercept of ground-water non-admission of saturation of soils in the space after retaining wall, as it increases ground pressure on a wall and diminishes local slop stability near-by a wall. The drainage system helps to avoid additional infiltration of atmospheric water additional getting up of water level in the piles zone.

The drainage system consists of two separate pipelines, located along retaining wall, which throw down water from opposite sides in a sink. From a sink the fault of water is foreseen by an underground pipe – collector in the existent overflow-pipe well of the drainage gallery system.

- Analysis of slope stability.

In obedience to the requirements of national building code, the value of normative factor of slope stability must be not less than 1.25.

For implementation of analysis of slope stability a design complex SLIDE-5 used. The complex has wide possibilities of calculations and interpretation of results – by 9 methods simultaneously (methods of Bishop, Yanbu, Spenser, Fellenius and others).

For the increase of reliability of results the analysis of slope stability were executed also by the program «BOBR», developed on the base of Terzaghi-Chugaev method. Comparison of the got results showed that they coincided in a sufficient degree. Thus, stability factors on lower and overhead areas by the «SLIDE-5» program are 1.015 and 1.229, by the «BOBR» program – 1.083 and 1.219.

On the basis of historical materials study, visual inspections of adjoining to the church building slopes and executed analysis, there was determined that considerable part of slopes of the St. Andrew's church hill are in the state close to the maximum equilibrium.

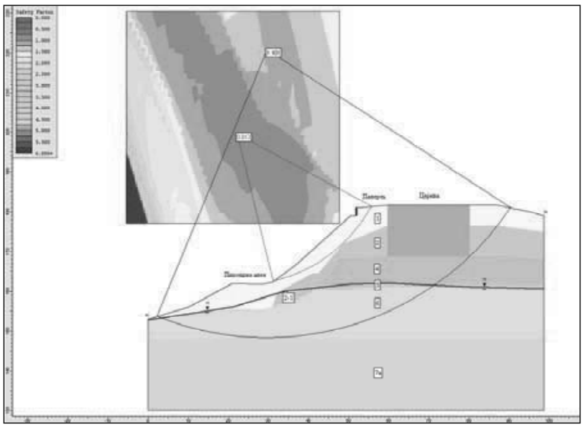

Fig. 10. The results of slope stability analysis
of the St. Andrew's church hill.

- Protection from erosive processes.

The water disposal system is designed as concrete chutes which intercept atmospheric water from the church parvis and give this water in the designed sink near the retaining wall.

The basic setting of the water disposal system is non-admission of saturation of soils on slopes of the St. Andrew's church hill, as it diminishes the local slope stability and promotes to water-wind erosions.

- Analysis of stress-strain state of building and ground basis.

Analysis of stress-strain state of building was carried out taking into account the deformation of the ground basis. As a result the values of stresses and deformations of bearings structures of building and their comparison with values of durability of materials are conducted.

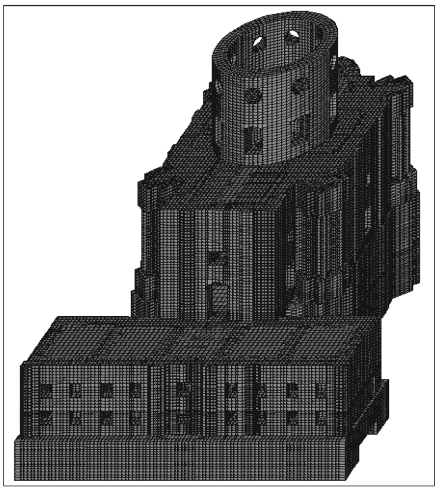

Fig. 11. Design model of the church building.

At the analysis of existence of the St. Andrew's church the followings groups of calculations of the system "building – basis" are executed:

Group 1 – analysis for determination of reasons of crack appearance in the walls of building and it stylobate part:

– at descriptions of soils in the natural state;

– design of saturation of basis under the whole building of church and its stylobate part;

– design of saturation of foundation basis of the north-eastern part of building;

– design of saturation of foundation basis of stylobate and the south-west part of building;

– design of saturation of foundation basis of the central part of building (under a dome).

Group 2 - analysis of actual stress-strain state of building structures taking into account damages fixed at inspection.

Group 3 - are analysis of forecast stress-strain state of building structures at the possible changes of the basis descriptions. Different variants of basis saturation under the whole building of church and its stylobate part are considered.

The modeling of soil saturation in calculations was carried out by setting to the soils, which bed in the foundation basis, the descriptions met the state of saturation. Thus takes into account also the appearance of zones of weakening and cavities in soils as a result of the suffusion to the gallery system which exists close to the foundations.

For the removal of subsequent uneven deformations of foundations and fixing of soils in the basis of bearings walls the stream cementation of soils (jet-columns) was executed. The design decision on strengthening of basis is showed on Fig. 12.

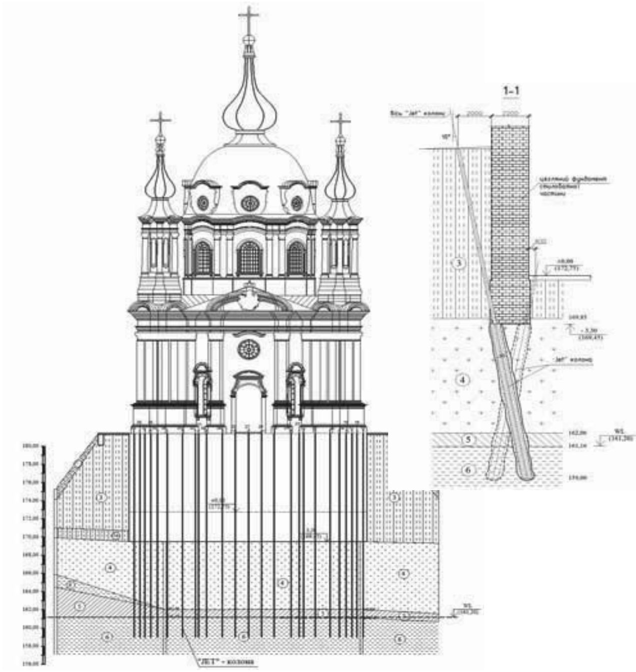

Fig. 12. Strengthening of the church foundations.

Analysis of the building taking into account the members of strengthening was executed on the basis of model in which there were taken into account existent through cracks in walls and overstrained areas of foundations. The results of analysis clearly showed the actual stress-strain state of structures after strengthening. In the design model the arranging of jet-columns under part of foundations was taken into account by substituting of the deformation modulus of soil in the natural state by the average deformation modulus of natural soil and jet-columns.

In addition to geotechnical measures, there were the executed works for restoration the integrity of building structures by strengthening of the damaged areas of masonry walls by the method of injection and reinforcement of cracks.

The monitoring of the state of building after implementation of reconstruction works showed that the deformations of the ground basis had stopped practically and the new damages of building did not arise up.

3. CONCLUSION

The modern methods of geotechnical defense for new and old buildings may provide the reliable protection from unfavorable geological processes and guarantee durable maintenance of these buildings.

Geotechnical problems related to the development of territories in the conditions of the Republic of Tajikistan

Problèmes géotechniques lies au développement de territoires dans les conditions de la République du Tadjikistan

Usmanov R.A., Saidov R.S.
Geotechnical society of Tajikistan, Dushanbe, Republic of Tajikistan

Mangushev R.A.
Saint-Petersburg state architectural and construction university, Saint-Petersburg, Russia

ABSTRACT: in this paper features of construction of buildings and constructions in difficult engineering-geological conditions of the Republic of Tajikistan are presented. Methods of design and construction of the bases and other foundations on loess collapsing soils, on weak water-saturated soil, and prospects of development of the hilly territories needing a difficult relief are considered.

RÉSUMÉ : Il est question dans cet article de la construction de bâtiments et de constructions dans des conditions difficiles à la fois d'ingénierie et de géologie rencontrées en république du Tadjikistan. On évoque les méthodes de calcul et de réalisation des radiers et autres fondations sur les sols lœssiques, sur les sols peu résistants saturés d'eau, ainsi que les perspectives de développement des territoires en terrains très accidentés nécessitant de difficiles reprises en sous-oeuvre.

KEYWORDS: loess collapsing soils, weak water-saturated soils, hilly territories, static and seismic influences.

1 INTRODUCTION

In the Republic of Tajikistan more than 90% of the territory are presented by a mountains, and the areas of plains are made by only 7%. The basis of development of a national economy of the republic is made by the agrarian sector which is based on irrigated agriculture under which about 70% of all flat territories are allocated. The deficiency of the earth being the main reserve for development of agricultural production, housing, industrial, etc. types of construction always represented a special problem and demands very reasonable and careful use.

Development of the country and growth of the population demands increase in volumes of agricultural production and construction of buildings of different function. Therefore, preservation and increase in land fund put before designers and builders of adoption of effective decisions. In this direction the most effective are:

- substantial increase of number of stores of buildings and constructions erected in flat territories that will allow to keep and free territories for development of agricultural production;
- development under construction of buildings and constructions of foothill (hilly) territories.

It should be noted that in the Republic of Tajikistan construction of buildings and constructions is carried out, generally in territories presented by loess collapsing and weak water-saturated soil, and in recent years as well on foothill (hilly) sites. Practically all territory of the republic is characterized by 8-9 mark seismic intensity. In the specified conditions design, construction and reliable operation of buildings and constructions is closely connected with use of effective methods of preparation of the artificial bases and devices of the foundations. Taking into account it in the republic the complex researches which results are generalized in considered article were conducted.

1.1 Construction on the loess collapsing soils

About 70% of flat territories of the republic are everywhere presented by loess collapsing soil which capacity changes from 5 to 300 m, and their thickness makes H_{sl} = 5…30 m, exceeds 30 m less often. More than 2/3 territories of the country are put by loess collapsing soil II of type, with the size of expected sag from a coefficient of relative collapsing ε_{sl} = 30…150 cm.

The majority of the cities, objects of civil and industrial function are erected in these territories. Thus till 80 years of the twentieth century, 4-6 floor buildings therefore for practical use researches were conducted were generally erected and the following superficial methods of consolidation of soil, the device of the bases and foundations (fig. 1) are developed(Musaelyan A.A. 1982, Krutov V. I. 1982, Galitsky V.G. and Popsuyenko I.K. 1985, Ruziyev A.R. and Usmanov R. A. 1991):

a) Consolidation by heavy tampers weighing 50…200 kN in combination with constructive and water protective measures. Advantages – simplicity and use of the simple equipment, rather low cost. Shortcomings – fast wear of the mechanisms, limited application in the conditions of dense building.

b) The device of the condensed soil pillows 3-5 m thick and more from a clay material in combination with constructive and water protective measures. Advantages – simplicity and use of the simple equipment, possibility of application in the conditions of dense building, rather low cost. Shortcomings – seasonality of work, big labor expenses when finishing soil to optimum humidity, increase in terms of construction at increase of thickness of a pillow.

c) Consolidation by energy of underwater explosions in combination with constructive and water protective measures. Advantages – simplicity and use of the simple equipment, low cost. Shortcomings – limited application in the conditions of dense building.

d) The device of the bases in tamping ditches with creation in their basis of broadenings from rigid materials. Advantages – use of the simple equipment, combination of processes of the device of a ditch and consolidation of collapsing soil, the minimum use of a timbering, decrease in reinforcing of the base to 50% and more, low cost. Shortcomings – fast wear of the mechanisms, limited application in the conditions of dense building.

e) Fixing of soil by way of silicification with activization of soil by carbon dioxide. Advantages – use of the simple equipment, high quality of fixing, possibility of fixing of soil in the basis of the emergency and deformed buildings. Shortcomings – very high cost and therefore, it is generally applied to strengthening of soil in the basis of the deformed buildings and constructions.

f) The device of the pile bases from lovering piles. Advantages – technological effectiveness, use of the high-performance equipment, ensuring appropriate quality. Shortcomings – difficulties at immersion of piles in soil of the firm and semi-firm consistence, limited application in the conditions of dense building, cost increase at increase in thickness of a collapsing layer of earth and removal of places of production of piles.

reduction of terms of consolidation of soil, rather low cost. Shortcomings - are similar to point “a”.

c) The accelerated consolidation by preliminary soaking in combination with deep explosions. Advantages – improvement of quality of consolidation and decrease in risk of development of seismic deformations. Shortcomings – are similar to point “a”.

d) Reinforcing of collapsing thickness by soil piles, including high-strength materials. Advantages – simplicity of production, use of the simple equipment, use of a local material, rather low cost. Shortcomings - application restriction in the conditions of dense building, fast wear of the equipment.

Note: at consolidation of soil on points “a”, “b”, “c” and “d” in the top part of the basis the buffer non condensed layer 3-5 m thick (h_f) which needs to be condensed further with heavy tampers is formed or to replace with the condensed soil pillow.

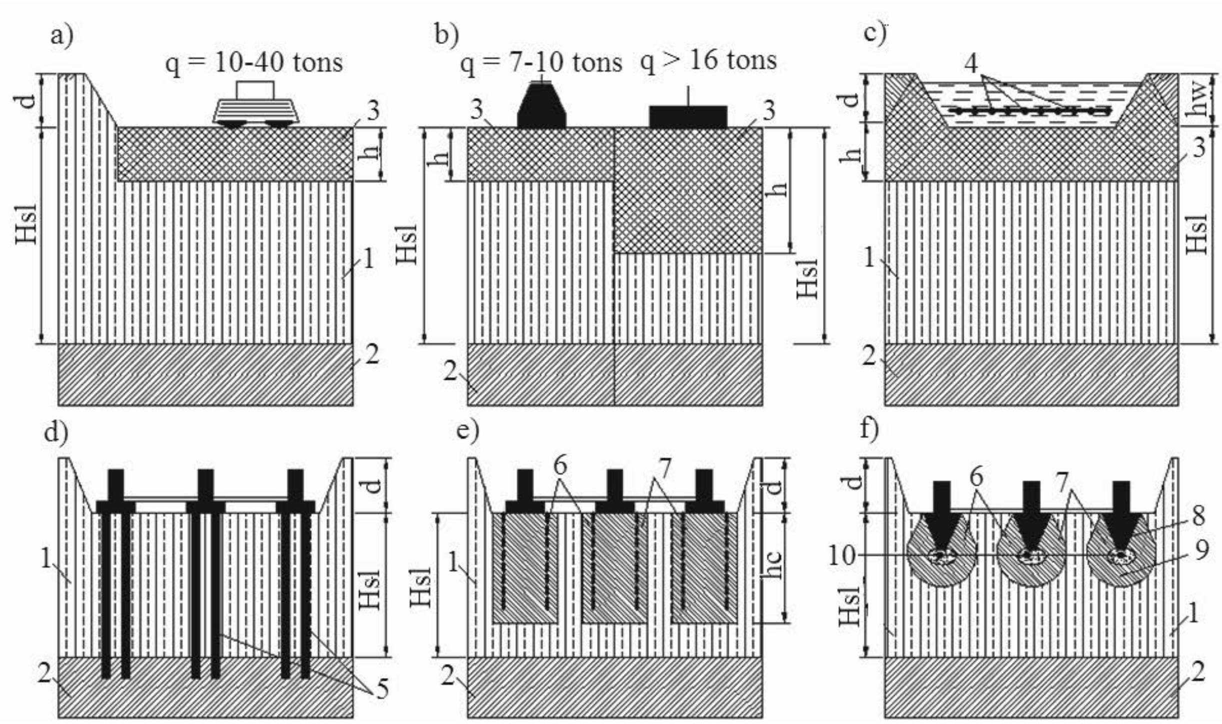

Figure 1. Methods of the device of the bases and the foundations on loess collapsing soil I of type:
1- loess collapsing soil; 2- non collapsing soil; 3- condensed soil pillow; 4- charges of explosive; 5- driven piles; 6- injektor for chemical fixing of soil; 7- fixed soil; 8- base in a tamping ditch; 9- condensed zone; 10- tamping rubble

All given methods of preparation of the bases and the device of the bases were investigated on joint action of static and seismic influences by intensity of 8-9 points on the basis of which the relevant normative documents on technology of the device and a calculation procedure were made. However the know-how showed on possibility of development of uneven deformations and violation of operational suitability of buildings and the constructions erected on the specified artificial bases. Use of these methods expediently and effectively in the conditions of collapsing soil I of type, and on collapsing soil II of type – in combination with deep methods of consolidation and fixing.

After the 80th years design and construction 9-12 floor and more buildings in this connection researches were conducted began and the following methods of deep consolidation of soil and a design of the pile bases are recommended for practical application:

a) Consolidation by preliminary soaking. Advantages – simplicity and low cost. Shortcomings – application restriction in the conditions of dense building, long terms of consolidation, need for large volume of water, need of the device of no filtration veils in the conditions of dense building.

b) The accelerated consolidation by preliminary soaking with application of drainage wells. Advantages – considerable

e) The device of the bored piles with a diameter from 0,5 to 1,2 m cutting all collapsing thickness. Advantages – possibility of the device in various conditions with use of the modern equipment. Shortcomings – use of the expensive equipment, complexity of quality control of works, need of carrying out expensive static tests of piles, rather high cost.

f) The device of the combined pile bases when in advance drilled well the pile of factory production is established, and a cavity of a well is filled with cement and sand solution. Advantages – simplicity of the device and use of the simple equipment, control and improvement of quality of the device of the pile bases, decrease in their cost. Shortcomings – restriction of possibility of application and cost increase at increase in length and distances of transportation of piles.

All above-mentioned methods were investigated on joint action of static and seismic influences by intensity of 8-9 points on the basis of which the relevant normative documents on technology of the device and a calculation procedure were made. Researches and operating experience testifies to opportunity and expediency of their application at the device of the bases and the foundations of high-rise buildings. In the conditions of the republic application of the slabby and pile bases which well proved in practice of high-rise construction of many countries is also expedient.

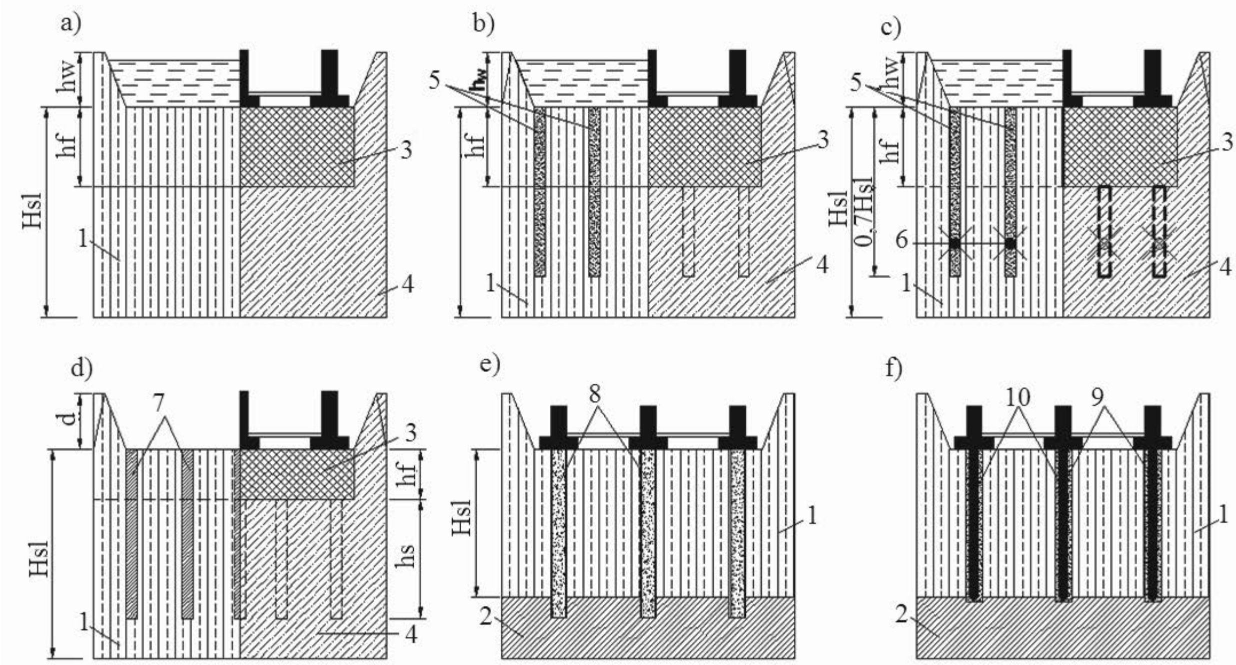

Figure 2. Methods of the device of the bases and the foundations on loess collapsing soil II of type:
1- loess collapsing soil; 2- non collapsing soil; 3- condensed soil pillow; 4- condensed thickness of soil; 5- drainage wells; 6- charges of explosive; 7- soil piles; 8- bored piles; 9- lowering driving piles; 10- cement and sand filler

1.2 Construction on weak water-satureted soils

In the Republic of Tajikistan, as a result of influence of a number of natural and technogenic factors sharp lifting of level of underground waters and flooding of the extensive territories put by big thicknesses of earlier low-damp loess soil owing to what they pass to category weak and strong compressibly ($R \leq 100$ kPa, $E \leq 5$ MPa) is observed. Thus processes of flooding of territories promote increase of seismic intensity of sites of construction on 1…2 points. Now about 40% of the mastered areas in the republic are presented by the specified soil and the steady tendency of their increase is observed.

Effective design, construction and operation of buildings on the specified soil are connected with application of various methods of the device of the artificial bases and the foundations taking into account high seismic activity of mastered sites. In this direction the corresponding researches were conducted and the following methods of the device of the bases and the foundations (fig. 3) are offered for practical application (Usmanov R. A. 2009):

a) The device high-condensed ($\rho_d \geq 2{,}2$ t/m^3) sandy, gravel and pebble pillows. Advantages – use of the simple equipment and simplicity of the device; low cost and small labor input; high reliability; existence of large volume of a local material. Shortcomings – difficulties at the device during the winter period; scope restriction with buildings to 6 floors.

b) The device of the bases from the driving and stuffed piles which are cutting through a weak layer of earth. Advantages – use of the modern equipment, reliability. Shortcomings – substantial increase of cost and restriction of a scope of driving piles at increase in thickness of weak soil; difficulties of quality control of production of a stuffed pile and increase of its cost at increase in length.

c) Fixing of soil by limy piles. Advantages – simplicity of technology of the device and low cost of a method, refusal of metal and cement application. Shortcomings – use of the special equipment, complexity of quality control of works.

d) Consolidation of soil by vertical sandy piles. Advantages – simplicity of technology of the device and low cost; existence of sufficient volume of a sandy material; refusal of metal and cement application. Shortcomings – use of the special equipment; difficulties of quality control of works; considerable labor inputs at the device and removal of a loading embankment.

e) Consolidation of soil by vertical sandy drains. Advantages – simplicity of technology of the device and low cost; existence of sufficient volume of a sandy material. Shortcomings – use of the special equipment; difficulties of quality control of works; considerable labor inputs at the device and removal of embankment.

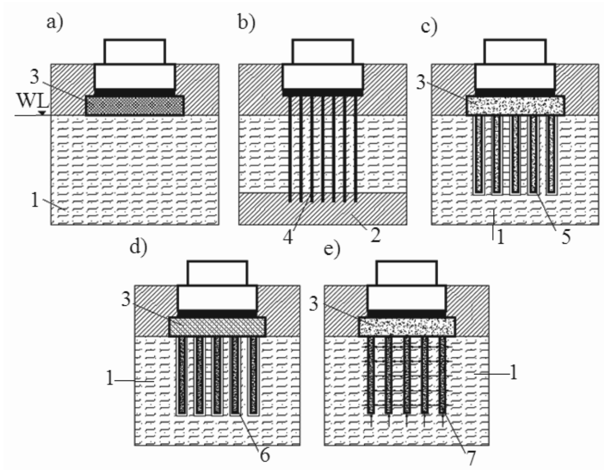

Figure 3. Methods of preparation of the bases and the device of the foundations on weak water-saturated loess soils
1- weak soil; 2- strong layer; 3- soil condensed pillow;
4- driving and stuffed piles; 5- limy piles;
6- sandy piles; 7- vertical sandy drains

All above-stated methods were investigated on joint action of static and seismic (seismoexplosive) influences by intensity of 8-9 points. Except the device of the high-condensed soil pillows, other methods of preparation of the bases and the device of the foundations can be recommended for the device of the bases and the foundations of high-rise buildings. And effective application of the slabby and pile bases also is expedient.

1.3 Development of foothill territories

Foothill (hilly) territories meet in all areas of the republic, are presented by the difficult (dismembered) relief and their area makes more than 5400 sq.km. Development of these territories under building of buildings and constructions of different function is one of the most effective directions of a solution of the problem of deficiency of the earth in the republic.

Hilly territories are characterized by existence of slopes by the steepness α = 20 … 65 ° and more, are put by loess collapsing soil thickness $H_{sl} \geq 20…30$ m relating to the II type on a collapse. Development of these territories under building represents very complex challenge and its effective decision is connected with development of such methods of the device of the bases and the foundations which allow to provide stability of slopes and at the same time are counter collapse actions in the conditions of essential change of humidity of the massif of soil and high seismic activity of sites of construction.

Purposeful development of hilly territories for housing, industrial and civil engineering began from 80th years of the last century. For the solution of this problem complex experimental and theoretical researches were conducted, the purpose and which tasks was identification of effective methods of counter collapse and protection of slopes against landslide. Methods of the device of the bases, allowing to eliminate collapse properties of soil and to provide stability of slopes are given in fig. 4 (Ruziyev A.R. and Usmanov R. A. 1991, Usmanov R. A. 2002, Akhmedov D. D. and Lekarkin V. K. 2002):

a) the device of the condensed pillows of the increased thickness with water protective measures;

b) thickness reinforcing by soil piles, including high-strength elements;

c) slotting loess collapsing soil driving and bored piles of big length;

d) consolidation of loess collapsing soil by preliminary soaking, including energy of deep explosions

In the conditions of the republic one of important questions is development of a method of calculation of stability of slopes of the various steepness, with identification of real surfaces of sliding since purpose of the relevant activities for ensuring its stability depends on it as a choice of rational methods of preparation of the bases and the device of the foundations, and. In practice the method of circular-cylindrical slip surfaces of sliding is widely used. However researches of the last years testify that in seismic conditions of the republic fluidifying landslides when there is a slipping of the top layer of a slope 5-7 m thick are often observed. Therefore, now one of key questions - the forecast and a method of calculation of stability of slopes of the various steepness with definition of real surfaces of sliding remains open and demands the decision.

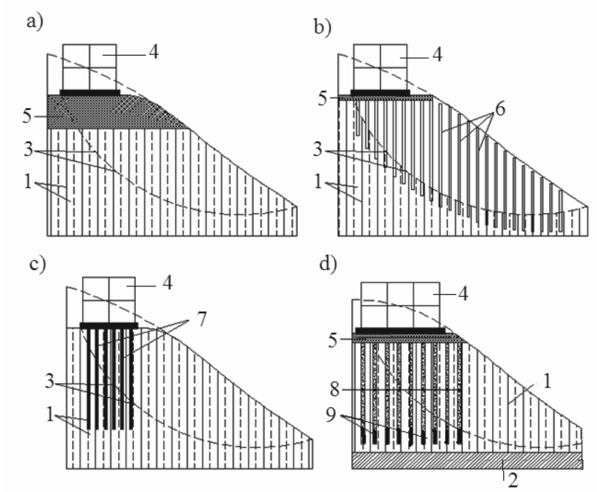

Figure 4. Methods of the device of the bases and the foundations in the conditions of a foothill territories:
1- loess collapsing soil; 2- non collapsing soil; 3- surface of sliding; 4- the projected building; 5- condensed soil pillow; 6- reinforcing elements; 7- driving or bored piles; 8- drainage and explosive wells; 9- charges of explosive

2 CONCLUSIONS

1. Design and construction of constructions in the Republic of Tajikistan is carried out in difficult geological and seismic conditions that considerably complicates and increases construction cost. Deficiency of the earth demands development under construction of unsuitable territories for agricultural production which are presented by problem soil, and also substantial increase of number of storeys of buildings and rational use of underground space of the cities.

2. One of the most effective directions is development of the foothill territories presented by a difficult relief and big thickness of loessial collapsed soil for which successful decision it is necessary to continue experimental and theoretical researches with application of modern technologies and calculation methods.

3 REFERENCES

Musaelyan A.A. 1982 . Improvement of methods of the device of the bases and the foundations in Tajik the Soviet Socialist Republic. Bases, foundations and mechanics of soil No. 6, 9-11.

Krutov V. I. 1982 . The bases and the foundations on loess collapsing soil. Kiev.

Galitsky V.G. and Popsuyenko I.K. 1985. Precipitation of industrial constructions on loess collapsing soil of Tajikistan. Bases, foundations and mechanics of soil No. 2, 9-11.

Ruziyev A.R. and Usmanov R. A. 1991. Experience of consolidation of loess collapsing soil by a hydroexplosive method in the conditions of a difficult relief. Bases, foundations and mechanics of soil No. 1, 13-14.

Usmanov R. A. 2002 . Condition and development prospect under building of hilly territories of the Republic of Tajikistan. Works of a republican seminar "Experience of studying of landslides and collapses on territories of Tajikistan and methods of engineering protection". Dushanbe, 117-120.

Akhmedov D. D. and Lekarkin V. K. 2002. Method of reinforcing of the slopes put by loess collapsing soil in seismic countries. Works of a republican seminar "Experience of studying of landslides and collapses on territories of Tajikistan and methods of engineering protection". Dushanbe, 117-120.

Usmanov R. A. 2009 . Water-saturated loessial soil as the bases of buildings and constructions in the conditions of the Republic of Tajikistan. Monograph. St. Petersburg.

The preservation of Agrigento Cathedral

La conservation de la cathédrale d'Agrigente

Valore C., Ziccarelli M.
DICAM - Dept. of Civil, Environmental, Aerospace and Materials Engineering – Università di Palermo – Italy

ABSTRACT: The Agrigento Cathedral was built about nine centuries ago on the edge of a steep slope made up of alternating inclined layers of soft calcarenites and fine-grained soils; its behaviour has never been satisfactory especially as far as the North aisle is concerned. Many corrective measures have been attempted during its lifespan and also a few years ago. They have been proved invariably to be unsuccessful. Recent geotechnical investigations, referred to in the paper, permitted to find out that the main cause of the Cathedral distress is a sliding mechanism involving the upper zone of the slope underlying the North aisle; consequently the essential requirement for the preservation of the Cathedral is the stabilisation of the slope.

RÉSUMÉ: Le Cathédrale d'Agrigente a été élevée voici environ neuf siècles sur le bord d'une pente raide, composée d'une alternance de couches inclinées de calcarénites tendres et de sols à grain fin. Le comportement de la Cathédrale n'a jamais été satisfaisant en particulier dans sa nef Nord. De nombreux remèdes ont été essayés au cours de sa vie et jusqu'à il y a quelques années. Ils se sont révélés toujours sans succès. De récentes investigations géotechniques, décrites dans le papier, ont permis de découvrir que la principale cause de la désordre de la Cathédrale est un mécanisme de glissement impliquant la zone supérieure de la pente située sous la nef Nord. En conséquence, la condition essentielle pour la préservation de la Cathédrale est la stabilisation de la pente.

KEYWORDS: Agrigento Cathedral; preservation; slope stability; clay; calcarenite.

1 INTRODUCTION

The Girgenti (now Agrigento, Sicily) gothic Cathedral was built in the XI century on the top of Agrigento Hill right on the edge of a steep slope about 40m high and inclined from 40 up to 50° towards North, Fig.1. The Cathedral has been profoundly changed during the XIV, XVI and XVII centuries as a consequence of structural damages caused by differential settlements of the foundations as well as by the horizontal thrust exerted on the northern masonry wall by the barrel vault which once covered the northern aisle. Other damages have been caused by earthquakes. Baroque superfetations were introduced during the XV century and were partially removed at the beginning of the XX century. A massive still unfinished bell tower, adjoining the church on the western side, was built in the XV century. The plan of the Cathedral is shown in Fig.1.

The building was originally smaller and located in the area of the present apse (East side); later extension towards the West required the construction of a rather high fill in order to keep unaltered the floor elevation. The present elevation of the nave floor is 327.54 m a.m.s.l.

The behaviour of the Cathedral has never been satisfactory: it has undergone settlements, tilting, distorsions, partial collapses. Many interventions, including partial demolitions and reconstructions, have been carried out in the last century. The most notable remedial measure was the underpinning of the columns and the northern wall by means of Fondedile "pali radice" (root piles) in 1976-1980 (Lizzi, 1993). Almost all interventions as yet carried out have been unsuccessful, and sometimes even self-defeating.

As a matter of fact, the fissuration pattern of the Cathedral observed after each intervention was a replica of the previous ones. The settlements and the horizontal outward movements of the North aisle have never stopped. In 2010, just a few years after the completion of the last stabilising works, the Cathedral has to be closed. Recently, systematic in situ geotechnical investigations and monitoring of ground movements as well as a precise survey of the Cathedral by the laser-scanner technique have been started. The main results of these investigations and an outline of the causes of the malfunctioning of the Cathedral are reported in the paper.

2 GEOTECHNICAL INVESTIGATIONS AND FIELD INSTRUMENTATION

The Cathedral foundation soils have been explored on many occasions, namely:

- in 1904, when an exploratory shaft 24m deep was excavated inside the Cathedral nearby its North -West corner; the shaft was filled with mass concrete intermingled with irregular calcarenite blocks;
- in 1976-80, when many vertical borings about 15m deep, were drilled inside and along the perimeter of the Cathedral, on the occasion of underpinning works by means of Fondedile root piles;
- in 2005: 8 vertical borings (marked with an asterix in Fig. 1) located on the area of the Cathedral parvis and around the ex Diocesan museum were drilled; 2 open standpipe piezometers and 5 inclinometer tubes were installed in the boreholes. Inclinometric measurements have been carried out in 2005-2006 and subsequently restarted in June 2011 with a new initial reading;
- in 2008: 20 vertical borings located inside and around the Cathedral were drilled (S12-S29 in Fig. 1); max depth: 62m; 3 Casagrande, 4 open standpipe piezometers and 6 inclinometer tubes were installed in the boreholes. Inclinometric measurements started only in June 2011;
- in 2012: 30 vertical and 6 inclined borings (S201-S227 in Fig.1) were drilled inside and around the

Cathedral as well as on the adjacent northern slope; (max depth of borings: 70m); 14 vibrating wire piezometric cells, 1 Casagrande piezometer, 2 open standpipe piezometers, and 7 inclinometer tubes were installed. Piezometric and inclinometric readings started in 2012 and are still carried out. Five exploratory pits were also excavated in the Cathedral.

During the 2012 investigation campaign: SPT, Menard pressurimeter and in situ permeability tests were carried out, and many undisturbed samples were taken for laboratory testing.

3 GROUND CONDITIONS

The Agrigento Hill is made up of layers of soils and soft rocks belonging to the northern limb of an asymmetric syncline with approximately E-W axis (Croce et al., 1980; Cotecchia et al., 2005). The core of the syncline is known as Agrigento Formation, AF, and dates back to Lower Pleistocene; it overlies Monte Narbone Formation, MNF, (Middle-Upper Pliocene). Within the area pertaining to the Cathedral the following layers have been recognised from bottom to top:

a) Grey, heavily overconsolidated clay with rare, thin lenses of silty sand, A; this layer is about 200 m thick and belongs to the MNF; its altered upper part A′ contains gypsum veins.

b) Soft, reddish biocalcarenites interbedded with yellowish calcarenitic sands, CLR. The thickness of this layer ranges from 24 to 37m. The contact with the underlying clay is sharp and dips approximately towards the South.

c) Grey clay AG, and grey-yellowish clay with thin subvertical veins or spars of minute crystals of secondary gypsum, AGG. The overall thickness of this layer (AG plus AGG) is about 12m. The contact with the underlying calcarenites is clearly defined by a thin transition layer, made up of clay intermingled with carbonatic shell shreds, and dipping 15-18° towars the South.

d) Silty sand and sandy silt, from grey to yellowish, SL. The thickness of this layer ranges from 4 to 6m.

e) Soft yellowish or reddish calcarenite interbedded with yellowish silty sand, CL. The rocks are frequently fractured. The thickness of this layer ranges from 4 to 12m. Small cavities have been found in these rocks in which an unlined passable adit has been excavated many years ago (Ismani hypogeum in Fig. 1).

Soil and rock b, c, d, e belong to AF.

A schematic vertical profile of the ground is shown in Fig. 2. It may be noted that the various layers bend down when approaching the slope. Similar ground conditions have been ascertained within the zone relevant to the Cathedral.

4 GEOTHECNICAL PROPERTIES OF SOILS AND ROCKS

Some data derived from results of laboratory and in situ tests are summarised in tables 1 and 2.

5 POREWATER PRESSURES

The few available piezometric data point out to the existence of a perched groundwater table within the fine-grained soils overlying calcarenites CLR. This hypothesis is consistent with the high permeability coefficient of calcarenites CLR and CL and with the observation that drilling water was systematically lost when boring in these rocks. A tentative groundwater table is drawn in Fig. 2.

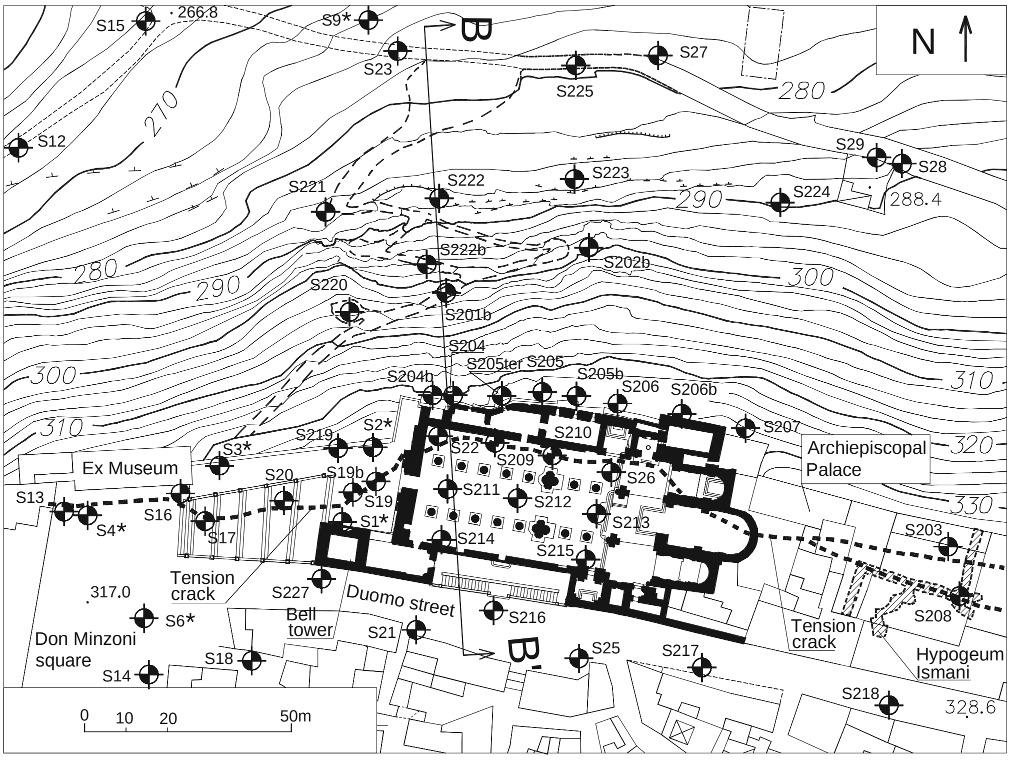

Fig. 1. Schematic plan of the Cathedral and of the adjacent slope, and location of the most relevant borings. It is also shown the longitudinal fracture or tension crack running through the northern aisle, the archiepiscopal palace and the Ismani hypogeum on the East side, and through the parvis and Don Minzoni square on the West side. Borings S201-S227 drilled in 2012; borings S12-S29 drilled in 2008; borings S1*-S9* drilled in 2005. Boreholes equipped with inclinometer tube: S1*, S2*, S3*, S4*; S13, S16, S20, S22, S26, S29; S203, S204, S207, S208, S209, S220, S221.

6 FOUNDATIONS OF THE CATHEDRAL

The columns and the southern wall have been founded directly on, or slightly above, the top surface of calcarenites

CL,whilst the northern wall and a small stretch of western (facade) wall rest on intensely fractured calcarenites or on silty sands SL, see Fig. 2. The columns have been underpinned by groups of fourteen "root piles" about 15 m long, slightly inclined to the vertical so to describe a ruled surface flaring downwards (Lizzi, 1993). Each root pile was reinforced with a single, 24 mm diameter, steel bar. Shorter root piles were used to underpin the northern wall of the Cathedral. Root piles groups under the nave columns have been tied at the top by a grid of reinforced concrete beams. It is clear from Fig. 2 that the foundation ground of the Cathedral is far from uniform and that the thickness of the soft calcarenite layer CL diminishes or vanishes as the northern slope is approached. During the underpinning works in 1976-1980 it was ascertained that the CL calcarenite layer was dissected by a long and deep fracture (or tension crack) located inside the Cathedral near the northern wall, as shown in figures 1 and 2; it was "stitched" by cement pressure grouting.

7 GROUND MOVEMENTS, FISSURATION PATTERN OF THE CATHEDRAL AND CAUSES OF ITS UNSATISFACTORY BEHAVIOUR

The most striking sign of ground movement is a longitudinal subvertical tension crack running in East-West direction through the floor of the northern aisle, and extending continuously to the parvis, the staircase and the Don Minzoni square, and in the opposite direction to the apse, the archiepiscopal palace and the Ismani Hypogeum as shown in Fig.1. This fracture has been firstly surveyed by Commissione del Ministero dei Lavori Pubblici for the investigation of the great "Addolorata landslide" (1968). The aperture of this fracture exceeds more than 20 centimeters in the Ismani hypogeum. After the restoration works completed in 2000, the fracture formed again in the Cathedral floor and in the parvis; its aperture slowly progresses and has now attained 4 cm. There is a step, from 2 to 3 cm high, between the northern and the southern walls of the fracture. The northern wall settled about 4 cm

The floor of the nave and the southern aisle have undergone negligible settlements.

Table 1. Geotechnical properties of soils R, SL, AG, AGG.

Soil	w_n (%)	w_l (%)	w_p (%)	S (%)	CF (%)	γ_s (kN/m^3)	γ_{sat} (kN/m^3)	c'_p (kPa)	φ'_p (°)	φ'_r (°)	E_{ed} (MPa)
R	/	/	/	/	/	/	/	0	30-35	/	/
SL	11-28	35-40	18-23	100	2-10	27-27.4	19.5-20.5	15-25	29-30	/	4-20
AGG	18-30	45-55	20-22	100	35-45	26.8-27.3	19.6-20.5	30-35	27-29	14	10-40
AG	18-30	43-51	20-23.3	100	31-43	26.9-27.4	20.2-20.7	30-40	28-30	16	20-60

Table 2. Geotechnical properties of calcarenites CL and CLR.

Calcarenite	n (%)	γ_s (kN/m^3)	γ_{sat} (kN/m^3)	σ_f (MPa)	k (cm/s)	E' (MPa)
CL and CLR	0.36-0.46	26.9-27.4	18.8-20.6	1.1-4.6	10^{-2} - 10^{-4}	300-700

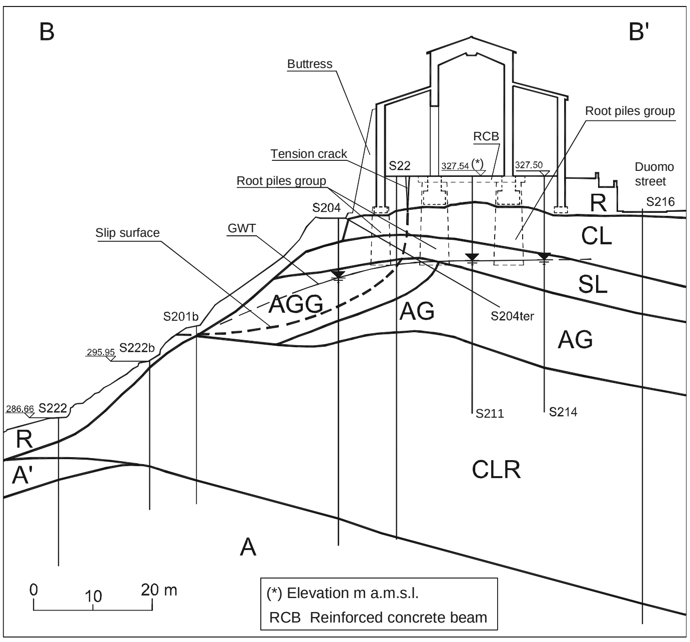

Fig. 2. Vertical cross ground profile B-B′. R: made ground or topsoil; CL: upper soft yellowish or reddish biocalcarenites interbedded with sand lenses; SL: silty sands and sandy silts; AG: grey clays; AGG: grey-yellowish or light brown clay with veins of minute crystals of secondary gypsum; CLR: lower soft reddish biocalcarenites with sand lenses; A: heavily overconsolidated grey clays; A′: grey-yellowish clays with gypsum veins.

An idea of the cumulative differential settlements and horizontal displacements towards the slope of the northern wall can be drawn from the deformed shape of an arch transversal to the axis of the northern aisle and adjacent to the transept. According to a fairly credible reconstruction depicted in Fig. 3, the northern springline of the arch might have undergone an horizontal displacement so large as 69 cm and a settlement of 93 cm relative to the other springline.

The pattern of the present-day fissuration and movements remarkably resembles that observed recurrently since 1904 as documented by photos and descriptions recorded in archival sources (Di Fede, 2011).

The relevant inclinometer readings, begun on June 2011 and summarized in Tab. 3, show that the ground mass located downhill of the longitudinal fracture undergoes significant horizontal displacements and point out the existence of shear surfaces at depths between 7 and 17m.

Based on these data and observations it is possible to identify a slide mechanism shown in Fig. 2. Similar mechanisms apply for the whole length of the Cathedral and the parvis zone, the archiepiscopal palace and Ismani hypogeum.

The above mechanism appear to be the main reason for the anomalous behaviour of the ground-Cathedral system. It has not been identified nor postulated up to now, and consequently the attempts to stabilise the Cathedral were unfounded. The sliding mechanism passes along the subvertical fracture and through silty sands SL and altered clays AGG. A stability analysis of this sliding mechanism, which involves the North aisle of the Cathedral, points out that the use of peak or residual shear strength parameters of soils SL and AGG is not warranted. In fact, if peak parameters are considered values of the factor of safety FS within the range 1.4-1.6 will be calculated, whether if residual strength is considered a value of FS much smaller that 1 is obtained: these values are inconsistent with the observed behaviour of the ground-Cathedral system. It is likely that the shear strength is gradually approaching the fully softened value for which the value of FS is 1.05.

Table 3. Superficial (top) horizontal displacement δh, and depth d of sliding surface indicated by inclinometric measurements from June 2011 to Dec. 2012. Location of inclinometer tubes relative to the longitudinal fracture. U: uphill; D:downhill. N: north; NW: north-west.

Inclinometer tube	δh *(mm)*	*Direction*	d (m)	*Location*
S1*	2	/	/	U
S2*	12.8	NW	7	D
S3*	6	N	15; 22	D
S4*	4	/	/	U
S13	3.2	/	/	U
S16	8	NW	11;16	D
S20	8.3	N	17	D
S22	10	NW	6; 11	D
S26	2.3	/	/	U

8 CONCLUSIONS

The behaviour of Agrigento Cathedral has been unsatisfactory since its construction in the XI century on the crest of a very steep slope. Many attempts to stabilise the ground-Cathedral system have failed because a sound diagnosis of its problems has not been formulated.

Recent geotechnical investigations permitted to identify a rather large sliding mechanism involving the North aisle of the Cathedral as well as long adjacent stretches of the edge of the slope. It is now evident that the preservation of the Cathedral requires prioritarily the stabilisation of the slope.

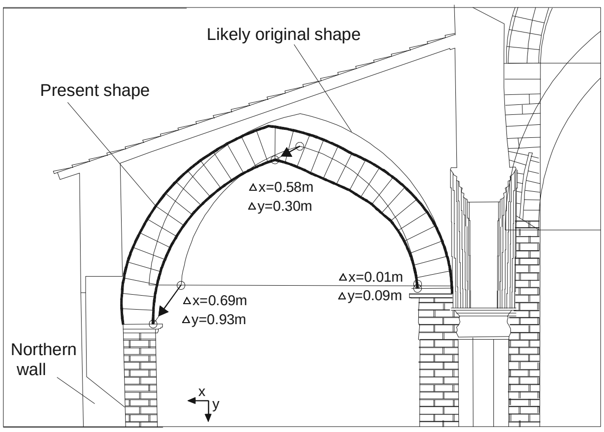

Fig. 3. Distorted arch located at the eastern extremity of the North aisle showing large differential movements between the springlines cumulated probably during some centuries. (Reconstruction by Arch. G. Renda).

9 REFERENCES

Commissione del Ministero dei Lavori Pubblici della Repubblica Italiana, 1968. *Technical Report on the 1966 Agrigento Landslide*. Città Spazio, N° 1-2. (In Italian).

Cotecchia V., Fiorillo F., Monterisi L., Pagliarulo R., 2005. Slope instability in the Valley of Temples, Agrigento (Sicily). *Giornale di Geologia Applicata*, 91, 91-101.

Croce A., De Miro E., Fenelli G.B., Jappelli R., Liguori V., Morandi R., Nocilla N., Pace E., Pellegrino A., Rossi Doria P., 1980. Agrigento town and the Valley of Temples. Problems of stability of the territory and of preservation of monuments. *Atti del XIV Conv. Naz. di Geotecnica*, Florence, 1, 109-124. (In Italian).

Di Fede M.S., 2010. L' "invenzione" della Cattedrale interventi di restauro nella prima metà del Novecento. In G. Ingaglio (editor): *La Cattedrale di Agrigento tra storia, arte, architettura*. Edizioni Caracol, Palermo, 167-186. (In Italian).

Lizzi F., 1993. 'Pali radice' structures. In S. Thorburn and G.S. Litteljohn (editors), *Underpinning and retention*. Blackie Academic & Professional, London, 84-156.

SYMBOLS

c'_p	peak cohesion intercept
E'	Young modulus
E_{ed}	constrained modulus
CF	clay fraction
k	coefficient of permeability
n	porosity
S	saturation degree
w_l	liquid limit
w_p	plasticity limit
w_n	natural water content
φ'_p	peak angle of shear strength
φ'_r	angle of residual shear strength
γ_s	specific weight
γ_{sat}	saturated unit weight
σ_f	uniaxial strength

Geotechnical characteristics of glacial soil deposits at Punta Arenas in Chilean Patagonia

Caractéristiques géotechniques des dépôts glaciaires du sol à Punta Arenas en Patagonie chilienne.

Vásquez A., Le Roux J.-P.
Universidad de Chile

Foncea C.
SRK Consulting (Chile) S.A

ABSTRACT: In the city of Punta Arenas, Chilean Patagonia, soils of glacial origin were deposited during the Last Glacial Maximum (LGM), with soft, organic and alluvial materials dominating during interglacials and the post-glacial period. The superposition of sedimentary environments together with glacial loading and unloading events, resulted in a heterogeneous stratigraphic succession with a variety of mechanical properties. This study proposes a geotechnical classification for the different deposits, which include tills, glacio-lacustrine and overbank materials observed in the urban and sub-urban areas of the city. Undisturbed samples obtained from excavations and open pits were tested for their index properties, shear resistance and compressibility. Additional tests included X-ray diffraction. For the geotechnical classification a composite mapping technique was used which included information of a great number of existing borings. It was established that low quality soils are located in depressions molded by glacial action as well as in overbank areas, which were filled by layers of normally consolidated clays and organic materials interbedded with coarser-grained deposits.

RÉSUMÉ: Dans la ville de Punta Arenas, Patagonie chilienne, les sols d'origine glaciaire ont été déposés au cours du dernier maximum glaciaire (DMG), dont des matières meubles, organiques et d'alluvions dominent pendant les périodes interglaciaires et la période post-glaciaire. La superposition des environnements sédimentaires avec des événements de chargement et de déchargement glaciaires, ont-ils abouti à une succession stratigraphique hétérogène avec une variété de propriétés mécaniques. Cette étude propose une classification géotechnique pour les différents dépôts, qui comprennent l'amas de débris mineral de la moraine et les dépôts glacio-lacustres. Des échantillons intacts provenant de fouilles ont été testés pour leurs propriétés d'index, de la résistance au cisaillement et la compressibilité. Des tests supplémentaires ont été inclus comment ceux de diffraction des rayons X. Pour la classification géotechnique nous avons utilisé une technique de cartographie composite. Il a été établi que les sols de mauvaise qualité sont situés dans des dépressions résultant du travail du glacier ainsi que dans les zones de débordement, qui ont été remplis par des couches d'argiles normalement consolidées et des matières organiques interstratifiés avec des dépôts de grain plus grossier.

KEYWORDS: Magellan Lobe, Patagonia, glacial clay, till, consolidation, composite maps

1 INTRODUCTION.

The city of Punta Arenas is situated on the western shore of the Magellan Strait, (see figure 5). The pressure of rapid urban development has led to building construction on soils that are almost always saturated, and due to their low bearing resistance, high compressibility and excessive variation, present unfavorable conditions for foundation design. The origin of the soils is mainly glacial, being due to the cyclic advance and retreat of a glacial lobe during the LGM, which caused stratigraphic successions that are highly variable both laterally and vertically. Temperate conditions during interglacial events and the post-glacial period, allowed the deposition of soft clays and the proliferation of peat bogs. Sand and gravel were also deposited within the channels of a drainage system.

The local physiography is one of the most important factors in the classification or zonation of the soils. In the context of surface hydraulics, Punta Arenas is crossed in an east-west direction by six natural channels: the Los Ciervos, La Mano, and Las Minas Rivers, and the D'Agostini or Pitet, Llau-Llau, and Bitsch Creeks (see figure 5). The drainage patterns are variable; the southern area is dominated by the relict glacial morphology, with the La Mano River mostly confined to a glacial valley. In the central area, the Las Minas River is dynamic and frequently overflows its banks, with occasional mud flows being considered a risk factor. Finally, in the north, the hydraulic pattern is more disperse with little incision. This is problematic with regard to the impermeable basal sediments that increase the risk of inundation. Fine overbank sediments and peat bogs are thus situated in areas with low gradients, mostly in the northern part of the city, whereas coarser sediments are deposited by the Las Minas River in the central area.

Understanding the complexity of the geological processes that operated in the area, allows the soils to be classified according to their origin and loading history, which is a key factor in their geotechnical characterization. We propose a paleogeographic interpretation method that includes SPT (Standard Penetrometer Test) values, and differentiates and demarcates soils of low bearing capacity.

2 THE LGM ADVANCE AND RETREAT

In the study area at least five glacial advances (A - E) of the Magellan Lobe are recorded, which were dated using ^{14}C and cosmogenic isotopes (Bentley 2005, Clapperton, 1995, McCulloch, 2005a). The LGM is represented by glacial advance B and is characterized by the evolution of the Juan Mazía Peninsula (figure 5), which happened after 31,250 calibrated years before present (Cal yr BP) and culminated between 25,200 – 23,100 Cal yr BP, followed by advance C of lesser extent, dated between 22,400 and 20,300 Cal yr BP. Glacial advance D, also of smaller extent, culminated between 17,700 and 17,600 Cal yr BP, succeeded by a glacial retreat. Glacial advance E caused the damming up of a lake between 15,500 and 11,770 Cal yr BP. The retreat of this glacier coincides with the maximum cooling period referred to as the Younger Dryas in the Northern Hemisphere, which was the last record of Pleistocene glacial advance (Bentley 2005, McCulloch, 2005a). The glacial processes deposited different sediments in the form of terminal, basal and lateral moraines, whereas glacial meltwater during the interglacial periods generated outwash plains. During warmer intervals peat bogs proliferated.

There is evidence that a large pro-glacial lake formed in the present Magellan Strait. Dating of a volcanic ash layer from the Reclus Volcano indicates that this happened before 12,640 ± 60 ^{14}C yr BP (McCulloch *et al*. 2005b). The low level of the Atlantic Ocean and the glacial barriers between the fjords, which did not allow the influx of waters from the Pacific Ocean, favored the deposition of varved clay and glacio-lacustrine clays in a freshwater environment, thus preventing the development of quick clays.

3 SOIL CHARACTERISTICS

3.1 General

The term "mazacote" is locally used to refer to a group of soft, bluish grey soils, considered in engineering as having poor geotechnical properties. Nevertheless, recognizing the complexity of depositional environments, events and structures that were superimposed during different geological periods, it is of prime importance to differentiate between push, basal and flood tills, outwash plains, lacustrine varved clays, organic clays, peat, and fine as well as coarse fluvial sediments with different compaction properties.

Till or moraine, a product of glacial erosion and plucking, is one of the most heterogeneous sediments because of its poor sorting. Its composition and structure depend on the manner in which it has been transported and the diagenetic history, so that it may vary from a dense till with a non-plastic matrix to a clay-rich till with a low consistency. Its sedimentary provenance is difficult to determine due to the fact that the material was transported from different, proximal or distal source areas, and subsequently suffered reworking. Geotechnically, it is important to differentiate between strongly pre-consolidated basal tills and melt-out till that is generally similar to normally consolidated clays.

The large pro-glacial lake and the presence of co-existing smaller lakes along the shores of the Magellan Strait provided the conditions for the deposition of lacustrine sediments, among which one of the most important types is varved clays.

The fine sediments associated with fluvial overbank areas with lower flow-regime currents, were deposited during modern inundation events, and geotechnically behave like normally consolidated clays (Vásquez 2012). These materials may show specific properties such as interbedded clay and silt, sedimentary structures including troughs and ripples (see figure 1), a high organic content (transported by water or formed *in situ* by local vegetation), laminas of coarse or fine sand with gravel lenses, the presence of sporadic gravel clasts with a maximum size of 1 cm, mica, carbon spheres, and strong oxidation.

Figure 1. Overbank fluvial sediments.

The glacial landscape, formed by rolling hills with abundant depressions, intermoraine channels and kettles, together with the Quaternary climatic changes, provided the necessary conditions for the evolution of peat bogs. Due to the fact that the area around the Strait was subjected to various glacial retreats, it is common to find significantly thick, vertically repeated peat bog deposits (see figure 4).

3.2 Structures

The soils derived from glacial environments show structures such as cracks, fractures, and complex deformation that depend on the material, the flow regime, the types of forces to which they had been subjected, as well as the water content. Sandy sediments deposited by slow currents may show undulating, continuous laminas, whereas soft sediments such as silty clay, if they have a high humidity content, develop structures like load casts, soft-sediment and recumbent folds, chaotic bedding, fluid escape structures, and polygonal mud cracks, *inter alia*. During field work it was common to observe slickensides, smooth oxidized surfaces caused by foliation slip in the tills, which indicate the intermittent laminar flow of fluids along discontinuities. At a macro-scale, the collapse of sub-vertical blocks in excavations could also be observed (see figure 2A). This can be explained by the vertical loading caused by the overlying glaciers and the subsequent lateral pressure-release within the excavations.

Another specific characteristic of the study area is the significant sub-glacial deformation of the sediments due to the shear force exerted by the overriding glaciers (see figure 2B). In road cuts, moraines show complex folds, faults and foliations with orientations indicating the direction of glacial advance.

Figure 2. Structures in glacial sediments, Punta Arenas. A) Collapse of sub-vertical blocks in excavations. B) Foliations in sub-glacial till.

3.3 Geotechnical characterization

Undisturbed soil samples were collected within the urban and sub-urban perimeter of the city, which were tested in the Laboratory of Solids and Particulate Matter of the Faculty of Physical and Mathematical Sciences of the University of Chile. Descriptions of the samples indicate specific components and structures such as the presence of carbon particles, plant roots, sedimentary structures such as ripples, micro-lamination, varved clay, laminas of coarse and fine sand with gravel lenses, the presence of gravel (which complicated the cutting of test cores), mica, and rapid oxidation in contact with the atmosphere.

The variety shown by the soils in terms of plasticity, (see figure 3) is surprising, which demonstrates that the glaciation left its mark in the extreme differentiation of the deposits. This ample spectrum reflects the percent of clay size materials, as well as the number and types of clay minerals, which vary according to the depositional environment, humidity, depth and amount of weathering.

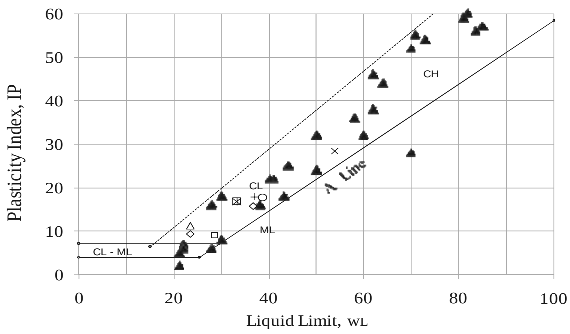

Figure 3. Casagrande Chart. Wide range shown by the types of soils, above line A.

Considering the above, granulometric tests were carried out with laser beam technology in the Sedimentology Laboratory of the University of Chile with a Mastersizer 2000, determining that the clay fraction, with a size less than 0.002 mm, does not exceed 15%. Because it is the clay fraction that largely controls the soil behavior, X-ray diffraction analysis was also carried out with a crystal powder diffractometer SIEMENS D5000, in the Crystallography Laboratory of the Department of Physics of the University of Chile. Of two samples analyzed, two types of clay minerals were identified: vermiculite and montmorillonite. Vermiculite is an alteration product of biotite (mica), whereas montmorillonite belongs to the smectite group, typically formed by the alteration of volcanic ash. Both minerals have a large cation exchange capacity and are expanding clays. The soils showed clay activities between medium and high (Vásquez 2012).

Using edometric tests and classifying the samples with reference to their sedimentary environment, one can determine that the soils that had not suffered geological loading, have larger initial void ratios (e_0) and compression indexes (Cc), whereas soils with a marked glacial deformation and a history of loading have lower e_0 and Cc values (see table 1), which directly influence their compressibility.

Table 1. Results of edometric tests, with soil samples classified by their origin (Vásquez 2012).

ID sample	Sedimentary environment	*Cc*	*Cr*	e_0
$M5LS_{40}$	Lacustrine	0.30	0.05	0.77
$M5LS_{20}$	Sub-aqueous, high energy	0.42	0.065	1.35
Planta Lana	Fluvial inundation	0.31	0.03	1.06
Chiloé-Briceño	Basal till	0.13	0.019	0.56
Cereco	Push till	0.12	0.04	0.63

Additionally, consolidated isotropically undrained triaxial compression tests (*CIU)* were carried out on cylindrical test cores of 5 cm by 10 cm. These were subjected to strain-controlled deformation with a load velocity of 0.13 %/min. Friction angles of 22º, 26º, 30º and 35° were recorded, with cohesions varying between 0 and 0.26 kg/cm^2. For stratified soils and/or those with clear sedimentary structures (troughs, ripples), the volume of coarse fraction is that which most influences the high shear strength, whereas the fine fraction depends on the type and volume of clay present, reducing the undrained strength. It is evident that the percentage of sand and/or silt in the mixture (i.e., varved clay, overbank soils) has a strong influence on the shear strength, which is why it would be common to find different results in series of triaxial tests.

An important aspect to consider in the field is the horizontal and vertical heterogeneity of the sediments. Figure 4 shows the wide variation that occurs over a distance of less than 50 m in boreholes 1 and 2. As regards the occurrence of peat at a depth of about 12 m, it is linked to more temperate geological periods, in a sub-basin where fine, soft sediments were deposited together with intercalated horizons of coarse sediments (gravel, sand).

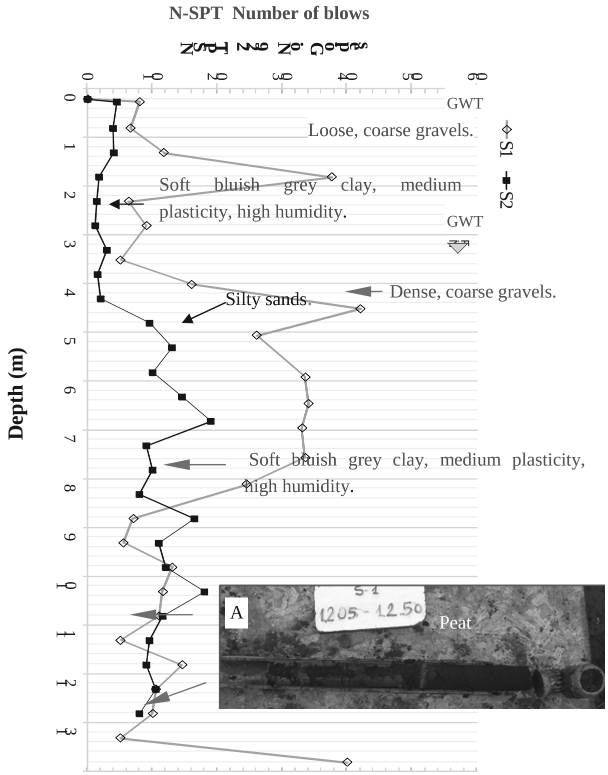

Figure 4. Two penetration tests, S1 and S2, separated by a distance of less than 50 m. A) Spilt-spoon sampler with peat, depth 12.0 m. (GWT) groundwater table.

4 TENTATIVE ZONIFICATION TROUGH COMPOSITE MAP

A composite map is the result of combining various maps of different types (e.g., topographic, sedimentological, paleontological) into a single map using a single set of contour lines. These maps accentuate parameters common in most or all of the contributing maps, and at the same time eliminate anomalies present in only one or a few of the latter. They can also show details which may not be visible in any of the contributing maps. The technique has been used in paleogeographic reconstructions and mineral exploration (Le Roux 1997). As applied here to a geotechnical problem, the soil strength characteristics were combined with SPT (Szigethi 1995-2010) and stratigraphic/sedimentological data, using 57 data stations distributed throughout the urban perimeter and the information of 110 geotechnical borehole data. The information was unified to a depth of 4 m.

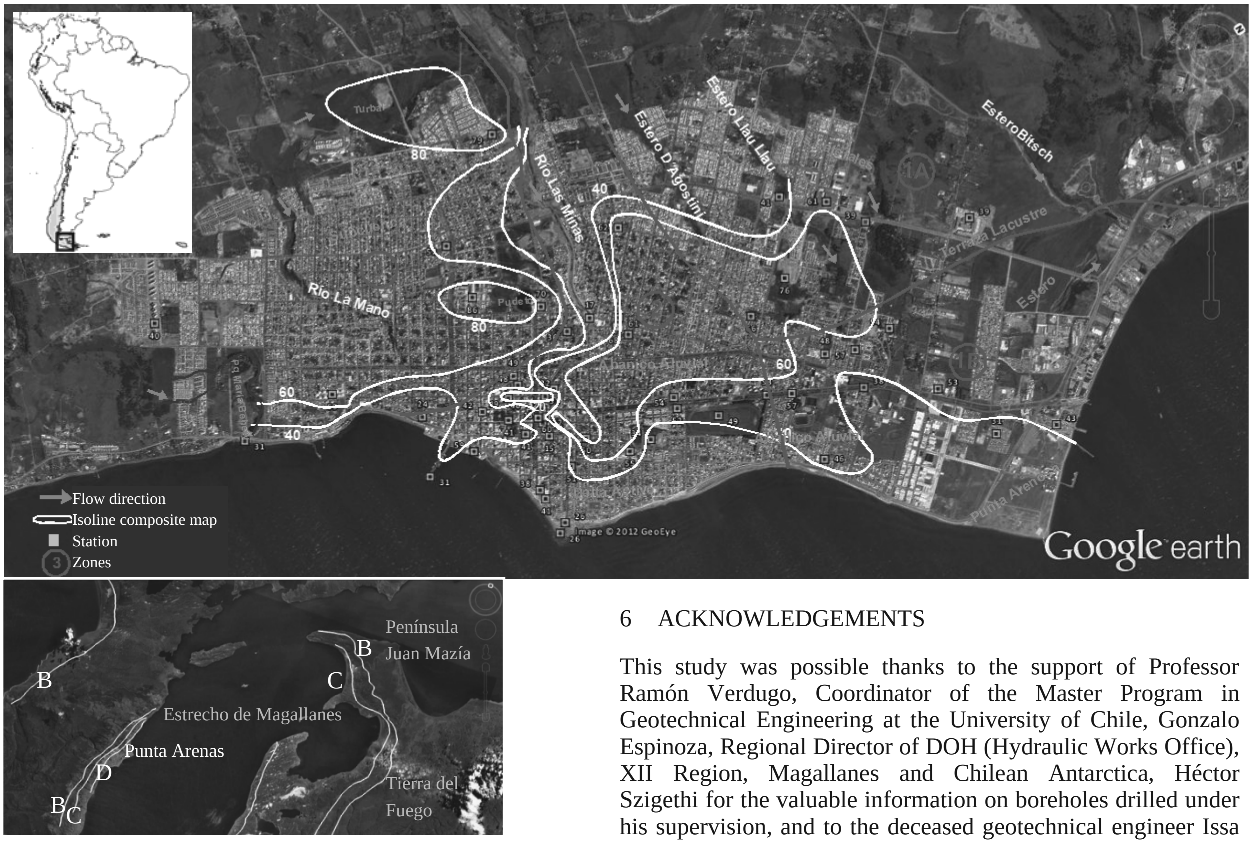

Figure 5. Location map of the study area. Composite map of Punta Arenas. Google Earth view of the city and Magellan Strait with stages of deglaciation labelled B-D, where B is the oldest and D the youngest moraine (after Bentley *et al*. 2005).

Using a spreadsheet and normalizing the data of topographic elevation, type of sediment (employing a scale of 1 to 7 for the coarsest to finest sediments, respectively) and the mean number of blows (N-SPT) for every station, the resultant composite value varies between 1 y 100 for the 57 stations. Finally, the composite values were contoured and interpreted (see figure 5).

The composite map technique highlights the sub-basins scoured by glacial action, in which soils of low bearing capacity (soft clays and peat) coincide with isolines having values higher than 60 and clearly demarcated by isolines having values above 80 (see figure 5). Additionally, the phreatic water levels in these areas are close to the surface, which is one of the most unfavorable conditions for foundation design.

4 CONCLUSIONS

Soils in the city of Punta Arenas show an extraordinary variation in their index and engineering properties, which makes them difficult to assess for sound geotechnical designs.

The combined, non-dimensional parameters of the composite map reveal the complex geological processes these areas have experienced. A study of the geological events during the Last Glacial Maximum allows the characteristics of the soils to be explained in terms of composition as well as in their effect on existing structures.

The composite map allows the definition of a tentative zonation which shows areas with more compressible soils and low shear strength associated with depressions containing lacustrine sediments such as clay and peat.

6 ACKNOWLEDGEMENTS

This study was possible thanks to the support of Professor Ramón Verdugo, Coordinator of the Master Program in Geotechnical Engineering at the University of Chile, Gonzalo Espinoza, Regional Director of DOH (Hydraulic Works Office), XII Region, Magallanes and Chilean Antarctica, Héctor Szigethi for the valuable information on boreholes drilled under his supervision, and to the deceased geotechnical engineer Issa Kort for his important support in the field.

5 REFERENCES

Bentley M.J., Sugden D.E., Hulton M.R.J., and Mcculloch R.D. 2005. The landforms and pattern of deglaciation in the Strait of Magellan, Bahía Inútil, southernmost South America. Geogr. Ann., 87 A (2): 313–333.

Clapperton, ch., Sugden D.E, Kaufman D., and Mcculloch R.D. 1995. The last glaciation in central Magellan Strait, southernmost Chile. Quaternary Research, 44:133-148.

Le Roux, J.P. 1997. Palaeogeographic reconstruction using composite maps, with case studies from three continents. Palageography, Palaeoclimatology, Palaeocology, 131: 51 – 63.

Mcculloch, R.D., Fogwill, C.J., Sugden, D.E., Bentley, M.J. and Kubik, P.W., 2005a. Chronology of the last glaciation in the central Strait of Magellan and Bahía Inútil, southernmost South America. Geografiska Annaler, 87 A (2): 289–312.

Mcculloch, R.D., Bentley, M.J. Tipping, R.M. and Clapperton, C.M. 2005b. Evidence for late-glacial ice-dammed lakes in the central Strait of Magellan and Bahía Inútil, southernmost South America. Geografiska Annaler, 87 A (2): 335–362.

Szigethi, H.; 1995-2010. Informes de laboratorio de mecánica de suelos y comunicaciones personales, Punta Arenas.

Uribe P.; 1982. Geología y consideraciones geotécnicas para el estudio de los suelos de fundación de la ciudad de Punta Arenas. Informe taller de título II. Departamento de Geología Universidad de Chile.

Vásquez, A.; 2012. Suelos de fundación de la ciudad de Punta Arenas. Tesis magíster en ciencias, mención ingeniería geotécnica. Santiago, Universidad de Chile. 136 p.

Geotechnical Issues of Megaprojects on Problematical Soil Ground of Kazakhstan

Questions géotechniques de mégaprojets sur sol problématique du Kazakhstan

Zhussupbekov A.Zh., Ling H.I.
Columbia University, New York, USA

Baitassov T.M., Lukpanov R.E., Tulebekova A.S., Yenkebayev S.B.
Eurasian National University, Astana, Kazakhstan

Popov V.N.
KarGIIZ, LTD, Karaganda, Kazakhstan

Krasnikov S.V.
Kazdorproject, LTD, Kazakhstan

Boominathan A.
Indian Institute of Technology, Madras, India

ABSTRACT: After the collapse of the Soviet Union, Astana has become the new capital of Kazakhstan. In the past decade, many modern architectural and engineering megaprojects have emerged (such as Khan-Shatyr, Peace Palace – Pyramid, house estate of "Severnoe Siyanie", Abu-Dhabi Plaza Hotel and so on). These modern megaprojects put forward new requirements to engineers utilizing more economical and technologically effective design and construction methodologies. The territory of the city of Astana is located on the Kazakh Steppe and the most apparent problem is the soil condition presented by inhomogeneous sandwich soil layers, characterized by various types of soft and dense soil, and hard soil bands, including freezing ground. At present, pile foundations are widely used, but it is very hard to use precast piles because they may break in the soil during driving or their heads may be damaged too, while the bearing capacity is not high. The best geoengineering solution in this case is the use of new pile technology like CFA (continuous flight auger), FDP (full displacement piles), DDS (drilling displacement system) and H-beam piles, that lead to increased bearing capacity. The present lecture includes static and dynamic, integrity piling test results and also data of numerical analysis of interaction of piles with soil ground.

RÉSUMÉ : Après l'effondrement de l'Union soviétique, est devenue Astana, la nouvelle capitale du Kazakhstan. Dans la dernière décennie, de nombreux mégaprojets modernes d'architecture et d'ingénierie ont vu le jour (comme Khan-Shatyr, Palais de la Paix - Pyramide, immobilier maison d'"Severnoe Siyanie", Abu-Dhabi Plaza Hôtel et ainsi de suite). Ces mégaprojets modernes proposer de nouvelles exigences pour les ingénieurs qui utilisent conception plus économique et techniquement efficace et méthodes de construction. Le territoire de la ville d'Astana est situé sur la steppe kazakhe et le problème le plus évident est la condition du sol présenté par inhomogènes couches de sol sandwich, caractérisées par différents types de sol souple et dense, et des bandes de sols durs, y compris congélation du sol. À l'heure actuelle, les fondations sur pieux sont largement utilisés, mais il est très difficile d'utiliser des piles préfabriquées, car ils peuvent se briser dans le sol pendant la conduite ou la tête peut être trop endommagés, tandis que la capacité portante n'est pas élevé. La meilleure solution dans ce cas, la géo-ingénierie est l'utilisation de la technologie nouvelle pile comme CFA (tarière continue), FDP (piles déplacement complets), DDS (système de déplacement de forage) et H-beam pieux, qui conduisent à augmenter la capacité portante. La conférence présente comprend statiques et dynamiques, les résultats de tests d'intégrité des pieux ainsi que les données de l'analyse numérique de l'interaction avec des tas de terre du sol.

KEYWORDS: pile technology, field and laboratory test, FEM modeling.

1 INTRODUCTION. FIRST LEVEL HEADING

During the last 20 years of independence, in the scopes of geoengineering, Astana had been grown significantly, many outstanding megaprojects have been raised for the relatively short time: Khan-Shatyr, Peace Palace – Pyramid, house estate of "Severnoe Siyanie", Abu-Dhabi Plaza Hotel, New Aktau city near the Caspian Sea and so on, and many other (Zhussupbekov A.Zh. 2012).

These modern megaprojects put forward new requirements to engineers and lead to proceed to best geoengineering solution in this case is the use of new pile technology like CFA (continuous flight auger), DDS (drilling displacement system) and H-beam piles. The short information about new and traditional pile technology are using in Kazakhstan is presented in Figure 1.

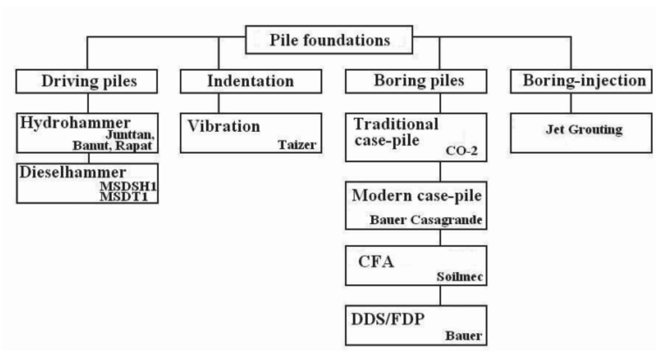

Figure 1. Pile foundations on construction sites of Kazakhstan

It has been mentioned previously that existing Kazakhstan standard of pile design is out of date and does not meet the modern geoengineering requirements. The preliminary design is performed based on the engineering and geological investigation of construction site. Accuracy of pile design generally depends on the accuracy of data presented in geological report. Final pile design project is corrected after approval by field tests. Nowadays conception of pile foundation Figure 2.

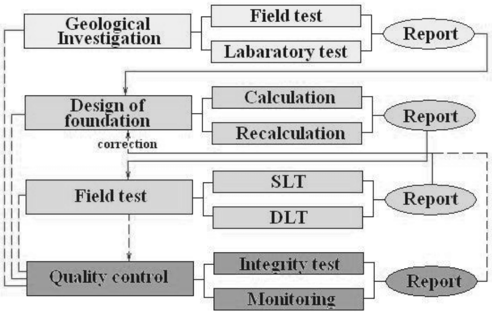

Figure 2. Pile foundation design concept

2 FEATURES OF NEW PILE TECHNOLOGIES

The DDS technology was established by Germany Company BAUER and undoubtedly presents practical values on Kazakhstan construction sites. The general advantages of this technology (comparing with traditional boring pile technology) are: fast installation of pile, economical efficiency, low noise during installation, absence of vibration, and high value of bearing capacity (Sultanov G.A. 2010).

Installation of DDS pile consists of four steps, as described below: place the boring machine to the boring place; bore the pile hole to the design level; fill the concrete under a pressure of 300 kPa; install the steel anchor into the pile body.

The principal feature of this technology is a special boring element. The pile hole is formed via two stages: during the moving down of boring element, the bullet teeth loosen the soil and the stabilizer displaces surrounding soil. During the moving up of boring element, the secondary compaction of hole takes place.

DDS technology allows installation of the pile up to 1200mm of diameter and 30m of length. During DDS pile design, it is required to take into account following parameters: diameter of pile, torque moment, indentation forces, density (strength, compaction of soil and power of concrete pump).

A CFA pile is a type of drilled foundation in which the pile is drilled to the final depth in one continuous process using a continuous flight auger. The use of the continuous flight auger rig avoids many of the problems of drilling and concreting piles experienced when using conventional power augers. The new CFA equipment can perform piles in most type of soils (including sand, gravel, silt, clay, chalk and weak weathered rock) with diameters up to 1200 mm and lengths down to 35-40 meters. So, with proper planning and design, performing equipment and skilled personnel, high production rates and high quality product can be achieved (Ashkey Y. 2008).

Installation of CFA pile consist of following steps: placing the boring machine to the boring place; boring the pile hole to the design level; removing the screw with simultaneous concrete filling under the high pressure and replace the boring machine, installation of steel anchor into the pile body with preparation of pile head.

The high quality of piles is ensured by not soil extraction for DDS and by high filling pressure for CFA.

Figure 3. New pile technologies

To analyze the bearing capacities obtained by SLT, the calculation of design bearing capacity by Kazakhstan Standards was performed by SNIP PK 5.01.01-2002. The classically bearing capacity is subdivided into two constituents: shaft and tip resistance. In Kazakhstan's Standard, the classical equation was modified and presented by following equation:

$$F_d = \gamma_c(\gamma_{cR} RA + u\sum \gamma_{cf} f_i h_i) \qquad (1)$$

where γ_c = safety factor; γ_{cR} and γ_{cf} = coefficients of soil work condition under the pile tip and around the pile, respectively.

Unfortunately, existing Kazakhstan Standards do not take into account soil compaction under the high concrete pressure in case of CFA technology and soil displacement without excavation in case of DDS technology that lead to reduction of settlement and increase in bearing capacities of pile foundation. Therefore it had been suggested to use following coefficients of soil working condition as presented in Table 1.

Table 1. Suggested coefficient of soil works for DDS and CFA piles

Type of pile	γ_{cR}	γ_{cf}
Driving Pile	1,0	1,0
Boring Pile	0,7-1,0	0,7
DDS (FDP) Pile	1,3	1,0
CFA Pile	1,0	1,0

3 TESTING OF PILE FOUNDATION

Many static and dynamic load tests were performed on this construction site. The SLT one of the more reliable field tests in analyzing pile bearing capacity in Kazakhstan. DLT is a fast bearing capacity analysis field test and give more or less reliable value of pile bearing capacity.

Dynamic load test (DLT). For definition of the bearing capacities of piles, it is required to use average refusal which are obtained during redriving of the piles after their "rest". The rest time depend on soil condition of site: for clayey soil 6 -10 days, for sandy and gravel soils up to 3 days.

Bearing capacity of the piles is defined by following empirical equation:

$$F_u = \frac{\eta AM}{2}\left[\sqrt{1+\frac{4E_d}{\eta AS_a}\cdot\frac{m_1+\varepsilon^2(m_2+m_3)}{m_1+m_2+m_3}}-1\right] \qquad (2)$$

where η=factor, dependent on concrete strength of the piles; A=cross section of tested pile; M=1 – factor, dependent on pile driving hammer's impact; E_d =effective energy of blows of the hammer, kNm.

According to Kazakhstan Standard at least 6 piles must be tested by DLT on each construction site.

Static Load Test (SLT). SLT one of the more reliable field tests in analyzing pile bearing capacity. SLT should be carried out for driving piles after the "rest" and for bored piles after achievements of the concrete strength, by more than 80%.

According to requirements of Kazakhstan Standard - SNiP RK 5.01-03-2002 (SNiP RK 2002) – ultimate value of settlement of the tested pile is depending on category of construction and is equal 16 or 24 mm. The last argument shows conditional character of SLT method.

According to Kazakhstan Standard 1% of constructed piles on construction site must be tested by SLT, but at least 2 SLTs in a site must be done.

Comparison of SLT and DLT. SLT and DLT both are practiced in Kazakhstan construction. According to experience on construction sites of Astana, some difference exists between SLT and DLT results. Moreover, results of bearing capacity of pile depend on type of hammer. Thus, DLT results obtained by using hydro-hammer are more approximate to the SLT results, namely more reliable than results obtained by using diesel hammer (Ashkey Y. 2008). The safety factor as defined by comparative analysis of many DLT and SLT data is presented in Figure 4.

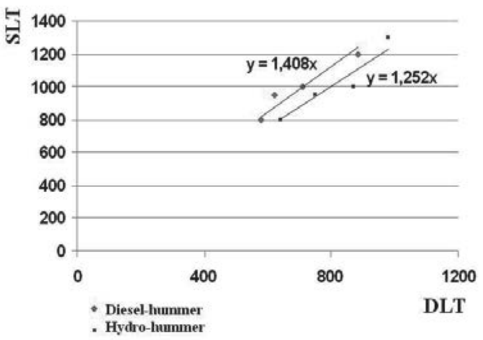

Figure 4. Comparison SLT and DLT

Alternative Load Test Method. From aforementioned it follows that SLT and DLT both have disadvantages. SLT required a lot of time, works and cost. Prescribed by Standard quantity of required SLT is not enough to adequately realize soil condition of construction site (2 SLT for 200 piles only). DLT is much faster but is not so reliable and is applicable to driving piles only.

Alternative load test method which precluded disadvantages of both SLT and DLT was used on this construction site – Pile Dynamic Analysis Method (PDA). PDA allows tests up to 10 piles per day and much cost effective than SLT. The comparison of SLT, DLT and PDA approved superiority of Pile Dynamic Analysis Method.

The O-cell bi-directional test of bored piles was firstly used on construction site of Astana. The general advantages of this method as compared with SLT and DLT are follows: no anchor piles, no external reaction system, no heavy transport is required, only half the stresses applied to the concrete, significant cost saving as loads increase.

Quality control of pile foundation. Pile integrity test is one of the non-destructive methods of pile quality control. This method allows analyzing integrity control for all existing types of piles (boring, injection, driving and so on). PIT is base on wave propagation theory in rigid body and is concerned with one of the modern quality control methods used world-wide. PIT allows detecting pile defects: approximate pile length, expansion and narrowing of pile cross section, modification of soil layers, heterogeneity of pile material, cracks in cross section of pile, extrinsic material in pile body.

Advantages of PIT are as follows: portable device is easy to carry. One operator will be able to test over 100 piles per day, depends on site condition, pile head preparation and approach to the pile; minimum influence to the construction work on the site; significant defects may be detected in the beginning of the construction. PIT has some limitations: reflection of the bottom of pile sometimes has errors depending on soil condition; little deflection (less than 5 %) of pile cross section cannot be identified.

According to Kazakhstan Standard requirements it is necessary to test 60% of boring piles and 50% of driving piles.

Geomonitoring. Geomonitoring for foundation settlement is one of the quality control methods that can be carried out during and after construction in exploitation period. Monitoring is indirect control of pile installation evaluation.

The principle of this method is monitoring the settlement of special marks which are installed to interested points of construction. Monitoring starts from the beginning of construction and allows revealing defects of foundation installation.

4 COMPARISON OF SLT RESULTS

SLT of different types of pile was performed with a view to compare bearing capacity of traditional (namely, boring casing pile and driving pile) (Zhussupbekov A.Zh. 2012).

All the piles were designed to the criteria of 2200kN bearing capacity. Designed parameters of piles (length and cross section) by Kazakhstan Standards are presented in Table 2.

Table 2. Designed pile characteristic

Type of pile	Required quantity, e.a.	Length of pile, m	Diameter or cross section, m
CFA	1	10	0.5
DDS	1	10	0.5
Casing	1	10	0.5
Driving	2	12	0.3 x 0.3

Results of comparison are presenting in Figure 5.

All of these coefficients show incapacity of accurate design of modern pile technology by out-of date Standards, otherwise this coefficients tending to 1. The results of SLT showed entirely expected regularity. CFA piles showed highest bearing capacity as long as during CFA pile installation it was expended much more concrete (in 2 times) than during casing pile installation. This factor was not considered during design; therefore coefficient equal 1.43. DDS pile approved effluence of compacted soil; therefore coefficient equal 1.22 (DDS versus casing). Differences between driving and casing pile neglected small, the reason of differences is empirical coefficients required by Standards.

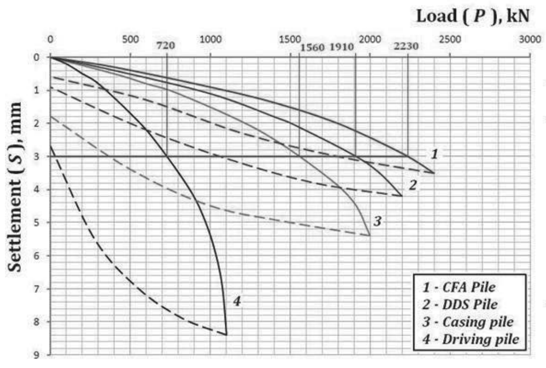

Description	Coefficient of reserve
F_{CFA}/F_{DDS}	1.17
F_{CFA}/F_{Casing}	1.43
$F_{CFA}/F_{Driving}$	1.55
F_{DDS}/F_{Casing}	1.22
$F_{DDS}/F_{Driving}$	1.33
$F_{Casing}/F_{Driving}$	1.08

Figure 5. Bearing capacity comparison of different piles

5 FEM MODELING OF BORED PILES

CFA Boring pile technology. The FEM elasto-plastic analysis was provided by computer program established by Prof. Tadatsugu Tanaka. It was used the mechanical properties of soil ground for the numerical calculation of bearing capacity and settlement. For analyzing bearing capacity of working as friction CFA and Casing piles were modeled and compared with results of static load test.

Taking advantage of the axi-symmetric nature of the problem, only a half domain of the model ground and pile were analyzed. The soil ground and pile were discredited into four noded quadrilateral elements. Number of nodal points are 675, number of finite elements are 606, number of materials are 4 (1is sand with gravel, 2 is hard clay, 3 is clay, 4 is bored pile).

During CFA pile installation the question of over-expenditure of concrete was appeared. The actual volume of borehole was about 1.3-1.4 times more than theoretical volume of borehole (Ashkey Y. 2008). After determination of preliminary average radius (r+∇r) increasing diameter of CFA piles and remodeled numerical mesh FEM analysis was repeated. It gives us increasing bearing capacity of CFA piles respectively "load-settlement" results of field static load test and stress and strain of soil around of single CFA pile through FEM computer program. The results of "load-settlement" through FEM illustrated in Figure 6.

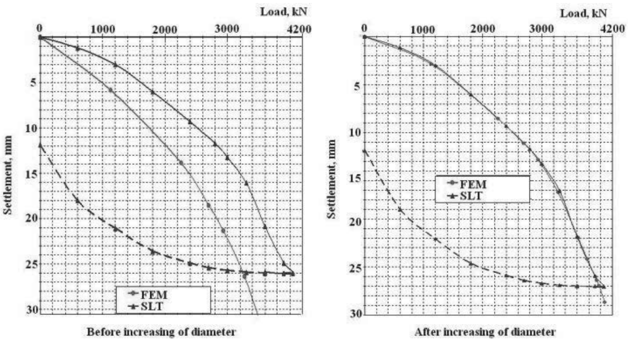

Figure 6. Results of CFA FEM analysis

DDS Boring pile technology. The FEM modeling of DDS pile was made in Plaxis 2D computer program (Figure 7).

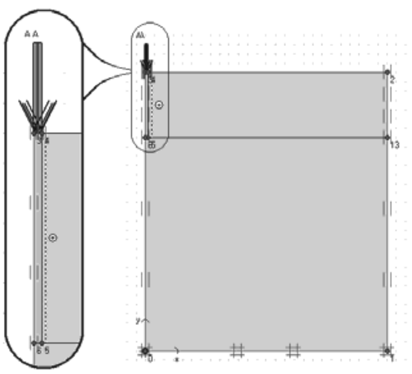

Figure 7. FEM modeling of DDS

The comparison diagram of bearing capacities of DDS and traditional bored piles by Plaxis is presented in Figure 8 (Expressed by $k=F_d/F_u$, where F_d – DDS bearing capacity, F_u – traditional bored pile bearing capacity). The points on diagram are lying above the diagonal line; it means that the values of DDS bearing capacity are exceeding traditional bored piles [2].

After some transformation it was got FEM coefficient of DDS pile works, which vary from 1.23 – 1.35 depends on type of soil (See Table 1).

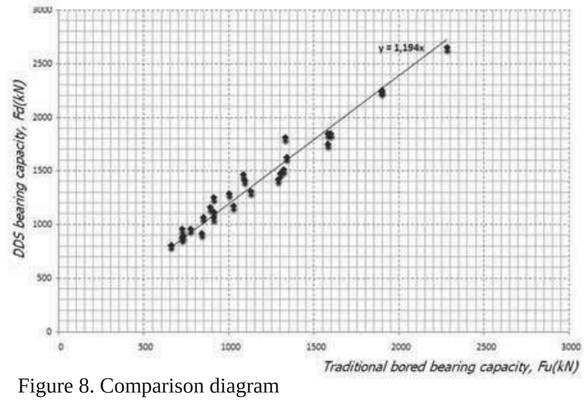

Figure 8. Comparison diagram

6 CONCLUSIONS

There were presented very short descriptions of geoengineering approach to the installation, testing and quality control of pile foundation which using on construction sites of Kazakhstan. This experience probable lead to the coming changes of the concept of Kazakhstan pile foundation design.

During designing of CFA pile of buildings and structures is need to consider volume of borehole expansion by result of additional pressure, as well as over-expenditure of the concrete which is depend on soil conditions and length of pile. Significant differences between bearing capacities of DDS and casing boring piles show incomplete usage of DDS technology resources. The coefficient of shaft work of DDS pile was defined and equal from 1.2 to 1.3 depending on soil condition.

PDA allows tests up to 10 piles per day, much cost effective than SLT, and more authentic than DLT. PDA is a type of DLT and is appropriate for any type of pile, but cannot be used to full extent on construction sites of Kazakhstan due to absence of Standard.

Pile integrity test is in the process of gaining official acceptance in Kazakhstan. PIT is a non-destructive method allowing make quality control of pile body whereupon of pile installation and even after many years of building exploitation. Geomonitoring for foundation settlement is indirect control of pile quality evaluation method and has become more relevant, especially for high-rise building construction.

Application of advanced technologies of pile foundations installation led to a significant economical efficiency. According to tests results, the piles installed by the above technologies showed high values of bearing capacity, which led to a decrease of pile length by 10 to 20% and increase economical efficiency by 20 to 30%.

7 REFERENCES

Zhussupbekov A.Zh. and Lukpanov R.E. 2012, Geotechnical issues of megaprojects on problematical soil in Kazakhstan, *Volume of Abstracts of ACEM`12*, Seoul, Korea, 127.

Sultanov G.A., Zhussupbekov A.Zh. Lukpanov R.E. and Enkebaev S.B. 2010, Research of Interaction between Displacement Pile and Soil Basement. *Proc. of Kaz-Kor joint geotechnical seminar*. Astana, Kazakhstan, 84-91.

Ashkey Y. 2008, Interaction of CFA bored piles with soil condition in Astana. *A dissertation submitted in partial fulfillment of the requirements for the PhD degree.*Astana, Kazakhstan.

SNiP RK 5.01-03-2002 "Pile foundation".

Zhussupbekov A.Zh. and Lukpanov R.E. 2012, Geotechnical issues of megaprojects on problematical soil in Kazakhstan, *Proc. of 3rd ICNDSMGE-ZM 2012*, Near East University, Nicosia, TRNC, 67-75.

General Report of TC 307
Sustainability in Geotechnical Engineering

Rapport général du TC 307
Durabilité en géotechnique

Basu D.
University of Waterloo, Canada

Puppala A.J., Chittoori B.
University of Texas at Arlington, U.S.A.

ABSTRACT: Sustainable geotechnics is an emerging sub-discipline within geotechnical engineering that covers a wide range of topics related to the sustainable development of civil infrastructure and society. In this general report, a brief overview of this new sub-discipline is provided with an aim to connect the broader scope of sustainability to geotechnical engineering research and practice. In addition, the papers allocated to the sustainability session (TC 307) of 18th ICSMGE are reviewed in the context of the big picture. Most of the papers deal with material recycling, reuse, and use of alternate materials in geotechnical engineering constructions. These apart, the topics covered in the allocated papers include use of geosynthetics, sustainable foundation engineering, subsurface remediation and site redevelopment, and sustainability assessment. Some of the important topics related to sustainable geotechnics not covered by the allocated papers are also mentioned.

RÉSUMÉ: La géotechnique soutenable est une nouvelle sous-discipline de la géotechnique qui couvre un large éventail de sujets liés au développement durable des infrastructures et de la société. On présente dans ce rapport général un bref aperçu de cette nouvelle sous-discipline avec l'objectif de relier le champ plus large du développement durable avec la recherche et la pratique en géotechnique. En outre, les articles de la session dédiée à la géotechnique soutenable (TC 307) de la 18e ICSMGE sont examinés dans un contexte plus large. La plupart des articles traitent de recyclage de matériaux, de réutilisation, et de l'utilisation de matériaux alternatifs dans les constructions géotechniques. En plus de cela, les sujets abordés dans les articles incluent l'utilisation des géosynthétiques, les travaux de fondation durable, la décontamination et le réaménagement de sites et l'évaluation de la durabilité. Certains sujets importants liés à la géotechnique soutenable non couverts par les articles considérés sont également mentionnés.

KEYWORDS: sustainable geotechnics, geosustainability, geohazard, resilience, life cycle assessment, recycling, reuse, remediation.

1 INTRODUCTION

Sustainability is a multi-scale, multi-disciplinary and multi-dimensional paradigm that aims at ensuring the well being of the world for the current and future generations. With its origin in the environmentalism of the nineteenth and early twentieth century, sustainability has come a long way since its inception in the later half of the twentieth century and is now widely recognized as a principle that advocates a balanced development maintaining harmony between the three Es — environment, economy and equity (Edwards 2005). The environmental aspect has mostly been the driver of sustainability movement because of global concerns regarding the rise in atmospheric carbon dioxide and temperature, rapid depletion of natural resources, and other similar environmental and ecological hazards. The construction industry accounts for about 40% of the global energy consumption, depletes large amounts of sand, gravel and stone reserves every year, contributes to desertification, deforestation and soil erosion, and causes land, water and air pollution (Dixit et al. 2010, Kibert 2008, Puppala et al. 2012, Saride et al. 2010). Therefore, green practices within the civil engineering industry can reduce the impact of construction on the environment. Geotechnical design and construction, being placed early in a typical civil engineering project, can significantly contribute to sustainable development by adopting environment-friendly, cost-effective and socially-acceptable choices and setting a precedent for the remainder of the project. The role of geotechnical engineering in sustainable development is being increasingly recognized, as evidenced by the formation of the ISSMGE technical committee "Sustainability in Geotechnical Engineering" (TC307) in 2012. In fact, the 18th ICSMGE has set a precedent by devoting a technical paper discussion session to the sustainability theme.

The purpose of this general report is (i) to provide a perspective on the new area of sustainable geotechnics, and (ii) to review the papers allocated to the sustainability session of the 18th ICSMGE in the context of the big picture.

2 SUSTAINABILITY AND GEOTECHNOLOGY

Engineered systems serve human societies by developing cost-effective products and, in the process, draw resources from natural systems and generate emissions and wastes that nature has to absorb. Thus, engineered systems are inextricably connected to the social, environmental, and economic systems. Because humankind is heavily dependent on engineered systems, sustainability of the physical world cannot be achieved without contributions from the engineered systems. This has been summed up by Basu et al. as the four Es of sustainability — engineering design, economy, environment and equity, as described in Figure 1.

Geo-structures and geo-operations often form important interfaces between the built and natural environments, and interact with and affect a wide variety of externalities. For example, dams and levees buffer the fluctuations in hydrologic cycles and affect water movement across regional and political boundaries; extraction of petroleum resources from the subsurface affects the natural environment and global economy; and landfill systems prevent contaminants from reaching groundwater across regional scales. Further, geotechnical engineering has a very important role in mitigating and containing disasters, and failure to do so is often catastrophic to the society. Breach of a levee system during a hurricane or tsunami, breakdown of underground water pipeline network during an earthquake, landslides triggered by rainfall or earthquake, disruptions and distress in an underground transit system due to terror attack are examples of disasters related to geotechnical systems. Thus, geotechnical engineering has a wide gamut and a global reach, and can influence the sustainable development of infrastructure and civil societies in a significant way. According to Long et al. (2009), there are seven categories where geotechnical engineering can contribute to improve the sustainability of the societal system. These include (i) waste management, (ii) infrastructure development and rehabilitation, (iii) construction efficiency and innovation, (iv) national security, (v) resource discovery and recovery, (vi) mitigation of natural hazards, and (vii) frontier exploration and development. A similar set of sustainability objectives for geotechnical engineering was also identified by Pantelidou et al. (2012): (i) energy efficiency and carbon reduction, (ii) materials and waste reduction, (iii) maintaining natural water cycle and enhancing natural watershed, (iv) climate change adaptation and resilience, (v) effective land use and management, (vi) economic viability and whole life cost, and (vii) positive contribution to society.

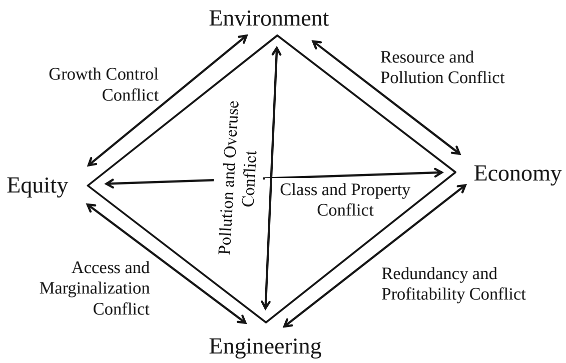

Figure 1. The four Es of sustainability in engineering projects (Figure 1 of Basu et al.).

On a project level, Basu et al. outlined the necessary steps to achieve sustainability objectives as (i) involving all the stakeholders at the planning stage of the project so that a consensus is reached on the sustainability goals of the project (such as reduction in pollution, use of environment friendly alternative materials, etc.), (ii) reliable and resilient design and construction that involves minimal financial burden and inconvenience to all the stakeholders, (iii) minimal use of resources and energy in planning, design, construction and maintenance of geotechnical facilities, (iv) use of materials and methods that cause minimal negative impact on the ecology and environment, and (v) as much reuse of existing geotechnical facilities as possible to minimize waste. In addition, emphasis should be put on proper site characterization so that geologic uncertainties can be minimized, on instrumentation so that proper functioning of a geotechnical facility can be ensured and required retrofitting can be performed, and on adaptive management strategies so that the resilience of the geotechnical facility can be enhanced and the vulnerability of the community linked with the facility can be reduced.

According to Basu et al. and Vaníček et al., sustainability related studies can be grouped into the following areas: (1) the use of alternate, environment friendly materials in geotechnical constructions, and reuse of waste materials, (2) innovative and energy efficient ground improvement techniques, (3) bio-slope engineering, (4) efficient use of geosynthetics, (5) sustainable foundation engineering that includes retrofitting and reuse of foundations, and foundations for energy extraction, (6) use of underground space for beneficial purposes including storage of energy, (7) mining of shallow and deep geothermal energy, (8) preservation of geodiversity, (9) environmental protection including protection of greenfields, (10) geohazard mitigation including mitigation of the effects of global climate change and multi-hazards, and (11) incorporation of geoethics in practice. Basu et al. emphasized the need for reliability- and resilience-based design as a part of sustainable geotechnical engineering. Additionally, Basu et al. summarized the different sustainability assessment tools available in geotechnical engineering and categorized them into (1) single criterion based metrics (e.g., carbon footprint), (2) multiple criteria-based tools (e.g., GeoSPEAR and life cycle assessment), and (3) point-based rating systems (e.g., I-LAST and GreenLites).

Based on the above discussion, it is evident that sustainable geotechnics is an emerging sub-discipline of geotechnical engineering that covers a wide area ranging from reliability- and resilience-based design and environment-friendly construction practices to energy geotechnics and geohazard mitigation. It also includes the development of sustainability assessment tools applicable to geotechnical engineering practice.

3 THEMES COVERED IN SUSTAINABILITY SESSION

There are 28 papers allocated to the sustainability session with authors from 20 countries representing all the ISSMGE regions. These papers cover a wide range of topics that can be broadly grouped into five areas.

3.1 Use of recycled and alternate materials

According to Vaníček et al., a variety of waste products are generated in the society that can be utilized in geotechnical constructions. These waste products can be categorized into industrial wastes (e.g., ash and slag), construction and demolition wastes (e.g., used bricks, concrete, and asphalt), mining wastes (mine tailings), and other wastes (e.g., tires, plastics, glass, and dredged material). Basu et al. provided an overview of the different waste utilization methods in geotechnical constructions and discussed about chemical soil treatment. Waste utilization and use of alternative material is one of the most widely researched areas in geotechnical engineering and it is not surprising that, out of the 28 papers allocated to this session, 20 papers contribute to this topic.

The papers on industrial waste recycling deal with a variety of geotechnical applications. Baykal investigated the use of silt-sized fly ash in manufacturing artificial, sand-sized pellets for use in construction projects (Figure 2). He reviewed the cold bonding pelletization technique, and studied the index and mechanical properties of the fly-ash pellets. The manufactured pellets behave like calcareous sands found in the nature.

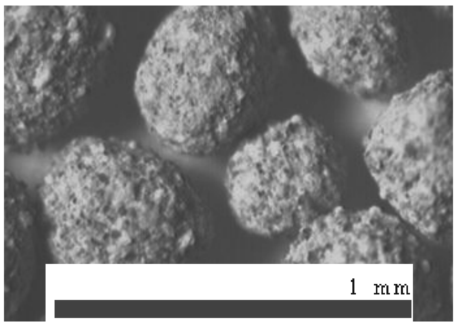

Figure 2. Manufactured fly ash pellets (Figure 7 of Baykal).

In another example of recycling of fly ash, Vukićević et al. investigated the reusability of a class-F fly ash (KFA) from a Serbian thermal power plant as a stabilizer in low plasticity silt and in high plasticity expansive clay. Several geotechnical engineering properties including grain size distribution, Atterberg limits, unconfined compression strength, moisture-density relationship, swell potential, and California bearing ratio (CBR) were determined for the control and treated soils. Based on the study, the authors concluded that the particular fly ash in question can be used as a stabilizer, and advocated a case-by-case approach with proper investigations for making decisions regarding the suitability of fly ash as a construction material.

Kikuchi and Mizutani proposed the use of granulated blast furnace slag (GBFS) as an alternative construction material for port structures because GBFS can reduce liquefaction potential and earth pressure when used as a backfill material for quay walls. The inherent ability of GBFS to solidify upon contact with seawater was explored and methods were proposed for its standardized application in the field. As GBFS solidification is a lengthy process and often the solidification is not uniform, Kikuchi and Mizutani proposed the use of powdered blast furnace slag (PBFS) in conjunction with prior homogeneous mixing treatment (PHMT) to accelerate the GBFS solidification process. In their experimental investigation, Kikuchi and Mizutani considered several issues, e.g., material separation after construction due to water flow, solidification of GBFS underground with flowing water, and the effect of the change in pore fluid chemistry due to a change from sea to fresh water on GBFS solidification, in determining the most appropriate mixture of GBFS and PBFS for accelerating the GBFS solidification. The authors found that PHMT treated GBFS-PBFS mixture is effective in reducing the amount of material separation in the GBFS-PBFS mixture and produced sufficient unconfined compression strength after about 2 months of curing in the seawater because of which it can be used to prevent liquefaction.

Nawagamuwa et al. investigated the properties of waste copper slag for use in vertical sand drains and sand piles as a substitute for sand. Geotechnical properties such as particle size distribution, hydraulic conductivity, shear strength, and stiffness were studied for the sand-sized waste copper slag particles mixed with poorly graded sand. It was observed that the particle size distribution, shear strength and hydraulic conductivity were not significantly affected due to the addition of the slag. However, the stiffness of the slag-sand mixture increased significantly. Based on the study, Nawagamuwa et al. concluded that waste copper slag can be safely and effectively used as a replacement for sand in vertical drains.

Vizcarra et al. (2013) investigated the applicability of municipal solid waste (MSW) incineration ash mixed with non-lateritic clay in pavement base layers. Chemical, physical, index, and mechanical tests were performed on the ash-soil mixture with 20% and 40% ash content, and the mechanistic-empirical design (Figure 3) for a typical pavement structure were carried out. The mechanical tests included modified Proctor test, resilient modulus test, and permanent deformation test. The addition of 20% fly ash to the non-lateritic clay soil improved the mechanical behavior and reduced the expansion of the clay. The fly ash mixed soil had a mechanical behavior compatible with the requirements for a low traffic volume.

Edil also focused on pavement geotechnics and provided an overview of different recycled waste products used in pavement construction. He discussed about the rapid characterization of industrial wastes like fly ash and bottom ash, and construction and demolition wastes (CDW) like recycled asphalt pavement and concrete aggregates with respect to their physical characteristics, geomechanical behavior, durability, material control, and environmental impact.

In another study related to pavements, Cameron et al. proposed the use of recycled concrete aggregates (RCA) blended with recycled clay masonry (RCM), obtained after demolition, in unbound granular pavements. The CDW were obtained from two local producers in South Australia, and conventional classification tests for soils and aggregates, Los Angeles abrasion test, Micro-Deval test, falling head permeability test, drying shrinkage test, undrained triaxial and repeated loading triaxial tests, and permanent strain rate modeling were performed. The test results were compared with the specifications from road authorities both within and outside Australia, and the RCA products were classified as Class 1 or base and the blended products as Class 2 or subbase materials.

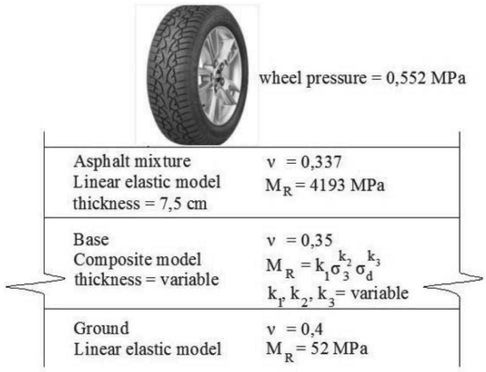

Figure 3. Pavement structure adopted in mechanistic-empirical analysis (Figure 1 of Vizcarra et al.).

Farias et al. also studied the feasibility of using CDW in paving of a shopping-center site in Recife, Pernambuco, Brazil. They performed a series of physical, chemical and mechanical tests with mixtures of different proportions of CDW obtained from the site and in situ excavated soil, and concluded that the recycled residues of civil construction (RRCC) alone and RRCC mixed with soil meet all the criteria of the local standard NBR 15.116:2004. Farias et al. (2013) also performed an economic analysis of different construction alternatives with the RRCC, which is described in section 3.5.

The study by Santos et al. also involves CDW. They presented a laboratory-scale experimental investigation on the performance of instrumented wrapped-faced retaining walls constructed using recycled construction and demolition wastes (RCDW) consisting of soil, bricks, and small particles of concrete. CDW is abundantly available in Brazil and approximately 70% by mass of municipal solid waste consist of CDW. CDW was found to have excellent mechanical and chemical properties for use as a back-fill material in geosynthetics reinforced walls. Consequently, two 3.6-m high, wrapped-faced retaining walls with facing batter angle of 13° were constructed at the University of Brasilia (UnB) Retaining Walls Test Facility. One retaining wall was constructed with geogrid and the other with geotextile with identical reinforcement lengths and spacings of 2.52 m and 0.6 m, respectively, using RCDW as the compacted backfill (Figure 4). The walls were instrumented along their central sections to measure strains, displacements, and earth pressures. The walls performed well during and after construction with the maximum horizontal displacement at the wall face being 150 mm. The only downside was the creation of uneven surfaces near the face due the presence of coarse particles. The use of a selected RCDW near the face for better aesthetic appeal was recommended.

Vaníček et al. presented an example of waste recycling in which a new construction material consisting of brick, fiber and concrete was used to reinforce dykes for flood protection and erosion control.

Winter discussed the use of lightweight tire bails (Figure 5) as a potential alternative for pavement foundation on soft soils. Tire bales comprise of 100 to 115 tires of light-goods vehicles and cars compressed into a lightweight block with a mass of about 800 kg and density of approximately 0.5 Mg/m^3. The bales measure approximately 1.3 m × 1.55 m × 0.8 m and are secured by five galvanized steel tie-wires running around the length and depth of the bale. The key advantage of tire bales is their modular nature which leads to potential savings in plant, labor, and time. These bales have been used in pavement constructions, slope protection, river bank erosion control, and lightweight embankment constructions. Winter described the different construction techniques and provided information regarding the measurement of properties, engineering properties and behavior associated with tire-bale use in construction, example applications, and end-of-service-life options.

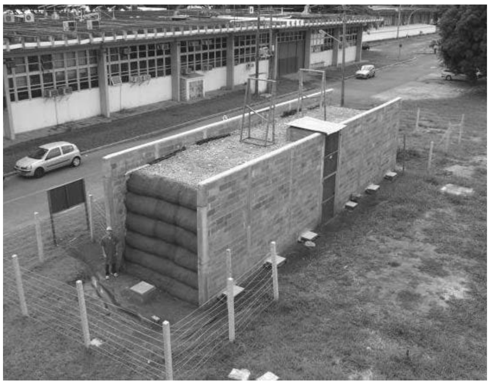

Figure 4. UnB retaining wall test facility (Figure 3 of Santos et al.).

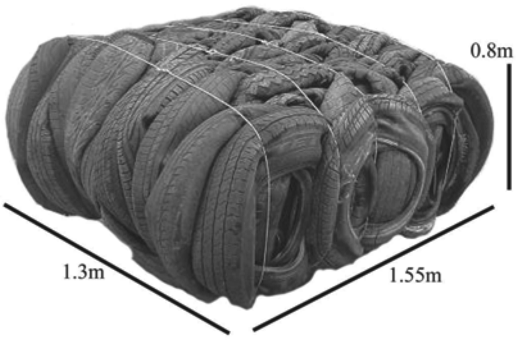

Figure 5. A typical tyre bale (Figure 1 of Winter).

Abdelhaleem et al. considered the use of recycled rubber and rubber-sand mixtures (RSM) as replacement soils in seismic areas due to the increased damping capacity of RSM. They performed site response analysis using the two-dimensional finite element method with equivalent-linear constitutive models for the geo-materials. Three earthquake ground motions of comparable magnitude and varying frequency content were applied to a deposit of sand with replacement soil and with different configurations of RSM. A parametric study was performed for investigating the effect of depth and thickness of the RSM layer and of the relative magnitudes of the natural period of the site and predominant period of earthquake on the sand-replacement soil-RSM system.

Kalumba and Chebet investigated the possibility of using discarded polyethylene shopping bags as soil reinforcement, and performed direct shear tests on Klipheuwel and Cape Flats sands mixed with perforated and non-perforated polyethylene strips of different lengths and of widths (Figure 6). Direct shear tests were performed with sand-polyethylene mixture and it was observed that there was an overall increase in the friction angle due to addition of the strips and that the increase in the friction angle depends on the length and width of the strips, perforations present in the strip, and percent weight of the strips (see, for example, Figure 7). Based on their results, Kalumba and Chebet suggested that the polyethylene strips can be used to increase the shear resistance of sandy soils.

Abdelrehman et al. performed a laboratory-scale study to investigate the efficacy of expanded polystyrene (EPS), a cellular polymeric material commonly used in the packaging industry, in reducing the heave in footings placed on expansive clay (Figure 8). They studied the compaction characteristics of EPS of different size and bead density mixed with silica sand. Subsequently, Abdelrehman et al. studied the response of circular footings of different diameters resting on a layer of sodium bentonite by replacing a part of the bentonite layer with the EPS-sand mixture. They performed a parametric study of the footing heave-settlement response as a function of different proportions of EPS-sand mixture, different replacement soil-layer thickness, footing size, and bead density. Abdelrehman et al. found that the swelling deformation of the footing decreases as the replacement-layer thickness increases.

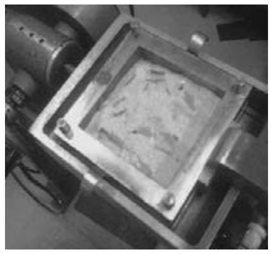

Figure 6. Direct shear tests with polyethylene chips from shopping bags (adapted from Figures 1b and 2b of Kalumba and Chebet).

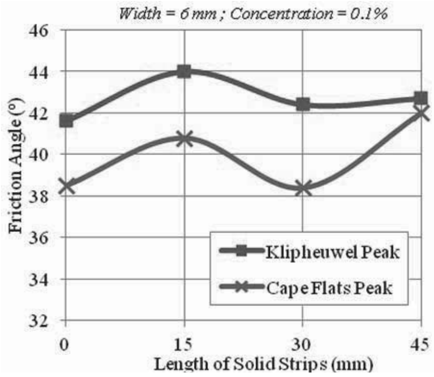

Figure 7. Friction angle of sand mixed with non-perforated polyethylene strips versus strip length (Figure 3a of Kalumba and Chebet).

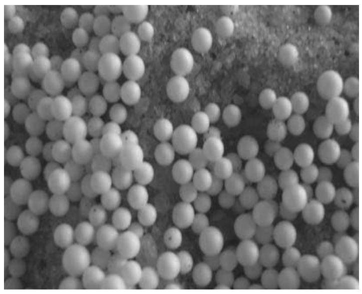

Figure 8. Expanded polystyrene (EPS) beads mixed with sand (Figure 1 of Abdelrehman et al.).

In another example of EPS recycling, Teymur et al. compared the performance of glass foam and EPS geo-foam as components of controlled low strength material (CLSM) often used as compacted backfill. They performed index tests, unconfined compression tests, and CBR tests, and found that glass mixtures have greater unit weight and strength than those of EPS foam mixtures. They concluded that glass foam CLSM can be used as pavement subbase, as fill for slopes and retaining structures, and to increase the strength and stiffness of soft clay deposits.

Drinking water sludge (DWS) discharged during water purification has potential use as a road infrastructure material (Watanabe and Komini). However, decomposition of the organic matter present in DWS decreases its shear strength because of which it is important to determine its durability for reuse. Watanabe and Komini collected DWS samples from Irabaki, Japan that contains aluminum and organic matters in the solid phase, and performed triaxial tests on the samples after subjecting them to aluminum leaching and biodegradation. They found that the shear strength of DWS decreases due to loss of organic matter and aluminum (Figure 9). Watanabe and Komini further quantified the effect of aluminum leaching and organic loss on the shear strength by modeling the leaching as a diffusion process and the organic loss as an exponential decay process. The study shows that DWS can be used in geotechnical applications.

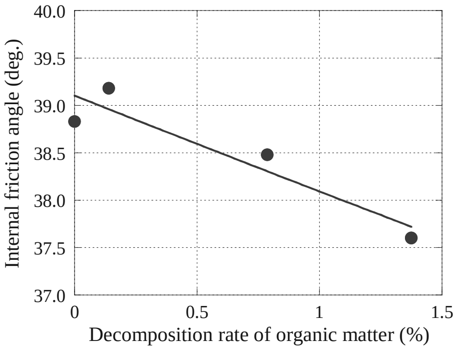

Figure 9. Friction angle of drinking water sludge as a function of decomposition rate of organic matter (Figure 7 of Watanabe and Komini).

Di Emidio et al. investigated the possibility of reusing dredged materials in landfill cover as a low-cost alternative. Enormous amounts of dredged material are generated from maintenance, construction, and remedial works related to water systems, and these materials are usually disposed of in landfills. Therefore, the reuse of dredged materials is important all over the world. For use in landfill cover, the dredged material must have low hydraulic conductivity and must retain the contaminants already present in it. In their study, Di Emidio et al. used dredged sediment obtained from Kluizendok in Ghent, Belgium and commercially processed kaolin Rotoclay® HB clay, and treated both with an anionic polymer Sodium CarboxyMethylCellulose (Na-CMC). Polymerization is particularly useful for dredged materials contaminated with metallic wastes. The authors investigated the mechanisms through which polymers can improve the efficiency of dredged sediments in waste containment impermeable barriers. Di Emidio et al. also conducted hydraulic conductivity and batch sorption tests to study the barrier performance and transport parameters of the treated dredged material and clay. The results showed that polymer treatment maintained low hydraulic conductivity of soil in electrolyte solutions and helped the material contain the spread of pollution. The results indicated that dredged sediments can be reused as alternative low-cost impermeable landfill cover.

Nakano and Sakai performed consolidation and triaxial tests on cement treated dredged soil samples collected from Nagoya Bay, Japan and modeled their elemental behavior using the SYS Cam-clay model. About 1.3 million m^3 of dredged soil is produced annually in Nagoya Bay, which has limited storage capacity because of which there is a pressing need for using the dredged soil as a geo-material. However, the clayey soil has low shear strength and high water content because of which cement is used as a stabilizer to improve its mechanical properties. The constitutive model of Nakano and Sakai reproduced the elemental test results reasonably well and the authors also performed finite element analysis using the software *GEOASIA* in order to capture the nonuniform deformation of triaxial test samples.

Air-foam treated lightweight soil, known as Super Geo-Material (SGM), is an example of an alternate material that is useful in harbor and airport constructions because of its light weight, safety features, and recyclability. Kataoka et al. mixed six different types of soils from Japan with seawater, blast furnace cement, and animal-protein hydrolyzed air-foam to prepare SGM specimens. They measured the unconfined compressive strength and small-strain shear modulus of the specimens, and studied their microstructure using a scanning electron microscope. Kataoka et al. observed that the strength and stiffness of the SGM samples increased with increase in the number of curing days, and attributed this increase to the growth and bonding of needle-like ettringite crystals within the SGM sample pores caused by the curing process.

Jefferis and Lam discussed the use of polymers as an alternative to bentonite in geotechnical construction fluids (slurries). Polymers have several advantages over bentonite in that polymer fluids require smaller preparation plants that can access congested urban areas, require shorter preparation time, and are environmentally less hazardous. In addition, constructions made with polymers have better performance than their bentonite counterparts. However, there are some limitations of polymers like reduction of fluid properties due to continued shear in recirculation systems and potential for loss of properties in saline soils. Therefore, Jefferis and Lam recommended that polymers should be used carefully with proper monitoring.

In order to investigate the reusability of in situ excavated soil with poor mechanical properties, Blanck et al. studied the effect of three non-traditional additives, an acid solution, an enzymatic solution, and a lignosulfonate, on the compaction characteristics and strength of silt. The test results showed that the acid solution did not improve the compaction characteristics and that adequate soil compaction can be achieved with low water content using the enzymatic solution and lignosulfonate. Blanck et al. concluded that enzymatic and lignosulfonate treatments would reduce water usage in constructions.

3.2 Efficient use of geosynthetics

The use of geosynthetics can reduce resource consumption and environmental impacts of geotechnical constructions, and can prevent soil erosion (Herteen 2012, Jones and Dixon 2011). Frischknecht et al. showed through life cycle assessment of pavement drainage systems that constructions using geosynthetics have less environmental impact.

Herteen et al. presented a general discussion on the use of geosynthetics, particularly geogrids, and pointed out that constructions with geosynthetics is more economical and environment friendly than traditional alternatives. According to Herteen et al., political reasons and population density and distribution often dictate the construction choices related to the national and international traffic routes within the European Union (EU), and geosynthetics can be used to advantage in many such constructions. The authors discussed about the use of geosynthetics in slope stabilization, reinforced earth walls, sound barrier walls, and embankments on soft clay, and pointed out the beneficial features of geosynthetics. They also discussed about the provisions given in Eurocode-7, German standards and British standards regarding constructions related to geosynthetics. Based on Herteen et al., it can be concluded that efficient, economic, aesthetically pleasing, and environment friendly constructions with minimal monitoring requirement are possible using geosynthetics.

3.3 Sustainable foundation engineering

Foundations form an integral part of geotechnical constructions, and sustainable design and construction of foundations are very important for overall sustainable development (Basu et al.). As part of sustainable foundation engineering, Basu et al. advocated the use of proper constitutive models and appropriate numerical analyses, adoption of reliability based design approach (e.g., LRFD), incorporation of spatial heterogeneity of soil in analysis and design, adoption of economical and environment friendly construction practices, reuse and retrofitting of existing foundations, and use of foundations in harvesting wind and geothermal energy.

Bourne-Webb et al. presented a case study of piled raft construction for a shopping center in Cambridge, UK as a cost-effective, time-saving and resource-efficient alternative to conventional pile foundations. Based on detailed site characterization that consisted of collection of data from adjacent sites, stress-path tests on bore hole samples, suction tests, and estimation of coefficient of earth pressure at rest, on monitoring of an instrumented basement of an adjacent hotel structure, and on linear and pseudo-nonlinear soil structure interaction analysis considering plate-on-spring approach, the piled raft foundation was designed with the piles used as settlement reducers. The design also ensured that there was minimal disturbance to the adjacent structures.

Reuse of foundations is often preferred over new foundations because reuse reduces waste disposal and environmental impact. Guilloux et al. presented three case studies of foundation reuse projects in Paris and Pantin. Figure 10 shows a cross section of one of the rehabilitation projects in Paris in which the existing pile foundations were strengthened by jet grouting and additional support was provided by newly installed micropiles. Guilloux et al. concluded that a site specific approach involving proper site characterization, condition assessment of existing foundations, delineation of existing and new foundation geometry, accurate estimation of changes in load, deformation and capacity during the construction process, consideration of different possible construction alternatives, proper choice of reinforcement technique, and proper monitoring is required for successful reuse of foundations. Vaníček et al. also advocated reuse of foundations particularly in the context of brownfield redevelopment.

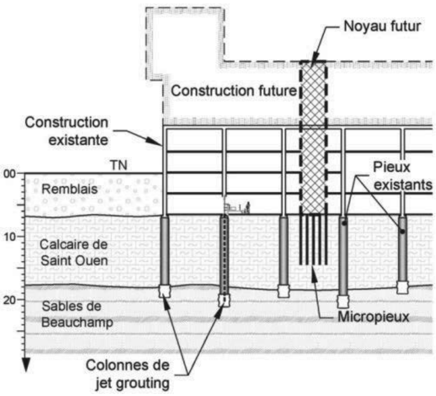

Figure 10. A cross section of foundation reuse project of Calberson warehouses, MacDonald Boulevard, Paris (Figure 1 of Guilloux et al.).

3.4 Subsurface remediation and site redevelopment

Redevelopment of contaminated sites including brownfield sites and landfills is an important part of sustainable geotechnics. According to Vaníček et al., brownfield redevelopment involves an initial reconnaissance study involving site characterization and economic feasibility study, followed by detailed site investigation, site remediation, and construction of new facilities at the site. Site remediation involves ground improvement by physical means (e.g., compaction and clay injection) and chemical treatment using encapsulation, permeable reactive barrier (Figure 11) and chemical stabilization. Vaníček et al. also provided an example of use of coal mine sites in Czech Republic where clayey overlays covering coal seams were excavated during mining activities and subsequently backfilled, and constructions were made on the mine sites using the mine-spoil heaps.

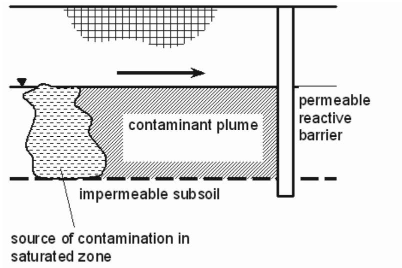

Figure 11. Site remediation by permeable reactive barrier (adapted from Figure 4 of Vaníček et al.).

McIntosh and Barthelmess provided a case study of reuse of a derelict (puticible waste) landfill site at Unanderra, NSW, Australia. Different geotechnical and geoenvironmental studies were conducted to assess the potential of the landfill site for construction. Environmental monitoring included testing of groundwater for contaminants and metals, and of gas monitoring wells for methane, hydrogen sulphate, and carbon dioxide. Monitoring for vibrations, noise and dust produced during site preparation was also conducted. The landfill density was increased by dynamic compaction, and environmentally neutral coal washery rejects locally present in the landfill site were used as cheap backfill material. A leachate control pond was constructed to receive the leachate during compaction and also to manage storm water on a long-term basis. Future civil and building services have been designed such that they do not penetrate the capping layer of the landfill. Driven steel piles bearing on underlying latite bedrock will be designed as building foundations. Flexible aprons will be provided between buildings and adjacent car parks, walkways and recreation areas, and raft slabs may be feasible for some lightweight, single-story buildings. The environmental design includes capping consisting of HDPE, GCL, geotextile fabric, 300 mm gravel gas drainage layer with a reinforcing geotextile, a gas drainage layer forming part of the cap, and leachate collection drains.

3.5 Sustainability assessment

The foregoing studies show that geotechnical engineering can contribute significantly to solutions of sustainability problems. Most studies are based on the common notions of sustainability like recycling, reuse, and use of alternate materials, technologies and resources. However, whether such new approaches are actually sustainable or not cannot be ascertained without proper assessment using, for example, whole life cost analysis and risk based performance analysis. Thus, a sustainability assessment framework is necessary for geotechnical projects to ascertain the relative merits of different options available for a project.

Frischknecht et al. performed a comparative life cycle assessment (LCA) of a pavement filtration system by comparing the performance of a gravel filter and a geosynthetics-based filter drain with the same hydraulic conductivity of 0.1 mm/s or more and with the same design life of 30 years. Life cycle inventory (LCI) of gravel and geosynthetics filter for a 1 m^2 functional unit was performed — Table 1 shows some key figures of LCI. Polypropylene granules was used as the basic material for the geosynthetics filter, and the LCI of geosynthetics manufacturing was performed using the ecoinvent data v2.2 based on the categories of raw materials, water, lubricating oil, electricity, thermal energy, fuel for forklifts and factory building. The environmental impact assessment (EIA) was performed considering eight impact indicators: cumulative energy demand, global warming potential, photochemical ozone formation, particulate formation, acidification, eutrophication, land competition, and water use. Based on the study, Frischknecht et al. found that the geosynthetics based filter layer causes lower environmental impact than the conventional gravel-based drain and that the environmental impact of geosynthetics manufacturing is mostly controlled by the impacts of raw-material production and electricity consumption during manufacturing.

Table 1. Selected key figures describing the constructions of one square meter of gravel and geosynthetics filter (Table 2 of Frischknecht et al.).

Material/Process	Unit	Gravel filter	Geosynthetics filter
Gravel	t/m^2	0.69	0
Geosynthetics layer	m^2/m^2	0	1
Diesel used in building machines	MJ/m^2	2.04	1.04
Transport, lorry	tkm/m^2	34.5	0.035
Transport, freight, rail	tkm/m^2	0	0.07
Particulates > 10 µm	g/m^2	4.8	0
Particulates > 2.5 µm and < 10 µm	g/m^2	1.3	0

Holm et al. developed an assessment and decision making tool for sustainable management of contaminated sediments in the Baltic sea, which included an emerging technology of solidification/stabilization. They presented the results of three case studies based on the ports of Oxelösund (Sweden), Gävle (Sweden) and Hamburg (Germany). Different management scenarios were considered at each port, and LCA were performed to choose the best options. Recycling of sediments, disposal in river and sea, energy use, and environmental impact were considered in the LCA. Holm et al. further developed a multicriteria decision analysis (MCDA) to integrate the three Es of sustainability in their decision making tool following a structured and balanced way.

Basu et al. also developed a multicriteria based sustainability assessment framework and applied it to pile foundation projects. The framework considers a life-cycle view of the pile construction process, and combines resource consumption, environmental impact, and socio-economic benefits of a pile-foundation project over its entire life span to develop a sustainability index (Figure 12).

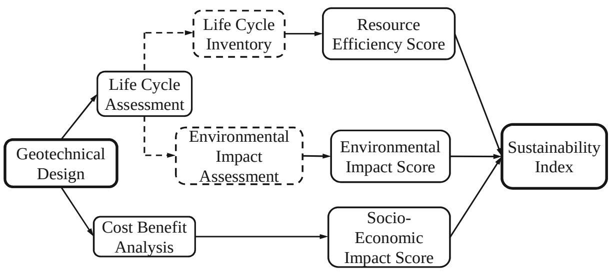

Figure 12. Multicriteria based sustainability assessment framework (Figure 3 of Basu et al.).

Edil provided an overview of the sustainability assessment tools used in pavement construction projects. He mentioned that LCA and life cycle cost analysis (LCCA) can be successfully used to assess the sustainability of pavement constructions. He further described a rating system for sustainable highway constructions known as Building Environmentally and Economically Sustainable Transportation-Infrastructure-Highways (BE^{2}ST-in-Highways^{TM}), which evaluates the sustainability of a highway project in terms of quantitative difference between a reference design and proposed alternative designs.

Farias et al. performed an economic analysis of different construction alternatives for their CDW paving project described in section 3.1. Although this is not a complete sustainability analysis, the environmental and social benefits are inherently present in the project. They considered two alternatives, first in which the CDW is completely disposed of in landfills and second in which the CDW and in situ soil mixture is used in paving the construction site. The high cost of disposal (Table 2) made the first option the most viable one with a direct cost savings of US$ 1.9 million, which does not even include the indirect cost-saving benefits from the reduced environmental impact that the project ensures.

Table 2. Costs for final disposition of wastes in licensed places (Table 6 of Farais et al.).

Disposition place	Unit	Unitary cost (US$)
Inert landfill	m^3	47.30
Processing plant	m^3	18.36

* Transportation cost not considered

In their study on the use of enzymatic solution and lignosulfonate as additives in silt (described in section 3.1), Blanck et al. performed LCA-EIA using 10 impact categories proposed in the NF P 01-010 standard. The analysis showed that the use of enzymatic solution reduces impacts in seven out of ten categories (Figure 13). The use of lignosulfate, however, did not produce sufficient environmental benefits.

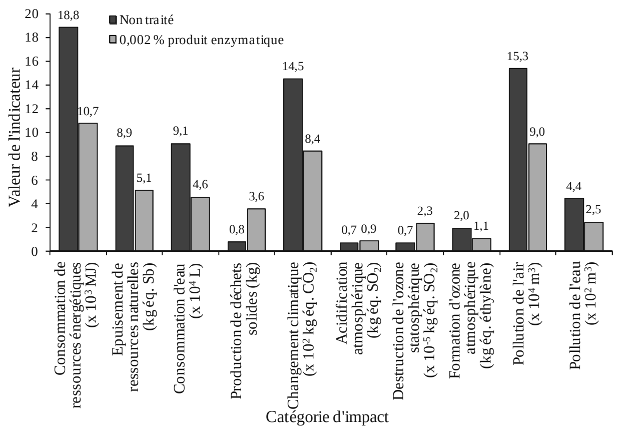

Figure 13. Results of environmental impact analysis for the use of enzymatic solution (Figure 3 of Blanck et al.).

4 IMPORTANT THEMES NOT COVERED

As sustainable geotechnics covers a wide range of topics, it is natural that the papers allocated to the sustainability session do not cover all the areas related to geosustainability. Some of the important topics not covered in details include sustainable site characterization, geohazard mitigation, reliability- and resilience-based analysis and design, geothermal energy foundations, geo-structures for wind and solar energy, sustainable ground improvement techniques, sustainable use of underground space, carbon sequestration, and ethical practices in geotechnical engineering. The other sessions and workshops of 18th ICSMGE cover some of these themes.

5 CONCLUSIONS

Sustainable geotechnics is a new sub-discipline focusing on geotechnical engineering practices that reduce the detrimental effects of geotechnical constructions and ensure the well being of the society and natural environment at all times. It not only includes environment-friendly practices that are cost effective and cause minimal financial burden to the present and future generations, but also promote reliability- and resilience-based design and adaptive management strategies so that social vulnerability is minimized and overall well being is upheld.

This general report provided an overview of this emerging area of geosustainability and reviewed the twenty eight papers allocated to the sustainability session of 18th ICSMGE. The authors of these papers represent 20 countries covering all the ISSMGE regions. Most of the papers emphasized the environmental aspect of sustainability, while some papers on sustainability assessment focused on the economic and social aspects. The topics covered by these papers can be broadly classified into five sub-themes: material recycling, reuse and use of alternate materials, efficient use of geosynthetics, sustainable foundation engineering, subsurface remediation and site redevelopment, and sustainability assessment. Although these papers deal with a variety of topics that contribute to the sustainable development of civil infrastructure and society, they do not cover all the important topics that are parts of sustainable geotechnics.

5 ACKNOWLEDGEMENT

Alain Corfdir helped us in interpreting the papers written in French for which we are grateful.

6 REFERENCES

Abdelhaleem A. M., El-Sherbiny R. M., Lotfy H. and Al-Ashaal A. A. 2013. Evaluation of rubber/sand mixtures as replacement soils to mitigate earthquake induced ground motions. *Proc. 18th ICSMGE*.

Abdelrahman G. E., Mohamed H. K. and Ahmed H. M. 2013. New replacement formations on expansive soils using recycled EPS beads. *Proc. 18th ICSMGE*.

Basu D., Puppala A. J. and Chittoori C. S. 2013. Sustainability in geotechnical engineering. *Proc. 18th ICSMGE*.

Baykal, G. 2013. Mechanics of manufactured soil using powder wastes. *Proc. 18th ICSMGE*.

Blanck G., Cuisinier O. and Masrouri F. 2013. Méthodes non traditionnelles de traitement des sols : apports techniques et impact sur le bilan environnemental d'un ouvrage en terre. *Proc.18th ICSMGE*.

Bourne-Webb P., Cunningham M. and Card G. 2013. Advanced testing and modelling delivers cost effective piled raft foundation solution. *Proc. 18th ICSMGE*.

Cameron D. A., Rahman M. M., Azam A. M., Gabr A. G., Andrews R. and Mitchell P. W. 2013. The use of recycled aggregates in unbound road pavements. *Proc. 18th ICSMGE*.

Di Emidio G., Verastegui Flores R. D. and Bezuijen A. 2013. Reuse of dredged sediments for hydraulic barriers: adsorption and hydraulic conductivity improvement through polymers. *Proc. 18th ICSMGE*.

Dixit M. K., Fernandez-Solis J. L., Lavy S. and Culp C. H. 2010. Identification of parameters for embodied energy measurement: a literature review. *Energy and Buildings* 42, 1238-1247.

Edil T. B. 2013. Characterization of recycled materials for sustainable construction. *Proc. 18th ICSMGE*.

Edwards A. R. 2005. *The sustainability revolution*. New Society Publishers.

Farias A., Fucale S., Gusmão A. and Maia G. 2013. Technical and economic analysis of construction and demolition waste used in paving project. *Proc. 18th ICSMGE*.

Frischknecht R., Stucki M., Blüsser-Knöpfel S., Itten R. and Wallbaum H. 2013. Comparative life cycle assessment of geosynthetics versus conventional filter layer. *Proc. 18th ICSMGE*.

Guilloux A., Le Bissonnais H., Saussac L. and Perini T. 2013. La réutilisation des fondations existantes dans les projets de réhabilitation de constructions anciennes. *Proc. 18th ICSMGE*.

Herteen G., Vollmert L. and Herold A. 2013. Modern geotechnical construction methods for important infrastructure buildings. *Proc. 18th ICSMGE*.

Herteen G. 2012. Reduction of climate-damaging gases in geotechnical engineering practice using geosynthetics. *Geotextiles and Geomembranes* 30 43- 49.

Holm G., Lundberg K. and Svedberg B. 2013. Sustainable management of contaminated sediments. *Proc. 18th ICSMGE*.

Jefferis S. A. and Lam C. 2013. Polymer support fluids: use and misuse of innovative fluids in geotechnical works. *Proc. 18th ICSMGE*.

Jones, R. and Dixon N. 2011. Sustainable development using geosynthetics: European perspectives. *Geosynthetics*, June 2011.

Kalumba D. and Chebet F. C. 2013. Utilisation of polyethylene (plastic) shopping bags waste for soil improvement in sandy soils. *Proc. 18th ICSMGE*.

Kataoka S., Horita T., Tanaka M., Tomita R. and Nakajima M. 2013. Effect of dredge soil on the strength development of air-foam treated lightweight soil. *Proc. 18th ICSMGE*.

Kiber C. J. 2008. *Sustainable construction – green building design and delivery*. John Wiley and Sons Inc.

Kikuchi Y. and Mizutani, T. 2013. Application of a method to accelerate granulated blast furnace slag solidification. *Proc.18th ICSMGE*.

Long J. C. S., Amadei B., Bardet J.-P., Christian J. T., Glaser S. D., Goodings D. J., Kavazanjian E., Major D. W., Mitchell J. K., Poulton M. M. and Santamarina J. C. 2009. *Geological and geotechnical engineering in the new millennium: opportunities for research and technological innovation.* The National Academic Press, Washington D.C.

McIntosh G. W. and Barthelmess A. J. 2013. Building on an old landfill: design and construction. *Proc.18th ICSMGE.*

Nakano M. and Sakai T. 2013. Interpretation of mechanical behavior of cement-treated dredged soil based on soil skeleton structure. *Proc. 18th ICSMGE*.

Nawagamuwa U. P., Senanayake A. and Rathnaweera T. 2013. Utilization of waste copper slag as a substitute for sand in vertical sand drains and sand piles. *Proc. 18th ICSMGE*.

Pantelidou H., Nicholson D. and Gaba A. 2012. Sustainable geotechnics. *Manual of Geotechnical Engineering* 1, Institute of Civil Engineers, U. K.

Puppala A. J., Saride S. and Williammee R. 2012. Sustainable reuse of limestone quarry fines and RAP in pavement base/subbase layers. *Journal of Materials*, ASCE, 24(4), 418–429.

Santos E. C. G., Bathurst R. J. and Palmeira E. M. 2013. Experimental reinforced soil walls built with recycled construction and demolition waste (RCDW). *Proc. 18th ICSMGE*.

Saride S., Puppala A. J., Williammee R. 2010. Assessments of recycled/secondary materials in pavement. *Ground Improvement Journal*, Thomas Telford, GI 163(GI1), 3-12.

Teymur B., Tuncel E. Y. and Ahmedov, R. 2013. Comparing the properties of EPS and glass foam mixed with cement and sand. *Proc. 18th ICSMGE*.

Vaníček M., Jirásko D. and Vaníček I. 2013. Geotechnical engineering and protection of environment and sustainable development. *Proc. 18th ICSMGE*.

Vizcarra G., Szeliga L., Casagrande M. and Motta L. 2013. Applicability of municipal solid waste (MSW) incineration ash in road pavements. *Proc.18th ICSMGE.*

Vukićević M., Maraš-Dragojević S., Jocković S., Marjanović M. and Pujević V. 2013. Research results of fine-grained soil stabilization using fly ash from serbian electric power plants. *Proc.18th ICSMGE*.

Watanabe Y. and Komine. H. 2013. Simplified prediction of changes in shear strength in geotechnical use of drinking water sludge. *Proc. 18th ICSMGE*.

Winter M. G. 2013. Road foundation construction using lightweight tyre bales. *Proc. 18th ICSMGE*.

Evaluation of Rubber/Sand Mixtures as Replacement Soils to Mitigate Earthquake Induced Ground Motions

Évaluation du mélange sable-caoutchouc comme sol de remplacement pour atténuer les mouvements sismiques

Abdelhaleem A.M.
Construction Research Institute, National Water Research Center, Egypt

El-Sherbiny R.M., Lotfy H.
Cairo University, Egypt

Al-Ashaal A.A.
Construction Research Institute, National Water Research Center, Egypt

ABSTRACT: Use of recycled rubber and rubber/sand mixtures (RSM) as lightweight material has been widely growing over the past decade. The increased damping capacity of RSM leads to considering its use as replacement soils in seismic areas to reduce the amplitude of earthquake induced ground motions. This paper presents a study on the effect of utilizing a layer of RSM within a replacement soil on the ground response during an earthquake. Site response analyses were performed using 2D finite element analyses applying an equivalent-linear constitutive model. Three earthquake ground motions of varying frequency content were applied to a deposit of sand with replacement soil having different configurations of RSM. Placing a layer of RSM within the replacement soil resulted in increasing the site natural period causing damping of spectral accelerations at low periods and amplification of spectral accelerations at high periods. Using a thin layer of RSM at deeper depths was more effective in than using thick but shallow RSM layers. The results indicate that RSM layers may be effective when the predominant period of the earthquake is lower than the site natural period, while the configuration is subject to the natural period of the intended structure.

RÉSUMÉ: Le caoutchouc recyclé et les mélanges sable-caoutchouc (MSC) en tant que matériaux légers ont eu une utilisation accrue au cours de la dernière décennie. L'augmentation de la capacité d'amortissement de MSC conduit à considérer son utilisation en tant que remplacement des sols dans les zones sismiques afin de réduire l'amplitude des secousses observées pendant les tremblement de terres. Cet article présente les résultats d'une étude sur l'influence des couches de MSC comme sol de remplacement sur la réponse du sol au cours d'un tremblement de terre. L'analyses de réponses du site ont été réalisées en utilisant la méthode d'éléments finis 2D appliquée sur un modèle constitutif du type « linéaire équivalent ». Trois régimes de tremblements de terre de fréquence variable ont été appliqués à un dépôt de sable avec terres de remplacement ayant différentes formulation de MSC. Placer une couche de MSC dans le sol de remplacement a eu pour effet d'augmenter la période naturelle du site; et ceci provoque une atténuation des accélérations spectrales à des périodes faibles et une amplification de la même accélération aux périodes fortes. L'application d'une mince couche de MSC à des profondeurs importantes a été plus efficace que d'utiliser des couches épaisses peu profondes. Les résultats indiquent que les couches MSC ne peuvent être efficaces que si la période dominante du tremblement de terre est inférieure à la période naturelle du site, et ceci en maintenant la configuration soumise à la même période naturelle de celle de la structure en question.

KEYWORDS: Recycled Material, Rubber-Sand Mixture, Replacement Soil, Earthquake Mitigation

1 INTRODUCTION

The use of recycled rubber and rubber/sand mixtures (RSM) as lightweight material in civil engineering applications has been widely growing over the past decade. Processed waste tires mixed with soils have been introduced as lightweight fills for slopes, retaining walls, and embankments. The mechanical properties of the mixture were discussed by (Edil and Bosscher, 1994; Ghazavi, 2004; Zornberg et al., 2004; and Mavroulidou et al., 2009), while dynamic properties of granulated rubber-sand mixtures were studied by (Feng et al., 2000; and Anastasiadis et al., 2012). Xu et al. (2009) performed numerical studies on protecting buildings from earthquakes hazards by RSM.

The utilization of RSM as replacement soils in seismic areas to reduce the amplitude of earthquake induced ground motions is addressed in this paper. The effect of changing the depth and thickness of the RSM layer will be investigated in this study. The results will be compared for a range of medium amplitude ground motions.

Data used in this parametric study is based on a comprehensive set of torsional resonant column tests performed for different dry and saturated specimens of sand-rubber mixture, (Senetakis et al., 2012). Based on these tests, the modulus reduction and damping curves can be generated for the sand-rubber mixture as a function of confining pressure. The parametric study is based on two-dimensional finite element analyses that can model seismic effects and site response of multilayered soil profile.

2 PROPERTIES OF PARENT MATERIALS

The properties of parent materials for the RSM used in this numerical analysis are based on results of the study by Senetakis et al. (2012). In this study, dry sand of specimen code (C3D06) and rubber material of specimen code (R3) were used as parent materials for the RSM of specimen code (C3D06-R3). The sand is natural of sub-rounded to rounded particles, whereas the rubber is granulated from recycled tire shreds. The properties of the parent materials is indicated in Table 1.

Table 1. Properties of sand and granulated rubber

Material	**Sand**	**Granulated rubber**
Unit weight, □ (kN/m3)	16.50	6.50
Specific gravity, Gs	2.67	1.10
Max. particle size, D_{max} (mm)	0.85–2.00	4.75–6.35
50% passing size, D_{50} (mm)	0.56	2.8
Coefficient of uniformity, Cu	2.76	2.29
Coefficient of curvature, Cc	1.23	1.18

The RSM used in the analyses herein was assumed to contain 35% rubber content (by weight) and a dry unit weight of 12.5 kN/m^2. The modulus reduction and damping curves of dry RSM (C3D06-R3) for different confining pressures (σ'_m) were generated according to Senetakis et al. (2012). The modulus reduction and damping curves of dry rubber-sand mixture (C3D06-R3), sand (C3D06), and the replacement soil at confining pressures (σ'_m = 50 kPa) are shown in Figure 1. The small strain shear modulii for the sand, RSM, and replacement soil are 65.6 MPa, 10.4 MPa, and 234 MPa, respectively.

3 NUMERICAL MODEL

A number of two-dimensional finite element models were built in QUAKE/W to evaluate the site response during an earthquake. The soil was modeled using an equivalent linear constitutive model. The baseline case representing the untreated site condition constitutes a 20 m thick layer of sand above bedrock. Two additional layers were inserted into the original model to simulate replacement soil and RSM layers in the different numerical analyses, as shown in Figure (2). The width of the RSM layers was assumed 20m.

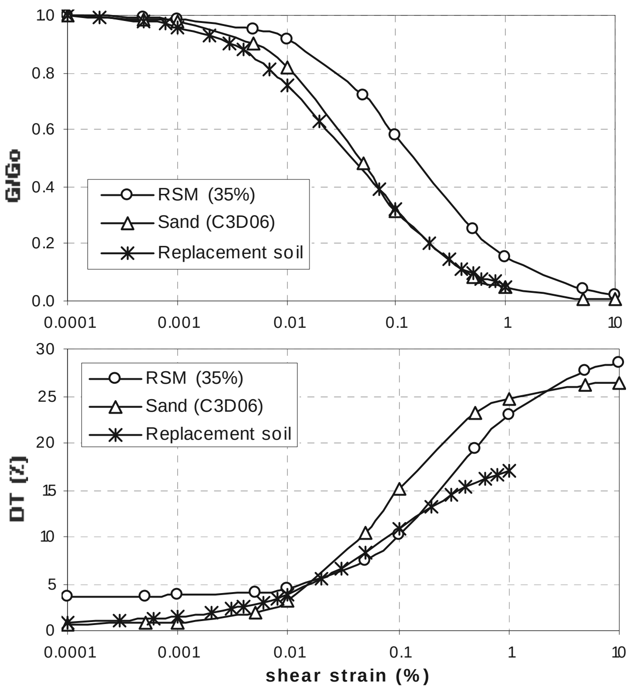

Figure 1. The modulus reduction and damping curves at ($\sigma'm$ = 50 kPa)

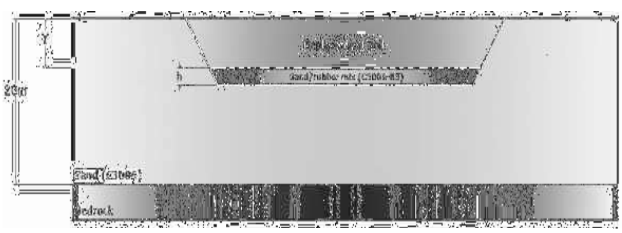

Figure 2. The FEM model used in the numerical study

The effect of changing the depth and thickness of the RSM layer and the replacement soil on top on the site response during earthquakes was investigated. An RSM layer 1 m thick was first assumed to be placed at depths of 1m, 2m, 4m, and 6m. The thickness of the RSM layer was then changed to 2m, 4m, and 6m at a depth of 2m to the top of the layer.

It is important to specify the geotechnical site category that helps us to determine the site natural period for the baseline case which consists of 20 m of pure sand above extended base bedrock. Site period can be obtained depending on the depth and characteristics of the soil deposit (Bray and Rodriguez-Marek, 1997). Because the sand soil deposit depth is greater than 6m and less than 30m, the site is classified as "Shallow Stiff Soil" and the site natural period will be around (0.5 sec), (Bray and Rodriguez-Marek, 1997).

4 EARTHQUAKE GROUND MOTIONS

Three earthquake ground motions of comparable magnitude and different frequency content were used to investigate the ground surface layer response in case of pure sand deposit (baseline case) and in cases of the existence of the RSM layer. The earthquake ground motions data were obtained from the ground motion database of the Pacific Earthquake Engineering Research Center (PEER). The ground motion database includes a very large set of ground motions recorded in worldwide shallow crustal earthquakes in active tectonic regimes. Figure (3) shows the response spectrum of earthquake input ground motions, and Table (2) summarizes their characteristics. The predominant period of the selected input ground motions varies between lower than the site natural period (T_{site} = 0.5 sec) such as in Lytel Creek (T_p = 0.08 sec) and San Francisco (T_p = 0.26 sec), and greater than the site natural period such as in Mammoth Lake earthquake (T_p = 0.925 sec) in order to cover a range of frequency contents for intermediate earthquakes.

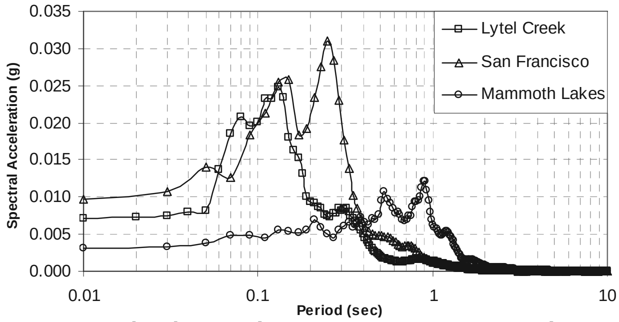

Figure 3. Earthquake ground motions response spectrum at damping ratio (5%)

Table (2): Earthquake ground motions characteristics

Event Name	Magnitude (M)	Peak Grnd. Accel. PGA (g)	Predominant Period, T_p (sec)	Station
Lytel Creek (1970)	5.33	0.070	0.130	Cedar Springs, Allen Ranch
San Francisco (1957)	5.28	0.095	0.260	Golden Gate Park
Mammoth Lake (1980)	4.73	0.031	0.925	USC Cash Baugh Ranch

5 RESULTS AND DISCUSSION

The influence of two parameters on the site response was studied, namely the depth of the rubber-sand mixture layer (Y) and the thickness of the rubber-sand mixture layer (h).

A. Depth of the rubber-sand mixture layer (Y)

The numerical simulations were performed for the baseline model (Pure sand) and for another three models in which a 1 m thick layer of RSM were placed at depths of 2m, 4m, and 6m. The three different input ground motions were applied to each model. The replacement soil on top of the RSM layer was modeled as a well compacted sand-gravel mixture layer with a unit weight of 20 kN/m^2. The modulus reduction and damping curves for the replacement soil are shown in Figure 1. The thickness of the replacement soil is the same as the depth of the RSM layer from ground surface (Y).

The response spectra at ground surface were plotted to investigate the effect of changing the depth of the RSM layer on the ground response. Figure (4) shows the results for the three earthquake ground motions. The results were divided into two groups. The first group is for earthquake ground motions that have a predominant period less than the site natural period (T_p < T_{site}), i.e. Lytel Creek (1970) and San Francisco (1957) earthquakes. The second group is for earthquake ground motions that have a predominant period grater than the site natural period (T_p > T_{site}), i.e. Mammoth Lake earthquake.

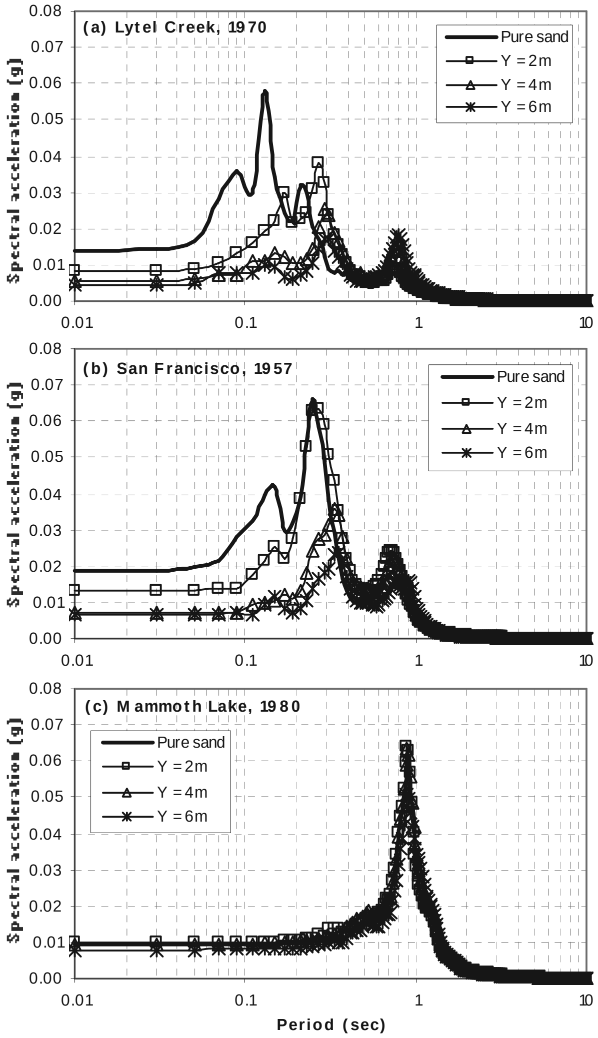

Figure 4. Response spectra of surface layer for variable RSM depth having thickness (h =1 m)

<u>*Group (1) - (T_p < T_{site})*</u>

This group contains two earthquake ground motions, Lytel creek and San Francisco. The response of this group due to increasing the depth of the RSM layer is summarized below.

Because the predominant period of the ground motion is less than the site natural period, amplification may occur at the fundamental or at secondary order periods of the site. The amplification factor between the spectral acceleration (Sa) at bedrock layer and at the surface layer has a maximum value at the fundamental period of the site. This value is reduced strongly in the successive secondary order periods.

Placing a layer of RSM resulted in increasing the site natural period causing shifting in the fundamental and secondary site periods to higher periods. Shifting of the site periods leads to maximum amplification at higher – more damped periods. This resulted in damping of spectral accelerations at lower periods and amplification of spectral accelerations at higher periods when using RSM compared to the baseline case (pure sand).

Increasing the depth of the rubber-sand mixture layer resulted in increasing the shifting towards the higher periods that leads to a higher order matching between site periods and ground motion predominant period (T_p). Thus, increasing the depth of the rubber-sand mixture layer resulted in highly damped response spectra of the surface layer at lower periods and amplification at higher periods (Figure 5). Increasing the RSM depth to 4m resulted in reduction in the maximum spectral acceleration reaching up to 56% to 45% in case of Lytel Creek and San Francisco earthquakes, respectively. Placing the RSM layer at 6m depth resulted in reduction in the maximum spectral acceleration ranging from 71% to 64% for the case of Lytel Creek and San Francisco earthquakes, respectively, compared to the baseline case (Pure sand).

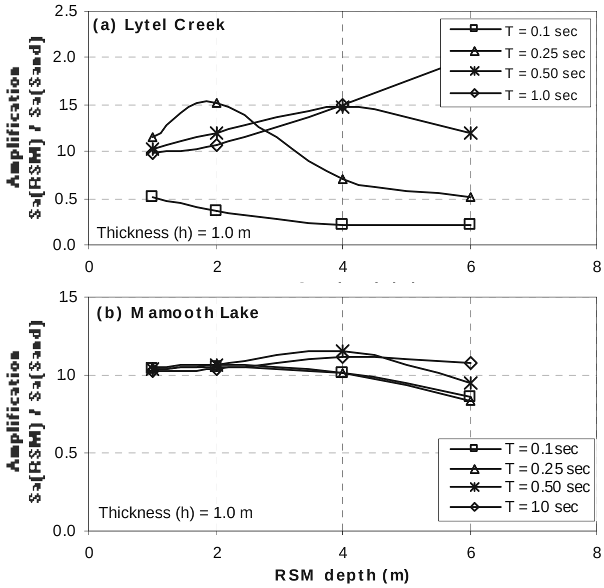

Figure 5. Effect of RSM depth on spectral acceleration

<u>*Group (2) - (Tp > Tsite)*</u>

This group contains only one earthquake ground motion, which is Mammoth Lake (1980). Because the predominant period of the ground motion is greater than the site natural period, significant amplification does not occur neither at the fundamental site period nor at secondary order periods. Increasing the depth of the RSM layer resulted in insignificant effect on the surface layer response spectrum. Placing the RSM layer at depths 2m and 4m resulted in approximately the same surface layer response spectrum of the baseline case (Pure sand). Placing the RSM layer at 6m depth resulted in a small reduction in the maximum spectral acceleration equals to 16 % compared to the baseline case (Pure sand), and this percentage may be slightly increased if RSM layer is put in deeper level.

B. Thickness of the rubber-sand mixture layer (h).

In this section, the numerical simulations were performed for the baseline model (pure sand) and for another three different models including RSM layers of varying thickness. Different values for the thickness of the RSM layer (h) were chosen to be 2m, 4m and 6m in the models, while the depth of the top of the RSM layer was constant at (Y=2 m) below ground surface in all simulations. The three different input ground motions were applied to each model. In case of Mammoth Lake earthquake, an additional simulation was performed with an RSM layer thickness of 9m.

The result of simulations was plotted in terms of the response spectrum of the ground surface layer to investigate its response to the change in the thickness of the RSM layer. Figure (6) shows the simulation results for the three different earthquake ground motions. Similar to the previous section, the results can be divided into two groups as follow:

<u>*Group (1) - (T_p < T_{site})*</u>

Increasing the thickness of the RSM layer caused decreasing of low period spectral acceleration and also caused considerable increasing in the high period spectral acceleration comparing by the base line case (balancing). This is evident from the amplification factors plotted in Figure (7) against different RSM thicknesses for different periods. Comparing to the baseline case (pure sand), at thickness of RSM layer equals to 6m a reduction in the maximum spectral acceleration in cases of Lytel Creek and San Francisco earthquakes ranged from 47% to 36%, respectively.

Group (2) - ($T_p > T_{site}$)

Increasing the thickness of the RSM layer from 1m to 4m caused increasing in the maximum spectral acceleration compared to the base line case. Increasing the thickness of the RSM layer from 4m to 6m resulted in a reduction in the maximum spectral acceleration decreased but still higher than the maximum spectral acceleration in the base line case. Increasing the RSM thickness to 9m resulted in reduction in the maximum spectral acceleration equals to 38% compared to the baseline case. Increasing the thickness of the RSM layer from 1m to 4m caused increasing in the spectral acceleration at low and high periods compared to the base line case (Figure 7). However, further increase in the thickness up to 9m resulted in a reduction in the amplification factor below the baseline case.

6 CONCLUSIONS

The following main points may be concluded based on the analyses presented herein:

- The effect of using RSM layer is dependant on the site natural period and the frequency content of the ground motion, while the effective configuration of the RSM layer is subject to the natural period of the intended structure.
- Placing a layer of RSM resulted in increasing the site natural period causing damping of spectral accelerations at low periods and amplification of spectral accelerations at higher periods compared to the baseline case.
- The deeper the RSM layer, the larger the shift in site natural period resulting in more effective damping and lower response spectrum at ground surface for a wider range of periods. Thus, the higher the natural period of the structure, the deeper the sand/rubber layer needed to achieve damping.
- For the same excavation depth, using a thin layer of RSM at the bottom of the excavation is more effective in damping the spectral accelerations at ground surface than using a thick layer of RSM.
- Settlements and creep in RSM layer should be studied in case of large thickness.
- Further investigation is needed to confirm the observation through physical and numerical modeling for earthquakes of different magnitude, amplitude, and frequency content.
- Soil structure interaction needs to be further investigated to examine the effect of the overlaying structure on the response.

7 REFERENCES

Anastasiadis, A., Senetakis, K., Pitilakis, K., Gargala, C., and Karakasi, I. (2012) "Dynamic Behavior of Sand/Rubber Mixtures. Part I: Effect of Rubber Content and Duration of Confinement on Small-Strain Shear Modulus and Damping Ratio," J. ASTM Int'l., 9(2).

Bray, J. D., and Rodriguez-Marek, A. (1997). "Geotechnical Site Categories." Proceedings First PEERPG&E Workshop on Seismic Reliability of Utility Lifelines, San Francisco, CA.

Edil, T.B. and Bosscher, P.J. (1994). "Engineering Properties of Tire Chips and Soil Mixtures," Geotech. Testing J., ASTM 17(4), pp. 453-464.

Feng, Z., and Sutter K.G. (2000). "Dynamic Properties of Granulated Rubber/Sand Mixtures," Geotech. Testing J., ASTM, Vol. 23, No. 3, September, pp. 338-344.

Ghazavi, M., (2004). "Shear Strength Characteristics of Sand-Mixed with Granular Rubber," Geotechnical and Geological Engineering, Vol. 22, pp. 401-416.

Mavroulidou, M., Etan, O., and Suntharalingam, M. (2009). "Mechanical Properties of Granulated Tyre Rubber-Sand Mixture," Proceedings of the 11th International Conference on Environmental Science and Technology, Crete, Greece, 3-5 September.

Senetakis, K., Anastasiadis, A., Pitilakis, K., and Souli, A. (2012). "Dynamic Behavior of Sand/Rubber Mixtures. Part II: Effect of Rubber Content on G/Go-g-DT Curves and Volumetric Threshold Strain," J. ASTM Int'l., 9(2).

Xu, X., Lo, S.H., Tsang, H.H., and Sheikh, M.N. (2009). " Earthquake Protection by Tire-Soil Mixtures: Numerical Study," New Zealand Society for Earthquake Engineering Conference Proceedings, Christchurch, New Zealand, April.

Zornberg, J.G., Cabral, A.R., and Viratjandr, C. (2004). "Behaviour of Tire Shred – Sand Mixtures," Canadian Geotech. J., Vol. 41, April, pp. 227-241.

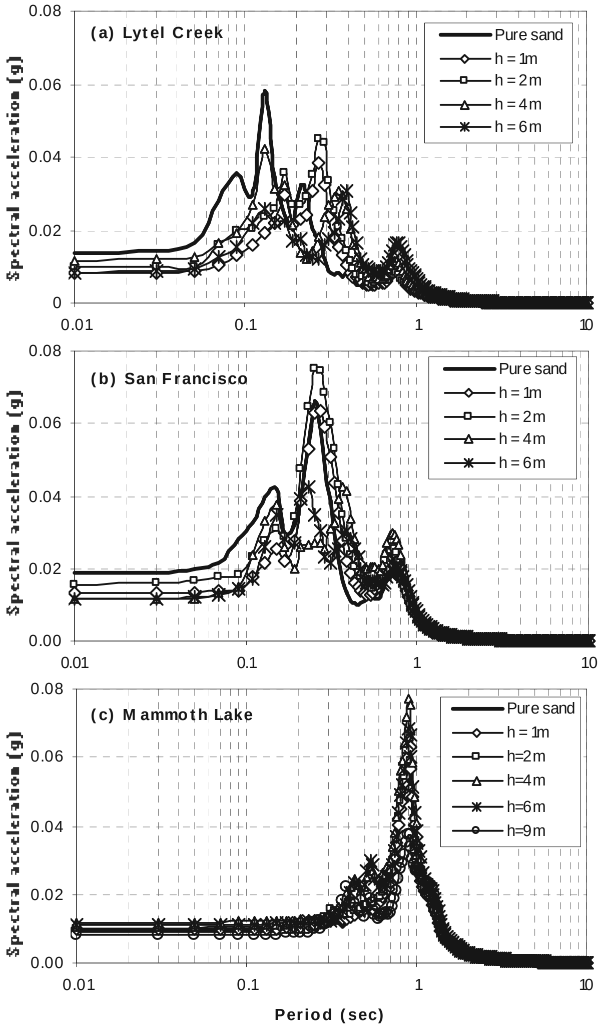

Figure 6. Response spectra of surface layer for variable RSM thickness having depth (Y = 1m) to top of RSM layer

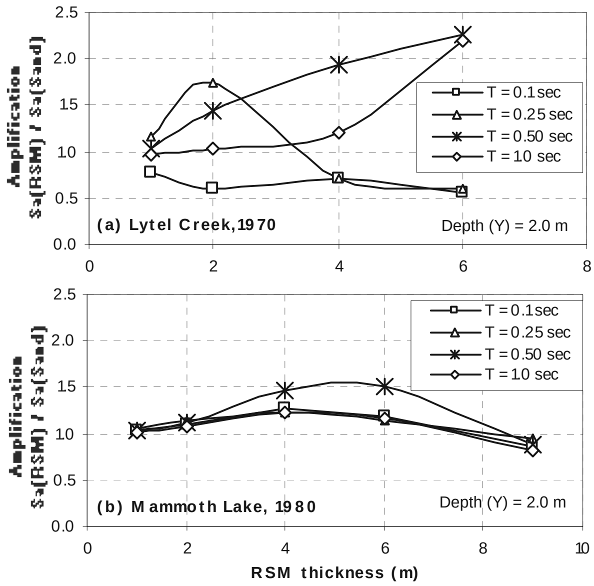

Figure 7. Effect of RSM thickness on spectral acceleration

New Replacement Formations on Expansive Soils Using Recycled EPS Beads

Remplacement sur les sols expansifs en utilisant des perles EPS

Abdelrahman G.E.
Civil Engineering Department, Faculty of Engineering, Fayoum University, Egypt

Mohamed H.K.
Soil Mechanics and Geotechnical Engineering Institute, Housing and Building National Research Center (HBRC), Egypt

Ahmed H.M.
Civil Engineering Department, Faculty of Engineering Cairo University, Egypt

ABSTRACT: One of the main problems encountered in constructing foundations on clays is volume change independent of loading caused by swelling of the soil. When the swelling is obstructed, large swelling pressures arise and that can cause damage to structures. This study examines the role of recycled expanded polystyrene (EPS) beads which is mixing with replaced soil in accommodating soil expansion and hence reducing swelling pressures on structures foundation. Laboratory tests are presented on the formation of expansive soil using Bentonite clay. Laboratory model was used to measure the decrease of the swelling, using replacement material which formed of blending sandy soil with recycled (Expanded Poly-Styrene) EPS-beads. The effect of different compositions and different ratios between EPS-beads, and sand as a replacement soil on the expansive soil (Bentonite powder, PI=95.4%, and G_s=2.55) which had free swell equal to 96.7% were studied. Results so far show that the EPS beads mixed with sand significantly reduces the volumetric change of the expansive soils. The parametric study showed that increasing EPS beads percentage in the replacement soil decreases bearing capacity and dry density γ_d, and increases OMC while for the Bentonite free swell decreases and settlement increases. Increasing footing breadth increases swelling and settlement. With increasing replacement layer thickness and beads density, the swelling and settlement decrease.

RÉSUMÉ : Un des principaux problèmes rencontrés dans la construction des fondations sur des argiles est le changement de volume indépendant de chargement provoqué par le gonflement du sol. Lorsque le gonflement est obstrué, les grandes pressions de gonflement surviennent et peuvent causer des dommages aux structures. Cette étude examine le rôle du polystyrène expansé recyclé (EPS) des perles qui est le mélange avec le sol remplacé en accueillant l'expansion du sol et donc la réduction des pressions sur le gonflement de fondation des structures. Des essais en laboratoire sont présentés sur la formation des sols expansifs avec de l'argile bentonite. Modèle de laboratoire a été utilisé pour mesurer la diminution de l'enflure, l'utilisation du matériel de remplacement qui a formé de l'assemblage avec des sols sablonneux recyclés (Expanded Poly-Styrène) EPS-perles. L'effet de différentes compositions et différents ratios entre les EPS-perles, et le sable du sol comme un remplacement sur le sol expansive (bentonite en poudre, PI = 95,4%, et GS = 2,55), qui avait sans égale gonfler à 96,7% ont été étudiés. Les résultats obtenus jusqu'ici montrent que les perles EPS mélangés avec du sable réduit considérablement le changement volumétrique des sols gonflants. L'étude paramétrique a montré que l'augmentation des EPS perles de pourcentage dans le sol de remplacement diminue la capacité portante et la densité sèche γd, et augmente OMC alors que pour la bentonite diminue la houle libres et augmente de règlement. L'augmentation de la largeur de fondation augmente l'enflure et de règlement. Avec une épaisseur de remplacement couche augmente et la densité des perles, l'enflure et la diminution de règlement.

KEYWORDS: Recycled expanded polystyrene, beads, expansive soils, swelling, sand, Bentonite.

1 INTRODUCTION

Problems related to expansive soils exist worldwide. Many buildings, light structures, highways, railways, airport slabs, water channels, pipelines, earth retaining walls, dams and bridges are damaged by expansive soils. One of the main problems encountered in constructing foundations on clays is volume change independent of loading caused by swelling and shrinkage of the soil. When the swelling is obstructed, large swelling pressures arise and that can cause damage to structures. There are many conventional treatments available for control of these problems. These include soil replacement with compaction control, moisture control, surcharge loading and thermal methods (Chen, 1988; Nelson and Miller, 1992). However, these methods have their own limitations with regards to their effectiveness and costs.

Expanded polystyrene (EPS) is a cellular polymeric material commonly used as a packaging medium for a variety of consumer appliances and electronic equipment. It is a lightweight material with a very low density (0.10 -0.20 kN/m^3) .Due to its convenience and low cost, EPS usage is increasing in the consumer market. That in turn results in a continuing increase in the availability of waste EPS products. Because of their lightweight and bulk nature, the waste EPS products occupy a substantial area of the landfill. Unlike other organic materials, EPS is not decomposable or biodegradable. Because of these problems, the European Union has restricted the disposal of EPS into landfills and set recycling targets (PPW Directive, 2005; UNEP, 2000). These impositions have forced manufactures to look for alternative reuse and recycle options. There are many recycling options available like thermal and compression methods. However, possible contamination of the products while in transportation and their limited usage make some of the products unsuitable for recycling. Hence there is a need to try other innovative applications for the bulk utilisation of waste EPS.

Since its inception, EPS composite soil has attracted the interests of many researchers. A few papers have been published regarding using EPS composite soil in reducing swelling pressures on structures foundation and behind retaining walls. Illuri & Nataatmadja (2007) and Illuri (2007) investigated the use of recycled EPS as a partial soil replacement and swell modifier for expansive soils. Artificially prepared expansive soils were manufactured in the laboratory by mixing fine sand with sodium bentonite of various proportions. Recycled EPS beads were mixed with these soils and the effects of varying the amount were investigated. The proposed soil improvement technique is thus showing great promise in sustainable construction. Nataatmadja and Illuri (2009) prepared an artificially reconstituted soils of different plasticity values by mixing fine sand and sodium bentonite. It has been found that the addition of EPS granules into these soils results in light-weight backfill materials, suitable for reducing swelling pressure behind domestic retaining walls.

The current research was conducted to investigate the recyclability of EPS packaging products in reducing swelling pressures on structures foundation by using recycled EPS beads as a mechanical admixer in replaced soils at their optimum-moisture contents. Mixing recycled EPS beads with soil replacement is introduced an environment-friendly geomaterials. The applications of recycled EPS as a swell shrink modifier as well as desiccation controller of expansive soils were considered in this study. The quantitative evaluation also whether recycled EPS beads provides significant benefits for use in soil replacement to reduce swelling pressures was done through an extensive experimental program.

2 MATERIALS

2.1 *Replacement Soil*

The replacement soil was sub-angular silica sand and classified according to the unified soil classification (USCS) system as a poorly-graded clean medium to fine sand (SP) with coefficient of curvature (C_c)= 1.73, coefficient of uniformity (C_u)=3.6 , max dry density (γ_{dmax}=19.2kN/m^3) and optimum moisture content (OMC)= 9%.

2.2 *Expansive Soil*

The expansive soil was a sodium Bentonite. The physical properties for the used Bentonite are summarized in Table 1.

Table 1. Physical properties of the used Bentonite

Liquid Limit (LL) %	143
Plastic Limit (PL)%	47.6
Plasticity Index (PI) %	95.4
Free Swell (FS)%	96.7
Specific Gravity (Gs)	2.55
Max Dry Density (γ_{dmax}) kN/m^3	14
Optimum Moisture Content (OMC) %	24

2.3 *Recycled EPS Beads*

For the present study, waste EPS beads were collected with three different beads densities and particle sizes. Photo 1 shows the beads's size compared to sand particles. The beads densities and particle sizes are summarized in Table 2.

Table 2. Properties of EPS Beads

EPS Beads	400	500	600
Density (KN/m^3)	0.10	0.16	0.20
Particle Size (mm)	5-6	4-5	1-3

3 COMPACTION CHARACTERISTICS OF SAND EPS MIX

To study the compaction characteristics, standard Proctor compaction tests were performed on a number of sand EPS mixes. With the addition of EPS beads, the density of the resulting composite is much lower than the original soils.

The EPS beads were added to the moist soil at a certain percentage of the soil’s dry mass. Compaction tests of the sand with EPS (SWEPS) composite were subsequently carried out immediately after mixing the sand and EPS.

Compaction curves for mixes of sand with different percentages of EPS beads are shown in Figure 1. From this figure, it can be observed that with the addition of EPS beads the dry density of the resulting mix varies considerably, it decrease with increasing the beads content but there is no significant variation in the optimum moisture content. This can be attributed to the low bulk density and very low moisture absorbency of the EPS beads. Since the beads are bulk in volume but very low in mass, the mass of the soil-EPS composite is generally controlled by the mass of the soil in the mix. Furthermore, as the moisture is held within the soil particles, the optimum moisture content of the mix is controlled by the optimum moisture content of the sand. From previous stud it is found that the increase of EPS-beads density increases the maximum dry density at the same beads ratio, Abdelrahman,(2009)

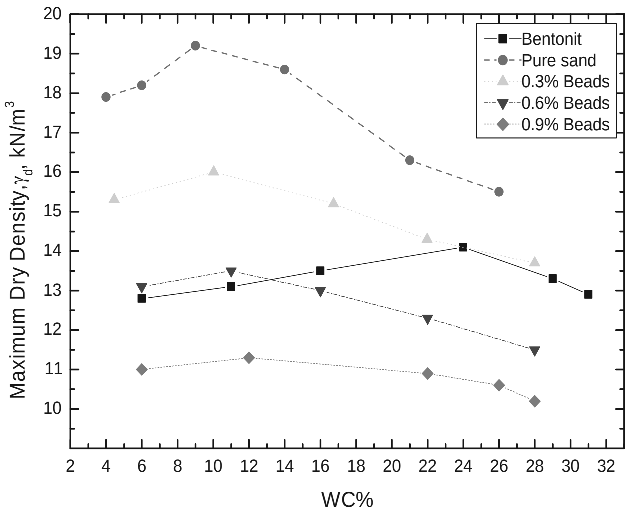

Figure 1. Compaction curves for mixes with sand and EPS contents at density of t EPS beads = 0.16kN/m^3

4 EXPERIMENTAL WORK

4.1 *Test Model*

Experimental model consists of cylindrical soil sample container with diameter is 15 cm and height = 18cm , two vertical dial gages to measure the settlement and swelling , circular footing with different diameters. Vertical stress equal to 30 kN/m^2 was applied on the footing which represented the applied stress of three stories building.

4.2 *Test Program*

A series of tests were performed on circular footing with different diameters rested on sand EPS mix replacement layer with different ratios of EPS beads and layer thickness above Bentonite layer both sand EPS mix replacement layer and Bentonite layer were compacted at their optimum moisture content (OMC). Mixing EPS beads with sand replacement layer leads to settlement under loading condition before adding water to the swelling layer cause EPS beads are compressible material and this explain why swelling and settlement are discussed together in the test results. The studied parameters are summarized in Table 3.

Table 3. The studied parameters

Diameter of footing (d) cm	5, 7, 10, and 12
Beads Density (γ_B) kN/m^3	0.1, 0.16 and 0.2
Beads Content (B) %	0, 0.3, 0.6, 0.9, and 1.2
Normalized Replacement Thickness (t_r/t_s) %	0, 12.5, 20, 25 and 33

4.3 Test Results and Analysis

4.3.1 Test results presentation

Swelling and settlement on surface soil and circular footing are presented in a set of curves with the different studied parameters.

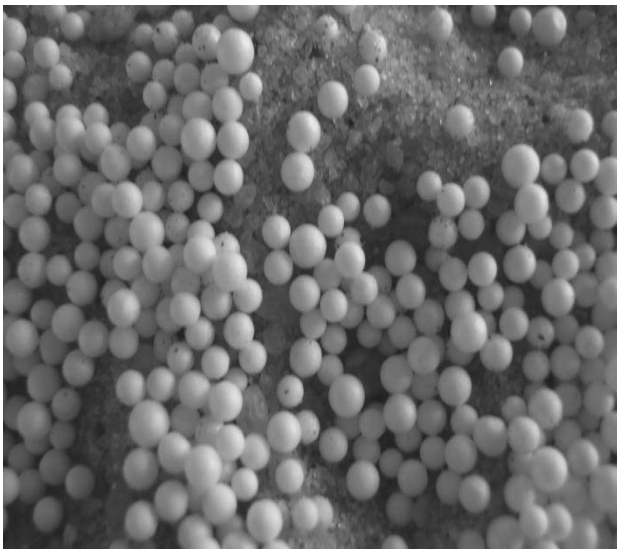

Photo 1. EPS beads mixed with sand

4.3.2 Effect of footing diameter (d) cm

Increasing rigid footing breadth causes increasing in settlement in soil. In case of swelling soil increasing footing breadth also causes increasing in swelling deformation even with existing of beads. But EPS beads may be leads to decrease the percent of the swelling and the settlement deformation as shown in Figure 2.

4.3.3 Effect of beads density (γ_B) kN/m^3

EPS density appears to be the main parameter that correlates with most of its mechanical properties. Compression strength, shear strength, tension strength, flexural strength, stiffness, creep behavior and other mechanical properties depend on the density. Higher density leads to improve its effect. As shown in Figure 3 increase beads density (γ_B) kN/m^3 leads to decrease each of the swelling and settlement on surface soil and circular footing.

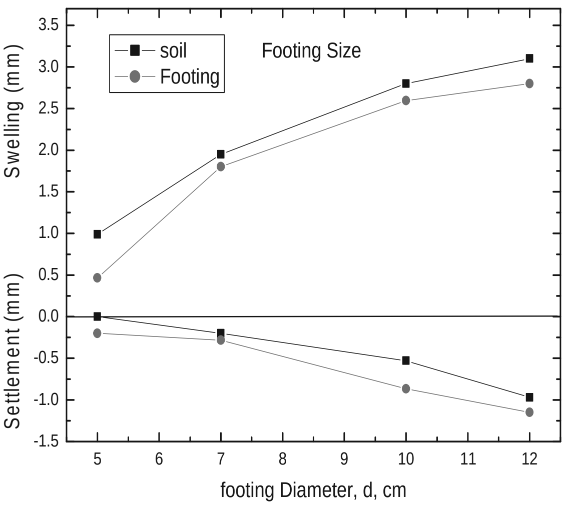

Figure 2.Relationship between increasing footing diameter (d) cm on settlement and swelling for soil and footing

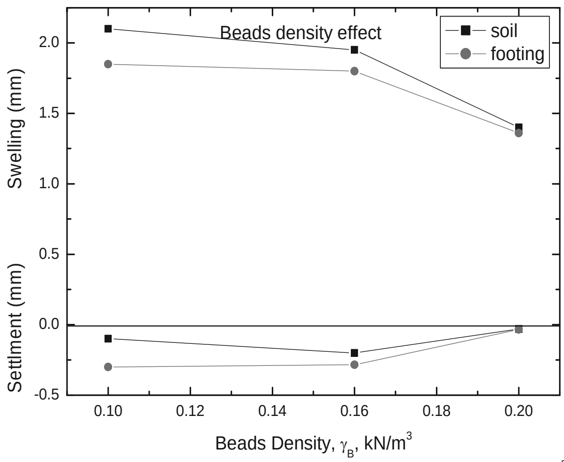

Figure 3.Relationship between increasing beads density (γ_B) kN/m^{3}on settlement and swelling for soil and footing

4.3.4 Effect of beads content (B) %

The EPS beads are highly compressible, with soft elastic nature, having only about 1% of the density of a typical soil.

As shown in Figure 4 increase beads content (B) % leads to decrease swelling pressure on the footing and decreases also the swelling settlement. EPS beads particles swelling energy absorption because of its compressible nature.

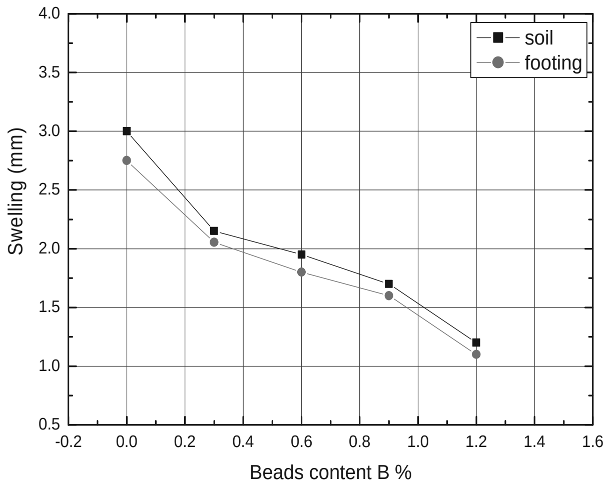

Figure 4.Relationship between increasing beads content (B) % on swelling for soil and footing

4.3.5 Effect of normalized replacement thickness (t_r/t_s) %

Replacement layer thinness t_r was chosen as a percentage of soil layer thickness t_s .As shown in Figure 5 increasing the replaced layer improve the resistance to the swelling pressure and decrease the swelling deformation. But economic point of view also is important taking in to account the swelling layer thickness. Increasing the normalized replacement thickness (t_r/t_s) % leads to decrease each of the swelling and settlement on surface soil and circular footing.

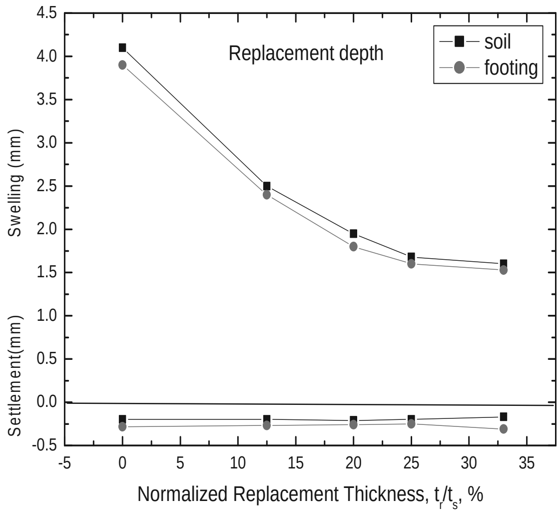

Figure 5.Relationship between increasing normalized replacement thickness (t_r/t_s) % on settlement and swelling for soil and footing

4.3.6 Effect of normalized replacement thickness (t_r/t_s) % at beads content (B) = 0.6%, footing diameter (d) = 7cm and of beads density (γ_B) = 0.16 kN/m^3

Figure 6 shows the detailed measurments for footing and replaced soil surrounded the footing during 24 hours. It obvious that at replaced soil with sand and EPS beads decreased the swilling more than 60% , also no big difference in settlement before adding water between different replacement ratios. Adding water after one hour to the model to saturate the soil caused swelling which increases with time. Increasing replacement layer thickness decreases the swelling.

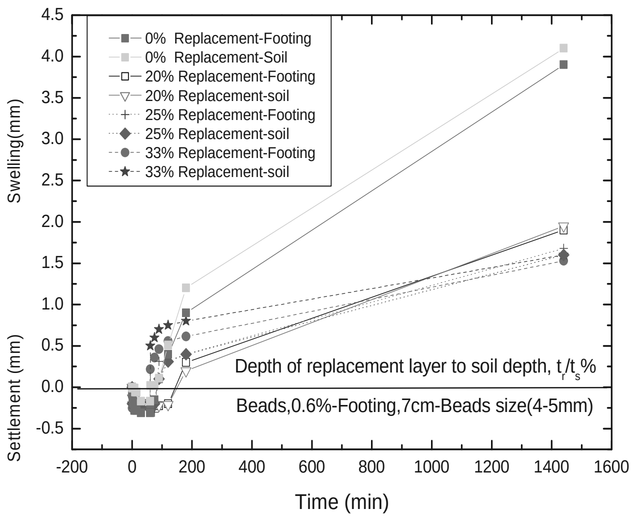

Figure 6 .Relationship between time (min) and settlement and swelling in (mm) for different normalized replacement thickness (t_r/t_s) % at beads content (B) = 0.6%, footing diameter (d) = 7cm and of beads density (γ_B) = 0.16 kN/m^3

5 CONCLUSIONS

The results of a study on the potential use of sand –EPS mix as soil replacement layer to reduce swelling of expansive soils below structure foundation have been presented. Different parameters affecting the swelling of structure foundation have been studied.

These parameters included the effect of footing diameter (d) cm where increasing rigid footing breadth caused increasing in settlement in soil but the presence of EPS beads lead to decrease the percent of the swelling and the settlement deformation. The second parameter was the effect of beads density (γ_B) kN/m^3 where increase beads density lead to decrease each of the swelling and settlement on surface soil and circular footing. The third parameter the effect of beads content in the sand replacement layer (B)% which was the most important parameter in this study where increasing this content lead to significant decrease in swelling. The fourth parameter was the effect of normalized replacement thickness (t_r/t_s) % where increasing the replaced layer improved the resistance to the swelling pressure and decrease the swelling deformation.

The innovative application of the recycled EPS beads mixed with sand replacement layer at optimum moisture content, so as to make a beneficial use of the waste EPS products, will offer a sustainable solution for both the housing and EPS industries.

6 REFERENCES

Abdelrahman G. E. 2009. Lightweight Mixture Using Clay, EPS-Beads and Cement. *Seventeen International Conference in Soil Mechanics and Geotechnical Engineering*, 17ICSMGE, Alex., Egypt.

Chen, F.H. 1988. Foundations on Expansive Soils. *Developments in Geotechnical Engineering* Vol.54, Amsterdam: Elsevier Science Publishing.

Illuri, H.K. and Nataatmadja, A. 2007. *Reduction of Shrink-Swell Potential With EPS Inclusion*. Proceedings 10th Australia New Zealand Conference on Geomechanics: Common Ground, Brisbane, Australia, pp. 90-95.

Illuri, H. K. 2007. Development of Soil EPS Mixes for Geotechnical Applications. *Ph.D. Disseration, School of Urban Development Centre for Built Environment and Engineering Research, Queensland University of technology*, Australia, 334p.

Nataatmadja, A. and Illuri, H. K. 2009. Sustainable Backfill Materials Made of Clay and Recycled EPS. *3rd CIB International Conference on Smart and Sustainable Built Environments*, Delft, Netherland.

Nelson, J.D and Miller, D.J. 1992. Expansive Soils Problems and Practice in Foundation and Pavement Engineering. *John Willey & Sons, Inc*, USA.

PPW Directive 2005. Directive 2005/20/E6 of the European Partiament and the Council of 9 March 2005 Amending Directive 94/62/EC on Packaging and Packaging Waste. *(OJL70 of 2005.03.16).*

United Nations Environment Program (UNEP) 2000. The Montreal Protocol on Substances that Deplete the Ozone Layer. *United Nations Environment Programme,* Nairobi, 47.

Sustainability in Geotechnical Engineering

Viabilité en géotechnique

Basu D., Misra A.
University of Waterloo

Puppala A.J., Chittoori C.S.
University of Texas at Arlington

ABSTRACT: This paper presents an overview of the different research studies performed in geotechnical engineering related to sustainable development. The philosophies of sustainability as applicable in geotechnical engineering are discussed. A review of the research and case studies performed in geotechnical engineering and how they can impact sustainable development is presented with particular emphasis on foundation engineering and ground improvement.

RÉSUMÉ : Cet article présente une vue d'ensemble des différentes recherches effectuées en géotechnique liée au développement durable. Les philosophies de la durabilité comme applicable en géotechnique sont discutées. Un examen des études de recherche et de cas réalisées en géotechnique et comment ils peuvent influer sur le développement durable est présenté avec un accent particulier sur les travaux de fondation et de l'amélioration du sol.

KEYWORDS: sustainability, waste recycling, life cycle assessment, multicriteria analysis, risk, resilience, carbon footprint.

1 INTRODUCTION

Civil engineering processes are both resource and fuel intensive. According to Dixit et al. (2010), the construction industry accounts for about 40% of the global energy consumption and depletes about two fifth of the sand, gravel and stone reserves every year. Construction activities also add to the problems of climate change, ozone depletion, desertification, deforestation, soil erosion, and land, water and air pollution (Kibert 2008). A geotechnical construction project not only has the above detrimental effects on earth's resources and environment but also changes the land use pattern that persists for centuries and affects the social and ethical values of a community. Thus, geotechnical projects interfere with many social, environmental and economic issues, and improving the sustainability of geotechnical processes is extremely important in achieving overall sustainable development.

This paper attempts to connect the broader scope of sustainable development with geotechnical engineering and presents a review of the research done on different aspects of sustainability in geotechnical engineering with particular emphasis on foundation engineering and ground improvement.

2 SUSTAINABILITY AND GEOTECHNOLOGY

Sustainability of a system is its ability to survive and retain its functionality over time. For an engineered system to be sustainable, it should be efficient, reliable, resilient, and adaptive. Efficiency requires that the resource use, cost and environmental impacts of the engineering system are minimal. Reliability ensures that the system is sufficiently far away from its predictable failure states. A resilient system has the ability to return to its original functioning state within an acceptable period of time when subjected to unpredictable disruptions. An adaptive system is responsive to gradual and natural changes within itself and in its environment, and is flexible to modifications and alterations required to cope with such changes. Together, these characteristics help in deciding whether an engineered system is capable of surviving in a complex and evolving socio-economic environment without losing its own character and function, and without violating the limits of the carrying capacity of the natural systems. Thus, the objective of sustainable engineering is to ensure the integration of an engineered system into the natural and man-made environment without compromising the functionality of either the engineered system or that of the ecosystem and society, and this harmony between the natural and built environments must be maintained at the local, regional and global scales. Therefore, in the engineering domain, sustainability can be looked upon as a dynamic equilibrium between four E's — engineering design, economy, environment and equity, as described in Figure 1.

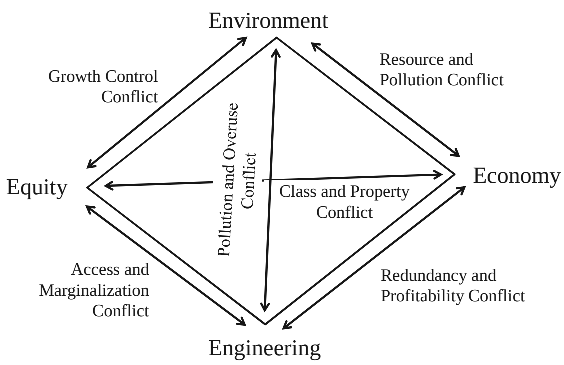

Figure 1. The four E's of sustainability in engineering projects.

In view of the four E's approach of sustainable engineering, the sustainability objectives that may be incorporated in geotechnical projects are: (i) involving all the stakeholders at the planning stage of the project so that a consensus is reached on the sustainability goals of the project (such as reduction in pollution, use of environment friendly alternative materials, etc.), (ii) reliable and resilient design and construction that involves minimal financial burden and inconvenience to all the stakeholders, (iii) minimal use of resources and energy in planning, design, construction and maintenance of geotechnical facilities, (iv) use of materials and methods that cause minimal negative impact on the ecology and environment, and (v) as much reuse of existing geotechnical facilities as possible to minimize waste. This approach aims at reaching a dynamic equilibrium between engineering integrity, economic efficiency, environmental effectiveness, and social acceptability and equity.

In an endeavor to incorporate sustainability in geotechnical design, three new trends have been identified (Iai 2011): (i) geo-structures are now designed for performance rather than for ease of construction, (ii) designs are now more responsive to site specific requirements, and (iii) the designs consider soil-structure interaction rather than just analysis of structural or foundation parts.

3 SUMMARY OF SUSTAINABLE GEOTECHNLOGY RESEARCH

Several research studies have been performed that aim at making geotechnical engineering practice sustainable. The areas in which research has progressed include (1) the use of alternate, environment friendly materials in geotechnical constructions, and reuse of waste materials, (2) innovative and energy efficient ground improvement techniques, (3) bio-slope engineering, (4) efficient use of geosysnthetics, (5) sustainable foundation engineering that includes retrofitting and reuse of foundations, and foundations for energy extraction, (6) use of underground space for beneficial purposes including storage of energy, (7) mining of shallow and deep geothermal energy, (8) preservation of geodiversity, and (9) incorporation of geoethics in practice.

Geohazards mitigation is another important aspect of sustainable geotechnical engineering — related studies include studies on the effects of global climate change and of multi-hazards on geo-structures. In this context, it is important to note that sustainable geotechnical engineering should not only focus on minimization of ecological footprints but also on making geo-structures reliable and resilient so that the effects of hazards, both natural and man-made, can be minimized. The aspect of reliability and resilience is particularly important for critical infrastructures (e.g., lifeline systems like transportation and power supply network without which other systems like cities cannot function) of which geo-structures like dams, embankments, slopes and bridge foundations are important components.

The recent research studies on geosustainability are mostly based on the common notions of sustainability like recycling, reuse and use of alternate materials, technologies and resources. However, whether such new approaches are actually sustainable or not cannot be ascertained without proper assessment using, for example, whole life cost analysis and risk based performance analysis. Therefore, a complete sustainability assessment framework is necessary for geotechnical projects to ascertain the relative merits of different options available for a project.

Any geosustainability assessment framework should have a life cycle view of geotechnical processes and products and should (i) ensure societal sustainability by promoting resource budgeting and restricting the shift of the environmental burden of a particular phase to areas downstream of that phase, (ii) ensure financial health of the stakeholders, and (iii) enforce sound engineering design. As the uncertainties associated with geotechnical systems are often much greater than those with other engineered systems, sustainability framework for geotechnical engineering should include an assessment of the reliability and resilience of the geo-system, and offer flexibility to the user to identify site specific needs.

From the environmental impact point of view, quantitative environmental metrics like global warming potential (Storesund et al. 2008), carbon footprint (Spaulding et al. 2008), embodied carbon dioxide (Egan et al. 2010), embodied energy (Chau et al. 2006) and a combination of embodied energy and emissions (carbon dioxide, methane, nitrous oxide, sulphur oxides and nitrogen oxides) (Inui et al. 2011) have been used to compare competing alternatives in geotechnical engineering. But, assessing the sustainability of a project based solely on metrics like embodied carbon dioxide or global warming potential involves ad hoc assumptions, puts excess emphasis on the environmental aspects and fails to consider a holistic view that must also involve technical, economic and social aspects (Holt et al. 2010, Steedman 2011).

Among the sustainability assessment tools that address the multidimensional character of sustainability, some are qualitative and represent the performance of a project on different sustainability related sectors pictorially (e.g., GeoSPeAR) (Holt 2011). The second category of multidimensional assessment frameworks consist of quantitative and life cycle based tools. Life cycle costing (LCC), life cycle assessment (LCA), multicriteria analysis and combinations of LCC and LCA have been used for this purpose. Assessment frameworks and metrics like Green Airport Pavement Index, BE^{2}ST-in-Highways and Environmental Sustainability Index fall under this category (Pittenger 2011, Lee et al. 2010b, Torres and Gama 2006).

The third approach to sustainability assessment is based on point based rating systems that provide a measure of sustainability of projects based on points scored in the different relevant categories. Rating systems like GreenLites (McVoy et al. 2010), I-LAST (Knuth and Fortman 2010), Greenroads (Muench and Anderson 2009), MTO–Green Pavement Rating System (Chan and Tighe 2010) and Environmental Geotechnics Indicators (Jefferson et al. 2007) fall under this category.

4 SUSTAINABLE GROUND IMPROVEMENT

A major part of the sustainability related research in geotechnical engineering has focused on ground improvement through the introduction of novel, environment friendly materials with particular emphasis on the reuse of waste materials. Puppala et al. (2009) proposed the use of alternate materials for soil stabilization including the use of recycled materials in geotechnical constructions. Other examples include the use of recycled glass-crushed rock blends for pavement sub-base and recycling of shredded scrap tires as a light-weight fill material.

Reuse of old pavements including asphalt and concrete pavements has been on the rise (Gnanendran and Woodburn, 2003). The old pavements are recycled into full and partial depth reclamation bases with cement or other additive treatment. Sometimes these pavements are recycled into aggregate materials which are termed as reclaimed asphalt pavement (RAP) materials. RAP materials have been used as bases with chemical stabilization, and several state DOT agencies in the USA has been using them in the new pavement construction projects. Puppala et al. (2009) performed a series of resilient modulus tests on cement and cement-fiber treated RAP for use as pavement base material. They reported that the structural coefficients increase with an increase in the confining pressure and these values are higher for cement and cement–fiber treated aggregates. The significant increase of structural coefficients with cement-fiber treatment (30%) was attributed to the tensile strength and interlocking properties offered by the fiber content.

Investments made on transportation and processing is reduced when native material after stabilization is used as a base or backfill material. This saves money that might otherwise be spent on fuels for transportation. The old pavement material if cannot be reused has to be landfilled, which increases the costs associated with the landfilling practices. Therefore, the use of old pavement materials as stabilized bases reduces the space used for landfills, which, in turn, reduces the overall carbon footprint of the project by not using aggregates from quarries.

The Integrated Pipeline (IPL) project which involves a long pipe line installation is a joint effort between the Tarrant Regional Water District (TRWD) and Dallas Water Utilities (DWU) that is aimed at bringing additional water supplies to the Dallas/Fort Worth metroplex. As a part of the pipeline layout and construction, large amounts of soil need to be excavated during the pipeline installation. Also, large amounts of material need to be imported for bedding and backfilling of the trenches. Both importing new fill material and exporting excavated trench material for landfilling will have serious implications on the economic and environmental aspects of the construction project.

As a result, a research study was initiated at the University of Texas at Arlington to identify chemical treatment of in-situ soil material that can be reused as either bedding, zone or backfill materials for the pipeline installation. Based on the comprehensive laboratory studies, the soils along the pipeline alignment are identified for potential reuse as backfill, bedding and zone materials after chemical amendment, and more details can be found in Chittoori et al. (2012). The cost and environmental benefits as well as emissions reductions of using in-situ native material versus imported fill materials are also explained.

5 SUSTAINABLE FOUNDATION ENGINEERING

Foundations form an integral part of geotechnical construction, and sustainable design and construction of foundations are very important for overall sustainable development. Sustainable foundation engineering entails robust analysis and design, economical and environment friendly construction that cause minimal disruptions to life and damage to adjacent properties, reuse and retrofitting of existing foundations as much as possible, and use of foundations in harvesting geothermal energy.

Robust design of foundations essentially involves a rigorous analysis (e.g., use of proper constitutive equations and analytical or numerical modeling of appropriate boundary value problems) and choice and execution of an appropriate design methodology (e.g., identification of all possible limit states and moving the design state sufficiently away from the limit states by either using a reliablity based method or by applying load and resistance factor design (LRFD) methodology). The recent trend in geotechnical engineering to incorporate LRFD is encouraging and several research studies have been conducted to rigorously develop resistance factors based on reliability analysis (e.g., Basu and Salgado 2012). Further, the incorporation of random fields to characterize spatial heterogeneity of soil in the probabilistic analysis of foundations and related soil structure interaction problems significantly contributes to sustainable foundation engineering (Haldar and Basu 2011, 2012).

Misra and Basu (2011, 2012) recently developed a multicriteria based sustainability assessment framework for pile foundation projects. The framework considers a life-cycle view of the pile construction process (Figure 2), and combines resource consumption, environmental impact and socio-economic benefits of a pile-foundation project over its entire life span to develop a sustainability index (Figure 3). The use of resources is taken into account based on the embodied energy of the materials used, the impact of the process emissions is assessed using environmental impact assessment and the socio-economic impact of the project is assessed through a cost benefit analysis. Three indicators are derived from the three aspects and are combined through weights to calculate the sustainability index (SI) for the different alternatives available for the project (Figure 3).

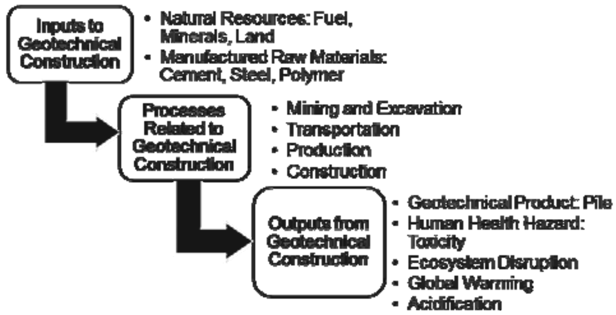

Figure 2. Flow chart showing the inputs, outputs, processes and impact categories in pile construction.

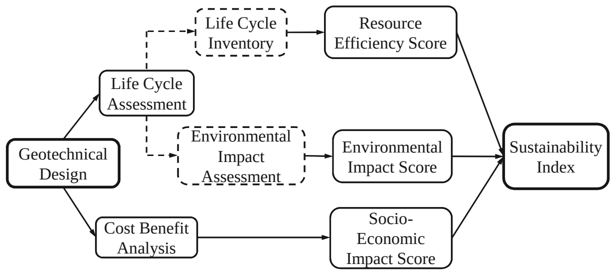

Figure 3. Multicriteria based sustainability assessment framework.

Reuse and retrofitting of foundations is a traditional practice for almost all refurbishment projects, but recently the concept has been extended for redevelopment projects as well (Butcher et al. 2006a). Reuse of foundations is an attractive option because the cost of removal of an old foundation is about four times that of construction of a new pile, disturbance to adjacent structures caused by foundation removal can be avoided, and backfilling of voids created by the removed foundation is not required. At the same time, the embodied energy consumed in reusing foundations is nearly half of that consumed in installing new foundations. Consequently, several case studies demonstrating the benefits of reuse of foundations have been documented (Anderson et al. 2006, Butcher et al. 2006b).

Foundation engineering has a prominent role in the alternative energy sectors like geothermal and wind energy. Case studies show that deep foundations can be used as energy storage and transmitting elements (Quick et al. 2005) while concrete surfaces in contact with the ground (e.g., basement walls) can act as heat exchangers (Brandl 2006). Research is in progress to develop proper characterization, analysis and design of energy related geo-structures like energy piles (Laloui 2011), wind turbine foundations (Doherty et al. 2010) and foundations for oil and gas drilling operations (Yu et al. 2011).

6 CONCLUSIONS

In recent times, a concerted effort is noted within the civil engineering industry in delivering built facilities that are eco-friendly and sustainable. Geotechnical construction, being resource intensive and by virtue of its early position in civil engineering projects, has a great potential to influence the sustainability of such projects. Incorporating sustainability in geotechnical engineering requires an understanding of the ideological conflicts that characterize sustainability and of the approaches that can make engineering processes sustainable. Philosophically, engineering sustainability can be looked upon as the balance between engineering design, economy, social equity and the environment (4 E's).

Sustainability related research studies in geotechnology essentially belong to two categories: those that contribute to global sustainability through the use of alternative materials and innovative engineering and those that develop sustainability assessment frameworks. A summmary of these research studies is provided with emphasis on two particular areas, ground improvement and foundation engineering. The focus of these studies is mostly on the environmental and economic aspects. It is recommended that a more holistic approach considering environmental, social, economic, reliability and resilience aspects (the 4 E's) should be developed for sustainable geotechnical practices.

7 REFERENCES

Anderson, S., Chapman, T. and Fleming, J. (2006). "Case history: the redevelopment of 13Fitzroy Street, London." Proc. of International Conference on Reuse of foundations for urban sites, Butcher, A. P., Powell, J.J.M., Skinner, H.D (eds.) 311-320.

Basu, D. and Salgado, R. (2012). "Load and resistance factor design of drilled shaft in sand." Journal of Geotechnical and Geoenvironmental Engineering, 138, 12.

Brandl, H. (2006). "Energy foundations and other thermo-active ground structures." Geotechnique 56(2), 81-122.

Butcher, A. P., Powell J.J.M. and Skinner, H.D. (2006b). "Stonebridge Park ─ a demolition case study", Proc. of International Conference on reuse of foundations for urban sites, Butcher A. P., Powell J.J.M., Skinner H.D (eds.) 321-330.

Butcher, A. P., Powell, J.J.M., Skinner, H.D. (eds.) (2006a). "Whole life cost and environment impact case studies", Reuse of foundations for urban sites: A best practice handbook, IHS BRE Press, Berkshire, United Kingdom, 116-119.

Chan, P. and Tighe, S. (2010). "Quantifying Pavement Sustainability in Economic and Environmental Perspective", Transportation Research Board 89th Annual Meeting, Washington, DVD.

Chau, C., Soga, K. and Nicholson, D. (2006). "Comparison of embodied energy of four different retaining wall systems." Proc. of International Conference on reuse of foundations for urban sites, Butcher, A. P., Powell, J.J.M., Skinner, H.D (eds,) 277-286.

Chittoori, B.S., Puppala, A.J., Reddy, R.K., Marshall, D. "Sustainable Reutilization of Excavated Trench Material." ASCE GeoCongress, 2012, Oakland, California, March 2012, 4280-4289.

Dixit, M.K., Fernandez-Solis, J.L., Lavy, S. and Culp, C.H. (2010). "Identification of parameters for embodied energy measurement: A literature review", Energy and Buildings, 42, 1238-1247.

Doherty, P., Casey, B. and Gavin, K. (2010). "Laying Foundations for Sustainable Energy", The Engineers Journal, 64(6), 262-266.

Egan, D. and Slocombe, B.C. (2010). "Demonstrating environmental benefits of ground improvement", Proc. of the Institution of Civil Engineers – Ground Improvement, 163(1), 63-70.

Gnanendran, C. T. and Woodburn, L. J. (2003). Recycled Aggregate for Pavement Construction and the Influence of Stabilization. Proceedings - Conference of the Australian Road Research Board, 21, 1755-1768.

Haldar, S. and Basu, D. (2011). "Beam on spatially random elastic foundation." In Proceedings of GeoRisk 2011, Atlanta, Georgia, U.S.A., CD-ROM, June 2011, GSP 224.

Haldar, S. and Basu, D. (2012). "Response of strip foundation on spatially random elastic foundation under variable column loads." In Proceedings of Geo-Congress 2012, Oakland, California, U.S.A., CD-ROM, March 2012.

Holt, D.G.A. (2011). "Sustainable Assessment for Geotechnical Projects", PhD. Thesis, University of Birmingham, U.K.

Holt, D.G.A., Jefferson, I., Braithwaite, P.A. and Chapman, D.N. (2010). "Sustainable Geotechnical Design", Proc. of Geocongress 2010, Florida, CD-ROM.

Iai, S. (2011). "Towards Global Sustainability", Geotechnics and Earthquake Geotechnics Towards Global Sustainability, Iai, S. (ed.), Springer.

Inui, T., Chau, C., Soga, K., Nicholson, D. and O'Riordan, N. (2011). "Embodied Energy and Gas Emissions of Retaining Wall Structures", Journal of Geotechnical and Geoenvironmental Engineering, 137(10), 958-967.

Jefferis, S.A. (2008). "Moving towards Sustainability in Geotechnical Engineering", Proc. of the Geo Congress 2008, GSP 178, 844-851.

Jefferson, I., Hunt, D.V.L., Birchall, C.A. and Rogers, C.D.F. (2007). "Sustainability Indicators for Environmental Geotechnics", Proc. of the Institute of Civil Engineers - Engineering Sustainability, 160(2), 57-78.

Kibert, C.J. (2008). Sustainable C

ment of I-LAST™ Illinois - Livable and Sustainable Transportation", Proc. of the Green Streets and Highways 2010 Conference, ASCE.

Laloui, L. (2011). "In-situ testing of heat exchanger pile", Proc. of

BE2ST In-Highways for Green Highway Construction Rating in Wisconsin", Proc. of the Green Streets and Highways 2010 Conference, ASCE.

McVoy, G. R., Nelson, D.A, Krekeler, P., Kolb, E., and Gritsavage, J.S. (2010). "Moving towards Sustainability: New York State Department of Transportation's GreenLITES Story", Proc. of the Green Streets and Highways 2010 Conference, ASCE.

Misra, A. and Basu, D. (2011). "A sustainable approach to foundation design." In Proceedings of 13th PanAmerican Conference on Soil Mechanics and Geotechnical Engineering and 64th Canadian Geotechnical Conference, Toronto, Canada, October 2011.

Misra, A. and Basu, D. (2012). "A quantitative sustainability indicator system for pile foundations." In Proceedings of Geo-Congress 2012, Oakland, California, U.S.A., CD-ROM, March 2012.

Muench, T.S. and Anderson, J.L. (2009). "Greenroads: A Sustainability Performance Metric for Roadway Design and Construction", http://www.transnow.org/publications/documents/TNW2009-13.pdf .

Pittenger, D.M. (2011). "Evaluating Sustainability of Selected Airport Pavement Treatments with Life-Cycle Cost, Raw Material Consumption, and Greenroads Standards", Journal of the Transportation Research Board, No. 2206, 61-68.

Puppala, A. J., Saride, S., Potturi, A. and Hoyos, L.R. (2009). "Resilient Behavior of Cement-Fiber Treated Reclaimed Asphalt Pavement (RAP) Aggregates as Bases." Proceedings of the International Foundation Congress and Equipment Expo, ASCE, 2009, GSP 187, 433-440.

Quick, H., Meissner, S., Michael, J., Quick, H.D.and Arslan, U. (2005). "Innovative foundation systems for high rise buildings." Proc. of the 1st Intelligent Building Middle East Conference, Bahrain.

Saride, S., Puppala, A. J., and Williammee, R (2010). Assessing Recycled/Secondary Materials as Pavement Bases. Ground Improvement 163, GI1, 3-12.

Spaulding, C., Massey, F. and LaBrozzi, J. (2008). "Ground Improvement Technologies for a Sustainable World", Proc. of the Geo Congress 2008, GSP 178, 891-898.

Steedman, R.S. (2011). "Geotechnics and Society: Carbon, a New Focus for Delivering Sustainable Geotechnical Engineering", Geotechnics and Earthquake Geotechnics Towards Global Sustainability, Iai S. (ed.), Springer.

Storesund, R., Messe, J. and Kim, Y. (2008). "Life Cycle Impacts for Concrete Retaining Walls vs. Bioengineered Slopes", Proc. of the Geo Congress 2008, GSP 178. 875-882.

Torres, V.N. and Gama, C.D. (2006). "Quantifying the Environmental Sustainability in Underground Mining", XV International Symposium on Mine Planning & Equipment Select, Torino, Italy.

Yu, O-K, Medina-Cetina, Z. and Briaud, J-L (2011). "Towards an Uncertainty-Based Design of Foundations for Onshore Oil and Gas Environmentally Friendly Drilling (EFD) Systems." Proc. of the GeoFrontiers 2011, Dallas, Texas, CD-ROM.

Mechanics of Manufactured Soil Using Powder Wastes

Mécanique des sols fabriqués à partir de déchets de poudre

Baykal G.
Bogazici University

ABSTRACT: Powder wastes like fly ash are produced in large volumes. They have handling, disposal problems and poor engineering performance due to their silt size. Manufacturing artificial sand and gravel from these silt sized powder wastes in large quantities will solve the associated problems of having silt size. Disc pelletizers with manufacturing capacities reaching one million ton a year makes this process economically feasible and practical for geotechnical applications. Fly ash is one of these powder wastes having silt size and easily available in many countries where they create huge disposal problems. Cold bonding pelletization technique is used to produce fly ash pellets of sand and gravel size and their mechanical properties are determined. The manufactured pellets are lightweight materials with adequate strength and can be used in many geotechnical projects. The fly ash pellets show similar behavior to that of calcareous sands. In addition to utilization of pellets as manufactured, it is also possible to manufacture soil to the desired specification by adding additives or apply surface treatment.

RÉSUMÉ : Déchets de poudre comme les cendres volantes sont produits en grandes quantités. Ils ont la manipulation, et l'élimination des problèmes de performance d'ingénierie pauvres en raison de leur taille limon. Fabrication de sable et de gravier artificielle à partir de déchets de limon ces poudres de taille en grandes quantités permettra de résoudre les problèmes associés ayant une taille de limon. Granulateurs à disques avec des capacités de production pour atteindre un million de tonnes par an rend ce processus économiquement faisable et pratique pour des applications géotechniques. Les cendres volantes sont un de ces déchets en poudre ayant une taille de limon et facilement disponible dans de nombreux pays où ils creat énormes problèmes d'élimination. Technique de granulation à froid de liaison est utilisé pour produire des boulettes de cendres volantes de sable et de gravier taille et leurs propriétés mécaniques sont déterminées. Les pellets sont fabriqués avec des matériaux légers résistance suffisante et peut être utilisé dans de nombreux projets en géotechnique. Les granulés de cendres volantes présentent un comportement similaire à celui des sables calcaires.

KEYWORDS: Powder wastes, cold bonding pelletisation, silt size, fly ash, calcerous sands, grain crushing.

1 INTRODUCTION

With increasing disposal costs, and growing ecological concerns, waste materials are utilized in geotechnical applications more and more each year. Due to its silt size, powder materials are hard to handle, transport, compact and dispose. Increasing the size of the powder wastes from silt size to sand and gravel size has a lot of benefits. Powder wastes like coal burning thermal power plant fly ash are used in many geotechnical applications. The pelletization cost for fly ash is around one to two Euros per ton and the capacity of one pelletizer can be as high as one million tons per year, making this approach a feasible and practical application in geotechnical engineering. Annual fly ash production for many countries is in the range of 1 to 100 million tons. This paper summarizes a series of research work about manufacturing sand and gravel from powder fly ash by cold bonding pelletization technique. The pelletization mechanism is explained and physical and engineering properties of the produced pellets are given.

The manufactured pellets behave like calcareous sands found in the nature. The source and shape difference of the natural calcareous sands do not exist in the manufactured pellets having nearly perfect sphericity and roundness. The crushing behavior of the manufactured soil is studied in detail. For potential applications like backfill for retaining walls, fill under the footings, pile installation in existing manufactured soil embankment, anchor installation in manufactured fills, the interface behavior and the influence of crushability on the interface behavior is also studied. Finally odometer tests, direct shear tests are conducted and the results are summarized.

1.1 *Mechanism of pellet formation*

Pelletization process is the agglomeration of moisturized fines in a rotating drum or disc. The product at the end of the process is called the “fresh pellet”. The crushing strength of the fresh pellet must be enough for hauling and stockpiling purposes. The pelletization technology is widely used in powder metallurgy engineering, and medicine industry.

The pelletization theory was developed in 1940’s. The performance of the pelletization process is a function of; i) the engineering properties of the material pelletized; ii) the amount of moisture in the medium; iii) the mechanical process parameters such as the angle of balling drum or disc to the normal and the revolution speed. Observations and analysis performed on these parameters with respect to mechanic and kinetic laws formed the theory of pelletization process (Baykal and Doven 2000).

When a fine grained material is moisturized, a thin liquid film forms on the surface of the grains, which forms meniscus between the grains. With the rotation in a balling drum or disc, they form ball shape structures with enhanced bonding forces between grains due to centrifugal and gravitational forces. The mechanism of pellet formation is presented in Figure 1. In the pendular state water is present only at point of contact of the grains. With more water addition some of the pores are filled with water in the funicular state. All intergranular space is filled with water in the capillary state. The most suitable state for pellet formation is the capillary state.

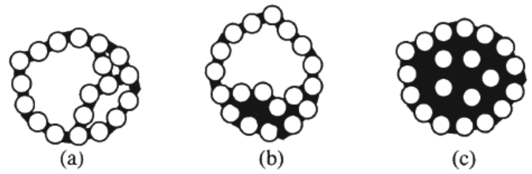

Figure 1. Mechanism of pellet formation; a) the pendular state; b) the funicular state; c) the capillary state.

The formation of capillary force between two grains is presented in Figure 2. The grain diameter of the powder material influences the magnitude of the surface tension force; small grain diameter is necessary to create enough pulling force to initiate agglomeration. Agglomeration can be achieved by drum or disc pelletizers. A typical disc pelletizer designed and manufactured for this study is presented in Figure 3 (Doven 1998).

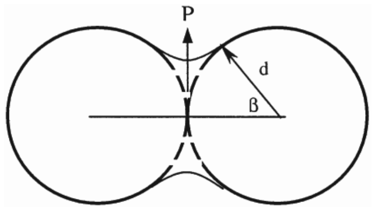

Figure 2.. Surface tension force created by water bridge between two particles.

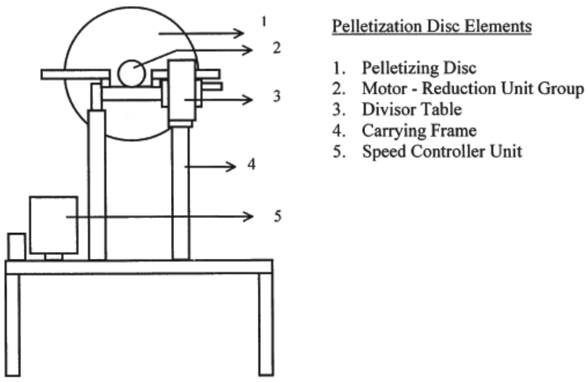

Figure 3. The sketch of disc pelletizer (back view).

The revolution speed of the disc can be controlled between 0 and 70 rpm and the angle of the disc plane to the normal can be adjusted between 0 and 90 degrees. The diameter of the disc is 0.40 meters and scraping blades are placed from center to one edge at 0.06 m intervals. During the revolution of the disc the grains pulled by surface tension are compacted further. The agglomerated grains hit to the scraping blades, falling free to the bottom section of the disc. This free fall action compacts the agglomerated product more. This repeated revolving and free fall action densifies and makes the agglomerated product stronger for handling. The motion of the grains in the disc is presented in Figure 4. The forces applied to the grains during pellet formation are presented in Figure 5. To achieve the most suitable pelletization process; the revolution speed and the angle of disc plane to the normal should be set in a manner to avoid the dominancy of gravitational or centrifugal forces (Figure 6).

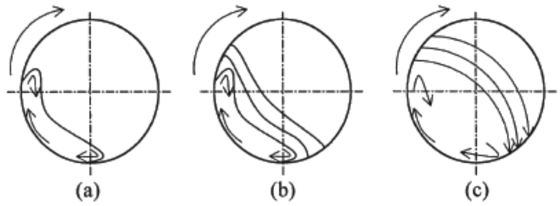

Figure 4. Motion of material in disc pelletizer revolving at various speeds.

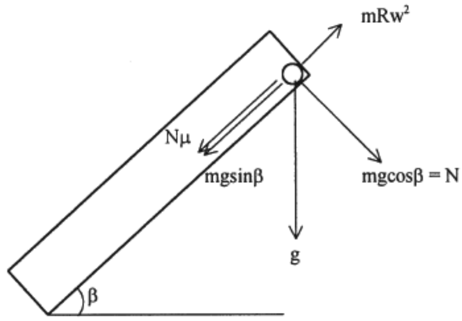

Figure 5. Forces acting on an individual pellet during pelletization process.

When the gravitational and centrifugal forces are in equilibrium then the normal force exerted by the pellet converges to zero and the following equation prevails.

$$m \times g \times \sin\beta = m \times R \times W^2 \qquad (1)$$

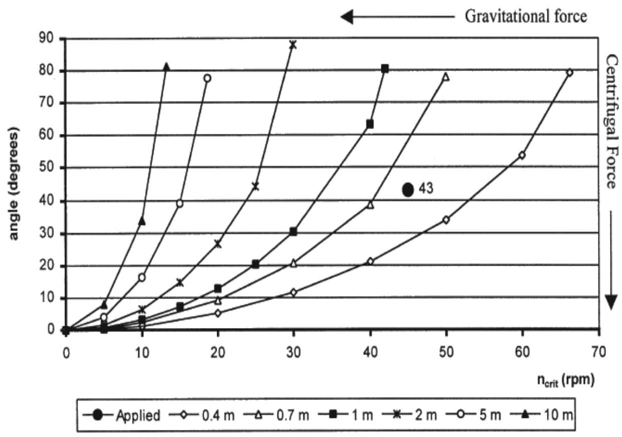

Figure 6. Variation of operation angle with respect to diameter of pelletization disc and critical revolution speed.

For various disc diameters the effect of operating angle and revolution speed on centrifugal and gravitational forces are presented in Figure 6.

2 PHYSICAL AND ENGINEERING PROPERTIES OF THE MANUFACTURED PELLETS

Turkey produces more than 17 million tons of fly ash annually. The fly ash used in the presented studies is obtained from Soma Coal Burning Thermal Power Plant in the west part of Turkey. The typical chemical composition of Soma fly ash is given in Table 1. The physical properties of manufactured fly ash pellets are presented in Table 2. The water absorption of the produced pellets is high.

Table 1. The chemical composition of Soma Fly Ash.

	Per cent
SiO_2	50.5
Al_2O_3	23.7
Fe_2O_3	5.8
CaO	9.3
MgO	2.6
SO_3	1.4
Loss on Ignition	2.2

Soma fly ash is self cementitious and it will harden without the need of another binder. The physical properties of the manufactured fly ash pellets are given in Table 2. The typical fly ash pellets are given in Figure 7.

Table 2. Physical properties of the fly ash pellets.

Unit weight	9.6 kN/m^3
Water absorption	31.4 %
Specific gravity	2.17
Bulk specific gravity	1.29

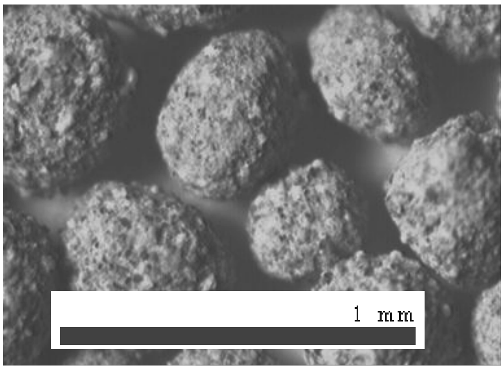

Figure 7. Manufactured fly ash pellets.

Table 3. Engineering properties of the fly ash pellets.

Optimum moisture content Dry unit weight (Standard Proct)	34.4 % 11.96 kN/m^3
Angle of internal friction	29.4°
California Bearing Ratio	58 %
Soundness loss of weight 9.5- 4.75 mm	9.0 %
Soundness loss of weight 19- 9.5 mm	7.9 %

Tables 1 through 3 show that fly ash pellets formed with cold bonding technique have similar engineering properties to that of soils. With no additional binder like lime or cement, self cementitious fly ash pellets have acceptable engineering properties. The soundness tests were conducted using sodium sulphate. Less than 12 percent weight loss after sodium sulphate treatment is allowable for concrete applications. The durability performance of the manufactured aggregates is adequate even for more demanding applications like concrete production.

From geotechnical point of view, the manufactured pellet aggregates have properties similar to those of granular soils except high water absorption value.

3 CRUSHING BEHAVIOR OF MANUFACTURED PELLETS

To demonstrate the effect of aggregate crushing sieve analyses were performed before and after direct shear testing of fly ash pellets at 50, 100 and 200 kPa normal stress. The change in grain size distributions before and after execution of the direct shear tests are given in Figure 8 (Danyıldız 2007).

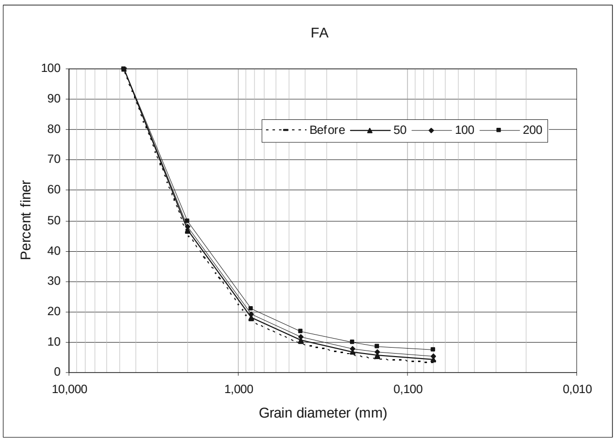

Figure 8. The grain size distribution of fly ash pellets before and after the conduction of direct shear test at a normal stress of 50, 100 and 200 kPa.

The fly ash pellets crushing behavior is similar to calcerous sands. The measured crushing behavior does not pose a threat for the engineering performance of the fly ash pellets for most geotechnical applications.

4 SHEAR STRENGTH OF FLY ASH PELLETS

Direct shear tests are conducted on manufactured fly ash pellet aggregates under 50,100 and 200 kPa normal stress applications. Interface tests are conducted on split samples of fly ash pellets and concrete. The internal friction angle and interface friction angle plots are presented in Figure 9.

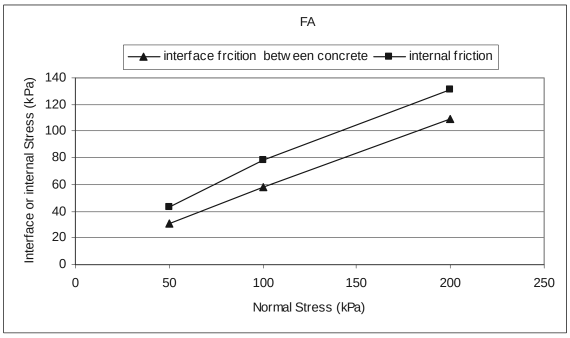

Figure 9. Internal and interface friction angles of fly ash pellets and pellet concrete interface.

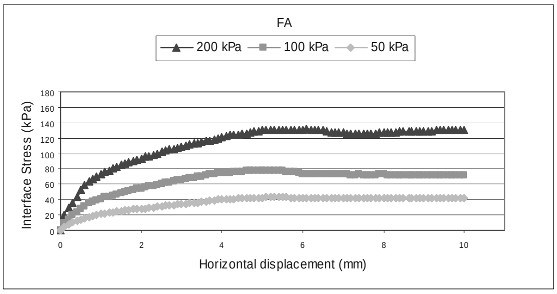

Figure 10. Shear stress vs. horizontal displacement of manufactured fly ash pellets.

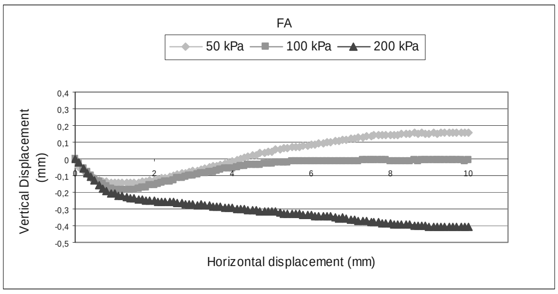

Figure 11. Shear stress vs. vertical displacement of manufactured fly ash pellets.

The shear stress vs. horizontal displacement and shear stress vs. vertical displacement values of fly ash pellet aggregates are presented in Figures 10 and 11 respectively. While dilation behavior is observed under 50 and 100 kPa, contraction behavior is seen under 200 kPa due to grain crushing.

5 SETTLEMENT BEHAVIOR OF PELLET AGGREGATES

Manufactured fly ash pellet aggregates are placed in an odometer and vertical stress of 25 to 1600 kPa is applied and removed. The corresponding void ratio values vs. the applied vertical stress are presented in Figure 12 (Erdurak 2011).

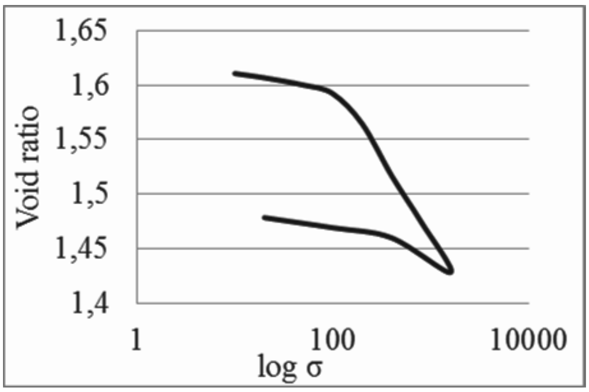

Figure 12. Odometer test results of fly ash pellets.

After the application of 100 kPa vertical stress the settlement increases. Even for high embankment fills the settlement magnitude is manageable.

6 CONCLUSIONS

The size of the silt sized powder wastes can be increased to sand and gravel size by pelletization technique in large volumes and low cost making the technique suitable for geotechnical applications. In this study experience with self cementing fly ash is presented, however the technique is applicable to other silt sized powder wastes provided that adequate capillary forces develop between the grains. For non self cementing fly ash, binders like hydrated lime or cement can be used for manufacturing. For higher performance needs the crushing strength of the fly ash pellets can be improved by using lime or cement additives. Surface treatment of pellets is possible using water glass at reasonable cost. High water absorbtion values(30 -35 per cent) place the manufactured granular material in an unique place in clasical soil classification. The durability of the aggregates is also satisfactory. With low unit weigh, free draining behavior, and ease of compaction, the manufactured soil has good potential for large volume utilization in geotechnical applications. The geotechnical properties of the manufactured soil ensures high stability. In addition to its potential for utilization in large volumes, the manufactured soil is a great tool for experimental research on crushable soils. It is possible to control the size, shape, surface texture, roundness, sphericity, crushing strength, unit weight, water absorption properties of the powder materials to produce soil with target engineering properties. This way by fixing one parameter at a time it will be possible to study the effects of each parameter on the engineering behaviour of natural soils. The cold bonding pelletization technology is a low tech technology which requires minimum capital investment and low operational costs. The whole process can be automated. If the manufactured aggregates are not used in a geotechnical application, a major reduction in disposal costs is achieved by improving handling, transportation, compaction and disposal in a dump site. Free draining property, high stability and potential for reuse when needed are other benefits of utilization.

7 ACKNOWLEDGEMENTS

The studies presented above are conducted by PhD student Ata Gurhan Doven; MSc students; Haydar Arslan, Egemen Danyıldız and Murat Cenk Erdurak with financial support provided by Bogazici University Scientific Research Fund and Turkish Scientific Research Council (TUBİTAK).

8 REFERENCES

Baykal G. And Doven A.G. 2000. Utilization of fly ash by pelletization process; theory, application areas and research results. *Resources Conservation and Recycling* 30, 59-77.

Doven A.G. 1998. Lightweight fly ash aggregate production using cold bonding technique. PhD Thesis. Bogazici University, İstanbul.

Erdurak M.C.2011. Artificial sand production for laboratory tests. MSc Thesis Bogazici University, Istanbul

Danyıldız E.2007. The interface behavior between granular soils and concrete. MSc Thesis, Bogazici University. Istanbul.

Arslan H. 2003. The effect of grain crushing on the behavior of granular materials. MSc Thesis. Bogazici University. Istanbul.

Méthodes non traditionnelles de traitement des sols : apports techniques et impact sur le bilan environnemental d'un ouvrage en terre.

Soil treatment with non traditional additives in earthworks: evaluation of the technical and environmental improvements.

Blanck G.
Agence de l'environnement et de la Maîtrise de l'Énergie, Angers, France
LEMTA (CNRS, UMR 7563), Université de Lorraine, France.

Cuisinier O., Masrouri F.
LEMTA (CNRS, UMR 7563), Université de Lorraine, France.

RÉSUMÉ : Dans le contexte actuel de fort développement des problématiques environnementales, la mise au point de techniques permettant de valoriser au mieux les matériaux de terrassement tout en limitant l'impact environnemental des chantiers est devenue un enjeu majeur. L'une des solutions innovantes proposées est d'utiliser des sous-produits industriels organiques en traitement des sols. Ainsi, l'objectif de cette étude est d'évaluer les apports de trois produits non traditionnels (un produit acide, un produit enzymatique et un lignosulfonate) sur le compactage et la portance d'un limon et d'en évaluer les effets sur le bilan environnemental d'un ouvrage en terre. Dans un premier temps, les résultats expérimentaux ont montré que les traitements enzymatique et au lignosulfonate permettaient d'augmenter les masses volumiques sèches atteintes et d'économiser de l'eau lors de la mise en œuvre du limon à condition que sa teneur en eau initiale soit faible. Dans un second temps, la comparaison des impacts environnementaux des deux traitements effectuée suivant la méthode d'analyse du cycle de vie, a permis d'identifier la variante ayant l'impact environnemental le plus restreint.

ABSTRACT: Sustainable development principles lead earthworks companies to use all natural materials on the construction site and to reduce the environmental impact of their activities. In this context, the use of industrial organic products has been proposed. The aim of this study is to characterize the modification of compaction and bearing capacity of a silt treated with three non-traditional additives (an acid solution, an enzymatic solution and a lignosulfonate). Observed modifications of the compaction properties showed interesting applications for the compaction of the silt when its natural water content is low. For the enzymatic and lignosulfonate treatments, savings of water could be expected during the construction stage. For these two treatments, a comparison of the global environmental impact was made thanks to a life cycle assessment study.

MOTS-CLÉS : Terrassement, traitements non traditionnels, compactage, analyse du cycle de vie, impact environnemental.

KEYWORDS: Earthworks, nontraditional treatments, compaction, life cycle assessment, environmental impact.

1 INTRODUCTION

La prise en compte des problématiques de développement durable tend à se généraliser dans le monde de l'entreprise tous secteurs confondus. Cette démarche conduit à proposer et à mettre en œuvre des solutions techniques toujours plus respectueuses de l'environnement et des populations sans mettre en péril l'économie des projets. Les entreprises du monde de la construction ont pleinement pris conscience de l'importance de bâtir en tenant compte de ce principe. Ainsi, les principaux acteurs du secteur de la conception, réalisation et maintenance des infrastructures routières se sont engagés début 2009 auprès du ministère en charge de l'écologie sur un ensemble de points à améliorer en vue d'atteindre les objectifs du développement durable dans ce secteur. Parmi les défis à relever, l'un revêt une importance primordiale pour les entreprises de terrassement : il s'agit de la valorisation de l'ensemble des matériaux naturels excavés sur chantiers pour atteindre d'ici 2020 l'objectif « zéro apport extérieur » (Ministère en charge de l'environnement 2009). En effet, parmi les sols extraits, tous ne peuvent pas être utilisés directement comme matériaux de construction, en raison de leur nature ou de leur état hydrique. Il s'agit par exemple de sols très argileux, ou de sols dont la teneur en eau est trop élevée, ou au contraire trop faible par rapport à l'optimum de mise en œuvre. Ne pas valoriser ces matériaux revient à les considérer comme des déchets et nécessite alors de les évacuer en dépôts. Le déséquilibre de volume ainsi créé est alors fréquemment compensé par un apport de granulats extraits de carrières dont l'impact environnemental est plus élevé.

Répondre à l'objectif de valorisation des matériaux du site passe à la fois par le développement des techniques traditionnelles de traitement des sols (chaux, liants hydrauliques) mais aussi par l'étude de solutions innovantes. Dans ce contexte de diversification des techniques, l'utilisation de produits non traditionnels organiques issus de diverses industries (pétrolière, papetière, sucrière, etc.) est proposée. Ces produits sont actuellement essentiellement utilisés pour la stabilisation de routes non revêtues (Scholen 1995, Surdahl 2007), ou dans une optique d'amélioration des performances mécaniques des sols (par exemple Tingle et Santoni 2003) et de réduction de leur potentiel de gonflement (Rajendran et Lytton 1997, Rauch *et al.* 2003). Cependant, l'emploi des produits non traditionnels relève essentiellement de l'empirisme laissant une part importante d'incertitude quant à l'anticipation du comportement des sols traités.

Au-delà des aspects uniquement techniques, il est également nécessaire d'aborder les traitements sous l'angle de leur bilan environnemental pour y intégrer plus amplement les aspects du développement durable. L'une des approches possibles est fondée sur les principes de l'analyse du cycle de vie (AFNOR 2006). La seconde phase de cette étude consiste à calculer et à comparer les bilans environnementaux des différentes variantes de traitement sur l'ensemble des phases du cycle de vie de la construction d'un ouvrage en terre. En effet, l'utilisation des produits non traditionnels se heurte à un verrou technique supplémentaire du fait de l'absence d'études ayant porté sur le bilan environnemental des opérations de traitement des sols.

2 MATÉRIEL ET MÉTHODES

Trois traitements non traditionnels ont été testés sur un limon. Suivant leur nature, une procédure spécifique est suivie.

2.1 *Produits de traitement*

Le produit classé dans la famille des produits acides est une solution aqueuse d'acide sulfurique contenant du limonène sulfonaté, sous-produit de l'industrie de la transformation des agrumes. Les résultats expérimentaux obtenus au laboratoire et ceux issus de la littérature (par ex. Tingle et Santoni 2003, Rauch *et al.* 2003) n'ayant pas montré de sensibilité des résultats mécaniques par rapport au dosage, un dosage classique de 0,01 % est utilisé.

Le produit enzymatique est une solution aqueuse organique dérivée de la transformation des mélasses, un sous-produit de l'industrie sucrière. Comme les propriétés mécaniques des sols traités ne semblent pas affectées par des modifications du dosage (Tingle et Santoni 2003, Velasquez *et al.* 2006), un dosage courant de 0,002 % est utilisé pour ce traitement.

Le troisième produit est une poudre de lignosulfonate de calcium, polymères organiques dérivant des lignines, sous-produit des industries papetières. Certaines études ont montré que les valeurs de résistance à la compression simple sont maximales pour un dosage de 5 % (Tingle et Santoni 2003, Santoni *et al.* 2002). Dans cette étude, les dosages massiques de 0,5 ; 2,0 et 5,0 % sont donc testés.

2.2 *Caractéristiques du limon étudié*

Le sol testé est un limon fin (87 % de passant à 80 µm), peu plastique (w_L = 34 % ; IP = 14) fréquemment rencontré lors de travaux de terrassement en France, en région parisienne.

2.3 *Procédure de traitement*

Pour les traitements au produit acide et à la solution enzymatique, la première étape de préparation consiste à humidifier le sol avec de l'eau distillée pour atteindre une teneur en eau de 3 % inférieure à la teneur en eau finale souhaitée. Le mélange est effectué à l'aide d'un malaxeur à couteaux puis est laissé reposé 24 heures en sacs hermétiquement fermés. Le produit de traitement est alors dilué dans la quantité d'eau requise pour atteindre la teneur en eau souhaitée puis ajouté progressivement au sol lors de l'opération de malaxage. Pour le traitement au lignosulfonate, le produit est directement ajouté au sol préalablement humidifié. Indépendamment du traitement, un temps de cure d'une heure est respecté avant compactage.

3 RÉSULTATS EXPÉRIMENTAUX

Les résultats expérimentaux présentés portent sur les caractéristiques de compactage et de portance du limon traité.

3.1 *Propriétés de compactage*

Les essais de compactage ont été menés conformément à la norme NF P 94-093 dans des moules CBR. Pour chaque teneur en eau, un essai de poinçonnement selon NF P 94-078 permet de déterminer la valeur de l'Indice Portant Immédiat (IPI) du sol. Pour le traitement au lignosulfonate, seul le dosage de 2,0 % est représenté sur la figure 1. Il s'agit du dosage pour lequel l'effet sur la courbe de compactage est maximal.

La figure 1 montre que le traitement à 0,01 % de produit acide n'entraine pas de changement significatif. En revanche, après ajout de 0,002 % de solution enzymatique et de 2,0 % de lignosulfonate, l'optimum Proctor est atteint pour des teneurs en eau optimales (w_{opt}) plus faibles et des masses volumiques sèches maximales (ρ_{dmax}) plus élevées. Ainsi, pour le traitement enzymatique, ρ_{dmax} est de 1,86 Mg/m^3 au lieu de 1,82 Mg/m^3 et w_{opt} de 14,5 % au lieu de 15,5 %. Du côté sec de l'optimum, les traitements au produit enzymatique et au lignosulfonate contribuent à augmenter les masses volumiques sèches dans une gamme de teneurs en eau allant de 8 à 15 %.

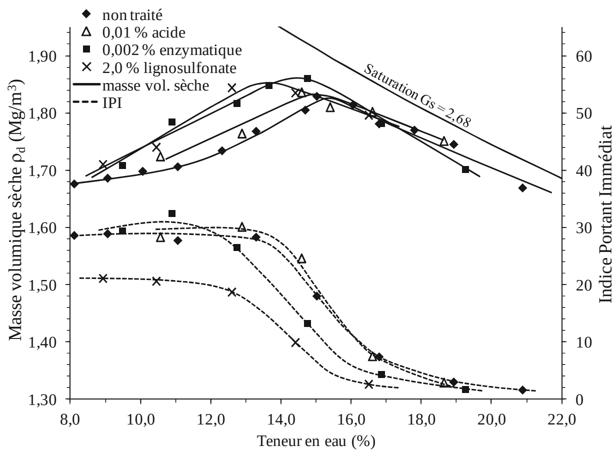

Figure 1. Courbes de compactage et de portance du limon traité avec trois produits non traditionnels.

3.2 *Exemple d'application au traitement d'un sol sec*

Les résultats expérimentaux montrent que certains traitements affectent la courbe de compactage en déplaçant l'optimum vers le côté sec et en augmentant les densités sèches obtenues. Cet effet peut trouver des applications intéressantes lors de la mise en œuvre de sols dont la teneur en eau initiale est située du côté sec de l'optimum. Ainsi, en supposant que la teneur en eau initiale du sol soit de 9,0 % (état très sec) et un objectif de compactage de 1,78 Mg/m^3, trois variantes de mise en œuvre peuvent être considérées pour un compactage à l'énergie Proctor normale (Figure 2) :

- le sol non traité est humidifié jusqu'à une teneur en eau de 14,0 % puis compacté,
- le sol est traité à 0,002 % de produit enzymatique, la teneur en eau de compactage requise est alors de 11,5 %,
- le sol est traité au lignosulfonate qui est épandu sous forme de poudre, puis mélangé au sol. Ensuite, la teneur en eau du sol est augmentée pour atteindre la valeur de 11,5 % puis le sol est compacté.

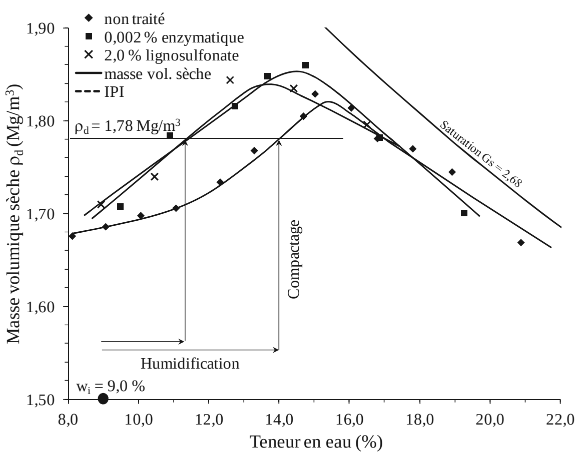

Figure 2. Comparaison des variantes de mise en œuvre du limon considérant une humidification puis un compactage à l'énergie Proctor normale.

Dans le cas du traitement au produit enzymatique et à 2,0 % de lignosulfonate, le compactage peut avoir lieu à une teneur en eau de 11,5 % au lieu de 14,0 % ce qui représente une économie d'eau de 44,5 m^3 pour 1000 m^3 de sol compacté.

Les résultats expérimentaux ont montré qu'il était possible, grâce aux traitements, d'atteindre un objectif de compactage donné pour une teneur en eau moindre ce qui permet de réaliser une économie d'eau. Toutefois, les étapes de production des substances utilisées, leur transport et leur mise en œuvre génèrent des impacts environnementaux qu'il est nécessaire d'évaluer sur l'ensemble des étapes du cycle de vie de l'ouvrage. L'objectif principal de la partie suivante est ainsi de définir dans quelle mesure les variantes traitées induisent une réduction de l'impact environnemental global par rapport à la mise en œuvre du sol non traité.

4 ANALYSE EN CYCLE DE VIE D'UN REMBLAI TRAITÉ

La démarche appliquée est celle définie dans les normes régissant l'analyse du cycle de vie. Le principe consiste à quantifier les intrants pour un système donné puis à calculer l'impact environnemental associé grâce aux données d'Inventaire du Cycle de Vie de ces intrants (ICV). L'impact environnemental est alors évalué à l'aide d'une méthode de calcul de l'impact. Au cours de cette étude, la méthode utilisée par la norme NF P 01-010 (AFNOR, 2004) est appliquée.

4.1 *Définition du système*

Le système étudié est un remblai dont la masse volumique sèche visée est de 1,78 Mg/m^3. La teneur en eau initiale du sol est supposée être de 9,0 % ce qui permet de se situer dans un contexte où les traitements présentent les meilleurs avantages (Figure 2). L'IPI minimal requis est fixé à 10 pour assurer une bonne traficabilité des engins de chantier. L'unité fonctionnelle choisie correspond à un volume compacté de 1000 m^3.
Définir le système revient à différencier les processus qui sont pris en compte dans l'étude et ceux qui en sont exclus. Au cours de cette étude, une démarche comparative a été adoptée ce qui a permis de réaliser un certain nombre de simplifications en ne considérant que les étapes qui diffèrent entre les variantes. Par exemple, l'ensemble des étapes préparatoires au chantier, les étapes d'extraction ou encore de transport du sol n'ont pas été prises en compte dans le calcul des impacts environnementaux car ces étapes sont identiques pour toutes les variantes.

4.2 *Calcul des intrants*

Les intrants considérés sont l'eau, les produits de traitement et les carburants. Les quantités des autres intrants (volume de sol par exemple) sont identiques pour toutes les variantes ce qui permet de les retirer du système.
La quantité d'eau requise est directement calculée à partir de la différence entre la teneur en eau initiale et finale. L'ICV de la production de l'eau dépend principalement de son origine. Par exemple, l'eau peut être prélevée sur des réseaux d'eau potable, dans des cours d'eau, ou encore être pompée dans un forage. Il est également possible d'anticiper les besoins en eau du chantier en créant des bassins pour y stocker les eaux de pluie. Compte tenu de la diversité des approvisionnements possibles et du manque de données statistiques relatives aux prélèvements d'eau sur chantiers, l'impact environnemental associé à l'étape de prélèvement de l'eau ne sera pas pris en compte et devra être discuté dans une étude de sensibilité.
Les quantités de produit enzymatique et de lignosulfonate requises sont directement calculées en considérant le volume de sol à traiter et les dosages appliqués. L'ICV du produit enzymatique n'est cependant pas disponible. Des hypothèses de substitution ont donc été être prises. Il a notamment été montré que le produit enzymatique possède des propriétés similaires à celles du Sodium Dodécyl Sulfate, un tensioactif courant, et qu'il agirait sur les sols selon un mécanisme similaire (Blanck *et al.* 2012). L'ICV du produit a donc été assimilé à celui du SDS dont l'ICV est connu (Stalmans *et al.* 1995, Hirsiger et Schick 1995).
L'ICV du lignosulfonate est issu d'une étude réalisée par Modahl et Vold (2011) à partir des données obtenues pour une usine située à Sarpsborg en Norvège.
Les étapes de transports consomment deux types de carburants : du diesel pour les poids lourds effectuant les transports routiers, et du fuel lourd pour les cargos chargés du transport maritime nécessaire à l'importation du produit enzymatique depuis les Etats-Unis. Connaissant la consommation de carburants nécessaire au transport des différents intrants, l'ICV de cette étape peut être calculé à partir des données du fascicule FD P01-015 (AFNOR, 2006). Quant à la consommation des engins de chantier, elles sont issues du retour d'expérience de DTP Terrassement.
Pour chacune des variantes, les intrants calculés sont résumés dans le tableau 1. Les résultats mettent par exemple en évidence que les variantes traitées consomment moins d'eau par rapport à la variante non traitée (44 500 L au lieu de 89 000 L). Pour le traitement au produit enzymatique, la consommation du pulvimixeur est deux fois moindre en comparaison avec la variante non traitée car une seule passe suffit pour effectuer le traitement contrairement à la variante non traitée où l'humidification doit être réalisée en deux passes. Le traitement au lignosulfonate nécessite quant à lui l'apport d'une masse de 35 600 kg de lignosulfonate dont le transport représente une consommation de carburant estimée à 379 L.

Tableau 1. Comparaison des intrants du système pour les trois variantes étudiées.

Intrant		*Non traité*	*0,002 % Produit enzymatique*	*2,0 % Lignosulf.*
Eau (L)		89 000	44 500	44 500
Produit (kg)		-	35,6	35 600
Diesel (L)	Camion	-	2	379
	Arroseuse	5,2	2,9	2,9
	Pulvimixeur	456	228	456
	Compacteur	30	30	30
	Épandeur	-	-	2,9
Fuel lourd (kg)		-	0,7	-

4.3 *Calculs des impacts environnementaux*

Pour le traitement au produit enzymatique (Figure 3), le calcul des indicateurs des 10 catégories d'impact proposés dans la norme NF P 01-010 montre que la variante traitée présente des impacts réduits dans 7 catégories sur 10 (consommation de ressources énergétiques, épuisement de ressources naturelles, consommation d'eau, changement climatique, formation d'ozone atmosphérique, pollution de l'air, pollution de l'eau). La consommation d'énergie est par exemple réduite de plus de 40 % et passe de $18{,}8.10^3$ MJ à $10{,}7.10^3$ MJ si le traitement au produit enzymatique est mis en œuvre. Au contraire, pour trois catégories, l'impact est augmenté, la production de déchets et la destruction de l'ozone stratosphérique en tête, suivie de l'acidification atmosphérique. Au-delà des valeurs calculées, il est nécessaire de se poser la question du caractère significatif des écarts observés. En effet, pour la production de déchets par exemple, la variante traitée présente un impact 4,5 fois plus élevé, cependant, l'augmentation de la production de déchet ne représente en valeur que 2,8 kg pour 1000 m^3 de sol compacté ce qui correspond à un volume très faible en comparaison aux 5200 kg/personne/an produite en moyenne en Europe (Eurostat 2008).

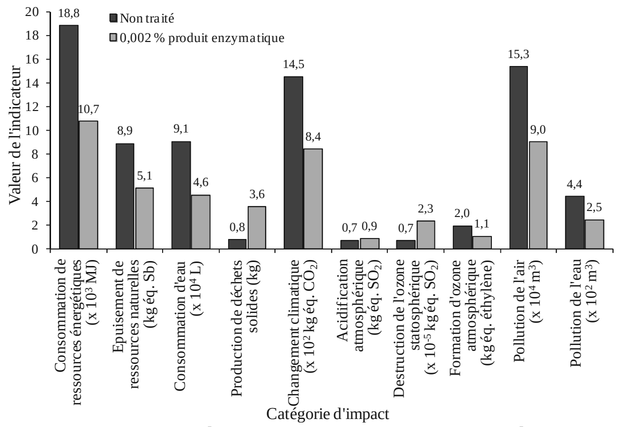

Figure 3. Comparaison des impacts environnementaux entre la variante non traitée et la variante considérant le traitement à 0,002 % de produit enzymatique.

Pour le traitement au lignosulfonate, le calcul des impacts révèle que le traitement conduit à dégrader fortement le bilan environnemental du système (Figure 4). À titre d'exemple, la consommation énergétique pour la variante considérant le traitement au lignosulfonate est évaluée à 927.10^3 MJ au lieu de $18,8.10^3$ MJ pour la variante non traitée.

Les résultats montrent également que malgré une réduction de la quantité d'eau consommée lors de l'étape de mise en œuvre, la consommation d'eau totale est plus élevée pour la variante traitée. En effet, sur l'ensemble du cycle de vie, la consommation d'eau est estimée à 460.10^4 L pour le traitement au lignosulfonate au lieu de $9,1.10^4$ L pour la variante non traitée. Cette différence est essentiellement due à la consommation d'eau nécessaire à la production du lignosulfonate.

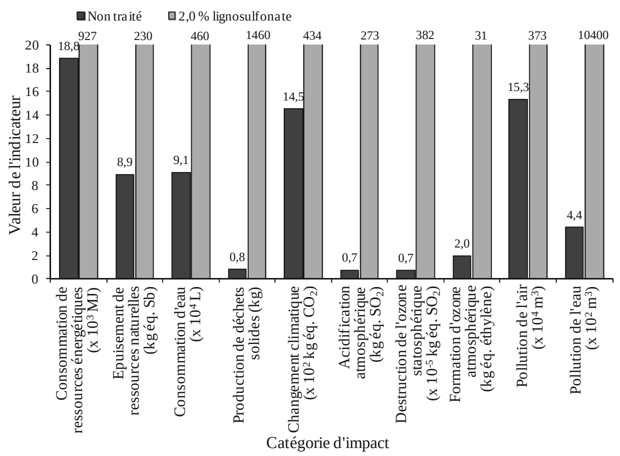

Figure 4. Comparaison des impacts environnementaux entre la variante non traitée et la variante considérant le traitement à 2,0 % de lignosulfonate.

5 CONCLUSION

L'étude présentée a l'originalité d'aborder des méthodes non traditionnelles de traitement à la fois sous l'angle des aspects géotechniques et sous celui des aspects environnementaux grace à une étude d'analyse du cycle de vie. Les essais de compactage et de portance ont permis d'identifier des variantes permettant de faciliter la mise en œuvre du limon et de réaliser des économies d'eau. Pour ces variantes, l'analyse du cycle de vie a montré que le traitement au produit enzymatique induisait une réduction de l'impact environnemental dans l'essentiel des catégories. Dans la situation étudiée, le traitement permet ainsi de combiner intérêt technique et environnemental. Au contraire, le traitement au lignosulfonate génère une forte augmentation de l'impact environnemental ce qui limite l'intérêt du traitement. Afin de confirmer la robustesse de l'étude environnementale, celle-ci devra être complétée par une étude de sensibilité portant sur les hypothèses et données d'entrées du système.

6 REMERCIEMENTS

Cette étude est financée par l'Agence de l'Environnement et de la Maîtrise de l'Énergie (ADEME) sous forme d'une thèse en partenariat avec Égis Géotechnique et DTP Terrassement. Les auteurs tiennent à remercier l'ensemble des personnes impliquées dans le comité de pilotage de la thèse pour leur participation et leur soutien.

7 REFERENCES

AFNOR NF EN ISO 14040. 2006. Management environnemental - Analyse du cycle de vie – Principes et cadre.

AFNOR NF P01-010. 2004. Qualité environnementale des produits de construction - Déclaration environnementale et sanitaire des produits de construction.

AFNOR FD P01-015. 2006. Qualité environnementale des produits de construction – Fascicule de données énergie et transport.

Blanck G., Cuisinier O., Masrouri F. 2012. Soil treatment with non-traditional additives in earthworks. WASCON 2012 – Göteborg.

Eurostat (2008), "Generation of waste", last update 06 March 2012. http://appsso.eurostat.ec.europa.eu/nui/show.do?dataset=env_wasgen&lang=en

Hirsinger F. and Schick K.P. 1995. A life cycle inventory for the production of alcohol sulphates in Europe. *Tenside Surfactants Detergents*. (2), 128-139.

Ministère en charge de l'écologie. 2009. Convention d'engagement volontaire des acteurs de conception, réalisation et maintenance des infrastructures routières, voiries et espace public urbain.

Modahl I.S., Vold B.I. 2011. The 2010 LCA of cellulose, ethanol, lignin and vanillin from Borregaard Sarpsborg. Ostfold Research.

Rajendran D., Lytton R.L. 1997. Reduction of sulfate swell in expansive clay subgrade in the Dallas district. Research Report TX-98/3929-1, Texas Transportation Institute, College Station.

Rauch A.F., Katz L.E. and Liljestrand H.M. 2003. An analysis of the mechanisms and efficacy of three liquid chemical soil stabilizers. Report FHWA/TX-03/1993-1, University of Texas, Austin.

Scholen D.E. 1995. Stabilizer Mechanisms in Nonstandard Stabilizers. *Conference Proceedings 6: Sixth International Conference on Low-Volume Roads* 2, 252-260.

Stalmans M., Berenbold H., Berna J.L., Cavalli L., Dillarstone A., Franke M., Hirsinger F., Janzen D., Kosswig K., Postlethwaite D., Rappert T., Renta C., Scharer D., Schick K.-P., Schul W., Thomas H., Van Sloten R. 1995. European life-cycle inventory for detergent surfactants production. *Tenside surfactant detergent* 32 (2), 84-109.

Surdahl R.W., Woll J.H. and Marquez H.R. 2007. Stabilization and dust control at the Buenos Aires national wildlife refuge, Arizona. *TRR: Journal of the Transportation Research Board* 1989 (1), 312-321.

Tingle J.S. and Santoni R.L. 2003. Stabilization of clay soils with nontraditional additives. *TRR: Journal of the Transportation Research Board* 1819 (2), 72-84.

Velasquez R.A., Marasteanu M.O. and Holzalski R.M. 2006. Investigation of the effectiveness and mechanisms of enzyme products for subgrade stabilization. *International Journal of Pavement Engineering* 7 (3) 213-220.

Santoni R.L., Tingle J.S. and Webster S.L. 2002. Stabilization of silty sand with nontraditional additives. *TRR: Journal of the Transportation Research Board* 1787, 61-70.

Advanced testing and modelling delivers cost effective piled raft foundation solution

Comment des essais avancés, associés à la modélisation, permettent d'obtenir une solution éconoomique de fondation sur pieux et radier

Bourne-Webb P.
Instituto Superior Técnico, Lisbon, Portugal

Cunningham M.
Shell Global Solutions Intl. BV, Den Haag, Netherlands

Card G.
GB Card & Partners, London, United Kingdom

ABSTRACT: A piled raft solution was proposed as an alternative to a conventional fully piled foundation for a new shopping development in Cambridge, UK. This paper demonstrates how the use of precedent knowledge, appropriately targeted investigation and modelling can provide cost effective and resource efficient foundation solutions.

RÉSUMÉ : Une solution radeau empilé a été proposé comme une alternative à une base conventionnelle entièrement empilés pour un développement nouveau point de vente à Cambridge, Royaume-Uni. Cet article montre comment l'utilisation des connaissances préalables, l'enquête ciblée et modélisation peut fournir rentables et efficaces des ressources des solutions de fondation.

KEYWORDS: Gault Clay, piled raft foundation, nonlinear stiffness, site characterisation.

1 INTRODUCTION.

1.1 *Piled rafts and settlement reducing piles*

There is a wide literature on the various methods of analysis and use of raft foundations generally (Cooke 1986, Price & Wardle 1986, Poulos 2001, Reul & Randolph 2003) and the use of piles as settlement reducers (Burland 1995, Love 2003).

In essence, where the soil underlying a structure is sufficiently stiff it is often the case that the use of a plain or piled raft solution will lead to economies when compared to the costs associated with a fully piled foundation system.

Effectively, load from the superstructure is first distributed through a plain raft to the subsoil and if the analysis predicts settlement in excess of that deemed to be acceptable, settlement reducing piles can be introduced at strategic points in order to stiffen the support to the raft and bring the expected settlements down to an acceptable level.

However, this solution is not often examined due to the sophisticated nature of the soil-structure interaction that needs to be analysed – the work involved in delivering the solution is too 'complicated' and the structural engineer prefers the ease, risk transfer and robustness of a fully piled option.

1.2 *Gault Clay and geological setting*

The Gault Clay is an over-consolidated clay that was laid down towards the end of the Lower Cretaceous period (c. 100 Ma), and its engineering behaviour lies between that of a soil and weak rock (Marsh & Greenwood 1995). In Cambridge, UK the Upper Gault sub-division predominates

In the Cambridge area, the strata over-lying the Gault, most significantly the Chalk of the Upper Cretaceous, have been largely removed by erosion, and the area was also subjected to a number of glaciations.

The removal of an estimated 150 m of overburden (Samuels 1975), in addition to the ice cover, has subjected the clay to significant stress relief with associated intense fissuring and softening and in addition, the stratum has experienced moderate levels of tectonic activity.

In engineering terms, the Upper Gault is a high plasticity clay (LL ~ 70 - 80%; PI ~ 45 - 55%) with moisture contents close to its Plastic Limit and a significant calcite content (30 – 40%).

At the site, the soil profile (Table 1), especially the distribution of the superficial soils and the upper surface of the Gault Clay, has been modified by historic construction that had reduced the original ground level.

Groundwater was found to be perched within the superficial soils at a level between 0.5 m and 1 m above the surface of the clay (noting that the surface of the clay undulated significantly), and water levels in the Lower Greensand were found to be in hydraulic continuity (Nash et al. 1996).

Table 1. Site specific soil profile

Top of layer: m OD	Thickness: m	Soil description
+5.8 to +11	0.3 to 3.3	Made Ground
	0.3 to 1.7	Brickearth
	0.1 to 2.4	Sand & Gravel
+3.2 to +8.5	0 to 3.6	Gault Clay (weathered)
	>34.7	Gault Clay
-30 approx.	Not proven	Lower Greensand

1.3 *Development at adjacent sites, Grand Arcade and foundation options*

Located in central Cambridge (Fig. 1), the Grand Arcade site is immediately adjacent to the Lion Yard shopping centre and the Crown Plaza Hotel (Lings et al. 1991, Ng & Nash 1995). The development covers a total area of about 1.4 hectares.

The excellent field and laboratory research work undertaken in relation to the deep basement excavation at the latter site, informed the decisions made during the development of the ground model for this project.

In addition to these relatively modern buildings, other structures of significance to the project were the Post Office (PO) and Telephone Exchange (BT) building(s) in the northeast corner of the site, and retained facades along the eastern boundary, facing St. Andrews Street; all of which had to be protected from damage during the works.

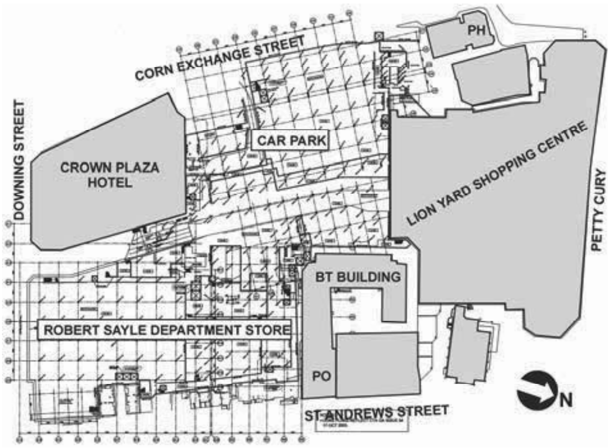

Figure 1. Plan of area surrounding Grand Arcade.

The re-development at the site involved the demolition of a number of existing buildings and because of the long history of occupation in the area, archaeological investigation was undertaken prior to the main construction works starting.

To form the basement substructure, zero sheet-pile and secant bored pile perimeter retaining walls were installed where needed, and ground levels were reduced generally by between 4 m and 7 m across the site.

The gross weight of the new structure was equivalent to a uniform loading of about 120 kPa which with an average unloading due to demolition and excavation of 80 kPa (ranging between 30 and 100 kPa), equates to a net loading of 40 kPa. However, this varied somewhat across the site and as a result in some areas, e.g. under core structures and some columns, net contact pressures locally were as high as 220 kPa.

During tendering, a value engineering exercise was undertaken and the option of replacing the conforming fully piled foundation with a piled raft was investigated, and this preliminary assessment suggested that significant savings were possible using this alternative.

2 SOIL CHARACTERISATION

2.1 *Site specific investigation and testing*

In order to develop the ground model for the proposed raft foundation it was necessary to supplement the site investigation and laboratory testing previously completed with further, high quality sampling and testing. Therefore, three additional 30 m deep boreholes were completed using rotary coring techniques and sub-samples were taken from the cores for stress path testing.

Prior to the stress path testing, the suction in each sample was measured using the IC suction probe, in order to be able to understand whether the samples may have been unduly disturbed when recovered or when in transit.

These measurements proved to be very interesting (Fig. 2) and while generally consistent they were significantly lower than what would be expected based on experience in for example the London Clay Formation, and imply much lower values of “at-rest” earth pressure coefficient, K_0 than might be expected based on a simple one-dimensional depositional and erosion environment.

It is thought that the post-depositional processes alluded to earlier and especially the lateral changes resulting from historic tectonics may have led to lateral stress relief and generally lower K_0 values in the Gault Clay. There is also the possibility that the clay simply cannot maintain suctions high enough to reliably represent the in situ stress conditions, although this is considered less likely - similar results in terms of suction measurement from large diameter (300 mm) samples of Gault Clay recovered from a site near Cambridge were seen by the Authors.

Stress path testing was undertaken on six samples to examine the changes in soil stiffness, during stress paths representative of the expected unloading during demolition and excavation, and reloading as the raft is constructed and loaded.

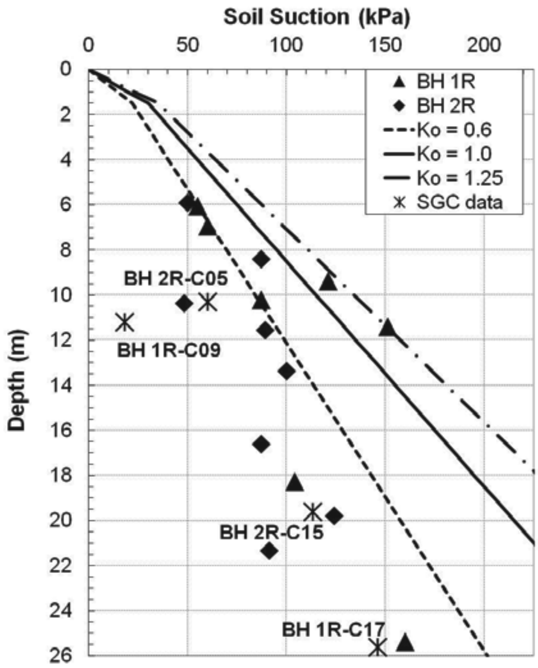

Figure 2. Sample suction profile and implied K_0 values

2.2 *Ground response at adjacent site*

When developing the ground model for design of the piled raft, it was recognised that next door there was effectively a full scale element test available in the form of the instrumented 10 m deep basement excavation created for the Crown Plaza Hotel (Fig. 3).

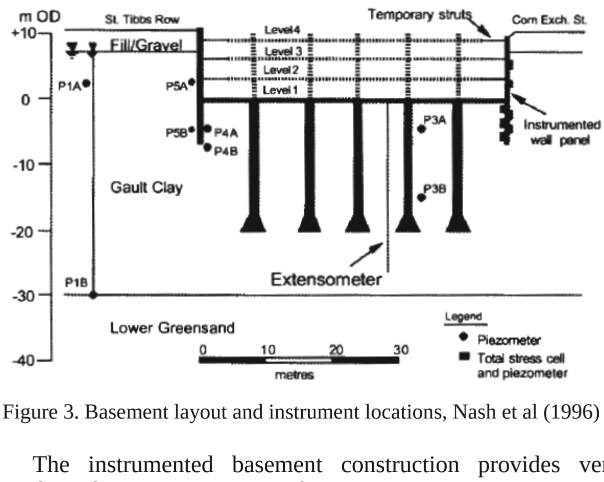

Figure 3. Basement layout and instrument locations, Nash et al (1996)

The instrumented basement construction provides very useful information in terms of the vertical ground movements associated with unloading during excavation and in the long-term (Nash et al. 1996, Lings et al. 1991). And while acknowledging that the piled foundations will have influenced the observations to a degree, the data (Fig. 4) was able to be used to make an independent assessment of the non-linear stiffness of the soil mass with depth and strain level. In particular the excavation to Level 2 was of interest as this represented the level of excavation in the new development.

During the basement excavation, block samples of the clay were recovered for laboratory characterisation of the soil. These studies examined the strength and deformation characteristics of the clay (Ng & Nash, 1995), Table 2 and its stiffness anisotropy (Pennington et al. 1997, Lings et al. 200). As with the field observations, this data informed the decisions made during the development of the ground model for this project as described in the following.

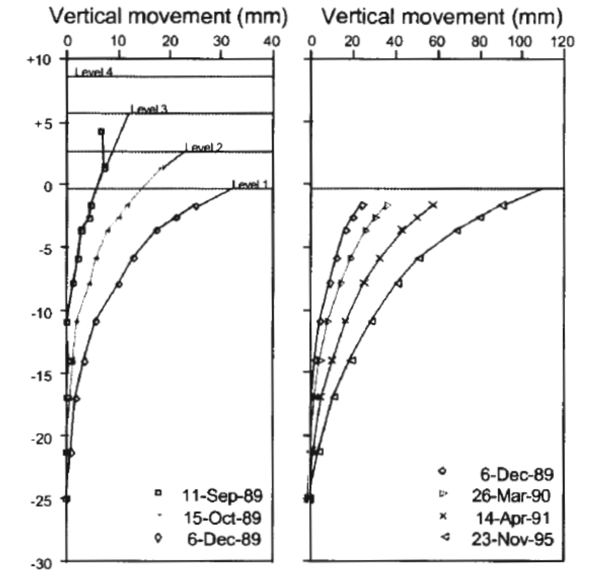

Figure 4. Observations of ground heave inside basement during and post-construction, Nash et al (1996)

Table 2. Typical Gault Clay geotechnical parameters

Parameter	Value
Natural moisture content: %	25 - 32
Liquid Limit, LL: %	70 - 80
Plasticity Index, PI: %	40 - 50
Liquidity Index, LI: %	0 ± 0.1
Undrained shear strength, c_u: kPa	75+5z [(1)]
Critical State angle of resistance, φ'_{CS}: deg	24° - 28°
Peak apparent cohesion, c'_{PK}: kPa	2 - 3
Peak angle of shearing resistance, φ'_{PK}: deg	32° - 34°
Initial shear modulus, G_0: MPa	80 - 120
Young's modulus at 0.2% strain, $E'_{0.2\%}$: MPa	c. 10

(1) z = depth below top of clay

2.3 *Integrated ground model*

In order to undertake the geotechnical calculations for the design of the piled raft, a ground model in terms of vertical stiffness, E was developed based on back-analysis of the observed heave response in the adjacent basement, Fig. 4 & 5 and stress path testing undertaken on high quality core samples from the site, Fig. 6. Data from the latter are summarised in Table 3.

The stiffness data from these two sources are compared in Fig. 6 – the comparison is remarkably good given the quite different sources and gave confidence in the use of the ground model for the design of the foundation system.

Table 3. Summary of stress path testing

Sample	1R-C09	1R-C17	2R-C05	2R-C17
Depth: m	11.2	25.6	10.3	19.6
$G_{max,i}$: MPa	37.5	180	45.5	104
$E_{u,0.01}/c_u$: -	1000	2200	1400	1200
$E_{u,0.1}/c_u$: -	475	860	300	560
$E_{u,0.5}/c_u$: -	190	220	100	280

The stiffness profile chosen for the design calculations is shown in right-hand side of Fig. 5 where it is compared to the 'average' line from the field data (dashed line in both sides of Fig. 5) and various values of constant E_u/c_u ratio ranging from 250 to 1500.

In the preliminary design at tender stage, anticipating strains in the region of 0.2% to 0.3%, a uniform modulus ratio E_u/c_u = 300 was used. It is clear from the figures below that this assumption quickly becomes unrepresentative of the response of the clay at depth and therefore any calculations are likely to overstate the movements that might be expected.

In the design calculations, use of the linear model yielded settlement predictions about one-third larger than that of the pseudo-nonlinear model. Thus peak settlements were reduced from 90 mm to 60 mm, and the area where settlements were considered excessive (i.e. greater than 40 mm), was greatly reduced.

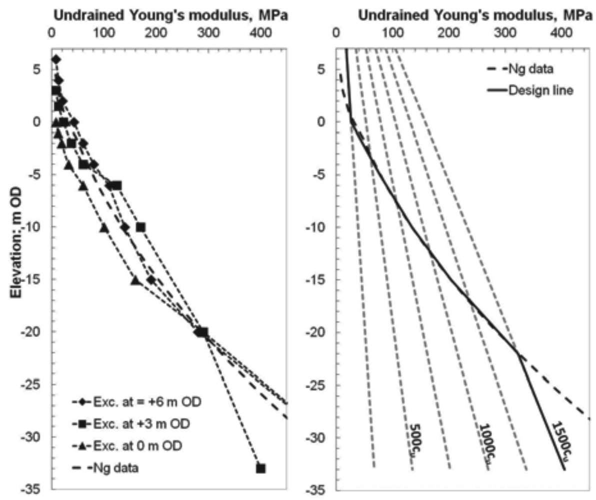

Figure 5. Back-analysis of ground stiffness model

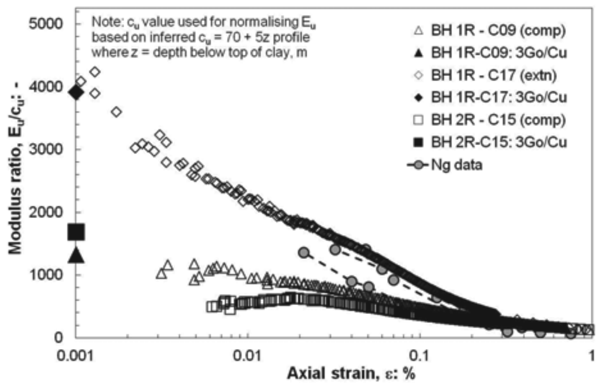

Figure 6. Nonlinear stiffness response from laboratory and back-analysed field data

3 FOUNDATION DESIGN

3.1 *Calculation method*

A number of simplified methods have been proposed for the evaluation of the load-settlement response of piled rafts but often these are difficult to apply to cases where the raft shape and/or load patterns are complex – as was the case here.

For this project, a plate-on-springs type structural analysis was undertaken in parallel with geotechnical analysis of ground movement using the pseudo-nonlinear elastic ground model described above. The analyses were iterated to achieve comparable movement predictions, the latter calculation providing subgrade stiffness values for use in the former that were consistent with the expected load changes and associated ground response across the raft footprint.

When including settlement reducing piles (SRP) in the calculation, rather than modelling them as a spring, it was assumed that they acted as a constant load. This was deemed acceptable on the basis that they would be settling 25 mm to 40 mm, at which point the shaft resistance would be fully mobilised.

Calculations were undertaken for three stages of loading / soil response:

1. Undrained excavation using the undrained stiffness profile in Fig. 5; this analysis suggested heave up to 30 mm might occur.
2. Semi-drained net loading using a stiffness profile based on $E' = 0.75E_u$ which was considered to be a reasonable estimate for the situation at the end of construction when it was estimated that 40±10% consolidation might have been achieved.
3. Drained net loading including uplift due to groundwater using a stiffness profile based on $E' = 0.50E_u$ which was assessed using elastic theory and the degree of anisotropy in stiffness suggested by Pennington et al. (1997), i.e. $G_{0(hh)}/G_{0(hv)} \approx 2$.

3.2 *Settlement control and role of SRP*

In the design, an overall factor-of-safety with respect to bearing capacity failure in excess of three was demonstrated for the raft. However, mitigation measures were required in order to:

- Reduce excessive contact pressures and limit raft settlements to less than 40 mm, as a plain raft was expected to settle 40 – 60 mm with local maxima of 60 – 90 mm under heavily loaded columns and building cores.

- Limit raft settlements along sensitive boundaries to less than 25 mm; in the absence of SRP where a similar range of settlement values as indicated above were expected.

- Minimise net load changes adjacent to the diaphragm wall on the hotel boundary which was achieved by introducing SRP to limit the contact pressures on this boundary to approximately the same values present prior to the redevelopment.

- Minimise movements of bearing piles supporting the hotel which with the measures introduced were estimated to be less than 1.5 mm.

This was achieved by the introduction of SRP at the required locations. Their use in the first instance is well documented however it is thought that this is the first such application in terms of mitigating potential impacts outside the site boundary.

4 CONCLUSIONS

Use of precedent knowledge of the ground's response to load change has allowed a calculation model to be derived that is better conditioned to predict ground movements in Gault Clay.

In this case, the use of a piled raft, though more complex to design, provided a clear cost and time advantage to a fully piled solution. Furthermore, the use of a well-conditioned pseudo-nonlinear elastic soil model allowed further savings by reducing the number of SRPs needed to achieve the performance criteria.

SRP have been employed in a novel way in order to limit vertical ground movements off-site by constraining those within the site boundary, and thus protect neighbouring buildings from potentially damaging movement.

5 ACKNOWLEDGEMENTS

The authors would like to thank Bovis Lend Lease and the Grand Arcades Partnership for allowing us to report on our contribution to this project, and Dr. David Nash of Bristol University with whom the first author spent a very interesting and productive afternoon discussing the Gault Clay.

The work presented here was undertaken while the authors worked at Card Geotechnics Ltd., UK.

6 REFERENCES

Burland J.B. 1995. Piles as settlement reducers, in – Proc. XIX Convegno Nazionale di Geotecnica, Pavia, 21–34.

Cooke R.W. 1986. Piled raft foundations on stiff clays – a contribution to design philosophy, Géotechnique 36(2), 169–203.

Lings M.L. Nash D.F.T. Ng C.W.W. and Boyce M.D. 1991. Observed behaviour of a deep excavation in Gault Clay: a preliminary appraisal, Proc. 10th European Conf. SMFE, 467–470.

Lings M.L. Pennington D.S. and Nash D.F.T. 2000. Anisotropic stiffness parameters and their measurement in a stiff natural clay, Géotechnique 50(2), 109–125.

Love J.P. 2003. Use of settlement reducing piles to support a raft structure, Proc. ICE Geotechnical Engineering 156(GE4), 177–181.

Marsh A.H. and Greenwood N.R. 1995. Foundations in Gault Clay, in – Geol. Soc. Spec. Publ. no. 10, Eng'g Geol. of Constr., 143–160.

Nash D.F.T. Lings M.L. and Ng C.W.W. 1996. Observed heave and swelling beneath a deep excavation in Gault Clay, Proc. Intl.Symp. on Geot. aspects of underground constr. in soft ground, London, 191–196.

Ng C.W.W. and Nash D.F.T. 1995. The compressibility of a carbonate clay, in - Compression and Consolidation of Clayey Soils, Yoshikuni & Kusakabe (eds), 281–286.

Pennington D.S. Nash D.F.T and Lings M.L. 1997. Anisotropy of G0 shear stiffness in Gault Clay, Géotechnique 47(3), 391–398.

Poulos H.G. 2001. Piled raft foundations: design and applications, Géotechnique 51(2), 95–113.

Price G. and Wardle, I.F. 1986. Queen Elizabeth II conference centre: monitoring of load sharing between piles and raft, Proc. ICE, Part 1 80(6), 1505–1518.

Reul O. and Randolph, M.F. 2003. Piled rafts in overconsolidated clay: comparison of in situ measurements and numerical analyses, Géotechnique 53(3), 301–315.

Samuels S.G. 1975. Some properties of the Gault Clay from the Ely-Ouse Essex water tunnel, Géotechnique 25(2), 239–264.

The Use of Recycled Aggregates in Unbound Road Pavements

L'utilisation d'Agrégats Recyclés en Revêtements de Chaussée sans Liant

Cameron D.A., Rahman H.H., Azam A.M.
University of South Australia (UniSA), School of Natural and Built Environments, Adelaide, Australia

Gabr A.G.
Mansoura University, Public Works Department, Faculty of Engineering, Egypt

Andrews R.
ARRB Group (South Australia), Adelaide, Australia

Michell P.W.
Aurecon Australia Pty Ltd, Adelaide, Australia

ABSTRACT: This paper argues for the acceptability for use in unbound granular pavements of recycled concrete aggregates (RCA) and recycled clay masonry (RCM) derived from demolition. Specifications from road authorities both within and outside Australia are considered, and results of tests carried out on specimens of RCA and RCM are compared with these specifications. The tests included conventional classification tests for soils and aggregates, Los Angeles abrasion value, Micro-Deval, falling head permeability, drying shrinkage, undrained triaxial tests and repeated loading triaxial testing for resilient modulus and permanent strain rate. The influence of matric suction on resilient modulus of the granular pavement materials is presented. Both RCA and RCA blended with RCM (20% by mass maximum) were found to meet existing specifications and therefore can be incorporated in road pavements. RCA was found to be suitable for use as a base course. In the case of RCA blended with RCM, as the proportion of RCM increases, the permanent strain rate increases and resilient modulus decreases, thereby compromising use of the blends as base material. However, RCA with up to 20% RCM is suitable for use as sub-base of a road pavement.

RÉSUMÉ : Ce document plaide pour l'acceptabilité, pour les revêtement de chaussée granulaires sans liant, des agrégats de bétons recyclés (ABR) et de la maçonnerie recyclée d'argile (MRA) provenant de la démolition. Les spécifications des autorités routières d'Australie et d'ailleurs sont considérées, et des résultats d'essais effectués sur des spécimens de ABR et de MRA sont comparés à ces spécifications. Les essais comprennent des essais conventionnels de classification pour sols et agrégats (valeur d'abrasion Los Angeles, Micro-Deval , perméabilité à charge variable, séchage et rétraction, essais triaxiaux non drainé et essais triaxiaux répétés pour le module résilient et la vitesse de déformation constante. L'influence de la succion matricielle sur le module résilient des matériaux granulaires de revêtement de chaussée est présentée. l'ABR et l'ABR mélangé avec le MRA (20% maximum en masse) se sont avérés satisfaire les spécifications existantes et peuvent donc être incorporés en revêtement de chaussée. l'ABR s'est avéré approprié pour l'usage comme couche de base. Dans le cas de l'ABR mélangé avec le MRA, à mesure que la proportion de MRA augmente, le taux de déformation permanente augmente et le module résilient diminue, compromettant de ce fait l'utilisation des mélanges en tant que matériau de couche de base. Cependant, l'ABR avec jusqu'à 20% RCM convient pour l'usage comme sous-couche de chaussée routière.

KEYWORDS: recycled aggregate, C&D waste, resilient modulus, permanent strain, matric suction, prediction

1 INTRODUCTION

Recycling of construction and demolition wastes can produce acceptable aggregates for civil engineering applications such as unbound granular pavements. Australian practice is well behind countries such as Japan, the United Kingdom, France, Germany and the Netherlands, but the recycling aggregate industry, which has emerged over the last decade, is growing. Quarry industries seem to feel challenged by recycling but should realise that even in Europe with its long history of recycling, recycled aggregate supply is unlikely to exceed 10 to 15% of total demand (Meininger and Stokowski 2011). Much of the research in Australia to date has focussed on Recycled Concrete Aggregates (RCA), Recycled Clay Masonry (RCM), recycled glass and waste rock. Much can be learned from the European experience, but this experience cannot be simply adopted as it is based on the range of climates, pavement construction practices and geology throughout Europe. Furthermore, the great majority of pavements in Australia are thinly surfaced, resulting in higher stresses being applied to the aggregates by passes of traffic.

Much of the work to date has been limited to the laboratory (e.g. Nataatmadja and Tan 2001, Aatheesan et al. 2009, 2010, Arulrajah et al. 2011, 2012a, 2012b and 2012c, Gabr et al. 2012, Gabr and Cameron 2012a, Azam and Cameron 2012, Azam et al. 2012, Jitsangiam et al. 2009, Leek and Siripun 2010). Gabr 2012 developed an empirical model for predicting permanent strain from testing of South Australian RCA, which he incorporated into Finite Element Analysis (FEA) to predict pavement life, similar to the approach of Huvstig et al. 2008. However the validation of this approach has not been made. Nevertheless a few field trials of roads constructed with C&D waste have been conducted (Ecocycle 1997 and Bowman & Associates 2009a and 2009b). The combination of laboratory and field data with FEA has much potential to improve pavement design generally.

This paper summarizes the work undertaken at the University of South Australia (UniSA) to evaluate aggregate produced from two local producers of recycled C&D waste, which consisted of either crushed concrete or RCA blended with fired clay masonry (RCM). All products were nominally 20 mm sized maximum aggregate. Variations in moulding moisture levels have been investigated, leading to some interesting findings relating soil suction to resilient modulus.

The South Australian Department for Transport, Energy and Infrastructure (DPTI, formerly DTEI) stipulates a range of material properties (DPTI, 2011), but includes minimum resilient modulus and maximum rate of permanent strain for Class 1 bases, based on a simplified, single stress stage Repeated Load Triaxial Test (RLTT). These performance based specifications are unique in Australia if not worldwide. In parts of Scandinavia, specifications require back-calculated resilient modulus from a falling weight deflectometer or Young's modulus from a plate bearing test (Gabr and Cameron 2011).

2 MATERIALS AND RANGE OF TESTS

Two RCA basecourse products, A and B, were tested, along with a comparable product (A20) of RCA with 20% by mass of RCM. Further materials were made at UniSA by blending product B with RCM to 10%, 20% and 30% (B10, B20 and B30). DPTI permit up to 20% by mass in RCA of "foreign material" consisting of clay brick tile, crushed rock and masonry for base course and subbase applications. Finally a virgin quartzite aggregate (Q) was evaluated, which is commonly used in Adelaide for construction of Class 1 bases.

The particle size distributions of the materials fell within DPTI specifications for Class 1 base. All the materials were well-graded gravel and sand mixtures with silty gravel; GW-GM according to the Unified Soil Classification System (USCS). Material A lay close to the coarse specification limit, while Material B20 crossed between the limits and had a fairly high proportion of fine sand-sized particles. The fines content of the two RCA products, A and B were just 5% and 7% respectively, while the quartzite base material (Q) had 11%.

Tests were conducted in line with the requirements of current Australian specifications. These included plasticity of fines, aggregate strength tests, Los Angeles abrasion, CBR tests on 4 day soaked samples and RLTT to the DTEI 2008 protocol. In addition, falling head permeability tests and shrinkage tests were conducted. Some concern has been expressed relating to the propensity of RCA to exhibit some cementation upon wetting and compaction. This self-cementation of RCA materials can produce increase of strength with time, but also the possibility of reduced permeability (AASHTO 2002) and shrinkage. Therefore shrinkage was investigated.

3 MATERIAL PREPARATION

All materials were compacted to a target Dry Density Ratio (DDR) of 98% of maximum dry density under Modified Proctor compactive effort. Static compaction, which is advocated by DTEI for unbound granular material, was used for compaction, largely because of the consistency of preparation. Moulding moisture variations are indicated for particular tests as follows. In South Australia, materials are commonly compacted at 80% of OMC and are allowed to dry back to 60% of OMC.

3.1 Falling Head Permeability

For the falling head permeability tests, the moulding moisture contents were 100 and 80% of OMC. Blended materials were tested; A20, B10, B20 and B30.

3.2 Drying Shrinkage

Samples were 200mm high by 100 mm diameter. Triplicate samples of materials A and B, and duplicate samples of A20 and B20, were prepared OMC. The target moisture content was reduced to 90% OMC if the material was found to be too fragile upon extrusion (e.g. samples B & B20). After compaction, the samples were extruded from the mould and sealed in plastic bags to cure for 7 days; the samples were then stored in a curing room (temperature 23±2°C and relative humidity 55±5%).

3.3 Undrained Triaxial and RLTT Testing

Duplicate samples were prepared.The resilient modulus and permanent deformation behaviour of RCA mixtures were investigated at different levels of moulding moisture contents, as was the undrained shear strength. Generally just one day of curing occurred before de-moulding and testing.

4 RLTT TEST METHODS

In Australia, there are two standard approaches to Repeated Load Triaxial Testing (RLTT); multi-stage stress testing and single-stage stress testing, e.g. the DTEI approach. DTEI 2008 specified application of a constant confining stress of 196 kPa and a vertical deviator stress of 460 kPa, pulsed over 50,000 loading cycles. AUSTROADS established a multi-stage stress RLTT under drained conditions to determine the permanent deformation and resilient modulus properties. Both these test protocols ahave been applied. In the RLTT program, deformations were measured with two pairs of inductance coils ("Emu" coils) mounted on the sample (Gabr et al. 2012).

5 INDEX VALUES AND OTHER PROPERTIES

The plasticity of fines of the various materials is indicated in table 1. The DPTI (2011) specifications call for a maximum Liquid Limit of 25% for Class 1 and 28% Class 2, and so A20 falls into Class 2, while all other materials would be acceptable for Class 1 applications.

Los Angeles Abrasion Value (LAA) and Micro Deval help to evaluate the abrasion resistance/toughness under traffic loading. The LAA values of the South Australian RCA examples ranged between 37% and 39%, which failed to meet the maximum of 30% proposed by DPTI. The Ile de France specifications (2003) for LAA allowed 35% for roads with the greatest traffic (GR4), increasing to 40% for GR3 and 45% for GR2. The values for RCM blends were in the range of 40 to 45%. The French Micro Deval limit of 30% for GR4 was met by both RCA products as the Micro-Deval values were 30% and 28% for products A and B, respectively. There is however a further requirement that the sum of LAA and Micro Deval must not exceed 55 for GR4 and 65 for GR3. Product B was on the limit for GR3, while product A, exceeded it (69). GR3 corresponds to a road with daily annual traffic of 85.

Average shrinkage curves with time are provided in Figure 1 for the four materials that were tested. Interestingly, shrinkage strains were similar for the RCA products, as they were for the blends (20% RCM); however, the addition of crushed masonry resulted in an appreciable drop in shrinkage. In the case of product B, a reduction of almost 60% was observed.

The permeability of blended recycled material when prepared at OMC was approximately 2 x 10-8 m/sec for blends based on RCA product B, but it was observed that A20 was ten times more permeable. Compaction to the same density but at just 80% OMC increased the permeability of all materials generally by a factor of approximately three.

Table 1. Selected properties of the recycled aggregate blends

Material	*A*	*A20*	*B*	*B10*	*B20*	*B30*
Liquid Limit (%)	26	27	23	24	23	23
Plastic Index (%)	2	2	1	3	3	2
LAA (%)	39	42	37	42	43	45
Micro Deval (%)	30	-	28	-	-	-

All materials met the specification of a minimum CBR of 80%, despite masonry content reducing the CBR significantly. Similarly the requirement of a maximum unconfined compression strength of 1 MPa after curing was met.

A study was undertaken of the matric suction–moisture content relationship, or soil water characteristic curve (SWCC) of the materials to enable estimation of matric suctions of RLTT samples from measured moisture contents. Initial matric suction was determined by the hanging column method for low suctions and the contact filter paper method (refer Azam and Cameron

2012 for details of the filter paper method) for suctions greater than 20 kPa. The SWCC plots of gravimetric moisture content against matric suction are provided in Figure 2 for the 2 blends with 20% RCM. Air entry values (u_{ae}) were the same for these two samples but the residual suction (u_r) differed (15 and 30 kPa). The air entry values were within the range reported for RCA by Rahardjo et al. 2010.

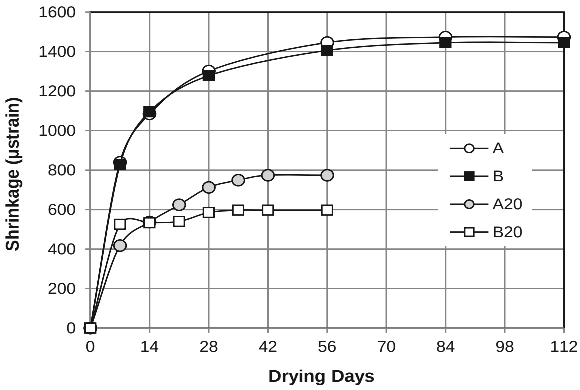

Figure 1. Shrinkage curves for the recycled materials

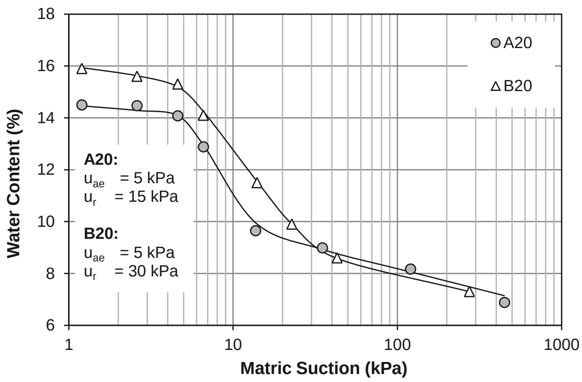

Figure 2. SWCC for materials A20 and B20

6 STATIC AND REPEATED LOADING RESULTS

Undrained shear strength data are indicated in Table 2 for material prepared at a target of relative moisture content of 80% OMC. The last row contains nominal shear strength values based on the shear strength parameters and a normal stress of 100 kPa. The nominal shear strength decreased generally with masonry content for the B samples, but the A samples seemed unaffected.

Shear strength increased with matric suction or decrease of relative moisture content. Between target moisture contents of 90 and 60% OMC, on average the nominal shear strength of the recycled materials increased by 13%, while the quartzite strength was improved by 9%.

The resilient modulus of the RCA products (materials A and B) varied between 500 and 950 MPa, clearly surpassing the DPTI 2011 requirement of 300 MPa. Generally resilient modulus decreased with moisture content although product A had a fairly constant modulus of approximately 600 MPa. The materials blended with crushed masonry performed well also. Even material B30 had a minimum modulus greater than 400 MPa. A relationship between initial matric suction and resilient modulus from the single stress stage of the DTEI test protocol, was developed and is illustrated in Figure 3. A simple power model fit the data for all materials adequately. The power function is consistent with the findings of Gupta et al. 2007. Further work is underway on predicting the resilient modulius from multi-stage triaxial stress testing (stress dependent model).

The DPTI specification for Class 1 material requires a minimum rate of permanent strain over the last 30,000 load cycles of $-1x10^{-8}$% per cycle. RCA performance was generally acceptable for Class 1 (refer Figure 4) although the blends with RCM were more appropriate for Class 2 applications. The quartzite material, Q, failed to make the DPTI Class 1 limit when prepared at 80% OMC or wetter.

Table 2. Undrained shear strength (80% OMC)

Material	*A*	*A20*	*B*	*B10*	*B20*	*B30*
Cohesion (kPa)	163	134	41	9	46	0
Friction angle (°)	48	55	60	53	44	53
Nom. strength (kPa)	277	274	214	142	143	133

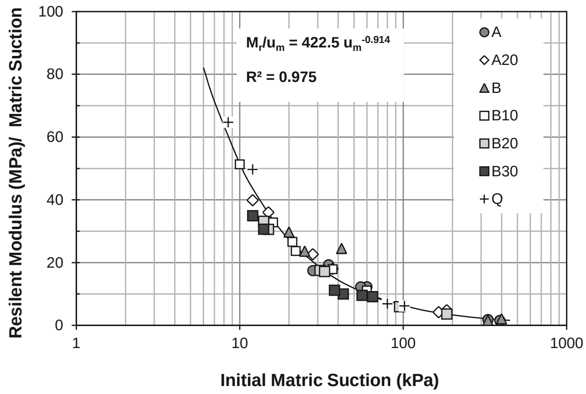

Figure 3. Resilient modulus as a function of initial matric suction

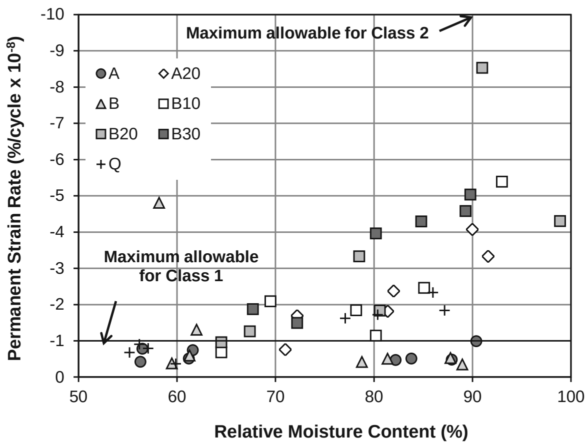

Figure 4. Permanent strain rate as a function of initial moisture content

7 PERMANENT STRAIN MODELLING

Gabr and Cameron 2012b proposed a predictive model for permanent strain from multi stage RLLT data on RCA materials A and B, and virgin aggregate, Q. Permanent strain increased with increase in either mean stress ratio (current stress to failure stress) or moisture content. The proposed model required mean normal stress, shear stress ratio, number of cycles, moulding moisture content, dry density and weighted plasticity index.

The model was found to fit very well the permanent strain for each material. An example is given in Figure 5. It was acknowledged by Gabr 2012 that the model attempeted to predict permanent strain over all material shakedown ranges, and so required further validation before confident application to prediction of rutting in pavements.Nonethless Gabr used finite element analysis of the impact of a single wheel load on a thin unsealed pavement, 320 mm thick, over a sand subgrade, to generate stresses for application of the permanent strain model and therefore predict pavement life. The life of a pavement constructed with material B was predicetd to improve 100 fold when the moulding moisture content was 60%, not 90% OMC.

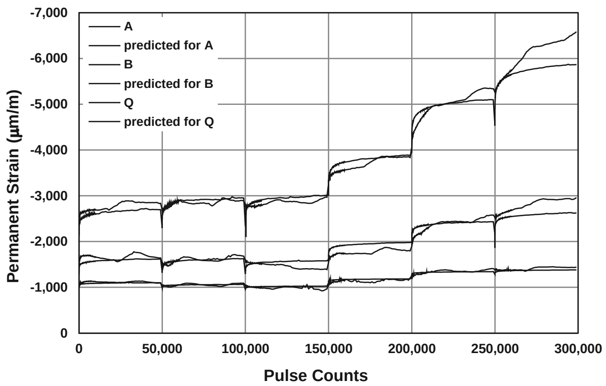

Figure 5. Permanent strain modeling of the materials at 80% OMC

8 CONCLUSION

From the evidence presented from RLTT data, the RCA products could be used as Class 1 base, while the blended products are more suited to Class 2 applications, or subbase. Other specification systems dependent on basic engineering properties, such as Los Angeles Abrasion and Liquid Limit may restrict the application of recycled materials to lesser applications. This paper has highlighted current research on recycled aggregates in South Australia, including the development of models for predicting both resliient modulus and permanent strain. Improvements to the models are being sought; for example matric suction should replace moisture content in the permanent strain model.

9 ACKNOWLEDGEMENTS

This research has been supported by industry partners ResourceCo and Adelaide Resource Recovery, as well as ZeroWaste and the Australian Road Research Board.

10 REFERENCES

AASHTO 2002. Standard specification for reclaimed concrete aggregate for unbound soil-aggregate base course. AASHTO, M319-02, Washington, D.C.

Aatheesan, T., Arulrajah, A., Newman, G., Bo, M.W. and Wilson, J. 2009. Crushed brick blends with crushed concrete for pavement sub-base and drainage applications. *J Australian Geomechanics*, 44 (2), pp. 65-72.

Aatheesan, T., Arulrajah, A., Bo, M.W., Vuong, B. and Wilson, J. 2010. Crushed brick blends with crushed rock for pavement system. *J Waste and Resource Management*, Vol. 163 (1), PP. 29-35.

Arulrajah, A., Piratheepan, J., Aatheesan, T., and Bo, M.W. 2011. Geotechnical properties of recycled crushed brick in pavement applications. ASCE *J Materials in Civil Engg*, 23(10): 1444 - 1542.

Arulrajah, A., Piratheepan, J., Younus, M. M., and Bo, M. W. 2012a, Geotechnical properties of recycled concrete aggregate in pavement sub-base applications. ASTM *Geotechnical Testing J*, 35 (5).

Arulrajah, A., Piratheepan, J., Disfani, M. M. and Bo, M. W. 2012b. Geotechnical and geoenvironmental properties of recycled construction and demolition materials in pavement subbase applications. *J Materials in Civil Engg*, (13th August 2012).

Arulrajah, A., Piratheepan, J., Bo, M. W. and Sivakugan, N. 2012c. Geotechnical characteristics of recycled crushed brick blends for pavement sub-base applications. *Canadian Geotech J*, 49(7), pp. 796-811.

Azam, A.M. and Cameron, D.A. 2012. Geotechnical properties of recycled clay masonry and recycled concrete aggregate blends in pavement. *J Materials in Civil Engg*, ASCE (29th June 2012).

Azam, A., Cameron, D.A. and Rahman, M.M. 2012. Blended recycled clay masonry and crushed concrete aggregate in bases. 2nd Int Conf on Transportation Geotechnics (ICTG), ISSMGE, eds Miura, Ishikawa, Yoshida, Hisari & Abe, Taylor & Francis Group, 10-12 September 2012, Sapporo, Hokkaido, Japan.

Bowman & Associates 2009a. Recycled concrete road base quality investigation. Strategic Waste Initiative Scheme (SWIS), Grant Scheme 4003 Report, Perth, Australia.

Bowman & Associates 2009b. Recycled concrete road base transport subsidy for test pavement trial. Strategic Waste Initiative Scheme (SWIS), Grant Scheme 5805 Report. Perth, Australia.

Cameron, D. A., Azam, A. and Rahman, M. M. 2011. Properties of recycled demolition waste for pavement construction. Proc, Int Conf on Advances in Geotechnical Engineering, ICAGE (CD).

Cameron, D. A., Azam, A. and Rahman, M. M. 2012. Recycled clay masonry and recycled concrete aggregate blends for pavements. Proc, GeoCongress, ASCE, San Francisco, March, pp 1532-1541.

DPTI (Department for Transport, Energy and Infrastructure) 2011. Part 215 Pavement Materials. Master specification, Division 2, Road Works,_http://www.dpti.sa.gov.au/documents/contractsandtenders/ specifications_-_division_2_roadworks

DTEI 2008. Determination of a characteristic value of resilient modulus and rate of deformation for unbound granular pavement materials. DTEI specifications, Materials group procedure, TP183, http://www.transport.sa.gov.au/materialstechnology

EcoRecycle 1997. Investigation Into the use of recycled crushed concrete for road base use. VicRoads, Alex Fraser, CSR Readymix Quarries and Independent Cement and Lime, Melbourne, Australia.

Gabr, A.G. 2012. Repeated load testing for primary evaluation of recycled concrete aggregate in pavements. PhD dissertation, University of South Australia, School of NBE.

Gabr, A.G., Cameron, D.A., Andrews, R. and Mitchell, P.W. 2011. Comparison of specifications for recycled concrete aggregate for pavement construction. *J ASTM International*, 8(10).

Gabr, A.G. and Cameron, D.A. 2012a. Properties of recycled concrete aggregate for unbound pavement construction. ASCE *J Materials in Civil Engg*, 24(6), pp 754-764.

Gabr, A.R. and Cameron, D.A. 2012b. Permanent strain modelling of recycled concrete aggregate for unbound pavement construction", *J Materials in Civil Engg*, ASCE, (25th September 2012).

Gabr, A.G., Mills, K.G. and Cameron, D.A. 2012. Repeated load triaxial testing of recycled concrete aggregate for pavement base construction. *Geotechnical and Geological Engineering*, SpringerLink, published online 30th Oct.

Gupta, S., Ranaivoson, A., Edil, T., Benson, C. and Sawangsuriya, A. 2007. Pavement design using unsaturated soil. Final Report, Minnesota Dept Transportation, Research Service Section, 245p .

Huvstig, A., Erlingsson, S., Hoff, I. and Saba, R. G. 2008. NordFoU – Pavement performance models. Part 2: Project level, unbound material. In Advances in Transportation Geotechnics – Ellis, Yu, McDowell, Dawson & Thom (eds), Taylor & Francis, pp 173-183.

Jitsangiam, P., Nikraz, H. R. and K. Siripun, K. 2009. Construction and Demolition (C&D) waste as a road base material for Western Australia roads. *Australian Geomechanics* 44 (3), pp 57-62.

Jitsangiam, P., K. Siripun, K., Nikraz, H. and Leek, C. 2012. Recycled concrete aggregate as a base course material in Western Australian road. Proc, 2nd Int Conf on Transportation Geotechnics (ICTG), ISSMGE, eds Miura, Ishikawa, Yoshida, Hisari & Abe, Taylor & Francis Group, 10-12 September 2012, Sapporo, Hokkaido, Japan.

Leek, C. and Siripun, K. 2010. Specification and performance of recycled materials in road pavements. Contract Report 001119-1, Curtin University, 72 pages.

Ile de France 2003. Guide techniques pour l'utilisation des mate´riaux re´gionaux d'Ile de France: les be´tons et produits de de´molition recycles. Ile-de-France, Paris, France.

Meininger, R. C. and Stokowski, S. J. 2011. Wherefore art thou aggregate resources for highways? *Public Roads*, FHWA, Sept/Oct, 75(2), http://www.fhwa.dot.gov/publications/publicroads/11septoct/

Nataatmadja, A. and Tan, Y. L. 2001. Resilient response of recycled concrete road aggregates. *J Transportation Engg*, 127 (5), pp 451-453.

Rahardjo, H., Vilayvong, K. and Leong, E.C. 2010. Water characteristic curves of recycled materials. ASTM *Geotechnical Testing J*, 34 (1), pp 89-96.

Vuong B.T. and Brimble R. 2000. AustRoads repeated load triaxial method – Determination of permanent deformation and resilient modulus characteristics of unbound granular materials under drained conditions. APRG Document 00/33 (MA), Australia.

Reuse of dredged sediments for hydraulic barriers: adsorption and hydraulic conductivity improvement through polymers

La réutilisation des sédiments dragués pour barrières hydrauliques: l'adsorption et l'amélioration de la conductivité hydraulique avec des polymères

Di Emidio G., Verastegui Flores R.D., Bezuijen A.
Ghent University, Zwijnaarde, Belgium

ABSTRACT: Environmental management and handling of dredged sediments is important worldwide, as enormous amounts of dredged material emerge from maintenance, construction and remedial works within water systems. Usually these materials, after temporary upland disposal in lagoons, are disposed in landfills. The aim of this study is to analyse the possible reuse of these sediments as a low-cost alternative material for landfill covers. The mechanisms through which polymers can improve the efficiency of dredged sediments for waste containment impermeable barriers were investigated. An anionic polymer was adsorbed to the surface of a dredged sediment. Hydraulic conductivity and batch sorption tests were executed to study the barrier performance and the transport parameters of this treated soil. Polymer treatment maintained low hydraulic conductivity of the soil to electrolyte solutions in the long term. The polymer treatment helped the soil to retain the spread of pollution.

RÉSUMÉ: La gestion de l'environnement et des sédiments dragués est important partout, parce que énormes quantités de matériaux de dragage sortent de l'entretien, la construction et les travaux de réparation dans les systèmes d'eau. Habituellement, ces matériaux, après le stockage dans les lagunes temporaires, sont déplacé dans les décharges. Le but de cette étude est d'analyser la possibilité de réutiliser ces sédiments en tant que matériau alternative à faible coût pour les couvertures d'enfouissement. Les mécanismes par lesquels les polymères peuvent améliorer l'efficacité des sédiments dragués pour les barrières de confinement des déchets imperméables ont été examiné. Un polymère anionique a été adsorbé à la surface des sédiments de dragage. Des essais de conductivité hydraulique et de sorption ont été exécutés pour étudier la performance de barrière et les propriétés de transport de cette terre traitée. Le traitement de polymère maintient une faible conductivité hydraulique du sol à le solutions électrolyte à long terme. Le traitement polymère contribué à résister la propagation de la pollution dans le sol.

KEYWORDS: reuse of dredged sediments, polymer treatment, low permeable hydraulic barriers.

1 INTRODUCTION

Soil contamination by heavy metals has been a long-term and worldwide environmental problem generated by anthropogenic activities of the past several decades. Heavy metals present in soils could find their way into human and animal populations through direct exposure or food chain/web, posing a serious risk to human health (Garcia-Sanchez et al. 1999; Gao et al. 2003; Ling et al. 2007). Heavy metals may be retained in clay soils by several soil phases or mechanisms, such as exchangeable, carbonate, hydroxide and organic phases (Griffin et al. 1976; Plassard et al. 2000; Sharma and Reddy 2004). The factors affecting the sorption of contaminants in soils are: (1) contaminant characteristics, such as water solubility, polar-ionic character, octanol-water partition coefficient; (2) soil characteristics such as mineralogy, permeability, porosity, texture, homogeneity, organic carbon content, surface charge, and surface area; and (3) fluid media characteristics, such as pH, salt content, dissolved carbon content.

Landfill sites for both chemical and industrial waste might be a serious threat for the environment, when not properly designed. To avoid pollution of the ground and groundwater, landfill sites are sealed with compacted clay liners (CCLs), geomembranes and Geosynthetic Clay Liners (GCLs). Suitable barriers must have a low permeability. To meet this property, the soil contained in CCLs and GCLs must fulfill some well-known physical and hydraulic criteria (Daniel 1993, Mitchell 1993).

Next to standard CCL and GCLs, there are emerging innovative barrier materials and systems, more efficient and/or less costly. Alternative evapotranspirative barriers (Malusis and Benson, 2006, Zornberg and McCartney 2010, Kison et al. 2012) or alternative barrier materials (such as, among others, paper sludge (Rajasekaran et al. 2000) dredged sediments (Di Emidio et al. 2006) can be necessary when: (1) high costs are associated with prescriptive materials and methods, (2) prescribed materials are not readily available, (Shackelford, 2005) and (3) when alternative materials are available in large quantities. In this regard, Di Emidio et al. (2006) studied the suitability of dredged materials to be used as alternative cover liner material for landfills. Different dredged materials were analyzed by means of laboratory tests, focusing on physical properties and hydraulic conductivity performance. As a result, acceptable zones (Daniel, 1993) based on hydraulic conductivity were established. Test results showed suitability of dredged sediments as hydraulic barrier alternative materials. Therefore, the use of dredged materials for cover liners represents an interesting opportunity for the future reuse of non-contaminated dredged materials.

On the other hand, dredged sediments are often polluted with contaminants, such as heavy metals (Singh et al. 2000, Mulligan et al. 2001, Peng et al. 2009). Methods to remove said metals from dredged sediment (Mulligan et al. 2001, Meegoda and Ruvini 2001, Bradl 2005, Peng et al. 2009) might be cumbersome and expensive. Therefore, alternative methods resulting in dredged sediments that retain heavy metals are highly needed.

Mazzieri et al. (2010) compared a polymer amended GCL with a conventional GCL permeated with a synthetic metal-rich acidic solution in order to compare the hydraulic, buffering and contaminant retention properties of the GCL materials. The breakthrough of metals occurred much earlier in the untreated GCL than in the polymer treated GCL, which was able to retain metals more effectively. Further insights are required to better understand the mobility of heavy metals in polymer treated clays and the ability of such clays to retain the heavy metals in the long-term.

This study involves the treatment of kaolin clay (as reference material) and dredged sediments with different percentages of an anionic polymer, Na-CMC (Sodium CarboxyMethyl Cellulose). This treatment is meant to improve their hydraulic performance as a lining material. This paper shows preliminary results (using $MgCl_2$ and sea water as reference solutions) to study the effects on both the hydraulic conductivity and the adsorption characteristics of polymer treated clays, such as kaolin and dredged sediments. The adsorption on polymer treated clays of heavy metals such as Zn, Cu and Pb is currently under investigation.

2 MATERIALS

A commercial processed kaolin Rotoclay® HB (Goonvean, St. Austell, UK) and a dredged sediment (DS) were used in this investigation. The kaolin was chosen as reference material because it has been largely used in previous laboratory research. The dredged sediment was obtained from Kluizendok in Ghent, Belgium. Table 1 shows some properties of the base materials used in this research. Both materials were treated with an anionic polymer, Sodium CarboxyMethylCellulose (Na-CMC) using different polymer dosages (2% and 8%) by dry weight of soil. The treatment consists of pouring a soil in a polymeric solution using a mechanical stirrer. The slurries obtained are then oven dried. After drying, the soils are ground using a mortar grinder (Di Emidio, 2010, 2012).

Deionised water, produced using a water purification system, was used as reference solution. A reference electrolyte compound, $MgCl_2$, was used for preliminary batch sorption tests on the treated and untreated soils. The electrolyte solutions were prepared by dissolving salts in deionised water. Moreover, natural seawater from the North Sea (near Oostende in Belgium) was used as permeant solution for the hydraulic conductivity tests on the treated and untreated soils. Table 2 and 3 show the chemical characteristics of deionized water and seawater.

3 METHODS

3.1 *Batch sorption test*

To study the adsorption of $MgCl_2$ on the treated and untreated soils, batch sorption tests were performed following the ASTM D4646. Different concentrations of $MgCl_2$ were used to prepare the equilibrium solutions for the batch sorption test. The untreated and treated soils were mixed for 24 hours in a rotatory table with $MgCl_2$ solutions of different concentrations (100 mg/l, 600 mg/l, 2000 mg/l, 6000 mg/l), using a soil-to-solution ratio 1:4. Then the slurries were separated by centrifugation. A centrifugation speed of 3000 rpm was sufficient to separate untreated soils from the solution, whereas a centrifugation speed of 10000 rpm was necessary to separate the treated soils from the solution. The sorption isotherms were obtained by plotting the sorbed mass of Mg^{2+} and Cl^- (meq/100g of soil, measured with a Spectroquant Photometer) vs. the equilibrium $MgCl_2$ concentration.

Table 1. Properties of the materials analyzed

Parameter	*kaolin*	*DS*
Type / source	Rotoclay®/Austell	Kluizendok
Specific gravity (-)	2.64	2.75
Liquid Limit (-)	59.0	44.1
Plastic Limit (-)	38.0	27.1
Swell index (ml/2g)	3.71	2.29
Silt content (%)	62.4	49.3
Clay content (%)	35.3	5.0
Sand content (%)	0.0	45.7

Table 2. Chemical analysis of the solutions used

Parameter	*Deionized water*	*Seawater*
EC (mS/cm)	0.0039	49.9
Salinity (-)	0.0	32.4
pH (-)	7.57	7.78
Na^+ (M)	-	0.455
K^+ (M)	-	0.012
Mg^{2+} (M)	-	0.053
Ca^{2+} (M)	-	0.012
Cl^- (M)	-	0.561
SO_4^{2-} (M)	-	0.024
HCO_3^- (M)	-	0.003
CO_3^{2-} (M)	-	0.0003
NO_3^- (M)	-	0.0007

Table 3. Chemical properties of the $MgCl_2$ solutions used for the Batch Sorption test

$MgCl_2$ (mg/L)	*EC (mS/cm)*	*Salinity (-)*	*pH*
100	0.301	0.0	6.87
200	1.382	0.5	7.04
2000	4.16	2.1	7.3
6000	12.13	6.46	7.7

3.2 *Hydraulic conductivity test*

Flexible wall hydraulic conductivity tests were conducted in order to investigate the impact of 8% of polymer addition on the hydraulic performance of the soils to a high concentrated electrolyte solution (natural seawater). The hydraulic conductivity tests were performed with an average effective stress of 30 kPa on 10 cm diameter samples with an initial porosity of about n = 0.718 (kaolin) and n = 0.542 (dredged sediment). To prepare the kaolin samples, the untreated and treated soil were poured dry in a stainless steel ring (0,45g/cm², as a standard GCL, 10 cm diameter) with a fixed height between two porous stones and submerged with seawater, with a sitting weight on top, for about one week. The dredged sediment sample was prepared by standard proctor compaction (ASTM D0698) with a water content two points higher than the optimum, to simulate a Compacted Clay Liner.

4 RESULTS AND DISCUSSION

4.1 *Batch sorption test results*

Figure 1 shows the sorption isotherms of the treated and untreated kaolin (a) and of the treated and untreated dredged sediment (b). The adsorbed mass of ions is plotted here vs. the equilibrium concentration of the $MgCl_2$ solutions. As shown in the graphs, batch sorption test results demonstrate that the sorbed mass of magnesium cations is higher onto the polymer treated soil compared to the untreated soil.

4.2 *Hydraulic conductivity test results*

Figure 2 shows the hydraulic conductivity test results of the treated and untreated soils. As shown in Figure 2.a, the hydraulic conductivity to seawater of the kaolin treated with 8% of the polymer was lower compared to that of the kaolin treated with 2% of the polymer. This result demonstrates that the hydraulic performance of a kaolin clay as barrier increases with increasing polymer dosage.

Figure 2.b shows that the hydraulic conductivity to seawater of the dredged sediment treated with 8% of the polymer is nearly two orders of magnitude lower compared to that of the untreated dredged sediment.

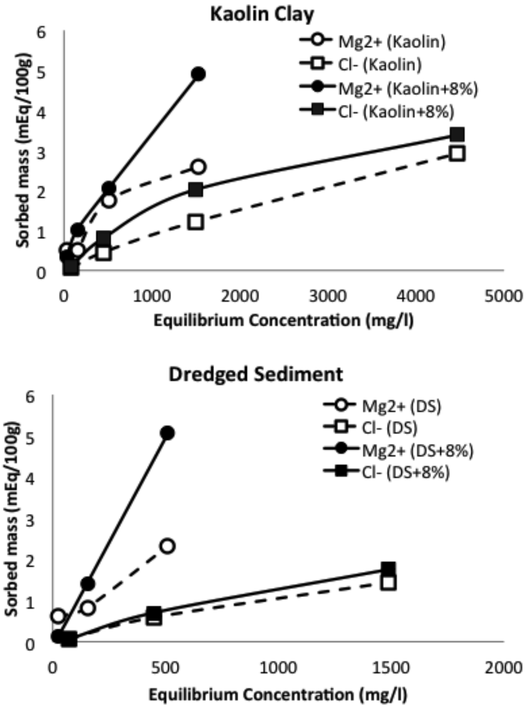

(a)

(b)

Figure 1. Sorption isotherms of kaolin (a) and dredged sediment, DS (b)

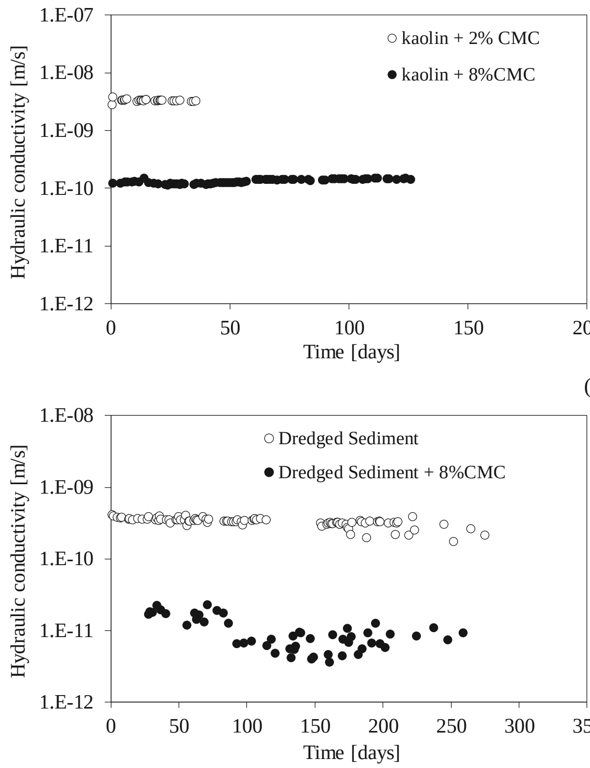

(a)

(b)

Figure 2. Hydraulic conductivity test results of (a) kaolin clay 2% CMC and 8% CMC, and (b) dredged sediment and dredged sediment treated with 8% CMC, permeated with natural seawater

5 CONCLUSION

The sorption isotherms of Mg^{2+} and Cl^- on the treated and untreated kaolin and on the treated and untreated dredged sediment were analyzed. The adsorbed mass of ions was plotted vs. the equilibrium concentrations. Batch sorption test results demonstrated that the sorbed mass of magnesium cations was higher onto the polymer treated soils compared to the untreated soils. These results are promising in view of metals retention in polymer treated dredged sediments. To further demonstrate the higher retention ability of polymer treated clays, the adsorption of heavy metals on kaolin, bentonite and dredged sediments is currently under investigation.

Hydraulic conductivity test results of treated and untreated soils were shown. The hydraulic conductivity to seawater of the kaolin treated with 8% of the polymer was lower compared to that of the kaolin treated with 2% of the polymer. This result demonstrates that the hydraulic performance of a kaolin clay increases (the hydraulic conductivity decreases) with increasing polymer dosage. The hydraulic conductivity to seawater of the dredged sediment treated with 8% of the polymer was significantly lower compared to that of the untreated dredged sediment. These results suggest the possible reuse of dredged sediments as alternative low cost impermeable barrier materials to isolate polluted sites and landfills.

6 ACKNOWLEDGEMENTS

The authors would like to acknowledge former thesis students (S. Lerno and R. Van den Steen) and technical staff (J. Van der Perre) for helping with the experiments.

7 REFERENCES

Bradl, H. 2005 *Heavy Metals in the Environment: Origin, Interaction and Remediation*. University of Applied Sciences, Neubrucke, Germany

Daniel, D.E, 1993. *Geotechnical Practice for Waste Disposal*. Chapman & Hall Ed.

Di Emidio, G., Van Impe, W.F., Van Impe, P. (2006). Geoenvironmental characterization of dredged sediment as alternative materials for covers. *5th ICEG, International Conference on Environmental Geotechnics*, 2006. Cardiff, UK

Di Emidio, G. 2010. *Hydraulic and chemico-osmotic performance of polymer treated clays*. PhD dissertation, Ghent University, Belgium.

Di Emidio, G. 2012. *Clayey barriers*. WO2012/025564 A1. PCT/EP2011/064542.

Kison, P., Malengier, B., Di Emidio, G., Peiffer, H., Van Keer, R. 2012. Inverse determination of soil characteristics with a bench-scale centrifuge. *Inverse Problems in Science and Engineering*.

Gao, Y.Z., He, J.Z., Ling, W.T., Hu H.Q., Liu, F. 2003. Effects of organic acids on copper and cadmium desorption from contaminated soils. *Environment International* 29, 613-618.

Garcia-Sanchez, A., Alastuey, A., Querol, X. 1999. Heavy metal adsorption by different minerals: application to the remediation of polluted soils. *The Science of the Total Environment* 242, 179-188.

Griffin, R.A., Shimp, N.F., Steele, J.D., Ruch, R.R., White, W.A., Hughes, G.M. 1976. Attenuation of pollutants in municipal leachate by passage through clay. *Environmental Science and Technology* 10, 1262-1268.

Ling, W., Shen, Q., Gao, Y., Gu, X., Yang, Z. 2007. Use of bentonite to control the release of copper from contaminated soils. *Australian Journal of Soil Research*, 2007, 45, 618-623.

Malusis, M, Benson, C. 2006. Lysimeters versus water-content sensors for performance monitoring of alternative earthen final covers. Geotechnical Special Publication, 147, 741-752, 2006, *Proceedings of the Fourth International Conference on Unsaturated Soils*

Mazzieri, F., Pasqualini, E;, Di Emidio, G; 2010. Migration of Heavy Metals Through Conventional and Factory-Prehydrated GCL Materials. *Proceedings of the 6xth ICEG, International Conference on Environmental Geotechnics*, 2010. Delhi, India

Meegoda, J.N., Ruvini, P. 2001. Ultrasound to decontaminate heavy metals in dredged sediments. *Journal of Hazardous Materials*, 85, 73-89.

Mitchell, J. 1993. *Fundamentals of soil behaviour*, John Wiley & Sons.

Mulligan, C.N., Yong, R.N., Gibbs, B.F. 2001. An evaluation of technologies for the heavy metal remediation of dredged sediments. *Journal of Hazardous Material* 85, 145-163.

Rajasekaran, G., Kamon, M., Katsumi, T., Inazumi, S. 2000. Evaluation of waste sludge as landfill cover. *Annuals of Disas. Prev. Res. Inst., Kyoto University*, No. 43 B-2, 2000

Peng, J., Song, Y., Yuan, P., Cui, X., Qiu, G. 2009. The remediation of heavy metals contaminated sediment. *Journal of Hazardous Materials*, 161, 633-640.

Plassard, F., Winiarski, T., Petit-Ramel, M. 2000. Retention and distribution of three heavy metals in a carbonated soil: comparison between batch and unsaturated column studies. *Journal of Contaminant Hydrology* 42, 99-111.

Shackelford, C.D. 2005. Environmental issues in geotechnical engineering. Keynote Lecture. *Proceedings of the 16th International Conference on Soil Mechanics and Geotechnical Engineering*. Osaka, Japan.

Sharma, H.D. and Reddy, K.R. 2004. *Geoenvironmental Engineering.* John Wiley & Sons, Hoboken, New Jersey.

Singh, S.P., Ma, L. Q., Tack F.M.G., Verloo, M.G. 2000. Trace Metal Leachability of Land-Disposed Dredged Sediments. *Journal of Environmental Quality* 29 (4), 1124-1132.

Zornberg, J.S., McCartney, J.G. 2010. Centrifuge Permeameter for Unsaturated Soils I: Theoretical Basis and Experimental Developments *Journal of Geotechnical and Geoenvironmental Engineering*, Vol. 136, No. 8, August 1, 2010.

Characterization of recycled materials for sustainable construction

Caractérisation des matériaux recyclés pour la Construction durable

Edil T.B.

University of Wisconsin-Madison, USA

ABSTRACT: Recyclable materials and industrial byproducts provide an environmentally and economical alternative to natural earthen materials when used safely and wisely in geotechnical construction. In particular, the construction of various elements of transportation systems requires large quantities of materials and locally available recyclable materials can be used extensively enhancing sustainability of construction. This paper addresses the rapid characterization required for this new class of materials such as recycled asphalt pavement, concrete aggregate, and coal combustion residues (fly ash, bottom ash). Recycled materials and industrial byproducts require an assessment of their environmental suitability in terms of potential impacts on surface and ground water quality for their acceptance. Finally, their field behavior need to be evaluated and their contribution to sustainability to be assessed.

RÉSUMÉ : Les matériaux recyclables et les sous-produits industriels fournissent ambiant et l'alternative économique aux matériaux de terre naturels une fois utilisés sans risque et sagement dans la construction géotechnique. En particulier, la construction de divers éléments des systèmes de transport exige de grandes quantités de matériaux et localement des matériaux recyclables disponibles peuvent être employés intensivement augmentant la durabilité de la construction. Ce document adresse la caractérisation rapide exigée pour cette nouvelle classe des matériaux tels que le trottoir réutilisé d'asphalte, l'agrégat concret, et les résidus de combustion de charbon (cendres volantes, cendre inférieure). Étant les matériaux réutilisés ou les sous-produits industriels, leur acceptation exige une évaluation de l'aptitude environnementale en termes d'impacts potentiels sur la qualité extérieure et d'eaux souterraines. En conclusion, leur besoin de comportement de champ d'être évalué et leur contribution à la durabilité à évaluer.

KEYWORDS: recycled materials, sustainable construction, recycled asphalt pavement, recycled concrete aggregate, coal ash.

1 INTRODUCTION

Development and growth need to be sustainable, in other words, integrate environmental, economic, and social dimensions towards global stewardship and responsible management of resources. Strategies need to evolve for sustainable development..Large quantities of natural and processed materials are used in construction activities such as buildings, transportation facilities, infrastructure, and environmental applications. These materials use natural resources and consume large quantities of energy to extract or process with associated green house gas emissions. Transportation facilities, such as highways, in particular use large quantities of materials in initial reconstruction and also during periodic rehabilitation. Recycling industrial byproducts and construction materials in highway construction can generate "green highways" where use of virgin materials and large amounts of energy and generation of green house gas emissions are minimized.

The necessary steps for characterization of widely used recycled materials (i.e., recycled asphalt pavement and recycled concrete aggregate) and industrial byproducts (i.e., coal combustion products such as bottom ash and fly ash) in highway construction are presented and discussed. The approaches for determining their physical characteristics, geomechanical behavior (i.e., resilient modulus), durability (i.e., freeze-thaw cycling, temperature effects, wet-dry cycling), constructability (i.e., compaction), material control, and their environmental suitability (i.e., leaching characteristics) for alternative beneficial uses are presented. Life cycle assessment (LCA) of the environmental benefits and the life cycle cost analysis (LCCA) for use of these materials are also discussed.

2 CHARACTERIZATION

We have been characterizing natural earthen materials systematically for nearly a century. Widespread use of these recycled materials is relatively new and time window to characterize them is short because of economical and environmental drivers. Testing methods developed for soils and construction specifications for natural aggregates and soils can be adapted to this new class of recycled materials and the existing pavement design procedures can be followed.

Material control in terms of variability of composition, grain size characteristics, inclusion of impurities are issues that need to be assessed for recycled materials, as they are products of anthropogenic processes rather than geological processes. There may be differences arising from basic material characteristics that may impact constructability in terms of compaction control. Modern pavement design requires resilient or elastic modulus as the primary geomechanical property. On the basis of this property layer thicknesses in a pavement and service life of a pavement can be determined. Durability under climatic effects, i.e., freeze-thaw and wet-dry cycles, is a critical quality for pavement materials because the pavements are surficial and directly influenced by the climate. Some of these materials have sensitivity to temperature in ways we are unaccustomed dealing with soils. Finally, while we do not question the environmental suitability of traditional materials like crushed aggregate, concrete and asphalt used in highway construction, use of recycled materials and industrial byproducts requires evaluation of environmental suitability, i.e., the leaching characteristics.

3 MATERIALS, APPLICATIONS & CRITICAL CHARACTERISTICS

The outstanding characteristics of a range of recycled materials widely used in highway construction are described along with typical applications.

3.1 Recycled Asphalt Pavement (RAP)

RAP (Figure 1) is produced by removing and reprocessing the hot mix asphalt (HMA) layer of existing asphalt pavement (Guthrie et al., 2007; FHWA, 2008). There is some ambiguity regarding the nomenclature involved in the production of RAP. Full depth reclamation (FDR) refers to the removal and reuse of the HMA and the entire base course layer; and recycled pavement material (RPM) refers to the removal and reuse of either the HMA and part of the base course layer or the HMA, the entire base course layer and part of the underlying subgrade implying a mixture of pavement layer materials (Guthrie et al. 2007, Edil et al. 2012). Unless specified, these three distinct recycled asphalt materials are collectively referred to as RAP. RAP is typically produced through milling operations, which involves the grinding and collection of the existing HMA, and FDR and RPM are typically excavated using full-size reclaimers or portable asphalt recycling machines (FHWA 2008, Guthrie et al. 2007). RAP can be stockpiled, but is most frequently reused immediately after processing at the site. Typical aggregate gradations of RAP are achieved through pulverization of the material, which is typically performed with a rubber-tired grinder.

RAP particles are coated with asphalt and its most value added use is in production of hot mix asphalt (HMA) with the benefit of reducing the fresh asphalt content. Seven RAP and 2 RPM samples collected from geographically diverse 7 states in the U.S.A. indicated a range of 5-7% asphalt content. RAP and RPM are widely used as unbound base material and the most common test used for specification is Grain Size Analysis. The most distinguishing physical characteristics are the grain size with some samples coarser and others finer. D_{50} of the 9 samples ranged 1.6 to 5.8 mm and the fines content was less than 2%. These materials all classified as A-1-a or A-1-b according to the AASHTO soil classification system. These samples had an average impurity (geotextiles, pavement markings, etc.) content of 0.2% for RAP, indicating that recycling industry has developed sufficient controls.

The compaction characteristics using the modified Proctor test indicated that the maximum dry unit weight (MDU) varies within a narrow range (19.4 to 21.5 kN/m^3) for RAP and the optimum moisture contents (OMC) (5.2 to 8.8%). OMC correlates significantly with the uniformity coefficient and percent moisture absorption and MDU correlates with OMC for RAP (Bozyurt et al. 2012).

Summary resilient modulus (SRM calculated at a bulk stress of 208 kPA, typical of base course layer) of the 9 RAP and RPM samples measured at OMC and 95% modified Proctor MDU, indicated that RAP/RPM has higher SRM (168 to 266 MPA) than natural crushed aggregate (152 MPa) and is significantly correlated with grain size characteristics (percent fines, D_{60}), asphalt content, specific gravity, and percent absorption (Bozyurt et al. 2012).

Application of freeze-thaw cycles indicated that SRM decreased in a range of 28 to 53% up to 20 cycles. However, RAP still had a higher stiffness than natural crushed rock aggregate regardless of the number of freeze-thaw cycles (Edil et al. 2012). Because of its asphalt content RAP can be expected to be sensitive to temperature changes. A decrease of approximately 30% in SRM was observed in RAP between the 23 and 35 °C. These temperature effects were absent in control specimens containing no asphalt. Micro-Deval and particle size distribution tests conducted on RAP after 5, 10, and 30 wet/dry cycles showed no apparent particle degradation (Edil et al. 2012).

RAP has excellent drainage capacity due to the hydrophobic nature of the asphalt coating and does not retain moisture (Nokkaew et al. 2012). Field leachate samples collected indicated that the concentrations of As, Se and Sb for RAP were slightly higher than the corresponding USEPA groundwater maximum contaiminant level (MCL) but decreased rapidly after the first flush (Edil et al. 2012). Falling Weight Deflectometer (FWD) tests were conducted at a test facility (MNROAD) on pavement with base course material of RAP indicated relatively small variation in stiffness and resilient modulus seasonally and indicated no deterioration over 4 years.

The investigations undertaken on RAP indicate that it is a suitable material for unbound base course applications and shows equal or superior performance characteristics compared to natural aggregates in terms of stiffness, freeze-thaw and wet-dry durability, and toughness. Their compositional and mechanical properties vary in relatively small range. The relative differences of RAP from natural aggregate such as temperature sensitivity, plastic deformations, and water absorption and retention characteristics are also well established. To determine the various properties of RAP (e.g., compositional characteristics, grain size distribution, compaction, resilient modulus), existing standard test methods employed for natural crushed aggregate can be used with added consideration for temperature control. There are no established standards for freeze-thaw and wet-dry cycling but published research methods can be adopted (Edil et al. 2012).

3.2 Recycled Concrete Aggregate (RCA)

The production of RCA (Figure 1) involves crushing structural or pavement concrete to a predetermined gradation. Fresh RCA typically contains a high amount of debris and reinforcing steel, and it must be processed to remove this debris prior to reuse (FHWA 2008). One of the value-added applications is use of RCA as a base course material although it can be used in constructing working platforms over soft subgrade and drainage medium. Depending on the crushing methods, the particle size distribution of an RCA can have a wide variability; with a lower particle density and greater angularity than would normally be found in more traditional virgin base course aggregates. Residual mortar and cement paste are typically found on the surface of the RCA, as well as contaminants associated with construction and demolition debris. The self-cementing capabilities of RCA are an interesting secondary property. The crushed material exposes un-hydrated concrete that can react with water, potentially increasing the materials strength and durability when used as unbound base course for new roadway construction. It follows that service life could also be extended as a result of these properties.

Seven RCA samples collected from geographically diverse 7 states in the U.S.A. indicated a range of 5-6.5% mortar content. The most distinguishing physical characteristics are the grain size with some samples coarser and others finer. D_{50} of the 7 samples ranged 1 to 13.3 mm and the fines content was less than 3-4% except two samples and higher than for RAPs. The mortar content was about 50% with small variation for these RCA samples. These materials classified mostly as A-1-a with some as A-1-b according to the AASHTO soil classification system. These samples had an average impurity (geotextiles, pavement markings, etc.) content of 1% for RCA, indicating that recycling industry has developed sufficient controls. The most predominant impurities for RCA were asphalt aggregate, aggregate with plastic fibers, brick, and wood chips. RCA derived from structures tend to have brick content. The effect of brick content up to 30% indicated no adverse effect on resilient modulus of RCA (Shedivy 2012).

The compaction characteristics using the modified Proctor test indicated that the maximum dry unit weight (MDU) varies within a narrow range (19.4 to 20.9 kN/m^3) for RCA and optimum moisture contents (OMC) (8.7 to 11.8%). OMC is greater than RAP's due the higher absorption capacity due to the porous nature of the mortar portion of RCA. OMC of RCA correlates significantly with the uniformity coefficient and percent moisture absorption and MDU correlates with OMC for RCA (Bozyurt et al. 2012)

RAP RCA

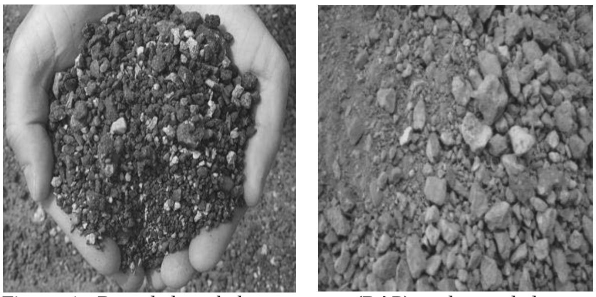

Figure 1. Recycled asphalt pavement (RAP) and recycled concrete aggregate (RCA)

Summary resilient modulus (SRM calculated at a bulk stress of 208 kPA, typical of base course layer) of the 7 RCA samples measured at OMC and 95% modified Proctor MDU, indicated that RCA has higher SRM (163 to 208 MPA) than natural crushed aggregate (152 MPa) and lower than RAP/RPM. SRM is significantly correlated with D_{30} and OMC (Bozyurt et al. 2012).

Application of freeze-thaw cycles indicated that SRM decreased 10-18% during the first five freeze-thaw cycles, but then an increased 30-38% above the initial SRM after 20 freeze-thaw cycles. The self-cementing properties of RCA and fines content generation over time could explain why an increase in stiffness after five freeze-thaw cycles occurred. (Bozyurt et al. 2011). Micro-Deval and particle size distribution tests were conducted on RCA after 5, 10, and 30 wet/dry cycles and no apparent trend was found between particle degradation and wet/dry cycling of the material

RCA has high drainage capacity but retains moisture more than RAP and natural aggregate base because of its hydrophilic cement mortar (Nokkaew et al. 2012). Laboratory batch and column leach tests and field leachate samples collected indicated that RCA base course has high alkalinity (pH = 10.8 to 12.9). As, Cr, Pb, and Se exceeded the maximum contaminant levels (MCLs) for the USEPA drinking water standard both at the field sites and in the laboratory column leaching tests. The concentrations of As, Pb, and Se for RCA exceeded the corresponding MCL only once or twice and the leaching behaviors were similar to that of the control natural crushed aggregate base course. As and Cr appear to be mainly sourced from the cement mortar based on the acid digestion results (Edil et al. 2012). Falling Weight Deflectometer (FWD) tests that were conducted at the MnRoad test facility on pavement with base course material of RCA indicated relatively small seasonal variation in modulus and no deterioration over 4 years.

The investigation undertaken on RCA indicate that it is a suitable material for unbound base course applications and shows equal or superior performance characteristics compared to natural aggregates in terms of stiffness, freeze-thaw and wet-dry durability, and toughness. Their compositional and mechanical properties vary in relatively small range. The relative difference of RCA from RAP and natural aggregate is its water absorption and retention characteristics. RCA displays high alkalinity thus oxyanions (As, Se, and Cr) should be given more attention to as they demonstrate enhanced leaching in a highly alkaline environment.

To determine the various properties of RCA (e.g., compositional characteristics, grain size distribution, compaction, resilient modulus), existing standard test methods employed for natural crushed aggregate can be used. There are no established standards for freeze-thaw and wet-dry cycling but published research methods can be adopted (Edil et al. 2012).

3.3 Coal Combustion Products (CCP)

CCPs of interest to highway construction include fly ash and bottom ash. When pulverized coal is burned in a dry bottom boiler, about 80 percent of the unburned material or ash is entrained in the flue gas and is captured and recovered as fly ash (Figure 2). The remaining 20 percent of the unburned material is dry bottom ash, a porous, glassy, dark gray material with a grain size similar to that of sand or gravelly sand (Figure 3). Although similar to natural fine aggregate, bottom ash is lighter and more brittle and has a greater resemblance to cement clinker. Beneficial use of bottom ash in highway applications, which is less than 50% of the material produced in the U.S.A., include structural fill (nearly half of all use), road base material, working platform material for construction of pavements over soft subgrade, fine aggregate in wearing surface in pavements and flowable fills, and as snow and ice control products. Bottom ash is predominantly well-graded sand-sized, usually with 50 to 90 percent passing a 4.75 mm (No. 4) sieve and 0 to 10 percent passing a 0.075 mm (No. 200) sieve (http://rmrc.wisc.edu).

Bottom ash has MDU of 11.8 to 15.7 kN/m^3 and OMC of 12-24%. Its internal friction angle varies from 32° to 45°. California bearing ratio (CBR) is typically 20 to 40. Summary resilient modulus (SRM calculated at a bulk stress of 208 kPA, typical of base course layer) for properly compacted bottom ash can be taken as 100 MPa. Bottom ash has similar drainage characteristic as sand with a hydraulic conductivity of 1x10^{-2} mm/s. All standard tests used to characterize natural granular materials like sand can be directly used for bottom ash.

The fly ash is a fine-grained, powdery particulate material that is carried off in the flue gas and usually collected by means of electrostatic precipitators, baghouses, or mechanical collection devices such as cyclones. Beneficial use of fly ash in highway applications, which is less than 50% of the material produced in the U.S.A., include cement replacement /additive in concrete (nearly half of all use), structural fill, stabilization agent for road subgrade and base material, working platform material for construction of pavements over soft subgrade, flow agent in flowable fills, and mineral filler in asphalt layers (http://rmrc.wisc.edu). Self-cementing coal fly ashes are suitable materials for the stabilization of subgrade soils, recycled pavement materials, and road surface gravel. Fly ash stabilization can result in improved properties, including increased stiffness, strength and freeze-thaw durability; reduced hydraulic conductivity, plasticity, and swelling; and increased control of soil compressibility and moisture. Fly ash stabilized materials may be used in roadway construction, such as working platforms during construction, stabilized subgrade, subbase, and base layers (Edil et al. 2006). Recently published ASTM standard practice provides guidance for testing and designing of stabilization of soil and soil-like materials with self-cementing fly (ASTM D7762 2011).

The possibility of groundwater contamination by trace elements that are commonly associated with coal combustion by-products is a concern. Areas with sandy soils possessing high hydraulic conductivities and areas near shallow groundwater should be given careful consideration especially

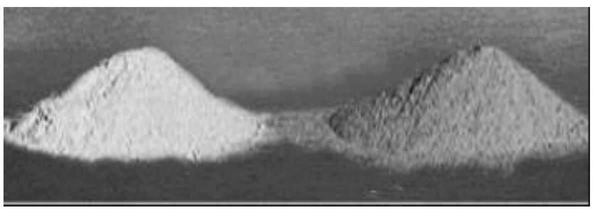

Figure 2. Fly Ash (different colors)

Figure 3. Bottom Ash

for large volume uses like structural fills. An evaluation of groundwater conditions, applicable state test procedures, water quality standards, and proper construction are all necessary considerations in ensuring a safe final product. There are several leaching tests and currently U.S. Environmental Protection Agency is nearing publication of new leaching standard appropriate for beneficial use application of CCPs and other similar materials (Kosson et al. 2002). U.S. EPA is currently reviewing its rules regarding beneficial use of CCPs.

4 ASSESSMENT OF SUSTAINABILITY

Assessment of sustainability involves the life cycle assessment (LCA) of the environmental benefits and the life cycle cost analysis (LCCA). LCA involves determining a variety of sustainability metrics (e.g., energy consumption, GHG emissions, water use, hazardous waste generation, etc.) associated with production of construction materials, their transportation to the construction site, and construction itself. These determinations can be made using available database programs such as the PaLATE model (Horvarth, 2004). LCCA evaluates life cycle cost of design alternatives including the initial construction and maintenance based on service life. A convenient computer code named RealCost can be used for this purpose (FHWA 2004). Service life is a crucial part of this analysis and materials with higher modulus typically result in a longer service life for the same thickness of pavement layers. Examples of LCA and LCCA are available (Lee et al. 2011).

A rating system for sustainable highway construction, named Building Environmentally and Economically Sustainable Transportation-Infrastructure-Highways, BE^{2}ST-in-Highways^{TM} was developed to provide a quantitative methodology for rating the benefits of sustainable highway construction (Lee et al. 2011). The methodology is grounded in quantitative and auditable metrics so that a transparent linkage exists between the project rating and the sustainable practices employed in construction. This rating system can be employed by the highway construction industry and agencies to quantitatively evaluate sustainable practices and to incorporate sustainable elements into projects.

The BE^{2}ST-in-Highways^{TM} system evaluates sustainability of a highway project in terms of a quantitative difference between a reference design and proposed alternative design(s). Thus, the reference highway design must be defined realistically. A conventional design approach in which sustainability concepts are not incorporated explicitly can be used as a reference design. The analysis assumes that the service life of conventional and alternative designs can be based on an international roughness index (IRI) prediction made with the Mechanistic Empirical Pavement Design Guide (M-EPDG) program (NCHRP) and that rehabilitation occurs at the end of the predicted service life.

5 CONCLUSIONS

1. It is imperative that industry-wide sustainable construction practices be adopted and recycled materials play a significant role in earthen construction where large quantities of materials are used such as in roadway construction.
2. Benefits of recycled materials include reduction in greenhouse gas emissions, energy, natural resources, and cost.
4. Wise use of recycled materials may create longer lasting structures and reduction in cost.
5. Conducting quantitative analyses using appropriate sustainability metrics to assess alternatives involving recycled materials is imperative.

6 ACKNOWLEDGEMENTS

The information and ideas presented were developed through numerous projects involving many associates and students, too long to list here. Prof. Craig H. Benson and the Recycled Materials Resource Center are acknowledged.

7 REFERENCES

ASTM. 2011. D7762 Standard Practice for Design of Stabilization of Soil and Soil-Like Materials with Self-Cementing Fly Ash.”

Bozyurt, O., Tinjum, J. M., Son, Y. H., Edil, T. B. and Benson, C. H. 2012. Resilient modulus of recycled asphalt pavement and recycled concrete aggregate. GeoCongress 2012, ASCE, GSP No. 225, Oakland, CA, 3901-3910.

Edil, T.B., Acosta, A.A. and Benson, C.H. 2006. Stabilizing soft fine-grained soils with fly ash. ASCE *Journal of Materials in Civil Engineering*, 18 (2), 283-294.

Edil, T.B, Tinjum, J.M. and Benson, C.H. 2012. Recycled Unbound Materials. TPF-5 (129) Final Report. MNDOT, MN, USA.

FHWA. 2008. User Guideline for Byproducts and Secondary Use Materials in Pavement Construction. FHWA-RD-97-148,VA, USA.

FHWA. 2004. Life Cycle Analysis RealCost User Manual. VA, U.S.A.

Guthrie, S. W., Cooley, D., and Eggett, D. L. 2007. Effects of reclaimed asphalt pavement on mechanical properties of base materials.” Jrnl. Transportation Research Board, NRC, No.2005, Wash. D.C., 44-52

Horvath, A. *Pavement Life-cycle Assessment Tool for Environmental and Economic Effects (PaLATE) User Manual*. http://rmrc.wisc.edu

Kosson D. S., Van der Sloot, H. A., Sanchez, F.,Garrabrants, A. C. 2002. An integrated framework for revaluating leaching in waste management and utilization of secondary materials. Env. Eng. Sci. 19, 159–204.

Lee, J. C., Edil, T. B., Benson, C. H. and Tinjum, J. M. 2011. Evaluation of variables affecting sustainable highway design using the BE^{2}ST-IN-HIGHWAYS^{TM} System,” *Jrnl. Transportation Research Board*, NRC, No. 2233, Wash. D. C., 178-186.

Nokkaew, K., Tinjum, and J.M., Benson, C. H. 2012. “Hydraulic Properties of Recycled Asphalt Pavement and Recycled Concrete Aggregate,” GeoCongress, ASCE, Oakland, CA, 1476-1485.

Technical and Economic Analysis of Construction and Demolition Waste Used in Paving Project

Analyse technique et économique des déchets dans la construction de pavage

Farias A., Fucale S., Gusmão A.
University of Pernambuco, Recife, Brazil

Maia G.
Gusmão Engenheiros Associados, Recife, Brazil

ABSTRACT: In this research, the technical and economic feasibility was analyzed as to the use of wastes originated from the deep excavation activity (continuous helical piles) and by demolition of old constructions for the application in layers of subgrade, sub-base and base in paving project. For such, laboratory tests were conducted for the verification of granulometry, real density, limits of consistence, compaction with intermediate energy, California Bearing Ratio (CBR) with measuring of expansion, which exposed the quality of the materials and its potentials. A comparative analysis was carried out between recycled material costs and the aggregate commonly used in paving project, discovering, besides the technical advantage, also the economic advantage of this alternative material.

RÉSUMÉ: Dans cette étude, nous avons analysé la faisabilité technique et économique de l'utilisation des déchets générés par l'activité des fondations profondes (type pieux CFA) et la démolition des anciens bâtiments pour une utilisation dans des couches de renforcement de la couche de forme, couche de fondation et le revêtement de base. Par conséquent, les tests de laboratoire ont été effectués afin de vérifier la taille des particules, les limites de densité réelles, avec compactage d'énergie intermédiaire, de soutien Californie Index pour mesurer l'expansion, qui a exposé la qualité des matériaux et de leur potentiel. Toujours en détention une analyse comparative entre le coût des matériaux recyclés et des agrégats couramment utilisé dans le revêtement, encontando, outre l'avantage technique, l'avantage de ce matériau alternative économique.

KEYWORDS: Construction and Demolition Waste, Recycling, Paving.

1 INTRODUCTION

The civil construction chain is one of the most important economic sectors in Brazil, between the years of 2004 and 2010, this sector grew 42.41%, representing an annual average of 5.18%. In 2011, between January and September, there was an increment of 3.8% over the same period last year, with the creation of 309 425 formal jobs during the first ten months of this year (CBIC, 2011). Moreover, constructive activities still have great social importance for countries, since they employ, direct or indirectly, a large percentage of manpower.

However, despite the economic importance, the construction industry has significant negative impacts to society, such as large waste generation, since the Construction and Demolition Waste - CDW, as it is in the city of Recife, capital of the state of Pernambuco, Brazil, represents 41% of all municipal solid waste (Gusmão, 2008).

Current Brazilian legislation, through the CONAMA Resolution 307/2002 predicts the principle of the polluter-payer for the civil construction sector, in other words, all the CDW is responsibility of the own sector, involving all the responsibility for waste management, including the final disposition only in places duly licensed.

In this scenario, it is essential that construction practices sustainable principles, with construction technologies that emphasize prevention, reduction, reuse and recycling of materials, besides the collection and disposal of waste committed.

In order to encourage the reuse and recycle of CDW in the construction itself, there are already technical rules to standardize and regulate the use of these materials, and one of them is the 15.116:2004 NBR, which deals with recycled aggregates from CDW – the use in preparation of concrete with no structural function and paving projects.

The paper presents a case of construction work to build a shopping center in Recife, where the waste from excavation (soil) of continuous helical displacement piles and the recycled CDW were used in an innovative way in the paving projects of the worksite itself, obtaining at the end of the construction, a significant economy of resources and materials.

1.1 Continuous helical displacement pile

The continuous helical displacement piles were introduced in Recife in the 1990s. At the time the equipment was brought from the Southeast region, with high mobilization costs. Its more frequent use in the construction of buildings started in the city in 2001 and is currently the most widely used type of pile in the construction of buildings in Recife. In 2010, it is estimated that the helical piles accounted for about three quarters of the pile market for buildings in the city (Gusmão, 2011).

The continuous helical piles have some peculiarities that popularized their use in the urban environment, especially the fact of not causing vibrations and for having great productivity compared to other solutions, such as pre-molded, metal and excavated piles.

However, there is one particular aspect which can be a limiting factor to its use: the production of excavation waste (soil). According to CONAMA Resolution 307/2002, the excavated soil is a CDW, and as such, it should be tracked throughout the whole building process: separation, storage, transportation, recycling and final disposal. Current legislation does not allow the soil to be disposed without any control.

Even in licensed areas, landfills of CDW occupy large areas, which could have a nobler purpose in the urban environment.

2 CHARACTERIZATION OF THE ENTERPRISE

It consists in the construction of a horizontal shopping center in Recife, Pernambuco, Brazil. The edification is formed by an pre-molded arched concrete structure with a total construction area (shopping areas and garages) of 255,500 m².

From the topographic point of view, the natural terrain did not possess pronounced leveling differences. As for the geological point of view, the land is located in the fluvial-marine plain, within the undifferentiated marine terrace.

On the terrain of the enterprise, there were 07 major warehouses and 10 smaller deposits, totaling an area of 20,949 m² of demolition, responsible for generating approximately 18,900 tons or 13,500 m³ of CDW. Considering also the temporary installations and concrete slabs of the service paths, it is estimated that globally 23,560 tons or 16,830 m³ of CDW were generated.

Given the geotechnical characteristics of the land and construction schedule, continuous helical piles were designed and implemented for the foundation of all edifications. Table 1 shows the total quantitative at the end of the work, as well as the production of excavated soil. A total of 25,013m ³ or 42,522 tons of soil (admitting an apparent specific weight of 17 kN/m³).

There is, therefore, a total waste (demolition + soil deriving from piling) of 66.082 tons. If all this material was taken to a licensed landfill, the cost of provision would be of US$ 28,00/ton, or a total of US$1.9 million, besides environmental costs.

Having this in mind and the large area of paving of the site, a technical and economic study for the reuse of waste from the excavation residues in the pavement layers of the work was proposed. The excavated material was then separated and stored in an area of the own work site.

Table 1 – Quantitative of piles.

Diameter of Pile	Quantity	Length Medium (m)	Excavated Soil (m^3)
400	504	21.68	1,713
500	2,965	23.30	17,506
600	692	22.67	5,794

3 PAVING OF THE ENTERPRISE

The total paved area of the work was of 96,463 m² and is in accordance with the specifications of the paving project, the sub-base layer in the circulation of the exterior parking lot (flexible pavement) should be stabilized granulometrically with sandy material, and have a thickness of 0.20 m and minimum California Bearing Ration (CBR) of 20%.

In the parking spaces outside (semi-rigid pavement), the sub-base layer should consist of improved soil with 4% cement, 0.10 m thick and minimum CBR of 20%.

Data showed that the paving and land leveling work would require 22,631 m³ of natural noble aggregates, in other words, there was a potential for the use of much of the residues in the work site.

4 METHODOLOGY

In order to enable the use of its own wastes in the paving projects of the work, the following actions were established:

i) Processing of waste from demolition of the warehouses through a mobile unit installed at the construction site. These wastes are in this paper called recycled residues of civil construction - RRCC;
ii) Separation and storage of excavated soil in the implementation of continuous helical piles;
iii) Conduction of laboratory tests to characterize the RRCC and the excavated soil.

For the study of the technical viability of the use of excavated soil in the paving process, several laboratory tests in four distinct phases were conducted, whose tests are summarized in Table 2.

Table 2 – Summary of the characterization tests and assayed samples.

Phase	RRCC or Mixture	Tests
1	Soil, RRCC, R30S70 and R60S40	Granulometry, CBR and Limits of Consistency
2	Soil, RRCC and R60S40	Granulometry, Limits of Consistency, Real Density of grains, Compactation, CBR, shape Index, Abrasion “Los Angeles” e Level of sulphates
3	R40S60 (samples collected in experimental field)	Granulometry, Compactation and CBR
4	RRCC, R60S40, R40S60 e R30S70 (samples collected in experimental field)	Compactation, Humidity *in situ*, Density in *situ* (Sand Flask)

RRCCR – recycled residues of civil construction; R30S70 – 30% RCCR + 70% pile soil; R40S60 – 40% RCCR + 60% pile soil; R60S40 – 60% RCCR + 40% pile soil

5 TECHNOLOGICAL CHARACTERIZATION OF THE MATERIAL

5.1 Composition of RRCC

Figure 1 shows the gravimetric composition of RRCC. It is observed that is predominant the concrete, since warehouses had large areas of concrete floor. In the small material, with diameter less than 4,8 mm, it was not possible to differentiate the waste just by sight.

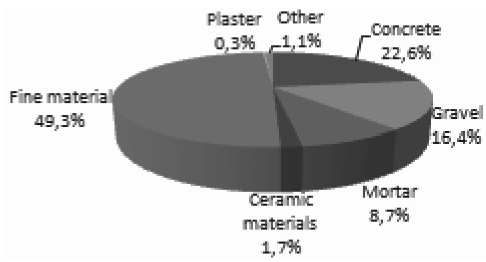

Figure 1 – Gravimetric composition of RRCC.

5.2 Composition of the excavation soil

For the development of the design of the foundations of the project, a total of 65 reconnaissance assays for percussion were performed. Initially, it was thought that the land would present deposits of soft soils, which are typical for this region of the city, but tests showed a basement formed by predominantly sandy soils.

Figure 2 shows the prediction of the type of excavated soil obtained from surveys conducted initially in the terrain. It is observed that sandy soils represent 85% of total soils present in the subsoil up to an average depth of 23m. The major difficulty in reusing soil from the excavation of a pile is that the excavated material is the result of full depth of the pile, and there are no means to segregate it. For a stratified profile, a completely heterogeneous material will be found.

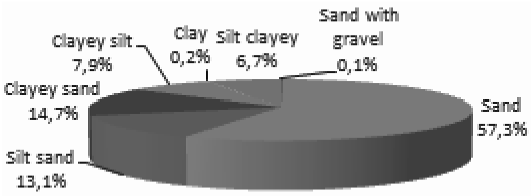

Figure 2 – Prediction of the excavated soil by piles through assays.

5.3 Granulometry

Figure 3 shows the granulometric curve of soil samples and of RRCC. It is observed that the RCCR is classified as gravel with thick and medium-sized sand. On the other hand, the soil is medium-sized and thin sand, which coincides with the prior prediction made by the assays.

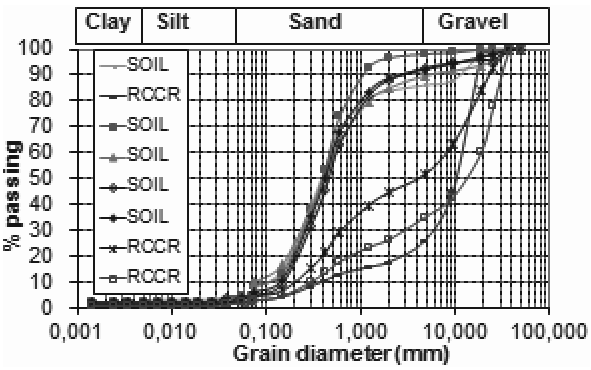

Figure 3 – Grain size curve of soil and of RRCC.

5.4 Compaction curves

Figure 4 shows some compaction tests with intermediate energy. It is observed that the optimum moisture varies between 4.1 and 9.1%, which are typical values for granular soils. It is also observed that the mixture soil + RRCC presented higher densities than the materials isolated, probably due to the fact that a higher degree of the group was reached.

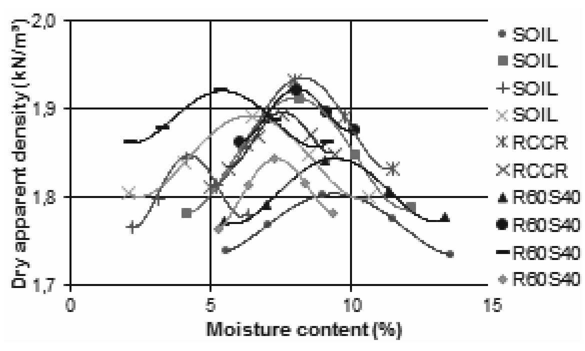

Figure 4 – Compaction Curves for soil, RRCC and mixture.

5.5 California Bearing Ratio (CBR)

Table 3 shows the CBR values obtained for the soil, RRCC and mixture of 60% RRCC and 40% soil (R60S40). The average values were equal to 39, 189 and 115%, respectively. The expansion values ranged from 0 to 0.2%.

Table 3 – Summary of the CBR values.

Material	CBR (%)	Avarage Value (%)	Variance Coefficient (%)
Soil	10 76 19 51	39	78
RCCR	191 188 84	189	1
R60S40	108 130 138	115	21

Regarding the NBR 15.116/04, for the possibility to use recycled material in the sub-base layers and pavement bases, CBR minimum is of 20% and 60%, respectively, implying that all mixtures have adapted to the requirements of the standard.

5.6 Shape Index

As the shape index approaches only the coarse aggregate with maximum characteristic dimension superior to 9.5 mm, only the RRCC samples were assayed. According to NBR 7809:1983, the maximum limit in the relation length/thickness is 3.0. This condition was met in both samples.

5.7 "Los Angeles" Abrasion

Just as in shape index, the "Los Angeles" abrasion test refers only to the coarse aggregate. For the two RRCC samples, the values were equal to 26.8 and 26.3% of depreciation, which are below the maximum limit of 50% set in the standard.

5.8 Sulphate levels

The maximum level of sulphate in relation to the mass of the recycled aggregate is 2%, according to NBR 15.116:2004. The values obtained in the assays of the soil and RRCC ranged between 0.04 and 0.09%, in other words, they were below the maximum limit set in the standard.

5.9 Technical Feasibility for using CDW in Paving Projects

Table 4 summarizes the results of some samples of soil, RRCC and the mixture soil-RRCC, comparing the values with the recommendation of NBR 15.116:2004. It was observed that only the soil did not meet the requirements for the use in paving layers. However, both the isolated RRCC as well as mixed with soil from the excavation of piles, meet all the criteria of the standard.

5.10 Economic feasibility of the use of CDW in paving projects

For the study of the economic feasibility of using CDW in paving layers in the project, an inquiry of the unitary cost of the acquisition of the aggregates specified in the paving project was initially performed, whose values are shown in Table 5. The costs of implementing the layers were not considered in the comparison, as it would be the same with the use of natural aggregates or CDW.

Table 6 shows the costs for the disposal at two sites licensed by the environmental agencies, which is an inert landfill or a processing plant for CDW. Both are located in the Metropolitan area of Recife.

Table 4 – Samples that did not meet the requirements of NBR 15.116:2004.

Parameters	NBR 15.116	Samples			
		i	i	ii	iii
Uniformity Coefficient (%)	≥ 10	**4.88**	**3.62**	39.28	14.88
Material through strainer Nº 40 (%)	Between 10 e 40mm	**53.47**	**45.76**	21.47	31.24
CBR (%) - Subgrade	≥ 12	**10.20**	**18.70**	190.5	129.7
CBR (%) - Sub-base	≥ 20	**10.20**	**18.70**	190.5	129.7
CBR (%) - Base	≥ 60	**10.20**	**18.70**	190.5	129.7
Subgrade Expansion	≤ 1	0.20	0.10	0	0
Sub-base Expansion (%)	≤ 1	0.20	0.10	0	0
Expansion (%) – Base	≤ 0,5	0.20	0.10	0	0
Maximum dimension of grains (mm)	63.5	19.10	19.10	38.10	38.10
Shape Index	< 3.0	*	*	2.20	*
Depreciation	< 50	*	*	26.76	*
Sulphate Content (%)	< 2.0	0	0	0.05	*

i – Soil; ii – RCCR; iii – R60S40
* *Not determined

Table 5– Costs of the acquisition of materials for paving project.

Material	Unit	Unitary cost of the acquisition (US$)
Sand for landfill	m^3	14,00
RRCC obtained with mobile plant onsite	m^3	14,00
RRCC obtained from processing plant outside the site	m^3	9,11
Simple graduated gravel (SGG)	m^3	20,41
Soil of the continuous helical pile	m^3	0*

* cost of transportation onsite disconsidered

Table 6 – Costs for the final disposition of wastes in licensed places.

Disposition place	Unit	Unitary cost (US$)
Inert Landfill	m^3	47,30
Processing plant	m^3	18,36

* cost of transportation onsite disconsidered

For the calculation of the financial impact of the use of the investigated materials in paving project, two scenarios for reuse of waste were considered:

- Scenario 1: all the brute RRCC is taken to the processing mill for recycling, and the pile soil is deposited in the inert landfill. The layers of paving are executed with natural aggregates;
- Scenario 2: use of mixture of pile soil with RRCC in the regularization of the terrain and the sub-base layer. The base layer is performed with the remaining available RRCC and another portion of natural aggregate (SGG).

In simulations, the volumes were calculated from the paving projects (flexible and semi-rigid), land leveling and gabion wall containment. In all cases, a bulking of 12% was admitted (project value) and apparent specific weight of RRCC and the soil is equal to 14 and 17 KN/m^3, respectively.

The estimation of Scenario 1 presented a cost of US$ 2.2 million, while Scenario 2 showed a total cost of US$ 320,498.21, in other words, the use of residues represent a direct saving of about US$ 1.9 million continuing to meet the technical requirements of the paving project, and allowing a very significant reduction of environmental impacts that were not valued.

In the implementation of the paving, the base layer only contained simple graduated gravel (SGG), as an option of the designer. Still, the direct saving obtained was almost the same as in scenario 2.

In summary, demolition residues and the soil from the excavation of helical piles were transformed into the "worksite quarry". The sustainable construction was cheaper than conventional work, showing the potential of the "green economy".

6 CONCLUSION

The article presents a case of building a shopping center in Recife where the excavation residues of the 4,000 helical foundation piles, in other words, about 25,000 m^3 of soil were used in the layers of the paving work (regularization of the terraind and sub-base). Demolition residues were also used from old existing warehouses on the land, which were transformed into recycled aggregates with a mobile plant installed at the worksite.

The demolition residues and soil from the excavation of the helical piles were transformed into the "worksite quarry". The sustainable work was cheaper than the conventional construction, showing the potential of the "green economy".

7 ACKNOWLEDGMENTS

The authors would like to thank the JCPM group for their trust throughout the development of the study, especially Dr. Francisco Bacelar. We also thank the Post-Graduation Program in Civil Engineering of the University of Pernambuco, CAPES (Brazilian funding agency) and FACEPE (funding agency of the state Pernambuco).

8 REFERENCES

CÂMARA BRASILEIRA DA INDÚSTRIA DA CONSTRUÇÃO – CBIC. Construção Civil: Desempenho e Perspectivas. Informativo Econômico. Brasília, 2011.

Gusmão, A. D. (2008). *Manual de Gestão dos Resíduos da Construção Civil*. 1a Edição. ISBN: 978-85-60917-04-4. CCS Editora. Camaragibe.

Gusmão, A. D. (2011). Prática de Fundações no Recife. Fórum da Construção do Recife.

NBR 7809:1983 NBR 7809:1983 – Agregado graúdo – Determinação do índice de forma pelo método do paquímetro – Método de ensaio. ABNT. Rio de Janeiro.

Comparative Life Cycle Assessment of Geosynthetics versus Conventional filter layer

Analyse de cycle de vie comparative d'une couche de filtre géotextile et conventionnelle

Frischknecht R., Büsser-Knöpfel S., Itten R.
Treeze Ltd., Kanzleistrasse 4, 8610 Uster, Switzerland

Stucki M.
Zurich University of Applied Sciences, Institute of Natural Resource Sciences, Campus Grüental, 8820 Wädenswil Switzerland

Wallbaum H.
Chalmers University of Technology, Civil and Environmental Engineering, 412 96 Göteborg, Sweden

ABSTRACT: Geosynthetics made from plastics can replace filter layers made of gravel. In this article goal and scope, basic data and the results of a comparative life cycle assessment of gravel and geosynthetics based filter layers are described. The filter layers of a road made of 30 cm gravel and a filter geosynthetic, respectively, form the basis for the comparison. The filter layers have the same technical performance and the same life time of 30 years. The product system includes the supply of the raw materials, the manufacture of the geotextiles and the extraction of mineral resources, the construction of the road filter, its use and its end of life phase. The life cycle assessment reveals that the geosynthetics based filter layer causes lower environmental impacts per square metre. The cumulative greenhouse gas emissions amount to 7.8 kg CO_2-eq (mineral filter) and to 0.81 kg CO_2-eq (geosynthetic filter). The variation of the thickness of the gravel based filter layer confirms the lower environmental impacts of a geosynthetics based filter layer. Environmental impacts of the geosynthetic production are dominated by the raw material provision (plastic granulate) and electricity consumption during manufacturing.

RÉSUMÉ : Les géotextiles sont utilisés pour remplacer le gravier dans les couches de filtres. Cet article contient une description de la définition de l'objectif et du champ d'étude, de l'analyse de l'inventaire et des résultats d'un analyse de cycle de vie comparative d'une couche de filtre géotextile et conventionnelle. La couche de filtre d'une rue est construite avec 30 cm de gravier ou avec une couche géotextile. Les deux couches de filtres ont les mêmes propriétés techniques et la même durée de vie de 30 ans. Les systèmes contiennent la provision des matériaux, la fabrication des filtres géotextiles et l'extraction du gravier, la construction, l'utilisation et l'évacuation de la couche de filtre. L'analyse de cycle de vie démontre qu'un mètre carré d'une couche de filtre géotextile cause moins d'impacts environnementaux qu'un mètre carré d'une couche de filtre gravier. Une couche de filtre gravier entraîne 7.8 kg CO_2-eq, celle de filtre géotextile 0.81 kg CO_2-eq des émissions des gaz à effet de serre par mètre carré. La variance de l'épaisseur de la couche de gravier n'influe pas sur la séquence environnementale des deux couches. La provision des matériaux et l'électricité utilisé dans la fabrication de la couche de filtre géotextile sont des facteurs primordiaux en ce qui concerne les impacts environnementaux de la couche de filtre géotextile.

KEYWORDS: filter layer, geosynthetics, gravel, life cycle assessment, LCA

MOTS-CLÉS : couche de filtre, géotextile, gravier, analyse de cycle de vie, ACV

1 INTRODUCTION

Geosynthetic materials are used in many different applications in civil and underground engineering, such as in road construction, in foundation stabilisation, in landfill construction and in slope retention. In most cases they are used instead of minerals based materials such as concrete, gravel or lime.

Environmental aspects get more and more relevant in the construction sector. That is why the environmental performance of technical solutions in the civil and underground engineering sector gets more and more attention.

The European Association for Geosynthetic Manufacturers (E.A.G.M.) commissioned ETH Zürich and Rolf Frischknecht (formerly working at ESU-services Ltd.) to quantify the environmental performance of commonly applied construction materials (such as concrete, cement, lime or gravel) versus geosynthetics (Stucki et al. 2011).

In this article, the results of a comparative Life Cycle Assessment (LCA) of a filter function in road construction are described. The filtration function is either provided by a gravel or a geosynthetic filter layer.

The environmental performance is assessed with eight impact category indicators. These are Cumulative Energy Demand (CED, Frischknecht et al. 2007), Climate Change (Global Warming Potential, GWP 100, Solomon et al. 2007), Photochemical Ozone Formation (Guinée et al. 2001a; b), Particulate Formation (Goedkoop et al. 2009), Acidification (Guinée et al. 2001a; b), Eutrophication (effects of nitrate and phosphate accumulation on aquatic systems, Guinée et al. 2001a; b), Land competition (Guinée et al. 2001a; b), and Water use (indicator developed by the authors). The calculations are performed with the software SimaPro (PRé Consultants 2012).

2 GEOSYNTHETIC FILTER VERSUS MINERAL FILTER

Filters systems in road construction assure that the base soil is retained with unimpeded water flow. In this article, the case of a geosynthetic filter layer is compared to the case of a mineral filter layer.

Polypropylene granules are used as basic material for the geosynthetic layer. They need to be UV stabilised to meet the requirements. The average weight of the polymer is 175 g/m^2.

The way of the construction of the filter depends on several factors. The basic conditions are shown in Tab. 1 and Fig. 1. The two alternative cases compare the environmental impacts of one square meter of the filter area below the road. The additional excavation needed at the boundary area of the mineral filter is not considered in the comparison.

Table 1. Design criteria of the two filter systems.

Parameter	*Unit*	*Gravel filter*	*Geosynthetic filter*
Filter size	m^2	1	1
Filtration geosynthetic	g/m^2	0	175
Gravel	cm	30	0

From these parameters it is calculated that the required thickness D of the mineral filter is 300 mm and the one with the geosynthetic filter layer is 1-2 mm. Fig. 1 shows a cross section of the filter profile as modelled in this LCA.
In a sensitivity analysis the thickness of the gravel filter is varied by +/- 10 cm.

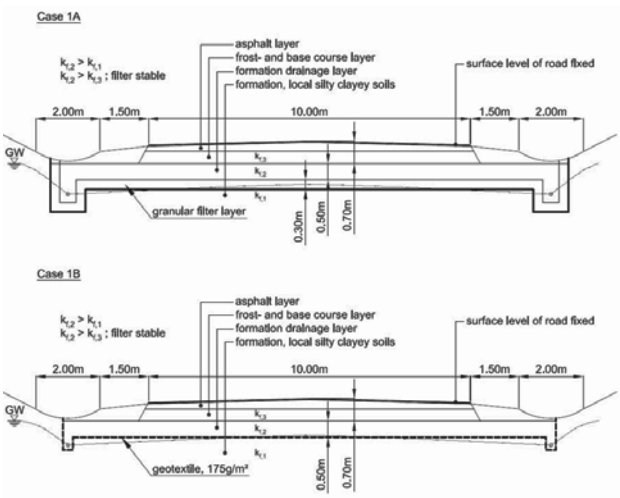

Figure 1. Cross section of the mineral filter (top) and geosynthetic filter system (bottom)

The functional unit in the comparative LCA is the provision of 1 m^2 of filter with a hydraulic conductivity (k-value) of 0.1 mm/s or more and an equal life time of 30 years.
The difference between the two cases lies in the amount of primary gravel used, the energy consumption that is related to the filter material used (material transportation, excavation etc.), and the use of geosynthetics. Recycled gravel is not considered for the filter system since no onsite recycled gravel is available when building a filter for the first time.
Some important key figures of the construction of the filter systems are summarized in Tab. 2. The information refers to one square meter filter and a life time of 30 years. The figures shown regarding the particulate emissions refer to emissions from mechanical processes (e.g., pouring, compacting of gravel). Direct land use is not included in this LCI because the type of land use under which the filter is being built in is not known.

Table 2. Selected key figures describing the two constructions of one square meter of filter

Material/Process	*Unit*	*Gravel filter*	*Geosynthetic filter*
Gravel	t/m^2	0.69	0
Geosynthetic layer	m^2/m^2	0	1
Diesel used in building machines	MJ/m^2	2.04	1.04
Transport, lorry	tkm/m^2	34.5	0.035
Transport, freight, rail	tkm/m^2	0	0.07
Particulates, >10 µm	g/m^2	4.8	0
Particulates, >2.5 µm & <10 µm	g/m^2	1.3	0

3 MANUFACTURING OF THE GEOSYNTHETIC LAYER

Data about geosynthetic material production are gathered at the numerous companies participating in the project using pre-designed questionnaires. The company specific life cycle inventories are used to establish average life cycle inventories of geosynthetic material.
The data collected include qualitative information of system relevant products and processes from the producer, information from suppliers of the producer (where possible) as well as data from technical reference documents (e.g. related studies, product declarations, etc.). Average LCI are established on the basis of equally weighted averages of the environmental performance of the products manufactured by the participating companies.
The primary source of background inventory data used in this study is the ecoinvent data v2.2 (ecoinvent Centre 2010), which contains inventory data of many basic materials and services.
In total, data from 13 questionnaires concerning the production of geosynthetic layers used in filter applications are included. The quality of the data received is considered to be accurate. The level of detail is balanced in a few cases before modelling an average geosynthetic layer.
Tab. 3 shows important key figures of the production of an average geosynthetic layer.

Table 3. Selected key figures referring to the production of 1 kg geosynthetic layer used in filter applications

Material	*Unit*	*Value*
Raw materials	kg/kg	1.05
Water	kg/kg	2.16
Lubricating oil	kg/kg	0.0026
Electricity	kWh/kg	1.14
Thermal energy	MJ/kg	1.49
Fuel for forklifts	MJ/kg	0.09
Factory building	m^2/kg	2.51E-5

4 LIFE CYCLE IMPACT ASSESSMENT

In this section the environmental impacts of 1 square meter filter over the full life cycle are evaluated. The life cycle includes the provision of raw materials as well as the construction and disposal phases.

In Fig. 2 the environmental impacts of the full life cycle of the filter are shown. The environmental impacts of the case with highest environmental impacts (mineral filter 1AS1) are scaled to 100°%. The total impacts are subdivided into the sections filter system, raw materials (gravel, geosynthetic layer), building machine (includes construction requirements), transports (of raw materials to construction site) and disposal (includes transports from the construction site to the disposal site and impacts of the disposal of the different materials).

Fig. 2 shows that the average geosynthetic filter system (1A) causes lower environmental impacts compared to the mineral filter system with regard to all indicators investigated. For all indicators the average filter with geosynthetics (1A) causes less than 25 % of the environmental impacts of a conventional gravel based filter (1B). The geosynthetic filter (1B) layer causes between 0.2 % and 14.3 % of the environmental impacts of the mineral filter layer (1A, water use, CED non-renewable). The greenhouse gas emissions caused by the geosynthetic filter (1B) are 10.4 % of the greenhouse gas emissions caused by the mineral filter (1A).

The non-renewable cumulative energy demand of the construction and disposal of 1 square meter filter with a life time of 30 years is 131 MJ-eq in case of the mineral filter and 19 MJ-eq in case of the geosynthetic filter. The cumulative greenhouse gas emissions amount to 7.8 kg CO_2-eq (mineral filter) and to 0.81 kg CO_2-eq (geosynthetic filter).

The main source of difference is the use and transportation of gravel. Hence, the use of geosynthetics may contribute to reduced environmental impacts of filter layers, because it substitutes the use of gravel.

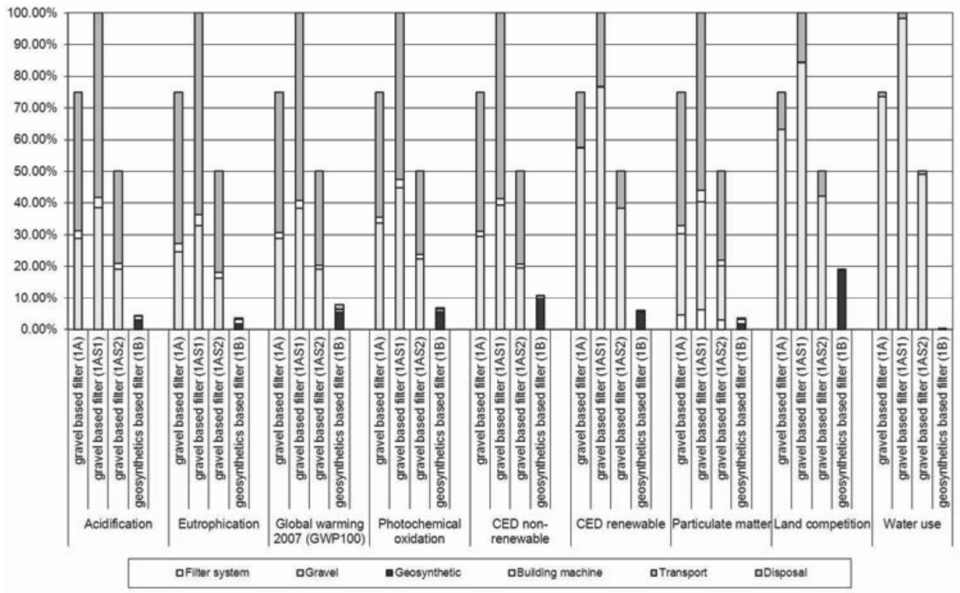

Figure 2. Sensitivity analysis: environmental impacts of the life cycle of 1 m2 of filter layer. 1AS1 and 1AS2 refer to the sensitivity analysis with a different thickness of the gravel based filter layer. For each indicator, the case with highest environmental impacts is scaled to 100°%.

4.1 *Sensitivity analysis*

In a sensitivity analysis, it is analysed how the results of the gravel filter layer change, if the thickness of the mineral filter is increased by 10 cm to a total thickness of 40 cm (1AS1) or if the thickness of the mineral filter is decreased by 10 cm to a total thickness of 20 cm (1AS2).

Fig. 2 reveals that, if a thicker filter layer is constructed, the environmental impacts of the gravel based filter increase by 33 % and if a thinner filter layer is constructed, the environmental impacts of the gravel based filter are decreased by 33 %. Nevertheless, in all cases the environmental impacts of a filter with geosynthetics (1B) are considerably lower than the environmental impacts of a gravel based filter (1A, 1AS1, 1AS2).

4.2 *Contribution Analysis Geosynthetic Production*

In this section the environmental impacts of 1 kg geosynthetic layer are evaluated. The life cycle includes the provision and use of raw materials, working materials, energy carriers, infrastructure and disposal processes. The category geosynthetic in Fig. 3 comprises the direct burdens of the geosynthetic production. This includes land occupied by the factory producing the geosynthetic as well as process emissions (e.g. NMVOC, particulate and COD emissions) from the production process but not emissions from electricity and fuel combustion.

The environmental impacts of the geosynthetic filter are shown in Fig. 3. The cumulative greenhouse gas emissions amount to 3.2 kg CO_2-eq per kg.

Environmental impacts are mostly dominated by the raw material provision and electricity consumption. Raw material includes plastics, chemicals, printing colours, and other additives. Plastic raw materials are responsible for between 4 % (land competition) and 80 % (CED non-renewable) of the overall impacts, printing colours, chemical and additives for between 2 % and 10 %.

Country-specific electricity mixes are modelled for each company and thus impacts of electricity consumption depend not only on the amount of electricity needed but also on its mix. The high share of electricity in CED renewable can be explained by the use of hydroelectric power plants in the electricity mixes of several factories.

Heating energy and fuel consumption for forklifts are of minor importance. With regard to land competition the geosynthetic production plays an important role (92 % of overall impacts). The impacts are dominated by the direct land use, i.e. land which is occupied by the manufacturer plant in which the geosynthetic is produced. Indirect land use, i.e. land occupation stemming from upstream processes, is significantly lower because no land occupation is reported in the inventories of plastic feedstock and no land intensive products such as wood are used in considerable amounts.

Water consumption (tap water, deionised water, decarbonised water) is included in the working materials. As a consequence, this category bears about 15°% of the total amount of water used.

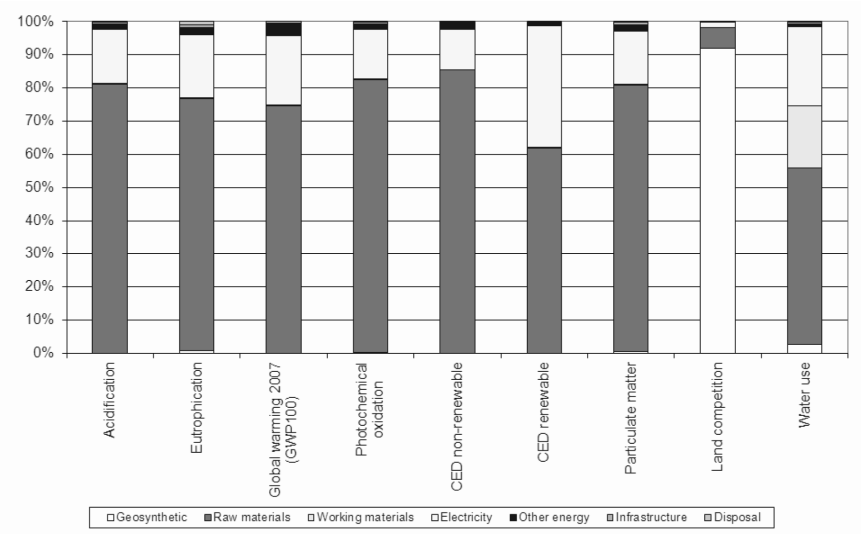

Figure 3. Environmental impacts of the life cycle of 1 kg geosynthetic layer. Geosynthetic includes direct burdens of the geosynthetic production. Raw materials include plastic, extrusion if necessary, and additives, working materials include water (tap and deionised) and lubricating oil, other energy includes thermal energy and fuels, infrastructure covers the construction of the production plant and disposal comprises wastewater treatment and disposal of different types of waste.

5 DISCUSSION AND CONCLUSION

A filter using a geosynthetic layer causes lower environmental impacts compared to a conventional gravel based filter layer with regard to all impact category indicators investigated. If 30 cm of gravel are saved, the specific climate change impact of the construction of 1 square meter filter using geosynthetics is about 7 kg CO_2-eq lower compared to the impacts from the construction of an equivalent gravel based filter.

The difference is considerable for all indicators (more than 85 %) and reliable. The difference in the environ¬men¬tal impacts arises mainly because the applied geosynthetic substitutes gravel, which causes considerably higher impacts when extracted and transported to the place of use. At least a layer of 8 cm of gravel must be replaced by geosynthetics used as a filter in order to cause the same or lower environmental impacts regarding all indicators.

The environmental impacts of the gravel based filter are significantly reduced, when constructing smaller filters (20 cm instead of 30 cm). Nevertheless, the sequence of the two cases does not change and the difference is still significant between the sensitivity cases of the mineral filter and the geosynthetic filter.

6 REFERENCES

ecoinvent Centre (2010) ecoinvent data v2.2, ecoinvent reports No. 1-25. Swiss Centre for Life Cycle Inventories, Duebendorf, Switzerland, retrieved from: www.ecoinvent.org.

Frischknecht R., Jungbluth N., Althaus H.-J., Bauer C., Doka G., Dones R., Hellweg S., Hischier R., Humbert S., Margni M. and Nemecek T. (2007) Implementation of Life Cycle Impact Assessment Methods. ecoinvent report No. 3, v2.0. Swiss Centre for Life Cycle Inventories, Dübendorf, CH, retrieved from: www.ecoinvent.org.

Goedkoop M., Heijungs R., Huijbregts M. A. J., De Schryver A., Struijs J. and van Zelm R. (2009) ReCiPe 2008 - A life cycle impact assessment method which comprises harmonised category indicators at the midpoint and the endpoint level. First edition. Report I: Characterisation, NL, retrieved from: lcia-recipe.net/.

Guinée J. B., (final editor), Gorrée M., Heijungs R., Huppes G., Kleijn R., de Koning A., van Oers L., Wegener Sleeswijk A., Suh S., Udo de Haes H. A., de Bruijn H., van Duin R., Huijbregts M. A. J., Lindeijer E., Roorda A. A. H. and Weidema B. P. (2001a) Life cycle assessment; An operational guide to the ISO standards; Part 3: Scientific Background. Ministry of Housing, Spatial Planning and Environment (VROM) and Centre of Environmental Science (CML), Den Haag and Leiden, The Netherlands, retrieved from: www.leidenuniv.nl/cml/ssp/projects/lca2/lca2.html.

Guinée J. B., (final editor), Gorrée M., Heijungs R., Huppes G., Kleijn R., de Koning A., van Oers L., Wegener Sleeswijk A., Suh S., Udo de Haes H. A., de Bruijn H., van Duin R., Huijbregts M. A. J., Lindeijer E., Roorda A. A. H. and Weidema B. P. (2001b) Life cycle assessment; An operational guide to the ISO standards; Parts 1 and 2. Ministry of Housing, Spatial Planning and Environment (VROM) and Centre of Environmental Science (CML), Den Haag and Leiden, The Netherlands, retrieved from: www.leidenuniv.nl/cml/ssp/projects/lca2/lca2.html.

PRé Consultants (2012) SimaPro 7.3.3, Amersfoort, NL, retrieved from: www.esu-services.ch/simapro/.

Solomon S., Qin D., Manning M., Alley R. B., Berntsen T., Bindoff N. L., Chen Z., Chidthaisong A., Gregory J. M., Hegerl G. C., Heimann M., Hewitson B., Hoskins B. J., Joos F., Jouzel J., Kattsov V., Lohmann U., Matsuno T., Molina M., Nicholls N., Overpeck J., Raga G., Ramaswamy V., Ren J., Rusticucci M., Somerville R., Stocker T. F., Whetton P., Wood R. A. and Wratt D. (2007) Technical Summary. In: Climate Change 2007: The Physical Science Basis. Contribution of Working Group I to the Fourth Assessment Report of the Intergovernmental Panel on Climate Change (IPCC), Cambridge University Press, Cambridge, United Kingdom and New York, NY, USA.

Stucki M., Büsser S., Itten R., Frischknecht R. and Wallbaum H. (2011) Comparative Life Cycle Assessment of Geosynthetics versus Conventional Construction Material. ESU-services Ltd. commissioned by European Association for Geosynthetic Manufacturers (EAGM), Uster and Zürich, CH.

La réutilisation des fondations existantes dans les projets de réhabilitation de constructions anciennes

Reuse of existing foundations for the rehabilitation of old buildings

Guilloux A., Le Bissonnais H., Saussac L.*, Perini T.
Terrasol, Paris, France
*(*à la date de publication : Geos, Paris, France)*

RÉSUMÉ : Lors de la réhabilitation de bâtiments existants, il est bien évidemment souhaitable de conserver dans la mesure du possible les fondations existantes de l'ancienne structure, quitte à les renforcer ou à créer des fondations supplémentaires si celles qui existent ne permettent pas de garantir la bonne tenue de la structure nouvelle. L'expérience, et notamment les trois exemples décrits dans cet article, montre que cette préoccupation conduit à développer une démarche de conception géotechnique originale : il convient de bien connaitre l'état des fondations existantes, de bien évaluer les variations de charges à tous les stades (depuis l'ancienne construction jusqu'à la nouvelle, en passant par les phases de chantier), de décider quelles sont les fondations à renforcer, puis d'étudier des techniques de renforcement adaptées aux conditions de chantier, dans des espaces souvent restreints et sans créer de désordres sur les parties d'ouvrages conservées, et enfin de s'assurer de la compatibilités des déformations et reports de charges.

ABSTRACT: For projects of rehabilitation of an existing building, it is obviously preferable to use as much as possible the existing foundations, including by reinforcing them or by creating additional ones when the existing ones cannot guarantee the safety of the new structure. Based on three case histories described in this paper, it is shown that a "new" geotechnical approach is required, including: deep knowledge of the state of the existing foundations, careful analysis of the load variations (from the old buildings to the new structure, together with the temporary stages), selection of the foundation to be reinforced, choice of reinforcement techniques, often to be implemented in narrow spaces and without any disorders on the structure left in place, and finally detailed analysis of load transfers and deformations compatibility.

KEYWORDS: Réhabilitation, renforcement, transferts de charges, compatibilité des déformations.
Rehabilitation, reinforcement, load transfer, deformation compatibility.

1 PRESENTATION

Les enjeux du Développement Durable sont à l'évidence très présents dans tous les projets de réhabilitation des constructions, qu'il s'agisse de bâtiments ou d'ouvrages d'art. Du point de vue du géotechnicien, il s'agit avant tout de rechercher une réutilisation maximale des parties de fondations existantes, afin de limiter les travaux souvent lourds de démolition et de reconstruction, avec consommation de matériaux « neufs ».

Ainsi, du point de vue du géotechnicien, cette préoccupation de Développement Durable conduit à se poser un certain nombre de questions, qui sortent quelque peu des problématiques géotechniques habituelles :

- pour réutiliser les fondations existantes, il est essentiel de bien les connaitre : quels sont les moyens d'investigation et de contrôle utilisables pour s'assurer de la géométrie de pieux par exemple, de la qualité du béton etc. alors que les plans de construction ne sont pas toujours disponibles ?
- lorsque le projet de réhabilitation conduit à une augmentation des descentes de charges, il faut soit renforcer les fondations existantes pour en augmenter la capacité portante soit en créer de nouvelles pour reprendre les charges additionnelles : comment alors évaluer la redistribution des charges, en intégrant les phasages de construction initiale, démolition et reconstruction ?
- même lorsque le nouveau projet ne conduit pas à une réelle modification des charges, on reste parfois confronté à une question d'évolution de la réglementation, qui est souvent devenu plus contraignante : ainsi, en l'absence de charges complémentaires, faut-il renforcer des fondations d'un ouvrage qui s'est toujours bien comporté, uniquement parce qu'il n'est plus conforme à la règlementation actuelle ?
- enfin, dans le cas où des renforcements de fondations existantes ou de nouvelles fondations sont rendus nécessaires, quelles sont les techniques de réalisation permettant à la fois d'intervenir dans des espaces souvent restreints et de minimiser les démolitions mêmes partielles sur l'existant ?

Ces différentes questions sont illustrées par trois projets en région parisienne, dont on présente les résultats des reconnaissances de l'existant, les études de conception des fondations et les méthodes de réalisation :

- La réhabilitation des entrepôts Calberson, boulevard Mac-Donald à Paris : la construction de nouveaux étages de superstructures et la détection d'anomalies géologiques en base des pieux existants ont conduit à la fois à renforcer les pieux existants par un traitement en jet-grouting sous leur base et à mettre en œuvre des fondations nouvelles par micropieux ;
- La réhabilitation du secteur Est de l'Université de Jussieu (Paris Vème) : le projet de réhabilitation ne conduisait en général pas à une augmentation des charges, mais les auscultations des pieux existants ont révélé des défauts localisés, en particulier en termes de longueur, qu'il a fallu traiter soit en reprenant une partie des charges par des micropieux nouveaux, soit par injections de terrain sous les fondations existantes. Un plot d'essai de traitement de sol a été réalisé avec essais de chargement statique axial sur des pieux existants pour quantifier l'effet du traitement ;
- La réhabilitation d'un ancien centre de tri postal à Pantin : sa transformation en vue de son réaménagement en Data Center a conduit à une augmentation importante des charges sur les pieux existants. Après une redéfinition des paramètres de sol pour s'approcher au mieux des conditions

de tassement observé depuis la construction de l'immeuble (phase calage), les pieux ont été traités toute hauteur par 2 colonnes de jet-grouting.

2 ENTREPÔTS MAC-DONALD

2.1 *La phase de conception*

Ce projet consiste à réhabiliter d'anciens entrepôts Calberson, construits dans les années 1970 sur une emprise de 600 x 60 m^2 située boulevard Mac-Donald à Paris, pour les transformer en bureaux, logements et équipements sociaux, conduisant à surélever la structure existante par la construction de nouveaux étages de superstructures. Le bâtiment existant est fondé sur pieux d'environ 10 m de profondeur et 1,0 à 1,6 m de diamètre.

L'ouvrage, comporte des sous-sols sur 6 m de profondeur environ, repose sur 10 m de calcaires de Saint-Ouen surmontant les sables de Beauchamp.

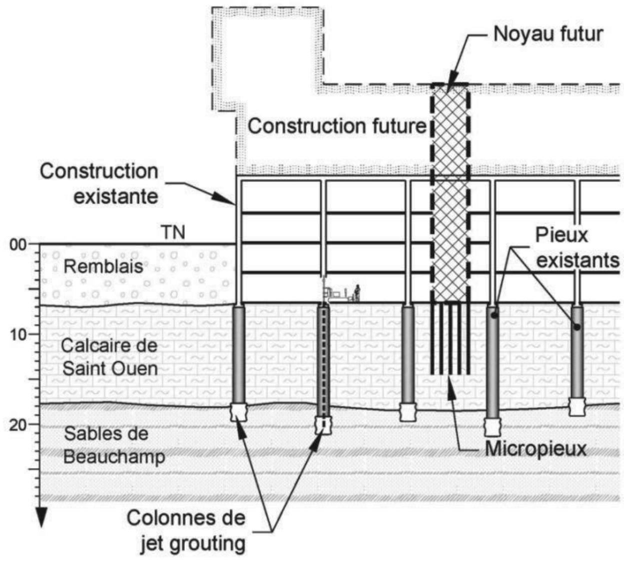

Figure 1 : coupe type du projet

Les études préalables se sont attachées à faire un diagnostic des pieux existants et à conduire des reconnaissances de terrain, qui ont révélé des anomalies géologiques en base des pieux existants.

Il était donc nécessaire :

- d'une part de renforcer les pieux existants pour optimiser leur portance, c'est-à-dire les faire travailler au maximum de la contrainte admissible dans le béton, fixée à 4,8 MPa après carottages et essais de compression sur le béton, et en respectant les tassements admissibles. Après examen de différentes solutions, la technique retenue a consisté à prolonger les pieux par des colonnes de jet-grouting sous leur pointe ;
- d'autre part de prévoir des fondations nouvelles par micropieux pour des structures nouvelles descendues en infrastructures, les noyaux.

En phase études, des essais de chargement statique des pieux existants ont également permis de définir des paramètres optimisés pour l'effort en pointe et le frottement latéral, mais également de mesurer en vraie grandeur la raideur des pieux, paramètre essentiel pour vérifier la distribution entre les pieux existants et les micropieux nouveaux des charges additionnelles, ainsi que la compatibilité des déformations.

2.2 *Suivi du chantier de renforcement*

Pour cet ouvrage, dont les pieux existants présentaient des défauts de portance vis-à-vis des futures charges, plus importantes que celles connues antérieurement, la solution retenue de renforcement des fondations consistait à prolonger la base des pieux par une colonne de jet-grouting de 1,3 m de diamètre et 3 m de longueur en général (deux colonnes pour les pieux de 1,6 m).

Sur la base de reconnaissances géotechniques approfondies, des essais de chargement des pieux existants et des nouvelles descentes de charges, nous avons pu déterminer les pieux nécessitant un renforcement et dimensionner ce dernier. C'est au total environ les ¾ des 500 pieux qui ont dû être renforcés.

Le chantier de jet-grouting a fait l'objet d'un suivi avec contrôle renforcé, pour la réalisation des forages inclinés traversant les pieux existants et permettant de réaliser les colonnes de jet-grouting sous leur base. En outre, s'agissant de travaux de reprise en sous-œuvre d'un ouvrage existant, il a fallu s'assurer que les travaux de jet ne conduisaient pas à des désordres sur les structures conservées, notamment vérification des soulèvements lors des phases d'injection (35 à 40 MPa) puis des tassements avant que la colonne ne fasse prise. De ce point de vue le chantier s'est déroulé sans désordres majeurs, avec des mouvements des poteaux ne dépassant pas quelques millimètres, ce qui a confirmé que la technique du jet-grouting, bien contrôlée et avec un phasage adapté, permettait d'intervenir en sous-œuvre sans créer de mouvements significatifs.

2.3 *Dimensionnement des fondations nouvelles*

Pour les parties de structures nouvelles (noyaux), nécessitant leurs propres fondations, compte tenu du contexte et de l'espace de travail contraint, c'est une solution sur micropieux qui a été retenue.

Le dimensionnement en termes de capacité portante de ces micropieux a conduit à prévoir des micropieux de longueur réduite, à 8 m en général après essais de chargement. Mais plus que la capacité portante, c'est en fait sur les redistributions des charges entre les pieux existants, de grande section, et les micropieux nouveaux, a priori plus souples, que l'attention a été portée. Cette problématique a nécessité une approche en déformations, pour s'assurer de la compatibilité des tassements sous charges entre les anciennes et nouvelles fondations.

Ainsi, après les essais de chargement des pieux existants qui avaient permis de définir les paramètres de raideur, des essais de chargement de micropieux ont été également réalisés, et il a même été réalisé un essai de chargement en vraie grandeur sur un groupe de 4 micropieux, pour mesurer l'incidence des effets de groupe sur la raideur. Un dispositif de chargement a été mis en place sur le site, dans l'intention d'évaluer un potentiel effet de groupe comportant quatre vérins, montés en parallèle et permettant d'appliquer un effort de 1000 kN sur chaque micropieux. L'essai a été concluant et n'a pas mis en évidence d'interaction significative entre les micropieux.

Puis les calculs ont été conduits avec une approche de plaque sur appuis élastiques, pour chacun des noyaux, les raideurs des appuis ayant été définies sur la base des essais de chargement. La Figure 2 montre un exemple de résultat pour l'un des noyaux avec charges concentrées, avec des tassements compris entre 1 et 4.5 mm, tout à fait compatibles avec ceux des pieux voisins.

C'est au total plus de 2700 micropieux qui ont été réalisés en complément du renforcement des pieux par Jet Grouting, et qui ont fait l'objet d'un suivi dans le cadre d'une mission géotechnique G4 selon la norme NF P94-500.

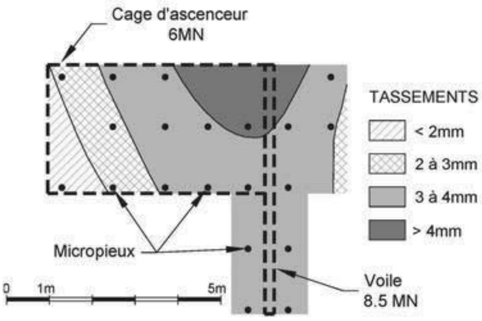

Figure 2 : Carte de tassements calculés

3 RÉHABILITATION DU SECTEUR EST DU CAMPUS DE JUSSIEU

Pour ce projet, la problématique était assez différente, dans la mesure où la construction nouvelle n'apportait pas de suppléments de charges sur les fondations par rapport à la construction ancienne. Les bâtiments datant des années 1970 se sont avérés fondés sur des pieux de 0.5 à 0.8 m de diamètre et d'environ 8 à 9 m de profondeur.

La Figure 3 montre que les pieux traversent 4 à 7 m de remblais et alluvions récentes limoneuses, puis 3 à 4 m d'alluvions anciennes sablo-graveleuses, de façon à venir « s'ancrer » sur l'horizon sous-jacent de calcaire grossier. Mais en pratique cet ancrage n'est pas toujours assuré, et la portance des pieux est donc variable.

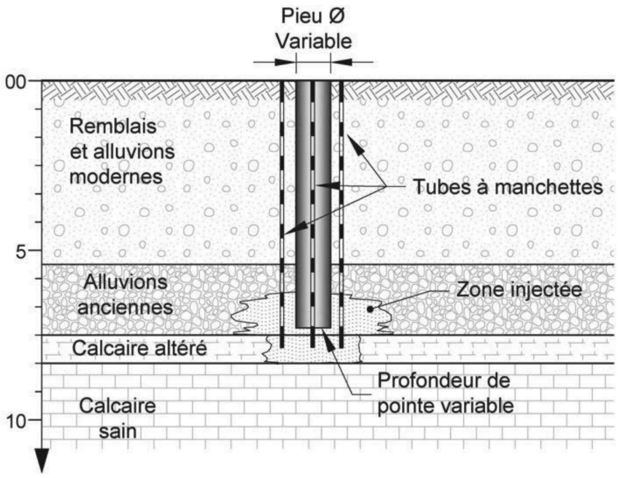

Figure 3 : coupe type des terrains et des principes de confortement

Ainsi dans le cadre de la réhabilitation de ce bâtiment, il a fallu « remettre à niveau » les niveaux de sécurité des fondations des différents appuis, ce qui a conduit à développer une méthodologie de projet suivant les différentes phases suivantes :

1. Des investigations des pieux existants, par exploitation des données d'archives et des puits de reconnaissance pour en déterminer le diamètre, complétées par méthodes géophysiques (impédance mécanique et sismique parallèle) pour en déterminer la longueur. Ces investigations ont montré que les pieux descendaient « plus ou moins » jusqu'au calcaire grossier, mais pas toujours avec un ancrage suffisant.

2. Des reconnaissances géotechniques et une réévaluation de la portance des pieux, avec les méthodes et moyens « modernes », afin de déterminer quels étaient les pieux à renforcer : essais pressiométriques de qualité, plots d'essais de traitement de terrain par injection sous la pointe, essais de chargements statiques de pieux avant et après injection, puis enfin calculs de pieux avec une approche en déformations et pas seulement en capacité portante, et enfin comparaison entre les résultats des modélisations et ceux des essais en vraie grandeur.

Ces premières comparaisons montraient en général que le comportement réel des pieux avant injection était beaucoup plus favorable que prévu, ce qui a conduit à faire de nombreuses retro-analyses pour finalement conclure à la nécessité de majorer les hypothèses géotechniques de frottement latéral par rapport aux règles usuelles.

Par ailleurs lors des essais de chargement après injection en pointe de pieu, l'un des pieux d'essai s'est rompu, correspondant à un dépassement de la contrainte admissible du béton du pieu, tandis que l'autre a montré un comportement largement amélioré par rapport à celui avant injection.

Cet ensemble d'essais et modélisations a permis de préciser quels étaient les pieux à renforcer, à valider la méthode de renforcement par injection sous la pointe, et à définir des hypothèses de calculs réalistes pour le projet final.

3. une revue des différentes méthodes de renforcement des pieux existants, micropieux, jet-grouting, injection en masse. Une analyse des avantages et inconvénients de chaque procédé a été conduite selon une approche multicritère, intégrant les conditions de mise œuvre, les risques de désordres sur la structure existante lors de leur mise en œuvre, la fiabilité du résultat, et bien sûr les coûts et délais

Ces approches ont conduit à retenir finalement la solution de traitement par injection en masse (Figure 3), validée par des plots d'essai qui ont été rigoureusement suivis, et complétée par des essais de chargement des pieux avant et après injection.

L'ensemble de la démarche, avec notamment des approches du comportement des pieux en déformations, a permis de réduire au stade projet d'environ 30 % le nombre total de pieux à traiter (environ 480). Les études détaillées d'exécution devraient encore conduire à une réduction très importante de fondations traitées.

4 RÉHABILITATION EN DATA CENTER D'UN ANCIEN CENTRE DE TRI POSTAL À PANTIN

Il s'agit toujours de la même problématique que pour les projets précédents : réhabiliter un bâtiment existant R + 5 avec un niveau de sous-sol, construit en 1973 et d'une emprise de 160 x 50 m, fondé sur 250 pieux environ, et qui devait être transformé en Data Center, avec une forte augmentation des descentes de charges.

Le contexte géologique comporte environ 6 m de remblais et limons, surmontant 3 à 4 m de marnes infra-gypseuses puis le calcaire de Saint-Ouen, les pieux étant ancrés dans l'un ou l'autre de ces deux derniers horizons,

Comme pour les cas précédents, la démarche suivie à conduit à identifier la géométrie des pieux existants et leur capacité portante. En l'absence de données d'archives, il a été procédé à des investigations des pieux existants par forages et méthodes géophysiques, qui ont permis d'établir la base de toute l'approche de conception de réutilisation des pieux existants, à savoir leur géométrie : il s'avère que leur diamètre est de 1.2 m et que leur profondeur est variable entre 9 et 11 m environ, c'est-à-dire que leur pointe se situe au voisinage de l'interface Calcaire de Saint-Ouen / sables de Beauchamp.

La vérification de la résistance à la compression simple R_c du béton des pieux a été faite par prélèvement de carottes de béton et essais sur échantillons. On a ainsi pu vérifier que le béton des pieux était de très bonne qualité avec des valeurs moyennes de R_c de l'ordre de 40 MPa.

Enfin les analyses de la capacité portante des pieux existants ont été faites à partir de nouvelles reconnaissances géotechniques : il s'est avéré qu'une proportion importante des pieux ne présentait pas la sécurité règlementaire. En effet les premiers calculs montraient que, selon les normes actuelles, et avec les hypothèses géotechniques déduites des essais, le bâtiment existant n'aurait pas du tenir pendant 40 ans sans déformations significatives, ce qui n'était à l'évidence pas le cas.

Nous avons donc été conduits à développer plusieurs approches en rétro-analyse (comparaisons entre les charges appliquées au cours de la vie de l'ouvrage et les capacités portantes théoriques, estimation du tassement réel subi par la construction…). Ces approches ont permis de réévaluer les propriétés géotechniques des terrains, et en pratique de les majorer par rapport aux résultats déduits des essais, ce qui a conduit à limiter le nombre de pieux existants à renforcer de façon lourde : la proportion de pieux qu'il a ainsi été décidé de renforcer est passée de 90% à 40 % environ.

Enfin nous avons examiné différentes conceptions de fondations pour la nouvelle structure, incluant soit des renforcements de pieux existants soit des fondations nouvelles, lorsqu'on avait un déficit de portance. Toutes ces solutions ont été étudiées en s'assurant de la compatibilité des déformations entre les différents types de fondations, et de l'incidence des phases provisoires (notamment la perte de portance provisoire lors de réalisation de jet-grouting, avant prise du coulis).

Le projet de base prévoyait de réaliser 4 à 6 micropieux autour de chacun des pieux présentant une portance insuffisante, avec une semelle de répartition liaisonnée aux pieux. Ces micropieux étaient destinés à reprendre tout ou partie de la différence de charge ramenée par la superstructure aux poteaux supportés par la fondation profonde. Cette solution bien que classique présentait néanmoins le désavantage :

- de multiplier les forages ;
- de nécessiter une semelle de forte épaisseur avec un ferraillage lourd afin de répartir correctement les charges et pouvoir ainsi solliciter les micropieux de rigidité bien moindre que celle des pieux.

Par ailleurs, elle ne permettait pas de tenir le planning imposé et dépassait le budget prévu initialement.

Ainsi, forts de l'expérience du chantier des entrepôts Calberson, Boulevard Mac-Donald à Paris, il a été décidé d'examiner une solution de confortement des pieux par jet-grouting. Après analyse de diverses solutions (solution mixte « micropieux + traitement de la pointe des pieux » - et solution de simple traitement en pointe), l'entreprise générale en charge de l'opération a opté pour la réalisation de deux colonnes de jet de renforcement de part et d'autres des fondations et de diamètre variable (entre 80 cm et 120 cm selon la profondeur) en prenant soin de rester au-dessus de la pointe des pieux existants selon le schéma de la Figure 4.

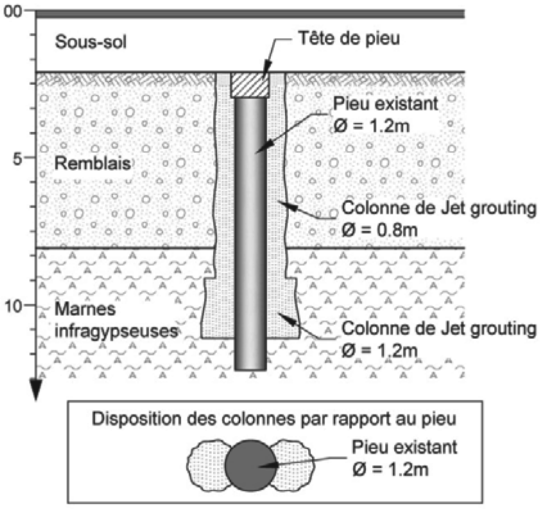

Figure 4 : principe du confortement par jet-grouting

Cette solution permettait de conserver la résistance en pointe pendant les travaux. Seule une perte de frottement a été prise en compte dans les calculs pendant la phase de jet-grouting proprement dite.

Le calcul de la fondation définitive a été mené en considérant que l'ensemble « pieu + jet » formait un monolithe permettant de recalculer ainsi le pieu renforcé avec une surface en pointe et un périmètre frottant majoré tout en vérifiant la part de charge passant dans le jet et la part de charge passant dans le pieux pour chaque section, à partir des raideurs relatives de chacun des matériaux.

La réussite de cette solution tenait principalement dans le bon accrochage entre pieux et colonnes de jet. Le planning ne permettant pas de mettre en œuvre un essai de chargement préalable, des colonnes d'essais de jet ont été néanmoins réalisées sur des pieux abandonnés puis dégagées sur 3,00 m de hauteur pour un constat visuel du contact pieu-jet et du diamètre des colonnes, qui s'est avéré tout à fait satisfaisant. Le frottement pieu-jet adopté était au final de $q_s = 500$ kPa.

Cette solution novatrice a permis de réutiliser les fondations existantes après traitement en vérifiant à la fois la portance et la compatibilité des tassements avec les impératifs de déplacement imposés par la structure.

5 SYNTHÈSE ET MÉTHODOLOGIE DE CONCEPTION

Le retour d'expérience de ces trois projets met en évidence une approche géotechnique spécifique, qui doit impérativement passer par les différents stades suivants :

- Etat des lieux et diagnostic des fondations existantes : type, géométrie, résistance intrinsèque, à partir de l'exploitation de données d'archives, d'investigations géophysiques (non destructives) et de reconnaissances destructives. Cette analyse doit intégrer également un diagnostic de l'état de l'ouvrage pour apprécier s'il a subi des dommages passés ;
- Analyse des descentes de charges sur les fondations, depuis l'état ancien jusqu'à la construction future, sans oublier les phases provisoires de chantier de réhabilitation ;
- Analyses géotechniques de la portance admissible des fondations existantes (intégrant les règlementations en vigueur), et donc des éventuels déficits de charge à reprendre pour l'état futur, ainsi que des déformations qu'elles ont pu subir par le passé ;
- Étude de différents scénarios pour la reprise de ces déficits, en envisageant plusieurs solutions combinant les fondations existantes, éventuellement à renforcer, et des fondations nouvelles à créer (pieux, micropieux ….) ; des plots d'essais en vraie grandeur sont souvent nécessaires à ce stade pour valider le choix des solutions et préciser le comportement en terme de raideur notamment ;
- Choix final des solutions, avec dimensionnement détaillé des différents systèmes : fondations anciennes conservées, renforcements et fondations nouvelles. Ce choix doit impérativement prendre en considération les conditions pratiques de mise en œuvre (travail en sous sols notamment), les compatibilités de déformations entre ces différents systèmes et l'histoire du chargement, y compris les phases intermédiaires de chantier.
- Et enfin un suivi géotechnique rigoureux du chantier, avec en particulier une attention toute particulière apportée aux mesures de déplacements de la structure conservée pendant l'exécution des fondations nouvelles et les traitements de terrain, afin de s'assurer que les travaux de fondations n'engendrent pas de désordres sur la structure existante.

Modern geotechnical construction methods for important infrastructure buildings

Méthodes de construction modernes des ouvrages géotechniques dans les grands projects d′infrastrcuctures

Heerten G.
NAUE GmbH & Co. KG, Gewerbestraße 2, 32339 Espelkamp, Germany

Vollmert L.
BBG Bauberatung Geokunststoffe GmbH & Co. KG, Gewerbestraße 2, 32339 Espelkamp, Germany.

Herold A.
IBH – Herold & Partner Ingenieure, Humboldtstr. 58 b, 99425 Weimar, Germany

Thompson, Dupond J.
Same affiliation

Alcazar G.
Other affiliation

ABSTRACT: Efficient traffic routes form the basis for a brisk economic trade and a close economic and social relationship of the European countries. Thus, the massive development of the national and international traffic routes is correspondingly important. Especially in densely populated areas the routes have to be designed and constructed in such a way that emissions remain compatible for the direct surroundings. In this case the modern construction management requires solutions which are well-engineered and which can be carried out economically. The visible parts of the constructions should correspondingly suit to the landscape in an ideal way. Thus, geosynthetics are used for the static design of high dams and noise protection barriers, in case of a foundation on extremely weak subsoils and for ground water protection measures. Large-scale projects actually realized as well as constructions monitored since years stand representatively for the possibilities and the importance which geosynthetics provide for the use in important infrastructural projects.

RÉSUMÉ : L'efficacité d'un réseau routier est la base d'échanges économiques rapides et de relations étroites en matière économique et sociale entre les pays européens. Ainsi, le développement massif des infrastructures routières nationales et internationales est par conséquent important. En particulier dans les zones fortement peuplées, les routes doivent être conçues et construites de sorte que les nuisances restent acceptables par le milieu environnant. Dans ce cas, la programmation de construction moderne exige des solutions qui soient bien conçues et réalisables de façon économique. Les parties visibles d'ouvrages devraient, également, s'adapter au paysage environnant de manière la plus naturelle possible. Pour ce faire, les géosynthétiques entrent dans la conception statique de grands ouvrages de retenue et des barrières anti-bruit, dans la construction de remblais sur des sols d'extrêmement faible portance et dans les ouvrages de protection des eaux souterraines. De grands projets aujourd'hui achevés ainsi que des ouvrages sous monitoring depuis plusieurs années sont représentatifs de l'étendue des possibilités qu'offrent les géosynthétiques dans les grands projets d'infrastructure.

KEYWORDS: geosynthetic reinforced soil, geogrid, design, regulation, Eurocode 7, infrastructure, costs, carbon footprint

1 INTRODUCTION

The reconstruction of existing and the design of new roads has to accept the geographic situation and has to take political and social based decisions into consideration. So not only bridges and tunnels, but also dams and cuttings are required in areas where the subsoil is not well suited and noise barriers have to be built using local soils.

Geosynthetics as modern construction material are relatively new in terms of understanding and are still not part of the standard education. Problems of understanding synthetics are often linked to the fact, that synthetics behave different compared to well-known materials as concrete and are not ideal elastic as e.g. steel. On the other hand, synthetics and wood, one of the eldest construction material ever used by civil engineers, are both polymers and comparable in many aspects. Additionally, synthetics are already used in many applications where concrete is not suitable and has to be protected against chemicals e.g. in pipelines.

It will be shown that geosynthetics have already become an important construction material in infrastructure applications and allow for modern and economic constructions, saving costs by lean structures, combining local soils, concrete and steel.

The significant reduction of the carbon footprint in many cases seems to be a future topic, but it has started right now. Several studies have been worked out actually, comparing classical solutions and structures using geosynthetics, as e.g. by Corney et al. (2009). Not only the economic effect becomes clear in this study by requiring less energy, but also the reduction of CO^2 during the whole process.

Egloffstein (2009) shows an example for an executed steep slope with an inclination of 60° for a road in a hilly region of Germany, using geosynthetics (Fig. 1). This construction had been planned with conventional cantilever walls, but had to be redesigned using a fully greened facing due to political reasons. Nevertheless, the budget for the construction has been reduced by factor 1.6 (Wessling & Vollmert). The carbon footprint - not being a topic in 2004 - has been calculated for the well documented wall respectively slope by Egloffstein (2009) as given in Fig. 2. The result 6:1 stands for its own.

2 EUROPEAN REGULATIONS – ACTUAL STATUS AND LINK TO GEOSYNTHETICS

Actually, Eurocode 7 (EC7) has become the decisive regulation in geotechnical works for all European countries linked to EU by law, but has not become well established up to now. All national standards have to be reduced to additional regulations, not being in any conflict to EC7. For Germany, the actual status for the normative range of regulations is given in Fig. 3. The

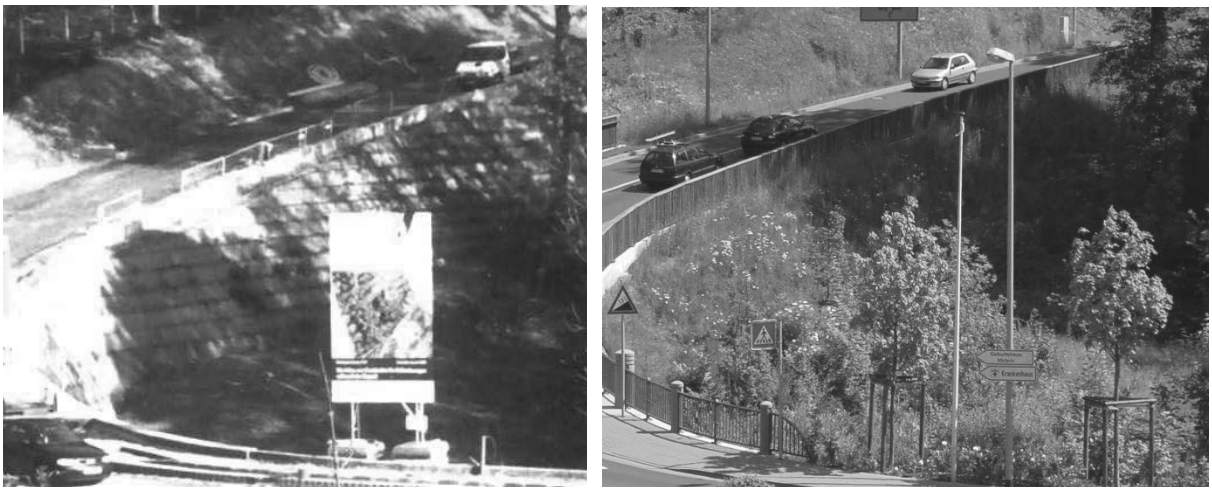

Figure 1. Steep slope in Idstein, under construction 2001 (left) and in service 2004 (right)

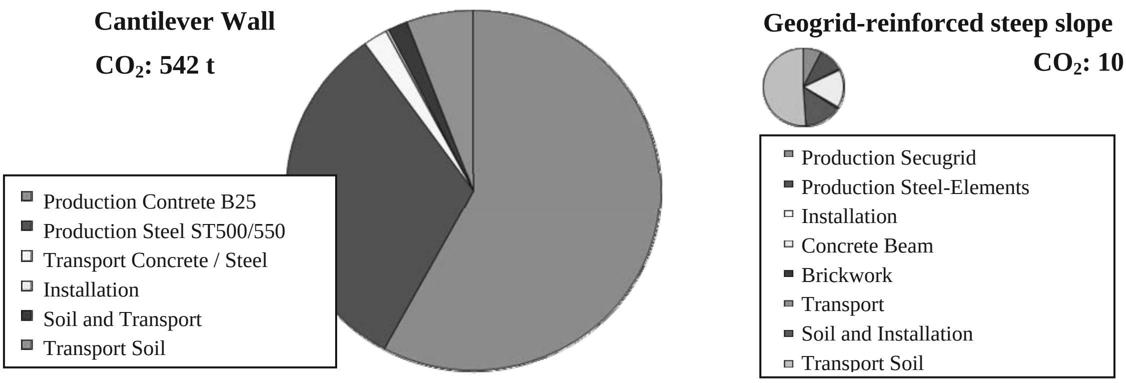

Figure 2. Carbon footprint comparison, example Idstein; cantilever wall (left) and executed geogrid reinforced steep slope (right)

current national standard DIN 1054 will be used as supplementary rule, but being reduced to fragments. The three parts of the rules will be combined to a normative handbook with blended text for practice aspects. DIN 1054:2010 refers to recommendations published by the German Geotechnical Society (DGGT).

The latest recommendation EBGEO dealing with geosynthetics is directly linked to DIN 1054:2010 and therefore also according to EC7; special hints are given how to use EBGEO in the EC7 concept. This recommendation is available as English translation (EBGEO, 2011). Substantial design instructions which meet the requirements of numerous practical applications are offered. These reflect the state-of-the-art considering the proven scientific findings.

In Great Britain, the comparable recommendation is called BS 8006. BS 8006 can also be read as a supplementary annex to the European Regulation and also hints are given how to use it in the EC7 context. So actually two finalized recommendations dealing with the use of geosynthetics are available and allow for design in accordance to EC7.

As it is well known, that EC7 allows for three different design approaches DA1, DA2 and DA3, used in different countries of the EU, it is of general interest whether the British and German recommendations lead to comparable results. Fig. 4 gives an example for a typical steep slope reinforced by geogrids. In both calculations the full set of partial factors as given by EC7 added by specific partial factors for geosynthetics as given by EBGEO and BS 8006 in addition to EC7 and the supplementary national regulations are used (Klompmaker & Werth, 2011).

It has to be stated here, that EC7 gives no full set of partial factors for the usage of geosynthetics. Therefore the authors strongly recommend the use of EBGEO in combination with DA3 and BS 8006 in combination with DA1 as long as no national regulations or recommendations exist in the other countries of the EU. Disregarding additional partial factors as given by EBGEO or BS 8006 can lead to significant excess of the ultimate and serviceability limit state.

For EBGEO and BS 8006 it can be stated that the outcome indicates that the codes are validated against practice, current scientific experience and result in well comparable utilization ratio.

3 LONG-TERM EXPERIENCE ON GEOSYNTHETICS REINFORCED WALLS AND CONCLUSIONS FOR DESIGN

Reinforced soil as one of the eldest construction techniques already used 1400ac in Iraq (Tower of Babylonia) has become popular with the availability of high strength wovens and the today's use of geogrids with perfect geosynthetic-soil-interaction properties. Herold (2007) documented seven high loaded structures that are under continuous supervision. The documented strain within the geosynthetic reinforcement is measured within the range of 0.05 % … 0.4 %. Various measurements from literature (Pachomow et al., 2007) show

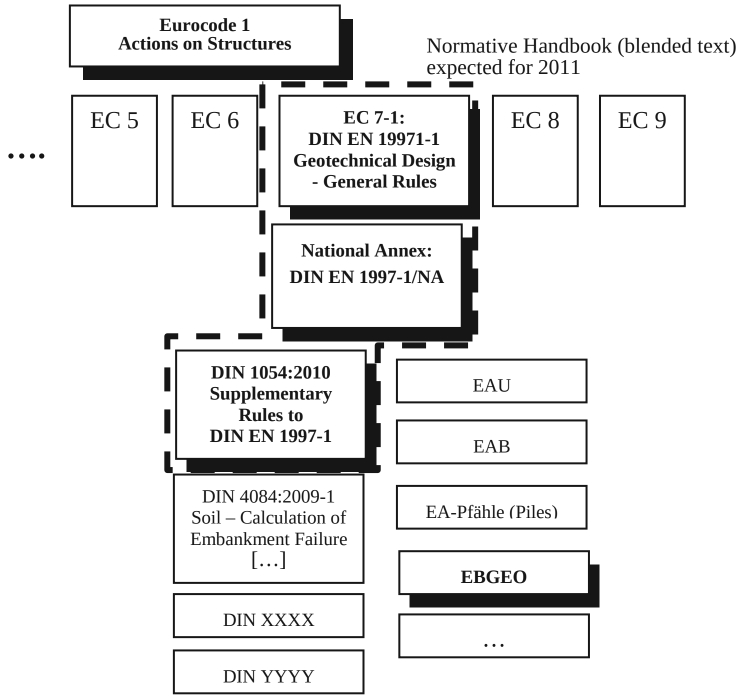

Figure 3. Normative range designing with geosynthetics (according to Kempfert, 2011)

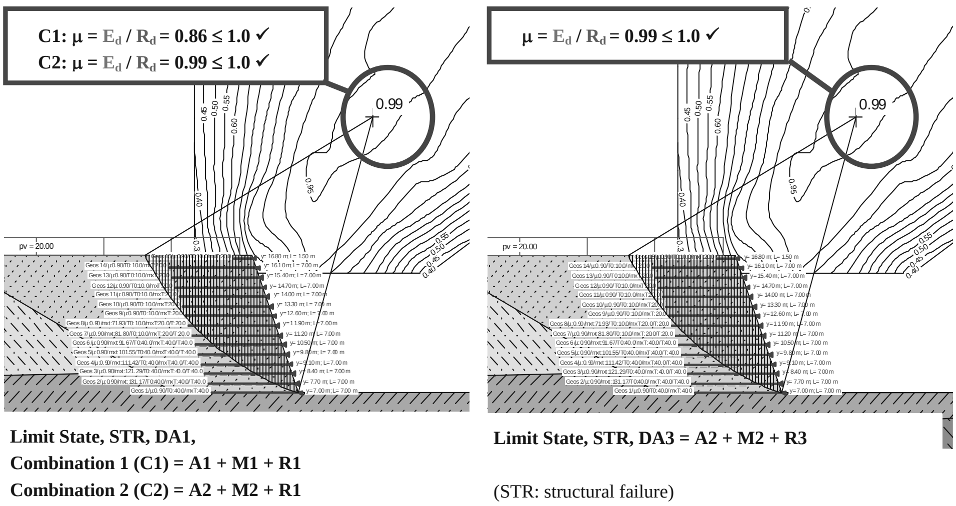

Figure 4. Example of a calculation of a steep geogrid reinforced slope, using BS 8006 (left) and EBGEO (right) with the same parameter set except partial factors according to the used Design Approach (according to Klompmaker & Werth, 2011)

also low strains less than 1.5 %. The strain therefore is less as expected by Ultimate Limit State Design (ULS), but in accordance to scientific approaches and actual understanding of compound material (Heerten et al., 2009).

Ruiken et al. (2010) managed to visualize the shear rotation of granular material in the front of a reinforced wall. The required deformation of the facing is very low and is depending on the degree of reinforcement respectively the vertical layer distance of the reinforcement. Secondary shear planes develop during deformation, showing significant differences as to be expected by active earth pressure theory. EBGEO has already used these findings on the basis of the publication by Pachomow (2007), allowing for a reduced earth pressure on the facing of a reinforced earth wall.

From back analysis of the constructions documented by Herold (2007), taking the actual design codes into consideration, general conclusions can be drawn and recommendations for further design are given concerning the expected deformation of a construction, see Table 1.

4 WORKED EXAMPLES FOR INFRASTRUCTURE DESIGN USING HIGH STRENGTH GEOGRIDS

The high ductility of reinforced soil structures and its economic benefit have raised a certain increase of usage in the last decade in Europe. Vollmert et al. (2010) document a structure, using approx. 6 ha of geosynthetics for noise barrier walls and embankments on weak subsoil in the Netherlands. Fig. 5 gives an partial overview of the construction with a total length of 2 km. The costs of the geosynthetics used are less than 1% of the total budget.

The visible and to environmental influences exposed part of the construction is the facing. Several facing types as gabions, wrap-around method as well as concrete blocks and panels are commonly used.

Table 1. Deformations to be expected for reinforced walls (according to Herold, 2007)

Max. horizontal deformation:		- H: max. height of construction;
Total:	h_{total} = 0.005 … 0.01 * H	h: horizontal deformation;
Post-construction:	h_{post} = 0.15 … 0.3 * h_{total} = 0.00075 … 0.003 * H	v: vertical deformation
		- all deformations within the construction;
Max. vertical deformation:		- to be added by subsoil settlements;
Total:	v_{total} = 0.01 … 0.02 * H	- lower boarder for walls without surcharge,
Post-construction:	v_{post} = 0.15 … 0.4 * V_{total} = 0.0015 … 0.008 * H	upper boarder with surcharge.

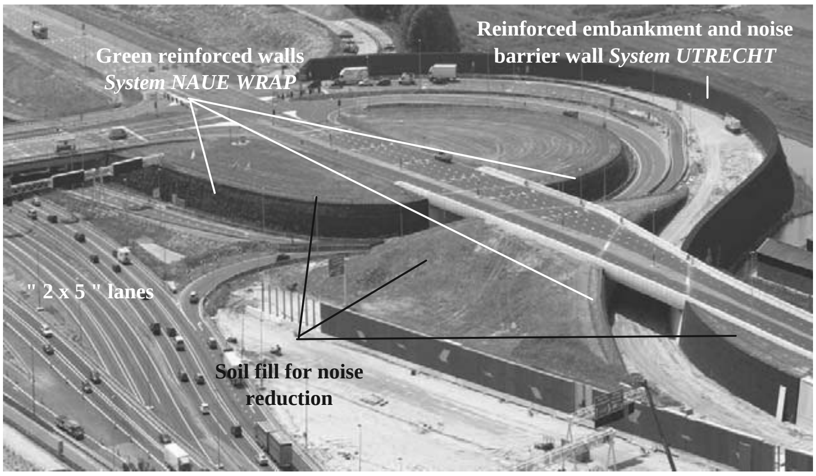

Figure 5. De Krul, Netherlands, overview (Vollmert et al., 2010)

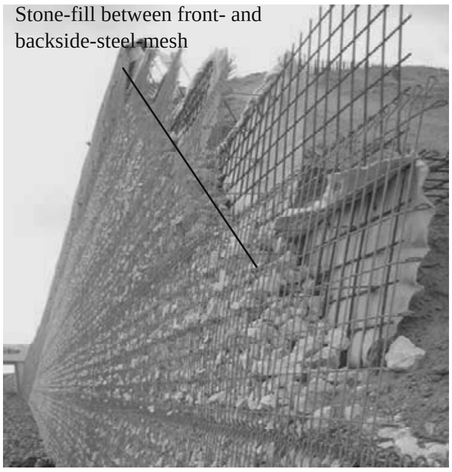

Figure 6. Double wall system (System NAUE DW)

The long-term serviceability depends therefore on usual and well known construction materials as steel and concrete. Nevertheless, the stability of the construction shall be ensured even in case of partial damage, e.g. following accidents, fire or vandalism or the construction has to be designed properly and protected by crash barriers.

It is the unique characteristic of reinforced walls that the internal stability can nearly never collapse by stress on the facing. Providing facing systems that can be repaired easily therefore give additional benefit for the maintenance of the structures.

An intelligent and lean facing system, combining the aspects of economic design and easy to maintain, has been realised at the project Wien (Fig. 6), differentiating the static support system on the soil side and the galvanised steel grid on the facing side. The gap is filled with natural stone in analogy to gabions. In case of a damage of the outer steel grid, the structure remains stable and just the filling and outer steel grids have to be reconstructed.

5 FINAL REMARK

Extending and reconstructing the infrastructure within the European countries as well as the international routes, structures for noise barriers and embankment foundations are required, fulfilling the economic requirements. Geosynthetics, namely geogrids, allow to use local soils and can be combined with steel elements as well as concrete and wooden elements.

The experience and scientific findings gained in the last two decades ensure a sophisticated level of engineering as documented in the design codes EBGEO and BS 8006, both in accordance with Eurocode 7. Nevertheless it should be noted that Eurocode 7 alone does not provide full sets of partial factors, so additional factors provided by EBGEO and BS 8006 are strongly recommended to be used depending on the specific national used design approaches.

6 REFERENCES

Corney, N., Cox, P., Norgate, S. & Thrower, A. (2009): Sustainable Geosystems in Civil Engineering Applications. WRAP, Banbury, July 2009.

Egloffstein, T. (2009): Bauverfahren mit mineralischen Baustoffen und Bindemitteln im ökologischen Vergleich mit dem Einsatz von Geokunststoffen. 6. Geokunststoff-kolloquium, NAUE GmbH & Co. KG, Bad Wildungen, January 2009.

Heerten, G., Vollmert, L. & Klompmaker, J. (2009): Geomechanical behaviour of geogrids – current design and future aspects of research linked to the rheological behaviour of compound material. 9th International Geotechnical Conference - Geotechnical Monitoring, Bratislava, June 2009.

Herold, A. (2007): 10 Jahre Verformungsbeobachtung an KBE-Bauwerken – Ist die Dehnsteifigkeit der Geokunststoffe der Schlüssel zur korrekten Prognose des Verformungsverhaltens von KBE-Stützbauwerken? geotechnik, Heft 30, 2007.

Kempfert, H.-G. (2011): Das Normenhandbuch. RuhrGeo Tag: Eurocode 7, Einführung in Deutschland, TU Dortmund, Heft 30, 2011.

Klompmaker, J. & Werth, K. (2011): Introduction of EC7 - Comparison of calculations following EBGEO and BS8006 in accordance to EC7. Parametric study for NAUE GmbH & Co. KG, unpublished.

Pachomow, D., Vollmert, L. & Herold, A. (2007): Der Ansatz des horizontalen Erddrucks auf die Front von KBE-Systemen. Tagungsband zur 10. FS-KGEO, München, 2007.

Ruiken, A., Ziegler, M., Vollmert, L. & Duzic, I. (2010): Recent findings about the confining effects of geogrids from large scale laboratory testing. 9th International Conference on Geosynthetics, Brazil, 2010.

Vollmert, L., Ramkema, A. & Verhoeff, G. (2010): Geokunststoffe und deren Bedeutung für großräumige Infrastrukturmaßnahmen am Beispiel des Knotenpunktes Hoogelegen der A2 Utrecht-Amsterdam. 31. Baugrundtagung, München, November 2010.

Wessling, A. & Vollmert, L. (2004): Geogitter bewehrte Steilböschung spart Kosten. Straßen & Tiefbau, Heft 11/2004.

Sustainable Management of Contaminated Sediments

Gestion durable des sédiments contaminés

Holm G.
Swedish Geotechnical Institute, Linköping, Sweden
Lundberg K., Svedberg B.
Luleå University of Technology, Luleå, Sweden

ABSTRACT: Increasing sea transport volumes require expansion of ports and due to longer, wider and more deep-draught ships considerable dredging of sediments often contaminated with heavy metals and organic contaminants has to be implemented. Handling options have to be identified in each actual case and the choice of option should be based on a sustainability approach, considering economy, environment and social aspects. In the EU-funded project "Sustainable Management of Contaminated Sediments in the Baltic Sea" (SMOCS; www.smocs.eu) within the Baltic Sea Region Programme 2007-2013, tools for assessment and decision making are developed, i. e. Life Cycle Analysis (LCA), Risk Assessment (RA) and Multi Criteria Decision Analysis (MCDA). To develop the tools a series of case studies have been performed comparing different handling options such as land disposal, sea disposal, confined aquatic disposal and beneficial use in port constructions utilizing the stabilization/solidification technology.

RÉSUMÉ : L'augmentation des volumes de transport maritime nécessitent l'extension des ports, et l'arrivée de navires plus longs, plus larges et à plus fort tirant oblige le dragage considérable de sédiments souvent contaminés par des métaux lourds et des polluants organiques. Différentes options de gestion doivent être identifiés dans chaque cas concret et le choix de l'option doit être fondé sur une approche de durabilité, compte tenu de l'économie, l'environnement et les aspects sociaux. Dans l'UE, un projet financé par «La gestion durable des sédiments contaminés de la mer Baltique "(SMOCS; www.smocs.eu) au sein du programme régional de la mer Baltique 2007-2013, des outils d'évaluation et de prise de décision sont développés, i. e. Analyse de Cycle de Vie (ACV), l'évaluation des risques (RA) et la multi-analyse des critères de décision (MCDA). Pour développer ces outils, une série d'études de cas ont été réalisées comparant diverses méthodes de manutention telles que l'enfouissement, l'immersion en mer, l'immersion confinée aquatique et l'utilisation bénéfique dans les constructions portuaires en utilisant les technologies de stabilisation / solidification.

KEYWORDS: Contaminant, sediment, mangement, sustainablility, stabilisation, solidification.

1 INTRODUCTION.

Sea transport is increasing due to its environmental and economic benefits. Ports are therefore a key part of the multi module transport system in the society. In Sweden, for example, the ports manage more than 90% of the tonnage in the trade. To enable to manage this amount of trade, ports have to run and operate a port infrastructure that is robust, cost effective and environmentally sustainable.

The increase in sea transport as well as longer, wider and more deep-draught ships cause huge needs of maintenance and development dredging of sediments in fairways and ports. In the coming years several million cubic meters of sediments need to be dredged in the Baltic Sea. A large volume of these sediments is contaminated with heavy metals and organic contaminants (HELCOM, 2009). This highlights a key issue for the society in the future - what is the sustainable management of these sediments? To approach sustainable management assessments should not be limited to site specific emissions but also include other categories such as use of energy, resources and climate impact (Arevalo, 2007). Handling options for dredged sediments have to be identified in each actual case and the choice of handling option should be based on a sustainability approach, considering economy, environment and social aspects, see Figure 1.

There are many possible options for managing contaminated sediments; the two major ones are either to take action or no action. In practice, action can include treatment in situ or ex-situ implying numerous options incl. capping of sea deposits, beneficial use of treated sediments as construction material or capping in-situ.

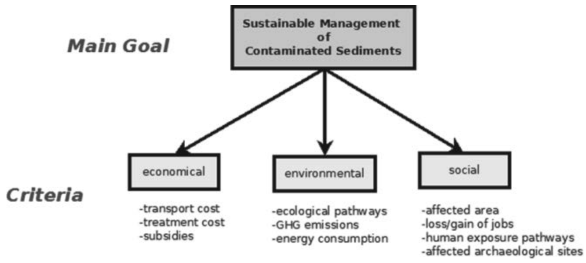

Figure 1. Sustainable management of contaminated sediments.

In the EU-funded project "Sustainable Management of Contaminated Sediments in the Baltic Sea" (SMOCS; www.smocs.eu) within the Baltic Sea Region Programme 2007-2013 tools for assessment and decision making are developed.

1.1 *Aim and objectives*

The aim of this paper is to presents results of case studies on assessment tools applicable in the sustainable management of contaminated sediments. The case studies include the stabilization/solidification (s/s) technology as one emerging sustainable handling option. Furthermore the authors present and invite stake holders to participate in networks to promote sustainable management in sediment handling and other port infrastructure.

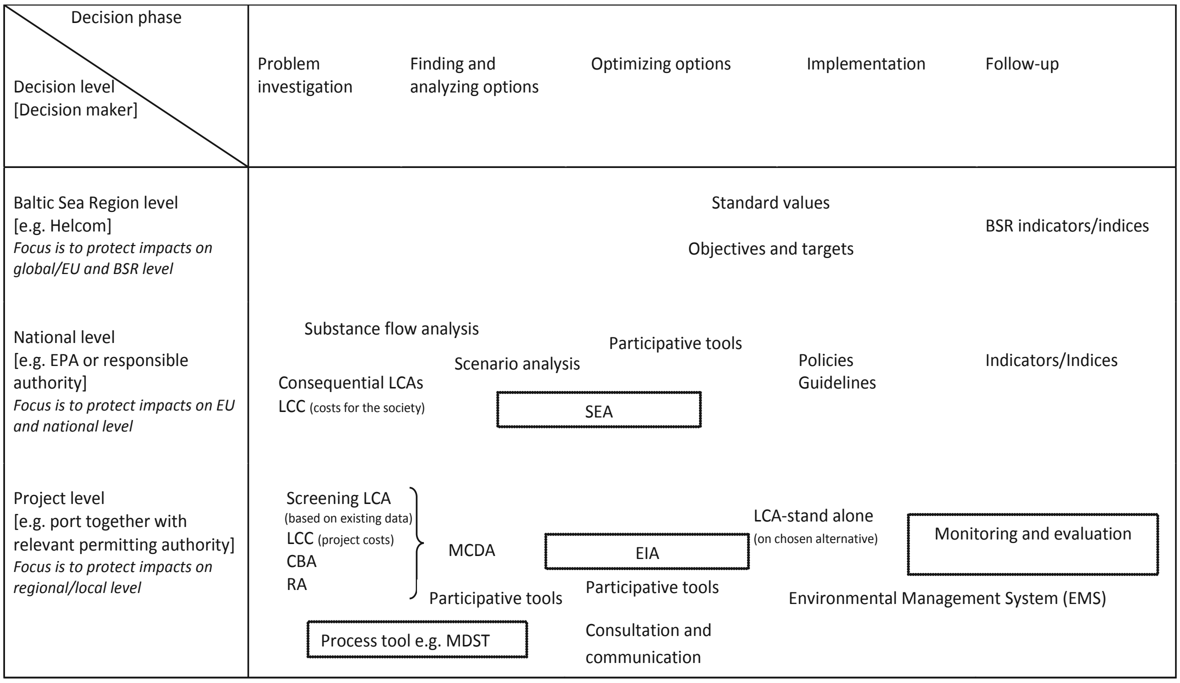

Figure 2. Examples of when different types of assessment tools which could be implemented in a decision process (Lundberg, et al, 2011).

2 TOOL-BOX FOR SUSTAINABLE MANAGEMENT

2.1 *Overview of tools*

There are several tools that could be used for sustainable assessment of contaminated sediments. The starting point for tools in decision making has to be based on an understanding of the nature of the decision that should be taken and the function and focus of the tool (de Ridder, et al., 2007). Therefore, the use of assessment tools depends on the decision level as well as the decision phase (se Figure 2).

Within the SMOCS project several case studies on assessment tools such tools have been performed. In this paper we present results from case studies using life cycle assessment (LCA) and multi criteria analysis (MCDA).

2.2 *Life cycle analysis (LCA)*

The purpose of a life cycle analysis (LCA) is to find out where in the life cycle the environmental load is the greatest and from what the impact is generated (ILCDA, 2011). This is mainly done through determining a material and substance flow. Thus is possible to assess the environmental impacts associated with all the stages of a product or a service/action life from-cradle-to-grave.

In the SMOCS project different management options of dredged contaminated sediments have been assessed by LCA (see Figure 3). The case studies have been based on sediment management in three ports; Port of Oxelösund, Sweden, Port of Gävle, Sweden and Port of Hamburg, Germany.

In the case studies of Port of Oxelösund and Port of Gävle, three possible management scenarios were compared. The scenarios were 1) utilization of sediment in quay construction by stabilization/solidification, 2) disposal in landfill and 3) disposal at sea. In the case study of Port of Hamburg, four management scenarios were compared. The scenarios were 1) disposal in river, 2) disposal at sea, 3) utilization of sediment in road construction or as landfill cover by METHA (Mechanical Treatment of Harbour Sediment), and 4) dewatering and disposal in landfill.

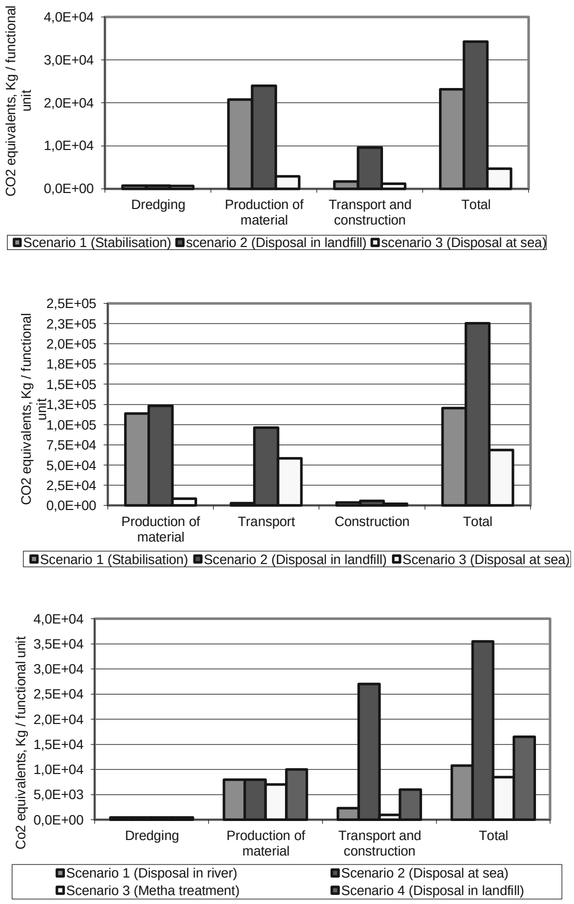

Figure 3. Port of Oxelösund, Port of Gävle, Sweden and Port of Hamburg, Germany (from top to bottom)

The system boundaries were chosen with a comparative LCA approach, i.e. identical activities in all scenarios were excluded, aside from dredging activities. The system boundaries were expanded and included also the beneficial utilization of the sediment. Hence, the functional unit included the handling of the sediment and also the production of the service that the sediment would provide when utilized in quay, road, bricks etc. Disposal scenarios also included the fulfillment of the service but sediment material was substituted with the production and use of conventional material.

LCA could provide the decision maker with a good view on environmental impacts for either a certain activity or for a comparison of different activities. The LCA could thus be used in an early decision phase for comparing relative differences in energy use and climate impact between different handling options.

LCA could also be used for displaying the relation between the energy use and climate impact from production of material, transport of material and construction work and maintenance respectively. This could be made with a stand-alone approach. With the standalone LCA approach, it could be possible to describe significant activities in each sediment management alternative. Such approach demands a more extensive data inventory but could provide information on which measures should be taken in each management alternative to reduce the energy use and climate impact. The stand-alone approach been tested in a SMOCS case study and the result is presented in Figure 4.

The data was collected from the cases of Oxelösund and Hamburg and completed with data on previously excluded activities such as dredging, transfers of dredged material.

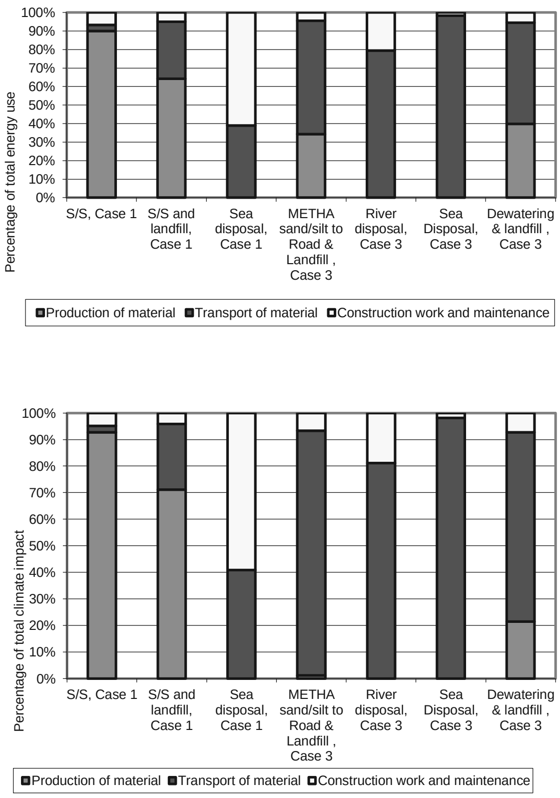

Figure 4. Percentage of total energy use (top) and climate impact (bottom) from the handling of sediments from in three categories of activities. Case 1 is Port of Oxelösund, Sweden and Case 3 is Port of Hamburg, Germany.

The overall conclusion from these LCA cases studies are that the selection of handling alternative for sediment management has major significance on the overall energy use and climate impact. Furthermore, the energy use and climate impact from transportation of materials and dredged material is often significant in the context of sediment management

2.3 *Multi Criteria Decision Analysis (MCDA)*

Multi criteria decision analysis (MCDA) is a tool that can integrate economic, environmental and social criteria and identifying the most sustainable handling alternative in a structured and rational way. Therefore, MCDA approach could be used at the project level for establishing the overall favorable handling alternative for management of contaminated sediments from a sustainability perspective. However, in order to be able to objectively score the performance of the different handling alternatives used in the MCDA other assessment tools are needed.

Within SMOCS MCDA case studies has been performed for the Port of Gothenburg and the Port of Lübeck integrating economic, social and environmental criteria for decision.

Fundamental steps in a MCDA are to (Belton and Stewart, 2001)

1. Identify possible handling options
2. Identify decision criteria and their indicators
3. Weight decision criteria's relative importance
4. Score the performance of the handling options in relation to each decision criterion
5. Calculate results

Results from the case study in the Port of Gothenburg are shown in Figure 5. A higher score should be interpreted as a better overall result, meaning that Rock chamber disposal and Solidification/stabilization are the most favorable options. A handling alternative scoring best on all decision criteria would result in the overall performance score 1.0. The bar colours show the contributions of environmental, social and economic criteria to the overall performance of each handling option. The impact of the port's weighting can be seen clearly: economic and environmental criteria are given 2 and 1.5 times the weight of social criteria, and hence these contribute more to the overall performance.

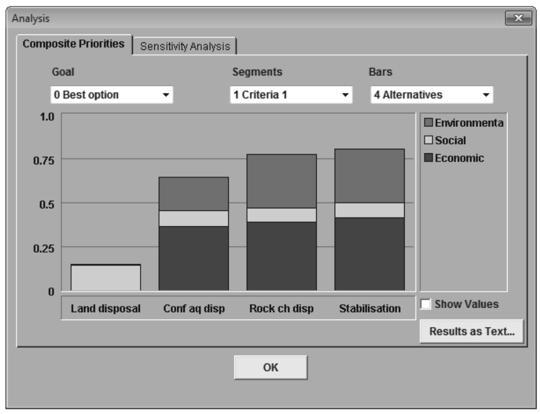

Figure 5. The MCDA results for the Port of Gothenburg case study showing the score of each handling option. A higher score means better overall performance.

3 CONCLUSION

MCDA provides a structured way of thinking through the whole range of decision criteria that should be taken into consideration when planning for handling contaminated sediments. MCDA can provide the transparency and documentation necessary for creating consensus between port owners and governmental organizations. This requires that a common opinion on decision criteria and weights can be established. It also requires that permit authorities embrace the concept of evaluating social, economic and environmental decision criteria together.

LCA is an appropriate tool for assessing energy and green house gas emission, information that give important input to the MCDA. The LCA could be used both for comparing different handling alternatives as well as displaying the relation between the energy use and climate impact from production of material, transport of materia, construction work, and maintenance.

The conclusion from the case studies using LCA and MCDA is that the selection of handling alternative for sediment management has major significance on the overall energy use and climate impact. Furthermore, it was shown that sediments utilized as construction material instead of disposed in landfill reduce energy use and climate impact significantly.

4 SMOCS DELIVERABLES AND A NETWORK ON SUSTAINABALE MANAGEMENT OF CONTAMINATED SEDIMENTS

The main deliverables of SMOCS consists of a guideline, tools for assessing sustainability and decision support, and a durable network. The guideline will address current and emerging technologies including verification of investigation and treatment technologies. The guideline will cover the whole process form planning to executing and control of treated sediments.

SMOCS has applied a highly participative approach. Therefore, the knowledge is compiled into the guideline in close cooperation with ports, maritime organizations, environmental authorities, construction industry as well as R&D performers. This approach is also a key starting point to establish a durable network.

The partners of the SMOCS project have agreed to establish a network for the period 2013-2017 on key issues and share experience, but also on development of further co-operation on identified issues. The topics covered are not limited to contaminated sediments thus including dredging and management of sediments in general as well as other port and authority issues if applicable.

The network is mainly based upon participants from the Baltic Sea Region. However as it exists in a European context, it is important that other regions can join and cooperate.

5 ACKNOWLEDGEMENTS

The SMOCS project is Part-financed by the European Union (European Regional Development Fund and European Neighbourhood and Partnership Instrument) the Baltic Sea Region Programme 2007-2013 and partly by the partners of the project being Swedish Geotechnical Institute, Luleå University of Technology, Sweden, Port of Gävle, Sweden, Lappenrannta University if Technology, Finland, Port of Kokkola, Finland, Maritime Institute, Gdansk, Poland, Port of Gdynia, Poland, Hamburg-Harburg University of Technology, Germany, Port of Klaipeda, Lithuania, and CORPI, Klaipeda, Lithuania

6 REFERENCES

Arevalo, E., Cesaro, R., Stichnothe, H., Hakstege, A.L., Calmano, W. 2007. Application of the principles of life cycle assessment to evaluate contaminated sediment treatment chains. *Sustainable Management of Sediment Resources* 2, 160-184.

Belton, V and Stewart, T J. 2001. *Multiple Critera Decision Analysis*. ISBN 9780792375050. Kluwer Academic Publishers. Dordrecht. 396p.

ILCDA 2011, *General guide for life cycle assessment – detailed guidance*. International reference life cycle data system, ISBN 978-92-79-19092-6.

Lundberg, K., Ohlsson, Y., Andersson Sköld, Y., Bergman, R., Falemo, S., Edeskär, T., Scheffler, A. 2011. *Dredging contaminated sediments in the Baltic Sea - A guide to sustainability assessment tools.* SMOCS Level 3 report [www.smocs.eu].

de Ridder, Wouter; John Turnpenny; Måns Nilsson et al. 2007. A Framework for Tool Selection and Use in Integrated Assessment for Sustainable Development. *Journal of Environmental Assessment Policy and Management*, Vol. 9, No. 4, 423-441.

Polymer support fluids: use and misuse of innovative fluids in geotechnical works

Les polymères: l'utilisation de nouveaux fluides de forage en travaux géotechnique

Jefferis S.A.
Environmental Geotechnics Ltd. and University of Oxford, United Kingdom

Lam C.
The University of Manchester, United Kingdom

ABSTRACT: Bentonite slurries have been used for over sixty years for the temporary support of excavations such as bored piles and diaphragm walls. At intervals over this time polymer products have been tried in place of bentonite but not always successfully. Recently it has become clear that, if used properly, polymer fluids offer many advantages over their bentonite counterparts, including improved foundation performance, lower environmental impacts, smaller site footprint and also simpler preparation, mixing and final disposal as they are used at much lower concentrations. They are also more easily managed than bentonite. However, successful use requires that the some specific characteristics of polymers are respected, in particular, it must be recognised that they are sorbed onto soils so that the polymer concentration in solution drops during use.

RÉSUMÉ: Les coulis de bentonite ont été utilisés depuis plus de soixante ans pour la mise en œuvre des pieux forés et parois moulées. Des boues polymères ont été testées pour remplacer ces suspensions d'argile mais les résultats n'ont pas toujours été conclusifs. Récemment, il est devenu évident que, si utilises correctement, les polymères offrent de nombreux avantages, entre autre une amélioration de la performance de fondation et une réduction de l'impact sur l'environnement; les procédés de préparation et de mélange sont facilités ainsi que la disposition de déchets car la quantité de polymères utilisée est plus petite que la quantité de bentonite nécessaire dans les coulis de bentonite. Cependant le succès de l'utilisation des polymères est limité par certaines de leurs propriétés – en particulier, le fait qu'ils s'adsorbent aux sols diminue leur efficacité durant le forage.

KEYWORDS: bentonite, diaphragm walls, piles, polymer, support fluids.

1 INTRODUCTION

1.1 *Background*

Bentonite slurries have been used for over sixty years for the temporary support of excavations for slurry trench cut-offs, bored piles and structural diaphragm walls and somewhat more recently for slurry tunnelling. At intervals over this time polymer alternatives have been tried but not always successfully, so that for some the word 'polymer' has become an anathema. However, recent developments have shown that, if used properly, polymer fluids offer many advantages over their bentonite counterparts, including improved foundation performance, smaller site footprint, reduced environmental impact and simpler mixing and final disposal as they are used at much lower concentrations than bentonite.

The many advantages polymer solutions offer can be achieved only if specifiers and users have a proper understanding of their properties and their in-situ behaviour and recognise that not all polymers are the same – the properties of the various polymers used in excavation works can vary very substantially. Unfortunately, it is still not unusual for users and/or specifiers to treat excavation support polymers as if they were a single material similar to bentonite. Polymer solutions are fundamentally different fluids to bentonite slurries and each type of polymer has distinct physical and chemical properties which must be respected to avoid misuse.

1.2 *Natural and synthetic polymers*

Early polymer fluids tended to be based on naturally derived products such as carboxymethyl cellulose, xanthan and guar gums but they had a limited range of properties, were easily biodegraded and thus short-lived unless treated with biocides which can have negative environmental impacts. Furthermore, like bentonite they could not inhibit the dispersion of fine soils such as clays into the excavation fluid and thus required cleaning before re-use.

In recent years, the advent of synthetic polymers has allowed the development of fluid systems with tailored properties. Systems can be designed to be bio-stable, environmentally benign and to inhibit clay dispersion so enabling repeated use without specialised soil-slurry separation plant such as hydrocyclones, dewatering screens and centrifuges. Today, with these benefits, synthetic polymers account for the vast majority of polymers used for foundation construction and in oil-well drilling (where bentonite free muds are regularly used). Natural polymers continue to be used for excavation projects where rapid biodegradation is useful such as the construction of permeable reactive barriers and deep drainage walls.

1.3 *Objectives*

To promote best practice in the use of polymer support fluids for the construction of deep foundations, this paper sets out the latest understanding of the behaviour of polymer fluids and also presents experience drawn from recent research and case histories from around the world.

2 SUCCESS THROUGH PROPER USE OF POLYMERS

2.1 *Operational benefits*

The operational benefits offered by polymer fluids traditionally have been one of the main reasons for contractors to switch from bentonite to polymers. For example, Lennon et al. (2006) note that the size and cost of the ancillary plant required for bentonite slurries make them relatively uneconomic for urban sites with restricted space and access such as those in city centres. Figure 1 shows such a site in central Glasgow, UK which although measuring just 24 m by 40 m required sixty-two 750 mm diameter bored piles, i.e., approximately one pile every 4 m. The size of the site and the scope of the work meant that polymer fluids were the only feasible option because they do not require multiple holding tanks for slurry hydration nor do they require separation plant to recover the used slurry. Unlike bentonite slurries, polymer fluids require only a short swelling and hydration time prior to use and indeed emulsion polymers develop their properties almost instantaneously after mixing. Powered polymers, after wetting out, for example, with a Venturi eductor can be hydrated in an open-top tank gently agitated with a compressed air lance.

Figure 1. The small site in Glasgow where a polymer fluid was used.

Anonymous (2001) note that during the construction of the Channel Tunnel Rail Link (CTRL) East Kent-Ashford to Cheriton section, polymers were chosen because setting up a bentonite plant on some of the sites would have been almost impossible due to space restrictions. The saving of time for site set-up is an associated advantage. Compact polymer plant can be moved from site to site relatively quickly whereas mobilising a bentonite set-up can absorb much valuable programme time.

2.2 *Environmental benefits*

Polymer fluids can offer significant environmental benefits when compared to their clay-based counterparts. For example, although used bentonite may be classified as a non-hazardous waste, it can be highly polluting if released into the aquatic environment. For projects near watercourses, polymer fluids are preferred over bentonite as they need not pose a danger to fish and in particular they do not build up on fish gills causing them to suffocate (Schünmann 2004).

As the disposal of liquid waste to landfill is banned in many countries, the final disposal of used bentonite slurries can be more costly than the purchase of the original bentonite powder. Polymers are used at perhaps one-fiftieth to one-twentieth of bentonite concentrations and the products can be broken down with readily available oxidising agents such as hypochlorite (bleach) so that after simple settlement the supernatant water can be disposed to sewer (with the undertaker's consent) and the settled fines added to the excavation spoil – ideally for re-use. Thasnanipan et al. (2003) report that in Bangkok the primary reason for switching to polymers was, in most cases, to minimise the environmental issues associated with bentonite fluids. Caputo (2009) also expressed concerns regarding the potential environmental impacts associated with the use of bentonite for the bored piles for a bridge across the Tagus River in Portugal.

2.3 *Improved foundation performance*

As outlined above, operational and environmental benefits are often cited as the main reasons for using polymers rather than bentonite. However, over the last two decades many field studies have been carried out to investigate the effects of polymer fluids and it is now appreciated that they can bring significantly improved load performance for piles, etc. The results of a recent UK case history are summarised below.

To assess the effects of different support fluids and of varying pile bore open times, Lam et al. (2010a) analysed the results from a full-scale field trial in East London, where the ground profile was a layer of made ground underlain by the Lambeth Group and then Thanet Sand. The trial involved the load testing of three instrumented piles, two of which were constructed under a polymer fluid and one under bentonite. The difference between the two polymer piles was the pile bore open time; one was concreted within 7.5 h of the completion of excavation (Pile P1) whilst the other was concreted at 26 h (Pile P2). The bentonite pile (Pile B1) was concreted at 7.5 h.

Figure 2 shows the load-settlement curves of the three piles; both polymer piles behaved similarly and significantly outperformed their bentonite counterpart at the maximum test load of 18 MN – and indeed the pile open for 26 h showed slightly better behaviour than that open to 7.5 h. Analysis of the data from the instrumentation on the piles and supporting laboratory tests demonstrated that the improvement in the load-settlement characteristics of the polymer piles was due to the higher shaft resistance and also the clean pile bases (Lam 2011). The effect of the polymer solution on concrete also was investigated. This showed that the polymer fluid had a similar effect on the strength and stiffness of hardened concrete as bentonite slurry – water from the fluids mixing with the surface concrete being the issue.

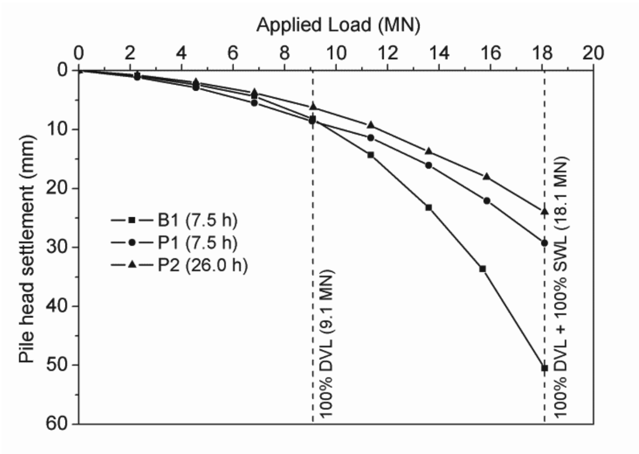

Figure 2. Load-settlement curves of bored piles at the East London test site. DVL: design verification load; SWL: specified working load.

Whilst the above results clearly demonstrate the potential benefits of polymer fluids, these will be realised only if suitable excavation tools are used and there is rigorous base cleaning prior to concreting. Figure 3 shows the auger used for the trial. This had twin flights which prevent suction developing in the fluid column as the auger is withdrawn. Spoil loads onto one flight and the other remains open allowing free fluid flow.

3 FAILURES THROUGH ABUSE OF POLYMERS

The literature reports many case histories of the successful use of polymer fluids. However, failures can still occur and polymer fluids can be used less than optimally as a result of lack of experience and/or understanding of the properties of the chosen polymer. In the following sections, a few examples of common polymer misuses are described.

Figure 3. A twin-flight auger used for the East London trial.

3.1 *Failure to use the polymer at the supplier's recommended concentration*

Suppliers typically recommend that polymer fluids should have a Marsh funnel viscosity somewhat higher than that for bentonite slurries. There is therefore a temptation for users to reduce the polymer concentration and/or for specifiers to require a lower viscosity. However, the Marsh funnel viscosity of an excavation fluid is not an indicator of its performance in the hole rather it is a control parameter to confirm that there is sufficient active material to develop the required fluid properties, such as control of fluid loss to the ground, suspension of cut spoil and inhibition of its dispersion of into the excavation fluid. Reducing polymer concentration may compromise fluid performance and should not be attempted.

3.2 *Viscosity degradation by fluid recirculation*

Lam et al. (2010b) report the results of an investigation of the effects of continued shear on the properties of polymer fluids. The work was carried out on-site using a typical bentonite slurry pipework configuration (Figure 4). The centrifugal pump runs continuously and the fluid is circulated back to the storage tank when the valve in the feed line to the excavation is closed so that the pump need not be repeatedly turned on and off during the excavation. This is an important aspect of plant operation as the storage tank may be at some distance from the excavation. Continuous circulation, although wasteful of energy, is generally regarded as beneficial for bentonite slurries as it prevents settlement and improves hydration.

Two commercially available polymer products based partially hydrolysed polyacrylamides (PHPAs) were used for the study. Each polymer fluid was prepared in accordance with the supplier's recommended procedure and allowed to stand overnight to ensure stable fluid properties. Recirculation through the pump system was then started with polymer drawn off for use in pile bores as required. The Marsh funnel viscosity of the fluid was measured at intervals and the results are shown in Figure 5. The overnight drop in viscosity was due to the escape of fine entrained air bubbles which were present in the fluids after mixing. The effect of air bubbles on fluid viscosity is not well recognised and initial viscosities can be mistaken for working viscosities so leading to under-dosage of polymers.

From Figure 5 it can be seen that once pumping started the viscosity of each of the fluids dropped and continued to do so up to the end of the test. Both PHPAs were of high-molecular-weight (i.e. they were long-chain molecules – longer chain lengths tend to give higher viscosities) and it seems that the chains were undergoing scission as a result of continuing shear in the centrifugal pump and pipework so reducing the fluid viscosity. Indeed the damage was so severe for Fluid B that the initial 65 s viscosity (after overnight ageing) had reduced to 35 s at 22.5 h (after approximately 8 h recirculation) and was tending to that of pure water (28 s).

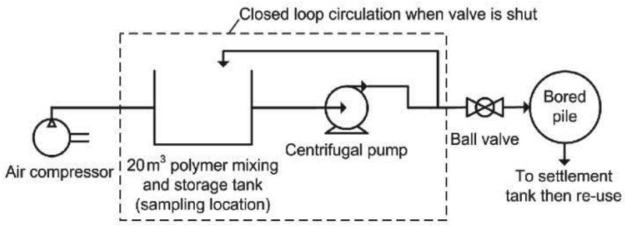

Figure 4. Schematic diagram of recirculation/delivery system.

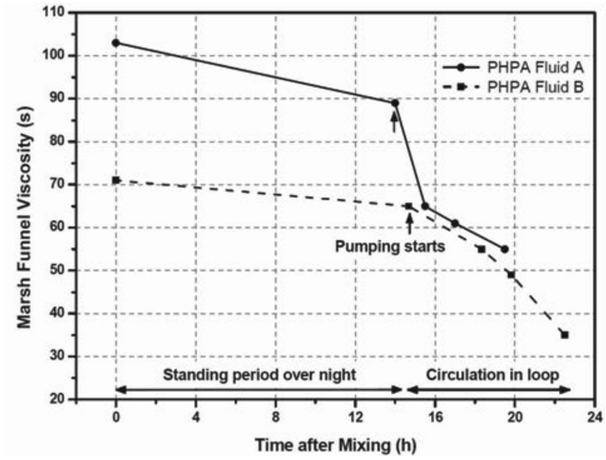

Figure 5. Reduction in viscosity of polymer fluids due to recirculation.

As the fluid was being used for pile excavations the viscosity was boosted by adding polymer directly to the pile bores to maintain stability and there were no collapses. However, had the monitoring programme not been in place, the contractor would not have been alerted to the problem and the pile bores might have collapsed due to the excessively low viscosity.

To avoid viscosity reduction due to prolonged shear in centrifugal pumps, it is recommended that diaphragm pumps are used as they induce less shear and can be designed to stop automatically (so also saving energy) when the pressure rises as a result of closure of the delivery valve. If diaphragm pumps are not available, fluid recirculation should be minimised.

3.3 *Fluid-soil/groundwater incompatibility*

The viscosity and hence other properties of PHPA fluids can be damaged by salts present in mix waters and in the ground. To investigate the effect of salts in mix water, Lam (2011) measured the viscosity of several commercial polymer products over a range of sodium chloride concentrations in the mix water using an Ubbelohde capillary viscometer. Figure 6 shows some of the test results. It can be seen that above about 100 mg/litre sodium chloride, the PHPA fluid lost about 60% of its viscosity in deionised water whereas the blended polymer lost only about 40%. However, for both fluids there was little further effect up to 1000 mg/litre. The effects of salts in mix water are recognised by suppliers and are compensated by increasing the polymer concentration and raising the solution pH with caustic alkalis – though increase in pH may give limited benefit.

In saline soils there should be regular monitoring of fluid viscosity to check for viscosity loss; there are case histories of collapses. For example, on the Vasco da Gama Bridge in Portugal two of the piles had to be re-drilled following collapses which were possibly due to fluid contamination (Bustamante et al. 1998, KB Technologies Ltd. 2000). Schwarz & Lange (2004) also report a case history of pile bore collapse due to high concentrations of salts at a site in Benin. Although simple PHPAs can be adversely affected by salts, engineered polymer systems are available which are more tolerant of ionic species in soils and these should be used in saline grounds.

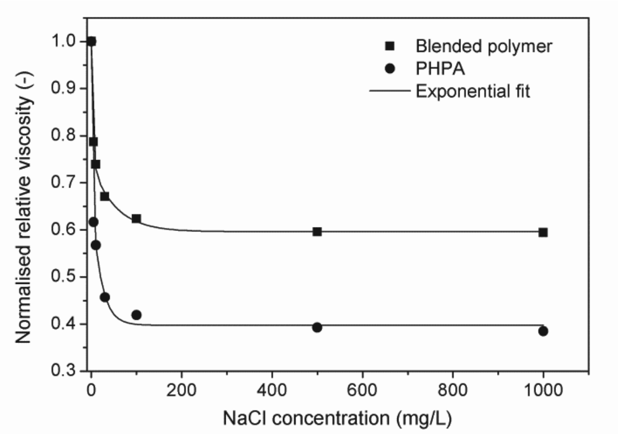

Figure 6. Effect of added sodium chloride on the viscosity of a commercial blended polymer product and a pure PHPA both mixed in deionised water.

3.4 *Loss of active polymer concentration due to repeated use*

The properties of polymer fluids depend on physical and chemical interactions between the polymer molecules in solution. An excavation polymer is thus an active chemical system. Whilst in use in an excavation, polymers tend to sorb onto soil surfaces, especially those of clays and this can beneficially reduce the break-up of lumps of cut soil and the resulting dispersion of fines into the fluid. However, it does follow that the concentration of active polymer drops with use and unless the concentration is regularly re-established the fluid will become little more than muddy water, a condition which the authors have dubbed as ‘flipped’. The system has ceased to be polymer solution with some suspended soil and become a soil slurry with little polymer remaining in solution.

Recognition of the effects of sorption is absolutely key to the management of polymer slurries. With hindsight it is now clear that a number of past problems with polymers can be traced to a lack of appreciation of the need to replenish the polymer lost by sorption and thus a wholly insufficient use of polymer.

To illustrate the effect of polymer sorption, Figure 7 shows the results of a series of tests on a PHPA-bentonite mix with increasing concentration of bentonite; the latter was used as a soil as it strongly sorbs PHPAs. It can be seen that as the bentonite concentration in the fluid increases, the polymer concentration drops and ultimately approaches zero.

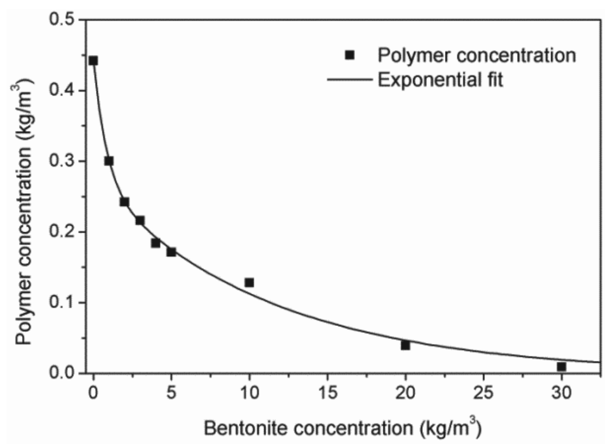

Figure 7. Reduction of polymer concentration by sorption.

4 CONCLUSIONS

Through the use of case histories and recent research findings, this paper has outlined some strengths and limitations of polymer fluids as potential replacements for bentonite slurries particularly for small or congested sites. Strengths include improved foundation performance, simpler site operations and reduced environmental impact. Limitations include reduction of fluid properties due to continued shear in recirculation systems, potential for loss of properties in saline soils and importantly sorption of polymers onto soils – which also can be a benefit as it reduces dispersion of fines into the fluid. To minimise the loss of fluid properties, fresh polymer must be regularly added to the system otherwise a significant degradation in performance of the fluid and potentially the foundation element will occur.

5 ACKNOWLEDGEMENTS

The work presented in this paper was undertaken as part of a research project jointly funded by the UK Engineering and Physical Sciences Research Council (EPSRC), Balfour Beatty Ground Engineering and KB International LLC. EPSRC grant reference nos.: EP/C537815/1 (Industrial CASE award) and EP/H50026X/1 (Knowledge Transfer Secondment). The authors would like to thank Messrs T. Suckling, V. Troughton, C. Martin, P. Martin and G. Goodhue for their help and advice throughout the project.

6 REFERENCES

Anonymous. 2001. Way out of a tight spot. *Ground Engineering* 34 (5), 16–17.

Bustamante, M., Gianeselli, L., Boato, R. and Conedera, A. 1998. Performance of polymer slurries in large diameter bored pile. *Proceedings of the 3rd International Geotechnical Seminar on Deep Foundations and Auger Piles (BAP III)*, Ghent, Belgium, A.A. Balkema, 119–127.

Caputo, A. 2009. Instrumented large diameter bored piles. *Proceedings of the 5th International Symposium on Deep Foundations on Bored and Auger Piles (BAP V)*, Ghent, Belgium, CRC Press, 213–227.

KB Technologies Ltd. 2000. *A SlurryPro CDP case history: Vasco da Gama Bridge, Lisbon, Portugal*. Trade literature.

Lam, C., Troughton, V., Jefferis, S. and Suckling, T. 2010a. Effect of support fluids on pile performance – a field trial in east London. *Ground Engineering* 43 (10), 28–31.

Lam, C., Jefferis, S.A. and Goodhue, K.G., Jr. 2010b. Observations on viscosity reduction of PHPA polymer support fluids. *Proceedings of Sessions of GeoShanghai 2010 International Conference*, Shanghai, China, Geotechnical Special Publications No. 205, American Society of Civil Engineers, 184–191.

Lam, C. 2011. *Properties and applications of polymer support fluids in geotechnical engineering*. DPhil thesis, University of Oxford, UK.

Lennon, D.J., Ritchie, D., Parry, G.O. and Suckling, T.P. 2006. Piling projects constructed with vinyl polymer support fluid in Glasgow, Scotland. *Proceedings of the 10th International Conference on Piling and Deep Foundations*, Amsterdam, the Netherlands, Deep Foundations Institute, 499–506.

Schünmann, D. 2004. Fisherman’s friend, *Ground Engineering* 37 (12), 17.

Schwarz, J. and Lange, U. 2004. Brückengründung mit 70 m tiefen flüssigkeitsgestützten gebohrten Pfählen in Benin/Afrika. *Proceedings of the 19th Christian Veder Kolloquium*, Graz, Austria, 73–89 (in German).

Thasnanipan, N., Aye, Z.Z. and Boonyarak, T. 2003. Behaviour of polymer-based slurry for deep-seated bored piles in multi-layered soil of Bangkok. *Proceedings of the 4th International Geotechnical Seminar on Deep Foundations on Bored and Auger Piles (BAP IV)*, Ghent, Belgium, Millpress, 267–274.

Utilisation of polyethylene (plastic) shopping bags waste for soil improvement in sandy soils

Utilisation des déchets de sacs en polyéthylène (plastiques) pour l'amélioration des sols sableux

Kalumba D., Chebet F.C.
University of Cape Town, South Africa

ABSTRACT: This study investigated the possibility of utilising polytheylene shopping bags waste to reinforce soils to pave way for its use in civil engineering projects such as in road bases, embankments and slope stabilisation. A series of direct shear tests was undertaken on soil-plastic composites of two selected sandy soils: Klipheuwel and Cape Flats sands. Strips of shredded plastic material were used as reinforcement inclusions at concentrations of up to 0.3% by weight. The effect of varying dimensions of the strips was investigated by using strip lengths from 15 mm to 45 mm and strip widths from 6 mm to 18 mm. Shear strength parameters were obtained for composite specimen from which analyses were done to identify the extent of soil improvement. The testing programme involved addition of solid strips as well as perforated strips with varied diameter of perforations to examine the effect of the openings on the strips. Laboratory results obtained favourably suggest that inclusion of this material in sandy soils would be effective for ground improvement in geotechnical engineering.

RÉSUMÉ : Cette étude a examiné la possibilité de l'utilisation des déchets des sacs d'épicerie en polyéthylène pour renforcer les sols afin de promouvoir son intégration dans les projets de génie civil tels que les couches d'assise des routes, les remblais et la stabilité des pentes. Une série d'essais de cisaillement direct a été réalisée sur des composites plastique-sols sur deux sols sableux sélectionnés : sable de Klipheuwel et de Cape Flats. Des lamelles de matériau plastique déchiqueté ont été utilisées comme intrants de renforcement à des concentrations allant jusqu'à 0,3% du poids. L'effet de la variation des dimensions des lamelles a été apprécié en modifiant leurs longueurs de 15 à 45 mm et leurs largeurs de 6 à 18 mm. Les paramètres de la résistance au cisaillement obtenus pour les spécimens de composites ont servi à faire des analyses pour l'estimation du degré d'amélioration des sols. Le procédé scientifique a été fait avec des lamelles pleines et des lamelles perforées à divers diamètres afin d'observer l'effet des interstices dans les lamelles perforées. Les résultats de laboratoire obtenus confirment favorablement que l'ajout de ce matériau dans les sols sableux serait efficace pour l'amélioration des sols dans les applications d'ingénierie géotechnique.

KEYWORDS: Plastic bags, Polyethylene, Waste minimisation, Soil reinforcement, Ground improvement, Shear strength

1 INTRODUCTION

Increased use of plastics in day to day consumer applications has resulted in municipal solid waste containing an ever growing fraction of plastic material used for a short time and discarded. Ever since their invention over 60 years ago, plastics have taken centre stage in daily life due to favourable attributes such as low weight, durability and lower cost as compared to other material types (Thompson et al. 2009, Andrady and Neal 2009). These attributes make plastics convenient and therefore highly demanded by consumers with production increasing substantially from about 0.5 million tonnes in 1950 to over 260 million tonnes by 2008 with higher projections expected in the future (Thompson et al. 2009). A large percentage of plastics produced are used for disposable applications like packaging and therefore reach the waste stream more quickly since their usage life is shorter than that of plastics used in the construction or automotive industry (Azapagic et al. 2003). Consequently about 10% by weight and 20% by volume of the municipal waste stream is composed of plastics destined for landfills (Barnes et al. 2009, Azapagic et al., 2003). Of the plastic material discarded, 50% is from packaging, a third of which consists of plastic shopping bags (Nhamo 2008).

Plastic shopping bags are water resistant materials mostly made of polyethylene, a non-biodegradable polymer produced from non-renewable petroleum and natural gas resources. The linear consumption patterns of plastic bags involving single usage and then disposal has led to environmental challenges such as diminishing landfill space, marine and urban littering. There is therefore a growing need to find alternative uses of reclaimed plastic bag waste to lengthen the usage time of the plastic material. This is so as to tap into the abundant plastic resource that possesses a great extent of versatility and yet in the same vein poses a danger to the environment if not well managed in terms of responsible disposal that involves resource recovery vital in contributing to sustainable development.

Chen et al. (2011) maintain that new approaches on the reuse of plastic waste in cities as alternative materials for urban developmental programs, referred to as urban symbiosis, could help reduce green house gas emissions and fossil fuel consumption. This study explored the possibility of utilising reclaimed plastic material from polyethylene bags as tensile inclusions to reinforce soil for ground improvement schemes in geotechnical engineering applications such as retaining walls, road bases, embankments and slope stabilisation.

Research into random inclusion of discrete polypropylene fibres in soil as reinforcement material have reported increases in peak shear strengths and reductions of post peak losses in soils (Zornberg 2002, Consoli *et al*., 2007, Falorca and Pinto 2011). Furthermore, these fibres have been found to improve compressive strength and ductility of soils (Maher and Ho 1994, Santoni *et al*., 2001, Miller and Rifai 2004). As a result, fibre reinforced soil consisting of polypropylene fibres have been successfully used on embankment slopes in the US (Gregory and Chill 1998) and in applications such as foundations for sport pitches, horse racing tracks and access for secondary roadways (Ibraim and Fourmont 2006).

The main objective of this study was therefore to investigate the effect of including plastic strips from polyethylene shopping bags on the shear strength of two locally sourced sandy soils. Additionally, perforations were introduced on selected strips to examine if increased bonding and interlocking of soil in the soil-plastic composite through the openings in the plastic material provided an additional effect on the shear strength parameters of the soil-plastic composite.

2 MATERIALS AND METHODS

2.1 *Soil Material*

The soil types used in the study were Cape Flats sand and Klipheuwel sand, both predominant in the region of Cape Town, South Africa. Cape Flats sand is a medium dense, light grey, clean quartz sand with round shaped particles while Klipheuwel sand is a medium dense, reddish brown sand with angular particles. Table 1 gives a summary of the physical properties of the sands.

Table 1. Engineering properties of the selected soils.

Soil Property	Cape Flats Sand	Klipheuwel Sands
Specific gravity, Gs	2.66	2.64
Particle Range (mm)	0.075-1.18	0.075-2.36
Mean Grain Size, D_{50}	0.5	0.72
Coefficient of uniformity, C_u	3.0	4.21
Coefficient of curvature, C_c	0.85	1.05
Angle of friction (°)	38.5	41.6

2.2 *Plastic Material*

The plastic bags (Figure 1a) were sourced from a local supermarket and shredded into strips of varying lengths and widths using a laser cutting machine. The bags were labeled as high density polyethylene (HDPE) according to the plastics identification code by the American Society of the Plastics Industry (SPI). The density was measured as 743 kg/m^3 with an average thickness of 40 μm and a tensile modulus of 389.7 MPa. The tensile strength obtained for the plastic material varied between 15 MPa and 20 MPa. Both the solid strips and perforated strips were included in the testing regime. For perforated strips, the laser cutting machine was used to make perforations of different diameters on the strips (Figure 1b).

Figure 1: a) Plastic Bag b) Shredded and perforated strips

2.3 *Experimental Work*

Soil samples for the tests were oven dried in order to eliminate any effects of moisture and the plastic strips mixed with the soil in a bowl to form a composite (Figure 2a). The plastic strips used were of lengths 15 mm, 30 mm, 45 mm, and widths of 6 mm, 12 mm, 18 mm. Perforations of diameter 1 mm and 2 mm were made on strips of width 6mm while their lengths varied. The strips were added to the soil at concentrations of 0.1% 0.2% and 0.3% by weight and the composite material placed into a 100 mm x 100 mm shear box for direct shear testing (Figure 2b). The specimen in the shear box was compacted to an average density of 1700 kg/m^3 and the tests performed for normal stresses of 25 kPa, 50 kPa, 100 kPa at a shear loading rate of 1.2 mm/min. The peak stress for each soil specimen was noted including the results obtained for the control experiment in which no strips were added to the soil.

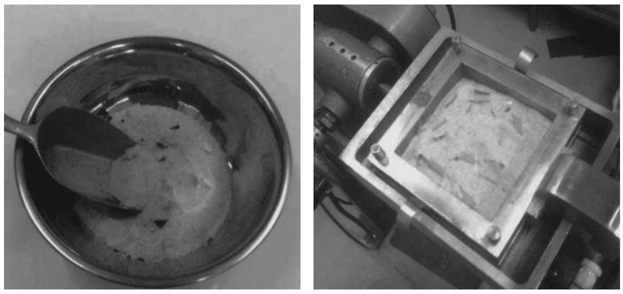

Figure 2: a) Soil-plastic composite b) Composite specimen placed in shear box for testing

3 RESULTS AND DISCUSSION

The peak shear stresses obtained from the direct shear tests were recorded and plotted against the respective applied normal stresses to determine the friction angles for each soil specimen tested. The results revealed a general increase in peak friction angles for both Klipheuwel and the Cape Flats sands on addition of both the solid and perforated plastic strips. The plastic parameters yielded a distinct effect on the soils as they were varied with both soils showing a unique response to each parameter. The relationship between the peak friction angle and the different strip variables of length, width, concentration and perforation diameter are presented in Figures 3 and 4.

3.1 *Solid Strips*

The results indicate that the peak friction angle for both Cape Flats and Klipheuwel sand is enhanced on addition of solid plastic strips (Figure 3a). An increase in friction angle from 38.5^o to 42.4^o was observed for the Cape Flats sand and from 41.6^o to 44^o in Klipheuwel sand. The higher values obtained for Klipheuwel sand was due to the better grading and thus giving a higher initial shear strength. The results reveal that maximum friction angles were obtained with 15 mm strips for Klipheuwel and 45 mm strips for Cape Flats sand. Therefore, there could be a limiting plastic strip length for the soil-plastic composite beyond which further lengthening results in a decrease in the shear strength on addition of the solid strips.

Further testing indicated that beyond the reinforcement width of 6 mm, the peak friction angle decreased which suggested that the soil strength decreases as the reinforcement strips widen (Figure 3b). This may be due to an increased interaction between the plastic strips caused by more overlapping for the case of wider strips in the test specimen resulting in reduced soil-plastic interaction in the composite.

An almost linear increase in the initial friction angle was observed for Cape Flats sand on increasing the strip content with a progressive improvement from 38.5^o at 0.1% to 42.4^o at 0.3% concentration (Figure 3c). Klipheuwel sand on the other hand responded with an increase on addition of 0.1% plastic and a decrease at higher concentrations. Higher plastic content seemed to affect the particle interlocking in the more angular shaped Klipheuwel sand resulting in a lower friction angle at greater strip concentrations.

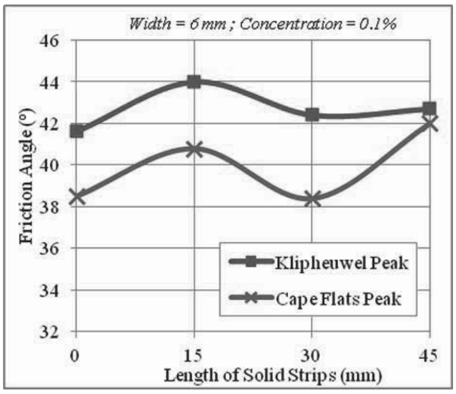

Figure 3a: Friction angle vs Solid strip length

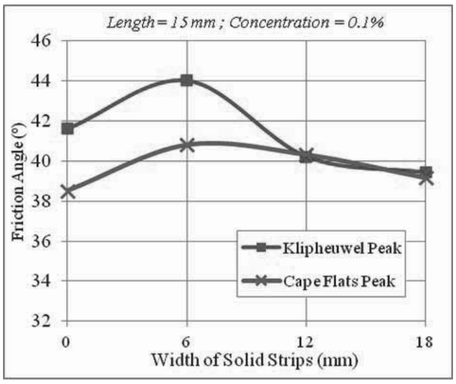

Figure 3b: Fiction angle vs. Width of solid strips

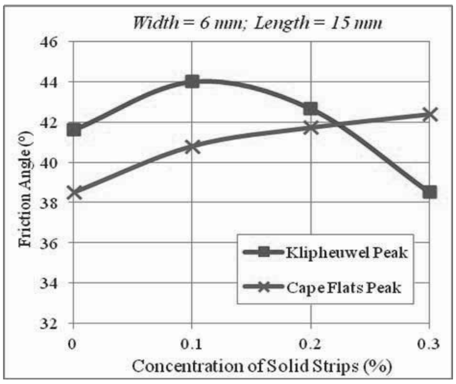

Figure 3c: Friction angle vs. Concentration of solid strips

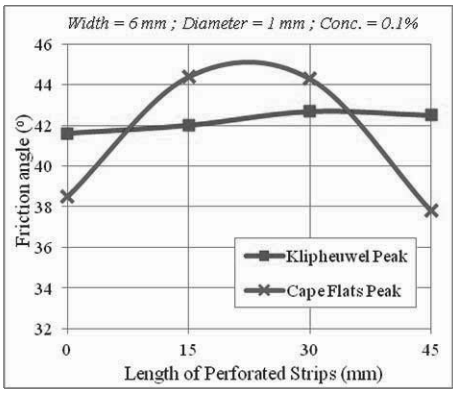

Figure 4a: Friction angle vs Perforated strip length

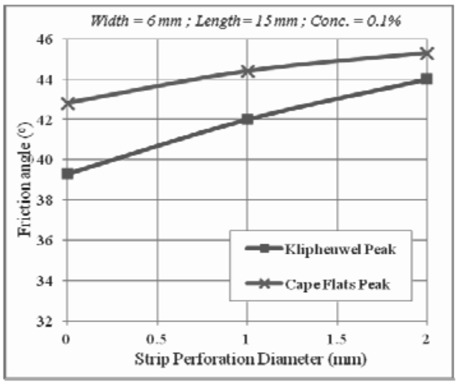

Figure 4b: Fiction angle vs. Perforation diameter

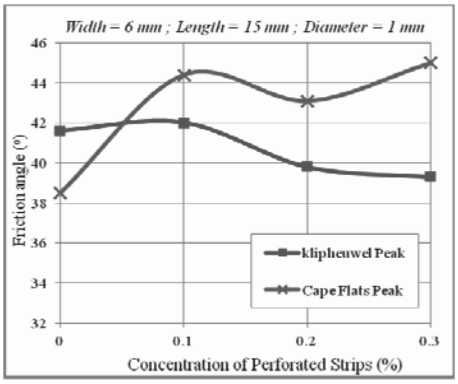

Figure 4c: Friction angle vs. Perforated strip concentration

3.2 *Perforated Strips*

Introducing perforations on the strips achieved higher friction angles with additional increases of 3.5% and 18.0% on inclusion of the perforated strips in Klipheuwel and Cape Flats sand respectively. This was represented by improvements from 41.6^o to 44^o for Klipheuwel sand and 38.5^o to 45.3^o for the Cape Flats sand (Figure 4a). The effect of varying the length of the perforated plastic strips was more significant in Cape Flats sand. Addition of the reinforcement generally had a bigger impact as regards improvement of the shear strength parameters for the more round shaped Cape Flats sand than for angular shaped Klipheuwel grains. This indicates an inherent requirement for reinforcement of the more poorly graded Cape Flats sand so as to enhance its strength properties.

Varying the strip perforation diameter provided an increase of up to 14.7% in Klipheuwel sand compared to using solid strips and for Cape flats sand a further increase of 8.5% was recorded (Figure 4b). This result indicated increases of 2^o for every additional mm in perforation diameter.

The improvement in friction angle with perforation diameter may be attributed to interaction between the soil and the plastic in the composite as well as better bonding and interlocking between the soil particles through the perforations in the plastic strips.

An increase in the peak friction angle from 38.5^o to 44.5^o for Cape Flats sand was obtained when perforated plastic strips were added to the soil at a 0.1% concentration as shown in Figure 4c. A concentration of 0.2% resulted in a slight decrease and a further increase in concentration to 0.3% provided a higher friction angle of 45.0^o. The pattern in Klipheuwel composites however indicated that addition of the perforated strips at a 0.1% concentration caused a slight improvement in friction angle but a decrease was observed for concentrations of 0.2% and 0.3%. This demonstrates that the influence of strip concentration could be soil specific due to the difference in soil properties like particle shape and size. Different soils would therefore require specific testing to determine the parameters particular to the soil type in order to obtain an optimal increase in the shear strength parameters on inclusion of the plastic strips.

3.3 *Deformation of Strips during Shear*

The plastic strips used in the composite specimen for the direct shear tests were assessed for physical deformations such as dents or rupture at the end of each experiment. The nature of deformations of the plastic strips was examined with respect to their location in the shear box. Visual inspections revealed that most of the elements that deformed were within or close to the shearing zone. The indentations on some of the strips may have been caused by soil particles as they pressed in to form surface attachments with the plastic strips (Figure 5a). This was mainly due to the particle shape and grading of the sandy soils used in the study that enhanced the frictional bonding between the soil and the plastic material. Other strips in the specimens were stretched and compressed due to the shearing action at or near the shear plane (Figure 5b). The stretched strips were located parallel to the shearing direction. This indicated that as the plastic strips were strained relative to the shearing direction, they improved the soil tensile strength by enabling transfer of forces arising from the loading conditions. None of the reinforcements in the composite were severely indented or ruptured during the shearing since the tensile strength of the plastic strips was greater than 15MPa compared to the generated shear forces in the test specimen under for a maximum applied normal stress of 100kPa.

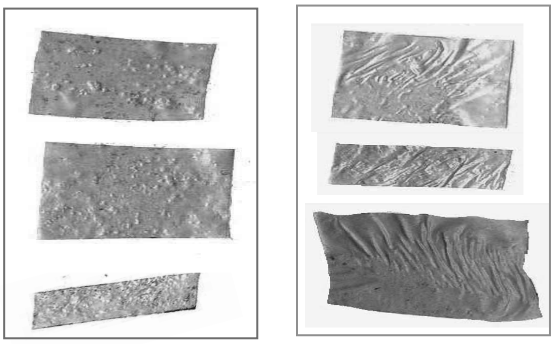

Figure 5 a): Dented Strips b) Stretched and Compressed Strips

4 CONCLUSION

A comprehensive laboratory direct shear testing programme was undertaken on composite specimens of sandy soils mixed with random inclusions of plastic strips obtained from high density polyethylene shopping bags. Two locally sourced soils, Klipheuwel and Cape Flats sands were selected for the research and the influence of plastic strips on the shear strength parameters of the sandy soils were studied. The effect of introducing perforations on the plastic strips was further examined. Parameters of the plastic strip inclusions such as length, width, concentration and diameter of perforations were varied to investigate the effect on the peak friction angle. The plastic strip lengths used in the study were 15 mm, 30 mm and 45 mm, strip widths 6 mm, 12 mm, 18 mm and perforation diameters of 1 mm and 2 mm made on the 6mm wide strips. The strips were added to the soil samples at concentrations of 0.1%, 0.2% and 0.3% by weight.

Results indicate an improvement in peak friction angle on addition of the solid strips and perforated strips of varied lengths and concentrations for the both sands. For the scope of experiments conducted, maximum values for the peak friction angles were obtained for strips of length 30 mm, concentration 0.1% and perforation diameter of 2 mm. Addition of perforations on the strips resulted in a further enhancement of the friction angle as compared to results obtained using specimens prepared with solid strips. An increase in the diameter of perforations resulted in higher values of friction angle at an average of 2^o for each mm in perforation diameter.

The laboratory results presented in the study favourably suggest the possibility of utilizing plastic material as tensile inclusions in sandy soil to increase the resistance to shear. As demonstrated in Chebet et al. 2012, the plastic inclusions can also improve the load bearing capacity and settlement characteristics of the sand. Additionally, introduction of perforations on the plastic material further aids in the interaction between the soil and plastic thereby boosting the soil's strength properties. However, a better understanding of the interaction mechanism in soils reinforced with the plastic material would be essential to properly document the engineering behaviour of the soil-plastic composite.

The influence of the soil physical properties, plastic properties and scale effects would need to be further investigated through more comprehensive testing in a wider range of stresses using larger scale tests to eliminate boundary effects. This could in turn contribute in the development of design methodologies for projects that may opt to incorporate this type of reinforcement material resulting in a reduction in project costs. Furthermore, successful application in the field could permit a reduction of plastic waste disposed of to landfills bringing along environmental benefits as a result of more efficient use of natural resources and reduction of CO_2 emissions.

5 REFERENCES

Andrady A. L. and Neal M. A. 2009. Applications and societal benefits of plastics. Philosophical Transactions of the Royal Society, B, 364: 1977 - 1984.

Azapagic A., Emsley A. And Hamerton L. 2003. Polymers, the Environment and sustainable sevelopment. John Wiley & Sons Ltd.

Barnes D. K. A., Galgani F., Thompson, R. C. And Barlaz M. 2009. Accumulation and fragmentation of plastic debris in global environments. Philosophical Transactions of the Royal Society, B, 364: 1985–1998.

Chebet F.C., Kalumba D. and Avutia D. 2012. Investigating the effect of plastic shopping bag waste material on load bearing capacity of foundation soils in civil engineering. Proceedings of the 21st WasteCon Conference and Exhibition, East London, South Africa, 376-383.

Chen X., Xi F., Geng Y. and Fujita T. 2011. The potential environmental gains from recycling waste plastics: Simulation of transferring recycling and recovery technologies to Shenyang, China. Waste Management (31) 168–179.

Consoli N. C., Casagrande M. D. T. and Coop M. R. 2007. Performance of a fiber reinforced sand at large shear strains, Geotechnique 57 (9), 751–756.

Falorca I. M. C. F. G. and Pinto M. I. M. 2011. Effect of short, randomly distributed polypropylene microfibers on shear strength behaviour of soils. Geosynthetics International 18 (1), 2–11.

Gregory G. H. and Chill D. S. 1998. Stabilization of earth slopes with fiber reinforcement. Proceedings of the Sixth International Conference on Geosynthetics, Atlanta, Georgia, USA.

Ibraim E. and Fourmont S. 2006. Behaviour of sand reinforced with fibres. Geotechnical Symposium on Soil Stress-Strain Behavior: Measurement, Modeling and Analysis, Roma, 807–818.

Maher M. H. and Ho Y. C. 1994. Mechanical properties of kaolinite fibre soil composite. ASCE Journal of Geotechnical Engineering 120 (8), 1381–1393.

Miller C.J. and Rifai S. 2004. Fiber reinforcement for waste containment soil liners. Journal of Environmental Engineering 130(8), 891-895.

Nhamo, G. 2008. Regulating Plastics Waste, Stakeholder Engagement and Sustainability Challenges in South Africa. Springer Science, Urban Forum 19: 83–101.

Santoni R. L., Tingle J. S. and Webster S. L. 2001. Engineering Properties of Sand-Fibre Mixtures for Road Construction, Journal of Geotechnical Engineering, ASCE 127 (3), 258–268.

Thompson, R. C., Moore, C. J., vom Saal, F. S. and Swan, S.H. 2009. Plastics, the Environment and Human Health: Current Consensus and Future Trends. Philosophical Transactions of the Royal Society B, 364: 2153–2166.

Zornberg J. G. 2002. Discrete framework for limit equilibrium analysis of fiber reinforced soil. Géotechnique 52 (8), 593–604.

Effect of dredge soil on the strength development of air-foam treated lightweight soil

Effets des sols de dragage sur le développement de la résistance des sols mélangés à de l'air

Kataoka S.
Hakodate National College of Technology, Hakodate, Japan

Horita T.
Kobe University, Kobe, Japan

Tanaka M.
Port and Airport Research Institute, Yokosuka, Japan

Tomita R., Nakajima M.
Koa Kaihatsu Corporation, Chiba, Japan

ABSTRACT: In this study, the unconfined compression strength, q_u, and the elastic shear modulus, G, from bender element test, were in detail examined in the laboratory by using the air-foam treated lightweight soil samples made from several kinds of soil. From the results of these tests, the values of the q_u and the G with curing period were different to the kinds of soils into the air-foam treated lightweight soil samples. In addition, it was found that the development of the q_u and the G were related to the increase / growth of the ettringite produced at the time of the reaction of hydration of the concrete. On the other hands, it has been shown that the relations between the q_u and the G are nearly proportional, and that this tendency remains always the same, whatever is the type of soil.

RÉSUMÉ : Dans cette étude, la résistance en compression simple, q_u, avec le module d'élasticité de cisaillement, G, du critère de l'élément bender, était en détail examinés en laboratoire à l'aide de l'air sous forme d'échantillons de sol traités légers fabriqués à partir de plusieurs types de sols. A partir des résultats de ces tests, les valeurs de la q_u et le G avec période de cure étaient différents des types de sols dans l'air sous forme d'échantillons de sol traité légers. En outre, il a été constaté que le développement de la q_u et le G sont liés à l'augmentation / la croissance de l'ettringite produite au moment de la réaction d'hydratation du béton. Dans le cas contraire, il a été montré que les relations entre la q_u et le G sont presque proportionnelle, et que cette tendance reste toujours le même, quel que soit le type de sol.

KEYWORDS: air-form treated lightweight soil, unconfined compression strength, elastic shear modulus.

1 INTRODUCTION

Air-foam treated lightweight soil is a ground material prepared by adding and mixing in a cement-type stabilizing agent and air foam made by a surfactant or animal-protein foaming agent to a source soil such as dredged soil and surplus construction soil. In recent years, there has been an increase in the number of construction projects using air-foam treated lightweight soil for the purpose of reducing earth pressure and containing land subsidence. This new type of ground material for harbor and airport construction that offers added value such as light weight, safety, and recyclability is called Super Geo-Material (SGM) (e.g. Thuchida et al. 1996).

When SGM is employed for a construction site, the required strength of the mix proportion is obtained by multiplying the design strength by an overdesign factor, and a mix proportion test is conducted in advance to determine the amount of stabilizing agent and air foam to be added to the source soil of which the moisture content has been adjusted with water. In some cases where the physical properties of the source soil are expected to vary from one sampling location to another, a mix proportion test is conducted in advance for each representative sampling location to adjust the amount of additives. Naturally, some variations are found in the strength of the soil samples (Nagatome et al. 2010). In fact, when the unconfined compression test and the bender element (BE) test were conducted on a large number of SGM samples taken from the same construction site and to which an equal amount of the stabilizing agent had been added, the unconfined compressive strength, q_u, varied from one sample location of the source dredged soil to another, albeit within the expected range of the design. It was confirmed that there is a high correlation between the shear wave velocity, V_s (or shear modulus, G) and q_u (Kataoka et al. 2011).

This study focused on the properties of the source soil within SGM. Six different types of source soil were used to prepare SGM in a room environment. The unconfined compression test and the BE test were conducted to examine the impact of curing time on the strength and stiffness of the soil. In addition, the microscopic structure of the specimens was observed using a Scanning Electron Microscope (SEM) in order to visually examine how the internal structure of SGM changed with the curing time.

2 SAMPLE PREPARATION AND TESTS PERFORMED

Table 1 shows the physical properties of the source soils used to prepare the SGM specimens. Six types of source soil were used: two types of dredged soil taken from the construction site of the Tokyo International Airport expansion project, one from the area where the odor of what was suspected to be hydrogen sulfide, biological decay and the like (hereafter "Tokyo Bay A") was relatively weak and the other from the area where the same odor was very strong (hereafter "Tokyo Bay B"); dredged soil taken from Kobe Port (hereafter "Kobe"); surface soil taken from a few meters below the seabed of the Sea of Okhotsk (hereafter "Okhotsk"); Kasaoka Clay; and Kuni-bond. The latter two are commercially available products. When liquid limit, w_L, a criterion used for the mix proportion design, was examined, the six types of source soil could be categorized as follows: Tokyo Bay A and B and Kobe, which had an approximately equal level of liquid limit; Kuni-bond, which had a higher w_L than the aforementioned three types; and Okhotsk Seabed Sediment and Kasaoka Clay, which had a lower w_L. While there were almost no differences between Tokyo Bay A and B in physical properties such as w_L and grain size composition, a major difference was observed in the pH level of pore water.

To prepare SGM specimens, seawater taken from Hakodate was used as the mixing water, blast furnace cement B as the stabilizing agent, and air foam (with a density of 0.05g/cm^3) prepared with hydrolyzed animal protein using the pre-foaming method as the foaming agent. These ingredients were then mixed with each of the source soils that had been passed through a sieve of 425μm and the resulting mixtures were put into plastic molds with a 5cm diameter and a 10cm height. With the top sealed by a plastic wrap, the mixtures were then cured in the air until the prescribed curing ages were attained. Table 2 shows the flow values of the specimens after the water content, w, of the source soils used to prepare the SGM specimens for this study was adjusted by sea water (hereafter "Adjusted Soil") and after the stabilizing agent and the air foam were mixed in. The required wet density and the amount of stabilizing agent added were respectively kept constant at ρ_t=1.1 g/cm^3 and 75 kg/m^3, with the water content ratio of the Adjusted Soil at 285%, equivalent to 2.5 w_L of Tokyo Bay A and B. While Tokyo Bay A, B and Kobe had similar w_L values, the flow value of Tokyo Bay B was slightly higher than those of the other two after the stabilizing agent was added to the specimens. In addition, the water content ratio of 285% was approximately five times higher than the already low w_L of Kasaoka Clay, causing its flow ability to rise. As a result, its flow value after the stabilizing agent was added exceeded the size of the acrylic plate (of 66 cm per side), which was used for the flow value measurement.

The SGM was taken out of two cylinders per specimen on each of the prescribed curing days to conduct the unconfined compression test and the BE test. In the BE test, bender elements were inserted in pairs at both vertical and horizontal ends, and the shear wave velocity was measured in both vertical and horizontal directions against the soil (V_{vh} , V_{hh}). From these values and the wet density of the specimens, ρ_t, the elastic shearing modulus ($G_{vh}=\rho_t \times V_{vh}^2$, $G_{hh}=\rho_t \times V_{hh}^2$) was obtained. An internal observation of the SGM specimens was made using an SEM on each of the prescribed curing days to examine the correlation between the strength development and the microscopic structure.

3 RESULTS AND DISCUSSIONS

3.1 *Strength and Shear modules of the SGM specimens*

Figure 1 shows the changes to the q_u and G_{vh} levels of the prepared specimens with the elapse of curing days. From the results, q_u and G_{vh} of all specimens showed a linear increase in the semi-log graph. However, a substantial degree of variability was observed from one source soil to another in the soil strength measured on the same curing day even though the mixing conditions, such as the cement quantity per unit volume and the w of the Adjusted Soil were identical. In particular, among the three types of dredged soil (Tokyo Bay A , Tokyo Bay B and Kobe) that shared almost identical physical properties such as w_L, the q_u level of Tokyo Bay B was much lower than the other two. It is suspected that the composition of the pore water was suppressing the strength development of Tokyo Bay B, given that its pH level was lower than those of the other two specimens. On the other hands, the w_L levels of Okhotsk and Kasaoka Clay were lower than those of the aforementioned three types of dredged soil. While Okhotsk showed large q_u and G_{vh} values, comparable to those of Tokyo Bay A, Kasaoka Clay had very low q_u and G_{vh} values, similar to those of Tokyo Bay B. The factors causing the large q_u and G_{vh} values of Okhotsk are suspected to be the large volume of silt in the soil. The small q_u and G_{vh} values of Kasaoka Clay are believed to be caused by the material separation that occurred after the cement and air foam were mixed in because of the high w ratio of the Adjusted Soil of 285 %, about 5 times greater than its w_L. The decrease in the strength of Kasaoka Clay is also likely to have resulted from its clay mineral components since the pore water composition

Table 1. Sample preparation

samples	Tokyo Bay A	Tokyo Bay B	Kobe	Okhotsk	Kasaoka Clay	Kuni-bond
ρ_s (g/cm^3)	2.62	2.70	2.64	2.56	2.71	2.70
w_L (%)	114.7	112.4	108.2	85.6	55.4	133.1
L_i (%)	10.4	11.5	9.7	7.2	8.2	7.8
pH	7.7	3.4	7.9	7.6	7.5	-
Grain size distribution (%)						
Sand	2	8	0	6	7	6
Silt	27	21	31	47	33	65
Clay (2~5μm)	38	32	33	23	16	16
Clay (~2μm)	33	39	36	24	44	12
clay mineral	Qtz Pl Ill Chl Sme	Qtz Pl Gp Ill Chl Kln	Qtz Pl Ill Chl Sme	Qtz Pl Ill Chl Sme	Qtz Pl Ill Sme Kln	Qtz Pl Sme

Table 2. Water contents and flow values of the SGM specimens

samples	Tokyo Bay A	Tokyo Bay B	Kobe	Okhotsk	Kasaoka Clay	Kuni-bond
w (%)	285 (2.5w_L)	285 (2.5w_L)	285 (2.6w_L)	285 (3.3w_L)	285 (5.1w_L)	285 (2.1w_L)
Frow value (cm)						
Adjusted soil	47.5	58.0	49.0	64.0	66.0 ~*	57.0
SGM	19.0	27.5	21.0	36.0	66.0 ~*	39.0

* : 66.0 ~ shows 66.0 over

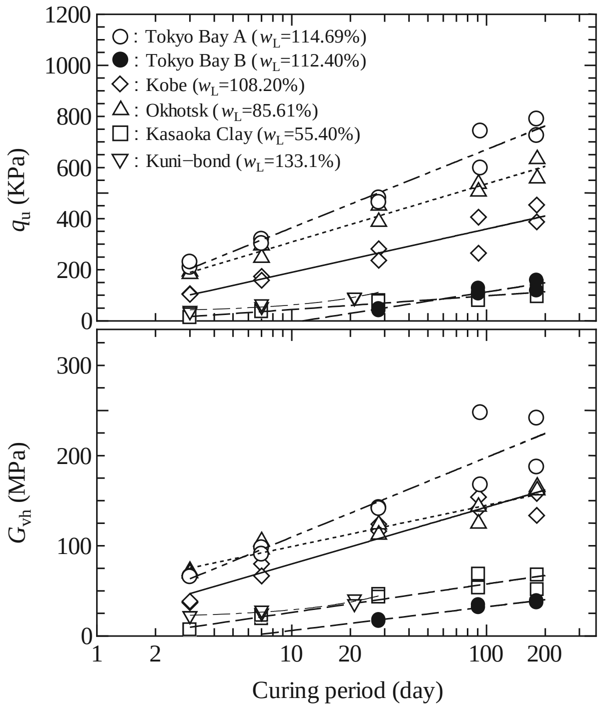

Figure 1. Variation of q_u and G_{vh} with the curing periods

probably did not play a role, as it likely did for Tokyo Bay B.

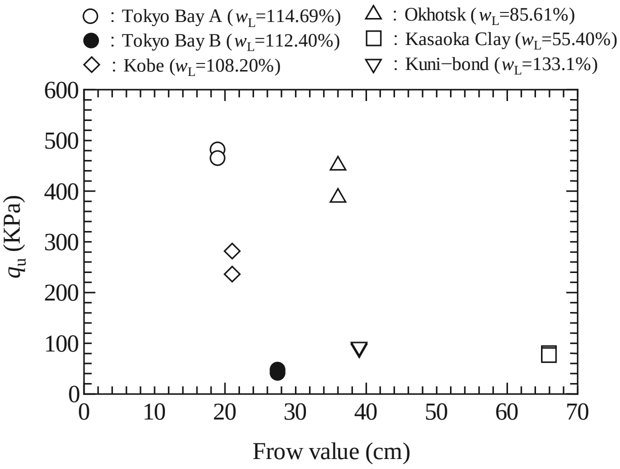

Figure 2. Relationship between flow values of the SGM and q_u (curing period of 28 day)

Figure 2 shows the relationship between the flow values of the SGM specimens and q_u on the curing period of 28 day. While it was believed that there is some relationship between flow values and soil strength, the lower q_u value of Tokyo Bay B than that of other specimens suggests that there is some relationship between the strength and the low pH level of Tokyo Bay B.

Figure 3 shows the relationship between G_{vh} and q_u. It is evident from the graph that there is a strong correlation between G_{vh} and q_u obtained from all the SGM specimens, with an approximately linear relationship between the two variables in each one of them. A previous study showed there is a linear relationship between q_u and Young's modulus in the small strain range of cement-treated sand, while another study demonstrated that there is a linear relationship, as it was found in this study, between the elastic shear modulus and the stiffness of cement-treated soil where cohesive soil was used as the source soil (Shibuya et al. 2001, Seng and Tanaka 2011). Based on these results, the relationship obtained in this study is believed to be a characteristic common to cement-treated soil. While changes to G_{vh} and q_u with the increase of curing days varied greatly from one soil type to another, it was confirmed that the relationship between the variables fell within a certain range, regardless of the type of source soil used. From this it can be concluded that in air-foam treated lightweight soils, where the amount of cement additive and the required ρ_t are approximately the same, the relationship between G_{vh} and q_u is approximately the same, regardless of the type of source soil.

Figure 4 shows the relationship between G_{vh} and G_{hh} obtained from the shear wave velocity propagating in horizontal and vertical directions. The slope is virtually uniform, regardless of the number of curing days and the soil type. However, the slope is smaller than that of natural clay deposits compacted to K_0 (Kawaguchi et al. 2008). Thus, a relatively uniform distribution of nearly spherical air foam inside SGM (Watabe et al. 2004) and a relatively loose (random) state in which the source soil has stabilized are believed to have made SGM an isotropic material in terms of stiffness.

3.2 *Micro structure observation of the SGM specimen*

The microscopic structure of SGM was observed using the SEM in order to examine the factors affecting the strength development of the SGM specimens from the changes to the internal structure with the passage of curing time.

Photos 1 show the internal structures of Tokyo Bay A, on the curing period of 3 (1a) and 182 days (1b), and Tokyo Bay B, on the curing period of 28 (2a) and 182 days (2b). It is observed

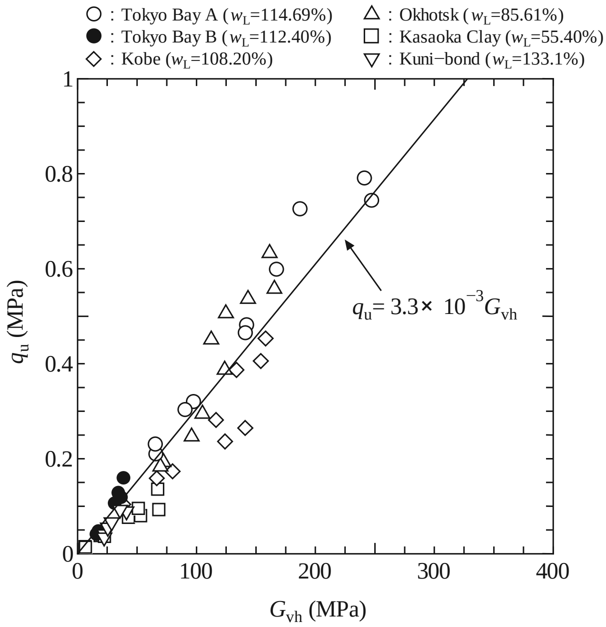

Figure 3. Relationship between G_{vh} and q_u

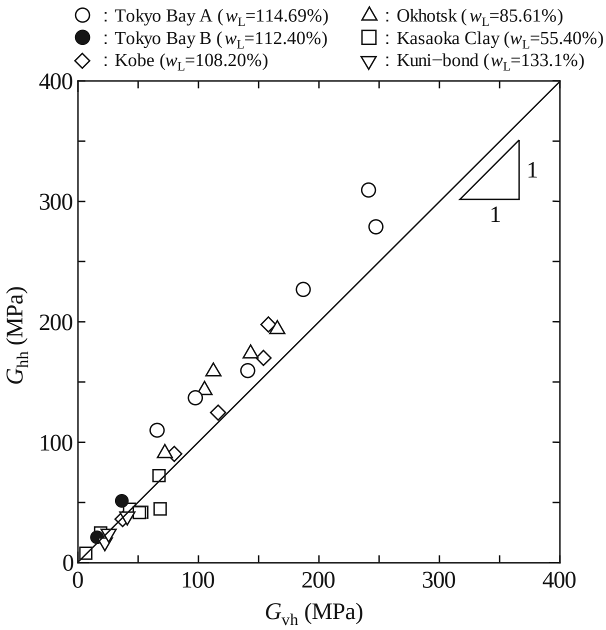

Figure 4. Relationship between G_{vh} and G_{hh}

that on the Tokyo Bay A, needle-like ettringite crystals were formed by the hydration process of the cement on the curing period of 3 day (see 1a), which was characterized by a higher level of strength. The photos also show how the needle-like crystals spread throughout the entire specimen by the 182 day (see 1b) and filled the void space. In the other hands, the ettringite in Tokyo Bay B were observed on the 28 and 182 day (see 2a, b), more void space was observed in the specimen's inner structure and the bonding of crystals did not seem very prevalent. The evidence raises the possibility that the formation, growth, and bonding of ettringite crystals play a major role in the development of the strength and stiffness of SGM.

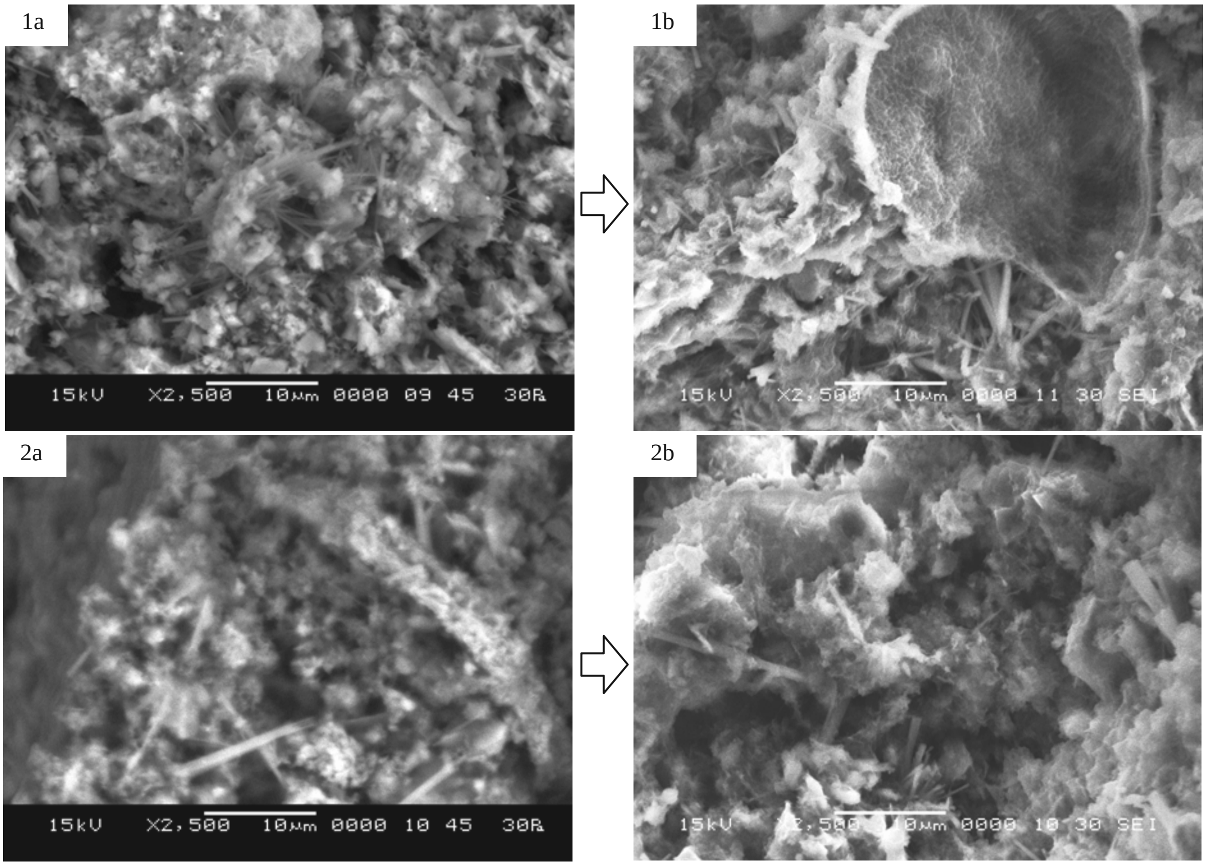

Photo 1. SEM observation of the Tokyo Bay A and B. Curing period of the Tokyo Bay A are 3 (1a) and 182 (1b) days, and curing period of the Tokyo Bay B are 28 (2a) and 182 (2b) days.

4 CONCLUSIONS

In this study the unconfined compression test, the BE test, and observations of the internal structure using an SEM were conducted on SGM specimens prepared with six different types of source soil to examine how different source soils would impact the strength development of SGM. The findings are summarized as follows:

- It was inferred that while the strength and stiffness of the SGM specimens increased with the elapse of curing days, there is a very large variation in their actual levels due to the mineral components and the constituents of pore water contained in the source soil used. In addition, it became clear that the SGM strength cannot be estimated from the flow values of the specimens.
- In SGMs with an approximately equal amount of cement additive and comparable target wet density, the strength and stiffness have a linear relationship as is the case in other cement-treated soil, and their slopes are approximately the same regardless of the soil type.
- The slope obtained from G_{hh} and G_{vh} is characterized by an approximately 1:1 relationship, showing that the air foam in the specimens makes SGM a very isotropic material in terms of stiffness.
- The observations of the internal structure of SGM using the SEM on the predetermined curing days suggested the possibility that the increase, growth, and bonding of needle-like ettringite crystals, formed by the hydration process of the cement, were a major factor contributing to the development of the strength and stiffness of the SGM specimens.

5 ACKNOWLEDGEMENTS

The authors thank Prof. Satoru Shibuya, Kobe University, Japan and Prof. Satoshi Yamashita, Kitami Institute of Technology, Japan for help to prepare the soil samples.

6 REFERENCES

Kataoka, S., Kawaguchi, T., Horita, T., Tanaka, M., Sakaiya, T. and Shibuya, S. 2011. Unconfined compression strength and elastic shear modulus of air-form treated lightweight soil. *Proc. of the 5th International Symposium on Deformation Characteristics of Geomaterials,* 2, 682-686.

Kawaguchi, T., Yamashita, S., Kataoka, S., Shibuya, S. and Kawajiri, S. 2008. Inherent and induced anisotropy of three natural sedimentary clays reflecting on the elastic shear modulus. *Proc. of the 4th International Symposium on Deformation Characteristics of Geomaterials,* 1, 575-579.

Nagatome, T., Mitarai, Y., Yamatoya, R., Kotou, T. and Noguchi, T. 2010. Unprecedented large scale of rapidly construction work of light weight soil with air form for Haneda D-runway Construction Project (Part 1: Validation of field mixing condition). *The 45th Annual Conference of JGS,* 2093-2094. (in Japanese)

Seng, S. and Tanaka, H. 2008. Properties of cement-treated soils during initial curing stages. *Soils and Foundations,* 51 (5), 575-579.

Sibuya, S. Mitachi, T. and Ozawa, H. 2001. Time/stress-history dependency of deformation-strength characteristics of cement-mixed sand. *Journal of JSCE,* 687 (III-56), 249-257. (in Japanese)

Tuchida, T., Okumura, T., Takeuchi, D. and Kishida, T. 1996. Development of light-weight fill from dredging. *Proc. of the 2nd International Congress on Environmental Geotechnics,* 1, 415-420.

Watabe, Y., Itou, Y., Kang, M.S. and Tuchida, T. 2004. One-dimensional compression of air-form treated lightweight geo-material in microscopic point of view. *Soils and Foundations,* 44 (6), 53-67.

Application of a Method to Accelerate Granulated Blast Furnace Slag Solidification

Une méthode de solidification accélérée des granulats issus de laitier de haut fourneau

Kikuchi Y.
Department of Civil Engineering, Tokyo University of Science, Noda, Japan

Mizutani T.
Geotechnical Engineering Field, Port & Airport Research Institute, Yokosuka, Japan

ABSTRACT: On-site observations indicate that granulated blast furnace slag (GBFS) solidifies over time, but the entire mass solidifies quite slowly. This means that if GBFS is to be relied upon to be solid, it must be treated in order to accelerate the solidification process. Adding blast furnace slag in micro powder form to GBFS effectively speeds GBFS solidification in seawater. To improve the material's resistance to separation, we recommend Prior Homogeneous Mixing Treatment (PHMT), which reduces the amount of separation of the material during pouring but does not interfere with the speed of the mixture's accelerated solidification. PHMT-treated GBFS tends to solidify better when inundated in seawater than in fresh water. It is strong enough to protect against liquefaction if it remains in seawater for about two months.

RÉSUMÉ : les observations in-situ indiquent que les granulats issus de laitier de haut fourneau (GLHF) se solidifient dans le temps, avec néanmoins une vitesse de prise assez lente. L'utilisation de GLHF solidifiés implique donc que ces derniers fassent l'objet d'un traitement afin d'accélérer ce processus de prise. L'ajout sous forme de poudre fine issue de laitiers accélère de manière efficace cette solidification sous l'eau. Afin de limiter la ségrégation, il est recommandé d'effectuer au préalable un mélange homogène avec la poudre. Cela réduit la ségrégation entre les matériaux durant le déversement du mélange tout en n'influençant pas l'augmentation de la vitesse de prise. Les GLHF traités avec de la poudre de laitier tendent après un mélange homogène à se solidifier de manière plus efficace lorsqu'il sont plongés dans de l'eau de mer plutôt que dans de l'eau douce. Ce mélange a alors assez de résistance pour résister à la liquéfaction si celui-ci reste immergé dans l'eau de mer plus d'une année et demi.

KEYWORDS: granulated blast furnace slag, solidification, backfill, quay wall

1 INTRODUCTION

Granulated blast furnace slag (GBFS) solidifies when it reacts with water. This property is known as latent hydraulicity. However, this characteristic of GBFS was ignored in the Japanese handbook for port construction engineers published in 1989 (CDIT, 1989) due to the lack of adequate information on the solidification of GBFS used in port construction. If used as a self-solidifying material, GBFS holds great promise for use in protecting against liquefaction and for earth pressure reduction.

Most GBFS used to backfill quay walls does solidify, but a post-construction follow-up survey showed that GBFS solidification is a lengthy process, it never solidifies uniformly, and some may remain unsolidified (Kikuchi et al. 2005). As a result, some treatment is necessary before GBFS can be used as a self-hardening material.

In this study, we examine a method to accelerate the solidification of GBFS and propose a practical way to apply that method.

2 PREVIOUS RESEARCH

GBFS is vitreous, and the silicate SiO_4 it contains is in an unstable condition compared with crystalline material (NSA 1980). GBFS has high chemical reactivity and therefore solidifies in the presence of water and under high pH conditions where the pH exceeds 11.

Nishi et al. (1982) concluded that the latent hydraulicity of GBFS is high in highly alkaline water but low in seawater, which has a pH of about 8.

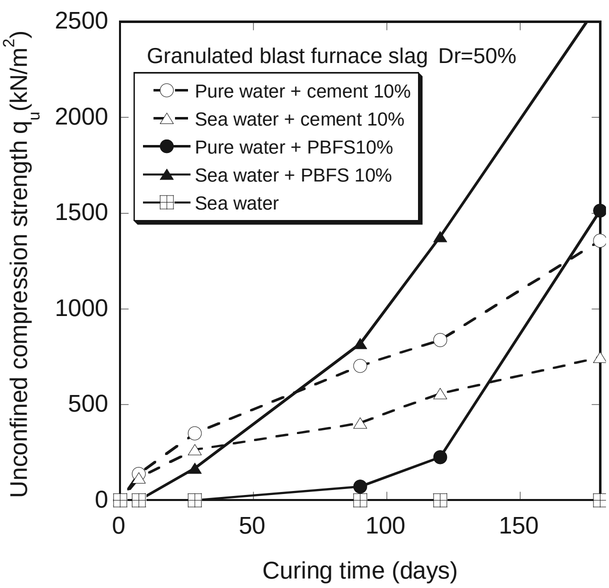

Figure 1. Acceleration of solidification achieved by mixing cement or PBFS with GBFS and by varying pore water type.

These facts suggest that solidifying GBFS in seawater is difficult because seawater acts as buffer solution with a very high buffering capacity (Christian 1986), and adjusting the pH of seawater is impractical.

A site investigation of GBFS placed as backfill 6-12 years previously showed that most of the GBFS had solidified, but its strength varied greatly (Kikuchi et al. 2006).

Kikuchi et al. (2011) tested various combinations of pore water and additives, attempting to speed GBFS solidification.

Figure 1 shows part of their results. Seawater and fresh water were tested with Portland cement and powdered blast furnace slag (PBFS) as additives. When fresh water was used, cement was more effective than PBFS in solidifying GBFS. But when seawater was used, PBFS was more effective than cement. Using seawater and PBFS was the most effective combination.

3 ISSUES REGARDING APPLYING THE GBFS SOLIDIFICATION ACCELERATION METHOD IN THE FIELD

There are several issues to consider when determining the most appropriate mixture of GBFS and PBFS for accelerating GBFS solidification: (1) the material can separate during construction, (2) it may separate after construction because of water flow (3) separation of the mixture is likely to affect how the GBFS solidifies, (4) the flow of pore water can affect solidification, and (5) GBFS may solidify differently when the pore water changes from sea water to fresh water (Kikuchi et al. 2010).

In the present study, we examine issues (1) to (5). First, we present experimental results regarding issues (2), (3), and (4). We then explain a way to prevent issue (1), and finally consider issue (5).

3.1 *Possibility of material separation after construction*

The physical properties of the GBFS used were ρ_s = 2.845 g/cm^3, ρ_{dmin}= 1.175 g/cm^3, ρ_{dmax}= 1.508 g/cm^3, D_{15} = 0.28 mm, and D_{50} = 0.38 mm. The physical properties of the PBFS used were ρ_s = 2.890 g/cm^3, with 5000 to 7000 cm^2/g of specific surface area. Artificial seawater was used as pore water.

The diameter of the PBFS was about 4 μm assuming spherical particles with no small holes. Thus, the GBFS and PBFS may separate when the mixture is poured onto the seabed. The ratio of D_{15} for GBFS to D_{85} for PBFS is more than 50. This ratio is an indicator of the possibility of material separation due to water flow through the material (Ishihara 2001).

We conducted experiments on the separation of the PBFS from the mixture. In this series of experiments, specimens with two layers were prepared. The lower layer of the specimen was a mixture of GBFS with 20% PBFS by weight. The upper layer was only GBFS. The relative density of each layer was 50%.

Water flowed from the bottom of the specimen with a hydraulic gradient of from 10 to 40. This test was conducted in a triaxial apparatus at a confining pressure of 50 kN/m^2 to prevent boiling. The outlet velocity of the water at a hydraulic gradient of 40 was 120 m/day. The total outlet water volume from the specimen was 6 times the void volume of the specimen.

Figure 2 shows close-up X-ray CT images of the boundary between the layers of the specimen, where the contrast reflects the density of the material. Comparing the images before and after water flow, small differences can be observed. This means that although there may be a little separation when the peak velocity of the water flow is 120 m/day, complete separation of the material does not occur under these conditions.

In practice, the water flow velocity in GBFS used as backfill for gravity quay walls is around several m/day. Thus, GBFS and PBFS will never separate after construction.

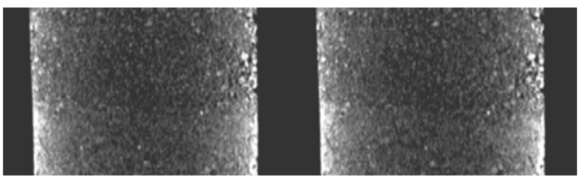

Before water flow After water flow of 120m/day
Figure 2. Close-up X-ray CT images at mid-height of the specimen.

3.2 *Solidification of GBFS after material separation*

The effect of material separation on the solidification characteristics of the material is examined in this section.

The GBFS and PBFS used here were the same as those used in section 3.1. The relative densities of the specimens were 50%. The pore water used was artificial sea water. In each specimen, 7.5% PBFS by weight was added to the GBFS. We tested four experimental mixing regimes: (1) GBFS and PBFS were mixed homogeneously (HMT), (2) PBFS was mixed with GBFS, then artificial sea water was added to achieve a 10% water content ratio and the mixture was cured in air for a week (prior homogeneous mixing treatment or PHMT), (3) One PBFS layer was sandwiched between two layers of GBFS, and (4) Two PBFS layers were sandwiched between three GBFS layers.

Each specimen was saturated with artificial sea water and sealed, then cured for a designated period at a constant temperature of 20 degrees centigrade. Each specimen's unconfined compression strength was measured after the designated curing period.

Figure 3 shows the relationship between the curing duration and unconfined strength. The unconfined compression strengths using HMT and PHMT exceeded 200 kN/m^2 after 14 days of curing. These strengths increased as the curing time lengthened. When the materials were separated, such as in cases (3) and (4), the unconfined compression strengths were very low. Figure 4 shows examples of the failure states for each case.

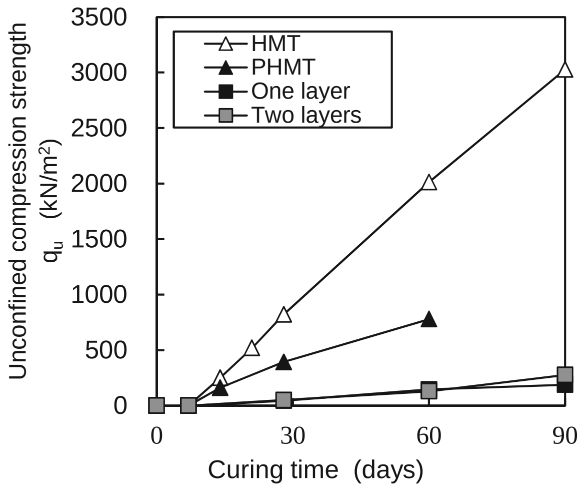

Figure 3. Change of unconfined compression strength with curing time.

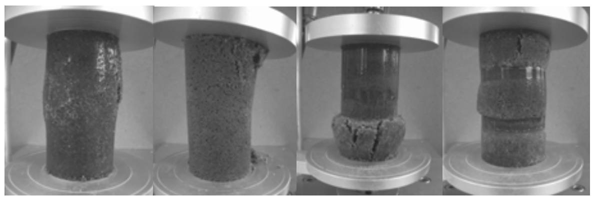

(a) HMT (b) PHMT (c) One layer (d) Two layers
Figure 4. Failure modes of specimens in each mixing regime

These results show the importance of thoroughly mixing the GBFS and PBFS in accelerating the solidification of the GBFS.

3.3 *Solidification of GBFS underground with flowing water*

In previous research, movement of pore water has been shown to prevent GBFS solidification (Kitayama 2003). In this section, we examine how pore water flow effects GBFS solidification. In this series of experiments, two water flow conditions and two mixing conditions were tested.

We used the same GBFS and PBFS as in section 3.1, and the HMT (1) and PHMT (2) mixing regimes from section 3.2.

In this series, sand boxes 30 cm wide, 30 cm long, and 50 cm high were fitted with a bulb for supplying water, located 3 cm from the bottom. Model ground 30 cm high was constructed of a mixture of GBFS and PBFS with 50% relative density. This was saturated with artificial sea water at the beginning of the test. Tests were run under static water and flowing water conditions. In the static water case, the pore water was never changed during the experiment. In the flowing water case, a volume of water equal to the volume of the voids in the ground was supplied slowly from the bottom of the ground once every three days. Curing continued for two months at a constant temperature of 20 degrees centigrade. After curing, the bearing strength distribution of the ground was measured using a soil hardness meter, and was converted to unconfined compression strengths.

The results show that the HMT-treated material subjected to static water conditions was the strongest. The material that had undergone HMT was weaker when cured in flowing water. However, for the PHMT-treated material, the opposite was true. With flowing water the PHMT material was stronger than the HMT material, meaning that PHMT has a higher potential to solidify GBFS than HMT under non-static water conditions.

3.4 *Improving resistance to separation during construction using PHMT*

For this series of experiments, we used GBFS with the following physical properties: ρ_s = 2.808 g/cm^3, ρ_{dmin}= 1.199 g/cm^3, and ρ_{dmax}= 1.562 g/cm^3. The median particle diameter (D_{50}) was 0.74 mm. The physical properties of the PBFS were ρ_s = 2.890 g/cm^3, with 5000 to 7000 cm^2/g of specific surface area. Artificial seawater was used as pore water.

As the GBFS and PBFS may separate when the mixture is poured onto the seabed, PHMT was used to counter this problem. With PHMT, some of the PBFS attaches to the GBFS granules, making the mixture more resistant to separation and decreasing the turbidity the mixture causes in water.

We mixed 10% seawater and 7.5% by weight of PBFS with GBFS and cured the mixture for a designated period in air. We measured the turbidity it caused after 0, 3, 7, 10, and 14 days of curing. In each test, about 0.460 N of the PHMT mixture was poured into 1000 ml of pure water and stirred well, then left to sit for 30 min. A turbidity meter was used for measurements.

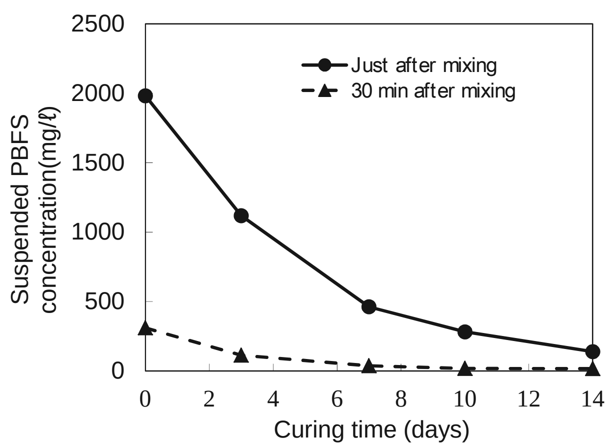

Figure 5. Change in suspended PBFS concentration with curing time.

Figure 5 shows how the suspended material concentration changed with curing time. The level just after mixing decreased to one-fourth of its initial value after 7 days of curing. The concentration 30 min after mixing became negligible after 7 days of curing.

A mixture of GBFS and PHMT is thus shown to be effective in reducing the amount of material separation during construction.

3.5 *Effects of changing from sea water to fresh water on the solidification of PHMT-treated GBFS*

Here, we address issue (5) described above. The follow-up survey about GBFS used as backfill noted in the introduction revealed that the pore water in the GBFS layer changed completely from seawater to fresh water over a period of 4 months (Kikuchi et al. 2005). This phenomenon occurs because the mean ground water level is higher than the mean sea level and rainfall supplies fresh water. Figure 1 shows that GBFS mixed with PBFS in seawater solidified in a month. With this in mind, we checked the effect of a pore water transition in a series of laboratory experiments.

Figure 6 shows how the experiment was set up. The box holding the sand was 800 mm long, 500 mm high, and 500 mm wide. We used PHMT cured for 7 days, made following the procedure described in section 3.2. The PHMT layer was made when wet and was covered by the sand layer. We used silica sand #4 (ρ_s = 2.644 g/cm^3, ρ_{dmin}= 1.342 g/cm^3, and ρ_{dmax}= 1.618 g/cm^3). The relative densities of the PHMT and sand were 50%. The water used to make the layers was artificial seawater, except for case 4 (Table 2.), in which fresh water was used. The shape of each layer is shown in Fig. 6. After making the model ground, 6 standpipes were installed at the positions marked No. 1, No. 2, and No. 3 to collect pore water. Two pipes were installed at each location to collect water from different depths. The open circles in Fig. 6 show the points where pore water was collected. Water was supplied as shown in the upper right part of the figure at a rate of 6 *l* per day. Effluent flowed from the bottom of the apparatus as shown in the figure. Since the void space in the model ground layer was about 84 *l*, the hydraulic retention time of the water in the apparatus was 14 days. Each experiment was conducted at 20 degrees centigrade. As the room was not perfectly temperature-controlled, its temperature was somewhat affected by the outside temperature.

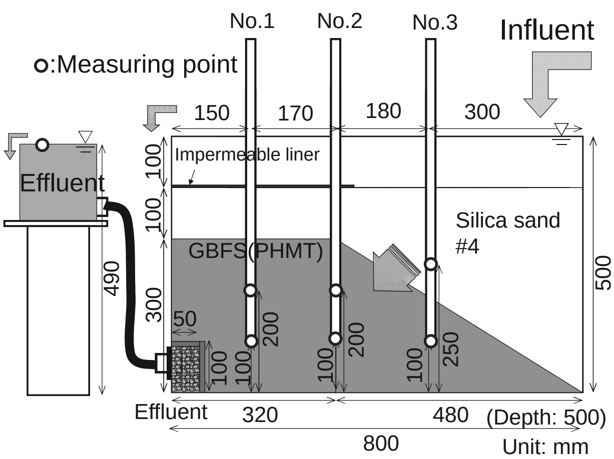

Figure 6. Experimental setup

During the experiment, pore water was collected from each point at designated times, and pH and salinity were measured. After 8 weeks, the strength of the PHMT-treated GBFS was measured with a Yamanaka soil hardness meter (Kikuchi et al. 2010). About 2000 strength measurements were made in each case. The data collected were converted to unconfined compression strengths using a relationship between strength and hardness determined before the experiment.

Table 1 shows the types of water supplied in each case.

Table 1. Experiment conditions

Case	Condition
Case 1	Sea water supplied for 8 weeks
Case 2	Sea water supplied for 6 weeks, then pure water supplied for 2 weeks

Case 3	Pure water supplied for 8 weeks
Case 4	Pure water used for making the model ground and Pure water supplied for 8 weeks

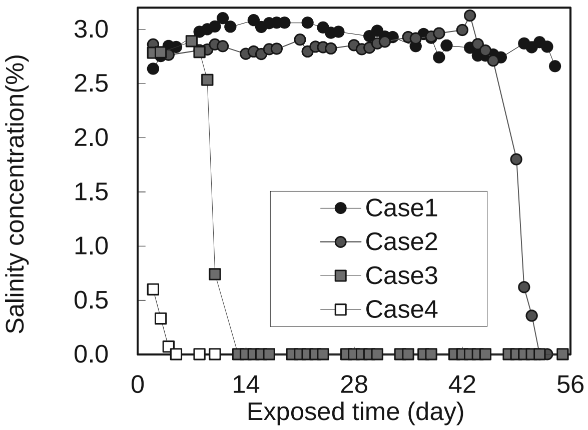

Figure 7. Change in salinity during the experiment (sampling location No. 1-100).

Figure 7 shows how the salinity changed during the experiments in standpipe No. 1, 100 mm from the bottom of the sand box. As shown in Table 1, fresh water was introduced starting at 42 days of exposure time in case 2. The salinity began to drop within about 1 week after the change and had almost vanished within 3 or 4 days after that point.

Figure 8 shows the converted unconfined compression strength distribution in each case. Table 2 shows the maximum and average strengths and the standard deviation for each case. The highest strength was observed in case 1, followed by cases 2 and 4, which were similar, and the lowest was in case 3. From these results, we see that about 2 months of curing time in seawater is important for accelerated solidification.

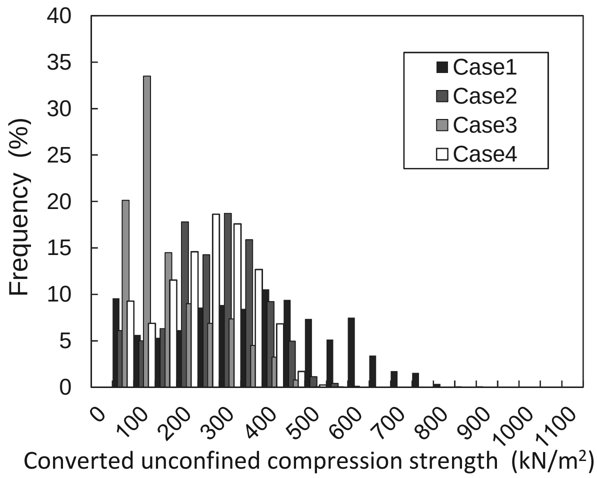

Figure 8. Distribution of converted unconfined compression strength.

An unconfined compression strength of more than 100 kN/m^2 is enough to prevent the liquefaction of sandy soil (Zen et al. 1990). The fractions of data below this level were 15%, 11%, 54%, and 16% in cases 1, 2, 3, and 4, respectively. This indicates that 80% of PHMT-treated GBFS cured in seawater for more than 2 months is strong enough to protect against liquefaction. This conclusion cannot be used to predict solidification levels in the field, but the results show that this technique can be used to accelerate the solidification of GBFS.

Finally, a series of permeability tests was conducted on solidified GBFS specimens in triaxial cells. After the permeability tests, the samples' unconfined compression strength was measured. These tests showed that the coefficient of permeability decreased with increasing strength. However, the coefficient of permeability was about 10^{-4} cm/sec even when the unconfined compression strength was about 1000 kN/m^2, indicating that the permeability of solidified PHMT-treated GBFS is about the same as that of ordinary sand.

Table 2. Converted unconfined compression strength (kN/m^2)

Case	Maximum	Average	Standard deviation
1	1060.2	331.4	189.4
2	550.8	244.9	107.9
3	500.7	130.5	99.5
4	493.9	213.4	102.9

4 CONCLUSION

The solidification of GBFS used in port structures can be accelerated by adding PBFS. However, mixing PBFS with GBFS presents some issues when used in actual construction sites. To overcome these problems, we subjected the GBFS to PHMT treatment. This paper demonstrates the superiority of this process. PHMT reduces the amount of separation of the GBFS/PBFS mixture and produces sufficient unconfined compression strength after about 2 months of curing in seawater, which occurs automatically when GBFS is used to backfill quay walls. We conclude that PHMT-treated GBFS solidifies at an accelerated rate and can be used to prevent liquefaction.

5 REFERENCES

Coastal Development Institute of Technology. 1989. - *Manual for granulated blast furnace slag used for port construction*, 71p. (in Japanese)

Christian, G. D. 1986. - *Analytical Chemistry*, 4th Edition.

Ishihara, K. 2001. *Soil Mechanics*, p.83. (in Japanese)

Kikuchi, Y., Ikegami, M., & Yamazaki, H. 2005. Field investigation on the solidification of granulated blast furnace slag used for backfill of quay wall. *Journal of JSCE* No.799/III-72. 171-182.

Kikuchi, Y., Oka, S., & Mizutani, T. 2010. Examining field application of solidification acceleration method of granulated blast furnace slag, *Report of PARI*, 49(2). 21-46.

Kikuchi, Y., Nakashima, K., & Mizutani, T. 2007. Acceleration of Solidification of Granulated Blast Furnace Slag. *13th Asian Regional Conference*. CD-ROM.

Kikuchi, Y., Nakashima, K., Oka, S., & Mizutani, T. 2011. Solidification acceleration and solidified shear strength evaluation of granulated blast furnace slag. *Journal of JSCE* C 67(1). 145-159.

Kikuchi, Y., Nakashima, K., Kimura, J., and Mizutani, T. 2006. - Solidification of granulated blast furnace slag used for port construction, *Report of PARI*, 45(2), 105-133. (in Japanese)

Kitayama, N. 2003. *Studies on application of granulated blast furnace slag to SCP method with low sand replacement ratio*. PhD thesis, Yamaguchi University, 155p.

Nippon Slag Association. 1980.- *Granulated blast furnace slag - Technical report on earth work material* -, 63-64. (in Japanese)

Nishi, M., Sato, Y. and Nanbu, M. 1982. - Strength characteristics of granulated blast furnace slag as a land reclamation material, *Tsuchi-to-Kiso*, JGS, 30(12), 41-48.

Zen, K., Yamazaki, H., & Sato, Y. 1990. Strength and deformation characteristics of cement treated sand by premixing method. *Report of PHRI*, 29(2). 85-118.

Building on an old landfill: design and construction

Construire sur une ancienne décharge : dimensionnement et exécution des travaux

McIntosh G.W.
Douglas Partners Pty Ltd, Unanderra, NSW, Australia

Barthelmess A.J.
Consulting Engineer, Wollongong, NSW, Australia

ABSTRACT: The Fo Guang Shan Nan Tien Buddhist Order commissioned the first stage of site investigations of the proposed Nan Tien Institute site at Unanderra, NSW Australia in 2000. Wollongong City Council donated the land which includes an old landfill. The site is located directly opposite the Nan Tien Buddhist Temple which opened in 1995 and is the largest Buddhist Temple in the southern hemisphere. The Institute is being developed in accordance with a masterplan which will ultimately cater for 3000 students and 360 staff. Geotechnical and environmental investigations have been undertaken to determine the extent of the remedial works that will be required for site development. The landfill (which closed in 1984), is some 5.7 ha in plan area and occupies nearly 50% of the total institute site. The results of the investigations have enabled geotechnical, environmental and civil design works to be completed for the initial stage of construction (the ground consolidation works) which were completed in March 2011. Stage 1 building works commenced in November 2012. Given within this paper are the investigation results, design overview and monitoring results (noise, odour, vibration, landfill gas and consolidation). Where relevant, comparison is given to predicted values.

RÉSUMÉ : L'Ordre Buddhist Fo Guang Shan Nan Tien confia l'étude géotechnique du future Institut Nan Tien, situé a Unanderra en Nouvelle-Galles du Sud en Australie, en 2000. La mairie de la ville de Wollongong a légué un terrain qui comprend une décharge qui occupe 5.7 ha, soit presque la moitié du site. La décharge a fermé en 1984. Le site se trouve en face du temple Buddhist Nan Tien, inauguré en 1995, le plus grand temple Buddhist de l'hémisphere sud. Le nouvel institut accueillera 3000 étudiants et 360 employés. Des études géotechniques et environmentales ont été menées avec pour but de déterminer l'ampleur des travaux de réhabilitation du site. Les résutats ont permis le dimensionnement géotechnique, environmental et civil pour la premiere phase de construction du projet, qui incluait la consolidation des sols entreprise en mars 2011. La construction des bâtiments a débuté en 2012. Ce document présente les résultats de l'étude, un apercu du dimensionnement et les résultats de surveillance (bruit, odeur, vibration, gas et consolidation des sols). Certains resultats sont comparés aux prédictions

KEYWORDS: landfill, dynamic compaction, methane drainage, leachate control, monitoring.

1 INTRODUCTION.

In September 2001, Wollongong City Council donated a 12 ha parcel of land at Unanderra to the Fo Guang Shan Nan Tien Buddhist Order on which is planned the Nan Tien Institute and Art Gallery. The site is opposite the existing Nan Tien Temple at Unanderra, NSW which was opened in 1995 and is the largest Buddhist Temple in the southern hemisphere. About half the Institute site includes a derelict (puticible waste) landfill which was operated by Wollongong Council up until its closure in 1984.

Geotechnical and environmental investigations have been ongoing since early 2000 with the overall masterplan of the site finalised in 2009. The project architects were commissioned to produce an environmentally sustainable design with development of the site to be undertaken in stages. Stage 1 works include the Cultural Museum, some limited teaching facilities and car parking areas.

Discussed within this paper are details on the geotechnical and environmental investigations, civil design, leachate collection and control, earthworks (including dynamic compaction results achieved during ground consolidation works completed in March 2011), the use of coal washery rejects as a fill source and environmental monitoring undertaken during earthworks (air, noise, dust, odour, landfill gas and vibration). Discussion is also given on foundation systems and gas drainage options that will need to be developed within the design of the future buildings.

2 BACKGROUND.

The existing Nan Tien Temple and the proposed Institute site are located on either side of the F6 freeway at Unanderra, NSW (refer Figure 1). The overall site area is around 15 ha with the derelict landfill occupying about half of the total site area. The main challenge to development of the site is primarily two fold – firstly, the assessment of both short-term and long term consolidation of the waste and then the design of buildings and civil works that can withstand the settlement estimates and secondly, the design of a system that will enable collection, treatment and discharge of landfill gases (of which methane is the biggest concern) and leachate in a safe and environmentally acceptable way over the life of the buildings.

3 THE PROJECT

The proposed Nan Tien Institute is being developed in accordance with a Masterplan which will ultimately cater for 3000 students and 360 staff. It will be a mixed use development comprising formal educational facilities, an art gallery, museum and other cultural facilities. The overall budget for Stage 1 of the project (including remediation of the landfill) is around $30 million AUD. Whilst architectural design is a work in progress, the first stage of the Institute will generally occur over several levels on the site, with basement carparking on the lower levels, then teaching and related facilities to a viewing platform at the higher locations on the site.

4 SITE INVESTIGATION AND RESULTS

4.1 *Geotechnical*

Investigations to establish a geotechnical model of the site included 103 test pits to depths of up to 5 m, 14 cored boreholes to depths of up to 12 m and the installation of 8 standpipe piezometers. In summary, the natural geological profile of the site comprised topsoil over residual clays with latite and sandstone bedrock (generally of medium to high strength) below depths of 1 – 1.5 m. The profile of the landfill included a coal washery rejects (CWR) and clay capping layer some 0.5 – 3.5 m in thickness (but generally less than 1 m) with the depth of the waste in the order of 4 – 12 m.

The landfill waste was interbedded with CWR and clays, as was expected given the conventional operation of a putrescible waste facility. The density of the landfill was generally loose with some denser sections as reflected by standard penetration test "N" values in the range 2 – 30. Perched water tables were also present. The extent of the landfill is shown in Figure 1.

Figure 1. Extent of landfill.

4.2 *Environmental (soil, water, air, noise)*

180 test locations were investigated across the site, most of which were in the landfill footprint. Contaminant concentrations were compared to the NSW DECC (2006) Health based Investigation levels. Within the soils, elevated levels of manganese and hydrocarbon (C10 – C36) were recorded. Testing of groundwater indicated elevated levels of iron, manganese, ammonia, nitrate and total phosphorus, typical of levels and contaminants found in landfill leachate. Methane, hydrogen sulphate and carbon dioxide were recorded in the gas monitoring wells with the methane levels within either the "explosive" range or exceeding the "explosive limits" and in a range that may cause asphyxiation.

In the areas outside the landfill footprint, no environmental concerns were recorded apart from random dumping of uncontrolled fill which was managed by conventional construction practices.

5 GROUND CONSOLIDATION WORKS

Site preparation was completed in March 2011 and included construction of a temporary leachate collection system, reshaping and benching of most of the site, dynamically compacting the landfill and undertaking of controlled earthworks to achieve design levels. Monitoring of air quality, noise, vibration levels and leachate was ongoing during the works.

5.1 *Civil Design and Leachate Control*

During initial site works, the expectation was that a relatively significant quantity of leachate would discharge from the landfill cell which would reduce after dynamic compaction. The reduced quantities were expected to be treated and managed long term by a membrane bio-reactor (prior to discharge off site or re-use on site). As the bio-reactor could not be sized to cater for the high loads during site preparation works, a 2ML leachate pond was constructed downslope of the landfill cell. Leachate was fed into the pond via a 2 m groundwater cut-off trench installed around the toe and flanks of the landfill cell. Once in the pond, leachate was then pumped through a treatment system consisting of pumps, sand filters, activated carbon filters and an automatic sampler prior to discharge into the sewer system via a Trade Waste Agreement with Sydney Water.

The leachate pond was designed to not only suit its purpose during dynamic compaction and site preparation (i.e. as a leachate pond), but to also double as an on-site detention (OSD) pond during the life of the Institute. This OSD pond assists with long-term management of stormwater on the site. The HDPE liner installed in the leachate pond during dynamic compaction was removed and the pond readily transformed for the OSD purpose. This saved having to build two very similar structures twice.

5.2 *Dynamic Compaction*

In order to improve the density of the landfill (and thus to improve longer term performance by limiting primary compression and secondary consolidation following progressive waste decomposition), dynamic compaction was selected as the appropriate method. The equipment (shown in Figure 2) included a 120 tonne crawler crane dropping a 25 tonne pounder from a height of (nominally) 20 m. Compaction was carried out in two phases. Following placement of a coarse "compaction layer" to provide stability for the crane, the primary phase comprised multiple drops of the concrete pounder (typically 3 – 4) on a 6 m x 6 m grid with the craters backfilled as the compaction proceeded. The final (or ironing) phase was carried out using a pounder of similar mass but a larger footprint (5 – 9 m2) with a drop height adjusted to the pounder size and compression achieved.

Using the methods of Hausmann (1990), an assessment was made of the degree of ground improvement with surface settlements of generally 1 – 2 m expected in the areas underlain by the deeper landfill. The survey results following completion of dynamic compaction and were predominantly within the range 0.5 – 1.5 m, in line with expectations and generally 10 – 12% of overall landfill depth.

Figure 2. Dynamic Compaction Equipment.

Following backfilling of the craters, earthworks were undertaken to reshape the surface of the various benches after which conventional fill placement was carried out to achieve design levels. In areas, this required the placement of up to 2 m of compacted fill which was placed under Level 1 geotechnical control to the requirements of Australian Standard AS3798 – 1996. As a result of the success of the dynamic compaction phase (which provided a solid base), the undertaking of additional earthworks was relatively straightforward with a compaction requirement of 100% of standard maximum dry density achieved in all fill areas. Fill materials included the use of coal washery rejects, a mining by-product from the coal washing process that is obtained at low cost (typical transport only) but has very good civil engineering properties for use as general fill and no negative environmental impacts.

5.3 *Site Monitoring*

Construction works for the ground consolidation contract were undertaken in accordance with a Construction Environment Management Plan (CEMP). The key objective of the CEMP was to develop a monitory programme for regulatory compliance and early detection of any significant environmental or community impacts.

Given the potential impacts due to dynamic compaction being carried out on the site and the presence of buildings on neighbouring properties, vibration trials were undertaken prior to commencement of compaction. An attenuation graph was prepared as shown in Figure 4 with a boundary buffer distance of 25 m nominated for a proposed vibration limit of 8 mm/sec (sector sum and component peak particle velocity). Texcel Vibration Monitors were installed for continuous data recording (one of which was in a neighbouring building) and adopting the buffer distances established by the trial, only nine exceedances were recorded during the 6 month construction period. No complaints were received from neighbouring properties.

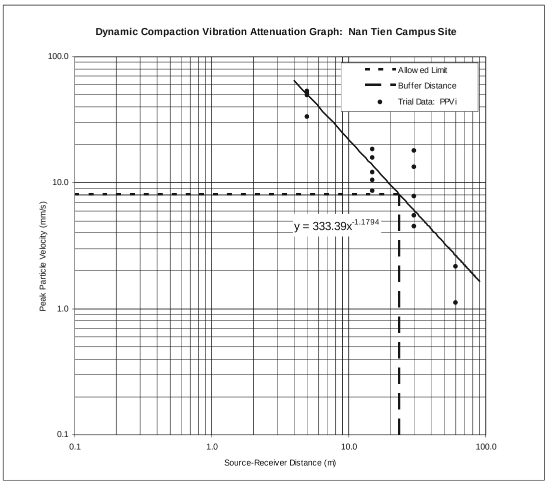

Figure 4: Dynamic Compaction Vibration Attenuation Graph

Whilst noise was considered to be the other major environmental impact that could cause community concern during compaction activities, monitoring over the 6 month period recorded a total of only 32 readings above the performance criteria of 75 dBA. Odour was primarily of concern during the initial excavation phase and was managed by minimising waste exposure time. Similarly, dust was managed by the implementation of good construction practices on site. Leachate and groundwater was monitored regularly with all outflow to the pre-determined requirements. Whilst results were typical of those expected from a landfill site, manganese and ammonia were flagged as elements of concern.

The obvious area of concern in all landfill projects is landfill gas (LFG). Methane, carbon dioxide and oxygen levels were monitored both inside and outside the landfill boundary as well as within site buildings. Daily monitory of landfill was undertaken using a GA2000 Gas Meter. Both surface and well measurements were taken as well as barometric pressure and lower explosive limit. Peak methane levels of up to 97% were recorded in wells in the landfill footprint, with levels generally in the range of 14 – 50%. Monitoring in wells adjacent to the landfill boundary was generally below threshold levels or 0% methane. Surface and enclosed space monitoring showed that LFG was not considered to be an issue at any time during the works.]

6 FUTURE WORKS AND BUILDING DESIGN

6.1 *Civil works, services and stormwater drainage*

All civil and building services (eg sewer, water, stormwater, electrical, gas) have been designed such that they will not need to penetrate the capping layer of the landfill. All service trenches and other works that require excavation (eg landscaping) will be within 'clean' material and limited to excavation depths of 2m. Earthworks associated with site reshaping will require construction of retaining walls up to 7m high. The walls have been designed as reinforced earth structures able to accommodate ground settlements of 300mm.

6.2 *Foundations*

The main advantage of dynamically compacting the landfill is that long term settlement of the landfill (post building construction) will be significantly reduced, but not eliminated (Thom 1998). As such, footing design for buildings located within the landfill footprint will be for driven steel piles founding in the underlying latite bedrock. Flexible aprons will be needed between the buildings (which will experience negligible settlement) and adjoining carparks, walkways and recreation areas (which will experience ongoing settlement). Whilst raft slabs may be feasible for some lightweight single story buildings, preliminary analysis has indicated that a 1 m thick reinforced earth raft will be needed to provide uniform bearing and to equalise the longer term settlements so that differential movements will be within acceptable limits.

6.3 *Leachate Control and Gas Drainage*

Leachate collection drains will be installed across the site and directed to the leachate treatment system. The current options for leachate collection include disposal to sewer, reinjection, spray or drip irrigation, removal by contractor, ammonia stripping, constructed wet lands and membrane bio reactor.

The primary elements of the environmental design are capping profile, methane drainage and leachate control. The requirement of the site capping is twofold; firstly – physical separation by covering contaminated materials and secondly – prevention of infiltration to the substrate, thereby minimising leachate recharge and mobilisation and upward migration of methane. Historically landfill capping systems have included a 0.5 m clay cap however this system alone was not considered intrinsically safe at this site in areas underneath buildings or pavements where piles will breach the cap and gas can accumulate in enclosed spaces.

The preliminary design for the capping consists of HDPE, GCL, geotextile fabric, 300 mm gravel gas drainage layer and a reinforcing geotextile, underlain by the existing waste, refer to Figure 5 below. Undercrofts will be constructed where possible to allow for suspension of services and cross-ventilation. In areas outside of the buildings an additional 1 m layer of clean fill material to further protect the cap from stormwater and root infiltration, drying out, cracking and accidental breaches will be installed. The preliminary design requires the landfill cap to extent 50 m beyond the landfill boundary or the site boundary whichever occurs first. At the landfill boundary within the site, the capping will be keyed in with a sump installed for leachate and landfill gas condensate collection.

Where the landfill extends over the site boundary a bentonite plug will be installed at the boundary to minimise migration of landfill gases through soils, refer to Figure 6.

Landfill gas drainage will consist of a gas drainage layer forming part of the cap. Collection pipes will be placed around the perimeter and across the benches with a maximum spacing of 50 m. An additional gas extraction filter layer and pipe work for the collection and discharge of LFG will be incorporated beneath the slab of all buildings where possible. Three remedial options for the management landfill gas were considered. The use of landfill gas for power generation was not considered feasible due to low gas flows as result of the age and stage of the decomposition of the waste present at the site this option

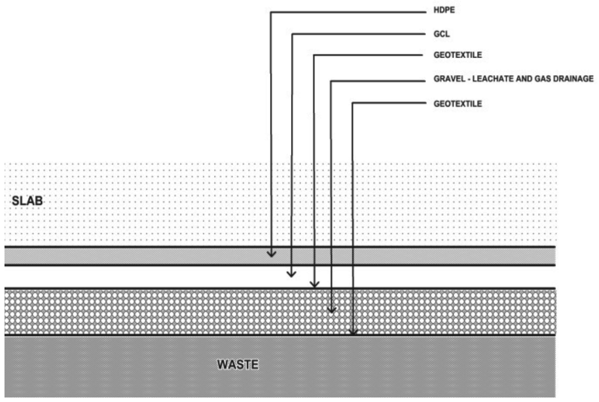

Figure 5: Preliminary design of cap for slab on ground

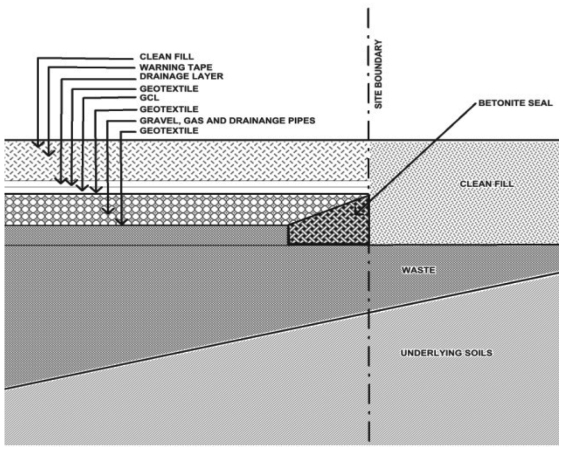

Figure 6: Preliminary design of cap at site boundary

Flaring of the gas, with ignition of the gas as it leaves the site was considered, given its advantage of reducing the landfill gas to a higher percentage of CO_2 and H_2O vapour, however the technical difficulties of operating the flare, the area required for a flare plant and the cost of setting up and maintenance of the plant, among others, far outweighed the advantages. The final remedial option, venting to the atmosphere, was chosen for the zero requirements for a specific treatment plant and operating costs. As such the preliminary design consists of the placement of turbine ventilator stacks around the site. Landfill gas discharge will occur through stacks that will extend 1 m above the proposed maximum building roof level across the site. To monitor the landfill gas and minimise the potential of migration off-site a series of monitoring wells will be installed.

7 LESSONS LEARNT DURING CONSTRUCTION

Of particular interest to those wanting to apply the techniques described in this paper for another site or project, are the lessons learnt during the construction of this project. Primarily, these are as follows:

1. The site was located within 50m of a main highway. A hazard was ‘fly rock’ being mobilized during dynamic compaction and hitting operators or leaving the site and colliding with a vehicle on the highway. To control this hazard, a no-go zone was established around the dynamic compaction rig and the rig was not allowed to operate near the highway.
2. The extent of consolidation during dynamic compaction was significant. At this site, the contaminated water make during dynamic compaction was also significant. Whilst this was predicted and readily catered for onsite (in accordance with the CEMP) it took a considerable amount of time to manage, sample for contamination and then subsequently discharge at an appropriate location. It was also relatively expensive.
3. The use of coal washery rejects, a mining by-product from the coal washing process, was entirely successful. This material was put to use on this site and would otherwise have ended up as landfill. The ability to use what would otherwise have been waste material, as fill material in the overall remediation of another landfill site, is considered best practice and an outstanding outcome environmentally.
4. The selection of an earthworks contractor must include an assessment of their ability to perform the work rapidly. Exposing the waste sections of the site created many hazards, and the contractors ability to perform the work and ‘cap’ the site ready for dynamic compaction in the shortest possible timeframe greatly reduces the exposure to those hazards and any expensive delays caused by (for example) inclement weather.

8 CONCLUSION

The use of dynamic compaction and construction of a landfill gas drainage system together with innovative civil solutions will allow the Fo Guang Shan Nan Tien Buddhist Order to develop their site and create a teaching and cultural facility as part of the existing Nan Tien Temple. Geotechnical and environmental performance was monitored during site preparation works and will be monitored during building construction.

9 ACKNOWLEDGEMENTS

The authors acknowledge the Fo Guang Shan Nan Tien Buddhist Order and affiliates for assistance in the project and their permission to use project specific data for this paper.

10 REFERENCES

Standards Australia. 1993. Determination of the penetration resistance of a soil – Standard Penetration Test. *Australian Standard AS 1289* 6.3.1 – 1993.

Standards Australia. 1996. Guidelines on earthworks for commercial and residential developments. *Australian Standard AS 3798 – 1997*.

Hausmann, M.R. 1990. Engineering Principals of Ground Modification. *McGraw Hill*.

Thom, M.J. 1998. The long term settlement behaviour of waste and its effect on future development. *3rd National Hazardous and Solid Waste Convention.*

Department of Environment and Conservation NSW. 2006. Guidelines for the NSW Site Auditor Scheme. *2nd Edition.*

Interpretation of mechanical behavior of cement-treated dredged soil based on soil skeleton structure

Interprétation des comportements mécaniques des sols dragués traités au ciment basée sur la structure squelette du sol

Nakano M., Sakai T.
International Member, Nagoya University,JAPAN

ABSTRACT: The objective of this study was to examine the mechanical behaviors of cement-treated dredged soil and evaluate them based on action of the soil skeleton structure through simulation of the behaviors by the SYS Cam-clay model. Besides, the behaviors were simulated by the ***GEOASIA*** soil-water coupled finite deformation analysis code. The new findings are summarized as follows; 1) As the soil is treated with high cement with low initial water content under shearing in high confining stress, its effective stress path moves up closer to the tension cut-off before failure. 2) The treated soil approaches the NCL of the remolded cement-treated soil. 3) The treated soil is regarded as a high structure and overconsolidated soil. 4) FEM analysis can describe softening behavior with shear banding through the triaxial compression test.

RÉSUMÉ: L'objectif de cette étude est d'examiner les comportements mécaniques de sols dragués traités au ciment et de les évaluer sur la base de l'action de la structure de squelette du sol par la simulation des comportements à l'aide du modèle SYS Cam-clay. Par ailleurs, les comportements sont simulés par GEODESIA, un programme d'analyse de déformations finies sol-eau couplées. Les nouveaux résultats sont résumés comme suit; 1) Comme le sol est traité avec du ciment haut à teneur en eau initiale faible avec cisaillement sous contrainte de confinement élevé, son chemin de contrainte effective se déplace plus près de la tension de coupure avant la rupture. 2) Le sol traité se rapproche de la NCL du sol traité au ciment et remoulé. 3) Le sol traité est considéré comme une structure haute et surconsolidée. 4) L'analyse par éléments finis peut décrire des comportements d'adoucissement avec bande de cisaillement lors d'essai de compression triaxiale.

KEYWORDS: cement stabilization, soil skeleton structure, elasto-plastic mechanics.

1 INTRODUCTION

About 1.3 million m^3 of dredged soil is produced annually in Nagoya Bay. However, the temporary storage capacity for the soil at Nagoya Port Island (PI) is limited, so effective use of the soil as a geomaterial has become a pressing issue. The water content of the soil is high, and the unconfined compressive strength is low, so to effectively use the soil as a geomaterial, it is necessary to add a stabilizer such as cement to improve the mechanical properties. Therefore, in this study, the mechanical behavior of cement-stabilized dredged soil (hereafter referred to as treated soil) was determined using laboratory tests and reproduced using an elasto-plastic constitutive model, with the objective of explaining the improvement effect.

Past constitutive equation study into cement-stabilized soil includes, for example, the study by Hirai et al. (1989), Yu et al. (1998), Kasama et al. (2000), Lee et al. (2004), and Wada et al. (2004). This study used the SYS Cam-clay model (Asaoka et al. 2002), an elasto-plastic constitutive model based on the action of the soil skeleton structure. It was assumed that the mechanical behavior for the criteria to define the soil skeleton structure was the mechanical behavior obtained from remolded samples of treated soil (hereafter referred to as remolded treated soil). The one-dimensional compression behavior was reproduced in addition to the shear behavior in order to explain the improvement effect of adding cement based on elasto-plastic mechanics, taking the soil skeleton structure into consideration. In addition, the effect of nonuniform deformation on triaxial test results was investigated by solving as a boundary problem (Asaoka et al. 1995), taking into consideration brittle behavior, which is a characteristic of the treated soil that was observed in the tests, in addition to the constitutive equation response considering the triaxial test to be an element test.

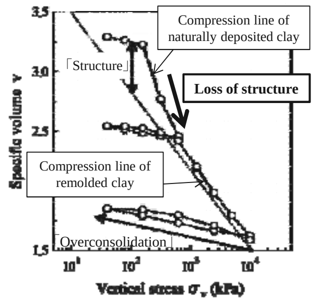

Figure 1. One-dimensional compression of natural deposited clay and definition of structure and overconsolidation

1 THE SYS CAM-CLAY MODEL

This section describes the SYS Cam-clay, the elasto-plastic constitutive model that was used to explain the mechanical behavior of the treated soil. Fig. 1 shows the oedometer test results for natural deposited clay and remolded clay. Natural deposited clay is defined as clay with structure, where the difference in specific volume v ($=1+e$; e is the void ratio) from remolded clay at the same vertical stress, in other words, the "bulk" is taken to be the extent of structure. As the vertical stress increases, the compression line of the natural deposited clay approaches that of remolded clay. The interpretation of this behavior in terms of the concept of soil skeleton structure is that there is decay/collapse of the soil structure due to shearing (plastic deformation) of the soil. A triaxial compression test is not shown here, but the critical state of natural deposited clay gradually approaches that of remolded clay as a result of shear. Basically, the structure collapses due to shear. Likewise, overconsolidation becomes normal consolidation as a result of plastic deformation. The SYS Cam-clay model defines structure, overconsolidation, and anisotropy as the soil skeleton structure, and an evolution rule is introduced that varies them in accordance with the plastic deformation to reproduce the mechanical behavior of natural deposited clay. This study focused on structure and overconsolidation, controlling the ease of change of their states using a degradation index of structure and a degradation index of OCR in accordance with their respective evolution rules (see Table 3), to explain the treated soil as natural deposited clay and the remolded treated soil as remolded soil.

Table 1 Physical properties of dredged soil

Soil particle density ρ_s [g/cm^3]	2.67
Natural water content w_n [%]	50–110
Liquid limit w_L [%]	52.5
Plastic limit w_p [%]	25.1
Plasticity index I_p [%]	27.4
Clay content [%]	60
Silt content [%]	36.6
Sand content [%]	3.4
Mean grain diameter D_{50} [mm]	0.002

2 REPRODUCTION OF THE MECHANICAL BEHAVIOR OF TREATED SOIL WITH SYS CAM-CLAY MODEL

2.1 *Physical properties of dredged soil and treated soil mixture conditions*

Table 1 shows the physical properties of PI dredged soil. Almost all of the soil is fine fraction with a high natural water content, and it does not achieve the required strength. Also, Table 2 shows the mixture conditions of the treated soil. In this study, the mixture conditions were assumed to be a water content w=120%, cement contents of C=30, 50, and 70 kg/m^3, and 28 days' curing in order to ensure fluidity and strength for the assumed Pneumatic Flow Method (Coastal Development Institute of Technology 2008).

Table 2 Mixture conditions used in the comparison of cement content

Dredged soil water content w_0 [%]	Cement content C [kg/m^3]	Water-cement ratio W/C
120	30	25.2
	50	15.0
	70	10.6

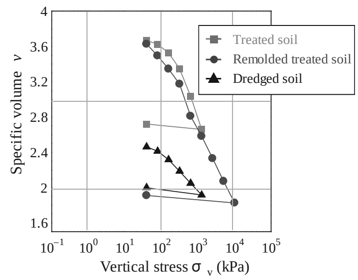

Figure 2. Comparison of uniaxial compression properties of treated soil, remolded treated soil, and dredged soil

2.2 *Mechanical behavior of treated soil (C=50 kg/m^3) and remolded treated soil and material constants*

Fig. 2 shows the oedometer test results for treated soil and remolded treated soil with C=50 kg/m^3, together with the results for dredged soil. Compared with dredged soil, treated soil has a high initial specific volume, and as a result of cement addition, it maintains the high specific volume state up to a certain vertical stress. When the vertical stress exceeds a pseudo consolidation yield stress, a high compressibility is exhibited. Compared with the remolded treated soil, there is a certain amount of structure up to the pseudo consolidation yield stress, and when the vertical stress increases further, it gradually approaches the compression line of the remolded treated soil. Fig. 3 shows the CU triaxial test results for the treated soil, and Fig. 4 shows the results for the remolded treated soil. The behavior exhibited in Fig. 3 resembles the behavior of overconsolidated and high structured clay (Asaoka et al. 2002). As shown in Fig. 4, the behavior of remolded treated soil resembles the behavior of dredged soil. However, the treated soil has a specific volume that is distinctly higher than that of dredged soil, so in Figs. 2 and 4, it is considered that remolded treated soil is a material that is different from dredged soil.

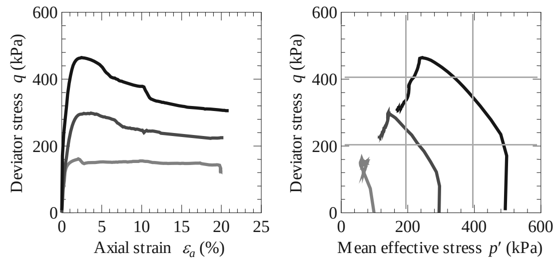

Figure 3. Consolidated undrained triaxial test results for treated soil

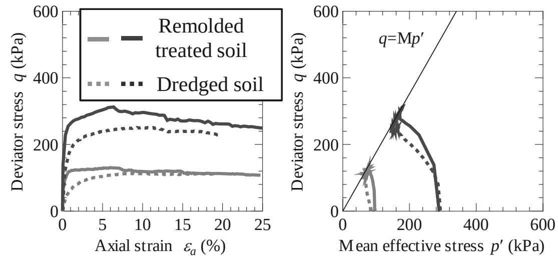

Figure 4. Consolidated undrained triaxial test results for remolded treated soil

2.3 *Reproduction of the mechanical behavior of 3 treated soils with different cement contents using the SYS Cam-clay model*

Treated soil was produced under the mixture conditions shown in Table 2, and mechanical tests were carried out on them and the remolded treated soil. Fig. 5 shows the results of oedometer tests on remolded treated soil. For all cement contents, the behavior was similar to that of remolded normally consolidated soil, and as the cement content increased, the slope of the NCL λ and the intercept N on the NCL increased. Fig. 6 shows the CU test results for remolded treated soil. For each of the cement contents, the behavior was similar to that of remolded soil, and differences in cement content did not cause a major change in the Critical state constant M. Based on the test results, the elasto-plastic parameters in accordance with the differences in cement content were assigned, as shown in Table 3.

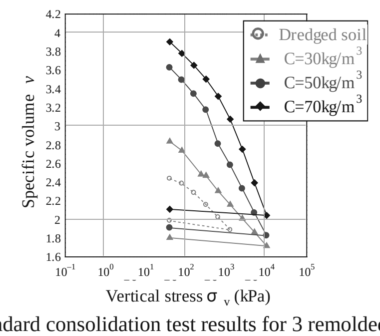

Figure 5. Standard consolidation test results for 3 remolded treated soils

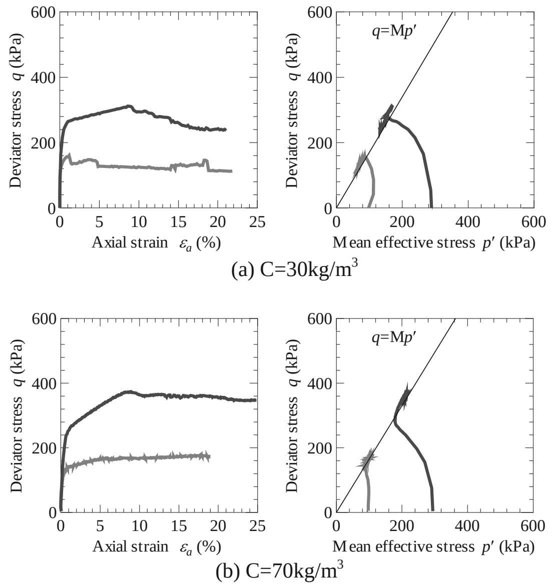

Figure 6. Consolidated undrained triaxial compression test results for remolded treated soils

Fig. 7 shows the oedometer test results for treated soil and the results reproduced using the SYS Cam-clay model. The test results show that as the cement content is increased, the consolidation yield stress increases, and in all cases, when the consolidation yield stress is exceeded, high compressibility is exhibited. For all the cement contents, it is considered that a high structure has been produced by the addition of cement. The analysis was generally capable of reproducing these trends. However, as the cement content increased, the accuracy was reduced.

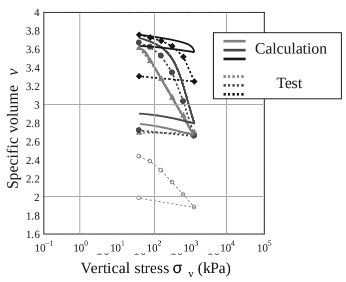

Figure 7. Treated soil standard consolidation test results and their analytical reproduction

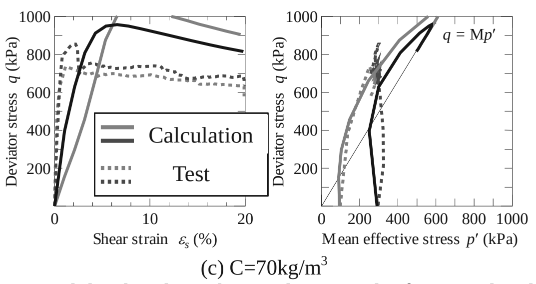

Fig. 8 Consolidated undrained triaxial test results for treated soil and their analytical reproduction

Fig. 8 shows the undrained shear test results and the reproduced results for treated soil. The critical state line CSL $q = \mathrm{M}p'$ for remolded treated soil is also shown in this figure. From the test results, the softening behavior occurs below $q = \mathrm{M}p'$ for treated soil with C=30 kg/m^3. For treated soil with C=50 kg/m^3, softening behavior occurs above $q = \mathrm{M}p'$ under high confining pressure. For treated soil with C=70 kg/m^3, there is distinct hardening behavior associated with plastic expansion and a high overconsolidation ratio. As the cement content is increased, the maximum value of the stress ratio q/p' easily exceeds M, and for C=70 kg/m^3, the effective stress reaches the tension cut-off line ($q = 3p'$). The analysis reproduced the behavior of the treated soil for low cement content, but it was difficult to reproduce the behavior above $q = \mathrm{M}p'$ for treated soil with a high cement content.

Table 3 shows the initial values of the material constants of the SYS Cam-clay model used in the analysis. The addition of cement produced high structure and pseudo overconsolidation. Also, the overconsolidation ratio increased as the cement content increased, but on the other hand, the extent of evolution of structure reduced. This is considered to be due to the fact that the water content of the dredged soil was constant in the mixture conditions used, so as the cement content increased, the water-cement ratio reduced, and this corresponds to the increase of N of the remolded treated soil as the cement content increased.

Table 3 SYS Cam-clay model material constants and initial values

Plasticity parameters		Treated soil		
Cement content (kg/m^3)		C=30	C=50	C=70
Water-cement ratio		25.2	15.0	10.6
Confining pressure (kPa)		98.1	98.1	98.1
Compression index	λ	0.21	0.36	0.51
Swelling index	κ	0.05	0.05	0.03
Limit state constant	M	1.70	1.60	1.65
NCL intercept	N	2.70	3.40	4.20
Poisson's ratio	ν	0.30	0.30	0.30
Evolution rule parameters				
Normal consolidated soil index	m	0.01	0.60	5.00
Structure degradation index	a	0.25	0.60	1.50
	b	1.00	1.00	1.00
	c	1.00	1.00	1.00
Plastic shear:plastic compression	c_s	0.20	0.50	0.10
Rotation hardening index	b_r	0.00	0.00	0.00
Rotation hardening limit index	m_b	0.50	0.50	0.50
Initial values				
Overconsolidation ratio	$1/R_0$	1.03	20.9	63.8
Extent of structure	$1/R_0$□	260	10.00	5.00
Vertical stress	σ_v	19.6	19.6	19.6
Specific volume	v_0	3.94	3.75	3.80
Stress ratio	η_0	0.00	0.00	0.00
Initial anisotropy	ζ_0	0.00	0.00	0.00

3 SOIL-WATER COUPLED FINITE DEFORMATION ANALYSIS FOR TRIAXIAL TESTS

In the above, we attempted to explain the mechanical behavior of treated soil from the point of view of considering the triaxial test as an element test. However, from observation of the failure mode of the test specimens, The characteristic brittle failure had occurred in the treated soil. Therefore, in this section, the effect of nonuniform deformation on the triaxial test results was investigated, taking the triaxial test to be a boundary problem.

3.1 *Analysis conditions for the soil-water coupled finite deformation analysis*

The soil-water coupled finite deformation analysis code ***GEOASIA*** (Noda et al. 2008), which incorporates the SYS Cam-clay model as the constitutive equation for soil structure, was used in the analysis. The analysis was carried out under plane strain conditions, and Fig. 9 shows the finite element mesh and boundary conditions. An undrained boundary was set around the test specimen, and frictional conditions were assumed at the top and bottom end surfaces with a rigid cap and pedestal. A primary asymmetric mode with a cosine curve (half period) having an amplitude of 0.005 cm (Asaoka et al. 1995) was applied as an initial geometric imperfection to the side surfaces of the test specimen. The shear velocity was 1.4×10^{-2}%/min, with a downward displacement velocity applied to the top end surface of the test specimen. The target test was C=50 kg/m^3 under confining pressure 294 kPa as shown in Fig. 3. The triaxial test was considered to be an a boundary problem, and the calculation was carried out using the material constants and initial values for the SYS Cam-clay model (Table 3).

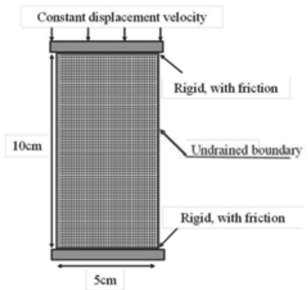

Figure 9. Finite element mesh and boundary conditions

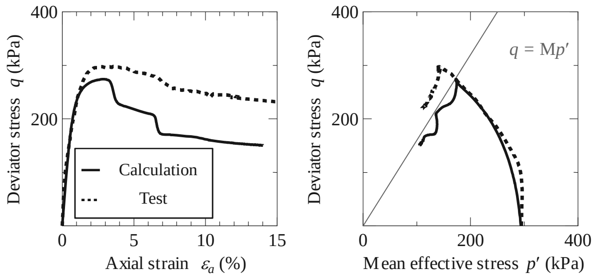

Figure 10. Consolidated undrained triaxial test results for remolded treated soil

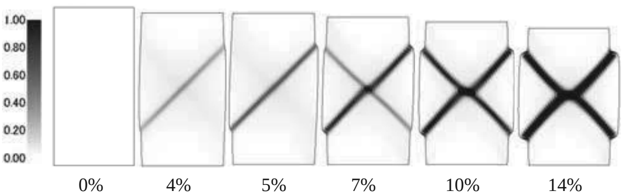

Figure 11. Consolidated undrained triaxial analysis results for remolded treated soil

Photograph 1 Failure shape of the test specimen

3.2 *Soil-water coupled finite deformation analysis results*

Fig. 10 shows the analysis results arranged considering the test specimen to be one element, together with the test results. Fig. 11 shows the shear strain distribution from the analysis. From the axial deviator stress-axial strain relationship in Fig. 10, it can be seen that at around 3% of axial strain and at around more than 6% of axial strain, the deviator stress suddenly drops. In the shear strain distribution in Fig. 11, ‘diagonal shear band’ occurs at about the same axial strain as in Fig. 10, then a shear band in the opposite direction occurs, and finally X-shaped shear bands are formed. The occurrence of shear bands and the drop in q coincide, so it can be seen that the cause of the drop in q is the occurrence of shear bands. In the test results, a clear load drop occurs at around 7–8% axial strain, but at around 5%, a small load drop can also be seen. Photograph 1 shows a view of the test specimen after shearing. X-shaped shear bands are formed as in the analysis.

4 CONCLUSIONS

We attempted to explain the mechanical behavior and improvement effect of treated soil due to the addition of cement based on test results, the SYS Cam-clay model, which is an elasto-plastic constitutive model that incorporates the concept of soil skeleton structure, and ***GEOASIA***. The following conclusions were obtained.

(1) Mechanical behavior of cement-stabilized treated soil: In the oedometer tests, as the cement content increased, the initial specific volume increased, the consolidation yield stress increased, and the compressibility was smaller up to the consolidation yield stress. In the triaxial tests, as the cement content increased, the maximum value of the stress ratio q/p' increased and approached the tension cut-off line.

(2) Mechanical behavior of remolded treated soil: In the oedometer tests, as the cement content increased, the intercept N and the slope λ of the NCL increased. In the triaxial tests, the M did not vary much with cement content.

(3) Reproduction using the SYS Cam-clay model: The addition of cement produces a higher structure and pseudo overconsolidation in the soil. Also, differences in cement content are easily reflected in differences in the overconsolidation ratio, and differences in water-cement ratio are easily reflected in the degree of structure. The analysis reproduced the mechanical behavior of treated soil, but for high cement contents, reproduction by analysis was difficult, which suggests that it is necessary to introduce a new model.

(4) Finite element analysis of the triaxial test: Although there were differences in the axial strain at occurrence of shear banding and the amount of drop in q, the analysis was capable of reproducing the trends of both occurrence of shear banding and the sudden drop in q. However, material constants and initial values used in the analysis were obtained by considering the triaxial test to be an element test. It is necessary to incorporate the viewpoints of both element tests and boundary problems in order to comprehend the natural behavior of the treated soil.

5 REFERENCES

Hirai, H. et al. 1989. An elastic-plastic constitutive model for the behavior of improved sandy soils. S&F 29 (2), 69-84.

Yu, Y. et al. 1998. A damage model for soil-cement mixture. S&F 38 (3), 1-12.

Kasama, K. et al. 2000. On the stress-strain behavior of lightly cemented clay based on an extended critical state concept. S&F 40 (5), 37-47.

Lee, K. et al. 2004. Constitutive model for cement treated clay in a critical state frame work. S&F 44 (3), 69-77.

Wada, M. et al. 2004. FEM Analysis of Stabilized Processed Soil Using a Superloading Yield Surface. Japan Society of Civil Engineers 59th Annual Conference, 1013-1014.

Asaoka et al. 2002. An elasto-plasticelasto-plastic description of two distinct volume change mechanisms of soils. S&F 42 (5), 47-57.

Asaoka et al. 1995. Imperfection-sensitive bifurcation of Cam-clay under plane strain compression with undrained boundaries. S&F 35 (1) 83-100.

Coastal Development Institute of Technology 2008. Technical Manual for the In-tube Mixed Stabilization Process Method (Revised Version).

Noda et al. 2008. Soil-water coupled finite deformation analysis based on a rate-type equation of motion incorporating the SYS Cam-clay model. S&F 48 (6), 771-790.

Utilization of waste copper slag as a substitute for sand in vertical sand drains and sand piles

Utilisation des scories de cuivre en tant que substitut pour le sable dans des drains et des colonnes de sable

Nawagamuwa U.P.
University of Moratuwa, Sri Lanka

Senanayake A.
University of Texas at Austin, USA

Rathnaweera T.
University of Calgary, Canada

ABSTRACT: Vertical sand drains are used as a method of expediting consolidation for ground improvement projects. Unfortunately, the installation of vertical sand drains have become less economically viable due to the high costs and limited availability of good quality sand. Particle size distribution analyses done on samples of waste copper slag obtained from the Colombo dockyard revealed that its gradation was similar to that of sand, which meant that waste copper slag could potentially be used as a substitute for sand, provided that it did not adversely affect the hydraulic conductivity of the resulting mixture. In this study, constant head permeability tests were done on "sand-copper slag" mixes of varying proportions and it was shown that up to 50% copper slag by weight could be added to sand without an appreciable loss in permeability. The performance of sand piles is dependent on strength and settlement characteristics of the sand. Hence, consolidation tests and direct shear tests were also carried out on the "sand-copper slag" mixes to explore how the mechanical properties of sand were affected by the copper slag.

RÉSUMÉ : Sable drains verticaux sont utilisés en tant que méthode d'accélérer la consolidation des projets d'amélioration des sols. Malheureusement, l'installation de drains verticaux sable sont devenues moins rentables en raison des coûts élevés et une disponibilité réduite de sable de bonne qualité. Analyses granulométriques effectuées sur des échantillons de scories de cuivre obtenu à partir des déchets du chantier naval Colombo a révélé que sa gradation était semblable à celle du sable, ce qui signifie que scories de cuivre des déchets pourrait être utilisé comme un substitut pour le sable, à condition que cela ne nuise pas la conductivité hydraulique du mélange résultant. Dans cette étude, des essais de perméabilité constants ont été réalisés sur la tête "sable-laitier de cuivre" mélange des proportions variables et il a été montré que jusqu'à scories de cuivre 50% en poids peuvent être ajoutés au sable sans perte notable de la perméabilité. La performance des piles de sable dépend des caractéristiques de résistance et de règlement du sable. Ainsi, des essais de consolidation et essais de cisaillement direct ont également été menées sur le sable-laitier de cuivre mélange d'explorer la façon dont les propriétés mécaniques de sable ont été affectés par les scories de cuivre.

KEYWORDS: waste copper slag, vertical drains, sand piles,

1 PARTICLE SIZE GRADATION

Laboratory sieve analyses were conducted on the waste copper slag. The material was first sieved through the No.4 (4.75mm) sieve to remove coarse particles which do not fall within the particle size range of sands. The results showed that the copper slag had a very small range of particle sizes. The material could be categorized as "poorly graded" according the USCS (C_u= 2.5 and C_c = 0.9).

The waste copper slag was mixed with a poorly graded sand (C_u =3, C_c =1.1) in proportions of 10%, 20%, and 40% by weight and tested how the geotechnical engineering properties of the sand would be affected.

The results of sieve analysis test conducted on the copper-sand mixes are shown in figure 1. It can be observed that the gradation curve is not greatly affected by the addition of waste copper slag. The only apparent change is a slight shift in the curves towards the right.

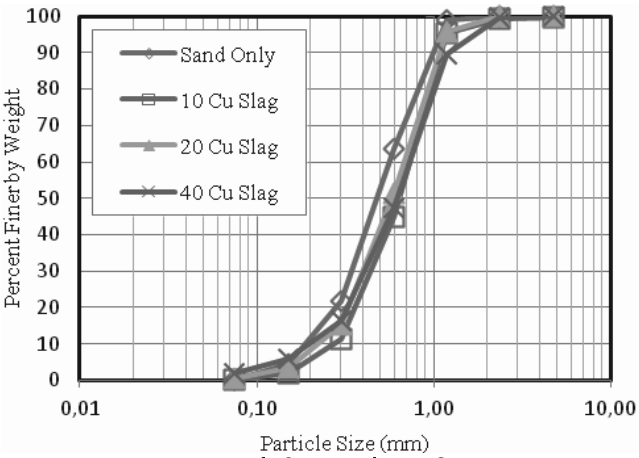

Figure 1: Particle Size Distribution Curves

2 HYDRAULIC CONDUCTIVITY

A poorly graded material will have a high void ratio as compared to a well graded material. Whilst this may be a undesirable attribute in many engineering applications, it can be an advantage if the material is to be used for sand drains. The purpose of sand drains is to provide a mechanism to expediting the dissipation of excess pore water pressures created in soil masses by acting as outlets for ground water to flow out. A key attribute of sand drains is to have very high hydraulic conductivities so that there is minimal resistance to water flowing them. High void ratios generally translate into high hydraulic conductivity thus, a material with high void ratio would be ideal for used in such drains.

The particle size gradation curves suggest that the hydraulic conductivity of the mixes should not deviate too much from that of the original sand. A series of constant head test were carried out on the each mix in order to check if this was true.

The permeameter was filled with air dried samples of the copper-sand mix by dropping the material through a funnel from a fixed height. Special care was taken during the preparation of the specimens in order to ensure that they were comparable and consistent among all the different copper-sand mixes. The funnel used in this case was one from a “Sand Cone” test used in estimating field compaction values and it was placed on top of the permeameter. The funnel was first filled to the brim and the tap was opened to let all the material fall in to the permeamter in a single step. This method could be estimated to produce samples slightly denser than those specified in ASTM D 4254. The unit weight of the specimen was found by weighing the permeameter and calculating the volumes occupied by the material.

Specific gravity of the waste copper slag was found to be 3.7 and that of the sand was around 2.65. The specific gravity of the copper-sand mixes were calculated as a weighted average based on the proportions of each component. The void ratio of each mix was then calculated .As expected, the void ratio are tightly grouped together, ranging between 0.7 – 0.8. There is a trend showing a peak void ratio at a mix proportion of 20% copper slag. However, these small differences in void ratios are not significant enough to affect the hydraulic conductivity of the materials as can be seen from **Figure 2**.

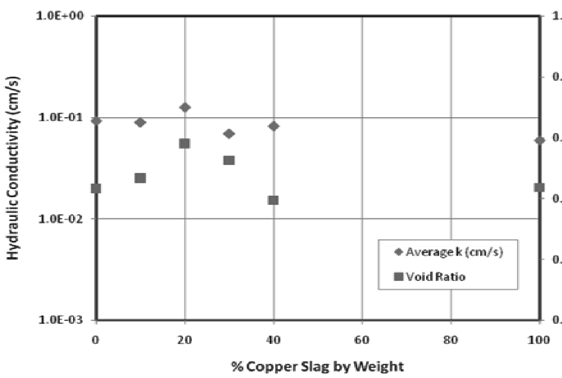

Figure 2: Hydraulic Conductivities and Void Ratios for Copper-Sand Mixes

3 SHEAR STRENGTH

The samples which were tested in the direct shear apparatus were prepared in ‘loose condition’ with no compacting. As expected, the plots on **Figure 3** are typical of ‘loose’ sand as they show a gradual gain in shear strength and then flatten out with no pronounced peak. It can also be seen that the axial strain required mobilizing maximum shear strength increases with the increase in the applied normal stress. Figure 6 shows the summary of Mohr Coulomb failure envelopes for various copper sand mixes and Table 1 provides friction angles those mixes.

The direct shear test results show that the addition of waste copper-slag does not affect the shear strength of the sand. A friction angle of 30 degrees is typical for a ‘loose’ sand and if need be, the friction angle can be increased further by densifying the material.

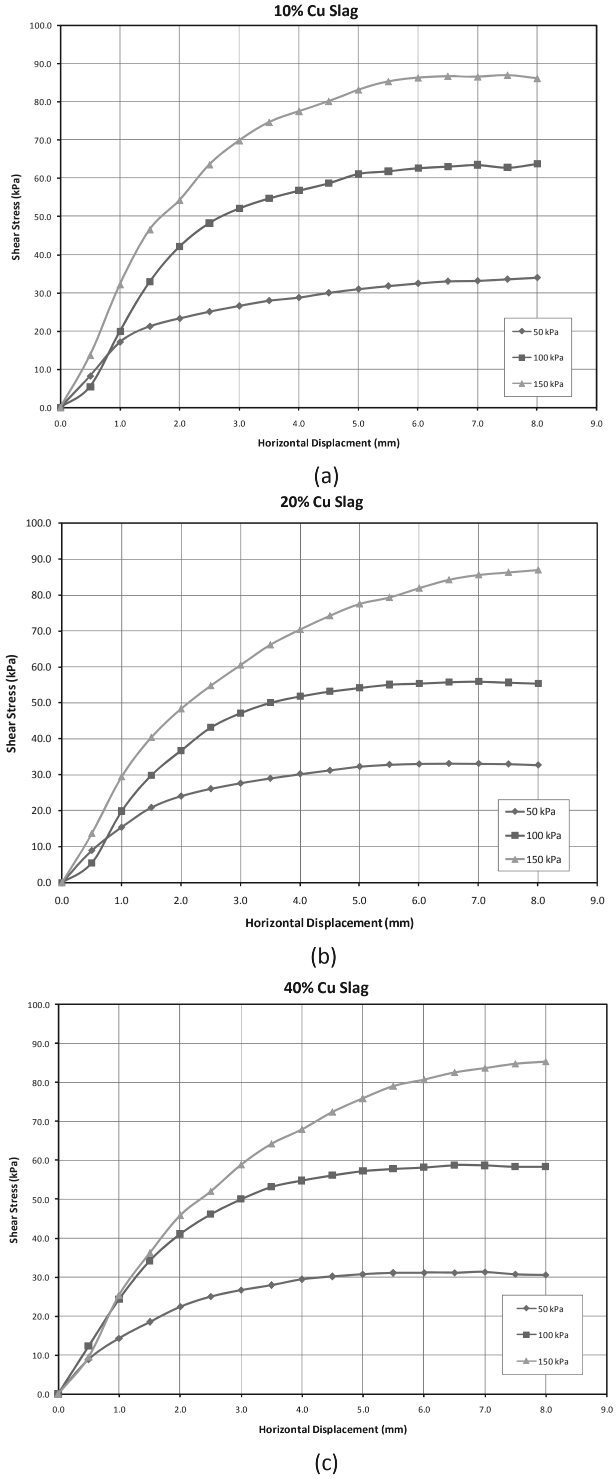

Figure 3: Direct Shear Test Results on Copper-Sand Mixes

Table 1: Friction Angles of Copper-Sand Mixes in ‘Loose’ State

% of Copper Slag by Weight	Friction Angle (degrees)
10	31.4
20	30.4
40	30.4

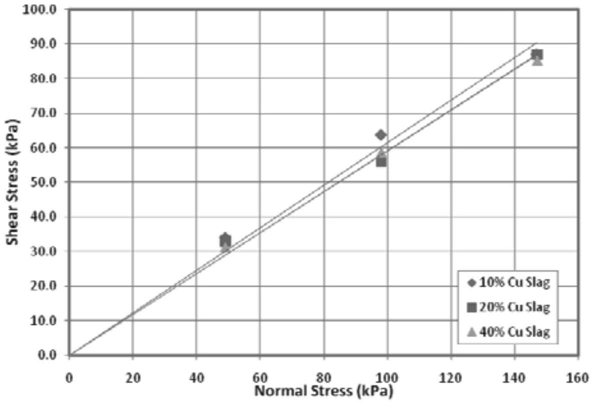

Figure 4: Mohr-Coulomb Failure Envelopes for Copper-Sand Mixes

4 STIFFNESS

The most significant effect of the addition of waste copper slag to sand was observed in confined compression tests. Dry specimens were tested in a consolidation apparatus to ascertain settlement and stiffness properties of the material. Standard consolidation tests with fully saturated samples were not warranted as the material had a very high hydraulic conductivity and consolidation would have occurred at a rapid rate. Strains were measured for different stress changes by applying loads on to the sample. **Figure 5** shows the results in the form of a typical strain vs log stress plot. There is clear distinction between the behavior of the sand and the copper-sand mixes. The addition of just 10% of waste copper slag drastically increases the stiffness of the material. All three curves for copper-sand mixes are tightly grouped which suggest that increasing the proportion of copper slag more than 10% does not have any further effect.

Figure 5: Compression Characteristics of Copper-Sand Mixes

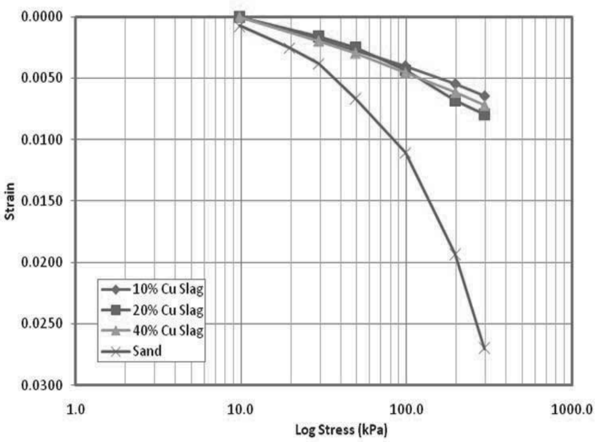

figure 6: Compression characteristics of copper-sand mixes

5 GEOCHEMICAL CHARACTERISTICS OF USED THE COPPER SLAG

Chemical properties of the used copper slag as a percentage of total weight are Iron Oxide-Fe_2O_3 55%, Silica-SiO_2 35%, Aluminium Oxide-Al_2O_3 3.01%, Calcium Oxide-CaO 0. 20%, Magnesium Oxide-MgO 0. 90%, Copper-Cu 0.42%, Titanium Di-oxide 0.60%, and Potassium Oxide 1. 02% (Hammarstrom et al.1999). The geochemical characteristic of used copper slag can be analyzed for its element content, pH, acid neutralization capacity (ANC), redox potential (Eh), and electrical conductivity (EC). According to the previous research done by Lim et al. (1997), it is clear that the pH of leachate generated from the used copper slag is around 8.4. This pH value is within the common pH range for soils and groundwater. Figure 6 shows the variation of pH- acid titration curves for used copper slag and natural soils (Moyer et al. 2000).

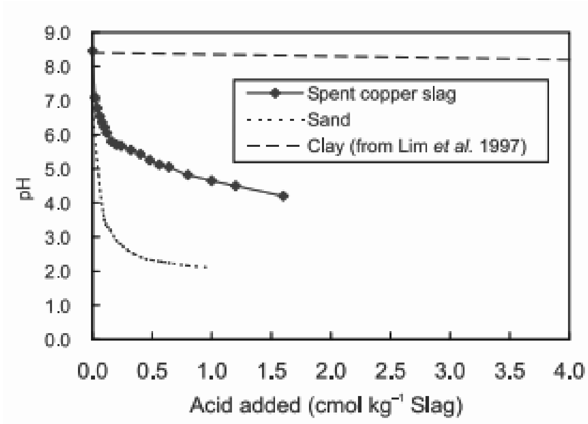

Figure 7: pH- acid titration curves for used copper slag and natural soils (After Moyer et al. 2000)

Figure 7 clearly illustrates that the used copper slag has a rather low ANC in comparison with the clay. Sand has practically negligible ANC. The low ANC value indicates that the spent copper slag is not resistant to acid attack. The concentration of Pb, Cd, Cr, Ba, As, Ag, Se, Cu, Zn, Ni and Hg in the used copper slag leachate are fairly low. The leachabilitie of Cu and Zn metals are much higher when compare with Cd, Pb, Cr and Ni. The impact of the heavy metals leachability would be nullified by dilution process under larger water: slag ratio. Another important property of the used copper slag is the Eh value. The initial Eh value for the used copper slag is 171 mV at a solid: water ratio of 1:1. The Eh would continue to decrease rapidly days after placing the copper slag. Due to the presence of sulphide minerals, the used copper slag can be oxidized under oxic condition and release H^+ into the pore water. As a result, there is a marginal drop in pH. The reduction can be expressed by the following reactions such as reactions of pyrite and ferrous. The amount of H^+ generated from this reaction is very low and do not have enough reaction power to make significant changes in double layer of clay minerals.

Pyrite oxidation:

$$4FeS_2 + 14O_2 + 4H_2O \longleftrightarrow 4Fe^{2+} + 8H^+ + 8SO_4^{2-}$$

Fe (11) oxidation:

$$4FeSO_4 + O_2 + 10H_2O \longleftrightarrow 4Fe(OH)_3 + 8H^+ + 4SO_4^{2-}$$

The variation in pH due to present of heavy metals can be affected to the groundwater pollution scenario. According to the previous research done on used copper slag, it is clear that the effect of groundwater pollution scenario is very unlikely to occur (Lim et al. 1997).

6 CONCLUSIONS

Results have show that the hydraulic conductivity of the tested sand was hardly affected by the addition of waste copper slag due to the void ratio and the hydraulic conductivity of the waste copper slag itself being very similar to that of the sand. Investigation of the geochemical characteristics of the used copper slag alleviates the concern of possible groundwater pollution by its use. Therefore, it can be concluded that used copper slag can safely and effectively be used as a replacement for sand in vertical drains.

The shear strength of properties of the tested sand-copper slag mix was found to be very insensitive to the amount of waste copper slag in the mix. In a “loose” state the sand-copper slag mix shows friction angles of 30.4° – 31.4°, which is a deviation of only 1°, even when the percentage by weight of waste copper slag changes from 0 to 40.

The stiffness of the sand was found to be clearly improved by the addition of waster copper slag. The addition of waste copper slag substantially reduced the settlement of the mix when tested in a conventional consolidation apparatus. This shows potential of waste copper slag to be successfully used as a replacement for sand in “sand piles” with the added advantage of improved performance.

It was puzzling to find that the stiffness of the sand-copper slag mix was insensitive to increases in the amount of waste copper slag beyond 10% by weight. However, the authors feel that shear strength and stiffness behavior holds the greatest potential for the use of waste copper slag hence, further testing is already underway.

7 ACKNOWLEDGEMENTS

Officials of Colombo Dockyard for providing waste copper slag for this research.

8 REFERENCES

Hammarstrom, J.M., Meier, A.L., Jackson, J.C., Barden, R., Wormington, P.J., Wormington, J.D., and Seal, R.R., II., 1999, Characterization of mine waste at the Elizabeth copper mine, Orange County, Vermont: U.S. Geological Survey OpenFile Rep. 99-564, 74 p.

Lim, Teik-Thye, and J. Chu. "Assessment of the use of spent copper slag for land reclamation." *Waste Management & Research*, 2006.

Lim, T. T., J. H. and Tech, C. I. (1997) Sorption and speciation of heavy metals from incineration fly ash in a marine clay. Journal of Environmental Engineering, 123 (11), 1107- 1115.

Moyer, T.C., Jourdan, R., Taylor, M., and Mozingo, J.T., Jr., 2000, Challenges of restoring an environment impacted by a century of copper mining: the Copper basin mining district, Tennessee: Geological Society of America, Abstracts with Programs, v. 32, no. 7, p. 476-477.

Tools for Natural Hazard management in a Changing Climate

Outils de gestion de désastres naturels dans un climat changeant

Rogbeck Y., Löfroth H., Rydell B., Andersson-Sköld Y.
Swedish Geotechnical Institute, Linkoping, Sweden

ABSTRACT: The paper will give an overview of some existing tools and models that can be used for risk analyses due to natural hazards (landslides, erosion and consequences of flooding) in a changing climate. Tools from several countries have been investigated by a literature survey and a questionnaire. A more comprehensive tool developed by Swedish Geotechnical Institute (SGI) will be presented more in detail. A compilation of tools has been carried out in the project "Baltic Climate", funded by the EU Baltic Sea Region Programme 2007-2013 and its partners. The investigation shows that there is a general lack of tools for soil movements in the countries in the Baltic Sea Region and that most of the existing ones don´t take climate change into consideration. The paper will present a model that can be used separately or as a complement to more general tools for spatial planning. The tool for soil movements considers the consequences of flooding, landslides and erosion in a changing climate and it can be used on both regional and local levels. The tool is described as a general method with examples from municipal level. The SGI tool has been used in several practical cases both on a regional and local level.

RÉSUMÉ: Cet article donne un aperçu de certains des outils et des modèles existants qui peuvent être utilisés pour l'analyses de risques reliés aux désastres naturels (glissements de terrain, l'érosion et les conséquences des inondations) dans un climat changeant. Des outils provenant de plusieurs pays ont été étudiés par une étude bibliographique et par questionnaire. Un outil plus complet développé par l'Institut Suédois de Géotechniquev (SGI) sera présenté plus en détail. Une compilation d'outils a été réalisée dans le projet «Climat Baltique», financé par le programme de l'UE de la mer Baltique 2007-2013 et de ses partenaires. L'étude montre qu'il y a un manque général d'outils pour les mouvements du sol et que les outils existants ne prennent pas en compte les changements climatiques. Cet article présente un modèle qui peut être utilisé séparément ou comme un complément à des outils plus généraux de l'aménagement du territoire. L'outil des mouvements de sol considère les conséquences d'inondations, de glissements de terrain et de l'érosion dans un climat changeant et il peut être utilisé au niveau régional ou local. L'outil est décrit comme une méthode générale avec des exemples au niveau municipal. L'outil SGI a été utilisé dans plusieurs cas pratiques aussi bien au niveau régional que local.

KEYWORDS: tool, natural hazard, landslide, erosion, climate change

1 INTRODUCTION

In order to establish resilient communities, mitigate damages, adapt the built environment and establish a sustainable society, there is a need for a sound decision basis for buildings, infrastructure, industry and the environment. One cornerstone to reach a sustainable development is to take natural hazards into account both for the situation today and for the consequences of climate change. The predictions of global climate change include sea level rise, in many countries increased precipitation and runoff and more intense and damaging storms which will increase the threats of natural hazards.

2 NATURAL HAZARD MODELS IN CLIMATE CHANGE

In this paper tools are presented that can be used in a climate change adaptation process, with focus on natural hazards such as landslides erosion and flooding, There are also review of more general tools, e.g. "The Baltic Climate Toolkit" which can be used for planning on the regional, local and detailed level. The main purpose of the toolkit is to highlight the importance of climate change mitigation and adaptation aspects in spatial planning [1].

The "The Baltic Climate Toolkit" is developed within the project Baltic Climate (BC) [1]. Adaptation to the future climate conditions, including flooding etc. should be one of the starting points of the planning process proposed in the BC-toolkit.

The comprehensive decision process model described in this paper focuses on natural hazards such as erosion and landslides (soil movements). It constitutes a part of the Baltic Climate project and can be used individually or as complement to the general toolkit for aspects regarding soil movements. It can be used for adaptation aspects especially for spatial planning or in built-up areas to ensure a safe, healthy and sustainable society. The investigation was done by a questionnaire sent to the partners and associated organisations in BC complemented by a brief literature survey.

In addition to the presentation of the decision process model, a practical application of the model in a municipality is presented. The investigation constituted a part of the BC project. According to the results provided by the respondents several countries have started investigations to identify risks of natural hazards such as coastal erosion, landslides and flooding, but the investigations do not always incorporate the effects of climate change. Furthermore, the investigations are normally restricted to currently developed areas [1, 2]. The investigation in the Baltic Sea Region showed that there is a general lack of tools for soil movements and they don't consider the impacts of climate change. However, in Sweden there is a model, developed by the SGI, which is presented in this paper.

The questionnaire survey of tools/models of soil movements was also expanded to outside the Baltic Sea Region. A questionnaire was completed by respondents in France, Hungary, Italy, Norway, Poland and Slovakia. In all responding countries models for soil movements are in use. The models presented from Hungary, Italy, Poland and Slovakia do, however, not take climate change into consideration.

The literature survey revealed that a large range of conference papers can be of interest when working with soil movements for example [3] describes the EU project *Response*: "Applied earth science mapping for evaluation of climate change impacts on coastal hazards and risk across the EU". The methodology employs commonly available digital data sets in GIS to assess regional-scale levels of coastal risk through production of series of maps. The outputs of the methodology comprise factual data maps and thematic maps and non-technical summary maps as planning guidance.

An on-going EU project is the KULTU-Risk project [4]. It will focus on water-related hazards. In particular, a variety of case studies characterised by diverse socio-economic contexts, different types of water-related hazards (floods, debris flows and landslides, storm surges) and space-time scales will be utilised [4].

In the UK there is a Climate Impact Programme (UKCIP) that contains a range of tools, methods and guidance which can be used for climate adaptation. The programme demonstrates how and where they fit into a risk-based planning process. There is also a National Appraisal of Assets and Risk from Flooding and Coastal Erosion, with adaption options on [5].

In France Baills et al. [6] have developed a method for integrating climate change scenarios into slope stability mapping. The climate factor treated as a variable in the stability calculation is the ground water level. Ground water levels are calculated from a conceptual hydrological model driven by rainfall data, and are described as filling ratio of the maximum ground water level [2].

3 THE SGI DECISION PROCESS MODEL FOR NATURAL HAZARDS

The SGI decision process model describes the potential risk related to a particular natural hazard, and makes it possible to establish a decision basis for spatial planning and climate adaption of built-up areas [7].

The model is partly based on the results of the Interreg Messina project [8] and the EU Life Environment Response project [9]. The model is based on identifying the prerequisites or probability for a natural hazard (P) combined with its associated consequences (C) which will determine the risk (R = PxC). The entire model can be used or only parts of it depending on the situation. The model aims to provide outcomes in the planning process that contributes to sustainable development including risk, environment, economy and social sustainability aspects as shown in Figure 1 [2].

At every stage in the decision process model (Figure 1), more detailed tools/models or suggestions exists that help to handle the questions that arise. For example under potential hazards the output can be a hazard map, and under the stage potential risk areas the output can be a risk map. Other relevant tools for identifying and assessing risk mitigation strategies can be databases or other information on previous experiences of strategies including pros and cons. It could also be a description on functionality and related costs for investment. In the long-term perspective, it could also be more holistic assessments such as life cycle and multi-criteria analyses. If there exists for example a mapping tool/model in another country it can be used instead of the one in this paper, and the other stages in the decision process model can be used together with that method.

For possible measures in spatial planning, or for adaptation of the built environment, socio-economic analyses and environmental assessments could be carried out. National and regional inventories of the natural hazards are necessary for spatial planning, to get an overview of risk areas or making priorities for preventive measures. At the local level the SGI tool can be used as a base for spatial planning, decision making of alternative measures in a municipality or at a specific location. The tool can also be used before investments are made in an area.

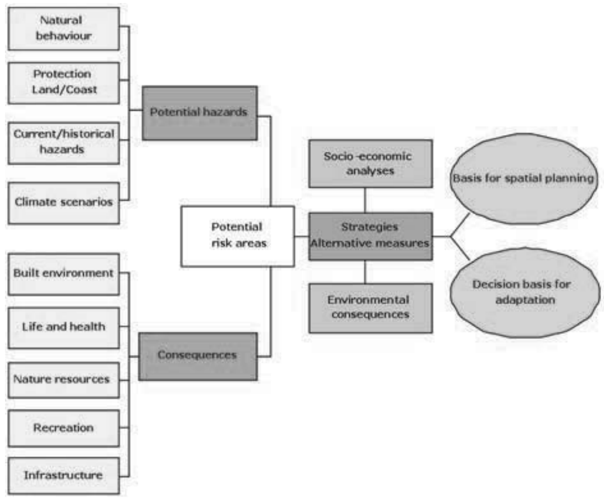

Figure 1. SGI decision process model.

Input to the model is for example Information on the site specific natural behaviour conditions which determine events that may lead to natural hazards. They can be topographical, bathymetrical, geological, water and wind conditions as well as vegetation. The high and low water levels in the sea and watercourses are important to determine. For water courses, also the streaming conditions must be estimated. These parameters are important to consider also for new climate scenarios. Also other input to the model has to be considered according to Figure 1[2].

3.1 Mapping of potential hazards/Probability

The susceptibility as an indication of the *probability* of hazards such as erosion, landslides and flooding can be estimated. In Sweden, national overview investigations of landslides, erosion and flooding are carried out and described briefly below.

The Swedish **landslide hazard mapping method for fine grained sediments** (clay and silt), is used in a nation-wide programme for landslide risk reduction in built-up areas administered by the Swedish Civil Contingencies Agency (MSB). The mapping method is divided in several stages which get more detailed and need more information for each stage. Initially a pre-study is carried out, with the purpose to identify sub-areas considered to be mapped. Thereafter, the mapped areas are divided into areas with and without prerequisites for initial slope failure. The next stage is to identify areas with satisfactory stability based on overview assessment and areas that need more investigations. The results are presented in a susceptibility map with three different zones. Other information of interest for slope stability, such as calculated sections, scars of old landslides, erosion in progress and the presence of quick clay can be shown on the same map [2, 10].

There is also a Swedish **landslide hazard mapping for till and coarse soils** [2, 11, 12] administrated by MSB, divided in stages in the same way. The susceptibility for landslides and debris-flows in slopes is carried out based on a combination of overview stability calculations (safety factor) and other influencing factors. The susceptibility for debris flows in gullies is based on already occurred debris flows and by mapping and compiling factors that could contribute to triggering of a debris flow. For both cases there is in general a combination of six main factors: topography, hydrology, soil conditions, land use, earlier soil mass movements and existing preventive constructions. It is necessary to calculate the peak discharge, determine the run-off conditions, the precipitation and the amount of available soil material. A classification is made and the results of the mapping and classification are reported on a map.

A **mapping for coastal areas** can also be performed. The hazards are identified by evaluation of the present state of the coast and a coastal geomorphologic model can be established. This includes the geomorphology, the topography and bathymetry as well as the driving forces such as water levels, waves, water currents and existing coastal protection. With climate change scenario for the chosen time period the probability for hazards such as erosion, landslides and flooding can be estimated. In Sweden, an overview mapping of the prerequisites of coastal erosion of the Swedish coasts, larger lakes and rivers has been carried out by SGI and maps will be found at [16] A model for risk analysis has also been developed at SGI, based on the principle of carry out analysis step by step depending on the need for decision basis [14] In many countries there are on-going works with **inundation mapping** due to EU directive. In many cases the mapping is done only for today's climate, but it is important to complement it with climate change scenarios.

3.2 Consequences

Potential consequences of a natural hazard can be described on overview or detailed levels. Within a governmental investigation on slope stability in the Göta River, SGI has developed a detailed method to identify, map and when possible assess consequences of potential landslides throughout the studied area [15, 16].

The method comprises:

- identification of consequences
- inventory/mapping of objects that may be affected
- assessment of the vulnerability, ie the probability of a certain consequence in case of a landslide
- method for monetary assessment

Relevant factors to consider are e.g. population, property, contaminated land, transportation network, industry. Monetary valuation of the consequences and estimation of the vulnerability are performed. The work has been divided in societal consequence sectors: buildings; transport, exposure, vulnerability and life; environmentally hazardous activities and contaminated sites; water and sewage systems; nature; culture; energy and electric supply systems; trade and industry.

The consequence is set to be the product of the inventory of elements at risk, value per unit area, the vulnerability and the exposure. The result is presented in a 2D map with five consequence classes given in MSEK/ha.

3.3 Potential risk areas

The principle is to identify risk areas based on the probability of an event and the consequences of such an event. Depending on the need of information risk analysis can be carried out on overview or detailed levels. In the Göta River investigation five classes of probability and consequence, respectively, are combined in a risk matrix from which three classes of risk are identified (Figure 2);

- low risk level
- medium risk level (investigation required)
- high risk level (preventive measures are required).

The outcome of the risk analysis can be presented in maps covering the investigation area illustrating the extent of the three risk levels. The method has been used in practice in e.g. the Göta river valley [17].

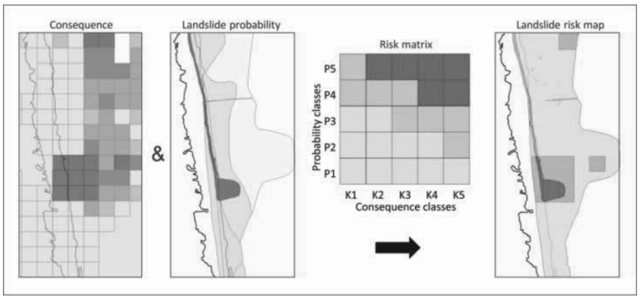

Figure 2. Illustration of risk analysis, where the consequences and probabilities for landslide are grouped into 5 classes and combined by GIS techniques in a risk matrix with three risk classes; low risk level, medium risk level (investigation required), high risk level [17].

3.4 Strategies and alternative measures

At the local level both for spatial planning and the built environment, the need for mitigation and adaptive measures must be identified, and data for the design and construction of such measures must be clarified. Requirements for remedial works can also be predicted using field-monitoring data, which may change the risk management philosophy from a reactive to a more pro-active one.

Mitigation measures for landslides, erosion and flooding risks often require levees, coastal protection and/or other stabilising measures. Such measures require geotechnical information during several stages of the planning and building process. In spatial planning, all factors that may cause risk for health and safety must be identified so that buildings and infrastructure will be located outside present and future risk areas or measures taken to secure these risk areas.

3.5 Socio-economic analyses and environmental impacts

For possible measures in spatial planning or for adaptation of the built environment socio-economic analyses are carried out. When socio-economic analyses are made they have to be based on correct actual data and valid methods to predict future development for different alternatives/scenarios. This is the basis for establishing the risk level that needs to be related to the acceptable risk level, the need of, and which, countermeasures that can be used to alleviate the potential problems. Also the stakeholders must be identified and the activities that are affected by possible changes to the land or coastal area. Analysis can be done for example by a Cost-Benefit Analysis (CBA). The basic way of working with a CBA model is to start by estimating total damage and loss for the "Do Nothing"-alternative. This value is later used as the benefit (or avoided damage) for the investigated options of preventive actions. The next step is to estimate the schedule and cost of implementing the options. Finally, if there still is a risk of damages for the investigated options; the cost of this is also calculated. For a CBA the selection criterion is that if the ratio between benefits and costs is greater than 1 (benefits divided by costs >1) the option is worth doing. The option with the highest benefit cost ratio gives "best value for money" [18].

Most of measures to reduce risks for natural hazards have to be built in environmentally and naturally sensitive areas close to the sea or rivers, in some cases consisting of Natura 200 areas. For that reason, all measures have to be evaluated due to the environmental impacts. For the proposed strategies and alternative measurements environmental consequences have to be considered.

3.6 Basis for spatial planning and adaptation

For spatial planning, following the stages in the model, the decision makers will have a proper and transparent basis for discussion with different stakeholders and the final decision of the best available way to establish sustainable land and coastal areas.

For the built environment, the decision makers will have a proper and transparent basis for the discussion with different stakeholders and the final decision of the best available way to adapt built environment on land and in coastal areas.

4 EXAMPLE ON THE LOCAL LEVEL

The model or parts of the model has been used in several climate and vulnerability analysis in Sweden, both on regional and local level.

The municipalities have to make comprehensive plans and detailed development plans, where risks for natural hazards must be investigated. In order to consider the consequences of climate change on the planned and existing built environment SGI and Swedish Metrological and Hydrological Institute have on behalf of Nynashamn municipality carried out an Overview Climate- and Vulnerability Analysis as a basis for the Municipal Comprehensive Plan 2010.

When working with comprehensive plans detailed data normally is not available, so the evaluation was made of the interface between areas with risk for natural hazards and consequences for important society constructions. The aim of the investigation was to clarify the consequences due to increased rain fall and sea level rise for different scenarios. Areas with risks for flooding, landslides or erosion have been investigated and the risk areas are illustrated in maps, see Figure 3. The interface between these areas and important society constructions has also been shown. The constructions can be e.g. special buildings, roads, railroads, dams. Environmental aspects have to be considered for e.g. flooding or landslides in contaminated areas or areas with enterprises with potential hazardous activities or dangerous substances.

An example of such a map is shown in Figure 3. The flooding from sea level rise is shown in the figure for different scenarios and the levels are also shown in Table 1.

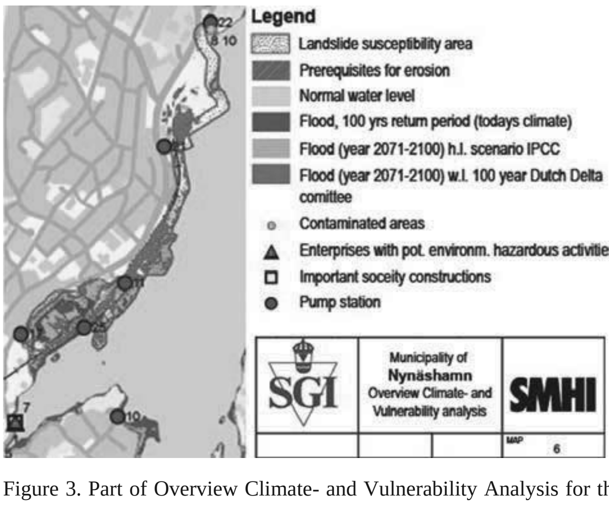

Figure 3. Part of Overview Climate- and Vulnerability Analysis for the Municipality of Nynäshamn in Sweden [2].

Table 1. The sea level for determination of flood along the coast of Nynashamn (given in meter in the Swedish height system RH00).

Case	*Level (RH00)*
1. Flood, 100 years return period (today's climate)	0.68
2. Flood calculated future (year 2071-2100) high level scenario according to IPCC	1.30
3. Flood, future (year 2071-2100) water level with 100 years return period, according to the Dutch Delta committee	1.71

As shown in the figure and table there can be rather different results depending on which scenario that are used. It is important to compare different scenarios and act for uncertainties. Recommendations have to be suggested for spatial planning. In built-up areas natural risks measures have to be taken to prevent damages on constructions. Strategies and measures are suggested, for example slope excavations, berms, levees, coastal protection or other stabilising measures.

REFERENCES

1. The Baltic climate project, financed by EU Baltic Sea Region Programme 2007-2013, http://www.toolkit.balticclimate.org
2. Rogbeck Y., Löfroth H. and Persson H. (2012) Baltic challenges and chances for local and regional development generated by climate. Swedish Geotechnical Institute, SGI. Varia 628, Linköping.
3. Fish P.R., Moss J.L., Jakeways J. and Fairbank H. (2007) Response: Applied earth science mapping for evaluation of climate change impacts on coastal hazards and risk across the EU; International conference on landslides and climate change. Challenges and solutions, Ventnor, Isle of Wight, UK, 21-24 May, 2007.
4. The KULTU-Risk project, www.kulturisk.eu
5. The UKCIP tool website, www.ukcip.org.uk/tools
6. Bailles A., Vandromme R., Desramaut N., Sedan-Miegemolle O. and Grandjean G. (2011) Changing patterns in climate-driven landslide hazard: an alpine test site. World Landslide Forum, 2, Rome, 3-7 October, 2011. Proceedings.
7. Rydell B., Persson M., Andersson M. and Falemo S. (2011) Sustainable development of near-shore areas. Planning and decision basis for prevention of natural hazards due to climate change. (In Swedish). Swedish Geotechnical Institute. Varia 608. Linköping.
8. Messina (2006) Monitoring and modelling the shoreline. Messina Component 2. Results from the Messina study. www.interreg-messina.org (2007-07-19).
9. McInnes R. (2006) Responding to the Risks from Climate Change in Coastal Zones. A good practice guide. Centre for the Coastal Environment, Isle of Wight Council, United Kingdom. www.coastalwight.gov.uk/response.html (2008-03-26).
10. Fallsvik, J. (2007). Zonation and landslide hazard by means of LS DTM - Deliverable 7, LESSLOSS - Risk Mitigation for Earthquakes and Landslides Integrated Project. Swedish Geotechnical Institute, SGI. Varia 578. Linköping.
11. Lundström K., Viberg L., Sundsten M., Andersson M, Fallsvik, J. and Sällfors G. (2007) Overview mapping of stability and run-off conditions in gullies and slopes in till and coarse-grained sediments. Mehtod description (In Swedish). Räddningsverket. Karlstad.
12. Rankka K. and Fallsvik J. (2005) Stability and run-off conditions – Guidelines for detailed investigation of slopes and torrents in till and coarse-grained sediments. Swedish Geotechnical Institute, SGI. Report 68. Linköping.
13. The SGI website, www.swedgeo.se
14. Rydell B., Blied L., Hedfors J., Hågeryd A.C. and Turesson S. (2012) Metodik för översiktlig kartering av risker för stranderosion. (Methodology for overview mapping of erosion). (In Swedish). Swedish Geotechnical Institute, SGI. Varia 641. Linköping.
15. Andersson-Sköld Y. (2011) Consequences of landslides in the Göta river valley – Sensitivity analysis, classification and application of the methodology throughout the study area. (In Swedish). Swedish Geotechnical Institute, SGI. Göta River Commission. Sub Report 13. Linköping.
16. Andersson-Sköld Y., Falemo S., Suer P. and Grahn T. (2011) Landslide risk and climate change – economic assessment of consequences in the Göta river valley. European conference on soil mechanics and geotechnical engineering, 15: Geotechnics of Hard Soils - Weak Rocks, Athens, 12-15 September, 2011. Proceedings, vol. 3, pp 1313-1318.
17. Landslide risk in the Göta river valley in a changing climate. Final Report 2 – Investigation conduct and methods. (In Swedish). Swedish Geotechnical Institute, SGI. Göta River Commission. Linköping.
18. Rydell B., Persson M., Rankka K. and Uytewall E. (2006) Guideline for socioeconomic valuation of the shoreline. Coastal innovations and initiatives, Littoral 2006, Gdansk, Poland, 18-20 September, 2006. Proceedings, vol. 1, pp 16-22.

Experimental reinforced soil walls built with recycled construction and demolition waste (RCDW).

Murs expérimentaux de sol renforcé construits avec résidus de construction et démolition recyclés

Santos E.C.G.
Polytechnic School of the University of Pernambuco

Palmeira E.M.
University of Brasília

ABSTRACT: In spite of its well known evolution, the Civil Engineering is yet pointed out as remarkable raw material consumer and one of the leading waste generators in modern society. Nowadays, construction and demolition waste became a complex problem to government authorities due to its economical and environmental impacts. Bearing in mind these aspects, the use of recycled construction and demolition waste (RCDW) in reinforced soil structures appears to be an interesting proposition. In order to investigate this proposal, two instrumented full-scale wrapped face geosynthetic reinforced walls were constructed using recycled construction and demolition waste as backfill material. The instrumentation plan consisted of more than 400 instruments and required the adoption of a careful installation process due to the presence of coarse particles of RCDW. The results have shown that RCDW has excellent mechanical properties - with low variation – which allow its use not just in the suggested proposal but in other geotechnical works. Additionally, based on lessons learned during the construction process, some recommendations are presented with the intention of promoting a better performance of reinforced walls built with this "novel construction material".

RÉSUMÉ : Malgré sa nette évolution, le génie civil est toujours indiqué comme un grand consommateur de matière première et un des leaders de la génération de résidus dans la société moderne. Actuellement, le résidu de construction et démolition est devenu un problème complexe pour les autorités municipales en raison des impacts économiques et environnementaux. Compte tenu de ces aspects, l'utilisation des résidus de construction et démolition recyclés (RCD-R) dans les structures de sol renforcé, émerge comme une proposition intéressante. Pour investiguer cette proposition, deux murs renforcés avec géosynthétiques de face enveloppé ont été construits avec RCD-R comme matériaux de remplissage. Les murs ont été construits à l'échèle réel et instrumentés. L'instrumentation consistait a plus de 400 instruments et elle a demandé l'adoption d'un procès minutieux d'installation en raison de la présence des cailloux du RCD-R. Les résultats ont montré que le RCD-R possède d'excellentes propriétés mécaniques – avec faibles coefficients de variation – qui permettent leur utilisation non seulement dans la proposition suggérée, mais aussi sur d'autres ouvrages géotechniques. De plus, basée sur les leçons apprises au cours du processus de construction, certaines recommandations ont été déposées dans le but de promouvoir une meilleure performance des murs renforcés construits avec ce "nouveau matériaux".

KEYWORDS: reinforced soil wall, geosynthetics, recycled construction and demolition waste, instrumentation.

1 INTRODUCTION.

The Geotechnical Engineering has provided the development of innovative solutions to complex Civil Engineering problems. This proves its technical capacity to face new challenges. However, besides its well known evolution, the Civil Engineering is yet pointed out as remarkable raw material consumer and one of the leading waste generators in our modern society. Nowadays, construction and demolition waste (CDW) became a complex problem to government authorities due to its economical and environmental impacts.

In this scenario, some aspects related to growth of cities and to the need for adoption of sustainable development concepts may threaten the technical and economical advantages of reinforced soil structures: i) lack of good quality backfill material near to site construction and ii) compliance with environmental laws, which became more strict with respect to exploitation of new raw materials deposits. Bearing in mind these aspects, the use of recycled construction and demolition waste (RCDW) in reinforced soil structures appears to be an interesting proposition.

In order to investigate this proposal, two instrumented full-scale wrapped face geosynthetic reinforced walls were constructed using RCDW as backfill material.

1.1 *RCDW geotechnical characterization for use in reinforced walls*

The Brazilian Environmental National Council (CONAMA), in its Resolution 307/2002, states that wastes generated in "[…] site preparation and excavation […]" are classified as construction and demolition waste (CDW). Due to this, huge amounts of soil stockpiles can be found in some Brazilian recycling plants. According to the Construction Waste Collecting Association (2011), in Brasília (capital city of Brazil) approximately 70% of mass of municipal solid waste consist of CDW. According to Santos (2011), approximately 65% of mass of the recycled construction and demolition waste (RCDW) produced in Brasília is composed of soil. This fact reveals an interesting perspective to the use of RCDW in geotechnical works.

Santos (2007), in order to evaluate the potential use of RCDW in geosynthetic reinforced walls, carried out a laboratory testing program focused on geotechnical characterization and pH tests. Furthermore, pullout tests with geogrids were performed using clayey sand [typical soil from the southeast part of Brazil] and sand obtained from a local supplier. Clayey sand was chosen in order to compare the behavior of RCDW to others materials. The sand material was compliant with FHWA recommendations for backfill materials.

The RCDW material revealed a low coefficient of variation with respect to geotechnical properties and low alkalinity applicable to be used with geogrid products. The mechanical properties were excellent for the proposed application. The results of pullout tests with RCDW showed that the recycled material yielded a better performance when compared with the standard sand.

Based on the facts listed above and results observed by Santos (2007) as well as on interesting perspective for the use of this waste in geotechnical structures, a research programme aimed at investigating the performance of reinforced soil structures using RCDW as backfill material started in 2009 at the University of Brasilia, Brazil.

2 EXPERIMENTAL REINFORCED RCDW WALLS.

2.1 *Recylced Construction and Demolition Waste (RCDW)*

The recycled construction and demolition waste (RCDW) used as backfill material consisted of the product of the crushing process of construction and demolition waste (CDW), which is composed mainly of mixed materials including soil, bricks, and small particles of concrete. The RCDW was sampled at the CDW Re-cycling Plant of Brasília-DF, located at Jockey Club Landfill (Figure 2). Usually, this material is used by the local government as cover for unpaved roads.

Figure 1. CDW Recycling Plant of Brasília-DF.

A large-scale equipment was used for the determination of the RCDW shear strength parameters. Because of the presence of coarse grained particles (Figure 2), the dimensions of the shear box used were 800x800x450mm. Table 1 presents the main geotechnical parameters of the RCDW tested.

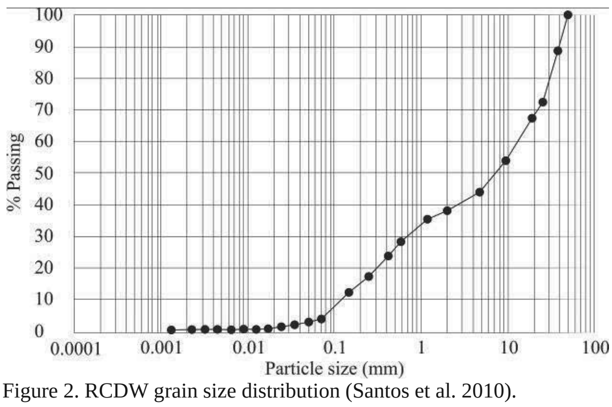

Figure 2. RCDW grain size distribution (Santos et al. 2010).

Table 1. Geotechnical properties of RCDW.

Parameter	*Value*
Specific gravity (g/cm^3)	2.74
Liquid limit (%)	35
Plastic limit (%)	28
Maximum dry unit weight (kN/m^3)	16.9
Optimum water content (%)	18
Friction angle (°)	38
Cohesion (kN/m^2)	14

2.2 *Geosynthetics*

The geosynthetics used as reinforcement for the walls in this investigation consisted of a polyester geogrid and a polypropelene nonwoven geotextile. Table 2 summarizes the main properties of the reinforcement.

Table 2. Geosynthetics properties.

Parameter	*Data/Value*	
	Geogrid	*Geotextile*
Polymer	PET	PP
Longitudinal tensile strength (kN/m)	20	19
Transverse tensile strength (kN/m)	9	21
Maximum tensile strain (%)	12	70

2.3 *UnB Retaining Wall Test Facility*

Experimental walls were constructed in the UnB Retaining Walls Test Facility located outdoor at the Foundation, Field Test and Geosynthetics Experimental Field area. The test facility was designed to allow two walls to be constructed up to 3.6 m high by 3.7m wide and extending up to 7.2m from the front edge of the facilityedge. The facility can contain up to 214 m3 of backfill material for the construction of two walls simultaneously. Figure 3 shows an overview of the test facility.

Figure 3. UnB Retaining Wall Test Facility (Santos et al. 2010).

3 CONSTRUCTION PROCEDURE AND INSTRUMENTATION.

The walls construction process was conducted using the moving formwork technique, which is a common method for the construction of wrapped-faced walls in the field. In order to reduce the side wall friction, the whole internal walls of the test facility were covered with three polypropylene sheets interspersed with lubrication (liquid silicone).

Three walls sections were named according to their cardinal orientation as West, Central and East. This configuration allows for the instrumented portion of the wall (Central section) to approach a plane-strain condition, free from side wall effects, as far as practical. This procedure has been adopted at Royal Military College of Canada (RMC) in a successful long-standing program on construction of full-scale reinforced walls (Santos et al. 2010).

The construction procedure consisted of placing the backfill material and compacting it in 200mm lifts. In order to provide a light compaction and a satisfactory surface leveling, a manual compaction roll was used. Near to the face, a hand tamping cylinder was used to minimize the effects of the compaction on the facing displacements. The total construction time was 29 days. Figure 4 and Table 3 present RCDW reinforced walls construction history and their main characteristics.

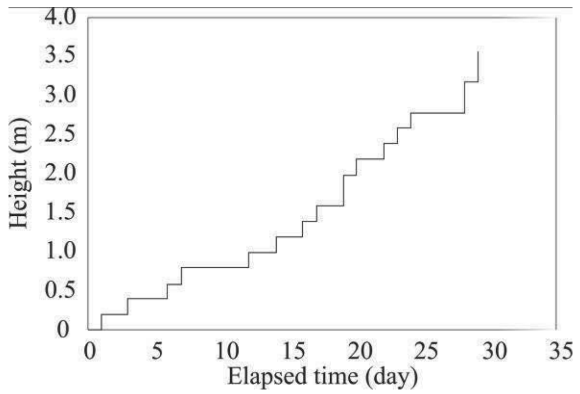

Figure 4. RCDW reinforced walls construction history (Santos et al. 2010).

Table 3. Main walls characteristics.

Characteristic	*Value*	
	Wall #1	*Wall #2*
Geosynthetics	Geogrid	Geotextile
Height (m)	3.60	
Facing batter (°)	13	
Reinforcement spacing (m)	0.60	
Reinforcement length (m)	2.52	

Approximately 400 instruments were installed in the two walls in order to record the following:

a. strain in reinforcement layers (strain gauges and wire-line extensometers installed in wall #1 and wall #2, respectively);
b. wall face displacements;
c. vertical earth pressure at the base of the RCDW (earth pressure cells - EPC);
d. horizontal earth pressure within the RCDW mass (EPC);
e. settlements along the surface of the RCDW mass (superficial marks);
f. horizontal displacement of the foundation soil (inclinometer).

Figure 5 shows the instrument distribution profile.

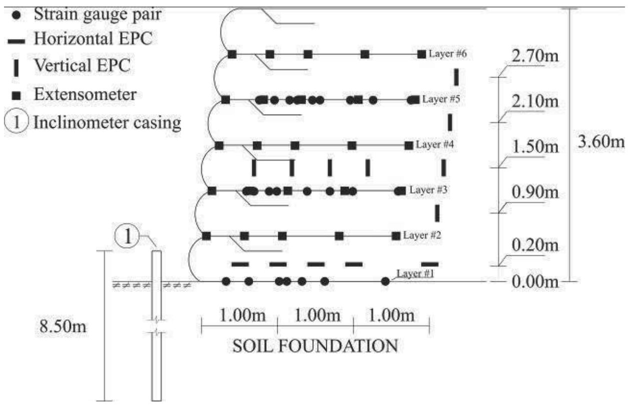

Figure 5.Instruments distribution profile.

Additional procedures were necessary to protect the instruments devices against mechanical damages during the walls construction. Because of the presence of coarse grained particles (Figure 2), the installation of the instrumented geogrid layers and earth pressure cells (EPC) were carried out using fine grained particles around the instruments. PVC tubes were used to create a region with selected fine RCDW - smaller than 2mm around EPC and strain gauges. Figure 6 presents a scheme of the region around strain gauges after geogrid layer installation process.

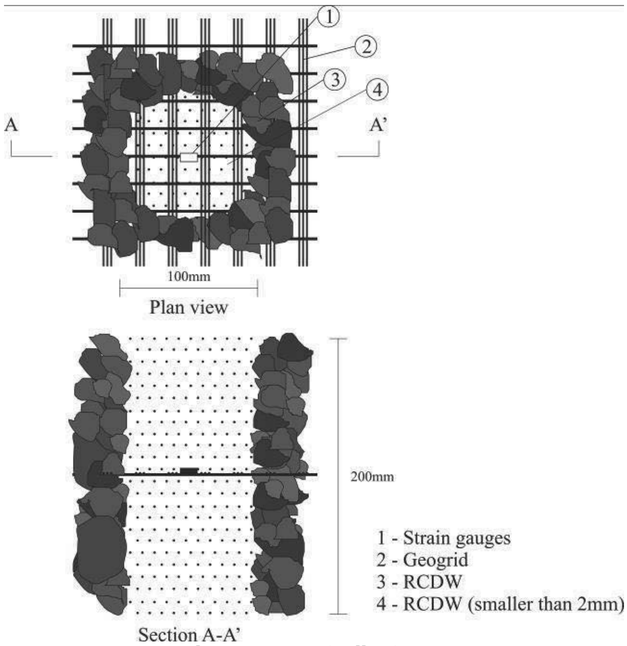

Figure 6.Region around strain gauges (wall #1).

The data recording after the walls construction revealed that just one strain gauge was mechanically damaged, which correspond to a survival level of 98% for installed strain gauges. This survival level kept stable until the end of research program even though the rainy seasons in Brasília. It was observed that all EPC survived to installation process but not to the first rainy season. After 110 days, all EPC failed.

Outward displacements of the walls faces during construction were measured. It was observed for the wall #1 (geogrid) a maximum end of construction face displacement measured with respect to formwork position of approximately 106 mm. Wall # 2 (geotextile) revealed a maximum end of construction face displacement - measured with respect to formwork position - approximately equal to 254 mm. Figure 7 shows wall #1 post-construction face profile.

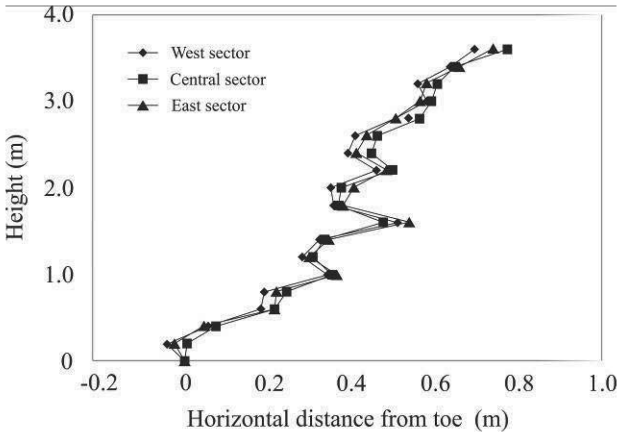

Figure 7. Post-construction face profile (Santos et al. 2010).

It was noticed for both walls that the presence of coarse particles near to face was responsible for the uneven surface and the different magnitude of facing displacements among the walls sectors at the same layer (Figure 8). Although this fact did not affect the mechanical performance of the walls, it is strongly advised to use a selected RCDW near the face in order to provide a better aesthetic aspect.

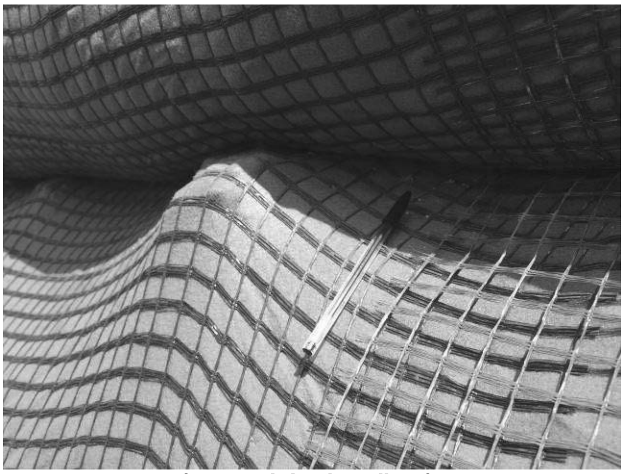

Figure 8. Uneven surface recorded at the wall #1 face.

4 CONCLUSIONS

The results obtained in the research programme have shown that the RCDW used has excellent mechanical properties - with low variation – which allow its use not just in the suggested proposal but in other geotechnical works. Additionally, the adoption of a careful installation process due to the presence of coarse particles of RCDW seemed to be successful once the strain gauges presented a high and stable survival level. Based on lessons learned during the construction process, some recommendations were presented with aiming at promoting a better performance of reinforced walls built with this “novel construction material”.

5 ACKNOWLEDGEMENTS

Funding for the research programme described here was provided by CNPq, FAP-DF and CAPES. The authors would like to acknowledge the contribution of the Geotechnical Research Group at RMCC, FURNAS, EMBRE, REFORSOLO, ORIGINAL, HUESKER, OBER, LINEA G, TORC, LINEA JR, ASCOLE, COOPERCOLETA and CAENGE AMBIENTAL.
.

6 REFERENCES

CONAMA – Brazilian Environmental National Council. Resolution nº 307 – Available in: http://www.mma.gov.br/port/conama/res/res02/res30702.html. Accessed at November 13th, 2006.

Santos, E.C.G., 2007. The Use of Recycled Construction and Demolition Waste (RCDW) in Reinforced Soil Structures. M.Sc. thesis, University of Sao Paulo, Sao Carlos, Brazil, 168 pp. (in Portuguese).

Santos, E.C.G, Palmeira, E.Marques, Bathurst, R. J. 2010 . Construction of a full-scale wrapped face geogrid reinforced wall using recycled construction and demolition waste as backfill material. In: *9th International Conference on Geosynthetics, 2010*, Guarujá-SP

Santos, E.C.G., 2011. Experimental Evaluation of Reinforced Soil Walls Built with Recycled Construction and Demolition Waste (RCDW) and Cohesive Soil as Backfill Materials. D.Sc. thesis, University of Brasília, Brasília, Brazil, 216pp. (in Portuguese).

Comparing the properties of EPS and glass foam mixed with cement and sand

Comparer les propriétés d'EPS et mousse de verre mélangé avec du ciment et du sable

Teymur B., Tuncel E.Y.
Istanbul Technical University

Ahmedov R.
BP, Baku

ABSTRACT: One of the formations in which the waste materials can be used as a component is controlled low strength material (CLSM). CLSM is a self-compacting cementious material that is generally used as back-fill as an alternative to compacted-fill. In this study, the availability of glass foam and Expanded polystyrene (EPS) geofoam as a component for CLSM production was investigated, some geotechnical properties including strength and unit weight characteristics of composite soils were explored using several laboratory tests. When the results are compared, EPS mixtures have lower unit weight and undrained shear strength values compared to glass foam mixtures. Therefore use of glass foam will have the advantage of higher strength compared to EPS mixtures and can be used as a subbase material. As a result, it was found that a mixture containing cement, polystyrene foam or glass foam and sand, can be successfully used in some applications such as improvement of slopes and reduction of embankment weight.

RÉSUMÉ : La formation dans laquelle les déchets peuvent être utilisés comme un composant est contrôlé par matériel de faible résistance (CMFR). CMFR est un matériau auto compactant ciment est généralement utilisé comme remblai comme alternative au remblai compacté. Dans cette étude, la disponibilité de verre de mousse et Expanded polystyrène (EPS) mousse géotechnique en tant que composant pour la production de CMFR a été étudiée. Certaines propriétés géotechniques, y compris la force et l'unité de poids caractéristiques des sols composites ont été explorées à l'aide de plusieurs tests de laboratoire. Lorsque les résultats sont comparés, mélanges de l'EPS ont poids unitaire inférieur et les valeurs de résistance au cisaillement non drainé par rapport aux mélanges de mousse de verre. Donc utilisation de mousse de verre auront l'avantage d'une résistance plus élevée par rapport à des mélanges d'EPS et peut être utilisée comme le matériau de remblai. En conséquence, il a été constaté qu'un mélange contenant du ciment, mousse de polystyrène ou mousse de verre et du sable, peut être utilisé avec succès dans certaines applications comme l'amélioration des pistes et réduction du poids de berge.

KEYWORDS: cement, EPS foam, glass foam, sand, soil improvement.

1 INTRODUCTION

With the rapid increase in the need for superstructure and the increase in demand for the multi-storey high-rise buildings, composite materials are used to improve weak soils. The use of environmental and industrial waste materials as raw material in composite soils helps protect environment with the recycling of these materials while providing more economic solutions. One of the formations in which the waste materials can be used as a component is controlled low strength material (CLSM). CLSM is a self-compacting cementious material that is generally used as back-fill as an alternative to compacted-fill. Use of the recyclable materials in civil engineering industry, especially in the geotechnical applications as raw materials, contributes to the economy and the environment.

In Turkey, a considerable sum of solid waste materials is made of glass (DPT, 2001). Glass foam is one of the waste glassware recycling products which are used in certain structural applications. With its porous structure and light weight, glass foam, generally used for thermal and acoustic isolation, is also a potential filling in geotechnical applications where lightweight is crucial. In Turkey, waste glass composes the significant part of solid wastes and one of the recycled glass product is glass foam. In this study, the availability of glass foam and expanded polystyrene (EPS) geofoam as a component for CLSM production was investigated, some geotechnical properties including strength and unit weight characteristics of composite soils were explored using several laboratory tests. A certain mixture design and some engineering properties of this lightweight composite fill were determined by unconfined compression and California Bearing Ratio (CBR) tests.

Lightweight fill materials can be used in geotechnical engineering for the consolidation and bearing capacity problems of very soft soils, for filling applications performed on potentially collapsible slopes generally. Expanded polystyrene (EPS) geofoam which is obtained from the oil is used in low strength and soft soil construction as a lightweight fill material in different places of the world today. Expanded polystyrene foam is supplied as raw materials in the form of small particles. EPS is widely used in various geotechnical applications such as embankments, retaining structures, slope stability, bridge piers and other applications (Aksoy 1998 and Aytekin 1997). EPS has advantages of low cost and durability properties for long years against other types of lightweight materials, as well. Due to these reasons, expanded polystyrene has been popular over time in civil engineering and widely used as light and compressible fill material in many geotechnical application areas.

Geotechnical properties of EPS-cement-sand mixture were determined by unconfined compression tests and CBR tests. Ratio in terms of weight for cement to material of mixture was measured as 12/1. As a result, it was found that a mixture containing cement, polystyrene foam and sand, can be successfully used in some applications such as improvement of slopes and reducing the weight of embankments.

2 EXPERIMENTAL RESULTS

Figure 1 shows the grain size distribution curve for the sand used in the experiments. Sand used is classified as poorly graded sand (SP). The sand has a specific gravity of 2.64, maximum and minimum void ratio of 0.85 and 0.54 respectively. D_{60} of the sand used is 0.35mm and the internal friction angle was found 41. Considering the weight proportions of cement and glass foam, mixtures with different weight ratios of cement, which is used as the binding material, and glass foam, which is regarded as the main component having the largest volume ratio in the mixture, were prepared. Cement and water were mixed first, sand was added next if denoted in the design, and after these components make up a rather homogenous mixture, glass foam is added to the mixture and stirred till homogeneity again.

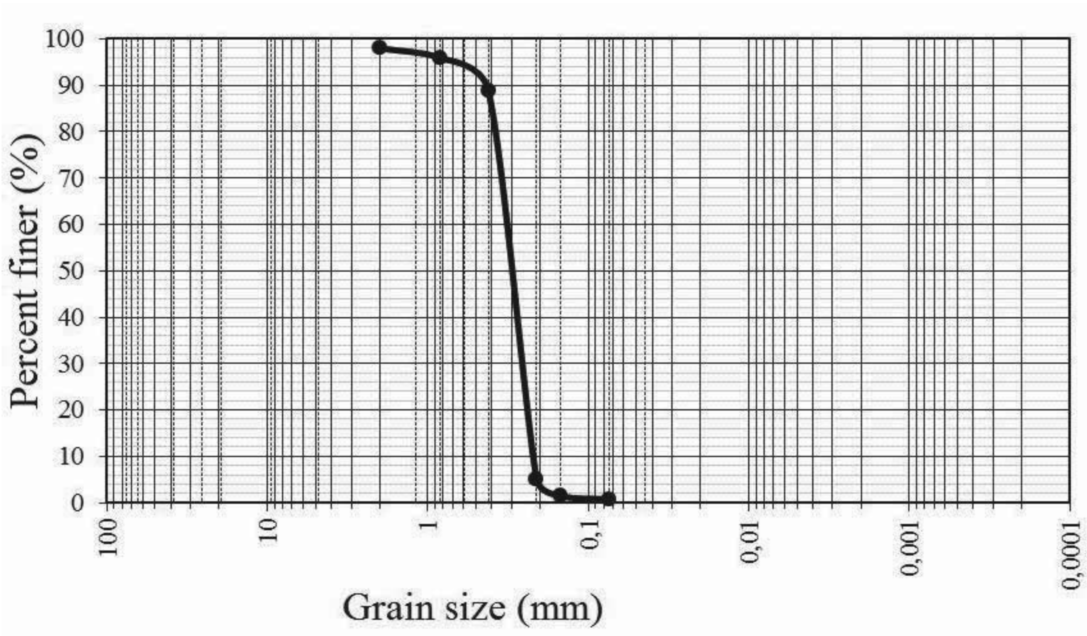

Figure 1. Grain size distribution curve for the sand used in the experiments.

When the 7-day experimental results of the mixtures that were produced using different sand ratios was examined, it has been observed that the optimum results were exhibited by the specimens which has equal sand and glass foam quantity and when cement over foamed sand mixture ratio is two. The water/cement ratio used is 0.45. Figure 2 shows the grain size distribution curve for the glass foam used in the experiments. The average value of the saturated unit weight of the glass foam mixture was found as 8.83 kN/m^3.

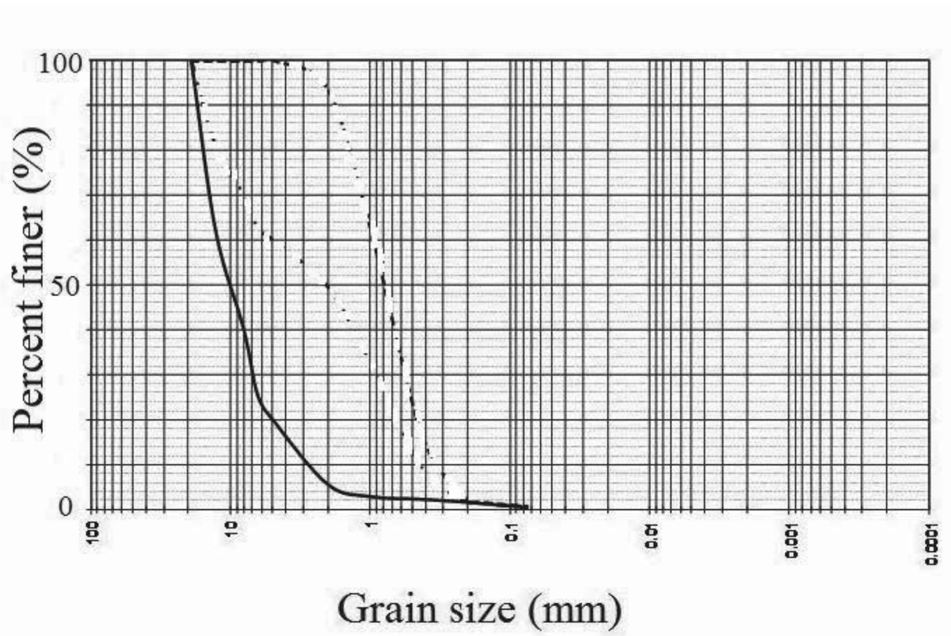

Figure 2. Grain size distribution curve for the glass foam used in the experiments.

Figure 3 shows the cement, sand and glass foam mixture sample used in the unconfined compression test. The average value of the typical 7-day unconfined compression strength of the mixture was determined as 0.75 MPa while the average of the 28-day unconfined compressive strength was 0.91 MPa. Figure 4 shows the results of these tests, as can be seen from the figure with time the strength of the sample increases. The CBR value of the 7-day mixtures was observed as 38.4 while this value was 78.9 for 28-day mixtures.

Figure 3. Cement, sand and glass foam mixture sample for the unconfined compression test (Tuncel, 2012).

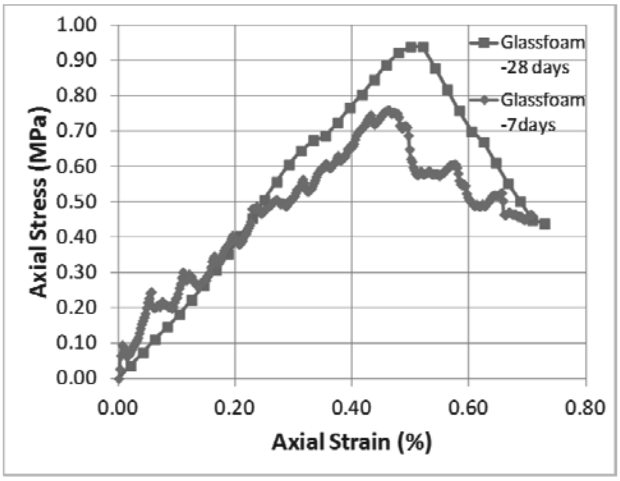

Figure 4. 7 and 28 days unconfined compression test results for the samples with glass foam.

The aim of the laboratory study of lightweight fill that consist of EPS-cement-sand mixture is investigation for its usability in geotechnical applications successfully. So for the solution of weak soils with low durability that have slope stability problems, it is tried to create more durable and compressible ligthweight soil than normal soils. The unit weight of the EPS mixture was 3.80 kN/m^3. Figure 5 shows the unconfined compression test sample of EPS, sand and cement mixture. Weight content of materials in mixture was selected, so different proportions such as 100%, 75%, 50% and 25% of EPS content of mixtures were prepared. To determine the ratio of EPS in the cementious material mixture, where sufficient shear strength is needed, unconfined compression tests were done. Prepared mixture samples were tested, then relevant percentage of expanded polystyrene content of material and cement/material ratio of mixture was determined. The relevant content of EPS in material is determined as 50% and ratio in terms of weight for cement/material of mixture was measured as 12/1. Unconfined compression value of 7 day sample is 0.22 MPa and of 28 day EPS mixed samples is 0.42MPa. According to the results, the mixture is defined as a low permeable lightweight fill and it also has CBR value that can be classified as medium. Figure 6 shows the results of these tests, as can be seen from the figure with time the strength of the sample increases.

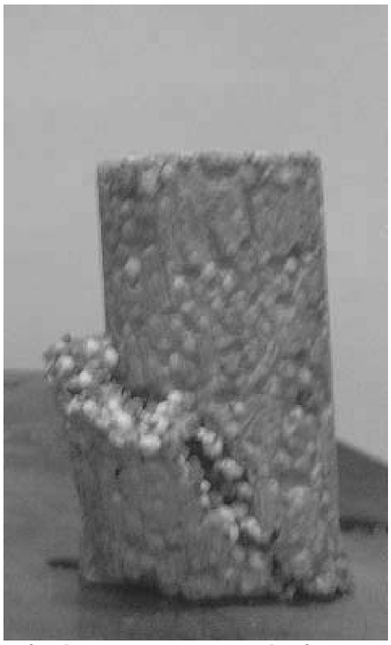

Figure 5. Unconfined compression test sample of EPS, sand and cement mixture (Ahmedov, 2012).

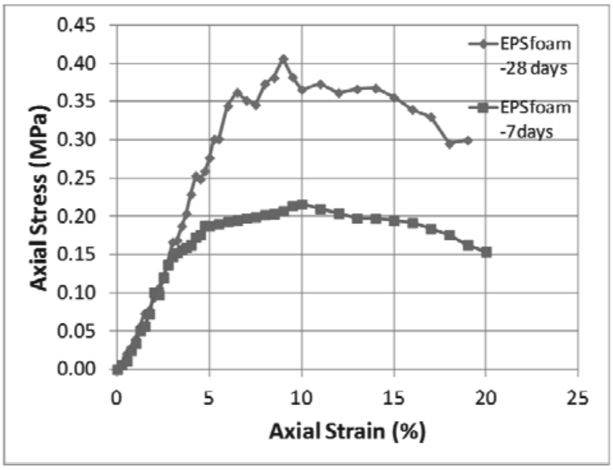

Figure 6. 7 and 28 days unconfined compression test results for the samples with EPS foam.

CBR tests showed that the glass foam-sand-cement mixtures have enough bearing capacity to be used as a subbase material. CBR values for 28 days old EPS mixture is 7 making it weak to be used as a subbase material. As a result, by producing lightweight fills with CLSM mixture produced using glass foam-sand-cement can be a solution for consolidation and bearing capacity problems of very soft soils which continually consolidate, constitution of geotechnical fills on potentially sliding slopes and reducing the stress distribution on retaining structures.

3 CONCLUSIONS

When the test results of the glass foam-sand-cement mixture compared with the other lightweight fill materials it was seen that glass foam-sand-cement mixture has a higher unconfined compressive strength and CBR value. The CLSM mixture produced using glass foam-sand-cement can be used as lightweight fills on very soft and continually consolidating soils for solving the consolidation and bearing capacity problems. It can be convenient to use this mixture as fill for potentially sliding slopes and for reducing the lateral stresses that received by soil retaining structures.

When the results are compared, EPS mixtures have lower unit weight and undrained shear strength values compared to glass foam mixtures. Therefore use of glass foam will have the advantage of higher strength compared to EPS mixtures and can be used as a subbase material.

4 REFERENCES

Ahmedov R. 2012. Determination of geotechnical properties of cement-EPS foam-sand mixture as a lightweight material fill, MSc Thesis, Istanbul Technical University, Turkey.

Aksoy İ. H. 1998. Use of polystyrene foam as a lightweight fill, Seventh national soil mechanics and foundation engineering conference, 2, 428 – 437, Istanbul.

Aytekin M. 1997. Numerical modelling of EPS geofoam used with swelling soil, *Geotextiles and Geomembranes*, 15(1–3), 133-146.

DPT 2001.Report on the eighth five year plan on water supply, waste water and waste materials, DPT Publications, Ankara.

Tuncel E.Y. 2012. Geotechnical Properties of Glass Foam-Cement-Sand Mixtures as a Lightweight Fill Material, MSc Thesis, Istanbul Technical University, Turkey.

Geotechnical engineering and protection of environment and sustainable development

Engineering géotechnique, protection de l'environnement et développement durable

Vaníček M., Jirásko D., Vaníček I.
Czech Technical University in Prague

ABSTRACT: The paper highlights the positive role of geotechnical engineering for protection of environment and sustainable development, first of all from the view of sustainable construction. The main attention is therefore focused on the problems which are sensitive to society in general as the construction on brownfields, utilization of waste and recycled materials for new construction and rehabilitation of territory affected by open pit mining process which is proposed as new development area. The first point is connected with the protection of greenfields and is defining basic phases of process of rehabilitation as the significance of first phase of geo-environmental investigation, remediation of contaminated subsoil and utilization of old foundation. The second point describes practical experiences with utilization of large volume waste as construction and demolition waste or ash in earth structures– not only from the view of mechanical behaviour but also from the view of potential impact on environment. The last point describes the utilization of the surface of the mining spoil heaps for new construction together with control of long term stability of slopes even for future expected ground water table and heavy rainfalls.

RÉSUMÉ : L'intervention souligne le rôle positif de l'engineering géotechnique dans la protection de l'environnement et le développement durable, et ceci essentiellement du point de vue de la construction durable. Elle se concentre surtout aux problèmes généralement perçus par la société comme sensibles : la construction sur les friches industrielles, l'utilisation de déchets et de matériaux recyclés dans la nouvelle construction, ainsi que le réaménagement du territoire affecté par l'exploitation minière à ciel ouvert. Le premier point est lié à la protection des greenfields et définit les phases principales du processus du réaménagement, comme la première phase de la prospection géo-environnementale, l'assainissement du sous-sol contaminé et l'utilisation des bases anciennes. Le deuxième point décrit des expériences pratiques avec l'utilisation des déchets volumineux comme p.ex. des déchets de construction et de démolition ou bien des cendres dans les ouvrages en terre, non seulement du point de vue des caractéristiques mécaniques, mais aussi de celui de l'impact potentiel sur l'environnement. Le dernier point décrit l'utilisation de la surface du terril pour les nouvelles constructions, tout en assurant le contrôle de stabilité de long terme des pentes, même pour la nappe d'eau souterraine attendue et les précipitations fortes.

KEYWORDS: brownfield, remediation, contaminant, waste, spoil heap, soil improvement

1 INTRODUCTION

Geotechnical Engineering is falling under the limited group of professions, which to the high extent are able to react not only on classical construction problems but also to new society demands, namely with respect to:

- Protection against natural hazards – first of all against floods, landslides and earthquakes;
- Energy savings – especially with respect of Geothermal energy, as with high potential energy (from large depth) or with low potential energy in the forms of earth aerial heat exchanger, systems utilizing heat pumps or systems utilizing heat reversible pumps either for heating or for cooling with help of energy piles or diaphragm walls;
- Raw materials savings – with high potential for waste and recycled material utilization, especially for large volume waste as e.g. ash, slag, construction and demolition waste etc;
- Protection of greenfields – as GE is playing significant role in the field of "Construction on brownfields";
- Environmental protection in general – e.g. from the view of safe deposition of waste (landfills, tailing dams, spoil heaps, underground repositories) or with respect to remediation of old ecological burdens – decontamination of subsoil.

However in a matter of fact all above mentioned problems can fall under the umbrella of Environmental geotechnics and are parts of the geotechnical engineering benefit to Sustainable Construction, (Vaníček I. 2012).

The branch of Environmental Geotechnics is now very well established, falling under the important part of Geotechnical Engineering which can be called Geotechnics, Geo-Technology and represents the third column by which Geotechnical Engineering is supported, (Vaníček, I. and Vaníček, M. 2008). Remaining three columns are Theoretical background, Geomechanics and Feeling for ground response, whereas the first column Theoretical background relies on the understanding of natural sciences such as geology, engineering geology and hydrogeology on the one hand, and on the understanding of mechanics, theory of elasticity on the other. The second column relies on the application of existing findings to the behaviour of soils and rocks under different stress - strain states – we are speaking about support from soil and rock mechanics and finally the fourth column relies on a certain feeling of geological environment which Terzaghi (1959) denotes as "capacity for judgment", and he says that "this capacity can be gained only by years of contact with field conditions", (see Figure 1), (Vaníček, I. 2010).

However with the respect of the limited range of the paper only three problems will be discussed further.

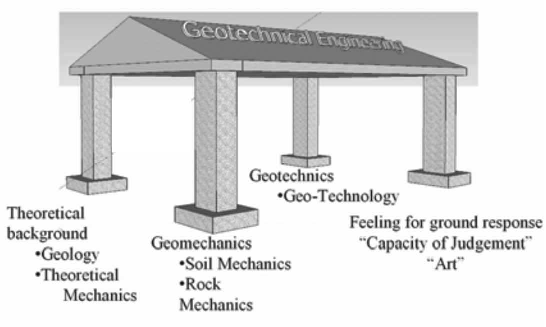

Figure 1. Four columns of Geotechnical Engineering

1 ROLE OF ENVIRONMENTAL GEOTECHNICS IN THE BROWNFIELDS REDEVELOPMENT

Very often the whole process of the brownfields redevelopment can be divided into the following individual steps, (e.g. Vaníček and Valenta 2009):

- site location identification,
- First phase of investigation,
- preliminary economic analysis,
- Second phase of investigation – detailed site analysis
- project of site development and methods of financing – feasibility study
- project and completion of site remediation
- project and completion of construction of new development (including foundation engineering, reuse of old foundations).

From these basic 7 steps, it is obvious that environmental geotechnics is strongly involved in the whole process. But typical for geotechnical engineers are four parts – 1st phase of investigation, 2nd phase of investigation – detailed site analysis, project and completion of site remediation and the problem of foundation engineering, respectively reuse of old foundations. These parts will be discussed further in more detail, (Vaníček 2010).

The first two steps are labelled as the first phase which can be also called the desk study, which is only supplemented by visual inspection. So this first phase mostly uses existing materials, where the study of archive materials and different maps composes the most important part of this phase.

The 2nd phase of the investigation encompasses site investigation, usually starting with borings, field tests, collection of samples and laboratory tests. Classical geotechnical data are useful from the foundation design perspective, geoenvironmental data from the view of site contamination.

The properties of the brownfields ground is usually affected by previous man made activity. These changes have character of physical, chemical or biological change. Owing to biological degradation some problems with gas (mostly with methane) are expected. However in most cases the subsoil remediation is connected with

- Physical improvement of the subsoil quality, with porosity decrease;
- Chemical improvement.

The main principle of physical improvement is to create top layer with much better quality than subsoil to be able to eliminate differential settlement of the subsoil and to guarantee the possibility to create good footing bottom for new foundations, see more in chapt. 4.

As the depth of the affected subsoil is usually deeper than the depth for which classical compaction rollers can be used it is necessary to apply other methods. The dynamic consolidation method was for example used for the subsoil improvement of old toxic landfill in Neratovice, (see Figure 2), where on the compacted material a new landfill was constructed, (e.g. Vaníček et al 2003).

Figure 2. Compaction of deposited waste by dynamic consolidation

In the north part of Bohemia, where there are many inner spoil heaps composed of uncompacted clay clods, a new method called "clay piles" was successfully applied.

A pre-driven profile is backfilled by clay of similar properties as is the surrounding material and subsequently compacted there, (see Figure 3).

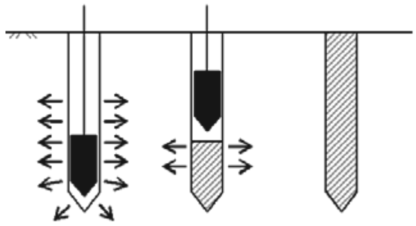

Figure 3. Ground improvement by "clay" piles

- The main aim of chemical improvement is to decrease the degree of subsoil chemical contamination on accepted level.

There is a very wide range of different methods which are used for site remediation. It is not the intention of this lecture to present the overview of these methods, because they are covered elsewhere, (e.g. Suthersan 1997), are summarized by US EPA or are a part of activities of ICEG – International Congresses on Environmental Geotechnics. Most of the methods utilize some geotechnical approaches, as drilling, pumping, hydraulic fracturing, and monitoring.

Nevertheless there are 3 methods preferably utilizing classical geotechnical methods as:

- Encapsulation – with the help of the underground sealing wall (Different types of cut-off walls) and the horizontal sealing system (CCL – compacted clay liner, GCL – geosynthetic clay liner, GL – geomembrane liner or composite liner), (Vaníček et al 1997),
- Permeable reactive barrier, e.g. (Jirasko and Vaniček 2009), where the vertical sealing wall regulates the contaminant plume to the permeable window –where contaminated water is cleaned – with the help of sorption, precipitation or degradation, (see Figure 4).
- Stabilization, solidification, - these methods are based on the principle of mixing waste with a bonding agent to create a stiff matrix where the contaminant is bonded. As a bonding agent the different combinations of cement, ash, lime and slag are usually applied.

Question about utilization of old foundations is the last geotechnical problem connected with brownfields redevelopment. This problem is especially sensitive for large cities as the average design life of office buildings is about fifty years.

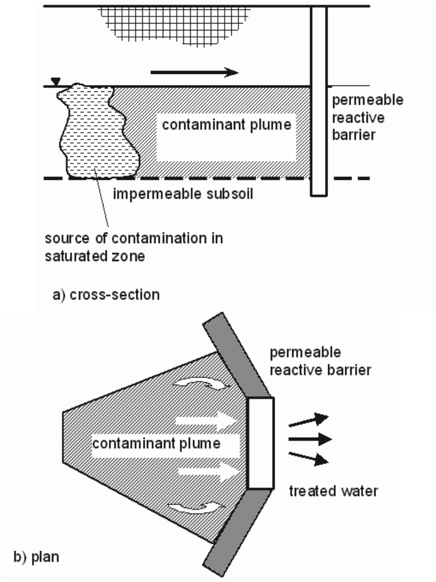

Figure 4. Remediation by in situ reactive barriers

So it means that buildings constructed in the 1950´s- 1960´s are now often demolished and reconstructed. Many of these large modern buildings have been designed with wide column spacing necessitating the use of deep piles or piled raft foundations, as was the case e.g. for London, (Chow 2003). Therefore the discussion is about three options – avoid, remove, reuse. The last option is now preferred as reuse of old foundations has many positive aspects from the environmental point of view, (e.g. Butcher, Powell and Skinner 2006).

Nevertheless we can reuse also spread foundations, which were used for old dwellings, e.g. prefab panel buildings; for farm buildings as well as for old industrial structures. Although the price for removal is not as problematic there as for pile foundations, the version of reuse is very attractive. Here the bearing capacity for subsoil composed of clays increased with time as the result of consolidation. Also the foundation settlement induced by new loading can be rather low, as some additional structural strength had chance to develop there with time for particle arrangement given by stresses from the old foundations.

Direction of the new research activity is therefore connected with observation of changes with time not only in subsoil surrounding existing foundations but also at the contact with this foundation. For bearing capacity and for settlement stress and strain paths are more complicated. Schematic drawing what is going on for selected layer below spread foundation is shown in Figure 5 and new laboratory and filed investigation should to prove some expected assumptions.

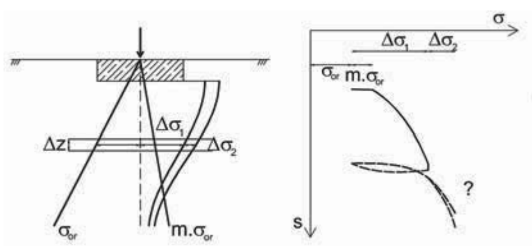

Figure 5. a) Scheme of vertical stresses below spread foundation; b) Expected settlement by additional loading $\Delta\sigma_2$

2 UTILIZATION OF LARGE VOLUME WASTE

Human activities produce a huge amount of different waste. Therefore the most important aim is to decrease the volume of such waste. Nevertheless for remaining waste the strategy should be defined and more efficient way is connected with reutilization of this waste. Civil engineering and first of all geotechnical engineering has a great chance to reuse large volume waste as:

- Construction – demolition waste – old bricks, concrete, ceramics, old asphalt pavement, gravel ballast.
- Industrial waste – ash, dross, slag;
- Mining waste – overlaying soils, waste rock, quarry waste, residues after washing china clay…

During last period the orientation is also on other relatively large volume materials as tyres, glass, polystyrene…

Only one example will be shown, which is combining the utilization of waste for the production of new construction material which can be used for better protection against floods. This new construction material is called brick – fibre – concrete which is composed from old bricks and concrete crushed particles together with classical additives for concrete – cement and water and with new additives – with synthetic fibres, (Vodička et al 2009).

After mixing together the final product looks like on the Figure 6a, where interconnection of individual components is visible. The degree of compaction can significantly determine the final result – what is for example very important from the view of permeability, as this property can be guaranteed in relatively wide range. The impact of the fibers can be seen from the Figure 6b, representing the result of bending test of prepared beam.

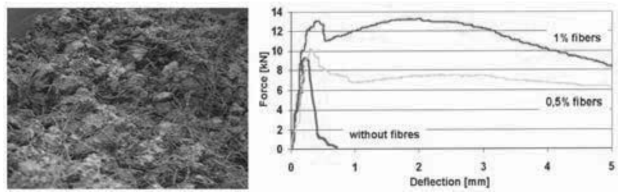

Figure 6. a) Mixture of brick – fibre – concrete; b) Influence of synthetic fibres on the strength parameters and behaviour after failure

After heavy floods there is usually huge amount of the construction and demolition waste and the new product can be applied for the reinforcement of reconstructed part of dikes. Laboratory models up to the scale 1:1 (see Figure 7) proved extremely high resistivity against surface erosion and such reinforced dikes can be applied not only for reconstructed parts but also in selected sections of dikes, where the crest is little bit lower than other part and overflowing can start there as higher resistivity is guaranteed.

Figure 7. Model of reinforced dike before and after the test

3 THE UTILIZATION OF THE SURFACE OF THE MINING SPOIL HEAPS FOR NEW CONSTRUCTION

Roughly 200 mil. m^3 of clayey material which overlay brown coal seam are removed and backfilled during open pit mining activity in the Czech Republic each year.

As extremely large part of the country in this area is affected by mining activity the construction of new structures on the surfaces of these spoil heaps is nearly necessity. The first condition is connected with long term slope stability as material properties are changing with time as well ground water level, (Vaníček and Chamra 2008). Second condition is connected with settlement, first of all with differential settlement, as this uncompacted clay fill has sometimes extreme elevation – more than 100 m. Typical example is Ervenice corridor, (Dykast et al 2003), with cross section shown in Figure 8. Only for top layer about 5 m little bit better material was applied and partly compacted. Nevertheless this layer significantly eliminated differential settlement, so that motorway on the top can be used without special limitation (see Figure 9) even when the total settlement exceeded 2 meters.

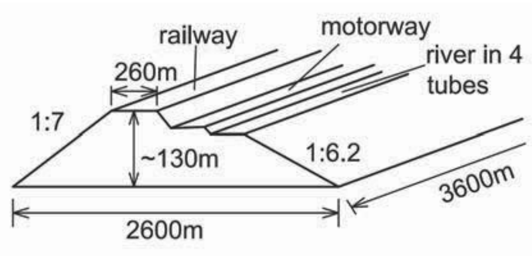

Figure 8. Schematic cross-section of Ervenice corridor

Figure 9. Photo of the top of Ervenice corridor

For classical objects founded on the spoil heaps surface the following approaches are applied:

Among passive measures we can count:

- postponing the new construction – however sometimes this condition is unacceptable;
- using some methods of deep foundations like piles – but solution can be limited by height of fill, by economical reasons and a negative skin friction should be taken into account;
- preconsolidation with additional load, which has to be removed after a certain time – very problematic as it is connected with huge volume of additional fill and with time needed for which this additional loading have to be applied.

Among active measures the different approach is usually chosen for total and for differential settlements. Higher value of total settlement can be accepted if:

- special technical solution is applied for engineering services as electricity, gas, sewage…,
- rectification can be applied e.g. for railway tracks, pipelines etc.

But most sensitive questions are connected with differential settlements with direct impact on damages to the structural elements and to the manner of the practical use of the structures. There we cannot so easily accept little bit higher values as for total settlement. Therefore if the probability that the expected different settlements will be higher than the accepted ones this situation has to be solved with the help of the following steps:

- to select such construction system which is not so sensitive to the differential settlements; or
- to improve the subsoil beneath foundations as was mentioned at the beginning of this chapter.

4 CONCLUSION

Short overview is stressing a significant role of the geotechnical engineering for environment protection, especially from the view of Sustainable construction, from the view which is very sensitive for all society. Three practical examples supported this general aspect from which new problems which our profession has to deal with are clearly visible.

5 REFERENCES

Dykast et al 2003 Ervěnice corridor – 130m high spoil heap from clayey material – with transport infrastructure on its surface. XIIIth European Conference on Soil Mechanics and Geotechnical Engineering, Volume 4. Praha: ČGtS ČSSI, p. 57–76. ISBN 80-86769-03-8.

Jirásko D. and Vaníček I. 2009. The Interaction of Groundwater With Permeable Reactive Barrier (PRB). *The Academia and Practice of Geotechnical Engineering.* Cairo: IFOS, p. 2473-2478. ISBN 978-1-60750-031-5.

Suthersan S.S. 1997. *Remediation Engineering. Design Concepts.* CRC. Lewis publishers, New York

Vaníček I. 2010. Urban Environmental Geotechnics Construction on Brownfields. *Geotechnical Challenges in Megacities*. St. Petersburg: GRF,. p. 218-235. ISBN 978-5-9902005-2-4.

Vaníček I. and Chamra S. 2008. The Influence of Extreme Raiinfall on the Stability of Spoil Heaps. *10th Int. Symp. on Landslides and Engineering Slopes.* London: Taylor and Francis, p. 1653-1658. ISBN 978-0-415-41196-7.

Vaníček I. and Valenta J. 2009. Examples of the use of environmental urban geotechnics for brownfield redevelopment. *Engineering Geology for Tomorrow's Cities*. London: The Geological Society of London. ISBN 978-1-86239-290-8.

Vaníček I. and Vaníček M. 2008.*Earth Structures in Transport, Water and Enviromental Engineering*. 1. ed. Berlin: Springer Science+Business Media. 637 p. ISBN 978-1-4020-3963-8.

Vaníček I.et al 2003. Remediation of Chemical Landfills in Neratovice and Chabarovice. *Geotechnical Problems with Man-Made and Man Influenced Grounds* - XIIIth European Conference on Soil Mechanics and Geotechnical Engineering, Volume 4. Praha: ČGtS ČSSI, p. 279-294. ISBN 80-86769-03-8.

Vodička et al 2009. Utilization of fibre-concrete in earth structures. *Sustainable construction 5*. CTU press, Prague, pp. 107-112.

Vaníček et al 2012. Sustainable Consruction. *Sustainable construction* CTU press, Prague ISBN 978-80-01-04873-3.

Vaníček et al 1997 Remedy of a chemical waste dump with foundation of a new dump on its surface. In Proc. 14th IC SMGE, Hamburg, vol 3, pp 1857–1860.

Chow 2003. Geotechnical aspects of tunnelling reuse of foundations and building on landfill in brownfield development. *Geotechnical Problems with Man-Made and Man Influenced Grounds* - XIIIth European Conference on Soil Mechanics and Geotechnical Engineering, Volume 3. Praha: ČGtS ČSSI, p. 343-348.

Butcher, Powell and Skinner 2006. *Reuse of foundations for urban sites.* A best practice handbook. IHS BRE Press. Bracknell.

Applicability of Municipal Solid Waste (MSW) Incineration Ash in Road Pavements Base

Utilisation de cendres d'incinération de déchets solides municipaux (MSW) dans la couche de base de chaussée

Vizcarra G., Szeliga L., Casagrande M.
Pontifical Catholic University of Rio de Janeiro, Rio de Janeiro, Brazil

Motta L.
Federal University of Rio de Janeiro, Rio de Janeiro, Brazil

ABSTRACT: This study presents the characteristics of Municipal Solid Waste (MSW) incineration ash, by-product obtained from electric energy generation power plant in Rio de Janeiro - Brazil, to evaluate its applicability in base road pavements layers through the ash mixture with a non-lateritic regional clay soil with very poor mechanical behavior. Chemical, physical, mechanical tests and the mechanistic-empirical design for a typical pavement structure were carried out on the pure soil and also in the soil mixtures with the addition of different ash content (20% and 40%). MSW fly ash reduced expansion of the material, showing increase in the resilient modulus value with time of cure, load cycle number and reduction of mixture water content. Permanent deformation tests showed mixture soil-MSW fly ash reached a state of plastic accommodation. A typical pavement design was carried out by comparing between pure soil and mixture soil-MSW fly ash; the results showed that it is feasible utilize it in low traffic road pavements, highlighting the positive work of MSW fly ash and its environmental advantages.

RÉSUMÉ: Cette étude présente les caractéristiques des cendres d'incinération des déchets solides municipaux (MSW), un sous-produit obtenu à partir d'une centrale de production d'électricité à Rio de Janeiro - Brésil, afin d'évaluer son applicabilité en tant que couche de base des chaussées en mélangeant la cendre avec un sol argileux non latéritique régional de comportement mécanique inacceptable à cet effet. Des essais chimiques, physiques, mécaniques,ainsi que la conception mécaniste-empirique d'une structure de chaussée typique ont été effectués sur le sol pur et aussi sur le mélange de sol avec addition de différentes concentrations de cendres volantes de MSW (20% et 40%). L'inclusion des cendres a réduit l'expansion du sol, indiquant une augmentation de la valeur du module résilient avec le temps de durcissement, le nombre de cycles de charge et la réduction de l'humidité du mélange. Des essais de déformation permanente ont montré que le mélange de sol-cendres volantes des déchets solides municipaux a atteint un stade de déformation plastique. La conception d'une chaussée typique a été réalisée pour comparer le sol pur et le mélange de sol-cendres volantes des déchets solides municipaux, les résultats ont montré que son utilisation est possible dans des chaussées de faible volume de trafic, mettant en évidence l'utilisation positive de ces cendres et ses avantages socio-économiques et environnementaux.

KEYWORDS: MSW fly ash, pavement, deformability properties, permanent deformation, resilient modulus.

1 INTRODUCTION.

This study evaluates the application of fly ash obtained from incineration of Municipal Solid Waste (MSW) use in base layers of pavements, by mixing the ashes with a non-lateritic regional clay soil. The Usina Verde is a privately held company located in the Federal University of Rio de Janeiro, and aims to provide environmental solutions for the disposal of municipal solid waste, through incineration with energy co-generation. The Usina Verde receives, daily, 30 tons of MSW Company's Waste Disposal of Rio de Janeiro. In sorting, recyclable materials are segregated manually along with the use of metal detectors; after this process, the composition of MSW is principally organic matter (88%), plastic (10%) and rubber (2%). The MSW is then crushed and separated as fine material and sent to drying. These wastes are sent to the incinerator, which operates at a temperature of 950ºC.

At the end of the incineration process are obtained fly ash and bottom ash, being from 8 to 10% by volume of the two ashes, which represent about 80% of bottom ash and 20% of fly ash (Fontes 2008).

2 OBJECTIVES

The objective of the investigations is to study the effect of MSW fly ash addition on the soil, evaluating deformability and expansibility properties, also thickness layer pavements base of soil with and without MSW fly ash

3 EXPERIMENTAL INVESTIGATION

3.1 Materials and properties

The non-lateritic clay soil in study came from a deposit located in the city of Campo Grande, Rio de Janeiro state. Fly ash comes from the burning of municipal solid waste (MSW) at Usina Verde, which is located on Rio de Janeiro / RJ. The tests performed at Pontifical Catholic University of Rio de Janeiro and Federal University of Rio de Janeiro, aiming to characterize and evaluate the soil and soil-MSW fly ash mixtures. Since there was no research evidence previous to this topic, 20% and 40% as percentages of fly ash were utilized to add to the soil. The symbols used in this study, which describe the materials and mixtures with percent in weight, are presented in Table 1.

Table 1. Material's symbols

Material	% Soil	% MSW fly ash	Symbol
Soil	100	0	S
MSW fly ash	0	100	CV
Mixture 1	60	40	S60/CV40
Mixture 2	80	20	S80/CV20

3.2 Experimental tests

3.2.1 Chemical and physical characterization

Tests such as X-Ray Fluorescence, Organic Matter Content, Lixiviation and Solubilization; Granulometric Analysis and Atterberg's Limit, MCT Test and Proctor Compaction Test were conducted.

3.2.2 Resilient modulus test

The tests were performed according to standardized test in the Geotechnical Laboratory of Federal University of Rio de Janeiro, into molds of 10 x 20 cm compacted at optimum moisture obtained in the compaction test.

In the cyclic load triaxial test, deviator stresses are applied in the sample top, always in the compression direction, furthering a load and unload, whereas the minor principal stress remains constant.

Each sample was subjected to eighteen stresses states were applied, with principal minor stress ranging from 0,021 to 0,137 MPa and deviator stress ranging from 0,021 to 0,412 MPa.

The Resilient Modulus (M_R) of soil is the relationship between the deviator stress (σ_d) applied repeatedly in a sample of soil in triaxial test and the corresponding specific recoverable or resilient strain (ε_r). As shown in Equation 1 (AASHTO TP46-94 1996).

$$M_R = \frac{\sigma_d}{\varepsilon_r} \tag{1}$$

Where:

M_R: resilient modulus;

σ_d: cyclic deviator stress (σ_1 - σ_3);

ε_r: resilient strain (vertical).

The composite model used in this study relates the resilient modulus of minor principal stress and deviator stress, as shown in Equation 2.

$$M_R = k_1 . \sigma_3{}^{k_2} \sigma_d{}^{k_3} \tag{2}$$

Where:

σ_3: minor principal stress;

σ_d: cyclic deviator stress (σ_1 - σ_3);

k_1, k_2 and k_3: correlation coefficients, derived from results of laboratory tests.

This model was chosen because it presents bigger correlation coefficients to the incorporating the minor principal stress and the deviator stress influence. The nonlinear least squares model estimation was utilized to obtain the correlation coefficients.

In order to evaluate the influence of cure time, optimal water content samples were prepared and next rolled into hermetically closed plastic bags for 7 and 21 days. Soon afterwards, these were proceeded to the resilient modulus tests.

3.2.3 Permanent deformation test

The tests were performed according to Guimarães (2009), using the same molds used in the Resilient Modulus Test. A total of 500,000 load cycles were applied for each specimen.

Three tests were conducted in the Mixture S60/CV40, in the condition of maximum dry density, at stress levels shown in Table 2.

Table 2. Permanent deformation tests

Test Number	σ_3 (MPa)	σ_d (MPa)
1	0,098	0,294
2	0,118	0,353
3	0,098	0,392

3.2.4 Pavement design

A pavement structure was assumed (Figure 1) considering Rio de Janeiro's weather, with the purpose of exploring the effects of adding MSW fly ash in soil on pavement project one. The thickness and mechanical properties of the coated asphalt and subgrade remain constant, so that only the the thickness of the base may be modified, according to the parameters of resilience for each material. As for the mechanistic-empirical analysis, the computer program SisPav (Franco, 2007) was used. Bernucci (1995) indicates for Brazilian low traffic roads an N value of 10^4 to 10^6 should be used. Thus, in this study, N value of 10^5 was assumed.

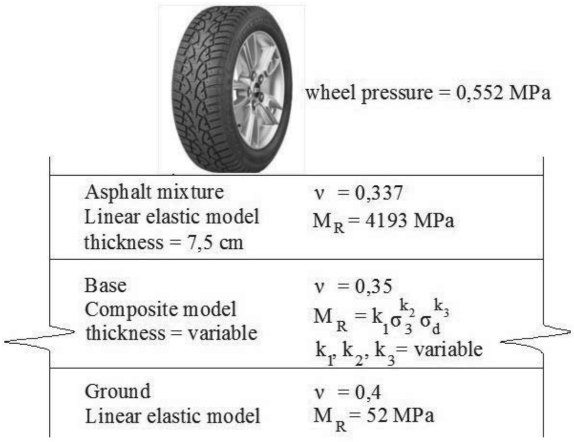

Figure 1. Pavement structure adopted.

4 RESULTS AND DISCUSSIONS

From the test conducted, the characteristics and effects of the addition of MSW Fly Ash into soil were studied.

4.1 Chemical characterization

The main chemical components of soil, which are normally found in residual soils, are SiO_2, Al_2O_3 and Fe_2O_3, such as showed in the Table 3. Lixiviation and Solubility tests performed according to Brazilian standards NBR 10005 and NBR 10006 for MSW fly ash and soil stabilized with 40% fly ash content. The mixture is classified non - dangerous and non-inert (Vizcarra 2010).

4.2 Physical characterization

MSW fly ash and mixtures can be noted as follows: first, the Atterberg Limits for pure MSW fly ash could not be performed due to the behavior of granular material, which during the test did not show plastic characteristics to their achievement. Second, the inclusion of MSW fly ash decreases the liquid limit and plasticity index, and increases the plastic limit of soil.

According the classification MCT (Nogami & Villibor 1995), the soil is classified as NG' behavior "non-lateritic-clay." When compacted under the conditions of optimum moisture content and maximum dry unit weight for normal energy compaction, these soils present characteristics of traditional highly plastic and expansive clays.

The use of these soils is related to restrictions resulting from its high expansibility, plasticity, compressibility and contraction when subjected to drying, its use is not recommended for base pavements, and some of the worst soil for the purpose of paving, from the tropical soils (Nogami & Villibor 1995).

From the curves of soil compaction and mixtures with fly ash obtained from the Modified Proctor tests, it can be stated that by increasing the level of ash in the mixture, the maximum dry density tends to decrease (Figure 2).

Table 3. Soil, MSW fly ash chemical composition

	Concentration (%)	
Compost	Soil	MSW Fly Ash
SiO_2	36 - 43	13 - 21
Al_2O_3	35 - 38	12 - 15
Fe_2O_3	13 - 21	5 - 7
SO_3	0 - 1	5 - 10
CaO	-	32 - 45
TiO_2	0,9 - 1,7	3 - 4
K_2O	2 - 4	2 - 4
Cl	-	4 - 6
Organic Matter	0,1	0,7

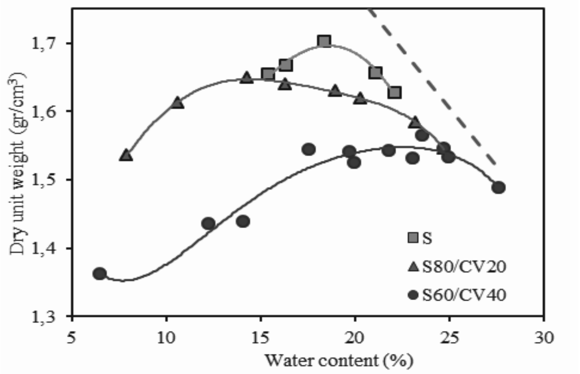

Figure 2. Compaction Curves of Soil and 20% - 40% Soil – Fly Ash Mixtures

4.3 Effect of MSW fly ash addition on resilient modulus

The results of Resilient Modulus tests (Figure 3) show that the Resilient Modulus of soil in study is dependent on the deviator stress and if the MSW fly ash is added, this behavior does not change. It is appreciated that the higher the deviator stress, the lower the value of resilient modulus.

The mixture with 20% MSW fly ash improved the mechanical behavior of pure soil, the mixture with 40% MSW fly ash downgraded the mechanical behavior, but it improved with cure time (Figure 4).

The mixture with 20% MSW fly ash was assessed with several different water contents. The results indicated the resilient modulus increased as the water content decreased.

4.4 Effect of MSW fly ash addition on permanent deformation

As shown in the Figure 5, the permanent deformation tends to stabilize reaching a plateau, it´s observed that Test 3 has a higher permanent deformation, this is due to increased tensions applied to the test.

The resilient modulus is increased with the number of load cycles (Figure 6), this can be explained by the diminution of elastic strain. The occurrence of the plastic accommodation (i.e. Shakedown) was investigated by using the behavior model developed by Dawson and Wellner, cited by Werkmeister (2003). The test results of permanent deformation test for the MSW fly ash – soil mixture were obtained and are displayed by the graph model of Dawson and Wellner cited by Werkmeister (2003) in Figure 7.

By analysis of this Figure it appears that all tests conducted with the MSW fly ash – soil mixture show a typical behavior for level A, i.e., demonstrated plastic accommodation, depending on the model proposed by Werkmeister (2003). The characterization of the level A behavior of both the shape of the curve, roughly parallel to the vertical axis, because when the rate of permanent deformation increase and have reached a magnitude of 10^{-7} (x 10^{-3} m/load cycle). I.e. at the final load cycles, the specimen´s permanent deformation increased by only 10 mm at each new cycle.

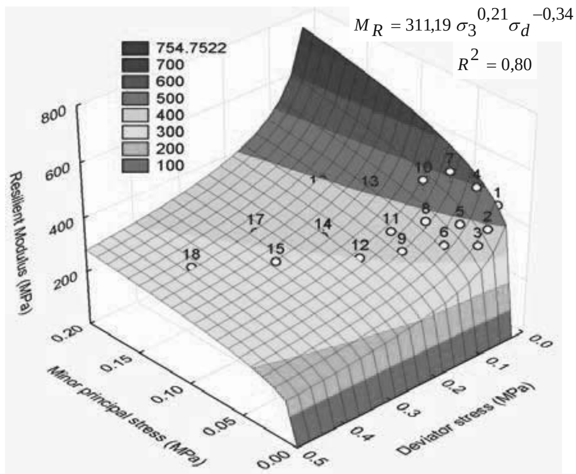

Figure 3. Soil with 40% MSW Fly Ash Resilient Modulus vs. Stresses (21 days of cure)

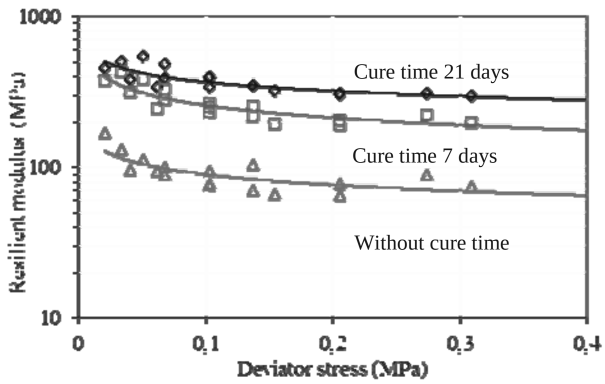

Figure 4. Resilient Modulus vs. Stress of Soil with 40% MSW Fly Ash – Cure Time Variation.

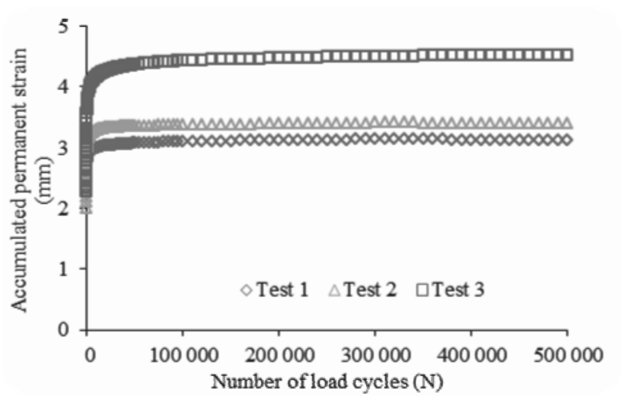

Figure 5. Accumulated Permanent Deformation Variation.

4.5 *Effect of MSW fly ash addition on expansibility*

The MSW fly ash decreases the expansion of the soil in study, which had an expansion of 4%, but with the addition of fly ash reduced it to 3.6% for 20% fly ash content and fell to 0.4% to a level of 40% fly ash. However, high content of fly ash when can deteriorate the mechanical behavior, resulting in a thicker layer.

4.6 *Effect of MSW fly ash addition in pavement base*

The mixture with 20% fly ash improved the mechanical behavior of pure soil, which is revealed by the decrease in thickness of the base compared to pure soil, for the same loading level and same parameters (criteria) for sizing. It is shown in Figure 8 the thickness of layers depending on the project period for each type of mixture, which was obtained by the computer program SisPav (Franco, 2007).

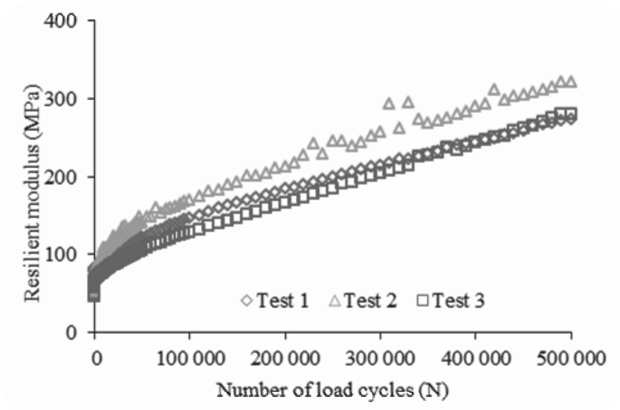

Figure 6. Resilient Modulus Variation.

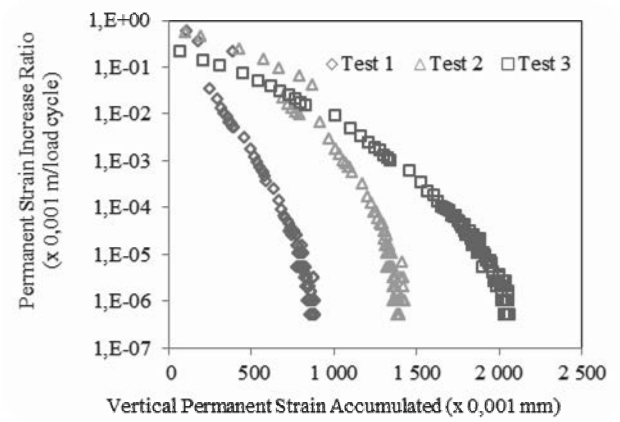

Figure 7. Shakedown´s occurrence search.

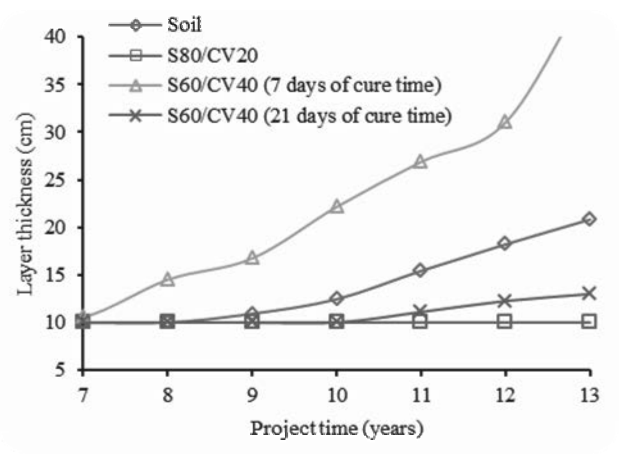

Figure 8. Layer Thickness according to Project Time

5 CONCLUSIONS

Mixtures with the inclusion of MSW fly ash had a mechanical behavior compatible with the requirements for a low traffic volume. The addition of 20% fly ash to the non-lateritic clay soil improved the mechanical behavior and reduced the expansion of the soil. The soil mixed with a content of 40% of fly ash decrease the mechanical behavior compared to pure soil, with the consequent increase in thickness; however, it improved with cure time and cycle loading number, decreasing significantly the expansion of the soil.

The results were satisfactory, being dependent on the ash content added, cure time and cycle loading number, highlighting the positive work of MSW fly ash for use in base layers of road pavements, eliminating the current problems of waste disposal in dumps and landfills.

6 ACKNOWLEDGEMENTS

The authors thank CNPq (MCT/CNPq 14/2009 # 480748/2009-8 project) for the financial support, as well as Usina Verde S.A. for the Municipal Solid Waste ash supply.

7 REFERENCES

AASHTO. 1996. TP46-94 - Standard Test Method for Determining the Resilient Modulus of Soils and Aggregate Materials. American Association of State Highway and Transportation Officials, Washington, D.C.

Bernucci, L. L. B. 1995. Considerations about pavement design using lateritic soils on low traffic volume roads. PhD Thesis. Polytechnic school of University of São Paulo, São Paulo, SP, Brazil (In Portuguese).

Brazilian Technical Standards Association ABNT. NBR 10005/04: *Procedure for obtention leaching extract of solid wastes*.

Brazilian Technical Standards Association ABNT. NBR 10006/04: *Procedure for obtention of solubilized extraction of solid wastes.*

Fontes, C. M. A. 2008. Utilization of the sewage sludge and urban solid waste ashes in high performance concrete. PhD Thesis. Federal University of Rio de Janeiro, Brazil (In Portuguese).

Franco, F. A. C. P. 2007. Mechanistical-empirical asphalt pavement design method - SisPAV. PhD Thesis. Federal University of Rio de Janeiro, Brazil (In Portuguese).

Guimaraes, A. C. R. 2009. A mechanistical empirical method to predict permanent deformation on tropical soils on pavements. PhD Thesis. Federal University of Rio de Janeiro, Brazil (In Portuguese).

Nogami, J. S., Villibor, D. F. 1995. *Pavimentos de Baixo Custo com Solos Lateríticos*, Editora Villibor, São Paulo. 240 p (In Portuguese).

Vizcarra, G.O.C. 2010. Aplicability of municipal solid waste for pavements base. M.Sc. Disssertation. Department of Civil Engineering, Pontifical Catholic University of Rio de Janeiro, Brazil (In Portuguese).

Werkmeister, S. 2003. Permanent Deformation Behavior of Unbound Granular Materials in Pavement Construction. These. Technical University of Dresden.

Research Results of Fine-Grained Soil Stabilization Using Fly Ash from Serbian Electric Power Plants

Les résultats de recherche de la stabilisation des sols de grains fins en utilisant les cendres volantes des centrales électriques serbes

Vukićević M., Maraš-Dragojević S., Jocković S., Marjanović M., Pujević V.
Faculty of Civil Engineering, University of Belgrade

ABSTRACT: This paper presents the results of laboratory research of fly-ash soil stabilization. Tests were conducted on mixtures with two types of fine-grained soils and fly ash sampled in Serbian electric power plant Kolubara. Used types of soils are low plasticity silty clay and very expansive, medium to high plasticity clay. Effects of fly ash on physical and mechanical properties of soil (grain size distribution, Atterberg limits, unconfined compression strength, moisture-density relationship, swell potential, CBR) were evaluated. Test mixtures were prepared at optimum water content from standard Proctor compaction test. Results of the research indicate that fly ash can effectively improve some engineering properties of soil.

RÉSUMÉ : Ce document présente les résultats de recherche en laboratoire de la stabilisation des cendres volantes. Les analyses effectuées concernent les mélanges avec deux types de sols de grains fins et de la cendre volante récupérée de la centrale électrique serbe « Kolubara ». Les types de sols utilisés sont de l'argile silteuse d'une plasticité faible et de l'argile très gonflante d'une plasticité moyenne à forte. Les effets des cendres volantes sur les propriétés physiques et mécaniques du sol (la distribution de la grosseur des grains, les limites d'Atterberg, la résistance à la compression uniaxiale, la relation entre la densité et l'humidité, les possibilités de gonflement, l'indice portant californien – CBR) ont été évalués. Les mélanges d'essai ont été préparés à teneur en eau optimale selon l'essai Proctor normal. Les résultats de la recherche signalent que les cendres volantes peuvent améliorer de manière efficace certaines propriétés techniques du sol.

KEYWORDS: soil stabilization, fly ash, fine-grained soil

1 INTRODUCTION

Fly ash makes the most of the combustion-by-products during the production of electricity in thermal power plants. A very small amount can be recycled, while significant amounts are disposed in landfills. The use of fly ash for soil stabilization can bring multiple benefits – protection of the environment, financial savings and it can also make the poorly-graded types of soils usable.

In Serbia, approximately 7 million tons of fly ash and slag are produced every year, of which only 3% is used in cement industry. The remaining products (about 300 million tons so far), are disposed on landfills, taking up the area of approximately 1600 hectares (Cmiljanić 2008, Cmiljanić 2010).

In Serbia, fly ash soil stabilization research was conducted for the first time during the preliminary design of the Serbian regional waste management center "Kalenic" (Report FCE Belgrade 2011). This research was performed by the authors during 2011. Waste management center "Kalenic" is located at open pit near thermal power plant "Kolubara". Disposal area of the "Kalenic" landfill is being formed by construction of the outer embankment, instead of soil excavation, which is the usual way. The construction of the embankment needs more than 1.5 million m^3 of material and costs are about 33% of total investment. Therefore, the possibility of using existing material from the site was analyzed in Laboratory for Soil Mechanics at Faculty of Civil Engineering in Belgrade. Results have shown that tested material is not appropriate for construction of the embankment. Because of this, the possibility of using fly ash from thermal power plant "Kolubara" for soil stabilization were considered.

This paper presents the results of fly ash soil stabilization laboratory research performed during 2011-2012, as the part of the research project funded by Electric Power Industry of Serbia.

2 MATERIALS

Materials used for the experimental research program include: fly ash from thermal power plant "Kolubara" (KFA) and silty clays from project "Kalenic" (Soil A) and from wind park project "Kosava" (Soil B).

2.1 *Fly ash*

Chemical composition of KFA was determined at the Faculty for Physical Chemistry in Belgrade and the results are shown in Table 1.

Table 1. Chemical composition of fly ash [%]

SiO_2	Al_2O_3	Fe_2O_3	CaO	MgO
50.21	23.83	9.89	4.79	3.12
K_2O	Na_2O	TiO_2	SO_3	P_2O_5
0.44	0.35	0.54	5.24	0.06

Because of the high percentage of SiO_2 and Al_2O_3, according to ASTM C 618, KFA belongs to Class F silica mineral ashes, with pozzolanic properties. Class C fly ash is not available in Serbia (Cmiljanic et al. 2010).

2.2 *Soils*

The soils used for this study are predominantly silty clays.

Soil A: Mineral composition consists of quartz, muscovite and soft minerals of montmorionite (testing performed at Faculty for Physical Chemistry, Belgrade). According to USCS, this soil, known as alevrite, is medium to high plasticity clay (CI/CH), with swell potential.

Soil B: Material was collected at the site of wind park near Vrsac, Vojvodina. Terrain at the site consists of Quaternary loess sediments. According to USCS, this soil is low plasticity clay (CL). Grain size distribution curves for used materials are given in Figure 1.

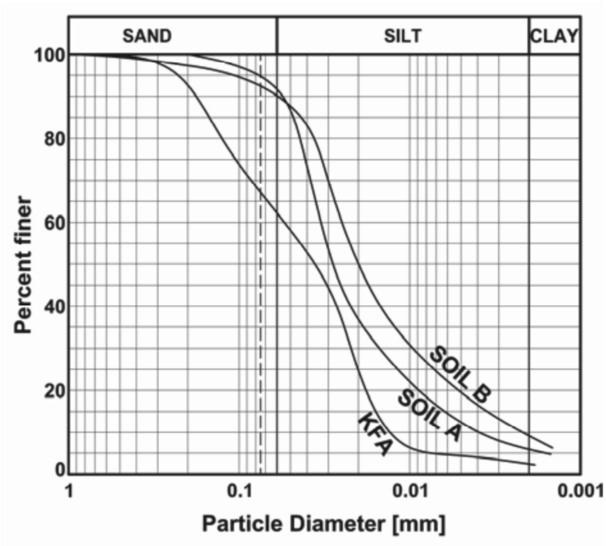

Figure 1. Grain size distribution curves

3 LABORATORY TESTING

Laboratory testing was conducted in the Laboratory for soil mechanics at Faculty of Civil Engineering in Belgrade. Testing samples were prepared by compaction, with moisture content equal to optimum moisture content from standard Proctor compaction test.

Fly ash soil mixtures were prepared at three fly ash-soil ratios (10, 15, 20% fly ash content by dry weight). After addition of water, mixtures were compacted without delay. According to (Terrel et al. 1979, Ferguson and Leverson 1999) compaction should start immediately after the mixing process and finish within a maximum of 2 hours. Samples were tested immediately after compaction (t=0), as well as after 7, 14, 28 and 60 days. Following engineering properties were determined: unconfined compression strength (UCS), California bearing ratio (CBR), effective shear strength parameters (c', φ') and compressibility modulus (M_v). All tests were performed according to SRPS Standards.

4 RESULTS AND DISCUSSION

4.1 *Soil plasticity*

In case of medium to high plasticity soil (soil A), it is observed that increasing of KFA percentage results in decreases in the liquid limit and plasticity index, which is not the case for low plasticity soil (soil B), as shown in Fig. 2.

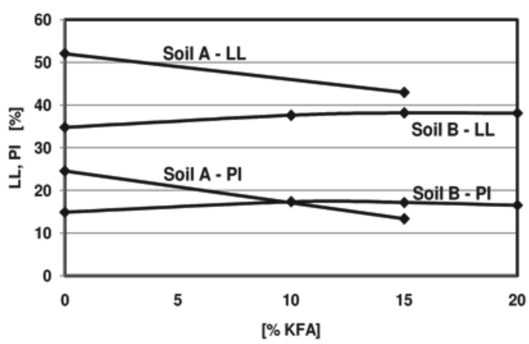

Figure 2. Variation in Atterberg limits for mixtures at t=0

4.2 *Compaction*

The results (Fig. 3) indicate that maximum dry density decreases and optimum moisture content increases as the fly ash content increases (for both soil types). The decrease in maximum dry density is associated with the fact that used fly ash has much lower weight than soil. Results are in line with Santos et al. 2011 and Sharma 2012, while opposite trend can be found for Class C fly ash stabilization (White et al. 2005 and Ramadas and Kumar 2012).

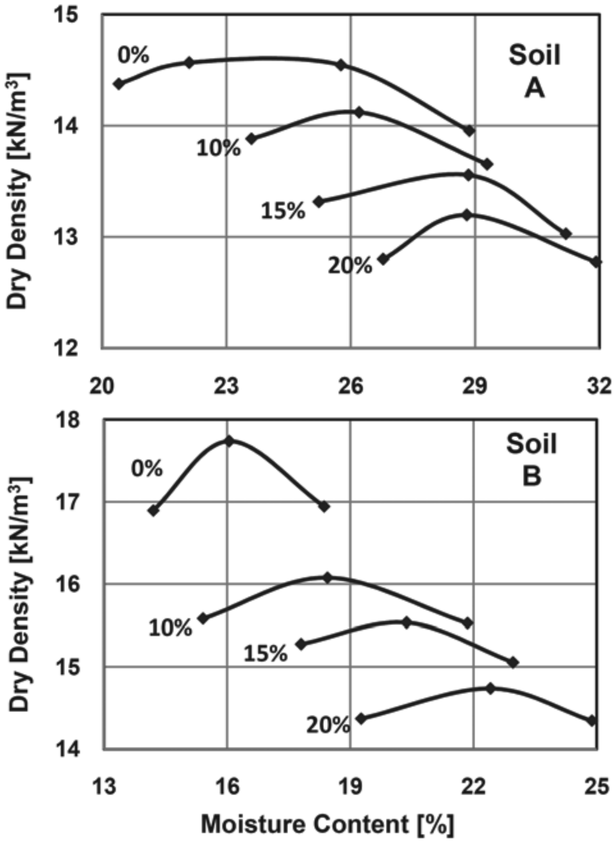

Figure 3. Moisture-density relationship of fly ash-soil mixtures

4.3 *Unconfined Compressive Strength (UCS)*

Increased soil strength is the main indicator of the successful soil stabilization. In previous studies (Ferguson and Leverson 1999, Ferguson 1993, Parsons 2002, Edil et al. 2006) strength of soil is usually determined by uniaxial compression test or bearing ratio test. The results of UCS tests shown in Fig. 4 indicate that maximum strength gain for soil A is obtained for mixture with 15% KFA. Soil UCS is increased by 15-25%, dependent of elapsed time.

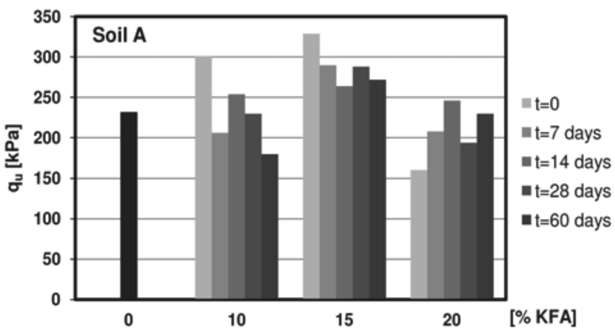

Figure 4. Strength gain of soil A for different percentages of KFA

UCS for soil B without stabilizer was around 400 kPa and addition of fly ash didn't result in strength gain.

4.4 *Effective shear strength parameters*

Effective shear strength parameters have been determined by using direct shear test. Obtained results (Fig. 5) show that long term friction angle doesn't substantially change with addition of fly ash, for both soil types. On the other side, cohesion significantly increases with time for all tested mixtures. This is associated with pozzolanic properties of used fly ash.

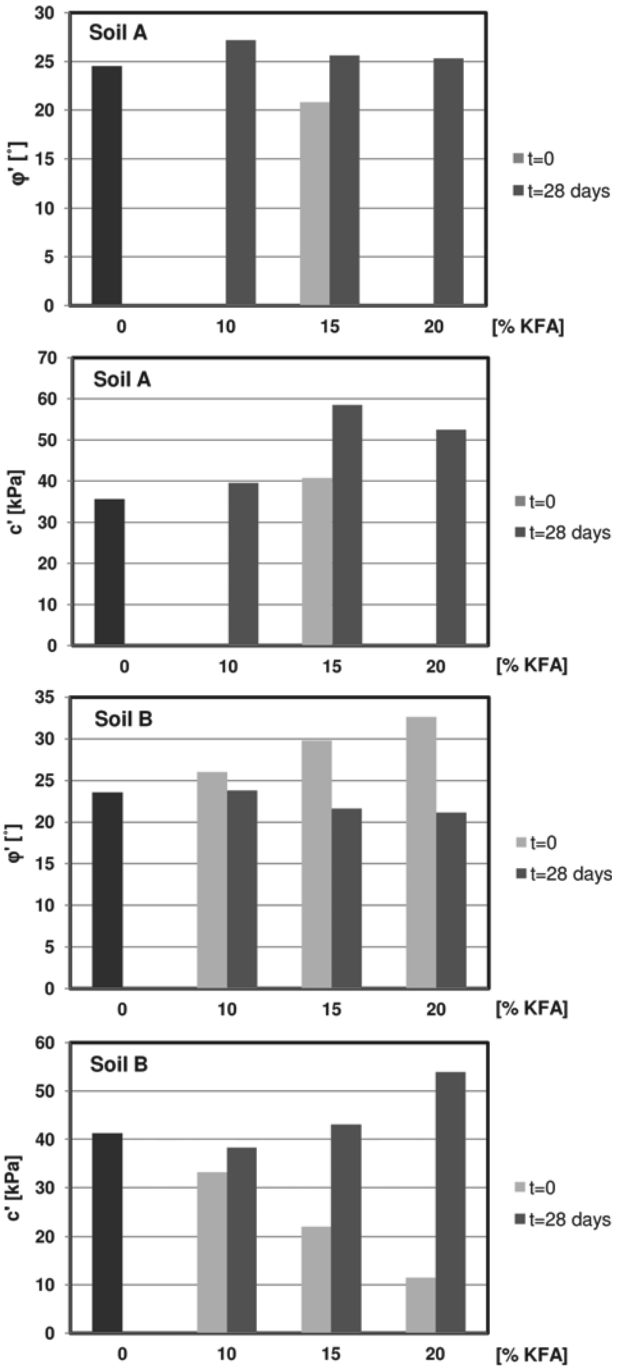

Figure 5. Variation in effective shear strength parameters

4.5 *California Bearing Ratio (CBR)*

For both soil types, California bearing ratio tests have been done on mixtures with 15% KFA, which is adopted as optimum. Compared with CBR values for base soils A and B, obtained results showed significant gain. In the case of soil A, CBR value increased nearly 300%, and 260-380% in the case of soil B (dependent on elapsed time). This is especially important for soil A, because it makes it usable for road construction (CBR value was increased from 2.1 to 5.8). CBR values are shown in Fig. 6, and are in line with Mackiewicz and Ferguson 2005, White et al. 2005 and Edil et al. 2006.

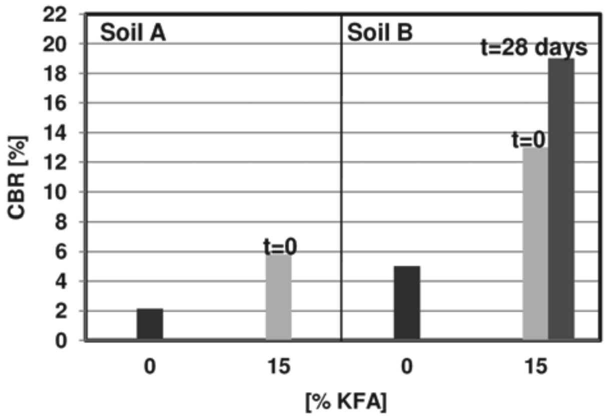

Figure 6. CBR values

4.6 *Deformation parameters*

Compressibility modulus (Fig. 7) for both soil types increase with addition of fly ash. Influence of time in this case was not significant. Overall modulus increase is around 15-35% for soil A and around 15% for soil B.

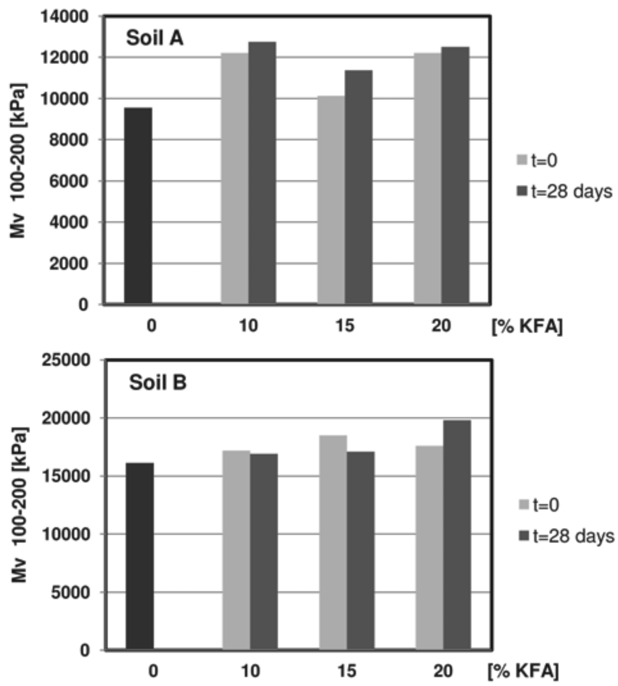

Figure 7. Compressibility modulus

4.7 *Swell potential*

Although strength and deformation parameters of soil A can be considered acceptable, this soil showed significant swell potential, which makes it unusable for most engineering purposes. This property is associated with the presence of expansive mineral montmorionite. Addition of 15% of fly ash, which is determined as optimum, resulted in significant decrease of swell deformation, from ε=8.6% to ε=1.8-3.1%. This results are in accordance with results of other autors

(Ferguson 1993, Zia and Fox 2000, Çokça 2001, Nalbantoglu and Gucbilmez 2002, Ramadas and Kumar 2012).

5 CONCLUSIONS

Although many scientific results show that Class F fly ash cannot be used for soil stabilization without addition of cement or lime, laboratory tests performed in this research have shown that fly ash from thermal power plant "Kolubara" is effective material for soil stabilization. Main conclusions of this research are as follows:

Additon of KFA decreases the plasticity index of medium and high plasticity soils (type A).

KFA impacts moisture-density relation of tested soils – optimum moisture content increases and maximum dry density decreases.

For soil A, based on UCS gain, amount of 15% KFA is identified as optimum. Strength gain was approximately 20%. There wasn't UCS gain for low plasticity soil B.

For both soil types, long term friction angle almost doesn't change with addition of KFA, while effective cohesion significantly increases with time for all tested mixtures.

CBR values increased around 260-380% for mixtures with 15% of KFA, which is adopted as optimum. This is main stabilization effect for soil B and very important effect for soil A.

Compressibility modulus for both soil types increase with addition of fly ash, without influence of time. Overall increase is around 15-35%.

Swell potential of very expansive soil A reduced with addition of 15% KFA. Swell deformation decreased from ε=8.6% to ε=1.8-3.1%.

Despite shown positive effects, the universal principle of soil stabilization using fly ash cannot be easily defined. It is necessary to perform detailed laboratory investigations, with certain types of ash and soil. It is the only possible way to precisely determine the optimal percentage of ash to be added, to determine strength gain and define the technology operations. The presented results of laboratory tests have confirmed the need to develop a research program in this field for Serbia, bearing in mind that the average annual production of fly ash that will be disposed on landfills is around 7 million tons.

6 REFERENCES

Cmiljanić S., Vujanić V., Rosić B., Vuksanović B., Tošović S., Jotić S. 2010. Physical-mechanical properties of fly-ash originating from thermo-electric power plants of Serbia. *Proc. of XIVth Danube-European Conference on Geotechnical Engineering: From Research to Design in European Practice*, Bratislava, Slovak Republic

Cmiljanić S., Jotić S., Tošović S. 2008. Prethodni rezultati istraživačko-razvojnog programa - primena elektrofilterskog pepela u putogradnji. *Simpozijum o istraž. i primeni savremenih dostignuća u našem građevinarstvu u oblasti materijala i konstrukcija*, 3-13

Çokça E. 2001. Use of Class C fly ashes for the stabilization of an expansive soil. *Journal of Geotechnical and Geoenvironmental Engineering* 127 (7), PWS Publishing Company, USA, 568-573.

Edil T.B., Acosta H.A. and Benson C.H. 2006. Stabilizing Soft Fine-Grained Soils with Fly Ash. *Journal of Materials in Civil Engineering © ASCE March/April 2006*, 283-294

Elaborat o geotehničkim istraživanjima terena za potrebe izgradnje regionalnog centra za upravljanje otpadom "Kalenić" u selu Kalenić (Report - Geotechnical investigation of the ground conditions for the construction of regional waste management center "Kalenic" in village Kalenic), 2011. Građevinski fakultet Univerziteta u Beogradu (Faculty of Civil Engineering University in Belgrade)

Ferguson G. 1993. Use of Self-Cementing fly ashes as a soil stabilization agent. *ASCE Geotechnical Special Publication* No. 36, ASCE, USA

Ferguson G. and Leverson S.M. 1999. *Soil and Pavement Base Stabilization with Self-Cementing Coal Fly Ash.* American Coal Ash Association, USA

Mackiewicz S.M. and Ferguson E.G. 2005. Stabilization of Soil with Self-Cementing Coal Ashes. *2005 World of Coal Ash (WOCA)*, Lexington, Kentucky, USA

Nalbantoglu Z. and Gucbilmez E. 2002. Utilization of an industrial waste in calcareous expansive clay stabilization. *Geotechnical Testing Journal* 25 (1), ASTM International, USA, 78-84.

Parsons R. L. 2002. Subgrade improvement through fly ash stabilization. *Miscellaneous Report*, Kansas University Transportation Center, University of Kansas, USA

Ramadas T.L., Kumar N.D. 2012. A study on strength and swelling characteristics of three expansive soils treated with fly ash. *Proc. of International Symposium TC 211 IS-GI. Recent Research, Advances & Execution Aspects of Ground Improvement Works, Vol. II,* Brussels, Belgium, from II-459 to II-466.

Santos F., Li L., Li Y., Amini F. 2011. Geotechnical Properties of Fly Ash and Soil Mixtures for Use in Highway Embankments. *World of Coal Ash (WOCA) Conference*, Denver, CO, USA

Sharma R.K. 2012. Subgrade Characteristics of Locally Available Soil Mixed With Fly Ash and Randomly Distributed Fibers. *Proc. of International Conference on Chemical, Ecology and Environmental Sciences (ICEES 2012)*, Bangkok, 177-181

Terrel R.L., Epps J.A., Barenberg E.J., Mitchell J.K., Thompson M.R. 1979. *Soil stabilization in pavement structures: A user's manual. FHWA-IP-80-2*, Vol. 2, Department of Transportation, Federal Highway Administration, USA

White D.J., Harrington D., Thomas Z. 2005. Fly ash soil stabilization for non-uniform subgrade soils, Volume I: Engineering properties and construction guidelines. *Report No. IHRB Project TR-461; FHWA Project 4.* Center for Transportation Research and Education, Iowa State University

Zia N. and Fox P.J. 2000. Engineering properties of loess-fly ash mixtures for road bases. *Transportation Research Record* 1717, Transportation Research Board, USA, 49-56

Simplified Prediction of Changes in Shear Strength in Geotechnical Use of Drinking Water Sludge

Prédiction simplifiée de changements dans la force du ciseau dans usage Geotechnical de boue de l'eau potable

Watanabe Y.
Central Research Institute of Electric Power Industry

Komine H.
Ibaraki University

ABSTRACT: Drinking water sludge is the aggregation of clay and organic compounds which is formed in flocculation and sedimentation process. This study focused on the decomposition of the bonding by flocculating agent and organic matter, and proposed a simplified method for the prediction of changes in shear strength caused by DWS decompositions. The changes in shear strength of DWS were investigated by triaxial compression tests. The specimens were produced using the DWS which was mainly decomposed by H_2O_2 solutions. As a result, volumetric strain became large in the large axial strain range, and the maximum deviator stress decreased concomitantly with the decrease in ignition loss. After the organic matter was decomposed until 1.38%, the internal friction angle decreased from approximately 38.8° to 37.6°. The changes of shear strength were related to the substantial period in geotechnical works such as road infrastructures. The decompositions of the mechanical bridging and organic matter were described based on diffusion-controlled Al leaching and aerobic biodegradation, respectively.

RÉSUMÉ : La boue de l'eau potable est l'agrégation d'argile et composés organiques qui sont formées dans le flocculation et processus de la sédimentation. Cette étude s'est concentrée sur la décomposition de la liaison par agent du flocculating et matière organique et a proposé une méthode simplifiée pour la prédiction de changements dans la force du ciseau causée par les décompositions DWS. Les changements dans la force du ciseau de DWS ont été enquêtés par les épreuves de la compression du triaxial. Les spécimens ont été produits utiliser le DWS qui était principalement décomposé par les solutions H_2O_2. En conséquence, la tension volumétrique est devenue grande dans la grande gamme de la tension axiale, et le stress du déviateur maximal a diminué de façon concomitante avec la baisse dans la perte de l'ignition. Après que la matière organique ait été décomposée jusqu'à 1.38%, l'angle de la friction interne a diminué d'approximativement 38.8° à 37. 6°. Les changements de force du ciseau ont été mis en rapport avec période substantielle dans le geotechnical travaille tel qu'infrastructures de route. Les décompositions de la mécanique qui lie et la matière organique a été décrite basé sur Al diffusion-contrôlé qui lessive et biodégradation aérobique, respectivement.

KEYWORDS: waste, sludge, reuse, organic matter, decomposition, aluminum, leaching, shear strength

1 INTRODUCTION

Drinking water sludge (DWS) which is discharged during water purification is presently classified as industrial waste in Japan. A microphotograph of DWS is represented in Fig. 1. DWS is the aggregation of clay and organic compounds which is formed in flocculation and sedimentation process. Reuse and disposal of DWS are an important viewpoint in the sound material-cycle society.

The geotechnical use of DWS such as a road infrastructure material is greatly anticipated. So far, mechanical and leaching characteristics of DWS have been investigated (Roque and Carvalho, 2006; Watanabe et al., 2009). Specifically, it is presumed that Al leaching results from the Al-type flocculating agent. Watanabe et al. (2011) showed that the organic matter decomposition decreased in shear strength of DWS. To reuse DWS safely, the evaluation of the durability is strongly required. Therefore, this study focused on the decomposition of the bonding by flocculating agent and organic matter, and proposed a simplified method for the prediction of changes in shear strength caused by DWS decompositions in geotechnical works.

2 DECOMPOSITION MECHANISM

The DWS formation during water purification process is based on two phases in Fig. 2. Less than 10^{-6} m diameter particles including organic matter were flocculated by chemicals as first binding, and floc settled and consolidated (Montgomery, 1985). Bonding force is generated by the

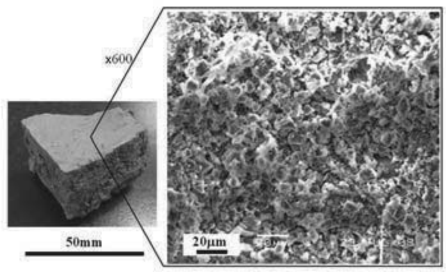

Figure 1. Microphotograph of DWS.

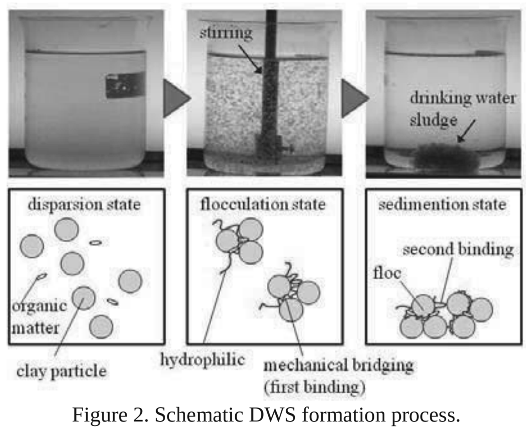

Figure 2. Schematic DWS formation process.

mechanical bridging of flocculating agent: polyaluminum

Table 1. Fundamental properties of DWS.

DWS	Particle density of soil (Mg/m^3)	Liquid limit (%)	Plastic limit (%)	Ignition loss(%)	Fulvic acid (%)	Humic acid (%)
A	2.58	224	145	17.6	0.039	3.14
B	2.61	178	104	18.8	0.032	2.39
C	2.52	269	151	26.6	0.034	9.27
D	2.45	113	91	27.3	0.040	4.31
E	2.54			17.1	0.016	1.20
F	2.65			22.1	0.049	3.90
G	2.45			19.1	0.036	5.14

chloride is frequently used in Japan. Some hydrophilic parts of flocculating agent remain and bind clods as second binding, then more than 10^{-5} m diameter clods presumably form DWS's porous structure as shown in Fig. 1.

In this study, DWS was sampled in Ibaraki, Japan. Approximate organic matter content of DWS was determined by ignition loss tests. The ignition loss and fundamental properties were listed in Table 1. Ignition loss of DWS was 17.6%−27.3%. The amount of humic and fulvic acids were determind by alkaline and acid isolation (Ohkubo et al., 1998). Specifically, humic acid content was dominant for DWS. It is indicated that organic matter exists in as a solid part and a bonding as well as the mechanical bridging. A main constituent of polyaluminum chloride is Al_2O_3. Previous study has been already confirmed Al leaching by column leaching tests in Fig. 3 (Watanabe et al., 2009). Organic matter decomposition at 30 degrees has been confirmed in Fig. 4 (Watanabe et al., 2011), which means the loss of DWS particles and binders. Consequently, engineering properties of DWS after the decomposition mentioned above are interest on a discussion of DWS durability.

3 RELATION BETWEEN SHEAR STRENGTH AND DECOMPOSITION

Shear characteristics of DWS after decomposition were investigated to elucidate the necessity of the mechanical bridging and organic matter on DWS's structure. The DWS which was mainly decomposed by H_2O_2 solution was used in triaxial compression tests.

3.1 Experimental procedure

Triaxial compression tests were executed using the DWS for which the mechanical bridging and organic matter had been decomposed by the H_2O_2 solution. The apparatus for the triaxial compression tests is portrayed in Fig. 5. The specimen had 100-mm height and 50-mm diameter. Specimens were produced by dynamic compaction using DWS-A. The dry density in CASES 1–4 was 0.815–0.825 Mg/m^3 which corresponds to compaction degree 76%. First, the specimen was isotropically confined by 10 kPa. Then the H_2O_2 solution (6%, 9%, 15%) was percolated through the specimen by 10 kPa of water pressure. Specimens in CASES 2, 3 and 4 were decomposed by the H_2O_2 solution. During H_2O_2 percolation, CO_2 was generated by oxidation. The CO_2 continuously flow into the sealed desiccator, and the CO_2 concentration was measured using a wireless CO_2 sensor. The completion of oxidation was confirmed as the CO_2 concentration converged, which prevented partial saturation of the specimen during shearing. The decrease in organic matter by H_2O_2 has been investigated in Table 2. The discharged water was collected, and Al concentration was measured. The distilled water was percolated after H_2O_2 percolation, and more than 0.95 of the B-value was confirmed for specimen saturation. The isotropic consolidation pressure was 50 kPa or 100 kPa. The triaxial tests were executed in the drainage condition with 0.1%/min of the strain rate.

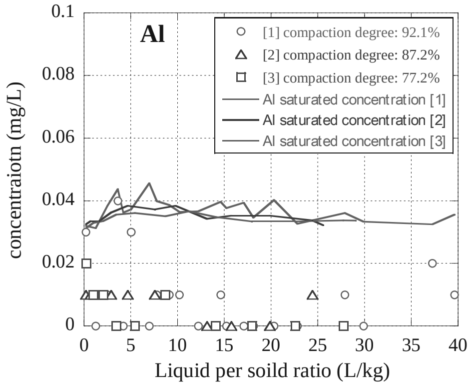

Figure 3. Al concentration in column leaching tests (Watanabe et al., 2009).

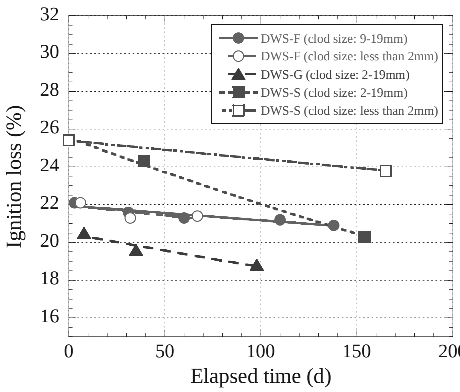

Figure 4. Changes of ignition loss of DWS at 30 deg. (Watanabe et al., 2011).

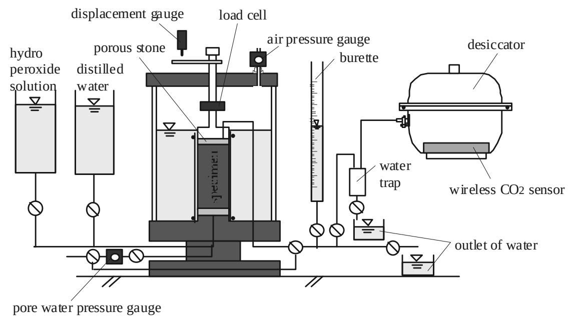

Figure 5. Apparatus for triaxial compression test.

Table 2. Decomposition rate of organic matter by 6% hydrogen peroxide solution for 24 h.

DWS	Decomposition rate (%)		
	Fulvic acid	Humic acid	Humin and soil particles
B	77.1	44.9	3.1
C	86.5	43.2	8.1
D	88.0	46.6	10.3
E	73.4	42.5	6.6

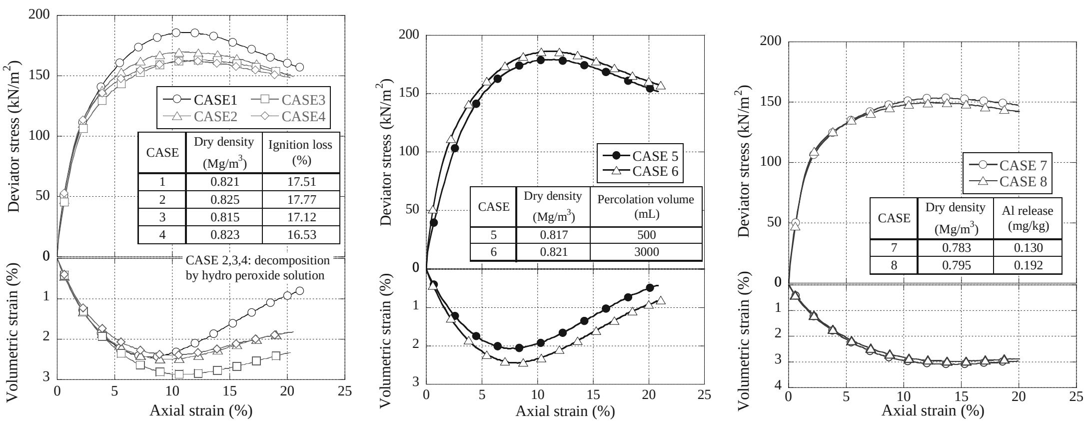

(a) H_2O_2 percolation (b) distilled water percolation (c) pH 4.0 water submergence

Figure 6. Relation between deviator stress and axial strain in triaxial compression tests using decomposed DWS.

As mentioned above, Al leaches during H_2O_2 percolation. The deformation of the mechanical bridging by Al leaching causes at the same time as organic matter decomposition. To distinguish the influence of Al leaching on the mechanical deformation from organic matter decomposition, shear characteristics of the DWS for which the mechanical bridging had been decomposed by leaching using distilled water adjust pH 4.0 using HNO_3 which was almost same pH as H_2O_2 solutions were also investigated in CASE 5 to 8. In acidic condition, humic acid almost remains in DWS, although fulvic acid is decomposed. In CASE 7 and 8, samples previously submerged in HNO_3 repeatedly, and the specimens were produced by dynamic compaction using the decomposed sample.

3.2 Experimental results

The respective relations between the deviator stress and the volumetric strain to axial strain at 50 kPa of confined pressure was presented in Fig. 6. Volumetric swelling was slight in the large axial strain range, and the maximum deviator stress decreased concomitantly with the decrease in ignition loss. For the cases of distilled water percolation, the influence of percolation volume was not obtained. The larger dry density typically showed higher shear strength. For the cases of pH 4.0 water submergence, maximum deviator stress slightly decreased and cumulative Al release increased with the increment of submergence. The influence of Al release on shear strength was relatively smaller than those of organic matter decomposition.

The internal friction angle and the cohesion of DWS after organic matter decomposition were, respectively, 38.6° and 0 kN/m^2. The mechanical bridging and the organic matter decomposition do not influence DWS cohesion. Assuming that the cohesion is 0 kN/m^2, the relation between the internal friction angle and the decomposition rate of organic matter was presented in Fig. 7. After the organic matter was decomposed until 1.38%, the internal friction angle decreased from approximately 38.8° to 37.6°. For the cases of pH 4.0 water submergence, the internal friction angle decreased from 37.2° to 36.7° although the dry density was smaller than any others. Consequently, results show that the decomposition of organic matter remarkably affects to the DWS shear strength. Chemical bonding between particles by the cementation of organic compounds is possible (Mitchell and Soga, 2005). Presumably, the strength of DWS clods decreased because the bonding was lost through organic matter decomposition.

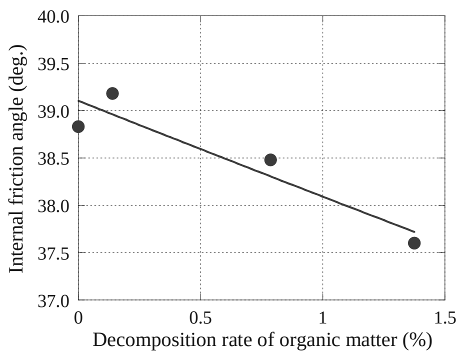

Figure 7. Relation between internal friction angle and decomposition rate of organic matter.

4 PREDICTION OF SHEAR STRENGTH TRANSITION

Al release and organic matter decomposition cause the decrease in shear strength of DWS. To evaluate the durability of DWS as a geo-material, this study related the change of its shear strength the decomposition to the substantial period in geotechnical works such as road infrastructures.

4.1 Shear strength transition addressing decomposition of mechanical bridging

Decomposition of the mechanical bridging is described as Al leaching behavior. When DWS is used as a subgrade material under groundwater level, Al diffusively leaches. Therefore, the Al leaching behavior is described as a diffusion equation based on the Fick's law.

$$\frac{\partial C}{\partial t} = D_e \frac{\partial^2 C}{\partial x^2} \tag{1}$$

In that equation, D_e is the coefficient of diffusion [m^2/s], C is the concentration [mg/L], and x signifies the distance from particle surface [m]. An initial condition and boundary conditions are shown as follows.

$$t = 0,\ x \leq 0; C = C_0$$
$$t > 0,\ x = 0; C = C_1, t > 0,\ x = -\infty; C = C_0$$

where C_0 represents the internal concentration of material [mg/L], and C_1 is the constant concentration [mg/L]. Assuming C_0 is sufficiently higher than C_1, the cumulative release M is derived.

$$M = 2C_0\sqrt{\frac{D_e}{\pi}}\left(t_2 - t_1\right) \tag{2}$$

D_e of Al is 4.77×10^{-15} m^2/s which was obtained by the serial batch leaching test (Watanabe et al., 2010). As t_1 is 0, the Eq. 2 transforms to Eq. 3, and it relates the cumulative Al release M_{exp} obtained in the triaxial tests to the elapsed time T.

$$T = \frac{M_{\exp}^{2} \cdot \pi}{4C_0^2 \cdot D_e} \tag{3}$$

Therefore, the transition of the internal friction angle caused by decomposing the mechanical bridging is calculated as shown in Table 3. Approximate 1.3% decrease in the internal friction angle supposedly causes during 38 years.

4.2 *Shear strength transition addressing decomposition of organic matter*

The organic matter decomposition of DWS as a subgrade material is able to be interpreted as following, assuming aerobic and unsaturated condition. Jenny (1941) described the decrease in soil organic matter as Eq. 4.

$$\frac{dX}{dt} = rX \tag{4}$$

where X is the mass of organic matter and r is the rate of decomposition. A solution of Eq. 4 is given by Eq. 5.

$$X = X_0 \cdot e^{-rt} \tag{5}$$

Assuming aerobic biodegradation, discharged CO_2 is originated from the carbon loss of decomposed organic matter approximately. From the results of constant temperature storage in aerobic condition of DWS (Watanabe et al., 2011), r is determined by fitting Eq. 5 into the experimental data as shown in Fig. 8. The daily CO_2 discharge during organic matter decomposition corresponds to the decomposition mass of organic matter, so the time integral of Eq. 5 approximately represents the total mass of decomposed organic matter Q_{dec}.

$$Q_{dec} = \frac{X_0}{r}\left(e^{-et_1} - e^{-rt_2}\right)\times\frac{12}{44} \tag{6}$$

Calculation results for the transition of the internal friction angle caused by decomposing the organic matter are listed in Table 4. Approximate 3.1% decrease in the internal friction angle by organic matter decomposition causes during 22 days in aerobic condition. Assumption of aerobic condition is not suitable for practice, so this study confirmed the organic matter decomposition in site. In the experimental construction that DWS was used as a backfill material of water pipe construction, the DWS layer was taken a position of -0.4 to -0.9 m depth under asphalt surface. The compaction degree was approximate 64–76%. The monitoring term was 19 months. As shown in Table 5, ignition loss slightly decreased at the end of the experiment. It is presumed that organic matter decomposition slowly progressed in contrast to the constant temperature storage because of anaerobic condition and lower temperature. The proposed method with aerobic condition excessively estimates the degradation in contrast of underground conditions.

5 CONCLUSIONS

DWS is the aggregation of clay and organic compounds. Focusing on the chemical bonding by flocculating agent and organic matter, a simplified method for the prediction of changes in shear strength of DWS in geotechnical works was proposed. The decomposition of the mechanical bridging and the organic matter was described based on diffusion-controlled Al leaching and aerobic biodegradation, respectively. The methodology proposed in this paper is significant to encourage safe geotechnical utilizations through estimations of the usable term for not only DWS but also available waste or by-products.

Table 3. Shear strength transition addressing decomposing the mechanical bridging.

Cumulative Al release (mg/kg)	Calculated elapsed time (y)	Internal friction angle (deg.)
0	0	37.2
0.130	17.4	37.6
0.192	38.0	36.7

Table 4. Shear strength transition addressing decomposing the organic matter.

Decomposition rate of organic matter (%)	Calculated elapsed time (d)	Internal friction angle (deg.)
0	0	38.8
0.14	2	39.2
0.79	12	38.5
1.38	22	37.6

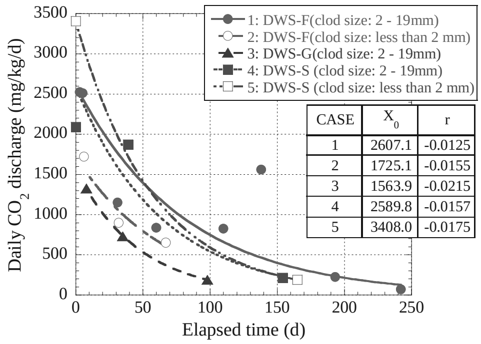

Figure 8. Results of constant temperature storage in aerobic condition of DWS (Watanabe et al., 2011).

Table 5. In-situ monitoring results of ignition loss of DWS

	Compaction degree (%)	CBR (%)	Ignition loss (%)	
			before construction	19 months later
Air-dried DWS	75.9	38.1	16.9	16.6
Filter-pressed DWS	64.3	55.3	24.7	24.0

REFERENCES

1) Jenny, H. (1941): *Factors of soil formation*, McGraw-Hill, New York.
2) Mitchell, J. K. and Soga, K. (2005): *Fundamentals of Soil Behavior*, third edition, John Wiley & Sons, Inc.
3) Montgomery J. M. (1985): *Water Treatment Principles and Design*, John Wiley & Sons Inc., pp.116-134.
4) Ohkubo, N., Yagi, O., and Okada, M.: Effects of humic and fulvic acids on the growth of microcystis aeruginosa, *Environmental Technology*, Vol. 19, pp. 611-617, 1998.
5) Roque, A. J. and Carvalho, M. (2006): Possibility of Using the drinking water sludge as geotechnical material, *Proc. of 5th International Congress of Environmental Geotechnics*, pp.1535–1542.
6) Watanabe, Y. et al. (2009): Environmental impact assessment of drinking water sludge, *Journal of Japan Society of Civil Engineering G*, Vol. 65, No. 3, pp. 188-201.
7) Watanabe, Y. et al. (2010): Serial Batch Leaching Test for Evaluating Degradation of Drinking Water Sludge in Geotechnical Reuse, *Proc. of 6th International Congress of Environmental Geotechnics*, pp.1073-1078.
8) Watanabe, Y. et al. (2011): Composition and decomposition of organic matter of drinking water sludge, *Proc. of 9th Geo-Environmental Engineering*, pp. 435–438.

Road foundation construction using lightweight tyre bales

Construction des assises de routes à l'aide de balles de pneus légères

Winter M.G.
Transport Research Laboratory (TRL), Edinburgh, United Kingdom

ABSTRACT: Road construction over soft ground presents considerable technical challenges. Such roads often serve remote communities and carry low levels of traffic; construction and maintenance must be achieved within very limited budgets. There are two main approaches to such construction: above ground (floating) and below ground (buried) construction. Floating construction is generally used where a relatively stiff material, such as fibrous peat, overlies a less competent material, such as amorphous peat. Buried construction is generally used in more competent materials, or in soft materials of shallower depth such that removal is viable. In both cases lightweight construction materials are desirable but can be costly. This paper describes tyre bales as a lightweight construction material and specifically addresses issues in relation to their use as a foundation material for roads over soft ground.

RÉSUMÉ : La construction de routes sur sol meuble présente des défis techniques considérables. Ces routes desservent souvent des collectivités éloignées et connaissent de faibles niveaux de trafic ; leur construction et leur entretien doivent respecter des budgets très serrés. Il existe deux méthodes principales pour ce type de construction : au-dessus du sol (construction flottante) et en dessous du sol (construction enterrée). La construction flottante est généralement employée lorsqu'un matériau relativement rigide, comme la tourbe fibreuse, repose sur un matériau moins compétent, tel que la tourbe amorphe. La construction enterrée est généralement privilégiée en présence de matériaux plus compétents, ou de matériaux souples moins profonds dont l'élimination est viable. Dans les deux cas, il est utile d'employer des matériaux de construction légers, qui peuvent cependant s'avérer coûteux. Cet article décrit les balles de pneus comme matériau de construction léger et traite spécifiquement des problématiques liées à leur utilisation comme matériau d'assise des routes sur sol meuble.

KEYWORDS: Sustainability, reuse, recycling, foundations, tyres, bales.

1 INTRODUCTION

The construction of roads over soft ground, such as peat, presents considerable technical challenges. Many such roads serve remote communities, carry only low levels of traffic, and must be constructed and maintained within limited budgets.

Where the depth of soft soil is significant, the approach to construction generally involves 'floating' the road on the existing subsoil. This may also involve the use of temporary surcharging and/or reinforcement at the base of the construction to help spread the load. If the depth of peat or other soft material is shallow then removal may be an option. The excavated material is then replaced by more competent materials. However, this does leave the issues of disposing of the excavated material and of preventing the adjacent material from flowing into the excavation. The resolution of either or both of these issues can prove costly, and such costs will increase rapidly with the depth of material excavated.

In both cases, the use of lightweight construction materials is desirable. This paper introduces lightweight tyre bales focusing upon their potential use as a road foundation material and draws on the author's experience in the UK and the USA. Relative to conventional lightweight foundation materials such as expanded polystyrene, the cost of tyre bale construction is relatively low.

2 TYRE BALES

Around 48M tyres (480,000 tonnes) are scrapped in the UK each year. However, the issue of scrap tyres is by no means unique to the UK and Europe. In the USA it has been estimated that over two billion used tyres are stockpiled, and that 285M are added each year (Winter et al. 2006). In the recent past the bulk of waste tyres in the UK was stockpiled, disposed of in landfill or illegally, or sent for energy recovery (Hird et al. 2001) or processed as waste-to-energy. In Europe the Landfill Directive outlawed the disposal of tyres in landfill, with UK exceptions being made for engineered works. In the USA a number of fires in waste dumps comprising whole tyres, and concerns regarding the potential flammability of tyre shreds and chips, led the drive towards alternative solutions.

The majority of R&D activity has addressed tyre shred, chip and crumb for use in construction works. An alternative is the baling of whole tyres to produce rectilinear, lightweight/low density, permeable, porous bales of high bale-to-bale friction.

2.1 *Composition, properties and behaviour*

Tyre bales comprise 100 to 115 car/light goods vehicle tyres compressed into a lightweight block of mass around 800kg and density *circa* $0.5 Mg/m^3$. The bales measure approximately 1.3m by 1.55m by 0.8m and are secured by five galvanized steel tie-wires running around the length and depth of the bale (Figure 1). They have considerable potential for use in construction particularly where their low density and ease of handling places them at a premium. A porosity of around 62% and permeability of approximately 0.02m/s through the length and 0.2m/s through the depth (Simm et al. 2005) makes them ideal for drainage applications. The bale-to-bale friction angle is around 35^o in dry conditions and stiffness in the vertical direction of Figure 1 is up to around 1GPa (Frielich & Zornberg, 2009; Winter et al. 2006). Furthermore, the process of tyre bale manufacture consumes around 1/16 of the energy required to shred a similar mass of tyres (Winter et al. 2006).

Substances that could potentially leach from tyres are already present in groundwater in developed areas. Studies suggest that leachate levels generally fall well below allowable regulatory limits and have negligible impact on water quality in close proximity to tyres (Hylands & Shulman, 2003) and that rates of release decrease with time (Collins et al. 2002). Similarly there is no evidence of significant deterioration of tyres buried in the ground for decades (Zornberg et al. 2004).

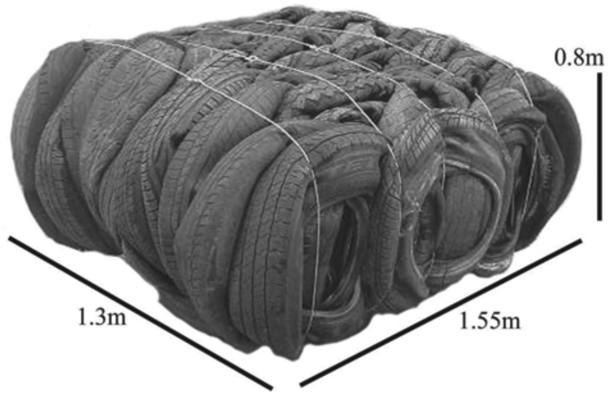

Figure 1. A typical tyre bale with dimensions.

Spontaneous fires in whole tyre dumps are not known to the author. In the USA, while combustion due to sparks from agricultural machinery and lightning have been reported, most observers suspect some form of arson in almost all cases. Baling whole uncompressed tyres reduces the volume by a factor of four to five, greatly reducing the available oxygen as well as the exposed rubber surface area as tyre-to-tyre contacts are formed, without exposing any steel reinforcing in the tyres. The exothermic oxidation reaction potential is significantly lower than for whole tyres and the risk of spontaneous combustion from tyre bales is viewed as extremely low. A modelled storage condition for a 17.5m by 6.0m by 3.0m volume of bales needed to reach and maintain a temperature of 188^{o}C for 39 days before spontaneous combustion became possible (Simm et al. 2005). In contrast reports have been made of internal heating of tyre shred and of apparently spontaneously combusted fires in large volumes in the USA (Sonti et al. 2000). Further details of tyre bale properties and behaviours are available (Anon. 2007).

Tyre bale use reflects positively on the sustainable use of materials and energy and other factors. In the last decade the application level has moved from domestic works/river bank erosion projects to slope failure repairs adjacent to a major Interstate Highway in the USA (Winter et al. 2009) and the construction of a lightweight embankment as part of the A421 A1-M1 link road construction which won the British Geotechnical Association's prestigious Fleming Award.

An adequate supply of tyres, and the resources to turn them into bales must be secured prior to the commencement of a project. As bales are around ¼ to ⅕ the volume of whole tyres it can be particularly difficult to gauge the volume of bales that will result from a stockpile of tyres. A series of nomograms was developed by Winter et al. (2006) and further refined (Anon. 2007) to rapidly describe the number of bales required to fill a given volume, the number of tyres likely to be used in their manufacture, and the number of eight hour (two man) shifts required to manufacture those tyre bales.

Tyre bales costs are similar to those of other road foundation materials (e.g. UK Type 1 Sub-Base). However, the main advantages of tyre bales are the much reduced plant and labour costs resulting from their rapid placement (Winter et al. 2006).

2.2 *British Standard*

The tyre baling industry in the UK reached a level of maturity with the production of a British Standard Publicly Available Specification (PAS) for tyre bales (Anon. 2007). It assists manufacturers to produce high quality, consistent and traceable products for use in construction by responsible and competent organizations, and demonstrate high and consistent quality via a Factory Production Control process. It covers activities and aspects of tyre bale manufacture, storage and use in construction, including: receipt, inspection and cleaning of tyres; handling and storage of tyres; production of bales (including a system for measuring and labelling bales to ensure traceability); handling and storage of the bales; transport, storage on site and placement of the bales; and factory production control.

Guidance is given to construction professionals in formulating preliminary design and construction proposals. Not all aspects of design are covered but information not available from other engineering documents is given. This includes: the measurement of properties; engineering properties and behaviours associated with tyre bale use in construction; example applications; and end of service life options.

3 METHODS OF CONSTRUCTION

There are two main approaches to road construction over soft ground: above ground (floating); and below ground (buried). Both use large volumes of granular fill.

It is important to decide whether or not a crust in, for example, peat may be breached or whether it must remain intact. Figure 2 illustrates advantages and disadvantages of floating and buried construction. The crust in peat will often be formed from fibrous vegetation. Similarly, many normally consolidated lowland clays in parts of Scotland and many Scandinavian 'quick clays' will have a stiffer crust. In general terms it is inadvisable to breach the crust of these materials and thus floating construction is preferred to buried construction.

3.1 *Floating construction*

In areas of deep soft soil, replacement techniques are unattractive as large volumes of material must be excavated, transported and disposed at both monetary and environmental cost. The surrounding soft material may create difficulties related to excavation support, basal heave and other factors, making the works uneconomic. Where the natural surface 'crust' is stiffer than the lower layers due to the presence of vegetation, desiccation, compaction and other factors, the surface may form the subgrade. Care is needed to ensure that the crust is not compromised during construction and that as the road is built the imposed loads are spread over a wide area.

In the past construction often utilised bundles of twigs (fascines), usually two layers orientated at 90^{o}, at subgrade level to resist differential movement. For greater loads logs were used on the fascines, working best for materials with stiff crusts (e.g. fibrous peat overlying softer amorphous, or humified, peat). The modern equivalent is a geosynthetic material; the use of tyre bales or other lightweight fill on the geosynthetic/sand layer lessens the applied load. The success of temporary surcharging is often limited in very soft soils such as peat due to the potential for long-term secondary and/or tertiary consolidation and the potential to breach any overlying stiffer layer.

3.2 *Buried construction*

The removal and replacement of in-situ materials with new, lightweight, fill is a costly option and may involve excavation below the water table. However, sidewall lateral restraint adds durable construction stiffness. The key to construction is to ensure that the fill adds minimal load.

Buried construction may be preferred in more competent materials, or in thinner layers of less competent materials for which removal is an option. Such materials include normally consolidated silts and clays, and soft predominately mineral soils (albeit with exceptions). A geotextile helps to spread the foundation load. Often the repair or reconstruction of an existing road over soft ground is required as a result of differential settlement which leaves an uneven surface with poor ride quality and an increased risk of flooding. The placement of material to raise and regulate the pavement surface increases the formation load causing further differential settlement; replacement of the existing material is thus necessary.

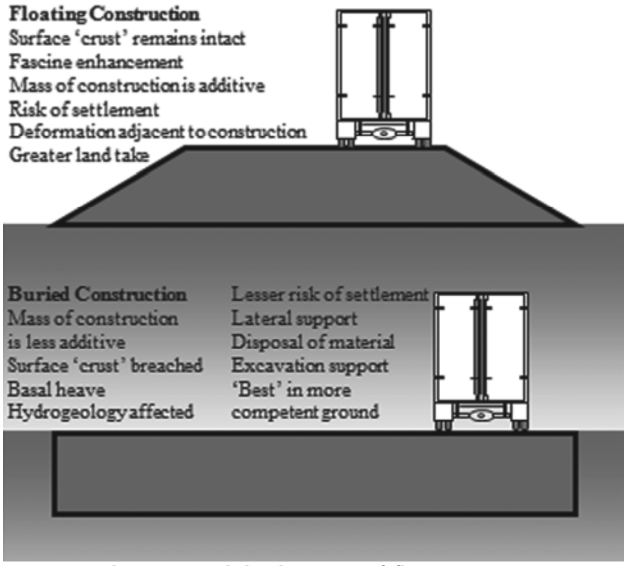

Figure 2. Advantages and disadvantages of floating construction (top) and buried construction (bottom).

4 CONSTRUCTION APPROACHES

The construction and rehabilitation of low-volume roads over soft ground is an ideal application for tyre bales. While there is currently little information to prove their use with higher traffic levels (in excess of a few hundred vehicles/day AADT) there are no pressing reasons why such uses should not be successful.

Low-volume tyre bale roads have been successfully constructed both above and below ground. A geotextile separator is used between the in-situ soil and the tyre bales, usually with a regulating layer of sand. The geotextile helps to prevent differential movement of the bales during and after construction. The decision as to whether the construction should be above or below ground is an important determinant of the approach to the design and construction.

Analytical input for low-volume road design on soft ground is often limited. The strength and stiffness properties of the soil involved are usually at or close to the lower limit of measurement, rendering input parameters subject to large errors. The sampling process may also disrupt the soil structure leading to values lower than the field condition. Accordingly many roads are designed on an empirical, specification-led basis.

The following sections summarises the main construction steps and issues and offer guidance based upon experience of successful projects and established good practice in constructing low-volume roads over soft ground using tyre bales. Further details are given by Winter et al. (2006) and Anon. (2007).

4.1 *Excavation and preparation*

For buried construction, excavation is the first construction activity. Low ground-pressure, tracked plant is preferred as is working in drier weather when the moisture content of the soil is minimised and strength and stiffness are maximised.

A suitable geotextile should be installed either at ground surface level or in the excavation followed by a regulating layer of sand if required. All geotextile-to-geotextile interfaces should have an overlap of 1m. The use of a geotextile has a number of advantages including aiding working conditions in soft soils, strengthening the structure by tying together the assembly of bales, and providing separation between the bales and the subsoil and thus preventing the ingress of fines. Randomly orientated, bonded, non-woven geotextiles have been found to be effective. Their main function is separation, with strength and resistance to clogging the most important properties. Geotextile design procedures should reflect local standards. The geotextile should be placed in the base of the excavation, or on the cleared ground. Sufficient excess should be allowed at either side to allow the bale assembly to be completely wrapped in the geotextile with a 1m overlap.

Rapid cellular construction minimises excavation size, exposure of the soil to weather and the likelihood of side slope failure. Bale sizes mean that excavations are unlikely to exceed 1m, but an assessment of the possibility of sidewall collapse and the associated risks to workers and others during the execution of such operations is essential.

4.2 *Placement and alignment*

Tyre bale handling must incur the minimum risk of damage to the steel tie-wires. The most successful means of handling tyre bales has been found to be a 'loggers'-clam', which can be attached to a variety of hydraulic equipment and provides an appropriate lift-and-place methodology while allowing the bale to be rotated to the correct alignment. Alternative forms of handling bales include brick-grabs and forklifts (Anon. 2007).

The manufacturing process renders tyre bales inherently heterogeneous. Information on the relative stiffness in each of the three directions is not currently available. Tyre bales exhibit a high stiffness when loads are applied vertically to the 1.3m by 1.55m plane (Figure 1); accordingly they are usually installed as illustrated in Figure 1 for applications that attract high vertical loads such as road foundations. The 1.55m by 0.8m plane is perpendicular to the load applied during manufacture and it is recommended that it is aligned perpendicular to the longitudinal confining stresses (i.e. with the tie-wires in line with the road.

While there are different layout options for the two-dimensional placement of tyre bales (i.e. in a single layer) a straightforward 'chessboard' pattern, as viewed in plan, is generally the easiest to construct and is recommended.

A regulating layer of sand is normally required between the top of the tyre bales and the geotextile wrapped over the top of the layer to help eliminate small variations in level.

The foregoing assumes that a single layer of bales is to support the road. If two or more layers are required then the second layer should be placed on top of the first, stepped in at either side to provide around half a bale width of overlap.

4.3 *Filling of voids*

The sub-rectangular shape of tyre bales means that voids remain at the corners of each bale even when they are butted up against one other. The design generally requires the stiffness and stability of the structure to be maximized and thus the voids should generally be filled (Figure 3). Coarse sand has been used successfully as have single-sized aggregate pellets. Crushed glass may be less likely to clog or arch than sand when wet, but is expensive. The most effective method of ensuring that the voids are filled has been found to be to bulldoze a 150mm to 300mm layer on top of the bale layer and then to apply a vibrating roller to the layer to vibrate the fill into the voids (Figure 3).

The fill material affects the density of the structure, with the voids taking up an estimated 4% to 8% (Anon. 2007) of the nominal rectangular bale volume, and must be allowed for in design calculations. The effects of regulating layer(s) above or below the tyre bale layer must also be taken into account.

Once the fill operation for a cell has been completed for a section of road, the geotextile should be wrapped around the bale-fill composite with an overlap of around 1m. A crushed rock sub-base should be placed and compacted on top of the completed section. A thickness of 150mm is likely to be sufficient to provide a construction platform for the works to continue without damaging the geotextile. The final thickness of sub-base must be assessed to ensure sufficient capacity during normal use and should be the subject of site-specific design. After these operations are completed the construction may proceed to the next cell, repeating the process described above until the road has been completed.

Figure 3. Bulldozing sand to fill voids, County Road 342 (CR342), 2000 (left); vibrating sand into inter-bale voids, CR647, 1999. (Courtesy Ken Smith, Chautauqua Co Dept of Public Facilities, NY.)

4.4 *Pavement construction and drainage*

Pavement construction is beyond the scope of this paper but further guidance is given by Winter et al. (2006) as is more detail on drainage considerations. The design should reflect local standards and climatic conditions.

5 SUCCESSFUL APPLICATIONS

Successful applications involving the construction of tyre bale road foundations have been achieved in both the USA (New York State) and the UK (Winter et al. 2005).

Chautauqua County Department of Public Facilities completed five projects using tyre bales as a lightweight subgrade replacement for roads over soft ground (Figure 4). The tyres result from the clean-up of a tyre dump and from a tyre amnesty programme. The geology of the County is characterised by sands and gravels in the river valleys with glacially deposited fine silty clays elsewhere, primarily on the hilltops which are often depressed forming high level swamps. These materials are stable if dry but are sensitive to moisture and to the freeze thaw cycle which can turn them into a material like ‘pottery slip’. Conventional unpaved roads constructed on them can turn into impassable quagmires. Tyre bale road construction was targeted on these roads.

Figure 4. Completed CR342 2004 after four years in service (left); B871 in Highland, UK (right, Courtesy G Smith, Highland Council.).

To date with the roads having been in service for up to nine years no major signs of distress have been observed that could be attributed to the presence of tyre bales. In the case of CR342 the traffic levels have been greatly increased (up to around 1,500 to 2,000 vehicles per day AADT) due to a new residential development in the vicinity.

A public road was constructed by Highland Council (UK) in late-2002 (Anon. 2003); performance has been satisfactory despite extreme loadings imposed by a very high proportion of heavy logging trucks using the route (Figure 4).

6 CONCLUSIONS

The use of lightweight tyre bales in the construction of road foundations over soft ground has the potential to satisfy the demand for low cost materials exhibiting such a beneficial property. Such uses also help to address society’s broader problem in respect of the large volumes of waste tyres which, in Europe at least, may no longer be sent to landfill for disposal; clearly such beneficial uses for waste tyres are required.

Supply and production issues are addressed and material costs shown to be comparable with conventional materials such as Type 1 sub-base. However, the key strength of tyre bales is their modular nature which leads to potential savings in plant and labour and the associated time savings. In some cases the low cost of tyre bales relative to other lightweight materials, such as expanded polystyrene, may allow the economic construction or rehabilitation of infrastructure in remote areas that would otherwise not be viable. An approach to the construction of low-volume road foundations on soft ground using tyre bales has been developed and is summarized herein.

Tyre bales offer a useful tool for the engineer across a wide range of construction applications that variously exploit their beneficial properties: namely low density, high permeability, high porosity and high bale-to-bale friction.

7 ACKNOWLEDGEMENTS

Copyright TRL Limited 2013. Funding was by the Veolia Environmental Trust Landfill Tax Credits Scheme supported by Inverness & Nairn Enterprise and Transport Scotland. The Royal Academy of Engineering part-funded (International Travel Award No. 04-301) a study visit to the USA.

8 REFERENCES

Anon. (2007). Specification for the production of tyre bales for use in construction, *PAS 108*. London: British Standards Institution.

Anon. (2003). The B871 tyre bale project – the use of recycled tyre bales in a lightweight road embankment over peat. Rovaniemi, Finland: Roadscanners.

Collins, K. C., Jensen, A. C., Mallinson, J. J., Roenelle, V. & Smith, I. P. (2002). Environmental impact assessment of a scrap tyre artificial reef. *ICES Journal of Marine Science* 59, S243-S249.

Freilich, B. & Zornberg, J. (2009). Mechanical properties of tire bales for highway applications. *Report FHWA/TX-10/0-5517-1*. The University of Texas at Austin.

Hird, A. B., Griffiths, P. J. & Smith, R. A. (2001). Tyre waste and resource management: a mass balance approach. *Viridis Report VR2*. Crowthorne: TRL Limited.

Hylands, K. N. & Shulman, V. (2003). Civil engineering applications of tyres. *Viridis Report VR5*. Crowthorne: TRL Limited.

Simm, J. D., Wallis, M. J. & Collins, K. (Eds.). (2005). Sustainable re-use of tyres in port, coastal and river engineering: guidance for planning, implementation and maintenance. *SR 669*. Wallingford: HR Wallingford.

Sonti, K., Senadheera, S., Jayawickrama, P. W., Nash, P. T. & Gransberg, D. D. (2000). Evaluate the uses for scrap tires in transportation facilities. Research Study 0-1808, Lubbock, TX: Texas Tech University.

Winter, M. G., Reid, J. M. & Griffiths, P. I. J. (2005). Tyre bales in construction: Case Studies. *TRL PPR 045*. Crowthorne: TRL Limited.

Winter, M. G., Watts, G. R. A. & Johnson, P. E. (2006). Tyre bales in Construction. *TRL PPR 080*. Crowthorne: TRL Limited.

Winter, M. G., Williammee, R & Prikryl, W. (2009). The application of tyre bales to the repair of slope failures. *Proceedings, Institution of Civil Engineers (Engineering Sustainability)*, 162(ES3), 145-153.

Zornberg, J. G., Christopher, B. R. & Larocque, C. J. (2004). Applications of tire bales in transportation projects. Recycled Materials in Geotechnics (Eds: Aydilek, A. H. & Wartman, J.). *Geotechnical Special Publication No 127, 42-60*. Baltimore, MA: American Society of Civil Engineers.

General report
Geotechnical problems of dikes (TC 201) and dams (TC 210)

Rapport général
Problèmes géotechniques dans les digues (TC 201) et barrages (TC 210)

Xu Z.
China Institute of Water Resources & Hydropower Research, State Key Laboratory of Simulation and Regulation of Water Cycle in River Basin

ABSTRACT: Among the papers submitted to the 18th International Conference on Soil Mechanics and Geotechnical Engineering (ICSMGE 2013), 11 papers are catalogued in the field of dike and dam, with 4 paper on dike and 5 papers on dam. By reviewing the submitted papers and recent development in related field, the general report for the joint session of TC201 (dike) and TC210 (dam) of ISSMGE Conference (Paris 2013) was presented. Besides the brief comments on the submitted papers, the general report discussed some selected geotechnical issues of dikes and dams. For dikes, the discussion is mainly focus on overtopping flow erosion, internal seepage instability and bank collapse. For dams, some key technologies for building high rockfill dam were presented, which includ properties of construction materials, foundation treatment, dam deformation control and hydraulic fracture of earth core.

RÉSUMÉ : Parmi les articles présentés au 18^e Congrès International de Mécanique des Sols et de la Géotechnique (CIMSG 2013), 11 articles sont catalogués dans le domaine des digues et barrages, avec 4 articles sur les digues et 5 sur les barrages. En passant en revue les articles présentés ainsi que les développements récents dans le domaine, le rapport général de la session conjointe des TC201 (digues) et TC210 (barrages) du congrès de la SIMSG (Paris 2013) a été présenté. En plus des brefs commentaires sur les articles présentés, le rapport général a examiné certains problèmes géotechniques des digues et des barrages. Pour les digues, la discussion est principalement ciblée sur l'érosion due au débordement, sur l'instabilité de l'écoulement interne et sur l'effondrement des rives. Pour les barrages, certaines technologies clés pour la construction de grands barrages en enrochement ont été présentées, qui incluent les propriétés des matériaux de construction, le traitement des fondations, le contrôle de la déformation du barrage et la fracturation hydraulique du noyau en terre.

KEYWORDS: dike, dam, gentechnical problems, general report

1 INTRODUCTION

Dike is a kind of very important structural approaches to flood management of rivers and lakes, and also to defense high tide alone seashores. To use dikes to protect land from annual floods date back centuries and in some places more than 2,000 years ago. Construction of a dike requires that it is high enough to exclude extreme flood and to avoid overtopping failure. Besides, as most of the dikes were constructed by earth materials and were normally found on natural riverbank, a common problem is seepage through the dike and foundation. The internal erosion by unfavorable seepage could lead to loss of dike or foundation materials and further lead to dike collapse and overtopping.

Rockfill dam is one of the most widely accepted and rapidly developed dam types in dam engineering. Rockfill dams in early stage were constructed by dumped rocks and face slabs. From 1920s to 1960s, with the progress of soil mechanics, earth core rockfill dam (ECRD) was well developed. The built dam height reached to 150m. After 1960s, with the application of vibrating roller and the technique of thin layer compaction, concrete faced rockfill dam (CFRD) was rapidly developed. Many high CFRD were constructed all over the world. At the same time, ECRD was further developed with the improvement of construction methods and equipment. At present, the dam height of CFRD has reached to 200m, while the height of ECRD has reached to 300m. CFRD and ECRD have become the main representative types of modern rockfill dam.

Dikes and dams are the important infrastructures in modern society. It is also an important field of the application of modern soil mechanics and geotechnical engineering. In conference ISSMGE 2013, there are 11 papers concerning dike and dam, which 5 paper on dikes and 6 papers on dams. For the papers on dikes, 2 papers are about seepage failure of dikes, with one paper for internal erosion and another paper for hydraulic failure; one paper is about settlement prediction; one paper for strength assessment of dike foundation material; one paper is about soil reinforcement of costal geotechnical engineering. For the papers on dam, two papers are about concrete faced rockfill dam, with one paper for numerical analysis and another paper for deformation control; two paper are about dam seepage, with one paper for the design of filter material and another paper for suffusion of loess material; one paper is about stability of earth dam; one paper is about the failure of tailing dam.

2 GEOTECHNICAL PROBLEMS OF DIKES

For dikes of flood defense, statistic analyses show that overtopping and internal erosion are the most common modes of dike failure. Besides, bank collapse is also one of the common threatens to the safety of dikes. All of these failure modes are the concern of geotechnical engineers in dike engineering.

2.1 *Flow erosion of overtopping*

When dike is not high enough to flood water level, overtopping will be happened. As most of the dikes are constructed by earth material, soil erosion by the flow of overtopping could cause the failure of the dike. Although no papers in ISSMGE 2013 have discussed this issue, it is still an important problem in dike engineering. In recently years, some overtopping cases were occurred and have finally led to the failure of the dikes. The dikes failure by Hurricane Katrina in 2005 in New Orleans, Louisiana, USA and Mississippi River levee failures by 2008 flood in USA are the typical cases of overtopping dike failure.

With occurrence of overtopping, the flow will erode the downstream side of the dike. Normally, soil erosion starts from the downstream toe of the dike, then develops upward to dike crest and finally lend to dike breach. The degree of damage depends on the depth and duration of overtopping as well as the soil properties. For geotechnical engineers, the more concerned issue is the impacts of soil properties on the flow erosion of overtopping. The overall index is the erodibility of the soil.

For the soils of dike, most of them are cohesive soil, the erodibility depends on its physic and mechanical properties, which include plasticity, water content, grain size, percent clay, compaction, and shear strength. In the study of soil erosion, Briaud has developed a method to determine the erosion function of a given soil (Briaud 2008). Based on this method, Michelle B. (2011) has conducted detailed investigation on the overtopping failure of Mississippi levee in the flood of June 2008 in USA. The studies have presented the levee overtopping case of the Winfield-Pin Oak site that was overtopped and severe erosion led to failure, and the Brevator site that was also overtopped but did not fail. By using Erosion Function Apparatus (EFA) (Briaud 2008), soil properties of plasticity index (PI), D50, and percent relative compaction were combined with EFA results to study the influence of these factors on the erosion resistance of a soil. Figure 1 presents the EFA results for the two levees. From the investigation and studies, it concluded that levee performance is influenced by the flood conditions, the site conditions, and the soil properties. Both sites in this study experienced large levels and durations of overtopping water, but it is proposed that the Brevator site survived because of its vegetative cover and more erosion resistant soils. Erosion is a very complicated phenomenon that cannot be described by any one parameter, but in all cases, dense and consistent native vegetative cover can greatly improve the overall levee performance.

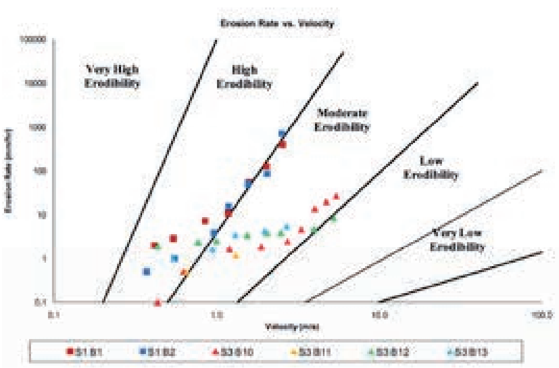

Figure 1 EFA results for Winfield-Pin Oak – S1 and Brevator – S3, Michelle B. (2011)

2.2 *Internal erosion*

Internal erosion caused by water seepage inside dike and foundation is a major failure mode of river dike damage. Actually, where there is a water head difference between upstream side and downstream side, there is seepage in the dike. With the rise of water level during flood period, the phreatic line is formed inside the dike and its position gradually rises up. At the same time, the seepage gradient in the dike and subsoil gradually increased. When the actual seepage gradient (J) is lager than the critical gradient of the subsoil (Jc), seepage failure is occurred.

As all the seepage failures are driven by hydraulic gradient, it could also be referred as hydraulic failure. The paper of H. Brandl has discussed the hydraulic failure of river dike, which include suffusion, contact erosion and internal erosion. The measures to avoid hydraulic failure are also presented in the paper. As internal erosion in dikes is not visible and difficult to be detected before the failure happened, the method of early diagnosis the possible internal erosion is significant in safety assessment of dikes. The paper of J. Monnet summarized the main methods for detecting dike internal erosion and presented the application of a new in-situ test, the Cross Erosion Test (CET), in Isère and Drac river levees in France.

Besides hydraulic conditions, the mechanism, procedure and the result of seepage failure have very close relation with the composition and properties of soil. Normally, dike seepage failures can be classified into 4 types: mass flow (all particles move by the force of flow), piping (fine grains flow though the channels of coarse particles), contact mass flow (erosion along the contact interface) and contact scouring. By analysis characteristics of soil gradation, the mode of seepage failure of each soil could be classified.

By large number of laboratory tests of different soils, Chinese scholars have summarized systematic methods to determine seepage mode of different soils.

According to the gradation, the non-cohesive soil can be classified into two types: homogeneous (Cu ≤ 5) and non-homogeneous (Cu > 5). For non-homogeneous soil, it can further be classified into two subtypes: discontinuous gradation soil and continuous gradation soil.

For homogeneous soil (Cu ≤ 5), there is only one failure mode: mass flow. For the non-homogeneous soil (Cu > 5), the failure mode depends on the gradation distribution. For soil with discontinuous gradation, the failure mode is determined by the content of fine grains (P). If P>35%, the failure mode is mass flow. If P<25%, the failure mode is piping. If P=25~35%, the failure mode is intermediate type. For the soil with continuous gradation, the failure mode is determined by content of fine grains method.

For the content of fine grains method, the content of fine grains at optimum gradation is introduced as an index. It is defined as:

$$P_{op} = \frac{0.30 - n + 3n^2}{1 - n}$$

n=porosity of the soil. If $P > 1.1P_{op}$, the failure mode is mass flow. If $P < 0.9P_{op}$, the failure mode is piping. If $P = (0.9\sim1.1)\,P_{op}$, the failure mode is intermediate.

The capability for resisting seepage failure is defined as the limit seepage force ($\gamma_w J$) that a unit volume of soil can be undertaken. The seepage gradient correspondent to this situation is the failure hydraulic gradient (J_n). Table 1 provides the summarization of allowed gradient and failure gradient.

Table 1 The range seepage gradient

J	Seepage failure modes				
	Mass flow		Intermediate	Piping	
	$C_u \leq 5$	$C_u > 5$		Continuous gradation	Discontinuous gradation
J_{fe}	0.8~1.0	1.0~1.5	0.4~0.8	0.2~0.4	0.1~0.3
J_a	0.4~0.5	0.5~0.8	0.25~0.4	0.15~0.25	0.1~0.2

For seepage safety of dikes, the primary goals of seepage control in dikes and foundation could be summarized as three aspects: (1) Decrease the quantities of seepage. (2) Release seepage pressure in advance for keeping the stability of foundation and geotechnical structure. (3) Prevent seepage failure of foundation and structure. Generally, the corresponding engineering measures are also includes three aspects:

·Seepage prevention: Put impermeable material in dike and foundation to cut the seepage passage and to decrease the water head in the dike and foundation.

·Drainage: Put permeable material as drainage at the certain places in the dike and foundation where the hydraulic gradient is relative large. To release the seepage pressure and let the seepage water freely discharge to downstream by the drainage.

·Filter protection: Filter is an effective measure for preventing seepage failure of soil. As it also has the drainage function, it is often as one part of the drainage. The materials for filter are natural sand and rock. But the material must satisfy following principals: □ filter material must be non-piping soil. □ the gradation relation between filter and protected soil must satisfy filter principals. □ the permeability coefficient of filter must larger than the protected soil. □ the coarse grains of the filter must hard and weathering resistant.

Figure 2 gives the typical engineering measures of seepage control applied in dike construction. The selection of theses engineering measures depends on the different situations of the dike.

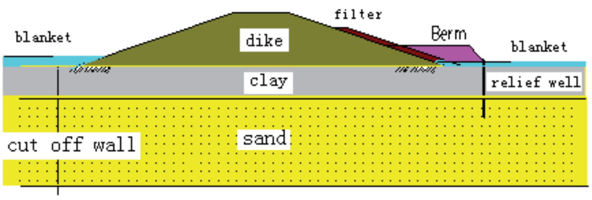

Figure2 Engineering measures of seepage control

2.3 *Bank collapse*

In nature rivers, the interaction of water flow and riverbank (upstream slope of dike) could cause bank erosion and bank collapse, which are the common damage to the safety of dikes. In USA, the total length of river channel is 5,600,000 km. About 800,000km riverbank were suffered of flow erosion, include bank collapse. In China, a severe bank collapse case has caused the lost of 115,000m^3 land. About half of a town was collapsed into river.

There are many factors that affect the occurrence of bank collapse, which include hydraulic features, properties of the materials of riverbed and river bank, features of river bank, impact of wind and wave, impacts of climate, impacts of human activities, etc. (Simons, 1982). For all these factors, water flow and boundary are the basic conditions.

For the mechanism of bank collapse, there are different viewpoints. Some scholars think water flow is the precondition of bank collapse. When the main stream of river approach riverbank, water flow will scour the bank and the bank slope will be steep. Some scholars believe the liquefaction of soil the cause of bank collapse. According to the force act on soil, the liquefaction of soil could be classified to shear liquefaction, seepage liquefaction and vibration liquefaction. If the dike is composed by non-cohesive sand or soils with less cohesion, its effective stress may drop to zero under the action of shear stress or seepage force. Some scholars explain the mechanism of bank collapse from the point of slope stability. Bank collapse occurred when upstream slope of the dike lost its stability. In flood season, soil of dike is submerged in water, which lead to the reduction of its shear strength. With the drop of upstream water level, the seepage force towards riverside and the reduced c, φ value could cause riverbank lost the stability.

As bank collapse is the result of the interaction of river flow and watercourse boundary condition, the engineering measures for avoiding bank collapse will mainly focus on water flow and watercourse boundary. For changing local water flow, groyne works are commonly employed. For improving boundary conditions, different bank protection method could be applied, which include riprap, concrete protection, geosynthetics, etc.

3 GEOTECHNICAL PROBLEMS OF ROCKFILL DAM

Rockfill dam is a widely applied dam type of dam engineering. The development of earth core rockfill dam in 1940s to 1960s is mainly based on the progress of the theory of soil mechanics. In recent years, more and more high rockfill dam will be constructed. New challenges on geotechnical engineering problems are encountered in the construction of those high dams.

3.1 *Construction material*

The construction materials of rockfill dam include impervious material, filter/transition material, and rockfill material. Proper application of the construction material according to its engineering properties is one of the key issues for rockfill dam design.

3.1.1 Impervious material of earth core

For high ECRD, earth core will subject to high stresses. Ordinary clay material could not meet the strength and compressibility requirements of high dam. Therefore, for most ECRD with the height above 200m, the core material uses gravelly soil. As for the composition, gravelly soil is mixture of clay and gravels with the grain size larger than 5mm (or 2mm). Soil of weathered rock and glacier deposit are also a kind of gravelly soil.

(1) Gradation adjustment for gravelly soil of core material

Generally, if the soil has more than 20% coarse grains content, i.e. the grain size larger than 5mm, it could be classified as gravelly soil. Those soils include various soils with gravels, clay gravel and weathered rocks.

The composition of nature formed gravelly soil is very inhomogeneous. When it is used as core material, its gradation and water content are often need to be adjusted by the requirement of design.

For nature gravelly soil with wide range of gradation, if the material is basically applicable, the oversize particles could be removed to increase the content of fine particles. The case for applying this measure is Pubugu ECRD in China.

The impervious material for the central core of Pubugou ECRD is the gravelly soil with wide range of gradation. The coarse grain content is 50%~65% and the content of particles with the size less than 0.1mm is 8.8~20%. In soil classification, the material is GP. The permeability of the material after compaction is 10^{-4}~10^{-5}cm/s, which is not fit the requirement of impervious material of high dam. With series studies, two measures were employed for improving the properties of the material, which are: adjust gradation by removing the particles with the size larger than 80mm (or 60mm) and use modified Proctor compaction energy to increase its density.

After removing the particles of the size larger than 80mm form the nature wide range gradation gravelly soil, the gradation of the material was improved significantly. The content of particles of the size less than 5mm was 50%, and the content of particles of the size less than 0.1mm was 22%. Classification of the material was change from GP to GC. Permeability of the material reached to 10^{-5}~10^{-6}cm/s. With the protection of filter material, the hydraulic gradient of seepage failure was 60~100.

By using heavy compaction standard (modified Proctor compaction), the compaction energy is increased from 604kJ/m^3 to 2704kJ/m^3. Accordingly, the maximum dry density of the material is increased from 2.23~2.32g/cm^3 to 2.375g/cm^3. The permeability of the material is less than 1×10^{-5}cm/s and the deformation modulus is also remarkably increased.

For borrow soil mainly composed by fine grains, the material usually cannot fit the stability and deformation requirement of high dam. In this case, gravels or crushed rock should be added to increase the content of coarse grains. The case for applying this measure is Nuozhadu ECRD in China.

The borrow materials of Nuozhadu ECRD is mixture of slope washed, residual soil and some strongly weathered rocks. The average grain composition is: 24% gravels with the size larger than 5mm, 44.3% fine grains with the size smaller than 0.074mm, 21.7% of the grains with the size smaller than 0.005mm. Most of the soils are classified as clay sand, low liquid limit clay with sand. As most of the grains are weathered sandstone and mudstone, grain particles are easily broken. After compaction, the content of grins with the size larger than 5mm could be reduced to 10%. The density, deformation parameters and shear strength of the material are very low. Thus, it is decided to add crushed hard rock to the nature borrow material.

The size range of crushed rock to be added in borrow material is 5~60mm. After optimization, proportion of the adding material is 35%. From the research results, after adding coarse particles, content of the grains with size larger than 5mm is 50%, content of the grains with size smaller than 0.074mm is 23.6%, content of the grains with size smaller than 0.005mm is 10%. The classification of the mixed material is GC. It is an idea impervious soil for high ECRD. Due to the breakage after compaction, the content of grains larger than 5mm could be 36%. Compare with the unmixed material, the maximum dry density could be increased from 1.7~1.8g/m^3 to 1.9~2.0g/m^3. The corresponding water content is about 10%~15%. The overall engineering properties of the material are greatly improved.

(2) Gradation and permeability of gravelly soil

The permeability of gravelly soil has close relationship with its gradation. For high ECRD, the general requirement is: the content of grains with size larger than 5mm should not above 50% (or should below 60%), the content of grains with size smaller than 0.075mm should not below 15%, and the content of clay grains should not below 8%. But in practices, due to the wide range gradation of natural gravelly soil, the above principles could be adjusted according to the real situations. By the analysis from the point of geotechnical engineering, the requirement of content of grains with size larger than 5mm should not above 50% is to guarantee the void of coarse grains could be filled by fine grains. The requirement of content of grains with size smaller than 0.075mm should not below 15% is to guarantee the low permeability and to keep internal stability of soil structure under seepage flow. As for the requirement of the permeability of impervious soil, when it is in the quantity of 10^{-5}cm/s, the actually leakage is quite small. It is unnecessary to request the permeability to be 1×10^{-5}cm/s. As for the seepage stability, normally, the gravelly soil with wide range gradation will have less clay grains. Thus, it has the same properties in seepage deformation as non-cohesive soil. The hydraulic gradient for seepage failure resistance of gravelly soil is mainly depends on the filter at the exit. With the protection of filter, the failure gradient can be improved significantly. Therefore, the content of clay grains above 8% could not be an unchangeable rule. For the case of Pubugou ECRD, the material has 17%~48% grains with the size smaller than 1mm and 4%~12% clay grains. Under normal compaction, the tested maximum hydraulic gradient could reach 90~140.

(3) Compaction of gravelly soil

The two methods for soil compaction quality control are dry density and compaction degree. In compaction, gravelly soil presents the properties of both gravel and clay. For the compaction of gravelly soil, it is required to get the maximum dry density of the full material and also to check the dry density of fine grains. By considering the variability of the soil, compaction degree is more often to be used as the index for quality control of gravelly soil compaction.

For the mixed soil with coarse and fine grains, besides the compaction degree of full material, it is also has the compaction degree of fine grins. As the compaction degree of fine grains mainly controlled the permeability and mechanical property of gravelly soil, it is unnecessary to conduct difficult large-scale compaction test for full material. When content of coarse grains is below 60%~70%, the dry density of full material will be increased with the increasing of coarse grains content. When content of fine grains is below 20%~30%, the coarse grains will not take the function of soil skeleton. The fine grains are fully compacted. Its dry density keeps unchanged. When content of fine grains reaches 30%, the coarse grains start to take function of skeleton. The more content of coarse grains, the stronger is its skeleton function. Thus, the fine grains inside void cannot be fully compacted. The dry density of soil will be reduced with the increase of coarse grains. When content of coarse grains is 60%~70%, the skeleton function of coarse grain is fully realized. The dry density of full material and fine grains reduced synchronously. All its mechanical properties are dropped in big scope and the permeability of soil are increased rapidly. Therefore, in the application of compaction degree control of fine grains, when content of coarse grains is below 25%, the compaction degree for fine grains could be controlled with 100%; when content of coarse grains is 25%~50%, the compaction degree control for fine grains could be reduced to 97%~98%.

3.1.2 Filter material

The process of seepage failure in soil is always started from exit, and gradually developed to the inside, then finally lead to local failure or whole structure failure. Using filter to control seepage exit is an effective seepage control measures in dam engineering. It could be a drainage zone and also to prevent fine grains flow out. For high ECRD with gravely soil as the core, although gravelly soils have certain content of clay grains, it is still belong to the soil without plasticity or with low plasticity. The filter design should also follow the principle of no fine grains been washed out. The paper submitted by S. Messerklinger discussed the functions of filter in geotechnical structures and summarized the main principles of filter design. Figure 3 is the summary of the design criteria of filter design (Messerklinger 2013). The paper submitted by R. Eerzariol presented the test studies on filter protection of loess, a kind of sandy silt that largely distributed in central Argentina. The studies suggested that filter with fines content between 15% and 25% perform the best condition of seepage stability for protecting silt core (Eerzariol 2013).

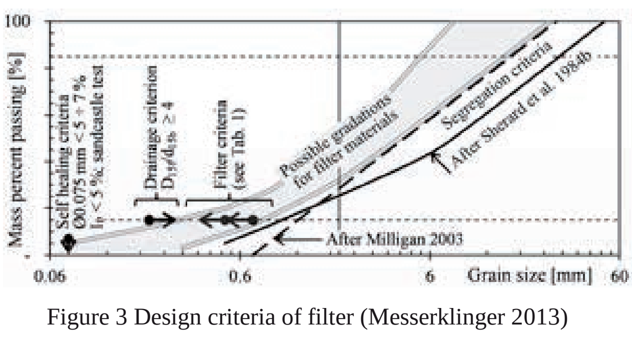

Figure 3 Design criteria of filter (Messerklinger 2013)

For high ECRD, the seepage stability of gravelly soil depends on many factors. Besides gradation, dry density, stress level and downstream protection are all have impacts on the internal stability of soil upon seepage flow. Normally, the mixture of sand, gravel and fine grains with good gradation will present good erosion resistance. For gravelly soil, if the content of coarse grains (>5mm) below 50%, the content of clay grains (<0.075mm) above 15%, and the material is well compacted, the gradient for resisting seepage failure will be relatively high. But in practice it should be aware that due to the variability of gravelly soil, the result obtained by calculation must be checked by filter test.

3.1.3 Rockfill material

Rockfill is the main construction material of rockfill dam. Its strength properties are related with dam slope stability and its stress-strain properties are related with dam deformation. From the experience of modern rockfill dam construction, deformation control is the most important issue to be considered. For high rockfill dam, rockfill with high or medium rock strength, i.e. the saturated uniaxial compressive strength is 30~80MPa, should be the best choice. For getting high compaction density, the rockfill should also have good gradation. From the point of deformation control and deformation coordination, rockfill for CFRD should have as high compaction density as possible. The purpose is to reduce the overall deformation quantities. For ECRD, the consideration in rockfill selection is more emphasized on deformation coordination between dam shell and earth core.

The particle shapes of rockfill material are usually polyhedron. Most of the particles are contacted by point. The compressibility of rockfill mainly depends on re-arrangement of particles, and it is also affected by other factors such as rock lithology, density, gradation, etc. Due to the granular characteristic of rockfill material, grain breakage and particles rearrangement is occurred at any moment during loading process. That means the status of rockfill material will be changed all the time. Therefore, the material properties will not be a constant value. For low dam, as the relatively low stress level of rockfill, the breakage of particles is not significant and most of the deformations are occurred during the stage of compaction. For high dam, due to the high stress level and complicated stress paths, the breakage and rearrangement of particles cannot be neglected. The process of the particles breakage and particles movement will lead to a significant increase of the post-construction deformation of rockfill. At present, this post-construction deformation of rockfill cannot be fully analyzed by existing models and methods. For correctly describe the change of status of rockfill material that caused by particles breakage and rearrangement, the properties of particles breakage of rockfill material must be fullly studied, and the new analysis models will be further developed.

For rockfill, another important characteristic is the wetting deformation property of the material. The mechanism of wetting deformation of rockfill is the inteneration and breakage of the edge of rockfill particles under the action of water. Besides, the lubricating action of water promotes the movement and rearrangement of the particles. Thus, it leads to the additional deformation. The wetting deformation of rockfill is directly related with its lithology. Normally, soft rockfill has relatively large wetting deformation. But it is noticed that even for the hard rockfill, such as limestone and tuff, the wetting deformation still cannot be neglected. The wetting deformation of rockfill will be reduced with the increasing of its density. In addition, the more of initial water content of rockfill, the less wetting deformation. Therefore, adding water during rockfill compaction will play an important role in speed up deformation completion and reducing post-construction of rockfill.

Correctly predict deformation of rockfill dam depends on the constitutive model used in numerical analysis. The paper submitted by Y. Chen used an elasto-plastic model that takes into account irreversible deformations of poorly or well-compacted rockfill under deviatoric and isotropic loading of rockfill, known as L&K-Enroch, developed by EDF-CIH (Chen 2013) to conduct 3D numerical analysis of Mohale CFRD in South Africa.

3.2 Foundation treatment

Foundation or subsoil condition is very important to the safety of dam. Before the construction of dam, the unfavorable layer in foundation must be properly treated. The paper submitted by J. Mecsi presented a failure case of tailing dam in Hungary (Mecsi 2013). The foundation of the dam has a sand-silt layer that may move under high water condition. Figure 4 is the summary of some effects for the failure of the tailing dam. It shows the impact of the unfavorable subsoil on the safety of the dam.

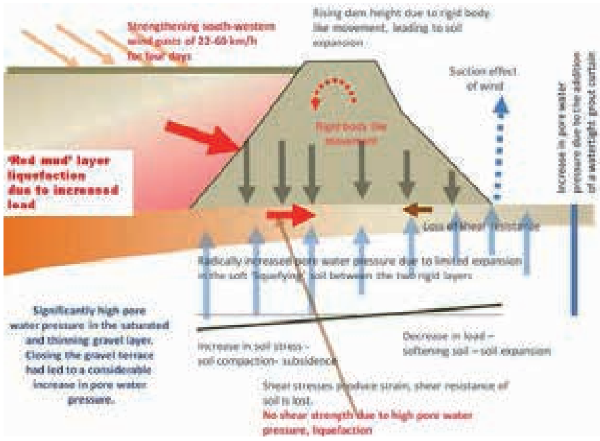

Figure 4 Summary of the effects for tailing dam failure

The foundation of high rockfill dam includes bedrock foundation and alluvium foundation of sandy gravel deposit. For the sandy gravel alluvium, if the alluvium has no soft, weak clay layers or silt, fine sand layers, the bearing capacity and stability of the foundation can be guaranteed. The main task of foundation treatment is seepage control. If the lower part of alluvium foundation exist sand layer, the possibility of sand layer liquefaction should be carefully assessed.

For high rockfill dams, the commonly accepted seepage control measure for foundation treatment is vertical cut off. It could effectively block the seepage though pervious alluvium foundation. With the measures of filter and drainage at downstream seepage exit, the foundation and dam body will not subject to seepage failure.

For high rockfill dam with deep alluvium foundation, the most effective vertical seepage control measures are excavation of all the alluvium layers under the impervious part of the dam or using concrete diaphragm wall to cut the seepage though foundation. Recently, concrete diaphragm wall is accepted for most of the high CFRD constructed on deep alluvium foundation. For this application, the diaphragm wall is connected with plinth via concrete slabs (Xu 2010). For high ECRD, both measures as alluvium excavation and concrete diaphragm wall are applied.

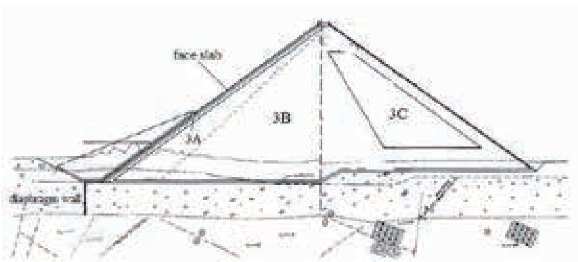

Figure 5 CFRD built on alluvium foundation

For high ECRD with the application of concrete diaphragm wall for seepage control, one of the key issues is the connection of diaphragm wall, earth core and gallery, and also the connection of gallery with abutments. Generally, directly insert diaphragm wall into earth core is more technically reliable. When the top of diaphragm wall is connected to earth core by gallery, differential displacement could be produced between the wall and gallery. Joints should be arranged for the connection. Also, the connection of gallery and abutments should also arrange joints for adapting large differential displacement.

For rock foundation, when bedrock exists geological defects such as permeable stratum, fault fissures filled with erodible materials, solution fissures or caverns, curtain grouting or curtain grouting combined with consolidation grouting are necessary. In design standard, the depth of grouting should reach to impermeable layer. The permeability of rock stratum is represented by Lugeon value (Lu). Usually, the value of 3~5 Lu could be applied for most of the rockfill dams foundation.

3.3 *Control and coordination of dam deformation*

In the design and construction of high rockfill dam, deformation control is the most important issue. The stress statuses of watertight barrier and dam operation performance are all related with dam deformation. Therefore, the concept of integrated deformation control and deformation coordination should be a principle for the design and construction of high rockfill dam. The main focus of this new concept includes two parts: (1) to reduce the total quantities of dam deformation, (2) to coordinate differential deformation between different zones.

Taking the example of CFRD, the ultimate purpose of deformation control and deformation coordination will be the safety of concrete face slabs and joint system. It could be expressed as:

$$\sigma_t < \begin{Bmatrix} \sigma_s \\ \\ \sigma_a \end{Bmatrix} < \sigma_c \qquad \begin{Bmatrix} \max(DP_o) \\ \max(DP_s) \\ \max(DP_d) \end{Bmatrix} < \begin{Bmatrix} D_o \\ D_s \\ D_d \end{Bmatrix}$$

Where: σ_t and σ_c are tensile and compressive strength of concrete; σ_s and σ_a are stress of face slab in the direction of dam slope and dam axis; DP_o, DP_s, DP_d are displacements of joint and D_o, D_s, D_d are upper limit of joint displacement.

For high CFRD, the general principles of the integrated deformation control and deformation coordination could be summarized as follows:

The deformation of rockfill is directly related to lithologic character, rockfill gradation, compaction density, dam height, valley shape, etc.

In the design and construction of high CFRD, the low compressibility and good gradation rockfill material should be selected, and the compaction density should be strictly controlled to reduce the overall deformation quantities of rockfill.

In the design of high CFRD, material zones should be arranged to achieve the coordination of deformations of different parts of the dam.

In the construction of high CFRD, the construction stages of rockfill and face slab should be well arranged to provide sufficient time for deformation stabilization of upstream rockfill.

The above principles could be expressed as:

$$S=F(H,H/A^2,n,S_c,C_s)$$
$$n \le n_l$$
$$g \le s_p, \quad E_u/E_d \le r$$
$$T \ge t_p$$

Where: S is the maximum settlement of rockfill, H is dam height, A is area of face slab; n is rockfill porosity (represent compaction density); S_c is uniaxial compressive strength of rock (represent lithologic character); C_s is coefficient of uniformity (represent gradation of rockfill).

From the analysis of monitoring data and numerical analysis, the control of rockfill deformation quantities could be represented by the ratio of maximum settlement of rockfill to the height of the dam. For CFRD with the height above 200m, d is recommended to be controlled to 0.8%~1.2%, that is:

$$S=dH \quad (d=0.8\%\sim1.2\%)$$

n_l is the standard for rockfill porosity control. For CFRD with the height above 200m, n_l is recommended to be controlled fewer than 20%. 18%~20% is more favorable.

S_p is the slope of the boundary between zone 3B and 3C. For high dam, the boundary line should incline to downstream side. The slope should not steeper than 1:0.5, i.e. $S_p \ge 0.5$.

r is the ratio of modulus of upstream and downstream rockfill. For CFRD with the height above 200m, the modulus ratio of upstream rockfill and downstream rockfill is recommended be controlled below 1.5 to coordinate deformation of upstream and downstream rockfill, i. e. $1.0 \le r \le 1.5$.

t_p is the time for upstream rockfill deformation completion. To reduce the impact of rockfill deformation on stresses of concrete face slab, certain period of time for rockfill deformation should be provided before the construction of concrete face slabs. Normally, the time is not less than three months, i.e. $t_p \ge 3$ months. On the other hand, as the criteria for assessing the completion of upstream rockfill deformation, monthly settlement rate of less than 3~5mm is the recommended as control values.

In addition to the control of deformation quantities, the new concept more emphasizes on the coordination of deformations between different dam zones. For high CFRD, it includes the deformation coordination for the rockfill of upstream and downstream, abutment area and riverbed area, upper part and lower part, and also, the deformation coordination of concrete face slab and upstream rockfill, and rockfill constructed in different stages. For high ECRD, the focus is on the coordination of deformation of rockfill shell and earth core to avoid harmful cracks on earth core.

In the paper submitted by N. Li, the methods for assessing deformation coordination of CFRD were proposed, which include settlement, horizontal displacement and deflection of concrete face slab (Li 2013). The propose concept was applied in the design and construction of Bakun CFRD. In the paper submitted by Y. Chen, three-dimensional numerical analysis of a high CFRD was presented. From the results of analysis, it is noticed that the large deformation of rockfill and differential displacement between rockfill and face slabs will cause the cracks on concrete face slabs (Chen 2013).

3.4 Hydraulic fracture of high ECRD

For high ECRD, the failure of earth core by hydraulic fracture is one of the key issues that concerned by dam engineers. And, it is also a controversial problem in geotechnical engineering. At present, the mechanism and criteria for hydraulic fracture are still questions and disputes among engineers and scholars.

From the analysis, the mechanism of hydraulic fracture is the crack developed under the condition of effective stress reduces to its tensile strength by the action of water load. The failure of hydraulic fracture is the process of outside water acting on the initial cracks to produce continuous extension of the cracks, and then finally run through the whole earth core. From the traditional point of view, when the increase of pore pressure leads to tensile effective stress of the soil, hydraulic fracture will be occurred. But, it should be noticed that many reasons could lead to the tensile effective stress. Only the reduction of effective stress is caused by external water load, the produced cracks are considered as hydraulic fracture.

From numerical analysis, it could be observed that the direction of principle stress on upstream surface of earth core is deflected due to the “arching effect” of dam shell. Upon reservoir impoundment, with the upstream water load, the direction of principle stress will be further deflected. The direction of major principle stress turns to parallel with the direction of water pressure. In this case, when the effective minor stress of the earth core reduced to the tensile strength of the soil by the action of water pressure, horizontal cracks will be produced. This could be the cause of hydraulic fracture.

When the initial cracks of hydraulic fracture are produced on the surface of the earth core, the further development of the cracks depends on many factors, which include hydraulic gradient, stress status and permeability of the soil, etc. The final failure mode of hydraulic fracture is soil erosion by seepage.

4 SUMMARY

Both in the field of dikes and dams, geotechnical problems are the essential engineering issues. Problems such as soil erosion by water flow, internal instibility by seepage, settlement and seepage control, foundation treatment are all related with the geotechnical properties of soils. With the changing situations and the development of modern dam engineering, more and more challenges will be encountered. Geotechnical engineering is a subject based on engineering practices. To solve the geotechnical problems in engineering, the basic principles of soil mechanics should be followed. Furthermore, the new concepts and methods are also need to be developed by systematic studies and careful observations.

The 11 submitted papers in the field of dikes and dams have covered relatively wide range of the studies and represented main concerns both in dike engineering and dam engineering.

5 REFERENCES

D. B. Simons, R. Li 1982 . Bank Erosion on regulated rivers. *Gravel-bed rivers, R.D.Hey, J.C.Bathurst, and C.R.Thorne, eds., John Wiley & Sons, Inc., Chichester, U.K.*.

H. Brandl, M. Szabo, Hydraulic failure of flood protectin dykes. *Proceedings of the 18th International Conference on Soil Mechanics and Geotechnical Engineering, Paris 2013*

J. Briaud, H. Chen, A. Govindasam, and R. Storesund. (2008). Levee erosion by overtopping in New Orleans during the Katrina Hurricane. *Journal of Geotechnical and Geoenvironmental Engineering.*

J. Mecsi, 2013. Some technical aspects of the tailing dam failure at Ajka Red Mud Reservoirs. *Proceedings of the 18th International Conference on Soil Mechanics and Geotechnical Engineering, Paris 2013*.

M. Bernhardt, J. Briaud, D. Kim, R. Storesund, S. Lim, R. G. Bea, J. D. Rogers, 2011. Mississippi river levee failure: June2008 flood. *International Journal of Geoengineering case history.*

N. Li, J. wang, Z. Mi, D. Li, Deformation safety of high concrete face rockfill dams. *Proceedings of the 18th International Conference on Soil Mechanics and Geotechnical Engineering, Paris 2013*

R. E. Terzariol, R. J. Rocca, M. E. Zeballos, 2013. Suffusion in compacted loessial ailts-interaction with granular filters, *Proceedings of the 18th International Conference on Soil Mechanics and Geotechnical Engineering, Paris 2013.*

S. Messerklinger, 2013. The design of filter materials and their importance in geotechnical engineering. *Proceedings of the 18th International Conference on Soil Mechanics and Geotechnical Engineering, Paris 2013*

Y. Chen, J.J. Fry, F. Laigle, Prédiction du comportement de barrage en enrochement de grande taille à l'aide d'une modélisation tridimensionnelle. *Proceedings of the 18th International Conference on Soil Mechanics and Geotechnical Engineering, Paris 2013*

Z. Xu, 2010. Progress in the construction of CFRDs on deep alluvium. *International Journal on Hydropower and Dams.*

.

Hydraulic failure of flood protection dykes

Défaillance du circuit hydraulique des levées de protection contre les inondations

Brandl H., Szabo M.
Vienna University of Technology, Vienna, Austria

ABSTRACT: The increase in frequency, magnitude and duration of floods during the past decades has become an outstanding challenge to geotechnical engineering. Appropriate measures against hydraulic fracture due to underseepage of dykes or levees require comprehensive knowledge of failure modes. This paper describes various forms of hydraulic failure and its critical values for different types of soil. Furthermore, measures to prevent hydraulic failure by placing berms or by installing relief elements at the landside dyke toe are discussed.

RÉSUMÉ : L'augmentation de la fréquence, l'ampleur et la durée des inondations au cours des dernières décennies, est devenu un défi exceptionnel à la géotechnique. Des mesures appropriées contre la fracturation hydraulique en raison de l´écoulement phréatique de barrage de rivière ou levées nécessitent une connaissance approfondie des modes de défaillance. Cet article décrit les différentes formes de défaillance du circuit hydraulique et de ses valeurs critiques pour différents types de sol. En outre, des mesures pour prévenir une panne hydraulique en plaçant des bermes ou en installant des éléments de relief à l'orteil terrestre digue est discuté.

KEYWORDS: dykes, flood protection, hydraulic failure, uplift, relief drainage.

1 INTRODUCTION

Floods have affected millions of people worldwide in recent decades. In several regions the magnitude and frequency of flood waves have increased dramatically since long-term measurements and historical reports have existed. In Austria, for instance a 2000 to 10 000-year flood event was back-calculated from the flood disaster in the year 2002. Such hitherto singular values cannot be taken as design values for flood protection dykes, but they underline the need for local overflow crests or spillway sections. Moreover, they clearly demonstrate that a residual risk is inevitable – despite most costly protective measures.

The risk of dykes or levee failure increases not only with the magnitude of a flood but also with its duration. For instance, the peak period of flood waves along the Austrian section of the river Danube usually lasts one to three days, whereas its tributary, the river March/Morava (Austria/Slovak border) frequently undergoes flood waves up to three or six weeks (Fig. 1). Figure 1 also illustrates the increase of magnitude and frequency of the floods since the 1990s.

Especially long-lasting flood waves exhibit in combination with a required groundwater communication below dykes a high risk potential regarding hydraulic failure. But also periodic short hydraulic loadings of flood protection dams and their subgrade can produce a failure caused by an inner erosion processes in a long-term.

2 FAILURE MODES OF DYKES

The knowledge of possible failure modes is an essential prerequisite for a reliable quality assessment of existing dykes and levees, and for an optimized design of new ones and for rehabilitation work. Moreover, it helps to optimize emergency measures during flood defence.

The dominating failure modes for typical ground conditions along rivers (near-surface, low-permeability sandy to clayey silts underlain by high permeability sand or gravel) are:

- overtopping or overflowing of the dyke/dam crest,
- hydraulic fracture,
- surface erosion and failure of the water-side slope due to wave action,
- piping due to animal activities, especially from beavers and rats,
- slope failure due to excessive pore-water pressures, seepage or inner erosion,
- slope failure due to a rapid drop of the flood water level,
- unsuitable planting of dykes (especially trees with flat roots).

Actually, it is often difficult to precisely determine the causes of a dyke failure. Several types of processes might be involved in a breach and multiple modes in a dyke failure. Statistical analyses show that overtopping and internal erosion are the most common modes of failure. While many of these failure mechanisms occur relatively fast, the erosion by underseepage develops more inconspicuously. If a groundwater communication below the dyke is possible, the aquifer or the overlaying low permeable layer can be progressively eroded during hydraulic loading. Hydraulic failure is critical because there may not be any external evidence, mostly only soil boiling can be found.

Due to this unpredictable behaviour hydraulic failure is frequently underestimated in practice and may occur in different forms (e.g. Eurocode 7; CEN 2004):

- By uplift (buoyancy). The pore-water pressure under the low-permeability soil layer exceeds the overburden pressure.
- By heave. Upward seepage forces act against the weight of the soil, reducing the vertical effective stress to zero; soil particles are then lifted away by the vertical water flow.

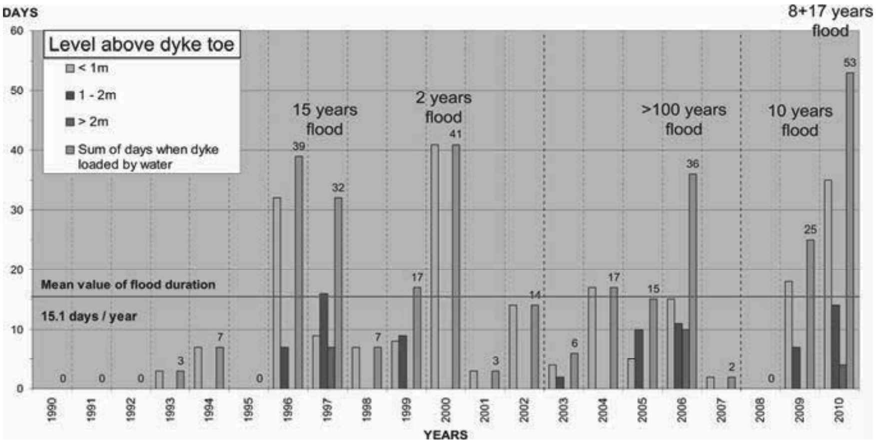

Figure 1. Duration of floods along the River March dykes (Water level at Dürnkrut – Austria/Slovakia; adapted after via donau). Two floods within three weeks in 2010.

This 'boiling' dominates in silty-sandy soil, and is combined with internal erosion.

- By internal erosion. Soil particles are transported within a soil stratum or at the interface of soil strata (Fig. 2). This may finally result in regressive erosion, leading to ground failure of the dyke, levee or dam.
- By piping. Failure by piping is a particular form of internal erosion, where erosion begins at the surface, and then regresses until a pipe-shaped discharge tunnel is formed. Failure occurs as soon as the water-side end of the eroded tunnel reaches the river bed or bottom of the reservoir. Frequently, several tunnels develop. This process may be induced or significantly promoted by animal activities, as field observations over many years have revealed.

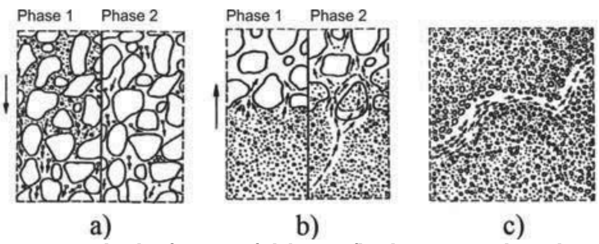

Figure 2. Hydraulic fracture of dykes or flood protection dams due to seepage through or beneath the dyke or dam (Ziems 1967): (a) suffusion (fine particles move into pore voids of coarse grain fractions); (b) contact erosion at the interface of soil strata; (c) internal erosion in steady-state flow condition.

Hydraulic failure may reach several tens of meters away from dykes or dams, as experience has shown (Fig. 3). This could be observed even for low flood protection embankments with a relatively small hydraulic gradient.

Eurocode 7 (CEN 2004) states that in situations where the pore-water pressure is hydrostatic (negligible hydraulic gradient) it is not necessary to check other than for failure by uplift. In the case of danger of material transport by internal erosion, filter criteria should be used. If the filter criteria are not satisfied, it should be verified that the critical hydraulic gradient is well below the design value of the gradient at which soil particles begin to move.

Experience has shown that the magnitude of the critical hydraulic gradient where internal erosion begins is frequently overestimated. Figure 4 summarizes the critical values on the basis of field observations, geotechnical measurements, literature and long-term experience for different soils. For comparison, the conventional criterion ($i_{crit} = \gamma '/\gamma_W$), Lane's criterion, and the critical zones after Eurocode 7 (CEN 2004) or Chugaev (1965) respectively are also plotted in the diagram.

Figure 3. Piping (soil boiling) far away from the dyke, and stabilizing measures to reduce the hydraulic gradient (photo: L. Nagy).

Hydraulic failure may occur despite cut-off walls, if they are "imperfect" walls in order to allow groundwater communication below the dykes or levees (for environmental reasons). Fine-grained cover layers with local "windows" and low residual shear strength favour such failure modes.

The need of underseepage control for permanent or temporary hydraulic loaded dams or levees is determined from the ground profile, soil mechanical properties and hydrological parameters. Seepage enters the permeable aquifer through the riverbed and through cracks and inhomogeneities in the waterside near-surface cover layer. Due to the hydraulic gradient the groundwater flows from the riverside to the landside of the dyke. This results into an artesian head at the base of the landside low permeable soil layer during the sustained flood stages. The overpressure may cause sudden uncontrolled heave or rupture of the landward fine-grained cover layer, especially at the dyke toe, followed by concentrated seepage flow and erosion in this area. If the seepage through the cover layer is possible then the hydraulic failure may occur without heaving and only through erosion of the fine-grained soil. The suffusion process is usually accompanied by piping of the aquifer and causes a gradual safety reduction.

Consequently, for the underseepage of dykes or levees safety analyses regarding hydraulic failure by erosion and/or heaving of the cover soil layer have to be performed.

Filter protection against hydraulic failure at the embankment toe is generally provided by the use of non-cohesive granular material (natural soil) that fulfils adequate design criteria for filter materials. Filter geotextiles have been

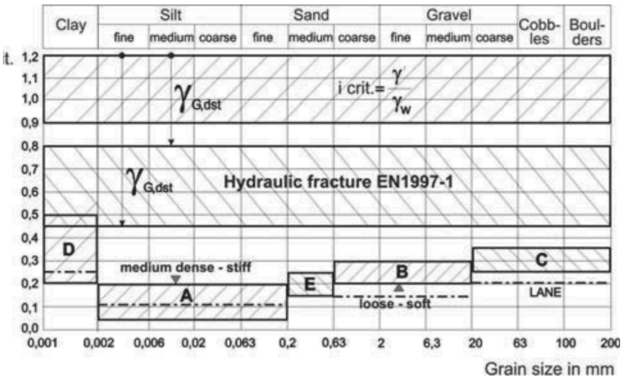

Figure 3. Critical hydraulic gradients for hydraulic fracture (internal erosion) (Brandl and Hofmann, 2006); $i_{crit.}$ depends not only on grain size distribution and density/stiffness but also on flow pressure; $\gamma_{G,dst}$ = partial safety factor for permanently unfavourable effects.

used increasingly since the early 1970s. Common filter criteria for soils are from Terzaghi and Sherard, and for geotextiles from Giroud (2010) and Heibaum et al (2006). All criteria have particular limitations, whereby non-cohesive and cohesive soils have to be distinguished. While two criteria are sufficient for granular filters (the permeability criterion and the retention criterion), four criteria are required for geotextile filters (Giroud 2010): the porosity criterion and the thickness criterion also have to be considered.

3 MAESURES AGAINST HYDRAULIC FAILURE

Hydraulic failure as an effect of underseepage may be prevented mainly by two permanent measures landward of a dyke or flood protection dam by

- installing trenches or relief columns or drainage wells,
- filling of berms, thus displacing the possible starting point of inner erosion or piping further away from the structure, and decreasing the hydraulic gradient at this point. Such berms should be constructed as access roads for quick and easy dam defence in the case of severe floods.

The function of the berm is to compensate through its counterweight the pressure which is acting at the base of the cover layer (Fig. 4a) and to prevent hydraulic failure of the dyke by seepage or uplift, or by internal erosion and piping. At the same time it must allow a free water outflow. Otherwise an excessive pore-water pressure would cause a sudden failure. Filter stable berms (filter geotextiles covered with sand, gravel, or other granular material) are often used as an emergency measure, when seepage occurs.

In many cases berms merely move the hydraulic problem further away from the dyke or dam, and retrogressive inner erosion may finally reach it in the long term (after several

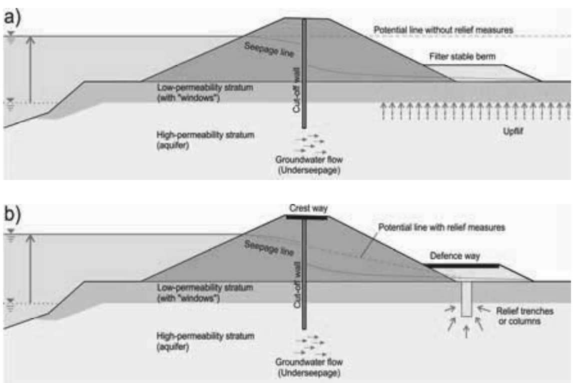

Figure 4. Permanent measures against hydraulic failure caused by underseepage of flood protection dykes: a) Filter stable berm as a counterweight; b) Relief drainage columns or trenches.

floods). Boiling and internal erosion have been observed up to 20 to 50 m away from dykes and dams, even though they were only 3 to 6 m high (Fig. 3). Moreover, wide berms are frequently not possible under confined space condition as well as in ecological sensible areas along rivers; therefore drainage trenches are preferred in these circumstances.

However, trenches excavated in very soft soil collapse immediately before geotextiles and fill material can be placed. The installation of trussed retaining panels would be too expensive. These problems could be overcome by developing 'relief granular columns', jacketed with a filter geotextile.

Jacketed (coated) stone or gravel columns have been installed in Austria since 1992. At first they were used mainly for drainage purposes, for instance as drainage walls to improve the stability of old flood protection earth dams. This method has significant construction advantages over conventional drainage trenches in loose or soft soil. In critical cases the coated columns are combined with other measures for dam refurbishment. The drainage material (usually clean 4/32 mm, 8/32 mm or 16/32 mm grain) is lowered by vibroflotation, whereby the vibrator is wrapped with a nonwoven geotextile (tied together at the toe of the vibrator).

The tops of relief columns should be covered with coarse drainage material, wrapped in filter geotextiles for longitudinal or transverse drainage. This drainage layer should carry an access road for easy dam defence in the case of severe floods.

Relief columns or trenches are filter stable elements at the landside embankment toe integrated into the dyke profile to reduce the pressure at the base of the low permeable cover layer during the critical flood stages (Fig. 4b). The safety factor against hydraulic failure (erosion or heaving) significantly increases through the controlled pressure relief. The negative effect of this measure is the concentrated groundwater outflow. This can lead under certain hydraulic gradients, soil/subgrade conditions and local topography to an earlier waterlogging of the hinterland.

Figure 4b illustrates also the typical cross-section through a new flood protection dyke after removal of the old one, which had been destroyed by a severe flood. The coated gravel columns (diameter 0.7 m) usually exhibit a spacing between 1.5 and 7.0 m, depending on local factors (geotechnical and ecological parameters, infrastructure, risk potential etc.); spacing is commonly about 4 m. The water-side dam slope is covered by a net for protection against beavers.

Another method to increase the stability against inner erosion is to reduce the hydraulic gradient by raising the water level at the landside in local reservoirs (Fig. 5). This method represents an emergency measure by placing sandbags around the erosion crack and is often used after indication of local hydraulic fracture in the beginning stage.

Figure 5. The giant piping at Tiszhasa/Hungary in 2000 and stabilizing measures (Nagy, 2011): Reduction of hydraulic gradient and lateral support of dyke slope.

4 DESIGN CRITERIA FOR RELIEF DRAINAGES AND ASSESSMENT OF WATTERLOGGING

Until now the design of relief measures (drainage columns or trenches) is based on rather insufficient basic principles, strong simplifications and idealizations. For the quantification of the water outflow from relief columns as well as for a pressure assessment beneath the cover layer only assumptions based on numerical models are in use. These approaches allow indeed comparative calculations of the quantity of seepage through and under the dyke (Fig. 6). But they do not allow an exact differentiation of the waterlogging from flood, precipitation and groundwater of the hinterland. Accordingly, the design of polders and pumping stations can be performed only based on estimated water outflows from the relief drainages.

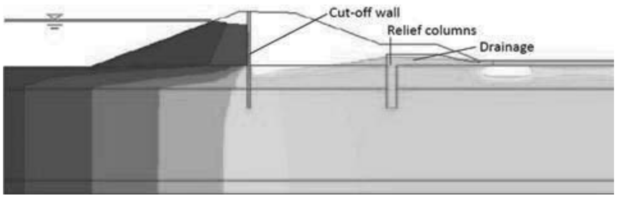

Figure 6. Simplified numerical model of a dyke with relief columns.

Nowadays the assessment of waterlogging is carried out mainly by mapping of water logged areas along the river after floods or heavy rainfalls in combination with digital elevation models (Fig. 7). The results are then combined with numerical simulation studies. Such a long-term monitoring gives some information about the outflow from the relief drainages as well as about the water distribution in the hinterland of the dyke. But it does not allow a detailed design of specific technical measures.

Figure 7. Mapping results for waterlogging with different origin.

Consequently, 1:1 scale model tests on dykes including the subgrade are the best solution to quantify the water outflow from the relief elements during flood stages. Experimental tests performed under laboratory conditions allow a higher degree of reliability than mere numerical simulations. Based on the results from physical modelling an exact calibration of numerical models can be performed.

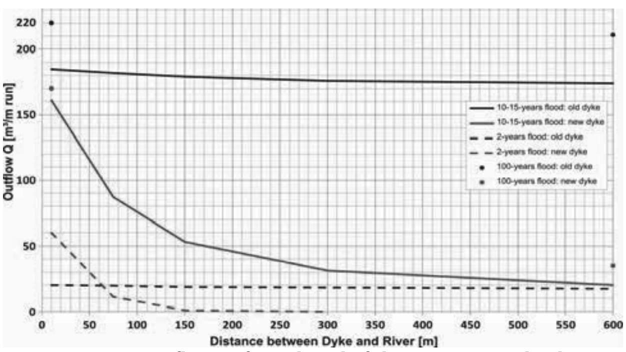

Figure 8. Water outflow Q from the relief drainage versus the distance between riverbed and old or new dyke resp. for different flood events.

In generally, the applicability of results from mere numerical modelling onto natural flow behaviour is strongly limited because of many parameters and boundary conditions. The quantity of water outflow through the relief columns is mainly influenced by subgrade/soil properties, flood wave characteristics, volume of unsaturated aquifer, distance between dyke and riverbed etc. Figure 8 shows the relation between the outflow and distance criterion for an old dyke (insufficient drainage) and the new one (with relief columns).

In the first phase of experimental underseepage studies small-scale (1:10) model tests were carried out at the Vienna University of Technology, Institute of Geotechnics (Fig. 9). The tests results were used for the design of an experimental station for 1:1 scale model tests.

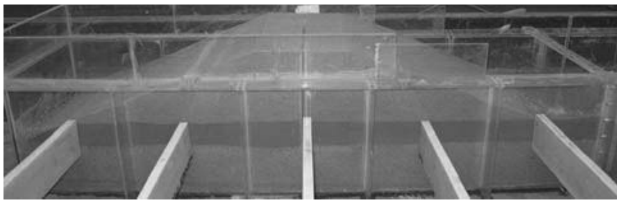

Figure 9. Small-scale model test of a flood protection dyke with simulated subgrade (fine-grained cover layer and permeable aquifer).

5 CONCLUSIONS

In the long-term underspeepage of dykes may lead to erosion processes of the fine-grained soil layers during floods. The hydraulic failure develops mostly very inconspicuously; therefore it is often underestimated in practice. Erosion criteria can be used to describe the critical state for different soil types found during soil investigation. For hydraulic failure prevention landside the dyke filter stable berms or relief columns or trenches have proven.

A technically and economically optimized design of relief measures can be achieved only by combining physical and numerical models. Such a combination takes the specific advantages of both methods. Based on physical model tests a calibration of the numerical model allows detailed parametric studies and makes an application of these results as design criteria generally possible.

6 REFERENCES

Darcy H. 1856. *Les fontaines publiques de la ville de Dijon.* Dalmont, Paris.

Brandl, H. & Hofmann, R. (2006). Erosionsstabilität und Standsicherheit von Schutzdämmen gegen Wildbäche und Murengänge mit besonderer Berücksichtigung von Einbauten. Sicherung von Dämmen, Deichen und Stauanlagen, Hermann, R. A., Jensen, J., Editors, Univ. Siegen, Germany, vol. I., pp. 139 – 171.

CEN (2004). EN 1997-1: Eurocode 7: Geotechnical Design – Part 1: General Rules. Comiteé Europeén de Normalisation, Brussels.

Chugaev, R. R. (1965). Calculation of the filter stability of the ground below dams. Gidrotechniceskoe Stroitel'stvo, No. 2 (in Russian).

Giroud, J. P. (2010). Development of criteria for geotextiles and granular filters. Prestigious Lecture 1. Proceedings of the 9th International Conf. on Geosynthetics, Guaruja´, Brazil, pp. 45 – 66.

Heibaum, M., Fourie, A., Girard, H., Karunararne, G. G., Lafleur, J. & McGrath, J. (2006). Hydraulic application of geosynthetics. Special Lecture. Proceedings of the International Conference on Geosynthetics (IGS), Yokohama, Japan, Millpress, Rotterdam, the Nether- lands, pp. 79 – 120.

Nagy, L. (2011). Investigation of soils outwashed from piping. Österreichische Ingenieur- und Architekten-Zeitschrift, Jhg. 156, No. 1-12/2011, p. 211-215.

Ziems, J. (1967). Neue Erkenntnisse hinsichtlich der Verformungsbeständigkeit der Lockergesteine gegenüber Wirkungen des Sickerwassers. Wasserwirtschaft – Wassertechnik 17, No. 7, 50 – 55 (in German).

Prédiction du comportement de barrage en enrochement de grande taille à l'aide d'une modélisation tridimensionnelle

Prediction of the behavior of very high CFRD using a 3D modelling

Chen Y., Fry J.-J., Laigle F.
EDF-CIH, Le Bourget-du-Lac, France

Vincens E., Froiio F.
Université de Lyon, LTDS, UMR CNRS 5513, École Centrale de Lyon, Lyon, France

RÉSUMÉ : Cet article montre comment une modélisation 3D permet de prévoir et de s'affranchir des pathologies observées sur les très grands barrages en enrochement. Ainsi, pour retrouver les pathologies du masque en béton observées sur un grand barrage, il faut utiliser un modèle tridimensionnel et considérer l'effet de la vallée, le zonage du corps du barrage, la séquence de construction, les interfaces entre la fondation et le remblai, la plinthe et le masque et celle entre le remblai et le masque et enfin une loi de comportement prenant en compte la forte non linéarité de la compressibilité et de la résistance avec la contrainte. La loi utilisée, L&K-Enroch, a été développée au sein d'EDF-CIH pour prendre en compte l'irréversibilité des déformations des enrochements bien compactés ou peu compactés sous charges déviatoires et isotropes pour les enrochements. La modélisation de la construction et de la mise en eau d'un barrage réel est prise comme exemple. Les résultats de la simulation expliquent, d'une manière plus convaincante, les pathologies des fissures sur le masque des grands CFRD.

ABSTRACT: This paper points out the key factors for detecting defects and avoiding them in the design of very high CFRD, based on a 3D modelling. In order to fit the observed cracks on the concrete slab on a high CFRD, a 3D modelling is required, taking into account the valley effect, the zoning of the dam body, the sequence of construction, as well as the interface between the foundation and the embankment, the interface between the plinth and the face slab, and that between the embankment and the face slab and finally a constitutive model able to catch the strong non linearity of compressibility and strength versus the state of stress. The constitutive model developed by EDF-CIH, known as L&K-Enroch, is an elastoplastic model that takes into account irreversible deformations of poorly or highly compacted rockfill under deviatoric and isotropic loading of rockfill. The 3D modelling of an existing CFRD is introduced in this paper as an example. The results of this modelling explain, in a rather convincing way, the pathology of cracks on the slab face of high CFRD.

MOTS-CLÉS : Grand barrage, CFRD, enrochement, modélisation, fissures, analyse numérique, loi de comportement

KEYWORDS: Large dam, CFRD, rockfill, modelling, cracks, numerical analysis, constitutive model

1 INTRODUCTION

Le barrage en enrochement à masque amont (CFRD) est en plein développement, car il a une grande stabilité et sa résistance remarquable au séisme. Le plus grand CFRD atteint 233 m à Shuibuya en Chine. Cependant, des fissures sur le masque amont en béton ont été souvent observées sur un grand nombre de très grands CFRD (Tianshengqiao-1, Aguamilpa, Campos Novos, Barra Grande, Mohale) attirant l'attention sur les limites de la conception traditionnelle basées principalement sur l'expérience et le jugement d'ingénierie.

Pour éviter de tels déboires, les experts disposent de la modélisation numérique pour mieux comprendre les pathologies observées sur ces ouvrages récemment construits, principalement des fissures, préciser ou compléter les solutions pour éviter ces désordres.

2 LOI DE COMPORTEMENT L&K-ENROCH

Afin de modéliser le comportement mécanique des très grands barrages en enrochement, une loi de comportement décrivant les déformations déviatoires et isotropes sous fortes contraintes adaptée est indispensable. Dans ce contexte, la loi de comportement L&K-Enroch a été développée au sein d'EDF-CIH (Laigle 2004, Silvestre 2007), afin d'améliorer la pertinence de la modélisation numérique des barrages en enrochement. Le modèle L&K-Enroch est une loi de comportement dérivée du modèle L&K, développé pour la modélisation des massifs rocheux. La plupart des concepts ont été conservés mais l'extrapolation de certaines notions aux enrochements en fait un modèle « dérivé ».

Selon la logique adoptée pour le développement du modèle L&K, la résistance de l'enrochement est uniquement régie par une composante de frottement et une composante de dilatance. D'un point de vue physique, l'hypothèse est faite que le corps d'un barrage en enrochement est assimilé, à moindre échelle et par homogénéisation, à un massif rocheux sans cohésion. Cette hypothèse justifie l'application du modèle L&K aux enrochements moyennant certaines adaptations. D'un point de vue rhéologique, le modèle L&K-Enroch est un modèle élastoplastique à écrouissage isotrope avec un mécanisme isotrope et un mécanisme déviatoire. La loi de comportement L&K-Enroch peut reproduire le comportement mécanique principal des enrochements comme observé au laboratoire :

- Un comportement non-linéaire et ductile sous chargement déviatoire. La partie réversible est très réduite, et la résistance au cisaillement est atteinte pour une déformation de cisaillement relativement élevée.

- Une phase de radoucissement possible au-delà de la résistance maximale, plus ou moins marqué en fonction du couple densité du matériau – contrainte de confinement.
- Un comportement ultime en grandes déformations représentant l'état critique.
- Un comportement volumique contractant ou dilatant en fonction de la densité du matériau et de l'état de contrainte.
- Un comportement volumique contractant significatif pour le matériau de faible densité, représentant des enrochements peu compactés ou non compactés, comme la plupart des CFRD construits au milieu du XX° siècle en France.
- Un mécanisme isotrope produisant les déformations volumiques induites par la charge hydrostatique, qui pourrait simuler la rupture des enrochements dans les grands CFRD.

3 HYPOTHÈSES DE MODÉLISATION

Afin de mieux comprendre les mécanismes de dégradation observés sur les grands CFRD, la modélisation 3D avec le code FLAC 3D de la construction et de la mise en eau du barrage de Mohale (Afrique du Sud) est prise en exemple.

3.1 *Géométrie de la vallée*

La prise en compte de l'impact de la forme de la vallée justifie le modèle 3D qui contient 29 874 mailles (Figure 1). Le maillage a été réalisé par le projet de recherche ECHO. Le modèle est séparé en 7 groupes distinguant les matériaux utilisés sur la partie amont ou aval: 3B (amont) ; 3C ; 3C1; 3C2 (aval) ; masque ; fondation, dans l'ordre des phases de construction. Cette distinction permet à tout moment de changer les caractéristiques des matériaux ou les phases de construction.

3.2 *Discontinuités cinématiques*

Les discontinuités du mouvement entre le remblai et sa fondation et le remblai et le masque sont prises en compte par des joints aptes à glisser ou s'ouvrir en vue de les reproduire.

3.3 *Historique de construction*

L'histoire du barrage doit être ensuite soigneusement reproduite. La construction du barrage est réalisée en 69 phases : la montée du remblai en 41 phases et le bétonnage du masque en 28 phases. La mise en eau est faite en 28 étapes

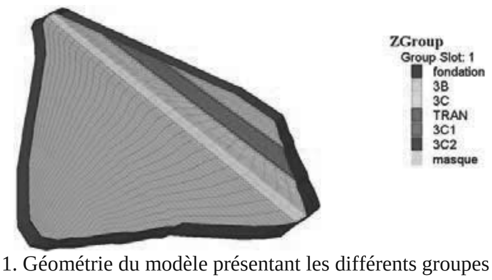

Figure 1. Géométrie du modèle présentant les différents groupes

3.4 *Choix de la loi de comportement*

Le comportement ductile des enrochements nécessite une loi de comportement adaptée. La loi L&K-Enroch est implantée dans le logiciel FLAC 3D.

3.5 *Calage des paramètres*

Peu de résultats expérimentaux (triaxiaux ou œdométriques) sont disponibles sur le matériau du barrage de Mohale pour identifier les paramètres de modèle. Le calage est fait en plusieurs étapes. Tout d'abord, il s'appuie sur le matériau « basalte de San Francisco (granulométrie No.2) » dont les propriétés sont voisines et accessibles. Les deux matériaux sont similaires au niveau de la géologie, du poids volumique, de l'indice des vides et de la forme des grains. Mais la dimension du matériau 3C du barrage de Mohale (d_{50}>25 mm) est plus grande que celle du Basalte San Francisco (d_{60}=19,8 mm).

Suite à un premier calcul, les déplacements apparaissent largement sous-estimés par rapport aux valeurs mesurées. Un ajustement sur les résultats d'auscultation est inévitable. Il concerne deux paramètres (Figure 2) : le module de Young (E) et la pression de consolidation initiale (P_{co}). Une fois que la pression moyenne dépasse la pression critique qui a un sens de pression de rupture plus que de pression de consolidation, l'indice des vides diminue rapidement et le module œdométrique se trouve fortement diminué.

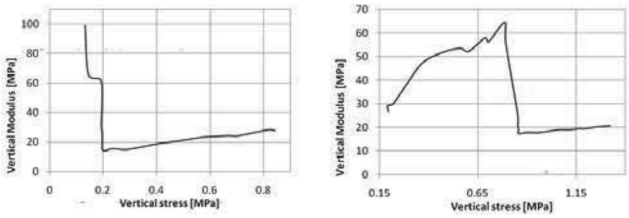

Figure 2. Module de déformation fonction de la contrainte verticale (à gauche : granulométrie serrée (3C) ; à droite : granulométrie étalée (3B), d'après Marulanda, 2009).

La pression critique est la pression isotrope en deçà de laquelle, la dilatance est visible et au delà de laquelle, il y a une forte hausse de la compressibilité par rupture des blocs. Elle est fixée au point de changement brutal du module vertical. Les valeurs ajustées pour le matériau amont (3B) et le matériau aval (3C) sont présentées dans le Tableau 1.

Tableau 1. Paramètres ajustés pour le modèle L&K-Enroch

Matériau	*3B*	*3C*
Module d'Young E (MPa)	35,2	22,5
Pression critique P_{co} (MPa)	0,8	0,2

4 INTERPRÉTATION DES RÉSULTATS

4.1 *Intérêt de la loi de comportement L&K-Enroch*

La comparaison avec le modèle de Mohr-Coulomb, calé avec la méthode de Barton et Kjaernsli (1981) et les mesures expérimentales pour le module de Young (Chen, 2012), montre que si ce dernier reproduit les tassements mesurés in-situ en phase de construction de manière satisfaisante, en ignorant l'impact de la pression hydrostatique sur le comportement de l'enrochement, il n'arrive pas à simuler correctement le comportement de l'ouvrage en phase de mise en eau. Il tend à sous-estimer l'influence de la Zone 3C en aval sur le comportement global du barrage et ne permet pas de simuler le déplacement en travers de la vallée. Le modèle L&K-Enroch intègre une surface de charge isotrope prenant en compte l'influence de la pression hydrostatique sur le comportement de l'enrochement. La surface de charge isotrope du modèle L&K-Enroch s'exprime avec le premier invariant de contrainte I_1 par :

$$f^i(\underline{\underline{\sigma}}; p_c) = \frac{I_1}{3} - p_c \qquad (1)$$

où p_c est définie par l'équation 2.

$$p_c = p_{c0}.e^{\beta.\varepsilon_v^p} \qquad (2)$$

Dans laquelle, p_c désigne la pression critique, ε_v^p, la déformation volumique plastique, p_{co} et β sont des paramètres du modèle. Ce mécanisme isotrope a un impact important sur les résultats de la modélisation : il est indispensable pour modéliser correctement le comportement des grands CFRD. En phase de construction, les résultats obtenus par les deux modèles correspondent bien aux mesures in-situ (7,4% d'erreur). A la fin de la mise en eau, l'écart entre les mesures et le calcul des maxima du déplacement amont-aval et du tassement avec le modèle de Mohr-Coulomb est de 117,3% et 42,5% respectivement au lieu de 6,5% et 25,8% avec L&K-Enroch.

Sauf mention spéciale, les résultats présentés sont obtenus en utilisant le modèle L&K-Enroch.

4.2 *Interprétation concernant l'origine des fissures de traction par flexion des grands CFRD*

La construction du masque amont du barrage de Mohale est effectuée en deux phases, afin d'avoir une protection vis-à-vis des crues. En effet, la première phase du masque achevée, permet de disposer d'un batardeau incorporé au CFRD.

Selon les résultats de l'analyse, aucune séparation entre le masque et le remblai n'est constatée lors de la première phase de construction du masque. Ensuite, la construction du remblai se poursuit, d'abord par la zone aval du remblai (zone 3C). Une fois que l'altitude de la partie amont du remblai et celle aval atteignent le même niveau (El. 2040 m). La construction se finit couche par couche (amont et aval en même phase) jusqu'à la crête (El. 2078 m). Pendant ces phases de construction, les enrochements du corps du barrage continuent à se déformer à cause du poids des couches rajoutées. En revanche, le masque amont en béton ne se déforme que très peu (le module de Young du béton est 100 à 1000 fois plus rigide que celui de l'enrochement), de telle sorte qu'une séparation horizontale importante (environ 26 cm) entre le masque et le remblai à l'altitude 2040 m se produit juste avant la construction de la deuxième partie du masque (Figure 3). C'est l'endroit où l'on a observé une fissure horizontale. Cette séparation a été également détectée sur les bords du masque.

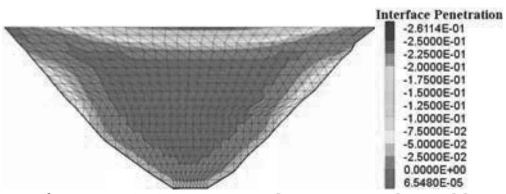

Figure 3. Séparation (<0) en m entre le masque et le remblai avant la deuxième phase de construction du masque

Pour valider l'hypothèse que le phasage de la construction est bien à l'origine de la fissuration, la construction intégrale du masque une fois achevée, la totalité de la construction du remblai a été modélisée. Aucune séparation significative n'y est constatée. Si le fluage des enrochements est négligé, le tassement des enrochements n'a alors aucune influence sur la déformation du masque et son possible détachement (Figure 4).

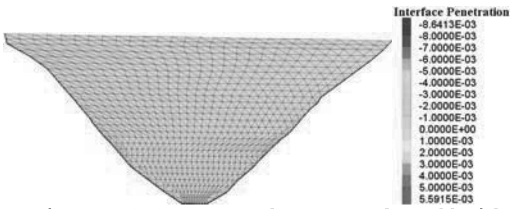

Figure 4. Séparation (<0) en m entre le masque et le remblai à la fin de la construction (Le masque construit après achèvement du remblai)

Une fois que le vide existe entre le masque et le remblai, le masque travaille en porte-à-faux, ce qui peut induire l'apparition de fissures horizontales dues au poids propre du masque et de la pression d'eau.

4.3 *Interprétation concernant l'origine des fissures de compression des grands CFRD*

Une fissure de compression a été souvent détectée au centre du masque lors de la phase de mise en eau. Ces fissures, qui ont ici une direction verticale, ont été observées dans plusieurs grands barrages tels que Tianshengqiao-I (Chine), Campos Novos (Brésil), Barra Grande (Brésil) ou Mohale (Lesotho).

D'après les simulations présentées, une forte contrainte de compression d'environ 22 MPa au centre du masque est constatée lors de la phase de mise en eau finale (Figure 5). L'orientation de la contrainte principale en compression est horizontale. Cette forte compression peut dépasser la limite de la résistance à la compression du béton (20-25 MPa) et produire cette fissure verticale constatée au centre du masque.

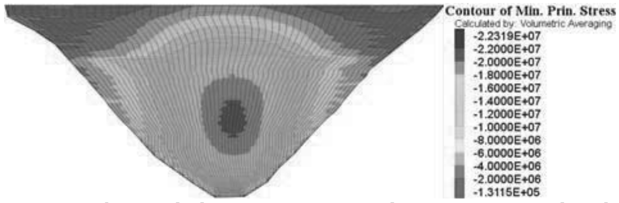

Figure 5. Champs de la contrainte principale majeure en Pa dans le masque en dernière phase de mise en eau

Le déplacement des enrochements vers le centre de la vallée accentué par la mise en eau entraine le masque et provoque une zone de compression et une zone de traction au sein du masque. Le déplacement maximal simulé de la rive gauche vers la rive droite est d'environ 5,8 cm et le déplacement maximal simulé de la rive droite vers la rive gauche est d'environ 6,0 cm (Figure 6). Le déplacement des enrochements vers le centre de la vallée induit une sollicitation tangentielle sur le masque par frottement. Il produit donc l'augmentation de contraintes de compression dans la partie centrale du masque et des contraintes de traction proches des rives.

Sous l'effet de ces contraintes de compression et de la gravité et du bourrelet du remblai qui apparait au pied du masque, des fissures de flexion inclinées en pied de masque peuvent s'ajouter aux fissures de compression.

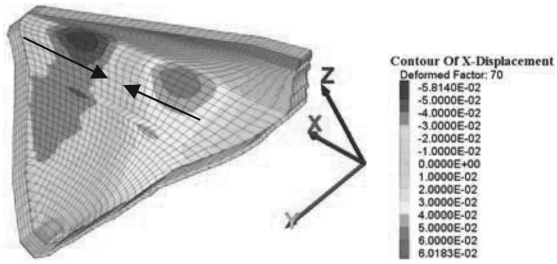

Figure 6. Déplacements longitudinaux (X) en m à fin de mise en eau

On peut aussi se poser la question de l'influence des joints verticaux du masque. En effet, l'épaisseur du masque diminue au niveau des joints, ce qui pourrait provoquer une concentration de contraintes à ces endroits là. Dans le cas de Tianshengqiao-1, l'épaisseur du masque est diminuée de 13 cm au niveau des joints verticaux (Cao et al., 2008).

4.4 *Interprétation concernant l'origine des fissures de traction pure des grands CFRD*

Le béton a une résistance à la traction de l'ordre de 2 MPa. En phase de construction, les simulations numériques révèlent l'existence de contraintes de traction d'environ 6 MPa dans le masque et le long des rives (Figure 7). Ces tractions sont générées par les déplacements des enrochements vers le centre de la vallée. Afin de résister à ces efforts de traction, une à deux rangées d'aciers sont mises dans le masque. Tandis qu'un joint le long de la plinthe relâche les tractions au contact des rives.

Figure 7. Traction (>0) aux bords du masque en fin de construction

A la fin de la mise en eau, on observe l'existence d'une bande horizontale à la cote El. 2040 m dans laquelle se développent des contraintes de traction verticales (Figure 8). D'autres contraintes de traction désolidarisent les bords du masque des rives.

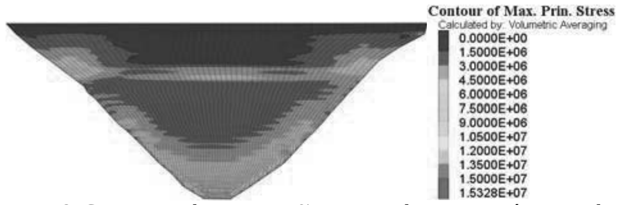

Figure 8. Contraintes de traction >0) en Pa sur la partie supérieure et les bords (rives) du masque amont à la fin de la mise en eau

Ces tractions peuvent générer des fissures horizontales du masque, identiques à celles de Aguamilpa, Mohale

4.5 *Interprétation concernant la qualité des enrochements de la zone 3C des grands CFRD*

Afin de vérifier l'impact de la déformabilité des enrochements aval sur le comportement global du barrage, trois simulations avec des modules différents de la zone 3C (aval) ont été réalisés. Les valeurs des modules de la zone 3C sont : 25 MPa, 50 MPa et 100 MPa. En revanche, le module de Young dans la zone 3B est constant et égal à 100 MPa. La comparaison entre les trois calculs est présentée ci-dessous.

Le détachement horizontal entre le masque et le remblai diminue lorsque le module en Zone 3C augmente. Si le barrage est construit avec un matériau de module identique en amont (3B) et en aval (3C), le détachement du masque sera moins fort. Le détachement augmente de 166% en moyenne, lorsqu'on utilise un matériau avec un module de 25 MPa au lieu de 100 MPa dans la zone de 3C. On peut aussi constater que la différence de l'ampleur du détachement entre les matériaux de 100 MPa et de 50 MPa est faible. On peut donc accepter que les matériaux utilisés entre la zone de 3B et la zone de 3C aient des modules différents, à condition de borner ce contraste. Selon l'analyse paramétrique précédente, un rapport maximum de 2 pourrait être toléré.

En phase de mise en eau, la traction au centre du masque augmente lorsque le module de déformation dans la zone 3C diminue. Ceci montre également l'effet positif d'un module fort dans la zone 3C sur le comportement du masque amont. En revanche, l'impact de la déformabilité de la Zone 3C sur la compression détectée au centre du masque est très faible d'après les résultats de notre simulation.

5 CONCLUSION

Les modélisations numériques présentées dans ce travail constituent une contribution à l'analyse du comportement mécanique des grands CFRD. Elles tentent d'expliquer les pathologies observées sur les grands CFRD, notamment la fissuration détectée sur le masque amont en béton.

D'après les résultats des simulations effectuées, les contraintes de compression générées en phase de mise en eau expliquent clairement la fissure verticale observée sur le masque amont. Pour y remédier, nous conseillons d'ajouter des joints verticaux de compression au centre du masque, qui dissiperont la compression concentrée et de renforcer les armatures dans le masque.

Les fissures horizontales observées, soit en phase de construction, soit en phase de mise en eau, proviennent de la compressibilité excessive des enrochements en 3B et 3C après la construction du masque. D'un point de vue mécanique, deux types de fissures horizontales sont à distinguer : la fissure de traction par flexion (due à une sollicitation de flexion engendrant de la traction en fibre tendue du masque) et la fissure de traction directe.

Les fissures de traction par flexion sont principalement causées par le détachement du masque de son support. Une fois que le masque perd son support, il travaille comme un système en porte-à-faux. Les fissures horizontales sont ensuite générées par le poids du masque ou la charge hydraulique. Les simulations montrent que le phasage de construction joue un rôle essentiel dans l'apparition de ce type de fissure. Si les conditions le permettent, il faudrait commencer la construction du masque après celle du remblai afin d'éviter l'impact des déformations différées des enrochements sur le masque amont. Selon les simulations numériques, l'impact de la déformabilité de la Zone 3C est significatif sur le comportement du masque. Cet impact est d'autant plus important que le barrage est haut. On conseille d'utiliser en Zone 3B et Zone 3C des matériaux dont les modules de déformation ne soient pas très différents.

Pour éviter les fissures de traction directe, on conseille d'utiliser un écran anti-adhérence pour éviter que les contraintes se transmettent de la bordure profilée au masque (Chen, 2012), de diminuer la déformabilité de la Zone 3C et d'ajouter un joint horizontal sur la partie supérieure du barrage (vers 1/3 de la hauteur du barrage).

6. RÉFÉRENCES

Cao K., Wang Y., Xu Y. and Liu S. 2008. Concrete Face Rockfill Dam, *China Water Power Press*

Chen Y., Fry J.J., Laigle F., Vincens E., and Froiio F. 2012. Numerical Analysis of High CFRD Using an Elastoplastic Constitutive Model *International symposium on dams for a changing world,* ICOLD 2012 Kyoto, Japon.

Barton N. and Kjaernsli B. 1981. Shear Strength of Rockfill, *Journal of the Geotechnical Engineering Division, Proceedings of the American Society of Civil Engineers.*

Laigle F. 2004. Modèle Conceptuel pour le Développement de Lois de Comportement adaptées à la Conception des Ouvrages Souterrains. Thèse de Doctorat, Laboratoire de Tribologie et Dynamique des Systèmes (LTDS), Ecole Centrale de Lyon.

Macedo-Gomez G., Castro-Abonce J. and Montanez-Cartaxo L. 2000. Behaviour of Aguamilpa Dam, *CFRD 2000*, Beijing.

Marsal R-J. 1967. Mechanical properties of rockfill, Embankment Dam Engineering, *Casagrande Volume*.

Marulanda C. and Anthiniac P. 2009. Analysis of a concrete face rockfill dam including concrete face loading and deformation. *10th Benchmark Workshop on Numerical Analysis of Dams,* Paris, France

Silvestre A. 2007. Modélisation numérique du comportement des ouvrages souterrains par une approche viscoplastique. Thèse de Doctorat, Institut national polytechnique de Lorraine.

Silvestre A. 2010. Projet ACABECE : Description de la loi de comportement retenue pour la modélisation rhéologique des enrochements.

Slope stability of the Włocławek Dam frontal earth dam in the light of the modernisation works carried out in the period 2000-2011

Stabilité de la pente du barrage en terre de Włocławek à la lumière des travaux de modernisation exécutés dans la période 2000-2011

Leszczynski M., Lipiecki B.
Ove Arup & Partners
Popielski P.
Hydro-Engineering And Hydraulics Department, Warsaw University of Technology

The authors of this paper carried out an analysis of archival data associated with the more than 40 years of Włocławek Dam exploitation for the needs of new dam design within the lower section of the Vistula River. The analysis was aimed at the issue of the existing dam safety and covered all its elements including the frontal earth dam. Archival geotechnical investigation were analysed as well as the monitoring results and all the modernisation and improvement works executed since the year 2000. As part of the task slope stability analyses were carried out for the frontal earth dam for various filtration conditions accounting for changes resulting from the modernisation works and improvements. The calculations were realised for variable sets of geotechnical parameters as a result of the interpretation of available archival geotechnical data in form of a sensitivity analysis in order to facilitate the comparison of the analysis outcome with the results of archival analyses done by others during the exploitation period of the structure. Within this paper the background for performing the analysis has been described as to explain the safety issues related with the existing structure in the light of the ongoing design of the new dam structure downstream.

Les auteurs de cet article ont conduit l'analyse des données concernant 40 ans d'exploitation du barrage de Włocławek, nécessaires pour élaborer le projet de construction d'un nouveau barrage situé en aval sur la Vistule. L'analyse a pris en considération avant tout la sécurité du barrage existant et tous ses éléments, y compris le barrage frontal en terre. On a analysé les informations géotechniques, les résultats d'observation et tous les travaux de la modernisation exécutés après l'année 2000. On a exécuté les calculs de la stabilité de la pente du barrage pour des conditions d'infiltration différentes. Les calculs étaient faits pour divers jeux de paramètres géotechniques (obtenus par interprétation de données géotechniques d'archives), sous forme d'analyse de sensibilité. Ce type de calcul a facilité la comparaison de nos résultats avec ceux d'analyses exécutées par d'autres pendant l'exploitation de l'ouvrage. L'article contient la description de la base de calcul et l'explicitation des problèmes de la sécurité du barrage à la lumière du projet de construction du barrage nouvel situé plus bas en cours du fleuve.

KEYWORDS: earth dam safety, seepage, piping effect, suffusion, internal erosion,

1 INTRODUCTION.

The analysed Dam structure is located at 674+500km chainage of the Vistula River in Poland. It consists of earth frontal dam (length of approximately 635m), 10 bay weir, fishpass, hydropower plant and navigation lock.

The soil profile beneath the dam and weir foundation level is formed by alluvial sands and partially by Tertiary deposits in form of clays, high plasticity clays and sands. The hydropower plant and navigation lock are founded on approximately 6 – 8m thick Pliocene clays and high plasticity clays overlying Miocene sands with lignite interbeddings. The earth dam body was formed partially as hydraulic fill (its centre and bank side) and partially as traditional fill (within the former river island zone).

The structure was originally designed as first of eight similar dams working in a cascade, however originally assumed system was never constructed, which basically resulted, in lack of downstream support to the analysed structure as assumed in the design process. In turn the structure has been operational since its construction in 1970 under unfavourable conditions compared to the design.

The key condition for establishment of cascade of dams along the Vistula River was, that downstream water level for each of the proposed dams to be formed by backwater from the downstream structure.

2 STUDY

Lack of the next structure downstream from Włocławek as discussed above induced major changes to the bottom of river valley immediately below and further downstream from the existing dam. Downstream erosion caused significant lowering of the river bottom within 40km distance from Włocławek, with obviously the most significant effect immediately below the dam cross-section. The observed effects of downstream water level lowering comprised among others:

- Abasement of the phreatic level within the earth dam,
- Increase of the hydraulic gradients below the weir and hydropower plant,
- Impact on hydropower plant blocks overall stability.

The induced areas of threats, to which Włocławek Dam has been exposed within passing years are the following:

- Decreasing density of the material within earth dam body,
- Hydraulic contact between up- and downstream levels within 6 of weir bays.

Since 1970s, when Włocławek Dam became operational, it was subject of continuous documentary, investigation, observations and modernisation works.

Within years of exploitation number of ground investigation campaigns and technical condition assessments was undertaken, starting from 1986, when first dynamic soundings through the earth dam were executed, supplemented by CPTs and georadar surveys in following years. Underwater observations and examinations were also carried out.

The processes of internal erosion of the dam body has been observed and degradation of its structure notified. These processes were described by W.Wolski and M.J.Lipiński, A.Furstenberg and T.Barański in “Influence of internal erosion on safety of old dams” 2000 and they generally consists of movements of soil particles within soil layers, form one soil to another, along boundaries of the layers or along the soil contact with rigid surfaces such as concrete etc.

“These movements of soil grains, irrespective of the aforementioned situations, are strongly dependent on the force of seeping water, characterized by the hydraulic gradient. The bigger the force of seeping water, the coarser the grains which can be moved. The movement of the soil particles is controlled by the geometry of the pores in the soil, particularly any constrictions the particles encounter during their movement. Certainly, if a particie is bigger than a constriction, the constriction will prevent its further movement (Kenney & Lan, 1985).

Nevertheless, whichever type of internal erosion takes place, the effect of the process is to increase the porosity of the soil zone thus influenced (Lafleur et al., 1993).

The effects of internal erosion most often detected are those located close to the drainage zones, which are characterised by higher gradients, particularly where the filters are not efficient. In these zones a large volume of particles may be washed out of the dam body or its foundation, thus creating sinkholes or caverns, often followed by regressive erosion - piping (Wolski, 1987).

Much more hazardous for dam safety, because more difficult to detect, are the internal erosion “Loose zones", which are characterized by increased (with respect to initial) porosity of the soil, which may develop without visible symptoms on the ground surface or the slopes of the dam. The internally eroded soil in the loose zones may be contractive during undrained shearing and therefore it has a high liquefaction potential. The phenomenon of liquefaction initiated in such loose zones "hidden" in the foundation or dam body can be triggered by any dynamic loading, e.g. during flood discharge, thus causing a flow slide usually with catastrophic consequences”

One of the elements being the subject of consistent observation and recording is the shape of phreatic level within the earth dam of Włocławek. This is supported by dense network of piezometers installed and automatically observed during the years of operation.

It has been identified that the observed phreatic level within the earth dam significantly differs from the designed one, calculated for stable downstream level (W.Wolski & others; 2000). Based on archival data analysis the scheme of low density material extent has been prepared (W.Wolski., J.Mirecki. 2011) within cross-section V – see Drawing 1. Drawing 2 presents the zones of loose material within dam body (with D_R<0,33). Based on the scheme of material zones the numerical model of the dam has been generated, taking into account the zones of low density material. Calculations have been performed using Z_SOIL2011v.11.13 software, the commonly used software based on final elements analysis method used for geotechnical, hydrotechnical and environmental engineering calculations (Data Preparation & Tutorials Z_SOIL PCv2010).

4 variants were considered for calculation purposes:

Variant 1 – the zones of low density material as shown on Drawing 3. The academic assumption (based on expert’s recommendation) was, that low phreatic level within the dam is being induced by proper work of surface insulation of upstream slope. The watertight facing adopted within zone of known upstream slope surface strengthening. The scheme of material zones as shown on Drawing 3.

Variant 2 – assumptions as per Variant 1. The watertight screen adopted within zone of known concrete panels location at upstream slope surface.

Variant 3 – the zones of low density material considered as per Drawing 3. The upstream slope surface insulation not considered, due to poor condition of the slope strengthening elements, qualified for repairs. The piping effect considered within dam base, as per expert’s recommendations (W.Wolski, J.Mirecki.2011). Location of the piping effect has been indicated within area, which was the subject of temporary partition during construction stage and where strong water flow was observed (K.Fanti, K.Fiedler, J.Kowalewski, S.Wójcicki, 1972)(page 352 drawing 5-5). Based on this assumption the zone of loose alluvium has been introduced within the model, that such effect has not been considered at design stage as induced during dam erection. This area has been prescribed for piping effect occurrence. Similarly, another zone of piping effect may take place in location of oxbow beyond the earth dam. Material zones scheme for Variant 3 as per Drawing 5.

Variant 4 – all assumptions as for Variant 3. Additionally, the watertight facing has been adopted within zone of known concrete panels location at upstream slope surface. Variant 4 assumes necessary repairs of concrete panels made.

At calculation stage, the different up- and downstream water level configurations were considered. Flooding conditions were modelled as per water states dated 23.05.2010, and normal working conditions dated 01.04.2012.

Boundary conditions were established based on both of records from existing piezometers and up- and downstream water levels. Two calculation cases were taken into consideration: normal working conditions and flooding conditions.

The piezometers network has been modelled, and after analysis completion, the results were compared with values observed in real. The seepages at upstream slope were also analysed, however only the ones having place above the existing downstream water level were considered. The above comparison was used for back analysis of the ground parameters and adequate modifications were made to meet the best matching to the real situation. The leading case for parameters verification was the normal working conditions of the dam.

The analysis results were presented in form of phreatic level projection across the dam body cross-section. Variant 1 is shown on Drawing 7. This drawing presents the low arrangement of groundwater level, which closely reproduces the one observed at the dam.

The arrangement of phreatic level is due from calculation based on the assumption that there is an impermeable facing on upstream slope. The aim of variant one of calculations was to demonstrate whether it is possible to achieve the low level of phreatic level as described in professional literature. Despite the convergence of a solution obtained from the calculations and the observed in nature above mentioned situation does not occur in the area of Wloclawek Dam. Structures situated on upstream slope were qualified to repair and do not meet conditions made in the calculations for Variant 1.

The results of phreatic level calculation in Variant 2 are presented on Drawing 8. This variant of calculations was based on the assumption that there is a watertight facing in the area of slope with reinforcing concrete panels. The results of numerical analysis for Variant 2 were not in the compliance with the position of phreatic level observed in nature.

The calculation results of phreatic level in Variant 3 are presented on Drawing 9. The appearance of piping effect in the base of the dam was considered in this variant. The position of phreatic level obtained in the calculations is the most consistent with the conditions observed in nature comparing to other variants. The differences relate to the initial filtration section where soil loosening effect may occur. It can cause the change of filtration factor and flow of water perpendicular to the surface of the model which is impossible to capture in 2D modelling.

The calculation results of phreatic level in Variant 4 are presented on Drawing 10. This variant was based on the assumption that there is piping effect and hypothetically watertight facing in the area of slope with reinforcing concrete panels. In calculations the position of phreatic level is different from what was observed in nature.

3 DRAWINGS

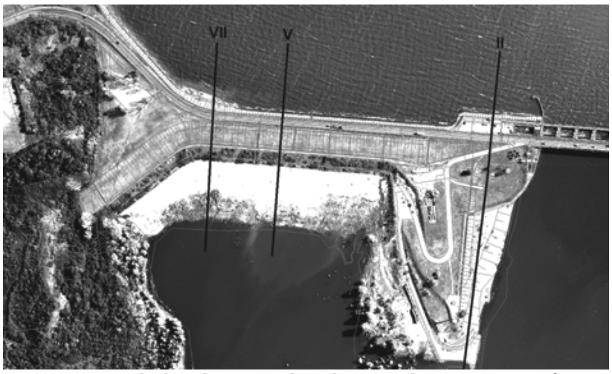

Drawing 1 Earth dam location plan showing the orientation of cross-section taken for calculations

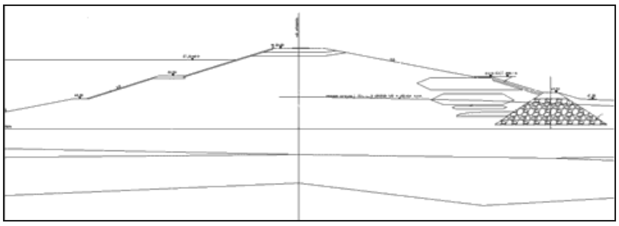
Drawing 2 Cross-section V with low density material zones marked

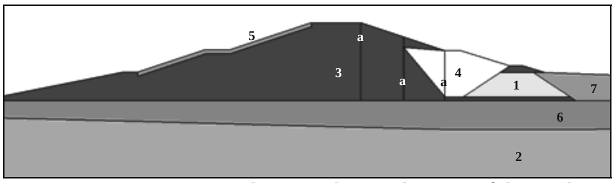

Drawing 3 Variant 1 Material zones scheme – location of the insulation at upstream slope

Material description – 1) dam drainage 2) impermeable layer 3) dam body – fine sand 4) loose zone within dam body 5) concrete panels/facing covering upstream slope of the dam 6) sands 7) berm 8)vertical piping – see drawings 5&6. 9)horizontal piping – see drawings 5&6 a) locations of piezometers taken into account for model establishment.

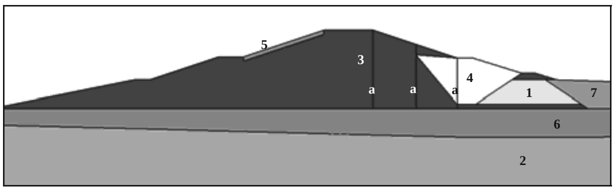

Drawing 4 – Variant 2 Material zones scheme – location of the insulation at upstream slope, within zone of concrete panels

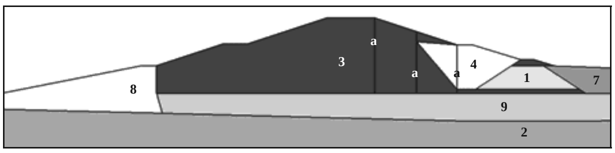

Drawing 5 Variant 3 Material zones scheme – piping effect at dam base

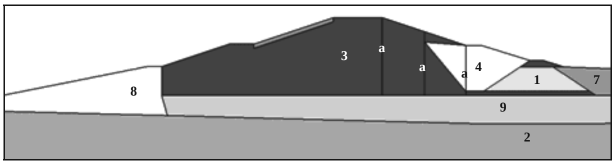

Drawing 6 Variant 4 Material zones scheme – piping effect at dam base plus watertight facing within zone of concrete panels installation

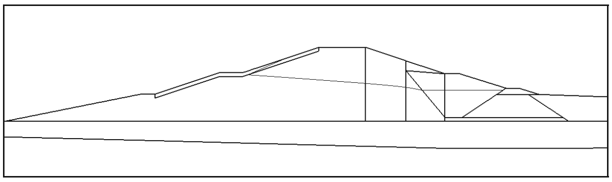
Drawing 7 Variant 1 Phreatic level across earth dam and material zones

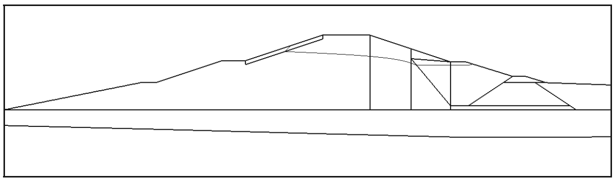
Drawing 8 Varian 2 Phreatic level across earth dam and material zones.

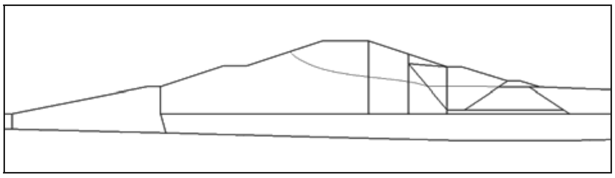
Drawing 9 Variant 3 Phreatic level across earth dam and material zones

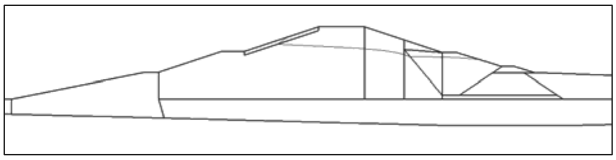
Drawing 10 Variant 4 Phreatic level across earth dam and material zones

4 CONCLUSIONS

The observed phreatic level course within the earth dam body differs significantly from the design values, which were assumed based on specified, stable downstream water level.

In Variant 3 the location of piping failure has been assumed based on known oxbow presence or base loosening indicated during the last phase of earth dam construction. These locations are hypothetical, however low phreatic level within dam body proves that phenomenon hazardous to Włocławek Dam exists.

In Variant 4, both of piping failure existence and parallel reinforcing of concrete panels at upstream slope induce deterioration of earth dam working conditions within the drainage zone (where interface between drainage and dam material not exists). It causes flow concentration and rising of the phreatic level and thus further development of suffusion phenomenon within ends of filtration paths through the dam.

Further, the seepage deformation might develop without strictly and immediately visible symptoms, and therefore might not be noticed during the operational activity of the entire structure.

This shall be also concluded, that construction of new dam, below the existing Włocławek Dam should improve its working conditions by reducing the differences between up- and downstream water levels, and thus pressure gradients which cause the suffusion within and below dam body.

Protection of the object against suffusion phenomenon development and piping effects shall be treated as the main element securing safety of Włocławek Dam.

For further observations of the loose zones and determination of the density change, periodic density control tests shall be introduced in the area of a site particularly exposed to high hydraulic gradients, as discussed above.

It is necessary to ensure that control tests are done with the use of equipment of internationally recognized standards in order to obtain the required accuracy of the density change determination and comparable results across worldwide known cases.

5 REFERENCES

Wolski W., Mirecki J. 2011. *Technical condition of Włocławek Dam assessment.* Warsaw.

Design documentation for establishment of geological conditions under Włocławek Dam.

Fanti K., Fiedler K., Kowalewski J., Wójcicki S. 1972. *Weirs*, Warsaw.

Data Preparation & Tutorials Z_SOILPCv2010. 2010. Lausanne

Wolski W., Lipiński M.J., Furstenberg A., Barański T. 2000*k*

Deformation safety of high concrete face rockfill dams

Calculs en déformations de la sécurité des grands barrages en rochement à masque amont en béton

Li N.
Nanjing Hydraulic Research Institute, Nanjing 210029

Wang J.
China Hydro Northwest Investigation Design & Research Institute, Xian 710065, China

Mi Z.
Nanjing Hydraulic Research Institute, Nanjing 210029, China

Li D.
Nanjing Hydraulic Research Institute, Nanjing 210029, China

ABSTRACT

Based on the analysis of the mechanism of serious damages of high concrete face rockfill dams (CFRDs), it is indicated that the causes of the cracking of cushion layer, the structural cracking and squeezed ruptures of concrete face slab are as follows: the deformations of the dam different zones are not coordinated and the deformations of the concrete face slabs are not coordinated synchronously with those of the dam body. The basis of empirical design that the water load on the concrete face enters the foundation upstream from the dam axis is not correct. Therefore the empirical design concept of CFRDs should be changed. The deformation safety is necessary for high CFRDs besides the stability safety and seepage safety for earth-rockfill dams. A new deformation coordination concept and the deformation safety design of high CFRDs including deformation coordination standards, judgment criteria and calculation methods are put forward. The deformation coordination design method for replacing the empirical design concept is shown to be important for high CFRDs through the application of Bakun Dam.

RÉSUMÉ

Dans l'analyse des problèmes de stabilité des barrages en enrochements à parement amont en béton de grande hauteur (CFRD), il a été remarqué que la cause de la fissuration du lit et du masque est le contraste de déformabilité entre les différentes zones constituant le barrage (massif et parement amont). La conception basée sur l'expérience considérant que la chargement dû à l'eau agissant sur le masque amont pénètre la fondation amont est incorrecte, et un changement dans le dimensionnement empirique des CFRDs devrait être envisagé. Il est aussi nécessaire d'assurer un calcul de stabilité en déformations en plus des calculs à la rupture et vis-à-vis des écoulements. Une nouvelle conception intégrant la compatibilité des déformations dans les analyses de stabilité des grands barrages en enrochements à masque amont en béton est établie à partir de normes de distinction et des méthodes de calcul à travers une application au projet de barrage de Bakun qui confirme l'intérêt de cette nouvelle approche par rapport à celles basées sur l'expérience.

KEY WORDs:CFRD, deformation safety, empirical design,deformation coordination, standard,judgment criterion.

1 INTRODUCTION

It takes only 46 years there are more than 500 concrete face rockfill dams(CFRDs) have been completed or under construction in the world. The safety and economic condition of CFRD are so good that CFRD has become the best dam type with the most competitive ability usually. But the design of the CFRD is empirical and is based on experience and precedent. Some serious damages as follows have happened at several high CFRDs since 1990's. Some cracks of cushion zone happened at Tianshengqiao No.1 Dam (178m high) and Xingo Dam(140m high). The top of concrete face slabs separated mostly from cushion layer and then more than 5000 cracks of concrete face slab occurred at Tianshengqiao No.1 Dam. A lot of cracks of concrete face slabs occurred then the seepage discharge reached 1700 L/s at Aguamilpa Dam(187m high). The serious cracks, squeezed ruptures and horizontal overlaps of concrete face slabs occurred at Campos Novos Dam(202m high), Barra Grande Dam(185m high)and Mohale Dam(145m high) then the seepage discharge increased an range from 600L/s to 1300L/s. The crack and squeezed rupture of concrete face slab occurred also at Tianshengqiao No.1 Dam and Shuibuya Dam(233m high).

The reason of cracking of cushion zone, separating of face slab top from cushion layer, and cracking of concrete face slab is that the deformation of dam different zones are not coordinated and the deformation of concrete face slab are not coordinated synchronously with the deformation of dam body. The modulus of deformation of main rockfill zone (upstream rockfill zone) is higher than that of downstream rockfill zone. The deformation of dam body is much larger than the deformation of concrete face slab. If the difference of deformation between dam body and concrete face slab was large enough to exceed the limit, the top of face slab would separate from cushion layer and then cracks of face slab would occur. The direction of the deformation of dam body faces the center of the valley and at this time the friction force facing the center of the valley occurs between concrete face slabs and cushion layer. If the compressive stress at the central area of concrete face slab exceeded the compressive strength limit of concrete that the squeezed ruptures, cracks and horizontal overlaps would occur. Therefore the deformation safety should be satisfied necessarily besides the stability safety and seepage safety for high CFRDs.

2 CONNOTATION OF DEFORMATION SAFETY OF HIGH CFRD

The deformation safety of high CFRD includes the deformation coordination of different zones of dam body and the deformation coordination synchronously between the deformation of dam body and the deformation of concrete face slab.

2.1 *Deformation coordination standards*

1）Coordination standard of dam body settlement

$$\left|\frac{S_{i+1}-S_i}{y_{i+1}-y_i}\right|<[I] \qquad (1)$$

$$\left|\frac{S_{i+1}-S_i}{x_{i+1}-x_i}\right|<[I] \qquad (2)$$

where S_i and S_{i+1} are settlement at i point and i+1 point of dam body (cm); y_i and y_{i+1} are coordinate at i point and i+1 point at direction of stream(m); x_i and x_{i+1} are coordinate at i point and i+1 point at direction of dam axis(m); [I] is limit of inclination(the difference of settlement)

2）Coordination standard of dam body horizontal displacement

$$\left|\frac{D_{Byi+1}-D_{Byi}}{y_{i+1}-y_i}\right|<[T] \qquad (3)$$

$$\left|\frac{D_{Bxi+1}-D_{Bxi}}{x_{i+1}-x_i}\right|<[T] \qquad (4)$$

where D_{Byi} and D_{Byi+1} are horizontal displacement at stream direction at i point and i+1 point of dam body(cm); D_{Bxi} and D_{Bxi+1} are horizontal displacement at dam axis direction at i point and i+1 point of dam body(cm); [T] is limit of displacement difference.

3) Coordination synchronously between dam body deformation and concrete face slab deformation

$$(D_{Bfi}\big|_j - d_{fi}\big|_j)_{\max} < [H_s] \qquad (5)$$

$$(D_{Bxi}\big|_j - d_{xi}\big|_j)_{\max} < [J] \qquad (6)$$

$$[H_s] = f(1/E_c, f_t, t_f, f_y \cdots) \qquad (7)$$

$$[J] = f(1/E_c, f_c, t_f, f_y, C_f \cdots) \qquad (8)$$

Where $D_{Bfi}\big|_j$ is displacement of dam body i point at normal direction of face slab at j time(cm); $d_{fi}\big|_j$ is deflection of face slab i point at j time(cm); $D_{Bxi}\big|_j$ is displacement of dam body i point at dam axis direction or at direction of face slab slope at j time(cm); $d_{xi}\big|_j$ is displacement of face slab i point at dam axis direction or at direction of face slab slope at j time(cm); [H_s] is limit of separation height of face slab(cm); [J] is limit of displacement difference between dam body and face slab at dam axis direction or at face slab slope direction(cm). E_c is elastic modulus of concrete; f_c is compressive strength of concrete; f_t is tensile strength of concrete; t_f is thickness of concrete face slab; f_y is compressive strength or tensile strength of reinforcement; C_f is friction coefficient between face slab and cushion layer.

2.2 *Deformation coordination judgment criteria*

The above-mentioned deformation coordination judgment criteria including [I], [T], [H_s] and [J] depend on the physical and mechanical properties of dam filling material and concrete, the dimension of face slab, as well as stress condition of dam body and concrete face slab. The above-mentioned judgment criteria could be decided by laboratory tests or back analysis based on prototype observation data. The laboratory tests include large scale simple shear test, large scale triaxial compression or extension test and large scale contact surface test. The real or modified material is used as dam filling material and face slab concrete in laboratory tests. The stress condition of sample in the test should imitate the real stress condition of dam body or face slab during construction or operation.

The prototype observation data from Tianshengqiao No.1 Dam, Aguamilpa Dam, Campos Noves Dam, Barra Grande Dam, Mohale Dam and Shuibuya Dam could be used to analyze the reasons for causing the above-mentioned serious damages.

The above-mentioned judgment criteria also could be obtained from back analysis.

2.3 *Calculation method and contact surface constitutive relation*

A three-dimensional finite element method (FEM) could be used as deformation coordination calculation method. NHRI (Nanjing Hydraulic Research Institute) double yield surface elastic-plastic model and Duncan E-B non-linear elastic model could be used to modeling dam filling material. A contact surface damage constitutive model could be used to modeling contact surface performance as the following formula.

$$\tau=\left(\frac{2\times e^{-\alpha\gamma^{n_1}\left(\frac{\sigma_n}{P_a}\right)^{n2}}}{e^{\alpha\gamma^{n_1}\left(\frac{\sigma_n}{P_a}\right)^{n_2}}+e^{-\alpha\gamma^{n_1}\left(\frac{\sigma_n}{P_a}\right)^{n_2}}}\right)\times\frac{\gamma}{\frac{1}{K_I\gamma_w\left(\frac{\sigma_n}{P_a}\right)^n}+\frac{\gamma}{\sigma_n\tan\delta_i}}+\frac{e^{\alpha\gamma^{n_1}\left(\frac{\sigma_n}{P_a}\right)^{n_2}}-e^{-\alpha\gamma^{n_1}\left(\frac{\sigma_n}{P_a}\right)^{n_2}}}{e^{\alpha\gamma^{n_1}\left(\frac{\sigma_n}{P_a}\right)^{n_2}}+e^{-\alpha\gamma^{n_1}\left(\frac{\sigma_n}{Pa}\right)^{n_2}}}\times\left(\sigma_n\tan(\delta_d)+c_n\right) \qquad (9)$$

Where τ is shear stress of contact surface; σ_n is normal stress of contact surface; γ is shear strain of contact surface; Pa is a standard atmospheric pressure; α、δ_i、δ_d、C_n、K_1、n、n_1、n_2 are model parameters. The model parameters of two typical CFRDs are shown in Table 1 Table 1. Parameters of contact surface damage constitutive model

Dam name	K_1	n	δ_i	δ_d	C_n	α	n_1	n_2
Houziyan (223.5m high)	23	0.49	1.2	0.50	5.42	0.040	2.0	-0.95
Jinchuan (112 m high)	20	0.55	1.2	0.47	2.02	0.045	1.6	-0.34

The effectiveness of fitting the contact surface damage constitutive model to contact surface test results for Houziyan Dam is quite good as shown in Figure 1.

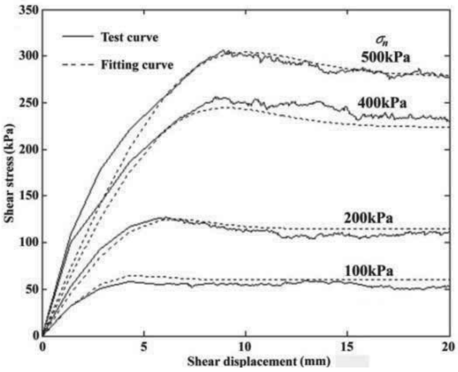

Figure1. Effectiveness of fitting contact surface model to contact surface test result for Houziyan Dam

3. APPLICATION OF DEORMATION COORDINATION DESIGN CONCEPT

The deformation coordination design concept has been applied in Bakun Dam. Bakun Dam is located on Balui River, Sarawak Malaysia. Bakun Dam is the second highest completed CFRD in the world with its height 202m. The former design of Bakun Dam was completed by H.S.Choi, Germany. The former dam zoning of Bakun Dam is shown in Figure 2.

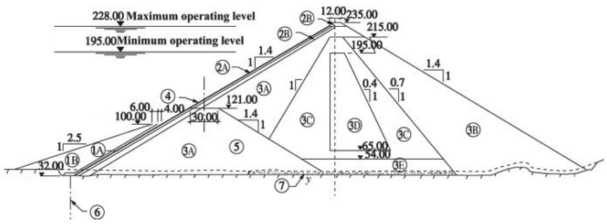

Figure 2 Zoning of Bakun Dam designed by empirical method (unit: m)

Bakun CWZ-Main Civil works tender had been obtained by Malaysia-China Hydro Joint Venture (MCH JV) in 2002. Bakun Dam design has been completed by China Hydro Northwest Investigation Design &Research Institute. Bakun Dam filling material test and 3D FEM analysis has been completed by Nanjing Hydraulic Research Institute. Based on deformation coordination design concept a new dam zoning for Bakun Dam has been put forward as shown in Figure 3.

The main difference between the former design and new deformation coordination design are as follows: The dry mass density of compacted rockfill is 2.09 g/cm^3 for the former and 2.22g/cm^3 for the latter. The water-stop of vertical joint of concrete face slab is bituminizing plate for the former and deformable Pulai Plate for the latter.

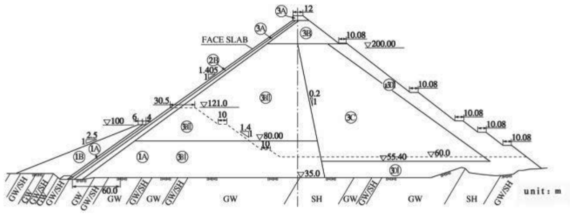

Figure 3 Zoning of Bakun Dam designed by new deformation coordination concept (unit: m)

The results of 3D FEM analysis and the comparison of dam behavior and deformation coordination level between the former design and new design are shown in Figure 4 to Figure 6.

The maximum settlement of dam body at completion is 376.4cm for the former and 230.6cm for the latter. The observed settlement is 227.5cm.The maximum displacement towards downstream of dam body during impoundment is 79.2cm for the former and 48.9cm for the latter. The observed displacement is only 13.0cm. The maximum deflection of face slab at impoundment is 105.7cm for the former and 84.7cm for the latter. The maximum compressive stress at dam axis direction of face slab at impoundment is 19.2MPa for the former and18.3MPa for the latter.

The following results could be obtained from Figures:

1) The dam deformation of dam body designed by empirical concept is uncoordinated especially at cushion zone and top of the first stage filling. Its maximum difference of dam body settlement is 4.55×10^{-2} (Figure 4) , its maximum difference of horizontal displacement of dam body is -2.94×10^{-2} (Figure 5) .Cracking of its cushion zone would occur probably.

2) The maximum displacement difference at normal direction between face slab and cushion designed by empirical concept reaches 113.5cm. Its top of face slab would separate from cushion and then cracks of face slab would occur probably.

3) The maximum compressive strain at dam axis direction of face slab designed by empirical concept is 670×10^{-6} (Figure 6) .which exceeded the limit of compressive stain (650×10^{-6}) from prototype data of Mohale Dam. In other words, squeezed rupture of concrete face slab would occur probably.

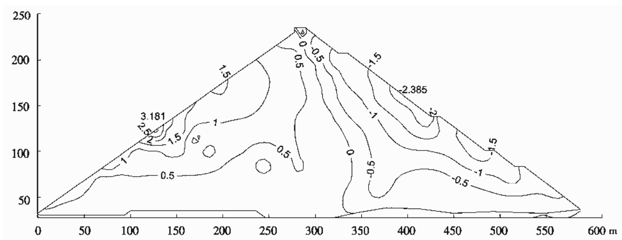

(a)Settlement difference of Bakun Dam body designed by deformation coordination method (unit:10^{-2})

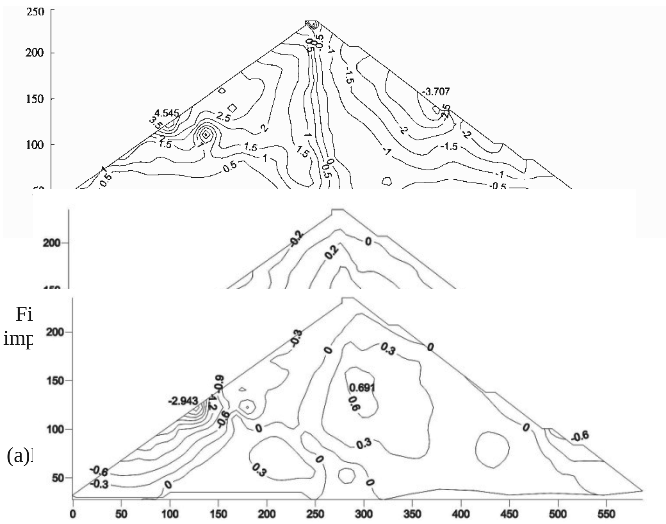

(b)Horizontal displacement difference of Bakun Dam body designed by empirical method (unit: 10^{-2})

Figure 5 Comparison of horizontal displacement difference of Bakun Dam body at water impoundment between empirical method designed and new deformation coordination concept method designed

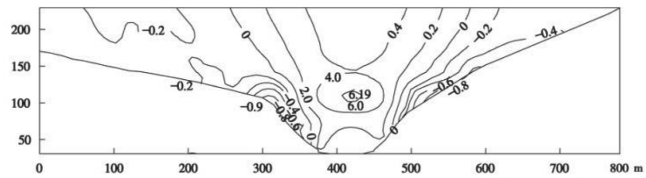

(a)Strain at dam axis direction of face slab of Bakun Dam designed by deformation coordination method (unit: 10^{-4})

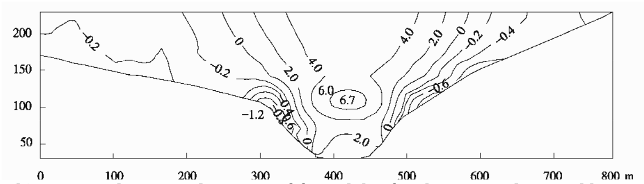

(b)Strain at dam axis direction of face slab of Bakun Dam designed by empirical method (unit: 10^{-4})

Figure 6 Comparison of strains at dam axis direction of concrete face slab at water impoundment of Bakun Dam between .empirical method designed and new deformation coordination concept method designed

4）Based on the calculation results and observation data of Bakun Dam designed by deformation coordination concept and constructed by MCHJV, it could be shown that the deformation of dam different zones is coordinated each other and the deformation of concrete face slab is coordinated synchronously with deformation of dam body. The maximum settlement difference of dam body is only 3.18×10^{-2}, decreasing 51% as compared with that designed by empirical method. The maximum displacement difference at normal direction between face slab and cushion is only 71.0cm, decreasing 60% as compared with that designed by empirical method. The observed maximum compression strain at dam axis direction of face slab is only 565×10^{-6}, decreasing 19% as compared with that designed by empirical method.

5）It could be considered based on Bakun Dam prototype observation data that the predicted behavior by 3D FEM analysis could reflect its real performance. This 3D FEM analysis method is effective and can be used for CFRD deformation coordination concept design.

4 CONCLUSIONS

The following conclusions could be obtained:

1）The reason of the cracking cushion layer, the structural cracking and squeezed rupture of concrete face slab is that the deformations of dam different zones are not coordinated each other and the deformations of face slab are not coordinated synchronously with the deformations of dam body.

2）The deformation safety should be satisfied necessarily for high CFRDs besides the stability safety and seepage safety for earth-rockfill dams as usually.

3）The deformation safety design method including deformation coordination standards, judgment criteria and calculation method is shown to be reasonable and important for high CFRDs through its application to Bakun Dam.

5. REFERENCES

Li, Neng-hui. 2007. *Recent technology for high concrete face rockfill dams*, Beijing: China Water Power Press, (in Chinese)

Cooke, J. B. 1984. Progress in rockfill dams, *Journal of Geotechnical Engineering, ASCE*, 110(10), 1383– 1414.

Cooke, J. B. 1998. Empirical design of concrete face rockfill dams, *Hydropower & Dam*, (6), 7– 11.

Li, Neng-hui. 2011. New concept of design for high concrete face rockfill dams, *Engineering Sciences*, 13(3), 12– 18.(in Chinese).

Li, Deng-hua, Li, Neng-hui. 2009. Experimental study on mechanical behavior of interface between soil and concrete slab. *Water Resources and Power*, 27(5),114– 118. (in Chinese)

Li, Neng-hui, Wang, Jun-li, Mi, Zhan-kuan, Li, Deng-hua. 2012. Connotation of deformation safety of high concrete face rockfill dams and its application. *Chinese Journal of Geotechnical Engineering*, 34(2),193-201 (in Chinese)

Safety of a protection levee under rapid drawdown conditions. Coupled analysis of transient seepage and stability

La sécurité d’une digue de protection en conditions de vidange rapide. Analyse couplée des écoulements transitoires et de la stabilité

López-Acosta N.P., Fuente de la H.A., Auvinet G.
Instituto de Ingeniería, UNAM, D.F., México

ABSTRACT: The rapid drawdown condition arises when submerged slopes of protection levees experience a rapid decrease of the external water level. In this paper the safety of a protection levee under rapid drawdown conditions is studied by numerically modeling this phenomenon as a coupled problem of transient seepage-deformation in a saturated/unsaturated medium. Analyses are performed based on finite element method by using the PLAXFLOW program for transient seepage analysis and the PLAXIS program for deformation, consolidation and stability analyses. The details of the proposed methodology are presented in this work. Also, recommendations for definition of material type (drained or undrained), type of soil constitutive model (Hardening Soil and Mohr Coulomb), boundary conditions and mesh generation of finite elements are provided. In the main part of the paper, the effects of multiple parameters such as position of phreatic surface, water drawdown ratio, drawdown rate and hydraulic conductivity are evaluated by a 2D model of stress-strain. Special emphasis is given to the study of the safety factor variation as a function of time obtained when assessing the stability of these earth structures. Finally, concluding comments about the results are exposed.

RÉSUMÉ: La condition de vidange rapide survient lorsque les pentes de digues de protection submergées expérimentent une réduction rapide du niveau d'eau externe. Dans cet article, la sécurité d'une digue de protection dans des conditions de vidange rapide est étudiée par modélisation numérique de ce phénomène comme un problème couplé de flux transitoire -déformation dans un milieu saturé / non saturé. Les analyses sont effectuées sur la base de la méthode des éléments finis en utilisant le programme PLAXFLOW pour l'analyse d'infiltration transitoire et le programme PLAXIS pour les analyses de déformation, de consolidation et de stabilité. Les détails de la méthodologie proposée sont présentés dans cet écrit. Également, des recommandations pour la définition du type de matériau (drainé ou non drainé), type de modèle constitutive de sol (Hardening Soil et Mohr Coulomb), conditions aux limites et de génération de maillage d'éléments finis sont fournis. Dans la partie principale de l'article, les effets de plusieurs paramètres tels que l'emplacement de la surface phréatique, le taux de vidange rapide, le rapport de vidange et la conductivité hydraulique sont évalués par un modèle 2D de contrainte-déformation. Une attention particulière est accordée à l'étude de la variation en fonction du temps des facteurs de sécurité obtenus lors de l'évaluation de la stabilité de ces structures en terre. Enfin, les observations finales sur les résultats sont données.

KEYWORDS: Protection levee, rapid drawdown, coupled analysis, transient seepage, slope stability, 2D model of stress-strain.

1 THE RAPID DRAWDOWN CONDITION

1.1 *The water drawdown phenomenon*

The water drawdown phenomenon can be divided in three modes (Fig. 1): a) *fully slow drawdown*, b) *fully rapid drawdown*, c) *general (transient) drawdown* (Duncan *et al.* 1990, Griffiths and Lane 1999, Lane and Griffiths 2000, Berilgen 2007, Huang and Jia 2009, Nian *et al.* 2011).

In the *fully slow drawdown* condition (Fig. 1a), the soil is assumed to be drained; in every moment of the drawdown the water level inside the levee (water table) equals the water level on the outside (the reservoir level), generating a steady-state flow condition, therefore the pore water pressure within the levee is hydrostatic condition. In the *fully rapid drawdown* mode (Fig. 1c), the soil is considered to be undrained, the water table is conserved at the initial level of the reservoir for every moment of the drawdown, so the pore water pressure inside the levee is the hydrostatic pressure. In both extreme cases, the water surface is assumed to be horizontal, except on the face of the slope for fully rapid drawdown mode, as shown in Figure 1c. For the *general (transient) drawdown* mode (Fig. 1b), a curvilinear water surface is generated within the soil structure whose position depends on the drawdown rate and the material properties (such as hydraulic conductivity, porosity, etc.), consequently the remaining pore water pressure within the levee is transient type (it varies as a function of time but also with the soil’s ability to retain water).

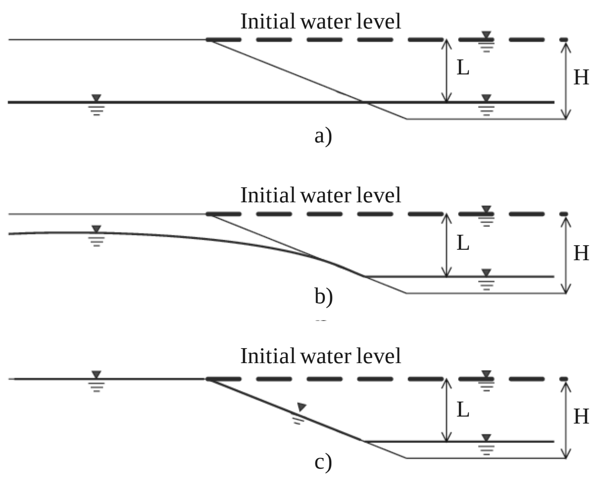

Figure 1. Water drawdown modes: a) Fully slow drawdown, b) Transient drawdown y, c) Fully rapid drawdown (Berilgen 2007).

1.2 *Classical methods for analyzing rapid drawdown*

Drawdown condition has been analyzed from different approaches depending on the progress in the field of classical soil mechanics. The analysis methods can be classified into two groups (Alonso and Pinyol 2008): a) water flow methods appropriated for and relatively permeable materials, b) undrained analysis methods applicable to low permeability materials.

The methods included in the first group solve the water flow problem within an earth slope subjected to changes of hydraulic boundary conditions as a function of time. According to these methods it is implicitly accepted that the solid skeleton of the materials involved in the drawdown phenomenon is rigid and no changes occur in the total stresses. Usually, recommendations for the study of relatively permeable materials are based on numerical, analytical or graphical groundwater flow techniques. However, these types of water flow methods do not consider the soil deformability which in the case of soft materials plays an important role in the velocity of dissipation of the pore water pressure.

The second approach considers only the pore water pressure change due to discharge of stresses associated to decrease of water level during the water drawdown phenomenon (mechanical problem). That is, the analysis is undrained type, in which water flow is negligible because of the significant drawdown rate compared with the permeability of material.

2 PROPOSED METHODOLOGY FOR ANALYSES

The stability analysis of a protection levee under rapid drawdown conditions requires the consideration of two effects: i) changes in total stresses due to external loads, such as hydrostatic pressure or overloading (e. g. bank protections sandbags, over-elevation on a levee height, etc.), and ii) seepage forces due to transient groundwater flow. According to the Terzaghi's principle (1943), the increase in total stresses in a saturated soil is equal to the sum of the effective stress plus the pore water pressure:

$$\Delta\sigma = \Delta\sigma' + \Delta p = \Delta\sigma' + (\Delta p_{seepage} + \Delta p_{excess}) \qquad (1)$$

Where $\Delta\sigma$ is the change in total stresses, $\Delta\sigma'$ is the change in effective stresses and Δp is the change in active pore water pressure, which is constituted by pore water pressure increases due to seepage ($\Delta p_{seepage}$) and pore water pressure increases due to changes in total stresses.

The pore water pressure due to seepage is computed by a water flow analysis. If the flow domain contains a water table that changes as a function of time, the problem becomes one of transient flow type. The excess pore water pressure due to changes in the total stresses is calculated by a stress-strain analysis. This pressure is not steady-state and changes with time (it increases or dissipates); therefore it also is a problem that requires be evaluated versus time. Additionally, during drawdown the dissipation of remaining pore water pressure (consolidation) may occur depending on material properties, drawdown rate and drawdown ratio. Consequently, to evaluate the stability of an earth structure subjected to rapid drawdown condition, it is required the coupling of the following analyses:

i) Transient-state seepage analysis.
ii) Deformation analysis.
iii) Consolidation analysis.
iv) Stability analysis.

Currently, numerical techniques are the most common solution, specially the finite element method. The preceding methodology is applied in the analyses performed herein, with a 2D plane-strain model using finite element programs: PLAXFLOW for the transient seepage analyses and PLAXIS for the deformation, consolidation and stability analyses (Delft University of Technology 2008), as shown below.

3 PARAMETRIC ANALYSES

3.1 *Problem statement*

In order to investigate the influence of rapid drawdown on stability of protection levees, analyses assuming the three different drawdown modes illustrated in Figure 1 were performed. For the *fully slow drawdown* mode, soil was assumed to be drained and only water flow analyses were carried out (uncoupled). For the *fully rapid drawdown* mode, soil was considered undrained and only undrained analyses were performed (uncoupled). For *transient drawdown* (Fig. 1b), a coupled analysis was performed and soil was assumed to be undrained.

3.2 *Geometric, hydraulic and mechanical properties, and initial and boundary conditions*

A homogeneous and isotropic levee (H = 6 m height and 2:1 slope) was considered in analyses, as illustrated in Figure 2.

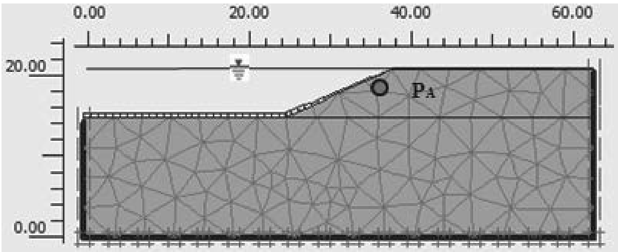

Figure 2. Simplified geometry of the analyzed levee.

The mechanical, hydraulic and rigidity properties of both the levee and the foundation soil were assumed in calculations as provided in Table 1. Similarly, in the analyses two different hydraulic conductivities (k=1×10^{-4} and 1×10^{-6} cm/s) and two drawdown rates (R=0.1 m/d and 1.0 m/d) were studied. The capacity of soil to retain water was defined by the *approximate Van Genuchten model* (1980).

For modeling the domain a fairly refined mesh was generated by using 15 nodes triangular finite elements, because they provide more accurate results in more complex problems, such as bearing capacity and stability analyses (Nagtegaal *et al*. 1974, Sloan 1981, Sloan and Randolph 1982). Standard boundary conditions were assumed (fixed bottom). The initial stress state was generated by using the K0 procedure. All model boundaries were considered to be impervious, except the surface of foundation soil, the slope and crown of the levee (see Fig. 2). It was also assumed that the reservoir level is initially located at the maximum elevation (21 m, corresponding to L=0).

3.3 *Numerical modeling*

For the numerical modeling of the problem, it was initially assumed that flow conditions within the embankment correspond to a steady-state (Δt = 0; L/H = 0), thus a steady-state flow analysis was firstly performed, which was followed by deformation and consolidation analyses. In this last analysis, a minimum pore water pressure was assumed within the levee (p_{excess} = 0.1 kPa), because the study is performed supposing that elapsed time is long enough to allow that the excess pore water pressure caused by the filling of the reservoir is dissipated. The relation L/H is called *drawdown ratio*, where L represents the position of the water level in the reservoir with respect to the crown of the levee at the end of each stage of the drawdown, and H is the height of the levee.

Subsequently, the drawdown phenomenon was simulated considering 5 stages (L/H = 0.2, 0.4, 0.6, 0.8 and 1), starting from level L = 1.2 m up to level L = 6 m (the total drawdown in this study). Each stage represents a time of the drawdown (Δt =

1.2, 2.4, 3.6, 4.8 and 6 days for drawdown rate R = 1.0 m/d and Δt = 12, 24, 36, 48 and 60 days for drawdown rate R = 0.1 m/d). Assuming these data, an iterative analysis was performed modeling in the following way:

i) *Transient-state seepage analysis*.- The variation of water level was evaluated by a transient-state flow analysis and the pore pressures induced by seepage ($p_{seepage}$) were calculated by using the PLAXFLOW program. In this analysis a linear variation of hydraulic head versus time was specified as a boundary condition.

ii) *Deformation analysis*.- The results obtained in the seepage analysis were used by PLAXIS and a deformation analysis in order to evaluate the excess pore water pressure induced by changes in total stresses was then performed.

iii) *Consolidation analysis*.- Finally, the dissipation of excess pore water pressure occurred during the drawdown condition was computed.

iv) *Stability analysis*.- After completing the drawdown stages, stability analyses were carried out for each stage (including the initial steady-state condition) using the results obtained in all previous analyses.

Table 1. Mechanical, hydraulic and rigidity properties of both the levee and the foundation soil.

Property	Unity	Value
γ (soil unit weight)	kN/m^3	20
k (hydraulic conductivity)	cm/s	1×10^{-4} and 1×10^{-6}
c' (effective cohesion)	kN/m^2	10
ϕ' (effective friction angle)	°	20
ψ (dilatancy angle)	°	0
E_{50}^{ref} (secant stiffness for CD triaxial)	kN/m^2	1000
E_{oed}^{ref} (tangent oedometer stiffness)	kN/m^2	1000
E_{ur}^{ref} (unloading/reloading stiffness)	kN/m^2	3000
ν (Poisson's ratio)	---	0.2
P^{ref} (reference stress)	kN/m^2	100
m (power for stress dependent on stiffness)	---	0.7

3.4 *Results of analyses*

With the aim of better understand the drawdown phenomenon, a material having a hydraulic conductivity of $k = 1\times10^{-6}$ cm/s and drawdown rate of $R = 1.0$ m/d was considered to initially study the influence of drawdown ratio on remaining pore water pressure within the levee. Figure 3 shows the progress of the pore water pressure computed at point P_A (which is illustrated in Figure 2), assuming the three drawdown modes mentioned before (Fig. 1). In this figure it can be observed that in the *fully slow drawdown* mode the pore water pressure significantly decreases as a function of the drawdown ratio L/H, whereas in the *fully rapid drawdown* the pore pressure remains constant and is equals to the initial pore pressure (steady-state), because in this case it is assumed that water surface is preserved at the initial level during each time of the drawdown. In the *transient drawdown*, the pore water pressure does not decrease at the same drawdown ratio as in the *fully slow drawdown*, but it is not conserved as high as in the *fully rapid drawdown* case. In this situation, the resulting pore water pressures are not in equilibrium with the new boundary conditions, so a transient flow regime is developed. This is due to the remaining water seepage within the body of the levee momentarily prevents the dissipation of pore pressures generated during the drawdown. In the same Figure 3 it can also be concluded that if an analysis taking into account the distribution of remaining pore water pressures and assuming *fully slow* or *fully rapid drawdown* modes is performed, the safety factors of the slope when external water level changes are underestimated or overestimated, respectively. Therefore, to analyze the stability of protection levees under drawdown conditions is recommended that a transient flow analysis type is applied.

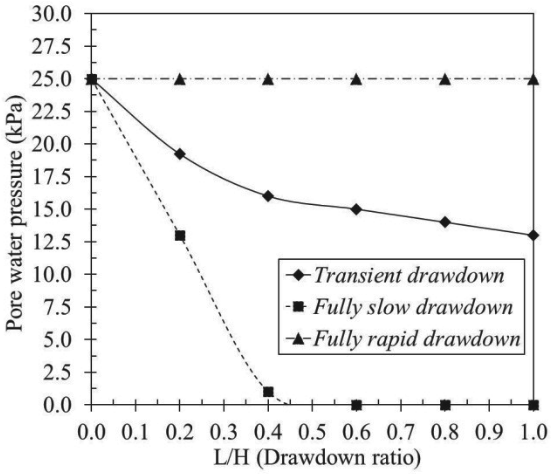

Figure 3. Pore water pressure versus drawdown ratio (L/H) considering different drawdown modes for H=6 m height, $k=1\times10^{-6}$ cm/s permeability and R=1.0 m/d drawdown rate.

Subsequently, the effects of hydraulic conductivity k and drawdown rate R on slope stability were analyzed. Figure 4 illustrates the variation of safety factor (FoS) as a function of the drawdown ratio (L/H) for different combinations of k and R assumed in analyses. From the above figure it can be seen that the behavior of low permeability soils ($k = 1\times10^{-6}$ cm/s) subjected to a relatively rapid drawdown rate ($R = 1.0$ m/d) is very similar to that showed in Figure 1c (the phreatic surface practically remains near the crown of the slope), consequently in this situation it can be supposed a *fully rapid drawdown* condition and an undrained method can be applied for calculations, that is, groundwater seepage analyses can be omitted. For more permeable soils ($k = 1\times10^{-4}$ cm/s) and a relatively slow drawdown rate ($R = 0.1$ m/d), the soil behavior is similar to Figure 1a (the water table practically descends at the same time than the reservoir water level), as a result, in this case a *fully slow drawdown* condition can be assumed and a water flow analysis (uncoupled) can only be utilized for calculations, this is because the excess pore water pressure generated by changes in the total stresses dissipates at the same velocity than the water level in the reservoir decreases. For intermediate conditions concerning to permeability and drawdown rate, calculations cannot be approximated to these two extreme cases, due to the computed safety factors differ from reality. For such cases, it is necessary to apply coupled transient flow-deformation analysis. From Figure 4 it can also be concluded that the dissipation velocity of pore water pressure mainly depends on the permeability of material and the drawdown rate.

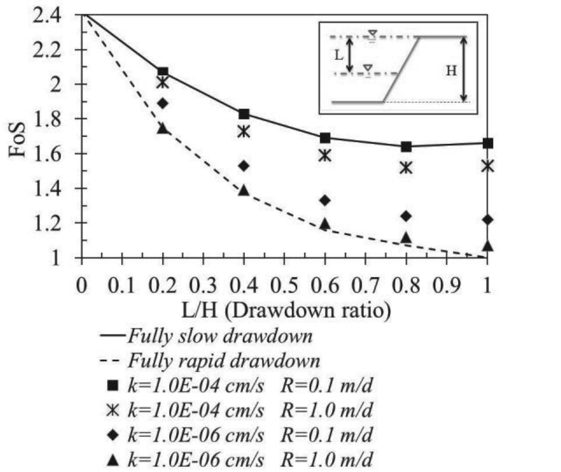

Figure 4. Variation of F○S with drawdown ratio (L/H) for H=6 m height and 2:1 slope.

Finally, the influence of varying the constitutive model and its parameters for predicting horizontal displacements was studied (Fig. 5). The safety factors in the analysis of the analyzed levee were also computed (Fig. 6). For these purposes, two constitutive models were assumed in analyses: Mohr Coulomb (MC) and Hardening Soil Model (HSM).

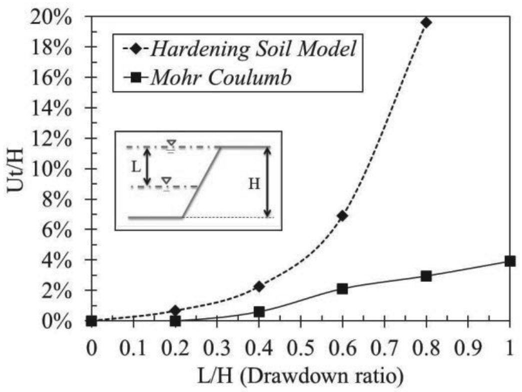

Figure 5. Horizontal displacements at the toe of the slope obtained by MC and HS constitutive models (k=1×10^{-6} cm/s and R=1.0 m/d).

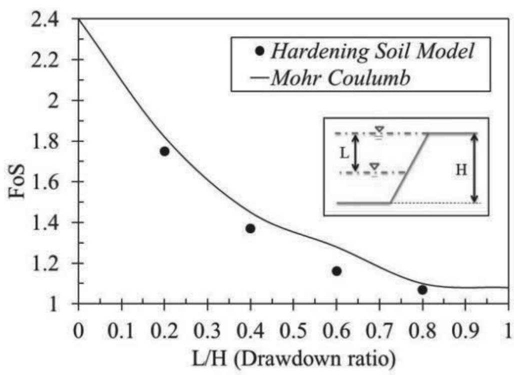

Figure 6. F○S as a function of drawdown ratio (L/H) computed by MC and HS models (k=1×10^{-6} cm/s and R=1.0 m/d).

From results presented in Figures 5 and 6 it can be drawn the following concluding comments:

- During the consolidation phase the MC model exhibits unrealistic horizontal deformations and lower than those obtained by the HSM model, due to: a) the HSM shows a plastic behavior at stress levels lower than the MC (Gens, 2012), b) in the loading and unloading process horizontal stresses in the HSM are larger than in the MC model, and c) the HSM has major peaks values of excess pore water pressure generated during loading or unloading process (Berilgen, 2007).

- When using the phi-c reduction method in combination with advanced constitutive models, these models behave such as the Mohr-Coulomb model, since stresses dependent on rigidity and the behavior obtained due to hardening effects are excluded from the analysis. In this case, the stiffness is calculated at the beginning of the calculation stage and remains constant until the calculation phase is completed.

4 GENERAL CONCLUSIONS

As demonstrated in this paper, the stability of a submerged slope under drawdown conditions (partial or total) is mainly affected by the properties of the material constituting the levee and the drawdown rate and drawdown ratio.

From results of parametric analyses it was observed that the *fully rapid drawdown* condition occurs when the water level of the reservoir descends more quickly than the remaining pore water pressures ($\Delta p_{seepage}$ and Δp_{excess}) are dissipated within the levee precisely caused by the drawdown, and no necessarily due to a total decrease of the water surface in a given period of time (minutes, hours or days). Finally, from slope stability analyses the safety factor was observed to decrease when the drawdown ratio (L/H) increases.

5 REFERENCES

Alonso E.E. and Pinyol N.M. 2008. Unsaturated soil mechanics in earth and rockfill dam engineering. *First European Conference on Unsaturated Soils*. Durham, Balkema.

Berilgen M. 2007. Investigation of stability of slopes under drawdown condition. *Computers and Geotechnics* Vol. 34, 81-91.

Duncan J.M., Wrigth S.G. and Wong K.S. 1990. Slope stability during rapid drawdown. *Proceedings of the H. Bolton Seed Memorial Symposium* Vol. 2, 253-272.

Gens A. 2012. Advanced Course on Computational Geotechnics 2D and 3D (PLAXIS and PLAXFLOW Users), Consolidation Section. UAQ, Santiago de Querétaro, Qro., México.

Griffiths D.V. and Lane P.A. 1999. Slope stability analysis by finite elements. *Geotechnique* 49(3), 387-403.

Huang M.S. and Jia C.Q. 2009. Strength reduction FEM instability analysis of soil slopes subjected to transient unsaturated seepage. *Computers and Geotechnics* 36(2), 93-101.

Lane P.A. and Griffiths D.V. 2000. Assessment of stability of slopes under drawdown conditions. *Journal of Geotechnical and Geoenvironmental Engineering* 126(5), 443–50.

Nian T., Jiang J., Wan S. and Luan M. 2011. Strength Reduction FE Analysis of the Stability of Bank Slopes Subjected to Transient Unsaturated Seepage. *Electronic Journal of Geotechnical Engineering*. Vol. 16, 165-177.

Nagtegaal J.C., Parks D.M. and Rice J.R. 1974. On numerically accurate finite element solutions in the fully plastic range. *Comp. Meth. Appl. Mech. Engng*. Vol. 4, 153-177.

PLAXFLOW Version 1.6 2008. Scientific Manual, Edited by R.B.J. Brinkgreve. *Delft University of Technology and Plaxis bv*. R. Al-Khoury, Plaxis bv and J.M. van Esch, GeoDelft. The Netherlands.

PLAXIS 2D Version 9.0 2008. Scientific Manual, Edited by R.B.J. Brinkgreve, W. Broere and D. Waterman, *Delft University of Technology and Plaxis bv*; The Netherlands.

Sloan S.W. 1981. Numerical analysis of incompressible and plastic solids using finite elements. Ph.D. Thesis. University of Cambridge, U.K.

Sloan S.W. and Randolph M.F. 1982. Numerical prediction of collapse loads using finite element methods. *Int. J. Num. Analyt. Meth. in Geomech.* Vol. 6, 47-76.

Terzaghi K. 1943. Theoretical soil mechanics. Art. 122: Effect of drainage on earth pressure and stability. pp. 338. John Wiley.

Van Genuchten MTh. 1980. A closed-form equation for predicting the hydraulic conductivity of unsaturated soils. *Soil Sci Am J* 44(5), 892-898.

Some Technical Aspects of the Tailing Dam Failure at the Ajka Red Mud Reservoirs

Quelques aspects techniques de la rupture d'une digue de retenue de boues à Ajka

Mecsi J.
University of Pécs, Engineering and Information Technology, Hungary

ABSTRACT: On October 4, 2010 at 12:25 the North-western part of the dam of the no. 10 red mud reservoir in Ajka (Hungary) has collapsed, and near one million m^3 alkaline red mud mixed with water has plunged in the valley of the Torna stream. The red mud flooded the valley-side parts of the village Kolontár and the town Devecser, then trough the Marcal river it has reached the river Danube in very short time. 10 people died, 123 injured, 260 houses became uninhabitable, and significant ecological damage occurred. This presentation aims at providing an informative fact-based description of the complex reasons resulting in dam ruptures.

RÉSUMÉ : Le 4. octobre 2010 à 12:25 la section Nord-Ouest de la digue de retenue du réservoir No 10 de boues rouges à Ajka, en Hongrie, s'écroulait. Environ 1 million m^3 de mélange de boues rouges alcalines et d'eau était déversé dans la vallée du ruisseau Torna. Les boues rouges recouvrirent les bords de la vallée dans le village Kolontár et dans la ville Devecser, puis atteignirent le Danube par le petit fleuve Marcal. Suite à l'accident, 10 personnes ont été tuées, 126 personnes blessées et 126 maisons sont devenues inhabitables. Egalement, les dégâts écologiques furent considérables. Le but principal de cette présentation est de donner une description objective des causes complexes de cette rupture du digue de retenue, basée sur les faits matériels.

KEYWORDS: tailing dam collapse, red mud reservoir,

1 INTRODUCTION

In Hungary three alumina plants have been built. One of them in the vicinity of Ajka town has been operational since 1942, and collected red mud in a reservoir in the valley of the Torna stream. The product of alumina production, 15.7 million m³ of red mud was deposited in 10 reservoirs in the valley of the Torna stream. The red mud is a waste product of the Bayer process. Bauxite is crushed and ground in mills and heated; alumina is precipitated by washing the bauxite with a hot solution of sodium hydroxide (NaOH) under pressure.

Fig.1.The site and affected localities, (http://www.bbc.co.uk/news)

Around 24-45 percent of red mud is ferrous oxide, but it also contains other metallic compounds. Red mud is not poisonous, but it is a hazardous material, due to its sodium hydroxide content. This highly alkaline (pH 12-13) material was transported by pipeline to reservoirs.

On October 4, 2010 the northwestern part of the dam of red mud reservoir No. 10 has collapsed, and near one million m^3 alkaline red mud mixed with water has plunged in the valley of the Torna stream. Fig. 1.-Fig4.

Fig.2. Natural-color satellite image of the area surrounding the spill

Fig.3. Natural-colour satellite image of the area surrounding the spill (http://redsludge.bm.hu)

The red mud flooded the valley-side parts of the villages, then trough the Marcal river it has reached the river Danube in very short time. 10 people died, 123 injured, 260 houses became uninhabitable, and significant ecological damage occurred.

Fig.4. Aerial photo with the flooded territory of Kolontár (photo: MTI)

2 GENERAL CONDITIONS

The embankment of the reservoir in question must be examined as part of the entire reservoir system, as the different parts of the system have a mutual impact on each another. The tragic tailing dam failure of the north-western corner of reservoir No. 10 highlighted the importance of a complex analysis.
Important aspects of the study are:

- the geological-geotechnical conditions and the morphological properties of the area;
- the conditions changed as a result of favourable technical interventions or technical interventions believed to be favourable;
- the extreme weather, precipitation and dynamic wind load conditions;
- the specific features of the substance stored in the reservoirs;
- the resistance reducing effects of pressures due to the transition of the substance from a more favourable condition to an unfavourable state of liquefaction;
- the different rigidity properties of the unfavourable embankment connections;
- and several other factors that could not have been considered by earlier regulatory systems.

3 HYDROGRAPHICAL AND SUBSOIL CONDITIONS

Figure 5 shows the subsoil conditions of the area based on detailed soil tests performed between 1975 and 1980. The territory had a basin-like character, fill with course gravel and sand and cover fine sand and silt, hence is had a swampy character, collected the water. The gravel terrace is gradually thinning towards the northern embankment. The „gravel basin" is bounded by a soft, easily liquefiable sludge layer of a plasticity index of Ip=6.8-8.5% and a water permeability of $k=10^{-5}$ cm/sec.
In the year 1989 soil excavations and geophysical measurements were conducted at the leg of reservoir No. 10.'s tailing dam, and the soil profiles were recorded. Figure 6 shows the soil profiles near the north-west corner. It is important to remark that near the north-west corner of reservoir No.10 sand-silt soils are to be found, and sandy-gravel layers above the fat clay. This soil layer unfavourable is that in fine sandy-silt fractions may move under higher water pressure conditions.

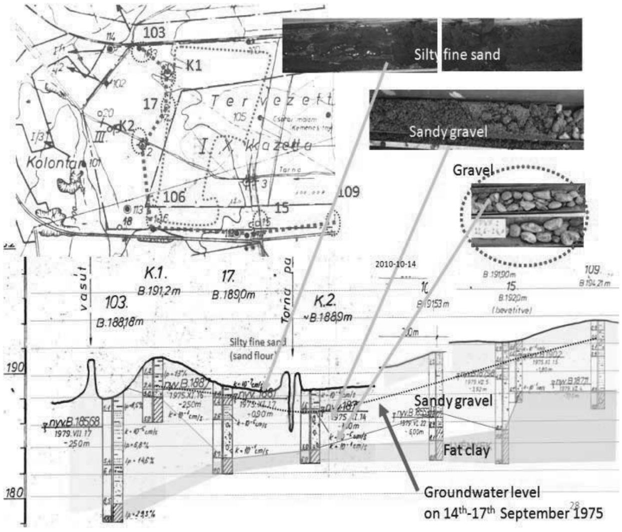

Fig.5. Illustration of the subsoil conditions of the reservoir system based on the original plans.

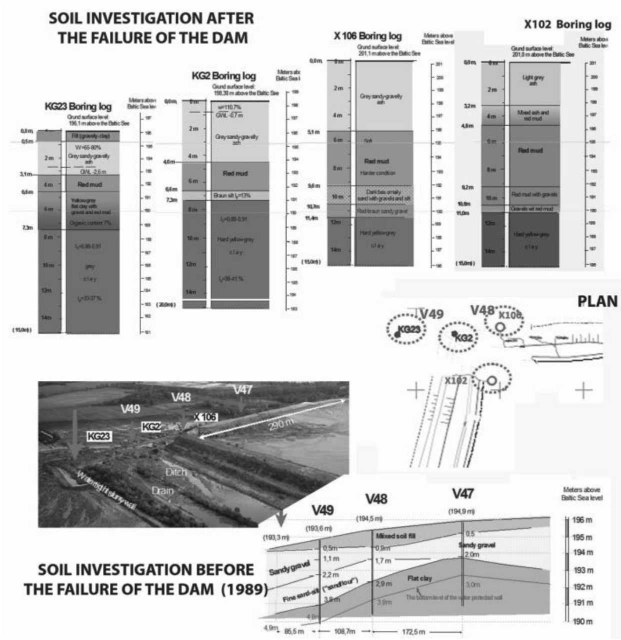

Fig.6. Soil profile near the West –North corner of the reservoir No. 10.

As a result, grain size becomes coarser on the inner side, while a „clay plug" may develop towards the edge of areas in motion. Such a clay plug is characterized by a sudden movement under a significant change in pressure and consequently a mudflow-like grain movement may evolve. Such a process may be extremely fast and unexpected.

4. THE CLOSURE OF THE RESERVOIRS

Water pollution was detected in the groundwater monitoring wells near the reservoir system in the 1970s–1980s. In compliance with the regulatory requirements, a watertight slurry wall was constructed to close down the southern and the western sides of the reservoir. Figure 7.
Later, as the pollution spread over towards the north, the construction of a new type of grout curtain was started around the reservoir system in 1999. Depths of 6.0-9.0-12.0 m appear on the south-eastern side.

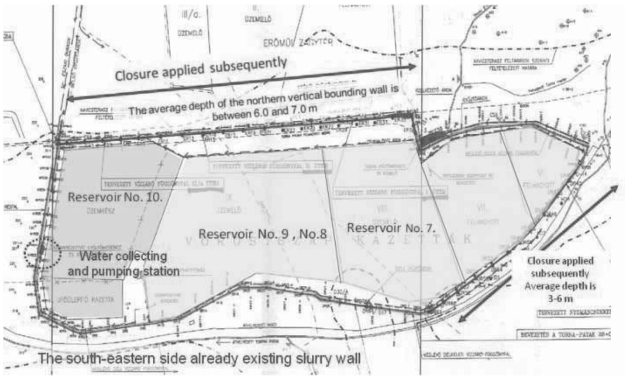

Fig.7. Soil profile near the West –North corner of the reservoir No. 10.

5. THE EMBANKMENTS MATERIAL

The boundary embankments show some special features. As they were made of slag and ash from the power plant, their weight is relatively low. Fig.8.

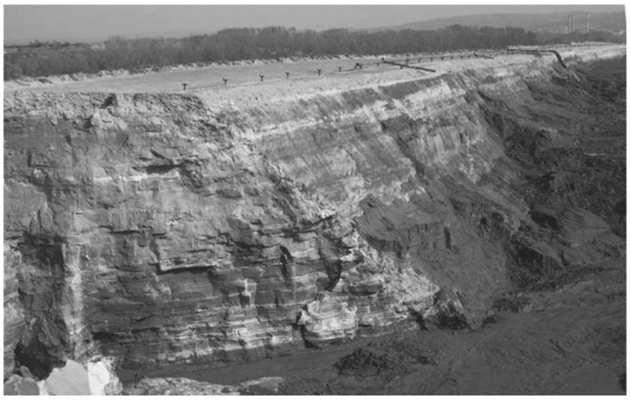

Fig.8. Material of the northern embankment of Reservoir No10 after the embankment failure.

Their average density is ρ= 1.5-1.55 gr/cm^3, while their dry density is ρ_s= 0,7-0,8 gr/cm^3, which is lower than that of water. The embankment is quasi-saturated with water. Due to the hydraulic chemical bond, the embankment is characterised by a relatively large strength. As a result of the construction technology applied, the embankment is layered and is of inhomogeneous structure, which manifests both in its strength and its water permeability characteristics.

6. PROPERTIES OF THE “RED MUD”

The description of the substance as „red mud” is not appropriate in terms of soil mechanics, as considering plasticity index, it belongs to the group of substances of medium to high plasticity and should be described as medium and fat clay.
Chemical effects, such as that of sodium hydroxide added to the swollen clay in the course of the technological process, may also have a role in the special behaviour of “red mud”.
It can conclusively be stated that the substance shows special thixotropic behaviour, it does not easily lose its water content and assumes the behaviour of a thick, plastic liquid upon significant loading. (Asbóth et al 1982.)

7. PRECIPITATION DATA

Comparing the total precipitation of the period between January and the end of September 2010 was 907÷980 mm, comparing the average of the 2000-2009 years data 513÷567 mm with 121÷131 mm standard deviation. (Fig 9.)

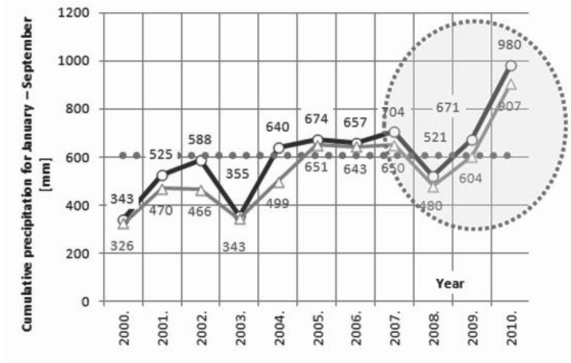

Fig.9. Total precipitation data in the 1st– 3rd quarter year between 2000 and 2010.

8. WIND SPEED AND WIND DIRECTIONS

The prevailing wind direction in the vicinity of Reservoir No. 10 is northern–north-western as shown in the wind direction frequency chart. Wind parallel with the direction of the embankment failure is very rare (Figure 10).

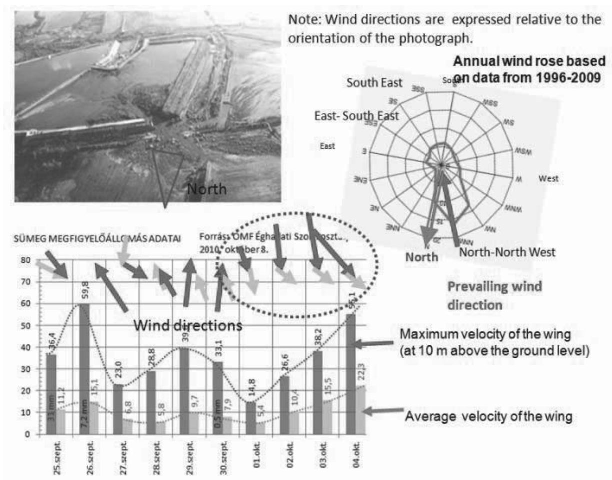

Fig.9. Vectors of prevailing wind directions and wind speeds between September 25.

Peculiar wind conditions were observed in the area between September 25 and October 4. Between October 1 and 4, a gradually strengthening, unfavourable wind speed toward the direction of the embankment failure was accompanied by casual wind gusts (Weather data services, National weather Services, October 8, 2010). The observations of the wind direction and speed were at 10 m over the ground surface, but the top surface the reservoir is 23-24m. It is mean that the wind speed in site should be significant more than the measured value. The highest wind speed values were measured on October 4, with an average of 22 km/h and occasion wind gusts of 60 km/h.
There is reason to assume that these unusual wind direction and wind speed conditions contributed to the development of the embankment failure. The sucking effect of the wind on the northern side of the embankment must be taken into consideration.

8. CIRCUMSTANCES OF THE EMBANKMENT FAILURE

The area is located in the lowest part of the drainage basin of the Torna stream, i.e. in the valley of the stream. In its original condition, the area, together with the subsurface stream valley formed a surface and subsurface water flow unit which was very sensitive to weather conditions. The area had been gradually involved in and shaped by industrial operations, through the construction of surface and subsurface structures. The northern, so called intermediate embankment of Reservoir No. 10, constructed in a smaller size with a view to the possible extension of the reservoir system, served as an external, i.e. boundary embankment. As a result, it was the surface run-off and flow conditions that were first changed significantly by the industrial use of the area in the stream valley.

It can be concluded that according to an engineering approach to finding the causes, the failure of the rigid embankment of large bearing capacity was a combined result of a number of unfavourable conditions.

The base width of the northern embankment is significantly different from the size of the other embankments, as it was considered a temporary structure, bearing in mind the possibility of a future extension. The slightly more than 20 m height of the solid part of the embankment is lower than the 26–27 m heights of the other embankments. Its effect manifested at the northern embankment – being by 25 m less in base width than the western embankment – as the resistance against displacement here was significantly lower, and also because the rigidity of the western and northern embankments showed significant difference at an unfavourable connection at the corner of the reservoir. (Figure 10.)

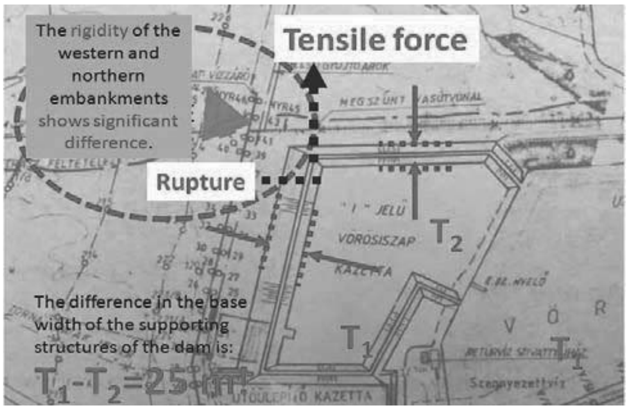

Fig.10. Dimensions of the western and southern dams.

The geotechnical conditions were determined by the fact that at the northern boundary embankment of the reservoir there are beds of easily liquefiable muddy fine sand (or sand flour as described earlier) in a layer of 3-4 m located in the closest vicinity of the critical corner of the reservoir, adjacent to a sandy-gravelly layer.

Significant pore water pressure may have developed in the soil layer underlying the embankment as a result of the geological properties of the enclosed gravel terrace functioning as a drainage basin and due to extremely high precipitation levels causing high water pressure conditions.

The increase of load on the slope surface of the embankment might have contributed to the excess load – and the increase of soil stress – in the subsoil on the inner side and as a consequence, to excess subsidence, while it probably caused a slighter rate of expansion on the outer side due to the rigid body like movement of the embankment.

The extremely rigid but light embankment and the soft, liquefiable subsoil provided highly unfavourable static conditions.

The liquefaction property and special thixotropic behaviour of the “red mud” may have also contributed to the disaster.

Chemical effects, such as that of sodium hydroxide added to the swollen clay in the course of the technological process, may also have a role in the special behaviour of “red mud”.

The extremely unfavourable wind direction and wind speed conditions may have given a final push toward the very sudden embankment failure.

It is also an important factor for the stability of the dam, that by what kind of filling technology is used. In what magnitude and distribution of water heights may occur within the area of the reservoir?

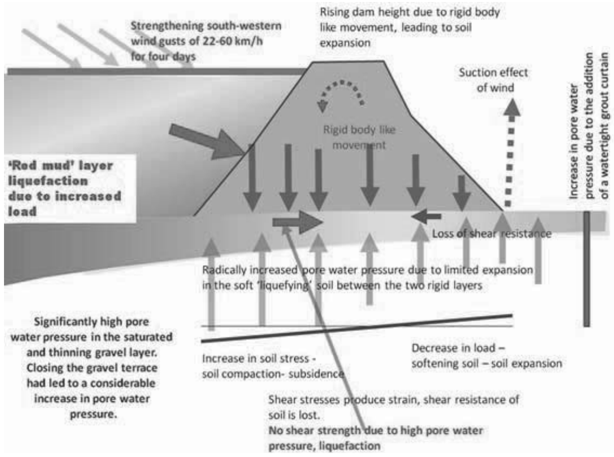

Fig.10. Summarizing some effects for the dam failure

The list of contributing factors could be further extended and it will readily be conceived that it is the accumulation of unfavourable conditions that led to the sudden rupture of the embankment.

9. SUMMARY CONCLUSIONS

The present study aims to provide a background to a non-exhaustive list of factors contributing to the embankment failure, while attempting to give a clear picture of the complex technical conditions.

The rupture of the embankment and the highly serious disaster emerging thereof serve as a lesson in several aspects for professionals performing technical or legislative tasks, as well as for those working in the area of the administration of justice and performing official control duties.

It is not an aim of the present study to identify scapegoats for the incident.

The findings and conclusions derived from the examinations may be further refined and supplemented in the future in light of further facts and data yet to be revealed.

The objective of the author of the present analysis is, led by deep sympathy for the victims and those who suffered damage, to provide an insight into the technical causes and the circumstances of the tragic incident, as well as to promote, with a humble approach to sciences, all endeavours to avoid such disasters in the future.

9. REFERENCES

Asbóth, J. et al (1982) Geotechnical aspects of hydraulic spoil banks, *Civil Engineering Review, Volume XXXII, 12/1982, pp. 538-546.*

Mecsi J. [2011]. “Red mud disaster - facts without comments- In Collapse Understanding to Solution Book (In Hungaian), *Edited by: J. Mecsi, Mérnöki Kamarai Kiskönyvtár 2nd edition ISBN 978-963-88358-1-9, ISSN 2062-5081 pp. 159-166*

Mecsi, J. (2012) Expert opinion on the examination of the embankment between Reservoirs No. 10 and 9) ME-SZI Engineering Expert Office. József Mecsi, October 15, 2011. (In Hungarian.)

Mecsi J. [2012]. “Engineering analysis of the Tragic Damage of a Reservoir dam *16th International Conference on civil Engineering and architecture Hungarian Technical Scientific Society of Transylvania, ISSN 1843-2123 pp. 263-271 (In Hungarian)*

The Design of Filter Materials and their Importance in Geotechnical Engineering

La conception de matériaux filtrants et leur importance en géotechnique

Messerklinger S.
Consulting Engineers, Poyry Energy Ltd., Zurich, Switzerland

ABSTRACT: The presence of water has a major influence on the design of soil structures as it reduces the effective stresses and hence shear resistance, and applies seepage forces in case of flow. This key topic is well known to every geotechnical engineer and the design principle for soil structure is to drain groundwater, infiltrated surface water or seepage water in a controlled manner from the soil. However, for soil structures whose purpose is to retain water, such as embankment dams impounding a reservoir, or dikes for flood protection along rivers and channels, both sealing and draining have to be ensured by the structures. With simple construction measures such as filter and drainage zones incorporated in earth structures composed of selected and treated materials, the stability and safety of these structures can be improved considerably. This paper discusses seepage control measures as well as the selection and design of appropriate filter materials.

RÉSUMÉ : La présence d'eau a une influence majeure sur la conception d'ouvrages géotechniques, car elle réduit les contraintes effectives et la résistance au cisaillement et donc applique des forces d'infiltration en cas de débit. Le sujet abordé est bien connu des ingénieurs en géotechnique. Le principe de conception des ouvrages est de drainer les eaux souterraines, les eaux de surface infiltrées ou les eaux d'infiltration de manière contrôlée à partir du sol. Toutefois, pour les ouvrages dont le but est de retenir l'eau, comme les barrages de retenue en remblai ou les digues de protection contre les inondations le long des rivières et des canaux, l'étanchéité et le drainage doivent être intégrés dans les ouvrages. Avec de simples mesures constructives telles que de des zones de filtrage et de drainage dans des ouvrages en terre, et composées de matériaux séléctionnés et traités, la stabilité et la sécurité de ces ouvrages est considérablement améliorée. Le présent document examine les mesures de contrôle d'infiltrations dans les ouvrages et la sélection et conception de matériaux filtrants appropriés.

KEYWORDS: filter design, seepage control, embankment dam failure

1 INTRODUCTION

1.1 *Effect of water in soils*

Soils are composed of single particles. The loads are transferred at the particle contacts with normal and shear forces[1]. The maximum shear force which can be transferred at the particle contact is proportional to the effective normal force at the contact, as defined by the total interparticle force and the pore water pressure, should the soil be saturated. The porewater pressures can correspond to the (a) hydrostatic head, should the soil skeleton be submerged, or (b) to an excess pressure which exceeds the hydrostatic head. Excess pressures develop for example (a) in loose deposits of low permeable granular soils, such as silts and fine sands, during an earthquake event (see e.g. Messerklinger et al., 2011a) or (b) by the application of an external load, e.g. during construction work, on compressible and low permeable soils such as clays and silts.

Summarizing: The water of a submerged soil skeleton reduces the effective interparticle forces and hence the shear resistance of the soil.

If the water in the soil skeleton is flowing with a velocity (v) at a hydraulic gradient (i), forces due to water flow are applied on the soil particles. These flow forces on the soil particles act in addition to the pore water pressures. The flow forces (F) act in the flow direction. Their magnitude is $F=i \cdot \gamma_w \cdot A$ where γ_w is the unit weight of the water and A is the cross-sectional area (in flow direction) of the soil body the water is flowing through. This is the average force on a soil body due to water flow at a hydraulic gradient of i. However, the flow forces acting on a single particle vary significantly. The flow velocity of the water in the pore space depends on the pore diameter and increases approximately with the square of the pore diameter. If the pore diameter changes, the pore flow velocity will also change. However, in permeability tests only the overall soil permeability, as defined by the permeability coefficient (k), is determined.

Summarizing: In case a hydraulic gradient is applied to the water in a submerged soil skeleton, the water will flow around the single particles, which applies flow forces in flow direction. These flow forces depend on the hydraulic gradient and are independent of the volume of water flowing through the soil.

1.2 *Effect of water on natural or man-made soil structures*

These effects of water on the soil influence the stability of soil structures, irrespective of whether they are natural or man-made. Natural soil structures are for example: (i) soil slopes; (ii) in-situ soils surrounding a man-made excavation or (iii) soil foundations of buildings or embankment dams. Man-made soil structures are for example the embankment dams[2] themselves. Subsequently, the effect of water on the stability and safety of such structures is discussed.

[1] For clays interparticle forces can act in addition to contact forces. The contact forces are defined by the self-weight of the soil and the external loads. Interparticle forces are e.g. (i) electromagnetic attractions, which are commonly called van der Waals forces or (ii) electrostatic repulsive or attractive forces at double layers.

[2] Note: Embankment dams can be used for different purposes such as road embankments, landfills, off-shore embankments e.g. for sea water intakes, shore protection or embankments surrounding reservoirs.

1.2.1 *Soil slopes*

Natural soil slopes are subjected to the natural groundwater flow conditions, and are formed of the given in-situ soil material which may have predefined slip surfaces with reduced shear strength, due to previous slides. These were subjected to earthquakes and weather conditions typical in the region and have correspondingly an overall factor of safety for slope stability of somewhat above one.

Constructing in or on natural soil slopes either reduces the resisting forces, e.g. by excavation, or applies driving forces, e.g. when structures are founded on the slope. For slopes within or next to man-made structures an overall factor of safety of well above one is desirable. Hence, the stability of natural slopes next to or within the construction area normally has to be improved.

The stability of slopes can be improved by man-made structures which apply resisting forces such as anchors, piles, etc. Or the slope stability can be improved by lowering the groundwater level in the slope to increase the effective stress and hence shear resistance at the drained soil. The water level can be lowered by drainage, e.g. with borings filled with filter and drainage materials and free or pumped outflow (see e.g. Messerklinger 2012).

1.2.2 *Soils surrounding a man-made excavation*

The excavation in saturated soil can be surrounded by an (i) impermeable or (ii) a permeable wall. For an impermeable wall, both the earth pressure and the water pressure act on the wall, and the pressure can be in the order of two to three times that for a permeable wall, on which only the effective earth pressure is acting. Lowering the water level behind the wall, e.g. by pumped wells or by drainage into the excavation pit, reduces the loads on the wall. However, this imposes a hydraulic gradient on the in-situ soil surrounding the excavation. This hydraulic gradient applies flow forces on the particles of the soil and these forces can cause transport of fine soil particles within the coarse soil particle skeleton for internally unstable soils (criteria see Chap. 2). At the surface where the water leaves the soil body, e.g. at the pumped drainage well or at other drainage points, the soil can be eroded unless the surface is protected with a filter and drainage material.

1.2.3 *Soil foundations of a dam impounding a reservoir*

With the impounding of the reservoir a hydraulic gradient and water pressure are applied on the soil foundation. The increased hydrostatic water pressure reduces the effective stresses and hence strength of the soil. The imposed hydraulic gradient applies flow forces onto the soil particles which can cause erosion within the soil skeleton or at the surface of the soil body where the water flows out of the soil. A layer of filter material at the water exit below a layer of drainage material will prevent erosion of soil particles and increase the effective stress. Examples are presented in Messerklinger et al. 2010 and 2011b.

1.2.4 *Man-made embankment dams for reservoirs*

With the impounding of the reservoir the hydraulic gradient and the water pressure are applied onto the man-made earth fill. Man-made earth structures allow for the placement of filter and drainage zones within the dam body. This is normally supported by a zone of reduced permeability (e.g. clay, concrete, asphalt, geomembrane) which reduces the volumes of water flowing through the structure (see Messerklinger 2011c). The incorporation of filter materials assures the stability and safety of embankment dams.

1.3 *Summary*

Water has a major influence on the stability and erosion resistance of natural and man-made soil structures as it reduces the effective stress and hence shear strength of the soil and applies forces in case water is flowing through the soil.

Hence, draining the water out of the soil structures improves their stability or the stability of structures built on or in the soil.

However, draining of the soil has to be done in a controlled manner. The hydraulic gradients and hence flow forces applied on the soil particles must not erode particles within the soil skeleton or at the surface.

For natural soils, this is assured by limiting the hydraulic gradient. For man-made structures the erosion is controlled by filter zones incorporated in the soil structure. The design of suitable filter materials is discussed in the next chapter.

2 DESIGN OF FILTER MATERIALS

For the design of state-of-the-art filter materials, the following six aspects are considered: (a) Filter ability (b) Internal stability (c) Self healing (d) Material segregation (e) Drainage capacity (f) Material durability.

2.1 *Filter ability*

With the identification of effective stresses in soils by Terzaghi and his co-workers in the early thirties of the last century, (Terzaghi 1936) a new era in soil mechanical engineering was initiated. This was the time when the effects of water on soil were investigated in depth, and resulted in the development of the consolidation theory (Terzaghi & Fröhlich 1936).

At the same time, Bertram (1940) proposed the criterion $D_{15\text{filter}}/d_{85\text{base soil}} \leq 6$ for soil filters based on laboratory investigations. This filter criterion was later modified to $D_{15\text{coarse-side filter}}/d_{85\text{fine-side base soil}} \leq 4$ and a drainage criterion of $D_{15\text{fine-side filter}}/d_{85\text{coarse-side base soil}} \geq 4$ was added by Terzaghi and Peck (1948), (Fig.1). These filter and drainage criteria were used for decades and are still today subjects lectured on to the bachelor and master students.

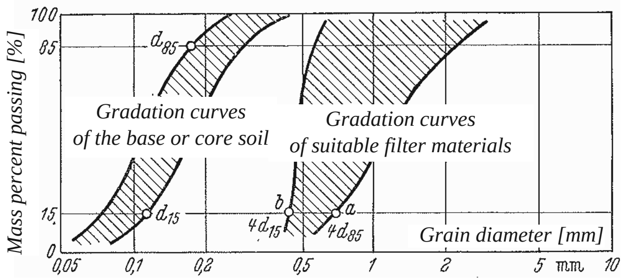

Figure 1: Filter and drainage criteria from Terzaghi & Peck (1948).

The filter design was reconsidered after incidents at and failures of major dam structures. E.g. after the Balderhead dam incident, where core material was eroded from an open fracture in the core zone into the filter material so causing sinkholes at the dam crest (Vaughan et al. 1970), Peter Vaughan and his co-workers searched for what they called the “perfect filter”. The idea was to hold back the smallest grain of a core material even under severe conditions such as concentrated seepage flow at high hydraulic gradients through e.g. a crack in the core. The approach towards the criterion was not via the gradation curve, such as adopted before by Terzaghi and his co-workers, but by the permeability coefficient of the filter material. Vaughan believed that “*..effectiveness of a filter may be defined by its permeability with more generality than by its grading.*” (Vaughan & Soares 1982, p.17). They proposed a linear correlation between the permeability coefficient (k in m/s) and the filtered particle diameter of $k = 6.1E\text{-}6 \cdot \delta^{1.42}$ (δ in µm, Note: The particle size of clays with flocculated structure is the floc-size.).

At the same time, James Sherard was investigating the cracking and failure of embankment dams built in the United States (Casagrande 1950, Sherard et al. 1963, Bertram 1967). In 1973 he wrote (p. 272): “*… at present it is well known that cracks have developed in the impervious sections of many dams*

…". He identified that the cracking was mainly caused by differential settlement of homogenous clay dams or by hydraulic fracturing of the core material due to the water pressure after impounding of the reservoir.

Numerous filter tests were performed (Sherard et al. 1984a), and based on the slot test data (Sherard at el 1984b) four soil categories with four individual filter criteria were identified:

1.) Sandy silts and clays (d_{85b}: 0.1-0.5 mm): $D_{15f}/d_{85b} \leq 5$
2.) Fine-grained clays (d_{85b}: 0.03-0.1 mm): $D_{15f} \leq 0.5$ mm
3.) Fine-grained silts (d_{85b}: 0.03-0.1 mm): $D_{15f} \leq 0.3$ mm
4.) Exceptionally fine soils ($d_{85b} < 0.02$ mm): $D_{15f} \leq 0.2$ mm

With the non-erosion filter test the filter criteria were further developed and termed criteria for "critical filter" (Sherard & Dunnigan 1985, 1989) as distinct from the "perfect filter" discussed above. For the critical filters four categories were defined based on the fines content (<0.075 mm, sieve 200) of the base soil (or core material). The fines content was determined on a gradation curve with a maximum grain diameter of 4.75 mm (sieve 4). For base soils with a maximum grain size exceeding 4.75 mm, the gradation curve was regraded to ≤4.75 mm in order to determine whether the base soil falls into category 1, 2 or 4. Whether the base soil falls into category 3 was determined on the original, non-regraded curve. For each of the 4 categories a filter criterion was defined (Tab. 1). These criteria still apply today. The current design approach is to use the conservative values of these criteria, as given in the right column of Tab. 1.

Table 1. Filter criteria.

Soil group	*Fines content <0.075mm*	*Filter criterion determined by tests after Sherard & Dunnigan (1989)*	*State-of-the-Art criteria in dam engineering*
1	85-100	$D_{15f} = 7d_{85b}$ to $12d_{85b}$	$D_{15f} \leq 9d_{85b}$
2	40-80	$D_{15f} = 0.7$ to 1.5 mm	$D_{15f} \leq 0.7$ mm
3	0-15	$D_{15f} = 7d_{85b}$ to $10d_{85b}$*	$D_{15f} \leq 4$ to 5 d_{85b}‡
4	15-40	Intermediate between group 2 and 3	Intermediate between group 2 and 3

*For subrounded grain shape 7 and for angular grains 10.
‡ Incorporates a factor of safety of two.

2.2 *Internal stability*

For filter materials to be internally stable means that within the soil skeleton the small particles do not move due to water flow forces. All soil particles should remain at their position even for water flow at high (>>1) hydraulic gradients such as occur at a fracture in the sealing zone of an embankment. A good definition of internal stability is given e.g. by Kenney & Lau (1985): "*Internal stability of granular material results from its ability to prevent loss of its own small particles due to disturbing forces such as seepage and vibration.*" In more recent literature, the term internal stability is used in a much broader sense[3]. However, in this paper the term will be used for the filter material design, and the internal stability of natural soils (in the foundation or dam fill) will be discussed at the end of this chapter.

Concerning the formation of sinkholes at the crest of zoned embankment dams, James Sherard (1979) studied the phenomenon and recommended use of a method proposed by Prof. Victor de Mello (1975) for the investigation of gap-graded soils, in order to assess the internal stability of filter materials.

In this method, which is also called "retention ratio criterion", the gradation curve of the filter material is divided into two curves at a selected grain diameter (d_S), gradation curves for the portions finer and coarser than d_S, respectively. For the two gradation curves the retention ratio (R_R) is calculated from the Terzaghi filter criterion: $R_R = D_{15f}/d_{85b}$. This is repeated for different values of d_S. All grains are considered to be stable if they satisfy the criterion $R_R \leq 7 \div 8$ for subrounded grains or $R_R \leq 9 \div 10$ for angular grains. The grain diameters (d_S) for which the retention ratio exceeds the given limits are potentially unstable and can be eroded by the water flow. Using this criterion to identify stable materials shows that gradation curves with a more or less straight line in the semi-logarithmic plot are stable.

Experimental investigations performed by Kenney & Lau (1985 and 1986) lead to a strict criteria in which the gradation curve of the fine part of the filter material (0<M%<30) should be on the more uniform side of the Fuller curve and the gradation curve of the coarser part of the filter material (30<M%<100) should be on the more uniform side of a straight line in the semi-logarithmic plot with a uniformity coefficient of $C_u \leq 12$ (Kenney & Lau 1986).

With this criterion, rather uniform filter materials are defined as internally stable. Such materials can be produced for man-made structures but they are rare in nature e.g. in soils present in the foundation of dams. Hence, for the assessment of natural soils with respect to internal stability, the approach is not to define the gradation but the critical hydraulic gradient. These studies were first done in Russia with the start of the construction of large run-of-river power plants in the 1920s (e.g. Pavlovsky 1922). Patrashev (1965) proposed a suffusion criterion and Pravedny (1976) a criterion for contact erosion. These criteria are not further discussed in the present paper as they are not applied for the design of man-made filter materials.

2.3 *Self healing*

Self-healing means that cracks which can form in the filter zone due to e.g. differential settlement, etc. do not stay open but close in case of water flow. Hence, the filter material must not have cohesion. This is assured by limiting the content of non-plastic (I_P<5%) fines to less than 5% (the latest ICOLD Bulletin on CFRD's, No. 141, allows 7% of fines). The sand-castle test (Vaughan & Soares 1982), confirms that the selected filter material meets the self-healing requirements.

2.4 *Material segregation*

When the filter material segregates, meaning that the coarser particles separate from the finer particles, the filter zone can no longer fulfill its purpose of preventing fine particles moving from the core to the filter zone or within the filter zone, because the segregated coarse grained components do not form a filter to the adjacent materials. Hence, the segregation of filter materials has to be avoided. Whether a material segregates depends on the handling and placement methods and on the gradation of the material. In the 50's and 60's of the last century, segregated material zones were improved manually. Later, the focus was put on the selection of appropriate gradation curves. One of the first discussions on segregation criteria is given in Sherard et al. (1984b) where they proposed a coarse boundary for filter materials (see also Fig. 2). It was generally agreed that a high content of sand and a small maximum grain size reduces the segregation. Based on observations and laboratory investigations (e.g. Sutherland 2002) a stricter criterion was presented by Milligan (2003), which specifies that wetted filter material with a gradation finer than the limit curve given in Figure 2 should be selected. The latter criterion is nowadays commonly applied.

[3] Fell and his co-workers in Australia (e.g. Foster and Fell 1999) discussed internal erosion by investigating the erosion process within the soil structure. They divided the erosion process into four steps: (i) initiation (ii) continuation (iii) progression (iv) breaching/ failure. The term internal erosion was divided into four sub-categories: (a) Concentrated leak erosion (b) Backward erosion (c) Contact erosion (d) Suffusion. These four sub-divisions were taken over by the latest ICOLD Bulletin "*Internal Erosion of existing Dams and their Foundations.*" Hence, what was previously termed internal stability of filters now falls into the sub-category (d) Suffusion.

2.5 *Drainage capacity*

The Terzaghi criterion $D_{15f}/d_{85b} \geq 4$ still applies and Sherard recommends $D_{15f} \geq 0.2$ mm.

2.6 *Material durability*

The durability of filter materials is typically investigated with standard tests such as the Los Angeles abrasion test (ASTM C535) or the wet and dry strength variation (typical limit $\leq$35%). However, for important dam structures a mineralogical and chemical investigation of the dam material is recommended. This can highlight if the material has inclusions of (i) swelling clay minerals or (ii) minerals which dissolve in water, e.g. gypsum or carbonate rocks. Latter materials cannot just dissolve but also re-cement at the particle contacts and create true cohesion. Materials with carbonate and sulphide content should be used with care for dam filter materials.

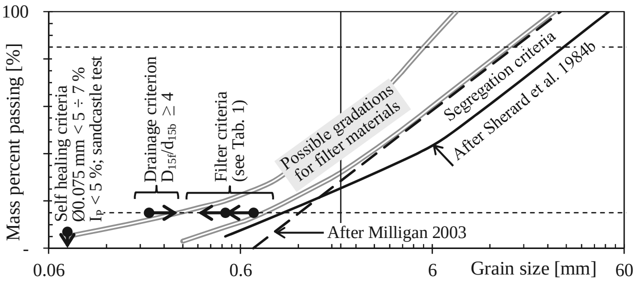

Figure 2: Summary of filter criteria.

3 CONCLUSIONS

Water has a major influence on the stability and erosion resistance of natural and man-made soil structures. Draining the water out of the soil structure improves its stability. However, draining of the soil has to be done in a controlled manner without erosion. This is achieved with filter materials placed in or on the soil structures. Filter materials have to have certain properties which are described by filter criteria, significant development of which took place during recent decades. Nowadays, these filter criteria are composed of six different parts and for each of these criteria are defined which have been discussed in this paper in detail.

Despite of all the efforts in filter design a significant number of failures still occurs due to erosion. Embankment dam failures are given e.g. in the ICOLD Bulletin "*Internal Erosion of Existing Dams and their Foundation*". About 4 of 10'000 large dams fail per year and 2 of these failures are caused by internal erosion. Overall about one embankment dam in 180 fail during its lifetime.

A recent example is the failure at the Prudencia hydro-power plant in Panama, where a homogenous dam made of residual soils failed at the contact to a concrete gravity structure. Neither in the dam body or at the dam toe, nor at the contact to the rigid concrete wall, was any filter material placed. This supported the failure mechanism which was triggered in the first place by leakage in the geo-membrane sealing (Messerklinger, 2013).

Although the design of filter materials and their application to soil structures is tought in undergraduate classes and is well known to geotechnical engineers, the lack of the design and placement of filter materials still causes numerous failures. Hence, further efforts on the selection of appropriate filter materials and their incorporation in soil structures are essential.

4 REFERENCES

Bertram, G.E. 1940. *An Experimental Investigation of Protective Filters.* Harvard Soil Mech. Series No.7.

Bertram, G.E. 1967. Experience with Seepage Control Measures in Earth and Rockfill Dams. *9th ICOLD Congress, Istanbul,* Vol. 3: 91.

Casagrande, A. 1950. Notes on the Design of Earth Dams. *J. Boston Soc. Civil Eng.* Oct. 1950, Vol. 37.

DeMello, F. 1975. Some lessons from unsuspected, real and factitious problems in earth dam engineering in Brazil. *6th Regional Conf. on Soil Mech. & Found. Eng.*, South Africa (11): 304ff.

Foster M. & Fell R. 1999. *A framework for estimating the probability of failure of embankment dams by internal erosion and piping using event tree methods.* UNICIV Report No. R-377, School of Civil and Environmental Engineering, Univ. New South Wales, Sydney.

Kenney, T.C. & Lau, D. 1985. Internal stability of granular filters. *Can. Geotech. J.* (22): 215-225.

Kenney, T.C. & Lau, D. 1986. Internal stability of granular filters. Reply. *Can. Geotech. J.* (23): 420-423.

Messerklinger, S., Brenner, R.P. & Zegele, Z. 2010. Safety and Maintenance Issues for a Long Embankment on a Karstic Foundation under Artesian Pressure. *2nd Int. Conf. on Dam Maintenance and Rehabilitation*, Zaragoza: 325-334.

Messerklinger, S., Straubhaar, R., Brenner, R.P., Herzog, R., Laue, J. & Springman, S.M. 2011a. Large-Scale Cyclic Triaxial Tests for the Seismic Safety Assessment of a high Earth Core Rockfill Dam. *15th ECSMGE*, Athen, 1171-1176.

Messerklinger, S., Brenner, R.P. & Zegele, Z. 2011b. Long-term Seepage behaviour of an Embankment dam founded on Rock Strata under Artesian Pressure. *Int. Symposium on Modern Technologies and Long-term behaviour of Dams*. Zhengzhou, China: 429-438.

Messerklinger, S., Aemmer, M. & Straubhaar, R. 2011c. Heightening of the Göscheneralp Earth-core Rockfill Dam. *Int. Journal on Hydropower & Dams*, 8(3): 43-50.

Messerklinger S. 2012. Erosion and Drainage Well Blowout in the Foundation of the Plavinas Powerhouse: Case History. *Geotechnical and Geological Engineering Journal*. 30(6): 1421-1433.

Messerklinger S. 2013. Failure of a Membrane-Lined Embankment Dam – Case Study. Submitted to *Geotextiles and Geomembranes.*

Milligan, V. 2003. Some uncertainties in embankment dam engineering. *ASCE.* 129(9): 785-797.

Patrashev A.N., Pravedny G.K. 1965. *Manual on designing of reverse filters for hydroengineering structures.* VSN-02-65/GPKE.

Pavlovsky N.N. 1922. *Theory of underground water motion beneath hydroengineering structures and their foundations and its basic application.* Research Land Reclamation Institute. St. Petersburg.

Pravedny G.K. 1976. *Guideline on calculation of seepage strength of dams made of soil materials.* P-55-76/VNIIG. Leningrad.

Sherard, J.L., Woodward, R.J. & Gizienski, S.F. 1963. *Earth and Earth-Rock Dams – Engineering Problems of Design and Construction.* John Wiley and Sons, New York.

Sherard, J.L. 1972. *Embankment Dam Cracking.* In Embankment Dam Engineering. John Wiley & Sons, New York: 271-348.

Sherard, J.L. 1979. Sinkholes in dams of coarse, broadly graded soils. *13th ICOLD Conf.*: 25-35.

Sherard, J.L., Dunnigan, L.P. & Talbot, J.R. 1984a. Basic properties of sand and gravel filters. *J. Geot. Eng.* 110(6): 684-700.

Sherard, J.L., Dunnigan, L.P. & Talbot, J.R. 1984b. Filters for silts and clays. *J. Geot. Eng.* 110(6): 701-718.

Sherard, J.L. & Dunnigan, L.P. 1985. Filters and leakage control in embankment dams. *Proc. Symp. on Seepage and Leakage from Dams and Impoundments. ASCE*, New York: 1-29.

Sherard, J.L. & Dunnigan, L.P. 1989. Critical filters for impervious soils. *J. Geot. Eng.* 115(7): 546-566.

Sutherland, K.J. 2002. *Quantifying and controlling segregation in earth dam construction.* MSc Thesis, University of Toronto.

Terzaghi, K. & Fröhlich, O.K. (1936). *Theorie der Setzungen von Tonschichten: Eine Einführung in die analytische Tonmechanik.* Deuticke, Leipzig.

Terzaghi, K. 1936. The Shearing Resistance of Saturated Soils. *Proc. 1st ICSMFE* 28(3):54-56.

Terzaghi, K. & Peck, R.B. 1948. *Soil Mechanics in Engineering Practice.* John Wiley&Sons, New York.

Vaughan, P.R. & Soares, H.F. 1982. Design of filters for clay cores of dams. *J. Geot. Eng.* 108(1): 17-31.

Vaughan, P.R., Kluth, D.J., Leonard, M.W. & Pradoura, H.H.M. 1970. Cracking and erosion of the rolled clay core of Balderhead dam and the remedial works adopted for its repair. *10th ICOLD*, Q.36-R.5.

Identification du risque d'érosion interne sur les digues de l'Isère et du Drac

Identification of erosion risk on the Isère and Drac river levees

Monnet J., Plé O., Nguyen D.M.
UJF-Grenoble 1, CNRS UMR 5521, Laboratoire 3SR, Grenoble

RÉSUMÉ : Dans cet article, nous présentons une synthèse des mesures utilisées pour le diagnostic des digues de l'Isère et du Drac (20km) vis-à-vis du risque de suffusion. Ces mesures comprennent des reconnaissances géophysiques par panneau électrique, des reconnaissances pressiométriques, des essais d'identification des sols et des essais avec un nouveau dispositif expérimental in situ l'Essai d'Erosion Transverse (Cross Erosion Test - CET). Cet essai comprend l'injection, dans un premier forage, de l'eau claire et du pompage dans un autre forage de l'eau chargée en particules de sol érodé. Les premiers résultats permettent d'identifier le risque de suffusion dans un matériau granulaire comme rencontré dans les digues de l'Isère et du Drac et de mesurer la masse des particules érodées de diamètre inférieur à 1,5 mm.

ABSTRACT: In this paper, we present a summary of the measurements carried out for the diagnosis of the Isère and Drac river levees (20km) for the risk of suffusion. These measurements include geophysical surveys by electrical panel, pressuremeter tests, identification of the soil and test with a new in-situ experimental device The Cross Erosion Test (CET). This test includes injection, in a first drilling of clean water and recovered in another one of water charged with particles. Preliminary results show that risk of suffusion can be characterized within a granular matter as found on the Isère and Drac river levees. Measurements of the mass of eroded particles have been undertaken for size smaller than 1.5 mm.

MOTS CLEFS : Erosion, Reconnaissance, Essai In-situ, Panneau-Electrique, Pressiomètre, Erosion Transverse

KEYWORDS: Erosion, Survey, In-Situ Test, Electrical panel, Pressuremeter, Cross-Erosion

1. INTRODUCTION

L'érosion interne se développe à partir de l'infiltration de l'eau dans le sol. Elle est la cause principale des incidents les plus graves observés sur les barrages et les digues. Une étude récente (Foster *et al.*, 2000) montre que pour les barrages présentant des ruptures hydrauliques, 46% des sinistres seraient dus au risque d'érosion interne. En France, 70 cas critiques ont déjà été détectés. A la suite des inondations de décembre 2003, les autorités ont décidé de développer des plans d'urgence pour empêcher tout accident majeur. Pour prévenir, il est nécessaire d'étudier et d'identifier les phénomènes d'érosion interne susceptibles de se développer dans les digues et les barrages. Quatre types d'érosion interne peuvent se développer : l'évolution des défauts dans la matrice de sol, l'érosion régressive, la suffusion interne et la suffusion à l'interface entre deux sols. La suffusion est un processus interne d'érosion où des particules fines de sol sont déplacées par infiltration à travers la matrice de sol. Un état de l'art peut être trouvé dans la littérature (Fell et Fry, 2007) et plusieurs études en laboratoire ont été réalisées sur le sujet (Wan et Fell, 2004) avec principalement la même technique expérimentale (Hole Erosion Test - HET).

1.1 Zone d'étude

Le site qui a été choisi comme zone d'étude par le SYndicat Mixte des Bassins Hydrauliques de l'Isère (SYMBHI) pour contrôler les digues et détecter les zones nécessitant un renforcement éventuel est la partie de l'Isère en amont de Grenoble, au niveau du campus de Saint Martin d'Hères (Figure 1). Dans cette zone une rupture potentielle a été identifiée au niveau des pépinières Paquet. L'étude a lieu sur les digues en rive droite et en rive gauche de l'Isère.

Sur cette zone, il a été réalisé :

- des essais pressiométriques à cycle,
- des reconnaissances par panneaux électriques,
- des prélèvements d'échantillons pour des analyses en laboratoire.

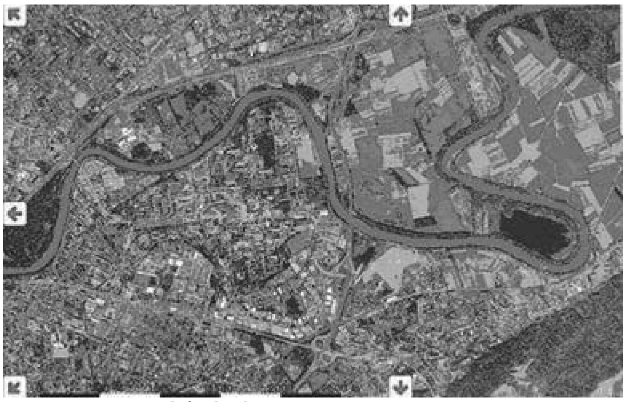

Figure 1 : La zone d'étude choisie

2. IDENTIFICATION DES SOLS PAR LA MÉTHODE DES CLUSTERS

2.1 Classement par cluster

Des essais pressiométriques cycliques (24) ont été réalisés lors des reconnaissances des digues de l'Isère sur 18 forages. Ils ont été regroupés avec les 185 essais pressiométriques de la reconnaissance du tunnel Nord de Grenoble, pour détecter les familles de sol auxquelles pourraient s'apparenter les sols des digues de l'Isère. Pour rendre automatique le classement des essais pressiométriques par couche géotechnique (avec des valeurs identiques de pression limite p_L et du module élastique E^e par couche) nous avons utilisé la méthode des clusters

(Monnet et Broucke, 2012; Monnet *et al.*, 2012). Cette méthode permet de classer des séries de données adimensionnelles en fonction de leur distance relative. Les distances ont été mesurées par la méthode Cosinus. Les résultats montrent que :

- la majeure partie des digues est constituée du cluster 3 (Figure 2), qui devrait correspondre à la famille 11 (sables gris et graviers),
- le reste de la structure des digues est constitué du cluster 1 qui devrait correspondre à la famille 8 (sables compacts) dans le haut des forages SC252, du cluster 6 qui devrait correspondre à la famille 1 (remblais de surface) dans le haut du forage SC252, du cluster 8 qui devrait correspondre à la famille 10 (sables gris faiblement argileux) pour le bas des forages SC230 et SC250 et du cluster 9 qui s'apparente à la famille 12 (sables gris) pour le milieu du forage SC136, et le haut de SC242 (Figure 2) et de SC248.

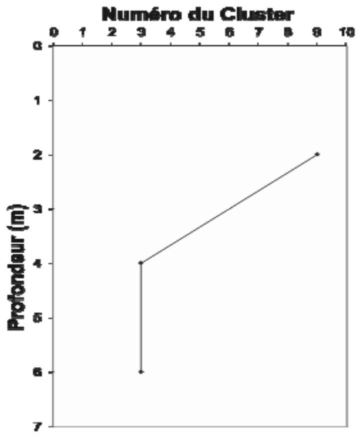

Figure 2 : Analyse par cluster du forage SC242

Tableau 1 : Relation entre les clusters et la résistivité des sols

Forage	Prof. (m)	N° Cluster	ρ (Ohm.m)
SD106	4	3	425
	6	3	425
SC230	2,5	3	1500
	5 ,25	3	1500
	7	8	425
SC238	2	3	1500
	4	3	1500
	6	9	1500
SC242	6	3	290
SC248	2	9	775
	4	3	1300
	6	3	1300
SC250	2,5	3	775
	5	3	775
	7	8	110
SD252	2	1	500-1500
	4	3	450
	6	3	450

2.2 Relation entre les clusters et la résistivité des sols

Une comparaison entre les numéros des clusters et la résistivité des couches a été entreprise (Tableau 1). On constate que :

- il n'y a pas de relation directe entre le cluster et la résistivité. Par exemple le cluster 3 correspond à une résistivité élevée (1500 à 1300 Ohm.m) dans les forages SC230, SC238, et SC248, mais à une résistivité faible (425 à 450 Ohm.m) dans les forages SD106 et SD252,
- le passage d'un cluster à un autre correspond généralement au passage d'une gamme de résistivité à une autre (SC230 de 5,25 à 7m ; SC248 de 2 à 4m ; SC250 de 5 à 7m ; SD252 de 2 à 4m).
- il existe une erreur d'interprétation liée à la précision de positionnement (± 1m) du forage sur la digue, et à l'incertitude inévitable liée à l'analyse inverse par panneau électrique (du simple au triple pour SD252 à 2m).

Tableau 2 : Résultats partiels (forages P252, P112, P120) de l'analyse de stabilité interne géométrique

	Indicateur	P252	P112	P120
Lafleur	$Rr = FOS/d_I$	0,63	13,92	9,64
	FOS (mm)	0,3	71,89	80,59
	Résultats	Instable	Suffusion	Suffusion
Kenney et Lau	H/F min	0,842	1,557	0,341
	Résultats	Instable	Instable	Instable
Kezdi	D'_{15}/d'_{85}	37,45	6,92	7,32
	Résultats	Instable	Instable	Instable
Kovacs	D'_{85}/O_{50}	0,146	0,088	0,107
	Résultats	Instable	Instable	Instable
Fell	Résultats	Stable	Stable	Stable

3. ANALYSE DES COURBES GRANULOMÉTRIQUES POUR QUANTIFIER LE RISQUE D'ÉROSION INTERNE

Le risque principal sur ces digues est celui de l'érosion interne identifié à l'aide de différents critères granulométriques issus de la bibliographie. Pour cela un programme a été construit pour calculer le gradient critique et le risque d'érosion à partir des critères granulométriques des différents sols. Les critères retenus sont ceux de Lafleur (1999), Kenney et Lau (1985), Kezdi (1979), Kovacs (1981) et Fell (2008). Les résultats sont rassemblés sur le Tableau 2. Sur les 18 forages, l'analyse précédente montre une large tendance à l'instabilité (voir Tableau 2). Dans un état sec ces digues (hors cas des crues exceptionnelles) restent stables.

4. CONCEPTION D'UN NOUVEL ESSAI IN SITU DE MESURE DE L'EROSION INTERNE – ESSAI CROSS EROSION TEST

4.1 Principe de l'essai

Le principe de l'essai est donné sur la Figure 3. Dans le premier forage, de l'eau claire est injectée avec une charge imposée (h_I) ou un débit volumétrique choisi (Q_I). Dans un second forage, l'eau chargée de particules est analysé. Le débit de sortie (Q_P) est produit par une pompe électrique de forage. Q_P et Q_I sont mesurées, le gradient hydraulique est calculé à l'aide de la formule de Bernoulli et comparé aux différents gradients hydrauliques critiques (Den Adel *et al.*, 1988; Khilar *et al.*, 1985; Terzaghi *et al.*, 1996; Vardoulakis et Papamichos, 2001). Ces paramètres permettent le contrôle des conditions hydrauliques de l'érosion interne. Dans un premier temps, le gradient hydraulique expérimental est comparé avec celui de Terzaghi mis sous la forme :

$$i_c = \rho_d/\rho_w - (1 - n) \quad (1)$$

où n est la porosité du sol, ρ_d la densité sèche du sol et ρ_w la densité de l'eau. Les résultats sont rassemblés dans le Tableau 3.

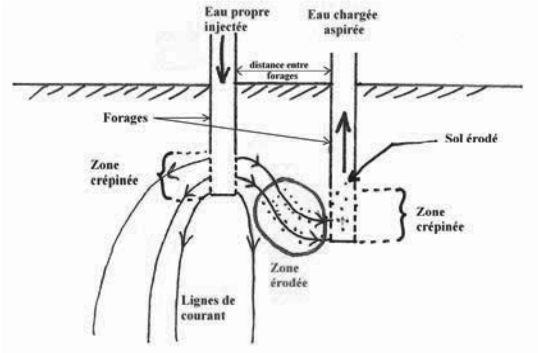

Figure 3 : Le principe de l'essai Cross Erosion Test

Une caméra placée à la sortie analyse (Figure 4-h) l'eau chargée de particules. L'appareil utilise une analyse spectrale. Le calibrage est effectué sur une solution standard de particules à différentes concentrations. La couleur rouge est utilisée pour ajuster la sensibilité de l'appareil. En sortie, les particules extraites du sol sont quantifiées à l'aide d'une balance de précision (± 0,01 g) (Figure 4-i).

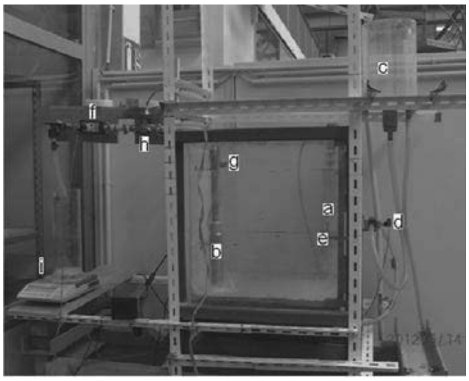

Figure 4 : Le principe de l'essai Cross Erosion Test

4.2 Sol testé

Deux mélanges de sol ont été testés (Tableau 3): le premier (S1) avec 60 % de sable (0/2 mm) et 40 % de gravier (2/20 mm) et le second (S2) avec 75 % de sable (0/2 mm) et 25 % de gravier (2/20 mm). Le coefficient d'uniformité C_u, rapport de d_{60} à d_{10} est respectivement égal à 15,3 pour S1 et à 3,7 pour S2. Ces sols granulaires sont couramment rencontrés dans les digues de l'Isère et du Drac. Le remplissage du réservoir nécessite une attention particulière. Trois techniques peuvent être utilisées, une pluviation dans l'air, un remplissage par saturation progressive et enfin, un remplissage après compactage par cloutage puis saturation progressive. La pluviation introduit de la stratification et des bulles d'air restent bloquées dans le sol. Le remplissage par saturation progressive permet d'atténuer la stratification mais introduit un défaut de compactage autour des forages. La troisième méthode palie aux défauts des deux précédentes et a été retenue pour les tests. La perméabilité du sol est obtenue directement dans le réservoir à l'aide de la méthode à charge variable. La perméabilité du sol (k) est donnée dans le Tableau 3.

4.3 Résultats expérimentaux

Trente-quatre tests ont été réalisés pour valider l'expérience.

Pour le premier essai avec le sol S2, la charge d'injection maintenue constante (Figure 1-c) est de 0,3 m. La fréquence de la pompe varie entre 25 et 35 Hz. Les paramètres expérimentaux sont mesurés en continu. Les résultats (Figure 5) sont traduits en termes de gradient hydraulique et comparés au gradient critique de Terzaghi. Pour cet essai aucune érosion interne n'a été détectée.

Tableau 3 : Caractéristiques des deux mélanges

	S1	S2
k (m/s)	$2.24\ 10^{-4}$	$1.45\ 10^{-4}$
n	0,33	0,25
ρ_d (kg/m^3)	1728	1935
d_{10} (mm)	0,26	0,20
d_{15} (mm)	0,33	0,25
d_{30} (mm)	0,517	0,38
d_{60} (mm)	4,00	0,75
d_{85} (mm)	9,67	9,58
C_u	15,3	3,7
i_c (m/m)	1,06	1,19

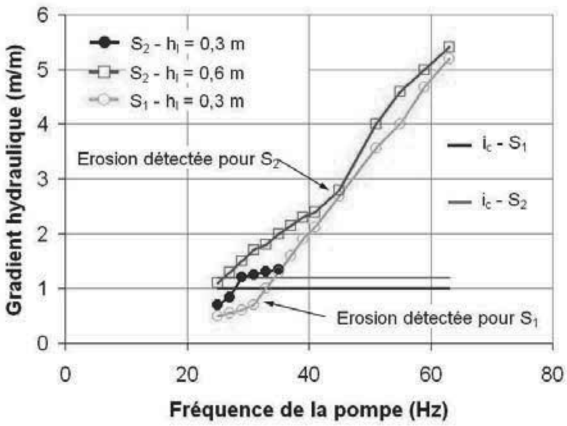

Figure 5 : Evolution du gradient hydraulique en fonction de la fréquence de la pompe – détection de l'érosion

Pour le second essai sur le sol S2, la charge d'injection constante est portée à 0,6 m. La fréquence de la pompe varie de 25 à 63 Hz. L'érosion interne est détectée pour une fréquence de 45 Hz. A partir de cet instant, le gradient hydraulique expérimental augmente (Figure 5), des particules érodées sont détectés avec la camera pour une concentration maximale de 43,3 g/l (Figure 6). La masse cumulée érodée est égale à 210 g (Figure 7).

Pour la dernière expérience avec le sol S1, la charge hydraulique (Figure 4-c) est imposée égale à 0,3 m. La fréquence de la pompe varie entre 25 et 63 Hz. L'évolution du gradient hydraulique est montrée sur la Figure 5. Ce gradient augmente rapidement après 35 Hz qui correspond au seuil d'érosion. L'érosion interne est détectée pour un gradient de 0,9 qui est inférieur au gradient de Tergaghi (Figure 6). Cela se traduit par une rupture de pente sur la courbe charge fréquence de la Figure 5 et indique une variation de perméabilité dans le milieu testé. La masse totale érodée mesurée est égale à 520g en fin d'essai (Figure 7).

4.4 Discussion des résultats expérimentaux

Parmi les critères (paragraphe 3) qui utilisent les diamètres respectifs des particules pour identifier un risque de suffusion, nous avons retenu le critère de Lafleur (1999) car il suppose l'existence d'un filtre à l'aval pour retenir un sol potentiellement suffusif à l'amont. Dans la mesure où la pompe est équipée d'une grille, ce critère semble plus particulièrement adapté. Il considère le rapport entre le diamètre de filtration FOS (Filtration Opening Size) et le diamètre d_I de la particule entrainée (calculée par le critère), pour prévoir soit un colmatage, soit une filtration, soit une suffusion (Equation 2).

Dans l'expérience considérée FOS est égal à 1,5 mm et d_I est le diamètre des particules érodées dépendant de C_u :

$$FOS/d_I < 1, \quad 1<FOS/d_I < 5, \quad 5<FOS/d_I \qquad (2)$$

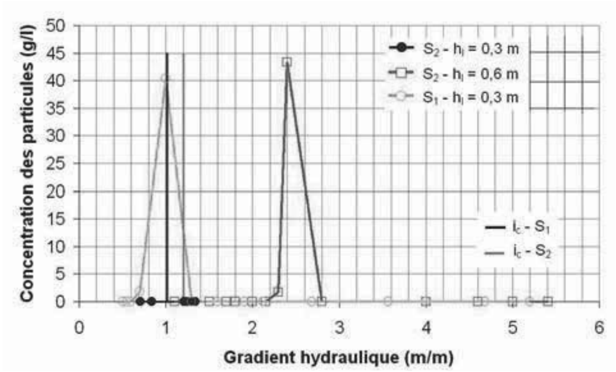

Figure 6 : Evolution de la concentration du sol érodé

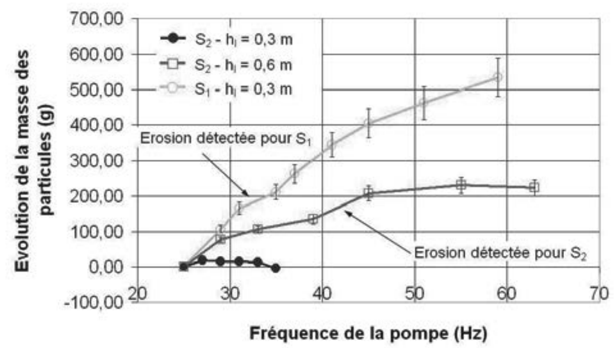

Figure 7 : Evolution de la masse de sol extraite

Tableau 4 : Critère d'érosion selon Lafleur (1999)

	FOS (mm)	C_u	d_I (mm)	FOS/d_I	Résultats
S_1	1,5	15	0,517	2,9	Auto-filtration
S_2	1,5	4	9,58	0,15	Colmatage

Pour le sol S1 la condition $C_u > 6$ est vérifiée et la valeur de d_I est égale à 0,517 mm, soit d_{30}. Le critère indique alors que le sol est en auto-filtration selon la terminologie de Lafleur (Tableau 4). Ce phénomène correspond à une suffusion puis à une stabilisation. Ce phénomène est effectivement observé expérimentalement pour un gradient hydraulique de 0,9. Par la suite, une stabilisation s'opère.

Pour le sol S2, la condition $C_u \leq 6$ est vérifiée et la valeur de d_I est égale à 9,58 mm, soit d_{85}. Le critère indique alors un colmatage (Tableau 4) la particule entrainée étant plus grande que l'ouverture du filtre. Cependant, l'expérience n'est pas en accord avec la théorie et l'érosion est effective pour un gradient hydraulique de 2,6 bien supérieur à celui de Terzaghi (1,19). Ce phénomène érosif a été observé par de nombreux auteurs (Arulanandan et Perry, 1983; Den Adel *et al.*, 1988; Khilar *et al.*, 1985; Terzaghi *et al.*, 1996; Vardoulakis et Papamichos, 2001; Faure *et al.*, 2006) qui montrent qu'un sol peut être stable du point de vue granulométrique mais qu'il devient instable pour des gradients hydrauliques trop importants.

5. CONCLUSIONS

Cet article traite des méthodes utilisées pour identifier les sols des digues de l'Isère, de façon à préciser le risque d'érosion. La méthode des clusters appliquée aux résultats pressiométriques, a été choisie pour définir les différentes couches de sols présentes dans les digues.

Par la suite, la corrélation avec les mesures de résistivité électrique a montré que les variations de résistivités permettent de définir les interfaces entre couches, et que la valeur de la résistivité n'est pas en relation directe avec la nature des couches.

L'analyse granulométrique du sol des digues de l'Isère, en utilisant les critères géométriques de la bibliographie a montré la susceptibilité de ces sols à l'érosion interne.

Un nouvel essai permettant de mesurer le risque de suffusion a été présenté. Cet appareil injecte de l'eau claire dans un forage et recueille l'eau chargée de particules dans un forage de prélèvement. Par une analyse d'images, il permet de détecter l'érosion (critère géométrique), mais il permet également d'imposer un gradient hydraulique au sol (critère hydraulique). Il combine en cela les deux paramètres principaux qui conduisent à une érosion interne du sol. Cet essai prédictif pour la suffusion, nous renseigne sur la valeur du gradient hydraulique à l'origine du phénomène. Il est donc particulièrement bien adapté aux reconnaissances sur les ouvrages hydrauliques. Il sera d'ailleurs prochainement utilisé in-situ pour caractériser le risque de suffusion des digues de l'Isère et du Drac.

6. REFERENCES

Den Adel H., Bakker K.J., Klein M., Breteler B., 1988, Internal Stability of Minestone, *Proceedings International Symposium on Modelling Soil–Water–Structure Interaction*, International Association for Hydraulic Research (IAHR) Balkema Publishers, pp. 225–231.

Faure Y.H., Baudoin A., Pierson P., Plé O., 2006, A contribution for predicting geotextile clogging during filtration of suspended solids, *Geotextiles and Geomembranes*, Vol. 24 N°1, pp. 11–20.

Fell R., Fry J.J., 2007, Internal Erosion of Dams and Their Foundations, Taylor & Francis Publishers.

Foster M., Fell R., Spannagle M., 2000, The statistics of embankment dam failure and accidents, *Canadian Geotechnical Journal*, Vol. 37, pp. 1000–1024.

Kenney T.C., Lau D., 1985, Internal stability of granular filters, Canadian Geotechnical Journal, Vol. 22, pp. 215–225.

Khilar K.C., Fogler H.S., Gray D.H., 1985, Model for piping-plugging in earthen structures, *Journal of Geotechnical Engineering*, Vol. 111 N°7, pp.833–846.

Kovacs G., 1981. Seepage hydraulics. In: Development in Water Science d 10. Elsevier Scientific Publishing Co., Amsterdam, The Netherlands, pp. 730.

Lafleur J., 1999, Selection of géotextiles to filter broadly graded cohesionless soils, *Geotextiles and Geomembranes*, Vol. 17, pp. 299–312.

Monnet A., 1998, Boulance, érosion interne, renard. Les instabilités sous écoulement, *Revue Française de géotech.*, Vol. 82, pp.3–10.

Monnet J., Broucke M., 2012, The use of a cluster analysis in a Ménard pressuremeter survey, ICE - Geotechnical Engineering ,London, Volume 165, Issue 6, 367 –377.

Monnet J., Huhes J., Dafin J., 2012, Cluster analysis and pressuremeter survey – the Gray Harbor case*; ISC4 Conference, Porto de Galinhas*, 911-919

Skempton A.W., Brogan J.M., 1994, Experiments on piping in sandy gravels, *Géotechnique*, Vol. 44 N°3, pp. 440–460.

Vardoulakis I., Papamichos E., 2001, A continuum theory for erosion in granular media, *Actes de la journées scientifique internationale*, Cermes 21, pp. 41–60.

Wan C.F., Fell R., 2004, Laboratory tests on the rate of piping erosion of soils in embankment dams, *Geotechnical Testing Journal*, Vol. 27 N°3, pp. 295–303.

Suffusion in compacted loessial silts. Interaction with granular filters.

Suffusion dans les limons lœssique compactés. Interaction avec les filtres granulaires

Terzariol R.E., Rocca R.J., Zeballos M.E.
Universidad Nacional de Córdoba, Argentina

ABSTRACT: Loess soils, which occupy much of central Argentina, are characterized by their high sensitivity to change in moisture. This condition categorized loess structure as internally unstable soil. Despite this natural condition, silts derived from loess are frequently used as material in roads and hydraulics constructions. In filtration processes, the soil should be shielded from erosion phenomena. The filter must have a particle size consistent with the ground to protect. In particular, sandy silts can be affected by phenomena of suffusion, or internal instability of the soil structure. The filter must control the loss of material and ensure the stability of flow. The present study shows the experimental results of flow applied to loessial silts, with low compaction. Tests have been conducted using filtration columns that simulate the soil-filter-drain. The test methodology applied aims to follow the research lines of similar studies worldwide. Studies have focused on analyzing the influence of variables such as degree of compaction, hydraulic gradient and composition of the filter material. The results obtained allow recommendations with reference to construction systems to be applied and the composition of the filter in order to properly control the suffusion.

RÉSUMÉ : Les lœss, qui occupent une grande partie de l'Argentine centrale, se caractérisent par une grande sensibilité au changement de teneur en eau qui permettent de classer ces sols dans la catégorie des sols à structure interne instable. En dépit de cet état naturel, les limons provenant des lœss sont fréquemment utilisés comme matériau pour les routes et les constructions hydrauliques. Dans les processus de filtration, le sol doit être à l'abri des phénomènes d'érosion. Le filtre doit avoir une granulométrie compatible avec le sol à protéger. En particulier, les limons sablonneux peuvent être affectés par des phénomènes de suffusion ou d'instabilité interne de la structure du sol. Le filtre doit contrôler la perte de matière et assurer la stabilité de l'écoulement. La présente étude montre les résultats expérimentaux de débit appliqués à des limons lœssique faiblement compactés. Des tests ont été effectués en utilisant des colonnes de filtration qui simulent le sol filtre de vidange. La méthodologie de test appliquée vise à suivre les lignes de recherche d'études similaires dans le monde entier. Les études ont porté sur l'analyse de l'influence de variables telles que le degré de compactage, le gradient hydraulique et la composition du matériau filtrant. Les résultats obtenus permettent recommandations par rapport à des systèmes de construction qui doivent être appliquées et la composition du filtre afin de bien contrôler la suffusion.

KEYWORDS: loess, sandy silts, filters, suffusion

1 INTRODUCTION.

In Argentina there are large deposits of sandy loam soils. These soil called loess, have been transported by wind. They have a high sensitivity to moisture changes, so they are considered unstable. One of the features of most interest is the hydraulic behavior of these soils. These silts can be used in the construction of cores in dams and embankments. On the road works in the central plains of Argentina, they are used in the formation of embankments. In these cases, the compacted soil is affected by infiltration processes and filtration through a porous medium. These processes, in some structures, generate erosions, which produce construction damage, or even in total failure.

This publication shows the characteristics of a soil protection system in order to avoid phenomena of erosion by filtration. The soil protection actions can be several. A classic action is granular filter construction. Other possible actions include changes in the internal structure of the soil, including the use of components that increase their internal resistance to erosion, or the construction of "barriers" formed by geosynthetics.

The behavior of natural filters has been one of the main subjects of study in geotechnical engineering. Terzaghi's original studies, since 1929, have been supplemented by Sherard and Dunnigan (1989), who made the most significant advances in the study of the behavior of filters.

Similarly, significant advances have been made by Khor and Woo (1989), Foster and Fell (2000) and Delgado and Locke (2008), Semar et al (2010). These authors have contributed to a better description of the behavior of soils in filtration problems, and have also generated recommendations on controlling erosion.

Erosion by filtration may start from the modification of the physico-chemical composition of the soil, resulting in dispersion phenomena. When soil structural organization, i.e. the accommodation of the particles, can lead to instability and erosion, the phenomenon is called suffusion, erodibility or internal erosion. Indraratna (1997, 2006, 2007), Wan and Fell (2004, 2008), Bonelli (2006), Bendahmane (2008), Indraratma et al (2008, 2011) and Benamar et al (2010), among others, have done important research in this field. These authors have developed new criteria for evaluating the potential of internal erosion, or suffusion in granular soils.

To understand the importance of this problem, we must analyze historical cases of dams whose cores have been constructed with silt. The most notable example is the Nurek dam in Tajikistan. A much discussed case is the Teton Dam in Idaho, USA failed in 1976 during the first fill. The failure is caused by internal erosion. In some cases of failure, it is considered that the material used in the construction of the core has a large influence. Smalley I.J. and Dijkstra T.A. (1991) indicated that the loess should not be used in cores of dams, because they lack the mineralogy and structural properties required for this application. Compacting the slime still remain dilatants and, consequently, their use represents a significant risk.In reply to this claim, Perry (1991) says that the highly erosive nature of the loess is well known. Accordingly, to avoid the dam core piping formed by silty soil, it requires the placement of an appropriate filter downstream. Thus Ririe Dam, built 35 kilometers of Teton Dam, has built a loess core and designed the appropriate filters, showing satisfactory performance.

In Argentina, loessial silts have been used in several dams and roadworks. The most important example is the Rio Hondo Dam, built in the 1960s, regardless dispersion problems (Grandi et al, 1961). The material used in this work is a silt with a clay content between 15 and 20% and plasticity index of 6% (Moretto et al, 1963). In structural revisions made several decades after its construction, it was concluded that the dam has adequate hydraulic behavior. Buraschi and Pujol (1999) have discussed the possibility of internal erosion in this dam.

This paper discusses the hydraulic stability sandy silt soil type, in the compacted state. The material is subjected to erosion situations under the application of several hydraulic gradients. For the protection of silt, it has been used natural filters with different particle sizes. One of the most discussed issues at the international level is the testing methodology. The authors have optimized an analysis methodology based on the use of a filter cell. The results of the test campaign performed with the technique developed by the authors of this publication are presented.

2 COMPOSITION OF THE STUDY

2.1 Soil involved in testing

The characteristics of the soil tested in these studies have been described by different authors, Reginatto (1970), Moll and Rocca (1991). Loessial soils of central Argentina are formed mainly by silt. The grain size composition comprising: sand (2% to 10%), silt (40% to 80%), and clay (20% to 35%). The composition is completed by calcium carbonate, variable between 2% and 10%, which exists in the form of nodules, called “toscas”, or precipitate in the contact between particles. These soils are alkaline, with pH> 8.

The physical properties of the soil tested are shown in Table 1.

Table 1.Properties of base material used

Property	Value
Natural moisture (ω), (%)	12.7 - 20.7
Dry Unit Weight (γ_d), (kN/m^3)	12.3
Specific Gravity (Gs)	2.65
Liquid Limit (ω_l), (%)	24.4
Plastic Limit (ω_p), (%)	21.0
Plastic Index (PI), (%)	3.4
Particles< 4.50 mm, (%)	100.0
Fines < 0.075 mm, (%)	93.4
Clay< 0.002 mm, (%)	14.0
USCS Classification	ML

Through compaction tests yielded a value of 15.5% optimum moisture and maximum dry unit weight of 17.6 kN/m^3. To simulate conditions of poor compaction, tests were conducted with the application of 90% of the energy corresponding to Standard Proctor test.

Fine grain sand was used as a base material for the construction of the filter. This type has been called SP, as the unified system. Zeballos et al (2010) have shown the unstable behavior of the system formed by compacted loess and filter, when it is formed only by sand. In the results presented in this paper, using filters formed by a combination of sand and silt loess, the filtration was measured. It has also been analyzing the operation of the set soil - filter, both under transient and steady flow. The mixtures tested as filters, have used combinations of sand and silt with a share of sand: 60%, 75%, 85% and 95%, relative to the total weight. The mixtures formed are presented in Figure 1. In the same Figure, the range corresponding to 15% pass filter (d_{15f}%) frequently recommended, is presented. Each of these mixtures was tested with the application of hydraulic gradients in the order of 20, 40 and 80. Figure 2 shows the location of the soil analyzed according to the classification of Burenkova (1993).

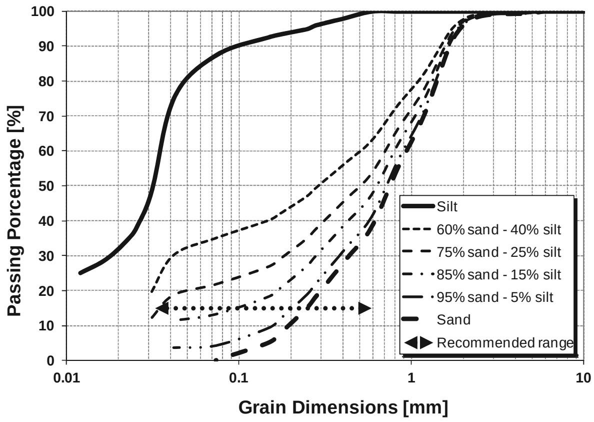

Figure 1.Particle size of the soils used in the study.

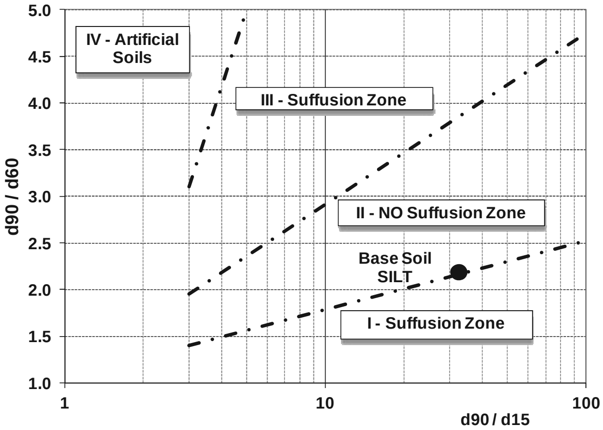

Figure 2.Burenkova chart for characterizing the potential of suffusion. Location of the studied silts.

For the materials used in this study, it is possible to make the following comments:

- Burenkova graph, locates the soil base tested (loess silt), in the limit of the erosive behavior.
- Several filter mixtures tested has fines content greater than that normally recommended for the treatment of these problems, (not exceeding 5% of passing sieve 200).

2.2 Tests Performed

A filtration chamber of large dimensions has been designed. The cylindrical chamber has a height of 500 mm with a span of 105 mm diameter. The chamber was constructed with transparent plastic, which allows visual monitoring of the filtration process. At its top, the chamber is connected with the water injection system pressure. In its lower part is connected to the flow registration system and containment system of solid particles. The chamber used, in schematic form, is presented in Figure 3.

In the upper part of the chamber is placed a granular material (drain) to facilitate the distribution of incoming water to the beaker. This allows the water to reach the probe evenly. The soil tested is located below the drain. The height of the cylinder is regulated depending on the applied hydraulic gradient. The filter is located below the probe, and then places another drain. The test apparatus has a bottom plate with an outlet hole that allows fluid control, and the collection of solid particles which migrate from the soil or filter.

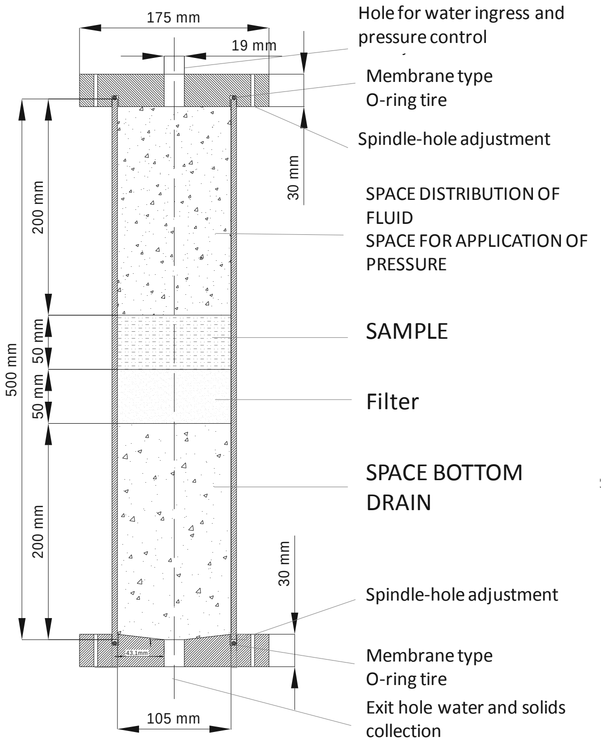

Figure 3. a) Schematic of the test system.

Prior to the execution of tests, a hole is drilled in the central part of the specimen to simulate a crack from uncontrolled erosion which could be initiated, or be achieved the overall instability of the material.

In the preparation of the test system, some difficulties have occurred in the installation of the filter and drain. An internal protocol was developed to avoid the complications caused by the lack of good contact between the various layers of the filtration column.

Tests have been carried out, in all cases, starting the process from the moisture condition of compaction. The filtered water volume and the weight of the solids passing through the filtration system were measured in all trials. In all cases, measurements were performed at intervals of time. Tests have lasted more than one day, until a leak was observed in steady state condition.

3 RESULTS

The variables in the set of tests were as follows: a) volume of water filtered vs. time, b) amount of filtered solids through the system, c) filtration rate, when the process is in steady state, d) steady state permeation.

Within the set of tests, the results for the filters with 60% of sand are not included in this paper. These filters have shown a highly unstable behavior, with great loss of material during filtration.

Figures 4a and 4b, for example, show the variation in the volume of filtered water to the various mixtures made and applied gradients. There is a growing trend for leaks with the gradient applied. The same trend was observed with the sand content in the filter.

In relation to the migration of particles, Figure 5 shows the percentage of solids that migrate with respect to the initial dry weight of the sample. The solids lost during the test tend to increase proportionally to the content of sand in the mixture. The losses are moderate for the filters having no more than 85% sand. For filters with 95% sand, the loss rate increases to more than double, compared to the previous cases. Much of the migration of solids occurs in the first minutes of the test. After the initial stage there is clear water seepage through the system.

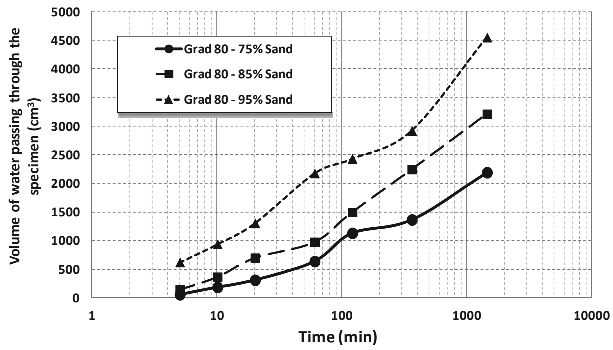

Figure 4.a. Changes in the volume of filtered water, as represented in logarithmic scale.

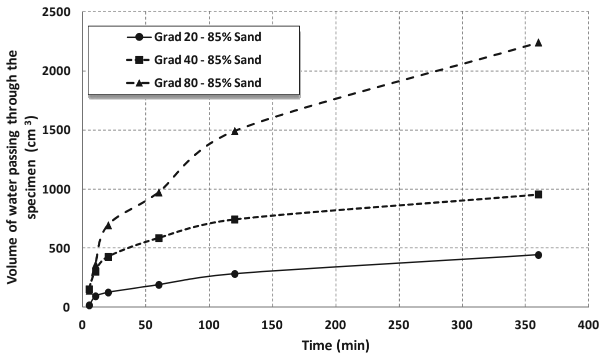

Figure 4.b. Representation of the evolution of the volume filtered, represented in full scale

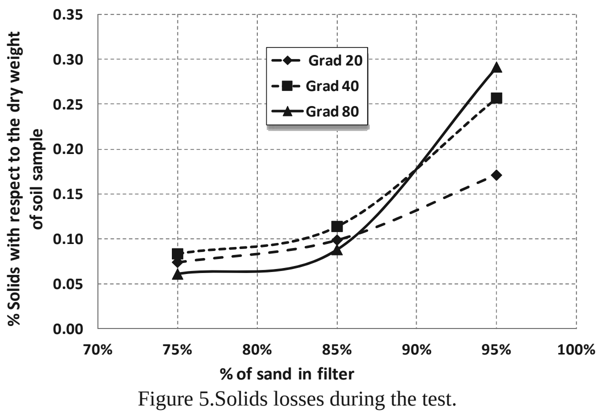

Figure 5.Solids losses during the test.

The filtration system tested shows a leak with the characteristics of a regular stationary regime after an initial transient stage.

The stability of the system can be seen through the identification of the mean values of permeability. These values are constant, even for different values of gradients.

The results, measured as rate of leak flux in the stationary phase and the permeability at this stage are shown in Table 2.

Table 2. Speed of filtration and permeability in the steady state phase.

Grad	Velocity of filtration (cm^3/s)			Permeability (cm/s)		
	75%	85%	95%	75%	85%	95%
20	0.009	0.014	0.017	5.5E-06	8.2E-06	1.0E-05
40	0.019	0.022	0.027	5.6E-06	6.3E-06	7.9E-06
80	0.034	0.050	0.070	4.9E-06	7.2E-06	1.0E-05

4 CONCLUSIONS

The results can be summarized in the following remarks:

- Sandy silt soils of low plasticity, typical "Loessical Formation" located on central Argentina, are in the limit suffusion unstable behavior, according with previous internationals studies.
- A test protocol for evaluation of the capacity of the filter for controlling suffusion instability was made based on set of measurements.
- In the construction of filters for hydraulic control of silty soils stability, materials with fines content greater than 5% have been employed. There has been a satisfactory performance with content not higher than 30%.
- The filter employed as mixtures with fines content between 15% and 25% showed the best conditions of stability. Under these conditions, there has been a small fraction of solid material lost. These losses occur mainly in the early stage, prior to achieving a steady flow.

5 ACKNOWLEDGEMENT

This research was sponsored by the Department of Science and Technology,(SECYT) Universidad Nacional de Cordoba.

6 REFERENCES

Banamar, A.; Beaudoin, A.; Bennabi, A & Wang, H. (2010). Experimental Study of Internal Erosion of Fine Grained Soils. *Scour and Erosion. Proceeding of the 5º International Conference. Geotechcnial Special Publication 210.* ASCE. Pp 368 -377.

Bendahmane F., Marot D., Rosquoët F., Alexis A., (2008). Experimental parametric study of suffusion and backward erosion, *Journal of Geotechnical and GeoenvironmentalEngineering ,134(1):57-67.*

Bonelli S., Brivois O., Borghi R., Benahmed N., (2006). On the modelling of piping erosion, *ComptesRendus de Mécanique, 8-9(334):555-559.*

Buraschi, J. y Pujol, A. (1999). Dique río Hondo: evaluación del comportamiento actual a 40 años de su puesta en operación. I Cong. Arg. de Grandes Presas y Aprovech. Hidroeléctricos. San Martin de los Andes. Vol. I: 311-320.

Burenkova, V. (1993).Assesment of suffusion in non-cohesive and graded soils.Filters in geotechnical engineering, Ed Braums, Heeramus and Schuler, Balkema, 357-360.

Delgado y Locke (2008). Delgado, F. P. (2008). Discussion of “A procedure for the design of protective filters. *Canadian Geotechnical Journal, 45*, 437-439.

Foster y Fell (2000). A method for assessing the relative likelihood of failure of embankment dams by piping. *Canadian Geotechnical Journal, 37*, 1025-1061.

Grandi,, A., Riva, J. Bolognesi, A y Moretto, O. (1961). Earth dams in argentina. Proc. V Intl. Conf. on Soil Mech Found. Eng. Paris vol II: 613-618.

Indraratna, B. (1997). Analytical Model for Particle Migration within Base Soil-Filter System. *Journal of Geotechnical and Geoenvironmental Engineering, 123*, 100 - 109.

Indraratna, B. (2006). Enhanced Criterion for Base Soil Retention in Embankment Dam Filters. *Journal of Geotechnical and Geoenviromental Engineering, ASCE , 1621 - 1627.*

Indraratna, B. (2007). Constriction-Based Retention Criterion for Granular Filter Design. *Journal of Geotechnical and Geoenvironmental Engineering, 133*, 266 - 276.

Indraratna, B; Aljorany, A. and Rujikiatkamjorn, C. (2008). "Analytical and Numerical Modelling of Consolidation by Sand Drains beneath a Circular Embankment" *Faculty of Engineering – Papers*.

Indraratna, B.; Trong Nguyen, V. and Rujikiatkamjorn, C. (2011). "Assessing the potential of internal erosion and suffusion of granular soils" *Faculty of Engineering - Papers* (2011): 550-554.

Khor y Woo (1989). Investigation of crushed rock filter for dam embankment. *Journal of Geotechnical Engineering, ASCE, Vol 115, 3, 399-412.*

Moll, L. y Rocca, R. (1991). Properties of loess in the center of argentina. Proc of IX Panam.Conf. on Soil Mech and Found Engng.Chile vol 1: 1-13.

Moretto, O., Bolognesi, A., López, A. y Nuñez, E. (1963). Propiedades y comportamiento de un suelo limoso de baja plasticidad. Proc. II Panam. Conf. SoilMech and Found. Eng. Brasil, vol II: 131-146.

Perry, E. (1991). Comments on the Teton dam (Idaho) Failure: problems with the use of loess material in earth dam structures. Eng. Geol. Vol 31, no 2, pp 205-206.

Reginatto, A. (1970). Propiedades mecánicas de algunos suelos de la ciudad de córdoba. 2º RAMSIF. Córdoba, Argentina

Semar, O.; Witt, K.J. & Fannin, J. (2010). Suffusion Evaluation – Comparison of Current Approaches. Scour and Erosion. Proceeding of the 5º International Conference. Geotechcnial Special Publication 210. ASCE. Pp 251-262.

Smalley I. and Dijkstra, T. (1991). The Teton dam (Idaho) Failure: problems with the use of loess material in earth dam structures. Eng. Geol. Vol 31, no 2:197-203.

Sherard y Dunnigan (1989). Critical Filters for Impervious Soils.*Journal of Geotechnical Engineering , ASCE, Vol 115: 927-947.*

Wan C.F., Fell R., (2004). Investigation of rate of erosion of soils in embankment dams, *Journal of Geotechnical and GeoenvironmentalEngineering ; 130(4):373-380.*

Wan y Fell (2008), Assessing the Potential of Internal Instability and Suffusion in Embankment Dams and Their Foundations. *Journal of Geotechnical and Geoenvironmental Engineering, 134,* 401 - 407.

Zeballos et al, (2010). Uso de limos loéssicos como material de núcleo de presa. Congreso Argentino de Mecánica de Suelos e Ingeniería Geotécnica 2010.

Predicting long-term settlements of coastal defences for the safeguard of the Venetian Lagoon

Évaluation des tassements de consolidation secondaire des structures côtières de protection pour la sauvegarde de la lagune de Venise

Tonni L., García Martínez M.F.
DICAM, University of Bologna, Italy

Simonini P.
DICEA, University of Padova, Italy

ABSTRACT: Over the last decades, a number of engineering solutions, including both nearshore and offshore structures, have been designed in order to protect human activities of the whole Venetian coastal environment as well as the invaluable historical and artistic heritage of Venice (Italy) from sea storms, high tides and recurrent flooding. In recent years, in the context of the ambitious mobile barriers system project known as MOSE, the existing jetties were extended and new breakwaters were set up in front of the three inlets connecting the lagoon to the Adriatic Sea. In order to preserve integrity as well as effectiveness, a key issue in the design of such structures is represented by the estimate of both short-term and especially long-term settlements. Indeed, field observations as well as laboratory evidence have shown that time-dependent phenomena cannot be considered as negligible in the predominantly silty sediments forming the Venetian lagoon basin. This paper focuses on the prediction of the long-term response of Venetian coastal defences, using a one-dimensional settlement method in conjunction with a $C_{\alpha\varepsilon}$ profile determined by piezocone tests and based on a formulation recently calibrated on field data from a Test Site located in the Venetian lagoon area.

RÉSUMÉ : Au cours de ces dernières décades, plusieurs mesures de protection contre la marée haute et les fréquentes inondations ont été mises en œuvre afin de protéger la ville historique de Venise (Italie) ainsi que les activités des communautés qui se sont développées au long de la lagune vénitienne. Récemment, lors du projet MOSE, qui consiste en un système de barrières mobiles placées auprès des trois bras de mer reliant la lagune à la mer Adriatique, les jetées existantes ont été remodelées et prolongées et de nouvelles structures de protection ont été construites. L'évaluation des tassements dus à la consolidation primaire et surtout secondaire est essentielle pour que ces ouvrages soient efficaces et en bon état au long des années. En effet, des études en laboratoire ainsi que des observations en place ont mis en évidence la contribution élevée de la consolidation secondaire aux valeurs totales des tassements des sols limoneux du bassin de Venise. Dans cet article on présente un calcul de tassement de consolidation secondaire d'un brise-lame, à l'aide d'une méthode qui permet d'évaluer $C_{\alpha\varepsilon}$ à partir des essais de pénétration statique (CPTU). La corrélation utilisée a été récemment établie sur une base de données assemblée auprès de la station d'essai de Treporti, située dans la lagune de Venise.

KEYWORDS: piezocone tests (CPTU); silt; sand; secondary compression; coastal defences; Venetian lagoon.

1 INTRODUCTION

Over the last decades, a number of engineering solutions, including both nearshore and offshore structures, have been constructed in order to protect human activities of the whole Venetian coastal environment as well as the invaluable historical and artistic heritage of Venice (Italy) from sea storms, high tides and recurrent flooding.

First in the late 19th century, several long jetties were built at the three inlets (Lido, Malamocco, Chioggia) connecting the lagoon to the Adriatic Sea (Figure 1). More recently, in relation to the ambitious project known as MOSE, consisting on a mobile barriers system for the temporarily closure of the lagoon inlets, the existing jetties were extended, reinforced and finally reshaped, new breakwaters were built in front of the inlets and a small island was realized within the Lido inlet.

In order to preserve both integrity and effectiveness, a key issue in the design of such structures is represented by the estimate of both short-term and especially long-term settlements, being the unexpected or underestimated reduction in the structure height a probable cause of flooding. Indeed, field observations as well as laboratory evidence have shown that time-dependent phenomena cannot be considered as negligible in Venetian sediments, hence the proper evaluation of the relevant parameters is of crucial importance for settlement predictions.

This paper focuses on the prediction of the long-term response of Venetian coastal defence structures, using a one-dimensional settlement method in conjunction with a secondary compression coefficient $C_{\alpha\varepsilon}$ profile determined from piezocone test data.

The approach is based on a formulation recently calibrated on field data assembled during approximately 6 years at the Treporti Test Site (*TTS*, Venice), within an extensive research

Figure 1. Satellite view of the Venetian lagoon.

project aimed at thoroughly analysing the stress-strain-time response of the predominantly silty sediments forming the Venetian lagoon subsoil.

The estimated settlements are compared with vertical displacement measurements provided by a very accurate monitoring system, based on an advanced technique known as Persistent Scatterer Interferometry.

The verification of empirical relationships using experimental data obtained from a different site of the Venetian lagoon is likely to constitute an important contribution to the practice of geotechnical engineering in this area.

2 THE VENETIAN LAGOON SUBSOIL

Over the last decades, the shallow Pleistocene sediments underlying the Venetian lagoon have been thoroughly investigated. First in the 1970s, in relation to the regional land subsidence and then in the 1990s, following the extensive site investigation programme related to the MOSE project.

From the large amount of data assembled over approximately 40 years, it turned out that the Venetian subsoil conditions consist of a complex assortment of interbedded normally consolidated or slightly overconsolidated silts, medium-fine silty sands and silty clays.

Despite grain size heterogeneity, research has shown that these sediments have a common mineralogical composition and that their mechanical behavior is mostly controlled by intergranular friction. Furthermore, as a consequence of their predominantly silty nature and high heterogeneity, undisturbed soil sampling is rather difficult to achieve, hence geotechnical characterization must essentially rely on in situ testing.

More recently, a new extensive research programme was carried out at the Treporti Test Site (*TTS*), located in the mainland beside Lido Inlet, with the aim of having a better understanding on the mechanical response of these intermediate sediments (Simonini 2004).

The valuable experience gained from the overall analysis of the data collected at *TTS*, including a large number of piezocone tests (CPTU) and subsoil strain measurements beneath a full-scale test bank, showed significant limitations of the existing approaches for the characterization of the predominantly silty sediments of the Venetian lagoon, thus suggesting a critical review of empirical and theoretical formulations with regard to their applicability to such soils (Tonni and Gottardi 2011).

It was also observed that such intermediate soils are often characterized by permeability values within the range in which partial drainage phenomena are likely to occur during cone penetration (Tonni and Gottardi 2010) and that the identification of this effect is of fundamental importance for a proper interpretation of CPTU measurements.

Furthermore, field observations showed that in these soils the decay of excess pore pressures is in general rather rapid and thus secondary compression plays an important role in the whole deformation process. As a result, the proper evaluation of the relevant parameters is crucial in settlement predictions.

3 EVALUATING SECONDARY COMPRESSION FROM CPTU

Unlike clayey deposits, the estimate of secondary compression behaviour of sandy and silty deposits is not routinely taken into account in the classical settlement calculation, although there is experimental evidence that time-dependent behavior of granular soils is not negligible. At low confining stresses the deformations are caused to rearrangement over time due to sliding and rolling between sand particles, whilst at high confining pressures the deformations are associated to continuous fracturing and deformation of grains (Augustesen *et al.* 2004).

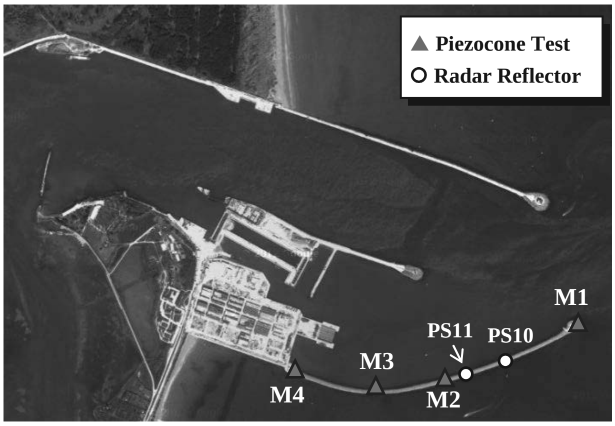

Figure 2. View of the Malamocco Inlet and location of the piezocone tests and radar reflectors (Persistent Scatterer, PS).

Secondary consolidation is typically characterized by the slope of the straight line portion of the vertical strain (ε_z) – logarithm of time (log*t*) curve obtained from oedometer tests, giving the secondary compression index $C_{\alpha\varepsilon}$:

$$C_{\alpha\varepsilon} = \frac{\Delta \varepsilon_z}{\Delta \operatorname{Log} t} \tag{1}$$

In recent studies (Bersan *et al.* 2012, Tonni and Simonini 2012), empirical, site-specific correlations, obtained from calibration on the *TTS* field data, have been proposed in order to estimate the secondary compression coefficient from cone resistance q_t. The approach is based on the experimental evidence that, in Venetian soils, frictional response governs both cone resistance and secondary compression, hence empirical correlations between $C_{\alpha\varepsilon}$ and q_t are likely to be a useful alternative on the classical laboratory tests for the estimate of creep characteristics.

Log regression analyses performed on the available data provided the following more significant relationships, both expressed in terms of the dimensionless normalized cone resistance Q_{tn}:

$$C_{\alpha\varepsilon} = 0.03 \cdot \left(Q_{tn}\right)^{-0.89} \tag{2}$$

$$C_{\alpha\varepsilon} = 0.077 \cdot \left(Q_{tn}\right)^{-1.14} \cdot \left(1 + \frac{\Delta u}{\sigma'_{v0}}\right)^{-0.74} \tag{3}$$

Here, an iterative nonlinear stress normalization procedure (Robertson 2009), accounting for the stress level and the soil class effects, was applied to the corrected cone resistance q_t in order to determine Q_{tn}.

It is worth mentioning that, according to the analyses based on the *TTS* data, the regression including a dependence on the stress-normalized excess pore pressure ($\Delta u/\sigma'_{v0}$) apparently gave a slightly better fit in comparison with eq. (2). Indeed, such additional independent variable allows accounting in some way for the different pore pressure response of soils in relation to the partial drainage conditions around the advancing cone.

4 CASE STUDY APPLICATION

Accurate measurements of long-term displacements of the coastal structures built along the Venetian coastline, next to the three lagoon inlets, have provided an opportunity to evaluate the predictive capability of the relationships described by eqs. (2) and (3).

Indeed, movements of coastal defense structures have been monitored using an advanced technique known as persistent scatterer interferometry (PSI), based on satellite-borne remote sensors. As explained in Tosi *et al.* (2012), the method is based on the identification and exploitation of individual radar reflectors, or persistent scatterers (PS), that remain coherent over long time intervals so as to develop displacement-time series. A significant advantage of PSI is represented by the possibility of detecting displacements with very high spatial and temporal resolution. According to ENVISAT ASAR and TerraSAR-X satellite images acquired from April 2003 to December 2009 and from March 2008 to January 2009 respectively, displacements of Venetian coastal structures turned out to range from a few mm/year for breakwaters and jetties older than 10 years to a maximum of 50-70 mm/year in the case of new or recently reshaped structures. Details on the whole PSI monitoring performed from Lido to Chioggia inlets are provided in Tosi *et al.* (2012).

In this paper, we will focus our attention only on the long-term vertical displacements measured from March 2008 to January 2009 at the Malamocco inlet, with special reference to the 1280 m-long, curved breakwater built in recent years just outside the inlet. This structure has shown settlement rates that vary in the range 5÷25 mm/year, with the higher values observed close to the seaward edge of the breakwater.

In order to apply the method described in section 3 and determine reliable values of $C_{\alpha\varepsilon}$, profiles of four piezocone tests located along the breakwater (Figure 2) have been interpreted. As an example, Figure 3 shows the corrected cone resistance q_t and pore pressure u measurements from CPTU M2, taken to 60 m depth.

All the soundings detail a complex soil profile of alternating silty sands, silts and silty clay, as recognized from prior studies performed at different sites of the Venetian lagoon. The pore pressure profiles rarely follow up the hydrostatic level, at times fall below it, but more often describe a slight contractive response, with generally moderate values of Δu.

Such stratigraphic complexity, typical of the whole Venetian lagoon subsoil, is confirmed by the well-known and newly revised piezocone-based classification framework proposed by Robertson (2009), aimed at identifying the *in situ* soil behavior

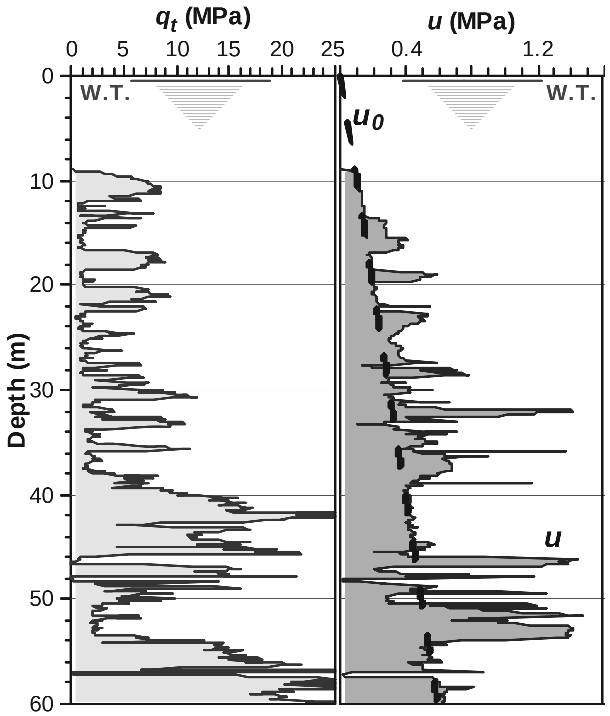

Figure 3. CPTU M2 log profiles.

type (SBT). Results from the application of the method to CPTU M2 data are shown in Figure 4. According to the SBT profile, the approach seems to predict a more pronounced clay-like behavior (zone 3) in comparison with the stratigraphic profiles obtained from nearby boreholes. Very thin layers of peat (zone 2) are at times detected, in particular from 22 to 48 m and from 51 to 53 m depth.

Results from the rather sophisticated classification approach developed by Schneider *et al.* (2008) are also plotted in Figure 4. This method, based on the normalized cone resistance ($Q = (q_t - \sigma_{v0})/\sigma'_{v0}$) and the stress normalized excess pore pressure ($\Delta u/\sigma'_{v0}$), was primarily derived to aid in separating whether cone penetration is drained, undrained or partially drained, hence the approach is recognized as superior to other classification charts when evaluating piezocone measurements in clayey silts, silts, sandy silts and transitional soils.

According to such classification framework, a large number of the CPTU M2 data fall in domains 1a and 3, this latter including a wide variety of mixed soil types.

Finally, Figure 5 provides the profile of the computed $C_{\alpha\varepsilon}$, as obtained from eqs. (2) and (3). Similar profiles have been obtained from the other available piezocone tests M1, M3 and M4. As evident from Figure 5, both formulations result in similar estimates of $C_{\alpha\varepsilon}$, although eq. (3) seems to provide lower values in the upper sandy layers.

In particular, the secondary compression coefficient in silts and silt mixtures (SBT zone 4) turns out to generally vary between 0.0015 ÷ 0.0035, rarely exceeding 0.004. Typical values of $C_{\alpha\varepsilon}$ in sand (SBT 6) fall in the interval 0.0005 ÷ 0.0008, whilst the range for sand mixtures (SBT 5) is somewhat higher (0.0007 ÷ 0.0018). Finally, $C_{\alpha\varepsilon}$ in clays-silty clays has been found to generally vary between 0.002 ÷ 0.006. It is worth observing that the computed values are in good agreement with the reference values of $C_{\alpha\varepsilon}$ derived from interpretation of long-term settlements observed at the Treporti Test Site.

Secondary compression of thin layers of peat, occasionally present throughout the stratigraphic profile, is described by rather high values of $C_{\alpha\varepsilon}$, such as 0.008 to 0.015. However, it is worth remarking that eqs. (2) and (3) have been not calibrated on such soil class, hence in this case the computed values of $C_{\alpha\varepsilon}$ cannot be applied without a great deal of uncertainty.

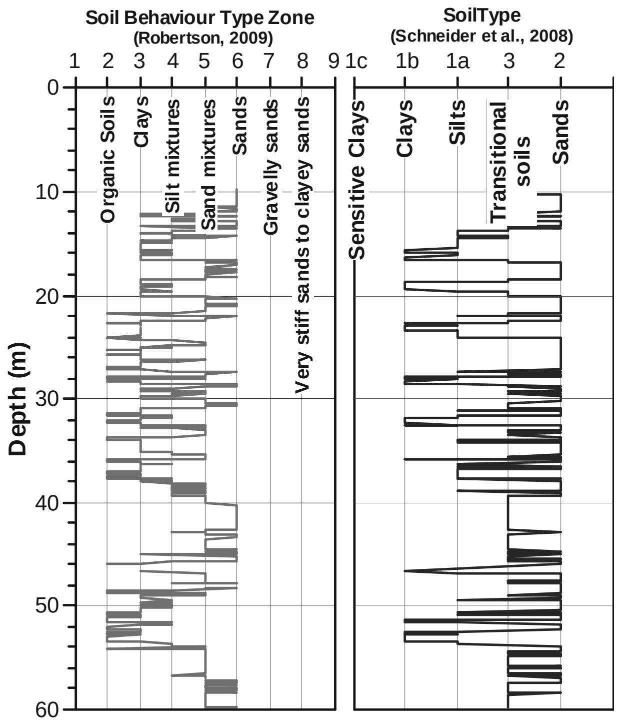

Figure 4. CPTU-based classification methods applied to test M2.

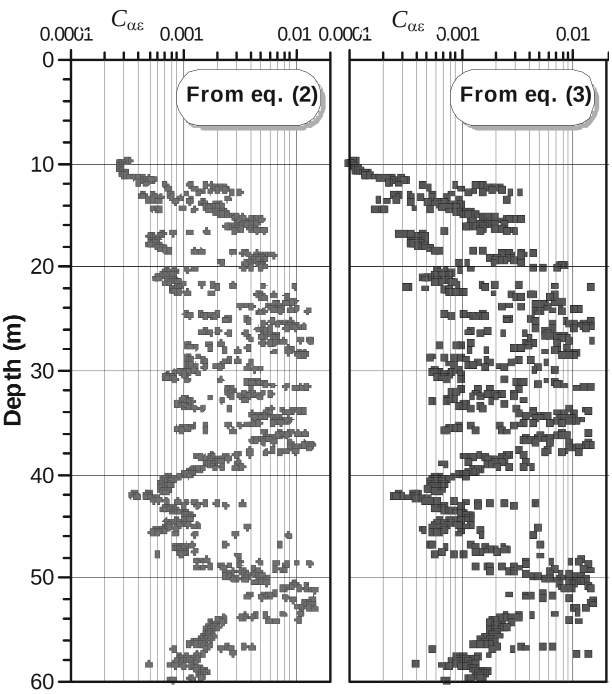

Figure 5. Profiles of the computed $C_{\alpha\varepsilon}$ from CPTU M2 data.

According to the so derived $C_{\alpha\varepsilon}$ values, a prediction of the secondary compression settlement S_{sec} occurred beneath the breakwater in the period March 2008–January 2009 has been carried out, using the well-known equation:

$$S_{\text{sec}} = -\sum_{1}^{n} \left(C_{\alpha\varepsilon}\right)_i \cdot H_i \cdot \log_{10}\left(\frac{t}{t_{ref}}\right) \qquad (4)$$

where n is the number of H_i-thick homogeneous soil layers considered in the calculation, t_{ref} = March 2008 and t = January 2009. On the basis of previous experiences on Venetian sediment behaviour, the analysis has been performed to a depth of approximately 40 m from sea bottom.

Figures 6 and 7 show the results obtained from the application of the method to CPTU M1 and CPTU M2 data respectively, together with vertical displacements measured for the radar reflectors PS10 and PS11, located between the selected piezocone tests (Figure 2). The figures clearly show that eqs. (2) and (3) result in similar settlement prediction and that the calculated trend fits fairly well the PSI-derived settlements.

5 CONCLUSIONS

Accurate measurements of long-term settlements of a breakwater built along the Venetian coastline, outside the Malamocco inlet, have allowed evaluating the predictive capability of two slightly different empirical relationships between piezocone measurements and the secondary compression coefficient, recently calibrated on independent data from the Venetian lagoon.

The application of the method has provided long-term settlement predictions which agree fairly well with measured displacements, thus confirming the effectiveness of both available correlations.

Research is currently focusing on the verification of such correlations at different areas of the Venetian lagoon, using site investigations and settlement measurements available from other defence structures located at the Chioggia and Lido inlets. Indeed, the validation of the proposed solutions to independent cases is likely to provide a useful contribution to the practice of geotechnical engineering in the Venice lagoon area.

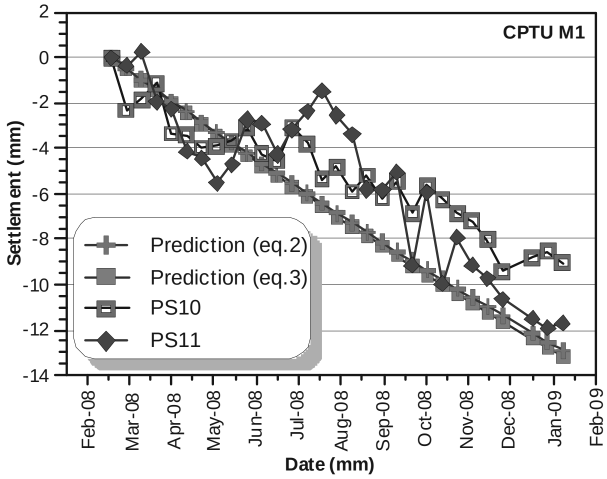

Figure 6. Settlement predictions using CPTU M1 data.

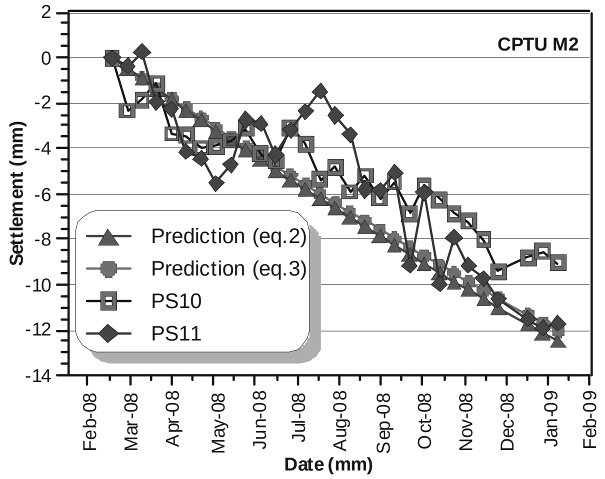

Figure 7. Settlement predictions using CPTU M2 data.

6 REFERENCES

Augustesen A., Liingaard M. and Lade P.V. 2004. Evaluation of time-dependent behaviour of soils. *Int. J. Geomechanics*, 4 (3), 137–156.

Bersan S., Cola S., Simonini P., Gottardi G. and Tonni L. 2012. Secondary compression of Venice lagoon sands and silts from CPTU. *Proc. 4th International Conference on Geotechnical and Geophysical Site Characterization, ISC-4*, Vol. 1, 383-389.

Robertson P.K. 2009. Interpretation of cone penetration tests – a unified approach. Can. Geotechnical J. 46 (11), 1337 – 1355.

Schneider J.A., Randolph M.F., Mayne P.W. and Ramsey N.R. 2008. Analysis of factors influencing soil classification using normalized piezocone tip resistance and pore pressure parameters. *J. Geotech. Geoenviron. Eng.*, 134 (11), 1569-1586.

Simonini P. 2004. Characterization of the Venice lagoon silts from in-situ tests and the performance of a test embankment. *2nd Int. Conf. on Site Characterization, ISC-2*, Vol.1, 187–207.

Tonni L. and Gottardi G., 2010. Interpretation of piezocone tests in Venetian silty soils and the issue of partial drainage. In: *Deep Foundations and Geotechnical In Situ Testing, ASCE Geotechnical Special Publication (205 GSP)*, 367–374.

Tonni L. and Gottardi G. 2011. Analysis and interpretation of piezocone data on the silty soils of the Venetian lagoon (Treporti test site). *Canadian Geotechnical Journal* 48, 616–633.

Tonni L. and Simonini P. 2012. Evaluation of secondary compression of sands and silts from CPTU. *Geomechanics and Geoengineering* i-First, 1-14. DOI:10.1080/17486025.2012.726748

Tosi L., Teatini P., Bincoletto, L., Simonini P. and Strozzi T. 2012. Integrating geotechnical and interferometric SAR measurements for secondary compressibility characterization of coastal soils. *Surveys in Geophysics* 33 (5), 907-926.

Full scale field tests for strength assessment of peat

Essais in situ en vraie grandeur pour évaluer la résistance d'une tourbe

Zwanenburg C., Van M.A.
Deltares

ABSTRACT: The costs for improving the safety of the Dutch Dike system are significant. The safety of about 40 km of dikes along the lake 'Markermeer' have to be increased according to the calculation methods based on current knowledge. However, the Markermeer dikes were already in place when the Markermeer was still part of the Zuiderzee. Water levels in the past have been higher then current design water levels. In this area, the subsoil consists mainly of peat and soft soils. The uncertainty associated with measuring the strength of soft soil (in laboratory testing) and constitutive behavior in computer models is a research issue in the safety assessment. In order to close the knowledge gap between the real dike and the small laboratory tests, full-scale field tests in the peat area have been executed. The large-scale field test, the so-called 'container tests' and intensive monitoring are executed in order to reduce the uncertainty of the strength parameters in the assessment of the stability of dikes on peat subsoil. This paper discusses results of the lab and field tests and shows how DSS tests and ball penetrometer tests correspond well to the actual strength found in the field tests.

RÉSUMÉ : L'amélioration de la sécurité du système de digues hollandaises a un coût significatif. La sécurité d'une quarantaine de km de digues le long du lac de Markermeer a été augmentée selon les méthodes de calcul basées sur nos connaissances actuelles. Cependant, les digues de Markermeer étaient déjà en place quand le lac faisait encore partie du Zuiderzee. Dans le passé, le niveau d'eau était plus haut que celui adopté dans les calculs faits à présent. En ce lieu, le sous-sol est constitué principalement de tourbe et de sols compressibles. L'incertitude associée à la mesure de la résistance de sols compressibles (en laboratoire) et aux lois de comportement dans les modèles numériques est le sujet de recherche dans le cadre de l'évaluation de la sécurité des digues. De façon à combler l'écart entre une digue réelle et les petits essais en laboratoire, des essais à échelle réelle ont été conduits dans une zone tourbeuse. L'essai in situ en vraie grandeur, appelé « essai au conteneur » a été exécuté et un système de surveillance intensive a été mis en place de façon à réduire l'incertitude sur les paramétres de résistance dans l'évaluation de la stabilité des digues construites sur les sols tourbeux. Le papier discute les essais en laboratoire et sur le terrain et montre que les résultats des essais de cisaillement simple direct et les essais au pénétromètre à balle correspondent bien à la résistance observée lors des essais in situ.

KEYWORDS: dike technology, peat, field tests

1 INTRODUCTION

Despite the fact that for centuries dikes have been built along rivers and lakes on soft ground, the stability assessment of these structures is still inaccurate. Due to uncertainties in sub soil behaviour and the daily practice of engineers making safe estimates of each not well known parameter, low factors of safety are calculated for dikes that have functioned properly for many years or even centuries. One of these examples is the dike between Amsterdam and Hoorn, approximately 30 km north of Amsterdam, along lake Markermeer. The dike originates from medieval times and its last reinforcement was made in 1926. Since the closure of the Zuiderzee, now known as IJsselmeer and Markermeer, occurrence of extreme high water levels is strongly reduced. As a consequence, present day design water levels are lower, but consist of a longer duration than occurred in the past. Despite the history of this dike, calculations show a low stability factor and indicate dike reinforcement. The design of the required reinforcement incorporates large stability berms with lengths up to 30 m. Such reinforcement has a strong impact on the villages and small towns along this dike section.

The calculated large stability berms followed from uncertainty in the peat characteristics. Laboratory tests on peat samples are difficult to interpret and result in a large scatter. To optimize the design, a series of field tests is conducted. The aim of these field tests is to make a comparison between the strength found in the field to the laboratory test results.

2 CHARACTERIZATION OF THE PEAT SUBSOIL

Figure 1 shows the subsoil profile. The depths in this profile are related to the reference datum NAP which is approximately main sea level. The ground level is approximately NAP -1.4 m. On top a thin clayey layer is found with a thickness of 0.2 to 0.5 m, followed by a peat deposit of approximately 4.5 m, a deposit of several clay layers with a thickness of 4.5 m, a thin basal peat layer and finally a thick pleistocene sand deposit. The water table is nearly at ground level, NAP -1.5 m to -1.6m.

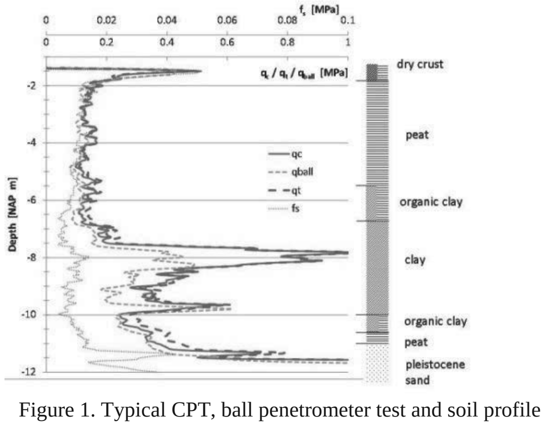

Figure 1. Typical CPT, ball penetrometer test and soil profile

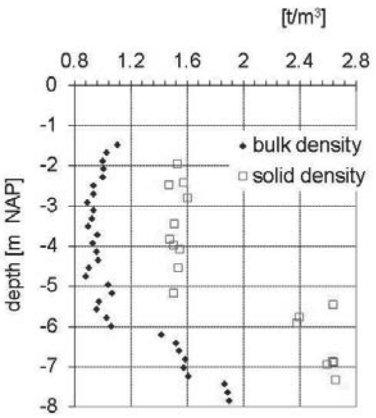

Figure 2. Bulk density and solid density, transition between peat and clay is found at NAP -5.5 m.

The peat layer is characterized as mainly sedge- reed peat. According to the von Post classification it is described as H2-H3, which means that the peat is only slightly decomposed. Figures 2, 3 and 4 give geotechnical characterisations of the peat layer.

Figure 2 shows the bulk density ρ and solid density ρ_s. For the peat samples $\rho = 0.98 \pm 0.08$ t/m^3, while for the clay layer the bulk density increases to $\rho = 1.8$ t/m^3 at a depth of NAP -8.5 m. Note that the peat bulk density is close to or even lower then the density of water. This can be explained by the large water content, the possible presence of gas in the peat samples and problems with re-saturating large pores in the laboratory before the bulk density measurement. The density of the solid particles, ρ_s is found by pycnometer measurements. The measurements on peat samples give $\rho_s = 1{,}52 \pm 0.04$ t/m^3 while for clay samples is found $\rho_s = 2.56 \pm 0.12$ t/m^3. The increase in bulk density at a depth of NAP -5.5 m gives a clear separation between the peat layer above NAP -5.5 m and the clay layers below.

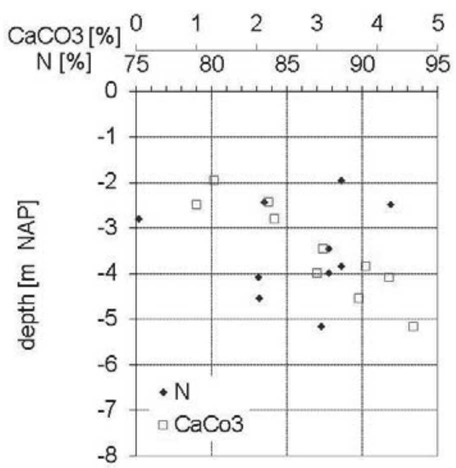

Figure 3. Loss on ignition, N and $CaCO_3$ content in peat layer

Figure 3 shows the loss on ignition N to be in the range of 75 to 90 % with an average value of N = 85.7 %, showing the high organic nature of the peat.

To check the validity of the data, ρ_s is calculated form N following the relation given by Skempton & Petley (1970):

$$\frac{1}{\rho_s} = \frac{1-1.04(1-N)}{1.4} + \frac{1.04(1-N)}{2.7} \tag{1}$$

Equation (1) gives for N = 0.857 [-], $\rho_s = 1.51$ [t/m^3] which is in good agreement with the measurements, $\rho_s = 1.52 \pm 0.04$ [t/m^3].

Samples from two borings were selected at 0.5 m depth interval for oedometer teststing, provide a profile of the pre-consolidation stress and water content with depth. Besides the series of oedometer tests a number of constant rate of strain tests, so-called CRS-tests are conducted. Figure 4 shows the pre-consolidation stress found by the oedometer and CRS tests. For the oedometer tests, the pre-consolidation stress is derived according to Becker (1987), for the CRS tests the procedure according to Den Haan (2007) is applied. The profile, presented in Figure 4, shows relatively high pre-consolidation stresses in the top layer, followed by lower values in the peat layer and organic clay layer. In the non-organic clay layer the pre-consolidation stress is larger than in the peat layer. There is a clear difference in the pre-consolidation stress at the top and lower part of the peat layer. For the oedometer tests the average pre consolidation stress in the range of NAP -2.4 m to NAP -4.0 m is 10.0 kN/m^2, with a maximum value of 13.4 kN/m^2 and a minimum value of 4.9 kN/m^2. For the lower part an average value of 7.5 kN/m^2 is found with a maximum value of 10.6 kN/m^2 and a minimum value of 5.0 kN/m^2. The same trend is found for the CRS tests.

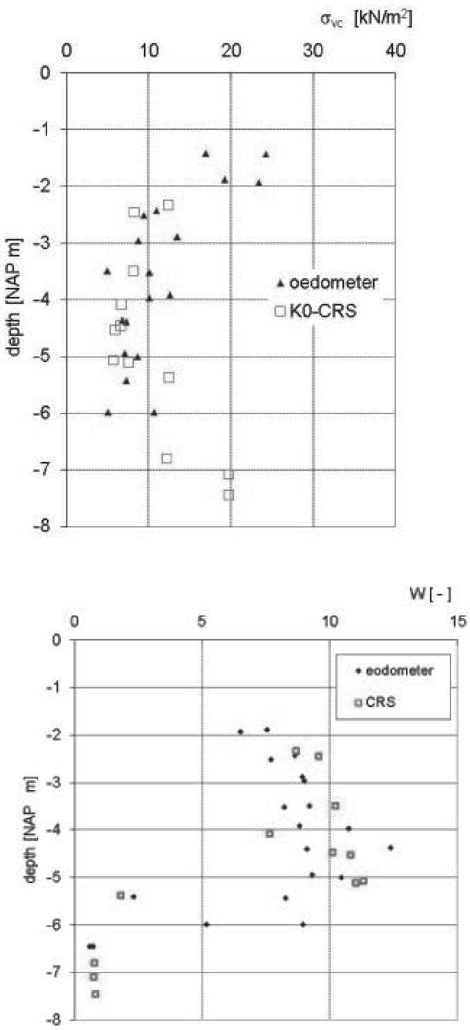

Figure 4. Oedometer and CRS test results, top: pre-consolidation stress, bottom: initial water content.

Figure 4 shows the profile of water content, defined as the mass of the pore fluid divided by the solid mass, with depth. The water content is measured before the execution of the oedometer and CRS tests. Note that the water content is given in absolute values and not expressed as a percentage. The average water content in the peat increases with depth from 6.45 (645%) to 12.4 (1240%). The organic clay layer shows lower values, with a large scatter. In the non-organic clay layer the water content reduces to 0.74 (74%).

A series of CPTs, including measurements with different cone types and ball penetrometer tests, finalises the subsoil characterisation. Figure 1 shows a typical CPT for the test field. In this CPT, the succession of subsoil layers can be recognized. According to Eurocode ISO/DIS 22476-1:2005,IDT the measurements represent a class 2 type CPT. For a class 2 CPT the accuracy of the tip resistance, q_c, equals 100 kPa. Figure 1 indicates for the peat a tip resistance of the same order of magnitude as the accuracy for which the CPT is conducted. This is typical for peat areas and also reported for other locations Den Haan & Kruse (2007) and Boylan et al. (2011). The low accuracy for these measurements makes the conventional class 2 CPT inadequate for accurate correlations with strength parameters. Ball penetrometer tests give a more accurate reading of the resistance in peat and are therefore used for correlation purposes.

3 LABORATORY TESTING

A large series of triaxial tests and Direct Simple Shear (DSS) tests were conducted. Discussion of all the test results is beyond the scope of this paper. This paper focusses on the DSS tests for which the sample was consolidated at approximately field stresses. The results of these tests were used to correlate the undrained shear strength, s_u, to ball penetrometer tests according to equation (2).

$$s_u = \frac{q_{ball}}{N_{ball}} \qquad (2)$$

in which q_{ball} represents the penetration resistance of the ball and N_{ball} represents the resistance factor.

In total 5 samples were tests at field stress conditions. Since the density of the peat is low and the water table reaches the surface the vertical effective stresses are also low, in the order of 2 – 7 kN/m^2. In the set-up of the field measurements for each boring, used to retrieve samples for DSS testing, a ball penetrometer test is executed at a distance of approximately 0.5 m. The DSS-strength is defined as the deflection point in the τ - σ’ diagram, representing the shear stress where the sample behaviour changes from compression to dilation. For each sample the DSS-strength is compared to the measured resistance in the nearby ball penetrometer test at the same depth. This led to the correlation of $N_{ball} = 17.9 \pm 1.2$.

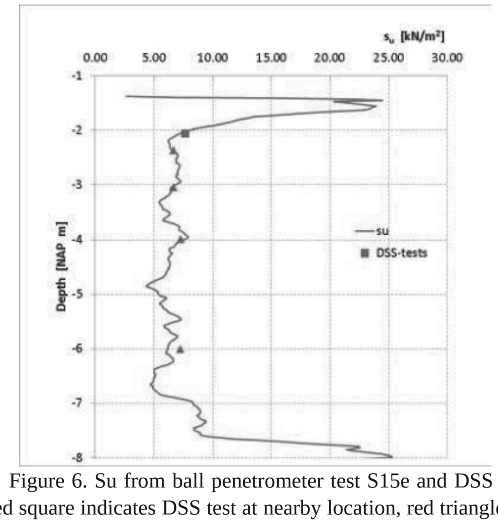

Figure 6. Su from ball penetrometer test S15e and DSS test results. Red square indicates DSS test at nearby location, red triangles other test results.

The undrained shear strength from the DSS tests ranges from 6.7 tot 7.7 kN/m^2 with an average value of 7.1 kN/m^2. The variation in the test results is small and the average value for N_{ball} found for the individual DSS test results fits well to the overall strength profile.

4 TEST SET-UP

In total 5 field tests are conducted. In the first two tests the peat is loaded in a few days to failure. The other 3 field tests include a two-periods loading procedure with several weeks of preloading before failure. This paper focusses only on the first two tests. For testing reproducibility the test loading is identical. Figure 7 shows the 3 loading phases of these tests.

In loading phase 1, a row of containers is placed and a ditch is excavated. The containers have the dimensions of 7.25 m (length) × 2.5 m (width) × 2.2 m (height). The ditch has a depth of 2.5 m and slope 1:1. After excavation, the ditch bottom rose due to swelling of the peat. The remaining depth during the test was approximately 2 m.

In loading phase 2, the containers were stepwise filled with water. Each load step consisted of a 0.25 m increase in water level. It was decided to start the next step if no failure had occurred in the previous step and deformation rates slowed down significantly.

In loading phase 3, the water level in the ditch was stepwise decreased. Each step consists of a 0.25 m lowering of the water table. Failure was found after lowering the water table in loading phase 3.

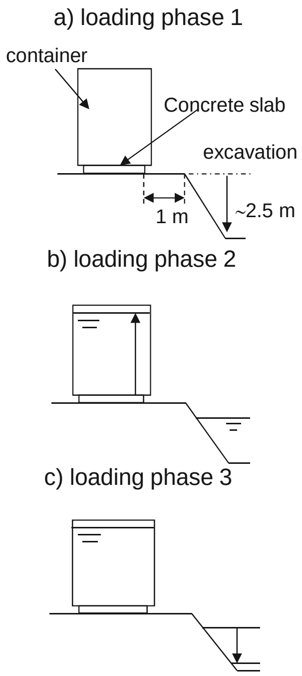

Figure 7. Planned test set-up

The instrumentation was concentrated in three measurement rows, see Figure 8. In figure 9 the location of the instrumentation placed in the second measurement row is shown. At three depths in the peat layer and at one depth in the clay layer, the pore pressure development was measured with Vibrated Wire Probes, VWPs and horizontal displacements were with a SAA unit, see Abdoun (2007), placed at the front of the container row. For measurement rows 1 and 2 the pore pressure development was measured at only two locations in the peat layer. Besides the instrumentation in the measurement rows the settlement under the middle two containers was measured with automated settlement plates, the water level in the container was measured for each container and the heave of the ditch after excavation was measurement with settlement plates.

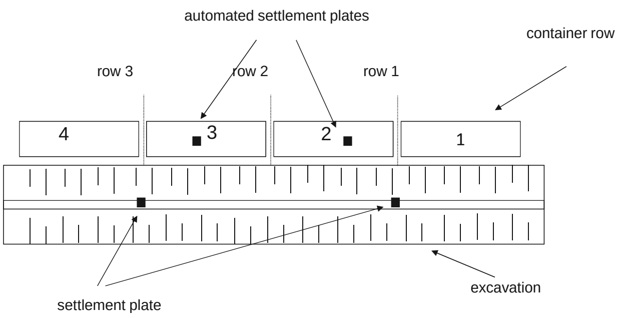

Figure 8. Top view

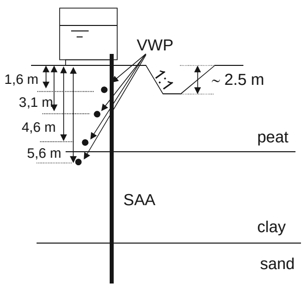

Figure 9. Instrumented cross section, VWP = vibrated wire probe.

5 RESULTS

The tests were run in approximately three days and this loading scheme resembles the loading velocity for river dikes, where high water levels rise and decline in a matter of days.

After the test was finished an excavation pit was made to study subsoil cracks and failure planes. These observations resulted in a reconstruction of the failure mechanism as shown in Figure 10 At the active side a clear and nearly vertical rupture plane was found accompanied with a secondary, backward running crack. This rupture plane intersected a nearly horizontal rupture plane. The horizontal rupture plane is only found at the active side of the failure. The maximum displacement found at the end of the test, measured at the front of the container row, is found at the same depth as the rupture plane was found at the active side. At the end of the test the slope of the ditch was nearly unaffected. This led to the conclusion that the horizontal displacements, measured at the front of the containers were followed by horizontal compaction of the peat between the containers and ditch.

Between the containers and horizontal rupture plane a series of minor horizontal and vertical cracks were found. It is not known whether these cracks were formed during the test, when the peat layer was loaded or after during swelling due to the removal of the load.

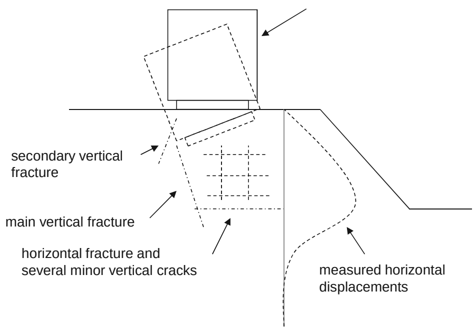

Figure 10. Sketch of failure mechanism.

6 ANALYSIS

After finalizing the field tests, an extended analysis was conducted including limit equilibrium analysis. Since the dimensions of the field tests are limited, 3D effects play a role. Based on the dimensions of the failure planes it is estimated that the friction along the sides of the failure mechanism adds approximately 10% extra friction to a plane strain assumed failure plane. So, failure is to be found for a calculated Safety Factor, SF = 0.9. For the analysis the Spencer and LiftVan method were applied. The LiftVan method, Van et al (2005), is a Bishop based method and includes a horizontal sliding plane between the active and passive parts of the slip circle with different radii. Back analysis with the conditions at which failure was found led to the average undrained shear strength, s_u, available at failure. Table 1 shows the results.

Table 1. Back analysis of test results, s_u in [kN/m^2] for which SF = 0.9.

Model	Test 1	Test 2
LiftVan	7.0	7.8
Spencer	7.3	8.0

7 CONCLUSIONS

The large scale field tests on the peat subsoil were conducted successfully. Measurements show an equivalent development of deformations and pore pressure in both tests. Together with the small differences found in the back analysis this indicates a good reproducibility of these tests.

The strength found in the DSS lab tests, in which the samples are consolidated at field stress level, correlate well to ball penetrometer tests. This resulted in a correlation between the ball cone field test and the DSS lab test.

The back analysis of the container tests shows that the average available shear resistance during the test is in the range of 7 to 8 kN/m^2. This corresponds well to the strength found from the DSS tests.

The combination of ball penetrometer tests and DSS tests, for which the sample is consolidated at field stress level, provide a valuable tool in obtaining peat strength parameters for safety assessments of dikes on peaty subsoil.

8 ACKNOWLEDGEMENTS

The research project, including the field tests, is initiated and funded by Hoogheemraadschap Hollands Noorderkwartier in cooperation with Rijkswaterstaat – Waterdienst.

9 REFERENCES

Abdoun T., Bennet V., DanischL., Shantz T. & Jang D. 2007 Field Installation details of a wire-less shape-acceleretion array system for geotechnical applications *Proceedings of SPIE, San Diego* volume 6529

Becker D.E., Crooks J.H.A., Been K., Jefferies M.G. 1987 Work as a criterion for determining in situ and yield stresse in clays *Can. Geot. J* **24**:549-564

Boylan N., Long M., Mathijssen F.A.J.M. 2011 In situ strength characterisation of peat and organic soil using full flow penetrometers *Can Geotech J.* **48**:1085-1099

Den Haan E.J. (2007) De intrinsieke tijd in het isotachenmodel *Geotechniek* **12**(1), 34-38 (in Dutch)

Den Haan, E.J. & Kruse, G.A.M. (2007) Characterisation and engineering properties of Dutch peats In: *Second international workshop on characterisation and engineering of natural soils Singapore* vol. 3 London Taylor & Francis p 2101 -2133

Skempton A.W., Petley D.J. 1970. Ignition loss and other properties of peats and clays from Avonmouth, Kings Lynn and Cranberry Moss, *Géotechnique* **20** (4), 343-356.

Van M.A., Koelewijn A.R., Barends F.B.J. 2005 Uplift phenomenon : Model, Validation and Design *international Journal of Geomechanics* 5:2, 98-106.

General Report TCs 307+212
Thermal Geomechanics with Emphasis on Geothermal Energy

Rapport général TCs 307+212
Géomécanique thermique avec une attention particulière portée sur l'énergie géothermique

Puppala A.J.
University of Texas, Arlington, Texas, USA

Choudhury D.
Indian Institute of Technology Bombay, Mumbai, India

Basu D.
University of Waterloo, Waterloo, Canada

ABSTRACT: Thermal geomechanics is an important area of soil and rock mechanics, and has applications in important areas related to sustainable development like energy extraction and storage, waste containment, forest fire, explosions in soil, and climate change. In this general report, a brief overview of thermal geomechanics is presented in the context of the papers allocated to the thermal geomechanics session of the 18th ICSMGE. A review of these papers is provided in the report. The topics covered by the papers can be broadly grouped into two sub-themes: thermal geomechanics and geothermal energy. The papers in the thermal geomechanics category focussed on the fundamental thermo-hydro-chemo-mechanical behavior of soil and rock while the papers on the geothermal category emphasized the application of thermal geomechanics in geothermal energy extraction through ground-source heat pumps and energy piles.

RÉSUMÉ: La thermogéomécanique est un domaine important la mécanique des sols et des roches avec des applications dans des domaines importants liés au développement durable, comme l'extraction et le stockage d'énergie, la maîtrise des déchets, les incendies de forêt, les explosions dans les sols et le changement climatique. Dans ce rapport général, on présente un bref aperçu de la thermogéomécanique basé sur les articles acceptés à la session correspondante du 18e CIMSG. Un examen de ces documents est présenté dans le rapport. Les sujets abordés par les articles peuvent être regroupés en deux sous-thèmes: thermogéomécanique et géothermie. Les articles de thermogéomécanique fondamentale sont consacrés à la thermo-hydro-chimio-mécanique des sols et des roches, tandis que les articles de géothermie traitent des applications de thermogéomécanique dans l'extraction de l'énergie géothermique par pompes à chaleur géothermiques et pieux énergétiques.

KEYWORDS: thermo-mechanics, geothermal energy, energy pile, sustainability, renewable energy, thermal conductivity.

1 INTRODUCTION

The 18th ICSMGE is being held at an interesting time of shifting paradigms at the backdrop of global climate change, economic downturn, population growth, advocacy for renewable energy use, and natural hazards. These factors have made governing bodies all over the world rethink the ways of day-to-day business, and the rather recent emphasis on sustainable development, that advocates a triple bottom line approach of balancing environment, economy and social equity, is an obvious outcome of such efforts. Consistent with this approach, the geotechnical profession has been motivated by the mantra of 'achieving maximum utilizing minimum', which is particularly important because the profession lies at the interface of the natural and built environments, and can significantly influence the economy, society and environment. Extraction of renewable energy, safe disposal of wastes, construction and maintenance of civil infrastructure and lifelines, and security against natural and man-made hazards are some of the far-reaching areas that geotechnical engineering contributes to, and this report on thermal geotechnics and its applications is, in part, a testimony of the variegated efforts that geotechnical engineers have put in towards sustainable development of civil infrastructure.

Thermal geomechanics is an important topic related to sustainable development. Heating and cooling of buildings using geo-structures like piles, walls and slabs, in situ burning of oil spill, oil recovery from reservoirs at high pressure and temperature, underground disposal of nuclear wastes, explosion on or inside the soil mass, forest fire, and global climate change affecting the freeze-thaw cycle of permafrost are some examples which may cause the soil temperature to vary from around −40°C to 300°C or more. It is well documented that temperature fluctuations have an effect on the soil strength and stiffness as well as on the pore pressure development. With an increase in temperature, the initial shear modulus and compressibility of clay increase and the drained and undrained shear strength decrease. Therefore, temperature fluctuations in soil may affect the stability of the civil infrastructure. Differential settlement of buildings due to heating and cooling using geothermal piles, changes in groundwater flow patterns and groundwater advection caused by geothermal heat pumps, temperature-imbalance induced seismic activities, distress in underground pipelines due to freeze-thaw cycles, debris flow and landslide are some examples in which the civil infrastructure is negatively impacted by alterations in soil temperature. It is thus imperative that research efforts are made toward understanding soil and rock behavior influenced by temperature change and heat flow.

An important application of thermal geomechanics is extraction of geothermal energy. Geothermal energy is a clean and renewable form of energy that is extracted from the deep and near-surface soil and rock strata by various means. Shallow geothermal energy is commonly extracted using ground-source heat pumps (GSHPs) from the shallow depths beneath the ground surface where the temperature remains stable within a narrow range of 7°-21°C. A GSHP typically consists of a heat pump, an air delivery system, and a heat exchanger, and uses the ground as a heat source and sink in winter and summer, respectively, to heat and cool buildings (Hughes 2008). Although several research studies have been performed on geothermal heat pumps, most of these studies focused on the thermal and thermodynamics aspects. It is only recently that the importance of the thermo-mechanical behavior of soil has come to the fore, particularly in the context of geothermal energy piles, which are now commonly used in some European countries to perform the dual role of supporting buildings and extracting shallow geothermal energy (Brandl 2006, de Moel et al. 2010). The thermo-mechanical stresses induced in the energy pile and the surrounding soil affect the pile-soil interaction and alter the pile capacity. Therefore, several research studies investigating the thermo-mechanical behavior of energy piles have been initiated in the recent past. It goes without saying that the practice of extraction of geothermal energy through heat pumps, pile foundations and other geo-structures can significantly reduce the use of fossil fuel and carbon dioxide emission, and is therefore an important part of sustainable geotechnical practices.

As mentioned previously, there are several applications of thermal geomechanics other than geothermal energy extraction, an important one being deep injection of nuclear wastes. For all these applications, it is important to understand the relevant thermo-hydro-chemo-mechanical behavior of soil and rock, and relate the fundamental behavior to the corresponding applications. Thus, studies related to thermal geomechanics can be classified into (i) study of elemental soil and rock behavior through laboratory tests and constitutive model development, and (ii) study of the applications using centrifuge and field experiments, and through theoretical modeling of the corresponding boundary value problems.

This general report provides a review of 18 papers related to thermal geomechanics that are accepted for publication in the proceedings of 18th ICSMGE. The topics covered by these papers can be grouped into the following broad areas: (i) thermal geomechanics, and (ii) geothermal energy. As the general theme in all these papers is closely linked with sustainable development and a few papers deal with geothermal piles, these papers were assigned to the Sustainability (TC 307) and Deep Foundations (TC 212) committees of ISSMGE with the responsibility of organizing a discussion session and producing a general report based on these papers. In the following section, a summary of the papers is provided and the salient information put forward by each paper are outlined.

2 REVIEW OF PAPERS

2.1 Thermal geomechanics

This sub-section includes the papers that describe the fundamental thermo-hydro-chemo-mechanical behavior of soil and rock through experimentation and modeling studies. Eight papers focus on this fundamental aspect of thermal geomechanics.

Tsutsumi and Tanaka studied the consolidation behavior of clayey soil under the combined effects of strain rate and temperature using a constant rate of strain (CRS) loading apparatus (Figure 1). The CRS apparatus was built based on the Japanese Industrial Standard (JIS) A 1227 (2009) and holds soil specimens with a diameter of 60 mm and an initial height of 20 mm. The water pressure was measured by connecting the bottom of the specimen to a transducer. The soil specimens were subjected to a back pressure of 100 kPa for ensuring full saturation. The displacement was obtained by counting the number of revolutions of the step motor and correcting for the deformation of the apparatus system. The displacement values were used to calculate the nominal strain, void ratio and nominal strain rate. The tests were conducted on reconstituted Louiseville clay samples (collected from Louiseville, Quebec, Canada) at temperatures varying between 10°C and 50°C with strain rates varying over 3×10^{-6} s^{-1} to 3×10^{-8} s^{-1}. Tsutsumi and Tanaka observed that the clay hydraulic conductivity was strongly dependent on temperature, that the preconsolidation stress decreased with increase in temperature, and that the viscous behavior disappeared with decrease in the void ratio (Figure 2). The authors also examined the ageing effects of the clay samples and inferred that it was caused by the acceleration of secondary consolidation wherein the clay particles are rearranged closely because an increase in temperature reduce the viscosity of the adsorbed water layer on the surface of the soil particles. Thus, the specimen developed a new structure exhibiting higher stiffness against subsequent loading.

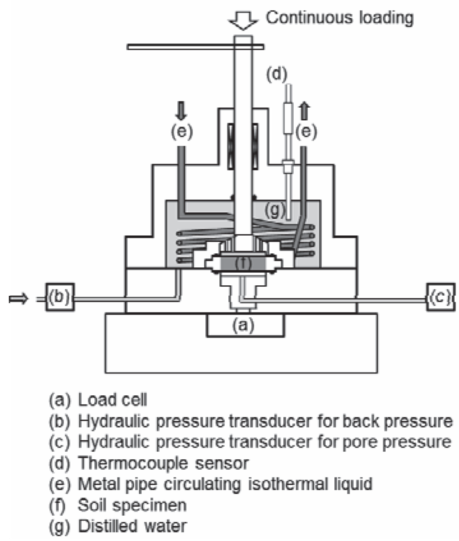

Figure 1. A schematic view of CRS testing apparatus for controlling temperature (Figure 2 of Tsutsumi and Tanaka).

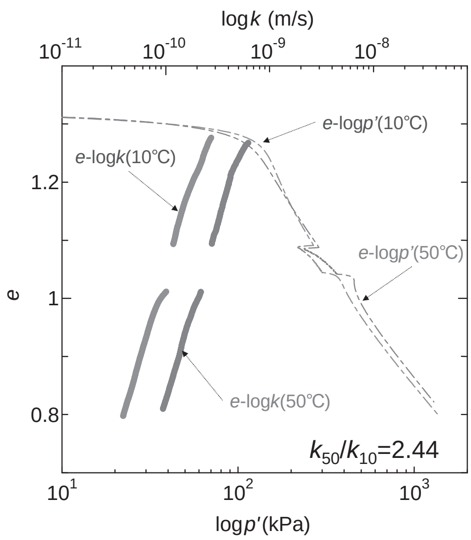

Figure 2. Variation of hydraulic conductivity k with void ratio e and effective stress p' (Figure 4 of Tsutsumi and Tanaka).

Zihms et al. described the effect of high temperature on soil properties. Soils are subjected to high temperatures due to several natural and man-made processes including wild fires, forest fires, and thermal remediation technologies. High temperature affects the particle size distribution, mass loss, mineralogy and permeability of soil. In sandy soils, the particle size decreases with increase in temperature because of mobilization of fines. In clayey soils, the overall particle size increases with increasing temperature owing to aggregation and cementation of the clay fraction. The authors studied the effects of moderate and high temperatures and of smoldering on soil properties and used the results to determine the changes in the soil composition due to temperature change and to predict possible complications that may arise during or after the remediation treatments. Both kaolin clay and its mixture with silica sand were tested, and it was observed that high temperature affects the shear-, plasticity- and infiltration-related soil characteristics. Zihms et al. recommended that more testing should be done to better understand the high-temperature effects on natural materials.

Monfared et al. presented an experimental work on the thermal pressurization of Boom clay, a host geologic formation for potential radioactive waste disposal in Belgium. Undrained heating test was performed under in-situ stress state conditions using a recently developed hollow cylinder triaxial apparatus (Figure 3) that offers a short water drainage path out of soil samples making it favorable for testing low permeability clay and claystone samples. During the heating phase, the thermal pressurization coefficient was determined from the change in pore pressure and the undrained thermal dilation coefficient was calculated from the measurement of volume change. Subsequently, a cooling phase was induced under drained conditions that allowed the determination of the thermo-elastic dilation coefficient. The parameters identified from the tests are important for modeling the thermal behavior of clay at the radioactive waste disposal site.

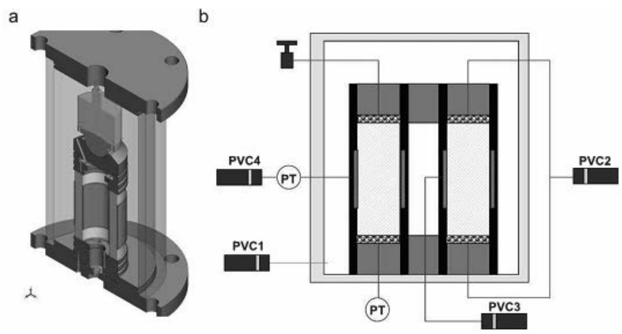

Figure 3. Schematic diagram of hollow cylinder triaxial apparatus (Figure 1 of Monfared et al.).

The study by Romero et al. also involves Boom clay. They investigated the thermal and hydraulic behavior of Boom clay by performing heating pulse tests on intact borehole samples using an axisymmetric and constant volume heating cell (Figure 4) with controlled hydraulic boundary conditions. The study focussed on the time evolution of temperature and pore pressure changes along heating and cooling paths including pore pressure development during quasi-undrained heating and subsequent dissipation according to the applied hydraulic boundary conditions (Figure 5). Romero et al. also performed a coupled thermo-hydro-mechanical (THM) finite element analysis to determine the thermal parameters by back-analysis and then to simulate the experimental results. The study helped in the identification of the main features of the hydro-thermal coupling under test conditions.

Low et al. focused only on the thermal aspects and described two methods to measure the thermal conductivity of soils. They compared the performance of two laboratory-test equipments: the thermal cell which uses a steady state method, and the needle probe which uses a transient method (Figures 6 and 7). Both the methods have their advantages and disadvantages. The needle probe provides results quickly, and hence, is not affected by moisture migration during testing. The thermal cell, on the other hand, requires longer time, and hence, the results from the thermal cell may be affected by moisture migration during testing. The authors performed the tests on London clay samples with the intent that these measurements will help in the analysis and design of energy foundations. They noted that the thermal cell approach is probably more suitable in the context of energy foundations as it can be used to measure the thermal conductivities of other relevant materials such as grout and concrete.

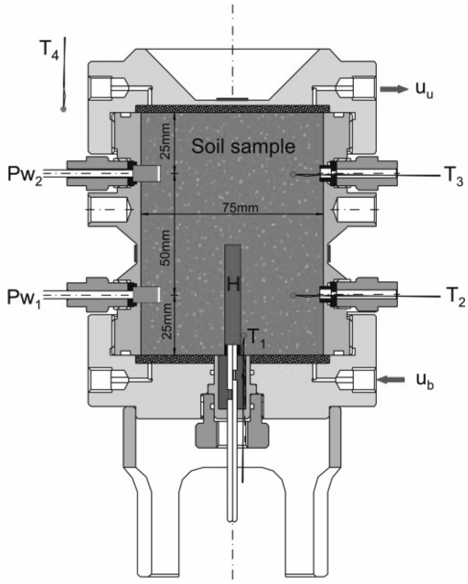

Figure 4. Axisymmetric heating cell and transducers (Figure 1 of Romero et al.).

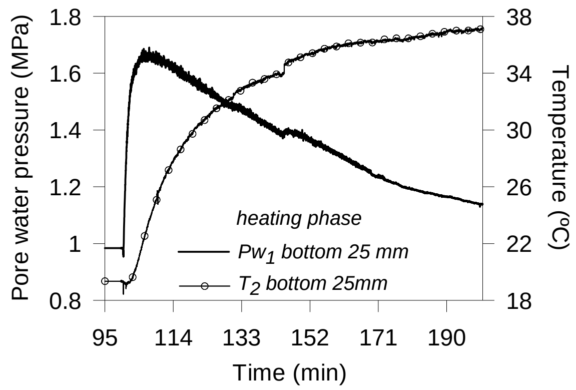

Figure 5. Time evolution of temperature and pore water pressure during heating (Figure 3 of Romero et al.).

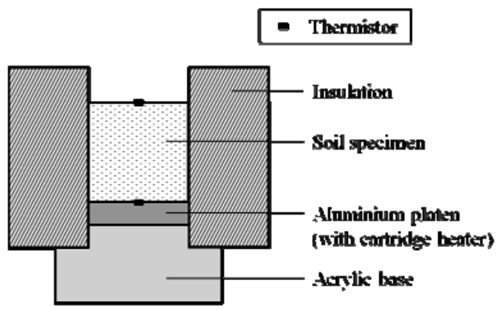

Figure 6. Thermal cell for thermal conductivity measurement (Figure 2 of Low et al.).

Xiong et al. developed a finite element software, SOFT, to simulate the THM behavior of soft rock. They simulated drained triaxial tests performed on soft rock and a field heating test performed by the Mont Terri underground laboratory in a soft rock known as Opalinus clay. The authors simulated the thermal heating isotropic drained triaxial test on soft rock as a boundary value problem with different values of overconsolidation ratio (OCR) and observed that the thermo-mechanical behavior of the soft rock depends on OCR. They simulated the field test with 4275 cubic iso-parametric elements using back-calculated model parameters obtained from a separate simulation of laboratory tests performed earlier on Opalinus clay. Xiong et al. studied the evolution of the temperature, excess pore pressure, and strain fields as functions hydro-thermal coupling under the test conditions can be adequately captured.

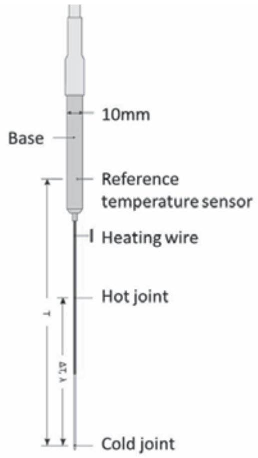

Figure 7. Needle probe for thermal conductivity measurement (Figure 1of Low et al.).

Nishimura et al. presented a multi-scale study in which a local-scale THM analysis of soil was connected to regional-scale geothermal analyses based on regional climatic prediction data, which was, in turn, obtained from the atmosphere ocean general circulation models (AOGCM) after applying statistical and locally informed down-scaling techniques. The purpose of the study was to develop an analytical framework for predicting soil-structure response to climate change in the cold regions. The main intent was to provide broad-scale predictions of geothermal responses at a regional scale that offer hazard zoning schemes related to permafrost thawing. The work will allow engineers to design infrastructure with better resistance to permafrost induced distress. The framework places climate prediction at the highest global level, and applies AOGCM data that is downscaled and calibrated against local climate datasets. The next (middle) level (Figure 8) combines engineering geology with nonlinear, one-dimensional thermal conduction finite element modeling to generate extensive analytical databases from which regional geocryological maps can be created that provide information on both hazard mapping and strategic planning of infrastructure. The lowest level of analysis includes soil-structure interaction modeling using a new THM constitutive model to help predict the complex soil-structure interactions expected as a consequence of temperature-change induced permafrost warming and degradation. The analysis approach and THM models were checked against regional geothermal maps in Eastern Siberia and against field tests on chilled pipelines in Calgary, Canada, and both the checks confirmed the predictions to be realistic.

Komine investigated the variations of swelling pressure and deformation of bentonites, sodium-type bentonite A, (Kunigel-V1) and calcium-type Bentonite C (Kunibond), that are produced in Japan and contain 57% and 80% montmorillonite, respectively. Bentonite is used as buffers for disposal of high-level radioactive wastes because its high swelling behavior helps in sealing wastes. However, the swelling characteristics of bentonite degrade because of the decay-heat from the radioactive wastes. Komine subjected the bentonite samples to different temperatures over different periods of time and then performed swell tests on the samples. The swelling pressure and strains were investigated as functions of the initial dry density and vertical stress and it was observed that the thermal effect on swelling deformation characteristics of sodium-type bentonite A is dependent on the vertical stress condition and that the swelling deformation characteristics of calcium-type bentonite C are markedly reduced by thermal exposure at vertical stress of 1000 kPa and by heating temperatures greater than 90°C for all heating durations (see, for example, Figure 9). Komine also performed chemical analyses such as measurement of cation concentration of water around the bentonite specimens, methylene blue absorption test, and X-ray powder method on the bentonite samples to study how the different cations influence the thermal behavior of the bentonites.

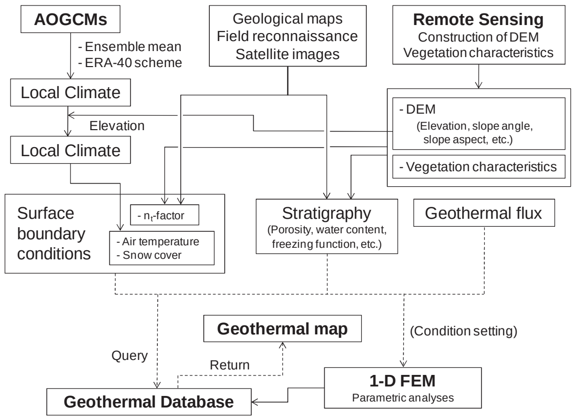

Figure 8. Structure of middle-level analysis to obtain local geothermal predictions based on climate predictions and local geography (Figure 2 of Nishimura et al.).

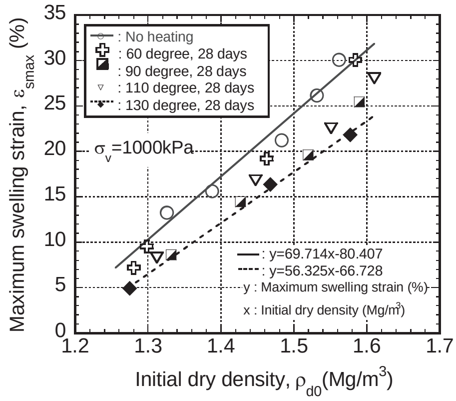

(a) Heating duration 28 days

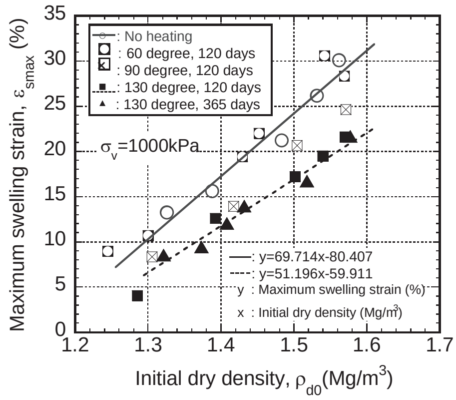

(b) Heating duration 120 days and 365 days

Figure 9. Relation between maximum swelling strain and initial dry density of calcium-type bentonite C at vertical stress of 1000 kPa (Figure 5 of Komine).

2.2 Geothermal energy

This sub-section includes the papers that deal with thermal energy extraction and storage. Out of the ten papers summarized here, four papers deal with different ground heat exchanger systems, five papers deal with geothermal piles, and one paper deals with thermal energy storage.

Bidarmaghz et al. studied the effects of different design parameters such as pipe configuration and fluid flow rate on the rate of heat extraction, and provided information that may aid engineers to design an energy-efficient and cost-effective ground heat exchanger (GHE) system. Finite element analyses were performed, as shown in Figure 10, to model different pipe-loop configurations, fluid flow rates and pipe separation, and to investigate their impacts on the total system efficiency.

Based on the analysis results on a large diameter borehole and for a given borehole length, Bidarmaghz et al. concluded that, as long as the same pipe length is embedded inside the borehole, thermal performance of the system is not significantly affected by pipe geometry placement. In small diameter ground heat exchangers (GHEs), the use of double and double cross U-pipe showed improved performance. The addition of a second U-pipe to both small and large diameter GHEs achieved significant additional (40-90%) thermal performance, and this can lead to major cost savings when compared to single pipe systems. The analysis also indicated that, when considering the size of the fluid circulating pump and its operational cost, highly turbulent fluid flow will not necessarily result in a more efficient system.

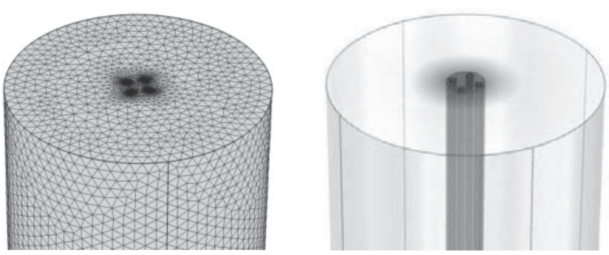

(a) (b)

Figure 10. Typical finite element model section: (a) mesh of a GHE with two U-pipes; (b) details of temperature distribution (Figure 2 of Bidarmaghz et al.).

Katzenbach and Clauss advocated the use of thermosiphon heat pipes in place of conventional heat exchanger U-pipes in GHEs because heat pipes eliminate the use of circulation pumps as the energy is driven through gravity and buoyancy in heat-pipe borehole heat-exchangers (Figure 11). The thermal performance of a heat pipe depends on a number of factors like driving temperature difference, mechanical and thermal properties (e.g., enthalpy) of the heat-carrying fluid, thermal conductivity and capacity, energy withdrawal rate on the condenser side, the geometric dimensions, and the inside pressure. The authors performed numerical analysis to investigate the sensitivity of various parameters like the length and diameter of heat pipe and borehole on the GHE performance. They found that the relationship between length and diameter has a large influence on the specific power (heat) and suggested an optimization of these dimensions in design. Katzenbach and Clauss concluded that the efficient energy transport within the heat pipe allows a relative increase in the coefficient of performance (COP) of 10% or more. They also collected temperature data from an instrumented geothermal heat pipe borehole heat exchanger system installed for new, single-family home. The data was used to compute the expected heat -power output and to assess the operation efficiency of the system.

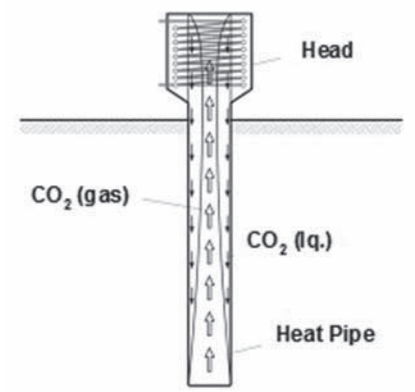

Figure 11. Geothermal heat pipe (Figure 2 of Katzenbach and Clauss).

Grabe at al. simulated the performance of a borehole heat exchanger operated in conjunction with air-sparging induced groundwater circulation using the multiphysics finite element software COMSOL. Groundwater circulation around GHE systems increases the heat-transfer efficiency because heat flow can then happen through convection in addition to the conductive flow that occurs in regular closed-loop GHEs. The authors considered a three-dimensional model in which the heat exchanger borehole is fitted with heat-exchanger and air-injection pipes (Figure 12). They neglected flow inside the well and heat pipes, and considered a homogeneous, sandy aquifer. The computations were performed by assuming that the hydraulic and thermal properties of soil are temperature independent, which implied that groundwater flow is not influenced by heat transport. Grabe at al. simulated the groundwater flow till the attainment of stationary conditions. The results obtained were superimposed with heat propagation in soil. A parametric study was performed by varying the density of air-water mixture inside the well, and the thermal and hydraulic conductivities of soil. A profitability analyses was also performed based on the numerical results. The authors concluded that air-sparging well combined with borehole heat exchanger increased the heat-abstraction capacity and that the system worked well for soil with high hydraulic conductivity.

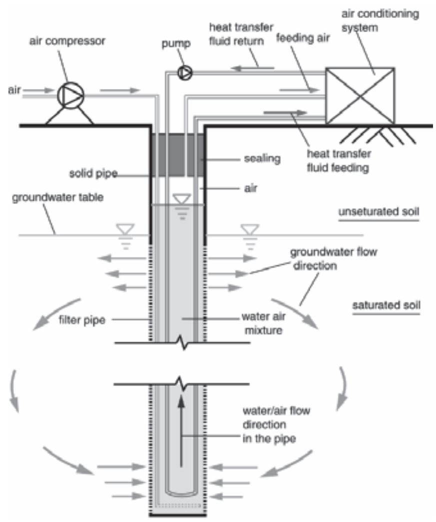

Figure 12. Combination of an air-sparging downhole heat exchanger with an air conditioning system (Figure 1 of Grabe at al.).

Ziegler and Kürten described two examples of novel geothermal energy utilization technique. In the first example, the thermal utilization of smouldering mining dump in the Ruhr area of Germany was described. Three heat-exchange fields consisting of borehole heat exchangers and temperature gauges were installed. Several thermal response tests determining the short-term behavior of the plants and long-term tests were carried out. Numerical simulations and analytical investigations were also performed to identify the important parameters that influence the heat output.

In the second example, Ziegler and Kürten described the use of thermo-active seal panels with integrated heat-exchange pipes (Figure 13) used in underground structures in direct contact with groundwater. The authors tested the efficiency of the panels through laboratory experiments. They noted the importance of heat transfer between soil and heat exchanger for achieving high efficiency. Because both these examples require plane heat-flow models (instead of axisymmetric models) to describe the heat flow, Ziegler and Kürten introduced a new equivalent thermal-resistance model (Figure 14) for describing heat transfer through plane structures.

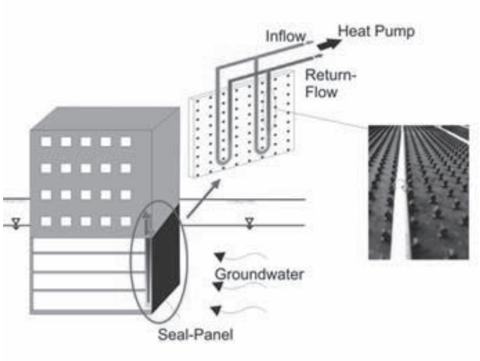

Figure 13. Thermo-active seal panel (Figure 2 of Ziegler and Kürten).

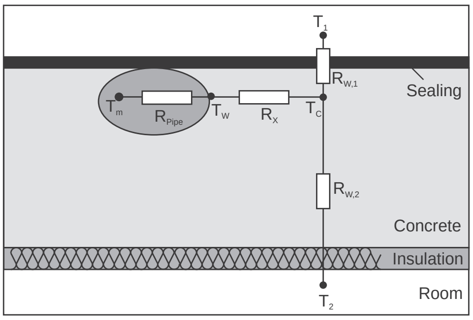

Figure 14. Equivalent star-network thermal resistance model for thermo-active seal panel (Figure 7 of Ziegler and Kürten).

The problem of energy piles is more complicated than that of geothermal heat pumps because of the coupled thermo-mechanical response. The coupled behavior of energy piles is highlighted in the study by McCartney et al. in which they investigated the impact of the pile-head boundary condition on the response of end bearing geothermal piles using a centrifuge test and monitoring a full-scale pile beneath an 8-story building at Denver, CO, USA. In the centrifuge test (Figure 15), the pile had a length of 533.4 mm and a diameter of 25 mm, and the scaling factor was 24. The pile was maintained at a constant temperature and then analyzed for thermally induced stresses and strains with load (no restraint) boundary condition at the head. The full-scale end-bearing drilled shaft (Figure 16) of length 14.8 m and diameter of 0.91 m has three heat-exchanger loops and is restrained at the head due to the presence of grade beams. The authors recognized the difference in the soil profiles and boundary conditions of the two piles and concluded that the boundary condition at the pile head has a significant effect on the magnitude and shape of stress distributions in energy piles.

Wang et al. also investigated through a field test the impact of the coupled thermo-mechanical response of energy pile on its capacity. A full-scale in situ geothermal energy pile equipped with ground loops for heating and cooling, multi-level Osterberg cells, thermistors, strain gages and transducers was installed at Monash University, Australia in an unsaturated, very dense sand profile. It was observed that the shaft capacity increased when the pile was heated and returned to its initial value when the pile was cooled (see Figure 17). The authors noted that energy piles have the potential to reduce the energy demand in built structures. They concluded that further research is required to understand the pile shaft behavior in different soil conditions and to assess the thermal properties of the energy pile ground heat exchanger and the surrounding soil for different field conditions.

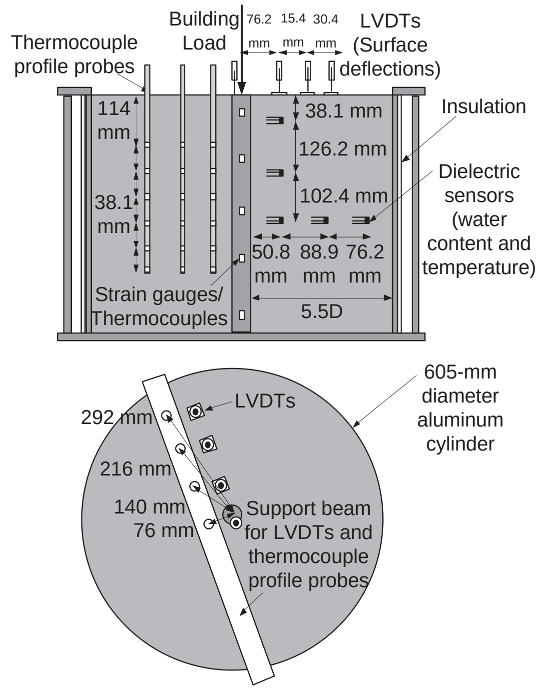

Figure 15. Schematics of the centrifuge-scale energy foundation test (Figure 2 of McCartney et al.).

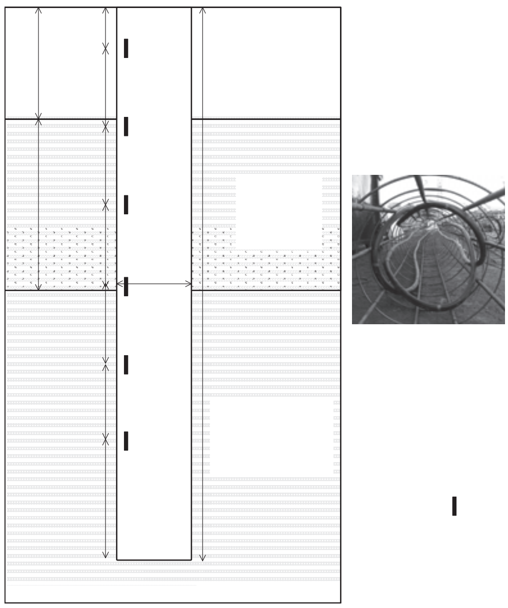

Figure 16. Soil stratigraphy and layout of energy drilled-shaft instrumentation (Figure 3 of McCartney et al.).

Suryatriyastuti et al. presented a theoretical analysis of geothermal piles subjected to heating-cooling cycles and mechanical loading. Two analysis methods were presented to predict the evolution of pile head displacement, axial stresses, and the mobilized soil resistance. The first method is commonly used for design of axially loaded pile, and is based on a model that describes the mobilization of the soil shear strength along the pile-soil interface. The effect of temperature is introduced in the calculation by imposing axial dilation or contraction of the pile corresponding to its thermal dilation or contraction. The analysis produced axial stresses along the pile and pile head displacement under different temperature changes and different pile head conditions. The second method takes into account the effect of thermal cycles. A more complex constitutive model Modjoin was used to simulate the soil-pile interface. Simulations using this model showed that thermal cycles can induce cumulative settlement at the pile head or generate axial stresses along the pile.

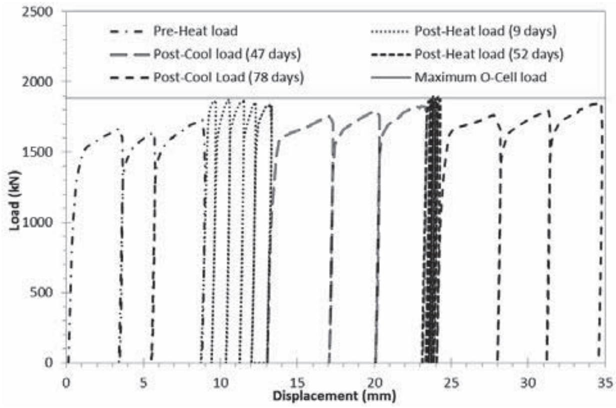

Figure 17. Load versus pile upper-section average shaft displacement – initial, after heating and after cooling (Figure 3 of Wang et al.).

Loveridge and Powrie focussed on the thermal aspects of energy piles. As part of their study, the authors monitored an instrumented pile heat-exchanger system in East London and presented the initial data from the first few months of operation of the energy system. Each pile in the system was installed with a pair of plastic U-pipes, which were inserted into the center of the pile (Figure 18) after the pile cage had been plunged into the concrete. Loveridge and Powrie described the ground conditions and the details of the instrumentation, and analyzed the initially collected data (Figure 19). The data demonstrated the transient nature of the heat transfer within the pile which is not taken into account in most existing design methods. The pile concrete was found to store thermal energy in the short term. The authors concluded that neglecting the short term storage capacity of concrete makes the design over conservative, underestimates the thermal capacity of the pile, and leads to an over estimation of the risk of ground freezing for large diameter piles.

Figure 18. Typical pile heat exchanger at the East London site (Figure 1 of Loveridge and Powrie).

Ponomarov and Zakhrov reported another energy pile foundation application in Russia. Field studies were carried out in a pilot site to determine the temperature distribution in the ground mass, the change of groundwater level, and the physical-mechanical and thermal-physical characteristics of the ground mass. The temperature distribution in the ground and its seasonal variations were obtained from the field monitoring data. In addition, numerical simulations were performed for quantitative evaluation of the thermal energy extracted from different energy foundations under the given climatic and hydro-geologic conditions.

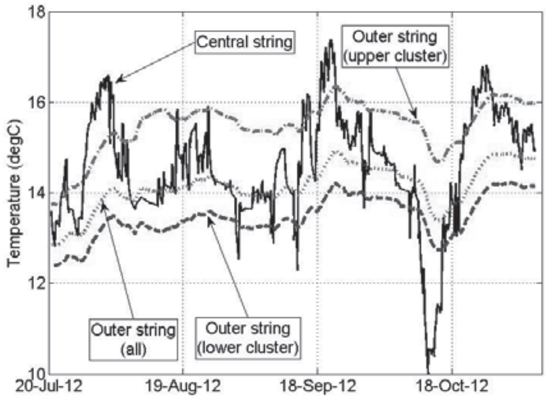

Figure 19. Mean thermistor string temperatures (Figure 6 of Loveridge and Powrie).

The study by Andersen et al. is not related to geothermal energy extraction but to thermal energy storage in an excavated pit in Marstal, Denmark. Thermal energy is usually stored by heating up a material using the available external source of energy (e.g., solar energy), and then this heat is recycled to the consumers using a heat pump. Several thermal energy storage systems using tanks, aquifer, pits, and boreholes are currently used or being considered in Denmark. Andersen et al. described the Marstal town pit-based thermal storage system (PTES), which aims at storing 100% renewable energies in the near future. The authors were involved with the various geotechnical difficulties that occurred during the construction of the PTES shown in Figure 20, which included the excavation stability, the groundwater and soil handling during the construction phase, and the long term consequences of thermal influence on deformations during the operational phase. According to the authors, PTES is applicable to other sites, and the utilization of renewable energy using PTES will enhance the renewable energy resources of other cities in Denmark.

Figure 20. PTES at Marstal, Denmark during completion of excavation and laying out of membrane (Figure 3 of Anderson et al.).

3 SUMMARY

Thermal geomechanincs is an important sub-discipline of geotechnical engineering that has applications in geothermal-energy extraction and thermal-energy storage, soil-structure response due to climate change, storage of nuclear wastes, and several other areas that contribute to the sustainable development of civil infrastructure. This general report summarizes 18 papers on thermal geomechanics and geothermal energy published in the proceedings of the 18th ICSMGE. The papers report a variety of studies encompassing laboratory and field experiments, and modeling. Out of these 18 papers, four papers were submitted from the UK, three from Japan, two each from Australia and France, and one each from Denmark, Russia, Spain, and USA. This indirectly shows the relative early stage of the current state-of-the-art on the thermal and geothermal energy related topics in geotechnical engineering. Eight papers focussed on the fundamental aspects of thermal geomechanics related to the thermo-hydro-chemo-mechanical behavior of soil and rock, four papers dealt with ground heat exchanger systems, five papers dealt with geothermal piles, and one paper dealt with thermal energy storage.

4 ACKNOWLEDGEMENT

Dr. Anh Minh Tang, Senior Researcher at Ecole des Ponts Paris Tech, France helped us in interpreting the papers written in French for which we are grateful.

5 REFERENCES

Andersen J, D., Bodker L. and Jensen M.V. 2013. Large Thermal Energy Storage at Marstal District Heating. *Proceedings of the 18th International Conference on Soil Mechanics and Geotechnical Engineering*, Paper No. 2398.

Bidarmaghz A., Narsilio G. and Johnston I. 2013. Numerical Modelling of Ground Heat Exchangers with Different Ground Loop Configurations for Direct Geothermal Applications. *Proceedings of the 18th International Conference on Soil Mechanics and Geotechnical Engineering*, Paper No. 2816.

Brandl, H. 2006. Energy Foundations and other Energy Ground Structures. *Géotechnique*. 56(2), 81-122.

de Moel, M., Bach, P. M., Bouazza, A., Rao, R. M. and Sun, J. O. 2010. Technological advances and applications of geothermal energy pile foundations and their feasibility in Australia. *Renewable and Sustainable Energy Reviews*, 14, 2683–2696.

Grabe J., Menzel F. and Ma X. 2013. Combination of borehole heat exchangers and air sparging to increase geothermal efficiency. *Proceedings of the 18th International Conference on Soil Mechanics and Geotechnical Engineering*, Paper No. 2356.

Hughes, P.J. 2008. Geothermal (Ground-Source) Heat Pumps: Market Status, Barriers to Adoption, and Actions to Overcome Barriers. *Oak Ridge Nat. Lab. Report* ORNL-2008/232.

Katzenbach R. and Clauss F. 2013. Geothermal Heat Pipe Borehole Heat – Exchangers Computational Simulation and Analysis of Measurement Data. *Proceedings of the 18th International Conference on Soil Mechanics and Geotechnical Engineering*, Paper No. 2373.

Komine H. 2013. Thermal influences on swelling pressure and swelling deformations of bentonites and investigations of its factors. *Proceedings of the 18th International Conference on Soil Mechanics and Geotechnical Engineering*, Paper No. 2010.

Loveridge F. and Powrie W. 2013. Performance of Piled Foundations Used as Heat Exchangers. *Proceedings of the 18th International Conference on Soil Mechanics and Geotechnical Engineering*, Paper No. 2521.

Low J. E., Loveridge F. A. and Powrie W. 2013. Measuring soil thermal properties for use in energy foundation design. *Proceedings of the 18th International Conference on Soil Mechanics and Geotechnical Engineering*, Paper No. 2492.

McCartney J.S., Murphy K.D. and Stewart M.A. 2013. Thermo – Mechanical Behaviour of Energy Foundations. *Proceedings of the 18th International Conference on Soil Mechanics and Geotechnical Engineering*, Paper No. 1822.

Monfared M., Delage P., Sulem J., Mohajerani M., Tang A.M. 2013. Pressurisation thermique dans l'argile de Boom. *Proceedings of the 18th International Conference on Soil Mechanics and Geotechnical Engineering*, Paper No. 1862.

Nishimura S., Jardine, R. J., Fenton C. H., Olivella S., Gens A. and Martin C. J. 2013. Development of a predictive framework for geothermal and geotechnical responses in cold regions experiencing climate change. *Proceedings of the 18th International Conference on Soil Mechanics and Geotechnical Engineering*, Paper No. 2481.

Ponomaryov A. and Zakharov A. 2013. Numerical simulation of the process of geothermal low-potential ground energy extraction in Perm region (Russia). *Proceedings of the 18th International Conference on Soil Mechanics and Geotechnical Engineering*, Paper No. 2672.

Romero E., Lima A., Gens A. and Vaunat J. 2013. Determination of the thermal parameters of a clay from heating cell tests. *Proceedings of the 18th International Conference on Soil Mechanics and Geotechnical Engineering*, Paper No. 2829.

Suryatriyastuti M., Mroueh H., Burlon S., Habert J. 2013. Analyse de la portance des pieux géothermiques. *Proceedings of the 18th International Conference on Soil Mechanics and Geotechnical Engineering*, Paper No. 1742.

Tsutsumi A. and Tanaka H. 2013. One – dimensional compressive behaviour of reconstituted clays under high temperature and small strain state. *Proceedings of the 18th International Conference on Soil Mechanics and Geotechnical Engineering*, Paper No. 2067.

Wang B., Bouazza A., Singh R. M., Barry-Macaulay D., Haberfield C., Chapman G. and Baycan S. 2013. Field investigation of a geothermal energy pile: Initial observations. *Proceedings of the 18th International Conference on Soil Mechanics and Geotechnical Engineering*, Paper No. 2622.

Xiong Y.L., Zhang F., Nishimura T. and Kurimoto Y. 2013. THM simulations for laboratory heating test and real – scale field test. *Proceedings of the 18th International Conference on Soil Mechanics and Geotechnical Engineering*, Paper No. 2290.

Ziegler M., and Kurten S. 2013. New Developments in near-surface geothermal energy systems. *Proceedings of the 18th International Conference on Soil Mechanics and Geotechnical Engineering*, Paper No. 2390.

Zihms S. G., Switzer C., Karstunen M. and Tarantitno A. 2013. Understanding the effects of high temperature processes on the engineering properties of soils. *Proceedings of the 18th International Conference on Soil Mechanics and Geotechnical Engineering*, Paper No. 2513.

Numerical Modelling of Ground Heat Exchangers with Different Ground Loop Configurations for Direct Geothermal Applications

Modélisation numérique des échangeurs de chaleur souterrains avec différentes configurations de boucles pour les applications géothermiques directs

Bidarmaghz A., Narsilio G., Johnston I.
Department of Infrastructure Engineering, The University of Melbourne, Australia

ABSTRACT: The design of ground heat exchangers (GHEs) involves the selection of detailed configuration options. However, there is limited understanding of the relative importance of different design choices on performance. This study investigates the effects of different design parameters such as pipe configuration and fluid flow rate on the heat extraction rate, and will be helpful to design a system which is energy efficient and cost effective. Different pipe configurations in vertical grouted boreholes including single U-pipe, double U-pipe, and double cross U-pipes for small diameter boreholes, and spiral and multiple U-pipes for larger diameter boreholes, are modelled in detail using state-of-the-art finite element methods. The effects of GHE configurations and fluid flow rate on system efficiency is determined and contrasted. Numerical results indicate that the thermal performance of the system is enhanced by transitioning from laminar to turbulent regime, and by increasing the volume of carrier fluid inside the pipes for a given GHE length (i.e., single versus double pipes). However, in larger diameter boreholes, GHE's thermal performance does not change significantly for different pipe configurations with similar pipe lengths inside the borehole (i.e., spiral versus multiple U-pipes).

RÉSUMÉ : La conception des échangeurs de chaleur souterrains (ECS) nécessite un choix parmi différentes configurations. Cependant, la compréhension de l'importance relative des différents choix de conception sur les performances est limitée. Cette étude examine les effets des différents paramètres de conception, tels que la configuration des tuyaux ou encore le débit du fluide sur le taux d'extraction de la chaleur. Elle sera utile pour concevoir un système éco-énergétique et rentable. Différentes configurations de tuyauterie dans des forages verticaux injectés, y compris le simple U-tube, le double U-tube et le U-tube en double croix pour forages de petit diamètre, et de multiples spirales et U-tuyaux pour forages de grand diamètre, sont modélisés en détail en utilisant des méthodes aux éléments finis. Les effets de la configuration d'un ECS et le débit du fluide sur l'efficacité des systèmes sont déterminés et comparés. Les résultats numériques indiquent que le rendement thermique est accru par la transition du régime laminaire au régime turbulent, et en augmentant le volume de fluide porteur à l'intérieur des tubes d'ECS d'une longueur donnée. Toutefois, dans les puits de grand diamètre, la performance thermique d'un ECS ne change pas de façon significative pour les configurations de tuyaux différents avec des longueurs de tuyaux semblables à l'intérieur du puits (par exemple, en spirale ou multiples U-tubes).

KEYWORDS : Direct Geothermal Energy, Vertical Ground Heat Exchangers, Ground Loop Configurations, Numerical Modelling

1 INTRODUCTION

In recent years, geothermal energy has become an alternative energy source with great environmental and economical benefits. Geothermal energy sources range from shallow depths to hot water and hot rocks a few kilometers below the ground surface. Ground source heat pump (GSHP) systems use shallow geothermal energy sources for heating, cooling or even hot water supply of commercial, industrial and residential buildings. The ground temperature below about 5 to 10 meters depth is nearly constant over the year and is close to the mean ambient temperature. Therefore, the ground is warmer than the atmosphere in winter and cooler in summer. GSHP technology takes advantage of this relatively constant ground temperature. In winter time, heat is extracted from the ground and transferred to the indoor area via GSHPs. This process is reversed in summer.

A critical part of GSHP systems is the ground heat exchanger (GHE), with vertical GHEs being a common choice due to their reduced footprint and significantly higher energy performance characteristics in comparison to horizontal systems due to smaller temperature fluctuations in the ground at depth (Banks 2008). The performance of GSHP systems depends on the amount of the heat transferred between the ground and the carrier fluid which circulates within the pipes embedded in the GHEs. Several design choices are required; however, only a relatively limited number of numerical, analytical and experimental studies have been conducted to assist in optimizing the design parameters.

Pipe loop configuration, fluid flow rate and pipe separation are some of many design parameters which affect system efficiency and they are numerically modelled here. Heat transfer and fluid flow are the two main physical processes combined in the numerical model. Heat exchange rates, which arise from temperature distributions in the ground, at the borehole wall and in the carrier fluid in different ground loop configurations, are discussed for a variety of ground loop configurations and operating conditions.

2 MODEL DESCRIPTION

A model of GHEs was developed from first principles, accounting for fluid flow and heat transfer through the various components of the GHE. The model represents GHEs that consist of grouted boreholes placed vertically in the ground, with water circulating within the pipes of these GHEs. Details of these models follow.

2.1 *3D finite element model*

The motion of the carrier fluid in the pipes is described by the well-known Navier-Stokes equations (NS). These equations are the formulation of the continuity law for an incompressible flow which represents the conservation of mass, and the formulation for conservation of momentum described in Eqs (1) and (2) respectively:

$$\rho\nabla.\mathbf{u} = 0 \tag{1}$$

$$\rho\frac{\partial\mathbf{u}}{\partial t} + \rho(\mathbf{u}.\nabla)\mathbf{u} = \nabla.\left(-PI + \mu(\nabla\mathbf{u}) + (\nabla\mathbf{u}^T)\right) + F \tag{2}$$

where ρ is the fluid density in kg/m^3, **u** represents the velocity field in m/s, P is pressure in Pa, I is the identity matrix, μ is the dynamic fluid viscosity in Pa.s, T represents the absolute temperature in K, and F is a volume force field of various origins (for example, gravity) expressed in N/m^3.

In a turbulent flow, all quantities in the previous equations fluctuate in time and space. The averaged representation of turbulent flow divides the flow quantities into an averaged value and a fluctuating part. The decomposition of the flow field into an average part and a fluctuating part, followed by insertion into the NS equations and then averaging, gives the Reynolds Average Navier Stokes equations (RANS), which allows a less expensive computational modelling of fluid flow in the turbulent regime, and is used herein:

$$\rho\frac{\partial\mathbf{u}}{\partial t} + \rho\mathbf{u} + \nabla\mathbf{u} + \nabla.\overline{(\rho\boldsymbol{u}'\otimes\boldsymbol{u}')} = -\nabla P + \nabla.\mu(\nabla\mathbf{u} + (\nabla\mathbf{u})^T) + F \tag{3}$$

Heat transfer from the ground to the heat exchanger and the carrier fluid can be modelled using conduction and convection equations. This process is the result of the flow of energy due to temperature differences. The generalized governing equation for heat transfer can be expressed as:

$$\rho_m C_{p,m}\frac{\partial T}{\partial t} + \rho_m C_{p,m}\mathbf{u}.\nabla T = \nabla.(k_m\nabla T) + Q \tag{4}$$

where ρ_m is the density of a given medium (i.e., fluid or solid) in kg/m^3, **u** is the velocity field in m/s, k_m represents the thermal conductivity of the given medium (i.e., fluid or solid) in W/(mK), $C_{p,m}$ represents the heat capacity of the medium (i.e., fluid or solid) in J/(kgK), and Q is an external heat source in W/m^3. Note that "solid" can refer to soil, rock, concrete, grout, steel or any other solid forming part of the subsurface components of the GHEs.

Heat transfer in the carrier fluid circulating in the pipes results from a combination of heat conduction and convection and can be modelled using Eq (4) in full. Here the fluid velocity field **u** is coupled to Eqs (1) and (2). In other words, the velocity field **u**, found by solving the governing Eqs (1) and (2), is used in Eq (4) when modelling the heat transfer by conduction and convection within the pipes.

On the other hand, heat transfer in solids, which occurs in the ground, in the borehole and in the pipe wall, also uses Eq (4), however, the second term of the left hand side vanishes as the velocity field is null (i.e., no fluid flow), thus Eq (4) reduces to a conduction only phenomenon. This is valid in the absence of groundwater flow.

2.1.1 *Numerical modelling of small diameter GHEs with single, double and double cross U-pipes*

The numerical models consist of 30 m long cylindrical vertical GHEs, 0.14 m in diameter, comprising high density polyethylene (HDPE) pipes embedded in grout, with assumed constant thermal properties (see Table 1 for details).

Table 1. GHEs' material thermal properties.

Material	Thermal conductivity [W/(mK)]	Heat capacity [J/(kgK)]
Soil/Rock	2	1300
Grout	2	854
Water	0.6	4200
HDPE pipes	0.45	-

A single, double or double cross HDPE U-pipe GHE with a pipe diameter of 0.025 m and wall thickness of 0.003 m is sequentially modelled to assess the thermal response of these different pipe configurations. The pipe separation (i.e., distance between inlet and outlet pipes) is set at its maximum value; in the other words, pipes are placed as close as possible to the borehole wall. This is known to render higher thermal efficiency than more closely spaced pipe placements and is common installation practice. The pipe cover, C, is kept equal in all cases modelled here (i.e., C_1 = C_2 = C_3). Therefore, the GHEs embedding single and double cross U-pipes have the same pipe separation $S_1 = S_2 = 0.11$ m, but due to geometry limitations, the pipe separation reduces to $S_3 = 0.07$ m in double U-pipe settings (see Figure 1). A soil cylinder with a diameter of 7 m surrounding the GHE completes the FEM model.

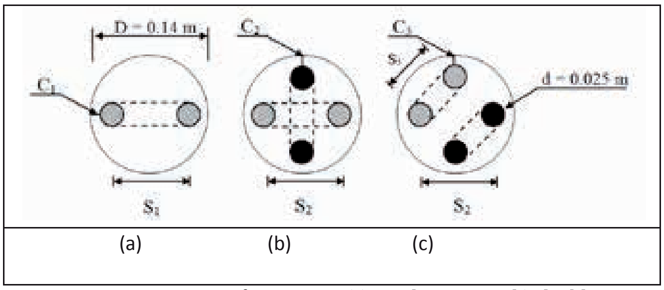

Figure 1. GHE pipe configurations: (a) single U-pipe, (b) double cross U-pipe, (c) double U-pipe.

A 5-day transient study with prescribed fluid flow rates varying from laminar to turbulent regime is conducted on these different GHE configurations. The recommended FEM mesh pattern consists of elements with higher mesh density near and in the pipes, becoming coarser in the radial direction, away from the center of the GHE and towards the ground. Figure 2 shows an example of a 3D model configuration and FEM mesh pattern for a GHE with two U-pipes.

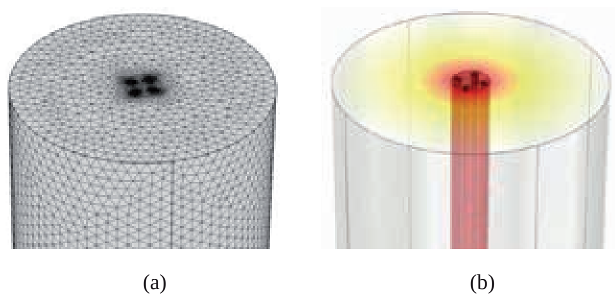

Figure 2. Example of a 3D FEM model section: (a) FEM mesh of a GHE with two U-pipes; (b) detail of temperature distribution.

2.1.2 *Numerical modelling of large diameter GHEs with spiral pipes and multiple U-pipes*

The numerical models consist of 30 m long cylindrical vertical GHEs, 0.46 m in diameter, comprising spiral and straight HDPE pipes embedded in grout. The GHE is surrounded by a soil cylinder of 7 m diameter.

A larger borehole diameter will be typically (but not always) required when HDPE pipes are used in a spiral configuration due to the stiffness of the pipe. GHEs with spiral pipes and with single, double or triple U-pipes are modelled for comparision.

HDPE pipes are 0.025 m in diameter and with a 0.003 m wall thickness. The spiral configuration consists of an inlet pipe with a 0.3 m spiral major diameter and axial pitches which are varied, sequentially, between 0.2 m to 1 m; and a straight outlet pipe (Figure 3-a). Consequently, different pipe lengths are modelled to investigate the effects on heat extraction rate. Numerical results obtained from the above modelling are compared to the results from 0.46 m diameter, 30 m long GHEs with single, double and triple U-pipes, 0.025 m in diameter embedded within, which render the same pipe lengths as the ones in the spiral configurations (see Figure 3-b through -d). The same assumed constant material properties are shown in Table 1. The FEM mesh in these model follows the same mesh density distribution as shown in Figure 2.

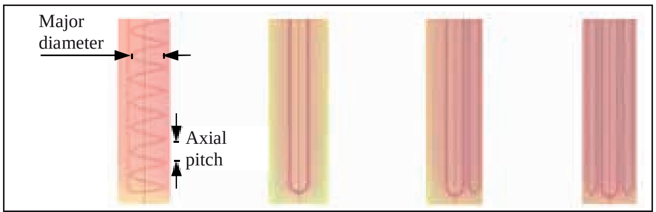

Figure 3. Detail of GHEs with (a) spiral pipe, (b) single U-pipe; (c) double U-pipe, (d) triple U-pipe.

2.2 *Initial and boundary conditions*

A depth dependent temperature, varying between 8.7°C at the ground surface and 18.6°C for the first 10 m below the ground surface, is applied over the entire model (the GHEs and the ground) as initial and far-field boundary condition. Below this relatively thin layer and from about 10 m to 30 m below the ground surface, a constant temperature of 18.6°C is applied to the rest of the model. To account for the thermal interaction between conductive and convective heat transfer, the inlet temperature and fluid flow rate are also specified as boundary conditions. The simulations are run in heating mode, that is, whilst extracting heat from the ground. For simplicity, a typical inlet temperature of 5ºC is prescribed in the inlet pipe(s) of the modelled GHEs. For the fluid flow simulation inside the pipes, a no slip boundary condition is applied on the pipe walls, in other words, the water velocity on the pipe wall is set to zero; and a reference atmospheric pressure is set in the outlet pipe(s) for the purpose of forced convection.

3 RESULTS

In this section a brief summary of the model validation is presented together with the results of the numerical simulations of the various ground loop configurations and fluid flow rates.

3.1 *Model validation*

Numerical results obtained from the transient study of GHE with a single U-pipe were validated against analytical solutions that are based on Infinite Line Source Model (ILSM), Finite Line Source Model (FLSM) and Cylindrical Source Model (CSM). Details of these solutions can be found elsewhere (Bernier 2001, Deerman 1990, Jun *et al.* 2009, Lamarche and Beauchamp 2007, Marcotte and Pasquier 2008). As an example, Table 2 summarises the results in terms of heat extraction rate q and outlet pipe(s) temperature T_{out} for the case of a 30 m long GHE, with 0.025 m diameter single U-pipe and water flow rate of ~14.5 l/min after 120 hrs of operation. Numerical results are in good agreement with the FLSM, which is the most reliable model among the previously mentioned models. The numerical results are also within the range of measurements reported for full scale experiments (Banks 2008, Gao *et al.* 2008, Hamada *et al.* 2007, Miyara *et al.* 2011).

Table 2 Comparison between analytical and numerical solutions.

Parameter	ILSM	FLSM	CSM	Field data	This work
q [W/m]	30.67	44.93	32.14	10-60	48.87
T_{out} [°C]	5.93	6.36	5.97	-	6.48

3.2 *Numerical results and discussion*

With the numerical model validated for the single U-pipe case, other GHE pipe configurations were then examined: the double U-pipe and the double cross U-pipe. Cross sections of all small diameter GHEs were shown in Figure 1. We studied the effects on the thermal performance of these GHE configurations caused by variations of water flow rate. Figure 4 shows a summary of the numerical results for GHEs with single, double and double cross U-pipes, expressed as the total average heat extraction of each GHE per meter depth of borehole.

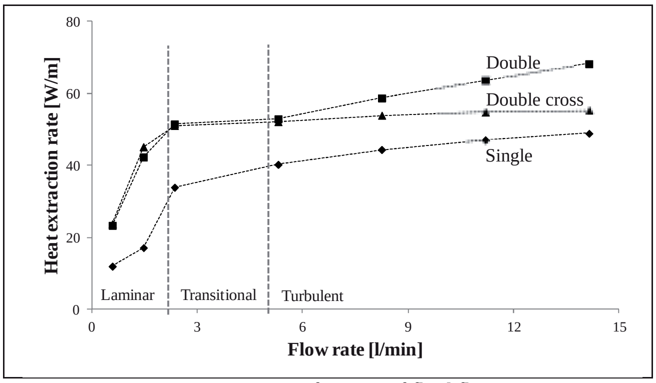

Figure 4. Heat extraction rate as a function of fluid flow rate.

As the average water flow rate increases in the pipe, heat extraction rate first tends to increase at a high rate for all GHE configurations considered here. However, above a flow rate of approximately 5.30 l/min (u = 0.18 m/s) the flow becomes turbulent and the increase in the heat extraction rate with flow (or Reynolds number) slows down in comparison with the laminar regime. Thus higher flow rates, do not necessarily results in significant increase in system's efficiency and the rate of increase declines with Reynolds number beyond a certain threshold. The addition of a second U-pipe to a single U-pipe configuration does not double the thermal performance but achieves between about 40% to 90% additional performance, depending on the volume of the water in contact with the ground heat source/sink. Nevertheless, savings may be achieved in terms of drillings costs, given the reduction in the total number or length of GHEs than would be needed with a single U-pipe. The comparison of double U-pipe and double cross U-pipe configurations shows that GHEs with double U-pipe perform about up to 23% better while the water fluid flow is in turbulent regime, and has nearly the same performance in laminar regime, for the pipe separations studied here.

For the case of large diameter GHEs, Figure 5 shows the effect of axial pitch in GHEs with spiral pipes. The figure shows that smaller axial pitches, which render longer pipe length, result in higher thermal performance since there is larger contact area between the water and the ground heat source/sink.

Comparing the thermal performance between large diameter GHEs with spiral pipes and U-pipes, Table 3 shows that for a given total water flow rate of 14.5 l/min in each GHE, and borehole length and diameter, GHEs with same pipe length embedded within have nearly the same thermal performance regardless of pipe geometry specifically when dealing with more than one U-pipe (i.e., spiral and multiple U-pipes with 0.14 m of pipe separation). Therefore, GHEs with multiple U-pipes instead of spiral pipes would be recommended, since (i) installation of GHEs with spiral pipes is, in general, not as easy to implement as with U-pipes due to HDPE pipe stiffness, and (ii) they have nearly the same thermal performance. In these large diameter GHEs, a relatively minor change in heat extraction rate is suggested by the numerical results when the total the flow rate through the GHE is increased. The rightmost column in Table 3 summarises the numerical results of doubling and tripling the flow rates in GHE with double U-pipes and triple U-pipes respectively (the same fluid flow rate is applied to each U-loop of the GHEs).

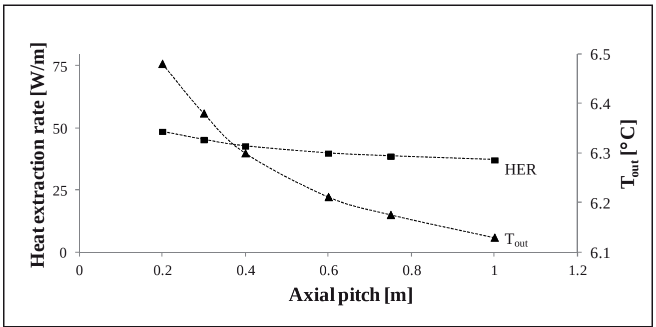

Figure 5. Heat extraction rate and outlet temperature in a spiral GHE with different axial pitches.

Table 3. Comparison of spiral and U-pipes GHE thermal performance for varying pipe lengths.

Geometry	Axial Pitch [m]	Pipe length [m]	Flow rate of 14.5 l/min in each GHE	Flow rate of 14.5 l/min in each U-pipe
			Heat extraction rate [W/m]	Heat extraction rate [W/m]
Spiral 1	0.2	180	48.63	48.63
Triple U	-	180	49.71	51.15
Spiral 2	0.3	120	45.35	45.35
Double U	-	120	44.07	45.10
Spiral 3	1	60	37.13	37.13
Single U-pipe	-	60	32.53	32.53

The previous observations will not vary significantly if different pipe separations in the U-pipes are used. To investigate the effects of pipe separation on GHEs thermal performance, single, double and triple U-pipes with different inlet-outlet pipe separations were simulated. Figure 6 shows variations of pipe separation for multiple U-pipe GHEs and how this affects the heat extraction rate. Pipe separation variations between S_S = 0.04 m and S_L = 0.28 m for the 0.46 m diameter GHE result in heat extraction rate increasing about 7% to 23%.

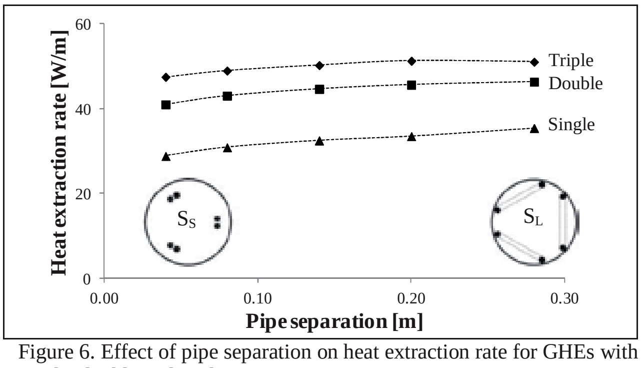

Figure 6. Effect of pipe separation on heat extraction rate for GHEs with single, double and triple u-pipes.

It is worth mentioning that pipe separation has a stronger influence on GHEs with single U-pipe than that of a triple U-pipe, the reason being that in multiple U-pipes, increasing the separation reduces the thermal interference between inlet and outlet pipe of one U-pipe but at the same time increases mutual interference between different U-pipes inside the GHE.

4 CONCLUSIONS

The outcomes of the multiple simulations performed in this work show that GHE configuration may affect system efficiency. Based on numerical results in a large diameter borehole and for a given borehole length, it seems that as long as the same pipe length is embedded inside the borehole, thermal performance of the system is not significantly related to pipe geometry placement, at least for the spiral and multiple U-pipes analysed here. However, comparison of small diameter GHEs with double and double cross U-pipe shows between 8% to 23% better performance of the former one. Nevertheless, the addition of a second U-pipe to both small and large diameter GHEs achieves significant (40-90%) additional thermal performance and could lead to important cost savings when compared with single pipe systems due to reduced drilling costs.

Heat extraction rates tend to increase rapidly as the Reynolds number increases in the laminar regime; however, the rate of increase reduces with Reynolds numbers once the flow becomes turbulent. This indicates that when considering the size of the fluid circulating pump and its operational cost, highly turbulent fluid flow will not necessarily result in a more efficient system overall. Regardless of number of U-pipes inside the GHE, larger pipe separation improves the system efficiency. However, as the number of U-pipes in the GHE increases, this effect becomes less pronounced due to thermal interference occurring between different U-pipes.

5 ACKNOWLEDGEMENTS

This work is partially supported by funding of $1.6 M from the Victorian Government's Energy Technology Innovation Strategy (ETIS) Pilot Demonstration Program (SEPD) and The University of Melbourne's Research Collaboration Grant.

6 REFERENCES

Banks, D. 2008. An introduction to thermogeology: ground source heating and cooling, Wiley-Blackwell.

Bernier, M.A. 2001. Ground-coupled heat pump system simulation. *ASHRAE Transactions* 107, 605-616.

Deerman, J. 1990. Simulation of vertical U-tube ground-coupled heat pump systems using the cylindrical heat source solution. *ASHRAE Transaction: Research* 3472, 287-295.

Gao, J., X. Zhang, J. Liu, K.S. Li and J. Yang 2008. Thermal performance and ground temperature of vertical pile-foundation heat exchangers: A case study. *Applied Thermal Engineering* 28(17), 2295-2304.

Hamada, Y., H. Saitoh, M. Nakamura, H. Kubota and K. Ochifuji 2007. Field performance of an energy pile system for space heating. *Energy and Buildings* 39(5), 517-524.

Jun, L., Z. Xu, G. Jun and Y. Jie 2009. Evaluation of heat exchange rate of GHE in geothermal heat pump systems. *Renewable Energy* 34(12), 2898-2904.

Lamarche, L. and B. Beauchamp 2007. A new contribution to the finite line-source model for geothermal boreholes. *Energy and Buildings* 39(2), 188-198.

Marcotte, D. and P. Pasquier 2008. Fast fluid and ground temperature computation for geothermal ground-loop heat exchanger systems. *Geothermics* 37(6), 651-665.

Miyara, A., K. Tsubaki, S. Inoue and K. Yoshida 2011. Experimental study of several types of ground heat exchanger using a steel pile foundation. *Renewable Energy* 36(2), 764-771.

The response of energy foundations under thermo-mechanical loading

La réponse des fondations thermo actifs sous chargement thermo mécanique

Bodas Freitas T.M., Cruz Silva F., Bourne-Webb P.J.
Instituto Superior Técnico, Lisboa, Portugal

ABSTRACT: The need to establish a sound basis for the understanding of the behaviour of geo-structures that are utilised for energy exchange within ground source heat pump systems has received increasing attention in recent years and a number of physical and numerical modelling studies of such systems have been undertaken. This paper details the results of a preliminary numerical study of the response of a foundation pile under steady-state heating, which when compared to the results of published observations, raises some interesting questions regarding the models of behaviour proposed in the literature and areas requiring further study in the future.

RÉSUMÉ : La nécessité d'établir une base solide pour la compréhension du comportement des géo-structures qui sont utilisés pour l'échange d'énergie dans les systèmes de pompe géothermique a reçu une attention croissante ces dernières années et un certain nombre d'études de modélisation physique et numérique de ces systèmes ayant été entrepris. Cet article détaille les résultats d'une étude numérique préliminaire de la réponse d'une fondation sur pieux sous chauffage stationnaire qui, lorsqu'il est comparé aux résultats de certaines observations publiées, soulève des questions intéressantes concernant les modèles de comportement proposés dans la littérature et les zones nécessitant une étude plus approfondie dans le futur.

KEYWORDS: pile, foundations, ground source energy, thermo-mechanical loading.

1 INTRODUCTION

The use of ground energy systems that employ heat-exchange loops within trenches and boreholes is well established and the technology is recognised as a key component for future sustainable energy use (Mackay, 2009).

While still a small component of the ground energy market, the use of civil engineering structures that are in contact with the ground (geo-structures) to replace the more convention heat-exchange methods is creating great interest. Bearing piles have been used for this purpose since the mid-1980s and more recently other elements have been used, e.g. retaining walls & tunnel linings.

Energy geo-structures and in particular, bearing piles are now often used in Austria, Germany and the UK, and there is increasing interest in their potential in many countries including the USA, Japan and China. However, the uptake of these alternative means for facilitating heat-exchange with the ground has been impeded by a lack of technical evidence regarding the impact of the thermal cycles on the serviceability and safety performance of the geo-structures.

This paper presents the results of a set of numerical analyses that were undertaken to evaluate the mechanisms of response of piles used for heat-exchange. First, to complete this introduction, observations of the thermo-mechanical (TM) response of piles and clay soil are reviewed. Then the basis for the analyses and the predictions that were obtained are presented, and the implications of the results are discussed. Finally, some ideas for future research in this field are suggested.

1.1 *Energy geo-structures*

Very few field or laboratory studies, where the TM response of energy geo-structures has been systematically observed, have been published. Energy geo-structures include load bearing piles, piled and diaphragm walls, and tunnels. To-date, published TM studies have involved only pile foundations (Brandl, 2006; Laloui et al. 2006; Bourne-Webb et al. 2009; McCartney & Rosenberg 2010).

The mechanisms of response seen in the pile tests appear to be broadly consistent and can be described in a simple schematic way (Amatya et al. 2012; Bourne-Webb, et al. 2013). Underlying this descriptive framework is the implicit assumption that the pile expands and contracts relative to the surrounding soil when heated and cooled, respectively. Thus, when heated the axial strain/forces in the pile become more compressive and when cooled less compressive (potentially even tensile pile axial response is seen), Fig. 1.

Associated with the pile axial response described above, the response at the pile-soil interface is also affected with the changes in mobilised pile shaft friction (shear stress) opposing the expansion and contraction of the pile, Fig. 1. These changes in pile axial response and mobilised pile-soil interface friction will occur on a daily and seasonal basis as the heating/cooling energy demand of the structure, that the ground energy system serves, varies.

1.2 *Thermo-mechanical characterization of clay*

The effect of temperature changes on the behaviour of soil is of interest in a number of fields including the sequestration of nuclear waste, buried high voltage electricity cables, buried pipelines, and increasingly energy geo-structures.

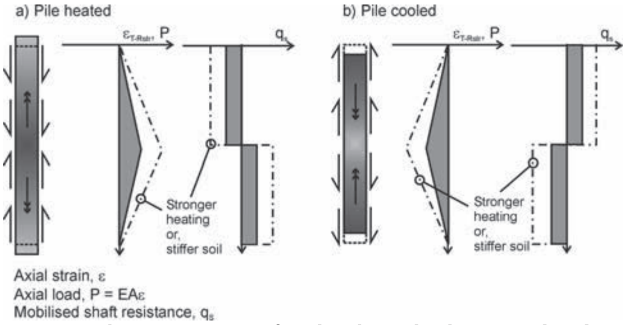

Figure 1. Schematic response of a pile subjected to heating and cooling, after Bourne-Webb et al. 2013.

In addition to the general impact on soil behaviour, the impact of temperature cycles at the pile-soil interface is also of interest in the case of energy geo-structures.

Experimentally, the effect of temperature on the mechanical behaviour of clayey soils has been found to be equivalent to that of strain rate, Marques et al., 2004. The effects are permanent and the soil behaviour can be described by a unique stress-strain-temperature law. In addition, it is found that while peak undrained strength increases with decreasing temperature, the critical state failure envelope is unique in stress space but temperature dependent in void ratio–mean effective stress space.

The thermal volumetric response of clay soil has been examined in a number of laboratory investigations (Campanella & Mitchell 1967; Baldi et al. 1988; Cekerevac & Laloui 2004) and it was found that the volume change of a clay sample in response to a change in temperature depends on the over-consolidation ratio (OCR). When heated, normally consolidated soil (OCR = 1) contracts (implying a negative coefficient of thermal expansion) and as the OCR increases, the soil becomes increasingly less contractive with moderately to highly over-consolidated (OC) clay being expansive, i.e. with positive values of the coefficient of thermal expansion, Fig. 2.

The testing also suggests that the thermal expansion of OC clay is reversible but there is a limit to the range of temperatures over which this occurs. At higher temperatures OC clay becomes contractive, e.g. at about 50°C in Fig. 2.

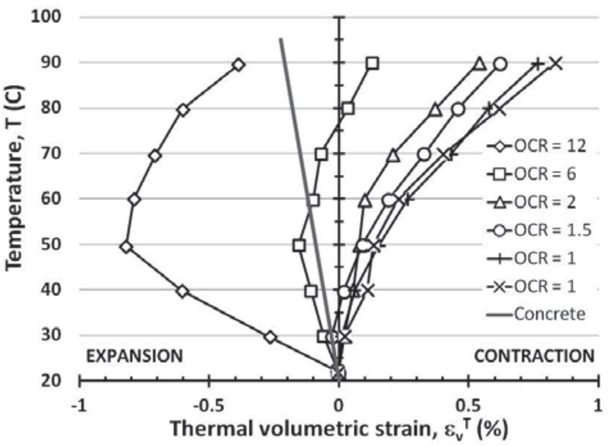

Figure 2. Effect of OCR on thermal volumetric response of Kaolin, after Cekerevac & Laloui, 2004.

Thus, a heavily OC clay such as the London Clay that supported the Lambeth College test pile, should expand more than concrete, perhaps by a factor of two or more.

The relative deformation of the pile with respect to the soil, in response to temperature change, is thought to be the source of the observed changes in pile response. Therefore, in this study, the effect of variations in the soil coefficient of thermal expansion relative to that of a concrete pile undergoing heating was evaluated. Table 1 summarises some typical values of this parameter for stiff over-consolidated clay found in the literature, and which formed the basis for selecting values for the numerical analyses, Table 2. Also, detailed in Table 1 are values of the coefficient of thermal expansion for water and concrete. The latter is primarily dependent on the type of aggregates that are used in the concrete mix.

Table 1. Typical values of volumetric coefficient of thermal expansion, β quoted for two clayey soils, concrete and water.

Material	β *(E-5, °K^{-1})*
Boom clay	4 to 6
Opalinus clay	
Concrete	2 to 4
Water (at 22°C)	27

2 BASIS FOR FINITE ELEMENT ANALYSES

2.1 *Geometry and boundary conditions*

A single pile with a diameter, D of 1.0 m and length, L of 30 m has been modelled in the program ADINA V8.5.0 assuming axisymmetry. After initial verification analyses, the side and bottom boundaries of the finite element mesh were set at a distance of 60 m (2L) and 90 m (3L) respectively, Cruz Silva, 2012.

No interface elements were introduced between the pile and soil solid elements, implying that the contact was perfectly rough. This also implies that the stiffness in the interface zone is the same as that for the soil, whereas the response on the pile-soil interface is known to be significantly stiffer.

Mechanical loading of the pile was modelled by applying a boundary pressure (6 MPa) that resulted in a pile settlement of about 1% of the pile diameter, i.e. about 10 mm. Displacement boundary conditions fix horizontal movement on the bottom and the two side boundaries while vertical movement is prevented only on the bottom boundary.

Thermal loading of the pile was modelled by the application of an increment of temperature ΔT=+30°C to all the elements making up the pile under steady state heat flow conditions. It is acknowledged that this is a simplification with respect to the actual temperature distribution in the pile cross-section and surrounding soil with time, but is considered to be reasonable with respect to the temperature along the pile which has been found to be almost constant, Bourne-Webb et al. 2009. Thermal boundary conditions ensured zero heat flow on the model centreline, and zero temperature change on the side and lower boundaries. Two scenarios were examined regarding the thermal boundary condition along the ground surface: zero heat flow and constant temperature. The resultant temperature fields are shown in Fig. 3. Again, these are acknowledged to be significant simplifications of the actual thermal conditions at the ground surface, although the latter is probably closest to reality.

2.2 *Material parameters*

In these analyses, both the pile and the soil were assumed to be elastic. This is considered to be a reasonable assumption for the structural element but is acknowledged to be a great simplification with respect to soil response which can be strongly nonlinear.

However, the aim of this study was to examine the pile response to temperature change on a simplified basis; additional layers of complexity may be added subsequently, including e.g. an interface with finite shear resistance, nonlinear TM/THM soil model(s), more realistic thermal loading and boundary conditions.

The adopted model parameters are shown in Table 2. In all the analyses undertaken, β for the concrete was held constant with a value of 3.0E-5°K^{-1} (note that the coefficient of linear thermal expansion, α = β/3). The values of β assumed for the soil were zero, half and double that for the concrete; representing a moderately OC clay.

In addition, the Young's modulus of the soil was increased by a factor of two from the base value of 30 MPa, in order to assess the effect of this parameter on the predicted thermal response of the pile.

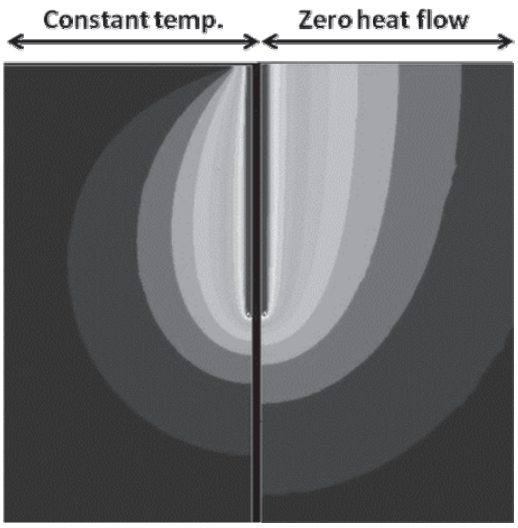

Figure 3. Steady-state temperature field as function of surface thermal boundary condition (contour interval: 2°C)

Table 2. Material parameters assumed for numerical analysis.

Parameter	*Concrete*	*Soil*
Young's modulus, E (MPa)	30000	30 or 60
Poisson's ratio, μ (-)	0.3	0.3
Coefficient of volumetric thermal expansion, β (E-5, °K^{-1})	3.0	0, 1.5 or 6.0
Thermal conductivity, k (kJ/hr.m.K)	8.4	4.0
Volumetric heat capacity, ρc_p (kJ/m^3.K)	1950	1500

3 PREDICTIONS

3.1 *Coefficient of thermal expansion*

The effect of changes in the value of the coefficient of volumetric thermal expansion, β of the soil, the stiffness of the soil and the thermal boundary condition on the ground surface of the model are illustrated, in terms of changes in pile axial stress, Fig. 4 and pile-soil interface shear, Fig. 5.

When comparing the plots, the dashed line for the β = zero case (the soil is thermally inert) provides a baseline for comparison, as the results are independent of the thermal boundary condition on the ground surface.

When the soil is less thermally expansive than the pile, i.e. β = 1.5E-5°K^{-1} and zero, heating the pile led to compressive axial stress with the maximum stress change for each β-value equating to about +12% and +15% of the stress that would be mobilised if the pile was fully restrained, P_{fix} (Table 3). The constant temperature boundary condition results in slightly greater (1 to 2%) restraint of the pile thermal expansion and thus, higher compressive axial stress are developed.

The effect of the thermal boundary condition on the ground surface becomes clearer when the soil is assumed to be more expansive than the pile (β = 6.0E-5°K^{-1}); when a zero heat flow condition was assumed, the pile went into tension (max. stress about -2% of P_{fix}) however, as identified above, the use of a constant temperature boundary condition resulted in greater restraint and the resulting stress changes were compressive (max. stress about +5% of P_{fix}) along the entire length of the pile.

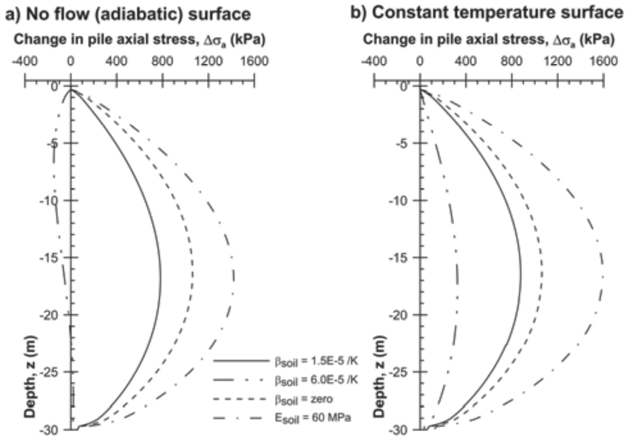

Figure 4. Change in pile axial stress due to temperature change of +30°C, Cruz Silva 2012.

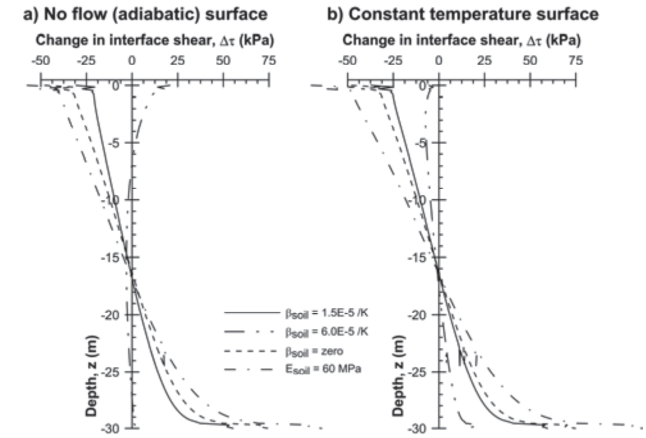

Figure 5. Change in pile-soil interface shear stress due to temperature change of +30°C, Cruz Silva 2012.

The shape of the profiles of predicted axial stress change (approx. parabolic) in Fig. 4 are directly related to the shape of the profile of mobilised friction at the pile-soil interface, Fig. 5 which is approximately linear (note that in Fig. 1 the mobilised friction was assumed constant and therefore the variation in axial stress was linear with depth).

Here again the effect of the coefficient of volumetric thermal expansion of the soil and the thermal boundary condition on the ground surface is seen. As the contrast in β-values of the pile and the soil increases, the magnitude of the predicted change in shear stress on the pile-soil interface, and the constant temperature condition leads to larger changes in shear stress compared to the zero heat flow condition.

As a consequence of the model being elastic and the interface not being modelled explicitly, i.e. with an appropriate stiffness and limiting strength, the shape of the interface friction (shear stress) profiles differs from that expected based on the simple model in Fig. 1 (which effectively assumes perfect plasticity) and the profiles inferred from observations in test piles, Amatya et al. 2012. The variation in shear stress along the pile-soil interface suggested here is only likely to be correct while the maximum stress values are below the yield strength on the interface.

3.2 *Soil stiffness*

In these analyses, the coefficient of thermal expansion in the soil was held at 1.5E-5°K^{-1}, and the soil Young's modulus was doubled from 30 MPa to 60 MPa. The predicted response in terms of change in axial stress and pile-soil interface shear for this case is also shown in Figs. 4 and 5 (dash-dot line) and can be compared to the analysis that used a soil Young's modulus of 30 MPa (solid line).

As the soil Young's modulus doubled from 30 MPa to 60 MPa, both the change in axial stress and interface shear stress increased, although the proportionality between the solutions was slightly less than two, due to relative pile-soil compressibility effects.

These results show that the operational stiffness in the soil mass will influence the response seen in the thermally loaded pile, and also illustrates how a stiffer shear response at the interface may lead to higher axial stresses in the pile.

4 DISCUSSION

Although a simple elastic model has been used to represent the pile and soil in the analyses presented here, the results presented highlight some interesting features.

The first relates to the compatibility of these results with observations and the simple descriptive models previously presented. The descriptive model was developed from and in order to explain the observed mechanisms of response in the few TM pile tests that have been reported in the literature and thus, implicitly assumes that the pile expands/contracts more that the soil.

In the analyses presented here when this assumption was met, the predicted response was inline with observations, with some differences due to the assumption of elastic soil response, i.e. linear variation of friction at pile-soil interface.

The predicted changes in axial stress were rather small when compared with the values measured in the field, and the theoretical value for a pile fully restrained against thermal deformation. Table 3 provides a comparison of the predicted (FEA) and observed restraining effect on two test piles, from Amatya et al. 2012.

This suggests that the pile as modelled in the FEA was almost completely free to expand and contract (the predicted deformation between the extremities of the pile confirms this), even when additional restraint in the form of either a larger differential in soil-concrete β-values or higher soil stiffness was considered.

Table 3. Thermal load and axial stress response of model and test piles.

Parameter	*FEA*	*Lambeth*	*EPFL*[2]
Temperature change, ΔT (°C)	+30	+29[1]	+21
Max. axial stress change as %-fully restrained value, P_{fix}[3]	10% - 20%	56%	36%

Notes: 1. First heating phase of Lambeth College heat sink pile;
2. First heating phase, Test T-1, EPFL
3. $P_{fix} = \alpha \Delta T A_{pile} E_{pile}$ (= 7069 kN for FEA results)

The second point of note relates to the importance and interdependence of the thermal boundary condition as demonstrated here by the assumption of either zero heat flow (perfect insulation) or constant temperature (no change relative to starting temperature) on the ground surface and the relative thermal expansion between the soil and the pile.

The results suggest that the thermal boundary conditions and thus the temperature field within the model impart their own form of restraint in the pile-soil interaction process, in addition to any mechanical restraint of the pile.

In particular, the cases examined here illustrate that the temperature field in the vicinity of the head of the pile was crucial in determining the form of response obtained from the analysis, i.e. while heating a pile in a soil with a higher coefficient of thermal expansion than the pile itself – as was the case in the Lambeth College test - compressive stresses where predicted only when a constant temperature boundary condition was specified at ground surface.

The constant temperature surface boundary condition meant that the soil near the surface and adjacent to the pile head was cooler, and despite the soil having a higher coefficient of thermal expansion, the pile was still able to expand relative to the soil mass and thus generate compressive axial stresses.

5 CONCLUSIONS

A linear elastic numerical model has been applied to the problem of the TM loading of piled foundations and the results have been found to generally reproduce observed mechanisms of behaviour.

The results presented here highlight that there is a complex interaction between the foundation and soil material's thermal characteristics, and the thermal boundary conditions. The sensitivity of the predicted response to these relationships needs to be investigated further.

Finally, the factors that determine the degree of fixity against thermal expansion that can be mobilised on the pile shaft also require deeper investigation, and future studies will focus on the pile-soil interface and the impact of thermal boundary conditions.

6 REFERENCES

Amatya B.L. Soga K. Bourne-Webb P.J. Amis T. and Laloui L. 2012. Thermo-mechanical behaviour of energy piles, Géotechnique, **62**(6), 503-519

Baldi G., Hueckel T. and Pellegrini R. 1988. Thermal volume change of the mineral-water system in low-porosity clay soils. Can. Geot. J., **25**, 807-825

Bourne-Webb P.J. Amatya, B. Soga K. Amis, A. Davidson, C. and Payne P. 2009. Energy pile test at Lambeth College, London: geotechnical and thermo-dynamic aspects of pile response to heat cycles, Géotechnique **59**(3), 237-248

Bourne-Webb P.J. Amatya B. and Soga K. 2013. A framework for understanding energy pile behaviour, ICE Proc. Geotechnical Engineering, 1-8 (http://dx.doi.org/10.1680/geng.10.00098)

Brandl H. 2006. Energy foundations and other thermo-active ground structures, Géotechnique **56**(2), 81-122

Campanella R.G. and Mitchell J.K. 1968. Influence of temperature variations on soil behavior. ASCE J. Soil Mech. and Fdtn. Div., ASCE, **94**, 709-734

Cekerevac C. and Laloui L. 2004. Experimental study of thermal effects on the mechanical behaviour of a clay. Int. J. Numer. Anal. Meth. Geom. **28**, 209–228

Cruz Silva F. 2012. Load-displacement behaviour of thermo-active piles. MSc Thesis, Instituto Superior Tecnico, Lisboa, Portugal, 105 pages (in Portuguese)

Laloui L. Nuth M. and Vulliet L. 2006. Experimental and numerical investigations of the behaviour of a heat exchanger pile. Intl J. Num. and Anal. Meth. in Geom., 30, 763 – 781.

McCartney J.S. and Rosenberg J.E. 2011. Impact of heat exchange on the axial capacity of thermo-active foundations. ASCE Geo-Frontiers 2011 : Advances in Geotechnical Engineering, GSP 211, 488-498

Mackay J.C. 2009. Sustainable Energy - without the hot air, UIT Cambridge Ltd., 383 pages (www.withouthotair.com)

Marques M.E.S. Leroueil S. and Almeida M.S.S. 2004. Viscous behaviour of St-Roch-de-l'Achigan clay, Quebec. Can. Geot. J. **41**, 25-38

Large Thermal Energy Storage at Marstal District Heating

Importante capacité de stockage de l'énergie thermique pour le chauffage collectif de Marstal

Dannemand Andersen J., Bødker L.
GEO (Danish Geotechnical Institute), Denmark

Jensen M.V.
PlanEnergi, Denmark

ABSTRACT: For many years the district heating system in the town Marstal in Denmark has been based on oil fuels. During the last decade Marstal District Heating has turned towards 100 % renewable energies, so that in 2012 a solar heat system – covering 10 hectares of land – will produce more than 50 % of the heat consumption and the rest from biomass energy. In Denmark solar heat production is very modest during the winter, contrary to the heat consumption. The large percentage of solar heat coverage is made possible by seasonal thermal energy storage large enough to preserve the solar energy produced during summertime until winter. For this purpose a 75,000 m^3 pit thermal energy storage has been established. The pit measures 88 meters by 113 meters at the top and has a depth of 16 meters, filled with water. The excavation for the pit goes through various layers of sand and clay below groundwater at steepest possible slopes to ensure an economical design. In this article the geotechnical challenges during the planning and execution of the pit are described.

RÉSUMÉ : Au cours de nombreuses années le système de réseau de chaleur de la ville de Marstal au Danemark a été basé sur les combustibles pétroliers. Au cours de la dernière décennie, le chauffage urbain de Marstal s'est tourné à 100% vers les énergies renouvelables, si bien qu'en 2012, un système de chauffage solaire, placé sur une superficie de 10 hectares de terrain, va produire plus de 50% de la consommation de chaleur, le reste devant provenir de l'énergie verte. La production de chaleur solaire au Danemark est très modeste au cours de l'hiver, contrairement à son besoin de consommation de chaleur. Le pourcentage élevé provenant de la chaleur solaire est rendu possible grâce à l'utilisation de stockage saisonnier de l'énergie thermique permettant de garder l'énergie solaire produite en été jusqu'en hiver. Dans ce but, une fosse de 75,000 m^3, oú l'énergie thermique est stockée, a été établi. Cette fosse remplie d'eau mesure 88 mètres par 113 mètres sur une profondeur de 16 mètres. L'excavation de la fosse passe au travers de couches de sable et d'argile au-dessous de la nappe phréatique, avec des pentes raides au possible pour assurer une conception économique. Dans cet article, les défis géotechniques au cours de la planification et de l'exécution de la fosse sont décrits.

KEYWORDS: Pit thermal energy storage; PTES; Seasonal thermal energy storage; Solar heat; Renewable energies.

1 INTRODUCTION

Denmark is placed in a climate where buildings need to be heated during most of the year. In urban areas district heating is dominating and district heating covers approx. 2/3 of the consumers in Denmark. The district heating systems are dominated by combined heat and power plants (CHP) widely spreaded in Denmark. Traditionally the district heating is based on mainly fossile fuels of coal, oil and gas, but waste and biomass heating are also used. The remaining 1/3 of the population is covered by individual heating dominated by gas or oil. A minor part is heated by other types of energy e.g., wood, geothermal energy, heat pumps etc.

A lot of district heating systems are turning from fossile fuels towards renewable energies. Especially use of solar heating is preferred for medium-sized plants as the technology is developed and well proved. The energy production of solar heating systems is though very dependent on the solar radiation, and in Denmark the radiation is very modest during the winter, almost inversely proportional to the need of heat consumption. In figure 1 the average solar heat radiation and the solar heat production during a year are illustrated.

In addition, the low heat consumption during summertime dictates the maximum size of the solar heating system, and consequently the solar heating system covers usually less than 10 - 20 % of the total heating consumption.

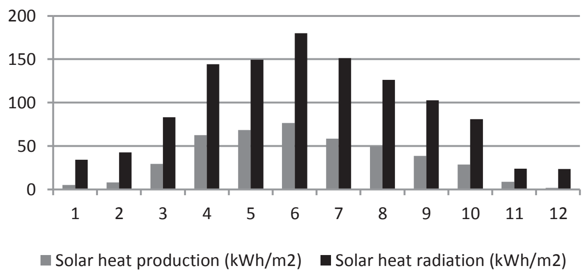

Figure 1. Monthly solar heat production and radiation at Marstal District Heating 2010-1012 (www.solvarmedata.dk).

The percentage of solar heat in the district heating may be increased by a seasonal thermal storage. The storage must be large enough to preserve the solar energy produced during summertime until winter.

Thermal energy is usually stored by heating up a material, and later on the heat can be recycled to the consumers using a heat pump. Water has shown to be an excellent heat storage material. Water is cheap and has a reasonable heat capacity compared to other materials. A relatively low value of the thermal conductivity of water is compensated as water is easily movable by pumping. Soil is also very cheap, but soil has poorer heat capacities and the heat is not easily movable. Figure 2 and 3 show typical values of the thermal conductivity and heat capacity for selected soils and water (Verein Deutscher

Ingenieure 2004). The figures show that the natural water content of the soils is very important for the thermal parameters.

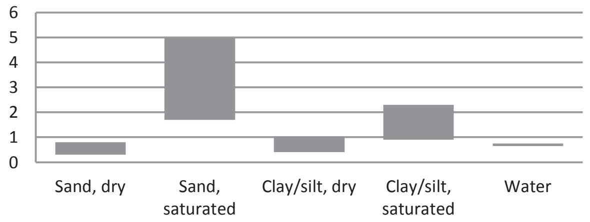

Figure 2. Typical values of thermal conductivity in W/(m·K).

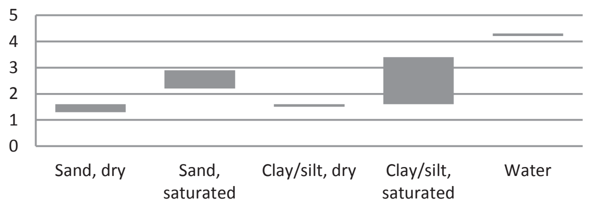

Figure 3. Typical values of volumetric heat capacity in MJ/(m^3·K).

The range of operational temperature must be as large as practically possible, as the range will impact on the necessary volume of storage.

Large seasonal thermal energy storages may be established as one of the following systems: TTES, PTES, ATES or BTES.

The TTES (Tank Thermal Energy Storage) system consists of an insulated steel tank filled with water and is widely used in the short-term regulation of the heat consumption against the heat production at heating plants. A volume of 1,000 – 5,000 m^3 is often adequate for most Danish medium-sized district heating systems. Typically operational temperatures are T = 30 - 90°C, i.e. $\Delta T \approx 60$°C.

The PTES (Pit Thermal Energy Storage) system is an excavated pit, which is lined by a membrane and filled with water. Operational temperatures are typically 30 - 90°C. The upper temperature affects the lifetime of the membrane and long term exposure of the upper temperatures therefore has to be avoided. The permissible level and exposure time of the upper temperature is a trade-off between the lifetime of storage and storage capacity. Usually the storage is not insulated towards the soil, as the energy loss through these areas is acceptable low under certain circumstances. The top of the storage – the water surface – is exposed to alternating climate conditions, including cooling by wind, which requires insulation. The insulation may be floating on the water or carried by a supporting system. For larger storages a PTES system is very cost-effective. In Denmark a few pilot PTES plants are in use with volumes up to 10,000 m^3, but larger plants are under construction, as this article describes.

The ATES (Aquifer Thermal Energy Storage) system stores the heat in a groundwater aquifer. The extend and characteristics of the aquifer must be well-known as the groundwater is pumped from a number of wells and – after passing a heat exchanger to impact or extract heat energy - infiltrated into the aquifer in another part of the aquifer. Typically operational temperatures are 5 - 30°C with $\Delta T \approx$ 25°C, i.e. the volume of water must be larger than for the above mentioned storages. This type of plant requires a groundwater aquifer with high permeability. In Denmark most of the drinking water supply is based on groundwater, and this implies that large ATES's will not be allowed in areas with special interest of drinking water supply. A growing number of ATES's have though been established, mainly initiated by a need of cooling during summertime of large building complexes.

The BTES (Borehole Thermal Energy Storage) system consists of a large number of boreholes with loops of heat pipes installed. The heat is transferred to the soil by circulating brine in the heat pipes and vice versa when the heat is to be consumed. As operational temperatures are 20 - 60 °C, i.e. $\Delta T \approx$ 40°C, and the heat capacity of soil is small compared to water, a larger soil volume is needed than for storages based on water. This is compensated as the boreholes usually go to 50 – 100 meters depth. The thermal conductivity of soil is moderate, and the response of the storage is thus relatively slow. At present only one pilot plant has been established in Denmark at a district heating plant.

2 SEASONAL ENERGY STORAGE IN MARSTAL

Marstal is a town with 2400 citizents on the Danish island Aeroe. For many years the district heating system in the city of Marstal has been based on oil fuels. During the last decade Marstal District Heating has turned towards 100 % renewable energies, so that from 2012 a solar heat system – covering 33,000 m^2 solar heat panels on 10 hectares of land – will produce more than 50 % of the heat consumption and the rest will come from biomass energy. At present the plant is the largest solar heat plant for district heating in the world, but this ranking will presumable only be held for a short period.

Marstal has been a Danish pioneer in thermal energy storage. In 1998 a 3,000 m^3 combined gravel and water pit has been built, and the plant was followed by a 10,000 m^3 PTES in 2003. Calculations have shown that the requested large percentage of solar heat coverage in Marstal needs a volume of 75,000 m^3 water in which case *all* surplus solar energy produced during summertime can be stored until winter. This volume is established by a PTES plant. The project is economically supported by the European Union (EU).

Performing a PTES has some preferred technical conditions in relation to an economic design in regards of both the establishment phase and the operation phase as described in the following:

The pit *must* be performed as an open pit without using e.g. a framing sheet pile wall which would increase the cost considerably. To minimize excavation costs the ground must consist of soils which can be excavated and handled by traditionally methods and with no significant groundwater handling.

To reduce heat loss into the air the pit must be covered by insulation with guaranteed resistance to temperatures up to 90°C for the lifetime of the storage. The top insulation and the bottom membrane (in this case a 2.5 mm HDPE liner) are some of the most expensive parts in a PTES and the area of the insulation must consequently be minimized.

Dry soils insulate better than moist or saturated soils, and moreover groundwater may introduce unwanted heat loss if heated groundwater flows across the site. Therefore, the groundwater level must be at a convenient depth below the bottom of the pit, alternatively a higher groundwater level is tolerated, but in that case no significant groundwater flow across the site is allowed.

The loss of heat is reduced to a theoretical minimum when the pit has a spherical shape. This is not obtainable in practice and excavation is often performed as an upturned frustum of pyramid. The width must be minimized, for which reason the slopes of the sides of pyramid must be as steep as practical possible. This reduces moreover the area of the expensive top insulation.

In order to establish soil balance in the project the excavated soil is to be used in building up embankments around the excavated pit. The excavated soil must be well suited and compactable for this purpose.

3 CONSTRUCTION AND SITE INVESTIGATIONS

In Marstal the PTES is placed on the top of a smooth hill in the outskirts of the town.

Due to area restraints the pit is slightly rectangular and measures 88 meters by 113 meters at the top, i.e. a bit larger than a football field. The water depth is 16 meters, of which approx. 12 meters go below the natural ground level and 4 meters are established by embankments of the excavated soil at the perimeter. As mentioned above the total volume of water is 75,000 m^3.

Early in the design process the slope of the sides was chosen to 1:2 which in a practically view is the steepest possible inclination for the installation works of the liner. This corresponds to an angle of 26.6° against horizontal level. Figure 4 shows a stylized cross section of the pit.

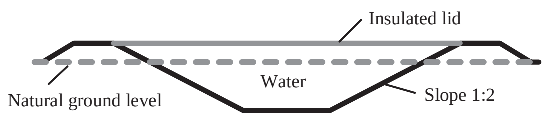

Figure 4. Stylized cross section of the PTES in Marstal.

A site investigation has been performed prior to the design phase. The investigation consisted of 10 borings, of which two borings in the centre were taken to 25 meters depth and 8 borings at the perimeter of the excavation were taken to 13 meters depth. The borings were performed as traditionally geotechnical borings with soil sampling, in-situ tests and installation of standpipes at adequate depths.

The investigation showed a thin layer of top soil covering various glacial deposits of primarily clay till and glacially relocated marine clay of interglacial origin (Cyprina Clay). At the northern side three meters of melt water sand were covering the clay. Besides, stripes and zones of melt water sand and sand till were found, apparently randomly in the clay.

In a geotechnical matter the marine clay was of special interest. The clay was of high to very high plasticity with plasticity index $I_P \approx 50$ %. The natural water content was w_{nat} = 21 – 30 % close to the plasticity limit. A fissured structure was detected in several samples, presumably caused by shear stresses during the glacial period and/or passive earth pressures at the end of the glacial period.

The clay deposits were generally stiff to very stiff. Field vane tests showed undrained shear strength c_{fv} between 250 and >700 kPa, thus with a slightly softened zone near the surface.

The effective strength parameters in the clay were estimated from a priori knowledge of similar soils. The characteristic value of the angle of friction of the marine clay was estimated to $\varphi \approx 20°$ and of the clay till to $\varphi \approx 30°$ with mean values approximately 5 degrees higher. Some effective cohesion in the clay must be expected, but according to Danish calculation practice the cohesion was limited to c' = 20 kPa in unfissured clay and c' = 0 kPa in fissured clay (on the safe side for decreasing stress level).

Standpipes had been installed at differing depths, separated by bentonite sealing materials. Groundwater levels were measured at very varying depths between a few meters depth and large depth (below excavation level). These measurements are assumed to be variably ground water build-ups depending on precipitation and season, whereas a stable ground water table in a primary aquifer is at large depth.

4 CONSIDERATIONS FOR THE CONSTRUCTION

Establishment of a PTES at the actual site was subject to four geotechnical concerns: the excavation stability, the groundwater and soil handling during the construction phase and the long term consequences of thermal influence on deformations in the operational phase.

4.1 *Excavation stability*

The stability of the excavation sides was to be sufficient during the construction phase. Provided that the ground water issue was handled, it was evident that a quickly performed excavation and refilling with water would be advisable as the clay would be stable in the short term undrained condition. On the other hand, calculations based on long term drained strength parameters showed unstable slopes in the marine clay, especially when adding prescribed safety factors according to Eurocode 7.

The period from starting excavation until fully filling the pit with water was planned to last 6½ months. One month had to be reserved the liner work, and as the available capacity for filling the pit with water was limited to 50 m^3/h the filling would itself take two months.

Undrained conditions were evaluated to last at least one month, but exceeding this period by several months caused severe considerations of the time for developing drained conditions and consequently collapses due to unstable slopes. It was evaluated that further tests and evaluations would not improve this engineering judgement significantly, and therefore the stability had to be evaluated for drained conditions.

Introducing less steep slopes than 1:2 was not an option, but a series of slope stability calculations based on different cross sections showed that it was possible to establish stable slopes of 1:2 by replacing layers of the marine clay until certain depths with sand or even clay till, see figure 5, forcing the rupture line at greater depth to involve more stable materials. The replacement of the marine clay would increase the volume of soil to be handled in the project by approximately 15 % which was acceptable.

During the excavation phase it was decided to abstain from replacements until indications of failures were observed. This reduced replacements to an absolute minimum.

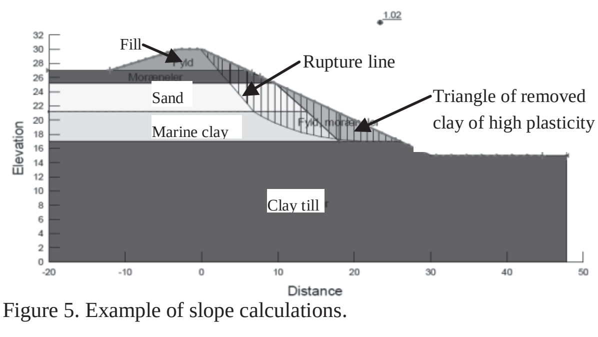

Figure 5. Example of slope calculations.

4.2 *Groundwater handling*

The potential energy loss due to groundwater flow across the site was evaluated to be very limited.

The groundwater build-ups had to be eliminated to enable dry excavation and a proper handling of the membrane. Furthermore groundwater lowering was necessary to prevent uplift, damages due to seepage from the excavation sides and sliding of the sides, which especially would be problematic if the sides were sliding after covering with the membrane.

The circumstance that the bottom of the pit was to be covered with a membrane implied that the groundwater lowering works was directed to take place on the outer side of the pit, i.e. at some distance from the excavation. This might reduce the draw-downs in the centre of the pit.

The chosen groundwater lowering system consisted of a combination of well-points, bored wells and a drainage system beneath the membrane.

The well-points were closely spaced at approx. 6 meters depth at the perimeter of the pit to deal with the groundwater flow in the upper layers of sand.

In addition eight bored wells were placed at the perimeter to deal with the deeper water built-ups. Besides pumping from the wells vacuum was applied to the wells to reduce pore water pressures in the soil and increase the effective stresses in the soil, at least to some distance from the wells.

Furthermore, a well in the centre of the pit was performed to prevent uplift. This well was initially installed with a pump, and during excavation the well was successively cut down to excavation level and the pump was removed.

Before covering up the bottom and the sides with the membrane, a drainage system in connection with the (weeping) well was established in the bottom. To prevent a lifting problem caused by accumulation of water beneath the membrane, pumping on the drainage system was made possible by traditionally well pumps mounted through two installed pipes laid in inclining ditches up the sides.

Pumping from the drainage system, the well-points and the bored wells at the perimeter of the pit was sustained until the pit was filled with water unto the measured highest natural ground water level approx. 1 meter below the surrounding level.

4.3 *Soil handling*

The excavated soil had to be built-in in the embankments around the pit. The soil mainly consisted of clay, where moisturing/weathering normally must be avoided in order to obtain reasonable compaction (more than 95 % Standard Proctor) and confined deformations of the embankments. Therefore, the earth works must take place during a period with favourable weather conditions, which in Denmark means the summer period.

Furthermore, the poor strength properties of the marine clay of high plasticity – especially in a remoulded condition - was dictating that the clay only had to be rebuilt in areas where the requirements to the soil were less critical.

4.4 *Consequences of thermal influence to the soil*

In the operational phase the temperature in the adjacent soil will increase, maybe up to 90°C close to the pit. This heating of the soil might cause a drying-up effect of the soil above the ground water table if no water is added from e.g. precipitation. In the actual case the clays seemed so preconsolidated that the natural water content was considered to be close to the shrinkage limit. Consequently the risk of development of a long term deformation problem was evaluated as a minor issue.

5 CONSTRUCTION PHASE

The PTES was established during the summer 2011 which happened to be very wet with precipitation more than twice the normal precipitation. In addition, a cloudburst occurred with more than 100 mm precipitation overnight which caused damages to the just finished surfaces and obstacles for the subsequent works. Consequently, the construction period was delayed 3 months into the winter.

This entailed that the preconditions for the project was severely challenged. Especially the maintenance of the stability of the sides was alarming. The predicted long term problem with poor drained strength parameter might be worsened if the efficiency of the ground water lowering system was reduced (due to clogging etc.). This problem period was not to end until the filling-in of water was above the surrounding ground level.

In spite of this no severe ruptures were recorded. Figure 6 shows a photo of the pit at a late stage of the excavation work.

Figure 6. Photo of pit during completion of excavation and laying out of the membrane in progress. The tower in the centre of the photo is a 16 m tall water in- and outlet for the operational phase of the PTES.

6 CONCLUSIONS AND PERSPECTIVES

The PTES project in Marstal has demonstrated that a thermal energy storage with 75,000 m^3 water is obtainable in connection with solar heat based district heating systems. The construction cost of the Marstal storage was 41 € per m^3 of water (exclusive VAT) including all pipe connection to the plant, control system, geotechnical support, etc. The construction cost also includes research and development costs of the storage and different lid designs. The costs are cost-competitive compared to other storage systems (e.g. TTES, ATES and BTES) and there is a potential to bring the costs further down.

The project has encountered difficulties in matters of soil and ground water conditions and challenges due to circumstances in the actual climate, but these challenges has been dealt with in order to minimize the costs of the PTES. Details in the project still needs to be optimized, but the project is a stepping stone in the development of the necessary techniques for decreasing the use of renewable energies.

The aim of the authors of this article is to pinpoint the challanges to be encountered during planning and execution of a PTES illustrated by an actual project. It is the authors' perception that a PTES is applicable for a lot of sites.

Denmark has approximately 400 district heating plants of varying size. Most of these plants are placed in rural areas, where establishment of solar heating plants supplemented by a PTES is an obvious solution. As an example the planning of a 60,000 m^3 PTES in connection with 35,000 m^2 solar heat panels at Dronninglund Destrict Heating in Denmark is ongoing and will presumable be established in 2013 - 2014. Some PTES's have been established in other countries, e.g. Germany, but none as large as in Denmark.

7 REFERENCES

GEO Danish Geotechnical Institute 2010-2011. Geotechnical reports for establishment of a PTES in Marstal (not published).

Mangold D, Schmidt T, The next Generations of Seasonal Thermal Energy Storage in Germany, www.solites.de.

Marstal District Heating 2010-2012. Monthly solar heat production and radiation, www.solvarmedata.dk.

Verein Deutscher Ingenieure 2004, 4640 Blatt 4.

Combination of borehole heat exchangers and air sparging to increase geothermal efficiency

Combinaison de sondes géothermiques et barbotage d'air pour augmenter l'efficacité géothermique

Grabe J., Menzel F., Ma X.
Technische Universität Hamburg-Harburg

ABSTRACT: Closed and open systems are available for the usage of shallow geothermal energy. In closed systems heat can only be transferred conductively for the case of no groundwater flow. Unfortunately heat conduction is a relatively slow heat transfer mechanism, which causes limited heat-abstraction capacities in geothermal systems. A patented method is presented, in which a closed system is combined with groundwater-circulation technology. In this way a groundwater circulation will be created artificially, which increases convective heat transfer in the soil and therefore the heat capacity of the geothermal system. In this paper a borehole heat exchanger combined with an air sparging well is numerically simulated. The induced groundwater circulation and the heat propagation are calculated sequentially. The heat capacity of this system is compared to a normal borehole heat exchanger. Furthermore, variation calculations are performed to investigate the influence of density of the water-air-mixture in the well, permeability and hydraulic conductivity of the soil. A profitability analysis is carried out based on the numerical results.

RÉSUMÉ : Des systèmes ouverts et fermés sont disponibles pour l'utilisation de l'énergie géothermique peu profonde. La chaleur, présente dans les systèmes fermés ne peut être transférée par conduction s'il n'y a pas un écoulement d'eaux souterraines. La conduction thermique est malheureusement un mécanisme de transfert thermique assez lent. Cela limite donc la capacité thermique dans ces systèmes géothermiques. On présente un procédé breveté où un système fermé est combiné avec une technologie de circulation des eaux souterraines. La circulation des eaux souterraines est artificiellement créée, ce qui permet d'augmenter le transfert thermique par convection dans le sol et, par conséquent, la capacité calorifique du système géothermique. Dans cet article, une sonde géothermique combinée à une injection d'air sont simulées numériquement. La circulation des eaux souterraines induite, ainsi que la propagation de chaleur, sont calculées de manière séquentielle. La capacité calorifique du système est comparable à celle d'une sonde géothermique normale. En outre, des calculs de variations sont effectués afin d'étudier l'influence de la densité de l'eau/air mélangé dans le puits de conductivité, de la perméabilité et l'état hydraulique du sol. Une analyse de rentabilité est ensuite effectuée à partir de ces résultats numériques.

KEYWORDS: shallow geothermal energy, air sparging, induced groundwater flow, numerical simulations

1 INTRODUCTION

Shallow geothermal systems use the energy that is available within the top 400 m of the Earth's crust. The relatively constant temperatures of the soil can be used to heat or cool buildings.

In closed systems without groundwater flow, heat is transported by conduction only. This is a very slow process and it limits the heat-abstraction capacity of the system. Systems that induce groundwater flow have the advantage of being able to use convection as a much faster heat transfer mechanism (Ma and Grabe 2009, Wang et al. 2009). These are open systems that, in spite of the higher efficiency, are rarely used because permissions for these systems are difficult to obtain. Also the hydrological boundary conditions for these systems can be hard to fulfill and limit the usage of open systems. Alternative methods are possible for closed systems.

Ma and Grabe (2009) suggest the combination of a groundwater-circulation system with a borehole heat exchanger. Several methods exist to induce groundwater circulation. For this example the air-injection well (Wehrle 1990) was chosen. The objective of this entry is to numerically show to what extent the efficiency of borehole heat exchangers can be increased through the use of air-injection at sites with low to zero groundwater flow (Ma and Grabe 2011).

2 NUMERICAL SIMULATION OF AIR-INJECTION BOREHOLE HEAT EXCHANGER

2.1 System description

Figure 1 shows the concept of the combined air-injection borehole heat exchanger. In this example the system is coupled with an A/C. Unlike with regular borehole heat exchangers the borehole in this case is not filled with grouting. Instead a drainage layer is installed below the water table and the heat exchanger pipes as well as the air-injection pipe are fitted into the borehole. Above the water table the borehole is sealed, save for a small opening to let the air escape.

For the following calculations summer usage is assumed as well as temperature independent thermal and mechanical characteristics. The results can easily be converted for a winter scenario as long as the fluid in the pipes does not reach temperatures below 0°C.

When the system is in use, air is injected to the lowest point of the well to create an air-water mixture with a density lower than that of the surrounding water. The water level in the well rises higher than the groundwater table. That way water can flow from the well into the aquifer in the top part of the well, while in the bottom part water is flowing from the aquifer into the well.

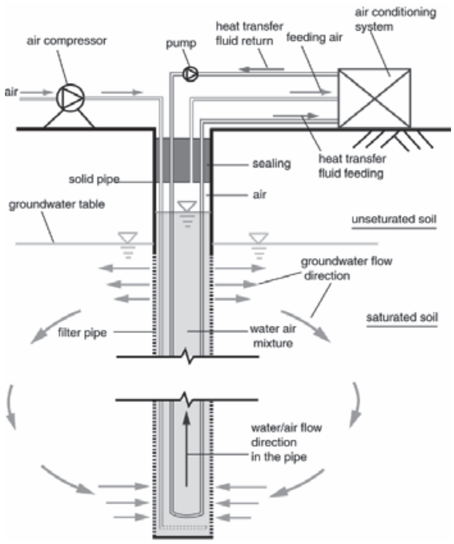

Figure 1. Combination of an air-sparging downhole heat exchanger with an air conditioning system

The combination of a borehole heat exchanger with an air-injection well increases the performance of the system shown in Figure 1 in three ways. First, the groundwater cools the air before it reaches the air conditioning system, therefore reducing the energy necessary for the A/C. Second, the vertical flow of the air-water mixture inside the well increases the heat exchange between the heat pipes and the groundwater (Gustafsson, Westerlund and Hellström 2010). And third, the circulation of the groundwater increases the heat convection in the subsurface which leads to a higher efficiency of the overall system.

2.2 *Numerical model*

The simulations of the air-injection borehole heat exchanger were done with the finite-element program COMSOL multiphysics. A three-dimensional model was used. The geothermal system has a radius of 10 cm and the thickness of the aquifer is 10 m. Prior to the air injection there is no groundwater flow. Four pipes are introduced into the well. The induced groundwater flow, as well as the convective heat transfer are modeled using the FEM. Flow inside the well itself and inside the heat pipes is neglected. The pipes are simplified represented as cylindrical heat sources with constant temperatures.

The aquifer is assumed to consist of homogeneous sand. Several variations concerning heat conductivity, permeability of the soil and density of the air-water-mixture are simulated with the model shown in Figure 2. The used thermal and hydraulic parameters are listed in Table 1. The bold values can be considered to be standard parameters.

Table 1. Applied thermal and hydraulic parameters of the soil and the air-water-mixture

Thermal conductivity sat. soil (W/(m · K))	*1.5/2.0/**2.5**/3.0/3.5*
Specific heat capacity sand (J/(kg · K))	**800**
Effective porosity (-)	**0,25**
Density of water (kg/m³)	**1000**
Density of air-water-mixure (kg/m³)	900/950/980/**990**
Density of sand grains (kg/m³)	**2650**
Permeability (m/s)	10^{-7} ~ $\mathbf{10^{-4}}$ ~ 10^{-3}

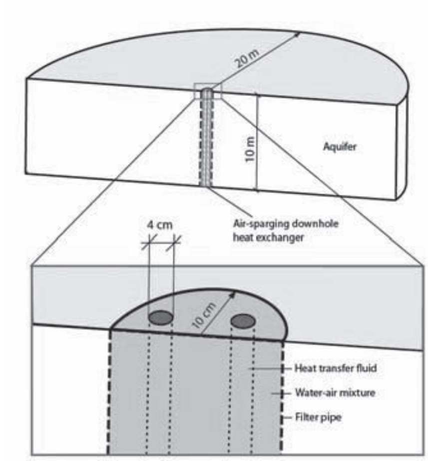

Figure 2. Numerical model for the simulation of an air-sparging downhole heat exchanger

The induced groundwater flow increases heat transport through convection. All calculations assume that the hydraulic and thermal parameters of the soil are temperature independent. This means that groundwater flow is not influenced by heat transport. Both mechanisms – groundwater flow and heat transport – are considered separately. The first step is to simulate the groundwater flow until stationary conditions are reached. The results are saved and in the second step the results are superimposed by the heat propagation in the soil in 90 days.

Before the air injection the well experiences a hydrostatic pressure distribution. As a boundary condition for the simulation the wall of the well experiences a constant pressure distribution from the air-water-mixture, which has a smaller density but a higher water level than the surrounding groundwater. Boundary conditions are shown in Figure 3 (Ma and Grabe 2011).

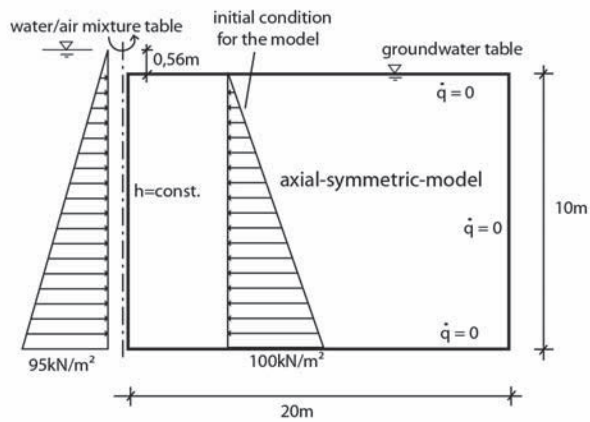

Figure 3. Boundary and initial conditions of the model for calculation of the groundwater circulation caused by air-sparging with an air-water-mixture with a density of 990 kg/m³

3 NUMERICAL RESULTS

3.1 *Groundwater flow*

The groundwater flow induced by the air injection is calculated until stationary conditions are reached. The arrows in Figure 4 show the calculated velocity vectors of the groundwater. The highest velocity (approx. $1.2 \cdot 10^{-5}$ m/s) can be found close to the well. With increasing distance to the well the velocity decreases. The flow lines show the groundwater circulation. The bold parameters from table 1 achieve a water exchange rate between well and soil of about 0.06 m³/h.

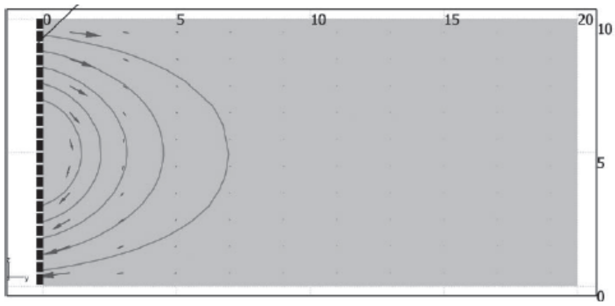

Figure 4. calculated velocity field (arrows) and particle tracing (lines) of the groundwater around the air-sparging downhole heat exchanger at a steady rate ($\Delta\rho$ = 10 kg/m³, k = 10^{-4} m/s)

3.2 *Heat transport*

Without the air injection the heat distribution around the borehole heat exchanger is uniform. The induced groundwater circulation transports heat away from the well and changes the shape of the temperature field. In the upper part of the aquifer the convective heat transport has the same direction as the conductive heat transport. This increases the heat spreading rate, which can be seen from the larger heat plume around the well. In the lower part of the well the groundwater flow direction is opposite the direction of heat conduction, which slows the heat spreading rate. At the bottom of the well the groundwater flow towards the well is so strong that the heat cannot spread outwards anymore.

The overall heat plume around the well is larger when air injection is active. This shows that more heat can be transported into the ground using an air-injection borehole heat exchanger than using a regular borehole heat exchanger.

3.3 *Efficiency of air-injection borehole heat exchanger with standard parameters*

The amount of heat $E(t_n)$ that the borehole heat exchanger transports into the ground at the time t_n equals the integral product of the temperature change along the entire body of soil with a soil density of ρ_B and the specific heat capacity c_B:

$$E(t_n) = \int \rho_B c_B \, [T(x,y,z,t_n) - T_0] dV \qquad (1)$$

The specific heat abstraction capacity per meter heat exchanger $P_s(t_n)$ is time-dependent:

$$P_S(T_N) = \frac{E(t_n) - E(t_{n-1})}{l \cdot (t_n - t_{n-1})} \qquad (2)$$

In this case l is the length of the borehole heat exchanger.

Figure 5 shows the specific heat abstraction capacity as a function of time, comparing a regular borehole heat exchanger and one that uses air injection. In both systems the heat abstraction capacity rapidly reduces within 20 days and changes only minimally afterwards.

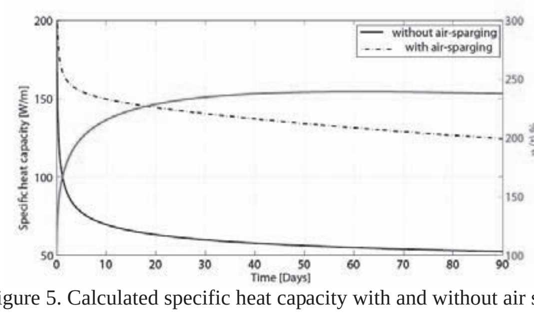

Figure 5. Calculated specific heat capacity with and without air sparging and efficiency increasing rate of the downhole heat exchanger compared with normal downhole heat exchanger ($\Delta\rho$ = 10 kg/m³, λ = 2.5 W/(m · K), k = 10^{-4} m/s)

3.4 *Variation calculations*

During the calculations three parameters were varied: density of the air-water-mixture inside the well, heat conductivity and permeability of the soil.

For low permeabilities of the soil (k < 10^{-5} m/s) the heat abstraction capacity depends only on the thermal conductivity of the soil. In permeable soils (k > 10^{-4} m/s), convection is the dominant heat transport mechanism and heat conduction has no influence. In between those parameters the heat abstraction capacity depends on permeabilty as well as on thermal conductivity.

The influence of the air injection depends on the ratio between thermal conductivity and induced convection. The decisive factor for thermal conductivity is the specific thermal conductivity of the soil (λ). The convection depends on the median groundwater circulation velocity (v_z) that can be calculated using Darcy's law.

$$v_z = k \cdot i \qquad (3)$$

Assuming a constant median flow distance the following relationship can be applied:

$$v_z = c \cdot k \cdot \Delta\rho \qquad (4)$$

Here, c is a constant. The efficiency increasing rate (η) is therefore mainly dependent on the three parameters k, λ and $\Delta\rho$. The relationship between η and λ shows that the five curves in Figure 6 fit very well when η is mutlilied by $\lambda^{0.7}$. The relationship between η, λ, k and $\Delta\rho$ is shown in Figure 7. The y-axis is labeled $\eta \cdot \lambda^{0.7}$ and the x-axis is labeled $k \cdot \Delta\rho$. All calculated points can be converged towards the adaptation curve.

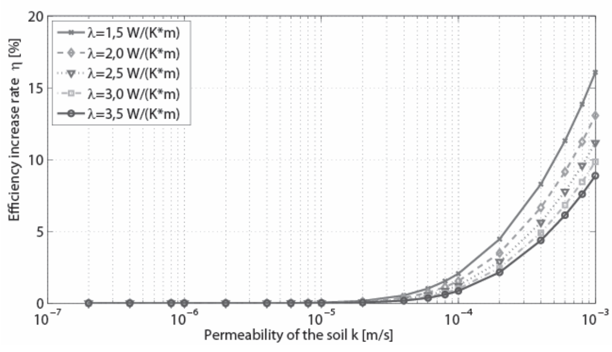

Figure 6. Calculated efficiency increasing rate of the air-sparging downhole heat exchanger against the conductivity and permeability of the soil ($\Delta\rho$ = 10 kg/m³)

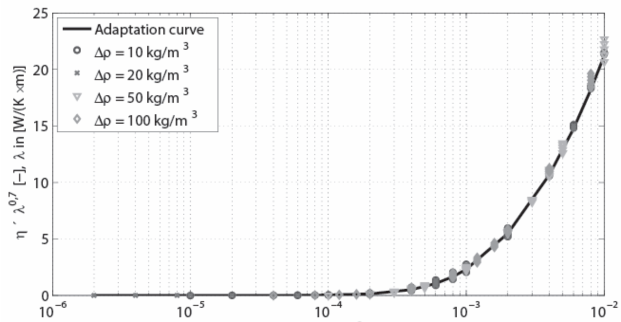

Figure 7. Presentation of the results of the variation calculations and the adaptation curve, x-axis: $k \cdot \Delta\rho$, y-axis: $\eta \cdot \lambda^{0.7}$

This phenomenon offers the possibility of estimating the efficiency increasing rate when the three parameters λ, k and $\Delta\rho$ are known.

4 PROFITABILITY ANALYSIS

To achieve a pressure difference between the well and the surrounding groundwater it is necessary to inject air into the well with an air compressor, which uses electricity. An air-injection borehole heat exchanger is only profitable when the increase of the heat abstraction capacity is higher than the energy used by the air compressor.

To calculate the energy necessary for the air compressor to work, two parameters are needed: operating pressure and air flow rate.

To calculate the injected air a perfomance record is chosen, which considers not only effective power for water production and air expansion but also includes a performance loss ratio (Rautenberg 1972):

$$N_L \pm N_W + N_R + N_S + N_B + N_{E,U}$$

With

N_L air expansion
N_W effective power for water production
N_R dissipation loss due to friction of the two-phase flow
N_S dissipation loss due to slip between air bubbles
N_B dissipation loss to accelerate the water
$N_{E,U}$ entry and exit dissipation loss

The dissipation loss $N_{E,U}$ is very small compared to the other factors and can be neglected.

By iteratively solving equation 5 the necessary air flow rate for inducing a groundwater circulation can be calculated. For a density of $\Delta\rho = 10$ kg/m³ the through air injection induced water flow rate is so low that effective power for water production can be disregarded. The amount of air necessary for achieving a pressure gradient in the well, which is the minimally necessary air flow rate (Luber 1999) and does not depend on soil permeability, is the decisive factor for calculating the total amount of air. This leads to a small-scale dependency of the total amount of air from the soil permeability.

Up until a permeability of $4 \cdot 10^{-5}$ m/s the coefficient of air injection (COA) is smaller than 1, which means that the amount energy used for air injection is higher than the increase in the heat abstraction rate and the use of the air injection technique is not favorable. With increasing k the COA also increases. In a soil with a permeability of $k = 10^{-3}$ m/s, the COA is expected to be about 100. In this case the 100 times of the energy used for the air compressor is converted into usable energy for air conditioning.

The coefficient of performance (COP) for ground coupled heat pumps can reach a maximum of 5 (Pahud and Hubbuch 2007, Wood, Liu and Riffat 2009). This value can already be exceeded by the COA-value of the air-injection borehole heat exchanger with a value for $k = 6 \cdot 10^{-5}$ m/s. In a permeable soil the COA shows the profitability of the air-injection borehole heat exchanger.

5 CONCLUSIONS

Combining an air-sparging well with a borehole heat exchanger offers the opportunity of increasing the heat-abstraction capacity of closed geothermal systems without pumping groundwater. The induced groundwater circulation accelerates the heat transfer through convection.

For a permeability of $k < 10^{-5}$ m/s, the induced circulation is too slow to have an effect on the heat transfer. But with increasing permeability the positive effect of the air injection increases as well. In soils with $k > 10^{-4}$ m/s convection is the dominant method of heat transfer. For soils with $k = 10^{-3}$ m/s and $\lambda = 2{,}5$ W/(m · K) the heat abstraction capacity can increase about ten times through use of air injection when $\Delta\rho = 10$ kg/m³.

Simulations so far have only been done for one air injection borehole heat exchanger and one operating period. Long term simulations as well as an in-situ test in Hamburg are planned (Ma und Grabe 2010).

With certain groundwater chemistries the use of this technique can lead to the sedimentation of iron ochre over time. This may lead to the necessity of cleaning the well with suitable methods (Herth and Arndts 1995). An alternative for this would be the usage of different gases like N_2 or CO_2. In those cases the air escaping the well should be collected and reused.

6 REFERENCES

Gustafsson, A., Westerlund, L. and Hellström, G. 2010. CFD-modeling of natural convection in a groundwater-filled borehole heat exchanger. *Applied Thermal Engineering* 30 (6-7), 683-691

Herth, W., and Arndts, E. 1995. Theorie und Praxis der Grundwasserabsenkung (3), Berlin

Luber, M. 1999. Luftinjektionsbrunnen zur in situ Grundwassersanierung, Hydraulik und Stoffdurchgang. Dissertation, Universität Karlsruhe

Ma, X. and Grabe, J. 2009. Modelling of usage of air injection well in a geothermal system. *COMSOL conference 2009*, Milano

Ma, X. and Grabe, J. 2010. Field test of a geothermal system in HafenCity Hamburg. *Proc. of Geoshanghai: Geoenvironmental Engineeringand Geotechnics* (204), 159-166

Ma, X. and Grabe, J. 2011. Steigerung der Effizienz von Erdwärmesonden durch Luftinjektion an Standorten ohne Grundwasserströmung. *Geotechnik* 34 (1), 42-50

Pahud, D., Hubbuch, M. 2007. Measured thermal performances of the energy pile system of the Dock Midfield at Zürich Airport. *Proceedings European Geothermal Congress.* Unterhaching

Rautenberg, J. 1972. Theoretische und experimentelle Untersuchungen zur Wasserförderung nach dem Lufthebeverfahren. Dissertation, Universität Karlsruhe

Wang, H., Qi, C., Du, H. and Gu, J. 2009. Thermal performance of borehole heat exchanger under groundwater flow, A case study from Baoding. *Energy and Buildings* 41 (12), 1368-1373

Wehrle, K. 1990. In situ Sanierung von CKW-Schadensfällen: Modellversuche zur Lufteinblasung (In-Situ-Strippen) in Lockergestein. *Altlastsanierung* 90, Dordrecht: Kluwer Publishers

Wood, C. J., Liu, H. and Riffat, S. B. 2009. Use of energy piles in a residential building, and effects on ground temperature and heat pump efficiency. *Geotechnique* 59 (3) 287-290

Geothermal Heat PipeBorehole Heat-Exchangers: Computational Simulation and Analysis of Measurement Data

Échangeurs thermiques à thermosiphon utilisés en géothermie : simulation numérique et analyse des mesures

Katzenbach R., Clauss F.
Technische Universität Darmstadt, Institute and Laboratory of Geotechnics, Germany

ABSTRACT: Shallow Geothermal Energy is a very promising alternative to fossil fuels, especially in the Residential and Commercial sectors, both including the heating and cooling of buildings. Among the available technologies in Shallow Geothermics, the Geothermal Borehole Heat-Exchanger equipped with a Heat Pipe is a particularly efficient optimization in comparison to conventional borehole heat-exchanger systems for two main reasons: Due to the gravity and buoyancy driven energy transport in the borehole heat-exchanger there is no need for a circulation pump. Hence, the consumption of by-energy is significantly reduced. Furthermore, the temperature distribution within the borehole heat-exchanger is advancing a high energy withdrawal rate much more than conventional systems. A method has been developed to estimate the heat transport of a Geothermal Heat Pipe Borehole Heat-Exchanger as computational simulations are used to determine the expected energy withdrawal rate. Furthermore, long-term measurement data have beencollected from a Geothermal Heat Pipe Borehole Heat-Exchanger installation. The analysis of measurement data allows proving the functionality.

RÉSUMÉ : L'énergie géothermique de surface comme alternative aux énergies fossiles est une source d'énergie prometteuse, en particulier dans les secteurs résidentiels et commerciaux incluant le chauffage et la climatisation des bâtiments. Parmi les technologies disponibles, les sondes géothermiques équipées d'un thermosiphon (conduite de chaleur) sont une solution particulièrement efficiente en comparaison des traditionnelles sondes géothermiques pour deux raisons principales. Il n'est d'abord pas nécessaire de disposer d'une pompe de circulation, à cause de la gravité et du transport d´énergie par la flottabilité dans la sonde, diminuant ainsi l'énergie d'alimentation. Ensuite, la distribution de température dans la sonde géothermique montre une consommation d'énergie moins importante que pour les systèmes conventionnels. Une méthode a été développée afin d'estimer le transport de chaleur assuré par un échangeur thermique sur le principe du thermosiphon utilisé en géothermie et des simulations numériques ont été effectuées afin de déterminer la consommation énergétique du système. Les données ont été collectées à long terme sur une installation utilisant une sonde géothermique à thermosiphon. L'analyse des données collectées permet de montrer la fonctionnalité de ce type d'installations.

KEYWORDS: shallow geothermal energy, heat pipe, thermosiphon.

1 INTRODUCTION

Geothermal Energy is a very promising alternative to fossile fuels, especially in the residential and commercial sectors, both including the heating and cooling of buildings: Almost 50% of the overall final energy consumption are being unsed for the tempering of buildings. As using the so-called "Shallow Geothermal Energy" – the thermal use of soil and groundwater in the uppermost spoil region for low-temperature applications – is almost everywhere applicable, decentral and in perfect conjunction with electirc power from other renewable sources, various applications scenarios in differenct climate regions, operational modes and building types in new construction and the existing building stock allow a wide range and large number of applications. Among the available technologies in Shallow Geothermics, the conventional geothermal borehole heat-exchanger, usually consisting of a double-u loop to circulate the energy carrying medium is most common. In order to optimize the overall energy performance of the heat exchanger and thereby of the entire geothermal facility a heat pipe is being used as main energy transport element of the borehole heat exchanger.

A heat pipe is a particularly efficient technology in comparison to conventional borehole heat-exchanger systems for two main reasons:

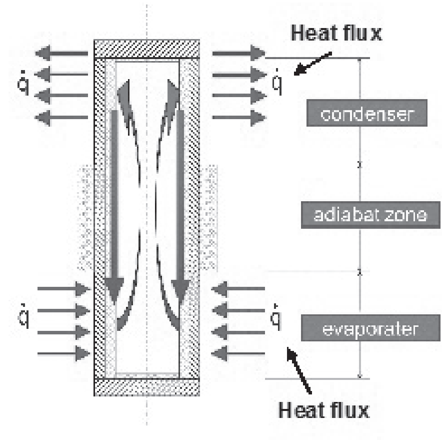

Figure 1: Heat Pipe: Working Cycle

Due to the gravity and buoyancy driven energy transport in the borehole heat-exchanger a high density of energy transport can be archived even without using a circulation pump.

Accordingly, the consumption of by-energy is being significantly reduced.

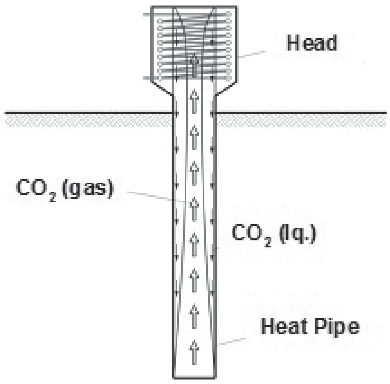

Figure 2: Heat Pipe: Geothermal Heat Pipe: Configuration

Furthermore, the temperature distribution within the borehole heat-exchanger is advancing a high energy withdrawal rate much more than conventional systems: The overall energy withdrawal rate is predominantly governed by the temperature difference between borehole heat-exchanger and ambient ground temperature, which by itself is limited in terms of its lower margin. Hence, a heat pipe borehole heat-exchanger is exploiting the usable temperature more efficient than conventional borehole heat-exchanger systems.

2 SIMULATION OF GEOTHERMAL HEAT PIPE OPERATION

The thermal performance of a heat pipe is dependent on a number of influencing parameters, e.g. driving temperature difference, mechanical and thermal properties of the heat carrier fluid – in the present case CO_2 – such as evaporation enthalpy, heat conductivity and capacity, viscosity, the energy withdrawal rate on the condenser side, the geometric dimensions and particularly the inside pressure and the amount of filling medium respectively, compare to Dunn and Reay (1993) and Lee and Mital (2003).

Based on a numerical algorithm and accounting for the conduction-governed energy transport from the soil to the cylinder and the convection-governed energy mechanism within the cylinder in vertical direction and considering both surface evaporation and boiling evaporation, an extensive number of computations were conducted in order to investigate the sensitivity to various parameters such as overall length, diameters of heat pipes and boreholes. The resulting specific power for a given set of parameters for a constant saturation pressure is plotted in Figure 3.

The exceptionally efficient energy transport within the heat pipe and the obsolete circulation pump in comparison to conventional borehole heat exchangers allow a relative increase of the coefficient of performance (COP) of up to more than 10°% (percentage).

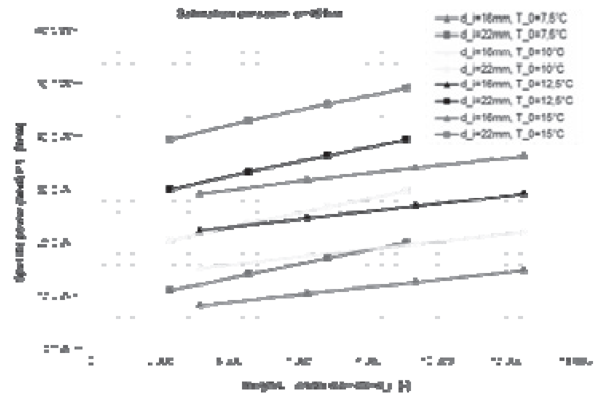

Figure 3: Simulated heat pipe performance: Energy withdrawal rate(specific power: heat)

During the operation of such a Two-Phase-Heat Pipe the thermal transfer resistance in film evaporation or condensation is significantly smaller in comparison to a system without phase change. Accordingly, a significantly smaller driving temperature difference between soil temperature and heat pump evaporator is necessary to archive the same overall heat flux density.

The relation between length and diameter has large influence on the specific power (heat). Accordingly, it is desirable to optimize this geometric relation during dimensioning and design.

3 CASE STUDY OF APPLICATION

Within a pilot project, a new-construction one-family home has been equipped with a ground-coupled heat pump in combinations with geothermal heat pipe borehole heat exchangers. These have been instrumented for long term measurements of ground temperatures and heat pump parameters(see Figure 4).

Figure 4: Measurement installation

The obtained temperature records (Figure 5) can be used to investigate the overall performance of the energy supply system as well as to analyse the operation and to control the functionality of the installation.

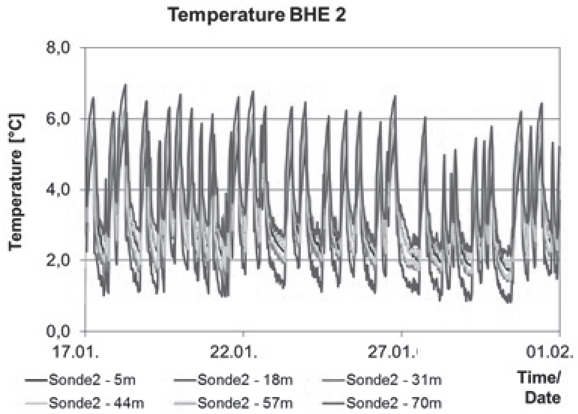

Figure 5: Temperature records

Especially the temperature distribution in depth and time along the heat-pipe borehole heat exchangers allows to identify the operation of the heat-pipes in detail:Figure 6 shows the temperature distribution at a specific borehole heat exchanger at different states of operation. One can observe that the temperature distribution is not linear. From this distribution information on the state of operation (bath or film evaporation) can be derived.

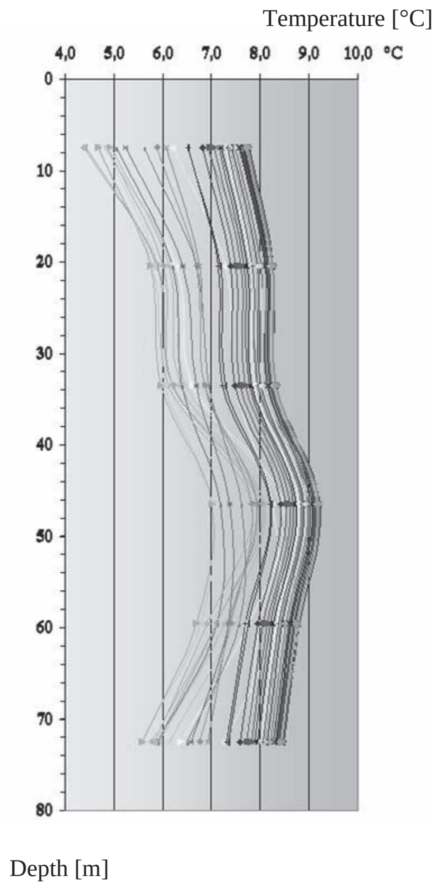

Figure6: Temperature profiles of a particular heat pipe borehole heat-exchanger within 24 h (30 min interval, the colors ranging red-yellow-green-blue-black)

4 SUMMARY

Geothermal Borehole Heat Exchangers using geothermal heat pipes for convective energy withdrawal and transport from and with the soil are a particularly efficient technology.

A method has been developed to compute the heat transport of a Geothermal Heat Pipe Borehole Heat-Exchanger.

Furthermore, long-term measurement data have been collected from a Geothermal Heat Pipe Borehole Heat-Exchanger installation. They have been successfully used to compute the expected heat power output and the systems' operation.

5 REFERENCES

Dunn, P.D.; Reay, D.A. (1993). Heat Pipes. University of Reading, Reading UK, Heriot-Watt University, Edinburgh, UK. Fourth Edition.

Lee, Y.; Mital, U. (2003). A two-phase closed thermosyphon. Department of Mechanical Engineering, University of Ottawa 2, Ottawa, Canada.

Analysis of the freeze thaw performance of geothermal heat exchanger borehole grout materials

Étude de la résistance au gel et dégel des sondes géothermiques verticales

Katzenbach R., Clauss F., Rochée S.
Technische Universität Darmstadt, Institute and Laboratory of Geotechnics, Germany

ABSTRACT: If the exposure of vertical borehole heat exchangers even to few freeze-thaw cycles may possibly lead to damage either of the body of backfill grout filling the borehole or it may lead to damage of the structure of the surrounding subsoil is subject of an ongoing discussion. Previous research has been focusing on the damage of the backfill grout body solely. The purpose of the research presented with this paper is to study the performance of the entire system subsoil-grouting body in terms of the freeze-thaw resistance by means of experimental analysis. As no standard procedure is available in codes or literature for these particular applications, a defined test setup and a reproducible procedure for the test conduction have been developed. Experiments were conducted in a cylindrical encasement with a sample of grout and saturated sand. Parallel, experiments with blank samples of each material were carried out. The samples were exposed to a temperature range varying between -20 °C and +20 °C. Analysis and interpretation of the results bases on grain size distributions before and after freeze thaw cycles, evaluation of weathering, temperature and strain measurements.

RÉSUMÉ : L'exposition des sondes géothermiques verticales à un nombre (même faible) de cycles de gel-dégel peut amener à une détérioration du mortier de remblayage assurant la jonction entre la sonde et le sol ou à une modification de la structure du sous-sol environnant. Les recherches antérieures se sont uniquement concentrées sur le mortier de remblayage. Il s'agit ici d'étudier expérimentalement la résistance aux cycles de gel-dégel du système complet constitué à la fois du coulis d'injection et du sol. Aucun protocole standardisé pour ce type d'applications n'est disponible actuellement dans les normes ou dans la littérature, un banc d'essai et un protocole reproductible ont donc été conçus pour réaliser l'expérience. Les tests ont été menés dans une gaine cylindrique sur des échantillons constitués de sable saturé en eau et de matériau de remplissage thermique. Des tests avec des échantillons témoins ont été menés en parallèle pour chaque matériau. Les échantillons ont été exposés à des températures variant entre -20 °C et +20 °C. L'analyse et interprétation des résultats est basée sur l'observation des courbes granulométriques avant et après les cycles de gel et dégel, l'évaluation de l'altération des échantillons et les mesures de températures et déformations.

KEYWORDS: geothermal energy, borehole heat exchanger, freeze thaw, grout material, subsoil, experimental.

1 INTRODUCTION

If the exposure of a borehole heat exchanger to freeze thaw cycles may lead to damage either the grouting or the circumfluent subsoil is subject of an ongoing discussion. Freeze-thaw-cycles occur because of an inaccurate dimensioning of the installation, of temporary high abstraction capacities or of modified terms of use, for example added apartments or buildings (Müller 2009).

Vertical borehole exchangers are composed of pipes in which flows a heat-transfer medium and of a backfill grout body between those cables and the surrounding subsoil. Grouting materials serve to stabilize the borehole during the setting up and to obtain a good thermal connection between heat transfer medium and subsoil. Moreover, those materials have to guarantee a sufficient sealing on target to avoid connections between groundwater aquifers.

Sealing of the borehole is related with the freeze-thaw-resistance of the grouting materials and more widely of the freeze thaw resistance of the whole system composed of grouting materials and circumfluent subsoil. Damages are principally due to the properties of water: volume of water contained in the pores of the material expands of 9 % by freezing, which may lead to deteriorate permanently the structure, even after thawing. Hence are connections between groundwater storeys possible which presents an environmental risk.

2 SET OF PROBLEMS

2.1 *Research significance*

Some cases of damage are documented in line with a project of the engineering companies GEOWATT AG and Ingénieurs-Conseils SA (Bassetti 2006). Various experimental analyses have been in addition carried out on the frost resistance of the backfill grout body in recent decades (Herrmann 2008, Müller 2009, Niederbrucker et al. 2008), but few investigations have been performed to evaluate the resistance of the whole system grouting-subsoil. Purpose is to design and develop a new test stand to determine the effects of the subsoil on the freeze thaw resistance of the whole system, focusing on the damages inside the materials as well as the alteration of contact surface, in accordance with conditions related to borehole heat exchangers.

2.2 *Influence parameters of frost in soils*

According experimental and theoretical analyses referenced in literature (Rückli 1950, Reutel et al. 1992), freeze penetration in the soil is influenced by following parameters:

- Grain structure
- Existing and mobilized water
- Temperature distribution during freeze and thaw periods
- Stress distribution

Presence of water in soil is given as main cause of degradations. Types of frost effects are different between fine and coarse grained soils: coarse grained soils presents some structure alterations after freeze thaw cycles, fine grained soils presents heaves and changes of plasticity index due to water pulling during freezing. Most damages in road structures occur when subsoil on ground surface is made of fine grained soils (ZTVE-StB 94).

Forages of vertical borehole heat exchangers attain depths in order of 100 m. Therefore, increasing of effective pressure with depth reduces the negative effects of freeze, as described by Ruckli (1950): for example, frost heave velocity for soils with a grain size between 0.005 mm and 0.010 mm decreases as pressure increases and is around equal to zero for pressures higher than 30 kN/m². Consequently, stress distribution in the soil and therefore on the borehole heat exchanger is considered as an important influence parameter. It leads to suppose that soil has a positive effect on frost resistance of the whole system, what should be verified here experimentally.

3 ACTUAL STANDARDS AND TESTS

There is actually no guideline for evaluating the frost resistance of vertical borehole heat exchangers. Developing a new procedure consists in defining the test experiments and the criteria regarding freezing resistance of the material. Following, an overview of the existing tests on freeze thaw resistance of different types of materials is given as base for possible procedures; under consideration that it should be further investigate with boundary conditions from vertical borehole heat exchangers.

German and international standards for freeze-thaw experiments on soils exist for natural stones and aggregates. The German standard DIN 52104:1982 which gives instructions regarding freeze-thaw behavior of natural stones was replaced by the standard DIN EN 12371, from which the latest edition appeared in 2010. Details about the determination of the freeze thaw resistance of aggregates are given in the German standard DIN EN 1367-1.

For unconsolidated material such as clay, silt and sand, there are no rules and standards. However, those types of soil are subject of research investigations (Rückli 1950, Simonsen and Isacsson 2001, Andersland and Ladanyi 2004).

For freeze thaw resistance of hardened concrete according to the common standards, a distinction between freeze-thaw-resistance on the one hand with and on the other hand without de-icing agents is made (pre-standard DIN CEN/TS 12390-9:2006). The first one corresponds to the resistance to repeated freeze-thaw cycles in contact with water. In case of the second one, the specimen is in contact with road salt. Usually the de-icing agent corresponds to a 3% NaCl solution. In the pre-standard DIN CEN/TS 12390-9 three methods are described: the slab test as a reference, the cube method and the CF and CDF testing (Capillary Suction) as alternatives. The difference between CF and CDF method is the test fluid (with water or with deicing agent).

Although no standards are available about freeze thaw resistance in application to borehole heat exchanger, some research reports deals specifically with freeze effects on grout materials (Herrmann 2008, Müller 2009, Niederbrucker et al. 2008).

Following test procedure takes care of those different standards and research reports and extends the actual analyses considering effects of freeze thaw with the surrounding soil.

4 EXPERIMENTS AND RESULTS

4.1 *Preliminary tests*

Experiments are conducted in a cylindrical encasement with a sample of grout material and soil. A more detailed description of the system for those tests is available in the next part. Preliminary tests has been conducted on samples with reduced dimensions in order to investigate the influence of water saturation of the surrounding soil and to validate the assembly procedure.

Two samples of cement and sand are represented on figure 1. In both cases, cement characteristics and assembly procedure remains the same. If the surrounding soil has a low saturation degree, a cone appears on the upper part of the cement cylinder. The cement part possesses in this case higher unconfined compressive strength and modulus of elasticity with an increasing rate in the order of 40 %.

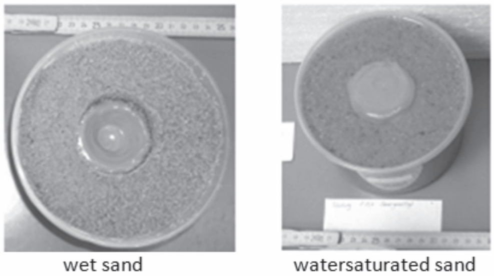

Figure 1: Influence of the water saturation of the surrounding soil

4.2 *Test procedure*

In order to avoid scaling factors, diameter of the grouting material cylinder is in the same range of diameters of real borehole heat exchangers, see figure 2 and 3. Dimensions of the cylindrical encasement were then selected taking in consideration the following statements: on one side, a large distance between rands of grouting material and rands of encasement limits the effects of deformations of the encasement on the grout material due to high temperature changes; on the other side, an increasing quantity of soil may lead to longer procedure time due to freezing and thawing periods and to more constraints regarding transport and storage due to an higher weight of the sample, which are to be considered for a reproductible procedure.

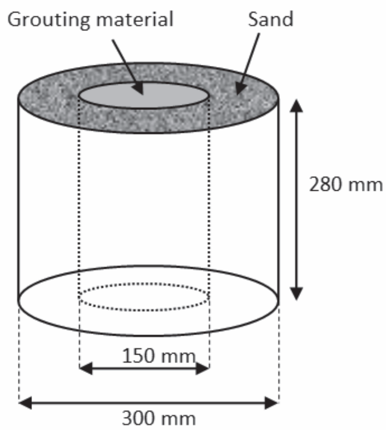

Figure 2: Dimensions of the samples of soil and grouting material

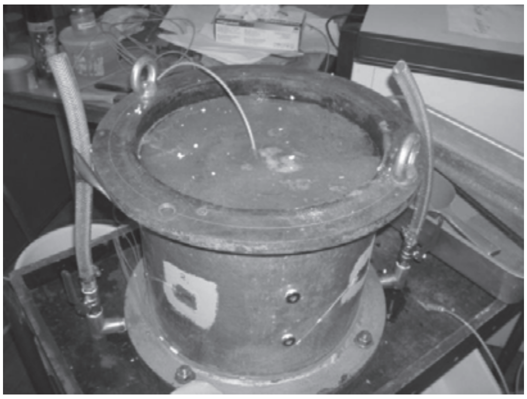

Figure 3: General view after assembly and hardening

As the development of the procedure requires many preliminary tests, the first experiments were conducted with sand for which time for consolidation and water saturation is reduced in comparison with fine grained soils.

The sample represented on figure 4 is as following assembled: firstly, filter plate (see figure 5) is laid in the encasement and the bored part covered with a filter paper. A PVC tube is then inserted in the cut-out of the filter plate, reproducing the use of a tubing casing. Sand is filled around this PVC tube and saturated from the bottom up. At last, grouting material is injected and the PVC tube is vertically removed. Grouting material hardens during 28 days before applying temperature loads. The assembly procedure has been validated and improved on base on experiments with reduced dimensions as related in the previous part.

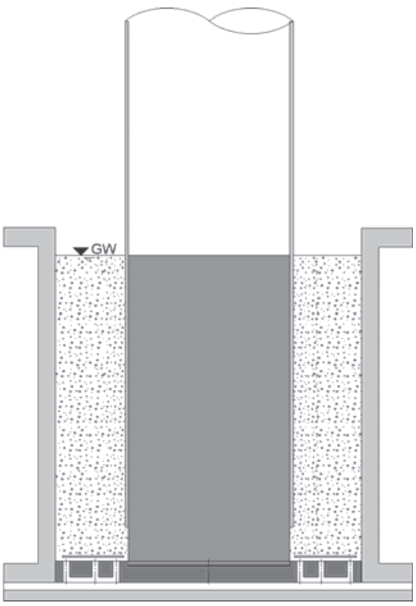

Figure 4: Sectional drawing of the sample during assembly

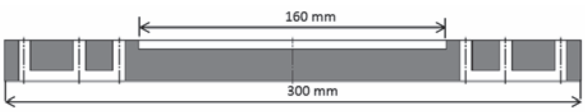

Figure 5: Sectional drawing of the filter plate

4.3 *Temperature measurements*

In case of a borehole heat exchanger, freeze-thaw cycles are mostly due to temperature changes inside the pipes. However, temperature varies during the tests outside the assembled unit in order to keep homogenous samples for performing unconfined compression tests. In the procedures referred in part 3 that deal with other boundary conditions and materials, temperature varies either between -10 °C and +10 °C or between -20 °C and +20 °C. The temperature range selected here between -20 °C and +20 °C is in accordance with the attainable temperatures inside the pipes of a borehole heat exchanger with an additional security factor.

Temperature measures are necessary before execution of the main experiments in order to fix the period of the freeze-thaw cycles, considering that freezing and thawing processes should attain a stable phase. A first sensor is used in order to control the environment temperature, a second sensor measures the temperature on the border of the encasement and a third sensor has been brought during the assembly inside the grouting material. According to those measurements (figure 6), the period of one freeze thaw cycle is fixed to 7 days. Investigations described in next part were carried out after two cycles.

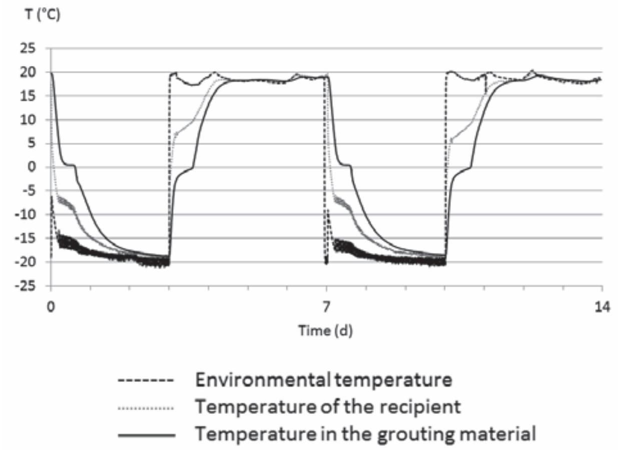

Figure 6: Temperature measurements during freeze thaw cycles on a sample of grouting material and saturated sand

4.4 *Further investigations*

An overview of the tests and investigations which were carried out in the framework of the procedure development is given in table 1.

Table 1: Types of investigations

Sample	Conditions	Investigations
Grouting material and watersaturated sand	With freeze-thaw cycles	Temperature measures, grading curve of sand
Blank sample with watersaturated sand	Without freeze thaw cycles	Grading curve
	With freeze-thaw cycles	Grading curve
Blank sample with grouting material	With freeze-thaw cycles	Surface alteration after each cycle, unconfined compression test
Blank sample with grouting material (in contact with water)	With freeze-thaw cycles	Surface alteration after each cycle, unconfined compression test

Figure 7: Alteration of a blank sample of grout material in contact with air (left) or with water (right) after two cycles

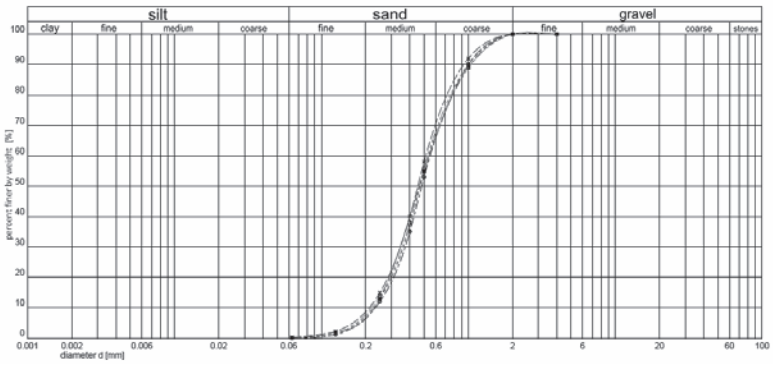

Figure 8: Grade curves of sand used for the experiments before and after freeze thaw cycles

Most frost damages at the surface of grouting material appear when the material is as blank sample directly in contact in water (see figure 7). The unconfined compression tests confirm the fact that freeze thaw cycles have more negative influence on the structure of blank samples of grouting material which are in contact with water, showing in fact a reduced compression strength.

In case of tests with grouting material and watersaturated sand, prelevements of the sand surrounding the grouting material would be carried out. The corresponding grading curves before and after the freeze thaw cycles are similar (figure 8), pointing out that the surface is less altered if sand surronds the sample despite a contact with water and that the presence of this type of soils has a positive effect on the resistance of grouting material regarding freeze thaw resistance. Due to the level of the effective pressure and permeability of the soil, water is pushed out the sample and pore volumes do not increase during icing.

5 CONCLUSIONS

Freeze thaw resistance of the system concerns not only the resistance of the grout material, but also of the surrounding soil and the interface between the two elements. Fine grained soils would be more critical than coarse grained soils regarding freeze thaw effects. Nevertheless, results presented in the literature for those types of soils show that such effects are fastly reduced with increasing effective pressure.

A real alteration of the system does not appear here, confirming a positive influence of the soil on the frost resistance of the system soil-grouting. Considering damages documented in reports, results from the literature and from the present experiments leads therefore to conclude that most frost damages would appear on the ground surface and concern more external elements such as distribution devices or pipes for the connection between building and borehole heat exchanger rather than grouting materials in the forage. Comparing the overall state of stress in the soil along a geothermal borehole heat exchanger with the stresses from freeze-thaw cycles observed in the presented investigations does not suggest the occurance of damages from the operation of a geothermal borehole heat exchanger even in peak load and with freeze-thaw cycles.

6 REFERENCES

Andersland, O., B., Ladanyi, B. 2004. *Frozen Ground Engineering*. John Wiley & sons, New Jersey, ‘Appendix C: Laboratory and Field Tests on Frozen Soils’, 315-367

Bassetti S., Rohner E. and Signorem S. 2006. *Dokumentation von Schadensfällen bei Erdwärmesonden*. Schlussbericht, Geowatt AG und Ingénieurs-Conseils SA, EnergieSchweiz.

DIN CEN TS 12390-9:2006. *Testing hardened concrete. Freeze Thaw Resistance*. (German Version). Deutsches Institut für Normung.

DIN EN 12371:2010. *Natural stones test methods – Determination of frost resistance*. (German Version). Deutsche Institut für Normung.

DIN EN 1367-1:2007. *Tests for thermal and weathering properties of aggregates. Determination of resistance to freezing and thawing*. (German Version). Deutsches Institut für Normung.

DIN 52104:1982. *Prüfung von Naturstein - Frost-Tau-Wechsel-Versuch*. Deutsches Institut für Normung.

Herrmann J. 2008. *Ingenieurgeologische Untersuchungen zur Hinterfüllung von Geothermie-Bohrungen mit Erdwärmesonden*. Dissertation , Fakultät für Bauingenieur-, Geo- und Umweltwissenschaften der Universität Fridericiana (TH), Karlsruhe.

Müller L. 2009. *Frost-Tau-Widerstand von Verfüllbaustoffen für Erdwärmesonden*. Beitrag „Der Geothermiekongress 2009“ Bochum.

Niederbrucker R., Steinbacher N. 2008. *Eignungsuntersuchung von Verpressmaterialien für Erdwärmesonden*. Technischer Endbericht, Land Oberösterreich.

Reuter, F., Klengel, J., Pasek, J. 1992. *Ingenieurgeologie. 3. Auflage*, Deutscher Verlag für Grundstoffindustrie GmbH, Leipzig-Stuttgart

Ruckli R. 1950. *Der Frost im Baugrund*. Wien Springer-Verlag.

Simonsen, E., Isacsson, U. 2001. *Soil behavior during and thawing using variable and constant confining pressure triaxial tests*. Canadian Geotechnical Journal, 38(4), 863-875

ZTVE-StB 94. Bundesministerium für Verkehr. 1994. *Zusätzliche Technische Vertragsbedingungen und Richtlinien für Erdarbeiten im Straßenbau*. FGSV Verlag GmbH.

Thermal influences on swelling pressure and swelling deformation of bentonites and investigation of its factors

Effets thermiques sur la pression et les déformations de gonflement des bentonites et facteurs d'influence

Komine H.
Ibaraki University

ABSTRACT: Because buffers for disposal of high-level radioactive wastes must have high swelling characteristics for sealing wastes, bentonite is currently designated for that use. High-level radioactive wastes generate decay-heat, and it is has been inferred that the swelling characteristics of bentonite decline because of the decay-heat of wastes. This study investigated swelling pressure and swelling deformation of bentonites during some thermal experiments conducted in the laboratory. Moreover, this study discusses the mechanism of thermal influences to bentonite-swelling by considering the above experimentally obtained results with chemical analyses such as measurement of cation concentration of water around the specimen, a methylene blue absorption test, and X-ray powder method for heated bentonites.

RÉSUMÉ : Parce que les bouchons pour le scellement de déchets radioactifs de haut niveau doivent avoir de fortes caractéristiques de gonflement pour fixer les containers, la bentonite est utilisée actuellement pour cet usage. Les déchets radioactifs de haut niveau produisent une chaleur décroissante, et ceci entraîne une baisse des caractéristiques de gonflement de la bentonite. Ce travail étudie la pression de gonflement et les caractéristiques de déformabilité des bentonites par des expérimentations thermiques menées en laboratoire. De plus, on discute le mécanisme des effets thermiques sur le gonflement de la bentonite obtenus ci-dessus par une analyse chimique incluant la concentration en cations, l'absorption du bleu de méthylène ou la diffraction de rayons X sur des poudres de bentonite chauffée.

KEYWORDS:Bentonite, Swelling, Radioactive waste disposal, Clay minerals, Chemical properties, X-ray diffraction analysis

1 INTRODUCTION

Because buffer materials for disposal of high-level radioactive wastes (HLWs) must have high swelling characteristics and very low permeability to seal the waste, bentonite is currently designated for that use.Ingeological disposal of high-level radioactive wastes, bentonite-based buffer fills spaces between the wastecontainer and bedrockbecause it has swelling properties and low permeability. High-level radioactive wastes generate decayheat. It is inferred that the swelling characteristics of bentonite declineby the decayheat of wastes.

The author assessed the swellingdeformationof one kind of sodium bentonite thathad undergonesome thermal exposure in a laboratory in an earlier study(Komine and Ogata, 1998) as preliminary research. Some researchers reported changes of soil behavior during heating (Akagi, 1994; Oscarson and Dixon, 1989). It appearspossible that bentonite receives decay heat of high-level radioactive wastejust as other soils do (see Fig. 1). In a disposal pit, as Fig. 1 shows, the swelling characteristics of bentonite might declinebecause of exposure to decay heat from wastes. It is therefore necessary to investigate thermal effectson swelling pressure and swelling deformation characteristics of somebentonitesfor buffer material development.

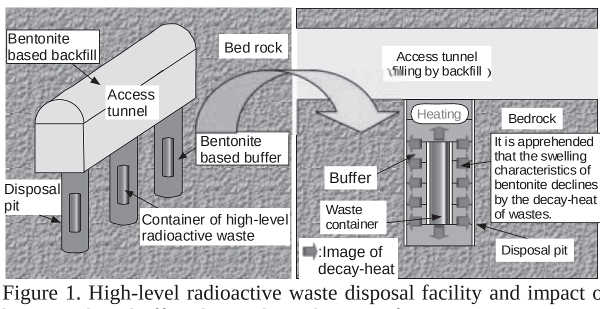

Figure 1. High-level radioactive waste disposal facility and impact on bentonite base buffers during decay-heating of wastes.

To elucidatethis problem, this study investigated swelling pressure and swelling deformation of bentonites that had undergone some heatexposure in the laboratory. Moreover, this study assessedmechanisms of thermal influences to bentonite-swelling by examiningthe experimentally obtained results using chemical analyses for the heated bentonites such as measuring cation concentrations of water around the specimen, methylene blue absorption tests, and X-ray powder method.

2 BENTONITE USED FOR THIS STUDY AND THERMAL EXPOSURE CONDITIONS

Commercial bentonitesof two kinds (Table 1) were used. Bentonite A, called Kunigel-V1, was produced at the Tsukinuno Mine in Yamagata prefecture, Japan. This sodium-type bentonite contains nearly 57% montmorillonite.It is used frequently in Japan to studyartificial barrier materials against radioactive waste. Bentonite C, called Kunibond, is produced at the Dobuyama Mine in Miyagi prefecture, Japan. This calcium-type bentonite hasnearly 80% montmorillonite content.

This study produced some bentonites that had undergone different thermal exposure by oven drying to investigate the thermal history influence onbentonite swelling characteristics. The heating conditions for producing the heated bentonites were 60, 90, 110, and 130°C.Heating periods were28, 120, and 365 days.Those heating temperatureswere used to simulate decayheating of HLWsbased on analytical results of maximum temperatures in bentonite-basedbuffers, whichare65–165°C (Japan Nuclear Cycle Development Institute, 2000) andon results of previous research (Japan Nuclear Cycle Development Institute, 2000) showing that montmorillonite will not be altered to illite at less than 130°C.

Table 1. Fundamental properties of bentonites A and C

Bentonite	A	C
Type	Sodium	Calcium
Density of soil particle(Mg/m^3)	2.79	2.71
Liquid Limit (%)	458.1	128.7
Plastic Limit (%)	23.7	38.4
Plasticity index	434.4	90.3
Montmorillonite content (%)	57	84
Cation Exchange Capacity (meq/g)	1.166	0.795
Exchange Capacity of Na^+ (meq/g)	0.631	0.119
Exchange Capacity of Ca^{2+} (meq/g)	0.464	0.585
Exchange Capacity of K^+ (meq/g)	0.030	0.019
Exchange Capacity of Mg^{2+} (meq/g)	0.041	0.072

After the bentonite heating described above, these samples werekeptat a constant temperature (22 ± 3°C) and constant humidity (70% relative humidity) until the water contents of samples stopped changing.

3 SWELLING PRESSURE AND SWELLING DEFORMATION OF BENTONITES AFTERSOMETHERMAL EXPOSURE

This study used the experimental apparatus presented in Fig. 2.The maximum capacity and the minimum scale of the load transducer were 10 kN and 0.0025 kN, respectively. The maximum capacity and the minimum resolution of the linear variable displacement transducer (LVDT)were, respectively, 25 mm and 0.002 mm. This study conductedswelling characteristic experiments of twokinds. The swelling pressure test measured the bentonites' swelling pressure as water was supplied to the confined bentonite specimen. The swelling deformation test measured the relationbetween the axial swelling deformation and the time from the start of water supply. Test proceduresweredescribed in an earlierarticle (Komine et al., 2009).

Figure 3 portrays the relation between maximum swelling pressure and the initial dry density of bentonites' thermal exposureduring swellingpressure tests. This figureshows that the influence of thermal exposureon swelling pressure characteristics of both bentonites is slight, provided that theheating temperature is less than 130°C and that the heating duration is less than 120 days.Regardingresultsobtained for calcium-type bentonite C depicted in Fig. 3(b), almost no influenceof thermal exposureon swelling pressure characteristics is shown for1.37–1.53 Mg/m^3initial dry density. However, a slightinfluenceof thermalexposure is apparentat 1.22–1.27 Mg/m^3.

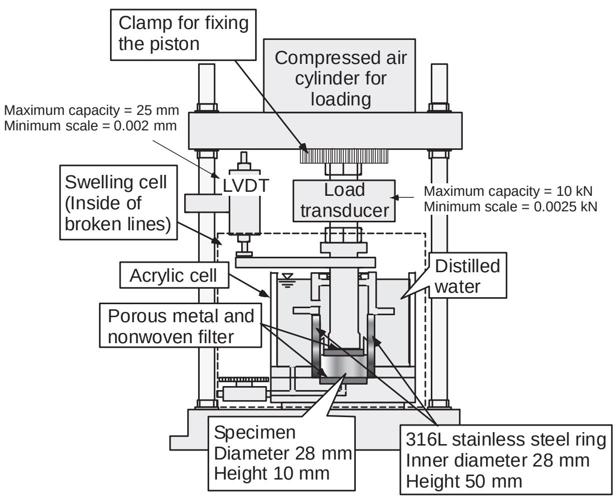

Figure 2. Experimental apparatus.

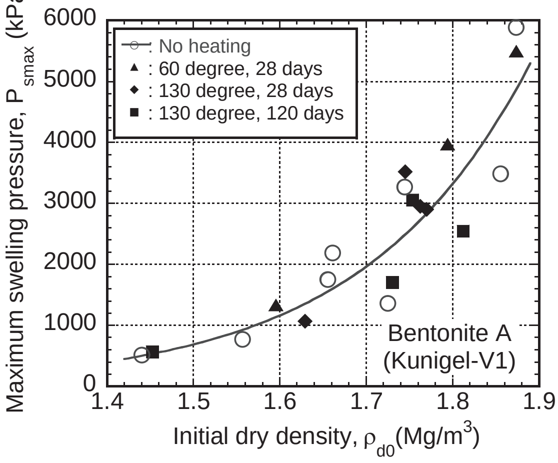

(a) Bentonite A

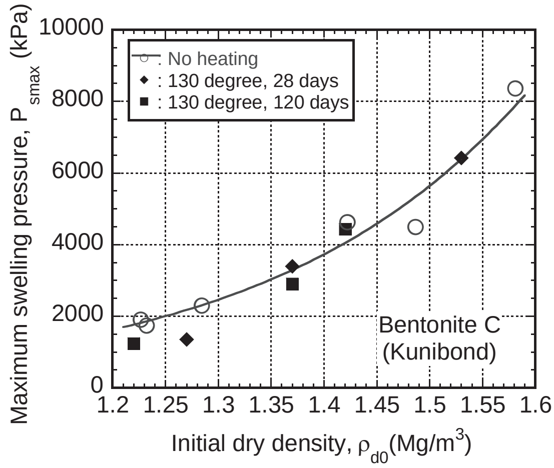

(b) Bentonite C

"No heating" in the legend denotes experimentally obtained results for bentonite with no thermal exposure. The temperature in the legend is the heating temperature by dryingoven. The days in the legend show the heating duration.

Figure 3. Relationbetween maximum swelling pressure and initial dry density of bentonites A and B withthermal exposure.

Figure 4 shows the relation between maximum swelling strain and initial dry density of sodium-type bentonite A at vertical stresses of 1000 kPa and 500 kPa. Results in this figureshow that maximum swelling strain increases linearly as theinitial dry density increases. For the sodium-type bentonite A, the swelling deformation property of bentonite after thermal exposure is almost unchangedunder 1000 kPa vertical stress. However, the swelling deformation property of bentonite isgreatlyreduced for heating at 90–130°C fora 365-day heating duration under conditions of 500 kPa vertical stress, as portrayed in Fig. 4(b). Those results indicate that the thermal influence to swelling deformation characteristics of sodium-type bentonite A is dependent onthe vertical stress condition. The influences of thermal exposureon swellingdeformation decrease for high vertical stresssuch as 1000 kPa. Thisdiscussion shows agreement with previously presenteddiscussionindicating that swelling pressure characteristics of bentonite Ashowalmost no change according to thermal exposure, as depicted in Fig. 3(a) and previously reportedexperimentally obtained results (Komine and Ogata, 1998) showing thatswelling deformation

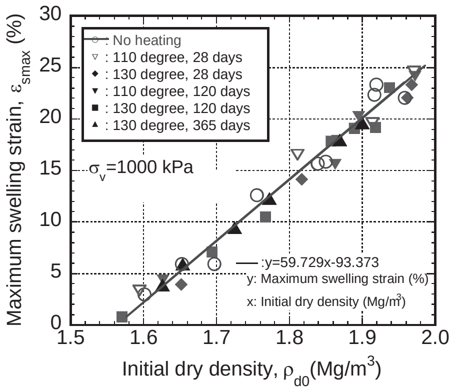

(a) Vertical stress = 1000 kPa

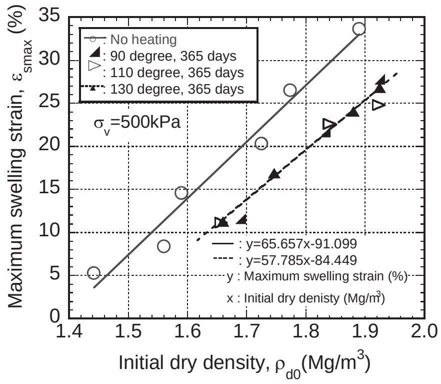

(b) Vertical stress = 500 kPa

Figure 4.Maximum swelling strain and initial dry density of sodium-type bentonite A with vertical stressof 1000 kPa and 500 kPa.

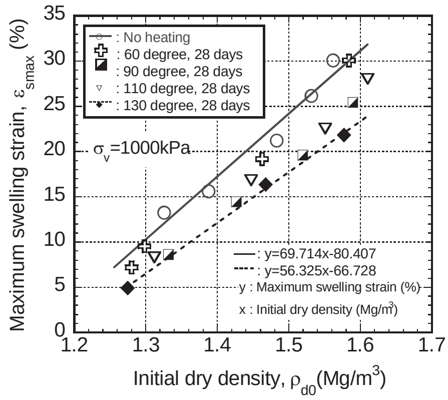

(a) Heating duration 28 days

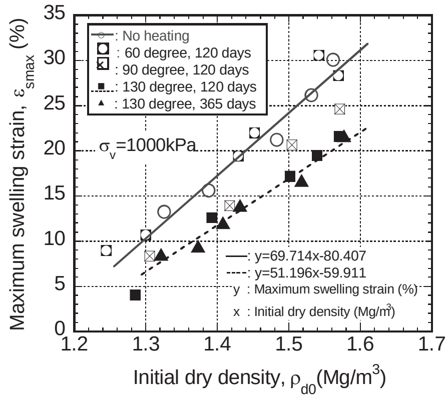

(b) Heating duration 120 days and 365 days

Figure 5. Relationbetween maximum swelling strain and initial dry density of calcium-type bentonite C at vertical stress of 1000 kPa.

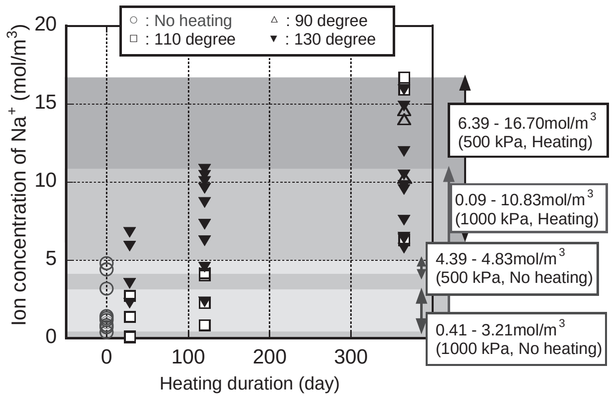

Figure 6. Results of sodium ion concentration of water around the compacted specimens of bentonite A after swellingdeformation tests.

Table 2. Results of sodium and calcium ions concentrations of water around calcium-type bentonite C after swelling pressure and swelling deformation tests.

Experiment	Heating temperature (°C)	Heating duration (day)	Na^+ ion concentration (mol/m^3)	Ca^{2+} ion concentration (mol/m^3)
Swelling pressure test	No heating		0.33–1.65	0.01–0.16
	130	28– 120	0.20–0.46	0.00–0.14
Swelling deformation test at 1000 kPa vertical stress	No heating		0.21–0.59	0.05–0.48
	90–130	28	0.03–1.27	0.01–0.45
	90–130	120	0.06–0.84	0.17–0.27
	130	365	0.50–0.78	0.12–0.25

characteristics of sodium-type bentonite are strongly reduced by thermal exposure at 9.8–10.0 kPa vertical stress.

Figure 5 showsthe relationbetween maximum swelling strain and initial dry density of calcium-type bentonite C at vertical stress of 1000 kPa. By comparing results presented in Fig. 5 with those in Fig. 4, the swellingdeformation characteristics of calcium-type bentonite C aremarkedlyreduced by thermal exposure at vertical stress of 1000 kPa. The swellingdeformation characteristics of calcium-type bentonite C are strongly reduced byheating temperatures greater than 90°Cfor all heating durations. Furthermore, the reduction ratio of maximum swelling strain attributable tothermal exposureincreases along with theinitial dry density.

4 THERMAL INFLUENCEON BENTONITESSHOWN BYCHEMICAL ANALYSIS RESULTS

Figure 6 presents sodium ion concentrations of water measured around the compacted specimen of sodium-type bentonite A after swelling deformation tests. This figure shows the relationbetween sodium ion concentration and heating duration with parameters of heating temperature and vertical stress.

Results depicted in Fig. 6 show thatthe sodium-ion concentration of water around the specimen is increasedby thermal exposure for sodium-type bentonite A. Especiallyfor higher heating temperatures and longer heating durations, the sodium-ion concentration of water around the specimen is higher. Moreover, Fig. 6 depicts that the sodium-ion concentration in water around the specimen at 500 kPa of vertical stress is greater than that at 1000 kPa of vertical stress. The measured results of calcium ion concentration are thesame results of sodium ion concentration. Those results show that exchangeable cations such as Na^+, Ca^{2+} are apt to elute to surrounding water around the bentonite specimen for the sodium-type bentonite A.In contrast, Table 2 presents results for calcium-type bentonite C which show thatthe sodium and calcium ionconcentrations are almost unchanged irrespective of thermal exposure. Therefore, the thermal influence on calcium-type bentonite differs from that on sodium-type bentonite.

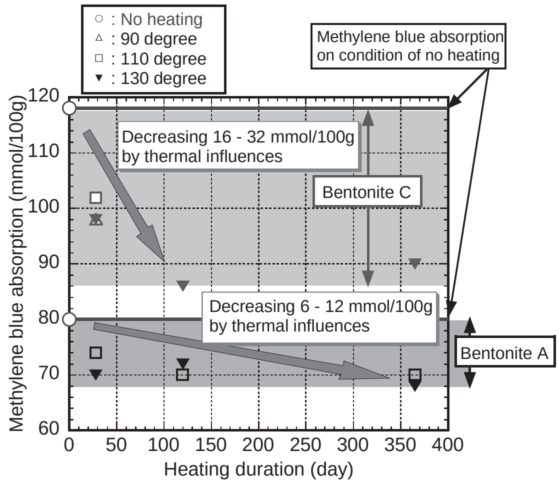

Figure 7.Methylene blue absorption for bentonites A and C with thermal exposure.

Figure 7 portrays the methylene blue absorption for bentonites A and C that had undergone thermal exposure. Results show thatthe absorbing capacities of methylene blue for bentonitesof both kinds are reducedby thermal exposure.

Figure 8 presents X-ray diffraction plots of bentonites A and C experienced thermal exposure. Results show thatthe X-ray diffraction plot of bentonite A hasalmost no change by thermal exposure.However, the plot for bentonite C shows a marked change because of thermal exposure. Therefore, the mechanism of thermal effects on sodium and calcium-type bentonites can be understood as shown in Fig. 9.

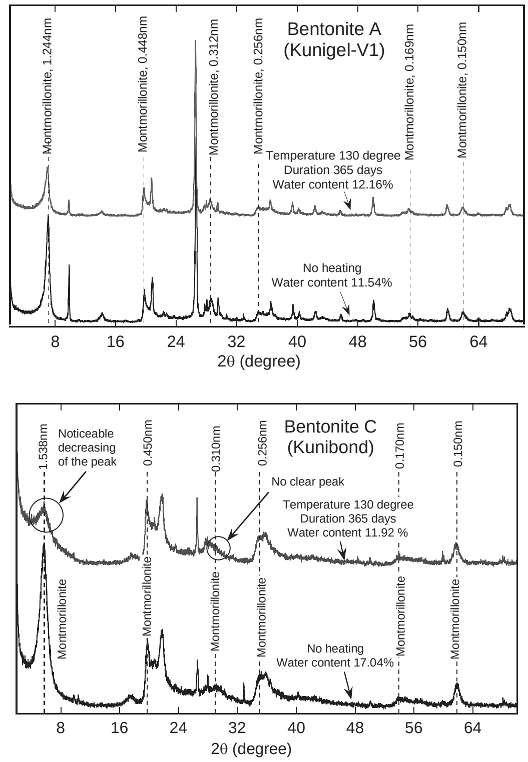

Figure 8. X-ray diffraction plots of Bentonite A and C with thermal exposure.

5 CONCLUSIONS

This study quantitatively assessedthermal exposure effects onthe swelling characteristics of sodium-type and calcium-type bentonites using swellingpressure and swellingdeformation testing of bentonites that had undergonethermal exposure. This reportdescribedmechanisms of thermal influences onswelling of these heated bentonites by consideration of the experimentally obtained results with measurements of cation concentrations of water surrounding the specimens, with methylene blue absorption tests, and X-ray powder method.

6 ACKNOWLEDGMENTS

This study was supported through funding by research funds of the Japanese Ministry of Education, Culture, Sports, Science and Technology and the TEPCO Research Foundation. The author alsothanks all members and students of the Geotechnical Laboratory, Ibaraki University, for their kind assistance and discussions.

7 REFERENCES

Akagi, H. 1994. A physico-chemical approach to the consolidation mechanism of soft clays, *Soils and Foundations* 34(4), 43-50.

Japan Nuclear Cycle Development Institute (Japan Atomic Energy Agency as of 2012) (2000). *H12: Project to establish the scientific and technical basis for HLW Disposal in Japan*, Project Overview Report, JNC TN1410 2000-001.

Komine, H. and Ogata, N. 1998. Thermal Influence on compacted bentonite for nuclear waste disposal, *Proceedingsof theThird International Congress on Environmental Geotechnics*1,39-44, 1998.

Komine, H.,Yasuhara, K. and Murakami, S. 2009. Swelling characteristics of bentonites in artificial seawater, *Canadian Geotechnical Journal* 46(2), 177-189.

Oscarson, D. W. and Dixon, D. A. 1989.The effect of steam on montmorillonite, *Applied Clay Science* 4, 279-292.

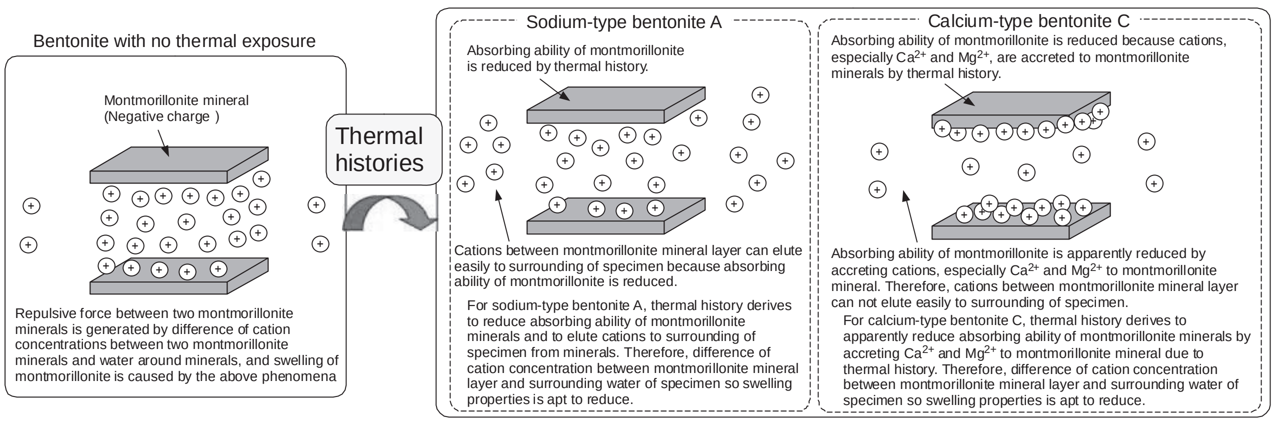

Figure 9. Mechanism of thermal influences to bentonite-swelling

Performance of Piled Foundations Used as Heat Exchangers

Performance des fondations sur pieux utilisées comme échangeurs thermiques

Loveridge F., Powrie W.
Faculty of Engineering and the Environment, University of Southampton, Southampton, UK

ABSTRACT: In closed loop ground energy systems, used to provide renewable heat energy to buildings, heat is transferred between a heat pump and the ground via ground heat exchangers. Fluid is circulated through pipes within the heat exchanger. Including these pipes within the concrete of piled foundations can give economies of excavation and materials. However, there remain few validated design approaches for determining the heating and cooling capacity of pile heat exchangers. There have also been concerns that inappropriate operation may cause extreme temperatures to develop in the ground, leading to loss of geotechnical performance. As a result most current design is conservative and does not fully utilise the thermal capacity of the pile-ground system. To permit validation of new design methods, instrumentation has been installed within a pile heat exchanger at a site in London. Initial results are showing the pile concrete to be making a substantial contribution to the short term storage of thermal energy. This is significant, as most design methods assume that the pile concrete merely acts to transfer heat to the surrounding ground. This heat storage also acts to protect the ground against larger fluctuations in the fluid temperature and is therefore beneficial for geotechnical performance.

RÉSUMÉ : Dans les systèmes de transfert d'énergie du sol en circuit fermé, utilisés pour la fourniture d'énergie thermique durable aux immeubles, les échangeurs thermiques transmettent la chaleur du sol à une pompe à chaleur. On peut obtenir des économies lors de l'installation si les tuyaux de l'échangeur thermique se trouvent dans le béton des fondations sur pieux. Il n'existe cependant guère d'approches conceptuelles validées pour la détermination des capacités thermiques des pieux à échangeurs thermiques et des préoccupations existent sur leur utilisation inappropriée ; la plupart des conceptions actuelles est donc conservative. Pour la validation de nouvelles méthodes de conception, on a installé de l'instrumentation dans un pieu à échangeur thermique sur un chantier à Londres. Les premiers résultats démontrent que le béton du pieu offre une contribution substantielle sur l'accumulation à courte durée de l'énergie thermique. Ceci est important pour l'amélioration de la performance géotechnique.

KEYWORDS: ground energy systems, piling, renewable energy, temperature effects

1 INTRODUCTION

It is becoming increasingly common for ground energy systems to utilise building piled foundations as the heat exchanger part of the system, facilitating heat transfer to the ground. In this arrangement, small diameter (<30mm) plastic pipes are cast into the piles, before being connected via larger header pipes to a heat pump. This forms the "source" side of the ground energy system. On the "delivery" side of the system, the heat pump is connected to heating and air conditioning units, which should be a low temperature system to maximise efficiency.

Design of pile heat exchangers is split into two main aspects. First the calculation of the thermal capacity of the pile heat exchanger, ie what heating and cooling power can be achieved from the pile or pile group. Secondly, it is important that additional checks are performed with respect to the geotechnical design so that any additional concrete stresses or displacements resulting from temperature changes induced in the piles can be taken into account in the structural design. These two design aspects do not, however, exist in isolation. The range of temperatures at which the heat pump system operates will directly influence both the available thermal capacity and the geotechnical design. It is therefore important that appropriate temperature limits are agreed between all parties. From a geotechnical perspective it is essential that the pile-ground interface does not reach freezing temperatures, while extreme higher temperatures may affect the efficiency of the heat pump.

While procedures for geotechnical design of pile heat exchangers are developing rapidly (GSHPA 2012; Amatya et al. 2012; Ouyang et al. 2011; Knellwolf et al. 2011), there remain few datasets available with which to permit validation of design methods for the heating and cooling capacity of piles (Loveridge & Powrie 2012). To address this important knowledge gap, the University of Southampton has commenced a programme of in situ monitoring of pile heat exchangers. This paper will present details of an instrumented pile heat exchanger in East London, along with initial data from the first few months of operation of the energy system.

2 SITE DESCRIPTION

The instrumented pile is part of the foundations for "The Crystal", Siemens' new landmark building adjacent to Royal Victoria Dock in East London. The Crystal is a multi-use development and contains an interactive exhibition on sustainable technologies as well as office space. It has been designed to be an all electric building, utilising solar power and ground source heat pumps to generate all the energy for the development.

The source side of the ground energy system comprises 160 pile heat exchangers and a field of 46 150m deep boreholes. The piles are 600mm, 750mm or 1200mm diameter and were constructed using contiguous flight auger techniques. Each pile was installed with a pair of plastic U-pipes, which were inserted into the centre of the pile (Figure 1) after the pile cage had been plunged into the concrete. The U-pipes were then connected together in series and usually joined into a single circuit with a neighbouring pile, before the pipework is continued to the header chamber and then on via larger pipes to the plant room for connection to the heat pumps.

Figure 1. Typical pile heat exchanger at the site (after breaking down to pile cut off level).

2.1 *Ground Conditions*

The site is underlain by a sequence of London Basin deposits. The piles are founded in the London Clay at 21m depth, but also pass through a significant thickness of superficial and man-made deposits (Table 1). As the site is located close to the confluence of the Thames and the River Lea in east London, the groundwater table is close to the ground surface, near to the base of the Made Ground.

Table 1. Table Ground Conditions.

Strata	Description	Depth (m)
Made Ground	Fine to coarse brick and concrete gravel; soft to firm black sandy gravelly clay.	3.3
Alluvium	Very soft clayey silt, sandy clay and peat.	6.3
River Terrace Deposits	Medium dense silty fine to coarse sand and fine to coarse gravel (mainly flint)	11.2
London Clay	Stiff thinly laminated fissured silty clay with silt partings	23.5

2.2 *Instrumentation*

One 1200mm diameter pile near the north east corner of the building was selected for monitoring. The pile was equipped with five thermistor strings. One of these was attached to the central bundle of plastic pipes, themselves inserted into the pile attached to a 40mm steel bar for stiffness (Figure 2). The U-pipes, the steel bar and the thermistor strings were installed to a depth of 20m within the pile. The other four thermistor strings were attached at equal spacings around the circumference of the steel reinforcing cage (Table 2). As the pile cage only extends to 8.5m below the pile cut off level it was not possible to extend the outer thermistor strings over the full 21m pile depth.

3 BACKGROUND DATA

Following construction of the pile, selected thermistors were monitored for approximately one month to provide an indication of the heat of hydration. During this period the groundworks beneath the building footprint were completed and all the pipe circuits were constructed as far as the header chambers. At this point it became possible to data log all the monitoring points to obtain information on the background soil temperatures at different depths.

These initial data are presented in Figure 3. It can be seen that during curing the pile reaches temperatures of almost 35°C at its centre, but that this reduces to approximately 30°C closer to the pile edge. In the main part of the pile, it takes over two months for the heat of hydration to dissipate fully and temperatures to return to between 13°C and 15°C. The near surface monitoring points (thermistor level 1, Figure 3) are influenced by the ambient air conditions. Within one month (when monitoring of these points first commenced) the thermistors at level 1 are already showing daily and longer term seasonal fluctuations reflecting the local air temperature.

Figure 2. Base of the central thermistor string prior to installation of the U-tubes and steel bar.

Table 2. Depths of thermistors installed with the pile.

Thermistor Level	Depth Below Pile Cut Off Level (m)	
	Central String	Outer Strings
1	0.7	0.75
2	3.6	3.25
3	7.1	6.6
4	11.1	-
5	15.1	-
6	19.1	-

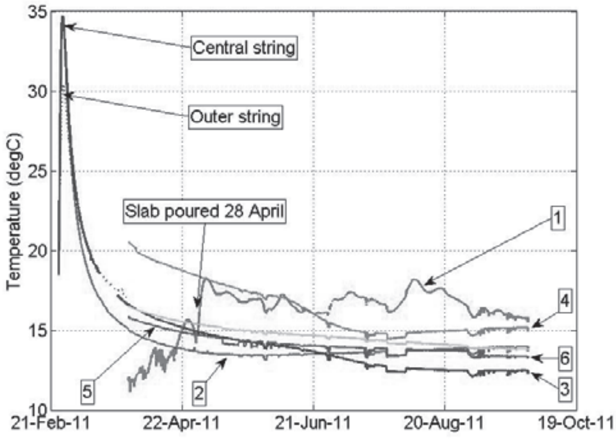

Figure 3. Initial pile temperatures during and after concrete curing (numbers refer to thermistor string levels).

The level 1 thermistors also show a distinct increase in temperature at the end of April 2011, coincident with the date at which the floor slab for the building was cast. This temperature increase will represent the additional heat of hydration from the concrete slab. Following this time, daily variations of temperature are also reduced due to the additional insulation. It is also interesting to note these level 1 temperatures appear to remain elevated for some time after the slab is cast; although it is difficult to separate this effect from that of the surface air temperature which would also be increasing at this time of year.

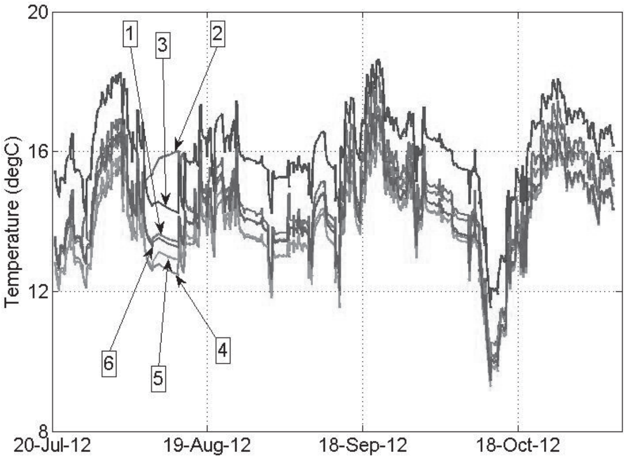

Figure 4. Operational temperatures from the central thermistor string (numbers refer to thermistor string levels).

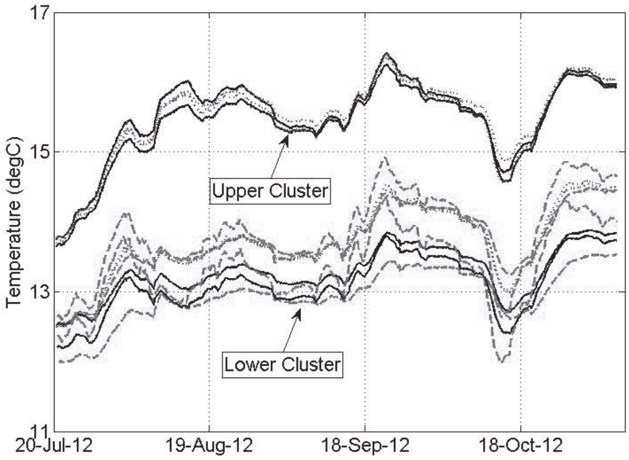

Figure 5. Operational temperatures from the outer thermistor string (dashed = thermistor level 1; solid = level 2; dotted = level 3).

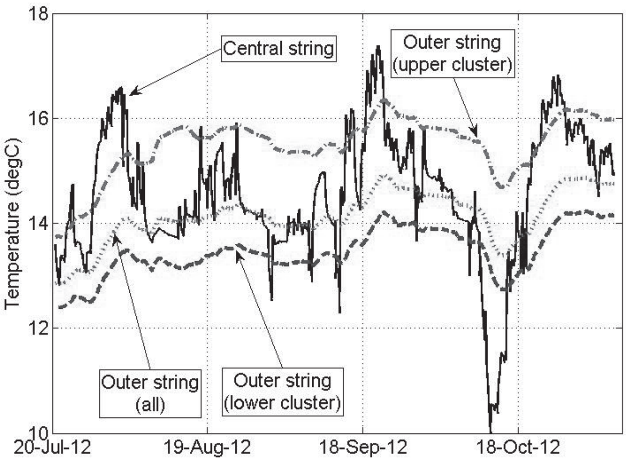

Figure 6. Mean thermistor string temperatures.

4 INITIAL RESULTS

Following collection of the background data it was necessary, due to construction constraints, to disconnect the datalogger until shortly after the Crystal was first occupied. Since collection of data recommenced we now have almost four months of temperature information for the pile under operational conditions.

Figure 4 and 5 present the temperature data from the central thermistor string and the outer thermister strings respectively. The central thermistor string records a greater range of temperatures than the outer strings, with ±4^{o}C and ±1^{o}C variation from the initial ground temperatures respectively. The central string also shows greater short term variation compared with the outer strings. This is because the temperature change of the central thermistors will closely follow that of the heat transfer fluid circulating within the U-tubes. However, by the time heat flow from the fluid reaches the outer thermistor strings any very short term variations will have smoothed out.

It is also noted that the outer thermistor readings are grouped into two distinct clusters. The upper cluster is approximately 2^{o}C warmer than the lower cluster, but follows a similar, although not identical trend. If both the U-tubes and steel cage were installed exactly centrally within the pile bore then, ignoring pile end effects and any variation in ground and concrete thermal properties, all the outer thermistors should read the same value. However, since an exactly central installation is not possible, it should be expected that there will be some variation in these values. However, what is surprising is that the upper cluster contains level 2 and level 3 thermistors from opposite sides of the pile, which should only have close to equal values if the cage and the pipes have been installed centrally. This could suggest that the readings in the upper cluster are erroneous.

This view is supported by looking at the average temperatures for the central and outer strings (Figure 6). Temperatures are generally rising with time as heat is rejected to the ground via the pile. Therefore the temperatures closer to the pile edge would be expected to be lower than those in the centre next to the pipes. In this context the upper cluster appears to be erroneously high, while the lower cluster shows temperatures in a more realistic range.

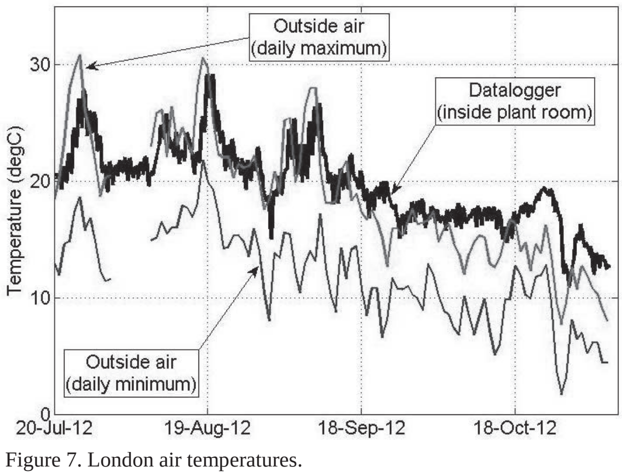

Figure 7. London air temperatures.

The general trend of increasing temperatures, despite the advent of cooler air temperatures as the autumn progressed (Figure 7) is a reflection of the complexity of both modern buildings and the heating-ventilation-air conditioning (HVAC) system in this building in particular. For a system where pile heat exchangers are either providing all of buildings heating and cooling demands, or covering only partial demand in combination with a traditional HVAC system, then the pile temperature would be expected to reflect the outside air temperatures and decrease throughout the winter months. However, in this case the energy needs of the building are being met by a combination of the pile heat exchangers, the borehole heat exchangers and a solar system. These means that the three components will be operated together to achieve the building heating and cooling demands and, for example, on some occasions excess solar thermal energy can be stored in the ground.

There is, however, one clear example of heat extraction visible in mid-October (Figure 6). Here the central thermistor readings dip markedly to around 10^oC on average. The corresponding change in the mean outer thermistor readings is much smaller, indicating that much of the heat energy required has actually been extracted from that temporarily stored in the pile concrete, rather than from the surrounding ground.

5 DISCUSSION

An important aspect of pile heat exchanger behavior is illustrated by the data presented in Section 4. As has been shown theoretically by Loveridge, 2012, large diameter piles can take many days to reach a thermal steady state. Therefore, for a heating/cooling demand which is varying on an hourly (or less) timescale the pile concrete will rarely be at thermal steady state. This is illustrated in Figure 6, which shows that the temperature change near to the pile edge is significantly damped compared to that close to the U-tubes and some subsidiary peaks/troughs are not reflected at all. If the pile was at steady state, as is assumed by all traditional design methods, then the temperatures near the pile edge would reflect all the temperature changes at the pipes.

This transient thermal behavior shown by the pile concrete is important for a number of reasons. First, if the pile is assumed to be at a thermal steady state then any ability of the pile concrete to store energy (rather than just transfer it to the ground) is being neglected. As a consequence steady state design will either 1) overestimate the temperature change predicted at the pile-soil boundary for a given heat flux, or 2) underestimate the available thermal energy capacity for a given temperature change. While this provides a safe conservative design it will significantly under-predict the thermal efficiency of the pile heat exchanger.

Taking a transient view of the pile concrete behaviour also shows there to be a reduced risk of extreme temperatures developing in the ground. Current practice (eg NHBC 2010; SIA 2005) tends to recommend that the lower limit on the heat transfer fluid temperature in pile heat exchangers should be kept above freezing with a 2^oC margin of error. However, given that the largest dips in the central thermistor temperatures shown in Figure 6 are not reflected to the same degree in the temperature changes of the outer thermistors, this approach clearly would be conservative in this case. This real behaviour is similar in nature to recent theoretical studies (Loveridge et al. 2012) which show that, for large diameter piles at least, temperatures lower than 0^oC can be sustained within the heat transfer fluid for short periods and have no detrimental effects on the ground. Similar conclusions were reached by Brandl in his Rankine Lecture (Brandl 2006), but do not seem to have been acted upon in general practice.

5.1 Further Work

The data presented in this paper is the beginning of a long term monitoring programme. The temperature data in the pile will subsequently be supplemented by energy data, both with respect to the heat transferred to the instrumented pile and for the balance of thermal energy between the different renewable energy systems in the building. This is essential for fuller interpretation of the pile data and will allow linking of the energy demand and pile temperature changes. This will provide a valuable dataset for validation of pile heat exchanger thermal design methods.

6 CONCLUSIONS

Temperature sensors have been installed within a working foundation pile which is also used as a heat exchanger within a ground energy system. Initial data from the pile is now available and demonstrates the transient nature of the heat transfer within the pile. This is significant, as most existing design methods for the thermal capacity of piles assume that the pile is at a steady state. For large diameter piles such as the one instrumented in this scheme, this is clearly not the case. Instead the largest fluctuations in temperature at the centre of the pile close to the pipe U-tubes are not reflected closer to the edge of the pile. This is due to the thermal buffering provided by the pile concrete, which acts as a short term energy store during short duration peaks in thermal demand.

The consequence of neglecting this short term concrete thermal storage is that design becomes over conservative and underestimates the thermal capacity of the pile. It also leads to an over estimation of the risk of ground freezing for large diameter piles.

7 ACKNOWLEDGEMENTS

The authors would like to thank Joel Smethurst and Harvey Skinner for assistance with installing the thermistors and datalogger respectively. The work would not have been possible without initial introductions and enthusiasm from Arup and Balfour Beatty Ground Engineering and subsequent support and commitment from Siemens Plc. We are also indebted to site support from ISG, Foundation Developments Ltd and Geothermal International Ltd. This work forms part of a larger project funded by EPSRC (ref EP/H0490101/1) and supported by Mott MacDonald, Cementation Skanska, WJ Groundwater and Golder Associates.

8 REFERENCES

Amatya B.L., Soga K., Bourne-Webb P.J. and Laloui L. 2012: Thermo-mechanical performance of energy piles. *Geotechnique* 62 (6), 503 -519.

Brandl H. 2006. Energy foundations and other thermo active ground structures. *Geotechnique* 56 (2), 81 – 122.

GSHPA 2012. *Thermal pile design, installation and materials standard.* Ground Source Heat Pump Association, Milton Keynes, October 2012.

Knellwolf C., Peron H. & Laloui L. 2011. Geotechnical analysis of heat exchanger piles. *Journal of Geotechnical and Geoenvironmental Engineering 1*37 (10), 890 - 902.

Loveridge F. 2012. *The Thermal Performance of Foundation Piles used as Heat Exchangers in Ground Energy System*s. Doctoral Thesis, University of Southampton.

Loveridge F. & Powrie W. 2012. Pile heat exchangers: thermal behaviour and interactions. *Proceedings of the Institution of Civil Engineers Geotechnical Engineering.* Available ahead of print at http://dx.doi.org/10.1680/geng.11.00042.

Loveridge F., Amis T. and Powrie W. 2012. Energy Pile Performance and Preventing Ground Freezing. *Proceedings of the 2012 International Conference on Geomechanics and Engineering (ICGE'12)*, Seoul, August, 2012.

NHBC 2010. *Efficient design of piled foundations for low rise housing, design guide.* BC Foundation.

Ouyang Y., Soga K. & Leung Y. F. 2011. Numerical back analysis of energy pile test at Lambeth College, London. *Proc ASCE GeoFrontiers 2011 Conference*, Dallas, Texas, http://dx.doi.org/10.1061/41165(397)46.

SIA 2005. *Utilisation de la chaleur du sol par des ouvrages de fondation et de soutènement en béton, Guide pour la conception, la réalisation et al maintenance.* Swiss Society of Engineers and Architects, Documentation D 0190.

Measuring soil thermal properties for use in energy foundation design

La mesure des caractéristiques thermiques du sol pour la conception des fondations énergie

Low J.E., Loveridge F.A., Powrie W.
Faculty of Engineering and the Environment, University of Southampton, Southampton, UK

ABSTRACT: Energy foundations incorporated into ground source heat pump systems provide a viable alternative to conventional building temperature regulation systems in the move towards sustainable building solutions. To design such a system, it is important to accurately model the heat transfer process between the foundations and the soil, which is largely governed by the soil thermal conductivity. This paper compares two laboratory test methods for determining soil thermal conductivity: the thermal cell which is a steady state method, and the needle probe which is a transient method.

RÉSUMÉ : Pour l'orientation vers des immeubles durables, les fondations énergie incorporées dans des systèmes de pompe à chaleur géothermique fournissent une alternative viable aux systèmes conventionnels de régulation de température des immeubles. La conception d'un tel système implique le modelage précis du processus, qui est en grande partie déterminé par la conductivité thermique du sol, de transfert thermique entre les fondations et le sol. Dans le texte qui suit l'on compare deux méthodes d'essai de laboratoire pour la détermination de la conductivité thermique du sol : la cellule thermique, méthode de régime établi, et sonde à aiguille, méthode de régime transitoire.

KEYWORDS: soil thermal conductivity, thermal cell, needle probe

1 INTRODUCTION

Ground source heat pump systems provide a viable alternative to conventional heating and cooling systems in the move towards sustainable building solutions (Banks, 2008). Heat is transferred between the ground and the building by means of a refrigerant which is pumped through a series of pipes buried in the ground. To minimize initial construction costs, the pipes can be cast into the foundations, eliminating the need to make further excavations. These systems are known as energy foundations. To design such a system, it is important to accurately model the heat transfer process between the foundations and the soil. This is largely governed by the soil thermal conductivity.

There are several different methods of measuring soil thermal conductivity (Mitchell and Kao, 1978). They fall into one of two categories: steady state or transient methods. At the laboratory scale, steady state methods involve applying one-directional heat flow to a specimen and measuring the power input and temperature difference across it when a steady state is reached. The thermal conductivity is then calculated directly using Fourier's Law of heat conduction. Transient methods involve applying heat to the specimen and monitoring temperature changes over time, and using the transient data to determine the thermal conductivity. This paper compares the two approaches using a thermal cell (steady state) and a needle probe (transient) apparatus. The tests were carried out on U100 samples of London Clay upon which a full soil classification was afterwards conducted.

2 BACKGROUND

There are several methods of measuring thermal conductivity which are considered as suitable for use with soils. For this study, the needle probe and thermal cell methods were chosen due to the simplicity of the apparatus.

2.1 *Needle probe*

The measurement of thermal conductivity using the needle probe method is based on the theory for an infinitely long, infinitely thin line heat source (Carslaw and Jaeger, 1959). If a constant power is applied to the heat source, the temperature rise ΔT at time t after the start of heating, at a radial distance r from the heat source, is:

$$\Delta T = -\frac{q}{4\pi\lambda} Ei\left(-\frac{r^2}{4\alpha t}\right) \quad (1)$$

where q is the power per unit length of heater, λ is the thermal conductivity, α is the thermal diffusivity and Ei is the exponential integral. After the power is switched off, the temperature difference is given by:

$$\Delta T = -\frac{q}{4\pi\lambda}\left[-Ei\left(-\frac{r^2}{4\alpha t}\right) + Ei\left(-\frac{r^2}{4\alpha\left(t-t_{heat}\right)}\right)\right] \quad (2)$$

where t_{heat} is the time at which the power is switched off. Equations (1) and (2) cannot be solved for λ and α explicitly, so a simplified analysis approximating the exponential integral is used which leads to (ASTM International, 2008):

$$\Delta T \cong \frac{q}{4\pi\lambda}\ln(t) \qquad 0 < t < t_{heat} \quad (3)$$

$$\Delta T \cong \frac{q}{4\pi\lambda}\ln\left(\frac{t}{t-t_{heat}}\right) \qquad t > t_{heat} \quad (4)$$

The needle probe used is the TP02 probe produced by Hukseflux Thermal Sensors (2003). It is 150mm long with a diameter of 1.5mm, and encloses a 100mm long heating wire with a thermocouple located midway along this heater measuring the temperature (see Figure 1).

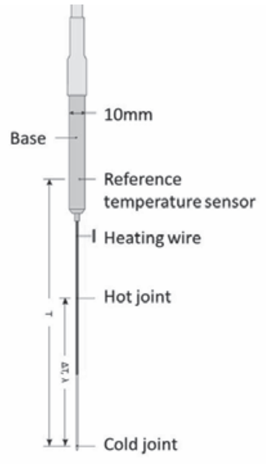

Figure 1. TP02 probe (Hukseflux, 2003).

2.2 *Thermal cell*

The thermal cell design was loosely based on Clarke et al. (2008). A diagram of the apparatus is shown in Figure 2. The thermal conductivity of a cylinder of soil is measured by generating one-directional heat flow along the axis of the specimen. The heat is generated by a cartridge heater embedded in the aluminium platen. Provided the specimen is well insulated so that radial heat losses can be neglected, the heat flow through the specimen during steady state is governed by Fourier's Law of heat conduction:

$$Q = -\lambda A \frac{\Delta T}{L} \tag{5}$$

where Q is the power input, A is the cross-sectional area, ΔT is the temperature difference across the length of the specimen, and L is the length of the specimen. If Q cannot be accurately determined, measurement of the temperatures in the specimen as it cools after the power is switched off (the recovery phase) can be used to determine the heat transfer coefficient between the top of the soil and the air and hence the power. This uses the lumped capacitance method, which is valid when the temperature difference across the soil is small compared with the temperature difference between the soil surface and the ambient temperature (Incropera et al., 2007):

$$\frac{T_{base} - T_{top}}{T_{top} - T_{amb}} < 0.1 \tag{6}$$

where subscripts *base*, *top* and *amb* refer to temperature at the base of the soil, top of the soil, and of the ambient air respectively. Where this is satisfied, the temperature of the soil at time t is (Clarke et al., 2008):

$$T = T_{amb} + \left(T_0 - T_{amb}\right)\exp\left(-\frac{hA}{mc_p}t\right) \tag{7}$$

where T_0 is the temperature of the soil at time t = 0 (when Equation (6) starts to apply), h is the convection heat transfer coefficient, m is the total mass of the soil, and c_p is the soil specific heat capacity. This is estimated from the properties of the soil constituents:

$$mc_p = \left(mc_p\right)_{soil} + \left(mc_p\right)_{water} \tag{8}$$

Equation (7) gives a theoretical decay curve which can be fitted to the experimental data by changing h until the two curves match. During steady state, conservation of energy dictates that the heat flow rate across the soil is equal to the heat flow rate at the top of the specimen from the soil to the air.

$$Q = \lambda A \frac{\left(T_{base} - T_{top}\right)}{L} = hA\left(T_{top} - T_{amb}\right) \tag{9}$$

This is used to calculate the thermal conductivity. It is worth noting that this method introduces an error associated with the estimation of the specific heat capacity from constituents whose properties may not be accurately known.

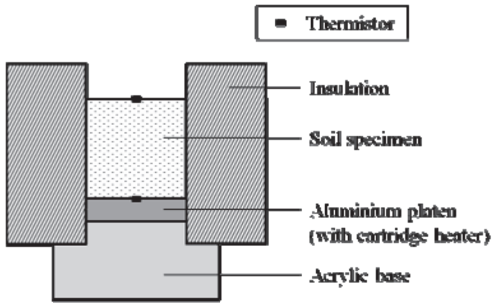

Figure 2. Thermal cell.

3 METHODOLOGY

3.1 *Measurement procedure*

The thermal conductivity of U100 samples of London Clay taken from a thermal response test borehole were tested using both techniques described in Section 2. Before any measurements were taken, the sealed samples were left in a temperature controlled room overnight to equilibrate. Each sample was treated as follows.

To accommodate the needle probe, a 200mm length specimen was prepared and secured in a rubber membrane. Shavings taken from the top of the sample were used to determine the initial moisture content at the top. The soil was found to be too hard to directly insert the probe. Therefore, a 5mm diameter hole had to be predrilled, and the hole filled with a high thermal conductivity contact fluid (in this case toothpaste was used) to reduce the contact resistance between the probe and the soil (Hukseflux, 2003). The probe was inserted into the hole, and secured with a clamp stand. It was then left for 20min to equilibrate with the soil. A constant power was then supplied to the needle probe heater for 300s, and then turned off. The temperatures during the heating and recovery periods were recorded. Using this procedure, five measurements were taken over the cross-sectional area of the specimen. One measurement was taken at the centre of the cross-section, the other four were equally spaced at a radial distance of 25mm from the centre.

To reduce the time it takes to reach steady state, the specimen was then cut in half and the top 100mm weighed and secured to the platen of the thermal cell (see Figure 2), and sealed at the top using aluminium foil to prevent moisture from leaving the top of the sample. Shavings taken from the bottom of the top half were used to determine the initial moisture content at the bottom. Insulation was then wrapped around the specimen. The temperature difference across the specimen is measured by two thermistors, one secured to the top of the platen, the other embedded at the top of the soil. The cartridge heater was then turned on, and the power controlled so that the platen remains at a constant temperature of 40°C. The power was measured using a MuRata ACM20-5-AC1-R-C wattmeter. Temperatures were monitored until steady state was reached and then maintained for at least 2hours. The power to the cartridge heater was then switched off, and the recovery period monitored. At the end of the test, shavings were taken from the top, middle and bottom of the specimen to determine the final moisture contents.

The holes drilled into the specimen and the contact fluid could potentially affect the thermal conductivity measurement using the thermal cell. To verify the result, the bottom half of the sample was also tested in the thermal cell, where these effects would be less significant.

A full soil classification was then conducted based on the British Standard 1377 (British Standards Institution, 1990), to determine the soil density, moisture content, liquid limit, plastic limit, particle density, and particle size distribution.

3.2 *Data analysis*

For the needle probe, using Equations (3) and (4) for heating and recovery respectively, graphs were plotted of temperature against the natural logarithm of time, and the gradient of the straight line section used to determine the thermal conductivity. A typical result is shown in Figure 3.

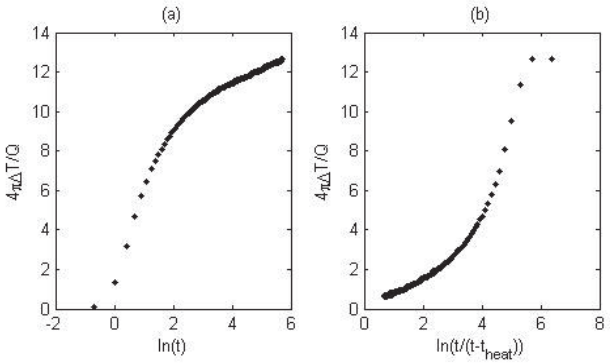

Figure 3. Graph of needle probe data for (a) heating and (b) recovery.

For the thermal cell, average temperatures during the steady state period were calculated for each thermistor. The average power supplied to the cartridge heater was also calculated. Equation (5) was then used to determine the thermal conductivity.

4 RESULTS AND DISCUSSION

The results of the tests are shown in Table 1, with the average value of the five needle probe readings given. The needle probe consistently gave lower values of thermal conductivity than the thermal cell. The sample properties are given in Table 2, where the moisture content given is the average of the values before and after testing. There is a decrease in thermal conductivity with depth. This may be due to a decrease in density, and also change in mineralogy. The top two samples were of firm slightly sandy clay. The bottom sample had a significant number of fissures, and a slightly greater sand content.

Table 1. Thermal conductivity measured using the needle probe for heating and recovery, and using the thermal cell.

Sample depth (m)	Thermal conductivity ($Wm^{-1}K^{-1}$)		
	Needle probe in heating	Needle probe in recovery	Thermal cell
8.00-8.45	1.47	1.30	2.01 (t)* 1.88 (b)
10.00-10.45	1.24	1.36	1.85 (t) 1.91 (b)
19.00-19.45	1.06	0.93	1.65 (t) 1.75 (b)

*t – top half; b – bottom half.

4.1 *Needle probe*

The variation in the five needle probe readings within the same sample was about ±10% for heating and ±15% for recovery. The sample at depth 19.00-19.45m had less variation. When the needle probe was previously tested using five identical agar gel samples, it gave a repeatability of ±2% for both heating and recovery, so most of the variation in results would seem to be due to natural variation in thermal conductivity of the soil.

The greatest disadvantage with the needle probe is in the interpretation of results relying on human judgement. The calculated thermal conductivity is highly sensitive to the selection of the part of the graph deemed to be a straight line. Another factor which may affect the results is the use of contact fluid. In theory, the contact fluid should only decrease the time it takes to reach the straight line section of the graph, i.e. it should have no effect on the calculated thermal conductivity. However, the fluid could potentially seep into cracks in the soil, and in doing so alter the thermal conductivity. After testing, the specimens were cut up to see if this was the case. The soil at depths of 8.00-8.45m and 10.00-10.45m did not contain many fissures, and the contact fluid seemed to have stayed within the drilled holes. It can therefore be assumed that the contact fluid had little effect on the needle probe results. However, for the sample at depth 19.00-19.45m there were a significant number of fissures, which contact fluid had seeped into. This could affect both needle probe and thermal cell measurements, giving higher thermal conductivity results than otherwise.

4.2 *Thermal cell*

In Section 2.2, two methods for calculating the thermal conductivity using the thermal cell were outlined. One involves measuring the power directly, the other uses the lumped capacitance method to calculate the power. Only the first method was deemed suitable for this study, as the temperature difference across the soil after the power is switched off was too great for lumped capacitance to apply i.e. Equation (6) was not satisfied.

The difference in thermal conductivity values between the top and bottom sections was about $0.1Wm^{-1}K^{-1}$. If the holes for the needle probe were to have a significant effect on the thermal conductivity values, the measurement for the top section would be expected to always be higher than for the bottom section, or vice versa. This is not the case, and as the area of the holes is only 1.25% of the total cross-sectional area, it can be assumed that the differences between the top and bottom sections are mainly due to the soil's natural variability.

The moisture content at the top of the specimens were measured before and after the thermal cell tests. The values after the test were consistently higher than those before the test. The greatest increase in moisture content was 5.2%. This shows that over the long heating period, moisture migration occurs in the direction of heat flow. This is where a temperature gradient causes the water to transfer latent heat through the pores as described by the liquid-island theory (Philip and de Vries, 1957). This theory suggests that in fairly dry media, the water is deposited in isolated pockets or 'islands', either filling small pores or attaching themselves between soil grains. When a temperature gradient is applied, there is a vapour flux in the direction of heat flow. Water evaporates from one island, and condenses at the boundary of the next island, thereby transferring heat from one island to the next.

4.3 *Comparing test methods*

The measured thermal conductivity for the thermal cell is higher than that of the needle probe by 40%, 45%, and 71% for a depth of 8.00-8.45m, 10.00-10.45m, and 19.00-19.45m respectively. This could be explained by a number of factors. The needle probe and thermal cell measure the thermal conductivity in the radial and axial directions respectively. It could be that the soil is anisotropic, and naturally has a higher thermal conductivity in the axial direction. However, the layers in the soil sample tended to be in the horizontal direction i.e. perpendicular to the cylinder axis. The thermal conductivity measured parallel to the layering should in general be higher than that measured perpendicular to the layering (Midttømme and Roaldset, 1998). If anisotropy was the reason behind the difference between needle probe and thermal cell values, then the needle probe would be expected to give higher values of thermal conductivity than the thermal cell. Therefore, it is unlikely that anisotropy is the reason behind these differences.

In the thermal cell calculations, the total power is used and any losses neglected. A simple finite element analysis was conducted, and indicated only minor losses. However, if losses are in fact significant, then the calculated thermal conductivities would be overestimates. A more thorough analysis would be necessary to determine whether this is the case.

The presence of contact fluid in the thermal cell test could potentially be aiding heat transfer. If the thermal conductivity of the contact fluid is determined, this would give a better indication as to what effect it could have. This should not be the main reason for higher thermal conductivity values, as the volume of contact fluid is comparatively small.

As previously mentioned, significant moisture migration occurs due to the large temperature gradient applied. As an additional mechanism for heat transfer, this may lead to higher measured values of thermal conductivity.

Table 2. Soil properties.

Sample depth (m)		Density (kgm^{-3})	Average moisture content (%)
8.00-8.45	Top	2092	23.4
	Bottom	2142	23.3
10.00-10.45	Top	2053	26.9
	Bottom	1951	27.1
19.00-19.45	Top	1783	26.3
	Bottom	1787	26.4

5 FURTHER RESEARCH

This study highlights the need for further investigation into the needle probe and thermal cell methods of thermal conductivity measurement for soils. With the needle probe, it is still unclear as to why heating and recovery gave different results for the thermal conductivity. As mentioned previously, the needle probe relies on human judgement in the interpretation of the results. Further research will be carried out to find a method which eliminates this source of error.

Some possible sources of error in the thermal cell method require investigation. A more detailed finite element analysis could be used to determine what power losses might be expected, so that this could be factored into the thermal conductivity calculation. The specimens were prepared by hand, so that the surface in contact with the platen may not be entirely flat. Tests on standard materials with and without a contact fluid between the platen and the soil could determine how significant the effects of this may be on the heat transfer. From the recovery data, there was a considerable temperature difference between the top and bottom of the soil for a long time after the power had been switched off. Clarke et al. (2008) was able to use the recovery curve to determine the power input, as the temperature difference was small. The reasons behind this discrepancy are unclear, so further tests using the thermal cell on different types of soil with a range of thermal conductivities will be beneficial.

The soil samples were taken from a borehole where a thermal response test was later conducted. Other samples were also taken to another laboratory to test for thermal conductivity using the thermal cell method. Once the results from these tests are known, a comparison will be made to the results gathered from this study.

6 CONCLUSION

Two test methods for thermal conductivity, the needle probe and thermal cell, have been compared. The needle probe takes less time to conduct, and the soil is only heated slightly and for a short period which means moisture migration is not expected to affect the results. However, hard soil samples may require predrilling, and the use of contact fluid which can seep into any existing fissures thereby potentially affecting the thermal conductivity measurements.

The thermal cell requires very little alterations to the soil sample, but raises some issues to do with power losses. The long heating time also means that moisture migrates towards the top of the specimen. Within the context of energy foundations, the thermal cell may prove more suitable for measuring the thermal conductivity of other relevant materials such as grout and concrete.

7 ACKNOWLEDGEMENTS

The authors would like to thank Harvey Skinner for his help in the design, build, and instrumentation of the apparatus. The soil samples were provided by Concept Engineering Consultants Ltd. The site work has been carried out by Arup, Canary Wharf Contractors Ltd, and Concept. This work forms part of a larger project funded by EPSRC (ref EP/H0490101/1) and supported by Mott MacDonald Group Ltd, Cementation Skanska Ltd, WJ Groundwater Ltd, and Golder Associates.

8 REFERENCES

ASTM International. 2008. *D 5334-08 Standard Test Method for Determination of Thermal Conductivity of Soil and Soft Rock by Thermal Needle Probe Procedure.* West Conshohocken, PA: ASTM International.

Banks D. 2008. *An introduction to thermogeology: ground source heating and cooling.* Oxford: Blackwell Publishing Ltd.

British Standards Institution. 1990. *BSI 1377:1990 Methods of test for soils for civil engineering purposes.* London: BSI.

Carslaw H.S. and Jaeger J.C. 1959. *Conduction of heat in solids.* 2nd ed. Oxford: Oxford University Press.

Clarke B.G., Agab A. and Nicholson D. 2008. Model specification to determine thermal conductivity of soils. *Proceedings of the Institution of Civil Engineers - Geotechnical Engineering* 161(3), 161-168.

Farouki O.T. 1986. *Thermal properties of soils.* Rockport, MA: Trans Tech.

Hukseflux Thermal Sensors. 2003. *TP02 Non-Steady-State Probe for Thermal Conductivity Measurement – manual v0908.* Delft: Hukseflux Thermal Sensors.

Incropera F.P., DeWitt D.P., Bergman T.L., and Lavine A.S. 2006. *Fundamentals of Heat and Mass Transfer.* 6th ed. Hoboken, NJ: Wiley.

Midttømme K. and Roaldset E. 1998. The effect of grain size on thermal conductivity of quartz sands and silts. *Petroleum Geoscience* 4, 165-172.

Mitchell J.K. and Kao T.C. 1978. Measurement of soil thermal resistivity. *Journal of the Geotechnical Engineering Division* 104, 1307-1320.

Philip J. R. and de Vries D. A. 1957. *Moisture movement in porous materials under temperature gradients.* Transactions, American Geophysical Union 38, 222-232.

Thermo-Mechanical Behavior of Energy Foundations

Comportement thermo-mécanique des pieux énergétiques

McCartney J.S., Murphy J.S., Stewart M.A.
University of Colorado Boulder

ABSTRACT: This paper focuses on the impact of the upper boundary condition on the thermo-mechanical response of end-bearin g energy foundations during heating. To support this discussion, results from tests performed on a centrifuge-scale energy foundation and a full-scale energy foundation beneath an 8-story building in Denver, Colorado are compared. Although the soil profiles differ in both tests, the centrifuge-scale foundation involved heating during a load-controlled (free displacement) scenario, while the full-scale foundation involved heating during the constraint associated with a real building. The stress distribution in the centrifuge test showed greater stresses near the toe of the foundation than near the head of the foundation, while those in the full-scale foundation were closer to being uniform along the length of the foundation. The soil in the centrifuge-scale test was unsaturated, compacted silt with uniform strength, while the soil in the field included unsaturated urban fill with relatively low side shear resistance underlain by claystone. This indicates that the constraint of the reinforced grade beams within the building foundation led to the higher thermally-induced stresses within the full-scale energy foundation.

RÉSUMÉ : Cet article met l'accent sur le rôle de la condition imposée à la limite supérieure pour la réponse thermo-mécanique des pieux énergétiques travaillant en pointe pendant le chauffage. Pour cette étude, les résultats de tests effectués sur des systèmes de fondations en centrifugeuse et à échelle réelle pour un immeuble de 8 étages à Denver sont comparés. Les profils de sols diffèrent dans les deux essais : la fondation utilisée dans la centrifugeuse nécessite de chauffer sous chargement contrôlé avec déplacement libre, tandis que la fondation à échelle réelle implique un chauffage sous la contrainte associée au bâtiment réel. La distribution des contraintes dans le test de centrifugation a montré des contraintes plus fortes à la base de la fondation que près de la tête du pieu, tandis que ceux de la fondation à grande échelle étaient plus uniformes sur toute la longueur de la fondation. Le sol de l'essai en centrifugeuse était saturé et constitué de limon compacté avec une résistance uniforme, tandis que le sol in situ était un remblai urbain de faible résistance au cisaillement surmontant une couche d'argilite. Ceci indique qu'il est nécessaire de prendre en compte les contraintes induites thermiquement dans les pieux énergétiques.

KEYWORDS:Energy foundations, soil-structure interaction, centrifuge physical modeling.

1 INTRODUCTION

Energy foundations are drilled shafts that incorporate ground-source heat exchange elements, which can be used to transfer heat to or from the ground to a building (Brandl 2006; Laloui et al. 2006; McCartney 2011). Ground-source heat exchange (GSHE) systems exploit the relatively constant temperature of the ground to improve the efficiency of heat pump systems for heating and cooling of buildings. Traditional GSHE systems typically require a network of boreholes installed outside of the building footprint, which can be cost-prohibitive (Hughes 2008). To counter this problem, heat exchange elements can be incorporated into deep foundation elements during construction to minimize GSHE installation cost. Although energy foundations may not provide all the energy required to heat and cool residential or commercial buildings, they may provide sufficient heat exchange to supplement a conventional system for little extra cost.Studies on full-scale foundations have established the efficiency of heat extraction and thermal properties of energy foundations (Ooka et al. 2007; Wood et al. 2009; Adam and Markiewicz 2009; Ozudogru et al. 2012).

Although important information has been collected regarding the thermo-mechanical behavior of energy foundations during heating and cooling, there are still questions to be answered. Several experimental studies have been performed in the laboratory using centrifuge-scale models of energy foundations which identified mechanisms of soil-structure interaction in energy foundations (McCartney et al. 2010; McCartney and Rosenberg 2011; Stewart and McCartney 2012). Further, several full-scale energy foundations have been installed throughout Europe and Asia, including two well-documented thermo-mechanical tests on full-scale foundations published to date; in Switzerland (Laloui et al. 2006), and in the UK (Bourne-Webb et al. 2009; Amatya et al. 2012). In these studies, proof load tests along with heating/cooling tests were used to evaluate the thermo-mechanical stress-strain response in the foundations. Data from these tests were used to develop soil-structure interaction design tools (Knellwolf et al. 2011). This paper addresses an important topic identified by Knellwolf et al. (2011), specifically the impact of the head boundary conditions on the distribution in thermally-induced axial stresses in energy foundations. This topic is investigated by comparing strain gauge data from two energy foundations having different head constraints (load-control and actual building constraint).

2 BACKGROUND

As a structural element is heated and cooled, thermally induced axial strains are superimposed onto already present mechanical strains. Thermal strains are induced in energy foundations due to thermoelasticity, although a combination of end bearing, side shear resistance, and head stiffness may provide constraint to the foundation, leading to the development of thermally induced stresses. A load transfer analysis may be used to represent these different features. A schematic of a load transfer analysis developed by Plaseied (2012) based on the work of Knellwolf et al. 2011) is shown in Figure 1. Different from a mechanical load transfer analysis, a spring at the head of the foundation is used to represent the constraint of a foundation by the overlying building and grade beams. During heating, the foundation will expand about a null point, the location of which depends on the distribution of side shear values (K_s) and the magnitude of the end stiffness (K_{base}) and head stiffness (K_h). An iterative approach can be used to ensure equilibrium between forces Q and compatibility between displacements ρ.

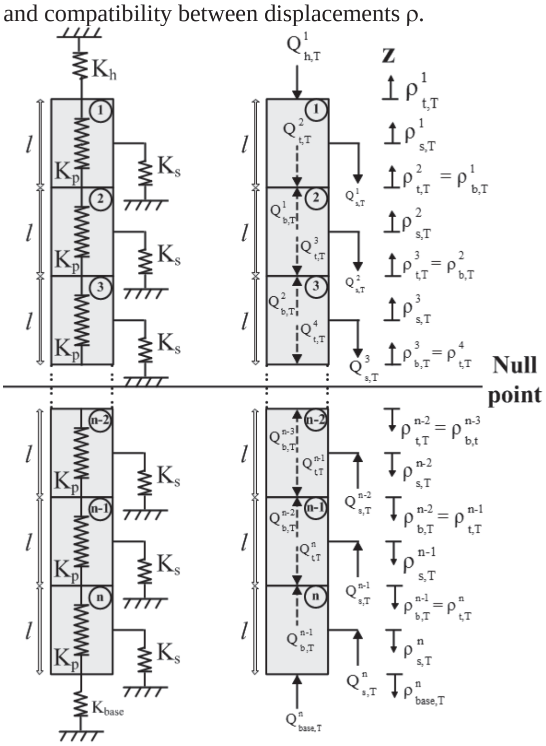

Figure 1. Thermo-mechanical load-transfer analysis (Plaseied 2012)

If strain gauges are used to monitor strains in the foundations, the thermal axial strains within a foundation can be obtained by subtracting the mechanical strains occurring due to an applied load (i.e., the weight of a building). Depending on the type of strain gauge, different thermal correction factors may need to be applied (McCartney and Murphy 2012; McCartney and Stewart 2012). The thermal axial stresses at any point in the foundation σ_T can be defined as follows:

$$\sigma_T = E(\varepsilon_T - \alpha_c \Delta T) \quad (1)$$

where E is the Young's modulus of reinforced concrete, ε_T is the measured thermalaxial strain, α_c is the coefficient of thermal expansion of reinforced concrete, and ΔT is the change in temperature. The value of $\alpha_c \Delta T$ represents the maximum axial strain possible in the energy foundationfor unrestrained conditions, and is negative (expansive) during heating.

3 FOUNDATION CASE STUDIES

3.1 *Centrifuge-Scale Energy Foundation*

The centrifuge-scale energy foundation evaluated in this study has a length of 533.4 mm and a diameter of 25 mm, and was installed in the center of a cylindrical container filled with a layer of unsaturated Bonny silt. The base of the foundation rests on the base of the container, providing a zero-displacement or end-bearing bottom boundary condition. The centrifuge test was performed at acentrifugal acceleration of 24, so the model-scale foundation is intended to represent a prototype-scale foundation having a length of 12.8 meters and a diameter of 1.2 meters. Although it is understood that heat flow cannot be scaled in a similar manner to geometry, stresses and strains, the thermally-induced stresses and strains are governed by the restraint provided by the surrounding soil, which depends on the stress state. Accordingly, it is expected that the thermally-induced stresses and strains will scale in a similar manner to mechanical stresses and strains. Accordingly, centrifuge tests involved maintaining the foundation at a constant temperature and waiting for thermally induced stresses and strains to stabilize.

The model energy foundation was precast outside of the soil layer due to the large amount of instrumentation, cables, and heat exchanger tubing within the assembly. This also permits the foundation to be tested outside of the soil layer to characterize their thermal and mechanical properties. The reinforcing cage for the model foundationwas constructed from a hoop of reinforced wire mesh. A cardboard tube having an inside diameter of 50.8 mm was used as a form for the foundation, permitting a concrete cover of 5 mm on the sides and 12.7 mm on the top and bottom. A total of three heat exchanger loops (3 inlets and 3 outlets) was installed in the foundation so that the distribution of heat across its circumference would be as uniform as possible. Embedded strain gauges and thermocouples were attached to the reinforcement cage of the model foundation at the locations shown in Figure 2. Linearly-variable deformation transformers were used to measure the axial displacement of the foundation and the soil surface. The distribution in temperature was measured using thermocouple profile probes and dielectric sensors (also used to monitor changes in volumetric water content of the soil). Additional details of the instrumentation are presented by McCartney and Stewart (2012).

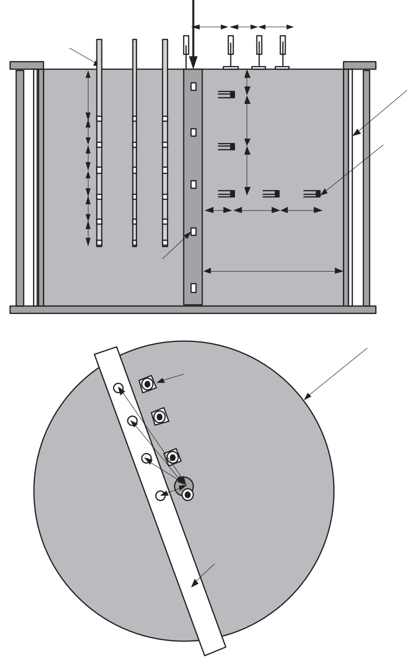

Figure 2.Schematics of the centrifuge-scale energy foundation test

A comprehensive set of characterization tests were performed on the pre-cast drilled shaft outside of the soil in a load frame at 1-gravity to determine the mechanical and thermal properties of the reinforced concrete. These results from these tests are reported in detail by Stewart (2012). The first test involved application of incremental axial loads under room temperature conditions, taking care to properly level the foundation and center the load to avoid bending. The mechanical strains encountered during application of an axial load of 700 kPa were variable. The Young's modulus determined using the corrected strain data was 7.17 GPa. The foundation was then heated to a temperature of 62 °C by circulating fluid through the heat exchange tubes within the foundation while maintaining a constant axial stress of 439 kPa. The foundation was permitted to freely expand under this axial stress, permitting definition of the coefficient of linear thermal expansion of the foundation (α_c = -7.5 με/°C, where με is micro-strain, with compressive strain defined as positive).

Heating tests were performed on the energy foundation in the layer of Bonny silt (USCS classification of ML) compacted at a gravimetric water content of 14% to a dry density of 1451 kg/m^3. An axial stress of 384 kPa was applied to the head of the foundation using a feedback-controlled electric motor. This motor permits the load to be maintained constant but permits free displacement. This implies that the value of K_h for the centrifuge-scale foundation should be close to zero. A heat pump, operated outside the centrifuge, was used to control the temperature of the fluid being circulated through the scale-model foundations. Details of the heat control system are provided by Stewart (2012).

3.2 *Full-Scale Energy Foundations*

Two drilled shaft foundations installed as part of the new Denver Housing Authority senior residential facilitywere converted into energy foundations. The energy foundations were coupled into a conventional GSHE system which was already being incorporated into the building. This paper focuses on the results of one of the drilled shafts,having a length of 14.8 meters and a diameter of 0.91 meters, that includes 3 heat exchanger loops. The shaft consists of a full-length reinforcing cage with nine #7 vertical reinforcing bars tied to #3 lateral reinforcing hoops spaced 0.36 meters on center. A schematic of the drilled shaft within the soil profile is shown in Figure 3. The drilled shaft functioned as rock-socketed, end-bearing elements in bedrock, with an expected load of 3.84 MN.The grade beams attached to the top of the foundation likely provided a non-zero stiffness to the head of the foundation (K_h> 0).

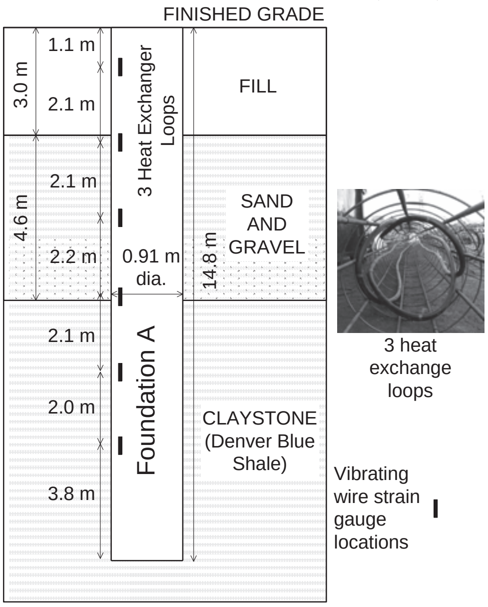

Figure 3.Soil stratigraphy and layout of foundation instrumentation

At the site, urban fill extends from grade to a depth of approximately 3 meters and consists of slightly moist, medium dense, clayey sand with gravel. Beneath the fill, non-expansive, medium dense, silty, sand and gravel extended to a depth of approximately 7.6 meters below grade. Following the sands and gravels, the subsurface conditions consisted of hard sandy claystone bedrock from the Denver formation. Because of the potential for caving during drilling through the overburden and possible perched ground water conditions, a cased-hole method was chosen for installation of the drilled shaft foundations at the site. Groundwater was observed near the depth of the claystone.

The heat exchanger system in the energy foundation consists of 44 mm-diameter polyethylene tubing attached to the inside of the reinforcing cages. The drilled shaft contains a total of 82.3 linear meters of tubing configured into three loops running the length of the reinforcing cage. The heat exchanger tubing was routed along the inside perimeter of the reinforcing cage to avoid crossing the diameter of the cage, which could block concrete flow or cause segregation of concrete. Equal angular spacing of the tubing was maintained to ensure relatively uniform temperature along the circumference of the shafts. Six vibrating wire concrete-embedment strain gauges with attached thermistors were incorporated into the foundation to monitor temperature and axial strain distributions with depth, although one gauge was damaged. The supply and return temperatures of the heat exchanger fluid were also monitored. More information is provided by McCartney and Murphy (2012).

4 STRAIN DISTRIBUTIONS

4.1 *Centrifuge-Scale Energy Foundations*

The axial thermal strain distributions in the centrifuge-scale energy foundation after heating to different changes in temperature above the ambient temperature of 20 °C are shown in Figure 4(a). Heating leads to a relatively uniform increase in negative axial strain throughout the foundation, indicating thermal expansion. The smallest strains are located near the toe of the foundation, which is as expected due to the rigid end restraint. The axial strains at the very top of the foundation represent the thermal strain for free expansion of the foundation ($\alpha_c\Delta T$). The measured strains are consistent with these theoretical values, and confirm that the top of the foundation can expand freely. An upward displacement in prototype scale of 1 mm was observed. The thermal axial stresses were calculated from the thermal strains using Equation 1. The location of minimum strain (and maximum stress) reflects the null point for the foundation, which is approximately at the bottom of the foundation. The trend in stress approaches zero at the top of the foundation, supporting the conclusion that K_h = 0.

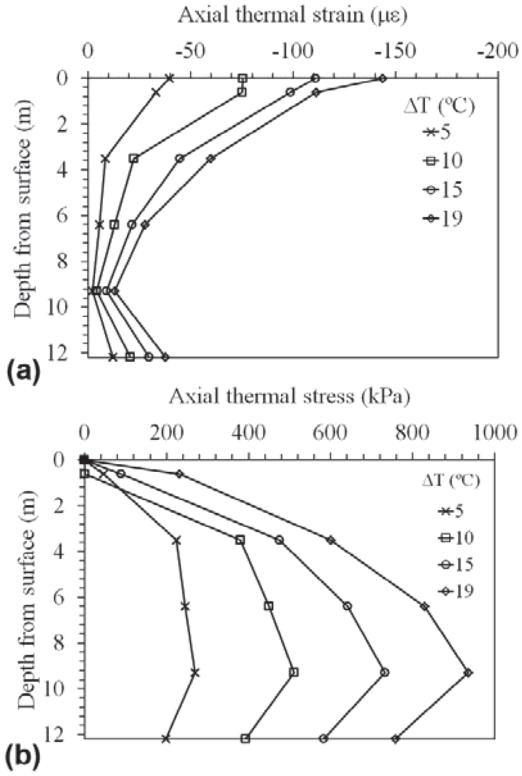

Figure 4. Centrifuge results: (a) Axial strains; (b) Axial stresses

4.2 *Full-Scale Energy Foundations*

During operation of the heat pump between March and May 2012, the temperature of the foundation was relatively uniform, and involved both heating and cooling. The strains induced in the foundation during different average changes in foundation temperature are shown in Figure 5(a). Similar to the centrifuge-scale foundation, the greatest strains were noted near the top of the foundation, resulting from the end-bearing boundary conditions at the toe. It was not possible to measure the displacement at the top of the foundation, but integration of the strains indicates that an upward displacement of approximately 0.18 mm occurred during a change in temperature of 3°C. Although the strain at the top of the foundation during heating is close to that expected for free expansion, this is not the case during cooling, where the strains are about 50% of free expansion conditions. During cooling of the foundation (heating of the building), the smaller axial strains are possibly due to the reinforcement connection to the grade beams at the ground surface. This indicates that K_h may be different for heating and cooling. The thermal axial stresses calculated using Equation 1 are shown in Figure 5(b). The coefficient of thermal expansion for the reinforced concrete was not measured, but is assumed to be -10 με/°C for the concrete mix design used in Colorado (Quartz aggregate with high slump). Similar to the centrifuge-scale energy foundation, the maximum stress is located near the toe of the foundation. In contrast to the results in Figure 4(b), the trend of the axial stresses indicates that the stresses do not tend toward zero at the top of the foundation. Based on the magnitude of stresses during heating, it is possible that the value of $K_h$is approximately half the stiffness of the end bearing spring at the toe of the foundation.

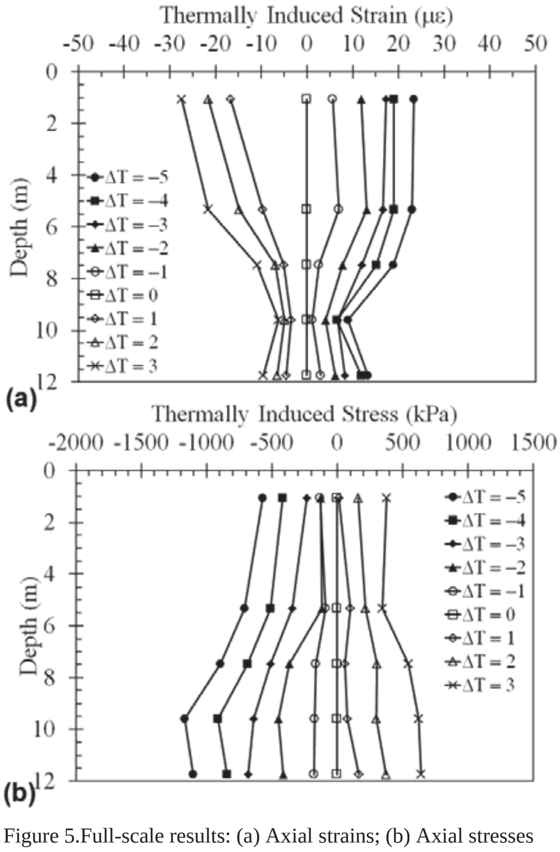

Figure 5.Full-scale results: (a) Axial strains; (b) Axial stresses

5 CONCLUSIONS

The results presented in this study indicate that the head boundary conditions of energy foundations have an important effect on the magnitude and shape of stress distributions in energy foundations. The results from an end-bearing centrifuge-scale foudation heated in load-controlled conditions indicate a similar shape to the thermal stress distribution but with negligible stresses at the head of the foundation. The results from a full-scale, end-bearing energy foundations during typical operation of a building in Denver, Colorado indicate that the thermal stresses are the greatest near the toe of the foundation, although the stresses near the head of the foundation are non-zero. The results indicate that even though a building applies a constant load to an energy foundation, the grade beam connections provide constraint to the head of an energy foundation, potentially with different magnitudes depending on whether the foundation is being heated or cooled.This is a subject of continued research being evaluated through further comparison of centrifuge- and field-scale foundations.

6 ACKNOWLEDGEMENTS

Financial support from the National Science Foundation grant CMMI 0928159 is appreciated.The authors acknowledge the support of Milender-White Construction Company, KL&A Structural Engineers, AMI Mechanical, Rocky Mountain Geothermal, and the Denver Housing Authority for agreeing to incorporate the energy foundations into the building.

7 REFERENCES (TNR 8)

Adam, D. and Markiewicz, R. (2009). “Energy from Earth-Coupled Structures, Foundations, Tunnels and Sewers.” Géotechnique. 59(3), 229–236.

Amatya, B.L., Soga, K., Bourne-Webb, P.J., Amis, T. and Laloui, L. (2012). “Thermo-mechanical Behaviour of Energy Piles.” Géotechnique. 62(6), 503–519.

Bourne-Webb, P., Amatya, B., Soga, K., Amis, T., Davidson, C. and Payne, P. (2009). “Energy Pile Test at Lambeth College, London: Geotechnical and Thermodynamic Aspects of Pile Response to Heat Cycles.” Géotechnique 59(3), 237–248.

Brandl, H. (2006). “Energy Foundations and other Energy Ground Structures.” Géotechnique. 56(2), 81-122.

Hughes, P.J. (2008). Geothermal (Ground-Source) Heat Pumps: Market Status, Barriers to Adoption, and Actions to Overcome Barriers. Oak Ridge Nat. Lab. Report ORNL-2008/232.

Knellwolf, C. Peron, H., and Laloui, L. (2011). “Geotechnical Analysis of Heat Exchanger Piles.” ASCE Journal of Geotech. and Geoen. Eng. 137(10). 890-902.

Laloui, L., Nuth, M., and Vulliet, L. (2006). “Experimental and Numerical Investigations of the Behaviour of a Heat Exchanger Pile.” International Journal of Numerical and Analytical Methods in Geomechanics. 30, 763–781.

McCartney, J.S., Rosenberg, J.E., and Sultanova, A. (2010). “Engineering Performance of Thermo-Active Foundation Systems. ASCE Geotechnical Practice Publication 6. pg. 27-42.

McCartney, J.S. and Rosenberg, J.E. (2011). “Impact of Heat Exchange on the Axial Capacity of Thermo-Active Foundations.” GeoFrontiers 2011. Dallas, TX. 10 pg.

McCartney, J.S. and Stewart, M.A. “Centrifuge Modeling of Energy Foundations under Cyclic Heating and Cooling.” ASCE Journal of Geotechnical and Geoenvironmental Engineering. In review.

McCartney, J.S. and Murphy, K. (2012). “Strain Distributions in Full-Scale Energy Foundations.” DFI Journal. In review.

McCartney, J.S. (2011). “Engineering Performance of Energy Foundations.” 2011 PanAm CGS Geotechnical Conference. Toronto, Canada. October 2-6, 2011. 14 pg.

Ozudogru, T., Brettmann, T., Olgun, G., Martin, J., and Senol, A. (2012). “Thermal Conductivity Testing of Energy Piles: Field Testing and Numerical Modeling.” ASCE GeoCongress 2012. Oakland, CA. March 25-29th 2012. 10 pg. CD ROM.

Plaseied, N. (2011). Load-Transfer Analysis of Energy Foundations. M.S. Thesis. University of Colorado Boulder. 90 pg.

Stewart, M. (2012). Centrifuge Modeling of Strain Distributions in Energy Foundations. MS Thesis. U. of Colorado Boulder. 110 pg.

Wood, C.J., Liu, H. and Riffat, S.B. (2009). “Use of Energy Piles in a Residential Building, and Effects on Ground Temperature and Heat Pump Efficiency.” Géotechnique 59(3), 287–290.

Pressurisation thermique dans l'argile de Boom

Thermal pressurization in Boom clay

Monfared M.[1], Delage P., Sulem J., Mohajerani M.[2], Tang A.M.
Ecole des ponts ParisTech, Navier/CERMES, Marne la Vallée, France
[1] now in BG Ingénieurs-conseils, Lausanne, Suisse
[2] now in CurisTech, Lyon, France

RÉSUMÉ : La pressurisation thermique dans l'argile raide de Boom au sein de laquelle est installé le laboratoire souterrain de recherche du SCK-CEN en Belgique (- 223 m) a été étudiée dans une cellule triaxiale thermo-hydro-mécanique (THM) à cylindre creux spécialement conçue pour les argiles et argilites à faible perméabilité et caractérisée par un court chemin de drainage (10 mm). Un essai de pressurisation thermique a été réalisé sous contraintes initiales proches des contraintes in-situ en augmentant en conditions non drainées la température (de 25 à 65°C à 1°C/h) et en mesurant l'augmentation de pression correspondante. Le coefficient de pressurisation thermique obtenu décroît avec la température entre 0.04 et 0.02 MPa/°C. La phase de refroidissement drainée permet de déterminer une valeur du coefficient de dilatation thermique drainé compatible avec celle de Sultan et al. (2000).

ABSTRACT: The phenomenon of thermal pressurization has been investigated in the Boom clay, the potential host rock presently considered in Belgium for radioactive waste disposal at great depth. Samples from the Mol underground research laboratory (- 223 m) have been used. Tests were conducted in a new hollow cylinder triaxial apparatus specifically developed. This device allows a short drainage length (10 mm) favourable in testing low permeability clays and claystones. A thermal pressurization test was carried out by increasing temperature very slowly (from 25 to 65°C at 1°C/h) in undrained conditions while measuring the changes in pore pressure in a sample submitted to in-situ stress conditions. The thermal coefficient measured decreased from 0.04 to 0.02 MPa/°C, in accordance with literature data. The drained cooling phase carried out afterwards provided a value of the drained thermoelastic coefficient in good agreement with that obtained by Sultan et al. (2000).

MOTS-CLES : argile raide, pressurisation thermique, chauffage, stockage de déchets radioactifs.
KEYWORDS : stiff clay, thermal pressurisation, heating, radioactive waste disposal

1 INTRODUCTION

La pressurisation thermique de l'eau interstitielle intervient en conditions non drainées ou faiblement drainées (sols peu perméables) dans les sols fins soumis à une élévation de température, du fait que le coefficient de dilatation thermique de l'eau est significativement plus fort que celui des minéraux. Le coefficient dilatation thermique α_s du quartz et des minéraux argileux est de l'ordre de $3{,}4 \times 10^{-5}$ $(°C)^{-1}$ (Palciauskas and Domenico 1982, McTigue 1986), celui de la calcite $1{,}38 \times 10^{-5}$ $(°C)^{-1}$ (Fei 1995) alors que le coefficient α_w de l'eau vaut 27×10^{-5} $(°C)^{-1}$ (Spang 2002).

La pressurisation thermique revêt une importance particulière dans le cas du stockage profond des déchets radioactifs exothermiques à haute activité, où sa connaissance est importante pour le dimensionnement des ouvrages de stockage. En réduisant la contrainte effective, une pressurisation excessive peut engendrer des instabilités dans le champ proche au niveau des galeries. D'autres applications concernent l'impact des techniques de récupération non conventionnelles de pétrole (avec injection de vapeur par exemple) sur les roches imperméables de couverture.

La pressurisation thermique dans l'argile raide de Boom au sein de laquelle est installé le laboratoire souterrain de recherche du SCK-CEN en Belgique (- 223 m) a été étudiée dans une cellule triaxiale thermo-hydro-mécanique (THM) à cylindre creux (diamètres extérieur et intérieur respectivement de 100 et 60 mm, hauteur 70 mm) spécialement conçue pour les argiles et argilites à faible perméabilité (Monfared et al. 2011). Cette cellule est caractérisée par un court chemin de drainage (la demie épaisseur du cylindre) permettant des conditions de drainage satisfaisantes même dans des conditions de très faible perméabilité (10^{-12} m/s pour l'argile de Boom).

Un essai de pressurisation thermique a été réalisé sous contraintes initiales proches des contraintes in-situ (contrainte moyenne de 3.25 MPa et pression interstitielle de 1 MPa) en augmentant en conditions non drainées la température entre 25 et 65°C à un taux de 1°C/h et en mesurant l'augmentation de pression correspondante.

2 DISPOSITIF D'ESSAIS ET MATÉRIAU

2.1 *Cellule triaxiale à cylindre creux*

Le schéma de la cellule est présenté en Figure 1 (Monfared et al. 2011).

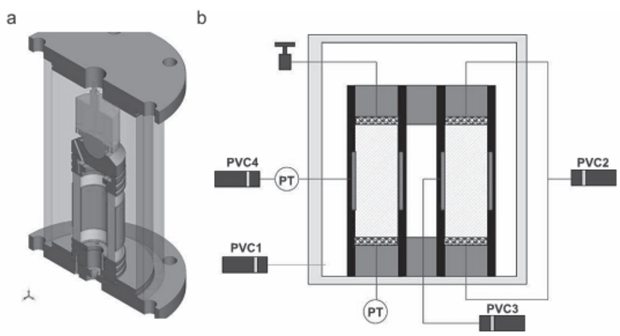

Figure 1. Cellule triaxiale à cylindre creux : a) schéma ; b) connexions aux contrôleurs pressions-volume et capteurs de pression.

Cette cellule permet l'application de conditions « triaxiales » classiques avec l'application d'une pression de confinement analogue à l'extérieur et à l'intérieur du cylindre creux.

Le diamètre extérieur est de 100 mm, l'intérieur de 60 mm et la hauteur de 70 mm. Grâce à des drainages latéraux sur les faces internes et externes de l'éprouvette, la longueur de drainage est réduite à 10 mm (demie épaisseur du cylindre creux), ce qui est essentiel pour assurer des conditions de drainage acceptables dans le cas des argiles et argilites de faible perméabilité (10^{-12} - 10^{-13} m/s) telles que celles considérées comme roches hôtes potentielles dans le stockage des déchets radioactifs.

Le chauffage est obtenu à l'aide d'une résistance électrique placée autour de la cellule de confinement (non représentée sur le Figure) avec un régulateur piloté par une mesure de la température du fluide de confinement (huile silicone), il permet une précision de 0,1°C. L'ensemble est d'isolé thermiquement de la température ambiante

Comme le montre également la Figure 1, l'éprouvette est reliée à 4 contrôleurs pression volume (PVC) pour l'application du confinement (extérieur et intérieur, PVC1), la contre-pression en haut et en bas (PVC2), la contrepression sur la face interne (PVC3) et externe (PVC4). La pression interstitielle peut être mesurée au niveau de l'embase inférieure et de la face extérieure. L'ensemble de ces conduits et les diverses connexions électriques (LVDTs, température,…) rendent l'embase assez complexe, comme on peut le voir sur la Figure 2.

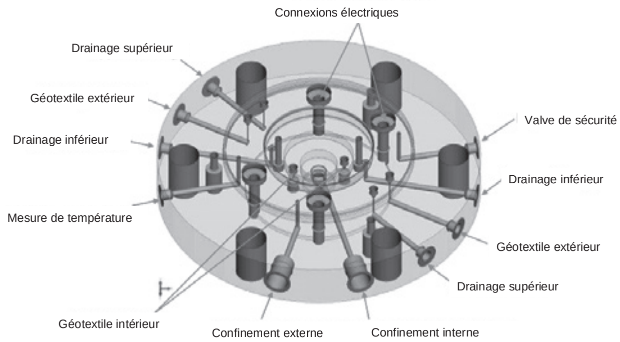

Figure 2. Schéma de l'embase de la cellule.

Les variations de volume sont suivies à l'aide de capteurs LVDT locaux permettant la mesure des déplacements axiaux et radiaux (Figure 3).

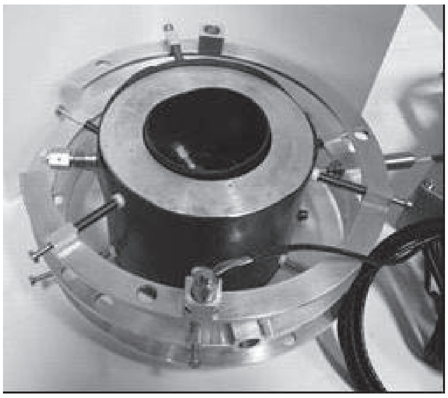

Figure 3. Mesures LVDT des déplacements locaux axiaux et radiaux

2.2 *Matériau étudié*

Les essais ont été effectués sur des éprouvettes prélevées dans la galerie de l'essai thermique Praclay excavée dans l'argile de Boom à une profondeur de 223 m dans le laboratoire souterrain du SCK-CEN (Centre d'études nucléaires) de Mol en Belgique (Bernier et al. 2007). Les caractéristiques de l'argile de Boom sont présentées au Tableau 1. Avec une certaine proportion de smectite (30%), l'argile de Boom présente des propriétés de gonflement.

Tableau 1. Caractéristiques de l'argile de Boom.

Porosité (%)	39
Teneur en eau (%)	25-30
Fraction argileuse (%)	55
Smectite (%)	30
Quartz (%)	25
Felspath, calcite, pyrite (%)	20

La taille de l'éprouvette s'est faite manuellement à la scie à bois à partir de carottes fournies de 100 mm de diamètre. Le cylindre intérieur a été taillé à l'aide d'une scie cloche à bois de 60 mm de diamètre. Pendant la taille, une membrane de néoprène était placée autour de l'éprouvette pour limiter le séchage.

3 RÉSULTATS EXPÉRIMENTAUX

3.1 *Resaturation de l'éprouvette*

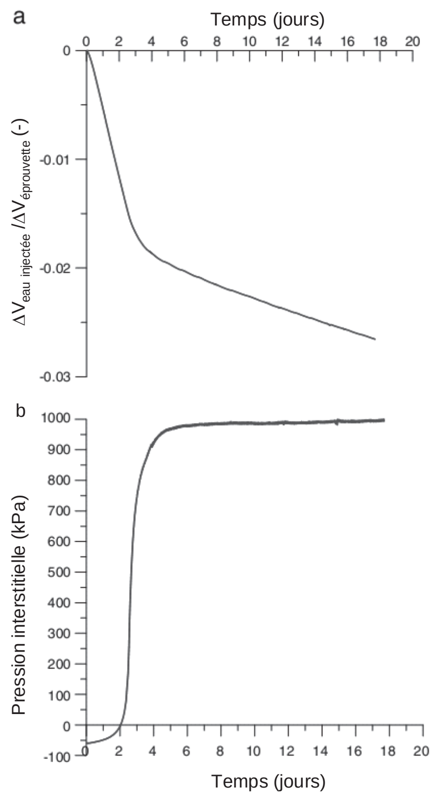

Figure 4. Resaturation de l'éprouvette d'argile de Boom

Afin de minimiser le gonflement (Delage et al. 2007), la saturation de l'éprouvette s'est faite sous contrainte effective en place (état proche de l'isotrope avec un K_0 de 0,9), définie par une contrainte moyenne p de 4,5 MPa et une pression interstitielle u de 2,25 MPa). La saturation s'est faite sous p = 3,25 MPa et u = 1 MPa en appliquant la contre-pression au sommet et à l'intérieur de l'éprouvette et en la mesurant à la base et sur la face extérieure avec les capteurs présentés en

Figure 1. La Figure 4 présente les variations d'échanges d'eau et de pression mesurées au cours du temps, montrant une bonne saturation après 4 jours à partir d'un état de succion dans l'éprouvette (pression initiale négative due au relâchement de contrainte lors de l'extraction). On observe que le volume injecté ne se stabilise pas malgré la saturation, signe d'une mobilisation de gonflement typique de ce type d'argile (0,5% en 15 jours).

3.2 *Essai de chauffage non drainé*

L'éprouvette a été soumise à une élévation de température à un taux de 1°C/h entre 25 et 65°C en conditions non drainées, toutes vannes fermées avec mesure de pression interstitielle à la base de l'éprouvette (Figure 1).

3.2.1 *Coefficient de pressurisation thermique*

La variation de pression interstitielle mesurée pendant cet essai est présentée en Figure 5. La comparaison avec les résultats obtenus par Horseman et al. (1987) avec un appareil triaxial classique est favorable. La pression interstitielle augmente de 1 MPa à 25°C à 2,1 MPa à 65°C.

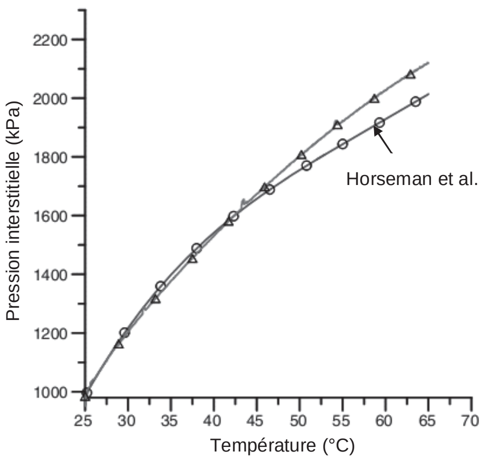

Figure 5. Pression interstitielle thermique, essai non drainé

Les réponses en pression interstitielle de la Figure 5 permettent de tracer les variations du coefficient de pressurisation thermique Λ en fonction de la température (Figure 6) qui, correspond à la pente de la courbe.

On observe en Figure 6 que le coefficient de pressurisation thermique mesuré décroit avec la température de 0.04 MPa/°C à 30°C à 0,02 MPa/°C à 60°C. Ces valeurs sont de l'ordre de grandeur de celles trouvées en bibliographie, égales à 0.06 MPa/°C (d'après des calculs effectués par Vardoulakis 2002 à partir de données de Sultan et al. 2000) et à 0.013 MPa/°C d'après Lima et al. (2010). Une telle décroissance a également été observée par Mohajerani et al. (2011) sur l'argilite du Callovo-Oxfordien considérée par l'ANDRA comme une roche-hôte potentielle pour les déchets en France. Une de ses raisons est la variation avec la température du coefficient de pressurisation thermique de l'eau sous la contrainte considérée présentée en Figure 8 (Spang 2002).

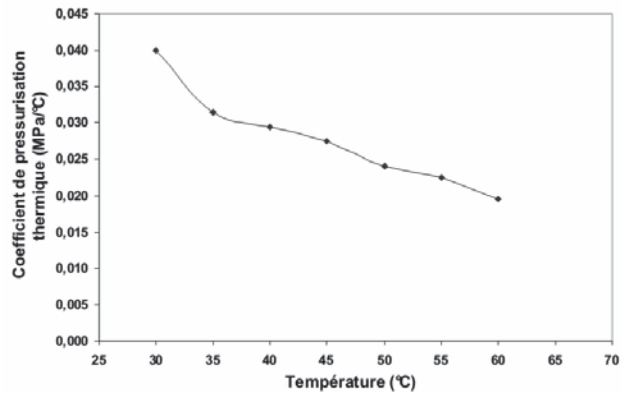

Figure 6. Variations du coefficient de pressurisation thermique avec la température.

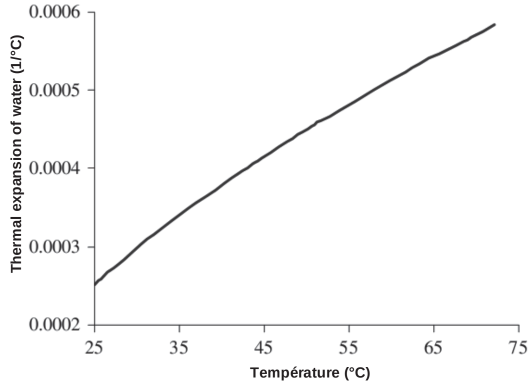

Figure 7. Variations du coefficient de pressurisation thermique de l'eau sous 4 MPa (Spang 2002)

La réponse en pression présentée en Figure 5 dépend en fait du couplage complexe de phénomènes thermiques (caractérisés par les coefficients de dilatation thermique α_i des phases solide et liquide) et mécaniques (caractérisés par les compressibilités des phases solide, liquide et de la compressibilité drainée de l'argile) sachant que ces paramètres varient également en fonction de la température (cf. Figure 7). Il convient de mentionner que la génération de surpressions thermiques pendant le chauffage non drainé engendre une diminution de la contrainte effective qui a pour conséquence un gonflement de nature mécanique.

En l'étape actuelle des travaux, on n'a pas encore d'éléments sur les variations avec la température de la compressibilité drainée de l'argile de Boom et les travaux se poursuivent dans ce sens pour une analyse plus détaillée.

3.2.2 *Coefficient de dilatation thermique non drainée*

La Figure 8 montre que l'échantillon s'est dilaté linéairement en conditions non drainées de 0,85%.

Cette valeur permet de déterminer le coefficient de dilatation thermique non drainé défini par la relation (1):

$$dV/V = \alpha_u \, dt \qquad (1)$$

avec $\alpha_u = 3,47 \times 10^{-4}$/°C

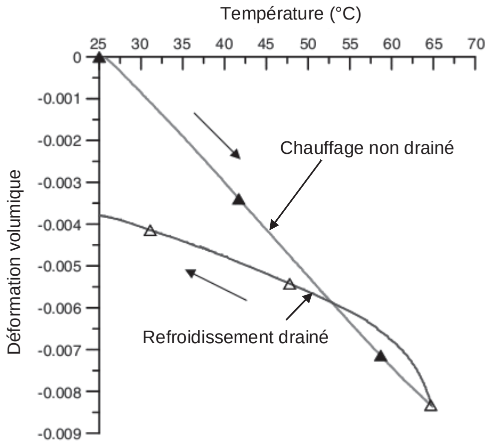

Figure 8. Variations volumiques lors des cycles en température.

3.3 *Essai de refroidissement drainé*

L'essai de chauffage non drainé a été suivi d'un refroidissement drainé sous les mêmes valeurs de contraintes constantes. Il a permis la dissipation des surpressions thermiques et s'est traduit par une contraction de l'éprouvette de 0,47% (Figure 8).

Il est possible que la courbure en début de refroidissement soit due à des adaptations des capteurs LVDT au changement de sens de déplacement. En utilisant la section linéaire observée entre 55 et 25°C, on obtient un coefficient de contraction thermoélastique (et donc d'expansion thermoélastique) $\alpha_d = 1{,}26 \times 10^{-4}$/°C comparable à la valeur de 1×10^{-4}/°C trouvée par Sultan et al. (2002).

4 CONCLUSION

Dans le cadre de recherches sur le comportement thermique de l'argile de Boom, roche-hôte potentielle pour le stockage à grande profondeur des déchets nucléaires en Belgique, un essai de chauffage non drainé suivi par un refroidissement drainé a été conduit sur un appareil triaxial cylindrique creux à faible longueur de drainage destiné à l'investigation expérimentale des phénomènes thermiques dans les argiles et argilites peu perméables.

L'essai réalisé a permis d'identifier des paramètres importants dans l'étude et la modélisation du comportement thermique de l'argile dans le champ proche des galeries;

Une valeur décroissante du coefficient de pressurisation thermique comprise entre 0,004 et 0,002 MPa a été déterminée. Cette décroissance, due en partie aux variations du coefficient de dilatation thermique de l'eau sous la contrainte considérée, résulte également des variations couplées avec la température de divers paramètres (dilatation thermique, compressibilité des phases solide et liquide, compressibilité drainée) qui ne sont pas encore tous identifiés. Les valeurs des paramètres obtenus sont en accord et complètent ceux déjà obtenus dans la bibliographie.

Il en va de même de la valeur de dilatation thermoélastique obtenue après l'essai de refroidissement drainé.

5 REMERCIEMENTS

Les travaux décrits dans cet article proviennent de la thèse du premier auteur, co-financée par la Commission Européenne dans le cadre du projet européen TIMODAZ (F16W-CT-2007-036449, coordonné par Dr. Li Xiang-Ling d'EURIDICE) et l'Ecole des Ponts ParisTech. Nous remercions aussi Dr. Li pour avoir fourni les échantillons d'argile de Boom..

6 REFERENCES

Delage P, Le T.T, Tang A.M, Cui Y.J, Li X.L. 2007. Suction effects in deep Boom clay block samples. Géotechnique, 57 (1), pp 239–244.

Fei Y. 1995. Thermal expansion. In: Thomas JA (ed) Mineral physics and crystallography: a handbook of physical constants. American Geophysical Union Online Reference Shelf 2, 29–44.

Horseman S.T., Winter M.G., Entwistle D.C. 1987. Geotechnical characterization of Boom clay in relatio,n with the disposal of radioactive waste. Commission of European Communities, EUR 10987.

Lima A.,Romero E., Gens A., Muñoz J., Li X.L. 2010. Heating pulse tests under constant volume on Boom clay. Journal of Rock Mechanics and Geotechnical Engineering 2 (2), 124-128.

McTigue D.F. 1986. Thermoelastic response of fluid-saturated porous rock, Journal of Geophysical Research, 91(B9), 9533–9542.

Mohajerani M., Delage P., Sulem J., Monfared M., Tang A.M., Gatmiri B. 2012. A laboratory investigation of thermally induced pore pressures in the Callovo-Oxfordian Claystone. International Journal of Rock Mechanics and Mining Sciences, vol. 52, 112-121

Monfared M., Delage P., Sulem J., Mohajerani M., Tang A.M. and De Laure E. 2011. A new hollow cylinder triaxal cell to study the behaviour of low permeable materials. International Journal of Rock Mechanics and Mining Sciences, 48 (4), 637-649.

Palciauskas V.V, Domenico P. A. 1982. Characterization of drained and undrained response of thermally loaded repository rocks. Water Resour, Res 18(2), 281–290.

Spang B. 2002. Excel Add-In for Properties of Water and Steam in SI-Units , http://www.cheresources.com/staff.shtml.

Sultan N., Delage P. & Cui Y.J. 2002. Temperature effects on the volume change behaviour of Boom clay. Engineering Geology, Vol. 64, 2-3, 135-145.

Vardoulakis I. 2002. Dynamic thermo-poro-mechanical analysis of catastrophic landslides. Géotechnique, 52 (3), 157-171.

Effet des conditions environnementales sur les propriétés mécaniques d'un ciment de puits géothermique

Effect of environmental conditions on the mechanical properties of geothermal well cement paste

Nauleau E., Martineau F., Kréziak C.
Université Paris-Est, IFSTTAR, Marne-la-Vallée, France
Ghabezloo S.
Université Paris-Est, Laboratoire Navier/CERMES, Ecole des Ponts ParisTech, France

RÉSUMÉ: Afin de remplir l'espace annulaire entre le tubage des puits de forage géothermiques et la formation géologique environnante, une gaine de ciment est utilisée et assure un rôle d'étanchéité. Des conditions environnementales comme la température, la pression et la présence de NaCl dans les eaux de l'aquifère du Dogger peuvent potentiellement influencer l'hydratation du coulis de ciment. Une cellule de maturation a été mise au point au sein de l'IFSTTAR afin d'étudier les effets de ces conditions sur l'hydratation et sur les propriétés de la pâte de ciment durcie. Des mesures de vitesse du son et de détermination du module de Young ont été réalisées sur la pâte de ciment durcie. Les éprouvettes sont préparées dans la cellule de maturation sous différents couples de pression/température, avec ou sans présence du NaCl dans le fluide environnant. Les résultats montrent une réduction significative des propriétés mécaniques de la pâte de ciment durcie avec l'augmentation de la température d'hydratation entre 20°C et 90°C. Une augmentation de la pression d'hydratation à 20MPa et la présence du NaCl à 20°C n'ont pas d'influence significative sur les propriétés mécaniques

ABSTRACT: In a geothermal well, a cement sheath is placed between the casing and geological formation for support and sealing purpose. Environmental factors such as temperature, pressure and the presence of NaCl in the fluids in Dogger aquifer can potentially affect the hydration of cement. A maturation cell is developed at IFSTTAR to study the effects of environmental conditions on the properties of the hardened cement paste. Ultrasonic wave velocity measurements and Young modulus tests are performed on specimens prepared in the cell under various pressure/temperature conditions, with or without NaCl in the surrounding fluid. The results show a significant reduction in the mechanical properties of the hardened cement paste with increasing hydration temperature between 20°C and 90°C. An increase in the pressure to 20 MPa and the presence of NaCl at 20°C show no significant influence on the mechanical properties

MOTS CLÉS : Pâte de ciment durcie, cellule de maturation, vitesse du son, module de Young, conditions d'hydratation
KEYWORDS: hardened cement paste, maturation cell, ultrasonic wave velocity, Young modulus, hydration conditions

1 INTRODUCTION

Le principe des puits géothermiques basse énergie consiste à extraire l'énergie géothermique contenue dans l'aquifère du Dogger (situé à 1800 mètres de profondeur à une température de 85°C) pour l'utiliser sous forme de chauffage. Dans un puits géothermique une gaine de ciment est placée entre la roche et le cuvelage d'acier pour assurer l'étanchéité et la stabilité de puits et protéger le cuvelage contre la corrosion. La tenue de cette gaine de ciment pendant la vie du puits est importante pour éviter tout problème de perte d'étanchéité qui pourrait causer des dégâts à l'échelle du puits mais aussi de pollution des nappes environnantes. Dans un puits, le gradient géothermique, les circulations d'eau chargée en éléments chimiques (Rojas et al. 1989, Ignatiadis et al. 1991), e.g. NaCl, au sein même de l'aquifère ainsi que les fortes contraintes dues à la profondeur sont susceptibles d'influencer l'hydratation du coulis de ciment et peuvent à long terme, contribuer à une dégradation prématurée du puits. Ces facteurs environnementaux (la température, la pression et les concentrations en NaCl) jouent un rôle prépondérant sur la cinétique d'hydratation, la composition chimique des hydrates et la microstructure de la pâte de ciment durcie (Theissing et al. 1978, Ramachandran et al. 1984, Escalante-Garcia et Sharp, 1997), ce qui modifie naturellement la perméabilité et les propriétés mécaniques du matériau et influence sa contribution dans l'étanchéité et la stabilité du puits. Afin d'étudier les influences de ces facteurs environnementaux sur le comportement de la pâte de ciment durcie, une cellule de maturation a été mise au point à l'IFSTTAR. Cette cellule de maturation permet de reproduire l'environnement d'un puits géothermique en combinant la pression, la température et la présence de NaCl.

Cet article s'intéresse donc, dans une première partie, à décrire le programme expérimental et le coulis de ciment utilisé, ses caractéristiques ainsi que les différents essais de caractérisation utilisés (détermination du module de Young et mesures de vitesse du son). La seconde partie de l'article est consacrée à la présentation de la cellule de maturation, de sa conception à son fonctionnement. Enfin la troisième partie s'intéresse aux résultats expérimentaux.

2 PROGRAMME EXPERIMENTAL

2.1 *Matériaux utilisés*

Un ciment de classe G (classification de l'American Petroleum Institute, API) a été utilisé pour la préparation des éprouvettes. Ce ciment est fréquemment utilisé pour la cimentation des puits de forage géothermiques ou pétroliers. Il s'agit d'un ciment à Haute Résistance aux Sulfates (teneur en C_3A inférieure à 3% d'après la norme 10A/ISO 10426-1 : 2000 de l'API). Le rapport eau/ciment choisi pour les essais est égal à 0.44 et la densité est égale à environ 1.9 (tous deux représentatifs des valeurs utilisés dans un puits). La composition du ciment de classe G utilisé est présentée dans le tableau 1.

Tableau 1 : Composition de ciment de classe G utilisé

Composants	C_3S	C_2S	C_3A	C_4AF
Pourcentage %	61.2	17.7	1.7	16.3

2.2 *Fabrication et conservation des éprouvettes*

Un mixeur équipé d'une cuve de 2.5 litres est utilisé pour la préparation de coulis de ciment. La première étape de fabrication est le malaxage de l'adjuvant anti-mousse avec l'eau pendant 5 min. Par la suite, deux autres adjuvants (un dispersant et un anti-sédimentation) ainsi que le ciment sont ajoutés et le tout est mélangé à haute vitesse (12000 t/min) pendant 35 secondes.

Le coulis de ciment est versé dans des moules cylindriques de 45 mm de diamètre et de 110 mm de hauteur. Pour être plus proche des conditions de puits, ces moules sont préparés avec un calcaire oolithique de 20% de porosité et de perméabilité égale à 10^{-15} m^2 (Figure 1). Ce choix s'explique d'une part par le fait que l'aquifère du Dogger est constitué d'un calcaire oolithique similaire, d'autre part, pour que le coulis de ciment soit en contact avec une solution saline, il était nécessaire d'utiliser un matériau poreux (figure 1 et 2).

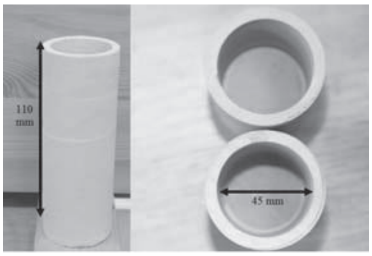

Figure 1. Moules préparés en calcaire oolitique

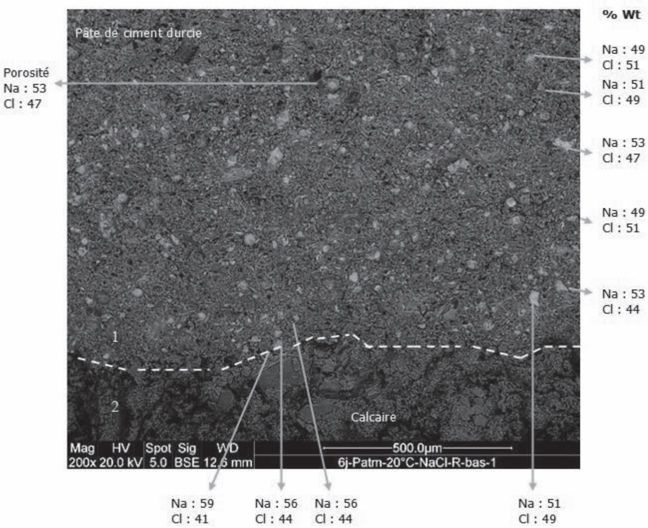

Figure 2. Image MEB de la pâte de ciment hydraté à 20°C à 6 jours avec présence de NaCl dans le fluide environnant.

C'est pour cette raison, que des essais au Microscope Electronique à Balayage (MEB) ont été réalisés afin de vérifier la pénétration du sel. En effet, la figure 2 représente une image MEB de la pâte de ciment hydratée à 20°C avec présence de NaCl dans le fluide environnant. Elle montre bien la migration des ions Na^+ et Cl^- (valeurs indiquées en pourcentage massique %Wt) du calcaire oolithique dans la pâte de ciment.

L'objectif est de simuler les conditions environnementales de l'hydratation du ciment (température, pression, présence du NaCl dans le fluide) dans un puits géothermique et de comparer séparément l'influence de ces facteurs sur les propriétés physico-mécaniques du matériau. Les moules sont ainsi soumis à différents couples de température et de pression pendant 7 jours. Les différents couples pression/température sont présentés dans le tableau 2. Les températures et les pressions choisies représentent le plus fidèlement possible les conditions environnementales pour l'hydratation en sub-surface, à environ 1000m et 2000m de profondeur (60°C et 90°C). Les cases grisées matérialisées par « x » représentent les couples réalisés et la notation « + sel » précise qu'il s'agit d'éprouvettes hydratées avec la présence de NaCl dans le fluide environnant. A noter qu'au minimum 4 éprouvettes ont été coulées pour chaque couple P/T. Tous les essais ont été réalisés sur des échantillons appartenant à une même préparation.

Tableau 2 : Descriptif du programme expérimental

	P_{atm}	10MPa	20MPa
20°C	x (+ sel)		x
60°C	x	x	x
90°C	x		x

Après 7 jours, les éprouvettes sont carottées au diamètre 40 mm, puis sont sciées et rectifiées pour obtenir une longueur de 80 mm. L'ensemble de ces opérations est réalisé à température ambiante et les éprouvettes sont par la suite conservées dans des bains à 20°C et à P_{atm} ou avec une teneur en NaCl pour les essais avec présence de sel.

2.3 *Essais réalisés*

Des essais de vitesse du son et la détermination du module de Young ont été réalisés pour connaitre les effets des conditions environnementales sur les propriétés mécaniques du ciment.

2.3.1 *Vitesse du son (NF EN 14579 (2005)).*

La vitesse de propagation du son dans les matériaux est une fonction directe de leurs propriétés élastiques et de leur compacité. Plus la porosité du matériau est faible, plus la propagation des ondes est rapide. Les mesures sont faites par transparence et longitudinalement car il est considéré que les éprouvettes étudiées ne présentent pas d'anisotropie. Afin d'assurer une bonne transmission du signal, du miel est utilisé comme produit couplant. Cet essai présente une bonne répétabilité inférieure à 3%.

2.3.2 *Détermination du module de Young (NF P 94-425 (2002)).*

L'essai s'effectue sur une éprouvette à section transversale circulaire d'un diamètre de 40 mm. Il consiste à appliquer, à l'aide d'une presse de 10 tonnes, un effort axial de compression avec un cycle de chargement/déchargement. Les déformations longitudinales ainsi que transversales de l'éprouvette sont mesurées durant l'essai qui est mené jusqu'à la rupture de l'éprouvette. Au départ, l'essai est contrôlé avec une vitesse de chargement de 0.25 kN/min. Un cycle de chargement/déchargement est réalisé (selon la norme la contrainte de début de décharge est comprise entre un tiers et deux tiers de la résistance à la compression estimée et la contrainte minimale lors du déchargement est environ égale à un tiers de cette contrainte). L'objectif est d'évaluer le module de Young sécant du matériau. Après ce cycle, l'essai est poursuivi en contrôlant le déplacement avec une vitesse de 0.0005mm/min jusqu'à la rupture. Pendant l'essai, le déplacement axial est mesuré à l'aide de 3 capteurs LVDT placés sur l'éprouvette grâce à un collier de mesure. Le module de Young est calculé par $E = \sigma_1 / \varepsilon_1$ avec σ_1 la contrainte axiale de l'éprouvette et ε_1 la déformation axiale de l'éprouvette.

3 CELLULE DE MATURATION IFSTTAR

3.1 *Présentation générale*

Un nouveau dispositif expérimental a été conçu à l'IFSTTAR avec pour objectif la reproduction des conditions de l'hydratation du ciment en terme de pressions, températures et des fluides chargés chimiquement dans un puits géothermique (Figures 3 et 4). Le système est composé d'une enceinte de 4 litres en inox formé d'un couvercle étanche d'une capacité maximale de 220 bars relié à un surpresseur, d'un manomètre sortie de 0-300 bars, d'une vanne d'isolement et d'une vanne d'impulsion. Le suppresseur est relié à une bouteille d'azote. La cellule d'hydratation peut accueillir quatre éprouvettes. Le groupe de surpression de 200 bars est constitué d'un filtre entrée gaz, d'un manomètre d'entrée 0-250 bars (0-25MPa) et d'un châssis en aluminium anodisé. Par ailleurs, des colliers chauffants sont disposés autour de la cellule et reliés à un boitier de régulation pour atteindre les températures souhaitées.

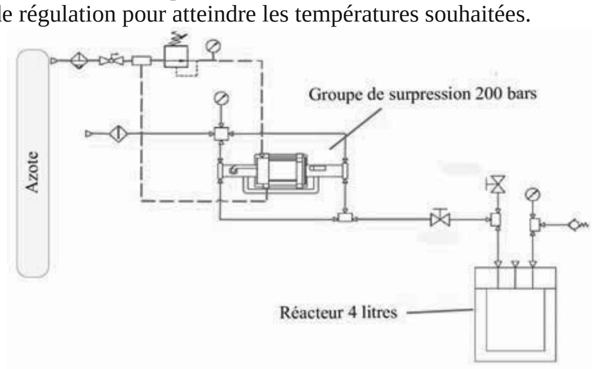

Figure 3. Schémas de principe de l'ensemble surpresseur/cellule (D'après le concepteur Maximator)

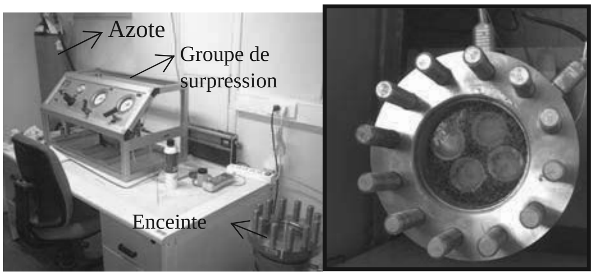

Figure 4 : Réacteur de maturation.

3.2. *Principe de fonctionnement*

Le principe de fonctionnement est le suivant : le gaz utilisé (dans ce cas de l'azote), est mis sous pression dans le surpresseur. Ce dernier est constitué d'une chambre et d'un piston de large diamètre. L'augmentation de la pression s'obtient en évacuant le gaz vers un piston de diamètre inférieur et à l'aide de clapets anti-retour. La pression souhaitée atteinte est envoyée dans la cellule *via* un circuit fermé. Des vannes pilotes permettent d'arrêter l'augmentation de la pression dans la cellule, le surpresseur régule lorsque la pression finale est atteinte.

La pression initiale à fournir pour atteindre une température et une pression souhaitée a été calculée en utilisant l'équation des gaz parfaits présentée dans la Figure 5. A titre d'exemple, si la température et la pression finale souhaitées sont respectivement de 60°C et 200 bars (20MPa), il est nécessaire de fournir une pression initiale de 176 bars.

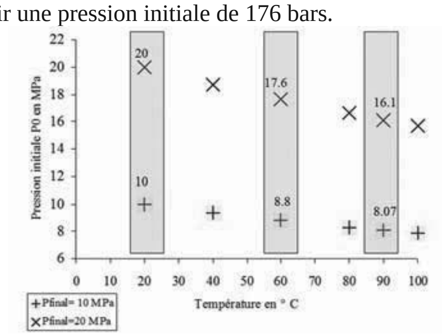

Figure 5 : Pression initiale à mettre en fonction de la température souhaitée

4 RÉSULTATS

Des mesures de vitesse du son et des modules de Young ont été effectuées sur les éprouvettes présentées dans le tableau 3. La Figure 6 présente les courbes contrainte-déformation des essais de compression uniaxiale réalisés sur trois échantillons hydratés sous une pression de 20 MPa à différentes températures : 20°C, 60°C et 90°C. Les modules de Young ont été évalués pour chacune des courbes et sont présentés dans le Tableau 3. Chaque essai a été réalisé pour au minimum trois éprouvettes. Les valeurs moyennes des résistances en compression simple (précision d'environ 3%), les modules de Young statiques (précision inférieure à 4%) ainsi que les mesures de vitesse du son (précision inférieure à 3%) sont présentés dans le Tableau 3.

On observe une diminution significative du module de Young, de la résistance en compression uniaxiale, ainsi que de la vitesse du son avec l'augmentation de la température d'hydratation. Ces diminutions sont principalement dues à une augmentation de la porosité de la pâte de ciment durcie avec l'augmentation de la température d'hydratation et sont en accord avec les conclusions présentées dans la bibliographie (Escalante-Garcia and Sharp 1997-1998, Verbeck and Helmuth, 1968, Jennings and al. 2007).

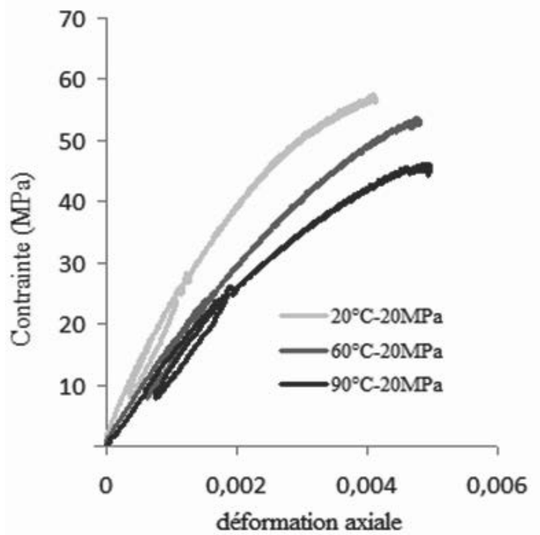

Figure 6 : Courbes de contrainte-déformation pour des échantillons hydratés à température différentes (20°C, 60°C et 90°C) et une pression de 20MPa.

Tableau 3 : Résultats du module de Young, de la résistance à la compression simple et de la vitesse du son évalués pour des échantillons hydratés sous 20MPa de pression à différentes températures.

Température (°C)	Module de Young (GPa)	Résistance à la compression (MPa)	Vitesse du son (m/s)
20°C	22.0	63.0	3526
60°C	16.6	53.2	3415
90°C	14.2	43.1	3243

La Figure 7 compare les courbes de contrainte-déformation entre deux éprouvettes hydratées à 20°C sous une pression atmosphérique et sous une pression de 20MPa. Les résultats présentés dans le Tableau 4 montrent que la pression d'hydratation n'a pas d'effet significatif sur les propriétés mécaniques de la pâte de ciment durcie, bien qu'elle joue un rôle d'accélérateur de prise (Yazici 2006).

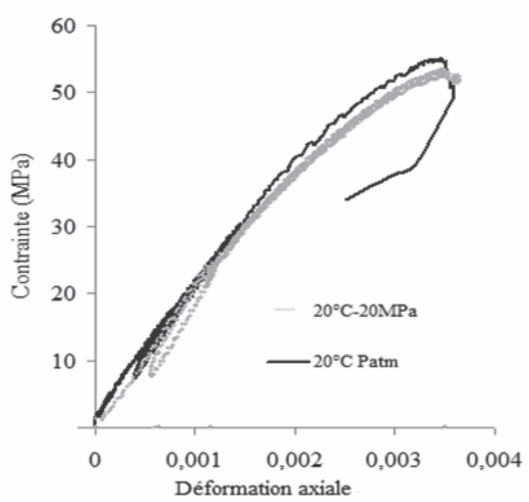

Figure 7: Courbes de contrainte-déformation pour des ciments hydratés à différentes pressions (pression atmosphérique et 20MPa) à une température de 20°C.

Tableau 4 : résultats du module de Young, de la résistance à la compression simple et de la vitesse du son pour des ciments hydratés à 20°C sous Patm et 20MPa

Couple P/T	Module de Young (GPa)	Résistance à la compression (MPa)	Vitesse du son (m/s)
20°C P_{atm}	21.2	65.0	3578
20°C 20MPa	22.0	63.0	3526

Les résultats expérimentaux concernant la présence du NaCl sont présentés dans le Tableau 5. La comparaison des modules de Young, des vitesses du son ainsi que des résistances à la compression entre les échantillons avec ou sans NaCl montrent que la présence du NaCl dans le fluide environnant n'a pas d'influence significative sur les propriétés mécaniques de la pâte de ciment durcie hydraté à 20°C. Les essais similaires sur les ciments hydratés à 90°C seront réalisés dans la suite de l'étude.

Tableau 5 Résultats des essais pour des ciments hydratés à 20°C-P_{atm} avec ou sans NaCl dans le fluide environnant

Couple P/T	Module de Young (GPa)	Résistance à la compression (MPa)	Vitesse du son (m/s)
20°C P_{atm}	21.2	63.0	3591
20°C P_{atm}+ sel	22.0	58.7	3506

5 CONCLUSION

Une cellule de maturation a été mise au point à l'IFSTTAR afin de reproduire les conditions environnementales de l'hydratation de coulis de ciment en température, pression de fluide et présence du NaCl dans un puits géothermique.

Un ciment de classe G a été utilisé pour la préparation des éprouvettes avec un rapport eau/ciment égale à 0.44 sous différents couples de pression/température ainsi que la présence ou non de NaCl dans le fluide environnant pendant l'hydratation. Afin de faciliter les échanges entre le ciment et le fluide interstitiel de la roche environnante, la pâte de ciment a été coulée dans des moules préparés avec un calcaire ayant une porosité de 20%. Ceci a permis une pénétration des ions Na^+ et Cl^- (visible au Microscope Electronique à Balayage). Différents couples de pression et température ont été appliqués pour la préparation des échantillons. Les résultats montrent un effet significatif de la température d'hydratation sur les propriétés mécaniques de la pâte de ciment durcie. La résistance à la compression et le module de Young montrent une diminution importante avec l'augmentation de la température d'hydratation entre 20°C et 90°C. Les résultats montrent également que la pression d'hydratation entre la pression atmosphérique et 20MPa n'a pas d'influence significative sur les propriétés mécaniques. De façon similaire, la présence du NaCl dans le fluide environnant à 20°C n'a pas d'influence significative sur les résultats.

6 RÉFÉRENCES

Escalante-Garcia J.I. and Sharp J.H. 1997. Effect of temperature on the hydration of the main clinker phases in Portland cements: part II, blended cements. *Cement and concrete research 28*, 1259–1274.

Ignatiadis I. Cheradame J.M. Lafforgue M. Castagne S. 1991. Evolution des concentrations en sulfures dissous dans les fluides géothermaux du Dogger du bassin de Paris. *BRGM R 33518 IRG SGN 91*, 134.

Jennings H.M. Thomas J.J. Gevrenov J. Constantinides G. Ulm F.J. 2007. A multi-technique investigation of the nanoporosity of cement paste. *Cement and Concrete Research 37*, 329–336.

Ramachandran, V.S. Seeley R.C. Polomark G.M. 1984. Free and comined chloride in hydrating cement and cement compounds. *Materials and Structures, vol. 19*, 285-289

Rojas J. 1989. Caractérisation et modélisation du réservoir géothermique du Dogger, Bassin parisien, France, rapport final. *Rap. BRGM R 30169 IRG SGN 89*, 239 p.

Taylor H.F.W. 1976. Hydraulic cement pastes : their structure and properties. *Cement and concrete Association*, 14-19.

Theissing E.M. Mebius-Van de Larr T. De Wind G. 1978. The combining of sodium chloride and calcium chloride by a number of different hardened cement pastes. *Cement and concrete Research, 8* (6), 683-692.

Verbeck G.J. and Helmuth R.A. 1968. Structures and physical properties of cement paste. *Proceeding of fifth international symposium on chemistry of cement*, 3, 1-32.

Yazici H. 2006. The effect of curing conditions on compressive strength of ultra high strength *concrete with high volume minerale admixtures*. *Building and Environment.42*. 2083-2089.

10A/ISO 10426-1 : 2000. Industries du pétrole et du gaz naturel – Ciments et matériaux pour la cimentation des puits- Partie 1 : Spécification.*American Petrolum Institut* (API).

NF EN 14579 2005. Méthodes d'essai pour pierres naturelles – Détermination de la vitesse de propagation du son.

NF P 94-425 2002. Détermination du module de Young et du coefficient de poisson.

Development of a predictive framework for geothermal and geotechnical responses in cold regions experiencing climate change

Développement d'un cadre conceptuel pour les réponses géotechniques et géothermales dans une zone polaire sous l'influence du changement climatique

Nishimura S.
Hokkaido University

Jardine R.J., Fenton C.H.
Imperial College London

Olivilla S., Gens A.
Universitat Politécnico de Catalunya

Martin C.J.
BP Exploration Operating Company Limited

ABSTRACT: Cold regions, which are expected to suffer particularly severe future climate effects, will pose very challenging geotechnical conditions in the 21st century involving ground freezing and thawing. Given the uncertainty of future environmental changes and the vast expanses of the cold regions, it is appropriate to address problems such as pipeline or road construction with analytical methods that have multiple scales and layers. High- and middle-level predictive tools are described that integrate climatic predictions from AOGCMs and their down-scaling schemes, geological and topographical (DEM) information, remotely-sensed vegetation data and non-linear finite element analysis for soil freezing and thawing. These tools output broad scale predictions of geothermal responses, at a regional scale, that offer hazard zoning schemes related to permafrost thawing. A more intensive local-scale predictive tool is then outlined that considers fully-coupled thermo-hydro-mechanical processes occurring at the soil-element level and outputs detailed predictions for temperature changes, pore water behaviour, ground stresses and deformation in and around geotechnical structures. Applications of these tools to specific problems set in Eastern Siberia and pipeline heave tests are illustrated.

RÉSUMÉ : Les conditions géotechniques des régions polaires représentent un défi pour le future car ces dernières sont plus susceptibles aux effets du réchauffement climatique, tels que les cycles de gel-dégel. Etant donné les incertitudes existantes concernant les futures variations climatiques ainsi que l'étendue des zones concernées, l'utilisation de méthodes analytiques multicouches est requise pour étudier les problèmes liés aux infrastructures linéaires. Cet article décrit un outil de prévision de haut niveau qui intègre : les prévisions climatiques des AOGCMs, des informations sur la géologie et la topographie (DEM) du terrain, des données sur la couverture végétale obtenues par télédétection et enfin des analyses par éléments finis des cycles de gel-dégel. Cet outil prédit approximativement la réponse géothermique à l'échelle régionale, et découpe la zone étudiée en fonction du risque de dégel du permagel. Un outil plus précis basé sur l'échelle locale est ensuite présenté. Il inclut un modèle avec couplage thermo-hydro-mécanique et prédit plus en détails les changements de température, les variations de pressions interstitielles et de contraintes ainsi que les déformations à l'intérieur et autour de structures géotechniques. Des applications pratiques de ces outils sont aussi présentées.

KEYWORDS: Climate change, permafrost, geothermal analysis, THM-analysis

1 INTRODUCTION

Anthropogenic climate change is expected to impact most severely in cold regions where the ground is currently frozen. Marked air warming may produce undesirable engineering consequences, including permafrost degradation over large areas where rich natural resources are being developed. Infrastructure design in such regions needs to consider how to cope with change through rational approaches that couple climatic, environmental, geotechnical, geological and structural modelling. Scale is a key problem in establishing such links. The powerful earth science predictive Atmosphere Ocean General Circulation Models (AOGCM) work at a much higher level, and over much broader areas, with consequently less spatial resolution than conventional geotechnical analyses. Moreover, the latter need to be relatively sophisticated to give realistic results. It appears infeasible to combine the two approaches directly in any monolithic, unified analysis package.

The present study considered three different scales, cascading predictions from the higher level analyses down as boundary conditions for each underlying tier. The highest-level involves manipulating data from AOGCM outputs, applying statistical and locally informed down-scaling techniques to produce regional climate change predictions. The middle-level starts with engineering geological ground modelling, classifying regions into broad stereotypes informed by local and remote sensing data. Regional climatic predictions are applied to this by using broad scale geothermal analyses to consider thermal changes through potentially great thicknesses of ground, accounting for background geothermal flux, local geology and topography. Annually varying thermal profiles and predictions of permafrost state emerge as inputs to smaller scale fully-coupled Thermo-Hydro-Mechanical (THM) analyses that predict engineering outcomes as ground displacement and/or stress responses to climate change. Such tools allow alternative infrastructure designs and mitigation measures to be assessed so that the most rational development strategies may be adopted.

The research described in this paper was part of a BP funded project to assess cold region climate change impacts. The initial focus was on Eastern Siberia. An interim overview and summary of approach was published by Clarke et al. (2008) while the detailed analytical treatments were set out by Nishimura et al. (2009a and b). This paper provides an updated summary of the project's outputs.

2 HIGH-LEVEL CLIMATIC PREDICTIONS

The study area considered is located in Eastern Siberia. A regional engineering geology evaluation was made first based on desk study data, remote sensing information and limited ground reconnaissance. A set of five stereotypical terrain units was established. Global climate data were derived for the area by considering the full ensemble of predictions from the 17 coupled AOGCM models included in the IPCC Fourth Assessment Report (IPCC, 2007). Their outputs depend on future greenhouse gas emission emissions using the SRES A2 scenario; a standard, marginally pessimistic projection. Statistical assessments were made by a team from Department of Physics at Imperial College to provide multi-model ensemble mean trends for future, seasonally varying, air temperatures (2 m above ground) and mean snow depth. These were compared with the locally observed dataset (ERA-40, from the European Centre for Medium-Range Weather) covering 1958–1998. Corrections were applied to the entire AOGCM ensemble time-series based on the differences between modelled and monthly mean temperatures over the observed period to eliminate model bias.

The AOGCM ensemble outputs were discretised into 2.5° x 2.5° (latitude and longitude) grid blocks, equivalent to ≈150km east-west by 280km north-south blocks in the study area. Ground elevation corrections were applied based on local topography to produce mean monthly air temperature and snow depth time-series, combined with models that described local orographic enhancement of precipitation and solar radiation. More details are given by Clarke et al. (2008) and Nishimura et al. (2009a). These processes led to time-series at set elevation intervals Above Sea Level (ASL) for each terrain type, which were fed directly into the middle-level analysis. Examples for the Rolling Hills terrain unit at 643mASL are shown in Figure 1.

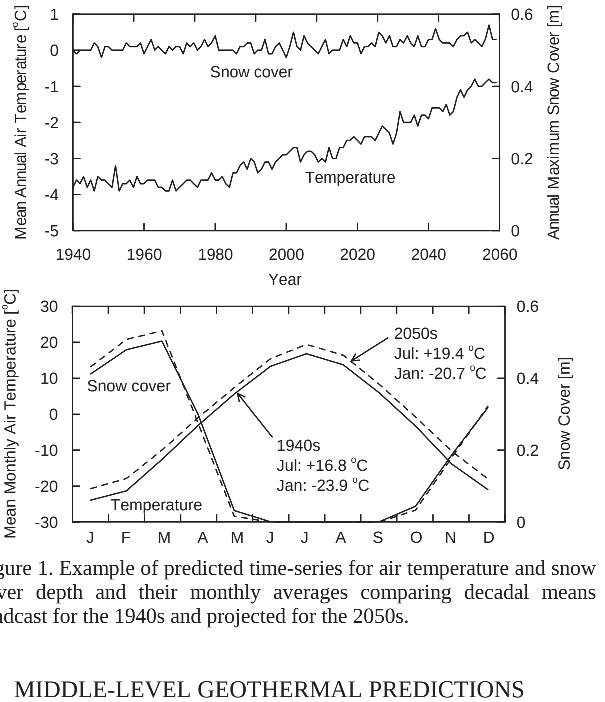

Figure 1. Example of predicted time-series for air temperature and snow cover depth and their monthly averages comparing decadal means hindcast for the 1940s and projected for the 2050s.

3 MIDDLE-LEVEL GEOTHERMAL PREDICTIONS

Horizontal heat flux is likely to be minor compared to vertical flow, except in very steeply sloping locations and other limited localities, so one-dimensional thermal finite element analysis offered a simple and efficient way of computing time-dependent, non-linear, ground responses to climatic changes. Air temperature, snow cover depth and upward background geothermal flux provided the key boundary conditions. However, quantitative analysis also required site-specific geotechnical profiles and topographic information, which is difficult to assign over wide areas involving variable climate and geography. The thermal analyses were therefore set into the broader scheme illustrated in Figure 2 in which a wide range of potential variables were considered analytically. For example, local climatic time-series were generated at Rolling Hills elevations of 343m, 643m, 943m and 1243mASL. Three different porosity-depth profiles were considered for each to represent a spread of stratigraphies. Six different ‘n-factors’ were assigned to each to defining a spread of the air-to-ground heat transfer efficiencies (Lunardini, 1978) that depend on surface characteristics, such as vegetation type. Finally, two underlying geothermal flux values were set and a total of 144 analyses run to cover the full range of conditions expected. The one-dimensional FE analysis outputs were stored and formatted so that specific information such as temperature at the active layer base (TTOP), temperature at Zero Annual Amplitude (TZAA) or permafrost table depth could be recovered swiftly from the analytical database.

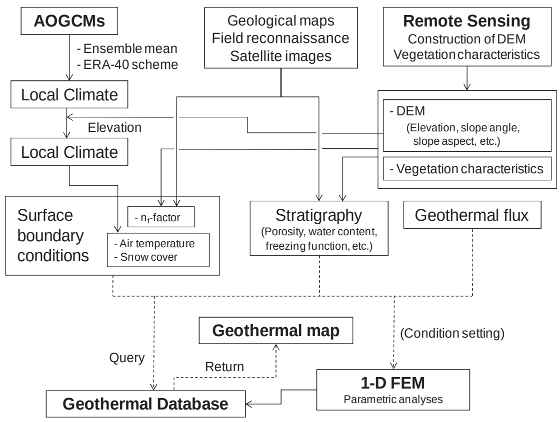

Figure 2. Structure of middle-level analysis to obtain local geothermal predictions based on climate predictions and local geography.

The one-dimensional thermal conduction finite element analysis involved a purpose-written code in which ground profiles were discretised as shown in Figure 3. Strong non-linearity in the geomaterials’ temperature-energy relationships and latent heat effects are captured as well as porosity/temperature-dependent thermal conductivity. The conductivity is expressed as a geometric mean of the soil mineral, liquid water and ice components; the unfrozen water content below 0^{o}C was expressed mathematically. The ground conditions expected for the 1940-50 decade were hindcasted by applying the 1940-1950 climate for around 1000 years before this date to obtain a fully stable initial state. From this point onwards the computed 1950 to 2050 climate time series were applied as boundary conditions and the ground response predicted; see Nishimura et al. (2009a) for details.

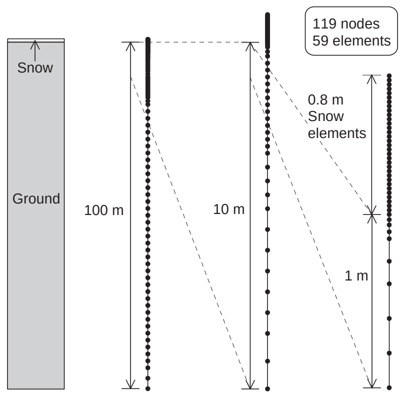

Figure 3. Discretisation of the ground in 1-D thermal analysis: Temperature boundary conditions are applied at different snow elements at different time of a year according to input snow cover depth data.

An example of the computational output is given in Figure 4, showing seasonally transient ground temperature-depth 'trumpet' curves for years 2000 and 2050. The climate warming effects are clear, with the permafrost table lowering and permafrost warming; effects are more dramatic near the surface than at depth.

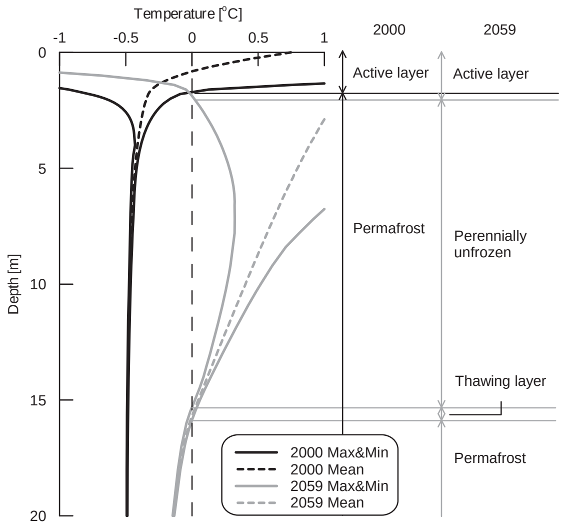

Figure 4. Computed annual temperature profiles for 2000 and 2059; Rolling Hills study area at 643mASL, n-factor = 0.6. Stratigraphy involves 1-m surface layer with porosity 0.4, decreasing to 0.04 at 15m depth.

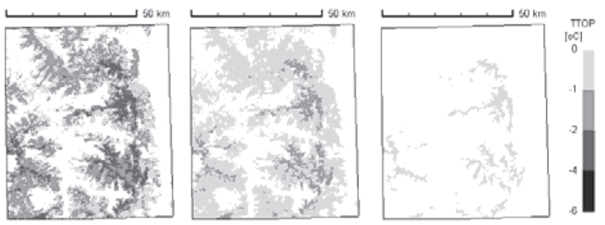

(a) 1940 (b) 2000 (c) 2059

Figure 5. Example of computed TTOP (annual mean temperature at active layer bottom) for a segment of studied area.

While site-specific geothermal computation is sufficient for small-scale engineering, strategic planning of large scale transport or pipeline infrastructure requires regional geothermal predictions for potentially changing permafrost characteristics. The three level approach generated maps of key parameters. The first step was to integrate primary data from remotely sensed Digital Elevation Models (DEMs) and ground information such as vegetation canopy cover with geological databases. These datasets are established with the aid of site reconnaissance and codified so that a best matching 1-D analysis case could be associated with any given landscape point. Once this correspondence has been made, thermal predictions could be retrieved for the given point from the 1-D analysis output database. Repeating the process and adopting a tight grid over the whole surface area allows maps to be drawn. The first task was to check whether the permafrost distributions predicted between the 1940s and present times matched current geothermal and permafrost conditions. Checks against the regional observations showed that the hindcasts were generally good, adding confidence to forward predictions. Figure 5 presents examples of TTOP maps at three stages of the analysis in a 60km by 80km study area showing clear warming of the permafrost being predicted at higher elevations of the Rolling Hills study area (after Nishimura et al., 2009a).

4 SOIL-STRUCTURE RESPONSE LEVEL PREDICTIONS

The lowest-level analyses aim to predict how soil-structure systems will respond to changing geothermal regimes. These interactions involve coupled physical processes, such as frost-heave in roads and around chilled pipelines, slope instabilities due to ground thawing and bearing capacity losses in piles and shallow foundations due to ground warming. Such problems are most rationally approached by adopting fully coupled THM analyses. The details of the THM model developed for this purpose are described by Nishimura et al. (2009b) and its essence is summarised below.

The broad framework of the proposed model involves the classical THM elements described by Gens (2007): equilibrium of forces; coupled mass and heat conservation; the Clausius-Clapeyron equation of phase equilibrium; permeability and thermal conductivity functions and a variety of models describing non-linear freezing and mechanical behaviour. The state variables include the total stresses, σ, the pore liquid water pressure, P_l, and the pore ice pressure, P_i. A novel feature of the proposed model is its mechanical constitutive mode expressing seamless transitions between frozen and unfrozen states. The mechanical model is developed from the Barcelona Basic Model (Alonso et al., 1990) for unsaturated soils, noting a close analogy between phase interactions in unsaturated soils and frozen soils. By adopting the 'net stress', σ-max(P_l, P_i), and the 'suction-equivalent', *max*(0, P_l -P_i), a Critical-State type elasto-plastic formulation was made possible while capturing temperature's effects via changes in these stress variables, as illustrated in Figure 6. The Clausius-Clapeyron equation is the key relationship relating pressure variables to temperature.

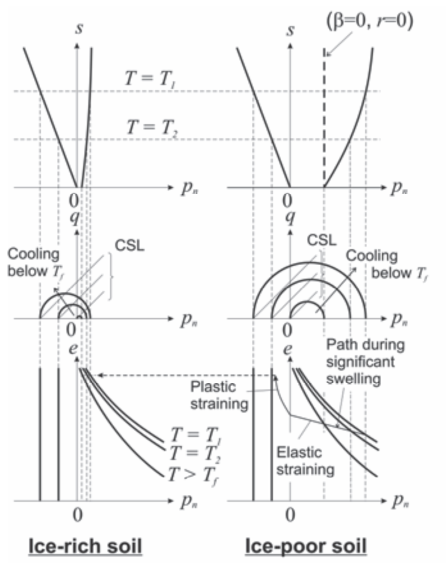

Figure 6. Schematic illustration of yield surface changes according to temperature changes in the newly developed mechanical model

Examples of the model's predictions for triaxial compression are shown in Figure 7. In the top-left diagram, higher strength develops at lower temperatures, a well-known feature of frozen soils. The stress-paths followed in accordance with the elasto-plastic scheme illustrated in Figure 6, are plotted in the right-hand side diagrams.

Validation of the THM-analysis was performed by simulating the Calgary field tests reported by Slusarchuk et al. (1978) on buried chilled pipelines. Pipes of 1.22m diameter were buried in initially unfrozen silty ground with the invert at 2.0m depth ('control' case C) and at 2.9m (the 'deep burial' case D). The pipelines were cooled internally from +6.5°C to -8.5°C over 50 days, after which the temperature was kept constant. Figure 8 shows the computed and observed ground

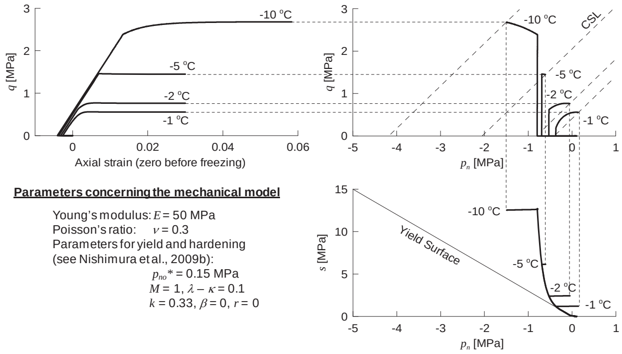

Figure 7. Example of model performance in triaxial compression at different temperatures; see Nishimura et al (2009b).

heave for the two cases, confirming the model's ability to capture the field heaving behaviour. The values of input parameters and the processes of their determination are described by Nishimura et al. (2009b). The control case was simulated with two different scenarios for the air temperature; it was set either constant at +6.5°C, or varied monthly, oscillating between +16.5°C in July and -8°C in January.

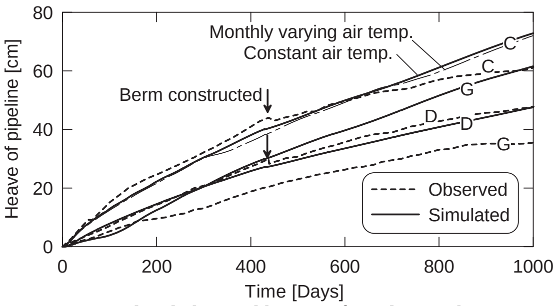

Figure 8. Computed and observed heaves of pipelines: Observation data from Slusarchuk et al. (1978). The 'G' case is a gravel-matted case; see the original literature for details.

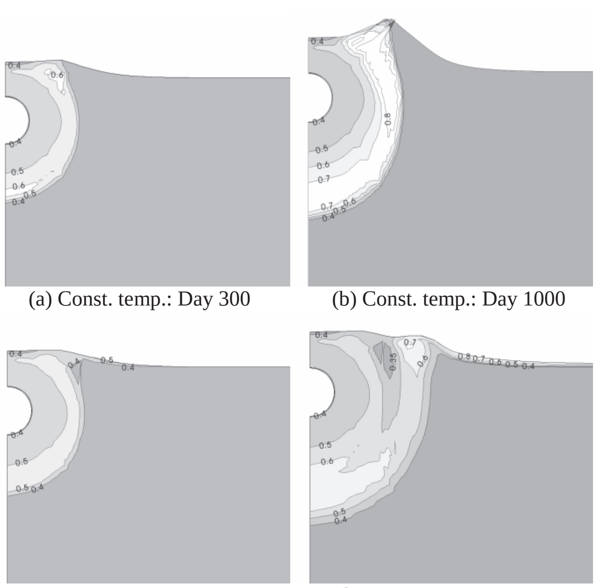

(a) Const. temp.: Day 300 (b) Const. temp.: Day 1000

(c) Varying. temp.: Day 300 (d) Varying. temp.: Day 1000

Figure 9. Computed geometry changes and porosity distributions.

The difference in the air temperature boundary conditions affected the surface movement patterns, as shown in Figure 9, despite the limited effect on overall pipe heave. Maintaining a fixed temperature difference between the ground surface and the chilled pipeline resulted in excessively large heave away from the centreline and movements that could not be considered reliably by the model's small-strain formulation. In the case with monthly variable ground surface temperature, surface freezing during winter disrupted the frost heave and permitted a more stable expansion of the frozen zones. The porosity distribution shown in Figure 9 indicate highly dilated, ice-rich areas around the pipeline, created by the influx of water drawn in by the 'suction' P_l -P_i,. The Calgary dataset allowed a critical validation of the-THM model's realistic performance. Inputting longer-time, transient future local climatic/geothermal trends from the middle-level analyses would allow the THM analyses to predict the site-specific soil-structure response against expected climate change.

5 CONCLUSIONS

A multiple-level analytical framework is proposed for predicting soil-structure responses to climate change in those cold regions where permafrost degradation plays an important role. The framework places climate prediction at the highest global level, and applies AOGCM data that is downscaled and calibrated against local climate datasets. The next level combines engineering geology with non-linear 1-D modelling to generate extensive analytical databases from which regional geocryological maps may be created that both inform hazard mapping and strategic planning of extensive infrastructure. As well as providing a middle-level screening tool, the geothermal analysis can set the conditions for lower-level, site-specific engineering analyses. A new THM-model with a novel mechanical constitutive model has been proposed to help predict the complex soil-structure interactions expected as temperature changes encourage permafrost warming and degradation. The mid-level approach was checked against regional geothermal maps in Eastern Siberia, while the THM analysis was tested against field tests on chilled pipelines in Canada, confirming the predictions to be realistic in both cases.

6 ACKNOWLEDGEMENTS

The research described was funded by BP. Their support and permission to publish the results is sincerely acknowledged.

7 REFERENCES

Alonso, E.E., Gens, A. and Josa, A. 1990. A constitutive model for partially saturated soils. *Géotechnique* 40 (3), 405-430.

Clarke, J., Fenton, J., Gens, A., Jardine, R., Martin, C., Nethercot, D., Nishimura, S., Olivella, S., Reifen, C., Rutter, P., Strasser, F. and Toumi, R. 2008. A multi-disciplinary approach to assess the impact of global climate change on infrastructure in cold regions, *Proc. 9th Int. Conf. on Permafrost*, Fairbanks, 279-284.

Gens, A. 2010. Soil-environment interactions in geotechnical Engineering. the 47th Rankine Lecture, *Géotechnique* 60 (1) 3-74.

IPCC, 2007. Climate Change 2007: The physical science basis. Contribution of Working Group I to the Fourth Assessment Report of the Intergovernmental Panel on Climate Change, Cambridge University Press.

Lunardini, V.J. 1978. Theory of n-factors and correlation of data. *Proc. 3rd Int. Conf. on Permafrost* , Edmonton, 41-46.

Nishimura, S. Martin, C.J., Jardine, R.J. and Fenton, C.H. 2009a. A new approach for assessing geothermal response to climate change in permafrost regions. *Géotechnique* 59 (3), 213-227.

Nishimura, S., Gens, A., Olivella, S. and Jardine, R.J. 2009b. THM-coupled finite element analysis of frozen soil: formulation and application. *Géotechnique* 59 (3), 159-171.

Slusarchuk, W.A., Clark, J.I., Nixon, J.F., Morgenstern, N.R. and Gaskin, P.N. 1978. Field test results of a chilled pipeline buried in unfrozen ground. *Proc. 3rd Int. Conf. on Permafrost*, Edmonton, 878-883.

An undrained upper bound solution for the face stability of tunnels reinforced by micropiles

Une solution en limite supérieure non drainée pour la stabilité du front de tunnels renforcés par micropieux

Pinyol N.M.
Centre Internacional de Mètodes Numèrics en Enginyeria (CIMNE).
Department of Geotechnical Engineering and Geo-Sciences. Universitat Politècnica de Catalunya (UPC)

Alonso E.E.
Department of Geotechnical Engineering and Geo-Sciences. Universitat Politècnica de Catalunya (UPC)

ABSTRACT: Tunnel in difficult soils may require procedures to prevent tunnel face failures. Face stabilization can be achieved by the installation of some structural elements. This paper presents an analysis of face stability of shallow tunnels in undrained soils reinforced by an umbrella of subhorizontal micropiles. Upper bound solutions for two dimensional plane strain conditions are given including the effect of micropiles. The micropile umbrella is embedded in the soil and supported on the tunnel lining. The kinematically admissible collapse mechanism defined to calculate the upper bound solution includes the action provided by a subhorizontal micropile at limiting conditions. The solutions are given in practical dimensionless charts which are useful to quantify easily the effect of the umbrella of micropiles. The plots provide a simple procedure to design the umbrella. The most relevant properties defining the umbrella are grouped into a single dimensionless coefficient which includes the yielding conditions and the geometry of the micropiles as well as the distance between them.

RÉSUMÉ : Les tunnels dans les sols difficiles peuvent nécessiter des procédés pour prévenir les ruptures du front du tunnel. La stabilisation du front peut être réalisée par l'installation de certains éléments structurels. Cet article présente une analyse de la stabilité du front dans des tunnels peu profonds en conditions non drainées renforcés par un parapluie de micropieux subhorizontaux. Des solutions de la limite supérieure pour des conditions bidimensionnelles de déformation plane sont présentées, y compris l'effet des micropieux. Le parapluie de micropieux est intégré dans le sol et soutenu sur le revêtement du tunnel. Le mécanisme de rupture cinématiquement admissible défini pour calculer la solution de la limite supérieure comprend la réponse prévue par un micropieu subhorizontal dans des conditions limites. Les solutions sont données dans des graphiques pratiques et sans dimensions qui fournissent une procédure simple de concevoir le parapluie. Les propriétés les plus pertinents qui définissent le parapluie sont regroupées en un seul coefficient sans dimension qui inclut les conditions de plastification et de la géométrie des micropieux, ainsi que la distance qui les sépare.

KEYWORDS: Tunnel, face stability, micropiles, upper bound, plasticity, undrained strength.

1 INTRODUCTION

Tunnel in difficult soils may require procedures to prevent tunnel face failures. In tunnel excavated by means of boring machines, a pressure can be applied against the face to counteract water and earth pressure. Several publications provide procedures to calculate the pressure required for stability. Well known solutions given initially by Davis et al. (1980) offer practical dimensionless charts for shallow tunnels in cohesive materials based on plasticity theorems (upper and lower bound solutions). This contribution was followed by several authors that presented similar solutions for frictional materials (Leca and Dormieux 1990) or improved solutions by using limit equilibrium, finite difference and finite element methods (Lyamin and Sloan 2002a,b, Augarde et al. 2003, Vermeer et al. 2002, Klar et al. 2007, among others).

Another calculation approach is to use Limit Equilibrium techniques (Anagnostou and Kovari 1996). They provide their results in terms of "bearing capacity" expressions. Finite Element and Distinct Element methods have been used extensively to examine face stability, in most cases under three dimensional conditions (Vermeer *et al*. 2002, Galli *et al*. 2003, Melis and Medina 2005). Among them, Vermeer *et al.* (2002) determined failure conditions of the face by means of a "c, ϕ reduction method" and provided three dimensional solutions for the drained case.

Face stabilization can also be achieved by the installation of some structural elements (bolts distributed in the front, concrete prevaults and umbrellas of micropiles). Several analysis of tunnel face stability taking into account the effect of a prevault and a reinforcement by bolts have been published (Peila et al. 1996, Wong et al. 2000, Yoo and Shin 2003, Lignola et al. 2008, 2010). However, limited attention has been paid to the reinforcement of tunnel faces by micropiles.

This paper presents a stability analysis of tunnel faces including an umbrella of sub-horizontal micropiles. The micropiles are considered as beams subjected to the kinematic motion imposed by the assumed failure mechanism. The limiting resistance of the supporting beams is first addressed. The failure mechanism imposes a displacement pattern on the beam, which reacts applying a critical combination of normal and shear forces on the boundary of the sliding body. These limiting supporting forces are calculated by assuming a Von Mises yield criterion for the micropile material. Then, they are introduced into the general minimization process associated with the upper bound formulation. Stability conditions are described in terms of dimensionless parameters and plotted in ready to use design charts. In particular, a dimensionless Micropile Coefficient, which includes all the relevant design parameters of the umbrella, could be isolated and plotted in terms of undrained soil strength and tunnel geometry.

2 UPPER BOUND SOLUTION INCLUDING SUBHORIZONTAL MICROPILES

2.1 *Collapse mechanism*

Consider the plane strain shallow circular tunnel of diameter D, having a cover depth C, represented in Figure 1. The soil around the tunnel is characterized by its unit weight (γ) and its undrained strength (c_u). A vertical stress, σ_S, is applied on the soil surface. In order to prevent a potential failure of the front, a pressure σ_T is applied on the tunnel face. In addition, a micropile supported on the already-built tunnel support is embedded in the soil. The micropile inclination with respect to a horizontal is defined by means of an angle η.

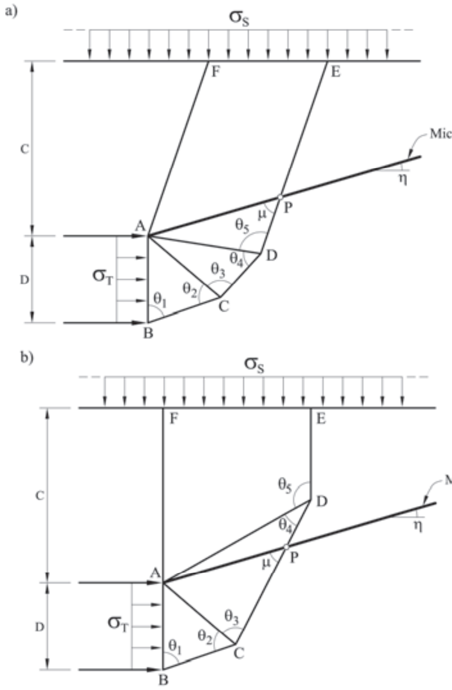

Figure 1. Collapse mechanism for upper bound calculation. (a) Micropile crossing DE side (upper wedge); (b) Micropile crossing CD side (lower wedge).

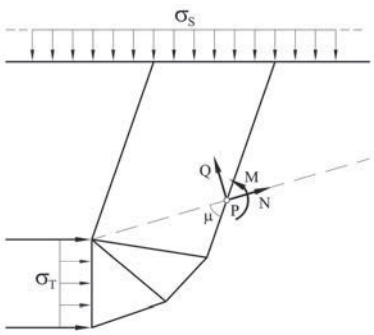

Figure 2. Micropile action on failure mechanism for upper bound calculation.

Under these conditions an upper bound solution for tunnel face failure is analyzed by means of a kinematically admissible collapse mechanism, defined by means of five degrees of freedom (the five angles θ_1, θ_2, θ_3, θ_4 and θ_5 in Fig. 1). Two possible collapse mechanisms are considered regarding the relative position between the micropile and the resulting collapse mechanism. In Figure 1a the micropile crossed the upper wedge on the DE side. This condition can be expressed by the following restriction: $3\pi/2-\theta_1-\theta_2-\theta_3-\theta_4-\eta<0$. Otherwise, the micropile will cross the side CD (Fig. 1b).

In the mechanism described, the micropile will react against the expected displacement imposed by the soil wedge. This effect will be included in the upper bound solution adding the work performed by the external forces transmitted by the micropile on the mobilized wedge. At point P (Fig. 2) he micropile action on the wedge will be characterized by a normal force *N*, a shear force *Q* and a bending moment, *M*. Notice that only *N* and *Q* will contribute directly to increase safety because the moment developed at point P will not produce any external stabilizing work.

2.2 Upper bound theorem

The upper bound theorem of plasticity is applied to the kinematically admissible failure mechanism shown in Figure 1. External work per unit of length performed by the external forces (weight, σ_S, σ_T and shear and tensile forces applied by the micropiles) due to a relative virtual rate of displacement is made equal to the internal dissipation of shearing work. The resulting equation is:

$$\frac{(\sigma_s-\sigma_T)}{c_u}-\frac{2C}{D}\frac{\sin\theta_2\sin\theta_4}{\sin\theta_1\sin\theta_3\sin\theta_5\cos(\theta_1+\theta_2+\theta_3+\theta_4+\theta_5)}-$$
$$\frac{1}{\tan\theta_1}-\frac{2}{\tan\theta_2}-\frac{2}{\tan\theta_3}-\frac{2}{\tan\theta_4}-\frac{1}{\tan\theta_5}- \tag{1}$$
$$\frac{\cos(\theta_1+\theta_2+\theta_3+\theta_4)}{\sin\theta_5\cos(\theta_1+\theta_2+\theta_3+\theta_4+\theta_5)}+\frac{\gamma D}{c_u}\left(\frac{C}{D}+\frac{1}{2}\right)-$$
$$\frac{\sin\theta_2\sin\theta_4}{\sin\theta_1\sin\theta_3\sin\theta_5 D c_u s}\left[N\cos\mu+Q\sin\mu\right]\Gamma=0$$

where *s* is the distance between two micropiles (assumed to be parallel) of the umbrella; μ is the relative angle between the micropile and the upper sliding wedge (Fig. 1) defined as:

$$\mu=5\pi/2-\theta_1-\theta_2-\theta_3-\theta_4-\theta_5-\eta \tag{2a}$$

when the micropile crosses DE; and

$$\mu=3\pi/2-\theta_1-\theta_2-\theta_3-\theta_4-\theta_5-\eta \tag{2b}$$

when the micropile crosses CD.

The parameter *A* in Eq. (1) is an auxiliary coefficient which also depends on the relative position between the micropile and the collapse mechanism:

$$\Gamma=1 \quad \text{when the micropile crosses DE} \tag{3a}$$

$$\Gamma=\frac{\sin\theta_5}{\sin\theta_4} \quad \text{when the micropile crosses CD} \tag{3b}$$

Any combination of external forces that verifies Eq. (1) will be either greater than, or equal to, the forces causing collapse. Notice that the first terms (except the last one) of Equation (1) identify the upper bound expression in the absence of micropiles (Augarde et al. 2003).

Forces exerted by the micropile on the critical wedge will be determined by an independent analysis in the following section. The micropile will be considered as a beam and subjected to the kinematic motion imposed by the assumed failure mechanism.

2.3 Micropile behaviour. Limiting conditions

The micropile is idealized as a beam subjected to a uniform imposed displacement δ due to the moving wedge of the expected collapse mechanism. Figure 3 shows the micropile isolated from the surrounding soil. In order to simplify the calculation of the beam, the effective embedded length *b* (distance between the crossing point P and a fixed, fully clamped, point X) of the micropile into the stationary soil will be assumed to be known. An estimation of the value of the clamping distance *b* may be obtained from the theory of piles embedded in an elastic half-space, subjected to a horizontal load and a moment at its head. This problem is described in Poulos and Davis (1980). According to this, *b* has been estimated in the range 0.2 to 0.1.

The displacement δ defines the type of deformation and the stresses of the beam. Its actual value will be found through the assumption that the micropile section will be taken to limiting conditions. Yielding conditions of the steel of the micropile will be assumed to follow a Von Mises criterion. (The grouting contribution is very small and it will be disregarded). The Von Mises criterion in plane strain can be expressed as follows:

$$\sigma^2+3\tau^2=\sigma_e^2 \tag{4}$$

where σ and τ are the normal and shear stress acting on a fiber of a cross section of the micropile and σ_e is the tensile strength of the steel. σ and τ will be expressed in terms of the normal force (N), shear force (Q) and bending moment (M).

The conditions leading to the maximum support provided by the micropile will be defined by those leading to the yielding of the most stressed fiber within the critically loaded steel cross section of the micropile. This section is point P in Figure 1.

Forces N and Q and moment M at point P, due to an imposed displacement δ, can be calculated if the mechanical and geometrical parameters of the micropile are known:

$$M=\frac{6EI_x}{b^2}\delta_v\,;\,Q=\frac{12EI_x}{b^3}\delta_v\,;\,N=\frac{AE}{b}\delta_h \qquad \text{(5a;b;c)}$$

where E is the steel elastic modulus, I_x is the moment of inertia with respect to the horizontal axis of the section and A is the cross-sectional area of the micropile (a steel tubular section has been choosen having a diameter d and thickness t). δ_h=δcos μ and δ_v=δcos μ are the horizontal and vertical components of the imposed displacement, δ, expressed in terms of the angle μ (Eq.(2)).

Under these conditions, normal and shear stresses due to the normal (N) and shear (Q) forces and moment (M) are calculated:

$$\sigma=\frac{N}{A}+\frac{M\,z}{I_x} \qquad \text{(6a)}$$

$$\tau=-\frac{QS_x}{2I_x t}=\frac{2Q\sqrt{d^2-4z^2}}{\pi d^2 t} \qquad \text{(6b)}$$

where z is the distance from the beam axis (x direction) to a particular point of the section and S_x is the static moment of the cross-sectional area above coordinate z**.**

Substituting N, Q and M from Equations (5) into Equations (6) and the resulting expressions for σ and τ into Equation (4), the Von Mises criterion can be written.

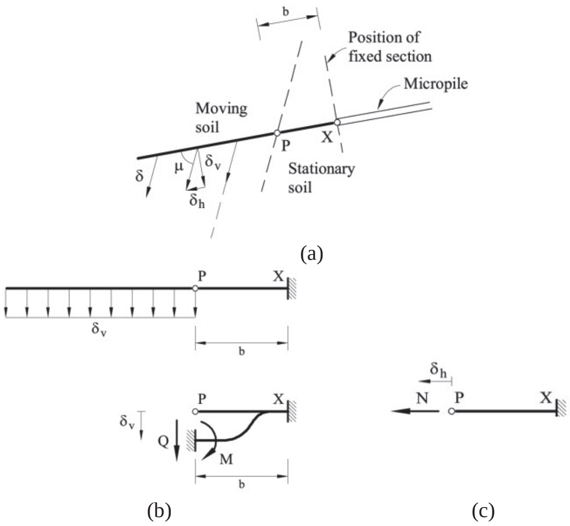

Figure 3. (a) Isolated micropile subjected to an imposed displacement δ; (b) bending behavior of the micropile; (c) tensile behavior of the micropile.

A conservative assumption is now introduced in the calculation. The available strength provided by the micropile is calculated as the value associated with the state in which the section starts to yield at some fiber. Therefore, the stress provided by the micropile beyond this point, due to the yielding of the rest of the section, is not considered here.

The shear stress τ reaches a maximum in the center of the section. On contrary, the stress σ due to N and M reaches a maximum at z = -R. Bending dominates the tensile stressing of the micropile for the particular problem we are considering due to the particular cross-section of the micropiles and the imposed loading mechanism. It turns out that the critical stress is located at the outer part of the cross section.

Applying Von Mises' criterion (Eq. 4) to the fiber characterized by z = -R the following expression for the displacement, δ, leading to the first fiber yielding in the micropile cross section at point P is derived:

$$\delta=\frac{\sigma_t b}{E}\frac{1}{\sqrt{f\left(d/b,\mu\right)}} \qquad (7)$$

where $f(d/b,\mu)$ is a function of the ratio between the diameter of the micropile (d) and the equivalent length of the beam (b) and the relative orientation between the micropile and the upper sliding wedge of the failure mechanism (μ) (Eq. (2)):

$$f\left(d/b,\mu\right)=6\cos\mu\sin\mu\left(d/b\right)+9\sin^2\mu\left(d/b\right)^2+\cos^2\mu \qquad (8)$$

Finally, when the value of δ given in Equation (7) is substituted into equation (5b and c), the following shear and tensile forces applied by the micropile on the sliding mechanism, at point P, are found:

$$N=\sigma_e td\pi\frac{\cos\mu}{\sqrt{f\left(d/b,\mu\right)}} \qquad \text{(9a)}$$

$$Q=\frac{3}{2}\sigma_e td\pi\left(d/b\right)^2\frac{\cos\mu}{\sqrt{f\left(d/b,\mu\right)}} \qquad \text{(9b)}$$

These expressions for N and Q are now introduced into Eq. (1) to find the external loads that leads to the defined failure mechanism. The resulting equation is:

$$\frac{\left(\sigma_s-\sigma_T\right)}{c_u}-\frac{2C}{D}\frac{\sin\theta_2\sin\theta_4}{\sin\theta_1\sin\theta_3\sin\theta_5\cos\left(\theta_1+\theta_2+\theta_3+\theta_4+\theta_5\right)}-\frac{1}{\tan\theta_1}-\frac{2}{\tan\theta_2}-\frac{2}{\tan\theta_3}-\frac{2}{\tan\theta_4}-\frac{1}{\tan\theta_5}-\frac{\cos\left(\theta_1+\theta_2+\theta_3+\theta_4\right)}{\sin\theta_5\cos\left(\theta_1+\theta_2+\theta_3+\theta_4+\theta_5\right)}+\frac{\gamma D}{c_u}\left(\frac{C}{D}+\frac{1}{2}\right)-\frac{\sigma_e td}{Dc_u s}\frac{\pi\left(\cos^2\mu+1.5\sin^2\mu\left(d/b\right)^2\right)}{\sqrt{f\left(d/b,\mu\right)}}\frac{\sin\theta_2\sin\theta_4}{\sin\theta_1\sin\theta_3\sin\theta_5}\Gamma=0 \qquad (10)$$

Notice that the fist term identifies the external forces without including the micropile. This term will be referred to as the "External Stress Coefficient". The reinforcement is identified by the dimensionless parameter $\sigma_e td/Dc_u s$ which combines in a simple expression the mechanical properties of the tubular reinforcement (σ_e, t and d), the undrained soil strength (c_u) and the spacing between micropiles axis (s). This ratio will be named the "Micropile Coefficient".

The most critical collapse mechanisms will be calculated optimizing the energy conservation equation with respect to the five angles describing the geometry.

2.4 *Upper bound solution for the External Stress Coefficient*

The coefficient (σ_s-σ_T)/c_u has been isolated from Equation (10) and minimized with respect to the angles in order to find the smallest upper bound solution linked to the mechanism proposed. The upper bound solution obtained depends on $\gamma D/c_u$, on the Micropile Coefficient and on the cover ratio C/D.

The set of parameters defining the problem have been collected in Table 1. The table indicates also the range of values typically encountered in practice. Three values of the Micropile Coefficient (0, 20 and 50) have been selected to plot the minimized values of the External Stress Coefficient (with respect to the five angles) against the cover ratio C/D for different values of the strength ratio $\gamma D/c_u$ (Fig. 4). The adopted values of b, that defines the clamped length of the micropiles (Fig. 2), is five times the micropiles diameter (d).

To visualize better the effect of the micropile umbrella, the unreinforced case is plotted in Figure 4. Note that the reinforcement leads to a reduction of the required pressure applied to the tunnel face of even to make it unnecessary.

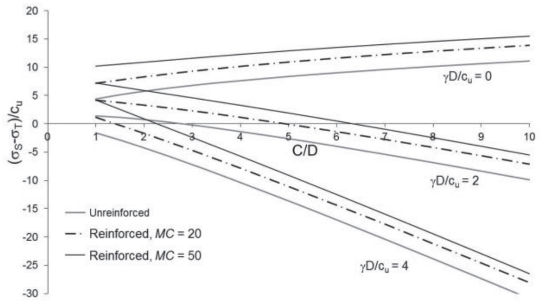

Figure 4. Upper bound solution of the External Stress Coefficient for the cases of Micropile Coefficient equal to 0 (reinforced case), 20 and 50. d/b = 0.1.

Table 1. Typical range of parameters.

Parameter	*Range of values*
Beam diameter d (m)	0.04-0.12
Beam thickness t (m)	0.0003-0.015
Distance between micropiles s (m)	0.1-1
Steel strength σ_e (MPa)	200-400
Soil undrained strength c_u	0.03-0.5
Tunnel diameter D (m)	2-12

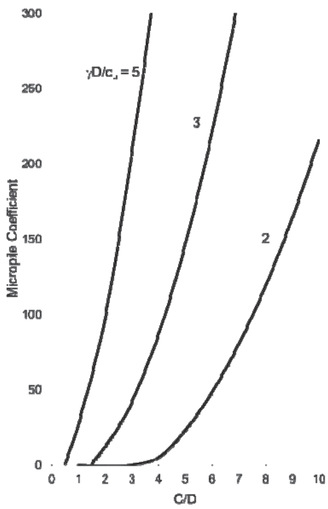

Figure 5. Upper bound solution of the Micropile Coefficient for the case of $(\sigma_s-\sigma_T)/c_u$ =0 and d/b = 0.20.

2.5 Upper bound solution of Micropile Coefficient

An upper bound solution is calculated now for the Micropile Coefficient assuming that the remaining external loads are known. The Micropile Coefficient is isolated in Equation (10). This expression provides values of the Micropile Coefficient leading to collapse. It is then interesting to find the maximum value of the Micropile Coefficient by mean of its optimization with respect of the angles and to find the critical failure mechanism.

The calculated critical value of the Micropile Coefficient has been plotted in Figure 5 in terms of C/D and $\gamma D/c_u$ and for the special case of =0. This is an interesting case in practice because it describes a conventional tunnel excavation procedure. In general, when boring machines are used micropiles reinforcement of the front is seldom used.

3 CONCLUSION

Tunnel face instability is a risk associated with open front construction methods. This paper presents an analysis of the face stability of tunnels reinforced with an umbrella of micropiles. Non-dimensional solutions based on the upper bound classical theorem of plasticity have been developed. The procedure is based on two aspects: a) defining the limiting resisting conditions of the individual micropiles and b) including the micropile forces within the formulation of the upper bound theorem. Micropiles limiting resisting forces have been calculated starting from a basic yield criterion (Von Mises) for tubular steel reinforcements. Also included in the analysis was the stabilisation of the tunnel head by a pressure applied on the tunnel face.

REFERENCES

Davis E.H., Gunn M.J, Mair R.J. and Seneviratne H.N. 1980. The stability of shallow tunnels and underground openings in cohesive material. *Géotechnique* 30, 397–416

Leca E. and Dormieux L. 1990. Upper and lower bound solutions for the face stability of shallow circular tunnels in frictional material. *Géotechnique* 40(4) , 581-606.

Lyamin A.V. and Sloan S.W. 2002a. Upper bound limit analysis using linear finite elements and nonlinear programming. *International Journal for Numerical and Analytical Methods in Geomechanics* 26(2), 181-216.

Lyamin A.V. and Sloan S.W. 2002b. Lower bound limit analysis using nonlinear programming". *International Journal for Numerical Methods in Engineering* 55(5), 573-611.

Augarde C.E., Andrei V.L. and Sloan S.W. 2003. Stability of an undrained plane strain heading revisted. *Computers and Geotechnics* 30, 419-430

Vermeer A., Ruse N. and Marcher T. 2002. Tunnel Heading Stability in Drained Ground. *Felsbau* 20 (6), 8-18

Klar A., Osman S. and Bolton M. 2007. 2D and 3D upper bound solutions for tunnel excavation using 'elastic' flow fields. *Int. J. Numer. Anal. Meth. Geomech*. 31, 1367–1374

Anagnostou G. and Kovàri K. 1996. Face Stability Conditions with Earth-Pressure-Balanced Shields. *Tunnelling and Underground Space Technology* 11(2), 165-173

Galli G., Grimaldi A. And Leonardi A. 2004. Three-dimensional modelling of tunnel excavation and lining. *Computers and Geotechnics* 31, 171–183

Peila D., Oreste P., Pelizza S. and Poma A. 1996. Study of the influence of sub-horizontal fibre-grass pipes on the stability of a tunnel face. *North American Tunneling'96*. Balkema: 425-432.

Wong H., Subrin D. and Dias D. 2000. Extrusion movements of a tunnel head reinforced by finite length bolts-a closed form solution using homogenization approach. International *Journal on Numerical and Analytical Methods in Geomechanics*, 24, 533-565

Yoo C.S. and Shin H.K. (2000) Behaviour of tunnel face pre-reinforced with sub-horizontal pipes. *Geotechnical aspects of underground construction in soft ground.* Kusakabe, Fujita and Miyazaki (eds). Balkema, 463–468

Lignola G.P., Flora A. and Manfredi G. 2008. A simple method for the design of jet grouted umbrellas in tunneling. *ASCE Journal of Geotechnical and Geoenvironmental Engineering* 134(12), 1778-1790

Melis M. J. and Medina L. E. 2005. "Discrete Numerical Model for Analysis of Earth Pressure Balance Tunnel Excavation". Journal of Geotechnical and Geoenvironmental Engineering 131(10), 1234-1242.

Numerical simulation of the process of geothermal low-potential ground energy extraction in Perm region (Russia)

Modélisation numérique du procès de la sélection géothermale d'énergie potentielle basse du sol dans les conditions de la région de Perm (Russie)

Ponomaryov A., Zakharov A.
Perm national research polytechnical university

ABSTRACT: The aim of our research is to study the interaction of energy foundations with the ground mass and to develop methods for their construction on the example of the city of Perm. Field studies of ground were carried out in a specially chosen pilot site to determine temperature distribution in the ground mass, change of ground-water level and physical-mechanical and thermal-physical characteristics of the ground mass. The diagrams of depth temperature distribution in the ground and its seasonal variations were obtained on the results of monitoring, and also the average groundwater level. To carry out numerical simulation, software-complex "GeoStudio" was selected. Its basic differential equation is the fundamental heat conduction equation with an internal heat source. The purpose of the numerical simulation was quantitative evaluation of the thermal energy extracted from different energy foundations under soil conditions in the city of Perm. By results of the spent numerical experiments the equations of regress and nomographs dependences of size of received thermal energy on geometrical parameters of the projected power bases to hydro-geological and climatic conditions of the Perm region are constructed.

RÉSUMÉ : Le but de notre recherche est l'étude de l'interaction des fondations énergétiques avec le sol et l'élaboration de leur méthode de construction sur l'exemple de la ville de Perm (Russie). Des études de la répartition des températures dans le sol, des changements du niveau de nappe aquifère, des propriétés physico-mécaniques et thermo physiques sont faites au cours de recherches in-situ sur un terrain expérimental choisi. Les résultats obtenus ont permis de déterminer des diagrammes de répartition des températures dans le sol et leurs changements saisonniers, ainsi que les changements du niveau des nappes aquifères. Pour la modélisation numérique nous avons choisi le logiciel Geostudio, dont l'équation différentielle de base est l'équation de conductivité de la chaleur avec une source de chaleur intérieure. Le but de la modélisation numérique était l'évaluation quantitative de l'énergie thermique en provenance des fondations énergétiques de différents types de sols de la ville de Perm. Selon les résultats des expériences numériques, nous avons construit des équations de régression et des nomogrammes de dépendance de la valeur de l'énergie thermique en fonction des paramètres géométriques des fondations énergétiques en conditions hydrogéologiques et climatiques de la région de Perm.

KEYWORDS: geothermal ground energy, ground thermal energy, energy foundation.

1 INTRODUCTION

One of the ways of increasing energy consumption efficiency when heating buildings is the use of renewable (alternative) energy sources. In developed countries ground thermal energy makes up a considerable proportion of energy used for heating.

Although studies of this problem have taken much time, technologies based on them are rather young. Nowadays, these technologies are widely used in many countries, such as Canada, Australia, the United States, and most European countries. Energy geothermal systems together with important environmental aspect have a great number of advantages:

- They allow reduced energy consumption for heating buildings by 50-70 %.
- The use of foundations as ground heat exchangers necessary from the structural point of view becomes possible.
- They have fewer current costs in operation.

Technologies that use geothermal energy have been used very rarely in Russia so far. Taking into account the advantages of the technology given and the state policy in the area of energy consumption we think that the problem of ground thermal energy investigation when laying foundations and building underground structures is pertinent.

The aim of our research is to study the interaction of energy foundations with the ground mass and to develop methods for their construction based on the example of the city of Perm.

2 PROBLEM STATEMENT

Heating system using ground thermal energy consists of three main parts: the system of pipelines embedded in the ground mass or in contact with the ground (primary circuit); the system of pipelines intended for heating or conditioning (secondary circuit) and a heat pump combining these pipeline systems (Grigorjev V.A. et al. 1982, Katzenbach R. et al. 2007).

The primary circuit is used to generate ground thermal energy and is located in the body of energy foundations. Piles, foundation plates, "slurry walls", diaphragms, anchors, walls of the underground floors and other constructions being in contact with ground can be used as energy foundations.

The advantage of energy foundations is that these structures (piles, foundation plates, etc.) are required for the conditions of constructional safety (that is, to ensure bearing capacity and deformability). Correspondingly, there is no need in their additional construction. Therefore, they are double-purpose structures acting as load-bearing elements and ground heat exchangers.

The secondary circuit is a closed heating system in the walls and slabs of a building.

The functions of the heat pump are to increase the temperature of the primary circuit heat carrier to the necessary one.

Ground is a multiphase system with a complex mechanism of heat transmission, which includes (Grigorjev V.A. et al.

1982): conductivity, convective transfer (convection), the processes of evaporation and condensation (latent heat transfer), heat radiation, ion exchange, freezing – thawing processes.

If the size of soil particles and pores is significantly small in relation to the total soil, the complex process of heat transfer in the ground can be reduced only to conductivity, which dominates in the case of energy foundations.

If there is an internal heat source (internal heat generation) in the concerned ground quantity, the basic equation of heat conductivity is as follows:

$$\frac{\partial t}{\partial \tau} = \alpha \Delta t + \frac{q_{\upsilon}}{\rho c} \quad (1)$$

where, α is thermal diffusivity, Δt is Laplace operator, q_{υ} is power of internal heat sources, t is temperature, τ is time, c is specific thermal capacity and ρ is density of solid medium.

Differential equations of heat conductivity show a character of the process and have many solutions. To obtain the solution of a specific task it is necessary to have initial and boundary conditions. Because of mathematical difficulties, the analytical solutions of these equations are possible only for simple cases. At present, a number of software packages that solve the problem of heat transfer in soils, including calculations of energy foundations have been developed.

3 EXPERIMENTAL INVESTIGATIONS

Field studies of ground were carried out at a specially chosen pilot site to determine temperature distribution in the ground mass, change of ground-water level and physical-mechanical and thermal-physical characteristics of the ground mass.

Engineering and geological structure of the site was defined by the results of the research done. Geologically, the experimental platform is composed of Quaternary alluvial-diluvial clay soils, at the base with pebbles up to 60-70 % of the total thickness of 11.6 m, overlapped by the thickness of filled-up ground of 6.0m thick. Bedrock is argillites, uncovered at a depth of 17.6 m.

The following physical-mechanical and thermal-physical characteristics of the experimental site ground were obtained on the results of laboratory work:

Table 1. Characteristics of the experimental site ground

№	Soil classification	Deep (m)	ρ (t/m^3)	w	e	c (kJ/ kg°C)	λ (W/ m°C)
1	Filled-up ground	0-6	1.91	0.25	0.73	1.27	1.33
2	Low plasticity loam	6-13	1.92	0.22	0.8	1.25	1.21
3	Gravel ground	13-17.6	1.69	0.007		0.85	0.41
4	Heavily weathered, cracked and waterlogged argillite	17.6	2.27	0.1	0.31	1.07	0.59

The diagrams of depth temperature distribution in the ground and its seasonal variations were obtained on the results of monitoring (Fig.1). Temperature fluctuations in the ground mass starting from the depth of 6.0 m are negligible. The maximum deviation from the mean temperature is less than 0.24°C. The temperature of the ground mass deeper than the depth of 6.0 m varies from 13° to 10° C, gradually decreasing with depth, being equal to 12°C before the depth of 12.0 m, 11°C from the depth of 10m to 16m and 10°C at the depth of more than 16m.

Positive surface temperature of the soil caused by the construction of overall housing for the recording equipment.

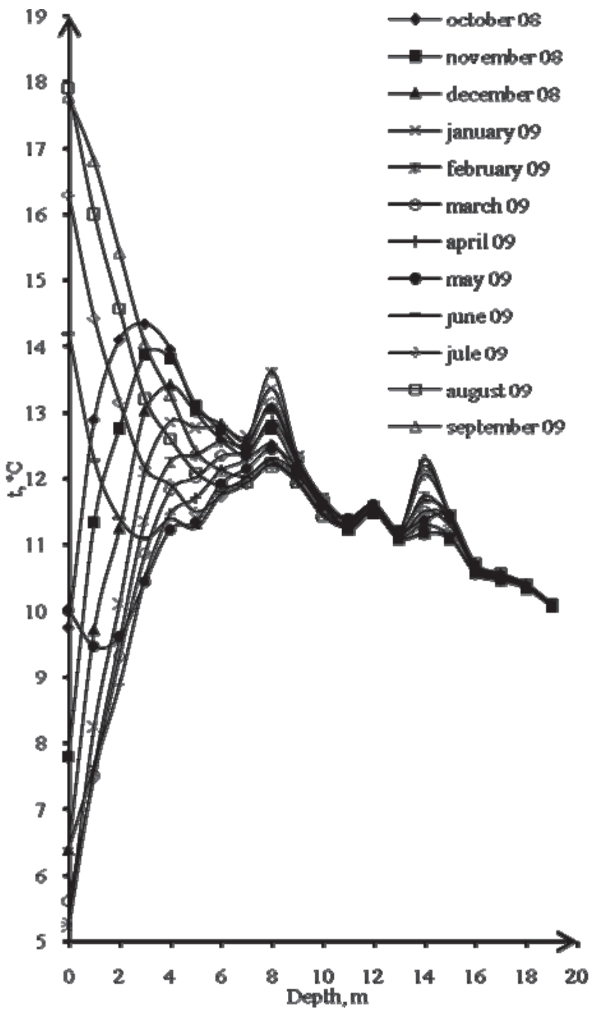

Figure 1. Diagram of depth distribution of temperature in the ground mass.

On the results of groundwater level monitoring it was established that the average groundwater level was 2.55 m. Groundwater level variations with time are negligible.

To carry out numerical simulation, software-complex GeoStudio was selected. Its basic differential equation is the fundamental heat conduction equation with an internal heat source (Grigorjev V.A. et al. 1982).

Test problems for three main types of underground structures being in contact with ground were preliminary solved:

- a pile with a diameter of 1.2m and 20m long;
- a 24m wide slab foundation, the depth of foundation is 20m;
- a slurry wall of 20m deep.

The temperature at each node in the initial period of time was taken as initial conditions. Boundary conditions were specified for the ground surface and for the lower boundary of the model. The boundary conditions of the lower boundary were taken as time-constant value of the heat flow density. The boundary conditions for the surface were set by applying climatic characteristics in the city of Perm in 2009.

Time parameters of the simulation (number of annual cycles) were taken on the condition of setting a “new” temperature regime of the ground mass taking into account the thermal energy that was extracted.

The boundary conditions for the surface of the construction situated below the soil freezing level as a time-constant temperature +1°C were additionally set. Thus, a maximal extraction of thermal energy through the surface of ground-structure contact was simulated.

To determine the minimal time parameters for the numerical simulations of various types of foundations, calculations were carried out and values of the heat flow density through the contact surface of the ground with the foundations were obtained for several calendar years. Figure 2 shows the values of the average heat flow density for the heating period.

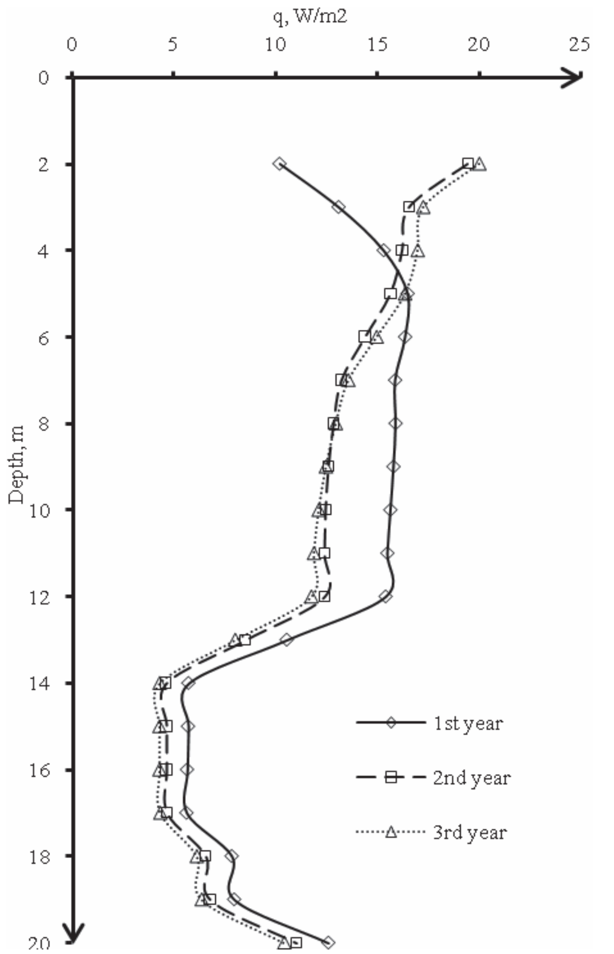

Figure 2. Diagram of average heat flow density through the contact surface of the soil with a 20 m long pile during the heating period

The minimal time parameters for the numerical simulation of different energy foundations maintenance were determined on the solution of the test problems. They are the following: 3 years for a single energy pile, 7 years for a slab foundation and 5 years for a slurry wall.

The purpose of the numerical simulation was quantitative evaluation of the thermal energy extracted from different energy foundations under soil conditions in the city of Perm. Thereto, main types of ground bases typical for the city of Perm were ascertained and numerical experiments were carried out. Based on them regression equations were obtained.

According to the studies done (Kaloshina S.V. et al. 2006), engineering-geological conditions in Perm can generally be reduced to two types. The first one is represented by low plasticity loam and gravel ground with sandy filling aggregate. The second type is medium sand, under which gravel ground with sandy filling aggregate lies. Low-compressible Upper Permian semi- rock occurs below gravel ground.

The experimental site refers to the ground base of the first type. When carrying out the numerical experiment, dependences on various factors of average heat flow density through the contact surface of the deep building parts with the ground were determined.

As two main types of ground conditions with concrete values of physical and thermal-physical characteristics of the ground were identified, their impact on energy foundations was taken into account through numerical calculations and obtaining the dependences for each type.

Therefore, geometrics parameters and underground structure depth were chosen as the main factors, namely:

- for a single pile: a pile radius (*r*) and pile tip depth (*d*);
- for a sunk slab foundation: foundation width (*b*) and foundation depth (*d*);
- for a slurry wall: foundation depth (*d*).

The following regression dependences based on numerical simulation results were obtained and nomograms were plotted. An example of a nomogram is shown in Fig. 3.

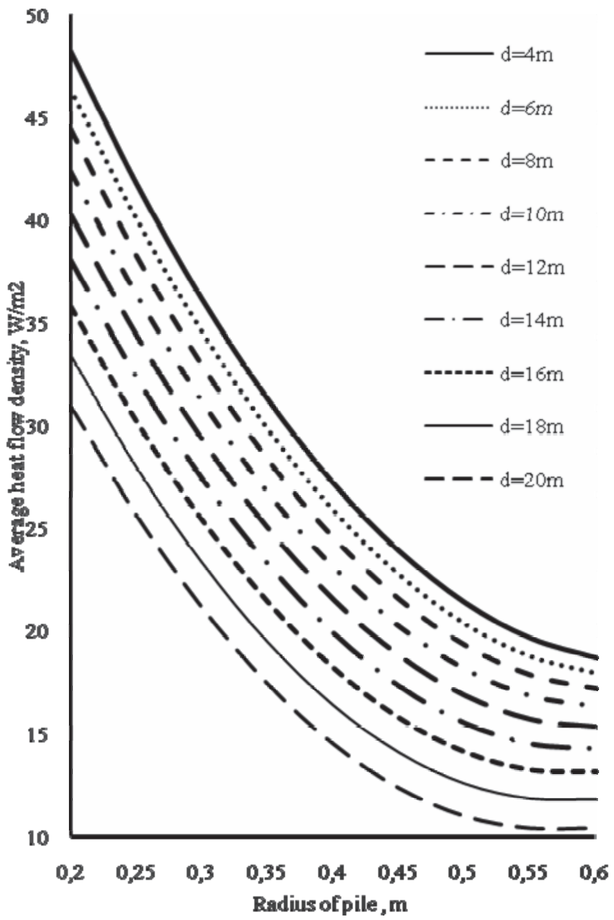

Figure 3. Nomogram of dependence of the heat flow density ($\bar{q}$) through the pile-ground contact surface on the radius (*r*) and the pile point depth (*d*). Engineering-geological conditions of the first type.

Example of distribution of temperature fields in the soil mass at work energy pile is shown in fig. 4.

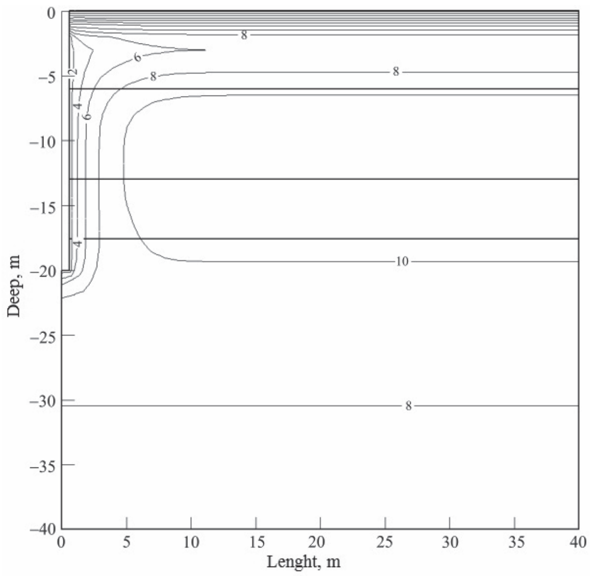

Figure 4. Distribution of temperature fields in the soil mass at work energy pile.

4 CONCLUSIONS

On the bases of the analysis of regression equations derived and nomograms plotted we can draw the following conclusions:

1. Heat flow density ($\bar{q}$) through the contact surface of an energy foundation will depend on:

- for a single pile – on its radius (r) and foundation depth (d). In this case, the heat flow density decreases with the increase of the radius and the length of the pile;

- for a sunken slab foundation – on its width (b) and foundation depth (d). In this case, the heat flow density decreases with the increase of the width and the foundation depth;

- for a slurry wall – on the foundation depth (d). In this case, the heat flow density decreases with the increase of the foundation depth.

2. The amount of heat flow density is higher for the engineering-geological conditions of the second type than for those of the first type, namely ≈ 10 % higher for a single pile and ≈ 6 % higher both for a slab foundation and a slurry wall.

5 REFERENCES

Grigorjev V.A., Emtsev B.E et al. 1982. *Heat and Mass Transfer. Heat-engineering experiment*: *Manual / edited by V.A. Grigorjev and V.M. Zorin.* Energoizdat, Moscow, 512 p.

Katzenbach R. et al. 2007. Hochleistungsenergiepfähle zur Nutzung der Geothermie im Hochhausbau. *Proceedings of the 6th Austrian Geotechical Conference*, Vienna, 18–19 January 2007, pp. 511-522.

Kaloshina S.V., Ponomaryov A.B. 2006. About engineering-geological conditions of construction in the city of Perm. *Proceed. of the International scientific and technical conference devoted to the 50th anniversary of Bashkir Scientific Research Institute for Construction*, Ufa, Vol. 2, pp. 119-124.

Determination of the thermal parameters of a clay from heating cell tests

Détermination des paramètres thermiques d'une argile à partir d'essais dans une cellule de chauffage

Romero E., Lima A., Gens A., Vaunat J.
Department of Geotechnical Engineering and Geosciences, Universitat Politècnica de Catalunya, Barcelona, Spain

Li X.L.
EURIDICE / SCK.CEN, Mol, Belgium

ABSTRACT: Boom Clay is being studied in Belgium in connection with the design of a repository for radioactive waste. Within this context, thermal impact may play an important role on the behaviour of this low-permeability clay. To evaluate this impact, heating pulse tests on intact borehole samples were carried out using an axi-symmetric and constant volume heating cell with controlled hydraulic boundary conditions. Attention is focused on the time evolution of temperature and pore water pressure changes along heating and cooling paths –i.e., pore pressure build-up during quasi-undrained heating and later dissipation to the applied hydraulic boundary conditions–. A coupled thermo-hydro-mechanical finite element program was used in a first stage to determine thermal parameters by back-analysis and then to simulate the experimental results.

RÉSUMÉ: L'argile de Boom est un matériau actuellement étudié en Belgique dans le cadre de la conception d'un centre de stockage de déchets radioactifs. Dans ce contexte, l'impact thermique est susceptible de jouer un rôle important dans la réponse de la formation argileuse, de faible perméabilité. Afin d'évaluer cet impact, des essais de chauffage par impulsion ont été réalisé sur des échantillons intacts, dans une cellule axisymétrique à volume constant qui permet de contrôler les conditions hydrauliques à sa frontière. Les mesures obtenues en termes d'évolution de température et de pression d'eau lors de cheminements de chauffage et de refroidissement indiquent le développement initial de pression de pores en conditions quasi-non drainées (cas du chauffage), suivi d'une dissipation postérieure vers un régime stationnaire équilibré avec les conditions hydrauliques appliquées. Un programme Éléments Finis couplés thermo-hydro-mécanique a été utilisé pour rétro-analyser, dans un premier temps, les paramètres de conductivité thermique et pour simuler, dans un deuxième temps, les résultats expérimentaux.

KEYWORDS: heating cell, clay, thermal conductivity, back-analysis, experimental results, numerical simulation

1 INTRODUCTION

Thermal impact may play an important role on the behaviour of low-permeability saturated clayey host formations in connection with the design of a repository for 'High-Level Radioactive Waste'. Boom Clay is currently the subject of extensive research on hydrothermal and mechanical phenomena that may possibly affect its performance as potential geological host formation.

There are a number of laboratory results concerning the saturated hydro-mechanical behaviour of Boom Clay under a constant temperature field and studies on this area are described -to cite but a few of them- in De Bruyn (1999), Le (2008) and Lima (2011). Nevertheless, there is less information on clay hydro-mechanical response on heating and cooling paths under controlled small-scale laboratory condition. To this end, the paper presents results from a comprehensive testing program performed on Boom Clay to determine thermal and hydraulic parameters using an axi-symmetric heating cell with measurement of temperature and pore pressure. Pore-pressure built-up and dissipation on fast heating pulse tests have been analysed using experimental results assisted by numerical simulations carried out with a coupled thermo-hydro-mechanical finite element code.

2 EXPERIMENTAL SETUP AND TESTED MATERIAL

Laboratory tests have been performed on Boom Clay (Mol, Belgium). Table 1 summarises the main properties of this Tertiary clay (20%-30% kaolinite, 20%-30% illite and 10%-20% smectite), which is slightly overconsolidated (Horseman *et al*. 1987, Coll 2005, Lima 2011).

Table 1. Main properties of Boom Clay.

Property	Value
Density, ρ	2.05 Mg/m^3
Dry density, ρ_d	1.65 to 1.67 Mg/m^3
Gravimetric water content, w	25 %
Density of soil solids, ρ_s	2.67 Mg/m^3
Void ratio, e	0.60 to 0.62
Degree of saturation, S_r	100 %
Liquid limit, w_L	56
Plastic limit, w_P	29
Vertical water permeability at 20ºC, k_{wv}	2.3×10^{-12} m/s
Vertical water permeability at 80ºC, k_{wv}	6.5×10^{-12} m/s
Horiz. water permeability at 20ºC, k_{wv}	4.5×10^{-12} m/s
Small-strain shear modulus, G_0	347 MPa
Poisson's ratio, ν	0.20

Figure 1 shows a scheme of a constant volume and axi-symmetric heating cell (Muñoz *et al*. 2009, Lima *et al*. 2010, Lima 2011), which has been used to perform heating pulse tests with controlled power supply and controlled hydraulic boundary conditions. Soil sample size is 75 mm in diameter and 100 mm high. A controlled-power heater (H in the figure) is installed along the axis of the sample in the lower part of the cell. Different transducers monitor the sample response, as shown in the figure: two miniature pore water pressure transducers (Pw_1 and Pw_2), and three thermocouples (T_1, T_2 and T_3). The cell is equipped with top and bottom valves to apply controlled hydraulic boundary conditions (u_u and u_b). The heater with controlled power supply remains switched on for 24 hours during the heating stage and later it is switched off to perform the cooling phase.

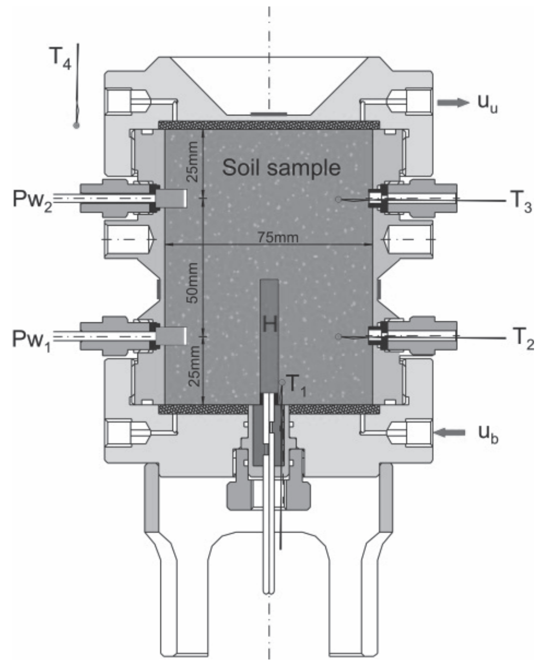

Figure 1. Axi-symmetric heating cell and transducers (Muñoz *et al*. 2009, Lima *et al*. 2010, Lima 2011).

3 EXPERIMENTAL RESULTS

Attention has been focused on the time evolution of temperature and pore water pressure changes during heating and cooling paths –i.e., pore pressure build-up during quasi-undrained heating and later dissipation to the applied hydraulic boundary conditions–. Throughout the course of the heating/cooling paths, the bottom drainage is maintained open at constant water backpressure (1 MPa) using an automatic pressure / volume controller, while the upper valve is kept closed. This backpressure is important since it allows measuring the pore pressure drop during the cooling phase without reaching the negative range (below atmospheric conditions). The initial and external temperatures are regulated by submerging the cell inside a temperature controlled water bath at temperature T_4 (Figure 1). Figure 2a shows the time evolution of temperature for different locations and along a heating and cooling cycle up to a maximum heater temperature of 54ºC. Figure 2b presents the corresponding time evolution of pore water pressures at different locations. During heating, pore water pressure increased due to the larger thermal expansion coefficient of water. The magnitude of the water pressure change depends on the rate of temperature increase / decrease, on soil compressibility and thermal-expansion coefficient, on water permeability and porosity, as well as on the hydraulic boundary condition applied. After the heating path, pore water pressure dissipates at constant temperature towards the hydraulic value applied at the boundary. Pore water pressure Pw_2 dissipates more slowly due to the larger distance to the draining boundary. An opposite pore pressure evolution is observed on cooling: an initial pore pressure drop followed by pressure recovery to the applied boundary condition (again, Pw_2 recovers more slowly).

Figure 3 shows a zoom of the early stage evolution of pore water pressure P_{w1} and temperature T_2 changes during another heating phase. These sensors are located close to the draining boundary (Figure 1). It can be observed that pressure changes develop at a faster rate compared to temperature changes. In fact, pore pressure starts to dissipate towards the applied hydraulic boundary condition well before the temperature reaches its maximum value.

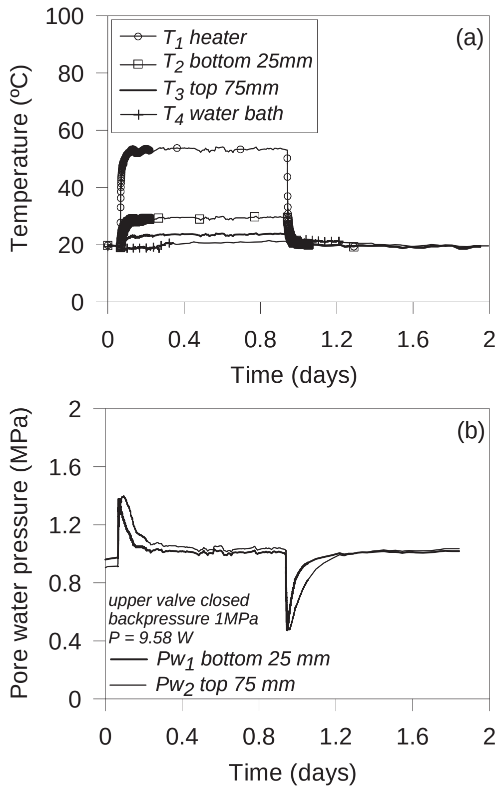

Figure 2. Temperature and pore water pressure evolutions during heating and cooling paths (Lima *et al*. 2010, Lima 2011).

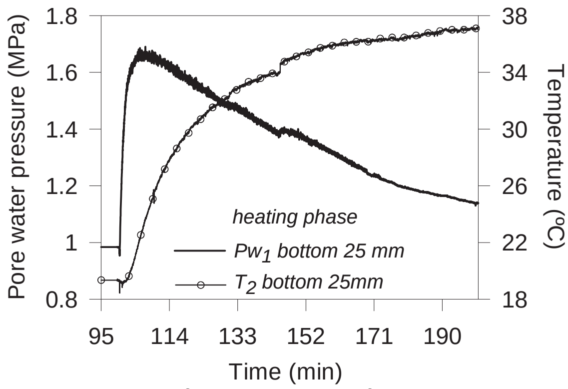

Figure 3. Zoom of time evolution of temperature and pore water pressure during heating (Lima *et al*. 2010, Lima 2011).

4 INTERPRETATION OF RESULTS

In the interpretation of the test results, it was assumed that temperatures and heat flux were not influenced by water pressure and flow, which means that heat convection was assumed to be negligible. The driving process for temperature change during the test is thus conduction only. This assumption is justified by the condition of constant overall volume prevailing in the heating cell that makes the change in porosity and the velocities of the solid phase very small. Moreover, the low permeability of the material prevents the existence of high velocities for the liquid phase. The flux of heat convected by the solid and liquid phases is, therefore, extremely low. In contrast, water pressure and flow were assumed to be influenced by temperature: as a consequence, while the thermal problem was decoupled from the hydraulic one, the hydraulic problem was coupled to the thermal one.

The test was then interpreted in two separated stages. First, a back-analysis of temperature measurements was carried out by performing uncoupled thermal simulations using the finite element program CODE_BRIGHT (Olivella *et al*. 1996); only the balance equation for energy was solved. Heat exchanged by the highly conductive stainless steel cell with the controlled water bath was accounted for as a convection-type boundary condition of the problem. This heat flux was assumed to be proportional to the difference between the temperature of the cell and the temperature of the water bath at each boundary node, through a convection coefficient h. Thermal optimisation was then aimed at identifying the values of the saturated thermal conductivity λ and the convection coefficient h. Calculations were performed for different combinations of λ and h. For each of them, a measure of the least squares difference between temperature simulation results and temperature experimental measurements ε was computed for different elapsed times. The three-dimensional plot in Figure 4 shows the least squares differences ε between simulation results and experimental observations. The best agreement was obtained for parameters λ=1.6 Wm^{-1}K^{-1} and h=24 Wm^{-2}K^{-1}.

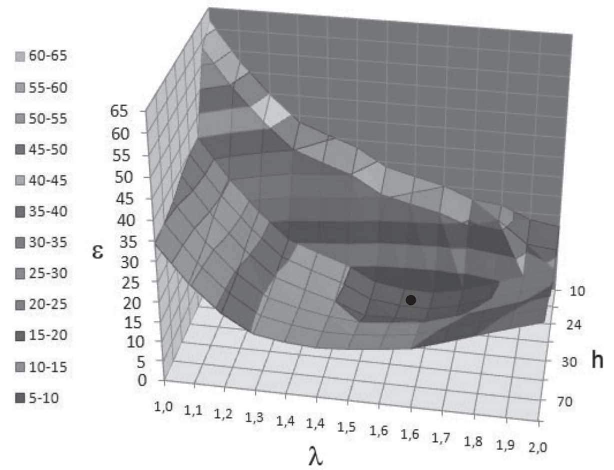

Figure 4. Three-dimensional graph showing the differences in temperature between observations and calculations in the back-analysis of the heating pulse test. Determination of thermal conductivity λ and convection coefficient h (Lima 2011).

Back-analysed thermal parameters were used to study the coupled thermal and hydraulic results. Water permeability and elastic soil parameters used in the simulations, which are reported in Table 1, were obtained from independent tests. Controlled-gradient tests at different temperatures and constant volume conditions for water permeability, as well as small-strain shear moduli with resonant column and bender element tests, have been reported by Lima (2011). Figure 5 displays the time evolution of temperature and pore water pressure (experimental and simulated results) during the same heating and cooling paths presented in Figure 2. A good agreement is observed in the pore water pressure response, which shows the consistency between the back-calculated and directly measured parameters from independent laboratory tests.

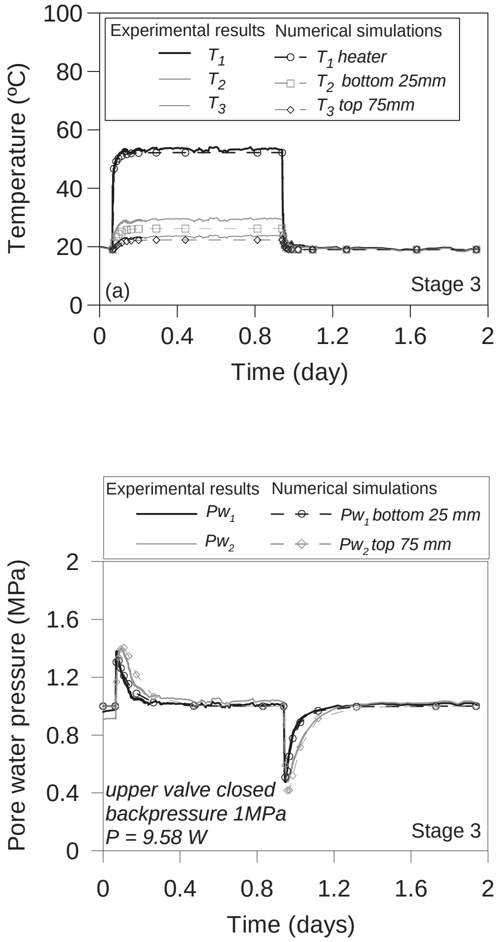

Figure 5. Time evolution of temperature and pore water pressure: experimental and simulated results (Lima 2011).

5 CONCLUSIONS

A series of heating and cooling paths were performed on Boom Clay –a reference host formation for potential geological disposal of 'High-Level Radioactive Waste' in Belgium– to study the impact and consequences of thermal loads on this low-permeability clay formation. Tests were performed in a fully-instrumented heating cell –with several thermocouples and pressure transducers– under constant volume and controlled hydraulic boundary condition: constant water pressure at the bottom drainage and top end with no flow condition. Selected results of a comprehensive experimental programme on intact borehole samples have been presented and discussed in terms of the joint measurements of temperature and pressure changes during the application of heating-cooling cycles.

Thermal and hydraulic results were calibrated and simulated using coupled thermo-hydro-mechanical analyses performed with a finite element code (CODE_BRIGHT). In particular, the thermal conductivity of the clay was determined by back-analysis of the thermal response. The coupled thermal and hydraulic results were also successfully simulated using parameters that had been back-calculated from previous heating pulse tests and also directly from independent laboratory tests. An overall examination of the results obtained allows the identification of the main features of the hydro-thermal coupling under the test conditions.

6 ACKNOWLEDGEMENTS

The authors acknowledge the financial support provided by EIG-EURIDICE / SCK.CEN (Belgium) through a PhD collaboration with International Centre for Numerical Methods in Engineering (Spain).

7 REFERENCES

Coll C. 2005. *Endommagement des roches argileuses et perméabilité induite au voisinage d'ouvrages souterrains*. PhD Thesis, Université Joseph Fourier, Grenoble, France.

De Bruyn D. 1999. *Influence of a temperature increase on the physical and mechanical behaviour of the Boom Clay in the framework of the HLW geological disposal*. PhD Thesis, UCL, Louvain-La-Neuve, Belgium.

Le T.T. 2008. *Comportement thermo-hydro-mécanique de l'argile de Boom*. PhD Thesis, CERMES, Ecole Nationale des Ponts et Chaussées, Paris, France.

Lima A., Romero E., Gens A., Muñoz J. and Li X.L. 2010. Heating pulse tests under constant volume on Boom clay. *Journal of Rock Mechanics and Geotechnical Engineering* 2 (2), 124–128.

Lima A. 2011. *Thermo-hydro-mechanical behaviour of two deep Belgian clay formations: Boom and Ypresian clays*. PhD Thesis. Universitat Politècnica de Catalunya, Spain.

Muñoz J.J., Alonso E.E., Lloret A. 2009. Thermo-hydraulic characterization of soft rock by means of heating pulse tests. *Géotechnique* 59(4), 293–306.

Olivella S., Gens A., Carrera J., Alonso E.E. 1996. Numerical formulation for a simulator (CODE_BRIGHT) for the coupled analysis of saline media. *Int. Journal Engineering Computations* 13 (7), 87-112.

Analyse de la portance des pieux géothermiques

Discussions about the bearing capacity of geothermal piles

Suryatriyastuti M., Mroueh H.
LGCgE, Villeneuve d'Ascq, France

Burlon S.
IFSTTAR, Paris, France

Habert J.
CETE Nord Picardie, Haubourdin, France

RÉSUMÉ : Les pieux géothermiques en plus d'être utilisés classiquement comme des éléments supportant des bâtiments permettent grâce à la circulation d'un fluide caloporteur de les chauffer ou les climatiser suivant la saison. Les pieux, sous l'effet des variations de température, subissent des chargements cycliques. Afin d'analyser ce problème et d'évaluer son impact sur le comportement des pieux géothermiques, deux types d'approches sont proposées : la première repose sur une modélisation conventionnelle de l'interaction sol-pieu, la seconde prend en compte les effets cycliques induits par les variations de température.

ABSTRACT: Geothermal piles are deep foundations providing not only structural support for the buildings but also heat exchanger elements from the ground to the buildings. Heat exchanges occur by the circulation of seasonal heat carrier medium, depending on the needs of heating or cooling the buildings. The pile foundations are then subjected to cyclic contraction and dilatation loading under the variation of temperature. To analyse this phenomenon and its impact to the structure stability, two types of studies are conducted, one by implementing a conventional method and an other by taking into account cyclic effects induced by temperature variations.

MOTS-CLES : pieu géothermique, capacité portante, effets cycliques, chargement axial, interface sol-pieu.

KEYWORDS: geothermal pile, bearing capacity, cyclic effects, axial loading, interface soil-pile.

1 INTRODUCTION

Les pieux géothermiques (pieux échangeurs de chaleur) présentent un intérêt particulier pour le chauffage et la climatisation des bâtiments afin de remplir les exigences fixées par les nouvelles réglementations thermiques. Dès lors que le sol présente en surface, entre 10 m et 50 m de profondeur, une température constante comprise entre 10°C et 15°C, ce qui est le cas dans la majorité des pays européens dont la France (Adam et Markiewicz 2009), l'efficacité des échanges thermiques est garantie. Ces pieux géothermiques sont constitués en général de béton armé et de tubes échangeurs de chaleur en U accrochés à la caisse de ferraillage. Le fluide caloporteur circulant dans le tube en U autorise des échanges thermiques entre le sol et la pompe à chaleur à laquelle le tube est lié, ce qui permet de chauffer ou climatiser le bâtiment. Sous l'effet des variations de température, les pieux géothermiques sont soumis à des variations répétitives de longueur qui peuvent s'assimiler à des chargements cycliques. En hiver, le fluide caloporteur injecté est plutôt froid (0 à 5°C) tandis qu'il est plutôt chaud en été (30 à 40°C).

Les connaissances acquises, à l'heure actuelle, dans le domaine des pieux échangeurs de chaleur concernent essentiellement le comportement thermomécanique des sols. Il apparaît que les propriétés mécaniques des sols en termes de déformation et de résistance ne sont pas affectées par les variations de température dans les gammes d'exploitation habituelle des pompes à chaleur 0°C – 40 °C (Böennec 2009, Cekerevac et Laloui 2004). Seule la pression de préconsolidation semble présenter des variations sensibles vis-à-vis de l'augmentation de la température.

En Europe, cette technologie s'est surtout développée en Autriche, en Suisse et en Allemagne (tunnel de Vienne, aéroport de Zürich, tour de Francfort, etc.). Toutefois, peu d'éléments méthodologiques existent ce qui conduit bien souvent à considérer des coefficients de sécurité plus importants que ceux utilisés pour les pieux classiques (Knellwolf *et al.* 2011, Bourne-Webb *et al.* 2009). Afin d'apporter des éléments complémentaires à l'analyse de la portance des pieux géothermiques, cet article propose des éléments méthodologiques fondés d'une part sur la mise en œuvre d'outils conventionnels de calcul et d'autre part sur l'utilisation d'outils numériques plus complexes dans le cas où les effets cycliques seraient significatifs pour la structure portée.

2 MODÉLISATION CONVENTIONNELLE

2.1 Principes de modélisation

Cette approche, utilisée couramment pour le dimensionnement des pieux sous charge axiale, est fondée sur la modélisation de l'interaction sol-pieu par des lois locales de mobilisation de la résistance du sol (loi *t-z*) (Frank et Zhao 1982). Le principe du calcul repose sur la décomposition de la déformation totale ε en une partie élastique ε^e et l'autre thermique ε^{th} selon l'équation (1). L'équation (2) présente l'équilibre mécanique du pieu :

$$\varepsilon = \varepsilon^e + \varepsilon^{th} \tag{1}$$

$$E_s S \frac{d^2 w}{dz^2} + f_{sol-pieu}(z, w) = 0 \tag{2}$$

où E_s est le module de Young du matériau constituant le pieu, S la section du pieu, w le déplacement vertical du pieu, $f_{sol-pieu}$ la loi de mobilisation du frottement axial ou de l'effort de pointe et z la profondeur.

2.2 Phasage de chargement et conditions en tête de pieu

Le chargement est réalisé systématiquement en deux phases : (i) une première phase de chargement « mécanique » et (ii) une deuxième phase de chargement thermique. Lors de la deuxième phase de chargement, une évolution homogène de la température est imposée à l'ensemble du pieu. L'observation des températures mesurées dans des pieux géothermiques instrumentés justifie cette approche (Bourne-Webb *et al.* 2009). Cette variation est intégrée dans le calcul en retenant une valeur du coefficient de dilatation thermique du béton α_T égale à $1{,}2\text{x}10^{-5}$ °C^{-1} et en imposant une déformation axiale. Seul le premier chargement thermique est considéré si bien que les éventuels effets cycliques ne peuvent pas être pris en compte. Le sol situé autour du pieu est supposé ne pas être soumis à des variations volumiques d'origine thermique, ce qui est valable quand l'écoulement de la nappe est suffisant (supérieur à 10 cm/jour) pour maintenir la température du sol constante (Fromentin *et al.* 1999).

Trois types de conditions en tête de pieu sont possibles : (i) pieu libre en tête (l'effort en tête de pieu n'est pas modifié lors de l'application du chargement thermique), (ii) pieu bloqué en tête (le déplacement en tête de pieu n'est pas modifié lors de l'application du chargement thermique) et (iii) prise en compte d'une rigidité en tête de pieu modélisant les conditions de liaison de ce dernier avec la structure portée.

2.3 Résultats obtenus

La méthode de calcul permet d'obtenir l'évolution des contraintes normales σ_n, des déplacements verticaux w et de la mobilisation du frottement axial q_s avec la profondeur. Les figures 1 et 2 présentent les « résultats-types » obtenus pour un pieu respectivement libre et bloqué en tête : par rapport à la situation où le pieu est simplement chargé mécaniquement, la déformation appliquée en hiver correspond à une diminution de la température de 12°C et celle appliquée en été à une augmentation de 20°C.

Ces comportements extrêmes permettent d'appréhender le comportement réel d'un pieu géothermique pour lequel la rigidité en tête est intermédiaire. Pour un pieu libre en tête, le refroidissement de ce dernier induit un tassement supplémentaire ainsi qu'une diminution de la contrainte normale dans les sections du pieu, voire dans certains cas, l'apparition de traction. Le réchauffement de la fondation conduit à un soulèvement de la tête de pieu accompagné d'une augmentation de la contrainte normale dans les sections du pieu. Dans tous les cas, les variations de température sont associées à des modifications de la répartition du frottement axial. Pour un pieu bloqué en tête, les résultats peuvent être interprétés de manière similaire.

2.4 Abaque de représentation du comportement global d'un pieu géothermique

Cet abaque (Figure 3) permet d'appréhender simplement les variations de déplacement vertical Δw_t et d'effort normal ΔNt en tête de pieu lors de l'application du chargement thermique, pour différentes gammes de température et de rigidité de la structure portée (Habert et Burlon 2012).

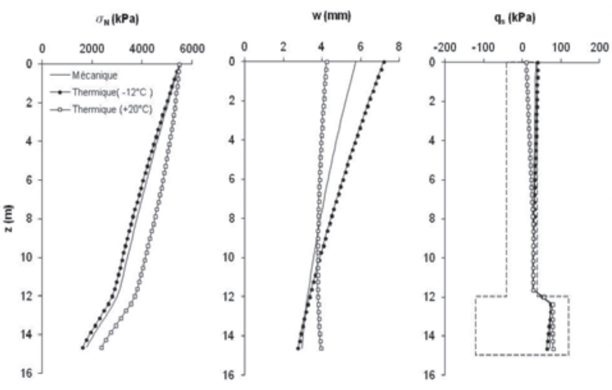

Figure 1. Comportement d'un pieu « libre en tête »

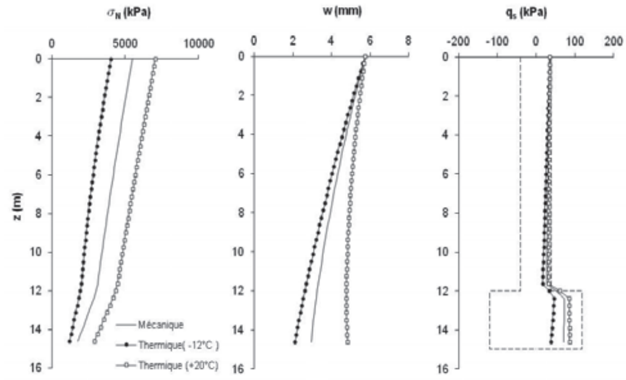

Figure 2. Comportement d'un « pieu bloqué en tête »

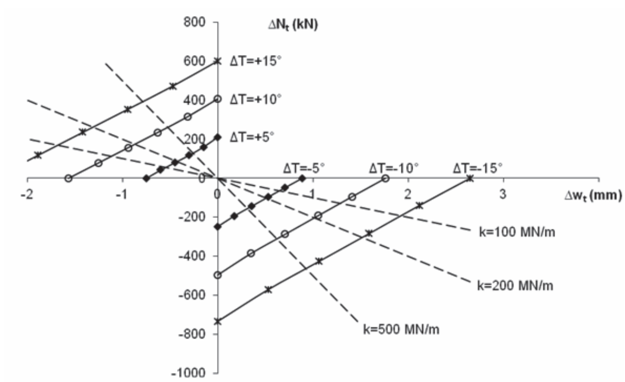

Figure 3. Abaque global de fonctionnement d'un pieu géothermique

3 PRISE EN COMPTE DES EFFETS CYCLIQUES

3.1 Introduction

La répétition des dilatations et des contractions du pieu sous l'effet des variations de température conduit à modifier plus ou moins significativement la répartition du frottement axial et de la contrainte à la base du pieu. Ces cycles sont alors susceptibles de provoquer des dégradations du sol et de l'interface sol-pieu et diverses stratégies de calcul peuvent être alors envisagées.

3.1.1 Modèle unidimensionnel : loi t-z cyclique

La loi *t-z* cyclique proposée est une loi d'interaction locale fondée sur les mêmes principes que la loi de Frank et Zhao (Frank et Zhao 1982, Suryatriyastuti *et al.* 2012). Elle permet de décrire de manière exhaustive chaque cycle de charge et de décharge. Elle est définie par l'équation (3) où n désigne le nombre de cycle de chargement, q_{si} [kPa] désigne le frottement mobilisé à l'inversion de charge (q_{si}=0 pour n=1), u_{ti} [m] et u_{ts} [m] désignent respectivement le déplacement de l'interface sol-pieu au cycle précédent (u_{ti}=0 pour n=1) et la somme des valeurs absolues des déplacements ($u_{ts} = \sum |u_{ti}|$). q_{sULT} [kPa] est le frottement maximal axial mobilisable lors du premier cycle, Δq_s [kPa] et ε [m] sont respectivement la variation positive ou négative du frottement maximal mobilisable et la vitesse de cette variation, et α [m] quantifie la rigidité de l'interface.

Les paramètres A et R (équations 4 et 5) permettent, à chaque inversion de chargement, respectivement, de limiter la valeur de frottement q_s et de quantifier l'éventuelle augmentation de rigidité de l'interface au cours des cycles (le paramètre ρ définit cette augmentation et le paramètre ξ indique la vitesse de cette augmentation). La formulation de la loi *t-z* cyclique permet de rendre compte des principaux phénomènes caractéristiques des effets cycliques (Lemaitre et Chaboche 2009) : relaxation et rochet.

$$q_s = q_{si} + A(-1)^{n+1}\left(q_{s0} + \Delta q_s\left(1 - e^{-\frac{u_{ts}}{\varepsilon}}\right)\right)\left(1 - e^{-R\left|\frac{u_t - u_{ti}}{\alpha}\right|}\right) \tag{3}$$

$$A = \left|\frac{q_{si} - (-1)^{n+1}\left(q_{s0} + \Delta q_s\left(1 - e^{-\frac{u_{ts}}{\varepsilon}}\right)\right)}{q_{s0} + \Delta q_s\left(1 - e^{-\frac{u_{ts}}{\varepsilon}}\right)}\right| \tag{4}$$

$$R = e^{-(n-1)\xi} + \rho\left(1 - e^{-(n-1)\xi}\right) \tag{5}$$

3.1.2 Modèle Tridimensionnel : Modèle d'interface Modjoin

La loi de comportement Modjoin (Shahrour et Rezaie 1997) est formulée dans le cadre de l'élastoplasticité avec deux systèmes d'écrouissage : l'un isotrope et l'autre cinématique non linéaire. La partie élastique est définie par deux paramètres k_n et k_t reliant d'une part la contrainte normale σ_n au déplacement relatif normal u_n et d'autre part la contrainte tangentielle τ au déplacement relatif tangentiel u_t. La surface limite f_l ainsi que la variable d'écrouissage isotrope associée sont définis par les équations (6) et (7) à partir de φ, *DR* et *ADR*. La surface de charge cinématique f_c ainsi que la variable d'écrouissage associée sont caractérisées par les équations (8) et (9) à partir des paramètres γ_c et β_c ainsi que du multiplicateur plastique λ. Enfin, la règle d'écoulement est présentée par les équations (10) et (11) à partir des paramètres ψ_c et a_c. La formulation de la loi Modjoin permet de rendre compte des principaux phénomènes cycliques (relaxation et rochet).

$$f_l = |\tau| + \sigma_n R_{\max} \tag{6}$$

$$R_{\max} = \tan\varphi + DR\left(1 - e^{ADR\, u_{tr}^p}\right) \tag{7}$$

$$f_c = |\tau - \sigma_n R_c| \tag{8}$$

$$dR_c = \lambda\left(\gamma_c |R_{\max} - R_c|^{\beta_c}\right) \tag{9}$$

$$\frac{\partial g}{\partial \sigma_n} = \left(\tan\psi_c - \left|\frac{\tau - \sigma_n R_c}{\sigma_n}\right|\right) e^{-a_c u_{tc}^p} \tag{10}$$

$$\frac{\partial g}{\partial \tau} = \frac{\tau}{|\tau|} \tag{11}$$

3.2 Application à l'étude d'un pieu géothermique

3.2.1 Présentation de l'exemple

L'exemple choisi concerne un pieu présentant une longueur *D* égal à 15 m et un diamètre *B* égal à 0.6 m. Les propriétés des terrains, des matériaux et de l'interface sol-pieu sont présentées dans le tableau 1. Le pieu est soumis à 20 cycles de chargement thermique d'une amplitude correspondant à une variation de température de 20°C (les cycles thermiques débutent par un refroidissement). La charge mécanique appliquée au pieu correspond au tiers de sa résistance limite définie conventionnellement par un enfoncement de la tête du pieu égal à *B*/10. Les calculs sont réalisés pour deux configurations : pieu libre en tête et pieu bloqué en tête.

Tableau 1. Propriétés des matériaux, des terrains et des interfaces (Hillel 2012)

Propriétés		*Sol*	*Béton*	*Interface*
Densité [kN/m^3]	ρ	1950	2500	
Module d'incompressibilité [MPa]	K	10	20000	
Rigidité normale [MN/m]	k_n			22
Module de cisaillement [MPa]	G	3.75	7500	
Rigidité tangentielle [MN/m]	k_t			8.33
Conductivité thermique [W/m^2]	λ_T	1.5	1.8	
Chaleur massique [J/kg °C]	C	800	880	
Coefficient de dilatation thermique [10^{-5} J/°C]	α_T	0.5	1.25	
Cohésion [kPa]	c			1
Angle de frottement [°]	φ			30

3.2.2 Résultats

Dans le cas du pieu libre en tête, les résultats obtenus montrent, pour les deux modèles, des variations similaires de déplacements en tête de pieu (Figure 4). Celle-ci a tendance à s'enfoncer au cours des cycles thermiques, avec toutefois, durant les cycles de réchauffement, un soulèvement qui correspond à une dilatation du pieu. Le rapport entre le déplacement induit seulement par les variations de température et par la dégradation de l'interface et le tassement initial du pieu atteint sur cet exemple 20%. Cet enfoncement résulte du choix des paramètres effectués pour les deux modèles et s'accompagne pour chaque section du pieu d'une diminution des frottements latéraux ainsi que d'une augmentation des déplacements tangentiels (Figure 5a et 5b). Les paramètres choisis rendent compte d'un phénomène de rochet pour le comportement de l'interface sol-pieu. La dégradation des propriétés du sol se traduit par une augmentation de l'effort normal dans le pieu pour les deux modèles (Figures 6a et 6b). Cette augmentation est toutefois faible puisqu'elle reste inférieure à 20%.

Dans le cas du pieu bloqué en tête, pour les deux modèles, les résultats obtenus montrent une diminution de l'effort normal en tête du pieu au cours des cycles thermiques (Figure 7). Cette diminution traduit un phénomène de relaxation qui est rendu possible par le choix des paramètres des modèles. Ce phénomène peut aussi être mis en évidence au niveau du comportement local de l'interface sol-pieu, particulièrement avec le modèle *t-z*. Le frottement latéral se dégrade sans enfoncement ni soulèvement notable du pieu (Figure 8a et 8b). Avec le modèle Modjoin, pour les deux sections de pieu considérées, une diminution du frottement latéral ainsi qu'un léger enfoncement sont constatés. La diminution de l'effort normal dans le pieu au cours des cycles de refroidissement est beaucoup plus importante qu'au cours des cycles de réchauffement (Figure 9a et 9b). Pour le modèle *t-z*, sur toute la hauteur du pieu, les efforts normaux diminuent uniformément dans le pieu. Pour le modèle Modjoin, les efforts normaux diminuent avec la profondeur hormis au niveau de la pointe du pieu. Pour ce modèle, la présence du sol autour du pieu autorise sans doute une répartition des forces qui limite la diminution de l'effort normal.

4 CONCLUSION

Les fondations profondes énergétiques supportent les charges transmises par les structures qu'elles portent et sont utilisées en même temps comme échangeurs thermiques. Elles présentent un fonctionnement particulier régi par les contractions et les dilatations qu'elles subissent. Les méthodes de calcul proposées permettent de prévoir l'évolution des déplacements en tête de pieu, de la contrainte normale et de la mobilisation de la résistance du sol en incluant le cas échéant des effets cycliques. L'instrumentation prochaine de pieux géothermiques permettra de valider ces modèles de calcul. Dans l'immédiat, les outils proposés permettent dès maintenant de justifier des pieux géothermiques selon les règles et les normes actuelles.

5 RÉMERCIEMENTS

Ces travaux sont réalisés dans le cadre du projet ANR « GECKO ». Les auteurs remercient vivement les différents partenaires du projet (ECOME, BRGM, IFSTTAR, CETE Nord Picardie, LGCgE, LAGEO, et EPFL) pour leur soutien.

6 REFERENCES

Adam D. et Markiewicz R. 2009. Energy from earth-coupled structures, foundations, tunnels and sewers. *Géotechnique* 59 (3), 229-236.

Boënnec O. 2009. Piling on the energy. *Geodrilling International* 150, 25-28.

Bourne-Webb P., Amatya B., Soga K., Amis T., Davidson C., et Payne P. 2009. Energy pile test at Lambeth College, London: Geotechnical and thermodynamic aspects of pile response to heat cycles. *Géotechnique* 59 (3), 237-248.

Cekerevac C. et Laloui L. 2004. Experimental study of thermal effects on the mechanical behaviour of a clay. *International Journal for Numerical and Analytical Methods in Geomechanics* 28, 209-228.

Frank R. et Zhao S. 1982. Estimation par les paramètres pressiométriques de l'enfoncement sous charge axiale de pieux forés dans des sols fins. *Bulletin Liaison Laboratoire Ponts Chaussées* 119, 17-24.

Fromentin A., Pahud D., Laloui L., et Moreni M. 1999. Pieux échangeurs : conception et règles de pré-dimensionnement. *Revue française de génie civil* 3(6), 387-421.

Knellwolf C., Peron H., et Laloui L. 2011. Geotechnical analysis of heat exchanger piles. *Journal of Geotechnical and Geoenvironmental Engineering* 37 (10), 890-902.

Lemaitre J. et Chaboche J.L. 2009. *Mécanique des Matériaux Solides*. Dunod, Paris.

Habert J. et Burlon S. 2012. Éléments sur le comportement mécanique des fondations géothermiques. *ACTES de Journées Nationales de Géotechnique et de Géologie de l'Ingénieur* (2), 617-624.

Hillel D. 2004. *Introduction to environmental soil physics*. Elsevier Science, USA.

Shahrour I. et Rezaie F. 1997. An elastoplastic constitutive relation for the soil-structure interface under cyclic loading. *Computers and Geotechnics* 21 (1), 21-39.

Suryatriyastuti M., Mroueh H., et Burlon S. 2012. Modélisation numérique du comportement thermomécanique d'un pieu échangeur de chaleur. *ACTES de Journées Nationales de Géotechnique et de Géologie de l'Ingénieur* (2), 593-600.

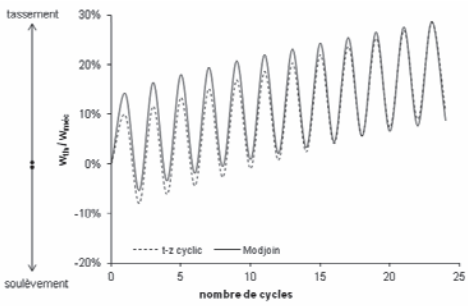

Figure 4. Pieu libre en tête – Variation relative du déplacement en tête du pieu

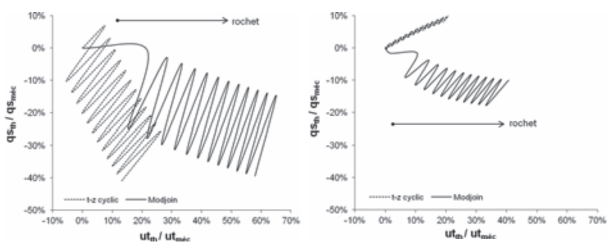

(a) (b)

Figure 5. Pieu libre en tête – Variation relative de la réponse de l'interface sol-pieu – (a) en profondeur ¼ L – (b) en profondeur ¾ L

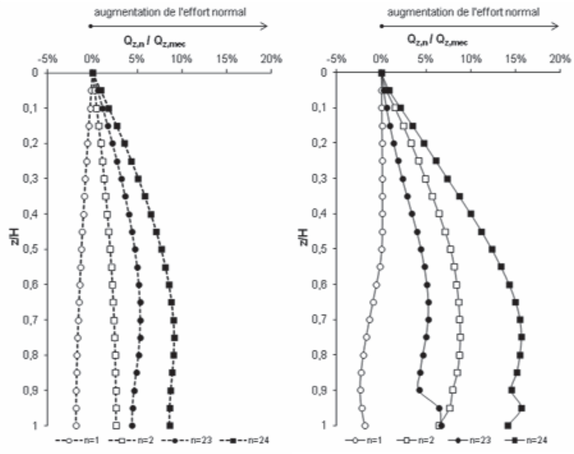

(a) (b)

Figure 6. Pieu libre en tête – Variations relatives des efforts induits par les variations de température dans le pieu – (a) Loi *t-z* – (b) Loi Modjoin

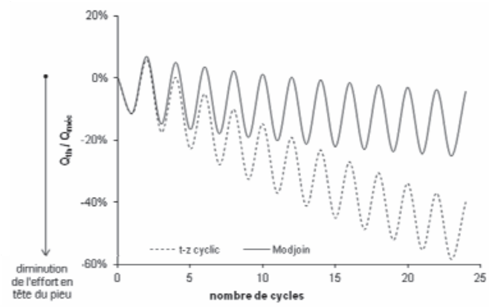

Figure 7. Pieu bloqué en tête – Variation relative de l'effort en tête du pieu

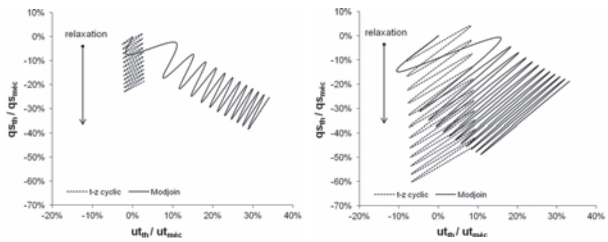

(a) (b)

Figure 8. Pieu bloqué en tête – Variation relative de la réponse de l'interface sol-pieu – (a) en profondeur ¼ L – (b) en profondeur ¾ L

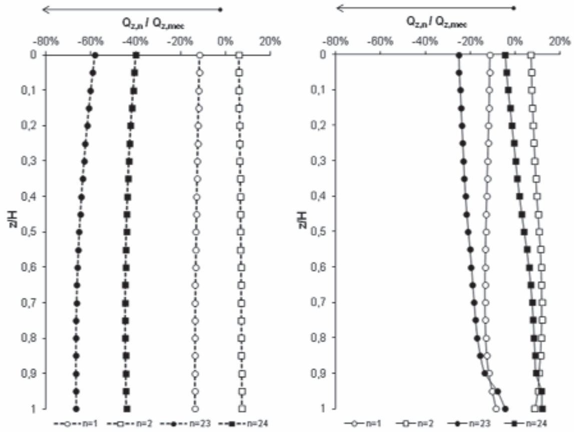

(a) (b)

Figure 9. Pieu bloqué en tête – Variations relatives des efforts induits par les variations de température dans le pieu – (a) Loi *t-z* – (b) Loi Modjoin

One-dimensional compressive behaviour of reconstituted clays under high temperature and small strain rate

Comportement oedométrique des argiles reconstituées sous fortes température et à faible vitesse de déformation

Tsutsumi A.
Foundations Group, Geotechnical Engineering Field, Port and Airport Research Institute, Japan

Tanaka H.
Division of Field Engineering for the Environment, Graduate School of Engineering, Hokkaido University, Japan

ABSTRACT: It is considered that a long term settlement of clay deposits so called secondary consolidation is caused by clay viscosity. In this paper, the viscous property of clayey soils is examined from two viewpoints of temperature and strain rate effects. To investigate these effects, constant rate of strain (CRS) loading test, in which the strain rate is changed during the test, was carried out at a temperature of 10℃ and 50℃for reconstituted Louiseville clay samples. It is found that as temperature is higher and the strain rate is smaller, the clay specimen does not follow conventional viscous behaviour, for example, the Isotache model, but the gradient of stress-strain curve considerably decreases. The reason for different behaviour from the Isotachemodel may be considered to be attributed to creation of a new structure to resist the external deformation, under high temperature and slow strain rate conditions.

RÉSUMÉ : On considère que le tassement à long terme de dépôts d'argile, appelé consolidation secondaire, est causé par la viscosité es argiles. Dans cette étude, on examine le comportement visqueux des sols argileux de deux points de vue : celui des effets de la température et celui des effets de la vitesse de déformation. Afin d'étudier ces effets, on a réalisé sur des échantillons d'argile de Louiseville reconstitués à des température de 10°C et 50°C un essai oedométrique avec une vitesse de déformation constante (CRS/Constant Rate of Strain), dans lequel la vitesse de déformation est modifiée durant l'essai. On a constaté que lorsque la température est plus élevée et la vitesse de déformation plus faible, l'échantillon d'argile ne suit pas le comportement visqueux conventionnel, par exemple le modèle Isotache, mais que la pente de la courbe de contrainte-déformation plastique diminue considérablement. On peut considérer que la raison de la différence de comportement par rapport au modèle Isotache doit être attribuée à la création d'une nouvelle structure pour résister aux déformations externes.

KEYWORDS:clay, one-dimensional consolidation, strain rate effect, temperature effect.

1 INTRODUCTION

In one-dimensional consolidation, the stress-strain relationships of clayey soils exhibit various viscous behaviours. One of them is well known behaviour depending on strain rate. It was reported that the stress-starin relationships of clayey soils were determined by strain rate (for example, Leroueil et al., 1985; Tanaka, 2005), and such strain rate effectwas simply described by Isotache model (Šuklje, 1957).On the other hand, the other viscous effect related to temperature is also observed. For example, Eriksson(1989)reported that the consolidation yield stress (p'_c) decreases with an increase in temperature as shown in Fig.1. These viscous effects, caused by strain rate and temperature, on stress-strain relationships of clayey soils arevery similar to each other, and they have been already reserached in previous studies.However, most of them focused on either one of the viscous effects: strain rate effect and temperature effectindividually, not simultaneously.

In this study, combined effects of strain rate and temperature on consolidation properties of clayey soils are examined. Especially, temperature effect on compressibility under smallstrain rate, which is observed in the field, is in detail discussed.

2 TESTING METHOD AND SAMPLES

In order to investigate combined effects of strain rate and temperature on consolidationproperties of clayey soils, a special constant rate of strain (CRS) loading test, in which the strain rate is changed during the test, was carried out at different temperatures.To observe the temperature effect, it is preferable to carry out CRS test using the same specimen, i.e., by changing the temperature during the testing, to avoid any differences in soil properties for different specimens. However, changing the temperature during the testing is very difficult in practice. When the temperature is changed, the measuring system as well as the specimen itself is influenced. One example is the zero drift of the sensors.For this reason, the CRS tests were carried out at two constant temperatures: 50℃and 10℃.

Figure 2 shows a schematic view of the CRS testing apparatus used in this study.The CRS apparatus followed JIS (Japanese Industrial Standard) A 1227 (2009): the specimen was 60 mm in diameter and 20 mm in initial height.The bottom of the specimen was connected to a transducer to measure the water pressure. The applied load was measured by a load cell at the bottom of the consolidation cell. A back pressure of 100 kPa was applied to assure good saturation of the specimen during the test. The effective vertical pressure (p') was calculated assuming that the excess pore water pressure in the specimen is distributed in a parabolic manner as expressed by Eq. (1):

$$p' = \sigma - \frac{2}{3}\Delta u \qquad (1)$$

where, σ is the total pressure on the specimen and Δu is the excess pore water pressure.

A loading apparatus consisted of a Step Motor System whose resolution is as accurate as 2,621,440 pulses per revolution, and this was controlled by a personal computer (see Tsutsumi and Tanaka, 2011).The displacement was not measured by a conventional dial gauge, but obtained directly by counting the number of revolutions of the step motor and corrected by the deformation of the apparatus system. The nominal strain (ε^{T}), the void ratio (e) and the nominal strain rate ($\dot{\varepsilon}^{\mathrm{T}}$)werecalculated using the displacement.

As shown in Fig. 2 a metal pipe was spiralled around the specimenand an isothermal liquid was circulated through this pipe to control the temperature(T), which was measured by a thermocouple attached to the upper side of the consolidation cell.To avoid the offset drift of measuring instruments due to changes in the temperature, the whole CRS testing apparatus was preliminarily kept under a testing temperature by circulating isothermal liquid.Then, the measuring instruments were initialized and the CRS test was started.

Reconstituted samples were used, to avoid the variability in soil properties for tested samples and to identify only the temperature effect. The samples were made from Louiseville clay, which was obtained from the Louiseville site along the St. Lawrence River in Quebec, Canada. Their main geotechnical properties are as follows: the liquid limit,the plastic limit and the density of soil particles are 71%, 22% and 2.767g/cm^3, respectively. Its detailed properties were referred by Tanaka et al. (2001).

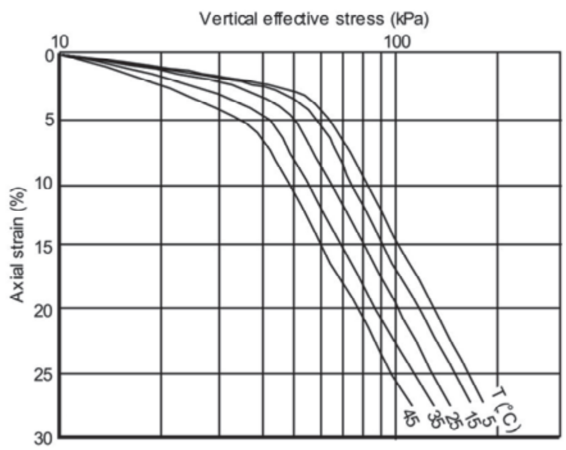

Figure1. A typical example of temperature effect on compression curves (after Eriksson, 1989).

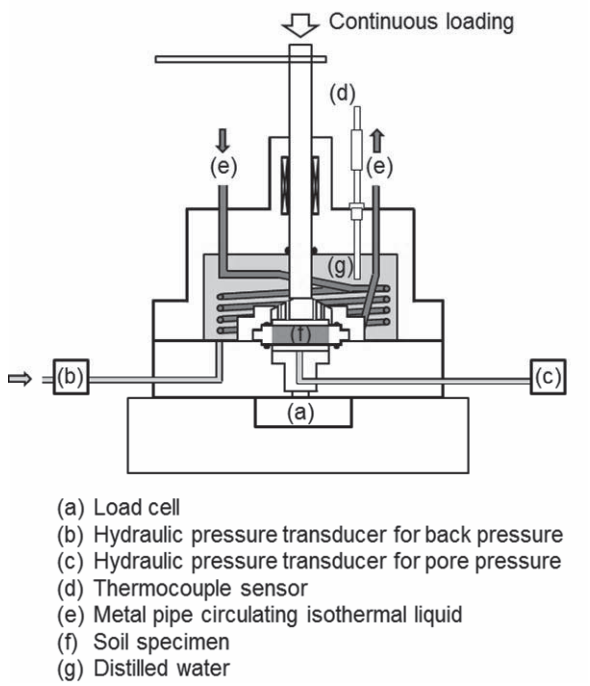

Figure 2. A schematic view of CRS testing apparatus for controlling temperature.

3 TEST RESULTS AND DISCUSSIONS

3.1 *Temperature effects on permeability*

Figure 3 shows therelationshipbetween$e$-log $p'$and Δu-log p'obtained from the CRS tests for Louiseville reconstituted samples. The testing was performed at a constant T value of 10 ℃ or 50 ℃, while the strain rate was changed during a test. The e-log p' curve segments between Points a and b as well as d and f were obtained under the reference strain rate of 3×10^{-6} s^{-1} ($\dot{\varepsilon}^{\mathrm{T}}$) and that between Points b and d under $\dot{\varepsilon}^{\mathrm{T}}$/100. In Fig.3,$\Delta u$ generated at 50℃ is clearly smaller than that at 10℃. It is considered that such a difference in Δu is caused by different hydraulic conductivity (k). According to JIS A 1227 (2009), k may be calculated by Eq. (2):

$$k = \frac{\rho_{\mathrm{wT}} g_{\mathrm{n}} \dot{\varepsilon}^{\mathrm{T}} H_0 H_{\mathrm{t}}}{2\Delta u} \tag{2}$$

where, ρ_{w}, g_{n}, H_0 and H_{t} are the unit weigh of water, the acceleration of gravity, specimen heights at initial and at each moment (t), respectively. The relationships of e-log k are shown in Fig. 4, where the k values were indicated at only normally consolidated (NC) states and they were not calculated in the phase “b-d”, because the strain rate was so small that the value of Δu was nearly zero andcould not be measured with sufficient accuracy. When k at 50℃ and 10℃ is denoted respectively as k_{50} and k_{10}, k_{50} is larger than k_{10} and the e-log k relationships for k_{50} and k_{10} are parallel to each other, as shown in the figure.This means that the ratio of k_{50}/k_{10} is constant at the same e value.

It is well known that the viscosity of water is strongly influenced by temperature. Indeed, in the testing method of permeability defined by JIS A 1218 (2009), the measured k value is calculated at 15℃ (k_{15}), taking account of the change in the water viscosity due to temperature. The ratio of k_{50}/k_{10} is represented by Eq. (3) with the viscosity coefficient of pure water (η_{T}).

$$\frac{k_{50}}{k_{10}} = \frac{\eta_{10}}{\eta_{50}} \tag{3}$$

The ratio η_{10}/η_{50} is calculated to be 2.39 based on η_{T} of pure water given in the Chronological Scientific Table (2004). As shown in Fig. 4, the ratio of k_{50}/k_{10} for Louiseville clay is 2.44, which is very close to the ratio η_{10}/η_{50}. Therefore, it may be concluded that the changes in k and Δu with T are caused by those of the water viscosity.

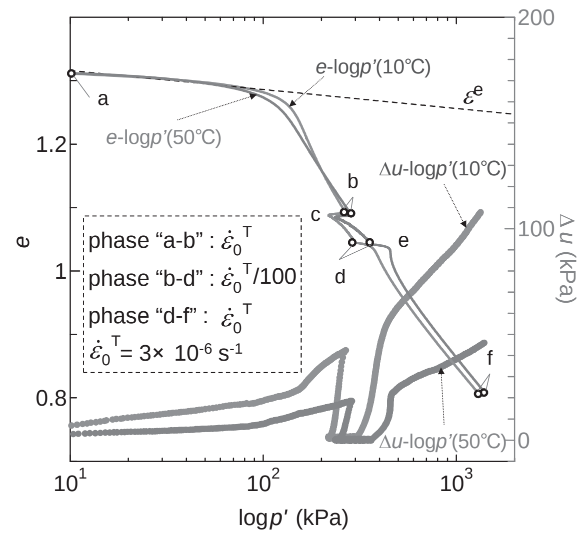

Figure 3. The e-log p'relationships obtained from CRS tests.

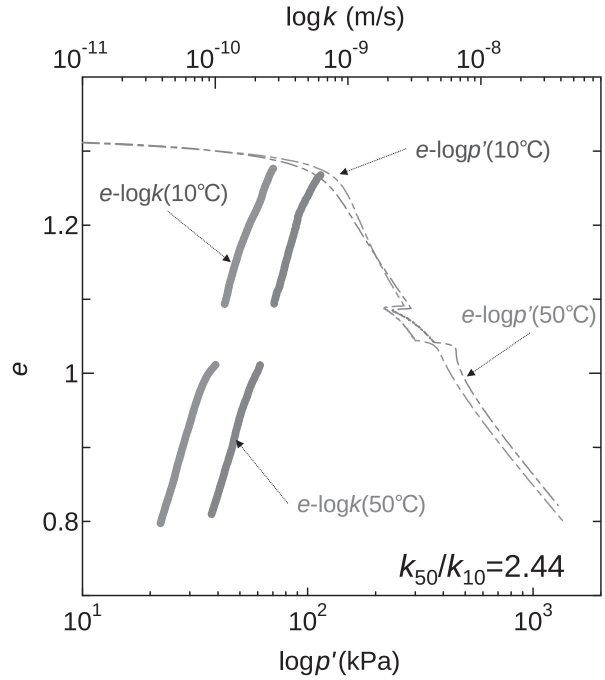

Figure 4. The variance of hydraulic conductivity with void ratio.

3.2 *Combined effects of strain rate and temperature on compressibility*

The temperature effect on compressibility beforedecreasing $\dot{\varepsilon}^{\mathrm{T}}$ is examined by comparing the *e*-log *p'* curves in the phase of"a-b" at 10℃ and 50℃, as shown in Fig. 3. It is observed that the *e*-log *p'* relationship at high temperature shifts to the left side: i.e.,p'_{c} decreases with an increase in *T*.In addition to the decrease in the p'_{c} value due to high temperature, it can be recognized that the*e*-log *p'* curve at 50℃ crosses the curve at 10 ℃: the gradient of *e*-log *p'* relationship at the normally consolidated state (C_{c})under the high temperature is smaller than that at low temperature. This behaviour is completely different from that presented in Fig. 1.

At Pointb in Fig. 3, a strain rate was instantly decreased during the tests.It is considered that the strain rate effectis relevant only to the viscous component of sample deformation.For example, in the Isotache model, the total strain (ε^{T}) is assumed to consist of the elastic strain (ε^{e}) and the visco-plastic strain ($\varepsilon^{\mathrm{vp}}$) indicated in Eq. (4):

$$\varepsilon^{\mathrm{vp}} = \varepsilon^{\mathrm{T}} - \varepsilon^{\mathrm{e}} \tag{4}$$

To evaluatethe strain rate effect on compressibility, *e*-log *p'* relationships are rearranged as the relationships between $\varepsilon^{\mathrm{vp}}$ and *p'*.It is assumed, in this study, that elastic strain is independent of temperature, andincremental ε^{e} is calculated using the slope of *e*-log *p'* relationships before reaching p'_{c}as shown in Fig. 3, where the *e*-log *p'* relationships for 10 and 50℃ are nearly identical.The relationships between $\varepsilon^{\mathrm{vp}}$ and *p'* are shown in Fig. 5, where the *p'* is normalized by the effective stress at Point b(p'_1), just before the strain rate is decreased.And the vertical axis indicates the incremental $\varepsilon^{\mathrm{vp}}$ from $\varepsilon^{\mathrm{vp}}$at Point b ($\Delta\varepsilon^{\mathrm{vp}}$). Here, the reference equi-strain rate line ($\mathrm{ESRL}_0^{\mathrm{vp}}$), which is presented by broken lines in the figure, is defined as$\varepsilon^{\mathrm{vp}}$-log *p'*relationship that a specimen may follow if visco-plastic strain rate ($\dot{\varepsilon}^{\mathrm{vp}}$) is not changed. Tsutsumi and Tanaka (2011) assumed that the $\mathrm{ESRL}_0^{\mathrm{vp}}$ can be expressed by a cubic function and the constants in the equation were obtained by the least square fitting.

The first interesting finding from Fig. 5 is that for both temperatures, *p'* decreases with a decrease in the strain rate due to the viscous effect, and this decrease in terms of the ratio p'/p'_1 is not significantly influenced by *T*.After p'/p'_1 attained the minimum value,the $\Delta\varepsilon^{\mathrm{vp}}$-log ($p'/p'_1$)relationship seen in Fig. 5is strongly influenced by temperature.In the phase of "c-d", where the strain rate becomes constant at $\dot{\varepsilon}_0^{\mathrm{vp}}$/100,the $\Delta\varepsilon^{\mathrm{vp}}$-log ($p'/p'_1$)curve at 50℃ approachesand crossesthe $\mathrm{ESRL}_0^{\mathrm{vp}}$. In the phase of "d-e-f", where the strain rate returned to the original rateof $\dot{\varepsilon}_0^{\mathrm{vp}}$, the curve considerably overshoots the $\mathrm{ESRL}_0^{\mathrm{vp}}$.On the other hand, the $\Delta\varepsilon^{\mathrm{vp}}$-log ($p'/p'_1$)curvein the phase of "c-d" at 10 ℃ does not cross the $\mathrm{ESRL}_0^{\mathrm{vp}}$ and the amount of the overshootdue to returning the original strain rate is considerably smaller than that at 50℃.Figure 6 shows a changein the gradient of $\Delta\varepsilon^{\mathrm{vp}}$-log ($p'/p'_1$)curve with increasing$\Delta\varepsilon^{\mathrm{vp}}$ in the phase of "d-e-f". In the Fig. 6, thegradient of $\Delta\varepsilon^{\mathrm{vp}}$-log ($p'/p'_1$)curve at 50℃ increases sharply at Point d, and then it decreases drastically after Point b. Such a drastic change of compressibility is often observed in the compression curves around p'_{c} of thestructured clays.

It can be considered that the specimen at high temperature and very small strain rate has gained the ability to resist the external deformation, as if the specimen has developed new structure. A similar phenomenon is observed even under the relatively fast strain rate. That is, as alreadymentioned in the phase of"a-b",C_{c} at 50℃ is slightly smaller than that at 10℃, although this difference is not significant. This tendency is more prominent under the extremely small strain rate of $\dot{\varepsilon}_0^{\mathrm{vp}}$/100.

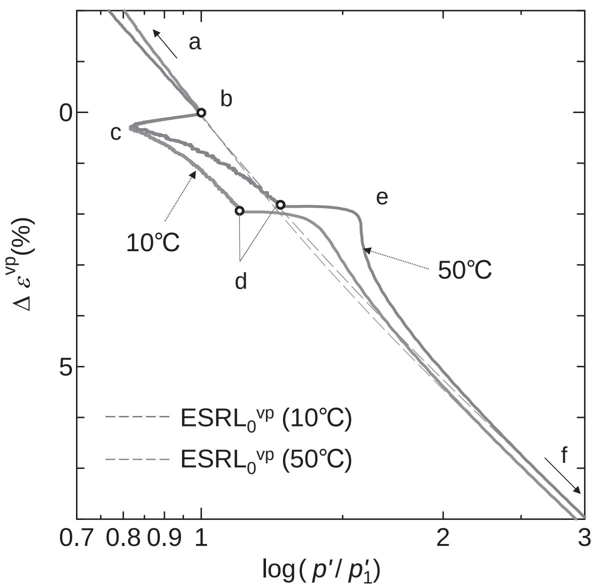

Figure5. The relationship between incremental visco-plastic strain and normalized effective stress.

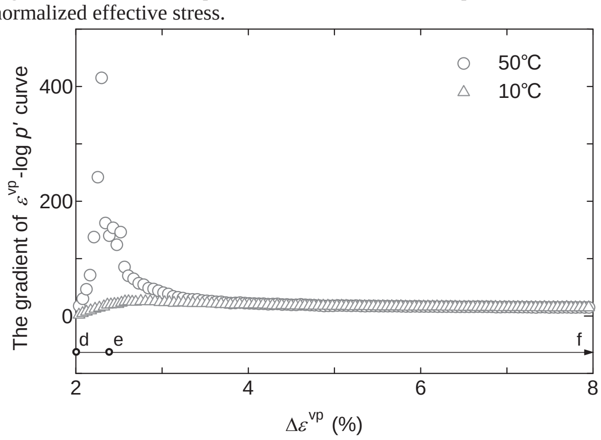

Figure 6. A change in the gradient of $\varepsilon^{\mathrm{vp}}$-log ($p'/p'_1$)curve with increasing $\Delta\varepsilon^{\mathrm{vp}}$ at the phase of "d-e-f".

3.3 *Discussions*

Two important effects on compressibility caused by the changing temperature were identified in this study. One is the so-called viscous behaviour due to high temperature conditions observed in the phase of "a-b" in Fig. 3: that is, p'_c decreases with an increase in *T*. Another effect is the gaining of the ability to resist deformation, i.e., decreasing C_c with an increase in *T*. This effect becomes much more prominent when the strain rate is smaller, as observed in the phase of "c-d" under $\dot{\varepsilon}_0^{vp}/100$ in Fig. 5; normalized *p'* at given $\Delta\varepsilon^{vp}$ is larger for higher *T*. As a result, in the phase of "d-e-f" in Fig. 5, the $\Delta\varepsilon^{vp}$-log (p'/p'_1) curve at 50℃ considerably overshoots the corresponding $ESRL_0^{vp}$, as if the clay specimen experienced ageing in the previous phase of "c-d". However, this overshoot is destructed by the faster loading under $\dot{\varepsilon}_0^{vp}$ and the $\Delta\varepsilon^{vp}$-log (p'/p'_1) curves return to their original trend.

According to Tsuchida et al. (1991), an increase in temperature provides the same effect as ageing on clay samples. They mentioned that this ageing is caused by cementation and this cementation is accelerated by an increase in temperature. A similar ageing effect was also reported byTowhata et al. (1993). In Fig. 7, cited from Towhata et al. (1993), clay samples were subjected by incremental step loadings after applying a load of 160kPa at 90℃ for various durations of time. The *e*-log *p'* relationship for heated samples shifts to higher *p'* in comparison to the reference relationship obtained by the end of primary consolidation indicated by the dotted line. They considered that such an ageing effect was caused by the acceleration of secondary consolidation: i.e., clay particles are closely rearranged because an increase in temperature reduces the viscosity of the adsorbed water layer on the surface of soil particles. As a result, the specimen develops a new structure, exhibiting higher stiffness against subsequent loading. It may be also considered that some types of structure are created during the loading process in the CRS test and its creation is considerably accelerated under high temperature conditions.

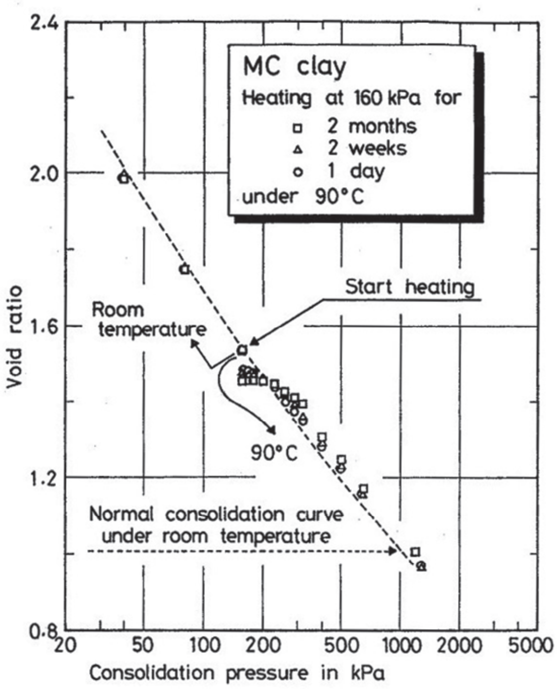

Figure 7. Thermal aging behaviour obtained from incremental loading consolidation test after Towhata et al. (1993).

4 CONCLUSIONS

To examine the combined effects of temperature and strain rates on the consolidation properties of clay, a series of CRS tests, in which the strain rate was not constant but changed during the test, was carried out at temperatures of 10℃ and 50℃for reconstitutedLouisevilleclay samples. The following conclusions were drawn:

1) The hydraulic conductivitywas strongly dependent on temperature. The reason for this is that the water viscosity increases with a decrease in temperature. As a result, the excess pore water pressure generated in the specimen at 10℃ was much higher than that at 50℃.
2) The yield effective stress decreased with increasing temperature, indicating that the clay specimens exhibited viscous behaviour by heating. However, such a viscous effect disappeared with a decrease in the void ratio (*e*) during a subsequent loading: under the higher level of the effective stress (*p'*). That is, the slope of the *e*-log *p'* curve at 50℃ at the normally consolidated state (C_c) was smaller than that at 10℃.
3) The tendency of a decrease in C_c, i.e., lowering compressibility, was more prominent under the loading condition of small strain rate.The reason for a decrease inC_c under high temperature at small strain rate may be attributed to the structure created.This explanation may be applied to the observed phenomenon of overshooting the *e*-log *p'*, when the strain rate was increased.

5 REFERENCES

Eriksson L.G. 1989.Temperature effects on consolidation properties of sulphide clays.*Proc.the 12th Int. Conf. on Soil Mechanics and Foundation Engineering*3,2087-2090.

Japanese Standards Association 2009. Test methods for permeability of saturated soils, *JIS A 1218: 2009*, 1-12 (in Japanese).

Japanese Standards Association 2009. Test method for one-dimensional consolidation properties of soils using constant rate of strain loading, *JIS A 1227: 2009*, 1-14 (in Japanese).

Leroueil S., Kabbaj M., Tavenas F. and Bouchard R. 1985.Stress-strain-strain rate relation for the compressibility of sensitive natural clays.*Geotechnique*35(2), 159-180.

National Institutes of Natural Sciences, National Astronomical Observatory of Japan 2004.Chronological Scientific Tables (in Japanese).

Šuklje L. 1957.The analysis of the consolidation process by the isotache method.*Proc. 4th Int. Conf. on Soil Mech. Found. Engng.*1, 200-206.

Tanaka H., Shiwakoti D.R., Mishima O., Watabe Y. and Tanaka M. 2001. Comparison of mechanical behavior of two overconsolidated clays: Yamashita and Louiseville clays.*Soils and Foundations*41(4), 73-87.

Tanaka H. 2005.Consolidation behavior of natural soils around p_c value –Inter-connected oedometer test–.*Soils and Foundations* 45(3), 97-105.

Towhata I., Kuntiwattanaku P. Seko I. and Ohishi K. 1993. Volume change of clays induced by heating as observed in consolidation tests.*Soils and Foundations* 33(4), 170-183.

Tsuchida T., Kobayashi M. and Mizukami J. 1991.Effect of ageing of marine clay and its duplication by high temperature consolidation.*Soils and Foundations* 31(4), 133-147.

Tsutsumi A. and Tanaka H. 2011.Compressive behavior during the transition of strain rate.*Soils and Foundations* 51(5), 813-822.

Field investigation of a geothermal energy pile: Initial Observations

Essai sur site d'un pieu géothermique : observations initiales

Wang B., Bouazza A., Singh R.M., Barry-Macaulay D.
Monash University, Melbourne, Australia

Haberfield C., Chapman G.
Golder Associates Pty Ltd, Melbourne, Australia

Baycan S.
Vibropile Pty Ltd, Melbourne, Australia

ABSTRACT: Shallow geothermal energy techniques integrated in structural pile foundation have the capability of being an efficient and cost effective solution to cater for the energy demand for heating and cooling of a building. However, limited information is available on the effects of temperature on the geothermal energy pile load capacity. This paper discusses a field pile test aimed at assessing the impact of coupled thermo-mechanical loads on the capacity of a geothermal energy pile. The full-scale in situ geothermal energy pile equipped with ground loops for heating/cooling and multi-level Osterberg cells for static load testing was installed at Monash University in a sandy profile. Strain gauges, thermistors and displacement transducer were also installed to study the behaviour of the energy pile during the thermal and mechanical loading periods. Thermal behaviour of the surrounding soils was also examined during the heating and cooling cycles of the energy pile. It has been found the pile shaft capacity increased when the pile was heated and returned to the initial capacity (i.e initial conditions) when the pile was cooled. Thus indicating that no loss in pile shaft capacity was observed after heating and cooling cycles.

RÉSUMÉ : Les pieux géothermiques ont la capacité d'offrir une solution efficace et rentable capable de réduire la demande d'énergie nécessaire pour le chauffage et le refroidissement des bâtiments. Cependant, peu d'informations sont disponibles sur les effets de la température sur la capacité de charge de ce type de pieux. Cet article présente les résultats d'essais in-situ de chargement visant à évaluer l'impact du couplage des charges thermomécaniques sur la capacité d'un pieu géothermique. Un pieu géothermique, équipé de tubes en polyéthylène pour la circulation du liquide nécessaire pour le chauffage/refroidissement du pieu ainsi que des cellules Osterberg multi-niveaux, a été installé dans du sable sur une profondeur de 16 m. En outre, ce pieu a été équipé de jauges de contrainte, thermistances et de capteurs de déplacement pour étudier son comportement pendant les périodes de chargement thermiques et mécaniques. Le comportement thermique des sols environnants a également été examiné lors des cycles de chauffage et de refroidissement du pieu. Ces essais ont montré que le frottement latéral du pieu augmente après qu'il ait été chauffé et retourne à la capacité initiale (c.-à-conditions initiales) après qu'il ait été refroidi. Ceci indique qu'aucune perte de la capacité n'a été observée après des cycles de chauffage et de refroidissement.

KEYWORDS: Energy piles, shaft resistance, Osterberg cells, thermal properties, in-situ pile load test, sustainable development

1 INTRODUCTION

Energy foundations widely known as energy piles can be defined as dual-purpose structural elements. They utilise the required ground-concrete contact element and the shallow solar energy flux, found within 100 m of the ground surface, to transfer the building loads to the ground as well as acting as heat exchanger units. Energy piles may be driven, bored or augered. Reinforced concrete piles have been found to be advantageous due to the material's high thermal storage capacity and enhanced heat transfer capabilities (Brandl, 1998).

Geothermal energy piles bring another dimension to pile design. The principle of energy piles is that energy is extracted from or sunk into the ground by a fluid, circulating via a Ground-Source Heat Pump (GSHP) similar to vertical borehole GSHP systems. The difference is where the energy pile foundation serves as an integral support to the superstructure in addition to heating and cooling the built structure (Bouazza et al., 2011). The advantages of energy piles are the cost saving over installing additional vertical boreholes and additional land areas generally required outside the perimeter of the built structure to accommodate other shallow vertical and horizontal GSHP systems.

Physical testing of pile foundations have been well documented on assessing the pile shaft and base capacity installed in various ground conditions with or without the influence of groundwater. However, the relatively new concept of energy pile foundations has introduced new parameters to be considered into pile design, to accurately predict the pile behaviour and reliability in modern structures.

2 BACKGROUND

Austria, Switzerland and Germany can be regarded as the pioneering countries that have investigated this technology for decades. Extensive use of energy geostructures have been featured in Austria. Brandl (2006) reported that more than 25,000 energy foundations (piles, etc.) were in use in Austria with installations dating as early as the 1980's.

Over the past five years, the installation of thermo active pile foundations has grown exponentially in the UK (Amis et al. 2008). There were approximately ten times more thermo-active foundations installed in 2008 than in 2005. The reason for this rise in production is mainly driven by the code for sustainable buildings that requires the construction of zero-carbon buildings by 2019 (Bourne-Webb et al. 2009). The implementation of the thermo active pile technology in the USA is very limited by comparison to Europe. Traditionally, reliance was on the use of ground source heat pumps (GSHPs) to reduce building energy consumption for heating and cooling (McCartney et al., 2010). Recently, the USA is experiencing a renewed interest in the use of energy piles as they have been identified as being a more cost effective solution compared to the use of other GSPHs systems

(McCartney et al., 2010). Countries such as China, Ireland and Japan are also experiencing an increased interest in the use of thermo-active piles (Hamada et al., 2007, Gao et al., 2008, Hemmingway and Long, 2011, Jalaluddin et al., 2011).

3 ENERGY PILE FIELD TEST

3.1 *Background*

The study conducted at Monash University is part of an international research effort aimed at obtaining a much better understanding of the thermo-mechanical effect on piles with the view of reducing the conservative approach taken so far in the design of energy piles. The study involves evaluation of the thermo-mechanical behaviour of soils, the thermal capacity of the pile, the built structure heat balance, soil thermal properties and influence of heat transfer on pile load capacity and shaft resistance. This paper reports on the pile field test undertaken at the Clayton campus of Monash University, Victoria, Australia.

3.2 *Site temperature profile*

To efficiently operate a heat exchanger pile system, the ground temperature needs to be warmer than the air temperature in winter and cooler than the air temperature during summer. This requires a ground with relatively constant temperature and knowledge of the magnitude of ground temperature changes for this system to operate efficiently. In-situ temperature profiling was conducted at the pile field test site. The site consists of 3 m thick clayey fill overlying Brighton Group materials from 3 m onward. The Brighton group consists mostly of fine to coarse very dense clayey sands and sands. Monitoring of ground temperature variation (Figure 1) indicates that the temperature of the surface zone (approximately 2 m below ground surface) and, to a lesser extent, that of the shallow zone (2 to 6 m) are influenced by short term ambient temperature changes. These variations begin to diminish upon reaching a depth greater than that of the shallow zone. Beyond 8 m (deep zone) temperatures are relatively constant (17-18 ºC) and are unaffected by seasonal temperatures changes making them suitable for heat exchanger pile systems.

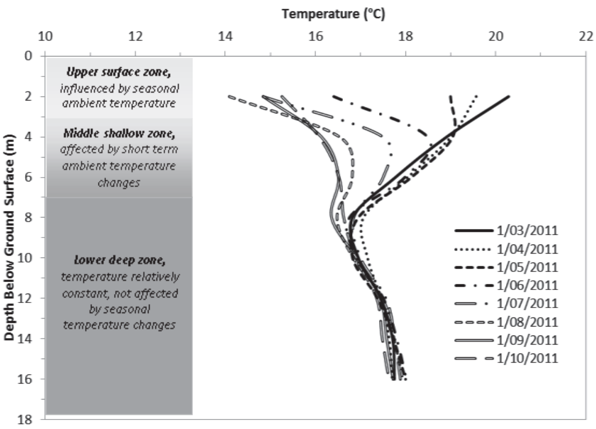

Figure 1. Typical ground temperature variation with depth, recorded at Clayton, Australia.

3.3 *Energy pile setup*

The Monash field heat exchanger or energy pile was installed in December 2010. It is a 600 mm diameter bored pile drilled to a depth of 16.1 m in Brighton Group materials. Groundwater was not observed during the installation process. Two levels of Osterberg cells (O-cells) were installed at 10 m and 14.5 m depth. By using two O-Cell levels, an accurate independent measurement can be taken for the material within the intermediate sections of the pile by observing the reaction of the relevant strain and displacement gauges with or without thermal loading. The use of O-cell also eliminates health and safety and other constraints associated with conventional static testing systems such as kentledge or anchor piles. The testing and monitoring equipment installed within the pile consisted of the following:

- Three loops of HDPE pipe (25 mm OD) attached to the pile cage, to 14.2 m, to circulate the heating transfer fluid.
- 10 vibrating wire strain gauges installed between the two O-cells levels and 6 vibrating wire strain gauges installed above the upper O-cell level.
- 12 vibrating wire displacement transducers installed within the pile to measure O-cell and pile movements.
- All vibrating wire instrumentations were fitted with a thermistor, and temperature of the concrete monitored at various levels.

Two boreholes were installed at a distance of 0.5 m and 2.0 m to the energy test pile, thermocouples were installed at 2 m intervals in each borehole to profile the temperature changes with depth and measure ground temperature during thermal loading.

4 FIELD PILE TEST RESULTS

4.1 *Thermal properties*

The ground thermal properties are paramount for an accurate design of a geothermal energy installation especially when it comes to sizing and costing the system. In this respect, in-situ ground thermal conductivity, pile thermal resistance and undisturbed ground temperature are key parameters for a successful design. The most important parameter required to optimise the design of energy piles or boreholes ground heat exchangers is the thermal conductivity of the ground (heat exchanger system and the surrounding soils). For the preliminary design of complex energy foundations or the detailed design of standard geothermal systems, sufficient accuracy of ground thermal properties can be obtained from field thermal response or laboratory testing. The thermal conductivity of the ground, which is directly relevant to the temperature-depth relationship, is sensitive to the local on-site geology and affected by its mineralogical composition, density, pore fluid and degree of saturation (Abuel-Naga et al., 2008, 2009). As a result, there is no constant depth at which all geothermal energy systems should be installed. Rather, factors such as local geology, climate and even surface cover must be considered in order to help determine a depth at which the ground temperature is relatively unaffected by seasonal temperature changes and to specify the required length of heat exchangers needed for the pile foundation.

Some of the thermal property parameters can be determined in laboratory tests but inclusion of site specific conditions such as groundwater flow and in-situ stresses are difficult to implement. Currently there is no testing standard available to conduct in-situ thermal conductivity of energy piles and assess their thermal resistance. However, the American Society of Heating, Refrigeration and Air Conditioning (ASHRAE) published a set of recommended procedures for undertaking formation thermal conductivity tests for geothermal applications (ASHRAE 1118-TRP). This procedure is popular with the borehole ground loop systems. However, the diameter of a borehole compared to a pile is a lot smaller and the number of piping loops is also lower.

Three Thermal Response Tests (TRTs) were carried out during the heating periods of the field testing program. The TRTs were carried out utilising a TRT unit consisting of a computerised logging system, control box, water pump, heating elements and a water reservoir. There is one outlet and one inlet on the TRT Unit. One TRT was carried out by circulating the heat transfer fluid through one loop of absorber pipes closest to the boreholes equipped with thermocouples. Two TRTs were carried out by transporting the fluid through all three loops of absorber pipes in a continuous series within the energy pile. Inflow and outflow temperature of the heat transfer fluid, ground temperature at every 2 m to 16 m depth within the two boreholes located at 0.5 m and 2.0 m from the edge of the test pile as well as the pile concrete temperature were recorded continuously during the heating periods. The test pile and the ground were cooled naturally by letting the induced heat dissipate into the surrounding environment following each TRT. The subsequent TRT did not start until the temperature readings within the pile and the boreholes were returned, as close as possible, to their initial undisturbed temperatures. The duration of each TRT are summarised in Table 1.

Table 1. Duration of Thermal Response Tests

TRT Name	*Test Duration (Heating)*	*Rest After Test (Cooling)*
1 loop (3 days)	3 days	5 days
3 loop ST (9 days)	9 days	47 days
3 loop LT (52 days)	52 days	78 days

Field research of in-situ measurement of the soil thermal conductivity was undertaken across Europe and USA on borehole ground heat exchangers for a number of years. Published literature (Gehlin, 2002; Austin, 1998) showed that during a TRT, based on the line source method, a defined energy was applied to the heat exchanger whilst the power input and the inflow and out flow temperature of the heat transfer medium was recorded. This measures the entire length of the ground heat exchanger, providing an effective thermal conductivity value whilst considering the borehole backfilling (or pile properties), variable ground and groundwater conditions. The effective thermal conductivity measured from a field TRT can be calculated by Equation 1:

$$\lambda_{eff} = \frac{Q}{4\pi k L_b} \qquad (1)$$

Where:

Q = constant heat power (W)

L_b = length of heat exchanger (m)

k = logarithmic relationship (slope of curve) between test duration (in log time), and the mean temperature of the heat transfer fluid

In-situ field estimation of the ground system's effective thermal conductivity consists of incorporating the energy pile ground heat exchanger and the surrounding soils as a whole system. This study presents an estimate of the effective thermal conductivity utilising the three TRTs. k is found by plotting the regression line derived from the time temperature series of a TRT, during the steady increase period of the fluid temperature. The average heat transfer fluid temperatures, with an applied Q of 2.4 kW, were plotted against time for each of the tests and the regression lines are shown in Figure 2.

The effective thermal conductivity calculated from Equation 1 was based on the heat exchanger and its immediate vicinity attaining steady-state conditions (Eskilson, 1987). This requires a minimum time criterion, as shown in Equation 2, to be satisfied.

$$t \geq \frac{5r_b^2}{a} \qquad (2)$$

Where:

t = "minimum-time" criterion for test duration (s)

r_b = borehole or pile radius (m)

a = thermal diffusivity (J/m^3 K)

The test data prior to this initial period, t = 100 hours for 3 loop TRTs, needs to be ignored to reduce errors as during this initial heating stage, the thermal front gradually reaches further beyond the heat exchanger wall. The average heating fluid temperature rises rapidly during this initial period, then as the thermal front travels further into the surrounding ground, the increase in average fluid temperature becomes steady. However, for the 1 loop TRT, the test was terminated after 3 days. Therefore, the first 48 hours of test data was ignored for comparison between the three TRTs.

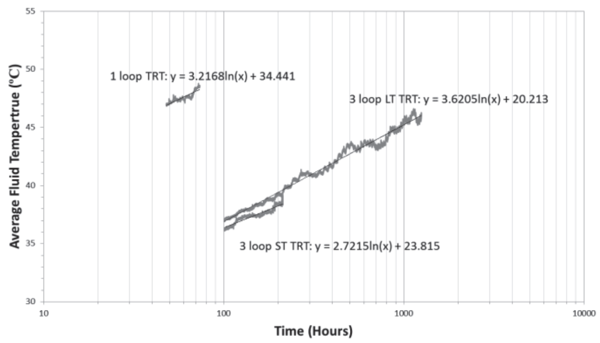

Figure 2. Estimation of effective thermal conductivity – slope of average fluid temperature vs. logarithmic of time

The results of effective thermal conductivity carried out in the three TRTs were not consistent. The 3 loop ST TRT achieved the highest value of 4.99 W/mK whilst the 3 loop LT TRT achieved the lowest value of 3.75 W/mK and the 1 loop TRT achieved an effective thermal conductivity of 4.19 W/mK for the energy pile system.

Austin (1998) showed that the line source model utilised by TRTs to estimate thermal conductivity were very sensitive to the temperature fluctuations. Figure 2 shows that there were fluctuations of the heat transfer fluid temperature during the heating periods of each TRT. The HDPE absorber pipes were insulated between the top of the energy pile to the testing unit with a combination of insulation foam, aluminium foil and soil. However, the top of the energy pile was exposed to the summer environment and direct solar energy. The fluctuation of average fluid temperature shown in Figure 2 was likely to be caused by solar radiation. The direct sunlight would heat up the concrete of the energy pile's upper surface section whilst increasing the average fluid temperature within the absorber pipes. Subsequently, during cooler nights where solar radiation was not present, the pile concrete cooled down significantly and decreased the average fluid temperature.

The estimated effective thermal conductivity found in this study is comparable to other published literature utilising energy piles as the ground heat exchanger. Published data (Brandl et al., 2006; Gao et al., 2008; Brettmann and Amis, 2011) shows that whilst utilising energy piles of at least 0.6 m in diameter during TRTs, effective thermal conductivity of the ground systems reached between 4 W/mK to nearly 7 W/mK in sandy and clayey soils. However, within smaller diameter piles the effective thermal conductivity was found to be between 2 W/mK and 3 W/mK. The long term TRT (3 loop LT) carried out over 52 days shown in this study is not a practical test to carry out due to the length of the testing period.

4.2 *Shaft resistance subject to thermo-mechanical loads*

The O-cell is a static form of testing although its application is inherently different to other existing pile load tests (i.e Statnamic, anchored loading system, etc.). The O-cell is a bi-directional, hydraulic driven, sacrificial loading jack installed within the test pile. It is capable of creating pressures which subsequently are applied to the pile shaft and base. The cell is capable of opening or expanding to 150 mm and is usually attached to the reinforcing cage that is cast within the pile. Where the O-cell is placed determines the testing schedule of the pile. The energy pile was subjected to mechanical load tests on its pile shaft, the first was performed prior to any thermal loading was introduced to the ground. At the end of each 3 loop ST and 3 loop LT heating and cooling periods the pile shaft was mechanically loaded and compared to the initial load test result.

Peak Upper O-Cell (UOC) load before and after thermal loading was carried out on the energy pile, the upper section of the pile shaft (10.1 m) was displaced in a upwards direction with the average displacement of the upper pile shaft for the mechanical pile tests shown in Figure 3. During loading (pressurising) of UOC the Lower O-Cell (LOC) was “closed” where the middle and lower section of the pile act as one whole section. This allowed the UOC to use the base resistance and the lower 6 m of the pile shaft resistance to react against the upper 10.1 m of the pile shaft resistance. The maximum applicable load on the 10.1 m pile upper section was approximately 1885 kN.

During mechanical loading of the energy pile, the shaft resistance can be variable. To evaluate the mechanical behaviour due to temperature change, consistent mechanical behaviour of the pile shaft is required before and after thermal loading to determine if there is any change in the shaft resistance. Load/unload cycles were applied until the loading behaviour was constant, thus, pile shaft reaching its ultimate residual resistance.

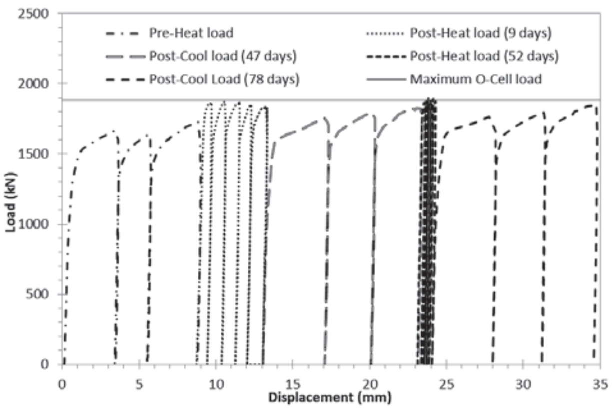

Figure 3. Load vs. pile upper-section average shaft displacement – initial, after heating and after cooling.

Figure 3 presents the pile loading tests carried out during the initial conditions, following the short-term and long-term thermal heating and cooling periods. The test results indicate that whilst the pile shaft of an energy pile undergoes thermal heating, the pile concrete slowly expands and the ultimate shaft resistance increases. However, as the energy pile was cooled following the heating period, the pile concrete slowly contracted back to its initial conditions, the ultimate shaft resistance decreased and returned closely to its initial conditions. Figure 3 also shows that the shaft resistance gained during the heating period was lost during the cooling period. However, ultimate shaft resistance did not decrease following the heating or cooling periods compared to its initial conditions.

5 CONCLUSIONS

Heat exchanger or energy piles have the potential to reduce energy demand in built structures and tackle the ever challenging climate debate. Energy piles are increasingly used in various parts of the world today, and the benefits, experiences and opportunities gained from these experiences can be adapted and applied to the local conditions. The energy pile testing works carried out at Monash University shows pile shaft resistance gained strength during thermal heating loads where the pile is founded in unsaturated, very dense sand. However, further research is required to understand the pile shaft behaviour in different soil conditions as well as assessing thermal properties of the energy pile ground heat exchanger and the surrounding soils in field conditions.

6 ACKNOWLEDGEMENTS

This study was part of a larger research program on geothermal energy piles funded by the Victorian Government Sustainability Fund, Vibropile Pty. Ltd., Golder Associates Pty. Ltd., GenesisNow, MIRVAC and GeoExchange Australia Pty. Ltd. Their support is gratefully acknowledged.

7 REFERENCES

Abuel-Naga, H.M., Bergado, D.T. and Bouazza, A., (2008). Thermal conductivity evolution of saturated clay under consolidation process. International Journal of Geomechanics, Vol.8, No2, pp. 114-122.

Abuel-Naga, H. M., Bergado, D. T., Bouazza, A. and Pender, M. J. (2009). Thermal conductivity of soft Bangkok clay from laboratory and field measurements. Engineering Geology, Vol. 105, pp. 211-219.

Amis, T., Bourne-Webb, P., Davidson, C., Amatya, B. and Soga, K. (2008). An investigation into the effects of heating and cooling energy pileswhilst under working load at Lambeth College, Clapham Common, U.K. Proceedings 11th Int. Conf. Deep Foundations, Deep Foundation Institute, CD Rom.

ASHRAE 1118-TRP. Methods for determining soil and rock formation thermalproperties from field tests.

Austin, W. A. (1998). Development of an insitu system for measuring ground thermal properties. Thesis, Oklahoma State University.

Bourne-Webb, P. J., Amatya, B., Soga, K., Amis, T., Davidson, C. and Payne, P. (2009). Energy pile test at Lambeth College, London: geotechnical and thermodynamic aspects of pile response to heat cycles. Géotechnique, Vol. 59, No. 3, pp. 237-248.

Brandl, H. (2006) Energy foundations and other thermo-active ground structures. Géotechnique, 56, No2, pp.81-122.

Brettman, T. and Amis, T. (2011). Thermal conductivity evaluation of a pile group using geothermal energy piles. Proceedings Geo-Frontiers 2011, Dallas , USA, pp. 499-508.

Bouazza, A., Singh, M., Wang. B., Barry-Macaulay. D., Haberfield. C., Chapman. G., Baycan. S., Carden. Y. (2011). Harnessing onsite renewable energy through pile foundations. Australian Geomechanics, 46, No 4.

Gao, J., Zhang, X., Liu, J., Li, K.S. and Yang, J. (2008). Thermal performance and ground temperature of vertical pile-foundation heat exchangers: A case study. Applied Thermal Engineering, 28, 2295-2304.

Gehlin, S. (2002). Thermal response test, method development and evaluation. Thesis, Lulea University of Technology.

Hamada, Y., Saitoh, H., Nakamura, M., Kubota, H. and Ochifuji, K. (2007). Filed performance of an energy pile system for space heating. Energy and Building, Vol. 39, pp. 517-54.

Hemmingway, P. and Long, M. (2011). Energy foundations-potential for Ireland. Proceedings Geo-Frontiers 2011, Dallas, USA, pp. 460469.

Jalaluddin, Miyara, A., Tsubaki, K., Inoue, S. and Yoshida, K. (2011). Experimental study of several types of ground heat exchanger using a steel pile foundation. Renewable Energy, vol. 36, pp.764-771

McCartney, J., Rosenberg, J, and Sultanova, A. (2010). Engineering performance of thermo-active foundations. Proceedings GeoTrends 2010, West Palm Beach, Florida, USA, pp.27-42.

THM simulations for laboratory heating test and real-scale field test

Simulations THM d'essais de chauffage en laboratoire et en vraie grandeur in situ

Xiong Y.L., Zhang F., Nishimura T., Kurimoto Y.
Nagoya Institute of Technology, Nagoya, Japan

ABSTRACT: In this paper, a program of finite element method (FEM) named SOFT, considering thermo-hydro-mechanical (THM) behavior of soft rock, has been developed to simulate the THM behavior of the soft rock in geological disposal based on a thermo-elasto-viscoplastic model. A thermal heating isotropic test for soil under drained condition in different over-consolidated ratio (OCR), is firstly simulated by the proposed numerical. Meanwhile, a real-scale field test is also simulated by the proposed method. The material parameters of the rock involved in the constitutive model are determined based on element tests for the rock. It is found that the proposed numerical method can well describe the THM behavior of the soft rocks, such as, the temperature change, the change of EPWP and the heat-induced deformation.

RÉSUMÉ : Dans cette étude, nous avons développé un programme aux éléments finis appelé SOFT intégrant le comportement thermo-hydro-mécanique de roches tendres basé sur un modèle thermo-élasto-viscoplastique de façon à simuler le comportement THM de ces roches constituant un site géologique de stockage. Un essai d'échauffement sous chargement isotrope en condition drainée avec différents rapports de surconsolidation a été tout d'abord simulé par le modèle numérique développé. Dans le même temps, un essai en vraie grandeur réalisé in situ a également été simulé. Les paramètres de la roche considérés dans le modèle ont été obtenus à partir d'essais élémentaires réalisés sur ce matériau. Les résultats obtenus montrent que le modèle est capable de bien décrire le comportement THM des roches tendres, incluant le changement en température, le comportement mécanique et les déformations induites par l'élévation de température.

KEYWORDS: THM behavior, thermo-elasto-viscoplastic model, FEM, soft rock, numerical analysis, geological disposal

1 INTRODUCTION

In considering the problem about deep geologic disposal for high level radioactive waste, not only artificial barrier, but also the thermo-hydro- mechanical (THM) behavior of natural barrier, most of which is sedimentary rock or granite, is also a very important factor to be studied. High radioactive substance might permeate with water through barrier systems to biosphere. The temperature emitting from nuclear waste canisters also requests the study of temperature effect on soft sedimentary rock. The water may induce swelling phenomenon which can yield to a damage of the nuclear waste containers due to the generated temperature. All the above phenomena need to be well understood in order to guarantee the safety and the efficiency of the waste sealing construction.

In this paper, a program of finite element method (FEM) named SOFT, considering soil- water-heat coupling problem, has been developed to simulate the above-mentioned THM behavior of geological disposal based on a thermo-elasto - viscoplastic model (Zhang and Zhang, 2009). In order to verify the applicability of the program, a thermal heating isotropic tests for soils under drained condition in different over-consolidated ratio (OCR), are firstly simulated by the proposed program. In the test, the thermal volume change is found to be dependent on OCR, which can also be found in other literature. In this paper, however, the element test is not regarded as an elementary behavior, but a boundary value problem due to the different thermal expansion of water and soil particles. The simulated results show that the THM phenomenon observed in the laboratory test can be explained well by the proposed numerical method.

Meanwhile, a real-scale field test reported by Gens et.al (2007) is also simulated by the proposed numerical method. The material parameters of the rock involved in the constitutive model are determined based on element tests for the rock.

2 SIMULATION OF ELEMENTARY HEATING TEST

Heat-induced volume strain of geomaterials has been investigated extensively in literature. Drained triaxial (isotropic) consolidation test is usually used to investigate this effect by heating the test specimen, in which a specimen is firstly consolidated to a given stress and then unloaded to reach a specified OCR state. After then it is heated to a prescribed temperature in a very slow rate in order to prevent generation of excessive pore water pressure (EPWP).

A very interesting result shown in the Figure 1 (a) was reported by Baldi et al. (1988), in which the heat-induced volumetric strain measured by the quantity of water discharge was dependent on OCR, that is, the specimen will change from contraction to dilation as OCR increases. Afterwards, some other researchers also reported the same test results, e.g., the works by Cekerevac and Laloui (2004) and Cui et al (2009).

In the present paper, the heating test for soft rock (Baldi et al.,1988) is simulated by the proposed THM-FEM program SOFT to explain the test results. The FEM model used in the THM analysis is shown in Figure 2. Though the test is regarded as a so-called element test of free thermal expansion test, its thermal-mechanical behavior, in the author's viewpoint, is a boundary value problem. In the simulation, all the boundary conditions are the same as those in the test. For instance, FEM model is only fixed in vertical direction (z) on bottom and other movements are totally free. The initial temperature is 22°C and the specimen is heated gradually up to 90°C with a rate of about 1°C /h. The material parameters and the physical properties of

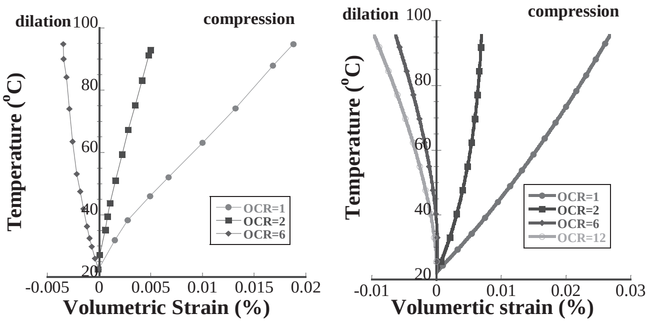

(a) Experimental result Measured by water discharge (Baldi et al,1988)
(b) Simulated result calculated by water discharge

Figure 1. Relationship between temperature and volumetric strain

the soft rock are listed in Table 1 and Table 2.

In the test, the heat-induced volumetric strain was measured with the amount of drained water indirectly, and its relation with temperature for different OCR is depicted in Figure 1(b). It is found that the thermal volume changes from contraction to dilation as the OCR value increases, which coincides well with the experimental results depicted in Figure 1(a). In Figure 3, however, it is found that volumetric strain of soil is always dilatant with the increase of temperature, no matter what OCR may be! This phenomenon just indicates that during heating, both water and soil particles expend but with different degree because the thermal expansion coefficient of water is much larger than those of soil particle, resulting in an apparent phenomenon of water discharge, which was explained as 'compression'. In high value of OCR, the expansion of soil particles becomes much larger than those of water, resulting in water absorption, which was explained as 'expansion' or dilatant. In conclusion, the observed phenomenon in the laboratory heating test is just a BVP of soil-water-heat interaction, rather than the inherent property of the soil itself.

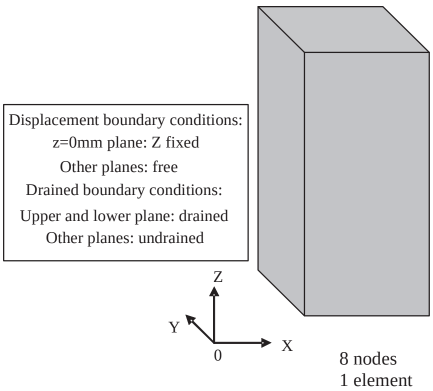

Figure 2. FEM model

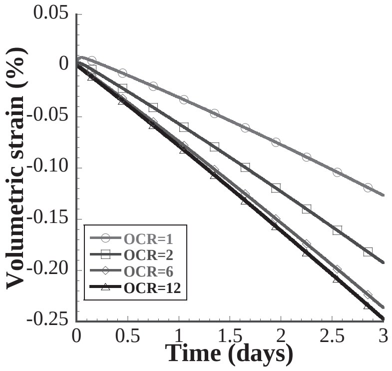

Figure 3. Change of volumetric strain of soil particle due to thermal effect calculated by FEM.

Table 1. Material parameters of rock

Young's modulus $\boldsymbol{E}$ (MPa)	300.0
Poisson's ratio $\boldsymbol{\nu}$	0.35
Stress ratio at critical $\boldsymbol{R_{CS}}(=\sigma_1/\sigma_3)$	10.9
Plastic stiffness $\boldsymbol{E_p}$	0.02
Potential shape parameter $\boldsymbol{\beta}$	1.5
Time dependent parameter $\boldsymbol{\alpha}$	0.42
Time dependent parameter $\boldsymbol{C_n}$	0.025
Overconsolidation parameter **a**	2000
Reference void ratio $e_0(\boldsymbol{\sigma_{m0}}$=98kPa)	0.85

Table 2. Physical properties of rock

Preconsolidation pressure (MPa)	0.6
Thermal expansion coefficient $\boldsymbol{\alpha_T}$ (1/K)	8.0×10^{-6}
$\boldsymbol{\alpha_{Water}}$ (1/K)	2.1×10^{-4}
Permeability $\boldsymbol{k}$ (m/s)	5×10^{-13}
Thermal conductivity $\boldsymbol{K_t}$ (kJ m^{-1} $K^{-1}Min^{-1}$)	0.18
Specific heat $\boldsymbol{C}$ (kJ Mg^{-1} K^{-1})	840
Heat transfer coefficient of air boundary $\boldsymbol{\alpha_c}$((kJ m^{-2} K^{-1} Min^{-1})	230
Specific heat of water $\boldsymbol{C_{water}}$ (kJ Mg^{-1} K^{-1})	4184

3 SIMULATION OF FIELD TEST

A field test of heating process (HE-D), carried out in a soft rock called as Opalinus clay by Mont Terri underground laboratory (Gens et al., 2007), is also simulated with the SOFT. For simplicity, only the case with symmetric condition is considered in this paper. Compared to the simulation by Gens et al. (2007), only 1/8 area is considered. Figure 4 shows 3D mesh that consisted of 4275 cubic isoparametric elements.

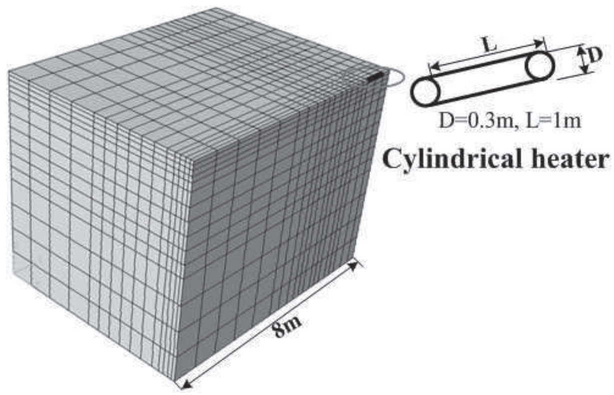

Figure 4. 3D FEM mesh

In order to investigate the mechanical behavior of the rock near HE-D experiment site, triaxial compression test under confining pressure of 8MPa was conducted by Jia et al (2007), whose results are first simulated by the proposed model and the results are shown in Figure 5. By this simulation, the parameters of the rock are determined and listed in Table 3 and Table 4. It can be seen that the proposed model can well describe the behavior of test rock.

Table 3. Material parameters of rock

Young's modulus $\boldsymbol{E}$ (MPa)	9800.0
Poisson's ratio $\boldsymbol{\nu}$	0.295
Stress ratio at critical $\boldsymbol{R_{CS}}$(=σ_1/ σ_3)	3.0
Plastic stiffness $\boldsymbol{E_p}$	0.002
Potential shape parameter $\boldsymbol{\beta}$	1.5
Time dependent parameter $\boldsymbol{\alpha}$	1.5
Time dependent parameter $\boldsymbol{C_n}$	0.005
Overconsolidation parameter **a**	8000
Reference void ratio e_0($\boldsymbol{\sigma_{m0}}$=98kPa)	0.159

Table 4. Physical properties of rock

Preconsolidation pressure (MPa)	900
Thermal expansion coefficient $\boldsymbol{\alpha_T}$ (1/K)	8.0×10^{-6}
$\boldsymbol{\alpha_{Water}}$ (1/K)	2.1×10^{-4}
Permeability $\boldsymbol{k}$ (m/s)	5×10^{-12}
Thermal conductivity $\boldsymbol{K_t}$ (kJ m^{-1} K^{-1}Min^{-1})	0.18
Specific heat $\boldsymbol{C}$ (kJ Mg^{-1} K^{-1})	840
Heat transfer coefficient of air boundary $\boldsymbol{\alpha_c}$((kJ m^{-2} K^{-1} Min^{-1})	230
Specific heat of water $\boldsymbol{C_{water}}$ (kJ Mg^{-1} K^{-1})	4184

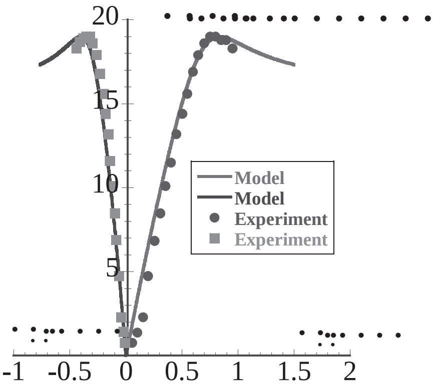

Figure 5. Simulation of triaxial test under confining pressure of 8 MPa for Opalinus clay

Figure 6 shows the change of temperature at the center of heater. The temperature reached about 40° at first heating phase, and then increased very sharply at the second heating phase up to the highest temperature of about 100°. When the power of heater is switched off, the temperature decreased sharply. It also can be seen that the calculated result can well describe the experimental data. Figure 6 also shows the change of temperatures at different position. On the whole, the THM-FEM analysis can well describe the HE-D experiment.

Figure 7 shows the change of temperature at different positions. It is known from the figure that the nearer the distance from heater is, the higher temperature will be. There is no prominent increase of temperature at the distance 5m far away from the heater due to the small heat conductivity of the rock.

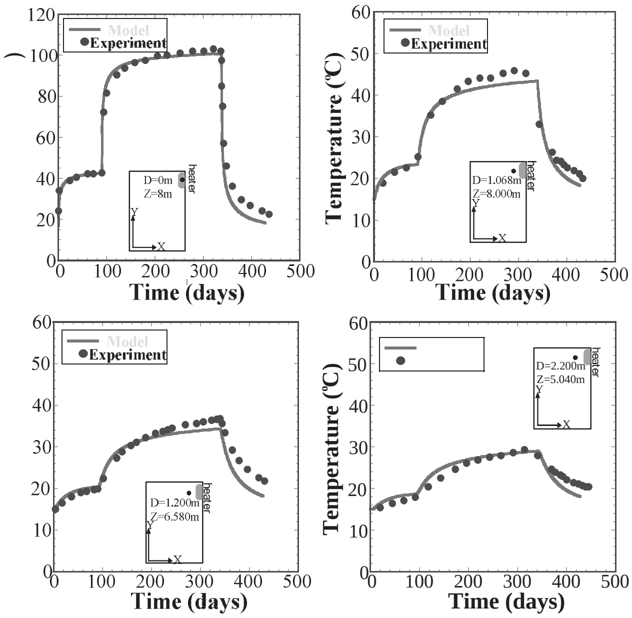

Figure 6. Change of temperature at different position

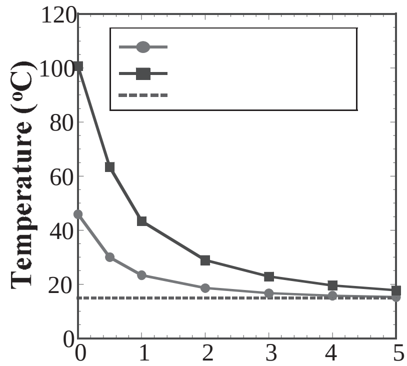

Figure 7. Computed temperature distributions at various times on cross section

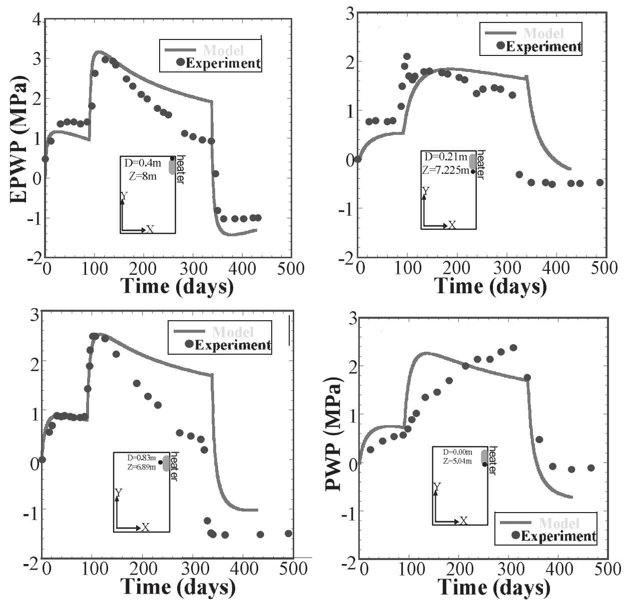

Figure 8. Variation of EPWP at different position

The evolution of EPWP with time is depicted in Figure 8 at the different sites. It is found that the EPWP increases sharply when temperature rises up suddenly, and then it will decrease with time even though the temperature is increasing. The highest value of EPWP is up to 3MPa. The increase of EPWP is due to the fact that thermal expansion coefficient of water is much higher than that of rock. Owing to the low permeability of rock, drainage is slow and the pore water expansion is impeded, resulting in the EPWP increase at the beginning. At later time, as mentioned above, migration of water from the heat source is gradually accelerated due to the increase of permeability, allowing pore pressure to dissipate.

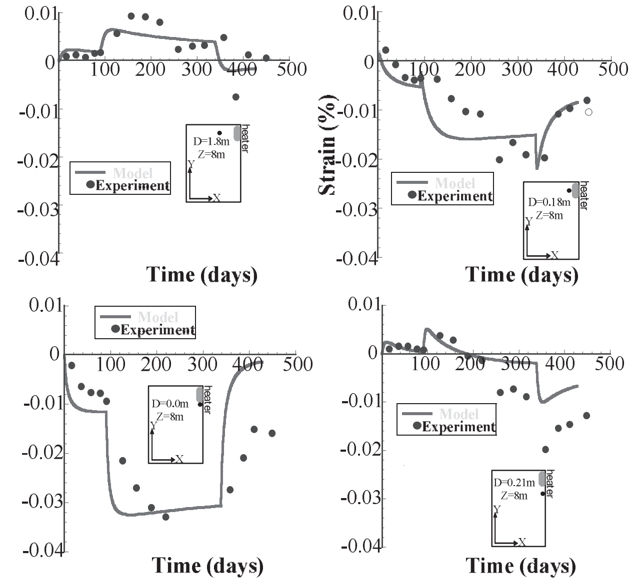

Figure 9. Variation of deformation at different position

At the same time, heat-induced deformation is also investigated. Figure 9 shows the calculated and test results at different positions. It is found that the calculation can describe the change of the deformation qualitatively if compared with the test data. The deformation of the rock near the heater is expansive; while the deformation of the rock far away from the heater is contractive. It is very easy to understand that the rock may behave expansive due to the significant increase of temperature; nevertheless, the change of temperature at the places far away from the heater is rather. Therefore, the dilation of the rock far away from the heater is very small compared with the rock in the vicinity of the heater. As the results, swelling force caused by the expansion of the rock near the heater will cause contraction of the rock far away from the heater.

4 CONCLUSIONS

In the paper, the following two conclusions can be made:

a) An isotropic element heating test is simulated by the proposed THM analysis based on an elasto-viscoplastic model. The calculation can well explain the phenomenon observed in the test that the heat-induced volumetric strain measured by water discharge changes from contraction to dilation with the increase of OCR in isotropic heating process. In the calculation with THM analysis, soil skeleton is always dilative with the increase of temperature regardless of what kind of OCR may be. The discharge of the water is just caused by different thermal expansion properties of the soil and the water! In a word, this phenomenon is merely a boundary value problem with soil-water interaction, not an inherent property of the rock itself!

b) A field test of heating process (Gens, 2007) is also simulated with the same THM analysis based on the same elasto-viscoplastic model. It is found that the proposed numerical method can well describe the THM behavior, such as, the temperature change, the change of EPWP and the heat-induced deformation.

5 REFERENCES

Baldi G, Hueckel T and Pelegrini R (1988): Thermal volume changes of the mineral-water system in low-porosity clay soils, *Canadian Geotechnical Journal*, Vol. 25, 808-825

Cekerevac C. and Laloui L. (2004): Experimental study of thermal effects on the mechanical behavior of a clay, *International journal for numerical and analytical methods in geomechanics*, Vol. 28, 209-228

Cui Y. J., Le T. T., Tang A. M., Delage P. and Li X. L. (2009): Investigating the time-dependent behavior of Boom clay under thermomechanical loading, *Getechnique*, 59, No. 4, 319-329

Gens A., Vaunat J., Garitte B. and Wileveau Y. (2007): In situ behavior of a stiff layered clay subject to thermal loading: observations and interpretation, *Geotechnique*, Vol.57, No.2, 207-228

Jia Y., Wileveau Y., Su K., Duveau G. and Shao J. F. (2007): Thermo-hydro-mechanical modeling of a situ heating experiment, *Geotechnique*, Vol.57, No.10, 845-855.

Zhang S. and Zhang F. (2009): A thermo-elasto- viscoplastic model for soft sedimentary rock, *Soils and Foundations*, Vol. 49, No. 4, 583-595.

New Developments in near-surface geothermal energy systems

Nouveaux Développements dans les systèmes géothermiques proches à la surface

Ziegler M., Kürten S.
Geotechnical Engineering, RWTH Aachen University

ABSTRACT: The geothermal utilization of the ground is a future oriented and environmental option to gain heat. In most cases borehole heat exchangers (BHE) are used. However, in the last years several researches which focussed on the development of new technologies are carried out. The Chair of Geotechnical Engineering (RWTH Aachen University) investigated new applications for the near-surface geothermal energy sector. In this regard, the geothermal utilization of smouldering mining dumps as well as the development of thermo-active seal panels are two main research topics. For both systems the description of the heat transfer between the geothermal system and the ground are important for an effective plant design. Mostly, the existing calculation models are based on the formulation of thermal resistances. For symmetric systems (such as a BHE) several approaches exist. However, these approaches cannot be transferred to plane structures directly. Therefore, a new model for plane structures is presented in this paper.

RÉSUMÉ : L'utilisation géothermique du sol est une option environnementale et orientée vers le futur pour obtenir de la chaleur. Dans la plupart des cas on utilise des sondes géothermiques; cependant, dans ces dernières années, plusieurs recherches orientées vers le développement de nouvelles technologies ont été réalisées. Le Département de l'Ingénierie Géotechnique (RWTH Aachen University) a fait des recherches sur des nouvelles applications pour le secteur de l'énergie géothermique proche à la surface. À cet égard, l'utilisation géothermique de terril couvant, ainsi que le développement de panneaux thermoactifs scellés sont deux des principaux thèmes de recherche. Pour tous deux systèmes, la description du transfert de la chaleur entre le système géothermique et le sol est importante pour une conception effective de l'équipement. La plupart des modèles de calcul existants sont basés dans la formulation de résistances thermiques. Pour des systèmes symétriques (comme un BHE) il y a de nombreuses approches. Pourtant, ces approches ne peuvent pas être transférées directement à des composants de grande étendue. Un nouveau modèle pour des composants de grande étendue est présenté dans cet exposé.

KEYWORDS: Geothermal Energy, Heat Transfer, Earth-Coupled Structures, Thermal Resistance, Numerical Simulation.

1 INTRODUCTION

The use of geothermal energy has been increased over the past years in Europe. Mostly, borehole heat exchangers (BHE) or horizontal ground heat exchangers (horizontal loops) are installed in the ground to gain heat. In some cases existing earth-coupled structures are thermally activated, e.g. piles, diaphragm walls or ground slabs (e.g. Brandl 2006). New developments focus on the thermal utilization of underground structures especially tunnels (e.g. Pralle et al. 2009, Adam and Markiewicz 2009). The main advantage of these systems are the low installations costs comparing to common geothermal systems due to the combination of structural and geothermal elements.

At the chair of Geotechnical Engineering at RWTH Aachen University new applications for the geothermal use of the ground are investigated. The geothermal utilization of smouldering mining dumps as well as the development and testing of new thermo-active seal panels are two main fields of research. For both systems an integrated approach has been carried out to enlarge the efficiency of respective systems.

In this paper the two research topics will be introduced. Furthermore, suitable models for the description of the heat transfer between the geothermal system and the ground will be shown for each topic.

2 GEOTHERMAL UTILIZATION OF SMOULDERING MINING DUMPS

Mining dumps are a common occurrence in coal-mining areas. Less well known is the fact that in many old dumps smouldering fires exist. Due to a poor processing technique in the past the amount of residual coal is high. In conjunction with a low compaction spontaneous combustion occurs.

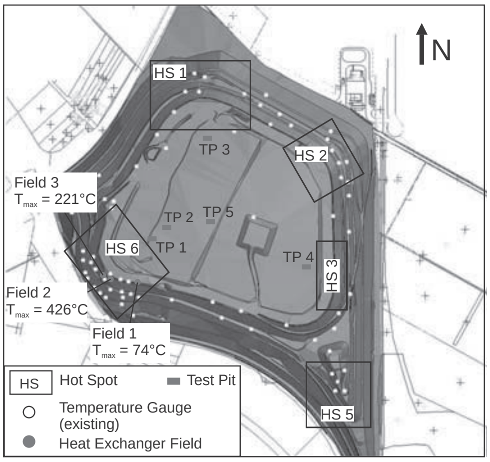

Figure 1. Schematic view of the smouldering mining dump

The smouldering leads to high temperatures inside the dump. These high temperatures imply a high energy potential, which isn't utilized until now. For determining the possible heat output from a smouldering a pilot plant on a mining dump in the 'Ruhr Area' in the western part of Germany has been operated over three years. An overview of the dump and the pilot plant is shown in Figure 1.

Three heat exchanging fields have been installed. Each field consists of a borehole heat exchangers (BHE) - designed as a coaxial probe – and five temperature measuring gauges, arranged in a semicircle around the BHE. Additional information on the plant can be found in Kürten et al. (2010). The heat exchanging fields were placed in a known Hot Spot (HS 6 in Figure 1). The maximum temperatures in each field varied between 75 °C (field 1) and 430 °C (field 2). The maximum values occurred in about 15m depth. So, the high energy potential of the dump can be confirmed.

Several Thermal Response Tests (determining the short-term behaviour of the plant, see e.g. Gehlin 2002) as well as long-term test were carried out. Additional, numerical simulations and analytical investigations were performed for estimating the main influencing parameters for the heat output. It could be shown, that a total heat output for the plant of 8kW could be achieved (Kürten et al. 2010). This corresponds to a heat requirement of two single family houses in Germany, approximately.

3 THERMO-ACTIVE SEAL PANELS

Based on the principle of thermo-active earth-coupled structures (e.g. Brandl 2006) thermo-active seal panels have been developed by the Chair of Geotechnical Engineering at RWTH Aachen University. For this, the required heat exchanging pipes were integrated in concrete protection plates made of PE-HD (PolyEthylene with High Density). Due to the thin plate the elements are characterized by a nearly contact to the ground. Furthermore, the wiring of the heat exchanging pipes is very flexible. The principle of the thermo-active seal panels is shown in Figure 2.

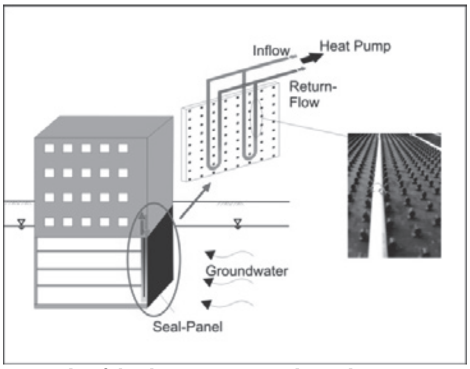

Figure 2. Principle of the thermo-active seal-panel

The main applications for the thermo-active seal panels will be underground structures with direct contact to groundwater. In this case a sealing of the structure is necessary anyway. By thermal activation of the system two functions (sealing and energetic function) can be combined. So, the additional installations costs for the geothermal plant are relatively low comparing to a common BHE.

The efficiency of the thermo-active seal panels was tested in large scale laboratory tests under different condition. The determined heat output varied between 30 W/m² and 300 W/m², whereby the higher values correspond to high flow rates in the heat exchanging system. The reason for this is that higher flow rates lead to a turbulent flow in the pipes and thereby to a better heat transfer between fluid and pipe. Additional, the thermal resistance of the system was measured approximately. The achieved values varied between 0.03 (mK)/W and 0.3 (mK)/W depending on the boundary and system conditions. According to the heat output the lowest values (optimum) belong to high flow rates.

In the laboratory tests different boundary conditions and system conditions were tested. The results have shown, that the decisive parameters for the heat output are the heat transmission area (characterized especially by the pipe distance, the leg distance between inflow and return flow and the pipe diameter), the flow rate in the heat exchanging system and the soil conditions (especially soil type, temperature, groundwater). More details can be found in Kürten et al. (2012).

4 HEAT TRANSFER BETWEEN GEOTHERMAL SYSTEM AND SUBSOIL

4.1 *Fundamentals*

For the planning and design of near surface geothermal plants the possible heat output of the systems for the existing boundary conditions has to be known. Empirical values are documented in the German guideline VDI 4640-2 (2009). These values are only valid for borehole heat exchangers and small installations (up to 30kW) as well as homogeneous conditions. For any other cases numerical simulations are necessary to guaranty a high efficiency of the system. Direct simulations (finite element methods, finite difference methods, etc.) are complicated and computationally very demanding. The reason is that the necessary scale (in time and space) for the explicit simulation of the heat exchanger and the simulation of the heat transport in the soil is different in a large order of magnitude. So, new methods are needed to reduce simulation time and the complexity of the model without losing accuracy.

One idea, which often has been used in the last years, is the transformation of the different processes to thermal resistances. The different thermal resistances can be superposed to a total thermal resistance. Then, the heat flow between geothermal system and soil can be calculated as the product of the total thermal resistance and the effective temperature difference. For the overall system the difference between soil and fluid temperature has to be used.

The difficulty in describing the heat transfer from the soil and the geothermal systems is therefore coupled to the accurate formulation of the total resistance of the systems. This value has to be formulated for each system depending on the relevant conditions. In the following the approach used for the BHE as well as the principles of a new model for plane structures developed by the authors will be shown.

4.2 *Heat transfer model for BHE*

In common literature many calculation models for the thermal resistance of a symmetrical system (such as BHEs) are documented and implemented in several software programs. Most of them are based on the work of Hellström (1991) as well as the applied model for determining the decisive parameters for the heat output from smouldering. A detailed model description can be found in Mottaghy and Dijkshoorn (2012). In the model the BHE is assumed as a 1D-Line-Element, which is integrated in a Finite-Difference-Mesh. The processes inside the BHE are modelled with the help of thermal resistances. The coupling with the software program is realized by passing over temperature boundary condition and heat flow rates. The model is implemented in the Finite-Difference-Program SHEMAT (Simulator for heat and mass transfer, see Clauser 2003). The program can simulate coupled heat and mass transfer (e.g. groundwater flow) and it has been proven for the simulation of geothermal systems.

Fundamentally, the thermal resistance for a coaxial probe depends on the pipe-diameter (inner and outer pipe), the pipe material, the flow rate, the heat exchanging medium and the backfill material (s. Figure 3). The main heat transport mechanisms are conduction (in the backfill material as well as in the inner and outer pipe) and convection (in the fluid). The conduction depends mainly on the material properties (characterized by the thermal conductivity) whereas the convection depends on the flow rate and the properties of the fluid (especially viscosity and density).

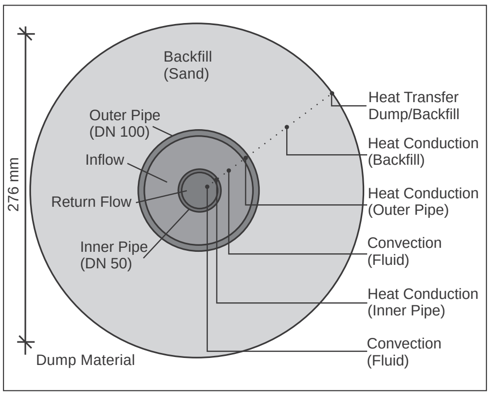

Figure 3. Heat transfer processes for the coaxial probe installed in the smouldering dump.

Every existing transport mechanism can be described with the help of thermal resistances. The different resistances can be combined with a series connection to a total connection and a total thermal resistance respectively. Details for the coaxial probe can be found in Mottaghy and Dijkshoorn (2012).

Post-test calculations of the in situ tests were performed to calibrate the applied model. After that, several analyses were carried out to identify the most important parameters for the geothermal utilization of a smouldering. As an example the influence of the thermal conductivity of the dump and the backfill material for each BHE is shown in Figure 4. The differences between the BHEs are caused by the different temperature regimes in the heat exchanging fields (see Figure 1). It can be seen that the thermal conductivity of the dump material is the most important parameter. In contrast, increasing the thermal conductivity of the backfill material has a less important influence.

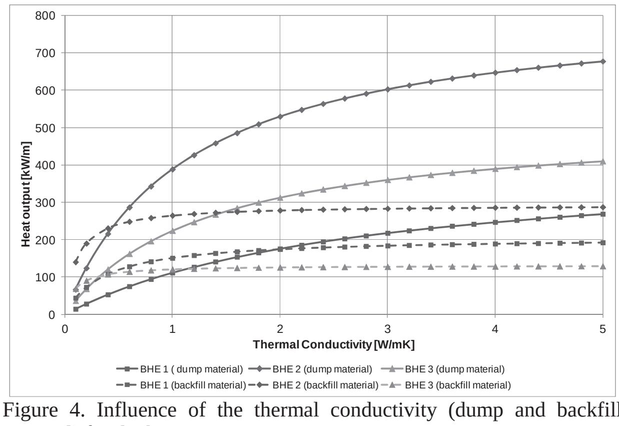

Figure 4. Influence of the thermal conductivity (dump and backfill material) for the heat output

The thermal conductivity of the existing dump material was determined in the laboratory. As a result, a value of 0.4 W/(mK) can be assumed. As expected the thermal conductivity of the material is very low. Additional, Thermal Response Tests (TRT) were carried out for each BHE. The resulting effective thermal conductivities varied between 1.0 W/(mK) (field 3) and 2.2 W/(mK) (Kürten et al. 2009). The effective thermal conductivity obtained by the TRTs cannot be equated with the thermal conductivity as a material property. It is rather a combination of all thermal processes involved. For the geothermal utilization of a smouldering the high underground temperature and the thermal radiation must be taken into account. For transferring the results to another site, the determining of the correct effective thermal conductivity will be the main problem.

In summary, the heat transfer inside the dump (heat replenishment) is the limiting factor the geothermal utilization of a smouldering. This is the reason why the achieved heat output of the pilot plant is relatively low comparing to the high temperatures inside the dump. Nevertheless, by the presented research project it could be shown that geothermal utilization of smouldering mining dumps is possible.

4.3 *Heat transfer models for plane structure*

For symmetric systems such as a BHE several approaches for the calculation of the heat transfer between ground and soil with the help of thermal resistances exist. In contrast, for plane structures there are no equivalent approaches documented. This may be due to the fact that the occurring processes are more complex due to the missing rotation-symmetry.

The developed thermo-active seal panels are characterized by a plane heat transfer. Nevertheless, in dependency of the boundary conditions the possible heat output of the systems must be describes realistically for an effective plant design. For this, a calculation model, which will be also implemented in the software program SHEMAT, has been developed by the Chair of Geotechnical Engineering at RWTH Aachen University.

The basic principle of the new calculation model corresponds to the existing model for a BHE (see section 4.2). The processes inside the thermo-active structure will be summarized to a total thermal resistance. The coupling between SHEMAT and the calculation model will be realized by passing over temperature boundary conditions and heat flows.

For the development of the calculation model two main aspects have to be considered. On the one hand, the heat transfer isn't symmetric. The heat transfer from the ground to the heat exchanging system should be the priority flow. Heat flows from the room have to be minimized to avoid a thermal circuit. On the other hand, the inflow and the return flow of the heat exchanging pipes are spatially separated. This means, that for a numerical simulation the heat exchanging systems cannot be design as a 1D-dimensional line-element only but rather as a 2D-dimensional element.

For determining the total thermal resistance for a plane structure the involved processes must be separated. The decisive single processes are shown in Figure 5.

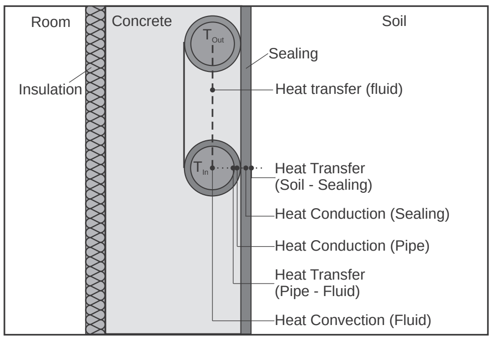

Figure 5. Heat transfer for a plane structure - thermal processes involved

The single processes can be transferred to a thermal resistance model (see Figure 6). It can be seen that there are three determining heat flows: heat flow due to the temperature difference between the two sides of the wall and the heat flow due the temperature difference between heat exchanger and ground and the room respectively. According to the superposition principle the two heat flows can be overlapped. The existing triangle mesh of the thermal resistances can be simplified to a star-network (see Figure 7).

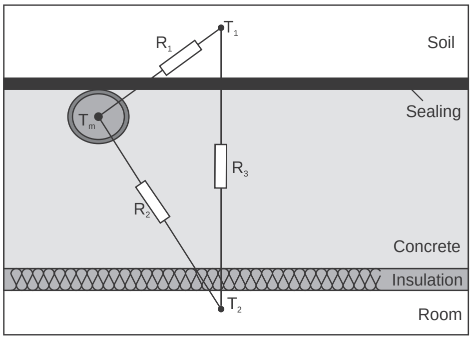

Figure 6. Thermal Resistance Model for the thermo-active seal panel (triangle mesh)

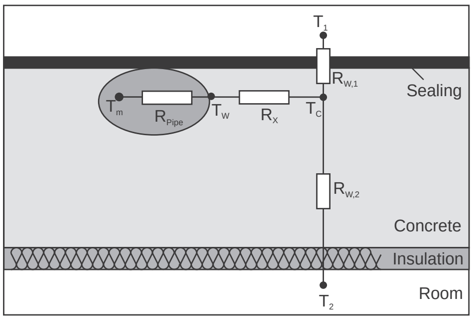

Figure 7. Thermal Resistance Model for the thermo-active seal panel (star-network)

The temperature in the heat exchanging pipe is assumed as an average temperature T_m between inflow and return flow. This simplification is very common in geothermal analyses. The thermal resistances due to the conduction in the pipe and the convection in the fluid flow are summarized to the resistance of the pipe R_{Pipe}. This leads to the temperature at the pipe wall T_W.

The interaction between the single heat exchanging pipes is represented by the so called 'structure resistance' R_x. Therefore, an approach will be taken which is adapted from the calculation of concrete core activation (see also Koschenz & Dorer 1999). By solving the differential equation for the heat conduction, the temperature distribution between two pipes can be determined. Then, the 'core temperature" T_C can be calculated as an integral of the temperature distribution. In this context, the decisive parameters will be the pipe distance, the embedded material (concrete) and the position of the pipe (overlaying material).

The advantage of this procedure is that all processes which are connected to the heat exchanging pipes can be summarized by calculation the core temperature. After calculation the core temperature the heat flow to both sides of the wall can be determined by using the well known assumption for the 1D-heat transfer through a wall. For the numerical coupling this approach has another advantage. The parameters which are used in the calculation model are the same values as the transfer values for SHEMAT (heat flows through both side of the wall and the resulting temperature at the outside of the wall T_1 and T_2 respectively).

5 CONCLUSION AND OUTLOOK

Near Surface Geothermal Energy is a good alternative to satisfy the heat requirement of buildings. To improve the efficiency of this renewable energy resource, new systems must be developed. It was shown that the thermal utilization of smouldering mining dumps is possible. The limiting factor is the poor transport inside the dump (due the low thermal conductivity) which can be compensated by the high temperature only for a bit. Nevertheless, the thermal utilization of the smouldering is a good alternative for the owner of the dump to deal with the smouldering.

The thermal activation of earth coupled structures is principle available for everyone. From the economic point of view, the boundary conditions (soil type, underground temperature, contact area, etc) have to be favourable. To achieve a high efficiency of this systems the heat transfer between soil and heat exchanger as to be described accurately. A calculation model for describing the heat transfer for plane structures between ground and thermo-active structures has been developed by the Chair of Geotechnical Engineering at RWTH Aachen University. This model is based on the combinations of thermal resistances, which is a common method in geothermal analyses. The model will be implemented in the software program SHEMAT. After that the calculation model should be verified by numerical simulations and calibrated with laboratory tests.

6 ACKNOWLEDGEMENTS

The research on the utilization of smouldering mining dumps was funded by the Federal Ministry of Education and Research (Germany). The work was done in collaboration with Unit of Technology of fuels (RWTH Aachen University, Germany), Fraunhofer Institute UMSICHT (Oberhausen, Germany), DMT – Department of Fire Protection (Dortmund, Germany) and Aix-o-therm GeoEnergien (Marl, Germany). The development of a Software tool for the calculation of the heat transfer of plane structures is funded by Deutsche Bundesstiftung Umwelt (DBU). This work is done in collaboration with Geophysica Beratungsgesellschaft mbH (Aachen, Germany) and NAUE GmbH & Co.KG. Sincere thanks are given to all.

7 REFERENCES

Adam D. and Markiewicz R. 2009. *Energy from earth-coupled structures, foundations, tunnels and sewers.* Géotechnique 59(3), 229-236.

Brandl H. 2006. *Energy foundations and other thermo-active ground structures*. Géotechnique 56(2), 81-122.

Clauser, C. 2003. *Numerical Simulation of Reactive Flow in Hot Aquifers. SHEMAT and Processing SHEMAT.* New York, Springer.

Gehlin, S. 2002. *Thermal Response Test – Methods, Development and Evaluation.* Ph.D. Thesis. Dep. of Environmental Engineering, Lulea University of Technology, Sweden.

Hellström, G. 1991. Ground heat storage. Thermal analysis of duct storage systems. Ph.D. Thesis; Dep. of Mathematical Physics, University of Lund, Sweden.

Koschenz, M., Dorer, V. 1999. *Interaction of an air system with concrete core conditioning.* Energy and Building 30, 139-145.

Kürten, S.; Ziegler, M.; Olischläger, V.; Ehrenberg, H. 2012. Untersuchungen zur Effizienz von thermo-aktiven Abdichtungs-elementen zur thermischen Nutzung des Untergrunds. In: Bautechnik 89 (3), p. 192-199.

Kürten, S., Feinendegen, M., Noel, Y., Gaschnitz, R., Schwerdt, P., Klein, A. 2010. *Geothermal Utilization of Smouldering Mining Dumps as a Substitute for Fossil Fuels.* Proceedings of ICCFR2 - Second International Conference on Coal Fire Research, Berlin, Germany.

Mottaghy, D. and Dijkshoorn, L. 2012. *Implementing an effective finite difference formulation for borehole heat exchangers into a heat and mass transport code.* Renewable Energy 45, 59-71.

Pralle N., Franzius J.N., Acosta F., Gottschalk D. 2009. *Using Tunneling Concrete Segments as Geothermal Energy Collectors.* Proceedings of the 5th Central European Congress on Concrete Engineering. Baden, Germany. 137-141.

VDI 4640-2 2009. *Thermal use of the underground – Ground source heat pump systems*. Beuth-Verlag, Berlin, Germany.

Understanding the effects of high temperature processes on the engineering properties of soils

Comprendre les effets des procédés a haute température sur les propriétés des sols

Zihms S.G., Switzer C., Karstunen M., Tarantino A.
University of Strathclyde, Glasgow, United Kingdom

ABSTRACT: High temperature processes such as in situ smouldering and thermal remediation techniques can achieve rapid removal of organic contaminants from soils in much shorter time periods than traditional remediation technologies. Thermal remediation processes use heat or heated water to volatilise the contaminant within the soil to enable its extraction. High temperatures affect the particle size distribution, mass loss, mineralogy and permeability of the soil. In sandy soils, the particle size decreases with increasing temperature due to a mobilisation of fines, which is likely due to the bond of fines to the sand grains being affected by temperature. In clayey soils, the overall particle size increases with increasing temperature due to aggregation and cementation of the clay fraction. Permeability seems to be affected by treatment type rather than temperature alone, comparing heat treated and smouldered samples showed an increase of sand permeability by approximately two magnitudes. This study illustrates the effects of high temperature and smouldering processes on soil characteristics and dynamic behaviour. Monitoring during and after aggressive remediation is advisable so that rehabilitation measures can be implemented before site redevelopment.

RÉSUMÉ : Des procédés a haute température tels que la combustion lente in situ et des techniques de traitement thermique peuvent achever une élimination rapide des contaminants organiques des sols en beaucoup moins de temps que les technologies de traitement traditionnelles. Les procédés de traitement thermique utilisent la chaleur ou de l'eau chauffée pour vaporiser les contaminants dans le sol pour permettre leur extraction. Des températures élevées affectent la distribution granulométrique, la perte de masse, la minéralogie et la perméabilité du sol. Dans les sols sablonneux, la taille des particules décroît avec l'augmentation de température due à une mobilisation des particules les plus fines, probablement dû à la liaison de ces particules aux grains de sable, affectée par la température. Dans les sols argileux, la taille des particules augmente avec l'augmentation de température due à l'agrégation et la cimentation de la fraction argileuse. La perméabilité semble être affectée par le type de traitement plutôt que par la température uniquement, des échantillons traités par la chaleur ont montré une augmentation de la perméabilité du sable d'environ deux ordres de grandeur par rapport à ceux traités par combustion lente.Cette étude montre les effets des températures élevées et des procédés de combustion lente sur les caractéristiques du sol et sur son comportement dynamique. Il est conseillé d'utiliser un système de surveillance pendant et après traitement agressif afin que les mesures de réhabilitation puissent être appliquées avant le réaménagement du site.

KEYWORDS: Thermal behaviour of soils, smouldering remediation, high temperature

1. INTRODUCTION

Soils can be exposed to elevated temperatures naturally through wild, forest or peat fires or through thermal remediation processes designed to mitigate contamination by hazardous organic chemicals. Most research on soil properties and their heat dependency is based on forest fires and therefore concentrates on erosion rates, ground stability and nutrients affected by fire severity. The effects of exposure to temperatures up to 500°C have been studied widely (Are et al., 2009; Certini, 2005; Rein, 2009; Rein et al., 2008). Literature published on heat treatments of clay evaluates the effects of temperatures up to 1000°C (Tan et al., 2004). Exposures of 200 – 850°C have been observed in soils during wildfires (Certini, 2005; DeBano, 2000; Mataix-Solera and Doerr, 2004; Rein et al., 2008). Moderate (300-400°C) and high (>450°C) temperature processes, such as hot water extraction, thermal desorption, soil heated vapour extraction, incineration or smouldering are used widely to treat contaminated soils (Araruna Jr et al., 2004; Chang and Yen, 2006; Gan et al., 2009; Kronholm et al., 2002; Lee et al., 2008; McGowan et al., 1996; Pironi et al., 2011; Pironi et al., 2009; Switzer et al., 2009; Webb and Phelan, 1997). Most research on soil remediation techniques focuses on the remediation result and less on the effects the process has on the soil properties itself. In some cases, the effects on soil properties may be a criterion for selection of the remediation technique (Chang and Yen, 2006; Pironi et al., 2011) or the soil properties may influence the results (Webb and Phelan, 1997). There is little research on the effects of thermal remediation processes on soil properties (Araruna Jr et al., 2004; Pironi et al., 2009). Based on the observations of soil erosion and subsidence after wildfires, further understanding of the effects of high temperature remediation processes must be developed.

The maximum temperatures observed in contaminant remediation vary by the process that is used. With the exception of smouldering remediation, all of these remediation techniques use heat or heated water to volatilise the contaminant within the soil to enable its extraction. Maximum temperatures for these technologies are typically adjacent to the heat source with more moderate target temperatures of 80-100^{o}C achieved within the wider treatment zone. The contaminant must be collected and treated (Chang and Yen, 2006; Gan et al., 2009; Kronholm et al., 2002; Lee et al., 2008; McGowan et al., 1996; Webb and Phelan, 1997). These processes maintain high temperatures in the soil for weeks to months or longer. In contrast, smouldering remediation uses the contaminant itself as fuel for the combustion reaction (Pironi et al., 2011; Pironi et al., 2009; Switzer et al., 2009). In laboratory studies, the soil particles are exposed to high temperatures on the order of 1000°C for coal tars and 600-800°C for oils for up to 60 minutes. Field scale efforts may result in exposure durations on the order of hours or longer.

Elevated temperatures have been shown to alter the mineralogical composition of soil. These effects have been studied extensively in relation to the effects of wildfires on soil properties. Colour change in soils has been observed after wildfire and after smouldering remediation. In most cases it changes from yellowish brown to reddish brown. This is due to the oxidation of soil iron content from goethite to maghemite or hematite (Goforth et al., 2005; Ketterings and Bigham, 2000). Decomposition of soil particles, especially clay minerals, starts at temperatures above 550°C (Certini, 2005). These temperatures are rarely reported for wild and forest fire, but temperatures up to 1200°C can be achieved during smouldering remediation (Pironi et al., 2009; Switzer et al., 2009).

This study aims to characterise the effects of moderate and high temperatures as well as smouldering on soil properties to determine the impact changes will have to the soil and predict possible complications that may arise during or after remediation treatment. Silica sand and kaolin clay are used as constituents of a synthesised simple soil. Clean untreated, heat-treated and contaminated/smouldered materials are evaluated to determine the impacts of the treatment conditions on soil properties.

2. MATERIALS AND METHODS

Coarse silica sand (Leighton Buzzard 8/16, Sibelco, Sandbach, UK) and kaolin clay (Whitchem Ltd, UK) were used as the base soil for all of the experiments. The sand contains 99% silicon-dioxide, has a mean grain size of 1.34 and a bulk density of 1.7g/cm^3 (Switzer et al., 2009). The sand and clay were accepted as received and the sand was subjected to the same pre-treatment. A programmable muffle furnace (Nabertherm L9/11/SKM, Nabertherm GmbH, Lilienthal, Germany) was used for all heating experiments. The sands evaluated after smouldering remediation were prepared in a 3m^3 experiment involving coal tar mixed with coarse sand. The initial concentration of this mixture was 31000 ± 14000 mg/kg total extractable petroleum hydrocarbons before treatment and the average concentration after smouldering remediation across the majority of the vessel was 10 ± 4 mg/kg (Pironi et al., 2009).

Table 1. Heat treatment programs

Sample Name	Pre-heating time (min)	Peak temperature for 60min	cooling down time (min)
Untreated			
105	**30**	**105°C (24h)**	**0**
250	**30**	**250°C**	**0**
500	**30**	**500°C**	**~ 60**
750	**60**	**750°C**	**~ 180**
1000	**60**	**1000°C**	**~ 240**

2.1 Sample Preparation and Heat Treatment

The silica sand was washed and wet sieved using a 425µm screen to eliminate any loose fines and air dried for several days. In case of mixed samples the dried silica sand was mixed with 10% mass kaolin clay and 5% moisture content before being heat treated. For each test, the required amount of samples was heated in the furnace following the heat treatment programmes listed in Table 1. After the required exposure duration, the samples were removed from the muffle furnace and placed in a desiccator to cool. Samples heated to temperatures above 500°C were allowed to cool in the furnace to 200°C before transfer to the desiccator.

2.2 Laboratory Testing

Particle density was measured using the gas-jar method suitable for coarse soils. Minimum density was measured using 1000g of sand in a 1L glass measuring cylinder with 20mL graduation BS1377-2:1990 and BS1377-4:1990). Maximum density was determined using the vibrating hammer method (BS1377-4:199). Particle size distribution for the sand was determined using a sieving method (BS1377-2:1990) using 1.18mm, 600µm, 425µm, 300µm and 212µm sieve sizes. The Atterberg Limits for the clay were determined using the cone penetration and rolling methods as outlined in BS1377-2:1990.

The sand-clay mixtures were prepared by dry-mixing 90% sand and 10% clay (by mass) and then adding distilled water to achieve a 5% moisture content. The sample was then thoroughly kneaded in a plastic bag by hand for 10 minutes and allowed to rest for 2 hours before any heat treatment.

3. RESULTS AND DISCUSSION

3.1. Mineralogy

During the heat treatment testing and after smouldering remediation, a colour change of the silica sand was observed (Figure 1). Exposure of this material to high temperatures results in colour change from yellowish brown to reddish brown with increasing temperature for the silica sand grains and a change from yellow to pinkish red for the crushed silica sand. This colour change is associated with the dehydration reaction of goethite with increasing temperatures to form hematite or maghemite. During the dehydration, the density of the iron-hydroxide increases from 4.3 mg/m^3 for goethite to 5.2 mg/m^3 for hematite (Wenk and Bulakh, 2004). The sand is comprised primarily of silicon dioxide; iron oxides make up a small fraction of its composition. High temperatures may cause additional changes in mineralogy that may be less likely to be detected by visual examination (Goforth et al., 2005; Pomiès et al., 1998). For example, silicon dioxide becomes unstable with high temperatures and forms silica polymorphs such as trydimite or cristobalite (Hand et al., 1998; Wenk and Bulakh, 2004). Thermal treatments (100-1200°C) on fly ash have transformed quartz minerals to cristobalite and smaller particles exhibit a characteristic glassy composition due their faster cooling time (Mollah et al., 1999).

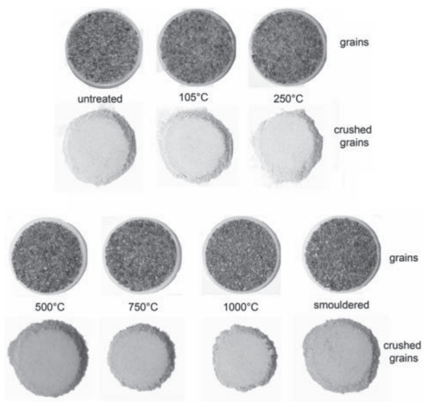

Figure 1. Silica Sand grains and crushed grains after heat treatment.

During testing that required the addition of distilled water, the clay was observed to discolour in the mixed samples, but the distilled water stayed clear (Figure 2). This is very likely associated with the iron oxidation reaction described above. It is possible that this surface reaction enables some of the iron oxides to become mobile and attach themselves onto the clay particles causing this discolouration (Zhang et al., 2011). In the clay-only samples, slight colour changes from white to greyish white were observed. In the smouldered samples for 10% clay and 20% clay mixtures with sand, the colour change was to a darker grey than the heat-only samples. This colour change was likely influenced by staining from the coal tar as well as the inherent colour change of the kaolin.

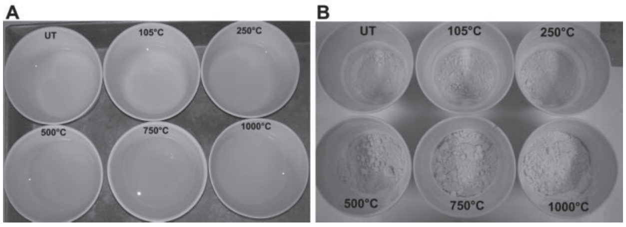

Figure 2. A: Kaolin clay (sand-clay mixture) fraction after heat treatment; B: Kaolin only after heat treatment.

3.2. Particle Size Distribution and Densities

In contrast to mineralogy, elevated temperatures did not seem to affect the particle density or minimum/maximum bulk densities of the silica sand. No real relationship was apparent between treatment temperature and density. For the particle density, the values are consistently near 2.65mg/m^3, which is a value that is widely used in geotechnical engineering calculations. The maximum and minimum densities are equally unaffected by heat treatment or smouldering. These observations are not consistent with the literature on wild and forest fire effects on soil properties, which suggests that bulk density would increase with temperature (Are et al., 2009; Certini, 2005). The lack of organic matter may explain the contrast. The results in this study, which show no significant change in density, suggest that the changes in soil density that are observed after wildfires are associated primarily with effects on organic matter and potentially the smaller silt and clay–sized particles.

Heat treatment has a small but appreciable effect on particle size distribution. As exposure temperature increases from 250 to 1000°C, the sample retained on the 1.18mm sieve increases. The variation in particle size distribution may be linked to the loss of mass beyond the initial moisture content. As temperature increases, mass loss increases. Although there is a dehydration reaction from goethite to hematite in the sand, the fraction of iron oxide relative to the total composition of the sand is too small for this reaction alone to account for the whole additional mass loss. For the silica sand kaolin clay mixture the trend is slightly different (Table 2). The sample retained on the 1.18mm sieve increases very slightly for 250°C, followed by an overall decrease for 250, 500, 750 and 1000°C. For 105 and 250°C the clay coats the sand grains allowing them to be retained on the 1.18mm sieve, for temperatures above 500°C this coating is destroyed resulting in less sample being retained. The coating effect increases the sand fraction >1.18mm by 7 to 16% compared to the higher temperature samples. This is not an increase in the sand fraction but an increase in grains the size of this fraction due to the additional clay coating. This coating could have an impact on the permeability and shear behaviour of these lower temperature samples after heat treatment depending on how easily it can be destroyed or removed by grain interaction or interaction with water.

Table 2. Sieve analysis results for silica sand – 10% kaolin clay mixtures (5% MC) for different heat treatments

Sample	**SIEVE ANALYSIS**	
	1.18mm	**<1.18mm**
	% retained	
105	**81.8 ± 1.9**	**18.2 ± 2.1**
250	**82.7 ± 0.8**	**17.3 ± 1.0**
500	**74.5 ± 3.2**	**25.5 ± 3.6**
750	**65.6 ± 3.6**	**34.4 ± 3.7**
1000	**67.7 ± 0.8**	**32.3 ± 1.5**

3.3. Atterberg Limits for kaolin clay

High temperature processes impact the dynamic properties of soils, particularly liquid and plastic limits at the highest temperatures. This impact on the clay fraction can lead to changes in dynamic behaviour for the clay – sand mixtures. The Atterberg limits for the temperature treatment up to 500°C are similar, especially the liquid limits are all within 64±2%, where the liquid limit for 750°C increases to 81% (Table 3) and this clay has a very high plasticity range compared to the lower temperatures. This is likely due to the increased dehydration of the clay at this temperature. These results are in contrast to Tan et al (2004) (Tan et al., 2004) who recorded an decrease in both liquid and plastic limits with increasing temperature treatment, including non-plastic behaviour for the clays above 400°C. This difference in behaviour can be two-fold. Firstly it can an affect based on the state of the tested sample, especially in regards to initial moisture content. Tan et al (5) uses over consolidated natural clays from Turkey, where this study investigated commercial loose kaolin powder with no moisture content. Secondly, the behaviour can be based on the main mineral contained in the sample, montmorillonite (2:1 clay) for the natural clays from Turkey compared to kaolinite (1:1 clay) for the commercial powder samples. Kaolininte does not swell in the presence of water whereas montmorillonite does swell. Based on this distinction, the responses of montmorillonite and other swelling clays to heat treatment may be different from the responses of kaolinite. Further work is necessary to explore the responses of montmorillonite and other clay minerals during thermal and smouldering remediation processes. The liquid limit test for the sample treated at 1000°C was not possible due to the clay not mixing properly with the water and behaving slightly non-newtonian, which means as the mixing motion stopped the sample liquefied and it was impossible to create a testable sample. Initially, the clay mixed well with the water and it was possible to produce a paste but with increasing water content the behaviour changed and the sample only stayed solid under a constant mixing motion, after stopping the mixing the sample quickly liquefied and dispersed. Storage in a sealed container did not yield different results. In contrast to the other samples (105-750°C treatments), no clay paste was formed. Instead, a stiff clay layer formed at the bottom of the bag with an overlying layer of clean water (Figure 3). This is an unexpected behaviour of the clay and no explanation has been found in the literature. It is likely that the temperature of 1000°C causes de-hydroxylation of the clay minerals, followed by aggregation of the particles and sintering (Fabbri et al.). The net result is that the kaolin particles seem to become hydrophobic. The induced hydrophobicity will affect dynamic properties of the soil such as grain-grain and grain-water interactions. In swelling clays, the effects are expected to be similar to those observed in kaolinite, though based on previous work (Tan et al., 2004), the shift toward hydrophobic particles may occur at lower temperatures. Because other clays are swelling, the effects of the dehydration and melting reactions are expected to have more substantial effects on clay volume as well as grain-grain and grain-water interactions.

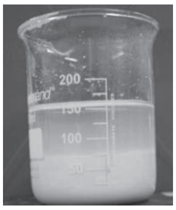

Figure 3. Kaolin clay after 1000°C treatment.

This work has demonstrated that high temperature remediation processes may have significant, long-term effects on soil properties and these effects must be taken into account as part of a holistic approach to aggressive, high-temperature soil remediation.

Table 3. Atterberg Limits and BSCS for kaolin clay for different treatment temperatures

Sample	Liquid Limit w_L	Plastic Limit w_P	Plasticity Index I_p	Plasticity Chart Classification
	%			
105°C	64.4	35.9	28.5	MH: silt, high plasticity
250°C	63.7	30.8	32.9	CH: clay, high plasticity
500°C	65.2	42.7	22.6	MH: silt, high plasticity
750°C	81.6	57.4	24.1	MV: silt, very high plasticity
1000°C	*ND*[1]	*ND*	*ND*	*ND*

[1]: Not Determined

4. CONCLUSIONS

High temperature exposure in the form of thermal treatment and smouldering remediation result in changes to soil properties. These changes are very likely to affect dynamic behaviour such as infiltration, permeability and shear behaviour. The impact appears to be different depending on the sample composition, sand only or sand-clay mixtures. This is due to the mineralogical composition and grain size of these two soil components. This study shows that some results are in contrasts to similar tests (kaolin compared to natural clays from Turkey) and this highlights the complexity of soils and their behaviour. This study gives a good insight into possible changes due to thermal or smouldering treatment. It shows that even lower temperatures (<500°C) can have an impact on the soil, especially on the clay-sand mixture samples. The observed coating of sand particles by clay can impact the infiltration and shear behaviour of the sample. If the coating can be easily removed than this can affect the structure of the sample and in turn weaken the sample or cause collapse after infiltration. This coating can also protect the sand grains from further impact by heat treatment and stabilise the sample. Further analysis is required to fully understand the effect of the clay coating and its stability. The change of Atterberg limits for the kaolin clay with increasing temperature shows that very high temperatures (1000°C) can severely change the behaviour of the soil. Further testing with other clays is necessary to fully understand the relationship between mineralogy and Atterberg Limits.

5. REFRENCES

Araruna Jr, J.T. et al., 2004. Oil spills debris clean up by thermal desorption. Journal of Hazardous Materials, 110(1-3): 161-171.

Are, K.S., Oluwatosin, G.A., Adeyolanu, O.D., Oke, A.O., 2009. Slash and burn effect on soil quality of an Alfisol: Soil physical properties. Soil and Tillage Research, 103(1): 4-10.

Certini, G., 2005. Effects of fire on properties of forest soils: a review. Oecologia, 143(1): 1-10.

Chang, T.C., Yen, J.H., 2006. On-site mercury-contaminated soils remediation by using thermal desorption technology. Journal of Hazardous Materials, 128(2-3): 208-217.

DeBano, L.F., 2000. The role of fire and soil heating on water repellency in wildland environments: a review. Journal of Hydrology, 231: 195-206.

Fabbri, B., Gualtieri, S., Leonardi, C.,2012. Modifications induced by the thermal treatment of kaolin and determination of reactivity of metakaolin. Applied Clay Science(0).

Gan, S., Lau, E.V., Ng, H.K., 2009. Remediation of soils contaminated with polycyclic aromatic hydrocarbons (PAHs). Journal of Hazardous Materials, 172(2-3): 532-549.

Goforth, B.R., Graham, R.C., Hubbert, K.R., Zanner, C.W., Minnich, R.A., 2005. Spatial distribution and properties of ash and thermally altered soils after high-severity forest fire, southern California. International Journal of Wildland Fire, 14(4): 343-354.

Hand, R.J., Stevens, S.J., Sharp, J.H., 1998. Characterisation of fired silicas. Thermochimica Acta, 318(1-2): 115-123.

Ketterings, Q.M., Bigham, J.M., 2000. Soil color as an indicator of slash-and-burn fire severity and soil fertility in Sumatra, Indonesia. Soil Science Society of America Journal, 64(5): 1826-1833.

Kronholm, J., Kalpala, J., Hartonen, K., Riekkola, M.-L., 2002. Pressurized hot water extraction coupled with supercritical water oxidation in remediation of sand and soil containing PAHs. The Journal of Supercritical Fluids, 23(2): 123-134.

Lee, W.-J. et al., 2008. Thermal treatment of polychlorinated dibenzo-p-dioxins and dibenzofurans from contaminated soils. Journal of Hazardous Materials, 160(1): 220-227.

Mataix-Solera, J., Doerr, S.H., 2004. Hydrophobicity and aggregate stability in calcareous topsoils from fire-affected pine forests in southeastern Spain. Geoderma, 118(1-2): 77-88.

McGowan, T.F., Greer, B.A., Lawless, M., 1996. Thermal treatment and non-thermal technologies for remediation of manufactured gas plant sites. Waste Management, 16(8): 691-698.

Mollah, M.Y.A., Promreuk, S., Schennach, R., Cocke, D.L., Güler, R., 1999. Cristobalite formation from thermal treatment of Texas lignite fly ash. Fuel, 78(11): 1277-1282.

Pironi, P., Switzer, C., Gerhard, J.I., Rein, G., Torero, J.L., 2011. Self-Sustaining Smoldering Combustion for NAPL Remediation: Laboratory Evaluation of Process Sensitivity to Key Parameters. Environmental Science & Technology, 45(7): 2980-2986.

Pironi, P. et al., 2009. Small-scale forward smouldering experiments for remediation of coal tar in inert media. Proceedings of the Combustion Institute, 32: 1957-1964.

Pomiès, M.P., Morin, G., Vignaud, C., 1998. XRD study of the goethite-hematite transformation: Application to the identification of heated prehistoric pigments. European Journal of Solid State and Inorganic Chemistry, 35(1): 9-25.

Rein, G., 2009. Smouldering Combustion Phenomena in Science and Technology. International Review of Chemical Engineering, 1: 3-18.

Rein, G., Cleaver, N., Ashton, C., Pironi, P., Torero, J.L., 2008. The severity of smouldering peat fires and damage to the forest soil. CATENA, 74(3): 304-309.

Switzer, C., Pironi, P., Gerhard, J.I., Rein, G., Torero, J.L., 2009. Self-Sustaining Smoldering Combustion: A Novel Remediation Process for Non-Aqueous-Phase Liquids in Porous Media. Environmental Science & Technology, 43(15): 5871-5877.

Tan, Ö., Yilmaz, L., Zaimoglu, A.S., 2004. Variation of some engineering properties of clays with heat treatment. Materials Letters, 58(7-8): 1176-1179.

Webb, S.W., Phelan, J.M., 1997. Effect of soil layering on NAPL removal behavior in soil-heated vapor extraction. Journal of Contaminant Hydrology, 27(3-4): 285-308.

Wenk, H.-R., Bulakh, A., 2004. Minerals Their Constitution and Origin. Cambridge University Press.

Zhang, S. et al., 2011. Mineralogy, morphology, and textural relationships in coatings on quartz grains in sediments in a quartz-sand aquifer. Journal of Contaminant Hydrology, 124(1-4): 57-67.

General Report
Shallow foundations

Rapport général
Fondations superficielles

Zerhouni M.I.
ARCADIS ESG – Le Plessis-Robinson - France

Demay B.
TRACTEBEL ENGINEERING- Gennevilliers - France

ABSTRACT: Ten papers, from different countries, were accepted to this Discussion Session on Shallow Foundations. This General Report reviews and summarizes the main contents and objectives of each of the submitted papers. This review shows that different themes are treated and studied. Most of them are related to the improvement of models for predicting settlements of shallow foundations in granular soils and in clayey soils. Accuracy and uncertainties in estimating settlements are assessed through probabilistic analyses in four of the accepted papers. The definition and the determination of moduli and elastic soil properties are also studied, like for instance the use of measured non-linear dynamic properties of soil. One paper addresses the settlement reduction by aggregate piers (stone columns) and defines, through a full scale loading program, the corresponding "improvement factor". Another theme related to the eccentrically and inclined loading of shallow foundations is treated in three papers. The interaction of nearby footings submitted to inclined loading is studied through Finite elements analyses. Foundations submitted to dynamic loadings are also emphasized through a paper presenting the study of an improved type of foundation combining massive block and plates.

RÉSUMÉ : Dix articles provenant d'auteurs de différentes nationalités ont été acceptés pour cette session de discussion sur les Fondations superficielles. Le présent rapport fournit une synthèse du contenu et des objectifs de chaque article. La revue montre que différents sujets ont pu être abordés. La plupart porte sur l'amélioration des modèles de prédiction des tassements de fondations aussi bien dans les sols granulaires que dans les sols argileux. La précision et les incertitudes associées à l'estimation des tassements sont évaluées au travers d'analyses probabilistes dans quatre des articles présentés. La définition et la détermination des modules et des propriétés élastiques des sols, comme par exemple, l'utilisation des propriétés dynamiques non linéaires, mesurées sont également abordées. Un article traite de l'amélioration des tassements par des colonnes ballastées et définit, sur la base d'un important programme de chargement de semelles en vraie grandeur, les facteurs de réduction des tassements. Trois des articles de la session concernent les semelles soumises à des charges inclinées et excentrées. L'interaction entre semelles rapprochées soumises à des charges inclinées est également étudiée par l'intermédiaire de modélisations aux éléments finis. Les fondations soumises à des chargements dynamiques sont également abordés par la présentation d'un système combinant un bloc massif associé à une ou plusieurs dalles.

KEYWORDS: shallow foundation, settlement, probabilistic approach, dynamic properties.

1 INTRODUCTION.

This general report reviews and summarizes the main contents and objectives of each of the papers submitted to the Shallow foundation session. Different themes are covered and studied by these papers.

Most of them are related to the study of settlements under shallow foundation either in granular soils or in clayey soils.

The definition and the determination of moduli and elastic soil properties are also studied. The use of non-linear dynamic properties, measured in-situ, to predict settlement is covered in one of the submitted papers.

Accuracy and uncertainties in estimating settlements are also assessed through probabilistic analyses.

The settlement reduction by using aggregate piers (stone columns) and a proposal for the definition, through the results of a full scale foundation loading program, of the corresponding "improvement factor" is given.

Another theme subject is related to the eccentrically and inclined loading of shallow foundations. The interaction of nearby footings submitted to inclined loading is studied through Finite elements analyses.

Foundations submitted to dynamic loadings are also emphasized through a paper presenting a study of an enhanced type of foundation combining massive block and plate.

2 SETTLEMENT OF SHALLOW FOUNDATIONS

2.1 *Settlement measurements*

In the paper of **Dapena & *al*.** from Spain, the settlements of major-scale shallow foundations of large biodigesters tanks of a Waste Water Treatment Plant have been recorded over the first ten years after they have been put in operation and loaded.

These biodigesters are located on top of a layer of dark gray silty clay alluvial sediments between 15 and 20 m thick

Dapena *& al*. discuss the amount of settlement recorded over the first 10 years and how it has developed over time. It also identifies how the pools have behaved differently, delimiting the areas with similar settlement rates.

The measured settlement values vary between 50mm and 200mm (figure 1).

They show (figure 2) that the settlement s, which occurs with time, fits the model $s = a\sqrt{ta} + b$, where ta is the time in years since the tank has been full.

Coefficient "a" is related to the rate of settlement and its distribution is similar to the settlement values.

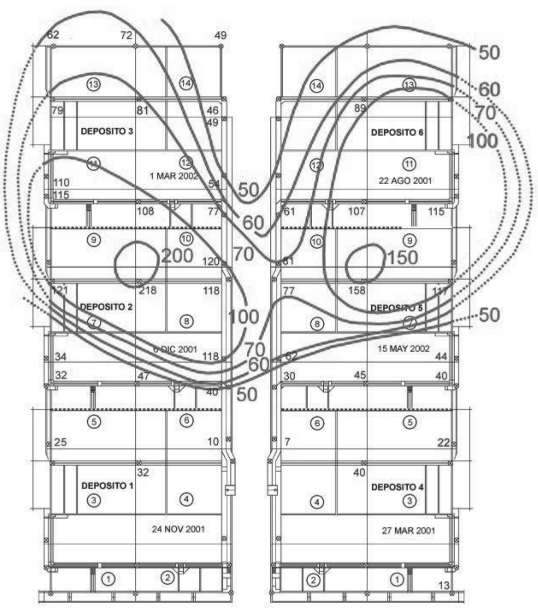

Figure 1. Contour lines for settlement at the biodigesters (in mm).

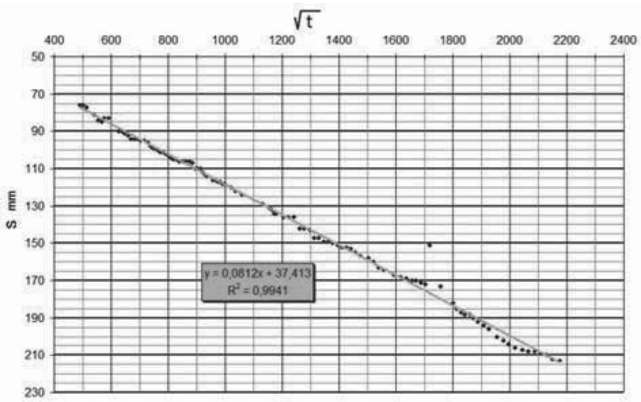

Figure 2. Settlement at point 53 of pool 2 based on the root of t (t= time in minutes) between 0.5 and 9 years and adjustment of the model.

2.2 *Settlement prediction*

In their paper, **Yang Guang-hua *& al***. from China, analyze the nonlinear settlement results of five plate loading tests carried out on the sand foundation in Riverside Campus (Texas A & M University) by using tangent modulus method.

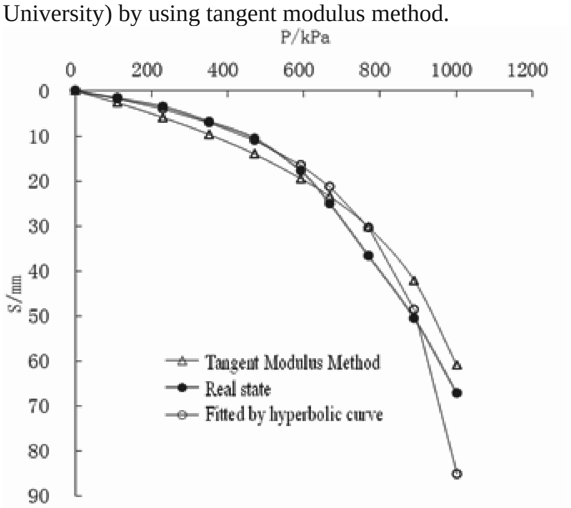

Figure 3. Example of experimental and calculated Loading curves for a 1.5m x 1.5m footing.

They show that the tangent modulus method can calculate the nonlinear settlement of foundation in a better way (see figure 3).

They also seek for simpler in-situ tests such as the Cone penetration test and the pressuremeter test to determine the soil parameters required in nonlinear settlement calculation.

Their paper attempts providing a more convenient way of using the tangent modulus method for calculation of the nonlinear settlement of foundations.

In the paper of **Stokoe *& al.***, an approach based on field seismic evaluation of small-strain ("elastic") shear modulus (Gmax) combined with nonlinear normalized shear modulus-shear strain (G/Gmax-log γ) relationships is presented. The effects of increasing confining pressure and strain amplitude on soil stiffness during loading of the footing are incorporated in this formulation.

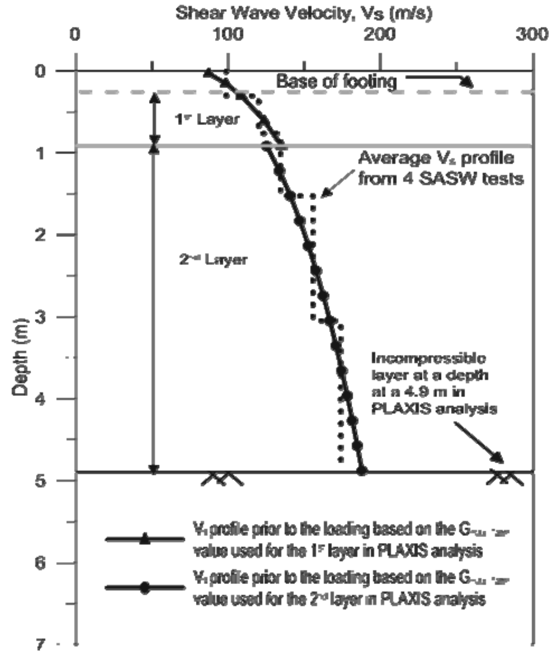

Figure 4. Average Vs profile from SASW tests and the two-layers model used in the finite element analysis..

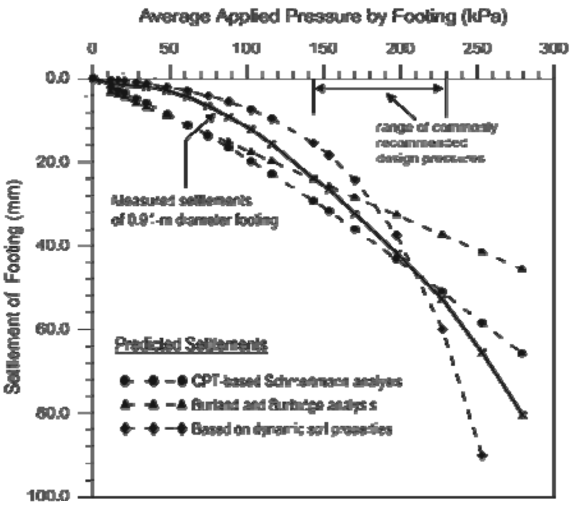

Figure 5. Measured and predicted load-settlement curves for the 0.91-m diameter footing.

The presented approach has several important benefits including: (1) in-situ seismic testing (figure 5), such as surface wave tests (SASW), which can readily be performed in all types of granular soils, including gravels and cobbles, (2) continuous load-settlement curves that are evaluated to stress states considerably above those expected under working loads, and (3) a methodology that is appropriate for all types of geotechnical materials, even those where the effective stresses change with time.

The method was investigated by comparing with a load-settlement test using a 0.91-m diameter footing. In the working stress range, predicted nonlinear footing settlements matched quite well with the measured ones (figure 6). The predicted nonlinear settlements in this range were also in reasonable agreement with predictions from traditional CPT and SPT procedures.

3 PROBABILISTIC APPROACHES

3.1 *Bearing capacity of shallow foundations*

In their paper, **Tian & Cassidy**, from Australia and **Uzielli**, from Italy, investigate the effect of the spatial variability in undrained shear strength S_u on the bearing capacity of a shallow strip footing on two-layered stiff-over-soft clay (see figure 6).

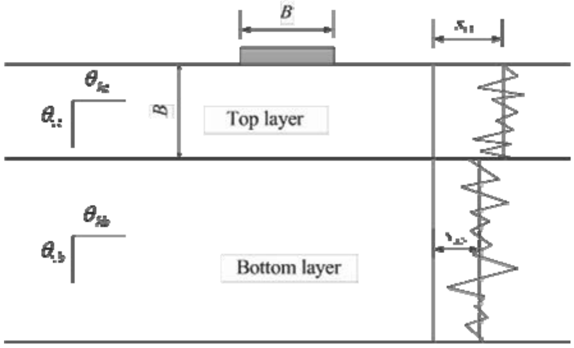

Figure 6. Definition of problem being investigated: stiff clay top layer over soft clay bottom layer.

They analyze the probabilistic assessment of the resistance factor N_c for bearing capacity for a strip footing on a stiff-over-soft clay profile. The analysis is performed by applying the Random Finite Element Method, which combines finite elements simulation, spatial variability analysis and Monte Carlo simulation.

Finite-element analyses are performed on meshes in which undrained strength values are assigned on the basis of quantitative estimates of the vertical and horizontal spatial variability and the probabilistically modeled scatter of undrained strength itself (see figure 7).

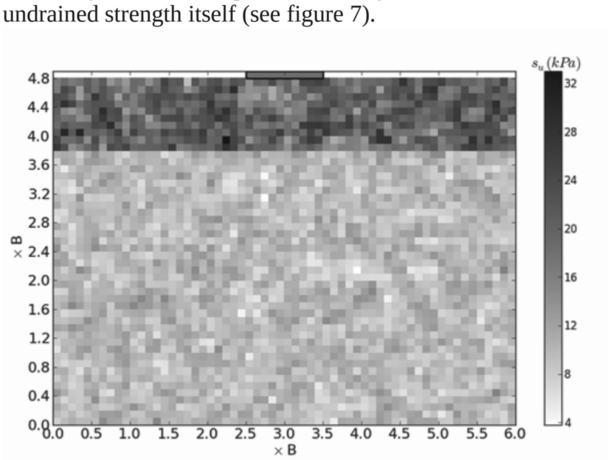

Figure 7. Example of random field mesh.

The study first results indicate that with high spatial variability in the undrained shear strength there is a significant reduction in the bearing capacity.

Mean bearing capacity factors and statistical distributions were provided for 12 cases of $s_{ut}/s_{ub} = 2$.

However, the 12 cases presented here represent a small subset of 1600 cases analyzed in a more ambitious numerical experiment.

3.2 *Settlement of shallow foundations*

Generally accepted methods for estimating immediate settlement of spread footings require the use of linear elastic models to simulate soil behavior; this approach does not capture the true non-linear behavior of soil. **Strahler & Stuedlein** present a statistical evaluation of a commonly used elasticity-based method and soil stiffness correlation using a load test database. Then, a simple non-linear model capturing observed load-displacement curvature in footing load tests is presented and its accuracy is characterized. The undrained initial elastic modulus is back-calculated using the load test database, and is found to vary as a function of overconsolidation ratio.

The use of a single undrained Young's modulus to predict the highly non-linear response of footings supported on cohesive soil has been shown to be slightly conservative at low displacements but increases in error with increasing displacement. A method to estimate displacements based on the non-linear Duncan-Chang model was shown to be slightly conservative and more accurately captures the overall load-displacement curve. The proposed method also allowed the estimation of an initial undrained Young's modulus, which appears to be correlated with OCR (see figure 8). This trend can be used to estimate the initial Young's modulus for use in the non-linear model or additionally modified to be used in elasticity based methods.

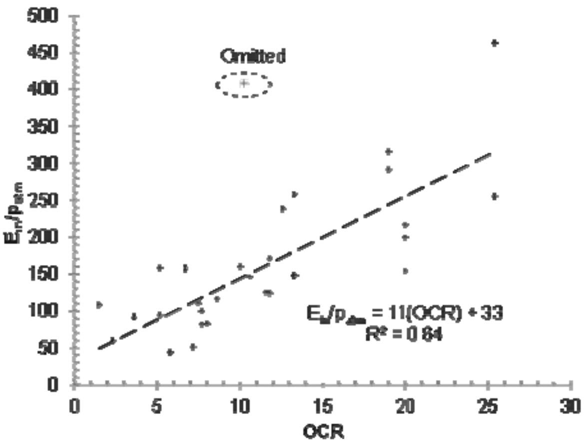

Figure 8. Back-calculated initial Young's modulus using Duncan-Chang model.

Despite the improvement in modeling footing response reported herein, significant uncertainty in the response remains without the adequate characterization of inherent soil variability, transformation error associated with correlations, and model error. Improved site characterization presents the best approach to reducing the uncertainty of footing load-displacement response.

Bungenstab *& al.* from Brazil, discuss about probabilistic settlement analysis of footings in sands, focusing on the load curve (estimated settlements). For this purpose, three methodologies that take the First and Second Order Second Moment (FOSM and SOSM), and Monte Carlo Simulation (MCS) methods for calculating mean and variance of the estimated settlements through Schmertmann's 1970 equation are discussed.

The deformability modulus (E_{Si}) is considered varying according to the division of the soil into sublayers and it is analyzed as the only independent random variable.

As an example of application, a hypothetical case in state of Espirito Santo, Brazil, is evaluated. Simulations indicate that there is significant similarity between SOSM and MCS methods, while the FOSM method underestimates the results due to the non-consideration of the high orders terms in Taylor's series. The contribution to the knowing of the uncertainties in settlement predictions can provides a more safety design.

Figure 9 shows the results for the probability of the predicted settlement to exceed different values of limiting settlements in a range between 10 to 50 mm. For example, the probability of the predicted settlement to exceed 25 mm is about 1,1%.

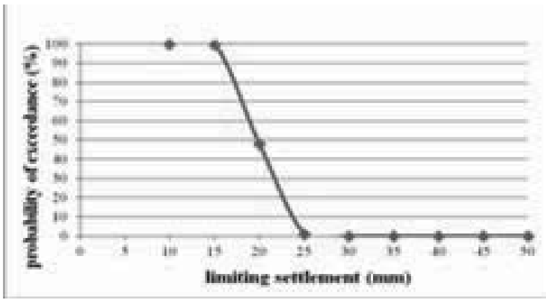

Figure 9. Probability for the predicted settlement, to exceed different values of limiting settlement.

The analysis of the sources of uncertainties indicates that about 80% of the settlement variance is influenced by the uncertainties due to inherent soil variability and measurement test errors.

4 SHALLOW FOUNDATIONS UNDER INCLINED LOADING

In their paper, **Atalar & *al.*** present laboratory model tests that were conducted in a dense sand to determine the bearing capacity of shallow strip foundation subjected to eccentrically inclined load. The embedment ratio (ratio of the depth of embedment *Df* to the width of the foundation *B*) was varied from zero to one.

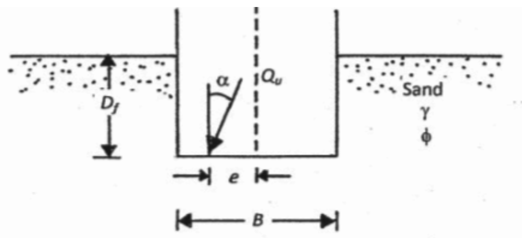

Figure 10. Shallow foundation on granular soil subjected to eccentrically inclined load.

Load eccentricity e was varied from zero to 0.15B and the load inclination with the vertical (α) varied from zero to 20 degrees. Based on the results of the present study, an empirical non-dimensional reduction factor *RF* has been developed. This reduction factor (see Eq. (1)) is the ratio of the bearing capacity of the foundation subjected to an eccentrically inclined load (average eccentrically inclined load per unit area) to the bearing capacity of the foundation subjected to a centric vertical load.

It was assumed that, for a given D_f/B:

$$RF = \text{reduction factor}$$
$$= \frac{q_{u(D_f/B,e,\alpha)}}{q_{u(D_f/B,e=0,\alpha=0)}} = \left[1 - a\left(\frac{e}{B}\right)^m\right]\left(1-\frac{\alpha}{\phi}\right)^n \quad (1)$$

The determined values of $a \approx 2$, $m \approx 1$ and $n \approx 2-(Df/B)$, based on the test results and within the range of parameters tested, have been proposed.

A comparison between the reduction factors obtained from the empirical relationships and those obtained experimentally shows, in general, a variation of ±15% or less. In a few cases, the deviation was about 25 to 30%.

The interaction of nearby footings resting on homogeneous soil bed and subjected to vertical and inclined loads has been studied by **Nainegali *& al.***, from India.

Two rigid strip footings of symmetrical width, *B* rest on the surface of the homogeneous soil layer of depth H, as shown in Figure 11.

The two footings are placed at a clear spacing, *S* and an inclined load, *P* is applied at an angle of inclination θ_L and θ_R with horizontal on the left and right footings, respectively. The effect of angles of inclination of load (θ_L and θ_R) and the clear spacing between the footings on the ultimate bearing capacity and settlement are analyzed.

A two dimensional finite element analysis is then carried out using the commercially available finite element software, ABAQUS.

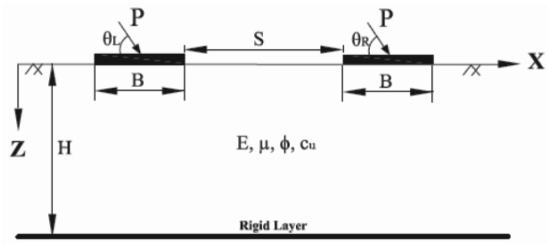

Figure 11. Problem definition for footings interaction.

Their study shows that the interference phenomenon has a considerable effect on the ultimate bearing capacity, increasing this capacity when footings are vertically loaded. For the cases where footings are subjected to inclined load the effect of interference on the bearing capacity has no significant effect. However for all cases of inclined loading condition, the interference effect on the settlement is quite significant. The settlement of interfering footings in the range of working load decreases with increase in the clear spacing between the footings and attains a value similar to isolated footing at greater clear spacing (S ≥ 5B).

5 IMPROVEMENT OF SHALLOW FOUNDATIONS

In their paper, **Kuruoglu & *al.***, from Turkey, study the settlement improvement factor for footings resting on rammed aggregate pier groups. They use a 3D finite element program, calibrated with the results of a series of full scale instrumented load tests.

Four large plate load tests were conducted with rigid steel plates of 3.0m by 3.5m. One of the load tests was on non-treated soil. Second load test was Group A loading on improved ground with aggregate piers of 3.0m length, third load test was Group B loading on improved ground with aggregate piers of 5.0m length and finally fourth load test was Group C loading on improved ground with aggregate pier lengths of 8.0m.

The aggregate pier groups under each footing, consisted of 7 piers installed with a spacing of 1.25 m in a triangular pattern. The pier diameter was 65cm. (See Figure 12)

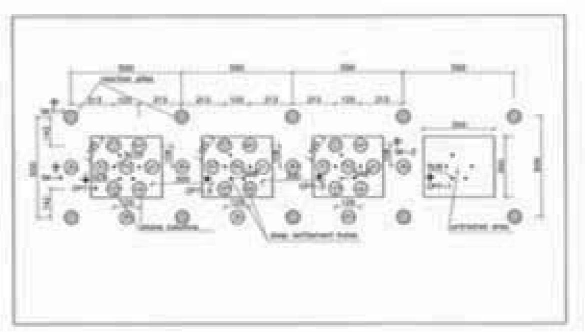

Figure 12. Location of aggregate piers at the test site.

A simplified 3D finite element composite soil model was then developed, which takes into account the increase of stiffness around the piers due to the ramming process. Design charts for settlement improvement factors of square footings of different sizes (B = 2.4m to 4.8m) resting on aggregate pier groups of different area ratios (AR = 0.087 to 0.349), pier moduli (Ecolumn = 36MPa to 72MPa), and with various compressible clay layer strengths (c_u = 20kPa to 60kPa) and thicknesses (L = 5m to 15m) were prepared using this calibrated 3D finite element model (see example in figure 13).

It was found that, the settlement improvement factor increases as the area ratio, the pier modulus and the footing pressure increase.

On the other hand, they observe that the settlement improvement factor decreases as the undrained shear strength and thickness of compressible clay and footing size increase.

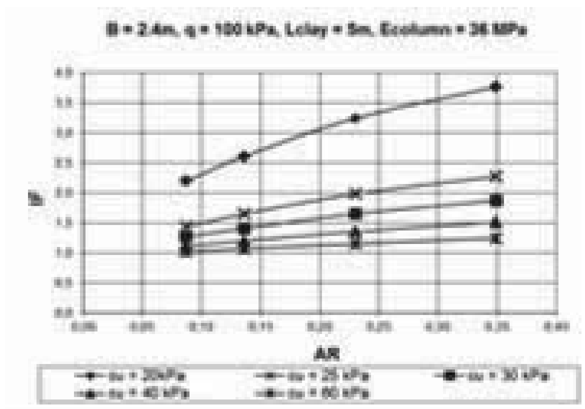

Figure 13. Settlement improvement factor (IF) vs. area ratio (AR) charts for a rigid square footing (B=2.4m) with a foundation pressure of q=100 kPa resting on end bearing rammed aggregate piers (L=5m, E=36 MPa).

Heavy machinery with rotating, reciprocating or impacting masses requires a foundation that can resist dynamic loadings and the resulting vibrations. **Y.Kirichek & V.Bolshakov** present in their paper new forms of foundations under machines with low dynamic loadings. They are named «Combined massive and plate foundations" (see Figure 14).

This type of foundations consists of deepened rigid solid mass, and attached to it in soil, thin horizontal plates.

Its natural frequencies can be sat in a wide frequency range by changing dimension and location of the attached thin horizontal plates in soil.

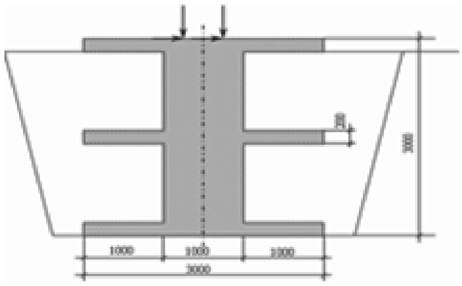

(a)

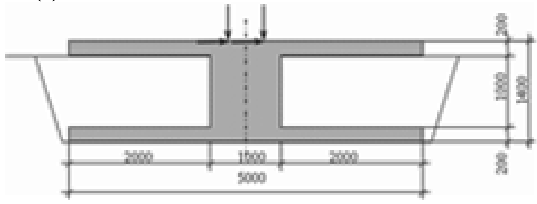

(b)

Figure 14. Combined massive and plate foundations: (a) – a solid block and three plates, (b) – a solid block and two plates.

As a result natural frequency of such foundation can be significantly higher in amount than of block-type foundation, and vibration level of the combined massive and plate foundations under low-frequency loading and impacting machinery generally is considerably lower.

For studying the behavior of the combined massive and plate foundations under low-frequency, large-scale field loading tests were conducted by **Kirichek & Bolshakov**. The comparison of the footing vibration tests with theory was done. For these tests, the vertical and horizontal dynamic forces on footing were generated by rotating mass vibrators. The large-scale models were 1.5 m in wide and 3.71 m in length.

The comparison of the amplitude-frequency responses of the combined massive plate foundations enable to evaluate influence of the dimension of plates on responses of foundation. It shows that the vibration amplitude decreases half as much with increasing of the plate area *F* twice as many.

The plate thickness *h* has less effect on the responses of foundation (see figure 15).

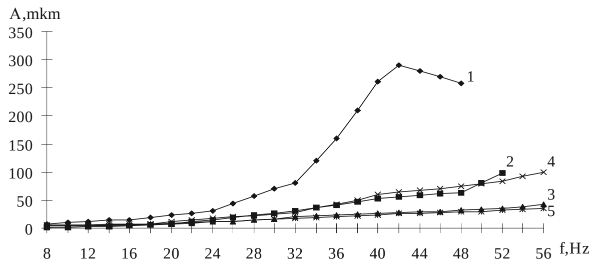

Figure 15. Amplitude-frequency responses of the combined massive and plate foundations with the plate on the top of the foundations to horizontal periodic load: 1 – amplitude-frequency response of the block, 2 – F=2.13, h=0.05, 3 – F=4.5, h=0.05, 4 – F=2.13m, h=0.1, 5 – F=4.5m, h=0.1m

It was experimentally determined that the effect of top plates was more effective under horizontal dynamic loading and the effect of bottom plates was more effective under vertical dynamic loading.

A thin plate on the soil can significantly reduce the vibration level of the block foundation.

6 ACKNOWLEDGEMENTS

We would like to thank the members of the Technical Commission of the CFMS "Comité Français de Mécanique des

Sols" for their contribution in reviewing the submitted papers to this session.

7 REFERENCES

Papers in this parallel session:

Atalar C., Patra C. R., Das B. M., Sivakugan N. 2013. Bearing capacity of shallow foundation under eccentrically inclined load.

Bungenstab F. C., Bicalho K. V., Ribeiro R. C. H. Aoki N. 2013. Estimating settlements of footings in sands – a probabilistic approach.

Dapena E., Roman F., Pardo de Santayana F. and Cuéllar V. 2013. Settlement velocity measured over ten years in major-scale shallow foundations on a preloaded 20-m thick silty alluvial layer.

Kenneth H., Stokoe K.H., Onur Kacar I., Kacar O., and Van Pelt J. 2013. Predicting Settlements of Shallow Footings on Granular Soil Using Nonlinear Dynamic Soil Properties.

Kirichek Y. and Bolshakov V. 2013. Combined massive and plate foundations under machines with dynamic loadings.

Kuruoglu O., Horoz A. and Erol O. 2013. Settlements Under Footings on Rammed Aggregate Piers.

Nainegali L. S. , Gosh P., Basudhar P. K. 2013. Interaction of Nearby Strip Footings Under Inclined Loading.

Strahler A. W. and Stuedlein A. W. 2013. Characterization of Model Uncertainty in Immediate Settlement Calculations for Spread Footings on Clays.

Tian Y., Cassidy M. J., Uzielli M. 2013. Probabilistic Assessment of the Bearing Capacity of Shallow Strip Footings on Stiff-Over-Soft Clay.

Yang G., Luo Y., Zhang Y. and Wang E. 2013. Application of The Tangent Modulus Method in Nonlinear Settlement Analysis of Sand Foundation.

Bearing capacity of shallow foundation under eccentrically inclined load

Capacité portante d'une fondation superficielle sous une charge inclinée excentrique

Atalar C.
Near East University, Nicosia, North Cyprus

Patra C.R.
National Institute of Technology, Rourkela, India

Das B.M.
California State University, Sacramento, USA

Sivakugan N.
James Cook University, Townsville, Australia

ABSTRACT: Laboratory model tests were conducted in a dense sand to determine the bearing capacity of shallow strip foundation subjected to eccentrically inclined load. The embedment ratio (ratio of the depth of embedment D_f to the width of the foundation B) was varied from zero to one. Load eccentricity e was varied from zero to $0.15B$ and the load inclination with the vertical (α) was varied from zero to 20 degrees. Based on the results of the present study, an empirical nondimensional reduction factor has been developed. This reduction factor is the ratio of the bearing capacity of the foundation subjected to an eccentrically inclined load (average eccentrically inclined load per unit area) to the bearing capacity of the foundation subjected to a centric vertical load.

RÉSUMÉ: Des essais ont été réalisés sur un sable dense en utilisant des modèles au laboratoire afin de déterminer la capacité portante d'une fondation superficielle filante sous chargement inclinée excentrique. Nous avons fait varier le rapport d'encastrement de la fondation (rapport entre la profondeur d'encastrement D_f et la largeur de la semelle B) entre 0 et 1. Nous avons également fait varier l'excentricité de la charge e de 0 à $0.15B$ et l'inclinaison de 0 jusqu'à 20 degrés. Sur la base des résultats de cette étude, un facteur empirique de réduction adimensionnel a été développé. Ce facteur de réduction est le rapport de la capacité portante d'une fondation soumise à une charge inclinée excentrique (charge excentrique inclinée moyenne par unité de surface) par rapport à la capacité portante d'une fondation soumise à une charge verticale centrée.

KEYWORDS: Load eccentricity, load inclination, sand, shallow foundation, reduction factor, ultimate bearing capacity

1 INTRODUCTION

On some occasions shallow foundations are subjected to eccentrically inclined load as shown in Fig. 1 for the case of a strip foundation of width B supported by sand. In Fig. 1, Q_u is the ultimate load per unit length of the foundation applied with an eccentricity e and inclined at an angle α with respect to the vertical. Meyerhof (1963) proposed a relationship for the vertical component of the average ultimate load per unit area of the foundation based on the effective area concept. For granular soil it can be expressed as

$$q_{uv(e,\alpha)} = \frac{Q_u \cos\alpha}{B} = \frac{B'}{B}(qN_q d_q i_q + 0.5\gamma B' N_\gamma d_\gamma i_\gamma) \quad (1)$$

where $q_{uv(e,\alpha)}$ = average vertical component of the ultimate load per unit area with load eccentricity e and load inclination α, $q = \gamma D_f$, γ = unit weight of sand, D_f = depth of foundation, N_q, N_γ = bearing capacity factors, B' = effective width = $B - 2e$, d_q, d_γ = depth factors, and i_q, i_γ = inclination factors.

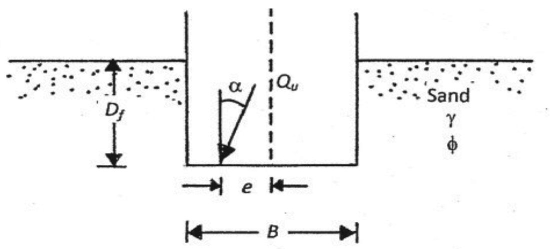

Figure 1. Shallow foundation on granular soil subjected to eccentrically inclined load.

The relationships for bearing capacity, depth and inclination factors are as follow,

$$N_q = e^{\pi \tan\phi}\left(\frac{1+\sin\phi}{1-\sin\phi}\right) \quad (2)$$

$$N_\gamma = (N_q - 1)\tan(1.4\phi) \quad (3)$$

$$d_q = d_\lambda = 1 + 0.1\left(\frac{D_f}{B}\right)\tan\left(45 + \frac{\phi}{2}\right) \quad (\text{for } \phi \geq 10°) \quad (4)$$

$$i_q = \left(1 - \frac{\alpha°}{90°}\right)^2 \quad (5)$$

and

$$i_\gamma = \left(1 - \frac{\alpha°}{\phi°}\right)^2 \quad (6)$$

where ϕ = soil friction angle.

Purakayastha and Char (1977) conducted stability analyses of eccentrically loaded strip foundations ($\alpha = 0$) supported by granular soil using the method of slices proposed by Janbu (1957). Based on their study it was proposed that, for a given D_f/B,

$$\frac{q_{uv(e,\alpha=0)}}{q_{uv(e=0,\alpha=0)}} = R = 1 - b\left(\frac{e}{B}\right)^c \quad (7)$$

where $q_{uv(e,\alpha=0)}$ = average ultimate vertical load per unit area of the foundation with load eccentricity e and load inclination α = 0, $q_{uv(e=0,\alpha=0)}$ = average ultimate bearing capacity with centric vertical load, R = reduction factor, b and c = functions of D_f/B only and independent of soil friction angle ϕ. The variation of b and c with D_f/B [Eq. (7)] is given in Table 1.

Table 1. Variation of b and c with D_f/B—Analysis of Purkayastha and Char (1977)

D_f/B	b	c
0	1.862	0.73
0.25	1.811	0.785
0.5	1.754	0.80
1.0	1.820	0.888

For D_f/B between zero and 1, the average values of b and c are about 1.81 and 0.8 respectively. So Eq. (7) can be approximated as,

$$\frac{q_{uv(e,\alpha=0)}}{q_{uv(e=0,\alpha=0)}} \approx R = 1 - 1.8\left(\frac{e}{B}\right)^{0.8} \tag{8}$$

Saran and Agarwal (1991) performed a limit equilibrium analysis to evaluate the ultimate bearing capacity of strip foundation subjected to eccentrically inclined load. According to this analysis, for a foundation on granular soil,

$$q_{u(e/B,\alpha)} = qN_{q(e/B,\alpha)} + \frac{1}{2}\gamma B N_{\gamma(e/B,\alpha)} \tag{9}$$

where $q_{u(e/B,\alpha)}$ = average inclined load per unit area with load eccentricity ratio e/B and load inclination α, $N_{q(e/B,\alpha)}$ and $N_{\gamma(e/B,\alpha)}$ = bearing capacity factors expressed in terms of load eccentricity e and inclined at an angle α to the vertical. They are available in tabular and graphical form in the original paper of Saran and Agarwal (1991).

The purpose of the present study is to present several laboratory model test results for the average ultimate inclined load per unit area of a strip foundation, $q_{u(e,\alpha)}$, supported by dense sand [i.e. $q_{uv(e,\alpha)}/\cos\alpha$]. A reduction factor has been proposed to estimate $q_{u(e,\alpha)}$ at a given D_f/B from the ultimate bearing capacity with centric vertical loading $q_{uv(e=0,\alpha=0)}$ at similar D_f/B.

2 LABORATORY MODEL TESTS

Laboratory model tests were conducted using a poorly graded sand with effective size D_{10} = 0.325 mm, uniformity coefficient C_u = 1.45 and coefficient of gradation C_c = 1.15. The model tests were conducted in a tank measuring 1.0 m (length) × 0.504 m (width) × 0.655 m (height). The two length sides of the tank were made of 12mm thick high strength fiberglass. All four sides of the tank were braced to avoid bulging during testing. The model foundation measured 100 mm (width B) × 500 mm (length L) × 30mm (thickness t) and was made from a mild steel plate. The bottom of the footing was made rough by applying glue and then rolling the steel plate over sand. Since the width of the test tank and the length of the model foundation were approximately the same, a plane strain condition roughly existed during the tests.

Sand was poured into the test tank in layers of 25 mm from a fixed height by raining technique to achieve the desired average unit weight of compaction. The height of fall was fixed by making several trials in the test tank prior to the model test to achieve the desired unit weight of sand. The model foundation was placed at a desired D_f/B ratio at the middle of the box. Load to the model foundation was applied by a loading assembly which was capable of applying eccentrically inclined load. It consisted of three units: (a) the electrical control panel, (b) hydraulic power pack and (c) loading device. The loading device was a combination of a beam, four cylinders, four supporting columns and a base. The hydraulic cylinder was the device that converted fluid power into linear mechanical force and motion. It converted fluid energy to an output force in a linear direction for executing different jobs. The capacity of the hydraulic cylinder in universal static loading setup was 100 kN. The load could be applied to the model foundation in the range of 0 to 100 kN with an accuracy of 1 N. The inclination of the load could be changed by forward and backward movement of the cylinder. The inclination of the load remained intact throughout the testing period by the provision of the check valve. Settlement of the model foundation was measured by dial gauges placed on two edges along the width side of the model foundation.

The average values of the various parameters during the model tests are given in Table 2.

Table 2. Model Test Parameters

Parameters	Values
Unit weight of compaction of sand	14.36 kN/m^3
Relative density of compaction	69%
Soil friction angle	40.8°
D_f/B	0, 0.5, 1
e/B	0, 0.05, 0.1, 0.15
Load inclination α	0, 5°, 10°, 15°, 20°

3 MODEL TEST RESULTS

Based on the load-settlement curves, the average ultimate inclined loads per unit area of the foundation $q_{u(e,\alpha)}$ (= Q_u/B; see Fig. 1) obtained from the present tests are given in Table 3.

4 ANALYSIS OF MODEL TEST RESULTS

Based on Eqs. (5), 6) and (7), it was assumed that, for a given D_f/B,

$$RF = \text{reduction factor}$$
$$= \frac{q_{u(D_f/B,e,\alpha)}}{q_{u(D_f/B,e=0,\alpha=0)}} = \left[1 - a\left(\frac{e}{B}\right)^m\right]\left(1 - \frac{\alpha}{\phi}\right)^n \tag{10}$$

In order to determine the values of a, m and n, the following procedure was used:

Step 1: For vertical loading conditions (i.e. α =0), Eq. (10) takes the form

$$RF = \left[1 - a\left(\frac{e}{B}\right)^m\right] \tag{11}$$

With α = 0 and, for a given D_f/B, regression analyses were performed to obtain the magnitudes of a and m.

Step 2: Using the values of a and m obtained in Step 1 and Eq. (10), for a given D_f/B, a regression analysis was performed to obtain the value of n for α > 0°.

The values of a, m and n obtained from analyses described above are given below,

- D_f/B = 0 — a = 2.23, m = 0.81, n = 1.98
- D_f/B = 0.5 — a = 2.0, m = 0.88, n = 1.23
- D_f/B = 1.0 — a = 1.76, m = 0.92, n = 0.97

From the values of a, m and n, It can be seen that the variations of a and m with D_f/B are very minimal; however, the value of n decreases with the increase in embedment ratio. The average values of a and m are 1.97 and 0.87 respectively.

Table 3. Experimental Average Ultimate Loads Per Unit Area and Reduction Factors.

D_f/B (1)	α (deg) (2)	e/B (3)	Experimental $q_{u(D_f/B,e,\alpha)}$ (kN/m^2) (4)	Experimental RF [Eq. (10)] (5)	Calculated RF [Eqs. (10), (12), (13) and (14)] (6)	Deviation— $\frac{\text{Col.6} - \text{Col.5}}{\text{Col.6}}$ (%) (7)
0	0	0	166.77	1.0	1	0.00
0	0	0.05	133.42	0.8	0.9	11.11
0	0	0.1	109.87	0.659	0.8	17.63
0	0	0.15	86.33	0.518	0.7	26.00
0	5	0	128.51	0.771	0.77	-0.13
0	5	0.05	103.01	0.618	0.693	10.82
0	5	0.1	86.33	0.518	0.616	15.91
0	5	0.15	65.73	0.394	0.539	26.90
0	10	0	96.14	0.576	0.570	-1.05
0	10	0.05	76.52	0.459	0.513	10.53
0	10	0.1	62.78	0.376	0.456	17.54
0	10	0.15	51.99	0.312	0.399	21.80
0	15	0	66.71	0.4	0.4	0.00
0	15	0.05	53.96	0.324	0.36	10.00
0	15	0.1	44.15	0.265	0.32	17.19
0	15	0.15	35.12	0.211	0.28	24.64
0	20	0	43.16	0.259	0.26	0.38
0	20	0.05	34.83	0.209	0.234	10.68
0	20	0.1	29.43	0.176	0.208	15.38
0	20	0.15	23.54	0.141	0.182	22.53
0.5	0	0	264.87	1.0	1.0	0.00
0.5	0	0.05	226.61	0.856	0.9	4.89
0.5	0	0.1	195.22	0.737	0.8	7.88
0.5	0	0.15	164.81	0.622	0.7	11.14
0.5	5	0	223.67	0.844	0.822	-2.68
0.5	5	0.05	193.26	0.73	0.74	1.35
0.5	5	0.1	165.79	0.626	0.658	4.86
0.5	5	0.15	140.28	0.530	0.575	7.83
0.5	10	0	186.39	0.704	0.656	-7.32
0.5	10	0.05	160.88	0.607	0.59	-2.88
0.5	10	0.1	137.34	0.519	0.525	1.14
0.5	10	0.15	116.74	0.441	0.459	3.92
0.5	15	0	151.07	0.57	0.503	-13.32
0.5	15	0.05	129.49	0.489	0.453	-7.95
0.5	15	0.1	111.83	0.422	0.402	-4.98
0.5	15	0.15	94.18	0.356	0.352	-1.14
0.5	20	0	115.76	0.437	0.364	-20.06
0.5	20	0.05	98.1	0.37	0.328	-12.80
0.5	20	0.1	85.35	0.322	0.291	-10.65
0.5	20	0.5	72.59	0.274	0.255	-7.45
1.0	0	0	353.16	1.0	1.0	0.00
1.0	0	0.05	313.92	0.889	0.9	1.22
1.0	0	0.1	278.6	0.789	0.8	1.38
1.0	0	0.15	245.25	0.694	0.7	0.86
1.0	5	0	313.92	0.889	0.877	-1.37
1.0	5	0.05	277.62	0.786	0.79	0.51
1.0	5	0.1	241.33	0.683	0.702	2.71
1.0	5	0.15	215.82	0.611	0.614	0.49
1.0	10	0	264.87	0.750	0.755	0.66
1.0	10	0.05	239.36	0.678	0.679	0.15
1.0	10	0.1	212.88	0.603	0.604	0.17
1.0	10	0.15	188.35	0.533	0.528	-0.95
1.0	15	0	225.63	0.639	0.632	-1.11
1.0	15	0.05	206.01	0.583	0.569	-2.46
1.0	15	0.1	179.52	0.508	0.506	-0.40
1.0	15	0.15	155.98	0.442	0.443	0.23
1.0	20	0	183.45	0.519	0.51	-1.76
1.0	20	0.05	166.77	0.472	0.459	-2.83
1.0	20	0.1	143.23	0.406	0.408	0.49
1.0	20	0.15	126.55	0.358	0.357	-0.28

Considering the uncertainties involved in any experimental evaluation of ultimate bearing capacity, we can assume without loss of much accuracy

$$a \approx 2 \tag{12}$$

$$m \approx 1 \tag{13}$$

$$n \approx 2 - \left(\frac{D_f}{B}\right) \tag{14}$$

The experimental values of *RF* defined by Eq. (10) are shown in Col. 5 of Table 1. For comparison purposes, the predicted values of the reduction factor *RF* obtained using Eqs. (10), (12), (13) and (14) are shown in Col. 6 of Table 3. The deviations of the predicted values of *RF* from those obtained experimentally are shown in Col. 7 of Table 3. In most cases the deviations are ±15% or less; however, in some cases, the deviations were about 25%. Thus Eqs. (10), (12), (13) and (14) provide reasonable good and simple approximations to estimate the ultimate bearing capacity of strip foundations ($0 \le D_f/B \le 1$) subjected to inclined eccentric loading. Or, for a given D_f/B,

$$q_{u(D_f/B,e,\alpha)} = q_{u(D_f/B,e,\alpha=0)} \times \left[1 - 2\left(\frac{e}{B}\right)\right]\left(1 - \frac{\alpha}{\phi}\right)^{2-(D_f/B)} \tag{15}$$

5 CONCLUSIONS

The results of a number of laboratory model tests conducted to determine the ultimate bearing capacity of a strip foundation supported by sand and subjected to an eccentrically inclined load with an embedment ratio varying from zero to one have been reported. Tests were conducted on dense sand. The load eccentricity ratio e/B was varied from zero to 0.15, and the load inclination α was varied from zero to 20° (i.e. $\alpha/\phi \approx 0$ to 0.5). Based on the test results and within the range of parameters tested, an empirical relationship for a reduction factor *RF* has been proposed [Eq. (15)]. A comparison between the reduction factors obtained from the empirical relationships and those obtained experimentally shows, in general, a variation of ±15% or less. In a few cases, the deviation was about 25 to 30%.

6 REFERENCES

Janbu, N. 1957. Earth pressures and bearing capacity calculations by generalized procedure of slices. *Proceedings, IV International Conference on Soil Mechanics and Foundation Engineering*, London, 2, 207-211.

Meyerhof, G.G. 1963. Some recent research on the bearing capacity of foundations. *Canadian Geotechnical Journal*, 1 (1), 16-26.

Purkayastha, R.D. and Char, R.A.N. 1977. Stability analysis for eccentrically loaded footings. *Journal of the Geotechnical Engineering Division*, ASCE, 103 (6), 647-651.

Saran, S. and Agarwal, R.K. 1991. Bearing capacity of eccentrically oblique loaded foundation. *Journal of Geotechnical Engineering*, ASCE, 117 (11), 1669-1690.

Estimating settlements of footings in sands – a probabilistic approach

Estimation des tassements de semelles dans les sables – une approche probabiliste

Bungenstab F.C., Bicalho K.V., Ribeiro R.C.H.
Federal University of Espirito Santo – UFES – Vitória/ES, Brazil.

Aoki R.C.H.
Engineering School of São Carlos – USP, São Carlos/SP, Brazil.

ABSTRACT: This paper discuss about probabilistic settlement analysis of footings in sands, focusing on the load curve (estimated settlements). For this purpose, three methodologies that take the First and Second Order Second Moment (FOSM and SOSM), and Monte Carlo Simulation (MCS) methods for calculating mean and variance of the estimated settlements through Schmertmann's 1970 equation are discussed. The deformability modulus (E_{Si}) is considered varying according to the division of the soil into sublayers and it is analyzed as the only independent random variable. As an example of application, a hypothetical case in state of Espirito Santo, Brazil, is evaluated. Simulations indicate that there is significant similarity between SOSM and MCS methods, while the FOSM method underestimates the results due to the non-consideration of the high orders terms in Taylor's series. The contribution to the knowing of the uncertainties in settlement predictions can provides a more safety design.

RÉSUMÉ : Cet article traite de l'approche probabiliste de l'estimation des tassements de semelles dans les sables, en se concentrant sur la courbe charge-tassements estimés. Pour ce faire, trois méthodes basées sur les moments du premier et deuxième ordre (FOSM et SOSM), des moyennes et écarts-types et sur des simulations de Monte Carlo (MCS) ont été utilisées pour le calcul du tassement moyen et sa variation à l'aide de l'équation de Schmertmann (1970) et sont discutées. Le module de déformabilité (ESi) est considéré variable dû à la division du sol en sous-couches et il est considéré comme le seul paramètre indépendant et aléatoire. Comme exemple d'application, une étude de cas situé dans l'état d'Espirito Santo, au Brésil, est discutée et évaluée. Les simulations montrent qu'il y a une similitude significative entre les résultats obtenus par les simulations SOSM et MCS, alors que les estimations FOSM sous-estiment les tassements en raison de la non-prise en compte des termes d'ordre élevé des décompositions en série de Taylor. La contribution à la connaissance des incertitudes dans les prédictions de tassement peut fournir un dimensionnement plus fiable.

KEYWORDS: Sandy soils, foundations (engineering), settlement of structures, reliability (engineering), probabilities.

1 INTRODUCTION

Probabilistic or reliability studies and risk evaluation have become increasing popular in geotechnical engineering only in the last decades (Sivakugan and Johnson 2004), while geotechnical analysis are still usually made by conventional deterministic approaches, based on safety factors. Most commonly studies in probabilistic analysis reported in the literature discuss the ultimate limit state (ULS), representing the probability of a foundation to failure, p_F. According to Aoki et al. (2002), this probability is function of relative position and scatter degree of the probability density curves of solicitation, fs(S), and resistance, F_R(R), as shown in figure 1, so:

$$p_F = \int_0^\infty F_R(R).f_S(S)dx \qquad (1)$$

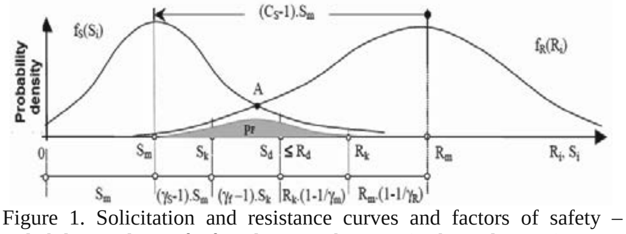

Figure 1. Solicitation and resistance curves and factors of safety – Reliability analysis of a foundation at the ULS (Aoki et al., 2002).

The same probabilistic concept can be applied to analyze the serviceability limit state (SLS) of a foundation (figure 2). In a foundation settlement analysis, the probability of failure becomes the probability of predicted or estimated settlement (calculated with service loads) to exceed limiting settlement (limiting movement affecting visual appearance, serviceability or function and stability). Here, solicitation and resistance functions assume the variability of predicted and limiting settlements, respectively, which are treated as dependent random variables. The probability of SLS to failure, p_E is then:

$$p_E = \int_0^\infty \rho(x).\rho_{\lim}(x).dx \qquad (2)$$

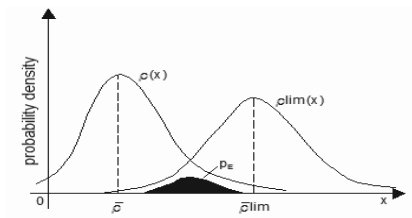

Figure 2.
Solicitation and resistance curves – Reliability analysis of a foundation at the SLS.

In the specific case of settlements of footings in sands, the predicted settlements can be evaluated through traditional methods, such as: Schmertmann (1970), Schmertmann et al. (1978), Burland and Burbidge (1984), Berardi and Lancellotta (1991). The limiting settlements evaluation can be made by using observational, empirical, structural or numerical modelling methods (Negulescu and Foerster 2010), but are beyond the scope of this paper.

This paper focuses on the solicitation curve and assumes, as a simplification, that the variability of the resistance (limiting settlement) curve is zero (i.e. it has been considered constant for some specific deterministic value). Thus, the probability of occurrence of limiting settlements becomes:

$$p_E[\rho \geq \rho_{\lim}] = \int_{\rho \lim}^{\infty} \rho(x).dx \tag{3}$$

The integrals of equations (1, 2 and 3) are commonly solved using analytical approximations (or reliability methods). In the following sections three methodologies using FOSM, SOSM and MCS methods with Schmertmann's (1970) equation are shortly presented and discussed as a simple and practical way to characterize the settlement solicitation curve for a case of a single footing in a sandy soil.

2 ANALYZED METHODOLOGIES

2.1 *Main concepts adopted*

The main concepts adopted on the analyzed methodologies are:

- The total predicted settlement (ρ) is given by Schmertmann's (1970), calculated through the sum of the settlement increments (ρ_i) of each sublayer:

$$\rho = \sum_{i=1}^{N} \rho_i \tag{4}$$

where: i=1, N and N is the number of adopted sublayers.

- If the increments (ρ_i) are statistically independents and $V[\rho_i]$ are the variance increments of the sublayers then, the total variance also can be calculated as the sum of $V[\rho_i]$:

$$V[\rho] = \sum_{i=1}^{N} V[\rho_i] \tag{5}$$

The proposed simplifications consider that the predicted settlement is function of only one random variable (E_{Si}, in each sublayer), and is completely described by its first two moments (mean and variance). The evaluation must have done considering the soil stratification, first through the evaluation of each sublayer, individually, and then accounting for the entire stratum of the subsoil (sum of the increments).

2.2 *The FOSM and SOSM methods*

Consider the given form of the performance function of the random variables x_1, x_2, x_3... x_i, independent, such as: $G[X]=G(x_1, x_2, x_3... x_i)$. Developing the function G[X] about its mean and the mean of the random variables x_i, using the Taylor's expansion series, gives (Baecher and Christian 2003):

$$G[X] = G[\bar{X}] + \frac{1}{1!}\frac{\partial G}{\partial x}(X - \bar{X}) + \\ + \frac{1}{2!}\frac{\partial^2 G}{\partial x^2}(X - \bar{X})^2 + \frac{1}{3!}\frac{\partial^3 G}{\partial x^3}(X - \bar{X})^3 + ... \tag{6}$$

The mean (E[ρ]) and variance (V[ρ]) of the predicted settlement can be obtained from equation (6), considering the Schmertmann's (1970) method as the performance function and assuming the parameter E_S as the unique random variable. For the FOSM method, gives:

$$E[\rho] = \rho = C_1 C_2 \sigma * \sum_{i=1}^{N} \left(\frac{I_{zi}\Delta_{zi}}{\bar{E}_{si}} \right) \tag{7}$$

$$V[\rho] = \left[C_1 C_2 \sigma^* \sum_{i=1}^{N} \frac{I_{zi}\Delta_{zi}}{\bar{E}_{si}^{\,2}} \right]^2 .V[E_{si}] \tag{8}$$

For the SOSM method, settlement mean and variance are:

$$E[\rho] = C_1 C_2 \sigma^* \sum_{i=1}^{N} \left(\frac{I_{Zi}\Delta_{Zi}}{\bar{E}_{Si}} \right) + \\ + C_1 C_2 \sigma^* \sum_{i=1}^{N} \left(\frac{I_{Zi}\Delta_{Zi}}{\bar{E}_{Si}^{\,3}} .V[E_{Si}] \right) \tag{9}$$

$$V[\rho] = \left[C_1 C_2 \sigma^* \sum_{i=1}^{N} \frac{I_{Zi}\Delta_{Zi}}{\bar{E}_{Si}^{\,2}} \right]^2 .V[E_{Si}] + \\ + 2\left[C_1 C_2 \sigma^* \sum_{i=1}^{N} \frac{I_{Zi}\Delta_{Zi}}{\bar{E}_{Si}^{\,3}} \right]^2 .V[E_{Si}]^2 \tag{10}$$

The first terms at the right side of equations (9 and 10) correspond exactly to the mean and variance calculated by the FOSM method, while the second terms represent the additional terms considered in the Taylor's series. This simple observation shows that the use of the FOSM method underestimates the results of mean and variance as increasing the importance of the second term of the considered performance function.

With the calculated values of settlement mean, variance and standard deviation (root square of variance) in hands, the probabilistic analysis can be made by setting the lognormal distribution to represent the predict settlement and specifying deterministic values to limiting settlement.

The lognormal distribution was used here for being a strictly positive distribution, while having a simple relationship with the normal distribution (Bredja et al. 2000, Fenton and Griffiths 2002, Goldsworthy 2006).

The methodologies assume the analysis of an isolated footing. Nevertheless, if two non-correlated footings are being evaluated, differential settlement can be obtained by:

$$E[\Delta\rho] = E[\rho_1] - E[\rho_2] \tag{11}$$

$$V[\Delta\rho] = V[\rho_1] + V[\rho_2] \tag{12}$$

where: $E[\rho_1]$ and $E[\rho_2]$ are mean predicted settlements of the footings and $V[\rho_1]$ and $V[\rho_2]$ are its variances.

2.3 *The MCS method*

The Monte Carlo Simulation method consists basically in the simulation of all random variables and the resolution of the performance function for all those generated values. Here again, deformability modulus is the only random variable.

As a simplification, is proposed a number of 1.000 simulations of modulus for each sublayer, using lognormal distribution. The simulation can be done by using random number generator algorithms for Microsoft Excel. The main steps are summarized below:

- Analysis of mean and variance of q_{ci} results, for each sublayer.
- Estimation of mean and variance of E_{Si}.
- Simulation of E_{Si} (using mean, variance and lognormal distribution).
- Calculus of settlement mean and variance increment for each sublayer.
- Calculus of total settlement mean and variance.
- Probabilistic settlement analysis using lognormal distribution and an adopted limiting settlement value(s).

2.4 *Evaluation of deformability modulus in the sublayers*

In reliability analysis, independent random variables are influenced by uncertainties and it must be appropriate quantified. In the proposed methodologies, only one random variable is adopted (E_{Si}) for each sublayer.

The uncertainties in E_{Si} can be analyzed by attributing values to E_{Si} variance ($V[E_{Si}]$), or by analyzing the sources of uncertainties in the E_{Si} estimations. Considering that the moduli E_{Si} are estimated from CPT, three sources of uncertainty are suggested to be accounted for:

(i) The uncertainties due to field measurements (q_{ci}, in this case) – in other words, the sum of inherent soil variability and equipments/measurement procedures errors of CPT. This variance is named $V_1[E_{Si}]$.

(ii) The uncertainties due to transformation models – in other words, the empirical correlations used to transform the field measurement results (q_{ci}) into required design parameters (E_{Si}). This variance is named $V_2[E_{Si}]$;

(iii) Statistical uncertainties – due to limited sampling or insufficient representative sampling data in the field. This variance is named $V_3[E_{Si}]$.

The sources of uncertainties represented by $V_1[E_{Si}]$ and $V_2[E_{Si}]$ are explicit in the E_{Si} x q_{ci} correlations. The typical form of those correlations is:

$$E_{Si} = \alpha . q_{Ci} \tag{13}$$

Observe that in equation (13) two variables can contribute for the uncertainties in E_{Si} estimations, which are: q_{ci} and α. It represents the uncertainties $V_1[E_S]$ and $V_2[E_S]$, as assumed before. The FOSM method is applied to equation (13) to give those sources of uncertainties. Then, $V_1[E_S]$ e $V_2[E_S]$ are:

$$V_1[E_{Si}] = \alpha_{average}{}^2 . V[q_{Ci}] \tag{14}$$

in which: $V[q_{ci}]$ is the sampling variance, calculated using q_{ci} results, of the i^{th} sublayer, and $\alpha_{average}$ is the average or mean α-value, from the choosed correlations.

$$V_2[E_{Si}] = q_{Ci\,average}{}^2 . V[\alpha] \tag{15}$$

in which: $V[\alpha]$ is the variance of α –values, supposed to be equally likely. To evaluate $V_2[E_{Si}]$, two or more empirical correlations are needed or, in other case, it results zero.

The third source of uncertainties evaluated is due to the representative of sampling data. Assuming that this source of uncertainties is function only of the amount of sampling (size of sample), it can be calculated using the following equation proposed by DeGroot (1986; apud Goldsworthy 2006):

$$V_3[E_S] = \frac{V_1[E_S]}{n} \tag{16}$$

in which: $V_1[E_S]$ is the sampling variance from E_S results; n is the number of data obtained from CPT.

Thus, the equation to account for all sources of uncertainties on the variance of E_{Si}, of the i^{th} sublayer is:

$$V[E_{Si}] = V_1[E_{Si}] + V_2[E_{Si}] + V_3[E_{Si}] \tag{17}$$

2.5 *Further discussions*

Comparative analysis has showed that the use of the FOSM method underestimates the results for $COV[E_S]>30\%$, reaching up to 50% error when $COV[E_S]=100\%$, due to the non-consideration of the higher orders terms in Taylor‘s series, while SOSM and MCS methods seems to converge, approximately, to same results for all $COV[E_S]$ values.

It has been also observed that the depth where the major variance contribution occurs is highly dependent of the E_{Si} values, with strong influence of the I_Z distribution factor, from Schmertmann's (1970). So, the significance of settlement variance contribution ($V[\rho_i]$), of the i^{th} sublayer, in total settlement variance ($V[\rho]$) increases as the lower the mean value of E_{Si} and the closer the sublayer is to I_{Zmax} depth.

As being simplified methods, is important to summarize the advantages and limitations of its use. Some advantages are:

- Easy application, trough electronic spreadsheets, without having finite element or advanced calculation software's.
- It's very helpful for giving guidance on the sensivity of design results (Griffiths et al. 2002), outcome from Schmertmann's (1970) equation, to variations of deformability modulus.
- Is possible to verify the distribution and the contribution of settlement variances in the sublayers.
- Despite the non-account for spatial correlations or scale of fluctuation of deformability modulus, the use of Taylor's methods is not against safety, as observed previously by Gimenes and Hachich (1992).

Some limitations are:

- It's assumed a single and isolated footing (i.e. there are no interaction among strain bulbs of adjacent footings and no soil-structure interaction effects).
- In a foundation SLS analysis is necessary to account for the variability of other important parameters as: geometry and load of footings, which were considered constants for the present study.

On the use of the proposed methodologies, is recommended that the sublayer thickness be considered as small as possible, so the influence of tendencies in vertical variability is minimal (Campanella et al, 1987). For example, in mechanical CPT with 20cm interval data, is indicated to set 20cm for sublayer thickness, so the vertical variability is already considered in the subsoil stratification and is not necessary to detrend the data (since the sublayers are treated as independent from each other). In this case, the evaluated uncertainties in moduli are only from horizontal variability of the sublayers.

3 EXAMPLE OF APPLICATION

This section presents an example of application of the SOSM methodology. The case considers one footing with 1600 kN centrally applied load, size of 2,0m x 2,0m, embedded 1,0m below ground surface. The subsoil stratum is showed in figure 3. This situation with shallow stratum composed by sand with varied relative density is a typical soil formation from the coastal of Vitoria/ES, influenced by the transgression/regression marine phenomena, occurred in Quaternaries' period.

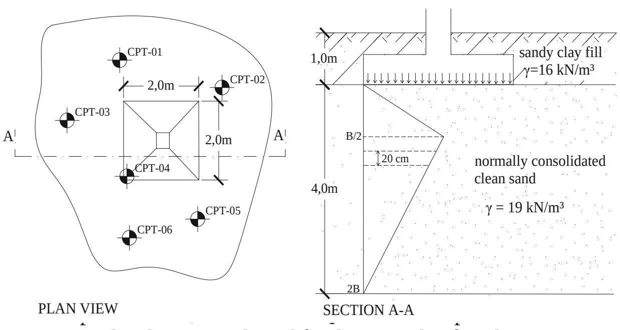

Figure 3. Subsoil stratum adopted for the example of application.

The results of 06 mechanical cone penetration tests (CPT), with 20 cm limit interval data, are hypothetically assumed to be available in a region around the footing, which is represented by the shown subsoil stratum.

For Schmertmann's (1970) equation, sublayer thickness was set at 20 cm. To account for soil variability in this region is firstly necessary to analyze statistically the CPT data. For each sublayer, q_{ci} mean and variance values must be calculated.

After that, deformability modulus has to be estimated for each sublayer, through the adopted(s) empirical correlation(s). Here, it's assumed the use of only one correlation, which is given by Schmertmann's (1970):

$$E_{Si} = 2 . q_{Ci} \tag{18}$$

The transformation must be done using mean q_{ci} values.

The next step is to calculate $V[E_{Si}]$. Observe that, as only one empirical correlation was adopted, $V[\alpha] = 0$ and then, $V_2[E_{Si}]$ becomes automatically null.

Following, the settlement mean and variance contribution of each sublayer has to be evaluated. Table 1 shows the main calculation steps and results for the given example, where: q_{ci} and E_{Si} are given in MPa and predicted settlements results (ρ, $\sigma[\rho]$) are given in mm. Variances are given in square units.

Table 1. Evaluation of CPT results, uncertainties in E_{Si}, and application of the SOSM method.

Sublayer	q_{ci}	$V[q_{ci}]$	E_{Si}	$V[E_{Si}]$	ρ_i	$V[\rho_i]$	% in $V[\rho]$
1	10,0	10,3	20,1	48,2	0,252	0,007	0,2
2	9,6	9,9	19,2	46,0	0,791	0,077	2,0
3	9,7	9,9	19,4	46,0	1,308	0,207	5,4
4	9,2	9,4	18,4	44,1	1,937	0,481	12,5
5	8,9	9,3	17,9	43,3	2,576	0,884	22,9
6	9,4	9,6	18,8	44,7	2,607	0,845	21,9
7	9,7	9,8	19,3	45,7	2,358	0,672	17,4
8	11,9	12,1	23,8	56,4	1,737	0,297	7,7
9	13,3	13,5	26,6	63,0	1,414	0,176	4,6
10	15,4	15,5	30,8	72,2	1,104	0,092	2,4
11	18,1	18,0	36,2	83,8	0,839	0,045	1,2
12	21,5	21,6	42,9	100,8	0,628	0,022	0,6
13	24,2	24,7	48,4	115,3	0,489	0,012	0,3
14	24,8	25,8	49,7	120,5	0,413	0,008	0,2
15	21,8	22,6	43,7	105,5	0,400	0,009	0,2
16	20,4	21,0	40,7	97,9	0,352	0,007	0,2
17	19,2	19,8	38,5	92,3	0,291	0,005	0,1
18	16,1	16,3	32,3	76,1	0,250	0,005	0,1
19	15,9	16,0	31,7	74,5	0,153	0,002	0,0
20	15,9	16,0	31,8	74,5	0,051	0,000	0,0
Sum	-	-	-	-	19,95	3,86	100,0
$\sigma[\rho]$	-	-	-	-	-	1,96	-
COV (%)	-	-	-	-	-	9,84	-

The mean and variance of the predicted settlement are then the sum of the increments of each sub-layer, as suggested by the sum at the bottom of the table 1. So, the predicted settlement can now be represented by the form:

$$\rho(mm) = 20 \pm 2 \tag{19}$$

For the complete characterization of the solicitation curve (predicted settlement) lognormal distribution was used. Figure 4 shows the results for the probability of the predicted settlement to exceed different values of limiting settlements in a range between 10 to 50 mm. For example, the probability of the predicted settlement to exceed 25 mm is about 1,1%. For exceeding values of over 40 mm, P [$\rho \geq 40$mm] ≈0.

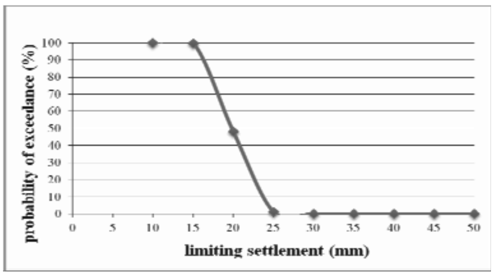

Figure 4. Probability of the predicted settlement to exceed different values of limiting settlement.

The analysis of the sources of uncertainties indicates that about 80% of the settlement variance is influenced by the uncertainties due to inherent soil variability and measurement test errors. It is important to emphasize that the uncertainties due to transformation model was not evaluated in the example.

4 CONCLUSIONS

It has been proposed and briefly discussed three simplified methodologies for probabilistic analysis of settlements of footings in sands, which adopts the soil stratification to compute the only considered random variable (deformability modulus).

Despite the presented limitations adopted on methodologies proposal, it can be assumed as a first approximation for evaluating the uncertainties (especially in deformability modulus) at the SLS analysis of a foundation. The association between probabilistic analysis and settlement predictions can become an interesting tool for geotechnical engineering in the knowing of soil variability and related uncertainties.

Therefore, any attempt to quantify the sources of uncertainties and its effects in geotechnical analysis, through probabilistic models, may become an important tool for helping engineers to make better and consistent design decisions.

5 REFERENCES

Aoki, N.; Cintra, J. C. A. and Menegotto, M. L. 2002. *Segurança e confiabilidade de fundações profundas*. 8th Congresso Nacional de Geotecnia, vol. 2, p. 797-806, Lisboa.

Baecher, G. B. and Christian, J. T. 2003. Reliability and statistics in geotechnical engineering. John Wiley and Sons, Chichester, England.

Berardi, R. and Lancellotta, R. 1991. Stiffness of granular soils from field performance. Gèotechnique 41, No. 1, p. 149-157.

Bredja, J. J. et al. 2000. Distribution and variability of surface soil properties at a regional scale. Soil Science Society of America Journal, 64, p. 974-982.

Burland, J. B. and Burbidge, M. C. 1985. Settlement of foundations on sand and gravel. Proceedings of Institution of Civil Engineers, Part 1, 78, Dec., p. 1325-1381.

Campanella, R. G.; Wickremesingue, D. S. and Robertson, P. K. 1987. Statistical treatment of cone penetrometer test data. Department of Civil Engineering, University of British Columbia, Vancouver B.C., Canada, p. 1010-1019.

Fenton, G. A. and Griffiths, D. V. 2002. Probabilistic foundation settlement on spatially random soil. ASCE Journal of Geotechnical and Geoenvironmental Engineering, 128(5), p. 381-390.

Gimenes, E. A. and Hachich, W. 1992. *Aspectos quantitativos em análises de risco geotécnico*. Solos e Rocha, São Paulo, 15, (1), p. 3-9.

Goldsworthy, J. S. 2006. Quantifying the risk of geotechnical site investigations. PhD. The University of Adelaide, Australia, January.

Griffiths, D. V.; Fenton, G. A. and Tveten, D. E. 2002. Probabilistic geotechnical analisys. How difficult does it need to be?, Proc. of the Int. Conf. on Probabilistics in Geotechnics: Technical and Economic Estimation, R. Pottler, H. Klapperich and H. Schweiger (eds.), Graz, Austria, United Engineering Foundation, New York, September.

Negulescu, C. and Foerster, E. 2010. Parametric studies and quantitative assessment of the vulnerability of a RC frame building exposed to differential settlements. Natural Hazards and Earth System Sciences. Sci., 10, p. 1781-1792.

Schmertmann, J. H. 1970. Static cone to compute static settlement over sand. Journal of the Soil Mechanics and Foundations Division, ASCE, vol.96, n° SM.3, p. 1011-1043.

Schmertmann J. H.; Hartman, J. P. and Brown, P. R. 1978. Improved strain influence factor diagrams. Journal of the Geotechnical Division, ASCE, 104(8), p. 1131-1135.

Sivakugan, N. and Johnson, K. 2004. Settlement predictions in granular soils: a probabilistic approach. Gèotechnique, LIV (07): p. 499-502.

Settlement velocity measured over ten years in major-scale shallow foundations on a preloaded 20-m thick silty alluvial layer

Velocité des affaissements mesurés sur dix ans, sur une foundation superficielle de grandes dimensions, sur une couche alluviale limoneuse de 20 m d'épaisseur préchargée

Dapena E.
Geotechnics Laboratory, CEDEX, Madrid Polytechnical University, Spain
Román F.
Confederation Hidrográfica del Norte, Ministry for the Environment, Spain
Pardo de Santayana F., Cuéllar V.
Geotechnics Laboratory, CEDEX, Madrid, Spain

ABSTRACT: The site of the GALINDO Waste Water Treatment Plant stands on a layer of alluvial deposits between 15 and 20 m thick which has been subjected to an average preloading of 2 Kg/cm^2 for over 20 years. The Phase 2 biodigester tanks take up two 62 x 195 m rectangles, separated by a 23 m wide central corridor in which the layer of alluvial sediment is 15 m thick. Construction of the slabs and walls of the deposits and the load of the water during normal operation of the plant bring about an increased load of 1.1 Kg/cm^2, giving rise to a net increase in load, as compared to that of the previous five years, of 0.14 Kg/cm^2, while still remaining below the preconsolidation pressure present from the beginning. According to the settlement measurements recorded, ten years after construction, three different areas can be seen at the site of these biodigester tanks: the area corresponding to Deposits 1 and 4, which has low compressibility, where the maximum settlement recorded was 32 and 40 mm; the area corresponding to Deposits 3 and 6, with average compressibility and maximum settlement recorded at 114 and 108 mm and that of Deposits 2 and 5, located in the intermediate area, with high compressibility and maximum settlement recorded at 217 and 156 mm. One obtains the settlement velocity distribution and analyzes them for each of the four deposits that have significant movement, comparing the average velocity corresponding to the period between 0.5 and 9 years, and the average velocity for the period between 8 and 10.3 years.

RÉSUMÉ : le site de la Station de traitement des eaux usées de GALINDO repose sur une couche de dépôts alluviaux de 15 à 20 m d'épaisseur qui a fait l'objet d'une surcharge moyenne de 2 Kg/cm^2 pendant plus de 20 ans. Les réservoirs du digesteur anaérobie de la Phase 2 utilisent deux rectangles de 62 x 195 m, séparés par un couloir central de 23 m de large dans lequel la couche des sédiments alluviaux mesure 15 m d'épaisseur. La construction des dalles et des parois des dépôts et le chargement de l'eau pendant le fonctionnement normal de la station entraînent un chargement supplémentaire de 1,1 Kg/cm^2, ce qui donne lieu à une augmentation nette du chargement de 0,14 Kg/cm^2, si nous le comparons à ceux des cinq années précédentes, tandis qu'il reste au-dessous de la pression de préconsolidation présente depuis le début. Conformément aux mesures de tassement enregistrées, dix ans après la construction, trois zones différentes peuvent être observées à l'endroit de ces réservoirs du digesteur anaérobie : la zone correspondant aux Dépôts 1 et 4 qui présente une faible compressibilité, où les tassements maximums enregistrés étaient de 32 et 40 mm ; la zone correspondant aux Dépôts 3 et 6 présentant une compressibilité moyenne et un tassement maximum enregistrés de 114 et 108 mm et ceux des Dépôts 2 et 5 qui se trouvent dans la zone intermédiaire, présentant une compressibilité élevée et un tassement maximum enregistré de 217 et 156 mm. Nous obtenons la distribution de la vitesse de tassement et nous l'analysons pour chacun des quatre dépôts qui présentent un mouvement significatif. Nous comparons la vitesse moyenne correspondant à une période de 0,5 à 9 ans et la vitesse moyenne sur une période de 8 à 10,3 ans.

KEYWORDS: settlement, alluvial sediments, waste-water treatment plant, blast furnace slag

1 INTRODUCTION

The foundations of the phase 2 biodigester tanks at the Galindo Waste Water Treatment Plant are located on top of a layer of dark gray silty clay alluvial sediments between 15 and 20 m thick. See Fig. 1. Beneath that is a compact layer of clay with gravel between 1 and 2 m thick, which extends down to solid rock.

This soil was preloaded for over 20 years with a layer of blast furnace slag, which transferred an average preload of 2 kg/cm^2. However, the distribution of the preload on the site of the phase 2 biodigesters was not known for certain, and this may explain the different behavior of the pools in response to settlement.

In addition, for the 6 years prior to construction of the phase 2 biodigesters, there was a uniform preload throughout the entire area on a scale equal to that which would be transferred by the biodigesters. However, when they were built, the initial design was modified and the load transferred was 0.14 kg/cm^2 greater than the load of the soil removed.

In Figure 1, it is possible to see that in the middle section of the site, precisely where pools 2 and 5 are located, the level of alluvial sediments is high, at the height of the support level for the foundation slab of pools 2 and 5. However, at the sites of pools 3 and 6, the surface of these deposits is 2.5 m below the foundation height, and the alluvial deposits are at an average depth of 3.5 m at pools 1 and 4.

The influence of preloading on settlement due to primary consolidation has been studied by Johnson (1970), Mitchell (1981), and Statmatopoulos and Kotzias (1983), among others. Secondary consolidation has been studied by Jamiolkowski, et al. (1983), Magnan (1984), Kousotfas, et al. (1987), Yu and Frizzi (1992), Alonso, Gens and Lloret (2000 and 2001), and Alonso (2004).

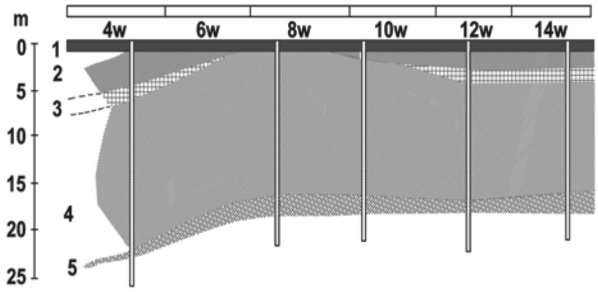

Figure 1. Stratigraphic profile of the soil under the biodigester foundation slabs. 1. Concrete. 2. Slag. 3 and 4. Silty clay. 5. Clay with gravel.

This paper discusses the amount of settlement recorded over the first 10 years since the biodigesters were put into operation and how it has developed over time. It also identifies how the pools have behaved differently, delimiting the areas with settlement and with similar settlement rates

2 SETTLEMENT RECORDED OVER THE 10 YEARS OF OPERATION

Figure 2 shows the total settlement recorded 10 years after the phase 2 biodigesters were constructed and filled. There are also lines connecting points with the same amount of settlement for the following values: 50, 60, 70, 100, 150 and 200 mm. The 50 mm settlement line includes pools 2, 3, 5 and 6. Pools 1 and 4 have settlement of less than 50 mm. Figure 2. The areas with the most settlement are in the center of pool 2, where it reaches 218 mm, and the middle of pool 5, where settlement reaches the level of 158 mm. Despite this significant settlement, no problems with the operation of the pools have become apparent

3 SETTLEMENT MODELS

Settlement development over the 10 years since the phase 2 biodigesters were constructed resembles the model $s = a_m \sqrt{tm} + b = a \sqrt{ta} + b$, where tm is the time since the biodigesters were first filled expressed in minutes, and ta is this time expressed in years.

This model was determined by adjusting the settlement values collected after 2.5 years, as contained in Dapena, et al. (2005). A least squares adjustment has now been applied to the settlement values collected for the period between 0.5 and 9 years after the pools were filled, using the computer program.

The corresponding a and b values at each point have thus been determined, as shown in Table 1.

The graph of how settlement developed at point 53 of pool 2, where the greatest settlement value was obtained, is shown in Figure 3, together with the corresponding model.

$$S_{53} = 0.0812 \sqrt{tm} + 37.4 = 58.9 \sqrt{ta} + 37.4;\ R^2 = 0.99$$

Because a decrease in the settlement rate was noted after 8 years, the model has also been adjusted for the settlement values measured between 8 and 10 years, obtaining the value $a_{8\text{-}10}$. Table 1.

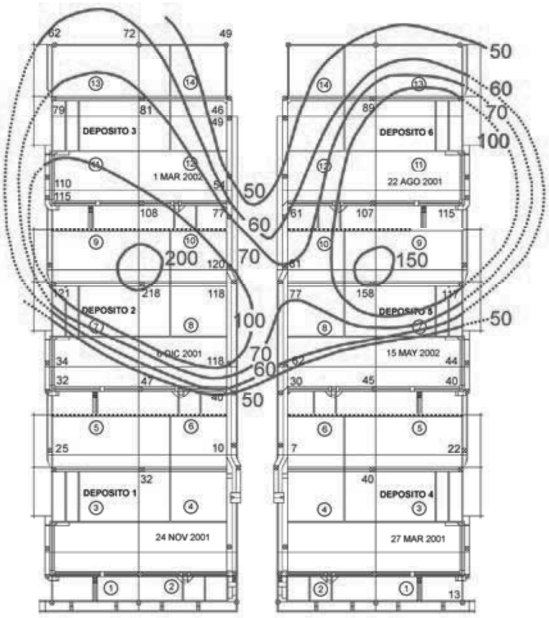

Figure 2. Contour lines for settlement at the biodigesters in mm. Settlement measured on March 12, 2012.

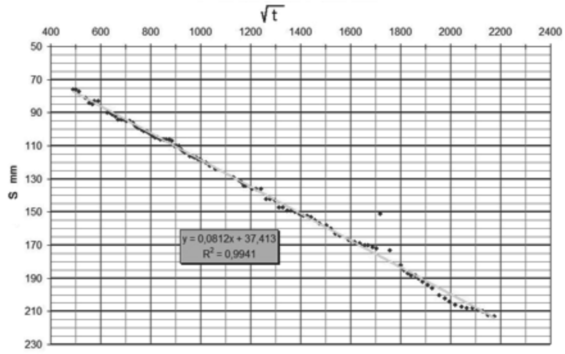

Figure 3. Settlement at point 53 of pool 2 based on the root of t (t= time in minutes) between 0.5 and 9 years and adjustment of the model.

4 DISTRIBUTION OF THE COEFFICIENT $\sqrt{ta}$

The increase in settlement over time is related to coefficient “a” of $\sqrt{ta}$ in the model used. The greater this coefficient is, the greater is the increase in settlement which will occur over a certain period of time.

The distribution of the $a_{0.5\text{-}9}$ coefficient for the biodigesters is shown in Figure 4. The lines connect points with the same value for this coefficient, separating different areas based on this value. The area of pools 1 and 4, where there was the least settlement, also has $a_{0.5\text{-}9}$ coefficients with lower values, less than $a_{0.5\text{-}9}=5$, whereas the center of pool 2 and pool 5, where the greatest settlement was recorded, have higher values for the coefficient: $a_{0.5\text{-}9}=58.9$ and $a_{0.5\text{-}9}=37.5$, respectively.

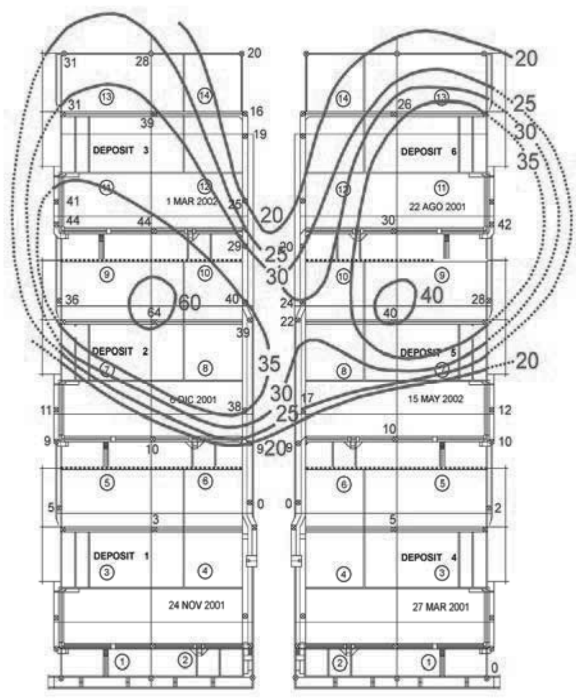

Figure 4. Distribution of values for the coefficient a.

5 SETTLEMENT DEVELOPMENT

According to the values for the coefficient a, shown in Table 1, in general, at each point the values for $a_{8\text{-}10}$ are lower than the values for $a_{0.5\text{-}9}$. This would seem to indicate that between 8 and 10 years after the biodigesters were first filled, there was a period of stabilization.

Dapena, et al. (2007) compared the settlement values for pool 5 measured after 4.5 years with the settlement values calculated for 4.5 years, using the model adjusted using the settlement values after 2.5 years. Except for point 8 of pool 5, where real settlement was clearly greater than calculations indicated, settlement at the remaining points of pool 5 matched that calculated using the model. The settlement measured at 10 years for pool 5 is shown in Table 2, together with the calculations. We can see that the real settlement is lower than the calculations, confirming the stabilization process.

6 SUMMARY AND CONCLUSIONS

The phase 2 biodigesters at the Galindo Waste Water Treatment Plant are located on a layer of silty clay between 15 and 20 m thick, which has been subjected to irregular preloading for 20 years, with average preconsolidation pressure of 2 kg/cm^2. However, for the site of the phase 2 biodigesters, the distribution of the preload was not known for certain.

Table 1. Values for coefficient a when the model s=a $\sqrt{ta}$ + b is adjusted using measurements between 0.5 and 9 years ($a_{-0.5\text{-}9}$) and measurements between 8 and 10 years ($a_{8\text{-}10}$).

Point	$a_{0.5\text{-}9}$	$a_{8\text{-}10}$	R^2_{8-10}	$b_{0.5\text{-}9}$
Tank 2				
40	38.5	23.7	0.96	2.4
41	38.3	24.7	0.97	-0.1
42	36.3	19.1	0.95	8.9
43	10.8	15.2	0.88	5.3
52	9.5	6.2	0.84	17.1
53	58.9	31.6	0.97	37.4
61	36.2	26.4	0.97	7.9
62	10.8	0	0.87	3.5
63	9.9	0	0.87	2.0
Tank 3				
35	18.1	10.9	0.98	-6.3
36	15.0	3.9	0.92	-0.3
37	13.5	9.6	0.91	+5.6
38	-	13.6	0.92	-
39	23.7	18.0	0.91	+0.9
54	28.9	23.3	0.97	14.5
55	21.0	9.0	0.95	16.1
56	21.8	27	0.92	-1.1
57	22.4	0	0.95	-4.1
58	26.0	11.3	0.97	-1.6
59	34.9	22.7	0.98	1.3
60	36.0	26.7	0.97	1.0
Tank 5				
6	7.7	6.7	0.59	7.1
7	12.7	5.9	0.70	5.8
8	35.2	29.7	0.96	8.1
16	37.5	23.3	0.97	46
17	7.8	4.4	0.08	22.0
26	7.5	2.9	0.52	6.6
27	17.5	13.6	0.92	8.3
28	22.8	15.6	0.96	8.0
29	22.8	12.0	0.96	11.6
Tank 6				
9	38.3	35.8	0.95	-6
14	21.5	16.1	0.89	32.2
15	28.9	28.7	0.94	21.5
30	20.3	18.4	0.95	0.5

Table 2. Tank 5. Settlement measured after 4.5 and 10 years and calculated for 4.5 and 10 years.

Point	4.5 years Measured mm	4.5 years Calculated mm	10 years Measured mm	10 years Calculated mm
26	24	26	30	36
17	41	41	45	52
6	33	31	40	42
27	46	46	62	65
28	57	56	77	79
16	128	128	158	171
8	84	76	117	105
29	61	74	81	104

For the 6 years prior to construction of the phase 2 biodigesters, a uniform preload equal to that which would be transferred by the biodigesters was kept on the entire area. However, when they were constructed, the initial design was modified and the load transferred was 0.14 kg/cm^2 greater than the load of the soil removed.

10 years after the biodigesters were constructed, tanks 1 and 4 have practically stabilized, as settlement is less than 50 mm in these areas. Tanks 2 and 5 are the areas with the greatest settlement, reaching 218 mm at tank 2 and 158 mm at tank 5, without any problems with the operation of the tanks having been detected. This settlement can be divided into zones, as shown in Figure 2.

The settlement which occurs based on time fits the model S = a $\sqrt{t_a}$ +b, where t_a is the time in years where the tank has been full.

Coefficient "a" is related to the rate of settlement and its distribution is similar to the settlement values as shown in Figure 4. Thus, at tanks 1 and 4, where the least settlement has occurred, the value of "a" is less than or equal to 5, while at the center of tank 2, it is $a_{0.5\text{-}9}$ =58.9, and at the center of tank 5, it is $a_{05\text{-}9}$ = 37.5.

By comparing the "a" values when the model is adjusted for the period of time between 0.5 and 9 years, and the "a" values when this period of time is between 8 and 10 years, it is possible to observe that the settlement is stabilizing, particularly in the areas with greater settlement.

7 REFERENCES

Alonso, E.E., Gens, A. y Lloret, A. (2000). *Precompresión design for secondary settlement reduction*. Geotechnique 50(6), 645-654.

Alonso, E.E., (2004). *Deformabilidad a largo plazo de suelos precargados.* 8º Simposio Nacional de la S.E.M.S.I.G., Valencia, págs 245 a 250.

Alonso, E.S., Lloret, A., Gens, A. y M. Salvadó (2001). *Overconsolidation effects on secondary compresión rates*. Proc. 15th International Conference on Soil Mechanics & Geotechnical Engineering.Istambul, 1:5-8.

Dapena, E., Román, E., San Salvador, J. (2005). Long term settlement of foundations made of 195 x 147 m slabs built on a layer of fluvial sediment. *Proc. 16th Int. Conf. Soil Mech. & Geotech. Engng. 1, 1033-1036.*

Dapena, E., Román, F. (2007). *Differential settlement measured over five years in major-scale shallow foundations on a preloaded 20 m. thick silty alluvial layer.* Proceedings of the 14th European Conference on Soil Mechanics and Geotechnical Engineering. Madrid. Vol. 2 pp.451-456

Jamiolkowsky, M., Lancellota, R. y Wolski, W. (1983). *Precompression and speeding up consolidation.* General Report. Proc. Europ. Conf. Soil Mech. Found. Engng. Helsinki, 3:1201-1226.

Johnson, S.J., (1970). *Precompression for improving foundations soils* J. Soil *Mech*. Found. Div. ASCE, 96(1): 111-114.

Koutsoflas, DC., Foott, R. y Hadleft, L.D. (1987). *Geotechnical investigations offshore Hong Kong*, J. Geotech. Enging. Dic. ASCE, 113(2): 87-105.

Magnan, J.P. (1994). *Methods to reduce the settlement of embankments on soft clay, a review*, In: Vertical and horizontal displacements. ASCE. Geotech. Special Pub. 40(1): 77-91

Mitchell, J.M. (1981). *Soil Improvement.* State of the art report. Proc. 10th *I*nt. Conf. Soil Mech. And Found. Engng. Stockholm. 2:509-565.

Stamatopoulos, A.C. y Kotzias, P.C. (1983). *Settlement-time predictions in preloading*. J. Geotech. Engng. Div. ASCE, 109(6): 802-820.

Yu, K.P. y Frizzi, R.P. (1994). *Preloading organic soils to limit future* settlements. Vertical and horizontal displacements of foundations and embankments, ASCE. Geotech. Special Pub. 40(1): 476-490.

Combined massive and plate foundations under machines with dynamic loadings

Des fondations combinées à blocs et plaques pour des machines avec charges dynamiques

Kirichek Y., Bolshakov V.
Pridnipronsk State Academy of Civil Engineering and Architecture

ABSTRACT: A new type of foundation under machines with dynamic loading is presented. The combined massive and plate foundation consist of deepened rigid solid mass and attached thin horizontal plates. Finite element analysis of the combined massive and plate foundation under machines with periodic loading is conducted. The analytical method of dynamic analysis of combined massive plate foundations under impact, rotating and reciprocal machines under dynamic loadings is applied. Experimental investigation of the combined massive and plate foundation interaction with a soil base was performed on large-scale models in the open ground. The analytical and numerical results are compared with large-scale models. It was shown that the combined massive and plate foundations are much more efficient compared to conventional block-type foundations under dynamic machines, such as turbo-pumps, compressors, fans, centrifuges, etc.

RÉSUMÉ: Il est proposé un nouveau mode de fondation pour des machines supportant des charges dynamiques appellée "la fondation combinée à blocs et plaques". Elle consiste en un bloc rigide, relié à des plaques de faible épaisseurnoyées dans le sol. Il a été réalisé des calculs de "fondations combinées à blocs et plaques" pour des machines soumises à des charges périodiques par la méthode des éléments finis. Les méthodes analytiques du calcul dynamique des "fondations combinées à blocs et plaques" ont été développées pour des machines subissant des impacts, des machines comportant des organes en mouvement rotatif et des bielles. L'interaction des "fondations combinées à blocs et plaques" et du sol a été étudiée expérimentalement à l'aide d'essais à grande échelle sur chantier. Les résultats des calculs analytiques et numériques sont comparés aux résultats des essais de modèles à grande échelle. Il est montré que des "fondations combinées à blocs et plaques" sont beaucoup plus efficaces que les fondations à blocs traditionnelles pour les turbopompes, les compresseurs, les ventilateurs, les centrifugeuses.

KEYWORDS: vibrations of foundations, dynamic loading, combined massive and plate foundations, dynamic analysis.

1 INTRODUCTION

Heavy machinery with rotating, reciprocating or impacting masses requires a foundation that can resist dynamic loadings and the resulting vibrations. A properly designed foundation is one that transfers the dynamic load on the soil without high vibration level. Depending on the types of load or dynamic equipment various types of foundations are used. A block-type foundation under machinery is simple and in common used. Its response depends on the foundation mass and area of foundation base (Barkan D.D.1962 and Brajama M.D., Bamana G.V. 2011). A heavy loaded foundation has extremely big weight and as a result its natural frequency is very low. Therefore, such foundation under low-frequency loading can have a very high level of vibration. Furthermore, in case operation of impact machines, it can be dangerous for building with low resonance frequency. No changes of dimensions of such foundations enable geotechnical engineers to decrease considerably the vibration level.

In the article new forms of foundations under machines with low dynamic loadings are presented. They were named «Combined massive and plate foundations" (Fig. 1). Foundations such as these consist of deepened rigid solid mass and attached to it in soil thin horizontal plates (Kirichek Y. 2011). Its natural frequencies can be sat in a wide frequency range by changing dimension and location of attached thin horizontal plates in soil. As a result natural frequency of such foundation can be significantly higher in amount then of block-type foundation and vibration level of the combined massive and plate foundations under low-frequency loading and impacting machinery generally is considerably lower.

2 LARGE-SCALE FIELD TEST

For studding behavior of the combined massive and plate foundations under low-frequency loading large-scale field tests were conducted. The comparison of the footing vibration tests with theory was done. For these tests, the vertical and horizontal dynamic forces on footing were generated by rotating mass vibrators. The large-scale models were 1.5 m in wide and 3.71 m in length (See Fig.2).

a)

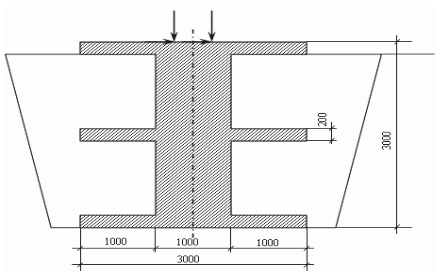

b)

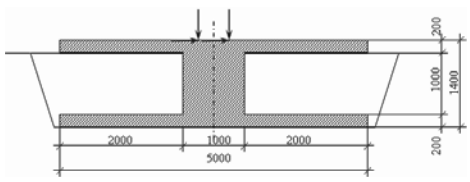

Figure 1. Combined massive and plate foundations: a – a solid block and three plates, b – a solid block and two plates.

Figure 2 shows the large-scale model of massive and plate foundations with the plate on the top or at the foot.

a)

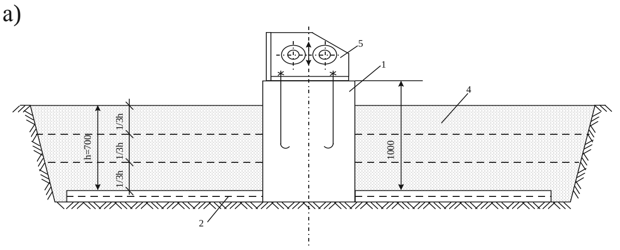

b)

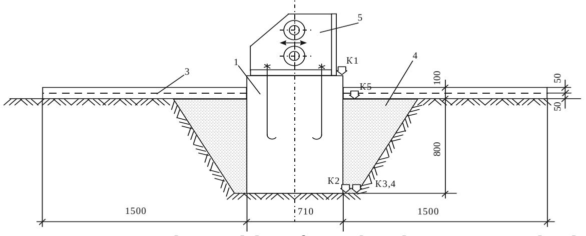

Figure 2. Large-scale models of combined massive and plate foundations: a – the plate is on the top of foundation, b – the plate is at the bottom of foundation. 1 – block, 2 – lower plate, 3 – upper plate, 4 – soil, 5 – vibrator.

The tests were performed on the silty clay with unit weight 19.7 KN/m^3, natural water content 0.22, voids ratio 0.85, Young's modulus 10 MPa. The block was 1 m high with the area of its foot equal 1m^2. The plates thickness was h=0.05m and h=0.1m. The area of the plates was F=2.13 m^2 and F=4.5 m^2. The foundations were placed at the centre of a hole excavated to the desired depth. Cyclic load was applied 12.7 – 25.4 KN under frequency 50 Hz. The amplitude-frequency responses of the combined massive and plate foundations under horizontal and vertical periodic loadings are shown in Figures 3 and 4.

a)

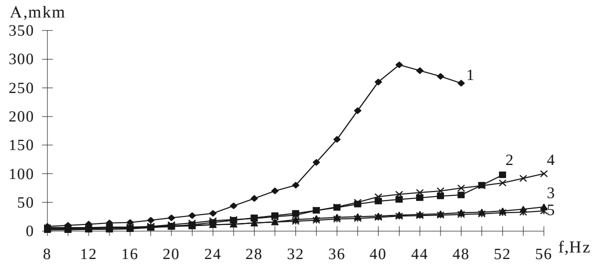

b)

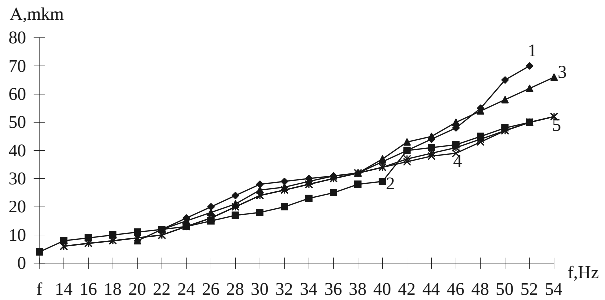

Figure 3. Amplitude-frequency responses of the combined massive and plate foundations with the plate on the top of the foundations: a – horizontal periodic load, b – vertical periodic load, 1 – amplitude-frequency response of the block, 2 – F=2.13, h=0.05, 3 – F=4.5, h=0.05, 4 – F=2.13m, h=0.1, 5 – F=4.5m, h=0.1m.

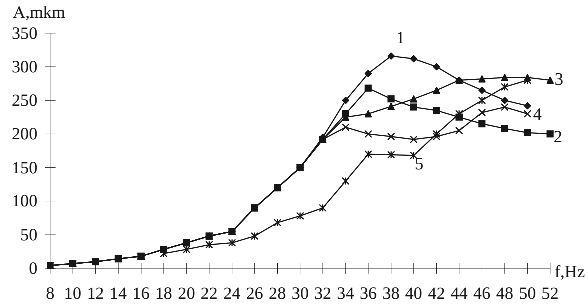

b)

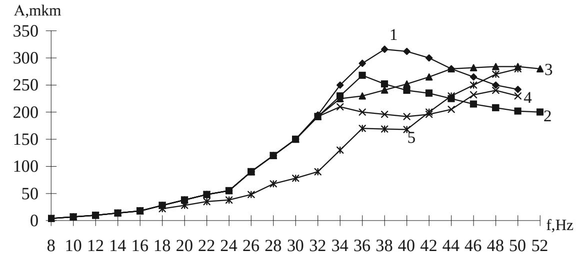

Figure 4. Amplitude-frequency responses of the combined massive and plate foundations with the plate at the bottom of foundations: a –, horizontal periodic load b - vertical periodic load, 1 – the amplitude-frequency response of the block, 2 – F=2.13, h=0.05, 3 – F=4.5, h=0.05, 4 – F=2.13m, h=0.1, 5 – F=4.5m, h=0.1m.

The comparison of the amplitude-frequency responses of the combined massive plate foundations enable to evaluate influence of the dimension of plates on responses of foundation. We note that the vibration amplitude decreases half as much with increasing of the plate area twice as many. The plate thickness has less effect on the responses of foundation. It was experimentally determinate, that the effect of top plates was bigger under horizontal dynamic loading and the effect of bottom plates was bigger under vertical dynamic loading.

A thin plate on the soil can significantly reduce the vibration level of the block foundation. Figures 5 and 6 present the results of such large-scale field test. Responses of the deepened block-type foundation with dimension 1m x 1m x1m became quite different after attaching a thin plate lying on the soil. So resonance frequencies became 42%-64% higher. As a result the high-frequency vibration amplitude decreased 3 – 4 times.

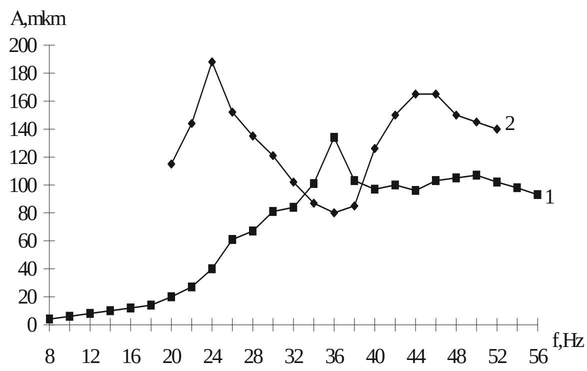

Figure 5. The amplitude-frequency responses of the block-type foundations under horizontal periodic loading: 1 – the plate with area 8m^2 is on the top of foundation, 2 – no plate.

a)

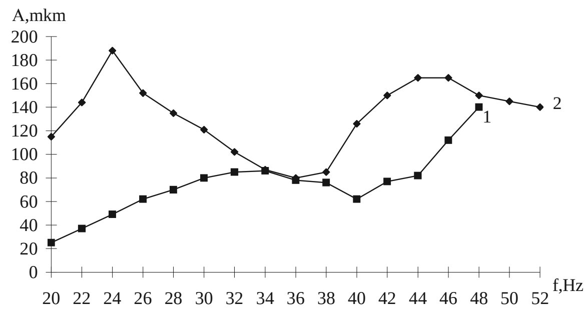

Figure 6. The amplitude-frequency responses of the block-type foundations under horizontal periodic loading: 1 – the plate with area $12m^2$ is on the top of foundation, 2 – no plate.

The vibration level of the plate extremely reduced with increasing the distance from the block. Figure 7 shows measuring on the large-scale model of block-type foundation with attached thin plate lying on the soil. Similar effect we can see on the slab around the block-type foundation of industrial machinery (See Fig.8).

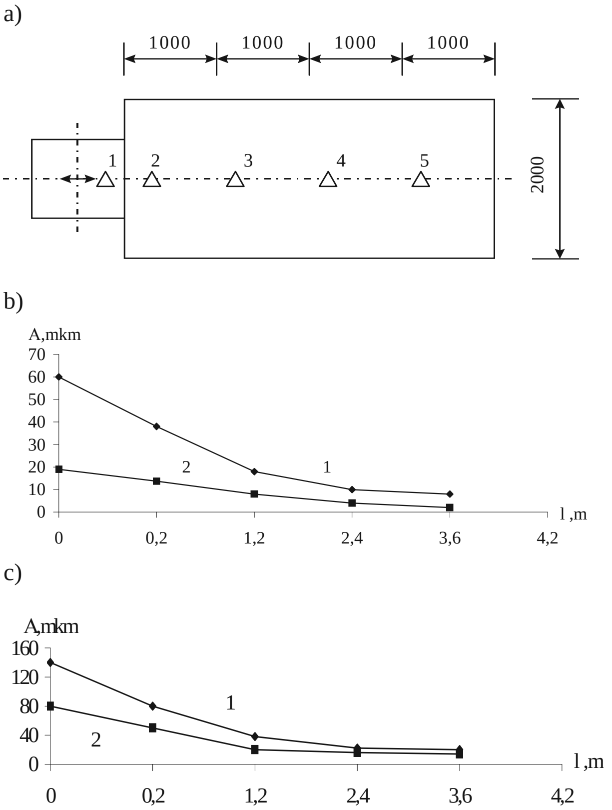

Figure 7. Decline of the vibration amplitude of the plate away the block: a – the large-scale model, b - vertical vibration amplitude, c - horisontal vibration amplitude, 1 – vibration frequency 40 Hz, 2 – vibration frequency 20 Hz.

The large-scale test results and the finite element analysis (Kirichek Y. 2000) present, that the combined massive and plate foundations have advantage over type-block foundations in frequency range 9 – 30 Hz, as their vibration level is considerably less. The slabs bring positive influence on the vibration level of block-type foundations in the low-frequency range. The vibration level of type-block foundations reduced two or three times as a result of increasing the natural frequency of system “block – slab”.

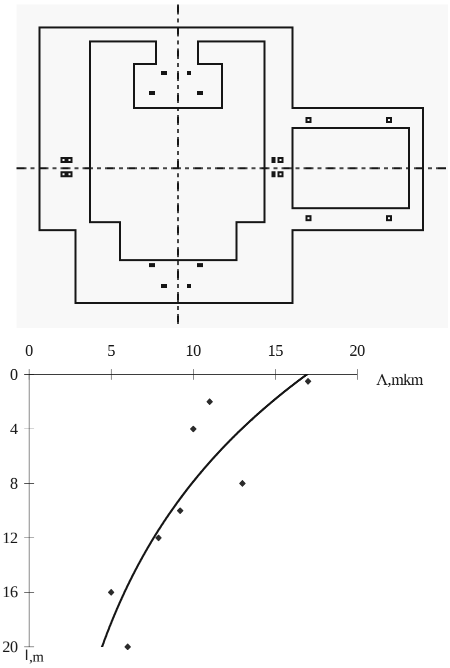

Figure 8. Decline of the horizontal vibration amplitude of the slab away the block-type foundation.

3 ANALITICAL SOLUTION

The mathematical model of the combined massive and plate foundations is a concentrated mass with either plates or beams on a viscoelastic base. Integral transformations for vertical and horizontal oscillations of the block and plates are considered as a problem of beams or plates on a viscoelastic base using asymptotic and transformation methods. The analytical

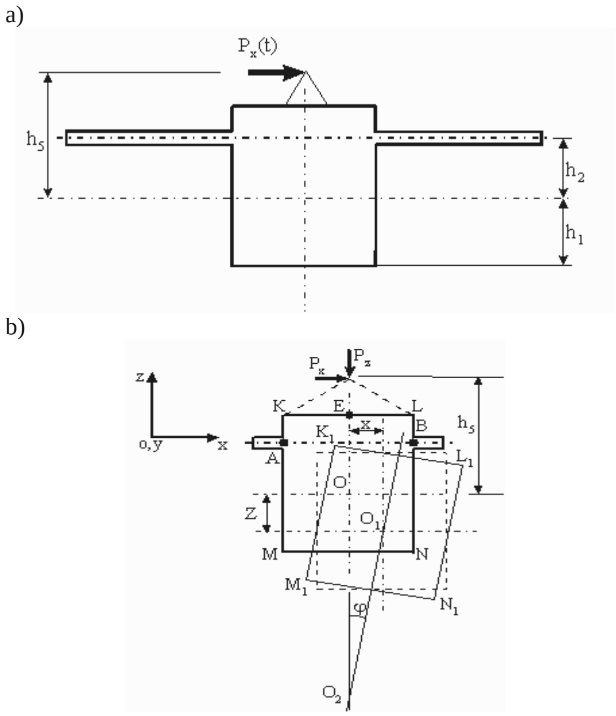

Figure 9. Design model of the combined massive and plate foundation

derivation of the complex problem is also given using a elementary system (Barkan D.D. 1962. and Verruijt A. 2010). Figure 9 shows the system consisted of a mass and some beams, supported by a linear springs.

Theoretical solution for such foundation subjected to sliding and rocking forced vibration is presented below. The vibration amplitude and natural frequencies of the block can be derived from displacement equation (see Eq. 1).

$$
\begin{aligned}
& m\ddot{x} + \left(K_x + K_{xn}\right)\cdot x - \left[K_x h_1 - (-1)^k K_{xn} h_2\right]\varphi = P_x(t) \\
& \theta\ddot{\varphi} + \left(K_\varphi + K_x h_1^2 + (-1)^k K_{xn} h_2^2 - Qh_1\right)\varphi + \\
& + \left(K_{xn} h_2 - K_x h_1\right)x = M_y\left[P_y(t)\right]
\end{aligned}
\tag{1}
$$

Where: m – mass of block;

K_x, K_{xn} - sliding subgrade modulus of the block and plate;

K_f – rocking subgrade modulus of the block;

For vibration amplitude the solution to Eg.1 can be given as:

$$
A_x = \frac{P}{\alpha}\left[1 + \frac{\alpha h_5 + \varepsilon}{\alpha\gamma - \beta\varepsilon}\left(\beta + h_5\alpha\right)\right] \tag{2}
$$

Where:

$$K_x + K_{x\pi} - m\omega^2 = \alpha;$$

$$K_x h_1 - (-1)^k K_{x\pi} h_2 = \beta;$$

$$K_\varphi + K_x h_1^2 + (-1)^k K_x h_2^2 - Qh_1 - \theta\omega^2 = \gamma;$$

$$K_x h_1 - K_{x\pi} h_2 = \varepsilon$$

The solution to Eg.1 of natural frequencies (see Eq. 3) can be written as

$$
\lambda_{1,2} = \sqrt{\frac{1}{2}\left(A \pm \sqrt{A^2 - 4B}\right)} \tag{3}
$$

Where

$$
A = \frac{K_x + K_{xn}}{m} + \frac{K_\varphi - Qh_1 + K_x h_1^2 + (-1)^k K_{xn} h_2^2}{\theta};
$$

$$
B = \frac{2(-1)^k K_x K_{xn} h_1^2 + \left(K_x + K_{xn}\right)\left(K_\varphi - Qh_1\right)}{\theta\cdot m}.
$$

Figure 10 shows the comparison of analytical solution (see Eq. 2) to field test result. The amplitude-frequency responses of the combined massive and plate foundation are shown. The plates with area 2.13 m^2 and 4.15 m^2 were located on the soil at the top of the foundation. This simple spring-mass system can be used for definition vibration level of the combined massive and plate foundation on the understanding that properties of dynamically loaded soil mast be correctly evaluated.

a)

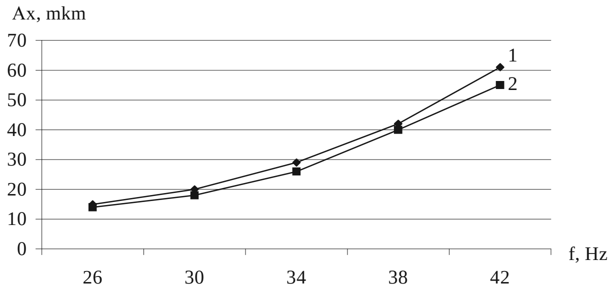

b)

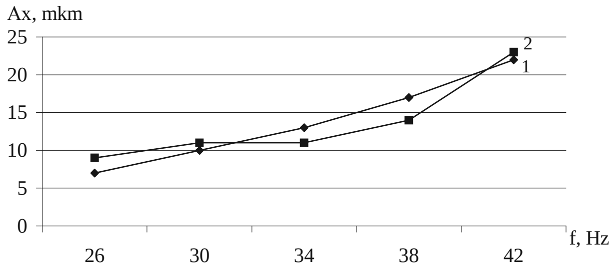

Figure 10. Comparison of analytical solution to field test result, amplitude-frequency responses of the combined massive and plate foundation with the plates on the top of foundation: a – area of the plate is equal 2.13 m^2, b – area of the plate is equal 4.15 m^2, 1 – analytical solution , 2 – field test result.

4 CONCLUSION

The new type of foundation under machinery with dynamic loading was developed. It was named the combined massive and plate foundation. The foundation consists of deepened massive block and attached in soil one or more horizontal plates. Finite element analysis and experimental investigation showed that the combined massive and plate foundations have advantage over block-type foundations in low-frequency range, as their vibration level is considerably less. The slab brings positive influence on vibration level of type-block foundations, their vibration levels get two or three times reduced and their natural frequency increases. For most problems the analytical derivation of solution is given using asymptotic and perturbation methods. The mathematical models for the oscillation of the combined massive and plate foundation are a lumped mass with beams or plates on the viscous-elastic basis. Integral transformations, Fourier series, averaging methods are applied for solution to such equations. The analytical and numerical results are compared with large-scale modeling test data.

5 REFERENCES

Barkan D.D. 1962. Dynamics of Bases and Foundations. MCGraw-Hill, Inc., New York.

Brajama M.D. and Bamana G.V. 2011. Princeples of soil dynamics. Cengaga Learning. 552p.

Kirichek Y. 2011. Analisys of the bechavior of massive plate foundations on viscoelastic base. Proc. of the 15-th European Conference on Soil Mechanic and geotechnical engineering. Athens, 557 – 562.

Kirichek Y. 2000. Combined Massive and Plate Foundations for Dynamic Loaded Machines, *Soil Mechanics and Foundations* 5, 292-299.

Verruijt A. 2010. An introduction to soil dynamik. Springer. Delft. 433p.

Settlements Under Footings on Rammed Aggregate Piers

Tassements sous des semelles sur pieux d'agrégats battus

Kuruoglu O., Horoz A.
Yuksel Proje International, Turkey

Erol O.
Middle East Technical University, Turkey

ABSTRACT: This study uses a 3D finite element program, calibrated with the results of a full scale instrumented load test on a limited size footing, to estimate the settlement improvement factor for footings resting on rammed aggregate pier groups. A simplified 3D finite element model (Composite Soil Model) was developed, which takes into account the increase of stiffness around the piers during the ramming process. Design charts for settlement improvement factors of square footings of different sizes (B = 2.4m to 4.8m) resting on aggregate pier groups of different area ratios (AR = 0.087 to 0.349), pier moduli (E_{column} = 36MPa to 72MPa), and with various compressible clay layer strengths (c_u = 20kPa to 60kPa) and thicknesses (L = 5m to 15m) were prepared using this calibrated 3D finite element model. It was found that, the settlement improvement factor increases as the area ratio, pier modulus and footing pressure increase. On the other hand, the settlement improvement factor is observed to decrease as the undrained shear strength and thickness of compressible clay and footing size increase.

RÉSUMÉ : Cette étude utilise un modèle de calcul en éléments finis 3D, calé à partir sur les résultats d'essais de chargement grandeur nature , totalement instrumentés, sur une semelle de dimensions limitées, dans le but d'estimer le facteur d'amélioration du tassement des semelles reposant sur des groupes de pieux en agrégats, battus. Un modèle simplifié par éléments finis 3D (modèle de sol composite) a été développé ; il prend en compte l'augmentation de la rigidité autour des piles pendant le processus de battage. Les abaques des facteurs d'amélioration de tassement d'une semelle carrée de dimensions variables (B = 2,4 m à 4,8 m) reposant sur des groupes de pieux en agrégats battus, avec des rapports de surface variés (AR = 0,087 à 0,349), modules de pile (Ecolumn = 36MPa à 72MPa), et avec différentes couche de renforcement d'argile compressible (c_u = 20 kPa à 60 kPa) et épaisseurs (L = 5m à 15m) ont été préparés en utilisant ce modèle en éléments finis 3D. D'une part, il a été constaté que le facteur d'amélioration du tassement croît en fonction de l'augmentation du rapport de la surface, du module de pile et de la pression des semelles. D'autre part, le facteur d'amélioration du tassement diminue lorsque la résistance au cisaillement non drainé, l'épaisseur de l'argile compressible ainsi que les dimensions des semelles croissent.

KEYWORDS: rammed aggregate pier, stone column, settlement improvement factor

1 INTRODUCTION

This study uses a 3D finite element program, calibrated with the results of a full scale instrumented load test on a limited size footing, to estimate the settlement improvement factor for footings resting on rammed aggregate pier groups. A simplified 3D finite element model (Composite Soil Model) was developed, which takes into account the increase of stiffness around the piers during the ramming process. Design charts for settlement improvement factors of square footings of different sizes (B = 2.4m to 4.8m) resting on aggregate pier groups of different area ratios (AR = 0.087 to 0.349), pier moduli (Ecolumn = 36MPa to 72MPa), and with various compressible clay layer strengths (c_u = 20kPa to 60kPa) and thicknesses (L = 5m to 15m) were prepared using this calibrated 3D finite element model.

2 CALIBRATION OF THE FINITE ELEMENT MODEL

The finite element model that is going to be used for the parametric studies that will be presented in the proceeding chapters of this study is calibrated with the results of full-scale field load tests detailed in Özkeskin (2004). The full scale field tests consist of load tests on both untreated soil and on three different groups of rammed aggregate piers with different lengths on the same site, and therefore offers the unique opportunity of calibrating geotechnical parameters for a finite element model.

The test area which is approximately 10m x 30m is located around Lake Eymir, Ankara. Site investigation at the test area included five boreholes which are 8m to 13.5m in depth, SPT tests, sampling and laboratory testing, and four CPT soundings. (see Figure 1)

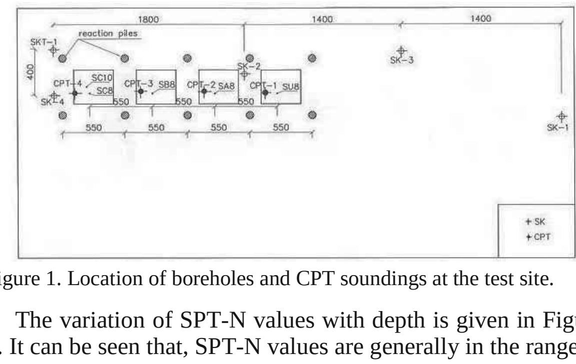

Figure 1. Location of boreholes and CPT soundings at the test site.

The variation of SPT-N values with depth is given in Figure 2. It can be seen that, SPT-N values are generally in the range of 3 to 10 in the first 8 m. After 8 m depth, SPT-N values are greater than 20, and the samples are identified as weathered graywacke. Based on the laboratory test results, the compressible layer, first 8 m, is classified as low plasticity clay (CL) and clayey sand (SC) according to USCS. The liquid limit of the compressible layer changes predominantly in the range of 27% to 43% with an average of 30%, and the plastic limit changes in the range of 14% to 20% with an average of 15%. The ground water is located near the surface.

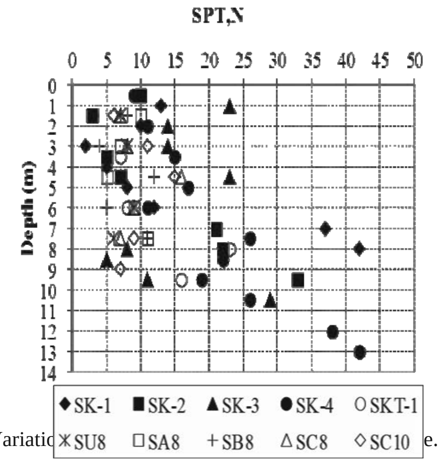

Variatic e.

Figure 2. Variation of SPT-N values with depth at the test site.

Four large plate load tests were conducted at the load test site. Rigid steel plates having plan dimensions of 3.0m by 3.5m were used for loading. First load test was on untreated soil. Second load test was Group A loading on improved ground with aggregate piers of 3.0m length, third load test was Group B loading on improved ground with aggregate piers of 5.0m length and finally fourth load test was Group C loading on improved ground with aggregate pier lengths of 8.0m. Each aggregate pier groups, i.e. Group A, Group B, and Group C, consisted of 7 piers installed with a spacing of 1.25 m in a triangular pattern. The pier diameter was 65cm. (See Figure 3)

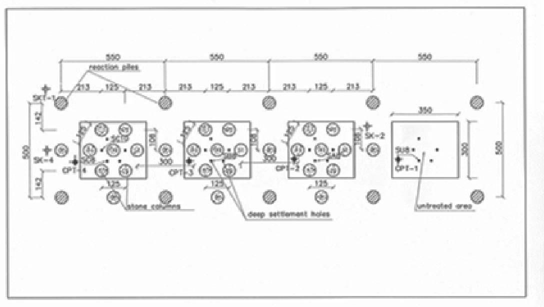

Figure 3. Location of aggregate piers at the test site.

For each group of aggregate piers, deep settlement plates were installed at 1.5m, 3m, 5m, 8m and 10m depths. 10cm thick fine sand layers were laid and compacted to level the surface before placing the total pressure cell on top of the center aggregate pier. The loading sequence for untreated soil load test was cyclic and at each increment and decrement, load was kept constant until the settlement rate was almost zero. For aggregate pier groups, the loading sequence was 50, 100, 150, 200, 250, 150, 0 kPa. Two surface movements, one at the corner and one at the center of the loading plate, and five deep movement measurements were taken with respect to time.

The data of the plate loading test on untreated soil was used for calibrating the finite element model. Geotechnical finite element software PLAXIS 3D Foundation which offers the possibility of 3D finite element modeling was used for the analysis. Loading plate, which has dimensions of 3.0mx3.5m, was modeled as a rigid plate and the loading was applied as a uniformly distributed vertical load on this plate according to the loading scheme used during the actual field test. The boundaries of the 3D finite element mesh was extended 4 times the loading plate dimensions in order to minimize the effects of model boundaries on the analysis. The height of the finite element model was selected as 12meters. The first 8 meters was the compressible silty clay layer and the remaining 4 meters was the relatively incompressible stiff clayey sand (weathered greywacke) layer. An isometric view of the 3D model is given in Figure 4.

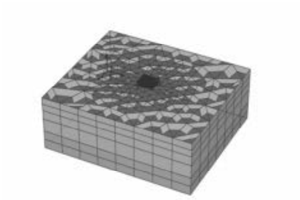

Figure 4. Isometric view of the 3D finite element model.

Both the compressible and relatively incompressible soil layers was modeled using the elastic-perfectly plastic Mohr-Coulomb soil model. Groundwater level was defined at the surface. The parameters of the relatively incompressible layer was set to high values, and various geotechnical parameters was assigned to the compressible layer until the surface load-settlement curve calculated from the finite element model matches with the field test data carried on untreated soil. The closest match, which is shown in Figure 5, was obtained with the parameters presented at Table 1.

Table 1. Calibrated soil parameters to be used in the finite element analyses.

Unit	γ (kN/m^3)	c (kPa)	ϕ(°)	E (kPa)	ν
Silty clay (0-8m)	18	22	0	4500	0.35
Clayey sand (8-12m)	20	0	40	50000	0.30

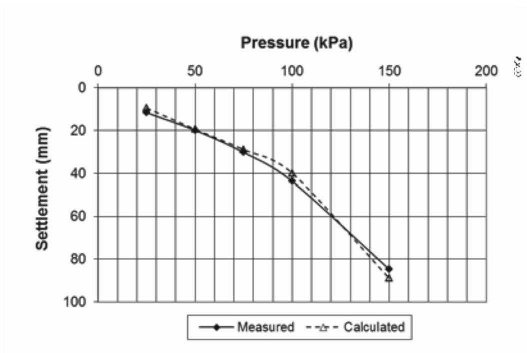

Figure 5. Comparison of surface load settlement curves for untreated soil

Once the geotechnical parameters of the native soil were determined, the next step was to model the field tests on three different rammed aggregate pier groups (i.e. Group A, Group B and Group C). In all three tests the rammed aggregate pier layout was similar (Figure 6) and the lengths of the aggregate piers were 3m, 5m and 8m for Group A, Group B and Group C, respectively. The size of the loading plate was 3.0mx3.5m, as it was the case at the field test on untreated soil.

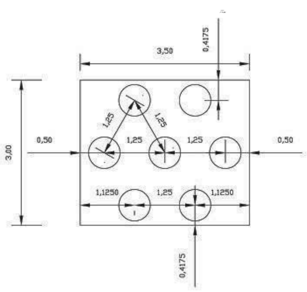

Figure 6. Field test rammed aggregate pier layout

The field load tests on rammed aggregate pier groups were again modeled by PLAXIS 3D Foundation. The size of the finite element mesh was kept the same as the model for the test on untreated soil for comparison purposes. Material model and geotechnical parameters derived from the calibration process were used for the native soil. Rammed aggregate piers were modeled with linear elastic material model and modulus of elasticity value was given as E = 39 MPa, as recommended by Özkeskin (2004), which is backcalculated from single pier load tests. Loading plate, which has dimensions of 3.0mx3.5m, was modeled as a rigid plate and the loading was applied as a uniformly distributed vertical load on this plate according to the loading scheme used during the actual field test. Calculated surface pressure-settlement curves for each aggregate pier groups are compared with the field measurements in Figure 7. (Surface pressure values are normalized with respect to the ultimate bearing capacity, q_{ult}, of the untreated soil.) The calculated surface settlements are larger than the measured ones for all cases.

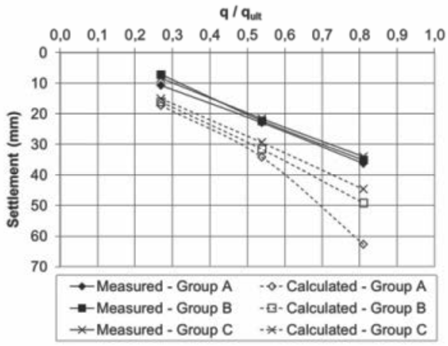

Figure 7. Comparison of surface load-settlement curves for loading on Group A rammed aggregate piers (Normal 3D FEM Model)

The observed stiffer and near-linear-elastic behaviour of aggregate pier groups can be explained by the increase of lateral stress in the matrix soil around the rammed aggregate piers caused by the ramming action during the installation of the piers. This increase in lateral stress of matrix soil results in improved stiffness characteristics as explained by Handy (2001). In order to match the observed stiffer and near-linear-elastic behaviour of actual field test measurements, it is decided to define linear elastic improved zones around the rammed aggregate piers at the 3D finite element model. It is assumed that a circular zone with a radius equal to two times of the rammed aggregate pier radius is improved around the rammed aggregate piers. (Modified Ring Model) This circular zone is also divided into two zones. (Figure 8) It is assumed that the modulus of elasticity value of the improved soil around the rammed aggregate pier increases to 2/3 of the modulus of elasticity value of the rammed aggregate pier at the first improved zone - $r = 1.5r_{aggregate\ pier}$ -, and to 1/3 of the modulus of elasticity value of the rammed aggregate pier at the second improved zone - $r = 2.0r_{aggregate\ pier}$ -.

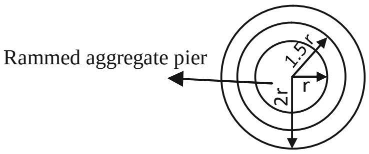

Figure 8. Geometry of the assumed improved zones around the rammed aggregate piers

Calculated surface pressure-settlement curves for each aggregate pier groups are compared with the field measurements in Figure 9. Calculated load-settlement curves fit to the expected near-linear-elastic behavior much better than before. The agreement with the measured surface settlement values are quite satisfactory for Group B and Group C loadings.

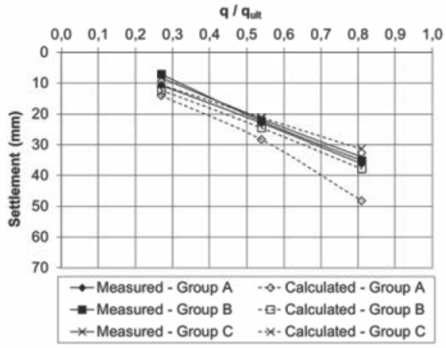

Figure 9. Comparison of surface load-settlement curves for loading on Group A rammed aggregate piers (Modified Ring Model)

The next step is to try to simplify this improved near-linear-elastic zone assumption (Modified Ring Model) so that it can be easily used for practical analyses. For this purpose, the area under the loading plate with the rammed aggregate piers is modeled as a composite soil block (Composite Soil Model). Linear elastic material model is used for the composite soil block and the modulus of elasticity of this composite zone is calculated as the weighted average of the rammed aggregate pier, improved zones around the rammed aggregate pier, and native soil, according to their respective areas. The improved modulus of elasticity values were selected as 2/3 of the modulus of elasticity value of the rammed aggregates pier at the first improved zone - $r = 1.5r_{aggregate\ pier}$ - , and to 1/3 of the modulus of elasticity value of the rammed aggregates pier at the second improved zone - $r = 2.0r_{aggregate\ pier}$ - , as concluded before. Calculated surface pressure-settlement curves for this case are compared with the field measurements in Figure 10. Calculated load-settlement curves with the Composite Soil Model yield more close results to the measured values than the Modified Ring Model, especially for floating pier groups. (i.e. Group A and Group B)

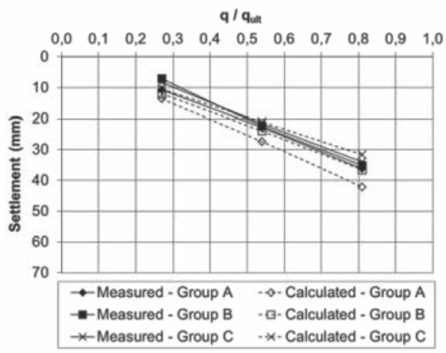

Figure 10. Comparison of surface load-settlement curves for loading on Group A rammed aggregate piers (Composite Soil Model)

As a result of the calibration process detailed in this chapter, it is concluded that the 3D finite element model, i.e. the Composite Soil Model, in which the area under the loading plate with the rammed aggregate piers is modeled as a composite soil block with equivalent linear elastic soil properties taking the stiffness increase around the piers during the installation process into account, satisfactorily models the surface pressure-settlement curves of uniformly loaded footings supported by rammed aggregate piers. It is to be mentioned that the model should be used cautiously for floating pier groups with pier lengths less than 1.5B (B = width of the footing), especially at high surface pressure levels , i.e. $q / q_{ult} > 0.5$, where q_{ult} = ultimate bearing capacity of the native soil.

3 DETAILS OF THE PARAMETRIC STUDY

Once the 3D finite element model (Composite Soil Model) to be used for the analysis of rigid footings resting on rammed aggregate piers was calibrated using the results of full-scale load tests as presented in the previous chapter, the next step is to carry out a parametric study using this finite element model to investigate the effect of both geometric parameters (area ratio of rammed aggregate piers, foundation load, width of foundation, rammed aggregate pier length) and material parameters (strength of foundation material, modulus of elasticity value of rammed aggregate piers) on the settlement improvement factor.

Three different footing sizes (2.4mx2.4m, 3.6mx3.6m and 4.8mx4.8m) were used for the parametric study. The thickness of the compressible clay layer under these footings was varied as Lclay = 5m, 10m and 15m for each different footing size. Four different area ratios (AR= 0.087, 0.136, 0.230 and 0.349) were used for the rammed aggregate pier groups under each different footing and compressible layer combination. Foundation pressures, q, were selected as q=25-50-75-100-125-150 kPa. Schematic representation of these parameters can be seen in Figure 11. The strength and deformation modulus values of the compressible clay layer were varied as shown at Table 2. The deformation modulus value of the rammed aggregate piers were selected as E_{column} = 36 MPa and 72MPa.

Table 2. Strength and deformation properties of the compressible clay layer used in the parametric study.

γ (kN/m^3)	c (kN/m^2)	ϕ (°)	ν	E_{clay} (kN/m^2)
18	20	0	0.35	4500
18	25	0	0.35	5625
18	30	0	0.35	6750
18	40	0	0.35	9000
18	60	0	0.35	13500

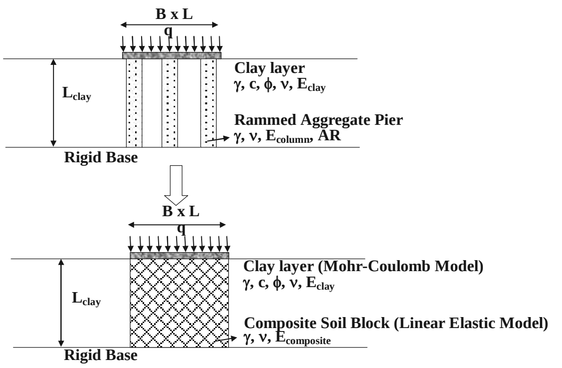

Figure 11 Schematic representation of composite soil model

For each case, first the untreated case is analyzed by modelling the uniformly loaded rigid footing on compressible clay using PLAXIS 3D Foundation. Untreated soil settlements were obtained by this way. Next, the rigid footings resting on rammed aggregate piers were modeled by PLAXIS 3D Foundation using the Composite Soil Block approach that was explained in detail in the previous section. Once the settlement values for the footings resting on rammed aggregate pier groups are calculated using this method, settlement improvement factors are calculated as:

$$IF = s_{untreated} / s_{treated} \quad (1)$$

where:

IF = settlement improvement factor

$s_{untreated}$ = settlement of rigid footing resting on untreated soil.

$s_{treated}$ = settlement of rigid footing resting on soil treated with rammed aggregate pier group.

The results of the parametric study detailed in this section are presented as design charts at Kuruoglu (2008). A sample design chart is shown in Figure 12. The design charts can be used to decide on the necessary area ratio of rammed aggregate piers for a target settlement improvement ratio for footings on compressible soils resting on rammed aggregate pier groups.

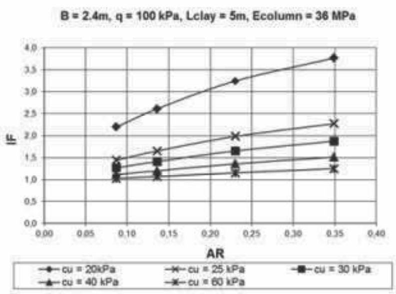

Figure 12. Settlement improvement factor (IF) vs. area ratio (AR) charts for a rigid square footing (B=2.4m) with a foundation pressure of q=100 kPa resting on end bearing rammed aggregate piers (L=5m, E=36 MPa)

As a result of the parametric study, it was found that, the settlement improvement factor increases as the area ratio, pier modulus and footing pressure increase. On the other hand, the settlement improvement factor is observed to decrease as the undrained shear strength and thickness of compressible clay and footing size increase.

4 CONCLUSIONS

A simplified 3D finite element model (Composite Soil Model) calibrated with the results of full scale load tests was developed, which shows that 3D models for estimating settlement improvement factor for foundations resting on rammed aggregate piers can be much simplified by modeling the area under the footing as a composite soil block with equivalent linear elastic soil properties, taking the stiffness increase around the piers during the installation process into account. It is to be mentioned that the model should be used cautiously for floating pier groups with pier lengths less than 1.5B (B = width of the footing), especially at high surface pressure levels , i.e. q / qult > 0.5, where qult = ultimate bearing capacity of the native soil.

Using this simplified model, design charts for settlement improvement factors of square footings of different sizes (B = 2.4m to 4.8m) resting on aggregate pier groups of different area ratios (AR = 0.087 to 0.349), pier moduli (Ecolumn = 36MPa to 72MPa), and with various compressible clay layer strengths (cu = 20kPa to 60kPa) and thicknesses (L = 5m to 15m) were prepared.

As a result of the parametric study, it was found that, the settlement improvement factor increases as the area ratio, pier modulus and footing pressure increase. On the other hand, the settlement improvement factor is observed to decrease as the undrained shear strength and thickness of compressible clay and footing size increase.

5 REFERENCES

Handy R.L. 2001. Does lateral stress really influence settlement. *Journal of Geotechnical and Geoenvironmental Engineering* 127 (7), 623-626.

Kuruoglu O. 2008. A new approach to estimate settlements under footings on rammed aggregate pier groups. *Thesis presented to the Middle East Technical University in partial fulfillment of the requirements for the degree of Doctor of Philosophy*. Ankara, Turkey.

Özkeskin A. 2004. Settlement reduction and stress concentration factors in rammed aggregate piers determined from full scale load tests. *Thesis presented to the Middle East Technical University in partial fulfillment of the requirements for the degree of Doctor of Philosophy*. Ankara, Turkey.

Interaction of Nearby Strip Footings Under Inclined Loading

Interaction de semelles rapprochées soumises à des charges inclinées

Nainegali L.S., Ghosh P., Basudhar P.K.
Department of Civil Engineering, Indian Institute of Technology-Kanpur, India

ABSTRACT: An attempt is made to study the interaction of two closely spaced rigid strip footings resting on homogeneous soil bed and find their ultimate bearing capacity (UBC) and settlement behaviour subjected to inclined loading. Finite element software ABAQUS is used for the analysis. The foundation soil is modeled as elasto-plastic material obeying the Mohr-Coulomb failure criterion. The soil domain is discretized with 4-noded bilinear plane strain quadrilateral elements. Parametric studies is performed by varying the angle of inclination of load with horizontal (θ) and clear spacing (S) between the footings. Both bearing capacity and settlement of interacting footings compared to that of an isolated footing increases with decrease in S for footings loaded vertically, whereas the effect on UBC for footings with inclined load is not significant.

RÉSUMÉ : Une étude a été réalisée pour analyser l'interaction de deux semelles filantes rigides rapprochées appuyées sur un sol homogène et déterminer la charge limite de rupture et les tassements lorsqu'elles sont soumises à une charge inclinée. Cette analyse a été réalisée avec le logiciel d'éléments finis ABAQUS. Le sol de fondation est modélisé par un matériau élasto-plastique satisfaisant le critère de Mohr-Coulomb. Les éléments de sol sont constitués de quadrilatères à 4 nœuds en contraintes planes. Des études paramétriques ont été réalisées en faisant varier l'inclinaison de la charge (θ) et l'espace entre bords de fondations (S). Il apparait que les capacités portantes et les tassements des fondations augmentent par rapport à ceux de fondations isolées lorsque l'espacement S diminue pour des semelles chargées verticalement, alors que la capacité portante n'est pas affectée pour des charges inclinées..

KEYWORDS: Interference, Inclined load, Bearing capacity, Strip footings, Homogeneous soil.

1 INTRODUCTION

The classical or conventional theories developed for bearing capacity and settlement of isolated shallow foundations have been studied exhaustively by several researchers in the early phase of the development of soil mechanics such as the theories postulated by Terzaghi 1943, Meyerhof 1963, Vesic 1973, etc have been a good representation of actual field conditions a few decades ago. But there are situations such as railway sleepers and foundations near the property lines wherein foundations are closely spaced. Under such conditions the stress isobars of the individual footings may interact and coalesce forming an overlapped stress isobar affecting a larger zone of foundation soil altering the behaviour of the individual foundations, which would be different from that of the isolated footings. Therefore, analysis of such problems should be carried out by considering all the factors that govern the interference behaviour of such closely spaced footings as realistically as possible. A number of investigations have been performed numerically as well experimentally to determine the interference effect of two nearby shallow foundations. Stuart 1962 was the pioneer to study the phenomenon effect on ultimate bearing capacity (UBC) of two nearby strip footings using limit equilibrium method. Most of the researchers (Graham et al. 1984, Kumar and Ghosh 2007, Kumar and Kouzer 2007, Kumar and Bhattacharya 2010, Mabrouki et al. 2010, Kouzer and Kumar 2010, Ghosh and Sharma 2010, Nainegali and Basudhar 2011, Lee et al. 2008, Nainegali et al. 2012) used numerical methods such as method of stress characteristics, upper or lower bound methods, finite difference and finite element methods to study the interference effect on UBC. Moreover laboratory model experimental tests were conducted by Khing et al. 1992, Das et al. 1993, Kumar and Sharan 2003, Kumar and Bhoi 2008, Ghosh and Kumar 2009. Most of the literature available on the subject is related to vertical loading however, in several situations interacting footings are subjected to inclined loading owing to vertical and horizontal loads transmitted through the superstructure or inclined columns or wind load.

Therefore, in this paper, an attempt is made to study the interaction of two closely spaced rigid strip footings resting on homogeneous soil bed and find their ultimate bearing capacity and settlement behaviour subjected to inclined loading.

2 PROBLEM DEFINATION

Two rigid strip footings designated as the left (B_L) and the right (B_R) footing of symmetrical width, B rest on the surface of the homogeneous soil layer of depth, H as shown in Figure 1. The two footings are placed at a clear spacing, S and an inclined load, P is applied at an angle of inclination θ_L and θ_R with horizontal on the left and right footings, respectively. The effect of angles of inclination of load (θ_L and θ_R) and the clear spacing between the footings on the ultimate bearing capacity and settlement are analyzed. The properties of the soil deposit are considered as specified by Ghosh et al 2011 for the first layer of soil deposit, wherein Young's modulus of soil, E is 2.06e+03 kN/m^2, Poisson's ratio, μ is 0.3, cohesion, c_u is 19.40 kN/m^2, soil friction angle, □ is 24.73^0, unit weight of soil, γ is 17 kN/m^3 and thickness of total soil deposit, H is 11.7 m. The loading cases are chosen such that the variation of load inclination leads to combination of symmetrical and asymmetrical loading conditions. The cases of loading are given in Table 1.

Table 1. Loading cases

Case	θ_L	θ_R	Layout
a	90^0	90^0	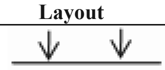
b	60^0	60^0	
c	60^0	120^0	
d	120^0	60^0	

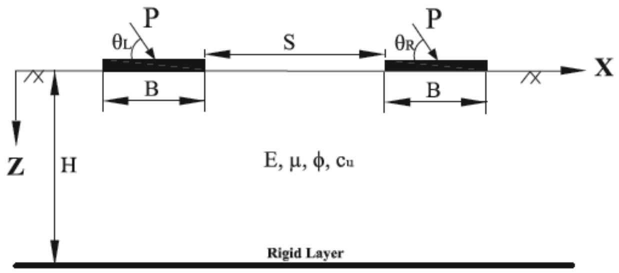

Figure 1. Definition of problem.

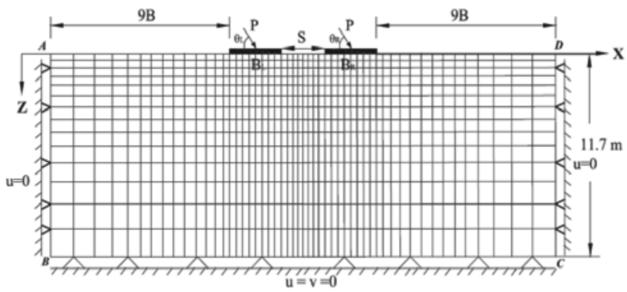

Figure 2. Discretized finite element domain and boundary conditions.

3 ANALYSIS

3.1 *Modeling*

The length of the strip footing is long enough compared to its width so the problem falls under plane strain condition. Henceforth two dimensional finite element analysis is carried out using the commercially available finite element software, ABAQUS 6.10. The soil is considered as elasto-plastic material obeying the Mohr Coulomb failure, where the parameter required for Mohr Coulomb plasticity model are prescribed in the previous section. The concrete footings are assumed to be linear elastic with a Young's modulus of 23.5e+6 kN/m^2 and a Poisson ratio of 0.2. The finite element mesh is generated with the use of CPE4R, a 4-node bilinear plane strain quadrilateral elements. The footings are placed on the surface of soil and have perfect contact with the soil. The nodes between footing and soil are tied using the tie constraints and no slip is allowed at the interface of footing bottom and soil. For the analysis of geotechnical problems, the initial state of stress is important and henceforth prior to application of external footing load the soil is analysed for initial state of stress with the use of geostatic step wherein the gravity load is applied. The static analysis may terminate when a few soil elements near the edge of the footings are distorted excessively which may happen at the ultimate state of failure. Hence the analysis is performed with dynamic implicit step where in the external footing load is applied very slowly to avoid the exciting the finite element model. The whole failure domain is considered in the present analysis to take care of both symmetrical and asymmetrical problems.

3.2 *Finite element domain, mesh and boundaries*

Figure 2, shows two (left and right) footings, size of failure domain, finite element mesh and boundary conditions. 4-noded bilinear rectangular plane strain elements are used to discretized the soil domain and suitable boundary conditions are assigned at the far end boundaries of the domain (Potts and Zdravkovic 1999). The bottom end BC is associated with fixed supports (no displacements are allowed) and side boundaries (AB and DC) are only fixed in horizontal direction. It is noted that the mesh is finer in the vicinity of the footings to take care of stress concentration. As the thickness of the soil deposit is of 11.7 m, so the domain in Z direction is fixed to 11.7 m. Thereby the sensitivity analysis is carried out to fix the domain size in X direction as discussed in Ghosh and Sharma, 2010. With B = 1 m, S = 0.5 m and subjected to vertical loads, the domain in X direction is varied in the range of 6B to 10B and thus the pressure displacements curves are obtained. It is seen that the pressure settlement curves almost converge beyond the domain size of 9B. Also same study is made for footings with inclined load; however convergence is obtained at 9B. Hence for all the cases as specified above, far boundaries in X direction (AB and CD) are considered at a distance of 9B from outer edges of the left and right footings. For the sake of space and brevity the details of sensitivity analysis are not presented.

3.3 Validation

The finite element model is validated prior to analyze the problem. For the validation the pressure settlement curves are obtained for isolated footing resting on soil surface and loaded with veritical and inclined (60^0 with horizontal) load and the same are presented in Figure 3 and Figure 4 respectively. The UBC (495 kPa) of vertically loaded footing obtained from the present analysis is seen to be close to the value (530 kPa) predicted by Terzaghi 1943 bearing capacity equation. For footing with inclined load, the UBC obtained is 145 kPa whereas the same is perdicted as 180 kPa by Meyerhof 1963 bearing capacity equation.

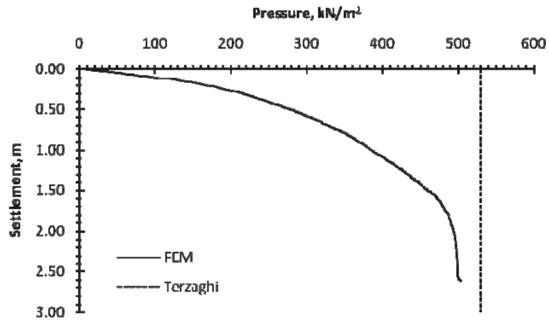

Figure 3. Comparison of FEM with Terzaghi 1943 equation for footing with vertical load.

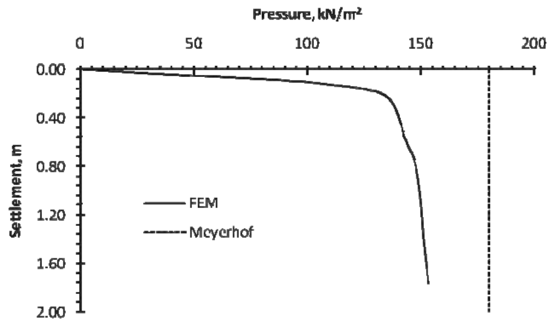

Figure 4. Comparison of FEM with Meyerhof 1963 equation for footing with inclined load.

3.4 *Results and Discussions*

Except case b, the rest of the cases (Case a, c and d) are symmetrical in condition and therefore, for the symmetrical cases the pressure settlement curves obtained both from the left and right footings are identical. It is to be noted that the pressure and settlements presented are obtained by averaging all the values obtained at all the nodes below the footing.

For case a, wherein the load is applied on the left and right footings at an angle of 90^0 with the horizontal, pressure settlement curves are obtained by increasing S/B ratio. The pressure settlement curves at S/B = 0.5 and 3.0 are presented in Figure 5, along with the curve for an isolated footing to ascertain the variation in the obtained curves. From the obtained pressure settlement curves of interfering footings, the ultimate bearing capacity of the soil is calculated at different S/B ratio and also the settlements, δ are obtained at the load intensity of

100 kPa assuming it to be in the range of working load. The same are presented in Table 2.

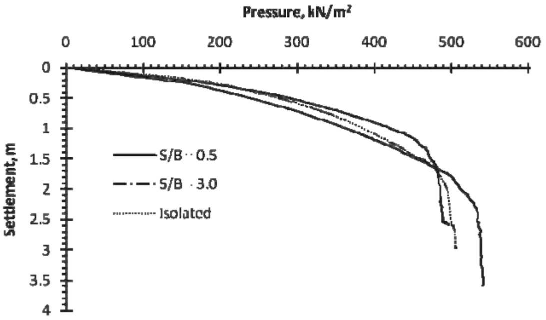

Figure 5. Pressure settlement curves for case a

Table 2. Bearing capacity and settlements of footing for case a.

S/B	0.5	1	1.5	2	2.5	3	3.5	5	Isolated
UBC, kPa	545	520	515	510	505	495	495	495	495
δ, mm (at 100 kPa)	156.5	148.1	141.3	135.9	131.4	127.8	124.7	118	105.7

It is observed from Table 2, that the UBC of interfering footings decreases with increase in S/B ratio and attains the value as that of isolated footing at higher spacing. At S/B = 0.5, the UBC is observed to be increased by about 10% compared to isolated footing. This is due the overlapping of the stress zones of individual footing when placed close to each other. The same can be observed from the stress contour plot as presented in Figure 6. Similar kind of variation is seen for the settlements at working load. The settlement is increased by 48% when the footings are placed at S/B = 0.5 and the percentage increase in the settlement decreases with increase in S/B ratio.

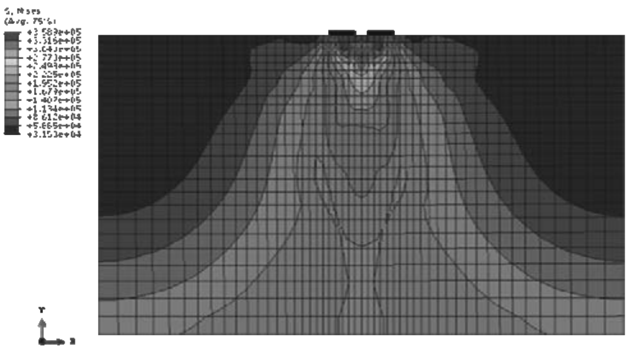

Figure 6. Stress contour for case a at S/B equal to 0.5.

As the case b, is unsymmetrical case the pressure settlement curves are obtained for both left and right footings at different S/B ratio and are seen to be non-identical. The pressure settlement curve for case b is obtained at S/B = 0.5 and shown in Figure 7. The UBC is calculated owing to the interference for left and right footings placed at different spacing and are presented in Table 3. Similarly the settlements, δ obtained at working load of 100 kPa are presented in Table 4. It is observed that the UBC of both footings decreases by 14% at S/B = 0.5 compared to that of isolated footing under same loading condition. However, at S/B = 2.5, the UBC of two footings attain a value as that of isolated footing and remains constant with further increase in S/B ratio. It is also observed that the settlement of left and right footing at working load is increased by 59% and 49% at S/B = 0.5 and decreases to 23% and 11%, respectively at S/B = 5.0 compared to that of isolated footing. The stress contour for case b at S/B = 0.5 is shown in Figure 8 and it is seen that the stress contours of right footing do not overlap much with that of left footing and hence negligible interference phenomenon is observed however the effect on settlement is higher.

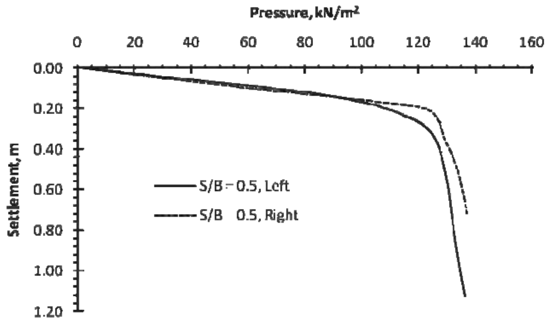

Figure 7. Pressure settlement curve of case b at S/B = 0.5.

Table 3. UBC (kPa) of interfering footings for case b, c and d.

S/B	Case			
	b		c	d
	Left	Right		
0.5	125	125	135	140
1.0	128	130	145	145
1.5	130	130	145	145
2.0	140	140	145	145
2.5	145	145	145	145
3.0	145	145	145	145
3.5	145	145	145	145
5.0	145	145	145	145
Isolated	**145**		**145**	**145**

Table 4. Settlement, δ (mm) obtained at 100 kPa load.

S/B	Case			
	b		c	d
	Left	Right		
0.5	166.79	155.52	155.96	155.04
1.0	162.61	145.84	148.28	146.46
1.5	157.10	140.21	141.69	140.95
2.0	151.56	135.44	131.91	136.38
2.5	146.94	130.85	130.95	132.52
3.0	142.59	126.93	127.16	129.11
3.5	138.66	123.57	124.04	126.10
5.0	128.95	116.13	117.03	118.97
Isolated	**104.70**		**104.70**	**104.70**

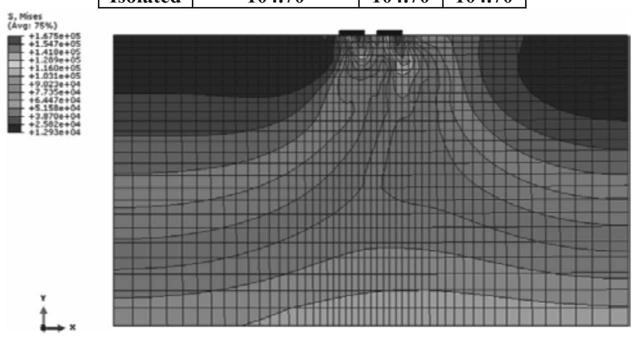

Figure 8. Stress contours for case b at S/B equal to 0.5.

Similarly, the pressure settlement curves are obtained for case c and case d. It is observed that the curves obtained from both left and right footings are exactly identical. From the obtained curves, the UBCand settlements at working load of 100 kPa are obtained and the same are tabulated in Table 3 and Table 4, respectively. The pressure settlement curves obtained for footings placed at S/B = 0.5 are shown in Figure 9 for case c and case d. The stress contour plot for case c and case d obtained by placing the footings at S/B = 0.5 are shown in Figure 10 and Figure 11 respectively. It is observed that the UBC of interfering footing decreases by 7% at S/B = 0.5 and at all S/B ratios the bearing capacity value remains same as that of isolated footing, revealing negligible or no effect of interference on the bearing capacity. However significant effect of interference on the settlement is observed. 49% increase in settlement of the footings as compared to the isolated footing is found. Similar observation is made for case d wherein the stress isobars diverge or are in opposite direction hence negligible or no overlap of stress contours is seen in the vicinity of footing edges where the stress concentration will be high and at greater depths of footings the stress contours overlap a bit. Henceforth, it is observed that the interference phenomenon has no significant effect on the bearing capacity; however it has certain considerable effect on the settlement of the footings. It is also observed that at the node point 1 m below the axis of symmetry, the vertical settlement obtained for case c is higher than that obtained for case d since in case c the footing loads on left and right footings converge towards the axis of symmetry and vice versa in case d.

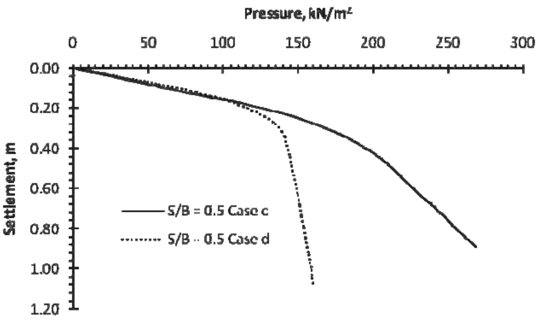

Figure 9. Pressure settlement curves of case c and case d at S/B equal to 0.5.

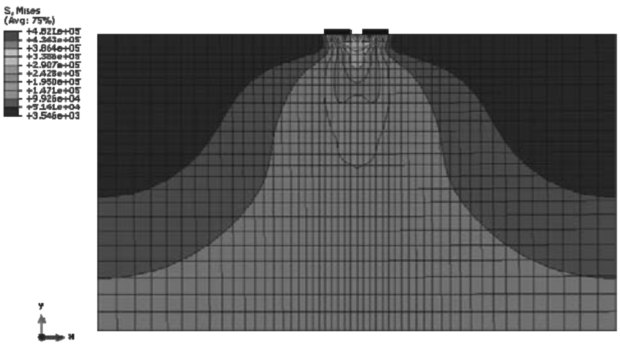

Figure 10. Stress contour for case c at S/B equal to 0.5.

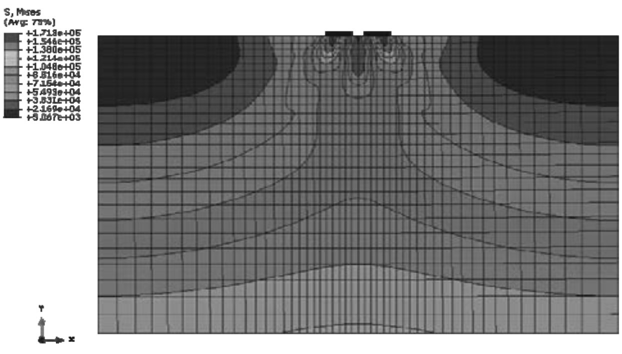

Figure 11. Stress contour for case d at S/B equal to 0.5.

4 CONCLUSIONS

A limited study is presented on the effect of two closely spaced rigid strip footings resting on the surface of homogeneous soil subjected to inclined load. The effect of interference phenomenon on ultimate bearing capacity and settlement at working load condition are studied. The phenomenon has certain considerable effect on the ultimate bearing capacity, increasing its capacity when footings are vertically loaded. For the cases where footings are subjected to inclined load the effect of interference on the bearing capacity has no significant effect. However for all the cases of inclined loading condition, the interference effect on the settlement is quite significant. The settlement of interfering footings in the range of working load decreases with increase in the clear spacing between the footings and attains a value as that of isolated footing at greater clear spacing ($S \geq 5B$).

5 REFERENCES

Terzaghi K. 1943. *Theoretical soil mechanics*. John Wiley and Sons, New York.

Meyerhof G.G. 1963. Some recent research on the bearing capacity of foundations. *Canadian Geotechnical J.* 1 (1), 16-26.

Vesic A.S. 1973. Analysis of ultimate loads of shallow foundations. *J. Soil Mech. and Found. Div.* 99 (1), 45-73.

Stuart J.G. 1962. Interference between foundations with special reference to surface footings in sand. *Geotechnique J.* 12 (1), 15-23.

Graham J. Raymond G.P. and Suppiah A. 1984. Bearing capacity of three closely-spaced footings on sand. *Geotechnique J.* 34 (2), 173-182.

Kumar J. and Ghosh P. 2007. Ultimate bearing capacity of two interfering rough strip footings. *Int. J. Geomech*. 7 (1), 53-61.

Kumar J. and Kouzer K.M. 2007. Bearing capacity of two interfering footings. *Int. J. Num. Analyt. Methods in Geomech*. 32, 251-264.

Kumar J. and Bhattacharya P. 2010. Bearing capacity of interfering multiple strip footings by using lower bound finite elements limit analysis. *Computers and Geotechnics* 37, 731-736.

Mabrouki A. Benmeddour D. Frank R. and Mellas M. 2010. Numerical study of the bearing capacity for two interfering strip footings on sands. *Computers and Geotechnics* 37(4), 431-439.

Kouzer K.M. and Kumar J. 2010. Ultimate bearing capacity of a footing considering the interference of an existing footing on sand. *Geotech. Geol. Eng*. 28 (4), 457-470.

Ghosh P. and Sharma A. 2010. Interference effect of two nearby strip footings on layered soil: theory of elasticity approach. *Acta geotechnica* 5, 189-198.

Nainegali L. and Basudhar P.K. 2011. Interference of two closely spaced footings: A finite element modeling. *ASCE Geotechnical Special Publiactions, Geo-forntiers: Advances in Geotechnical Engineering*, Dallas, Tx.

Lee J. Eun J. Prezzi M. and Salgado R. 2008. Strain influence diagrams for settlement estimation of both isolated and multiple footings in sand. *J. Geotech. Geoenviron. Eng*. 134 (4), 417-427.

Nainegali L.S. Basudhar P.K. and Ghosh P. 2012. Analysis of nearby rigid strip footingson elastic soil bed subjected to inclined load. *Indian Geotechnical Conference: Advances in Geotechnical Engineering* NewDelhi, India.

Khing K.H. Das B.M. Yen S.C. Puri V.K. and Cook E.E. 1992. Interference effect of two closely spaced shallow strip foundations on geogrid reinforced sand. *Geotech Geolog Eng*. 10, 257-271.

Das B.M. Puri V.K. and Neo B.K. 1993. Interference effects between two surface footings on layered soil. *Transportation Research Record* 1406, 34-40.

Kumar A. and Saran S. 2003. Closely Spaced Footings on Geogrid-Reinforced Sand. *J. Geotech. Geoenviron. Eng*. 129 (7), 660-664.

Kumar J. and Bhoi M.K. 2009. Interference of two closely spaced strip footings on sand using model tests. *J. Geotech. Geoenviron. Eng*. 135 (4), 595-604.

Ghosh P. Kumar P. 2009. Interference effect of two nearby strip footings on reinforced sand. *Contemporary Eng Sciences* 2 (12), 577-592.

Ghosh. P. Magistris. F. and Fabbrocino. G. 2011. Seismic response of pier foundations of an existing roadway bridge. 5th International Conference on Earthquake Geotechnical Engineering (5ICEGE) Santiago, Chile.

ABAQUS User's Manual. 2010. ABAQUS/Standard user's manual, volume II version 6.10. Hibbitt Karlsson and Sorenson Inc. Rhode Island.

Potts D.M. and Zdravkovic, L. 1999. *Finite element analysis in geotechnical engineering*. 1, 2, Thomas Telford Publications, London.

Over a decade of experience with computer aided learning in geotechnical engineering

Plus d'une décennie d'expérience dans le domaine de l'enseignement assisté par ordinateur dans le domaine de l'ingénierie géotechnique

Springman S.M., Herzog R., Seward L.
Institute for Geotechnical Engineering, ETH Zürich, Wolfgang-Pauli Strasse 15, 8093 Zürich, Switzerland

ABSTRACT: While Computer Aided Learning has become a valuable part of the palette of tools available in developing and teaching university courses in geotechnical engineering, it is not the universal panacea and requires careful planning, didactic considerations and high quality in the delivery. The 'Institut für Geotechnik' (IGT) at ETH Zürich has been using an e-learning platform for the last 12 years to teach basic soil mechanics to students at the bachelor level in German. The notes are embedded with quizzes, virtual and real laboratory exercises, frontal lectures and accompanying lecture videos. A second generation knowledge-based platform GEOTip (GEOTechnical Information Platform) was developed inhouse using PHP and MySQL to stay abreast of advances in web technology and to ensure ongoing sustainability. All materials have been translated into English and extended using podcasts and accompanying videos to cover additional multidisciplinary courses for students in geophysics, environmental sciences and engineering. This paper describes concepts, key features and technical background for GEOTip. A summary of the students' course evaluations is also presented and the change in the students' perception of the platform over the years is analysed as well.

RÉSUMÉ : Bien que l'enseignement assisté par ordinateur (EAO) soit devenu un élément précieux de la palette d'outils à disposition pour développer et enseigner des cours d'université dans le domaine de l'ingénierie géotechnique, il ne s'agit pas d'une panacée universelle. L'EAO demande une planification attentive, des considérations didactiques et une haute qualité de distribution. L'« Institut für Geotechnik » (IGT) à l'ETH Zürich utilise une plate-forme d'e-learning depuis 12 ans pour enseigner en allemand les bases de mécanique des sols aux étudiants de niveau bachelor. Les notes de cours sont incorporées à des quizz, des exercices virtuels et réels en laboratoire, des cours magistraux et des vidéos de cours. Une plate-forme de connaissances de deuxième génération, GEOTip (GEOTechnical Information Platform) a été développée en interne en utilisant PHP et MySQL afin de se maintenir à la pointe des avancées dans le domaine de la technologie du web et d'en assurer la durabilité. Tous les documents ont été traduits en anglais et complétés à l'aide de podcasts et de vidéos d'accompagnement pour couvrir les cours multidisciplinaires supplémentaires pour les étudiants en géophysique et sciences de l'environnement. Cet article décrit les concepts, les caractéristiques-clé et le contexte technique pour GEOTip. Un résumé des évaluations des cours par les étudiants est aussi présenté et le changement de la perception de la plate-forme par les étudiants est aussi analysé.

KEYWORDS: knowledge-based platform, embedded multi-threaded geotechnical resources, e-learning

1 INTRODUCTION

Early developments for Computer Aided Learning in geotechnical engineering existed as part of the GeotechniCAL reference package funded by the UK Higher Education Funding Council Teaching and Learning Technology Programme and were led by Dr Leslie Davison, Professors David Muir Wood and John Atkinson. Subsequently, a pilot project for an introductory course in German in soil mechanics at Bachelor level, CALICE (Computer Aided Learning in Civil Engineering), was funded in 2000 ((Sharma *et al.*, 2001; Springman *et al.*, 2003). This was part of a Swiss-British initiative under the umbrella of the ETH World Virtual Campus, to promote a step-change in the students' development, understanding and acquisition of knowledge. The resources developed included:

- online reference material for information,
- simulations designed to encourage reflection,
- open ended questions linking theory to practice,
- multiple choice descriptive and numerical questions to consolidate learning and assess progress.

All Bachelor and Masters courses from the Chair for Geotechnical Engineering have been mounted on the second generation, inhouse knowledge-based platform GEOTip (GEOTechnical Information Platform) since 2007. Subsequently, the introductory Bachelor course in soil mechanics has been extended for several different versions of multidisciplinary Masters' courses in geophysics, environmental sciences and engineering, in English. This paper describes concepts, key features and technical background and the students' evaluation of the progress.

2 GEOTIP: CONCEPT FOR THE GEOTECHNICAL INFORMATION PLATFORM

2.1 *Key features*

GEOTip was developed in house using PHP and MySQL to host the existing multi-threaded geotechnical resources. These included videos of the frontal lectures for streaming for later viewing, a script with embedded media, online quizzes, practical site-specific challenges and virtual laboratory demonstrations with associated questions for ongoing assessment of learning. Each student's performance is summarised on their personalised home-page.

Eight chapters of the bachelor's course soil mechanics listed below form the basis of the content with quizzes, virtual laboratory tests and challenges associated with each one. A final chapter about the construction of the Monasavu Dam in Fiji provides a useful opportunity to apply a simple form of 'problem-based' learning.

- 1. The ground
- 2. Stresses in the ground

- 3. Groundwater
- 4. General deformation behaviour of soils
- 5. Shear strength
- 6. Slope stability
- 7. Settlement
- 8. Compaction
- 9. Monasavu dam: fundamentals

The Masters' courses in English are running at capacity and students from a variety of engineering and science backgrounds are more inclined to choose virtual resources that suit their respective needs, learning styles, and language, while using the same core learning materials. A further range of innovative learning opportunities including online laboratory guides, pod- and vod-casts, which have been embedded in mindmaps to improve the clarity of the overview, efficiency of delivery and to empower students to access a variety of resources, each fulfilling several different didactic needs.

The pedagogical aim of the courses offered is to provide students with a variety of didactic methods, so each individual may choose the resources that suit their learning style best, and therefore learn efficiently. Assessment is then made through the quizzes (automatic, meaning students receive their marks instantly), challenges and virtual laboratories (wholly or partly marked by hand).

Students must solve all the quizzes, scoring a minimum of 40% of the total points, in order to earn credit for the course. These interactive animations illustrate some of the most complex geotechnical processes, supported by probing questions. These animations are a part of the mandatory exercises that the students have to complete successfully. Challenges are more complex problems derived from real life projects. These projects are explained using pictures, video-clips, blueprints, geological profiles and text. Helping students to understand from a practical, rather than just a theoretical, standpoint is a challenge in all engineering courses. It is with this issue in mind that the Monasavu dam chapter, online laboratories (chapter 3.2) and other challenges were written.

Exercises are a compilation of multiple-choice questions and arithmetical problems. They offer the student a chance to test their knowledge and to prepare for the quizzes. While solving the problem, the student receives immediate feedback whether their answer is correct or not. A hyperlink provides easy access to the corresponding chapter in the script.

Student course evaluations are enabled so that ongoing feedback can be obtained, although the frequency of responses has dropped off in recent years. Consistently high marks were gained from student evaluations, although there has been change in the students' perception of the platform over the years, which is analysed as well.

2.2 *Technical background*

GEOTip is an in-house developed database driven website using PHP and MySQL. Since both programs are open source and widely used, ongoing sustainability is ensured. In addition, an Adobe Media server is being used to stream the video material.

Technically, GEOTip consists of three parts:

1. the knowledge based system, where text parts, pictures, videos, animations and equations are stored in a common categorized tree structure (multiple categories are possible) combined with Meta tags;
2. the exercise questions, which are also stored using the same tree structure;
3. the e-learning courses then make use of the contents stored in first two parts.

New e-learning courses can easily be put together through the integrated Content Management System by accessing the knowledge base part to create an online script. Virtual laboratory exercises, challenges and recorded lectures can be added in the same way.

The platform has been programmed as a multi-language system using German and English to serve the needs of international students better. Users can choose the language of the platform in the profile settings, while the language of the content can be changed at any time. Adding a further platform language could be done at any time, without needing a major re-write of the base code.

GEOTip uses a multi-level access system, allowing IGT to retain control of intellectual property. While unregistered guests only have access to limited selected content, registered users, who are taking a course, have access to all the content stored in the knowledge base part of the website.

To make it as simple as possible for authors to create content for the platform, a Content Management System (CMS) has been incorporated. Through the CMS text parts can be written and pictures and videos uploaded. The CMS also includes an inhouse developed intuitively usable equation editor based on Adobe Flash (Fig. 1).

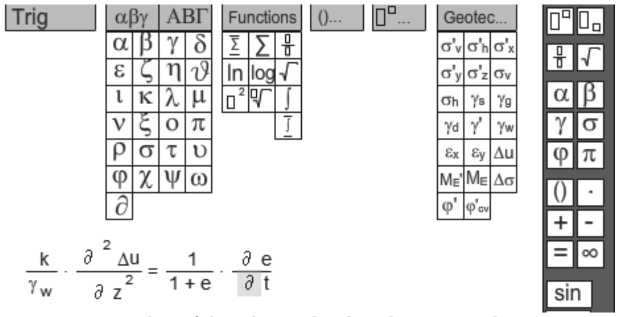

Figure 1: Screenshot of the inhouse developed equation editor.

An Adobe Media server is used for all the video streaming services. An inhouse developed flash player interface is used to access the videos on the Media server. From the client-side only, a browser with the Adobe Flash plugin (animations and video services) and Java (virtual lab exercises) is needed. To maximise browser compatibility, the website does not use java-script for the student pages. This solution enabled the development of a double screen feature for the lecture videos showing the recorded projector picture in a large screen and the lecturer in a smaller screen. About a third of the lectures are re-recorded for the German course in "soil mechanics" every year, to ensure the material is up to date.

Single and multiple choice questions and calculation exercises can be created through the CMS. The numbers in the question for the calculation exercises and corresponding answer can be varied from student to to discourage copying in two different ways. The first, classical option is to upload a csv formatted file containing different numbers and the solution per line. The second option makes use of an adapted equation editor, in order to store the equation for the solution in the platform. This reduces the time to develop a calculation question. The accuracy demanded for the solution can be set for each calculation exercise or globally for the whole course.

2.3 *Summary of course evaluations*

An anonymous course evaluation system was implemented in order to assess student acceptance and to be able to continue to improve the platform. It is possible to display multiple-choice questions with this system, as well as to give free answers to text questions in the context dependent frame to the right of the main content on the webpage.

The survey consists of approximately 110 questions about course understanding, assessment of the quizzes, virtual labs and challenges and about the handling and layout of the platform itself for the bachelor-level course "soil mechanics". In order to have the best quality answers, the survey is not just shown at the end of the semester but questions are gradually introduced over the course of the semester shortly after the corresponding topic has been covered. Nevertheless, the participation of the students significantly decreases over the course of the semester.

Student participation has also decreased over the years. While in 2007, the year GEOTip was introduced to the students, 38 % of all possible questions were answered; this percentage decreased to 12 % in 2011 and then rose again to 19 % in 2012 (see Figure 2).

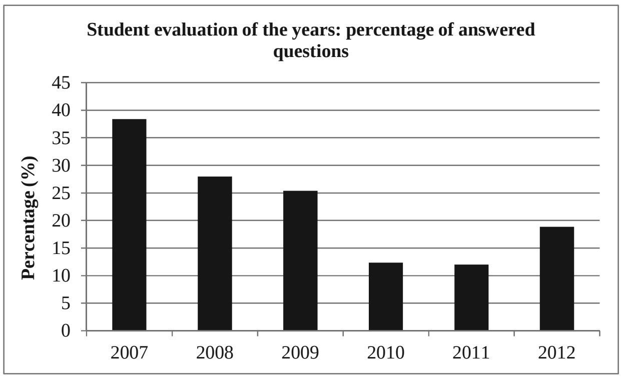

Figure 2: Student participation over the years since 2007.

Figure 3 shows that students generally judge GEOTip to be better than other computer aided learning systems. Astonishingly, the number of students without prior experience of computer aided learning systems increases over the years since its introduction.

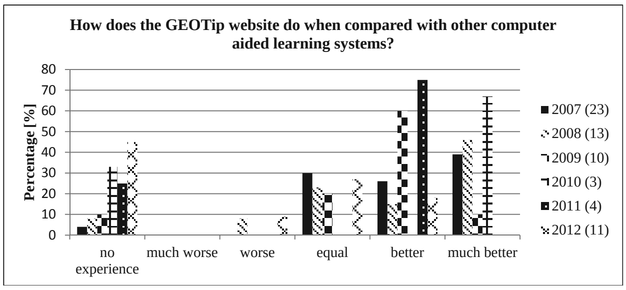

Figure 3: Development of the comparison of GEOTip with other computer aided learning systems over the years. The number of answers is given in parentheses.

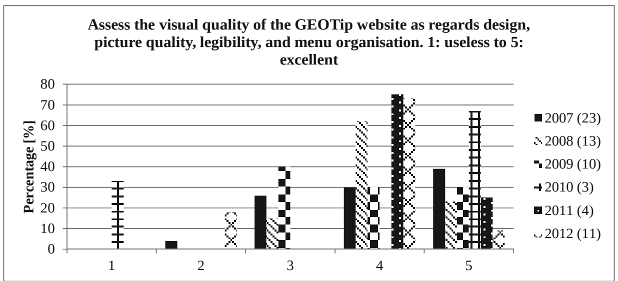

Figure 4: Development of the assessment of the design, picture quality, legibility and menu organisation over the years. The number of answers is given in parentheses.

The GEOTip website is mainly given marks of 4 and 5 out of 5 for design, picture quality, legibility and menu organisation (Figure 4). It can be seen though that a decreasing number of students award the mark 5 (excellent) although objectively the content and design of the website has not changed. This could be a hint that students' perception changes with time and that continuing improvement is needed to keep students' acceptance at a high level.

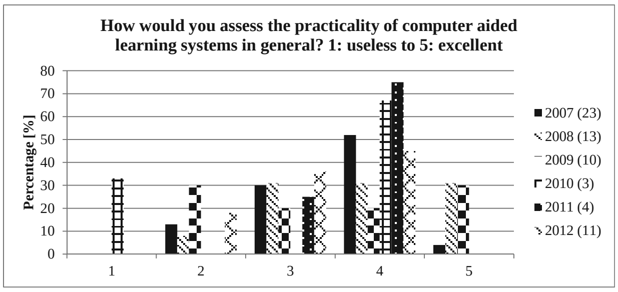

Figure 5: Development of the assessment of the practicality of computer aided learning systems over time. The number of answers is given in parentheses.

3 INNOVATIONS

Funding from an ETH Zürich Innovedum grant was received in August 2011, in order to upgrade the services offered by GEOTip for students from outside civil engineering, who study soil mechanics as a part of their course. Work began on a series of recorded lectures based on a set of mindmaps, which were designed to introduce basic concepts, and also on a series of recorded experiments, designed to explain to students and new staff members how each experiment works and how to use the equipment within the IGT laboratory. Work also began on revising and updating the script – a bilingual purpose written textbook, designed to take students through the course.

3.1 *Recorded lectures*

In order to reduce time burdens on professors and assistants, a series of online lectures, based on mindmaps and the online scripts have been created using a combination of voiceovers over moving images, taken using screengrab software, displaying the section of the mindmap, the script or the graphic being discussed. Each of the 7 lectures is between 1-3 hours long. Since fundamental but complex issues are covered, it is pieced together so that single sections may be used as stand-alone lectures in order to allow students to focus in on one issue rather than being side-tracked by confronting many topics at once. The main aim was to give students a method of learning basic concepts from geotechnical engineering at their own pace, and allowing them to revisit some of the more complex ideas as many times as required. "Jump points" embedded both into videos and corresponding mindmaps allow students to go straight to a chosen section and revisit the same section on multiple occasions.

3.2 *Online laboratories*

Online laboratories are recorded videos of an assistant performing many experiments (such as oedometer, Proctor and plastic index tests) used to produce one of a series of commonly-used engineering parameters.

The rationale behind the online laboratories was twofold – firstly it allows bachelors and masters students to learn how data that they will use throughout their career is produced, and what common inaccuracies and mistakes are. Secondly, it will allow project students and new members of staff to understand how to use the equipment in the laboratory, while reducing commitments for the laboratory manager and technician.

Within the recorded demonstrations explanations of how to perform the experiment, reasons why the experiment is done in a particular way, and common mistakes made are embedded. The demonstrations are not designed to be watched whole, but to be used as reference guides, with viewers skipping through sections and repeating other sections.

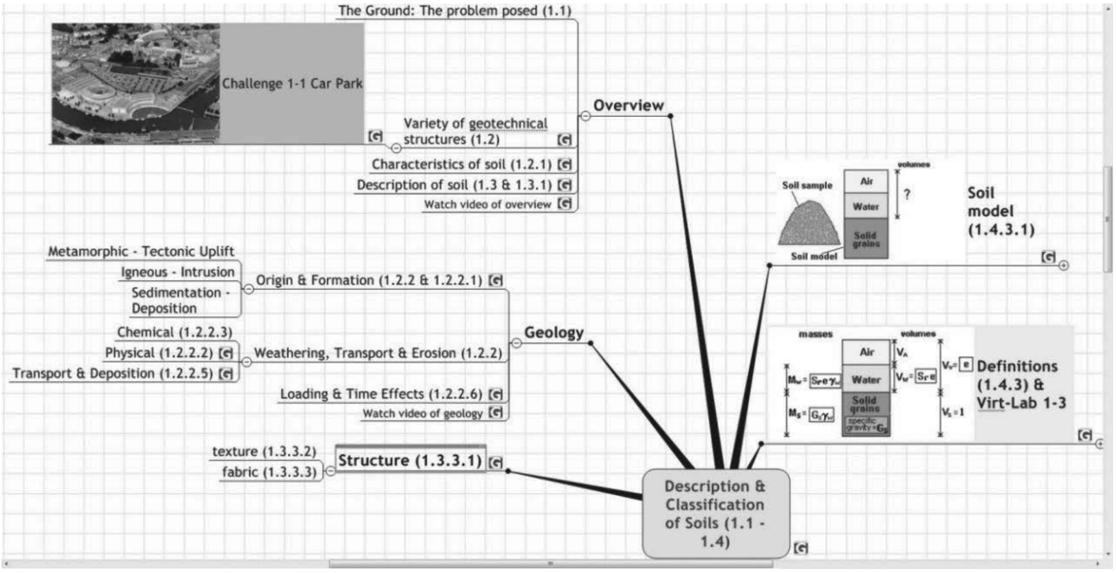

Figure 6: Part of a central mindmap, which forms the basis of courses taught using GEOTip.

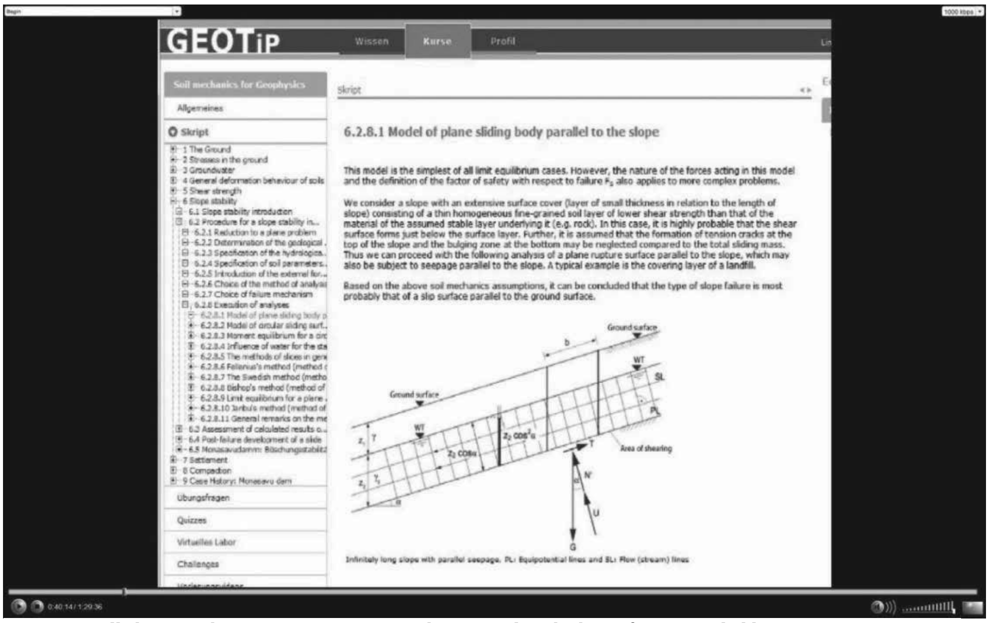

Figure 7: Still showing the purpose written script being used as the basis for a recorded lecture.

4 CONCLUSIONS

An online learning platform has been developed and evolved successfully to optimise teaching of the fundamentals of Geotechnical Engineering to bachelors and masters students. The site was developed using state of the art inhouse methods and freeware PHP and MySQL, allowing for constant regeneration and updating, and recent work has provided more base material in the form of lecture videos, vod-casts and on-line labs to allow students to learn at their own speed.

Evaluations have shown that GEOTip is well received by students, who are able to learn using one or more of the many didactic methods available (lectures, exercises, script, mindmaps), however responses are becoming less positive with time, showing the need for constant updating.

5 ACKNOWLEDGEMENTS

The authors would like to thank Dr Les Davison, Prof Jitendra Sharma, Robert Banjac, ETH NET, ETH World, FILEP, INNOVEDUM for input and financial support.

6 REFERENCES

Sharma, J.S., Springman, S.M. and Davison, L.R. 2001. An Internet-based Multi-threaded Approach to Computer-aided Learning in Civil Engineering. *7th International NETTIES Conference. 3rd International Conference on New Learning Technologies*. 7.2.1-7.2.8.

Springman, S.M., Mayor, P.A. and Banjac, R. 2003. CALICE: Entwicklung und Erfahrungen. Frühjahrestagung, EDV-Programme in der Geotechnik, Zürich. *Schweizerische Gesellschaft für Boden- und Felsmechanik SGBF 146*, 28.3.2003: 28-36.

Predicting Settlements of Shallow Footings on Granular Soil Using Nonlinear Dynamic Soil Properties

Prédiction des tassements de fondations superficielles sur des sols granulaires en utilisant des propriétés dynamiques non linéaires du sol.

Stokoe K.H., Kacar O.
University of Texas at Austin, Texas, USA

Van Pelt J.
CDM Smith, Inc. Dallas, Texas, USA

ABSTRACT: The governing design criterion for shallow foundations in freely draining granular soils is usually permissible settlement. Due to difficulties in obtaining undisturbed samples of granular soils composed of mainly sands and gravels, settlement predictions are generally based on correlations with in-situ penetration tests. In this study, field seismic measurements are used to evaluate small-strain ("elastic") shear moduli of granular soils (G_{max}). These small-strain moduli, combined with nonlinear normalized shear modulus-shear strain (G/G_{max}-log γ) relationships, are used to predict settlements of shallow foundations under working loads. The G/G_{max}-log γ relationships are based on models developed from dynamic resonant column (RC) tests of reconstituted sands and gravels. The combination of field G_{max} results and laboratory G/G_{max}-log γ relationships have been implemented in a finite element program (PLAXIS) via a subroutine. Settlement predictions with this approach are illustrated by comparison with a load settlement test using a 0.91-m diameter footing. At working stresses, nonlinear footing settlements were predicted quite well, similar to predictions with traditional CPT and SPT procedures.

RÉSUMÉ: Le critère de dimensionnement pour des fondations superficielles sur sols granulaires est, souvent, le tassement admissible. A cause de la difficulté à obtenir des échantillons intacts de sols sableux et graveleux, les prévisions de tassement sont basées sur des corrélations déduites des essais in-situ. Dans la présente étude, des mesures sismiques in situ sont utilisées pour évaluer les modules de cisaillement elastique en petites déformations des sols granulaires (Gmax). Ces modules, combinés avec des relations de variation non-lineaire module-distorsion, G/Gmax-log γ, sont utilisés pour prévoir les tassements des fondations. Les relations G/Gmax-log γ sont basées sur des modèles développés à partir d'essais à la colonne résonante (RC) sur des éprouvettes reconstituées de sables et graviers. La combinaison des mesures de Gmax in-situ et des relations G/Gmax-log γ obtenues en laboratoire sont introduites via une sous-routine dans un programme d'éléments finis (PLAXIS). Les prédictions des tassements obtenues avec l'approche proposée sont présentés en les comparant aux résultats d'un essai de chargement utilisant une fondation de 0.91m de diamètre. Sous contraintes de service, les previsions de tassements non-lineaires sont bonnes. Elles sont similaires à celles déduites des procédures SPT et CPT traditionnelles.

KEYWORDS: in-situ seismic testing, nonlinear dynamic properties, granular soil, footing settlement

1 INTRODUCTION

In shallow foundation design, bearing capacity and settlement are the two main criteria considered. For freely draining granular soils, permissible settlement becomes the governing factor in most cases. Laboratory tests to predict the stress-strain behavior of soils generally require an undisturbed sample which is nearly impossible and/or very expensive to recover from the field for granular soils. Therefore, settlements of shallow foundations on such soils have traditionally been predicted using empirical correlations that relate in-situ penetration test results with load-settlement tests or case histories. In this article, an approach based on field seismic evaluation of small-strain ("elastic") shear modulus (G_{max}) combined with nonlinear normalized shear modulus-shear strain (G/G_{max}-log γ) relationships is presented. The effects of increasing confining pressure and strain amplitude on soil stiffness during loading of the footing are incorporated in this formulation. The approach has several important benefits including: (1) in-situ seismic testing which can readily be performed in all types of granular soils, including gravels and cobbles (2) continuous load-settlement curves that are evaluated to stress states considerably above those expected under working loads, and (3) a methodology that is appropriate for all types of geotechnical materials, even those where the effective stresses change with time.

2 TRADITIONAL AND RECENT SETTLEMENT-PREDICTION METHODS

One of the first methods of predicting footing settlements on granular soils was proposed by Terzaghi and Peck (1948). They conducted plate-load tests on 300-mm square plates on sand and then predicted the settlements of full-size footings using an empirical relationship. Meyerhof (1965) proposed a method where the settlements were predicted based on standard penetration test (SPT) blow count, N_{60}. One of the most widely used methods today was originally proposed by Schmertmann (1970). He used elastic theory, model load tests, field cone penetration tests (CPT) and finite element analysis to develop the approach. In Schmertmann's method, the soil stiffness is expressed as an equivalent elastic modulus which is based on CPT results. Burland and Burbidge (1985) reviewed a data set of case histories and developed a method using corrected SPT results. In all methods, a key parameter, the strain dependency of the soil stiffness, is not directly considered.

One of the earliest methods to take the strain dependency of the soil stiffness into account was proposed by Berardi and Lancellotta (1991). They proposed an iterative scheme where the soil stiffness was evaluated based on the corrected

SPT blow count and varied according to the calculated relative strain levels. Lee and Salgado (2001) proposed a model where soil stiffness is reduced based on the tolerable settlements and relative density of the soil. A simplified method was proposed by Lehane and Fahey (2002) which takes the soil nonlinearity into account by reducing the small-strain Young's modulus with increasing axial strain.

None of these methods incorporate field seismic testing to estimate soil stiffness near the base of footing where much of the settlement occurs. In addition, none of the methods considers the combined effects of shear strain level, stress state and gradation on nonlinear stress-strain behavior of granular soils. In this study, an approach implementing dynamic nonlinear soil behavior and field seismic testing is proposed to estimate the settlement of footings as discussed below.

3 NONLINEAR BEHAVIOR OF GRANULAR SOIL

The stress-strain behavior of granular soil ranges from linear ("elastic") at small strains to highly nonlinear at large strains. The shear strain below which the shear modulus is constant is defined as the elastic threshold strain, γ_t^e. For granular soils with no plasticity, γ_t^e varies with effective confining pressure, σ_0', and gradation, usually expressed by the uniformity coefficient, C_u (Menq, 2003). For working stresses associated with shallow foundations, γ_t^e likely ranges from 0.0001 to 0.003%. Advances in in-situ seismic measurements, especially development of surface wave tests like the Spectral-Analysis-of-Surface-Waves (SASW) test (Stokoe et al.,1994), permit small-strain shear wave velocity (V_s) and shear modulus (G_{max}) to be evaluated very near the surface and in granular soils, even soils with gravel and cobbles. Other dynamic laboratory testing methods, such as the torsional resonant column, have made it possible to investigate the nonlinear shear modulus of granular soils over a wide strain range. For instance, Hardin and Drnevich (1972) conducted the first comprehensive study of nonlinear soil behavior and the parameters affecting nonlinearity. They proposed a hyperbolic model to define nonlinear soil behavior. This hyperbolic model was modified by Darendeli (2001) based on a large dataset of combined resonant column and torsional shear tests (RCTS) as follows:

$$G/G_{max} = \frac{1}{1+\left(\frac{\gamma}{\gamma_r}\right)^a} \tag{1}$$

where $a =$ curvature coefficient; $\gamma_r =$ reference shear strain at $G/G_{max} = 0.5$; and G is the shear modulus at shear strain $= \gamma$. The value of the reference shear strain depends on plasticity, confining pressure and overconsolidation ratio. The modified hyperbolic model was further refined by Menq (2003) for sands and gravels with no plasticity by defining reference strain, γ_r, and curvature coefficient, a, as follows:

$$\gamma_r = 0.12{C_u}^{-0.6}\left(\frac{\sigma_0'}{P_a}\right)^{0.5{C_u}^{-0.15}} \tag{2a}$$

$$a = 0.86 + 0.1\log\left(\frac{\sigma_0'}{P_a}\right) \tag{2b}$$

where γ_r is in %; $C_u =$ uniformity coefficient; $\sigma_0' =$mean effective confining pressure in the same units as P_a; and $P_a =$ reference mean effective confining pressure (1 atm).

A subroutine using the modified hyperbolic model described by Equations 1 and 2 was written and implemented in a commercially available finite element program (PLAXIS). The subroutine uses a small-strain reference shear modulus (discussed below and represented by Equation 3) adjusted to the increasing stress state and the G values in the G/G_{max}-log γ relationship are adjusted to the increasing shear strain level. The subroutine is used to perform equivalent linear calculations (Kacar, 2013).

4 FIELD LOAD-SETTLEMENT TEST

To begin to develop a database of measured footing settlements at granular sites with in-situ seismic and nonlinear dynamic laboratory measurements, a small-scale footing was constructed at a site in Austin, Texas. A detailed geotechnical investigation was carried out at the site, including soil sampling, cone penetration testing (CPT), Spectral-Analysis-of-Surface-Waves (SASW) seismic tests, and crosshole seismic tests.

4.1. *Soil Properties at Test Site*

Based on standard laboratory tests, the soil at the field site is a lightly overconsolidated, non-plastic silty sand with a friction angle of 39 degrees and a cohesion of 6.1 kPa (likely resulting from capillary stresses). Results from SASW and crosshole seismic tests and CPT tests are presented in Figure 1. The friction ratio averages about 1.1% between depths of 0-2.1m and about 0.7% between depths of 2.1m-4.9 m.These friction ratios are indicative of nonplastic granular soils (Lunne et al., 2002). As seen in Figure 1, good agreement exists between the crosshole and SASW results. Therefore, the average V_s profile from four SASW tests was used to model the soil. With this profile and the average mass density of the soil determined from intact samples (1.70 g/cm^3), the small-strain shear modulus (G_{max}) versus depth profile before loading the footing was modeled as:

$$G_{max} = G_{\max\_1atm}\left(\frac{\sigma_0'}{P_a}\right)^{n_G} \tag{3}$$

where $G_{\max\_1atm} =$ small-strain shear modulus at an effective confining pressure of 1atm; $\sigma_0' =$ mean effective

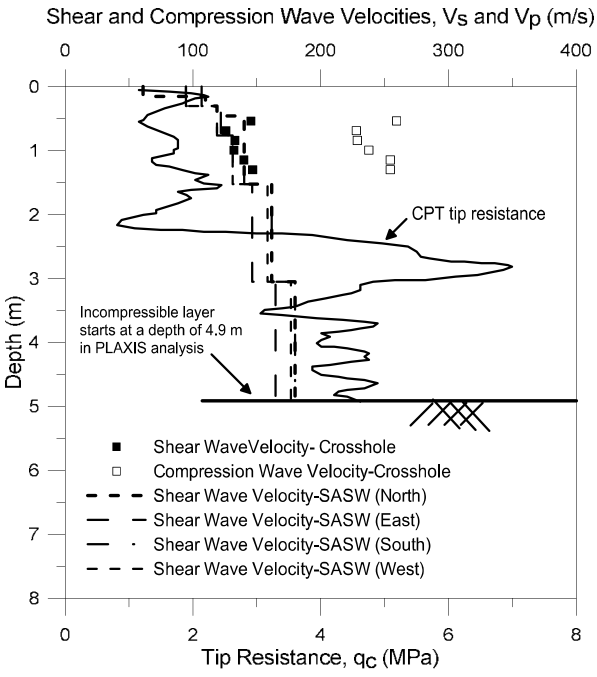

Figure 1. In-situ seismic and CPT test results at the field site of the load-settlement tests with a 0.91-m diameter footing

confining pressure (calculated using $K_0 = 0.70$ and a capillary stress of 3 kPa); $P_a =$ reference mean effective confining pressure, 1 atm; and $n_G =$ slope of the $\log G_{max}$–$\log \sigma_0'$ relationship. The modeling represented by Equation 3 resulted in the two-layer profile presented in Figure 2. The G_{max_1atm} and n_G parameters for each layer are: layer 1 - G_{max_1atm} = 86.2 MPa and 0.48; layer 2 - G_{max_1atm} = 74.2 MPa and 0.51, respectively. The values of n_G close to 0.5 indicate that the soil in each layer is uncemented.

4.2. *Load-Settlement Test*

A reinforced concrete footing with a diameter of 0.91 m and a thickness of 0.30 m was constructed at the site after removing the upper 0.25 m of soil. Linear potentiometers, attached to a reference frame were used to measure footing settlements. The load was applied by a hydraulic jack reacting against the weight of a tri-axial vibroseis truck, named T-Rex, as shown in Figure 3a. The load was measured with a 50-kip load cell and was applied to the top of the footing through a loading frame (see Figure 3b). The load–settlement test was performed in March, 2010. The measured load-settlement curve is presented in Figure 4 by the solid line.

5 COMPARISON OF PREDICTED AND MEASURED LOAD-SETTLEMENT CURVES

To investigate the settlement prediction methods, predicted and measured load-settlement curves are compared. The prediction methods are: (1) Schmertmann et al. (1978) CPT-based method, (2) Burland and Burbidge (1985) SPT-based method and (3) the method based on dynamic soil properties presented herein. The predicted and measured load-settlement curves are presented in Figure 4 and are discussed below.

For the Schmertmann et al. method, the elastic moduli were calculated based on the CPT results using:

$$E_s = 2.5q_c \qquad (5)$$

where $E_s =$ modulus of elasticity of the soil; and $q_c =$ cone penetrometer tip resistance. The upper 2 m of soil under the footing was divided into 5 layers and an average value of 1.53 MPa of q_c was assigned to each layer. Additional details on the procedure can be found in Van Pelt (2010). As seen in Figure 4, the predicted load-settlement curve is not as nonlinear as the measured curve, but predicts quite well in the working-load range.

For the Burland and Burbidge (1985) method, settlements are estimated using the SPT blow count, N_{60} in the correlation:

$$s = \frac{1.71qB^{0.7}}{{N_{60}}^{1.4}} \qquad (6)$$

where $s =$settlement (mm); $q =$applied bearing pressure (kPa); $B =$footing diameter (m); and $N_{60} =$ average SPT blow count over the depth of influence which is about 1 m for a footing with B = 1m, uncorrected for overburden pressure. As no SPT tests were performed at the field site, the CPT tip resistance values were correlated to SPT blow count using the correlations proposed by Robertson et al. (1983). For an average q_c value of 1.53 MPa, this correlation gives an average value of 5 for the SPT blow count. As seen in Figure 4, the predicted load- settlement

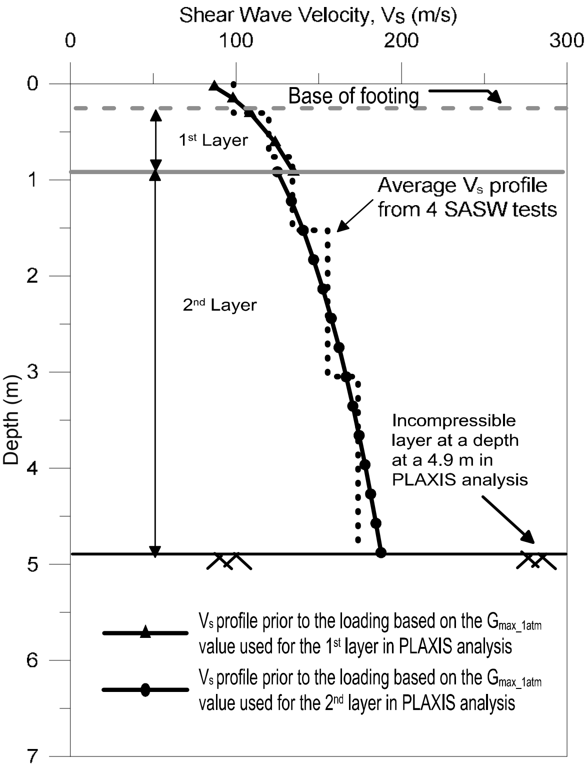

Figure 2. Average V_s profile from SASW tests and the two-layer model used in the finite element analysis

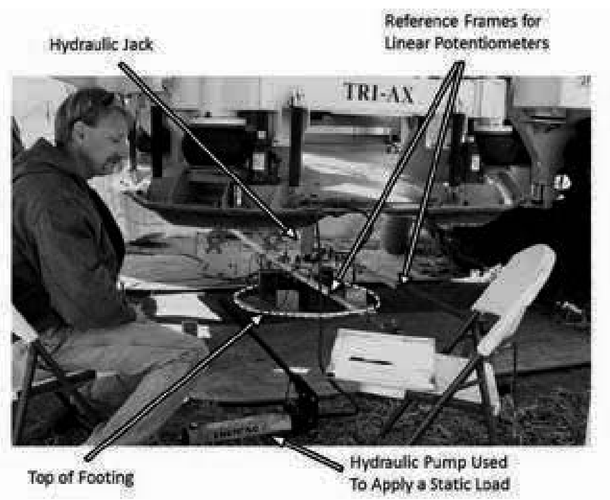

(a)

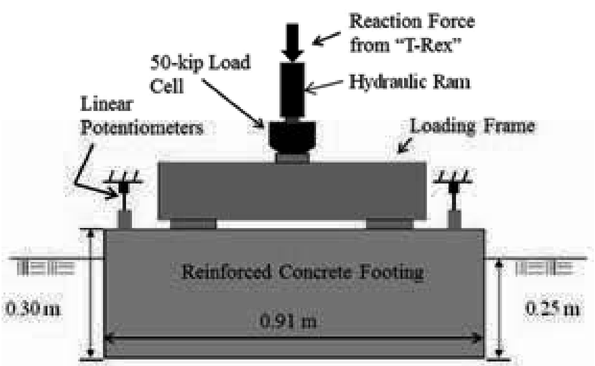

(b)

Figure 3. Field Load-settlement test: (a) T-Rex in position during loading (b) Cross-section of the load-settlement arrangement

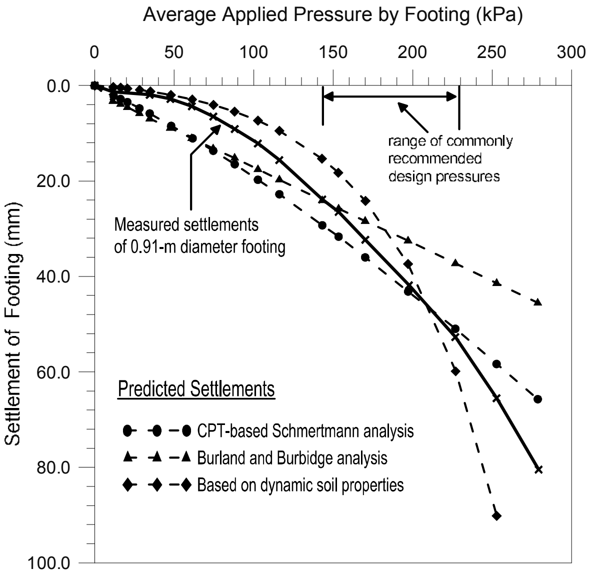

Figure 4. Measured and predicted load-settlement curves for the 0.91-m diameter footing

curve is linear while the measured settlements are nonlinear. Also, the predictions underestimate the measured settlements at higher working loads.

For the method based on dynamic soil properties, a two-layer G_{max} profile was developed from the two-layer V_s profile presented in Figure 2. A thickness of soil beneath the footing of 5B was used in the settlement analysis to eliminate boundary effects (Brinkgreve et al, 2011). With the subroutine that incorporates Equations 1, 2 and 3 in PLAXIS, a finite element analysis was performed. As noted earlier, the G_{max} values were adjusted to the increasing stress state and the G values in the G/G_{max}-log γ relationships were adjusted to the increasing shear strain during loading. As seen in Figure 4, the predicted load-settlement curve captures much of the nonlinearity exhibited in the load-settlement curve. The primary point of concern is that the predicted curve is more nonlinear than the measured curve, particularly above settlements around 70 mm. This difference is being investigated. However, it must be pointed out that the predictive method based on dynamic soil properties worked quite well in this case study with fine-grained granular soils and, in theory, should be just as readily applied to coarse-grained granular soils with gravel and cobbles.

6 CONCLUSIONS

A new method for predicting settlements of shallow footings on granular soils is presented. The method is based on field seismic measurements to evaluate the small-strain shear moduli (G_{max}) combined with nonlinear normalized shear modulus-shear strain (G/G_{max}-log γ) relationships determined in the laboratory from dynamic resonant column testing. Important factors in the model are that: (1) G_{max} values are adjusted to the increasing stress during loading and (2) the G values in the G/G_{max}-log γ relationships are adjusted to increasing strain levels. A subroutine was written to incorporate this formulation in a commercially available finite element program, PLAXIS. The method was investigated by comparing with a load-settlement test using a 0.91-m diameter footing. In the working stress range, predicted nonlinear footing settlements compared quite well with the measured ones. The predicted nonlinear settlements in this range were also in reasonable agreement with predictions from traditional CPT and SPT procedures.

The new predictive method has several advantages over traditional CPT and SPT methods. First, field seismic measurements are used to characterize the soil in-situ. Field seismic measurements, especially those done with surface-wave tests, are readily applied to all granular soils, including soils containing gravel and cobbles which are difficult to test by CPT and SPT methods. Second, the nonlinear characterization of granular soil modeled with G/G_{max}-log γ relationships captures the nonlinear stress-strain curve of the granular soil during loading. Third, in the case of field seismic measurements with surface-wave tests, all equipment is placed on the ground surface (no boreholes). The V_s profile is nearly continuous with depth. They are quickly performed, cost effective and begin evaluating stiffness within centimeters of the surface. Finally, the new method is applicable to all geotechnical materials, even cemented gravelly soils and fine-grained soils that are consolidating under the footing loads. Work is presently underway with large-grained cemented alluvium.

7 REFERENCES

Berardi R. and Lancellotta R. 1991. Stiffness of granular soil from field performance. *Geotechnique* 41(1) 149-157

Brinkgreve R.B.J., Swolfs W.M and Engin E. 2011. Plaxis 2D 2011. *Tutorial Manual*

Burland J.B. and Burbidge M.C. 1985. Settlement of foundations on sand and gravel. *Proceedings, Institution of Civil Engineers*. 78(1) 1325-1381

Darendeli M.B. 2001. Development of a new family of normalized modulus reduction and material damping curves. *Ph.D. Dissertation, University of Texas at Austin*, 362 p.

Hardin B.O. and Drnevich V.P. 1972. Shear modulus and damping in soils; Design equations and curves. *Journal of the Soil Mechanics and Foundation engineering Division, ASCE* 98(7) 667-692

Kacar O. 2013 (expected) Predicting settlement of shallow footings on granular soil using field seismic and laboratory dynamic nonlinear soil properties. *Ph.D. Dissertation, University of Texas at Austin*

Menq F. 2003. Dynamic properties of sandy and gravelly soils. *Ph.D. Dissertation, University of Texas at Austin,* 364 p.

Meyerhof G.G. 1965. Shallow foundations. *Journal of the Soil Mechanics and Foundations Division, ASCE* 91(SM2), 21-31

Lehane B. and Fahey M. 2002. A simplified nonlinear settlement prediction model for foundations on sand. *Canadian Geotechnical Journal* 39(2) 293-303

Lee J. and Salgado R. 2001. Estimation of footing settlement in sand. *International Journal of Geomechanics* 2(1) 1-28

Lunne T., Robertson P.K. and Powell J.J.M. 2002.*Cone Penetration Testing in Geotechnical Practice,Spon Press, New York*

Robertson P.K., Campanella R.G. and Whightman A. 1983. SPT-CPT correlations. *Journal of Geotechnical Engineering* 109(11) 1449-1459

Schmertmann J.H. 1970. Static cone to compute static settlement over sand. *Journal of the Soil Mechanics and Foundations Division, ASCE* 96(3), 1011-1043

Schmertmann J.H., Hartman J.P. and Brown P.R. 1978. Improved strain influence factor diagrams. *Journal of the Geotechnical Engineering Division, ASCE* 104(8), 1131-1135

Stokoe K. H., II, Wright S.G., Bay J.A., and Roesset J.M. 1994. Characterization of geotechnical sites by SASW method. *Geophysical characteristics of sites,ISSMFE, Techical committee 10 for XIII ICSMFE, International Science Publishers, New York* 15-25

Terzaghi K. and Peck R.B. 1948. *Soil Mechanics in Engineering Practice,* 1st edition, John Wiley & Sons, New York

Van Pelt J. 2010.Predicting of settlements of shallow foundations on cohesionless, granular soil using dynamic soil measurements. *M.S. Thesis. University of Texas at Austin*, 363 p..

Characterization of Model Uncertainty in Immediate Settlement Calculations for Spread Footings on Clays

Caractérisation de l'incertitude des modèles de calculs du tassement immédiat de semelles reposant sur des sols argileux

Strahler A.W., Stuedlein A.W.
Oregon State University

ABSTRACT: Immediate settlement calculations for spread footings supported by clay soils are generally based on displacement influence factors derived from elastic stress fields and soil stiffness estimated from triaxial compression strength tests or correlations to various measureable characteristics such as plasticity, strength, or stress history. As a consequence of the linear elastic design models, curvature in load-displacement behaviour cannot be characterized unless the stiffness degradation of the subgrade is explicitly incorporated. This paper uses a load test database of spread footings on clay to evaluate the accuracy of an elasticity-based immediate settlement estimation method, which was shown to significantly reduce in accuracy with increasing magnitudes of displacement and exhibit significant variability. A method to predict immediate settlements using a non-linear constitutive model set within an elastic stress field is presented, and is shown to capture the general non-linear shape of footing load tests and maintain its accuracy over a broad range in displacements with similar uncertainty to that of the elasticity-based method. Recommendations are made to estimate an appropriate initial stiffness for use with non-linear and linear elastic models based on back-calculated undrained soil modulus.

RÉSUMÉ: Les modèles acceptés de prévision du tassement immédiat des semelles de fondation reposant sur les sols argileux sont généralement basés sur des facteurs d'influence de déplacement calculé à partir de champs de contraintes élastiques en conjonction avec la rigidité du sol estimée à partir d'essais triaxiaux, ou de corrélations avec des paramètres mesurables comme l'indice de plasticité, la résistance au cisaillement non drainé, et la contrainte de préconsolidation. En raison de l'utilisation de modèle élastique linéaire, la non-linéarité de la relation charge-déplacement ne peut pas être caractérisée sauf si la dégradation de la rigidité du sol de fondation est incorporée explicitement dans le modèle. Cet article utilise une base de données d'essais de chargement de semelles sur des sols argileux afin d'évaluer la précision d'une méthode d'estimation du tassement immédiat en élasticité. La performance de cette méthode en termes de précision se dégrade sérieusement avec l'augmentation du déplacement. Elle est aussi caractérisée par une grande variabilité. Dans cet article, une méthode de prévision des tassements immédiats à l'aide d'un modèle de comportement non linéaire en champ de contrainte élastique est présentée. On montre qu'elle reproduit la forme générale non linéaire des essais de chargement de semelles de fondation et qu'elle présente une bonne précision sur un grand intervalle de déplacements avec une incertitude similaire à celle de la méthode basée sur l'élasticité. Des recommandations ont été faites pour estimer le module initial utilisé avec les modèles élastiques non linéaires et linéaires qui sont fonction des modules de sols non drainés obtenus par retro-calculs.

KEYWORDS: elastic settlement, settlement, shallow foundations, clay soils, undrained loading.

1 INTRODUCTION

Spread footings are used throughout the world as viable foundation support systems for structures. They are typically constructed of reinforced concrete, can assume any shape, and generally meet the following criteria (Vesic, 1973; Das, 2011):

1. The depth of footing embedment, D_f, lies between the ground surface and up to four times the footing width, B, below the adjacent grade, and
2. Additional support, such as driven piles or drilled shafts, are not located beneath the footing.

Designers must evaluate two conditions to ensure that the foundation will perform adequately (Perloff and Baron, 1976): safety against overall bearing failure in the supporting soil, and displacements leading to unsatistfactory structural performance must not occur. The first condition is often considered the most critical limit state; however, immediate settlement can lead to a serviceability limit state and must be included in design.

Generally accepted methods for estimating immediate settlement of spread footings require the use of linear elastic models to simulate soil behavior; this approach does not capture the true non-linear behavior of soil. This study presents a statistical evaluation of a commonly used elasticity-based method and soil stiffness correlation using a load test database. Then, a simple non-linear model capturing observed load-displacement curvature in footing load tests is presented and its accuracy is characterized. The undrained initial elastic modulus is back-calculated using the load test database, and is found to vary as a function of overconsolidation ratio.

2 IMMEDIATE SETTLEMENT OF SHALLOW FOUNDATIONS ON CLAY

2.1 *Elasticity-based design methodology*

Carrier and Christian (1978) found that stress distributions developed from finite element analyses (FEA) used in conjunction with embedment factors proposed by Burland (1970) produced the most reasonable values of displacement assuming an undrained Poisson's ratio, ν_s, equal to 0.5 for clay. Mayne and Poulos (1999) modified Burland's work and developed an improved distortion settlement estimation approach for circular foundations that accounts for variations in Poisson's ratio, soil modulus, foundation rigidity, and embedment effects. The resulting expression for immediate settlement can be constructed as (Mayne and Poulos 1999):

$$\delta_i = \frac{q_{app} B_{eq} I_E I_F I_G}{E_s}\left(1-\nu_s^2\right) \tag{1}$$

where q_{app} = applied bearing stress, B_{eq} = equivalent diameter of the footing, I_E, I_F, I_G are displacement influence factors that control the magnitude of displacement (described below), and E_s is the Young's modulus of the soil.

The stresses below a spread footing, and therefore the immediate settlement, are affected by the amount of footing embedment. Burland's embedment influence factor, I_E, is used to modify the stress distribution for embedment effects.

Regression analyses on Burland's charts yielded a simple representation of I_E (Strahler 2012):

$$I_E = 1 - \frac{1}{3.5e^{(1.22\nu_s - 0.4)}\left(\frac{B_{eq}}{D_f}\right)} \quad (2)$$

In addition to embedment effects, stresses below a spread footing are also affected by the rigidity of the foundation. The rigidity correction factor, I_F, is used to modify the stress distribution to account for foundation rigidity and is given by (Mayne and Poulos 1999):

$$I_F = \frac{\pi}{4} + \frac{1}{4.6 + 10K_f} \quad (3)$$

where K_f = the foundation flexibility factor (Brown, 1969) and is a function of the modulus of the soil as well as the modulus, thickness and radius of the foundation.

Soil profiles that exhibit a linear increase in modulus with depth, termed a Gibson profile (e.g., Mayne & Poulos, 1999), may be modeled using the Gibson displacement influence factor, I_G, given by:

$$I_G = \frac{1}{\left[1.27 + 0.75\left(\frac{E_o}{k_E B_{eq}}\right)^{-0.8}\right]} \quad (4)$$

where E_o is Young's modulus of the soil directly beneath foundation, k_E is the rate of increase of modulus with depth.

The use of Eqn. (1) requires an estimate of soil stiffness; for undrained loading of footings on clay the appropriate stiffness for linear elastic models is the undrained Young's modulus, E_u. Although many correlations to E_u exist (e.g., Kulhawy and Mayne 1990), Duncan and Buchignani (1987) suggested that E_u was linearly proportional to undrained shear strength, s_u, and proposed the following commonly used expression:

$$E_u = Ks_u \quad (5)$$

where K = the constant of proportionality and is a function of stress history and soil plasticity. Duncan and Buchignani (1987) proposed Figure 1 to indicate the sensitivity of K to plasticity index (PI) and overconsolidation ratio (OCR).

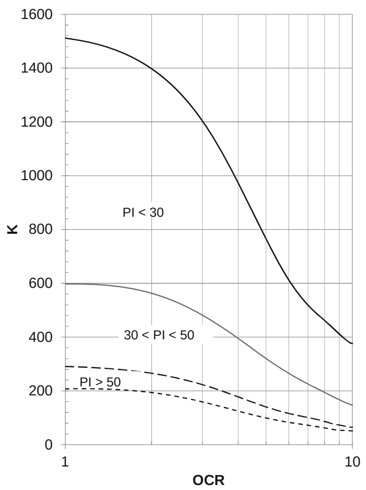

Figure 1. Variation in the K-factor based on OCR and PI (adapted from Duncan and Buchignani 1987).

2.2 *Non-linear distortion displacement models*

Several researchers have pointed to the limitations of linear elastic-perfectly plastic model behavior and developed non-linear distortion displacement models that attempt to more accurately estimate displacements (Osman and Bolton, 2004; Elhakim and Mayne, 2006; Foye, et al., 2008). These methods are either computationally intensive, require significant or potentially expensive subsurface information, or rely on FEAs that assume homogeneous or isotropic soil conditions and are limited to specific stress conditions. As a result they may not be applicable to many realistic design scenarios and are limited in their appropriate uses.

3 LOAD TEST DATABASE AND STATISTICAL APPROACH FOR IMMEDIATE SETTLEMENT MODEL EVALUATION

3.1 *Development of load test database*

To evaluate the uncertainty in the linear elastic distortion settlement calculation and provide the basis for a new model, a database of case histories was developed. The database was initially populated with 24 case histories and was subsequently reduced to 12 with 30 individual footing load tests based on the quality of soil and load test information. The stress histories represented in the database largely consist of lightly to heavily overconsolidated soil profiles, with just one true normally consolidated soil profile. The database included 13 square foundations and 17 circular footings. Twenty-eight of the footings were embedded below the ground surface. Further details on the load test database are given in Strahler (2012), and are not described here for brevity.

3.2 *Statistical approach*

The accuracy of the immediate settlement models evaluated herein was characterized using the mean bias, λ, defined as the ratio of an observed and calculated displacement, and its distribution. Distributions of the sample bias values were assessed using goodness of fit metrics, and appropriate second moment statistics were determined. The coefficient of variation (COV) of the bias, defined as the standard deviation in bias divided by its mean, is used herein as a convenient representation of dispersion. Details regarding distribution fitting are given by Strahler (2012).

4 EVALUATION OF THE ELASTICITY-BASED APPROACH

Equation (1) was rearranged to compute the elasticity-based bearing pressure, q^e_{app}, for each displacement, δ_i, for a given load-displacement curve:

$$q^e_{app} = \frac{E_u \delta_i}{B_{eq} I_G I_F I_E \left(1 - \nu_s^2\right)} \quad (6)$$

To evaluate the performance of Eqn (6) using the footing load test database, the undrained shear strength was averaged over B_{eq} and the constant of proportionality, K, was linearly interpolated from Figure 1 for data pairs of PI and OCR. The upper dark line was assumed to correspond to a PI = 0, whereas the lower dashed line was assumed to correspond to a PI = 100. For case histories with soil layers characterized with OCRs greater than 10, K was assumed to be equal to the value at OCR = 10 (Figure 1).

Following the computation of bearing pressures, the sample biases were calculated and their statistical distribution determined. The mean bias for a displacement of 10 mm was 0.85, indicating that the undrained Young's modulus estimated using Figure 1 and Eqn. (6) is moderately un-conservative (i.e. the calculated bearing pressure for 10 mm of displacement is greater than that measured). However, the model exhibited significant variability, with COV = 85 percent. The accuracy in the selected approach decreases significantly with increases in magnitude of displacement. For example, at displacements of 25 and 50 mm, Eqn. (6) and Figure 1 produced mean biases and COVs of 0.46 and 88 percent, and 0.17 and 54 percent, respectively. The COV at 50 mm is somewhat smaller due to the reduction in the number of bearing pressure-displacement data pairs at larger displacements available in the database.

5 DEVELOPMENT OF PROPOSED MODEL

The evaluation of the elasticity-based approach presented above indicated a need for more accurate immediate settlement calculations. An accurate model should account for the non-linear response of footings loaded rapidly on clays. An approach that incorporates common triaxial strength test data within an elastic stress field is described below.

5.1 *Selected constitutive response*

The Duncan-Chang hyperbolic model (Duncan and Chang, 1970; Duncan et al. 1980) is a non-linear soil constitutive model that expresses the development of the principal stress difference as a function of axial strain, initial Young's modulus, and effective confining pressure. The stress path that develops below the center of a footing is similar to an undrained triaxial compression stress path (Stuedlein and Holtz, 2010). The failure criterion can be defined as the point at which half of the principal stress difference exceeds the available shear strength:

$$(\sigma'_1 - \sigma'_3)_{ult} = 2s_u \tag{8}$$

where $(\sigma'_1 - \sigma'_3)_{ult}$ is the principal stress difference at failure. The original hyperbolic model developed by Kondner (1963) is given as:

$$\sigma'_1 - \sigma'_3 = \frac{\varepsilon}{\dfrac{1}{E_{in}} + \dfrac{\varepsilon}{(\sigma'_1 - \sigma'_3)_{ult}}} \tag{9}$$

where σ'_1 and σ'_3 can represent the vertical and horizontal stresses below the center of a footing, respectively, ε is the axial strain and E_{in} is the initial undrained Young's modulus, which remains constant during undrained loading (Duncan, et al., 1980). Note that E_{in} represents the initial tangent Young's modulus and is typically measured at small strains; the range in strain associated with E_u as reported by Duncan and Buchignani (1987) is not known.

5.2 *Calculation of footing displacements*

The distribution of vertical, horizontal, and shear stress beneath the center of the footing was generated for each footing in the load test database using elasticity theory assuming undrained conditions (v_s = 0.5). During loading, the change in vertical and horizontal stresses, $\Delta\sigma_1$ and $\Delta\sigma_3$, can be modeled as the change in vertical and radial stresses, $\Delta\sigma_v$ and $\Delta\sigma_r$, respectively, by assuming that square footings can be treated as equivalent circles (Davis and Poulos, 1972).

Substitution of Equation (8) into Equation (9) and rearranging for axial strain produces an expression for displacement based on the integration of strains over the assumed depth of influence. This study considered an effective depth of $2B_{eq}$ for the integration of strains. The displacement resulting from an applied load, δ_i, can be calculated using:

$$\delta_i = \int_0^{2B_{eq}} \frac{\Delta\sigma_{vr_{\Delta Z_j}}}{E_{in_{\Delta Z_j}} + \dfrac{\Delta\sigma_{vr_{\Delta Z_j}}}{2s_{u_{\Delta Z_j}}}} d\Delta Z_j \tag{10}$$

where $\Delta\sigma_{vr}$ is the principal stress difference and ΔZ_j = an increment of depth. Pertinent soil parameters (s_u, OCR, and PI) were averaged over a depth of B_{eq} below the footing where the majority of the large strains develop.

Due to the asymptotic nature of the constitutive model adopted, unreasonable displacements are computed when the applied shear stress approaches s_u within a given ΔZ_j. To mitigate this effect, the shear stresses were limited to 99 percent of the available s_u (i.e., $\Delta\sigma_{vr}/2 < 0.99s_u$). Although, excessive displacements result at higher loads, the calibrated hyperbolic model may be used to estimate the non-linear pre-failure displacements without performing a time-consuming numerical study.

5.3 *Displacement prediction using the non-linear model*

Bearing pressure-displacement curves were calculated using the Duncan-Chang model and elastic stress fields. The E_u was estimated using Figure 1 and Equation (5). The observed and predicted q-δ curves were compared statistically with the bias. Bearing pressure-displacement points corresponding to $\Delta\sigma_{vr}/2 \geq 0.99s_u$ were omitted.

On average, the non-linear approach produced a slight under-prediction of displacements for a given bearing pressure, with a mean λ = 1.13 for each bearing pressure-displacement curve in the database, but exhibited significant variability (COV = 105 percent). The relatively large COV is the result of the inherent variability in soil strength, transformation model error in the calculation of undrained modulus, and model error. The tendency for the selected non-linear constitutive model and elastic stress-field to under-predict the displacement at a given bearing pressure resulted from excessive strains calculated as the mobilized shear stresses approached the undrained shear strength.

6 BACK-CALCULATION OF INITIAL MODULUS

Another application of a non-linear constitutive model within an elastic stress field is the estimation of the initial Young's modulus of the soil. Equation (10) can be rearranged for initial Young's modulus and its value back-calculated using least squares regression on the observed bearing pressure-displacement curve:

$$E_{in} = \int_0^{2B_{eq}} \frac{\Delta\sigma_{vr_{\Delta Z_j}}}{\delta_{\Delta Z_j}\left(1 - \dfrac{\Delta\sigma_{vr\Delta Z_j}}{2s_{u_{\Delta Z_j}}}\right)} d\Delta Z_j \tag{11}$$

where E_{in} is the initial undrained Young's modulus averaged over a depth B_{eq}. Again, data-pairs corresponding to shear stresses approaching the ultimate stress difference were omitted.

The back-calculated initial Young's modulus depends on the shape of the predicted bearing pressure-displacement curve. In some cases the predicted curvature of the bearing pressure-displacement curve was not in agreement with the observed curvature and in these instances the fitting procedure was modified to estimate the initial portion of the bearing pressure displacement curve. This was done to focus on the initial stiffness characteristics (Strahler 2012).

6.1 *Young's modulus comparison*

The calculated undrained Young's modulus and back-calculated initial Young's modulus, E_{in}, were compared using the bias and its distribution. In general, the E_u calculated using the Duncan and Buchignani (1987) correlation under-predicts the back-calculated initial modulus (mean λ = 3.05) and exhibits a significant amount of variability (COV = 99%). This level of under-prediction is not surprising, given that the Duncan-Chang model uses an initial undrained Young's modulus that is typically based on the first 0.1 to 0.25% of axial strain or less. The type or strain level of the Young's modulus referenced by

Duncan and Buchignani (1987) is not specified, but the relationship was developed from in-situ testing and could potentially represent a tangent or secant modulus at 50% of peak strength. Thus, the strain levels for the estimated E_u and E_{in} may not be similar, and could explain the inaccuracy and uncertainty shown in Figure 2.

A new K was calculated using the back-calculated E_{in} and the results are presented in Figure 2. The relationship proposed by Duncan and Buchignani (1987) has been overlaid on the data for comparison and appears to be independent of *PI*.

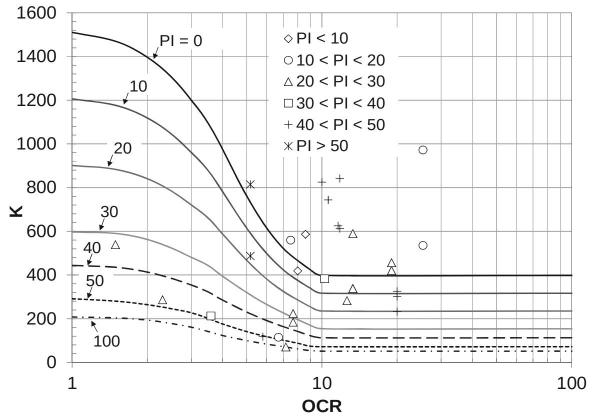

Figure 2. Back-calculated *K*-factor using non-linear model compared to Duncan & Buchignani (1987).

6.2 *Correlation to initial undrained Young's modulus*

When plotted against OCR, the back-calculated initial Young's modulus normalized by the atmospheric pressure, p_{atn}, exhibits a linear trend line. The stiffness appears to increase with *OCR*. A single footing used a 21 cm diameter tendon extended to bedrock beneath the center of the footing in order to develop displacements (Bauer 1976). The tendon likely interfered with the failure mechanism of the soil beneath the footing and produced a higher initial Young's modulus. It was included in the database because it was not considered a support mechanism (drilled shaft, driven pile, etc.); however, it was omitted in Figure 3 due to its clear departure from the trend.

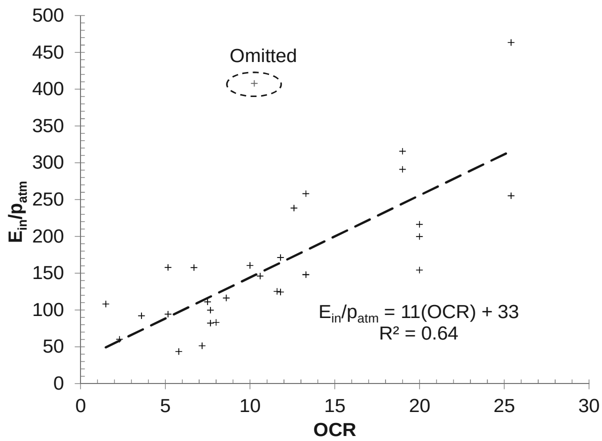

Figure 3. Back-calculated initial Young's modulus using Duncan-Chang model, based on Duncan & Buchignani (1987).

7 SUMMARY AND CONCLUSIONS

The use of a single undrained Young's modulus to predict the highly non-linear response of footings supported on cohesive soil has been shown to be slightly conservative at low displacements but increases in error with increasing displacement. A method to estimate displacements based on the non-linear Duncan-Chang model was shown to be slightly conservative and more accurately captures the overall load-displacement curve. The proposed method also allowed the estimation of an initial undrained Young's modulus, which appears to be correlated with *OCR*. This trend can be used to estimate the initial Young's modulus for use in the non-linear model or additionally modified to be used in elasticity based methods.

Despite the improvement in modeling footing response reported herein, signficant uncertainty in the response remains without the adequate characterization of inherent soil variability, transformation error associated with correlations, and model error. Improved site characterization presents the best approach to reducing the uncertainty of footing load-displacement response.

8 REFERENCES

Bauer, G. E., Shields, D. H. and Scott, J. D., 1976. Predicted and Observed Footing Settlements in a Fissured Clay. Ottawa, Pentech Press, pp. 287-302.

Brown, P., 1969. Numerical Analyses of Uniformly Loaded Circular Rafts on Deep Elastic Foundations. Geotechnique, 19(3), pp. 399-404.

Burland, J., 1970. Discussion, Session A. London, British Geotechnical Society, pp. 61-62.

Carrier, D.I. and Christian, J., 1978. Janbu, Bjerrum and Kjaernsli's chart reinterpreted. Canadian Geotechnical Journal, Volume 15, pp. 123-128.

Das, B., 2011. Principles of Foundation Engineering. Seventh ed. Stanford, CT: Global Engineering.

Davis, E. and Poulos, H., 1972. Rate of Settlement under two- and three- dimensional conditions. Geotechnique, 22(1), pp. 95-114.

Duncan, J.M. and Buchignani, A., 1987. An Engineering Manual for Settlement Studies, Berkeley: University of California.

Duncan, J.M. and Chang, C., 1970. Nonlinear Analysis of Stress and Strain in Soils. Journal of the Soil Mechanics and Foundations Division, 96(SM3), pp. 1629-1653.

Duncan, J.M., Byrne, P., Wong, K. and Mabry, P., 1980. Strength, Stress-Strain and Bulk Modulus Parameters for Finite Element Analyses of Stresses and Movements in Soil Masses, Berkeley: University of California.

Elhakim, A. and Mayne, P.W., 2006. Foundation Load-Displacement Response from Small-Strain Stiffness. Atlanta, ASCE, pp. 1-6.

Foye, K., Basu, P. and Prezzi, M., 2008. Immediate Settlement of Shallow Foundations Bearing on Clay. International Journal of Geomechanics, 8(5), pp. 300-310.

Holtz, R.D., 1991. Stress Distribution and Settlement of Shallow Foundations. In: H. Fang, ed. Foundation Engineering Handbook. 2nd ed. New York: Chapman and Hall Inc., pp. 167-222.

Kondner, R., 1963. Hyperbolic Stress-Strain Response: Cohesive Soils. Journal of the Soil Mechanics and Foundations Division, February, 89 (SM1), pp. 115-144.

Kulhawy, F.H. and Mayne, P.W., 1990. Manual on Estimating Soil Properties for Foundation Design, Palo Alto: Electric Power Research Institute.

Mayne, P.W. and Poulos, H., 1999. Approximate Displacement Influence Factors for Elastic Shallow Foundations. Journal of Geotechnical and Geoenvironmental, 125(6), pp. 453-460.

Osman, A. and Bolton, M., 2004. A New Approach to the Estimation of Undrained Settlement of Shallow Foundations on Soft Clay. Engineering Practice and Performance of Soft Deposits, pp. 93-98.

Perloff, W. and Baron, W., 1976. Soil Mechanics: Principals and Applications. First ed. New York: Ronald Press Company.

Stuedlein, A. W. and Holtz, R. D., 2010. Undrained Displacement Behavior of Spread Footings in Clay, pp. 653-669.

Strahler, A. W., 2012. Bearing Capacity and Immediate Settlement of Shallow Foundations on Clay.

Vesic, A., 1973. Analysis of Ultimate Loads of Shallow Foundations. Journal of the Soil Mechanics and Foundations Division, 99(1), pp. 45-73.

Probabilistic Assessment of the Bearing Capacity of Shallow Strip Footings on Stiff-Over-Soft Clay

Evaluation probabiliste de la capacité portante de semelles filantes peu profondes sur couche d'argile rigide recouvrant une couche d'argile molle

Tian Y., Cassidy M.J.
Centre for Offshore Foundation Systems, UWA Oceans Institute & ARC CoE for Geotechnical Science and Engineering, University of Western Australia, Perth, Australia

Uzelli M.
Georisk Engineering S.r.l., Florence, Italy

ABSTRACT: This paper focuses on the probabilistic assessment of the resistance factor for bearing capacity for a strip footing on a stiff-over-soft clay profile. The analysis is performed by applying the Random Finite Element Method, which combines finite element simulation, spatial variability analysis and Monte Carlo simulation. Finite-element analyses are performed in the program ABAQUS on meshes in which undrained strength values are assigned on the basis of quantitative estimates of the vertical and horizontal spatial variability and the probabilistically modelled scatter of undrained strength itself. The stochastic implementation of the numerical analyses results in samples of bearing capacity factors which, when normalized by a deterministic bearing capacity factor, provide a set of tabulated factors calibrated to user-defined target reliability levels. The results have application for the prediction of foundation punch-through, where the footing pushes the upper strong layer of soil into the softer clay beneath.

RÉSUMÉ : Cet article porte sur l'évaluation probabiliste du facteur de résistance de la capacité portante d'une semelle filante posée sur une couche d'argile rigide recouvrant une couche d'argile molle. L'analyse applique la méthode des éléments finis aléatoires, qui associe simulation par éléments finis, analyse de variabilité spatiale et simulation par la méthode de Monte Carlo. Les analyses par éléments finis sont réalisées avec le programme ABAQUS, en utilisant des maillages pour lesquels la valeur de résistance au cisaillement non drainée est déterminée sur la base de l'estimation quantitative des variabilités verticale et horizontale, ainsi que sur la dispersion de la résistance au cisaillement non drainée modélisée de façon probabiliste. L'implémentation stochastique des analyses numériques conduit à des facteurs de capacité portante qui, lorsqu'on les normalise par le facteur de capacité portante déterministe, fournit un ensemble de facteurs étalonnés pour des niveaux de fiabilité prédéfinis. Les résultats obtenus trouvent une application pour la prédiction du poinçonnement des fondations, dans le cas où la fondation pousse la couche supérieure de sol dur dans la couche de sol mou située en dessous.

KEYWORDS: Bearing capacity, shallow foundation, spatial variability, probability, random finite element analysis, strip footing

1 INTRODUCTION

The bearing capacity of a shallow foundation on two layered clay soil is a classical problem in soil mechanics and one of importance to many applications, including the punch-through of offshore foundations. The problem being analyzed in this paper is defined in Figure 1: what is the vertical load carrying capacity of a strip footing of width (B) on a top layer of soil of undrained shear strength (s_{ut}) overlying a weaker bottom layer (s_{ub}). Using finite element analysis in conjunction with limit theorems, Merifield et al. (1999) published extensive bearing capacity factors (N_c*) defined to predict the vertical capacity as a function of the strip footing width and the undrained shear strength of the top clay layer. Conditions of varying top layer thickness and shear strength ratio were analyzed. However, these solutions were only provided for deterministic properties of soil with no spatial variability accounted for.

This paper makes use of the Random Finite Element Method (RFEM) (see Fenton and Griffith, 2008) to investigate the effect of the spatial variability in undrained shear strength on the bearing capacity of a shallow strip footing on two-layered stiff-over-soft clay. In the RFEM the characterization of the spatial variability enables the generation of random fields with spatially varying values, all of which are mapped onto a finite element mesh. The generation of multiple random fields associated with the soil domain allows the repeated implementation of finite element analysis, yielding multiple samples of outputs. These can subsequently be analysed statistically.

Although RFEM has been used to estimate the statistical distribution of the vertical undrained bearing capacity of a strip foundation on a single layer (Paice et al. 1996, Nobahar and Popescu 2000, Griffiths and Fenton 2001, Griffiths et al. 2002, Fenton and Griffiths 2003, Popescu et al. 2005, Kasama and Whittle 2011, Cassidy et al. 2012) it has yet to be applied to the two-layered condition. The aim of this paper is to (i) provide a methodology for doing so, (ii) discuss preliminary trends due to changing variation in undrained shear strength distributions, and (iii) estimate quantitatively the degree of unconservatism in using deterministic bearing capacity factors.

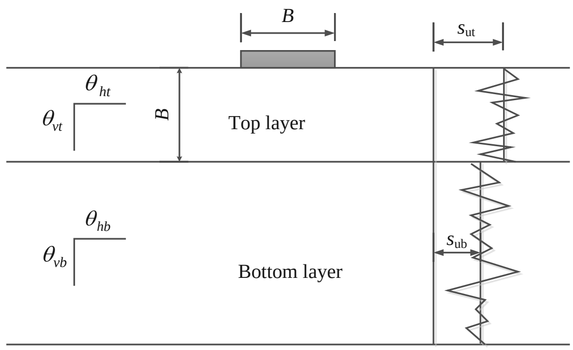

Figure 1. Definition of problem being investigated.

2 METHODOLOGY

The FE analysis model used in this paper is illustrated in Figure 2. Two-dimensional plane strain conditions were assumed and the commercial ABAQUS finite element package utilised (version 6.10, Dassault Systèmes 2010). A shallow foundation with width B was founded on the surface of the two-layered soil, which was modelled by a linear-elastic perfectly-plastic Tresca constitutive law with an undrained shear strength (s_u). The elastic response was defined by the Young's modulus ($E = 500s_u$) and the Poisson's ratio set as 0.49. Corresponding to one of the analysis cases of Merifield et al. (1999), the soil contained a top layer of $1B$ thickness. For efficiency the infinite bottom layer of Merifield et al (1999). was shortened to $3.8B$; a depth deep enough, however, to ensure no boundary effects. The analysis width was $6B$. The lateral soil boundaries were roller supported and the bottom was pinned. The top surface was assumed to be free. A fully bonded foundation/soil interface was used to model the undrained behaviour.

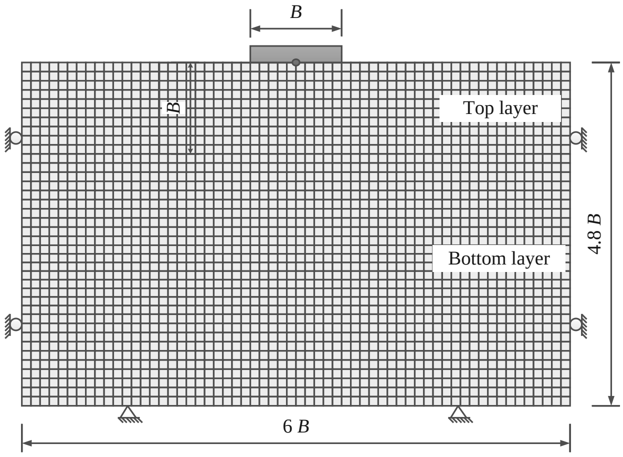

Figure 2. The FE model used

The soil domain was divided into 60 by 48 square zones of width $0.1B$, as shown in Figure 2. In each zone the soil properties were constant and defined by an undrained shear strength s_u and Young's modulus $E = 500s_u$. However, these properties changed from zone to zone representing the spatial variability of the soil. For the majority of the soil domain a zone was represented by one finite element. However, in a region of size 3B by 1B close to the strip footing (as bounded by heavy lines in Figure 2) nine smaller finite elements per zone were used. These smaller elements, each with the same material properties, were required to improve the numerical accuracy of the solution. Therefore, in total there are 5280 finite elements in the mesh but only 2880 zones of spatially varying soil properties.

The spatially variable undrained shear strength s_u of both top and bottom layer was modelled as a normally distributed random field with a mean μ_{s_u} and standard deviation $\sigma_{s_u} = COV \cdot \mu_{s_u}$. Consistent with the deterministic values of Merifield et al. (1999), the mean shear strength of the top layer was set as twice the bottom layer, with values of $\mu_{s_{ut}} = 20$kPa and $\mu_{s_{ub}} = 10$kPa assumed in this paper. The COV, vertical and horizontal correlation length θ_v and θ_h for both top and bottom layer vary systematically. Table 1 details the random variables assumed for the 12 cases presented.

For each case, 1000 realisations of the random fields of undrained shear strength s_u were generated using the Local Average Subdivision algorithm (Fenton and Vanmarcke 1990; Fenton 1994). One of the 1000 realisations of the random field of case 1 ($COV_t = COV_b = 0.3$ $\theta_{vt} = \theta_{ht} = \theta_{vb} = \theta_{hb} = 0.1B$ see Table 1 for details) is illustrated in Figure 3.

3 RESULTS

3.1 *Deterministic Case*

The modified bearing capacity factor $N_c^* = Q_u/Bs_{ut}$ was defined in Merifield et al. (1999) as the ultimate bearing capacity Q_u normalised by the footing width B and top layer shear strength s_{ut}. Merifield et al. (1999) reported N_c^* as 4.44 (lower bound), 4.82 (upper bound) and 4.63 (average) for the situation considered in Figure 2. A deterministic case was first conducted in this paper with uniform undrained strengths of 20 kPa and 10 kPa for the top and bottom layer, respectively. An N_c^* of 4.66 was obtained. This good agreement implies that the FE analyses in this paper are reliable and comparable to the Merifield et al. (1999) analyses.

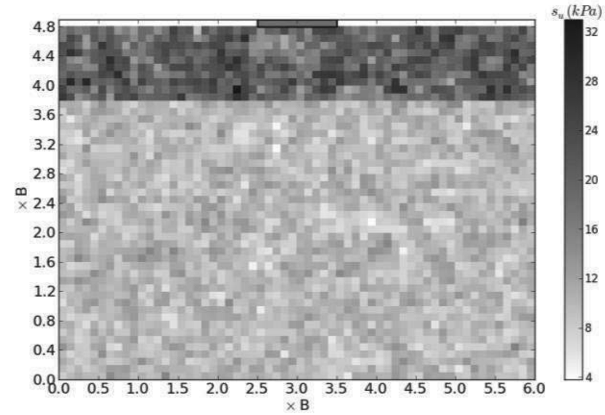

Figure 3. Example random field (for case 1)

Table 1. Calculation cases and summary results

Case	Input parameters						Analysis results		
	Bottom layer			Top layer					
	Θ_{vb}	Θ_{hb}	COV_b	Θ_{vt}	Θ_{ht}	COV_t	$N^*_{c\,m}/N^*_c$	$\sigma(N^*_{c\,r}/N^*_c)$	P_e
1	0.1	0.1	0.3	0.1	0.1	0.3	0.93	0.02	$5.0 \cdot 10^{-4}$
2	0.1	0.1	0.1	0.1	0.1	0.1	0.98	0.01	$1.3 \cdot 10^{-3}$
3	0.1	0.1	0.1	0.1	0.1	0.3	0.95	0.02	$5.6 \cdot 10^{-3}$
4	0.1	0.1	0.3	0.1	0.1	0.1	0.96	0.01	$1.0 \cdot 10^{-4}$
5	0.1	0.1	0.3	0.1	10	0.3	0.94	0.07	0.144
6	0.1	0.1	0.3	0.1	1	0.3	0.93	0.05	0.057
7	0.1	0.1	0.3	1	10	0.3	0.93	0.18	0.277
8	0.1	0.1	0.3	1	1	0.3	0.89	0.12	0.133
9	0.1	10	0.3	0.1	0.1	0.3	0.92	0.04	0.022
10	0.1	1	0.3	0.1	0.1	0.3	0.92	0.03	$4.0 \cdot 10^{-4}$
11	1	10	0.3	0.1	0.1	0.3	0.90	0.09	0.149
12	1	1	0.3	0.1	0.1	0.3	0.90	0.05	0.054

Note: $\Theta = \theta/B$

3.2 *Stochastic soil cases: variation of COV, constant θ*

The mean undrained shear strength of the top layer μ_{sut} is used to defined a modified bearing capacity factor for the stochastic cases (N_{cr}^*) and where

$$N_{cr}^* = Q_{ur}/B\mu_{sut} \quad (1)$$

in which Q_{ur} is the stochastic ultimate bearing capacity. The values of N_{cr}^* of the 1000 realisations random field for each case were ordered and the sample median value denoted as N_{cm}^*. The standard deviation of the N_{cr}^*/N_c^* for the 1000 random field realisations is calculated as $\sigma(N_{cr}^*/N_c^*)$. The values of N_{cm}^* and $\sigma(N_{cr}^*/N_c^*)$ evaluated for all the cases presented in this paper are provided in Table 1. The histogram of N_{cr}^*/N_c^* from the 1000 random field realisations for case 2 ($\theta = 0.1B$ $COV = 0.1$ see Table 1) is depicted in Figure 4, with $N_{cm}^* = 0.98\,N_c^*$ and $\sigma(N_{cr}^*/N_c^*) = 0.01$. The empirical cumulative distribution functions for cases 1-4 are shown in Figure 5.

In order to investigate the influence of changing the COV for both or one of the layers, the cumulative curves for cases 1~4 are shown in Figure 5. In these cases the horizontal and vertical correlation lengths of both top and bottom layers were kept constant as $\theta = 0.1B$. As shown in the figure, the average bearing capacity factor for all of the stochastic cases (represented by N^*_{cm}) is less than the deterministic case. This is consistent with the reports of Nobahar and Popescu (2000), Griffiths et al. (2002) and Cassidy et al. (2012). Further, when the COV of both layers is increased from 0.1 to 0.3 the average bearing capacity reduces from 0.98 to 0.93 and the normalised standard deviation increases from 0.01 to 0.02. This is as expected and is shown in the two extremity curves of Figure 5. Comparing the cases where the COV of only the top layer (case 3: COV_b=0.1, COV_t=0.3) and only the bottom layer (case 4: COV_b=0.3, COV_t=0.1) provides more insight into the mechanisms of failure. We can see from Figure 5 that the COV of the top layer has a more significant effect with case 3 trending towards case 1 where both layers are 0.3. Moreover, the similarity of the shapes of case 2 and case 4 as well as case 3 and case 1 implies that the top layer COV determines the variation (standard deviation) of the curves.

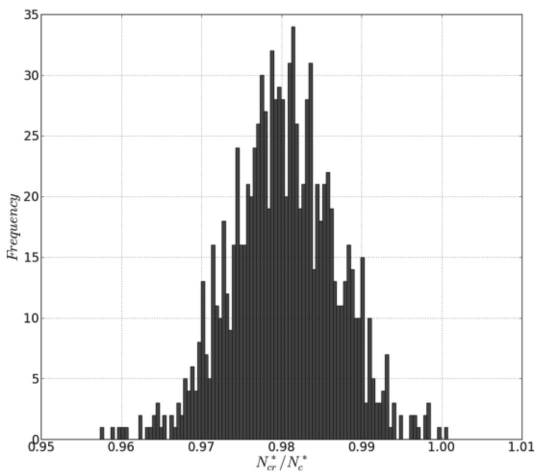

Figure 4 Histogram of N^*_{cr}/N^*_c for case 2

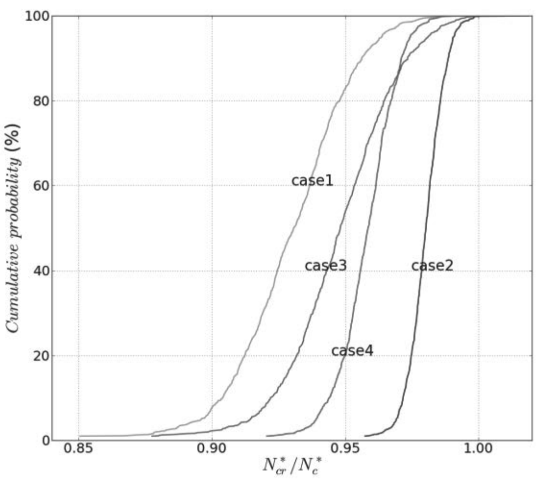

Figure 5 Cumulative probability curves for varying COV of cases 1 to 4

The output samples of stochastic bearing capacity factor normalized by the deterministic value were analysed with the aim of estimating the frequentist probability of exceedence of unity, i.e., the probability that the stochastic bearing capacity factor exceeds the deterministic bearing capacity factor. This assessment is important in the context of engineering design, as it provides a measure of the unconservatism in using deterministic bearing capacity factors, i.e., in neglecting uncertainty and spatial variability. In only 6 cases out of the 12 analyzed, output samples resulted to be lognormal at the 95% confidence level using the Anderson-Darling test. Hence, estimating the probability of exceedence of unity from cumulative values of fitted lognormal samples would not allow confident assessement for all cases. Empirical cumulative distribution functions were calculated for each sample. The empirical probability P_e of exceedence of unity for each case is noted in the rightmost column in Table 1.

The failure mechanisms of three selected realizations of case 1 ($\theta = 0.1B, COV = 0.3$) are shown in Figure 6. These represent the minimum, median and maximum N^*_{cr} cases and are shown alongside the deterministic failure mechanism (uniform and mean parameter values). In all three cases the existence of the random field results in a non-symmetric failure mechanism, with the minimum bearing capacity case most unsymmetrical. With the increasing of bearing capacity, the failure mechanism tends to resemble the deterministic case. The importance of spatial variability in the top layer can be observed, with the majority of the failure mechanism residing in that layer. Further, with higher variability and potential for weaker zones the mechanism for lower bearing capacity is both more unsymmetric and shorter (pulling it further into the top layer).

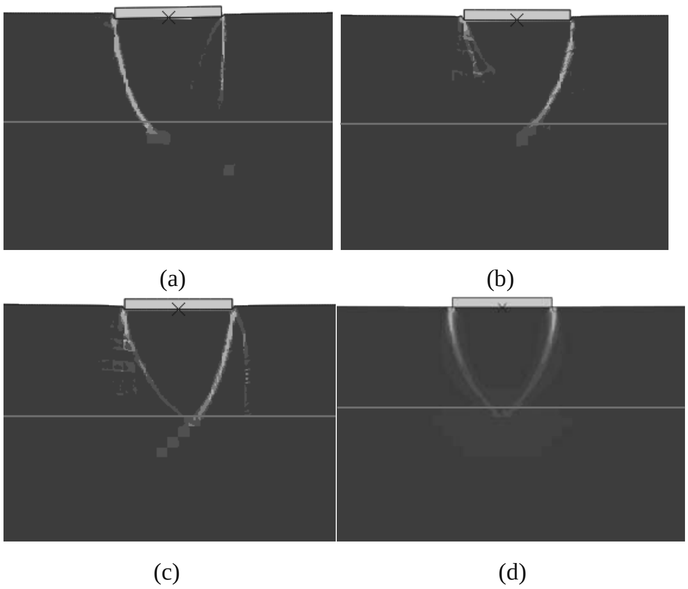

Figure 6. Failure mechanisms from finite element analysis for (a) lowest, (b) median and (c) highest bearing capacity, and (d) deterministic uniform case (for clarity only a section of 3*B* width and depth 2*B* show)

3.3 *Stochastic soil cases: variation of correlation length in top layer*

With the top layer determined to play a more significant role in the problem configuration of this paper further concentration on the effect of top layer correlation length is discussed. The results for correlation length varying from 0.1B to 10B are presented as cumulative probability curves in Figure 7. These represent cases 5, 6, 1, 7 and 8 in Table 1. As for the $\theta_{vt}/B = 0.1$ cases (cases 5, 6 and 1), the largest bearing capacity corresponds to the largest horizontal correlation length $\theta_{ht} = 10B$ (case 5) while the minimum corresponds to $\theta_{ht}/B = 1$ (case 6). This is consistent with the observation of Griffiths et al. (2002) for the single layer case. In general, a large correlation length results in greater standard deviation of the bearing capacity, i.e. the foundation becomes more "nonuniform". The minimum bearing capacity occurs at $\theta_{vt}/B = \theta_{ht}/B = 1$.

3.4 *Stochastic soil cases: variation of correlation length in bottom layer*

Comparison of the results of case 9, 10, 1, 11 and 12 indicates the correlation length effect of the bottom layer. It again shows that increasing horizontal correlation length tends to increase the standard deviation of the bearing capacity factor (see Table 1 and Figure 6). However, the largest average bearing capacity corresponds to the minimum correlation length case (case 1: $\theta_{vt}/B = \theta_{hb}/B = 0.1$). This differs to what is occurring in the top layer. The maximum average bearing capacity corresponds to the largest correlation length case 11, which is consistent with the results of changing the correlation length of the top layer.

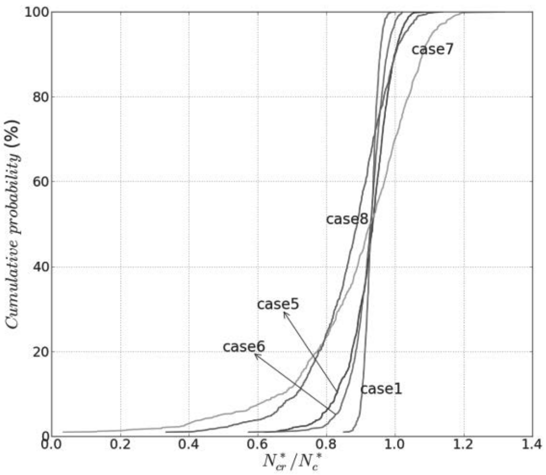

Figure 7. Cumulative probability curves for variation of correlation distance in the top layer (cases 1, 5, 6, 7 and 8)

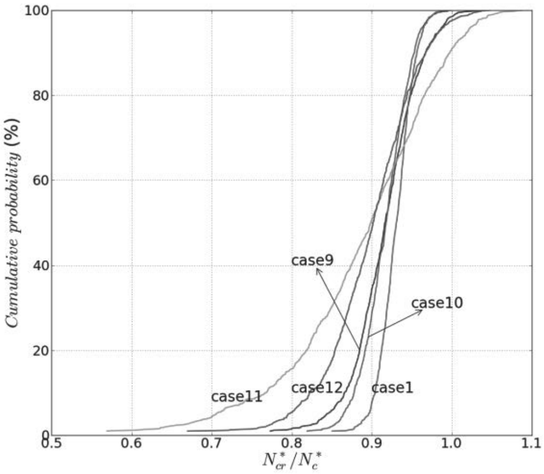

Figure 8. Cumulative probability curves for variation of correlation length in bottom layer (cases 9, 10, 1, 11 and 12)

4 CONCLUSIONS

In this study, finite element analysis of the vertical bearing capacity of a strip footing penetrating stiff-over-soft clay was conducted by taking the spatial variability of undrained strength into account. The results indicate that with high spatial variability in the undrained shear strength there is a significant reduction in the bearing capacity. Mean bearing capacity factors and statistical distributions were provided for 12 cases of s_{ut}/s_{ub} = 2, COV = 0.1 and 0.3, and θ_v/B and θ_h/B = 0.1, 1 and 10. For the case of top layer thickness equal to the strip footing width presented it was shown that variation in the top layer had a greater effect on reducing the bearing capacity (when correlation distance was held constant). This was due to the unsymmetric bearing capacity shortening further into the top layer.

The empirical probabilities of exceedence of the deterministic bearing capacity factor in the stochastic case differ from case to case, ranging from on the order of 10^{-4} to 0.277, thus attesting for the influence of the magnitude of spatial variability and uncertainty on the effects of stochastic modelling. The maximum value observed for case 7 is well below a "central" value of 0.5; hence, overall, it is assessed that the deterministic case is significantly unconservative from an engineering standpoint.

The conclusions drawn in this paper may be specific for the geometery and soil conditions analysed. The 12 cases presented here, however, represent a small subset of 1600 cases analysed in a more ambitious numerical experiment. Cases of (i) $\mu_{s_{ut}}/\mu_{s_{ub}}$ = 4/3 and 2, (ii) COV = 0.1 and 0.3, (iii) θ_v/B and θ_h/B = 0.1, 1 and 10, as well as (iv) a gradient of increasing undrained shear strength with depth, and (v) a footing embedded to 0.5B into the top layer, make up the full programme. The results of the larger study will be published in due course.

5 ACKNOWLEDGEMENTS

This research is being undertaken with support from the Australia-China Natural Gas Technology Partnership Fund and The Lloyd's Register Educational Trust.

6 REFERENCES

Cassidy, M.J., Uzielli, M. and Tian, Y. (2012) "Probabilistic Combined Loading Failure Envelopes of a Strip Footing on Spatially Variable Soil". Computers and Geotechnics, In Press. http//dx.doi.org/ 10.1016/j.compgeo.2012.10.008

Dassault Systèmes (2010) "Abaqus Analysis User's Manual"

Fenton, G. A. (1994). "Error Evaluation of Three Random-Field Generators". *J. Eng. Mech.*, 120(12), 2478–2497.

Fenton, G. A. and Griffiths, D. V. (2003). "Bearing-Capacity Prediction of Spatially Random C-Phi Soils." Canadian Geotechnical Journal 40(1): 54-65.

Fenton, G. A. and Griffiths, D. V. (2008). "Risk Assessment in Geotechnical Engineering". Hoboken, N.J., John Wiley & Sons.

Fenton, G. A. and Vanmarcke, E. H. (1990). Simulation of Random Fields via Local Average Subdivision. *J. Eng. Mech.*, 116(8), 1733–1749.

Griffiths, D. V. and Fenton, G. A. (2001). "Bearing Capacity of Spatially Random Soil: The Undrained Clay Prandtl Problem Revisited." Geotechnique 51(4): 351-359.

Griffiths, D. V., Fenton, G. A. and Manoharan, N. (2002). "Bearing Capacity of Rough Rigid Strip Footing on Cohesive Soil: Probabilistic Study." Journal of Geotechnical and Geoenvironmental Engineering 128(9): 743-755.

Kasama, K. and Whittle, A. J. (2011). "Bearing Capacity of Spatially Random Cohesive Soil Using Numerical Limit Analyses." Journal of Geotechnical and Geoenvironmental Engineering 137(11): 989-996.

Merifield, R. S., Sloan, S. W. and Yu, H. S. (1999). "Rigorous Plasticity Solutions for the Bearing Capacity of Two-Layered Clays." Geotechnique 49(4): 471-490.

Nobahar, A. and Popescu, R. (2000). "Spatial Variability of Soil Properties - Effects on Foundation Design". Proceedings of 53rd Canadian geotechnical conference, Montreal, Quebec.

Paice, G. M., Griffiths, D. V. and Fenton, G. A. (1996). "Finite Element Modeling of Settlements on Spatially Random Soil." ASCE Journal of Geotechnical Engineering 122(9): 777-779.

Popescu, R., Deodatis, G. and Nobahar, A. (2005). "Effects of Random Heterogeneity of Soil Properties on Bearing Capacity." Probabilistic Engineering Mechanics 20(4): 324-341.

Residual Soils and the Teaching of Soil Mechanics

Les sols résiduels et l'enseignement de la mécanique des sols

Wesley L.D.
University of Auckland, Auckland, New Zealand

ABSTRACT: There is a serious gap in the teaching of soil mechanics because of its failure to include coverage of residual soils as an integral part of such teaching. A rough estimate suggests that at least half of the earth's surface is covered by residual soils, and in today's world the most rapid growth and development is occurring in countries that contain a very high proportion of these soils. Civil engineering students are graduating from universities around the world having studied soil mechanics to varying levels, but without even being aware of the existence of residual soils, let alone having any understanding of their properties. The purpose of this paper is to highlight the fact that while much of what is taught in soil mechanics courses is common to both soil groups, there are significant and important areas where concepts applicable to sedimentary soils are completely irrelevant to residual soils.

RÉSUMÉ: L'omission de l'enseignement des sols résiduels est une lacune grave dans l'enseignement de la mécanique des sols. Une estimation approximative laisse à penser qu'au moins la moitié de la surface terrestre est recouverte par des sols résiduels, et la croissance et le développement les plus rapides dans le monde actuel a lieu dans des pays qui contiennent une proportion très élevée de ces sols. Les étudiants en génie civil terminent leurs études à travers le monde en ayant étudié la mécanique des sols à des niveaux variables, sans même être au courant de l'existence des sols résiduels ou de leurs propriétés. Cet article vise à mettre en évidence le fait qu'alors qu'une grande partie de ce qui est enseigné dans les cours de mécanique des sols est également valable pour les sols résiduels, il y a des chapitres significatifs et importants de l'enseignement où les concepts applicables aux sols sédimentaires sont complètement hors sujet pour les sols résiduels.

KEYWORDS: Residual soils, soil mechanics teaching, stress history, formation, compressibility, slope stability

1 INTRODUCTION

Although residual soils are found on the earth's surface almost as commonly as sedimentary soils, their existence and properties are rarely mentioned in soil mechanics courses and text books. The result is that certain concepts developed from sedimentary soil behaviour are routinely applied to residual soils and routinely result in a mistaken understanding of their behaviour. This is surely an indictment on those who teach soil mechanics in our universities. It is well past the time when residual soil behaviour should be an integral part of mainstream soil mechanics, especially of its syllabus in university courses. This paper is an attempt to highlight some significant aspects of residual soil behaviour that should be essential material in basic soil mechanics courses.

2 FORMATION

Figure 1 illustrates residual and sedimentary soil formation. Residual soils are formed directly from their parent rock by physical and chemical weathering, while. sedimentary soils undergo further processes including transportation by streams and rivers, sedimentation in lakes or in the sea,.followed by consolidation.

Their formation method has some obvious influences on the properties and behaviour of these two soil groups, the main ones being the following:

(a) sedimentary soils undergo a sorting process during erosion and re-deposition that give them a degree of homogeneity that is not present in residual soils.

(b) residual soils do not undergo a consolidation process, and their properties cannot be related to stress history. The terms normally and over-consolidated have no relevance to residual soils. Strictly speaking the parameters C_c and C_s are not applicable to residual soils. The parameter C_c is defined as the (log) slope of the virgin consolidation line. It is readily apparent from their formation process that there is no such thing as a virgin consolidation line for a residual soil.

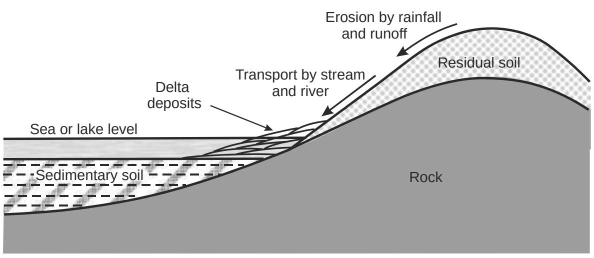

Figure 1. Soil formation (after Wesley, 2012)

(c) Some residual soils, especially those derived from volcanic parent material consist of unusual clay minerals not found in sedimentary soils

(d) Residual soils generally have much higher permeability than sedimentary soils, which has important implications for behaviour in oedometer tests and in estimates of short term and long term stability of cut slopes.

3 CONSOLIDATION BEHAVIOUR

Figure 2 shows results of oedometer tests on samples of a residual soil derived from the weathering of Peidmont formation in southeastern USA. Figure 2(a) shows the results plotted using the conventional log scale for pressure. This convention arises from the behaviour of sedimentary clays when deposited and consolidated under water. Values of pre-consolidation pressure and over-consolidation ratio have been determined from these graphs and are listed in the figure. As noted earlier, stress history has no significant relevance to residual soils, and assumptions that they should display pre-consolidation pressures are erroneous.

There is no reason at all to use a log scale for pressure when illustrating the compression behaviour of residual soils. The graphs have therefore been re-plotted using a linear scale in Figure 2(b). These graphs show a very different picture; there is no indication at all of "pre-consolidation" pressures. Those inferred from the log plot are not soil properties; they are purely the product of the way the data are plotted

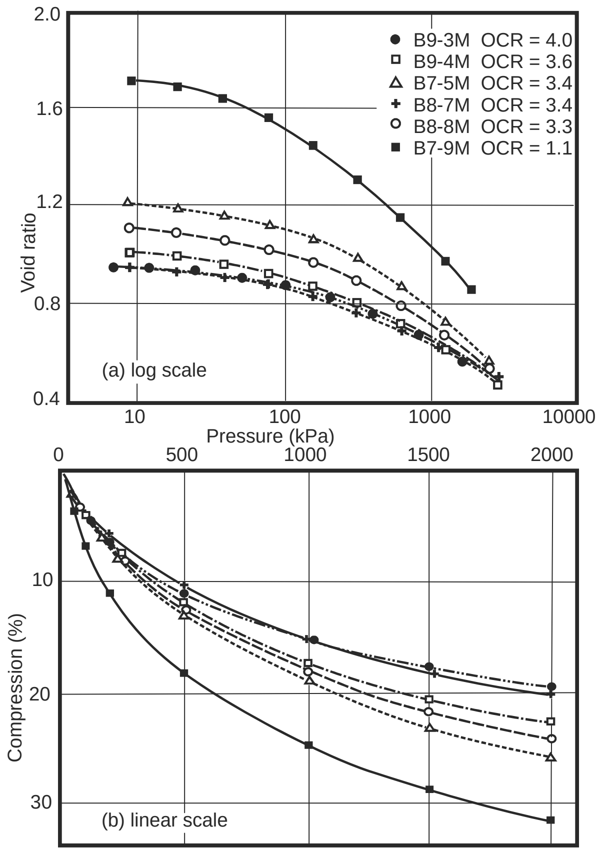

Figure 2. Misinterpretation of the e-log(p) graph (after Wesley, 2000).

A second example of the misleading nature of log plots is given in Figure 3, which shows the results of oedometer tests on a residual clay found in the Auckland region of New Zealand. The graph using a log scale suggests the existence of a pre-consolidation pressure at about 600 kPa, while the linear plot shows no trace of this; in fact the behaviour is almost linear.

While residual soils, by definition, cannot have pre-consolidation pressures because they are not formed by a consolidation process, they may still show a significant increase in compressibility at certain stress levels. This arises because some residual soils are highly structured and at a certain stress level this structure begins to collapse causing the increased compressibility This stress is best termed a vertical yield pressure rather than a pre-consolidation pressure.

Some residual soils can show extremely variable compression behaviour, such as that illustrated in Figure 4 which shows oedometer tests on three samples of clay derived from the weathering of andesitic volcanic ash. When plotted using a log scale, the behavour appears similar, and yield pressure could be inferred from all three graphs. However, when re-plotted using a linear scale the picture is very different.

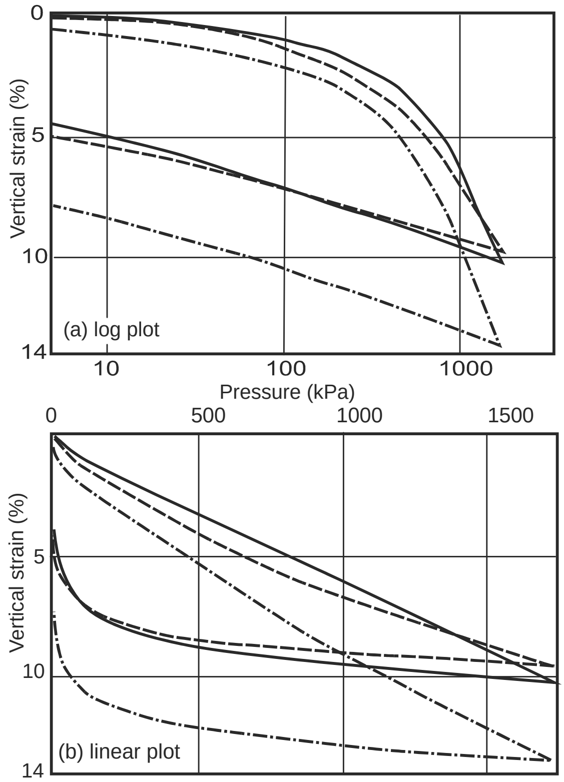

Figure 3. Behaviour of an Auckland residual soil (after Pender et al, 2000)

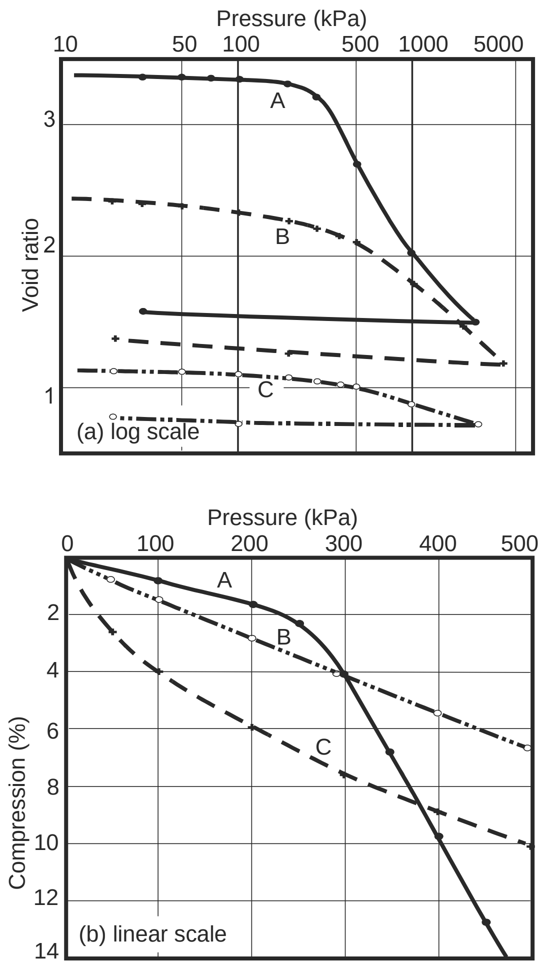

Figure 4. Behaviour of volcanic ash soils

It is now seen that only Sample A shows a yield pressure, of about 250 kPa. Sample B shows almost linear behaviour, while Sample C shows steadily decreasing compressibility, or “strain hardening” characteristics.

A general representation of soil compressibility, especially over the pressure range of interest to geotechnical engineers, is shown in Figure 5. This gives a far more realistic picture than the conventional e-lot(p) plot. The almost universal use of the log plot has created the belief that the compressibility of all soils can be adequately represented by two straight lines on a log graph, which is certainly not the case.

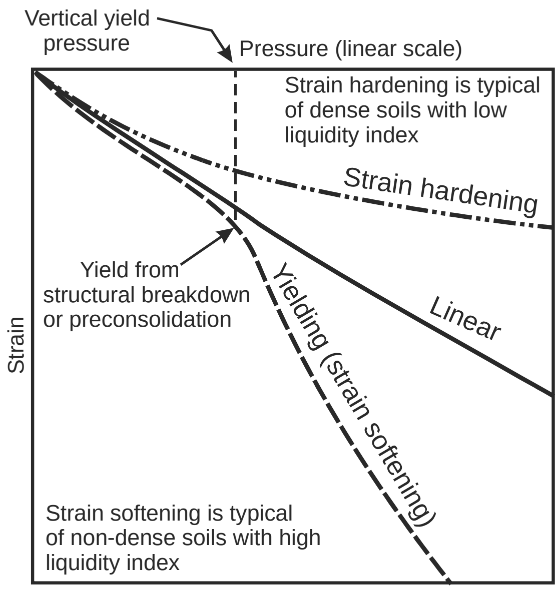

Figure 5. A better representation of soil compressibility, valid for all soils. (after Wesley, 2010).

It is a regrettable that the profession and those who teach soil mechanics have not taken more notice of what Professor Nilmar Janbu has been saying for many years. His message is summarised in the following statement (Janbu, 1998):

“--- *it remains a mystery why the international profession still uses the awkward e-log p plots, and the incomplete and useless coefficient C_c which is not even determined from the measured data, but from a constructed line outside the measurements* ---”.

Janbu made the above comments based on experience with sedimentary soils. The mystery remains even greater with residual soils. There is little doubt that if teachers of soil mechanics always plotted results of oedometer tests on undisturbed soils using both linear and log scales they would very quickly realise how misguided the continued use of the log scale is.

4 INFLUENCE OF HIGH PERMEABILITY

The high permeability of residual soils is caused by various factors, including their relatively coarse nature, the presence of unusual clay minerals, and particular forms of micro structure. The high permeability has various practical implications and students should be made aware of these in basic soil mechanics courses. Only two will be described here; the first is the determination of the coefficient of permeability from oedometer tests, and the second is the short and long term stability of cut slopes in clay.

Figure 6 shows typical root time graphs from conventional oedometer tests on residual soils. According to one dimensional consolidation theory these graphs should show an initial linear section, from which the well known Taylor construction can be used to determine the coefficient of consolidation. The graphs in Figure 6 do not display this linear section, simply because the pore pressure dissipates almost as soon as the load increment is applied, and the shape of the graphs is a creep phenomenon unrelated to the rate of pore pressure dissipation.

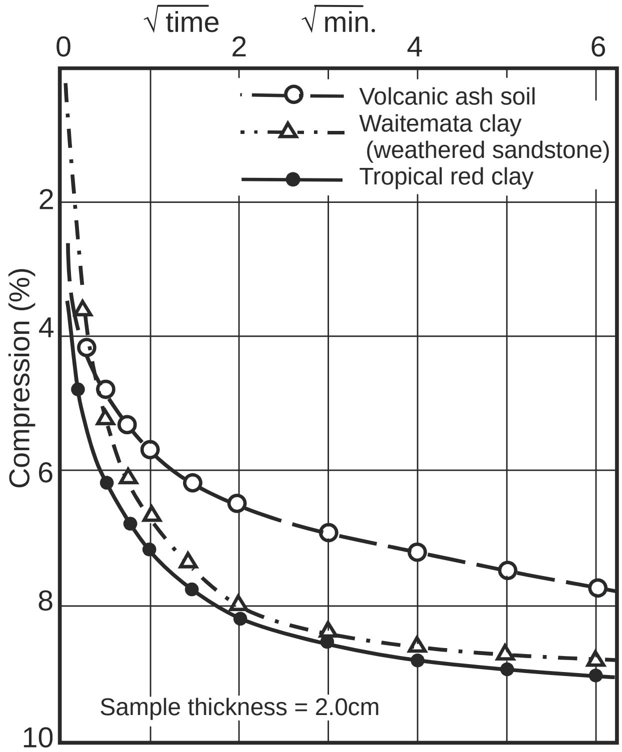

Figure 6 Root time graphs from tests on residual soils.

It is not difficult to show that the highest value of the coefficient of consolidation that can be reliably determined from an oedometer test with a sample thickness of 2.0cm is approximately $0.1m^2$/day (= $0.012cm^2$/sec.). Readings taken in the first minute will only lie on a straight line if the c_v value is less than $0.1m^2$/day; many residual soils have higher values. Because most geotechnical engineers and laboratory technicians are unaware of this, the Taylor construction continues to be regularly applied to graphs such as those in Figure 6, and erroneously low values of c_v are determined.

5 SLOPE STABILITY

The main trigger for slips or landslides in residual soil slopes is intense and prolonged rainfall, a fact that reflects the relatively high permeability of such soils. In the case of cut slopes, therefore, it is very unlikely that behaviour during excavation will be undrained. It is much more likely that a new long term seepage pattern will develop as excavation proceeds. However, this pattern will only be an average state, and there will be frequent changes with time reflecting the weather changes. This situation is illustrated in Figure 7, alongside the commonly assumed behaviour of sedimentary soils. In residual slopes changes in the water table and pore pressure occur in both a regular seasonal pattern and in a random and unpredictable manner as a result of sudden storm events. The challenge to the geotechnical engineer is to estimate the worst case situation.

A further significant feature of slopes in residual soils is that they are often much steeper than those in sedimentary soils. This means that water tables may also be relatively steep, and if analytical methods are used to assess stability, then care is needed in the way the pore pressure is included in the analysis. The example in Figure 8 illustrates this point.

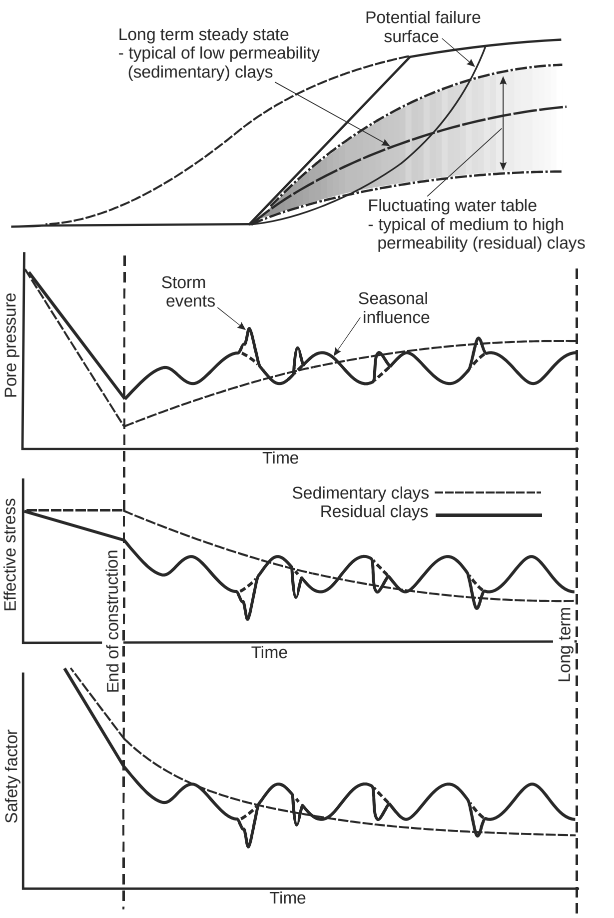

Figure 7 Short and long term stability of cut slopes (after Wesley, 2010).

This figure shows a steep cut slope subject to variable weather patterns. One way in which the worst case pore pressure state can be determined analytically is to assume that rainfall continues long enough for the water table to rise to the surface and create a stable seepage state. This may be excessively conservative, but does at least put a lower limit on the theoretical safety factor.

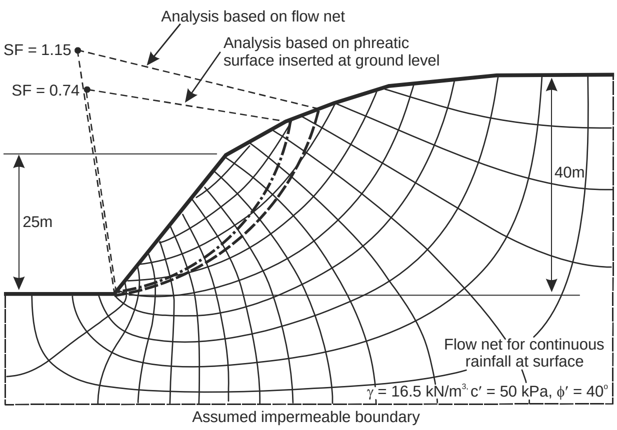

Figure 8 Influence of pore pressure assumptions on the estimate of safety factor.

There are then two ways of including the pore pressures from this state in a slip circle analysis. The first, and normal, method is to determine the pore pressure directly from the vertical intercept between the phreatic surface and the slip surface – the "vertical intercept" assumption. In this case it will be the vertical distance from the ground surface to the slip surface. Almost all computer programmes make this assumption, which may be reasonable in gentle slopes but can give very misleading results in steep slopes, which is what the example in Figure 8 illustrates.

The second method is to consider the practical situation realistically and determine a flow net compatible with the boundary conditions. The pore pressures can then be determined from this flow net. It is evident from Figure 8 that the vertical intercept assumption, which implies that equipotential lines are vertical is physically impossible. The short section of level ground at the top of the slope is an equipotential line and flow lines will begin perpendicular to this. The flow net shows that most of the equipotentials along the slip surfaces are far from vertical.

The safety factors determined by the two methods, using the computer programmes SeepW and SlopeW, are the following:

Vertical intercept assumption SF = 0.74

From the correct flow net: Safety Factor = 1.15

The difference is very large, and although many slopes in residual soils may not be as steep as that in Figure 8, there are many, especially in places like Hong Kong that are considerably steeper Thus the error in the safety factor could be even greater than that indicated in the Figure 8 analysis.

6. CONCLUSIONS

Although residual soils occupy about half the world's surface very few universities cover them in their soil mechanics courses. This includes many universities surrounded on all sides by residual soils. The result is that geotechnical engineers routinely apply concepts valid only for sedimentary soils to residual soils and gain a mistaken understanding of their behaviour.

It is long past the time when residual soil behaviour should be part of mainstream soil mechanics and an integral part of university courses. The importance of this cannot be overemphasised. Education today is globalised in a way it hasn't been in the past and large numbers of students from Asia, Africa and Latin America are obtaining their education in the universities of Western countries. Residual soils tend to be predominant in the former counties, but only sedimentary soil behaviour is covered by degree courses in the latter. Students thus return to their home countries unaware that significant parts of the soil mechanics they have been taught do not apply to the residual soils they are highly likely to encounter in their own countries.

7. REFERENCES

Janbu, N. 1998. Sediment deformation. *Bulletin 35, Norwegian University of Science and Technology,* Trondheim, Norway.

Pender, M.J., Wesley, L.D. Twose, G., Duske, G.C., and Satyawan Pranjoto 2000. Compressibility of Auckland residual soil. Proc. *GeoEng2000 Conf,* Melbourne.

Wesley, L.D. 2000. Discussion on paper: Influence of in situ factors on dynamic response of Piedmont residual soils. *ASCE Journal of Geotechnical and Geoenvironmental Engineering*. 126 (4), 384-385.

Wesley, L.D. 2010a, Fundamentals of Soil Mechanics for Sedimentary and Residual Soils. John Wiley & Sons Ltd, New York.

Wesley, L.D, 2010b. Geotechnical Engineering in Residual Soils. John Wiley & Sons Ltd New York.

Wesley, L.D. and Pender, M.J. 2012. Aspects of soil mechanics teaching. *Proceedings, 11th Australia New Zealand Conference on Geomechanics,* Melbourne.

Application of The Tangent Modulus Method in Nonlinear Settlement Analysis of Sand Foundation

Application de la méthode du module tangent dans le calcul du tassement non-linéaire de fondations sur sol sableux

Yang G.-H.[1, 2, 4], Luo Y.-D., [2, 3], Zhang Y.-C.[1,4], Wang E.-Q.[1,4]

1.Guangdong Research Institute of Water Resources and Hydropower, Guangzhou 510610, China; 2. School of Civil and Architectural Engineering, Wuhan University, Wuhan 430072, China; 3. Shenzhen Geotechnical Investigation & Surveying Institute Co. Ltd., Shenzhen，518028, China；4. The Geotechnical Engineering Technology Center of Guangdong Province, Guangzhou 510610, China

ABSTRACT: Foundation settlement computation method is always a hot and difficult issue in geotechnical engineering for the difficulty in which soil parameters obtained from laboratory test are quite different from undisturbed soil in the field. Especially for sand foundation and stiff clay foundation with strong structure, settlement calculating with laboratory test parameters makes distinct error from actual situation. The tangent modulus method, based on calculation parameters determined from in-situ plate loading test, can overcome this shortcoming, and can be used in analyzing nonlinear foundation settlement. This method makes a new progress in foundation settlement computation. In this paper, systematic geotechnical test data from Texas A&M University Riverside Campus are utilized to test the hyperbola model of soil and the tangent modulus method. Then, methods for soil parameter determination in different depth are studied through such simple in-situ tests such as pressuremeter test and cone penetration test, and these methods are verified through plate loading test with different size. The analysis results prove that the tangent modulus method has better accuracy of nonlinear settlement computation. Also, it is feasible to obtain the computation parameters for the tangent modulus method from some simple in-situ tests, which provides an easier way in determining parameters of the tangent modulus method.

RÉSUMÉ : Le calcul de tassement des fondations est toujours un problème difficile dans les études géotechniques, et la difficulté réside dans la différence très grande entre les paramètres géotechniques obtenus à partir d’essais de laboratoire et ceux obtenus à partir d’essais in-situ, en particulier pour les fondations sur sol sableux et les fondations sur argile raide surconsolidée. L'erreur entre les résultats du calcul de tassement basés sur les paramètres issus d’essais de laboratoire et la valeur réelle du tassement peut être très grande. La méthode du module tangent, basée sur le calcul de paramètres déterminés à partir d’essais de plaque, permet de s’affranchir de ce défaut, et peut être utilisée dans une analyse non-linéaire du tassement des fondations. Cette méthode représente un nouveau progrès dans le calcul du tassement des fondations. Dans cet article, on a utilisé les données d’essais géotechniques systématiques réalisés au Campus Riverside de l’Université A & M au Texas pour valider un modèle hyperbolique de comportement du sol et la méthode du module tangent. Puis on a déterminé des méthodes de calcul des paramètres géotechniques à différentes profondeurs à partir d’essais in-situ simples comme l’essai pressiométrique ou le CPT, et on a validé ces méthodes au moyen de résultats d’essais de chargement de fondations superficielle (plaques de différentes tailles). Les résultats montrent que la méthode de module tangent utilisé pour le calcul de tassement non linéaire de la fondation a une meilleure précision. Egalement, il est possible d’obtenir les paramètres de calcul de la méthode au module tangent à partir d’essais in-situ comme l’essai pressiométrique ou le CPT.

KEYWORDS: foundation settlement; tangent modulus method; in-situ test; nonlinear; sandy soil subgrade

1 INTRODUCTION

Due to the complexity of the geomaterial, the calculation of foundation deformation is not accurate, which can be specifically attributed to the unreasonable calculation method and less accurate value of geotechnical parameters. Due to the disturbance of undisturbed soil in the sampling and sample making preparation process, the foundation deformation parameters accessed by the laboratory test will be seriously distorted. Therefore, the development of settlement deformation calculation method based on the in-situ tests has practical significance on the improvement of accuracy of the ground deformation calculation. As to sand foundation, due to the sand-sampling difficulties, currently the international recognized way - Schmertmann semi-empirical method is based on the experience of cone penetration test to determine the deformation modulus of the sand, using the layer-wise summation method to calculate foundation settlement[1]. The existing methods are difficult to fully calculate the nonlinear settlement of the foundation. Based on plate loading test, Yang Guanghua[2~6] proposed that the tangent modulus method can better solve the problem of the accuracy of the foundation settlement calculation. However, as parameters are derived from the plate loading test which has high cost and can not apply to deep soil. Therefore, to explore other simple tests instead of in-situ plate loading test to determine the required parameters is very important. This paper[7]discusses how to use the pressuremeter test to determine the required parameters.

American scholar Briaud JL, Gibbens R M., et, al [8]have carried out the plate loading test with five different sizes’ plates, static cone penetration test, pressuremeter test and other systematic soil tests on the sand foundation in Riverside Campus, Texas A & M University. The shape of plates are square and the sizes are 1m, 1.5m, 2.5m, 3m, 3m. The purpose is to test the effectiveness of a variety of foundation settlement calculation methods. By making use of these valuable test data, this paper further testifies the applicability of the tangent modulus method[4] for nonlinear settlement computaion and studies how to use the static cone penetration test and pressuremeter test and other simple in-situ tests to determine the parameters of the foundation parameters required in the tangent modulus method, and it can further develop and improve the tangent modulus method.

1.1 *Calculation Principle of Tangent Modulus Method*[4]

The tangent modulus method is a new method based on the in-situ plate loading test to create the P-S curve of soil, in order to calculate the settlement of foundation. Assuming that the basis load - settlement curves can be fitted by using the hyperbolic curve, we create the hyperbolic curve method, as formula (1):

As a and b are the parameters of test, the nonlinear tangent modulus of soil can be calculated as hyperbolic curve formula (1), as formula (2):

$$p = \frac{s}{a+bs} \quad (1) \quad E_t = (1 - R_f \frac{p}{p_u})^2 \cdot E_{t0} \quad (2)$$

E_{t0} is the initial tangent modulus, p is the additional stress of soil, p_u is the ultimate capacity of foundation soil, R_f is the damage ratio coefficient which is similar to that of the Duancan-Chang model.

While the tangent modulus E_t along the depth is solved by formula(2), we could use layer-wise summation method to calculate the settlement. It is a good method to determine the parameters of soil because the soil is undisturbed and the nonlinear properties of soil are well considered, this method can calculated the nonlinear settlement of soil accurately.

Assuming soil layer is Δh_j load increment Δp_i , the amount of compression of this soil layer is as formula (3):

$$\Delta s_{ij} = \frac{\Delta p_i \cdot \alpha \cdot \Delta h_j}{E_{ij}} \qquad (3)$$

α is the additional stress of distribution coefficient, and E_{ij} is the tangent modulus on the soil layer corresponding to the load p. After the amount of compression of each layer is calculated, according to layer-wise summation method, the total settlement under added load is , as formula (4):

$$\Delta s_i = \sum_{j=1}^{n} \Delta s_{ij} \qquad (4)$$

When using this method to calculate the nonlinear settlement of foundation, the key is to determine three parameters, including the tangent modulus value E_t of the each foundation layer of soil, and the strength parameters - c and φ required in Formula (2) calculation as well as the initial tangent modulus E_{t0} , which are simple.

Please put one open line before a Figure (centered, see Figure 1) or a Table (use the Figure tag or use paintbrush).

1.2 *Foundation settlement calculation parameters determined by plate loading test*

As to the p-s curve measured by the plate loading test, it can inversely calculate the internal friction angle φ of foundation settlement parameters, cohesion c and the initial tangent modulus E_{t0} , resulting in a more reasonable calculation parameters.

Loading test site is located in the Riverside Campus, Texas A & M University, with 0 to 10.5m depth of sand and black stiff clay as the sublayer. The main physical and mechanical parameters of the indoor tested silty sand are shown in Table 1.

Tab.1 physical mechanic index of ground soil

γ (kN/m^3)	w (%)	Gs	e	c (kPa)	φ (°)	depth(m)
15.6	5.0	2.66	0.75	0	34.2	0.6
				0	36.4	3.0

A total of five plate loading tests are conducted in the site, and the plates are square with width of 1~3m. The test is carried out at depth of 0.76 m.

We use two methods to forecast the p-s curve, e.g. the first method uses the aforementioned fitted hyperbolic parameters a and b to directly draw p-s curve based on the assumption[2] that p-s curve complies with the hyperbolic model; the second method is the aforementioned tangent modulus method: first calculate the tangent modulus E_t under different loads as formula(2), then calculate the amount of compression of each layer as(3), and lastly make summary of the foundation settlement under different load by layer-wise summation as (4), and draw p-s curve [4]

When calculating the amount of compression of each layer by tangent modulus method, the ultimate bearing capacity of each layer is determined by the Terzaghi formula (5). The cohesion $c = 0$, and the internal friction angle φ is inversely calculated by loading test data in Formula (5).

$$P_u = \frac{1}{2}\gamma B N_\gamma + q N_q + c N_c \qquad (5)$$

By using the above two methods, the p-s curves of the five plates are drawn respectively, and compared with the actually measured data shown in Figures 2 to 6.

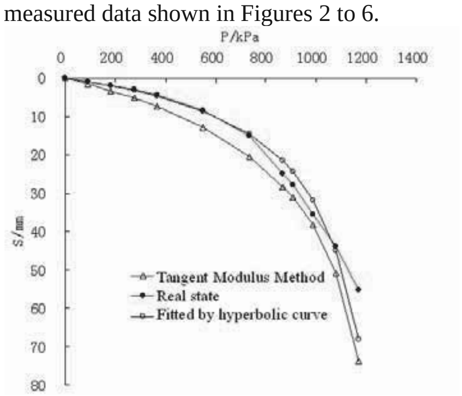

Fig.2 The P-S curve of 5#footing(1.0m×1.0m)

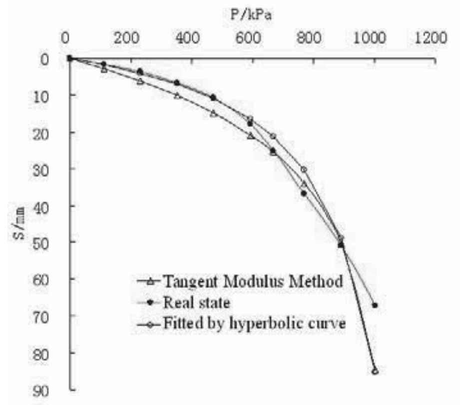

Fig.3 The P-S curve of 2# footing(1.5m×1.5m)

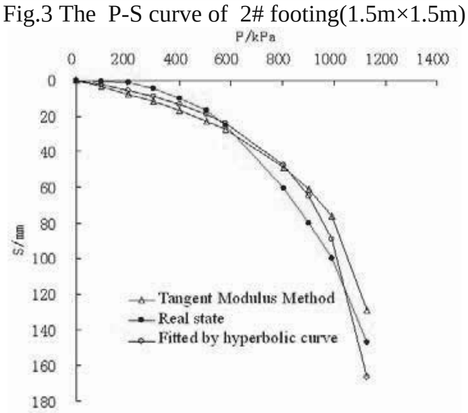

Fig.4 The P-S curve of 4# footing(2.5m×2.5m)

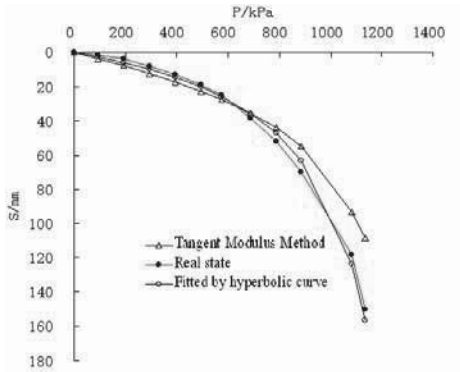

Fig.5 The P-S curve of 1# footing(3.0m×3.0m)

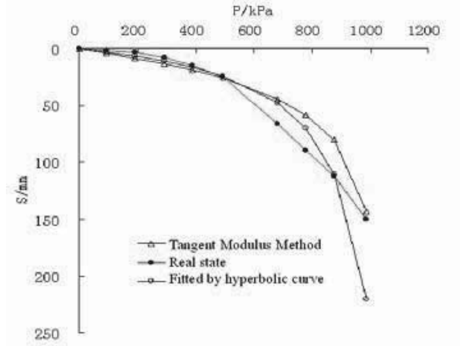

Fig.6 The P-S curve of 3# footing(3.0m×3.0m)

From the predictions of the above two methods, they all get good results. For homogeneous foundation formed by only one category of soil, the two methods result in the same effect, but as to the non-homogeneous layered soil expressed directly by hyperbolic curve, when the small-size plate loading test results are used for the large-size foundation, its reflection of the deep soil is not enough.

When using the second method to calculate the layered foundation settlement by the tangent modulus method, it can adopt different c and φ for different soil layers, as well as the initial tangent modulus E_{t0} of soil to reflect the effect on the deep soil and the soil of different layers, which has better adaptability for the foundation generally composed by the multi-layer soil.

The parameters of different test points inversely calculated by the tangent modulus method are shown in Table 2.

Table 2. Foundation soil parameters of 5 plates inversely calculated by loading test data

Plate loading test Number	E_{t0} **/MPa**	p_u **/kPa**	c **/ kPa**	φ /°
5#(1.0m×1.0m)	83.4	1399	0	37.2
2#(1.5m×1.5m)	84.4	1202	0	35.5
4#(2.5m×2.5m)	84.7	1340	0	34.8
1#(3.0m×3.0m)	90.9	1405	0	37.0
3#(3.0m×3.0m)	86.4	1128	0	35.6

The average of soil parameters in Table 2 are as follows:E_{to}=86Mpa,φ=36°. The settlement load curve of each plate calculated by taking these soil parameters and using tangent modulus method is shown in Figures 7 to 11.

The figures show that the calculation and test results are in consistent to a large extent. But the accuracy is less than that of Figures 2 to 6. This is mainly because the soil parameters in Figures 2 to 6 are inversely calculated by each pilot point, while Figures 7 to 11 are calculated by using the average value of inversely calculated parameters at each test point. In actual engineering, this heterogeneity makes it unlikely to conduct plate loading test for each foundation location. Therefore, this paper further explores the use of easier pressuremeter test to determine the initial tangent modulus E_{to} of tangent modulus method in the soil at different depth by using static cone penetration test (CPT) to determine the angle of internal friction φ in the tangent modulus method in sand of different layers. And c = 0.

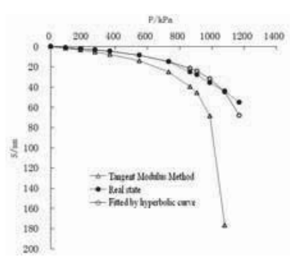

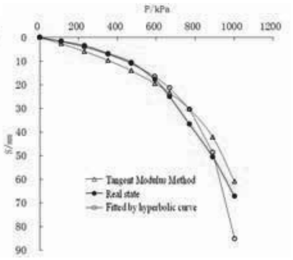

Fig.7 5#footing(1.0m×1.0m)Fig.8 2#footing(1.5m×1.5m)

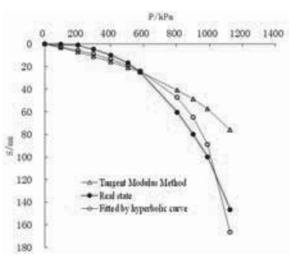

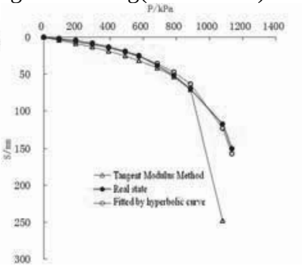

Fig.9 4#footing(2.5m×2.5m)Fig.10 1#footing(3.0m×3.0m)

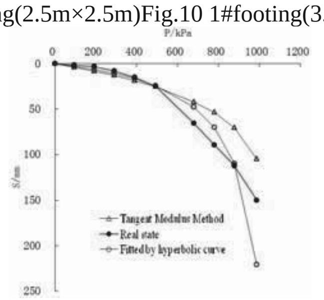

Fig.11 3#footing(3.0m×3.0m)

1.3 *The initial tangent modulus of soil layer determined by pressuremeter test*

The formulation of the initial tangent modulus can be determined by the curve of pressuremeter test:

$$E_{t0} = \frac{(p_l - p_0)}{(p_l - p_0) - (p_f - p_0)} \cdot E_m = \frac{(p_l - p_0)}{(p_l - p_f)} \cdot E_m \quad (6)$$

The initial tangent modulus of foundation E_{to} can be determined by using the corresponding loading interval (p_0, p_1), critical edge pressure p_f , limit pressure p_l and the pressuremeter modulus E_m .

It should be pointed out that the above calculated tangent modulus is the level indicator. If the sand foundation is recognized as isotropic media, then the above calculation results can be used as the vertical indicators in settlement calculation.

According to the typical pressuremeter test curve (PMT-2, the standard method of test execution standard [8]) on loading test sites in Riverside Campus, Texas A & M University, $p_l = 400kP_a$, $p_f = 280kP_a$, $p_0 = 20kP_a$. After substituting in to the above formula, it can get:

$$E_{t0} = \frac{(400-20)}{(400-280)} \cdot E_m = 3.2E_m \quad (7)$$

1.4 *Foundation strength parameters determined by static cone penetration test*

In the process of static cone penetration test (CPT), the foundation soil strength failure occurs. The test data can vividly reflect the strength indicators of the different stratigraphic depths.

If it can figure out the mechanism of the mechanical destruction of the foundation soil by the CPT test, thereby establishing the relationship of the CPT test foundation and strength indicator, it will help to use the CPT data to a more rational extent.

In accordance with the numerical analysis method, it selects different soil strength indicators φ to calculate the tip resistance and lateral resistance, then the total penetration resistance of CPT test is transfered. As to the comparison between $\varphi \sim p_s$ data determined by the numerical analysis and the empirical relationship proposed by the Chinese railway specifications shown in Figure 19, φ determined by the numerical calculation is slightly larger than the value recommended by railway specifications. After fitting the $\varphi \sim p_s$ data by power function, they have good correlation and the fitted empirical relationship is shown as follows:

$$\varphi = 29.352 \times p_s^{0.0915} \tag{8}$$

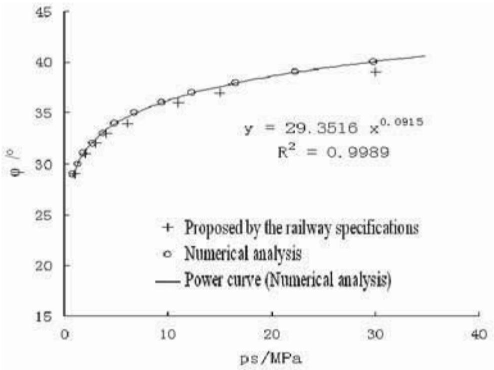

Fig.12 the fitting relationship of $\varphi - p_s$

1.5 *Foundation settlement calculations based on pressuremeter test and the static cone penetration test parameters*

With using the method motioned above, the initial tangent modulus E_{t0} along the depth can be determined by in-situ pressuremeter test, the shear strength indicator along the depth determined by static cone penetration test. With the parameters of tangent modulus method , we calculated the settlement of each footing by layer-wise summation method based on tangent modulus method, and compare with the measured results and the calculated results of each plate by the tangent modulus method when average foundation inversely calculated value E_{t0} =86MPa , φ =36°in the loading test, the result is good. The result of 2# footing is showed as figure 13.

From the settlement of each plate, after using the simple in-situ tests such as pressuremeter test and static cone penetration test to determine the calculated parameters of each foundation layer, the calculated settlement curves match well with the measured curves, which indicates that it is feasible to use pressuremeter test and static cone penetration test to determine the tangent modulus parameters of each foundation layer, thus calculating the nonlinear settlement of the foundation. These ways are easier to be achieved than the plate loading test, as well as easier to obtain the deep soil parameters.

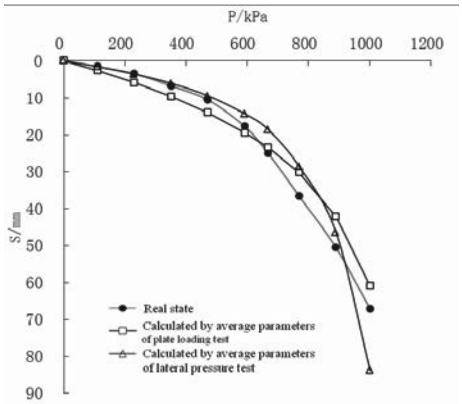

Fig.13 2# footing(1.5m×1.5m)

2 CONCLUSIONS

By analyzing the nonlinear settlement results of five plate loading tests by tangent modulus method on the sand foundation in Riverside Campus, Texas A & M University, this paper shows that the tangent modulus method can calculate the nonlinear settlement of foundation in a better way. At the same time, this paper also seeks more simple in-situ tests such as the static cone penetration test and pressuremeter test to replace the plate loading test to determine the foundation parameters required in nonlinear settlement calculation, which achieves a better effect. Therefore, this paper provides a more convenient way to promote the use of the tangent modulus method to calculate the nonlinear settlement of foundation, which is of great significance to the improvement on the design level of the foundation.

3 REFERENCES

[1] Schmertmann, J. H., Static cone to compute settlement over sand, J. Soil Mech. Found. Div., ASCE, 96(8), 1011, 1970.

[2] YANG Guang-hua. The hyperbolic model for estimating nonlinear settlement of foundation[J].Ground Improvement,1997(1):50-53. (in Chinese)

[3] YANG Guanghua. The simplified nonlinear settlement computation method for soft foundation[J]. Guangdong Water Resources and Hydropower,2001,(1):3–5.(in Chinese)

[4] YANG Guang-hua. Nonlinear settlement computation of the soil foundation with the undisturbed soil tangentmodulus method[J]. Chinese Journal of Geotechnical Engineering, 2006, 28(11): 1927-1931. (in Chinese)

[5] Yang Guanghua, New computation method for soil foundation settlements[J], Journal of Rock Mechanics and Geotechnical Engineering, 2008, (4): 679-686. (in Chinese)

[6] Yang Guanghua, Wang Junhui, Application of undisturbed soil tangent modulus method for computing nonlinear settlement of soil foundation[J], Rock and Soil Mechanics, 2011, 32(S1): 33-37. (in Chinese)

[7] Nonlinear Settlement Computation of the Soil Foundation Based on in-Situ Testing. Guangdong Water Resources and Hydropower. no.7,2010. (in Chinese)

[8] American Society for Testing and Materials Committee on Standard. Standard test method for prebored pressuremeter testing in soils[S]. ASTM D4719, 2000